THE 18TH INTERNATIONAL SYMPOSIUM ON WIRELESS PERSONAL MULTIMEDIA COMMUNICATIONS (WPMC)

3rd GLOBAL WIRELESS SUMMIT GWS-2015

THE 5TH INTERNATIONAL CONFERENCE ON WIRELESS COMMUNICATIONS, VEHICULAR TECHNOLOGY, INFORMATION THEORY, AEROSPACE & ELECTRONIC SYSTEMS (WVITAE)

THE 3rd INTERNATIONAL CONFERENCE ON COMMUNICATIONS, CONNECTIVITY, CONVERGENCE, CONTENT & COOPERATION (IC5)

Proceedings
Volume-2: WPMC-2015
December 13-16, 2015, Hyderabad, India

THE 18TH INTERNATIONAL SYMPOSIUM ON WIRELESS PERSONAL MULTIMEDIA COMMUNICATIONS (WPMC)

3rd GLOBAL WIRELESS SUMMIT GWS-2015

THE 5TH INTERNATIONAL CONFERENCE ON WIRELESS COMMUNICATIONS, VEHICULAR TECHNOLOGY, INFORMATION THEORY, AEROSPACE & ELECTRONIC SYSTEMS (WVITAE)

THE 3rd INTERNATIONAL CONFERENCE ON COMMUNICATIONS, CONNECTIVITY, CONVERGENCE, CONTENT & COOPERATION (IC5)

Proceedings
Volume-1: WVITAE-2015
December 13-16, 2015, Hyderabad, India

Proceedings Co-edited by :

Dr. Ambuj Kumar

Department of Business Development and Technology,
School of Business and Social Sciences
Aarhus University, Herning,
Denmark

Prof. Peter Lindgren

Department of Business Development and Technology,
School of Business and Social Sciences
Aarhus University, Herning,
Denmark

and,

Prof. Ramjee Prasad

Knight ("Ridder") of the order of Dannebrog, a distinguished award by the Queen of Denmark

FELLOW IEEE, IET, IETE, WWRF
Founder President, CTIF GLOBAL CAPSULE
Founder Chair, GISFI
Founder Chair/Co-Chair, GWS/ WPMC Steering Board
Founder President, VISHWANIKETAN

Founder Editor-in-Chief, Int. J. Wireless Personal Communications (Springer)

Distinguished Professor, Department of Clinical Sciences and Translational Medicine, University of Rome "Tor Vergata", Italy

Professor, Future Technologies for Business Ecosystem Innovation (FT4BI), Aarhus University, Herning, Denmark

About Wireless Personal Multimedia Communications (WPMC)

The Wireless Multimedia Personal Communications (WMPC) was inaugurated as a global platform which aims at enabling collaboration in the field of wireless information and multimedia communications. The Wireless Multimedia Personal Communications (WMPC) International Symposium was started way back in 1998, with about 200 participants and about accepted 100 papers. Thereafter, in four years span, the number of participants has reached and exceeded 400 and the number of papers more than 300 for each Symposium. In every WPMC International Symposium, high-quality technical sessions, workshops, tutorials as well as product exhibitions are organized. Since the first WPMC in YRP (Japan), seventeenth WPMCs were held through the world in Asia, Europe, North and South Americas.

In the year 2007, this event was held in Jaipur (India). The quality of the presentations is also very high. It is indisputable that WPMC has become one of the major international conferences in the field of wireless Communications. Some of the themes of earlier Symposia were (i) Communications, Networking and Applications for the Internet of Things, (ii) Autonomous Communication and Networking for Promoting Human Living, and (iii) Orchestrating Wireless Personal Multimedia Communications for Digital Services etc.

Every year is witnessing rapid change in the field of wireless communications with the development and deployment of new technologies and solutions in the field of wireless technologies. Every aspect of wireless communications right from physical layer, resource management including alternative methods of spectrum management, interference management, IoT & M2M, smart antenna, MIMO, multimedia QoS & traffic management, visible light communications, cloud computing, security & privacy, vehicular networks, radio propagation & channel modelling, cognitive radio & SDR, mobile multimedia & mobile TV, wellness & health care, ICT for energy efficiency etc. WPMC is becoming more and more important every year. Against such a backdrop, it was truly gratifying that the 18th International Symposium of WPMC was held in Hyderabad during December, 2015. This Symposium was supported by National Institute of Information and Communications Technology (Japan), and YRP (Japan).

About Global Wireless Summit

The Global Wireless Summit (GWS) had been conceptualized in bringing together wireless media communication/personal communication, etc. The First GWS was successfully held in Princeton (USA), in 2013, followed by the Second one in Aalborg (Denmark), in 2014. As has been the tradition for this Summit, it continues to feature a high-quality technical program across a wide range of research in the wireless communications and related areas. Under the theme "Democratizing Communications", the GWS-15 brought together academia, industry and standardization bodies working on green and secure communication. The conference explored activities, trends and future challenges towards ICT globalization including energy and security issues in existing and future wireless technologies. The Global Wireless Summit-15 presented high-level technical sessions; tutorials, and special sessions on advance topics; workshops; and panel discussions.

Under the theme of 'Democratizing Communications,' the 18th International Symposium on Wireless Personal Communications (WPMC), and the 3rd Global Wireless Summit (GWS) are jointly organized, encompassing the 5th International Conference on Wireless Communication, Vehicular Technology, Information Theory and Aerospace & Electronics Systems (WirelessVITAE), The 12th World Wide Security and Mobility Conference (WWSMC), and the 3rd International Conference on Communications, Convergence, Content and Cooperation (IC5).

About Wireless VITAE

The Wireless Vehicular Technology, Information Theory Aerospace & Electronics Systems (VITAE) is the only international conference broadly addressing the wireless developments in the world by merging the communities from four different IEEE societies. The 1st Conference was held in 2009 in Aalborg (Denmark) followed by 2nd in 2011 in Chennai (India). The 3rd was held in 2013 at Atlantic City, NJ, USA. The 4th was co-located with GWS-2014 in 2014 at Aalborg (Denmark). The primary event in Aerospace, Information Technologies and Databases & Information Systems category centerpieces to Aerospace, Wireless Communication, Information Theory, Vehicular Technology and Electronics Systems issues. Wireless VITAE joined hands with GISFI to provide a platform to gather the different facets of the wireless into a single event and to exchange ideas and knowledge among the different research communities that address the various aspects of the wireless theme. The International Wireless VITAE conference is Global one that addresses the trends, challenges and future roadmaps within a conglomerate of existing and novel wireless technologies, including cellular, short-¬range, sensor and embedded ones. Cognitive and self-¬organizing networks, nano-sensors, positioning and localization, Internet of Things (IoT), positioning and localization, recent advances in information theory and its applications, space technology for very high data rates, and techno-¬economic aspects of telecommunications are part of the scope, among others.

Committee Members

RAMJEE PRASAD,

- Steering Board Chair/Co-Chair of WPMC, GWS, and Wireless VITAE;
- Founder Director, CTIF Global Capsule (CGC), Aarhus University, Herning, Denmark;
- Founder Chairman, Global ICT Standardisation Forum for India (GISFI).

RATNAM VARADA RAJAKUMAR,
General Chair, Global Wireless Summit 2015
Director, Indian Institute of Technology,
Bhubaneswar, Odisha, India

ASHOK CHANDRA,
Executive Chair, TPC , Global Wireless Summit 2015
Former Wireless Adviser to the Government of India

Masao Sakauchi,
President, National Institute of Information and Communications Technology, Japan
WPMC Organizing Committee

Mitsutoshi Hatori,
Chairman, YRP R&D Promotion Committee, Japan
WPMC Organizing Committee

Shingo Ohmori
Co-chair of WPMC Steering Board
President, YRP International Alliance Institute, Japan
Vice President, YRP R&D Promotion Committee, Japan
WPMC Organizing Committee

NEELI R. PRASAD,
TPC Co-Chair, Global Wireless Summit 2015
International Technological University (ITU), USA

ERNESTINA CIANCA,
Publication Chair, Global Wireless Summit 2015
University of Rome Tor Vergata, Italy

AMBUJ KUMAR,
Web Co-chair, Global Wireless Summit 2015
Aarhus University, Denmark

Welcome Speeches

On behalf of the Steering Committee of the WPMC 2015, Global Wireless Summit (GWS) 2015, and Wireless VITAE 2015, it is my great pleasure to bid you all a warm welcome to these highly renowned events in the beautiful historic city of Hyderabad, India.

Under the theme of '**Democratizing Communications**,' the 18th International Symposium on Wireless Personal Communications (WPMC) and 3rd Global Wireless Summit (GWS) are jointly organized, encompassing the 5th International Conference on Wireless Communication, Vehicular Technology, Information Theory and Aerospace & Electronics Systems (Wireless VITAE), The 12th World Wide Security and Mobility Conference (WWSMC), and the 3rd International Conference on Communications, Convergence, Content and Cooperation (IC5).

Wireless communications have evolved over the years to open great potential for monetizing on multimedia data and diversified user-generated content, making them a ubiquitous means of connecting people and businesses. Democratization of hardware, software and connectivity is the necessary enabler to benefit all stakeholders and provide a stable platform for creating profits out of technology disruption.

The setting of WPMC 2015 jointly with GWS2015 was in the heart of the City of Pearls, as Hyderabad historically been known for its blooming pearl industry. Today, Hyderabad is also a major center for the technology industry. The WPMC and GWS2015 program featured an unusually distinguished group of keynote and invited speakers, as well as a strong technical program with novel research contributions from the relevant thematic areas from all over the world. In addition, an extensive list of social events were scheduled to allow for a break from the exciting technical sessions. Please, take the advantage of the many opportunities to network and expand your technical and cultural horizons.

I would like to extend my appreciation to my global colleagues for their dedication and effort to put together a strong event.

Ramjee Prasad,

Steering Board Chair/Co-Chair of WPMC, GWS, and Wireless VITAE

It is my great pleasure to host the 18th International Symposium on Wireless Personal Multimedia Communications (WPMC'15) in Hyderabad, India.

The WPMC symposia series first commenced in 1998, as a unique international conference dedicated to wireless multimedia communications aiming for global collaboration. In cooperation with YRP, we hold the symposium in a location in Asia, Europe, America or Australia each year.

This year's host country, India, has shown remarkable developments in the information and communications technology (ICT) field, in particular, in mobile phones, since the 10th WPMC Symposium held in Jaipur in 2007. During that time attention to wireless technology has also increased and a broad range of R&D activities have been advanced. Against such a backdrop, it is truly gratifying that the WPMC Symposium is being held here.

As Japan's sole national research institute in the field of ICT, the National Institute of Information and Communications Technology (NICT), promotes research and development in fundamental technologies in the fields of networks, including wireless communication, universal communication, advanced ICT, and electromagnetic sensing. Through these technologies, we aim to contribute to improving and resolving various challenges that society faces.

In particular, NICT positions big data of a public nature that helps to contribute to society as "Social Big Data." We focus on R&D of such Social Big Data, with the goal of having it used throughout society as social infrastructure, and ensuring that the knowledge and information gained from it is further disseminated. Additionally, efforts leading to the Internet of Things (IoT) and Internet of Everything (IoE), where all things and all data become connected, are advancing, and NICT is actively contributing to the IoT Acceleration Consortium, which represents Japan's efforts in this area, and its technology development working group, the Smart 'IoT Acceleration Forum'. Furthermore, learning from the response to the Great East Japan Earthquake that devastated Japan in March 2011, we are also engaging in research and development to swiftly deploy a wireless telecommunications network in the aftermath of a disaster.

For this symposium, NICT has set up a Wi-SUN workshop, 5G workshop, and Resilient Wireless Network Technologies workshop as themes related to such areas of research and development at this symposium. Currently, data gathering through networks using wireless technology is being conducted in various fields and industries across the globe. At the same time, the diversification of ICT had made wireless communications technology increasingly available to people. Given this situation, I believe that holding

this ICT workshop here in India will be extremely effective and holds great significance.

Lastly, I sincerely hope that WPMC'15 will be a significant forum that promotes extensive collaborations and interchanges among those engaged in the R&D of wireless communications, towards the realization of a society where people can live with a sense of security and comfort.

Masao Sakauchi,

President, National Institute of Information and Communications Technology, Japan

On behalf of YRP R&D Promotion Committee, one of the co-organizers of the 18th International Symposium on Wireless Personal Multimedia Communications (WPMC 2015), it is my great pleasure to welcome you in Hyderabad, India.

Since the first WPMC was held in our Yokosuka Research Park (YRP), Japan, in 1998, this symposium had been held in various cities in the world every year providing researchers of wireless communications with opportunities to gain new knowledge and information and also to exchange with each other. We are excited that this year the WPMC is held in India for the second time after the WPMC 2007 held in Jaipur owing to the great cooperation of Global ICT Standardization Forum in India (GISFI), Indian Institute of Technology Bhubaneswar and Kharagpur, Jawaharlal Nehru Technological University Hyderabad, and other Indian colleagues, and we truly appreciate hard work and great efforts of all people concerned. YRP has developed as an international R&D hub for radio and telecommunications technologies since its establishment in 1997. Currently, about 58 organizations with 5,200 researchers and engineers gather in YRP, and the member of our Committee, one of the promoting bodies of YRP, has reached to around 150. We have also concluded memorandums of understanding for research exchange with research parks and ICT institutions, totaling 51 organizations in 15 countries and one region.

Now, in YRP, in addition to the R&D of the 4th generation mobile communication systems, discussions and studies on the 5th generation mobile communication systems that are to be introduced in 2020 are under way. In Broadband Wireless Forum, which was established in our Committee in 2009, discussions on practical application of wireless power transmission technologies are going on, and last year in May, we also established a new Committee to promote application of Wireless Smart Utility Network, Wi-SUN. YRP intends to use the fruits of these activities as a foothold to lead the world's R&D in ICT and further enhance YRP's function. We also would like to further strengthen wide-ranging international collaboration encompassing Europe, America, Asia and Oceania, and other regions, and we expect WPMC to be the very important platform for international exchange.

I hope that this WPMC2015 will be fruitful and enjoyable to all participants.

Mitsutoshi Hatori,

Chairman, YRP R&D Promotion Committee, Japan

At the outset, as the Executive Chairman of the Technical Program Committee (TPC) of the third Global Wireless Summit (GWS-2015), it gives me an immense pleasure to heartily welcome you to this Summit being held in the City of Hyderabad, India during December 13-16, 2015.

The Global Wireless Summit (GWS) has been conceptualized in bringing together wireless media communication/personal communication, etc. The First GWS was successfully held in Princeton (USA), in 2013, followed by the Second one in Aalborg (Denmark), in 2014. Under the theme "Democratizing Communications", the GWS-15 brings together academia, industry and standardization bodies working on green and secure communication. The conference will explore activities, trends and future challenges towards ICT globalization including energy and security issues in existing and future wireless technologies.

Global Wireless Summit 2015 is hosting 18th International Symposium on Wireless Personal Multimedia Communications (WPMC); 5th International Conference on Wireless Communications, Vehicular Technology, Information Theory Aerospace & Electronics Systems (WirelessVITAE) 2015, IC5 and World Wide Security & Mobility Conference (WWSMC). The WPMC-15 and WirelessVITAE 2015 are the major events and both are held second time in India. The 1st International Symposium on WPMC was held in 1998, and since then it is held every year with an objective of providing a 'global platform' for discussions on the latest trends in the wireless multimedia communications. In the year 2007, this event was held in Jaipur (India). Wireless VITAE is the only international conference broadly addressing the wireless developments in the world by merging the communities from four different IEEE societies. The 1st Conference was held in 2009 in Aalborg (Denmark) followed by 2nd in 2011 in Chennai (India).

The Global Wireless Summit-15 presented high-level technical sessions; tutorials, and special sessions on advance topics; workshops; and panel discussions. All the submitted contributions received for technical and special sessions have been thoroughly reviewed by the TPC including other leading experts and only the best quality of papers have been accepted for presentations. It may be mentioned that each paper was reviewed by at least three experts. TPC of GWS-15 has 15 Co-chairs and over 70 members, from a wide variety of academic, industrial, and research organizations around the globe.

As has been the tradition for this Summit, it continues to feature a high-quality technical program across a wide range of research in the wireless communications and related areas.

I would like to take this opportunity to profoundly thanks the TPC Co-chairs; TPC members; Chairpersons of Special Sessions, Workshops; reviewers; and authors.

I request you all to take the advantage of this grand Summit and have thought provoking 4 days in the City of Hyderabad.

Ashok Chandra

Technical Program Committee (TPC) Executive Chair, WPMC 2015 and GWS 2015

Former Wireless Adviser to the Government of India

Welcome to Hyderabad, India to join WPMC2015.

On behalf of the Steering Board of WPMC, I would like to express my deep gratitude to all the delegates for coming from all over the world, and expect you will be having exciting experiences at WPMC2015 in Hyderabad.

The WPMC2015 is the 18th WPMC held for the second time in India, one of the most fantastic and attractive countries in the world.

The WPMC was inaugurated in 1998 to establish a global platform for mutual cooperation and discussions in the field of wireless multimedia communications with a strong financial supports by National Institute of Information and Communications Technology (NICT). The first WPMC was held at Yokosuka Research Park (YRP) in Japan in honor of the opening of YRP in 1997.

Since the first WPMC in YRP, seventeenth WPMCs were held through the world in Asia, Europe, North and South Americas.

With the continued and close support by numerous organizations and human relationships, the WPMC has grown into an international symposium widely recognized by industries and academic societies.

I wish to take this opportunity to thank all supporting committee members and staffs of WPMC2015, especially for General Chair, Prof. R.V Rajakumar, Director IIT Bhubaneswar, India, and TPC Chair, Dr. Ashok Chandra, Former Wireless Advisor, to the Government of India.

Shingo Ohmori

Co-chair of WPMC Steering Board

President, YRP International Alliance Institute, Japan

Vice President, YRP R&D Promotion Committee, Japan

Venue Map

Central Events

09:30-11:30

December 14-16, 2015

Workshops and Special Sessions

11:30 until End of the day

December 14-16, 2015

1.1 & 1.2

HICC
GROUND FLOOR PLAN

Technical Papers, 11:30 until End of the day, **December 14-16**

Workshops and Special Sessions, 11:30 until End of the day, **December 14-16**

Rooms: MRG .01 to MRG .06

ENTRANCE TO THE HICC & CONFERENCE HALL

Please Contact GWS Event Management Personnel or HICC Reception for queries and guide to HALLS/ Rooms

Program at a Glance

Sunday, December 13

Day 1

"Tutorials"

Time Slot	Day1: Sunday, December 13| Tutorials	
08:30-19:00	Registration	
	Morning Tutorial Session	
09:00-13:30 Coffee Break 11:00-11:30	**WPMC Tutorial Session on "TV White Space for Affordable Broadband Access "** **Kentaro Ishizu**, *National Institute of Information and Communications Technology*, **Japan; Abhay Karandikar,** *Indian Institute of Technology Bombay*, **India; Takeshi Matsumura,** *National Institute of Information and Communications Technology*, **Japan**	**MR 2.01**
	WPMC Tutorial Session on "Optimal Filtering and Parameter Estimation Techniques for Statistical Models" **Laxminarayana Pillutla,** *Dhirubhai Ambani Institute of Information and Communication Technology*, **India**	**MR 2.02**
	WPMC Tutorial Session on " Antennas for Millimeter-wave Wireless Communications" **T Rama Rao,** *SRM University*, **India**	**MR 2.03**
	WVITAE Tutorial Session on "IoT and Low Voltage Analog Design for Wireless Applications" **Sudhanshu S. Jamuar,** *University Malaysia Perlis*, **Malaysia**	**MR 2.04**
	WVITAE Tutorial Session on "Energy-Spectral Efficiency in Cooperative Cognitive Radio Network with Challenges in Security" **Santi Prasad Maity,** *Indian Institute of Engineering Science and Technology, Shibpur*, **India**	**MR 2.05**
13:30-14:30	**LUNCH**	
	Afternoon Tutorial Session	
14:30-18:30 Coffee Break 16:30-17:00	**WPMC Tutorial Session on "Road to 5G Wireless Systems: Challenges Ahead vis-à-vis Progress Made "** **Amitava Mukherjee,** *IBM Pvt. Limited*, **India; Debashis Saha,** *Indian Institute of Management Calcutta*, **India**	**MR 2.01**
	WPMC Tutorial Session on "Wireless Channel Impairments Removal Techniques" **Sanjay Kumar,** *Birla Institute of Technology*, MESRA , **India**	**MR 2.02**
	WVITAE Tutorial Session on "Transmission Technologies for 5G" **Suvra Sekhar Das,** *Indian Institute of Technology, Kharagpur*, **India**	**MR 2.03**
	WVITAE Tutorial Session on "Visible Light Communication for Road Safety in the Intelligent Transportation Systems" **Navin Kumar,** *Amrita University & School of Engineering*, **India**	**MR 2.04**
	WVITAE Tutorial Session on "ICT for Health Care" **Vishwanath Sinha,** *M. N. National Institute of Technology, Jaipur,* **India**	**MR 2.05**
19:00-20:00	Welcome Reception in Foyer/ Pool Side Lawns	

Monday, December 14

Day 2

"Workshops, Special Sessions, Contributed Papers"

Time Slot	Day2: Monday, December 14 | Grand Opening Program		
08:30-19:00	**Registration**		
09:00-10:00	**GRAND OPENING**		**HALL 1**
	Ceremony	**Lighting of the Lamp Ceremony: Presided by B.N. Bhandari, Local Organizing Chair, WPMC/ GWS 2015**	
	Welcome Speech	**Ratnam Varada Rajakumar**, *General Chair*, WPMC/GWS 2015	
	Inaugural Speech	**Ramjee Prasad**, *Steering Board Chair/Co-Chair of WPMC, GWS and Wireless VITAE; Founder Chair, GISFI*	
	Introduction Speech	**Ashok Chandra, TPC Executive Chair, WPMC/ GWS 2015**	
	Opening Speech-1	**Fumihiko Tomita**, Vice President, *NICT*, **Japan**	
	Opening Speech-2	**Mitsutoshi Hatori**, Chairman, *YRP*, **Japan**,	
	Opening Speech-3	**Smriti Dagar**, *President, IETE*, **India**	
	Round Table Discussions: "India Knowledge Economy- Transformation through Digitization and Innovation"		
10:00-11:00	**Discussion**	Moderator:-**Sudhir Dixit**, WWRF, **USA**, **Anand R. Prasad**, NEC Corporation **Japan,** **Dina Simunic,** *University of Zagreb***, Croatia** **Ashok Chandra,** *TPC Executive Chair, WPMC/ GWS 2015*, **India** **Kiritkumar Lathia, GISFI/CTIF, Denmark,**	
	Vote of Thanks	**Sandip Inamdar**, Finance Chair, **WPMC/ GWS 2015**	
11:00-11:30	**Coffee Break**		
11:30-19:00		**Technical Sessions**	
19:30-22:30	END of DAY 2 || Cultural Program (Mridangam and Kuchipudi Group Dance Recital), GALA DINNER & Best Paper Award: HALL1		

Time Slot	Day2: Monday, December 14 || HALL 1.1 Activities || Workshops & Special Sessions (I-A)		
08:30-19:00	Registration		
09:00-11:00	**GRAND OPENING**		**HALL 1**
11:00-11:30	**COFFEE BREAK**		
11:30-13:30	**WPMC Special Session on "Mobile applications for Management of the Digital Business, Implications for the Infrastructures and Organisations"** **Session Organizer and Chair: Zoran Veljovic,** *University of Montenegro,* **Montenegro**		HALL 1.1
	Invited Talk	Manufacturing and Standardization in India**, Arun Golas**, *former DDG, Ministry of Communications, Government of India, New Delhi,* **India**	
	1570231052	Dynamic Pathloss Model for Future Mobile Communication Networks; **Ambuj Kumar, Albena Mihovska, Ramjee Prasad**; *CTIF, Aalborg University,* **Denmark**	
	1570228076	Challenges and Opportunities for Enhancing User Privacy and User Empowerment; **Prashant Dhotre, Samant Khajuria , Henning Olesen**; *Center for Communication, Media and Information Technologies (CMI),Aalborg University Copenhagen,* **Denmark (***)**	
	1570228069	Sensitive Association Rules Hiding Methods: A Survey; **Geeta Navale, Suresh Mali**; *Sinhgad Institute of Technology and Science, Pune,* **India**	
13:30-14:30	LUNCH		
14:30-16:30	**WPMC Workshop on "Vision and research activities toward the Fifth Generation Mobile Systems (5G)"** **Workshop Organizer and Chair: Kentaro Ishizu,** *Association of Radio Industries and Businesses (ARIB) & National Institute of Information and Communications Technology (NICT),* **Japan**		HALL 1.1
	Activities on 5th Generation Mobile Communications System in Japan ;**Kohei Sato;** *Association of Radio Industries and Businesses (ARIB),* **Japan**		
	5G Prospects in India; **VikramTiwathia**; *The Cellular Operators Association India (COAI),* **India**		
	5G research activities and key enabling technologies ;**Haesik Kim**; *VTT,* **Finland**		
	Small-cell Structured Wireless Networks for 5G: Centralized vs Decentralized Architecture ;**Fumiyuki Adachi**, *Tohoku University,* **Japan**		
	The Unified 5G Platform; **J. VinoshBabu James**, *Qualcomm,* **India**		
16:30-17:00	COFFEE BREAK		
17:00-19:00	**WPMC Special Session on "Combedded Systems"** **Session Organizer and Chair: Abhay Gandhi,** *Viswesarayya National Institute of Technology, Nagpur,* **India**		HALL 1.1
	1570227356	Artificial intelligence auto-mobility in material handling & fork-lift manufacturing; **Ajinkya Vasant Nichit①, Kedar S. Joshi①, Sachin B. Rao ②, Sushant S. Gaidhani ①, Shrinivas Vasantrao Shinde③**; ①*Sandip Institute Of Engg, & Management, Nashik,* ②*G.H. Sapat College Of Engg., Nashik,* ③*Jawahar Institute Of Technology, Nashik;* **India**	
	1570227801	Interference Analysis and Mitigation Techniques in Wireless Body Area Network; **Subhojit Moitra, P.H.Ghare, A.G. Kothari**; *VNIT, Nagpur,* **India**	
	1570227808	Implementation of Low Cost IoT Based Smart Home using Open Source Platform; **Varun Tiwari, Avinash Keskar** □; *Visvesvaraya National Institute of Technology, Nagpur,* **India**	
	1570227846	Performance Comparison of DCT based Entropy Coding Techniques; **Samruddhi Y. Kahu, Kishor M. Bhurchandi**; *Visvesvaraya National Institute of Technology, Nagpur,* **India**	
	1570227857	UWB Sensing antenna, Reconfigurable transceiver and antenna based Cognitive Radio Test bed; **S. Manoj, Sumin. D. Joseph**□, **Chetan. Waghmare, Nandakumar. K., Ashwin Kothari**; *Department of Electronics VNIT, Nagpur,* **India**	
	1570227987	Methods of Frequency Offset Estimation in OFDM Based System; **A. P. Rathkanthiwar①, A.S.Gandhi②**; ①*Priyadarshini College of Engineering Nagpur,* ②*Visvesvaraya National Institute of Technology, Nagpur* , **India**	
19:30-22:30	END of DAY 2 || Cultural Program (Mridangam and Kuchipudi Group Dance Recital), GALA DINNER & Best Paper Award: HALL1		

Time Slot	Day2: Monday, December 14 || HALL 1.2 Activities || Workshops & Special Sessions (I-B)		
08:30-19:00	Registration		
09:00-11:00	**GRAND OPENING**		**HALL 1**
11:00-11:30	**COFFEE BREAK**		
11:30-13:30	**WVITAE Special Session on " mHealth and Medical Informatics"** **Session Organizer and Chair: Albena Mihovska, Aalborg University, Denmark**		HALL 1.2
	Opening Talk	**Shyam Chakrabortty,** *Oy Trinnect Ltd.,* **Finland**	
	Invited Talk	Role of ICT for the Advancement of Dentistry **, Gianpaolo Sannino,** *University of Rome, Tor Vergata,* **Italy**	
	Invited Talk	Patient centered learning and Early clinical exposure of medical students to 'Diabetes and Metabolic syndrome**, Yogesh Sharma①, Ankur Joshi②, Dept of Medicine③, Rakesh Biswas;** *①LNMCH,②dept of Medicine, GMC,③dept of Medicine, LNMCH;* *Bhopal Madhya Pradesh*, **India**	
	Invited Talk	Review of telemedicine technologies in India**, Sumit Gautam***①***, Shyam Chakraborty②;** *① IIIT Hyderabad, India;* ***②****Trinnect Ltd.,* **Finland**	
13:30-14:30	LUNCH		
14:30-16:30	**WPMC Workshop on "Resilient Wireless Network Technologies" (I)** **Workshop Organizer and Chair: Ryu Miura,** *National Institute of Information and Communications Technology (NICT)*, **Japan**		HALL 1.2
	1570213366	On-going Field Experiment of NerveNet in Shirahama Town for Resilient Town Network; **Masugi Inoue, Yasunori Owada , Kiyoshi Hamaguchi** *; Resilient ICT Research Center,* *National Institute of Information and Communications Technology (NICT)*☐, **Japan**	
	1570213263	Pilot testing and demonstration of self-management network and applications by NerveNet; **Yasunori Owada , Kiyoshi Hamaguchi, Masugi Inoue;** *Resilient ICT Research Center,* *National Institute of Information and Communications Technology (NICT)*☐, **Japan**	
	1570213055	Development and Field Experiment of Distributed Peer Aware Communication Networks; **Lin Shan, Huan-Bang Li, Takashi Matsuda, Ryu Miura**; *Wireless Network Research Institute, National Institute of Information and Communications Technology (NICT)*☐, **Japan**	
	1570213332	A hybrid multi-hop network by small-unmanned aircraft and satellite telecommunication systems; **Fumie Ono①**; **Byeong-pyo Jeong②, Yasunori Owada②, Shan Lin ①, Ryu Miura①**; *①Wireless Network Research Institute,* ***②****Resilient ICT Research Center, National Institute of Information and Communications Technology (NICT)*☐; **Japan**	
16:30-17:00	COFFEE BREAK		

16:30-17:00	(Continued: Hall 1.2 Activities) COFFEE BREAK		
17:00-19:00	**WPMC Workshop on "Resilient Wireless Network Technologies" (II)** **Workshop Organizer and Chair: Ryu Miura,** *National Institute of Information and Communications Technology (NICT)***, Japan**		HALL 1.2
	1570213462	QZSS SS-CDMA Location and Short Message Communication System; **Noriharu Suematsu, Suguru Kameda, Yuji Miyake, Tomohide Takahashi , Akinori Taira, Tadashi Takagi, Kazuo Tsubouchi**; *Research Institute of Electrical Communication, Tohoku University*, **Japan**	
	1570213016	Disaster Countermeasure Experiments using WINDS; **Takashi Takahashi①, Kazuyoshi Kawasaki①, Akira Akaishi①, Toshio Asai①, Maki Akioka①, Tomoshige Kan①, Morio Toyoshima①, Byongpyo Jeong②, Hajime Susukita②, Shuji Murakami②**; ①*Wireless Network Research Institute,* ②*Resilient ICT Research Center; NICT,* **Japan**	
	1570195491	A Path Ordering and Reference Selection Method for the Differential Delay Tomography; **Takehiro Otsuka① , Shinsuke Hara①②, Takahiro Matsuda③②, Kenichi Takizawa③, Fumie Ono‡ , Ryu Miura‡**; ①*Graduate School of Engineering,* ②*Osaka City University,* ③ *Graduate School of Engineering, Osaka University*; **Japan**	
	1570205987	Experimental Evaluation on Wireless Tomography with Compressed Sensing in a Three-Dimensional Space**; Kengo Yokota; Kengo Yokota① , Shinsuke Hara① , Takahiro Matsuda②, Masaki Mukamoto②, Yuki Uemura②, Kenichi Takizawa③, Fumie Ono④, Ryu Miura④** □; ①*Graduate School of Engineering, Osaka City University ,Sugimoto, Sumiyoshi-ku, Osaka,* ②*Graduate School of Engineering, Osaka University 2-1 Yamadaoka, Suita, Osaka,* ③*Strategic Planning Office, National Institute of Information and Communications, Koganei, Tokyo ,* ④*Wireless Network Research Institute, National Institute of Information and Communications Technology ,Kanagawa*; **Japan**	
19:30-22:30	END of DAY 2 || Cultural Program (Mridangam and Kuchipudi Group Dance Recital), GALA DINNER & Best Paper Award: HALL1		

Time Slot	Day2: Monday, December 14 || MRG .01 Activities || Contributed Papers: Cognitive Radio Networks and Spectrum Management (I)		
08:30-19:00	Registration		
09:00-11:00	**GRAND OPENING**		**HALL 1**
11:00-11:30	COFFEE BREAK		
11:30-13:30	**Cognitive Radio Networks and Spectrum Sensing & Management (I-A) | CRN, Relay and Routing : WVITAE & WPMC || *Session Chair: K.T.V. Reddy, TPC Chair, IETE, India***		MRG .01
	1570213275	C2R2M: Cluster-based Cognitive Radio Routing Mechanism; **Shriram Kulkarni, Shriram Markande**; *University of Pune*, **India**	
	1570209919	Adaptive Cooperative Spectrum Sensing and Access in Cognitive Radio Networks; **Kayalvizhi G;** *SSN College of Engineering*, **India**	
	1570212756	Evaluation of Channel Assembling Strategies with Single-Class Users in Cognitive Radio Networks; **Ebenezer Esenogho, Tom Walingo**; *University of KwaZulu-Natal*, **South Africa**	
	1570188607	Evaluating the Effect of Selfishness on Flooding Based DTN Routing Algorithms; **C Sobin**, **Vaskar Raychoudhury**; *IIT Roorkee*, **India**	
	1570213104	**WPMC:** Throughput of Secondary User in Underlay Cognitive Relay Network with Energy Harvesting; **Binod Prasad, Sanjay Dhar Roy, Sumit Kundu**; *National Institute of Technology, Durgapur*, **India**	
	1570207535	**WPMC:** Quality of Service Enforcing Centrally Optimized Routing for Delay Tolerant Networks; **Abhishek Thakur, Chittaranjan Hota**; *BITS Pilani, Hyderabad Campus* , **India**	
13:30-14:30	LUNCH		
14:30-16:30	**Cognitive Radio Networks and Spectrum Sensing & Management (I-B): WPMC || *Session Chair: Masahiro Umehira, Ibaraki University, Japan***		MRG .01
	1570193943	A Compressive Sensing-based Channel Estimation via GAMP in FBMC/OQAM System; **Meng Lin, Yunzhou Li, Limin Xiao, Yan Zhang, Xibin Xu, Jing Wang**; *Tsinghua University*, **China**	
	1570206001	New Pricing Model for Dynamic Dual-operator Spectrum Sharing in GSM; **Meghan Saitwal, Yuva Kumar, Brij Mohan Baveja, Mohammed Zafar Ali Khan, Uday B Desai;** *Indian Institute of Technology, Hyderabad*, **India**	
	1570192957	Improved p-norm Energy Detector with Soft Combining in AWGN Channel for Spectrum Sensing; **Vaibhav Kumar, Deep Kandpal, Ranjan Gangopadhyay, Soumitra Debnath;** *L.N.Mittal Institute of Information Technology, Jaipur*, **India**	
	1570213925	Selective Sensing Framework for Opportunistic Mobile Phone Sensing Networks; **Thejaswini M, Pachamuthu Rajalakshmi, Uday B Desai**; *Indian Institute of Technology, Hyderabad*, **India**	
	1570193867	Investigation on Listen-Before-Talk Mechanism of Licensed-Assisted Access to Unlicensed Spectrum; **Yu Jiang①, Hiroki Harada②, Liu Liu①, Huiling Jiang① ,Satoshi Nagata††**; ① *DOCOMO Beijing Communications Laboratories Co., Ltd*, **China**, ② *NTT DOCOMO, INC*, **Japan**	
	1570213278	CDF Based Spectrum Occupancy Rate Measurement Using Least Square Estimation of Gaussian Noise Period; **Shota Rachi, Akira Saito, Masahiro Umehira, Shigeki Takeda;** *Ibaraki University*, **Japan**	
16:30-17:00	COFFEE BREAK		

16:30-17:00	(Continued: MRG .01 Activities) COFFEE BREAK		
17:00-19:00	**Cognitive Radio Networks and Spectrum Sensing & Management (I-C): WPMC** ***||Session Chair: Sumit Kondu, NIT DurgapurA Leti, France***		MRG .01
	1570208599	Detection Performance of Soft Data Fusion in Rician Fading Channel for Cognitive Radio Network; **Srinivas Nallagonda[1][2], V Chandra Sekhar[1], Aniruddha Chandra[3][4], Sanjay Dhar Roy[4], Sumit Kundu[4];** *[1]M V S R Engineering College ,[2]Osmania University,[3]Brno University of Technology, [4]National Institute of Technology, Durgapur, WB*;**[1][2][4]India, [3]Czech Republic**	
	1570213378	Evaluation of permutation entropy detection for cognitive radio networks; **Srinu Sesham, Amit Kumar Mishra**; *University of Cape Town, Cape Town*, **South Africa**	
	1570208853	Optimization of Cooperative Spectrum Sensing in Cognitive Radio over Erroneous Reporting Channel; **Narasimha Rao Banavathu, Mohammed Zafar Ali Khan**; *Indian Institute of Technology, Hyderabad*, **India**	
	1570213111	Distributed Token Based MAC for Multi-Channel Multi-Interface Cognitive Radio WMN; **Mohammed A R Quadri, Ramesh Babu Battula, Manoj Singh Gaur, Dinesh Gopalani, Meenakshi Tripathi**; *Malaviya National Institute of Technology Jaipur*, **India**	
	1570209789	Path and Load Aware Routing Algorithm for Cognitive Radio Wireless Mesh Network**; Ramesh Babu Battula, Manoj Singh Gaur, Dinesh Gopalani, Emmanuel Shubhakar Pilli**; *Malaviya National Institute of Technology, Jaipur*, **India**	
	1570213374	Fractal dimension of spectral estimates for spectrum sensing under noise variance uncertainty; **Srinu Sesham[1], Amit Kumar Mishra[1], Siba Kumar Udgata [2], Samrat Sabat[2]**; *[1]University of Cape Town, Cape Town* ,**South Africa,** *[2]University of Hyderabad, Hyderabad*, **India**	
19:30-22:30	END of DAY 2 || Cultural Program (Mridangam and Kuchipudi Group Dance Recital), GALA DINNER & Best Paper Award: HALL1		

Time Slot	Day2: Monday, December 14 || MRG .02 Activities || Contributed Papers: Next Generation Networks & Internet of Things (I)		
08:30-19:00	Registration		
09:00-11:00	**GRAND OPENING**		**HALL 1**
11:00-11:30	COFFEE BREAK		
11:30-13:30	**Next Generation Networks (I-A) | 5G and Device to Device Communications: WPMC || *Session Chair: Sri Ganesh Rao, Tata Consultancy Services, Bangalore, India***		MRG .02
	1570194953	The impact of Network Neutrality on the OTT Service of 5G WISDOM; **Yapeng Wang, Ramjee Prasad**; *Center of TeleInFrastrukur, Aalborg University,Aalborg*, **Denmark**	
	1570206855	Efficient Device-to-Device (D2D) Offloading Mechanism in LTE Networks; **Bighnaraj Panigrahi, Rashmi Ramamohan, Hemant Kumar Rath, Anantha Simha**; *Tata Consultancy Services*, **India**	
	1570208181	Survey of Device-to-Device Communications Infrastructure-less in IEEE 802.15.8 Task Group; **Marco Hernandez, Ryu Miura**; *NICT*, **Japan**	
	1570208909	Link Adaptation Strategies for Cellular Downlink with low-fixed-rate D2D Underlay; **Afonso Eduardo, Ivo Sousa, António J. Rodrigues**; *Instituto de Telecomunicações (IT) Instituto Superior Técnico (IST), Universidade de Lisboa Lisbon*, **Portugal**	
	1570210057	A Pattern Division Multiple Access Scheme for 5G wireless communication systems; **Zhang Kai, Jin Xu**; *Beijing University of Posts and Telecommunications*, **China**	
	1570213212	Coexistence of Systems with Different Multicarrier Waveforms in LSA Communications; **Mirza Golam Kibria, Gabriel Porto Villardi, Kentaro Ishizu , Fumihide Kojima**; *Wireless Network Research Institute, National Institute of Information and Communications Technology*, **Japan**	
13:30-14:30	LUNCH		
14:30-16:30	**Next Generation Networks (I -B) | Spectrum Issues and Intelligent Approach: WVITAE || *Session Chair: S.K. Agarwal, Former Director, DIETY, Government of India, India***		MRG .02
	1570213573	Spectrum Scarcity at the Extensive and Intensive Edges: From White Space to 5G; **Benoît Pierre Freyens**; *University of Canberra*, **Australia**	
	1570210051	Real Time Evaluation of Energy Detection and Covariance based Spectrum Sensing Algorithms; **Sunil Devanahalli, Samrat Sabat**; *University of Hyderabad*, **India**	
	1570213985	Self Configurable Intelligent Distributed Antenna System; **Ambuj Kumar, Albena Mihovska, Ramjee Prasad**; CTIF, *Aalborg University*, **Denmark**	
	1570209885	Distributed Forward-Backward Pursuit Algorithm for Distributed Compressive Sensing; **Suchithra Sudhakaran, Neelakantan PC**; *Adi Shankara College of Engineering and Technology*, **India**	
	1570210103	Spectrum for 5G Services; **Purnendu Shekhar Mani Tripathi①②, Ramjee Prasad②**; ①*Ministry of Communications* & IT, **India**, ②*Centre for TeleInFrastructure(CTiF),Aalborg University, Aalborg*, **Denmark**	
	1570209977	On Performance of Eigenvalue based Detectors for Spectrum Sensing under Different Fading Conditions; **Ashwini Deshmukh①, Madhukar Deshmukh②, Flemming Bjerge Frederiksen②, Ramjee Prasad②③**; ①*Trinity College of Engineering Research Pune*, **India**, ②*RATE, Department of Electronic Systems,* ③*CTIF; Aalborg University*, **Denmark**	
16:30-17:00	COFFEE BREAK		

16:30-17:00	(Continued: MRG .02 Activities) COFFEE BREAK		
17:00-19:00	**Next Generation Networks (I- C) | Future Vision and IoT: WVITAE & WPMC ||*Session Chair: Raja Rajeswari, IETE, India***		MRG .02
	1570213430	Access for Internet of Things using Smartphone as a Gateway utilizing LTE and WiFi; **Prateek Mathur[1], Rasmus Hjorth Nielsen[2], Neeli Rashmi Prasad[3], Ramjee Prasad[1]**; *[2]Cisco Systems* , **USA,** *[3]Center for TeleInFrastructure (CTIF)*, **USA**, *[1]Center for TeleInFrastructure (CTIF), Aalborg University*, **Denmark**	
	1570213454	Cognitive framework for flexible queuing strategy in Next Generation Networks; **Hanuma Chitti[1], Neeli Rashmi Prasad[2], Knut Ovsthus[3], Ramjee Prasad[1]**; *[2]Center for TeleInFrastructure (CTIF)*, **USA**, *[3]Bergen University College*, **Norway**, *[1]Center for TeleInFrastructure (CTIF), Aalborg University*, **Denmark**	
	1570215979	Service Interaction through Gateways for Inter-Cloud Collaboration within the Arrowhead Framework; **Pál Varga[1], Csaba Hegedus[2]**; *[1]Budapest University of Technology and Economics, [2] AITIA International Inc.*; **Hungary**	
	1570191635	Single Thing Sign On Identity Management for Internet of Things; **Vanya Zdravkova, Mihail Mihaylov, Albena Mihovska, Ramjee Prasad**; *Department of Electronic Systems, Center for TeleInfrastruktur, Aalborg University*, **Denmark**	
	1570191687	**WPMC:** Towards Internet of Services - SDN-enabled IMS Architecture for IoT Integration; **Anton Katov[1], Bayu Anggorojati[1], Sofoklis Kyriazakos[1], Albena Mihovska[1], Neeli Rashmi Prasad[2]**; *[1]Center for TeleInFrastructure (CTIF), Aalborg University*, **Denmark,** *[2]Center for TeleInFrastructure (CTIF), Aalborg University*, **USA**	
	1570195595	**WPMC:** Packet Scheduling Scheme to Guarantee QoS in Internet of Things; **Reema Sharma[1], Navin Kumar[2], Namratha Gowda[1,3], Srinivas Talabattula[4];** *[1]The Oxford College Of Engineering, [2]Amrita University & School of Engineering, [3]Visvesvaraya Technological University, Karanataka, [4]Indian Institute of Science, Bangalore*; **India**	
19:30-22:30	END of DAY 2 || Cultural Program (Mridangam and Kuchipudi Group Dance Recital), GALA DINNER & Best Paper Award: HALL1		

Time Slot	Day2: Monday, December 14 || MRG .03 Activities || Contributed Papers: Vehicular & Mobile Ad-hoc Networks (I)		
08:30-19:00	Registration		
09:00-11:00	GRAND OPENING		HALL 1
11:00-11:30	COFFEE BREAK		
11:30-13:30	**Vehicular & Mobile Ad-hoc Networks (I-A)| Aerial and Sensor Ad-Hoc Networks: WVITAE|| *Session Chair: Sanjay Kumar, Birla Institute of Technology, Ranchi, India***		MRG .03
	1570214001	Embedded Video Processing and Data Acquisition for Unmanned Aerial Vehicle; **Vrunal Mhatre, Akshay Patil, Siddhesh Chavan, Ashish Chittimilla, Aaron Samuel;** *Fr. Conceicao Rodrigues College of Engineering*, **India**	
	1570194189	HANET: Millimeter wave based intelligent radio architecture for serving place time capacity issue; **Purnima Lala Mehta[①②③④], Troels B. Sørensen[①③], Ramjee Prasad[①②③]**; *[②]Center for TeleInFrastructure (CTIF),* **Denmark**; *[③]Department of Electronic Systems, [①]Aalborg University,* **Denmark**; *[④]HMRITM, New Delhi,* **India**	
	1570195421	GSHMAC: Green and Secure Hybrid Medium Access Control for Wireless Sensor Network; **Pranav Pawar[①], Rasmus Hjorth Nielsen[②], Neeli Rashmi Prasad[③], Ramjee Prasad[①]**; [②]Cisco Systems , **USA**; [③]Center for TeleInFrastructure (CTIF), **USA**; [①]Center for TeleInFrastruktur, Aalborg University, Aalborg, **Denmark**	
	1570214751	Automatic Household Power Measurement & Control System based on Wireless Sensor Networks; **Jameel Ahamed;** *Aligarh Muslim University, Aligarh,* **India**	
	1570213872	Conducted EMI Analysis of Vehicle Positioning System and Strategies to Reduce Conducted EMI; **Shreenivas Ramesh Jog, Nidhi Chaturvedi**; *D. Y. Patil Institute of Engineering & Tech.*, **India**	
	1570213870	Study of Radiated Emission from Wireless Positioning System and the strategies to minimize it; **Shreenivas Ramesh Jog, Suvidha Chitnis**; *D. Y. Patil Institute of Engineering & Tech.*, **India**	
13:30-14:30	LUNCH		
14:30-16:30	**Vehicular & Mobile Ad-hoc Networks (I-B) |Wireless Sensor Networks: WPMC || *Session Chair: Vishwanath Sinha, M N National Institute of Technology, Jaipur, India***		MRG .03
	1570210123	An Interdependent Source-Channel Coding for Energy Efficient Communication in WSNs**; Resmi N C, Sonali Chouhan**; *Indian Institute of Technology Guwahati,* **India**	
	1570194199	Impact of Network Coding on Distributed Indoor Target Tracking using Wireless Sensor Networks; **Laxminarayana Pillutla, Shourya Gupta, Dushyant Singh**; *Dhirubhai Ambani Institute of Information and Communication Technology (DA-IICT)*, **India**	
	1570195119	Mobility-aware Hybrid Synchronization for Wireless Sensor Network; **Dnyaneshwar Mantri, Neeli Rashmi Prasad, Ramjee Prasad**; *Center for TeleInFrastructure (CTIF), Aalborg*, **Denmark**	
	1570195013	Characterization for Reporting Rate of Adaptive Sectoring Scheme to Improve Reliability in WSN; **Manohar S. Chaudhari [①], Vivek Shankar Deshpande[②], Ramjee Prasad[③]**; *[①]Sinhgad Institute of Technology, Pune University,* **India**; *[②]University of Poona & MIT College of Engineering,* **India**; *[③]Center for TeleInFrastructure (CTIF), Aalborg University,* **Denmark**	
	1570195063	Q-MOHRA:QoS Assured Multi-Objective Hybrid Routing Algorithm for Heterogeneous WSN; **Nandkumar Kulkarni[①], Neeli Rashmi Prasad[②], Ramjee Prasad[①]**;*[①]Center for TeleInFrastructure (CTIF),* ***Denmark****; [②]Center for TeleInFrastructure (CTIF),Aalborg University*, **USA**	
	1570213289	Performance Analysis of Total Power Consumption in Linear Multi-hop Networks; **Satoshi Yamazaki[①], Kouji Ohuchi[②]**; *[①]Numazu National College of Technology & Department of Control & Computer Engineering, Numazu, Shizuoka, [②]Shizuoka University Johoku, Hamamatsu, Shizuoka;* **Japan**	
16:30-17:00	COFFEE BREAK		

16:30-17:00	(Continued MRG .03 Activities) COFFEE BREAK		
17:00-19:00	**Vehicular & Mobile Ad-hoc Networks (I-C)|Vehicular and Mobile Ad-Hoc Networks: WPMC || *Session Chair: Vladimir Poulkov, Technical University of Sofia, Bulgaria***		MRG .03
	1570188641	Transmission Capacity Analysis for Linear Vehicular Ad Hoc Networks; **Xinxin He, Weisen Shi, Tao Luo;** *Beijing University of Posts and Telecommunications*, **China**	
	1570199753	Trust based Detection and Elimination of Packet Drop Attack in the Mobile Ad-hoc Networks; **Vishvas Kshirsagar[1][2], Ashok Kanthe[1][3], Dina Simunic[3]**; *[1]Sinhgad Institute of Technology, Lonavala,* **India**, *[2]Savitribai Phule Pune University,* **India,** *[3]Faculty of Electrical Engineering and Computing (FER), University of Zagreb*, **Croatia**	
	1570199757	The Behavioral Based Gray Hole Attack Detection in Mobile Ad-hoc Network (MANET); **Parineet Shukla[1][2], Ashok Kanthe[1][3], Dina Simunic[3]**; *[1]Sinhgad Institute of Technology, Lonavala,* **India**, *[2]Savitribai Phule Pune University*, **India**, *[3]Faculty of Electrical Engineering and Computing (FER), University of Zagreb*, **Croatia**	
	1570194567	On Supporting Integrated Multimedia Traffic in TDMA based Mobile Ad hoc Networks; **Mallesham Dasari[1], Himanshu Sindhwal[1], Naresh Vattikuti[1], Bheemarjuna Reddy Tamma[2]**;*[1]Uurmi Systems Pvt. Ltd. Hyderabad, [2]IIT Hyderabad, Hyderabad;* **India**	
	1570194813	Intrusion Detection System Against Colluding Misbehaviour in MANETs; **Pragya Mishra, Karm V Arya, Hardev singh Pal**; *ABV-Indian Institute of Information Technology & Management, Gwalior*, **India**	
	1570195073	Two-Party Key Agreement Protocol for MANETs based on Verifiable Secret Sharing Scheme; **Cheruku Asha Jyothi, Narsimha Gugulotu**; *Jawaharlal Nehru Technological University College of Engineering, Jagtial, Karimnagar, Telangana,* **India**	
19:30-22:30	END of DAY 2 || Cultural Program (Mridangam and Kuchipudi Group Dance Recital), GALA DINNER & Best Paper Award: HALL1		

Time Slot	Day2: Monday, December 14 || MRG .04 Activities || Contributed Papers: Technology Applications (I)		
08:30-19:00	Registration		
09:00-11:00	**GRAND OPENING**		**HALL 1**
11:00-11:30	COFFEE BREAK		
11:30-13:30	**Technology Applications (I-A) | Human Applications : WVITAE & WPMC || *Session Chair: Vladamir Poulkov, Technical University of Sofia, Bulgaria***		MRG .04
	1570213423	Behavior State Feature Extraction through Single Channel EEG Device for Medical Application; **Sravanth Kumar Ramakuri, Vivek Kumar, Bharat Gupta**; *Birla Institute of Technology Mesra, Ranchi*, **India**	
	1570206439	Real-time Detection of EEG Electrode Displacement for Brain-Computer Interface Applications; **Giulia Cisotto, Silvano Pupolin**; *University of Padua*, **Italy**	
	1570213165	Remote Heart Rate Evaluation by Variational Mode Decomposition**; Bogdan Gavriloaia[1], Octavian Fratu[1], Simona Halunga[1], Gheorghe Gavriloaia[2], Constantin Mara[2], Radu Vizireanu[1]**; [1]University Politehnica of Bucharest, [2]University of Pitesti; **Romania**	
	1570210205	Speech Feature Analysis and Selection for Emotion Classification; **Angel Manolov, Ognian Boumbarov, Agata Manolova, Vladimir K. Poulkov, Krasimir Tonchev**; *Technical University of Sofia*, **Bulgaria**	
	1570213386	Public Auditing and Data Dynamics in Cloud with Performance Assessment on Third Party Auditor; **Snehal Sawant[1,2], Aaradhana Arvind Deshmukh[1,2], Albena Mihovska[1], Ramjee Prasad[1];** [1]*CTIF, Aalborg University*, **Denmark,** [2]*Smt.Kashibai Navle College of Engineering, Vadgoan BK, Pune*, **India**	
	1570195309	**WPMC:** Non Audio-Video gesture recognition system; **Razvan Craciunescu[1,2], Cristian Ionut Dita[1], Albena Mihovska[1], Octavian Fratu[2], Sofoklis Kyriazakos[1], Ramjee Prasad[1]**; [1]*CTIF, Aalborg University*, **Denmark**, [2]*University Politehnica of Bucharest*, **Romania**	
13:30-14:30	LUNCH		
14:30-16:30	**Technology Applications (I-B) | Human Applications : WPMC || *Session Chair: fred Harris, San Diego State University, USA***		MRG .04
	1570207155	Fuzzy Logic based Human Detection in Video; **Manojkumar M Gawali, Dipti R. Pawar**; *Sinhgad College of Engineering, Pune*, **India**	
	1570207563	Improving Segmentation Accuracy for Motion Detection using Bidirectional Video Processing**; Abhishek Thakur, Ankesh Kumar**; *BITS Pilani , Hyderabad Campus*, **India**	
	1570194919	Automatic Speaker Detection and Recognition in a multi classroom E-Learning System; **Amitha Vijayan, Balaji Hariharan**; *AMRITA Vishwa Vidyapeetham Amritapuri, Kollam*, **India**	
	1570213262	Real-time EEG Monitoring and Transmission over Low Bandwidth Wireless Networks; **Kaushik Lahiri[1], Amitava Mukherjee[1], Mrinal Kanti Naskar[2]**; [1]*IBM India Pvt Ltd;* [2]*Jadavpur University*; **India**	
	1570194425	Adaptive priority based network bandwidth throttling for a Virtual Classroom System**; Jobina Varghese, Balaji Hariharan**; *AMRITA Vishwa Vidyapeetham Amritapuri, Kollam*, **India**	
	1570213445	Minimal Error IEEE 802.15.4 Communication Module for Heart Monitoring Data Transmission in IoT; **Subrahmanyam Vuddagiri, Mohammed Abdullah Zubair, Ajay Yadav, Pachamuthu Rajalakshmi**; *Indian Institute of Technology Hyderabad*, **India**	
16:30-17:00	COFFEE BREAK		

16:30-17:00	(Continued MRG .04 Activities) COFFEE BREAK		
17:00-19:00	**Technology Applications (I-C) | Multiple Areas: WVITAE || *Session Chair: Hiroshi Harada, Kyoto University, Kyoto, ICT, Koganei,* Japan**		MRG .04
	1570207041	Design of Amateur Radio Wireless Transceiver to Reduce the Impact of Natural Calamities; **Ashwini Shingate[1], Rushikesh Borse[2], Shubham Tiwari[3], Arvind Jawale[4]**; [1][2]*Savitribai Phule Pune University*, [2]*Savitribai Phule Pune University*, [2]*Shubhra Energy*, [4]*Scout Satara*; **India**	
	1570210199	Deep Sea Exploration Recovery and Transport [DESERT] Vehicle and its Modes of Communication; **Aileen Sengupta[1], Pavel Sengupta[2]**; [1]*Techno India College of Technology, Rajarhat,* [2]*Dr. Sudhir Chandra Sur Degree Engineering College, Dum Dum, Kolkata* □; **India**	
	1570208685	Energy Efficient Lighting System for Indoor Parking with Ubiquitous Communication; **Mahesh Jha[1], Navin Kumar[2]**; [1]CMRIT, VTU, [2]Amrita University & School of Engineering; **India**	
	1570210063	Recent Progress in Radioclimatological Modeling in Equatorial and Tropical Africa; **Thomas Afullo, Akintunde Alonge**; University of Kwazulu-Natal, Durban, **South Aftrica**	
	1570210261	Digital door lock using fingerprint, webcam and GSM - a novel approach for smart homes; **Ashish Patwari, Karuna Yepuganti, Arpit Omar, Shekhar Thakur, Kaushik Kumar**; *VIT University, Vellore*, **India**	
	1570209921	Marine Vessel Detection Comparing GPRS and Satellite Images for Security Applications; **Sajan Ambadiyil[1], Dintu Thomas[2], V P Mahadevan Pillai[3]**; [1]*Optical Image Processing Division, C-DIT,* [2]*SCMS School of Engineering and Technology,* [3]*University of Kerala, Thiruvanthapuram, Kerala*; **India**	
19:30-22:30	END of DAY 2 || Cultural Program (Mridangam and Kuchipudi Group Dance Recital), GALA DINNER & Best Paper Award: HALL1		

Time Slot	Day2: Monday, December 14 || MRG .05 Activities || Special Sessions on WWRF & GISFI and; Contributed Papers: Physical and Fundamentals (I)		
08:30-19:00	Registration		
09:00-11:00	**GRAND OPENING**		**HALL 1**
11:00-11:30	COFFEE BREAK		
11:30-13:30	**WPMC Special Session on "Selected Topics"** **Session Organizer and Chair: Shinsuke Hara,** *Osaka City University*, **Japan**		MRG .05
	Invited Talk	"Home neuro- rehabilitation: an ICT near Future Service", **Silvano Pupolin**, *University of Padua*, **Italy**	
	Invited Talk	" **Lakhshmi Mukunkutla**, *USA/Aalborg University*, **Denmark**	
	Invited Talk	"Convergence Techniques for Future Communications", **M. Jankiraman**, *Larsen & Toubro Ltd. (L&T), Bangalore*, **India**	
	Invited Talk	" Making a Safe and Secure 4 G World", **Debu Nayak**, *Huawei Telecommunications India Pvt. Ltd*, **India**	
13:30-14:30	LUNCH		
14:30-16:30	**Physical and Fundamentals (I-A) | LTE and Multiple Access Techniques (OFDMA/OFDM/SC-FDMA, MIMO, SISO): WPMC & WVIATE || *Session Chair:* ", M. Jankiraman, *Larsen & Toubro Ltd. (L&T), Bangalore, India***		MRG .05
	1570196365	Joint Transceiver Design for QoS-Constrained MIMO Two-Way Non-Regenerative Relaying; **Rohit Budhiraja, Bhaskar Ramamurthi**; *Department of Electrical Engineering, IIT Madras*, **India**	
	1570190883	New virtual 8x1 MISO scheme with QOSTBC; **Ugljesa Urosevic, Zoran Veljovic, Milica Pejanovic-Djurisic**; University of Montenegro, Podgorica, **Montenegro**	
	1570212700	Limited Feedback Scheduling For MIMO-OFDM Broadcast Network; **Prabina Pattanayak, Preetam Kumar;** *Indian Institute of Technology, Patna*, **India**	
	1570193823	An Efficient Deterministic Scheme for Blind CFO Estimation in SC-FDMA; **Vinay Kumar Trivedi, Vidya Sagar, Preetam Kumar**; *Indian Institute of Technology, Patna*, **India**	
	1570209997	**WVIATE:** Capacity Analysis of MIMO BC Channels in Presence of Spatial Correlation; **Ashok Panda①, Swadhin Kumar Mishra②, Ajit Kumar panda②**; ①IIIT Bhubaneswar,② *NIST Berhampur*; **India**	
	1570212704	**WVITAE:** Error Rate Performance for Multiuser scheduling in MIMO downlink system with imperfect CSI; **Prabina Pattanayak, Diwakar Pandey, Preetam Kumar;** *Indian Institute of Technology, Patna*, **India**	
16:30-17:00	COFFEE BREAK		
17:00-19:00	**WVITAE Special Session: Wireless World Research Forum (WWRF):** **Knud Erik Skouby,** Aalborg University **, Denmark and Sudhir Dixit,** WWRF**, USA**		MRG .05
	Theme : **Mobile History of India**		
	Opening Speech	**Knud Erik Skouby,** *Aalborg University* **, Denmark**	
	Keynote Speech	**Sudhir Dixit,** *WWRF*, **USA**	
	Invited Talk	**Krishna Sirohi,** *NIKSUN*, **India**	
19:30-22:30	END of DAY 2 || Cultural Program (Mridangam and Kuchipudi Group Dance Recital), GALA DINNER & Best Paper Award: HALL1		

Time Slot	Day2: Monday, December 14 || MRG .06 Activities || Second International Workshop on Innovation and Entrepreneurship(IWIE) (I)			
08:30-19:00	Registration			
09:00-11:00	**GRAND OPENING**			**HALL 1**
11:00-11:30	COFFEE BREAK			
11:30-13:30	**Second International Workshop on Innovation and Entrepreneurship(IWIE) :(I-A) || Entrepreneurship Contest** Second International Workshop on Innovation and Entrepreneurship(IWIE) | (I –A) Organizer and Chair: Sofoklis Kyriazakos, CTIF, Aalborg University, Denmark **Introduction to the Workshop and Entrepreneurship Contest**			MRG .06
	Mayank Kumar Mittal, **SaleYourBooks.com** Mayank Semwal , **Genralsorts** Shilpa Chaudhary, **Car security Systems** Meenakshi Gupta, **MNY PRO** Jafar Mapara, **Identity Management System** Akskay Radke, **Smart Indian railways**	Mayank Semwal, **App for professional Help** Deepak Sharma, **Instant Presentation and Converter** Mukesh Wadile, **SecureChip** Heramb Pawar, **Clear Vision** Naman Vashishth, **Find ME!!!!** Darshan Vyas, **CLOTH TESTER using IMAGE PROCESSING** Shashank Roy, **Electronic Refigerator**	Adarsh Mishra, **Virtual PPM-1** Utkarsh Trivedi, **Service Providers Support** Irram Patharwat, **Methane Extraction Digester** Manoj Radadiya, **Gesture and Voice based Television Control System** Nikhil Prabhu, **Smart Electric Car using AMR7** Jafar Mapara, **Connected Homes** Madhukesh Heggannavar, **Design and Development of Magnetron Power Source**	
13:30-14:30	LUNCH			
14:30-16:30	**Second International Workshop on Innovation and Entrepreneurship(IWIE) :(I-B) || Entrepreneurship Contest** Second International Workshop on Innovation and Entrepreneurship(IWIE) | (I –B) Organizer and Chair: Sofoklis Kyriazakos, CTIF, Aalborg University, Denmark IWIE Activities			MRG .06
16:30-17:00	COFFEE BREAK			
17:00-19:00	**Second International Workshop on Innovation and Entrepreneurship(IWIE) :(I-C) || Entrepreneurship Contest** Second International Workshop on Innovation and Entrepreneurship(IWIE) | (I –C) Organizer and Chair: Sofoklis Kyriazakos, CTIF, Aalborg University, Denmark **Results and Discussion of Entrepreneurship Contest of the IWIE Workshop Day -1**			MRG .06
19:30-22:30	END of DAY 2 || Cultural Program (Mridangam and Kuchipudi Group Dance Recital), GALA DINNER & Best Paper Award: HALL1			

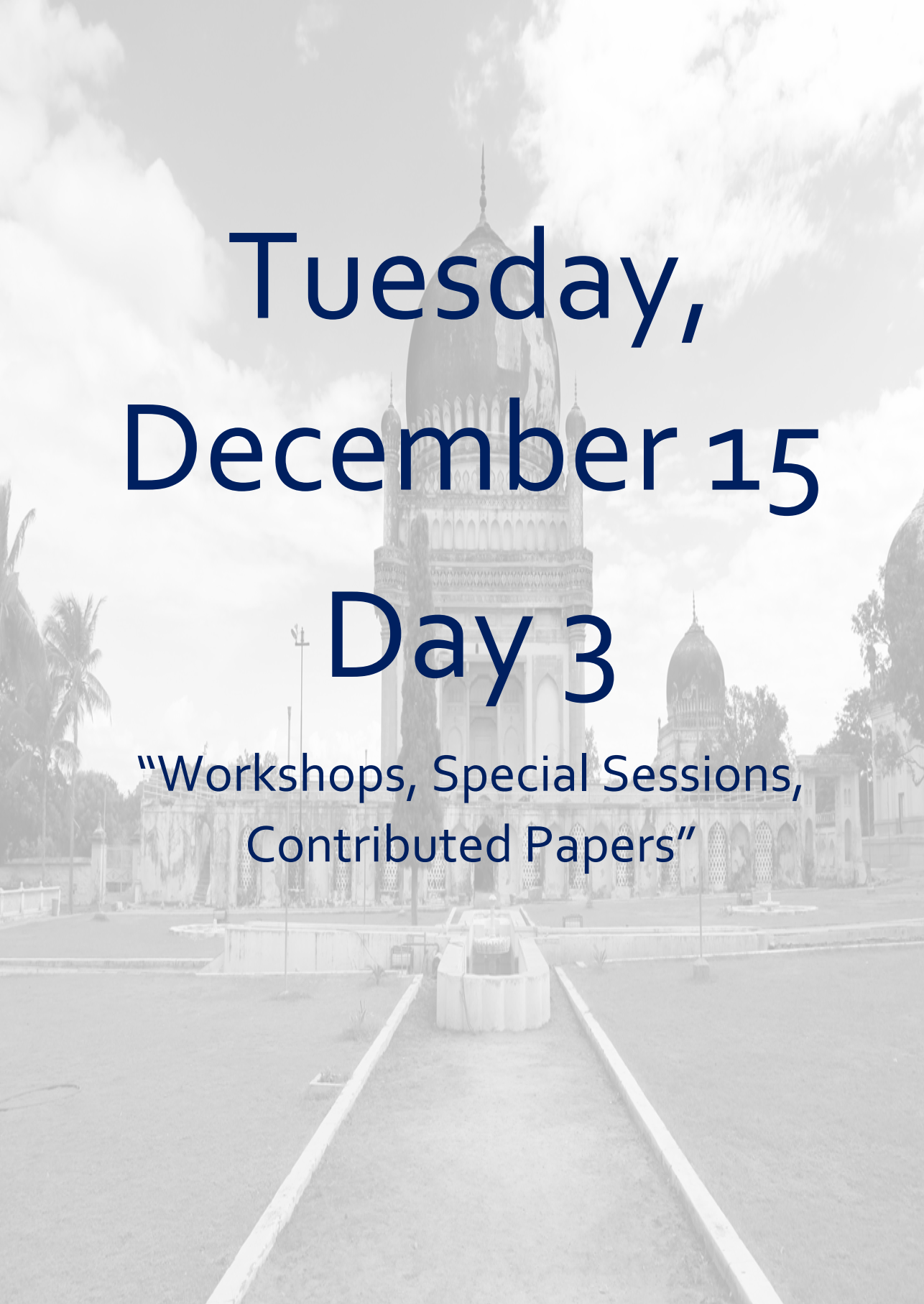

Tuesday, December 15

Day 3

"Workshops, Special Sessions, Contributed Papers"

Time Slot	Day3: Tuesday, December 15 || HALL 1.1 & 1.2 Activities || Workshops & Special Sessions (II-A)			
08:30-19:00	Registration			
09:00-11:00	**Keynote Speech || Chair: Ashok Chandra, TPC Executive Chair, WPMC/ GWS-2015** **Lars Kiekegaard**, Teracom, **Denmark** **Ramesh Rao**, University of California, San Diego, **USA**			**HALL 1**
11:00-11:30	**COFFEE BREAK**			
11:30-13:30	**WPMC Special Session on "Smart Village 'Rural Model': Basic Unit for a Digital India" || Session Organizer and Chair: Mayur Dave,** *IETE*, **INDIA**			HALL 1.1
	1570227716	Demonstrating SWiFiIC - Sustainable WiFi for Rural Communication; **Abhishek Thakur, Aarthi J, Amit Chawla, Chittaranjan Hota**; *BITS Pilani, Hyderabad Campus,Hyderabad*, **India**		
	1570234273	"IoT" based Smart Village: An Indigenous step towards 'Digital India'; **Madhukant Patel①, Piyush Yadav②**; *①MD, Reve Automation LLP, ②Green Cloud iSoft P. Ltd., Dehradun*, **India**		
	1570234316	Rurbanisation of India; **Bipin Pradeep Kumar**, *Gaia Smart Cities*, **India**		
	WVITAE Special Session on "Persuasive Multi Business Model Innovation in a World of Persuasive Technologies" **Session Organizer and Chair: Peter Lindgren,** *Multi Business Model Innovation and Technology, Aarhus University*, **Denmark ||Session Co-organizers: Troels Christian, K. Andersen, Torben Bjerrum, Annabeth Aagaard, Ole Horn Rasmussen, Morten Karnøe Søndergaard** *Aarhus University*, **Denmark; Theodoor van Dongen,** *VDMBee, Veenendaal*, **The Netherlands**			HALL 1.2
	1570228216	Persuasive Technology and Business Models; **Morten Karnøe Søndergaard, Peter Lindgren, Niels Einar Veirum;** *Stanford Peace Innovation Lab, Department of Business Development and Technology, Aarhus University*, **Denmark**		
	1570228627	Service and Big Data business model in a world of persuasive technologies; **Troels Christian K. Andersen, Torben Cæsar Bisgaard Bjerrum**; *Aarhus University, Herning*, **Denmark**		
	1570228634	Secure Persuasive Business Models and Business Model Innovation in a World of 5G; **Peter Lindgren, Katharina Wuropulos**; *Aarhus University*, **Denmark (###)**		
13:30-14:30	LUNCH			
14:30-16:30	**WPMC Workshop on " Advanced Technologies and Promotion Strategies for Wi-SUN and the Wireless Grid Systems" || Workshop Organizer and Chair:** *Fumihide Kojima*, **Japan**			HALL 1.1
	Wi-SUN Alliance -Promoting open interoperable industry standards for smart utility networks; **Hiroshi Harada**, NICT, Japan		NICT's R&D, Standardization and Promotion Avtivities on Wi-SUN and the wireless grid systems; **Fumihide Kojima**, NICT, Japan	
	Wi-SUN RLMM Profile for Sensor Network Application; **Ryota Yamada**, Omron, Japan		Wi-SUN Alliance Activity in India; **Amarjeet Kumar**, Wi-SUN Alliance, India	
	WVITAE Workshop on "Wearable and Nearable Internet of Things (WaNIOT 2015)"|| Workshop Organizer and Chair: Balamuralidhar P, *Tata Consultancy Services (TCS)*, **Bangalore, India**			HALL 1.2
	Introduction by the workshop chair: Dr. Balamuralidhar P., TCS Innovation Lab, Bengaluru Wearables for Newborns": Prof. Bharadwaj Amrutur, Indian Institute of Science, Bengaluru Wearables for Safety: Mr. Ganesh Suryanarayanan, GTIO, Tata Group, Bengaluru		Data-driven Healthcare using Affordable Sensing", Dr. Arpan Pal, TCS Innovation Lab, Kolkata RF based Sensing of Cardiopulmonary Vital Signs": Mr. R.P.Pinto, SAMEER, Mumbai IoT in healthcare: Applications to neurology: Dr. Jayavardhana Gubbi, TCS Innovation Labs, Bengaluru	
16:30-17:00	COFFEE BREAK			

16:30-17:00	(Continued Hall 1.1 and 1.2 Activities) BREAK				
17:00-19:00	**Matchmaking session – Indian industry meets Global Industry || Organizer and Chair: Krishnal Sirohi,** *GISFI*, **India**				HALL 1.1
	Lars Kierkegaard, *Teracom*, **Denmark**	**Srinivasa Gutta, INVECAS,** *Hyderabad,* **India**	**Sivabalan Arumugam,** *NEC* **, Japan**	**Kiritkumar Lathia, GISFI/CTIF, Denmark**	
	Sandip Inamdar, *WISDOM Pvt. LTD.*, **India**	**Balaji Kanigicherla,** *Ineda Systems, Hyderabad,* **India**	**Gangadhar Gude, SoCtronics,** *Hyderabad,* **India**	**Subbarangaiah,** *VEDA IIT, Hyderabad*, **India**	
	WVITAE Special Session on " Fiber-Wireless Convergence for broadband Connectivity in 5G perspective" || **Session Organizer and Chair: Jayashree Ratnam,** International Institute of Information Technology, *Hyderabad*, **India**				HALL 1.2
	Invited Talk	Journey to World Wide Wireless and its Deployment Challenges**, D.S. Rao**, Tata Communications Ltd, Hyderabad, India			
	1570228022	Participation of Optical Backbone Network in Successful Advancement of Wireless Network; **Rajarshi Mahapatra**; *CVR College of Engineering*, **India**			
	1570228026	On 5G Cellular Backhaul Networks; **Mahima Mehta**, *Intel Mobile Communications India Pvt. Ltd., Bangalore*, **India**			
	1570228029	Telecom Regulatory Issues in Converged Era; **G. Muralidhar , Robert Ravi**; *Telecom Regulatory Authority of India*, India **(***)**			
19:30-22:30	END of DAY 3 || NETWORKING DINNER: FOYER				

Time Slot	Day3: Tuesday, December 15 || MRG .01 Activities || Workshops & Special Sessions (II-B)		
08:30-19:00	Registration		
09:00-11:00	**Keynote Speech**		HALL 1
11:00-11:30	COFFEE BREAK		
11:30-13:30	**WVITAE Special Session on" Internet of Things (IoT)"** **Session Organizers: Birger Andersen①, Knud Erik Skouby②, ② Samant Khajuria,** ①*Technical University of Denmark, Copenhagen*, ②*Aalborg University, Copenhagen*, **Denmark** **Session Chair: Birger Andersen,** *Technical University of Denmark, Copenhagen*, **Denmark**		MR G.01
	Keynote Talk	IoT in Theory and Practice**, Birger Andersen,** *Technical University of Denmark, Copenhagen*, **Denmark**	
	1570227404	Heuristic Trust in IoT; **Bipjeet Kaur①, Henrik Tange②;** ①*Denmark Technical University* , ②*Wireless Center CTIF Copenhagen*; **Denmark (###)**	
	1570228109	Cyber security for M2M Smart Grid; **Sarmistha De Dutta①, Prof. Ramjee Prasad②**; ①*NIKSUN, Inc.*, **USA** ②*Center For TeleInFrastruktur , Aalborg University*, **Denmark**	
	1570228247	GET IoT- Green Computing and Energy Harvesting technology in Internet of Things (IoT); **Jetendra Joshi, Anshumali Singh, Lakshya Gourav Moitra , Manash Jyoti Deka**; *NIIT University, Neemrana, Alwar, Rajasthan*, **India**	
	1570228361	An Energy Efficient Adaptive Wireless Link for Farms based on IoT technologies**; T. Blaszczyk①, P. Lynggaard②**; ①*Technical University of Denmark,* ②*CMI, Aalborg University Copenhagen*; **Denmark**	
	1570231008	Implementation Of Internet Of Things Using Near Field Communication For Parking Automation; **Aishwarya Sanjay Ikhe, Sagar Jayant More, Priyanka Sanjay Suranglikar, Prashant S Dhotre;** *Sinhgad Institute of Technology and Science, Pune*, **India**	
13:30-14:30	LUNCH		
14:30-16:30	**WVIATE Special Session on "Spectrum Management and Networking for Multi-link Satellite and Terrestrial Communication Systems"** **Session Organizers and Chairs: Preetam Kumar, Vinay Kumar Trivedi, Akash Agarwal;** *Indian Institute of Technology Patna*, **India**		MR G.01
	Invited Talk	Vimal Bhatia, *Associate Professor, IIT Indore*, **India**	
	Invited Talk	Preetam Kumar, *Assistant professor, IIT Patna*, **India**	
	1570221151	Cancellation of Inter-Cell Interference in Downlink with No Backhaul Information Exchange; **Shuvabrata Bandopadhaya①, Jibendu Sekhar Roy②**; ①*Silicon Institute of Technology, Bhubaneswar, Odisha,* ②*School of Electronics Engineering, KIIT University, Bhubaneswar, Odisha*.; **India**	
	1570226980	Performance Analysis Of Interference Cancellation In MIMO-FBMC; **V.Padmapriya , N.Venkateswaran**; *SSN College of Engineering, Chennai*,**India**	
	1570227724	Measurement and Identification of White Space using Low Cost SDR for Rural Wireless Broadband; **Vinit Sharswat, Pradeep Godara, Abhijeet Bishnu, Vimal Bhatia;** *Indian Institute of Technology Indore*, **India**	
16:30-17:00	COFFEE BREAK		

16:30-17:00	(Continued MRG .01 Activities) COFFEE BREAK		
17:00-19:00	**WVITAE Special Session on " eWALL"** **Session Organizer and Chair: Sofoklis Kyriazakos, CTIF,** *Aalborg University***,** *Aalborg,* **Denmark**		MR G.01
	1570224200	Improving the Trustworthiness of Ambient Assisted Living Applications; **Elias Z. Tragos①, Pavlos Charalampidis①, Alexandros Fragkiadakis①, George Lambropoulos②, Sofoklis Kyriazakos②;** ①FORTH-ICS,② Converge SA**; Greece**	
	1570224206	Requirements and Challenges in Evaluation of Systems for Independent Living of Senior Citizens; **Antun Kerner, Antonija Marinčić, Ana Koren, Dina Šimunić ,Ramjee Prasad**; *Faculty of Electrical Engineering and Computing, University of Zagreb,* **Croatia**	
	1570224166	Virtual sensing environment for care at home; **Aristodemos Pnevmatikakis;** *Athens Information Technology, IRIS Laboratory, Athens,* **Greece**	
	1570224167	Expression recognition using graph based feature selection; **Krasimir Tonchev, Nikolay Neshov, Agata Manolova ,Vladimir Poulkov**; Technical University of Sofia, **Bulgaria**	
	1570213206	Participatory Heuristic Evaluation of the First Iteration of the eWALL Interface Application**; Clara Schaarup①, Louise Bilenberg Pape-Haugaard①, Stine Veje Hangaard①, Albena Mihovska② ,Ole Hejlesen①; ①Department of Health Science and Technology, ②Center for TeleInfrastruktur □;** *Aalborg University, Aalborg,* **Denmark**	
	1570195309	Non Audio-Video gesture recognition system; **Razvan Craciunescu, A. Mihovska ; Center for TeleInfrastruktur □;** *Aalborg University, Aalborg,* **Denmark**	
19:30-22:30	END of DAY 3 || NETWORKING DINNER: FOYER		

Time Slot	Day3: Tuesday, December 15 || MRG .02 Activities || Workshops & Special Sessions (II-C)		
08:30-19:00	Registration		
09:00-11:00	**Keynote Speech**		HALL 1
11:00-11:30	COFFEE BREAK		
11:30-13:30	**WPMC Special Session on "Manufacturing Engineering"** **Session Organizer and Chair: Dnyandeo Dattatray Shinde,** *Sandip Foundation, Sandip Institute of Engineering & Management, Nashik, Maharashtra*, **India**		MR G.02
	Invited Talk	Total Productive Maintenance (TPM) an overview; **Rajendra G. Tated**; *Sandip Foundations, Sandip Institute of Engineering and Management, Nashik*, **India**	
	Invited Talk	Application of KK pillar of TPM – An Industrial Case study; **J. P Yavalkar;** *TPM-Learning center, Bajaj auto ltd. Waluj Aurangabad*, **India**	
	Invited Talk	Lean Six Sigma - Success Story of Kavach; **Jadhav Ganesh A.;** *Gabriel India Ltd. Pune*, **India**	
13:30-14:30	LUNCH		
14:30-16:30	**WPMC Special Session on "Manufacturing Engineering" (Contd.)** **Session Organizer and Chair: Dnyandeo Dattatray Shinde,** *Sandip Foundation, Sandip Institute of Engineering & Management, Nashik, Maharashtra*, **India**		MR G.02
	1570226974	Identifying Root Causes for Students Problems in Technical Education using Fishbone Diagram; **Dnyandeo Dattatraya Shinde①, Shwetambari Sanjay Ahirrao①, Prachi Dilip Shinde①, Rajendra G. Tated①, Morten Falch②**; ①*Sandip Foundations, SIEM, Nashik, India,* ②*Center for Communication, Media and Information Technologies (CMI), Aalborg University Copenhagen*, **Denmark**	
	1570226994	Effect of Newly Designed Burnishing Tool on Surface Micro hardness of AA6351; A. S. Maheshwari①, Dr. R. R. Gawande②; ①*Sandip Institute of Technology & Research Centre, Nashik. (Maharashtra),* ②*Bapurao Deshmukh College of Engineering, Wardha (Maharashtra)*; **India**	
	1570228066	Application of Principal Component Analysis to Magnetic Abrasive Finishing**; Sandip B. Gunjal, P. J. Pawar**; *K.K.W.I.E.E. & R, Nasik*, **India**	
	1570227495	Metric Based Efficiency Analysis Of Educational ERP System Usability - Using Fuzzy Model; **Anil Kumar, Reza Tadayoni, Lene Tolstrup Sorensen**; *Department of Electronic Systems, Aalborg University*, **Denmark**	
	1570227534	A Brief Review on Process Parameter Optimization of GMAW Process and Grey-based Taguchi Method; **U. V. Patil, G. R. Naik**; *KIT's College of Engineering, Shivaji University, Kolhapur*, **India**	
	1570227977	Vehicle Monitoring and controlling system using CAN protocol; Mosam Sangole□, **Vicky Chaudhary, Vishakha Nighute, Priyanka Satpute;** *Sandip Foundation Nashik, Maharashtra*,**India**	
16:30-17:00	COFFEE BREAK		

16:30-17:00	(Continued MRG .02 Activities) COFFEE BREAK		
17:00-19:00	**WPMC Special Session on "Manufacturing Engineering" (Contd.)** **Session Organizer and Chair: Dnyandeo Dattatray Shinde,** *Sandip Foundation Sandip Institute of Engineering & Management, Nashik, Maharashtra,* **India**		MR G.02
	1570227004	Application of Real Coded Genetic Algorithm to Dynamic Layout Benchmark Problem; **Kailas V. Chandratre, P.J. Pawar**; *, K.K.W.I.E.E. & R, Nasik*, **India**	
	1570227011	Model Development for Preventive Maintenance and Replacement Policy; **Anand S. Relkar, Keshav N. Nandurkar**; *S. I.T.R.C., Nashik, K.K.W.I.E.E.R, Nashik*; **India**	
	1570227290	Vacuum Gripper Design For An Industrial Handling System; **Ajinkya Vasant Nichit, Suraj Ramesh Jadhav, Anirudh Arun Desai, Vishal Eknath Patil,Vishal Sonowane**; *Sandip Institute Of Engg. & Mangt. Nashik*, **India**	
	1570228555	Automatic Ration Distribution System-A Review; **Swapnil R. Kurkute, Dipak P. Patil, Chetan Medhe, Ashwini Kshirsagar, Ashlesha Revgade** □; *SIEM Nasik*, **India**	
	1570227469	Self -Balancing Platform for Personal Transport; **Yogesh Risodkar , Ganesh Shirsath, Monali Holkar, Mayur Amle**; *SIEM, Sandip Fondation, Nashik*, **India**	
	1570228052	Decommissioning of Nuclear Facilities and Dose Rate Calculations for Nuclear Power Plant Staff; **Pushkar Prashant Lachake, Dnyandeo Dattatraya Shinde**; *Sandip Institute of Engineering and Management, Nashik*, **India**	
19:30-22:30	END of DAY 3 || NETWORKING DINNER: FOYER		

Time Slot	Day3: Tuesday, December 15 || MRG .03 Activities || Contributed Papers: Physical and Fundamentals (II-A)		
08:30-19:00	Registration		
09:00-11:00	**Keynote Speech**		**HALL 1**
11:00-11:30	COFFEE BREAK		
11:30-13:30	**Physical and Fundamentals (II-A-1) | Antenna & Circuit Design, Analysis and Investigation: WPMC || *Session Chair: Laxminarayana Pillutla; Dhirubhai Ambani Institute of Information and Communication Technology, India*** 1570213114	Design Optimization and SAR Evaluation of SS-UWB Patch Antenna for WBAN; **Vivek Kumar, Sravanth Kumar Ramakuri**; **Bharat Gupta**; *Birla Institute of Technology Mesra, Ranchi,* **India**	MRG .03
	1570210207	Radar Range and Range Resolution Enhancements; **Uma S Jha, Erik Chowdhury**; *Space & Airborne Systems, Raytheon Co, El Segundo, California,* **USA**	
	1570209793	SIW based Antipodal Linear Tapered Slot Antenna for Inter-Satellite Communication Links at 60 GHz; **Nishesh Tiwari, T Rama Rao, Purva Shrivastava**; *SRM University,Chennai,* **India**	
	1570192429	SAR and Thermal effects of a Body Wearable Microstrip Antenna at UHF and UWB frequencies; **Varshini Karthik, T Rama Rao**; *SRM University,Chennai,* **India**	
	1570213460	Antenna Radiation Pattern Based 3D Localization Technique; **Amarlingam Madapu[1], Pachamuthu Rajalakshmi[1], Vinod Kumar Netad[1], Masaya Yoshida[2], Kiyohito Yoshihara**; [1]Indian Institute of Technology Hyderabad, Hyderabad, **India,** [2]*KDDI R&D Laboratories Inc., Green and M2M Application Laboratory Iidabashi,* **Japan**	
13:30-14:30	LUNCH		
14:30-16:30	**Physical and Fundamentals (II-A-2) | LTE & Multiple Access Techniques (OFDMA/OFDM/SC-FDMA, MIMO, SISO): WPMC || *Session Chair: Uma S. Jha, Raytheon Co., California, USA*** 1570213429	Distributed Spatial Modulation-OFDM in Uplink Relay-assisted Cellular Network; **Kunal Sankhe, Rama Garimella**; *International Institute of Information Technology, Hyderabad,* **India (***)**	MRG .03
	1570213444	Simultaneous Transmission of Information and Energy in OFDM Systems; **Sumit Gautam, P. Ubaidulla**; *International Institute of Information Technology-Hyderabad,* **India**	
	1570210151	Blind Channel Length Estimation for OFDM Systems using Cumulant Features; **Ajay Kambhampati, Udit Satija, Baratram Ramkumar, M Sabarimalai Manikandan**; *IIT-Bhubaneswar,* **India**	
	1570213302	A Feasibility Analysis of LTE-CommSense; **Amit K. Mishra[1], Mohammed Zafar Ali Khan[2], Santu Sardar[3]**; [1]*Department of Electrical Engineering, University of Cape Town,* **South Africa**, [2]*Department of Electrical Engineering, IIT Hyderabad,* **India,** [3] *ANURAG, Defence Research & Development Organization*, **India**	
	1570167111	An Efficient Resource Block Allocation Algorithm in LTE-Based Systems with User Rate Constraints; **Vijay Gutta, AmruthMuddana, T K Ramesh**; *Amrita VishwaVidyapeetham,* **India**	
	1570213529	LTE-Advanced Radio and Network Optimization: Basic Coverage and Interference Constraints; **Fernando J. Velez, Sofia Sousa, Jessica Acevedo ,Daniel Robalo**; *Instituto das Telecomunicações - DEM Universidade da Beira Interior,Faculdade de Engenharia, Covilhã,* **Portugal**	
16:30-17:00	COFFEE BREAK		

16:30-17:00	(Continued MRG .03 Activities) COFFEE BREAK		
17:00-19:00	**WPMC Special Session on " Selected Topics in Physical & Fundamentals-1"** **Session Organizer and Chair** : **T Rama Rao,** SRM University, **India**		MRG .03
	1570160791	Performance of MIMO Detection Techniques with Spatial Multiplexing**; Soma Umamaheshwar①, Tipparti Anil Kumar②, K Srinivas Rao③**; ①*SR Engineering College,* ②*SVS Group of Institutions,* ③*TRR College of Engineering, Telangana*, **India (###)**	
	1570213390	Reducing memory consumption with a lossless image compression algorithm based on predictive coding; **Rupali S. Vairagade**; *Sinhgad Institute of Technology and Science, Pune*, **India (***)**	
	1570209839	Enhancement in Spectral Efficiency using Circular Convolution in MIMO FBMC towards Wireless Network 5G; **Payal P. Tayade, Vandana M. Rohokale**, *SKNSITS, Lonavala*, **India (###)**	
	1570209843	Performance Analysis of Group based Cooperative Sensing Schemes; **K Jyostana①, N. Vandana②, Swathi Roja②, B. N. Bhandari②**; ①*VNR Vigana Jyothi Institute of Engineering and Technology,* ②*Jawaharlal Nehru Technological University*; Hyderabad, **India (###)**	
	1570238199	A Comparative Study of Channel Estimation for MIMO-OFDM system; **G Surendher**, Sree Chaitanya *Institute of Technological Sciences, Karimnagar,* **India (###)**	
19:30-22:30	END of DAY 3 || NETWORKING DINNER: FOYER		

Time Slot	Day3: Tuesday, December 15 || MRG .04 Activities || Contributed Papers: Physical and Fundamentals (II-B)		
08:30-19:00	Registration		
09:00-11:00	**Keynote Speech**		**HALL 1**
11:00-11:30	COFFEE BREAK		
11:30-13:30	**Physical and Fundamentals (II-B-1) | Channel Fading and Selection :WVIATE || *Session Chair-Ernesthina Cianca, University of Rome, Tor Vergata, Italy***		MRG .04
	1570208291	Joint Channel Estimation and CCI Cancellation for STBC-OFDM System in Fast Fading Channel; **Jyoti P Patra, Prasanta Kumar Pradhan,, Poonam Singh, Sarat Kumar Patra**; *National Institute of Technology Rourkela*, **India**	
	1570210195	Rate Independent Multicarrier Variable Rate Scheme over Frequency Selective Channel; **Akash Agarwal**, **Vijay Mukati**, **Preetam Kumar**; *Indian Institute of Technology, Patna*, **India**	
	1570210219	Performance of Amplify-and-Forward Cooperative Diversity under Ricean Fading; **Maja Delibasic, Milica Pejanovic-Djurisic, Zoran Veljovic**; *University of Montenegro*, **Montenegro**	
	1570213163	Performance of a space-time coded MC-CDMA system in a Rayleigh fading channel; **Olanrewaju B Wojuola**, **Stanley H. Mneney**, **Viranjay M Srivastava**; *University of KwaZul-Natal*, **South Africa**	
	1570194569	A new shaping code for PAPR Reduction in Single-Carrier Modulation; **Yonathan Tate, Dan Raphaeli;** *Tel Aviv University*, **Israel**	
	1570207637	PAPR Reduction Comparison of the MC-CDMA System with Various Companding Techniques; **Sarala Beeram①, Bhagya sree Vonguru②, BN Bhandari③, Dronam Raju Venketeswarlu③**; *①M V S R Engineering College, Hyderabad & Osmania University*; *②B E & Osmania University, Hyderabad*; *③JNT University Hyderabad;* **India**	
13:30-14:30	LUNCH		
14:30-16:30	**Physical and Fundamentals (II-B-2) | Physical Channel: WPMC || *Session Chair-Thomas J. O. Afullo, University of KwaZullu-Natal, South Africa***		MRG .04
	1570213381	On Detection Improvement in MC-CDMA Image Watermarking on Fading Channel; **Santi Prasad Maity①, Seba Maity②**; ①Indian Institute of Engineering Science and Technology, Shibpur, ②CEMK, Kolaghat, **India**	
	1570213387	On the Backhaul Reduction in Joint Transmission Network with Channel Uncertainty; **Zhangxing Liu, Hui Tian, Cheng Qin** ; *Beijing University of Posts and Telecommunications*, **China**	
	1570212327	Variable Encoding and Sequencing Pattern Driven Multiple Image Bit Watermarking for Wireless Domain; Soumit Chowdhury①, Nabin Ghoshal ②; ①Govt. College of Engineering & Ceramic Technology, Kolkata, ② University of Kalyani, India	
	1570177831	Improving Performance of Impulsive Noise Canceller Under Class A Impulsive PLC Channel; **Hirotomo Yasui, Akira Nakamura, Makoto Itami**; *Tokyo University of Science*, **Japan**	
	1570211271	A Generic and Compatible Implementation for 2D and 3D Geometry-based Stochastic Channel Models; **Zhenzi Liu, Tian Lei, Yuming Bi, Pan Tang, Wei Chen, Jianhua Zhang**; *Beijing University of Posts and Telecommunications*, **China**	
	1570209407	Low Rate Common Control Channels with Distributed Cross-Layer Optimization via Genetic Algorithm; **Pranoti Balki, Kishor P. Patil**; *Sinhgad Academy of Engineering, Pune*, **India**	
16:30-17:00	COFFEE BREAK		

16:30-17:00	(Continued MRG .04 Activities) COFFEE BREAK		
17:00-19:00	**Physical and Fundamentals (II-B-3) Performance, Analysis and Ranking: WPMC || *Session Chair- Mqhele Dlodlo, University of Cape Town, South Africa***		MRG .04
	1570194241	Analysis of Data Transmission Management through Software Defined POX Controller; **Vaishnavi Moorthy, Revathi Venkatraman**; *SRM University, Chennai*, **India**	
	1570193591	Design and Performance Analysis of a Penta-band Spiral Antenna for Vehicular Communications; **Ramya R, T Rama Rao;** *SRM University, Chennai*, India	
	1570194537	Performance Analysis of Energy Detector in Correlated Log-normal Fading Channels for IR-UWB Systems; **S. Josephine, Anil Mahanta, P. R. Sahu**; *IIT Guwahati*, **India**	
	1570208727	Performance Comparision of Various Detection Methods for QO-STBC over Time Selective Channel; **Jyoti Patra, Poonam Singh**; *National Institute of Technology Rourkela*, **India**	
	1570211595	Design and Data Analysis of a Signal Measurement System Based on Variable Signature Sequences; **Ji-Hyun Moon, Jeong-Ho Kim, Na-Hyung Kim, and Bing Yuan Chen**; *Ewha Womans University*, **Republic of Korea**	
	1570191499	Ranking of Total Productive Maintenence pillars using Analytical Hierarchy Process; **Dnyandeo Shinde[1][2][3], Morten Falch[2], Rajendra Tated[3], Ramjee Prasad[4];** [1]*Center for Communication, Media and Information Technologies (CMI), Aalborg University Copenhagen,* **Denmark**, [2]*Aalborg University Copenhagen,* **Denmark,** [3] *Sandip Foundations, Nashik***, India,** [4]*CTIF, Aalborg University*, **Denmark**	
19:30-22:30	END of DAY 3 || NETWORKING DINNER: FOYER		

Time Slot	Day3: Tuesday, December 15 || MRG .05 Activities || Contributed Papers: Efficient Wireless Communications		
08:30-19:00	Registration		
09:00-11:00	**Keynote Speech**		**HALL 1**
11:00-11:30	COFFEE BREAK		
11:30-13:30	**Efficient Wireless Communications (A) | Energy Harvesting: WPMC || *Session Chair- Sudhanshu S. Jamuar, University of Malaysia Perlis*, Malaysia**		MRG .05
	1570213231	Energy-Efficient Resource Allocation for Hybrid Services with QoS Requirements in Cellular Network*;* **Yuhao Zhang, Ning Wang, Baoling Liu***; Beijing University of Posts and Telecommunications*, **China**	
	1570192925	DEAR: An Energy-centric Adaptive Region of Interest Mechanism for Wireless Mobile Devices; **Hrishikesh Venkataraman①, Ting Bi②, Ting Wu②, Gabriel-Miro Muntean②;** ①*Center for Smart Cities, Indian Institute of Information Technology (IIIT), Chittoor, Sricity, AP,* **India,** ②*Performance Engineering Laboratory, Dublin City University (DCU), Glasnevin, Dublin 9,* **Ireland**	
	1570192965	EDAS- Energy-Efficient Device-based Adaptive Cross-Layer Scheme for Wireless Multimedia Transmission; **Hrishikesh Venkataraman①, Shen Wang②, Gabriel-Miro Muntean②;** ①*Center for Smart Cities, Indian Institute of Information Technology (IIIT), Chittoor, Sricity, AP,* **India,** ②*Performance Engineering Laboratory, Dublin City University (DCU), Glasnevin, Dublin 9,* **Ireland**	
	1570194465	Energy Efficient Scheduling Algorithm for the Real-time Multicast and Unicast Services; **Min Wang①, Qiaoyun Sun①, Shuguang Zhang①, Yinlong Liu②, Yu Zhang②;** ①*Information School, Beijing City University;* ②*Institute of Information Engineering Chinese Academy of Sciences, Beijing;* **China**	
	1570213117	Secrecy Outage of a Cognitive Relay Network with Energy Harvesting and Imperfect CSI; **Pranabesh Maji, Binod Prasad, Sanjay Dhar Roy, Sumit Kundu;** National Institute of Technology, Durgapur, **India**	
	1570213446	Analytical Model of Relay Node Integrating IEEE 802.15.4 MAC and Energy Conserving State Behaviour; **Rajavaraprasad Yerra, Malyala Pavana Ravi Sai Kiran, Pachamuthu Rajalakshmi**; Indian Institute of Technology Hyderabad, **India**	
13:30-14:30	LUNCH		
14:30-16:30	**Efficient Wireless Communications (B) | Security, Trust, Privacy and Authentication: WPMC || *Session Chair- Vandana Rohokale , SIT, Lonavala, India***		MRG .05
	1570194123	Elliptic Curve Cryptography based Key Management for the M2M Local Cloud Platform; **Bayu Anggorojati①, Neeli Rashmi Prasad②, Ramjee Prasad①;** ①*Center For TeleInFrastruktur , Aalborg University*, **Denmark**; ②*Center For TeleInFrastruktur*, **USA (***)**	
	1570210161	Privacy-Preserving Friend Matching Protocol approach for Pre-match in Social Networks; **Shubhangi S.Ople①, Aaradhana A. Deshmukh②, Albena Mihovska②, Ramjee Prasad②;** *Savitribai Phule Pune University*, **India,** ②*CTIF, Department of Electronics Systems Aalborg University, Aalborg*, **Denmark**	
	1570195039	A certificate-driven Approach to Access Control in Future Internet; **Nancy Ambritta①, Poonam Railkar②, Parikshit Narendra Mahalle①;** ①*Sinhgad Institute of Technology and Sciences & Smt. Kashibai Navale College of Engineering,* ②*Smt. Kashibai Navale College of Engineering of Engineerin, Pune University*; **India (***)**	
	1570195141	A Modified RFID Authentication Protocol Using Elliptic Curve Cryptography; **Rajesh Dochania, Nirmal Roberts, Karm V Arya***; ABV-Indian Institute of Information Technology and Management, Gwalior*, **India**	
	1570213335	Secure and Privacy Enabled Anonymous Computing for Heterogeneous (SPEACH) IoT; **Meena Singh, Rajan M A, Shivraj Vl , P. Balamuralidhar**; *Tata Consultancy Sevices Limited*, **India**	
16:30-17:00	COFFEE BREAK		

16:30-17:00	COFFEE BREAK		
17:00-19:00	**Efficient Wireless Communications (C)	Security, Trust, Privacy and Authentication: WVITAE || *Session Chair-K.V. Arya, AVIIITM, Gwalior, India***		MR5 .05
	1570213434	Architectural Integration for Security in Advanced Metering Infrastructure; **Priyanka D.Halle[1], Vandana Rohokale[1], Ramjee Prasad[2]**; [1]E&TC SKNSITS, Lonavala, **India** [2] *Center For TeleInFrastruktur , Aalborg University*, **Denmark**	
	1570194669	Trustbook: A Trust-based access control in Online Social Networks; **Vedashree Takalkar, Parikshit Narendra Mahalle**; Savitribai Phule Pune University, STES, Pune, **India**	
	1570210113	Daubechies Wavelet based Effective Data Authentication in Wireless Domain; **Anirban Goswami[1], Nabin Ghoshal[2]**; [1]*Techno India*, [2]*University of Kalyani*; **India**	
	1570211897	Mesh IP Video Surveillance Systems Model Design and Performance Evaluation; **Smart Lubobya[1], Mqhele E. Dlodlo[1], De Jager Gerhard[1], Ackim Zulu[2]**; [1]*University of Cape Town*, **South Africa**; [2]*University of Zambia*, **Zambia**	
	1570210201	Secret Transmission through Audio Signal with Reduced Distortion for Wireless Communication (STASRD); **Dipnkar Pal[1], Nabin Ghoshal[2]**; [1]*Techno India*, [2]*University of Kalyani*; **India**	
	1570209931	Secure E- Voting System with integration of NFC, Biometrics and Cloud Computing; **Amol Potgantwar[1], Tejas Upasani[2]**; [1] *Sandip Foundation*, [2]*Savitribai Phule*,[1][2]*Pune University*; **India**	
19:30-22:30	END of DAY 3 || NETWORKING DINNER: FOYER		

Time Slot	Day3: Tuesday, December 15 || MRG .06 Activities || 23rd GISFI Standardization Series Meeting Meeting on Security and Privacy/ WWSMC	
08:30-19:00	Registration	
09:00-10:30	**23rd GISFI Standardisation Meeting on Security and Privacy/ WWSMC:** *Session Chair:* ***Anand R. Prasad****, NEC Corporation* ***Japan****; Session Organiser:* ***Anand R. Prasad,*** *NEC Corporation* ***Japan****;* ***Krishna Sirohi****, NIKSUN,* ***USA;*** ***Sivabalan Arumugam,*** *NEC Mobile Network Excellence Centre(NMEC), NEC India Pvt Ltd,* ***India*** Opening by Co-Chairs: **Anand R. Prasad**, Chief Advanced Technologist, Executive Specialist, NEC Corporation ; **Krishna Sirohi**, Senior Advisor, Niksun **Session 1: Cyber Security ||** Moderator**: Krishna Sirohi**, NIKSUN Topic: Cyber Security**, Ramamurthy Gemini,** *Chairman , Cyber security & privacy foundation***, India** **Session 2: IoT Security ||** Moderator: **Krishna Sirohi**, NIKSUN Topic: Internet of Things – Security**; Sivabalan Arumugam,** NEC Mobile Network Excellence Centre(NMEC), NEC India Pvt Ltd	MRG .06
10:30-11:00	COFFEE BREAK	
11:00-13:00	**GISFI Special Session on Security and Privacy/ WWSMC-1** **Session 3: Communication System Security ||** Moderator: Anand R. Prasad, NEC Corporation Topic: Telecom Security **; Vijay Madan,** Chief Mentor - IT & Technology, Network Operation, Tata Teleservices Limited Topic: Telecom Security **; Alf Zugenmaier,** Professor, Munich University of Applied Sciences Topic: Mobile PKI , **Zia Saquib**, Scientist, CDAC, Hyderabad Topic: Wired & Wireless Security **G.K. Satyanarana;** Head, Telecom, ECIL, Hyderabad	MRG .06
13:00-14:00	LUNCH	
14:00-16:00	**GISFI Special Session on Security and Privacy/ WWSMC-1** **Session 4: Cloud & Platform Security ||** Moderator: Sivabalan Arumugam, NEC India Pvt Ltd Topic: Information Security - Cloud Environment ; **Gopala Rao Jammi**, Professor , MEC (A Group of TechM), Hyderabad Topic: Personal Safety: Next Frontier in Mobile Security ; **Kulkarni Dattatraya**, Intel Security Group, Bangalore Topic: NFV Security**; Prabhu T**, NEC India, Chennai, **India** Topic: Monitoring Aspects**; Krishna Sirohi,** Senior Advisor, NIKSUN	MRG .06
16:00-16:15	COFFEE BREAK	
16:15-17:15	**GISFI Special Session on Security and Privacy/ WWSMC-2** **Session 5: Panel Discussion "What are the pains? What is needed?" ||** Moderator: **Anand R. Prasad**, NEC Corporation, **Japan** **Vijay Madan,** Chief Mentor - IT & Technology, Network Operation, Tata Teleservices Limited **G.K. Satyanarana,** Head, Telecom, ECIL, Hyderabad **Krishna Sirohi,** Senior Advisor, NIKSUN **Alf Zugenmaier,** Professor, Munich University of Applied Sciences	MRG .06
19:30-22:30	END of DAY 3 || NETWORKING DINNER: FOYER	

Wednesday, December 16

Day 4

"Workshops, Special Sessions, Contributed Papers"

Time Slot	Day4: Wednesday, December 16 || HALL 1.1 & 1.2 Activities || Workshops & Special Sessions (III-A)		
08:30-19:00	Registration		
09:00-11:00	**Keynote Speech || Session Chair : Ramjee Prasad, Center for TeleInFrastructure , Aalborg University, Denmark** **fred Harris**, San Diego State University, **USA** **Harish Mysore**, *IEEE*, **India** **Dinesh Chand Sharma,** *SESEI*, **India**		HALL 1
11:00-11:30	COFFEE BREAK		
11:30-13:30	**Second International Workshop on Innovation and Entrepreneurship(IWIE)- III** **Workshop Organizer and Chair: Sofoklis Kyriazakos,** CTIF, Aalborg University, **Denmark**		HALL 1.1
	WVITAE Special Session on "Communication, Navigation, Sensing and Services (CONASENSE)" - I **Session Organizers and Chairs: *Leo Ligthart, Tu-Delft, the Netherlands; Ernestina Cianca, University of Rome Tor Vergata, Italy***		HALL 1.2
	1570227732	Modified RAR and PLSR-based artifact removal for stroke detection in UWB radar imaging; **E. Ricci, A. Colucciello, S. Di Domenico, E. Cianca, T. Rossi**; University of Rome "Tor Vergata",Rome, **Italy**	
	1570228263	Communication Framework for Tele-rehabilitation Systems with QoS Guarantee; Plamen Semov, **Nikolay Dandanov, Georgi Balabanov, Krasimir Tonchev and Vladimir Poulkov**; *Technical University of Sofia*, **Bulgaria**	
	1570230189	vNet Zero Energy for Radio Base Stations- Balearic Scenario①; Pere Sabater Frau①, Albena Mihovska①, Ramjee Prasad①, Andreu Moia Pol② ,Angel Igelmo Ganzo②, Xavier Canals Solé③, Jaume Ochogavia Colom④; *Center for TeleInFrastruktur (CTIF) Aalborg University, **Denmark**; ②Universitat Illes Balears (UIB), ③Telefonica España S.A., ④Balearic Islands Government*, **Spain**	
	1570236132	Reliable Frame Selection for Speaker Identification under Voice Disguise Scenario; **Swati Prasad, Ramjee Prasad**; *Centre for TeleInfrastruktur (CTIF), Aalborg University, Aalborg*, **Denmark**	
	1570228151	Performance Analysis of SOFDM Transmission Scheme over Integrated Satellite/Terrestrial Network; **Akash Agarwal□①, B. M. Bhaveja②, Preetam Kumar①**; ①*Indian Institute of Technology Patna□*, ②*Department of Electronics & Information Technology (DeitY) New Delhi*, **India (***)**	
13:30-14:30	LUNCH		
14:30-16:30	**Second International Workshop on Innovation and Entrepreneurship(IWIE)- III (Contd)** **Workshop Organizer and Chair: Sofoklis Kyriazakos,** CTIF, Aalborg University, **Denmark**		HALL 1.1
	WVITAE Special Session on "Communication, Navigation, Sensing and Services (CONASENSE)" -II **Session Organizers and Chairs: *Leo Ligthart, Tu-Delft, the Netherlands; Ernestina Cianca,** University of Rome Tor Vergata, **Italy***		HALL 1.2
	1570226963	Efficient Filtering Technique for Chronic Wound Image Processing under Tele-Wound Network; **Chinmay Chakraborty, Bharat Gupta**; *Birla Institute of Technology Jharkhand*, **India**	
	1570227100	End-to-End Delay Analysis of IEEE 802.15.6 Standard for WBAN Medical Paradigm; **Vivek Kumar, Bharat Gupta**; *Birla Institute of Technology Jharkhand*, **India**	
	1570227212	Relevance of signal processing of the voice in diagnosing human tuberculosis; **Giovanni Saggio①, Santosh Bothe②**; ①University of Rome "Tor Vergata",Rome, **Italy, ②***Bharati Vidyapeeth University , Pune*, **India**	
	1570227247	A P2P architecture for Mobile Assisted Logistic Operations; **Pierpaolo Loreti* , Lorenzo Bracciale* , Francesco Zampognaro* , Massimo Povia† , Gianluca Gargiulo‡;** **NITEL - University of Rome Tor Vergata, †Technosky Via del Casale Cavallari, §NAIS Via Andrea Noale; Rome*, **Italy**	
	1570238200	GeoLocation Aware Dynamic Spectrum Sensing in Cognitive Radio Networks; **Usha Kurumaddali,** *GGS Indraprastha University*, **India**	
17:30	END OF WPMC-2015 & GWS-2015		

Time Slot	Day 4: Wednesday, December 16 || MRG .01 Activities || Contributed Papers: Wireless Communications		
08:30-19:00	Registration		
09:00-11:00	**Keynote Speech**		**HALL 1**
11:00-11:30	COFFEE BREAK		
11:30-13:30	**Wireless Communications (A) | Spectrum for Future Radio Networks: WPMC || *Session Chair: Albena Mihovska, CTIF, Aalborg University, Denmark***		MRG .01
	1570235616	Preliminary performance evaluation of the FBMC based future IEEE 1900.7 Standard; **D. Noguet, J.-B. Doré and B. Miscopein**; *Minatec Campus CEA Leti 17, rue des Martyrs – 38054 Grenoble Cedex 9*, **France**	
	1570213121	Long-haul Communication Trial in London TV White-space with IEEE 802.11af-based High Power Prototype; **Takeshi Matsumura[1] , Kentaro Ishizu[1] , Keiichi Mizutani[2], Tran Ha Nguyen[1], Homare Murakami[1][3], Fumihide Kojima[1][3], Hiroshi Harada[2][3]**; *[1]NICT, Yokosuka, [2]Kyoto University, [3]Kyoto, ICT, Koganei*, **Japan**	
	1570192849	Outage Analysis of Cellular Two-Way Relaying with Spectrum Sharing in Nakagami-m Fading; **Ronshee Chawla, M. Mounika Reddy, Prabhat Kumar Upadhyay**; *IIT Indore*, **India**	
	1570213448	Field Experiments for Broadband Mesh Network Operating in TV White Space; **Kentaro Ishizu, Fumihide Kojima**; *National Institute of Information and Communications Technology*, **Japan**	
	1570210145	TVWS Regulations and the first IEEE 802.11af indoor experiments in Singapore; Dien Vinh Hoang[1], Takeshi Matsumura[2], Kentaro Ishizu[2], Homare Murakami[2], Fumihide Kojima[2]; [1]*Singapore Smart Wireless Lab, National Institute of Information and Communications Technology* (NICT), **Singapore**, [2]*NICT*, **Japan**	
	1570194697	Novel Closed form Expression for Multi Cell Cooperation using MHCP to Reduce Interference; **Suman Yadav, S Pratap Singh**; *Galgotia College of Engineering and Techolongy*, **India**	
13:30-14:30	LUNCH		
14:30-16:30	**Wireless Communications (B) | Algorithms and Innovative Approach: WVITAE || *Session Chair: Sri Chandrasekaran, IETE, India***		MRG .01
	1570210211	Classification Based Automatic Assessment for Web Based Learning; Wacharawan Intayoad, Punnarumol Temdee; Mae Fah Luang University, **Thailand**	
	1570188921	Comparative analysis of load balancing algorithms for LTE/LTE-A Hetnets; **Diego Castro-Hernandez**, **Raman Paranjape**; *University of Regina*, **Canada**	
	1570208745	Fuzzy based Moving Object Detection and Classification in Video; **Manojkumar M Gawali**, *Sinhgad College of Engineering*, Pune, **India**	
	1570213914	Swarm Optimization Based on Genetic Algorithm & Relevance Feedback Technique for Data Clustering; **Gandamalla Malini, M.Seetha, K.V.N.Sunitha**; *GNITS, Hyderabad*, **India**	
	1570212950	Downlink Joint Processing for Non Orthogonal Multiple Access; **Islam Atef, Essam Sourour;** *Alexandria University, Alexandria*, **Egypt**	
	1570197177	The Studies of Millimeter Waves at the frequencies of 60 GHz in Outdoor Environments- A Survey; **Hitesh Singh**; *HMRITM, Delhi*, **India**	
16:30-17:00	COFFEE BREAK		
	Networking		
	END OF WPMC-2015 & GWS-2015		

Time Slot	Day 4: Wednesday, December 16 || MRG .02 Activities || Contributed Papers: Physical and Fundamentals (III)		
08:30-19:00	Registration		
09:00-11:00	**Keynote Speech**		**HALL 1**
11:00-11:30	COFFEE BREAK		
11:30-13:30	**Physical and Fundamentals (III–A) | Signal Processing-1: WPMC & WVITAE || *Session Chair: Navin Kumar, Amrita University, Bangalore, India***		**MRG .02**
	1570194245	Blind Image Quality Assessment Based on Phase Congruency and Spatial-spectral Entropies; **Maozheng Zhao, Yanping Lu, Cuiwei Li, Ran Gao, Qin Tu, Bo Yang, Aidong Men**; *Beijing University of Posts and Telecommunications*, **China**	
	1570195699	Opinion-unaware blind image quality assessment based on sparse representation; **Maozheng Zhao[1], Xiaoqiang Guo[2], Ran Gao[1], Bo Yang[1], Aidong Men[1]**; [1]*Beijing University of Posts and Telecommunications*, [2]*Academy of Broadcasting Science*, **China**	
	1570208027	QoE Based Pseudo Heartbeat Message Compression Mechanism for Wireless Networks; **Zhiqun Hu, Xiangming Wen, Zhaoming Lu, Zhaoxing Li**; *Beijing University of Posts and Telecommunications*, **China**	
	1570213506	**WVITAE**: On CS Reconstruction Images using LDPC code over Radio Mobile channel; **Ankita Pramanik, Santi Prasad Maity**; *Indian Institute of Engineering Science and Technology, Shibpur*, **India**	
	1570210061	Modeling of Modified Erlang-k Distribution for Raindrop Size Distribution over South Africa; **Akintunde Alonge, Thomas Afullo**; *University of KwaZulu-Natal, Durban*, **South Africa**	
	1570192393	Enhanced Turbo Equalizer Using 2 Dimensional Iterative Soft Decision Interference Cancellation; **Doron Shinbox, Dan Raphaeli**; *Tel-Aviv University*, **Israel**	
13:30-14:30	LUNCH		
14:30-16:30	**Physical and Fundamentals (III –B) | Design and Development: WPMC & WVITAE || *Session Chair: Venkatapathy Prithviraj, Rajalakshmi Institute of Technology, Chennai, India***		**MRG .02**
	1570209863	Modeling & Simulation for complex System of systems design, test, and verification; **Uma Jha, Jon Wada**; *Space & Airborne Systems, Raytheon CoEl Segundo, California* , **USA**	
	1570213885	Design Of Low Voltage Bandgap Reference Circuit Using Subthreshold MOSFET; Sushma Sangolli, Rohini Hongal; *B.V.B College of Engineering and Technology, Hubli*, **India**	
	1570194201	Eight-Path Harmonic Rejection Mixer for Full Band Mobile TV; **Kiran B, Roy P Paily**; *Indian Institute of Technology Guwahati*, **India**	
	1570209947	Database Assisted Automatic Modulation Classification Using Sequential Minimal Optimization; **K. Pavan Kumar Reddy, Lakhan Shiva, Kadiri Abhilash, Yoganandam Yeleswarapu**; *Birla Institute of Technology and Science, Hyderabad Campus*, **India**	
	1570212671	Design and Development of a Mobile Wireless Video Streaming Mote; **Bhuvanesh D, Manjunath Hegde, Manikandan J**; *PES Institute of Technology*, **India**	
	1570213484	Design of BiCMOS based low temperature coefficient bandgap reference; **Deepa Talewad, Anilkumar Nandi, Ramesh Karmungi**; *B.V.B College of Engineering and Technology, Hubli*, **India**	
16:30-17:00	COFFEE BREAK		
	Networking		
	END OF WPMC-2015 & GWS-2015		

Time Slot	Day 4: Wednesday, December 16 || MRG .03 Activities || Contributed Papers: Wireless Networks		
08:30-19:00	Registration		
09:00-11:00	**Keynote Speech**		**HALL 1**
11:00-11:30	COFFEE BREAK		
11:30-13:30	**Wireless Networks | WPMC & WVITAE || *Session Chair: G S Tomar, MIR Labs, Gwalior, India***		MRG .03
	1570184143	A Fine Grained Position for Modular Core NoC; B. **Naresh Kumar Reddy, M.H.Vasantha, Y.B.Nithin Kumar, Dheeraj Sharma**; *National Institute of Technology, Goa*, India **(***)**
	1570191965	Analytical Evaluation of Frequency Reuse For Hybrid Full-/Half-Duplex Cellular System; Wenping Bi, Limin Xiao, Xin Su, Shidong Zhou; *Tsinghua University*, **China**
	1570192715	A New Approach for Crossed Sector Detection in Live Mobile Networks based on Radio Measurements; David Duarte①②, Pedro Vieira①②, António J. Rodrigues③, André Martins, Nuno Silva③; ①*Instituto Superior de Engenharia de Lisboa (ISEL),* ②*Instituto de Telecomunicac¸˜oes (IT), Lisbon,* ③*Instituto Superior T´ecnico (IST), Lisbon,* **Portugal**
	1570213280	A Revolutionary Rural Agricultural Participatory Sensing Approach Using Delay Tolerant Networks; **Prateek Gupta, Bhushan Gurmukhdas Jagyasi, Bighnaraj Panigrahi, Hemant Kumar Rath, Srinivasu Pappula, Anantha Simha**; *Tata Consultancy Services*, **India**
	1570213277	**WVITAE:** Performance Analysis of EPC with IMS Network Architecture; **A Bagubali①, Prithiviraj Venkatapathy②, Pathak Mallik①**; ①*VIT University, Vellore,* ②*Rajalakshmi Institute of Technology , Chennai,India,* **India**
	Invited Talk	Role of Cyber Security for Digital Business; **T. R. Dua**, *GISFI*, **India**
13:30-14:30	LUNCH		
14:30-16:30	**Wireless Networks | WPMC || *Session Chair: Hrishikesh Vankataraman, Indian Institute of Information Technology, Chittoor, India***		MRG .03
	1570213596	IEEE802.15.4g based Wide Area and Mobile Wi-SUN Communication Systems; **Hiroshi Harada, Keiichi Mizutani, Kentaro Mochizuki, Kentaro Obata**; *Kyoto University*, **Japan**
	1570207517	Hierarchical Mesh Based Energy Efficient Multicast Routing on IEEE 802.15.4 based networks; **Verotiana Rabarijaona①, Fumihide Kojima①, Hiroshi Harada②**; ①*National Institute of Information and Communication Technology,* ②*Kyoto University & Graduate School of Informatics,* **Japan**
	1570192635	Efficient Visibility Modeling for Free-Space Optical Systems Design; **Ivo Sousa①③, António J. Rodrigues②, Maria Paula Queluz②**, ①*Instituto de Telecomunicac¸˜oes (IT), Lisbon,* ②*Instituto Superior T´ecnico (IST), Lisbon,* **Portugal**
	1570187749	Reliable Link Layer Packet Reconstruction for Rotating Polarization Based Radio Communication; **Ritesh Kumar Kalle**, *HITACHI*, **India**
	1570213414	SUN-RAN Orchestrating Resource Management using Superframe Division Data Aggregation Technology; **Fumihide Kojima, Chang-Woo Pyo, Masayuki Oodo**; *National Institute of Information and Communications Technology(NICT),* **Japan**
	1570176791	Green Indoor Network In A Passive Way; Yu Liu, *Jiangsu Automation Research Institute*, **China**
16:30-17:00	COFFEE BREAK		
	Networking		
	END OF WPMC-2015 & GWS-2015		

Time Slot	Day 4: Wednesday, December 16 || MRG .04 Activities || Workshops & Special Sessions (III-B); IC5		
08:30-19:00	Registration		
09:00-11:00	**Keynote Speech**		**HALL 1**
11:00-11:30	COFFEE BREAK		
11:30-13:30	23rd GISFI Standardization Meeting- 5 G Innovation in India **Session Chair: Ashutosh Dutt**		
	Presentation1	5G Framework for a Personalised Network; **Nitish Mittal**, *5G Company, Vishawaniketan*, **India**	
	Presentation2	5G Model in WISDOM; **Sounak Moulik**, *5G Company, Vishawaniketan*, **India**	
	Presentation3	Security Challenges in a 5G Network; **Nidhi** , *5G Company, Vishawaniketan*, **India**	
	Presentation4	5G Concept; **Sandeep Mukherjee**, *,5G Company, Vishawaniketan*, **India**	
13:30-14:30	LUNCH		
14:30-16:30	**IC5: Third International Conference on Communications, Connectivity, Convergence, Content and Cooperation** **Session Chair: Swrana Ravindra Babu, IETE, India**		MRG .04
	1570213308	Survey on Service Discovery Mechanisms; **Gitanjali Shinde Henning Olesen**; *Center for Communication, Media and Information Technologies (CMI) Aalborg University Copenhagen*, **Denmark**	
	1570191301	Multislotted Microstrip Patch Antenna for Dual Band and UWB Applications; **Shailendra Kumar Dhakad, Dr. Neeraj Kumar, Keshav Kumar, Swapnil Mengade, Rohit Gupta**; *Birla Institute Of Technology and Science Pilani, Goa*, **India (***)**	
	1570194207	An application of Internet of Things in Transportation System; **Ganesh Balaraman, Harisudha Kuresan**; *SRM University*, **India (***)**	
	1570195047	Analysis of Audio Watermarking Techniques for Cyber Security in Copyright Infringement; **Sushma Ambekar① □, Vandana Rohokale①, Ramjee Prasad②;** ①SKNSITS, Lonavala, **India**, ②CTIF, Aalborg University, **Denmark**	
	1570208707	30-Second Integration Time Power Law Conversion Model for Rainfall Attenuation in South Africa; **Mary N. Ahuna,, Thomas J. Afullo, , Akintunde A. Alonge**; *University of KwaZulu Natal Durban*, **South Africa**	
	1570209327	Illumination, Indoor Localization and Very High Speed Data Communication using VLC; **Anusha Addanki, Navin Kumar**; *Amrita Vishwa Vidyapeetham (University) Bangalore*, India	
16:30-17:00	COFFEE BREAK		
	Networking		
	END OF WPMC-2015 & GWS-2015		

Time Slot	Day 4: Wednesday, December 16 || MRG .05 Activities || Workshops & Special Sessions (III-C)		
08:30-19:00	Registration		
09:00-11:00	**Keynote Speech**		**HALL 1**
11:00-11:30	COFFEE BREAK		
11:30-13:30	**WVITAE Special Session on " Wireless Communications"** **Session Organizer and Chair** : *Mqhele Dlodlo, University of Cape Town, South Africa*		MRG .05
	1570227491	Hard-combined Cooperative spectrum sensing using Time-frequency method; **S M Hiremath①, Sarat Kumar Patra①, Amit Kumar Mishra②;** ①*National Institute of Technology Rourkela, Odisha,* **Indiadlodlo,** ②*University of Cape Town*, **South Africa**	
	1570228229	The Implementation of the Modified AODV Routing Protocol in Mobile Ad-Hoc Networks; **Vekani Reviet Baloyi, Lesiba Kola**; *University of Limpopo*; **South Africa (###)**	
	1570228530	Enlarged QR-LRL Based Massive MIMO Detector for Soft Output Generation; **Sukriti Garg, Krati Mittal, Divyang Rawal**; *LNM Institute of Information Technology, Jaipur*, **India**	
	1570230967	Interference Management in Heterogeneous and Small Cell NetwPerorks; **M. Bala Krishna, Puneet Bansal**; *Guru Gobind Singh Indraprastha University , New Delhi,* **India**	
	1570233114	Mesh IP Video Surveillance System - A System Perspective and Performance Evaluation; **M .E. Dlodlo, C. S. Lubobya, S Lubobya, O Osanaiye, E Okumu, H Ohize,** *University of Cape Town*, **South Africa**	
13:30-14:30	LUNCH		
14:30-16:30	**WPMC Special Session on " Selected Topics in Physical & Fundamentals -2"** **Session Organizer and Chair** : ***Bharat Gupta, Birla Institute of Technology, Ranchi, India***		MRG .05
	1570210153	An ingenious framework for solving cold start problem in recommender system; **Pankaj Chaudhary① , A. A. Deshmukh②**; ①*Smt. Kashibai Navale College of Engineering, Pune* **India**, ②*Department of Electronics Systems, Aalborg University*, **Denmark (***)**	
		Area-Power Analysis of Carry Selected Adder using Transmission Gates; **Ch. Rajendra Prasad①, T. Anil Kumar②**; ①*SVS Institute of Technology*, ②*SR Engineering College*; Warangal, **India (###)**	
		Privacy Preserving Friend Matching Protocol for Pre match in Social Networks; **Shubhangi Ople, Aradhna Deshmukh**; *Smt. Kashibai Navale College of Engineering, Pune* **India (###)**	
		Self-Programmable Variable Digital Filter (VDF) Design Based of FPGA; **T. Anil Kumar;** *SR Engineering College,* Warangal, **India (###)**	
		Design of High Performance Phase Locked Loop for Clock Synchronization; A. Rajesh①, B.L. Raju①, K. Chenna Kesava Reddy②; ①ACE, Engineering College, ②*Jawaharlal Nehru Technological University College of Engineering*; Hyderabad, **India** (###)	
	1570237867	Object Detection, Passive tracking and Active Tracking; **Shreeya Shevade**, *Government College of Engineering, Aurangabad, Maharashtra,* **India (***)**	
16:30-17:00	COFFEE BREAK		
	Networking		
	END OF WPMC-2015 & GWS-2015		

Time Slot	Day 4: Wednesday, December 16 || MRG .06 Activities || Workshops & Special Sessions (III-C)	
08:30-19:00	Registration	
09:00-11:00	**Keynote Speech**	**HALL 1**
11:00-11:30	COFFEE BREAK	
11:30-13:30	**Networking Meeting**	MRG .06
13:30-14:30	LUNCH	
14:30-16:30	**GISFI Future Strategy Meeting**	MRG .06
16:30-17:00	COFFEE BREAK	
	Networking	
	END OF WPMC-2015 & GWS-2015	

Note:

***** paper withdrawn and/or resubmitted with different title**

paper was not presented by authors

Index of Papers
WVITAE-2015

INDEX OF PAPERS SUBMITTED IN WVITAE 2015

Conference	Paper ID	Paper Title	Page #
WVITAE 2015	1570188607	Evaluating the Effect of Selfishness on Flooding Based DTN Routing Algorithms	68
WVITAE 2015	1570188921	Comparative analysis of load balancing algorithms for LTE/LTE-A Hetnets	73
WVITAE 2015	1570188927	Performance Analysis of Multiband Tapered Feed Single-Arm Spiral Antenna for Vehicular Communication	78
WVITAE 2015	1570191635	Single Thing Sign On Identity Management for Internet of Things	82
WVITAE 2015	1570192393	Enhanced Turbo Equalizer Using 2 Dimensional Iterative Soft Decision Interference Cancellation	87
WVITAE 2015	1570194189	HANET: Millimeter wave based intelligent radio architecture for serving place time capacity issue	92
WVITAE 2015	1570194569	A new shaping code for PAPR Reduction in Single-Carrier Modulation	97
WVITAE 2015	1570194669	Trustbook: A Trust-based access control in Online Social Networks	102
WVITAE 2015	1570195047	Analysis of Audio Watermarking Techniques for Cyber Security in Copyright Infringement	107
WVITAE 2015	1570195421	GSHMAC: Green and Secure Hybrid Medium Access Control for Wireless Sensor Network	112
WVITAE 2015	1570197177	The Studies of Millimeter Waves at the frequencies of 60 GHz in Outdoor Environments- A Survey	117
WVITAE 2015	1570206439	Real-time Detection of EEG Electrode Displacement for Brain-Computer Interface Applications	121
WVITAE 2015	1570207041	Design of Amateur Radio Wireless Transceiver to Reduce the Impact of Natural Calamities	126
WVITAE 2015	1570207637	PAPR Reduction Comparison of the MC-CDMA System with Various Companding Techniques	131
WVITAE 2015	1570208291	Joint Channel Estimation and CCI Cancellation for STBC-OFDM System in Fast Fading Channel	136
WVITAE 2015	1570208685	Energy Efficient Lighting System for Indoor Parking with Ubiquitous Communication	141
WVITAE 2015	1570208707	30-Second Integration Time Power Law Conversion Model for Rainfall Attenuation in South Africa	146
WVITAE 2015	1570208745	Fuzzy based Moving Object Detection and Classification in Video	151
WVITAE 2015	1570209327	Illumination, Indoor Localization and Very High Speed Data Communication using VLC	156
WVITAE 2015	1570209885	Distributed Forward-Backward Pursuit Algorithm for Distributed Compressive Sensing	161
WVITAE 2015	1570209919	Adaptive Cooperative Spectrum Sensing and Access in Cognitive Radio Networks	165
WVITAE 2015	1570209921	Marine Vessel Detection Comparing GPRS and Satellite Images for Security Applications	170
WVITAE 2015	1570209931	Secure E- Voting System with integration of NFC, Biometrics and Cloud Computing	175
WVITAE 2015	1570209977	On Performance of Eigenvalue based Detectors for Spectrum Sensing under Different Fading Conditions	179
WVITAE 2015	1570209997	Capacity Analysis of MIMO BC Channels in Presence of Spatial Correlation	183
WVITAE 2015	1570210051	Real Time Evaluation of Energy Detection and Covariance based Spectrum Sensing Algorithms	187
WVITAE 2015	1570210061	Modeling of Modified Erlang-k Distribution for Raindrop Size Distribution over South Africa	192
WVITAE 2015	1570210063	Recent Progress in Radioclimatological Modeling in Equatorial and Tropical Africa	197
WVITAE 2015	1570210103	Spectrum for 5G Services	202
WVITAE 2015	1570210113	Daubechies Wavelet based Effective Data Authentication in Wireless Domain	207

WVITAE 2015	1570210195	Rate Independent Multicarrier Variable Rate Scheme over Frequency Selective Channel	212
WVITAE 2015	1570210199	Deep Sea Exploration Recovery and Transport [DESERT] Vehicle and its Modes of Communication	217
WVITAE 2015	1570210201	Secret Transmission through Audio Signal with Reduced Distortion for Wireless Communication (STASRD)	222
WVITAE 2015	1570210205	Speech Feature Analysis and Selection for Emotion Classification	227
WVITAE 2015	1570210211	Classification Based Automatic Assessment for Web Based Learning	232
WVITAE 2015	1570210219	Performance of Amplify-and-Forward Cooperative Diversity under Ricean Fading	236
WVITAE 2015	1570210261	Digital door lock using fingerprint, webcam and GSM - a novel approach for smart homes	241
WVITAE 2015	1570211897	Mesh IP Video Surveillance Systems Model Design and Performance Evaluation	246
WVITAE 2015	1570212327	Variable Encoding and Sequencing Pattern Driven Multiple Image Bit Watermarking for Wireless Domain	251
WVITAE 2015	1570212671	Design and Development of a Mobile Wireless Video Streaming Mote	256
WVITAE 2015	1570212704	Error Rate Performance for Multiuser scheduling in MIMO downlink system with imperfect CSI	261
WVITAE 2015	1570212756	Evaluation of Channel Assembling Strategies with Single-Class Users in Cognitive Radio Networks	266
WVITAE 2015	1570212950	Downlink Joint Processing for Non Orthogonal Multiple Access	271
WVITAE 2015	1570213163	Performance of a space-time coded MC-CDMA system in a Rayleigh fading channel	276
WVITAE 2015	1570213165	Remote Heart Rate Evaluation by Variational Mode Decomposition	281
WVITAE 2015	1570213275	C2R2M: Cluster-based Cognitive Radio Routing Mechanism	286
WVITAE 2015	1570213277	Performance Analysis of EPC with IMS Network Architecture	291
WVITAE 2015	1570213308	Survey on Service Discovery Mechanisms	296
WVITAE 2015	1570213386	Public Auditing and Data Dynamics in Cloud with Performance Assessment on Third Party Auditor	301
WVITAE 2015	1570213423	Behavior State Feature Extraction through Single Channel EEG Device for Medical Application	306
WVITAE 2015	1570213430	Access for Internet of Things using Smartphone as a Gateway utilizing LTE and WiFi	311
WVITAE 2015	1570213434	Architectural Integration for Security in Advanced Metering Infrastructure	315
WVITAE 2015	1570213454	Cognitive framework for flexible queuing strategy in Next Generation Networks	320
WVITAE 2015	1570213484	Design of BiCMOS based low temperature coefficient bandgap reference	325
WVITAE 2015	1570213506	On CS Reconstruction Images using LDPC code over Radio Mobile channel	330
WVITAE 2015	1570213573	Spectrum Scarcity at the Extensive and Intensive Edges: From White Space to 5G	335
WVITAE 2015	1570213870	Study of Radiated Emission from Wireless Positioning System and strategies to minimize Radiations	340
WVITAE 2015	1570213872	Conducted EMI Analysis of Vehicle Positioning System and Strategies to Reduce Conducted EMI	345
WVITAE 2015	1570213885	Design of Low Voltage Bandgap Reference Circuit Using Subthreshold MOSFET	350
WVITAE 2015	1570213914	Swarm Optimization Based on Genetic Algorithm & Relevance Feedback Technique for Data Clustering	355
WVITAE 2015	1570213985	Self Configurable Intelligent Distributed Antenna System	360
WVITAE 2015	1570214001	Embedded Video Processing and Data Acquisition for Unmanned Aerial Vehicle	365
WVITAE 2015	1570214751	Automatic Household Power Measurement & Control System based on Wireless Sensor Networks	370

WVITAE 2015	1570215979	Service Interaction through Gateways for Inter-Cloud Collaboration within the Arrowhead Framework	376
WVITAE 2015	1570221151	Cancellation of Inter-Cell Interference in Downlink with No Backhaul Information Exchange	382
WVITAE 2015	1570226963	Efficient Filtering Technique for Chronic Wound Image Processing under Tele-Wound Network	387
WVITAE 2015	1570226980	Performance Analysis Of Interference Cancellation In MIMO-FBMC	392
WVITAE 2015	1570227100	End-to-End Delay Analysis of IEEE 802.15.6 Standard for WBAN Medical Paradigm	397
WVITAE 2015	1570227212	Relevance of signal processing of the voice in diagnosing human tuberculosis	402
WVITAE 2015	1570227247	A P2P architecture for Mobile Assisted Logistic Operations	406
WVITAE 2015	1570227491	Hard-combined Cooperative spectrum sensing using Time-frequency method	411
WVITAE 2015	1570227724	Measurement and Identification of White Space using Low Cost SDR for Rural Wireless Broadband	416
WVITAE 2015	1570227732	Modified RAR and PLSR-based artifact removal for stroke detection in UWB radar imaging	421
WVITAE 2015	1570228022	Participation of Optical Backbone Network in Successful Advancement of Wireless Network	426
WVITAE 2015	1570228026	On 5G Cellular Backhaul Networks	431
WVITAE 2015	1570228109	Cybersecurity for M2M Smart Grid	436
WVITAE 2015	1570228216	Persuasive Technology and Business Models	441
WVITAE 2015	1570228247	GET IoT- Green Computing and Energy Harvesting technology in Internet of Things (IoT)	446
WVITAE 2015	1570228263	Communication Framework for Tele-rehabilitation Systems with QoS Guarantee	451
WVITAE 2015	1570228361	An Energy Efficient Adaptive Wireless Link for Farms based on IoT technologies	456
WVITAE 2015	1570228530	Enlarged QR-LRL Based Massive MIMO Detector for Soft Output Generation	461
WVITAE 2015	1570228627	Service and Big Data business model in a world of persuasive technologies	466
WVITAE 2015	1570230189	vNet Zero Energy for Radio Base Stations- Balearic Scenario	471
WVITAE 2015	1570230967	Interference Management in Heterogeneous and Small Cell Networks	476
WVITAE 2015	1570231008	Implementation Of Internet Of Things Using Near Field Communication For Parking Automation	481
WVITAE 2015	1570233114	Wireless Mesh IP Video Surveillance System - A Systems Perspective	485
WVITAE 2015	1570235616	Preliminary performance evaluation of the FBMC based future IEEE 1900.7 Standard	490
WVITAE 2015	1570236132	Reliable Frame Selection for Speaker Identification under Voice Disguise Scenario	496
WVITAE 2015	1570238200	GeoLocation Aware Dynamic Spectrum Sensing in Cognitive Radio Networks	500
WVITAE 2015	1570238521	Technical Background for Quality Long-Term Care Services in Europe	505

Technical Papers
WVITAE-2015

THE 5TH INTERNATIONAL CONFERENCE ON WIRELESS COMMUNICATIONS, VEHICULAR TECHNOLOGY, INFORMATION THEORY, AEROSPACE & ELECTRONIC SYSTEMS (WVITAE-2015)
December 13-16, 2015, Hyderabad, India

Evaluating the Effect of Selfishness on Flooding Based DTN Routing Algorithms

Sobin C C
Dept. of Computer Science and Engineering
IIT Roorkee, Uttarakhand, India - 247667
Email: sobincc@gmail.com

Vaskar Raychoudhury
* Dept. of Computer Science and Engineering
IIT Roorkee, Uttarakhand, India - 247667
Email: vaskar@ieee.org

***Abstract*—Delay Tolerant Networks (DTNs) are sparse mobile networks in which a complete end-to-end path may not exist. Routing is challenging in such networks, because of the frequent network disconnections, which will result in frequent change in network topology. Most of the existing DTN routing algorithms consider that all the nodes are honestly participating in message delivery. But in many real scenarios, nodes are selfish, and not willing to forward the message further in the network. We observed that in many real scenarios, neither all nodes are altruistic nor selfish, and classified the selfishness present in the network into individual selfishness and social selfishness. In case of individual selfishness, a node may behave selfishly because of some external reason, such as limited buffer space, limited power, etc. A node will forward the message only to nodes, who are friends, or having similar interests, or belongs to same community, etc., in case of social selfishness, In this paper, we have analyzed the impact of both individual and social selfishness on exiting flooding based routing algorithms such as Epidemic routing and Spray and Wait routing and proposed a method to detect and resolve selfishness to improve their routing performance.**

I. Introduction

Delay Tolerant Networks (DTNs) are sparse wireless networks where mobile nodes work in an ad-hoc manner and forward data opportunistically upon contacts. DTNs allow communication between nodes in the absence of network infrastructure and continuous network connectivity. Therefore, they are widely used in many applications like social networking [1] [2], wildlife tracking [3] [4], remote village networks [5] [6], vehicular communication [7] [8] and underwater networks [9], etc.

In DTNs, different types of user behavior will result in different network conditions. DTN based short message service has become very popular these days because it offers a more convenient way to exchange information in a mobile way. DTNs are marked by their mobile nodes with their contact sequences in order to exchange the packets. DTN Routing can be divided into opportunistic routing, social based routing and incentive based routing. In opportunistic routing, the relay node is selected based on its opportunity of meeting the destination node. In social based routing, the relay is selected based on social relationship with the destination node. In incentive based routing, credits are given to the relay node for forwarding the message.

A node in a DTN is considered as selfish when that node is not willing to forward the packet further in the network. There can be various scenarios present in which few nodes in a network can act selfishly. The nodes in DTN can act individually or socially selfish. Nodes show individual selfishness because of the small buffer space and less battery power and they act socially selfish because they do not want to act as a relay for the nodes with which it does not have social ties with it or does not belong to same communities, etc. For successful working of DTNs there is a need that all nodes in the network communicate honestly, but in reality nodes are not willing to participate in the network which hinders the performance of the network.

In this paper, we have discussed two types of selfishness, individual and social, that can be present in the network. We then analyze the effects of these two types of selfishness on flooding based DTN routing algorithms such as Epidemic routing and Spray and Wait routing, and proposes a technique to improve the packet delivery ratio of the existing algorithms by mitigating the selfishness involved.

II. Related Works

The routing in DTN can be done with the help of the social characteristics of the nodes, like friendship, community, etc.; or by forcing the nodes to participate in the routing process by giving credit to them; or it can be done just by mere exchanging the packets when encountered with other nodes. Selfishness can be divided as individual selfishness and social selfishness. In individual selfishness the nodes behave selfishly because of its own interest, the nodes in this category are only interested in forwarding their own packets. In the social selfishness, the nodes do they not forward the packet to the nodes with which they do not have any social connection.

Three types of individual selfishness are considered in the previous works. In the first category, non-participation, there are two types of nodes present in the network, the one who explicitly do not take part in the routing process and the other one, who after accepting the packet drops it from the network. In the second category, energy-preservation, the nodes do not participate to save their device energy. In the last category, storage-preservation, the nodes act selfishly even when the storage space is available to save their buffer space for their own use.

Chen, et al. [10] proposed a trust management protocol in which, not only the quality of service is considered, but, also considers the social properties of the network. The social properties include the honesty and unselfishness of the nodes.

They propose two models, equal weight QoS and also the social trust management protocol. When compared with epidemic routing, the trust based protocol gave a higher delivery ratio than epidemic routing.

Wu, et al. [11] uses a theoretical framework to analyze the effect of the social selfishness. A social graph is considered as an overlay above the actual physical graph. A social graph is a graph in which two nodes are connected if they are friends with each other. It is then assessed that the links of a node in the social graph follow a power law distribution. A relation between nodes can be of strong link and weak link as nodes are more willing to help their friends. The system is modeled as a Markov process. The results of the analysis show that the different degree of social selfishness has different performance of the routing algorithm.

Miao, et al. [12] calculates the effect of binary Spray and Wait protocol when selfish nodes present in the network. Two types of nodes are assumed to be present in the network, the nodes which specifies explicitly for non participation and the nodes which drops the packet after receiving the same. They calculated that the delivery probability of the routing algorithm reduced to 40 % when all the nodes are selfish with the help of Random Way Point Model.

Wu, et.al. [13] gives a theoretical model to simulate the presence of individual and social selfishness in Epidemic Routing. The model was based on Markov process. Their simulation results show that the presence of selfish nodes reduces the performance of epidemic routing significantly, also, if there are nodes which are present in two or more communities which in turn improves the delivery performance of the same.

III. Epidemic Routing

Vahdat, et al. [14] have proposed a flooding based forwarding approach, called as Epidemic routing with an aim to maximize the delivery rate while minimizing the delivery delay. For reducing the total network resources consumed while routing the message from source to destination, they suggest to put a limit on either the message hop count or the buffer space allocated at each node. Therefore, the message will be dropped after its TTL (Time-To-Live) expires or if the buffer at the peer is full. This scheme is based on the idea that the message will eventually find its destination through transitive exchanges between nodes, if they are spread in the connected portion of the network.

The primary goal of epidemic routing is to deliver messages with high delivery probability to the destination node. As it can be seen from figure 1, that the source of the message floods the message to C_1 and C_2, which are in its range; C_2 then stores the message till it meets another node C_3. Then C_3 stores the message and finally deliver it to the destination D. So, the overall goal of epidemic routing is to escalate the delivery rate and minimize the delivery latency.

All nodes are assigned a unique node identifier. Every node stores a summary of the messages it has cached locally in a summary vector. Whenever some node *A* comes in the communication range of node *B*, the node with smaller identifier, say node *A*, starts an anti-entropy session with the

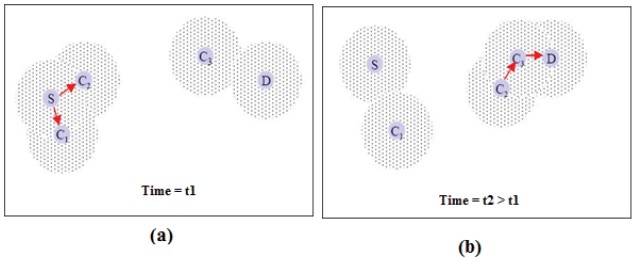

Fig. 1. Epidemic Routing

node *B*, as shown in figure 2. During this, *A*, provides its summary vector to *B*. Node *B*, finds which messages present in *A*s cache are not present locally and makes a request for them. Then, the initiator of the anti-entropy session, here node A, provides the requested messages to node *B*. Some messages may find their destination in this step only (i.e., messages destined to *B*), while others have to be similarly relayed across the network.

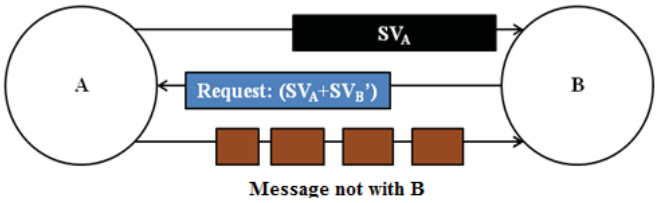

Fig. 2. Summary vector exchange in Epidemic Routing

Flooding results in high resource consumption in terms of both power and storage. Hop count can be set to lower values to avoid this. By setting a low value of hop count, the delivery ratio will decrease and average delivery time will increase. On the other hand, if hop count is high, messages will be dispersed in the network more quickly, resulting in a higher delivery ratio and lower average delivery time. Bounding the buffer space at every node is another trick to reduce resource consumption. Epidemic routing can have a delivery rate of 100% in partitioned networks where ad-hoc routing protocols fail entirely.

A. Epidemic Routing With Selfishness

Epidemic routing is the flooding based algorithm, no decision making scheme is required while choosing the relay, to decrease the resource consumption. Whenever node *A*, meets a peer *B*, all the messages which node *A*, have, are forwarded to node *B*. As the contact time is small in these types of networks and when the nodes in the network are showing the selfish behaviors, the packets should be sent to those nodes first who does not show the selfishness property. Every node in the network maintains a table *R*, which is used to store history of receipt of messages from its neighbors. Suppose, a source node *S*, wants to send a message to destination node *D*. Let *X*, be the set of neighbors of the node *S*, then the node *S*, sorts the list its neighbors in increasing order with respect to

the value of corresponding *R*, as shown in equation 1. Then a node sends the messages to the connections in order according with the sorted list.

$$\underset{i \in X, i \neq S}{\forall} Sort_{ascending}(X, R) \tag{1}$$

IV. Spray and Wait Routing

Spray and Wait is a limited flooding-based approach [15], a betterment of Epidemic Routing. It is also a multi-copy scheme where the message is replicated with encountered nodes for routing to the destination. The strength of this scheme is that it is simple, does not require any knowledge about the network and does not even use the past encounter records.

Whenever a node has a message to send to some other node, it replicates the message into *L* different nodes. This is called as the spray phase, because the source node, without any network information, copies its message to other nodes. If the destination of the message is not met during the spraying process, these *L* nodes transmit a single copy directly to the destination node. Transmitting the message directly means that the nodes will buffer the message till they see its destination or its TTL expires. This is the wait phase of the algorithm.

There may be different variations of the algorithms based on the distribution of initial *L* copies on the network. In the simplest form, *L* copies can be distributed to first *L* distinct nodes the source encounters. Another variation of the algorithm, called Binary Spray and Wait, is to distribute half of the copies to the encountered node and keeping the remaining half at every step of relaying. This means, if a node A has *n* copies of the message and encounters a node B, it sprays *n/2* copies to B and keeps the remaining *n/2* copies with itself and repeats this until it is left with just a single copy when it switches to direct transmission. Spray and Wait is a ticket-based forwarding scheme, in which, every message is assigned logical tickets. Tickets depict the number of relays the message is to be forwarded.

We have worked on Binary Spray and Wait algorithm, in which, if a node have multiple copies of a packet and if it has a connection with node B, then the former node gives half of the copies to the later node and keeps half of it. And when a node is left with one instance of the packet, it can do only transmission to the destination node.

We can see an example, in figure 3, in which node *S*, sprays, 3 copies to node 1, 2 and 3 respectively. Node 7 sprays 2 copies to node 11 and 8 and is left with half of the copies. Nodes 11 and 8 send their copies to node 10 and so on. Node 14 and 16 is the nodes who were finally left with only one copy and they send it directly to the destination, *D*.

The advantages of this algorithm are :

• It has less number of transmissions when compared with other flooding-based schemes

• When the load is high in the network, it gives less delivery delay

• It is scalable, as the number of nodes in the network increases, the number of transmissions per node decreases

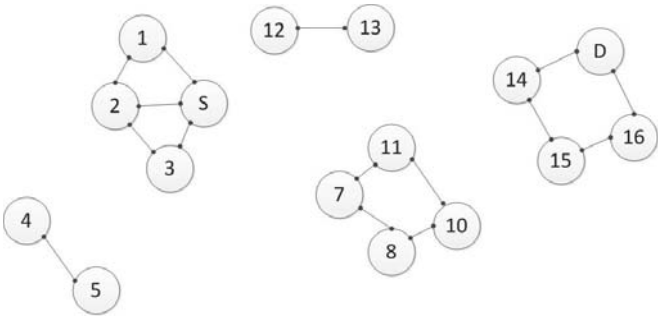

Fig. 3. Spray and Wait Routing

• It is a very simple algorithm and requires no knowledge of the network

A. Spray and Wait With Selfishness

As Spray and Wait routing is the modified version of epidemic routing, it is also a type of flooding based technique. The only difference lies in the fact that instead of disseminating the message to all the connections, it sprays or sends only L copies to all the active connections it has. Similar to epidemic routing, the method sort all its neighbors, *X*, in the increasing order of table *R* as in equation 1, where *S* is the node who is seeking the next relay.

V. Results

Evaluating the various DTN protocols requires some proper tool and the ONE simulator [16] is one such tool. The ONE simulator is mainly used for the modeling of the nodal movement, inter node contacts, message handling and routing. We have done the empirical analysis for Epidemic Routing and Spray and Wait with the help of ONE Simulator.

We have considered that there are three types of nodes present in the network, vehicular nodes, pedestrian nodes and tram nodes. The simulation time is the total number of time span which have considered for node communication. The transmission speed of the node is the data rate at which the packets are transmitted from one node to another. Time to live is the total number of seconds after which the packet will get dropped from the network. A message creation interval is the time range in which the nodes creates packet for each other. Wait time is the time for which each node waits before moving to the next location.

TABLE I. Simulation Settings

Parameters	Values
Simulation time	43200s=12h
Transmission Speed of nodes	250kBps
Number of nodes	125
Time To Live (TTL) of a message	300 minutes
Message Creations Interval	25-30 Seconds
Wait Time	10-30 seconds
Interface	Bluetooth and high speed interface

To model the real-world mobility, we have used two types of map based mobility and random movement models for simulation.

TABLE II. EPIDEMIC ROUTING RESULTS

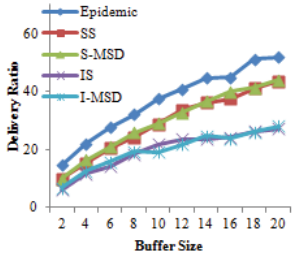

(a) SPMBM, pnc =0.9, pnf =0.1

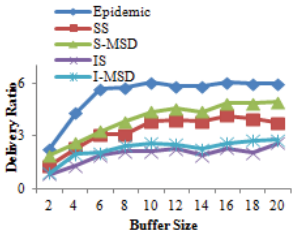

(b) RWPM, pnc =0.9, pnf =0.1

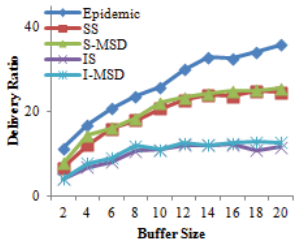

(c) MBM, pnc = 0.9, pnf = 0.1

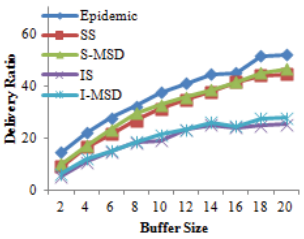

(d) SPBM, pnc =0.5, pnf =0.5

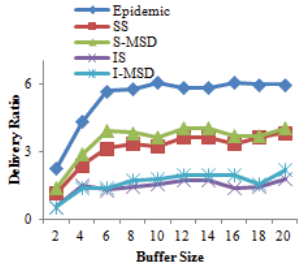

(e) RWPM, pnc =0.5, pnf =0.5

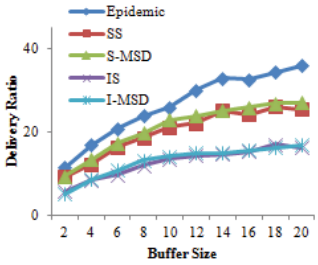

(f) MBM, pnc =0.5, pnf =0.5

TABLE III. SPRAY AND WAIT ROUTING RESULTS

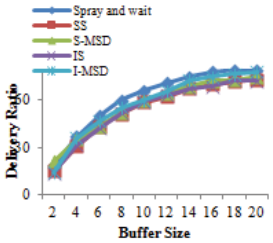

(a) SPBM, pnc=0.9, pnf=0.1

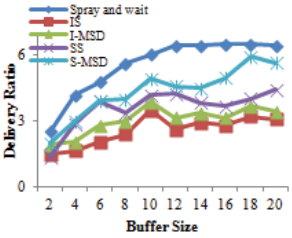

(b) RWPM, pnc=0.9, pnf =0.1

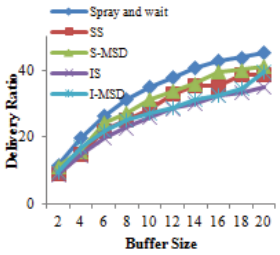

(c) MBM, pnc =0.9, pnf =0.1

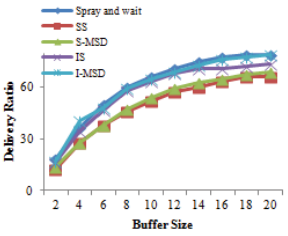

(d) SPMBM, pnc = 0.5, pnf =0.5

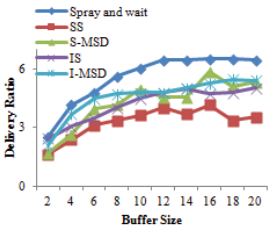

(e) RWPM, pnc =05, pnf =0.5

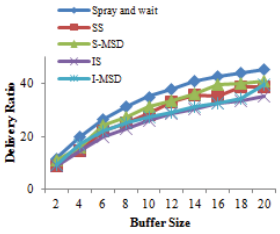

(f) MBM, pnc =0.5, pnf =0.5

• Random Movement Mobility Model: In this type of models the nodes move randomly and freely without restrictions, and their location, velocity and acceleration changes with time. It is a famous model because of its simplicity. The destination for a node, its speed and direction are all chosen randomly. The drawback with this type of model is that, it is not close to the real world movement.

• Map-Based Movement Mobility Model: This mobility model is different from the random movement model in a way that all the node movement is confined to the underlined paths of the graph. We have used Helsinki downtown area, both roads and pedestrian walkways.

Figure (a) to (c) in Table II shows the performance of Epidemic Routing when the buffer threshold is 30% and the value of pnc=0.9 and pnf=0.1 with ShortestPathMapBased Movement (SPMBM), Random Waypoint Movement (RWPM) and MapBasedMovement (MBM). Figure (d)-(f) shows the same but with variation with probabilities, pnc=0.5 and pnf=0.5.

It can be concluded from the above results that the effect of social and individual selfishness is different on the delivery probabilities of the Epidemic routing. I-MSD and S-MSD gives good performance with SPMBM and RWPM model and, I-MSD does not gives good results with MBM model, as this mobility model does not follow any path property and the relations between the nodes could not be created. Whereas S-MSD gives better results with MBM because the friends of a node does not change and is irrespective of the node mobility.

Figure (a)-(c)in Table III shows the performance of Spray and Wait Routing when the buffer threshold is 30% and the value of pnc=0.9 and pnf=0.1 with ShortestPathMap-Based Movement (SPMBM), Random Waypoint Movement (RWPM) and MapBasedMovement (MBM). Figure (d)-(f) shows the same but with variation with probabilities, pnc=0.5 and pnf=0.5.

It can be seen from the above results that the effect of social and individual selfishness is different on the delivery probabilities of the Spray and Wait routing. The effect of social selfishness on the delivery performance is more than individual selfishness which is not the case in epidemic routing. I-MSD and S-MSD gives good performance with SPMBM and RWPM model and, I-MSD does not gives good results with MBM model as this mobility model does not follow any path property and the relations between the nodes could not be created. Whereas S-MSD gives good results with MBM, because no matter the mobility, the friend in the network does not change.

VI. CONCLUSION

In many real scenarios of DTN applications, selfishness may be present in the network. In such cases, a node will not forward the packet to ray node or to the destination. There can be various scenarios present in which few nodes in a network can act selfishly such as individual selfishness and

node selfishness. Individual selfishness is when selfish nodes do not want to store messages of other nodes because of their limited buffer space. Social selfishness is when a node acts selfishly towards another node only if the latter is not a friend of the former. In this paper, we have evaluated the impact of both individual selfishness and social selfishness on flooding based DTN routing algorithms such as Epidemic routing and Spray and Wait and proposed a technique to improve the packet delivery ratio of the existing algorithms by mitigating the selfishness involved. As part of future work, we would like to conduct the empirical and real test bed analysis of the proposed method.

REFERENCES

[1] H. Ntareme, M. Zennaro, and B. Pehrson, "Delay tolerant network on smartphones: applications for communication challenged areas," in *Proceedings of the 3rd Extreme Conference on Communication: The Amazon Expedition*, p. 14, ACM, 2011.

[2] S. M. Allen, G. Colombo, and R. M. Whitaker, "Uttering: Social micro-blogging without the internet," in *Proceedings of the Second International Workshop on Mobile Opportunistic Networking*, pp. 58–64, ACM, 2010.

[3] P. Zhang, C. M. Sadler, S. A. Lyon, and M. Martonosi, "Hardware design experiences in zebranet," in *Proceedings of the 2nd international conference on Embedded networked sensor systems*, pp. 227–238, ACM, 2004.

[4] R. C. Shah, S. Roy, S. Jain, and W. Brunette, "Data mules: Modeling and analysis of a three-tier architecture for sparse sensor networks," *Ad Hoc Networks*, vol. 1, no. 2, pp. 215–233, 2003.

[5] A. S. Pentland, R. Fletcher, and A. Hasson, "Daknet: Rethinking connectivity in developing nations," *Computer*, vol. 37, no. 1, pp. 78–83, 2004.

[6] A. Doria, M. Uden, and D. Pandey, "Providing connectivity to the saami nomadic community," *generations*, vol. 1, no. 2, p. 3, 2009.

[7] A. Balasubramanian, Y. Zhou, W. B. Croft, B. N. Levine, and A. Venkataramani, "Web search from a bus," in *Proceedings of the second ACM workshop on Challenged networks*, pp. 59–66, ACM, 2007.

[8] B. Hull, V. Bychkovsky, Y. Zhang, K. Chen, M. Goraczko, A. Miu, E. Shih, H. Balakrishnan, and S. Madden, "Cartel: a distributed mobile sensor computing system," in *Proceedings of the 4th international conference on Embedded networked sensor systems*, pp. 125–138, ACM, 2006.

[9] T. Small and Z. J. Haas, "The shared wireless infostation model: a new ad hoc networking paradigm (or where there is a whale, there is a way)," in *Proceedings of the 4th ACM international symposium on Mobile ad hoc networking & computing*, pp. 233–244, ACM, 2003.

[10] R. Chen, F. Bao, M. Chang, and J.-H. Cho, "Trust management for encounter-based routing in delay tolerant networks," in *Global Telecommunications Conference (GLOBECOM 2010), 2010 IEEE*, pp. 1–6, IEEE, 2010.

[11] Y. Li, P. Hui, D. Jin, L. Su, and L. Zeng, "Evaluating the impact of social selfishness on the epidemic routing in delay tolerant networks," *Communications Letters, IEEE*, vol. 14, no. 11, pp. 1026–1028, 2010.

[12] J. Miao, O. Hasan, S. B. Mokhtar, L. Brunie, and K. Yim, "An investigation on the unwillingness of nodes to participate in mobile delay tolerant network routing," *International Journal of Information Management*, vol. 33, no. 2, pp. 252–262, 2013.

[13] Y. Wu, S. Deng, H. Huang, and Y. Deng, "Performance analysis of epidemic routing in delay tolerant networks with overlapping communities and selfish nodes," *International Journal of Computers Communications & Control*, vol. 8, no. 5, pp. 744–753, 2013.

[14] A. Vahdat, D. Becker, *et al.*, "Epidemic routing for partially connected ad hoc networks," tech. rep., Technical Report CS-200006, Duke University, 2000.

[15] T. Spyropoulos, K. Psounis, and C. S. Raghavendra, "Spray and wait: an efficient routing scheme for intermittently connected mobile networks," in *Proceedings of the 2005 ACM SIGCOMM workshop on Delay-tolerant networking*, pp. 252–259, ACM, 2005.

[16] A. Keränen, J. Ott, and T. Kärkkäinen, "The one simulator for dtn protocol evaluation," in *Proceedings of the 2nd international conference on simulation tools and techniques*, p. 55, ICST (Institute for Computer Sciences, Social-Informatics and Telecommunications Engineering), 2009.

THE 5TH INTERNATIONAL CONFERENCE ON WIRELESS COMMUNICATIONS, VEHICULAR TECHNOLOGY, INFORMATION THEORY, AEROSPACE & ELECTRONIC SYSTEMS (WVITAE-2015)
December 13-16, 2015, Hyderabad, India

Comparative analysis of load balancing algorithms for LTE/LTE-A Hetnets

Diego Castro-Hernandez, Raman Paranjape
Department of Electronic Systems Engineering, University of Regina, Canada
Email: castrohd@uregina.ca, raman.paranjape@uregina.ca

***Abstract*—The performance of load balancing algorithms in HetNets is investigated in this paper. We performed a comparative analysis of three load balancing algorithms, including our previously proposed algorithm based on local optimization. We evaluated the offloading capabilities, fairness of the distribution of the load among base stations and downlink data rate gains. We also evaluated the practicality of these algorithms in terms of the required amount of coordination and exchange of information among base stations (e.g. handover triggering). An excessive exchange of signaling messages is undesired and leads to an increase in power consumption, this type of analysis has usually been overlooked in past studies. We tested these algorithms in a typical HetNet deployment in a university campus, subject to realistic traffic and load distribution. Our results show that all three algorithms were able to provide significant data rate gains. However, our load balancing algorithm was substantially superior in terms of practicality due to a minimum level of coordination and exchange of information among base stations.**

I. Introduction

Heterogeneous networks (HetNets) are becoming the preferred choice of network operators to meet the ever increasing demand of mobile data traffic in LTE/LTE-A networks. HetNets are particularly useful and a cost-effective solution to provide high quality service to traffic hotspots. One of the main objectives of HetNets is to offload users from the already congested macrocells.

In conventional mobile networks, users are associated with the base station that provides the strongest received signal or the highest signal-to-interference-plus-noise ratio (SINR). These types of user association mechanisms tend to overload macrocells, due to their high transmission power compared to microcells or picocells. This situation leads to unbalanced load distributions, causing congestion in macrocells and under-utilization of the resources provided by small cells. Several authors have studied the load balancing problem in HetNets. Different strategies based on *traffic transfer* have been proposed, e.g. cell breathing techniques and cell biasing methods. A detailed description of these strategies can be found in [1]. In recent years, authors in [1] and [2] have proposed approaching the load balancing issue as a convex optimization problem. A utility function is formulated, typically in terms of the user's achievable data rate and the user association that maximizes the network-wide sum of the utility is found. Iterative algorithms that can be implemented in a distributed manner were proposed in [1], [2]. In [3], we proposed a distributed load balancing algorithm based on the local optimization of the sum of the utility values, such maximization is performed by each base station (BS) considering only local information regarding its currently associated users.

In this paper, we performed a comparative analysis of the performance of three load balancing algorithms. The algorithms considered in this study are the one proposed by Ye *et al.* in [1], by Shen and Yu in [2] and our load balancing algorithm proposed in [3]. The evaluation scenario consisted of a typical HetNet deployment in a university campus venue under realistic traffic and load conditions. Our results confirmed the benefits of balancing the load in HetNets. Significant data rate gains were achieved by all the algorithms. However, our load balancing algorithm is substantially superior in terms of practicality due to the minimum amount of exchange of information among eNBs, a situation that leads to lower power consumption compared to the other two algorithms.

II. System model

In this paper, we are interested in the evaluation of the performance of load balancing algorithms subject to typical conditions in a two-tier LTE/LTE-A HetNet deployment. Our analysis focuses on downlink transmissions. The implications of load balancing in the uplink are not considered in this study. Furthermore, in this paper we do not consider inter-layer interference since we have selected a HetNet deployment with dedicated spectrum per layer, i.e. non-cochannel deployment.

Effective load balancing in HetNets is directly related to the user association scheme being applied. User association is the process of selecting the serving BS for a mobile user (UE). An indicator variable x_{ij} has been typically used to describe the association of the UE i to eNB j [1]–[3]. The variable x_{ij} takes the value of 1 when user i is associated to eNB j, otherwise it takes the value of 0 .

We denote as $\mathcal{I}$ the set of all active users in the network, and as $\mathcal{J}$ the set of all base stations. The total number of active users is denoted as N_U, while the total number of BSs is denoted as N_B. The set of users associated with base station j can be expressed as $\mathcal{I}_j = \{i | x_{ij} = 1, i \in \mathcal{I}\}$.

We now define the instantaneous downlink data rate offered by the j^{th} eNB to the i^{th} user as [3]:

$$r_{ij}(k) = \omega^o_{ij}(k) \cdot b_{ij}(k) \tag{1}$$

Where $\omega^o_{ij}(k)$ is the bandwidth in Hz scheduled (offered) for downlink transmissions to the i^{th} UE during the k^{th} subframe. The term $b_{ij}(k)$ corresponds to the normalized rate of the UE in b/s/Hz and is, in general, a function of the SINR$_{ij}$. Where SINR$_{ij}$ is the ratio of the received power from the j^{th} eNB and the total power of the received interference from neighbouring cells belonging to the same tier plus noise. The value $b_{ij}(k)$ has been typically calculated with the well-knwon Shannon Hartley theorem [1], [2]. However, in our analysis we follow the approach proposed in [3]. Where the value of b_{ij} is determined by the *Channel Quality Indicator* (CQI) periodically reported by each UE to its serving BS. Our simulator uses a SINR-to-CQI mapping for a 10% block error rate (BLER) [3].

A. Load of eNBs

In a LTE/LTE-A network, all active UEs that connect to an eNB have to share the available bandwidth. Each one of the UEs demands a specific quality of service depending on the running application. The task of the scheduler is to distribute the available bandwidth such that the demanded quality of service of each user is satisfied, while keeping a sense of fairness. The load of an eNB can be quantified in terms of the demanded load index L^D_j calculated as [3]:

$$L^D_j = \frac{\sum_{i \in \mathcal{I}_j} \bar{\omega}^D_{ij}}{W_j} \tag{2}$$

Where $\bar{\omega}^D_{ij}$ is the average demanded bandwidth of user i and W_j corresponds to the total bandwidth of the j^{th} eNB. A demanded load index higher than 1 indicates that the total demanded bandwidth is higher than the available bandwidth, i.e. the base station is overloaded.

III. Problem formulation

The load balancing problem has been typically defined in terms of an optimization problem. Such problem consists of the maximization of a network-wide aggregate of a utility function $U(\cdot)$, usually such function is defined in terms of the long-term data rate R_{ij} as in [3] or in terms of the achievable data rate as in [1], [2]. The optimal user association $\hat{\mathbf{X}} = \{x_{ij} | i \in \mathcal{I}, j \in \mathcal{J}\}$ is then the solution to:

$$\begin{aligned} \hat{\mathbf{X}} = \arg\max_{X} \quad & \sum_{i \in \mathcal{I}} \sum_{j \in \mathcal{J}} x_{ij} \cdot U_i(R_{ij}) \\ \text{s.t.} \quad & \sum_{j \in \mathcal{J}} x_{ij} = 1, \forall i \in \mathcal{I} \\ & x_{ij} \in \{0,1\}, \forall i \in \mathcal{I}, \forall j \in \mathcal{J} \end{aligned} \tag{3}$$

The optimal user association $\hat{\mathbf{X}}$ is the one that maximizes the network-wide sum of the utilities, with the constraint that each user must be associated to only one eNB. This optimization problem is a combinatorial problem whose computation has been shown to be intractable for real-size networks [1].

IV. Load balancing algorithms

We start this section with a description of the two load balancing algorithms based on convex optimization. These algorithms were proposed by Ye *et al.* in [1] and by Shen and Yu in [2]. Both these algorithms approximate the solution to the problem formulated in (3) by applying Lagrangian dual decomposition analysis. The algorithm proposed in [1] is based on the subgradient method, the one proposed in [2] is based on the dual coordinate descend method. We finish this section with a description of our load balancing algorithm based on local optimization, proposed in [3].

A. Algorithm based on the Subgradient Method (SGM)

The use of Langrangian dual decomposition to solve the load balancing problem formulated in (3) was initially proposed in [1]. Two dual variables are defined: $\boldsymbol{\mu} = [\mu_1, \ldots, \mu_{N_B}]^T$ (which can be interpreted as BS-specific prices), and ν. The maximization of the Lagrangian function in the dual domain is achieved with the following user association rule: [1]:

$$j^{(i)} = \arg\max_{j'} (a_{ij'} - \mu_{j'}), \ \forall \ j' \in \mathcal{J} \tag{4}$$

With a_{ij} being the achievable utility that user i would obtain if it is associated with eNB j. It is given by:

$$a_{ij} = \log\left(W_j \log\left(1 + \text{SINR}_{ij}\right)\right) \tag{5}$$

According to (4), UE selects as its serving cell the eNB that provides the highest value of its utility minus the BS-specific price. The values in $\boldsymbol{\mu}$ should be calculated in such a way that the load among eNBs is balanced. This pricing interpretation of the dual variable $\boldsymbol{\mu}$ is further discussed in [1], [2]. In [1], the subgradient method is proposed to calculate the values of the dual variables in an iterative manner. During the $(t+1)^{th}$ iteration of the algorithm, the BS-specific prices are updated according to [2]:

$$\mu^{(t+1)}_j = \mu^{(t)}_j - \beta^{(t)} \left(e^{\mu^{(t)}_j - \nu^{(t)} - 1} - \sum_i x^{*(t)}_{ij} \right) \tag{6}$$

The variable $\beta^{(t)}$ is a step size that can be calculated with a self-adapted scheme as proposed in [1]. Such scheme depends on many parameters whose selection greatly affects the speed of converge as shown in [2]. The other dual variable $\nu^{(t+1)}$ is given by:

$$\nu^{(t+1)} = \log\left(\frac{\sum_j e^{\mu^{(t)}_j - 1}}{N_U} \right) \tag{7}$$

For the algorithm to converge, all BS-specific prices μ_j have to be calculated with the same value of the step size, hence tight synchronization between eNBs is needed. Finally, the primal variable $\hat{\mathbf{X}}$ is obtained from the dual variables by applying (4).For a more detailed description of this method we refer the reader to [1].

B. Algorithm based on Dual Coordinate Descend (DCD)

Similarly as in [1], authors in [2] also apply a Lagrangian dual analysis to obtain the network-wide user association that approximates the solution to (3). However, the use of a dual coordinate descend approach is proposed as the mechanism to update the BS-specific prices μ_j. The values of the BS-specific prices are updated according to [2]:

$$\mu_j^{(t+1)} = \sup\left\{\mu_j \mid f_2^{(t)}(\mu_j) - f_1^{(t)} \leq 0\right\} \tag{8}$$

With $f_1^{(t)}$ being the number of UEs currently associated to eNB j and $f_2^{(t)} = e^{\mu_j^{(t)} - \nu^{(t)} - 1}$.

The resulting algorithm for load balancing is then identical to the SGM method, with the exception that (8) must be used to update the BS-specific prices as opposed to (6) used by the SGM method. A key advantage of the dual coordinate descent method is the fact that it does not depend on a step size and convergence is faster. However, as stated in [2], this is in general a suboptimal approach and a tight duality gap can exists. Additional details about this method as well as an upper bound of the duality gap can be found in [2].

C. Load balancing algorithm based on local optimization (LOM)

Our proposed load balancing algorithm is based on the observation that the network-wide optimization problem described in (3) can be simplified by letting the overloaded base stations determine their own local optimal user association. Where such local user association is constrained by a desired level of demanded load. The simplified version of the optimization problem can be expressed in terms of a local indicator variable $\tilde{x}_i$ as [3]:

$$\begin{aligned} \hat{\mathbf{X}}_j = \underset{\tilde{X}_j}{\arg\max} \quad & \sum_{i \in \mathcal{I}_j} \tilde{x}_i \cdot U_i(R_{ij}) \\ \text{s.t.} \quad & \sum_{i \in \mathcal{I}_j} \tilde{x}_i \cdot \bar{\omega}_{ij}^D < \alpha W_j \\ & \tilde{x}_i \in \{0,1\}, \forall i \in \mathcal{I}_j, \alpha \geq 1 \end{aligned} \tag{9}$$

Where R_{ij} is the long-term rate and $\tilde{\mathbf{X}}_\mathbf{j} = \{\tilde{x}_i | i \in \mathcal{I}_j\}$. The local optimal user association $\hat{\mathbf{X}}_\mathbf{j}$ can be calculated by each overloaded base station considering the demand of the UEs currently associated to it. The main objective of the optimization problem in (9), is to allow an overloaded BS to select which users would maximize its sum of the utility while keeping its total demanded load under a desired level, i.e. the total demanded load of the selected users must not exceed the value αW_j. The parameter α can take a value higher or equal than 1. A value of α closer to unity will provide a stricter selection of UEs. Such parameter can be setup by the network operator.

Based on the set $\hat{\mathbf{X}}_j$, an overloaded eNB classifies its currently associated users in two sets $\mathcal{S}_j$ and $\mathcal{T}_j$. With $\mathcal{S}_j = \left\{i | \tilde{x}_i = 1, \tilde{x}_i \in \hat{\mathbf{X}}_j\right\}$ and $\mathcal{T}_j = \left\{i | \tilde{x}_i = 0, \tilde{x}_i \in \hat{\mathbf{X}}_j\right\}$. The set $\mathcal{S}_j$ contains the subset of users that will continue to be associated with eNB j after such eNB has estimated $\hat{\mathbf{X}}_j$. The set $\mathcal{T}_j$ contains the subset of users that the base station will attempt to transfer to other underloaded eNBs via handover operation.

Similarly as in [1] and [2], we have selected a logarithmic utility function. A logarithmic function has the advantage that it yields high increase in utility values if more resources are provided to users with low rates (cell-edge users), as opposed to providing the same amount of resources to users already with good rates. This encourages cell-edge user associated with overloaded eNBs to be transferred to underloaded base stations where they can receive more spectrum resources, hence improving the balance of the load among eNBs. In our case we define the logarithmic utility function as:

$$U_j(R_{ij}, \bar{\omega}_{ij}^o) = \log\left(\frac{R_{ij}}{\bar{\omega}_{ij}^o}\right) \tag{10}$$

The quantity $R_{ij}/\bar{\omega}_{ij}^o$ represents the average normalized long-term rate for the i^{th} UE in b/s/Hz. We approximate the solution of the problem formulated in (9) with an approach based on greedy heuristics as described in [3]. The pseudocode of this process is presented in Algorithm 1.

Algorithm 1 Get $\hat{\mathbf{X}}_j$

Require: $\mathcal{U} = \{U_i | i \in \mathcal{I}_j\}, \mathcal{W}^D = \{\bar{\omega}_{ij}^D | i \in \mathcal{I}_j\}, \alpha$
1: $demanded_load \leftarrow 0$
2: Sort($\mathcal{U}$) in descending order
3: **for** $n = 1$ to $|\mathcal{I}_j|$ **do**
4: $\quad UE_n \leftarrow Get_UE(\mathcal{U})$
5: $\quad$ **if** $demanded_load + \bar{\omega}_{nj}^D < \alpha W_j$ **then**
6: $\quad\quad \tilde{x}_n = 1$
7: $\quad\quad demanded_load = demanded_load + \bar{\omega}_{nj}^D$
8: $\quad$ **else**
9: $\quad\quad \tilde{x}_n = 0$
10: $\quad$ **end if**
11: **end for**
12: $\hat{\mathbf{X}}_j \leftarrow \{\tilde{x}_n\}$

After executing Algorithm 1, an overloaded BS can determine the sets $\mathcal{S}_j$ and $\mathcal{T}_j$. Then, the base station must submit handover requests for each UE in $\mathcal{T}_j$ to neighboring cells with spare capacity and whose RSRP (Reference Signal Receive Power) and SINR satisfy the cell selection criteria defined by the operator. In order to identify a base station with spare capacity, all base stations must periodically broadcast their demanded load index. The

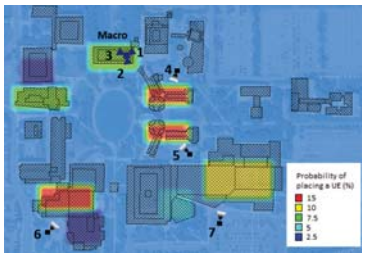

Fig. 1. Traffic map and location of base stations

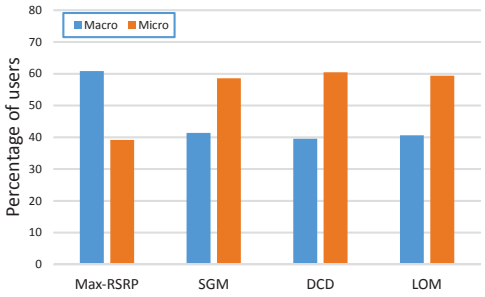

Fig. 2. Distribution of users between macrocell and microcell layers

exchange of this information is a functionality expected to be part of Self-Optimizing Networks (SON) [3].

V. Performance Evaluation

The performance evaluation of the three load balancing algorithms described in Sect. IV was carried out considering a two-tier HetNet deployment in the University of Regina campus, in Saskatchewan, Canada. This university campus corresponds to a urban environment with irregular distribution of buildings over a flat terrain. A 3D model of the environment, including 18 buildings, was created with a resolution of 1 m. The area under study has dimensions 600 m by 700 m. The distribution of the buildings is shown in Fig. 1.

The two-tier HetNet considered in this paper consists of one three-sector macrocell (cells 1,2 and 3) and four outdoor microcells (cells 4,5,6,7) as shown in Fig. 1. The macrocell is located on the rooftop of a building at a height of 36 m, its transmission power was set at 47 dBm and it operates at 2.1 GHz. All microcells are mounted on lamposts with a height of 6 m, their transmission power was set at 30 dBm and their carrier frequency is 2.6 GHz. Users were distributed spatially according to a traffic map derived from network statistics and knowledge of the users' distribution. The traffic map is presented in Fig. 1. A proportional scheduler was applied in our simulations.

The propagation model applied in this study corresponded to a site-specific path loss model based on the Uniform Theory of Diffraction and geometrical optics, this model is similar to the one proposed in [4]. A total of 350 runs were simulated, 130 users were considered in every run. The baseline of our analysis was provided by the Max-RSRP user association scheme, i.e. UEs associate to the eNB with strongest RSRP. The demanded downlink rate for each user was randomly generated between 0.5 Mbps and 10 Mbps.

A. Distribution of users

Fig. 2 shows the distribution of users between the macrocell and the microcell layers. The Max-RSRP rule clearly shows an unbalanced distribution of users, where the macrocell tends to be overloaded and the microcells are under-utilized. For the Max-RSRP rule, most of the users were associated to the macrocell, only 40% were associated to the microcells. The three load balancing algorithms were able to revert this situation, they were capable of offloading the macrocell by approximately 20%. The DCD method showed a slightly better offloading percentage, around 1% higher than the SGM and LOM methods. Therefore, regarding the offloading of the macrocell, all three load balancing algorithms perform equally good.

TABLE I
Fairness Indexes

	Max-RSRP	SGM	DCD	LOM
Fairness index	0.6	0.87	0.82	0.86

B. Distribution of the load among eNBs

The distribution of users per layer in a HetNet is not enough to measure the effectiveness of the load distribution among eNBs, especially in the case where the demand of all users is not assumed constant. It is important to quantify how fair is the sharing of the load between base stations. This can be done with the calculation of the Jain's fairness index $F(\mathbf{L})$. Where $\mathbf{L} = [L_1^D, \ldots, L_{N_B}^D]^T$ is a vector containing the load indexes of the N_B base stations in the network. The fairness index is calculated according to:

$$F(\mathbf{L}) = \frac{\left(\sum_{j\in\mathcal{J}} L_j^D\right)^2}{N_B \cdot \sum_{j\in\mathcal{J}} \left(L_j^D\right)^2} \tag{11}$$

The fairness index $F(\mathbf{L})$ takes the maximum value of 1, under the idealistic situation where the total load is equally shared by all base stations.

Table I shows the results. The Max-RSRP rule showed the lowest value of the fairness index, reaching only 0.6, this indicates a poor distribution of the load. On the other hand, the load balancing algorithms achieved a fairer load sharing among base stations since the value of the fairness index was increased above 0.8. In particular, the SGM method achieved the highest value of the fairness index, reaching 0.87. The other two load balancing methods achieved slightly lower fairness indexes.

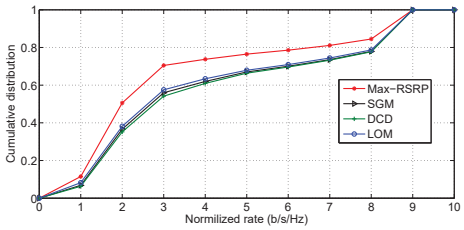

Fig. 3. Cumulative distribution of the normalized long-term rate

C. Cumulative distribution of the normalized long-term rate

As an additional performance metric, we were interested in quantifying the overall data rate gain after balancing the load. In Fig. 3 we provide the cumulative distribution of the normalized long-term data rate for the overall HetNet. It can be observed that the CDFs obtained by the load balancing algorithms show a significant improvement in the normalized data rate. This means that a higher spectral efficiency was achieved. Therefore, a more efficient use of spectrum resources was possible compared to the case when the user association was defined by the max-RSRP scheme. The three load balancing algorithms showed a similar improvement of the normalized rate. All percentiles experienced a gain, this is specially important for the low percentiles, since they represent users receiving the worst downlink rates in the network (i.e. cell-edge users).The rate gain for the 10^{th} percentile reached a value between 1.22x to 1.3x. This means data rates were improved by 22% to 30% due to a more balanced load distribution among base stations. The data rate was almost doubled for the 70^{th} percentile.

These results show that our load balancing algorithm (LOM) provide data rate gains that are very close to the ones provided by the other two methods SGM and DCD, however our algorithm is significantly less complex. It is important to mention that these two methods SGM and DCD are very close to optimality as shown in [1], [2].

D. Evaluation of the practicality of the algorithms

In this final subsection of the performance evaluation of the load balancing methods, we focus our attention on the complexity and practicality of the algorithms considered in this study.

The SGM and DCD methods require the exchange of at least $m(N_B + N_U)$ messages where m is the number of iterations [1]. On the other hand, our load balancing algorithm only requires each base station to broadcast its demanded load index. An overloaded base station would proceed to execute Algorithm 1 and select the UEs that would be transfered to lightly loaded base stations (i.e. set $\mathcal{T}_j$), at this point only UEs currently associated with overloaded base stations would be handed over, there is no need to update the network-wide user association as it is done in every iteration of the SGM and DCD methods. Therefore, our load balance algorithm requires the exchange of $N_B + \sum_{j\in\mathcal{J}} |\mathcal{T}_j|$.

TABLE II
AVERAGE EXCHANGE OF MESSAGES

	SGM	DCD	LOM
Number of messages	7065	785	36

Table II shows the average number of additional exchanged messages due to the application of the load balancing algorithms. The SGM method requires an extraordinary amount of exchanged messages due to the fact that its convergence is slow, as opposed to the DCD method. Our load balancing algorithm requires a minimal amount of exchange of messages among base stations, this leads to lower levels of required coordination and lower impact on the signaling load of the network. Furthermore, our algorithm would have a reduced impact on power consumption as opposed to the DCD and SGM methods. Therefore, it is evident that in terms of practicality as well as impact on power consumption, our algorithm is superior.

VI. Conclusion

In this paper, we performed a comparative analysis of the performance of three load balancing algorithms. We evaluated the effectiveness of these algorithms considering a typical two-tier HetNet deployment subject to a realistic traffic distribution. The load balancing algorithms were able to offload up to 20% of the users from the macrocell layer, this led to a fairer distribution of the demanded load among base stations. The three algorithms provided significant data rate gains for all percentiles, reaching a value up to 2x gain for the 70^{th} percentile. Particularly important is the evaluation of the number of exchanged messages and triggered handovers, since this factor is related to the practicality of the algorithms. Our load balancing algorithm is substantially superior since it requires a minimal amount of exchange of messages among base stations, this leads to lower levels of coordination and lower impact on the signaling load of the network.

References

[1] Q. Ye et al., *User Association for Load Balancing in Heterogeneous Cellular Networks*, IEEE Trans. Wireless Commun., vol.12, no.6, pp.2706,2716, June 2013

[2] K. Shen, W. Yu, *Distributed Pricing-Based User Association for Downlink Heterogeneous Cellular Networks*, IEEE Journal on Selected Areas in Communications, vol.32, no.6, pp.1100,1113, June 2014

[3] D. Castro-Hernandez and R. Paranjape, *A Distributed load balancing algorithms for LTE/LTE-A Heterogeneous Networks*, Wireless Comm. and Networking Conf. Workshops (WCNCW), pp.380-385, March 2015

[4] D. Castro-Hernandez and R. Paranjape, *Estimation of coverage areas in microcells*, IEEE Intl. Conf. on Advanced Networks and Telecommunications Systems, pp.1,6, Dec. 2013.

THE 5TH INTERNATIONAL CONFERENCE ON WIRELESS COMMUNICATIONS, VEHICULAR TECHNOLOGY, INFORMATION THEORY, AEROSPACE & ELECTRONIC SYSTEMS (WVITAE-2015)
December 13-16, 2015, Hyderabad, India

Performance Analysis of Multiband Tapered Feed Single-Arm Spiral Antenna for Vehicular Communications

Ramya and T. Rama Rao
RADMIC, Department of Telecommunication Engineering,
SRM University,
Chennai, India.
vijaramya@gmail.com; ramaraotr@gmail.com

***Abstract*—Significant developments in automotive industries ensures safety and entertaining journey by sharing information among the vehicles and inside vehicles utilizing wireless networks available. A new printed single arm spiral antenna with tapered feed is proposed to cover the navigational wireless frequencies viz., 1.2 GHz, 1.5 GHz (Indian Regional Navigation Satellite System and Global Positioning System) and Wireless Communication frequencies viz., 2.45 GHz, 3.3 GHz (Wi-Fi & WiMAX) and Dedicated Short Range Communication (DSRC) frequency, 5.8 GHz for vehicular communications. To achieve better impedance matching and multiple frequencies, tapered feed is introduced at the edge of single arm spiral. Antenna is designed using 3D Electromagnetic (EM) software tool and validated using RF equipment. Compact size, omnidirectional radiation pattern and improved circular polarization make this antenna an appropriate candidate for vehicular wireless communications.**

Keywords—Multiband antenna;tapered feed;spiral antenna; circular polarization;impedance matching;Vehicular wireless communications.

I. INTRODUCTION

The remarkable growth in the present communication technologies increases the usage of communication systems for automotive applications. The intelligent transport system (ITS) ensures better quality travel by providing vehicle safety information through broad communication technologies. In addition, ITS expects multimedia data exchange through internet connection among the moving vehicles [1]. ITS includes short-range and long-range communication to allow a vehicle to interact with the outside world for information exchange. Nowadays, the vehicles upcoming with GPS, GSM, Wi-Fi, Bluetooth, WiMAX, DSRC and more. These services which functions at different frequency necessitate a number of dedicated antennas to be integrated in the vehicle. Hence, the vehicle antennas are likely to be of compact, low cost and with multiband operations.

Researcher around the globe explored different methods of resonating multiband with single radiator. This includes slot antennas [2], inverted F antennas [3, 4]. In [5 - 7] author proposed stacked antennas to resonate in multiband for vehicular applications that occupies more space in roof of the vehicle. In [8], two separate radiator shared aperture to reduce the space occupation by proposing PIFA antenna integrated with 'Y' shaped monopole. In [9], author proposed a fractal multiband antenna for vehicular radar and imaging system.

Now a days, printed monopole antenna became prevalent for automotive systems because it could meet the benefits of omnidirectional pattern, compact in size, low cost, ease to fabricate and achieve ITS requirements [10]. In [11], coplanar monopole (cactus shaped) antenna is proposed to resonate at 2.4 GHz and 5.8 GHz. In [12], two – hook facing opposite side in one plane and cross shaped monopole at the back plane is introduced to operate at 2.4 GHZ, 5.2 GHz and 5.8 GHz. The antennas observed in literature does contain omnidirectional pattern with linear polarization. The European standard EN 12253 [13] provides the requirement for vehicular communication antenna. As per EN 12253, omnidirectional radiation pattern with circular polarization helps to maintain better communication between moving vehicles.

A key to miniaturize the antenna is maximizing the current flow in the conducting element. Hence we have chosen the spiral structure in our proposal. Added to that one of the characteristics of spiral antenna is circular polarization which satisfies the requirements of vehicular communication antenna. Several spiral monopole antenna are proposed to achieve multi band, circular polarization and omnidirectional radiation pattern [14 - 17]. In spiral antennas impedance matching is not uniform at all bands especially at lower bands. A tapered feed helps to improve the impedance matching [18]. This paper gives solution for the mentioned issues of multiband, circular polarized and omni directional radiation pattern with better impedance matching.

In this paper, we propose a printed spiral antenna with tapered feed which supports wireless communication services along with navigation services operates at IRNSS (1.2 GHz), GPS (1.5 GHz), Wi-Fi (2.4 GHz), WiMax (3.3 GHz) and DSRC (5.8 GHz). IRNSS is a regional navigation satellite system being developed by India to offer precise position information service to users [19]. Further the paper is organized as, in Section II defines the design of the

proposed antenna and the effects of tapered feed on impedance matching followed by Section III, the discussion on performance of the antenna.

II. ANTENNA DESIGN

A. Construction of the Proposed Antenna

The proposed printed spiral antenna with tapered feed is shown in Fig. 1. The size of the proposed antenna is 51 x 35 x 1.574 mm3 with ground plane size of 4.5 x 35 mm2 designed on the Rogers's RT Duroid 5880 substrate with permittivity(ε_r) of 2.2 and loss tangent(δ) of 0.0009. The dimensions of the dielectric substrate is obtained using (4) and (5) [20].

$$W_p = \frac{c}{2f_r}\sqrt{\frac{2}{\varepsilon_r+1}} \quad (1)$$

$$L_p = \frac{c}{2f_r\sqrt{\varepsilon_{reff}}} - 2\Delta \quad (2)$$

$$\Delta L = \frac{h(0.412)(\varepsilon_{reff}+0.3)(\frac{W_p}{h}+0.264)}{(\varepsilon_{reff}-0.3)(\frac{W_p}{h}+0.8)} \quad (3)$$

$$L = L_p + 6h \quad (4)$$

$$W = W_p + 6h \quad (5)$$

For our desired multiband operation, we have considered circumference of the inner and outer circle of the planar spiral as $\lambda/4$ with respect to the lower and upper frequencies. The inner and outer radius of the circles are obtained using (6) and (7). The Table 1. gives the dimensions of the antenna.

$$r_1 = \frac{c}{8\pi f_{high}} \quad (6)$$

$$r_2 = \frac{c}{8\pi f_{low}} \quad (7)$$

$$s = w = \frac{r_2 - r_1}{4N} \quad (8)$$

B. Effects of Tapperd Feed

In spiral antennas the impedance matching is not uniform at all bands. In order to achieve better impedance matching we introduced taper feed. Fig 2 and Fig. 3 shows the effects on impedance due to taper feed at lower and higher frequency band.

In Fig.2. , the slope 1 defines without tapering. We could observe that there is less effect of tapper feed on impedance at lower frequency bands and significant variation at higher frequency bands. As the slope increases there is a decrement in impedance value. In our proposed design we have chosen taper slope of 1.6.

TABLE I. DIMENSIONS OF THE PROPOSED ANTENNA

Label	Dimensions (mm)
L	51
W	35
L1	18.1
L2	4.5
S	1.25

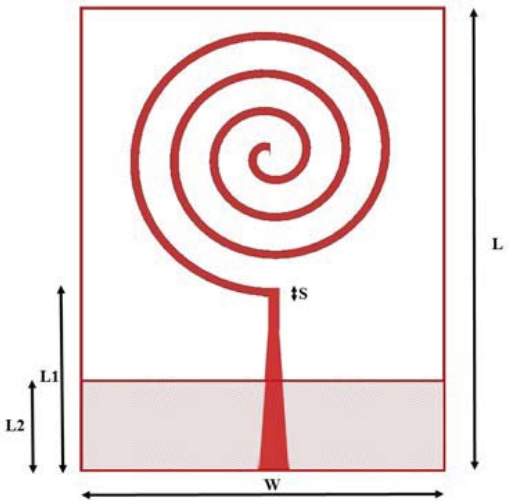

Fig. 1. Geometry of the proposed antenna

III. RESULTS AND DISCUSSIONS

The proposed antenna is designed and simulated using the 3D Electromagnetic tool HFSS. Keysight's N9925A Vector Network Analyzer is used to validate the antenna performance. The comparison of simulated and measured return loss of the proposed antenna is shown in Fig. 4. It shows, there is good agreement between measured and simulated results.

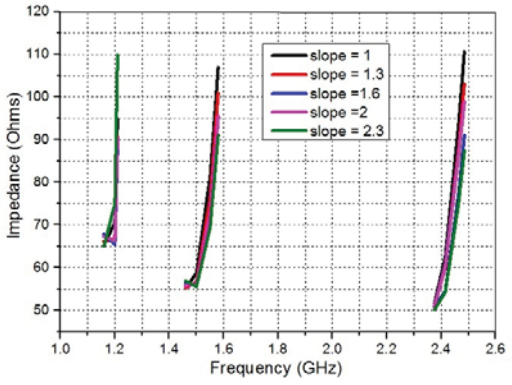

Fig. 2. Impedance variation based on slopes at lower frequency bands

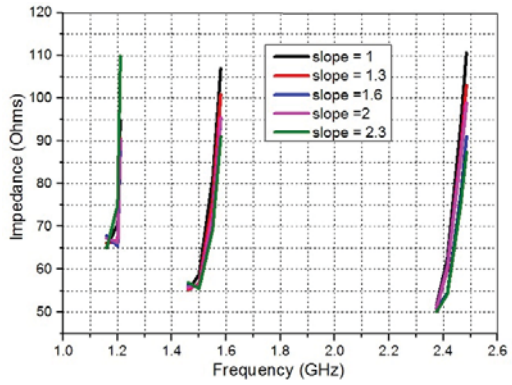

Fig. 3. Impedance variation based on slopes at lower frequency bands.

Fig. 5 shows 2D plot of the axial ratio verses frequency of the proposed antenna. It can be observed that, axial ratio is less than 3dB at all desired frequency bands implies that the proposed antenna is circularly polarized. Axial ratio bandwidth of 50 MHz, 60 MHz, 110 MHz, 170 MHz, and 370 MHz at 1.2 GHz, 1.5 GHz, 2.4 GHz, 3.3 GHZ and 5.8 GHz are achieved.

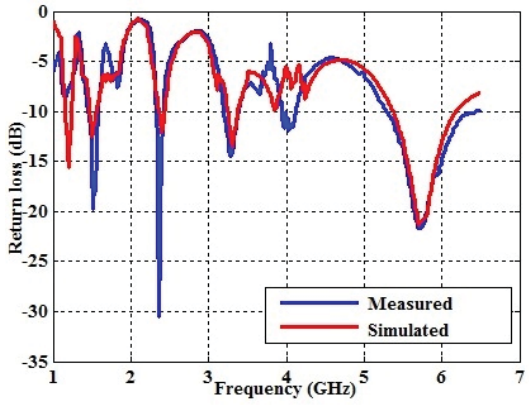

Fig. 4. Return loss versus frequency of the proposed antenna.

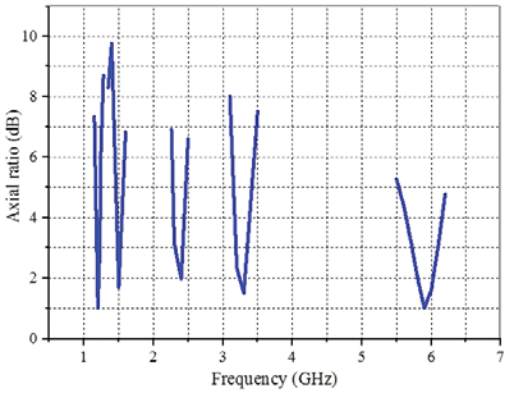

Fig. 5. Axial ratio versus frequency of the proposed antenna

Fig. 6 shows the radiation pattern at lower frequency bands (1.2 GHz, 1.5 GHZ and 2.4 GHZ) of the proposed antenna. At all three desired bands, antenna radiates in omnidirectional. Gain is found to be 1.07 dB, 1.75dB, 1.88 dB, 1.52 dB and 5.48 dB at 1.2 GHz, 1.5 GHz, 2.4 GHz, 3.3 GHZ and 5.8 GHz respectively.

The near omnidirectional radiation pattern at higher frequency bands (3.3 GHz and 5.8 GHz) of the prosed antenna is shown in Fig. 7.Table. 2 lists the performance comparison of simulated and measured antenna. It can be inferred from the table that the measured and simulated results are with good agreement. Prototype of the proposed antenna is shown in Fig.8.

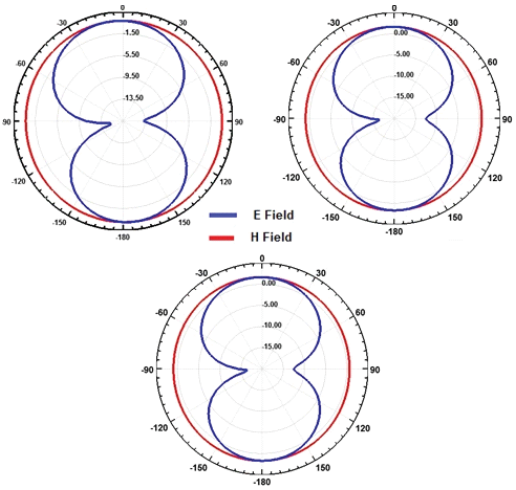

Fig. 6. Radiation pattern of the proposed antenna at lower frequency bands.

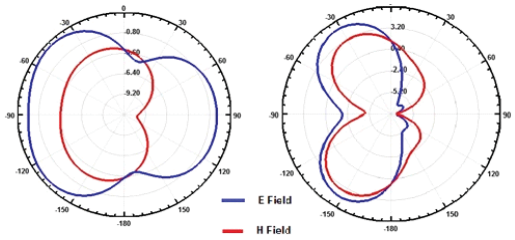

Fig. 7. Radiation pattern of the proposed antenna at higher frequency bands.

Fig. 8. Prototype of the proposed antenna.

TABLE II. ANTENNA PERFORMANCE

Parameters M –MEASURED S – SIMULATED		**Frequency in GHz**				
		1.2	***1.5***	***2.4***	***3.3***	***5.8***
Impedance BW (GHz)	M	0.05	0.11	0.09	0.19	1.10
	S	0.07	0.08	0.07	0.13	0.81
Return loss (dB)	M	10.80	15.43	13.85	14.2	20.4
	S	15.6	12.50	12.30	13.6	20.5
Gain (dB)	S	-1.30	0.17	1.20	1.61	5.32
AR BW (%)	S	4.16	4.00	4.58	5.15	6.37
Radiation Efficiency (%)	S	82.1	89.7	89.8	85.0	94.7

IV. CONCLUSIONS

The design of penta-band based circularly polarized, single arm spiral antenna is presented with a compact size of size 51 x 35 x 1.574 mm3 to address Vehicular Wireless Applications for Navigational Communications and Terrestrial Wireless Network Communications. By the introduction of tapering in the feed line, better impedance matching is achieved at all desired bands. It is inferred that there is a healthier agreement between measured and simulated results. Further, it is observed efficiency with the multiband spiral antenna varied from 82.13 ~ 94.74%. Thus the multiband, omnidirectional pattern and circular polarization at all desired frequency makes the proposed antenna an appropriate applicant for the various applications of Vehicular Wireless Communications.

REFERENCES

[1] T. Ijiguchi, D. Kanemoto, K. Yoshitomi, K. Yoshida, A. Ishikawa, S. Fukagawa, & Kanaya, H. “Circularly Polarized One-Sided Directional Slot Antenna With Reflector Metal for 5.8-GHz DSRC Operations”, .IEEE Antennas and Wireless Propagation Letters, 13, 778-781, 2014.

[2] Wen-bo, Zeng, L. Xiang-yang, and L. Ji-xiang. "A dual-band RFID slot tag antenna for ITS application." In Consumer Electronics, Communications and Networks (CECNet), 2013 3rd International Conference on, pp. 5-7. IEEE, 2013.

[3] M. T. Le, Q. C. Nguyen, T. P. Vuong, and C. Defay. "New metamaterial structure for the design of a high gain antenna at 5.8 GHz." In 2012 IEEE International Conference on Wireless Information Technology and Systems ,2012.

[4] Hossain, Md Robiul, and D. K. Karmokar. "Dual-band Inverted-F Antenna for Military and Intelligent Transportation System Applications." International Journal of Advancements in Research & Technology, Volume 1, Issue 6, November-2012 .

[5] Rafi, Z. Gh , M. Mohajer, A. Malarky, P. Mousavi, and S. Safavi-Naeini. "Low-profile integrated microstrip antenna for GPS-DSRC application." Antennas and Wireless Propagation Letters, IEEE 8, 44-48., 2009.

[6] Fujimoto, Takafumi, and D. Tanaka. "An L-Probe Fed Stacked Rectangular Microstrip Antenna Combined with a Ring Antenna for Triple Band Operation in Its." Progress In Electromagnetics Research C 37 , 1-13., 2013.

[7] Fujimoto, Takafumi, and R. Nakanishi. "Stacked rectangular microstrip antenna for triple band (GPS/VICS/ETC) operation in ITS." In Antennas and Propagation (APSURSI), IEEE International Symposium on, pp.175-178. IEEE, 2011.

[8] Alsath, M., and K. Malathi "A Shared-Aperture Multiservice Antenna for Automotive Communications." IEEE Antennas and Wireless Propagation Letters 13 , 1417-1420., 2014.

[9] Raj, V. Dhana, A. M. Prasad, M. Satyanarayana, and G. M. V. Prasad. "Implementation of printed microstrip apollonian gasket fractal antenna for multi band wireless applications." In Signal Processing And Communication Engineering Systems (SPACES), 2015 International Conference on, pp. 200-204. IEEE, 2015.

[10] N. Koch, Antennas for Automobiles. INTECH Open Access Publisher,2012.

[11] Gamage, K. H. Jagath , M. Engjom, and I. A. Jensen. "Design of a low profile multi-band antenna for vehicular communication system." In Antennas and Propagation (EuCAP), 2013 7th European Conference on, pp. 1273-1277. IEEE, 2013.

[12] Rahman, Toyobur, Y. Zhaowen, and H. Youcef. "A dual band monopole microstriop printed antenna for WLAN (2.4/5.2/5.8 GHz) application." InMicrowave Technology & Computational Electromagnetics (ICMTCE), 2013 IEEE International Conference on, pp. 204-207. IEEE,2013.

[13] CEN, “Road Transport and traffic telematics – dedicated short range communication – physical layer using microwave at 5.8 GHz, 2004.

[14] H., T. Lee, W. Jang, and J. Lee. "Miniaturization of planar spiral monopole antennas with parasitic elements for terrestrial DMB application." In IEEE Int. Symp. Antennas and Propag.(ISAP), pp. 573-576.

[15] Zhang, Fu-Shun, Yang-Tao Wan, Dan Yu, and Bing Ye. "A Microstrip- Fed Multiband Spiral Ring Monopole Antenna with Improved Radiation Characteristics at Higher Resonant Frequencies." Progress In Electromagnetics Research C 41 , 97-109., 2013.

[16] Haridas, T. Nakul, Arslan, and A. T. Erdogan. "Multiband Antenna for Space Based Reconfigurable Satellite Sensor Node." In Wideband, Multiband Antennas and Arrays for Defence or Civil Applications, 2008.

[17] Zhang, Yangjun, T. Nakata, and T. Miyashita. "A miniature circular disc monopole UWB antenna with a tapered feed line and a circular ground." In Microwave Conference, 2008 China-Japan Joint, pp. 411-414. IEEE, 2008.

[18] L. Liu, X. J. Yang, and S. W. Cheung. "Design of Wideband Monopole Antennas Using a Simple Tapered Feed Line and Slot." In Progress in Electromagnetics Research Symposium, pp. 474-478. Electromagnetics Academy. The Journal's web site is located at http://www. piers. org/piersproceedings/, 2013.

[19] www.irnss.isro.gov.in

[20] Microstrip and Printed Antenna Design”, Randy Bancroft, Second Edition, Institution of Engineering and Technology, 2009.

THE 5TH INTERNATIONAL CONFERENCE ON WIRELESS COMMUNICATIONS, VEHICULAR TECHNOLOGY, INFORMATION THEORY, AEROSPACE & ELECTRONIC SYSTEMS (WVITAE-2015)
December 13-16, 2015, Hyderabad, India

Single Thing Sign On Identity Management for Internet of Things

Vanya Zdravkova, Mihail Mihaylov, Albena Mihovka, Ramjee Prasad
Department of Electronic Systems, Center for TeleInfrastruktur
Aalborg University
Aalborg, Denmark
{vzdrav,mrm,albena,prasad}@es.aau.dk

Abstract*—Within the context of heterogeneous Internet of Things (IoT) network driven by Machine-to-Machine (M2M) communications there is a need for a proper user identification and Identity Management (IdM) mechanisms which to involve all of the objects in the IoT. The paper addresses user identification by proposing Single Thing Sign On (STSO) IdM architecture for IoT, where the end-user is in the middle of a user-centered services ecosystem. The proposed scheme enables user recognition and services access only by identification of one of the "things" related to the user such as personal computing devices, sensors etc. The authors propose a novel user identification method driven by computing device recognition algorithm (CDR algorithm). To better illustrate the use case of the STSO IdM and CDR algorithms they are analyzed in context of the eHealth platform for Ambient Assisted Living – eWALL.*

Keywords—IoT, STSO, IdM, CDR, user identification, eWALL(or eHealth platform)

I. INTRODUCTION

Internet of things (IoT) represents a unique interconnected system, which enables devices to communicate globally using set of standard protocols and connecting various heterogeneous networks. By means of a unique identifier (ID) IoT objects are able to communicate directly with each other [1]. In the context of IoT, the concept of identity extends to things. Identities can be considered as end points so that it is easy to ensure access to that thing endpoint independently [2].

The user identification process can be explained as an interaction whereby the user identity is provided to the security system. The identification provides access to and the modification of data by a certain personal, and enables services and communications to be customized [3]. In IoT context, identification can be explained as an association of attributes which represents identifiers. To make the communication within IoT more efficient, one common device and object identifier would be beneficial [2] [3].

Various methods for user identification and attractive Identity Management (IdM) mechanisms, such as Single Sign On (SSO) have been proposed [2] [4]whereby the user effort of remembering passwords is simplified on a web level. L. Some early solutions to IoT IdM [5] are now being implemented but they still need improvement and standardization [4][6]. TIdM for M2M is represented by authentication of multiple user's devices where the user can access a particular single service with all of his/her devices after performing initial authentication only on one device. The scenario adopted here assumes that the user will be able to access multiple services on a number of different devices by authenticating only to one of those devices. The access to connected shared devices, will enable gathering contextual metadata and sensors data and will enable user centered responsive services. The enabling IdM feature is introduced in this paper as Single Thing Sign On (STSO), which addresses challenges, such as heterogeneous networks with minimum human interaction, how to enable successful communication among personalized devices, and privacy.

Based on the published research [6] [7] [8], a number of generic system requirements of relevance to the STSO integrated IdM system were summarized in Table I.

TABLE 1. GENERIC SYSTEM REQUIREMENTS

Goal	Description
Flexibility	To enable support of various network devices
Scalability	To scale easily to envisioned use-cases and provides global communication through discoverable identifiers which are unique within various domains
Extensibility	To provide integrity and proper APIs for integration of novel for the system devices
Reliability	To provide reliable communication on-time reaction.
Privacy	To keep and protect the personal user information from unauthorized access.

To address the identity issues related with the proposed STSO IdM in IoT Computing Device Recognition (CDR) algorithm for automated and secured user and device identification.

This paper is organized as follows: Section II proposes the IdM system model for IoT. Section III proposes a Computing Device Recognition algorithm for automated user identification. Section IV discuss about the implementation of the STSO IdM in eHealth platform scenario. Section V summarizes the improvements and finally Section VI concludes the paper.

II. STSO IDM SYSTEM MODEL

A. IdM system Architecture

The proposed idea is to enable IdM for the identification of the user across multiple domains. The STSO IdM is based on

the federated IdM system model proposed in [2]. The high-level system architecture is shown in Fig.1

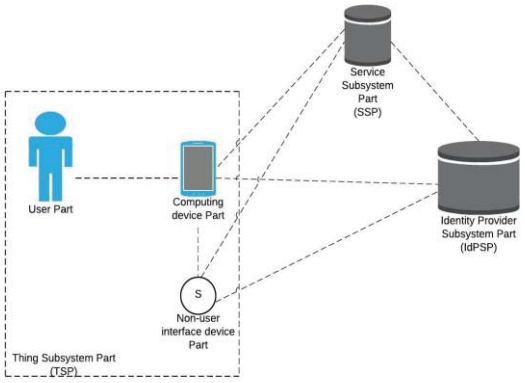

Fig. 1. High - level IdM system structure

The main physical entities of the system in Fig. 1 are the following:

1) Thing Subsystem Part (TSP) - it represents the "things" in IoT such as users, smart computing devices, sensors and actuators. All of these take an important role in the user identity process by providing identities to the Identity Provider Subsystem Part (IdPSP). TSP is divided into three separate subsystems as follows:

a). User as a Part (UP) - in the proposed IdM system, the user is an actor, being a part of the system, who access multiple services by using his/her device(s). User identity data is obtained and provided by IdPSP.

b*). Computing Device Part (CDP)* - it is a functional layer residing in a user device and serve for providing middleware functionalities for the system. From security point of view, this part is needed to prevent unauthorized data modification and corruption.

c*). Non-user interface Device Part (Non-userIntDP)* - this part is responsible for collecting accurate information from personal and/or shared non-user interface devices regarding users' needs. In that way, it supports SSP to provide always on time responsive services to the users.

2) Identity Provider Subsystem Part (IdPSP) - the responsibility of the IdPSP is to store all the identity data. In addition, it is also responsible for the user, device and service authentication. Also, access to the non-user interface devices is managed by IdPSP. It can be remotely or locally located and one of the main benefits is that the IdPSP can provide communication and different functionalities automatically.

3) Service Subsystem Part (SSP) - is a part of the proposed IdM service layer that enables authentication of a user or "things" both for local or remote services.

The design of the proposed IdM system allows multiple IdPSs management by multiple IdPs. The IdPSPs provides identity storage information, features for searching and discovering from a device perspective in an easier way and thus the latter is able to establish dynamic connections.

The regular user can create a private subsystem of identifiers for his devices and established identities, which can be further provided to an IdPSP to manage them.

B. STSO Connection Procedure

The general STSO connection procedure is shown in Fig. 2.

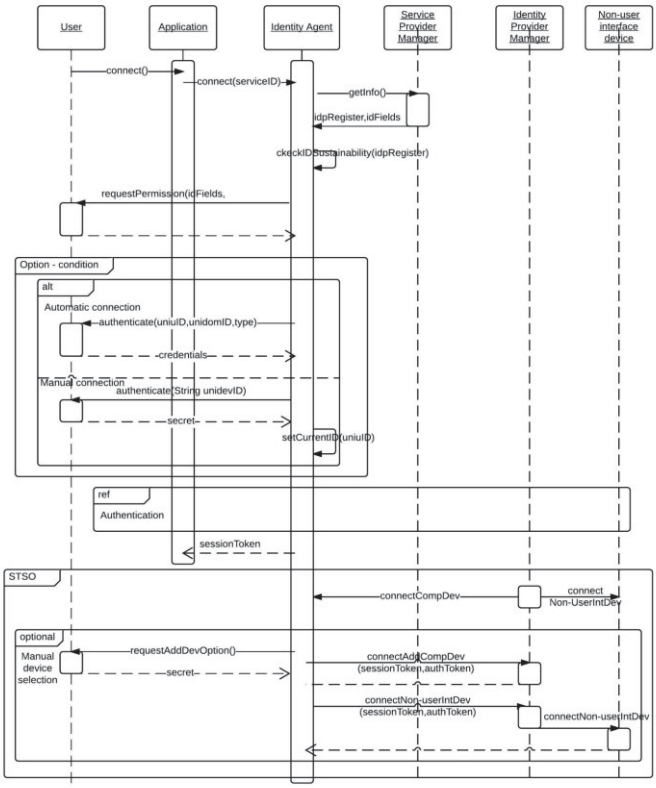

Fig 2. STSO connection sequence diagram

Let us consider a case where a given computing device is utilized by a human user and the latter intends to connect locally or remotely to an available service through a certain application. The user may use beforehand applications, which require an automatic connection to the service, independently of the user's intentions. The sequence flow is as follows:

1) *Application* sends connect request to *IdentityAgent* providing service ID or alternative information related to requested service.

2) *IdentityAgent* uses the provided service information in order to establish communication with related *ServiceManager* and learn about IdPs relationships with the service and the required identity fields.

3) *IdentityAgent* obtains certain information associated to desired service from *ServiceProviderManager*.

4) *IdentityAgent* checks whether the provided computing device identity is active (if there is any) and appropriate for the service by using IdP list related to the service.

5) Subsequently, *IdentityAgent* notifies the user about the required identity data fields and gives an option for identity switch based on service requirements.

There are two possible alternative login mechanisms as shown in Fig. 2 The first one is an optional automated connection where all of the devices related to the user are automatically connected based on only one thing identification. If certain computing device(s) is (are) recognized by IdPs regarding user's preferences, STSO is activated.

The second is a manual connection procedure, whereby the user may manually confirm the identity and choose a device. Then, the provided thing's credentials should be checked by the *IdentityAgent* or IdP, which are required parties in the authentication procedure

Once the authentication is successfully completed, *sessionToken* is being set from *IdentityProviderManager* and send to the *IdentityAgent*. The latter sends a received *sessionToken* to the *Application,* which needs that token in order to establish its own communication to the service without elaborating with *IdentityAgent*.

The connection procedure includes an STSO feature where the *IdentityProviderManager* sends the connection device a request to, both, the computing and non-user interface devices groups related to the current user profile. That allows the automatic connection to the other user-related devices, after one of the things (user or computing device) is identified and connected. The procedure is enabled by a recorded connection in the *ConnMsg* class managed by the *IdentityManagerProvider*.

As an optional step, the user can choose manually devices, which he/she would like to utilize. In this case, either the *IdentityAgent* would ask whether they would like to access the service by means of the personal devices, or the user might agree and choose some additional devices and specify a secret key derived as an *authToken.* The latter will be used in the message send to the *IdentityProviderManager* afterwards.

When the *ServiceManagerProvider* requests authentication from the *IdentityProviderManager*, then:

1) The *IdentityAgent* sends a message to the *IdentityProviderManager* to request a connection to the additional computing devices and non-user interface devices as per the user's preferences. The message contains the *authToken* and *sessionToken*.

2) The *IdentityManagerProvider* receives the message for connecting to the additional devices, performs the authentication and sends a connection message to the targeted devices, if the authentication is successful.

III. COMPUTING DEVICE RECOGNITION ALGORITHM

In order to support STSO IdM, we propose a Computing Device Recognition (CDR) algorithm for user identification. The CDR algorithm does not exclude the most commonly adopted method for identification - *username* and *password*. It can be considered as an additional feature that simplifies the authentication (automatic and less user intervention) but manual authentication can still optionally be used.

The CDR algorithm is given in Fig. 3.

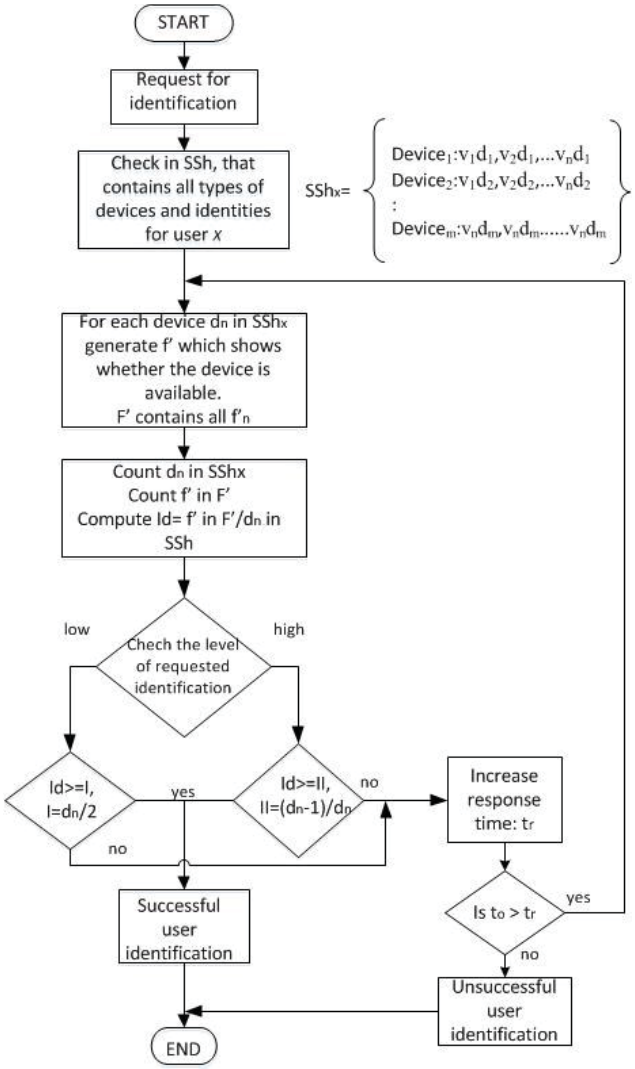

Fig. 3 CDR identification algorithm

The user's types of device identities (v_nd_m) are stored in a Smart Sheet (*SSh*). SSh_x is unique list of devices pointing to user *x*. Each device *d* is recorded to the SSh_x list with a reference number within the interval *[1-m]*. For each device in the *SSh* list, there is a set of different types of identifiers *v*, with a reference number within the interval *[1-n]*, which is assigned to the particular device d_m. If a request for identification from one of the listed and registered devices in a certain domain is received, the register automatically starts to search if there are other user devices and how many of them are available in the local domain. The user is able to define the level of security by manipulating the number of the devices needed for a proof of user identity. For example a certain user may create a policy for 3 out of 5 personal devices simultaneous recognition for automatic user identity recognition. The user is a part of the Internet of people whereby he/she plays the role of manager of

the rules in the system, regarding his/her preferences and wishes.

The available user's computing devices are counted and written in *F'sheet*. After that, the algorithm computes the *Id* index which shows the ratio between the entire devices stored in the SSh and those which are available in the *F' sheet* at a certain moment. Then, the level of required identification is checked. Here, two scenarios are available – for high and low level of identification depending on the user's or services' rules. If the level is low, the algorithm compares whether *Id* is bigger or equal to *I*. In that case, the ratio *I* is equal to at least half of the declared devices in *SSh* which must be discovered and recognized.

If that expectation is true, the identification of the user is successful. If not, the response time t_r is increased and compared with the timeout t_o for the service so the the process is started again until $t_o > t_r$. If the level is high – that the *Id* should be compared to *II index* which allows only one of the user computing device to be unavailable. If that expectation is true, the identification of the user is successful. If not, the process is started again until the timeout t_o for the service expires.

A coefficient which defines the identification rate of the computing device is proposed in order to be used for the identification assessment within the CDR algorithm, $\boldsymbol{Ir_{cd}} = \boldsymbol{N_{cd}/M_{cd}}$, where Ir_{cd} is an identification rate coefficient of the computing device N_{cd} is a number of identified computing devices *(cd)* related to the particular user M_{cd} is a total number of predefined computing devices *(cd)* required for the identification

Ircd is equal to the number of identified computing devices related to the particular user over the total required number of predefined computing devices necessary for the identification procedure.

The identification rate of the CDR algorithm depends on the number of correctly identified computer devices, related to a particular user and it must be equal or close to '1' in order to recognize the user itself.

IV. STSO IDM EHEALTH SCENARIO

This section proposes an implementation and use of STSO IdM in an eHealth scenario. The key requirements for enabling a sustainable eHealth system, are the personalization and adaptation to specific needs and preferences, the efficient data and context sharing between the different required services and artefacts, including the handling of multiuser identification, auto configuration and calibration systems [9]. Typically, a myriad of wireless and wired communication and data processing technologies and networked devices need to interoperate in order to provide highly personalized services.

The funded under the European Union's Framework Program Seven (FP7) project eWALL[1] (eWall for Active Long Living, 2013) has proposed a system platform able to sense and "learn the needs of the user who in order to provide personalized support to healthcare and unobtrusive daily activities [10]. In the context of eWALL, IdM would allow for real-time user and device recognition regardless of the presence of other users around. IdM would allow for more efficient use of resources and would eliminate the need to deploy personal sensor nodes specifically to cater for the needs of the user under observation.

The eWALL system is composed of two main subsystems: the eWALL Sensing Environment and the eWALL Cloud.*The eWALL Sensing Environment* - is deployed over a physical space and interacts with the primary user. A Home Sensing Environment, operates in the domestic surroundings of the user. It monitors the status of environmental parameter such as humidity, temperature, luminosity, motion etc. A Mobile Sensing Environment would operate around the user and collect data from wearable devices. The data would be transferred to the home device gateway wirelessly when the user is within the communication range of it. Such wearables could be smartphones, pulse and blood oxygen saturation sensors, body temperature sensors, ect.

The eWALL Cloud would handle the data processing and storage whereby the eWALL Cloud is connected to the home environment of each user. Based on actions performed within the Cloud environment, personalized services and applications will be offered to the corresponding user.

A. Implementation of STSO IdM in eWALL

The implementation of STSO IdM is proposed as subsystems components to be included in the eWALL architecture shown in Fig. 4 with the benefits of improved eWALL user identification, better mobility and more responsive eWALL applications

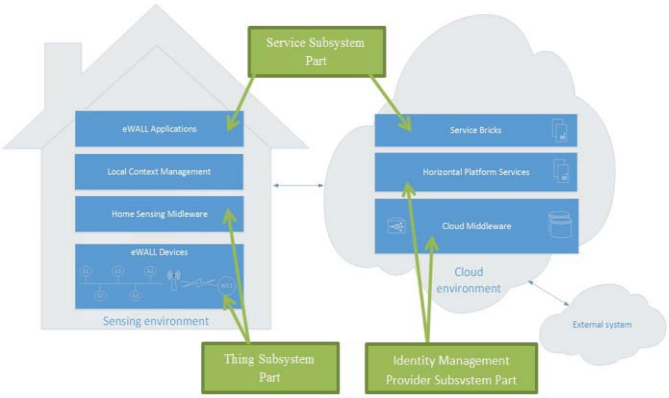

Fig. 4. Implementation of STSO IdM subsystem parts in eWALL

TSP resides on the eWALL devices and Home Sensing Middleware components of eWALL where the eWALL users, sensors and computing devices could be assumed as part of the infrastructure, when referring to IoT and IdM. The Identity

[1] EU FP7 Project eWALL http://ewallproject.eu/

Agent should be installed on the eWALL primary user's computing devices, in order to enable the STSO feature.

IdPSP should be deployed as part of the Cloud Middleware and as a part of the Horizontal Platform Services where the user profile information is stored and managed at a cloud level. The IdentityManagerProvider should be implemented on a cloud middleware level to enable identity functionalities such as thing identity creation, management and deletion. What is missing for the eWALL system on a cloud level is a device identity management related to a certain user.

SSP is already represented in eWALL by User profiling functionalities the respective applications and services assignment to a certain user.

It is proposed to include the implementation of the STSO IdM within eWALL as a part of the holistic architecture of the platform, rather than as a single component or plug in. This would affect the overall architecture and would require dedicated C++ components to be implemented on a DeviceGateway level while other Java software artefacts should be deployed on a cloud level. The implementation may also cause changes in the JSON data format used for the sensors and actuators data representation and exchange, as well as it will require storing of additional device identity data both on the homePC (CouchDB) and eWALL cloud (MongoDB) databases.

V. IMPROVEMETS

By introducing and implementing the IdentityAgent and IdentityProvider, eWALL will be able to extend further with adoption of the CDR algorithm where the user input efforts will be minimized. The password retyping and remembering will be substituted by the algorithm, which will contribute for simplifying the system and improving the privacy and security.

A number of advantages should be summarized as follows:

- CDR algorithm will improve the eWALL system in terms of usability and ease of use. It also is a way of performing better user experience, improved personalization and minimizing the need of user input which is important from senior or cognitive impaired users' point of view.
- STSO IdM will improve the eWALL system in terms of mobility and inner system sites roaming – by ensuring user identification and eWALL application access.
- STSO will add value to the eWALL system by providing Service orientation and ensuring always responsive services
- Personalization and privacy of services by improved ability for the user to create the rules for identification within the eWALL system.
- STSO IdM and CDR algorithm will improve the security by reducing the possibility for personal data abuse or unwanted system intrusion.

With introducing the STSO IdM in eWALL both the users and the business parties will benefit from better utilized sensing infrastructure, seamless roaming between eWALL sensing environments, improved personalization and security of the services and better monitoring of the patients.

Another advantage is that based on only one profile for STSO IdM, the user could be identified and be able to utilize various services by using myriad of devices. Furthermore, the user will be able to define and manage his/her own rules in the stage of profile creation such as: device connectivity type (automatically or manually), services access permissions, number of computing devices as an input data for CDR procedure.

VI. CONCLUSION

Referring to proper and meaningful scenarios for implementation of STSO IdM, good examples are the e-Health and, in particular, the Ambient Assisted Living (AAL) services The introduced STSO IdM system is a novel solution addressing the communication and interactions between all of the things involved in IoT in automated, time- and efford-saving manner. The STSO feature enables access to services through only one thing sign on without need of separate identification on web level or any additional manual actions. The proposed CDR identification algorithm ensures automated user identification. Privacy and security supportive technologies like the proposed from the author STSO IdM and CDR algorithm have the potential to fill in this gap for proper technology solutions.

REFERENCES

[1] "The internet of things" [Online]. Available: http://www.iot-i.eu/iot/public/news/resources/TheThingsintheInternetofThings_SH.pdf. [Accessed: June-2015].

[2] P. Mahalle, N. R. Prasad, and R. Prasad, "Identity Management Framework towards Internet of Things. CTIF Aalborg, November 2013.

[3] D. Todorov, Mechanics of User Identification and Authentication: Fundamentals of Identity Management. CRC Press, 2007.

[4] Ingo Friese, "Concepts of Identity within the Internet of Things - DG - Identities of Things - Kantara Initiative." [Online]. Available: http://kantarainitiative.org/confluence/display/IDoT/Concepts+of+Identity+within+the+Internet+of+Things.[Accessed: Jul-2015].

[5] "Final: OpenID Authentication 2.0 - Final." [Online]. Available: http://openid.net/specs/openid-authentication-2_0.html. [Accessed: May-2015].

[6] M. V. Moreno, J. L. H. Ramos, and A. F. Skarmeta, "User role in IoT-based systems," 2014 IEEE World Forum on Internet of Things (WF-IoT), pp. 141–146.

[7] R. Prasad, Ed., My personal Adaptive Global NET (MAGNET). Dordrecht: Springer Netherlands, 2010..

[8] Signals and Systems Telecom, "The Wireless M2M & IoT Bible: 2014 – 2020 - Opportunities, Challenges, Strategies, Industry Verticals and Forecasts." May-2014.

[9] A. Mihovska, M. Mihaylov, S. Kyriazakos, R. Prasad, "Standardization and Innovation for Smart e-Health Monitoring Services," in SmartMedDev, Lisbon, 2015.

[10] A. Mihovska, S. Kyriazakos and R. Prasad, "eWall for Active Long Living: Assistive ICT Services for Chronically Ill and Elderly Citizens," in Systems, Man and Cybernetics (SMC), San Diego, CA, 201.

THE 5TH INTERNATIONAL CONFERENCE ON WIRELESS COMMUNICATIONS, VEHICULAR TECHNOLOGY, INFORMATION THEORY, AEROSPACE & ELECTRONIC SYSTEMS (WVITAE-2015)
December 13-16, 2015, Hyderabad, India

Enhanced Turbo Equalizer Using 2 Dimensional Iterative Soft Decision Interference Cancellation

Doron Shinbox and Dan Raphaeli
Dept. EE-Systems, Tel-Aviv University, Israel

***Abstract*—In this paper, a novel iterative equalizer applying soft feedback is introduced, the 2 dimensional ISDIC (2D ISDIC) equalizer. The 2D ISDIC is the first equalizer that bridges the gap between the low complexity ISDIC equalizer which has poor performance, to the high complexity inverse channel equalizing methods, such as the LMMSE and the MMSE ISDIC equalizers, which has better performances. The 2D ISDIC will be incorporated into the turbo equalization scheme, resulting in an enhanced turbo equalizer, that performs better than the conventional, state of the art, linear turbo equalizer, with lower complexity and lower amount of iterations.**

I. Introduction

Inter symbol interference (ISI) is a well known phenomena affecting single carrier (SC) communication system, requiring the need on an equalizer. Various solutions to the ISI problem were widely investigated in literature throughout the years, from the maximum likelihood sequence estimator (MLSE) through different linear equalizers and to decision feed back (DFE) equalizers. One of latest class of equalizers are the iterative equalizers applying soft decision feedback. This type of equalizers consist of a two parts, linear part and a soft decision calculation part, which in not linear. The soft decision symbols are fed back to the linear equalization part and thus adding a non linear information for the symbol estimation which improves the equalizer's performance. This scheme is done in an iterative manner until it converges.

The optimal, in the sense of minimum mean square error (MMSE), iterative equalizer applying soft feedback is the MMSE ISDIC equalizer [1]. The MMSE ISDIC uses the information of the soft decision symbols in order to compute the LMMSE filter. Then a soft decision is made on the LMMSE output. The computation of an LMMSE filter of minimum twice the channel size every symbol estimation, makes it to be high complexity equalizer, and not practical to implement. On the other hand, the ISDIC equalizer [2], is a low complexity iterative equalizer applying soft feedback. The ISDIC equalizer uses a matched filter as a feed forward filter in order to concentrate the overall impulse response at one sample. Then, an ISI cancellation is made on that sample, followed by a soft decision. The application of a matched filter, instead of a channel inverse filter, makes it a very low complexity equalizer. However, it was shown that this equalizer performs well only on long random channels, with impulse like auto correlation functions.

In 1993, the novel turbo code scheme was introduced [3] and the concept of passing information between two decoders gave rise to the turbo equalization scheme [4]. In the turbo scheme an iterative receiver repeat the equalization and decoding on the same set of received data, where the feedback information from the decoder is incorporated into the equalizer in an iterative manner. The first turbo equalizer scheme was presented using a maximum a posteriori (MAP) equalizer. However the MAP equalizer suffers from high computational load for channels with long memory or large constellation size. Replacing the MAP equalizer with an LMMSE equalizer was proposed in [5], [6], and is widely known as the linear turbo equalizer. This approach performs almost as well as turbo equalizer based MAP algorithm, only requiring more iterations to achieve similar BER results.

In this paper, we introduce the novel 2 dimensional ISDIC (2D ISDIC) equalizer. The 2D ISDIC is based on a patent from 2005 [7] which was never published as a paper, and was implemented as an ASIC for use in power line communications. In the 2D ISDIC equalizer, we use a matched filter, in order to concentrate the overall impulse response at two samples, hence 2D. Then a partial ISI cancellation is made on the two matched filter's output samples, leaving two symbols uncanceled. A minimal 2 length LMMSE filter is then used to cancel the ISI left. Finally, a soft decision is made on the LMMSE output. The use an LMMSE filter improves the performance on much more difficult channels, with minimal increase in complexity. The main reason for the performance improvement of the 2D ISDIC is that the errors in the fed back symbols are less amplified in return to some increase in noise enhancement. If we take $D = 1$, we get the ISDIC equalizer, and if we take D to be the block length, we get the LMMSE equalizer. Therefore, the 2D ISDIC, may be considered as the bridge between both equalizers.

The 2D ISDIC will be then incorporated into the turbo scheme, resulting in an enhanced turbo equalizer. The enhanced turbo equalizer has two feedback. The feedback from the inner 2D ISDIC equalizer and from the decoder. The results show that the performance of the resulting 2D ISDIC turbo equalizer is better than the conventional, state of the art, linear turbo equalizer, with lower complexity and lower amount of iterations.

Before proceeding, Some frequently used notation is introduced. Vector are written in bold letters and are considered to be column vectors. Matrices are specified by capital letters. The vector $H_{(m,:)}$ represent the m^{th} row vector of the matrix H . The LLR operator $L_{obsevation}(x)$ is given by:

$$L_{observation}(x) \triangleq ln\left[\frac{P(x=1/observation)}{P(x=-1/observation)}\right] \quad (1)$$

The observation represents either the equalizer output which will be denoted by $L_e(x)$ or the decoder output denoted by $L_c(x)$. The soft decision of a symbol x_n will be defined as $s \triangleq E[x/observation]$. In this paper we will use a very simplified approximate model for the observations as $observation = x + z$ where z is a white Gaussian noise with zero mean and variance σ_z^2. Then, the relation between $L_{observation}(x)$ and the soft decision which is also the MMSE of x given an observation: $E[x/observation]$, is

$$s = tanh\left(\frac{L_{observation}(x)}{2}\right) = tanh\left(\frac{observation}{\sigma_z^2}\right) \quad (2)$$

II. System model

Fig 1, depicts the transmitter structure of our model. First the data bits are passing through a convolutional encoder and then through an interleaver, followed by a modulator. In this paper, for simplicity, e consider a real, discrete, time invariant impulse channel response $\mathbf{h} = [h_0, ..., h_{L-1}]$, perfectly known to the receiver. We will use the matrix notation for the received sequence $\mathbf{r}$

$$\mathbf{r} = H\mathbf{x} + \mathbf{w} \quad (3)$$

where H is an $N + L - 1 \times N$ size toeplitz matrix, describing the channel h. $\mathbf{x}$ is a length N transmitted coded data sequence $\mathbf{x} = [x_0, ..., x_{N-1}]$ taken from a BPSK alphabet $x_n \in \{+1, -1\}$ and $\mathbf{w}$ is a $N + L - 1$ length i.i.d Gaussian noise vector with zero mean and σ^2 variance. In order to develop the equations for the 2D ISDIC equalizer, we will define the matched filter output $\mathbf{u}$

$$\mathbf{u} = C\mathbf{x} + H^T\mathbf{n} \quad (4)$$

where$C$ is the channel's auto-correlation matrix $C = H^T H$.

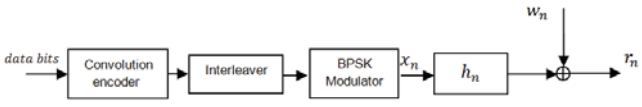

Figure 1. Transmitter and channel configuration

III. 2 Dimensional ISDIC Equalizer (2D ISDIC)

The 2D ISDIC equalizer is a combination of the ISDIC equalizer and a 2 size LMMSE filter. Like the ISDIC operation, the received signal is passing through a matched filter followed by an ISI cancellation. However, in the 2D ISDIC we choose two matched filter's outputs to perform a partial ISI cancellation on. For the estimation of x_n we will choose the outputs u_n and u_{n+d} , where d is chosen according to the channel characteristics. The number of matched filter's outputs selected, will be denoted by D, and will be referred as the dimension of the ISDIC equalizer. In this scheme, the ISI is not tempted to by fully canceled like in the ISDIC equalizer. Instead a number of symbols are left uncanceled and therefore we refer it as a partial ISI cancellation. The number of uncanceled symbols will be equal to the dimension of the equalizer D. Next, an LMMSE equalizer of length D is used to estimate the current symbol since the ISI of the uncanceled symbols remains. Finally, a soft decision is made on the LMMSE output. The parameter D is a trade-off between the ISI cancellation part and the LMMSE part, where $D = 1$ leads to the conventional full cancellation ISDIC equalizer, will be referred from now on as the 1D ISDIC, and $D = N$ leads to the conventional LE. The LE suffers from noise enhancement, and the conventional ISDIC suffers from error propagation (feeding wrong estimations), so some value in between can give best performance. We analyzed the trade-off, and found out that the value $D = 2$ gives good performance in most of the channels tested, and is also leads to the lowest complexity.

Every estimation of the symbol x_n , the partial ISI cancellation is done using the soft decision symbols vector $\mathbf{s}_n^\mu$, defined as

$$\mathbf{s}_n^\mu = \quad (5)$$

$$\left[\ s_0^\mu, \quad ... \quad s_{n-1}^\mu, 0, s_{n+1}^{\mu-1}, ..., 0, s_{n+d+1}^{\mu-1} \quad , ... \quad s_{N-1}^{\mu-1}\ \right]^T$$

where s_k^μ is the soft decision of the symbol x_k at the μ^{th} iteration, $\mu \in \{0, ..., \mu_{max}\}$, with initial conditions $s_k^0 = 0, \forall k$. Note that we exclude the soft symbols $s_n^{\mu-1}$ and $s_{n+d}^{\mu-1}$, where for the 1D ISDIC equalizer this vector excludes only $s_n^{\mu-1}$. The choice of d is done according to next highest peak (in absolute value) of the channel's auto correlation function defined as

$$\rho_n = \sum_{k=0}^{L-1} h_k h_{n+k} \quad (6)$$

Since $\rho_n = \rho_{-n}$ we can take d to be either positive or negative. For example, in both channels auto correlation functions, depicted in Fig 5, we can choose d to be ± 1. Furthermore, we know that the soft decision symbols vector $\mathbf{s}_n^\mu$ is updated sequentially, meaning that the pre soft symbols $\mathbf{s}_k^\mu, \forall k < n$ passed one more iteration than the post soft symbols $\mathbf{s}_k^{\mu-1}, \forall k > n$, and probably more accurate. Therefore, we choose d to be positive in order to use the soft symbol $\mathbf{s}_{n-d}^\mu$ instead of $\mathbf{s}_{n+d}^{\mu-1}$ for the partial ISI cancellation part, and leave the ISI from the symbol x_{n+d} to be treated by the LMMSE filter.

After choosing the two matched filter's $u_n$and u_{n+d} we perform a partial ISI cancellation according to

$$q_0 = u_n - C_{(n,:)}\mathbf{s}_n^\mu \quad (7)$$

$$q_1 = u_{n+d} - C_{(n+d,:)}\mathbf{s}_n^\mu \quad (8)$$

Assuming normalized channel, i.e. $\rho_0 = 1$, the matrix notation for the partial ISI cancellation output $\mathbf{q}$ is

$$\mathbf{q} = G\mathbf{x}_n + \mathbf{e} \quad (9)$$

where

$$\mathbf{q} = \begin{bmatrix} q_0 \\ q_1 \end{bmatrix} \quad G = \begin{bmatrix} 1 & \rho_d \\ \rho_d & 1 \end{bmatrix}$$

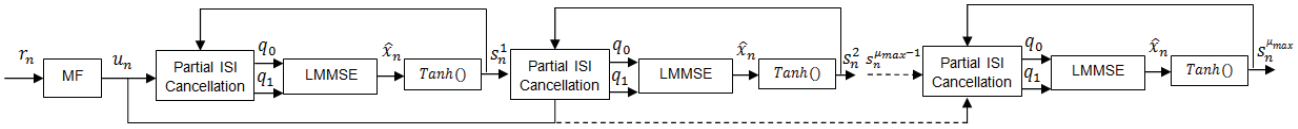

Figure 2. 2D ISDIC Equalizer

$$\mathbf{x}_n = \begin{bmatrix} x_n \\ x_{n+d} \end{bmatrix} \quad \mathbf{e} = \begin{bmatrix} e_0 \\ e_1 \end{bmatrix}$$

and $\mathbf{e}$ is the error term due to Gaussian noise and estimation errors.

The way we chose to compute the LMMSE coefficients follow the basic idea which was presented in [1], and states that the computation of the coefficients should be done given the past soft decisions and should be carried out on every symbol i.e new LMMSE coefficients are calculated for each symbol. The LMMSE solution for estimating x_n from the vector $\mathbf{q}$ is

$$\mathbf{w}^T = E[x_n \cdot \mathbf{q}^T / \mathbf{s}_n^\mu] \cdot \left(E[\mathbf{q} \cdot \mathbf{q}^T / \mathbf{s}_n^\mu]\right)^{-1} \tag{10}$$

Neglecting the conditional (given the vector $\mathbf{s}_n^\mu$) statistical dependencies between $x_i, x_k \forall k \neq l$ and between $x_k, n_l \forall k, l$ and using the following relations:

$$E[x_n / \mathbf{s}_n^\mu] = E[x_n] = 0 \tag{11}$$

$$E[x_{n+d} / \mathbf{s}_n^\mu] = E[x_{n+d}] = 0 \tag{12}$$

and

$$E[x_k / \mathbf{s}_n^\mu] = s_k^\mu, \forall k < n \tag{13}$$

$$E[x_k / \mathbf{s}_n^\mu] = s_k^{\mu-1}, \forall k > n,\ k \neq n+d \tag{14}$$

$$E[x_k^2 / \mathbf{s}_n^\mu] = 1, \forall k \tag{15}$$

we can derive the LMMSE coefficients

$$\mathbf{w}^T = G_{(1,:)} \left(GG^T + \Sigma_e\right)^{-1} \tag{16}$$

where Σ_e is the covariance matrix of the error term vector $\mathbf{e}$. (the covariance matrix elements will be presented in the journal paper). The biased LMMSE output is

$$\hat{x}_n = \mathbf{w}^T \mathbf{q} \tag{17}$$

We now approximate $\hat{x}_n$ as white Gaussian noise added to the symbol and the soft decision is computed according to

$$s_n^\mu = tanh\left(\frac{\hat{x}_n}{1-\alpha}\right) \tag{18}$$

where $\alpha = \mathbf{w}^T G_{(:,1)}$ is the LMMSE biased term. Note that in the 1D ISDIC $1-\alpha$ is replaced with the variance of the error signal after the ISI cancellation $\widehat{\sigma}_\mu^2[n]$, given in [2]. The scheme of the 2D ISDIC is presented in Fig 2.

IV. The Enhanced Turbo Equalizer Architecture

The conventional turbo equalizer scheme is depicted in Fig.3. and will be used here as the basis for the development of the new enhanced algorithm. $L_e(x_n)$ and $L_c(x_n)$ represents the LLR of the symbols at the output of the equalizer and at the output of the decoder, respectively. $L_p(x_n)$ represents the prior information of the symbols from the decoder (independent of the channel observations for a sufficient long block length) and is equal to

$$L_p^i(x_n) = L_c^i(x_n) - (L_e^i(x_n) - L_p^{i-1}(x_n))$$

where the superscript i represents the outer iteration number. The iterations begin with initial conditions of $L_p^0(x_n) = 0, \forall n$.

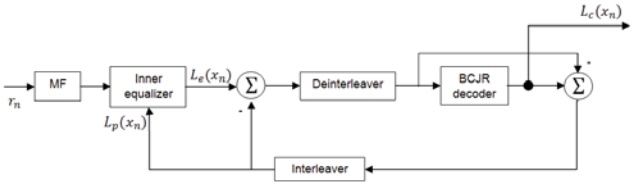

Figure 3. Turbo equalizer receiver

In the enhanced turbo equalizer scheme we use the ISDIC algorithm as a inner equalizer (1D or 2D). When using the ISDIC algorithm in the turbo scheme, we have two sources of feedback for each symbol. The feedback from the equalizer iteration (inner iterations) and from the decoder (outer iterations). We use the information from the decoder to update the soft symbols vector every outer iteration. Furthermore we use the information from the decoder when computing the soft symbol $s_n^{\mu,i}$ which is the soft symbol in i^{th} outer iteration and in the μ^{th} inner iteration where $i \in \{1, ..., i_{max}\}$. We also use the information from the decoder for the a priori information on the x_{n+d} symbol in the 2D ISDIC algorithm as will be explained. The enhanced turbo equalizer scheme is depicted in Fig .4.

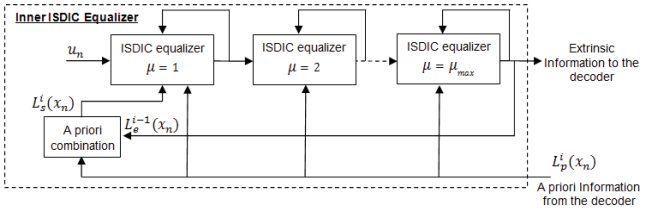

Figure 4. Enhanced Turbo equalizer receiver

where we have two observations for each symbol: $L_e^{i-1}(x_n)$ and $L_p^i(x_n)$, assuming that$L_e^{i-1}(x_n)$ and $L_p^i(x_n)$ are independent for a sufficient long block length, we simply combine the two sources

$$L_s^i(x_n) = L_e^{i-1}(x_n) + L_p^i(x_n) \tag{19}$$

where $L_s^i(x_n)$ is the combined prior to be used in the inner equalizer.

A. 1D ISDIC Turbo Equalizer

In order to incorporate the ISDIC into the turbo scheme we need to make the following modifications. After each outer iteration, new prior information $L_p^i(x_n)$ is given from the decoder. The soft symbols are initialized every outer iteration according to

$$s_n^{0,i} = tanh\left(\frac{L_e^{i-1}(x_n) + L_p^i(x_n)}{2}\right) = \tag{20}$$

$$= \frac{s_n^{\mu_{max},i-1} + tanh\left(\frac{L_p^i(x_n)}{2}\right)}{1 + s_n^{\mu_{max},i-1} tanh\left(\frac{L_p^i(x_n)}{2}\right)}, \forall n$$

with initial conditions $s_n^{0,1} = 0, \forall n$. The a prior information from the decoder is in addition used in the soft decision calculation, and the soft decision calculation of the 1D ISDIC becomes

$$s_n^{\mu,i} = tanh\left(\frac{y_n^{\mu,i}}{\widehat{\sigma}_\mu^2[n]} + \frac{L_p^i(x_n)}{2}\right) \tag{21}$$

B. 2D ISDIC Turbo Equalizer

In order to incorporate the 2D ISDIC to the turbo scheme we need to make the following modifications. First we need to update the soft symbols vector (5) which is done in the same way as in (20). Second we need to modify the LMMSE coefficients. Recall that the 2D-ISDIC principle is not to use the soft symbol of the symbol $n+d$ in the ISI cancellation, however, when incorporating the 2D ISDIC into the turbo scheme we wish to use the a prior information from the outer iteration available for this symbol and therefore equation (12) is modified to

$$E[x_{n+d}/\mathbf{s}_n^{\mu,i}] = E[x_{n+d}] \triangleq m_{n+d} \tag{22}$$

, where

$$m_{n+d} = tanh\left(\frac{L_p^i(x_{n+d})}{2}\right) \tag{23}$$

and the LMMSE solution is now

$$\mathbf{w}^T = G_{(1,:)}\left(G\begin{pmatrix} 1 & 0 \\ 0 & 1 - m_{n+d}^2 \end{pmatrix} G^T + \Sigma_e\right)^{-1} \tag{24}$$

$$b = -m_{n+d} \cdot \mathbf{w}^T G_{(:,2)} \tag{25}$$

Finally the soft decision equation (18) is modified according to

$$s_n^{\mu,i} = tanh\left(\frac{\hat{x}_n}{1-\alpha_n} + \frac{L_p^i(x_n)}{2}\right) \tag{26}$$

V. Complexity Comparison

An important aspect of the ISDIC equalizers is their low computational complexity. We will compare the computational complexity per received symbol of the ISDIC Equalizers to the Linear Equalizer. For our comparison we do not consider the computation of the LLRs and the soft decision (the $tanh()$ operator) which can be done with a lookup and it is 1 operation.

The number of multiplications and additions for the Linear Equalizer was given in [6] and is $O(M^2)$ where M is the length of the LMMSE filter and is usually twice the channel size. For both 1D and 2D ISDIC Equalizers the matched filter operation the ISI cancellation part and the calculation of σ_n^μ and Σ_e consist of $O(M)$ multiplications and additions. Furthermore the 2 size LMMSE filter in 2D ISDIC scheme requires a constant number of multiplications and additions and therefore the overall computational complexity of the 1D and 2D ISDIC Equalizers is $O(M)$.

VI. Results

We present the BER performance results by simulating data transmission using the system introduced in section 2. We examine the performances of the different schemes on two channels examples. The first channel was taken from [8] and was used in [5]. We took this channel for comparison reasons. The second channel is twice the size of the first channel and was randomly chosen from a Gaussian fading distribution.

$$h_1 = [0.407, 0.815, 0.407] \tag{27}$$

$$h_2 = [0.65, -0.56, 0.08, -0.36, 0.34, -0.1] \tag{28}$$

The absolute value of the auto-correlation function of the two channel is shown in Fig.5.

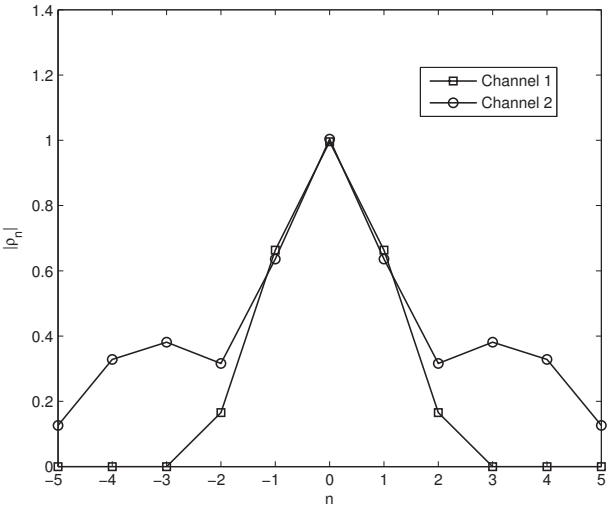

Figure 5. Channels auto correlation functions

The decoder and the interleaver/deinterleaver are identical to all methods. They differ only in the inner equalizer, which is either LMMSE, 1D-ISDIC, 2D-ISDIC or MAP Equalizer. For the LMMSE in the first channel we took a filter of 5 taps and for the second channel we used a 12 taps filter. The Linear Turbo Equalizer is the state of the art Turbo Equalizer [6] and [5]. The performance of the equalizers is lower bounded by the coded AWGN channel BER and by the MAP Turbo Equalizer [4] and they serve as a reference for evaluating the performance of our algorithm. We used a recursive, systematic encoder for the rate 0.5 code G=[7 5] where the first polynomial is used for the feedback and the second for the output bit. This code was chosen for comparison with other papers that used the same code[6] and [5]. For the interleaver we used the S-Random permutation [9] with S=20 and we took the block length to be 1024 ($N = 2048$) . We present our results after 2 outer iterations (1 iteration of separate equalization and code and one iteration with feedback from the code) and 1 inner iteration per outer iteration.

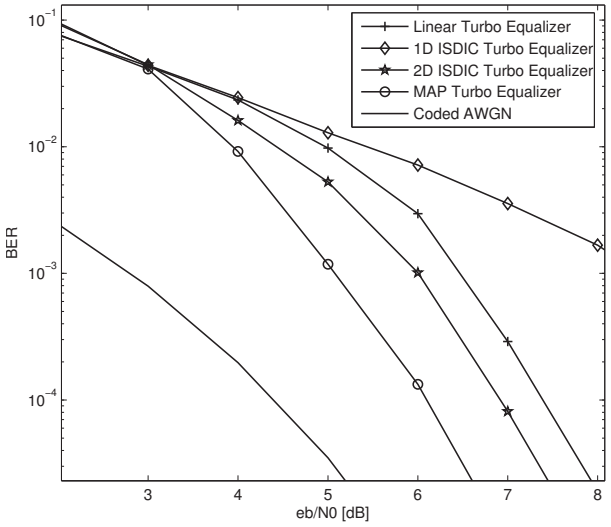

Figure 6. First channel BER Performance

Fig .6. shows the BER results of the 3 different equalizers on the first channel. The 2D ISDIC Turbo Equalizer perform better than the Linear Turbo Equalizer while the 1D ISDIC Equalizer performs poorly. There is less than 1dB gap from the MAP Turbo Equalizer.

Fig .7. shows the BER results of the second channel. Again the 2D ISDIC Turbo Equalizer performs better than the Linear Turbo Equalizer and it has 1dB gain over it. The gap from the MAP Turbo Equalizer is still about 1dB. The 1D ISDIC still performs poorly.

VII. Conclusions and Further research

A new approach for iterative soft decision feedback equalizers with a 2 coefficients length LMMSE estimation was proposed. This type of equalization is suitable for a inexpensive systems working with a single carrier but suffer from strong ISI. Due to the high performance after only few iterations we can suggest it for even for a latency limited applications. We have shown that our method improves the BER performance drastically with only few iterations made. Further optimizations that we will present in later publications will include optimization of the cancellation part, other than using only two symbols as shown in this paper, and in the case for two symbols we will present an optimization on the selection of the symbol $n + d$. An adjustments to spectrum efficient constellations such as high rate QAM will be also presented. One more interesting point that will be elaborated in the journal paper is the convergence of those iterative equalizers and their analysis using EXIT charts.

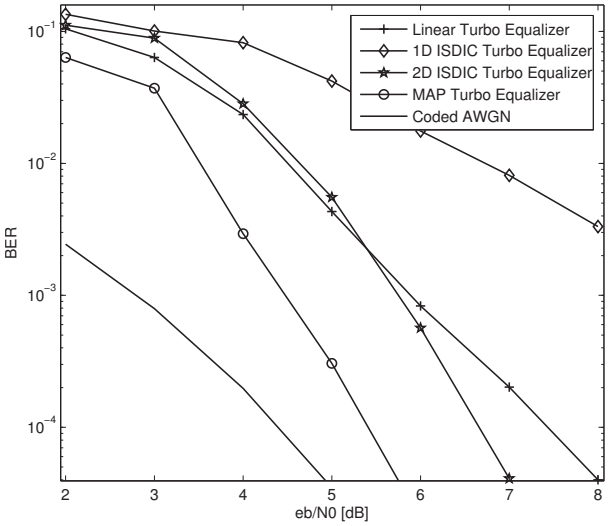

Figure 7. Second channel BER Performance

References

[1] J. F. Roßler, W. H. Gerstacker, A. Lampe, and J. B. Huber, "Matched-filter-and mmse-based iterative equalization with soft feedback for qpsk transmission," in *Broadband Communications, 2002. Access, Transmission, Networking. 2002 International Zurich Seminar on*. IEEE, 2002, pp. 19–1.

[2] W. H. Gerstacker, R. Muller, and J. B. Huber, "Iterative equalization with adaptive soft feedback," *Communications, IEEE Transactions on*, vol. 48, no. 9, pp. 1462–1466, 2000.

[3] C. Berrou, A. Glavieux, and P. Thitimajshima, "Near shannon limit error-correcting coding and decoding: Turbo-codes. 1," in *Communications, 1993. ICC '93 Geneva. Technical Program, Conference Record, IEEE International Conference on*, vol. 2, May 1993, pp. 1064–1070 vol.2.

[4] C. Douillard, M. Jézéquel, C. Berrou, D. Electronique, A. Picart, P. Didier, and A. Glavieux, "Iterative correction of intersymbol interference: Turbo-equalization," *European transactions on telecommunications*, vol. 6, no. 5, pp. 507–511, 1995.

[5] M. TuĬĹchler and A. C. Singer, "Turbo equalization: An overview," *Information Theory, IEEE Transactions on*, vol. 57, no. 2, pp. 920–952, 2011.

[6] M. Tuchler, R. Koetter, and A. C. Singer, "Turbo equalization: principles and new results," *Communications, IEEE Transactions on*, vol. 50, no. 5, pp. 754–767, 2002.

[7] D. Raphaeli, "Equalizer for communication over noisy channels," Aug. 30 2005, uS Patent 6,937,648.

[8] J. G. Proakis, *Digital communications. 1995*.

[9] S. Dolinar and D. Divsalar, "Weight distributions for turbo codes using random and nonrandom permutations," 1995.

THE 5TH INTERNATIONAL CONFERENCE ON WIRELESS COMMUNICATIONS, VEHICULAR TECHNOLOGY, INFORMATION THEORY, AEROSPACE & ELECTRONIC SYSTEMS (WVITAE-2015)
December 13-16, 2015, Hyderabad, India

HANET: Millimeter wave based intelligent radio architecture for serving place time capacity issue

Purnima Lala Mehta
Center for TeleInfrastruktur (CTIF),
Aalborg University,
Aalborg, Denmark,
pla@es.aau.dk

Prof (Dr.) Troels B. Sørensen
Department of Electronics Systems,
Aalborg University,
Aalborg, Denmark,
tbs@es.aau.dk

Prof. (Dr.) Ramjee Prasad
Center for TeleInfrastruktur (CTIF),
Aalborg University,
Aalborg, Denmark,
prasad@es.aau.dk

***Abstract*— Small Unmanned Aerial Vehicles (UAVs) are advancing their scope beyond military applications. Most of the work has been concentrated in adopting multi-UAV systems in providing cellular services to enhance the network coverage. However, little or no attention has been considered in serving moving hotspot conditions aka Place Time Capacity (PTC). In this paper, we explore a disparate way of employing multi-UAV systems by proposing a concept of Hovering Ad-Hoc Network (HANET) distinctively to solve PTC congestion using millimeter wave communication. We present a suitable architecture based on airborne HANET members as load balancing assistance to the primary network to offload user traffic to the nearby base station. The paper also presents a conceptual physical design of a HANET member to endorse further the proposed architecture.**

Keywords*— *WISDOM; Place Time Capacity; UAVs; HANET; Millimeter waves

I. BACKGROUND

Wireless Innovative System for Dynamic Operating Megacommunications (WISDOM) concept as asserted by Dr. Ramjee Prasad in [1], predicted the need for design and development of wireless infrastructure to serve the massive capacity with high data rates as high as 1 Tbps for the future 5G networks. However, a key challenge for telecom operators has always been serving hotspot areas that are densely packed by potential subscribers. Large subscriber base trying to access the radio resources at the same time is a major cause of network congestion leading to connection failures. Nonetheless, when such subscribers move in a group attempting to use mobile internet concurrently at events like festivals, carnivals, etc., they tend to create capacity demand at every position they traverse. Ambuj et al. have termed this condition of moving hotspot, even more precisely capacity-in-motion with respect to time as Place Time Capacity (PTC) [2].

As reviewed in [3] and [4], adding low power Pico nodes have been proposed to be a promising proposal in enhancing network coverage and capacity to meet the high user traffic and data rate demand. However, under PTC situations, deploying small pico base stations does not seem to be an appropriate solution as capacity in demand is erratic and tend to cease with time. Moreover, the number of handovers might increase posing a burden to the pico base stations. PTC congestion does not occur all-round the year and adding permanent base stations will be under-utilized at all other times.

Recent trends in UAV based applications indicate in employing autonomous small aerial based radio nodes as a solution to assist the existing fixed infrastructure to provide cellular services to the ground users [5][6]. Exploiting the current advances in compact physical structures, mountable small radio equipment along with small antenna array and accurate sensors are making it feasible for the aerial cells to communicate reliably with the ground nodes. We believe that deploying such multi-UAV radio devices working in teams can greatly solve PTC congestion in countries with potentially dense subscribers, e.g. India.

In this paper, we propose Hovering Ad-Hoc Network (HANET) as a solution to serve PTC. This swarm based architecture employs multi-layered communication paradigm including Millimeter-Wave Communication (MMWC). Emphasizing on MMWC, first is the MMWC between aerial radio nodes and ground-based existing infrastructure. And, second is a millimeter wave (MMW) assisted communication link between radio nodes and users on the ground for traffic offloading assistance to ground-based infrastructure. Also, the conceptual physical design of the flying HANET member is proposed to endorse the proposed concept.

This paper is organized as follows: The related work is given in Section II. In Section III, we present the HANET concept architecture. Finally, we conclude the paper and indicate future work in section IV.

II. RELATED WORK

Recent years have seen increasing growth in research and implementation of UAV based deployments for a number of applications. Ongoing industrial projects like Facebook Drone [7] and Google Loon [8] are in development to lay high altitude platforms to extend web access and internet connectivity to the ground users. Also, low altitude platforms are being scrutinized for emergency operations and

communication services. In [9], a quadcopter based prototype was implemented to bridge two end systems using small single-UAV and multi-UAV relays depending upon the distance between them. The authors have also discussed the positioning of such UAVs forming a Wireless Mesh Network. The work presented in [10] describes a power efficient radio resource allocation mechanism based on game theory approach using Low-Medium Altitude Aerial Platforms (LMAPs) for Aerial LTE uplink and downlink. Low Altitude 3G Small UAVs (SUAVs) functioning as mobile relays have also been investigated for urban and rural areas. In [11], the authors have compared existing load balancing and static relaying techniques with the performance of 3G SUAVs and a significant improvement in throughput and QOS was observed when deployed with multi SUAVs in target areas. Tom et al. [12], have presented Octocopter based GSM infrastructure for establishing field communications in the absence of commercial services and argued upon improvised cost, power and, spectral efficiency in comparison to existing GSM radio interface.

There are only a couple of studies that have considered moving subscriber hotspots. One of them has tested a set of adaptive base stations deployed on a rail at the ceiling of an airport building to service the moving user hotspot at the arrival of an airplane [13]. Authors proposed stigmergy based distributed algorithms to identify the need for changes in position and configuration of the railing base stations autonomously according to the dynamic user demand. A Swarm of UAVs equipped with LTE-4G to offload traffic into neighboring cells for cell outage compensation was suggested in [6]. Their proposed work incorporated aerial UAV relays to reduce the downlink system loss for a given outage scenario and suggested that it can also be applied to moving traffic overload situations (parade, etc.). A similar implication was made in [14] for natural disaster recovery management and user traffic offloading during massive moving of crowds using Low Altitude Platforms (LAPs). Wherein, a statistical propagation model for predicting the air-to-ground path loss between a low altitude platform and a terrestrial terminal was proposed, however, no specific case in handling moving crowd situations was outlined.

Some other related projects like AVIGLE [15], SMAVNET [16], ABSOLUTE [17], etc. are also dealing with UAV/Drone based implementation in the areas of surveillance, disaster management, civil security and cellular communication services. Further, the AIRBEAM project [5] have proposed a role based connectivity management to maintain reliable communication between UAV swarms for emergency operations and ground user services. However, none of the work has been propounded distinctly for servicing moving hotspot situations using aerial devices. In this paper, we propose the applicability of UAV-MM wave based cellular communication service through a concept of HANET exclusively to serve the Place Time Capacity problem.

III. PROPOSED HANET ARCHITECTURE

A. Hovering Ad-Hoc Network (HANET)

We coin HANETs as *a team of self-itinerant, intelligent and adaptive hovering radios to serve the dynamic traffic need of moving subscriber hotspots by optimally positioning themselves at the Area of Event (AoE). We consider Area of Event as an area where a moving crowd accumulation is potentially high.*

In comparison to other classes of ad-hoc networks, namely Mobile Ad-hoc Networks (MANETs) and Flying Ad-Hoc Networks (FANETs), HANETs mainly differ by having lower mobility, LOS connectivity between the devices in the HANET, and ability to provide cellular services to the ground mobile users. We will assume cellular services in the International Mobile Telecommunications (IMT) communication bands currently defined, as well as the possible future use of the millimeter wave bands. Table 1 summarizes a comparison of HANETs from MANETs and FANETs [18].

Table I

Parameter	MANETs	FANETs	HANETs
Node Mobility	Low	Very high	Low
Mobility Model	Random	Regular (predetermined paths) /Special (autonomous multi-UAV systems)	Nomadic (mobility follows PTC)
Node Density	Low	Very low	Low
Topology Change	Slow	Fast	Quasi-constant
Radio Propagation (node altitude)	Close to ground, NLOS for most cases	High above ground, LOS for most cases	Both above and close to ground (LOS)
Mobility type	Quasi-Stationary, ground	Flying	Hovering (ground & flying)
Inter-member distance	Short	Long	Shorter
Communication Band	On-demand, Unlicensed	Unlicensed/ Cellular	IMT and Millimeter-wave
Application type	Specific user scenario	Multi-UAV applications	PTC load dispersion

B. HANET Network Architecture

A Hovering Ad-hoc Network (HANET) is a network of aerial radio nodes that collaborate and coordinate to serve accumulated PTC situations at the AoE. To understand the working of HANET, fig. 1 depicts a conventional network architecture with an AoE served by two conventional base stations (following a PTC congestion and overloading), BS1 and BS2. The modified architecture will comprise additional elements that are:

1) HANET Members
2) HANET Gateway Base Station (HGBS)

The flying HANET members that include HANET Serving Members (HSM) and/or HANET Relay Members (HRM) is defined under HANET Base Station Subsystem (HBS) and is a separate network subsystem other than conventional Base Station Subsystem (BSS) involving the overloaded Base Stations BS1 & BS2. A team of HRM that are connected to a HGBS form a HANET Relay Subsystem (HRS). The role of HSM is to provide service to the mobile users underneath and the HRM are used to relay user data from HSM to HGBS. Each HANET member is capable of being a part of either HSM or HRM or both.

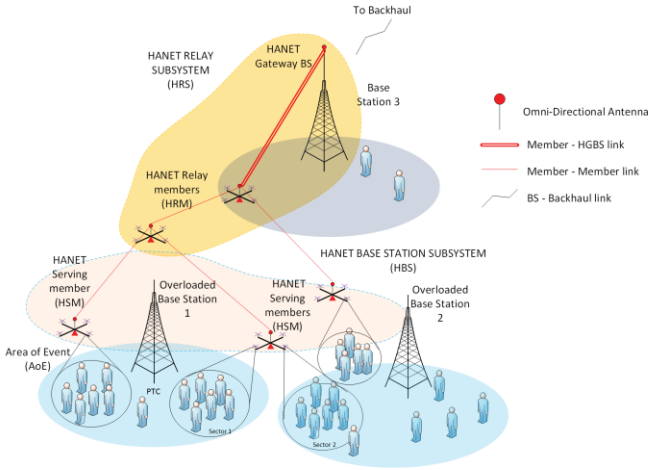

Fig 1. HANET complementing Primary Network

Each HANET member will service the subscribers using four sectors comprising of directional antennas. As we can see from fig. 3, the four sectors are mainly taking advantage of the proposed HANET design with a quadcopter base with four arms. Covering these arms with aerodynamic carbon based casing will provide sufficient room for sticking metallic wafers to form a directional antenna and therefore, we can have four directional antennas for each of the technology (IMT and MM). Further, having more sectors per 360-degree span will provide better control on the dynamic subscriber movements in the HANET member's vicinity. Also, the higher number of sectors will provide the opportunity to increase the antenna gain by narrowing the beamwidth without losing coverage at the sector boundaries. Depending on many propagation related factors, more sectors will likely also give us better confinement of interference in the system.

In dense urban, urban and suburban scenarios, it is inevitable to face severe propagation loss due to shadowing, diffraction, reflection, etc. Therefore direct backhaul from HSM may lead to loss of communication. In this case, the HRM can relay the user data to the nearby base station (HGBS). The communication in the HBS requires member to user communication that will be provided through IMT channels and possible future millimeter wave cellular channels by the HSM. User data will be relayed by the HRM to service the moving crowd continuously. By making HANET follow the moving subscribers, the number of handovers that could have possibly occurred in the network otherwise would eventually reduce thereby potentially relieving the bulk handover issues within the overloaded network. Further, the backhauling will be done through millimeter wave channels only. The member to member control information containing their placement coordinates, IDs, etc. for maneuvering control and optimal positioning of each member will also be communicated through millimeter wave channels.

For our research, we particularly delve into laying mm-waves for a member to member/HGBS and member to mm-user devices as an overlay to traditional IMT layer. This is because i) no interference with any of the IMT channels, ii) higher bandwidth to serve mm-user devices and for relaying user data to the nearest base station (both IMT and mm data), and, iii) member to user communication likely to be in LOS at all times as HSM will be closer to the users underneath. The HSM might not be necessarily in LOS with the HGBS, which is why HRM forming a network chain will come into play to relay the user data from HSM to HGBS.

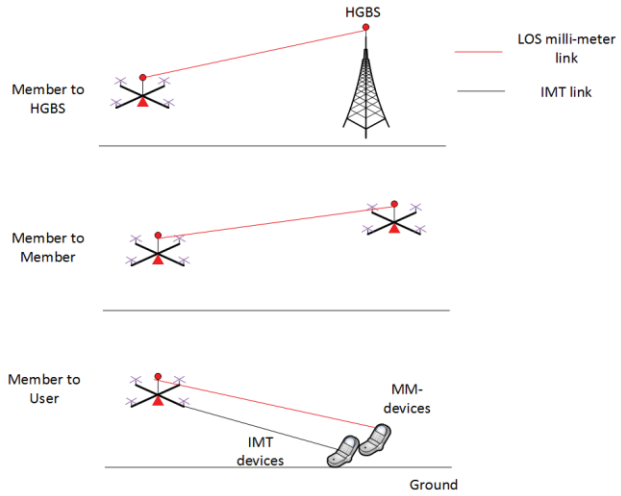

Fig 2. HANET Communication Links

There is one challenge that needs consideration when HANET members are airborne using mm-waves. Mm-waves need more power due to short aperture antennas and higher transmission losses. Advancement in using arrays of multiple antennas producing highly coherent and directional beams can overcome this challenge [19]. However, this comes at the cost of more intelligence required by the HSM to keep the beams highly directional and focused. Even for HRM to communicate, an LOS is important to maintain. Further, Rappaport et.al have further concluded that significant non-line-of-sight (NLOS) outdoor, street-level coverage is possible up to approximately 200 m from small base stations at 28 & 73 GHz [20]. In addition to this, it has been estimated that there will be 50 billion devices including mm-future phones, which would be connected to mobile networks with multi-gigabit data rates by 2020 [19]. The millimeter wave

communication is surely paving its way onto serving cellular communication in 5G and hence a separate layer of mm-waves has been proposed with the architecture.

Fig.2 summarizes the connecting links between HANET members and with the user devices and HGBS. As it is possible to know the time and place of events where PTC might arise, base stations nearby the subscriber hotspots can be strategically exploited to service the overloaded user traffic. We propose an additional transceiver architecture that will reside on such base stations to act as HANET Gateway Base Stations (HGBS) thereby exclusively communicating with the HANET members. A HANET member closest to the HGBS will be the Point of Interconnect (PoI) and will act as HRM and further relay the user data to the backbone network. Although the HGBSs can be placed at uniform locations across the city/region but doing so will put an extra load on the Capital Expenditure (CAPEX) to the service operators. The events that trigger PTC problems occur at some particular areas or, at open spaces hence the base stations around only those areas only can be put to function as HGBSs.

The HANET will be a formation of Wireless Mesh Network (WMN) that uses multi-hop communication. Routing plays a fundamental role, and selecting a routing protocol is a challenge for the HANET to ensure which is needed for reliability in routing the data and control information between the members. The configuration of the members might change in lieu of dynamically changing mobility patterns of the subscriber hotspots. The inter-member communication protocol will focus on sustaining a temporary itinerant hovering network in dynamic weather conditions to deliver high data rate to the PTC. For the proposed architecture, the communication protocol will address a reliable and efficient, power aware, time synchronized network topologies like star or mesh.

Furthermore, the idea of employing HANET to serve PTC requires some form of intelligence to be assimilated into such devices to sense the network environment and the PTC region. The intelligence would assist them to decide their network footprint by electronically/mechanically steering their antennas. The HANET members must aim to i) maximally cover the AoE with required QOS to users, ii) establish continuous connectivity among themselves such that no voids/overlaps are created, and iii) maintain network dynamics while moving with respect to subscriber hotspot movements.

C. Physical Framework

A robust, reliable and compact physical structure is important to design and build to be executed as a complement to fixed base stations, with the purpose of delivering adequate Quality of Service (QOS) to a real-time moving hotspot event. Here we present a thought generated physical design of HANET structure shown in fig. 3. Apart from the basic components of a UAV-quadcopter structure, Table II elaborates the radio communication equipment in HRS/HBS for a HANET device required to serve PTC-driven network conditions.

Table II

System members	Component Usage	Description
	Communication Equipment	
HBS	Panel Antenna	Directional antenna for Member-User communication in IMT band
HBS	Patch Antenna	MM-wave antenna for Member to MM-based user device communication
HRS, HBS	Omni-Antenna	MM-wave antenna for Member-Member communication
HRS	Omni-Antenna	MM-wave antenna for Member-HGBS communication
Morphologic & Subscriber Sensing		
Real Time Image Analysis using cameras & sensors to identify physical environment and human clusters		

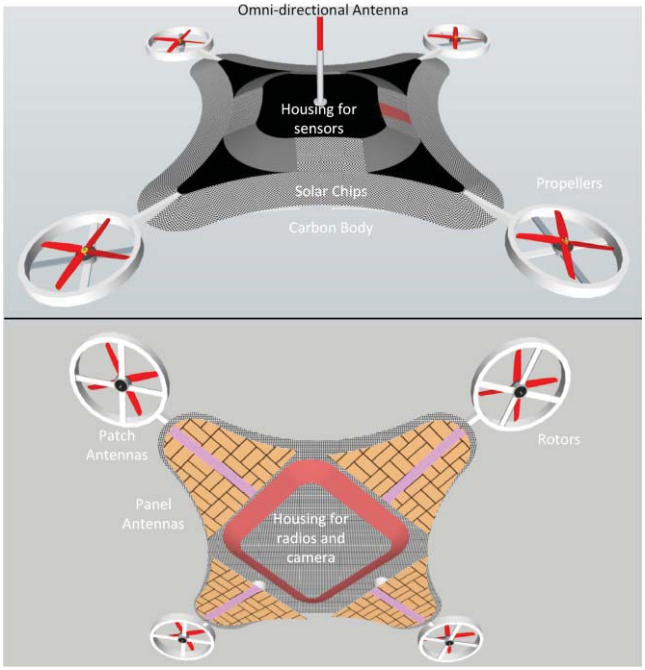

Fig 3. HANET member proposed physical design

As depicted in the fig. 3, we have proposed a quadcopter based HANET device design consisting of four brushless rotors with propellers wide in diameter for better stability and low power consumption. The contour of the propeller chassis extrudes a carbon fiber panel that will consist of both panel (IMT devices) and patch (mm devices) antenna's metallic wafers to provide coverage underneath the hovering altitude. The wings of the quadcopter will affix four such assemblage of panel and patch antennas to cater four sectors with four distinct carriers to serve different clusters of subscribers. The coverage area to be served by each of the panel antennas can be steered depending upon the cluster of users within the

communication range of the quadcopter. Furthermore, the top surface of the frame will mount the omni-directional millimeter wave antenna for the member to member/HGBS communication. As the lower surface of the wing frame is utilized for serving antennas, consequently the upper surface of the frame can be used to mount solar panels that will keep charging the Lithium Polymer (LiPo) batteries thereby increasing the longevity of device service per period of operation.

The lower part of HANET device structure will encapsulate all the radios (IMT & MM) and the Inertial Measurement Unit (IMU) consisting of sensors along with GPS and cameras. The IMT radio will be connected to the port of panel antennas, and similarly millimeter wave radio will be connected to the port of patch antennas on each of the quadcopter wings. The carriers of the HANET member can be distributed among its four sectors thus improvising frequency re-use at the local level.

The members have a Control and Maneuvering Unit (CMU) that is connected to the rotors and propellers for adjustment of angular velocity to perform operations like turn, hold, hover, etc. The IMU will be composed of sensors to measure the physical parameters like direction, speed, and coordinates of the HANET device structure. The CPU of the member will account for all the information from radios and IMU to instruct CMU to move the mechanical parts of the device and to control further the physical parameters of the radios.The power requirements of quadcopter based aerial devices need to be addressed to increase the flight hours during its single operation. We propose adding multiple solar chips over its upper body to charge the quadcopters continually. The weight of the device should be sufficient to carry communication equipment and sensors for its operation during PTC situation and still bearing high-level endurance.

IV. Conclusion

This paper proposed a concept of Hovering Ad-Hoc Network (HANET) as a different prospect of using small multi-UAV based network deployment to deal with Place Time Capacity (PTC) problems. User capacity is not static but in motion and varies dynamically at events like carnivals, festivals, etc. and therefore, providing service with HANET as an assistance to the primary base stations can be useful to balance heavy traffic conditions. A physical framework based on quadcopter structure forming a suitable network architecture is also presented. Further, the paper proposed an adoption to millimeter wave mobile service delivery by HANET members keeping in view the future 5G networks incorporating millimeter wave devices by 2020. The HANET concept introduced in this paper can be extended to devise artificial intelligence based HANET for decision making in hovering control and positioning. Furthermore, the swarm of such hovering members can be utilized in specific scenarios like defense applications and disaster management.

REFERENCES

[1] R. Prasad, 5G: 2020 and Beyond. River Publishers, 2014.

[2] Kumar, A.; Mehta, P.L.; Prasad, R., "Place Time Capacity- A novel concept for defining challenges in 5G networks and beyond in India," Wireless Computing and Networking (GCWCN), 2014 IEEE Global Conference on, vol., no., pp.278,282, 22-24 Dec. 2014

[3] Ericsson White Paper 284 23-3165 Uen, February 2012 "Heterogeneous networks"

[4] Stanze, Oliver; Weber, Andreas, "Heterogeneous networks with LTE-Advanced technologies," Bell Labs Technical Journal, vol.18, no.1, pp.41,58, June 2013,doi: 10.1002/bltj.21592

[5] Goddemeier, N.; Rohde, S.; Wietfeld, C., "Experimental Performance Evaluation of Role-Based Connectivity Management for Cooperating UAVs," Vehicular Technology Conference (VTC Spring), 2014 IEEE 79th, vol., no., pp.1,5, 18-21 May 2014

[6] Rohde, S.; Wietfeld, C., "Interference Aware Positioning of Aerial Relays for Cell Overload and Outage Compensation," Vehicular Technology Conference (VTC Fall), 2012 IEEE, vol., no., pp.1,5, 3-6 Sept. 2012

[7] Facebook, "Connecting the World from the Sky," Facebook, Technical Report, 2014.

[8] "Project Loon," Wikipedia, the free encyclopedia. 04-Jun-2015.

[9] Morgenthaler, S.; Braun, T.; Zhongliang Zhao; Staub, T.; Anwander, M., "UAVNet: A mobile wireless mesh network using Unmanned Aerial Vehicles," Globecom Workshops (GC Wkshps), 2012 IEEE, vol., no., pp.1603,1608, 3-7 Dec. 2012

[10] Liqiang Zhao; Chi Zhang; Hailin Zhang; Xiaohui Li; Hanzo, L., "Power-Efficient Radio Resource Allocation for Low-Medium-Altitude Aerial Platform Based TD-LTE Networks," Vehicular Technology Conference (VTC Fall), 2012 IEEE, vol., no., pp.1,5, 3-6 Sept. 2012

[11] Weisi Guo; Devine, C.; Siyi Wang, "Performance analysis of micro unmanned airborne communication relays for cellular networks," Communication Systems, Networks & Digital Signal Processing (CSNDSP), 2014 9th International Symposium on, vol., no., pp.658,663, 23-25 July 2014

[12] Wypych, T.; Angelo, R.; Kuester, F., "AirGSM: An unmanned, flying GSM cellular base station for flexible field communications," Aerospace Conference, 2012 IEEE, vol., no., pp.1,9, 3-10 March 2012 doi: 10.1109/AERO.2012.6187134

[13] H. Claussen, "Autonomous Self-Deployment of Wireless Access Networks in an Airport Environment," Proc. 2nd Internat. Federation for Inform. Processing (IFIP) Internat. Workshop on Autonomic Commun.

[14] Al-Hourani, A.; Kandeepan, S.; Jamalipour, A., "Modeling air-to-ground path loss for low altitude platforms in urban environments," Global Communications Conference (GLOBECOM), 2014 IEEE, vol., no., pp.2898,2904, 8-12 Dec. 2014

[15] S. Rohde, N. Goddemeier, C. Wiefeld, F. Steinicke, K. Hinrichs, T. Ostermann, J. Holsten and D. Moormann, "AVIGLE: A System of Systems Concept for an Avionic Digital Service Platform Based on Micro Unmanned Aerial Vehicles," in Proc. of IEEE International Conference on Systems, Man, and Cybernetics (SMC), 2010.

[16] S. Hauert, S. Leven, J.-C. Zufferey and D, Floreano, "Communication-based Swarming for Flying Robots," International Workshop on Self-Organized System, Zurich, Switzerland, 2010.

[17] "EU-FP7 ICT IP Project ABSOLUTE," 2013. [Online]. Available: http://www.absolute-project.eu/reports/publicationsI

[18] İlker Bekmezci, Ozgur Koray Sahingoz, Şamil Temel, Flying Ad-Hoc Networks (FANETs): A survey, Ad Hoc Networks, Volume 11, Issue 3, May 2013, Pages 1254-1270, ISSN 1570-8705, http://dx.doi.org/10.1016/j.adhoc.2012.12.004.

[19] A. Bleicher, "The 5G phone future [News]," IEEE Spectrum, vol. 50, no. 7, pp. 15–16, Jul. 2013.

[20] Rangan, S.; Rappaport, T.S.; Erkip, E., "Millimeter-Wave Cellular Wireless Networks: Potentials and Challenges," Proceedings of the IEEE , vol.102, no.3, pp.366,385, March 2014 doi: 10.1109/JPROC.2014.2299397

THE 5TH INTERNATIONAL CONFERENCE ON WIRELESS COMMUNICATIONS, VEHICULAR TECHNOLOGY, INFORMATION THEORY, AEROSPACE & ELECTRONIC SYSTEMS (WVITAE-2015)
December 13-16, 2015, Hyderabad, India

A new shaping code for PAPR Reduction in Single-Carrier Modulation

Yonathan Tate
Dept. of EE-Systems, TAU
Tel Aviv, Israel
Email: tateyoni@post.tau.ac.il

Dani Raphaeli
Dept. of EE-Systems, TAU
Tel Aviv, Israel
Email: danr@eng.tau.ac.il

***Abstract*—A novel PAPR shaping technique for single carrier transmission with high spectral efficiency is presented. This technique applies puncturing of error correction redundancy bits to achieve a desired Markovian symbol transmission probability distribution, which avoids symbol sequences with high peak values. To measure the overall gain of a peak reduction transmission, a link-gain metric, which takes into account both PAPR reduction and average energy loss, is presented. For a 16-QAM system with transmission rate of 3 bits/symbol and a SRRC pulse shape with roll-off factor 0.1 and duration of 4 symbols, a link gain of 1.87 dB is demonstrated using a pragmatic binary Turbo code for error correction. The technique can be used to improve any single carrier communication link limited by the PA peak power. It is in particular attractive to satellite communications by maximizing the rate of a given transponder, or given terminal hardware.**

I. Introduction

In practical communication systems power amplifiers (PA) are commonly used to enable wireless transmission over long distances. When using such a PA, it is crucial to keep the input signal's power within the PA's linear region in order to avoid saturation of the transmitted signal, which leads to both in-band and out-band disturbances. Transmission signals at the PA input are therefore backed-off (BO) so that instantaneous high peak power values will not cause saturation. The cost of the BO is that the average power of the signal is lower, thus compromising the transmission rate. This effect is especially severe in transmission signals with wide dynamic range, such as OFDM. However, in band limited single carrier transmission, which is common in satellite communication systems, high Peak to Average Power Ratio (PAPR) is also common. The PAPR problem in satellite communication is significant due to the high cost of PA, and due to the limited satellite resources even 1dB loss is critical.

Since the length of the pulse shape exceeds the symbol duration, high instantaneous peak power values are the result of certain symbol sequences. A possible approach to reduce the PAPR is therefore to try to avoid such sequences.

The method of Trellis shaping (TS), first suggested by Forney to reduce the average transmission power in high orders constellation signaling [1], has been shown to be useful for the purpose of PAPR reduction as well [2]. Originally, TS was shown to work well with Trellis Coded Modulation (TCM) [1]. Several attempts have been made to combine TS with other ECC schemes [3] [4]. In [4], LDPC code as inner code was combined with TS for power reduction. In [3] TS for PAPR reduction was combined with convolutional ECC. The reported gain in [3] was 1.8 dB PAR gain with 1.5 dB loss in SNR, resulting in an overall link gain of 0.3 dB. However, the SNR loss was calculated theoretically and may be higher in practical schemes. Additionally, the information rate was 1 bit/symbol, and higher rates were not investigated.

TS is based on adding shaping bits, usually one bit per symbol, to create redundancy in the possible symbol sequences representing a given information word, and a Viterbi decoder which is used to select the symbol sequence with the minimal PAPR cost. Although PAPR gain can be achieved in this way, several issues are not fully addressed by PAPR reduction using TS. First, TS adds an integer number of bits per symbol, which does not allow a complete rate/shaping trade-off. Second, it is not clear whether the PAPR reduction achieved by TS for a given rate is optimal. And third, the combination of TS with modern error correcting codes (ECC) such as Turbo codes or LDPC, which is crucial for enabling a reliable communication system, has not been optimized, leading to lower gain.

This paper addresses all three issues by proposing a novel PAPR shaping technique, which is based on puncturing of ECC redundancy bits to achieve a non-uniform Markovian symbol distribution which completely avoids symbol sequences with high peak values, but allows transmission of all other symbol sequences and thus

maximizes the information rate for a given peak constraint. Also, this technique is shown to perform well when applied with pragmatic Turbo codes, compared to a non-shaped system. The method can be regarded as a generalization of a previous work by the authors [8], obtaining a power reduction gain in a similar way.

We obtained encouraging results. For a turbo coded 16-QAM system with transmission rate of 3 bits/symbol and a SRRC pulse shape with roll-off factor 0.1 and duration of 4 symbols, a shaping gain of 2.81 dB is demonstrated by simulation. Since the scheme had also loss of 0.94 dB in Eb/N0, the resulting link gain is 2.81-0.94=1.87 dB. We also compared shaped 16-QAM to unshaped APSK and even 8PSK, and achieved gain, though lower than compared to unshaped QAM.

The rest of the paper is organized as follows: In section 2 some background and notations are given. In section 3 the process of deriving a practical symbol distribution with peak constraint is presented. In section 4, the combination of TCM with the shaping process is defined, both for the Tx and Rx parts. Section 5 presents simulation results of the shaped system, compared to a non-shaped reference system. In section 6 conclusion remarks are given.

II. System Model

Let C be a 2-dimensional constellation with cardinality $|C| = M$. Let $\boldsymbol{c} = (c_0, ..., c_{n-1})$ where $c_i \in C$ be a frame of n symbols transmitted over an AWGN channel. The transmission sequence $\boldsymbol{c}$ is passed through an over-sampled Square Root Raised Cosine (SRRC) pulse shape filter $h[n]$ with effective duration spanning over K_s symbols. The resulting transmission signal $x[n]$ is given by

$$x[n] = \sum_{k=\lfloor n/N_s \rfloor}^{\lfloor n/N_s \rfloor + K_s - 1} c_k \cdot h\big(T(n/N_s - k)\big) \qquad (1)$$

Where T is the duration of a symbol and N_s is the number of samples taken in a symbol period.

The instantaneous power of the signal is given by $p[n] = |x[n]|^2$. The PAPR is the ratio between the peak and the average values of $p[n]$, where the peak value is defined as the value of $p[n]$ which is exceeded with probability P_{peak}. In this paper we use the value $P_{peak} = 10^{-4}$.

Generally, when applying shaping for PAPR reduction both PAPR and average power of the transmitted waveform are affected. Since any reduction in PAPR allows for an equivalent increase of average power, the overall gain of a shaped system is the sum of the PAPR and average power gains. This gain is denoted from here on as "link gain".

III. Markovian Symbol Distribution With Peak Constraint

A. Optimal Symbol Distribution

A *channel state* at time k, denoted s_k, is defined as the length $K_s - 1$ symbol sequence $(c_{k-K_s+1}, .., c_{k-1})$. The combination of a channel state and a symbol c_k determines N_s samples of $p[n]$. Consider a peak constraint $p[n] < p_{peak}$ on the signal's power samples. Let $\mathcal{C}$ be a codebook of length n frames, which consists of all the frames which do not include a sequence exceeding p_{peak}. $\mathcal{C}$ is a one-to-one mapping function which associates information words of length $\log_2(M) n R_s$ bits to frames of n symbols, where R_s is the shaping rate. Taking $n \to \infty$ and calculating the marginal distribution $P^* \triangleq \Pr(s_k|s_{k-1})$ gives the maximal entropy symbol distribution given the peak constraint. P^* can be derived analytically using the conditional limit theorem [5]. Specifically, if $W(s_k|s_{k-1})$ is the Markov representation of the uniform transmission, then according to theorem 4 remark 2 in [5] the desired Markov I-projection P^* is given by

$$P^*(x,y) = \begin{cases} \lambda^{-1} u(x) W(y|x) v(y) & \text{if } (x,y) \in E \\ 0 & \text{if } (x,y) \notin E \end{cases} \qquad (2)$$

Where E is the set of all (s_{k-1}, s_k) combinations of consecutive channel states for which the resulting samples of $p[n]$ do not exceed p_{peak}, λ is the largest eigenvalue of the matrix obtained from W by replacing the entries $(s_{k-1}, s_k) \notin E$ by zeros, and u and v are the corresponding left and right eigenvectors.

In general, an additional constraint on the average power of the distribution may be considered to attempt an increase in shaping gain. However, previous work by the authors has shown that given a peak constraint, the optimal distribution is achieved when no further constrains are applied [6].

To simplify the following notations, from here on any stationary distribution $P(s_k|s_{k-1})$ is denoted by $P(c|s)$ instead, since given s the next channel state is uniquely defined by the symbol c.

B. Practical Symbol Distribution

To apply the theoretical distribution on a practical scheme, first it is required that the symbol transition probabilities will be of the form 2^{-k}. Since the maximal entropy distribution P^* in general does not hold this property, a quantized version of P^*, denoted as $\bar{P}^*$, is used instead. Specifically, for a conditional distribution

$\Pr(c|s)$ the quantized probability $\bar{\Pr}(c|s)$ is obtained by rounding $\Pr(c|s)$ to the closest 2^{-k}. If required, the lowest probabilities are manipulated to ensure that the sum of the quantized distributions equals 1.

Since a 0 probability is rounded to 0, it is ensured that no illegal symbol transition occurs when applying $\bar{P}^*$. The only effect of the quantization process is therefore a reduction of the transmission entropy, and thus it's rate. This reduction however was found to be negligible in most cases.

C. Theoretical Gain

The channel capacity of transmission with Markovian constraint generally cannot be found analytically. Instead, it can be derived by monte-carlo simulation as described in [7]. In our case the state depends on the input sequence only, therefore the recursion of $\mu_k(s_k)$ reduces to

$$\mu_k(s_k) = \sum_{s_{k-1}} \sum_{c_k} \Pr(y_k|c_k) \Pr(c_k|s_{k-1}) \delta(s_k, s_{k-1}, c_k) \mu_{k-1}(s_{k-1}) \quad (3)$$

Applying this method on the distributions $\bar{P}^*$ for various peak constraints, and comparing to the capacity of uniform un-shaped transmission, yields the theoretical SNR gain of each $\bar{P}^*$. In addition, the PAPR gain can also be found analytically, as both p_{peak} and p_{avg} are known for each $\bar{P}^*$, and can be compared to the PAPR of the uniform transmission. Such comparison is presented in figure 1 for the case of transmission in rate of 3 bits/symbol over a 16-QAM constellation, with an SRRC filter with roll-off factor 0.1, $K_s = 4$ and $N_s = 8$. The constellation is normalized such that the average (uniform) symbol energy is 1. It can be seen that the maximal link gain in this case is expected for peak constraint of 2.2. Note that comparing to a different constellation would not change the optimal peak constraint, as only the reference PAPR and SNR would differ.

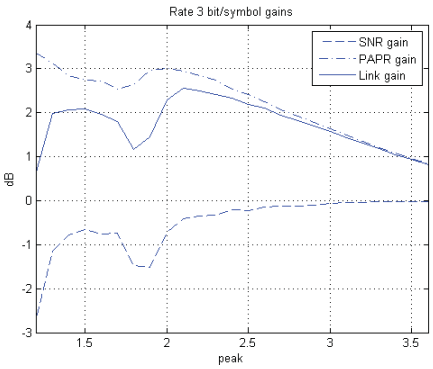

Fig. 1: Theoretical SNR gain, PAPR gain and link gain for different peak constraints of 3 bits/symbol transmission over a 16-QAM constellation, with an SRRC filter with roll-off factor 0.1, $K_s = 4$ and $N_s = 8$.

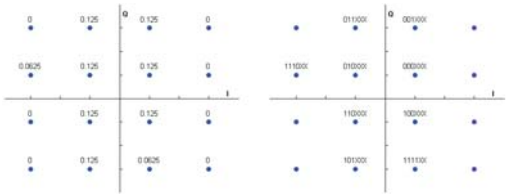

Fig. 2: Example of a 16-QAM bit-mapping. On the left are quantized probabilities, on the right are bit values assigned to each symbol. 'X' marks a don't-care value, which translates to an erased bit.

IV. Applying with Pragmatic Binary TCM

A. General Method

The nonequiprobable signaling is now applied in the following way. After adding error correction redundancy bits to the information sequence, the resulting bit sequence is divided into m-tuples, where the first d bits of each tuple are information bits and the last $m-d$ bits are redundancy bits. The m-tuples are then sequentially mapped into symbols using a channel-state dependent mapping table. The table contains for each state the quantized values of $P(c|s)$. The channel state is updated with the new symbol and the process is repeated with the next m-tuple. An example of a mapping table is illustrated in figure 2.

B. Bit Labeling

For a given channel state, each symbol is transmitted with a different probability. The method to apply different symbol probabilities is adopted from [8]. A larger probability is obtained by assigning to that symbol a bit sequence with smaller number of bits, while taking the rest of the bits of the label as "dont care. For example assuming the number of bits used for bit labeling is $m = 6$. A symbol with assigned bits of 11xxxx will have a probability of 0.25 since all the words 110000-111111 will be assigned to it. An example of a mapping table is illustrated in figure 2.

The bit labeling problem is not trivial. A straight forward Gray bit labeling is not well defined. Additionally, the bit-mapping is different for each state, which implies that the bit labeling of a symbol depends on the channel state. On the receiver side, a Trellis decoder must be used to keep track of the channel state. Consider a scenario in which a symbol error occurred at the receiver; because the channel state is the sequence of the last $K_s - 1$ symbols, a single symbol error results in an error in the evaluation of $K_s - 1$ consecutive states.

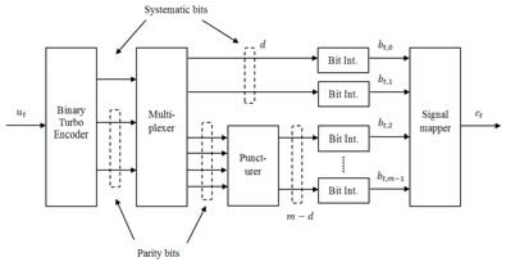

Fig. 3: Pragmatic turbo encoder. In the shaped case, the signal mapper saves the current channel state and applies additional puncturing to achieve non-uniform signalling.

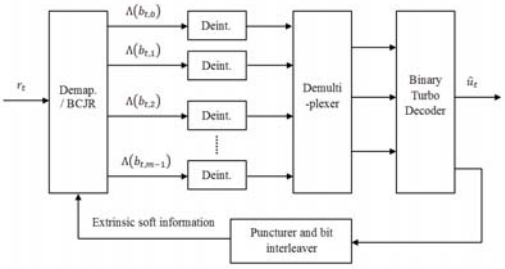

Fig. 4: Pragmatic turbo decoder. In the shaped case, the de-mapper is replaced by a BCJR decoder which runs over the channel state progression.

Since each state holds a different bit labeling, even if all other symbols are evaluated correctly their bits might be in error due to their state dependent labeling.

Following these observations, when constructing the symbol bit-maps two objectives are to be taken under consideration: first, that for each state the labeling of the symbols would be as close to Gray as possible and second, that for "close states", which differ by one symbol, the labeling would be as close as possible, to minimize the bit error probability in the correct-symbol incorrect-state scenario.

C. Combining with Pragmatic TCM

The nonequiprobable signalling is now applied to TCM. In pragmatic binary TCM [10], a single binary turbo code of rate 1/3 is used as the component code. The encoder outputs are multiplexed and punctured to obtain m bits per symbol, with d systematic information bits and $m-d$ parity bits, as shown in figure 3. The signal mapper then maps each m-tuple into a symbol from C. In the non-shaped system $m = \log_2(M)$ and the mapping is a constant Gray code. In the shaped system $m > \log_2(M)$ and the mapping depends on the channel state. Due to "X" mapping digits the mapping itself applies an additional puncturing, therefore this scheme is in fact a variable-rate turbo code, since the number of parity bits given to each information bit varies as a function of the input combination.

At the receiver side, shown in figure 4, the noisy symbols are received by a demapper module in the non-shaped case, or a BCJR module in the shaped case. In both cases, the LLR values $\Lambda(b_t)$ are produced for each encoded bit. The LLR values are used, after appropriate bit de-interleaving, as an a-priory input to a binary turbo decoder. In each iteration, the turbo decoder produces extrinsic LLRs which are used as an a-priory input to the demapper/BCJR module, which in turn calculates new extrinsic LLRs which are sent back to the turbo decoder. After a pre-determined number of iterations has been reached, the bit estimations $\hat{u}_t$ are determined by performing hard decision on the turbo decoder's a-posterior LLRs.

V. Simulation Results

The pulse shape tested in all our simulations is an SRRC filter with effective duration $K_s = 4$, roll-off factor 0.1 and an over-sampling factor $N_s = 8$. The shaping was applied on a 16-QAM constellation. This setup results in a Trellis with 4096 states. To reduce the complexity of the channel state BCJR decoder, states with alpha value smaller than 1e-6 were disregarded. This approximation was found to have negligible effect on performance. In addition, all constellations were normalized such that the average (uniform) symbol energy is 1. In the shaped transmission, power samples caused by inter-frame symbol sequences were ignored. In practice, peak samples caused by such sequences can be avoided in several ways, such as using tail-biting on the BCJR, applying proper termination with small rate cost or extending the frame length so that these peaks become negligible.

The code used with all schemes is a standard rate 1/3 turbo encoder [11], made up of two elementary encoders with memory size 4 and the same generator polynomial 37-23 (octal number 37 represents the feed-forward connections and 23 the feedback connections). This code is known to be an optimal code with memory size 4 for various turbo-code rates [12]. The Turbo decoding was ran for 18 iterations on block length of 4096 information bits with pseudorandom interleaving.

As was shown in section III-C in the case of rate 3 bits/symbol the maximal gain is expected at peak constraint of 2.2. This peak constraint was indeed found to achieve the highest link gain also in simulations. The shaped transmission is compared to non shaped 16-QAM and 16-APSK transmissions with the same pulse shape. The resulting FER curves and PAPR distribution are presented in figures 5, 6 respectively. The SNR at which FER 10^{-2} is reached and the PAPR corresponding to cross-over probability of 10^{-4} are summarized

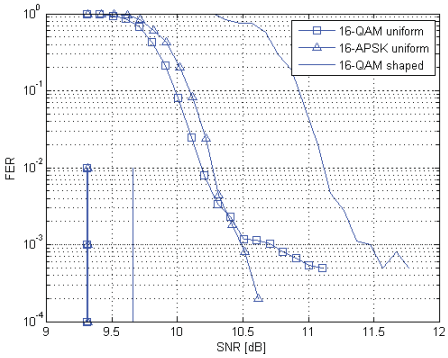

Fig. 5: FER to SNR performance comparison for rate 3 bits/symbol. All schemes used the same pragmatic binary TCM code with data length = 4096 bits. The loss of the 16-QAM shaped transmission is 0.943 dB and 0.845 dB compared to uniform 16-QAM and 16-APSK respectively.

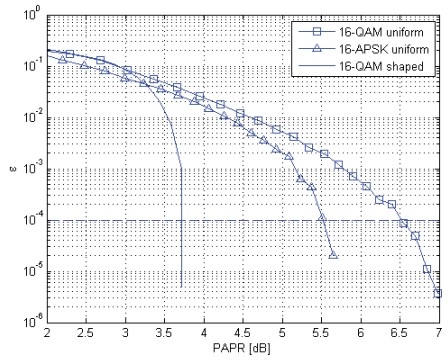

Fig. 6: PAPR comparison for rate 3 bits/symbol. For each scheme the CCDF of the peak power is presented, where the x-axis are normalized by p_{avg} to reflect the PAPR. At crossover probability of 10^{-4} the shaped transmission has a gain of 2.81 dB and 1.84 dB over uniform 16-QAM and 16-APSK respectively.

in table I. It can be seen that the shaped transmission achieves an overall link gain of 0.99 dB compared to uniform 16-APSK transmission and 1.87 dB compared to uniform 16-QAM transmission. Comparing the 10^{-2} SNR to the capacity, it can be seen that the uniform transmission distance from capacity is 0.89 dB and 0.97 dB for uniform 16-QAM and 16-APSK respectively, while the shaped transmission is 1.48 dB from capacity. This indicates that a loss of about 0.5 dB is suffered due to the proposed practical scheme.

System	Capacity	SNR 10^{-2}	PAPR 10^{-4}
16 QAM shaped	9.65 dB	11.13 dB	3.71 dB
16 QAM uniform	9.3 dB	10.19 dB	6.53 dB
16 APSK uniform	9.32 dB	10.28 dB	5.56 dB

TABLE I: Rate 3 bits/symbol FER and PAPR summary

VI. Conclusion

In this letter we have presented a novel technique for reducing the PAPR of single carrier transmission with high spectral efficiency. The main cost of this technique is loss of SNR and an additional BCJR decoder which replaces a simpler de-mapper module. However, this technique was shown to operate well with modern ECC scheme, namely turbo codes, and reduce the PAPR of the transmission signal such that an overall gain is achieved compared to uniform transmission. In the rate of 3 bits/symbol when using a 16-QAM constellation, this gain was demonstrated to be up to 1.87 dB compared to uniform transmission. This technique also allows for SNR loss to PAPR gain tradeoff by choosing different peak power values to be avoided.

References

[1] G. D. Forney, Jr., "Trellis Shaping", *IEEE Trans. Inf. Theory, vol. 38, No. 2, pp. 281–300, Mar. 1992.*

[2] M. Tanahashi and H. Ochiai, "Trellis Shaping for Controlling Envelope of Single-Carrier High-Order QAM Signals", *IEEE JOURNAL OF SELECTED TOPICS IN SIGNAL PROCESSING, vol. 3, pp. 430–437, Jun. 2009.*

[3] Tanahashi, M. and Ochiai, H., "Turbo decoding of concatenated channel coding and trellis shaping for peak power controlled single-carrier systems", *IEEE Transactions on Communications, vol. 58, pp. 9–15, Jan. 2010.*

[4] Shilpa, G. and Thangaraj, A. and Bhashyam, S., "Dirty paper coding using sign-bit shaping and LDPC codes", *Proceedings (ISIT), 2010 IEEE International Symposium on Information Theory, pp. 923–927, Jun. 2010.*

[5] Csiszar, I. and Cover, T.M. and Byoung-Seon Choi, "Conditional limit theorems under Markov conditioning", *IEEE Transactions on Information Theory, vol. 33, pp. 788–801, Nov. 1987.*

[6] D. Raphaeli and S. Achtenberg, "Achievable Gains in Peak Power Reduction via Single-Carrier Distribution Shaping", *IEEE International Symposium on Information Theory Proceedings, 2012.*

[7] Arnold, D.M.; Loeliger, H.-A.; Vontobel, P.O.; Kavcic, A.; Wei Zeng, "Simulation-Based Computation of Information Rates for Channels With Memory", *IEEE Transactions on information theory, vol. 52, pp 3498–3508, Aug. 2006.*

[8] D. Raphaeli and A. Gurevitz, "Constellation Shaping for Pragmatic Turbo-Coded Modulation With High Spectral Efficiency", *IEEE Trans. Commun., vol. 52, pp. 341–345, Mar. 2004.*

[9] Bahl, L. and Cocke, J. and Jelinek, F. and Raviv, J., "Optimal decoding of linear codes for minimizing symbol error rate", *IEEE Transactions on Information Theory, Mar 1974, pp. 284–287.*

[10] S. Le Goff, A. Glavieux, and C. Berrou, "Turbo codes and high-efficiency modulation", *Proc. IEEE Int. Conf. Communications, New Orleans, LA, May 1994, pp. 645–649.*

[11] C . Berrou, A. Glavieux, and P. Thitimajshima, "Near-optimum error-correcting coding and decoding: Turbo codes", *IEEE Trans. Commun., vol. 44, pp. 1261–1271, Oct. 1996.*

[12] S. Benedetto, R. Garello, and G. Montorsi, "A search for good convolutional codes to be used in the construction of turbo codes", *IEEE Trans. Commun., vol. 46, pp. 1101–1105, Sept. 1998.*

Trustbook: A Trust-based access control in Online Social Networks

Vedashree .K.Takalkar, Parikshit N.Mahalle
Department of Computer Engineering
Smt.Kashibai Navale College of Engineering
Savitribai Phule Pune University
Pune-411041, India
vedatakalkar@yahoo.com,aalborg.pnm@gmail.com

Abstract*—In recent years Online Social Networks (OSNs) like Facebook, Twitter have become very popular. As a result, lot of data is uploaded and generated. The privacy settings that are offered are very cumbersome for user. Hence, the data that is uploaded should be imposed with certain access control policies. This paper discusses the trust-based approach for OSN. Also, it discusses the novel model for calculating the Trust value. Further it discusses the performance of the 'Trustbook' showing that the system is scalable. This paper solves the problem of data confidentiality in OSN by building a user friendly application where more of the task is shifted from user to system.

***Index Terms*— Access control, Data confidentiality, Social network, Trust**

I. INTRODUCTION

Online Social Networks (OSNs) are becoming popular day by day. The popularity is tremendously increasing as social networks help to establish the relationships between different people around the globe. As mentioned in [1], the architecture of OSN puts light on the various components of OSN. Fig 1 [1] shows the architecture of OSN. It includes applications at the top which are developed by third party and use the OSN services. OSN is primarily made of users who are identified by their profiles. All the users are connected to each other through the relationships like friends, close friends. OSN service provider [1] is finally responsible to provide all the OSN specific functionalities and data management. As per the study [3] there are 3.14 billion users who actively use Facebook which is one of the popular OSN and this number continues to grow exponentially. Thus, data uploaded by them also grows and hence should be given a secured access. A Facebook survey of 325 users [4] was conducted and it was found that 69.2% keeps their posts public giving no privacy to it. This may be because of cumbersome privacy settings. Also only 19.4% users are concerned about the privacy policies on Facebook. Hence, the survey shows that people are not much concerned about the data confidentiality attack that may happen due to weak privacy settings. In real world, all the relations are based on trust between the people. Same trust is now proposed to be used in the access control of the data in OSN. Hence, a trust-based access control strategy is formulated so as to make the access control more efficient and user friendly. Various attributes are used to decide a trust value between the user and his each friend.

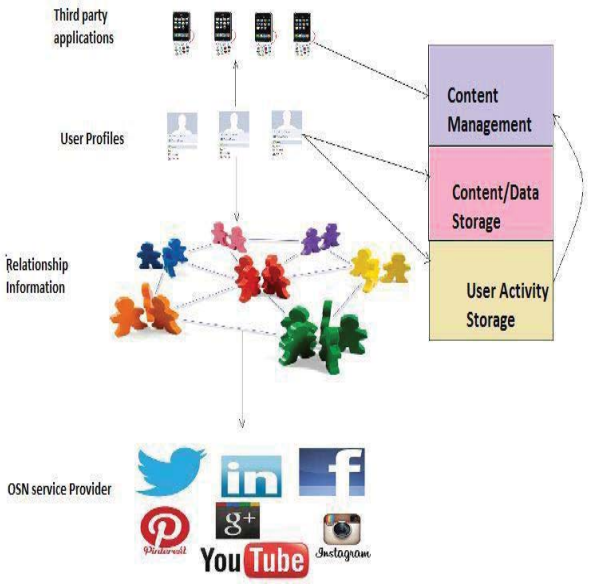

Fig.1 Generalized OSN Architecture [1]

In current scenario, whenever data is uploaded it can be viewed by all the friends. However, it may happen that some data is highly secured and the user may not want it to be seen or accessed by all the friends in the friend list. In the current OSN scenario like in Facebook, it lets you to take a binary decision about whether to keep your data public or private [5]. Also to customize the privacy settings is a cumbersome and time consuming job for the user. Hence, it is very important to develop an access control mechanism that will automate the access control decision effectively and also be user-friendly.

II. RELATED WORKS AND EVALUATION

Table I discusses the various literatures that have been studied and surveyed from the perspective of trust. Few literatures used

the trust but did not use it for data access control. In [5] multiparty access control was proposed which was used to achieve data confidentiality. However, trust between the user and friends were not considered for the formulating the access control policies. [6] uses the concept of trust in OSN by calculating credibility which is dependent on the interactions between the user and his friends. However, the interaction cannot be a sole attribute to decide the trust between the users. [7] takes into consideration the distance metric to decide the trust. This trust is used to filter out the content. It uses the clustering techniques to compute trust value. [8] mentions the different propagation models and classification schemes for trust metrics .[7] discusses different techniques to evaluate trust such as behavioral, machine-based ,statistical and heuristic techniques. In [9] Appleseed is used to compute trust in a local group. [10] uses the hop distance to calculate the trust. New algorithm is proposed in [11] for trust-based inference in social network. To find optimal trust path, [12] mentions the heuristic based approach which otherwise is a difficult task. The user's

Facebook usage patterns were studied in [15]. Thus the literature was specifically studied from the required point of view of trust. It has been observed from the study that there is less application of trust in OSN. Even if it is used, it is not applied for data access control. Hence, a novel approach for Trust value calculation is proposed to be applied in the field of OSNs.[13] – [19] were studied to understand the current work in security in OSN.

IV PROPOSED WORK

In order to reduce the user efforts and also to achieve automated and efficient access control mechanism, trust-based access control has been used. The notable contribution of the work lies in establishing an access control mechanism which is effective as well as simple from the user's point of view. Trust-based access control involves the design of the system that involves the access of the user's data to be given only to the trusted friends in the friend list. The three attributes are taken into consideration for calculating the trust value. They are Experience (EX), Context information (CI), and interaction (I). The reason for considering these three attributes is the surveys that were studied. According to [2] almost 82% users give importance to experience while accepting the friend request. Also [15] mentions that the user unfriend those users who are not active on OSN as every OSN has a limit upto which the friends can be added. Hence, another parameter CI was considered. [6] considers the interaction for establishing the trust between the users. The importance given by the user for every factor while accepting the friend request was studied. This means that these are the factors that are important from the user's perspective when it comes for showing the trust.

The Trust value is calculated using the derived formula from the survey results. Hence, trust value is calculated from every user to every friend. More the Trust value more secured data can be shared. Now, the decision of denying or allowing the access to a particular data is defined by a Trust Rule. While uploading any data like a photo as mentioned in [4], security level is attached to every data that is uploaded. The Trust Rule compares the trust value and the security level of each data that is given as an input by the user. If the trust value is greater than or equal to the security level then access to the data is allowed else the access is denied. Permission to access the data means that the data like photos, videos, posts can be seen on the home page of the friend. Thus Trust Rule works with the security level of the data and the Trust value that is calculated by the formula.

Table 1. Specific Evaluation of Related Work

Reference	Technique used to achieve trust	Is Trust used for Access control ?	User opinion considered?	Consideration of Characteristics of friends in OSN
Multiparty Access Control for Online Social Model and Mechanisms [5]	Trust is not considered	No	No	No
Estimating trust value: A social network perspective [7]	Clustering methods, user generated ratings	No	Yes	No
New Algorithm for Trust Inference in Social Networks [11]	Probabilistic models	No	No	No
Experimental Analysis on Access Control Using Trust Parameter for Social Network[6]	Interactions between users and friends	Yes	No	No
Propagation Models for Trust and Distrust in Social Networks[8]	Propagation models	No	No	No
Finding the Optimal Social Trust Path [12]	Heuristic algorithms	No	No	No
Operators for Propagating Trust and their Evaluation in Social Networks[9]	Trust metrics	No	No	No
Trust based approach for protecting user data in social networks[10]	Hop based technique	Yes	No	No
Proposed Scheme	Using EX,CI and I	Yes	Yes	Yes

There are different components of the architecture.

A. Activity Tracker

Activity Tracker is required to track how much the user is active on the OSN. It considers various parameters like frequency of logins, number of posts posted by the user. This tells that how much the user is active on the OSN. Thus this is defined as the context information. The Activity Tracker mainly computes the activity of the user in the OSN.

B. Trust Manager

The Trust Manager is responsible for the calculation of the trust value of every user. Also it executes the formulated equation to calculate the Trust value. As and when the CI changes, the Trust value also changes. This work of modification and calculation of Trust value is done by the Trust Manager.

C. Decision Maker

The Decision Maker is responsible for taking the decision of permission to grant or deny the access to the data.

This component executes the Trust Rule. Trust Rule works as follows:

If Trust_Value > = security_level of the data then access is allowed
Else
Access Denied.

This is the mathematical representation of the Trust Rule which includes a simple comparison between the security level and the trust value of the friend. The Trust Rule is designed based on the concept of data confidentiality. In real life we like to share our confidential data with the trusted people. Hence, mathematically a direct variation exists between the trust value and the security level.

D. Data Center

The data center is responsible for storing data that has been uploaded by the user as well as the relationship information. The access to the data is controlled by decision maker from the data center. It consists of all the details such as the frequency of logins, number of posts, photos uploaded by the user. Also, it stores all the user activities like comments, likes given by the users. All these information is helpful to calculate the context information and hence further calculation of the Trust value.

II. MATHEMATICAL MODEL

Mathematically, system can be represented as a trust function. Let T(X) be the trust value of friend X of user U. Hence, T(X) depends on three values EX, CI and I. Thus,

T(X)=F(EX, CI, I) (1) The survey of Facebook users [21] was studied and few literatures were studied to understand the parameters that users consider while accepting a friend request. Those parameters were considered while calculating the Trust value. The percentages were used to calculate the weights for each parameter. These weights show the effect on the action of accepting a friend request. Hence, the weights depict the importance given by every user for trusting someone as a friend. The Trust value is calculated as follows:

T_{val}=0.614EX+0.277CI+0.109I (2) All the parameters have been given a fuzzy value and which has a crisp value which is put into (2) to get the trust value.

VI RESULTS AND DISCUSSION

The proposed system named ‘Trustbook’ is implemented in JSP, PHP and at the backend MySql is used. The aim of the system is to make the access control of the data on the social network simpler and less tedious to the user. The developed system only accepts the EX from the user while accepting the friend request of a new friend. The rest of the parameters are calculated by the values stored in the database. The database has tables to store the photos uploaded by the user, likes, comments, posts of the users. Also online-offline details, login details are maintained. All these counts were maintained for the calculation of CI. To the best of our knowledge, this is the first system that is developed which calculates and implements the CI for the Trust value calculation.

The Trust Rule is implemented as a join query and depending upon which the access control is decided. Trustbook is designed in such a manner that it bestows less efforts for the user for the access control. User chooses the EX by selecting one of the three categories for the friend while accepting a friend request. Also, the user while uploading a photo selects a security level for the photo and then the trust Rule is executed.

Following are the modules that play an important role in the efficient execution of ‘Trustbook’.

A User Interface

OSNs provide lot of functionalities starting from the basic to the advanced like third party applications and different games. However, Trustbook has only implemented the required functionalities of OSN like sending and accepting a friend request, uploading photos, posts, liking, commenting on the data. The User interface is kept simple to increase usability of the application. A mechanism to input EX is just a matter of click. Also to add a security level to a photo before it is being uploaded, a slider is provided which makes user easy to change the security level.

B Trust Value Calculation

The database holds tables to store I and CI of the user. Also the response of a user while accepting a friend request is stored in the database as EX. This fuzzy value is matched with the corresponding crisp value and then stored in the database. This is done for rest of the parameters and using (2) the final trust value is calculated.

The Trust Rule is applied as a query that implements this rule. The rule is implemented on the Home page of every user because all the photos, videos are seen at the home page. The security level is also stored in the database along with the data for which that security level is submitted by the user.

Thus the user has only 2 inputs to the system as far as trust calculation is required. First is EX which is an experience of the user while accepting the friend request and second one is the security level that is attached with every photo that has been uploaded by every user.

The results of the system have been studied with only photos but the Trust rule and sensitivity level is not dependent on the type of data for which it is put to use. It defines an approach to implement stricter and simpler access control mechanism.

The system was implemented and then checked for the performance with the current system. The implemented system outstands in following aspects:

- User friendliness
- Scalability
- Design of Dynamic Access Policies

The current scenario expects the user to frame the access policies mentioning the names of the friends who can view a particular data. It becomes cumbersome for the user if he has many friends in the friend list. Also even if the user has made groups of friends, some of the photos can be expected to be viewed by the intersection of friends from those groups. Hence, it makes the task more cumbersome and tiring for the user. The implemented scenario makes this task easier. The access control is defined using Trust Rule. Hence using only two input values of EX and security level the Trust policies are implemented. Other job is not the responsibility of the user.

The other performance measure is the scalability. The system was checked for the performance of different number of users. The observations stated that the time remains almost constant with the growing number of users. The time was recorded for calculating Trust value through the database.

.

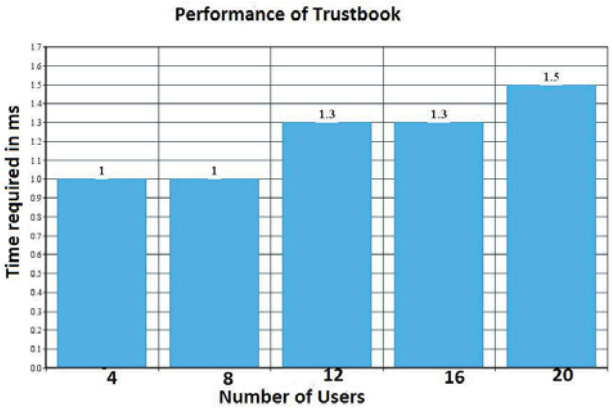

Fig 2.System Performance to calculate Trust Value

Fig 2 depicts the performance of the system. X axis mentions the number of users considered for every experiment. For every turn of an experiment, the required numbers of user profiles were created. After that, their profiles were built and then the actual OSN activities such as sending and accepting friend requests, commenting, liking, uploading photos etc was initiated.

This made the entries in database regarding the CI and I. EX was made to be inserted in the database when the owner of the profile accepts friend request. Thus through the time readings given by the MySql to execute the query that finds the CI,EX and I values, the total time was calculated by the summation of the time required to get EX,CI and I from database. These values retrieved from the database are further used in (2) to calculate the Trust Value.

Ti(Tr_Val) = Ti(CI)+Ti(I)+Ti(EX) (3) In (3), Ti is the function to calculate time. Since, the Trust value depends on the specified three parameters, the time required to calculate trust will also depend on the time required to calculate the three parameters.

Additionally there were some observations made in the system. The Trust Value is the dynamic parameter which keeps on changing. The system takes EX as the input only once. However, it can be made updatable anytime is a future work. However, CI measures the dynamicity of the user. As long as he is dynamic the Trust value will be positively affected. But if he is not active on OSN for some days or month, the CI will be dropped adversely affecting the Trust value. Hence Trust value is dynamic in nature. The system has also implemented the Trust value dynamically. Whenever, the related sub parameters (dynamicity, number of friends of CI change) change so does change the Trust value. This gives rise to the dynamic access control policies where user's involvement and effort is reduced giving more accurate and efficient results than it would have been done in the current scenario (manually).

VIII CONCLUSIONS AND FUTURE WORK

Trustbook performs the access control by adding a flavor of Trust to it. Trust-based access control with the specified parameters is a novel approach. It solves the problem of defining the access control policies in the current OSN. The users spend lot of time to design the access control policies making the task tedious. To solve this problem, 'Trustbook' is developed which generates the access control policies depending on the Trust Rule that is defined. Every time the system generates the new access control policies depending on the user's input for EX and security level for the data. However, the access control policies are governed by the Trust Rule only. The system has been proved to be more user-friendly and efficient as far as access control is concerned.

'Trustbook' has efficiently achieved the data confidentiality in OSN through efficient Trust-based access control.

The future work aims at implementing a data confidentiality attack as mentioned in [20]. The data can be leaked due to data dissemination. To avoid this [20] has proposed the threat

handling mechanism using Trust. This threat handling mechanism will be implemented in the future work. Also, the results regarding the efficiency of the threat handling mechanism need to be found out and validated for efficiency. Moreover, the current system can be improved in terms of security of maintaining the trust values at the data center. Some stringent encryption techniques can be used for the same.

REFERENCES

[1] Vedashree Takalkar,PN.Mahalle," Data confidentiality in Online Social Networks: A Survey",IJSR,Vol 4 issue 1 Jan 2015

[2] http://mashable.com/2011/12/19/friend-unfriend-facebook

[3] http://www.pewinternet.org/2012/02/03/why-most-facebook-users-get-more-than-they-give-2

[4] https://www.stonetemple.com/how-are-peopleusing-facebook/

[5] HongxinHu,Gail-Joon, Jan Jorgensen," Multiparty access control for online social model and mechanisms", IEEE Transactions On Knowledge And Data Engineering, Vol. 25, No. 7, July 2013

[6] SaumyaOmanakuttanand MadhumitaChatterjee,'Experimental Analysis on Access Control Using Trust Parameter for Social Network', Springer-Verlag Berlin Heidelberg 2014

[7] Wei-Lun Chang & Arleen N. Diaz & Patrick C.K. Hung, 'Estimating trust value: A social network perspective', Springer Science+Business Media New York 2014

[8] Cai-Nicolas Ziegler and Georg Lausen, 'Propagation Models for Trust and Distrust in Social Networks', 2005 Springer Science + Business Media, Inc. Manufactured in The Netherlands

[9] Chung-Wei Hang,Yonghong Wang, Munindar P. Singh,' Operators for Propagating Trust and their Evaluation in Social Networks',2009, International Foundation for Autonomous Agents and Multiagent Systems

[10] Wilfred Villegas, 'A Trust Based Approach For Protecting User Data In Social Networks', cascon '07 proceedings of the 2007 conference of the center for advanced studies on collaborative research

[11] UgurKuter, Jennifer Golbeck,'SUNNY: A New Algorithm for Trust Inference in Social Networks Using Probabilistic Confidence Models', Copyright 2007, Association for the Advancement of Artificial Intelligence (www.aaai.org)

[12] Guanfeng Liu, Yan Wang, Mehmet A. Orgun, Ee-PengLim,'Finding the Optimal Social Trust Path for the Selection of Trustworthy ServiceProviders in Complex Social Networks', IEEE Transactions On Services Computing, Vol. 6, No. 2, April-June 2013

[13] Lo-Yao Yeh,,Yu-Lun Huang,, Anthony D. Joseph, , Shiuhpyng Winston Shieh, , and Woei-Jiunn Tsaur, *Member, IEEE,"*A Batch-Authenticated and Key Agreement Framework for P2P-Based Online Social Networks*",* IEEE Transactions On Vehicular Technology, Vol. 61, No. 4, May 2012

[14] Duong Van Hieu, Nawaporn Wisitpongphan, and Phayung Meesad, 'Analysis of Factors which Impact Facebook Users' Attitudes and Behaviours using Decision Tree Techniques", 11th JCSSE (International Joint Conference in Computer Science and Software Engineering

[15] JunbeomHur, "Improving security and efficiency in attribute based data sharing", IEEE Transactions On Knowledge And Data Engineering, Vol. 25, No. 10, October 2013

[16] Shucheng Yu, Cong Wang, KuiRen, and Wenjing Lou," Achieving Secure, Scalable, and Fine-grained Data Access Control in Cloud Computing", INFOCOM, 2010 Proceedings IEEE DOI: 10.1109/INFCOM.2010.5462174 PublicationYear: 2010

[17] Mohamed Shehab , Anna Squicciarini , Gail-JoonAhn ,IriniKokkinou ," Access control for online social networks third party applications",Elseveir 897e911 computers & security 31 (2012)

[18] JunbeomHur," Attribute-Based Secure Data Sharing with Hidden Policies in Smart Grid", IEEE Transactions On Parallel And Distributed Systems, VOL. 24, NO. 11, NOVEMBER 2013

[19] Vipul Goyal, Cong Wang, KuiRen, Wenjing Lou,"Attribute Based Data Sharing with Attribute Revocation", ASIACCS'10, Beijing, China. Copyright 2010 ACM 978-1-60558-936-7, April 13–16, 2010

[20] Vedashree Takalkar,Parikshit.Mahalle," Handling Data Confidentiality Attack Due to Data Sharing using Trust-based Approach in Online Social Networks", International Journal of Engineering Research and Technology", Volume 4,Issue 5 May 2015

THE 5TH INTERNATIONAL CONFERENCE ON WIRELESS COMMUNICATIONS, VEHICULAR TECHNOLOGY, INFORMATION THEORY, AEROSPACE & ELECTRONIC SYSTEMS (WVITAE-2015)
December 13-16, 2015, Hyderabad, India

Analysis of Audio Watermarking Techniques for Cyber Security in Copyright Infringement

Sushma Ambekar
SKNSITS, Lonavala, India
sushma.ambekar91@gmail.com

Vandana Rohokale
SKNSITS, Lonavala, India
vmr.301075@gmail.com

Ramjee Prasad
CTIF, AAU, Denmark
Prasad@es.aau.dk

***Abstract* — With the enormous intensification in the development of internet technology and rapid growth in usage of digital multimedia, the problem such as copyright infringement has emerged. Copyright infringement occurs when someone other than the copyright holder or copyright owner use or distribute information without permission. In recent times, due to great developments in computer and internet technology, multimedia data i.e. audio, video, images have found wide applications. Digital watermarking has been considered as a powerful technique for copyright protection of multimedia data. As compared to the image and video watermarking, less research attention is given to audio watermarking techniques. As audio watermarking has not been investigated in details, this paper performs a comparative analysis of different audio watermarking techniques for copyright protection.**

Keywords— Copyright infringement, Audio watermarking, Robustness, Security, complexity, imperceptibility. Copyright infringement, Audio watermarking, Robustness, Security, complexity, imperceptibility.

I. INTRODUCTION

In today's world, the number of internet users has vastly increased with the parallel growth of information and digital technology. With the internet development and rapid growth in usage of digital multimedia, it has become very easy to generate unauthorized copies of digital data. In many areas this has become very problematic. Therefore it has created new challenges to protect intellectual property rights (IPR). Nowadays, protecting the electronic documents from unauthorized copying is an important issue. Due to the rapid growth of evolving technologies, there is an increase in the risk of different cyber-crime attacks. The problems such as copyright infringement and intellectual property rights (IPR) violation have emerged due to the growth of information and digital technology.

Copyright infringement occurs when someone other than the copyright holder or copyright owner use or distribute information without permission. For example illegally downloading music, image or cartoon on website or in a document. It is not easy to avoid copyright infringement. By using new technologies, virtually anything can be copied easily and nearly perfectly. Digital watermarking is one of the best solutions to prevent illegal copying, modifying and redistributing multimedia data. Security is the degree of protection from loss, damages, criminal activity and resistance to harm. Nowadays, it's very important to provide security for the electronic documents. It is common for many people to share and transfer the multimedia data due to rapid growth of Internet and networks technique. This multimedia data is easily copied and modified due to which necessity for copyright protection is increased.

Digital Watermarking has been proposed as technique for copyright protection of multimedia data. Digital Watermarking is a process of embedding digital signals or pattern into a multimedia object without affecting in any way the quality of the original file. While sending a message to destination, it should be watermarked to protect this message from illegal copying and it also provides the security. In digital watermark mechanism, information is invisibly inserted into audio or video, image. Digital Watermarking is nothing but hiding digital signal message such as image, audio (song), video within the signal itself. The hiding process has to be robust in such a way that the modifications of the media are hardly possible. Digital Watermarking is used to prevent or avoid illegal copying, redistributing and modifying multimedia data. By using digital watermarking, we can provide the copyright protection, covert communication, content identification and data authentication.

.

II. CLASSIFICATION OF DIGITAL WATERMARKING TECHNIQUES

Digital watermarking techniques classification is based on type of document. Using this criterion, techniques can be classified into three types:

- Image watermarking
- Video watermarking
- Audio watermarking

Several digital watermarking techniques are proposed which include watermarking for images, audio and video.

1) *Image Watermarking*: This adds watermark to image. It is used to hide the information into image and this information is later detected and extracted for author's ownership.
2) *Video Watermarking*: Here watermark is applied to individual frames of a video. Video Watermarking is nothing but the extension of image watermarking. Video watermarking imposes real or near real-time watermarking system.

3) *Audio Watermarking*: Digital audio watermarking is used for protecting audio files against illegal copying. It embeds the watermark to audio files such as music, MP3, etc.

Primarily, the research of image watermarking was started, and then the watermarking techniques were developed for audio. There is less research on the development of audio watermarking techniques. Less watermarking techniques are proposed for audio compared to the image/video. As Human Auditory System (HAS) is more sensitive than the Human Visual system (HVS), it is very difficult to add watermark data in audio file as compared to the image file. The audio watermarking algorithms are not easy. Also the available studies on audio watermarking are far less than that of video watermarking or image watermarking. Applying watermarks on audio data by using various algorithms is known as audio watermarking.

III. PROPERTIES OF DIGITAL WATERMARKING

Properties of digital watermark are as listed below:

1) Robustness: Robustness is nothing but the watermark embedded in data has the ability to withstand non-malicious distortions. Watermark data should be robust so that it should not be eliminated by unauthorized distributors and watermark data should resist many attacks such as filtering, compression and filtering with compression, noise addition, cropping, resampling, Re - quantization.
2) Imperceptibility: The watermark should be invisible, inaudible to human eyes/ears, only be detected by an authorized person. Imperceptibility is nothing but hiding a watermark so that the watermark should not affect the quality of the original signal.
3) Capacity and data payload: Capacity is nothing but the number of bits that can be embedded in one second of the host signal. If multiple watermarks are embedded into an data, then watermarking capacity of the image is the sum of all individual watermarks data payload.
4) Security: Security of a watermark is the ability that watermark should only be extracted by authorized person. Security resists malicious attacks. Security provides watermark access only to the authorized parties and thus able to achieve the purpose of copyright protection. If we provide security then hacker cannot remove the watermark without having knowledge of detector, composition of watermark and embedding algorithm.
5) Computational cost: If the watermarking method is less complex then the computational cost of the watermark should reduce. If computing resources such as hardware and software required for watermarking method are with high complexity algorithms then it incurs more computational cost. If the watermarking method is simple then limited resource will be required and also computational cost should be less. Thus the computational cost and complexity of watermark methods are directly proportional to each other and vice-versa.

We need to make a trade-off between all these requirements/ properties because they are often contradictory with each other.

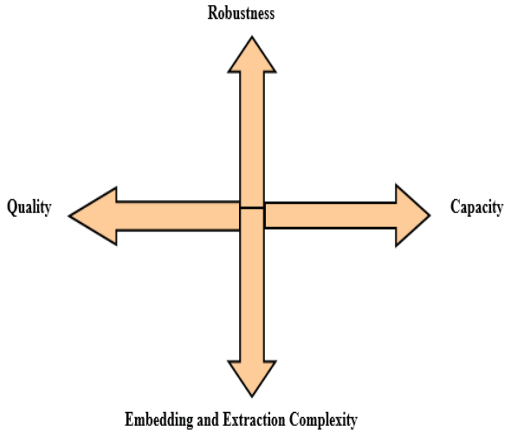

Figure 1 - Properties tradeoff

For example increasing data rate or capacity in watermark system results in reduces the robustness against attacks and also degradation of quality of the watermarked signal.

IV. STATE OF THE ART

The audio watermarking method by using Generalized Spread Spectrum Watermarking scheme (GSSW) was proposed in one. The big advantage of this scheme is that it is having large maximum capacity as compare to the Traditional Spread Spectrum method [1]. Audio watermarking using lifting wavelet transform (LWT) and QR decomposition method (QRD) has high data payload and good imperceptible and also this method is highly robust against various attacks. Here in this method first audio signal is divided into non-overlapping frames. Then watermark information is embedded in each frame of audio signal. From low frequency LWT coefficients of frame we can obtain upper triangular matrix. The largest or highest element of the upper triangular matrix watermark data can embed. Also this method has high robustness [2].

Time-spread Echo based audio watermarking for audio signal provides good imperceptibility but for this method there is need to further enhance the robustness against de-synchronization attacks. In this method robustness optimization and imperceptibility optimization has been performed simultaneously. Also here coefficients of echo filter are obtained by using finite-impulse-response (FIR) filter design [3]. Blind audio watermarking method based on DWT-SVD also provides the robustness. Audio watermarking is providing for the copyright protection [4]. In Audio watermarking using DWT and SVD method, two secret keys are used for encryption and description. Therefore this method can provides better security. In this method initially original audio signal is segmented by Discrete Wavelet Transform (DWT).

Table 1- State of the art in digital watermarking techniques for Audio Signals

Sr. No.	Paper Title	Publication year	Method used	Features
1	Channel Capacity Analysis of the Generalized Spread Spectrum Watermarking in Audio Signals	2015	Generalized spread spectrum watermarking (GSSW) scheme	maximum capacity of the GSSW scheme is larger than that of the traditional spread spectrum scheme
2	A Blind Audio Watermarking Method Based on Lifting Wavelet Transform and QR Decomposition	2014	lifting wavelet transform (LWT) and QR decomposition (QRD)	highly robust, high data payload and provides good imperceptible
3	Time-Spread Echo-Based Audio Watermarking With Optimized Imperceptibility and Robustness	2015	FIR with HAS	provides imperceptibility but need to enhance robustness
4	DWT-SVD Based Blind Audio Watermarking Scheme For Copyright Protection	2014	DWT-SVD	Robust
5	A Blind LWT-Based Audio Watermarking Using Fast Walsh Hadamard Transform and Singular Value Decomposition	2014	LWT using FWHT and SVD	robust, high perceptual quality audio, high imperceptibility, high data payload
6	Digital watermarking in audio for copyright protection	2014	DWT and SVD	high robustness, provides security by using 2 secret keys
7	Patchwork-Based Audio Watermarking Method Robust to De-synchronization Attacks	2014	discrete cosine transform(DCT)	higher embedding capacity, robust
8	An Improved Patchwork-Based Digital Audio Watermarking In CQT Domain	2014	CQT, ICQT, frame pairs, patchwork	better signal quality and robust
9	Fast and low-complexity Audio watermarking	2014	FFT	high capacity, robustness, low-complexity
10	A High Capacity Quantization-Based Audio Watermarking Technique Using the DWPT	2014	QIM (Quantization Index Modulation) technique on the DWPT (Discrete Wavelet Packet Transform) coefficients.	high embedding capacity, robustness
11	An Audio Watermarking Method Using Pitch-Transformed Sound of Original Music	2014	phase coding phase coding	sound quality increased
12	A Novel Audio Watermarking Algorithm Based On Neighboring Samples	2014	Time domain and Neighboring Samples	robustness, imperceptibility
13	Robustness Enhancement of Quantization Based Audio watermarking Method Using Adaptive Safe-band	2014	Adaptive safe-band based method	enhance robustness
14	A High Payload Audio Watermarking Algorithm Robust against Mp3 Compression	2014	Discrete wavelet transform (DWT)	Very good robustness, high embedding capacity, High Payload, good imperceptibility, high perceptual transparency
15	Spread Spectrum Audio Watermarking: Enhancement of Detection and Watermarking Capacity	2014	spread spectrum; LPC	high capacity and less robust
16	Audio watermarking system based on Frequency Hopping modulation	2014	Frequency hopping modulation, spread spectrum.	reliability increases

Then singular value decomposition (SVD) is applied on non--overlapping blocks and then in each block of singular values watermark information or watermark data is embedded. The advantage of this method is it having high robustness [6]. The audio watermarking based on Patchwork is robust to de-synchronization attacks. Initially in this method watermark Information is embedded in audio signal in Discrete Cosine Transform domain (DCT) and then in watermark signal synchronization bits are added in logarithmic DCT (LDCT) domain. The embedding capacity of this scheme is high [7]. In the research of audio watermarking in CQT domain includes improved patchwork method. This watermarking technique

provides the better signal quality and robustness is enhanced in this technique. Also this scheme ensures the imperceptibility [8].

Fast and low complexity audio watermarking based on Fast Fourier Transform (FFT) algorithm initially the FFT spectrums are segmented into short frames and then by using Fibonacci numbers the magnitude of the FFT samples changed. This scheme provides the high embedding capacity. The main advantage of this method is it's having low complexity. Also this scheme provides the high capacity. This method has good robustness [9]. Audio watermarking scheme based on high capacity quantization in Discrete Wavelet Packet Transform (DWPT) provides robustness and it's having high embedding capacity. Here in this method the audio signal is segmented into number of sub bands using Discrete Wavelet Packet Transform (DWPT). This method ensures the transparency [10].

Table 2 – Various Research Parameters for Audio Watermarking Techniques with Different Algorithms

Paper No	Method used	Robustness	Imperceptibility	Security	Capacity and data payload	Low complexity	Reliability	Quality
[1]	Generalized spread spectrum watermarking (GSSW) scheme			Not Addressed till now	Yes	Not Addressed till now		
[2]	Lifting wavelet transform (LWT) and QR decomposition (QRD)	Yes	Yes		Yes			
[3]	FIR with HAS		Yes					
[4]	DWT-SVD	Yes						
[5]	LWT using FWHT and SVD	Yes	Yes		Yes			Yes
[6]	DWT and SVD	Yes		Yes				
[7]	Discrete cosine transform(DCT)	Yes		Not Addressed till now	Yes			
[8]	CQT, ICQT, frame pairs, patchwork	Yes						Yes
[9]	FFT	Yes			Yes	Yes		Yes
[10]	QIM (Quantization Index Modulation) technique on the DWPT (Discrete Wavelet Packet Transform) coefficients.	Yes			Yes	Not Addressed till now		
[11]	Phase coding phase coding							Yes
[12]	Time domain and Neighboring Samples	Yes	Yes					
[13]	Adaptive safe-band based method	Yes						
[14]	Discrete wavelet transform (DWT)	Yes	Yes		Yes			
[15]	Spread spectrum; LPC				Yes			
[16]	Frequency hopping modulation, spread spectrum.						Yes	

Audio watermarking using the Pitch-Transformed sound of music improves the quality of sound. The key idea is use of phase coding and processed sound for audio watermarking for copyright protection [11]. Audio watermarking using Neighboring samples method was proposed. It uses the watermarking in time domain. This method provides the robustness and imperceptibility characteristics of watermarking. In this method the frame with three samples is used. These samples define the amount of distortion to be added. If middle sample is distorted then the middle sample of frame is made equal to '1' of the neighboring samples. This scheme provides the good signal quality [12].

The adaptive safe band based method is also used for audio watermarking. This scheme enhances the robustness. In this

paper fixed size safe-band is used between two quantization steps. Just by changing the size of safe band the robustness of watermarking can be improved [13].

Audio watermarking scheme using Discrete Wavelet Transform (DWT) gives very good robustness. Also it enhances the embedding capacity of watermarking. It improves the imperceptibility. Also it has high perceptual transparency and high payload. In this scheme the non-overlapping frames uses in Discrete Wavelet Transform [14].The research in audio watermarking performs by using spread spectrum and linear predictive coding algorithm (LPC). This method provides the high capacity of watermarking. But this scheme is less robust against various attacks. In this method at the receiver the linear predictive coding (LPC) and high pass filtering is used to reconstruct the embedding signal [15]. Audio watermarking using frequency hopping modulation technique and spread spectrum increased reliability is studied in [16].

V. PROPOSED WORK

Table 2 lists various research parameters for Audio Watermarking Techniques with Different Algorithms. It reveals from the table that lot of research work is done in the audio watermarking techniques with consideration of parameters such as robustness, imperceptibility, capacity, data payload and quality. But the security, complexity reduction and reliability are the least attended issues which are very important for the safety from various cyber attacks. This research work proposes the combination of Discrete Wavelet Transform (DWT) and singular value decomposition (SVD) with Fast Fourier Transform (FFT) using Frequency Hopping Spread Spectrum mechanism which will be able to provide security with low complexity and reliability with good quality of audio watermarking.

VI. CONCLUSIONS AND FUTURE SCOPE

Cyber Security is very critical issue for the forthcoming fifth generation mobile communication where huge data will be generated. To save that data from various cyber attacks is the real challenge. Negligible amount of attention has been given towards the security and reliability of the audio data which contains very important information. Development of robust and secure audio watermarking techniques is the need of the forthcoming converged internet age. This research work aimimg towards Analysis of Audio Watermarking Techniques for Cyber Security in Copyright Infringement will be further extended in the direction of the combination of Discrete Wavelet Transform (DWT) and singular value decomposition (SVD) with Fast Fourier Transform (FFT) using Frequency Hopping Spread Spectrum mechanism which will be able to provide security with low complexity and reliability with good quality of audio watermarking.

REFERENCES:

[1] Ying Zhang, Zhengguang Xu, and Benxiong Huang, “Channel Capacity Analysis of the Generalized Spread Spectrum Watermarking in Audio Signals,” IEEE SIGNAL PROCESSING LETTERS, VOL. 22, NO. 5,May. 2015, pp. 519–523.

[2] Pranab Kumar Dhar,” A Blind Audio Watermarking Method Based on Lifting Wavelet Transform and QR Decomposition”, 8th International Conference on Electrical and Computer Engineering, December, 2014,pp.136-139.

[3] Guang Hua, Jonathan Goh, and Vrizlynn. L. L. Thing,” Time-Spread Echo-Based Audio Watermarking With Optimized Imperceptibility and Robustness”, Ieee/Acm Transactions On Audio, Speech, And Language Processing, Vol. 23, No. 2, February 2015, pp.227-239.

[4] Krishna Rao Kakkirala, Srinivasa Rao Chalamala, Bala Mallikarjuna Rao G,” DWT-SVD Based Blind Audio Watermarking Scheme For Copyright Protection”, IEEE ICALIP2014,pp.180-183.

[5] Pranab Kumar Dhar, Tetsuya Shimamura,” A Blind LWT-Based Audio Watermarking Using Fast Walsh Hadamard Transform and Singular Value Decomposition”, 2014 IEEE,pp.125-128.

[6] Mustapha Hemis and Bachir Boudraa,” Digital watermarking in audio for copyright protection”, ICACSIS 2014, pp.189-193.

[7] Yong Xiang, Iynkaran Natgunanathan, Song Guo,” Patchwork-Based Audio Watermarking Method Robust to De-synchronization Attacks”, IEEE/ACM TRANSACTIONS ON AUDIO, SPEECH, AND LANGUAGE PROCESSING, VOL. 22, NO. 9, SEPTEMBER 2014, pp.1413-1423.

[8] Peng Hu, Qin Yan, Luan Dong, Meng Liu,” An Improved Patchwork-Based Digital Audio Watermarking In Cqt Domain”,IEEE 2014,pp.920-923.

[9] Mehdi Fallahpour, David Megías,” Fast and low-complexity Audio watermarking”, 2014 10th International Conference on Mobile Ad-hoc and Sensor Networks,IEEE-2014,pp.329-325

[10] El bahi, Abdellah Adib,” A High Capacity Quantization-Based Audio Watermarking Technique Using the DWPT”, IEEE, july-2014.

[11] Harumi Murata, Akio Ogihara,” An AudioWatermarking Method Using Pitch-Transformed Sound of Original Music”, 2014 Tenth International Conference on Intelligent Information Hiding and Multimedia Signal Processing,pp.268-271.

[12] Shahid Md. Asif Iqbal, Alok Kumar Chowdhury, Amina Akhter, Kingshuk Dhar,” A Novel Audio Watermarking Algorithm Based On Neighboring Samples” 16th Int'l Conf. Computer and Information Technology, 8-10 March 2014, pp.473-477.

[13] Iynkaran Natgunanathan, Yong Xiang, Tianrui Zong, and Yang Xiang,” Robustness Enhancement of Quantization Based Audio Watermarking Method Using Adaptive Safe-band”, IEEE ICC 2014 - Communication and Information Systems Security Symposium,pp.890-895.

[14] Arashdeep Kaur, Malay Kishore Dutta, K.M.Soni and Nidhi Taneja, “A High Payload Audio Watermarking Algorithm Robust against Mp3 Compression”, 2014 IEEE,April-2014.

[15] Hosein Fami Tafreshi, Ali Asghar Soltani Farani,” Spread Spectrum Audio Watermarking: Enhancement of Detection and Watermarking Capacity” The 22nd Iranian Conference on Electrical Engineering (ICEE 2014), May 20-22, 2014,pp.1477-1482.

[16] Mohammed Khalil, Abdellah Adib,” Audio watermarking system based on Frequency Hopping modulation”, 2014 IEEE,july-2014.

[17] AparnaJR, Sona! Ayyappan,” Comparison of Digital Watermarking Techniques”, 2014 International Conference On Computation Of Power, Energy, Information And Communication (ICCPEIC), IEEE, Janeaury-2014.

[18] Haikun Liu, Member, Hai Jin,” Hotplug or Ballooning: A Comparative Study on Dynamic Memory Management Techniques for Virtual Machines”, IEEE Transactions On Parallel And Distributed Systems, VOL. 26, NO. 5, MAY 2015,pp.1350-1363.

THE 5TH INTERNATIONAL CONFERENCE ON WIRELESS COMMUNICATIONS, VEHICULAR TECHNOLOGY, INFORMATION THEORY, AEROSPACE & ELECTRONIC SYSTEMS (WVITAE-2015)
December 13-16, 2015, Hyderabad, India

GSHMAC: GREEN AND SECURE HYBRID MEDIUM ACCESS CONTROL FOR WIRELESS SENSOR NETWORK

Pranav M. Pawar[1], Rasmus H. Nielsen[2], Neeli Rashmi Prasad[3], Ramjee Prasad[1]
[1]Center for TeleInFrastruktur, Aalborg University, Aalborg, Denmark
[2]Cisco Systems, San Jose, USA
[3]Center for TeleInFrastruktur, Aalborg University, Princeton, USA
{ pmp, prasad }@es.aau.dk[1], rhnielsen@ieee.org[2], neeli.prasad@ieee.org[3]

Abstract— **The cost efficiency of wireless platforms and their easy deployment enable the applicability of it in widespread application domains. Wireless sensor networks (WSNs) are not excluded from it. Their application domains vary from industrial monitoring to military applications. A WSN is a resource-constrained network and energy of the WSN node is a valuable resource. Like every other network, WSNs are also vulnerable to security attacks. A security attack can results in networks consuming more resources, leading to earlier depletion of node energy. A significant part of the resource consumption in a WSN is controlled by the medium access control (MAC) mechanism. This paper focuses on WSN MAC mechanisms and countermeasures for attacks targeting the MAC layer in a WSN. Denial of sleep attacks are the most relevant for WSN MAC as these types of attacks have shattered effects, which bring down the sensor lifetime from years to days. This paper proposes a secure hybrid MAC mechanism, Green and Secure Hybrid Medium Access Control (GSHMAC) to overcome the devastating effect of WSN MAC attacks. The proposed mechanism provides features such as collision threshold-based MAC mode control and countermeasures on WSN MAC using internal MAC mechanisms. GSHMAC shows improved energy-efficiency, delay, and throughput in the presence of attacks, as compared with state-of-art secure MAC mechanisms.**

Keywords- Wireless sensor network (WSN), medium access control (MAC), cluster, hybrid-MAC, security, denial of sleep attack, energy efficiency, throughput, delay.

I. INTRODUCTION

WSN applications in areas related to everyday life are speedily increasing and at the same time, the use of WSNs in industrial use cases is becoming still more widespread. Every application of sensors can significantly improve aspects of living and help to increase productivity and efficiency of the domains in which they are deployed [1]. However, as applications of WSNs are becoming still more widespread and broader, and their demands are increasing, the chances of the network to be attacked or compromised by malicious users are also increasing. Proper security measures while deploying WSNs are, therefore, a necessity to take full advantage of the deployment of new applications [2].

WSNs are subject to many different attacks at different layers of the communication stacks. Attacks on the medium access control (MAC) layer are some of the most severe as the MAC layer allocates resources for communications, which accounts for a significant part of the overall energy consumption of the system. Therefore, it is necessary to implement countermeasures to protect the MAC layer from security attacks. The literature suggests different security solutions for MAC layer attacks, a majority of which are cryptographic solutions. However, such solutions are computational heavy for a resource constrained WSN system. More lightweight solutions for the WSN MAC layer security can be achieved by organizing the internal MAC mechanisms of a WSN [3, 4].

This paper proposes a novel MAC layer mechanism, Green and Secure Hybrid Medium Access Control (GSHMAC), to countermeasure different attacks, specifically the collision attack, replay attack, and full domination attack [3]. The proposed mechanism is a cluster-based [4] hybrid MAC mechanism [5], which uses a mix of time division multiple access (TDMA) and carrier sense multiple access (CSMA) mode for intra-cluster communication and TDMA mode only for inter-cluster communication. During intra-cluster communication, MAC mechanism shifts the mode according to a collision threshold value. GSHMAC is inherently secure; as it implements cluster-based networking, where an attack in one cluster will not easily penetrate into another cluster. The other security perspective in GSHMAC is the use of TDMA mode for inter-cluster communication and mixed TDMA and CSMA mode for intra-cluster communication. If a node shifts to TDMA mode, it will communicate only during consigned slots and an attack will, therefore, only be successful if malicious nodes succeed in stealing those slots.

In addition, GSHMAC modifies the internal MAC mechanism (Mode shift mechanism of hybrid MACs according to traffic conditions and cluster-based topology used) further to enhance the security. In this respect, use of collision threshold value [6] is introduced to detect collision attacks along with the maintenance and analysis of a replay counter to detect replay attacks. In addition, the security relating to a full domination attack is improved by combining the two countermeasures. The proposed secure mechanism shows better performance in the presence of different kinds of denial of sleep attacks as compared with state-of-art secure MAC solutions. It shows improved energy efficiency, delay, and throughput.

The remainder of the paper is organized as follows. Section 2 presents the related work in secure MAC mechanisms and different countermeasures for MAC layer security attacks. Section 3 describes the assumptions and system model. Section 4 gives a detailed background of GSHMAC with the mechanism used. Section 5 gives insight of the security countermeasures used in GSHMAC. Section 6 discusses the

simulation details and comparative results of GSHMAC. Last section concludes the paper with future work.

II. Related Work

Qingchun Ren et al. [7] presented a secure MAC mechanism using a soft decision theory approach. It is developed by considering a request to send (RTS)/clear to send (CTS) based MAC mechanism. The proposed mechanism works for defending against collision, unfairness, and exhaustion attacks. A disadvantage of the proposed work is that it considers too many parameters for attack decision that leads to increased computational complexity. Brownfield et al. [8] studied energy resource vulnerabilities of WSNs and led WSN MAC mechanisms and proposed a new MAC mechanism, Gateway-MAC (G-MAC), for alleviating the effects of denial of sleep attacks. G-MAC uses centralized cluster management to defend against denial of sleep attacks, and the gateway node is responsible for relaying all inter- and intra-network traffic. G-MAC shows good energy savings in the presence of denial of sleep attacks as compared to other MAC mechanisms. The mechanism shows increased computational and communication overheads because of continuous transfer of gateway responsibilities and authentication of the packet at gateway. David R. Raymond et al. [9] developed a cluster adaptive rate limiting (CARL) approach to defending against denial of sleep attacks. It considers the denial of sleep attack involving unauthenticated and replay packets. It improves the defense against attacks by limiting active periods of high rate malicious traffic. The disadvantages of CARL are that the network designer has to set the various threshold values to control the rate-limiting behavior and an increase in control traffic. David R. Raymond et al. [10] made a significant contribution in the area of denial of sleep attacks for WSN MAC mechanisms. They proposed the denial of sleep attacks classification method according to the attacker's knowledge of the MAC mechanism and the capabilities to evade authentication and encryption mechanisms. Raghavendra V. Kulkarni et al. [11] proposed a secure MAC mechanism based on generalized neurons. The proposed solution is applicable to denial of service attacks on CSMA-based MAC mechanism. Here, the neurons are trained by using particle swarm optimization mechanism. The algorithm shows improved network lifetime in the presence of an attack. The algorithm is complex and requires the extensive training of neurons for attack detection. Chen Chen et al. [12] proposed a defense mechanism for S-MAC. It mainly considers defense against those attacks, which are having information of the victims such as collision attack, unfairness attack, exhaustion attack, and broadcast attack. The mechanism shows decreased packet drops in an attack situation. The disadvantage is that the solution increases the energy consumption and transmission delay because of fake schedule switch scheme. P. Sankara Rao et al. [13] presented a multi-layer perception based mechanism for securing CSMA-based MAC. It increases the security of the MAC by continuously monitoring for attack situations. The mechanism assures for improved performance in the presence of an attack, but the author had not given any experimental proofs for it. Ching-Tsung Hsueh et al. [14] proposed the two-tier receiver-initiated secure MAC (TE2S) for WSNs denial of sleep attacks. It presents a simplified authenticating process for improving the performance of MAC countermeasures. The proposed scheme is considered as a cross-layer receiver-initiated secure scheme. The proposed scheme shows improved defense against attacks, and it shows reduced energy consumption. The mechanism increases the computation overheads because of the used cryptographic solutions. Tapalina Bhattasali et al. [15] presented a distributed collaborative mechanism for detecting sleep deprivation torture in WSNs. The proposed solution uses a hierarchical network framework for heterogeneous sensor field. The mechanism promises for improved energy efficiency but has not provided any experimental evidences for it.

The review of related work illustrates that currently available secure MAC mechanisms are based on neural networks, fuzzy, and cryptographic approaches. These approaches countermeasure the denial of sleep attack but increase the computational complexity, which raises the overheads on resource constrained WSNs. These proposed solutions are also not tested by considering multiple malicious nodes in the network. Therefore, the motivation of the proposed work is to develop less computational intensive, energy, delay, and throughput efficient, secure MAC mechanism by considering internal features of hybrid MAC mechanisms.

III. Prerequisites

A. System Model

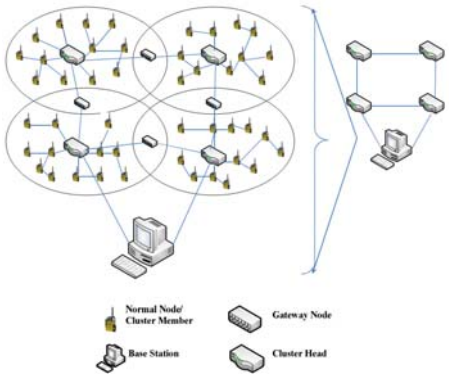

Figure 1. System model for GHMAC

The system model for the proposed mechanism is as shown in Figure 1. The proposed mechanism considers a cluster-based network, which is an effective way to improve the scalability and energy efficiency of WSNs. The clusters are collection of the cluster node (or cluster member) and cluster head (CH). Every node in the cluster has an equal amount of initial energy. Each cluster consists of a CH. The CH maintains the data counter and collision threshold value. The data counter will be incremented when the CH will receive a sensed information (or data) with different packet-id. The collision threshold value is the average amount of collisions allowed in the cluster. Every node in the network sends sensed information to the CH that aggregates it and sends it towards BS.

B. Assumptions

The secure and energy efficient MAC is developed by considering common network and node assumptions for WSNs. The considered assumptions for proposed MAC mechanism are described as above. All nodes have similar competencies and identical significance. Nodes are location un-aware without any global positioning system (GPS) capabilities. Every node has a unique identification (ID). The network is divided into clusters; every cluster has a CH and cluster members. BS, CH, and cluster members are assumed

static. There is a single BS in the network. The clusters are considered as multi-hop clusters, to achieve better energy efficiency and scalability in the clustered environment. The system considers the multi-hop communication for inter- and intra- cluster communication. There are mixed uni- and bi-directional links. The nodes in the network periodically elect the CHs. The nodes will transmit a message to the network after some particular interval of time.

IV. Green and Secure Hybrid Medium Access Control (GSHMAC)

GSHMAC is a green and secure hybrid MAC mechanism, which uses both TDMA and CSMA mode of communication according to the requirement of the network. The different blocks in GSHMAC are,

- ✓ Cluster-based topology
- ✓ GCF scheduling algorithm
- ✓ Hybrid synchronization mechanism
- ✓ MAC mode control
- ✓ Countermeasures on WSN MAC attack

- Cluster-based topology: Cluster-based topology helps to improve the scalability, energy efficiency, and contributes to reducing the effect of security attacks because of its inherent security. GSHMAC uses the Enhanced Multihop Clustering Algorithm (EMCA) [16] for forming the cluster-based topology.
- Green Conflict Free (GCF) scheduling algorithm: Scheduling algorithm is the essential part of the hybrid MAC mechanism, which helps to decide the particular conflict free slot for communication. The hybrid MAC mechanism proposed here uses GCF [17] as a scheduling algorithm. GCF is a three-hop conflict-free scheduling algorithm for WSN.
- Hybrid Synchronization Algorithm: Synchronization is necessary to achieve the timing accuracy during the node communication and slot assignment. GSHMAC uses hybrid synchronization for achieving it efficiently. The hybrid synchronization algorithm uses approximate diffusion-based synchronization for intra-cluster communication and tight sender-receiver synchronization for inter-cluster communication [18].
- MAC mode control: GSHMAC uses TDMA mode for inter-cluster communication and TDMA or CSMA mode for intra-cluster communication. It considers that initially all clusters are using a CSMA mode. The MAC mode control is responsible for shifting of mode from TDMA to CSMA and vice versa. The shifting of MAC mode depends on a collision threshold value. If the amount of collision inside the cluster goes beyond the collision threshold value, then the cluster will shift the node from CSMA to TDMA. Every time a node will experience a collision, it will send a CSE message to the CH.
- Countermeasures on WSN MAC attack: The proposed secure hybrid MAC mechanism includes the countermeasure against WSN MAC layer attack. The solution gives countermeasure for collision-, replay-, and full-domination- attacks. The proposed solution uses the internal characteristics of the hybrid MAC mechanism such as the collision threshold value for the counter measuring the collision attack and data counter value for the counter measuring the replay attack.

V. Security Countermeasures for WSN MAC Attacks

A. *Countermeasure for Collision Attack*

The proposed countermeasure is developed by considering the hybrid MAC layer mechanism, which changes its mode from CSMA to TDMA and vice-versa. The mode changes according to the amount of traffic in the network. If the number of collision in the cluster goes beyond the collision threshold value, the cluster shifts the mode from CSMA to TDMA. The typical collision threshold considered here is 5% [6], which is the normal collision rate considered in the literature. If the collision experience by a node is above the collision threshold, the node shifts the mode. An attack on a network increases the malicious traffic, which leads to increased collisions. The large amount of collisions in a network shifts the mode from CSMA to TDMA. In TDMA mode, every node will communicate only in consigning slots, and it is expected that collisions in the network should reduce. However, as the malicious users have knowledge of the MAC layer mechanism used. Therefore, a malicious user will not be stop and introduces collisions into the network. Hence, if a collision is introduced in TDMA mode and it is going beyond the collision threshold value, then a collision attack will be held on the network, and the network will take necessary care of it. Figure 2 shows the mechanism to countermeasure the collision attack. The proposed GSHMAC mechanism considers that if nodes in a cluster experience a collision, it will inform the CH using a CSE message. If the amount of collisions goes beyond the collision threshold value, the cluster will shift the mode from CSMA to TDMA, and otherwise the cluster will work in CSMA mode. Once the mode will be shifted to TDMA, nodes will start to transmit in TDMA mode. If nodes experience the collision in TDMA mode, that will inform it to the CHs. If the amount of collisions goes beyond the collision threshold value in TDMA mode, the collision attack on the network, otherwise no attack in the network and network shifts to CSMA mode. The CSE message transmitted from a node contains node ID and information about the collision. Once the collision attack in a network, the system will analyze the CSE message and the node that sent highest number of CSE messages to the CH is declared as a malicious node and isolate it from the network. The malicious node is isolated from the network by removing all incoming and outgoing links from node and updating the routing table of the network.

The other situation is when collisions are introduced due to misconfiguration of nodes or interference by some other sources. The proposed countermeasure considers such situations as malicious if the collision is caused due to crossing of collision threshold value. The same previously described mechanism will be used to detect misconfigured or interfering node. The proposed countermeasure is not using any cryptographic mechanism to detect the attack. It detects the attack by using the internal MAC mechanism considered the hybrid MAC mechanism.

B. *Countermeasure for Replay Attack*

The countermeasure for replay attack on the WSN MAC layer is built up by considering that data generated by the node have a unique ID. Every data packet considered here consist of the node ID, data ID, and information. If a node will receives the data with same data ID and node ID, it is not in sequence and not following the packet interval gap set in the network; then

the network will detect the replay attack. Here, two conditions are checked for node being malicious i.e. packet interval gap and data ID and node ID of the current packet.

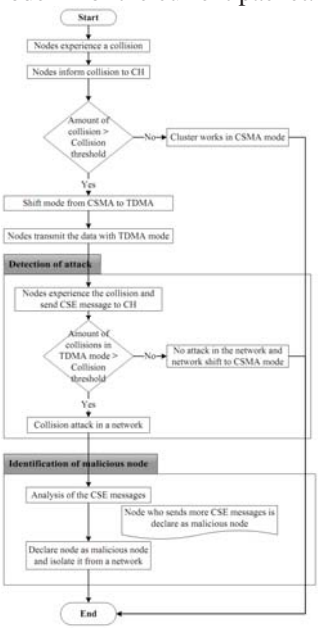

Figure 2. Countermeasure for collision attack

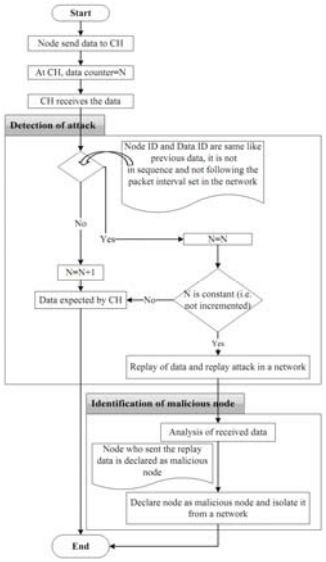

Figure 3. Countermeasure for replay attack

Here, the CH of each cluster maintains a data counter. The initial value of data counter is *N*, whenever the network is initialized. The data counter will be incremented by one when the event is not a replay event. The mechanism for detecting the replay attack is as shown in Figure 3. Here, the node sends a packet to the CH, and if the received packet on CH have the same node ID and data ID, like previously received packet, it is not in expected sequence and not following the packet interval set in the network then data counter will not be incremented. If the data counter is not incremented, it means there is the replay of the same event inside the cluster. Replay event is one of the signs of replay attack. Once the replay event is detected, the system will analyze the replayed packets. The node who replayed maximum number of packets is declared as a malicious and isolates it from the network.

C. *Countermeasure for Full Domination Attack*

The full domination attack will be detected on the network by combining countermeasure of collision attack and replay attack. Full domination attack dominates the network by introducing collisions and replays of a large number of events in the network.

VI. SIMULATION RESULTS AND DISCUSSIONS

A. *Simulation Details*

The simulation of the algorithm is performed using Network Simulator-2 (NS-2) and the parameters considered for the simulation are presented in Table I. The simulation considers that WSN nodes are deployed uniform randomly in an area of 100m by 100m. The simulations are carried out under the assumption that the attacker can initiate an attack from multiple nodes randomly from 1 to 20 malicious nodes in the network. The simulation considers the packet interval as 0.1s.

TABLE I. SIMULATION PARAMETERS

Parameter Name	Setting Used
Network Interface Type	Wireless Physical
Radio Propagation Model	Two-Ray Ground
Antenna Type	Omni-directional Antenna
Channel Type	Wireless Channel
Interface Queue	Priority Queue
Buffer size of IFq	50
MAC	GSHMAC, GMAC, TE2S
Routing Protocol	Ad-hoc Routing
Initial Energy (Joule)	100
Idle Power (mW) [3,5]	14.4
Receiving Power (mW) [3,5]	14.4
Transmission Power (mW) [3,5]	36.0
Number of Nodes	100
Number of sources	99
Number of BS	1
Placement of nodes and BS	Nodes are placed uniform randomly in a given area, and the BS is placed at the center of the area.
Clustering Algorithm	EMCA
Number of simulation runs	50

B. *Results and Discussions*

Figures 4, 5, and 6 show the average energy consumption, delay, and throughput of GSHMAC, TE2S, and GMAC under different attack situations respectively. Here, the experimentation considers the interference on the same slot. The graph shows that the performance of GSHMAC is better than the other two mechanisms in attack situations because GSHMAC countermeasure the attacks by using the internal MAC mechanism. GSHMAC shows 31.80% and 38.87% of improvement in average energy consumption as compared with state-of-the-art mechanism TE2S and GMAC respectively. It also improves delay by 18.41% and 22.61%, and throughput by 30.28% and 43.39% as compared with TE2S and GMAC respectively. Here, the GSHMAC shows better improvement in energy consumption and throughput but not significant improvements in delay. The reason for such tradeoff is time required for mode shifting and TDMA scheduling in hybrid MAC mechanisms. GSHMAC detects the attacks using collision threshold- and data counter value and mitigates the attack by isolating the malicious node. TE2S is receiver-initiated secure MAC mechanism. It also countermeasures the different kinds of denial of sleep attack, but its performance is less than GSHMAC as it uses cryptographic mechanism.. The cryptographic approaches use by the TE2S increases the communication and key maintenance overheads, which reduces the overall performance of MAC mechanism. TE2S shows better

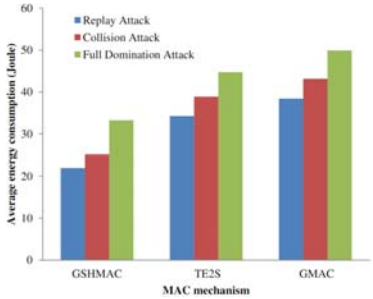

Figure 4. Average energy consumption of MAC mechanisms under attacks

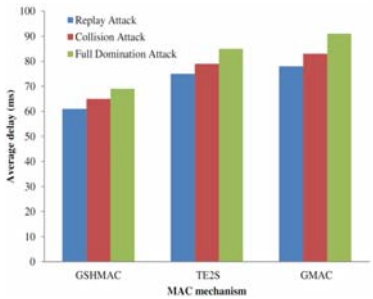

Figure 5. Average delay of MAC mechanisms under attacks

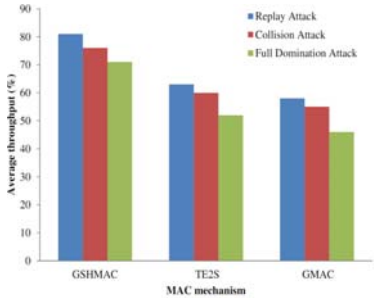

Figure 6. Average throughput of MAC mechanisms under attacks

performance than GMAC as TE2S is LPL (Low Power Listening MAC), where it overcomes GMAC. GMAC is a cluster-based approach, which shows good performance in the presence of attacks because of its frame architecture and cluster-based approach used.

The cluster-based approach helps to bring down the penetration of an attack by maintaining a hierarchy of nodes for communication. The MAC mode control mechanism used in GSHMAC also helps to countermeasure a collision attack at extent because as collisions are increasing in the network it shifts to TDMA mode. Another reason that GSHMAC is better than the other two mechanisms is that GSHMAC is more accurate to detect a collision- and domination attack. GSHMAC detects a collision- and domination attack if a collision is present in TDMA mode too. The primary reason for its enhancing throughput is counter-measuring of an attack at the required time, which leads to better throughput. The communication delay of the system is also better than attack situations, as it countermeasure the attack by internal MAC mechanisms and stops the attack.

CONCLUSIONS AND FUTURE WORK

The great extent of WSN research had concentrated towards the security issues of WSN as vast numbers of malicious attacks are making devastating effect on to the performance of WSN. The performance of WSN is majorly depended on to the amount of available resources and mechanisms for allocating or using the resources. MAC layer plays a significant role in it, and WSN MAC layer attacks (denial of sleep) are the most devastating one as they attack on resource allocation mechanisms of WSN. Hence, the paper makes a contribution in the area of the secure MAC mechanism for WSN. First, the paper studies the different kinds of secure MAC mechanism and WSN MAC attack countermeasures. The study shows that state-of-art available mechanisms are providing efficient security, but the amount of overheads introduced by them are larger. Second, the paper proposes the secure hybrid MAC mechanism GSHMAC to improve the performance of WSN in existence of WSN MAC attacks. GSHMAC provides the lightweight solution by using internal MAC mechanisms. The comparative evaluation of mechanism with the state-of-art work shows reduced energy consumption, and delay, with improved throughput in different attack situations. The future work includes exploring the solutions for other WSN layer attacks using the internal working mechanism of a particular layer-protocol. The work can also be extended to propose the secure framework for WSN, which helps to spread the horizon of WSN applications.

REFERENCES

[1] Giuseppe Anastasi, Marco Conti, Mario Di Francesco, Andrea Passarella, “Energy Conservation in Wireless Sensor Networks: A Survey”, Elsevier Ad hoc Networks. Vol. 7, Issue 3, 2009, pp. 537–568.

[2] Xiangqian Chen, Kia Makki, Kang Yen, Niki Pissinou, “Sensor Network Security: A Survey”, IEEE Communications Surveys & Tutorials’, Vol. 11, No. 2, Second Quarter, 2009, pp. 52-73.

[3] Pranav M. Pawar, Rasmus H. Nielsen, Neeli R. Prasad, Shingo Ohmori, Ramjee Prasad, “Activity Modelling and Comparative Evaluation of WSN-MAC Security Attacks”, Journal of Cyber Security and Mobility, River Publisher’s, Vol. 1, Issue 3, 2012, pp. 205-225.

[4] Ammeer Ahmed Abbasi, Mohamed Younis, “A Survey on Clustering Algorithms for Wireless Sensor Network”, Elsevier Computer Communication. Vol. 30, Issue 14-15, 2007, pp. 2826-2841.

[5] Pranav M. Pawar, Rasmus H. Nielsen, Neeli R. Prasad, Shingo Ohmori, Ramjee Prasad, “Hybrid Mechanisms: Towards an Efficient Wireless Sensor Network Medium Access Control”, WPMC, Brest, France, 2011, pp. 1-5.

[6] M. E. a. R. L. Hal Stern, “Chapter 17: Network Performance Analysis. Managing NFS and NIS”, O'Reilly, 2001, pp. 168-216.

[7] Qingchun Ren, Qilian Liang, “Secure Media Access Control (MAC) in Wireless Sensor Networks: Intrusion Detections and Countermeasures”, PIMRC, Barcelona, Spain, 2004, pp. 3025 - 3029.

[8] Brownfield M., Yatharth Gupta, Davis N., “Wireless Sensor Network Denial of Sleep Attack”, IEEE IAS, West Point, NY, USA, 2005, pp. 356-364.

[9] Raymond David R., Midkiff S.F., “Clustered Adaptive Rate Limiting: Defeating Denial-of-Sleep Attacks in Wireless Sensor Networks”, MILCOM, Orlando, FL, USA, 2007, pp. 1-7.

[10] Raymond David R., Marchany R.C., Brownfield M.I., Midkiff S.F., “Effects of Denial-of-Sleep Attacks on Wireless Sensor Network MAC Protocols”, IEEE Transactions onVehicular Technology, Vol.58, Issue 1, 2009, pp. 367-380.

[11] Raghavendra V. Kulkarni, Ganesh K. Venayagamoorthy, Abhishek V. Thakur, Sanjay K. Madria, “Generalized Neuron Based Secure Media Access Control Protocol for Wireless Sensor Networks”, MCDM, Nashville, TN, USA, 2009, pp. 16-22.

[12] Chen Chen,Li Hui,Qingqi Pei,Lv Ning,Peng Qingquan, “An Effective Scheme for Defending Denial-of-Sleep Attack in Wireless Sensor Networks”, In the Proceedings of IEEE 5th International Conference on Information Assurance and Security , Xi'an, China, 2009, pp. 446-449.

[13] P.Sankara Rao, K.V.S.R.P.Varma, Ravikanth Satapati, E.Vamsidhar, “Multilayer Perceptron based Secure Media Access Control Protocol for Wireless Sensor Networks”, ICCIC, Coimbatore, India, 2010, pp. 1-5.

[14] Ching-Tsung Hsueh, Chih-Yu Wen, Yen-Chieh Ouyang, “Two-Tier Receiver-Initiated Secure Scheme for Hierarchical Wireless Sensor Networks”, ITST’ 12, Taipei, Taiwan, 2012, pp. 254-258.

[15] Tapalina Bhattasali, Rituparna Chaki, Sugata Sanyal, “Sleep Deprivation Attack Detection in Wireless Sensor Network”, International Journal of Computer Applications Vol. 40, Issue 15, 2012, pp. 19-25.

[16] Qian, Jinfang Zhou, Liping Qian, Kangsheng Chen, “Highly Scalable Multihop Clustering Algorithm for Wireless Sensor Networks”, ICCCAS’ 06, Guilin, Guangzi, China, 2006, pp. 1527-1531.

[17] Pranav M. Pawar, Rasmus H. Nielsen, Neeli R. Prasad, Shingo Ohmori, Ramjee Prasad, “GCF: Green Conflict Free Scheduling Algorithm for WSN”, ICC-E2Nets’ 12, Ottawa, Canada, pp. 5795-5799.

[18] Pranav M. Pawar, Rasmus H. Nielsen, Neeli R. Prasad, Ramjee Prasad. (2014) ‘A Hybrid Algorithm for Efficient Wireless Sensor Network Time Synchronization’, Wireless VITAE’ 14, Aalborg, Denmark, pp. 1-5.

THE 5TH INTERNATIONAL CONFERENCE ON WIRELESS COMMUNICATIONS, VEHICULAR TECHNOLOGY, INFORMATION THEORY, AEROSPACE & ELECTRONIC SYSTEMS (WVITAE-2015)
December 13-16, 2015, Hyderabad, India

The Studies of Millimeter Waves at the frequencies of 60 GHz in Outdoor Environments- A Survey

Hitesh Singh
Assistant Professor)
HMRITM, Delhi
Delhi, India
Email: Hitesh.singh.85@gmail.com

Ramjee Prasad
Founder Director, (CTIF)
Aalborg University
Aalborg, Denmark
Email: prasad@es.aau.dk

Ashok Chandra
Former Wireless Adviser
to the Govt. of India
New Delhi, India
Email: drshokchandra@gmail.com

***Abstract*—With the tremendous growth of commercial mobile communication networks world over, the radio frequency becomes more valuable natural resources. The Radio spectrum is an essential tool for economic and social growth of a country. The shortage of bandwidth forces researchers for the exploration of the underutilized millimeter wave spectrum for designing the communication broadband networks. Very little research has been done in the areas of cellular mm-wave propagation in densely populated indoor and outdoor environments. For the design of future 5G network it is very necessary to obtain vital information regarding mm-wave propagation characteristics and its behavior in various environmental conditions. This paper describes the various studies carried out earlier in the field of radio wave propagation at 60 GHz in outdoor environment.**

***Index terms*: Millimeter waves, Wireless Propagation, 5 G, 60 GHz**

I. Introduction

Advancement in wireless technology has driven the demand for more radio spectrum bandwidth from every sector of the wireless applications. It is further accelerating day by day, and we are heading towards greater mobility with ever-increasing demand of higher data rates. The growth of internet has further fueled the demand for wireless services, due to which the available radio spectrum is becoming a scare and congested. Various studies have shown that the increasing demand for spectrum is due to the regulatory schemes introduced by authorities to protect rapid increase of spectrum users [2]. Various researchers are working hard on devising a methodology for resolving forthcoming spectrum crisis. Recently various regulators have shown interest in sponsoring free radio channels to allow access for unlicensed devices. For example Industrial, Scientific and Medical (ISM) radio band in 2.4 GHz frequency are allocated freely for public usage. This was very successful in short range low powered radio communications in wireless local area network.

Most of the terrestrial commercial applications are below 3GHz and have already been assigned to different radio communications services which are working with non-spectrum efficient, technologies. Lower spectrum bands provide better coverage, simpler hardware and good mobility. If we go to higher spectrum bands , situation would be just reversed, i.e. it provide less coverage, complexity in hardware and less mobility. Currently, no vacant spectrum especially below 3 GHz is available for newer wireless technologies. Radio spectrum, being natural resource, cannot be created. Therefore, its efficient use is inevitable.

The 5th generation wireless systems denote the next major phase of mobile telecommunications standards beyond the current 3G/4G/IMT-Advanced standards.

II. Concept of WISDOM

Today presence of various devices incorporates productivity and quality of life of human beings, in all technological domains. In most cases these devise work in isolation or with very little cooperation among each other, and serve a well-defined single purpose for which they have been designed.[5] The recent innovation of device manufacturing and communication technologies have enabled personalized and mobile connectivity of various devices, making them smart and their penetration is expected to grow exponentially in the next years such a huge growth is already creating an unprecedented opportunity for novel applications and services that grow far beyond the mere purpose of each user, but are based on interconnectivity and interworking. Users are benefiting from services in the public or private sphere, while more and more personalized digital content is being generated. This novel concept of connectivity and mobility is called WISDOM [1]. The Wireless Innovative System for Dynamically Operating Mega Communications, which is proposed to provide ubiquitous terabit wireless connectivity enabling human- centric mega-communication applications over a dynamic, interoperable and secure network.

WISDOM is developed to enable the growth of an interconnected society, bridge the physical and virtual worlds by offering a seamless personalized rich digital experience for the end users, while creating the optimal conditions for capitalizing on future internet innovations [4].

The three founding pillars of WISDOM are:

- An information theoretic performance/ capacity estimation of different types of networking paradigms.
- Design of protocols based on end-to-end, cross-network-domainperformance optimization
- Cognitive radio network based self organizing networks for management of possible usage scenarios and to minimize the spectrum and energy requirements [1,6]

WISDOM aims to design and develop technologies, system that could globally integrate, interconnect and communicate into a flexible and dynamic system for the human centric and machine centric communications in 2020 and beyond [1,11].

III. Importance of 60 GHz

With the increase in the demand of higher frequencies various researchers have shown their interest in millimeter wave mainly in 60GHz. The 60 GHz frequency band has many advantages over lower frequency bands. One of the reasons for increasing craze in the availability of huge bandwidth. The 60 GHz provides continuous and less restricted bandwidth in terms of power limit. With the huge potentials of capacity and flexibility 60 GHz bandwidth became a good candidate for high transmission rate future communication systems [13].

The regulations allows high transmission power for 60 GHz as compared to other less frequency bands in order to overcome high power losses due to oxygen and rain. As due to limited range of network in 60 GHz, it is confined to very limited areas which in turn provide higher frequency reuse which allows high throughput network. The form factor of 60 GHz systems is 140 times smaller than the systems which use lower frequencies.

With various advantages provided by 60 GHz bands it also has some of the limitations which need to be resolved. The IEEE 802.15.3c has provided various applications in the millimeter wave technology with various data rates and ranges. It is very challenging task for 60 GHz systems to provide sufficient power margins for reliable and efficient communication link. Another challenge for 60 GHz is the delay spread of the channel. Larger delay spread increases the complexity of the system which makes its practical implementation difficult.

IV. Studies done so far in outdoor Environment

Various researches have carried out studies in the areas of millimeter wave propagation in outdoor environment, but are limited especially for 60GHz. As in outdoor environments these waves faces various challenges like rate of rain drop size, dust and snow particles causing attenuation, de-polarization and noise. There are various types of outdoor environments and have different effects on propagation of radio waves. Different types of environments are:

URBAN ENVIRONMENTS

1) Less Dense
2) Highly Dense

The less dense areas consist of city streets with less population, road tunnels, empty parking area, grass fields etc. where as in highly dense urban areas consist of pedestrian walkway in densely populated city, Multistoried buildings etc. in the rainy conditions various factors affects the propagation like drop size, rain intensity etc. vegetation also plays an important role as size and types of trees, shape of leaves, trunk size etc. affect the radio wave propagation.

A. URBAN OUTDOOR ENVIRONMENTS

The urban environments consist of a city which, contain buildings, streets, lampposts, vehicles and people. There are also variations in urban environments which includes less dense and highly dense urban environments. Researchers had done various studies in these types of environments. Less dense urban environments consist of cities which are moderately populated. Their streets are not over crowded. Few high rise buildings are there with considerable distance between them. Roads are broader and lots of open spaces are available. Highly dense urban area consists of overcrowded cities. Their streets are full of traffic and lots of people are moving in pedestrian walkways. Considerable amount of high rise buildings are presents.

B. LESS DENSE URBAN ENVIRONMENTS

Various researchers have done propagation studies in this type of environments. Mostly include university campus, grasslands, empty parking area etc.

The outdoor 60GHz frequency measurements done by Duscan M. Matic, Ramjee Prasad et al [7] in the outdoor environments of Delft University, Netherlands. They had chosen grass fields outside the building and empty parking area. Here there were no obstacles. They present the results of frequency fading over 100 MHz bandwidth centered around 59.9 GHz. from the experimental results they obtained the k factor of the Rice distribution and path loss coefficients. By fixing the position of TX and moving the RX different spatially distributed locations throughout the test area was used. The experiment setup used in [13] consists of synthesizes signal generator named Marconi 2024, 60 GHz TX and RX and spectrum analyzer named Anritsu MS2651A. From spectrum analyzer to PC, data was transferred by general purpose information bus. The frequency response consists of 500 amplitudes samples at a frequency sampling of 0.2MHz. [13]. The TX consists of 120 degrees flat omnidirectional antenna and RX consists of 120 degree omnidirectional and 15 degree patch directional antenna was used.

The measurements are carried out outside building in open grassland. The receiver antenna was moved away in a straight line from 27 m distance apart from the receiver. The receiver was moved away from the TX and measurements were taken at the intervals of every one minutes. So we get 27 different measurements. The height of antenna was 1.59 meters.

Another measurement was done in an open empty parking area which includes some trees. The antenna height was 1.59 m the experiment was conducted with both type of antennas on distance of 3 to 25 meter with 25 points of observations in a straight line and 12 on the side of the parking.

From all the experimental results the average value of k and standard deviation s of rice factor k are calculated. For experiment done on grass field the value of k was 84.25 and s was 87.94. for parking area value of k was 80.71 for omnidirectional antenna and 423.85 for directional antenna. The value of s was 79.87 for omnidirectional antenna and 165.35 for directional antenna.

It was observed from the experiment that the average decay with distance is small. This is because of many reflections and they sum up together. Although this leads to small k factor and to the fact that the modeling is not so good.

Smulders. et.al. [12] has performed both narrowband and wideband measurements at outdoor environments for 60 GHz. The experimental results which they obtained are compared with deterministic model which they developed. They had conducted different experiments in different outdoor environments like airport fields, urban streets and city tunnels.

They had used a channel sounder which was based on correlation. The RF frequency was centered around 59.0 GHz with bandwidth of 200 MHz, corresponding to a resolution of 5 ns. For transmitter 90 degree horn antenna was used and 20 degree biconical horn used as a receiver. The height of TXwas kept at 4m and RX was 2.2m. The different parameters which was considered during measurements was mean delay (MD), RMS delay spread (RDS), delay interval (DI), delay window (DW) and sliding delay window (SDW).

The observation made in city streets do not represent multipath situation. Values of RDS and 90% SDW was lower than 20ns and 50ns respectively. In the case of city square the 90% SDW may be 150 ns or more. A read tunnel had many similarities to the city streets environments. A bad multipath situation was observed by parking garage because of the large dimensions and the relatively smooth surfaces creating strong reflections.

For the simulation purpose, a ray tracing tool was developed. It includes the features like direct and reflected rays which are up to the third order and diffuse reflections and diffractions are neglected. Rays are interpreted by non-reflected objects such as foliage. A dielectric canyon having a rough surface type of scenario was described. For both transmitter and receiver antennas polarization and radiation patterns are taken into account. This simulation tool was developed in order to understand the behavior of outdoor environments more specifically in urban streets, and allow the estimation of both narrowband and wideband channel characteristics. The results obtained were good except 90% SDW. This is because sensitivity of this parameter toward reflected rays with low amplitude, therefore yielding large differences between simulation and real results.

C. HIGHLY DENSE URBAN ENVIRONMENTS

Eshar Ben Dor. Et .al in [14] described 60 GHz wideband propagation measurements in cellular peer to peer outdoor environments. They presented a channel sounder which was operated at 38 and 60 GHz with a pass band bandwidth of 1.9 GHz. The channel sounder provides RMS delay spread measurements resolutions and angle-of-arrival (AoA). [14].

They have developed 750 mega chips per second spread spectrum sliding correlator channel sounder for 38 and 60 GHz. This has a 1.5 GHz null to null bandwidth and uses a 1.9 GHz RF pass band centered at 59.4 GHz carrier frequency in order to provide 1.3 ns multipath time resolution.

The experiment was performed in outdoor courtyard with pedestrian in University of Texas campus. The campus is consisting of various buildings and some trees. Another experiment was conducted for the investigation effect of vehicular communications. It was conducted in a parking area which includes various vehicles, several lampposts and surrounded by tall multistoried buildings with few vegetation. The TX and RX were placed 1.5 m above ground.

The experiment done in the courtyard showed that the path loss exponents are slightly greater than free space for LOS paths. For NLOS paths when exited for particular antenna orientation they produce a link which was 15 40 dB weaker than LOS. It was also observed that for all outdoor locations some of NLOS antenna pointing scenarios could make a link. For NLOS scenarios, the RMS delay spread was observed as 36.6 ns. In courtyard the mean RMS delay for both LOS and NLOS scenarios was 6.02 ns. For the experiments done in parking area, where transmitter was fixed on a ground and receiver was fixed inside a car and moving in a confined parking area. The mean RMS delay was observed as 2.73 ns and maximum of 12.3 ns for 17 measured LOS and NLOS scenarios in parking area. It was observed that in a free space path loss LOS pointing scenarios offered less than 1 ns RMS delay spread. On the other hand NLOS antenna pointing scenarios produce much higher multipath delay spread and path loss.

Rappaport.et.al. [15] has carried out propagation measurements at 38 GHz and 60GHz frequencies at various outdoor environments. Their measurements show time delay spread and path loss as a function of separation distance and antenna pointing angles.

They use channel sounder which has variable rate PN sequence generator. For 38 GHZ they had 400 Mcps and for 60 GHz they had 750 Mcps. The millimeter wave up down convertor get the input of IF frequency of 5.4 GHz. These convertors contain mixer and LO frequency multipliers which give output of 37.625 GHz and 59.4 GHz. The 38 GHz Tx and Rx used vertically polarized horn antennas with gain of 25 dB and half power beam width of 7 degree. The 60 GHz Tx and Rx used vertically polarized antenna whose gain is 25dB and contain beamwidth of 7.3 degrees.

In this work two different types of experiments are done. In the first type TX and RX was placed at the same level. There was single TX and 10 RX was placed at different locations. The area was surrounded by various buildings which are of 1 to 10 stories long. The receiver moved away from the transmitter to about 19 to 129 meters. There are various obstacles presented in the scenarios like automobiles, brick and aluminum sided buildings, foliage, lamppost, handrails and signs.

The second type of experiment was done in scenario where TX was placed on a roof top and receiver are placed at ground level. Rests of the situations were similar as described in first experiment.

The experimental results obtained for LOS link was free path loss with no RMS delay spread. In NLOS there was

higher RMS delay spread of 122 ns for first experiment and 107 ns for second experiment. It was also observed that as if the azimuth pointing angels increased from the bore sight the RMS delay spread is also increases in NLOS.

In [16] Jonathan S. Lu. et. al. has performed experimentation on diffraction and scattering on 60 GHz radio wave. Diffraction was measured at building corners whereas scattering was observed at car, lamppost and buildings. Human obstruction was also measured.

The TX used in this was consisting of SMF100A microwave signal generator of 10 GHz frequency which was attached to frequency multiplier SMZ90 which multiplies by 6. Then it was connected to V-Band horn antenna of 24dBi gain and 11 degree beam width. The Rx system consists of same antenna system used in TX. It was then connected to low noise amplifier NIZ 3387. The signal was then sentto harmonic mixer FS Z90. Then signal was down converted and sent to vector signal analyzer FSQ26.

For the conduction of outdoor measurements on cars, lamppost and buildings the TX and RX are placed on a moving cart and then moved according to some fixed angles. The height of antennas was kept at 1.33m.

The diffraction measurements were done for building corners. For this purpose two different sites were chosen one was the corner made up of concrete while another was made up of concrete and windows. In the first experiment TX cart was placed at a distance of 3.75 meter from the corner and the angle inclination was 18 degree. The Rx was placed at a distance of 2.8 meters in the shadow region and moved in an arc. The movement was done on angles between 200 and 260 degrees and recording was made at every 10 degree intervals. In the second experiment the TX was placed at a distance of 6.1 meters from the corner with inclination of 10 degree. The RX was placed at a distance of 4 meter in a shadow region and again moves in an arc with an angle of 200 to 260 degrees with an interval of 15 degrees.

The scattering measurements were done for a car in an empty parking area. The transmitter was placed at a distance of 23 meters from car. The transmitter bore sight was centered on the side of car and normal to the surface of car. The receiver was moved in an arc of 23 meters and scattering angles relative to the normal of car surface in ranges from 14 to 75 degrees.

For the study of human blocking two scenarios was taken. In the first scenario it was assumed that the TX and RX were at same height which was 1 meter and moving from one place to another. The observation was made within the LOS distance of TX and RX of 7 meters. In another scenario the TX was at roof top with height of 2.65 meters and RX at ground at the height of 0.9 meters. They are moving within the radius of 7 meters.

It was observed that scattering measurements done from cars and lampposts was higher near the specular direction. The diffraction results suggest that the scattering from lamppost and cars are higher than diffraction from corners of buildings.

It was observed from scattering measurements of buildings that received power was higher when TX and RX were placed in horizontal plane and in specular direction. In case of non-specular direction best results was found in case of ridges and columns.

The results of human blockings suggests that the absorbing screen models used in the work was quite accurate with the actual results obtained with standard deviation of prediction error not more than 5 dB.

V. CONCLUSION

This work had explored various studies done in radio wave propagation at 60 GHz. It had concluded that the higher frequencies specially 60 GHz are the very sensitive in nature for propagation in various outdoor environments. It was observed that results are different for different environmental conditions. In order to develop new technologies a thorough propagation studies are required in Indian environments.

REFERENCES

[1] Ramjee Prasad, 5G: 2020 and Beyond, published by River Publishers, 2014.
[2] Purnendu S. M. Tripathi and Ramjee Prasad, Spectrum Trading in India and 5G, Journal of ICT Standardization, Vol. 1, 159-174, August 2013.
[3] R. Prasad, WISDOM: Wireless Innovative System for Dynamically Operating Mega communications ITU-T Technology Watch Report, to be published in 2012.
[4] Ramjee Prasad, Global ICT Standardization Forum for India (GISFI) and 5G Standardization, Journal of ICT standardization, 1(2), 123-136, 2013.
[5] Ramjee Prasad, Future Networks and Technologies supporting innovative communications, published in proceedings of IC-NIDC2012, 2012.
[6] Ramjee Prasad, Keynote Speech Wireless Innovative System Dynamic Megacommunications (WISDOM), in IEEE CongART08, First IEEE International Workshop on Cognitive Radio and Advanced Spectrum, February, 2008.
[7] Dusan M. Matic, Hiroshi Harada and Ramjee Prasad, Indoor and outdoor frequency measurements for mm waves in the range of 60 GHz, Vehicular Technology Conference 1998, VTC 98, 4819 IEEE. Vol.1, pp 567 571,IEEE, 1998
[8] F. Davarian, D. Rogers and R. Crane, Special Issue on: Ka-Band Propagation Effects on Earth-Satellite Links, Proceeding of the IEEE, Vol. 85, No. 6, pp. 805-1024, June, 1997
[9] ITU Recommendation ITU-R P.676, International Telecommunication Union Radio Sector, Geneva, 1997.
[10] R.K. Crane, "Propagation phenomena affecting satellite communication systems operating in the centimeter and millimeter wavelength bands," Proceedings of the IEEE, vol.59, no.2, pp. 173-188, Feb. 1971.
[11] http://wpc.dot.gov.in/Docfiles/National%20Frequency%20Allocation%20Plan-2011.pdf.
[12] P.F.M. Smulder and L.M. Correia, Characterisation of propagation in 60 GHz radio channels, Electronics and Communication Engineering Journal, April 1997.
[13] Su-Khiong Yong, Pengfei Xia and Alberto Veldes Gracia, 60 GHz Technologies for Gbps WLAN and WPAN: From Theory to Practice, John Wiley and Sons, Ltd, 2011.
[14] Eshar Ben-Dor, Theodore S. Rappaport, Yijun Qiao, Samuel J. Lauffenburger, Millimeter wave 60 GHz outdoor and vehicle AOA propagation measurements using a broadband channel sounder, proceedings of IEEE Globecom 2011.
[15] Theodore S. Rappaport, Eshar Ben_Dor, James N, Murdock, Yijun Qiao, 38 GHz and 60Ghz Angle dependent propagation for cellular and peer to peer wireless communications, published in proceedings of 2012 IEEE International Conference on Communications, Ottawa, Canada, June 2012.
[16] Jonathan S. Lu, Patrick Cabrol, Daniel Steinbach and Ravikumar V. Pragada, Measurements and characterization of various outdoor 60 GHz Diffraction and Scattering paths, published in the proceedings of IEEE Miitary Communication Conference 2013.

THE 5TH INTERNATIONAL CONFERENCE ON WIRELESS COMMUNICATIONS, VEHICULAR TECHNOLOGY, INFORMATION THEORY, AEROSPACE & ELECTRONIC SYSTEMS (WVITAE-2015)
December 13-16, 2015, Hyderabad, India

Real-time Detection of EEG Electrode Displacement for Brain-Computer Interface Applications

Giulia Cisotto and Silvano Pupolin
Department of Information Engineering
University of Padua
{giulia.cisotto & silvano.pupolin}@dei.unipd.it

***Abstract* – Electroencephalography (EEG) has a relatively old history since Hans Berger in 1929 recorded the human brain activity for the very first time. Since then, a number of experiments had led to a strengthened employment of this technology both in the clinical practice and in the most advanced research platforms. Although amazing developments have already been achieved, no gold standards are available for the processing of EEG signals. However, EEG signal processing used in several applications of Brain-Computer Interface (BCI) has already promised unbelievable progresses. In the context of a specific BCI application, this paper deals with a particular kind of artifact due to electrode-pops that can degrade the EEG recordings and, consequently, make BCI give wrong outputs to patients operating it for their benefit in recovery or in daily life.**

Keywords – EEG, BCI, electrode-pop artifact, online algorithm.

I. Introduction

Electroencephalography (EEG) [1] has a relatively old history and nowadays all Hospitals, clinical Institutes and even Universities have an EEG system to perform daily clinical assessments of several kinds of patients or to study the cerebral activity of healthy and impaired people in a relaxation status or during a task execution. Although its widespread availability, no gold standards for the analysis of the EEG traces are recognized all over the world. Instead most clinicians analyze by-eye only the cerebral activity of their patients being satisfied to observe macroscopic changes like epileptic seizures or alternating phases of more or less reactive awareness represented by larger or smaller oscillations in the frequency band around 10 Hz, the so-called α band. However research has already shown, in many years of study, that an amount of information is hidden in this complex combination of waves that EEG is.

One of the most amazing fields of EEG employment is the Brain-Computer Interface (BCI): after a training period, a subject can learn to operate a computer to communicate in an alternative way with the external world or to move again by controlling a wheelchair or a robotic arm [2].

This paper deals with a specific kind of EEG artifact that can arise from the displacement of an electrode during recordings. This event can cause the subject to fail in operating a BCI – at least for a limited period of time - because of the artefactual analysis of the correspondent EEG signal affected by the huge abnormal peak and oscillations following the displacement.

II. Electrode-pop artifact in EEG recordings

EEG recordings at the scalp of a subject are a combination of useful signal and disturbance. To be precise, the former is constituted by the neural response of the subject to an experimental task or, simply, it carries the information about the status of the individual, and the latter is the sum of all the other components of the EEG traces. As mentioned before, there can be several causes of disturbance but, generally, they are classified as follows:

a) external interferences. The main element of this set is the power line noise that usually corrupts the EEG recordings. For this reason, a notch filter around 50 Hz or 60 Hz is implemented to remove this considerable interference during EEG evaluations or experimental sessions.

b) *physiological interferences*. They can be further divided into two subclasses: muscular and neural noises. Eye-blinks, eye-gaze changes, chewing, gnashing, swallowing and head slight movements are muscles activations that can compromise the whole recordings. Skin sweat can be also a relevant phenomenon to cope with sometimes. Finally, distractions, habituation and other collateral cognitive phenomena can elicitate neural populations of different cortical regions to spike and, at the scalp level, to show interfering waveforms. The latter are considered disturbance and are usually removed on the basis of their spatial and/or frequency occurrence.

Then artifacts can occur either accidentally or along the whole recording. For instance, artefactual activity due to mains is usually present along the entire registration while muscular contraction is in the most cases a very short phenomenon that can seriously corrupt a relatively short-lasting recording segment. One of the most impacting causes of artifact is the so-called *electrode-pop*: although quite rare, this kind of noise can be completely superimposed over the low amplitude useful signal and make the identification procedure of the EEG characteristics almost impossible for a long time (tens of seconds). A typical example of its shape is captured by Fig.1 where the usual abrupt negative fall, overshoot and slow-oscillating return to baseline values are clearly visible.

It can be easily expected that such an artefactual activity compromises any kind of automatic features identification.

Cautions in order to avoid this kind of artifacts can be taken during the recording preparation: clinical technicians are trained to pay attention on this type of occurrence. Nevertheless electrode-pops can sometimes happen anyway. A hardware solution to cancel out this artifact has been proposed in [3] although without any quantification of its performance.

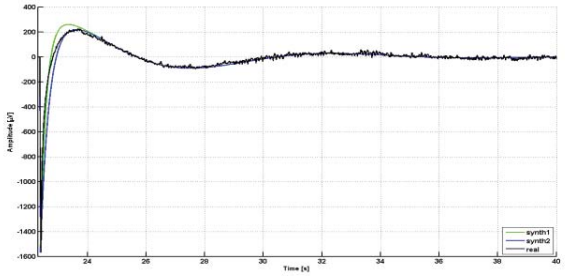

Fig. 1 Signal with electrode-pop artifact. A detail.

Several software solutions to remove artifacts have appeared in the past years [4-9]. The main objective of these solutions was to obtain a clear EEG signal for clinician eye-analysis. Our objective is somewhat different because we want to extract from EEG some real-time features to be used as feedback in BCI applications.

Hereafter a new real-time signal processing algorithm is presented with the aim to identify and remove this electrode-pop artifact before to estimate the EEG features required to assess the patient's status or to operate an EEG-based external device in a BCI fashion scheme.

III. Real-time algorithm for electrode-pop artifact

We consider the BCI treatment for motor recovery of the upper limb in stroke survivors described in [10], where the signal processing unit runs the world-spread software BCI2000 [11] which does not care about the electrode-pop artifact. Unfortunately, some recorded sessions of the whole BCI treatment were affected by this electrode displacement. We remark that feedback to the patient should be given in real-time based on *Movement-Related Desynchronization* (*MRD*) [12] of EEG signal. The presence of artifact prevents us to properly detect the MRD for several seconds. A new algorithm was designed and implemented with the goal to be performed in real-time during the BCI experiment and to reduce the time where MRD cannot be detected as short as we can. This algorithm has to be little time-consuming to allow the BCI system to process the remaining on-line analysis and provide the robotic feedback to the subject performing the experiment before he/she starts to execute the movement task.

In order to quantify the algorithm performance, the signal-to-disturbance-ratio (SDR) has to be computed. This would be possible only if a version of the same signal with and without the disturbance is available. To this purpose, a synthetic electrode-pop artifact was constructed and then added to a real EEG signal where no disturbance affected the trace. Then, the SDR is computed.

The artifact shown in Fig.1 is typical for each class of EEG amplifiers. Indeed, the first part, spanning few tens of milliseconds, is directly related to the amplifier bandwidth, while the second part, which shows a damped oscillation, is due to the AC coupling of the electrode to the amplifier.

Two different shapes of synthetic artifacts, similar to the real one, have been chosen for the following analysis and are displayed in Fig. 2 with a detail in Fig. 3.

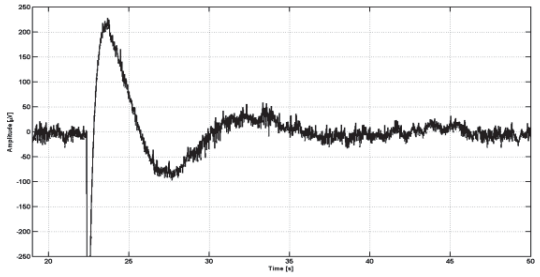

Fig. 2 Raw signal (black) and two different examples of synthetic artifacts.

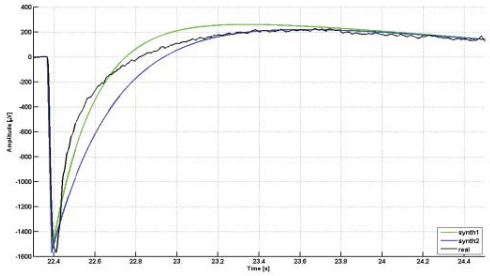

Fig. 3 Detail of Fig.2.

We remark that the artifact has an amplitude two order of magnitude larger than the EEG signal. To cancel the effects of this large disturbance only a nonlinear procedure works. We considered two different algorithms: i) estimate the main pulse and canceling it or ii) detect the time instant when the main pulse starts and set the signal to zero until it returns to zero. The first solution would be more precise but it would require a bunch of computations and an accurate model of the artifact to estimate the main pulse with enough precision. On the contrary the second algorithm has two main steps: 1) compute the first derivative of EEG signal as the difference between each sample and the previous one, and 2) determines where the absolute value of the derivative is higher than a threshold for N consecutive samples. Indeed, the electrode-pop could be represented as the impulse response of the amplifier filter. The rise-time t_r is related to the 3dB bandwidth B_s of the filter by the approximated relationship $t_r \approx 1/(3B_s)$. Hence, the rise-time span over $N=F_c t_r$ consecutive samples, where F_c is the sampling rate of the EEG. As an example, if F_c is set to 512 Hz and B_s is 20 Hz, N is about 8. The beginning of the artefact is given by the first sample where the derivative is higher than the threshold and the end by the sample where the EEG signal returns to zero. Then, the EEG samples between these points are replaced by zeros and discarded from the MRD detection. The zeros substitution between the two zero-crossing points is justified by the concern that filtering can give rise to transient signals due to possible abrupt signal discontinuities at the artefactual interval edges. During the interval of time where artifact is removed no feedback is intended to be provided to the subject but the system is thought to be waiting for new reliable values. An example of application of this method is reported in Fig.4 where the sum of an original artifact-free signal (recorded from the FZ site on the scalp) and a synthetic electrode-pop (black curve) is displayed along with its first

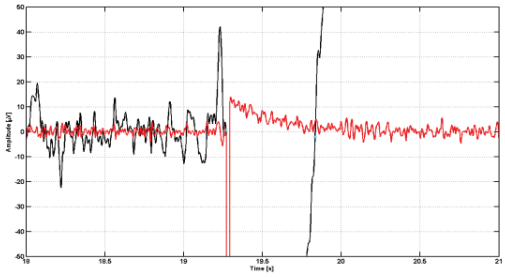

Fig. 4 Artifact-addicted EEG signal (black), its derivative (red) and the artefactual interval edges (cyan dots).

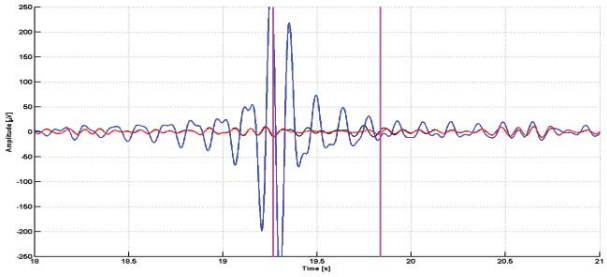

Fig. 5. The original raw signal filtered in the (7,14) Hz band (black curve), the filter output after the application of the proposed algorithm (red curve), the filter output without any artifact detection algorithm (blue curve) and the artefactual interval (magenta vertical lines).

derivative (red curve), and the two time instants labeled as the edges of the artefactual period are highlighted with cyan dots.

After these two first steps, the standard BCI2000 or another procedure involving a high-pass filtering above 1 Hz can be run as usual. The latter leads to the cancellation of the large remaining slow oscillation following the huge negative abrupt fall just removed, bringing back the signal to fluctuate around reliable values again. The zeros-fulfilled artefactual interval is filtered too and small oscillations arise at the filter output: however this does not represent an issue since this period of time is completely discarded from the following analysis. The difference between the (7,14) Hz band filter output with a previous step of artifact detection and removal and the same output without that preliminary operation is plotted in Fig.5. The (7,14) Hz band filtered version of the original raw signal without the synthetic artifact is also reported in both figures as a comparison. Moreover, two magenta vertical lines define the artefactual interval that is discarded from the following analysis.

Fig.5 shows that ideally-filtering a signal with an electrode-pop artifact causes an evident non-causal response that compromises the following analysis. Moreover, a real case filter would also introduce a significant delay that must be limited to make the BCI feedback reliable. On the contrary, filtering the EEG signal with the artifact removed does not cause any significant disturbance. The latter considerations are confirmed by the analysis of the performance presented later on.

Let us denote the original EEG signal filtered in the (7,14) Hz band as x while the filter output without the algorithm application as y_1 and the same quantity with the artifact previously detected and removed as y_2. Then e_1 and e_2 are defined as the following differences:

$$e_1 = y_1 - x \quad \text{and} \quad e_2 = y_2 - x$$

represent the errors between the filter output and the original artifact-free signal.

In order to quantify the algorithm performance, the error energy M_e, the signal energy M_x and the SDR (computed as the ratio between M_x and M_e) at the filter output was computed over 256 samples-wide time windows. Such a window width was chosen to be the same as that used by the BCI2000 software currently operating in the online procedure during the BCI experiment.

Then the new algorithm was employed in an offline analysis to assess its effectiveness. The goal of this analysis was to detect the presence of MRD during the BCI experiment described in [10].

III. Results

Let s be the original raw EEG signal and a the synthetic artifact. The latter was implemented as the formula below:

$$a(t) = A_1 \exp(-t/\tau_1) + A_2 \exp(-t/\tau_2)\cos(2\pi f_0 t + \varphi_0),\ t>0$$

where the constants A_1, A_2, τ_1, τ_2, f_0 and φ_0 are reported in Table I for the two synthetic artifacts shown in Figs.2 and 3 as an example.

In both the cases the synthetic artifact shapes are pretty close to that of the real one, but the "blue" artifact was selected to perform the following computations.

Then the linearly combination of signal s with signal a (s+a) drives the filter in the (7,14) Hz band. If the signal s+a has been previously processed by the algorithm for the electrode-pop artifact detection and removal, the filter output is y_2, otherwise y_1 is obtained. The above mentioned signal x is the filter output when the raw signal s drives the filter. The energy of the two errors e_1 and e_2, and the correspondent SDR_1 and SDR_2 were computed on the limited time intervals of 256 samples and compared to assess the advantage of the application of the new algorithm. Fig.6 shows indeed the energy of the two different errors computed within the above defined windows shifting by 8 samples at time.

The correspondent SDRs behaviors are displayed in Fig.7 where the ratio between the signal energy M_x and the error (either e_1 or e_2) energy M_e is computed over the same 256 samples time interval. Fluctuations of the SDRs curves are due to those of the original EEG signal. From Fig.6 and the next Fig.7 the advantage to apply the algorithm to remove the electrode-pop artifact becomes definitely clear.

In fact, from Fig.7 it can be noted that SDR_2 is constantly 30 dB larger than SDR_1 and is suddenly higher than 0 dB after the artefactual interval where the signal was reset and its values discarded from the following MRD analysis. Indeed, it has to be incidentally mentioned again that the part of the EEG trace between the magenta edges is not taken into account for the following analysis of the MRD and, since the signal in the same interval was canceled, the correspondent SDRs values

are unreliable. After proving the quantitative advantage of the proposed procedure, the algorithm will soon be tested in a real BCI application.

TABLE I. PARAMETERS OF SYNTHETIC ELECTRODE-POP ARTIFACT.

	A_1 [μV]	A_2 [μV]	τ_1 [s]	τ_2 [s]	f_0 [Hz]	φ_0 [rad]
Blue artifact	-1866	350	-0.3	-4	0.10352	0.55287
Green artifact	-1866	350	-0.2	-4	0.10352	0.55287

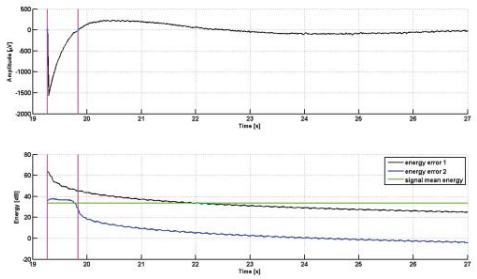

Fig. 6 Energy of the errors at the filter output along with the mean energy level of the original artifact-free signal x (green line) and the artefactual interval (magenta lines).

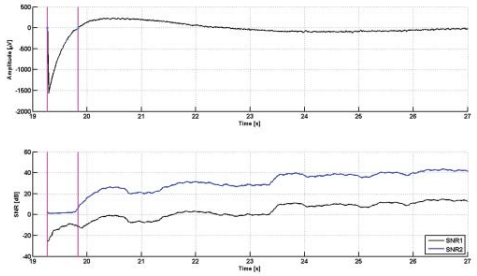

Fig. 7 SDRs at the filter output with the artefactual interval (magenta lines).

It has to be recalled that the BCI platform taken into consideration was described in [10] and its aim was to improve the reaching movement accuracy in mild-impaired post-stroke chronic patients by means of a force feedback that acts as a *mirror* of the cerebral activity related to that action: roughly speaking, while the patient is performing a reaching task on a plane, a force feedback helps him/her in completing the movement only if the expected neural pattern, i.e. spatial and frequency features, is activated. In particular, the MRD is computed in real-time by the BCI2000 software as the normalization of the spectral power around 10 Hz estimated at the current time instant on mean and standard deviation of the analogous quantity gathered during the initial relaxation period. Moreover, these computations are performed on the basis of the recordings coming from specific locations, i.e. the sensorimotor cortex, on the subject's scalp.

If an electrode-pop occurs, all these estimations become affected by abnormal values obtained by filtering the huge impulse present in the signal due to the temporary electrode displacement. Figs.8 to 10 shows the mean energy values obtained during the initial relaxation period, the movement and the correspondent MRD estimation. It has to be recalled from [10] that the more negative the values of the MRD, the more efficient the BCI training. Specifically, Fig.8 is plotted by analyzing the artifact-free dataset where x represents the signal coming from the FZ location.

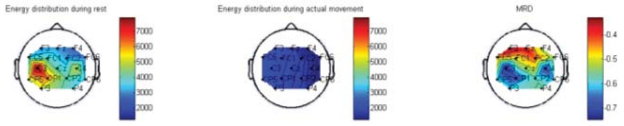

Fig. 8 MRD topography of an artifact-free EEG recording.

Then, Fig.9 shows the disastrous effect of an electrode-pop artifact occurred in the FZ sensor during the initial rest period. The MRD values of this artefactual signal were computed based on y_1.

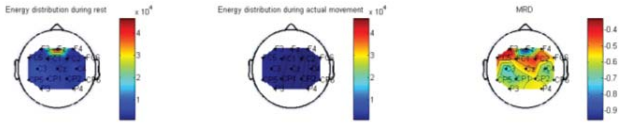

Fig. 9 MRD topography of an artifact-addicted EEG dataset with a synthetic electrode-pop artifact on the FZ site.

As clearly visible from Fig.9, an artefactually huge energy value is focused at the FZ location in the scalp frontal area. While energy distribution during the movement periods of all the following trials is almost within the range of normality, it can be easily expected that the normalization process based on the rest period will lead to unreliable estimation of the patient's cerebral activity, i.e. the MRD values, with a consequent feedback production not related to the physiological activity of the subject and thus useless for him/her motor training.

Finally, Fig.10 reports the analogous energies distributions and MRD estimations gathered after the application of the proposed algorithm that removes the artefactual peak and correctly filters the remaining slow and large overshooting oscillation. Therefore the MRD value of the FZ termination was computed based on y_2. The figure assesses, then, the benefit of such preliminary procedure to remove this kind of artifacts. Indeed, a focus of the activity in C3, Cp1 and C4 is a reasonable expectation since those sites are locations above the sensorimotor cortex: in fact, they belong to the cerebral area where the sensory and motor information is received from the external world, processed and transmitted again to the muscles, the final movement actuators. Moreover, energy values of the rest period are significantly lower than those of the previous case (Fig.9) when the electrode-pop artifact destroyed the EEG physiological waveforms.

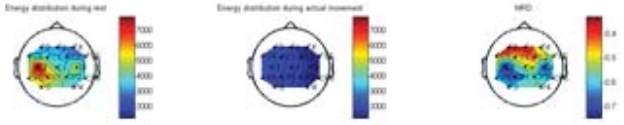

Fig. 10 MRD topography after removing the synthetic electrode-pop artifact from the same EEG dataset of Fig. 8.

DISCUSSION

The previous results assessed the necessity and the effectiveness of the algorithm proposed by the authors to detect and remove the electrode-pop artifact in real-time. From the topographical distribution of the MRD values displayed in Figs.8 to 10 it can be noted that a huge artifact like an electrode-pop occurred in one location of the scalp can compromise the MRD identification and, in particular, increase the number of false positive or false negative detections. Moreover, the effectiveness of the algorithm is also based on its real-time application: in fact, a simple difference operation between consequent amplitude samples (the first derivative step) and the check of its large decrease in few samples (less than 10, i.e. 20 milliseconds) allow the detection of the artifact due to an electrode pop. Furthermore this online identification comes at a very good performance since, as shown in Fig.7, the SDR_2 is constantly much better than the procedure that excludes this detection (SDR_1 curve). As expected, a constant increase of the SDR can be observed as far as the impact of the artifact on the informative signal decreases. As seen from Figs.6 and 7: the first part of the artefactual interval has to be excluded from the following analysis of the MRD because of its artifact abrupt negative slope. An additional interval of time where signal values have to be discarded can be roughly estimated in 1/B, where B is the filter bandwidth (B = 7 Hz in this particular case, then 1/B = 150 ms). In this prolonged period of time - lasting at most one second - the SDRs values are unacceptable (SDR_1) because of the artifact presence or unreliable (SDR_2) because of the signal cancellation in that period. But the most interesting note is that the proposed algorithm suddenly regains a good SDR into respect to the procedure without the artifact detection. As clearly visible from Fig.6, the error energy of the signal preprocessed with the electrode-pop algorithm becomes smaller than the mean energy of the signal immediately after the above defined interval, allowing a much early MRD identification. Concluding, it has to be one more time remarked that the proposed procedure removes only one second of the signal content from the analysis which is a fairly trade-off to have an artifact-free signal, while the current procedure should discard much longer time to wait for the SDR_1 to reach 20 dB (that is the minimum value to have the error energy less than 1% of the useful signal energy, a satisfactory threshold for the MRD evaluations). Finally, it can be observed that if an artifact occurs during the initial long rest period (40 seconds long), both the standard procedure and the new one can correctly estimate the MRD value from the artifact-free remaining part of the rest recording. On the contrary, if it happens during a movement trial (lasting at most one second) it disastrously impacts and the current procedure can not estimate the MRD along several trials, while the new algorithm allows this operation just one second later, that is losing at most one trial (where the BCI feedback would be not provided).

CONCLUSION

In the context of the BCI platform described in [10] an algorithm to detect and remove in real-time rare but huge electrode-pop artifacts was implemented and tested. In particular the shape of this kind of artifacts was mathematically proposed and the performance of the algorithm shown in terms of SDR computed at the band-pass filter output that estimates the signal energy content in the (7,14) Hz band, the typical cerebral rhythms associated with a movement, its planning, observation or even imagination. The energy of the error at the filter output was also computed and this outcome further proves the reliability and efficiency of the algorithm: while the current online BCI procedure provides non-physiology-related and, as a consequence, useless feed-backs to the stroke patient performing the rehabilitative exercise, the presented procedure allows to exploit the EEG data as early as one second after the electrode pop up event. This therefore confirms the convenience of the application of the new algorithm during the online BCI operations since it ensures a more reliable BCI feedback to the patient operating the system.

REFERENCES

[1] E. Niedermeyer, F.H. Lopes da Silva (eds.) *Electroencephalography: basic principles, clinical applications and related fields*, 4th edition, pp. 958–967. Williams and Wilkins, Baltimore, MD, 1999.

[2] N. Birbaumer and L.G. Cohen, "Brain-computer interfaces: communication and restoration of movement paralysis", *J Physiol*, vol.579, pp.621-636, 2007.

[3] J. S. Barlow, "Automatic elimination of electrode-pop artifacts in EEG's", *IEEE Trans Biomed Eng*, vol. BME-33, pp.517-521, 1986.

[4] T.P. Jung, S. Makeig, M. Westerfield, J. Townsend, E. Conchesne, T.S. Sejnowski, "Removal of eye activity artifacts from visual event-related potentials in normal and clinical subjects", *Clin Neurophysiol.*, vol.111, pp. 1745-1758, 2000

[5] P. J. Durka, H. Klekowicz, K. J. Blinowska, W. Szelenberger and S. Z. Niemcewicz, "A simple system for detection of EEG artifacts in polysomnographic recordings", *IEEE Trans Biomed Eng*, vol. 50, pp. 526-528, 2003.

[6] A. Delorme, S. Makeig, "EEGLAB: an open source toolbox for analysis of single-trial EEG dynamics including independent component analysis", *J. Neuroscience Methods*, vol. 134, pp. 9-21, 2004

[7] A. delorme, T.J. Sejnowski, S. Makeig, "Enhanced detection of artifacts in EEG data using higher-order statistics and independent component analysis, *Neuroimage,* vol. 34, pp. 1443-1449, 2007

[8] H. Nolan, R. Whelan, R.B. Reilly, "FASTER: Fully automated thresholding for EEG artifact rejection", *J. Neuroscience Methods*, vol. 192, pp. 152-162, 2010

[9] W.O. Tatum, B.A. Dworetzky, D.L. Schomer, "Artifact and recording concepts in EEG", J. *Clin Neurophysiology*, vol.28, pp. 252-263, 2011

[10] G. Cisotto, S. Silvoni, M. Cavinato, M. Agostini, F. Piccione and S. Pupolin, "Brain-Computer interface in chronic stroke: an application of sensorimotor closed-loop and contingent force feedback", , *Proc of IC-C'13*, Budapest, Hungary, pp.2972-2976, 2013.

[11] G. Schalk, D.J. McFarland, T. Hinterberger, N. Birbaumer and J.R. Wolpaw, "BCI2000: A general-purpose brain-computer interface (BCI) system", *IEEE Trans Biomed Eng*, vol. 51, pp. 1034-43, 2004.

[12] G.Pfurtscheller and F.H.Lopes Da Silva, "Event-related EEG/MEG synchronization and desynchronization: basic principles.", *Clin. Neurophysiol.*, vol.110, pp.1842-1857, 1999.

THE 5TH INTERNATIONAL CONFERENCE ON WIRELESS COMMUNICATIONS, VEHICULAR TECHNOLOGY, INFORMATION THEORY, AEROSPACE & ELECTRONIC SYSTEMS (WVITAE-2015)
December 13-16, 2015, Hyderabad, India

Design of Wireless Transceiver for Amateur Radio to Reduce the Impact of Natural Calamities

Ashwini Shingate
Student of M.E. (Digital Systems)
Sinhgad Academy of Engineering
Savitribai Phule Pune University
Pune, India
ashwinishingate@gmail.com

Rushikesh Borse
Associate Professor, Department of E&TC Engineering
Sinhgad Academy of Engineering
Savitribai Phule Pune University
Pune, India
rpborse@gmail.com

Shubham Tiwari
Founder and Director
Shubhra Energy Pvt. Ltd
Indore, India
vu3sxn@gmail.com

Arvind Jawale
Assistant District Commissioner
Scout
Satara, India
asjawale25@gmail.com

***Abstract*— Communication is the major problem during catastrophe. To address this problem the technology called amateur radio is used. During calamities and natural disaster times, amateur radio is recurrently used as an emergency communication system when wired line, cell phones and other contemporary means of communications goes down. This paper shows the design and implementation of wireless transceiver based on amateur radio. It also describes the concept of ham radio station. In this proposed work every block is designed for a 50 Ω impedance for input and output stage. The blocks in transceiver can be exchanged to any other frequency band, so it is like a universal block design. Here the design of transceiver is made to work within 14 to 14.35 MHz HF spectrum of amateur radio. It outlines specially the transceiver and antenna used in ham radio station.**

Keywords*— Amateur radio; Antenna; Arduino Uno; Wireless transceiver.

I. INTRODUCTION

Natural calamities like earthquake, flash flood, storms, tsunami, etc. are beyond human control. A major consequence of these calamities is to damage the existing communication infrastructure. If the infrastructure damaged, people do not get any help because their location cannot be conveyed [6]. Many people died during flash flood in Uttarakhand, India, in the year 2014, because the rescue team could not reach the stranded people in time, due to failed communication links. A potential solution to this situation is the Amateur Radio. Recently, in April 2015, in Nepal because of earthquake all communication links failed. For communication in Nepal many hams were invited, and all communication was carried on amateur frequencies.

Amateur Radio operators are called ham. HAM stands for Hertz, Armstrong, Marconi which are the inventors of the HAM. HAM also known as Help All Mankind. It is a non-commercial, non-profit radio service, friendly and a technical hobby enjoyed by nearly 6 million hams all over the world. The amateur radio service is found on an oath that includes public service, and radio amateurs [4], [6].

Ward Silver in his book [1], "Ham Radio for Dummies" explains architecture of HAM radio. Fig. 1 shows a typical ham station's components and gadgets. The radio is connected with a feedline to one or more antennas. Antenna switch allows the ham operator to select one of the antenna. An antenna tuner is used between the antenna and the transmitter to operate at peak efficiency.

One can use headphones and microphone to communicate using the various methods of transmitting speech. If Morse code (Continuous Wave) is preferred, operator use the traditional straight key, it is an old-fashioned Morse code transmission device, but recently more commonly use paddle and keyer [1].

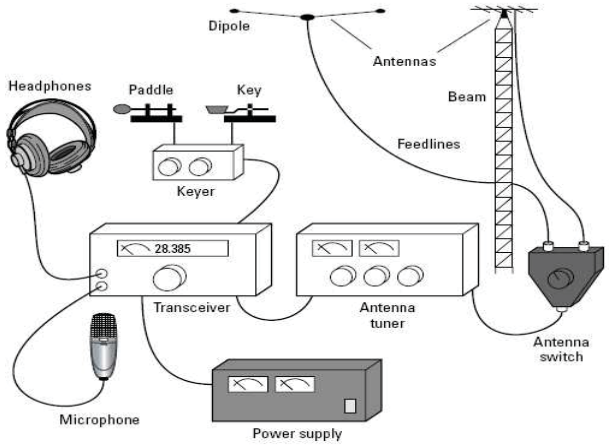

Fig. 1. Architecture of ham radio station
(Courtesy of Ward Silver [1])

There are different available frequency bands for HF, VHF and UHF. Ham voice modes are amplitude modulation (AM),

which includes the narrower-bandwidth single sideband (SSB), and frequency modulation (FM). For the most part, SSB is heard on HF, while FM is the typical voice mode used for VHF, UHF and microwave bands [6].

This paper, demonstrates the design and implementation of SSB transceiver for 14-14.35 MHz HF frequency spectrum. The paper is structured as follows: Section II describes the importance of amateur radio in wireless communication. Section III explains designing of ham radio transceiver. The result is shown in section IV followed by conclusion in Section V.

II. Importance of Amateur Radio in Wireless Communication

To provide wireless communications to an entire world, capacity of users is increased when Bell Laboratories developed the cellular concept in 1960s and 1970s [10]. During first generation the radio techniques used analog communication, which had high efficiency and easy to build. In second generation standards use digital modulation and multiple access techniques. Multi-megabit Internet access provided by third generation wireless networks [9], [10]. In 3G system users having ability to receive live music, conduct interactive network sessions, simultaneous voice and data access. with multiple access with multiple communication nodes. at the same time by using a single mobile handset at any circumstances [5]. Mobile 4G LTE (Long-Term Evolution), LTE Advanced provides faster and better Mobile Broadband, which have more data capacity [9].

During disaster only amateur radio is used, because all 2G, 3G and 4G trends depends upon BTS (Base Transceiver Station), BSC (Base Station Controller), MSC (Mobile Switching Center), PSTN (Public Switched Telephone Network) which are failed down during disaster. As a worldwide communication medium, spectrum utilization and allocation of the HF band is regulated by the International Telecommunication Union (ITU). A portion of the HF band is allocated for the use of people interested in radio technology as a hobby known as amateur radio, which follows ionospheric propagation [4], [6]. The ham radio works on the high-frequency (HF) band (2-30 MHz). The propagation is via direct wave, surface wave, near-vertical incidence sky wave (NVIS), and ionospheric propagation provides a means of communication, from line-of-sight (LOS) to beyond-line-of-sight (BLOS) and over-the-horizon (OTH) ranges [3]. For amateur communication it requires only transceiver, battery and antenna, which can be mounted very easily. Hence it can prove very effective tool when other media of communication systems are fails.

III. Designing of Amateur Radio Transceiver

Fig. 2 shows the block diagram of the proposed system. It includes both transmitter and receiver sections.

Following are the different blocks of the transceiver:

A. Antenna

Antenna is connected to the transceiver with a piece of coaxial cable. During transmission, it radiates signal in space

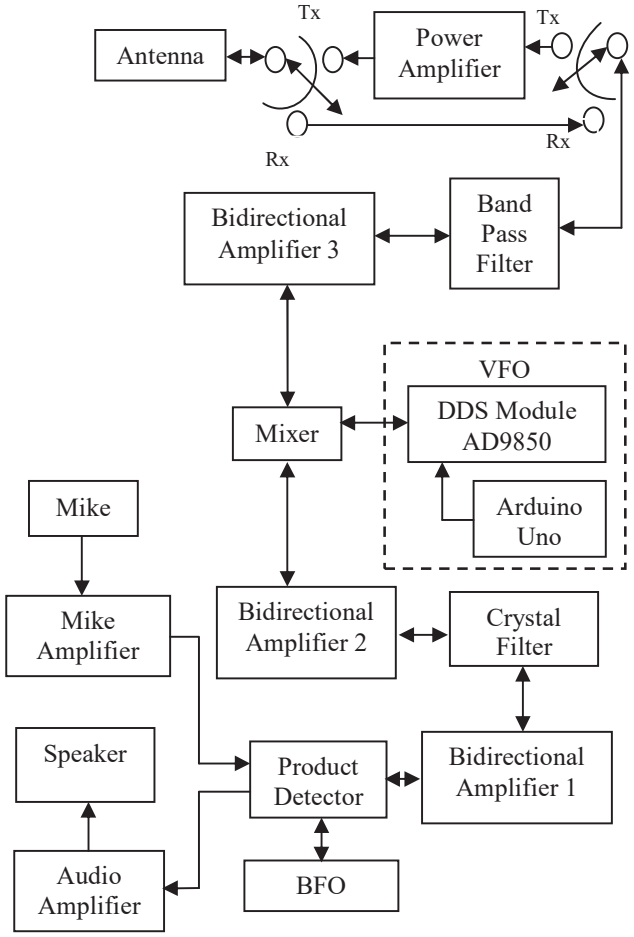

Fig. 2. Block diagram of the proposed system

and during reception it receives signal through the space. Typically, yagi, dipole and vertical antennas are used for HF, verticals for VHF and UHF, and dish antennas for the microwave frequencies [3], [4], [5]. In proposed work, we have used inverted-V dipole antenna. The halves of a dipole sloped to form an inverted-V. For dipole, antenna length is half the wavelength. It is calculated by the following equation:

$$\lambda = \frac{C}{F} \quad (1)$$

where C=Speed of the light in free space, F= Frequency

For 14 to 14.35 MHz frequency bandwidth, its center frequency is 14.175 MHz. The speed of light in free space=3×10^8 m/s, wavelength (λ), for 14.175 MHz frequency is 20.39m.

So the antenna length is given by:

$$L = \frac{\lambda}{2} \quad (2)$$

Therefore each arm of dipole is of 5.1 m length.

B. Microphone

A microphone called a mike is an acoustic-to-electric transducer or sensor which converts sound waves in air into an electrical signal [2]. In proposed work condenser microphone is used.

C. Mike Amplifier

The balanced modulator and the audio speech processor need a certain optimum level, which can be in the range of 0.3 to 0.6 V AC. For getting this level signal from microphone is passed to the mike amplifier.

D. BFO (Beat Frequency Oscillator)

To create an audio frequency signal and making transmission audible, a beat frequency oscillator or BFO is used. The signal from the BFO and modulating intermediate frequency is mixed to create a beat frequency. BFO frequency is heard as a tone in the speaker. It is used to demodulate single sideband (SSB) signals. The signal from BFO is comprehensible, by essentially replacing the missing carrier signal [10]. In proposed work BFO produced a carrier frequency of 10 MHz.

E. Product Detector

The output of product detector is the mathematical product of the BFO and the audio modulating signal. The BFO must be tuned to the same frequency as the suppressed carrier to prevent distortion of the recovered audio [2]. It produces double sideband (DSB) with carrier.

F. Bidirectional Amplifier

As the name suggests it amplifies signal in both direction, during transmission as well as reception. Direction of signal flow determined by the control voltage applied to an amplifier. Only one amplifier operates at one time [8]. In this amplifier input and output impedance is same, at both port it is matched. In proposed work, for amplifier input stage is feedback amplifier and output circuit is a Darlington emitter follower which has unity voltage gain [11].

G. Crystal Filter

A band pass frequency response is produced when group of crystals, of the same nominal frequency connected into a ladder network [11]. In proposed system ladder crystal filter is used. For selection of crystals, its parameters must be checked. To pass 10 MHz signal 4 crystals of 10 MHz are used in proposed system for making ladder network. A mesh is one loop of a ladder consisting one crystal and two shunt coupling capacitors on either side of it [12]. Capacitance of coupling capacitor is calculated as:

$$C_{jk} = \frac{C_m F}{k_{jk} B} = \frac{1}{4 k_{jk} B \pi^2 F L_m} \quad (3)$$

End terminating resistance is given by

$$R_E = \frac{2\pi B L_m}{q} \quad (4)$$

where C_m is motional capacitance, F is center frequency, k_{jk} is normalized coupling coefficient, B is bandwidth and L_m is motional inductance and q is normalized value of filter.

H. Mixer

Mixer is a nonlinear circuit or device that accepts its input as two different frequencies and produce output as a mixture of signals at several frequencies [5], [11]. In proposed work double balanced diode ring quad configuration is used that consist of four diodes. This arrangement ensures that only two diodes conduct in each cycle of AC signal. In proposed work two frequencies fed to mixer are 10 MHz from BFO and 4 - 4.35 MHz from VFO which produced desired output during transmission and reception.

I. VFO (Variable Frequency Oscillator)

For frequency control during communication it is necessary to have a frequency-tuning knob that covers the entire band and not just a few hertz. Its hard because, without the stability, an ordinary RF oscillator will drift hundreds of Hz during sending [2]. To build a VFO in proposed system, direct digital synthesizer AD9850 using Arduino microcontroller board based on ATmega328 is used. It generates frequency as an analog output sine wave. By using the frequency varying knob on front panel on metal box of transceiver, entire bandwidth of desired range is achieved. The details of Arduino Uno board and AD9850 are as follows:

1) Arduino Uno

Arduino is an open-source electronic prototyping platform. It is a microcontroller board based on the ATmega328. The functionality of Arduino contains Atmel microcontroller, USB programming/communication interface, voltage regulator and power connections, breakout I/O pins, in-circuit serial programmer (ICSP) connector [8].

2) AD9850

The AD9850 is a highly integrated device. To form a complete, digitally programmable frequency synthesizer function in AD9850, the direct digital synthesizer (DDS) technology coupled with an internal high speed, high performance D/A converter. Output tuning resolution of 0.0291 Hz for a 125 MHz reference clock input provided by a 32-bit frequency tuning word. It uses CMOS technology and performance on 155 mW power dissipation of 3.3V supply. It is available in a space-saving 28-lead SSOP, surface-mount package [8].

Algorithm for frequency generation of VFO is shown in Fig. 3:

J. Bandpass Filter

A bandpass filter is an electronic device that allows signals to pass between two special frequencies and discriminates against signals at other frequencies [11]. In proposed system triple tuned LC bandpass filter is used. By selecting center frequency F, bandwidth B in Hz. Inductance, L is calculated as L=10/F. The capacitance at both end of load is calculated as:

$$C_o = \frac{1}{\omega} \cdot \frac{1}{\sqrt{R_0 Q_E \omega L - R_o^2}} \quad (5)$$

$$Q_E = \frac{qFQ_u}{BQ_u - qF} \quad (6)$$

where ω is angular frequency as 2ΠF, Q_u is unloaded inductor and q is normalized value, R_o is load value at both ends.

Algorithm: VFO Frequency Generation

1. *Start*
2. *Define pre-processor directives*
3. *Define variables*
4. *Define setup functions*
5. *Frequency selection*
6. *Initialize LCD*
7. *If Frequency = 1 MHz*
8. *Then increment frequency*
9. *Else*
10. *Initialize the starting frequency for 14 MHz*
11. *End if*
12. *Set the flag indicating frequency change*
13. *Transfer frequency to AD9850*
14. *Send 32 bit bit frequency*
15. *Dividing the given 32 bit frequency into 4 bytes*
16. *Transferring a byte taking 1 bit at a time*
17. *Frequency update*
18. *Sine of desired frequency obtained*
19. *Display result on LCD*
20. *End*

Fig. 3. Algorithm for frequency generation of VFO

K. Audio Amplifier

For getting the good output from speaker it is possible to use op amps as low power audio output driver [2]. In proposed work LM386 audio driver IC is used for amplification.

L. Speaker

A loudspeaker is an electro-acoustic transducer that produces sound in response to an electrical audio signal input [2]. In proposed work 80 Ω speaker is used.

M. Linear Power Amplifier

For getting more output power at load a linear amplifier is used. Linearity of linear power amplifier refers to the ability of the amplifier to increase power levels of signals that are accurate reproduction of the input signal. Load impedance, supply voltage, input bias current, and power output capabilities affected on efficiency of linear amplifier [11]. In proposed work, the low-cost medium power NPN transistor 2N2218 is used as pre-linear driver. It drives an IRF510 MOSFET as a main driver for 10 watts of power at 14 – 14.35 MHz for getting desired result.

IV. Results

A. Hardware of System

The hardware of transceiver is built. Fig. 4 shows the hardware of the system developed. Three different PCB are made. The section in the top left of the image is the main transceiver. VFO section is directly below it with Arduino board and AD9850. The entire section on the right side is linear amplifier.

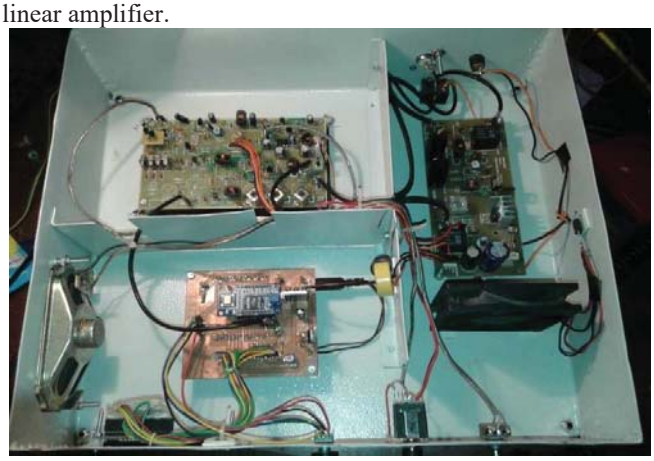

Fig. 4. Hardware of a system

Hardware is tested at the frequency range of 14 – 14.35 MHz. The system works on 13.5 V. Table 1 shows output of different parts in transceiver.

TABLE I. Output of Different Blocks

Block	Output
VFO	4 – 4.35 MHz
BFO	9.9989 MHz
Mike Amplifier	2 KHz
Audio Amplifier	2.5 KHz
Modulation Index	1
Pre-Linear Amplifier (Frequency)	14 – 14.35 MHz
Pre-Linear Amplifier (V_{PP})	4 V_{PP}
Linear Amplifier Voltage (Without load)	146 V_{PP}
Linear Amplifier Voltage (With load)	6 V_{PP}
Power of Linear Amplifier	10 Watts

Fig.5 shows the BFO frequency that is nothing but the carrier frequency as shown on DSO, getting result of 9.9989 MHz.

Fig.6 shows the VFO frequency as shown on DSO getting result from 4 to 4.35 MHz by moving the frequency varying knob on front panel of hardware box. In image it shows about 4.2025 MHz.

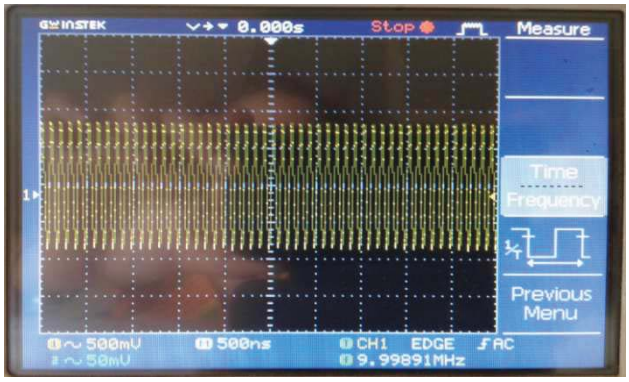

Fig. 5. BFO frequency

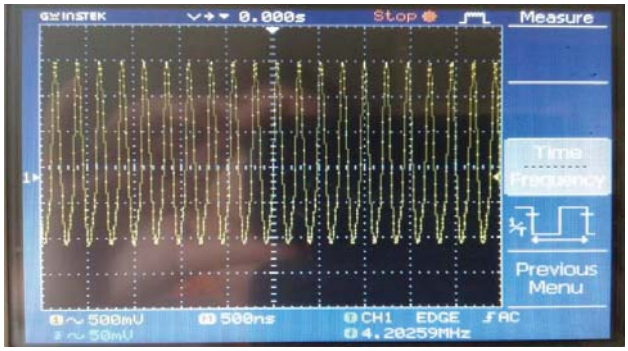

Fig. 6. VFO frequency

Fig.7 shows the frequency which is nothing but the SSB signal obtained at output of transceiver which is passed to the linear amplifier. Its frequency is from 14 to 14.35 MHz by varying the VFO frequency knob. In image by checking result on DSO we get result of 14.0408 MHz.

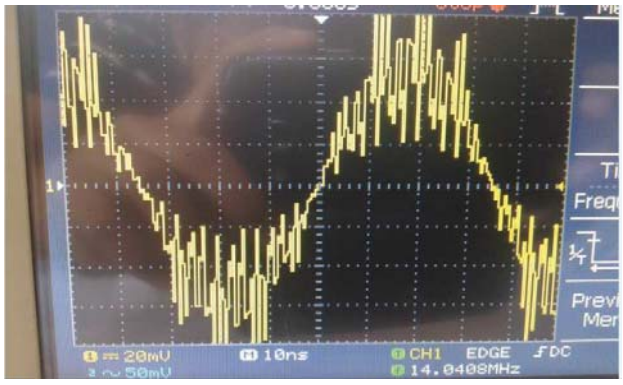

Fig. 7. Final output frequency from transceiver

B. Antenna Implementation

As the frequency of system is 14 – 14.35 MHz. In this proposed work, antenna used for this frequency bandwidth is inverted dipole antenna. Hardware implementation of antenna is done as shown in Fig.8. The halves of a dipole are sloped at apex angle greater than 90**°**, standing wave ratio(SWR) is 1.1. The centre of two arms of dipole connected to feedline cable. In proposed work coaxial cable RG58 of 50 Ω is used for connection between antenna and transceiver.

Fig. 8. Implementation of inverted-V dipole antenna mounted at SAE, Kondhwa, Pune.

V. CONCLUSION

Hardware implementation of proposed system is done to achieve desired aim. DDS VFO provides frequency between 4 to 4.35 MHz. BFO frequency obtained is 10 MHz. Output frequency from transceiver is 14 to 14.35 MHz. As VFO is implemented with DDS technology, it is effortless to tune whole band during communication with good stability. Combination of analog and digital methods gives good results. From the result it is seen that DDS VFO, SSB generation is easy, and it gives 90% efficiency of modulation. As it use only single upper side band so power required is less. Output power from linear amplifier is 10 watts. With rapid advancements in technology, it is now possible to design whole transceiver with digital concept. In future this work can be extended to design and implementation of transceiver for SDR and WSPR mode. Also by putting some extra switching functions, it can be used for multiband access of frequency during communication.

REFERENCES

[1] Ward Silver, “Ham Radio for Dummies,” Wiley Publishing, pp. 22–24 Indiana, 2004.

[2] Joseph J. Carr, “RF Components and Circuits,” 1st ed., Planta Tree, Great Britain, 2002.

[3] David Sumner, “The Arrl Antenna Book,” ARRL the national association for amateur radio, Newington, USA, 2007.

[4] Kristen Haring, “Ham radio's technical culture,” Gary Frost, vol. 4, pp. 10–19, December 2007.

[5] Jim Brown, “A ham's guide to rf ferrites, baluns, and audio interfacing,” Audio Systems Group, 2010.

[6] Bart Lee, “Amateur radio in disaster relief,” ARRL the national association for amateur radio, California, 2010.

[7] K.Sindhura, V.Mounika, G.Ravali and V.Sindu, “Implementation of direct digital synthesizer ad9850 using arduino uno,” Gokaraju Rangaraju Institute of Engineering and Technology, India, 2013.

[8] Jochen H. Schiller, “Mobile Communications,” 2nd ed., Pearson Education, Great Britain, 2003.

[9] Theodore S. Rappaport, “Wireless Communications Principles and Practice,” 2nd ed., pp. 1–55, Pearson Education, India, 2002.

[10] Wes Hayward, Rick Campbell and Bab Larkin, “Experimental Methods in RF Design,” ARRL the national association for amateur radio, Newington,USA,2004.

THE 5TH INTERNATIONAL CONFERENCE ON WIRELESS COMMUNICATIONS, VEHICULAR TECHNOLOGY, INFORMATION THEORY, AEROSPACE & ELECTRONIC SYSTEMS (WVITAE-2015)
December 13-16, 2015, Hyderabad, India

PAPR Reduction Comparison of the MC-CDMA System with Various Companding Techniques

B.Sarala[1]
Department of ECE,
M V S R Engineering College,
Hyderabad.
b.sarala@rediffmail.com

V.Bhagya sree[2]
Department of ECE,
B.E, ECE, MECS
Hyderabad.
vongurubhagya03@gmail.com

B.N.Bhandari[3]
Department of ECE,
JNTUH,
Hyderabad
bnb@ieee.org

D.S.Venketeswarlu[4]
Department of ECE
Retired professor, BHU
Hyderabad
dsv4940@gmail.com

***Abstract*---In a single carrier system, a deep noise of fading can cause the entire link to fail but within a multi-carrier system, only a small percentage of the subcarriers will be affected. High Peak to Average Power Ratio (PAPR) of the transmitted signal is a major problem in the MC-CDMA system. It deteriorates the system performance due to large number of subcarriers and also reduces power amplifier efficiency, the battery life and resolution. Several methods are proposed for the PAPR reduction in the literature, such as μ-law, Exponential and Linear Non Symmetrical Transform (LNST) companding techniques. These techniques are implemented for the OFDM system over AWGN channel only. A-Law generates distortion at small signals and μ-law companding technique enlarges only small signals so that average power increases and causes spectral side-lobe generation. The PAPR reduction capacity of the exponential companding technique is very significant factor but there is an increased latency and system complexity. The LNST companding technique offers more bandwidth. In this paper, a few methods are used to reduce the PAPR, the system complexity, processing delay, distortion, noise and interference and improve the BER performance and quality of the channel. The existing and Modified Exponential Companding with Clipping Transform (MECCT) and Modified Linear Non Symmetrical Transform (MLNST) methods are implemented for the MC-CDMA system over AWGN channel.**

Keywords—MC-CDM; PAP; system; LNST; companding; MECCT; MLNST

I. INTRODUCTION

The combination of the CDMA and the OFDM based MC-CDMA system was initiated in 1993 [1]. It is a multiple access system used within the OFDM telecommunication schemes which supports many users simultaneously. The main idea of the MC-CDMA system relies on transmission of data by dividing the high rate data stream into an *N* number of low data rate parallel streams to transmit all of them on a separate subcarrier [1]. The MC-CDMA system spreads every user signal in the particular frequency domain. The MC-CDMA system transmits a single data bit at many narrowband subcarriers and every subcarrier is encoded with a phase offset from 0 to π based on a spreading code. The band of frequency offsets form code to differentiate users. Frequency domain spreading systems wherein the chips of spread data symbols are allocated across the subcarriers and are also projected independently by Yee et.al (1993), Fazel and Papke (1993) and Chouly et.al (1993) [2].

The merits of the MC-CDMA system are used in high data rates, simpler frequency domain equalization, higher spectral efficiency with better BER performance and minimum delay spread which also reduces the multipath effects.

The MC-CDMA system is employed to combat channel spreading, thereby strengthening the system capacity to accommodate a large number of users. The Long Term Evolution (LTE) gives a large range of data rates from 100 Mbps to 1 Gbps. The high PAPR result in the multi-carrier modulation is caused by the multiple subcarrier sinusoidal signals added simultaneously to form the large amplitude signal. The large amplitude signal causes IBR and increased BER and also degrades the system performance. An advanced counter is to stop the incidence of the non-linear distortion by the reduction of the PAPR of the transmitted signal. One of the challenging issues in the MC-CDMA system is high PAPR.

The signal pre-distortion method to decrease the PAPR which is based on companding was first projected by Wang [3]. A number of companding techniques are proposed by several authors. Among these the μ-Law companding expands merely small signals so that it increases the average power and causes spectral side-lobe generation and reduces the PAPR. The exponential companding is a non-linear scheme. It has less spectral side-lobe generation [4]. The linear companding transform by inflexion point, that is, the Linear Non Symmetrical Transform (LNST) can be better in performance than the μ-Law companding [5]. Clipping is easy and efficient and causes IBR and increased BER. The companding transforms are superior to clipping as they decrease distortion significantly. The main objective of this study is to reduce the PAPR and BER and improve the power efficiency of the MC-CDMA system without additional bandwidth using MECCT and MLNST companding techniques.

This paper is organized into five sections. Section I describes the introduction of the MC-CDMA system and companding function. Section II, the PAPR problem in the MC-CDMA system is described. Section III the block diagram of the MC-CDMA system is described. In section IV the existing companding techniques and also the modified companding techniques such as MECCT and MLNST are presented. In section V computer simulation results are presented. In section VI conclusions are listed.

II. THE MC-CDMA SYSTEM

Fig 1 shows the MC-CDMA transceiver system. It transmits binary data bit of a κ^{th} user concurrently on a number of narrow band subcarriers. The κ^{th} user data bits are spread, modulated and mapped within the frequency domain with the Inverse Fast Fourier Transform (IFFT) [2].

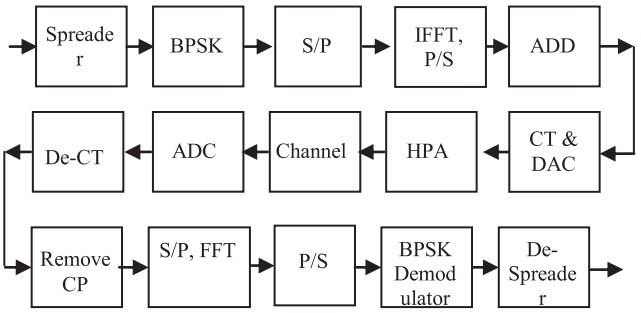

Fig 1: The MC-CDMA Transceiver

The companding techniques are proposed for the PAPR reduction and are able to increase the BER performance and minimize Outer Band Interference [OBI]. The Companding Transform (CT) output is fed to the parallel to serial converter and guard insertion block. The sequence is passed through a DAC and the High Power Amplifier (HPA). The transmitted signal is represented as

$$x^{\mathrm{K}}(t)=\sqrt{\frac{2P}{N}}\sum_{i=0}^{I-1}\sum_{l=0}^{N-1}d_i^{\mathrm{K}}c_l^{\mathrm{K}}e^{j\left(2\pi\left(f_c+\frac{1}{T_d}\right)\right)t*P_{T_d}} \quad (1)$$

Where d_i^K represents the i^{th} input data bits of the user κ and d_i^K is presumed to be an arbitrary variable which assumes values +1 or -1 by the same probability. c_l^K is the l^{th} spreading code of the κ^{th} user, P_{Td} represents the rectangular modulation, P is the power of data bit, I indicates the number of data bits, N correspond to the number of the subcarriers, f_c is the lowest subcarrier frequency, $1/T_d = f_d$ is the subcarrier separation [6]-[7].

At the receiver the de-companding transform (De-CT) is applied before CP removal and Fast Fourier Transform (FFT) block, to pick up the unique signal. This is developed through an FFT block to demodulate several subcarriers.

The demodulator demodulates the PSK signal and then de-spreads the code synchronization to accomplish fully the initial path of the desired signal. The process of the original data of the received signal at the output of the intended user can be determined by substituting base band transmitted signal with the phase shift. The received signal is obtained as

$$Y(t)=\sqrt{\frac{2P}{N}}\sum_{\kappa=0}^{\mathrm{K}-1}\sum_{i=0}^{I-1}\sum_{l=0}^{N-1}\beta_l^{\mathrm{K}}\,d_i^{\mathrm{K}}\,C_l^{\mathrm{K}}\left(e^{-j\left(2\pi\left(f_c+1/T_d\right)t+\varphi_l^{\mathrm{K}}\right)p_{T_d}(h)+W(t)}\right) \quad (2)$$

Where $h=\left(t-lT_d+\varphi_l^{\mathrm{K}}\right)$

$$\varphi_l^{\mathrm{K}}=\phi_l^{\mathrm{K}}-\theta_l^{\mathrm{K}} \quad (3)$$

φ_l^{K} Shows the phase difference between the transmitter and the receiver, $W(t)$ is the AWGN with a double sided Power Spectral Density (PSD), β_l^{K} denotes outcomes of the channel. The MC-CDMA system can handle N concurrent users by excellent BER with typical receiver methods [8]-[9] and [10].

III. PAPR PROBLEM IN THE MC-CDMA SYSTEM

The high PAPR of the transmitted signal depreciates the performance of the MC-CDMA system. The high PAPR signal is transmitted through a nonlinear amplifier which causes spectral widening and power efficiency degradation. Hence, to prevent the spectral broadening of the MC-CDMA system its power amplifier is controlled in the linear region.

In general, the PAPR of the above system signal x(t) is described as the ratio of maximum instantaneous power to its average power[11].The PAPR of the MC-CDMA system is expressed as

$$PAPR=10Log_{10}\frac{\max\left[|X(t)|^2\right]}{E\left[|X(t)|^2\right]}dB \quad (4)$$

Where $E\left[|X(t)|^2\right]$ denotes average power. It is easy to manipulate the above equation by decreasing the numerator $\max\left[|X(t)|^2\right]$ or increasing the denominator $E\left[|X(t)|^2\right]$ or both. As a large number of subcarriers (N) exist, they result in high PAPR. The relation between The Crest Factor (CF) and the PAPR is given as

$$CF=\sqrt{PAPR} \quad (5)$$

The CCDF of the PAPR of the data block with Nyquist rate sampling is given as

$$P(PAPR>X_0)=1-P(PAPR\leq X_0) \quad (6)$$

X_0 is the PAPR threshold value and N is equal to the number of subcarriers. This equation is not accurate for a small number of subcarriers [12].

IV. COMPANDING TECHNIQUES

In companding, small signals are amplified and large signals are attenuated and compression occurs. It increases the Signal to Noise Ratio (SNR), as the input signal is low and therefore reduces the effect of system noise source. Let N indicate the number of subcarriers used for parallel transmission and let x_n $(0\leq k\leq N-1)$ indicate n^{th} complex modulated data symbol in a block of N information symbols. Here, k is the discrete frequency component and n is the discrete time component. The output x_n of the N-point IFFT of X_K are the MC-CDMA signal samples over one symbol interval. This is mathematically represented as

$$X_n=\frac{1}{\sqrt{N}}\sum_{n=0}^{N-1}X_K e^{\frac{2\pi kn}{N}},k=0...N-1 \quad (7)$$

The amplitude $|x_n|$ has a Rayleigh distribution with the Cumulative Distribution Function (CDF) as follows-

$$F_{X_n}(X)==1-\exp\left(\frac{-X^z}{\sigma^z}\right),X\geq 0 \quad (8)$$

The peak power results as *N* modulated symbols are added with equal phase [4].

A. The μ-law companding

The μ-Law companding is a linear companding method which amplifies only small signals in order to increase the average power and cause spectral side-lobe generation and reduces the PAPR [11]. The μ-Law companded signal is given as

$$\begin{aligned} Y(n) &= CX(n) \\ &= \frac{V}{\ln(1+\mu)} \ln\left(1+\frac{u}{V}|X(n)|\right) \operatorname{sgn}(X(n)) \end{aligned} \tag{9}$$

Where *v* is the average amplitude of the signal and μ is the companding factor. The de-companding signal is specified as

$$\begin{aligned} \hat{X}(n) &= C^{-1} r(n) \\ &= \frac{v}{\mu}\left\{\exp\frac{\left[|y(n)|\ln(1+\mu)\right]}{V}-1\right\}\operatorname{sgn}(Y(n)) \end{aligned} \tag{10}$$

B. The exponential companding

The exponential companding is a non-linear companding scheme that regulates both high and low peak signals and can maintain the average power at the same level, with less spectral side-lobe generation and better phase error performance. The companded signal is obtained by using the exponential companding function specified by

$$C(x) = \operatorname{sgn}(x)^d \sqrt{a\left(1-\exp\left(\frac{-X^z}{\sigma^z}\right)\right)} \tag{11}$$

Where $C(x)$ is the companded signal of the exponential companding transform, sgn(x) is signum function, α is a positive constant which determines average power of output signal, $x(n)$ is the original MC-CDMA symbol [4].

To maintain input and output signals at the same average power level α is given by,

$$\alpha = \left[\frac{E\left(|X(n)|^z\right)}{E\left[\sqrt[d]{\left(1-\exp\left(\frac{-|x(n)|^2}{a^z}\right)\right)}\right]^2}\right]^{\frac{d}{2}} \tag{12}$$

At the receiver, the de-companding function of $C(x)$ is used in inverse operation, i.e.

$$c^{-1}(x) = \operatorname{sgn}(x)\sqrt{-\sigma^2 \log\left(1-\frac{x^d}{\alpha}\right)} \tag{13}$$

C. MECCT Companding

The MECCT technique combines the clipping concept and the exponential concept. It uses an algorithm known as Modified Exponential Companding with Clipping Transform (MECCT) [13]. The MECCT companding algorithm is explained below-

$$\begin{aligned} x_m &= x_n, \text{ When } 0 \le |x_n| \le T_1 \\ &= T_1 + \log\left(|X_n| - T_1 + 1\right) \text{ , when } |X_n| > T_1 \end{aligned} \tag{14}$$

The final output is expressed as

$$X_{mn} = |X_m| e^{j\theta} \tag{15}$$

Where $\theta = \tan^{-1}\left(\frac{b}{a}\right)$ and x_n is in the form of $ax_n + jbx_n$, the threshold value at the transmitter is calculated as $T_1 = \frac{median(|x_n|)}{\sigma_{x_n}}$, where, σ_{x_n} is the standard deviation, $|x_n|$ is the modulus of the MC-CDMA transmitted symbol and T_1 is the threshold value.

At the receiver, the de-companding transform operates on the received signal to obtain an estimation of the transmitted signal. The MECCT de-companding algorithm is as given below-

The original received signal after de-companding is

$$\begin{aligned} \hat{x}_n &= r_n e^{j\theta}, \text{ When } |r_n| \le T_2 \\ &= \left(T_2 - 1 + 10^{|r_n|-T_2}\right) e^{j\theta} \quad \text{When } |r_n| > T_2 \end{aligned} \tag{16}$$

The threshold value at the receiver is given by $T_2 = \frac{median(|r_n|)}{\sigma_{r_n}}$. Where, σ_{r_n} is the standard deviation, $|r_n|$ is the modulus of the MC-CDMA received symbol.

D. The MLNST companding

The Modified Linear Non Symmetrical Transform (MLNST) is an idea of the LNST with phase angle, which can outperform the LNST companding The MLNST algorithm is as follows-

$$\begin{aligned} Y(n) &= \frac{1}{\mu} X(n) e^{j\theta}, \text{When } |X(n)| \le TM \\ &= \mu X(n) e^{j\theta}, \text{When } |X(n)| \ge TM \end{aligned} \tag{17}$$

Where, $\theta = \tan^{-1}\left(\frac{b}{a}\right)$ and $x(\mathrm{n})$ is in the form of $ax(\mathrm{n}) + jbx(\mathrm{n})$, where the ranges of μ and *TM* are $0 \le \mu \le 1$ and $0 \le TM \le \max\{|X(n)|\}$. . Since $X(n)$ is complex valued, the companding function should be applied to real and imaginary parts separately [5]. At the receiver, the unique signal can be recovered as stated by

$$\begin{aligned} \hat{X}(n) &= \mu R(n) e^{j\theta}, \text{When } n \varepsilon \varphi_1(TM) \\ &= \frac{1}{\mu} R(n) e^{j\theta}, \text{When } n \varepsilon \varphi_2(TM) \end{aligned} \tag{18}$$

V. RESULTS

The MC-CDMA with *A*-Law, μ-Law, LNST and exponential and also modified MECCT and MLNST companding schemes are simulated using MATLAB with 1024 symbols. The IFFT size is 256 with 64 subcarriers and Quadrature Phase Shift Keying (QPSK) modulation and GOLD codes. The performance of the MC-CDMA system in terms of the PAPR and BER is investigated with the different companding techniques. The PAPR performance can be evaluated by using cumulative distribution function of the MC-CDMA signal.

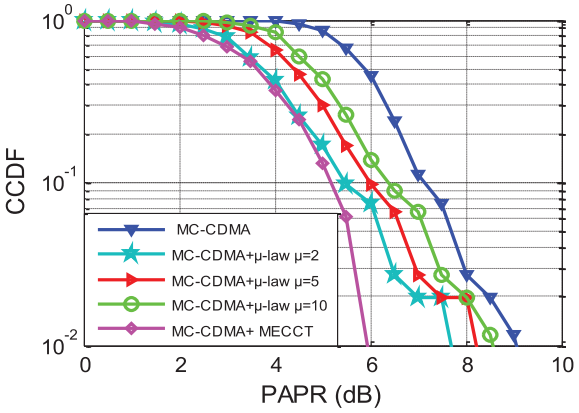

Fig 2. The MC-CDMA with μ-Law

The MECCT based system has better PAPR performance for Gold codes. The MECCT based system reduces the PAPR by 1.75 dB than the μ-law based system at μ=2 as shown in Fig 2.

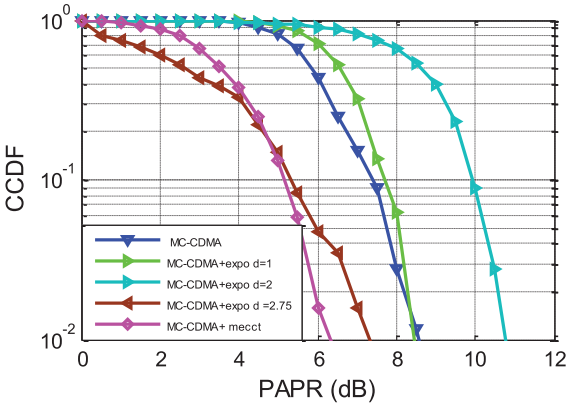

Fig 3. The MC-CDMA with exponential companding

In the MC-CDMA system with exponential companding with GOLD codes the PAPR reduces by 2.5 dB as compared to the MC-CDMA system at *d* =2.75 as shown in Fig 3. The PAPR performance of this system is better than that of the MECCT companding based system. When *d* value is above 3.0, its PAPR reduces by a maximum value.

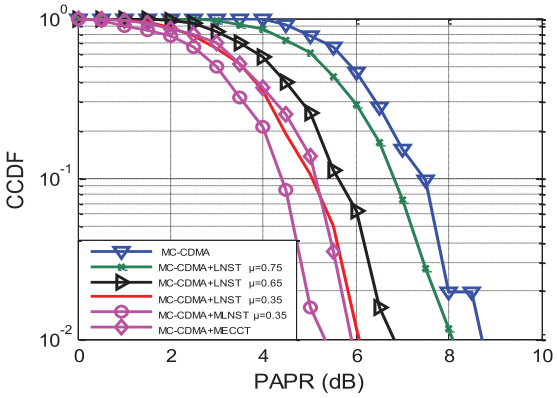

Fig 4. The MC-CDMA with LNST

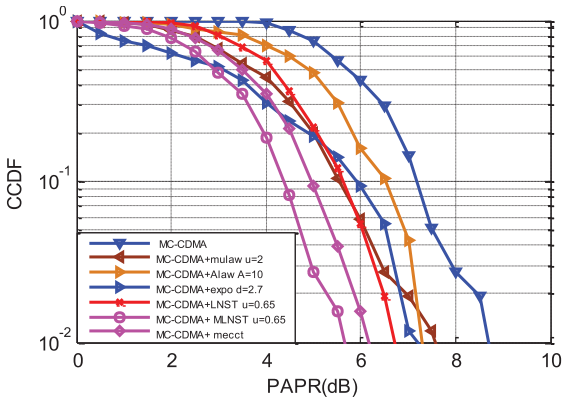

Fig 5. The MC-CDMA with different companding techniques

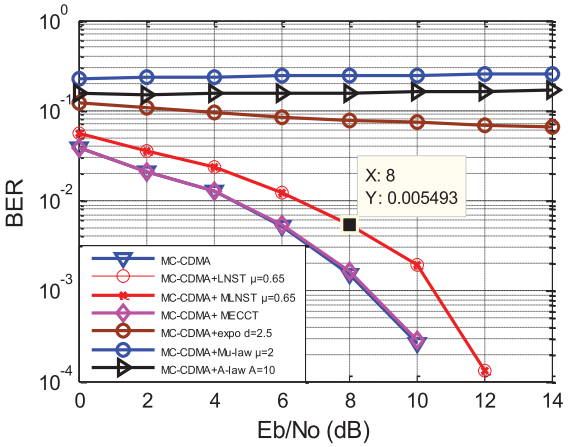

Fig 6. The BER performance of the MC-CDMA with different companding techniques over AWGN channel

The Fig 4 shows the MC-CDMA with LNST companding with Gold codes. In the MC-CDMA system with MECCT and MLNST companding, PAPR performance is better than in the LNST companding based system. MLNST companding based system, reduces the PAPR by 0.75 dB at μ=0.35 as compared to MECCT and LNST companding based system.

TABLE 1: Comparison of different companding techniques

MC-CDMA System with companding	Parameter		
	PAPR reduction in dB	*Power saving %*	*AWGN BER at 10 dB*
No companding	---	23	0.0002472
A-law	2.0	23	0.1606
μ-law	2.0	23	0.2488
Exponential	1.5	18.64	0.0729
LNST	1.0	11.76	0.001993
MLNST	3.0	35	0.001993
MECCT	2.50	29	0.0002472

In the MECCT companding based system PAPR reduces by 0.75 dB than in the MC-CDMA system with LNST companding. MC-CDMA system with MLNST companding reduces the PAPR by 0.5 dB as compared to the MECCT based system and 1.0 dB than the LNST based system as shown in Fig 5. The MECCT has lesser BER than the LNST, MLNST, Exponential, A-law and μ-law companding techniques. The MECCT based companding system has less BER than the LNST and other companding based systems as shown in Fig 6 and their parameters in Table 1.

VI. CONCLUSION

MECCT and MLNST companding techniques are employed with the MC-CDMA system to reduce the PAPR and to increase the BER performance over traditional techniques. Hence, this improves spectral efficiency. The MECCT based MC-CDMA system has less PAPR as compared to the MC-CDMA system.

This implemented method reduces the PAPR substantially by 2.5 dB as compared to MC-CDMA system. It saves bandwidth of 2.0 dB at the receiver as compared to the MC-CDMA system with LNST companding system over AWGN channel. The MECCT based MC-CDMA system has lesser spectral side-lobe generation as compared to the MC-CDMA and MC-CDMA system with LNST companding. The MECCT companding technique is of much less implementation complexity as compared to the exponential companding.

REFERENCES

[1]. V.Jagan Naveen, K.Murali Krishna, K.Raja Rajeswari, "Performance analysis of MC-CDMA and OFDM in wireless Rayleigh channel", International Journal of Advanced Science and Technology, volume 25, December, 2010.
[2]. Hara and S. Prasad R, "Overview of multi-carrier CDMA", IEEE Communications Magazine, Volume 35, No.12, pp 126 – 133, Dec 1997.
[3]. Chin-Liang Wang and Sheng-Ju Ku (2006)" A Low –Complexity Companding Transform for Peak to Average Power Ratio Reduction in OFDM Systems", ICASSP, Vol.-IV,pp329-332.
[4]. T.Jiang, Y.Yang,and Y.Song, (2005)"Exponential companding technique for PAPR reduction in OFDM signals," IEEE Transactions Broadcast, Vol.51,no.2,pp244-248.
[5]. Suleiman A. Aburakhia, Ehab F.Bardan, and Darwish A.E Mohamed (2009) "Linear Companding Transform for the Reduction of Peak-to-Average Power Ratio of OFDM signals" IEEE Transactions Broadcast, Vol.55,no.1,pp 155-160.
[6]. Ramjee Prasad, " OFDM for Wireless Communication System" Artech House, Boston. pp184-204.
[7]. Chang, R. W., and R. A. Gibby "A Theoretical study of the Performance of an Orthogonal Multiplexing Data Transmission Scheme". IEEE Tran., vol.com.16, no.4, pp 527-540, August 1968.
[8]. Joy Iong-Zong "Theoritical Analysis of an MC-CDMA system in cellular Environments", Journal of Science and Engineering Technology, (2010), vol.6, no.1, pp37-50.
[9]. Joy Iong-Zong Chen (2006), "Performance Analysis of MC-CDMA Communication Systems over Nakagami-M Environments", Journal of Marine and Technology, vol.14, no.1, pp 58-63, 2006.
[10]. K.Fazel, S. Kaiser, "Multi-Carrier and Spread Spectral Systems"-From OFDM and MC-CDMA to LTE and WiMAX, second edition, DOCOMO communication Laboratories, Europe, Germany, pp 60-61, A John Wiley and sons, Ltd, 2008.
[11]. Zhongpeng Wang, (2011) "Combined DCT and companding for PAPR reduction in OFDM Signals", Journal of Signal and Information Processing, Vol.2, pp 100-104.
[12]. S.H.Han and J.H.Lee, (2005) "An overview of Peak to average Power Ratio reduction techniques for multi-carrier transmission", IEEE Wireless Communication Magazine, Vol.12, No.2, pp 55-65.
[13]. B.Sarala and D.S.Venketeswarlu, and B.N.Bhandari "MC-CDMA PAPR Reduction Using a Modified Exponential Companding Transform with clipping" Global Journals Research in Engineering, volume 13, issue 10, version 1.0, July 2013.

THE 5TH INTERNATIONAL CONFERENCE ON WIRELESS COMMUNICATIONS, VEHICULAR TECHNOLOGY, INFORMATION THEORY, AEROSPACE & ELECTRONIC SYSTEMS (WVITAE-2015)
December 13-16, 2015, Hyderabad, India

Joint Channel Estimation and CCI Cancellation for STBC-OFDM System in Fast Fading Channel

Jyoti P Patra[1], Prasanta Kumar Pradhan[2], Poonam Singh[3], Sarat Kumar Patra[4]
E mail1: jyotiprasannapatra@gmail.com, E mail2: dearprasanta@gmail.com, E mail3 psingh@nitrkl.ac.in, E mail2: skpatra@nitrkl.ac.in
Dept. of Electronics and Communication
National Institute Of Technology
Rourkela-769008, India

Abstract— The performance analysis of Alamouti space time block code (STBC) based orthogonal frequency division multiplexing (OFDM) assumes that the channel is constant over Alamouti code period (two consecutive OFDM symbol block). However, in fast fading channel, this assumption does not hold good and causes Co-channel Interference (CCI).To cancel the CCI effect, different detection methods are proposed earlier namely Successive Interference Cancellation (SIC), Zero Forcing (ZF), Decision Feedback (DF) and Maximum Likelihood (ML). These detection methods are performed by assuming that the complete channel knowledge is known at the receiver side. But, in practical scenario, the channel is unknown to the receiver. Hence, we have proposed a new channel estimation technique which estimate the channel and thereby cancel the CCI effect jointly.

Keywords—OFDM; STBC;CCI; Channel EStimation;

I. INTRODUCTION

Recently, the wireless communication system is more focused on reliability and spectral efficiency [1]-[2]. The link reliability is solved by STBC technique which is proposed by Alamouti [3]. Originally, the STBC technique is applied to flat fading channel and it is assumed that the complete channel knowledge is known at the receiver. But in practical scenario, the channel is frequency selective fading rather than flat fading and the channel knowledge is unknown to the receiver. This problem can be solved by applying OFDM technique to the STBC system as OFDM converts the frequency selective fading channel into many narrow parallel flat fading channels [4]. However, in time varying fast fading channel the Alamouti STBC-OFDM system undergoes two types of interfering namely inter-carrier interference (ICI) and CCI [5]. The ICI is occurred due to the loss of orthogonality among the subcarrier within the OFDM block. The CCI occurs due to the variation of channel frequency response (CFR) over Alamouti code period. Due to the CCI effect, the two consecutive transmitted OFDM symbol blocks are coupled with each other at the receiver side. Both the ICI and CCI cause significant performance degradation in time varying fast fading channel. However the power of CCI is proved to be 7 - 8 dB greater than the power of ICI regardless of the channel variation [5]. Hence, we only consider the CCI effect on the Alamouti coded OFDM system. In previous literatures, various detection methods have been addressed for cancelling the effect of CCI [5]-[8]. In [6], a diagonalized maximum likelihood detector (DMLD) is proposed to remove the CCI. But the DMLD method is more computational complexity. Hence, a similar performance with low computational complexity ZF detector is proposed in [7]. In [5] SIC method is proposed. The SIC method has a low computational cost but its performance is not accurate enough due to the error propagation problem. The decision feedback (DF) method is proposed for STBC/SFBC OFDM system in [8]. These detection methods are applied by assuming that the complete channel knowledge is known at the receiver side.

However, in such systems, CSI is required to be known at the receiver side in order to recover the transmitted signal. There are two approaches for channel estimation namely the blind channel estimation and pilot aided channel estimation. In blind channel estimation, the statistical properties of the received signal are required to recover the transmitted signal. Such system has high spectral efficiency as no pilot symbol is used for channel estimation. In case of pilot aided channel estimation, pilot symbols are known a prior to the receiver and are multiplexed with the transmitted data streams for channel estimation. As compared to pilot aided channel estimation, the blind channel estimation is limited to slow time varying channel, has higher complexity and poorer performance. Hence, in this paper, pilot aided channel estimation is carried out for channel estimation purpose. One of the main problems in pilot symbol aided channel estimation for MIMO OFDM systems is the inter-transmitter-antennas-interference (ITAI) [9]. The ITAI arises when two transmitted signal are mixed at the receiver side and hence it is difficult to separate these transmitted signals. There are two approaches to handle the ITAI problem namely zero-form and non-

zero form pilot pattern. This paper proposes a modified zero form pilot arrangement based on Alamouti principle to avoid the ITAI effect. Another important criterion of channel estimation is the interpolation techniques. Linear, spline, second order, low pass interpolation (LPI) methods have been investigated in [10] and demonstrated that pilot aided channel estimation based on low pass interpolation LPI gives the best performance among all the interpolation technique.

The proposed channel estimation is based on least square (LS) algorithm with modified zero-form of comb type orthogonal pilot structure at pilot subcarriers while the low pass interpolation method is applied at data subcarriers for STBC-OFDM system in time varying multipath fading channel.

The rest of the paper is organized as follows. In Section II, the system model for the STBC based OFDM system along with the channel model is discussed. The proposed channel estimation technique is presented in Section III. In Section IV, the performance of the developed channel estimation is analyzed. Finally, Section V concludes the paper.

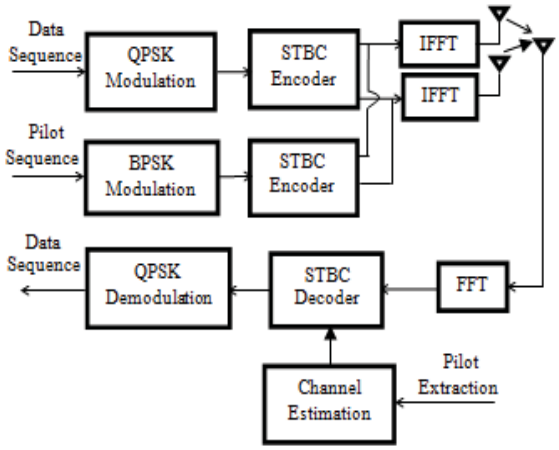

Fig. 1 Block diagram of STBC-OFDM system model

II. SYSTEM MODEL

Consider the QO-STBC proposed in [3] with 4 transmit In this section, an STBC based OFDM system with two transmit antennas and one receive antennas is described along with the exponential decaying Power Delay Profile (PDP) channel model as multipath Rayleigh fading channel.

A. System Model

The system model for STBC-OFDM with two transmit antenna and one receive antenna is shown in the Figure1. At the transmitter side, a random data sequence is generated and modulated according to any specific modulation scheme such as BPSK, QPSK or 16QAM. Then the output modulated data are passed through the STBC encoder. The STBC encoder converts the single input modulated information data into two parallel encoded output data according to Alamouti STBC scheme [3]. The Alamouti STBC scheme is described as follows. At the first time instant $X_1(k)$ and $X_2(k)$ are transmitted from the transmit antenna 1 and 2 respectively. In the second time instant $-X_2^*(k)$ and $X_1^*(k)$ are transmitted from antenna 1 and 2 respectively. Hence, the output of the STBC encoder can be written in matrix form and is given in bellow

$$X(k) = \begin{bmatrix} X_1(k) & X_2(k) \\ -X_2^*(k) & X_1^*(k) \end{bmatrix} \quad (1)$$

where $k = 0,1,2,\ldots\ldots N-1$

$X_1(k)$ is the k^{th} subcarrier for the transmitting antenna 1 before the IFFT operation and N is the number of subcarrier in a single OFDM symbol block. Then both the encoded output signal are passed through the serial to parallel converter(S/P) and finally reached at the Inverse Fast Fourier Transformation (IFFT) block. Finally, the resulting signals are transmitted from the antennas after insertion of the cyclic prefix (CP) which is assumed to be larger than delay spread of the multipath channel in order to avoid inter symbol interferences (ISI).At the receiver side, at first the CP is removed and then the received signal is processed by a Fast Fourier Transformation (FFT). The FFT output of the received signal after the removal of CP can be written in the matrix form and is given here

$$Y(k)=\begin{bmatrix} Y_t(k) \\ Y^*_{t+T}(k) \end{bmatrix} = \begin{bmatrix} H_{1,t}(k) & H_{2,t}(k) \\ H^*_{2,t+T}(k) & -H^*_{1,t+T}(k) \end{bmatrix} \begin{bmatrix} X_1(k) \\ X_2(k) \end{bmatrix} + \begin{bmatrix} Z_t(k) \\ Z^*_{t+T}(k) \end{bmatrix} = HX+Z \quad (2)$$

where $H_{1,t}(k)$ and $H_{2,t}(k)$ are the CFR for the first and second transmit antenna at the first time instant respectively. $Z_t(k)$ is the additive white Gaussian noise with zero mean and unit variance after the FFT operation.

It is to be noted that the channel is taken to be ideal where it is assumed that the perfect channel knowledge is known at the receiver side. According to Alamouti scheme, the channels are considered to be static over two consecutive OFDM symbol block, i.e., $H_{1,t} = H_{1,t+T}$ and $H_{2,t} = H_{2,t+T}$. The STBC decoding operation is performed by multiplying H^H on both the side of the equation (2), the original transmitted signal can be recovered after taking the hard decision of the decoded signal and can be written as

$$\hat{X}(k) = Q\left(\frac{\tilde{X}(k)}{\Phi(k)}\right) \quad (3)$$

where $\tilde{X} = H^H(k)Y(k)$

$$\Phi(k) = |H_{1,t}(k)|^2 + |H_{2,t+T}(k)|^2 = |H_{1,t}(k)|^2 + |H_{2,t+T}(k)|^2$$

$\tilde{X}$ is the decoded signal and Q denotes the hard

decision function. Hence, the two estimated signals $\hat{X}(k)$ are decoupled from each other at the receiver side.

However, in the fast fading channel, the channels are not same for two different time slots. Hence, $H^H H$ is no longer a orthogonal matrix and is given by

$$G = H^H H = \begin{bmatrix} \alpha_1(k) & \beta(k) \\ \beta^*(k) & \alpha_2(k) \end{bmatrix} \quad (4)$$

where $\alpha_1(k) = \left|H_{1,t}(k)\right|^2 + \left|H_{2,t+T}(k)\right|^2$

$$\alpha_2(k) = \left|H_{1,t+T}(k)\right|^2 + \left|H_{2,t}(k)\right|^2$$

$$\beta(k) = H^*_{1,t}(k)H_{2,t}(k) - H^*_{1,t+T}(k)H_{2,t+T}(k)$$

$\alpha_1(k)$, $\alpha_2(k)$ are the desired diversity gain terms and $\beta(k)$, $\beta^*(k)$ are the CCI terms. By multiplying G with FFT output of the received signal Y, the detected output signal vector can be written as

$$\tilde{X} = \begin{bmatrix} \tilde{X}_1(k) \\ \tilde{X}_2(k) \end{bmatrix} = \begin{bmatrix} \alpha_1(k)X_1(k) + \beta(k)X_2(k) + Z'_t(k) \\ \beta^*(k)X_1(k) + \alpha_2(k)X_2(k) + Z'_{t+T}(k) \end{bmatrix} \quad (5)$$

$\alpha_1(k)X_1(k)$ and $\alpha_2(k)X_2(k)$ are the desired signal. $\beta(k)X_2(k)$ and $\beta^*(k)X_1(k)$ are the CCI signal which are coupled with the desired signal at the receiver side. Hence, in order to accurately recover the original transmitted signal, these two CCI signal are to be cancelled.

B. Channel Model

In this paper, an exponential decaying PDP channel [11] is adopted for the STBC-OFDM system model. The channel is modeled as finite impulse response (FIR) with total L+1 non-zero path with zero mean and average power σ_l^2.

The channel can be expressed by

$$h_l = N(0, \frac{\sigma_l}{2}) + jN(0, \frac{\sigma_l}{2}) \quad (6)$$

where $N(0, \frac{\sigma_l}{2})$ is the zero mean with variance σ_l^2.

The power of multipath component decreases exponential. The first path of the model is chosen to be

$$\sigma_0^2 = \frac{1-\lambda}{1-\lambda^{L+1}} \quad \lambda = e^{\frac{T_s}{\tau_{rms}}} \quad (7)$$

The T_s and τ_{rms} are the sampling period and root mean squared delay of the channel. The energy of the l^{th} path can be written as

$$\sigma_l^2 = \sigma_0^2 \lambda^l. \quad (8)$$

Furthermore, each multipath is modeled as uncorrelated Rayleigh fading channel with Jakes sum-of-sinusoidal (SOS) model [12].

C. STBC-OFDM Detection Method

In the time varying fast fading channel, multiplying H^H with H does not give an orthogonal matrix. Therefore, a transform matrix (Ω) is multiplied with H matrix to make (4), an orthogonal matrix, and is given by

$$\Omega H = \mathrm{diag}(\varphi_1, \varphi_2) \quad (9)$$

where φ_1 and φ_2 are the complex number

After simplification of the equation (9), Ω can be written in the matrix form and is given here

$$\Omega = \begin{bmatrix} H^*_{1,t+T}(k) & H_{2,t}(k) \\ H^*_{2,t+T}(k) & -H_{1,t}(k) \end{bmatrix} \quad (10)$$

The φ_1 and φ_2 have the same value and is given by

$$\varphi = \varphi_1 = \varphi_2 = H^*_{1,t+T}(k)H_{1,t}(k) + H_{2,t}(k)H^*_{2,t+T}(k) \quad (11)$$

Substituting Ω in the place of H^H, the equation (2) becomes

$$\tilde{X} = \Omega Y = \mathrm{diag}(\varphi, \varphi)X + \Omega Z \quad (12)$$

The estimated original transmitted signal can be obtained by dividing the value of φ on both the side and taking the hard decision

$$\hat{X}_1(k) = Q(\frac{\tilde{X}_1(k)}{\varphi(k)}) = X_1 + Z \quad (13)$$

$$\hat{X}_2(k) = Q(\frac{\tilde{X}_2(k)}{\varphi(k)}) = X_2 + Z \quad (14)$$

The ZF method is simple and gives better result than Alamouti method as it simply forces the two CCI terms to zero.

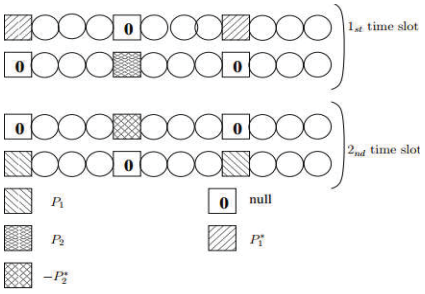

Fig. 2 Proposed pilot arrangement pattern

III. Coventional Detection Methods

The channel estimation for STBC OFDM is generally performed by assuming that the channel is constant over two consecutive OFDM symbol blocks. But in fast fading channel, the CSI are not identical for two different time slots i.e. $H_{1,t} \neq H_{1,t+T}$ and $H_{2,t} \neq H_{2,t+T}$. Hence, in order to perform perfect data detection, all the entire four channels ($H_{1,t}$, $H_{1,t+T}$, $H_{2,t}$ and $H_{2,t+T}$)

have to be estimated. To estimate the above mentioned four channels, we propose a new pilot scheme that avoids ITAI thereby facilitating perfect channel estimation. The proposed pilot scheme is shown in the Fig.2. The pilot subcarriers are designed in such a way that when one transmitting antenna transmits the pilot the other antenna is assumed to be silent and vice-versa. This assumption prejudicially avoids the ITAI effect. In this proposed method, the four channels are estimated independently thus cancelling the effect of CCI. The channel estimation is carried out by LS algorithm. After estimating the channel at pilot subcarriers LPI has been applied to estimate the channel at data subcarriers. LPI method is chosen for its better performance in fast fading scenario. The position of the pilot subcarriers during first time slot at antenna 1 is P_1 and at antenna 2 is P_2 respectively. Arrangement of P_1 and P_2 can be given as Equation (15) and (16) respectively

$$P_1 = \lfloor p_1, 0, p_3, 0, p_5, ...2N_p - 1 \rfloor \quad (15)$$

$$P_2 = \lfloor 0, p_2, 0, p_4, 0, p_6 .....2N_p - 1 \rfloor \quad (16)$$

Where, N_p stands for the total number of pilot subcarriers in a single OFDM symbol block. During 2nd time slot, antenna 1 transmits $-P_2^*$ and antenna 2 transmits P_1^*. The received signal in the frequency domain at pilot sub-carriers for 1st time slot (t = t) and 2nd time slot (t = t+T) can be written in Equation (17) and (18) respectively

$$Y_{t,p} = H^p_{1,t} P_1 + H^p_{2,t} P_2 + Z_t \quad (17)$$

$$Y_{t+T,p} = -H^p_{1,t+T} P_2^* + H^p_{2,t+T} P_1^* + Z_{t+T} \quad (18)$$

P_1, P_2 are inserted uniformly (with zero padded at alternate locations) in each OFDM symbol block. The H_{11}^p, H_{21}^p, H_{12}^p and H_{22}^p are the four CFR at the pilot subcarrier of the four different channel paths.

The four channels after LS algorithm are given by

$$H^p_{1,t} = Y_{t,p}(\text{odd postions}) / P_1(\text{odd Positions}) \quad (19)$$

$$H^p_{2,t} = Y_{t,p}(\text{even postions}) / P_2(\text{even postions}) \quad (20$$

$$H^p_{1,t+T} = -Y_{t+T,p}(\text{even postions}) / P_2^*(\text{even postions}) \quad (21)$$

$$H^p_{2,t+T} = Y_{t+T,p}(\text{odd postions}) / P_1^*(\text{odd postions}) \quad (22)$$

In order to estimate the channel at data subcarrier by using channel information at pilot subcarrier, the interpolation technique is needed. The LPI technique is applied as it performs the best in time varying channel [10]. After getting the four CFR at data subcarriers ZF detection technique has been applied to recover the original transmitted signal. We call the proposed channel estimation combined with ZF and Alamouti method as ZF and Alamouti estimated method respectively.

IV. SIMULATION RESULTS

The performance comparison of different detection methods including Alamouti, ZF methods for STBC based OFDM system is carried out on the basic of SER over various mobile speeds. The total simulation parameter used for simulation is listed on the Table1. The SER performance comparison of Alamouti and ZF detection method with perfect and proposed channel estimation scheme for normalized Doppler spread 0.03, 0.06 and 0.12 and are shown in the Fig 3, Fig 4 and Fig 5 respectively. The simulation result shows that Alamouti method suffers severe performance degradation due to CCI effect. The performance of ZF method is better than Alamouti detection method as it simply forces the CCI term to zero. The simulation results show that ZF estimated method gives better result than estimated Alamouti method. From the Fig 3 - Fig 5, it is seen that, when, the normalized Doppler frequency increases the SER increases drastically. From the simulation result, we also see that as the normalized Doppler spread increases, the estimated ZF method outperforms the perfect Alamouti method at high SNR.

Table1.Simulation Parameters

Parameter	Value
FFT Size	128
Number of Subcarrier	112
Number of CP	16
Pilot Spacing	1:8
Data Modulation	QPSK
Pilot Modulation	BPSK
Carrier Frequency	5GHz
Channel BW	1MHz
Subcarrier Spacing	7.8125KHz
Channel Model	Exponential decaying
Number of Multipath	3
Mobile speed	50/100/200 Km/h
Normalized Doppler frequency (F_dNTs)	0.03/0.06/0.12

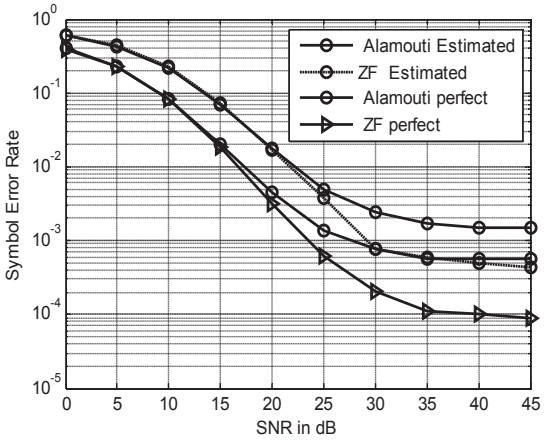

Fig. 3 SER performance comparison of Alamouti and ZF method with perfect and proposed channel estimation for normalized Doppler spread 0.03

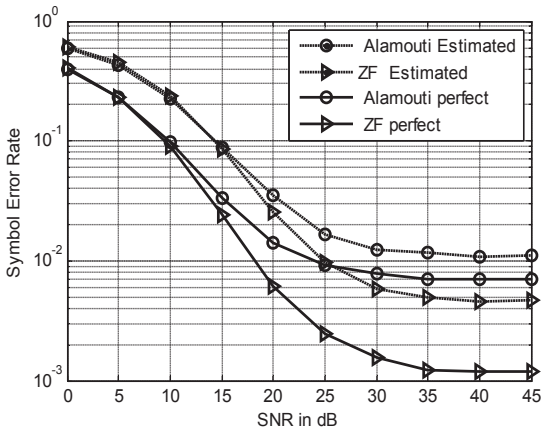

Fig. 4 SER performance comparison of Alamouti and ZF method with perfect and proposed channel estimation for normalized Doppler spread 0.06

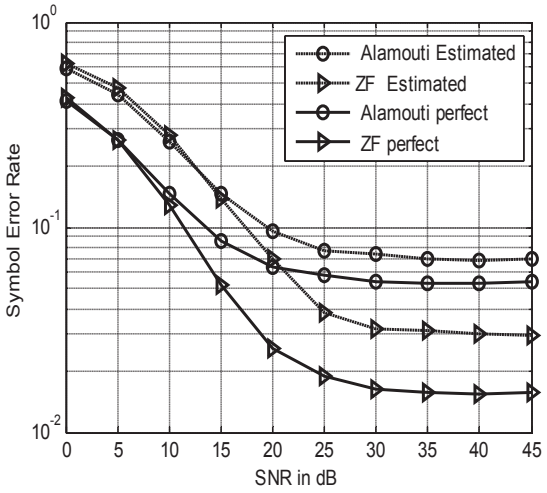

Fig. 5 SER performance comparison of Alamouti and ZF method with perfect and proposed channel estimation for normalized Doppler spread 0.12

V. CONCLUSIONS

In this paper, we have studied a combined effect of CCI cancellation and channel estimation for high mobility STBC-OFDM scheme. The proposed channel estimation method is based on LS algorithm with a modified zero form pilot arrangement based on Alamouti principle to avoid ITAI and there by facillating to estimate the entire four channels at pilot subcarrier and LPI method is applied at data subcarrier. Thus, by using the entire four channels, ZF detection technique has been implemented to recover the original transmitted signal by cancelling CCI effects. The disadvantage of the developed channel estimation method is that it suffers from spectral efficiency due to the insertion of zeros at alternative pilot location. This scheme can also be extended to other CCI cancellation schemes to improve the system performance.

REFERENCES

[1] G. Stuber, "Broadband MIMO-OFDM Wireless Communications", *IEEE Transaction on Signal Processing*, vol.92, pp. 271-294, 2004.

[2] A. F .Naguib, N. Seshadri and A. R Calderbank, "Increasing data rate over wireless channels: Space–time coding and signal processing for high data rate wireless communications", *IEEE Communications Magazine*, vol.17, pp.76–92, 2000.

[3] S. M Alamouti, "A simple transmitter diversity scheme for wireless communications", *IEEE Journal of Selected Areas in Communications*, vol.16, pp.1451–1458, 1998.

[4] K. F. Lee and D. B. Williams, "A space-time coded transmitter diversity technique for frequency selective fading channels," *IEEE Sensor Array and Multichannel Signal Processing Workshop*, Cambridge, MA, pp. 149-152 ,2000.

[5] J. W. Wee, J. W. Seo, K. T. Lee, Y. S. Lee and W. G. Jeon, "Successive Interference Cancellation for STBC-OFDM systems in a Fast Fading Channel," *IEEE Vehicular Technology Conference*, pp. 841-844 ,2005.

[6] H. Kanemaru and T.Ohtsuki, "Interference cancellation with diagonalized maximum likelihood decoder for space-time/space-frequency block coded OFDM," *IEEE Vehicular Technology Conference*, pp. 525-529, 2004.

[7] C.M. Li , I.T. Tang and G.W. Li " Performance Comparison of the STBC-OFDM Decoders in a Fast Fading Channel" *IEEE International Symposium on Intelligent Information Technology Application*, pp.791-795, 2008.

[8] D. Lin, P. Chiang and H. Li, "Performance analysis of two branch transmit diversity coded OFDM systems in time varying multipath Rayleigh fading channels," *IEEE Transaction on Vehicular Technology*, vol. 54, pp. 136 - 148, 2005.

[9] H. Zhang, J. M. Chen, Y. X. Tang and S. Q. Li, "Analysis of pilot-symbol aided channel estimation for MIMO-OFDM systems", *IEEE International Conference on ICCCAS*, Jan- 2004, pp. 299-303, 2004.

[10] S. Coleri, M. Ergen, A. Puri and A. Bahai, "Channel estimation techniques based on pilot arrangement in OFDM systems", *IEEE Transaction on Broadcasting*, vol.48, pp.223–229, 2002.

[11] G. L. Stüber, *Principles of Mobile Communication*, London: Kluwer, 2001.

[12] W. C. Jakes, *Microwave Mobile Channels*, New York: Wiley, 1974.

THE 5TH INTERNATIONAL CONFERENCE ON WIRELESS COMMUNICATIONS, VEHICULAR TECHNOLOGY, INFORMATION THEORY, AEROSPACE & ELECTRONIC SYSTEMS (WVITAE-2015)
December 13-16, 2015, Hyderabad, India

Energy Efficient Lighting System for Indoor Parking with Ubiquitous Communication

Mahesh Kumar Jha
Dept. of Telecommunication Engg.
CMR Institute of Technology
Bangalore, India
mahesh.kumarjha.in@ieee.org

Navin Kumar
Dept. of Electronics and Communication Engg.
Amrita Vishwa Vidyapeetham (University)
Bangalore, India
navinkumar@ieee.org

***Abstract*— This paper presents visible light communication (VLC) based energy efficient lighting system in indoor parking area for illumination and at the same time the system would offer ubiquitous communication. Light emitting diodes (LEDs) based VLC is used for communication and illumination simultaneously. An attempt is made to optimize the positioning of LED emitters in the parking area on the ceiling to obtain the desired signal-to-noise ratio (SNR) and bit error rate (BER). Two lighting configurations in the parking area are discussed. We compare the power transmission from LED emitters, number of emitters, SNR distribution, BER and cost for both the configurations. Multi level pulse amplitude modulation (M-PAM) is used for modulation. Further, we compare M-PAM with on-off keying (OOK) to get the required SNR and power requirement to achieve the same BER.**

Keywords*—visible light communication, information and communication technology, light emitting diodes, multiple pulse amplitude modulation, Energy efficiency.*

I. INTRODUCTION

Providing lighting is one of the most important and expensive responsibilities of a city. Lighting can account for 10–38% of the total energy bill in typical cities worldwide [1]. The modern smart and intelligent information and communication technology (ICT) infrastructure plays very important role in developing a smart city which includes designing energy efficient public illumination systems such as road, street, parking, and offices [2]. It will save huge energy and budget for the city in developing countries because of its strategic importance for economic and social stability. This smart lighting system can be used simultaneously for illumination as well as ubiquitous communication.

Though various domains are targeted, an intelligent energy efficient parking system can be used towards the development of smart cities. This illumination system enables communication in the indoor parking area offering users to be connected with high data rate networks. The indoor parking system can be designed such that users are informed at the entrance about the availability of parking slot and assists in reaching to the slot smoothly. The networked illumination system can adjust the brightness accordingly in saving some additional energy. This is possible with LED-based illumination system which has already been said to be the future lighting system [4-5].

Recent advancements in solid state lighting (SSL) have triggered research in the domain of optical wireless communication (OWC) especially visible light communication (VLC) [3]. VLC uses visible light spectrum (380nm-780nm) normally emitted from LEDs. LED, being semiconductor device has inherent characteristic of high speed switching which makes this device suitable for data communication. LED-based VLC offers many other distinctive advantages such as low cost design, free from most popular radio frequency (RF) based system, harmless to human health and of course usage of license free spectrum. Furthermore, the LED is power efficient illuminating device. LED-based VLC can be used to offer ubiquitous communication even in the places where RF is not reachable such as underground, subway and even in indoor parking area. In these situations, remaining always connected becomes challenging.

Normally, the VLC LED emitter is designed with multiple LEDs to provide necessary illumination by the use of high brightness (HB) or white LEDs. Also, multiple LEDs can be used as multiple-input and multiple-output (MIMO) technique [7] which would support high data rate communication and would help designing a robust communication system.

In this paper, we have considered energy efficient illumination for indoor parking system. This illumination system can be used for data communication within parking area. We have optimized the positioning of LED emitters in a given parking area to achieve desired signal-to-noise ratio (SNR) for enabling communication as well as making the system energy efficient. Furthermore, we have analyzed the BER performance and power requirement. The M-PAM modulation technique is used and compared with OOK modulation performance.

The remainder of this paper is organized as follows. In section II, LED based visible light communication system discussed. The parking layout, related work and analysis are presented in the section III, while in section IV the results are discussed. Finally, conclusion is given in section V.

II. LED BASED VISIBLE LIGHT COMMUNICATION SYSTEMS

Visible Light Communication normally employs lighting sources (LEDs) as transmitters and utilizes photodiodes as receivers. In this analysis we consider only line of sight (LoS)

link. VLC transmitters modulate intensities of light at such high speed that human eyes cannot perceive any difference between before and after modulation. As a result, VLC transmitter can be used for lighting and data communication simultaneously. The emitted light travels through LoS link and intercepted by photodiode based receiver. The photodiode converts light intensity into electrical signal, which is then amplified and processed to obtain final output. The received power will normally be a function of transmitted power, distance between transmitter and receiver, receiver collecting area, field of view (FOV) of the receiver, channel gain and so on. We discuss this next.

A. Channel DC gains

The radiation pattern of LEDs approximates Lambertian pattern and Lambertian radiant intensity is given by [8-9]:

$$R_o(\emptyset) = \left[\frac{(k+1)}{2\pi}\right] cos^k(\emptyset) \quad (1)$$

where k is the order Lambertian emission, and given by semi-angle at half illuminance of an LED $\emptyset_{1/2}$ as:

$$k = -ln2/\ln(cos\emptyset_{1/2}) \quad (2)$$

The irradiance and incident angles are denoted as $\emptyset$ and φ respectively.

In an optical link, the channel direct current gain (DC) is given as:

$$H(O)_{LOS} = \begin{cases} (A_{rx}/d^2)\, R_o(\emptyset)\cos(\varphi) & 0 \le \varphi \le \varphi_c \\ 0 & \varphi > 0 \end{cases} \quad (3)$$

where A_{rx} is the detector area, d is the distance between the transmitter and receiver and φ_c is the field of view (FOV) of the photodiode.

B. Received power

At the receiver, light passes through the optical filter and concentrator, so the received power is:

$$P_{rx} = (P_{LOS} + P_{diff}) \times T_f(\varphi) \times g(\varphi) \quad (4)$$

where $T_f(\varphi)$ is the transmission coefficient of the optical filter, $g(\varphi)$is the concentrator gain. P_{LOS} is the total received power of i LEDs in directed path, given as:

$$P_{LOS} = \sum_{i=1}^{LEDs} P_{tx} H^i_{LOS}(0) \quad (5)$$

Here $H^i_{LOS}(0)$ is the i^{th} LED channel DC gain and P_{tx} is the transmitted power. P_{tx} is given as: $P_{tx} = P_{LED} \times R_o(\emptyset)$. The power emitted by the LED is P_{LED}. The received diffused power with receiving area A_{rx} is given as $P_{diff} = A_{rx} I$, where I is the total intensity.

C. Signal to Noise Ratio (SNR)

At the photodiode, the received optical power is converted into the electric current which is given as:

$$i = P_{rx} \times r \quad (6)$$

where r is the responsivity (A/W) of the photodiode. The SNR is given by:

$$SNR = \frac{(r \times P_{rx})^2}{\sigma^2_{total}} \quad (7)$$

where σ^2_{total} is the total noise variance and it is given by:

$$\sigma^2_{total} = \sigma^2_{shot} + \sigma^2_{amplifier}$$
$$= 2qR(P_{rx} + P_n)B_n + i^2_{amplifier} B_a \quad (8)$$

where $B_n = I_2 R_b$ is the noise bandwidth, P_n is the noise power of ambient light, R_b is the data rate, I_2 is the noise bandwidth factor and B_a is the amplifier bandwidth.

III. INDOOR PARKING SYSTEM MODEL

The layout of the parking system is considered as shown in Fig.1. It is consider as one way parking system i.e. car will enter at one end and will exit from the other end. The LEDs light will be fixed on the ceiling at different positions.

The system is investigated for two cases/scenarios: first, we consider that lights are placed on both sides (boundary wall) and second, over the aisle width on the ceiling towards the aisle length. The aisle length and module width are considered 100m and 16.5m respectively on x- and y- axis. The module width of parking area is selected based on both sided parking and one way aisle width. The space length and space width are considered 6.5m and 3.5m respectively. The height of the light from the surface is considered at 4.5m. The photodiode receiver is considered to be installed in front of the driver glass. The important parameters are listed in Table1. In this analysis we consider only LoS link.

A. Modulation Scheme

In this paper, M-level pulse amplitude modulation (M-PAM) is considered, where M denotes the constellation size with spectral efficiency of $R = log_2(M)$ bits/s/Hz. The M-PAM is compared with OOK modulation. The BER of unipolar M-

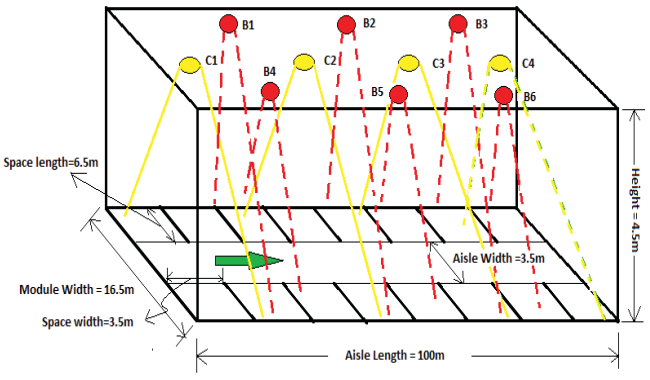

Fig.1: Parking layout/Model

PAM is given by:

$$\mathrm{BER_{M-PAM}} = \frac{2(\mathrm{M}-1)}{\mathrm{M}\log_2(\mathrm{M})}\,\mathrm{Q}\left(\frac{1}{\mathrm{M}-1}\sqrt{(\mathrm{SNR})}\right) \quad (1)$$

The BER for the case of OOK modulation is given as:

$$\mathrm{BER_{OOK}} = \mathrm{Q}\left(\sqrt{(\mathrm{SNR})}\right) \quad (2)$$

TABLE I. THE PARAMETERS OF THE SYSTEM MODEL

Parking area	$\boldsymbol{100m \times 16.50m \times 4.50m}$
Transmitters height	$4.50m$
Receiver height	$1m$
Semi-angle at half power	$22.5\ deg.$
FOV at the receiver	$15\ deg.$
Detector physical area of PD	$1\ cm^2$
Transmission co-efficient of optical filter	1
Refractive index of lens at PD	1.5
Photodiode responsivity	0.4
Amplifier bandwidth	$50\ MHz$
Wall reflectivity	0.7
Floor reflectivity	0.15
Ceiling reflectivity	0.8
Bit rate	$4\ Mbps$
Noise bandwidth factor	0.562
Amplifier noise density	$5pA/\sqrt{Hz}$
Ambient light photo current	$5840\mu A$

IV. RESULTS AND DISCUSSION

Investigation in this paper considers $\boldsymbol{100m \times 16.5m \times 4.5m}$ layout for the indoor parking system as shown in Fig.1. We tried to optimize the positioning of LED lights in a given area for the uniform SNR for the purpose to obtain acceptable data rate communication and uniform illumination. The transmitted power from each LED light is 25W. First, we consider that lights are placed on both side of the parking area. In this case, we placed 6 LED lights at the positions of $\boldsymbol{B1}$(17.5m, 3m, 4.5m), $\boldsymbol{B2}$(50.5m, 3m, 4.5m), $\boldsymbol{B3}$(83.5m, 3m, 4.5m), $\boldsymbol{B4}$(30m, 13.5m, 4.5m), $\boldsymbol{B5}$(60m, 13.5m, 4.5m), $\boldsymbol{B6}$(90m, 13.5m, 4.5m) on x-, y- and z-axis respectively.

The simulation result of SNR distribution is shown in Fig.2. It is observed that the desired SNR is obtained throughout the area. The minimum SNR is about 23dB which is at any corner and maximum SNR is about 48dB (just below the lamp), which is obvious. In fact, when we consider the data communication in the parking area and car/vehicle onboard, we have taken into account the driver seat place of the corner most vehicles which would be the furthest where the SNR is expected to be the minimum. Sometimes, it so happens that people stay back in the car and continue accessing Internet. In this situation also, we ensured that SNR value is high enough to enable BER performance. At the same time, the area is sufficiently illuminated to light up the entire space.

In the second case, we tried to place the lights on the ceiling over the aisle width area by considering 3-LED lights and 4-LED lights. 3-LED lights are placed at the positions of $\boldsymbol{C1}$(17.5m, 8.25m, 4.5m), $\boldsymbol{C2}$(50.5m, 8.25m, 4.5m), $\boldsymbol{C3}$(83.5m, 8.25m, 4.5m) on x-, y- and z-axis respectively. The layout is seen in Fig.1. The simulation result of SNR distribution for this case is shown in Fig.3. For this, we found the minimum SNR is about 20dB which is at corner end and maximum SNR is about 47.5dB. Furthermore, we placed the 4-LED lights at the positions of $\boldsymbol{C1}$(12.5m, 8.25m, 4.5m), $\boldsymbol{C2}$(37.5m, 8.25m, 4.5m), $\boldsymbol{C3}$(62.5m, 8.25m, 4.5m), $\boldsymbol{C4}$(87.5m, 8.25m, 4.5m) on x-, y- and z-axis respectively. The simulation result of SNR distribution for this case is shown in Fig.4. In this case, we observed the minimum SNR is about 24dB which is at the corner and the maximum SNR is about 47.5dB.

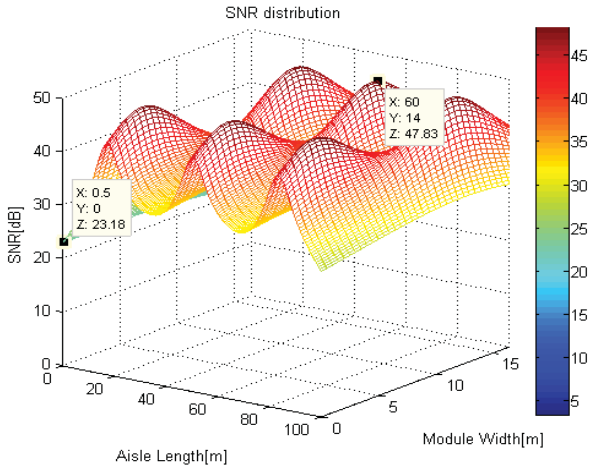

Fig.2: SNR distribution when both side LED lights are placed

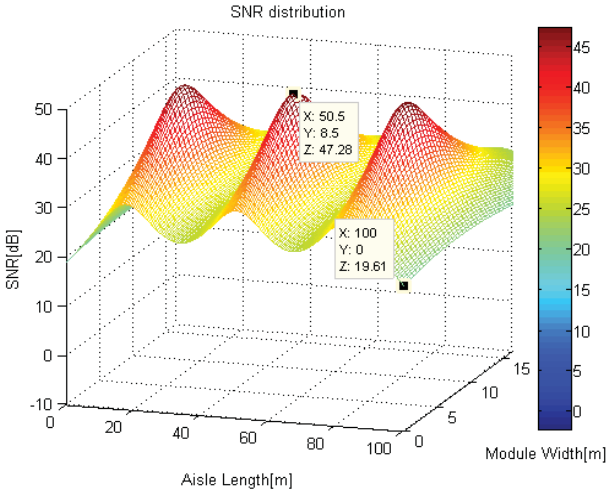

Fig.3: SNR distribution when 3-LED lights are placed over Aisle width

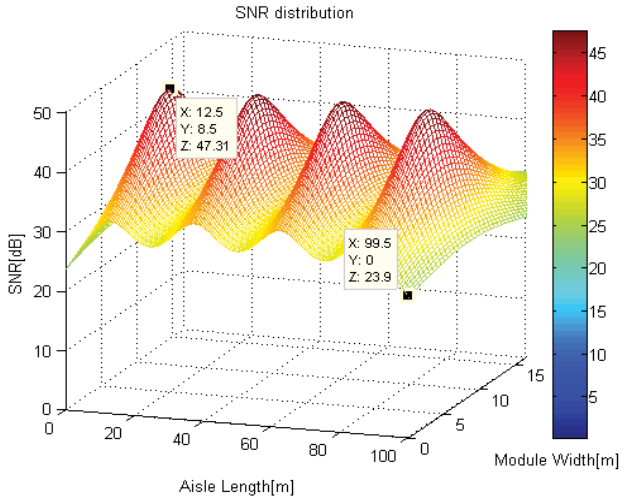

Fig.4: SNR distribution when 4-LED lights are placed over Aisle width

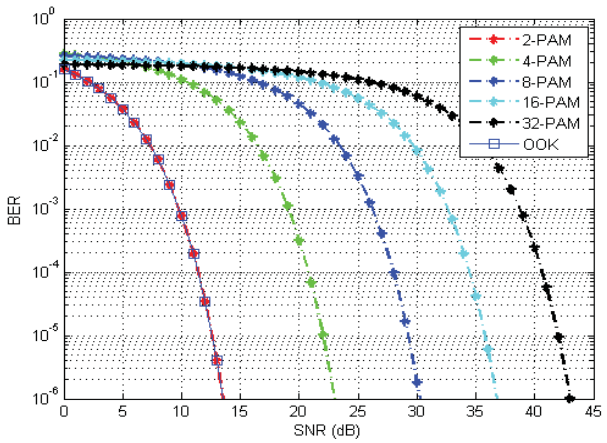

Fig.5: BER analysis of M-PAM and OOK

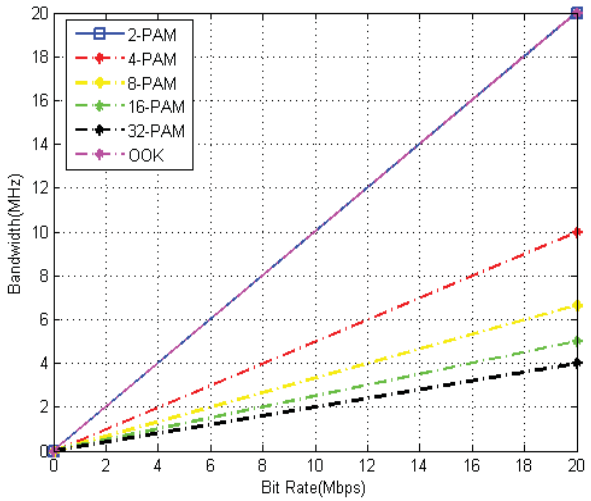

Fig.6: Analysis of bandwidth and bit rate

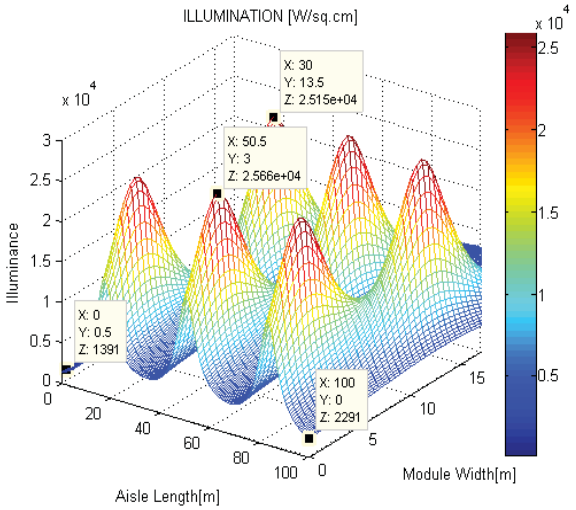

Fig.7 (a): Illumination with 6-LED lights

It is found that the desired SNR on overall surface in the parking area including corner points are obtained. And, it can be said that the second arrangement, where lamp posts are over aisle width, is found to be efficient in terms of energy.

We also investigated SNR value to support BER performance. We considered M-PAM for the modulation. The simulation result for BER for M-PAM is shown in the Fig.5. For the 2-PAM modulation, an SNR of about 14dB is needed to obtain a BER of 10^{-6} which is the same as OOK modulation technique. However, to obtain same BER, M-PAM needed SNR of about 23dB, 30dB, 36dB and 43dB when M = 4, 8, 16 and 32 respectively. However, M-PAM will offer high data rate transmission.

The bandwidth required to achieve the desired bit rate is shown in Fig.6. The OOK and 2-PAM gives the same performance in terms of bandwidth required for the bit rates. But with increase in *M*, bit rate improves and bandwidth decreases.

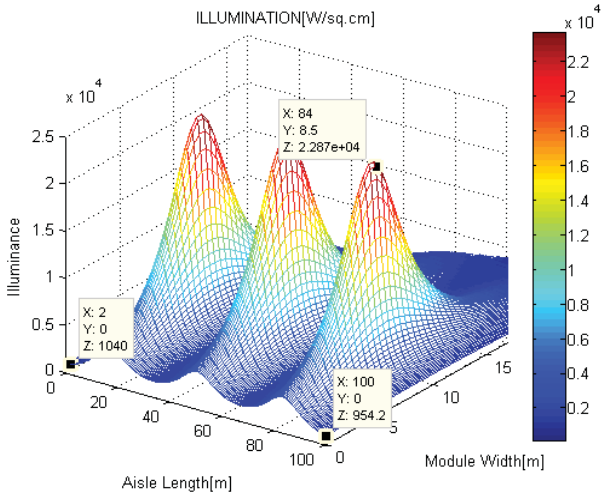

Fig.7 (b): Illumination with 3-LED lights

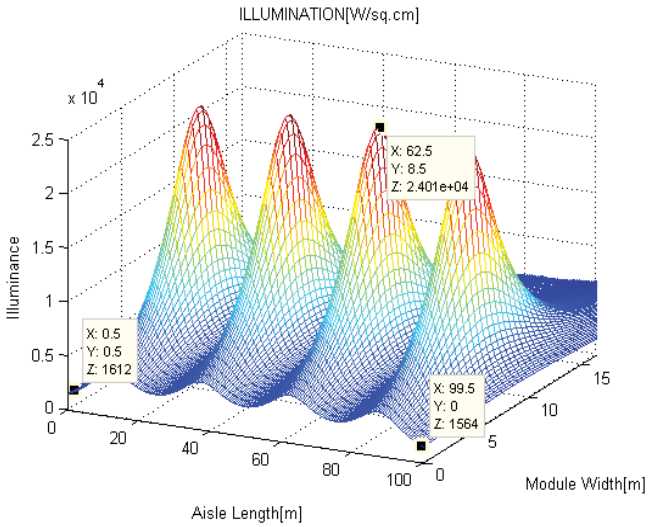

Fig.7(c): Illumination with 4-LED lights

TABLE II. CONFIGURATIONS ANALYSIS

Configurations	SNR(dB)		Illumination(W/cm^2)	
	Minimum	Maximum	Minimum	Maximum
6-LED LIGHTS	23	48	1391	2.566×10^4
4-LED LIGHTS	24	47.5	1564	2.401×10^4
3-LED LIGHTS	20	47.5	954.2	2.287×10^4

The illuminations for all the cases as discussed in section III are shown in Fig.7 (a)-(c). From the simulation, it is found acceptable illumination in all the cases over the surface. The SNR and Illumination analysis for the different cases are summarized in Table II. The minimum SNR and illuminance is observed at extreme corner area of the parking which is obvious. The minimum SNR of about 20dB is observed in all the considered configurations which is suitable for communication in the parking area. The maximum and minimum illuminations are observed about 2.566×10^4 W/cm^2 and 954.2 W/cm^2 respectively which will give proper illuminance over the surface in the parking area. Thus, LED lights can be used for illumination and at the same time for ubiquitous communication for the indoor parking systems. At the same time, the system is highly energy efficient.

V. CONCLUSION AND FUTURE WORK

The Illuminance over the surface in the parking area is analyzed for two different positionings of LED emitters. For all these positions, SNR distribution and BER performance is studied and analyzed with multi level PAM modulation technique. Further, it is compared with OOK modulation technique. The power transmission for each LED emitter is equal. So the transmitted power will be low if less number of LED emitters is placed and relatively it will be cost effective. We are in the process of finding an algorithm for automatization of placement of LED emitters for any given area depending on some inputs such as irradiation angle of emitters, receiver position and so on. We are also looking at devising suitable coding mechanism which can be efficiently and effectively used. We are also working on intelligent lighting in which all the lighting (VLC emitters) will be connected and intelligently switch adjust the intensity depending on ambient lights and motion detectors.

REFERENCES

[1] USAID-India," Energy efficient street lighting guidelines," Version 2.0, June, 2010.

[2] Navin Kumar, " Smart and Intelligent energy efficient public illumination system with ubiquitous communication for smart city," ISSS conference, March 28-30, 2013.

[3] D. O'Brien, H. L. Minh, L. Zeng, G. Faulkner, K. Lee, D. Jung, Y. Oh, and E. T. Won, "Indoor visible light communications: challenges and prospects," *Proc. SPIE, Free-Space Laser Commun. VIII*, vol. 7091, no. 1, p. 709106, 2008.

[4] M. S. Shur and R. Zukauskas, "Solid-State Lighting: Toward Superior Illumination," *proceeding of the IEEE*, vol. 93, pp. 1691-1703, 2005.

[5] T. Komine and M. Nakagawa, "Fundamental analysis for visible light communication system using LED lights," *IEEE Trans. consumerElectron.*, vol. 50, no. 1, pp. 100–107, Feb. 2004.

[6] J. Gancarz, H. Elgala, T.D.C. Little, "Impact of Lighting Requirements on VLC Systems", *IEEE Communications Magazine*, Decemer 2013.

[7] O'Brien, "Multi-input multi-output (MIMO) indoor optical wireless communications," in *Conf. Record 2009 Asilomar Conf. Signals, Syst., Comput.*, pp. 1636–1639, 2009.

[8] Joseph M.Kahn and John R.Barry, "Wireless Infrared Communications", *Proc.IEEE*, Vol. 85, No. 2, PP. 265-298, 1997.

[9] Yanrong Pei, Shaoxin Zhu, Hua Yang, Lixia Zhao, Xiaoyan Yi, Junxi Wang, Jinmin Li, "LED Modulation Characteristics in a Visible-Light Communication System", Optics and Photonics Journal, Vol3, 139-142, 2013.

THE 5TH INTERNATIONAL CONFERENCE ON WIRELESS COMMUNICATIONS, VEHICULAR TECHNOLOGY, INFORMATION THEORY, AEROSPACE & ELECTRONIC SYSTEMS (WVITAE-2015)
December 13-16, 2015, Hyderabad, India

30-Second Integration Time Power Law Conversion Model for Rainfall Attenuation in South Africa

Mary N. Ahuna[1], Thomas J. Afullo[2], Akintunde A. Alonge[3]
Discipline of Electrical, Electronic and Computer Engineering
University of KwaZulu Natal
Durban, South Africa

[1]215000279@stu.ukzn.ac.za, [2]afullot@ukzn.ac.za, [3]alongea@ukzn.ac.za

***Abstract*—Measured data for 5-minute, 1-minute and 30-second integration times are used to derive the power law model for 1-minute and 30-second data. These measurements are carried out in Durban (29°52'E, 30°55'S), South Africa over a period of 15 years, but segmented into three periods corresponding to the three different integration times. The measured conversion factors for conversion from 5-minute to 1-minute integration time are compared to global parameters and errors show that the global parameters may not be generalized for use globally. Furthermore, this paper proposes 30-second conversion factors for Durban. In addition, specific attenuation values on terrestrial networks are estimated for selected microwave and millimeter wave bands, namely Ku, Ka and 60 GHz.**

Keywords— Rain rate, specific attenuation, integration time, conversion factors

I. INTRODUCTION

Globally, both large and small corporate businesses are yearning for high speed and high capacity communication links for their business activities [1]. Additionally, Internet Service Providers (ISPs) and online broadcast companies rely on bandwidth scalability to provide high speed communication and high capacity data transfer to their clientele [2], [3]. This need can be fulfilled via the utilisation of high frequency communication channels available in the microwave and millimetre-wave bands. However, rainfall attenuation becomes more prominent when frequencies above 10 GHz are used - especially in tropical, sub-tropical and equatorial regions - which are often characterised by heavy rainfalls during some months of the year [3]. For successful design of satellite and terrestrial microwave systems, design engineers require sufficient information on rainfall attenuation for the region in consideration. This information can be estimated by analysis of rain rate data collected over that region for a relatively long period of time [1-4]. There is agreement that rainfall data with lower integration times provide more information for accurate prediction of rainfall attenuation. Consequently, for effective prediction of rainfall effects over radio links at microwave and millimetre bands, measured data with integration times at 1-minute and or lower, are important. They can be utilized to obtain rainfall distributions and useful conversion factors for effective radio planning.

Significant research work has been carried out associated with rainfall attenuation over South Africa, particularly in Durban, for radio propagation in microwave and millimetre wave bands [2], [4]-[7], [9]-[12]. Studies conducted on rainfall attenuation in this region were based on the microphysics of rain. In one of these studies, Odedina and Affulo [7] proposed rainfall zones for attenuation prediction based on International Telecommunication Union (ITU) recommendation P.837-4 nomenclature [8]. In their work, [7] also suggested that rain fading is severe in the north eastern provinces of South Africa compared to the western provinces. In a further experimental campaign on rainfall over South Africa, Owolawi [9] was able to develop rainfall rate contour maps for South Africa's locations for 5-minute to 1-minute integration times. This study buttressed the earlier investigations of Odedina and Afullo [7]. In addition, the rainfall drop size distribution (DSD) technique approach in [13] enhanced initial efforts on rain rate campaign over Durban. Alonge and Afullo [10] applied parameter estimation techniques to confirm that the lognormal and gamma DSDs gave the best characteristics of drop sizes over Durban. They further used this approach to establish the seasonal variability of DSDs in Durban. Their results predicted that summer and autumn seasons are periods associated with high probabilities of outages in wireless networks. A thorough examination of the overall work done in South Africa reveals that rainfall data used are mainly of one minute integration time [6], [11]. However, it has been shown that rainfall data with lower integration time of 30 seconds or less are important in outage prediction analysis for wireless networks [3]. It is with respect to this observation that this current study is undertaken.

Integration time, also referred to as resolution time, generally refers to the sampling interval of data archiving which is often dependent on the choice of the measuring instrument. In a number of research, integration times of 15 minutes, 10 minutes and 1 minute are mostly used [3], [9]. In locations where the equipment is incapable of sampling rainfall data at these high rates, one hour sampling time is often utilized – although this is not widely encouraged because resultant attenuation estimates are likely to be underestimated. Rainfall measurements with less than one hour sampling time provide better time series analysis of rainfall rate variation in the time domain. This is important for radio engineers

particularly in the determination of sufficient fade margins required to counter rain attenuation effects in microwave bands [4].

Rainfall rate measurements at any location could be obtained by collecting data over a period of time from national meteorological administrations. Alternatively, these measurements can be obtained from independent rainfall rate measurements by means of rain gauges, distrometers or radar with small integration times [12]. Among the choice of equipment, the rain gauge is prominent because it is easily installed and it is also inexpensive. Gauges at the surface measure the point accumulation of rain-water with a known time interval and provide the result as point rain rate i.e. accumulation per unit time averaged over some measurement [13]. Most common types of rain gauges include the standard (graduated cylinder) rain gauges, tipping bucket rain gauges, weighing precipitation gauges and an optical rain gauges.

In this study, rainfall data measurements were collected using the Joss-Waldv□gel (JW) RD-80 distrometer installed at the University of KwaZulu Natal, Durban, and the rain gauge data obtained from the South African Weather Service (SAWS). From these sets of data over Durban, inferences are made from rain rate cumulative distributions and their required conversion factors. The rest of this paper shall be as follows: Section II discusses the measurements and data processing; Section III examines rainfall cumulative distributions and conversion factors; Section IV discusses results associated with specific attenuation and Section V provides the conclusion of this study.

II. Measurements And Data Processing

Rainfall data collected over Durban are mainly archived data from the distrometer and the rain gauge over a period of time. These equipment have varying levels of accuracy and measurement errors and it is widely accepted that the distrometer has an improved sensitivity to rainfall measurements than the rain gauge [14]. The distrometer unit basically has two components: outdoor and indoor units. The outdoor unit is designed with droplet receiving area of 0.005 m^2 and is capable of processing rainfall data into 20 categorized channels via the indoor unit [15]. Each of these channels have rain drops with diameters ranging from 0.3 mm to 5.4 mm. The computation of rainfall rate is given by [6], [16]:

$$R = \frac{6\pi \times 10^{-4}}{A \times T} \sum_{i=1}^{20} {D_i}^3 C_i \quad [mm/h] \qquad (1)$$

where C_i and D_i are the number of rain drops and mean drop diameter (mm) in the ith class, respectively, A is the sample area (0.005 m^2), T is the sampling time given as 60 seconds and $v(D_i)$ is the terminal velocity of rain drop in m/s.

On the other hand, the tipping rain gauge measures the amount of rain when a reed sensor is triggered, signalling the tipping sequence. The rain gauge has a poor sensitivity especially at very low rainfall rates (< 2 mm/h), but, on the other hand, it is gives a more inexpensive way of collecting the rainfall data across the world.

In this study, rainfall measurements obtained from these equipment have integration times of 5-minutes, 1-minute and 30-seconds. The set of 1-minute (60-seconds) and 30-second data are both retrieved from the JW RD-80 distrometer. The 1-minute data was collected between October 2008 to December 2010, while the 30-second data was obtained between April 2013 and March 2015. The 5-minute rainfall data from SAWS over Durban was collected in the period 2001 to 2011 (11 years). Representative number of samples, as well as their periods of collection are summarized in Table I.

III. Cumulative Distributions and Conversion Factors of Rainfall Rate over Durban

This section discusses the analysis of rainfall data measurements at different integration times collected over Durban with the aim of obtaining their cumulative distributions. Furthermore, we employ regression analysis to determine relationships between data at different integration times.

The cumulative distribution represents an evaluation technique of identifying the percentage exceedence probability of rainfall rate required for optimal wireless service in a rainy medium. These probabilities enable communication engineers to determine the permissible fade margin levels required by base stations to reduce network outages during rainy periods. Generally, rainfall rate values for different locations, corresponding to 0.01% exceedence are of major interest to viability of satellite and terrestrial communication links. Hence this parameter is often referred to as $R_{0.01}$. From the data collected cumulative distributions are obtained for three categories of rainfall integration times as seen in Fig. I.

A. Rainfall Cumulative Distributions for Different Integration Times

Fig.1 shows the cumulative distributions for three integration times from 0.004% <P < 9.5% of rainfall rate exceedence. The three distributions have a similar shape profile, with the 30-second graph being a scaled version of the 5-minute graph with a factor greater than 1. It is then evident from Fig. 1 that the rainfall rate is proportional to integration time. This further proves that an instrument with a long sampling time can easily miss logging shorter peaks in the rain intensity, resulting in lower measured rainfall intensities per unit length of time.

In Table II, R_1 value for 30-second integration time is determined as 6.5 mm/h, $R_{0.1}$ = 24.7 mm/h and $R_{0.01}$ = 64.3 mm/h. For the 1-minute integration, R_1 = 5.8 mm/h, $R_{0.1}$ = 23.2 mm/h and $R_{0.01}$ = 59.5 mm/h. For 5-minute integration time, are R_1 = 3 mm/h, $R_{0.1}$ = 16.8 mm/h and $R_{0.01}$ = 55.2 mm/h. It is observed that the 30-second integration time presents more information by giving a higher value of $R_{0.01}$ of 64.3 mm/h. Thus, there is need to convert other higher rain rates to 30-seconds integration time.

TABLE I. Rainfall Measurement over Durban from Different Equipment

DATA SAMPLING TIME	SAMPLES	NUMBER OF YEARS	INSTRUMENT USED
30 seconds	45,657	2	Distrometer
1 minute	56,463	2	Distrometer
5 minute	20,459	11	Rain Gauge

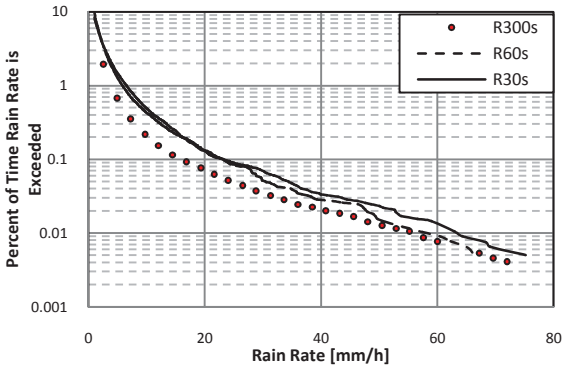

Figure 1: Cumulative distributions of rainfall rates for T-second integration time

TABLE II. PERCENTAGE OF RAIN RATE EXCEEDANCE FOR VARIOUS INTEGRATION TIMES OVER DURBAN

INTEGRATION TIME (sec)	PERCENTAGE OF RAIN EXCEEDENCE (%)					
	1	0.3	0.1	0.03	0.01	0.003
30	6.5	13.6	24.7	43.9	64.3	84.3
60	5.8	12.5	23.2	38.7	59.5	70.0
300	3.0	8.5	16.8	32.0	55.2	79.2

The $R_{0.01}$ determined was comparable to the ITU-R P.837-1 [11] predicted value of 63 mm/h for this region.

A summary of rain rate values of different integration times obtained over Durban for exceedence between 0.003% and 1% is presented in Table II.

B. Determination of Conversion Factors

In cases where data collection is done using other times, models have been developed for conversion of $R_{(\tau\ \mathrm{min})}$-values into $R_{(1\ \mathrm{min})}$-values as highlighted by [9], [17]-[19]. Conversion from a higher integration time values to 1-minute or lower rainfall rate integration time is very useful for development of rain rate models applicable in the prediction of rainfall attenuation at a given region [3], [20]. From the work of Ajayi and Ofoche [3], it was established that a power law relationship exists between the equiprobable rainfall rates of two integration times, given by:

$$R_\tau = u(R_T)^v \quad [mm/h] \tag{2}$$

where R is the rainfall rate, τ and T are integration times at the required and available rainfall rates respectively.

Segal [21] proposed a method of conversion that was expressed as the proportion of the equally probable rainfall rate,

$$\rho_\tau(P) = \frac{R_1(P)}{R_\tau(P)} \tag{3}$$

with conversion factor, $\rho_\tau(P)$, expressed as a power law

$$\rho_\tau(P) = aP^b \tag{4}$$

where $R_1(P)$ represents the rainfall rate at 1-minute integration time with the probability of occurrence P, $R_\tau(P)$ is the rainfall rate in τ-minute integration time, and the parameters a and b are coefficients regression analysis of rainfall data.

There are two main approaches used for rain rate conversion: use of equivalent rainfall rates or same probability of occurrence [22]. The method adopted in this paper is the use of same probability of occurrence. This approach is used on 5-minute data, 1-minute data and 30-second data collected over Durban. The three sets of data collected were used to generate conversion factors from higher to lower integration times using the power-law fit and are shown in Fig. 2 (a) - (c). These conversion factors are later compared in Table VI with those determined by other researchers in various regions of the world.

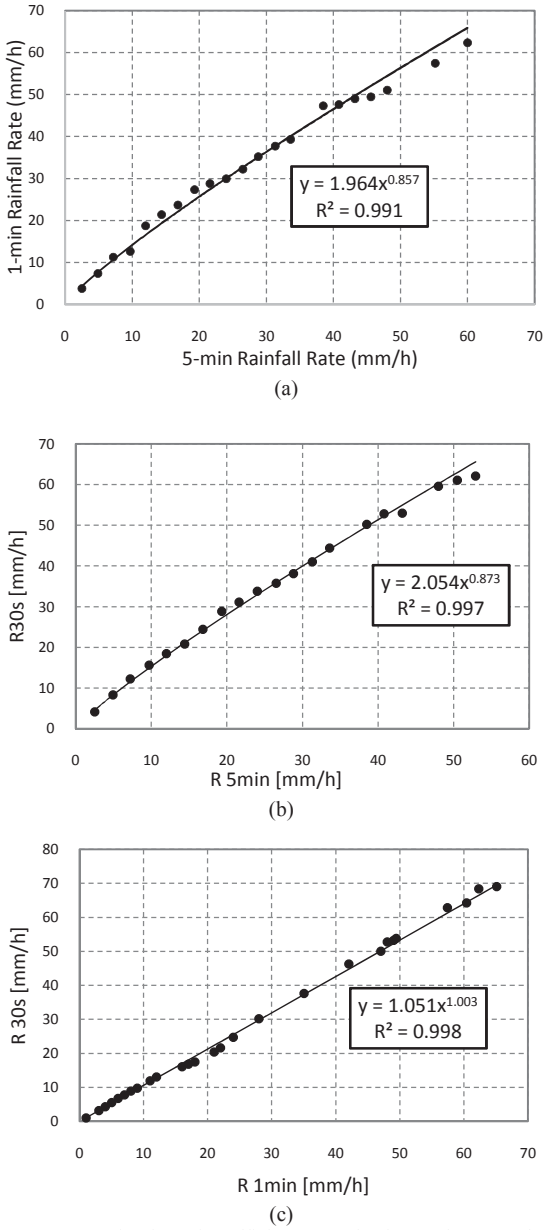

Figure 2: Determination of coefficients u and v for Durban, South Africa, in the conversion from (a) 5-minute to 1-minute, (b) 5-minutes to 30-seconds and (c) 1-minute to 30-seconds

Using (2), conversion coefficients for Durban were determined to be the following:

$$R_{30s} = 1.051{R_1}^{1.003} \quad (5)$$

$$R_{30s} = 2.078{R_5}^{0.868} \quad (6)$$

$$R_1 = 1.964{R_5}^{0.858} \quad (7)$$

where R_{30s} is the rainfall rate in 30 seconds while R_1 and R_5 are 1-minute and 5-minute times, respectively.

Estimates from our proposed rainfall rate conversion models should be representative of actual measurements. In this regard, our models in (5) - (7) were validated using the chi squared statistics (χ^2) test for goodness of fit. The function describing χ^2 is given in [23] as,

$$\chi^2 = \sum_{i=1}^{N} \frac{y_i - f(x_i)^2}{y_i} \quad (8)$$

where y_i and $f(x_i)$ are the measured and predicted values respectively, with N being the sample size.

Results from error analysis and power-law models describing the power-law conversion models are presented in Table III and Table IV. The chi-squared test was carried out at a confidence level of 0.05 and we obtained values of 2.0371, 1.0193 and 0.8452 from the three models in (5), (6) and (7) in that order. A comparison with chi-squared table showed that the three models passed the test and can be used for rainfall rate conversions in Durban.

From the power law relationship, Table V highlights comparisons of regression coefficients u and v obtained in this study with those determined previously by Ajayi and Ofoche [3] at Ile-Ife, Nigeria and Flavin [24] in Australia, USA, Europe and Canada. It is seen that the proposed model's coefficient u is higher than its counterparts from other regions of the world. Error analysis was done using $R_{0.01}$ value of 55.2 mm/h of the measured 5-minute data over Durban and the ITU-R P.837-1 [11] predicted $R_{0.01}$ value of 63 mm/h for Region M.

TABLE III. POWER-LAW CONVERSION COEFFICIENTS TO 1 MINUTE

Coefficients for $R_\tau = u(R_T)^v$, for τ = 60s					
T (Sec)	***a***	***b***	**R^2**	**RMS**	**CHI**
300	1.964	0.858	0.992	1.883	2.037[a]

[a]Significant level is given as 30.144, at DF = 19

TABLE IV. POWER-LAW CONVERSION COEFFICIENTS TO 30 SECONDS

Coefficients for $R_\tau = u(R_T)^v$, for τ = 30s					
T (Sec)	***u***	***v***	**R^2**	**RMS**	**CHI**
60	1.051	1.004	0.998	1.051	1.019[b]
300	2.079	0.868	0.997	1.324	0.845[c]

[b]Significant level is given as 38.885, DF = 26 [c]Significant level is given as 31.41, DF = 20

TABLE V. COMPARISON OF POWER LAW REGRESSION COEFFICIENTS WITH THOSE OBTAINED IN OTHER PARTS OF THE WORLD COEFFICIENTS

Coefficients for $R_\tau = u(R_T)^v$, for τ = 1 min				
Model	T (Min)	*u*	*v*	Error (%)
AJAYI [3]	5	0.991	1.098	28.6
OWOLAWI [7]	5	1.062	1.051	13.9
FLAVIN [25]	6	0.990	1.054	7.7
Proposed	5	1.964	0.858	2.6

Ajayi and Ofoche [3] model resulted in an error of 28.6%, the Owolawi [7] 13.9%, Flavin [24] model 7.7% and the proposed model in (7) produced an error of 2.6%. The highest error is thus observed from Ajayi and Ofoche [3] model. The tropical climate of Ile Ife, characterized by heavy rainfall, is largely a factor contributing to this large error. From Table V, it is observed that the Flavin [24] model is closer to the measurements in Durban with an error of 7.7%.

IV. CALCULATION OF SPECIFIC ATTENUATION VALUES OVER DURBAN, SOUTH AFRICA

Arising from the need for high capacity and high speed communication links, Ku, Ka and V bands are utilized for both terrestrial and satellite communications such as wireless broadband access (WBA), multipoint video distribution services (MVDS) and other broadband services [1]. The major challenge in operating at these higher frequencies is high signal attenuation resulting from signal absorption in high intensity rain rates. To address this setback, specific attenuation values were determined at Ku, Ka and 60 GHz bands as summarized in Table VI. The 60 GHz channel is unlicensed band that has been identified for use in short range wireless communications due to its high speed capability and frequency reuse [25].

ITU-R P.838-3 [26] provides the procedure for the calculation of specific attenuation on the link as given in (9):

$$\gamma_R = kR^{\propto} \quad [dB/km] \quad (9)$$

where R is the rain rate in mm/h at probability of exceedence while k and α are functions of polarization and frequency provided by [26].

Results of calculated specific attenuation at 1-minute integration time for Durban at Ku (12 GHz), Ka (30 GHz) and 60-GHz bands are presented in Fig. 3. From this figure, it is observed that the three curves have the same shape profile but with specific attenuation values at 60-GHz band being higher than those at 12 GHz and 30 GHz. As an example, at the same probability percentage exceedence of 0.01%, the specific attenuation is 2.99 dB/km at 12 GHz, 11.58 dB/km at 30 GHz band and 19.65 dB/km at 60 GHz band. This shows that specific attenuation due to rainfall increases as frequency of operation increases as expected. This implies that a consequent increase or decrease in rainfall rate also affects the system availability. As a result, the occurrence of high rainfall

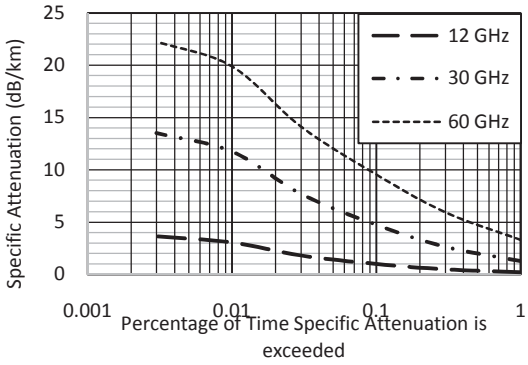

Figure 3: Computed specific attenuation exceeded for different percentages of time using 1-minute integration time data over Durban

rate in Durban will affect the performance of radio links due to measured attenuation caused by rain.

V. CONCLUSION

Using the power law relationship between equiprobable rain rates of two different integration times, we have obtained measured and predicted values of rainfall rate exceeded for 0.01% of the average year at 1-minute integration time that are comparable to ITU-R P.837-1 predicted value of 63 mm/h for Durban, South Africa. Power law models obtained at Durban, South Africa, can be used by other regions in similar climatic regions to convert rainfall rate statistics from higher integration times of 5 minutes and 1 minute to 30 seconds, respectively for more accurate prediction of rainfall attenuation especially in South Africa.

ACKNOWLEDGMENT

The author is grateful to the Centre for Radio Access and Rural Technologies (CRART) and the Discipline of Electrical, Electronics and Computer Engineering, University of KwaZulu-Natal, South Africa, for their support.

REFERENCES

[1] D. L. Emiliani, L. Luini, and C. Capsoni, "Analysis and parameterization of methodologies for the conversion of rain rate cumulative distributions from various integration times to one minute," IEEE Antennas and Propagation Magazine, Vol.51, No.3, 70-84, June 2009.

[2] M. R. UI Islam, T.A Rahman, S.K.A. Rahim, K. F. Al-tabatabaie and A. Y. Abdulrahman, " Fade margins prediction for broadband fixed wireless access (BFWA) from measurements in tropics," Progress In Electromagnetics Research C, Vol. 11, 199-212, 2009.

[3] G. O. Ajayi, and E.B.C Ofoche, "Some tropical rain rate characteristics at Ile-Ife for microwave and millimeter wave applications," Journal of Climate and Applied Meteorology, Vol. 23, 562-567, Apr. 1984.

[4] S. J. Malinga, P.A. Owolawi and T.J.O. Afullo, "Computation of rain attenuation through scattering at microwave and millimeter bands in South Africa," Progress In Electromagnetics Research Symposium Proceedings, Taipei, pp 959-971, 2013.

[5] P. A. Owolawi, T.J. Afullo and S.B. Malinga, "Effect of rainfall on millimeter wavelength radio in Gough and Marion Islands," Progress in Electromagnetics Research Symposium, Beijing, China, March 23-27, 2009.

[6] A. A. Alonge and T.J. Afullo, "Seasonal analysis and prediction of rainfall effects in eastern South Africa at Microwave Frequencies," Progress in Electromagnetics Research B, Vol. 40, 279-303, 2012

[7] M. O. Odedina and Thomas J.O. Afullo, "Characteristics of seasonal attenuation and fading for line-of-sight links in South Africa," SATNAC, pp 1-6, 2008.

[8] ITU-R P.837-4 Recommendation, "Characteristics of precipitation for propagation modelling," Geneva, 2003

[9] P. Owolawi, "Derivation of one-minute rain rate from five-minute equivalent for the calculation of rain attenuation in South Africa," PIERS Online, Vol.7, No.6, pp 524-535, 2011

[10] A. A. Alonge and T.J. Afullo, "Regime analysis of rainfall drop-size distribution models for microwave terrestrial networks," IET Microwave, Antennas and Propagat., Vol. 6 (4), March, 2012.

[11] ITU-R P.837-1 Recommendation, "Characteristics of precipitation for propagation modelling," Geneva, 1994

[12] P. O. Akuon, and T.J.O. Afullo, "Rain cell sizing for the design of high capacity radio link systems in South Africa," Progress in Electromagnetics Research B, Vol.35, 263-285, 2011

[13] T.J.O. Afullo, "Raindrop size distribution modeling for radio link design along the eastern coast of South Africa," Progress In Electromagnetics Research B, Vol. 34, 345-366, 2011

[14] J. Wang, B.L. Fisher and D.B. Wolff, "Estimating rain rates from tipping-bucket rain measurements," Journal of Atmospheric and Oceanic Technology, 2006.

[15] Distromet system, The Joss-Waldvogel Distrometer Handbook, Basel, Switzerland, 2000

[16] R. Gunn, and G.D. Kinzer, "Terminal velocity of fall for water drops in stagnant air," J. Appl. Meterology, Vol.6, 243-248, 1949.

[17] F. Moupfouma, "More about rainfall rates and their prediction for radio systems," IEEE Proceedings, Vol. 134 (6), Pt. H, 527-537, 1987

[18] R. K. Crane, " Electromagnetic Wave Propagation through Rain", Wiley Interscience, New York, 1996

[19] T. Milda, and Z. Mindaugas, "Atmospheric attenuation due to humidity, electromagnetic waves," Chapter 8, pp 158-172.InTech, 2011

[20] ITU-R P.618-11 Recommendation, "Propagation data and prediction methods required for the design of Earth-space telecommunication systems," Geneva, 2013

[21] B. Segal, "The influence of the raingauge integration time on measured rainfall-intensity distribution functions", Journal of Atmospheric and Oceanic Technology, Vol.3, 662-671, Dec. 1986

[22] C. W. Ooi, and J. S. Mandeep, "Empirical methods for converting rainfall rate distribution from several higher integration times into a 1-minute integration time in Malaysia," GEOZIFIKA, Vol. 30, pp. 143-154, Nov. 2013.

[23] M. Galoie, G. Zenz and A. Motamedi, "Rainfall analysis for the Schoeckelbach Basin (Australia) and determining its best-fit probability distribution model," DOI:10.5675/ICWRER_2013, 43-52

[24] R. K. Flavin, "Rain attenuation considerations for satellite paths," Telecom Australia Research Laboratories Report No 7505, 1982.

[25] N. Guo, R.C. Qui, S. S. Mo and K. Takahashi, "60-GHz Millimeter-Wave Radio: Principle, technology and new results," Research Article, EURASIP Journal on Wireless Communications and Networking, Volume 2007, 1-8, December, 2004.

[26] ITU-R P.838-3 Recommendation, "Specific attenuation model for use in prediction methods," Geneva, 2005

THE 5TH INTERNATIONAL CONFERENCE ON WIRELESS COMMUNICATIONS, VEHICULAR TECHNOLOGY, INFORMATION THEORY, AEROSPACE & ELECTRONIC SYSTEMS (WVITAE-2015)
December 13-16, 2015, Hyderabad, India

Fuzzy based Moving Object Detection and Classification in Video

Mr. Manojkumar M. Gawali
Dept. of Computer Engineering
Sinhgad College of Engineering
Pune, India-411041
gawalimanojkumar1@gmail.com

Prof. Dipti R. Pawar
Dept. of Computer Engineering
Sinhgad College of Engineering
Pune, India-411041
dvshitole.scoe@sinhgad.edu

***Abstract*—Human detection is one of the important and fundamental steps in advanced applications like human activity analysis, gait recognition, human centric surveillance, intelligent video surveillance system, etc. Inaccurate detection of human in all these application leads to false alarms. The proposed method consists of four steps namely; moving object detection, blob detection, feature extraction and classification. Moving object detection is done by performing background subtraction technique which uses fuzzy logic approach. After performing background subtraction blobs are identified. Then blob feature extraction is done by using simple and efficient features like height, width, number of black and white pixels. These features are trained using Support Vector Machine (SVM). The Support Vector Machine is capable to learn all features of blob, and it is used for human or non-human classification. The system is tested on INRIA and PETS 2000 standard data-set.**

Keywords*—Object Detection; Blob Detection; Feature Extraction; SVM classification

I. Introduction

Over the recent years, detecting human beings accurately from video scene of a surveillance system is attracting field due to its wide range of applications in event detection, human gait characterization, person identification, gender classification, etc. Video surveillance system having two sub-problems, one is detection of moving objects and another one is determining whether moving object is human or not.

For moving object detection there are three basic approaches used: Background subtraction, Temporal differencing, and Optical flow. Background subtraction is one of the most popular approach for moving object detection. This method consists in finding the difference of current frames with respect to a background frame in order to detect pixels whose difference is greater than threshold value [1]. A popular mixture of gaussian technique for background subtraction approach consists in modeling each pixel with a Gaussian distribution [2]. The adaptive version of this algorithm works well when the background is dynamic. Temporal differencing approach for moving object detection simply takes difference between previous and next frame, if this difference is greater than threshold value, then moving object is detected [3]. Optical flow is another approach for moving object detection. This approach calculate motion of field, and flow distribution characteristics of image using different methods to estimate optical flow. Optical flow approach is sensitive against noise, and it is highly complex [4]. Lijun, Xiao proposed an approach for moving object segmentation using fuzzy logic algorithm [5]. Basically the fuzzy logic algorithm is used for thresholding as well as background updation part. Object segmentation is done using background subtraction which uses fuzzy approach, that is responsible for improving segmentation accuracy and reducing under-segmentation problem. In [6] Gambhir, D and Manchando presented an algorithm that automatically segment moving object in video by creating multiplicative mask, and it contains less number of noisy, false pixels. The segmented object tracked via color features, and then position of moving object predicted using kalman filter. In [7] Kalyan Kumar, and Pankaj Kumar has presented an approach for moving object detection using simple thresholding technique for background subtraction. This scheme depends on two basic algorithms; the first algorithm models background depends on first few frames, and second algorithm extract moving object based on simple thresholding. The strength of this simple thresholding technique is lies in it's simplicity, and intensity range for each pixel location define in background.

There are different methods to detect human beings from video. Template based human detection method is based on predefined template dataset defined by users. In [8] Zhujie and Yu has presented face recognition method based on eigen face technique. This face recognition method works in two part. The first part is responsible for constructing eigen faces of training images, and second part include test images that is recognized by computing the euclidean distance. In [9] Ali, Syed Sohaib and Zafar has presented method for human detection and recognition. This approach uses very effective features such as area, perimeter, centroid, principal axis of inertia for classification part. In [10] Osuna, Edgar, and Federico Girosi has presented an application for face detection using support vector machine. Support vector machine is responsible for determining appropriate class, either human or non-human. Kong, Yinghui, and Lei wang [11] proposed a method for moving object classification based on feature combination and Support Vector Machine. The method for moving object classification includes various steps such as object detection, post processing, feature extraction and SVM classification. Mahapatra, Tusar Kanti Mishra [12] proposed scale and view invariant approach for human detection based on template dataset. Scale and view invariant contour features like distance, angle, and cord to arc ratio are effective for template based human detection from video. The proposed human detection method requires following four steps; (a) Moving Object Detection, (b) Blob Detection, (c) Feature Extraction, (d)

SVM Classification. Rest of the paper is presented as follows. Section II is the discussion about system architecture and it's implementation details. Section III introduces comparative analysis and discussion. Section IV is all about experimental evaluation part. Section V is all about conclusion and future scope of the work. Fig. 1 shows flow for proposed human detection system.

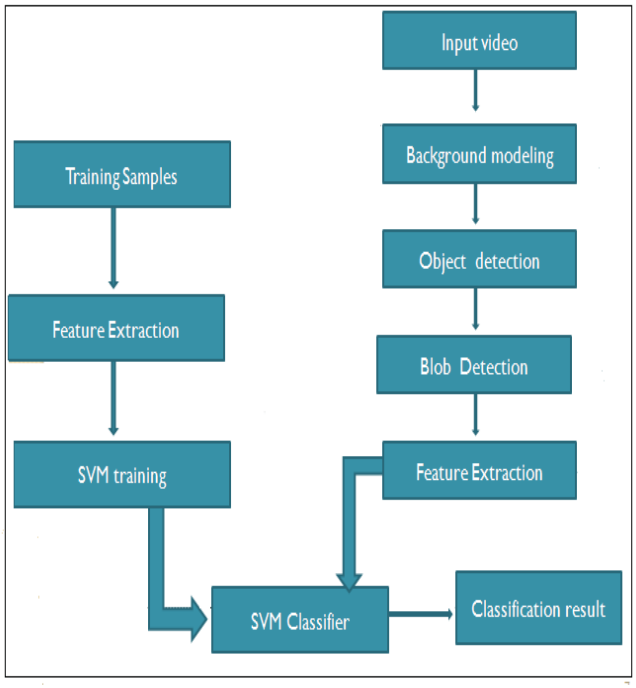

Fig. 1. Human Detection System

II. System Architecture

For human detection, the first essential step is to detect moving object from video, and then classifies it to human or non human.

A. Frame Extraction

The frame extraction module takes video as input and produces number of frames based on time delay between frames. The number of maximum frames depends on length of video and time delay between frames. Mathematically, this is shown in eq (1).

$$X_n: n>1 \ \& \ n = \text{Video length} / td, \ \& \ td > 1 \qquad (1)$$

Where,

- X_n is the n^{th} frame.
- n is the number of frames required.
- td represents time delay between frames.

Table I shows number of extracted frames that mainly depends on video length and delay factor.

TABLE I. Frame Extraction

Video Set	Size(MB)	Length (sec)	fps	Time delay(msec)	Number of frames
1	6.23	58	19.40	50	1161
2	6.23	58	25.0344	40	1452
3	6.23	58	33.3793	30	1936
4	6.23	58	1	1000	58
5	6.23	58	2	500	116

B. Background subtraction

Background subtraction is process of separating out foreground objects from maintained background model. The proposed background subtraction method uses fuzzy logic approach for calculating background frames. A foreground object is an entity that is separated based on minimum and maximum frame. For background model creation, consider first N numbers of frames are background frames, where all these background frames doesn't contain foreground objects. Apply fuzzy logic on these background frames. Let {f1, f2,..., fN} be the fuzzified background frames, which are used for background modeling part. After getting fuzzified background frames, calculate minimum and maximum background modeling frames. When new frame comes with foreground object each pixel of frame is applied to fuzzy inference system, if pixel value is in between minimum and maximum then consider background pixel, otherwise foreground pixel. Mathematically foreground or background separation is shown below in eq (2).

$$a(i, j) - \alpha < i < b(i, j) + \alpha \qquad (2)$$

where α is very useful parameter in variety of illumination conditions, and it's value is constant, a (i, j) is the minimum frame, while b (i, j) is maximum frame, and i is the fuzzified pixel value of current frame. The value of minimum frame a (i, j) and maximum frame b (i, j) is calculated from first N fuzzified background frames. The proposed fuzzy background subtraction approach directly works on color video, so that is the main reason, this background subtraction approach is efficient one. Using this proposed background subtraction method, there is no need for post processing of frames. Each pixel having three different values (i.e. for red, green, and blue) are given to fuzzy inference system for calculating fuzzified pixel value as shown in Fig. 2. A fuzzy inference system consists of four main parts: fuzzification, rule base, inference engine, and defuzzification. The basic steps required for fuzzy logic algorithm are shown in below:

1) Define the linguistic terms and variable, that comes under initialization part.
2) Then construct the membership functions, that comes under initialization part.
3) Then construct the fuzzy rules, that comes under initialization part.
4) First step is convert the crisp input data to fuzzy values using defined membership functions, that is the part of fuzzification.
5) Second step is to evaluate the rules in the rule base.
6) Third step is to combine the results of each rule, that is the part of inference engine.
7) Last step is convert the output data to non-fuzzy values, that is the part of defuzzification.

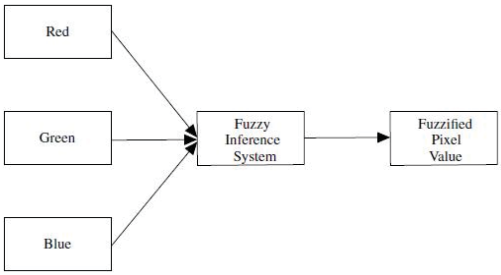

Fig. 2. Fuzzified pixel value calculation

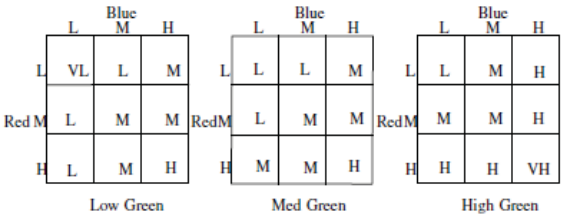

Fig. 3. Fuzzy Rules

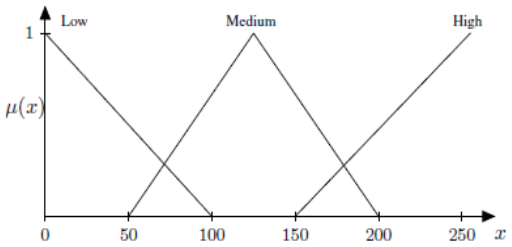

Fig. 4. Membership function for red color

Fig. 3 shows fuzzy rules, and the abbreviation for these rules are L-Low, M-Medium, H-High, VL-Very Low, VH-Very High. There are various types of membership function such as Triangular, Trapezoidal, S, Gaussian etc. [13]. Fig. 4 shows Triangular membership function for red color. This membership function having three linguistic term Low, Medium, and High. After fuzzifying inputs, fuzzy rules in the form of (if.... then) are applied for calculating final crisp value. The proposed fuzzy background subtraction method is compared with simple thresholding technique [7]. Fig. 5 shows the result of simple

Fig. 5. Result of Simple background subtraction technique using thresholding method. [7]

background subtraction technique using thresholding approach, while Fig. 6 shows proposed fuzzy logic based background

Fig. 6. Result of proposed fuzzy logic based background subtraction technique (without any post processing (a) with α = 5, (b) with α = 10 and (c) with α = 20).

subtraction approach.

C. Blob Detection

After completion of background subtraction method, object is detected. Once moving object gets detected, then capture the blob of respective moving object as shown in Fig. 7. Blob is defined as a collection of bunch of pixels within region. Whereas blob is analysed based on the identification

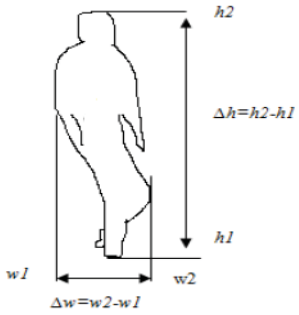

Fig. 7. Identified Blob

of connected pixel regions from the image. The blob detection algorithm distinguishes pixels by their value and mark them in two categories: white blob (foreground) or black blob (background).

D. Feature Extraction

Feature extraction holds an important stepping stone to pattern recognition and machine learning problems. To recognize and classify an object in an image, first extract useful features out of the image. Feature extraction is necessary step for extracting image attribute, to identify or interpret meaningful object from image. Four important features like height, width, number of black and white pixels are extracted from blobs of human and car. These four features are converted into two features i.e. aspect ratio of height to width, and aspect ratio of number of black to number of white pixels.

1) Width: This feature is calculated having difference of Leftmost pixel and Rightmost pixel.
$$\Delta w = w2 - w1$$
2) Height: This feature is calculated having difference of Topmost pixel and Bottommost pixel.
$$\Delta h = h2 - h1$$
3) Aspect Ratio (W/H): It is the ratio of width to height.

$\Delta w/\Delta h$

4) Aspect Ratio (B/W): It is the ratio of number of black pixel to number of white pixel.

E. SVM Classification

In recent years, SVM classifier is very effective for solving classification and regression problems [14]. The features of human and non-human blobs are given to support vector machine training part. Support vector machine is capable to learn all those features. In training part these features are divided into two classes using SVM linear kernel function i.e positive and negative class. In proposed method of human detection, SVM is based on a linear classifier in a high dimensional feature space, which has allowed the development of somewhat fast training techniques, even with a large number of input variables and training datasets. In proposed method support vector machine classifies the objects either as a human or non-human.

III. Comparative Study and Discussion

In the recent, there were several systems have been developed for human detection from videos. That are almost similar approaches, the proposed algorithm performed better in terms of detection accuracy rate. Lipton et.al. [14] used

TABLE II. Comparison of Classification Accuracy With Existing System

Sr.No	Algorithm	Detection Accuracy
1	Moving Target Classification and Tracking From Real Time Video [14]	82.80 %
2	Moving Target Classification in Video Sequences based on Feature combination and SVM [15]	80%
3	Human Motion Detection Using Fuzzy Rule base Classification of Moving Blob Regions [16]	93.75%
4	Proposed Method	95.22 %

a simple multi-feature classification approach with features like dispersedness, area and detection rate of 82.8%. Kong, Lei Wang [15] had obtained 80% detection rate of human and car. Table II shows comparative analysis with existing system. See, J., Lee [16] had obtained 93.75 % detection rate of human motion. On other hand, we introduced a novel and efficient approach for moving object detection using fuzzy logic algorithm, and support vector machine classifier gives 95.22 % classification rate of human and non human.

IV. Experimental Evaluation

The proposed system uses standard dataset INRIA and PETS 2000. The dataset comprises .avi or .mp4 videos having any size, duration 1-58 seconds, and with 2-27 frames per second. The SVM classifier was trained using 800 blobs. Among these, 500 were positive samples indicating human blobs and rest 300 were negative samples indicating car blobs for training. Table III shows classification rate of moving object. INRIA and PETS 2000 dataset used in this experiment is tested over 8 different videos that contain 2 objects (i.e human and car). Among these 6 videos contain only human and other 2 videos contain only car. Results analysis for all these scenarios are given in Table III.

TABLE III. Classification Rate of Different Moving Objects

Sr.No	Moving Object Class	Total number of blobs	Detected human blobs	Detected car blobs	Classification accuracy
1	Human	48	44	4	91.66 %
2	Human	77	72	5	93.50 %
3	Human	58	55	3	94.82 %
4	Human	62	59	3	95.16 %
5	Human	64	60	4	93.75 %
6	Human	80	74	6	92.50 %
7	Car	38	0	38	100 %
8	Car	80	3	77	96.25 %

A. Sample output

In output part video contains human. The red line depicts detected blob, that gives result human. Figure 8 gives classification result.

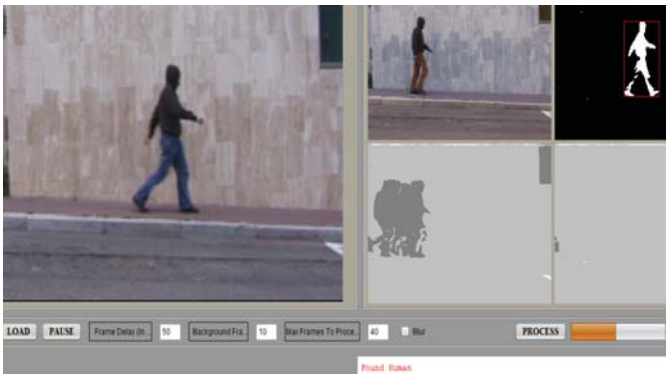

Fig. 8. Classification result of sample video

V. Conclusion and Future Work

A method for human detection in video sequences is based on mainly two aspects: Fuzzy approach for moving object detection, and Support Vector Machine is used for moving object classification. In this paper, a novel and efficient approach for background subtraction using fuzzy logic is presented. Features are extracted after detecting the blobs. These features are given as input to Support Vector Machine (SVM) to classify the object, whether it is human or non-human. SVM is used as a binary classifier, means it is used for human and non-human classification. The proposed human detection system have many aspects that can be improved in future. This system will further used for object tracking and recognition purposes. The background subtraction approach for moving object detection can be extend to various image conditions (lighting or long-term scene changes), and moving camera dataset. The objects detected are classified for only two classes, in future this could be extended to multiple classes.

References

[1] Seki, M., Fujiwara, H., & Sumi, K. (2000).“A robust background subtraction method for changing background.” *In Applications of Computer Vision, 2000, Fifth IEEE Workshop on. (pp*. 207-213). IEEE.

[2] Stauffer, Chris, and W. Eric L. Grimson. “Adaptive background mixture models for real-time tracking.” *Computer Vision and Pattern Recognition, 1999. IEEE Computer Society Conference on*. Vol. 2. IEEE, 1999.

[3] S. Fejes, L.S. Davis, "Detection of independent motion using directional motion estimation," *Technical Report, CAR-TR-866, CS-TR 3815, University of Maryland*, August 1997.

[4] Kinoshita, K., Enokidani, M., Izumida, M., & Murakami, K. (2006, December). "Tracking of a moving object using one-dimensional optical flow with a rotating observer." *In Control, Automation, Robotics and Vision, 2006. ICARCV'06. 9th International Conference on* (pp. 1-6). IEEE.

[5] Lijun, X. (2011, August). "Moving object segmentation based on background subtraction and fuzzy inference." *In Mechatronic Science, Electric Engineering and Computer (MEC), 2011 International Conference on (pp. 434-437).* IEEE.

[6] Gambhir, D., & Manchanda, M. (2014, February). Adaptive threshold based segmentation for video object tracking. In Advance Computing Conference (IACC), 2014 IEEE International (pp. 1127-1132). IEEE.

[7] Hati, Kalyan Kumar, Pankaj Kumar Sa, and Banshidhar Majhi. "Intensity range based background subtraction for effective object detection." *Signal Processing Letters, IEEE* 20.8 (2013): 759-762.

[8] Turk, Matthew A., and Alex P. Pentland. "Face recognition using eigenfaces." *In Computer Vision and Pattern Recognition, 1991. Proceedings CVPR'91., IEEE Computer Society Conference on*, pp. 586-591. IEEE, 1991.

[9] Ali, Syed Sohaib, M. F. Zafar, and Moeen Tayyab. "Detection and Recognition of Human in Videos Using Adaptive Method and Neural Net." *In Soft Computing and Pattern Recognition, 2009. SOCPAR'09. International Conference of*, pp. 604-609. IEEE, 2009.

[10] Osuna, Edgar, Robert Freund, and Federico Girosi. "Training support vector machines: an application to face detection." *In Computer Vision and Pattern Recognition, 1997. Proceedings., 1997 IEEE Computer Society Conference on*, pp. 130-136. IEEE, 1997.

[11] Soumya Varma, Sreeraj M. "Object detection and classification in Surveillance System." *In recent advances in Intelligent computational system*, 2013 IEEE conference.

[12] Mahapatra, Ansuman, Tusar Kanti Mishra, Pankaj K. Sa, and Banshidhar Majhi. "Background subtraction and human detection in outdoor videos using fuzzy logic." *In Fuzzy Systems (FUZZ), 2013 IEEE International Conference on*, pp. 1-7. IEEE, 2013.

[13] J.Jang and M. C-T, "Neuro-Fuzzy and Soft Computing " . *Prentice-Hall*, 1997.

[14] Lipton, A. J., Fujiyoshi, H., & Patil, R. S. (1998, October). "Moving target classification and tracking from real-time video." *In Applications of Computer Vision, 1998. WACV98. Proceedings., Fourth IEEE Workshop on (pp*. 8-14). IEEE.

[15] Kong, Yinghui, and Lei Wang. "Moving Target Classification in Video Sequences Based on Features Combination and SVM." *In Computational Intelligence and Software Engineering (CiSE), 2010 International Conference on, pp.* 1-4. IEEE, 2010.

[16] See, J., Lee, S., & Hanmandlu, M. (2005). "Human motion detection using fuzzy rule-base classification of moving blob regions." *In Proc. Int. Conf. on Robotics, Vision, Information and Signal Processing (Vol. 2005, pp*. 398-402).

THE 5TH INTERNATIONAL CONFERENCE ON WIRELESS COMMUNICATIONS, VEHICULAR TECHNOLOGY, INFORMATION THEORY, AEROSPACE & ELECTRONIC SYSTEMS (WVITAE-2015)
December 13-16, 2015, Hyderabad, India

Illumination, Indoor Localization and Very High Speed Data Communication using VLC

Anusha Addanki
ECE Dept, School of Engineering
Amrita Vishwa Vidyapeetham (University)
Bangalore, India
Anushaaddanki8@gmail.com

Navin Kumar
ECE Dept. School of Engineering
Amrita Vishwa Vidyapeetham (University)
Bangalore, India
navinkumar@ieee.org

***Abstract*—In this paper, a visible light communication (VLC) is analyzed for highly accurate indoor localization, high data rate information transmission while performing the function of illumination. All the functions are simultaneously achieved. The light emitting diodes (LEDs) working as VLC emitters are installed on ceiling which are placed at optimal position in order to provide uniform signal-to-noise ratio (SNR) in the entire considered area. Through analysis and simulation work, it is shown that with simplified overall system, the performance for all the functions can be optimized. The positioning error is small maximum to a few centimeters and at the same time bit error rate (BER) performance is very high.**

Keywords-visible light communications; indoor localization; received signal strength

I. INTRODUCTION

Visible light communication (VLC) is an emerging noble kind of optical wireless (OW) broad band communication technology [1]. VLC uses unregulated and unlicensed visible spectrum (380nm-760nm) of light normally emitted from light emitting diodes (LEDs) for information transmission wirelessly. VLC is particularly becoming popular for its simultaneous dual function i.e. illumination as well as high data rate transmission. In addition, it offers many other advantages leveraging from the advancement and usage of LEDs. For example, promotion of green technology, power efficient, cost effective design, no electromagnetic interference, highly secured and many more.

LED-based VLC has a number of interesting and novel applications both indoor and outdoor. While in outdoor, it can be an integral part of intelligent transportation systems (ITS) [2], road illumination and communications; in the indoor VLC can be designed for high data communication system, such as offloading data along with WiFi for upstream data in simple system, parallel communication and so on. In addition, VLC is also being considered for indoor localization. Some of the recently reported studies [3-5] reveal high accurate localization using same LED-based illumination system. This particular application of VLC is drawing reasonable attention from researchers worldwide since the most popular and widely used global positioning system (GPS) does not guarantee the accuracy in the indoor or even unable to find position of the object. Though, there are different methods based on WiFi, Bluetooth in association with cellular like GSM being examined and investigated [4]. Even radio frequency identification (RFID), Infrared (IR) and ultrasound based system is also reported [6]. These methods include variation in regard to accuracy, complexity and cost. In other hand, the optical wireless especially VLC can offer very high accuracy positioning in terms of centimeter (cm) and millimeter (mm) without significant change in existing infrastructure. Indoor navigation using LED-based VLC offers eco-friendly illumination based communications.

Indoor localization is an interesting and potential application of VLC. It would help a person to track an object within a museum or shopping mall by making use of handheld devices incorporated with VLC receiver. On considering the future scope many organizations focus on research based activities into indoor localization. LED light bulbs acting as VLC transmitters utilize its excellent characteristics for indoor localization with photo-detector as optical receiver.

There are different positioning algorithms such as triangulation and proximity [5-8] and they have different accuracy and complexity. We have used the triangulation, a more generic and relatively accurate method for location estimation. It consists of lateration and angulations. The former estimates the target location by measuring received signal strength (RSS) to find distances between the target (object integrated with VLC receiver) and several reference points (light source working as VLC emitter in this case). The later, angulations measure angles relative to several reference points and finds out estimated distance to find the location.

Authors Zhang et al [5] used RSS based triangulation techniques to find the estimated location. However, they did not consider communication aspect and the main focus was precise location detection. Authors have neither considered the energy optimization of the system. Though they used 4-set of LED illuminated lights but they are not optimized for energy. In the paper [3], authors used different set of emitter-receiver pair for data communication in addition to emitter-receiver for localization. In this also, the signal-to-noise ratio (SNR) distribution is not uniform and energy is not optimized for data communication. This results in different data rate across the considered area and relatively higher estimated error in the corner of the room.

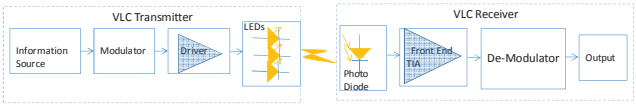

Fig.1: VCL System Architecture

In this paper, we use the same set of emitter-receiver and they are used for simultaneous function of localization and data communication. In addition, the illuminating LED lights placed in the desired area for the uniform SNR distribution and optimized transmitted power from each reference point so that energy is not wasted. The uniform SNR not only results in the greater accuracy in the entire area for location detection but also enhances the bit error rate (BER) performance when used for high data rate communication.

The contents of the rest of the paper are as follows. Section II describes overall VLC system architecture in brief. The algorithm and analysis is presented in section III while section IV discusses the results. Finally, section V concludes the paper with the intention of continued future work.

II. Overall System Architecture and Configuration

In this section, we briefly describe the overall system and then discuss the channel characteristics.

A. Overall VLC System

A generic VLC system is shown in Fig.1. The system comprises a set of LED lights which form VLC emitter. The array of LED is required for high intensity lights for relatively longer data communication range as well as sufficient light intensity in the working area. The emitter (set of LEDs) requires driver to provide sufficient current to drive the LEDs or the array of LEDs. The LED emitter must be modulated for data communication. Most widely used modulation technique is intensity modulation and direct detection (IM/DD) or on off keying (OOK). Thus in the transmitter, the data information source is modulated which is applied to the driver amplifier to deliver necessary drive current to the LEDs emitter.

The receiver is based on photo detector (PD). The amount of light falls on the collecting area of PD will get converted to electrical signal which must be amplified. Normally, transimpedance amplifier (TIA) [9] is used as front end in optical domain. A blocking capacitor is used to block the direct current (DC) resulting from natural lights. The amplified signal is low pass filtered, demodulated to get back the original signal at the receiver.

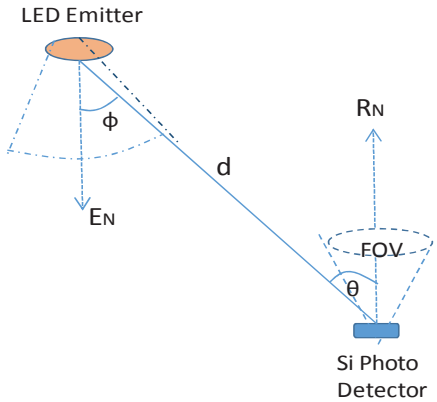

Fig.2: Channel Model

The light emitted from the array of LEDs carries the data information wirelessly and forms the channel (optical wireless channel). Normally, line-of-sight (LoS) link is considered in VLC system design.

B. The Channel Characterization

Fig.2 shows the illustration for LoS channel. The direct distance between LED emitter and receiver is considered to be *d*. The optical wireless link is characterized by direct current gain and given by:

$$H(0) = \begin{cases} \frac{m+1}{2\pi d^2} A_r . \cos^m(\Phi) . Ts(\theta) . g(\theta) . \cos(\theta), & 0 \le \theta \le \theta_c \\ 0, & \theta > \theta_c \end{cases} \quad (1)$$

where A_r area of the detector, θ is the angle between the normal of receiver to the direct distance from the emitter, $T_s(\theta)$ is the gain of optical filter, $g(\theta)$ is the concentrator gain. θ_c is semi-angle of FOV. The Lambertian order m is given by $m = -\ln 2 / \ln(\cos \Phi)$, where Φ is the half power angle of the LED. The received optical power at the detector is given by:

$$P_r = H(0) . P_t \quad (2)$$

where P_t denotes optical power of the LED.

III. Design and Analysis

In this section, we discuss the system model, frame structure and details of the algorithm.

A. System Model

The overall system model is illustrated in Fig. 3.There are five LED light points installed on the ceiling of the room. Each one of the light point with specific co-ordinates transmits its own unique identity (UI) followed by the information data

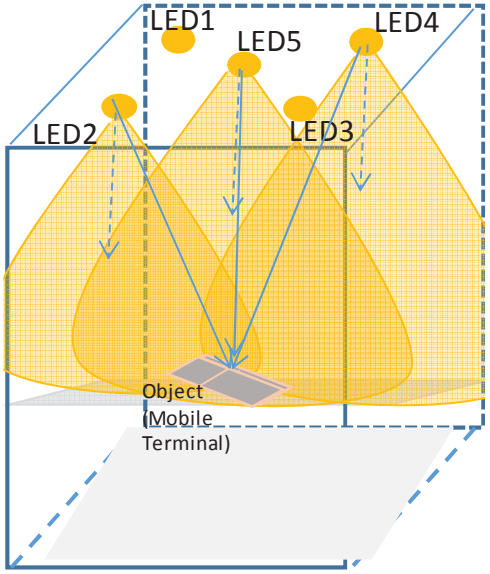

Fig.3: System Configuration for Location determination

when modulated. The position (coordinates) of the LED lights are automatically calculated by designed algorithm based on other parameters such as irradiation angle of the LEDs, field of view (FoV) of the PD, maximum dimension of the area and the desired SNR at the extreme point (corner) in the room. This not only enables the high data rate transmission in the entire area but also the least estimated positioning error. For the uniform SNR distribution, we use 5 set of LED lights of the same emitted power as shown in the system layout in Fig.3. The object which is to be detected incorporates the VLC PD receiver and at the same time has the capability to receive the information in the entire room area. We consider the PD receiver to be placed at a height of 1-m (table) from the surface (ground) within the room. However, system is designed to perform almost the same performance even the receiver is placed on the surface. The parameters for system model are shown in Table-1.

B. Channel Access and Frame Structure

To access the channel, we rely on asynchronous mechanism [5] to reduce the complexity. We use a frame slotted additive on-line Hawaii (FS-ALOHA) protocol which is approximately similar to the ALOHA (shown in Fig.4). In this, the frame is divided into a fixed number of time slots (relatively higher, over 200). Each transmitter then selects the slot randomly and transmits its data frame. It is likely that sometimes two or more transmitters select the same slot and therefore resulting in collision. This is shown in Fig.5. It is also possible that two or more emitter's transmission overlap. In this case also, there will be collision resulting in failure in location determination. As described in [5], if the number of slots (N) is relatively large (N>200), the performance of synchronous [4] and asynchronous is approximately the same. Therefore, we choose N = 250. It is also important to discuss that that N should not very large and neither be small in number. If N is small, more collision will occur degrading the performance but if N is large, it is possible to see more emptied slot. Thus,

TABLE 1: System Model Parameters

Parameters	Values
Considered room dimension (L x W x H)	3 x 3 x 3 m^2
Position of LED light	A (0.5, 0.5, 3); B(2.5,0.5,3); C(0.5,2.5,3); D(2.5,2.5,3); E(1.5,1.5,3)
Receiver Height	1m
Receiver detector area (A_r)	1cm^2
Field of View	55 degree
Responsivity of receiver	0.54 (A/W)
LED transmitted power from each emitter	6W

Fig.4: Frame Structure

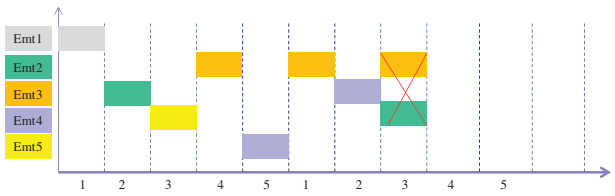

Fig.5: Illustration of frame transmission and collision of FS-ALOHA

with this number of slot, the performance of location positioning is the same as the synchronous based.

Each LED emitter is assigned a coordinate (x,y,z) based on optimized placement for uniform illumination in the given area. The coordinates are encoded into three 16-bit return to zero (RZ) codes. We use on-off-keying modulation to send the information. Normally, the transistor driver is biased so that the average power (P_0) is always transmitted and during modulation, the respective LED emitter will transmit higher intensity that is peak power (P). The receiver placed anywhere in the area will detect the signal, segregate the UI from data from any of the three LED emitter to calculate the triangulation. Thus information data and location information is separated.

C. Location Determination

Each of the LED transmits its UI modulated in OOK format to the receiver. The power difference at the receiver end is measured to find out the estimated distance. We find out the estimated distances from all the reference points and calculate the estimated location and positioning error (if any). Considering any three co-ordinates for positioning, we would have ten random ways to find the position for our system. On finding out the estimated average error for our system we would be able to define the position. This defines the object with very less positioning error. If the modulation depth of OOK at the transmitter end is η_{ook}, the power difference (P_{df}) between the transmitted ON and OFF pulse could be:

$$P_{df} = \eta_{ook} . P_{cnst} \tag{3}$$

where P_{cnst} is the optical power emitted from LED without modulation. The power difference at the receiver side (P_{dfr}) is given by:

$$P_{dfr} = H(0) . P_{df} \tag{4}$$

The direct distance d between LED emitter and the receiver from Eq. (1) is given as:

$$d = \sqrt{\frac{(m+1)A_r . \cos^{m}(\Phi) . \cos(\theta) . P_{df}}{2\pi P_{dfr}}} \tag{5}$$

The optical concentrator gain and filter gain is normalized. We also consider that the transmitter and the receiver axes are perpendicular to each other the estimated distance is given as:

$$d_{est} = \sqrt{d_{est-xy}^2 + H^2} \tag{6}$$

$d_{\text{est-xy}}$ is the horizontal distance between transmitter and the receiver, H is the vertical distance (height) between transmitter and receiver:

$$d_{est-xy} = \sqrt{\sqrt{\frac{A_r.\mathrm{P}_{df}.H^2}{\pi \mathrm{P}_{dfr}}} - H^2} \quad (7)$$

So, with the help of estimated horizontal distance we would be able to find the estimated co-ordinate by triangulation.

To estimate the unknown position, a set of two equations would be enough with the assumption that after the estimated distance between the LED's and the receiver is known. These set of equations would be helpful to solve for (*x, y*). The (x, y) would be the estimated position of receiver.

In the system described above, we have five transmitters A, B, C, D and E. The entire equations group formed by any three points can be solved and the estimations can be averaged.

$$(x - x_A)^2 + (y - y_A)^2 = d_A^2 \quad (8)$$

$$(x - x_B)^2 + (y - y_B)^2 = d_B^2 \quad (9)$$

$$(x - x_C)^2 + (y - y_C)^2 = d_C^2 \quad (10)$$

$$(x - x_D)^2 + (y - y_D)^2 = d_D^2 \quad (11)$$

$$(x - x_E)^2 + (y - y_E)^2 = d_E^2 \quad (12)$$

On solving for eq. (10), (11) and (12), we get an equivalent linear set of equations to solve for (x, y). The final averaged estimation could be helpful to find out the equivalent positioning (x,y) error given as:

$$e_r = \sqrt{(x_{\mathrm{real}} - x_{est})^2 + (y_{\mathrm{real}} - y_{\mathrm{est}})^2} \quad (13)$$

where x_{real}, y_{real} are the real position of the receiver in *x* and *y* direction respectively.

D. Data Transmission Rate

As shown in Fig.4, the frame comprises 8-bit start and 8-bit stop bit. The preamble 48-bit is the UI of individual LED emitter. We also use 16-bit cyclic redundancy check (CRC). With each frame a data of 256-bit is appended. Thus, the frame length is:

Frame Length (L) = (8+8+16+48+256) = 336-bits. (14)

Each LED emitter transmits a frame in one slot. If we repeat the transmission 40 times per second, the data rate will be:

$$\mathrm{R} = 40.\mathrm{L}.\mathrm{N} = 3.36\mathrm{Mbps} \quad (15)$$

The high brightness (HB) LED with tens of MHz switching is commercially available and we are using in our design for the demonstration. However, much higher data rate is possible with other high speed HB LED.

E. Bit Error Rate Analysis

One of the parameters to determine the performance of data communication system is the bit error rate which is the function of signal to noise ratio and it varies depending on the modulation technique. For simple OOK modulation, the probability of error is given as:

$$P_{eook} = Q(\sqrt{SNR}) \quad (16)$$

where *Q(.)* is the error function given as:

$$Q(x) = \frac{1}{\sqrt{2\pi}} \int_x^{\infty} exp\left(-\frac{u^2}{2}\right) du = \frac{1}{2}\left(1 - \mathrm{erf}\left(\frac{\mathrm{x}}{\sqrt{2}}\right)\right)$$

SNR Analysis

Uniform SNR is necessary in the given area for accurate detection of the position of the object as well as for the acceptable and uniform data rate. The signal component is given by:

$$S = \mathcal{R}^2 P_{dfr}^2 \quad (17)$$

where $\mathcal{R}$ specifies the detector responsivity.

The noise is described to be Gaussian with a total of shot and thermal noise. The shot noise is dependent on background current induced by light (I_{bg}).

$$N = \sigma_{th}^2 + \sigma_{st}^2 \quad (18)$$

where the shot noise is given as:

$$\sigma_{st}^2 = 2q\mathcal{R}(P_{rc})B + 2qI_{bg}I_2B. \quad (19)$$

where q is the electronic charge, B is the equivalent noise bandwidth, same as that of modulation bandwidth, I_{bg} is the background current which can vary depending on Sun lights. The I_{bg} is maximum of around 5100μA under direct sunlight exposure and 740μA under indirect sunlight exposure; the noise bandwidth factor I_2=0.562. Following [1], the thermal noise is calculated to be very small. We considered this value to be -225dBm.

The received power P_{rc} is given as:

$$P_{rc} = \sum_{i=0}^{5} H_{\mathrm{i}}(0)\mathrm{P}_{\mathrm{i}} \quad (20)$$

where $H_{\mathrm{i}}(0)$ is the instantaneous DC channel gain and P_i is the instantaneous emitted power from the i'th LED emitter respectively.

As can be observed from the figures (Fig.7 and 8), the SNR is uniformly distributed within the room due to the presence of five LED's positioned precisely. This kind of positioning would lead to evaluation of significant SNR even at the corners of the room. The positioning error would also be relatively less even at the corners of the room. From Fig.7, we can observe SNR is relatively higher due to indirect sunlight exposure where noise contribution would be relatively less.

IV. PERFORMANCE RESULTS AND DISCUSSIONS

Different performance results are presented in this section. We plotted for location as estimated error. Similarly, we plotted for SNR and BER.

The positioning error is shown in Fig.6. It can be seen that the error is much smaller in most of the area. However, at extreme corner the error is relatively larger but still much small.

SNR distribution is given in Fig.7. It can be seen that in the entire given area the SNR value is much larger than the acceptable value of BER for data communication. We also see that the minimum and maximum variation of SNR is around 2dB which suggests emitters are also uniformly distributed.

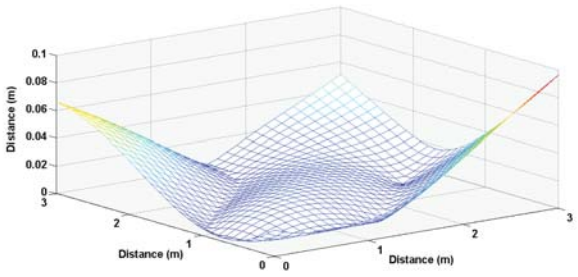

Fig.6: The positioning error in the given area

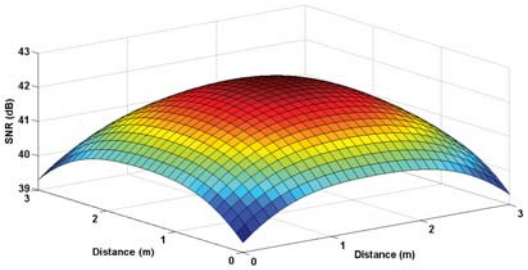

Fig.7: SNR distribution without background noise

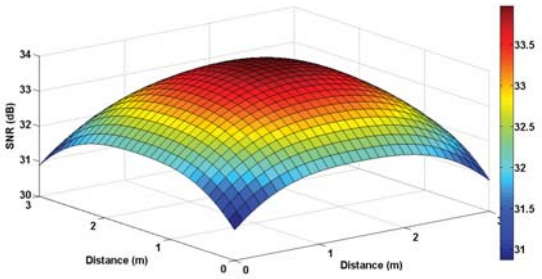

Fig.8: SNR distribution with background noise.

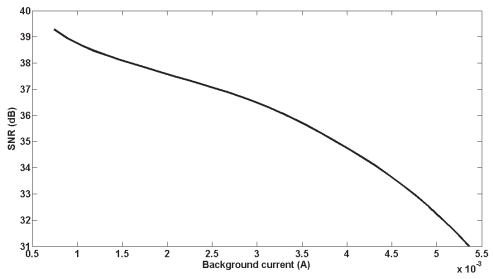

Fig.9: SNR variation with background noise.

The distribution of SNR remains the same, however, the value decreases with maximum of background noise as shown in Fig.8.

Overall variation in SNR with varying background current is also given in Fig.9. With the increase in background current, the SNR decreases which is obvious, however, with a range of background current the SNR is still enough to give the necessary data rate and BER performance.

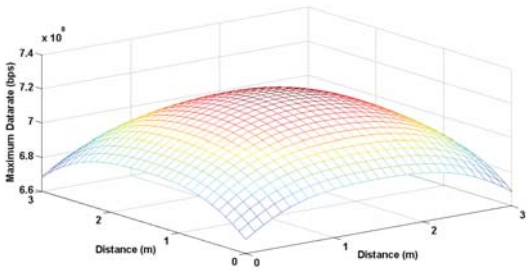

Fig.10: Data rate in the given area

The data rate for which can be achieved is shown in Fig.10. It can be seen that much higher data rate is possible in terms of few tens of MHz. However, as stated above in VLC the data rate is limited to the switching characteristics of opto-electronics circuit.

V. CONCLUSION

Studies are performed on indoor localization based on visible light communication. A simplified system is analyzed which can perform simultaneous all three functions of data transmission, localization and illumination. It is shown that high accuracy localization can be achieved and at the same time uniform SNR ratio offers better BER performance.

In fact, the paper should be supported by hardware demonstration but it is not complete. The receiver is being designed for its performance. We are also trying to further improve optimization of location of LED emitter for better SNR distribution based on few parameters only. There are possibilities for further improvement in respect of both emitter as well as data transmission. We are addressing these issues.

REFERENCE

[1] Toshihiko K. and Masao Nakagawa, “Fundamental Analysis for Visible-Light Communication System using LED Lights”, IEEE Transactions on Consumer Electronics, Vol. 50, No. 1, February 2004

[2] Navin Kumar, Nuno Lourenço, Domingos Terra, Luis N. Alves, Rui L. Aguiar, “Visible Light Communications in Intelligent Transportation Systems”, IEEE Proc.Intelligent Vehicles Symposium, Spain, June 3-7, pp.748-753, 2012

[3] Se-Hoon Yang, Eun-Mi Jeong, Deok-Rae Kim, Hyun-Seung Kim, Yong-Hwan Son and Sang-Kook Han, “Three-Dimensional Localization Based on Visible Light Optical Wireless Communication”, IEEE Proc. ICUFN 2013, pp.468-469, 2013.

[4] Weizhi Zhang, M. I. Sakib Chowdhury and Mohsen Kavehrad, “Indoor positioning algorithm using light-emitting diode visible light communications”, SPIE Optical Engineering 51(8), August 2012.

[5] Weizhi Zhang, M. I. Sakib Chowdhury and Mohsen Kavehrad, “Asynchronous indoor positioning system based on visible light Communications”, SPIE Optical Engineering 53(4), April 2014.

[6] Giulio Cossu, Marco Presi, Raffaele Corsini, Pallab Choudhury, Amir Masood Khalid and Ernesto Ciaramella,”A Visible Light Localization Aided Optical Wireless System”, IEEE Proc. 2nd IEEE Workshop on Optical Wireless Communications, Itally, pp. 828-833, Nov. 2011.

[7] K. Panta and J. Armstrong, “ Indoor localisation using white LEDs, ” Electron. Lett. 48(4), pp. 228 – 230, 2012.

[8] Tero Kivimäki, Timo Vuorela, Pekka Peltola and Jukka Vanhala, “A Review on Device-Free Passive Indoor Positioning Methods”, International Journal of Smart Home Vol.8, No.1, pp.71-94, 2014.

[9] R. L. Aguiar, A. Tavares, J. L. Cura, E. De Vaaconcelos, L. N. Alves, R. Valadas, and D. M. Santos, "Considerations on the design of transceivers for wireless optical LANs," in OWC, IEE Colloquium, pp. 2/1-231, 1999.

THE 5TH INTERNATIONAL CONFERENCE ON WIRELESS COMMUNICATIONS, VEHICULAR TECHNOLOGY, INFORMATION THEORY, AEROSPACE & ELECTRONIC SYSTEMS (WVITAE-2015)
December 13-16, 2015, Hyderabad, India

Distributed Forward-Backward Pursuit Algorithm for Distributed Compressive Sensing

Suchithra P Sudhakaran
PG Scholar
ASIET, Kalady
suchitrapampala@gmail.com

Dr. Neelakantan P C
Professor
ASIET, Kalady
neelakantan.ec@adishankara.ac.in

Abstract— ***A greedy Pursuit algorithm is developed for solving distributed compressive sensing problem in a connected network. This algorithm is based on Forward-Backward Pursuit algorithm that does not require any prior knowledge of sparsity and also gives better performance than Subspace Pursuit algorithm. So theoretically when Forward-Backward Pursuit algorithm comes in distributed scenario, it will give better performance than Distributed Subspace Pursuit algorithm. Through an experimental evaluation, we show that the proposed Distributed Forward-Backward Pursuit algorithm gives 6 dB higher Signal to Reconstruction Error Ratio (SRER) than Distributed Subspace Pursuit algorithm.***

Keywords—Distributed Compressive Sensing; Greedy Pursuit algorithm; Sparsity; Forward-Backward Pursuit algorithm; Subspace Pursuit algorithm

I. INTRODUCTION

Of late, Compressive Sensing (CS) is became a hot research topic among researchers since it is a new method which capture and compress signals at a rate below Nyquist rate. Compressive Sensing (CS) is a sampling paradigm which samples the signals at a rate below the Nyquist rate [1] [2] [3] [4]. One of the main application of CS is in the field of Wireless Sensor Networks (WSNs). There are limiting parameters on WSNs such as power consumption, life time, cost, bandwidth and traffic. The WSNs need independent energy resources and so energy consumption is one of the most important factor to determine the life time of wireless sensors. As WSNs continue to grow, there is a need for new mechanisms to reduce these limiting parameters. The compressive sensing techniques optimizes energy consumption and holds promising improvements to these parameters [5].

For a multiple-sensor scenario, most effective case is a distributed setup where several CS-based sensors are connected through a distributed (decentralized) network [5]. Several CS reconstruction algorithms have been developed, which includes convex optimization and Bayesian algorithms [6]. An important class of reconstruction algorithms is the Greedy Pursuit (GP) algorithm which gives good performance with low complexity. The GP algorithms use linear algebraic tools to estimate the underlying support-set of the sparse signal vector followed by estimating associated signal values from a measurement vector [6]. Various Greedy Pursuit Algorithms developed for distributed Compressive Sensing are Distributed Parallel Pursuit Algorithm (DIPP) [7], Distributed Orthogonal Matching Pursuit algorithm (Di OMP) [6] [9] [10], Distributed Subspace Pursuit algorithm (Di SP) [6] [8] [9] [10], Distributed Predictive Subspace Pursuit (DPrSP) [9], Distributed Forward-Reverse Orthogonal Greedy Search (Di FROGS) [6] [9] [10].

Greedy Pursuit algorithms like Subspace Pursuit algorithm and CoSaMP algorithm require a prior knowledge of sparsity level [3]. Backward Pursuit algorithm, Subspace Pursuit algorithm and Orthogonal Matching Pursuit algorithm start to fail at around Sparsity level, K = 25 [11]. This disadvantage is overcome by a new algorithm called Forward-Backward Pursuit algorithm (FBP). FBP does require any prior knowledge of sparsity level (K) and it starts to fail only when sparsity K is greater than 30 [11]. So theoretically when Forward-Backward Pursuit algorithm comes in distributed scenario, it will give better performance than Subspace Pursuit algorithm. The proposed Distributed Forward-Backward Pursuit algorithm gives 6 dB higher Signal to Reconstruction Error Ratio (SRER) than Distributed Subspace Pursuit algorithm and this has been verified through simulations.

II. DISTRIBUTED COMPRESSIVE SENSING

For observing the Distributed Compressive Sensing problem (DCS) consider the i^{th} sensor node. Then the sparse signal $x_i \in R^N$ is measured as

$$y_i = A_i x_i + w_i \quad (1)$$

where $y_i \in R^M$ is the observation vector, $A_i \in R^{MxN}$ is the measurement matrix and $w_i \in R^M$ is the measurement noise, M < N. There has been K_i non zero components with indices $T_i = \{l: x_i(l) \neq 0\}$ in signal vector x_i. This T_i is known as support set of x_i. The DCS reconstruction problem endeavors to reconstruct or x_i for all i by exploiting some common structure among i sensors well-defined by the signal model

and exchanging some information among sensor nodes over the network topology [6] [8] [9] [10].

A. *Mixed Support Set Signal Model*

The mixed support set signal model has a shared structure where the signal vector x_i consist of two parts

$$x_i = a_i^c + a_i^p \ , \ \forall \ i \in \{1, 2 \ldots I\} \qquad (2)$$

a_i^c is the common sparse component and a_i^p is the innovative component. Both a_i^c and a_i^p in (2) have independent non-zero components. There are K_i^p non-zero values in a_i^p. The non-zero values are located uniformly at random over the support set $T_i^p \in \forall \ i \in \{1, 2 \ldots I\}$. With the constraint that the support set $T_i^c = T^c$ is shared, there are similarly K^c non-zero components for a_i^c. The elements of T^c are common to all signals, but it is unknown to the reconstruction part. For the i^{th} sensor node, this contributes a support set T_i for each x_i as

$$T_i = T^c \ \cup \ T_i^p \ , \ \forall \ i \in \{1, 2 \ldots I\} \qquad (3)$$

B. *Network Topology*

The DiFBP algorithm described in this paper can work in any network topology. If the network is well connected, then this algorithm will give better performance. The effects of the network topology on the performance of DiFBP is not considered in this paper. Here, we emphasis on the development of DiFBP suitable for any network.

C. *Algorithmic Notations*

We define four algorithm functions in the algorithm. The functions are given as follows

max_indices(x, k) ≜ {the set of indices corresponding to the k largest amplitude components of x} (4)

min_indices(x, k) ≜ {the set of indices corresponding to the k smallest amplitude components of x} (5)

resid(y, C) ≜ y-$CC^{\dagger}$y, for some matrix C (6)

and

add_1(s, T) ≜ {∀ j ∈ T, performs $s_j = s_j + 1$}, (7)

where s= [s_1, s_2….,s_N] and $s_j \geq 0$

For the i^{th} sensor node, I_i^{out} denotes the set of indices corresponding to the connected outgoing nodes and I_i^{in} denotes the set of indices corresponding to the connected incoming nodes.

III. DISTRIBUTED GREEDY PURSUITS ALGORITHMS

Some of the existing distributed greedy pursuit (Di GP) algorithms are Distributed Parallel Pursuit algorithm (DIPP) [7], Distributed Orthogonal Matching Pursuit algorithm (Di OMP) [6] [9] [10], Distributed Subspace Pursuit algorithm (Di SP) [6] [8] [9] [10], Distributed Predictive Subspace Pursuit (DPrSP)[12], Distributed Forward-Reverse Orthogonal Greedy Search (Di FROGS) [6] [9] [10]. There are two principles [6] for working of Di GP algorithms. First, each CS node transmits its own full support set estimate to the neighbouring connected nodes. It also receives a set of full support-set estimates from the neighbouring connected nodes. Second, using the set of all received support-set estimates and by invoking a voting mechanism [7] [12] [6], each CS node finds an estimate of the common support-set, either serially or parallelly. Then, using the common support-set estimate as the initial knowledge, each CS node finds a new estimate of the full support-set and then again exchange the full support-set information.

DiSP [6] [8] [9] [10] is based on the existing subspace pursuit [12] algorithm and it use parallel support set construction mechanism. First modify the SP algorithm and then use it for developing DiSP. The principle strategy of DiSP [8] is to improve the common support set estimation by exchanging full support set estimates over iterations. Like DiSP [8], we can develop all other distributed algorithms.

IV. DISTRIBUTED FORWARD-BACKWARD PURSUIT

Distributed Forward-Backward Pursuit algorithm is designed based on Forward-Backward algorithm. Forward-Backward Pursuit algorithm (FBP) is an r-support algorithm, so we can develop DiFBP by using the same approach in DiSP [13]. To implement Distributed Forward-Backward Pursuit (DiFBP) algorithm, we have to first modify the FBP algorithm. Using the modified FBP algorithm presented in Algorithm 2, DiFBP algorithm is carried out in each node. By calling FBP(.), DiFBP algorithm executed in each node is presented in Algorithm 1.

Algorithm 1 (Distributed FBP (DiFBP)): Executed in the i^{th} node, where I_i^{out} and I_i^{in} are set of outgoing and incoming nodes respectively.

Input: $\mathbf{C_i}$, $\mathbf{y_i}$, $K_i^{(p)}$, $K^{(c)}$

Initialization:

1. $K_{i,max} = K_i^{(p)} + K^{(c)}$
2. $(\widehat{T}_i, \hat{\mathbf{x}}_\mathbf{i}, n_i) \leftarrow$ MODFBP ($\mathbf{C_i}$, $K_{i,max}$, $\mathbf{y_i}$, ∅)
3. $n_i^{old} \leftarrow n_i$
4. $\widehat{T}_i \leftarrow \emptyset$, $\forall \ i^* \in I_i^{in} \backslash$ i (i.e. except i)

Iteration:

1. **repeat**
2. **if** $n_i > n_i^{old}$ **then**

3. $(\widehat{\mathrm{T}}_\mathrm{i}, \hat{\mathbf{x}}_\mathbf{i}, \mathrm{n_i}) \leftarrow (\widehat{\mathrm{T}}_\mathrm{i}^{\mathrm{old}}, \hat{\mathrm{x}}_\mathrm{i}^{\mathrm{old}}, \mathrm{n_i^{old}})$
4. **end if**
5. $(\widehat{\mathrm{T}}_\mathrm{i}^{\mathrm{old}}, \hat{\mathrm{x}}_\mathrm{i}^{\mathrm{old}}, \mathrm{n_i^{old}}) \leftarrow (\widehat{\mathrm{T}}_\mathrm{i}, \hat{\mathbf{x}}_\mathbf{i}, \mathrm{n_i})$
6. $\hat{T}_{i^*}^{old} \leftarrow \hat{T}_{i^*}, \ \forall \in I_i^{in}\backslash \mathrm{i}$
7. {**Transmit:** $\widehat{\mathrm{T}}_\mathrm{i}$ to all nodes i $\in I_i^{out}$}
8. {**Receive:** $\hat{T}_{i^*}$ from all nodes i $\in I_i^{in}$ }
9. $s_i \leftarrow 0_{Nx1}$
10. for each $i^* \in I_i$ do
11. $s_i \leftarrow add_1(s_i, \hat{T}_{i^*})$
12. **end for**
13. $\widehat{\mathrm{T}}_\mathrm{i}^{(\mathrm{c})} \leftarrow$ max_indices(s_i, $K^{(c)}$)
14. $(\widehat{\mathrm{T}}_\mathrm{i}, \hat{\mathbf{x}}_\mathbf{i}, \mathrm{n_i}) \leftarrow$ MODFBP ($\mathbf{C_i}$, $\mathrm{K_{i,max}}$, $\mathbf{y_i}$, $\widehat{\mathrm{T}}_\mathrm{i}^{(\mathrm{c})}$)
15. **until** $(n_i \geq n_i^{old})$ **and** $(\hat{T}_{i^*}^{old} \ \forall \ i^* \in I_i)$

Output: $\hat{\mathbf{x}}_\mathbf{i}$, $\widehat{\mathrm{T}}_\mathrm{i}$

Inputs to Algorithm 1 is i^{th} node's sensing matrix $\mathbf{C_i}$, the measurement vector $\mathbf{y_i}$ and the number of elements in the private and common support sets ($\mathrm{K_i^{(p)}}$and $\mathrm{K^c}$). In the initial phase of the algorithm, first estimate of the i^{th} sensor node's support set is achieved by executing the function MODFBP(.). The residual norm $\mathrm{n_i}$ is stored to use as the performance measure and an empty set $\emptyset$ is initialized as the support set of neighboring nodes. There are four functionalities in the iteration phase of the algorithm. They are: (1) Steps 2-4 will prevent the result deviating from better solution if intermediate estimated support set in step 10 is worse than the estimated support set in the previous iteration (denoted by 'old'). (2) Step 7 and 8 establish the communication phase where the estimated support sets are exchanged among the nodes. (3) An estimate of the common support set with cardinality $K^{(c)}$ is achieved. (4) Using the common support set obtained, MODFBP is executed to estimate a new full support set. These four functionalities are iteratively performed until a stopping criterion based on two conditions is fulfilled together: (a) the residual norm in the i^{th} node does not decrease and (b) no new support set estimates from connected node arrive.

A. Modified Forward-Backward Pursuit(MODFBP)

Here, we describe the modified FBP in Algorithm 2. An initial support set T_{ini} is provided to the MODFBP.MODFBP will continue to improve this initial support set building the final support set. When T_{ini} =∅, MODFBP will reduce to standard FBP [3]. At k-th iteration stage, modified FBP forms the matched filter $C^T r_{k-1}$, identifies indices of alpha (forward step size) largest amplitudes and merge with old support set (step 3 and 4). This step is known as forward step. Then projection coefficients of y onto $C_{\tilde{T}^k}$ are computed and identifies the indices corresponding to the beta (backward step size) smallest amplitudes (steps 5 to 7). This step is known as backward step. This produces the final estimate of k-th iteration. Then the projection coefficients and the residue are updated until some halting condition (steps 8 to 10) is satisfied.

Algorithm 2: Modified FBP (MODFBP):

Input: C , alpha, y, T_{ini}

Define: beta, ε

Initialization:

1. $T^0 = T_{ini}$
2. r^0 = resid(y,C_{T_0})
3. k← 0

Iteration:

1. repeat
2. k← k+1;

Forward step:

3. T_f= max_indices ($C^T r_{k-1}$, alpha)
4. $\tilde{T}^k = T^{k-1} \cup T_f$
5. w= $C_{\tilde{T}}^{\dagger}$ y, projection

Backward step:

6. T_b= min_indices (w, beta)
7. $T^k = \tilde{T}^k - T_b$
8. w=$C_T^{\dagger}$ y
9. r^k= resid(y,C_{T_k}), [r^k = y- C_{T_k}w = y-C_{T_k} $C_{T_k}^{\dagger}$ y]
10. until ($\|r_k\| \leq \varepsilon \| r_{k-1}\|$)
11. k← k-1

Output:$\hat{T}$, $\hat{x}$, n

Functional form: ($\hat{T}$, $\hat{x}$, n) ← MODFBP(C, alpha, y, T_{ini})

V. SIMULATIONS AND RESULTS

In the simulation we are comparing four algorithms (SP, FBP, DiSP, and DiFBP). The results are taken for clean and noisy measurement cases. For noisy measurement, we have chosen Signal to Measurement Noise Ratio (SMNR) as 20 dB ($10log_{10}\frac{E\{||x||_2^2\}}{E\{||w||_2^2\}}$). To compare the performance of algorithms, performance measure taken is Signal to Reconstruction Error Ratio (SRER).

$$\mathrm{SRER} = 10\ log_{10}\frac{E\{||x||_2^2\}}{E\{||x-\hat{x}||_2^2\}} \quad (8)$$

We define fraction of measurement as

$$\alpha = \frac{M}{N} \quad (9)$$

For the plots given in the paper, we have chosen that each node is connected to exactly two nodes i.e. one fixed

connection matrix. The signal parameter is taken as N=500; the cardinality of private support set is taken as $K^{(p)} = 10$ and cardinality of common support set is taken as $K^{(c)} = 10$. We have chosen I=10 nodes and for each node there are Q=100 number of sensing matrices (c_i) and number of data sets x taken for each node is P=100. The total number of data for statistics is P.Q.I = 100000. The forward step size (alpha) is taken as 20 [11], termination parameter ϵ is taken as 1e-7 [11] and backward step size (beta) which is alpha-1 is taken as 19 [11].

In the figures given in this paper, there are four algorithms compared SP, FBP, DiSP and DiFBP. SP and FBP are standard Subspace Pursuit and standard Forward-Backward Pursuit algorithms respectively. For clean measurements in Fig.1, we have observed that DiFBP gives better performance than DiSP. At $\alpha = 0.16$, DiFBP gives 3 dB better performance than DiSP. For noisy measurements in Fig.2, we have observed that DiFBP gives better performance than DiSP. At $\alpha = 0.16$, DiFBP gives 6 dB higher performance than DiSP and also DiFBP gives 10 dB higher SRER compared to FBP.

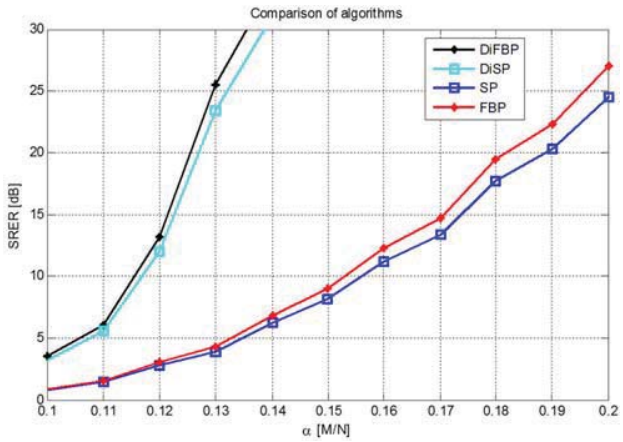

Fig.1: SRER versus fraction of measurements for clean measurements.

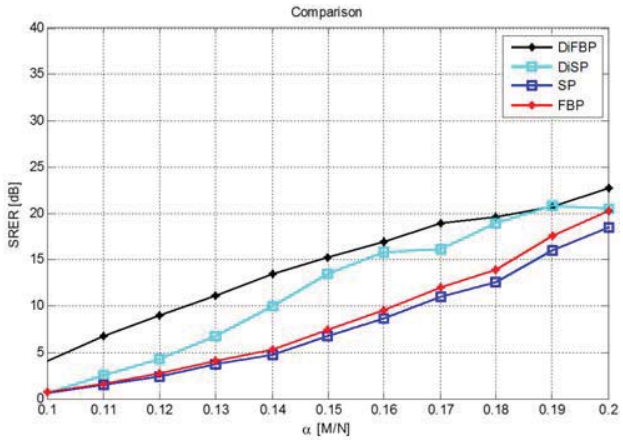

Fig.2: SRER versus fraction of measurements for noisy measurements (SMNR = 20dB)

VI. CONCLUSION

In this paper, a distributed greedy pursuit algorithm called DiFBP (Distributed Forward-Backward pursuit) is developed. Using the mixed support set model, it is shown how this algorithm can be developed based on the standard Forward-Backward Pursuit algorithm. By experimental evaluation in a well-connected network, we conclude that the DiFBP significantly improves the performance compared to the DiSP and standard FBP algorithms.

REFERENCES

[1] D. Donoho, "Compressed sensing," *IEEE Transactions on Information Theory*, vol. 52, no. 4, pp. 1289–1306, April 2006

[2] E. J. Candes, "Compressive sampling," *International Congress of Mathematics*, vol. 3, pp. 1433–1452, 2006

[3] E. J. Candès and M B. Wakin, "An Introduction to Compressive Sampling,'' *IEEE Signal Processing Magazine*, March 2008

[4] R. Baraniuk, "Lecture Notes on Compressive sensing ," *IEEE Signal Processing Magazine*, vol. 24, no. 4, pp. 118–121, July 2007

[5] Chong Luo et.al, "Compressive Data Gathering for Large-Scale Wireless Sensor Networks," *Mobicom '09*, September 20-25,2009.

[6] Dennis Sundman et.al, "Distributed greedy pursuit algorithms," *Elsevier Signal processing*, pp.298-315, May 2014.

[7] Saikat Chatterjee et.al, "DIPP: A Distributed Greedy Algorithm based on Democratic Voting Principles," J*ournal Of Latex Class Files*, Vol.6, No.1, January 2007.

[8] Dennis Sundman et.al, " A greedy Pursuit algorithm for Distributed Compressed Sensing," *IEEE International Conference on Acoustics, Speech, and Signal Processing, pp.* 2729-2732, 2012.

[9] Dennis Sundman , " Greedy Algorithms for Distributed Compressed Sensing," *Doctor Thesis in Telecommunication*, 2014

[10] Saikat Chatterjee et.al, "Methods for Distributed Compressed Sensing," *Journal of Sensor and Actuator Networks*, December 2014.

[11] Nazim Burak Karahanoglu et.al "Compressed Sensing Signal Recovery via Forward-Backward Pursuit," *Elsevier Digital Signal Processing*, July 2013.

[12] Wei Dai et.al, "Subspace Pursuit for Compressive Sensing Signal Reconstruction," *IEEE Transactions on Information Theory*, No.5, 2009

[13] M.F. Duarte, S. Sarvotham, D. Baron, M.B. Wakin, and R.G. Baraniuk, "Distributed compressed sensing of jointly sparse signals," *Proc. Asilomar Conf. Signals, Sys., and Comp.*, pp. 1537 – 1541, Oct. 2005

THE 5TH INTERNATIONAL CONFERENCE ON WIRELESS COMMUNICATIONS, VEHICULAR TECHNOLOGY, INFORMATION THEORY, AEROSPACE & ELECTRONIC SYSTEMS (WVITAE-2015)
December 13-16, 2015, Hyderabad, India

ADAPTIVE COOPERATIVE SPECTRUM SENSING AND ACCESS IN COGNITIVE RADIO NETWORKS

[1]G.Kayalvizhi, [2] K. Muthumeenakshi, [3] Dr. S.Radha

Dept. Of ECE, SSN College of Engineering
Chennai, Tamil Nadu, India.
[1] kayalgowtham@gmail.com, [2] muthumeenakshi@ssn.edu.in,[3] radhas@ssn.edu.in

Abstract—**Frequency spectrum is an essential resource in wireless communication. Due to the rapid growth in wireless technology and increasing number of wireless users, the demand for spectrum has increased. This increased demand for spectrum leads to a problem of spectrum underutilization. The solution to this problem is accomplished through the use of cognitive radio technology, which has provided a different way to increase the efficiency of the spectrum utilization. Spectrum sensing is an indispensible function of cognitive radio to identify the available spectral holes. Energy detection is considered as a preferred technique for spectrum sensing in cognitive radio networks. Upon identifying the free spectrum, the technique to access the primary user spectrum for data transmission is dynamic spectrum access. This paper proposes an adaptive cooperative spectrum sensing and access scheme for cognitive radio networks. The main objective of this work is to improve the spectrum sensing and access and also to increase the access probability of each user. Detection accuracy decreases due to low signal to noise ratio (SNR) at the secondary user in cooperative spectrum sensing and also due to fixed collection period scheme. Low SNR secondary users are excluded in order to improve the detection probability and efficiency of spectrum sensing and access. It also uses adaptive collection period. The simulation results shows that the adaptive sensing and access with high SNR secondary user performs better when compared to all other schemes and also increase the access probability of each user.**

Index Terms **-** Adaptive collection, Cognitive radio, Cooperative sensing, Spectrum access.

I. INTRODUCTION

Radio spectrum is a limited and scarce resource in wireless technology and it is completely regulated by authorized bodies such as the Federal Communication Commission (FCC). As the usage of wireless technology increases, the demand for the spectrum is also increasing. The portion of the radio spectrum that is being allocated by the FCC to the licensed users has not been utilized fully. Cognitive radio has been proposed as a solution to improve the spectrum utilization. Cognitive radio is a radio that intelligently recognizes the status of the radio spectrum and adaptively changes the transmission parameter such as frequency, bandwidth, transmission power and modulation [1]. In cognitive radio terminology, licensed users are called the primary users and unlicensed users are called the secondary users. When the primary user is idle or not making use of the radio spectrum the secondary user equipped with cognitive radio may in future able to sense and opportunistically utilize the radio spectrum. Thus the main challenge in cognitive radio is to identify the presence or absence of primary user in radio spectrum this method is known as spectrum sensing. Spectrum sensing is the estimation of the instantaneous occupancy of the frequency spectrum and it act as an important key factor for cognitive radios. Various techniques exist for performing spectrum sensing.

The most common three spectrum sensing techniques are as Cyclostationary feature detection, Matched filtering and Energy detection (ED) based spectrum sensing technique is the mostly widely used technique for analyzing the sensing performance. This technique is commonly utilized for detecting the presence of unknown signals. The main advantage of this technique is that it does not require a prior knowledge about the signal to be detected [1]. The most widely used ED can be implemented in the time domain or frequency domain, the basic principle is to compare the energy of the signal to a threshold over a given bandwidth within

a specific sensing period. The ED in frequency domain such as Welch periodogram based estimation provides flexibility to access a multiple channels of different frequency [2]. Spectrum access is the technique mainly used to access the unutilized portion of primary user spectrum for data transmission. In [6] secondary user checks the Primary user signal based on Request to send (RTS) /Clear to send (CTS) before transmitting data, which reduces the interference to primary user. In [5], 3-phase RTS/CTS exchange is proposed. In the first phase, two secondary users exchange contention RTS(C-RTS)/contention CTS(C-CTS) messages for contention and spectrum reservation another secondary users hearing these messages are kept from accessing the medium. In the second phase, the secondary users exchange channel availability information using sensed RTS/CTS (S-RTS/S-CTS) messages. Finally, Transmission RTS/CTS (T-RTS/T-CTS) messages notify the completion of data transmission. Relationship between spectrum sensing time and access delay is analyzed using RTS/CTS exchange of each secondary user. In order to minimize the access delay, optimal sensing time and channel access are derived. Here the collection period are fixed [7]. In another study, the fixed collection period method is improved by introducing the adaptation of the collection period [4]. In the adaptive collection period scheme, the optimal stopping time of the collection period is adaptively determined based on the SRTS packets collected so far. This adaptive collection scheme is studied in a situation in which all the SNR values of primary user signal at the secondary users are equal. This paper proposes an improved spectrum access scheme which increases the access opportunity of each user.

In cooperative spectrum sensing, the decision is based on the entire secondary user participating in the network. The network consists of both the high SNR and low SNR secondary users. The low SNR secondary user doesn't contribute much to the sensing performance and hence the performance gets reduced. In proposed scheme, the low SNR value of secondary user are excluded and considering only the decision based on high SNR value of secondary user. This scheme improves the detection probability. In this method, the number of secondary user reduces, thereby increasing the access probability of each user.

Further, this paper is organized as follows. System model for adaptive cooperative spectrum and access is presented in section II. Section III presents the concept of adaptive collection period scheme. Simulation results and performance analysis are discussed in section IV and section V is the conclusion of the paper.

II. SYSTEM MODEL FOR ADAPTIVE COOPERATIVE SENSING AND ACCESS

In this system model, SU0, SU1, SU2 and SU3 are the secondary users participating in this network. Each secondary user performs spectrum sensing using Welch periodogram ED technique [2]. SU0 acts as a collecting user or fusion center. Its main function is to collect the sensed information from each secondary user and make the decision accordingly. It is assumed that the location of the primary user is known to all the secondary users. Based on this, each secondary user calculates its SNR and transmits both the sensed information and the SNR to the fusion center. In Fig.1 TX and RX represents transmission and reception.

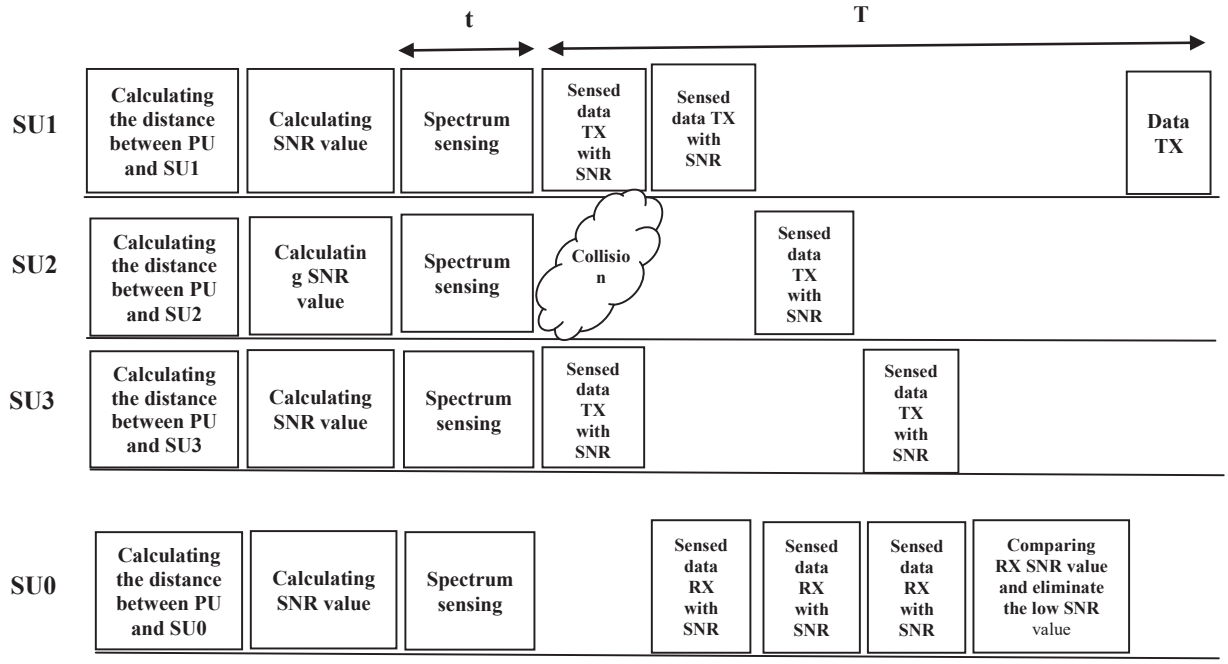

Fig.1. System model for Adaptive cooperative spectrum sensing and access in Cognitive radio

The collection period starts at the end of the spectrum sensing. The secondary user which has least spectrum sensing time will start sending the data to the collecting user. If other user sends the sensed information at the same slot then the collision occurs and information is lost. Then another secondary user having the next least sensing time will transmit its sensed information along with its corresponding SNR value. It is assumed that the each secondary user transmits its sensed information with a probability *p,* where *p* is (1/M), M is the number of secondary users. Spectrum sensing time is denoted as t. Thus the duration of the combined sensing data collection and data transmission period is fixed to *T* whose corresponding number of slots is *K*.

Proposed scheme does not make the decision based on all the secondary users and here the collection period is not fixed. The collection period stops only when the collecting user decides that sufficient number of sensed information are collected. After collecting the sensed information and their corresponding SNR, it compares the received SNR value and excludes the sensed information of low SNR secondary user. The collecting user decides the decision only based on high SNR secondary user and provides the access to that user for transmitting its data.

III. ADAPTIVE COLLECTION PERIOD SCHEME

When the collection period is used it is necessary to determine the length of the collection period. The length of the collection period is not known at the start of the collection period. Instead each slot of the collecting user decides whether to extend the collection period by one more slot or stop the collection period. This decision is based on the revenue of the collected information.

Here it is assumed that there are *q* slots remaining till the next spectrum sensing and the number of sensed information packet received at the collecting user is denoted as *r*. Consider a secondary user has sent its sensed information and SNR value to the collecting user. After receiving the fusion centre, checks whether to extend or stop the collection period based on the following [3]:

$$a(r,q)=\begin{cases} stop\,(=0) & if\ ER(r,q,end)\geq ER(r,q,extend) \\ extend\,(=1) & otherwise \end{cases} \quad (1)$$

$$ER(r,q,end)=q(1-Pf_r)$$

$$ER(r,q,extend)=(P_{s,r})ER(r+1,q-1)+(1-P_{s,r})ER(r,q-1)$$

where $a(r, q)$ represents the action of the state (r, q). The collecting user will stop collecting the sensed information when the value of expected revenue to stop is greater than the value of expected revenue to extend. Else, it will extend the collection period until revenue to stop value becomes greater. $ER(r, q, end)$ is the expected revenue to stop collection period. When it stops the collection period the remaining q slots are used for data transmission when the sensing decision results the primary user signal is absent. Pf_r represents false alarm probability of the received secondary user. $ER(r, q, extend)$ is the expected revenue to extend the collection period by one more slots or it waits for sensed information from another secondary user. $P_{s,r}$ is the probability that another sensed information are received in the next slot. $ER(r+1,\ q-1)$ represents the expected revenue when one more sensed information packet is received. $ER(r,\ q-1)$ represents expected revenue when no sensed information packet is received in next slot. The state probability is given by

$$P_{s,r}=1-(M-r)*p*(1-p)^{M-r-1}$$

The average collection period length (TC) and number of information packet collected (N_a) are given in equation (2) and (3) [5],

$$TC=\sum_{r=0}^{M}\sum_{i=1}^{\binom{M}{r}}\sum_{q=1}^{T-1}(T-q)\ P(s_r,q)\ (1-a(r,q)) \quad (2)$$

$$Na=\sum_{r=0}^{M}\sum_{i=1}^{\binom{M}{r}}\sum_{q=1}^{T-1}(r)\ P(s_r,q)\ (1-a(r,q)) \quad (3)$$

$$P(s_r,q)=\left(1-(M-r)*p*(1-p)^{M-r-1}\right)^{K-q}$$

The net normalized throughput is given by,

$$R=\frac{T_d*l}{t+(T*l)} \quad (4)$$

where T_d is the average number of slots used for data transmission incorporating the effect of sensing error probability for derivation of net normalized throughput are given in equation (5) .Where in equation (5) P_0 denotes the probability that the primary user signal does not present and P_1 represents the probability that the primary user signal is present, where l time duration of each slots which is assumed as 0.25 ms [4].

$$T_d=\sum_{r=0}^{M}\sum_{i=1}^{\binom{M}{r}}\sum_{q=1}^{T-1}q\,P(s_r,q)\left(1-a(r,q)\right)*((1-Pf_r)P_0+P_{mdr}*P_1) \quad (5)$$

IV. SIMULATION RESULTS

The simulation results describe the performance of adaptive cooperative spectrum sensing and access in

cognitive radio networks. The primary user signal is a QPSK with frequency of 6 MHZ. Here location of primary user is fixed. The secondary users are randomly located within an area of 1000 x 1000 m. Here the total number of secondary user participating in spectrum sensing is considered as 5. The location of secondary user is not fixed it keeps on changing each and every time. Fig.2. shows the random number of secondary user and its corresponding location

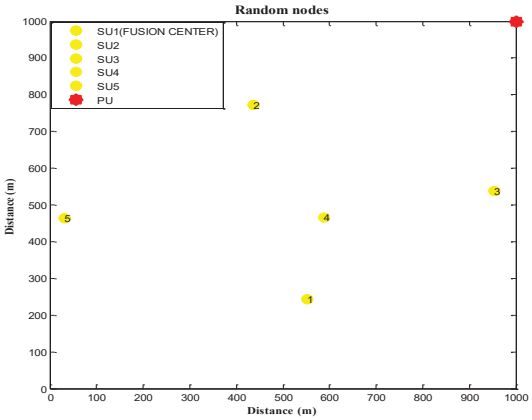

Fig. 2. Random number of secondary user, M= 5

After each secondary user calculates the SNR based on distance, each user starts sensing the spectrum and then transmits the sensed information based on adaptive collection period. Here the transmit SNR of primary user is assumed as 100dB and path loss is assumed as 2. Fig.3. shows the adaptive collection period for different number of secondary user received at the collecting user or fusion canter.

Fig.4. shows the data transmission slots against sensing time for different number of secondary user received. It clearly shows that the when the sensing time increases the number of slots used for data transmission decreases based on received number of secondary user. Here the sensing time ranges from 1 to 9 ms. when r is less, the number of slots used for data transmission will be more. There are totally 20 slots out of which one slot is used for calculating SNR value and then when the r is 2 the maximum number of slots it can obtain is 17 and the minimum of 9 slots for data transmission.

Fig.5. shows the normalized throughput against the varying sensing time for different number of received secondary users. P_0 is set to 1.The simulation results show that when only one high SNR secondary user is received in the collection period, the throughput performance is better than others. When the information from all the secondary users is collected, it becomes the adaptive scheme without excluding the low SNR secondary user. Fig.6. shows the normalized throughput when the probability that primary user signal is absent, P_0 is varied from 0 to 1. The proposed adaptive high SNR secondary user schemes show best performance for all the P_0 values because the detection probability will be more in high SNR secondary user.

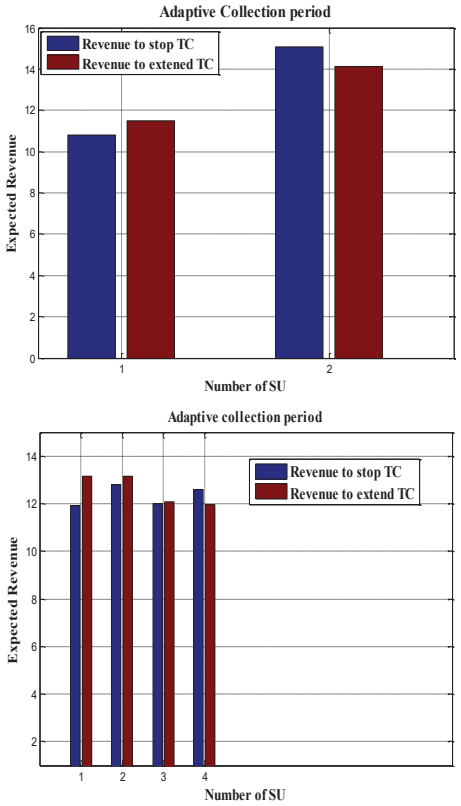

Fig.3 Adaptive collection period for different number of secondary users

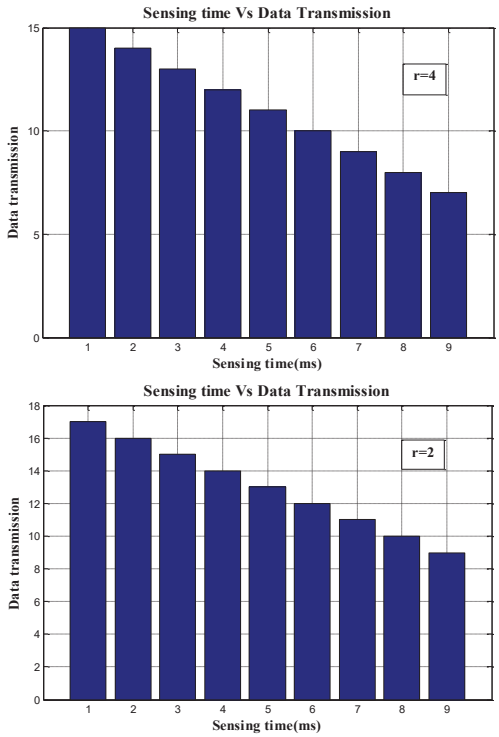

Fig.4. Sensing time Vs Data transmission for different number of secondary users

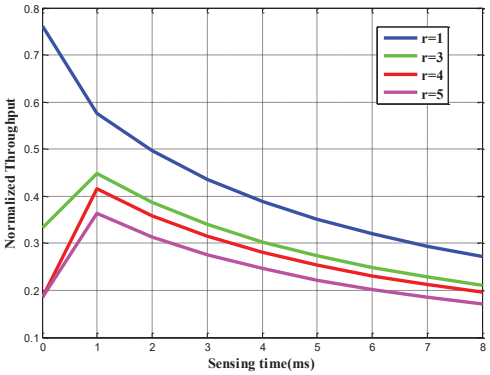

Fig .5.Sensing time Vs Normalized throughput for different value of r.

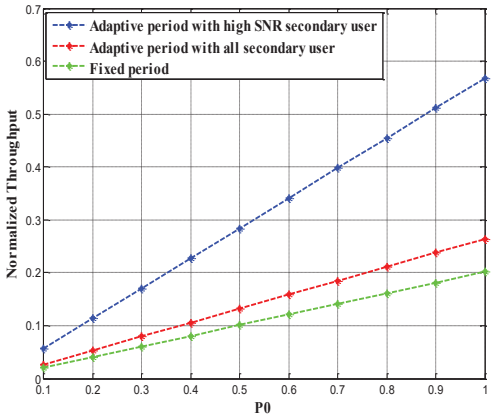

Fig.6. P0 Vs Normalized throughput, M=5, t = 1.5 ms

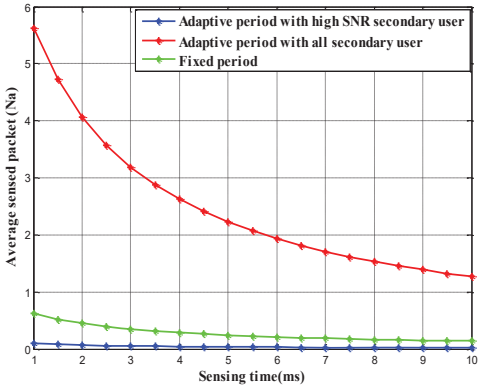

Fig.7. Sensing time Vs Average sensed packet (Na), M=5, t = 1.5 ms

Fig.7. shows the sensing time Vs average sensed packet. The proposed scheme shows the best performance when compared to all other schemes. In adaptive high SNR secondary user scheme, the number of collected and information packet are not larger compared to other schemes. The performance of normalized throughput when the combined collection and data transmission period, T, is changed is shown in Fig.8. T Vs Normalized throughput, M=5, t = 1.5 ms. The high SNR secondary user scheme shows the best performance for all the values of T. As T increases, the portion of the sensing time and collection period decreases compared with the data transmission time and hence the throughput increases.

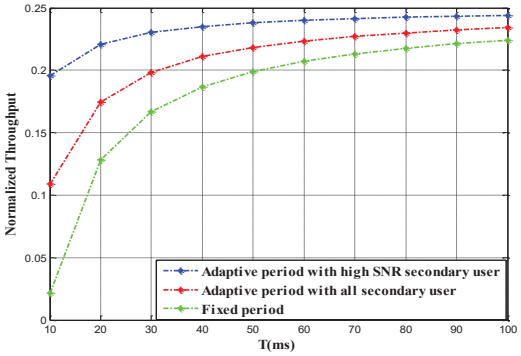

Fig.8. T Vs Normalized throughput, M=5, t = 1.5 ms

V. CONCLUSION

The proposed method uses an adaptive collection period in cooperative spectrum sensing which includes only the high SNR secondary users. In order to enhance the detection probability and spectrum efficiency the adaptive collection period scheme is used and here the low SNR secondary users are eliminated. The fusion center decides whether to stop or extend the collection period based on the expected revenue calculated at that time. The user which has the high SNR value can access the spectrum for data transmission hence the problem of interference is reduced is also reduced. Simulation results confirm that the adaptive high SNR secondary user performs better when compared to other schemes. In future, an adaptive cooperative spectrum scheme with fair policies for spectrum allocation for all secondary users can be designed.

REFERENCES

[1] Akyildiz, Ian F, et al. (2006) 'Next generation/dynamic spectrum access/cognitive radio wireless networks: a survey', Computer Networks 50.13: 2127-2159.

[2] Andrade, A. G. (2013) 'Performance evaluation of Welch's periodogram-based ED for spectrum sensing', Communications, IET 7.11.

[3] D.J. Lee, (2013) 'Adaptive cooperative spectrum sensing using random access in cognitive radio networks', IEEE 24th International Symposium on Personal, Indoor and Mobile Radio Communications: MAC and Cross-Layer Design Track.

[4] D.J.Lee, (2015) 'Adaptive random access for cooperative spectrum sensing in cognitive radio networks', IEEE Transactions on Wireless communication, vol.14,no.2, pp. 831-840.

[5] J. Jia, Q. Zhang, and X. Shen, (2008) 'HC-MAC: A hardware constrained cognitive MAC for efficient spectrum management', IEEE J. Sel. Areas Communication., vol. 26, no. 1. pp. 106-117. .

[6] Q. Zhao, L. Tong, A. Swami, and Y. Chen, (2007) 'Decentralized cognitive MAC for opportunistic spectrum access in ad hoc networks: a POMDP framework', IEEE J. Sel. Areas Communication., vol. 25, no. 3, pp. 589-600.

[7] D.-J. Lee and H. Wu,(2011) "Spectrum sensing time minimizing the access delay of IEEE 802.11-like MAC in cognitive radio networks," *IEEE Communications Letters*, vol. 15, no. 11, pp. 1249-1251.

THE 5TH INTERNATIONAL CONFERENCE ON WIRELESS COMMUNICATIONS, VEHICULAR TECHNOLOGY, INFORMATION THEORY, AEROSPACE & ELECTRONIC SYSTEMS (WVITAE-2015)
December 13-16, 2015, Hyderabad, India

Marine Vessel Detection Comparing GPRS and Satellite Images for Security Applications

Sajan Amabdiyil
Optical Image processing & Security products,
Centre for Development of Imaging Technology,
Thiruvanthapuram-695027,
Kerala, India
Email:ambadycdit@gmail.com

Dintu Thomas
Communication Engineering Department,
SCMS School of Engineering and Technology,
Ernakulum, Kerala, India
Email: dintuthomas91@gmail.com

V.P.Mahadevan Pillai
Department of Optoelectronics,
University of Kerala,
Kariavattom,
Thiruvanthapuram-69558,
Kerala, India
Email:vpmpillai9@gmail.com

***Abstract*—Unauthorized and unregistered sea going fishing vessels are being used for criminal activities in the coastal areas. The issue of piracy against merchant ships using illegal fishing vessels poses a significant threat to world shipping. Unfortunately counter piracy efforts and maritime security by the own and other nation enforcement often affects the innocent fishermen who go for trans-border fishing. Hence a proper vessel monitoring system is required to protect the maritime security without tampering the routine fishing activity of the sea going fishermen. This paper reports a system for the detection of genuine marine fishing vessels comparing the satellite images and GPRS signal information.**

***Index Terms*—Vessel Monitoring Systems, Satellite images, GPRS, Trans-border fishing.**

I. Introduction

Monitoring the marine vessels is crucial for increasing the safety and security of the maritime traffic and preventing illegal activities on the waters. For example, immigration, illegal fishery, pollution, smuggling and piracy. Poaching is also getting a serious problem since it will cause environmental crisis in coastal zones. As we are aware ninety per cent of the worlds commerce travels by sea. Now the issue of piracy against these merchant ships is a significant threat to the international economy. Day by day pirate attacks and merchant vessels hijack is increasing. Once a vessel has been hijacked, the pirates demands a large ransom amount for the safe return of the crew, vessel and cargo. Unfortunately counter piracy efforts and maritime security by the own and other nation enforcement often affects the innocent fishermen who go for trans-border fishing. So going beyond that limit for fishing is hazardous to the fishermen. Many fishermen got injured and even died as part of the counter piracy efforts and maritime security [1]. Though the measures to combat piracy and illegal activities cannot be unlawful, it has to be analyzed whether there is at least reasonable apprehension of a pirate attack or encroachment. Hence a proper vessel monitoring system is required to protect the maritime security without tampering the routine fishing activity of the sea going fishermen.

There are many vessel monitoring systems, that are used in commercial fishing to allow environmental and fisheries regulatory organizations to monitor, the position, time, speed and course of fishing vessels [2], [3]. For example, the Automatic Identification System (AIS), which transmits the location of the ship to the center via radio communication. The limitation of this equipment is that all fishing vessels may not be equipped with AIS transponders. The AIS might be purposely switched off, defected or simply a smaller vessel (e.g. sailboat, fishing boat) is not equipped with this system since they are very expensive [4], [5].Hence to monitor the fishing vessels and detect illegal activities it is important to locate all the vessels with or without functioning AIS. This required a proper cost effective vessel monitoring system to protect the maritime security without tampering the routine fishing activity of the sea going fishermen. This paper explains a study on cost effective GPS-GPRS based vessel tracking system [6] and also detection of marine vessels from satellite images for a comparison with GPRS signal information.

In India, there are nine marine states and four Union Territories [7]. The length of national coastline is about 7516.6 km. Name of the state and length of each coastline in kilometer is as follows. Gujarat (1214.70), Maharashtra (652.60), Goa (101.00), Karnataka (208.00), Kerala (569.70), Tamil Nadu (906.90), Andhra Pradesh (973.70), Odisha (476.70) and West Bengal. (157.50).The union territories are Daman & Diu (42.50), Lakshadweep (132.00), Puducherry (47.60) and Andaman & Nicobar Islands (1962.00). According to UN convention on the law of sea, the limits for the various maritime zones are divided into three such as

- 12 nautical miles (NM)- Territorial Sea,
- 24 nautical miles (NM) -Contiguous Zone and
- 200 nautical miles (NM) - Exclusive Economic Zone.

Beyond 200 NM are the international waters [8].

II. GPS, GPRS and Imaging Satellite - an Overview

A. Global Positioning System (GPS)

The Global Positioning System (GPS) is a satellite-based system that can be used to locate positions anywhere on the earth. It was first developed by the United States Department of Defense. The official name of GPS is NAVSTAR (Navigation Satellite Timing and Ranging).It provides a 3-dimensional

positioning, continuous, real-time, navigation and timing all over world. The GPS system consists of three segments, they are: a)The space segment: i.e. the GPS satellites b) The control segment, which is operated by the U.S. military, and c) The user segment, which includes both civilian military and users and their GPS equipment [9], [10].

B. General Packet Radio Service (GPRS)

GPRS is a Mobile Data Service accessible to Global System for Mobile Communication (GSM) and IS-136 mobile phones users. It provides packet-switched service and several number of users can divide the same transmission channel for transmitting the data. It is a third-generation step towards internet access. It replaces the wired connections which makes the system more intelligible access to the packet data networks like the internet. The principle employed by GPRS is the packet radio to transport the user data packets in a structured way between external packet data networks and GSM mobile stations. These packets can be routed directly to the packet switched networks from the GPRS mobile stations. It provides an end-to-end wireless architecture.

C. Imaging satellites

Imaging satellites which have been used for maritime security, have mostly involved Synthetic Aperture Radar (SAR) sensors as sources of the images, Indian satellites using these sensors include RISAT-I and RISAT-II. SAR sensors like other radars send successive pulses of microwaves or radar waves, from a moving platform like a satellite or an aircraft. The distance the SAR device travels over a target creates a large synthetic antenna aperture. The larger the aperture is, the higher the image resolution becomes, regardless of whether physical aperture or synthetic aperture.

This allows SAR to create high resolution images with comparatively small physical antennas. The synthetic aperture is caused by the movement of the source of the radar. As the SAR device on board the aircraft or spacecraft moves, the antenna location relative to the target changes over time. Signal processing of the recorded radar echoes allows it then to combine the recordings from the multiple antenna locations. This forms the synthetic antenna aperture, and allows it to create finer resolution image than what would be possible with the given physical antenna aperture. Usually SAR imagers find use in a lot of remote sensing applications. Fig.1 below shows the sample images.

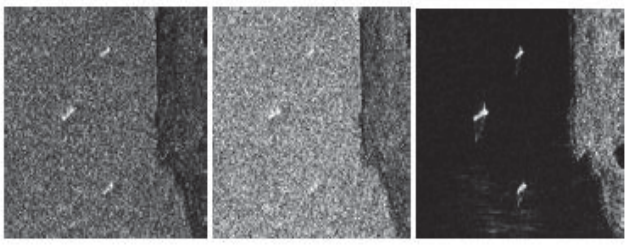

Fig. 1. Image patches from vancouver POLSAR data [11]

As these are RADAR images, there are some inherent problems in these kinds of images, these are listed below:

- Spatial resolution is limited.
- They cannot be used to detect images of length greater than 15m.
- Revisit time of the satellite to the target area is too long, hence making it difficult to use for surveillance unless many are present.
- Human interpretation of these images is very tough and involves polarimetric techniques to color the image first.

SAR imagery also has some advantages, because which it is preferred for identifying water vessels: [12], [13]

- Since the vessels are typically made of metal and their structure contains sharp edges they reflect the radar rays intensively, thus on the SAR images the vessels on open waters are bright dots and edges.
- The characteristics of SAR images enable reliable operations also by rainy and cloudy weather independent from the sun light conditions.

Optical satellite images can be used for the detection of marine vessels from satellite images. Optical imagers use mostly the visible light spectrum for the imaging purpose. Optical imaging satellites which are used for image analysis, includes SPOT which is a constellation of 7 satellites with optical imaging sensors, which together enable larger swaths while taking an image. It has an imaging swath of 60 km and high resolution enabling the detection of smaller vessels. The examples of optical images are shown in fig. 2.

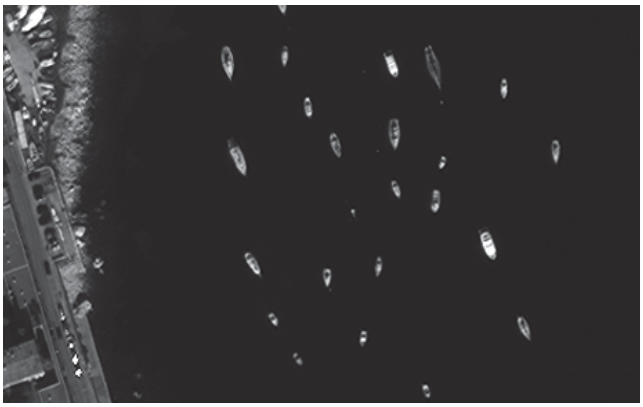

Fig. 2. Image patches from vancouver POLSAR data [13]

The advantages Optical satellite images (OSI) are as follows:

- OSI can have a higher spatial resolution, thus enabling the detection of smaller vessels and enhancing the vessel type classification.
- The human interpretation is easier than a SAR image, without the use of polarimetry.
- The tasking of an optical satellite is more simpler.

The main disadvantages of optical satellites is that they heavily depend on the weather and they can work only during daytime [14].

III. Proposed system

In the proposed system, a unit consists of GPS based location identification hardware and GPRS data communication facility along with a micro-chip that contain the whole information regarding the vessel and sailors/fisherman will attached to the sea going vessels [6]. Using this location and identity of the sea-going vessels can be easily traced and tracked out in the connectivity area in online mode with any of the enforcement authorities. The signals from the system will automatically activate immediately as the vessel start to sail and the position of the vessels will be regularly updates in the Central Monitoring System (CMS). The precompiled database of the CMS will contain all the details regarding the registered boats such as engine and hull numbers, its owners name, operating state, details regarding the dimensions, capacities and power along with fishing technique undertaken. The entire registered vessel will have specific area, scope and duration to fish. This will be regularly updated in the CMS along with current status and condition of the vessel. While the fishing vessel travelling beyond the connectivity area the communication network between the CMS and the vessel will be lost. Though the built in GPS and memory device in the system records the positions wherever the vessel roaming in the sea area, it will be communicated to the CMS while it come back to the connectivity area.

Usually the sea going fishing vessels stay in the deep sea (non-connectivity area) for fishing around 10-15 days. During this period CMS is unaware regarding their activities in the deep sea as there is no communication network. In this circumstance only enforcement teams like Coast Guard, Coastal police and Navy can monitor the fishing boats using Government approved registration number. Daily thousands of vessels will stay in the deep sea and take part in the fishing activity as fishing is one of the major incomes for the people living in the coastal areas of India. If any Unregistered fishing boats and those displaying fake registration numbers is being used for any illegal activities in the national sea boundary (deep sea) it is very difficult to identify and cross check the same by the enforcement authorities. Usually larger sea going marine vessels is always equipped with the Automatic Identification System, which might be purposely switched off, or simply a smaller vessel is not equipped with this system. In order to detect the illegal fishing vessels, it is important to locate the vessels also without functioning AIS.

Hence to detect the illegal fishing vessels, it is designed to uses the satellite images for the detection of marine vessels in comparison with GPRS signal information. Knowing the advantages and disadvantages, it has been chosen in this system to use optical images rather than SAR images because of easier access and implementation, as polarimetry is an additional step which is removed. The schematic representation diagram is shown in fig. 3.

Fig. 4 shows the flow chart of vessel detection by comparing the GPRS signal information and Satellite image.The GPS-GPRS system will automatically activate immediately as the vessel starts to sail. The GPS receiver in the system identifies the location and position of the vessels and it is send to the CMS via GPRS network. The network coverage area of GPRS in the maritime area of India is about 25-30 km. Beyond this area, i.e. GPRS non connectivity area, satellite images of the coastal territory are used to detect the vessels. From the satellite image, it is able to detect the number,time and position of the vessels using image extraction algorithms and update it to the CMS.Then compare the information obtained from GPRS signal and Satellite image. If the information same, no alert to CMS. Unless check whether the vessel is within the GPRS connectivity area or in the non connetcivity area. If it is in the connectivity area,an alert is given to CMS as well as to the enforcement auothorities. if it is in the GPRS non connectivity area, check whether the vessel is permitted in that area using the satellite image of the coastal territory.If the information of the vessels are same then send the updates of position to the CMS otherwise give an alert to the enforcement auothorities and CMS.

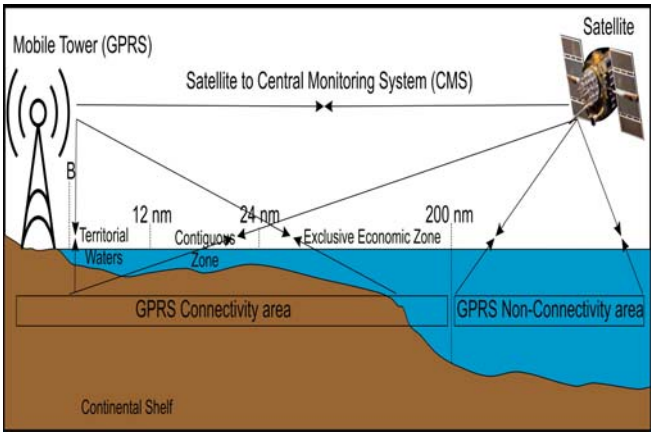

Fig. 3. Schematic representation diagram for proposed system.

The various steps involved in the digital processing of Satellite Images to isolate and identify the images of the fishing vessels are: Image rectification and restoration, Image enhancement, Information extraction [15].

Image rectification and restoration: Geometric distortions apparent themselves as errors in the position of a pixel relative to other pixels in the image. If it is left uncorrected, these distortions give any data extracted from the image is useless. Distortions occur for many reasons. For example, due to changes in platform attitude, altitude, earth curvature, earth rotation, detector delay and panoramic distortion. Most of them can be solved mathematically and are removed before you buy an image. Altitude changes are however difficult solved mathematically and thus a procedure called image rectification is performed. Satellite systems are however geometrically quite stable.

Image Enhancement:These techniques are used to improve the quality of an image as distinguished by a human. It is a most useful technique because many satellite images when

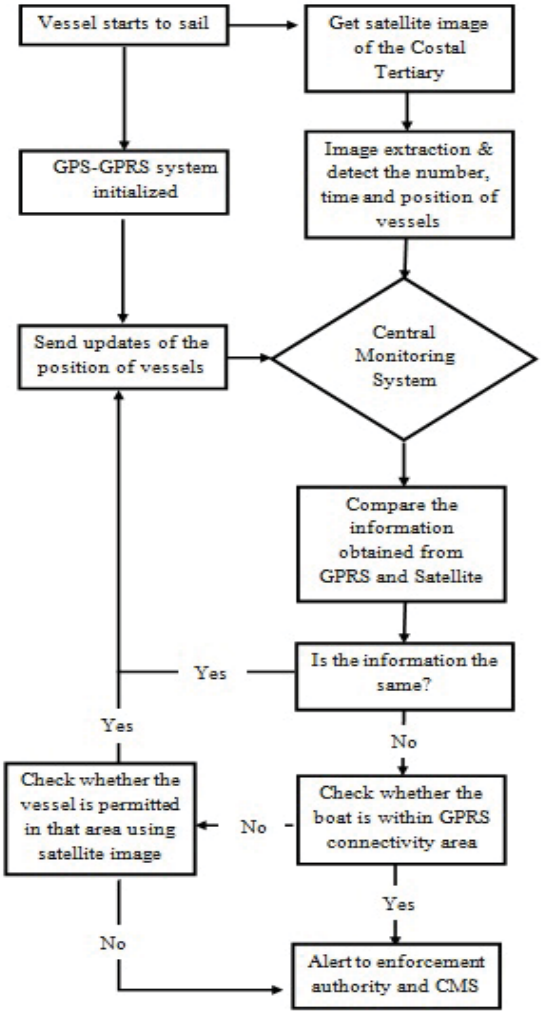

Fig. 4. Flow chart of comparion of GPRS signal & satellite image

considered on a color display give inadequate information for image interpretation. There are various kinds of techniques used for improving image quality such as contrast stretch, edge enhancement, density slicing, and spatial filtering. Image enhancement is attempted after the image is corrected for geometric and radiometric distortions.

Information extraction:It includes image classification in which it classifies the images automatically and categorizes all pixels in an image into land cover classes and themes. The term classifier refers to a computer program uses statistics and training data to divide the data into groups. There are wide varieties of techniques for classifiers, which are used for different purposes. Information extraction algorithms are specific to application. These will mostly be shape and feature detection algorithms [16].

The vessel detection problem mainly reduces to two distinct problems. One regarding the isolation of components in an image and the other regarding the classification of the isolated components as being vessel or other. Many component isolation methods are available and the most used is thresholding method. But it perform poorly on maritime vessel detection problems. So, the component isolation method can be used which is based on the image component tree algorithm. In this method two processes are used for identifying and isolating boats from satellite images. The first method is Isolation of likely candidates which can be done using Component tree formation and then deciding a height (related to the value of a component), using which we decide the components which are to be processed further. The second method is Random Forest Classifiers which are used to detect the vessel. Artificial Neural Network (ANN) method can also be used. The classifier needs to be constructed based on some training data in order to predict the data. This means that a human must identify a number of vessel targets to be used as training data.

IV. Analysis and Discussion

The major drawbacks of the existing security systems like Automatic Identification System (AIS) are: they are not cost effective, systems are very bulky, it is applicable only for the ships and not for the fishing boats and it is based on radar communication. Hence it requires large power and high gain antennas. To overcome these problems a new technology, GPS-GPRS system is proposed which is feasible and cost effective for the sea going fishing vessels. The system consists of a GPRS, GPS, and a micro-chip containing all the information about the vessels and fishermen. The position, location and identity of the seagoing vessels can be easily traced and tracked out by the enforcement authority. It can be provided with a two battery system which helps to provide long life to the equipment. Also, if one of them is tampered it automatically sends message to the CMS and the other one automatically switched on. The advantages of the proposed system are: Cost effective, Portable, Long battery life, Handy, Requires less power. But the coverage area of the GPRS network is limited. The GPRS network coverage in the maritime area is about 25-30 km and beyond this area, satellite images are used to detect illegal fishing vessels.

There are lot of algorithms for identifying boats and other water vessels. The paper [13] describes two steps for detecting water vessels. The first step involves detection of features using haar wavelet. The main purpose of using this is to reduce the in-class while increasing the out-of-class variability compared to the raw data and thus making classification easier. In the second step again a classifier is used, a more complex classifier called Adaptive Boosting. The described detection method can detect the vessels with a good quality if the water mask is accurate and the water doesnt contain large waves. The classifier is complicated to implement. Another paper [14] mainly explain with two process for identifying and isolating boats from satellite images:(1) Isolation of likely candidates is done using Component tree formation and then deciding a height (related to the value of a component), using which we decide the components which are to be processed further. (2) Machine Learning algorithm and Random Forest Classi-

fiers are used to detect the vessel. At most optimal penalty parameters, false positives were 10%. It is easy to implement but maybe not the most efficient as high resolution images were taken and image enhancement technique is also required to improve the result. Also in paper [16], it deals first with the Pre- processing using three steps: tiling, removing cloud masking using thresholding, contrast enhancement. In the next process Segmentation is done using mathematical morphology and connected components. And again a component tree and height based technique is used to filter and divide the image. In the third step Discrete Wavelet Transform and Radom Transform are performed to make certain parts more visible, further a regressive predictor is used to classify candidates. It all depends on the probability threshold. As the threshold is increased the number of false positives decreases otherwise increases. This method is also complicated to implement and the results are seemingly inefficient as the classifier used is little rudimentary. In this paper the method described in Patrik Johansson, [14] is used to detect the marine vessels which are less complicated when compared to other detection methods.

V. Conclusion

In this paper an efficient and cost effective method for marine vessel detection comparing GPRS and Satellite Images is proposed. This will definitely benefit the poor fisherman to secure their life while fishing and also enforcement to protect the coastal area, which in turn provides the national and international security. In this paper a detailed review on various algorithms for identifying marine boats from satellite images has been done. Further work is needed to fully explore the capability of the approach under a wider range and weather conditions. This study is a good basis for further development of methods that might be useful in real world applications of maritime surveillance.

References

[1] https://en.wikipedia.org/wiki/Enrica_Lexie_case

[2] Emmanouil Detsis, YuvalBrodsky, PeterKnudtson, Manuel Cuba, Heidi Fuqua, Bianca Szalai, "Vessel monitoring system", *International Space University (ISU), 1 rue Jean Dominique Cassini, Illkirch-Graffenstaden, France*, 2012.

[3] Mr. Pradip Vanparia, Dr. Y. R. Ghodasara, "Review Paper On To Study and Enhance Coastal Security System Using GIS/GPS Tool", *International Journal of Computer Applications & Information Technology* Vol. I, Issue II, September 2012.

[4] Kurt Schwehr, "Vessel Tracking Using the Automatic Identification System (AIS) During Emergency Response", *Lessons from the Deepwater Horizon Incident Center for Coastal and Ocean Mapping / Joint Hydrographic Center*, 2011.

[5] M. Surekha, R. Preethi, K. Padma priya, T. Devika, N. Divya, "Arm Based Fishing Boat Security System", *International Journal Of Innovative Research In Electrical, Electronics, Instrumentation And Control Engineering*, Vol. 2, Issue 2, February 2014.

[6] Sajan Ambadiyil, V. P. Mahadevan Pillai, V. Praveen, K. G. Jayan, S. K. Sudheer. "Holographic Registration Plates with GPRS (HRPG) network for sea-going vessels to augment the coastal security". *Proceedings of the International Conference on Ultra Modern Telecommunications, ICUMT 2009*, 12-14 October 2009.

[7] Pushpita Das, "Coastal Security" *IDSA Monograph* no. 22, September 2013.

[8] P. K. Ghosh, "India's Coastal Security Challenges and Policy Recommendations", *ORF ISSUE BRIEF*, August 2010.

[9] C. Swaykos, J. Swett, R. Kastler, "OCEANS 2010", *MTS/IEEE Biloxi - Marine Technology for Our Future: Global and Local Challenges*, pp. 1-5 , GPS based navigation, 2010.

[10] S. Ganesa vadivu, R .Lavanya, P. Meenakshi Vidya, K.S. Sujath, "Tracking coastal region using ZigBee technology", *Proceeding of 5th National Conference on VLSI, Embedded and Communication & Networks*, April 17, 2014.

[11] Su Xuwu. et al, "Ship Detection in Polarimetric SAR Based on Support Vector Machine", *research Journal of Applied Sciences, Engineering and Technology*, September 2012.

[12] Changren Zhu, Hui Zhou, Runsheng Wang, and Jun Guo, "A Novel Hierarchical Method of Ship Detection from Spaceborne Optical Image Based on Shape and Texture Features", *IEEE Transactions on Geoscience And Remote Sensing*, Vol. 48, No. 9, September 2010.

[13] Mattyus G, "Near Real-Time Automatic Marine Vessel Detection on Optical Satellite Images", *International Archives of the Photogrammetry, Remote Sensing and Spatial Information Sciences*, May 2013.

[14] Patrik Johansson, "Small vessel detection in high quality optical satellite imagery", *Chalmers University of Technology Gothenburg*, May 31, 2011.

[15] Sreenivas. B, B. Narasimha Chary, "Processing of Satellite Image using Digital Image Processing", *Geospatial World Forum*, 2011.

[16] Christina Corbane, Laurent Najman, Emilien Pecoul, Laurent Demagistri and Michel Petit, "A complete processing chain for ship detection using optical satellite imagery", *International Journal of Remote Sensing*, Vol. 31, No. 22, 20 November 2010.

THE 5TH INTERNATIONAL CONFERENCE ON WIRELESS COMMUNICATIONS, VEHICULAR TECHNOLOGY, INFORMATION THEORY, AEROSPACE & ELECTRONIC SYSTEMS (WVITAE-2015)
December 13-16, 2015, Hyderabad, India

Secure E- Voting System with integration of NFC, Biometrics and Cloud Computing

Tejas Upasani[1] Mrunal Satbhai[2] Ankit Panchal[3] Madhuri Taunk[4]
Department of Computer Engineering
SITRC, Nashik

***Abstract*— Smart Phones have become essential in today's digital era. Many technologies like RFID, QR Codes, Barcodes, Bluetooth and other proximity devices have been used. Out of these, NFC is an emerging technology. NFC is short range technology that enables communication between two NFC enabled devices. These devices operate at very close distance from each other, at around 3.9 and below. Moreover, cloud computing being an efficient storage technology, servers can be implemented using cloud. Biometrics has also proved to be a measure for verification and validation. Biometric results are unique and an accurate identification factor.**

Efficiency and accuracy are two important aspects of any E-voting system. Use of NFC leads to easy and secure e-voting. It makes the system easy to understand for the general public that have no technical knowledge, along with increasing its usability for all users. So NFC based E-voting can not only offer accuracy and increased usability but also reduce the scalability issues. It can bring out transparency, accuracy and efficiency.

But, in today's digital world scenario, it is very important to efficiently handle the network traffic while working with servers. Overhead may cause the failure of server, which leads to loss of critical data of the voter. The Cloud Computing Approach provides a splendid solution to this issue to efficiently maintain and access data. The proposed system uses NFC for secure voting, provides cloud computing for the database servers and biometrics for authentication.

***Keywords*— NFC Tag, NFC Reader, Biometric, Cloud computing, Secure Element.**

I. INTRODUCTION

The foundation for democracy is election. Election is the process of choosing right person for the right job. According to tradition procedure of voting huge equipments and paper work is required. The voting process is too tedious and time consuming as well is the tallying process. In the existing system, voter has to go to the voting booth, which becomes a geographical limitation. The proposed system overcomes this limitation. The resources being reusable, the system becomes inexpensive. The system also satisfies efficiency measures like scalability, authentication, voter privacy, confidentiality, integrity, accuracy, verifiability and mobility. The proposed system fits into the quality measures of an Efficient E-voting system. An effective system must give accurate results. It must provide provisions to vote beyond geographical limits. It needs to be secured and should include technology that maintains accuracy and increase user interaction and usability. The system proposed here includes NFC as the core technology for voting is proposed. In this system, an Android based NFC enabled Smart phone and posters of candidate contesting the elections containing NFC tags are used for voting. The voter will first enter their biometric information. Then the mobile device containing NFC has to be tapped on the poster of respective candidate to cast a vote to the desired candidate. Now, the voter information obtained by the biometric recognition kit and the vote from the Smartphone is sent to the authentication server on cloud. If the casted vote is valid, then the recorded vote is counted in the database on cloud. If this vote is invalid that is casted due to any illegal activity, then this recorded vote is discarded during the authentication phase.

II. REVIEW OF LITERATURE

It is important that any e-voting system has to be efficient and should fulfill the basic measures of ideal e-voting. These required measures are described as follows:

Accuracy: The vote so entered should not be altered before or after it is been counted.

Privacy: The link between the voter and the casted vote must be completely finished, so as to hide the identity of the voter after the casted vote is counted.

Verifiability: Every voter can verify whether their casted vote is been counted.

Mobility: A voting system may provide provisions to the voter to vote anywhere, breaking the geographical barriers.

Democracy: Only eligible voters can cast a vote, and authentication of every voter is necessary before voting. Verification has to be done in case of double voting by the same candidate [1].

These measures are of great importance and have to be completely satisfied. Earlier, E-voting was implemented using electronic ballot system. Some systems used touch panels and printers. Such systems were vulnerable to tampering of vote information which led to the use of Barcodes or QR codes for voting. Later RFID emerged to be used for e-voting. Yet the issue of security, remained unsolved. NFC being more secure for data transmission, it is proposed to use NFC for e-voting [2] [4]. Near Field Communication is wireless communication technology which works for radio frequency of short range. Near Field communication creates a point-to-point network for data communication. Near Field Communication works on unlicensed radio frequency band of 13.56 MHz available. When NFC enabled devices brought within close proximity i.e. a small distance around 4 cm to 20 cm, data transfer at rate of up to 424 Kbps can be achieved. It permits data transfer in the chunks of 106 Kbps and 212 Kbps as well. It can provide a bandwidth of approximately 2 MHz [8] [9].

Near Field Communication provides contactless communication. NFC technology is based on Radio Frequency Identification (RFID). It uses the magnetic field induction that is emitted by NFC enabled devices to actuate communication between them. NFC technology is emerging faster as its applications are increasing day by day in every sphere of life. And importantly, if NFC technology is being used in combination with mobile phone, then it can offer great opportunities. NFC technology provides users to just wave his mobile phone near NFC enabled tag and the task is done [13].

NFC work on frequency for data across is 13.56 megahertz and data which can be sent at 423, 212, 106 kilobits per second. NFC technology is based on two side interaction - initiator and target where initiator starts communication by producing magnetic induction field wave. While target plays the role of receiver by using

this magnetic field wave to activate it and performs necessary communication. Communication node Initiator and Target can be tags, stickers, or cards that do not require any batteries [17] NFC readers include a secure element or secure access module in their hardware. This is just a simple processor that's attached to the NFC controller. The secure element can be programmed to verify a code sent by the reader using public key encryption and decryption. Because the secure element of a reader/writer (or of a smart card) is capable of running small programs on its own (called applets or taglets), it can even generate new hashes on the fly. Along with NFC, Biometrics is also integrated into the system for accurate user identification and authentication. Face recognition, hand geometry biometrics, iris scanning, signature matching, voice analysis, vein printing and fingerprint recognition are the variants of Biometrics. Face and vein printing techniques are attain universality but are poor at uniqueness. Iris scanning provides uniqueness, but cannot be acceptable widely for every individual. Hand geometry matching matches the structure of an individual's hand, but gives average resulting performance. However, Fingerprint recognition is one such technique that offers uniqueness, high matching performance and permanence [7].

Using cloud computing users and enterprises get capability to store and process their data in third party centers. It share the resources. Cloud computing focuses on maximizing the effectiveness of the shared assets. Cloud assets are normally shared by a number of customers and in addition dynamically reallocated per demand. With cloud computing, a number of customers can entry a single server to retrieve and replace their knowledge with out buying licenses for various purposes.

Cloud companies give distant supply of computing sources using internet. Particularly Cloud environments are the place prospects get hold of companies from a third-party Cloud supplier. Cloud providers encompass computing capabilities supplied by Cloud infrastructure and communications capabilities supplied by the Web.

Networking can be a key component for offering knowledge communications in Cloud knowledge facilities in addition to amongst information facilities distributed at totally different places [14].

Measures of cloud computing:

1. Availability -Information needs to be accessible whenever required.
2. Confidentiality -Knowledge ought to be stored confidential.
3. Reliability - Information must be dependable four. Safety - Safety of information and software program interfaces ought to be maintained [15].

Cloud computing fashions [16]

A) Public cloud: Public cloud is one primarily based on the usual cloud computing mannequin, wherein a service supplier makes assets out there over the web. Public cloud providers could also be free or provided on a pay-per mannequin.

Benefits of public cloud companies:

1. Straightforward and cheap set-up
2. No wasted assets since you pay for what you employ.

B) Neighborhood cloud (inner or company cloud):- additionally referred to as inner cloud or company cloud.

Any such cloud supplies hosted companies to a restricted variety of individuals.

C) Hybrid cloud: Hybrid cloud is a Cloud Computing surroundings through which a corporation gives and manages some assets in-house and has others supplied externally. The hybrid strategy permits an enterprise to reap the benefits of the scalability and cost-effectiveness.

D) Personal cloud: A neighborhood cloud could also be established the place a number of organizations have related necessities and search to share infrastructure in order to appreciate a number of the advantages of cloud computing. However these choices are dearer for offering increased degree of privacy so as an alternative of neighborhood cloud non-public cloud is used [16].

The secure element resists the attacks that can be found in any smart card. The secure element provides storing area in smart phones and it built with different hardware and software. The SE has many different key fields for security mechanism and also provide process for authentication in system.

III. PROPOSED SYSTEM

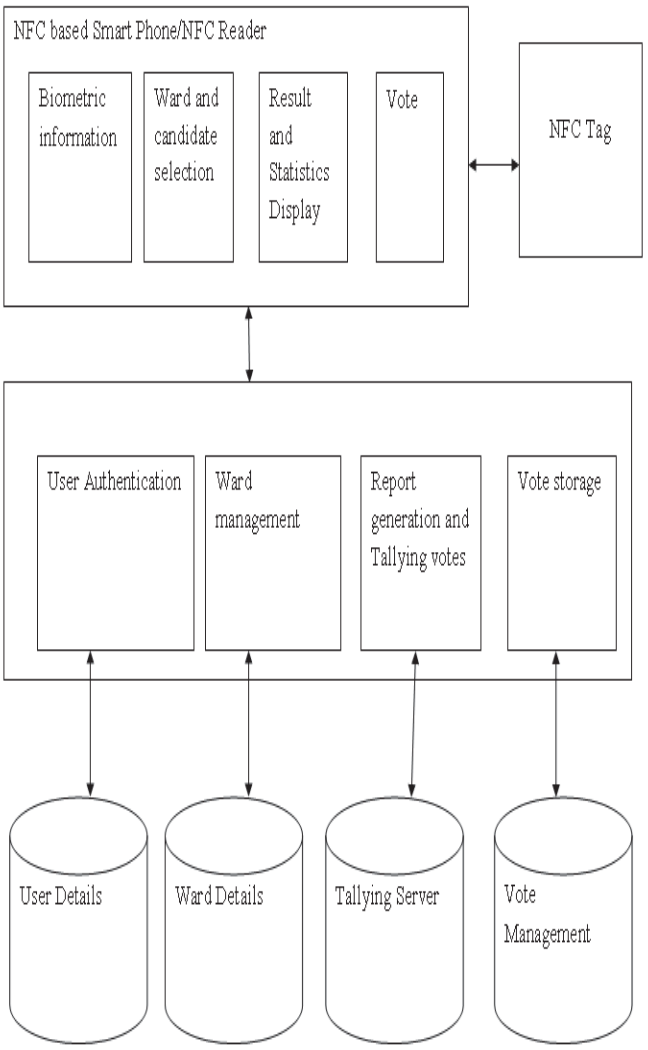

Fig 1. Overview Architecture of Secure E- Voting System with integration of NFC, Biometrics and Cloud Computing

The proposed system utilizes NFC enabled mobile device/NFC reader for casting the vote. Along with this an NFC card will be used for storing the candidate information. The user's biometrics is given an ID corresponding to that of his voter ID. This information will be stored on cloud prior to the voting process. To vote, the voter must provide their NFC enabled devices in the proximity of the NFC tag for data exchange and once the NFC device is identified, the voter is asked to present their biometric details. The biometric system sends the received information received to be checked to the corresponding ID card. If the two match, the voter is allowed to select their choice of candidate from the buttons in the selection panel from a particular ward. After a vote has been casted the ID card is marked for future referencing, this prevents the voter from casting multiple votes. The

voter's information is also marked in the database of the system. The tally for each candidate's vote is stored in the database, and once the voting process has ended, the results may be obtained.

IV. SEQUENCE DIAGRAM

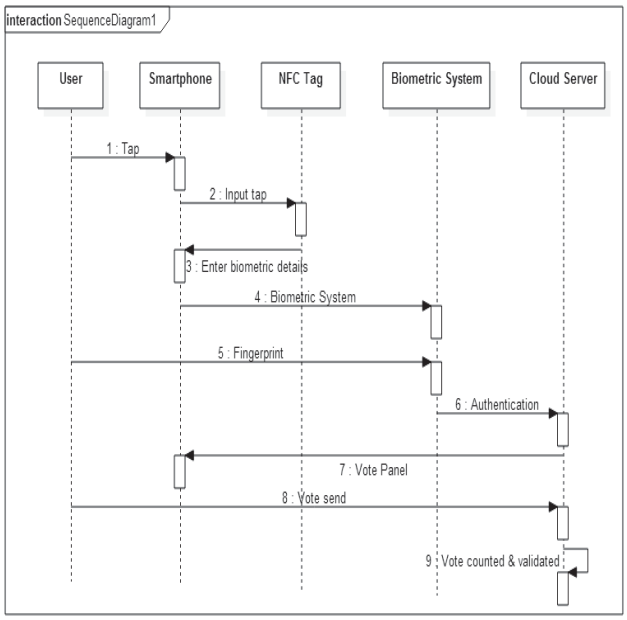

V. STATE CHART DIAGRAM

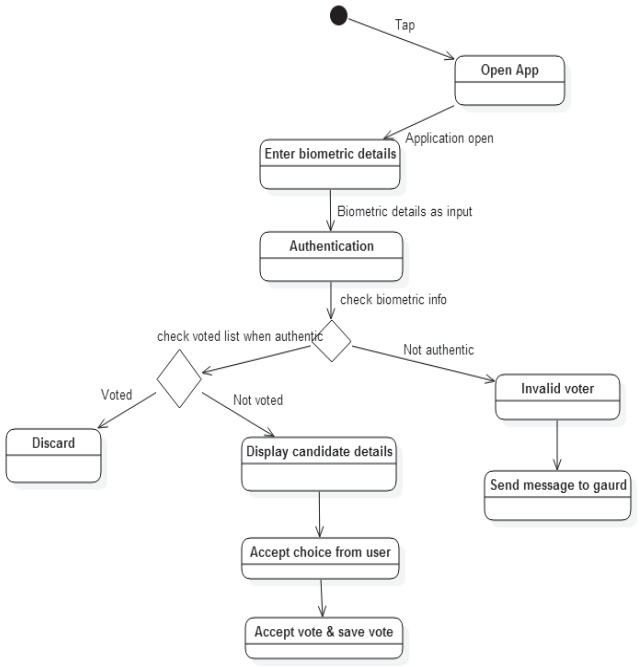

VI. MATHEMATICAL FOUNDATION

Let B represent the set of Biometric Recognition System:

B = {Fingerprint Scanning System}

Let M represent the set of Mobile Application to be used:

M = {{Java}, {Android}…}

Let NFC tags in the Smart Posters be denoted as,

T = {Details of Candidate}

Therefore, Let 'E' represent all the equipment used in the concerned system,

E = {{B}, {M}, {T}}

Let all the users associated with the system be represented by U:

U = {{Voter}, {Candidate}}

Hence,

Interactive Relation between the user and the equipment used in the system can be defined by Relation set 'R',

R = {(Voter, B), (Voter, M), (Candidate, T), (M, T)}

Now, the vote information and the candidate data as well as the voter Identity is sent to the Verification server.

Therefore, the entire verification process can be denoted as follows:

Let,

Event p: Vote Information

Event q: Candidate Data

Event r: Voter Identity

Therefore,

Event S should denote the validation and correct verification of the above provided details.

The Event S is true only for the TRUE Values of 'p', 'q' and 'r'. This also means that the Verification is TRUE only if the vote information and the candidate data as well as the voter Identity is VALID and TRUE.

$$S \rightarrow \{(p \wedge q) \wedge r = : \text{TRUE}$$

By integration of the above two systems, the entire logic behind the proposed system can be explained.

Therefore,

The integrated system can be denoted as:

$$\int R.S = \lim_{n \to \omega} \sum r.s$$

Where, (r, s) are the input values to the entire system and

ω is the number of votes being entered into the system.

CONCLUSION

As voting is a crucial process in democracy; it has to be conducted in a secure and fair manner, avoiding security breaches. The proposed system, in this paper, uses NFC technology for efficient E-voting system with minimum use of resources. NFC provides greater security for transmission of the sensitive data regarding the elections. Biometrics is integrated for correct identification and authentication of voter. Moreover, to avoid the server overhead and failure, Cloud computing is included. It is necessary to achieve ideal election goals like scalability, authentication, voter privacy, confidentiality, integrity, accuracy, verifiability and mobility; which will be achieved in the proposed system.

ACKNOWLEDGMENT

Prof. Amol D. Potgantwar
HOD Computer Engineering,
Sandip Foundation's SITRC, Nashik.

REFERENCES

1. Kerem Ok, Vedat Coskun, Mehmet N. Aydin "USABILITY OF MOBILE VOTING WITH NFC TECHNOLOGY" ISIK University, Department of Information Technology 34980, Sile, Istanbul, Turkey, IASTED international conference on software engineering 2010, 151-158
2. Punam Dhamale Varsharani Jagtap Pooja Ranjane Shraddha Thorat "Mobile Voting System Using Advanced NFC Technology" (IJSRD/Vol. 2/Issue 08/2014/091) 400-401
3. Syed Mahmud Hasan, Arafa Mohd. Anis, Hamidur Rahman, Jennifer Sherry Alam, Sohel Islam Nabil and Md. Khalilur Rhaman "Development of Electronic Voting Machine with the Inclusion of Near Field Communication ID Cards and Biometric Fingerprint Identifier" School of Engineering and Computer Science BRAC University Dhaka, Bangladesh, 978-1-4799-6288-4/14/$31.00 ©2014 IEEE, 383-387
4. Carlos Vegas González "The New Belgian E-voting System" PhD Reseacher on Constitutional Law EVOL2 / eVoting Legal Lab (DER2010-16741), Spain, 199-211
5. Stavros Valsamidis, Athanasios Mandilas, Sotirios Kontogiannis, Alexandros Karakos, " ELAN, an alternative approach to e-voting systems, focused on elections data analysis" Kavala Institute of Technology, Democritus University of Thrace, MIBES 2011 – Oral, Valsamidis-Mandilas-Kontogiannis-Karakos, 347-359
6. Shruthi.B.M, Pooja Mohnani, Mallinath, Ashwin.R.G "Multimodal Biometric Authentication Combining Finger Vein and Finger Print" Dept of Telecommunication Engg. CMRIT Bangalore, Dept of Electronics & Communication Engg., RLJIT Doddaballapur, Dept of Electronics & Communication Engg., MSRIT Bangalore International Journal of Engineering Research and Development e-ISSN: 2278-067X, p-ISSN: 2278-800X, www.ijerd.com Volume 7, Issue 10 (July 2013), PP. 43-54
7. V. S. Jahagirdar, Naresh Sen, Santosh Kumar Tiwari, "Near Field Communication", 2014, Available at URI: http://hdl.handle.net/123456789/658.
8. C. Mulliner, "Vulnerability Analysis and Attacks on NFC-enabled Mobile Phones", International Conference on Availability, Reliability and Security, IEEE Computer Society, Proceedings of the 1st International Workshop on Sensor Security (IWSS), 2009.
9. A. Alzahrani, A. Alqhtani, H. Elmiligi, F. Gebali, M. S. Yasein, "NFC Security Analysis and Vulnerabilities in Healthcare Applications", IEEE Pacific Rim Conference on Communications, Computers and Signal Processing (PACRIM), ISBN: 978-1-4799-1501-9, 27-29 Aug. 2013, pp. 302 – 305.
10. R. Ramanathan and J. Imtiaz, "NFC in Industrial Applications for Monitoring Plant Information", Fourth ICCCNT, IEEE-31661, Tiruchengode, India, July 4-6, 2013.
11. Bekir Bilginer and Paul-Luis Ljunggren, "Near Field Communication", Master"s Thesis, Lund University, February 2011.
12. M. Mareli, S. Rimer, B. S. Paul, K. Ouahada, and A. Pitsillides, "Experimental evaluation of NFC reliability between an RFID tag and a Smartphone", IEEE AFRICON, 2013, pp. 1-5.
13. X Yu-ning, "Research on NFC and SIMpass Based Application", Proceedings of the International Conference on Management and Service Science, IEEE, ISBN: 978-1-4244-4638-4, 20-22 September 2009, Wuhan, China, pp. 1-4.
14. Qiang Duan, Yuhong Yan, and Athanasios V. Vasilakos "A Survey on Service-Oriented Network Virtualization Toward Convergence of Networking and Cloud Computing", IEEE TRANSACTIONS ON NETWORK AND SERVICE MANAGEMENT, VOL. 9, NO. 4, DECEMBER 2012.
15. Kiranjot Kaur, Sheveta Vashisht "Data Separation Issues in Cloud Computing", Department of Computer Sciences and Engineering,Lovely Professional University, Phagwara, Punjab, India- 144411 kiranjot70@gmail.com Department of Computer Sciences and Engineering, Lovely Professional University,Phagwara, Punjab, India- 144411 sheveta.16856@lpu.co.in, Vol. 1, Issue X, Nov.2013 ISSN 2320-6802.
16. Pankaj Arora, Rubal Chaudhry Wadhawan Er. Satinder Pal Ahuja, "Cloud Computing Security Issues in Infrastructure as a Service"M.Tech CSE, IGCE. Asstt.prof (CSE), IGCE Associate Professor & HOD (CSE),IGCE Punjab Technical univ. Punjab technical univ. Punjab technical Univ, Volume 2, Issue 1, January 2012.
17. Coskun, V., Ozdenizci, B., & Ok, K. (2013). A Survey on Near Field Communication (NFC) Technology. Wireless personal communications, 71(3), 2259-2294.

THE 5TH INTERNATIONAL CONFERENCE ON WIRELESS COMMUNICATIONS, VEHICULAR TECHNOLOGY, INFORMATION THEORY, AEROSPACE & ELECTRONIC SYSTEMS (WVITAE-2015)
December 13-16, 2015, Hyderabad, India

On Performance of Eigenvalue based Detectors for Spectrum Sensing under Different Fading Conditions

Ashwini Deshmukh
Department of E & TC
Trinity College of Engineering and Research,Pune, India
(ashwinideshmukh1991@gmail.com)

Madhukar Deshmukh
CTIF, Department of Electronic Systems, Aalborg University
Aalborg, Denmark
(mmd@es.aau.dk)

Flemming B. Frederiksen
RATE, Department of Electronic Systems,Aalborg University
Aalborg, Denmark
(fbf@es.aau.dk)

Ramjee Prasad
CTIF, Department of Electronic Systems,Aalborg University
Aalborg, Denmark
(prasad@es.aau.dk)

***Abstract*—After advent of Cognitive Radio networks, spectrum sensing and signal detection has received wide attention. It has been observed that simple energy detectors do not perform as desired under very low SNR regime. The radiometer performance further degrades due to noise uncertainty. Eigenvalue based detectors performs better due to their larger independence on received signal SNR. Authors have used an algorithm from their earlier work for detection of Chi-Sq distributed independent random signals using Wishart matrix which model the sample covariance matrix. The Wishart matrix has been computed by using algorithm given by Odell and Feiveson (1966). The performance of Wishart modelled MME detector is evaluated when received signal undergoes fading. Different signal fading models like Rayleigh, Rician are considered and performance is evaluated in form probability of detection.**

I. Introduction

Opportunistic Spectrum Sharing (OSA) has gained importance due to higher bandwidth requirements due to large number of digital devices. The cognitive radio technology is visualized as enabling technology for flexible usage spectrum [1], [2], [3]. In this regard, spectrum sensing is the fundamental function of Cognitive Radio (CR) wherein radio detects the current electromagnetic spectrum environment to identify unutilized idle spectrum of licensed users or Primary Users (PU) [2]. In case of IEEE 802.22 standard, due to passive DTV network and primary protection requirement, there are stringent requirements on detection at very low SNR ($-20dB \equiv -114dBm$) and entire spectrum sensing duration to be 2 seconds [4]. These constraints mandate continuous scanning of the TV spectrum [5], [4]. Furthermore, spectrum sensing by single cognitive radio has limitations due to hidden node problem [1]. Quadratic form for energy detector is realized by Urkowitz [6] wherein linear filter followed by squaring and integration system has been used. Such an operation can be described as a filtered energy detector. Test statistics for detection has generally unknown distributions. It can be observed that, signal-to-noise ratio (SNR) is an important parameter which affects the performance energy detector [6]. As distribution is unknown, characteristics of hypothesis is also unknown so generally estimation of mean and variance is carried out for designing of detection algorithm.When signal and noise power is not known apriori, generalized likelihood ratio test (GLRT) is designed for this case, which uses empirical second-order statistics of the received data. GLRT gives suboptimal detection performance. However, in spite of its simplicity, energy detector employed for spectrum sensing in very low SNR regime do not give desired performance and its performance further deteriorates under noise and interference uncertainty. Hence, Eigenvalue based detector for which detection performance is largely independent of received signal SNR, can be a better choice. Other algorithms like Cyclostationary detection algorithm, are either difficult to implement or require signal information which is not possible due to legacy considerations in case of Cognitive Radio Networks (CRN).

Pioneering work in this context has been done by Nadakuditi and Silverstein [7] and Zeng et al. [8] who made use of multivariate statistics in terms of sample covariance matrix for detection of independent random signals. Covariant matrix was used for the detection and Wishart distribution [9] and [8] is considered only for calculating the detection threshold. In this paper, the algorithm using maximum-minimum eigenvalue based detection approach with Wishart random matrices is adapted from the work of Deshmukh et al. [10]. Wishart matrix is simulated in MATLAB by using algorithm given by Odell and Feiveson (1966) [11]. This algorithm uses a centering matrix to scale sample covariance matrix which has

always a Wishart distribution [12]. Hence, a sample covariance matrix can be modeled as Wishart matrix. In the present work, different signal fading models have been considered while evaluating the performance of Wishart based MME detection algorithm.

A. Detection Model

A generalized detection model assuming multiple input signals from J sources is proposed. Detection is assumed to be carried out at K receivers. It also assumed that N number of samples collected by each k receiver during the sensing time [5]. Received discrete signal at k receivers is denoted by

$$y_k(n) = \sum_{j=1}^{P} h_{kj}(n)s_{kj}(n) + \eta_k(n) \tag{1}$$

be a kx1 vector containing k received samples at time 'n' where $n = (1, 2, ...N)$. This detection problem is posed as binary hypotheses testing problem such that [8], [13]

$$\begin{array}{c} H_1 := Y = y_k(n) = \sum_{j=1}^{P} h_{kj}(n)s_{kj}(n) + \eta_k(n) \\ H_0 := Y = y_k(n) = \eta_k(n) \end{array} \tag{2}$$

where; $S_{kj}(n) = (j = 1, 2, 3, ..., P)$, $P \geq 1$ source signals, $h_{kj}(n)$ is the channel response from signal source j to receiver k and $\eta_k(n)$ represents noise sample and the noise is assumed to be Additive Gaussian White Noise(AWGN)s.t. $\eta(n) \sim \mathcal{N}(0, \sigma_n^2)$. Furthermore, channel is assumed to be flat fading for the sensing duration [9], [8].The probability density function Y corresponding to each hypotheses are $f_{Y|H_0}(y|H_0)$ and $f_{Y|H_1}(y|H_1)$ where y is particular value of the random variable Y.If $D = D_0, D_1$ is decision space and $H = H_0, H_1$ is Hypotheses, then conditional density functions representing the different decisions are

$\mathbb{P}(D_i|H_j); i, j = 0, 1$ in terms of decision regions is given by $\mathbb{P}(D_1|H_1) = [\int_{Z_1} f_{Y|H_1}(y|H_1)dy]$ equivalently.

$$\int_Z f_{Y|H_1}(y|H_1)dy = \int_Z f_{Y|H_0}(y|H_0)dy = 1 \tag{3}$$

this allows to change the decision regions such that;

$$\int_{Z_1} f_{Y|H_j}(y|H_j)dy = 1 - \int_{Z_0} f_{Y|H_j}(y|H_j)dy; j = 0, 1 \tag{4}$$

Generalized Probability of detection P_d is given by [13], [14]

$$P_d = \mathbb{P}(T_{GD} > T|H_1) = Q(\frac{T - \mu_1}{\sigma_1\sqrt{N}}) \tag{5}$$

where; T_{GD} is a of test statistic for generalized detector, T is predetermined threshold, σ_1^2 is variance under hypothesis H_1, μ_1 is mean of T_{GD} under H_1, where

$$\mu_1 = \frac{(2(1 + \gamma_r))^{P/2}}{\sqrt{\pi}}\Gamma(\frac{P + 1}{2})\sigma^P \tag{6}$$

$$\sigma_1^2 = \frac{(2(1 + \gamma_r))^P}{\sqrt{\pi}}[\Gamma(\frac{2P + 1}{2}) - \frac{1}{\sqrt{\pi}}\Gamma^2(\frac{P + 1}{2})]\sigma^2 P \tag{7}$$

where, γ_r is average received SNR, $P > 0$ and $\Gamma(.)$ is a Complete Gamma function [14] Requirement on P_d and P_{fa} depends upon applications. Generally P_{fa} is considered to be $P_{fa} \leq 0.1$ for spectrum sensing in TV white space (TVWS) based Cognitive Radio Network(CRN).

1) Calculation of Detection Threshold: At very low SNR values, derivation of threshold become very difficult if it is based on value of P_d [15], [8] because of unknown signal. As P_{fa} is related with hypothesis H_0 [13], hence sample covariance matrix of noise is,

$$C(N) = \frac{1}{N}\sum_{n=L}^{L-1+N} \hat{\eta}(n)\hat{\eta}'(n) \tag{8}$$

where; C is special Wishart matrix. The expression of the joint PDF of the ordered eigenvalues is complicated. The derivation for the threshold can be found in Tracy and Widom [15], [8]. The distribution of largest eigenvalues of the real random matrix are given by the following Theorem-1.1. Extreme eigenvalues are calculated according to Theorem-1.2.

Theorem 1.1: If noise is assumed to be real and let $A(N) = \frac{N}{\sigma_n^2 C(N)}$, $\mu = (\sqrt{N-1}+\sqrt{d})^2$, $\nu = (\sqrt{N-1}+\sqrt{d})(\frac{1}{\sqrt{N-1}} + \frac{1}{\sqrt{d}})^{1/3}$ and assume that $\lim_{N\to\infty}\frac{d}{N} = x(0 < x < 1)$, then $\frac{\lambda_{max}(A(N)-\mu)}{\nu}$ converges with probability one(1) to Tracy-Widom distribution of order 1, dimension $d = ML$ where; M is oversampling rate and L is smoothing factor.

Let $\beta = \frac{N}{d}$, then the First order Tracy-Widom Cumulative Distribution Function (CDF) is given by [11], [15],

$$\begin{array}{l} F_1(c) = exp(-\frac{1}{2}J(c; q(c))[F_2(c)]^{1/2} \\ \text{where, } F_2(c) = exp(-I(c; q(c)) \\ I(c; q(c)) = \int_c^\infty (y - c)q(c)^2 dy \\ J(c; q(c)) = \int_c^\infty q(y)dy \end{array} \tag{9}$$

where $q(.)$ is Painlevé-II equations.

Theorem 1.2: Assuming that $\lim_{N\to\infty}\frac{d}{N} = x(0 < x < 1)$, then $\lim_{N\to\infty}\lambda_{min} = \sigma_\eta^2(1 - \sqrt{x})^2(0 < x < 1)$

Extreme eigenvalues of random matrices are calculated based upon Theorem- 1.1 and Theorem-1.2 and Sawyer [11] such that,

$$\begin{array}{l} \lambda_{max} \approx \frac{1}{N}(1 + \beta^{-1/2})^2 \\ \lambda_{min} \approx \frac{1}{N}(1 + \beta^{-1/2})^2 \end{array} \tag{10}$$

Note that $d = ML$ and $\beta = N/d$

$$\begin{array}{l} \lambda_{max} \approx \frac{1}{N}(\sqrt{N} + \sqrt{d})^2 \\ \lambda_{min} \approx \frac{1}{N}(\sqrt{N} - \sqrt{d})^2 \end{array} \tag{11}$$

Tracy-Widom distribution for the asymptotic eigenvalues of certain random matrices of order 1, denoted by $F - 1$ and it is a cumulative distribution function(CDF) of the Tracy-Widom distribution of order 1 can found in Tracy and Widom [15]. For real values of noise, probability of false alarm of MME is given as;

$$P_{fa} = \mathbb{P}(\frac{\lambda_{max}}{\lambda_{min}} > \gamma) \tag{12}$$

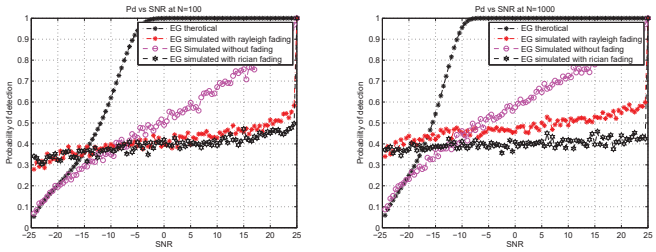

Fig. 1. Energy based detection: (a) for N=100, (b) for N=1000

Plugging in the values of λ_{max} and λ_{min} from Eq. (11), decision threshold is taken such that:

$$P_{fa} = 1 - F_1\left(\frac{\gamma(\sqrt{N}-\sqrt{d})^2 - \mu}{\nu}\right)$$

$$\text{This implies, } F_1\left(\frac{\gamma(\sqrt{N}-\sqrt{d})^2 - \mu}{\nu}\right) = 1 - P_{fa}$$

$$\frac{\gamma(\sqrt{N}-\sqrt{d})^2 - \mu}{\nu} = F_1^{-1}(1 - P_{fa}) \tag{13}$$

by putting values of μ and ν from Theorem-1.1 detection threshold is given as

$$\gamma = \frac{(\sqrt{N}+\sqrt{d})^2}{(\sqrt{N}-\sqrt{d})^2}\left(1+\frac{(\sqrt{N}+\sqrt{d})^{-2/3}}{(Nd)^{1/6}}F_1^{-1}(1-P_{fa})\right) \tag{14}$$

II. Performance of Detectors

The performance of the energy detector, covariance based MME detector and Wishart modelled MME detector is evaluated for SNR=-20dB and Pfa=0.1 are obtained for different number of samples. Signal undergoes different fading environment.

For minimum number of samples, performance of detector under Rayleigh and Rician fading conditions nearly acheives the same response 1. Detector performance enhances for signal under Rayleigh fading than that under Rician. It is observed that, energy detector shows better performance under nonfading (AWGN)channel conditions than other two fading channels. Performance is evaluated in the form of probability of detection with respect to SNR.

Covariance based MME detector performes better under Rician fading in comparision with Rayleigh case 2 and 3.

Performance under AWGN and Rician fading channels closely follows each other. For larger number of samples, detector performance improves for AWGN channel case compared to other two fading conditions. In general, Wishart modelled MME detector 4 and 5 performes better under different fading conditions than energy detector and Covariance based MME detector. Furthermore, as number of samples are increased, effect of fading is nearly nullified and detector achieves same performance under Rayleigh, Rician and AWGN fading conditions.

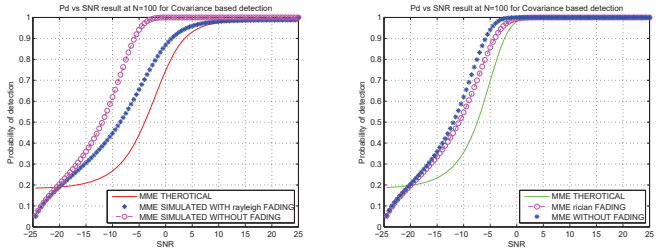

Fig. 2. Covariance based MME detection: (a) Rayleigh (N=100), (b) Rician (N=100)

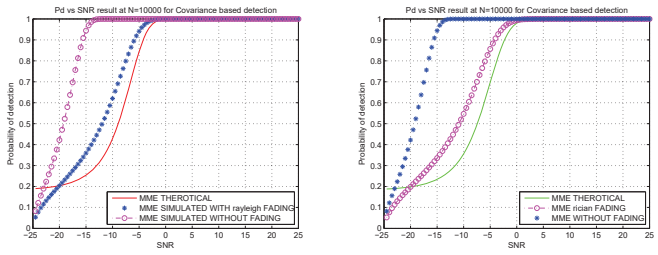

Fig. 3. Covariance based MME detection: (a) Rayleigh (N=10000), (b) Rician (N=10000)

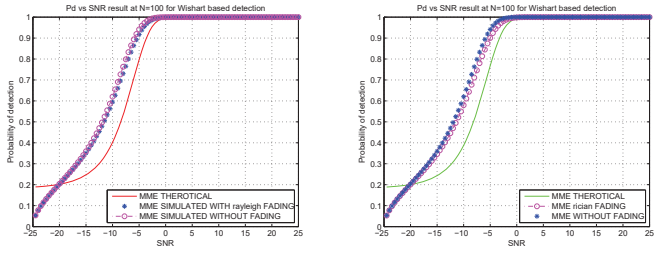

Fig. 4. Wishart base MME detection: (a) Rayleigh (N=100), (b) Rician (N=100)

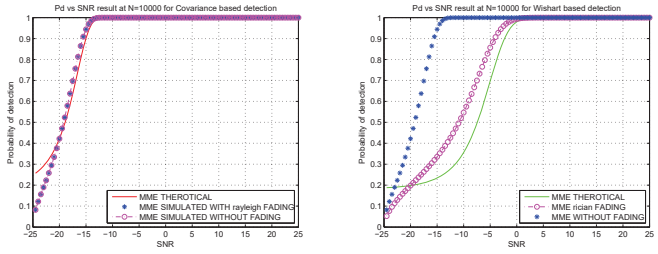

Fig. 5. Wishart base MME detection: (a) Rayleigh (N=10000), (b) Rician (N=10000)

III. Conclusion

The performance of detection algorithm for spectrum sensing in cognitive radio is presented. In this context, Maximum-Minimum Eigenvalue based detection has been reviewed. Performance of algorithm developed earlier exploiting Wishart random matrices and faster Odell and Fevison algorithm for computing the Wishart matrices is investigated under different fading conditions. The fading and non-fading environments are considered for signals to be detected. It has been observed that detector needs more number of required samples in fading environment to attain the same detection performance. It can be observed that, Wishart modelled MME detector performs better under different fading conditions than energy detector and Covariance based MME detector.

Acknowledgment

Authors appreciate the guidance and help of Dr. Vinayak L. Patil, Professor at Dept. of Electronics & Telecommunication, Trinity College of Engineering & Research, Savitribai Phule Pune University in writting this paper.

References

[1] S. Haykin, "Cognitive radio: Brain-empowered wireless communications," *IEEE Journal on Selected Areas in Communications*, vol. 23, no. 2, pp. 201–220, February 2005.

[2] Y. Zeng, Y. Liang, A. T. Hoang, and R. Zhang, "A review on specrum sensing for cognitive radio:challenges and solutions," *Hindawi Publishing Corporation EURASIP Journal on Advances in Signal Processing*, 2010, Article ID 381465.

[3] A. Kortun, T. Ratnarajah, M. Sellathurai, C. Zhong, and C. B. Papadias, "On the performance of eigenvalue-based cooperative spectrum sensing for cognitive radio," *IEEE Journal of Selected Topics in Signal Processing*, vol. 5, no. 1, Feb 2011.

[4] N. Han, S. Shon, J. H. Chung, and J. M. Kim, "Spectral correlation based signal detection method for spectrum sensing in ieee 802.22 wran systems," Feb.20-22 2010.

[5] T. Yucek and H. Arslan, "A survey of spectru sensing algorithms for cognitive radio applications," *IEEE Communications Survy and Tutorials*, vol. 11, no. 1, First Quarter 2009.

[6] H. Urkowitz, "Energy detection of a random process in colored gaussian noise," *IEEE Transactions on Aerospace and Electronic Systems*, vol. AES-5, no. 2, pp. 156–162, March 1969.

[7] R. R. Nadakuditi and J. W. Silverstein, "Fundamental limit of sample generalized eigenvalue based detection of signals in noise using relatively few signal-bearing and noise-only samples," *IEEE Journal of Selected Topics in Signal Processing*, vol. 4, no. 3, June 2010.

[8] Y. Zeng and Y. C. Liang, "Maximum-minimum eigenvalue detection for cognitive radio," *18 Annual IEEE International Symposium on Personal, Indoor and Mobile Radio Communications (PIMRC 07)*, 2007.

[9] F. Penna, R. Garello, and M. A. Spirito, "Cooperative spectrum sensing based on the limiting eigenvalue ratio distribution in wishart matrices," *IEEE Communications Letters*, vol. 13, no. 7, July 2009.

[10] M. Deshmukh, A. Deshmukh, F. B. Frederiksen, and R. Prasad, "Extreme eigenvalue based detection for spectrum sensing in cognitive radio under impact of noise and interference uncertainty," *Signal Processing (Under review)*, 2015.

[11] S. Sawyer, "Wishart distributions and inverse wishart sampling," *Washington University*, April 2007.

[12] A. Bejan and J. Warren, "Largest eigenvalues and sample covariance matrices," *,University of Warwick,Department of Statistics*, September 2005.

[13] Y. Zhao, M. Lizdabel, J. Gaeddert, K. Bae, J. Um, and J. H. Reed, "Signal detection and estimation," in *Second Edition by Mourad Barkat.*

[14] S. Kalamkar and A. Banerjee, "On the performance of generalized energy detector under noise uncertainity in cognitive radio," *Indian Institute of Technology Kanpur 208016, India, IEEE 2013*, 2013.

[15] C. A. Tracy and H. Widom, "On orthogonal and symplectic matrix ensembles," *Comm. Math. Phys.*, vol. 177, pp. 727–754, 1996.

THE 5TH INTERNATIONAL CONFERENCE ON WIRELESS COMMUNICATIONS, VEHICULAR TECHNOLOGY, INFORMATION THEORY, AEROSPACE & ELECTRONIC SYSTEMS (WVITAE-2015)
December 13-16, 2015, Hyderabad, India

Capacity Analysis of MIMO BC Channels in Presence of Spatial Correlation

Ashok Vamsidhar Panda
Department of ETC
IIIT
Bhubaneswar,India
Email: ashok.v.panda@gmail.com

Swadhin Kumar Mishra
Department of ECE
NIST
Berhampur,India
Email:swadhin@nist.edu

Ajit Kumar panda
Department of ECE
NIST
Berhampur,India
Email:akpanda62@hotmail.com

***Abstract*—In this paper a scheduling algorithm for multi-user multiple-input-multiple-output (MU-MIMO) system is considered. Users are selected at the base station(BS) based on the received signal to interference plus noise ratio(SINR). The M transmit antennas at the base-station(BS) selects M most favorable antennas from the receiver side and transmit parallel and independent data streams to them. A spatially correlated channel model is assumed. The effect of spatial correlation between channels on the average channel capacity is discussed. The distribution functions for the SINR values at the receiver side as well as the achieved sum-rate for a MIMO system with correlated channels are presented and compared with a system with independent and identically distributed (IID) channel model. The loss in achieved sum-rate in the MU-MIMO system with spatial correlation is also analyzed.**

I. Introduction

MIMO (Multiple Input Multiple Output) is one of the widely used technologies now a day. The reasons for the huge demand for MIMO are the high achieved data rate and reliable transmission of data. One of the key features that enable MIMO to achieve the large channel capacity is spatial multiplexing [1]. By using spatial multiplexing the transmitter sends data independently and in parallel so that the link capacity increases. If there are M transmit antennas at the base station(BS) and N receive antennas at the receiver side, then the capacity increases by a factor *min* $\{M, N\}$. Spatial diversity technique is implemented in MIMO systems to ensure reliable transmission. The optimal throughput in a MIMO system can be achieved by using Dirty Paper Coding (DPC) at the transmitter side[2]. But to implement DPC we need full channel state information (CSI) at the transmitter and very complex hardware circuitry is needed. To provide full CSI at the transmitter (CSIT) the reverse channels must be heavily loaded. To overcome these problems in implementation of DPC many sub-optimal user selection algorithms are proposed which are very simple to implement and which try to reduce the load on the reverse channels. Another feature that enables MIMO to increase the link signal-to-noise-ratio (SNR) and range is beamforming. Various authors discuss many suboptimal user selection algorithms using beamforming technique.

Zeroforcing beamforming(ZF-BF) technique along with a sub-optimal scheduling algorithm is presented in [3]. The proposed scheduling algorithm is called as semi orthogonal user selection(SUS) in which users orthogonal to each other are selected. In [4] a scheduling scheme is proposed for MU-MIMO system where the authors have implemented beamforming independently at the trasnmit side as well as receive side. A comparison is done to find out which of the beamforming,i.e transmit or receive achieves better result in terms of capacity.

The system performance of a MIMO system is characterized by the number of transmit and receive antennas. It also depends on the existence of channel correlation. Because in many practical scenario, correlations exist between signals from antenna elements due to the scattering environment. Correlation between channels exist between each antenna element at the transmitter and/or each element at the receiver. The degree of correlation among the channels is a function of scatters in the environment and the antenna spacing at the transmitter and receiver[5]. In [6] it is shown that with spatial correlation between channel elements there is loss in the channel capacity. Many works are also carried out where authors have carried out scheduling algorithm on spatially correlated channels. A MU-MIMO scheduling scheme for a spatially correlated channel is introduced in [7]. Here the user selection criteria is based on the Eigen values of the users. A limited feedback scheduling scheme for a MU-MIMO spatially correlated broadcast channel system is proposed in [8]. Here the scheduling algorithm is designed with an aim to maximize the sum-rate achieved by ZFBF.

In this paper we present a sub-optimal user scheduling algorithm in which we assume that each user is able to estimate its channel perfectly. Each user finds out the maximum achieved *SINR* values at its receive antennas. The maximum *SINR* values are feedback by each user to the transmitter side. At the transmitter side each of the transmit antenna selects the most favorable user and then transmit the symbol/frame to the selected antenna of that user. So only scalar feedback is used. The presentation in [8] is for users with single antenna whereas our proposed scheme is for users with multiple antennas. Another difference lies in the way in which CSI is calculated. The broadcast channels are assumed to be spatially correlated with each other. We compare the achieved throughput of the proposed scheduling algorithm in a spatially correlated channel environment with that of a system where the channel

is assumed to be IID.

The paper is organized as follows: Section II presents the system model for the MU-MIMO system. A brief introduction to spatial correlation is also made in this section. The scheduling algorithm is described in Section III. The simulation results and the corresponding analysis are done in Section IV. Finally the conclusion is presented in Section V.

II. System Model

We consider a multi-user MIMO broadcast system having M number of transmit antennas at the base-station and R_n is the number of receive antennas of n^{th} user at the receiver side where $n = 1, 2, \cdots, N$ as shown in the Fig. 1. As the usual case for any general cellular system, we assume that $N \times R_n >> M$. The objective of the scheduling scheme is to choose a set of favorable antennas/users S from the user side such that $|S| \leq M$ and then the transmit antennas transmit M parallel data streams to the selected set of antennas. The received signal at user n is represented as

$$\mathbf{y}_n = \overline{\mathbf{H}}_n \mathbf{x} + \mathbf{w}_k \tag{1}$$

where $\mathbf{x}$ is the transmitted vector of size $M \times 1$ in a given time slot t and $\mathbf{w}_k$ is an additive white Gaussian noise(AWGN) vector of size $R_n \times 1$ with zero mean and unit variance. $\overline{\mathbf{H}}_n$ is the channel matrix of user n of size $R_k \times M$. The channel matrix of n^{th} user can equivalently represented as [8]

$$\overline{\mathbf{H}}_n = \mathbf{H}_n^{iid} \times \mathbf{R}_n^{1/2} \tag{2}$$

where $\mathbf{R}_n$ is an $M \times M$ *spatially correlation* matrix of user n and $\mathbf{H}_n^{iid}$ is the usual independent and identically distributed(IID) channel matrix of n^{th} user with size $R_n \times M$. The individual elements of channel matrix $\mathbf{H}_n^{iid}$ are assumed to be Rayleigh fading coefficients which implies that the components between j^{th} receive antenna of user n and i^{th} transmit antenna $h_{j,i}^{(n)}$ is complex Gaussian distributed having zero mean and unit variance i.e. $h_{j,i}^{(n)} \sim CN(0,1)$. The channel is assumed to be flat i.e. for a symbol interval t, the signal components experience constant response from the channel. We consider a equal power allocation scheme. The total transmit power P follows the constraint $E\|\mathbf{x}_n\|^2 = P$. Here we assume a transmission scheme where the total transmit power is equally divided between the transmit antennas. Hence the allocated power to each of M transmit antenna is P/M.

User n calculates its signal-to-interference-plus-noise-ratio(*SINR*) values according to

$$SINR_{i,j}^{(n)} = \frac{|\overline{h}_{j,i}^{(n)}|^2}{\frac{M}{\alpha_n} + \sum_{i' \neq i} |\overline{h}_{j,i'}^{(n)}|^2} \tag{3}$$

where $i = 1, 2, \ldots, M$ and $j = 1, 2, \ldots, R_n$. α_n is the average *SNR* of user n. i' terms are the interference terms. $\overline{h}_{i,j}^{(n)}$ are the components of the channel matrix $\overline{\mathbf{H}}_n$. The individual components of the spatial correlation matrix are found out as[6]

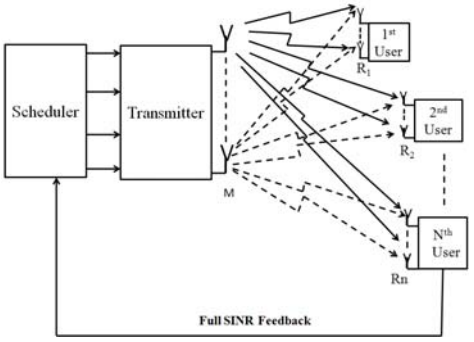

Fig. 1. System model for MU-MIMO system with M transmit antennas at BS, N users with user n having R_n antennas

$$R_{mn} = \frac{1}{2\Delta} \int_{\phi-\Delta}^{\phi+\Delta} \exp\left[j\tau(i-k)\sin\beta\right] d\beta \tag{4}$$

where $\tau = \frac{2\pi d}{\lambda}$ and d and λ are the distance between elements and wavelength of the signal respectively. The angel spread by the incoming multipath is described as 2Δ and the average arrival angle is represented as ϕ.

III. Scheduling Algorithm

A sub-optimal scheduling algorithm is discussed which is based on selecting users with highest *SINR* values. The algorithm is presented in two parts. In the first part each user calculates the achieved *SINR* values at each of its receiving antennas according to (3), i.e. each user calculates $R_n \times M$ *SINR* values. As the main objective of the algorithm is to reduce the load on the feedback channel each user, instead of making available all *SINR* values, finds out the maximum *SINR* value and feed it back to the transmitter side. Each user also finds out the indices of transmit and receive antenna corresponding to the maximum *SINR*. Along with the *SINR* value the transmit antenna index is also feedback by each user. The scheduling is performed at the base-station side in the second part. After getting all the feedback from the user side each transmit antenna selects one of the favorable user based on the *SINR* value.

We also present the achieved sum-rate capacity by the scheduling algorithm. The probability distribution function (*PDF*) of the *SINR* values at the receiver side is also presented subsequently.

A. Throughput Analysis

Once each of the transmit antenna m selects the favorable user n^* and the corresponding receive antenna B_n, the total sum-rate capacity can be found out by

$$R = \sum_{m=1}^{M} \log_2\left(1 + SINR_{m,B_n}^{(n^*)}\right) \tag{5}$$

where $SINR_{m,B_n}^{(n^*)}$ is the *SINR* of the selected user n^* at the receive antenna B_n from transmit antenna m.

Algorithm 1 Scheduling Algorithm

FEEDBACK PART

Set $\kappa_t = 1, 2, \cdots M$, and $\kappa_r = 1, 2, \cdots N$

For $n = 1, 2, \cdots N$

1: User n calculates its SINR values using equation (3). Maximum SINR values are calculated:

$$V_n = \max_{i \in \kappa_t, j \in \kappa_r} SINR_{i,j}^{(n)}$$

2: The corresponding transmit and receive antenna indices are obtained as:

$$T_n = \arg_i \max_{i \in \kappa_t, j \in \kappa_r} SINR_{i,j}^{(n)}$$

$$B_n = \arg_j \max_{i \in \kappa_t, j \in \kappa_r} SINR_{i,j}^{(n)}$$

3: Each user n feedback the corresponding V_n and T_n to the base-station.

SCHEDULING PART

After getting all the feedback from the user side, the BS performs the following:

4: For $m = 1, 2, \cdots M$

Set J_m is formed which contains the user whose $V_n = m$.

5: Antenna m at the BS selects one user from J_m randomly.

B. PDF Analysis

In this section we present the distribution function for the maximum *SINR*(V_n)values of each user. Assuming $R_1 = R_2 = \cdots = R_n = R_N$, $SINR_{m,B_n}^{n^*}$ can be written as [10]

$$SINR_{m,B_n}^{n^*} \approx \max Z_p \tag{6}$$

where

$$Z_p = \frac{|q_p|^2}{\frac{M}{\alpha_p} + \sum_{j=1}^{M-1} |q'_{p,j}|^2} \tag{7}$$

the elements of Z_p in the numerator and denominator i.e. $q_p, q'_{p,j} \sim CN(0,1)$ $p = 1, \cdots, NR_n$, and $j = 1, \cdots, M-1$.

We can write

$$Z = \frac{A}{\frac{M}{\gamma_p} + B} \tag{8}$$

as the Z_p^is are IID. A and B are chi-squared distributed as $A \sim \chi^2(2)$ and $B \sim \chi^2(2M-2)$.

We take

$$P_d = \max_{n \in J_m} \max_{i \in \kappa_t, j \in \kappa_r} SINR_{i,j}^{(n)} \tag{9}$$

Then the *PDF* of the Z_p is given by

$$f_Z(t) = \frac{e^{-Mt/\alpha_p}}{(1+t)^M} \left(\frac{M}{\alpha_p}(1+t) + M - 1 \right), t \geq 0 \tag{10}$$

IV. Results and Analysis

We consider a MU-MIMO BC system with M=2 and $R_1 = R_2 = \cdots, R_N = R = 2$. All the simulations are performed by taking 10000 realizations. First the simulation is done considering the channel to be simple Rayleigh fading

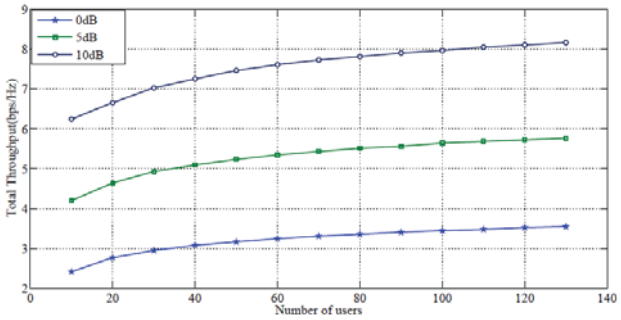

Fig. 2. Sum-rate capacity Vs. number of users for SNR=0 dB, 5dB and 10dB for a system with $M = 2, R_n = 2$ with spatially correlated channels

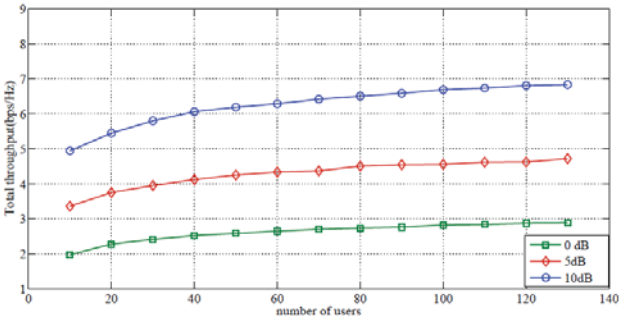

Fig. 3. Sum-rate capacity Vs. number of users for SNR=0 dB, 5dB and 10dB for a system with $M = 2, R_n = 2$ with IID Rayleigh fading channels

Gaussian channel. We find the achieved throughput using the scheduling algorithm as discussed above and Fig.2 represents the the throughput Vs number users is for *SNR* values of 0dB, 5dB and 10dB. The same scheduling algorithm is simulated for a spatially correlated channels and the achieve throughput for the system is obtained for various set of users. The spatial correlation matrix is found out as mentioned in (4). Fig. 3 present the corresponding curve for a spatially correlated channel. We compare the achieved throughput using the scheduling algorithm considering spatial correlation between channel elements (i.e. spatially correlated channel)and IID channel for *SNR*=10 dB and presented the curves in Fig. 4. It is observed from both Fig. 2 and Fig. 3 that as the

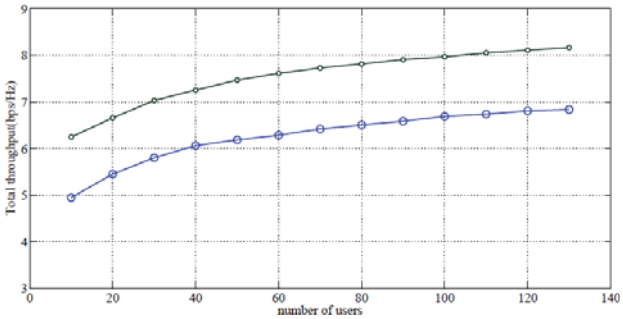

Fig. 4. Sum-rate capacity comparison between spatially correlated channels and IID Rayleigh fading channels with $M = 2, R_n = 2$ and SNR=10dB

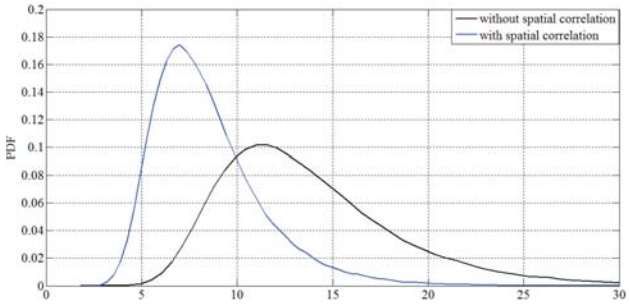

Fig. 5. Comparison between PDF of the highest SINR values of users between a system with IID channels and a system with spatially correlated channels for $N = 130$,$M = R_N = 2$, and SNR=10dB

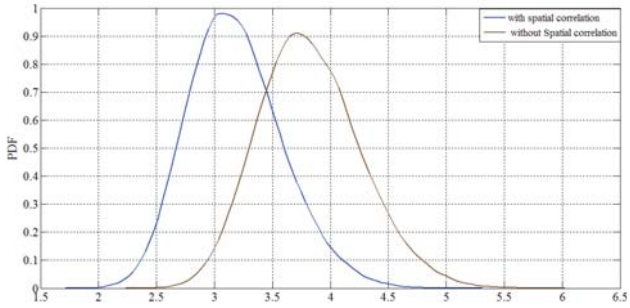

Fig. 6. Comparison between PDF of the achived sum-rate between a system with IID channels and a system with spatially correlated channels for $N = 130$,$M = R_N = 2$, and SNR=10dB

number of users are increasing the sum-rate capacity is also increases. But in Fig. 4 it is observed that if we consider the spatial correlation between channel elements, there is loss in the sum-rate capacity. For *SN*R=10dB and $N = 130$, we get a throughput of 8.1 bps/Hz without taking correlation,i.e if the channel is assumed to be IID. But if correlation is taken into consideration then throughput is scaled down to 6.8 bps/Hz.The loss in the sum-rate capacity remains nearly uniform for different set of users.

The probability distribution analysis for the $SINR^n_{m,B_n}$ is done in section (III-B). The P_d is simulated for 100000 random times and the PDF $f_P(f)$ is plotted in Fig. 5. In the same figure we also present the PDF of same P_d considering a spatially correlated channel matrix. The PDF of the total throughput for both type of channel models, i.e. spatial correlated channel and IID channel is also generated and presented in Fig. 6. It is observed Fig. 6 the probability distribution of sum-rate for both the cases are nearly equal.

V. Conclusion

We consider a MU-MIMO broadcast system in which a simple limited feedback scheduling algorithm is implemented. The scheduling algorithm is based on selecting users with highest *SINR* values. When the algorithm is considered for a system where the channel is IID, it is observed that as the number of users is increased, the sum-rate achieved also increases. We get the same observation when we run the simulation for spatially correlated channels. But the achieved sum-rate capacity for a system with spatially correlated channel element is less than the case for an IID channel element. As the number of users increases the loss in the sum-rate capacity maintains nearly a constant level. We also compare the PDF of *SINR* at the user side and the achieved sum-rate for both the cases. From the plots depicting the PDF of the achieved sum-rate in both the cases, it is clear that the probability distribution if of same type with difference statistical parameters. So work can be carried out to find out some weighing factor so that the sum-rate capacity achieved in the case of a spatially correlated channel approaches to the achieved sum-rate capacity in case of IID channels.

References

[1] A. Goldsmith, S.A. Jafar,N. Jindal, S. Viswanath, "Capacity limits of MIMO Channels", *IEEE J. Select. Area.Commun.*, vol. 21, no.5, pp. 684-702, Jun. 2003

[2] M. Costa, "Writing on dirty paper," *IEEE Trans. Inf. Theory*, vol. 29, no. 3, pp. 439441, May 1983

[3] T. Yoo, A. Goldsmith, "On The optimality of multiantenna broadcast scheduling using zero-forcing beamforming," *IEEE J.Select.Areas.Commun.*, vol. 24, no. 3, pp. 528-541, Mar. 2006.

[4] L. Wang,C. Yeh, "Scheduling for multiuser MIMO broadcast systems: Transmit or Receive Beamforming?", *IEEE Trans. Wireless Commun.*, vol. 9, no. 9, pp. 2779-2791, Sep. 2010

[5] C. Oestges,"Validity of the Kronecker model for MIMO correlated channels" *IEEE 63rd Vehicular Tech. Conf*, VTC 2006- Spring.

[6] S. Loyka, G. Tsoulos, "Estimating MIMO system performance using the correlation matrix approach," *IEEE Commun. Letters*, vol. 6, no. 1, pp. 19-21, Jan. 2002

[7] H. Lee, M. Shin,C. Lee, "An eigen-based MIMO multiuser scheduler robust to spatial channel correlation," *IEEE 61st Vehicular Tech. Conf.*, Spring. 2005, vol.2, pp.1134-1137.

[8] W. Xu,C. Zhao, Z. Ding, "Limited feedback multiuser scheduling of spatially correlated broadcast channels," *IEEE Trans. on Vehicular Technology*, vol. 58, no. 8, pp. 4406-4418, Oct. 2009

[9] J.W. Wallace, M. A. Jensen, "Modeling the indoor MIMO wireless channel," *IEEE Tran. Antennas and Propagation*, vol. 50, no. 5, pp. 591-599, May 2002

[10] M. Sharif, B. Hassibi "On the capacity of MIMO broadcast channels with partial side information," *IEEE Trans. Inform. Theory*, vol. 51, no. 2, pp. 506-522, Feb. 2005

THE 5TH INTERNATIONAL CONFERENCE ON WIRELESS COMMUNICATIONS, VEHICULAR TECHNOLOGY, INFORMATION THEORY, AEROSPACE & ELECTRONIC SYSTEMS (WVITAE-2015)
December 13-16, 2015, Hyderabad, India

Real Time Evaluation of Energy Detection and Covariance based Spectrum Sensing Algorithms

D.K.Sunil, Samrat.L.Sabat

***Abstract*—Spectrum sensing is one of the major components in cognitive radio architecture. Many algorithms are being reported for spectrum sensing by restricting the study to only theoretical simulation. In this paper we propose a detailed methodology for real time implementation and evaluation of spectrum sensing algorithm. We compare the real time performance of two algorithms namely Energy Detection(ED) and CAV (Covariance Absolute Value) on a Virtex 6 FPGA platform. BFSK signal corrupted with Additive White Gaussian Noise (AWGN) is used for real time performance evaluation. The probability of detection, sensing time and resource utilisation are used as the metrics for measuring the efficiency of algorithm. It is observed that the real time results are lower than simulation results by 5 dB and 1 dB for ED and CAV respectively. The sensing time varies between 2 to 4 milliseconds within their SNR range of detection. Simulation on a DVBT signal demonstrates that ED algorithm can achieve SNR_{wall} of -8dB SNR, whereas CAV fails to detect, due to lack of correlation in the signal. However when the signal is correlated, CAV outperforms the ED algorithm.The FPGA resource utilization is lower for ED compared to CAV.**

***Index Terms*—Cognitive radio, Spectrum Sensing, Field Programmable Gate Array (FPGA)**

I. Introduction

Cognitive radio (CR) is the technology proposed to overcome the spectrum scarcity problem in wireless communication by using its unique feature of dynamic spectrum acess. Spectrum sensing is first and critical component of Cognitive radio. In this stage, the channels are scanned to determine whether it is occupied or vaccant. Many signal processing algorithms such as energy detection, moment based, matched filtering, cyclostationary, covariance absolute value, wavelet based have been reported for spectrum sensing [1], [2], [3], [4], [5], [6]. Among them energy detection is computationally simple and fast. However its performance degrades for low Signal to Noise ratio signal. In practice, the sensing algorithm needs to be implemented in the hardware. Thus a spectrum sensing algorithm preferrably should be computationally simple and able to detect the signal at low SNR. In literature, there exists many algorithm limited to theretical analysis only, where as its real time implemetation analysis are limited. A few studies have been reported about the real time implemetation of sensing algorithm for cognitive radio [7], [8], [9], [10], [11], [12], [13]. A detailed hardware implementation methodolgy is also missing in the literature. Thus it is necessary to study the performance of sensing algorithm in the real time and provide a detailed methodology for its implementation. Although energy detection algorithm has low computational complexity, it is sensitive to noise variance. The performance of sensing algorithm is improved by exploiting the correlation in the samples using covariance absolute value algorithm. The reported simulation study shows that the CAV algorithm can achieve much better perfromance than ED and cyclostationary algorithm. This paper presents the performance comparison of ED and CAV algorithm on XILINX Vertex 6 FPGA development board. BFSK signal and noise are generated using signal and noise generator and detected pulses are observed in the oscilloscope. From the detected signal the sesnig time and probability of detection for different SNR are reported.

The paper is organised as follows: Section II gives the sensing model , Section III the details of the two Sensing schemes, Section IV details the hardware, calibration and signal processing and Section V gives results and Section VI concludes.

D.K.Sunil is with HAL and is pursuing Ph.D under the supervision of Samrat.L.Sabat who is with Centre for Advanced Studies in Electronics Science and Technology (CASEST),University of Hyderabad, Hyderabad, India. e-mail: (dksunil@uohyd.ac.in, slssp@uohyd.ernet.in)

978-1-4244-8953-4/11/$26.00 © 2015 IEEE

II. Sensing model

Let the received signal $y(t)$ be defined by :

$$y(t) = hx(t) + w(t) \quad (1)$$

$x(t)$ is the transmitted signal and $w(t)$ is a zero mean Gaussian random variable with unit variance , h is the channel gain (a random variable with a known or unknown probability density function). The channel is assumed to be flat fading with no Doppler shift. The sampled signal is denoted by $y(n)$. The detection is a

binary hypothesis test between the two hypotheses:

$$H_1 : y(n) = hx(n) + w(n); \quad (2)$$

$$H_0 : y(n) = w(n); \quad n = 1, 2, ...N; \quad (3)$$

where N is the number of samples related to the observed duration. The decision logic is

$U(k) > \gamma$; choose H_1 ; signal present

$U(k) < \gamma$; choose H_0 ; signal absent

where $U(k)$ is the test statistic and γ is the threshold.

III. Spectrum Sensing Methods

A. Energy Detection(ED) Algorithm

Energy detection is a simple technique for detecting the presence of a signal. The hardware requirements are low; but its sensitivity is poor [1]. In ED the frame energy is computed as follows:

$$U(k) = \frac{1}{N} \sum_{n=1}^{N} y(n)^2 \quad (4)$$

where $U(k)$ is the frame energy for the k^{th} frame, k and n are the frame and sample indices respectively and N is the number of samples per frame. $U(k)$ is the test statistic. Under H_0, the test statistic has a Central Chi-square distribution with N degrees of freedom and under H_1 it has a non-central Chi-square distribution with N degrees of freedom and the non-centrality parameter proportional to the SNR. For low SNR conditions ; $N = O(1/SNR^{-2})$. For detection under low SNR conditions N is large. If N is large, as per the Central Limit theorem, the test statistic can be approximated as a Gaussian [14]:

$U(k) : N(\sigma^2, 2\sigma^4/N)$; under H_0

$U(k) : N(P + \sigma^2, 2(P + \sigma^2)^2/N$; under$H_1$;

The threshold γ can be set as:

$$\gamma = Q^{-1}(P_f)\sigma^2(2/N)^{-2}; \quad (5)$$

where P is the average signal power, P_f is the desired probability of false alarm, $Q(.)$ is the Gaussian tail probability function.

B. Covariance Absolute Value Detection Algorithm

The CAV algorithm works on the concept that the covariance matrix of a totally un-correlated signal is diagonal [5]. In this method, the test statistic is the ratio between $T1$ and $T2$, where $T1$ is the sum of all the elements of the sample covariance matrix and $T2$ is the sum of the diagonals. Both are scaled by a smoothing factor L which is the number of lags selected for computing the sample autocorrelation. The statistical covariance matrix is approximated by the sample covariance matrix $R_x(N)$ [5]:

$$R_x(N) = \begin{pmatrix} \lambda(0) & \lambda(1) & \cdots & \lambda(L-1) \\ \vdots & \ddots & \dots & \vdots \\ \lambda(L-1) & \lambda(L-2) & \cdots & \lambda(0) \end{pmatrix} \quad (6)$$

$$\lambda(l)) = \frac{1}{N} \sum_{m=0}^{N-1} x(m)x(m-l)); l = 0, 1..L-1 \quad (7)$$

$$T1(N) = \frac{1}{L} \sum_{n=1}^{L} \sum_{m=1}^{L} |r_{nm}(N)| \quad (8)$$

$$T2(N) = \frac{1}{L} \sum_{n=1}^{L} |r_{nn}(N)| \quad (9)$$

$$\gamma = T1/T2 \quad (10)$$

where, r_{nn} and r_{nm} are the diagonal and other elements of the Covariance matrix R. $\gamma > 1$ indicates the presence of a signal, else there is no signal in the scanned band.

IV. Experimental setup

A. Hardware details

The experimental setup in shown in Fig. 1. A BFSK signal of bandwidth 200kHz centred at 70 MHz is generated using Agilent 4430B signal generator. Random noise of fixed power is generated using a noise generator (RS SMBV 100A). The signal power is combined with the noise power in a power combiner (Pasternak 2000).The signal of desired SNR is generated by keeping the noise power fixed while varying the signal power to the combiner using attenuator. The test conditions of the signal and noise are given in Table I. The resultant signal of desired SNR is input to an analog bandpass filter of centre frequency 70 MHz with a bandwidth of 10 MHz. The filtered signal is input to an Add-On FMC 150 Mezzanine card [15] on the ML605 FPGA board [16]. Here it is sampled at 61.44 MHz. This results in an aliased signal at 8.56 MHz.The signal of interest is extracted by applying this to a digital bandpass filter centred at 8.56 MHz and with a bandwidth of $\pm$ 3 MHz. Rate reduction is obtained by decimating the signal by a factor of 10. Due to rate reduction the signal is effectively resampled with a sampling frequency of 6.144 MHz thus resulting in the signal getting translated to 2.416 MHz. This input is fed to a mixer with a local oscillator frequency of 2.416 MHz. The local oscillator is generated by a high accuracy Drect Digital Synthesizer (DDS). The resulting baseband signal is low pass filtered with a corner frequency of 200 KHz. This is followed by a rate decimation by a factor of 10 for generating the baseband $I(n)$ and $Q(n)$ samples at 614.4 KHz rate. The signal flow is shown in Fig. 2.

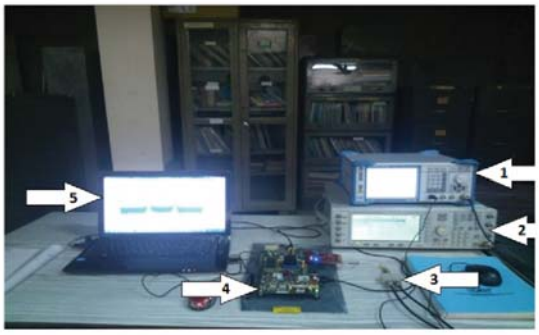

Fig. 1. Realtime Spectrum Sensing evaluation Setup: (1) Noise Generator RS SMBV 100A, (2) Signal Generator Agilent 4430B, (3) Pasternak 2000 Power Combine, 70 MHZ BPF and attenuator, (4) Xilinx ML605 with Virtex-6 XC6VLX240T-1FFG1156 FPGA and FMC-150 ADC/DAC add-on card, (5) ISE running on Laptop

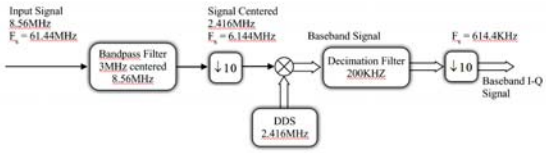

Fig. 2. Digital downconversion , filtering, decimation and spectrum sensing implemented on the Virtex-6 FPGA.

B. Digital downconversion and SNR Calibration

A calibration is carried out to ensure that the noise added to the signal is resulting in the desired SNR. To validate this a 64 k FFT is computed on the sampled data and the SNR is computed. The 64K FFT of the captured signal at SNR of -11.5dB is shown in Fig. 3. This figure clearly indicates that the 70 MHz carrier is positioned at 8.56 MHz as expected. The agreement between actual and computed SNR is less than 0.4 dB as listed in Table II.

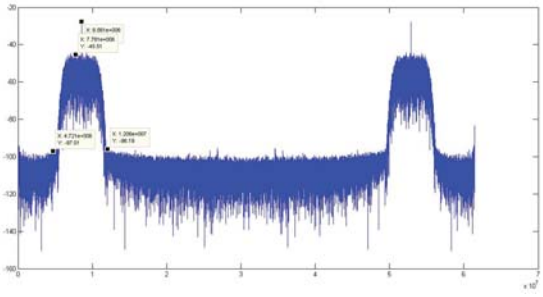

Fig. 3. 64 K FFT of the noisy signal at an SNR of -11.5 dB. The carrier can be seen at 8.56 MHz above the noise. The X axis values are from zero to 70 MHz. The spectrum has a distinct bandpass shape due to the filtering action of the 70 MHz Bandpass filter.

TABLE I
SIGNAL CAPTURE CONDITIONS

sl	Description	Conditions
1	Signal frequency	70 MHz
2	Signal power level	-20 dBm
3	Noise Band width	6 MHz
4	70 MHz Bandpass filter	+/- 3 MHz @ - 3dB
5	70MHz BPF loss	-5.17 dB
6	Power Combiner loss	-3 dB
7	FFT	64 K
8	Sample rate	61.44 MHz
9	Aliased frequency	8.56 MHz

TABLE II
SNR CALIBRATION : ACTUAL VS COMPUTED ON FPGA

At Power Combiner			AFTER FFT		
Signal Generator power, dBm	Noise Generator power, dBm	Input SNR, dB	Computed Signal Power, dBm	Computed Noise Power, dBm	Computed SNR, dB
-20	-8.27	-11.73	-28.17	-16.69	-11.48
-20	-13.27	-6.73	-28.17	-21.63	-6.54
-20	-18.27	-1.73	-28.17	-26.81	-1.36
-20	-23.27	3.27	-28.17	-31.73	3.56

C. Simulation and Realtime test

For computer simulation random burst of a BFSK modulated signal of 450 frames, of 512 samples each, are created. The modulated signal power is normalised to unity. Flat Rayleigh fading is added to the signal and the necessary SNR is created by adding random noise, of unit variance, to the scaled signal power. The SNR is varied from -20 dB to +10 dB. The received $I(n)$ and $Q(n)$ are generated and the energy is computed for energy detection . The leading and trailing edges of the burst are detected. The first and second edges indicating that the channel is occupied or vacant respectively. The number of frames between the two detected edges is the sensed length. The ratio of sensed length to total burst length gives the probability of detection (Pd). For the CAV simulation the sample covariance matrix is computed and the ratios of $T1$ and $T2$ are computed. Rising and falling edges are detected when $T1/T2 > 1.1$ and < 0.8 respectively.

For the real time burst generation the signal generator is set to pulsed mode, with BFSK modulation. The gating clock is set to 1 KHz and this is fed to the

TABLE III
DETECTION SENSITIVITY VS NUMBER OF SAMPLE PER FRAME

Number of samples	ED	CAV
32	+2	–
64	0	-12
256	-4	-15
512	-4	-16
1024	-6	-16
2048	-8	-16

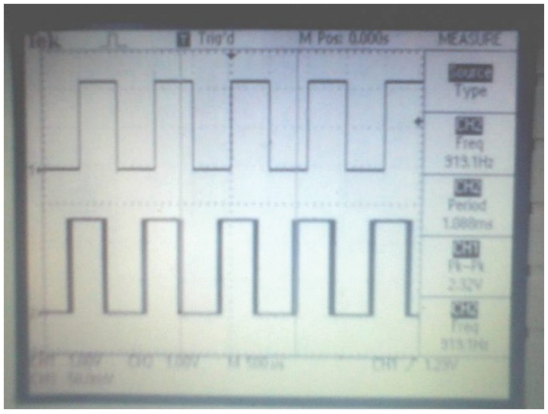

Fig. 4. Real time sensing capture on digital oscilloscope. Top trace is the Pulsed input waveform and bottom trace is the output from the FPGA after detection. The offset from the leading edge of the first pulse on the top trace to the leading edge of the second pulse on the botom trace is the sensing time. Note the jitter on the bottom trace, which will not be seen in simulation, due to variation in sensing time on hardware. The jitter is about 75 μSec.

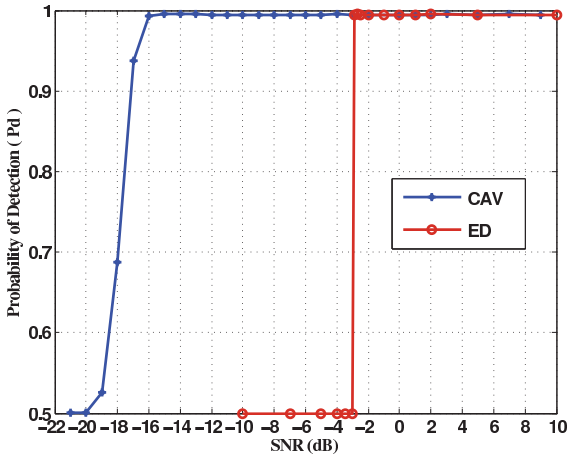

Fig. 5. Pd vs SNR Comparison of two schemes in real time on FPGA with pulsed input.

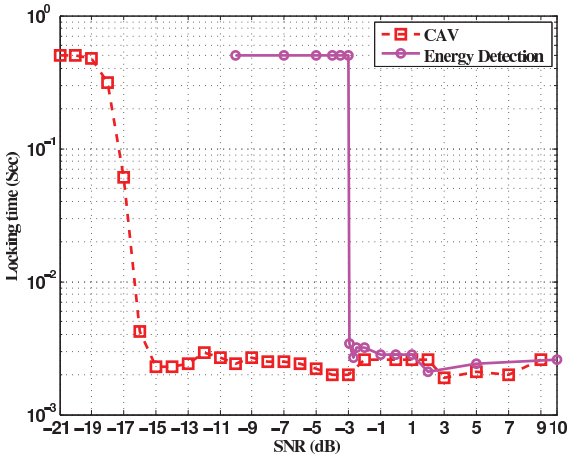

Fig. 6. Sensing time vs SNR of the pulsed signal in real time on FPGA. The sensing times are 2- 3 mSec for ED and CAV.

external trigger of the signal generator. The output is therefore pulsed with an ON time of 0.5 mS and an OFF time of 0.5 mS. This gating clock is fed to the Channel A of the oscilloscope. The FPGA executes the algorithm and outputs a discrete which goes high on the rising edge and goes low on the falling edge. This is fed to Channel B of the Oscilloscope. This is shown in Fig. 4. The ratio of the ON time of the input pulse and detected pulse is used to calculate the Pd. Table III shows the detection sensitivity of the two schemes as a function of number of samples. Beyond 512 samples there is little improvement in sensitivity. Therefore all real time implementations were carried out at a frame size of 512 samples.

V. Results and Discussion

For performance comparison (SNR vs Pd) of the two algorithms namely ED and CAV are implemented on the FPGA and the results are shown in Fig. 5. It is observed that Pd=0.9 was achieved at SNR of -3 and -17 dB for ED and CAV algorithms respectively. For energy detection the threshold is fixed and a function of only the number of samples per frame [17]. Therefore the detection performance falls suddenly below -3 dB SNR when the frame energy falls below the threshold. The $SNR\ Wall$ phenomenon [18] is valid for energy (radiometer) detection. Fig. 6 plots the sensing(locking) time for the two algorithms. The ED and CAV take about 2-3 mS for execution. The processing time changes sharply and becomes large at the SNR where the algorithm starts failing. Considering that normally a burst to be detected will last for tens of seconds this delay is not significant. This result indicates that about 1000 channels can be scanned in the 2 seconds allowed by the standard and their occupany decided for use.

Fig. 7 shows performance comparison using Matlab simulation, Simulink with SYSGEN blocks, Hardware Cosimulation and in Real time (RT). From this figure it is inferred that Pd = 0.9 occurs at SNR of -8 and -18 dB for ED and CAV algorithms respectively. The degradation from simulation to real time is 5 dB for ED and less than 1 dB for CAV indicating its robustness. It is clear that the degradation in sensitivity from Matlab simulation to real time can range from 1 to 5 dB. This margin has to be built into system design to ensure reliable performance. Table IV gives the resource utilization on the FPGA for the real time implementation of the two algorithms. As expected the ED utilizes the least-resources followed by CAV. Fig. 8 shows the performance of ED and CAV algorithms for BFSK and DVBT signals. ED performs identically for BFSK and DVBT whereas CAV detects BFSK but fails

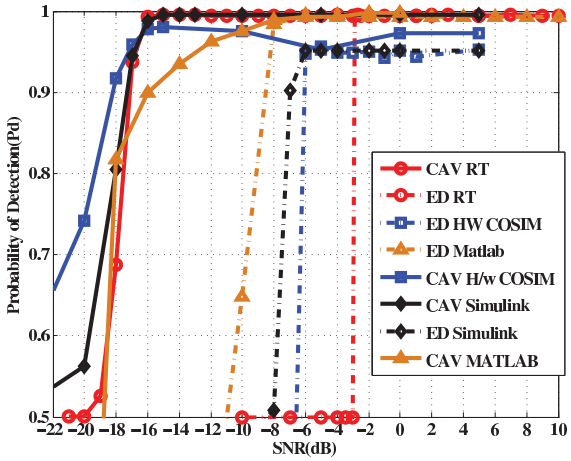

Fig. 7. Pd vs SNR Comparison of two schemes in all four stages. This plot is combination of four plots. Note the spread of the traces , going from simulation to Real time.

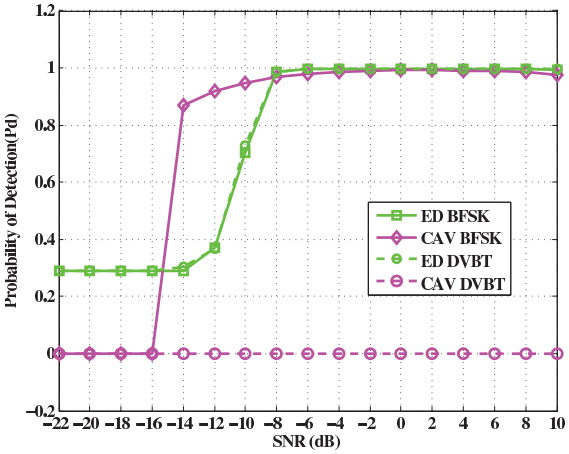

Fig. 8. Pd vs SNR for ED and CAV for BFSK and DVBT. Note that ED works for both BFSK and DVBT whereas CAV fails in the case of DVBT , due to lack of correlation.

to detect the DVBT signal. This can be attributed to the lack of correlation in the DVBT signal.

TABLE IV
RESOURCE UTILIZATION ON FPGA

sl	Resource on Virtex 6 FPGA	Available	Utilization		Percentage	
			CAV	ED	CAV	ED
1	Number of Slice Registers	301,440	8,442	1800	2	1
2	Number of Slice LUTs:	150,720	8,502	1401	5	1
3	Number of occupied Slices:	37,680	2,552	519	6	1
4	Number of bonded IOBs:	600	76	25	12	4
5	Number of RAMB36E1/FIFO36E1s	416	0	0	0	0
6	Number of RAMB18E1/FIFO18E1s:	832	1	1	1	1
7	Number of DSP48E1s:	768	129	44	16	5

VI. CONCLUSION

We have implemented two spectrum sensing algorithms on a Virtex 6 FPGA and have demonstated a calibration method for proper evaluation of spectrum sensing algorithms in real time. We have shown that real time results could be many dB off from the simulation for ED whereas CAV performance is consistent. However, CAV would fail if the signal lacks correlation whereas ED algorithm would still perform. Future work will focus on optimising the FPGA resource utilization for these algorithm.

REFERENCES

[1] H. Urkowitz, "Energy detection of unknown deterministic signals," *Proceedings of the IEEE*, vol. 55, no. 4, pp. 523–531, April 1967.
[2] F. Digham, M.-S. Alouini, and M. K. Simon, "On the energy detection of unknown signals over fading channels," in *IEEE International Conference on Communications, 2003. ICC '03.*, vol. 5, May 2003, pp. 3575–3579.
[3] T. Cui, J. Tang, F. Gao, and C. Tellambura, "Moment-based parameter estimation and blind spectrum sensing for quadrature amplitude modulation," *IEEE Transactions on Communications*, vol. 59, no. 2, pp. 613–623, February 2011.
[4] K. Kim, I. Akbar, K. Bae, J.-S. Um, C. Spooner, and J. Reed, "Cyclostationary approaches to signal detection and classification in cognitive radio," in *2nd IEEE International Symposium on New Frontiers in Dynamic Spectrum Access Networks*, April 2007, pp. 212–215.
[5] Y. Zeng and Y.-C. Liang, "Spectrum-sensing algorithms for cognitive radio based on statistical covariances," *IEEE Transactions on Vehicular Technology*, vol. 58, no. 4, pp. 1804–1815, May 2009.
[6] Z. Tian and G. Giannakis, "A wavelet approach to wideband spectrum sensing for cognitive radios," in *1st International Conference on Cognitive Radio Oriented Wireless Networks and Communications*, June 2006, pp. 1–5.
[7] A. Tkachenko, D. Cabric, and R. Brodersen, "Cognitive radio experiments using reconfigurable bee2," in *Fortieth Asilomar Conference on Signals, Systems and Computers*, Oct 2006, pp. 2041–2045.
[8] Y. Tachwali, M. Chmeiseh, F. Basma, and H. Refai, "A frequency agile implementation for ieee 802.22 using software defined radio platform," in *Global Telecommunications Conference, 2008. IEEE GLOBECOM 2008. IEEE*, Nov 2008, pp. 1–6.
[9] Z. Chen, N. Guo, and R. Qiu, "Demonstration of real-time spectrum sensing for cognitive radio," *Communications Letters, IEEE*, vol. 14, no. 10, pp. 915–917, October 2010.
[10] O. Mian, R. Zhou, X. Li, S. Hong, and Z. Wu, "A software-defined radio based cognitive radio demonstration over fm band," in *Proceedings of the 2009 International Conference on Wireless Communications and Mobile Computing: Connecting the World Wirelessly*. ACM, 2009, pp. 495–499.
[11] G. Chaitanya, P. Rajalakshmi, and U. Desai, "Real time hardware implementable spectrum sensor for cognitive radio applications," in *Signal Processing and Communications (SPCOM), 2012 International Conference on*, July 2012, pp. 1–5.
[12] Z. Wen, Z. Meng, Q. Wang, L. Liu, J. Zou, and L. Wang, "An fpga real-time spectrum sensing for cognitive radio in very high throughput wlan," vol. 7719, pp. 606–616, 2013. [Online]. Available: http://dx.doi.org/10.1007/978-3-642-37015-1_53
[13] S. Koley, V. Mirza, S. Islam, and D. Mitra, "Gradient-based real-time spectrum sensing at low snr," *Communications Letters, IEEE*, vol. 19, no. 3, pp. 391–394, March 2015.
[14] R. Tandra and A. Sahai, "Snr walls for signal detection," *IEEE Journal of Selected Topics in Signal Processing*, vol. 2, no. 1, pp. 4–17, Feb 2008.
[15] Xilinx, "FMC 150 datasheet," http://www.4dsp.com/FMC150.php, 2012.
[16] ——, "UG534 (v1.8),"ML605 Hardware User Guide," www.xilinx.com/support/documentation/boardsandkits/ug534.pdf, 2012.
[17] D. Cabric, "Cognitive radios: System design perspective," in *Ph.D Thesis,University of California,Berkeley*, 2007.
[18] R. Tandra and A. Sahai, "Fundamental limits on detection in low snr under noise uncertainty," in *International Conference on Wireless Networks, Communications and Mobile Computing*, vol. 1, June 2005, pp. 464–469 vol.1.

THE 5TH INTERNATIONAL CONFERENCE ON WIRELESS COMMUNICATIONS, VEHICULAR TECHNOLOGY, INFORMATION THEORY, AEROSPACE & ELECTRONIC SYSTEMS (WVITAE-2015)
December 13-16, 2015, Hyderabad, India

Modeling of Modified Erlang-k Distribution for Raindrop Size Distribution over South Africa

Akintunde A. Alonge, *Graduate Member*, *IEEE* and Thomas J. Afullo, *Fellow*, *SAIEE*
Discipline of Electrical, Electronic and Computer Engineering,
University of KwaZulu-Natal,
Durban, South Africa
{alongea, afullot}@ukzn.ac.za

***Abstract*—Rainfall parameters are required to understand the effects of precipitation over satellite and terrestrial links operating at microwave and millimeter wave bands. Among these parameters is the rain Drop Size Distribution (DSD) in which the contributions of rain droplets in the atmosphere are considered in estimating attenuation due to rainfall. In this paper, we present the three-parameter modified Erlang-*k* distribution as an alternative approximation of rainfall DSD. The Method of Moments (MoM) parameter estimation technique is applied to evaluate the required input parameters from rainfall measurements over subtropical Durban (29°52′S, 30°58′E) archived between 2008 and 2010. Estimates from the proposed Erlang distribution at different rain intensities are compared to other popular existing DSD models like the lognormal and gamma distributions. Our proposed distribution – is seen to conform to acceptable Self-Consistency (SC) rule and minimal error statistics – compared to other existing models. This is evident in the Root Mean Square Error (RMSE) and Chi statistics obtained from simulations. It is inferred from investigations that the proposed Erlang-*k* distribution offers a better computational advantage of rainfall DSD over subtropical locations.**

Keywords—Rainfall attenuation; Erlang-k DSD model; Method of Moments; Rainfall rate; Rainfall DSD

I. INTRODUCTION

Precipitation features prominently among the major source of attenuation for satellite and terrestrial communication systems operating at microwave and millimeter wave bands [1]. Exhaustive literature is available on the adverse role of rainfall phenomena in transmission systems operating above 10 GHz, particularly in the tropical and equatorial regions [2], [3]. An approach applied in the prediction of rainfall attenuation requires the knowledge of rainfall DSD. The DSD approach presents a unique way of estimating attenuation by accounting for the populations of varied rain drops in the atmosphere – vis-à-vis the theory of scattering and absorption. There is however, a huge preference for modified gamma and lognormal distributions in the modelling of rainfall DSDs, particularly in tropical and equatorial regions with high rainfall [4]. These models have also been shown to give good estimates in subtropical regions, to which South Africa belong [5]-[6].

The process of DSD formation over terrestrial and satellite radio links during rainfall events is of significance importance. From recent propagation studies, it has been empirically shown that rainfall processes over radio links rmanifest as a semi-Markovian queue, with individual rain spikes possessing Erlang-*k* distributed service times [7], [8]. This discovery may imply that several elements of the rainfall process, including rainfall rate and rainfall DSD also exhibit similar probability behaviour representative of the generic Erlang family of distribution. It is on this premise that a further investigation on the suitability of this distribution for DSD modeling is importantly undertaken. It is expected that Erlang distribution will provide some form of DSD approximation, since it is closely related to gamma distribution.

In this paper, an investigation is undertaken on the suitability of the modified Erlang-*k* distribution for DSD modeling using rainfall measurements in Durban, South Africa. The input parameters are obtained by applying the parameter estimation technique of Method of Moments (MoM). The proposed model is later compared with existing models applied in subtropical regions. The Self-Consistency (SC) rule, alongside error statistic tests, is applied to comparably determine its performance.

II. ERLANG-K DROP SIZE DISTRIBUTION MODEL

For this study, the Erlang-*k* distribution is proposed for the modeling of rainfall DSDs. The Erlang-*k* DSD represents a *scaled* Probability Density Function (PDF) belonging to the family of multiplicative PDFs, in which several stages are encountered, in a system [9]. The popularity of this model is attributed to its high-end application in classical telephone networks as advocated by *Agner Krarup Erlang* (1878-1929). In contemporary communication engineering, it is predominantly applied in queueing systems and complex teletraffic analysis [10].

The Erlang-*k* DSD is a statistical distribution mathematically given by (1):

$$N(D) = N_m \frac{\lambda^k D^{k-1}}{\Gamma(k)} exp(-\lambda D) \text{ for } \lambda > 0, \forall k \in \mathbb{Z}^+ \quad (1a)$$

and,

$$\lambda = k\mu \qquad [mm^{-1}] \qquad (1b)$$

where N_m is the scaling parameter in mm^{-1}, k is the number of stages or shape parameter, μ is the scale parameter and D is the average diameter of rain drops per channel ranging from 0.3 mm to 5.4 mm. The Erlang-k distribution is a special case of the gamma distribution, such that $\lambda = \frac{1}{\theta}$ and k is always a real positive integer. In relation to the popular modified gamma DSD, the parameters from (1) are such that $m = k - 1$ and $N_o = \frac{N_m \lambda^k}{\Gamma(k)}$.

The Moment Generating Function (MGF) of the Erlang-k distribution is given by:

$$M_n = N_m \left(1 - \frac{n}{\lambda}\right)^{-k} \cong N_m \sum_{i=0}^{\infty} (-1)^i \binom{-k}{i} \frac{n^i}{\lambda^i} \qquad (2a)$$

where n is a positive integer representing the moment number. (2) gives a clear definition of the Erlang-k MGF as a power series where nth raw moments are related to derivative of specified series terms when n is set to zero [11]. In literature, a much more modified form of determining the exact nth moment as proposed in [12] is given by:

$$M_n = N_m \frac{\Gamma(k+n)}{\Gamma(k)} \frac{1}{\lambda^n} = N_m \frac{(k+n-1)!}{(k-1)!} \frac{1}{\lambda^n} \qquad (2b)$$

The eventual MGF arising from several stages as obtained in (2b) gives credence to the multiplicative characteristics of Erlang-k distribution. This function contains all the known information of the layered Erlang-k PDF as embedded in the parameters of N_m, k and λ.

III. Data Measurement, Modelling and Simulation

The rainfall measurements applied in this study are obtained from RD-80 Joss-Waldvögel distrometer installed at the University of KwaZulu-Natal, Durban at geographic coordinates of 29°52′S, 30°58′E. The processed data applied represents drop size spectra (of one-minute sampling time) collected over a period of October 2008 and December 2009. The spectra signature consists of rainfall rates ranging between 0.0003 mm/h to 117.49 mm/h. For the sole purpose of this experiment, only rain rates above or equal to 1 mm/h are processed. This reduces the available dataset to 7366 minutes of processed data. This is to discourage the presence of measurement errors arising from dead time and noisy low rain rates which are predominant. An effective way of processing the filtered dataset at this location is to determine the averaged values of similar rain rates as undertaken in [5]. Using this approach, a total of 52 unique rain drop size spectra (all averaged) were obtained in Durban.

The computational procedure for estimating the input parameters of the proposed distribution is undertaken by Method of Moments (MoM) as applied in related literature [4], [13]. This technique involves equating the theoretical moments of the Erlang-k DSD as given in (2b) to the computed moments from measurements. The nth moment of measurement is obtained with the knowledge of the DSD such that:

$$M_n = \sum_{i=1}^{20} {D_i}^n N(D_i) \Delta D_i \qquad (3)$$

where $N(D_i)$ is the rainfall DSD and $\Delta D_i$is the interval between the average diameters of the different channels, D_i.

The accrued rainfall DSD from measurements is computed directly from the dataset given by [16]:

$$N(D) = \frac{c_i}{s \times T \times v_t \times \Delta D} \ [mm^{-1} m^{-3}] \qquad (4)$$

where c_i is the number of drops per channel, s is the sampling area of the conical surface of the distrometer in m^2, T is the sampling interval in seconds and v_t is the terminal velocity in *m/s*.

With regard to the theoretical moments to be generated from (2b), certain combinations of moments are expected to give appropriate results. Researchers in radar and microwave studies have identified specific combinations, with guaranteed moment numbers related to radio engineering [13]. For example, the combination of the 3rd, 4th and 6th moments (MM346) for resolving three-parameter probability distributions has long been described as the most suitable [4], [13]. This is mainly due to the stability and kernel similarity of this combination to unique rainfall indices such as rainfall rates, rain attenuation and radar reflectivity. Using this combination, it is inferred from (2b) that:

$$M_3 = N_m \frac{k(k+1)(k+2)}{\lambda^3} \qquad (5a)$$

$$M_4 = N_m \frac{k(k+1)(k+2)(k+3)}{\lambda^4} \qquad (5b)$$

$$M_6 = N_m \frac{k(k+1)(k+2)(k+3)(k+4)(k+5)}{\lambda^6} \qquad (5b)$$

By solving (5*a*), (5b) and (5c) as simultaneous equations, solutions of related Erlang-k DSD parameters are given as:

$$k = round\left\{\frac{(6\alpha - 9) - \sqrt{1 - 8\alpha}}{2(1-\alpha)}\right\} \qquad (6a)$$

where,

$$\alpha = \frac{M_6 {M_3}^2}{{M_4}^3} \qquad (6b)$$

$$\lambda = \frac{M_3(k+3)}{M_4} \qquad (7)$$

$$N_m = \frac{M_3 \lambda^3}{k(k+1)(k+2)} \quad (8)$$

IV. Results and Discussions

In this section, derivation of parameters for the proposed Erlang-*k* DSD, as well as its performance over different rain rates are discussed.

A. Derivation of Parameters for Erlang-k DSD model

By applying results from the MoM solutions as proposed in (6) – (8), scatterplots are obtained as seen in Fig. 1. For each of these scatterplot, the plotting of Erlang-*k* input parameters and their corresponding rainfall rates are undertaken. From Fig. 1, it is observed that each of these parameters form a unique relationship with rainfall rate as implied from their scatterplots. For example, the parameter, N_m, is observed to be positively correlated to rainfall rate as seen in Fig. 1a. However, the parameters, μ and *k*, are found to be negatively correlated to the rainfall rate as seen in Fig. 1b and 1c. This suggests that the drop concentration (N_m) increases as higher rainfall rates are attained. This is expected as total drop contributions present along the radio links or radar paths increases as rain builds up. In any case, it also confirms that moments considered in this work *i.e.* M_3, M_4 and M_6 similarly follows this same trend. For parameter μ, the scatterplot in Fig. 1b implies that the mean diameter of Erlang-*k* DSD will shift leftward as rainfall rate increases. This is mainly reliant on the premise that this input parameter is always the reciprocal of mean of the data. Finally, parameter *k* as seen in Fig. 1c follows the same trend as μ. This is possible because their product always result in λ (see Eqn. 1b). This parameter generally refers to the number of stages for the proposed modified Erlang-*k* DSD. Our results show that *k* should range between the values of 3 and 6, depending on the maximum recorded rain rate. Infact, *k* gives 3 at low rainfall rates (R < 5 mm/h). For medium rain rates (5 mm/h ≤ R < 17 mm/h), *k* is predominantly 4. For high rain rates under shower and thunderstorm conditions (17 mm/h ≤ R < 50 mm/h), *k* is mainly 5. For much higher rain rates (R > 50 mm/h), *k* is typically given as 6 (and above in some cases).

It follows from the scatterplot results that suitable expressions for the proposed model could simply be obtained by regression analysis. By applying this procedure, the following expressions are derived as input parameters of the Erlang-*k* DSD in (1) as follows:

$$k + 3 = round\{2.6105R^{0.19}\} \quad (9)$$

$$N_m = 808.99R^{-0.087} \quad (10)$$

$$\mu = 2.3326R^{-0.334} \quad (11)$$

where R is the rainfall rate in mm/h.

On the general approach applied, we can indeed affirm that the combination of the 3rd, 4th and 6th moments (MM346) gives a good approximation of the estimated input parameters for other models. Kozu and Nakamura [13] and Timothy *et al.* [4] independently considered these combinations in their publication on modified gamma DSDs in Japan and lognormal DSDs over Singapore respectively. Several other researchers estimated statistical DSDs from distrometers in India [4], Nigeria [14], Malaysia [15] and South Africa [5]–[6] using either the lognormal, modified gamma or Weibull distribution.

B. Performance of the Erlang-k DSD model

As obtained from the combination of regression functions as derived in (10) – (11), the performance of the proposed Erlang-*k* DSD is undertaken. This is analysis is undertaken over four averaged rainfall rates namely 5mm/h, 25 mm/h, 75 mm/h and 120 mm/h. These selected rainfall rates are representative of different regime conditions of rainfall in Durban: drizzle, widespread, shower and thunderstorm [5].

These results presented in Fig. 2 show that the proposed model gives good fits at different rainfall rates. The modification to the shape parameter in (9) *i.e.* (k + 3), is seen to improve the robustness of the model especially in conjunction with N_m. This modification is significant because it demonstrates the similarity between the modified version of gamma distribution in [13] and the currently proposed modified Erlang-*k* distribution. At high rainfall rates (Figs. 2c and 2d) for instance, our proposed model however gives a good approximation of both smaller and larger diameters of rain drops over our location in Durban.

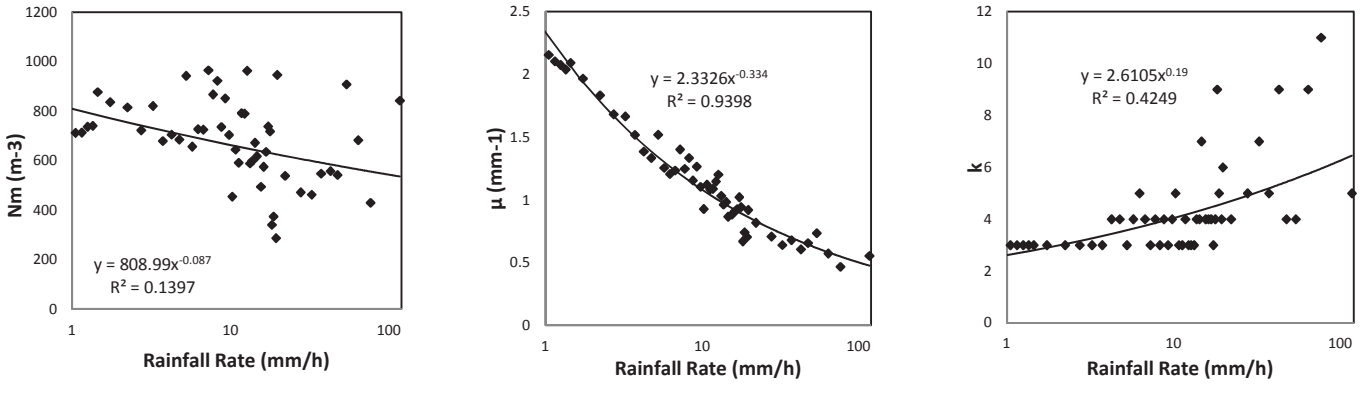

(a) (b) (c)

Fig. 1. Scatterplot of proposed Erlang-k DSD parameters from distrometer measurements over Durban, South Africa (a) N_m (b) μ (c) *k*

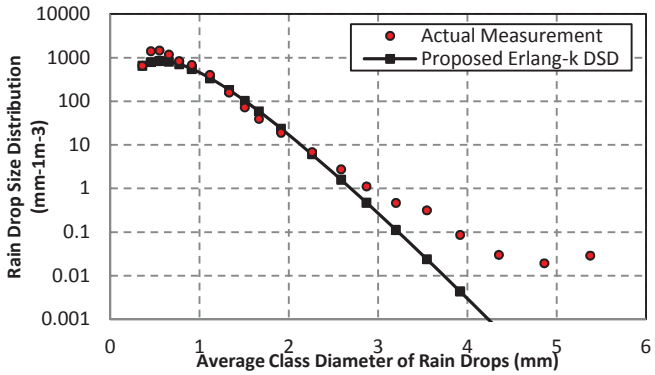

(a)

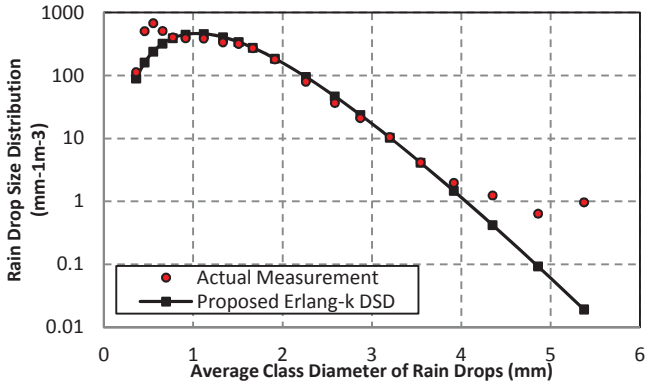

(b)

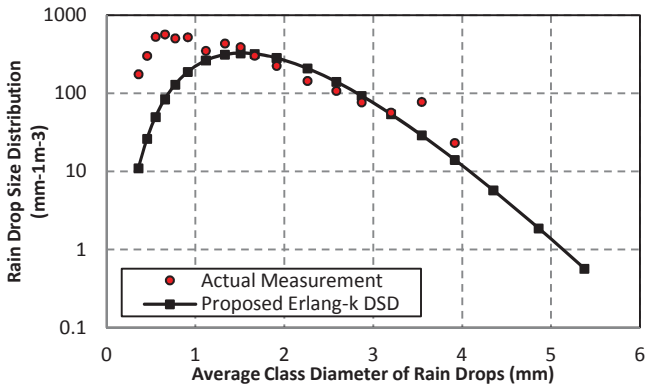

(c)

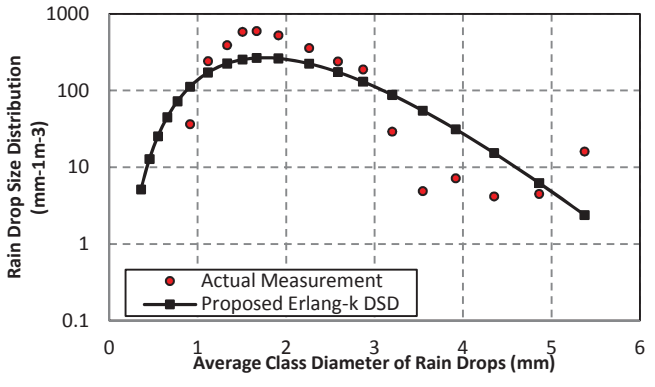

(d)

Fig 2. Performance of proposed Erlang-*k* DSD models at different rain rates. (a) 5 mm/h (b) 25 mm/h (c) 75 mm/h (d) 120 mm/h

C. Comparison of Proposed Model over Existing Models over Durban

The development of Erlang-*k* DSD model as undertaken in this work requires a valid comparison with other useful DSD models applicable in this field. For the purpose of this comparison, the modified gamma DSD and lognormal DSD models are applied based on their wide applications for DSD estimation at tropical, subtropical and equatorial regions. The modified gamma DSD model given in [13]; in this study, m is approximated to the values of 2 and 3. The statistical function for lognormal DSD model is given in [14].

A summary of the input parameters for compared Erlang-*k*, gamma and lognormal DSD models in Durban, derived from MoM, is given in Table I. To make a valid comparison, the Self-Consistency (SC) rule is applied for each of these different DSD models. The SC rule implies that any probability distribution must be able to estimate accurately the random variable that generated its input parameters. In this case, the random variable is rainfall rate, as the input parameters are dependent on rainfall rate. The estimated rainfall rate from the DSD models to be compared is obtained from given by:

$$R_{estimated} = \frac{6\pi}{10^4}\sum_{i=1}^{20} {D_i}^3 N(D_i) v_t \Delta D_i \quad [mm/h] \qquad (12)$$

where v_t and $\Delta D_i$are the terminal or fall velocity and diameter interval respectively.

In Fig. 3, we compare the linear plots obtained from actual rain rates and the estimated rain rate from self-consistency rule. It is observed that all the compared models have closer predictions at lower rain rates. However, at higher rainfall rates, the Erlang-*k* DSD model gives a more accurate prediction, with the lognormal and gamma ($\lambda = 2$) DSD models predicting less accurately. This is also confirmed in the error statistics for each of these models. The error statistics is determined by considering the error deviations between the estimated rain rate from DSD models and actual rain rate by applying both the Root Mean Square Error (RMSE) and Chi Square statistic (χ^2). The corresponding expressions for these error statistics are thus given:

$$RMSE = \left[\frac{1}{n}\sum_{i=1}^{n}\left(R_{actual,i} - R_{estimated,i}\right)^2\right]^{1/2} \qquad (13)$$

$$\chi^2 = \sum_{i=1}^{n}\frac{\left(R_{actual,i} - R_{estimated,i}\right)^2}{R_{actual,i}} \qquad (14)$$

where *n* refers the total number of samples compared for each DSD model which is taken as 52.

At 5% significant level, the critical value for this work is taken as 68.669 [16], which imply that compared DSD models' hypothesis are valid. From the computed error statistics results in Table I, it can be seen that the proposed Erlang-*k* DSD

TABLE I. INPUT PARAMETERS OF DIFFERENT DSD MODELS IN DURBAN, SOUTH AFRICA

DSD MODEL	PARAMETERS	INPUT PARAMETER FUNCTIONS	RMSE	CHI
ERLANG (Proposed)	N_m, k, μ	$N_m = 808.99R^{-0.087}$ $\mu = 2.3326R^{-0.334}$ $round(k+3) = 2.6105R^{0.19}$	1.52	2.84
GAMMA (μ = 2)	N_o, Λ, λ	$N_o = 1.1031 \times 10^5 R^{-0.732}$ $\Lambda = 6.6731R^{-0.259}$ $\lambda = 2$	2.62	3.92
GAMMA (μ = 3)	N_o, Λ, λ	$N_o = 3.609 \times 10^5 R^{-0.991}$ $\Lambda = 7.7853R^{-0.259}$ $\lambda = 3$	2.17	2.84
LOGNORMAL	N_T, μ, σ	$N_T = 1145.2\, R^{-0.136}$ $\mu = -1.1063 + 0.3654\, ln(R)$ $\sigma = 0.5408 - 0.035\, ln(R)$	2.57	4.05

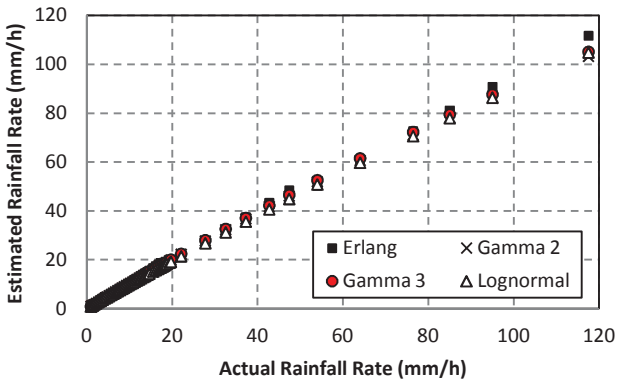

Fig. 3. Self-consistency plots for different DSD models in Durban

model gives the lowest RMSE at 1.52 at all compared rain rates in Durban. This suggests that Erlang-*k* distribution gives an improved prediction of rainfall DSD over all known existing models applied in subtropical South Africa.

V. CONCLUSION

In this paper, the Erlang-*k* distribution is proposed as a suitable model for predicting rainfall DSD over Durban. Results obtained in this work clearly imply that this model gives a better performance compared to existing models. This proposed DSD model can be applied in the design of efficient and viable microwave and millimeter wave communication links, for both terrestrial and satellite purposes.

REFERENCES

[1] R.K. Crane, Propagation Handbook for Wireless Communication System Design, CRC Press, Florida, pp. 74–76, 2003.

[2] H.E. Green, "Propagation Impairment on Ka-Band SATCOM in Tropical and Equatorial Regions," *IEEE Antennas Propag. Magazine*, Vol. 46, No. 2, pp. 31-44, 2004.

[3] S. Das, A. Maitra and A. K. Shukla, "Rain attenuation modeling in the 10-100 GHz frequency using drop size distributions for different climatic zones in tropical India," *Progress In Electromagnetics Research B*, Vol. 25, pp. 211-224, 2010.

[4] K.I. Timothy, J.T. Ong and E.B.L. Choo, " Raindrop size distribution using method of moments for terrestrial and satellite communication applications in Singapore", *IEEE Antennas Propagat.*, Vol. 50, pp. 1420–1424, October 2002.

[5] Afullo, T. J. O. (2011), "Raindrop size Distribution Modeling for Radio Link Design along the Eastern Coast of South Africa," *Progress in Electromagnetic Research B*, Vol. 34, pp. 345-366.

[6] A.A. Alonge and T.J.O. Afullo, "Seasonal Analysis and Prediction of Rainfall Effects in Eastern Southern Africa at Microwave Frequencies," *Progress in Electromagnetic Research B*, Vol. 40, pp. 279-303, 2012.

[7] A.A. Alonge and T.J. Afullo, "Fractal Analysis of Rainfall Event Duration for Microwave and Millimetre Networks: Rain Queueing Theory Approach," *IET Microwave Antennas Propag*., Vol. 9(4), pp. 291-300, March 2015.

[8] A.A. Alonge and T.J. Afullo, "Characteristics of rainfall queues for rain attenuation studies over radio links at subtropical and equatorial Africa," *Radio Science*, Vol. 49, pp. 583-596, August 2014.

[9] J.A. White, J.W. Schmidt and G.K. Bennett, *Analysis of Queueing Systems*, Academic Press, New York, 1975.

[10] G. Bolch, S. Greiner, H. de Meer and K.S. Trivedi, Queueing networks and Markov chains, John Wiley and Sons, New York, 1998.

[11] S. Keshav, "Mathematical Foundations of Conmputer Networking," Addison-Wesley Professional Computing Series, Pearson Education, New Jersey, 2012.

[12] J. Wang, H. Zhou, F. Xu and L. Li, "Hyper-Erlang Based Model for Network Traffic Approximation," Parallel and Distributed Processing and Applications Lecture Notes in Computer Science, Vol. 3758, pp. 1012-1023, 2005.

[13] T. Kozu and K. Nakamura, "Rainfall parameter estimation from dual-radar measurements combining reflectivity profile and path-integrated attenuation", *J. of Atmos. and Oceanic tech.*," pp. 259–270, 1991.

[14] I.A Adimula and G.O. Ajayi, "Variation in raindrop size distribution and specific attenuation due to rain in Nigeria", *Ann. Telecom*, Vol. 51, No. 1-2, pp. 87–93, 1996.

[15] H.Y. Lam, J. Din and S.L. Jong, "Statistical and Physical Descriptions of Raindrop Size Distributions in Equatorial Malaysia from Disdrometer Observations," *Advances in Meteorology*, Vol. 2015, Article ID 253730, pp. 1-14, 2015.

[16] Chi Square Distribution Table accessed at http://www.medcalc.org/manual/chi-square-table.php.

THE 5TH INTERNATIONAL CONFERENCE ON WIRELESS COMMUNICATIONS, VEHICULAR TECHNOLOGY, INFORMATION THEORY, AEROSPACE & ELECTRONIC SYSTEMS (WVITAE-2015)
December 13-16, 2015, Hyderabad, India

Recent Progress in Radioclimatological Modeling in Equatorial and Tropical Africa

Thomas J.O. Afullo, *Fellow*, *SAIEE* and Akintunde A. Alonge, *Graduate Member*, *IEEE*
Discipline of Electrical, Electronic and Computer Engineering,
University of KwaZulu-Natal,
Durban, South Africa
{Afullot, alongea}@ukzn.ac.za

***Abstract*—This paper presents recent developments in the area of radioclimatological modeling over equatorial and tropical Africa. The work mainly highlights current efforts targeted at understanding the effects of precipitation over microwave and millimetric wave propagation. Interpretation and analysis of rainfall measurements undertaken at two African sites of subtropical and equatorial climate are examined in the context of new investigations. The determination of critical diameters of rain drops responsible for total specific attenuation of rainfall over South Africa and Rwanda is presented. Under time series analysis of rainfall processes, the novel approach of queueing theory to determine the underlying characteristics of rainfall over radio links at these locations is discussed. Conclusions from these diverse studies show that these locations exhibit similar precipitation characteristics in terms of critical diameters and semi-Markovian rainfall queues.**

Keywords—Radioclimatological modeling; Critical diameters; Specific Attenuation; Rainfall rate; Queueing theory

I. INTRODUCTION

The increasing global demand for larger bandwidths in the microwave and millimeter bands is a contemporary issue in the communication industry [1]. In sub-Saharan Africa, this is complicated by rapidly increasing customer base for broadband connectivity and high-quality data content. The technical panacea for this recurring problem requires the adoption of tripartite transmission conditions: migrating to higher frequency bands, utilizing complex modulation schemes and compensating for power losses [2]. Migration to higher frequency bands vis-à-vis power compensation falls into large-scale propagation requirements, which can be optimised by radioclimatological modeling. Therefore, the need for accurate propagation studies is therefore an advantage in the availability of communication systems, especially in areas with exceptional climatic phenomena in Africa.

A history of propagation measurement campaigns and efforts already undertaken at different locations of the Southern Africa were presented in [3]. In this current work, recent progress on the investigation of the role of precipitation in radiopropagation is discussed based on results obtained from subtropical and equatorial Africa [4] – [9]. Precipitation belongs to the group of hydrometeors, which affects the performance of wireless systems, operating at microwave and millimeter wave bands [10]. Its effects dangerously become dominant at transmission frequencies from 10 GHz and above, especially in areas of tropical, subtropical and equatorial climatic characteristics.

In this paper, recent investigations on two principal concepts are primarily discussed to understand the effects of precipitation over radio links at Durban (29°52′S, 30°58′E), South Africa and Butare (2°36′S, 29°44′E), Rwanda.

II. CRITICAL DIAMETER ANALYSIS OVER EQUATORIAL AND SUBTROPICAL AFRICA

The subject of rainfall attenuation is particularly a topical one, especially in regions characterized with intense rainfall. Subtropical and equatorial regions of Africa fall among these locations, where signal disruptions could affect the availability of communication systems [2], [10]. In theory, attenuation due to rainfall is the result of the mechanism of scattering and absorption effects on rain drops in the atmosphere. There have been discussions on the actual contributions of rain drops of different sizes to signal attenuation. The earliest works on this subject was undertaken by Lee *et al.* in Singapore [11], Lam in Malaysia [12], Marzuki in Equatorial Indonesia [13] and Fiser in Czech Republic [14]. In these studies, certain sizes of raindrops were classified as being important contributors to the resulting rain attenuation over radio links.

A. Critical Diameters for Rain Attenuation in Durban

In subtropical and equatorial Africa, an initial study undertaken in Durban, South Africa [4] confirmed the observations in [11] - [14]. The so-called specific ranges of rain drops mainly associated with rainfall attenuation are described as the critical diameters for rainfall attenuation [11],[12]. These diameters are found to be strongly dependent on the Drop Size Distribution (DSD). Mathematically, rainfall DSDs have been found to be approximated in many tropical, subtropical and equatorial regions with minimal errors, by lognormal and modified gamma distributions [10]-[12]. By putting this into consideration, Adetan and Afullo [4] computed the critical diameters for rainfall specific attenuation in Durban by applying [15]:

$$A_s = 4.343 \times 10^{-3} \int_0^{D_{max}} Q_{ext}(D, \lambda, m).N(D)dD \; [dB/km] \quad (1)$$

where Q_{ext} is the extinction cross section dependent on diameter, D, wavelength, λ, and the complex refractive index, m. $N(D)$is the rainfall DSD.

In [4], the incremental total specific attenuation for lognormal DSD model computed numerically is given by:

$$dA_s = 4.343 \times 10^{-3} \frac{\kappa N_T}{2^{\alpha}\sigma\sqrt{2\pi}} \left[D_j{}^{\alpha-1}.e^{-t}\right] \quad (2a)$$

where,

$$t = \frac{1}{2}\frac{\left[ln(D_j) - \mu\right]^2}{\sigma} \quad (2b)$$

where κ and α are the Mie coefficients obtained at 20°C over Durban. N_T, μ and σ are the inputs of the lognormal DSD.

Similarly, for the gamma DSD for μ = 2, the incremental specific attenuation from [4] is likewise given as:

$$dA_s = 4.343 \times 10^{-3} \frac{\kappa N_o}{2^{\alpha}} \left[D_j{}^{\alpha+2}.e^{-\Lambda D_j}\right] \quad (3)$$

where N_o and Λ are the inputs of the gamma DSD.

Plots arising from the numerical solution of (2a), (2b) and (3) over different frequencies are shown in Fig. 1 at $R_{0.01} = 60\ mm/h$ over Durban. The peaks of these plots indicate the maximum critical diameter(s) responsible for the highest contributions to specific attenuation. It is evident from the conclusions of Adetan and Afullo [4] that the overall critical diameters of rain drops responsible for total specific attenuation in Durban lies between 0.5 mm ≤ D ≤ 2.5 mm.

B. *Comparison of Critical Diameters over South Africa and Rwanda*

A further comparison of critical diameters over subtropical African location of Durban and equatorial African location was undertaken in [6] over different microwave and millimeter bands. In this work, the critical diameters contributing to total specific attenuation were examined. By considering the rainfall availability at 99.99% at these two locations (Durban = 66.25 mm/h; Butare = 73.88 mm/h), the effects of bin removal was also considered. This systematic approach considers the gradual removal of unimportant bins while examining their overall effect on total specific attenuation. Results from this experiment are found in Table I. Using this approach, results from investigations on effects of critical diameters over subtropical and equatorial Africa was thus concluded in [6] as:

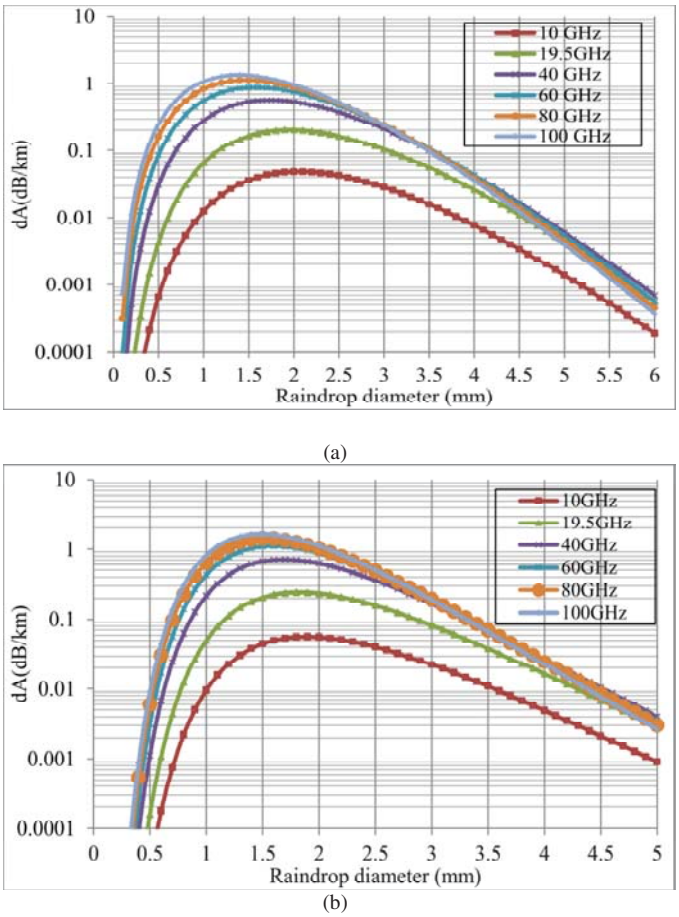

Fig. 1. Overall specific attenuation against the drop size diameters at various frequencies at $R_{0.01}$ = 60mm/h (a) Lognormal DSD model (b) Gamma DSD model.[5]

> *"The largest contribution to the total attenuation is observed at the diameter range 1.5 ≤ D ≤ 3.5 mm at Butare and for Durban, at frequencies below 40 GHz. At frequencies above 40 GHz, the maximum contribution to the rain attenuation is observed in the diameter range 1.0 ≤ D ≤ 3.0 mm in Durban. A minimal percentage contribution is observed at larger diameters as the frequency increases"*

TABLE I. PERCENTAGE FRACTION OF THE TOTAL SPECIFIC ATTENUATION FORMED BY RAIN DROPS DIAMETERS AT SELECTED FREQUENCIES [6]

CRITICAL RANGE (mm)	DURBAN (SOUTH AFRICA)				BUTARE (RWANDA)			
	10 GHz	40 GHz	80 GHz	150 GHz	10 GHz	40 GHz	80 GHz	150 GHz
0.1 ≤ D ≤ 2.0	5.66	10.47	16.32	21.50	27.84	40.33	51.59	59.46
0.5 ≤ D ≤ 2.5	18.16	28.02	37.86	45.34	52.46	65.70	75.45	81.28
1 ≤ D ≤ 3.0	36.14	48.82	59.56	66.73	72.20	82.00	87.68	90.22
1.5 ≤ D ≤ 3.5	54.29	66.83	74.15	78.50	79.98	81.65	79.19	75.49
4.0 ≤ D ≤ 7	32.54	21.96	14.85	10.87	8.58	4.39	2.33	1.43

III. Rainfall Queueing Theory Over Equatorial and Subtropical Africa

One of the dynamic problems facing wireless communication systems, especially in Radio Resource Management (RRM) is the issue of adaptive power management in rainy medium [16]. This problem becomes more critical, when combined with the availability of communication systems operating at microwave and millimetric bands, under the harsh conditions of precipitation. The issue of adaptive power management in rainy medium, often deployed in the form of Adaptive Power Control (APC), clearly offers improved signal reception in both terrestrial and satellite communication. However, certain time domain characteristics of the rainfall process must be considered to achieve seamless power control in real time. It is from this perspective that recent studies on rainfall at equatorial and subtropical Africa were approached in [7] - [9].

The major objective of describing the underlying characteristics of rainfall over radio links was firstly hypothesized as a queueing problem [7]. In this work, an established radio link is assumed to exist between any two fixed points, either from the terrestrial or satellite communication perspective. A rainfall process is said to occur when rain clouds, while producing rain droplets, are propelled across the radio link by advective forces. This scenario is depicted in Fig. 1 as a First In, First Out (FIFO) process. In the pioneer effort of Alonge and Afullo [7], [8], the problem of a queue in rainfall process became evident when several arrivals of rain clouds, and consequently rain rates are encountered within a rainfall event. This overall mechanism results in two possibilities: fluctuation of rainfall rate values, whose time domain probabilities are often stochastic in the time domain, and, the existence of unique rain spikes in a typical rainfall time series. These two possibilities reflect the need to ascertain the existence of queues in any rainfall process.

Initial studies on the existence of queues was first undertaken using the rain rate time series data (at one minute sampling time) obtained from the Joss-Waldvogel RD-80 distrometer installed at the University of KwaZulu-Natal, Howard College, Durban [7], [9]. The rainfall time series

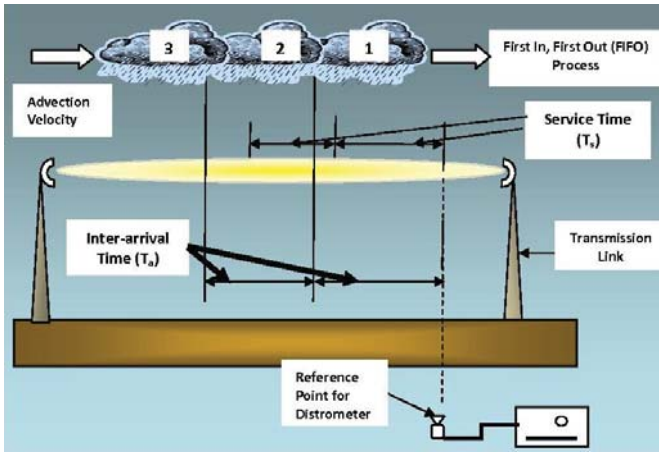

Fig. 2. The concept of rainfall process as a queue [7]

measurements were partitioned into rainfall events, and the rainfall events segmented into sub-events [7]. This procedure follows the earlier assumptions of validating the components of the queue process, which in this case manifests as rain spikes. The individual queue parameters for each of the retrieved spike were estimated accordingly. In this regard, three major queue parameters were considered: service time, inter-arrival time and overlap time [7].

A. Modeling of Queue Distributions of Rainfall Time Series in Durban

The basic assumption would be that the queue discipline is either Markovian or non-Markovian, with time as the independent variable. Based on this knowledge, two distributions considered in the modeling of queue parameters over radio links in Durban belong to the group of exponential family. The simplest distribution in a Markovian queue process is the exponential distribution given by [7]:

$$f(t) = \lambda \ exp\,(-\lambda t), \quad \text{for } t \geq 0, \qquad \forall t \in \mathbb{R} \qquad (4)$$

where λ could be the service, arrival or overlap rate as the case may require. The variable, t, could represent the service, inter-arrival or overlap time.

The most appropriate distribution for a non-Markovian queue process is the Erlang-k distribution given by [7]:

$$f(t) = \frac{k\mu\,(k\mu t)^{k-1}\ exp\,(-k\mu t)}{\Gamma(k)} \quad \text{for } t \geq 0 \qquad (5)$$

where k refers to the number of stages and μ could assume the service, arrival or overlap rate.

Fig. 3 depicts the queue modeling undertaken for service time and inter-arrival time in Durban. This modeling clearly implies that the service time distribution for shower rainfall regimes over Durban is unimodal and non-exponential as seen in Fig. 3a. This suggests that this process is non-Markovian process. On the other hand, Fig, 3b clearly implies that the inter-arrival time distribution is an exponential curve, suggesting a Markovian process. A summary of the overall results in Durban showing estimated error statistics, as well as strengths and weaknesses of the two distributions for different regimes are shown in Table II [8]. According to Table II, RMSE refers to Root Mean Square Error, χ^2 is the Chi statistic, DF is the Degree of Freedom and SL is the significant level (related to the critical value). These results clearly shows that Erlang-k distribution is the most preferred in the modeling of rainfall process over radio links when considering the service and overlap times. However, the exponential distribution is undisputably preferable in modeling the inter-arrival time distribution.

The results clearly described the underlying process of rainfall over radio links as a semi-Markovian queue, with Erlang-k distributed service time (E_k) and exponentially distributed inter-arrival time (M). Clearly, this confirms that

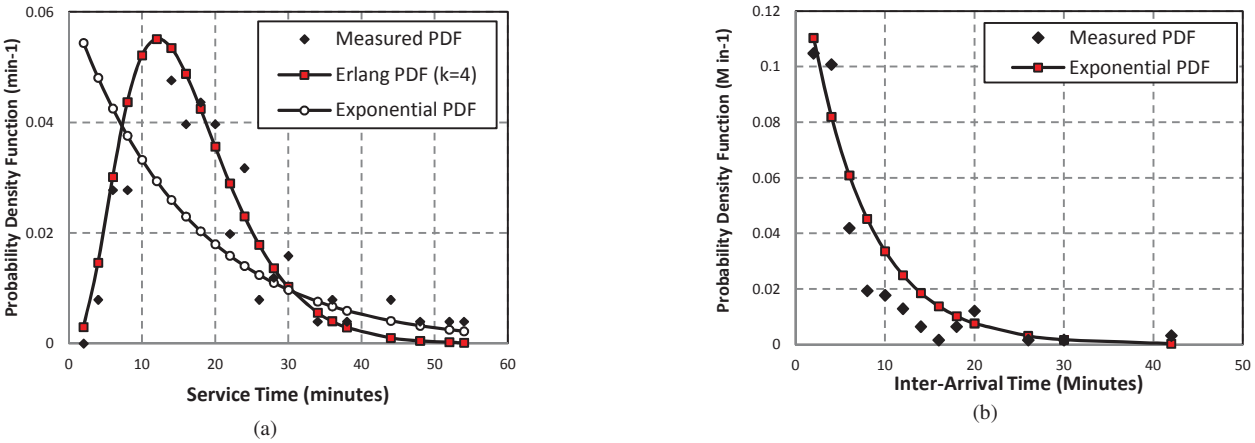

Fig. 3. Distribution modeling for queue parameters for shower regime in Durban, South Africa (a) Service time (b) Inter-arrival time [7]

TABLE II. ERROR ANALYSIS OF FITTED QUEUE DISTRIBUTIONS OVER DIFFERENT REGIMES IN DURBAN, SOUTH AFRICA [8]

QUEUE PARAMETER	REGIME	PROPOSED MODEL	RMSE	χ^2	DF	SL
SERVICE TIME	DRIZZLE	M	0.0246	0.3004	145	174.10
		E_k^*	0.0094	0.7226		
	WIDESPREAD	M	0.0268	0.3413	174	205.78
		E_k^*	0.0077	0.1224		
	SHOWER	M	0.0216	0.3188	125	152.09
		E_k^*	0.0084	0.2648		
	T/STORM	M	0.0159	0.2983	100	124.34
		E_k^*	0.0104	0.3470		
INTER-ARRIVAL TIME	DRIZZLE	M	0.0151	0.0860	125	152.09
	WIDESPREAD	M	0.0118	0.0594	156	186.15
	SHOWER	M	0.0129	0.0919	123	149.89
	T/STORM	M	0.0128	0.2118	88	110.89
OVERLAP TIME	DRIZZLE	M	0.0357	0.1368	125	152.09
		E_k^*	0.0292	0.2913		
	WIDESPREAD	M	0.1739	0.9053	155	185.05
		E_k^*	0.0099	0.0441		
	SHOWER	M	0.0197	0.0648	123	149.89
		E_k^*	0.0084	0.0204		
	T/STORM	M	0.0135	0.0768	88	110.89
		E_k^*	0.0087	0.0215		

queues are present in the overall process of precipitation over subtropical Durban.

B. Comparison of Queue Parameters over South Africa and Rwanda

The confirmation of queuing characteristics over Durban, South was further compared with queue characteristics at the tropical location of Butare. Alonge and Afullo [8], [9] found that the same queueing conditions generating rainfall rates over radio links in Durban was clearly present in Butare. This led to the designation of rainfall process according to the Kendall notation of $M/E_k/s/\infty/FCFS$, which is representative of a semi-Markovian process. The stability of the rainfall process as a self-generating queue is of utmost important. The queue stability is mainly determined by applying the condition [8]:

$$\rho = {}^{\lambda_a}/_{\mu_s} \leq 1 \qquad (6)$$

where λ_a and μ_s is the arrival rate and service rate.

TABLE III. GENERAL COMPARISON OF QUEUE PARAMETERS IN DURBAN AND BUTARE [8]

SERVICE TIME							
LOCATION	μ_s	t_s	k	RMSE	χ^2	DF	SL
DURBAN	0.0659	15.1801	5	0.0033	1.218	547	605.52
BUTARE	0.0653	15.3152	6	0.0053	0.3578	445	495.17
INTER-ARRIVAL TIME							
LOCATION	λ_a	t_a		RMSE	χ^2	DF	SL
DURBAN	0.1425	7.0169		0.0076	0.0095	495	547.86
BUTARE	0.1476	6.7754		0.0788	0.0521	385	431.73
OVERLAP TIME							
LOCATION	σ_o	t_o	k	RMSE	χ^2	DF	SL
DURBAN	0.2053	4.8714	3	0.0065	0.0168	494	546.81
BUTARE	0.2267	4.4097	4	0.2278	0.1209	383	429.61

From results obtained in [7]-[9], it was generally concluded that the rainfall queueing process over Durban and Butare are clearly unstable semi-Markovian queues. It would appear that the inherent meteorological mechanism of rainfall conditions simultaneously provides some form of natural servers. The numbers of these natural servers tend to be around 5 or 6 at the both locations. A summary of the queue parameters obtained from time series measurements in Durban and Butare is presented in Table III. From the set of results available, the queue parameters obtained for service, inter-arrival and overlap time are very similar in South Africa and Rwanda. This implies that there is virtually no difference in the queue conditions in subtropical and equatorial Africa. However, there is a clear difference in the number of stages required to estimate the service time and overlap time distributions. In addition, it is observed that distribution model errors (from RMSE) for service time, inter-arrival time and overlap time may not exceed values of 0.5%, 0.8% and 12% respectively.

V. CONCLUSION

In this paper, we present the current status of research in the area of radioclimatological modeling in Southern and equatorial regions of Africa. The study is based on measurements undertaken in Durban, South Africa, and in Butare, Rwanda. The critical diameters for rain attenuation at microwave and millimetric waves are presented for the two regions. In addition, we present the queuing theory approach to rain attenuation studies, in which the inter-arrival rate, the service rate are presented for the various rainfall regimes. Further studies are being undertaken to further refine the model, and thus properly interpret all parameters obtained.

REFERENCES

[1] H.E. Green, "Propagation Impairment on Ka-Band SATCOM in Tropical and Equatorial Regions," *IEEE Antennas Propag. Magazine*, Vol. 46, No. 2, pp. 31-44, 2004.

[2] D. Foty, B. Smith, S. Sinha and M. Schröter, "The Wireless Bandwidth Crisis and the Need for Power-Efficient Bandwidth," *IEEE AFRICON conference*, Livingstone, Zambia, pp. 1-6, 13-15 Sept. 2011.

[3] T.J.O. Afullo, "Progress in Radioclimatological Modeling for Southern Africa," Proc. 2nd IEEE International Conference on Wireless Communcication, Vehicular Technology, Information theory and Aeropace and Electronic systems technology (Wireless Vitae), Chennai, India, 28 Feb – 3 March, 2011.

[4] O. Adetan and T.J.O. Afullo, "The Critical Diameters For Rainfall Attenuation In Southern Africa," *Progress in Electromagnetic Research B*, Vol. 46, pp. 275-297, Dec. 2012.

[5] O. Adetan and T.J.O. Afullo, "Raindrop Size Distribution and Rainfall Attenuation Modelling in Equatorial and Subtropical Africa: The Critical Diameters," *Annals of Telecommunications*, Vol. 69, pp. 607-619, 2014.

[6] O. Adetan, Modeling of Raindrop Size Distirbution and Critical Diameters for Rainfall Attenuation over Microwave Links in Southern Africa, PhD Thesis submitted to the University of KwaZulu-Natal, Jan. 2014.

[7] A.A. Alonge and T.J. Afullo, "Fractal Analysis of Rainfall Event Duration for Microwave and Millimetre Networks: Rain Queueing Theory Approach," *IET Microwave Antennas Propag*., Vol. 9(4), pp. 291-300, March 2015.

[8] A.A. Alonge, Queueing Theory Approach to Rain Fade Analysis at Microwave and Millimeter Bands in Tropical Africa, PhD Thesis submitted to the University of KwaZulu-Natal, Dec. 2014.

[9] A.A. Alonge and T.J. Afullo, "Characteristics of rainfall queues for rain attenuation studies over radio links at subtropical and equatorial Africa," *Radio Science*, Vol. 49, pp. 583-596, August 2014.

[10] G.O. Ajayi, S. Feng, S.M. Radicella and B.M. Reddy, Handbook on Radiopropagation Related to Satellite Communications in Tropical and Subtropical Countries. Trieste: ICTP, pp. 5–7, 1996.

[11] Y. Lee, S. Lakshmi and J. Ong, "Rain drop size distribution modelling in Singapore-Critical diameters," in *Antennas and Propagation, 2007. EuCAP 2007. The Second European Conference on*, pp. 1-5, 2007.

[12] H.Y. Lam, J. Din, L. Luini, A. D. Panagopoulos and C. Capsoni, Analysis of raindrop size distribution characteristics in Malaysia for rain attenuation prediction," *IEEE Xplore General Assembly and Scientifc Symposium, XXXth URSI*, Aug. 13-20, 2011.

[13] M. Marzuki, T. Kozu, T. Shimomai, W. L. Randeu, H. Hashiguchi and Y. Shibagaski, "Diurnal Variation of Rain Attenuation obtained from Measurement of Raindrop Size Distribution in Equatorial Indonesia," *IEEE Transactions on Antennas and Propagation*, Vol. 57(4), pp. 1191-1196, Apr. 2009.

[14] O. Fiser, "The Role of Particular Rain Drop Size Classes on Specific Rain Attenuation at various Frequencies with Czech Data Example," in *Proceedings of ERAD*, 2002.

[15] A. Maitra, "Rain Attenuation Modelling from Measurements of Rain Drop Size Distribution in the Indian Region," IEEE Antennas Propag., Vol. 57(9), pp. 1191-1196, April 2009.

[16] Y.H. Lee and S. Walker, "Effects of Rain Attenuation on Satellite Video Transmission," 73rd Vehicular Technology Conference (VTC Spring), Yokohama, Japan, 15-18 May 2011.

THE 5TH INTERNATIONAL CONFERENCE ON WIRELESS COMMUNICATIONS, VEHICULAR TECHNOLOGY, INFORMATION THEORY, AEROSPACE & ELECTRONIC SYSTEMS (WVITAE-2015)
December 13-16, 2015, Hyderabad, India

Spectrum for 5G Services

P S M Tripathi
Centre for TeleInFrastructure(CTiF)
Aalborg University
Aalborg, Denmark

Ramjee Prasad
Centre for TeleInFrastructure(CTiF)
Aalborg University
Aalborg, Denmark

***Abstract*—The phenomenal growth in mobile data traffic calls for a drastic increase in network capacity beyond current IMT (3G/4G) networks. There is a call for the next generation mobile communication system (5G). The 5G network envisages data speed of 1Tbps and beyond. Presently, mobile communications are operating between 700 MHz to 2.6 GHz. These spectrum bands do not have the capacity to carry such enormous data. Millimeter (mm) frequency band beyond 10 GHz is the obvious and the most preferred band for 5G. In this paper, we analysed frequency bands for 5G communication services.**

I. Introduction

Advancement in mobile communication has made peoples life easier, whether it is ordering a pizza, accessing internet, searching an address in a city or connecting with others via social networking site. Essential services such as e-commerce, e-banking, e-governance, e-health etc. will continue expanding their coverage and heading towards more mobility. These expansions will lead to need for enormous wireless traffic in future. Ericsson has predicted that the wireless traffic would be increased by 1000 times in 2020 than seen in 2010. This traffic is primarily driven by increased usage of mobile multi-media services [1]. Todays wireless traffic is largely contributed by human centric applications. Machine centric traffic will contribute equally (or even more than human centric) in the future as there is a forecast of approximately 50 billion connected devices by 2020 [2]. The combination of human and machine centric applications will diversify the landscape of the telecom industry in terms of size, cost, energy dissipation and services. Machine centric applications require data delivery of high reliability, and on the other side human centric applications require data delivery at high speed and always connected. Therefore, the next generation of mobile communication will be moving towards to a future state of everything everywhere and always connected with reliability [3]. The existing 4th generation mobile communications (also known as IMT-A [International Mobile Telecommunications-Advanced]) is all IP based network with packet switched delivery for efficiently meeting the needs of the future generation networks with high data rates of 100 Mbps (high mobility) /1Gbps (low mobility). Various networks such as the wired (PSTN - Public Switched Telephone Networks), LAN (Local Area Networks), IP based mobile network, cellular (2G/3G), WiMAX (Worldwide Interoperability for Microwave Access), nomadic, ad-hoc and sensor networks are able to communicate with the core network. The 4G network is fulfilling the present demands. However, the needs for high throughput will continue to increase in future wireless networks due to high bandwidth demanding applications such as entertainment, multimedia, Intelligent Transport Systems (ITS), telemedicine, emergency, safety/security applications and other futuristic applications. These applications will push the demand for real-time, symmetric, wireless ubiquitous connectivity to an individual with a data rate that far exceeds the capacity offered by the current 4G network [4]. The vision of the 5G communication system is universally deployable converging technologies, which enable wireless services and applications at a data rate more than one terabit per second (Tbit/s) with coverage extending from a city to a country to the continents and to the world that will enable user-centric mega-communications [4]. The growth of 5G network would drive substantial economic benefits by serving as a platform for innovation in many areas of public and commercial importance, and benefits will lead to more investment, faster economic growth and new jobs. Radio spectrum is a prime factor in driving the growth of mobile services. The success of 5G network is based on the unconstrained availability of spectrum. About 1200 MHz of spectrum in the frequency bands below 5GHz has been identified for IMT services during the World Administrative Radio Conference (WARC) -92, World Radiocommunication Conference (WRC) -2000 and WRC-2007. These frequency bands are 450-470 MHz, 698-960 MHz, 1710-2025 MHz, 2110-2200 MHz, 2300-2400 MHz, 2500-2690 MHz, and 3400-3600 MHz. The identified spectrum is non-contiguous and scattered in different frequency bands from 450 MHz to 3.4 GHz. However, the actual allocation is ranging between the frequency band 700 MHz to 2.6 GHz. The spectrum available for cellular mobile services does not exceed a total of 780 MHz, and an operator has approximately 200 MHz spectrum across all IMT bands for providing telecom services with different access technologies from GSM to LTE [5]. However, 1200 MHz non-contiguous spectrum would not hold the pressure of high mobile data growth, demand for convergence of different varieties of services and speed. Therefore, more spectrum bands would need to be explored. Presently, frequency bands under consideration are: 470-698 MHz, 1300-1400 MHz, 1427-1 527 MHz, 1695-1700 MHz, 2025-2110 MHz, 2200-2290 MHz, 2700-3100 MHz, 3400-4200 MHz, 4400-5 000 MHz, 5350-5 470 MHz and 5725-6425 MHz. Some of them will be finalised during WRC-15 and thereafter will be earmarked for IMT-A services.

II. CONCEPT OF 5G NETWORK

The 4G network offers a convergence of heterogeneous wireless network of different access technologies and wireless networks and has the ability to connect anywhere and anytime. The future network will be the extension of the existing 4G network. The 5G wireless network will have capabilities for supporting high capacity and massive connectivity for an increasingly diverse set of services, application and users, and flexible

and efficient use of all available contiguous/non-contiguous, licensed/unlicensed spectrum. Convergence of technologies, ultra-high capacity, universal coverage, minimum energy usage and cost-efficiency are key characteristics of the 5G wireless system concept. At the core of 5G applications are M2M communications enabled by technological breakthroughs in a plethora of scientific areas, wireless and wired communications, artificial intelligence, the Internet, robotics and space [4]. Currently, operators are providing services using multiple RATs (2G, 3G, WiMAX, LTE, WLAN, Bluetooth and other emerging access technologies, etc.). For example, operators rely on unlicensed Wi-Fi network to offload traffic demand at hot-spots. Devices are equipped with multiple RATs like cellular, Wi-Fi and Bluetooth to connect the peripheral devices and internet. The 5G network should have the capability to integrate multiple radio access technologies seamlessly and to choose a suitable one among them, and to switch over between various access technologies, combine different streams coming from different technologies during a session to meet capacity demands [6].

The constant decrease in cell size enhances the cell capacity, spectral efficiency by exploiting spatial reuse and brings the communication services closer to the user [7]. The small cell with low transmit power provides flexibility in managing high data traffic hot spots. The future 5G network will have a relatively large number of small cell sites with different cell size from macro to femto and with low transmit power to meet the high traffic demand. The low-powered small cell sites will use to enhance the capacity, whereas macro cells will use to enhance the coverage. The 5G networks offer multiple options in respect of transmit power, coverage, capacity, spectrum usage and choice of RATs, and move towards cost reduction, green energy and better resource utilisation.

The network would also create a dynamic environment to cover D2D and M2M communications so that such communication takes place directly between user equipment or between machines (in the context of Internet of Thing) without use of base stations or core network [7]. Such type of communications will coexist dynamically within the network and will help to improve the area spectral efficiency, cellular coverage and reduce end-to-end latency and power consumption.

Therefore, the 5G network would be an integrated wireline/wireless network, where the wireless part comprises a dense network of small cells with capacity enhanced through high-order spatial multiplexing (MIMO), cell data rates of the order of 10 Gbps and round-trip latency of 1 ms. With these attributes, the combined network will support everything from simple M2M devices to immersive virtual reality streaming, with monitoring and control of literally billions of sensors and multiple simultaneous streaming services, and will support the massive data collection and distribution needs of the Internet of Things (IOT) [3]. There are three main aspects to realizing 5G communication systems in figure 1 [4].

Enabling 5G intelligent core: Intelligent core will be the soul of the 5G network. M2M and IoT are keys for realizing the intelligent core which provides seamless ubiquitous networking and connectivity in the 5G network.

Enabling ubiquitous connectivity: Ubiquitous connectivity will be for coverage under high mobility and data rates,

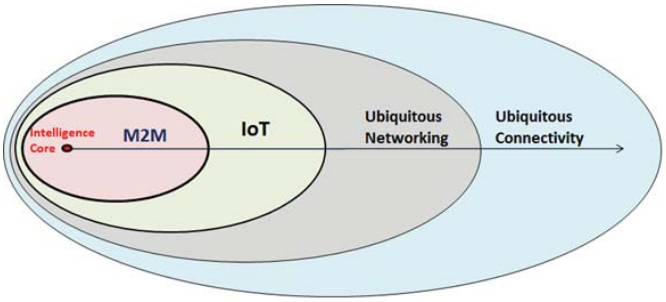

Fig. 1. Concept of 5G network

and to moving application from device to device without any content interruption. Use of millimeter wave links, high-order spatial multiplexing (MIMO) antenna, virtualization, small cell deployments and novel spectrum usage methods, are some of the keys for ubiquitous connectivity.

Enabling Ubiquitous networking: The ubiquitous networking will provide the same quality of services to end users, regardless of how many access networks, and spectrum bands are integrated for connectivity purposes.

The 5G network is conceptualized as a multi-layers heterogeneous network. Primary layer will be a macro layer which responsible for ubiquitous connectivity. Secondary layers, embedded in the primary layer, will be a combination of small cells (micro, pico and femto) to provide additional capacity to end users. This additional capacity will be in the form of extra spectrum on the same carrier, different access technology or an additional stream on a different carrier. The network will be controlled by an intelligent unit WISDOM [4], [8], [9]. The function of multilayer network is conceived as initially, a user will be connected to the primary layer. When data requirements go beyond the primary layer network capacity after providing the additional spectrum (if available) and change in radio access technology available within the primary layer, the user will also get connected to the nearest secondary layer through the WISDOM network. This has been depicted in the figure 2, where three users A, B and C have been shown. The requirements of the user A and B is beyond the capacity of primary layer, they have also been connected to secondary layers, whereas the user C requirement is within the capacity of primary layer.

With the above- mentioned features, a modification in 4G networks could make the best candidate for 5G network. Based on this assumption, the concept of 5G has been introduced as integration of 4G with WISDOM as given below [8], [9]:

$$4G\&WISDOM = 5G$$

The Wireless Innovative System for Dynamic Operating Mega Communications (WISDOM) is a communication system for ubiquitous trustworthy human-centric connectivity via an arbitrary infrastructure support. The WISDOM, as shown in Figure 3, principle brings unlimited wireless world interconnection, convergence, and cooperation (geographically including cities, countries, continents, and finally, the whole world), together with a large variety of multimedia services

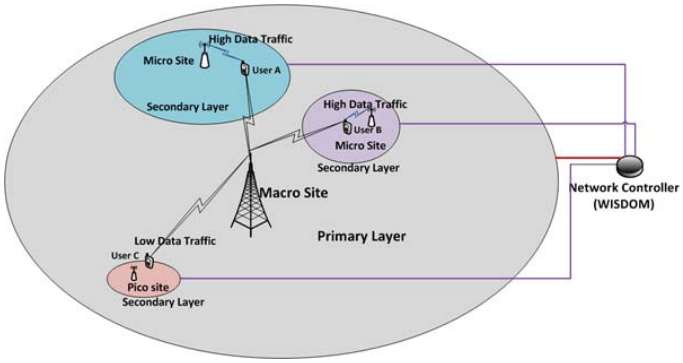

Fig. 2. 5G Network: Primary and secondary layers

at very high data rates, and becomes the main 5G definition point.

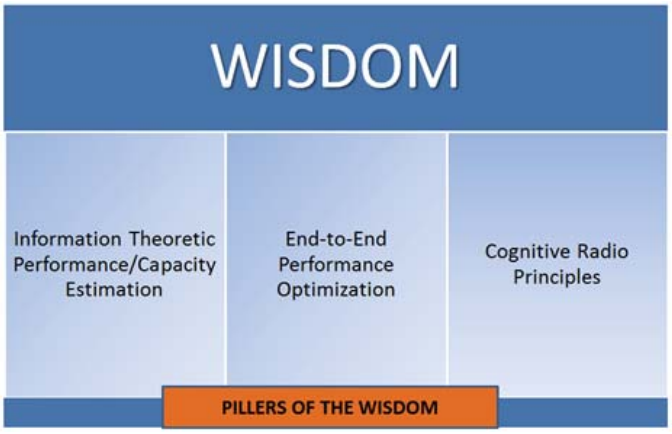

Fig. 3. WISDOM Principle [4]

The three founding pillars of WISDOM are [9]:

- An information theoretic performance/capacity estimation of different types of networking paradigms
- Design of protocols based on end-to-end, cross- layer and cross-network-domain performance optimization
- Cognitive radio (CR) network based self-organizing networks for management of possible usage scenarios and minimize the spectrum and energy requirements.

WISDOM aims to design and develop technologies, system that could globally integrate, interconnect and communicate into a flexible and dynamic system for the human-centric and machine centric communications in 2020 and beyond [8]. The operational domain of WISDOM concept requires well-defined network protocols, architecture for heterogeneous network, integration between different kinds of terrestrial and satellite network to provide applications upto 1Tbps link rate at short distance or as system aggregate operating in burst mode, and at least 250 Mbps to the end user for real time applications with coverage extending from a city, to a country, the continent and the world (4). The WISDOM concept will lead wireless communications beyond the emerging technologies and towards the realization of that new paradigm, based on the combination of five independent elements, Communication, Connectivity, Convergence, Content and Cooperation [9].

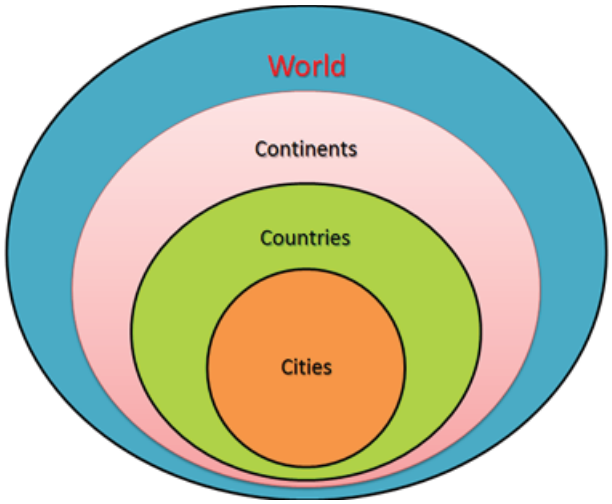

Fig. 4. Globel connectivity through WISDOM

III. IMPLEMENTATION CHALLENGES

5G network is basically delivery of services at any user platform using various wireless access technologies over any kind of network (all kinds of wireline, wireless, satellite networks) and spectrum band with a speed of more than 250 Mbps at end user. Therefore, a general framework should be developed to evaluate the performance of 5G wireless systems, taking into account as many performance metrics as possible from different perspectives. Besides, coexistence study between heterogeneous, the following implementation challenges should also need to be addressed:

In order to offer the services in a personalized form, the 5G technology must know some primary information about its users: identity, location, and privacy issues. 5G will have the hard task of operating an ever-growing number of heterogeneous networked devices that can communicate with each other or with people or robots to satisfy dynamic and high-level user expectations. 5G standardization must define uncertainties relating, for example, to new threats to cyber security, trust or privacy; trends in economic growth around the world; public acceptance of wireless and applied-field technologies; and legislative restrictions.

5G network envisages delivery over any kind of network. Therefore, a realistic channel models with proper accuracy complexity trade-off are required for 5G network. Massive MIMO channel model is an option. The technical challenge in developing massive MIMO systems is the signal processing complexity. Simplification of algorithm in massive MIMO system is a challenge. The massive MIMO should have the capability [12]: i) to support 10-100 times more devices than today ii) to allow very long battery lifetimes of the wireless device iii) to incur minimum signalling overhead iv) to enable low cost wireless devices v) to support efficient transmission of small payloads with fast setup and low latency.

At the same, it is desirable to have 99.999% coverage, while energy consumption and cost for the infrastructure should not increase.

The network should be energy efficient. Energy efficiency has two aspects; the first one is energy spend for maintaining infrastructure, which have a direct link with operational overhead and the other one is energy consumption in the end users devices. There are communication strategies, which require high energy for computation. Such applications will drain users device battery. To reduce energy consumption, two different approaches are under consideration. The first approach is creation of small cells with high capacity density. The main challenges of this approach are related to providing an economic backhaul solution and to minimise the additional deployment cost. The second one is use of massive MIMO system. The challenges of massive MIMO include the diffusion of energy due to scattering in NLOS scenarios, limiting the achievable directivity, and the complexity of spatial multiplexing of users.

The interference-tolerant CR networks is very much part of the 5G network. Reliable and practical management of the mutual interference of CR and primary systems is essential for 5G network. Therefore, regulation of the transmit power is essential for the CR system to coexist with other licensed systems.

5G network will be a step further towards low cost, plug and play, self-configuring and self-optimising networks. 5G system will be combination of macro and several micro, pico and femto cells embedded within the macro cell and will be deployed dynamically and in a heterogeneous manner, combining different radio technologies. Such configuration will improve spectral efficiency and coverage within an area. A massive deployment of small access nodes induces several challenges such as an adverse interference scenario or additional backhaul and mobility management requirements, which 5G needs to address. Different levels of coordination/ cooperation among small cells are keys to enhance the network capacity and keep interference at an adequate level, to manage mobility and spectrum, to ensure service availability and response to non uniform traffic distribution between neighbouring access points [13].

IV. SPECTRUM FOR 5G SERVICES

The network capacity depends on the number of base stations, radio access technology and frequency bandwidth. The 5G network will have several short range cell base stations for capacity boosting, which works alongside macro cells. The spectrum requirements for macro cell and short range cells are different. Macro cells will be for ubiquitous connectivity, and small cells will be for capacity booster [7]. Low frequency waves are suitable for macro cells due to its wide coverage and better penetration, and high frequency waves are suitable for booster cells due to large data carrying capacity. Therefore, spectrum requirements for the 5G networks could be divided into two different categories, low and high frequency waves.

A. LOWER SPECTRUM BANDS

As stated above, approximately 1200 MHz of spectrum has been identified for IMT-A services in the different frequency bands below 5GHz. These frequency bands are suitable for macro cell sites due to better propagation and penetration properties. If we look at the frequency allocation table, almost 50% of the total spectrum between 300 MHz to 6 GHz has been earmarked for mobile services as primary services. It means that this 50% of the total spectrum can be utilized for mobile services alone or in sharing with other primary services. The frequency bands below 6 GHz have already been allocated to legacy services long back. Therefore, no vacant spectrum is available below 6 GHz at present. The two options are available to enhance the spectrum availability for 5G communications; spectrum re-farming and spectrum sharing.

The spectrum re-farming is basically allowing existing license holders to utilise the allocated spectrum for some other purpose or migration of license holders from the existing band to some other band and reuse of the current band for other radio services. For example, re-farming of 900 MHz or 1800 MHz band, which was earlier allotted for 2G GSM services, is now being replaced by 3G or 4G network. Another example is the vacation of spectrum in the 700 MHz band by broadcasting services due to the digital switch over. Re-farming is a cumbersome process involves protracted negotiation with existing operators for migration, and also invites additional expenditure in migration.

Spectrum sharing is another option, where two or more than two operators share the same spectrum in frequency, time and geographic dimensions for providing same or different services. For example, there are several services, which use spectrum for a certain period of time or at certain locations. Such spectrum could be considered vacant, during the period or at the locations, where existing licensed operator is not using and the same could be utilised by mobile operators to provide IMT services. This type of sharing is known as static spectrum sharing. Another possibility is the dynamic spectrum access (DSA) that allows to access spectrum in opportunistic manners. CR is the basic tool for exploiting DSA. The CR enabled system sense the vacant spectrum and operates from the vacant spot, and retreat occupied spectrum on arrival of the primary user. A big chunk of already identified 1200 MHz spectrum has not yet been freed for IMT services worldwide. If we allow DSA, the spectrum crunch for the 5G network in lower bands would get resolved without doing large scale spectrum re-farming.

B. Higher Spectrum Band: MM-WAVES

The spectrum bands identified under the IMT umbrella do not have the capacity to carry such enormous data which required for 5G services. Therefore, mm-waves could be the candidate bands for 5G mobile communications, especially for second layer network due to high data carrying capacity. The mm-waves have the following advantages [11]:

1) Not much operation at mm-waves so more spectrum is available at mm-waves
2) Very large blocks of contiguous spectrum to support future applications
3) Due to high attenuation in free space, frequency reuse is possible at short distance
4) Spatial resolution is better at mm-waves hardware with CMOS technology

5) Advancement in semiconductor technology allows low cost
6) Small wave-length makes possible use of large antenna arrays for adaptive beam forming
7) The small size of the antenna at mm-waves facilitates easy integration on chip and installation at suitable locations.

Millimeter waves allow larger bandwidth and offer high data transfer and low latency rate that are suitable for high speed reliable internet services. The small wavelength facilitates small size antenna and other part of radio hardware, which reduces costs and also easy to install. The transmitters antenna would be like a lamppost, which could be installed on building, street lamppost, etc.

At such high frequency, waves are more prone to rain and other atmospheric attenuation. The wavelength is in the order of millimeters, and rain drops are also of the same size. Rains absorb high frequency waves and make it difficult for propagation. However, the experimental results show that in heavy rain condition, attenuation is 1.4 dB and 1.6 dB for 200 meters distance at 28 GHz and 38 GHz respectively [5]. A proper link design with slight high transmit power may take care of rain attenuation.

Wavelength at such high frequencies is in the range of millimetres. Any slight change in the position would affect the signal strength at the receiving end, due to which mm-waves are deeply affected by scattering, reflection and refraction. The r.m.s. delay spread for mm-wave is of the order of few nano seconds, and it is high for are non-line of sight (NLOS) links than line of sight (LOS) links[6]. Similarly, path loss exponent for NLOS links is higher than LOS links. Due to higher path loss and r.m.s delay spread, it is assumed that mm-waves are not suitable for non-line of sight (NLOS) links. However, these difficulties could be managed by using carrier aggregation, high order MIMO, steerable antenna, beamforming techniques. Propagation feasibility studies for mm waves have been carried out at research institutes, and concluded that propagation is feasible upto 200 meters of distance [5], [11] in both the conditions i.e. line of sight (LOS) and non-line of sight (NLOS) with transmit power of the order of 40-50dBm in a difficult urban environment. The cell size in dense urban areas normally varies between 100 meters to 300 meters. Therefore, mobile cellular is possible at mm-waves.

The traditional uses of the mm-waves include radio navigation, space research, radio astronomy, earth exploration satellite, radar, military weapons and other applications. The backbone/backhaul networks (point to point network) for existing telecom network to connect base station to main switching centre (MSC), Local Multipoint Distribution System (LMDS), indoor WLAN, high capacity dense networks are also present in the mm-waves. The typical microwave backhaul bands are at 6.0 GHz, 11.0 GHz, 18.0 GHz, 23.0 GHz, and 38.0 GHz frequency bands.

The Radiocommunication Sector of International Telecom Union (ITU) is responsible for management of radio spectrum at international level. As per ITU-R frequency allocation plan, the frequency band 10 40 GHz has been earmarked for satellite based services in all the three regions along with Fixed and mobile services. Local Multipoint Distribution System (LMDS), WLAN, Satellite services and High capacity dense network etc. are main services present in mm-waves. Several point to point fixed microwaves links are also working in this band. These links are basically for backbone/backhaul network for GSM and other services. A good amount of vacant spectrum is available at mm-waves which could be utilised for 5G communications services. 5G services may transmit high power approximately 40 -50 dBW. Therefore, coexistence study needs to be carried out with existing LMDS and satellite services, which working in neighbouring spectrum bands.

V. Conclusion

In this paper we discussed frequency bands for 5G mobile communications services. Lower band is suitable for the primary layer due to better propagation characteristics. Exclusive spectrum below 6 GHz is not available. The availability can be increased through spectrum sharing as primary and secondary user concept. The Millimetres waves are most suitable candidate bands for secondary layer of 5G network. Analysis of candidate bands shows that sufficient spectrum is available, which could be allocated for the 5G services. However, extensive co-existence study with existing usage is required to be carried out for making provision for the 5G communications services.

References

[1] Ericsson, More than 50 billion connected devices, White Paper, February 2011

[2] Osseiran Afif, et.al., The foundation of the Mobile and Wireless Communications System for 2020 and beyond. METIS white paper. www.metis2020.com

[3] Agilent, Current Activity in 5G. www.agilent.co.in/about/ news-room/tmnews/background/5g/

[4] Prasad R., Global ICT Standardisation Forum for India (GISFI) and 5G Standardization. Journal of ICT Standardization, Vol. 1, 123136. doi:10.13052/jicts2245-800X.12a. 2013 River Publishers.

[5] Rappaport T.S et.al. Millimeter Wave Mobile Communications for 5G Cellular: It will work. Open Access, IEEE.(2013). DOI: 10.1109/ACCESS.2013.2260813.

[6] C I Badoi et.al.5G based on Cognitive Radio. Wireless Personal Communications (2011) 57:441-464. DOI 10.1007/s11277-010-0082-9

[7] Demestichas, P., et.al. Jing Yao, "5G on the Horizon: Key Challenges for the Radio-Access Network," Vehicular Technology Magazine,IEEE,vol.8,no.3,pp.47,53,Sept.2013.

[8] Prasad R., Introducing 5G Standardisation, 11th GISFI Standardisation Series Meeting, 17-12-2012, Bangalore, India

[9] Prasad, R., "Convergence: A step towards unpredictable future," Wireless Technology Conference, 2009. EuWIT 2009. European , vol., no., pp.187,191, 28-29 Sept. 2009

[10] Y.Yu et al. Integrated 60 GHz RF Beamforming in CMOS. Springer Science+ Business Media. DOI 10.1007/978-94-007-0662-0-2.

[11] Geng S. et.al.Millimeter-Wave Propagation Channel Characterisation for Short-Range Wireless Communication.IEEE Transaction on Vehicular Technology Vol. 58, No.1, January 2009.

[12] Radio Access and Spectrum FP7FutureNetworksCluster. http://www.academia.edu/9872297/Radio_Access_and_Spectrum_FP7_FutureNetworksCluster

[13] Rui Wang; Honglin Hu; Xiumei Yang, "Potentials and Challenges of C-RAN Supporting Multi-RATs Toward 5G Mobile Networks," Access, IEEE , vol.2, no., pp.1187,1195, 2014 doi: 10.1109/ACCESS.2014.2360555

THE 5TH INTERNATIONAL CONFERENCE ON WIRELESS COMMUNICATIONS, VEHICULAR TECHNOLOGY, INFORMATION THEORY, AEROSPACE & ELECTRONIC SYSTEMS (WVITAE-2015)
December 13-16, 2015, Hyderabad, India

Daubechies Wavelet based Effective Data Authentication in Wireless Domain

(DWEDAWD)

Anirban Goswami
Dept. of Information Technology, Techno India
EM 4/1 Salt Lake, Sec -V
Kolkata-700091, India
angos.kol@gmail.com

Nabin Ghoshal
Dept. of Engineering and Technological Studies,
University of Kalyani, Kalyani
Nadia-741235, India
nabin_ghoshal@yahoo.co.in

***Abstract* — the proposed paper demonstrates an improved data authentication technique based on Daubechies Discrete Wavelet Transform (DWT). The primary concern is to maintain uncompromising visual quality and prevent unauthorized manipulation of the secret data during wireless communication. The secrecy of hiding is inflated by hiding the secret data in the high frequency transformed coefficients of two distinct levels concurrently. Proper measures are taken to increase the imperceptibility of the added noise. At the receiver's end, a blind reverse process is applied to obtain the secret information from authenticated image and authenticity of the extracted data is verified by using a message digest. The algorithm has been tested against some related attacks and also may prove effective in designing a secured smart health card. Extensive experimental results show better performance over other similar techniques.**

Keywords—image authentication; daubechies 2; message digest; ssim; copy attack.

I. INTRODUCTION

In modern days there is an incremental advancement in the use of technology for facilitating day to day activities. So, the biggest challenge is information security when sending information from one place to another with the aid of wireless technology. Efficient security techniques evolved from time to time and digital data authentication [1, 2] is considered as one of the techniques for safe transmission. The technique is implemented by hiding information generally with other information that is only known to the intended receiver. Hiding involves two factors: 1) perceptual transparency and 2) the volume of payload data [3] and robustness of embedding [4].

Recently, algorithms are designed using Discrete Wavelet transforms (DWT) for its two prominent features namely Multi-resolution analysis (MRA) and rectification of the problem of time - frequency resolution as mentioned in the theoretical aspects of Human Visual System (HVS). A wavelet transform can be represented as a function using wavelets and termed as daughter wavelets. These are then scaled and translated copies of the main oscillating waveform is called the mother wavelet. Some of the recent works shows involvement of DWT coefficients at different levels. Souvik Bhattacharyya et al. [5] implemented 1-level resolution using DWT and embedded in all the four coefficients. In another algorithm, Vanitha T et al. [6] considered only the LSB positions of DWT coefficients to embed the message bits. An attempt had been made by Aayushi Verma et al. [7] to insert the secret data in the LL sub-band of the transformed coefficients. Embedding of secret messages in high frequency coefficients and utilizing the unchanged low frequency coefficients for improving the image quality was proposed by Po-Yueh Chen et al. [8]. To improve the quality of the reconstructed image, different compression thresholds for the wavelet coefficients was proposed by P. Raviraj et al. [9].

Some of the above algorithms used lossy compression technique [10], some used 1-level decomposed coefficients for embedding and in others there is a degradation in the image quality after the embedding of secret data. In the proposed algorithm, Daubechies Wavelet Transform [11] is used because the feature of orthogonality increases the bandwidth efficiency. The wavelet is more robust to narrowband interferences than the Orthogonal Frequency-Division Multiplexing (OFDM) modulation in wireless communication and also proves efficient in compression [12], image analysis [13] and classification of signals [14]. The next section deals with the mathematical representation of Daubechies DWT.

II. CONCEPT OF DAUBECHIES WAVELET TRANSFORM

The Discrete Wavelet Transform of a signal is implemented by passing a signal through a series of filters called filter bank. The Daubechies wavelets generally have the highest number i.e. A of vanishing moments, for given support width (2A – 1). These are more accurate, since change in the input data set is reflected in the high pass filter results at each transform step. In the proposed algorithm we have used D4 or db2 wavelet transform where there are 2 vanishing moments. In D4, a polynomial with two coefficients i.e. constant and linear signal components is encoded. Mathematically the coefficients are represented as

$$b_k = (-1)^k a_{(N-1-k)} \quad (1)$$

where *k* is the coefficient index, *b* is a coefficient of the wavelet sequence, a coefficient of the scaling sequence and N is the wavelet index (here N=4). In D4 the coefficients for the scaling functions are taken as {0.6830127, 1.1830127, 0.3169873 & -0.1830127}. The wavelet coefficients are derived by reversing the order of the scaling function coefficients and then reversing the sign of every second one, i.e. {-0.1830127, -0.3169873, 1.1830127, -0.6830127}.

The forward transform is implemented as: Let us consider a list S with 2 halves. The first half (S_0 to $S_{(1/2-1)}$) contains even elements and the second half ($S_{1/2}$ to $S_{(N-1)}$) contains odd elements. In the forward transform S[1/2 + n] references an odd element and S[n] references an even element. The steps are:

- U1: for n=0 to (1/2 -1), S[n] = S[n] + √3S[1/2+n].
- P1: S[1/2] = S[1/2] – (√3/4) S[0] – ((√3-2)/4)S[1/2-1].

  For n=1 to (1/2 -1)

  S[1/2+n] = S[1/2+n] - (√3/4) S[n] -((√3-2)/4)S[n-1].
- U2: for n=0 to (1/2 -2), S[n] = S[n] – S[(1/2) +n+1].

  S[(1/2)-1]= S[(1/2)-1] – S[1/2].
- N: for n=0 to (1/2 -1), S[n] = ((√3-1)/ √2) S[n].

  S[n+1/2] = ((√3+1)/ √2) S[n+1/2]. (2)

In the above steps U1 and U2 stand for Updates, P1 stands for Predicate and N stands for Normalize.

The inverse transform is the mirror reflection of the forward transform.

Section III deals with encryption of the payload, embedding of encrypted data, adjustment for maintaining proper image property, extraction of the encrypted data and decryption of the payload after receiving the authenticated cover image via wireless communication.

III. THE TECHNIQUE

Separate sub sections are defined for different aspects in data authentication in wireless domain. In sub-section A, the secret data is encrypted with the help of 4 keys to increase the robustness of imperceptibility. The sub-section B deals with the proposed embedding technique for authentication in HH block of the transformed cover image. The high frequency coefficient set HH include the edges and textures of the image and HVS is insensitive to changes in such coefficient sets. So, HH block of both the levels are used for embedding the encrypted payload. Hiding for authentication is done at pseudorandom position without distorting the image quality. In the third sub-section C, accurate measures are taken to bind all the pixels within proper image property even after embedding the payload in a transformed block. The above procedures are framed keeping in mind that the secret data is to be transmitted through a wireless communication medium and there is be a chance of unauthorized interference. Lastly, the sub-sections D and E are responsible for proper extraction and presenting authentic payload to an intended receiver.

A. Encryption of the payload image

Pre-calculated size of blocks taken from the payload image are encrypted within its boundaries one at a time. The rearrangement of blocks defines a transformation of reallocation of blocks in such a manner that the correlation of a pixel with the neighboring pixel decreases. The process is done in two steps:

- Firstly every pixel location is modified to a new location with the help of 2 keys each of size 2 bytes. The equations are:

  $X` = (K_0 \times X + K_1) \oplus N$ and

  $Y` = (K_0 \times Y + K_1) \oplus N.$ (3)

  (X, Y) is the original location of a pixel, (X`, Y`) is the modified location of a pixel and N denotes the length of the image. Two keys (K_0, K_1) are used to authentic the process.
- In the second step, the output image is divided into a set of 2 x 2 non overlapping blocks. The pixels of each of the blocks undergo ⊕ operations with 2 more keys (K_2, K_3) each of size 2 bytes to produce a new set of pixels. The equation is:

  $X` (i, j) = X (i, j) \oplus (K_2/ K_3)$ (4)

  The values of i and j are both (0, 1), X (i, j) is the original value of a pixel and X` (i, j) is the modified value. If (i == j) then K_2 is used, otherwise K_3 is used.

B. Embedding procedure

An image as cover and the encrypted image as payload are taken as input. The output is an authenticated image. A message digest (SHA-1) of size 160 bit is generated from the encrypted payload and the cover image is considered as a set of 4x4 non overlapping sub-images.

Repeat the following steps until the payload gets fully fabricated.

- Each of the sub-images is converted to transform domain by applying 2-level Daubechies DWT (D4/ db2).
- The integer part of the target frequency coefficients (i.e. HH2 and 4 coefficients of HH1) of a block are chosen for embedding.
- The current block number is represented as a combination X_i (i =0 to 16) of bits. A pseudo-random position is generated by the expression: ipos = ($X_3 \oplus X_2 \oplus B_p$) where B_p is the last embedded bit.
- The payload bits are scanned one at a time and is fabricated in pseudo-random position in each of the target frequency coefficients.
- In some cases, an adjustment is required to reduce the degree of the embedded noise. The bit of the binary representation on the right of s (1 to 0) is altered, where

s is the current modified bit in the target frequency component.

- The authenticated pixels are generated by applying Inverse Daubechies DWT (D4/ db2) on the respective sub-image block.
- To restore proper image property, necessary readjustments are applied on the adverse authenticated block.
- The correct spatial block is returned back into the output image in the same location.

C. Retention of image property

Some authenticated pixel values may contradict the image property. Rectification is done on the required authenticated pixels of a block and the embedding algorithm is repeated for that block. A threshold value T determined after experimentation on a number of images is considered to ease the process. The possible causes and the remedies are mentioned below:

- If the spatial pixel values lie either in [0, T]/ [255-T, 255] / [0, 255], and there is a generation of either (-) ve authenticated pixels/ (+) ve authenticated pixels/ both. Then as per the range a value A = [0- (highest (-) ve pixel value)] is added, a value B = [(highest (+) ve pixel value) – 255] is subtracted and [2 x max (A, B)] is either added or subtracted from the default pixel values in the respective range.
- If the spatial pixel values are in the range (0, T)/ (255-T)/ 255) and there is generation of both (-) ve and (+) ve pixel values. The spatial pixel values are adjusted as: 1) values below T by the value (2 x max (A, B)) and 2) the values above T by the value max (A, B).
- If the spatial values are in the mid-range [(T+1), ((255-T) - 1)], then no rectification is necessary.

D. Extraction procedure

The input is an authenticated image and the output is an encrypted image (payload).

- Non-overlapping blocks of size 4 x 4 are read in sliding window pattern from the authenticated image.
- Each of the sub-images is converted to transform domain by applying 2-level Daubechies DWT (D4/ db2).
- The integer part of the target frequency components is chosen and the pseudo-random positions are generated.
- The embedded bits are extracted from the designated areas.
- The bits are arranged sequentially to form payload size, message digest (SHA–1) of size 160 bit and the encrypted payload itself.
- From the extracted payload, a message digest (SHA-1) of size 160 bit is also generated.
- The extracted and the generated message digest is compared to check the authenticity of the extracted encrypted payload.

E. Decryption of the extracted payload

- In the first step, the extracted payload is divided into a set of 2 x 2 non overlapping blocks. The pixels of each of the blocks undergo $\oplus$ operations with the two keys (K_2, K_3) to re-produce the original set of pixels. The equation is:

$$X(i, j) = X`(i, j) \oplus (K_2/ K_3), \quad (5)$$

The values of i and j are both (0, 1), X` (i, j) is the modified value of a pixel and X (i, j) is the original value. If (i == j) then K_2 is used, otherwise K_3 is used.

- In the second step, the modified pixel location is reallocated to the original location by using the equations:

$$X = ((X` \oplus N) - K_1) / K_0$$

$$Y = ((Y` \oplus N) - K_1) / K_0 \quad (6)$$

(X`, Y`) is the modified pixel location, (X, Y) is the original pixel location and N denotes the length of the image. K_0 and K_1 are the two keys.

The above two steps help to frame the desired payload at the receiver's end.

A flowchart for the technique is shown in Fig. 1.

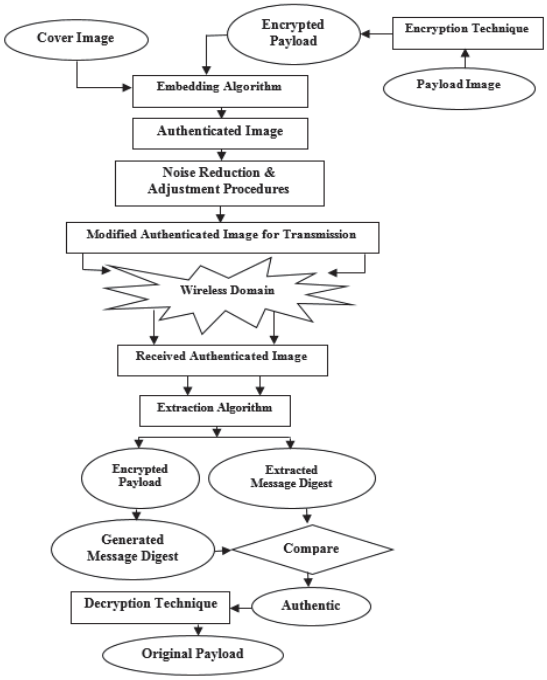

Fig. 1. *The TECHNIQUE of DWEDAWD*

IV. Result, comparison and analysis

A number of gray scale images are considered to test the effectiveness of the proposed algorithm. The experimentation has been done in a system with 4 GB of main memory, processor of at least 1 GHz clock speed, 1 GB of graphics memory and 4 GB of free disk space. The imperceptibility of data hiding is measured in terms of Peak Signal to Noise Ratio (PSNR) [15], Image Fidelity (IF) and Structural Similarity Index Metric (SSIM) [16]. The computed metric values are shown in Table I.

TABLE I. ANALYSIS OF PSNR, MSE, IF AND SSIM

Source Images	Capacity (Byte)	PSNR	IF	SSIM
Monalisa	12100	38.01	0.9934	0.9979
Lenna	12100	37.24	0.9345	0.9960
Baboon	12100	37.90	0.9919	0.9976
Oakland	12100	37.68	0.9952	0.9932
Woodlad	12100	37.54	0.9927	0.9969
Peppers	12100	37.19	0.9890	0.9968
Tiffany	12100	35.87	0.9949	0.9887
Airplane	12100	36.76	0.9856	0.9956
Sailboat	12100	37.91	0.9918	0.9964
Average	**12100**	**37.34**	**0.9854**	**0.9954**

The degradation level of an authenticated image is considered to be quite acceptable if the PSNR value is greater than 35 dB. The proposed algorithm is quite successful in achieving a decent average PSNR value i.e. 37.34 dB in spite of hiding quite a volume of secret data in both the levels of resolution simultaneously. Moreover the average values of IF and SSIM i.e. 0.9854 and 0.9954 respectively proves that the authenticated image more or less resembles the cover image.

The visual interpretation of some gray cover images used for experimentation are shown in Fig. 2. The dimension of each such grayscale image is 512 x 512 and that of the payload image 'Earth' is 110 x 110. From the figure it can be observed that there is hardly any difference between the source and embedded images in terms of HVS.

Source Images	Authenticated Images	Magnified Source Images	Magnified Authenticated Images
Fig. 2a.giraffe	**Fig. 2d.**	**Fig. 2g.**	**Fig.2j.**
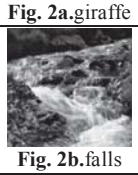 **Fig. 2b.**falls	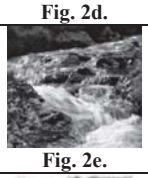 **Fig. 2e.**	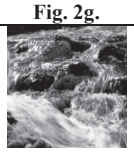 **Fig. 2h.**	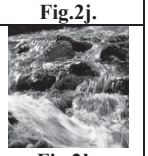 **Fig.2k.**
Fig. 2c.kaya	**Fig.2f.**	**Fig. 2i.**	**Fig.2l.**

Fig. 2q
Embedded Payload (Earth)

Fig. 2q
Extracted Payload (Earth)

Fig. 2. *Visual Interpretation of images in DWEDAWD*

In addition to this, a performance comparison is also done with some of the existing algorithms as shown in Table II.

TABLE II. COMPARATIVE ANALYSIS OF PSNR

No	Algorithm	Level of Resolution	Avg. PSNR (in dB)
A	[5]	1	34.60
B	[17]	1	38.52
C	[18]	2	26.30
D	[19]	2	33.08
E	[20]	2	36.04
F	**DWEDAWD**	**2**	**37.34**

In the above table, the proposed algorithm shows an increase in the average PSNR value (i.e. 37.34 dB) even with 2-level of resolution as compared to the algorithms A and B with 1-level of resolution and less or similar embedding capacity. The algorithm also proves an enhancement in data authentication as compared with the algorithms C to E, with 2-level of resolution and similar embedding capacity.

The proposed algorithm also proves its grittiness against some of the related attacks and is also effective in smart health card technology as discussed below.

A. Attacks

- Visual Attack: An initiative is taken to resist this attack by eliminating certain issues like 1) embedding in a sequential order and 2) length is less than the maximum size of the bit plane.
- Statistical Attack: A histogram analysis is done on both the cover and authenticated images and it may be inferred that the proposed algorithm shows resistance against this kind of attack.

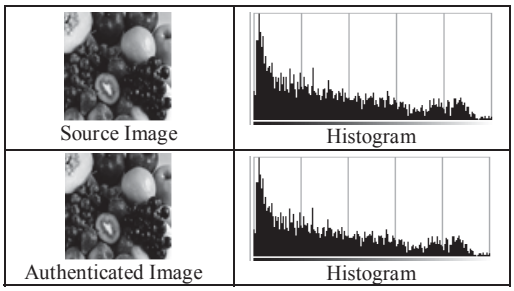

Fig. 3. *Histogram Analysis of Source and Authenticated Images*

- Copy Attack: The embedding of payload is dependent on a self-defined pseudorandom function which establishes a link between the payload and the cover

image. The link can only be verified by an authorized receiver during the extraction of the payload. This will cause a problem in terms of the marked target cover image and also helps to restrict protocol attack.

- Collusion Attack: Every copy of a cover image have different embedding policy, and the attacker cannot predict the embedding location and hidden data by colluding many copies of the authenticated image. Only the owner has the record of different embedding policies and can always extract the payload from the attacked authenticated image by applying the different policies.

B. Social Implication

Smart Health card is a useful option to define basic health information of an individual like blood group, current health problems and current medications while treating an accident or medical emergency. Citizens having certain health problems and are constantly on the move are at a high risk. Since the cards have up-to-date information, doctors can have access to all the information they need during emergencies which will reduce chances of medical errors. Every Smart card is linked via wireless communication to an online Personal Health Record that is created when the patient gets registered in a hospital and given the Smart card. To enhance the robustness of data authentication the patient's information will be encrypted before being fabricated into the smart card.

V. CONCLUSION

The proposed algorithm defined in frequency domain helps to enhance the security in wireless communication. Use of gray images helps efficient routing in terms of energy. Efficient authentication prevents attenuation of the signal strengths. Pseudo-random embedding position obstructs tracing a payload by unauthorized user and the control technique helps to optimize the noise integration. Due to the effectiveness of encryption procedure, the proposed scheme may be more robust against brute force attack applicable in wireless systems.

ACKNOWLEDGEMENT

The authors express their deep sense of gratitude to the faculty members of the Dept. of Engineering and Technological Studies, University of Kalyani, West Bengal, India, where the work has been carried out.

References

[1] I. Cox, M. Miller and J. Bloom, Digital Watermarking, Morgan Kaufmann Publishers, 2002.

[2] M. Borda and I. Nafornita, "Digital Watermarking - Principles and Applications", The International Conference on Communications, 2004 Bucharest, pp. 41-54.

[3] Ghoshal N., Mandal, J. K., Sarkar A. and Chakrabarty D, "Image Authentication by Hiding Large Volume of Data and Secure Message Transmission Technique using Mask", The IEEE International Advanced Computing Conference (IACC'09), Thapar University, Patiala, India, March 6-7th, 2009, ISBN: 978-1-4244-2928-8, pp. 3177-3182.

[4] Ghoshal N., Mandal J. K. and Khamrui A, "A Framework for Block based Image Authentication (FBIA)", The Fourth IEEE International Conference on Industrial and Information Systems (ICIIS'09), Peradeniya University, Sri Lanka, December 28th -31st, 2009 ISBN: 978-1-4244-4837-1, pp. 343-348.

[5] Souvik Bhattacharyya and Gautam Sanyal, "Data Hiding in Images in Discrete Wavelet Domain Using PMM", Academic Journal, World Academy of Science, Engineering & Technology, Aug 2010, Issue 44, pp. 376 - 384.

[6] Vanitha T, Anjalin D Souza, Rashmi B and Sweeta Dsouza, "A Review on Steganography - Least Significant Bit Algorithm and Discrete Wavelet Transform Algorithm", IJIRCSE, October 2014, Vol.2, Special Issue 5, pp. 89-95.

[7] Aayushi Verma, Rajshree Nolkha, Aishwarya Singh and Garima Jaiswal, "Implementation of Image Steganography Using 2-Level DWT Technique", International Journal of Computer Science and Business Informatics, May 2013, Vol. 1(1), pp. 1-14.

[8] Po-Yueh Chen and Hung-Ju Lin, "A DWT Based Approach for Image Steganography", International Journal of Applied Science and Engineering, 2006, Vol. 4, No. 3, pp. 275-290.

[9] P. Raviraj and M.Y. Sanavullah, "The Modified 2D-Haar Wavelet Transformation in Image Compression", Middle-East Journal of Scientific Research, IDOSI Publications, 2007, Vol. 2, No. 2, ISSN 1990-9233, pp. 73-78.

[10] Amir Said and William A. Pearman, "An Image Multi-resolution Representation for Lossless and Lossy Compression", IEEE Transactions on Image Processing, 1996, Volume: 5, Issue: 9, pp. 1303-1310.

[11] Daubechies I., "Ten Lectures on Wavelets", SIAM, Philadelphia (1992) , pp. 357–367.

[12] Kuduvalli, G.R., Rangayyan, R.M., "Performance analysis of reversible image compression techniques for high resolution digital teleradiology", IEEE Trans. Med. Imag. 11, 1992, 430–445.

[13] Lina, J.M., "Image Processing with Complex Daubechies Wavelets", Journal of Mathematical Imaging and Vision 7, 1997, 211–223.

[14] Patnaik, L.M, "Daubechies 4 wavelet with a support vector machine as an efficient method for classification of brain images", Journal of Electronic Imaging 14(1), 2005.

[15] Sumathi Poobal and G. Ravindran, "The Performance of Fractal Image Compression on Different Imaging Modalities Using Objective Quality Measures", IJEST, Jan - Feb 2011, Vol. 2, Issue 1, pp. 239-246.

[16] Zhou Wang, Alan Conrad Bovik, Hamid Rahim Sheikh et al., "Image Quality Assessment: From Error Visibility to Structural Similarity", IEEE Transactions on Image Processing, 2004, Vol. 13, No. 4, pp. 600-612.

[17] Pallavi Patil and D.S. Bormane, "DWT Based Invisible Watermarking Technique for Digital Images", IJEAT, April 2013, ISSN: 2249 – 8958, Volume-2, Issue-4, pp.603-605.

[18] Yedla Dinesh and Addanki Purna Ramesh, "Efficient Capacity Image Steganography by Using Wavelets", IJERA, Jan-Feb 2012, Vol. 2, Issue 1, ISSN: 2248-9622, pp. 251-259.

[19] Ashish Chawla and Pranjal Shukla, "A Modified Secure Digital Image Steganography Based on DWT Using Matrix Rotation Method", International Journal of Computer Science and Communication Engineering, May 2013, Volume 2, Issue 2, ISSN 2319-7080, pp. 20 – 25.

[20] Li Li, He-Huan Xu, Chin-Chen Chang and Ying-Ying Ma, "A novel image watermarking in redistributed invariant wavelet domain", The Journal of Systems and Software, 2011, Doi: 10.1016/j.jss.2011.01.025, pp. 923–929.

THE 5TH INTERNATIONAL CONFERENCE ON WIRELESS COMMUNICATIONS, VEHICULAR TECHNOLOGY, INFORMATION THEORY, AEROSPACE & ELECTRONIC SYSTEMS (WVITAE-2015)
December 13-16, 2015, Hyderabad, India

Rate Independent Multicarrier Variable Rate Scheme over Frequency Selective Channel

Akash Agarwal* Vijay Mukati†, Preetam Kumar‡
Department of Electrical Engineering
Indian Institute of Technology Patna
Bihar 800013, India
Email: {*akash.agarwal,†vijay.mtee13, ‡pkumar}@iitp.ac.in

***Abstract*—In order to support Variable Bit Rate (VBR) data transmission in frequency selective channel, we propose a rate-independent multicarrier based scheme. The purpose of the present work is to implement rate independent transmission scheme over the frequency selective channel while maintaining the desired QoS. In this paper, the VBR Spread Orthogonal Frequency Division Multiplexing (SOFDM) transmission scheme is proposed and compared with Variable Spreading Length (VSL)-OFDM. For all the schemes, three Variable Rate classes are considered for analysis and simulation. Results show that the BER performance of SOFDM is independent of rate. It is shown that, SOFDM outperforms VSL-OFDM for all the considered VBRs. Hence, SOFDM transmission scheme could be a suitable candidate for variable rate communication system.**

***Index Terms*—SOFDM, VBR, Multicarrier, VSL-OFDM**

I. Introduction

In wireless communication, various services like voice, image, data and video etc. need to be integrated to support multimedia services in 3G and beyond systems. Hence variable rate systems aim to provide broadband services and require a great amount of integration among available schemes. The bottleneck to provide such services include higher bandwidth and hostile wireless channel, while maintaining required QoS and reliability [1].

Based on the rigorous research in the past the combination of multiplexing schemes namely Orthogonal Frequency division Multiplexing (OFDM) and Code Division Multiple Access (CDMA), termed as Multicarrier (MC-CDMA) had been proved to be suitable to combat such difficulties [2]. MC-CDMA was first proposed in [3], and analyzed in [4] over the frequency selective channel. Later, in order to support reliable multi-user communication, Group Orthogonal (GO) MC-CDMA [5], GO-OFDMA [6], Variable Spreading Length (VSL) MC-CDMA [7] etc. transmission schemes were proposed and analyzed over the frequency selective channel. In [7], both variable rate Multi-Code and Variable Spreading Length (VSL) access schemes of MC-CDMA are implemented over the slow Rayleigh fading channel. It is illustrated that Multi-Code MC-CDMA has better BER performance than VSL MC-CDMA for higher data rates. In this work, the Multi-code and VSL spread MC-CDMA schemes are implemented and compared for the single user case, terming it as spread-OFDM and VSL-OFDM respectively. Although, the concept of SOFDM has also been discussed in [8].

Till date, to the best of our knowledge no analytical/simulation work employing variable rate multicarrier transmission schemes, for such system has been discussed in the literature. In this paper, variable rate SOFDM and VSL-OFDM schemes for single user are implemented over slowly varying frequency selective fading channel. It is shown that the BER performance of SOFDM scheme is independent of transmission rate.

Section II describes about the system model and performance analysis of VBR single user spread-OFDM. In Section III, the system model of VBR VSL-OFDM is presented. In Section IV, the simulation results are shown. Finally, Section V concludes the paper.

II. Variable Rate Single User Spread-OFDM

A. Proposed System Model

In this work, spread OFDM technique has been used as VBR transmission scheme. Walsh Hadamard (WH) code has been employed as spreading code. Spreading provides the diversity in the frequency domain and thus improves the error performance of the wireless communication systems. The transmitter model of the variable rate spread-OFDM scheme is shown in Figure 1. The incoming serial modulated data bits $d_r = \left\{d_0, d_1, \cdots, d_{\frac{r}{R}-1}\right\}$ are converted into parallel form with symbol duration T, depending upon the transmission rate $r \in \{4R, 8R, 16R\}$, where R is the basic rate. For higher rate transmission, $\frac{r}{R}$ is taken to be higher value and vice versa. Each parallel stream of rate r, is spread by a row of orthogonal Walsh Hadamard (WH) code matrix $C_r = [C^0_{1\times N}; C^1_{1\times N}; \cdots C^{\frac{r}{R}-1}_{1\times N}]$ of dimension $\frac{r}{R} \times N$, and then modulated over N different subcarriers. Cyclic prefix (CP) of length $\frac{N}{4}$ is added to form the OFDM symbol to avoid the Inter Block Interference (IBI) caused due to multipath propagation of the signal [9]. This length of cyclic prefix is considered so as to insure that the cyclic prefix duration is4 greater than the delay spread due to the channel.

The transmitted signal employing spread-OFDM scheme for particular r is expressed as:

$$s_r(t) = \sqrt{2P}\sum_{k=0}^{N-1}\sum_{p=0}^{\frac{r}{R}-1} d_p(t)C^k_p(t)exp(2\pi j f_k t) \quad (1)$$

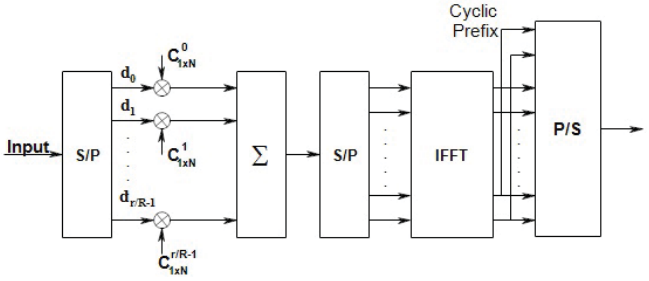

Figure 1: Transmitter model for the variable rate Spread-OFDM

where, $f_k = f_0 + \frac{k}{T}$.

B. Analysis over AWGN Channel

Spread-OFDM system is considered with N subcarrier and rate r. The sum of the parallel spread data is represented as

$$X_r(i) = \sum_{p=0}^{\frac{r}{R}-1} d_p C_p(i), \qquad 0 \le i \le N-1 \tag{2}$$

Equation (2) can be written in the vector form of order $1 \times N$ as,

$$\mathbf{X}_r = \mathbf{d}_r \mathbf{C}_r \tag{3}$$

In the above equation, $\mathbf{d}$ is of order $1 \times \frac{r}{R}$ and $\mathbf{C}$ is of order $\frac{r}{R} \times N$. For instance, if r =8R then the dimensions of $\mathbf{d}$ and $\mathbf{C}$, and hence $\mathbf{X}_r$ are 1×8, $8 \times N$ and $1 \times N$ respectively. Thus for any rate r, the sum $\mathbf{X}_r$ would be modulated onto all N orthogonal subcarriers. For any considered data rate, the spreading length of the code remains same. The difference lies only with the number of the codes employed based on the number of parallel substreams as shown in Fig. 1.

After IDFT operation, users data can be represented as,

$$s_r(n) = \frac{1}{N} \sum_{k=0}^{N-1} X_r[k] e^{\frac{j2\pi kn}{N}}, \qquad n = 0, 1, ..., N-1 \tag{4}$$

Considering only the effect due to AWGN noise with zero mean and variance of $N_o/2$, the received signal will be

$$v_r(n) = s_r(n) + w_r(n) \tag{5}$$

where, $w(n)$ is the AWGN noise vector. Received signal after DFT operation at the receiver gives

$$v_r[k] = \sum_{n=0}^{N-1} v_r(n) e^{\frac{-j2\pi kn}{N}}, \quad 0 \le k \le N-1 \tag{6}$$

From equation (5) and (6),

$$v_r[k] = \sum_{n=0}^{N-1} \left[\frac{1}{N} \sum_{l=0}^{N-1} X_r[l] e^{\frac{j2\pi ln}{N}} \right] e^{\frac{-j2\pi kn}{N}} + W_r(k) \tag{7}$$

$$v_r[k] = \underbrace{\frac{1}{N} \sum_{n=0}^{N-1} \sum_{l=0}^{N-1} X_r[l] e^{\frac{j2\pi(l-k)n}{N}}}_{F} + W_r(k) \tag{8}$$

where,

$$F_r = \begin{cases} X_r(k), & for\ \ l = k \\ 0, & otherwise \end{cases} \tag{9}$$

Final recevied vector at all the subcarriers are as,

$$v_r = [X(0)+W(0),\ X(1)+W(1),\ ....X(N-1)+W(N-1)]_{1\times N} \tag{10}$$

$$\mathbf{V}_r = \mathbf{X}_r + \mathbf{W}_r \tag{11}$$

At the receiver, particular data rate is obtained as

$$\begin{aligned} \tilde{\mathbf{V}}_\mathbf{r} &= \mathbf{V}_r [\mathbf{C}_r^T]_{N \times \frac{r}{R}} \\ &= \mathbf{X}_r . \mathbf{C}_r^T + \mathbf{W}_r \mathbf{C}_r^T \\ &= \mathbf{d}_r \mathbf{C}_r \mathbf{C}_r^T + \mathbf{W}_r \mathbf{C}_r^T \\ &= \mathbf{d}_r + \mathbf{W}_r \mathbf{C}_r^T \end{aligned}$$

Now finding the mean of the decoded signal over a particular subcarrier g assuming zero mean noise,

$$\begin{aligned} E[\tilde{V}_r^g] &= E[d_r^g] + C^T E[W_r^g] \\ &= E[d_r^g] = \pm\sqrt{E_b} \end{aligned}$$

The variance of the decoded signal,

$$\begin{aligned} Var[\tilde{V}_r^g] &= Var[W_r^g C^T] \\ &= C_r C_r^T Var[W_r^g] = \tfrac{N_o}{2} \end{aligned}$$

Therefore, the average error probability for BPSK modulated signal is given as [10],

$$P_e = Q\left(\sqrt{\frac{2E_b}{N_o}}\right) \tag{12}$$

Equation (12) is independent of data rate and hence the performance is same for the three rates considered. Analytical and simulation results over AWGN for three rates (i.e. 4R, 8R and 16R) are shown in Figure 2.

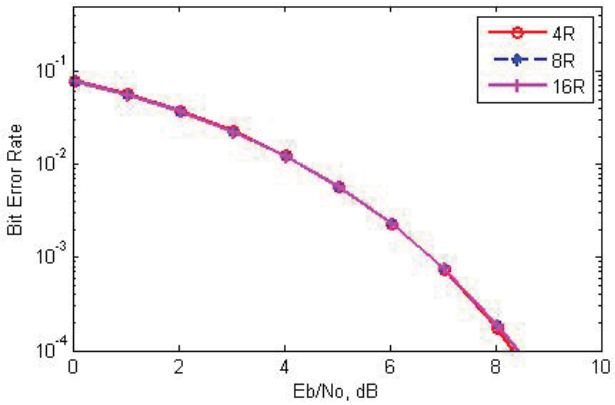

Figure 2: BER Performance of spread-OFDM over AWGN Channel

C. Analysis over Frequency Selective Channel

User's rate dependent data after multiplying with the code matrix of dimension $\frac{r}{R} \times N$ yields a summation of dimension $1 \times N$, and is expressed as,

$$\mathbf{X}_r = \sum_{p=1}^{\frac{r}{R}-1} \mathbf{d}_p \mathbf{C}_p(i) = [\mathbf{d}_r \mathbf{C}_r]_{1\times N}^T \tag{13}$$

The output of N point IDFT unit for particular rate can be expressed as

$$\mathbf{S}_r = \mathbf{D}^N \mathbf{X}_r \tag{14}$$

where $\mathbf{D}^N$ is the IFFT matrix of dimension $N \times N$. The transmitted signal gets linearly convolved with the channel implse response and is additionaly affected by the AWGN noise at the receiver.

$$\mathbf{V}_r = \mathbf{S}_r \otimes \mathbf{h} + \mathbf{n} \tag{15}$$

The output of N point DFT unit at the receiver can be expressed as

$$\mathbf{V}_{r_F} = \mathbf{H}\mathbf{X}_r + \mathbf{n}_F \tag{16}$$

where, $\mathbf{H}$ denotes the diagonal $N \times N$ channel impulse response (CIR) matrix in frequency domain as

$$\mathbf{H}_{k,k} = \sum_{n=0}^{L-1} h_n e^{-j2\pi(k-1)n/N} \tag{17}$$

Let us consider σ_s^2 and σ_z^2 denotes the variance of signal and noise respectively. The output of the N point DFT at the receiver is given to an $N \times N$ MMSE equalizer denoted by $\tilde{\mathbf{H}}$ as [11]

$$\tilde{\mathbf{H}}_{k,k} = \frac{(\mathbf{H}_{k,k})^*}{\left|\mathbf{H}_{k,k}\right|^2 + \frac{\sigma_n^2}{\sigma_s^2}} \tag{18}$$

$$\tilde{\mathbf{X}}_r = \underbrace{\tilde{\mathbf{H}}\mathbf{H}}_{\mathbf{F}}\mathbf{X}_r + \tilde{\mathbf{H}}\mathbf{n}_F \tag{19}$$

where, $\mathbf{F}$ is a $N \times N$ matrix,

$$\mathbf{F}_{n,r} = \frac{1}{N}\sum_{k=0}^{N-1} \frac{|\mathbf{H}_k|^2}{|\mathbf{H}_k|^2 + \frac{\sigma_n^2}{\sigma_s^2}} \tag{20}$$

$$\Lambda = diag[\mathbf{F}] \tag{21}$$

from equation (19), we get

$$\tilde{\mathbf{X}_r} = \Lambda\mathbf{X}_r + \tilde{\mathbf{H}}\mathbf{n}_F \tag{22}$$

Multiplying the above equation (22) with the code matrix $\mathbf{C}_r^T$ of order $N \times \frac{r}{R}$ to get back the actual information bits

$$\begin{aligned} \tilde{\mathbf{d}}_r &= \tilde{\mathbf{X}}\mathbf{C}_r^T \\ \tilde{\mathbf{d}}_r &= \Lambda\mathbf{X}_R\mathbf{C}_r^T + \tilde{\mathbf{H}}\mathbf{n}_F\mathbf{C}_r^T \\ \tilde{\mathbf{d}}_r &= \Lambda\mathbf{d}_r + \tilde{\mathbf{H}}\mathbf{n}_F\mathbf{C}_r^T \end{aligned} \tag{23}$$

In equation (23), first term denotes the desired signal and the last term denotes the noise component.

From equation (23), for a particular subcarrier g assuming β_0

$$P_e(\tilde{\mathbf{d}}_r^g < 0) = erfc\left(E\left[\tilde{\mathbf{d}}_r^g\right] / \sqrt{\left(2 * Var\left[\tilde{\mathbf{d}}_r^g\right]\right)}\right) \tag{24}$$

$$\gamma = \frac{\left(E\left[\tilde{\mathbf{d}}_r^g\right]\right.}{\sqrt{\left(2 * Var\left[\tilde{\mathbf{d}}_r^g\right]\right)}} = \beta_0\sqrt{\frac{E_b}{No}} \tag{25}$$

Instantaneous received SNR of equation (25) is determined using equation (23) through MATLAB simulation. Then, the probability of error for BPSK transmission in general can be calculated as,

$$P_e = \frac{1}{2}\int_0^\infty erfc(\gamma)p(\gamma)d\gamma \tag{26}$$

where, $p(\gamma) = \frac{1}{E_b/N_o}e^{\frac{-\gamma}{E_b/N_o}}$

The results obtained using equations (23), (24), (25) and (26) for different rates are shown in Fig. 4.

III. Variable Rate VSL-OFDM

In this paper, single user VSL-OFDM is considered for the purpose of comparison with the proposed scheme. The transmitter model of VBR single user VSL-OFDM transmission scheme is shown in Figure 3. Unlinke SOFDM, the modulated data bits are converted from serial to P parallel streams depending upon the specific transmission rate r, where $r \in 2^n R, n \in I^+$ and $P \in \frac{r}{R}$. Each parallel output symbol is copied onto $F = \frac{N}{P}$ branches and then respectively multiplied bit-by-bit by the row of orthogonal WH code matrix of order $F \times F$, where $F \in 2^n, n \in I^+$.

Irrespective of any data rate, there are a total of PF parallel symbol outputs after such frequency domain spreading, which are then transmitted simultaneously by modulating over PF orthogonal sub-carriers. In this scheme, the value of P and F are selected such that PF equals to the N-point IFFT size or the number of subcarriers onto which the data is modulated. The length of CP is same as that considered for SOFDM.

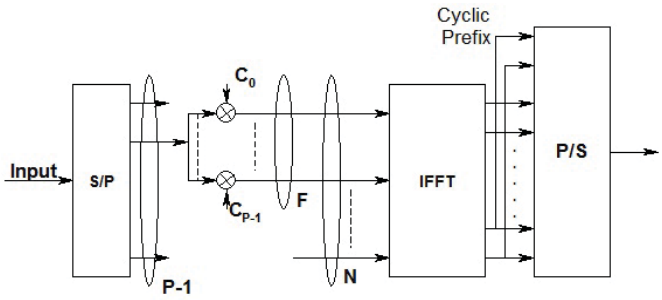

Figure 3: Transmitter model for the variable rate VSL-OFDM

The transmitted signal employing VSL-OFDM scheme, for particular r, as shown in Fig. 3 is of the form

$$s_r(t) = \sqrt{2P}\sum_{p=0}^{P-1} d_p(t)\sum_{k=0}^{\frac{N}{P}-1} C_p^k(t) exp\left[2\pi j\left(\frac{N.p}{P} + k\right)\frac{t}{T}\right] \tag{27}$$

IV. Simulation and Results

The Simulation Results for the variable rate Spread-OFDM and VSL-OFDM are shown in this section. All the simulations are done over frequency selective pedestrian channel-A [12] in MATLAB using Monte-Carlo simulations. In this paper, three different data rate (4R, 8R and 16R) are considered for simulation and analysis. In this work, BPSK modulation scheme is considered for both the VBR schemes. For each data rate, the energy per bit varies i.e. the highest rate users will transmit at reduced energy compared to lower bit rate users. Fig. 4. shows the simulation results for the three different rates (4R, 8R and 16R) of spread-OFDM scheme over the considered channel. From Fig. 5., it could be observed that the

BER performance for all the rates, are identical and match well with the analytical results. Such identical performance is due to the proportionate increase in the number of codes employed as the data rate (parallel substreams), which leads to the higher coding gain. For higher data rates such as 16R, higher number of orthogonal rows of WH code matrix are employed which leads to higher coding gain, and hence compensates for the performance degradation caused due to the lower received SNR. Thus, the trade off exists between the system complexity due to the usage of increased number of codes, and the data rate.

In Fig. 6, the bit error rate performance of the spread-OFDM scheme is compared with the VBR VSL-OFDM. Results obtained clearly shows that the performance of VSL-OFDM varies with data rates, the performance degrades as the rate increases. Even the performance of lowest rate (4R) VSL-OFDM is considerably poor than all rates of spread-OFDM. Around 7.5 dB of SNR gain is achieved by spread-OFDM over the lowest rate VSL-OFDM. This gain is even greater when compared to higher rate VSL-OFDM.

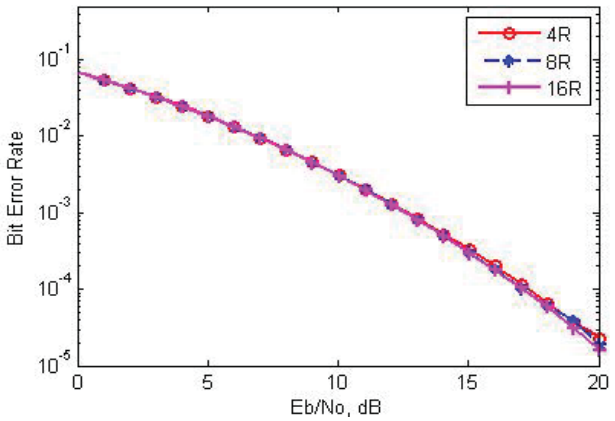

Figure 4: BER Performance of spread-OFDM over Pedestrian Channel

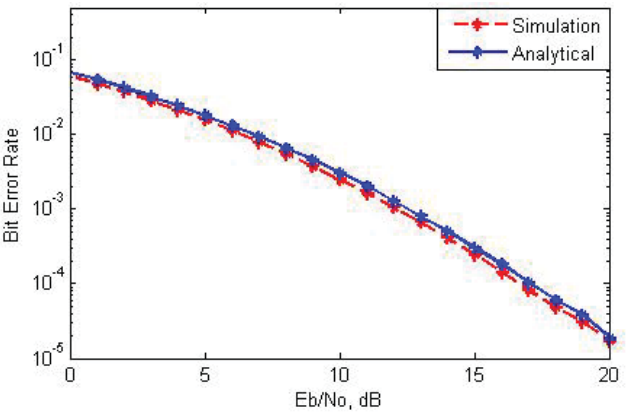

Figure 5: BER Performance of spread-OFDM for all rates over Pedestrian Channel

The maximum rate which spread-OFDM can support depends on the number of available subcarriers N and is equal to NR. For example, in this paper the number of available

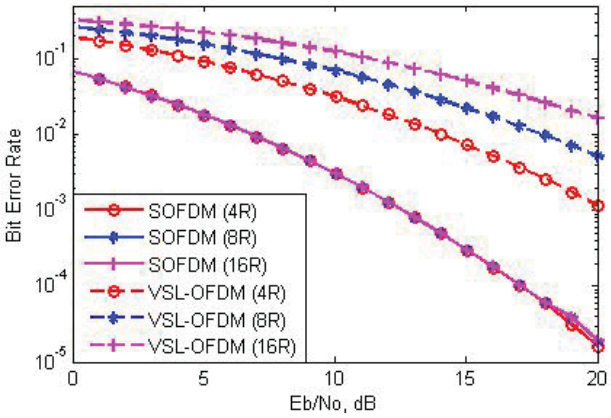

Figure 6: BER Performance comparison of spread-OFDM with VSL-OFDM over Pedestrian Channel

subcarriers are 64. Therefore, spread-OFDM can support maximum rate up to 64R. Moreover any rate can be supported by spread-OFDM which is not possible in case of VSL-OFDM due to the design constraint. Maximum rate supported by spread-OFDM can even increase by using higher modulation order. For example, in QPSK modulated maximum rate spread-OFDM, the will be double (128R). But as the modulation order increases the performance of spread-OFDM also degrades, as shown in Fig. 7. So there exists a trade-off between the date rate and the modulation order.

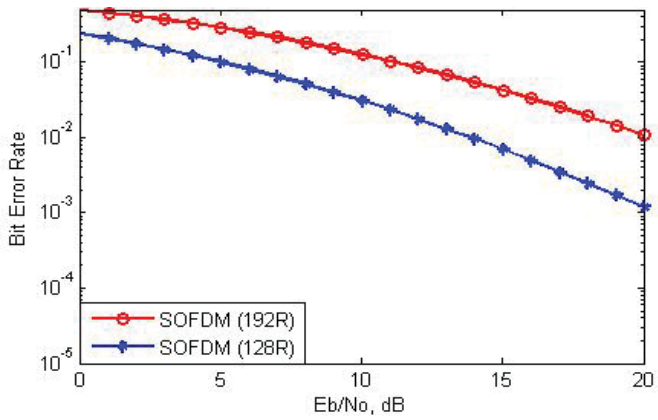

Figure 7: BER Performance of spread-OFDM with different modulation order

V. Conclusion

In this paper, the rate-independent spread-OFDM scheme has been discussed. Detailed analysis of the proposed scheme has been presented over AWGN and frequency selective channel. Further, simulation results match with the analytical results. Spread-OFDM is then compared with the VSL-OFDM and the results obtained clearly shows the performance improvement of spread-OFDM over VSL-OFDM. BER performance is independent of the transmission rate in case of spread-OFDM, while for VSL-OFDM the performance degrades as the rate increases. For spread-OFDM, SNR gain of about 7.5 dB is observed over the lowest rate VSL-OFDM.

The gain is even higher when compared with the higher rate VSL-OFDM. Later, for SOFDM, a trade-off between the transmission rate and modulation order is highlighted. These results clearly indicate that spread-OFDM can be a potential bandwidth efficient variable rate scheme for the wireless multipath environment.

ACKNOWLEDGMENT

This work is part of the project funded by DEITY, Government of India. We sincerely acknowledge the support of DEITY.

REFERENCES

[1] A. Goldsmith, *Wireless Communication.* New York: Cambridge Univ. Press, 2005, ch. 2.
[2] S. Hara and R. Prasad, "Overview of multicarrier CDMA," *IEEE Commun. Mag.*, vol. 35, no. 12, pp. 126-133, Dec. 1997.
[3] Y. Nathan, J.-P. M. Linnartz, and G. Fettweis, "Multi-carrier CDMA in indoor wireless radio networks," *IEICE Transactions on Communications*, vol. 77, no. 7, pp. 900-904, 1994.
[4] S. Hara and R. Prasad, Design and performance of multicarrier cdma system in frequency-selective rayleigh fading channels, Vehicular Technology, IEEE Transactions on, vol. 48, no. 5, pp. 15841595, Sep 1999.
[5] X. Cai, S. Zhou, and G. Giannakis, Group-orthogonal multi-carrier cdma, in MILCOM 2002. Proceedings, vol. 1, Oct 2002, pp. 596601 vol.1.
[6] Y. Xu, J. Weng, and T. Le-Ngoc, Group-orthogonal ofdma in fast time-varying frequency-selective fading environments, in Vehicular Technology Conference, 2004. VTC2004-Fall. 2004 IEEE 60th, vol. 1, Sept 2004, pp. 488492 Vol. 1.
[7] P.-W. Fu and K.-C. Chen, "Multi-rate multi-carrier CDMA with multiuser detection for wireless multimedia communications," *in 2003 IEEE Wireless Communications and Networking, 2003*. WCNC 2003, 2003, vol. 1, pp. 385-390
[8] M. Debbah, P. Loubton, and M. De Courville, "Spread OFDM performance with MMSE equalization," in *IEEE International Conference on Acoustics, Speech, and Signal Processing, 2001. Proceedings. (ICASSP'01)*. 2001, vol. 4. IEEE, 2001, pp. 2385-2388.
[9] H. Schulze and C. Luders, *Theory and applications of OFDM and CDMA: Wideband wireless communications*. John Wiley & Sons, 2005.
[10] J. Proakis and M. Salehi, *Digital Communications*. McGraw-Hill Education, 2007.
[11] H. V. Poor, S. Verdu, "Probability of error in MMSE multiuser detection," *IEEE Transactions on Information Theory*, vol.43, no.3, pp.858-871, May 1997
[12] 3GPP standardization group,"3rd Generation Partnership Project; Technical Specification Group Radio Access Networks; Deployment Aspects," *3GPP Tech. Rep*. 25.943, v.4.2.0, June 2002.

Deep Sea Exploration Recovery and Transport [DESERT] Vehicle and its Modes of Communication

Pavel Sengupta
Department of Mechanical Engineering
Dr. Sudhir Chandra Sur Degree Engineering College, Dum Dum
Kolkata, West Bengal
pavel.warrior.within@gmail.com

Aileen Sengupta
Department of Electronics and Communication Engineering
Techno India College of Technology, Rajarhat
Kolkata, West Bengal
aileensengupta@gmail.com

Abstract: Man has explored less than 5% of three-fourths of the water on Earth [1]. This is mostly due to lack of cheap and effective under-water transportation. Submarines and other deep sea modules have a wide range of problems and have limited our exploration capabilities and reach. After recent disasters requiring a wide range of under water rescue operations, it has become clear that we do not possess the means to efficient and effective under water travel. The Deep Sea Exploration Recovery and Transport (DESERT) Vehicle is an attempt to bridge that gap. Modeled on sharks, the fastest and most aerodynamic creatures in the seas, the underwater vehicle takes cues from nature and uses to its advantage. Deep and long ranged underwater travel and communication, using an engine and propeller system which uses sea water as a fuel [2], are the main points of discussion in this paper.

This study mainly focuses on the theoretical framework and design of DESERT, a undersea vehicle and the difficulties in attempting to do so. The ideas behind its mode of communication under-water have also been put forward and explored. Using new technological advancements, a first-of-its-kind model has been put forward with an inclination towards making it feasible.

Keywords: Aerodynamic, AUV, DESERT, Flapping flight, ROV, Sharks, SWIPE, Under Water Acoustic Communication, UUV

1. Introduction

In the present, underwater travel has expanded beyond submarines to personal submarines, *Unmanned Underwater Vehicles (UUV), Autonomous Underwater Vehicles (AUV), Remotely Operated Vehicles (ROV)* and many more such robotic submersibles [3]. A variety of creative uses of these high-tech vehicles has been found, which works as an alternative to sending humans down into the depths. Hundreds of different AUVs have been designed over the past 50 or so years [4]. Large vehicle have advantages in terms of endurance and sensor payload capacity; smaller vehicles benefit significantly from lower logistics [5]. The future of AUV is evolving and changes in design are expected. These include hover-capable AUVs, ultra-low-power, long-range variants such as underwater gliders [6] or hybrid AUV/ROV design that switch between roles as part of their mission profile.

However, bionic AUVs are best suited for under water travel. These vehicles are able to achieve higher degrees of efficiency in propulsion and maneuverability by copying successful designs in nature. The DESERT is a first venture into combining the best of both bionic AUVs and underwater gliders.

Fig 1: Sharks are the most aerodynamic, fast and longest surviving sea creatures known to man [7]

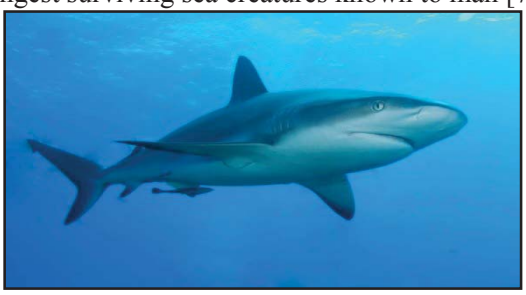

DESERT is an aerodynamic vehicle which is built on the model of sharks and mimic shark

movements. It has fins which work by providing flapping movement thus helping in movement. Propulsion is provided by an underwater engine, which works primarily using sea water as a fuel [2]. It is a green engine as is the technology. Newer technologies have helped in making design changes to existing AUVs and ROVs, thereby making way for DESERT and other future underwater vehicles.

2. Theory

The DESERT is shaped like sharks and uses their streamlined shape. This shape is known as the *Sears – Haack* body. The *Sears–Haack* body is the shape with the lowest theoretical wave drag in supersonic flow, for a given body length and given volume. Sharks have a body shape and skin type to have minimum pressure drag in supersonic flow [8].

Fig 2: The Sears – Haack body shape. The most aerodynamic shape having lowest drag [9]

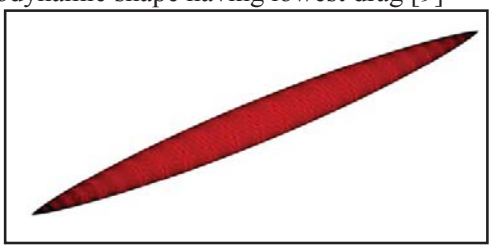

3. Design

DESERT features all the equipments and modern sensors found in any AUVs, UUVs or ROVs. It will host a collection of new systems for underwater communication under both manned and unmanned conditions. The design of DESERT has been divided into a number of individual components. The figure 3 below shows a rough outline of the DESERT. It is powered and propelled by the Sea Water Immersed Propulsion Engine (SWIPE) [2]. The entire underbelly of the vehicle has ballast tanks, like in a submarine, and for the same purpose. The entire outer skeleton is made by carbon fiber reinforced polymer and also uses carbon fiber and Aluminum. In addition, the outermost skin of the vehicle is covered with a graphene lacquer.

Fig 3: Rough outline of the DESERT model based on the similarities of a shark body

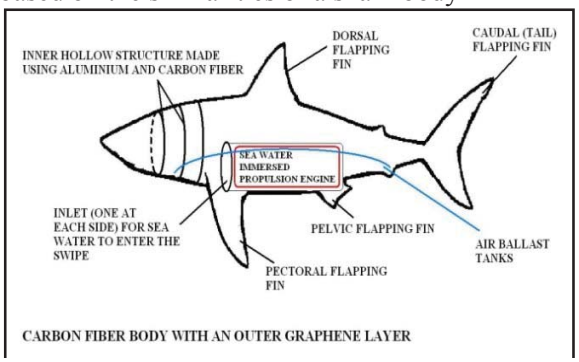

The theoretical design of each component has been elaborated under each section.

3.1 Outermost skin

The outer skin of the DESERT has a graphene layer which can generate electricity when salty sea water flows over it [10]. The electricity generated from the flowing sea water over this Graphene layer is collected by the engine SWIPE or any internal storage unit inside the DESERT. Although the amount of electricity generated is small, it can be harnessed to run any medium or small system within the vehicle.

The graphene coating will be present on the DESERT as a scaly skin coating, which resembles the shark scales and are known as *placoids* (slate-like) as in fig 4. The tiny ridges arranged parallel to the swimming direction - known as *riblets* - decrease drag in water, explaining the amazing speed that some sharks reach with minimal effort [11].

Fig 4: The scaly shark skin known as placoids serve as a means of streamlining movement

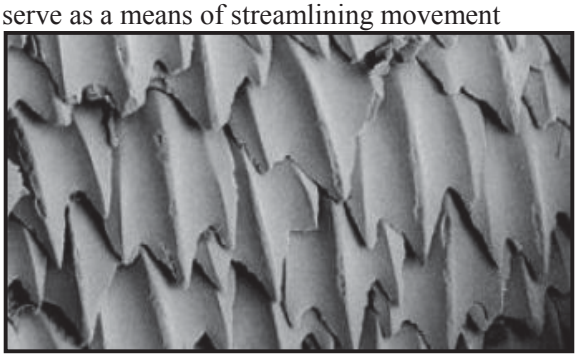

This scaly hide will serve as both a suit of armor and a means of streamlining movement. A new coating system to imitate this riblet effect has been tried and used by researchers and is a new prototype that combines a suitable lacquer and the technology for applying it [11]. The graphene layer applied must be present in that lacquer.

3.2 Exterior and Interior Framework of DESERT

The exterior and interior framework of the vehicle is made of Carbon Fiber Reinforced Polymer (CFRP) and Aluminum. CFRP is strong and light and is used where high strength-to-weight ratio and rigidity are required. Aluminum is lightweight and moldable. Before using these materials, they must be tested for high pressure conditions [12]. So the use of Kevlar or Fiber Glass can also be possible.

CFRP finds an excellent use in the fins of DESERT. It is a flapping wing or fin [14] and is used to impart motion and direction to the vehicle while underwater. Research is ongoing to make the effective and optimum flapping wings. The flapping fins move in all three axes to provide motion. These fins propel and guide DESERT. The outer wings/fins, attached to the body can function as a mechanism to impart a flapping movement to the vehicle.

Fig 5: The skeletal structure of DESERT

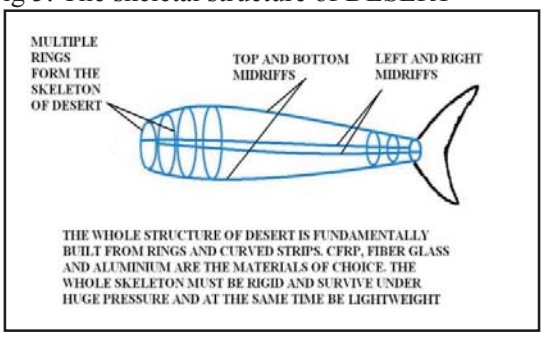

The whole inner skeleton of the DESERT will be constructed of thick rings as shown in fig 5. They will be well connected by a central midriff on the top, bottom, left and right, to provide rigidity to the structure. Multiple midriffs can be made as per design criteria. Inside the vehicle, the wall is CFRP.

The outer diameter of DESERT will be limited to 500-1000 mm. This impacts its towing capacity and speed. The aim will be to reduce the payload and increase speed. The provision of air ballast tanks, occupying a small area of the underbelly of the vehicle is beneficial. One or more air ballast tanks must be present to lift or sink the vehicle when pressurized air is forced into or out of it.

3.3 External Flapping Fins

The five flapping fins comprise of a Dorsal Fin, a Pelvic Fin, two Pectoral Fins on two lower sides and a Tail Fin. Fig 3 outlines the wings/fins. The fins must be carefully designed and behave like that of a shark fin and each fin must function independently. To propel the DESERT, the tail will swing back and forth to move forward. Much like an airplane, this forward movement pushes water around the fins to create lift. This is the same principle used by sharks. The tail fin must be built to create this movement of flapping.

DESERT also has two sets of paired fins on the sides, similar to the pectoral fins of sharks. The shark can position these fins at different angles, changing the path of the water moving around them. When the shark tilts a fin up, the water flows so there is greater pressure below the fin than above it. This creates upward lift. When the shark tilts the fin down, there is greater pressure above the fin than below it. This pushes the shark downward. This is the same method the DESERT must use. The DESERT also has one or two vertical dorsal fins on its back and a vertical anal fin on its underside, just like in a shark. These fins are flapping in nature and work like the vertical stabilizer wing on an airplane. They help the shark keep its balance as it moves through the water. They can be moved from side to side to help turn the vehicle left and right. The fin arrangements give sharks amazing speed and maneuverability. They can cruise or stop suddenly and make sharp turns in every direction. The same must be expected from DESERT.

3.4 Propulsion and Power

The vehicle is driven by an engine and propeller system known as the Sea Water Immersed Propulsion Engine (SWIPE) [2]. The power

produced by the SWIPE is not huge. This is why two of such engines must be carried by the vehicle. Although it makes the vehicle bulky, the benefit of added power is required. In addition, the engine uses sea or salt water as fuel and does not require surfacing at all. It is also a green technology and causes no form of pollution. The DESERT has been built using the benefits of both AUV and underwater gliders. It has got external flapping fins and an engine with propeller system and together it serves to cover all aspects of propulsion and power.

4. Communication and Navigation

Above the sea, the DESERT must be equipped with radio wave transmission system and GPS. Below the sea however, radio and GPS do not work effectively so DESERT can rely on Dead Reckoning (Dead reckoning is the process of calculating the current position by using a previously determined position, in our case by GPS, and advancing that position based upon known or estimated speeds over elapsed time and course.)

Fig 6: The navigator plots their 9am position, indicated by the triangle, and using their course and speed, estimates their own position at 9:30am and 10am [15]

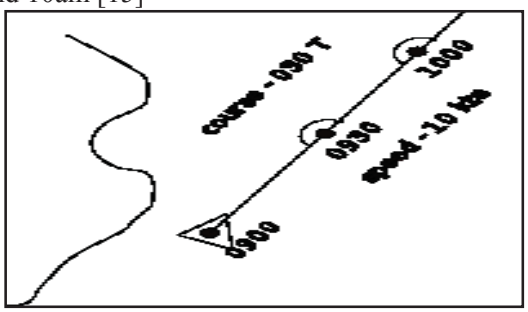

DESERT can also use LBL navigation wherein, when a ship is available over the surface, ultra-short baseline or short-baseline positioning can be used to calculate where the DESERT is, relative to the earlier known position. For fixing the position more accurately, an Inertial Navigation System on DESERT will calculate its position and velocity, and these estimates can be improved by adding acoustic Doppler current profiler - ADCP (this is a hydro-acoustic current meter which measures the velocity of water over a range using the Doppler effect, within that column of water, the device contains piezoelectric oscillators to be used as a trans-receiver but in addition we need to use an ADC and digital signal processing to measure the Doppler's shift and a microprocessor need to be used to determine the sound velocity). The vehicles can intercommunicate with each other through under water acoustic network using hydrophones arranged in array, and FSK modulation can be used for further signal processing. The DESERT can also use vector sensors with a specific signal processing algorithm, for better perception of sound.

Under water acoustics network is a process of transmitting and receiving messages under the water [16]. Among several ways the DESERT can use hydrophones as it has acoustic impedance match with water and the hydrophones can be set up in three dimensional arrays wherein spatial filtering can be used to achieve spatial selectivity (in this arrangement the hydrophones are arranged in such an angle that some of the signal interfere constructively and some destructively and this arrangement can be implemented at the transmitter and receiver to obtain directional signal transmission).

FSK (Frequency shift key) is a form of modulation where digital information is transmitted through the change of frequency and DESERT can use the simplest form of FSK, the binary FSK, wherein we have two frequency sets, each representing 0's and 1's and at the receiving end there can be filter and a level detector to detect whether a 0 or 1 has been sent. Another emerging method is through vector sensors.

Fig 7: The vector sensor indicating the pressure sensors and the flow sensors [17]

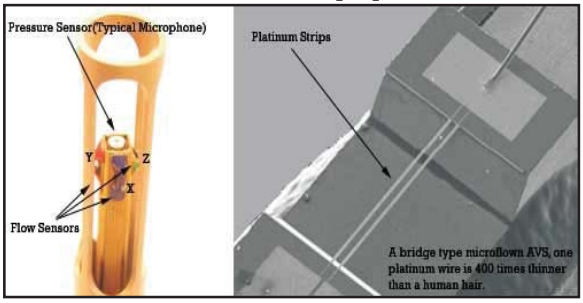

A vector sensor, if employed in DESERT, would help to measure the wave velocity which cannot be done by the pressure sensor. These types of sensors can measure both the scalar and the vector components of the field at a single point in the water. DESERT could use the inertial vector sensors which measures the velocity by acoustic medium motion.

4. Conclusion

Like AUVs, the DESERT must show capability to collect data for scientific and military purposes. To reduce the overall time and cost of acquiring data over large areas, multiple vehicles must be used. Through recent research, AUVs were capable of communication and cooperation without the intervention of an above-water operator. The DESERT having the same features must be able to do so too. The vehicles must perform cooperative operations autonomously i.e. without intervention by an external operator.

Flying in formation, deployment, replacement of missing vehicles, divert of a single vehicle from a formation to a position of interest, and replacement of the formation leader can all be done by DESERT, co-operating with other vehicles. In such missions, inter-vehicle communication is an important requirement upon which co-ordination strategy and intelligence decision making functions can be built, similar to AUVs.

5. References

[1]http://oceanservice.noaa.gov/facts/exploration.html

[2]Sea Water Immersed Propulsion Engine. By P. Sengupta and A. Sengupta, ICMPE 2015 Pune. 28th IRF ISBN: 978-93-85465-29-1 (7th June, 15)

[3]http://www.mbari.org/topics/technology/tech-vehicles.htm

[4]http://auvac.org/resources/infographic/timeline/

[5]https://en.wikipedia.org/wiki/Autonomous_underwater_vehicle

[6]https://en.wikipedia.org/wiki/Underwater_glider

[7]Image (Caribbean reef shark) courtesy - https://en.wikipedia.org/wiki/Portal:Sharks/Selected_articles

[8] Bodies having Minimum Pressure Drag in Supersonic Flow - Investigating Nonlinear Effects. By Karthik Palaniappan and Antony Jameson, Department of Aeronautics and Astronautics, Stanford University, Stanford, CA

[9]Image courtesy - https://en.wikipedia.org/wiki/Sears%E2%80%93Haack_body#/media/File:Sears-Haack.png

[10]http://phys.org/news/2014-04-team-electricity-saltwater-graphene.html

[11]http://news.softpedia.com/news/The-Shark-Coating-42520.shtml

[12] Investigation of Burst Pressure on Carbon / Glass Fiber Reinforced Polymer Metal Tube for High Pressure Applications. By B.G. Sumanaa, H.N. Vidya Sagara, M. Krishnab, G.R. Rajkumarb

[13]Image courtesy - www.naro.ethz.ch

[14] Research on Birds Flapping-Wing Bionic Mechanism. By Bingbing Liang, Jiankun Cui, Liyang Zhang. http://www.ccsenet.org/journal/index.php/mer/article/view/13944

[15]Image courtesy: https://en.wikipedia.org/wiki/Dead_reckoning

[16] Under Water Acoustics: https://en.wikipedia.org/wiki/Underwater_acoustic_communication

[17] Image Courtesy: http://ese.wustl.edu/ContentFiles/Research/UndergraduateResearch/CompletedProjects/WebPages/sp09/JoshuaYork/avs.html

THE 5TH INTERNATIONAL CONFERENCE ON WIRELESS COMMUNICATIONS, VEHICULAR TECHNOLOGY, INFORMATION THEORY, AEROSPACE & ELECTRONIC SYSTEMS (WVITAE-2015)
December 13-16, 2015, Hyderabad, India

Secret Transmission through Audio Signal with Reduced Distortion for Wireless Communication (STASRD)

Dipankar Pal
Dept. of Computer Science and Engineering
Techno India
Kolkata, India
mail2dpal@yahoo.com

Nabin Ghoshal
Dept. of Engineering and Technological Studies
University of Kalyani
Kalyani, West Bengal, India
nabin_ghoshal@yahoo.co.in

***Abstract*—The work proposed in this paper deals with secret wireless transmission of sensitive data or message using a digital audio signal as carrier with reduced distortion in the modulated audio signal for enhanced imperceptibility of the added noise. This algorithm decomposes the carrier audio samples into small non-overlapping frames and uses Discrete Fourier Transform (DFT) to convert them into frequency domain. Payload data bits are inserted in transformed frequency coefficients at pseudo-random bit positions, generated by an unique generator function, to protect the secret data from any potential hacking attempt as the bits can only be retrieved accurately by reproducing the exact sequence of bit positions at extraction time with the help of the same pseudo-random number generator. Also a 160 bit message digest of the hidden message is inserted into the carrier to verify the integrity of the extracted message at the receiving end. The proposed algorithm has been experimented with various types of carrier audio signal and message data. Test results, compared with the previous version of this algorithm, show significant performance improvement in terms of both subjective and objective metrics.**

Keywords—Data security; Audio Steganography; Wireless Transmission; DFT; HAS; MSE; SNR; PSNR; MOS

I. INTRODUCTION

In the last decade we have noticed a major boost in the segment of wireless communication technologies which has become a widely accepted platform for transmission of digital data of all types across the globe. But, at the same time secured transmission of sensitive data has also become a prime concern for every organization. Secured data transmission involves consideration of three influencing factors of data security. These are, 1) confidentiality, which ensures the secrecy of data that must not be revealed to anybody except the intended parties, 2) integrity, which guarantees that the data is not modified during transmission or storage and 3) authenticity, which assures that the received data has been sent by a legitimate sender.

Till date secured data transmission is mainly achieved through cryptographic techniques, which are based on presenting the content of a message garbled to unauthorized people. But these techniques are unable to avoid the suspicion of any third party about the existence of the sensitive data or message being transmitted. So, to explore better or complementary new techniques, researchers has focused on techniques based on steganography, which hide sensitive data in another innocent looking cover medium, e.g. digital audio signal, in an attempt to completely avoid any suspicion about the existence of the hidden data along with the information of its sender and receiver as well. As a result, digital audio steganography has emerged as a prominent source of data hiding across novel telecommunication technologies such as covered voice-over-IP, audio conferencing, etc.

Hiding data in audio signals is more challenging compared to the techniques involving images or video sequences. This is due to the wider dynamic range of human auditory system (HAS) in comparison to human visual system (HVS) [1]. Audio-based steganography exploits the property of masking effect of HAS [2]. HAS perceives sounds over a range of power greater than 109:1 and a range of frequencies greater than 103:1. The sensitivity of HAS to the additive white Gaussian noise (AWGN) is high as well. White Gaussian Noise in a sound file can be detected as low as 70 dB below ambient level [3].

The quality of audio steganographic methods are influenced by various factors [4]. The importance and the impact of each factor depend on the application area and the transmission environment. The most influencing factors are, imperceptibility, robustness to noise, compression, security and hiding capacity. Generally, robustness and hiding capacity hardly coexist in the same steganographic system. This is due to the tradeoffs imbalance between these two criteria i.e. increase in robustness results in decrease in data hiding capacity [2].

Primarily data hiding in audio signals can be performed in three ways, a) using time domain techniques [5, 6], b) using frequency-transform domain techniques [7, 8] and c) using a combination of both [9]. Performance of these techniques varies with respect to the robustness and imperceptibility (inaudibility) of the added noise. Time-domain techniques include the Least Significant Bit (LSB) substitution, echo

hiding techniques and many others. Frequency domain techniques employ human perceptual properties and frequency masking characteristics of the human auditory system. The phase and magnitude of the transform domain coefficients are modified to embed the secret message. This procedure [15, 16] offers high level of robustness i.e. attempt to remove the watermark results in introduction of serious distortion in the original audio signal fidelity. To get back the payload, inverse frequency transform is applied. Popular transforms include Discrete Fourier Transform (DFT) [10, 11, 12], Discrete Cosine Transform (DCT) [13] and Discrete Wavelet Transform (DWT) [14].

II. THE TECHNIQUE

The proposed algorithm uses one dimensional Discrete Fourier transform and is a combination of two main procedures: insertion of the payload and extraction of the payload. In the context of this algorithm payload consists of three types of data, which are, 1) size of the actual message in bytes (length: 32 bit), 2) SHA-1 message digest of the message data (length: 160 bit) and 3) message data itself.

The algorithm is capable of hiding any form of message, be it a text, image, audio or any other file type into the uncompressed cover audio signal and produces the corresponding stego audio, which has the same size as that of the original audio.

In the insertion process the payload is treated as a sequence of bits $b_1, b_2, ..., b_N$, where N is the total length of the bit sequence, $b_k \epsilon (0,1)$ and $k = 1$ to N. The original cover audio signal is decomposed into non-overlapping equal sized frames each consisting of two audio samples. Due to non-stationary behaviour of audio signals it is necessary to analyse them in short time intervals (frames) in order to apply signal-processing rules [17, 18]. To convert each of these frames into transform domain one dimensional discrete Fourier transform is applied, resulting in two corresponding DFT coefficients. Out of them only the second coefficient value is considered for embedding as embedding in the first coefficient value results in perceptible noise in the final stego audio.

A payload data bit is inserted into the binary converted value of the integer part of the real component of the frequency coefficients. The insertion position is generated pseudo-randomly in the range of 0 and 3 i.e. the 1st LSB layer to 4th LSB layer. After replacing the target bit t_p in the target binary sequence T at position p by a payload bit b_k some or all of the bits on the left and/or right (depending on the magnitude of T) of the target position p in T are flipped to minimise the difference in the magnitude of the resulting binary sequence T'. Thus the value of T' remains closest to the original value of T. For example, if $T = 00001000_2 = 8_{10}$, and if we embed 0 into 4th LSB layer, result will be $T' = 00000000_2 = 0_{10}$, making the difference huge, which is $T - T' = 8$. To minimise the difference between T and T' we use our proposed method and then the modified value of T' becomes $00000111_2 = 7_{10}$, which is closer to the original value T, with a difference of only 1. To get back the corresponding time domain values when inverse DFT is applied on the modified frequency component frames consisting of resultant binary sequence T' this technique greatly reduces the distortion (due to the added noise component in the form of payload) in the final stego audio.

The extraction process is pretty straight-forward, which involves DFT transformation of the stego audio samples to frequency domain. Payload bits are then extracted from the integer part of the real frequency components by reproducing the same pseudo-random number sequence used in the insertion process. The extracted sequence of bits are reconstructed sequentially to get the three components of the payload i.e. message size, message digest and message data. The extracted message digest is then compared with the message digest generated from the extracted message at receiving end to ensure the integrity and authenticity of the received message. The extraction process is completely blind as it does not require the original cover audio for the purpose of extraction. The overall process of the proposed technique is graphically illustrated in Fig. 1 below.

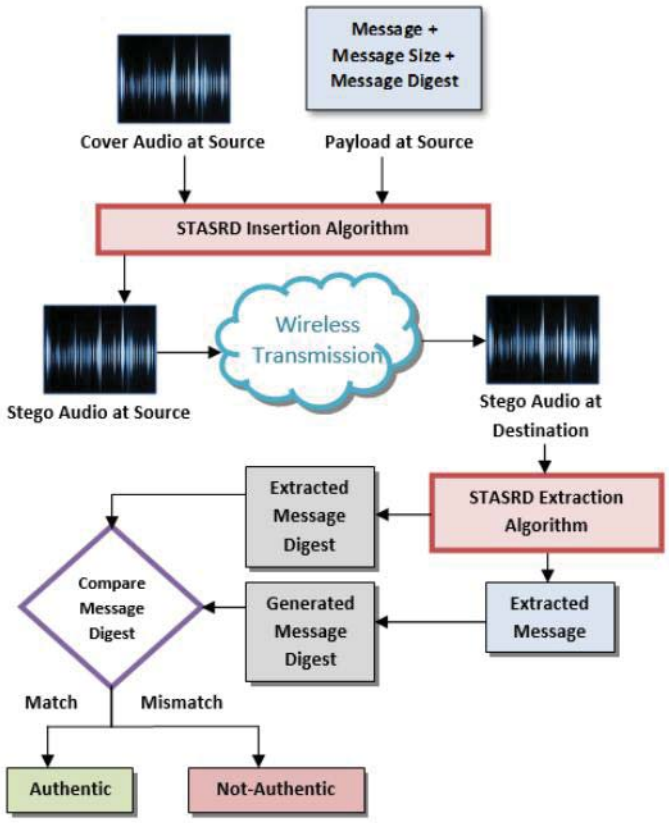

Fig. 1. Insertion and Extraction Process of STASRD

A. Insertion Algorithm

Input: A PCM WAVE cover audio and a message file of any type.

Output: A stego PCM WAVE audio.

Steps:

1. Copy the header information from the input cover audio into the output audio.

2. Generate a 160-bit message digest (SHA-1) of the message file.
3. Repeat the following steps until all the bits of the payload are embedded,
   3.1. Read a pair of sample amplitude values from the input audio into a two element frame.
   3.2. Apply 1-D Discrete Fourier Transformation on the frame to get the corresponding frequency coefficients.
   3.3. Generate a number (between 0 and 3) using a pseudo-random function to determine the insertion position of the payload bit.
   3.4. Replace the original bit, at the position obtained in the previous step, of the binary counterpart of real integer part of the 2nd frequency coefficient with the payload bit.
   3.5. Flip the bits on the left and/or right of the replaced bit to make the magnitude of the modified frequency component closest to the original value, which reduces distortion in the final stego component.
   3.6. Apply Inverse Discrete Fourier Transformation on the modified frame to get the corresponding amplitude values in time domain.
   3.7. Write the new sample values into the output audio in the same sequence as they have been read.
4. Copy rest of the samples from the input audio (if any) into the output audio.
5. Stop.

B. Extraction Algorithm

Input: A stego PCM WAVE audio.

Output: The extracted payload.

Steps:

1. Repeat steps 1.1 to 1.5 until all the bits of the payload are extracted,
   1.1. Read a pair of sample amplitude values from the input audio into a two element frame.
   1.2. Apply 1-D Discrete Fourier Transformation on the frame to get the corresponding frequency coefficients.
   1.3. Generate a number (between 0 and 3) using the same pseudo-random function to determine the insertion position of the payload bit.
   1.4. Extract a payload bit from the real integer part of the 2nd frequency coefficient using the bit position obtained in the previous step.
   1.5. Construct a byte of the payload data by eight consecutive extracted bits to form the payload data incrementally.
2. Generate a 160-bit message digest (SHA-1) of the extracted message.
3. Compare the generated message digest with the one extracted as part of the payload to verify the integrity and determine the authenticity of the extracted message.
4. Stop.

III. Experimental Results and Discussion

Thorough experimentation has been done using the proposed algorithm taking various types of cover audio as well as message to test the performance in different scenarios. After performing the insertion algorithm on each set of cover audio and message file type the quality of the resulting stego audio is examined using various objective and subjective metrics [19, 20], which are briefly discussed below.

A. Objective Metrics

1) Mean Squared Error (MSE): Computes an error signal by subtracting the test signal from the reference, and then computing the average energy of the error signal.

2) Signal to Noise Ratio (SNR): It is a measure that compares the level of a desired signal to the level of background noise. It is defined as the ratio of signal power to the noise power and a ratio higher than 1:1 indicates more signal than noise.

3) Peak Signal to Noise Ratio (PSNR): Defined as the ratio between the maximum possible power of a signal and the power of corrupting noise that affects the fidelity of its representation.

B. Subjective Metric

Objective metrics are considered as the most common procedure for the measurement of noise difference between the original and stego audio signals, but one drawback is that they do not prove authentic during consideration of some specific characteristics of HAS. So a different metric named Mean Opinion Score (MOS) is used as the subjective measure of the quality of audio signals. To determine MOS, a number of listeners listen to both the original and stego audio signals and rate them according to the grades shown in table 1.

TABLE I. MOS Grading Scale

MOS Grade	1	2	3	4	5
Remarks	Very Annoying	Annoying	Slightly Annoying	Perceptible, Not Annoying	Imperceptible

The final MOS is the arithmetic mean of all the individual scores, and may range from 1 (worst) to 5 (best).

C. Results

A variety of CD quality stereo audio signals with 16 bits/sample resolution have been used in the test phase. Three types of message, text, image and audio were separately inserted in each of the four types of cover audio signals i.e. instrumental, pop, rock and speech. Some example audio

signals and messages involved in the experimentation are visualised in Fig. 2.

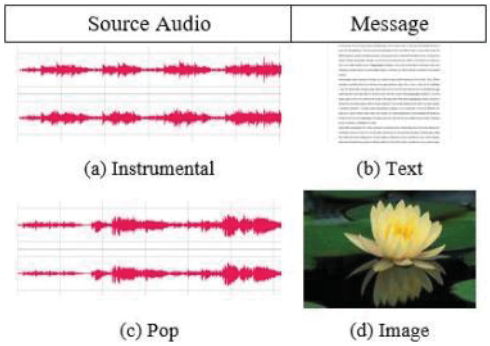

Fig. 2. Source Audio Signals and Messages used in STASRD

The results obtained in various objective tests as well as the subjective test are discussed in the following sub-sections.

1) Objective Tests – Table 2 shows the maximum hiding capacity of each type of cover audio and actual number of bytes embedded for each type of message along with test results of STASRD in terms of MSE, SNR and PSNR.

TABLE II. RESULTS OBTAINED USING STASRD

Cover Audio	Capacity (Bytes)	Message Type - Size	MSE	SNR (dB)	PSNR (dB)
Instrumental	166472	Text - 159464 Bytes	0.4996	73.4605	93.3221
Pop	170492		0.4719	74.0745	93.5699
Rock	165455		0.5005	78.7894	93.3142
Speech	160117		0.4770	73.8736	93.5236
Instrumental	166472	Image - 158856 Bytes	0.5085	73.3844	93.2460
Pop	170492		0.4786	74.0136	93.5090
Rock	165455		0.5019	78.7776	93.3024
Speech	160117		0.4741	73.8996	93.5497
Instrumental	166472	Audio - 152686 Bytes	0.4663	73.7606	93.6221
Pop	170492		0.4560	74.2230	93.7184
Rock	165455		0.4660	79.0998	93.6246
Speech	160117		0.4579	74.0506	93.7006
Average		**157002 Bytes**	**0.4799**	**75.1173**	**93.5002**

It can be observed from the above results that despite of embedding a substantial amount of message data (1,57,002 bytes in average) the proposed algorithm shows an impressive performance with an average SNR value of 75.1173 dB and PSNR value of 93.5002 dB.

Moreover, the comparison presented in the following table exhibits the superiority of STASRD in terms of imperceptibility over the previous algorithm Secured Data Transmission Through Audio Signal (SDTAS) [21], which has no mechanism to reduce the distortion level in resulting stego audio signals. Thus, STASRD is quite appropriate in wireless transmission of secret data with reduced distortion level.

TABLE III. COMPARISON OF RESULTS OBTAINED USING SDTAS AND STASRD

Parameters (Average)	SDTAS	STASRD
Embedded Bytes	157002	157002
MSE	2.5442	0.4799
SNR (dB)	67.8725	75.1173
PSNR (dB)	86.2554	93.5002

2) Subjective Test – Twenty five pairs of source and stego audio, produced by the proposed algorithm, were put to tests and more than 35 listeners were involved to test the resulting audio signal pairs (Original and Stego). The listeners were requested to listen to the pairs very attentively. The final grades for the respective pairs are shown in table 3 and reveal high imperceptibility of the inserted noise (message) in the cover audio signals.

TABLE IV. SUBJECTIVE MEASURE OF AUDIO SIGNALS USING STASRD

Cover Audio	Message Type	MOS Grade
Instrumental	Text	5
Pop		5
Rock		5
Speech		5
Instrumental	Image	5
Pop		5
Rock		5
Speech		5
Instrumental	Audio	5
Pop		5
Rock		5
Speech		5

The values in the above table exhibit the subjective quality of the stego audio signals where there is no perceptible distortion in the resulting cover audio after embedding the payload data. This result is achieved due to the treatment done on the modified frequency components at the time of insertion of payload bits to keep the impact of the inserted noise negligible. And this is also evident from the above comparison in table 3.

IV. CONCLUSION

The proposed algorithm STASRD greatly enhances the imperceptibility of the transmitting secret data of any form, text, image or audio using an audio signal as cover. It adds a bit adjustment mechanism to reduce the distortion level of the resultant stego audio signal at the time of inserting the payload. The extraction process is also very straight-forward and blind. Performance of the algorithm has been evaluated by both objective and subjective metrics and the results show significant improvement in comparison with the previously proposed technique by the authors. Thus, this novel algorithm proves to be quite appropriate for secret transmission of data over the wireless domain.

ACKNOWLEDGMENT

The authors express their deep sense of gratitude to the faculty members of the Dept. of Engineering and Technological Studies, University of Kalyani, West Bengal, India, where the work has been carried out.

REFERENCES

[1] W Bender, D Gruhl, N Morimoto, A Lu, "Techniques for data hiding", IBM Syst. J 35(3 and 4), 313–336 (1996).

[2] E Zwicker, H Fastl, "Psychoacoustics", Springer Verlag, Berlin, 1990.

[3] Nedeljko Cvejic, "Algorithms for audio watermarking and steganography", Oulu 2004, ISBN: 9514273842.

[4] Fatiha Djebbar, Beghdad Ayad, Karim Abed Meraim and Habib Hamam, "Comparative study of digital audio steganography techniques", EURASIP Journal on Audio, Speech and Music Processing 2012, 2012:25.

[5] Nedeljko Cvejic, Tapio Seppnen, "Increasing the capacity of LSB-based audio steganography", FIN-90014, University of Oulu, Finland ,(2002).

[6] Dipankar Pal, Anirban Goswami, Nabin Ghoshal, "Lossless audio steganography in spatial domain", Int. Conf.on Frontiers of Intelligent Computing:Theory and Applications, AISC 199, pp. 575-582. DOI: 10.1007/978-3-642-35314-7 65, Springer, 2012.

[7] Acevedo A., "Digital watermarking for audio data in techniques and applications of digital watermarking and content protection", Artech House, USA, 2003.

[8] Arnold M., "Audio watermarking: features, applications and algorithms," in proceedings of the ieee international conference on multimedia and expo, pp. 1013-1016, 2000.

[9] Foo S.W., Ho S.M., Ng L.M., "Audio watermarking using time-frequency compression expansion", IEEE Inter-national Symposium on Circuits and Systems, 201-204, 2004.

[10] Ghoshal N., Mandal J. K., "Discrete Fourier Transform based multimedia color image authentication for wireless communication (DFTMCIAWC)", 2nd International Conference on Wireless Communications, Vehiculare on EmeTechnology, Information Theory and Aerospace & Electronic Systems Technology, Wireless Vitae 2011, ISBN: 978-1-4577-0787-2/11, Le Royal Meridian Chennai, India, 28th Feb.- 3rd March, 2011.

[11] Ghoshal N., Mandal J. K., "Controlled data hiding technique for color image authentication in frequency domain (CDHTCIAFD)", 2nd International Conference on Emerging Applications of Information Technology, EAIT-2011, ISBN: 978-1-4244-9683-9, CSI Kolkata Chapter at Science City, Kolkata, India, February 19-20th, pp. 284-287, 2011.

[12] Senbin Yang, Wei Tan, Yanpu Chen, Wenjun Ma, "Quantization-Based digital audio watermarking in discrete Fourier transform domain", Journal Of Multimedia, Vol. 5, No. 2, April 2010.

[13] Pranab Kumar Dhar, Mohammad Ibrahim Khan and Saif Ahmad, "New DCT based watermarking method for copyright protection of digital audio", International journal of computer science & information Technology (IJCSIT), Vol.2, No.5, October 2010, pp. 91 -101.

[14] Ali Al-Haj, Ahmad Mohammad, Lama Bata, "DWT–Based audio watermarking", The International Arab Journal of Information Technology, Vol. 8, No. 3, pp. 326 – 333, July 2011.

[15] Zhang Y, Lu ZM, Zhao DN (2010b). "Quantization based semi-fragile watermarking scheme for H.264 video". Inf. Technol. J., 9(7): 1476-1482, 2010.

[16] Cox I. J., Kilian J, Leighton FT, Shamoon T, "Secure spread spectrum watermarking for multimedia", IEEE Trans. Image Process., 6(12): 1673 -1687, 1997, 1997.

[17] Ghoshal N., Mandal J. K., Sarkar A., Chakraborty D., Ghosh S., "Image authentication by hiding large volume of data and secure message transmission technique using mask (IAHLVDSMTTM)", Proceedings of IEEE International Advanced Computing Conference IACC'09, ISBN: 978-1-4244-2928-8, Thapar University, Patiala, India, pp. 3177-3182, March 6-7th, 2009.

[18] Ghoshal N., Mandal J. K., Khamrui A., "A framework for block based image authentication (FBIA)", Proceedings of 4th IEEE International Conference on Industrial and Information Systems, ICIIS09, ISBN: 978-1-4244-4837-1, Peradeniya University, Sri Lanka, pp. 343-348, December 28th -31st, 2009.

[19] Nedeljko Cvejic, Tapio Seppnen, "Digital audio watermarking techniques and technologies: applications and benchmarks", InformatIon Science Reference, Hershey, New York, ISBN 978-1-59904-515-3 (ebook), 2008, pages - 79, 239.

[20] Dermot Campbell, Edward Jones, Martin Glavin, "Audio quality assessment techniques - A review and recent developments", Journal of Signal Processing, Elsevier, 0165-1684/2009 Elsevier B.V. doi:10.1016/j.sigpro.2009.02.015.

[21] Dipankar Pal and Nabin Ghoshal, "Secured Data Transmission Through Audio Signal (SDTAS)", 9th International Conference on Industrial and Information Systems (ICIIS2014), ABV-Indian Institute of Information Technology and Management, ISBN: 978-1-4799-6498-7, Gwalior, India. 15th – 17th December, 2014.

THE 5TH INTERNATIONAL CONFERENCE ON WIRELESS COMMUNICATIONS, VEHICULAR TECHNOLOGY, INFORMATION THEORY, AEROSPACE & ELECTRONIC SYSTEMS (WVITAE-2015)
December 13-16, 2015, Hyderabad, India

Speech Feature Analysis and Selection for Emotion Classification

Angel Manolov, Ognian Boumbarov, Agata Manolova, Vladimir Poulkov, Krasimir Tonchev
Faculty of Telecommunications
Technical University of Sofia
Sofia, Bulgaria
angel.manoloff@gmail.com, {olb, amanolova, vkp, k_tonchev}@tu-sofia.bg

The increasing role of spoken language interfaces in human-computer interaction applications has created conditions to facilitate a new area of research - namely recognizing the emotional state of the speaker through speech signals. This paper proposes a text independent method for emotion classification of speech signals used for the recognition of the emotional state of the speaker. Different feature selection criteria are explored and analysed, namely Mutual Information Maximization (MIM) feature scoring criterion and its derivatives, to measure how potentially useful a feature or feature subset may be when used in a classifier. The proposed method employs different groups of low-level features, such as energy, zero-crossing rate, frequency bands in Mel scale, fundamental frequency or pitch, the delta- and delta-delta regression and statistical functions such as regression coefficients, extremums, moments etc., to represent the speech signals and a Neural Network classifier for the classification task. For the experiments the EMO-DB dataset is used with seven primary emotions including neutral. Results show that the proposed system yields an average accuracy of over 85% for recognizing 7 emotions with 5 of the best performing feature selection algorithms.

***Index Terms*—speech emotion recognition, feature selection, affective space, human-computer interaction, neural network classifier**

I. Introduction

SPEECH is the fastest and most natural method of communication between people. For this reason, researchers define it as being an efficient way to interact with machines. For this to be fulfilled, however, computers must possess sufficient knowledge and intelligence to separate the content from the human voice and speech. Speech recognition or the process of converting human speech into a series of words is the basic discipline in this area, where the success achieved so far is greatest. Information about emotional state is expressed via speech through numerous cues, ranging from low level acoustic ones to high level linguistic content. Several approaches to speech based automatic emotion recognition, each taking advantage of few of these cues have been explored [1]–[4]. It is believed that this would help to extract additional semantic aspects of speech that would improve work systems and speech recognition.

The main goal of this paper is to present the results of an extensive study and comparative analysis of different methods for voice feature selection criteria and to measure how potentially useful a feature or feature subsets may be when used in a classifier for emotion classification.

The rest of the paper is organized as follows: the next section describes the state of the art for the problem of recognizing the emotional state of the speaker through speech signals. Section III introduces the EMO-DB dataset used for research purposes in this paper. Then in Section IV a description of the proposed algorithm is given. In the following section the experimental results are illustrated. The final section draws the conclusion and suggests the scope of future work.

II. State of the art

A. Models of affective space

The selection of induced emotions is a crucial design feature of any human-computer interactive system dealing with voice recognition, and should be guided by a clearly specified theoretical model of the affective space. These models generally fall into one of three categories: categorical, dimensional and appraisal-based.

Categorical models focus on universal set of primary emotions (e.g. *fear, anger* or *disgust, happiness, sadness, surprise*), which are typically seen in terms of their evolutionary adaptive value [5]. These models are more easily understood and better suited for research purposes because they can be combined with facial expression for multi-modal recognition.

The more natural model is the dimensional [6] because a single label might not describe the complexity of an affective state very well. So to represent emotional signals in a more natural way a continuous rather than a categorical view of emotions is used. This way the emotion is modeled as a point in a multidimensional space describing emotionally relevant dimensions like arousal or activation, pleasantness or valence and dominance.

The appraisal-based model is based on the emotion being quantified with different evaluation checks, such as the novelty, intrinsic pleasantness, goal-based significance, coping potential and compatibility with standards [6].

Each model, categorical, dimensional or appraisal has its advantages and disadvantages [7]. In the categorical approach, mixed emotions cannot adequately be described with one label. In the dimensional approach, the reduction of emotion space to two or three dimensions may be not suitable for classification purposes because of the loss of information. The appraisal-based approach requires complex, multi-componential and sophisticated measurements with a panel of experts.

Even though neither model is not claimed to be sufficient for differentiating all possible emotions, we have chosen to

use in our research the categorical model and we try to classify emotions in the 7 basic categories mentioned above. In our context, the object of analysis will be a short phrase, digitally encoded and stored in an appropriate audio format. The phrases are segmented and separated into separate files according to certain criteria ergo specific emotional class.

B. Feature description

An important problem in systems for recognizing emotion in speech is the selection of features that effectively provide differences between affective classes, but also this process must not dependent on the speaker or lexical content of the speech. Although many have studied such features in the scientific community there is no agreement on which are the best ones.

Audio signals carrying speech are not fixed, often during processing speech there is a need to divide the signal into small segments called frames. The aim is to explore small enough areas where the signal is assumed to be stationary. Prosodial speech features such as the fundamental frequency or pitch (F_0) and energy of the signal are extracted from each frame and are called local features. On the other hand, the use of statistical analysis for the whole phrase gives the global features of the signal. There are disputes about which of the two types is more effective in these systems. Most scientists agree that global features outperform local in terms of training time of the classifier and the total accuracy of classification [8]. One of the reasons for that is global features being much fewer in number than the local. However, the researchers argue that global features are only effective in separating the classes with high activation [9] such as *anger, fear, joy* and classes with low activation as *sadness*. It is argued that global features do not do well between classes with a similar level of activation, for example anger against joy. Another problem with global features is that the timing information contained in the speech signal is completely lost in this presentation. An alternative solution in the same direction is to obtain feature vectors for sections with voice activity. Using only these selected parts of the signal the features of speech can be grouped into four main categories: continuous, voice quality-based, spectral and features based on Teager Energy Operator (TEO-based). Continuous features are used very frequently in recognition of emotion. According to [10] these features can be further classified into the following sub-categories: 1) pitch-related features; 2) formant frequencies; 3) timing features; 4) voice-quality parameters; 5) articulation parameters.

The voice quality is a special feature, because the human perception is subjective and its affected by many variables. According extensive study done in [11], acoustic correlates associated with voice quality, are grouped into the following categories: 1) voice level: signal amplitude, energy and duration; 2) voice pitch; 3) phrase, word, phoneme, and feature boundaries; 4) temporal structure which refers to measures at the pitch contour level and related structures in the intensity domain.

Besides the acoustic features in the time domain such as fundamental frequency and energy of the signal there are also discriminative features that can be selected in the frequency domain such as the spectral distribution, the speaking rate and the fundamental frequency contour. It has been found that the emotional impact of a phrase has an impact on the distribution of energy in the frequency spectrum of a signal [9]. Examples are: happiness sections have high energy values for the range, treble, while those with sadness have low levels of the same range [12]. Spectral features can be extracted in several different ways such as through Fourier transform, but also through the following methods: Linear Predictive Coding (LPC), one-sided autocorrelation LPC (OSALPC) [13], Short- time coherence method (SCM) or least-squares modified Yule- Walker equations (LSMYWE) [14]. There are also the cepstral-based features derived from appropriate transformations of linear features such as cepstral-based OSALPC (OSALPCC) and cepstral-based LPC and mel-frequency scale coefficients (MFCC) [13].

The current most commonly used short-term spectral features are the LPC-derived cepstral coefficients and their regression coefficients. As for the regression coefficients, typically the first- and second-order coefficients, that is, derivatives of the time functions of cepstral coefficients are extracted at every frame period to represent spectral dynamics (the delta- and delta-delta-cepstral coefficients). In [13] is noted that the addition of delta-cepstral features strongly improves speech recognition accuracy, and a further but smaller improvement is provided by the addition of double- delta cepstral features. For these reasons some form of delta and double-delta cepstral features are part of nearly all speech recognition systems.

C. Feature extraction

In [15] the authors have proved that the right choice of features for recognizing emotion in speech strongly depends on the nature of the specific classification task, which is considered. For example if we consider the classification of affective states with high levels of activation against such with low level, generally continuous features based on the voice tone or pitch are used for description. It is believed that more complex tasks require an approach build on a combination of different types of features. Also, there are certain interrelationships between the aforementioned types of features, for example spectral features are related to voice quality and the spectral envelope show patterns of evolution of speech articulation.

During feature selection the primary objective is to determine a subset of all extracted features that can provide the best classification results. An appropriate subset is typically evaluated using a feature selection criterion such as cross-validation error and mutual information between annotation class and the specific descriptor [16]. On the other hand, feature transformation, is finding a suitable uniquely linear or non-linear transformation of the original feature vector space into another abstract space with a small number of dimensions. This must be achieved so that useful information is preserved. Feature extraction algorithms are one of the main components of the emotion detection system.

The methods for feature selection can be associated into two broad groups in terms of their dependence on the classifier:

classifier-dependent - ”wrapper” and ”embedded” methods, and classifier-independent called filter methods. For the purpose of this work the latter approach will be used. The filter methods [16] separate the classification and feature selection components, and define a heuristic scoring criterion to act as a proxy measure of the classification accuracy. Intuitively, such a criterion may be selected on the basis of the determination of the correlation between the attribute and the label of the class on the assumption that a better correlation would be associated with a better recognition. In our case we use but not limit ourselves with the Mutual Information Maximization (MIM) feature scoring criterion to measure how potentially useful a feature or feature subset may be when used in a classifier. An extended description of this criterion is given in [16] along with different derivatives of the algorithm. The different criteria, compared in this research, are mentioned in Table I, section IV.

III. Database

In the design of an emotion recognition system, one important factor upon which the performance of emotion recognition system depends is the emotional database used to build its representation of human emotions.

Emotional behavior databases have been recorded for investigation of emotion, where some are natural while others are acted or elicited. For the analysis of vocal expressions of emotions, audio databases such as Belfast naturalistic database, Berlin Database of Emotional Speech (EMO-DB) [17], and Montreal Affective Voices have been researched [15].

The EMO-DB chosen for the current research purposes is a German acted database, which consists of recordings from 10 actors (5 male, 5 female). The data consist of 10 German sentences recorded in *anger, boredom, disgust, fear, happiness, sadness* and *neutral*. The final database consists of 535 utterances after listeners' judgement. The phrases have a length of 1-2 seconds and they are approximately equally divided between the key emotional classes, gender of the actor, text the phrase and etc. This dataset was chosen because of the nature of the annotation done on the entire phrase, i.e. the phrase is the smallest discrete unit of meaningful research. This allows the use of global features for the whole phrase.

IV. Description of the algorithm

The block diagram on Fig.1 represents the idea of the general algorithm for solving the classification problem using the selected dataset. Illustrated are all key phases in the processing of the signal information. In each of the major phases are presented various processes grouped by the software used for this research.

All the software applications used for the development of the proposed algorithm are open source platforms. The experimental environment chosen for this research is GNU Octave version 3.8.1. openSMILE (an abbreviation of The Munich open Speech and Music Interpretation by Large Space Extraction - http://www.audeering.com/research/opensmile) is a modular tool for extracting features for applications in digital signal processing and machine learning. The focus is on

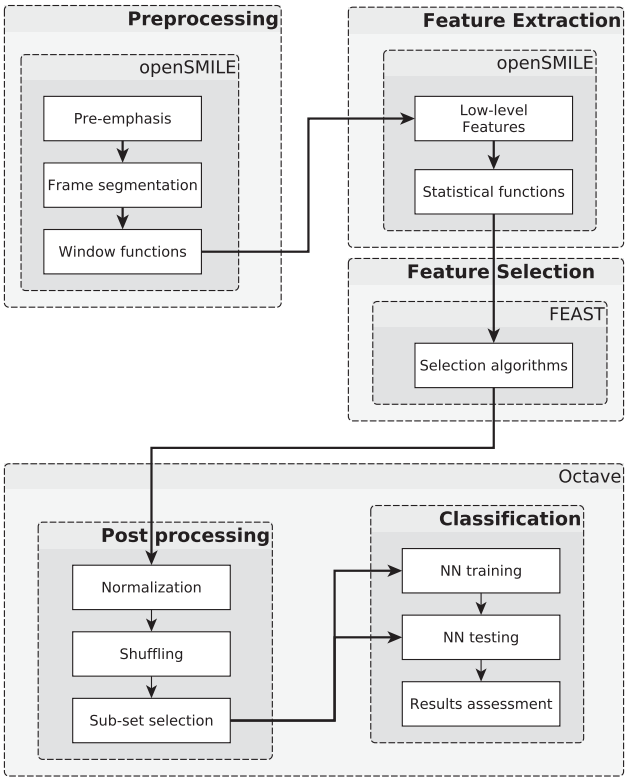

Fig. 1. Block diagram of the proposed algorithm

features associated with audio signals. We use openSMILE for the preprocessing step where different types of pre-emphasis algorithms are used to de-noise the signal, for calculating the frequency spectrum and for the extraction of the low level features such as energy, zero-crossing rate, frequency bands in Mel scale, pitch and 14 MFCC. Using these features the delta- and delta-delta regression are calculated together with the statistical functions such as regression coefficients, extremums, moments etc.

FEAST (http://www.cs.man.ac.uk/~gbrown/fstoolbox/) is freely redistributable software package capable of integrating in MATLAB/Octave and includes implementations of known algorithms for feature selection, namely those based on mutual information some of them are mentioned in Table I.

After the feature selection step for the classification we use the Neural Network (NN) classifier with different number of hidden layers and k-fold cross validation.

V. Experimental results

A. Analysis of the criteria for feature selection

Extensive testing is done for the parameters of the NN using feature vectors with 384 elements (16 low level features + their 16 delta coefficients * 12 statistical functions) as described in [2]. High accuracy is achieved primarily for networks with number of neurons in the hidden layer roughly between 30 and 50, while for larger networks with more than 100 neurons, the outcome in terms of recognition rate is very low.

TABLE I
LIST OF ALGORITHMS IMPLEMENTED IN THE FEAST PACKAGE

Criterion	Full name	Authors
RELIEF	Relevant Features via Statistical Method	Kira and Rendell (1992)
MIM	Mutual Information Maximisation	Lewis (1992)
MIFS	Mutual Information Feature Selection	Battiti (1994)
JMI	Joint Mutual Information	Yang and Moody (1999)
CMIM	Conditional Mutual Information Maximisation	Fleuret (2004)
ICAP	Interaction Capping	Jakulin (2005)
MRMR	Max-Relevance Min-Redundancy	Peng et al. (2005)
DISR	Double Input Symmetrical Relevance	Meyer and Bontempi (2006)
CIFE	Conditional Infomax Feature Extraction	Lin and Tang (2006)
CONDRED	Conditional Redundancy	Pocock et al. (2011)

TABLE II
DISTRIBUTION OF SELECTED FEATURES BY GROUPS

Group	Features	Group count	CMIM [a]	Total [b]
Energy	LOGenergy	1	17	69
MFCC	mfcc(0-12)	13	131	821
Mel-spectrum	Mag_melspec(0-25)	26	132	493
Time	zcr(zero-crossing)	1	20	52
Pitch	voiceProb,F0env,F0	3	8	67
Spectrum	fband(0-250,0-650,250-650, 1000-4000,3010-9123); RollOff(25.0,50.0,75.0,90.0); Flux;Centroid MaxPos;MinPos	13	76	418

[a] For the single criterion yielding top recognition score (CMIM).
[b] For the criteria with the best results: CMIM, JMI, DISR, ICAP RELIEF.

After setting the optimal parameters for the NN classifier, the next phase is to compare the behavior of the feature selection criteria mentioned in Table I. The new feature vector is composed of 56 low-level features, delta coefficients of first and second order, all of them multiplied by 39 statistics functions. The final number is 6669 global attributes (large dataset). So the selection criterion must downsize the number of attributes to 384 - to compare the results with [2]. For each of the algorithms in FEAST we deploy 10 times 10-fold cross- validation. Highest accuracy is achieved with features selected by CMIM, JMI, ICAP, DISR and RELIEF, with very similar values - just under 86%. These results are comparable with the EMO-DB accuracy in the evaluation of annotation by an independent panel of experts [17] and with the published results in [18]. In other words, the resulting combined models (large number of features + selection + classification) reach the precision with which a person recognizes the emotional state of the actor.

We must note that the top 20 of the most common features used by the different criteria are belonging to almost all major groups. For this reason, further analysis was performed with respect to distribution groups shown in Table II. In it all low-level features used in the large dataset are accounted. Based on the results from the experiments described in the previous paragraph, was selected CMIM criterion for the subsequent experiments (the highest score in the cross-validation - 85.72% for all classes). Distribution groups are clearly shown in pie charts of Fig.2.

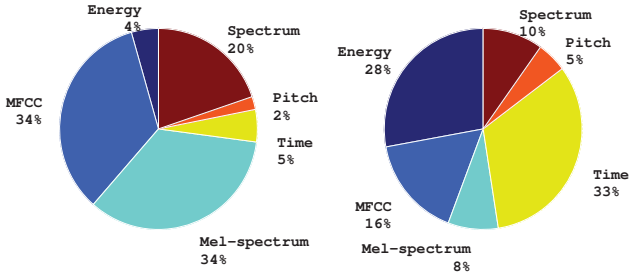

(a) (b)

Fig. 2. Pie charts of the shares of selected feature groups of CMIM criterion a) number selected features from a group; b) relative share of the group (obtained as the number of the selected features is divided by the number of the low-level features in the group before the selection).

B. Recognition accuracy

The previous sub-section discusses the results in terms of feature selection criteria, features and their main groups. At this point, we assess the feasibility of the models in terms of emotional categories for the selected dataset. In Table III are presented the recognition rate results for each class of emotion with cross validation. As expected, anger is the most accurately recognized class, followed by sadness (both with over 90% accuracy). Weaker recognition rate display those of boredom, fear, disgust and neutral, but still the accuracy is over 80%.

TABLE III
RECOGNITION RATE BY CLASSES

Criterion	Anger	Boredom	Disgust	Fear	Happiness	Sadness	Neutral
MIM	90.83	84.06	77.07	79.09	72.59	88.80	83.72
MRMR	84.49	71.57	53.97	60.09	47.88	83.42	75.26
MIFS	83.20	47.74	31.66	46.57	42.51	71.97	49.94
CMIM	93.34	88.71	79.83	80.03	74.89	91.72	83.70
JMI	92.38	89.28	83.30	82.34	68.61	89.87	86.06
DISR	92.52	89.76	83.88	82.99	70.19	87.81	85.73
CIFE	87.60	69.21	58.17	54.24	51.49	72.68	65.47
ICAP	92.82	87.84	79.87	80.38	75.99	92.01	82.63
CONDRED	83.79	80.25	70.52	69.14	56.00	80.36	71.79
RELIEF	92.39	90.64	81.18	77.13	72.49	90.39	87.68

Table IV depicts the top selected features in particular. Those were ordered by a mutual score, we defined as $S = \sum_{i \in \mathcal{B}} (384 - F_i + 1)$, where $\mathcal{B}$ is the subset of the five selection criteria yielding best recognition accuracy and F_i is the corresponding rank as selected by criterion i.

TABLE IV
TOP 20 SELECTED FEATURES BY THE FIVE BEST SELECTION CRITERIA

Feature	Score	CMIM	JMI	DISR	ICAP	RELIEF
zcr_sma_quartile2	1536	✓	✓	✓	✓	
mfcc_sma_de[12]_iqr1-3	1424	✓	✓	✓	✓	
mfcc_sma[1]_quartile2	1410	✓	✓	✓	✓	
mfcc_sma_de_de[1]_nzqmean	1391	✓	✓	✓	✓	
mfcc_sma[0]_quartile3	1335	✓	✓	✓	✓	
LOGenergy_sma_de_quartile3	1335	✓	✓	✓	✓	
mfcc_sma_de_de[4]_linregerrA	1320	✓	✓	✓	✓	
Mag_spectralMinPos_sma_qmean	1302	✓	✓	✓	✓	✓
Mag_spectralRollOff75.0_sma_minameandist	1246	✓	✓	✓	✓	
mfcc_sma_de[7]_nzgmean	1188	✓	✓	✓	✓	✓
mfcc_sma_de_de[7]_stddev	1137	✓	✓		✓	✓
mfcc_sma_de_de[7]_nzabsmean	1126	✓	✓	✓	✓	✓
mfcc_sma_de[1]_percentile95.0	1079	✓	✓	✓	✓	✓
mfcc_sma_de[12]_nzgmean	1079	✓	✓	✓	✓	✓
mfcc_sma_de_de[12]_iqr1-3	1062	✓	✓	✓	✓	

The last stage of the current study was done in exploring fewer features based on the ordered lists returned by the selection criteria algorithms. From Fig.3 it is obvious that almost the same success in terms of recognition rate can be achieved with about 200 features.

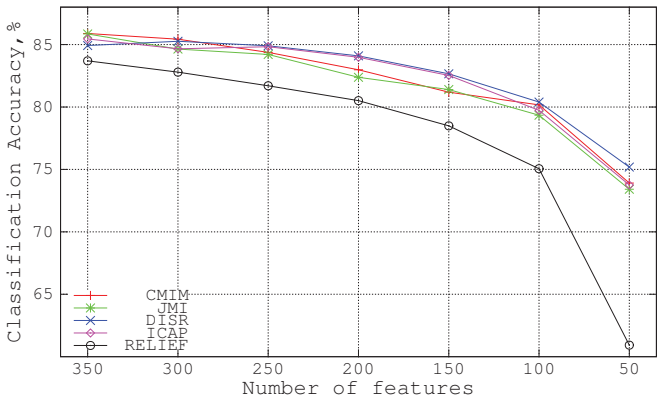

Fig. 3. Analysis of reducing the number of features

VI. CONCLUSION

This paper explores different feature selection criteria such as Mutual Information Maximization (MIM) feature scoring criterion and its derivatives to measure how potentially useful a feature or feature subset may be when used for classification purposes. A text independent method of emotion classification of speech is proposed in this paper. The proposed method employs different groups of low-level features and statistical functions, to represent the speech signals and a NN classifier for the classification task. For the experiments the EMO-DB dataset is used with seven primary emotions. Results show that the proposed system yields an average accuracy of over 85% for recognizing 7 emotions with 5 of the best performing feature selection algorithms.

We plan to expand our work by including in the classification step the Support Vector Classifier and to compare its recognition accuracy to the current NN classifier. The most important challenge remains the fusion between the two modalities speech and face emotion recognition. There are two way of fusion of the modalities: 1) at the feature level (before running the classifier) and 2) at the results level (combining results from classifier from each modality). By fusing the multimodal data we expect an increase in the recognition rates in comparison to the unimodal systems.

ACKNOWLEDGMENT

This work was supported by contract DFNI I02/1 for research project: "Intelligent man-machine interface for assistive medical systems in improving the independent living of motor disabled users" of the Bulgarian Research Fund of the Ministry of Education and Science.

REFERENCES

[1] M. El Ayadi, M. S. Kamel, and F. Karray, *Survey on speech emotion recognition: Features, classification schemes, and databases*, Pattern Recognition, vol. 44, pp. 572-587, 2011.
[2] B. Schuller, et al., *Recognising realistic emotions and affect in speech: State of the art and lessons learnt from the first challenge*, Speech Comm. (2011), doi:10.1016/j.specom.2011.01.011
[3] Ververidis, D. and Kotropoulos, C., *Emotional speech recognition: Resources, features, methods, and applications*, Speech Communication, vol. 48, issue 9, pp. 1162-1181, 2006
[4] K. Han, D. Yu, and I. Tashev, *Speech emotion recognition using deep neural network and extreme learning machine*, Proceedings of INTERSPEECH, ISCA, Singapore, pp. 223-227, 2014
[5] R. Plutchik, *The Psychology and Biology of Emotion*, New York: HarperCollins College, 1994.
[6] H. Gunes and B. Schuller, *Categorical and dimensional affect analysis in continuous input: current trends and future directions*, Image and Vision Computing, 2012.
[7] F. Ringeval, A. Sonderegger, J. Sauer, D. Lalanne, *Introducing the RECOLA multimodal corpus of remote collaborative and affective interactions*, Automatic Face and Gesture Recognition (FG), 2013 10th IEEE International Conference and Workshops on, pp.1-8
[8] H. Hu, M.-X. Xu, W. Wu, *Fusion of global statistical and segmental spectral features for speech emotion recognition*, International Speech Communication Association8th Annual Conference of the International Speech Communication Association, Interspeech 2007, vol. 2, 2007, pp. 10131016
[9] T. Nwe, S. Foo, L. De Silva, *Speech emotion recognition using hidden Markov models*, Speech Commun. 41 (2003) 603623
[10] C. Lee, S. Narayanan, *Toward detecting emotions in spoken dialogs*, IEEE Trans. Speech Audio Process. 13 (2) (2005) 293303
[11] Ch. Peter, R. Beale, *Affect and Emotion in Human-Computer Interaction: From Theory to Applications*, vol. 4868 on Lecture Notes in Computer Science Information Systems and Applications, Springer 2008
[12] Kr. Izdebski, *Emotions in the Human Voice, Volume 1: Foundations*, Plural Publishing, 2007
[13] S. V. Arora, Effect of Time Derivatives of MFCC Features on HMM Based Speech Recognition System, ACEEE Int. J. on Signal and Image Processing , Vol. 4, No. 3, Sept 2013, pp.50-55
[14] S. Bou-Ghazale, J. Hansen, *A comparative study of traditional and newly proposed features for recognition of speech under stress*, IEEE Trans. Speech Audio Process. 8 (4) (2000) 429442
[15] Ayadi, M. E., M. S. Kamel, and F. Karray, *Survey on speech emotion recognition: Features, classification schemes, and databases*, Pattern Recognition, vol. 44, issue 3, pp. 572-587, 2011.
[16] G. Brown, A. Pocock, Z. M. Zhao, M. Luján *Conditional Likelihood Maximisation: A Unifying Framework for Information Theoretic Feature Selection*, Journal of Machine Learning Research 13 (2012) 27-66
[17] F. Burkhardt , A. Paeschke , M. Rolfes , W. Sendlmeier , B. Weiss, *A database of german emotional speech*, Proceedings of Interspeech, Lissabon (2005), pp 1517–1520
[18] Siqing Wu, Tiago H. Falk, Wai-Yip Chan, *Automatic speech emotion recognition using modulation spectral features*, Speech Communication 01/2011; 53:768-785. DOI:10.1016 j.specom.2010.08.013

THE 5TH INTERNATIONAL CONFERENCE ON WIRELESS COMMUNICATIONS, VEHICULAR TECHNOLOGY, INFORMATION THEORY, AEROSPACE & ELECTRONIC SYSTEMS (WVITAE-2015)
December 13-16, 2015, Hyderabad, India

Classification Based Automatic Assessment for Web Based Learning

Wacharawan Intayoad
School of Information Technology
Mae Fah Luang University
Chiang rai, Thailand
wacharawan.int@mfu.ac.th

Punnarumol Temdee
School of Information Technology
Mae Fah Luang University
Chiang rai, Thailand
punnarumol@mfu.ac.th

***Abstract*— Web based learning plays a vital role in the global education since it can support learner from anywhere and anytime. The automatic assessment is required for web based learning to provide the individual support for each learner. The challenging is to serve the large numbers of learners with appropriate individual support. Therefore, there is the necessity to determine the effective automatic assessment so that the appropriate feedback can be given. This paper thus aims to determine the appropriate classification method for providing the automatic assessment for a large numbers of learners through web based learning. The interaction between the learners and the learning objects is used for classification. Two classification methods which are k-nearest neighbors and decision tree are studied and compared in this paper. The case study with 419 learners enrolling the course "Introduction to Information Technology", Mae Fah Luang University shows that both classification methods are suitable for employing as the automatic assessment classifiers because k-nearest neighbors provides 93.08% and decision tree provides 91.16% accuracy respectively.**

Keywords*— *automatic assessment; classification method; KNN; Decision Tree; web based learning

I. INTRODUCTION

The Information Communication Technology (ICT) establishes new strategy to achieve the learning objectives in education system. The ICT has created the major shift in education system, the roles of teacher, learner, curricula and new media in the past decades [1]. The integration of ICT in teaching and learning creates a possibility for learner to learn from anywhere and anytime with wired and wireless communications. The learning model that goes beyond classroom enhances the life-long and the effective of learning for both learners and teachers [2] for modern education system. Web based learning has been introduced for many years as the new delivery form of e-learning and become a common way for modern education systems nowadays. To promote effective learning of the web based learning, some issues need to be considered such as the effectiveness of knowledge transferring, learning lifestyle supporting, and learning efficiency evaluation.

Many outstanding theories such constructivism and situated cognition aim to design the learner-centered environment. These theories have the common assumption that the learners are active participants. They gain the knowledge from the relevant context and they also contribute or respond to learning objects [3] appropriately. Supporting the variety of learning theories in web based learning is even more important and challenging especially when it has to serve a large numbers of learners. Each learner has different learning abilities, personal interests, background knowledge and the ability to learn [4]. The learning styles of each individual in web based learning, such as how they interact with the learning objects and do their practice can be used to analyze learner's behavior in many areas [5] especially in implementation of web-based learning system[4]. Because the learning style affects learning outcome such as passing or failing the course, analyzing learning style could predict the learning achievement. The learners who have the difference background could have difference learning style [6]. Therefore, it will be an advantage, if the learners can be classified as who are going to pass or fail the course so that the assistant can be made appropriately on time. The classification of learners will enhance the learning efficiency of the learner and it is necessary for automatic assessment and feedback [7].

Therefore, the objective of this paper is to determine the appropriated methods for classifying the students who will potentially pass or fail the course. The interaction between students and learning objects is mainly used for classification in this paper. The k-nearest neighbor (KNN) and decision tree are examined and compared since they have been successfully applied in several classification problem domains [8]. The result from this paper will be useful in the improvement of the automatic assessment and feedback for web based learning.

II. LITERATURE REVIEWS

A. ICT for Education

ICT has affected the working process in many sectors, including the education sectors. It changes the way of teaching and learning [9]. It establishes the flexible learning strategies. The flexible learning strategies means that the flexible of time, place, content selection and delivery of instructions [1]. The ICT can enhance the teaching and learning process in higher education [10]. With the network, it makes possible for learners and teachers to access to the content in any place and time, which is also known as distributed learning. The key factor of the distributed learning is the web-based instruction [1]. There are a different types of learners and some learners might not be satisfied with the instruction or content that be provided. Even the ICT is a productivity tools in education system but to fulfill the different types of learner satisfaction, the learning software is the key competencies [1].

B. Automatic Assessment for Web Based Learning

The automatic feedback and assessment is the useful tools for self-learning and distance learning [7]. The advantages of the automatic feedback are enabling the instance feedback to the learner, consistency of evaluating assignment and reducing task and time for instructors [3]. The research found that the automatic assessment could enhance the learning result [11]. Moreover, the automatic assessment has applied many machine learning methods for many different purposes [12] including this paper.

C. K-Nearest Neighbor

K-Nearest Neighbor (KNN) is a method for data classification based on the similarity measure. It is used for measuring the distance among data attributes. Classification process consists of examining the features of a newly or unknown data and assigning it to one of the predefined set of class. The training dataset is the predefined set of class coming from the historical records. It is essential that the training dataset is big enough to cover all of the populations so that KNN is suitable for classification [13].

Generally, the KNN is suitable for numeric data. However, it can be applied with discrete data. There are two main operations commonly used for KNN including distance function and combination function. The distance function calculates the distance between two records to measure the similarity of data. The combination function combines the result of the distance then sorts the distance by ascending. The value of k identifies the numbers of the nearest neighbors. There are two main decision rules in KNN which are similarity voting and majority voting schema [14]. Many research has been used the KNN method in classification purpose. For example, Chang et al. purpose a mechanism for classifying learning style and identifying learners' learning styles. Some research goes further than applying the method because they also purpose the improvement the classification methods [14].

D. Decision Tree

Decision tree is a hierarchy data structure for using in decision support. It looks like a real tree model with the root node on the top and leaf node at the bottom of the tree. The decision tree diagram consists of node, branch, and leaf. Each node has its own attribute. The node at the top of the tree is called root node. Branch represents the possible attributes. Leaf is at the bottom of the tree which represents a class, or the result of prediction [13].

There are some famous versions of the decision tree methods such as ID3 and C4.5. The C4.5 method is suitable with an uncertain class label and can be applied pre-pruning and post-pruning to reduce the least reliable branches. Furthermore, the C4.5 applies the Information gain method as well as ID3 and the C4.5 can solve some disadvantages of ID3 [13]. There is Gain ratio criterion in the C4.5. The Gain ratio is used to decide which attribute should be selected and it helps reducing the bias for selecting attribute process by taking the number and size of branches into account when choosing an attribute [13]. Finally, the Split information of the attribute is applied to determine gain ratio [13].

Decision Tree has been adapted in many kinds or classification problems especially in web based learning. For example, the decision tree can be used to analyze learning profile from the data source such as web log to classify the learners' learning styles [15], analyzing the learners' activities [16], predicting learning effectiveness [16], enhancing learning outcome [17], etc.

III. RESEARCH METHODOLOGY

A. Data Gatheing

Mae Fah Luang University has been fully deployed the web based learning for "Introduction to Information Technology" course. This course is required as the general education course for every first-year student. There are more than 3,000 enrolling this course every year. The data used in this paper is collected from Web based learning course in 2013 academic year. The training dataset comes from 419 students. These students are from difference majors. These majors are categorized into two group, science (sc) and none science (nsc) majors. The training dataset is gathered from 2 parts. The first part is gathered from weblogging data which record the student's interactions with learning objects. The Introduction to Technology course consists of 6 modules. The spreadsheet module is selected for this paper, because there are a significant numbers of failure students. There are totally 18 learning objects in this module. The learning objects are available for students to access in any order and anytime. Finally, the second part data is the student assessment result which are passing or failing this module. This data is used for both the classifiers. TABLE I demonstrates the example of the training dataset.

TABLE I. EXAMPLE OF TRAINNING DATA

Std. no	**1**	**2**	**3**	**4**	**5**	**6**	**7**	**8**	**9**	**10**
Area	nsc	nsc	nsc	nsc	nsc	nsc	sc	sc	sc	sc
Grade	f	f	p	f	p	p	p	p	f	f
LO99	2	0	1	5	0	0	0	2	1	3
LO102	1	0	0	0	1	1	1	4	1	0
LO103	0	0	0	0	0	0	0	0	0	0
LO104	0	0	0	0	1	0	1	5	2	0
LO105	0	1	0	0	1	1	2	1	2	0
LO106	0	0	0	0	1	2	2	1	3	0
LO107 to LO113	0	0	0	0	0	0	0	0	0	0
LO114	0	0	0	0	0	1	1	2	2	0
LO115	0	0	0	0	1	1	0	2	2	1
LO116	0	0	1	0	0	0	1	2	1	0
LO120	0	0	1	2	0	0	0	2	2	0
LO121	7	1	1	7	0	0	0	3	2	0

The first-row "std. no" presents 10 examples. The second row presents the study areas which are science (sc) and none-science (nsc). The third row shows learning outcome of each student which are pass (p) or fail (f). The rows from LO99 – LO121 demonstrate the frequencies that the student interacts with these learning objects. For example, the first student who is student number 1 is from none-science major and did not pass the module. This student interacts with LO99, LO102 and LO121 two times, one time and seven times respectively.

B. *Accuracy of Correctly Classified*

The accuracy of the classifier method has to be tested. The formula for evaluating the total classification accuracy is defined as equation no. (1) [18].

$$\text{accuracy} = \frac{\text{no. of all correct classified samples}}{\text{no. of all examples}} \quad (1)$$

C. *KNN Classifier*

The Euclidean distance is applied in this KNN process. Euclidean distance calculates the difference between the sample data and training data. The Euclidean distance is defined as shown in equation no. 2 [19].

$$\left(d(x_m, x_n) = \sqrt{\sum_i (x_{m,i} - x_{n,i})^2} \right) \quad (2)$$

Where x is data for classifying which is defined as a vector x= (x1, x2, x3,….,xn), n is the number of the example's attributes, x1 is the example's attribute. "i" is from 1 to k. The smaller $d(x_{m,}x_{n)}$ means that these two examples are more similar [18].

TABLE II. EUCLIDEAN DISTANCE CALCULATION

Student No.	Major	Lo99	Lo102	Lo103	…	Distance
D(1,10)	0	1	1	0	…	1.73
D(2,10)	0	3	0	0	…	3.32
D(3,10)	0	2	0	0	…	2.24
D(4,10)	0	2	0	0	…	2.24
D(5,10)	0	3	1	0	…	3.74
D(6,10)	0	3	1	0	…	4.00
D(7,10)	1	3	1	0	…	4.36
D(8,10)	1	1	4	0	…	6.63
D(9,10)	1	2	1	0	…	4.69

TABLE II demonstrates how to calculate Euclidean distance of the testing data who is the student no.10 from other 9 students. According to TABLE II, the first column is the student no. 1-9. The second column is the student major. The column "99" to" …" are the learning objects which the Euclidean calculates in the process of $(x_{m,i} - x_{n,i})^2$. The distance column shows the result of the calculation. The value of k is the numbers of nearest neighbors for classification. This number identifies how many neighbors effect classification which will choose from the distance matrix. The k is usually an odd number. The number of k influences the accuracy of the result. If k is smaller, then the result will be higher variance or less stable. If k is larger, then the result will be higher biased and less stable. The lists below are the example results of KNN with different k values in this paper.

- If k value is 3, then the nearest neighbor is student no1 (fail), no3 (pass) and no4 (fail), so there are 1 pass and 2 fail, then student no. 10 is classified as fail the module.
- If k value is 5, then the nearest neighbor are student no 1(fail), no3 (pass), no4 (fail), no2 (fail) and no5 (pass), so there are 2 pass and 3 fail, then student no. 10 is classified as fail the module.

D. *The Decision Tree Classifier*

This paper has adapted the C4.5 method since there are 2 class types, "pass" and "not pass". From the training dataset, there are 419 instances. The students are categorized into two classes including, passing and not passing the course. The attributes for calculating the decision tree is a number of times accessing learning objects and the major of studying. There are total 19 attributes used in this paper. After running the decision tree, there are 9 attributes is accounted for classifying. Each attribute has 2 classes including pass and not pass statuses.

Fig. 1 demonstrates the decision tree results from the training data. The gain ratio is the criteria for selecting the split point. Each branch is created by comparing the value between the split point and split attribute. In this paper, the root node is LO104 which is selected because of its maximum gain ratio. From LO104, the dataset is divided into left and right branches. If split attribute value ≤ split point value (4.5), otherwise another branch which is LO121 becomes necessary. In another hand, if split attribute value split > point value (4.5), then the LO99 needs to be performed. The method will repeat the process to build a decision tree for the sub-dataset, until the dataset is empty or the terminated condition is satisfied.

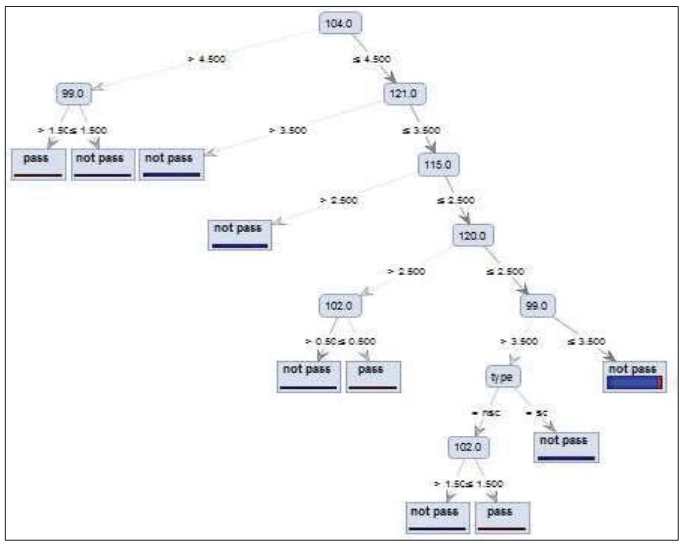

Fig. 1 Decision Tree Classification Results

IV. RESULTS AND DISCUSSION

A. *KNN Classification Accuracy*

In this paper, KNN classifier is tested for k = 1, k = 5, and k=9 respectively. According to the classification accuracy of KNN from TABLE III, k=9 has the highest accuracy which is 93.08% where k=1 and k=5 have 83.30% and 92.85% accuracies respectively.

TABLE III. CLASSFICATION ACCURACY

	K=1	K=5	K=9

Accuracy rate	83.30	92.85	93.08

TABLE IV demonstrates the classification result of KNN with k=9. The KNN predicts the failing student with 93.08% accuracy. However, 29 students who actually pass the course but they are classified as fail the course. For the pass, accuracy is 0.00%. The method could not predict 29 cases of pass students. Following equation (1), the accuracy of correctly classified examples is 93.08% and standard deviation is 1.04%.

TABLE IV. PRECISION OF KNN WITH K=9

	True fail	True pass	Class precision
Pred. fail	390	29	93.08%
Pred. pass	0	0	0.00%

B. Decision Tree Classifier Accuracy

TABLE V demonstrates the accuracy result of decision tree which is evaluated by the cross-validation evaluation technique. There are 382 students predicted as fail who actually fail the course. The 8 students are predicted to pass but they actually fail. There is no student has been classified as passing the course. However, 29 students who actually pass the course but they are classified as fail the course. Therefore the accuracy for predicting the failing student is 93.06%. The accuracy for predicting the passing student is 0.00%. There are 8 students who fail the module, but the method predicts as passing the module. Following equation (1), the accuracy of correctly classified examples is 91.16% and standard deviation is 1.91%.

TABLE V. PRECISION OF DECISION TREE

	True fail	True pass	Class precision
Pred. fail	382	29	93.06%
Pred. pass	8	0	0.00%

The result shows that both classification methods provide high classification accuracies although the accuracy of KNN is slightly higher than that of the decision tree. Therefore, both classifiers are potentially appropriate for automatic assessment in this paper. The training data composes of many examples for more numbers of failure than passing students. Therefore, this will probably lead the biasing for a classifier for the majority class. The future work will be improving the classification accuracy. In addition, the future study will also be focusing on protecting data security while retaining student's privacy.

V. CONCLUSION

This paper aims to determine the appropriate classification method for automatic assessment in web based learning by using the interaction between the learners and the learning objects. KNN and decision tree are studied in this paper for identifying the effective classifier. The case study is conducted with 419 learners enrolling the course "Introduction to Information Technology", Mae Fah Luang University, which is the web based learning course. The results shows that both classification methods are suitable for employing as the automatic assessment in web based learning by providing 93.08% and 91.16% accuracies for KNN and decision tree methods respectively.

VI. REFERENCE

[1] S. Majumdar , " Emerging Trends in ICT for Education & Training," 2015
[2] G. Attwell, "The Personal Learning Environments - the future of eLeaming?," eLearning Papers, vol. 2, no. 1, pp. 1-8, 2007.
[3] J. F. Bowring, "A new paradigm for programming competitions," in Proc. 39th Tech. Symp. Comput. Sci. Educ , pp. 87–9, 2008.
[4] Ye, D. Xing, "A construction of personalized network education system based on web usage mining. Computer Application Software," Computer Applications and Software 8, 2002.
[5] R. M. Felder, and R. Brent, "Understanding Student Differences," Journal of Engineering Education, vol. 94, no. 1, pp. 57-72, 2005.
[6] P. Temdee, W. Intayoad, "Discovering and analyzing learning pattern on web based learning using social network analysis," Asia-Pacific Signal and Information Processing Association, 2014 Annual Summit and Conference (APSIPA). IEEE, p1-4, 2014.
[7] L. Malmi, A. Korhonen, "Automatic feedback and resubmissions as learning aid," In Advanced Learning Technologies, 2004. Proceedings. IEEE International Conference, pp. 186-190, August 2004.
[8] I. H. Witten, and F. Eibe, "Data mining: Practical machine learning tools and techniques with Java implementations 2nd Edition," San Francisco, CA: Morgan Kaufmann, 2000
[9] P. Anderson, "What is Web 2.0? Ideas, technologies and implications for education," vol.1, no.1, Bristol, UK;JISC, 2007
[10] A. Sife, E. Lwoga, C. Sanga, "New technologies for teaching and learning: Challenges for higher learning institutions in developing countries. International Journal of Education and Development using ICT,",3, no. 2, 2007.
[11] P. Resta,(Ed.), "Information and Communication Technologies in Teacher Education: A Planning Guide. UNESCO" , Paris, 2002
[12] M. Cristian, B.D. Dan, "From Decision Trees to Classification Rules with Data Representing User Traffic from an e-Learning Platform," In Information and Communication Technologies 2006, ICTTA'06, 2nd, vol. 1, pp. 702-707,2006.
[13] Han, Jiawei, M. Kamber, J. Pei, "Data mining: concepts and techniques: concepts and techniques," Elsevier, 2011.
[14] C. Lee, SK .Yoo, Y. Park, N. Kim, K. Jeong, B. Lee, "Using Neural Network to Recognize Human Emotions from Heart Rate Variability and Skin Resistance," IEEE Engineering in Medicine and Biology 27, 2005
[15] Y.-C. Chang, W.-Y. Kao, C.-P. Chu, and C.-H. Chiu, "A learning style classification mechanism for e- learning," Computers & Education, vol. 53, no. 2, pp. 273–285, 2009.
[16] G. Chen, C. Liu, K. Ou, and B. Liu, "Discovering Decision Knowledge from Web Log Portfolio for Managing Classroom Processes by Applying Decision Tree and Data Cube Technology," Journal of Educational
[17] M. Ueno, "Animated pedagogical agent based on decision tree for e-learning," Advanced Learning Technologies, ICALT 2005. Fifth IEEE International Conference, pp. 188-192, July 2005.
[18] Rapid Miner Documentation, Performance. Available: http://docs.rapidminer.com/studio/operators/evaluation/performance/classification_and_regression/performance_binominal_classification.html
[19] K.Q. Weinberger and L.K. Saul, "Distance metric learning for large margin nearest neighbor classification," The Journal of Machine LearningResearch, vol. 10, 2009, pp. 207-244

THE 5TH INTERNATIONAL CONFERENCE ON WIRELESS COMMUNICATIONS, VEHICULAR TECHNOLOGY, INFORMATION THEORY, AEROSPACE & ELECTRONIC SYSTEMS (WVITAE-2015)
December 13-16, 2015, Hyderabad, India

Performance of Amplify-and-Forward Cooperative Diversity under Ricean Fading

Maja Delibasic, Milica Pejanovic-Djurisic, Zoran Veljovic
Research Centre for ICT, Faculty of Electrical Engineering
University of Montenegro
Email: majai@ac.me

***Abstract*—This paper presents a study on the bit error rate performance of cooperative diversity system under Ricean fading environment. Single-antenna nodes (relays) operate in variable-gain amplify-and-forward (VG AF) mode. Destination node receives two copies of information signals, from source and from relay, and combines them applying maximal ratio combining (MRC). We develop a novel analytical model for bit error rate performance, which is applicable to various fading scenarios described with different Ricean *K* factors and average signal to noise ratios (SNR). Finally, we determine the level of system performance improvement, or equivalently the signal-to-noise ratio gain, due to the existence of line of sight signal component between the network nodes and nodes cooperation. Numerical results show that the Ricean *K* factor have significant influence on overall system performance. Simulation results confirm the validity of the proposed analytical model.**

I. Introduction

In the previous years, the number of applications using wireless communication systems has remarkably increased. Such growth demands higher data rates and higher reliability of wireless systems. However, it is well known that wireless signal transmission imposes serious challenges in fulfilling these demands, due to the complex nature of wireless radio channel. To mitigate the negative effect of multipath signal propagation, various technical solutions for wireless networks are proposed. One of the most commonly used techniques for efficiently coping with the negative effects of multipath fading and for providing significant improvements in reliability and throughput is diversity. It is a relatively simple solution based on the usage of multiple antennas placed at the transmitter and/or receiver. However, the size, cost and hardware constraints in the use of multiple antennas may not always be feasible, especially in small portable devices. To overcome this problem, the concept of cooperative diversity became the focus of various research efforts, [1]. Such concept assumes that multiple (single antenna) nodes share their antennas in order to transfer the information from one to another. Through their cooperation, distributed antenna system is created, providing diversity gain without the necessity for multiple antennas.

Cooperative diversity has been in the research focus in recent years, since such concept offers significant performance benefits, including improved wireless link performance, increased spatial diversity, capacity and extended network coverage, [1]–[4]. In such wireless network infrastructure additional network nodes, called relays (R), are introduced in order to assist in signal transmission from source (S) to destination (D). Through cooperation among the network nodes, a virtual antenna array is created and by combining signals received through multiple signal paths certain diversity gain can be achieved. Such idea was first proposed by Meulen [5] and Cover [6].

Relay usually performs one of the two main relaying methods: Amplify-and-Forward (AF) or Decode-and-Forward (DF), [3]. AF relaying is a popular method for implementing in relay systems because of relatively simple processing of the received signal. Namely, the received signal from the source is amplified at the relay and then retransmitted towards the destination. Depending on the source-relay channel information, R can perform fixed gain (FG), also called average power scaling [3], or variable gain (VG), or instantaneous power scaling [7]. In this work we consider dual-hop variable gain AF cooperative relay system operating in an asymmetric Ricean fading environment, meaning that fading parameters (average SNRs and Ricean *K* factors) of the S-R and R-D channels are not necessary identical.

In order to determine performance of cooperative diversity systems, good knowledge of wireless channel is of the great importance. Thus, extensive studies are done assuming different communication scenarios and various fading statistics. Cooperative diversity systems operating in Rayleigh and more general Nakagami-*m* fading environment are studied in [8]–[12], having identical or non-identical fading channel parameters. At the same time, Ricean fading is also commonly used in the technical literature to model wireless propagation comprising a LoS (Line-of-Sight) component and multiple scattered components, [13]. However, despite the obvious practical importance of such Ricean channel model that is typical for micro/macro cellular communication, as well as indoor radio channels [14], only a few works have analyzed the performance of cooperative diversity systems in such LoS fading conditions, [15]–[21]. The lack of general model for performance analysis of such systems in an asymmetric Ricean fading environment represents the main motivation for the research presented in this paper. We propose appropriate analytical model which leads toward deriving the exact expression for system end-to-end bit error rate (BER) given in the form of infinite, but fast converging sum. We also compare the theoretical results with Monte Carlo simulations for different scenarios considered.

Section II describes the model of the analyzed system and associated channel distributions. In Section III we derive the BER expression for the received signal at destination, at the output of MRC combiner. The obtained results are showed in Section IV. Concluding remarks are given in Section V.

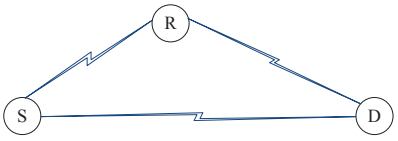

Fig. 1. Two hop cooperative relay system

II. System Model

A simple example of wireless cooperative diversity system is shown in Fig 1, in which source (S) sends the information to destination (D) using intermediate relay node (R). The destination will receive two copies of the information signal, one from source directly and the other from the relay. By proper combination of these two versions of the same signal, cooperative diversity can be achieved. The main advantages of cooperative communication are higher spatial diversity, reduced transmitted power, higher throughput and adaptability to network conditions, [22].

Each transmission period is divided into two time intervals. In the first time slot, S broadcasts the information signal to R and D. In the second time slot, R amplifies and forwards the scaled version of the signal to D, and the source keeps silent. Since D receives two versions of the same signal, one from S and the other from R, spatial diversity is achieved, with the received signals being combined by applying MRC.

It has been found in practice that by introducing the intermediate node (relay) between S and D, and by carefully planning its position, different links of a relay system could experience LoS fading conditions. In such circumstances, Ricean distribution is more suitable to describe statistical properties of the S-R and R-D fading channels, [13]. Furthermore, Ricean fading channels on the two hops are assumed to have different values of *K* factors and average received powers (or equivalently average SNRs). At the same time, the channel between S and D is assumed to follow Rayleigh fading distribution, because there are multiple paths due to buildings, trees and other objects and thus fading should be considered as more severe.

The instantaneous SNR of the signal received after maximal ratio combining done at the destination node can be written as:

$$\gamma_t = \gamma_0 + \frac{\gamma_1 \gamma_2}{\gamma_1 + \gamma_2 + c}. \quad (1)$$

γ_0 represent the instantaneous SNR of the direct S-D channel, while γ_1 and γ_2 represent the instantaneous SNRs of the first (S-R) and second (R-D) hop of the relaying channel, respectively, defined as $\gamma_i = \frac{|h_i|^2}{\Omega_i}$, $i = 0, 1, 2$. $\Omega_i = E[|h_i|^2]$, where h_i, $i = 0, 1, 2$ represent mutually independent complex channel gains of the S-D, S-R and R-D channel, respectively. Furthermore, it is assumed that additive white Gaussian noise (AWGN) has zero mean with respective noise powers N_0, N_1 and N_2 for S-R, R-D and S-D links. c is the constant which can have value 1, for the exact SNR of S-R-D link, or its good approximation for $c = 0$, [23]. Without loss of generality, in further analysis we consider automatic gain control (AGC), thus ignoring the noise at the relay, [24]. In that case $c = 0$.

Based on the above assumptions, the instantaneous SNR of direct link, γ_0, is distributed according to exponential distribution with the PDF (Probability Density Function), [14]:

$$p(\gamma_0) = \frac{1}{\overline{\gamma}_0} e^{-\frac{\gamma_0}{\overline{\gamma}_0}}. \quad (2)$$

For wireless links on the two hops experiencing Ricean fading, γ_i, $i = 1, 2$, are distributed according to non-central χ^2 distribution with two degrees of freedom, [25]. In that case PDF of the instantaneous SNR of *i*-th hop, $i = 1, 2$, is:

$$p(\gamma_i) = a_i e^{-K_i} e^{-a_i \gamma_i} I_0\left(2\sqrt{K_i a_i \gamma_i}\right). \quad (3)$$

In the above equation we put $a_i = (1 + K_i)/\overline{\gamma}_i$, where K_i is the Rician *K* factor of the *i*-th hop, $i = 1, 2$, and $I_0(\cdot)$ is the zero-th order modified Bessel function of the first kind. Ricean factor *K* represents the measure of the fading severity, and it is defined as the ratio of the LoS component power to the power of scattered components, [14]. For the special case of $K = 0$ (non LoS scenario), the Rician fading distribution becomes the Rayleigh fading distribution, while for $K \to \infty$, the distribution approximates that of an AWGN (no fading) channel. Typical values of the *K* factor in indoor/outdoor land mobile applications normally range from 0-12 dB, [13].

III. Performance Analysis

Average bit error rate (BER) is a useful criteria for evaluating performance of wireless communication systems. Traditionally, BER can be computed either using MGF (Moment Generating Function) based approach, or averaging the conditional bit error probability over the SNR distribution [14, Eq.(1.8)]. The latter (PDF-based) approach can be applied only if combined SNR per bit can be determined in a form feasible for further use. However, finding the PDF of the combined SNR in a tractable form is more difficult if the combined paths have different fading distributions and different fading parameters. Since the total SNR is given with (1), in this paper we will use the MGF based approach to determine BER of the analyzed cooperative diversity system operating in asymmetric Ricean fading environment.

To compute the average error probability, it is necessary to evaluate the following integral, [14]:

$$P_b(\gamma_t) = \int_0^\infty Q\left(\sqrt{2g\gamma_t}\right) p(\gamma_t)\, d\gamma_t, \quad (4)$$

where $Q(\cdot)$ is Gaussian Q function, defined as $Q(x) = 1/\sqrt{2\pi}\int_x^\infty e^{-t^2/2} dt$, while $p(\gamma_t)$ is PDF of the total received SNR. Parameter g is determined by the specific modulation scheme employed. If MPSK (M-ary phase shift keying) of the transmitted signal is assumed, $g = sin^2\pi/M$. Using the alternate representation of Gaussian Q function, defined as:

$$Q(x) = \frac{1}{\pi}\int_0^{\pi/2} \exp\left(-\frac{x^2}{2sin^2\theta}\right) d\theta, \quad (5)$$

BER can be represented over MGF of the total received SNR. Knowing the fact that MGF of the sum of two independent random variables is equal to the product of their MGFs, BER of the analyzed cooperative diversity system can be presented in a form of single, finite range integral:

$$P_b = \frac{1}{\pi}\int_0^{\frac{M-1}{M}\pi} M_{\gamma_0}\left(-\frac{g}{sin^2\theta}\right) M_{\gamma_{SRD}}\left(-\frac{g}{sin^2\theta}\right) d\theta. \quad (6)$$

In the case of Rayleigh fading, MGF is given in the following form, [14]:

$$M_{\gamma_0}(s) = \frac{1}{1 - s\bar{\gamma}_0}. \quad (7)$$

In order to proceed with the performance analysis of the considered cooperative diversity system, it is necessary to find SNR statistic of the S-R-D link. Previously, in [26] we derive statistical properties of the total received SNR at D, for the two-hop AF VG relay system operating in Ricean fading environment. We have shown that the PDF of the total received SNR of two hop AF VG relay system is given with (8). It is clear that (8) is presented in a form of infinite sum. However, it is dominated by the first few terms, and can be computed with sufficient accuracy with only few terms of a summation, as given in [26]. Calculating the Laplace transformation of the PDF, with the aid of [27, Eq. (6.621.3)], MGF can be also derived in a form of infinite but fast converging sum, given in (9). $F(\cdot,\cdot;\cdot;\cdot)$ denotes Gauss hypergeometric function [27, Eq. (9.100)], while $\Gamma(\cdot)$ is Gamma function. In the case when fadings on the two hops are characterized with Rayleigh distribution ($K_1 = K_2 = 0$), the infinite summation in (9) reduces to only one summation term, i.e. $n = m = 0$.

After deriving MGF of the total SNR at D, we can obtain the average BER for a variety of modulation types using the MGF based approach, by putting (9) and (7) in (6).

The above described analytical model for exact determination of the two-hop cooperative diversity systems BER performance in the chosen propagation scenario, to the best of authors knowledge, is new. There are some similar performance analyses of cooperative diversity systems operating under mixed Ricean/Rayleigh and Ricean/Nakagami-*m* fading channels, but the case of having Ricean fading on both hops of relaying channel is not considered. Model presented in this paper is general, and includes a whole range of fading severity, from non LoS ($K_1 = K_2 = 0$) to ideal case of no fading ($K_i \to \infty$).

IV. Results

This section presents the numerical and simulation BER results for the analyzed cooperative diversity system having arbitrary fading channels parameters.

In all considered scenarios we have assumed that the channel between S and R as well as the one between R and D have LoS communications, with arbitrary chosen Ricean *K* factors, and the channel between S and D experience multipath Rayleigh fading. That is why in the Monte Carlo simulations, three independent channel variables are created following Ricean and Rayleigh distribution. Signal at R is amplified and forwarded to D, where the signals from S and R are combined using MRC. The AWGN is modelled as complex Gaussian random variables having zero mean and variance N_i, $i = 0, 1, 2$.

The obtained BER performance curves are plotted versus the average SNR of S-R link. BPSK mapping of the information signal is assumed ($M = 2$). Analytical results are evaluated numerically and presented with lines, while the simulation results are shown by different markers.

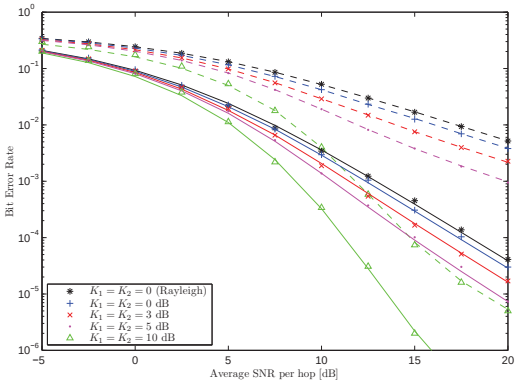

Fig. 2. BER versus average SNR per hop, identical channel parameters on S-R and R-D links; solid line - cooperative diversity; dashed line - relay system without cooperation

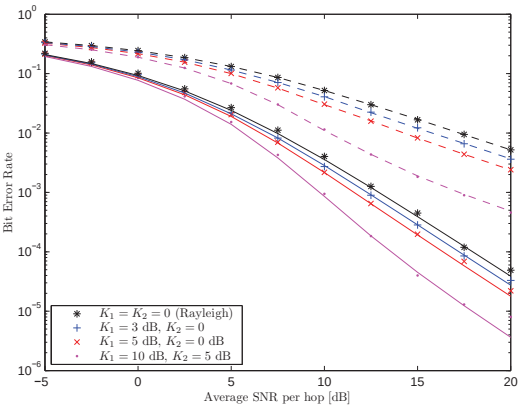

Fig. 3. BER versus average SNR per hop, non-identical *K* factors on S-R and R-D links, $\bar{\gamma}_0 = \bar{\gamma}_1 = \bar{\gamma}_2$; solid line - cooperative diversity; dashed line - relay system without cooperation

Fig. 2 presents BER values of the considered cooperative communication system in the case that fadings on S-R and R-D links have identical parameters. The average SNRs of all three links are assumed to be equal ($\bar{\gamma}_0 = \bar{\gamma}_1 = \bar{\gamma}_2$). BER results for the non-cooperative scenario (no direct communication between S and D) are also presented. It is observed from the figure that the existence of LoS between the S and R as well as R and D have significantly improves overall system performance. As *K* factors increase BER decreases. Furthermore, even if the direct channel is strongly influenced by multipath fading, its contribution in diversity combining is of great importance.

Fig. 3 illustrates the BER performance when the S-R link has different *K* factor than R-D link. Here we assume that the *K* factor of the first (S-R) link is greater thant the *K* factor of the second (R-D) link. However, knowing that γ_{SRD} is symmetrical to the SNRs of the individual hops, γ_1 and γ_2, the statistic of the total SNR, and thus the BER of the considered system will be the same as in the case when the *K* factor of the R-D link is greater than *K* factor of the S-R link.

Even in the case of different fading severities on the individual links, benefits of nodes cooperation is undoubted. The system with cooperative diversity offers significant gain

$$p(\gamma) = 2a_1a_2e^{-(K_1+K_2)}e^{-(a_1+a_2)\gamma}\sum_{n=0}^{\infty}\sum_{m=0}^{n}\frac{(a_1K_1)^m(a_2K_2)^{n-m}\gamma^{n+1}}{(m!(n-m)!)^2}\sum_{k=0}^{n+2}\binom{n+2}{k}\left(\frac{a_1}{a_2}\right)^{\frac{n-m-k+1}{2}}K_{n-m-k+1}\left(2\gamma\sqrt{a_1a_2}\right) \quad (8)$$

$$\begin{aligned}M_{\gamma_{SRD}}(s) = a_1a_2e^{-(K_1+K_2)}\sum_{n=0}^{\infty}\sum_{m=0}^{n}\frac{{K_1}^m(K_2a_2)^{n-m}}{(m!(n-m)!)^2}\sum_{k=0}^{n+2}\binom{n+2}{k}\frac{{a_1}^{n-k+1}\sqrt{\pi}2^{2n-2m-2k+3}}{\left(a_1+a_2+2\sqrt{a_1a_2}-s\right)^{2n-m-k+3}}\\ \times\frac{\Gamma(2n-m-k+3)\Gamma(m+k+1)}{\Gamma(n+5/2)}F\left(2n-m-k+3, n-m-k+\frac{3}{2}; n+\frac{5}{2}; \frac{a_1+a_2-2\sqrt{a_1a_2}-s}{a_1+a_2+2\sqrt{a_1a_2}-s}\right)\end{aligned} \quad (9)$$

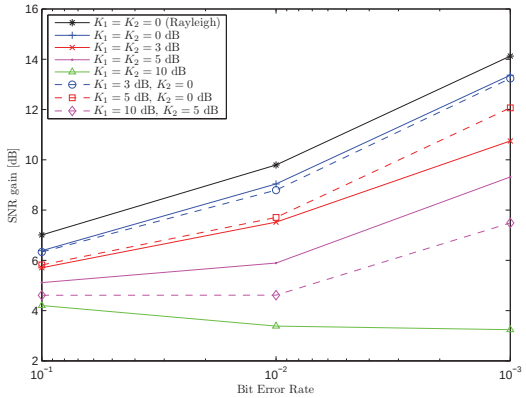

Fig. 4. SNR gain, $\bar{\gamma}_0 = \bar{\gamma}_1 = \bar{\gamma}_2$

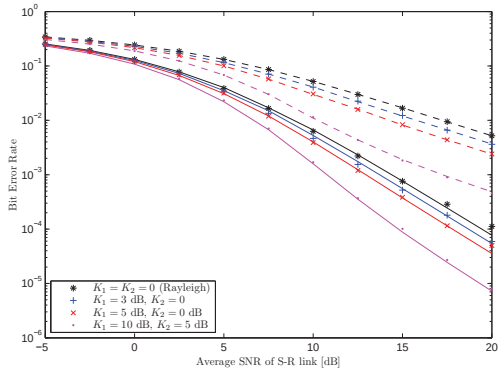

Fig. 5. BER versus average SNR of S-R link, $\bar{\gamma}_1 = \bar{\gamma}_2 = 2\bar{\gamma}_0$; solid line - cooperative diversity; dashed line - relay system without cooperation

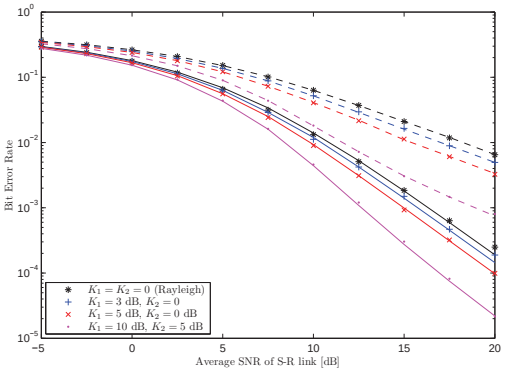

Fig. 6. BER versus average SNR of S-R link, $\bar{\gamma}_1 = 1.5\bar{\gamma}_2 = 4\bar{\gamma}_0$; solid line - cooperative diversity; dashed line - relay system without cooperation

compared to the system without cooperation. Fig. 4 presents the SNR gain, i.e the SNRs difference of cooperative and non-cooperative relay systems needed for achieving the same level of BER performance. The lowest SNR gain is obtained in the case of high K factors, because the contribution of direct (S-D) signal in the diversity combining, compared to the relay link is neglected. However, in the more severe fading conditions (lower K), as K factors of relay links decrease, the obtained gain increases, since the influence of direct link in diversity combining becomes greater.

When considering wireless cooperative diversity, the realistic assumption is that SNRs on the three links are not always equal. In particular, the S-D link is generally longer than S-R and R-D links, thus the signal power received at D from S, and equivalently the average SNR of the S-D link, is likely to be lower than the average SNRs of S-R and R-D link. Accordingly, in further analysis we assume that $\bar{\gamma}_1 = \bar{\gamma}_2 = 2\bar{\gamma}_0$ and $\bar{\gamma}_1 = 1.5\bar{\gamma}_2 = 4\bar{\gamma}_0$. The obtained BER results are presented in Fig. 5 and Fig. 6, as a function of $\bar{\gamma}_1$. BER results for the system with no cooperation are also presented. The appropriate SNR gains are shown in Fig. 7.

Presented results confirms the fact that in all the cases, even when the direct link is influenced by more severe fading than the relaying link, its contribution to diversity combining is not neglected. Even in the case that the average SNR of direct link is 4 time less than the average SNR of one of the relay links, for achieving the BER of 10^{-3} 6-12 dB less SNR is needed compared to non-cooperative scenario.

Furthermore, it can be seen that all the analytical results exactly match with the Monte Carlo simulations, confirming the accuracy of the presented analysis.

V. Conclusion

This paper presents novel analytical model for BER performance analysis of cooperative diversity system. Signals received at D directly from S, and from two hop variable gain AF relaying are combined using MRC. Signals transmitted over the S-D, S-R and R-D channels may experience different fadings. Thus, we assume that S-R and R-D channels are characterized with Ricean fading, while direct S-D link is under more severe fading and characterized with Rayleigh fading distribution. First we derive the MGF of the combined

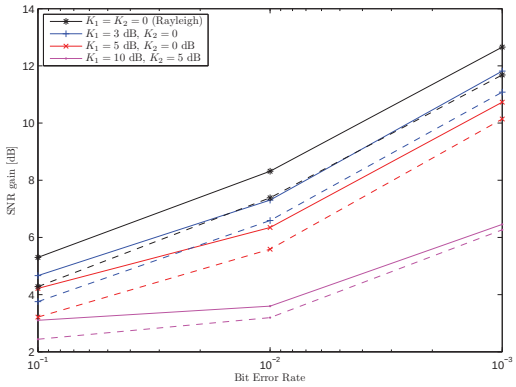

Fig. 7. SNR gain for non-identical channels; solid line - $\bar{\gamma}_1 = \bar{\gamma}_2 = 2\bar{\gamma}_0$; dashed line - $\bar{\gamma}_1 = 1.5\bar{\gamma}_2 = 4\bar{\gamma}_0$

SNR at D, in a form of infinite, but fast converging sum. Based on this expression, the average bit error rate of M-ary PSK signal is derived, using maximum 25 summation terms, for all the considered values of Ricean K factor.

The presented results clearly demonstrate that the considered system exhibits considerable improvements in system BER performance for various values of fading channels parameters, compared to the non-cooperative scenario. Furthermore, it has been shown that the existence of LoS between S and R and/or R and D influences the overall system performance. The obtained results can be useful to the system design engineers when planning the relay position.

Such system model is sufficiently general to encompass various fading channel conditions, as well as different communications scenarios which include both cooperative and non-cooperative communication. Furthermore, the generality of our analysis and numerical examples enables that the BER performance of a digital communications scheme using cooperative diversity can be also evaluated for other coherent modulation schemes and a variety of wireless fading channels. The performance of the proposed system may also be extended to other relaying schemes, such as FG-AF, or DF.

ACKNOWLEDGMENT

This research is supported by the project Advanced solutions for performance improvements of wireless cooperative e-service infrastructures, funded by the Ministry of Science of Montenegro, REGPOT project Fostering innovation based research for e-Montenegro (Fore-Mont) and the HERIC project through the BIO-ICT Centre of Excellence (Contract No. 01-1001).

REFERENCES

[1] A. Sendonaris, E. Erkip, and B. Aazhang, "User cooperation diversity. Part I. system description," *IEEE Trans. Commun.*, vol. 51, no. 11, pp. 1927–1938, 2003.

[2] J. N. Laneman, D. N. Tse, and G. W. Wornell, "Cooperative diversity in wireless networks: Efficient protocols and outage behavior," *IEEE Trans. Information Theory*, vol. 50, no. 12, pp. 3062–3080, 2004.

[3] M. O. Hasna and M.-S. Alouini, "A performance study of dual-hop transmissions with fixed gain relays," in *Proc. IEEE Int. Conf. Acoustics, Speech, and Signal Processing (ICASSP'03)*, vol. 4, 2003, pp. IV–189.

[4] G. K. Karagiannidis, T. A. Tsiftsis, and R. K. Mallik, "Bounds for multihop relayed communications in Nakagami-*m* fading," *IEEE Trans. Communications*, vol. 54, no. 1, pp. 18–22, 2006.

[5] E. C. Van Der Meulen, "Three-terminal communication channels," *Advances in applied Probability*, pp. 120–154, 1971.

[6] T. M. Cover and A. E. Gamal, "Capacity theorems for the relay channel," *IEEE Trans. Inf. Theory*, vol. 25, no. 5, pp. 572–584, 1979.

[7] H. Mheidat and M. Uysal, "Impact of receive diversity on the performance of amplify and forward relaying under APS and IPS power constraints," *IEEE Communication Letters*, vol. 10, no. 6, pp. 468–470, June 2006.

[8] S. N. Datta and S. Chakrabarti, "Unified error analysis of dual-hop relay link in Nakagami-*m* fading channels," *IEEE Commun. Lett.*, vol. 14, no. 10, pp. 897–899, 2010.

[9] S. Ikki and M. H. Ahmed, "Performance analysis of cooperative diversity wireless networks over Nakagami-*m* fading channel," *IEEE Communications Letters*, vol. 11, no. 4, pp. 334–336, 2007.

[10] B. Maham and A. Hjørungnes, "Asymptotic performance analysis of amplify-and-forward cooperative networks in a Nakagami-*m* fading environment," *IEEE Commun. Letters*, vol. 13, no. 5, pp. 300–302, 2009.

[11] J. Zhang, T. Zhang, J. Huang, and R. Yuan, "ABEP of amplify-and-forward cooperation in Nakagami-*m* fading channels with arbitrary *m*," *IEEE Trans. Wireless Commun.*, vol. 8, no. 9, pp. 4445–4449, 2009.

[12] S.-I. Chu, "Performance of amplify-and-forward cooperative diversity networks with generalized selection combining over Nakagami-*m* fading channels," *IEEE Commun. Letters*, vol. 16, no. 5, pp. 634–637, 2012.

[13] J. Parsons, *The mobile radio propagation channel*. John Wiley, 2000.

[14] M. K. Simon and M.-S. Alouini, *Digital communication over fading channels*. John Wiley & Sons, 2005.

[15] T. Q. Duong, H. Shin, and E.-K. Hong, "Effect of line-of-sight on dual-hop nonregenerative relay wireless communications," in *IEEE 66th Vehicular Technology Conference VTC Fall*, 2007, pp. 571–575.

[16] J. Adeane, M. R. Rodrigues, and I. J. Wassell, "Characterisation of the performance of cooperative networks in Rician fading channels," in *IEEE Int. Conf. Telecommunications (ICT2005)*, May 2005.

[17] M. Ilic-Delibasic and M. Pejanovic-Djurisic, "Performance improvement of two-hop cooperative relay system under correlated Ricean fadings," in *IEEE Int. Conf. Wireless VITAE*, 2014, pp. 1–4.

[18] A. Iqbal and K. M. Ahmed, "A hybrid satellite-terrestrial cooperative network over non identically distributed fading channels," *Journal of Communications*, vol. 6, no. 7, pp. 581–589, 2011.

[19] A. Gurung, F. Al-Qahtani, Z. Hussain, and H. Alnuweiri, "Performance analysis of amplify-forward relay in mixed Nakagami-*m* and Rician fading channels," in *IEEE Int. Conf. Advanced Technologies for Communications (ATC)*, 2010, pp. 321–326.

[20] H. Katiyar and R. Bhattacharjee, "Performance of two-hop decode-forward multi-antenna cooperative relaying in Nakagami-*n* fading channel," in *Proc. IEEE India Conference (INDICON)*, 2009.

[21] H. Ding, J. Ge, and Z. Jiang, "Asymptotic performance analysis of amplify-and-forward with partial relay selection in Rician fading," *Electronics letters*, vol. 46, no. 3, pp. 248–250, 2010.

[22] P. Liu, Z. Tao, Z. Lin, E. Erkip, and S. Panwar, "Cooperative wireless communications: A cross-layer approach," *IEEE Wireless Communications*, vol. 13, no. 4, pp. 84–92, 2006.

[23] T. A. Tsiftsis, G. K. Karagiannidis, P. T. Mathiopoulos, and S. A. Kotsopoulos, "Nonregenerative dual-hop cooperative links with selection diversity," *EURASIP Journal on Wireless Communications and Networking*, vol. 2006, no. 2, pp. 34–34, 2006.

[24] P. Anghel, M. Kaveh *et al.*, "Exact symbol error probability of a cooperative network in a Rayleigh fading environment," *IEEE Trans. Wireless Communications*, vol. 3, no. 5, pp. 1416–1421, 2004.

[25] J. G. Proakis, *Digital communications*. McGraw-Hill, 2000.

[26] M. Delibasic and M. Pejanovic-Djurisic, "Dual-hop amplify and forward relay system over non-identical Rician fading channels," *Wireless Personal Communications*, pp. 1–12, 2014.

[27] I. Gradshteyn and I. Ryzhik, *Table of Integrals, Series and Products 7th edn.* New York: Academic, 2007.

THE 5TH INTERNATIONAL CONFERENCE ON WIRELESS COMMUNICATIONS, VEHICULAR TECHNOLOGY, INFORMATION THEORY, AEROSPACE & ELECTRONIC SYSTEMS (WVITAE-2015)
December 13-16, 2015, Hyderabad, India

Digital door lock using fingerprint, webcam and GSM

A novel approach for smart homes

Ashish Patwari[2] , Arpit Omar[1], Shekhar kumar Thakur[1] and Kaushik kumar[1]
[1] Final year students B.Tech ECE, [2] Assistant Professor, School of Electronics Engineering
VIT University
Vellore, Tamilnadu, India
E-mail: ashish.p@vit.ac.in

***Abstract*— This paper explains the design and implementation of an electronic door lock using microcontroller and suitable peripherals. Home security has gained a lot of significance in the present day world owing to increased crimes, nuclear families and busy lifestyles. The proposed system provides a secure setup consisting of a fingerprint detection module, a webcam, microcontroller AT89S52, a GSM module, an LCD display and a DC motor. Fingerprints of 4 to 5 family members are registered in the fingerprint device. A user who wishes to enter the home shall get his/her fingerprint authenticated. Unauthorized users are denied access and the GSM module interfaced to the microcontroller sends an SMS to a predefined mobile phone (preferably, of the family head). The novelty of this project which differentiates it from the existing solutions [1-6] is that the webcam captures the image/scene in both the cases, irrespective of whether access is granted or denied. This feature helps in capturing any attempts made by burglars to gain access into the home by forcing children or elderly family members to undergo the fingerprint authentication. The webcam is serially interfaced to a personal computer and captures the events at the door. An optional LCD module displays the status of authentication or denial of access as the case may be. Upon authentication, the motor rotates and the door opens.**

Keywords—Microcontroller; fingerprint recognition R305; intelligent door lock; secure homes; GSM module SIM900; webcam; Proteus software.

I. INTRODUCTION

Modern households need foolproof security measures to provide access into the home. Smart homes call for digital or electronic solutions which offer reliability, ease of access, correctness and affordability. A digital door lock offers secure access through electronic and electromechanical components.

This project uses the most reliable biometric technique; namely, the fingerprint verification method. Other forms of biometric recognition include Iris scan, face recognition, voice recognition etc., Fingerprint techniques are simple, reliable and provide non-invasive means for personal identification as the patterns are unique to each individual.

Any biometric technique consists of two basic procedures, namely *Enrollment* and *Authentication* [1]. As a starting point, fingerprints of the family members are registered (enrolled) into the fingerprint module which is interfaced to the microcontroller through serial communication UART (Universal Asynchronous receiver transmitter). The complete system consists of a webcam, an optional LCD display, GSM SIM900 modem and a DC motor. Legitimate users are granted access whereas imposters are denied access.

The system provides accurate results for fingerprint scanning as the R305 scanner has False Acceptance Rate (FAR) 0.0001% and False Rejection Rate (FRR) 0.1% which are quite reasonable. Details about FAR and FRR can be found in [1].

The system was first simulated in the Proteus ISIS software. Since all the hardware components are not supported in the software, a keypad module was used instead of the fingerprint scanner and a virtual terminal was used in place of the GSM module just to ensure that the design and programming were correct. Once the desired functionality was achieved through software simulation, hardware interfacing was carried out.

II. EXISTING METHODS OF SECURE ACCESS

Authors in [2] propose a similar thought of biometric access using fingerprints but use an MMS mechanism to notify the house owner about imposters. Authors in [3-4] propose multi-factor authentication using fingerprint, RFIDs and one-time passwords (OTP) for secure ATM booth access. Authors in [5] and the references therein propose secure home access using the face recognition technology.

Other systems such as the traditional mechanical lock and key were replaced by electronic microcontroller locks which have passwords. These have been superseded by the use of smart cards (ID cards, RFID tags). Different modes of providing access are discussed in [6].

III. PRESENT PROJECT OR PROPOSED METHOD

The proposed system is built by interfacing suitable peripherals such as the fingerprint sensor (R305), webcam, 16x2 LCD display (optional), DC motor (with relay) and GSM modem with the microcontroller AT89S52. Users who wish to enter the home, have to clear the authentication procedure at

the fingerprint module (R305 optical fingerprint sensor) upon which, the microcontroller turns the motor ON and opens the door. In case of unauthenticated users, the access is denied, microcontroller sends an SMS to the house owner's mobile phone using the SIM900 modem. The optional LCD display shows 'Authenticated Door Opening' in case of authorized users and 'Access Denied' when the authentication fails. The webcam captures pictures at all instances of fingerprint access.

A. *Merits*

Our system is simpler than the one proposed in [2] as it uses SMS feature and eliminates the need of sending MMS links which are quite awful for general public as they need internet connectivity and complex mobile configuration settings. SMS based systems do not need internet connectivity or high-end mobile handsets.

Multi-factor authentication systems proposed in [3-4] are slightly expensive as they need additional circuitry and 32-bit microcontrollers. The only advantage of these systems is that they provide foolproof security because of multi-factor authentication.

Our system offers an inexpensive solution and low power operation compared to the above solution.

It also overcomes the drawbacks of password based systems by eliminating the need for memorizing complex passwords and gives the freedom from stolen password/smart card crimes. Fingerprints are time invariant and are not vulnerable to memory loss/hacking attacks. They do not require complex image processing techniques which are used for face recognition such as in [5].

B. *Uniqueness*

The novelty or uniqueness of this project comes from the fact that the webcam captures the images in all cases i.e., access grant or denial and forms a powerful repository of images which may be useful in cases of burglary to identify the culprits. Incidences of forceful authentication at ATMs and other places have been reported in many countries and are common examples of crime where the accused force the victims to login by threatening or manhandling. The proposed system provides an edge by capturing the images during successful authentications too, thereby providing an option to track events of forced entry into the homes.

IV. DESIGN AND IMPLEMENTATION

The design of any Embedded system is carried out by following the design lifecycle which involves identifying the requirements of the system, laying down specifications regarding the usage of hardware and software tools, optimization, detailed design of hardware and software coding, integration of hardware and software modules, testing and manufacturing followed by maintenance and upgrade. We take the same approach to explain about this project though the last two steps may not be applicable in this context.

A. *Requirements*

The requirement of the system is a fingerprint scanner which authenticates or declines the user requests, a webcam which takes pictures, a provision to send SMS to a pre-defined mobile number and a motor which runs to open the door.

B. *Specifications*

Hardware specifications

- AT89S52
- Fingerprint scanner R305_V1.6
- GSM modem SIM 900A
- Webcam (Genius video cam model NB1)
- 16x2 LCD display (HD44780)
- DC motor (100 rpm)
- Power Supply for 5V
- Top win universal programmer

Software specifications

- Keil IDE
- Proteus ISIS Professional
- Express PCB or OrCAD

C. *Hardware and Software Design*

Hardware flow

Initially a block diagram of the entire system was made and then the circuit level schematic was designed.

The following Fig. 1, shows the block diagram

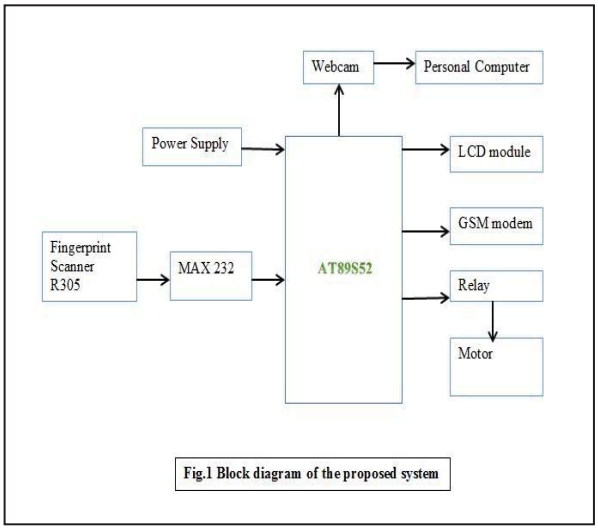

Fig.1 Block diagram of the proposed system

The fingerprint scanner operates with TTL logic. So a voltage level converter i.e., MAX 232 was used to interface. The LCD display unit is optional.

Software flow

A flowchart describing the sequence of operations was drawn and then the programming was done in Embedded C using the Keil IDE and the HEX code was generated.

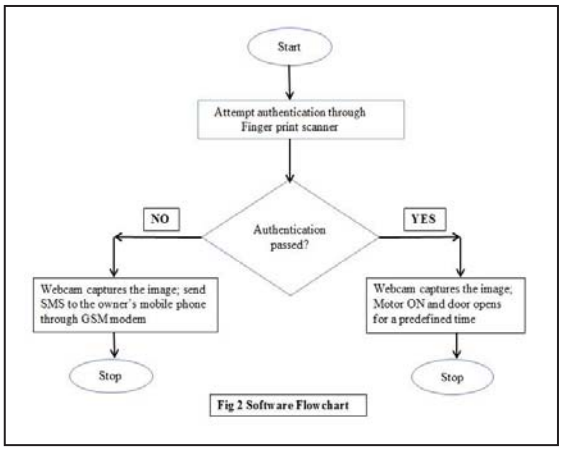

Fig 2 Software Flow chart

Hardware design

The circuit level design was implemented in the Proteus software. Keypad, virtual terminal were used in place of fingerprint scanner and GSM modem respectively. The Hex code which was generated through Keil was ported to the microcontroller in the Proteus environment. Simulation was carried out to verify the functionality of the concept.

The figures 3,4 below show the Proteus ISIS screenshots

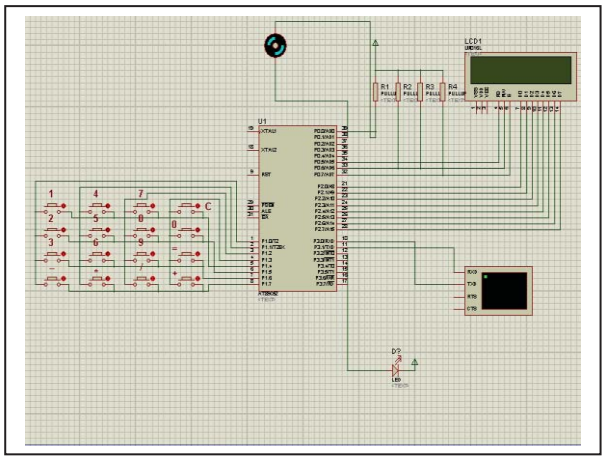

Fig 3. Circuit level schematic in Proteus ISIS

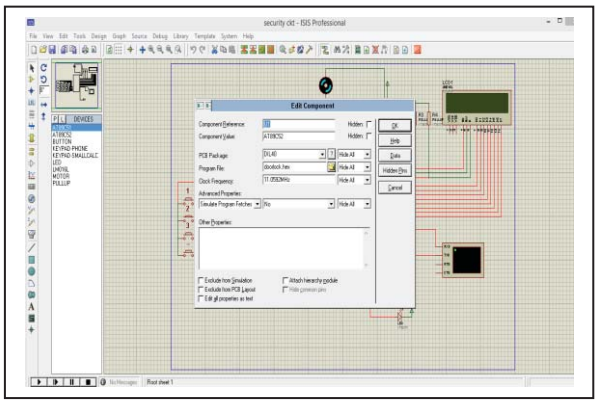

Fig 4. Porting HEX file into Proteus ISIS

After the simulation, the hardware prototype was implemented. All the required peripherals were procured and the interfacing was carried out.

Software design

The programming routines for the fingerprint module, webcam, LCD display and GSM module (using AT- attention commands) were being developed simultaneously.

D. Hardware software Integration

After successful code development and hardware interfacing, the hardware software integration was done by burning the HEX file into the microcontroller through the Top win programmer. An evaluation board for AT89S52 was made use of; to which the fingerprint, GSM and webcam were attached and the system prototype is shown in Fig 5.

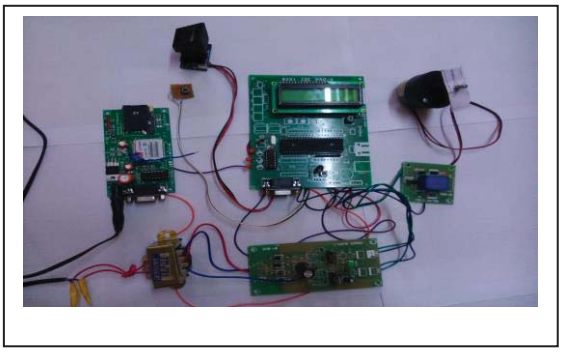

Fig 5. Hardware Prototype

E. Testing

The hardware model was tested by registering the fingerprints of different users. In case if the features are not registered properly, the device asks to undergo scanning once again. After the enrollment phase, the device was ready for operation. Figures 6-10 show that under different conditions, the circuit has functioned in the desired manner.

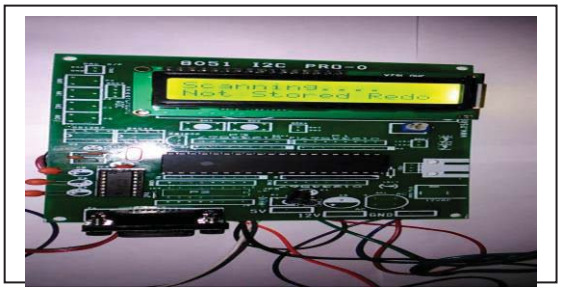

Fig 6. Circuit prompts the user to re-scan

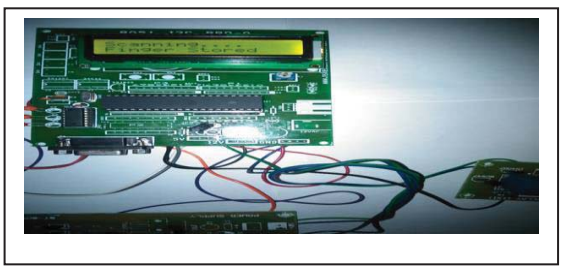

Fig 7. Scanning successful, fingerprint stored

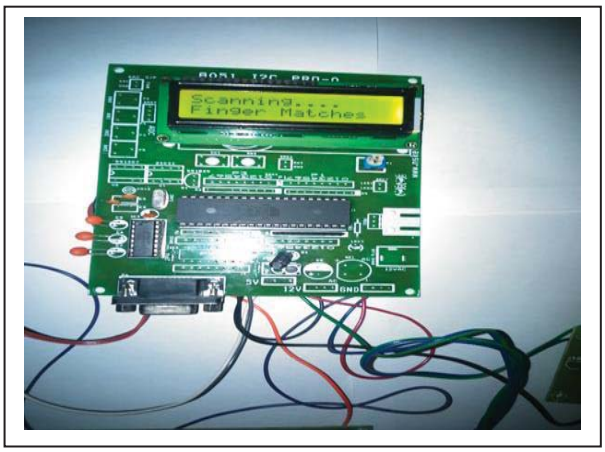

Fig 8. Authenticated user

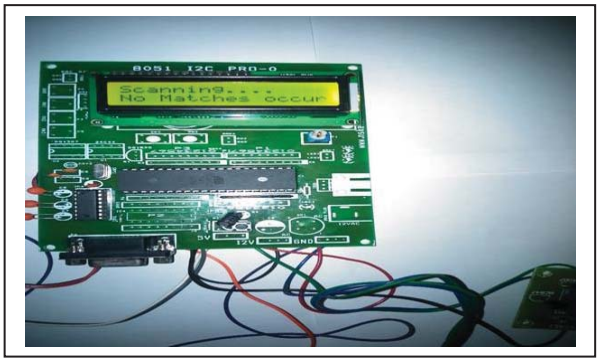

Fig 9. Authentication fails

Fig 10.SMS on owner's phone in case of imposters

Thus the desired functionality was obtained from the hardware prototype. After successful authentication, the microcontroller activates the DC motor through the ULN driver and relay circuit which opens the door for a predefined time of 30 seconds (which may be programmed as per the user's choice) and then closes the door. If the person misses out the entry during this time, he/she has to undergo the authentication test again.

The following Table I gives a brief description of the important hardware components used in this project.

TABLE I: KEY HARDWARE MODULES

Hardware module	**Specifications**		
	Description	***Product number***	***image***
Fingerprint sensor	Optical sensor, 500 dpi, can hold 250 fingerprints, 1:N matching	R305_V1.6	
GSM modem	Dual-band,GPRS capability, SIM holder, RS 232 serial communication, variable baud rate, AT commands	SIM 900A GSM/GPRS modem	
Webcam	Wired USB, 0.1MP, image recording BMP, JPEG format	Genius video cam model NB	

V. CONCLUSION AND FUTURE SCOPE

We would like to conclude that the digital door lock was designed and implemented using fingerprint, webcam and GSM modules. The working model was designed and tested. The system meets the desired requirements. The system offers a reliable and simple method to provide secure access to homes. It operates in real time and interacts with the real world. It ensures correctness and accuracy. The final product has to be manufactured by considering real world constraints such as the form factor, power consumption, cost, speed of operation etc.,

Future Scope

As discussed in [3], a mechanism of OTP authentication may also be used in addition to the fingerprint module. Other improvements such as interfacing a real-time clock (RTC) to the microcontroller to keep track of the events and corresponding calendar daytime. A pressure or vibration sensor may be interfaced such that the sensor can detect any event of tampering with the machine and raise an alarm using a sound buzzer. Using IoT (Internet of Things), the webcam can send email to the house owner's smartphone which is a viable option compared to the SMS or MMS techniques.

ACKNOWLEDGMENT

The authors would like to acknowledge the facilities and infrastructure available at the microcontroller lab and embedded systems lab in the School of Electronics Engineering, VIT University, Vellore. We would also like to appreciate the expertise and guidance obtained from the TIFAC core, VIT Vellore.

REFERENCES

[1] Mary Lourde R, Dushyant Khosla, "Fingerprint Identification in Biometric security systems," International Journal of Computer and Electrical Engineering, Oct 2010, 1793-8163.

[2] B. Anubala, M. Rahini, T. Bavithra, "Intelligent door locking system," International Journal of Engineering Research and Applications (IJERA), International Conference on Humming Bird, March 2014.

[3] D. Vinod kumar, Prof.M R K Murthy, "Fingerprint Based ATM Security by using ARM7," IOSR Journal of Electronics and Communication Engineering (IOSRJECE), ISSN: 2278-2834 Volume 2, Issue 5 (Sep-Oct 2012), PP 26-28.

[4] Raghu Ram.Gangi, Subhramanya Sarma.Gollapudi, "Locker opening and closing system using RFID, fingerprint, password and GSM," International Journal of Emerging Trends & Technology in Computer Science (IJETTCS), Volume 2, Issue 2, March – April 2013.

[5] I.Yugashini, S.Vidhyasri, K.Gayathri Devi, "Design and Implementation Of Automated Door Accessing System with Face Recognition," International Journal of Science and Modern Engineering (IJISME), ISSN: 2319-6386,Volume-1, Issue-12, November 2013.

[6] Pavithra.B.C, Myna.B.C, Kavyashree.M, "Fingerprint Based Bank locker system using Microcontroller," Proceedings of IRF International Conference, 05th April-2014, Pondicherry, India, ISBN: 978-93-82702-71-9.

[7] Mazidi and Mazidi, The 8051 Microcontroller and Embedded Systems using Assembly and C, 2nd Edition, Pearson India, 2007.

[8] Rajkamal, Microcontrollers: Architecture, Programming, Interfacing and System Design, 1st Edition, Prentice Hall of India, 2009.

[9] PCB Design Tutorial –David.L.Jones, 2004.

THE 5TH INTERNATIONAL CONFERENCE ON WIRELESS COMMUNICATIONS, VEHICULAR TECHNOLOGY, INFORMATION THEORY, AEROSPACE & ELECTRONIC SYSTEMS (WVITAE-2015)
December 13-16, 2015, Hyderabad, India

1570211897

Mesh IP Video Surveillance Systems Model Design and Performance Evaluation

C. S. Lubobya , M .E. Dlodlo, G. De Jager and A. Zulu, *Members, IEEE*

***Abstract*— This paper proposes a model for Internet Protocol (IP) mesh video surveillance systems and presents the performance evaluation of AODV and OSPF routing protocols in wireless mesh video surveillance system. A wireless mesh video surveillance network consists of IP cameras linked to mesh routers which are then linked to the mesh gateways. Local monitoring can be done by inserting a switch or router between the gateways and the Internet while remote monitoring can be done through the Internet. Routing provides selection, constructing and management of routes in order to maximise Throughput and minimise video Packet Losses, End-to-End delays and Jitter. Results show that the OSPF routing protocol outperformed the AODV in Throughput, Packet Loss, End-to-End delay and Jitter terms with a throughput advantage of 35%.**

***Index Terms*— Wireless Mesh Networks; Video Surveillance; Routing Protocols ; Throughput; End-to-End delay; Jitter.**

I. INTRODUCTION

There is an increased use of wireless mesh network (WMNs) in homes, industries and service organizations for data and voice applications. Wireless Mesh Networks are communication networks consisting of wireless devices, with single or multiple radio interfaces, for the purpose of receiving and transmitting defined information type. Video streaming, broadcasting and video surveillance applications are some of the applications in which wireless Mesh networks can be used. WMN have the advantage that they provide large coverage area, have low backhaul connection costs, prolong battery life for end-users and above all provide connectivity to users without line of sight[1]. The architectural design differs depending on application and number of source nodes connected or anticipated to be connected. Three common network architecture designs have been proposed in [1] [2]: infrastructure/backbone, client and hybrid infrastructure-client type. Devices making up the WMN architecture include a combination of: mesh clients (MCs) and /or non-mesh clients, Access Points (APs), Mesh Routers (MRs) and Mesh Gateways (MGs).

For the infrastructure/backbone based WMN, mesh clients and mesh routers connects to the Internet through mesh gateways using wired cables. Mesh routers relay information from mesh clients to the mesh gateways, which routes the information to the Internet. Both the mesh routers and gateways have multiple interfaces. Fig.1 illustrates the infrastructure based WMN.

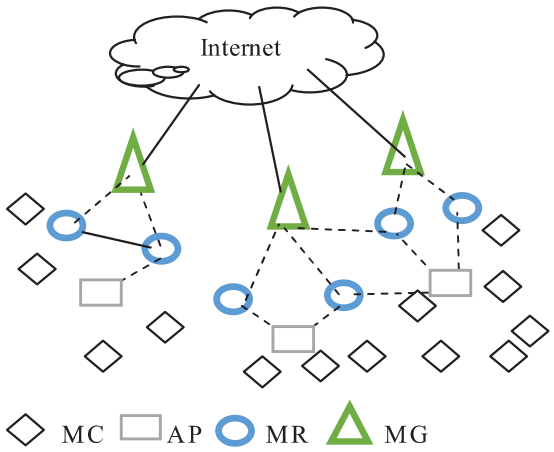

Fig. 1: Wireless Mesh Network Infrastructure

In client WMN, mesh clients connects to each other as peers. There are no wired connections, mesh routers and gateways as each mesh client is a standalone device with routing functions [3]. The hybrid WMN combines the infrastructure and client WMN whereby internet, Wi-Fi, sensor and connectivity is provided by the infrastructure component while the client WMN part provides routing and configuration functions.

Routing protocols provides selection, construction and management of routes. It also maximises throughput and minimises video packet delays[2]. Additionally, Jun and Sichitiu suggested that general Mobile Ad-hoc Networks (MANET) routing protocols can be used in WMN[4].

This paper proposes a model for IP mesh video surveillance system and presents the performance comparison of AODV and OSPF routing protocols for a meshed video surveillance system operating in the Meshed Wi-Fi environment. The next section gives related work on routing in mesh networks. Section III, discusses the wireless mesh IP video surveillance system in detail and explains the functions of each unit. The detailed description of the ad-hoc and dynamic routing

This work is supported by the University Science, Humanities and Engineering Partnerships in Africa (USHEPiA) Fund.

C. S. Lubobya is with the faculty of Engineering and Built Environment , Electrical Engineering, University of Cape Town, P/B X3, South Africa, (e-mail: lbbsma001@myuct.ac.za.)

M .E. Dlodlo is with the faculty of Engineering and Built Environment , Electrical Engineering, University of Cape Town, P/B X3, South Africa, (e-mail: mqhele.dlodlo@uct.ac.za.)

G. De Jager is with the faculty of Engineering and Built Environment , Electrical Engineering, University of Cape Town, P/B X3, South Africa, (e-mail: gerhard.dejager@uct.ac.za.)

A. Zulu is with the School of Engineering, Department of Electrical & electronics Engineering, University of Zambia, Box 37392, Zambia, (e-mail: ackim.zulu@unza.zm.)

1570211897

protocols is given in section IV. Section V describes the simulation set up in details while section VI discusses the results obtained in simulations. The conclusion is given in section VII.

II. RELATED WORK

A new Mesh Routing Protocols (MRP) was proposed and its performance evaluated and compared to the traditional mobile ad-hoc network routing protocols in the work by Jun and Sichilui [4]. MRP outperformed the general purpose MANET protocols in terms of routing overhead, packet delivery ratio, network throughput, end-to-end delay, and average hop-count [4]. Broch et al.[5] did a performance comparison study of multi-hop wireless ad hoc network routing protocols. They configured 50 mobile nodes connected in multi-hop fashion and observed that the Dynamic Source Routing (DSR) and Ad-hoc On-demand Distance Vector (AODV) performed particularly well, delivering over 95% of the data packets regardless of mobility rate compared to Temporarily Ordered Routing Algorithm (TORA) and Destination-Sequenced Distance Vector (DSDV) protocols. Shubat and Essied [6] compared the performance of the AODV protocol for single and multi-radio scenarios. They observed that the AODV performed well in a multi radio in terms of throughput, end to end delay and packet loss. Campista et al.[7] evaluated the performance of different WMN routing metrics; Hop count, Expected Transmission Count (ETX), Expected Transmission Time (ETT), and ML metrics. They implemented and assessed them using the OLSR routing protocol. Chissungo and Blake [8] in their review on ad hoc routing protocols categorised and discussed the inner workings of proactive, reactive and hybrid ad- hoc routing protocols.

This paper makes the following contribution: firstly it proposes a network model for wireless mesh IP video surveillance by exploiting the advantages of mesh networks discussed in section I. Secondly, the paper investigates the performance of OSPF and AODV routing protocols for such a model in terms of throughput, jitter, packet loss and delay.

III. WMN VIDEO SURVEILLANCE MODEL

Fig.2 shows a wireless mesh video surveillance model. It consists of several Wi-Fi IP cameras; wireless Mesh Routers (MRs) and Mesh Gateways (MGs) to form an infrastructure based video surveillance system. The IP cameras are not meshed clients, that is, they do not send surveillance video from one IP camera to the other. The cameras connect directly to the mesh routers. This way the hop count is minimized as Video surveillance information routed to the MRs only hops from IP cameras to each of the MRs and the MGs. Hop count is the number of hops between the IP cameras and the MGs [1]. A detailed description of each unit in the model now follows.

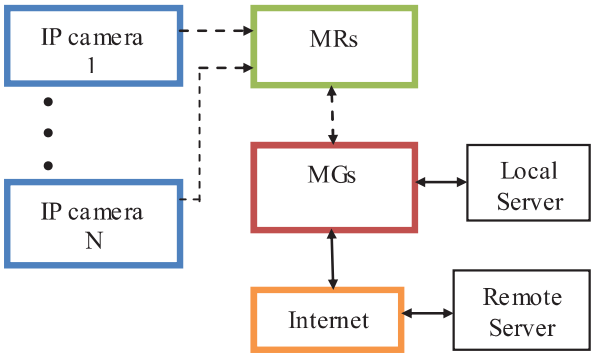

Fig. 2: Block Diagram of a Mesh IP Video Surveillance System

A. IP cameras

An IP camera or network camera , is a device that digitizes and processes analog images or videos, encodes them internally and then transmits the video information digitally over a wired or wireless connection to a computer or similar device [9].The Wi-Fi video surveillance IP cameras consists among other components the lens, the Charge Coupled Device (CCD) or the Complementary Metal Oxide Semiconductor (CMOS), the analogue to digital converter (A/D) and the Digital Signal Processor (DSP). There are various types of IP cameras: dome, box, bullet, covert, Pan Tilt Zoom and the like cameras. Some of these camera types have Wi-Fi functionality.

In general, the network bandwidth (B) can be calculated from the knowledge of number of IP cameras, frame size and frame rate as:

$$B = \frac{FS \times FR \times N \times 8}{1024} \quad (1)$$

Where the frame size in Kilobytes is, is the frame rate and is the number of IP cameras. The constant 8 is included since there are eight bits per byte. However, the actual bandwidth consumed by each router in the network can be measured and is called the flow throughput. Flow throughput (T_{flow}) is the summation of the traffic sent by MRs and received by the MGs over the observation period [10]. It is a measure of the bandwidth consumed by each router in the network.

$$T_{flow} = \frac{\sum_{k \in K} \left| \, rec.bits(n \to k) \, \right|}{t} \quad (2)$$

B. Mesh Routers and Gateways

These are wireless multi-interface devices operating in the ISM band of frequencies. Typically, in this model we used 2.4GHz unlicensed frequency. Mesh routers provides the first access or contact point for the IP cameras. They then relay the surveillance information to the mesh gateway routers. The mesh gateway has Ethernet connectivity to the internet. This

1570211897

work involved creating custom mesh routers and mesh gateways. We created multiple radio interfaces and configured the new devices for video surveillance use.

C. Internet

Surveillance information can be routed to the local storage servers and monitoring displays or to the remote monitoring devices via the internet. A category 5 or 6 Ethernet cable is recommended for the MG-switch-Internet link connectivity. The Internet can be accessed anywhere using web connectivity and therefore it provides a link for remote monitoring.

D. Local and Remote Monitoring

Local monitoring can be placed anywhere between the mesh gateways and the internet. Practically, that would mean inserting a switch or router (not shown) between the mesh gateways and the internet. The local and remote monitoring consists of video servers, one or several display units and/or personal computers. Some modern, Wi-Fi IP cameras do have provisions for a memory card through which surveillance information can be stored before transmission to the nearest mesh router."

IV. AD-HOC AND DYNAMIC ROUTING PROTOCOLS

In this section, a detailed discussion of ad-hoc and dynamic routings protocols is done in order to determine the possibility of use in WMN video surveillance systems.

A. Ad-hoc Routing Protocols

Ad-hoc networks are infrastructure-less networks in which every node in the network can communicate to the next node via a wireless link. Ad-hoc routing protocols are primarily employed in Ad-hoc networks. We investigate their performance in this work considering that part of WMN design is infrastructure-less. These protocols are broadly classified as proactive, reactive and hybrid ad-hoc routing protocols.

In proactive or table-driven routing protocols, each node continuously updates it routes to every other node in the network and keeps at least one route to any destination in the network[7][10]. Routers periodically transmit routing information throughout the network and maintain a consistency routing table. Examples of proactive ad-hoc routing protocols includes: DSDV, Wireless Routing Protocol (WRP), Global State Routing (GSR) and Cluster-head Gateway Switch Routing (CGSR). One major drawback of these type of ad hoc routing protocols in highly dynamic network topology is that a large amount of resources is needed to keep routing information up to date [11].

With Reactive or On-Demand Routing protocols, a node only requests the route to the destination if it has a packet to send [7] [11]. The major advantage of on-demand protocols is that communications overheads are reduced as requests are only send when there is a packet to transmit. However, that potentially increases delay during transmission due to route research process. Examples of reactive protocols include AODV, DSR, Cluster Based Routing Protocol (CBRP), Temporally Ordered Routing Algorithm (TORA), Associativity-Based Routing (ABR), Location Aided Routing (LAR) and Signal Stability Routing (SSR).

Alternatively, they can be classified as source initiated, power aware, hybrid, location aware, multicast and the like as categorised by Boukerche *et al* [12]. Hybrid protocols combine features of proactive and reactive protocols. The fundamental roles of these protocols are essentially the same: increasing or maximising throughput while reducing packet loss, control overhead and energy usage [12].

B. Dynamic Routing Protocols

Dynamic routing protocol are a class of routing protocols in which a router learns about the network topology by announcing its presence and sharing its available routes with other routers on the network [13]. Existing routers update their routing tables every time there is new router addition on the network; thus routers learn about each other on the network. Dynamic routing protocols have two major advantages over static routing protocols: scalability and adaptability [13]. As Scalable routing protocols they enable network to grow more quickly and in a large way, and adapts well to network topology growth or failure of one or more network components[13]. Other advantages are that configurations are less prone to error and consume less time to configure and maintain.

Dynamic routing protocols are divided into interior and exterior gateway protocols. Interior gateway protocols are used for routing inside an autonomous system.ie within the network systems. Exterior routing protocols are used for routing between autonomous systems and example is the BGPv4 routing protocols. Interior gateway protocols are further divided into Link State Protocols and distance vector protocols.

Link state protocols selects the best routing path by calculating the state of each link in a path and finding the path that has the lowest total metric to reach the destination [13]. The best route for data is calculated based on cost. Once convergence occurs, protocol traffic is limited to changes in specific links. Examples include: Intermediate-System to Intermediate-System (IS-IS), Open Shortest Path First (OSPF), etc. With OSPF a complete topological database of all connections in the local network is maintained and each router calculates from its data structure the shortest path tree. This path tree describes the shortest path to each destination address and specifies the nearby router to send to for each communication [13].

Distance Vector Protocols selects the best routing path based on a distance metric and an interface [13]. It uses a distance calculation plus an on-going network interface to choose the best path to the destinations network. Examples of distance vector protocols are Routing Information Protocol (RIP) versions one and two, Interior Gateway Routing Protocol (IGRP) and Enhanced Interior Gateway Routing Protocol (EIGRP). When a change occurs in the network, the router with the change informs other routers.

V. PERFORMANCE EVALUATION METHODOLOGY

For evaluating the performance of the model under varying routing protocols and channels assignment schemes, we used an H.264/AVC CIF video with 352x268 resolutions,

1570211897

10 frame per second video and having a payload of 3216 bytes. OPNET Modeller 14.5 network simulator tool was used in simulations.

Two scenarios were adopted in our simulation based on the model of Fig.2. Scenario one consists of a mesh video surveillance system with 28 IP cameras with half of the cameras clustered around and linked to MR1 and the other half around MR2. All IP cameras are single mode, consisting of one wireless LAN interface in the IEEE 802.11g, 2.4GHz unlicensed ISM frequency band. The two mesh router MR1 and MR2 are also wirelessly linked to the two mesh gateways, MG1 and MG2. Like the IP cameras, mesh routers and mesh gateways are all operated in the IEEE 802.11g and the buffer size set to 1,024,000 bits. Further, the MR and MG have all been custom created with multiple wireless interfaces and have been configured as illustrated in Table 1. Care has been made to disable wireless access functionality on the IP cameras since the intention is to transmit video surveillance information in one direction, typical of surveillance systems. We then configure OSPF routing protocols and IP addresses on the mesh and non-mesh device interfaces. The system is run for 20 minutes and throughput, end to end and jitter values plotted and compared to the second scenario.

TABLE 1: CONFIGURATION OF MESH DEVICES

Mesh device	Interface	channel	Frequency (MHz)
IP camera cluster 1	1	1	2412
IP Camera cluster 2	1	2	2417
MR1	3	1 4 6	2412 2427 2437
MR 2	3	2 5 7	2417 2432 2442
MG1	2	5 6	2432 2437
MG2	2	4 7	2427 2442

The second scenario is duplicated, retaining the IP cameras and mesh devices parameters setup, including geographical position of all devices. The only change made is the type of routing protocol; the AODV ad-hoc routing protocols is now configured. The start time for all simulations was 100s and end time was 1200s.

For a valid video transmission packet loss should not exceed 1% [14], otherwise throughput needs would not be satisfied. End to end delay should be less than between 150ms and 200ms [14] [15] while jitter delay for one way traffic should be less 60ms [14]. The two scenarios are run under strict assumptions that: no other programme is running during simulations, including web browsing. Simulating devices are assumed not to have any external interfering signals.

VI. RESULTS AND DISCUSSION

Fig.3 shows the results of the throughput measurement over the simulation time of 1200s or 20minutes based on (2) for 28 cameras. As seen from the figure when the mesh surveillance system was configured with OSPF routing protocol, an average throughput of 6.63Mbps was measured in contrast with 4.31Mbps for the AODV routing protocol. That represents a 35% throughput increase for OSPF under similar conditions. This can be attributed to the fact that with AODV protocol, Mesh routers gets flooded with surveillance video information bits. Flooding tends to make the network inefficient since connections happen on nodes that are close to each other, in this case IP cameras and mesh routers. OSPF controls flooding of mesh devices. Control packets should be sent to close nodes in order to make the network efficient thereby improving capacity.

The throughput versus number of IP cameras is shown in fig. 4. The throughput under OSPF routing protocol increases linearly with increase in number of IP cameras upto 28 cameras. Beyond 28 cameras the throughput maintains a constant value of 6.62Mps. With AODV protocol, throughput too increases with increase in number of IP cameras. However, beyond 28 cameras throughput begins to drop. OSPF performs better than AODV regardless of the number of IP cameras. Throughput for either routing protocols type does not exceed the calculated capacity (B) plot based on (1).

In fig. 5, we show the packet/bit loss comparison between the two routing protocols for the two scenarios. Both scenarios are loaded with 6.63Mbps. A bit loss of 0.44mbps was recorded for the AODV and none for the OSPF. AODV packet loss percentage of the total load was 6.58% which is above the accepted percentage of below 1%. These bit loss results when compared to results of fig. 4, further explains why throughput is low.

Fig. 6 shows the measured results for End-to-end delay. The OSPF routing protocol outperformed AODV with 0.31ms End-to-end delay compared to the 6.24ms measured for the AODV. The AODV and OSPF performance are all within the acceptable limit of 150ms. However, increasing the number of IP cameras, frame size and frame rate could possibly make AODV End- to- End delay values exceed the 150ms limit.

The average jitter variations measured results is shown in fig. 7. For easy comparison, a logarithmic scale has been used. AODV has a high log average jitter value than the OSPF. In time terms this represents an average jitter of 18ms for AODV compared to 5.34 μs for OSPF with both values within recommended limit of less 60ms for video transmission. The good performance of the OSPF can be attributed to the shorter hop network formed thus reducing the size of the mesh topology and creating sub-optimal routes. AODV Queues video packets when discovering new routes causing packets to be dropped, minimising throughput and increasing latency.

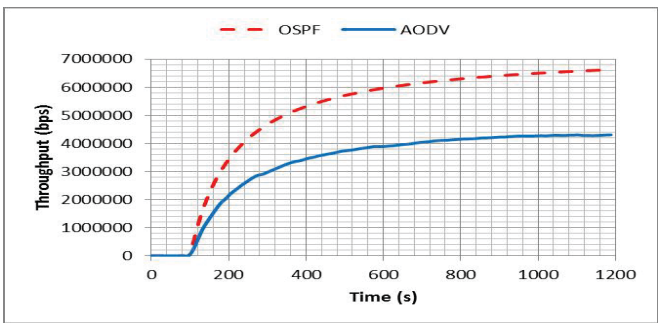

Fig.3: Throughput measurement for OSPF and AODV Routing Protocols

1570211897

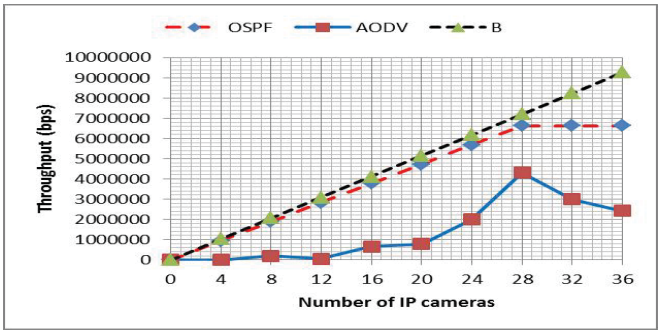

Fig.4 Throughput variations as number of cameras increases

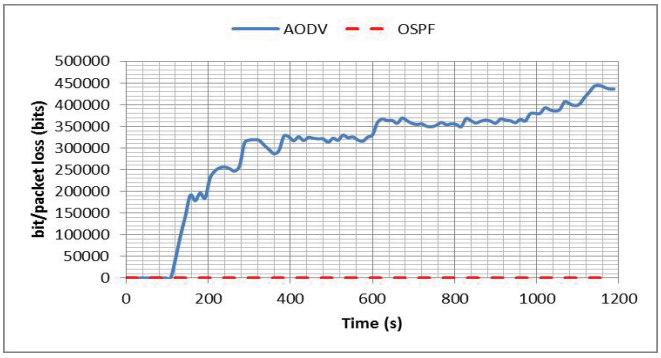

Fig.5: Bit Loss Measurements at the Buffer

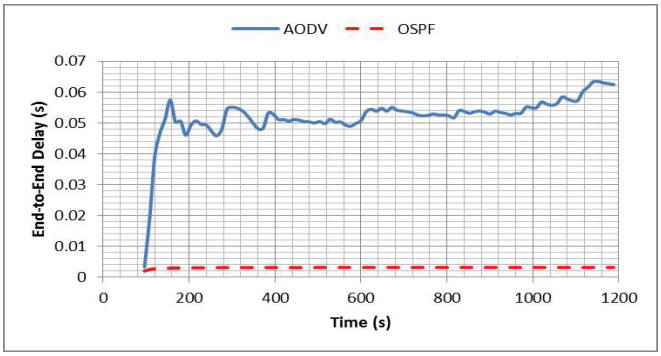

Fig.6: End-to-end Delay measurement

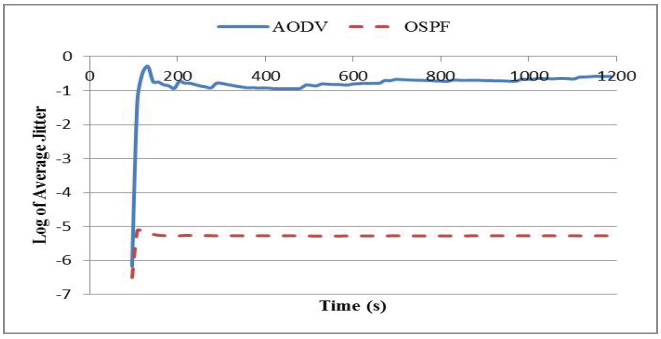

Fig.7: Jitter measurements for the two scenarios

VII. CONCLUSION

This paper has proposed a mesh IP video surveillance model and presented the performance comparison between OSPF and AODV routing protocols in the IEEE 802.11g, 2.4GHz mesh environment. The OSPF routing protocols outperformed the AODV routing protocols in throughput by 35% for 28 cameras; OSPF performs better than AODV regardless of the number of IP cameras. The OSPF routing protocols also has better packet loss, End-to-End delay and jitter values than the AODV, making OSPF a better routing protocol for video surveillance applications. Going forward, an investigation on effect of mesh topologies and routing algorithms on throughput, packet loss and jitter is suggested.

REFERENCES

[1] D. Benyamina, A. Ha, and M. Gendreau, "Wireless Mesh Networks Design — A Survey," vol. 14, no. 2, pp. 299–310, 2012

[2] S. Odabasi and A. Zaim, "A Survey on Wireless Mesh Networks, Routing Metrics and Protocols," *International Journal Of electronics, mechanical and mechatronics engineering,* vol. 2, pp. 92–104, 2010.

[3] I. F. Akyildiz, "A survey on wireless mesh networks," *IEEE Commununications Magazine*, vol. 43, no. 9, pp. S23–S30, 2005.

[4] J. Jun and M. L. Sichitiu, "MRP: Wireless mesh networks routing protocol," *Comput. Commun.*, vol. 31, pp. 1413–1435, 2008.

[5] J. Broch, D. Maltz, D. Johnson, Y.-C. Hu, and J. Jetcheva, "A Performance Comparison of Multi-Hop Wireless Ad Hoc Network Routing Protocols," *4th Annu. ACM/IEEE Int. Conf. Mob. Comput. Netw.*, pp. 85–97, 1998.

[6] S. S. Ahmeda and E. A. Essied, "Routing Protocols for Wireless Mesh Networks," Iecture Notes Softw. Eng., vol. 1, no. 1, pp. 35–38, 2013.

[7] M. E. M. Campista, P. M. Esposito, I. M. Moraes, L. H. M. Costa, O. C. M. Duarte, D. G. Passos, C. V. N. De Albuquerque, D. C. M. Saade, and M. G. Rubinstein, "Routing Metrics and Protocols for Wireless Mesh Networks," *IEEE Netw.*, vol. 22, pp. 1–30, 2008.

[8] E. Chissungo, H. Le, and E. Blake, "Routing Protocols and Metrics used on Wireless Mesh Networks,"[Online].Availab: http://people.cs.uct.ac.za . [Accessed:15-June, 2015].

[9] J.Cabasso, "Analog vs. IP Cameras." [Online]. Available: http://www.aventuracctv.com/newsletter/DOCS/Aventura_Newsletter_02_Analog_vs_IP_Cameras.pdf. [Accessed: 02-Jun-2014].

[10] A. Ouni, H. Rivano, and F. Valois, "Capacity of wireless mesh networks: determining elements and insensible characters.," PlanNet 2010, Int. Work. Plan. Optim. Wirel. Commun. Networks (IEEE WCNC2010 Work., 2010.

[11] A. K. Gupta, H. Sadawarti, and A. K. Verma, "Performance analysis of AODV, DSR & TORA routing protocols," IACSIT Int. J. Eng. Technol., vol. 2, no. 2, pp. 226–231, 2010.

[12] A. Boukerche, B. Turgut, N. Aydin, M. Z. Ahmad, L. Bölöni, and D. Turgut, "Routing protocols in ad hoc networks: A survey," Comput. Networks, vol. 55, no. 13, pp. 3032–3080, 201

[13] S. G. Thorenoor, "Dynamic routing protocol implementation decision between EIGRP, OSPF and RIP based on technical background using OPNET modeler," 2nd Int. Conf. Comput. Netw. Technol. ICCNT 2010, pp. 191–195, 2010.

[14] J. M. Hamodi and R. C. Thool, "Investigate the performance evaluation of IPTV over WIMAX Networks," vol. 5, no. 1, pp. 81–95, 2013.

[15] Y. Chen, T. Farley, and N. Ye, "QoS Requirements of Network Applications on the Internet," Information-Knowledge-Systems Manag., vol. 4, pp. 55–76, 2004.

THE 5TH INTERNATIONAL CONFERENCE ON WIRELESS COMMUNICATIONS, VEHICULAR TECHNOLOGY, INFORMATION THEORY, AEROSPACE & ELECTRONIC SYSTEMS (WVITAE-2015)
December 13-16, 2015, Hyderabad, India

Variable Encoding and Sequencing Pattern Driven Multiple Image Bit Watermarking for Wireless Domain

(VESPDMIBWWD)

Soumit Chowdhury
Department of Computer Science & Engineering
Government College of Engineering & Ceramic Technology
Kolkata, India, Pin 700010, West Bengal, India
sc_study123@yahoo.in

Nabin Ghoshal
Department of Engineering & Technological Studies
University of Kalyani
Kalyani, Nadia, Pin 741235, West Bengal, India
nabin_ghoshal@yahoo.co.in

***Abstract* - The paper presents a novel color image authentication scheme by variably watermarking bits of four secret images within the carrier image imparting multi verification criteria applicable for the wireless platform. Secret bits are hidden into all the pixel bytes of the sub image block using distinctly different dynamically variable bit insertion approaches on each of them within the spatial domain values. Additionally bits are also inserted with different sequencing patterns on the pixel bytes of the sub blocks involving the bits of the same or the different secret images injecting robustness and reliable authentication. Apart from that secret bits are randomly rotated on these pixel bytes ensuring strong security and resistance against the image processing attacks. Threshold based highly variable and randomized coding ranges are further adopted on these pixel bytes eventually strengthening the robustness against the attacks in combination with the secure bit insertion policies needed for the wireless domain. Delicate noise adjustment on these bit embedded pixel bytes optimizes the distortions against the attack fragility limits and ultimately improving the watermarked image quality even with very high data pay load capacity. This dynamically randomized separate encoding strategies for the different multi-image secret bits actually enhancing the watermark sustainability as well as secure authentication scenarios. Experimental results have confirmed outstanding watermark imperceptibility by far as compare to the other existing schemes while pretty decent robustness is also achieved against the image processing operations with the multi watermark insertion concept encouraging utilization of the approach under the public wireless environments.**

Keywords—Steganography;Multiple-Image-Hiding;Image Authentication;Multi-Image-Watermarking;Variable-Bit-Hiding–Sequence;Variable-coded-watermarks.

I. INTRODUCTION

Advancement in digital transmission demands secure communication as well as strong authentication scenarios where Steganographic approaches are often utilized for hiding the secret images within the carrier image authenticating its ownership. In this context color image authentication can be considered more suitable due to their wider ranges of color variations and having enough redundant information for hiding the secret bits [2-4]. In extension of this multiple image watermarking is further explored in recent times involving multiple verification phases and they are relatively robust as compare to the single image watermarking concept [5,6]. This idea actually encourages reasonable recovery of at least one of the hidden images under the common image processing operations [7-10] and is quite useful for synchronously embedding the watermarks for the multiple users [5-15].

In the present scenario image authentication with multiple watermarks can be considered very vital in the wireless domain in order to reliably and efficiently validating the transmission of digital e-documents. Wireless environment is basically susceptible to illegal unauthorized access and its signal transmission also suffers from severe distortions due to the heavy noise inclusion within the host signal [17]. So multi image watermarking within the transmitted host image not only resists the total destruction of the hidden watermarks but also introduces strong authentication for this domain [5-9,17].

A. Related Works

Among the existing works [3], in 2009 divided and encrypted multiple parts of a binary watermark image and embedded them into the blue components of the host color image for achieving robustness but the process is somewhat non blind in nature. Then [4], in 2010, watermarked three small grey-scale images in the Red, Green, and Blue channel with their respective encryption keys using a chaotic map based technique where embedding positions and the watermark bits are encrypted using the pair coupled maps. The approach reflects marginal watermarked image quality while the authenticating images are mostly affected by attacks. Reference [5], in 2010 embedded 24 binary images within the mid frequency components of the DCT as the RGB watermark and also inserted 12 binary images using the different LSB substitution techniques while the watermark images are

differently scrambled for different domains before embedding. Then [6], in 2011 suggested a multiple grey-scale based watermarking scheme for medical images using DWT and repetitive BCH encoded watermarks which are destroyed under the cropping and contrast attacks. Reference [7], in 2013, developed a technique using DWT where two small watermarks are embedded successively one after the other and also they are segmented between the odd rows and the even rows but the qualities of the images were affected to an extent even with the small watermarks. Then [8], in the same year proposed a technique for embedding multiple gray scale watermarks in the DCT and spatial domains separately with fuzzy-c means clustering that identifies the small zones of watermark embedding. Although the approach shows robustness but the watermark imperceptibility is not very high. Reference [9], in 2013 added multiple grey scale watermarks by segmenting the host image into non overlapping blocks by means of space filling curve and block DCT energy. Watermarks are added by modifying the respective block singular values but 3-level ENOPVD decomposition introduces greater overhead with increasing distortions also. On recent concepts [10] in 2014 showed binary double image watermarking based on the position property of the grey scale cover image although it has not resulted relatively good quality of the extracted images. Reference [11] in 2014 also highlighted watermarking of four binary images where DWT is applied on the non-overlapping sub blocks while the most densely packed information blocks are identified based on the texture for watermark insertion. Reference [12], in the same year demonstrated gray scale based invisible multiple biometric watermarking approach in the different frequency bands with re-watermarking concept where the interference of the different watermarks are to be reduced considerably. Reference [13] in the same year embedded two watermarks one after the other on the host image with different embedding methods like additive, multiplicative and hybrid using the DWT but the quality of the extracted images under the noise attacks are not that great. Then [14], in 2015 proposed a technique where three combined binary watermarks in a 3-D watermarking sequence were added into the sub image blocks with best abundant texture information and the approach shows at least one watermark recovery against the common image processing attacks. Reference [15], in 2015 introduced two level watermarking for biometric images where the sparse measurement information on fingerprinting while the iris bio-metric template using CS theory was generated for secure watermarking but the watermarked image quality was low.

B. Motivation

Existing works [3-15] are mainly focused on binary or gray scale images supporting very little data pay load capacity while every pixel bytes of a sub image block are not considered for watermarking that would have eventually increased the availability or robustness aspects of the secret bits. In addition these works have very rarely highlighted the different bit sequencing patterns on the sub block pixel bytes involving the secret bits of the same or the different images for further tackling the robustness issues. Although some approaches have adopted different bit insertion techniques for embedding successive watermarks but hardly any work that proposes distinctly different dynamically variable bit insertion policies on each of the different pixel bytes of the sub image blocks. In fact this successive watermark insertion does not guarantee the quality of the watermarked image while they are destroyed with severe cropping attacks.

In view of these unaddressed issues especially for the wireless domain the work adopts distinctly different dynamically variable secret bit insertion strategy for each of the pixel bytes of the sub image block with extreme randomization. Also multi-watermark bit embedding is done sequentially through the threshold based variable range driven bit insertion approach that somewhat enhances the robustness as compare to the successive watermark embedding policy. Additionally different secret bit sequencing patterns involving the bits of same or the different watermark images are incorporated in a more randomized manner onto the separate pixel bytes of the sub image blocks. This idea basically strengthens the availability cum robustness aspects of the secret bits and even adding an extra layer of security on the authentication scenarios apart from the secure bit insertion criteria. Avove all partial noise adjustment on the bit inserted pixel bytes not only optimizes the distortions against the robustness but actually imparts further randomizations as well.

The paper is organized as follows; sec.2 describes the bit insertion and extraction process, sec.3 shows the experimental results, sec.4 presents the social application, sec.5 gives the conclusion followed by acknowledgement and references.

II. The Technique

A. Bit Insertion Algorithm

Input: One color cover image and four secret color images.
Output: One watermarked color image having hidden images.
Method: Cover image is divided into 2x2 non overlapping sub block of pixel bytes for inserting one secret bit into each pixel byte resulting four bit insertion per sub matrix block. These four bits are hidden on a random rotational sequence starting from the pixel byte position 'I' of the sub matrix decided from the matrix number 'Mat' as I=[sum of the digits of Mat+Digit reverse value of Mat+(Mat+digit reverse value of Mat)%4]%4
Steps:
1. Secret Bit Insertion for the First matrix Element-
1.1 Last two digits of the matrix number D2D1 written in a reverse manner and the resultant decimal number is then modulo with 4, while the mod value resulted between 0-3 is added with 3 to obtain the range value M as M=(D2D1)%4+3.
1.2 The upper(U) and lower(L) multiple value of M with respect to the first matrix element number is then considered and the respective reference point R of the range is calculated as the round off value for the expression R=(L+U)/2.
1.3 Now for inserting the secret bit '1' or '0', the output coding C will be performed as – for inserting '1', if M=3, then C=R, otherwise C=R+1, but for inserting '0', C=R-1 always.
1.4 The coded value C thus obtained will be written in the first element position of the sub matrix block as the output value.
2. Secret Bit Insertion for the Second matrix Element-

2.1 Lower (L) and upper (U) multiple number of 6 with respect to the second element value is considered. **2.2** Matrix number (Mat) is then modulo with L and the resultant value is again modulo with 3 to obtain value v1(0-2). **2.3** The value v1 is then added with 2 to generate v2 (2,3,4) **2.4** Now add the value of v2 with L to obtain the reference R. **2.5** For inserting bit '1' coding C=R+1, and for inserting '0' coding C=R-1, and C is written in the second element place.
3. Secret Bit Insertion for the Third matrix Element-
3.1 Lower (L) and upper (U) multiple number of 6 with respect to the third element value is considered. **3.2** Matrix number (Mat) is then modulo with U and the resultant value is again modulo with 3 to obtain value v1(0-2). **3.3** The value v1 is then added with 2 to generate v2 (2,3,4). **3.4** Now add the value of v2 with L to obtain the reference R. **3.5** For inserting bits '1' coding C=R+1, and for inserting '0' coding C=R-1, and C is written in the third element place.
4. Secret Bit Insertion for the Forth matrix Element-
4.1. Lower (L) and upper (U) multiple number of 4 with respect to the fourth element is considered and the average of these two values are taken for identifying the reference point. **4.2** For inserting bits '1' coding C=R+1, and for inserting '0' coding C=R-1, and C is written in the fourth element place.
5. Step 1 to 4 is repeated until all the secret bits are finished.
Bit Insertion Example- Let the matrix number N=24 with its pixel byte elements are [21,19,23,15] and the secret bits are to be inserted as (1,0,1,0) in the given element sequences. Now for the first element M=[(42)%4+3]=5, L=20,U=25, and R=Round[(20+25)/2]=23, hence C=(R+1)=24. Then for the second element L=12, U=18, gives v2=[(24%12)%3+2]=2, and R=12+2=14, hence C=R-1=13. Now for the third element L=18, U=24, so v2=[(24%24)%3+2]=2, and R=18+2=20, hence C=R+1=21. For the fourth element L=12, U=16, so R=(12+16)/2=14, produces C=R-1=13. So the final secret bit inserted matrix is [24,13,21,13] which will be transmitted.

B. Bit Extraction Algorithm

First of all the correct random circular sequence of inserted bits are identified through the derivation of starting index number I, as it was computed in the sender side part since the concerned matrix number 'Mat' is known to the receiver also.
1. Bit Extraction from the First Matrix Element-
1.1 Repeat step 1.1 and 1.2 as defined in the bit insertion process where the upper and lower multiple number values are determined with respect to the received coded value C for computing the same reference point R since the concerned matrix number is known to the receiving end also. **1.2** If code C≥R, then 1 is extracted; otherwise '0' is extracted.
2. Bit Extraction from the Second Matrix Element -
2.1 Identify upper and lower multiple value of 6 with respect to the received coded value 'C' as it lies within this range. **2.2** Repeat steps 2.2 to 2.4 as defined in the bit insertion process for computing the same reference point R since the concerned matrix number is also known at the receiving end. **2.3** If code C≥R, then 1 is extracted; otherwise '0' is extracted.
3. Bit Extraction from the Third Matrix Element-
3.1 Identify upper and lower multiple value of 6 with respect to the received coded value 'C' as it lies within this range. **3.2** Repeat steps 3.2 to 3.4 as defined in the bit insertion process for computing the same reference point R since the concerned matrix number is also known at the receiving end. **3.3** If code C≥R, then 1 is extracted; otherwise '0' is extracted.
4. Bit Extraction from the Fourth Matrix Element-
4.1 Identify immediate upper and lower multiple value of 4 with respect to the received code 'C' as it lies in this range. **4.2** Compute the average of these two values as obtained in step 4.1 to obtain the same sender side reference point R. **4.3** If code C≥R, then 1 is extracted; otherwise '0' is extracted.
Bit Extraction Example- The received matrix [24,13,21,13] is used for extraction of four hidden bits with its elements are coded C values. For the first element L=20, U=25, based on C value, so R=23 as computed like the sender side, and Since C>R, hence '1' will be extracted. For the second element L=12, U=18 based on the C value, and R=14 calculated like the sender side. Now C<R implies '0' will be extracted here. For the third element L=18, U=24 based on the C value, and R=20 determined just like the sender side. As C>R so '1' will be extracted. Then for the fourth element L=12, U=16, based on C value, gives R=14 just like the sender side. Here C<R extracts '0' and the whole extracted secret bit set are (1010).

C. Bit Insertion Sequences

Three different cases of secret bit sequncing patterns are considered in Fig1. where the first case shows embedding of each secret image within one of the four equally partitioned non overlapping region of the cover image and hence the four pixel bytes of the sub-matrix belonging to a partcular region will hold secret bits of the same image. Another option is to embed the secret images one after the other where secret bits of the same image is actually hosted by the consecutive set of submatrices. Alternatively four different secret image bits can be inserted into the four different pixel bytes of the submatrix block satisfying the parallel bit embedding concept which actually takes care of the noise related attacks while sequntial bit insertion policy performs well under the cropping attack.

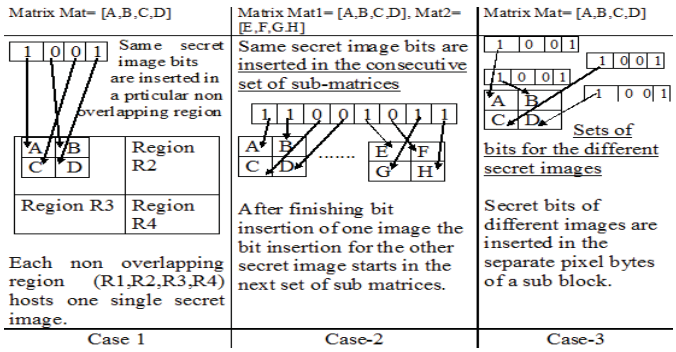

Fig.1 Different pattern of bit insertion sequences on the pixel bytes.

III. EXPERIMENTAL RESULTS

Four equal sized secret color images are watermarked within the host color image of size 512x512 maintaining its identical visual qualities as shown in Table-I. Systems are developed under LINUX using the PPM images and tested in the public wireless network platform (Wi-Fi) with Table-II reflecting excellent watermark imperceptibility in terms of higher PSNR (db), SSIM, CC and Similarity Factor (SF)[1-15] values.

TABLE I. VISUAL QUALITIES OF WATERMARKED IMAGES [16]

Original Image with Bit Insertion sequences used	Embedded image sizes 32x32	Embedded image sizes 64x64	Embedded image sizes 80x80
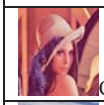 Case1-(Lena)			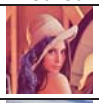
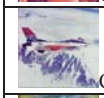 Case2-(airplane)			
Case3- (baboon)			

Identical histograms for the watermarked images are given in Table IV whereas Table V shows the secret watermark images used in this experiment. Since the coded pixel byte values are maintained close to their original values in several cases randomly with smaller variable coding ranges so the resulting PSNR and the other similarity parameter values are relatively higher or better than the other related existing approaches. This observation was thoroughly confirmed in Table-III which actually establishes far superior watermark imperceptibility of this scheme basically supporting very high data pay load embedding capacity as compare to most of the other recent existing works. Overall the approach has definitely guaranteed outstanding watermarked image quality and hence it is free from any kind of visual, statistical or copy attack making the scheme perfectly suitable for the vulnerable wireless domain applications. The watermarking strength in the public wireless domain is explored in Table-VI under the attacks and noise integration by studying the qualities of the extracted images.

TABLE II. WATERMARKED IMAGE QUALITY ASSEMENT

Image	Secret image sizes 32x32 (total 12288 bytes of data embedding)	Secret image sizes 64x64 (total 49,152 bytes of data embedding)	Secret image sizes 80x80 (total 76,800 bytes of data embedding)	Bit pattern sequence used
lena	PSNR=51.91	PSNR=47.25	PSNR=45.23	Case 1
	SSIM=0.9992	SSIM=0.9975	SSIM=0.9959	
	CC=0.9999	CC=0.9997	CC=0.9995	
	SF=0.9999	SF=0.9998	SF=0.9997	
baboon	PSNR=52.22	PSNR=46.94	PSNR=45.07	
	SSIM=0.9999	SSIM=0.9996	SSIM=0.9993	
	CC=0.9999	CC=0.9998	CC=0.9996	
	SF=0.9999	SF=0.9999	SF=0.9999	
lena	PSNR=51.82	PSNR=47.12	PSNR=45.05	Case 2
	SSIM=0.9991	SSIM=0.9972	SSIM=0.9953	
	CC=0.9998	CC=0.9992	CC=0.9994	
	SF=0.9999	SF=0.9998	SF=0.9996	
baboon	PSNR=52.05	PSNR=47.20	PSNR=44.95	
	SSIM=0.9997	SSIM=0.9994	SSIM=0.9972	
	CC=0.9998	CC=0.9998	CC=0.9991	
	SF=0.9999	SF=0.9999	SF=0.9998	
lena	PSNR=51.95	PSNR=47.12	PSNR=45.22	Case 3
	SSIM=0.9998	SSIM=0.9971	SSIM=0.9961	
	CC=0.9998	CC=0.9997	CC=0.9995	
	SF=0.9999	SF=0.9998	SF=0.9997	
baboon	PSNR=51.75	PSNR=47.11	PSNR=45.15	
	SSIM=0.9998	SSIM=0.9995	SSIM=0.9935	
	CC=0.9999	CC=0.9997	CC=0.9997	
	SF=0.9999	SF=0.9999	SF=0.9999	

TABLE III. COMRARISON OF WATERMARK IMPERCEPTABILITY

Applied Techniques / Algorithms		Embedding capacity (bits/ bytes)	PSNR (db)
Color Image Watermarking with Fourier Transform[2]	SCDFT	3,840 bytes	30.1024
	QFT	3,840 bytes	30.9283
	DCT	3,840 bytes	30.4046
Multiple-Watermarking Scheme on Improved Chaotic Map [4]		6,144 bytes	30.11
Robust and Efficient Multiple Watermarking Scheme. [9]		5,120 bytes	33.8506 (Max)
Robust Multi watermarking Scheme for Multiple Input Digital Images [11]		4,096 bits	28.44 (max.)
A Novel Three-Tier Protection for Digital Images Using Blind Watermarking Scheme[14]		3,072 bits	40.76
Compressive Sensing Based Multiple Watermarking Technique [15]		320 byte	30.79
Proposed Approach		76,800 bytes	44.95 (Min).

TABLE IV. HISTOGRAM COMPARISON OF WATERMARKED IMAGE

Hidden Secret Image Sizes 32x32	
Original Image	Watermarked image
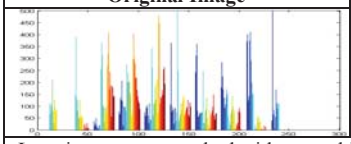	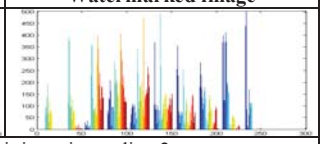
Lena image watermarked with secret bit insertion policy 2	
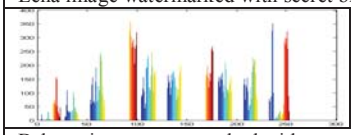	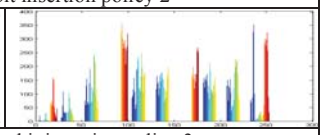
Baboon image watermarked with secret bit insertion policy 3	

TABLE V. SECRET WATERMARK IMAGES USED AS PAY LOAD [16]

Map	Oakland	Ocean	Earth

TABLE VI. PERFOMANCE AGAINST IMAGE PROCESSING ATTACKS

Extracted secret hidden images[16] of size 80x80				
Attacked Lena (with bit sequence)	Map	Oakland	Ocean	Earth
case=1				
Cropping- 200x300 block cut from the upper right corner	SF=1.0, CC=0.99	SF=0.12, CC=0.15,	SF=1.0, CC=1.0	SF=1.0, CC=0.99
case=2				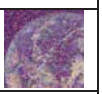
Pick noise-random speed=12, randomize=22%, Repeat=1.	PSNR= 16.75db, SF=0.33, CC=0.70	PSNR= 14.82db, SF=0.29,C C=0.69	PSNR= 18.25db, SF=0.35, CC=0.75	PSNR= 17.92db, SF=0.31, CC=0.72
case=3				
Gaussian random noise- speed=7%, randomization=9%	PSNR= 19.85 db, SF=0.38, CC=0.76	PSNR= 18.25db, SF=0.35,C C=0.74	PSNR= 19.17db, SF=0.33, CC=0.79	PSNR= 23.72db, SF=0.49, CC=0.81

Due to the dynamically variable ranges of bit encoding concept the scheme is mostly robust against the noise attacks while the region based embedding performs well under the cropping attack as shown in Table-VI. The approach encourages partial recovery of at least one of the secret images under sustainable randomized attacks maintaining sufficient visual quality of the watermarked image during transmission.

IV. Application In Wireles Platform

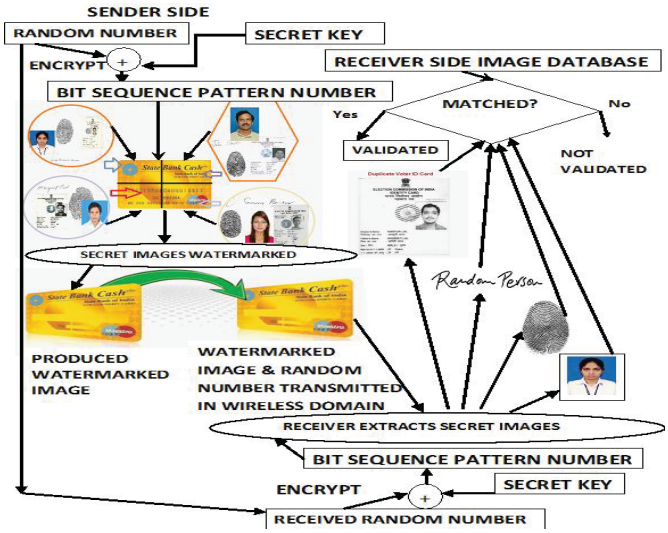

Fig2. Authenticating Digital Documents in Wireless Domain

The proposed concept can be effectively utilized for authenticating the transmitted digital documents within the wireless environment as shown in Fig2. The idea is to transmit a random number along with the watermarked image containing hidden secret images of biometric features of its owner. This random number is used to encrypt the secret key of the owner for generating the secret bit insertion sequence number used during the watermarking. These secret key and secret images are also available at the receiver side Data Base (DB) against a particular user where the received random number is again encrypted with the concerned secret key in order to identify the appropriate secret bit sequencing pattern. Using this pattern the hidden secret images are extracted from the watermarked image and then matched properly with the respective images stored in the DB to judge the authenticity.

V. Conclusion

The proposed work focuses on a secure and reliable color image authentication scheme for the wireless domain by watermarking different secret image bits with dynamically variable encoding strategies and also using different randomized secret bit sequencing patterns. Variably coded values has in fact established superior watermark imperceptibility as compare to the other approaches while the robustness is also achieved against the image processing operations promoting partial recovery of at least one of the secretly hidden images. Additionally different secret image bit sequencing patterns are quite useful for strongly authenticating the cover image under the wireless environment where the security is often compromised. So this enhanced form of color image authentication scheme for the wireless systems capable of resisting the brute force attack while also maintaining the better watermarking strength under the signal interference.

Acknowledgment

The author(s) expresses the deep sense of gratitude to all the associated staff members of the Dept. of Engineering and Technological Studies (DETS), University of Kalyani, West Bengal, India, where the work has been carried out.

References

[1] M. Kutter, F. A. P. Petitcolas, "A Fair Benchmark For Image Watermarking Systems" Electronic Imaging 99, Security and Watermarking of Multimedia Contents, vol. 3657, pp. 1-14, Sans Jose, CA, USA, 25-27 January 1999, The Int. Society for Optical Engg.

[2] T.K Tsui , Res. In Motion, Waterloo, Xiao-Ping Zhang, Androutsos D., "Color Image Watermarking Using Multidimensional Fourier Transformation", IEEE Transactions on Information Forensics and Security, ISSN: 1556-6013, vol. 3, no. 1, pp. 16-28, Mar 2008.

[3] Ibrahim nasir, Ying weng, Yianmin jiang, stanley ipson, "Multiple Spatial Watermarking Technique In Color Images", signal, image and video processing., (springer), vol.4, issue 2, pp. 145–154, June 2010.

[4] S. Behnia, M. Teshnehlab, P. Ayubi, "Multiple-Watermarking Scheme Based On Improved Chaotic Maps", Comm. in Nonlinear Sc. & Numerical Simul.(Elsiver), vol. 15, issue 9, pp. 2469-2478, sep 2010.

[5] K.Ganesan and Tarun Kumar Guptha, "Multiple Binary Images Watermarking in Spatial and Frequency Domains", Signal & Image Processing An International Journal (SIPIJ), Vol.1, No.2, Dec. 2010.

[6] A.Kannammal, S.Subha Rani, "Authentication of DICOM Medical Images Using Multiple Fragile Watermarking Techniques in Wavelet Transform Domain", IJCSI, Vol. 8, Issue 6, No 1, Nov. 2011,

[7] N. Mohananthini, G. Yamuna, R. Vivek, "Comparison of Successive and Segmented Watermarking Techniques for Color Images", pp 13-16, IJCA, IJCA Proc. on NCETICT 2013.

[8] Sameh Oueslati, Adnane Cherif, and Bassel Solaiman, "Multiple Binary Images Watermarking in Spatial and Frequency Domains", Int. Journal of Computer Theory and Engg., Vol. 5, No. 4, pp 598-602, Aug. 2013,

[9] Gaurav bhatnagar, Q.M. Jonathan wu, "A New Robust and Efficient Multiple Watermarking Scheme", Multimedia Tools & Appl. (Springer), ISSN: 1573-7721(Online), 1380-7501 (Print), Sep 2013.

[10] Gil–Je Lee, Kee-Young Yoo, "An Improved Double Image Watermarking Scheme Using The Position Property",. Multimedia Tools & Applications (Springer), ISSN: 1573-7721(Online), April 2014.

[11] Mahdi Babaei, Kok-why ng, Hossein Reza Babei, Hamid Ghorbani Niknajeh, "Robust Multi watermarking Scheme for Multiple Digital Input Images in DWT Domain", International Journal of Computer and Information Technology, Vol.3, Issue 4, pp 834-840, July 2014.

[12] Vandana Inamdar, Priti P Rege, "Dual Watermarking Technqiue with Multiple Biometric Watermarks", Sadhana, Vol. 39, pp. 3–26, Feb 2014.

[13] Mohananthini Natarajan, Yamuna Govindarajan, "Performance Comparison of Single and Multiple Watermarking Techniques", I.J. Comp. Net. and Info. Sec., 2014, vol. 7, pp. 28-34, June 2014 in MECS (http://www.mecs-press.org/), DOI: 10.5815/ijcnis.2014.07.04.

[14] K. Karthik, Dr M. A. Dorai Rangaswamy, "A Novel Three-Tier Protection for Digital Images Using Blind Watermarking Scheme", I. J. of Adv. Trends in Comp. Sc. and Engg. Vol. 4 No.1, pp. 15 – 19 Feb10. Special Issue of ICACET 2015 - Held on February10, 2015.

[15] Rohit M. Thanki, Komal R. Borisagar, "Compressive Sensing Based Multiple Watermarking Technique for Biometric Template Protection", I.J. Image Graphics and Signal Proc., 2015, vol. 1, pp. 53-60, Dec. 2014.

[16] http://sipi.usc.edu/services/database/Database.html.

[17] Nabin Ghoshal, J.K. Momdal, "Discrete Fourier Transform based Multimedia Colour Image Authentication for Wireless Comm.", 2nd IEEE Intl. Conf. Wireless VIATE 2011, Chennai, Feb. 28 2011-March 3 2011, pp. 1-5, ISBN: 978-1-4577-0787-2.

THE 5TH INTERNATIONAL CONFERENCE ON WIRELESS COMMUNICATIONS, VEHICULAR TECHNOLOGY, INFORMATION THEORY, AEROSPACE & ELECTRONIC SYSTEMS (WVITAE-2015)
December 13-16, 2015, Hyderabad, India

Design and Development of a Mobile Wireless Video Streaming Mote

Bhuvanesh D†, Manjunath Hegde† and Manikandan J‡

† Department of Telecommunication Engineering, PES Institute of Technology
‡ Professor and Domain Head (Signal Processing), Crucible of Research and Innovation (CORI), PES University, 100-Feet Ring Road, BSK Stage III, Bangalore 560085, India
{email : manikandanj@pes.edu}

***Abstract*— Video streaming is considered as one of the best compelling sources of information for several applications ranging from vehicular technology, security systems, biomedical systems to aerospace applications. Video streaming using wireless network is quite challenging and a lot of research is in progress. In this paper, design and development of a low-cost real-time wireless video streaming mote is proposed which is an outcome of a funded project. Two different variants of the proposed system are designed and tested. One uses an Arduino YUN board and the other uses a Raspberry PI board. The proposed wireless video streaming mote is aimed at moving around an area under surveillance, gathering images and transferring the same to control station. The proposed system has potential applications including assistance to vehicle drivers during reversing, parking, autonomous driving of the vehicles, driving vehicles using mobile application etc. The proposed system designed has a myriad of real-time applications for domestic requirements with social cause too.**

Keywords- Electronic Systems; Vehicles; Video Streaming; Wireless.

I. INTRODUCTION

Videos in the form of recorded videos, off-line videos and real-time video streaming are considered as the best sources of information for various applications ranging from rear-end collision warning system for cars in [1], surveillance and home security in [2], personal protection and kidnapping detection in [3], automatic detection of crimes in [4], Helmet Mounted Display Systems (HMDS) in [5], to Curiosity rover landing event from Mars in [6]. Live video streaming using wireless network is quite challenging and a lot of research is in progress.

In this paper, design of a low-cost wireless mote is proposed as shown in Fig. 1, which is capable of moving around an area under surveillance and can perform live video streaming of its path onto a mobile phone as well as laptop using Wi-fi network. This can be widely used for security purposes such as around VIP buildings and high-alert zones/ offices, wherein the mobile mote would be continuously roaming around these zones and performing live video streaming. These mobile motes can also be programmed to roam around and collect data from stationary access points in a wireless sensor network area as shown in Fig. 1.

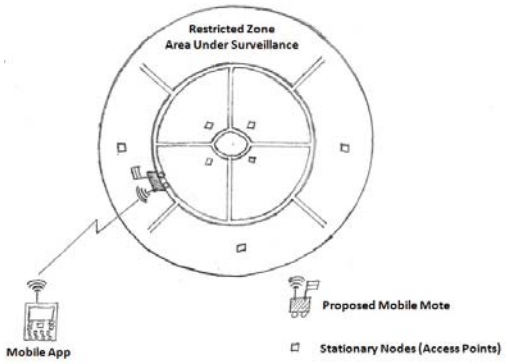

Fig. 1. Working of proposed Mobile Mote

The organization of the paper is as follows: Section II explains the design of the proposed mote using Raspberry Pi board and Section III explains the design of the system using Arduino Yun board. Experimental results and comparison between the two systems is reported in Section IV followed by conclusion, acknowledgement and references.

II. DESIGN OF PROPOSED MOTE USING RASPBERRY PI

Raspberry Pi [7] is a credit-card sized single board computer, running open-source Linux as operating system, which is designed and developed by the non-profit charitable Raspberry Pi foundation, UK. The board is designed using Broadcom BCM2835 system on a chip processor which includes an ARM1176 processor with an operating speed of 700MHz. Different models and variants of Raspberry are available in the market with the Raspberry Pi Model B+ being the latest version and the details about the comparison between different Raspberry models (Model A, Model B, Model A+, Model B+, Pi 2 and Compute) are reported in [8]. Raspberry Pi boards are being used for various applications such as design of miniaturized cloud data center in [9], novel education platform in [10], interactive home automation in [11] and many more. Considering the capabilities and features of Raspberry board, the same is employed for the proposed work.

A. Hardware Design

The block diagram of proposed wireless mote designed using Raspberry Pi with live video streaming capability is shown in Fig. 2. The Raspberry Pi board is powered using a 6600mAh power bank and the motors are powered using a 12V 1.3Ah battery to establish a complete wireless mote which is capable of moving in an area under surveillance. A Logitech make C170 USB camera is connected to the board for capturing video and an Edimax make EW-7811 wireless adaptor is used to establish wireless connectivity to other wireless nodes including phone and laptop. Texas Instruments make L293D based motor driver circuitry is designed to power the 12V DC motors for the mobility of the proposed wireless mote. Fig. 3 shows the snapshot of the hardware designed as per the block diagram shown in Fig. 2.

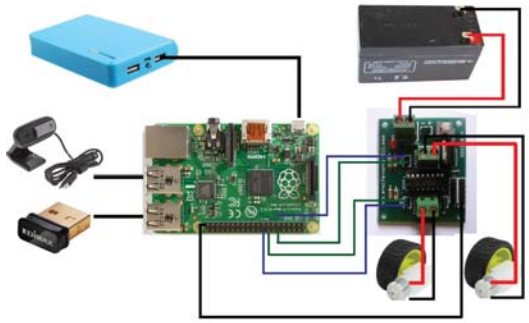

Fig. 2. Block diagram of proposed Mobile Wireless Mote

Fig. 3. Snapshot of the Mobile Wireless Mote designed

B. Software Design

Once the hardware is designed as shown in Fig. 3, the software design is initiated as per the design flow explained below. The first step is to install an operating system for the Raspberry board. Raspbian OS is downloaded from [12] and installed for the proposed work. In order to install drivers and write python script for Raspberry Pi board, the board should be connected to a monitor. The two alternative approaches for doing the same are connecting the board to a HDMI monitor or by using putty software to get remotely connected to the board. Once OS is installed on the Pi board, two libraries/frameworks are installed for the proposed design. One is the WebIOPi, which is a fully integrated Internet of Things framework for the Raspberry Pi and is considered as the perfect Swiss-knife to control, debug and use Raspberry Pi's GPIO locally or remotely from a browser or any app. In the proposed work, communication between android smartphone and Pi board based mobile mote is established through this library using HTTP client services. The WebIOPi library is downloaded from [13] and the following commands are used to install the WebIOPi library in the Pi.

pi@raspberrypi ~ $ wget webiopi.googlecode.com/files/WebIOPi-0.6.3.tar.gz
pi@raspberrypi ~ $ tar xvzf WebIOPi-0.6.3.tar.gz
pi@raspberrypi ~ $ cd WebIOPi-0.6.3
pi@raspberrypi ~ $. /setup.sh

The second framework is Gstreamer, which is a pipeline based multimedia framework that allows programmer to create a variety of media-handling components. The Gstreamer framework is used in the proposed work to decode the video information from USB webcam connected to Raspberry Pi board. Before installing the Gstreamer library/packages, the Raspbian OS should be updated using the following commands

pi@raspberrypi ~ $ sudo apt-get update
pi@raspberrypi ~ $ sudo apt-get upgrade

Once the OS is updated the Gstreamer packages are installed using the following command

pi@raspberrypi ~ $ sudo apt-get install gstreamer-tools gstreamer0.10-plugins-bad gstreamer0.10-plugins-good v4l-utils

After installing the packages, a python script is written which serves as the main program residing on the Raspberry Pi board to perform the functional requirements of a mobile mote with wireless video streaming capability. This is followed by a shell script written for video streaming and commands are given to run both the scripts on boot.

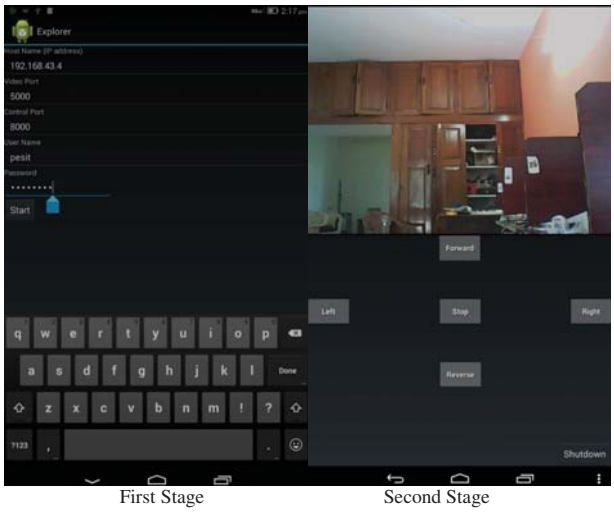

First Stage Second Stage

Fig. 4. Android App designed for the proposed mobile mote

An android application using Eclipse IDE [14] is designed as shown in Fig. 4 for the proposed work which has two stages of operation. The first stage demands the user authentication and successful authentication leads to the second stage for navigating the mobile mote towards a desired direction using buttons and live video streaming as shown in Fig. 4.

III. Design of Proposed Mote using Arduino Yun

Arduino Yun [15] is a microcontroller board based on the ATmega32u4 microcontroller and the Atheros AR9331 processor. The Atheros processor onboard operates at 400MHz and supports OpenWrt-Yun linux distribution. The board has built-in Ethernet and WiFi support. Arduino boards including Arduino Yun are being used for various real time applications such as design of portable wireless indoor air monitoring system in [16], wireless sensor node for outdoor pollution monitoring in [17], Human-Computer Interface for Users with disabilities in [18] and many more. Both, Arduino and Raspberry Pi boards are considered as two powerful devices in the market with each one having its own followers and supporters and hence a mobile mote with video streaming is developed using Arduino Yun too and the performances are evaluated in the proposed work.

A. Hardware Design

The block diagram of proposed wireless mote designed using Arduino Yun with video streaming capability is same as shown in Fig. 2 where Raspberry Pi board is replaced by an Arduino Yun board and the USB Wifi adaptor is replaced by the Wifi available on-board. The other interfaces and functionalities are same as mentioned for Raspberry Pi based mobile mote.

B. Software Design

Once the hardware is designed using Arduino Yun board, the software design is initiated as per the design flow given below. Two approaches of video streaming are explored in this work. The first approach discusses video streaming using both python script (for Atheron processor) as well as arduino sketch (for ATmega32u4 microcontroller). The Yun board runs a distribution of Linux for embedded systems named OpnWrt-Yun based on OpenWrt and a full install of Python 2.7 is included as well. In order to install few drivers required for the proposed work, the Yun board is connected via secure shell (SSH) as shown in Fig. 5 after giving following command in the terminal.

ssh root@yourYunName.local

An Open PacKaGe Management (opkg) considered as a lightweight package management system based upon ipkg is written in C, which is intended for use on embedded Linux devices such as Arduino Yun. The package manager is first updated using the following command

opkg update

Fig. 5. Snapshot of the OpenWrt Terminal for Arduino Yun board.

The USB video class (UVC) drivers provide driver support for video streaming functionality on the USB such as webcams, video recorders etc. These drivers are installed using the following command

opkg install kmod-video-uvc

The fswebcam utility is required to take pictures from the terminal and the same is installed using the following command

opkg install fswebcam

In order to stream videos online, mjpg streaming library is installed using the following command

opkg install mjpg-streamer

The final software comprises of two parts. The first one is a python script that will upload the pictures captured using camera onto the Dropbox from micro SD card. Second part of the code is an arduino sketch which calls the python script to take pictures via the bridge library of the Yun. The video streaming requirement is met by initially streaming the video locally and then transmitting it to Youtube using Wirecast software.

The second approach discusses video streaming handled using Arduino sketch (for ATmega32u4 microcontroller) and libraries for Atheron process that can be used along with arduino sketch. This avoids the need of python script. The Bridge library's Process class is used to run Linux processes on the Atheron AR9331 processor. The first step of this approach demands the configuration of the Wifi network on the Arduino Yun board, which includes establishing Wifi connection between Arduino Yun and smartphone/tablet/ laptop. Google chrome browser is used to monitor the video streaming onto a PC/laptop and an easy auto refresh plug-in for Google chrome is installed for auto refresh of the screen. Similarly Dolphin browser is used to monitor the video streaming onto android phones with auto tab reload plug-in.

IV. Results and Observations

A rough breakup of the budget required to develop the proposed system using Raspberry Pi and Arduino Yun is reported in Table I. It may be observed from Table I that the

design using Arduino Yun is expensive over the system designed using Raspberry Pi board and hence the final mobile mote with wireless video streaming and control prototype is designed using Raspberry Pi board. Snapshot of the working of mobile mote using Raspberry Pi board is shown in Fig. 6. It may be observed that the video in front of the mobile mote is displayed on the android app. Also the mobile mote is successfully controlled using the four buttons visible on the mobile application for navigating the robot in all four directions and halt. Snapshot of the wireless video streaming from Arduino Yun onto a mobile phone as well as laptop is shown in Fig. 7. In Fig. 7, the USB cable connected to laptop is only for powering the Arduino Yun board and video streaming onto mobile phone and laptop is achieved using Wifi network.

TABLE I. EXPENSES INCURRED FOR THE PROPOSED SYSTEM

Hardwares ↓	Raspberry Pi Based System	Arduino Yun based System
Raspberry Pi	$40	NA
Arduino Yun	NA	$75
USB Webcam	$15	$15
12V Battery	$10	$10
6600mAh Power Bank	$15	$15
WiFi Adaptor	$10	NA
Robot Chassis and Misc.	$10	$10
Total	**$100**	**$125**

V. CONCLUSION

In this paper, design of mobile motes with live video streaming capabilities is discussed using two recent boards, Raspberry Pi board and Arduino Yun board. Details about the hardware and software design for both these variants are discussed. It is concluded that the design using Raspberry Pi board is economical over the design using Arduino Yun board. The proposed system has huge potential in vehicular technology and automotive industry towards designing an autonomous and mobile application based vehicle driving assistance for specially challenged. The system can also be used for assistance towards reverse parking the vehicles and for use of rear-end anti-collision warning. The proposed design can be easily adapted for designing home-security systems, industrial applications related to long-armed pick and place robots with video capability and many more applications.

ACKNOWLEDGEMENTS

This work is funded by the All India Council for Technical Education (AICTE) under the Research Promotion Scheme (RPS) vide project grant No. 8-138/RIFD/RPS/POLICY-3/2013-14.

Fig. 6. Snapshot of Video streaming from Raspberry Pi based mobile mote

Fig. 7. Snapshot of Video streaming from Arduino Yun for the proposed mote

REFERENCES

[1] Tang-Hsien Chang and Chen-Ju Chou, “Rear-end collision warning system on account of a rear-end monitoring camera”, in Proc. IEEE Intelligent Vehicles Symposium, Xi’an, China, June 2009, pp. 913-917.
[2] Yi Gu, Myoungjin Kim, Yun Cui and Hanku Lee, “Design and Implementation of UPnP-based Surveillance Camera system for Home Security”, in Proc. Int. Conf. on Information Science and Applications, Suwon, South Korea, June 2013, pp. 1-4.
[3] Miyahara A and Nagayama I, “An Intelligent security camera system for kidnapping detection”, Journal of Advanced Computational Intelligence and Intelligent Informatics, Vol. 17, pp. 746-752.
[4] Goya K, Zhang X, Kitayama K and Nagayama I, “A Method for Automatic Detection of Crimes for Public Security by using Motion Analysis”, in Proc. Fifth Int. Conf. on Intelligent Information Hiding and Multimedia Signal Processing, Kyoto, Sep 2009, pp.736-741.
[5] Yokokohji Y, Sugawara Y and Yoshikawa T, “Accurate image overlay on video see-through HMDs using vision and accelerometers”, in Proc. IEEE Virtual Reality, New Brunswick, NJ, March 2000, pp.247-254.
[6] George B, Shams K, Knight D and Kinney J, “Mission critical cloud computing in a week”, in Proc. IEEE Aerospace Conference, Big Sky, Montana, March 2013, pp. 1-7.
[7] Raspbrry Pi – Teach, Learn, and Make with Raspberry Pi. https://www.raspberrypi.org/.
[8] Raspberry Pi Model Specifications, http://www.element14.com/community/docs/DOC-68090/l/raspberry-pi-2-b-a-a-compute-module-dev-kit-comparison-chart.

[9] Fung Po Tso, White D.R., Jouet S, Singer J and Pezaros D.P., "The Glasgow Raspberry Pi Cloud: A Scale Model for Cloud Computing Infrastructures", in Proc. 33rd Int. Conf. on Distributed Computing Systems Workshops, Philadelphia, July 2013, pp. 108-112.

[10] Ioannou N.K., Ioannidis G.S., Papadopoulos G.D. and Tapeinos A.E., "A novel educational platform, based on the Raspberry-Pi: Optimized to assist the teaching and learning of younger students", in Proc. Int. Conf. on Interactive Collaborative Learning, Dec 2014, Dubai, pp. 517-524.

[11] Jain S, Vaibhav A and Goyal L, "Raspberry Pi based interactive home automation system through E-mail", in Proc. Int. Conf. on Optimization, Reliability and Information Technology, New Delhi, Feb 2014, pp. 277-280.

[12] Raspberry Pi Downloads – Software for the Raspbrry Pi. https://www.raspberrypi.org/downloads/

[13] WebIOPi, http://sourceforge.net/projects/webipoi/files/

[14] Android Tutorial, www.tutorialspoint.com/android.

[15] Arduino Yun, https://www.arduino.cc/en/Main/ArduinoBoardYun.

[16] Qianqian Yang, Guangyao Zhou, Wenhui Qin and Bin Zhang, "Air-kare: A Wi-Fi based multi-sensor, real-time indoor air quality monitor", IEEE Int. Wireless Symposium, Shenzhen, China, Apr 2015, pp.1-4.

[17] Manikandan J, Niladri C, Venugopal S, Krishnamurthy V and VK Agrawal, "Wireless Sensor node for Green Environment", in Proc. Int. Conf. on Human Computer Interactions, Chennai, Aug 2013, pp.1-5.

[18] Davide Mulfari, Antonio Celesti, Maria Fazio and Massimo Villari, "Human-Computer Interface Based on IoT Embedded Systems for Users with Disabilities", in Proc. Int. Conf. on IoT as a Service, Oct 2014, Rome, Italy. pp. 376-383.

THE 5TH INTERNATIONAL CONFERENCE ON WIRELESS COMMUNICATIONS, VEHICULAR TECHNOLOGY, INFORMATION THEORY, AEROSPACE & ELECTRONIC SYSTEMS (WVITAE-2015)
December 13-16, 2015, Hyderabad, India

Error Rate Performance for Multiuser scheduling in MIMO downlink system with imperfect CSI

Prabina Pattanayak*, Diwakar Pandey†, Preetam Kumar‡
Department of Electrical Engineering, Indian Institute of Technology Patna, Bihar 800013, India
Email: {*prabina, †diwakar.mtee13, ‡pkumar}@iitp.ac.in

***Abstract*—In this paper, the bit error rate(BER) performance of downlink multiuser scheduling (MUS) for multiple-input-multiple-output (MIMO) transceiving systems is analysed with imperfect channel state information (CSI) caused by feedback delay over Rayleigh fading channel. Two transceiving schemes, i.e., space time block codes (STBC) and selective transmission maximum ratio combining (ST/MRC) has been studied with normalized signal-to-noise ratio (SNR) based scheduling in heterogeneous environment and serving M number of users at a time, where M is the number of transmit antennas. Also the performance under perfect and imperfect CSI is studied for the two transceiving schemes which shows different performances for different schemes. In frequency selective channel, orthogonal frequency division multiplexing (OFDM) performs well to transform it from frequency selective to frequency flat. Therefore error rate performance of MUS-MIMO downlink system integrated with OFDM is studied in heterogeneous user environment with imperfect CSI and STBC transceiving scheme and a considerable gain in error rate performance is observed.**

I. Introduction

Single antenna systems do not utilize the channel efficiently as single user is being served by the base station (BS). Hence, multiple antenna systems have gained momentum as they ensure efficient spectrum utilization. In fading channels, multiuser diversity (MUD) and antenna diversity results in both higher spectral efficiency and better bit error rate (BER) performance [1]. In multiuser (MU) enviornment, MUD can be exploited in case of channel state information (CSI) feedback by receivers to BS. According to multiuser scheduling (MUS), the spectral efficiency of broadcast channel (BC) can be maximized by sending real data to users with the best channel conditions [1].

Dirty paper coding (DPC) and zero-forcing (ZF) precoder in multiuser multiple-input multiple-output (MU-MIMO) environment result in optimal usage of channel by pre-cancelling the interference at users. However, these schemes are not implementable in real time as perfect CSI at transmitter (CSIT) is required. In literature limited feedback scheduling schemes are discussed [2]–[4]. In recent past, soft computing techniques are also used for scheduling [5], [6]. The bit error rate (BER) performance of user scheduling for MU MIMO broadcast system with heterogeneous users is less studied in past. Hence, in this paper, the BER performance of MIMO MUS is studied for imperfect CSI caused due to feedback delay is considered where BS serves multiple users (equal to the number of transmit antennas at BS) simultaneously.

MUD gain with opportunistic scheduler is analysed in [7], [8]. Wong [9] investigated the performance analysis of both single and multiuser MIMO diversity channels using Nakagami-m distribution. Antenna diversity and MUS is jointly investigated for the generalized Nakagami fading channels along with the derivation of unified capacity formula for MUS with different transceiving schemes in [10]. BER and capacity expressions with MUS for heterogeneous and homogeneous users are presented in [11], [12]. MUS system capacity is analysed in [13], [14] by taking delayed CSI into account. BER performance analysis for MUS-MIMO system with imperfect CSI and heterogeneous network is presented in [15] with space time block code (STBC), selective transmission maximum ratio combining (ST/MRC) and selective transmission selective combining (ST/SC) combining schemes. However, only the user with highest SNR is being served at a time using time division multiplexing (TDMA) technique. This results in inefficient spectrum utilization by not exploiting the advantage of spatial multiplexing gain, where the capacity of the wireless channel can be increased linearly by a factor of $min\{M, N\}$. M and N are the number of transmit and receive antennas respectively.

Hence, it will be interesting to observe the performance of the MUS-MIMO downlink system with imperfect CSI and heterogeneous users when M users are served simultaneously according to DPC. Moreover, integrating orthogonal frequency division multiplexing (OFDM) with MIMO can convert a frequency selective channel into a frequency flat channel. This can result in better BER performance of the MU MIMO-OFDM BC. Here, BER performance of MUS-MIMO-OFDM downlink system with frequency selective channel and heterogeneous users is analysed for various transceiving schemes like STBC, and ST/MRC for perfect and imperfect CSI through extensive simulation resuls.

Section II describes the system model along with the MUS scheme. Simulation results are presented and discussed in Section III. Finally, Section IV concludes the paper.

II. System Model and Multiuser Scheduling Scheme

A. MUS-MIMO downlink system

Consider multiuser scheduling for MU MIMO downlink system. It consists of one BS with M number of transmitting antennas. There are K number of users each one having N number of receiving antennas. The wireless channel between

BS and users is assumed to be flat Rayleigh fading channel. The users feed back the CSI to the BS. Depending upon this feedback the transmitter schedules the users for transmitting data. The channel between the transmitter and receiver is represented by an $N \times M$ channel matrix $H^k = h_{ij}^{(k)}$, where the complex element $h_{ij}^{(k)}$ is the gain between the jth transmit and the ith receive antenna for the kth user. The channel elements are independent and identically distributed ($i.i.d.$) complex Gaussian random variables (RVs) with zero mean and 0.5 variance per dimension. The MIMO transceiving scheme namely STBC and ST/MRC has been used for multiuser scheduling. It has been assumed that the channel is quasi static, i.e., the channel parameters do not change for one STBC frame but varies from one frame to another. For the STBC scheme the received SNR per symbol of the kth user can be expressed as below [16], [17]:

$$\begin{aligned}\gamma_{STBC}^k &= (P_t^k/rM\sigma_n^2) \times \sum_{j=1}^{M}\sum_{i=1}^{N} \left|h_{ij}^k\right|^2 \\ &= \frac{\bar{\gamma}^k}{rM}\sum_{j=1}^{M}\sum_{i=1}^{N}\left|h_{ij}^k\right|^2 = \frac{\bar{\gamma}^k}{rM}\left\|H^k\right\|_F^2, \quad (1)\end{aligned}$$

Where r is the code rate, P_t^k is the total transmit power, $\sigma_n^2$is the noise variance, $\bar{\gamma}^k$ is the average SNR at the kth user, and $\left\|H^k\right\|_F^2$ is the square of the Frobenious norm of $\{h_{ij}^k\}$. According to this scheme, all transmit antennas are utilized for transmitting data.

For the ST/MRC case the received SNR per symbol of the kth user is given by:

$$\begin{aligned}\gamma_{ST/MRC}^k &= max(P_t^k/\sigma_n^2 \sum_{i=1}^{N}|h_{ij}|^2) \ \forall\ j = 1, 2, ...M \\ &= max\left(\bar{\gamma}^k \sum_{i=1}^{N}|h_{ij}|^2\right) \\ &= max\left(\bar{\gamma}^k \left\|h_j^k\right\|_F^2\right) \ \forall\ j = 1, 2, ...M, \quad (2)\end{aligned}$$

where $\left\|h_j^k\right\|_F^2$ is the Frobenious norm of jth column of H^k. According to this scheme, the BS selects the transmit antenna which results in $max\left\|h_j\right\|_F^2 \forall j$ = 1, . . ., M.

The received SNR (γ^k) may be expressed as the largest order statistic of LQ scheme of L *i.i.d.* received SNRs as discussed in [15]

$$\gamma^k = \max_{m=1,\ldots,L}\{r_m^k\}, \quad (3)$$

where

$$r_m^k = \begin{cases} \rho^k \left\|H^k\right\|_F^2, & \text{L = 1, Q = MN for STBC} \\ \rho^k \left\|h_j^k\right\|_F^2, & \text{L = M, Q = N for ST/MRC} \end{cases}$$

where the average receive SNR, i.e., ρ^k will be expressed for different transceiving schemes as $\rho^k = \frac{\bar{\gamma}^k}{rN}$ for STBC, and $\rho^k = \bar{\gamma}^k$ for ST/MRC.

Here complete knowledge of the channel is considered based on the CSI received from the receiver. Also the feedback channel is assumed to be error free but there is delay in received CSI value. In multiuser scheduling each user feeds back its maximum SNR value along with the corresponding transmit antenna index to the BS. After attaining the complete feedback from all users, BS schedules M distinct users with highest SNR values corresponding to each transmit antenna. However, in case of STBC, users do not send the index of the transmit antenna (which is not required). The BS will perform multi-user scheduling using delayed CSI denoted as $\hat{\gamma}^k = \max_{m=1,\ldots,L}\{\hat{r}_m^k\}$, where $\hat{r}_m^k = \hat{\rho}^k \left\|\hat{H}^k\right\|_F^2$ for STBC, and $\hat{r}_m^k = \hat{\rho}^k \left\|\hat{h}_j^k\right\|_F^2$ for ST/MRC. $\hat{H}^k$ is the τ delayed form of H^k having same Gaussian distribution as H^k and the correlation coefficient between their elements is $c_k = J_0(2\pi f_d^k \tau_k)$ where J_0 is first order Bessel function of the first kind. τ_k, and f_d^k are feedback delay and the maximum Doppler frequency of user k respectively. Also, the relationship between the actual channel and its delayed form as discussed in [18] can be expressed as below:

$$H^k = c_k\hat{H}^k + \sqrt{(1-c_k^2)}E^k, \quad (4)$$

where E^k is the channel error matrix which is independent of $\hat{H}^k$, and its entries are $i.i.d.$ complex Gaussian RVs with zero mean and variance $\sigma_k^2 = 1 - c_k^2$. The signal received at each user k is given as below:

$$y^k = H^k s + n^k. \quad (5)$$

In this paper, BER performance is compared through simulation for the below mentioned two scenarios as:

- The user with the best received SNR is being served by the BS. and
- The M users with the M best received SNRs are being served simultaneously by the BS.

Moreover, the BER performance for heterogeneous network is compared for both perfect and imperfect CSI at BS.

B. MUS-MIMO-OFDM downlink system

In a multiuser MIMO−OFDM downlink system, a single cell has been considered where the transmitter is furnished with M transmitting antennas and there are K heterogeneous users each having N antennas as receiver. The scheduling process for users at the BS allots a sub-carrier to a particular user at the initialization of each frame for which the user has reported the highest received SNR value. The BS then selects the best M users, who have reported the highest M SNR values. The signal is then transmitted to that M users over their l_{th} subcarrier on which they have reported highest SNR. The SNR value of the k^{th} user over the l_{th} subcarrier is shown below in (6) for STBC transceiving scheme:

$$\begin{aligned}\gamma_l^k &= (P_t^k/rM\sigma_n^2) \times \sum_{j=1}^{M}\sum_{i=1}^{N}\left|h_{ij}^{k,l}\right|^2 \\ &= \frac{\bar{\gamma}^k}{rM}\sum_{j=1}^{M}\sum_{i=1}^{N}\left|h_{ij}^{k,l}\right|^2. \quad (6)\end{aligned}$$

A mobile user will be able to detect the signal forwarded to it by utilizing point-to-point MIMO spatial multiplexing, if and only if N is equal to or larger than M as discussed in [20]. The channel has been considered to be frequency selective and has been modelled as a length P finite− impulse response (FIR) filter as described in [19]. The space frequency channel at the l_{th} tone for the kth user can be written as below as described in [20]:

$$H_l^k = \sum_{p=0}^{P-1} \sigma_p F[k,p] exp(-j2\pi \times p), \tag{7}$$

where $F[k,p]$ is $M \times M$ square matrix and MIMO channel impulse responses of the kth user with each $F[k,p]$ contains independent $\mathcal{CN}(0,1)$ elements. σ_p^2 represents the channel power delay profile normalized by assuming $\sum_{p=0}^{P-1} \sigma_p^2 = 1$. The channel is expected to be quasi-static, which remains same for one coherence time duration. Here one coherence time is equal to the length of one OFDM frame. Also each frame consists of a number of OFDM symbols. Correlation coefficient between the channel elements on two arbitrary subcarriers r and s is given as in [21]

$$\begin{aligned} \beta_{r,s} &= E[(H_r^k)(H_s^k)^*_{i',j'}] \\ &= \sum_{p=0}^{P-1} \sigma_p^2 exp(-j2\pi(r-s)p/L)\delta[i-i'] \\ &\quad \times \delta[j-j']]. \end{aligned} \tag{8}$$

The received signal by kth user over the lth sub-carrier can be expressed as below:

$$y_l^k = H_l^k s_l + n_l^k, \tag{9}$$

where H_l^k is given by (7), x_l is signal vector transmitted over the lth sub-carrier and n_l^k is the normalized noise vector with $\mathcal{CN}(\iota, \infty)$ elements. The BS will perform multiuser scheduling by calculating the SNR values at each of the user and for each subcarrier given by (6).

III. Simulation Results and Discussions

In this section, BER performance of MUS for MIMO and MIMO-OFDM BC over quasi static Rayleigh flat fading channels is discussed. Monte-carlo method is used for simulation for various scenarios. An exponentially decaying profile expressed as $\{\bar{\gamma}^k = \bar{\gamma} e^{-\varepsilon(k-1)}, k = 1, \ldots, K\}$, is used for heterogeneous case to compute the average SNRs of users. Here ε is the power decaying factor [12], and its value has been taken as 0.2 for all the simulation results. For heterogeneous case normalized SNR based scheduling is used for user selection. The channel estimation and antenna selection time is set to be $190mus$ as used in [22] for all simulations presented in this paper. The correlation coefficient of any user k is given by relation as $c_k = J_0(2\pi f_d^k \tau_k)$. Here, we have considered a heterogeneous network consisting of four users. The Doppler frequencies for the these users are assumed to be $f_d^k = 200$, 300, 400, and $500Hz$ corresponding to their speed of 43.2 , 64.8 , 86.4, and $108Km/h$. The carrier frequency is assumed to be $5GHz$. Assuming τ_k value as $190mus$, the correlation coefficients are obtained as $c = \{0.98, 0.96, 0.94, \text{and } 0.91\}$ for these users. For this entire section the various simulations are performed for 2×3 MIMO system with four users as discussed earlier.

A. Numerical result for MUS-MIMO downlink system

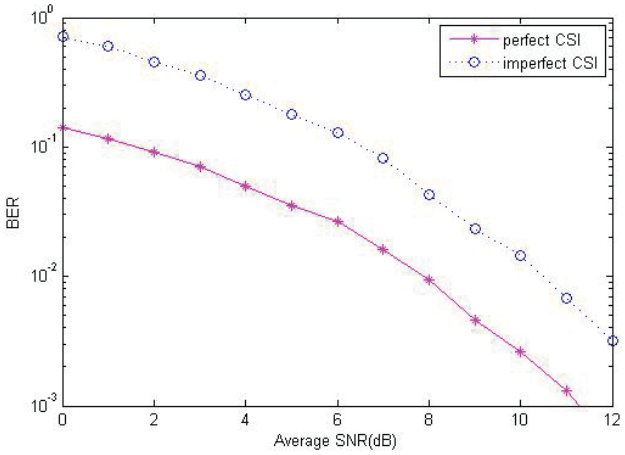

Fig. 1. Performance comparison for perfect and imperfect CSI

In Fig.1, performance comparison for perfect and imperfect CSI has been plotted, using binary phase shift keying (BPSK) modulation in MUS-MIMO environment and using the discussed scheduling algorithm. From the Fig.1 it is clear that the BER performance under imperfect CSI case is worse than that in case of perfect CSI.

In Fig.2, simulation results are plotted for BER performance comparison for the case when the BS serves single user with the maximum SNR and multiple users(equal to the number of transmit antennas) with imperfect CSI. BPSK is used as the modulation scheme. It is important to observe from this is that there is very less increment in BER, i.e., approximately 1 dB loss while we are serving to M users simultaneously. However it is observed that the capacity increases M-fold by serving M users simultaneously.

In Fig.3, performance comparison for STBC and ST/MRC transceiving schemes are given for imperfect CSI at the BS. For both the schemes BPSK modulation is used. For ST/MRC scheme performance is better because only user selection gets affected by delayed CSI in case of STBC however for ST/MRC both user and antenna selections are affected. However, for the case of perfect CSI at BS, the BER performance is as shown in Fig.4. In this case the performance of ST/MRC is better than STBC as more diversity gain is achieved by ST/MRC in the presence of perfect knowledge of channel condition at the transmitter.

B. Numerical result for MUS-MIMO-OFDM downlink system

The BER performance achieved by MUS for MIMO-OFDM frequency selective BC channel is shown in Fig.5. The exponential power delay profile σ_p^2 is used to model the channel

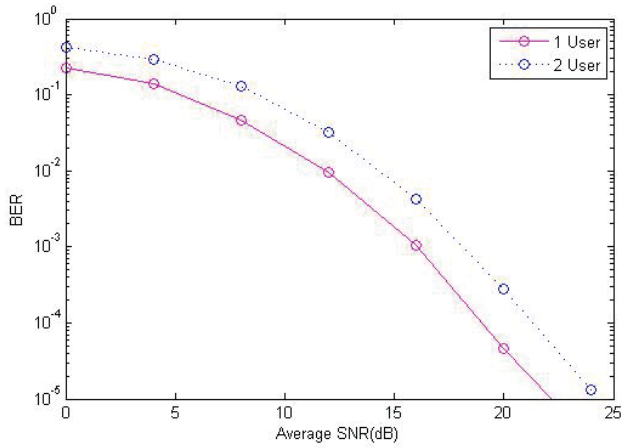

Fig. 2. Performance comparison for the case when the BS serve single user and multi users (depending on number of transmit antennas), With imperfect CSI.

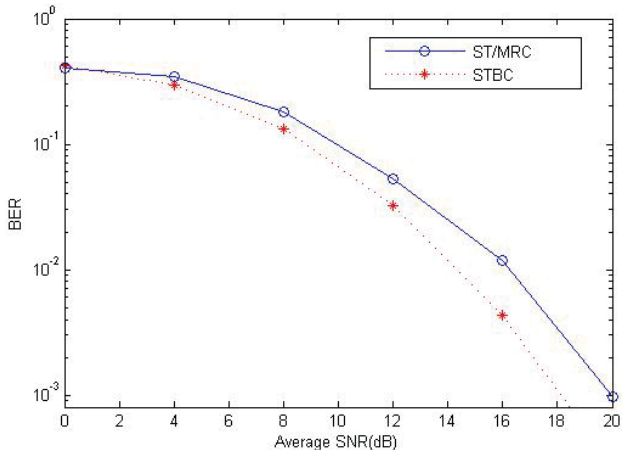

Fig. 3. Performance comparison for STBC and MRC with imperfect CSI

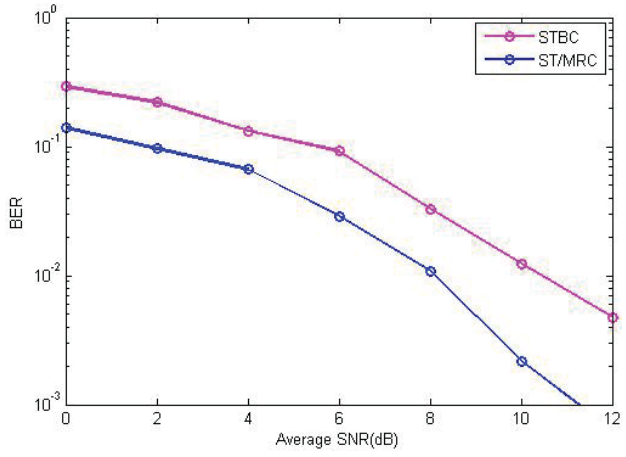

Fig. 4. Performance comparison for STBC and MRC with perfect CSI

for simulation results. It is given by (10) as discussed in [20]

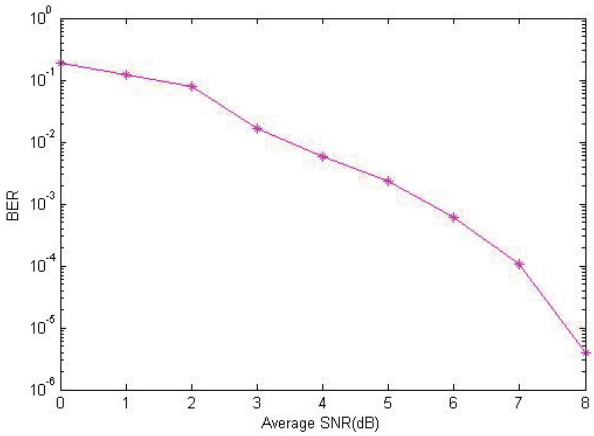

Fig. 5. Performance of MUS-MIMO-OFDM downlink system

as:

$$\sigma_p^2 = \frac{1 - exp(-1/D_{exp})}{1 - exp(-P/D_{exp})} exp(-p/D_{exp}),\ 0 \leq p \leq P-1, \tag{10}$$

where P is the number of resolvable paths which is taken as P = 4 and total sub-carriers are assumed to be 16, i.e., L = 16. Also the D_{exp} is considered to be 2 for the simulation purpose. STBC coding scheme is used with BPSK modulation over frequency selective channel for which the system model is provided in section II. It can be observed from the plot that a reasonably good BER performance of 10^{-6} is achieved at an SNR of 8 dB.

IV. Conclusion

In this paper, we have presented an error performance study of MUS for both MIMO, and MIMO-OFDM downlink system with imperfect CSI at the transmitter end. The BER performance by MUS for MIMO broadcast network over Rayleigh flat fading channel with heterogeneous users is studied with two transceiving schemes like STBC, and ST/MRC. BER performance is done for both the cases of perfect and imperfect CSI. The effect of serving multiple users simultaneously on BER performance is also observed. It is interesting to observe that the BER performance of serving M users with the M best SNRs degrades insignificantly (by approximately 1 dB) as compared with serving only the user with the highest SNR. It is observed for the case of perfect CSI that the BER performance of ST/MRC is better than STBC due to more diversity gain provided by ST/MRC. Moreover, it is observed for the case of imperfect CSI that the BER performance of STBC is better than ST/MRC because the delayed CSI affects only selection of user in case of STBC while in case of ST/MRC it affects both user and antenna selection. Later in the paper, the BER performance attained by MUS is studied for MIMO-OFDM downlink system over a frequency-selective channel. The performance is very intriguing in frequency-selective channel environment.

V. Acknowledgement

This work is part of the project funded by DEITY, Government of India. We sincerely acknowledge the support of DEITY.

References

[1] L. Yang and M.-S. Alouini, "Performance analysis of multiuser selection diversity," *IEEE Transactions on Vehicular Technology*, vol. 55, no. 6, pp. 1848–1861, 2006.

[2] G. Wunder, J. Schreck, and P. Jung, "Nearly Doubling the Throughput of Multiuser MIMO Systems Using Codebook Tailored Limited Feedback Protocol," *IEEE Trans. on Wireless Commun.*, vol. 11, no. 11, pp. 3921 –3931, 2012.

[3] M. Min, D. Kim, H. Kim, and G. Im, "Opportunistic Two-Stage Feedback and Scheduling for MIMO Downlink Systems," *IEEE Trans. Commun.*, vol. 61, no. 1, pp. 312–324, 2013.

[4] P. Pattanayak, K. M. Roy, and P. Kumar, "Analysis of a new MIMO broadcast channel limited feedback scheduling algorithm with user grouping," *Wireless Personal Commun.*, vol. 80, pp. 1079–1094, 2015.

[5] M. Naeem and D.C. Lee, "A joint antenna and user selection scheme for multiuser MIMO system," *Applied Soft Computing*, vol. 23, pp. 366–374, 2014.

[6] P. Pattanayak and P. Kumar, "A computationally efficient genetic algorithm for MIMO broadcast scheduling," *Applied Soft Computing*, vol. 37, pp. 545–553, 2015.

[7] P. Viswanath, D. N. C. Tse, and R. Laroia, "Opportunistic beamforming using dumb antennas," *IEEE Transactions on Information Theory*, vol. 48, no. 6, pp. 1277–1294, 2002.

[8] J. Jiang, R. M. Buehrer, and W. H. Tranter, "Antenna diversity in multiuser data networks," *IEEE Transactions on Communications*, vol. 52, no. 3, pp. 490–497, 2004.

[9] K.-K. Wong, "Performance analysis of single and multiuser MIMO diversity channels using Nakagami-m distribution," *IEEE Transactions on Wireless Commun.*, vol. 3, no. 4, pp. 1043–1047, 2004.

[10] C.-J. Chen and L.-C. Wang, "A unified capacity analysis for wireless systems with joint multiuser scheduling and antenna diversity in Nakagami fading channels," *IEEE Transactions on Communications*, vol. 54, no. 3, pp. 469–478, 2006.

[11] M. Torabi, D. Haccoun, and W. Ajib, "BER performance analysis of multiuser diversity with antenna selection in MRC MIMO systems," in *IEEE, Global Telecommunications Conference, 2009, GLOBECOM 2009* IEEE, 2009, pp. 1–6.

[12] M. Torabi and D. Haccoun, "Performance analysis of joint user scheduling and antenna selection over MIMO fading channels," *IEEE Signal Processing Letters*, vol. 18, no. 4, pp. 235–238, 2011.

[13] J. L. Vicario and C. Anton-Haro, "Analytical assessment of multi-user vs. spatial diversity trade-offs with delayed channel state information," *IEEE Communications Letters* , vol. 10, no. 8, pp. 588–590, 2006.

[14] L. Yang, "Achievable rate of MIMO systems with multi-user diversity and delayed feedback," *Electronics letters*, vol. 45, no. 15, pp. 783–785, 2009.

[15] X. Yu, X. Dang, S. Leung, Y. Liu, and X. Yin, "Unified analysis of multiuser scheduling for downlink MIMO systems with imperfect csi," *IEEE Transactions on Wireless Commun.*, VOL. 13, NO. 3, pp. 1344-1355, MARCH 2014.

[16] H. Shin and J. H. Lee, "Performance analysis of space-time block codes over keyhole nakagami-m fading channels," *IEEE Transactions on Vehicular Technology*, vol. 53, no. 2, pp. 351–362, 2004.

[17] E. G. Larsson and P. Stoica, *Space-time block coding for wireless communications*. Cambridge university press, 2008.

[18] V. Sharma, K. Premkumar, and R. N. Swamy, "Exponential diversity achieving spatiotemporal power allocation scheme for fading channels," *IEEE Transactions on Information Theory*, vol. 54, no. 1, pp. 188208, 2008.

[19] H. Bolcskei, D. Gesbert, and A. J. Paulraj, "On the capacity of OFDM-based spatial multiplexing systems," *IEEE Transactions on Communications*, vol. 50, no. 2, pp. 225–234, 2002.

[20] M. Eslami and W. A. Krzymien, "Net throughput maximization of per-chunk user scheduling for MIMO-OFDM downlink," *IEEE Transactions on Vehicular Technology*, vol. 60, no. 9, pp. 4338–4348, 2011.

[21] M. R. McKay, P. J. Smith, H. A. Suraweera, and I. B. Collings, "On the mutual information distribution of OFDM-based spatial multiplexing: exact variance and outage approximation," *IEEE Transactions on Information Theory*, vol. 54, no. 7, pp. 3260–3278, 2008.

[22] G. Oien, H. Holm, and K. J. Hole, "Impact of channel prediction on adaptive coded modulation performance in rayleigh fading," *IEEE Transactions on Vehicular Technology* , vol. 53, no. 3, pp. 758–769, 2004.

THE 5TH INTERNATIONAL CONFERENCE ON WIRELESS COMMUNICATIONS, VEHICULAR TECHNOLOGY, INFORMATION THEORY, AEROSPACE & ELECTRONIC SYSTEMS (WVITAE-2015)
December 13-16, 2015, Hyderabad, India

Evaluation of Channel Assembling Strategies with Single-Class Users in Cognitive Radio Networks

Esenogho Ebenezer and Tom Walingo
School of Electrical, Electronic and Computer Engineering
University of KwaZulu-Natal
213573292@stu.ukzn.ac.za

Abstract— **Channel assembling (CA) strategies which allows several Primary User (PU) idle or unused channel-slot to be aggregated into combinations of usable secondary user (SU) channels have been deployed in cognitive radio networks. However, many of these schemes have been implemented without considering the varying nature of a wireless link that incorporates adaptive modulation and coding (AMC). This paper develops and compares two channel assembling strategies which are the Immediate Blocking Strategy (IBS) and Readjustment Based Strategy (RBS) in single-class SU traffic on a dynamic wireless link. The performance is evaluated through extensive simulation and the results demonstrate that, in a single class SU traffic, capacity and throughput is improved with significant reduction in blocking and Forced Termination .**

Keywords—AMC, channel assembling, cognitive radio networks, homogeneous traffic.

I. INTRODUCTION

Radio spectrum is the most precious and scarce resources in wireless communication systems given the facts that the existing licensed band are almost exhausted as a result of exponential growth in wireless applications and services both in multimedia and voice services[1][2]. Studies have shown that busty Primary User (PU) behaviour has been characterized as ON/OFF (utilizing and non-utilizing) given rise to un-used spectrum in time domain and spatial domain as in the TV white space (TVWS). In a radio network comprising of PU and Secondary User (SU), the primary users have high priority to use their spectrum while SU periodically sense to identify un-used channels [4]. Based on the sensing outcome, SUs tune their transceivers to communicate among themselves without interfering with the PU. The un-used PU channels/time slots need some organization to meet the demand of the SUs hence, the need for channel assembling. An effective channel assembling strategy must take into account the PU behaviour models and several of them were investigated in [3]. Network traffic has evolved from simple to more dynamic scenario such that, each SU requires different Quality of Service (QoS) at different signal to noise ratio. Hence, the need to aggregate PU un-used channels/slots to improve SU throughput and capacity since the channel is opportunistically used. This paper develops and compares two channel assembling strategies which incorporate the dynamics of a wireless link with adaptive modulation and coding (AMC) against No-assembling strategy (NA) in a homogeneous SU traffic. Moreover, the number of the channel/slot to be assembled for a particular SU with corresponding assembling strategy dependents on their signal to noise ratio (SNR).

II. RELATED WORK

Significant research work on channel assembling strategies has been done so far and they are aimed at developing novel schemes that exploits the scarce resources. In [6]. Channel assembling (CA) strategies with different spectrum adaptation strategies were proposed. In their work, two strategies which dynamically adjust channel occupancy of ongoing traffic flows are developed. In [10] Two channel aggregation schemes for wideband cognitive radio networks were proposed which are, a Constant Channel Aggregation scheme (CCA) and a Variable Channel Aggregation scheme (VCA) are presented. In the variable channel aggregation scheme, the bandwidth of the cognitive user is aggregated with a probability distribution or aggregated on the basis of the number of the residual channels. [6] [7]. Implements a dynamic CA strategy designed for heterogeneous traffic environment and spectrum adaptation by employing channel sharing and spectrum assignment among elastic users (real time) and non-elastic (non-real time). In [11] The authors incorporate priority queuing in CA such that, real-time SU are queued and serviced before non-real SU if no resources are available with the aim of avoiding or minimizing instant blocking. Combined queuing based CA and channel fragmentation is proposed in [9]. The protocol work in such a way that in any event, of batch arrival of SU, a secondary user channel can be split and share amore other SUs to accommodate other SU which cannot tolerate delay. However, none of these strategies considered the varying nature of a wireless link that incorporates adaptive modulation and coding (AMC). This paper develops and compares through simulation study, two channel assembling strategies which are the Immediate Blocking Strategy (IBS) and Readjustment Based Strategy (RBS) in a similar SU traffic on a dynamic wireless link.

III. SYSTEM MODEL AND ASSUMPTIONS

Consider an infrastructure based network consisting of a PU base station (TV mast), a cognitive radio base station (CRBs) and its users of similar class operating in the same frequency band as shown in Fig.1. The PU has full priority to utilize the spectrum and can pre-empt the SUs at any time irrespective of the class. The SU traffic operates in a first come first serve (FIFO) model since they are all of equal class. However, the first SU has higher priority to in terms of channel access and can pre-empt others if need arise. SU opportunistically utilizes the PU channels by employing any of the channel assembling schemes (IBS or RBS).

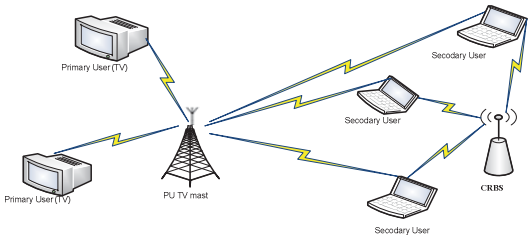

Fig. 1. Network Architecture

The licensed spectrum is divided into M frequency channels. Each channel frame consists of β slots and channel utilization per frame is on a slot basis. The PU utilizes one channel on an ON/OFF slot basis while SU can opportunistically assemble multiple adjacent or non-adjacent channels/slots, in frequency and time domain of the spectrum. The channel frame utilization map for a determined PU's ON/OFF behaviour is shown in Fig 2. The dynamic SU frame results in a heterogeneous system with variable frame channel/slot capacity and the SU traffic requires a particular transmission rate/number of channels. The CRBS decides to admit, block/ forcefully terminate the SU based on resources availability as dictated by channel assembly strategies deployed. The available capacity is determined by the conditions of the wireless link in terms of the SU SNR.

A. *Wireless Channel and AMC*

The Nakagami- m channel model is used to model the wireless link due to its versatility of spanning a wide range of fading channels [8].

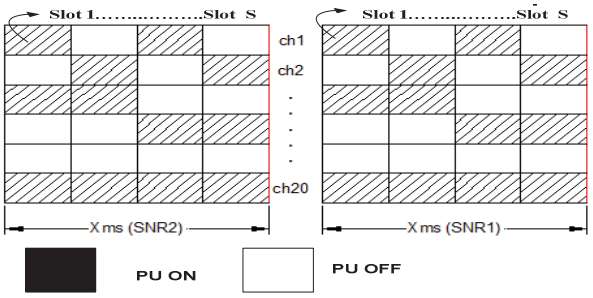

Fig. 2. Wireless frame utilization

The differing channel conditions are captured by the Finite State Markov Chain (*FSMC*) whose analysis for slow fading channel conditions is well known [9]. The entire SNR range is partitioned into Good, Moderate and Bad shown in Fig. 3. However, the specific modulation and coding modes for the AMC scheme as per IEEE 802.22 standard is adopted from [12]. The transition matrix of the FSMC, P is given by,

$$P = [p_{ij}]_{(N+1)\times(N+1)} \qquad (1)$$

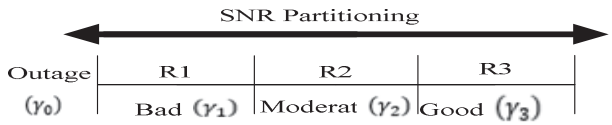

Fig. 3 SNR Partitioning

AMC is used in maximizing data rate with respect to the channel state thus, maintaining a prescribed packet error rate (PER) as adopted in [8]. The numbers of slot/channel a SU aggregate for data transmission decreases with increase in received SNR. [15]. Mode 1, Mode 2, Mode 3 Corresponds to QPSK, 16-QAM and 64-QAM representing assumed three states.

B. *Channel Slot Capacity*

Consider slot duration T_n in second as the minimum time to transmit a packet of length $\emptyset$ bits and R_n be the transmission mode in the slot while R_N is the highest transmission mode. The number of slots/channel in a fixed frame S is a variable function of the dynamic SNR with S being more when the SNR is good and less when bad. The number of slots of a frame in mode/state n, *(n=1, 2…)*, β_n, is given by,

$$\beta_n = \left(\frac{R_N \emptyset}{R_n \varepsilon_s R_1}\right) \qquad (2)$$

Where $\varepsilon_s$the constant channel is symbol rate per second and T_f is the frame duration in seconds. The channel state utilization is characterised by two-state Markov chain as shown in Fig. 4. Where ∂_i is the transitional probability from ON state to OFF state and σ_i be the transitional probability from the OFF state to the ON state for the i^{th} channel.

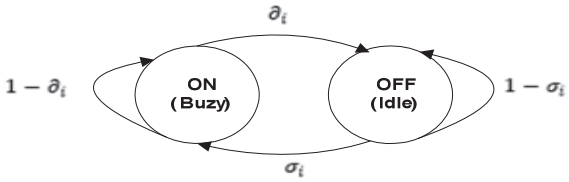

Fig. 4. The ON-OFF channel usage model for PU

The PUs slot/channel capacity, $\theta_{pu}$is given as,

$$\theta_{pu} = \beta_n \sum_{i=1}^{M} P_i \left(\frac{\sigma_i}{\sigma_i + \partial_i}\right) \qquad (3)$$

Where $P_i = \begin{cases} 1, & i \le N_{su} \le M \\ 0, & otherwise \end{cases}$, N_{su} is the number of frequency channel that have the presence of SU

Note that $\gamma_i = \sigma_i/(\sigma_i + \partial_i)$ is the channel utilization ratio. The SU system capacity (slot capacity/OFF capacity) $\theta_{su}(n)$, is given by,

$$\theta_{su} = (M * \beta_n) - \theta_{pu} \qquad (4)$$

IV. CHANNEL ASSEMBLING STRATEGIES

In this section, three strategies are presented. They are, the Immediate Blocking Strategy (IBS), the Readjustment Based Strategy (RBS) and the No-assembling scheme.

A. IBS ($\theta_{pu}, \theta_{su}, \theta_i, \theta_j$)

In this scheme, a SU which does not manage to assemble sufficient channels are immediately blocked. However, a SU that arrives first is given higher priority to the SU which arrives last. All the SUs are pre-empted by the arrival of a PU. Let Z be the total number of SUs in the system and the resource requirements for first $SU\ \ i$ be θ_i and next SU $\ j$ be $\ \theta_j$ respectively [13]. The assembly procedure is shown as Algorithm 1 below:

Algorithm I *for the CA using IBS*

CRBs check wireless link $\boldsymbol{\gamma_{su}}$;// cognitive radio base station checks wireless link state (SNR)

CRBs check $\boldsymbol{\theta_{su}}$;// cognitive radio base station checks available recourse for SUs

Access condition for i users

If ($\overbrace{\boldsymbol{\theta_{su} \geq \sum_{i=1}^{Z} \theta_i}}$); // resource assembly test as a function of SNR/mode pair.

$SU_{i,j}$_admit = true; // admit SU_s admit SU_i and assemble with a probability

else

$SU_{i,j}$_admit=false;//**block** the SU_s

if $[(\boldsymbol{\theta_{su} \geq \sum_{i=1}^{Z} \theta_i}) - \boldsymbol{\theta_{pu}}]$; // PU arrival, interrupts SU_i

$SU_{i,j}$_forced termination =true;//**forced-terminate** of ongoing SU_s

End If ;// terminate if no event

Go to start.

B. RBS ($\theta_{pu}, \theta_{su}, \theta^i_{min}, \theta_i, \theta^i_{max}$)

In this scheme, both SU_i and SU_j requires a minimum of $\theta^{min}_{i,j}(\theta^{min}_i, \theta^{min}_j)$ and maximum of $\theta^{max}_{i,j}(\theta^{max}_i, \theta^{max}_j)$ number of channels to commence or stop assembling respectively. When a SU_i require service, the assembling mechanism (CRBs) checks for resource availability similar to the IBS scheme. If the resources are available and sufficient, SU_i is admitted, otherwise, Readjustment Algorithm II is executed. However, because of the system is design in FIFO model, SU_i given preferential treatment.

Algorithm II *for the CA using RBS*

CRBs check wireless link $\boldsymbol{\gamma_{su}}$;// cognitive radio base station checks wireless link state (SNR)

CRBs check $\boldsymbol{\theta_{su}}$;// cognitive radio base station checks available recourse for SUs

condition for i user access

if ($\overbrace{\boldsymbol{\theta_{su} \geq \sum_{i=1}^{Z} \theta_i^{min}}}$); **);** // test for SU_{s1} resources

SU_i_admit = true; // admit SU_i

else

if $\left[\begin{array}{c}(\boldsymbol{\theta_{su} - \sum_{i=1}^{Z} \theta_n^{min}}) < \boldsymbol{\theta_{n,new}^{min}}) \\ \boldsymbol{or} \\ (\boldsymbol{\theta_{su} - \sum_{i=1}^{Z} \theta_n^{min}}) - (\boldsymbol{\omega})) \end{array}\right]$;// test for new SU arrival or PU arrival

Do $(\boldsymbol{\theta_i^{max} - 1})$, ++ *j:*// donation and iterate over i^{max} user resources

$SU_{i,j}$_admit = true; // admit $SU_{i,j}$ and assemble for both users

else

SU_i_admit =false; //**block** new SU_i no-free slot or insufficient

else

if all condition cannot be meet

$SU_{i_}$ FT=true;// force-terminate on going SU_i

End if; // start the process.

C. No-Assembling Strategy (NA)

This is the convectional communication system where transmitters and receivers communicate with each other without application of any special scheme or techniques. Even when enough idle channels are available, it is wasted.

V. SYSTEM MODEL PERFORMANCE MEASURES.

Let λ_p, λ_s be the arrival rates of the PU and SU respectively. Service time is exponentially distributed with the service rates defined as μ_p , μ_{su} for the PU and SU, respectively as in [10-11]. The total rate for a user is assumed to be the product of the users channel/slot service rate and the number of assembled channels/slot $\theta_i\mu_{si}$ or $\theta_j\mu_{sj}$ respectively.

A. The Performance Measures

a) *The blocking probability* P_b of SU traffic class is the probability that a new SU is denied access to the spectrum if it cannot meet the condition in the algorithms. If total SU blocked and arrived are Ω_{Ts} and λ_{Ts} respectively, then , It is expressed as,

$$P_b = \frac{Total\ \ SU\ blocked}{Total\ SU\ arrivals} = \frac{\Omega_{Ts}}{\lambda_{Ts}}$$

b) *The forced termination probability* P_f of traffic is the probability of an ongoing SU being pre-empted by a PU arrival however, in this paper, forced termination probability represents the fraction of the forced commenced SU services. Also, If total SU forced terminated and admitted are η_{Ts} and ζ_{Ts} respectively, then , It is expressed as,

$$P_f = \frac{Total\ SU\ forecd\ terminated}{Total\ \ admitted\ SUconnections} = \frac{\eta_{Ts}}{\zeta_{Ts}}$$

c) *Throughput* (T_P) is define as the fraction of SUs packet that successfully delivered (average service completion upon PU arrival), after meeting the necessary conditions in the algorithm. It can be given as,

$$T_P = \lambda_s(1 - P_b) \qquad (5)$$

d) *Capacity* ρ_{su}: The capacity of the homogeneous SU network is the average number of SUs service completion per unit time. Thus, ρ_{su} of admitted SUs at a particular time is a function of the SNRs/modes pair. It is expressed as,

$$\rho_{su} = \frac{Average\ number\ of\ SUs\ service\ completion}{Time(seconds)}$$

$$\rho_{su} = \{T_P = \lambda_s(1 - P_b)\}/T_n \qquad (6)$$

VI. NUMERICAL RESULTS AND DISCUSSIONS

To illustrate the performance evaluation of the CA strategies with AMC, the numerical results based on simulation are presented in this section for a homogeneous SU traffic. The parameters are configures as, $\lambda_p = 0.5$, $\lambda_s = 1.5\ \mu_s = 0.85$, $\mu_s = 0.6, Z = 6, P_b = 0.55$ $P_f = 0.65, T_P = 2.5, \rho_{su} = 2.2$ $\theta_i = 4$. MATLAB tool was used to run the simulations for each of the strategies. However, comparing the strategies of the RBS with the IBS strategies one can argue that there is a significant improvement of the RBS scheme over the IBS due to its flexibility. Precisely, the RBS scheme outperformed the IBS scheme in terms of SU capacity, throughput blocking and forced termination probability respectively.

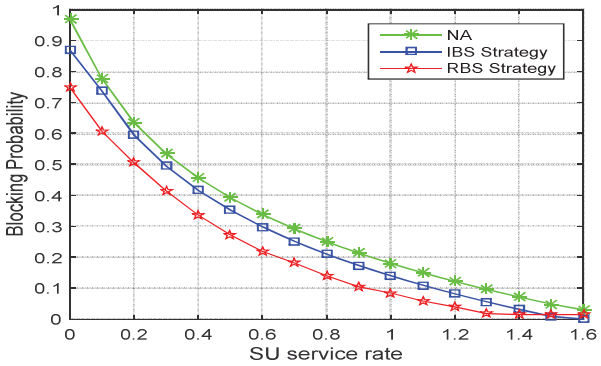

Fig.5a blocking probability P_b vs μ_{su}

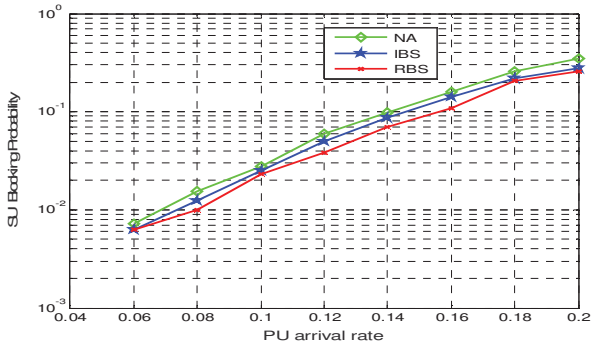

Fig.5b blocking probability of SU as a function of λ_p

Fig. 5a shows that, when the service rate μ_{su} of the SUs grows as a result of good channel condition, the blocking probabilities decreases since more SUs will be served. However, in both case (Fig. 5a and Fig. 5b), RBS scheme has a lower blocking probability as compared to the IBS while the NA strategy has a higher blocking probability. Moreover in Fig. 5b, as more PUs arrives, empty channel slot will not be available so, more SUs will not be given access.

In an event of batch arrivals of PUs, the SUs will experience decrease in throughput because very few slots will be available for the SUs to use and as such, not much will be sent by the SU as shown in Fig. 6a. Similarly, throughput improved as PU departs and more channels/slots are assembled by the SUs. However the RBS still shows better performance as compared to the two other strategies (IBS and NA) due it adaptability with respect to PU arrival as shown in Fig. 6a and 6b.

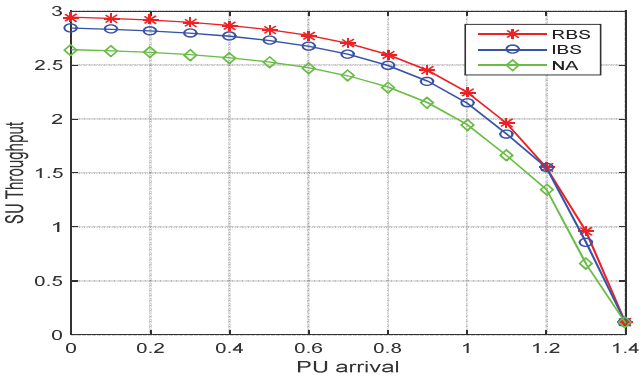

Fig.6a Throughput of SU as a function of λ_p

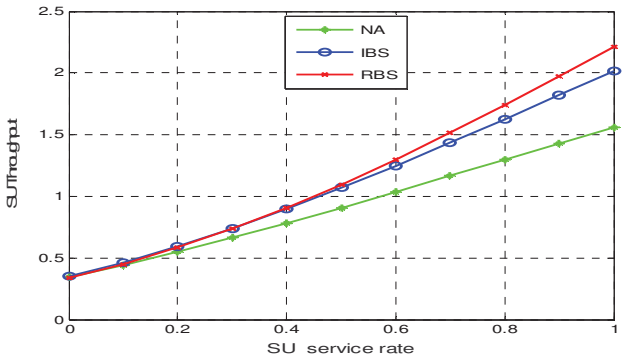

Fig.6b Throughput of SU as a function of λ_p

Fig.7a and Fig, 7b illustrates gradual increase in SU capacity with respect to the service rate and SNR irrespective of the scheme deployed. Incorporating AMC in channel assembling strategies helps improve service completion rate because more data will be sent as the SNR becomes better. However, in both results, the RBS showed a better characteristic due to its flexibility as compared to IBS and NA respectively.

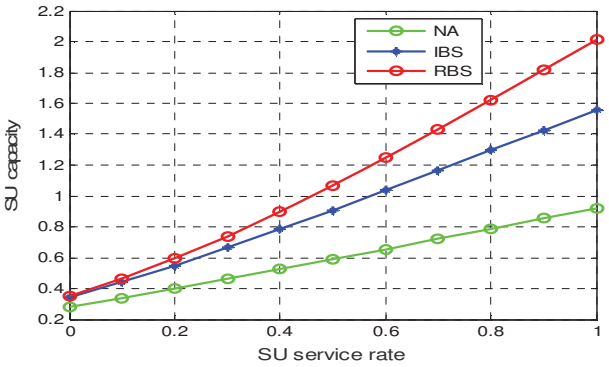

Fig.7a SU capacity as a function of μ_{su}

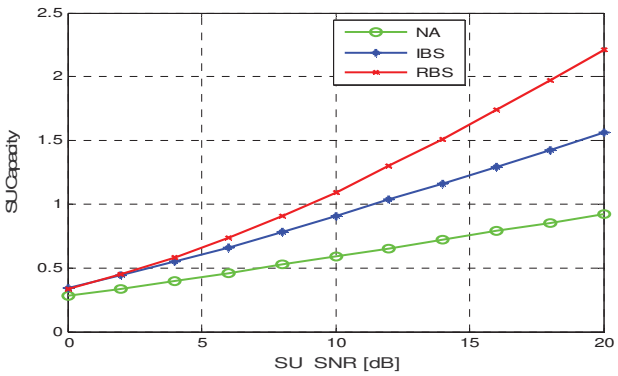

Fig.7b SU capacity as a function of SNR [dB]

In Fig.8a, PU activity has a significant effect on the behaviour of the SUs in terms of when to assemble channels and when to drop already assembled SU channels slot. When PUs arrives either in batch or individually, an ongoing SU must forcefully terminate its transmission if idle channel does not exist elsewhere within the network. Likewise in Fig.8b, when an SU arrives and enough channels exist, it is serviced and as such, the probability to force terminate these SU will drop. Moreover, the RBS scheme emerge a better scheme than the IBS and the NA as shown in the results.

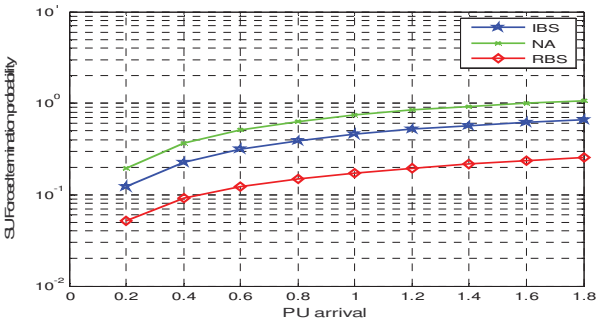

Fig.8a SU FT as a function of λ_p

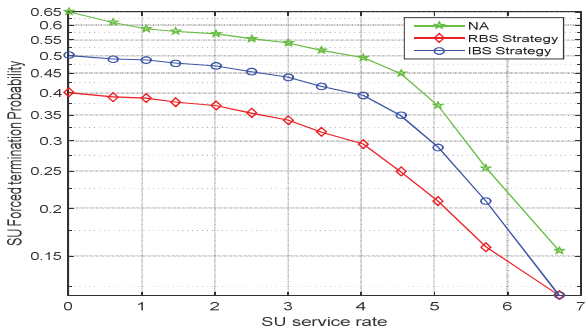

Fig.8a SU FT as a function of μ_{su}

VI. CONCLUSION

In this paper we have shown and compare through a simulation study, the performance measures of two channel assembling techniques for cognitive radio network, considering the dynamics of a wireless link with AMC against NA. The result obtained from our simulation shows that, the RBS techniques perform better than the IBS and the NA techniques in the sense that, it has lower blocking and force termination probabilities respectively. Also, it demonstrates that AMC is a robust technology in improving channel allocation schemes if incorporated. However, our future work will be focus in two folds: The selection of secondary users with two traffic running simultaneously.

ACKNOWLEDGEMENT

This work is sponsored by Telkom SA and Alcatel lucent under the Centre for Radio Access and Rural Technology (CRART), UKZN.

REFERENCES

[1] L. Zhai, K. Liu, Y. Liu, M. Yang and L. Zhuang "A Slot-Based MAC Protocol in Cognitive Radio Wireless Networks" *Wireless Communications, Networking and Mobile Computing*, WiCOM '08. 4th International Conference on Page(s): 1- 4.

[2] M. M. Rashid, M. J. Hossain, E. Hossain, V. K. Bhargava. "Opportunistic spectrum scheduling for multiuser cognitive radio: a queueing analysis" Wireless Communications, *IEEE Transactions on* Vol: 8, Issue: 10, 2009, Page(s): 5259- 5269.

[3] E. Ebenezer and T. Walingo "Primary Users ON/OFF Behaviour Models in Cognitive Radio Networks" 2rd *International Conference on Wireless and Mobile Communication Systems (WMCS '14)* Lisbon, Portugal, 2014. pp. 209-214.

[4] C. Cormio and R. Kaushik, Chowdhury, "A survey on MAC protocols for cognitive radio networks" *Elsevier Ad Network 7* (2009) 1315-1329.

[5] Su H., and X. Zhang Cross-layer based opportunistic MAC protocols for QoS provisioning over cognitive radio wireless networks .*IEEE Journal on Selected Areas in Communications* 2008; 26(1):118–129.

[6] L. Jiao, F. Y. Li, and V. Pla, "Dynamic Channel Aggregation Strategies in Cognitive Radio Networks with Spectrum Adaptation" *IEEE Globecom 2011 proceedings*. 2011 pp.1-6

[7] L. Jiao, F. Y. Li, and V. Pla, "Modelling and performance analysis of channel assembling in multi-channel cognitive radio networks with spectrum adaptation," *IEEE Trans. Veh. Technol.*, vol. 61, no. 6, pp.2686–2697, July 2012.

[8] X. Wang, Q. Liu, and G. B. Giannakis, "Analyzing and Optimizing Adaptive Modulation Coding Jointly With ARQ for QoS-Guaranteed Traffic" *IEEE Transactions On Vehicular Technology,* vol 56, no. 2, March 2007 pp.710-720

[9] L. Li, S. Zhang, K. Wang and W. Zhou "Queuing Method in Combined Channel Aggregation and Fragmentation Strategy for Dynamic Spectrum Access" 23rd *IEEE Symposium on personal, Indoor, and Mobile Radio Communication-(PIMRC*), 2012, pp.1214-1219.

[10] J. Lee and Jaewoo So "Analysis of Cognitive Radio Networks with Channel Aggregation" *IEEE Wireless Communications and Networking Conference (WCNC)* 2010 proceedings. Page(s): 1 - 6

[11] A. M. I. Balapuwaduge L. Jiao, F. Y. Li, and V. Pla, "Channel Assembling with Priority-Based Queue in Cognitive Radio Network: Strategy and Performance" *IEEE Transaction on wireless Communication*, vol.13, NO. 2, FEBUARY 2014, Pp.630-644.

[12] N. M. Apurva and G. Chounard "Enabling Rural Broadband Wireless Access Using Cognitive ratio Technology" doc.: *IEEE 802.22 - 10/0073r03 2010-06-15*.

[13] Esenogho E. T. Walingo "Performance Evaluation of Channel Assembling Strategies with Multi-Class Secondary Users in Cognitive Radio Networks", *Southern Africa Telecommunication, Networking and Application Conference (SATNAC)* 2015, Cape Town, September 6th - 9th pp.81-86. ISBN978-0-620-67151-4.

THE 5TH INTERNATIONAL CONFERENCE ON WIRELESS COMMUNICATIONS, VEHICULAR TECHNOLOGY, INFORMATION THEORY, AEROSPACE & ELECTRONIC SYSTEMS (WVITAE-2015)
December 13-16, 2015, Hyderabad, India

Downlink Joint Processing For Non Orthogonal Multiple Access

Islam Atef
Faculty of Engineering
Alexandria University
Alexandria, Egypt
Islamaf81@yahoo.com

Essam Sourour
Faculty of Engineering
Alexandria University
Alexandria, Egypt
sourour@ieee.org

***Abstract*—Cooperative communication is one of the emerging technologies that promise significantly higher reliability and spectral efficiency in wireless networks. It is a new form of diversity that allows users or nodes to share resources to create collaboration via distributed transmission and processing of messages. As candidate multiple access for future radio access, Non orthogonal multiple access (NOMA) over orthogonal multiple access (OMA) are adopted as downlink access scheme for future 5th generation mobile communication. In this paper, we compare user throughput when using orthogonal multiple access (OMA) and NOMA in macro femto network. We show through computer simulation the effect of imperfect interference cancellation on user throughput. We assist the performance of user selection when using fixed power allocation. Finally, we propose NOMA with COMP scenario whose performance improvement lead for user and cell throughput.**

Keywords—NOMA; JP; Heterogeneous.

I. INTRODUCTION

Heterogeneous Network (HeNet) is one of new technologies defined by 3GPP to improve LTE advanced network performance, it consists the deployment of macro cell with different cells such as microcells, femtocells, and picocells which enhance cellular network capacity [1].

Femtocells, also known as home eNodeB were first introduced in 3rd Generation Partnership Project (3GPP) Release 8, signaling that it had become a mainstream wireless access technology [2].

Femtocells promise improved indoor coverage and increased throughput for mobile data services while off-loading traffic from expensive macro radio access networks onto the low cost public Internet [3].

Femtocells access mode defines which user is allowed to use each femtocell. Two modes are defined, open access mode which every registered and unregistered user can access that femtocell but disadvantage of this mode is increased of signaling overhead. In the closed access mode only registered users are served by femtocell. Even femtocell provide higher signal quality than open access mode, the disadvantage of this type leads to high cross interference [4], [5].

Power control of HNB is interference management technique which mitigates interference to both macro user equipment (MUE) and home (femto) user equipment (HUE), it can be achieved by minimizing total transmission power of HeNB [6], [7]. The downlink transmission from HeNB will affect on nearby MUE when using co-channel deployment between macro and femto cell, strong interference from HNB may cause the received signal from macro to MUE degraded and unacceptable.

The enhanced Inter Cell Interference Coordination (eICIC) in heterogeneous networks is an efficient inter cell interference scheme compared to ICIC in LTE release 8 and 9 which that ICIC only consider data channels and didn't focus in interference between control channels [8], but in LTE release 10 solve this problem by two main solution, one in time domain multiplexing such as almost blank subframe (ABS), the other in frequency domain multiplexing such as carrier aggregation (CA).

The design of radio access technology (RAT) is one important aspect of improving system capacity. Radio access technology are characterized by multiple access scheme such as code division multiple access (CDMA), time division multiple access (TDMA), frequency division multiple access (FDMA), or orthogonal frequency multiple access (OFDMA), which indicate how multiple users access and share the system resources [10].

Non orthogonal access code division multiple access (CDMA) is widely used in the 3rd generation mobile communication system. Orthogonal frequency division multiple access (OFDMA) is adopted in 4th generation mobile communication system e.g., LTE and LTE-advanced for achieving good system throughput.

As candidate multiple access for future radio access, Non orthogonal multiple access (NOMA) over orthogonal multiple access (OMA) are adopted as downlink access scheme for future 5th generation mobile communication. In NOMA multiple users are multiplexed in power domain in base station (transmitter side) and in receiver side serial interference cancellation (SIC) are used to separate multiuser signals [11].

Cooperative MIMO (Co-MIMO) technique also referred to as coordinated multi-point transmission (CoMP) has emerged as a key enabling technique to improve system spectral efficiency and effectively mitigate inter cell interference (ICI). The cooperative transmission techniques involve two categories i.e. joint processing (JP) and coordinated beamforming (CB). Coordinated joint processing uses simultaneous transmissions of data from multiple transmission points to a single user in order to improve its received signal

quality and actively cancel the interference from other cells. It involves sharing of data and channel state information (CSI). In coordinated beamforming, data for a single user is instantaneously transmitted from one of the transmission points; however, coordinated beamforming/scheduling is performed to reduce the interference caused to other cells [12].

In this paper we showed the effect of imperfect interference cancellation on user throughput when using serial interference cancellation in receiver side. We compare through computer simulation between two users selection schemes when using fixed power multiplexing allocated to users in transmitting side using non orthogonal multiple access. We showed improvement of using NOMA over OMA in heterogeneous network downlink. Proposed Joint Processing with NOMA scenario will be shown as the method which improves user and cell throughput. The remainder of this paper is organized as follow: NOMA concept described in section II. Mitigation interference scheme and COMP are described in section III and section IV, respectively. Section V describes our proposed NOMA with Joint transmission. System simulation model are presented in section VI, followed by simulation results in section VII. Conclusion of paper is shown in section VIII.

II. NON ORTHOGONAL MULTIPLE ACCESS

NOMA is the one of the most promising technologies that it will play a central role in the 5th generation network. NOMA is a combination of OFDMA with superposition and interference cancellation techniques. It uses new path loss profile which utilizes pathloss difference for user multiplexing purposes and is proved more efficient than OFDMA.

A) NOMA Transmission

The basic concept of NOMA downlink as the eNB select two users have different channel gain and send two signals to each users but in different power allocation. For NOMA transmitter side, the total power for any multiplexed two users is the same. User whose channel gain is better condition than the another user is allocated less power, so power allocated to each user and selecting two pair users affect not only to user throughput but also other user due to inter-user interference.

B) NOMA Receiver

At the receiver side, where user 2 has a better channel than user 1 and hence can decode any data that user 1 can successfully decoded. Using superposition coding scheme, user 1 treats signal of user 2 as noise and decodes its data from y_1. User 2, which has better channel, performs successive interference cancellation (SIC): it decodes the data of user 1 (treats its data as interference) and then proceeds subtract signal of user 1 from y_2 and decode its data, with each possible split power $P=P_1 + P_2$, [12], [13]. The following throughput of two users as:

$$R_1 = log_2\left(1 + \frac{P_1|h_1|^2}{P_2|h_1|^2+N_{0,1}}\right) \quad (1)$$

$$R_2 = log_2\left(1 + \frac{P_2|h_2|^2}{N_{0,2}}\right) \quad (2)$$

Where P_1 and P_2 are transmitted power for users i=1,2. h_1 and h_2 are channel gain for two users, N is power of additive white Gaussian noise, R_1 and R_2 are throughput for two users.

C) Imperfect successive interference cancellation

In fact not all interference power is removed under cancellation; the parameter $\varepsilon \rightarrow [0, 1]$ gives the residual power of user after cancellation. The equation (2) after considering imperfect interference cancellation will be:

$$R_2 = log_2\left(1 + \frac{P_2|h_2|^2}{\varepsilon_1 P_1|h_2|^2 + N_{0,2}}\right) \quad (3)$$

Where ε is imperfect interference cancellation, $\varepsilon = 0$ for perfect interference cancellation. In simulation we show different values of ε.

D) Transmit power allocation

Due to power domain multi user multiplexing, the transmit power allocation (TPA) is important consideration in NOMA downlink, it affects the achievable throughput not only that user but throughput of system. In our simulation we compare between two transmit power allocated schemes, first used in [14], which called Pre defined user group and per group fixed power allocation (FPA) and our proposed scheme is user sorting power allocation (USPA). In first scheme, the users are divided into two different user groups according to their channel gains and pre defined threshold. In FPA, the users can be paired together only if they belong to different user groups. In the second scheme; the user sorting power allocation (USPA) is described as follow:

- PF scheduling calculates maximum priority for each user and sorts Users corresponding to their maximum priority.
- Users which will be selected by PF are sorted in descending order according to their signal to interference ratio (SIR), so high SIR users are the top of this list.
- The Scheduler Divides this list into two groups
- The users can paired together from different group (top of group 1 will be paired with top of group 2,etc)

III. MITIGATION INTERFERENCE SCHEME

In heterogeneous network, when macrocell network operates on the same carrier as HeNBs, HeNB-macrocell interference can result degrading performance in some scenario, indoor MUE which can't be associated to HeNB due to presence of CSG (closed subscriber group) nodes, MUEs are affected by interfering signal coming from HNB, also MUEs close to building (near outdoor) may experience to interference then may lead to degrade signal to interference ratio. Inter femto interference is other interference will be taken account in our simulation, since due HUE can be associated to HeNB in the same apartment or macrocell, the interference comes from HeNB neighbor apartment may be strong. Two mitigation interference schemes will be used in our simulation; Autonomous power control method and

enhanced ICIC in time domain which named as almost blank subframe (ABS).

A) Power control

To limit the impact interference of femtocell on existing heterogeneous network, it desired to limit transmission power control of CSG HeNBs; we used method which described in [15]. The following equation represents the power control algorithm for HeNB

$$P_{TX} = \max(P_{TX,min} , \min(P_{TX,max} , P_{RX} + PL - \lambda)) \quad (4)$$

Where P_{TX} is HeNB transmission power, $P_{TX,min}$, $P_{TX,max}$ are the minimum and maximum transmission powers which values are -10 dBm and 20 dBm, respectively. P_{RX} is the power received from the strongest macro (MNB), PL is the assumed pathloss in dB, and λ is the target minimum C/I value in dB. The target is to minimize interference to macro network, while the pathloss determines the desired HeNB coverage; it should be set to maximum pathloss for any link between HeNB and its HUE in same apartment (the value in our simulation is 60dB)

B) Almost Blank Subframe (ABS)

The basic idea is to have some subframe which femtocell is not allowed to transmit data. This scheme is called Almost blank subframe (ABS), ABS is TDM (time domain multiplexing) scheme for enhanced inter-cell-interference coordination (eICIC)[9]. To alleviate this issue, subframe resources are split among macrocell and femtocell to improve reliability [15], it means that macrocell can use all resources but femtocell can use only half of all subframe.

IV. Coordinated MultiPoint Transmission

Depending on whether the user data is shared among all the transmission points within a CoMP cluster, downlink CoMP transmission schemes can be divided into two main categories: coordinated scheduling/beamforming and joint processing.

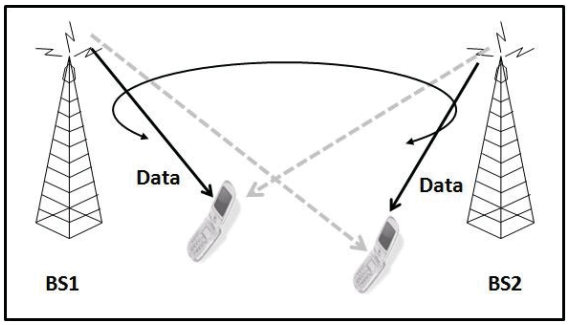

Fig. 4.Coordinated Scheduling/Beamforming Scheduling

A) Coordinated Scheduling/Beamforming Scheduling (CS/BS)

In CS/BS as shown in figure 4, user data is only available in one cell, and coordinated beamforming and scheduling is done between cells to reduce interference to other cells

B) Joint Processing (JP)

In joint processing approach, user data is available simultaneously at all transmission cells. JP is further categorized into Joint Transmission (JT) and Dynamic Cell selection (DCS) as shown in figure 5a and 5b respectively.

In JT the same resource block (RB) of physical downlink shared channel (PDSCH) is transmitted from multiple cells among coordinated cells. In DCS, RB of PDSCH is transmitted from one cell among the coordinated cells. The unique cell is dynamically selected by fast scheduling where minimum pathloss is considered [16] and [17].

V. Proposed NOMA with Joint Transmission

We extend our simulation with NOMA to base station (BS) cooperative cellular downlink for future radio access. Since the MIMO capacity is increased as the numbers of transmitter and receiver antennas are increased, while the allowable numbers of these antennas per BS and user terminal are limited, employing a combination of BS cooperation and multiuser MIMO is an effective way to enhance the cellular system performance.

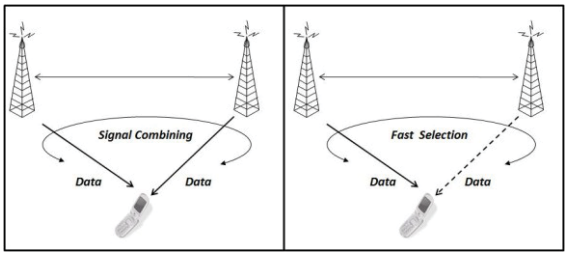

a) Joint Transmission b) Dynamic cell selection

Fig. 5.Joint Processing

For the proposed NOMA in a BS cooperative scenario, we employ NOMA with Joint transmission in this paper. We show that the proposed NOMA scheme with BS cooperation achieves better system-level throughput compared to OMA. We also show that the effect of the proposed NOMA scheme is more significant when BS cooperation is assumed since the BS cooperation improves the channel conditions of the cell-edge users, which are appropriate for obtaining a higher non-orthogonal user multiplexing gain. Figure 6 shows the flow chart of proposed NOMA with Joint Transmission.

VI. System Simulation Model

Simulation model is Macro-Femto cell deployment (heterogeneous network) which according to model described in [16] which some assumption and parameters used in simulation.

We employed 19-hexagonal macrocell with an inter site distance (ISD) of 500m; each macro node cell site includes three cells with antenna boresights pointing in the three horizontal directions separated by 120 degrees. The system bandwidth is 10 MHz, it means 50 RBs (Resource blocks).Macro transmission power in each cell equal to 46 dBm.25 macro UEs are dropped randomly following a uniform distribution in each cell dropped within the cell site

area. Dual strips model of HeNBs are randomly dropped in each cell, dual strips are composed of two building separated by one strip as shown in Figure. 5. A uniformly distributed is independently generated for each apartment.

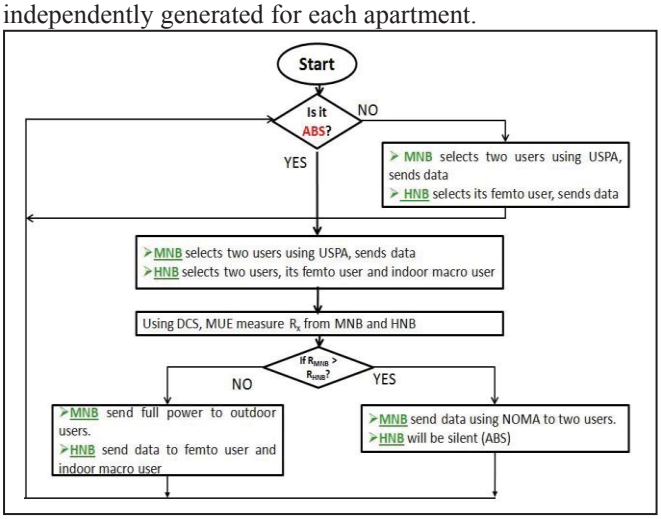

Fig. 6.The flow chart of proposed NOMA with Joint Transmission

HeNB and associated HUE are dropped in random location with minimum separation 3 m for each apartment, note that HeNB are assumed to be closed subscriber group (CSG) cells, we assume that both HeNBs and macro are synchronized in both time and frequency domain.

HUEs may associate to either its HeNB in its apartment or macrocell depending on received power, while MUE (macro user equipment) can only associate to MNB (macrocell), minimum distance between MNB and MUE is 35 m [15]. In our simulation we use 35% of MUEs are dropped indoor in random location. We assume two transmit antennas at the eNBs and two receive antennas at the UEs. UEs are assumed to be served using transmission mode 4 (TM4) as described in the LTE terminologies [6]. The maximum HeNB transmission power is 20 dBm. The deployment configuration channel is co-channel for both macro eNBs and HeNBs; they share the same spectrum. 5ms reporting periodicity is assumed while mobile speed is assumed to be 3m/s. Proportional fair is downlink scheduler in our simulation that at each Transmission Time Interval (TTI).

VII. System Results

We show in figure 8 comparison of cumulative distribution function for our heterogeneous network (macro and femto) model using orthogonal multiple access (OMA) and non orthogonal multiple access (NOMA) and see how NOMA boost user throughput comparing to OMA, this is because user throughput of orthogonal multiple access is limited by orthogonal bandwidth allocation. Figure 9 shows comparison between two schemes; Pre defined user group and per group fixed power allocation (FPA) and; user selection power allocated (USPA).Due to using high difference in channel gain USPA scheme lead improvement in user throughput than FPA. It shows that MUE throughput improve when using USPA, 90% of users in USPA are getting more than 0.5 Mbps versus 87% of users are getting more than 0.5 Mbps in FPA.

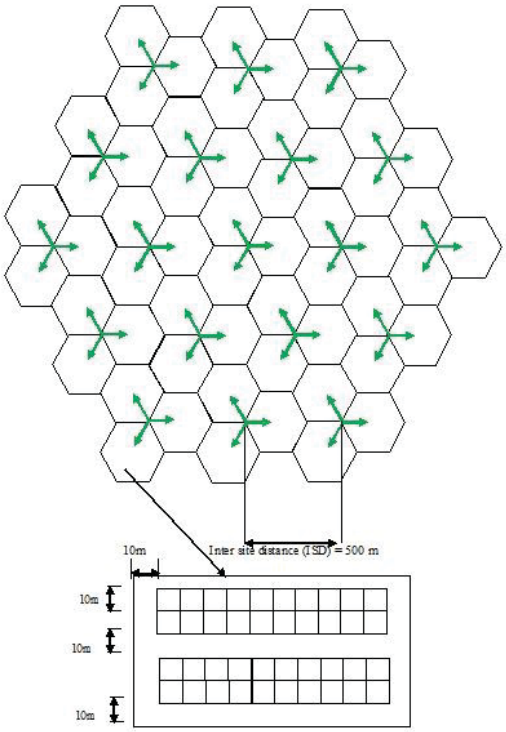

Fig. 7. System simulation model

In fact not all interference power is removed under cancellation; the parameter ε → [0, 1] gives the residual power of user after cancellation. ε =0 for perfect interference cancellation. Figure 10 compares between the effects of different imperfect interference cancellation on macro users throughput, it shows the throughput improves when imperfect interference cancellation decreases. Figure 11 shows the comparison between macro users throughput with COMP and without COMP, with COMP; only 40 percent are getting lower than 3 Mbps but without COMP, approximately 80% are getting lower than 3Mbps.

VIII. Conclusion

In this paper, we evaluate LTE heterogeneous network (macro femto network) with closed femto cells. We propose user selection with fixed power allocation scheme for NOMA downlink in heterogeneous network (USPA) and compare with FPA scheme. We propose Joint transmission as COMP techniques with NOMA in heterogeneous network and show how downlink Joint processing with NOMA improves average user throughput and cell throughput .

REFERENCES

[1] H.Liang, I.Z.jovacs, P.Moensen, O.Klein, and W. Stormer, “Optimal New Site Deployment Algorithm for heterogeneous Cellular Networks”, IEEE VTC, pp.1-5, 2011.

[2] V. Chandrasekhar, J. G. Andrews, and A. Gatherer, Femtocell Networks:A Survey, in IEEE Comm. Mag., pp. 59-67, Sept. 2008.

[3] Physical layer procedures, 3GPP TSG TS 36.213, V10.2.0, June 2011,
[4] J. Zhang, G.Roche, Femtocells: technologies and deployment, .1st edition, 2010

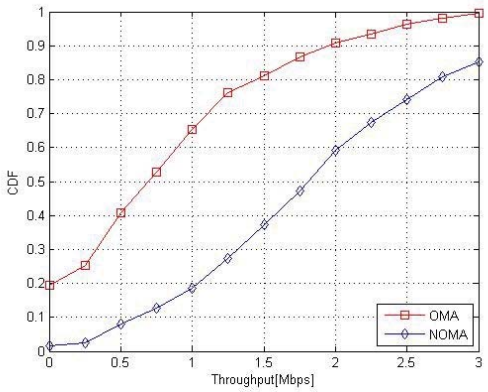

Fig. 8. Compare Macro users throughput when using OMA and NOMA

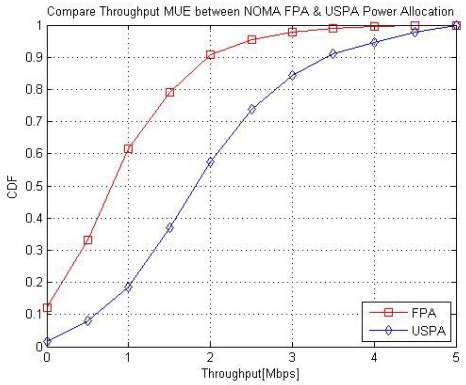

Fig. 9. Compare throughput of MUE between FPA and USPA

[5] 3GPP TS 25.467 V10.1.0, 3rd Generation Partnership Project; Technical Specification Group Radio Access Network; Stage 2 (Release 10),March.2011
[6] L. Xiangfang,L. Lijun, K. Deepak, " Downlink Power Control in Co-Channel Macrocell Femtocell Overlay", Information Sciences and Systems, pp.383-388, Mar 2009
[7] FDD Home eNB Radio Frequency (RF) requirements analysis, 3GPP TSG TR 36.921, V10.0.0, Apr. 2011,.
[8] F. Xiangning, C. Si, Z. Xiaodong, "An Inter-Cell Interference Coordination Technique Based on User's Ratio and Multi-level Frequency Allocations", IEEE WiMOB, pp.799-802, Sept. 2007.
[9] P.Monogioudis,J.Miernik,J.Seymour, "Algorithms for Enhanced Inter-Cell Interference Coordination (eICIC) in LTE HetNets ", IEEE/ACM Transactions, pp.137-150, Feb.2014
[10] Y.Saito, Y.Kishyama,A,Benjebbour, A.Li , and K.Higuchi, "Non-Orthogonal Multiple Access (NOMA) for future radio access", Proc.of IEEE VTC, pp.1-5, june 2013.
[11] A,Benjebbour, Y.Kishyama Y.Saito, T.Nakamura, A.Li , and A.Harada, "Concept and practical considerations of non-orthogonal multiple access (NOMA) for future radio access", ISPCS IEEE ,pp.770-774, NOV 2013.
[12] 3GPP TR 36.819 "Technical Specification Group Radio Access Network; Coordinated multi-point operation for LTE physical layer aspects" (Release 11), V11.1.0, Dec.2011

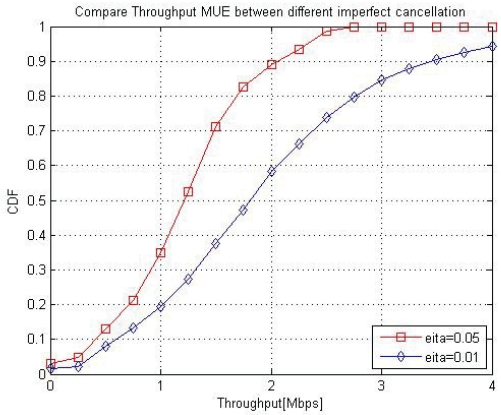

Fig. 10. Compare Macro users throughput when using imperfect IC

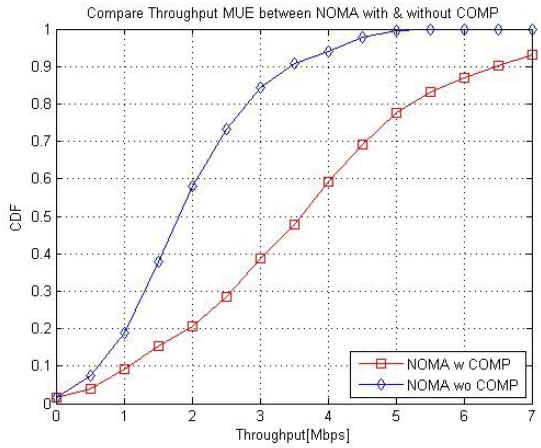

Fig 11.Compare throughput of MUE between NOMA with and without COMP

[12] D.Tse, P.Viswanath, Fundamental of Wireless Communication, .Cambridge University Press, 2005
[13] T.M. Cover, J.A.Tomas, Elements of Information Theory, 2nd edition, 2006
[14] A,Benjebbour, Y.Kishyama Y.Saito, T.Nakamura, A.Li , and A.Harada, "System-level performance evaluation of downlink non-orthogonal multiple access (NOMA)", PIMPRC IEEE 24th International Symposium, Sep 2013,pp.611-615
[15] A.Barbieri, A.Damnjanovic, J.Tingfang, J.Montojo, Y.Wei, "LTE Femtocells: System Design and Performance Analysis", IEEE VTC Spring, 2011, pp.1-5
[16] D.Lee,H.Seo, B.Clerckx, E.Hardouin, D.Mazzarese, S.Nagata,K.Sayana,"Coordinated multipoint transmission /reception techniques for LTE-advanced"Wireless Communications, pp. 26 – 34,June 2010,
[17] D.Lee,H.Seo, B.Clerckx, E.Hardouin, D.Mazzarese, S.Nagata, K.Sayana, "Coordinated multipoint transmission and reception in LTE-advanced: deployment scenarios and operational challenges", Comm. Mag., , pp.148–155,Feb 2012

THE 5TH INTERNATIONAL CONFERENCE ON WIRELESS COMMUNICATIONS, VEHICULAR TECHNOLOGY, INFORMATION THEORY, AEROSPACE & ELECTRONIC SYSTEMS (WVITAE-2015)
December 13-16, 2015, Hyderabad, India

Performance of a space-time coded MC-CDMA system in a Rayleigh fading channel

Olanrewaju B Wojuola, Stanley H Mneney and Viranjay Srivastava
School of Engineering
University of KwaZulu-Natal
Durban, South Africa
wojuolao@ukzn.ac.za, mneneys@ukzn.ac.za and viranjay@ieee.org

***Abstract*—Increasing demand for wireless services requires fast and robust broadband wireless communication for efficient utilisation of the scarce electromagnetic spectrum. Multi-carrier modulation and the use of multiple antennas coupled with multiple-access techniques have emerged as one of the promising solutions for high-speed future wireless communication. In this paper, we investigate the performance of a multi-antenna space-time block-coded (STBC) multi-carrier code-division multiple-access (MC-CDMA) system in a frequency-selective channel using Gold codes as spreading sequences. Results show that for a STBC CDMA system in a flat-fading channel at low signal-to-noise ratio, the coding gain provided by the codes surpasses the diversity advantage provided by the use of multiple antennas. The combination of diversity gain from the use of multiple antennas, coupled with coding gain provided by the Gold codes, plus the diversity gain resulting from frequency diversity of multi-carrier transmission and spectrum-spreading makes the composite STBC MC-CDMA system resilient to channel fading. This fact is particularly the case for long codes.**

Keywords— Space-time block coding, code-division multiple-access, orthogonal frequency-division multiplexing, multi-carrier transmission, Gold codes, spatial diversity, coding gain.

I. INTRODUCTION

The limited radio frequency spectrum, the harsh mobile environment, and the ever-increasing demand for wireless applications calls for advanced techniques for combatting the hostile environmental factors and for more efficient use of the scarce radio spectrum. One of the promising techniques for future wireless communication is the deployment of multi-input multi-output (MIMO) antenna system with orthogonal frequency division multiplexing (OFDM) coupled with multiple-access techniques. The combination of these techniques guarantees a much more reliable and robust transmission over the hostile wireless channel. This paper models the performance of a MIMO space-time block-coded (STBC) OFDM-CDMA system in a fading channel. The motivation for investigating space-time coded OFDM-CDMA system is because of the robustness of OFDM-CDMA against channel fading [1], and space-time coding in harnessing diversity and coding gain for improved system performance [2]. OFDM converts a frequency-selective channel to a flat-fading channel. Furthermore, the combination of OFDM and CDMA, as found in a multi-carrier (MC) CDMA, lowers the symbol rate in each subcarrier, the advantage being that a longer symbol duration makes it easier to quasi-synchronise the transmission. It also enables the use of a guard interval which helps in eliminating inter-symbol interference (ISI) [1-3].

Space-time coding (STC) is known to be an effective diversity technique for combating channel fading without bandwidth penalty. STC combines transmit diversity with coding scheme. In recent years, different types of space-time coding schemes, including space-time block codes (STBC), space-time trellis codes (STTC), concatenated STBC-STTC, and super-orthogonal STTC (SOSTTC), have been studied [4-6]. STBC, first proposed by Alamouti in 1998 [7], and later generalised by Tarokh [8, 9], provides diversity gain but no coding gain. However, the attractiveness in STBC includes its ability to achieve maximum possible diversity advantage, coupled with the simplicity of its implementation and decoding algorithm [10].

Although significant amount of work has been done on space-time-coded MC-CDMA systems, available literature shows that existing works have been largely limited to the use of Walsh-Hadamard codes as spreading sequences. Only a few reported works [11-14] involving the performance of Gold codes in such systems are available, and we seek to add to this small collection. In this paper, we investigate the performance of a series of Gold codes in a space-time coded CDMA system.

The rest of this paper is organised as follows. A description of the communication system is given in Section II. Results of software simulations are presented and discussed in Section III. The paper concludes with a summary of important results in Section IV.

II. SYSTEM MODEL

A space-time coded MC-CDMA system combines the positive advantages of space-time coding, multicarrier modulation with that of a CDMA system. Fig. 1 shows system block of a space-time coded MC-CDMA system for a single user. Here, the user source signal, represented by the vector $\boldsymbol{X}$, is first space-time coded by the STC encoder into parallel sub-streams. The CDMA encoder then encodes each sub-stream using a user's unique code. Each of the encoded sub-streams is placed on a subcarrier for onward transmission via the multiple transmit antennas through the wireless channel. The transmitted sub-streams convolves with the channel, and are then picked up by the receive antennas. At any time instant, the signal detected by each receive antenna is a summation of all the signals coming from the transmit antennas. To recover the original signal, the receiver carries out the reverse process on the detected signal.

Fig. 2 is another block diagram of the STC MC-CDMA system showing details of signal transformation through the communication system. This is described as follows. In the transmitter, the source signal is first space-time coded by the STC encoder into sub-streams. Each sub-stream is converted from serial to, say, N_p parallel symbol streams, having a symbol duration T_s. Each symbol stream is multiplied by the user code $c_k(t)$, after which the resulting signal for the pth

symbol stream modulates a subcarrier f_p. The subcarriers are orthogonal on the symbol duration and are given by $f_p = f_o+p/T_s$, where f_o is RF frequency. The multicarrier signal is obtained from addition of the different subcarrier signals. The resulting OFDM symbols are transmitted simultaneously from the individual transmit antennas. The received signal *r(t)* is a convolution of the multicarrier signal and the channel impulse response corrupted by noise. To recover the original data, the receiver carries out the reverse of what the transmitter does. In actual implementation, inverse fast Fourier transform (IFFT) and fast Fourier transform (FFT) are normally employed by the OFDM modulator at the transmit and the receive end respectively for improved system efficiency.

Starting from basic principles, we will now be developing a mathematical description of the communication system. The treatment begins by considering a simple direct-sequence (DS) CDMA system.For a multi-user DS-CDMA system comprising *K* users, the received signal *r(t)* at time *t* is a linear superposition of the signals for all users. We can show that the received signal *r(t)* is given by Equation (1), where user *k* is user index, c_k(t) is the code sequence for the user, $b_{k,t}$ is the user binary data, ω_c is carrier frequency, and θ_k is phase angle, $\beta_{kl,}$ is path gain for user *k* and path *l*, τ_{kl} is propagation delay, γ_{kl} *is* phase shift, *l* is path index, *L* is number of paths, and $n_{k,t}$ represents channel noise.

Now consider a space-time coded CDMA system with a transmit diversity scheme having n_T transmit antennas. Let $\boldsymbol{b_{k,t}}$ be the user data, space-time coded onto the n_T transmit antennas. The user data can be represented by a vector as

$$\begin{aligned} \boldsymbol{b_{k,t}} &= \left\{ b_{k,t}^{i} \right\}, \qquad i = 1, 2, \ldots, n_T \\ &= \left\{ b_{k,t}^{1}, b_{k,t}^{2}, \ldots, b_{k,t}^{n_T} \right\} \end{aligned} \tag{2}$$

where $b_{k,t}^{i}$ is the user data for antenna *i* at time *t.* For a multi-user system comprising *K* users, we can show that the received signal *r(t)* is a linear superposition of the signals for the users, and is given by Equation (3).

The space-time coded CDMA system above involves multiple transmit but single receive antenna. Now consider a space-time coded system with both transmit and receive diversity involving multiple antennas at both ends: multiple n_T transmit and n_R receive antennas. Received signal $r_{k,t}^{j}$ at j^{th} receive antenna and time *t* is a superposition of the signals

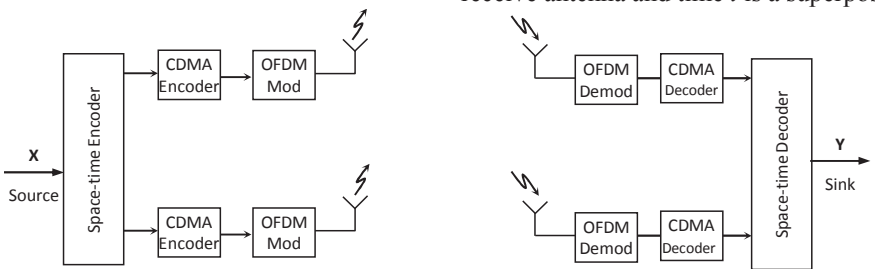

Fig. 1. Space-time coded MC-CDMA system.

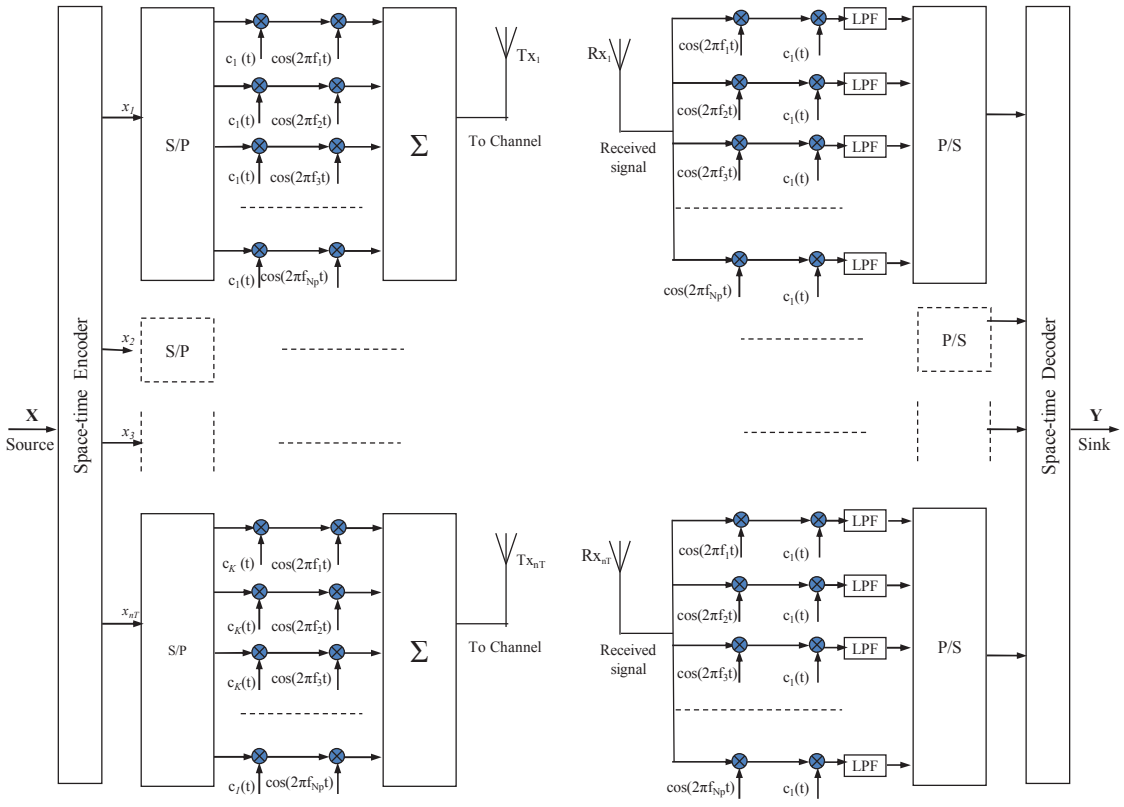

Fig. 2. Space-time coded MC-CDMA system showing details of signal transformation

coming from all the transmit antennas. Received signals for the all the receive antennas can be represented by

$$\begin{aligned} \boldsymbol{r}_{k,t} &= \left\{ r_{k,t}^{j} \right\}, \qquad j = 1, 2, \ldots n_R \\ &= \left\{ r_{k,t}^{1},\ r_{k,t}^{2}, \ldots, r_{k,t}^{n_R} \right\} \end{aligned} \tag{4}$$

Following a similar argument to that of the previous section, we can show that the signal received at the j^{th} receive antenna at time t for a multi-user system comprising K users is given by Equation (5). The array of signals $\left\{ r_{k,t}^{1},\ r_{k,t}^{2}, \ldots, r_{k,t}^{n_R} \right\}$ from the n_T transmit antennas can be combined using receive diversity technique such as maximal ratio combining, equal gain combining or selection combining.

Consider a space-time block code transmit diversity scheme involving two transmit antennas. Its generator matrix G for complex orthogonal design is given by [7, 8]:

$$G_2 = \begin{pmatrix} x_1 & x_2 \\ -x_2^* & x_1^* \end{pmatrix} \tag{6}$$

where columns signify transmit antennas and rows signify time instances. Thus, at time $t = 1$, x_1 and x_2 will be transmitted from antenna 1 and 2 respectively, while at time $t = 2$, $-x_2^*$ and $-x_1^*$ will be transmitted from antenna 1 and 2 respectively. Assuming a single receive antenna, and fading coefficient to be constant over two consecutive time slots, the received signal is given by

$$r_1 = h_1 x_1 + h_2 x_2 + \eta_1 \tag{7}$$

$$r_2 = -h_1 x_2^* + h_2 x_1^* + \eta_2, \tag{8}$$

where h_1 and h_2 signify the coefficients of the channel, and η_1 and η_2 the channel noise. For a space-time block code scheme involving four transmit antennas, transmission matrix G for real orthogonal design is given by [4, 5, 8]

$$G_4 = \begin{pmatrix} x_1 & x_2 & x_3 & x_4 \\ -x_2 & x_1 & -x_4 & x_3 \\ -x_3 & x_4 & x_1 & -x_2 \\ -x_4 & -x_3 & x_2 & x_1 \end{pmatrix} \tag{9}$$

Gold codes are a type of pseudo-noise (PN) sequences derived from combination of certain pairs of *m*-sequences called the *preferred sequences*, implemented using Linear Feedback Shift Registers (LFSR). A Gold code has a period $N = 2^n - 1$, where n is the length of the shift register.

III. Results and Discussion

Software simulations were carried out to investigate the performance of an OFDM-modulated as well as a STBC MC-CDMA system in a Rayleigh frequency-selective fading channel. The channel was assumed to be quasi-static, meaning that the fading process remained constant during transmission of each data frame.

A. STBC versus CDMA system

This section compares the performance of a transmit diversity system with that of a CDMA system for a 31-chip Gold code. Looking at Fig. 3, it can be seen that the Gold code provides a coding gain of about 14 dB, relative to the uncoded, no-diversity case. However, the code provides no diversity gain. Another look at this figure shows that in terms of bit-error-rate (BER), at low Eb/No the coding gain provided by the Gold code surpasses the diversity advantage provided by the use of the multiple antennas.

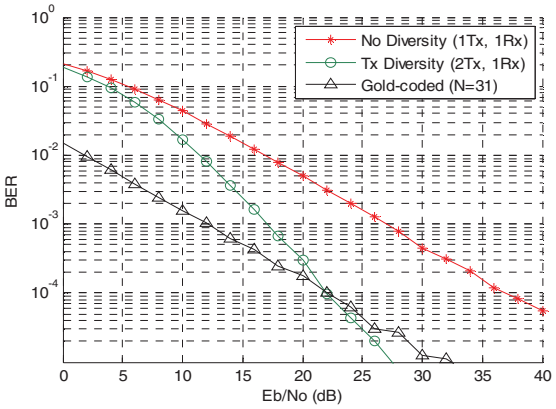

Fig. 3. Performance of a STBC system versus a Gold-coded system

B. STBC-CDMA system

This section presents the performance of a STBC CDMA system. Fig. 4a shows the results for a 31-chip Gold code. Looking at this figure, it can be seen that the STBC-CDMA system provides both diversity and coding gain. The curve for the plain 2x1 system is seen to be parallel to that of the STBC-CDMA system, which clearly shows that space-time coding is solely responsible for the diversity gain, while Gold code encoding is responsible for the coding gain. In the composite STBC-CDMA system, the diversity advantage of the STBC is complemented by the coding gain of the CDMA, giving better system performance. Diversity decreases the asymptotic error rate as a function of signal-to-noise ratio (SNR), while coding gain provides vertical shift of the error performance curve. At a BER of 10^{-3}, there exists about 12 dB difference between the coding gain of a CDMA-only system and its space-time-coded counterpart. This difference in coding gain grows with decent in BER. Apart from these, the figure also shows that the coding gain between the no-diversity link and its Gold-coded counterpart is the same as that between the transmit-diversity link and its Gold–coded counterpart.

$$r(t) = \sum_{k=1}^{K} \sum_{l=1}^{L} A \beta_{kl} e^{j\gamma_{kl}}\ c_k (t - \tau_{kl})\, b_k (t - \tau_{kl}) \cos\left(\omega_c (t - \tau_{kl}) - \theta_{kl}\right) + n_{k,t} \tag{1}$$

$$r(t) = \frac{1}{\sqrt{n_T}} \sum_{k=1}^{K} \sum_{i=1}^{n_T} \sum_{l=1}^{L_i} \beta_{kl}^{i} e^{j\gamma_{kl}^{i}}\ c_k \left(t - \tau_{kl}^{i}\right) b_k \left(t - \tau_{kl}^{i}\right) \cos\left(\omega_c \left(t - \tau_{kl}^{i}\right) - \theta_{kl}^{i}\right) + n_{k,t} \tag{3}$$

$$r^{j}(t) = \frac{1}{\sqrt{n_T}} \sum_{k=1}^{K} \sum_{i=1}^{n_T} \sum_{l=1}^{L_{i,j}} \beta_{kl}^{i,j} e^{j\gamma_{kl}^{i,j}}\ c_k \left(t - \tau_{kl}^{i,j}\right) b_k \left(t - \tau_{kl}^{i,j}\right) \cos\left(\omega_c \left(t - \tau_{kl}^{i,j}\right) - \theta_{kl}^{i,j}\right) + n_{k,t}^{j} \tag{5}$$

Fig. 4b shows simulation results for a 127-chip Gold code. It can be seen that this figure has similar features with Fig 4a of 31-chip Gold code. However, the 127-chip provides greater coding gain than the 31-chip Gold code. This is expected, consequent to difference in process gains of the codes.

C. *Performance in a frequency-selective channel*

We shall now be looking at results of the system performance in a frequency-selective Rayleigh fading channel. A four-path channel with fixed path delays and path gains were considered for a sample frequency of 10 kHz and a maximum Doppler shift of 83.3 Hz. Table 1 shows the simulation parameters. The performance of a space-time coded OFDM system as well as a MC-CDMA system were investigated for a single user. The number of subcarriers was kept fixed at 64. Cyclic prefix was added after IFFT at the transmitter, and removed at the receiver before FFT. The simulation results shall now be presented as follows.

D. *Space-time coded OFDM system*

Here, the performance of a space-time coded OFDM system in the frequency-selective channel is considered. For comparison, the results, Fig. 5, show the performance for a single-antenna, no-diversity (1x1) case for transmit diversity and MRC receive diversity. The water-fall region of this figure shows that the transmit and the receive diversity schemes provide the same diversity gain. This agrees with expectation, both being second-order diversity schemes. However, the figure shows that the receive diversity has a 3-dB advantage over the transmit diversity. This is because total transmitted power is modelled to be the same in both cases, such that the power transmitted from each transmit antenna of the latter is half that of the former. If the transmitted power is made to be the same in both cases, then the performance would be identical. It is noteworthy that these features are similar to those observed for a flat-fading channel.

Another important feature of Fig. 5 is the appearance of error floor. This error floor cannot be attributed to multi-user interference, as there is no interferer here. Rather, it originates from multi-paths characteristics of a frequency-selective channel. The figure shows that the receive diversity's 3-dB advantage is lost in the error floor region, such that both the transmit and the receive diversity schemes exhibit the same level of error floor. Compared to no-diversity scheme, the benefit of using multiple-antenna is obvious, as revealed by the lowering of error floor by the latter. A close look at the performance curves shows that whereas the error floor for no-diversity is about 0.1479, it is about 0.0740 for transmit diversity (see data tips). Dividing the former by the latter gives 1.9995, which indicates that the diversity scheme reduced the error floor by a factor of two.

TABLE I. SIMULATION PARAMETERS

Modulation type	QPSK
Frame size	64 QPSK symbols
No. of subcarriers	64
Cyclic extension (25%)	16 symbols
Carrier frequency	900 MHz
Max Doppler shift	83.33 Hz
Sample Frequency	10 kHz
Number of paths	4
Path gains(dB)	0 -20 -30 -40
Path delays (μs)	0 1 5 10

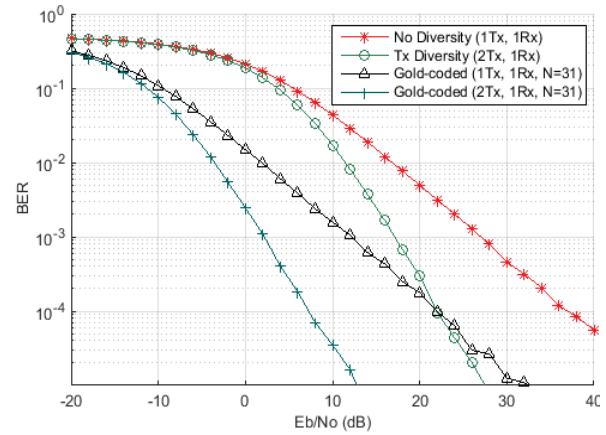

(a)

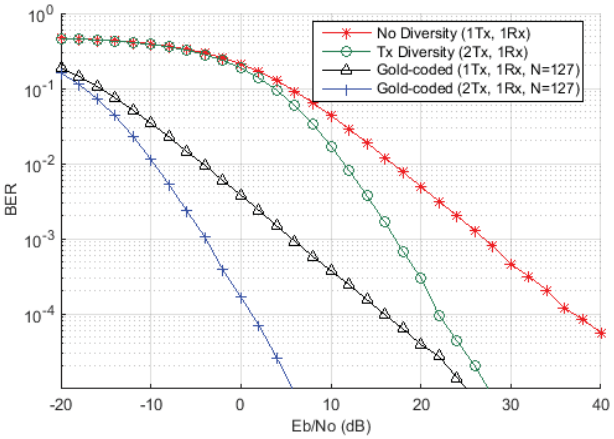

(b)

Fig. 4. Performance of a STBC-CDMA system for (a) 31- and (b) 127-chip

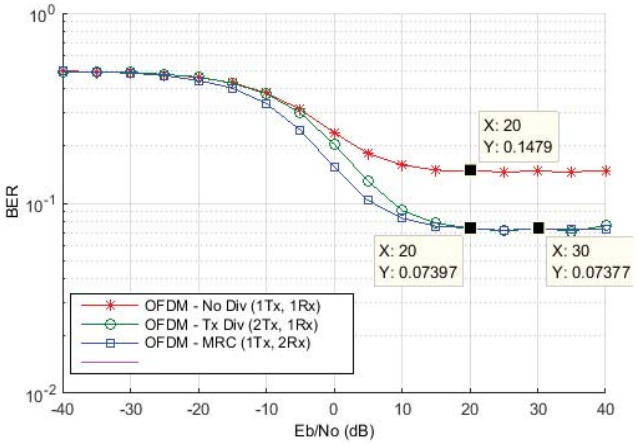

Fig. 5. Performance of a STBC OFDM system in a four-path frequency selective Rayleigh channel.

E. *Space-time block-coded MC-CDMA system*

This section presents results on the performance of a STBC MC-CDMA system in the frequency-selective channel. Results for STBC-OFDM are also included for the purpose of comparison. Simulations were carried out on the system performance for Gold codes of different lengths. Fig. 6 shows results for a 31-chip Gold code. It is obvious from this figure that a STBC MC-CDMA system has better performance than its STBC-OFDM counterpart. Comparing no-diversity transmission shows that at a BER of 10^{-1}, the use of the 31-chip Gold codes in the MC-CDMA system provides a coding gain of about 16.272 dB relative to the OFDM system (Fig. 5). For the transmit diversity scheme, the STBC MC-CDMA provides

a coding gain of about 15.516, relative to the OFDM system. Another look at the figure shows that the performance curves of STBC MC-CDMA and the STBC OFDM has similar slopes in the waterfall region. This indicates that the MC-CDMA provides no additional diversity gain to the STBC MC-CDMA system. That is, for the 31-chip Gold-coded STBC MC-CDMA system, diversity gain originates solely from the use of the multiple antennas, while coding gain comes from Gold codes.

Another important feature in this figure is the level of error floor. It is obvious from Fig. 6 that the STBC MC-CDMA system has lower error floor than the SBTC-OFDM system. For the no-diversity scheme, error floor is about 0.1479 (Fig. 5) for OFDM transmission, and 0.1271 for MC-CDMA. For transmit-diversity scheme, error floor is about 0.0738 for OFDM transmission, and 0.0591 for MC-CDMA. For the MC-CDMA system, the results show that the use of transmit diversity provides about 2.164 reduction in error floor.

We shall now consider simulation results for a 127-chip Gold code, as shown by Fig. 7. Looking at this figure, it is obvious that this longer code gives a better performance than its 31-chip counterpart in terms of BER, coding gain, diversity gain and level of error floor. For the no-diversity transmission at a BER of 0.2, the 127-chip Gold codes provides a coding gain of about 24.944 dB relative to the OFDM system. Looking at the results for the transmit diversity scheme shows that for the 127-chip code, the performance curve for the STBC MC-CDMA has steeper slope in the waterfall region than its STBC-OFDM counterpart. This implies that the former has a higher diversity gain than the latter. This can be compared to the results for 31-chip Gold code, for which the two systems have similar slopes in the waterfall region. The extra diversity gain observable in the 127-chip system could only be attributed as coming from MC-CDMA. For the 127-chip code, MC-CDMA provides not only coding gain, but also diversity gain.

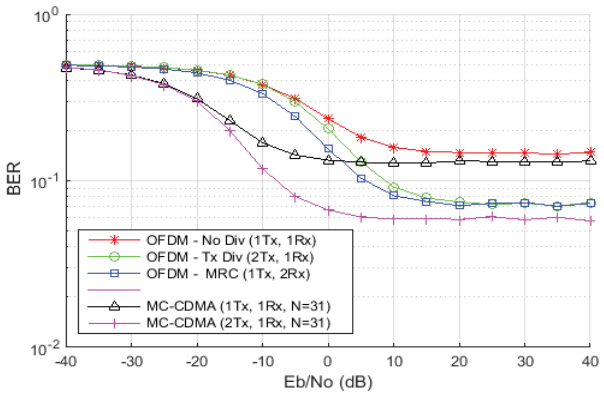

Fig. 6. Performance of a STBC MC-CDMA system for a 31-chip Gold code.

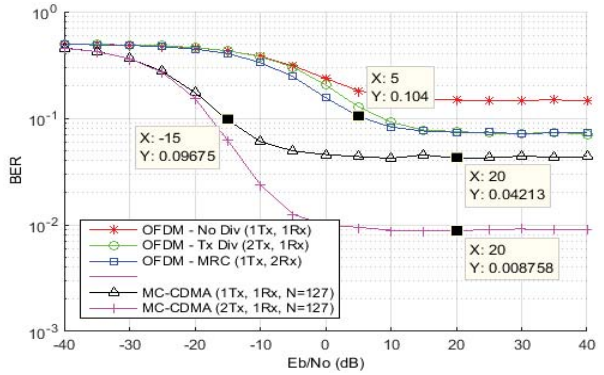

Fig. 7. Performance of a STBC MC-CDMA system for 127-chip Gold code

Now turning to the level of error floor, the results show that for the no-diversity case, error floor is about 0.04214 for 127-chip MC-CDMA system. With reference to the OFDM system, this is equivalent to a factor of about 3.51 reduction in error floor. For transmit-diversity scheme, error floor is about for 0.0088 for the 127-chip MC-CDMA, which is equivalent to a factor of about 8.4164 reduction in error floor

IV. Conclusion

This paper presented the performance of a space-time block-coded multi-carrier CDMA system using Gold codes as spreading sequences. Results on the performance of a space-time block-coded OFDM system in a frequency-selective channel showed that the receive diversity's 3-dB advantage over its transmit diversity counterpart was lost in the error floor region, such that both the transmit and the receive diversity schemes exhibited the same level of error floor. The results also showed that with reference to no-diversity transmission, the transmit diversity reduced the system error floor by a factor of two. The outcome of investigation of the performance of a space-time block-coded multi-carrier-CDMA system showed that the composite system is resilient to fading particularly for long codes, resulting in significant lowering of error floor.

References

[1] Z. Wei, X.-G. Xia, and K. Ben Letaief, "Space-Time/Frequency Coding for MIMO-OFDM in Next Generation Broadband Wireless Systems," *IEEE Wireless Communications,* vol. 14, pp. 32-43, 2007.

[2] Q. M. Rahman and A. B. Sesay, "Non-coherent MT-CDMA system with diversity combining," in *Canadian Conference on Electrical and Computer Engineering*, 2001, pp. 1351-1356.

[3] S. Hara and R. Prasad, "Overview of multicarrier CDMA," *IEEE Communications Magazine,* vol. 35, pp. 126-133, 1997.

[4] H. Jafarkhani, *Space-time coding: theory and practice*: Cambridge university press, 2005.

[5] B. Vucetic and J. Yuan, *Space-time coding*: John Wiley & Sons, 2003.

[6] I. B. Oluwafemi and S. H. Mneney, "Review of Space-time Coded Orthogonal Frequency Division Multiplexing Systems for Wireless Communication," *IETE Technical Review (Medknow Publications & Media Pvt. Ltd.),* pp. 417-426, 2013.

[7] S. Alamouti, "A simple transmit diversity technique for wireless communications," *IEEE Journal on Selected Areas in Communications,* vol. 16, pp. 1451-1458, 1998.

[8] V. Tarokh, H. Jafarkhani, and A. R. Calderbank, "Space-time block codes from orthogonal designs," *IEEE Transactions on Information Theory,* vol. 45, pp. 1456-1467, 1999.

[9] V. Tarokh, H. Jafarkhani, and A. R. Calderbank, "Space-time block coding for wireless communications: performance results," *IEEE Journal on Selected Areas in Communications,* vol. 17, pp. 451-460, 1999.

[10] L. K. Bansal and A. Trivedi, "Comparative Study of Different Space-Time Coding Schemes for MC-CDMA Systems," *Intl. J. of Communications, Networks and System Sciences,* vol. 3, pp. 418-24, 2010.

[11] X. Chong, M. El-Hajjar, R. G. Maunder, Y. Lie-Liang, and L. Hanzo, "Performance of the Space-Time Block Coded DS-CDMA Uplink Employing Soft-Output ACO-Aided Multiuser Space-Time Detection and Iterative Decoding," in *71st IEEE Vehicular Technology Conference (VTC 2010-Spring)* 2010, pp. 1-5.

[12] N. Kumaratharan and P. Dananjayan, "STSIC detection for multi-user MIMO MC-CDMA systems," in *TENCON IEEE Region 10 Conference*, 2008, pp. 1-6.

[13] G. Senthilkumar and R. Amutha, "Capacity enhancement of multicarrier code division multiple access (MCCDMA) using orthogonal complete complementary codes and adaptive constellations," *Scientific Research and Essays,* vol. 9, pp. 153-161, 2014.

[14] H. Xiaoyu and C. Yong Huat, "On the capacity of multicode and variable spreading gain multirate space-time block coded multicarrier CDMA systems over frequency selective Rayleigh fading channel," in *IEEE 60th Vehicular Technology Conference (VTC2004-Fall)*, 2004, pp. 353-357

THE 5TH INTERNATIONAL CONFERENCE ON WIRELESS COMMUNICATIONS, VEHICULAR TECHNOLOGY, INFORMATION THEORY, AEROSPACE & ELECTRONIC SYSTEMS (WVITAE-2015)
December 13-16, 2015, Hyderabad, India

Remote Heart Rate Evaluation by Variational Mode Decomposition

Bogdan Gavriloaia, Octavian Fratu, Simona Halunga
Telecommunications Dept.
University Politehnica of Bucharest
Bucharest, Romania
bogdan.gavriloaia@gmail.com

Gheorghe Gavriloaia, Constatin Mara, Radu Vizireanu
Electronics, Communications and Electric Engineering
University of Pitesti
Pitesti, Romania
ggavriloaia@gmail.com

***Abstract*— Vital signs (heart rate, respiratory rate, body temperature, and blood pressure) are features of physiological functions expressing the physical condition. The doctors use them during early diagnoses. The information about the heart rate is the primary vital sign which needed on a human approach in both emergency and clinical situations. Noncontact detection and monitoring of the human heart are well-accepted solutions for intensive care monitoring or home health care applications. This paper deals with the remote assessment of the heart (pulse) rate by facial color processing. The information is obtained by processing a certain color from the video signal. There is a maximum difference in spectral absorption of the colors for the two min components of the blood: oxy-hemoglobin and deoxy-hemoglobin. Biological signal was recorded from a video camera during 20 s, and it was associated with an important component of background noise. Results using variational mode decomposition (VMD) algorithm for determining heart rate (HR) of the facial color processing are presented and are compared with those obtained by using the empirical mode decomposition (EMD) algorithm. HR values are similar to those measured with a pulse oximeter in the same time period when the level of the signal to noise ratio is high. At small level of this ration, the EMD algorithm did not work properly.**

Keywords*— heart rate, facial expression, pattern recognition, computer vision, biomedical signal processing

I. INTRODUCTION

Status human health can be judged by measuring physiological parameters, which usually are interdependent. The most important common medical tests consist in verifying work of heart, respiratory system, and body's temperature. The accurate measurement and monitoring of these physiological parameters plays an important role in a wide variety of applications in healthcare, psycho-physiological examinations, sports training, and so forth. Abnormal levels of these parameters represent important risk factors for health.

Cardiovascular disease is the leading cause of death in almost all countries. Aging is another risk factor. The aging process involves various chemical and physical alterations which contribute to cognitive decline. There is a difference between natural cognitive decline and cognitive impairment [1]. Mild cognitive impairment (MCI), for example, is the earliest detectable stage. MCI may aggravate functioning daily life. For example, symptoms of memory loss and difficulty subtle in execution of complex cognitive tasks may occur [1, 2]. Early detection of these vulnerabilities could allow more successfully applying of preventive treatments. Pulse rate (PR) and heart rate variability (HRV) are important physiological markers to identify these higher risks [3].

The influences from many sources: physiological, behavioral, affective, cognitive, social, and environmental shape the heart activity under brain control. There are many studies in the literature that shows significant correlations between HR and cognition. Early HR control is important to reduce the development of cognitive symptoms in later life. A high HR suggests a major risk factor (especially midlife) [3, 4], and a low BP is more detrimental (particularly in older age) [5]. The brain is connected bidirectionally with the heart by the central autonomic network (CAN). The HR is the interplay between the parasympathetic (high frequency (HF)) and sympathetic (low frequency (LF)) branches. In the case of the short-term time series, the power spectrum contains two major components, a high (0.15–0.40 Hz) and low (0.01–0.15 Hz) frequency components. The poor cognition is linked to a low HR because the system autonomy is less reactive to changes in the external environment and is therefore less adaptable. The effects of the sympathetic nervous system neurotransmitters like norepinephrine are the slow time scale of seconds, while the parasympathetic nervous system effects using acetylcholine are fast, millisecond time scale.

Vital signs are parameters of physiological functions expressing the physical condition and are used for making initial diagnoses, and heart rate is considered as the primary vital sign information which is needed on a human approach in both emergency and clinical situations. There are many sensing principles and monitoring methods for HR evaluation, but the simplest method is palpation of some arteries. Traditional techniques for the HR measurement are contact-based and require sensors to be placed on certain positions on the body surface by finding certain points on the skin where the artery's pulsation is transmitted to the surface. The evaluation process of HR is a little bit difficult for certain people like premature neonates, infants at risk of sudden infant death syndrome, burn victims, and elderly. Sometimes, these methods may influence the underlying physiological parameters being measured.

Public compliance depends in part on the monitoring being contactless, non-obtrusive, and noninvasive. Based on working principle, in recent years four categories of contactless methods have been proposed for the heart monitoring: electromagnetic-based monitoring systems, laser-based monitoring systems, image-based monitoring systems, and other methods [6].

The two monitoring systems based on electromagnetic and laser can achieve high performances, but the price of equipment and mobility are limiting factors.

In the context of recent advances in video technology, the video cameras ability to measure physiological parameters, including HR, has been reported [6, 7]. The image-based methods for heart rate monitoring is based on the observation that the deflection of a human vessels due to heartbeats can be visually observed from the consequent deflection that the skin surrounding an important vase [8]. In [9] Takano reported the results of using the brightness data from a time-lapse image of a CCD camera. The data were measured for 30s. Chen et al. [10] investigated the Hilbert-Huang transform of the face reflectance for the HR measurement. Parra and Da Costa proposed to video acquire the deflections when the skin is illuminated by a 2 mW HeNe laser beam in the neighborhood of the vein [11]. McDuff et al. [12] used a DSLR camera capturing five color bands for remote HVR evaluation, Balakrishnan, et al. [13,14] have studied the subtle head oscillations accompanying the cardiac cycle from videos and performed the principal component analysis to decompose the trajectories into a set of mono-dimensional component motions, and identified the picks of the most periodic component for HR.

This paper addresses remote measurement of subtle changes in facial color due to HR by processing a certain color in the visible spectrum where there is the highest difference of skin color during a cardiac cycle.

In the remainder of this paper we will: 1) present materials and a novel numerical method for nonlinear processing of biosignals; 2) demonstrate that this method can allow remote evaluation of HR, and 3) compare our measurements with other results.

II. Materials and Methods

Many data about the skin morphology, composition or physiology could be obtained by investigation its optical properties. In vivo examination is noninvasive and widely used by clinicians for getting real time information about individual state of health. Light scattering and absorption properties of the skin are caused by various chromatophores, and hemoglobin in blood is one of the most important. Blood can reach up to 50 μm below skin surface. The pressure and the oxygen concentration of the blood are variable during heart cycle. Hemoglobin has two important components: oxy-hemoglobin, having a higher affinity for oxygen, and deoxy-hemoglobin that has a higher affinity for carbon dioxide. Their absorption spectra are shown in Fig. 1 [15, 16]. The biggest difference between the spectra of the two components of hemoglobin, oxygened and deoxygenated, occurs at about 560 nm. The amount of arterial blood (oxigened) to the skin surface varies over time due to the pressure generated by the heart rate. At the same time, the amount of deoxygenated blood from the superficial veins is constant. As a result, the reflected signal will contain information on the activity of the heart.

Unfortunately, the noise level is very high and the reflectance variation is small. Moreover, both the amplitude and frequency vary during investigation period, and filtering methods based on Fourier Transform cannot be used [17].

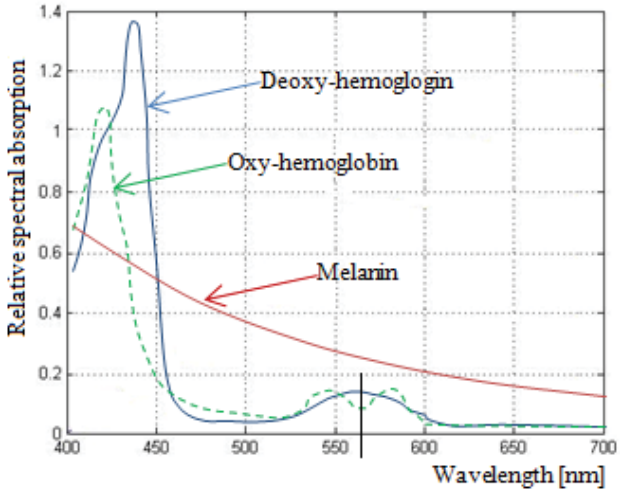

Fig. 1. Relative spectral absorption of melanin, oxy-hemoglobin, and deoxy-hemoglobin in the visible spectrum

New methods for nonlinear and nonstationary signals processing have been investigated in recent literature [17, 18]. They include time domain methods and frequency domain methods.

The Empirical Mode Decomposition (EMD) method is a novel and representative method for time signal analysis [17, 18, 19]. Nearly any signal can be decomposed into a finite set of intrinsic mode functions (IMF) whose Hilbert transforms give instantaneous values by their characteristic time scales in the data empirically [20, 21]. These intrinsic modes, obtained through a recursive process of sifting operations, have a limited bandwidth.

Dragomiretskiy has described a new method to decompose a signal in frequency domain, Variational Mode Decomposition (VMD) [22]. The problem was inspired by EMD algorithm and consists in signal decomposition into a small number of k modes (k imposed from the beginning design), that have a very limited bandwidth around their characteristic center frequency ω_k, which is to be determined along with the decomposition [22].

The bandwidth assessment of the u_k mode is realized in three steps: 1) the associated analytic signal is computed by means of the Hilbert transform in order to obtain a unilateral frequency spectrum; 2) the mode's frequency spectrum is shifted to "baseband" by mixing with an exponential tuned to the respective estimated center frequency; 3) the bandwidth is now estimated through the H^1 Gaussian smoothness of the demodulated signal, i.e. the squared L2-norm of the gradient. The variational problem can be formulated as follow [22]:

$$\min_{u_k,\omega_k}\left\{\sum_k\left\|\partial_t\left[\left(\delta(t)+\frac{j}{\pi t}\right)*u_k(t)\right]e^{-j\omega_k t}\right\|_2^2\right\}$$
$$\text{s.t.}\quad \sum_k u_k = f \tag{1}$$

where $*$ denotes convolution.

In [22] is presented the algorithm for the reconstruction constraint by using both a quadratic penalty term and Lagrangian multipliers. The augmented Lagrangian is as follows [22]:

$$\mathcal{L}(u_k,\omega_k,\lambda)=\alpha\sum_k\left\|\partial_t\left[\left(\delta(t)+\frac{j}{\pi t}\right)*u_k(t)\right]e^{-j\omega_k t}\right\|_2^2 + \left\|f-\sum u_k\right\|_2^2+\left\langle\lambda, f-\sum u_k\right\rangle. \tag{2}$$

The minimization problem can be solved in spectral domain as follow [22]:

$$\hat{u}_k^{n+1}=\underset{\hat{u}_k,\hat{u}_k=\hat{u}_k^*}{\arg\min}\left\{\alpha\left\|j\omega\left[(1+\operatorname{sgn}(\omega+\omega_k))\hat{u}_k(\omega+\omega_k)\right]\right\|_2^2 + \left\|\hat{f}-\sum\hat{u}_i+\frac{\hat{\lambda}}{2}\right\|_2^2\right\}. \tag{3}$$

The role of the Lagrangian multiplier is to enforce the constraint, while the quadratic penalty improves convergence. In the case of signals that are both finite in time and resolution a certain window is necessary.

III. Experiment and Results

The input sensors were a video camera and a pulse oximeter. The same person has been investigated during about 20 seconds.

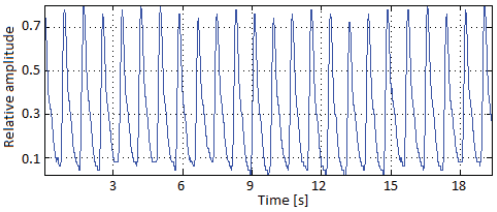

(a)

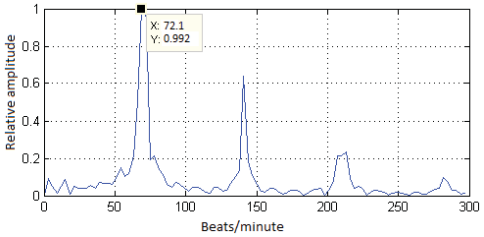

(b)

Fig. 2. The pulse oximeter output (a) and its Fourier Transform (b)

The output of the pulse oximeter was recorded to have a reference for the other sensor. The time evolution and its Fourier Transform of the signal from pulse oximeter are shown in Fig. 2a and 2b. The frequency value of about 72 beats /minute (from Fig. 2 b) represents the HR reference value. Also, the signal has still three important harmonics

Two methods were used to decompose this signal. In the first case, this signal was decomposed into 9 IMFs by using the EMD algorithm [17]. The time evolutions of the first 4 IMFs are shown in Fig. 3a. The first two IMFs are due to noise components. Their amplitudes are not too big. The IMF_3 looks like a clear harmonic of the input signal, and can be used to evaluate the HR.

The results of the signal decomposition in four oscillation modes by using VMD algorithm [22] are shown in Fig. 3 b. Harmonic structure of these modes is much more visible. The K2 oscillation mode looks like the IMF3 that was previously investigated by EMD algorithm. The assessment of the center frequencies of these modes is a recursive process, and after a number of iterations their values stabilize. In Fig. 4 is shown the variation of the central frequencies for the four oscillation modes using VMD.

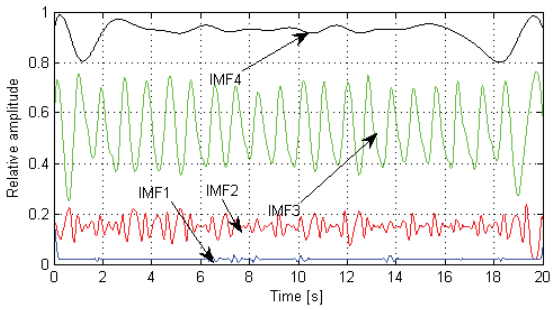

(a)

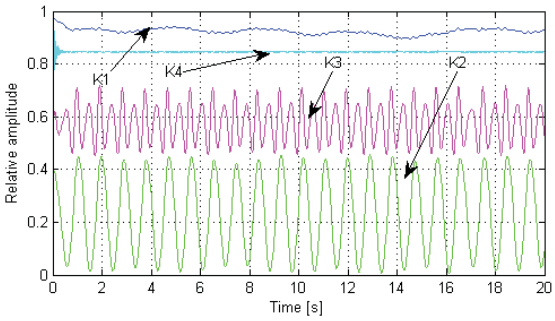

(b)

Fig. 3. The mode decomposition of the signal with EMD (a) and VMD (b)

The iterative process may be stopped after about 70 iterations. HR value is about 72 beats / minute, the same as indicated by pulse oximeter.

The signal component from video stream having 560 nm is formed by using the following weighted mixing of the three colors: red (R), green (G) and blue (B) [8]:

$$I(x,y)=0.254*R(x,y)+0.659*G(x,y)+0.087*B(x,y) \quad (4)$$

The forehead area was selected by using the Viola Jones face detector from OpenCV 2.4.10 library in MATLAB [23].

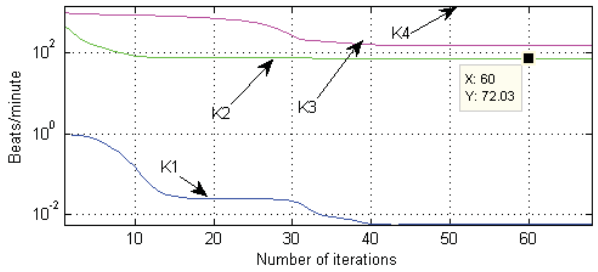

Fig. 4. The oscillation mode dependence versus number of iterations

The pixel having the biggest intensity value is chosen and the spatial position was maintained for the whole video stream of 20 s. This signal is shown in Fig. 5a. After applying a Hamming window [20], four oscillation modes were extracted by using VMD algorithm. Their time evolutions are shown in Fig. 5b, and their dependence on the number of iterations is shown in Fig. 5c. Iterative process stabilizes after a greater number of iterations (about 140).

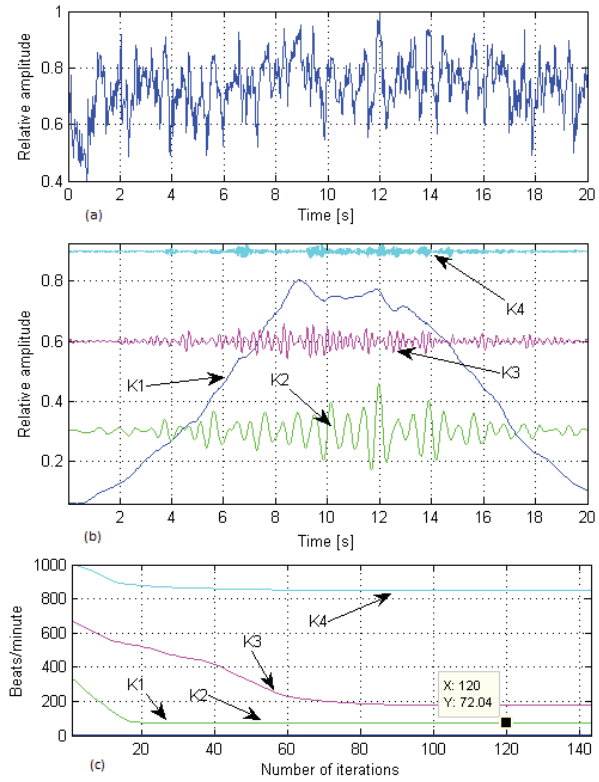

Fig. 5. Variational mode decomposition of the input video signal (a), the time variation of the four oscillation modes (b), and their evolution versus number of iterations.

The investigated signal is corrupted by noise, the signal to noise ratio is very low. K1 oscillation mode is very high and is due to application of Hamming window. The useful component is K2 and is seen that as its value (value corresponding HR of about 72 beats/minute) is identifiable even at this rapport signal to noise having a small value.

Unfortunately, EMD algorithm has not led to satisfactory results which may reveal a harmonic component to assess HR. 21 IMFs were obtained, but all were corrupted by noise. The EMD algorithm fails to extracts the harmonics accurately if the signal is affected with noises [24, 25].

IV. CONCLUSIONS

The remote evaluation of HR from face reflectance was investigated. The output RGB data from a video camera during 20 s have been converted in a mono-dimensional signal corresponding to the wavelength of 560 nm. In the same time the data from a pulse oximeter were recorded.

The two biosignals carrying information about HR were investigated using specific algorithms. EMD method provides decomposition into time domain components, and VMD method generates the signal components into frequency domain. The signal from the pulse oximeter had a high signal to noise ratio, and it was used to check the accuracy of the two methods. HR value displayed by the pulse oximeter was about the same as obtained by expansion the digital signal in Fourier series, 72 beats /minute. Also, this signal is composed of four distinct harmonics.

After that, the two methods have ensured an effective decomposition in several IMFs or oscillation modes of the pulse oximeter signal. Every decomposition was recovered the frequency components approximately the same as measured by pulse oximeter.

In the next step, mono-dimensional signal from the video camera, having a small level of the signal to noise ratio, was broken down into components using the two algorithms previously tested. The VMD algorithm has allowed the signal decomposition into four oscillation modes, one of them with frequency of about 72 beats / minute, after a double number of iterations. The EMD algorithm has allowed the signal decomposition into 21 IMFs, but no one contains the frequently noted by pulse oximeter.

ACKNOWLEDGMENTS

The work has been funded by the EC through the FP7-IP project eWALL no. 610658, and by UEFISCDI through the FP7 eWALL support project no. 262/EU.

REFERENCES

[1] J. Jacobs, P. Embree, M. Glei, S. Christensen, P. Sullivan, “Characterization of a novel heart and respiratory rate sensor”. Conference Proceedings IEEE Engineering in Medicine and Biology Society, San Francisco, pp. 2223-2226, 2004

[2] J. Thayera, F. Ahsc, M. Fredriksonc, J. Sollers, T. Wagere, “A meta-analysis of heart rate variability and neuroimaging studies: Implications

for heart rate variability as a marker of stress and health", Neuroscience and Biobehavioral Reviews 36p; p. 747–756, 2012

[3] S. Suzuki, T. Matsui, Chapter 21: Remote sensing for medical and health care applications. In: Escalante-Ramirez, B., Ed., Remote Sensing—Applications, InTech, Rijeka, 479-492, 2012

[4] G. Demiris, D. Oliver, J. Giger, M. Skubic, M. Rantz, "Older adults' privacy considerations for vision based recognition methods of eldercare applications". Technol Health Care, 17(1), pp.41-48, 2009.

[5] D. Vizireanu, R Preda, "Is "five-point" estimation better than "three-point" estimation?", Measurement 46 (1), 2013,pp. 840-842, Elsevier.

[6] M-Z., Poh, D., McDuff, R., Picard, "Advancements in noncontact, multiparameter physiological measurements using a webcam," Biomedical Engineering, IEEE Transactions on, vol. 58, no. 1, pp. 7–11, 2011. B. Martinez, M. F. Valstar, X. Binefa, and M. Pantic, "Local evidence aggregation for regression-based facial point detection," IEEE Transactions on Pattern Analysis and Machine Intelligence, vol. 35, no. 5, pp. 1149–1163, 2013.

[7] B. Jing, L. Haiyun, " A Novel Thermal Measurement for Heart Rate", Journal of Computers, Vol 8, No 9, 2013, pp. 2163-2166,

[8] B. Gavriloaia, R. Vizireanu, O. Fratu, C. Barca, C. Mara, "Remote Assessment of Heart Rate by Skin Color Processing ", BlackSeaCom Conference, Romania, 2015, in press.

[9] C. Takano, Y. Ohta, "Heart rate measurement based on a time-lapse image", Med Eng Phys. 2007, pp.:853-860.

[10] D. Chen, et al., "Image sensor-based heart rate evaluation from face reflectance using Hilbert–Huang transform " IEEE IEEE Sensors Journal, Vol. 15, No. 1, 2014, pp. 618 – 627

[11] J. Parra, G. Costa, "Optical remote sensing of heartbeats", in Visualization of Temporal and Spatial Data for Civilian and Defense Applications, Glenn O. Algood, Nickolas L. Faust, Editors, Proceedings of SPIE Vol. 4368, pp. 113-121 (AEROSENSE, SPIE International Symposium, Orlando, Florida, USA, 16-20 April 2001,

[12] D. McDuff, S. Gontarek, and R. Picard, "Improvements in remote cardio-pulmonary measurement using a five band digital camera," Biomedical Engineering, IEEE Transactions on, 2014.

[13] G. Balakrishnan, F. Durand, and J. Guttag, "Detecting pulse from head motions in video," in Computer Vision and Pattern Recognition (CVPR), 2013 IEEE Conference on. IEEE, 2013, pp. 3430–3437.

[14] G. Balakrishnan, Analyzing pulse from head motions in video Ph. D thesis, Massachusetts Institute of Technology, 2013

[15] R.J. Scheuplein, "A survey of some fundamental aspects of the absorption and reflection of light by tissue", J Soc Cosmet Chem 1964 15, pp. 111–122.

[16] E. Edwards, S. Duntley, "The pigments and color of living human skin", Am. J. Anat., 65, , pp. 1–33, 1939

[17] N. Huang, et al., "The empirical mode decomposition and the Hilbert spectrum for non-linear and non-stationary time series analysis", Proc. R. Soc., Lond. A 454, 1998, pp. 903–995

[18] J. Huang, S. Yu, H. Syu, A. See, "The non-contact heart rate measurement system for monitoring HRV", Conf Proc IEEE Eng Med Biol Soc. 2013; 2013, pp. 3238-3241.

[19] Q. Chen, N. Huang, S. Riemenschneider, and Y. Xi, "A B-spline approach for EmpiricalMode Decomposition," Adv. Comput. Math., vol. 24, pp. 171–195, 2010.

[20] D. Vizireanu, C Pirnog, V Lăzărescu, A Vizireanu, "The skeleton structure—an improved compression algorithm with perfect reconstruction", Journal of digital imaging, Vol. 14, No. 1, pp. 241-242, Springer, 2001

[21] M. Torres, M. Colominas, G. Schlotthauer, P. Flandrin. "A complete ensemble empirical mode decomposition with adaptive noise". Proc. IEEE Int. Conf. Acoust., Speech Signal Process.(ICASSP). p. 4144–4147, 2011.

[22] K., Dragomiretskiy,"Variational Mode Decomposition" Signal Processing, IEEE Trans., Vol. 62 Issue:3, 2014, pp 531 – 544

[23] P. Viola, M.. Jones, "Rapid Object Detection using a Boosted Cascade of Simple Features", Proceedings of the 2001 IEEE Computer Society Conference on Computer Vision and Pattern Recognition, 2001. Vol. 1, pp.511–518.

[24] K., Dragomiretskiy, D., Zosso "Two-Dimensional Variational Mode Decomposition" Energy Minimization Methods in Computer Vision and Pattern Recognition Lecture Notes in Computer Science Volume 8932, 2015, pp 197-208;

[25] C. Aneesh, K. Sachin, P. Hisham, K. Soman, "Performance comparison of Variational Mode Decomposition over Empirical Wavelet Transform for the classification of power quality disturbances using Support Vector Machine", Procedia Computer Science 46, 372 – 380, 2015.

THE 5TH INTERNATIONAL CONFERENCE ON WIRELESS COMMUNICATIONS, VEHICULAR TECHNOLOGY, INFORMATION THEORY, AEROSPACE & ELECTRONIC SYSTEMS (WVITAE-2015)
December 13-16, 2015, Hyderabad, India

C2R2M: Cluster-based Cognitive Radio Routing Mechanism

Shriram Kulkarni
IT Department, Sinhgad Academy of Engineering
Research Scholar, Sinhgad College of Engineering
Pune, India

Shriram Markande
E&TC Department, NBN Sinhgad School of Engineering
Pune, India

Abstract— **Cognitive Radio (CR) technology enable nodes to use unutilized portions of the spectrum for communications. It increases the efficiency of spectrum usage. But CR introduces new challenges in design of protocols at different layers of the protocol stack. Use of clustering in Cognitive Radio Networks (CRNs) provides better network-wide performance. This paper introduces a new routing protocol for CRNs called Cluster based Cognitive Radio Routing Mechanism (C2R2M). In C2R2M, cluster formation is based on Low Energy Adaptive Clustering Hierarchy (LEACH) algorithm. LEACH is further modified to select more suitable Cluster Head (CH). The use of channel assignment algorithm and co-existence of Secondary Users (SUs) and Primary Users (PUs) in route decision improves the performance of C2R2M. Simulation results show that C2R2M achieves better network performance in terms of throughput, delay and routing overheads as compared with Ad-hoc On-demand Distance Vector (AODV) routing protocol in CRNs.**

Keywords—Cognitive Radio Network, Routing, Clustering, Cluster Head

I. INTRODUCTION

Regulation of today's wireless networks is carried out using a fixed spectrum assignment policy. Regulating authorities in respective countries distribute the spectrum to different license holders for specified duration and geographical areas. The license holders provide the services to end users which are called as the licensed users. This policy served well earlier.

While unlicensed spectrum bands are always crowded, the licensed spectrum remains underutilized or unutilized as the licensed users are not using it all the time. Thus, fixed spectrum assignment policy results in an inefficient usage of spectrum. According to Federal Communications Commission (FCC) the average usage of spectrum ranges in between 15% and 85% i.e. the spectrum utilization is not well [1]. On the other hand, due to tremendous increase in wireless devices and applications in recent years, the demand for spectrum is increasing rapidly.

To deal with spectrum scarcity and/or inefficient usage of spectrum, researchers introduced a device called as Cognitive Radio (CR). CRs can be networked to form the Cognitive Radio Networks (CRNs). In CRNs the CRs are known as the Secondary Users (SUs) and the licensed users are called as Primary Users (PUs). CR can sense the spectrum to find unused portions of it, known as white spaces. Also, CR can change its operating parameters to make use of these white spaces for its operation provided it is not interfering with the PUs. CR needs to switch to another white space if PU requires the same band of frequencies. This is called as the opportunistic use of the spectrum which increases spectrum utilization.

Research in CRNs has mainly focused at lower layers of the protocol stack even though the CR paradigm was introduced long back in 1999. Routing at network layer is one of the main issues in CRNs [2]. It is different and challenging than normal wireless networks due to variable nature of the available spectrum. Also, different sets of channels used by SUs increase the routing challenges. Tight coupling between the routing module(s) at network layer and the protocol(s) at lower layers is required. Use of clustering in CRNs provide network-wide performance enhancement. Clustering increases the scalability, stability of the CRNs and helps in balanced distribution of resources.

This paper proposes a Cluster-based Cognitive Radio Routing Mechanism (C2R2M) which finds out the efficient path form source node (PU or SU) to the destination sink node or Base Station (BS). Its working is divided in two parts. In first part it goes for Cluster Head (CH) selection and cluster formation. And in second part it carries out the channel assignment and discovers an efficient route from source to destination.

The remainder of the paper is organized as follows: Section II presents previous work in cluster based CRN routing. System model and assumptions are given in Section III. Section IV describes the proposed technique C2R2M. Performance evaluation of C2R2M is given in Section V and finally the conclusions are presented in Section VI.

II. RELATED WORK

Ghalib A. Shah et al. [3] introduced a spectrum-aware clustering for efficient multimedia routing in cognitive radio sensor networks. In this paper, CH selection is based on

the energy and relative spectrum awareness such that non-contiguous available spectrum bands are clustered and scheduled to provide continuous transmission opportunity. It uses a hybrid Medium Access Control (MAC) for data routing. Each node computes a joint energy spectrum rank in which a high rank node is elected as a CH that controls the spectrum access and data routing. Simultaneously it performs inter- and intra- cluster routing which exploits the performance. However, the use of hybrid MAC for data routing increases the routing overheads.

Rojin Tizvar et al. [4] proposed a collision and energy aware routing method for cognitive radio wireless sensor networks. It considers two main phases: next hop selection and channel selection. The routing is performed hop-by-hop with local information and decisions. Local reduction of collision probability leads to reduce in energy consumption. It also reduces the packet delay in terms of hop cost.

Anna Vizziello et al. [5] introduced a location based routing mechanism that combines location-based routing protocol and RSSI based localization algorithm. Routing consist of intra- and inter- cluster phase. It considers the existence of heterogeneous PUs and jointly selects spectrum and route. It also helps to reduce the interference to PUs. But it assumes similar spectral characteristics in different locations in a given cluster.

A cluster-based link recovery mechanism for spectrum aware on-demand routing in cognitive radio ad hoc networks projected by Chih-Chieh Tang et al. [6] recovers failed links locally and does not change the original routes. It uses buffer to cache the data packets during route recovery. SUs which are in the intersection area of all PUs' radio coverage form a cluster. CH chooses an available channel and assigns it as communication channel to all cluster members. Performance of this scheme is good particularly if there is an intersection area of all PUs' radio coverage in the network. It provides higher throughput in more congested environment. But route recovery mechanism adds the extra message overheads.

Nayyer Panahi, et al. [7] proposed adaptation of Low Energy Adaptive Clustering Hierarchy (LEACH) routing protocol to cognitive radio sensor networks. Here, by using the physical layer information and preserving the feature of random CH selection in LEACH, it has been tried to both move the position of CHs to appropriate locations and make their quantity optimal. Transfer of CHs to appropriate locations increases the network lifetime. However, it increases the network instability because of continuous transfer of CH location.

The cluster based control channel allocation in cognitive radio networks given by Sisi Liu et al. [8] uses an architecture that allocates different channels for control at various clusters in the network. It reduces the frequent need of re-clustering and takes into account the channel availability in deciding cluster memberships. Drawback of this technique is that it is limited only to cellular cognitive radio network. Also, it considers that CRN have same communication range for each channel.

United nodes, a cluster-based routing protocol for mobile cognitive radio networks proposed by A.C. Talay et al. [9] uses spectrum availability cost and interference metrics for route decision in cluster-based network. It uses router preservation method to repair the defective routes. It shows better adaptability with increased throughput and reduced data delivery latency. But it does not use any co-operation among the primary and secondary users during route decision, which may lead to inefficient routes.

Thus, clustering is a good solution to improve the performance of routing in CRN. The clustering helps to improve routing in terms of stability of route, route discovery and maintenance, rediscovery of route in case of link failure, reduction in routing overheads and improve the security.

III. SYSTEM MODEL

A. Assumptions

The proposed algorithm considers certain assumptions which are given in this section. Every node in the network has spectrum sensing capabilities [10, 11], which sense the available number of channels correctly. The whole network has network-wide Common Control Channel (CCC) [10, 11]. The network is divided into clusters, each cluster consist of CH, gateway nodes and member nodes. Every node in the network has distinctive identification (IDs). All nodes in a network are considered as homogeneous i.e. every node has same communication and data gathering capabilities. Every node in the network has same transmission and interference range. The network considers stationary PUs and SUs. The network considers the BS or sink node. It collects information from all nodes in the network. The sink node is considered as stationary.

B. System Model

Generalized system model is shown in figure 1 while intra- and inter- cluster communication is shown in figure 2.

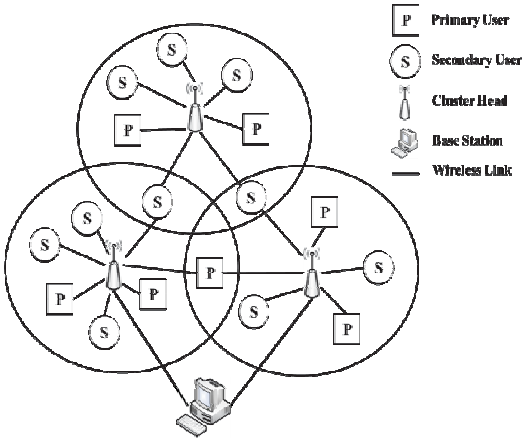

Figure 1. Generalized system model

Figure 1 shows the cluster-based [12] system model considered for the proposed routing algorithm. It considers *N* number of nodes randomly deployed in the specified area and collecting the information with some specific interval. The network consists of *C (C = {1,2,3,….})* data channels and one common control channel. The network considers the presence of both PUs and SUs. PU uses the licensed channel assigned to it. The mapping of licensed channel with number of PUs is one to one. PUs are in active state if they are using their own licensed channel. SUs can use this channel if PUs are not using it. The mapping of channel with SUs is one to many. Every SU node has spectrum sensing ability to know the available channels and it has capability to calculate the probability of PUs' presence on channel.

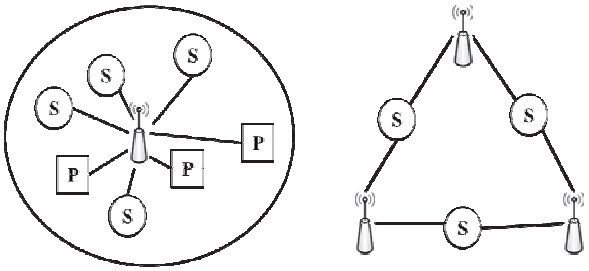

Figure 2. Intra-cluster and inter-cluster communication

Here, the network is divided into *n* clusters. Each cluster consists of CH, cluster members, and gateway nodes. The cluster members can directly communicate with CHs. The CH acts as the coordinator node for particular cluster. It gathers the information from cluster members. It also plays an important role in channel sensing decisions, which is required during routing. The member nodes like all PUs and SUs are associated with CHs. The communication between the members of a cluster is called as intra-cluster communication which is shown in figure 2 (a). The number of hops in between member nodes and CH is single. The gateway nodes are common nodes in between two or more clusters, they act as the bridge in between two clusters. They have capabilities two listen from both clusters. Hence, they are used during inter-cluster communication as shown in figure 2(b). The communication pathway from any CRN node to BS is,

$$Member\ node \rightarrow Local\ CH \rightarrow Gateway\ node \rightarrow Remote\ CH \rightarrow BS$$

IV. Cluster-based Cognitive Radio Routing Mechanism (C2R2M)

The aim of Cluster-based Cognitive Radio Routing Mechanism (C2R2M) is to find out the efficient path form source node (PU or SU) to the destination sink node or BS. To find out the efficient path, algorithm is divided into two phases. In first phase it goes for CH selection based on LEACH algorithm, node degree and available idle channels. It also completes cluster formation in this phase. In second phase it finds an efficient route from source to destination and also carries out channel assignment.

A. CH Selection and Cluster Formation

The proposed routing mechanism forms the clusters using LEACH clustering algorithm. According to the general LEACH [12, 13] algorithm, probability of *node i* to be a CH is denoted by $P_i(n)$. It is given as,

$$P_i(n) = \begin{cases} \dfrac{k_{CH}}{N - k_{CH} * \left(r \bmod \dfrac{N}{k_{CH}}\right)} & ; T_i(n) = 1 \\ 0 & ; T_i(n) = 0 \end{cases} \quad \ldots\ldots\ldots(1)$$

where, N is the number of nodes in a network, k_{CH} is the probable number of CHs per round, r signifies the present round number and is an indicator function which determines that either node i has been a CH for the most recent rounds or not. Most recent rounds are calculated by using following formula.

$$\left(r \bmod \frac{N}{k_{CH}}\right) \ldots\ldots\ldots(2)$$

This formula has probability to select each node as a CH once per cycle.

Here, the LEACH algorithm is used by considering number of available idle channels and the degree of each node. These two are used as extra factors for choosing the more appropriate CH in CRN environment. The probability of a node to become a CH is more which has higher number of available idle channels and has highest node degree in the available nodes. Let, c_i be the number of available idle channels on *node i* and d_i is the degree of *node i*. Therefore, new probability that node i to a be a CH is,

$$P_i(n) = \begin{cases} \dfrac{k_{CH} * c_i * d_i}{\left[N - k_{CH} * \left(r \bmod \dfrac{N}{k_{CH}}\right)\right] * \sum_{a=1}^{N} c_a d_a} & ; T_i(n) = 1 \\ 0 & ; T_i(n) = 0 \end{cases} \quad \ldots(3)$$

The calculated probabilities are useful to determine CHs according to the availability of channels and degree of node. This work considers the node with probability $P_i(n)$ greater than or equal to 0.5 as a CH. Once the CH decision is performed the nodes in the transmission range of CH will be considered as the cluster members.

B. Route Discovery

The route discovery phase finds the route from source node to destination node. It starts when any node (either PU or SU) want to transmit data to BS. As discussed in the system model path from cluster member to BS goes via CH. Therefore, route discovery phase is divided into two sub-phases: intra-cluster route discovery and inter-cluster route discovery. Intra-cluster route discovery finds the path from

source node to CH and inter-cluster route discovery finds the path from CH to BS. The basic procedure of both sub-phases is same; it only changes the source and destination node.

A sender node broadcast a request message through CCC. Request message consist of source node ID, receiver node ID, and the available channel information. The intermediate node who receives the request message updates its route table and forwards the request to the next intermediate node. Every time when node sends request to next intermediate node it also updates the reverse routing table. Here, route will be stored in route table only when both intermediate nodes have common communication channel. If there is no common communication channel in-between the two nodes then it will drop the request message, and route will not be stored in the route table. In this situation, intermediate node should rebroadcast the request message.

When the destination node will receive the request message transmitted via intermediate nodes, it will generate the reply message. The reply message will be unicast towards the node, which have generated the route request message. The reply message consists of ID of source node and destination with the channel information of destination node. The reply message goes through each intermediate node and stores and updates the forwards routing table of the intermediate nodes. Every intermediate node maintains the forward routing table and reverse routing table.

Now, the channel assignment will be done by using receiver channel list and the sender's channel list. The sender and receiver channel list is obtained from the route request and reply messages. The work selects a suitable common available channel from sender and receiver for transmission. The algorithm first makes the list of available common channels and then for improving the utilization of channel, the channel with low utilization will be given a high priority. Here, the channel with less than 50% utilization is given as high priority. If there is no single channel with less than 50% utilization then any one channel will be assigned randomly from available common channels.

V. SIMULATION RESULTS

The implementation is performed by using discrete event simulator NS-2 (Network Simulator-2) [14]. The parameters set during simulations are shown in Table 1. The simulation considers the area of network as 1000m * 1000m. The nodes are distributed uniform randomly in the given area. The simulation considers the following parameters for measurement,

- Average End-to-End Delay: The delay of one packet is time difference between packet's receive time at BS and packet's send time from source node. The total delay in the network is considered as sum of delays of all received packets. The average end-to-end delay is sum of delays of all received packets divided by total number of received packets.
- Average Throughput: Throughput is computed in terms of packet delivery ratio (PDR). PDR is the ratio of number of packets received by sink node divided by number of packets sent by source nodes. It is considered in percentage.

TABLE I. SIMULATION AND NODE PARAMETERS

Parameter Name	Setting Used
Network Interface type	Wireless Physical
Radio Propagation Model	Two-Ray Ground
Antenna	Omni-directional
Channel Type	Wireless Channel
Link Layer	Link Layer (LL)
Interface Queue	Priority Queue
Buffer size of IFq	50
MAC	CRMAC [14]
Routing Protocol	AODV [15], C2R2M
Transport Layer	UDP
Traffic Model	CBR
Number of Nodes	Varying from 50 to 200
Node Placement	Random
Size of Packet	100 bytes
Number of Packets	100
Number of Simulation Runs	10

The proposed algorithm addresses the open issues like scalability and route stability. Figures 3, 4, and 5 show the average end-to-end delay, average throughput, and routing overheads of Ad-Hoc On-demand Distance Vector (AODV) routing protocol and C2R2M respectively by varying number of nodes in the network. Here, the evaluation considers the nodes, which are varying from 50 to 200 with an interval of 50, number of channels considered is two (2), and packet time interval is one (1) second.

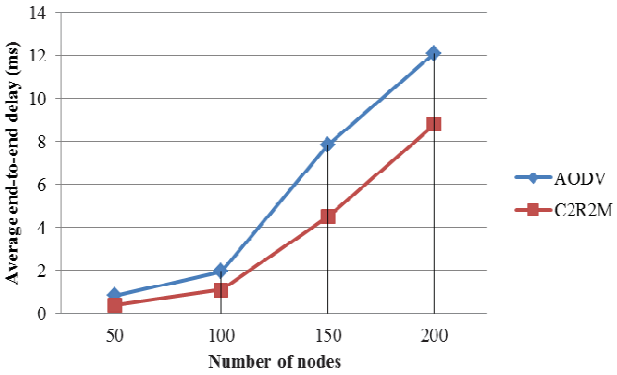

Figure 3. Number of nodes vs. average end-to-end delay

The result shows that the performance of C2R2M is better than the performance of AODV. The reasons for better performance of C2R2M than AODV are, the clustering algorithm used which decides the clusters according to the node degree and number of channels, co-existence of SUs and PUs during route decision, and channel assignment algorithm used. The reduction in routing overhead of C2R2M is because of local level (cluster-level) route decisions, which in turn helps to reduce the average end-to-end delay in the network.

The average throughput is also increased because of better selection of CHs and co-existence of SUs and PUs.

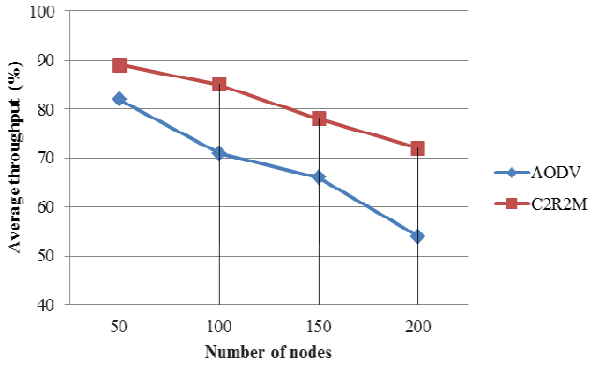

Figure 4. Number of nodes vs. average throughput

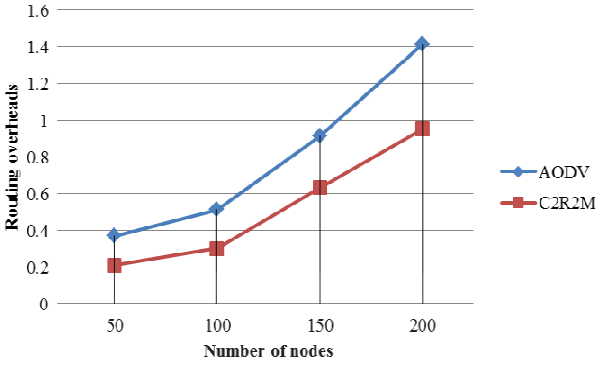

Figure 5. Number of nodes vs. routing overheads

VI. CONCLUSIONS

In this paper, a new routing technique called Cluster based Cognitive Radio Routing Mechanism (C2R2M) is proposed which improves network performance in terms of routing. This scheme utilizes LEACH algorithm to form clusters and modifies it to provide better CH. The impact of varying number of nodes on the operation of C2R2M in terms of throughput, delay and routing overheads is presented. Also the comparison of the performance of C2R2M with AODV is carried out and shown that the proposed C2R2M achieves better results than AODV for CRNs. It improves the route stability and supports scalability which is shown with the results. In the future the authors of the paper will explore the effect of varying number of available channels and the possibility of link failure due to mobility of nodes which will improve link stability.

REFERENCES

[1] F. Akyildiz, W. Lee, M. C. Vuran, S. Mohanty, "NeXt generation/dynamic spectrum access/cognitive radio wireless networks: A survey", Elsevier Computer Networks, Vol. 50, Issue 13, pp. 2127–2159, September 2006.

[2] Moustafa Youssef, Mohamed Ibrahim, Mohamed Abdelatif, Lin Chen, and Athanasios V. Vasilakos, "Routing Metrics of Cognitive Radio Networks:ASurvey", IEEE Communications Surveys & Tutorials, Vol. 16, No. 1, First Quarter 2014.

[3] Ghalib A. Shah, Ozgur B. Akan, "A Spectrum-aware Clustering for Efficient Multimedia Routing in Cognitive Radio Sensor Networks", IEEE Transactions on Vehicular Technology, Accepted, 1-12, 2014.

[4] Rojin Tizvar, Maghsoud Abbaspour, Mahdi Dehghani, "CR-CEA: A Collision- and Energy-Aware Routing Method for Cognitive Radio Wireless Sensor Networks", Springer Wireless Networks, Issue May 14, 1-16, 2014.

[5] Anna Vizziello, Sanaz Kianoush, Lorenzo Favalli, Paolo Gamba, "Location based Routing Protocol exploiting Heterogeneous Primary Users in Cognitive Radio Networks", IEEE ICC, Budapest, Hungary, 2890 – 2894, 2013.

[6] Chih-Chieh Tang, Kuo-Feng Ssu, and Chun-Hao Yang, "A Cluster-Based Link Recovery Mechanism for Spectrum Aware On-Demand Routing in Cognitive Radio Ad Hoc Networks", Springer Smart Innovation, Systems and Technologies, Vol. 20, 601-610, 2013.

[7] Nayyer Panahi, Ali Payandeh, Hojat Olah Rohi, Hojat Olah Rohi, "Adaptation of LEACH Routing Protocol to Cognitive Radio Sensor Networks", IEEE IST, November 6-8, Tehran, Iran, 541 – 547, 2012.

[8] Sisi Liu, Loukas Lazos, Marwan Krunz, "Cluster-Based Control Channel Allocation in Opportunistic Cognitive Radio Networks", IEEE Transactions on Mobile Computing, Vol. 11, No. 10, 1436-1449, 2012.

[9] A.C. Talay D.T. Altilar, "United nodes: cluster-based routing protocol for mobile cognitive radio networks", IET Communication, Vol. 5, Issue 15, 2097–2105, 2011.

[10] Sazia Parvin, Farookh Khadeer Hussain, Omar Khadeer Hussain, Song Han, Biming Tian, Elizabeth Chang, "Cognitive radio network security: A survey", Elsevier's Journal of Network and Computer Applications, Vol. 35, 1691–1708, 2012.

[11] Hasan A. A. Al-Rawi, Kok-Lim Alvin Yau, "Routing in Distributed Cognitive Radio Networks: A Survey", Springer Wireless Personal Communication, Vol. 63, 1983–2020, 2013.

[12] Kok-Lim Alvin Yau, Nordin Ramli, Wahidah Hashim, Hafizal Mohamad, "Clustering algorithms for Cognitive Radio networks: A survey", Elsevier Journal of Network and Computer Applications,Vol. 45, 79–95, 2014.

[13] Wendi Rabiner Heinzelman, Anantha Chandrakasan, and Hari Balakrishnan, "Energy-Efficient Communication Protocol forWireless Microsensor Networks", IEEE International Conference on System Sciences, Hawaii, USA, 1-10, 2000.

[14] Network Simulator-2, www.isu.edu

[15] Perkins ,C.E., Royer E. M, Ad-Hoc On-demand Distance Vector Routing, IEEE WMCSA, New Orleans, LA, USA, 99-100, 1999.

THE 5TH INTERNATIONAL CONFERENCE ON WIRELESS COMMUNICATIONS, VEHICULAR TECHNOLOGY, INFORMATION THEORY, AEROSPACE & ELECTRONIC SYSTEMS (WVITAE-2015)
December 13-16, 2015, Hyderabad, India

Performance Analysis of EPC with IMS Network Architecture

A.Bagubali
School of Electronics Engineering
VIT University
Vellore, Tamilnadu 632014
Email: bagubali@vit.ac.in

V. Prithiviraj
Professor and Principal
RIT
Chennai, Tamilnadu
Email: profvpraj@gmail.com

P.S. Mallick
Professor and Dean
SELECT
VIT University, Vellore, India
Email: psmallick@vit.ac.in

***Abstract*—The IP Multimedia subsystem is a core network used with telephony services and multimedia. It has made it possible to use common standardized system for different multimedia services such as video conferencing, simultaneous media transfer etc. IMS represents a reusable way to integrate and deploy several voice and data services. This advanced technique of IMS is being widely used with LTE(Long Term Evolution) standardized by Third Generation Partnership Project(3GPP). It has been proposed in order to overcome the limitations of existing technologies 2G and 3G. LTE is an advanced technology but still it also uses IMS for multimedia delivery over LTE networks. This paper deals with integrating IMS with EPC (Evolved Packet Core) architecture to analyse different parameters based on Quality of Service(QoS). These parameters include call setup time, bandwidth usage, jitter, throughput and session management. To analyze the performance, a prototype of EPC was deployed. This has been further deployed on Linux test bed while carrying out the proposed approach. The results of this paper have been demonstrated in a different manner. Instead of inducing live traffic, It analyzes the usage of bandwidth reduction in long run.**

***Keywords*-IMS, EPC, LTE, VOIMS**

I. Introduction

Wireless cellular networks have been widely used for the past few years. People mostly relied on digital networks for different multimedia services. This technique has been quite successful in alternating among different active units and endpoints in the network. This path of wireless standards have been evolved focusing on building the next generation of all IP- network infrastructures[1][7]. The IMS and EPC were designed as an important steps towards the next generation networks to fulfil this need. It provides higher bandwidth, and lower operational costs of the whole network, and it also gives maximum convergence with the internet.

A. IP-Multimedia Subsystem

IMS is defined to be a mediator which enables the delivery of simultaneous multimedia services such as voice, data, video etc. Basically, it acts as an intermediate network which constitutes different entities to make this network functional. Few important features of IMS that separates it from others are:

- It maintains Quality of Service (QoS) by adopting several mechanisms.
- IMS has the ability to provide multimedia based new experience to its users.
- SIP signalling is provided by IMS network from one user end to another.
- It does not depend on access techniques.
- IMS has the inbuilt efficiency to offer both packaged and compound services.

B. Evolution of IMS

As mentioned in the earlier section, IMS standards have been maintained and written by the community related to next generation networks i.e. 3GPP. IMS was first introduced by the 3GPP in Release 5 for the standards of UMTS network. The initial phase concentrated on defining the entities which were considered as the core elements. Later on, various IMS protocols were defined for session control, management and authentication as well as for multimedia transfer and media processing. Release 6 by 3GPP included integration of WLAN(Wireless Local Area Network) and broadband networks to maintain the fact that voice call should be in continuation. It also enables the use of several multimedia related services like conferencing, push-to-talk, simultaneous video sharing etc. During Release 7, basis of specifications was provided to maintain the standards. Release 8 focused on defining the areas which were not addressed earlier such as Operations, Administration and Maintenance (OAM) and mainly works on optimization of IMS to overcome the limitations of 3rd generation networks[10][12]. The evolution of IMS network keeps the service providers more active and competitive.

C. The IMS Architecture

Architecture of IMS constitutes the entities or functional elements that enable it to act as an intermediate network. Defining architecture also includes the interaction process among these functional elements and the protocols need to carry out such interaction. With the associated functionality, these entities can also be viewed as layers or planes shown in fig.1. These entities have interfaces externally to the application, user and other networks[11].

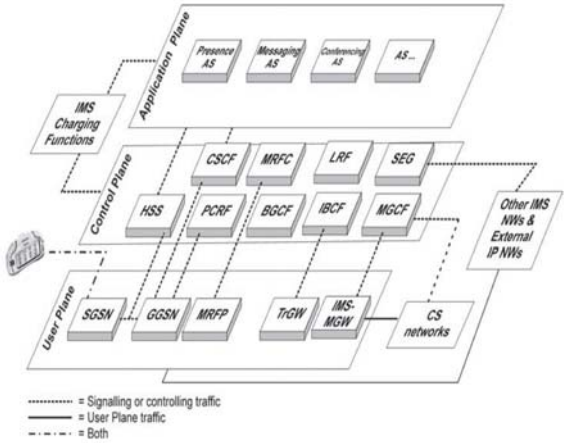

Fig. 1. IMS Architecture

1) Planes: There are certain protocols which make it possible to communicate among different entities. These packets have data flow which either takes the form of signals or media. The control plane consists of certain functional entities which have functions to perform related to signalling. They provide function for session establishment, maintenance and operation. The media planes contains the entities giving the resource and adaptation functions. Access to the application along with the service logic is given by service plane. Application and billing servers, Operational Support System (OSS) and service access functions are included in these entities[2].

D. EPC network Architecture

Fig.2 shows that Evolved Packet Core Architecture (EPC): EPC provides a converged data and voice networking frame work to provide LTE connections to the users. Main components of EPC consists of MME, S-GW, P-GW. The Signaling Gateway(S-GW):one of the main function it performs routing and forwarding Packets, and also it acts as a anchor point for inter e-node B handovers[3][13]. It offers a data path between the PDN gateway and enodeBs via S5 Interface, which supports either the GPRS tunneling protocol (GTP) or the proxy mobile(PMIPv6) protocol. Packet data interface termination point called PDN-GW:It performs anchoring functions of sessions for external packet data networks via SGi interface[5][6]. The main function of PDN-GW is to provide a packet filtering per user based and rate enforcement policies as well as service level charging[7].

II. Proposed Work

The proposed EPC with IMS Integration Architecture shown in fig.3. All-IP mobile core network for LTE is an EPC,

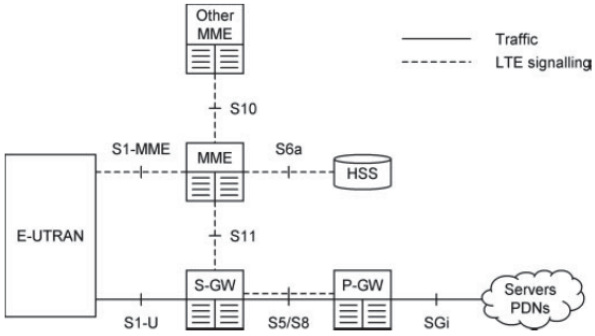

Fig. 2. EPC network Architecture

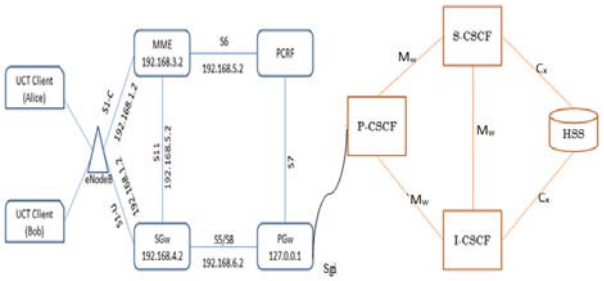

Fig. 3. EPC with IMS Integration Architecture

authorizing the mobile and fixed convergence of real time and non real time packet dependent services. The integration of Open IMS core with Evolved Packet Core is done in the steps by Running all the services of Open IMS core like P-CSCF, S-CSCF, I-CSCF and FHoSS using the terminal.

A. Methodology

Here,the IMS provides the delivery of voice services across the clients while the EPC provides the network framework for providing data packets at a high rate[9]. Therefore the interworking of both the networks can improve the existing QoS (Quality of Services) and support additional services that require high bandwidth. The integration approaches/methodologies for delivering voice services in EPC[8][14]:

- CS Fallback
- VoLGA
- VoIMS

B. Methodologies comparison

The comparison of all these methods is shown in table 1. VoIMS approach gives huge benefits of Internet and it is also capable to provide utilities related to mobile field. This helps us to choose the approach/methodology of VoIMS to deploy on the test bed along with the Evolved Packet Core (EPC) for delivering voice services.

Requirement	CS Fallback	VoLGA	VoIMSLTE
Network Requirement	None	VANC, Security gateway, AAA Server	IMS core,IP-SM-GW
Legacy Network upgrades	All MSCs overlaying Coverage	None	None
EPS/IMS Upgrades	E-UTRAN, MME	E-UTRAN, MME	HSS
Terminal changes	CS Fallback support	VoLGA SRVCC	IMS client

TABLE I
NETWORK IMPLEMENTATION UPGRADES

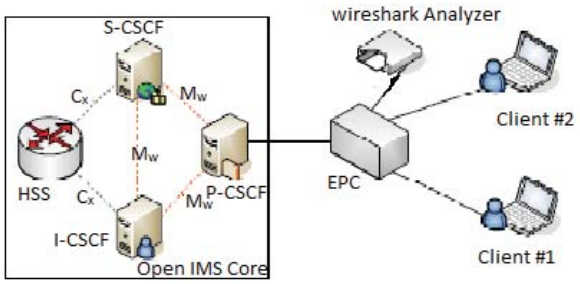

Fig. 4. Testbed setup with QoS Guarantees

C. Quality of Services (QoS) scenarios

We have designed a cloud computing environment which creates an environment of virtual servers and clients, eliminating the need of any physical resource. Further,a few open source tools were deployed in the Linux Virtual machine to consider the parameters related to QoS, by starting different configured profiles and evaluating the QoS parameter within the network[5].To measure the effect of various QoS scenarios, wire shark has been used to monitor the system traffic while observing the IP addresses and labelled PORT numbers.

III. EPC-IMS IMPLEMENTATION

The EPC-IMS implementation took place in four stages. Stage One: Configuration and Deploying of Open IMS core services in the test bed. Stage Two: Installation and Deploying of EPC components. Creating virtual IP addresses for integration of IMS with EPC[4][5]. Stage Three: Deploying the UCT IMS client and registering it with the core network. Stage Four: Deploying the wireshark for packet capture, Iperf and Jpref for measuring QoS parameters shown in fig.4. In the results we check the following parameter for the 6 QoS scenarios created by changing the Quality of Service required by the clients. given in table 3.

- Bandwidth usage
- SIP packets generated
- Call setup times and
- jitter

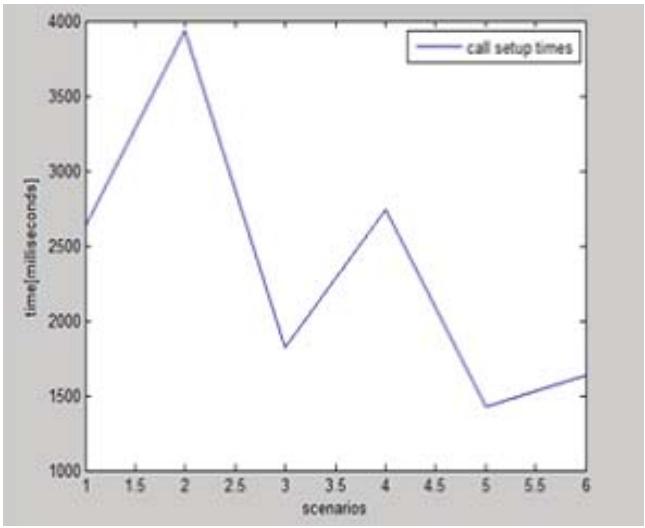

Fig. 5. Analysis of Call Setup Time

IV. SIMULATION RESULTS

A. Analysis of Call Setup Time

It is observed that in fig.5 the call setup time increases with additional QoS parameters induced, when we look at scenario 1 and scenario 2. But when we compare scenario 3 and scenario 5 the call setup time has decreased, this is because, as QoS has been chosen to be non-compulsory for one of the clients, therefore the sequence came to 3rd scenario. Due to this, call setup time drops critically low. however, the client having compulsory QoS, still transmits the additional messages.

B. Analysis of Bandwidth Usage

fig.6 shows that as the QoS requirement increases the bandwidth usage increase because of the additional messages sent by the client to compare scenario 1 and scenario 3 increase in the bandwidth usage.To compare scenario 3 and scenario 5 the bandwidth usage is decreased despite the additional messages sent by the client for which QoS is mandatory. Drop in bandwidth can also be observed with scenario 2 and scenario 4 although additional messages(SIP) still exists. The reason behind this, is that the segmented SIP messages, allowed by provisional ones that were used to enforce QoS. Due to this, the size of the SIP message and the total bandwidth used by the client gets reduced.

Parameter	Scenario 1	Scenario 2	Scenario 3	Scenario 4	Scenario 5	Scenario 6
Bandwidth usage [kbps]	10390367	10136722	10480340	10315013	10446540	11171559
Call Setup Time [milliseconds]	2636	3933	1824	2740	1426	638
SIP Jitter [milliseconds]	0.14	0.07	0.08	0.07	0.03	0.05
no.of Packets Generated	75	85	138	274	480	694
RTP Jitter [milliseconds]	1.53	1.85	2.05	1.89	1.93	3.27

TABLE II
COMPARISON OF ALL THE SCENARIOS

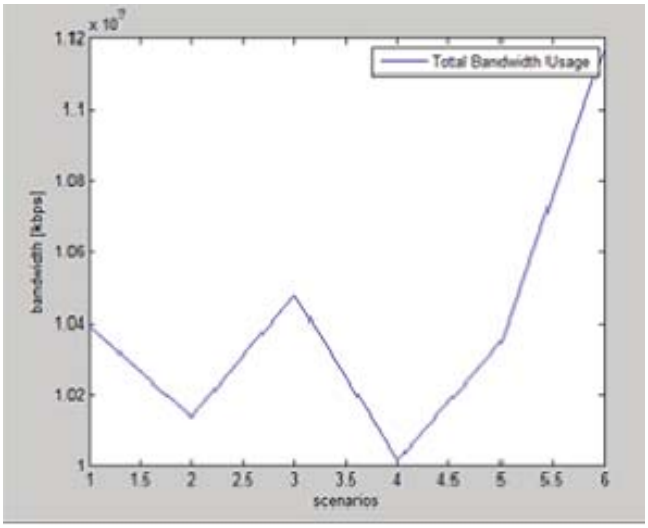

Fig. 6. Analysis of Bandwidth Usage

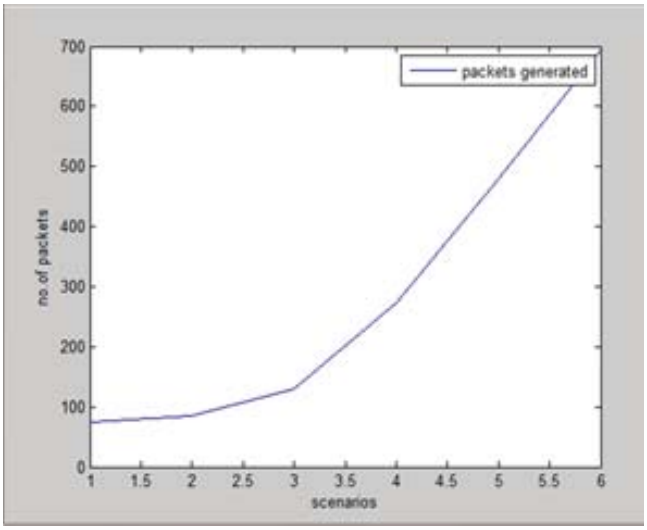

Fig. 7. Analysis of Packets Generation

C. Analysis of Packets Generation

The above fig.7 clearly indicates that the number of packets generated increases with the increase in the QoS enforcement priority. This is because additional messages were sent by client as the required QoS increases. So we can see a steady increase in number of packets generated as the scenarios rises and due to the different QoS parameter required by the clients of the particular scenario.

S.NO	Client#1 QoS	Client#2 QoS
1	Compulsory	Compulsory
2	Non-Compulsory	Non-Compulsory
3	Non-Compulsory	None
4	Compulsory	None
5	Compulsory	Non-Compulsory
6	None	None

TABLE III
EXPERIMENTAL QOS MATRIX

V. SUMMARY AND CONCULUSION

This paper has presented the experimental measurements for the IMS and the LTE/SAE integration. We have conducted experiments on three approaches on providing voice over LTE: CS Fallback, Voice over LTE Generic Access (VoLGA), and Voice over IMS (VoIMS). While, each approach has been associated with some advantages and disadvantages, it was concluded that VoIMS is the best suited approach for delivering voice over LTE network because of its less complexity, widely accepted delivery platform and also standardized by the 3GPP standards. The complete effect of QoS parameters on the IMS SIP signalling load has been observed, while negotiation takes place for IMS session between two users. Scenarios with no QoS, with non-compulsory QoS and with compulsory QoS have been considered for the analysis. From the experimental results, it has been observed that, the amount of data transferred by clients and the core network increases in which some QoS parameters present between 30% and 70%, But the amount of bandwidth usage reduces on the long run, Which could be used by some other clients or we can induce few services for the same client along with the voice services. So it is found that Evolved Packet Core (EPC) provides higher bandwidth, lower latency compared to other core networks. Based on this stsudy, It is suggested that LTE/SAE-EPC integrated with IMS is the best option for 4G telephony services.

REFERENCES

[1] Manabu Itol,Kiyohide Nakauchil,"Service-Specific Network Virtualization to Reduce Signaling Processing Loads in EPC/IMS",journal for rapid open access publishing, IEEE Transactions,volume-2,pp-1076-1084, 2014
[2] SIP Protocol Overview, Ravinson Ltd., United States, 2001
[3] Magnus Olsson, Shabnam Sultana, Stefan Rommer, Lars Frid, Catherine Mulligan, SAE and the Evolved Packet Core, first edition, 2009, USA
[4] Deployment of EPC, White paper by CISCO, USA, 2010

[5] Introduction to Evolved packet Core, Strategic White Paper, Alcatel-Lucent, 2010
[6] Jing Han Haiming Wang,"Principle and Performance of TTI Bundling For VoIP in LTE FDD Mode Nokia Device R&D/Wireless System Research", Nokia (China) Investment Corporation, Limited, 100176, Beijing, China
[7] R. Rajavelsamy, V. Jeedigunta, B. Holur, M. Choudhary, and O. Song, Performance evaluation of VoIP over 3G-WLAN interworking system,Wireless Communications and Networking Conference, 2005 IEEE, vol. 4, 2005.
[8] I. Tanaka, T. Koshimizu, and K. Nishida, CS Fallback Function for Combined LTE and 3G Circuit Switched Services, NTT DOCOMO Technical Journal, vol. 11, no. 3, pp. 1319, 2009.
[9] Sibonelo Madlopha, Offering Voice Services in the Evolved Packet Core and Ensuring Service Continuity during Handoff , Neco Ventura Department of Electrical Engineering, University of Cape Town Rondebosch, Cape Town, South Africa.
[10] Alcatel-Lucent, Options for Providing Voice over LTE and Their Impact on the GSM/UMTS Network, 2009.
[11] Cathal Mc Daid, Overview and Comparison of QoS Control in Next Generation Networks, 2009
[12] The LTE Network Architecture, Alcatel- lucent, Strategic White paper, 2010
[13] M. Sauter," Voice over LTE via Generic Access (VoLGA)", A Whitepaper, pp1-16, Aug. 2009.
[14] The VoLGA Forum http://www.VOLGA-forum.com/

THE 5TH INTERNATIONAL CONFERENCE ON WIRELESS COMMUNICATIONS, VEHICULAR TECHNOLOGY, INFORMATION THEORY, AEROSPACE & ELECTRONIC SYSTEMS (WVITAE-2015)
December 13-16, 2015, Hyderabad, India

Survey on Service Discovery Mechanisms

Gitanjali Shinde and Henning Olesen
Center for Communication, Media and Information Technologies (CMI)
Aalborg University Copenhagen
DK-2450 Copenhagen SV, Denmark
gis@es.aau.dk, olesen@cmi.aau.dk

***Abstract*— Massive number of web services are available, with a deployment of huge number of the Internet of Things (IoT) applications e.g. smart homes, smart cities, intelligent transport, e-health and many more. In the IoT paradigm, almost every device around us will be on the Internet to provide specific services to end users. A large number of services will be available to help end users however providing and selecting appropriate service from a massive number of available services is the challenge of IoT. Service discovery plays a vital role in web service architecture. Traditionally, keyword search has been used for service discovery. The traditional approaches of service discovery couldn't be applied as it is for web services in the IoT environment as devices providing, and accessing services are resource constrained in nature. E.g. limited size, limited energy source, limited computational capability and limited memory. Hence, there is need of a lightweight and semantic service discovery approach for the IoT. This work analyzes different service discovery approaches. This analysis will focus on the key requirements of service discovery mechanism needed for the IoT environment.**

***Keywords*— Internet of Things, Service Description, Service Discovery, Semantic Service Discovery, User Preference.**

I. INTRODUCTION

In the IoT environment devices around us are connected to the Internet to provide services to the end users. IoT devices could be anything around us. i.e. sensors, RFID tag, RFID reader, actuators. The different IoT devices may use different wireless/wired technology to transmit data to cluster head i.e. WLAN, ZigBee, NFC, Zwave, WiFi [1]. These devices may be different in sizes, computational capability hence heterogeneity will major challenge to design WS. IoT will be deployed in large number and almost in all application domains i.e. e-health, smart home, the smart city [2], intelligent transport, logistics and many more. Hence, large number of devices will be working with each other over the Internet to provide services to the end users. End users access a web service (WS) depending on their requirements hence selecting appropriate service from a large number of available services is essential design parameter for WS.

Remainder of this paper is structured as follows the motivation is discussed in the Section II, the detailed literature of service discovery mechanisms is discussed in Section III, comparative analysis of literature work is presented in Section IV and discussion is summarized in Section V.

II. MOTIVATION

Predicting and providing appropriate service depending on context and user preference is the necessity of IoT environment. User may be mobile and will require to access services via his/her Smartphone hence the lightweight WS discovery process is the important design parameter of WS architecture for IoT. In the IoT environment devices around us sense information and depending on this information services are built. Every IoT device is not capable of building and providing WS as IoT devices are resource constrained in nature. Hence, few devices are grouped together as a cluster, and one computationally strong device is selected as cluster head to perform complex task [3]. i.e. building and providing WS. The information senses by the IoT devices are raw and unstructured in nature, so there is need of describing services depending on the raw and unstructured information by converting it into structured format. The need of clustering IoT devices and lightweight WS discovery is shown in figure 1.

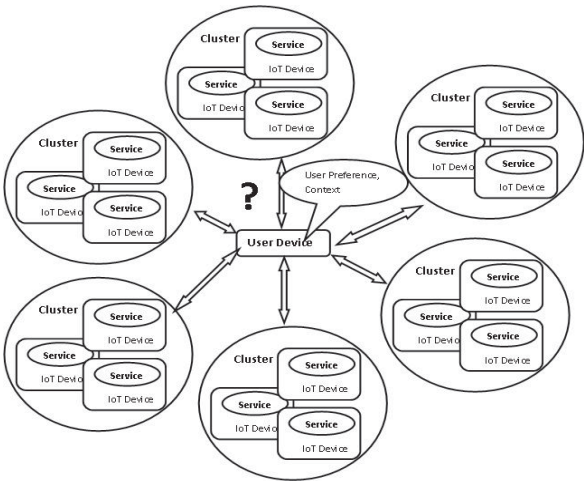

Figure 1. Requirement of service discovery mechanism for IoT environment

Traditional WS discovery methods are not applicable to IoT environment due to its different requirements, hence it is

important to review different WS discovery mechanisms. WS are the description of operations that perform a certain task. WS are language and platform independent. WS could perform a simple task or complex task. A WS has three components service provider, service registry, and service requestor. Service provider describes services using standard extensible markup language (XML) i.e. web service description language (WSDL). Services are advertised by publishing it to a registry. Universal Description Discovery and Integration (UDDI) is the registry used to publish web services. End users are the service requestor, requesting for web service using find operation. WS has four phases of the life cycle. i.e. Build, Deploy, Run, and Mange depicted in fig 2.

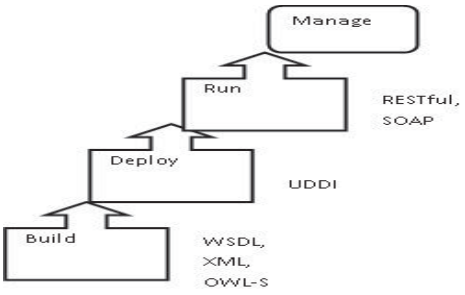

Fig.2. Life Cycle of WS

Build phase of life cycle plays very important role in the WS life cycle, to provide appropriate service to end user the description of WS is matched with requirements of the end user. WS uses the Simple Object Access Protocol (SOAP) to access WS, and it is not suitable for the WS architectures in the IoT environment as SOAP based approach are heavyweight in nature. Traditionally, syntactic service discovery mechanism is used to discover the WS. A syntactic service discovery mechanism result in a list of services among that user has to select appropriate service depending on his/her requirement, and this is not feasible approach for IoT environment. To provide appropriate service to end user, the service description should be done in the semantic way so that in the service discovery phase service could be searched very efficiently.

WSDL, SOAP and UDDI standards are used to build service architecture. However, the WSDL is not designed for semantic description. WSDL describes WS in the form of port, port type, and bindings. Hence, it is very difficult to specify semantic details about WS i.e. nonfunctional requirements, QoS requirements, availability, reliability, throughput, response time and mean time before failure. This invokes the need of a semantic description of services. To provide the semantic descriptions, different approaches are invoked i.e. OWL-S, WSDL-S. However these methods have few limitations i.e. huge number of services exists are described using WSDL format and it is not feasible to add semantic in the existing services, every new service can't have semantic description with it and service requestor may be unaware of terms related to the service. UDDI is used to publish a WS, however the runtime parameters cannot be stored in the UDDI and there is no universal registry for storing WS. Hence, it is very difficult to store runtime parameters to improve WS description [4].

Few challenges for WS architectures for IoT environment as follows:

- Information sensed by IoT device is heterogeneous, raw and unstructured
- IoT devices are resource constrained in nature i.e. limited energy source, limited computational capability, limited memory and limited size
- Traditional WS discovery mechanism is heavyweight and keyword search based
- User-centric approach is not considered in the traditional service discovery mechanisms
- The semantic service description is required for WS.

In the near future IoT devices around us offer a huge number of services to end users for betterment and comfortable life. The end user must get services depending on their requirement. However, IoT comes with challenges mentioned above. This invokes the need of a lightweight and semantic service architecture for IoT. In the next Section review of different approaches of service discovery is done. This analysis helps to find out design parameters of service architecture for IoT environment.

III. Related Work

The service description is the first and important step of service architecture as the efficiency of service discovery is dependent on the service description. In the literature, service description is done by three different approaches. i.e. functional, non-functional and data structural [5]. To provide appropriate service depending on user's requirement the need of betterment in a service description is invoked. The semantic service description is the step to fulfill the need mentioned above. The semantic service description can be done in two ways i.e. annotation based and semantic language based. The annotation based approach improves the expressivity of service description by providing an annototional description for data types, inputs and output of WS. In the IoT paradigm, devices around us will provide services to end users. A large number of services will be available as IoT applications will be deployed in all domains. To provide appropriate and useful service to the end user, efficient service discovery mechanisms are needed. Traditionally, services are registered in the UDDI registry then services are searched using the keyword search mechanism. The UDDI based service architecture faces the limitation due to a centralized approach, hence different ways of deploying service architectures are discussed by Demian et al. [6]. i.e. centralized and distributed. Centralized approach categorized into portal and UDDI based architecture. UDDI based architecture further categorized into hybrid and portal based. Distributed architecture approach categorized into three different ways. i.e. Agent based, Internet based and Point to

Point(P2P) based architecture. Among these different ways of WS architecture, appropriate architecture is used depending on the requirement of the application.

The ontology-based services discovery is proposed by Paliwal et al. [7]. Service discovery is achieved by functional level service categorization and semantic enhancement of service request. The service categorization is done at UDDI by performing two steps. i.e. parameter based service refinement and semantic similarity based matching. Service refinement is done by combining semantic characteristics with syntactic characteristics in WSDL description. In this approach, each service is represented as vector i.e. Service Description Vector (SVD). Service refinement is done by improving semantic contents of the SVD. Services having similar functionality may be grouped in different categories at UDDI, such services from different categories are grouped together in the cluster. These clusters are labeled depending on their functionality for efficient service discovery. To label the cluster, an ontology concept is used. Services from cluster are mined to find the pattern to satisfy the user's request. Hyperclique patterns are used for this purpose. User's request is enhanced using Latent Semantic Indexing (LSI) technique. In this approach, the service refinement and discovery is dependent on the WSDL file. It is impractical that every existing service will have a semantic description with WSDL file.

Logic-based and knowledge based service search and discovery are proposed by Cassar et al. [8]. The latent factor based approach is used to describe the service. Latent factors are recovered from service description by probabilistic machine learning approach. A latent factor is related to the semantic description of web service and can be expressed as probability distribution function. In this Ontology web language for services (OWL-S) is used for service description. To retrieve latent factor from the description, it is converted into Service Transaction Matrix (STM). STM provide a training set, and it is served as input to probabilistic machine learning technique to extract latent factors. Clustering of relevant services is done on the basis of latent factors using Latent Drichlet Allocation (LDA). Service discovery process works efficiently on clustered services.

Meditskos et al. [9] proposed service profile ontology-based service description. Object-based structural matching technique and logic reasoning methods are used for match making process of service discovery. Ontology roles are combined with description logic reasoning for improved service discovery process. The comparison between the complex concept (CC) and service profile (SP) description of WS description is proposed in this wok. The four ontology levels are used to describe WS i.e. Service, Service Profile, Service Process and Service Grounding. In the profile based discovery mechanisms, the service request and service advertisement both represented as the profile. Profile based discovery gives discovery results very efficiently.

Bootstrapping Ontology mechanism for service discovery is proposed by Segev et al. [10]. Term Frequency and Inverse Document Frequency (TF/IDF) methods are used to evaluate WSDL description. These methods review the service description from internal and external perspective. Lastly, free text description method is used to resolve the inconsistencies in the service description ontology. It works in four steps. i.e. token extraction, token evaluation, concept evocation and ontology evolution. Initial filtering and extraction of the labels from WSDL document is done in the token extraction step. In the second step the tokens are evaluated by TF/IDF and web context extraction (WCE) method. TF/IDF method searches for the token that present most frequently in its WSDL document but least present in other service's WSDL documents i.e. token that can represent service in a unique way. In a WCE method group of tokens are extracted from WSDL file of service that can represent the context of service. In the concept evocation, step tokens extracted from both methods are evaluated, and tokens present in both methods are selected to describe the service. In the last step i.e. ontology evolution current ontology is compared with newly extracted descriptors. In this work the description of WS is improved for efficient discovery.

Chakraborty et al. [11] proposed service discovery for pervasive computing. In the pervasive environment usually services are advertised in the broadcast way. However the global broadcasting has limitations i.e. broadcasting of services couldn't be applied for the large-scale network as it works poorly with increasing network size and it uses the more resources and power. In the proposed method solution to overcome the drawbacks of global broadcasting is discussed. It works in two steps. i.e. service caching and group based advertisement of service request. Services are cached at every peer and service requests are forwarded in the group-based approach. Every group of nodes advertises the services provided by the group in abstract way. Hence service request could be easily forwarded to the appropriate group. Group based approach minimizes the efforts to search appropriate node that providing the service demanded by user.

WS description, advertisement, execution and discovery using DARPA agent Markup Language (DAML) is discussed by McIlraith et al. [12]. Descriptive API is used to provide service specification, service capabilities, interfaces and prerequisites for service execution. DMAL Agent based technology is used in this work to discover WS depending on the user preferences and constraints. Zisman et al. [13] proposed the need and solution of runtime service discovery. Service replacement is needed due to various reasons i.e. Unavailability or malfunctioning of service, changes in structure of interface or functionality of service, better service is available to complete associated task. The pull and push model of run time service discovery is used to replace the service that no longer needed. Requirement of Quality of Service (QoS) parameters for WS description and discovery are discussed by Kritikos et al.[14]. QoS parameters are categorized into two types. i.e. domain dependent and domain independent. QoS broker service architecture is proposed in this work. The broker plays the middle layer between user and WS. Analysis of different QoS parameters helps to describe WS semantically with non-functional qualities. Guinard et al. [15] proposed the RESTful service architecture. Proposed

approach is targeted for the IoT environment. IoT devices are resource constraints in nature hence RESTful approach is used for WS. Device profile (DP) is generated for each IoT device that provides services. DP provides services to the users with minimal user interaction. The minimal user interaction is the need of the IoT environment to achieve lightweight service architecture. The context awareness is used as key parameter for service discovery as in future network large number of services will be available. Among such large number of services only appropriate service should be provided to the user hence user preference and context are the parameter for service discovery. In the proposed work these requirements of future network are focused. i.e. RESTful services, Context and user preferences. However access methodology for WS is not addressed in this work. Universal Presence Server (USP) based lightweight RESTful WS architecture is discussed by Chunyan et al.[16]. Proposed architecture includes three entities. i.e. Request Manager (RM), Publication Manager (PM) and Subscription Manager (SM). PM publishes the service description in publication database. SM retrieves the list of services present from the USP database. SM dynamically decides the interface agent to interact with the end user. Dynamic decision of message interface makes this approach lightweight for accessing and interacting with WS.

A vast literature work is done in the area of service architecture to achieve the dynamic, on demand, lightweight and context aware service discovery. Thirteen different approaches of service discovery are analyzed by Debajyoti et al.[17]. i.e. context aware WS discovery, publish subscribe model, keyword clustering, service request expansion method, graph ranking, layer based semantic discovery, WS discovery techniques for heterogeneous networks, WS indexing, structural case based reasoning, agent and QoS based discovery, collaborative tagging, using finite automaton and hybrid approach for WS discovery. When service discovery method is not capable of discovering service based on user's requirement then approximate WS is suggested, for such type of process the behavioral matching of WS is required. The user's requirements are described using behavioral graph and the WS discovery process is converted into graph matching process. From the analysis of different techniques of WS discovery in this work the importance of QoS parameters is focused. As using different semantic and syntactic discovery approach large number of services could be discovered for same type of function. Selecting one WS for user's requirement will be more dependent on the nonfunctional parameters. i.e. QoS parameters. Survey of QoS based WS discovery approaches is done by Phalnikar et al. [18]. The detailed categorization of QoS parameters is discussed in this work. Ontology and syntactic approaches of WS discovery with QoS parameters are compared and the requirements of ontology based WS discovery are proposed in the work i.e. the automatic WS discovery, WS invocation and WS composition. WS description is the base of WS discovery process, efficiency of discovery process increases with semantic description of WS. Bitar et al.[19] reviewed different ways of WS description methods. The need of lightweight semantic description is proposed in this work. WS described using semantic method then that can be efficiently discovered through semantic discovery. In the near future huge number of WS will be present around us hence need of semantic WS discovery is invoked, tremendous research work is going in the direction to discover efficient protocol for WS discovery. Review of different semantic WS discovery approaches is discussed in the [20], [21].

Ibrahim et al. [22] categorized the service matching processes into three types depending on the heterogeneity level in the matching process. i.e. algebraic, deductive and hybrid approach. In an algebraic approach, the degree of similarity between WS descriptions is taken as a parameter to discover appropriate service for user's requirement. Structured graphs are used to find out the degree of similarity between WS descriptions. In a deductive approach, the WS discovery is based on logic i.e. description logic and first-order logic. In this approach instead of semantic different other elements of WS description are considered for service matching process i.e. preconditions and effect matching (PE matching), input and output matching (IO matching), and input, output, precondition and effect matching (IOPE).

IV. COMPARATIVE ANALYSIS

In the above section, different prominent techniques of WS discovery are discussed. In view of realizing IoT application, there is need of dynamic WS architecture hence this literature survey will help to figure out the designing parameters of WS architecture for IoT environment. IoT paradigm requires the major focus on the user's requirement as IoT application will be deployed for the betterment for end user's life. WS will be available in large number as IoT devices providing services are large in number. Hence, appropriate service discovery will play an important role in near future. Thinking ahead, the IoT devices that will provide and access WS are resource constraint in nature hence there is a requirement of lightweight WS architecture. Table 1 summarizes the applicability of WS discovery approaches for IoT environment. Comparative analysis is based on three important requirements of future network. i.e. User preference, context awareness and lightweight framework. In the IoT environment end user may be mobile and may not be aware of services provided at that location. In each location there may be large of services presents among these services end user must be made aware of only few services that are required by end user. Hence the context aware and user preference aware WS framework is required in the IoT environment.

TABLE I. ANALYSIS OF WS DISCOVERY APPROACHES

Approaches	Discovery Technique	UPref	CAW	LW
[7]	Semantic with Latent Semantic Indexing	No	Yes	No
[8]	Semantic with Service Transaction Matrix and Latent Drichlet Allocation	No	Yes	No
[9]	Service profile ontology-based	No	Yes	No

[10]	Term Frequency and Inverse Document Frequency and web context generation	No	Yes	No
[11]	group-based service request forward approach	No	No	Yes
[12]	DARPA agent Markup Language	Yes	Yes	No
[13]	pull and push model	No	Yes	No
[14]	Quality of Service	Yes	Yes	No
[15]	RESTful Approach	Yes	Yes	Yes
[16]	Universal Presence Server	No	No	Yes

UPerf- User Preferences, CAW- Context Awareness and LW- Lightweight

Requirements of WS architecture for IoT environment as follows:

- Semantic description of WS
- Automatic on demand WS discovery
- User-centric approach
- Context awareness approach
- Lightweight registration process for WS
- RESTful approach

V. Conclusions and Future Work

In order to provide WS framework for IoT environment it is important to determine the requirements of WS architecture for IoT network. Hence we have reviewed the literature for service description and service discovery methods. In the literature tremendous work is done for service architecture however this approaches are not appropriate to apply for IoT settings as devices that will provide and access services in IoT paradigm are resource constrained in nature. This survey work will help to determine the designing parameters for WS architecture for IoT network. The user centric approach is the needed in the near future as large number of services will be available, among such huge number of services user must get appropriate service depending on user's requirements. Future plan is to explore a semantic service description method and lightweight, user centric and context aware service discovery methods for IoT network.

References

[1] Jayavardhana Gubbi, Rajkumar Buyya, Slaven Marusic, Marimuthu Palaniswami, " Internet of Things (IoT): A vision, architectural elements, and future directions." Journal Future Generation Computer Systems,Volume 29 Issue 7, Pages 1645-1660, September, 2013.

[2] A. Zanella, N. Blui, A. Castellani, L. Vangelista, and M. Zorzi, "Internet of Things for Smart Cities," IEEE Internet Things J., vol. 1, no. 1, pp. 22–32, Feb. 2014

[3] G. Shinde and Henning Olesen, " Interaction between users and IoT clusters: Moving towards an Internet of People, Things and Services (IoPTS)", WWRF 34th meeting, 21st -23rd April 2015. Page No:

[4] Mydhili K Nair, Mydhili K Nair, "Look Before You Leap: A Survey of Web Service Discovery", International Journal of Computer Applications ,Volume 7, Issue No.5, September 2010

[5] Hajar Omrana, Ibrahim El Bitar, Fatima-Zahra Belouadha, Ounsa Roudiès, "A Comparative Evaluation of Web Services Description Approaches", 10th IEEE International Conference on Information Technology: New Generations, 2013, Pages 60-64

[6] Demian Antony D'Mello and Ananthanarayana V. S, "A Review of Dynamic Web Service Description and Discovery Techniques", First IEEE International Conference on Integrated Intelligent Computing, 2010, pages 246-251.

[7] Paliwal, A.V, Shafiq, B, Vaidya, J., Hui Xiong; Adam, N," Semantics-Based Automated Service Discovery", Transactions on Services Computing, IEEE Year: 2012, Volume: 5, Issue: 2, Pages: 260 - 275,

[8] Cassar, G, Barnaghi, P, and Moessner, K," Probabilistic Matchmaking Methods for Automated Service Discovery", IEEE Transactions on Services Computing, Year: 2014, Volume: 7, Issue: 4, Pages: 654 - 666

[9] Meditskos, Georgios; Bassiliades, N, " Structural and Role-Oriented Web Service Discovery with Taxonomies in OWL-S", IEEE Transactions on Knowledge and Data Engineering, Year: 2010, Volume: 22, Issue: 2, Pages: 278 - 290

[10] Segev, A., Sheng, Q.Z, " Bootstrapping Ontologies for Web Services", IEEE Transactions on Services Computing, Year: 2012, Volume: 5, Issue: 1, Pages: 33 - 44

[11] Chakraborty, D, Joshi, A, Yesha, Y. Finin, T, "Toward Distributed service discovery in pervasive computing environments", IEEE Transactions on Mobile Computing, Year: 2006, Volume: 5, Issue: 2, Pages: 97 - 112

[12] McIlraith, S.A., Tran Cao Son, Honglei Zeng, " Semantic Web services", IEEE Intelligent Systems, Year: 2001, Volume: 16, Issue: 2, Pages: 46 - 53

[13] Zisman, A., Spanoudakis, G, Dooley, J, Siveroni, I, "Proactive and Reactive Runtime Service Discovery: A Framework and Its Evaluation", IEEE Transactions on Software Engineering, Year: 2013, Volume: 39, Issue: 7 Pages: 954 - 974

[14] Kritikos, K., Plexousakis, D, "Requirements for QoS-Based Web Service Description and Discovery", IEEE Transactions on Services Computing, Year: 2009, Volume: 2, Issue: 4, Pages: 320 - 337

[15] Guinard, D, Trifa, V, Karnouskos, S. Spiess, P, Savio, D, " Interacting with the SOA-Based Internet of Things: Discovery, Query, Selection, and On-Demand Provisioning of Web Services", IEEE Transactions on Services Computing, Year: 2010, Volume: 3, Issue: 3, Pages: 223 - 235

[16] Chunyan F, Belqasmi, F, Glitho, R, "RESTful web services for bridging presence service across technologies and domains: an early feasibility prototype", IEEE Communications Magazine, Year: 2010, Volume: 48, Issue: 12, Pages: 92 - 100

[17] Debajyoti Mukalhopadhyay, Archana Chougule, "A survey on web Service Discovery Approaches ".

[18] Phalnikar, R.; Khutade, P.A, "Survey of QoS based web service discovery", World Congress on Information and Communication Technologies (WICT), Year: 2012, Pages: 657 - 661

[19] El Bitar, I, Belouadha, F.-Z, Roudies, O, "Review of Web services description approaches", 2013 8th International Conference on Intelligent Systems: Theories and Applications (SITA), Year: 2013, Pages: 1 - 5

[20] Malaimalavathani, M.; Gowri, R,"A survey on semantic web service discovery", 2013 International Conference on Information Communication and Embedded Systems (ICICES), Year: 2013,Pages: 222 - 225

[21] Priyadharshini.G, Gunasri.R, and Saravana Balaji.B, " A Survey on Semantic Web Service Discovery Methods", International Journal of Computer Applications (0975 -8887) Volume 82 , Issue No :11, , November 2013

[22] Ibrahim El Bitar, Fatima,Zahra Belouadha, and Ounsa Roudies, " Semantic Web Service Discovery Approaches : Overview And Limitations", International Journal of Computer Science & Engineering Survey (IJCSES) Vol.5, No.4, August 2014

THE 5TH INTERNATIONAL CONFERENCE ON WIRELESS COMMUNICATIONS, VEHICULAR TECHNOLOGY, INFORMATION THEORY, AEROSPACE & ELECTRONIC SYSTEMS (WVITAE-2015)
December 13-16, 2015, Hyderabad, India

Public Auditing and Data Dynamics in Cloud with Performance Assessment on Third Party Auditor

Snehal P. Sawant
PG student, Dept. Of Computer Engineering
Smt.Kashibai Navle College of Engineering, Vadgoan BK.
Pune, India
snehalsawant19@gmail.com

Aaradhana A. Deshmukh, Albena Mihovska, Ramjee Prasad
Center for TeleInfrastruktur (CTIF),
Aalborg University,Aalborg, Denmark
{aad,albena,Prasad}.es.aau.dk

***Abstract*—Cloud computing allows the user to outsource their computation and storage overhead to a public cloud, managed by cloud service providers. Data stored in the cloud may reside on remotely servers and this raises security issues. This paper addresses the issue of data storage integrity. The scheme presented in this paper uses the concept of an external Third Party Auditor (TPA). TPA is an external party who is going to perform integrity verification of the user's data on behalf of the user. The proposed scheme assures integrity verification with a dynamic data support, to ensure that changes made to the data are reflected properly. In addition to a simultaneous approach of integrity verification and data dynamics, this scheme enables to determine the performance of the TPA.**

***Index Terms*—Data storage integrity, public auditing, data dynamics, cloud computing, Performance Assessment.**

I. Introduction

Cloud computing is an Internet-based service, which allows the users to access services from a shared pool of configurable network resources[1],while paying only for the portion of the usage. Cloud services have been categorized into three types: (1) SaaS (Software as a Service), (2) IaaS(Infrastructure as a Service), and (3) PaaS (Platform as a Service). Cloud computing enables the users to outsource their tasks of data storage and computation to a public cloud, managed by a cloud service provider. In this paper the major focus is on the cloud storage integrity. When users store their data in the cloud, the user hands over the data to the Cloud Service Provider(CSP). The CSP may have data centers at geographically different places. The benefit of the cloud is that the users can access their data in cloud anytime, and anywhere with a single Internet connection. But the drawback is, that the user has no knowledge or control about where the data is being stored. Data integrity at untrusted servers is an important issue[1]. Data integrity is an act of making sure that the user's data stored in the cloud is correct and consistent. It is an action, which makes sure that data can only be accessed and altered by those who have been authorized to do so. Sometimes to efficiently manage the storage space and to save expenses, the service provider might be a bit negligent to rarely accessed ordinary users data[1]. Hence, it becomes very essential to be able to check the status of the data stored in the cloud. In order to perform data integrity verification, different schemes have been proposed till now[2]. All these prior work considers different parameters in their schemes(e.g. efficiency of the scheme, etc.). Fundamentally, we can distinguish between two categories, public auditing and private auditing. Private auditing schemes are more proficient than public auditing schemes. Public auditing schemes allow for not just the user but anyone to challenge the cloud server for the accuracy of the data. This paper takes the public auditing into consideration. It is not possible for a user to carry out an integrity check on a timely basis. We propose an external Third Party Auditor (TPA),whose task is to verify the user's data stored in the cloud, on behalf of the user. Public auditing is nothing but a verification of the user's data performed by an external TPA, on behalf of the user. For security purposes, the TPA will perform stateless verification, i.e. verification will be performed without retrieving the user's data stored in the cloud. This paper also addresses the issue of dynamic data operations. When the user stores his data in the cloud, the user also makes some modifications to the data,whenever necessary. Data dynamics is an ability to support block level operations, such as block insertion, block deletion, block modification on the data stored. It is necessary to check whether the changes made to the data by the user are replicated properly to the data stored in the cloud. This paper proposes public auditing and dynamic data support for ensuring cloud data storage integrity. Further, we aim to assess the performance of the TPA by enabling to calculate the time required to accomplish each verification request by the TPA.

II. RELATED WORK

Prior to this scheme, a lot of work has been done for remotely stored data integrity verification. Ateniese et. al.[1] are the first to consider public auditing in their scheme 'Provable Data Possession'(PDP) for safeguarding the possession of files stored remotely. In their work they have applied the concept of RSA-based homomorphic tags for auditing remotely stored data. But Ateniese et. al. did not consider dynamic data support. Later in their subsequent work [2], the authors extended the concept of PDP to propose a dynamic form of PDP. This scheme provides efficient and secure provable data possession with less computation overhead. It supports secure and limited dynamic operations on the data. The drawback of this scheme is that it supports only a prefixed number of

verifications. Further, it supports only a limited number of basic block level dynamic operations and does not support block insertion operation. In [3], Wang et.al. considered the dynamic data support in a distributed environment. The authors applied Erasure correcting codes, to support the dynamic operations for the data update, delete and append. This scheme is efficient against Byzantine failure, malicious attacks etc. Though this scheme supports dynamic data operations, it does not support insertion of data blocks in between the data. In [4], Jules and Kaliski, proposed a "Proof of Retrievability" (PoR) scheme. The authors applied the concept of spot checking and error correcting codes, to guarantee both the 'Possession' and the 'Retrievability' of the files stored remotely. The authors used special purpose precomputed encrypted blocks known as 'sentinels', which were included in a file randomly for detection purposes. However, the use of sentinels stops the detection of data dynamics updates. This scheme does not support public auditing properly[11]. In [5], Shacham and Waters proposed an improved PoR Scheme. The authors used the concept of homomorphic authenticators constructed based on BLS-signatures, to aggregate a security proof into a small authenticator value, and to achieve public verifiability. This scheme works only on static files. Erway et.al.[6] were the first to consider 'Dynamic Provable Data Possession '(DPDP), which is an extended version of the PDP scheme. They applied the concept of Authentication Directories with ranking schemes. To provision block insertion, the authors removed the index information in the 'tag' calculation of the existing PDP scheme. This scheme enables efficient proof of the entire file system by providing verification at different levels for different users without downloading the whole data. Though this scheme focuses on both the audit and the dynamic operations of data, its efficiency is unclear. Though various schemes have been proposed for remote data integrity verification, the issue of supporting both public auditing and data dynamics has not been fully addressed. In [7],Wang et.al. have proposed a scheme, which supports both public auditing and data dynamics. They combined the concept of PDP and POR schemes. An external TPA for the verification of the user's data was introduced to the scheme. This scheme is beneficial as it reduces the tasks of the user. The authors have used the concept of homomorphic authenticators and Merkle hash tree, to verify that the values and positions of the data blocks are unmodified. Our scheme uses the same concept of TPA but using zero knowledge proof and CRC-64 techniques rather than Elliptical Curve Cryptographic (ECC) techniques. Our scheme efficiently reduces the time required to perform the verification of the remotely stored data.

III. SYSTEM ARCHITECTURE

The System Architecture is shown in Fig. 1. The following blocks can be defined:

a. User: The user is an entity, who has some data to be stored in the cloud. The user stores his data to the cloud, and depending on the cloud for the computation and the maintenance of the data. The user can be an individual person or an organization. In this paper, we will use terms 'user' and 'client' interchangeably. Whenever the user wishes to perform a verification of his data, he sends a challenge request to the server via the TPA.

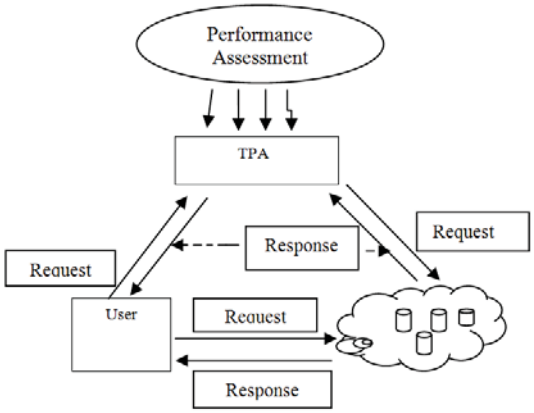

Fig. 1. System Architecture

b. Cloud Storage Server (CSS) or Server: This is an entity who possesses massive amount of storage space and resources needed to manage the user's data. It allows the users to store their data in the cloud storage and to manage the user's data. When the server receives a challenge request from a client, a proof of correctness gets generated and returned to the client.

c. TPA: This is an external entity whose task is to perform the verification of the user's data, on behalf of the user. The TPA performs the verification by challenging the server, to verify that the user's data is unaltered [7]. Though the TPA is going to perform the verification on behalf of the user, it should not retrieve the user's data i.e. the TPA should perform 'blockless verification'. The TPA verifies the user's data without retrieving it[12]. In the cloud model, by keeping larger files to the remote servers, the user can be relaxed from the load of storage and maintenance. As data stored in the cloud can be stored on any geographical distant server, the user does not possess any data locally. Therefore, it is essential for the user to ensure that the data are accurately stored and maintained[9][15]. The user should be able to perform check data accuracy periodically without having any local copies of the data. Practically, it is not possible for the user to take audits on a periodical basis. The user can hand over this task to the TPA[13]. Any TPA with the public key can become a verifier. This scheme assumes that the user can communicate with the cloud server via the CSP, to access, to modify or to retrieve their data. The user or the TPA can challenge the server on a timely basis to check the accuracy of the data. In response to this challenge the server returns proof of correctness.

A. *Proposed Scheme*

This section provides a proposed scheme for the cloud storage integrity. The proposed system supports both data dynamics and public auditing. For public auditing this scheme uses the concept of Zero Knowledge Proof (ZKP) and CRC-64

hashing technique. In general, a ZKP is a way by which the prover (i.e. the server) can demonstrate to the verifier (i.e. the TPA) that a given statement is true, without disclosing any information apart from the fact that the statement is really true. Basically, CRC-64 is an error sensing code, which is mostly used to verify the data transmitted over a network. CRC-64 is used to check that data travelling through the network (cloud) is unaltered. In addition to the efficient provisioning of public auditing with blockless verification, the scheme uses the homomorphic authenticator technique. The homomorphic authenticators are nothing but metadata produced from distinct data blocks, which can be safely combined in such a way to assure a verifier that a linear arrangement of data blocks is properly calculated by verifying only the aggregated authenticator. In the proposed scheme, CRC-64 is used for hashing purposes, where the existing scheme uses merkle hash tree for hashing. Basically, the proposed scheme operation is divided into four steps, as follows:

1. KeyGen(): The KeyGen operation is carried out between the user and the cloud server. By using this step, public and secret keys are generated.

2. SigGen() : The SigGen operation is used to perform the preprocessing of the user's data . In this step, metadata of the user's file is generated and these metadata are signed using a secret key.

3. GenProof(): In the GenProof operation, the TPA gives a challenge message to the cloud server to prove that the data stored in the cloud is accurate and unmodified. The server generates the proof for the respective challenge message.

4. Verify Proof():In verify proof operation, the TPA returns the proof generated by the server to the user. After that, the user verifies his data by using a secret key.

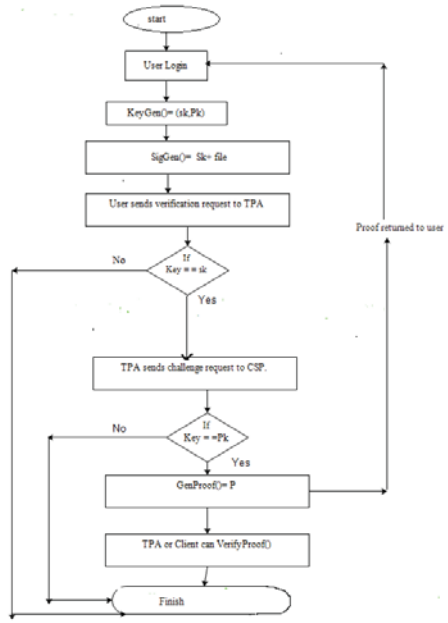

Fig. 2. Flowchart representing public auditing and data dynamics

The Flowchart procedure is shown in Fig. 2. This procedure is used to create security keys, such as a private key and public key. It is achieved by invoking KeyGen(). In the pre-processing, it makes use of the homomorphic authenticators and the metadata. The procedures need two parameters, namely, the file and the key. The contents of the file are divided into several blocks. A hash code is calculated for each block. The hash code of two blocks is then combined. The combined key is further combined with other keys made up of two combined keys. The following steps are carried out for the overall integrity verification and dynamic data operations. For public auditing and data dynamic support this scheme uses the concept of Merkle Hash Tree(MHT). MHT is an authentication structure, which is used to verify the values of data blocks. But in this scheme MHT is used to verify both the values and the positions of the data blocks. MHT is proposed to proficiently and safely prove that a set of elements are untouched and unchanged. MHT is a binary tree, where leaf nodes are hashes of accurate data value. In the top of MHT there is a root value. The authentic root value is acquired from reliable source. Whenever a hash tree is received from any party, the authentic root value acquired from reliable source is compared with the root of hash tree received from other source, to confirm that the set of elements are untouched and unaltered.During the verification phase the following steps are carried out:

1. Let chalmsg be the challenge message. Message chalmsg specifies the blocks to be challenged .The TPA sends a chalmsg message to the server and generate the random set Chalmsg (i,Bi), where i ϵ I.

2. When the server receives the request chalmsg = (i,Bi) the server computes the following:

$\Psi = \sum B_i \; m_i \; \epsilon \; Z_p$ ..... (1)
where ψ is a data set.

3. compute $\Phi = (\Pi i \; \emptyset i)^{Vi}$ ..... (2)
where Φ is a signature set.

Here both the data blocks and the corresponding signature block are combined into a single block. Additionally, the prover will also provide the verifier with a small amount of auxiliary information ω_i. This is the information about the nodes that reside on the path between the root and the requested node i.e. information about neighborhood nodes.

4. The Prover responds to the verifier with a proof

P=(ψ,Φ,H(mi),ω,Sigsk(H(R)))..... (3)

When the client receives the response proof from the server, it verifies the proof by computing the root R using (H(mi),ω) where iϵ I and ω is auxiliary information;then the root would be verified by using sigsk(H(R))else output false if fails. Finally, it verifies the data block mi:

mi,(mi) i.e. (Φ .g) = e(Φ Π H(mi)^{Bi} u$^{\psi}$,V) ..... (4)

To ensure that changes made to the data by user have

been reflected properly, this scheme provides support on data operations such as block insertion, block deletion, block modification, dynamically. To support the dynamic operations on the data, the following steps are carried out.

B. Data modification

1.To modify block mi to mi' generate a new signature for that corresponding block is

Φ'=(H(mi' $u^{mi'}$)$^{\alpha}$.....(5)

2.Upon getting this modification request, the server updates the file F and computes R' and returns

Pupdate = (ω,H(mi)),sigsk(H(R).R') ..... (6)

3.Upon receiving Pupdate, the client computes R usingH(mi),ω).

4. Then it performs the verification Sigsk(H(R)) and the output is 'False' if the verification fails. The following operations Are then performed Compute Rnew using(ω ,H(mi'))Verify update by checking if(Rnew = = (R')sign R' by succeed then finally server update R' signature.

C. Performance Assessment

The existing scheme supports both public auditing and data dynamics .but in the case of failure the TPA becomes the bottleneck to the single point failure. Hence, in the proposed scheme the main focus is on how to assess performance of the TPA. For that purpose this scheme maintains a queue[10][8] . Let λ be the arrival time of customer's request.

Let μ be the service time of customer's requests.

Let Δ be the delay in the queue.

Let the time at which service begins is Sb.

Let the waiting time be Wi.

Let the Total time be T.

Let P be the utilization factor = λ /μ.

The goal is to determine the time taken by the TPA to verify each verification request. Each verification request is placed in the queue before the TPA processes it. Before computing total time we need to consider delay in the queue. We need to compute the time at which service begins is Sb.

Sb = λ + Δ .....(7)

Let the Service time be μ.

Let the Wi be the waiting time and computed as:

Wi = Δ + μ .....(8)

Finally Let T be the total time taken to complete each request can be computed by:

T= λ + Wi .....(9)

Where, T- Total Time

λ - Arrival Time

Wi- Waiting Time

μ - Service time

Sb - time at which service begins. Δ - Delay in the queue.

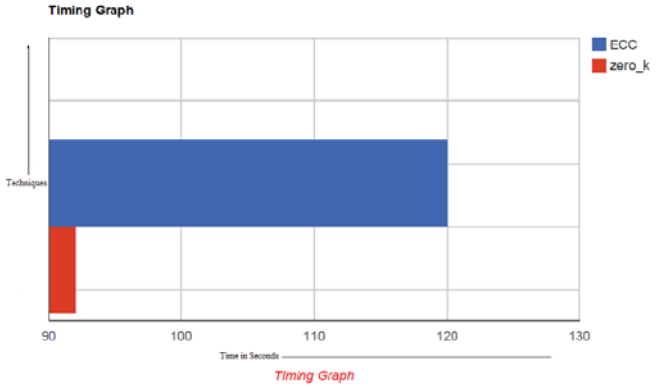

Fig. 3. Graph representing time required to process each user request

Fig. 3 shows the timing graph that represents the time taken by the TPA to perform the verification of each request. Fig. 3 shows the comparison between the time taken by the ZKP technique and the Existing Elliptical Curve Cryptographic (ECC) technique. The ZKP takes less time than the ECC technique.

IV. CONCLUSION

For integrity verification the existing system provides the public auditing scheme using a TPA. The TPA performs the auditing of the client's data on behalf of the client using the challenge response protocol. In addition to the auditing, the existing scheme also supports data dynamics operations, such as block insertion, block deletion, block modification etc. to check whether the changes done by the client are incurred properly to the data stored on cloud. As the TPA is going to perform a number of auditing tasks simultaneously it becomes essential to determine the performance of the TPA, so that it can perform properly in the event of failure. For this purpose the proposed scheme provides a functionality to supervise the performance of TPA for smooth functioning.Our Proposed scheme mainly focuses on Time reduction. As ZKP are probabilistic rather than deterministic, it becomes essential to achieve higher level of security. Though ECC techniques takes much time for verification , they are more secure.Hence to improve the efficiency of algorithm can be considered as a future work.

REFERENCES

[1] G. Ateniese, R.Burns, R.Curtmola,J.Herring,L.Kissner,Z.Peterson,D.Song " Provable Data Possession at Untrusted Stores," 14th ACM Conference on Computer and Communications Security (CCS 2007).

[2] G. Ateniese, R.D. Pietro, L.V. Mancini, and G. Tsudik, "Scalable and Efficient Provable Data Possession," Proc. Fourth Int'l Conf. Security and Privacy in Comm. Networks (SecureComm'08), pp. 1-10,2008.

[3] C. Wang, Q. Wang, K. Ren, and W. Lou, "Ensuring Data Storage Security in Cloud Computing," Proc. 17th Int'l Workshop Quality of Service (IWQoS '09), 2009.

[4] A. Juels and B.S. Kaliski Jr., "Pors: Proofs of Retrievability forLarge Files," Proc. 14th ACM Conf. Computer and Comm. Security (CCS '07), pp. 584-597, 2007.
[5] H. Shacham and B. Waters, "Compact Proofs of Retrievability,"Proc. 14th Int'l Conf. Theory and Application of Cryptology andInformation Security:Advances in Cryptology (ASIACRYPT '08),pp. 90-107, 2008.
[6] C. Erway, A. Kupcu, C. Papamanthou , and R. Tamassia,"Dynamic Provable Data Possession," Proc. 16th ACM Conf. Computer and Comm. Security (CCS '09), 2009.
[7] Qian Wang, Cong Wang, KuiRen , Wenjing Lou And Jin Li " Enabling Public Auditability and Data Dynamics for Storage Security in Cloud Computing" IEEE transaction Paper on Parallel and Distributed Systems vol 22 No 5, pp. 847-859, May 2011.
[8] Aaradhana A. Deshmukh, Dr.Albena Mihovska, Dr.Ramjee Prasad Center for" A Cloud computing security schemes:- TGOS [Threshold Group-Oriented signature] and TMS [Threshold multisignature schemes] "Tele-Infrastruktur (CTIF), Dept of Electronic Systems, Aalborg University Aalborg, Denmark,2012.
[9] E.-C. Chang and J. Xu, "Remote Integrity Check with Dishonest Storage Server," Proc. 13th European Symp.Research in Computer Security (ESORICS '08), pp. 223-237, 2008.
[10] Gowtham Kanagaraj, Naveen Shanmugasundaram And Sathish Prakash "Adaptive Load Balancing Algorithm Using Service Queue", 2nd International Conference on Computer Science and Information Technology (ICCSIT'2012) Singapore April 28-29, 2012 .
[11] K.D. Bowers, A. Juels, and A. Oprea, "Proofs of Retrievability: Theory and Implementation," Report 2008/175, Cryptology ePrint Archive, 2008.
[12] Q. Wang, C. Wang, J. Li, K. Ren, and W. Lou, "Enabling Public Verifiability and Data Dynamics for Storage Security in Cloud Computing," Proc. 14th European Symp. Research in Computer Security (ESORICS '09), pp. 355-370, 2009.
[13] Qian Wang, Cong Wang, KuiRen , Wenjing Lou And Jin Li " Enabling Public Auditability and Data Dynamics for Storage Security in Cloud Computing" IEEE transaction Paper on Parallel and Distributed Systems vol 22 No 5, pp. 847-859, May 2011.
[14] Snehal P. Sawant , Aaradhana. A. Deshmukh," Survey on Public Auditing and Data Dynamics in Cloud Data Storage" International Journal of Science and Research (IJSR),ISSN (online) 2319-7064.
[15] T. Schwarz and E.L. Miller, "Store, Forget, and Check: Using Algebraic Signatures to Check Remotely Administered Storage,"Proc. 26th IEEE Int'l Conf. Distributed Computing Systems (ICDCS'06), p. 12, 2006.

THE 5TH INTERNATIONAL CONFERENCE ON WIRELESS COMMUNICATIONS, VEHICULAR TECHNOLOGY, INFORMATION THEORY, AEROSPACE & ELECTRONIC SYSTEMS (WVITAE-2015)
December 13-16, 2015, Hyderabad, India

Behavior State Feature Extraction through Single Channel EEG Device for Medical Application

Sravanth Kumar and Vivek Kumar
Research Scholars: dept. of ECE,
Birla Institute of Technology Mesra
Ranchi, India
Srava2010@gmail.com, mr.vivek.1988@ieee.org

Bharat Gupta
Associate Professor: dept. of ECE
Birla Institute of Technology Mesra
Ranchi, India
bharatg@bitmesra.ac.in

Abstract— **presently researchers are working on the development of EEG-based human computer interface for enhancing the quality of life in medical as well as non-medical applications. Such technology can be incorporated to psychology, anesthesiology, gaming, security system and for real-time patients monitoring. The Neurosky Mind wave headset devices are generally utilize to detect and measure electrical activity of the user's forehead and transmit the collected data wirelessly, to a computer for further processing. After processing EEG signal, it is categories into various frequency bands for feature extraction. This paper mainly deals in extracting the feature of EEG signal in Openvibe. In this paper, we have proposed an algorithm to extract the features like frequency band, amplitude and power spectral density. Based on the feature extraction, we can characterize the EEG signal and use it for different real-time applications. Furthermore, we have discussed the mental or behavior state of the person (Eye Blink, Meditation, Attention levels) through the NeuroSky Mind wave (MW001) device using Openvibe.**

Keywords— EEG Sensor, BCI, Signal Processing, Openvibe

I. INTRODUCTION

Recently, a new attribute human-centric communication and human-computer interaction is incorporated with digital media has been revolutionized the numerous fields like medical, sports, entertainment, including wellness and quality of life. Most importantly, such technologies are the key interest to the vast potential for various medical applications. Monitoring brain activities with brain-computer interfacing (BCI) has enabled real-time healthcare monitoring applications for much neurological disorder and disabled patients. This field has the potential to shift clinic centric technologies to patient-centric technologies by monitoring brain activities. Generally BCI utilized to performs four distinct tasks. Converting neurological input signals into electrical signals; extracting features; gathering important information, and combine all meaningful information for useful purposes [1].

In BCI system, the user sends the information through the brain signals on the receiver side these signals will be received and apply for target applications. The application then converts these signals into commands that cause movements. The BCI has been used for a widening variety of such applications. The initial applications have been aimed at helping disabled people utilize machines. These days, many researchers consider that wireless BCI systems are a very important step towards getting BCI applications out of laboratories. Recent advances in embedded system, sensor technology, digital signal processing techniques and wireless Communication technology has made real-time brain activity monitoring possible [2]-[3]. The information (brain signal) is transmitted either wired or wirelessly to the computer system using a multiple distributed EEG (electroencephalogram) electrodes or sensors placed over the human head [4]. We have characterized wired and wireless devices based on literature work, recent advances, and their applications. These devices help to improve the quality of life paralyzed or mentally disabled patients in a hospital and home [6].

In this paper, we focus on the different type of EEG systems and their applications. We have also mentioned the state of the art available wireless EEG devices and their features. Initially, researchers proposed wired BCI system to diagnose disease [6] which is very uncomfortable for the patients. Currently, wireless BCI system helps people's life more comfortable. These systems are able to offer improvements in entertainments, games, medical engineering, rehabilitation, and daily life because such systems have obvious advantages. They are simple, convenient, and flexible to use because of wireless.

The NeuroSky MindWave headset is used to collect raw signal from the human brain. The accessed Data from the Neurosky headset are then plotted through the Application Program Interface of Neurosky Inc. using a processing based program. We assign a subject to perform facial gestures and mental activities tasks like smooth and fast opening and closing eye, blink, concentration, and meditation. The real-time raw data was recorded during the subject performed these actions using Openvibe software, Further development of process-based algorithms of concentration and meditation level of recognition for Medical applications.

The rest of paper is as follows Literature Survey on EEG signal and its characteristics are given in section II. Section III provides the proposed work and Section IV provides Results and Discussion on Feature Extraction through Behavior state Monitoring using Neurosky Mindwave Device.

II. LITERATURE SURVEY

EEG is the representation of the electrical signal of the brain activity from the scalp. The first neural activity of the human brain published in Hans Berger (1924) [2] using a simple galvanometer. EEG is generally described in frequency band vary of amplitude and frequency of the wave represent various brain states which depend on internal brain behavior state and external simulation [3]. In recent years, clinical use of EEG 21 electrodes is used to identify 5 fundamental waves.

Generally, brainwaves are classified in five frequency bands i.e., Delta, Theta, Alpha, Beta, and Gamma. Delta signal (0.1-3.5Hz) associates with a deep sleep condition. Theta (4-8Hz) signal consist of with dreams, imaginary, idling, drowsiness. Alpha (8-12Hz) represents relaxed, reflection and pattern appears in wakefulness. Beta (>13 to 30Hz) alert, working active, busy, thinking and concentration and Gamma (30 to 100Hz) is associated with the rhythms for high-level information processing as shown in Table1.

Table 1. Frequency band classification based on Brain Activity

Brainwave Type	**Frequency range**	**Mental states and conditions**
Delta	0 to 4Hz	dreamless sleep, unconscious
Theta	4Hz to 8Hz	recall, fantasy, imaginary, dream, creative
Alpha	8Hz to 13Hz	Relaxed, but not drowsy, tranquil, conscious
Low Beta	13Hz to 15Hz	relaxed yet focused, integrated
Midrange Beta	16Hz to 20Hz	Thinking, aware of self & surroundings
High Beta	20Hz to 30Hz	Alertness, agitation
Gamma	30Hz to 100Hz	Motor Functions

Now a day's great development is happening in wireless EEG devices for patient monitoring, gaming, and other applications. Previously, researchers are using wired EEG devices for patient monitoring but now easily handling through wireless EEG devices [5]. These EEG devices have been developed by Neurosky, OCZ technology, InteraXon, PLX devices and Emotive systems [3]-[4].

III. METHODOLOGY

A. Utilized Resources: Hardware

The main hardware used for this study is NeuroSky MindWave Device, having a single-channel headset and its cost around $100. The device consists of eight main parts - ear clip, ear arm, battery area, power switch, adjustable headband, sensor tip, sensor arm and thinks gear chipset [5]. The main principle of this device is very simple. In this device, two sensors are used to detect the EEG signals and filter out the noise. First sensor tip detects electrical signals from the forehead of the brain, through the electrode positioning (FP1) according 10-20 system of the EEG [2]-[6].

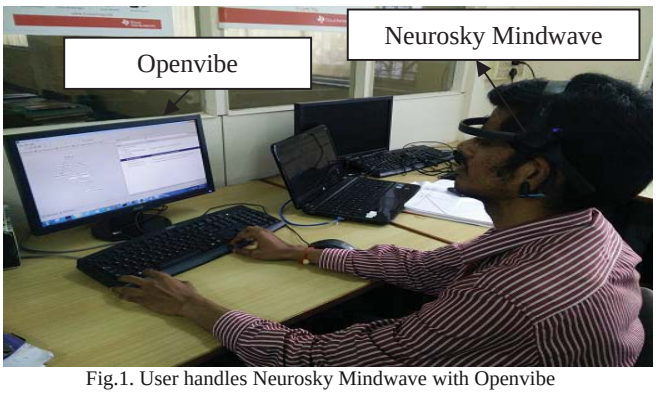

Fig.1. User handles Neurosky Mindwave with Openvibe

The second sensor ear clip is used for ground reference to filter out the electrical noise. Signals from this sensor are receiving via the electrode placed in the left ear lobe, where the data obtained at 512 Hz of sampling rate with each sample there is a 16-bit ADC resolution [7]. User handles Neurosky Device with the computer as shown in Figure 1.

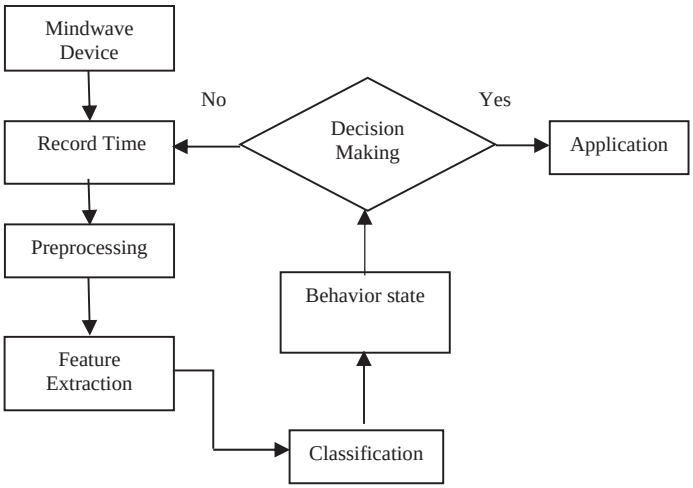

Fig.2. Proposed Algorithm for Behavior state Monitoring

We have proposed an algorithm for behavior state monitoring as shown in Figure 2, with the help of Neurosky Mindwave system. The First step is to setup Mindwave Wireless EEG Device to system/laptop through the wireless communication technology such as Bluetooth through the serial port. Next we have recorded the EEG data for certain time period. Normally these recorded data contains a lot of external noises, so first we have to eliminate this noise using preprocessing techniques. In preprocessing techniques, we are eliminating the artifacts and external noise using filtering techniques. We are setting up the frequency 0 to 40 Hz. After this we normalize the received data and then extract the features from EEG signal such as amplitude, frequency band, power spectral density based on the classification methods

such as Linear discriminant analysis (LDA) and Support Vector Machines (SVM).

B. Utilized Resources: Software

More simplify signal processing techniques and data analysis is possible through the Openvibe software [9]. It is a computing language using software programming designed for data analysis, computation and visualization [8]. Openvibe allows 2D and 3D visualization of data through the topology. In this paper, Openvibe is used to process the EEG signal. Normally EEG machines electrodes are placed on the head of the subject and transmits EEG signal to computer with huge external noise, artifacts and interference but in Openvibe software are easily tackled these issues [11]-[16].

First we setup the Neurosky Mindwave device to the computer over Openvibe platform for acquiring brain signal according to the steps shown in Figure 4. In next step, acquiring server of Openvibe with Neurosky device and device properties will transfer the data after pairing with Bluetooth to the system/laptop. It allows Bluetooth connection which send data in the form of packets. Then, we design our proposed algorithm for behavior state/mental state in Openvibe.

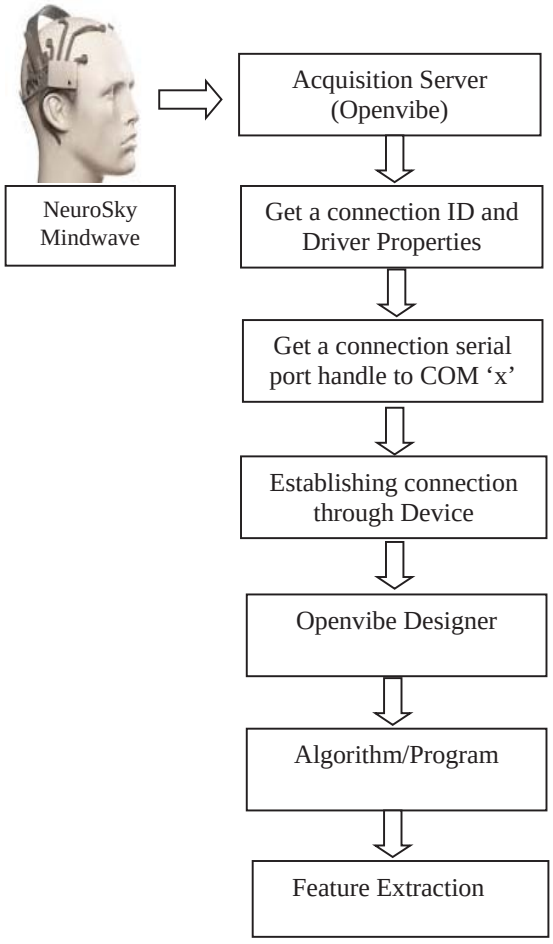

Fig.3. NeuroSky MindWave Communication protocol

IV. RESULT & DISCUSSION

Initially, we setup the Neurosky device setup with Openvibe software which is mathematical and graphical programming language. In Openvibe, it is easy to drag and drop the inserting options. First initiate the acquisition server of Openvibe with Neurosky Mindwave device, sample per count is 32, a connection port is 1024 and sampling frequency of the device is 512Hz. Then open the openvibe designer for programming, we design a simple program for acquisition and signal display as shown in Figure 4. For obtaining raw EEG signal of a user through neurosky mindwave device with a single electrode (Fp1) placed on the forehead. The raw EEG signal is shown in Figure 5.

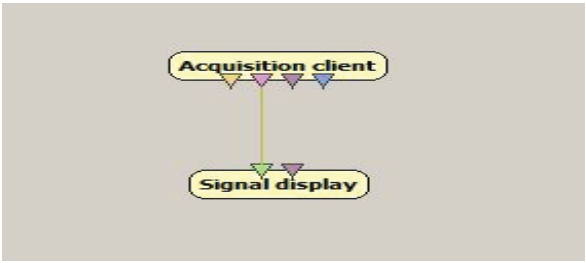

Fig.4. Acquisition of EEG signal in openvibe

The signal shown in Figure 5 is the result of eye blinking of the subject, which is clearly visible.

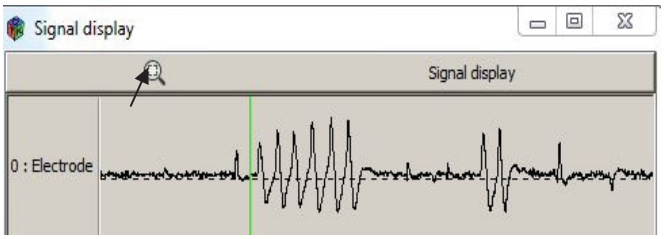

Fig.5. Raw EEG signal

Next we are storing the acquired data into Geographic Data Files (GDF) format shown in Figure 6. Normally stored data is for certain time period. Openvibe is efficient software for storing data into different formats.

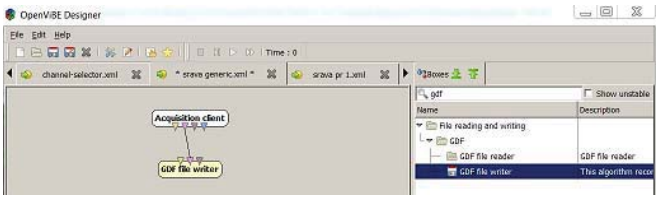

Fig.6. Stored Raw EEG data in GDF format

Brain waves have different types of activity measures in different frequency bands as shown in Table 1. The stored data is classified in different frequency bands as shown in Figure 7. We can observe that only Delta wave and Theta wave are point of concern for further processing.

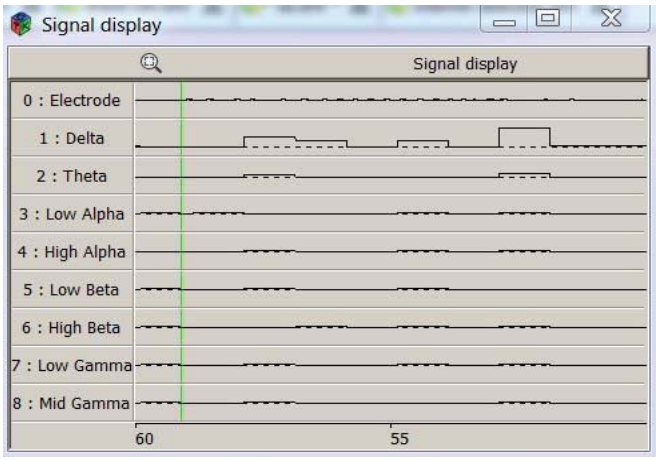

Fig.7. EEG Signal in Frequency Band Spectrum

Next step is to extract features from the stored data with an algorithm shown in Figure 8. The feature for behavior state are amplitude, frequency range and the power contain in these signals. According to the Figure 8, we import the GDF file and place it for reading. Next we are selecting the channel selector for the appropriate frequency band.

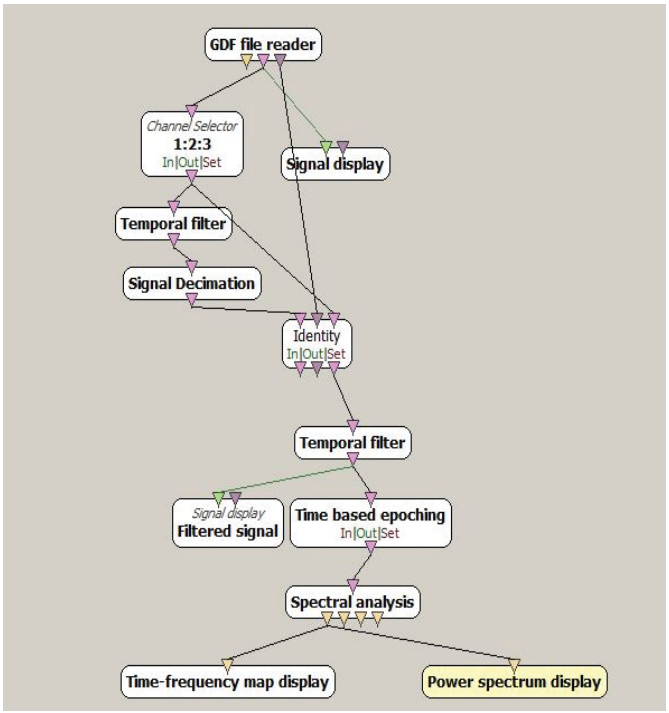

Fig.8. Step used in Feature Extraction from EEG Signal in Openvibe

We are selecting only two frequency bands of the brain signal. One is Delta wave and another Theta wave because Mindwave device has single channel device which is put on the forehead (Fp1) it reads only Frontal lobe of the brain. This device gives sampling frequency 512 Hz and data block size is 32 per samples per second. We are giving the delta and theta wave to identity as input data. EEG signal are non-stationary signal which contains a lot of noise. We remove such noise using a temporal filter. By using Band-pass filter for extracting the required frequency bands. The range for lower cut-off frequency is 0Hz and upper cut-off frequency 40Hz. After filter and eliminate the noise from the signal look like in Figure 9.

Fig. 9. Filtered EEG signal.

Then we are using time-based epoch to divide the signal into time-based epoch that is its gives every second 512 samples and blocks of 32 samples (32/512 = 1/16). Next we are applying time-based epoch signal to spectral analysis. It gives the signal amplitude. Finally, the signal applied to power spectrum display in this we are applying minimum frequency as 0Hz and maximum frequency set to the 40Hz, observing output in Figure 10.

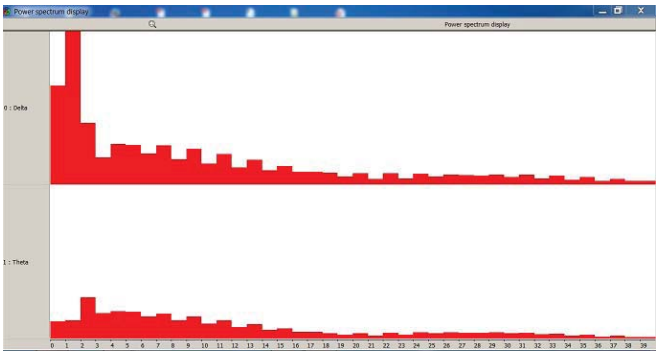

Fig. 10. Power Spectral Density of filtered EEG signal

In this spectrum, we are observing user's recorded data in relaxation state shows user's concentrate or in deep meditation level. Next we have proposed Time-frequency map, it generally measures power spectra of a signals gives over with a time. It displays power spectra of signals over time, making it possible to track changes in amplitudes over a given time span shown in Fig. 11.

From the Figure 11, we can conclude that with our proposed algorithm, we would be able to find the behavior state of the user. Mainly it gives behavior state like attention or meditation levels, Motor skills like hand/Eye Condition and conscious thoughts.

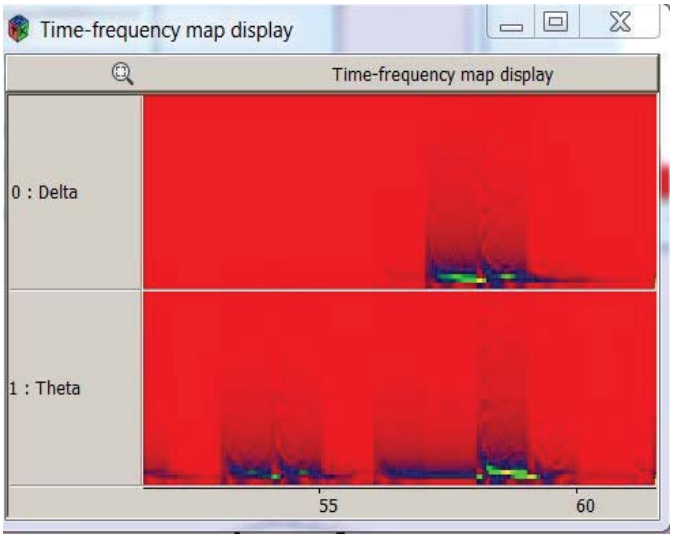

Fig. 11. Time-frequency map display of filtered EEG signal

V. Conclusion

We have proposed an algorithm for the feature extraction from EEG signal in Openvibe environment. First we observe the raw EEG data for a certain time period in Openvibe. Next we have shown how to store the data through a Neurosky Mindwave device in GDF format. We have extracted the feature of EEG signal as amplitude, frequency and power. Behavior state monitor through the single channel device used on the forehead is possible. We would observe the subject attention or meditation levels, motor skills like hand/Eye movement. Generally, health care provider, doctors, and nurses are able to get the status of the patient's health only after the occurrence of the emergency. By analyzing the EEG signal of Subject, we would get the relevant data of patient's disease status before the occurrence of any emergency like heart attack, brain injuries, etc. Literature suggests that proper analysis of brain signal will be very helpful for the improvement of medications and other nonmedical purposes. Our proposal, to somewhat enhance the level of medication given to the patient will be done by the knowledge of what has happened in neuron activity.

References

[1] R. Palaniappan, C. S. Syan, and R. Paramesran, "Current Practices in Electroencephalography-based Brain Computer Interfaces", IGI Global, vol. 143, pp- 1-14, 2009.

[2] B. I. Morshed, and A. Khan, "A brief Review of Brain Signal Monitoring Technologies for BCI Applications: challenges and Prospects", Journal of Bioengineering and Biomedical Science, vol. 4, no. 1, pp. 1-10, May 2014.

[3] J. P. Donoghue, "Connecting Cortex to Machines: Recent Advances in Brain Interface", Nature Neuroscience, vol.5, pp. 1085-1088, November 2002.

[4] Y. Lieu, O. Sourina, and M. K. Nguyen, "Real-time EEG-based Huamn Emotion Recognition and Visualization", international Conference on Cyberworlds, pp. 262-269, October 2010.

[5] Sourina O,wanq Q,Nguyen M k 'EEG-Based 'serious' game and monitoring tools for pain management'studies in health technology and informatics, 2011.

[6] S. Debener, F. Minow, R. Emkes, K. Gandras, and M. D. Vos, "How about taking Low-cost, Small, and Wireless EEG for a Walk", Psychophysiology, vol. 49, no. 11, pp. 1617-1621, November 2012.

[7] G. Eason, B. Noble, and I. N. Sneddon, "On certain integrals of Lipschitz-Hankel type involving products of Bessel functions," Phil. Trans. Roy. Soc. London, vol. A247, pp. 529–551, April 1955.

[8] Jasper, H., 'Report of committee on methods of clinical exam in EEG', Electroencephalogr. Clin. Neurophysiol., 10, 1958, 370–375.

[9] Barrett, G., Blumhardt, L., Halliday, L., Halliday, A. M., and Kriss, A., 'A paradox in the lateralization of the visual evoked responses', Nature, 261, 253–255.1976.

[10] Effects of electrode placement', http://www.focused-technology.com/electrod.htm, California. Accessed on 22/2/2014.

[11] Mindwave,http://developer.neurosky.com/docs/lib/exe/fetch.php?media=mindwave_user_guide_en.pdf accessed on 4/3/2015.

[12] Emotiv,https://emotiv.com/.../Emotiv%20EPOC%20Specifications%202014.pdf accessed on 4/3/2015.

[13] Wojciech SAŁABUN 'Processing and spectral analysis of the raw EEG signal from the MindWave' PRZEGLAD ELECKTROTECHNICZNY, ISSN 0033-2097, R. 90 NR 2/2014.

[14] M.Murugappan,M.Rizon, RNagarajan, S.Yaacob, I.Zunaidi, and D.Hazry EEG feature Extraction for classifying Emotions using FCM and FKM International Journal Of Computers And Communications, issue 2, Vol. 1, 2007.

[15] Panagiotis C. Petrantonakis, Leontios J. Hadjileontiadis Emotion Recognition from Brain signals using Hybrid Adaptive filtering and higher order crossing Analysis IEEE transactions on Affective Computing Vol 1, No 2 July-December 2010.

[16] Sravanth Kumar Ramakuri, Vivek Kumar, and Bharat Gupta, "Extraction for Human Behavior from EEG Signal for Medical Application", 2nd International Conference on Microelectronics, Circuits and Systems (Micro 2015), Kolkata, 11- 12, July 2015.

THE 5TH INTERNATIONAL CONFERENCE ON WIRELESS COMMUNICATIONS, VEHICULAR TECHNOLOGY, INFORMATION THEORY, AEROSPACE & ELECTRONIC SYSTEMS (WVITAE-2015)
December 13-16, 2015, Hyderabad, India

Access for Internet of Things using Smartphone as a Gateway utilizing LTE and WiFi

Prateek Mathur*, Rasmus H. Nielsen†, Neeli R. Prasad*, Ramjee Prasad*
*Center for TeleInFrastruktur (CTIF), Department of Electronic Systems
Aalborg University, Aalborg 9220, Denmark
{in_pm,np,prasad}@es.aau.com
†Cisco Systems, San Jose, USA
{rhnielsen}@ieee.org

***Abstract*—Communicating the Internet of Things (IoT) data relying on Long-Term Evolution (LTE) and WiFi has been been presented in the relevant literature. However, this necessitates devices to have LTE/WiFi capability of their own, that has limitations in the form of power consumption, and radio access congestion. Alternatively, Bluetooth, ZigBee, and Near Field Communication (NFC) are promising technologies for low power personal area network communication, and used for IoT devices. These technologies have not been truly examined for their capacity for IoT as they require a custom gateway to communicate the data to the Internet. In this paper we present a system model wherein the smartphone functions as a gateway for the IoT devices operating on NFC, ZigBee and Bluetooth. The smartphone functioning as a gateway for transferring IoT data. The system modelled in the form of a Markov Chain based on the operational states of the smartphone is presented.**

***Index Terms*—internet of things, LTE, WiFi, gateway**

I. Introduction

The Internet of Things (IoT) and the machine type communication (MTC) devices are expected to bring a paradigm shift in the communication world. A largely accepted notion has been that IoT devices would be operated relying on the Long-Term Evolution (LTE). Similarly use of WiFi has been proposed as an effective means for access and traffic relaying pertaining to IoT. Although utilizing LTE for all IoT devices is challenging considering certain aspects such as that IoT devices have low data rate and can collectively exhibit very bursty behaviour, *i.e.*, many devices reporting the same physical parameter at the same time. They could also be highly variable over a given period of time. Further, the devices are expected to be operated on batteries, and therefore performing the desired utility over extended periods of time is highly desirable.

Enhancements in LTE have been brought in the form of discontinuous reception (DRX/DTX) mechanisms that allow the devices to power on and off as per the requirement [1]. LTE as a gateway for IoT devices to transfer data is presented in [4]. In the paper LTE based data transmission (gateway functionality) is considered in the form of a smartphone, home router, and a road side unit, and the performance analysis of devices served is presented. This paper, however, does not consider the possible utility of WiFi based gateway functionality. Authors in [2] present a mechanism to distribute the devices into clusters such that all devices in a given cluster share similar properties, and access is granted to a cluster through LTE, this however may be hard to implement considering the operational diversity of devices. Authors in [3] present a mechanism for granting access to devices using device to device (D2D) connections between the MTC devices and the smartphone (user equipment (UE)), with the data uploaded using UE along-with the human centric communication data. This is a similar approach to the proposed system in this paper, however, the authors consider that all the MTC devices have the same transmit power with a packet arrival rate represented a Poisson distribution. In the presented system by the authors the operational homogeneity of the IoT devices is not considered. Using WiFi for providing access to the IoT devices has been dealt with in the some of the research works, especially with the advent of the IoT specific communication standard 802. 11ah [5]. Utilizing Bluetooth and its low energy variant Bluetooh low energy (BLE) have been stated as promising technologies for transferring IoT data [6]. Authors in [7] present a Semi Markov Model to represent the traffic flow of IoT data demonstrated through a sensor based event detection application. The paper however does not examine the communication of data through LTE/WiFi or the use of UE as a gateway. Interestingly, to the best of authors knowledge no work has looked onto how ZigBee, Near Field Communication (NFC) and Bluetooth based devices could be brought within the IoT ecosystem utilizing the UE as a gateway device. These technologies are useful considering the fact that they have a low power consumption and offer long term reliable operational capacity. Further, LTE and WiFi have been looked as competing technologies for providing access to the devices and not as complementary technologies that could be utilized collectively to serve the purpose of providing access to the devices. Femtocells and evolved NodeBs to connect WiFi and LTE based devices have been presented in [8] but nowhere is the utility of UE as a gateway discussed. This gains even more prominence considering the fact that current UE's are capable of having parallel connections to WiFi and LTE, in addition to their capacity to communicate with the IoT devices using ZigBee, Bluetooth, and NFC technologies. This is specifically relevant in a home/office environment where the number of devices is expected to be just a handful.

Lately, the immense utility of offloading of human centric

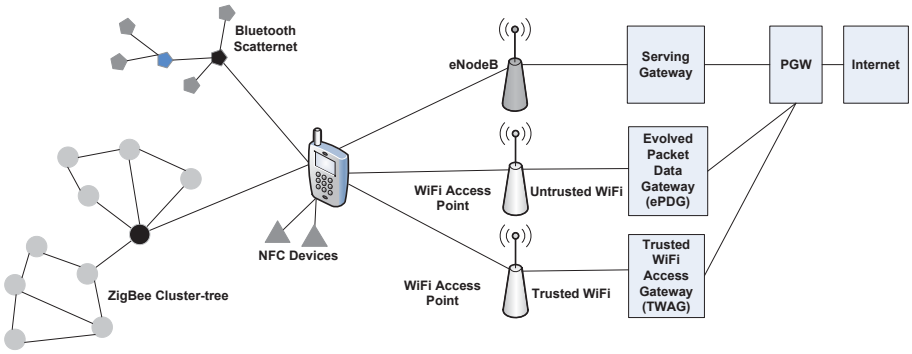

Fig. 1. System model for data transfer using the UE

excess traffic relying on device to device communication has been gaining prominence [9]. Instead of offloading human centric communication data, offloading IoT data has not been considered till date to the best of authors knowledge. This work presents a system model wherein the UE is expected to garner the data from IoT devices relying on the low power technologies and transfer it using WiFi or LTE to the Internet serving as an overall gateway device.

The communication for the devices relying on UE as a gateway should be delay tolerant and it is considered that adherence to the strict delay budget as stated say in [1] regarding guaranteed bit rate and delay budget are not necessary. It is assumed that there is just one UE through which these IoT devices can communicate their data to the Internet. As it is shown through the table the latency in establishing a connection is of the magnitude of maximum few seconds (Table I).

The rest of the paper is organized as follows. Section II presents the proposed system model for collection of data from IoT devices at the UE and transmission to the Internet, and modelling of the various states in the process as a Markov Chain are presented in Section III. Conclusions are presented in Section IV of the paper.

II. System Model

The system for collecting the data from the IoT devices, processed at the UE, and transferred to the Internet using LTE and WiFi is discussed in individual sub-sections. In the system it is considered that the data traffic from the devices is delay tolerant to a certain extent. For a device which requires strict delay budget, this system model would not be appropriate. Such a device should be enabled to transfer its data directly using LTE/WiFi chipset.

A. Bluetooth

As stated earlier Bluetooth, specifically BLE, is regarded as a key technology for IoT. The Bluetooth devices usually operate in a piconet formation wherein one of the device functions as a master and the rest function as slaves, there can be seven slaves for each master device. Additionally, piconets can be merged to work together forming a scatternet [10]. The Bluetooth devices are expected to relay their data traffic to the UE through a master device for the overall scatternet as shown in Fig. 1, master device is shown as a black pentagon, while the blue pentagon shows the device working as slave/master merging the piconets to form the scatternet. The data transferred to the UE is thus the aggregated data from all the devices in the scatternet.

B. ZigBee

ZigBee based PAN comprises of two types of devices, *i.e.*, full functional devices (FFD) and reduced-function devices (RFD). The FFD can operate as an overall coordinator for the PAN, coordinator, or just as a device [11]. ZigBee supports three topologies for operation i.e. cluster-tree, star and mesh. The IoT devices are expected to work as a cluster-tree with the elected PAN coordinator would communicating for all the nodes with the UE [12]. Zigbee is often considered as the communication base for sensor networks, therefore the Zigbee devices could be a sensor network that would communicate relying on the UE [13].

C. Near Field Communications

The NFC communication could take place between a passive tag and the UE. The UE can also communicate with another NFC enabled phone directly. The UE can read and write data on to a passive NFC tag following the NFC Data Exchange Format (NDEF). There are many variations in NDEF format data records, usually a small set of record type definitions are used [14]. The communication between the NFC tags and the UE can only take place if the distance is too short (10 cm), therefore it is assumed that data from the NFC tags would be obtained whenever the UE is in close proximity of the NFC devices.

D. UE - Data Processing

As stated earlier the UE has capabilities to connect with Bluetooth, ZigBee and NFC based devices. In addition, the

TABLE I
IOT DATA COMMUNICATION TECHNOLOGIES

	ZigBee	Bluetooth	Bluetooth Low Energy	NFC	WiFi	LTE
Data rate	250 /40 / 20 kbps	3 Mb/s	1 Mb/s	106/212/424 kbps	54 Mb/s	50 Mb/s
Network join time	30 ms	3 s	3 ms	-	-	-
Number of devices	2^{16}	8	unlimited	-	-	-
Power consumption	30 mW	100 mW	10 mW	-	-	-
Topology	Star/mesh/cluster tree	Piconet/scatternet	Piconet/scatternet	Peer to peer	-	-

UE is capable of concurrently connecting with LTE and WiFi. The data from the Bluetooth, ZigBee or NFC devices comes to the UE as a data stream with the establishment of a connection. The connection time for transferring the data from the devices to the UE is stated in the Table I. It is expected that representing device (master device in ZigBee and Bluetooth) would communicate with UE to transfer the data periodically based on the data generated by the devices that it represents. As all the technologies utilize different packet/frame formats the UE organizes the data in uniform data streams and places them in a buffer. The UE is expected to be capable of establishing connections with the IoT device leader (Bluetooth, ZigBee) or the NFC devices in round-robin manner based on the occurrence of an event/update. The connection establishment times are fairly low for the UE to communicate with the devices following such an order. The UE is expected to only serve one type of IoT devices at a given point of time, if other type of IoT devices try establishing a connection at that instant of time, they would have to reattempt the connection at a later time instant.

E. LTE Transfer

The uplink and downlink transmissions are governed by the eNodeB. The eNodeB provides the resources to each UE as time-frequency domain radio resources referred as resource blocks (RBs) [2]. The RBs span 0.5 ms, *i.e.*, half length of a sub-frame and 180 kHz (12 sub-carriers). The uplink data transmission takes place using the physical uplink shared channel (PUSCH). The possible RBs for PUSCH are provided in the downlink by physical download shared channel (PDSCH). The possible allocations permitted for future states are notified to the UE in preceding downlink channels, the RBs allocated vary for every allocation round [15]. The data if transferred through LTE is send to the eNB that forwards it to the Internet through serving and packet gateway (shown in Fig. 1).

F. WiFi Transfer

The WiFi based access point could be trusted or untrusted and that accordingly whether the connection would be access point and the evolved packet gateway or the trusted gateway. They in turn communicate with the packet gateway which in turn connects with the Internet. The transfer through WiFi would take place under two conditions, primarily, if the UE determines that the RBs needed for data transfer would be more than what is allotted by the eNodeB. This could happen if the allotted RBs would be utilized for transferring human centric traffic (voice and data). Additionally, the data transfer with WiFi is expected to be governed by policies set by the access network discovery and selection function (ANDSF) entity of the LTE core network based on the UE based quality of cellular connection and WiFi. The IP based connection is expected to migrate following mobility with IP address preservation (IPFLOW) or simultaneous IP connectivity to 3GPP and WiFi access networks (MAPCON) [16].

The benefit of relying on the UE for transferring the IoT data would be the difference in resources that would be utilized to transfer through the proposed system and alternatively with each device transmitting its data individually relying on WiFi and LTE. This should be looked into considering the fact that data from few IoT devices if communicating on their own with an end-to-end connectivity on LTE could cause severe radio congestion, involve higher power consumption, and a higher operational cost.

III. MARKOV CHAIN

The data transfer using the UE can be modelled as Markov Chain since the future state is independent of the past system instances. The overall system can be represented as a Markov Chain with four states:

- Idle state
- Processing state
- Transmission state - LTE
- Transmission state - WiFi

1) Idle State: The idle state refers to the state wherein the UE has no incoming data from the IoT device(s). However, the UE could be busy transmitting the human centric communication data. The UE would continue to check periodically for any incoming data in a round-robin manner from the IoT devices.

2) Processing State: The processing state would be the wherein UE is involved in processing the data stream received from IoT device(s). The transition from idle state to processing state would be governed by the probability (p_{ip}) of a data transmission arriving from the IoT device(s). The data to be transmitted is readied by the UE in this state and placed in a transmission buffer.

3) Transmission State - LTE: The transmission of the data from the UE to the Internet would take place preferably through LTE. The probability of transmitting the data using LTE (p_{pl}) would be governed by the conditions stated earlier in Section II-F. Once the transmission is completed the system is expected to transit back to the idle state (p_{li}) or processing state (p_{lp}) depending on the whether the UE has data ready in

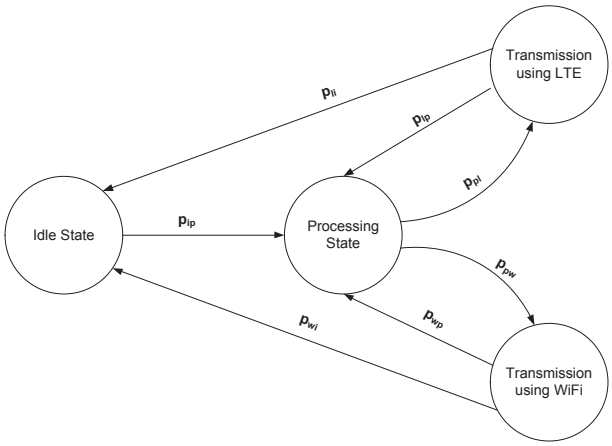

Fig. 2. Markov chain states of the UE for transferring IoT data

the buffer to upload or there will be some data available very soon, alternatively the system transits to the idle state.

4) Transmission State - WiFi: The transmission will take place using WiFi if the data could not be transmitted using LTE governed by the conditions stated earlier. The probability to transfer between the states: processing to transmit with WiFi (p_{pw}) and transmit state to processing (p_{wp}) or transmitting state to idle (p_{wi}) would be in a way similar to those concerning LTE. The actual probability states can be determined by determining the operational characteristics of the IoT devices and based on the human centric data traffic characteristics. Since, the number of IoT devices (Bluetooth, ZigBee, and NFC) in the typical home/office environment would not be many, these characteristics can be approximated fairly well. Subsequent to determining the state transition probabilities the state holding probabilities can be determined. They can be utilized to compare with system operating on end-to-end transmission done through LTE or WiFi.

IV. Conclusions

The presented system model for utilizing UE to transfer IoT data is very promising, especially considering the capacity to avoid the need of placing LTE/WiFi chipset on all devices or designing gateways for individual technologies, viz., NFC, ZigBee, and Bluetooth. The presented UE based gateway system offers additional utility for the UE utilizing functionalities that it is capable of undertaking. Additionally, with the presented system model better utility can be derived for the low power communication technologies that are well positioned for dealing with IoT traffic. Further work would involve comparing the presented system with end-to-end communication of IoT data relying on LTE/WiFi.

References

[1] J.-M. Liang, J.-J. Chen, H.-H. Cheng, and Y.-C. Tseng, "An energy-efficient sleep scheduling with qos consideration in 3gpp lte-advanced networks for internet of things," *Emerging and Selected Topics in Circuits and Systems, IEEE Journal on*, 2013.

[2] S.-Y. Lien and K.-C. Chen, "Massive access management for qos guarantees in 3gpp machine-to-machine communications," *Communications Letters, IEEE*, 2011.

[3] P. P. R. F. Giovanni Rigazzi, Nuno K. Pratas, "Aggregation and trunking of M2M traffic via D2D connections," in *Communications (ICC), 2015 IEEE International Conference on*, 2015.

[4] L. Costantino, N. Buonaccorsi, C. Cicconetti, and R. Mambrini, "Performance analysis of an lte gateway for the iot," in *World of Wireless, Mobile and Multimedia Networks (WoWMoM), 2012 IEEE International Symposium on a*, 2012.

[5] S. Aust, R. Prasad, and I. Niemegeers, "Ieee 802.11ah: Advantages in standards and further challenges for sub 1 ghz wi-fi," in *Communications (ICC), 2012 IEEE International Conference on*, 2012.

[6] Bluetooth 4.2 smarter, faster, enables iot. [Online]. Available: http://www.bluetooth.com/SiteCollectionDocuments/4-2/bluetooth4-2.aspx

[7] N. Nikaein, M. Laner, K. Zhou, P. Svoboda, D. Drajic, M. Popovic, and S. Krco, "Simple traffic modeling framework for machine type communication," in *Wireless Communication Systems (ISWCS 2013), Proceedings of the Tenth International Symposium on*, 2013.

[8] M. Condoluci, M. Dohler, G. Araniti, A. Molinaro, and K. Zheng, "Toward 5g densenets: architectural advances for effective machine-type communications over femtocells," *Communications Magazine, IEEE*, 2015.

[9] S. Andreev, A. Pyattaev, K. Johnsson, O. Galinina, and Y. Koucheryavy, "Cellular traffic offloading onto network-assisted device-to-device connections," *Communications Magazine, IEEE*, 2014.

[10] E. Georgakakis, S. Nikolidakis, D. Vergados, and C. Douligeris, "An analysis of bluetooth, zigbee and bluetooth low energy and their use in wbans," in *Wireless Mobile Communication and Healthcare*, ser. Lecture Notes of the Institute for Computer Sciences, Social Informatics and Telecommunications Engineering, J. Lin and K. Nikita, Eds. Springer Berlin Heidelberg, 2011, vol. 55, pp. 168–175.

[11] J.-S. Lee, Y.-W. Su, and C.-C. Shen, "A comparative study of wireless protocols: Bluetooth, uwb, zigbee, and wi-fi," in *Industrial Electronics Society, 2007. IECON 2007. 33rd Annual Conference of the IEEE*, 2007.

[12] S. Jung, A. Chang, and M. Gerla, "Comparisons of zigbee personal area network (pan) interconnection methods," in *Wireless Communication Systems, 2007. ISWCS 2007. 4th International Symposium on*, 2007.

[13] M. De Sanctis, C. Stallo, S. Parracino, M. Ruggieri, and R. Prasad, "Interoperability solutions between smartphones and wireless sensor networks," in *Satellite Telecommunications (ESTEL), 2012 IEEE*, 2012.

[14] R. Want, "Near field communication," *Pervasive Computing, IEEE*, 2011.

[15] S. Kumar, E. Hamed, D. Katabi, and L. Erran Li, "Lte radio analytics made easy and accessible," in *Proceedings of the 2014 ACM Conference on SIGCOMM*, 2014.

[16] D. Flore, "3gpp & unlicensed spectrum," Chairman of 3GPP TSG-RAN (Qualcomm Technologies Inc.), Tech. Rep., 2015.

THE 5TH INTERNATIONAL CONFERENCE ON WIRELESS COMMUNICATIONS, VEHICULAR TECHNOLOGY, INFORMATION THEORY, AEROSPACE & ELECTRONIC SYSTEMS (WVITAE-2015)
December 13-16, 2015, Hyderabad, India

Architectural Integration for Security in Advanced Metering Infrastructure

Priyanka D.Halle
E&TC SKNSITS,
Lonavala, India
hallepriyanka2011@gmail.com

Vandana Rohokale
E&TC SKNSITS,
Lonavala, India
Vmr.301075@gmail.com

Ramjee Prasad
CTIF, Aalborg University
Denmark
prasad@es.aau.dk

Abstract— At present, cyber security has become very significant dilemma. The worldwide security integration gives number of cyber security standards. These standards provide different digital security techniques which are developed to avoid cyber security attacks. These standards propose general outlines and accurate techniques for implementing cyber security. For Architectural integration the cyber security standards play vital role. In this paper, authors are trying to improve security by providing reliable architectural integration. Improvement in security for Advanced Metering Infrastructure (AMI) will make it more reliable and advanced. Smart grid can be defined in one sentence but AMI cannot be defined so. AMI integrates number of technologies to reach its goal. AMI is responsible for collecting all data and information from loads and consumers. Smart architectural integration is very essential for AMI. Infrastructure of AMI consists of basic steps like power generation, substation and distribution. Different attacker attacks on AMI infrastructure. By improving architecture we can make AMI more secure.

Keywords— Architectural integration, AMI, Security, Communication Standard.

I. INTRODUCTION

For Architectural integration cyber security standards play an important role. To protect the cyber infrastructure, National Cyber Security Division (NCSD) has acknowledged two important objectives: To construct and maintain a successful national cyberspace response system and to apply a cyber-risk management program for protection of critical infrastructure [1]. A security strategy should have three goals:

1. To avoid the hacker from getting access to critical data
2. To slow down the hacker enough to be caught
3. To frustrate the hacker enough to cause him or her to quit the hacking attempt

When designing a security policy, care is needed to be taken to identify precisely what you are trying to protect and while we think about the architecture for security above mentioned three security policies should be considered. Table 1 gives brief idea about standards for cyber security which is helpful for architectural integration [1]. These standards give policies for security purpose in architectural integration. Fig. 1 gives the overall idea about cyber security essential for architectural integration. This paper discusses the architectural changes occurring at both the centre and the substation control levels for security purpose [2]. AMI security has become a demanding problem now days because of its integration with the external networks, remote system, and Internet world. Today's metering infrastructure employs computer based monitoring and control operations to enable application of one network to exchange data with other application of different network. Communication protocol, network topologies, and computerization plays vital role to make the metering infrastructure advanced and it is supplementary to make a grid smarter.

Smart Grid has become a necessary requirement of the utilities and its patrons for the reason that digitization of the grid system provides important benefits like wealthy information at minor cost, greener power, greater than before efficiency etc. Metering infrastructure plays significant role in the smart grid and acts as an vital interface between utilities and its consumers. A metering network comprises a large number of different types of energy meters like advanced meters and legacy meters. To achieve the vision of smart grid, similar metering network can be integrated for exchanging the usage data and taking necessary control actions [4]. Cyber-attacks are always linked with the computer networks and communication protocols. It can easily affect the communication of AMI applications [4].Thereby it can degrade the performance. Hence by providing smart architectural integration, cyber-attacks can be removed. This paper further describes different architecture integration techniques, various communication standards for security, parameters for controlled architecture and different algorithms and methodologies.

Fig. 1 illustrates the conceptual structure of cyber security for architectural integration. CIA is nothing but confidentiality, integrity and availability and the main aim of this paper is to provide cyber security by considering improved architectural integration. At present, the transportation of the power system is becoming larger and more complex. At the same time, as the computer networks constitute a core component in the infrastructure, these information and communication components may bring more failures of operations and controls to the power system. By

TABLE1: CYBER SECURITY STANDARDS AND POLICIES PROVIDED BY THE STANDARDS

Cyber Security Standards	Policies/Services provided by the standards
ISO/IEC 27001:2013 International Organization for Standardization (ISO) and the International Electro-technical Commission (IEC).)	It specifies a management system that is intended to bring information security under explicit management control.
Standard of Good Practice	The Information security Forum (ISF) published a comprehensive list of best practices for information security.
North American Reliability Corporation (NERC)	These standards are used to secure bulk electric systems although NERC has created standards within other areas.
National Institute of Standard and Technology (NIST)	It provides computer security policy.
ISO 15408	It allows many different software applications to be integrated and tested in a secure way.
Request for Comments (RFC)	The RFC 2196 provides a general and broad overview of information security including network security.
ISA/IEC-62443 (formerly ISA-99)	It defines procedures for implementing electronically secure Industrial Automation and Control System.
Information Assurance at Small-to-Medium Enterprises (IASME)	It provides criteria and certification for small-to-medium business cyber security readiness.

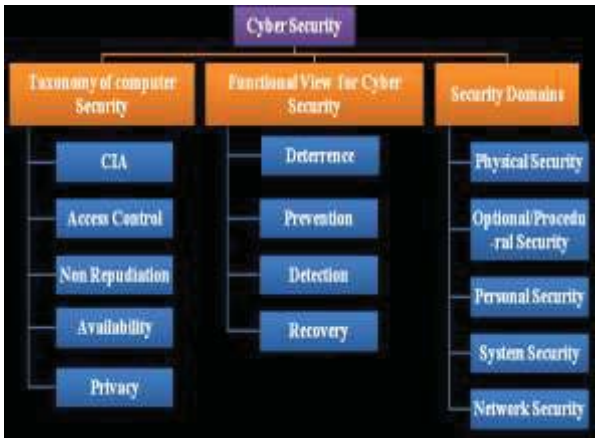

Figure 1- Cyber security for Architectural Integration

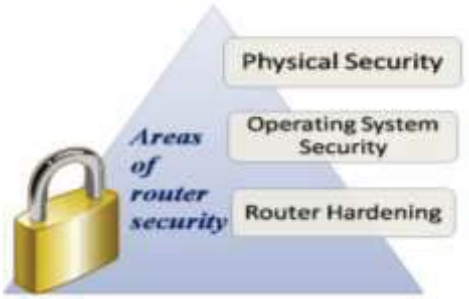

Figure 2- Areas of router Security

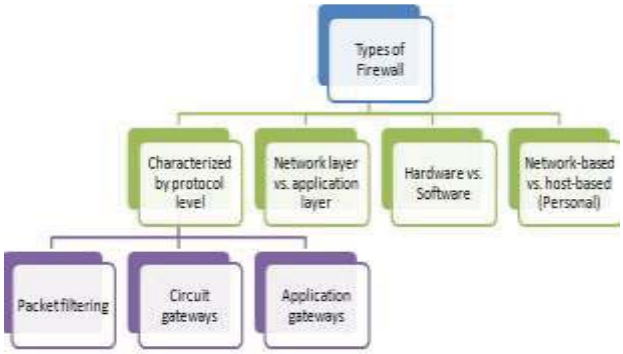

Figure3- Different types of firewall

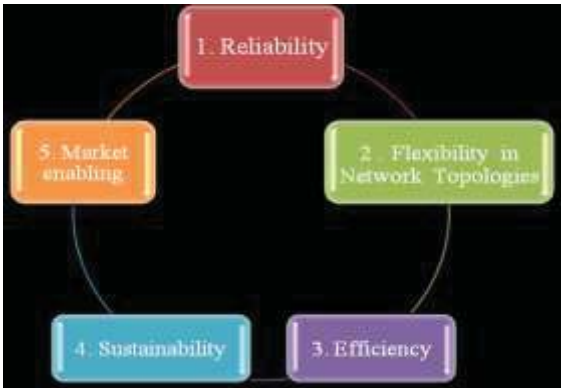

Figure 4- Features of AMI

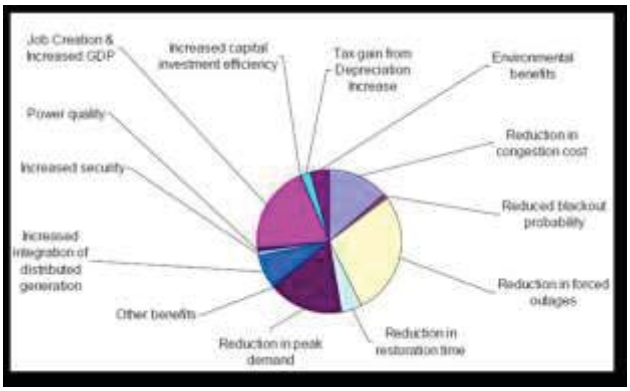

Figure 5- Breakdown of Smart Grid benefits[17]

TABLE 2: EVALUATION OF STATE OF THE ART IN TERMS OF SECURITY

Paper No.	Flow of process considered	Technology considered for integration	Communication Standards/methodology for security	Parameters for control architecture	Methodology/ Algorithm
[1]	The integration of DER (Distributed Energy Resource)	New SCADA architecture	IEC communication Standards and IEC/NIST	Medium Voltage regulation	State Estimator function, algorithm is based on an AC Optimal Power Flow
[2]	Substation	Microprocessor-based Intelligent Electronic Devices and standardized protocol and TCP/IP over wide area networks	Firewalls, cryptography schemes	provide a remote configuration change and control with default passwords	Optimal Power Flow (OPF) algorithm
[3]	Energy distribution (customer user interface)	Key distribution server (KDS)	Digital Signature, Encryption/Decryption, Key Management, Message Digest, Station-to-Station Protocol	Network services, AMI network, devices like meter, gateway, and lED, communication channel	Diffie-Hellman algorithm
[4]	Generation ,substation and distribution	Attack Modeling and Security Evaluation Component (AMSEC), Attack Graph Generator Manager of Service Dependencies	Personal firewalls, and host-based vulnerability scanners	Security policy, fixed events and alerts; possibility of estimating the influence of configuration and policy data on the security level	Attack Modeling and Security Evaluation Framework, real time algorithms
[6]	Power networks	FDI approach, FDI framework	FDI filter	Automatic Generation Control signal	Model based fault detection and isolation (FDI) method
[7]	Substation	Network-based cyber intrusion detection system (NIDS)	IEC 61850, e.g., Generic Object Oriented Substation Event (GOOSE) and Sampled Value (SV)	Monitors anomalies and malicious activities of multicast messages, Cyber physical security	Specification-based detection algorithms, IDS algorithms, network-based anomaly detection algorithm
[8]	Substation, Generator and Transmission lines	A forced outage rate (FOR) Model, SCADA system, (AAWP) model and worm spreading detection model	Worm spreading model, , Monte Carlo simulation methodology	Power system reliability, loss of load probability	Anomaly inference algorithm

initiation of malicious cyber-attacks, cascading failures may be triggered from the control system in the substation, thus components in the power system can be de-energized and operation can be irritated. Cyber attacks may hamper the tripping of a breaker or even shut down the generator. The security of the power system is dependent on its ability to resist the cyber attacks targeting the generator and transmission lines [8]. Also cyber security depends upon the architectural integration. Therefore in this paper, authors are trying to provide more reliable and secure AMI by providing different architectural integration.

II. STATE OF THE ART

The architectural solution of the Attack Modelling and Security Evaluation Component is discussed in details here. There is a variety of literature, which considers different approaches for attack modelling and security evaluation taking into account various classes of attacks. We briefly analyse current state-of-the-art with respect to flow of process considered, technology considered for integration, communication standards, parameters for control architecture and different methodologies or algorithms which are shown in Table 2 [5]. Routers, Firewalls and DMZ (demilitarized zone) Hosts provide security to the entire network by configuring policies. Router is a very essential device in networking. The Architectural integration should try to provide security to the router. Areas of router security as shown in fig. 2.

Firewall provides secure connectivity between networks. It is used to implement and insist on a security policy for communication between networks. Fig. 3 depicts various types of firewalls.

Different firewalls help to provide security. Table 2 gives state of the art for cyber security for AMI with architectural integration.

There is lot of literature which has considered different architectural integration for security purpose in power grid. Table 2 gives overall idea about architectural integration, some researchers have considered substation process, and some of them have considered generation and distribution. Still entire smart grid or AMI infrastructure consideration for security purpose is missing**.** Power Generation, Distribution and Harvesting where smart systems convert energy from different sources to electricity, store and distribute it to the users. Energy harvesting usually refers to the process by which energy is derived from external sources, captured and stored for small, autonomous devices at a low scale. Sensor-based systems for control of wind turbines and portable, multipurpose energy harvesting bracelets are just some examples of this increasingly studied field in the today's efforts aimed at lowering the carbon footprint [9].

III. FUTURE SCOPE

From the literature survey it is clear that, at present, there is a big issue of cyber security. In this paper authors are trying to improve security in different processes of smart grid basically for AMI. There are different processes in smart grid like generation, transmission, substation or distribution substation. By considering following benefits researchers should try to improve security:

1. More efficient transmission of electricity.
2. Quicker restoration of electricity after power disturbances.
3. Reduced operations and management costs for utilities.
4. Reduced peak demand, which will also help lower electricity rates.

Fig. 4 gives features of AMI; these features should be taken into account by researchers. The number of researcher have worked on architectural integration for AMI but still no any full proof security in terms of confidentiality, integrity, availability, accountability has come up. Therefore in future the researchers have lot of scope in this field to do research in terms of security.

The researchers should consider risk analysis (identify threats, assess threat's impact and likelihood), risk treatment (compute threat prevention, detection and mitigation actions) and risk monitoring (evaluate risk evolution over time) [10]. For security purpose one of the researchers has considered the principle of false data injection and proposed two distributed detect algorithms. One is DOID (Distributed Observable Island Detection algorithm), which is based on observable islands theory. If a line connected by two nodes is passed through different observable islands, false data injection is detected in this line. The other algorithm is DTAD (Distributed Time Approaching Detection algorithm). For one measuring point, if the state estimation values vary a lot, then attack is detected [11].

Some papers discuss challenges in assuring the trustworthiness (performance, dependability, and security) of the rising smart grid, using example of research started at the DOE and HHS-funded Trustworthy Cyber Infrastructure for the Power Grid (TCIPG) Centre. The objective of TCIPG is to provide trustworthiness in the nation's electric grid cyber infrastructure such that it continues to transport electricity and maintain significant operations even in the presence of cyber attacks. Achieving this objective will involve the extension, integration, design, and development of IT technologies swallowed with key properties of real-time availability and security. This research area provides many opportunities for dependability analysts and engineers to apply and extend their work [12]. Fig. 5 shows breakdown of smart grid benefits.

From the Fig. 5 it is clear that, increased security portion is very small and due to this reason, cyber security becomes essential issue nowadays. Therefore researchers can do lot of work in this field by considering different architectural integration. Some researchers have worked on the dependability issue of control centre networks in Smart Grid. There have been several works in the fields of smart grid security and dependability analysis [13]. Cyber- physical

energy systems is a hot research topic, and this is not likely to change in the near future. Still, there are white spots in this domain, especially in scalability, analytic description, and numeric handling of the used models. This collection of research papers shall serve as a help for researchers on their way in mastering these important but complicated systems [14].

Compliance, Risk Assessment and Security Testing Improvement Profiling CRSTIP as a dissemination tool for RASEN technologies, as it allows identifying maturity levels with respect to key security and compliance areas. Ideally, a concise description for each of the key areas should be available that denote the techniques and tools that can be used to drive the improvement as well as the requirements to other key areas that are the precondition to improve from one level to the next. As future work, our desire is to provide a web-based implementation where users are able to fill in their assessment and obtain information regarding the requirements for moving to the next level in their areas of interest [15].

To achieve cyber situation awareness, the role of human cyber analysts should be considered explicitly important into the design of security tools, algorithm, and techniques, such as attack graph [16]. Therefore, based on existing theories of situation awareness, a cyber situation Awareness (SA) model and an embedded SKRM (Situation Knowledge Reference Model) model are constructed to enhance the coupling of current techniques for situation awareness to enable security analyst's effective analysis of complex cyber-security problems. Current and future work is to demonstrate the potential capabilities of SKRM model for enabling cyber situation awareness.

REFERENCES

[1] "DHS National cyber security Division", DHS government 2010-10-03 Retrieved 2012-05- 12.

[2] Giovanna Dondossola , Fabrizio Garrone, Gianluigi Proserpio , CarloTornelli , " Impact Of DER Integration On The Cyber Security Of SCADA Systems –The MediumVoltage Regulation Case Study", CIRED Workshop – Lisbon 29-30 May 2012.

[3] Junho Hong, Alexandru Stefanovy, Chen-Ching Liu_y, Manimaran Govindarasuz, " Cyber-Physical Security in a Substation", 2012 IEEE Trans.

[4] Mini S. Thomas, Senior Member, IEEE, Ikbal Ali, Senior Member, IEEE, and Nitin Gupta, " A Secure Way of Exchanging the Secret Keys in Advanced Metering Infrastructure", 2012 IEEE Trans.

[5] Igor Kotenko and Andrey Chechulin, " Common Framework for Attack Modeling and Security Evaluation in SIEM Systems", 2012 IEEE International Conference on Green Computing and Communications, Conference on Internet of Things, and Conference on Cyber, Physical and Social Computing.

[6] Erasmia Evangelia Tiniou, Peyman Mohajerin Esfahani, and John Lygeros, "Fault detection with discrete-time measurements: An application for the cyber security of power networks", 52nd IEEE Conference on Decision and Control December 10-13, 2013. Florence, Italy.

[7] Junho Hong, Chen-Ching Liu, "Detection of Cyber Intrusions Using Network-Based Multicast Messages for Substation Automation", 2014 IEEE Trans.

[8] Yichi Zhang, Lingfeng Wang, Weiqing Sun, " Reliability Evaluation of Power Grids Considering Worm Spreading Pattern in SCADA", 2013 IEEE Trans.

[9] Marco Crepaldi ,Michelangelo Grosso ,Alessandro Sassone, Stefano Gallinaro, Salvatore Rinaudo,Massimo Poncino, Enrico Macii, and Danilo Demarchi, " A Top-Down Constraint-Driven Methodology for Smart System Design", 2014IEEE I, first QUART ER 2014, IEEE circuits and systems magazine.

[10] Henrik Sandberg, Saurabh Amin and Karl Henrik Johanss, " Cyber physical Security in Networked Control Systems", IEEE Control Systems Magazine , Februwary 2015.

[11] Yun Liu, Lei Yan, Jian-wei Ren, Dan Su, " Research on Efficient Detection Methods for False Data Injection in Smart Grid", 2014 IEEE Trans.

[12] William H. Sanders, "Keynote Talk Assuring the Trustworthiness of the Smarter Electric Grid",IEEE Trans.

[13] Ming Xiang, Sotharith Tauch and William Liu, " Dependability and Resource Optimation Analysis for Smart Grid Communication Networks", 2014 IEEE Fourth International Conference on Big Data and Cloud Computing.

[14] Edmund Widl, Peter Palensky, Pierluigi Siano, Christian Rehtanz, " Guest Editorial Modeling, Simulation, and Application of Cyber-Physical Energy Systems", IEEE Trans. On Industrial Infomatics, VOL. 10, NO. 4, November 2014.

[15] Arthur-Jozsef Molnar, J¨urgen Großmann, " CRSTIP - An Assessment Scheme for Security Assessment Processes", 2014 IEEE International Symposium on Software Reliability Engineering Workshops.

[16] Xiaoyan Sun, Jun Dai, Peng Liu, " SKRM: Where Security Techniques Talk to Each Other",2013 IEEE Trans.

[17] www.ieeexplore.com,Wikipedia.org.

THE 5TH INTERNATIONAL CONFERENCE ON WIRELESS COMMUNICATIONS, VEHICULAR TECHNOLOGY, INFORMATION THEORY, AEROSPACE & ELECTRONIC SYSTEMS (WVITAE-2015)
December 13-16, 2015, Hyderabad, India

Cognitive Framework for Flexible Queuing Strategy in Next Generation Networks

Sri Hanuma Chitti*, Neeli R. Prasad*, Knut Øvsthus†, and Ramjee Prasad*
*Center for TeleInfrastructure, Aalborg University, Aalborg, Denmark
Email: {shc, np, prasad}@es.aau.dk
†Faculty of Engineering, Bergen University College, Bergen, Norway
Email: knut.ovsthus@hib.no

***Abstract*—Adaptive and intelligent concepts are being employed in the networks to handle increasing dynamic traffic. Incorporation of Cognitive functionality in network nodes is one of the emerging techniques. This paper proposes a cognitive framework for next generation networks to enable flexibility in order to handle the traffic in dynamic manner. The framework is applied to the drop-tail queuing algorithm strategy which is the simplest queuing mechanism for efficient link utilization and congestion avoidance. Additional improvements that transform the networks to be flexible and scalable are presented. The results of the proposed method are compared with drop-tail algorithm in the context of packet loss, queuing time, and queue length. The results promise optimized and flexible operation by reducing up to 60% packet loss and queuing time while solving the problem of buffer-bloat. In addition, the possibilities of extending the proposed framework with target parameters such as energy efficiency, stability, and cost efficiency are discussed.**

***Index Terms*—Cognitive algorithms, queuing strategies, data analytics, next generation networks**

I. INTRODUCTION

THE growth in number of mobile devices is at a rapid pace in the recent years. This growth is assisted by a number of innovative applications that are incorporated in mobile devices. Together with the increase in number of devices and usage scenarios, the mobile internet traffic is ever growing [1]. In the context of increase and variety in mobile traffic, the demands from heterogeneous applications are increasingly stringent. For instance, the rise in services like online gaming and video streaming demands low packet loss. Consequently, providing better quality of service (QoS) to users with effective congestion avoidance mechanisms has been the primary objective for the operators.

Together with the provisioning of QoS and Quality of Experience (QoE) to users, customer differentiation is another important objective for the operators. New business models are evolving on the basis of customer and service differentiation to generate additional revenue for the operators [3]. It is wiser in the operator's point of view to investigate intelligent approaches to gauge traffic dynamics. Time is one of the important parameter to gauge user expectation on a particular service delivery. As all the subscribers are not very active all the time, it is observable to see the separation in peak traffic for different services at different time instances.

Cognitive functionality is one of the emerging approaches in making the radio networks flexible and self-reliant [4]. In the process of developing futuristic network architectures, the concept of cognitive framework was presented in this paper. It is applied to the context of queuing strategies which are designed to handle the congestion in network elements. Congestion is a major problem in next generation networks and is a result of converging services like data, voice, multimedia, etc. [2]. A number of algorithms like Drop-tail, Random Early Detection (RED), RED with In and Out (RIO) were proposed in the past to avoid congestion but very few of them like Drop-tail and weighted RED (WRED) are successful to make their way into the network elements because of their simple yet effective approaches [2], [10]-[12].

The application of proposed framework differentiates itself from all of the existing queuing strategies by reconfiguring the queuing parameters dynamically depending on the operator requirements. In the existing approaches, the queuing parameters are fixed during the initial configuration of the device. Some adaptive algorithms calculate the queuing parameters based on the incoming traffic which incurs additional computational complexity. By using the cognitive cycle, the proposed framework simplifies the process of parameter estimation and further reducing the computational complexity within the network elements.

The paper is distributed as follows: Section II summarizes the background of cognitive framework and related work in the area of queuing algorithms. The framework have been proposed and described in Section III and flexible queuing concept based on proposed framework is presented in Section IV. Simulation and evaluation results are discussed in Section V. Extension of the model is described in Section VI and conclusion is presented in Section VII.

II. BACKGROUND

Cognitive functionality has been addressed in research works for the primary objective of increase in usage efficiency with prior knowledge on the surroundings. The cognitive cycle can be divided in three parts: cognitive learning, decision making, and enforcing action. The cognitive learning phase involves the process of acquiring knowledge by sensing or other methods. The decision making phase includes analysis of the knowledge acquired to draw the decisions. In the last phase, the decisions are implemented in the system with the

corresponding methods. The phases mentioned above are basic building blocks of cognitive cycle since its inception [4].

The utilization of scarce resources like frequency spectrum is in the forefront in employing cognitive functionality. It has been applied to many areas in the communication link namely spectrum sharing, power control, relaying etc [4]. In this paper, cognitive functionality is applied to active queue management (AQM) algorithms. The motives behind queue management algorithms are to reduce the packet loss, queuing time, and improve link utilization. There was a lot of research and proposals in the field of AQM algorithms which is briefed in the following. The algorithms have been divided under two categories:

- *Adaptive parameter tuning:* Many of the first generation AQM schemes were static with fixed thresholds to control the queuing operations. The traditional drop-tail algorithm has evolved by employing fuzzy and adaptive techniques in defining the buffer lengths [2]. Another method, RED is the basis for many of its variants like adaptive random early detection (ARED), weighted random early detection (WRED) and so on. RED is based on dropping the packets before the buffer is full. The packet drop probability is calculated adaptively based on factors like queue length, flow differentiation etc. Algorithms like drop-tail are very simple in operation by dropping all the incoming packets when the buffer space is full [13], [14].

  The above mentioned algorithms are designed to optimize some of the performance parameters. At the same time, the complexity of implementation increases with the optimization of performance parameters. The higher complexity limits the real time implementation as it involves higher computation power and thereby power consumption.

- *Adaptive sizing algorithms:* Some algorithms are focused on changing the buffer size in an adaptive way [5], [9]. They are developed mainly to find the minimum buffer size for parameter optimization. The constraints for the optimization are calculated based on real time measurements. The computational complexity is different for several buffer sizing algorithms but have superior complexity when compared to simple algorithms like drop-tail. They also have the complexity of changing the physical memory segments.

III. PROPOSED FRAMEWORK

As mentioned earlier, the non-uniform dynamic nature of the peak traffic has been the motivation in developing the proposed framework. The proposed cognitive framework can be divided in three parts: cognitive analytics, cognitive engine, and reconfiguration. They can be attributed to the phases of the cognitive cycle: cognitive learning, decision making, and enforcing action respectively.

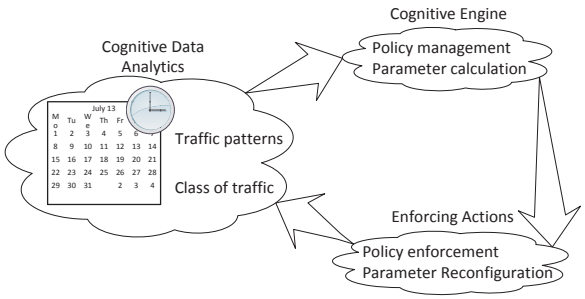

Figure 1. Phases in the proposed cognitive framework

a. *Cognitive data analytics*

In the context of the proposed framework, cognitive analytics is a database which contains the information about user traffic with reference to time axis. The traffic information may include the number of sources based on their priority, type of the traffic, service delivery information, and so on. Cognitive data analytics can provide the data about the time intervals of traffic load for a particular class type. It can be updated at a changeable rate that can be controlled remotely.

b. *Cognitive Engine*

The cognitive engine is a decision making entity which does the calculation of parameters based on the data from cognitive analytics. It analyses the data obtained from the database of cognitive analytics and compute the parameters for the particular node. The computations by cognitive engine are against the required performance parameters that are set by the operator. The cognitive engine is capable of working autonomously in addition to having operator controllability. After computing the required calculations, the cognitive engine sends the data to the corresponding network node.

The location of the cognitive engine is of operator's interest. It can be operated from a centralized hardware or from the cloud. It is also possible to integrate the cognitive engine in individual nodes. In integrated scenario, the cognitive analytics database has to be accessible from the cloud. The number of nodes under single cognitive engine is scalable depending on the computational and connection capabilities of it.

c. *Enforcement of Actions*

The individual network nodes implement the actions defined by the cognitive engine. This kind of enforcement involves, changing the parameters, configuring the buffers, allowing the modules in sleep mode etc. To perform the required actions, the nodes should have the capability of self-configuration. Each of the individual nodes which are implementing the actions may feedback to the cognitive engine and/or cognitive analytics database.

IV. FLEXIBLE QUEUING

In the context of the communication network infrastructure, the cognitive framework is applied to AQM algorithms. A new method of simple queuing strategy, flexible queuing is presented in this section. The flexible queuing strategy works on the principle of cognitive cycle, which was described

earlier. The phases in the framework are mapped to the process of queue management.

a. *Cognitive Learning*

As described in the cognitive data analytics phase of the framework, the learning phase collects the information about the rate of traffic flow with respective to time scale. As mentioned earlier, in real time, not all sources are active at the same time. So, to exploit that separation in the rate of traffic, the traffic is classified in time scale. The cognitive analytics database which was used to validate the framework is shown in the following table.

TABLE I
TRAFFIC LOAD IN DIFFERENT TIME SLOTS

	0-30s (t1)	30-60s (t2)	60-90s (t3)
host1	ON	ON	ON
host2	ON	ON	ON
host3	OFF	OFF	ON
host4	OFF	OFF	ON

The traffic from 4 different sources which have equal priority has been categorized in different time slots, as shown in Table 1. The priority can be different depending on the QoS metrics. For example, real time traffic with latency and packet drop rate constraints may benefit in the presence of non-real time traffic. The case of equal priority has been considered to highlight the benefits of flexible queuing. The time scale in this context is taken as *90s,* which is the simulation time. *Host1* and *host2* are scheduled to send the data in all of the 3 mentioned time slots (*t1, t2,* and *t3*) whereas *host3* and *host4* are scheduled to start sending the data only in the third time slot (*t3*). The duration of the time slots varies as per the need and requirements of the operators. The frequency of cognitive analytics database update is configurable by the cognitive engine. In this context, it updates at the beginning of the simulation as the traffic information is known beforehand. It is also possible to have reservations from the users for particular time slots. The advanced level of differentiation like type of traffic, information on service and customer differentiation can be developed within the cognitive analytics database.

b. *Decision Making*

Being the decision making entity, the cognitive engine implements the algorithms and in this context a flexible queuing method. The corresponding flow chart is presented in Figure 2.

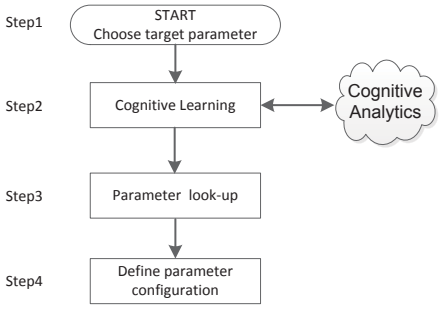

Figure 2. Flowchart of cognitive engine

The target performance parameters for this study are queuing time and packet loss. The queuing time in this context is the time for a packet to pass through the queue in a particular network element. The queuing time is one of the significant contributors to the round trip time. The delays in the network should be minimal to support the interactive multimedia content and other such data services from next generation user devices. The network node drops a packet based on some predefined conditions depending on a particular queuing strategy. In the current context, the packet will be dropped when the available queue length is null. Optimization of packet loss is important to avoid TCP global synchronization problems [6]. Majority of the internet traffic is of transmission control protocol (TCP) type and better handling of such traffic saves the network from serious issues like global synchronization, high packet losses, and high queuing delays [4].

To establish the operation of proposed framework, queuing time is optimized in *t1* and *t2* whereas packet loss is optimized in *t3*. So, the framework optimizes queue length parameter by decreasing or increasing it to improve queuing time or packet loss respectively. With the mentioned parameters, the method operates as follows when a packet arrives.

Step1: queuing time during low traffic from *host1* and *host2*; packet drop for high traffic from *host3* and *host4.*

Step2: cognitive engine acquires the information about data traffic from cognitive analytics. From Table I, it is expected that low traffic from *host1* and *host2* is up to *t2* and host3 and host4 starts sending traffic in *t3* resulting high traffic.

Step3: the cognitive engine read the current queue length parameter (q_{len}) of the node, threshold queue length (q_{thr}) and maximum queue length (q_{max}) which are defined during initial configuration.

Step4: if the threshold queue length (q_{thr}) is smaller than q_{len}, the queue size should be q_{thr} for the duration until *t3*. Otherwise, the q_{len} is maintained as queue size for the same duration. The queue size should be configured as q_{max} from *t3* to reduce the packet loss.

c. *Reconfiguration of parameters*

The new parameters defined by cognitive engine are reconfigured in the nodes either by the nodes or the cognitive engine. In this context of the simulation scenario, the cognitive engine reconfigures the necessary parameters in the nodes. In real time, the nodes should have the capability of self-configuration to enforce the actions themselvesfigures.

V. SIMULATION AND RESULTS

The simulation setup is in OMNET++ environment [7] with 4 hosts and 4 destinations connected through a bottleneck link is shown in Figure 3 and parameters are provided in the following table:

Table II			
Simulation Parameters			
q_{max}	20	*a*	100 Mbps
q_{thr}	10	*b*	1 Mbps
Simtime_tot	90s	*mss*	1000B

The setup generates TCP traffic from the hosts. The hosts employ TCP Reno algorithm in generation of the traffic with no sack support and no delayed ACK support. The simulation time is set as *90s* and the hosts send the traffic as mentioned in Table 1, where the *green* indicates ON state and *red* indicates OFF state. Each of *host1* and *host2* is scheduled to send *1000MB* of data whereas *host3* and *host4* are scheduled to send *500MB* with the maximum segment size as 1000B.

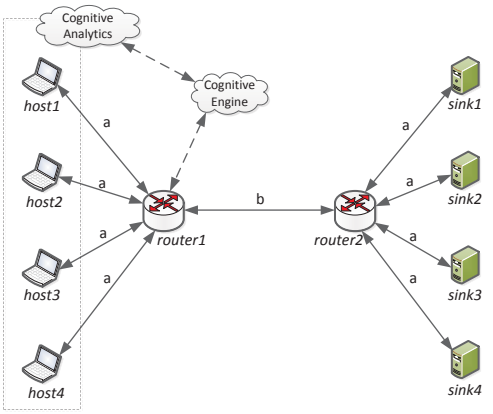

Figure 3. Simulation setup

The hosts send the traffic to corresponding sink nodes like *host1↔sink1, host2↔sink2* and so on. The end nodes are connected by a bottleneck link between *router1* and *router2* as shown in Figure 3. The data rate of *a* links is of 100 Mbps and 1 Mbps for *b* link with 10ms delay.

Drop-tail algorithm is used to collect the results for the cognitive framework setup. Drop-tail is widely considered as simple algorithm with lowest complexity but suffers from high packet drops. By applying cognitive framework in that context, the packet drops can be controlled by selecting appropriate queue size in different time instants.

The cognitive engine configures the *router1* with appropriate queue length based on the simulation time. When $0 \leq simtime_t < 60$, the parameter *pktdroprate* = FALSE and *queuetime* = TRUE. When $simtime_t \geq 60$, the parameter *pktdroprate* = TRUE and *queuetime* = FALSE. The queue parameters are $q_{max} = 20$, $q_{thr} = 10$, and $q_{len} = 20$. To establish the philosophy of flexible queuing, static thresholds are considered for queue lengths. It is up to the Operator to design the strategy with dynamic thresholds which is our future direction of research.

The results for queue length, queuing time, packet drops are compared with the cases of with and without cognition. The plots are downscaled by using exponential moving average with the scaling factor $\alpha = 0.01$ for queuing time comparison, $\alpha = 0.005$ for queue length comparison. By applying the exponential moving average, more weights are given to the recent samples. The moving average is applied to improve the visibility compared to raw plots generated within OMNET++ simulator.

a. Queue Length

The plot in Figure 4 shows the averaged queue length in number of packets corresponding to the simulation time for the drop-tail algorithm with two cases (for the queue size of 10 and 20) and flexible queuing method. In the flexible queuing method, the queue length is configured by the cognitive engine based on the simulation time.

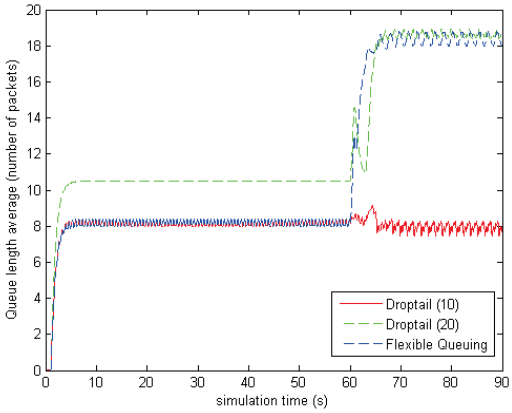

Figure 4. Comparison of queue length variation

In this simulation, the cognitive engine configures the queue size to q_{thr} until *60s* and q_{max} after 60sec to accommodate the traffic from additional hosts. By reducing the q_{len} until *t3 (60s),* it is possible to save some buffer space which can be used for other additional purposes like to store special-type packets and speed-up the system.

b. Packet loss

The packet loss for different methods is presented with a bar chart in Figure 6. As it is mentioned the shorter queue method suffers with high packet loss. With the current schedule of the data transmission, by doubling the queue size, almost 75% of the packet drops can be avoided. By employing flexible queuing, the overall packet loss can be lowered to 40% and at the same time saving the buffer space that can be used for other purposes within the system. So, the proposed method is suitable for avoiding packet loss to reduce retransmissions and TCP synchronization issues with optimal buffer adjustment mechanism.

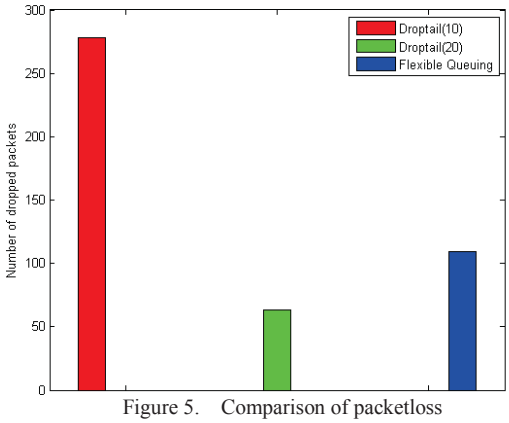

Figure 5. Comparison of packetloss

c. Queuing time

The queuing time is proportional to the queue length. By reducing the buffer length until t3, the queuing time is

optimized. As the *queuetime* parameter is set to *1*, the queue length is set to q_{thr} which reduces the queuing time. It is clear that by employing the flexible queuing method, the *queuetime* is optimized for the required duration as shown in Figure 7. The queuing time for the smaller buffer method is on the lower side of the remaining two methods throughout the simulation time but it suffers higher packet drops.

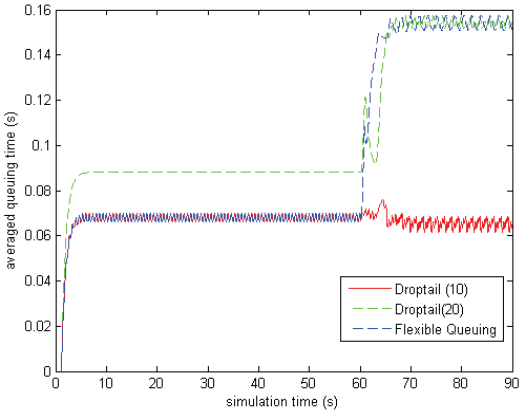

Figure 6. Comparison of queuing time variation

VI. EXTENSION AND FUTURE SCOPE

The cognitive framework is applicable to overall network infrastructure to achieve many objectives like energy efficiency, network stability, cost efficiency and much more. The framework can be extended to improve the energy efficiency of the network element by setting up several components into sleep mode. In that context, the cognitive engine takes up the additional responsibility of controlling sleep periods according to the data traffic. By the same token, network stability and other target parameters can be optimized. In addition to applicability, the location of cognitive engine is an area of research.

Our future work includes investigation of efficient utilization of buffer space in the context of dynamic queue length adjustment. It is much more important when the traffic involves multiple classes of service. The framework is extendable for longer duration of time with advanced functionalities like multiple class of service (CoS), service differentiation, and so on.

VII. CONCLUSION

The cognitive framework is expected to play an important role in automating the networks in the way of realizing flexible, scalable and intelligent networks. The cognitive framework has a number of advantages in terms of costs, operability, service differentiation, and so on. The framework is applied to queuing algorithms for validation. It proves to be a simple framework to deploy with many benefits. The advantages include reduction in packet loss rate, queuing time, throughput, and at the same time promising flexibility to optimize a particular parameter in a particular time. From the observation of the results, the proposed strategy, with intelligent design, benefits real time traffic to a great extent which has constraints on delay and other issues.

The proposed framework plays an important role in the process of instilling self-organization capability in the nodes. To implement the facilities like customer differentiation and service differentiation, traffic engineering on the basis of time scale is the enabling factor. So, the availability of time based traffic dynamics is the key issue for the success of the framework.

ACKNOWLEDGMENT

The authors would like to acknowledge fruitful discussions with Ceragon Networks, Bergen, Norway in defining the system model.

REFERENCES

[1] Cisco Systems, “Cisco Visual Networking Index: Global Mobile Data Traffic Forecast Update, 2011-2016.” Cisco Systems, February 2012

[2] Adams, R., "Active Queue Management: A Survey," *IEEE Communications Surveys & Tutorials,* vol.15, no.3, pp. 1425-1476, October2012
doi: 10.1109/SURV.2012.082212.00018

[3] Lott, M.; Karppinen, J.; Kross, J., "Service differentiation for enhanced consumer experiences," *Proceedings of* 15th *International Conference on Intelligence in Next Generation Networks (ICIN)*, pp.58-63, October 2011

[4] Wang, B.; Liu, K.J.R., "Advances in cognitive radio networks: A survey," *IEEE Journal of Selected Topics in Signal Processing*, vol.5, no.1,pp.5-23,February2011
doi: 10.1109/JSTSP.2010.2093210

[5] Zhang, Y.; Loguinov, D., "ABS: Adaptive Buffer Sizing for Heterogeneous Networks," *Proceedings of 16th International Workshop on Quality of Service (IWQoS 2008)*, pp.90-99, 2-4 June 2008

[6] L. Kleinrock, "The Latency/Bandwidth Tradeoff in Gigabit Networks," *IEEE Communications Magazine*, vol. 30, no. 4, pp. 36–40, April 1992.

[7] Varga, A., “OMNeT++ User Manual”, ver 4.2.2, 2011

[8] Nakauchi, K.; et. al., "Virtual cognitive base station: Enhancing software-based virtual router architecture with cognitive radio," *Proceedings of 2012 International Conference on Communications (ICC 2012),*pp.2827-2832,June2012.
doi: 10.1109/ICC.2012.6364496

[9] Vishwanath, A.; Sivaraman, V.; and Thottan, M; “Perspectives on router buffer sizing: recent results and open problems,” *Proceedings of SIGCOMM Computer Communications vol.* 39, no. 2, pp.34-39, March 2009

[10] Floyd, S.; Jacobson, V., "Random early detection gateways for congestion avoidance," *IEEE/ACM Transactions on Networking,* vol.1, no.4, pp.397-413, August 1993. doi: 10.1109/90.251892

[11] Seungwan Ryu; Rump, C.; Chunming Qiao, "Advances in internet congestion control," *IEEE Communications Surveys & Tutorials,* vol.5, no.1,pp.28-39, Third Quarter 2003. doi: 10.1109/COMST.2003.5342228

[12] Chatranon, G.; Labrador, M.A.; and Banerjee, S; “A survey of TCP friendly router-based AQM schemes,” *Computer Communications*, vol. 27, no. 15, pp. 1424–1440, 2004.

[13] Arpaci, M; and Copeland, J.; “An adaptive queue management method for congestion avoidance in TCP/IP networks,” in *Proceedings of the IEEE Global Telecommunications Conference (Globecom ’00)*, vol. 1, San Francisco, CA, USA, 2000, pp. 309–15.

[14] S. Floyd, R. Gummadi, and S. Shenker, “Adaptive RED: An algorithm for increasing the robustness of RED,” 2001.Available: citeseer.ist.psu.edu/floyd01adaptive.htm

THE 5TH INTERNATIONAL CONFERENCE ON WIRELESS COMMUNICATIONS, VEHICULAR TECHNOLOGY, INFORMATION THEORY, AEROSPACE & ELECTRONIC SYSTEMS (WVITAE-2015)
December 13-16, 2015, Hyderabad, India

Design of BiCMOS based low temperature coefficient bandgap reference

Deepa Talewad, Anilkumar Nandi, Ramesh Karmungi
Student, B.V.B College of Engineering and Technology, Hubli, India, ditalewad@gmail.com
Professor, B.V.B College of Engineering and Technology, Hubli, India, anilnandy@bvb.edu
Manager in Analog domain, SmartPlay Technologies, Bangalore,India, ramesh.karmungi@smartplayin.com

***Abstract*—BiCMOS bandgap reference which having advantage over MOS based BGR in terms of its accuracy at its reference output and very less temperature coefficient. This paper presents bandgap reference circuit with folded cascode operational amplifier(opamp) in order to improve the final Vref output of bandgap reference. The temperature stability of output can be improved by using an extra trimming circuit in voltage mode architecture of bandgap reference still operating with less power consumption. Using only first order temperature compensation technique the proposed circuit gives output voltage of 1.181V with 0 °C to 100 °C temperature variation which corresponds to temperature coefficient of 19ppm/ °C.A single stage folded cascode opamp which is included in the proposed bandgap which improves power supply rejection ratio of BGR and input common mode range, output swing and stability at opamp and BGR output. The simulation results shows that power supply rejection ratio of proposed BGR is -43db from dc to 30KHz frequency, gain of folded opamp is 78db,Phase margin is 70, input offset of opamp is 1.96μV and closed loop gain of opamp in BGR is 118db.The proposed bandgap reference is simulated using MentorGraphics pyxis tool, EldoSpice simulator in 130nm CMOS technology. The proposed BGR output will be used in low dropout regulator circuit which is operating at 3.3 supply and gives regulated output of 1.8V.**

***Index Terms*—Voltage mode architecture, PSRR, Temperature coefficient, PTAT, CTAT voltage, trimming.**

I. Introduction

A stable high performance bandgap reference circuit plays vital role in the high performance circuits like ADC, DAC, LDO, Charge pump circuit. A voltage reference must be highly precise and stable with respect to temperature, supply, process and load variations. High power supply noise rejection ratio (PSRR) of LDOs which merits the noise immunity, since high PSRR of LDOs mostly depends on PSRR of voltage reference [1]. This paper presents design of BiCMOS based voltage reference with good PSRR and low temperature coefficient(TC) which is most important in terms of accuracy of system [3]. A Brokaw CMOS bandgap reference presented by Yongsheng Yin [6], using current mode architecture which gives Vref of 0.5V and better PSRR but drawback of circuit is Vref output is very sensitive with respect to temperature because of sensitivity of resistor at the output and power dissipation in terms of mill volts. This paper presents CMOS bandgap reference with voltage mode architecture with trimming circuit in order to get low temperature coefficient with better PSRR and also start up problem in the conventional bandgap reference (BGR) is avoided using simple startup for proper operation of circuit. The proposed BGR uses PNP bipolar transistor instead of NPN transistor. Since NPN bipolar transistor contributes high current gain, high matching precision, and its difficult to implement the NPN transistor on CMOS process [6]. The proposed circuit produces the reference voltage of 1.181V, to meet the requirements of design under less voltage. By using voltage mode architecture and bipolar transistors, the proposed circuit produces very less TC of Vref with only first order temperature compensation and greatly reduces the circuit complexity as compared to the papers [4] [5]. Compared to conventional BGR which uses two stage operational amplifier(opamp) [8], the proposed circuit uses single stage folded cascode opamp in order to get highly stable output at the output of BGR with low TC since opamp input offset is very low(in terms of 1.96μV) , single stage can give very high gain and PSRR of BGR.

The section II describes conventional BGR principal, section III discusses about proposed BGR principal, section IV includes Simulation results, section V gives conclusion and references.

II. Conventional BGR Principal

The basic principal is V_{BE} (Base to emitter) voltage of bipolar transistor which generates complementary to absolute temperature (CTAT) voltage with negative temperature coefficient and difference between V_{BE} of two bipolar transistor (Thermal voltage V_T) which carrying unequal current densities which exhibits proportional to absolute temperature voltage with positive temperature coefficient (PTAT). The final Vref output is addition both PTAT and CTAT voltage with near zero temperature coefficient is generated [7]. The typical output of BGR is 1.181V, which is close to bandgap voltage of silicon at room temperature.

A. Negative TC Voltage generation

Generally the forward voltage of pn junction diode exhibits negative temperature coefficient (TC), and also the base to emitter voltage of bipolar transistor exhibits the similar characteristics. For bipolar device we can write as

$$I_C = I_S e^{\frac{V_{EB}}{V_T}} \tag{1}$$

Where

$$V_{EB} = V_T ln \frac{I_C}{I_S} \tag{2}$$

where, VT=Thermal voltage =kT/q and Is=The saturation current

$$I_S = bT^{4+m}e^{\frac{E_g}{kT}} \tag{3}$$

b= proportionality factor and m= material constant proportional to electron mobility. Therefore negative TC is given by

$$\frac{\partial V_{EB}}{\partial T} = \frac{V_{EB} - (4+m)V_T - \frac{E_g}{q}}{T} \tag{4}$$

Assuming Ic is constant

$$\frac{\partial V_{EB}}{\partial T} = \frac{V_{EB} - (3+m)V_T - \frac{E_g}{q}}{T} \tag{5}$$

Assuming Ic to be a function of temperature

B. Positive TC voltage generation

If two bipolar transistors operate in unequal current densities then difference between their base to emitter voltage directly proportional to their absolute temperature [7]. While positive TC is given by

$$\Delta V_{EB} = V_{EB1} - V_{EB2} = V_T ln(n) \tag{6}$$

$$\frac{\partial \Delta V_{EB}}{\partial T} = \frac{V_T ln(n)}{T} \tag{7}$$

Now the BGR reference voltage is described as,

$$V_{ref} = V_{EB} + IR_2 = V_{EB} + R_2(\frac{\Delta V_{EB}}{R_1}) \tag{8}$$

The second term in the above equation IR2 has positive temperature coefficient of +0.086mV/$^\circ$C, and first term V_{EB} has negative temperature coefficient of -2mV/$^\circ$C at room temperature. R2/R1 ratio is adjusted such that near zero temperature coefficient of Vref is achieved theoretically [7]. The temperature coefficient of final Vref output is given by

$$\frac{\partial V_{ref}}{\partial T} = \frac{V_{EB} - (3+m)V_T - \frac{E_g}{q}}{T} + \frac{R_2 V_T ln(n)}{R_1 T} \tag{9}$$

After putting

$$\frac{\partial V_{ref}}{\partial T} = 0 \tag{10}$$

in above equation the final BGR output is given by

$$V_{ref} = \frac{E_g}{q} + (3+m)V_T \tag{11}$$

Where Eg is bandgap of silicon at room temperature =1.12eV, V_T=25mV thermal voltage, m is constant factor= -1.5 for silicon. After putting all values Vref=1.25V at room temperature. The conventional BGR uses two stage operational amplifier (opamp) but output of BGR is having high temperature coefficient, which is not a good design [7]. The proposed BGR uses folded cascade opamp , which is highly stable because of single dominant pole which is located near to 3db BW of opamp will explain in next section.

III. PROPOSED BGR PRINCIPAL

The drawback conventional architecture is the opamp output is not stable [8] and hence BGR output, and also start up problem in the circuit. In current mode architecture output is very sensitive with respect to temperature and high power dissipation in the circuit which is in terms of mill volts [1] [6].The proposed voltage mode architecture consists of startup circuit, folded cascode opamp, and core BGR shown in figure 1.

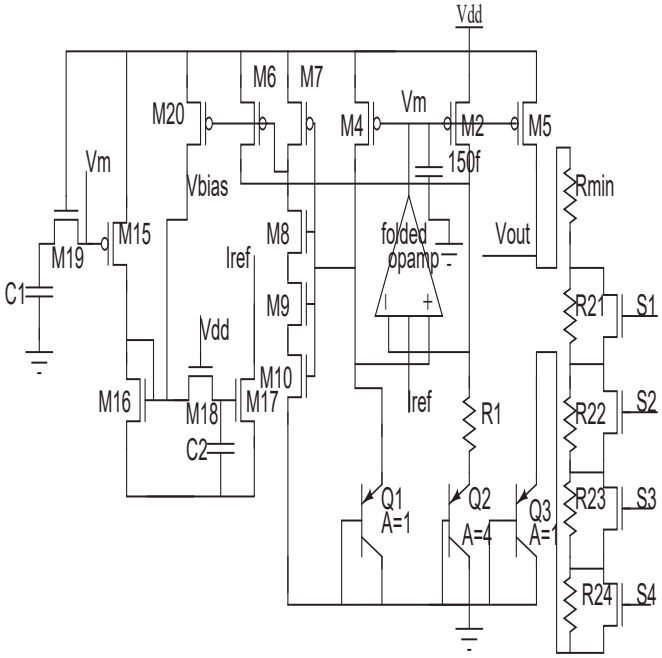

Fig. 1. Proposed voltage mode BGR architecture

For the operation of circuit there are two voltages V_{EB} and ΔV_{EB} are generated with negative and positive TC respectively. A diode connected PNP transistor Q3 at the output generates V_{EB} voltage which having negative TC(CTAT characteristics) and the pnp transistors Q1, Q2 which carries equal currents and having their areas in ratio of 1:4. Since both transistors Q1 and Q2 are unequal sizes which exhibits difference voltage(ΔV_{EB}) across resistor(Difference between node a and b). The voltage across resistor ΔV_{EB} exhibits PTAT characteristics. The R1 resistor decides current flowing in branch-3 and 4(Both carries equal current) and same current is mirrored in the output branch. The voltage across R2 is PTAT voltage and V_{EB} of Q3 exhibits CTAT voltage, the final output is addition of both voltages [7]. The value of R2 is selected such that the Vref output is having very less temperature coefficient.After trimming R2 is sum of R_{MIN}, R21,R22,R23 and R24 are as shown in figure.

A. Trimming circuit

The trimming circuit is added to reduce the temperature coefficient of Vref output at different supply and corners. A 4 bit series trimming circuit is used [10], with resistors

values are selected by calculating fine and coarse variations of resistors at different supply and process corners. The fine resistor value is selected for minute variations and coarse resistor value is selected for large variation of resistor at different supply variations and corners. R_{MIN0}, R_{MIN1} and R_{MIN2} are minimum resistors values obtained at SS, TT and FF corners in order to get required BGR output voltage.Coarse resistors are selected as

$$R_{coarse0} = R_{MIN1} - R_{MIN0} \tag{12}$$

and

$$R_{coarse1} = R_{MIN2} - R_{MIN1} \tag{13}$$

and fine resistors are selected to adjust the resistors at different process corners and supply for minute variations in order to get proper BGR output.From the figure R_{MIN0}=R_{MIN},$R_{coarse0}$=R21,$R_{coarse1}$=R22, R23 and R24 are fine resistors.These values are chosen by NMOS switches in accordingly by their turn on and turn off which is driven by digital circuit [10].

B. Startup circuit

The devices M6,M7 and M8 forms a startup circuit, M7, M8 forms inverter, which is part of startup circuit as shown in figure 1 [1]. Initially when there is no current in core circuit, the top two PMOS M2 and M4 are turned on, which makes input to inverter is one and output is zero. The zero input which turned on the PMOS M6 device, and initiates the current in core circuit. Once the core BGR turned on then startup will turned off and carrying very less current(In terms of pA). The devices M6 in sub threshold region, M7 in triode and M8 in saturation region always for the proper operation of startup [6].

C. I_{REF} generation circuit

The current reference of 1μA for folded cascode opamp is generated from BGR PMOS current mirror as shown in figure 2.The biasing for M15 device is selected from BGR PMOS current mirror by properly adjusting aspect ratio of M15 and same current is mirrored to nmos M16 and connected to I_{REF} of opamp. Now opamp will not work because startup circuit is not included, to aviod this problem an extra PMOS M20 is biased from startup circuit and connected to I_{REF} genaration circuit. So that once startup will initiates the current in Iref circuit, opamp will work properly. The extra RC circuit is included in reference generator to aviod an ac signal coming from opamp cascode structure.A ac signal is coming from opamp output because the circuit is not symmetry at its both cascode branches, so no ac signal cancellation at the output of opamp.There is a loop formed from output of opamp through bias circuit which degrades the phase margin due to additional poles. RC circuit is used to push these poles outside UGB.

D. Operational amplifier

The proposed circuit uses single stage folded cascode operational amplifier(opamp) with high gain and CMRR(Common mode rejection ratio) as shown in figure 2.

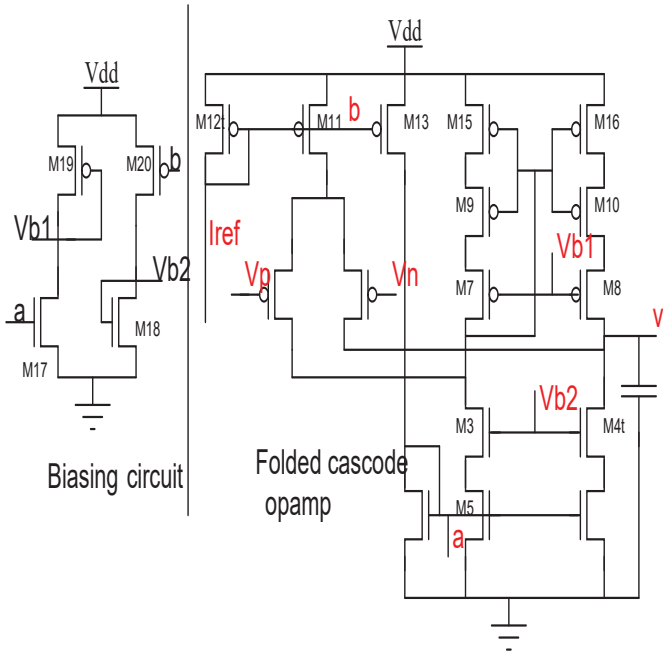

Fig. 2. Folded cascade opamp with biasing circuit

The sufficient high gain improves the PSRR of BGR [1]. The pmos input pair folded cascode opamp is chosen in order to meet the gain, stability[11]. The biasing voltages for opamp cascode stages are generated by using current mirrors as shown in left half of figure 2 [9]. The devices M1 and M2 are input pair of opamp, the inputs to opamp are driven by BGR a and c nodes as shown in figure 1. M11 is the top tail device which carrying 2μA current. Devices M3 to M10 are cascode loads to opamp which carrying 0.5μA current. M5 and M6 are bottom tail devices which carries currents from both input devices and cascode stage. Load capacitance of opamp is taken from adding all capacitance associated with M2 and M3 devices. The overall opamp which carries current of 7μA and operating all devices in saturation [11]. The gain of folded cascode opamp is given by

$$A_V = \frac{gm_2 gm_4 gm_8 R_1}{gds_8 gds_{10} gm_4 R_1 + gds_4 gm_8} \tag{14}$$

The first order gain bandwidth (UGB) is given by

$$\frac{gm_4 gm_8 c_L (gds_8 gds_{10} gm_4 R_1 + gds_4 gm_8)}{gm_2 (gds_8 gds_{10} {gm_4}^2 c_4 R1 + c_2 gds_4 {gm_8}^2 + c_4 gds_4 gm_4 gm_8)} \tag{15}$$

The location of first real pole or domiant pole is given by

$$P_1 = -\frac{gds_8 gds_{10} gm_4 R_1 + gds_4 gm_8}{gm_4 gm_8 c_L R_1} \tag{16}$$

The location of second real pole is given by

$$P_2 = -\frac{gm_4 gm_8}{gm_8 c_2 + gm_4 c_4} \tag{17}$$

The location of third real pole is given by

$$P_3 = -\frac{gm_8c_2 + gm_4c_4}{c_2c_4} \tag{18}$$

The location of high frequency zero is given by

$$Z_1 = -\frac{gm_8}{c_4} \tag{19}$$

IV. SIMULATION RESULTS

Simulations have been carried out using MentorGraphics Pyxis tool with EldoSpice simulator in 130nm CMOS technology with supply of 1.8V with 10 % variations. The operational amplifier used in the proposed BGR is single stage folded cascade opamp, has given gain of 77.6db and phase margin of 72 degree as shown in figure 3.Simulation results shows that after connecting an opamp into BGR, the input offset voltage of opamp is very less voltage around 1.96μV. Figure 4 shows startup behavior of BGR output. The time required for BGR to produce a stable output is 200ns(at typical,27 °C) [1]. The simulation is carried out by performing transient analysis when supply voltage is given as ramp signal varying between 0V to V_{DD} within 10ns, 100ns and corresponding output voltage, which gives the startup behavior of BGR when vdd is ramped up.

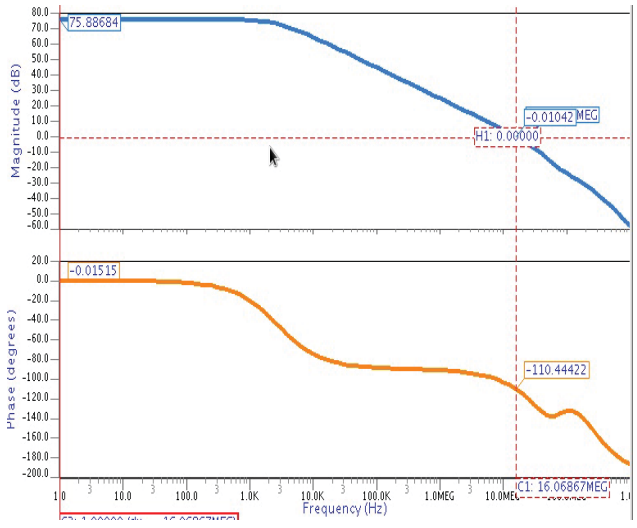

Fig. 3. Gain and Phase plot of folded opamp

The variations of Vref versus temperature at different process corners before trimming, which gives variations of Vref at process corners is 43mV. Figure 5 shows Vref Vs Temp curve at different process corners after trimming ciruit is used, which gives variations at TT, SS and FF are 1.8mV, 4.7mV and 4.5mV leads to TC of 30ppm/ °C, 39.8ppm/ °C and 38ppm/ °C respectively. The overal variation of Vref at different process corners(TT, SS, FF) with supply variations(1.62V ,1.8V, 1.98V) is 4.7mV and TC of 39.9ppm/ °C.

Therefore folded cascode opamp is self compensated and is highly stable without using any compensation techniques [8].

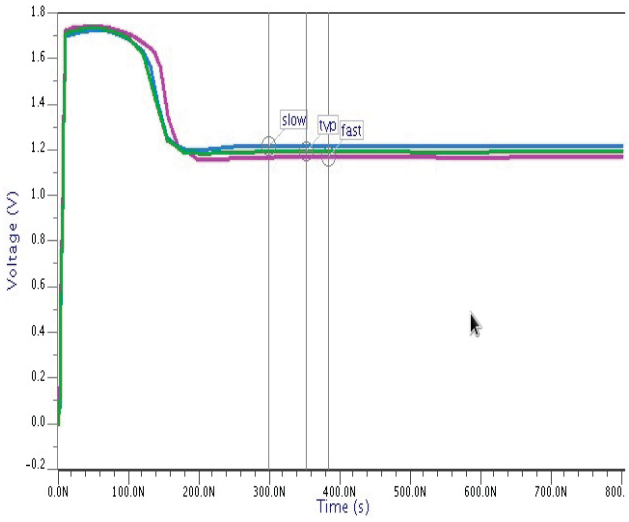

Fig. 4. Start-up behavior of the BGR output voltage with VDD ramp

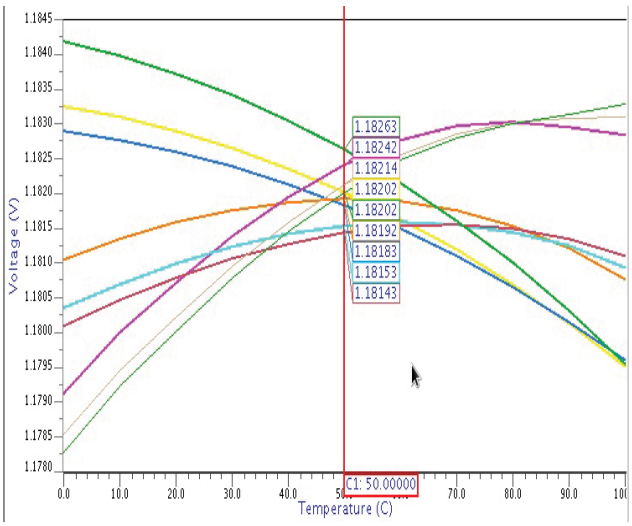

Fig. 5. BGR output after trimming

Table 1 shows the comparision table of Folded cascode opamp performance parameters between theoretical and simulated values. Theoretical values are optained by half circuit smal signall analysis of folded cascode opamp using Maxima tool.As given in equations 14 to 19 which includes approximated gain, UGB and all pole-zero equations.From the table 1 it shows that the percentage of error between theoretical and simulated values is very less and pole1 is domiant pole and it will decides the stability of opamp. The next poles(pole2 and pole3) and zero are located at very high frequency, i.e after UGB, Which all together leads to phase margin of 70 degree. The performance metric of different architectures of bandgap reference are shown in table3 [2] [4]. From the table it can be seen that the proposed circuit got a standard Vref output of 1.181V with bipolar structure which is good reference output as compared to other papers[5] [6]. The

TABLE I
COMPARISION OF PERFORMANCE PARAMETERS BETWEEN THEORETICAL AND SIMULATED VALUES OF OPAMP

Parameters	Theoretical	Simulated
Av(db)	74.8	77.6
UGB(MHz)	15.48	16
pole1(KHz)	−2.74	−2.47
pole2(MHz)	−57	−52
pole3(MHz)	−74.4	−80

variation of Vref curve across temperature is 1.18mV, which is good value as compared to paper [3] and [5].The PSRR of proposed architecture is good value [5] and which is enough for given application (Low dropout regulator).By using voltage mode architecture the proposed circuit achieved temperature coefficient of 19 ppm/°C [5].

The layout of proposed bandgap reference is as shown in figure 6. Which includes opamp, startup circuit, RC filter circuit, trimming and Iref generation circuit. The PNP transistors are used in the ratio of 1:4:1 and layout includes resistors as rnpolyhi and capacitor as mimcap 3x3. The overall area of layout is 80μmX40μm.

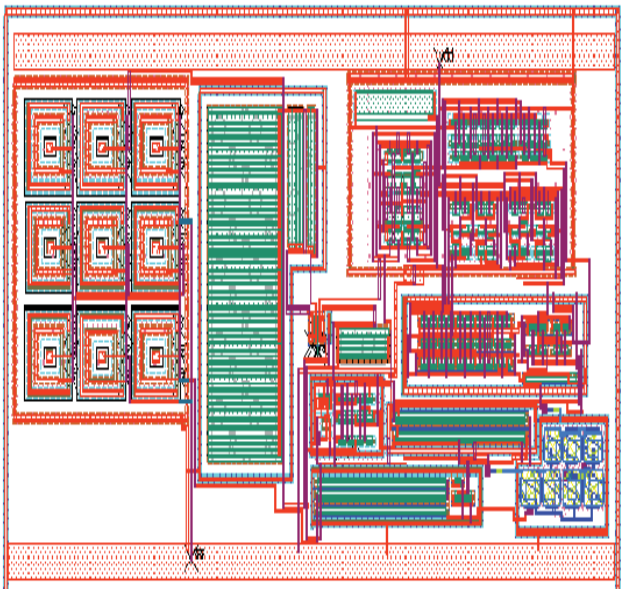

Fig. 6. Layout of BGR

V. CONCLUSION

A BiCMOS voltage mode bandgap reference is designed and simulated with good PSRR and low temperature coefficient. The proposed circuit is simulated with supply of 1.8V with 10% variations, which produced Vref output of standard 1.181V using bipolar version and TC of 19ppm/°C. A single stage folded cascode opamp generates gain of 78db, with very less input offset of 1.96μV because of closed loop gain of opamp in BGR is 118db. The PSRR of overall design is -43db up to frequency range of 30KHz, its good value for given application. The total current drawing from supply is 12.5μA and the overall power consumption in the circuit is 18.4μW. The proposed BGR is well suited for CMOS system on chip applications for its power flexibility, temperature and supply variations stability of reference voltage and its power supply rejection ratio.The proposed BGR output will be use in LDO circuit, which is operating at 3.3V supply and gives regulated output of 1.8V.

TABLE II
PERFORMANCE COMPARISON OF BANDGAP REFERENCE CIRCUITS

Parameters	[2]	[3]	[4]	[5]	[6]	Proposed Design
CMOS Tech(μm)	0.8	0.8	0.35	0.18	0.18	0.13
VDD(V)	1	-	3.3	1.8	1.8	1.8
Vref(V)	0.54	1.2	1.18	0.62	0.5	1.181
Vref variations	0.3V	2.8mV	1mV	1.4mV	0.9mV	1.18mV
Temp range(°C)	0/80	−40/125	10/90	0/70	−40/125	0/100
TC(ppm/°C)	7.5	14	10.5	32.5	9	19
PSRR(db)	-	110	-	35	100	43
CL Gain(db)	-	108	-	-	112	118

VI. ACKNOWLEDGEMENT

The authors are very thankful to SmartPlay Technologies Pvt. Ltd, Bangalore, India for its resources and facilities

REFERENCES

[1] Abhisek Dey and Tarun Kanti Bhattacharyya, *"Design of a cmos bandgap reference with low temperature coefficient and high power supply rejection performance"*,VLSICS,Vol2, No3, September 2011.
[2] Piero Malcovati, Franco Maloberti, Carlo Fiocchi, and Marcello Pruzzi, *"Curvature- Compensated BiCMOS Bandgap with 1-V Supply Voltage"*,IEEE Journal of Solid-State Circuits, 2001, vol.36,No. 7, pp. 1076 1081.
[3] P Siew kuok Hoon,Jun Chen,Franco Maloberti "An improved bandgap reference with high power supply regection",The University of Texas,Inc,USA,2002.
[4] Mitrea, O., Popa, C., Manolescu, A. M., and Glesner, M "A curvature-corrected CMOS bandgap Reference",Adv. Radio Sci., 1, 181-184, doi:10.5194/ars-1-181-2003.
[5] Ro-Min Weng, et al. "A 1.8-V High-Precision Compensated CMOS Bandgap Reference",IEEE Conference on Electron Devices and Solid-State Circuits, 2005, pp. 271 273.
[6] Jun Hu, Yongsheng Yin,Honghui Deng*"Design of a High-performance Brokaw Band-gap Reference"*,Hefei University of Technology
[7] Behzad Razavi *" Design of analog cmos integrated circuits"* McGraw-Hill, 2001.
[8] Miss Rohini Hongal,Mr. Rajashekar B. Shettar*"DESIGN AND IMPLEMENTATION OF CURVATURE CORRECTED BANDGAP VOLTAGE REFERENCE-1.1V using 180nm Technology"*,IEEE,2010.
[9] Arivazhagan P*"Design and Implementation of Op-Amp Based Low Power CMOS Bandgap Voltage Reference with Minimum Supply oF 0.8V"*,ISSN,Vol3,No2, June 2013.
[10] Juan Martinez Brito, Sergio Bampi, H. Klimach*"A 4-Bits Trimmed CMOS Bandgap Reference with anImproved Matching Modeling Design"*,supported by the National Science Foundation.
[11]] I. Toihria and T. Tixier*"Improved PSRR and Output Voltage Swing Characteristics of Folded Cascode OTA"*,International Journal of Electronics and Electrical Engineering Vol. 3, No. 4, August 2015.
, China,IEEE,2010.

THE 5TH INTERNATIONAL CONFERENCE ON WIRELESS COMMUNICATIONS, VEHICULAR TECHNOLOGY, INFORMATION THEORY, AEROSPACE & ELECTRONIC SYSTEMS (WVITAE-2015)
December 13-16, 2015, Hyderabad, India

On CS Reconstruction Images using LDPC Code over Radio Mobile Channel

Ankita Pramanik
Electronics & Telecommunication Department
IIEST, Shibpur,
India
Email: ankita@telecom.iiests.ac.in

Santi P. Maity
Information Technology Department
IIEST, Shibpur,
India
Email: santipmaity@it.iiests.ac.in

***Abstract*—Compressed Sensing or Compressive Sampling (CS) is the process of signal reconstruction using the samples obtained at a rate far below the Nyquist rate from sparse representation on suitable basis. Reconstruction by CS has gained wide spread application in many practical problems that demand satisfactory reconstruction of images from partial sensed data. In literature CS problem is mostly addressed as reconstruction problem done at the place of sensing. But in reality, many applications like Magnetic Resonance Imaging (MRI), Body Area Network (BAN) need data reconstruction at a place far away from the place of sensing. In this work, the effect of additive white Gaussian noise (AWGN) noise and fading channel is shown on the reconstruction process. To overcome the effect of noise and fading, the sensed samples are encoded by low density parity check code (LDPC) before transmission is done. It is observed that longer is the length of the LDPC codes better (lower) is the bit error rate (BER) performance. Here a method to construct larger length but 4 cycle free irregular LDPC codes from IEEE WiMAX standard is also proposed. Extensive simulation results show the efficacy of the use of LDPC codes and the trade-off in code rate and measurements on reconstruction quality.**

I. Introduction

Compressed Sensing (CS) revolves around the idea of reconstructing the original signal from very few measurements [1], [2]. It assumes that the original signal is sparse in some suitable representation space i.e. basis function. It picks up few of these sparse signals from that domain and then reconstructs the original image from these samples. Hence CS overcomes the problem of high speed sampling, reduces transmission delay and saves storage space at the cost of computation for finding a solution to an under-determined system of linear equations. Various methods of reconstruction have been used in CS, namely L_1 optimization [3], Basis Pursuit (BP) [4], algebraic reconstruction technique or stochastic approximation. A standard approach in solving under-determined or ill-conditioned linear systems of equations consists of minimizing an objective function which includes a quadratic (l_2) error term combined with a sparseness-inducing (l_1) regularization term. BP, the Least Absolute Shrinkage and Selection Operator (LASSO) [5], wavelet based de-convolution etc are a few well-known examples of this approach.

The methods stated above are known as parametric reconstruction techniques. Most often a closed form solution is difficult to achieve or they get stuck at local optima. The sparse signals can also be reconstructed by another approach- iterative non-parametric modelling. This method is implemented by the use of spatially denoising adaptive filter based on Robbins-Monro (RM) stochastic approximation algorithm [6]. RM is a family of iterative stochastic optimization algorithms that attempt to find zeros or extrema of functions that cannot be computed directly but can be solved through estimation via noisy observations. In RM-CS reconstruction problem [6], along with the observed space, random noise is inserted on the unobserved portion of the spectrum on each iteration [6]. Adaptive filter is then used to attenuate noise and reveal features i.e. to improve the visual quality of the image. In literature, majority of CS techniques assume that the reconstruction is done at the place of sensing itself. But in reality, reconstruction is often done at a place far away from where the sensing is done, for example, MRI, Computed Tomography (CT) scan, body area network (BAN) etc. All these applications need transmission of sensed data over radio mobile channel with low error rate and possibly in an energy efficient form.

In this work, image reconstruction on CS is done through transmission of measurement using Low Density Parity Check Codes (LDPC) over noisy and fading channel. Here, LDPC is chosen as the error control code as it is capacity achieving, ubiquitous codes i.e. can be applied in any scenario. Irregular LDPC code of length 10 million bit and rate (R) -1/2, has achieved capacity of 0.045 dB from the Shannon limit [7]. First a larger length but 4 cycle free irregular LDPC codes is proposed and is used on CS reconstruction transmission problem. Then a trade off between the number of measurements and code rate on reconstruction quality is studied.

Section II makes a literature review on CS and LDPC. Section III presents the system model the channel mode, the non- parametric CS reconstruction technique used and the proposed extended LDPC codes. Simulation results are shown in Section IV while conclusions are made in Section V.

II. Literature Survey

This work deals with the effect on CS reconstruction quality after transmission of sensed samples through a radio mobile channel using LDPC. So, the literature survey focuses mainly on the works which deal with CS and LDPC codes.

LDPC codes are block codes with parity-check matrices that contain only a very small number of non-zero entries. The parity check matrix is sparse and hence the name low density. LDPC codes are decoded iteratively and may be used for progressive reconstruction of image/video signal. The LDPC

code-words satisfy a set of linear parity-check constraints. One issue in construction of LDPC codes, is that 4 cycles within the parity check matrix or H matrix should be avoided. Presence of 4 - cycle delays the convergence of the decoding procedure. The other important issue is the length of the code. Larger the length of the LDPC code, closer it is to the Shannon limit in error bound.

Of late LDPC codes have been explored on CS. In [8], LDPC codes have been used on CS as a sensing matrix. The H matrix of the LDPC code has been used as the sensing matrix of CS and the sensed samples are reconstructed in situ (at distant place i.e. far away) by Orthogonal Matching Pursuit (OMP). In [9], a relationship between channel coding and CS is established. It shows that parity-check matrices of good channel codes can be used as *good* measurement matrices under BP. In [10], the system design of CS based source encoding system for data compression in wireless sensor applications is described. In [11], a unified CS - EC channel model is given for sparse and almost sparse channels. The decoding of LDPC codes based on CS reconstruction has been attempted in most of the work involving CS and LDPC. To the best of our knowledge this is the first work in which LDPC is considered for channel coding while transmitting CS samples through a radio mobile channel. Furthermore, the present work uses non-parametric method of reconstruction of signal [6] unlike the other existing LDPC-CS unification schemes that use various parametric approaches. The LDPC codes, by providing redundancies, improve the bit error rate (BER) performance. Due to the improved (lower) BER value achieved by adding redundancies, data can be transmitted even at lower SNR. So, energy saving can be achieved. Energy is an important natural resource. In the multi-hop wireless path with battery driven sensors and relays are to be used for image acquisition and end-to-end transmission.

III. System Model

A. RM-CS via recursive spatially adaptive filtering

Energy saving in processing part can be achieved using algorithms that have low computational complexity and hence are less power hungry. Transmission power can be saved by reducing the number of samples to be transmitted i.e. by compressing the signal. This alternative paradigm for CS signal reconstruction replaces the implicit regularization imposed by l_p norms by explicit adaptive filtering. Performance of this approach overcomes the problem of regularization criteria by advanced spatially adaptive (both local and non-local) method [12]. The empirical results presented in [6] show that this approach is able to reconstruct images with improved visual quality from highly incomplete measurements provided that sensing matrix captures low frequency components (high valued sparse coefficients).

Let the original signal x is transformed to y by applying some appropriate transformation basis, assuming that y is sparse in that transformed domain. The work in [6] introduced a binary valued sampling operator S, with values 0 or 1 of the available portion Ω of the spectrum. Thus, the point-wise products $S. * y$ and $(1$ - S$). * y$ produce a decomposition of the spectrum into two complementary parts, $y_1 = S. * y$ and $y_2 = (1$ - S$). * y$. The total signal y can thus be written as,

$$y = y_1 + y_2 = S. * y + (1 - S). * y \tag{1}$$

Here, y_1 and y_2 are the observed (known) and the unobserved (unknown) parts of y, respectively. The goal is to reconstruct θ (or equivalently y_2) from the available data y_1. An estimate of y_2 can be obtained by the following recursive formula after the k^{th} iteration.

$$\begin{aligned} \hat{y}_2^{(0)} = 0,\ (initialization)\ k = 0, \\ \hat{y}_2^k = \hat{y}_2^{k-1} - \gamma_k[\hat{y}_2^{k-1} - (1 - S). * T(\phi(T^{-1} \\ (y_1 + \hat{y}_2^{k-1}))) + (1 - S). * \eta_k], k \geq 1 \end{aligned} \tag{2}$$

From the estimate of y_2, the estimate of the image signal y can be obtained as:

$$\hat{y}^{(k)} = y_1 + \hat{y}_2^{(k)}$$

Taking the inverse transform of the estimate of y gives back the original image.

During the recovery of CS samples transmitted through noisy radio mobile channel, the parametric reconstruction is done not on y_1 but on $Hy_1 + \eta$, where H is the channel fading co-efficient and η the channel noise. For AWGN channel fading parameter $H = 1$.

B. Channel Model

The reconstruction of the original image by RM gives appreciably good results when the reconstruction is done at the same place i.e. reconstruction done at the place where the samples are sensed. If the reconstruction of the original image from the sensed samples is done at a place far away from the place where the samples are sensed, then the samples are corrupted with noise during transmission. During transmission, noise gets added to these sensed samples. In the absence of any error correcting codes (ECC), the samples are decoded by hard decision decoding. So, the reconstruction procedure gets greatly affected due to the noise samples. To improve the reconstructed image quality at the far end, the sensed samples after quantization are encoded with LDPC code for protection from channel errors. The sensed samples can pass through a fading channel instead of the AWGN channel. Image degradation is more severe where transmission through radio mobile channel that creates fading channel. The fading channel degrades the samples more than AWGN noise.

C. LDPC Codes

In IEEE 802.16-2009 standard, LDPC code currently consists of six different code classes spanning four different code rates i.e., 1/2, 2/3, 3/4 and 5/6 [7]. The maximum length of theses codes is 2304. In this work we propose a technique to extend the codes given in the standard. Each entry of the H matrix of the final LDPC code obtained from the IEEE 802.16-2009 standard is expanded by an identity matrix. So, if the original size of the H matrix is m X n and if the size of the identity matrix be p X p, then the size of the extended matrix will be mp X np. The extended parity check matrix H_{ext} can be obtained from the base parity check matrix H by the following formula:

$$H_{ext} = H \otimes B \tag{3}$$

where $\otimes$ stands for Kronecker product and B is the identity matrix of size p X p. H_{ext} can be calculated as follows

$$A \otimes B = \begin{bmatrix} a_{11}B & \dots & a_{1n}B \\ \vdots & \ddots & \vdots \\ a_{m1}B & \dots & a_{mn}B \end{bmatrix}$$

Multiplication of the identity matrix does not introduce 4 - cycle. If the original LDPC code is 4- cycle free then the expanded matrix will not have 4 - cycle. Let the length between two nodes i.e., two entries of the H matrix be L. When each entry of the H matrix is extended by unity matrix, equivalently the nodes are shifted by 1. So, the length L remains constant. But these nodes do not cause any 4- cycle with the existing nodes. Thus by multiplication of the standard H matrix with unit matrix the length of the H matrix is extended without introduction of 4- cycle for H matrices given in the WIMAX standard. As we know that larger the length of the codeword, better is the error protection capability. By the above mentioned method, the length of the H matrix can be increased to get better CS reconstruction i.e. low probability of error. The probability of error of reconstructed data varies with the rate of the error control coding used. Let us define the following notation for a code of rate R:
E_c = SNR per code bit
E_b = SNR per information bit = $\frac{E_c}{R}$.
The probability of error for soft decision decoding for BPSK in AWGN channel is upper bounded as follows:

$$P_e \leq Q(\sqrt{\frac{2E_c}{N_o}\Sigma_{l=1}^{n} c_{j,l}}) \tag{5}$$

where the information vector x_i is mapped to the codeword $c_i = c_{i,1}, c_{i,2}, , c_{i,n}$ [13]. For coded BPSK on Rayleigh fading channel and with Soft decision decoding the probability of error can be given as follows [13]

$$P_e \leq Q(\sqrt{2\Sigma_{l=1}^{n} c_{j,l} E_{j,l}}) \tag{6}$$

Deriving the bounds of the probability of error for CS reconstruction with LDPC is an interesting problem.

IV. Results and Discussion

This section presents performance results. The sensed signals are quantized, then BPSK modulated and transmitted through the AWGN channel. Simulation is done over large number of images but due to space limitation few images are shown. In Fig. 1 (a) and (b), the sensed samples (CS measurement space, K = 80% are taken) are transmitted through AWGN channel, SNR is 2 and 3 dB, respectively. The samples received through the noisy channel are used to reconstruct the image. The Structural Similarity Index (SSIM) of the reconstructed images are 0.0877 and 0.1220 and Peak Signal to Noise Ratio (PSNR) are 10.41 dB and 12.25 dB, respectively. Image considered for simulation is (256 X 256), 8 bits/pixel.

The same 80% samples of the image Lena are encoded by LDPC and then transmitted through the same AWGN channel. The images can be reconstructed to visually satisfying values if

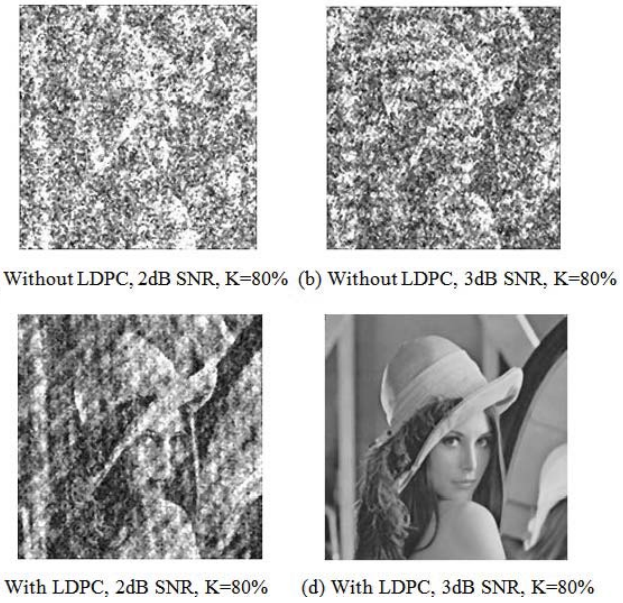

(a) Without LDPC, 2dB SNR, K=80% (b) Without LDPC, 3dB SNR, K=80%

(c) With LDPC, 2dB SNR, K=80% (d) With LDPC, 3dB SNR, K=80%

Fig. 1: Image reconstruction after transmission through AWGN channel

the sensed samples are encoded by LDPC before transmitting, as is evident in Fig. 1 (c) and (d). The SSIM values are 0.2753 and 0.9340 and the PSNR of the reconstructed images are 17.1752dB and 32.0725 dB, respectively.

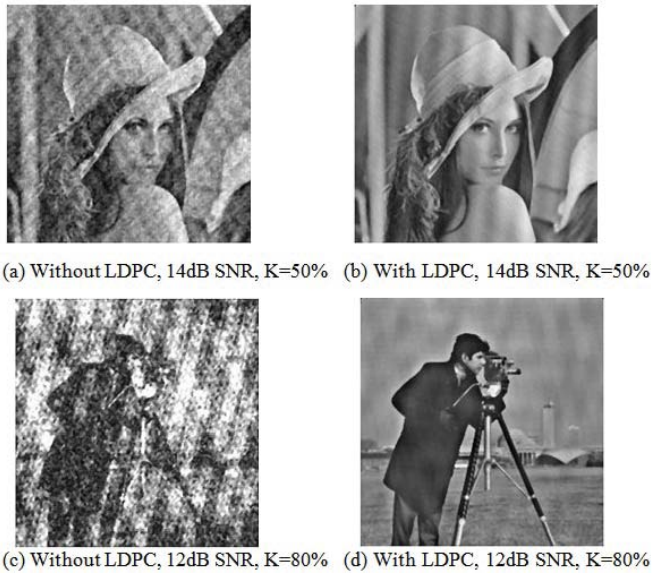

(a) Without LDPC, 14dB SNR, K=50% (b) With LDPC, 14dB SNR, K=50%

(c) Without LDPC, 12dB SNR, K=80% (d) With LDPC, 12dB SNR, K=80%

Fig. 2: Image reconstruction after transmission through Rayleigh fading channel

The effect of fading on reconstruction without and with LDPC is shown in Fig. 2. As an example to demonstrate the effect of fading, 50% samples of the image Lena is sensed by CS. The samples are transmitted directly through a Rayleigh fading channel at 14dB and also after encoding the samples with LDPC. The SSIM and PSNR of the reconstructed images

without and with LDPC are 0.4959, 0.8418 and 21.5860 dB and 26.9992 dB and are shown in Fig. 2 (a) and Fig. 2(b) respectively. Simulation is also done on the cameraman image by taking 80% samples and the SNR of the channel is set as 12dB. The SSIM and PSNR of the reconstructed images without and with LDPC are 0.3249, 0.7592 and 17.2472 dB and 25.4037 dB and are shown in Fig. 2 (c) and Fig. 2(d), respectively. The effect of noise with the percentage of varying CS samples encoded with LDPC is also studied. The CS samples of the image Lena are picked up from 10% to 50% in steps of 10% and passed through AWGN channel and the SNR of the channel varies from 0 to 4.5 dB in steps of 0.5 dB. The LDPC code chosen is the proposed LDPC code. The basic LDPC code is rate 2/3 taken from the IEEE 802.16 standard. To improve the BER performance, this LDPC code is extended by Kronecker product with an identity matrix of weight 4. Performance comparison with and without LDPC is given in Fig.3.

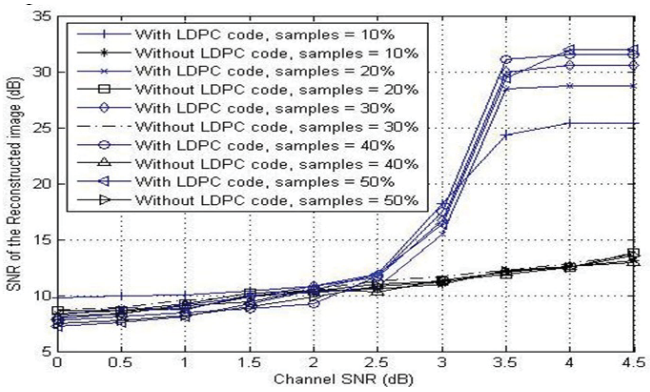

Fig. 3: PSNR of the reconstructed images vs channel SNR

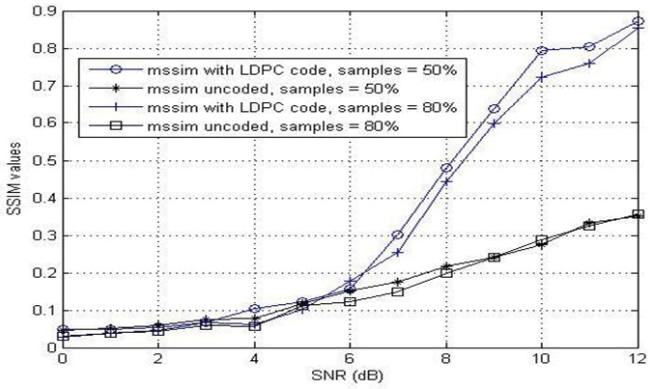

Fig. 4: SSIM of CS reconstructed image vs SNR in Rayleigh fading channel

The effect of Rayleigh fading channel on CS reconstruction with the variation in measurements is also studied. The SSIM values of the reconstructed image of the cameraman in comparison with the original image when 50% and 80% samples are sensed and reconstructed are plotted and shown in Fig. 4. The LDPC code used is the proposed extended standard LDPC code. From the simulation results, it is clearly evident that LDPC codes improve the quality of the reconstructed images not only in AWGN channel but also in Rayleigh fading channel.

These days with the advent of Wireless Health Monitoring System, far end reconstruction of medical images has become a necessity. Fig. 5 (a) shows the reconstructed image of MRI head image for CS measurements, K = 50%. The samples are transmitted through Rayleigh fading channel at 16 dB with LDPC coding rate 2/3. Fig. 5 (b) shows the reconstructed image without use of ECC. The SSIM values are 0.9069 and 0.3008 with and without LDPC coding, respectively.

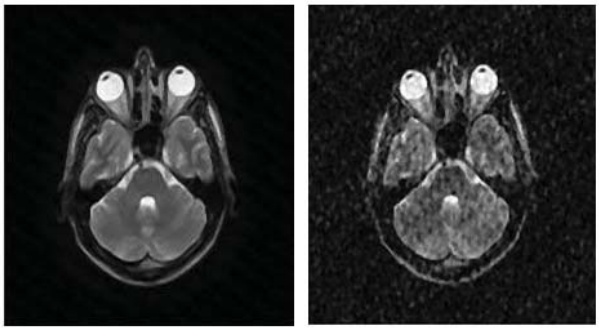

(a) With LDPC, K = 50% (b) without LDPC, K = 50%

Fig. 5: Reconstruction at far end of MRI head image at 16 dB Rayleigh fading channel

The effect of variation in code rates of LDPC was also studied. The SSIM values obtained after encoding the sensed data with different rates of LDPC and transmission through an AWGN channel is shown in Fig. 6. The LDPC codes used were constructed by the proposed LDPC construction technique from IEEE 802.16 standard. From Fig. 6 it is evident that as the code rate increases, the SSIM of the CS reconstructed images increases.

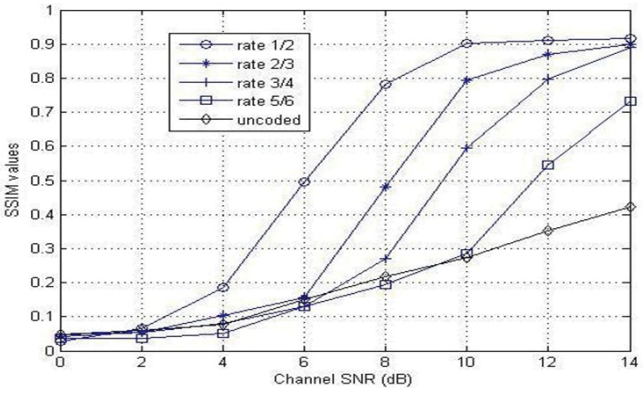

Fig. 6: Varying the rates of LDPC in Rayleigh fading channel

A three dimensional (3D) plot relating SNR vs BER vs SSIM is shown in Fig. 7. Simulations are done over a large number of test images. Numerical values shown are obtained by taking average over 50 images. In Fig. 7, 50% samples of the images are used to study the effect of BER of LDPC

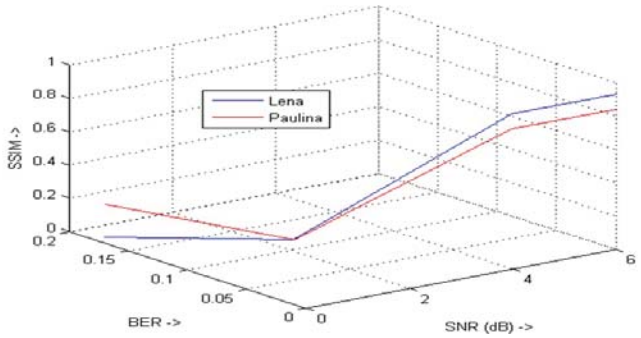

Fig. 7: Effect of channel SNR on SSIM and BER in AWGN channel

on SSIM of CS reconstructed image. As expected, with the channel SNR increases, BER values decrease and hence SSIM values increase.

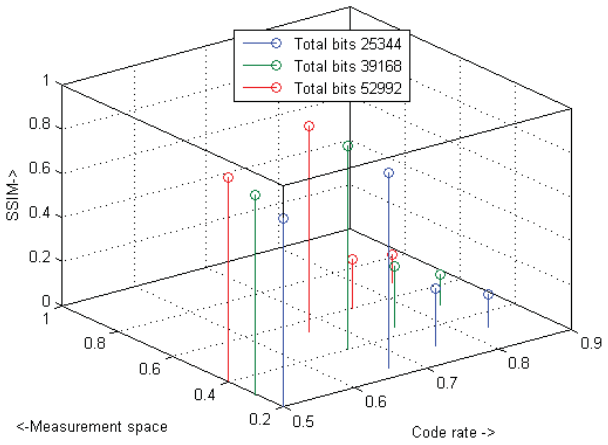

Fig. 8: Variation of SSIM with different LDPC rates and varying sample space keeping total number of bits constant at 4dB SNR

In Fig.8, a plot of SSIM vs the code rates and the number of measurements but keeping the total number of bits constant is shown. The 1st set of data is for rate(R) = 1/2 and measurement space (K) = 0.2; R = 2/3, K = 0.25; R = 3/4, K = 0.3; R = 5/6, K = 0.325. The SSIM obtained are 0.8554, 0.8851, 0.2607 and 0.1474 respectively. The total number of bits = 25344. The 2nd set of data is for R = 1/2 and K = 0.3; R = 2/3, K = 0.4; R = 3/4, K = 0.45; R = 5/6, K = 0. 5. The SSIM values obtained are 0.9023, 0.9232, 0.2774 and 0.1384, respectively. The total number of bits = 39168. The 3rd set of data is for R= 1/2 and K = 0.4; R = 2/3, K = 0.54; R = 3/4, K = 0.6; R = 5/6, K = 0.675. SSIM values obtained are 0.9232, 0.9325, 0.2191 and 0.1239 respectively. The total number of bits = 52992. From the plot it is seen that if the measurement space is increased and a higher rate LDPC code is used then the reconstruction (SSIM) is not good. On the other hand, SSIM of rate 1/2 code is slightly less than that of rate 2/3. Thus simply increase in the sample space or decrease in the code rate does not increase the SSIM. An optimal value of the code rate and sample space/ measurements needs to be obtained.

V. Conclusions

This work studies the effect of a radio mobile channel on CS reconstruction image using RM scheme. It also proposes a method to construct a larger length LDPC code from IEEE 802.16 standard. This work shows that better CS reconstruction is achieved when the CS samples are encoded by LDPC before transmission. LDPC codes lower the BER of the received CS samples. BER of transmitted CS samples, without LDPC coding is sufficiently high. With the increased percentage of CS sample space transmitted through the channel, better reconstruction is obtained. For a fixed CS sample space better reconstruction is obtained when the rate of the LDPC code is increased. Under constant power constraint, simulation results show a trade off relationship between the code rate and the number of measurements on SSIM values. Extensive simulation results show that a moderate CS space encoded by rate 2/3 LDPC code gives significantly improved SSIM values. The proposed work may be extended as a rate and an energy efficient system design.

References

[1] E. J. Candes, J. K. Romberg, and T. Tao, Robust uncertainty principles: Exact signal reconstruction from highly incomplete frequency information, IEEE Trans. Inf. Theory vol. 52, pp. 489 - 509, 2006.

[2] E.J. Cands and M. B. Wakin, An Introduction To Compressive Sampling, IEEE Signal Processing Magazine, vol. 21, pp. 21 - 30, March 2008.

[3] Y. Zhang, Theory of compressive sensing via 1-minimization: A non-RIP analysis and extensions, Ph. D Thesis, Department of Computational and Applied Mathematics, Rice University, Houston, TX, Tech. Rep. TR08-11 (revised), 2008.

[4] S. S. Chen, D. L. Donoho, M. A. Saunders, "Atomic decomposition by basis pursuit", SIAM Journal on Scientific Computing, vol. 20, pp. 33 - 61, 1998.

[5] R. Tibshirani, The Lasso page "Regression shrinkage and selection via the lasso".Journal of the Royal Statistical Society, Series B 58 (1): pp. 267 - 288, 1994.

[6] K. Egiazarian, A. Foi, and V. Katkovnik, Compressed sensing image reconstruction via recursive spatially adaptive filtering, IEEE International Conference on Image Processing, vol. 1, pp. 549 - 552, 2007.

[7] A. Pramnik, G. Patil, L. Borman, Small length Quasi-Cyclic LDPC code for wireless applications, IEEE AICERA/ICMiCR, pp. 1-5, 4-6 June 2013.

[8] W. Lu, K. Kpalma and J. Ronsin Sparse Binary Matrices of LDPC codes for Compressed Sensing, Data Compression Conference, Snowbird, United States, 2012.

[9] A. G. Dimakis, R. Smarandache and P. O. Vontobel, LDPC Codes for Compressed Sensing, arxiv 1012.0602.

[10] F. Chen, F. Lim, O. Abari, A. Chandrakasan and V. Stojanovi, Energy-Aware Design of Compressed Sensing Systems for Wireless Sensors Under Performance and Reliability Constraints, IEEE Transactions on Circuits and Systems I, vol. 60, no. 3, pp. 650 - 661, March 2013.

[11] H. Z orlein, D. Lazich and M. Bossert, Performance of Error Correction Based on Compressed Sensing, International Symposium on Wireless Communication Systems, Aachen,pp. 301 - 305, 2011.

[12] K. Dabov, A. Foi, V. Katkovnik, and K. Egiazarian, Image denoising by sparse 3-d transform-domain collaborative filtering, IEEE Transactions on Image Processing, vol. 16, no. 8, pp. 2080 - 2095, 2007.

[13] V. V. Veeravalli, Error Control Coding for Fading Channels class handout, Available at, vvv.ece.illinois.edu/ece559/handouts/notes5.pdf

THE 5TH INTERNATIONAL CONFERENCE ON WIRELESS COMMUNICATIONS, VEHICULAR TECHNOLOGY, INFORMATION THEORY, AEROSPACE & ELECTRONIC SYSTEMS (WVITAE-2015)
December 13-16, 2015, Hyderabad, India

Spectrum Scarcity at the Extensive and Intensive Edges: From White Space to 5G

Benoît Pierre Freyens
Economics, Faculty of BGL
University of Canberra,
ACT 2601 AUSTRALIA

Abstract[1]— **as with previous generations of networks, future 5G deployments will need to use much larger blocks of spectrum to deliver their services. This additional spectrum can either be found at the extensive edge (e.g. the digital dividend) or at the intensive edge (e.g. spectrum sharing). The successful nature of spectrum sharing in UHF white spaces in the US offers a promising lead to expand the latter, and should be contrasted with far more exclusive spectrum rights in the UHF (and other bands) prevailing in other countries, and which are currently being re-assessed by regulators. This short paper revisits the key mechanisms of the white space model in which spectrum usage rights recognise a primary user, broadcasters, but tolerate opportunistic usage by symbiotic secondary users such as PMSE users, and potentially, much less symbiotic users such as providers of mobile broadband and telecommunications applications. It then draws inference to help define critical spectrum sharing arrangements needed for future 5G deployment and implications for regulatory reforms to highly prescriptive spectrum rights arrangements.**

Keywords **– Spectrum Sharing; White Spaces; 5G; Mobile Broadband; Broadcasting**

I. INTRODUCTION

The massive spectral efficiency gains achieved by the advent of digital transmission technology are slowly dissipating against a backdrop of ever surging demand for spectrum by mobile broadband and other telecommunications industries, which keep exerting pressure on a finite quantum of broadcasting spectrum. In early 2008, the Federal Communications Commission (FCC) auctioned and re-allocated 62 MHz of UHF broadcasting spectrum in the 700 MHz band, known then as the digital dividend 1.0 [1, 2]. Since 2012 the FCC has sought to further recover and re-allocate broadcasting spectrum in the lower 600 MHz band through a 'carrot-and-sticks' package known as the Incentive Auction and Repacking Program [3]. Pursuit of digital dividends 2.0 and 3.0 is also currently underway in Australia and New Zealand [4].

Concurrent to this search for additional spectrum at the *extensive* edge, there has also been successful development at the *intensive* edge. The high economic value of white spaces (unassigned UHF broadcast spectrum) has fuelled competing demands by wireless services with varying capacities to impose- and suffer from interferences. Prominent amongst those services were `symbiotic' devices (land mobile, wireless microphones), `invasive' devices (mobile broadband applications), and carrier services in search of additional UHF spectrum to test for- and prepare future 5G deployments.

The paper takes stock from the regulatory arrangements put in place by the FCC to authorise or, better put, tolerate access of high-quality broadcast spectrum resources by competing services; licensed broadcasting stations (the incumbents), program making and special event (PMSE) users, unlicensed mobile broadband devices, and telecommunications networks. The motivation for the paper is to inform the spectrum scarcity debate that is intensifying in the United States and elsewhere as future requirements for 5G networks are being laid out.

This question is of particular importance because a number of countries such as New Zealand, Australia, and the UK that had legislated or otherwise authorised highly exclusive spectrum rights in 1989, 1992 and 2006 (including property rights regimes) are now pondering the potential negative implications of high exclusivity rights for the spectrum requirements of future network developments. There is increasing understanding that any plan to address spectrum scarcity in the future must necessarily include lowering the extent of these rights to some degree, to allow for instance blanket or conditional permission for secondary users to intervene and exploit even very-short term spectrum opportunities. So, this new development contrasts with the regulatory

[1] Contact details: Ben Freyens, Associate Professor of Economics, Faculty of BGL, University of Canberra, Email: ben.freyens@canberra.edu.au. The views presented in this paper should not be assumed to represent the views of University of Canberra.

orthodoxy prevailing just one or two decades ago in spectrum reforms countries, which emphasised certainty and exclusivity over flexibility and sharing [5]. The white space model is an example of the latter, tolerating secondary usage of assigned but temporary idle spectrum as long as opportunistic users conform to non-interfering etiquette. Although this model has attracted very different types of users and led to no shortage of controversy between regulators and primary users it offers one of the main avenues to reduce spectrum scarcity at the intensive edge for 5G networks.

II. SHARING AT THE INTENSIVE EDGE

The high economic value of white space spectrum and the apparent tolerance of broadcasters for early `symbiotic' white space users soon attracted new generations of innovative wireless technologies, particularly designed for mobile broadband applications (with Microsoft and Google, two major players). Mobile broadband devices generally operate at higher power, use far more sophisticated technology than their predecessors and generate much higher economic value than older, symbiotic devices such as wireless microphones. Concerned about the potential for interference - through critical mass effects - broadcasters have opposed these new `invasive' white space users and, in a high-profile legal action, sued the US regulator (the FCC) for initially authorising their operations [6]. The FCC has since recognised the potential for interference between broadcasters and mobile broadband white space users and has settled the matter by requiring the use of geo-location databases for the operation of low power unlicensed wireless devices (ET Docket 04-186 & ET Docket 10-174) and for unlicensed mobile broadband devices (47 C.F.R. §§ 15.701-.707). The FCC rulings specifically require white space users to identify vacant channels through their devices' geo-location database accessibility capabilities [7]. Similar developments are underway in the UK, with plans for opportunistic use of unused DTT UHF spectrum by the end of 2015 [8].

Market demand for access and use of UHF spectrum holes will only worsen over time. On the one hand, the quality of UHF white space spectrum is such that there is and will be increasing demand for secondary usage of unused UHF spectrum by an ever larger array of wireless services - particularly for `last mile' rural broadband access, machine to machine communications, and for urban broadband architectures. On the other hand, broadcasters and white space users will also soon have to contend with added competition from 4G and 5G networks operators. In the US, Germany and Sweden, the digital dividend (the spectrum made available through higher spectral efficiency of digital technologies) was auctioned to telecommunications carriers. By clawing back UHF spectrum from broadcasters and reallocating the digital dividend to cellular services, regulators now face the arduous task of allocating licences (or unlicensed rights) in ways that maximise the overall economic value generated by three very different types of services on a fixed quantity of very high value spectrum. Broadcasting, mobile broadband and cellular networks vary considerably in the transmission power they use (and implied potential for interference), in their economic nature (public, private or mixed goods) and in the value they generate through company profits and consumption benefits. Consequently, the socially desirable partitioning of this fixed, non-substitutable amount of spectrum (the UHF Band) amongst these three services ranks as one of the most important contemporary policy questions for regulatory agencies such as the FCC, OFCOM and various others.

Regulators have so far threaded cautiously. Except for the FCC's 2008 momentous decision, no other regulatory agency has authorised mobile broadband devices on TV white spaces yet. Except for Australia's 2010 decision to reduce the degree of exclusivity of its property rights regime there are also few indications that regulators would tolerate white space devices in spectrum licensed to cellular network carriers. In their post-digital switchover band planning exercises, regulators have also been careful to assign high power (DTV broadcasters) at the lower end of the UHF band and low-power services (LTE networks) at the higher end, whilst separating the two services with a large guard band. Yet, engineering research suggests that broadcasters 'use of existing cellular infrastructure could release further spectral gains, but would require specific guard space arrangements with carriers, which mobile broadband devices could further exploit (see for instance various contributions to IEEE DySPAN2011).

A. Symbiotic and Invasive Usage of White Spaces

A defining characteristic of white spaces is that they consist of UHF channels *allocated* to broadcasting but not *assigned* to the provision of broadcasting services. Analog TV needs to keep free, unencumbered channels between used channels in any one city in order to warrant sufficient control on interference from signals transmitted by adjacent bands' services. As guard spaces, white spaces are therefore specifically assigned to buffer against interferences from neighbouring broadcasts at the edge of a license area. A device, which opportunistically uses these available channels, is commonly referred to as a white-space device. Historically, there has been two types of devices: (i) symbiotic and (ii) invasive devices, and two approaches

to unlicensed spectrum-sharing: (i) overlay (cognitive radio-based: sensing and occupying idle spectrum, which is vacated upon usage by the primary user) and (ii) underlay (low/spread power but permanent operations under the noise floor of many primary users).

Symbiotic devices have long co-existed with broadcasters on unused UHF guard bands. The best profiled example is wireless microphones used for Program Making and Special Events (PMSE). Wireless microphones are mostly used by stage performers (e.g. for concerts) but also by TV performers (e.g. reality shows), using idle television channels in given locations. Wireless microphones combine a `quasi-overlay' approach - as their operators determine the idle channels that they can safely operate in - with an underlay approach - they are quite low power and operate below the noise floor of many broadcasts transmissions. In the US, the relationship was always based on tolerance rather than legitimacy. Officially part of the American Broadcast Auxiliary Service, wireless microphones are theoretically subject to licensing. However, due to the overlay/underlay nature of the equipment, interferences have been rare, mild and have proved impossible to detect in real time anyway. Consequently, licensing requirements never saw much enforcement by the US regulator (the FCC) and a well-funded corporate media constituency, now politically difficult to disenfranchise, has emerged. To a large extent, this constituency was not perceived as harmful and was quietly tolerated by broadcasters. For many years, the two services have co-existed pacifically on licensed broadcast spectrum. The status-quo was challenged in 2008, when the FCC auctioned the 700 MHz licences clawed back from broadcasters through digital switchover, which required PMSE users to migrate to lower segments of the UHF Band. In Australia as in the UK, the use of wireless microphones for PMSE usage in white space is licensed but subject to refarming after digital switchover. In the UK, for instance, PMSE usage will be migrated out of the 800 MHz band at a significant re-equipment cost to the industry.

Invasive devices followed in the wake of symbiotic devices' lasting success in establishing a niche in white space spectrum. Initially, around 2002, these devices took an `underlay' approach to spectrum sharing, transmitting under the noise floor of primary users. Ultra-wide band devices provide the most obvious examples of underlay signal devices. Ultra-wide band technology operates on very large bandwidths and across a number of bands used by licensed equipment. It is mostly used for personal local area networks, radar, and imaging and surveillance applications. The devices' power density (power per MHz) is so low that they do not cause interference to high power equipment such as broadcasters' transmitters. Although these devices have been allowed in a number of bands in the US, the UK and some Continental European nations, broadcasters remain wary of ultra wide band technology and have successfully obtained regulatory limits to the range of frequencies it can use (in most cases in much higher frequencies than UHF).

However, invasive white space usage re-emerged soon afterwards with the FCC's 2008 decision [6] to open up TV channel white spaces to unlicensed cognitive radio technologies for mobile broadband applications. The degree of technological sophistication, cutting-edge innovation and the high economic value of these applications was the main rationale driving the FCC decisions. For instance, use of TV white spaces by these new technologies has proved highly suited for (i) the deployment of `Wi-Fi on steroids' urban networks (Wi-Fi is low-power and transmits on microwaves, which restricts both range and wall penetration); (ii) the provision of `last mile' broadband in rural services where fibre is too expensive and where, again, long signal propagation properties are needed; and (iii) machine to machine communications, where again white spaces' wall penetration properties could enable automatic utility metering in buildings.

B. Promoting Spectrum Sharing in the White Space Model

Early ideas proposed including GPS receivers and programming each invasive white space device with a database of all TV stations in an area, however this would not have avoided other non-stationary or unlicensed users in the area, or any stations licensed or altered after the device was made. In early 2009, US Broadcasters asked a Federal Court to rescind the 2008 FCC authorization for white space usage by invasive white space devices on the ground that testing of white space sensing devices had been insufficient. Initial tests performed by the FCC in early 2008 showed that portable, unlicensed personal broadband devices operating in the same band as TV broadcasts could indeed cause interference. The FCC subsequently agreed on some device restrictions, including using geo-location technology to allow invasive devices to compare their location against an established database of TV stations. Invasive devices that did not incorporate geo-location capabilities would be considered for authorisation on a case by case basis and have to submit to a rigorous application process for FCC certification. For a while, the deployment of invasive white spaces devices appeared impeded by uncertainties over future reallocation of TV bands, over the certification of technologies intended to identify white spaces, and slow progress on the establishment of a system of geo-

location facilitated database consultations. However, the US Congress then drafted legislation in July 2011 advocating use of incentive auctions[2]as a way to make more UHF spectrum available for mobile broadband devices. Both the FCC and OFCOM have since moved on to a regime allowing non-interfering access through geo-locational capability [7, 8] Finally, Australia has in December 2011 passed legislation amending its Radiocommunications Act 1992 to develop the regulatory discretion to authorise secondary usage of invasive white space devices in spectrum protected by property rights (such as used to license telecommunications networks).

III. SHARING AT THE EXTENSIVE EDGE: SERVICES COEXISTENCE

The deployment of mobile white space technologies on primary and secondary basis is now well underway. In its 2010 National Broadband Plan, which mostly targeted alleviating spectrum scarcity at the *extensive* edge the FCC expressed the need to make 300 MHz of spectrum available for mobile broadband within 5 years, of which 120 MHz should come from TV Bands. Given the fixed physical constraints on the amount of UHF spectrum available such objectives can only be achieved through more efficient use of frequencies allocated to broadcast TV (470-698 MHZ) and auctioned to network services (various blocks between 698 and 806 MHz). Implicitly, improving the economic usage of these blocks of spectrum will require planning for some form of co-existence between the various services involved.

Improved usage efficiency at the extensive edge will also require carefully balancing the economic value created by new services against the interference costs they may generate (or suffer from). These trade-offs will soon emerge in other countries than the United States. A worldwide process of UHF reallocation from broadcasting to telecommunications technologies requiring a high degree of licence certainty (e.g. HSPA, WiMAX and LTE networks) is currently underway in a large number of other OECD countries. There too, the reallocation process will transform the increasingly difficult relationship between broadcasters and white space devices into a triangular, more complex and interactive contest over UHF spectrum rights.

Coexistence will be difficult. In particular, broadcast services (such as DTV) and telecommunications networks (such as 3G) are fundamentally incompatible technologies. Broadcasting uses a small number of sites to transmit at extremely high power over a large area. By contrast, network carriers deploy a much larger number of base stations (usually in cellular-like pattern) and operate at very low power levels. The potential for broadcasters to interfere with networks is large and the general regulatory approach adopted so far in many countries is to separate is to separate the UHF Band in a lower segment (for digital broadcasting) and a higher segment (for telecommunications networks), with a large guard band in between the two services and smaller guard bands between each licensed operator.

An alternative approach is to interleave broadcasting and network services with medium to large guard band separating licensed spectrum blocks from one another. While this approach may appear inefficient due to the larger guard space requirements, the fact that these guard spaces can be used by white space devices to generate important economic benefits suggests the presence of trade-offs so far ignored by regulators. There may also be synergies between broadcasting and network services that have not been explored so far. For instance, Ericsson Research has recently pioneered several experiments in various regions of the US showing the suitability and higher spectral economy of designing alternative transmission architectures for TV broadcasters based on using existing telecommunications networks infrastructure [9]. Whereas the development of new cellular networks for broadcasters would be highly uneconomical, having broadcasters use existing carrier infrastructure would be feasible and more efficient than current broadcasting systems.

These findings spell out a possible future in which TV broadcasters could relinquish a large amount of UHF spectrum for network and broadband applications whilst operating viably and more efficiently using existing cellular infrastructure. Whereas such an arrangement would reduce the power requirements of broadcasters, they would still require regulating large guard bands between TV and telecommunications services. Since mobile broadband devices make a high-value usage of the unused guard bands separating the other two services, there seems to be no economic rationale for regulating against the operations of white space devices in those guard bands. Instead, regulators should be encouraged to find optimal trade-offs between the value generated by mobile broadband applications and the interference cost imposed on the primary users of the UHF Band (especially networks, which are considerably more sensitive to interference).

Of course, entrenched secondary rights for - and widespread use of - invasive white space devices in the UHF band could seriously constrain reallocation of the band from broadcasting to telecommunications if a full-scale migration of broadcasting out of UHF was to proceed later on (a possible digital dividend 2.0 in the

[2] Incentive auctions differ from mainstream auctions in that the FCC manages the auctions, but the seller is a broadcaster acting on a voluntary basis.

medium to long-term). In other words, developments at the intensive edge may thwart or significantly slow down progress at the extensive edge. This would particularly be the case if the regulatory requirements for white space devices are based on the assumption that the UHF band will continue to be used for digital terrestrial television, rather than for a mixed environment also including telecommunications networks. If the former prevails, white space devices may have few incentives to develop a capacity to operate in a telecommunications environment without causing interference. Alternatively, if developers of white space devices invest in the capacity to cooperatively share the UHF band with advanced telecommunications technologies (hypothetically in shared-infrastructure arrangements with broadcasters), the deployment of innovative white space technologies in the UHF band could allow early realisation of the economic potential of the UHF band without compromising higher value use in the medium term.

IV. CONCLUDING REMARKS

The ITU decision at WRC-12 to allow mobile use of 694-790 MHz in Europe, Africa and the Middle East is a clear example of how demand for mobile data is driving regulatory change. Broadcasters initially understood the telecommunications industry to be a competitor for their UHF spectrum resource, but the emergence of mobile broadband devices and standards used e.g. for machine communications present such growth areas for existing networks that we can confidently predict that competition for spectrum (as well as customers) and therefore spectrum scarcity will intensify.

In this context, where then will the new spectrum requirements be met for future network developments, which will have to offer higher throughput, extended device autonomy and much improved latency responses? Without looking too far into the future, how will we release spectrum to run trials on temporary assignments? In this article I have underpinned this question in quantity terms (extensive edge) and quality terms (intensive edge). At the extensive edge, the main challenge is technological (finding new spectrally-efficient technologies) and political (refarming smaller operators). At the intensive edge, the main challenge is no longer technological (the capacity to access spectrum opportunistically in milliseconds is well established) but regulatory: designing licensing arrangements that do not preclude, and ideally encourage spectrum sharing opportunities. Neither an administrative approach nor an exclusive property rights approach to white space assignments would have resulted in the observed successes of this spectrum-sharing model. Any spectrum sharing model in which a primary user keeps the discretion to deny spectrum sharing opportunities to secondary or third users to restrict competition would also be bound to fail.

As the first wave of regulatory arrangements for invasive WSD is finalised and implemented, care must be taken to ensure that regulatory arrangements developed at the intensive edge blend seamlessly with developments at the extensive edge. More specifically, a piecemeal approach consisting of encouraging spectrum sharing by lowering primary users' rights may run into difficulties if these rights remain defined at a much higher degree of exclusivity at the extensive edge.

REFERENCES

[1] B. P. Freyens and M. Loney, "Digital switchover and regulatory design for competing white space usage rights " *New Frontiers in Dynamic Spectrum Access Networks (DySPAN), 2011 IEEE Symposium*

[2] B. P. Freyens, "A Policy Spectrum for Spectrum Economics," *Information Economics and Policy,* vol. 21, pp. 128-44, 2009.

[3] FCC. (2014, 25 March 2012). Expanding the Economic and Innovation Opportunities of Spectrum Through Incentive Auctions. *GN Docket No. 12-268, June2, 2014, FCC 14-50, Washington, DC:*

[4] B. P. Freyens and M. Loney, "Projecting Regulatory Requirements for UHF White Space," in *Wireless Networks in the TV White Space: Concepts, Techniques and Applications*, R. A. Saeed and S. J. Shellhammer, Eds., ed Boca Raton, FL: Taylor & Francis/CRC Press, 2012.

[5] B. P. Freyens, "Shared or Exclusive Radio Waves? A Dilemma Gone Astray," *Telematics and Informatics,* vol. 27, pp. 293-304, 2010.

[6] FCC, "In the Matter of Unlicensed Operation in the TV Broadcast Bands: Second Report and Order," Federal Communications Commission, Washington, D.C ET Docket 08-260A, 2008.

[7] ITU. (2014, 15 May 2009). Overview of FCC's New Rules for TV White Space Devices and Database Updates. *ITU-R SG 1/WP 1B Workshop: Spectrum management issues on the use of white spaces by cognitive radio systems*.

[8] OFCOM, "Implementing TV White Spaces " Office of Communications, February 2015.

[9] J. Huschke, J. Sachs, K. Balachandran, and J. Karlsson, "Spectrum requirements for TV broadcast services using cellular transmitters," *New Frontiers in Dynamic Spectrum Access Networks (DySPAN), 2011 IEEE Symposium*

THE 5TH INTERNATIONAL CONFERENCE ON WIRELESS COMMUNICATIONS, VEHICULAR TECHNOLOGY, INFORMATION THEORY, AEROSPACE & ELECTRONIC SYSTEMS (WVITAE-2015)
December 13-16, 2015, Hyderabad, India

Study of Radiated Emission from Wireless Positioning System and the strategies to minimize the Radiations

Shreenivas Jog
Dept. of Electronics & Telecommunication Engineering
Dr. D.Y. Patil Institute of Engineering & Technology
Pimpri, Pune, India.
srjog_etc@bsnl.in

Suvidha Chitnis
Dept. of Electronics & Telecommunication Engineering
Dr. D.Y. Patil Institute of Engineering & Technology
Pimpri, Pune, India.
suvidhachitnis@gmail.com

***Abstract*—This paper presents the measurement of Radiated Emission from GPS based Vehicle Positioning and Localization System and implementation of the mitigation techniques in order to make the system compatible with the EMC requirements as per CISPR EMI/EMC Standard. In current scenario, the GPS based Vehicle Positioning System is essential part in the application areas like Logistics, Public Transports, Naval Ships, Railways etc. Due to its usefulness in daily life, the system has been taken as the test model for this research work. The Radiated Emission test for GPS based Vehicle Positioning System has been conducted at the Centre for Electronics Test Engineering (CETE), Pune, India.**

This model was first tested in the GTEM Cell after which it was found that some of the readings were above the limits specified as per the EMC standard. In this paper, the techniques have been proposed to reduce the level of Radiated Emission. The shielding by Aluminum Enclosure has been implemented. The results of re-testing the GPS based system with Aluminum Enclosure are presented. After re-test it was found that the Radiated Emission level was found to be reduced by 10 to 15 dB making the system compatible with the EMC requirements.

***Index Terms* —Radiated Emission, GPS based VTS, EMI receiver, CISPR, Positioning, Localization, Vehicular Communication**

I. INTRODUCTION

Modern electronic equipment operates on high frequency signals. EMI is the major issue as far as the performance of electronic equipments is concerned. Hence, it is essential to overcome the EMI problem and to meet the EMC requirements. The emission from wireless / electronics equipments must be restricted within specified limits as per EMI/EMC standard like CISPR or MIL-461E.

For this research work GPS based Positioning and localization system has been taken as a model. The GPS based system consists of a GPS receiver (Pro Gin SR87), a microcontroller 89S52 to process the positional data and LCD to display the information. This GPS module transmits current position of vehicle with the help of GSM Module (SIM 300) in the form of latitude and longitude via SMS to the registered mobile phone [1]. The accuracy of GPS receiver (10 to 15 meters) can be improved by using Differential GPS (DGPS) up to 3 to 5 meters.

In this research paper Aluminum Enclosure is designed and implemented after comparing the shielding effectiveness of various metals. The block diagram of GPS based Wireless Positioning System is shown in Figure 1.

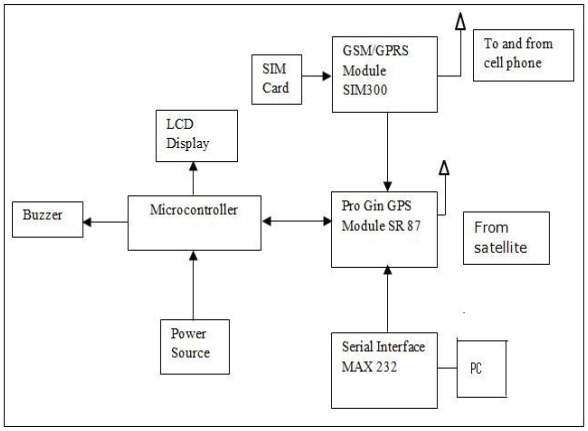

Fig.1: Block diagram of GPS based Wireless Positioning System

II. RADIATED EMISSION TEST IN GTEM CELL

The structure of GTEM (Giga-hertz transverse electromagnetic) cell resembles like a big horn antenna. It can be described as flared coaxial line terminated at one end. The walls form outer shield of the coax, while the inner conductor takes the shape of a septum. While making a connection with an EMI receiver, walls are connected to the shield of the coaxial cable and the septum to the inner conductor.

The septum is terminated at the other end by a resistive termination. The termination is essential to avoid reflection and maintain uniform field. Such terminations can work up to 200MHz. Termination above 200MHz is affected by conical absorbers. It extends the range of GTEM cell up to 40GHz. The termination maintain uniform field and avoid reflections [2].

During the test EUT (Equipment under Test) is placed on a EUT manipulator. The emission from the device is measured and readings from all three axes have been measured. These readings are then fed to the correlation software, from which we get final values. Measurement in a GTEM cell is an alternative to OATS (Open Area Test) [2].

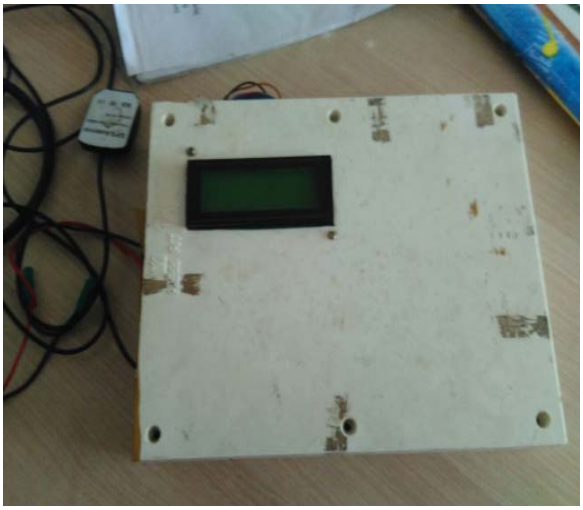

Fig. 2: View of GPS based Wireless Positioning System before shielding

Figure 2 shows GPS based Vehicle Positioning and Localizing system before shielding.

III. Methods to Reduce Radiated Emission

The following methods have been proposed to reduce the radiated emission [3, 4, 5].

A. Shielding with metal enclosures:

Metallic enclosures made from Copper, Aluminum, Mu-metal or magnetic materials could be used to shield entire assembly. The selection of metal depends on the type of wave, amount of attenuation required and the cost of shielding metal.

B. Grounding and Bonding:

Grounding is essential to control EMI. Single point or multipoint grounding techniques can be used depending upon frequency of application. Bonding is processes in which components, equipment, or several systems are electrically connected and further grounded to system earth point.

C. Design of PCB:

Increasing usage of printed circuit board in complex electronics requires unique shielding solutions. Solving EMI problem at PCB level is less expensive compared to further lab testing. When the frequency is greater than 2 GHz, the board-level shielding can be enhanced with the addition of microwave absorbers. From EMI point of view, multilayer PCB is recommended for getting better results [6].

D. Filtering:

RFI Filters can also be added in power supply lines to reduce the radiation. EMI filters can be classified as power line filters and data filters. Power line filters are incorporated into power mains to allow only power frequency while blocking all other frequencies.

IV. Shielding Effectiveness

While exploring the materials for enclosures, various materials like Copper, Aluminum, Mu-metal, Stainless Steel, Mild Steel etc were considered and compared on the basis of various parameters like shielding effectiveness, mechanical strength and immunity to corrosion. Aluminum has less relative conductivity (0.61) than Copper, but it is good option for corrosive environment. Aluminum is a good shielding material specially meant for EMI/EMC conditions. Mild Steel and Stainless Steel having less shielding effectiveness are popular materials used in commercial equipment since they have a good mechanical strength. However, Mild Steel is susceptible to corrosion. Hence Aluminum shielding enclosure has been designed and implemented [7].

The total shielding effectiveness of a shielding material (*SE*) equals the sum of the absorption loss (*A*), the reflection loss (*R*) [3].

$$SE\ (dB) = R\ (dB) + A\ (dB) \quad (1)$$

where,

$$A = 3.34t \sqrt{(f \mu_r \sigma_r)}\ dB \quad (2)$$

$$R = 168 + 10 \log (\sigma_r / \mu_r f)\ dB \quad (3)$$

Thickness of Al enclosure is $t = 0.254$ inch (1mm),

μ_r is relative permeability,

f is the frequency, and

σ_r is relative conductivity

TABLE I: SPECIFICATIONS OF METALS

Material	Relative Conductivity (σ_r)	Relative Permeability (μ_r)
Cu	1	1
Al	0.61	1
Mild Steel	0.178	2000
Mu-metal	0.03	20000

With above mentioned values [3] as indicted in Table I, shielding effectiveness of Al, Mu-metal, Mild-Steel and Copper enclosure is calculated over entire frequency range with the help of MATLAB and plotted as shown in figure 3.

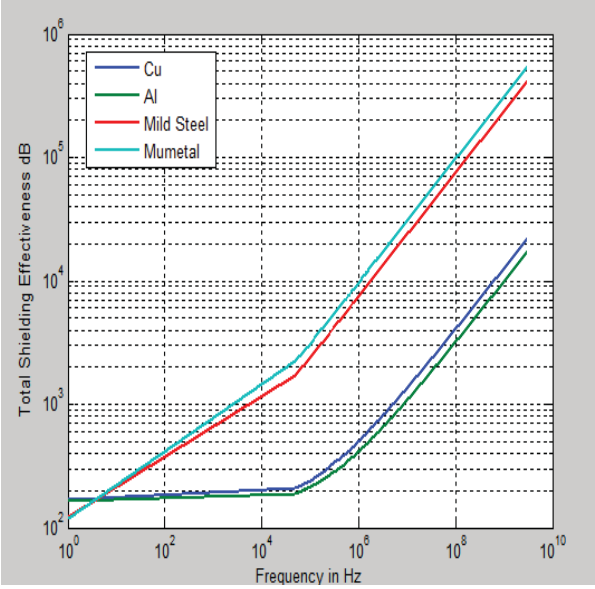

Fig. 3: Graph of Shielding Effectiveness (SE) of Al, Cu and Mu-metal and Mild-steel

.

V. DESIGN OF SHIELDING ENCLOSURE

Aluminum enclosure has been designed with opening for cables and LCD. Dimensions are: (l) =165mm, (b) =115mm, (h) =73mm, thickness (t) = 1mm.

Figure 4 shows Aluminum Enclosure as per the dimensions indicated above, implemented for PCB of GPS based Vehicle Positioning System.

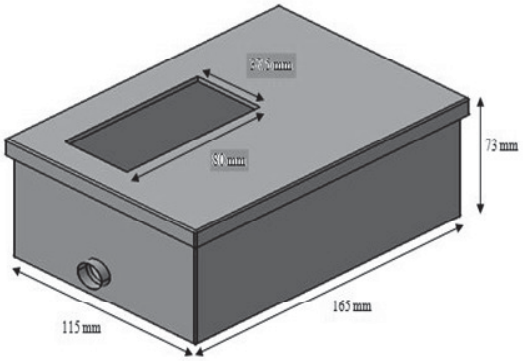

Fig. 4: Aluminum Enclosure for GPS based Wireless Positioning System

The conductive gaskets serve as effective shielding material used in gaps, holes, small openings of enclosures. A gasket may be required if the gaps, slots and holes around the metal plate interface allow excessive radiation of the internally generated electromagnetic waves [3, 4]. Such emissions cause the equipment to radiate more than specified values as per the EMI/EMC standards. The Aluminum EMI Enclosure has been sealed by Silver filled conductive gaskets to avoid any leakage of radiation through holes, gaps and openings. Silver filled Silicon gasket has wider operating temperature range (-55^0 to 165^0C) and good shielding effectiveness (110dB) with lower volume resistivity (0.008 ohm-cm) [8].

Fig. 5: View of GTEM Cell with testing of GPS Model

Figure 5 presents model kept in the GTEM cell for testing of Radiated Emission at CETE, Pune.

TABLE II: RE LEVEL WITHOUT SHIELDING AND WITH AL SHIELDING

Frequency in MHz	E-Field Readings Before Shielding (dBuV/m)	E-Field Readings After Shielding (dBuV/m)
33.12	37.05	26.22
39.76	35.47	32.66
49.76	34.25	20.62
56.80	36.04	21.94
60.88	42.34	25.57
79.28	43.51	37.44
93.52	29.35	25.24
100.72	25.42	17.79
115.20	24.91	14.9
127.20	25.72	20.64
132.74	24.69	21.54
154.80	22.27	20.17
178.80	28.07	27.49
184.32	26.03	21.0
195.32	26.10	22.76
212.00	22.07	20.72

VI. OBSERVATION AND RESULTS FOR VEHICLE POSITIONING AND LOCALIZATION SYSTEM

The model was tested in GTEM cell at Centre for Electronics Test Engineering (CETE), Pune, India. Radiated Emission readings were taken in three orthogonal axes for frequency ranges of 30MHz to 1GHz. In this case, CISPR 11 standard of class A has been taken as a reference. Class A standard is defined for the industrial equipments. Standard level specified is 40dBuV/m for 30-230MHz and 47dBuV/m for the range of 230-1000 MHz frequency.

For initial frequencies up to 300MHz, some of the readings exceed the standard level specified as 40dBuV/m. Shielding Effectiveness is found by MATLAB Simulation. The GPS model has been enclosed with Aluminum shielding cabinet with 1 mm thickness with conductive gaskets and whole assembly was again re-tested. Table II shows RE level before and after shielding.

Radiated Emission from the model was found to be more than specified limits as per the standard for a particular frequency range without Al Enclosure. The radiated Emission was found to be reduced around 10 to 15 dB with Al Enclosure shielding. Table II shows the some of the observations with and without Al shielding. Figure 6 shows the plots of Radiated Emission with and without Al shielding.

It was observed that some readings without Enclosure were above the standard limit hence model was not complying with the EMC standards. Hence, it was essential to implement an appropriate metallic enclosure shielding to the PCB of this model.

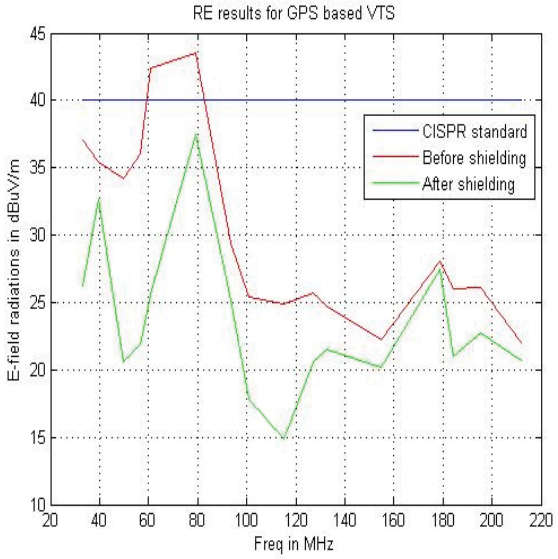

Fig. 6: Graph of observations of E-field Radiated Emission before and after shielding with and without Al Enclosure for GPS Model

The reading without enclosure was exceeding specified level at a frequency of 33MHz. This RE level was due to third harmonic of crystal oscillator (11MHz) of model. The second peak was found at 79MHz frequency. It was also due to harmonic of crystal oscillator. After shielding with Al Enclosure, RE level was found to be reduced below specified level. For further improvement in the results, it is proposed that crystal should be covered with Copper clamps grounded to the system / PCB earth. Figure 7 represents model with Aluminum shielding.

`

Fig. 7: Photograph of GPS based Wireless Positioning System with Al Shielding

VII. Conclusion

The Radiated Emission from the GPS Positioning system model was found to be more than specified limits as per CISPR EMI/EMC standard specifically at frequency band of 60 MHz to 80 MHz. Aluminum Enclosure of 1 mm thickness using conductive gaskets has been designed and implemented for the GPS based Vehicle Positioning System. With the implantation of Al Enclosure, it was found that Radiated Emission level was reduced by 10 to 15 dB. The Model with Enclosure was found to be compatible with CISPR EMI/EMC Standard.

Acknowledgement

The authors wish to sincerely thank Dr.R.K. Jain, Principal, Dr. D.Y. Patil Institute of Engineering and Technology, Pimpri, Pune, Savitribai Phule Pune University, Shri Krishna Murari and Shri Chetan Kathalay from Centre for Electronics Test Engineering (CETE), Pune for their valuable help for this research proposal.

References

[1] Shreenivas Jog, M.S. Sutaone, Bhushan Joshi, VrushaliBahirat, Jinesh Nair and AstitvaKarunesh, "Implementation Of a System for Localisation and Positioning of Vehicles Using GPS and GPRS Technology" International Journal Of Future Computer and Communication ,vol 3,No.1, pp.18-21, February 2014.

[2] Chetan Kathalay "A Practical Approach to Electromagnetic Compatibility", EMC publications, Pune, Edition 1.

[3] Henry Ott, "Electro-Magnetic Compatibility Engineering", A John Wiley & Sons, INC., publications, 2009.

[4] B. Keiser, "Principles of Electromagnetic Compatibility" 3rd edition Artech House, 1987.

[5] Tim Williams, "EMC for product design" Newness *Publications*, 4th Edition, 2007.

[6] Eric Benedict, PCB Design for EMI/EMC Compliance, WEMPEC Seminar 21st July 2000.

[7] Shreenivas Jog, M.S. Sutaone, V.V. Badawe "Performance Comparison of EMI Enclosures for GPS based Vehicle Tracking System", published in ACEEE, *International Journal for Recent Trends for Engineering and Technology (IJRTET)* Volume 6, Issue 2, pp. 274 to 278, February -2012.

[8] Application Notes: SSD Polymers EMI Elastomer Shielding Gaskets.

THE 5TH INTERNATIONAL CONFERENCE ON WIRELESS COMMUNICATIONS, VEHICULAR TECHNOLOGY, INFORMATION THEORY, AEROSPACE & ELECTRONIC SYSTEMS (WVITAE-2015)
December 13-16, 2015, Hyderabad, India

Conducted EMI Analysis of Vehicle Positioning System and Strategies to Reduce Conducted EMI

Shreenivas Jog
Dept. of Electronics & Telecommunication Engineering
Dr. D.Y. Patil Institute of Engineering & Technology
Pimpri, Pune, India.
srjog_etc@bsnl.in

Nidhi Chaturvedi
Dept. of Electronics & Telecommunication Engineering
Dr. D.Y. Patil Institute of Engineering & Technology
Pimpri, Pune, India.
nidhi2308@gmail.com

***Abstract*— The main objective of this paper is to measure the Conducted Emission (EMI) and propose mitigation techniques in order to meet the Electromagnetic Compatibility (EMC). For this research work, GPS based vehicle positioning system has been taken as a model. The Conducted Emission test for GPS based system has been performed using SCHAFFNER make Line Impedance Stabilization Network (LISN) and SCHAFFNER SCR 3501 Spectrum Analyzer at the Centre for Electronics Test Engineering (CETE), Pune, India which is Government of India undertaking. This model was first tested without RFI (Radio Frequency Interference) filter. The EMC standard is specified for the frequency range of 150 kHz to 30 MHz for Conducted Emission measurement. The CE level has been reduced by using filtering method. The results obtained were compared with the CISPR standard in order to investigate the effectiveness of the applied EMI mitigation techniques. The analysis and experimental results finally shows that the Conducted Emission has been reduced by 20 dB using the EMI filter.**

***Keywords*— GPS, Conducted Emission, CE, EMI/EMC, RFI, EMC Testing, Vehicular Communication**

I. INTRODUCTION

Electromagnetic Interference (EMI) is an electromagnetic pollution caused by the generation of electromagnetic energy that is unwanted. This energy can interfere with the normal operation of electronic equipment resulting in the degradation of its functionality. EMC stands for Electromagnetic Compatibility and is defined as the ability of equipment to perform satisfactorily in its intended environment without introducing intolerable interference. EMI/EMC is used as a combined term as we try to achieve EMC by limiting EMI. Electromagnetic Emission is defined as the phenomenon by which electromagnetic energy releases from a source. This emission can be in the form of a current via conducting wires known as Conducted Emission (CE) and can also be in the form of radiation through openings like displays, cable entries; ventilation holes etc. and is known as Radiated Emission [1].

Conducted Emission (CE) is the EMI emitted by equipment in the form of a current through any conductor that interfaces the equipment with the outside environment. Conducted Emission measurement is generally carried out over a frequency range from a few kilohertz to tens of megahertz. The term Conducted Emission is actually used by MIL standard 461, while CISPR/IEC based standards use the terms like terminal disturbance voltage or conducted disturbance voltage. The CISPR based test standards specify Conducted Emission (CE) measurement from 150 kHz to 30MHz on the mains cable [1].

II. GPS BASED VEHICLE TRACKING SYSTEM

As numbers of vehicles are increasing day by day, the GPS based positioning system is very useful in order to:

- Track the location of the vehicle,
- Provide protection of vehicle from thieves,
- For security and road assistance,
- For monitoring of delivery time,
- For emergency help.

The areas where GPS based vehicle tracking system is commonly used are: Schools, Public Transports, Railways, Logistics, Rented Taxis etc. The vehicle tracking system is designed using GPS (Global Positioning System) technology. The GPS system works on the principle of "Triangulation". There are 24 satellites available in the space, out of which it is guaranteed that minimum 3 active satellites are available at any time. The GPS based vehicle tracking system consists of a GPS receiver which receives the signals from the satellites. The calculation is based on the time taken by a signal to reach from each satellite. Based on this time calculation, GPS receiver can not only locate the exact location of the vehicle but also it can compute the velocity and time. It also provides details such as longitude, latitude, height from sea level [2]. Figure 1 shows the block diagram for the GPS based vehicle tracking system.

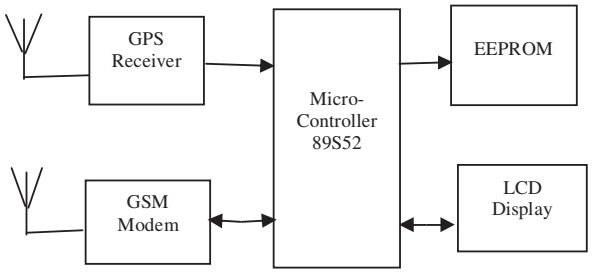

Fig. 1: Block Diagram of GPS Based Vehicle Tracking System

The GPS receiver (ProGin SR87) receives signals from the satellites, and then calculates its current location. This information is then communicated to the microcontroller (89S52) which processes this data using serial interfaces. The GSM module (SIM 300) receives request for sending vehicle location from registered cell phone. The GSM module sends reply SMS to same cell phone giving the vehicle location [2].

III. Test Setup for CE Measurement

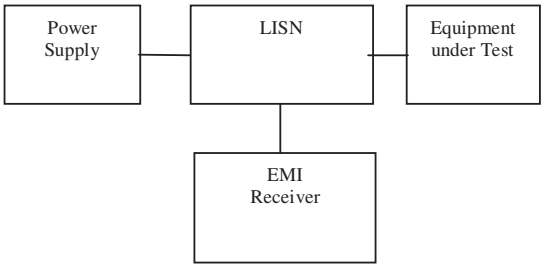

Fig. 2: Block Diagram of Laboratory Test Set Up

A basic test setup for Conducted Emission (CE) measurement is shown in figure 2. The equipment under test is connected to the power supply through a Line Impedance Stabilization Network (LISN). The LISN performs three main functions: First, it acts as a buffer and isolates the EMI receiver from the mains. Second, it functions as a filter and ensures that EUT is fed with a pure mains supply and third, the LISN stabilizes the impedance of mains to 50Ω to match the input impedance of the EMI receiver. For ensuring accurate measurement, the output impedance of the LISN must be constant and equal to the input impedance of the EMI receiver over the entire frequency range of measurement. Any mismatch between these two will result into the measurement error. The output of LISN is fed to the EMI receiver which is a double or triple super-heterodyne radio receiver [1]. The Conducted Emission test for GPS based system has been performed using SCHAFFNER make Line Impedance Stabilization Network (LISN) and SCHAFFNER SCR 3501 Spectrum analyzer at CETE Pune, India.

Conducted Emission Limits:
All EMC standards specifies that the Conducted Emission of an equipment shall be below certain limits. The CISPR standards specifies different limits for industrial use equipment, called as Class 'A' and domestic use equipment, called as Class 'B'. While performing an actual CE measurement, the limits are superimposed on the plotted graphs [1].

TABLE I: CISPR CLASS-A LIMITS (FOR INDUSTRIAL USE)

Frequency (MHz)	Limits dB(uV)	
	Quasi-Peak	*Average*
0.15 to 0.5	79	66
0.5 to 30	73	60

TABLE II: CISPR CLASS - B LIMITS (FOR DOMESTIC USE)

Frequency (MHz)	Limits dB(uV)	
	Quasi-Peak	*Average*
0.15 to 0.5	66 to 56	56 to 46
0.5 to 5	56	46
0.5 to 30	60	50

IV. Results For Conducted Emission Testing Without Filter

Table III gives the readings for GPS based system without filter while tested for Conducted Emission.

TABLE III: FINAL SCAN RESULTS FOR GPS BASED SYSTEM WITHOUT FILTER

Frequency MHz	Avg. Level dBuV	Avg. Limit dBuV	QP Level dBuV	QP Limit dBuV
0.1640	57.49	66.00	60.86	79.00
0.2160	58.65	66.00	60.87	79.00
0.2210	52.50	66.00	55.94	79.00
0.3250	63.90	66.00	65.90	79.00
11.0570	58.87	60.00	61.85	73.00
16.5920	45.98	60.00	49.65	73.00
22.1180	63.83	60.00	65.77	73.00

The Microcontroller 89S52 used in this GPS system consists of a crystal oscillator to provide clock pulses to the microcontroller. The oscillation frequency at which crystal oscillator operates is 11.0592 MHz. After analyzing the test results, it is found that the CE level which exceeded the limit was appearing at the frequency of 22.1180 MHz which is the 2nd harmonic of the crystal oscillation frequency hence

crystal oscillator is the component causing exceeded CE level.

The power supply of the GPS system consists of 1000uF electrolytic capacitor which is the part of the filter, so the other peaks which are occurring below 1MHz frequency range are due to the power supply ripple and its harmonics however these peaks are within limits. Figure 3 shows the graph of Frequency v/s. CE level for GPS system without filter.

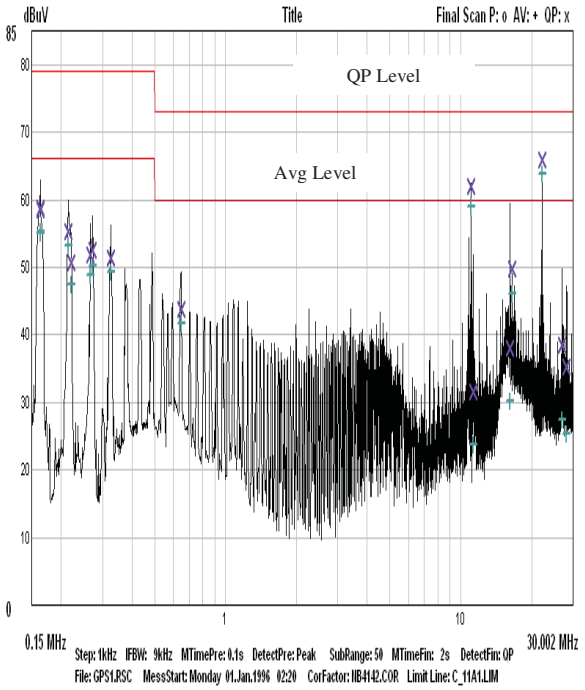

Fig. 3: Graph of Frequency vs. CE for GPS based positioning system without Filter

V. Mitigation Techniques for Conducted Emission

In order for a device to meet the EMC requirements, it must satisfy the requirements set by the American FCC, or European CISPR standards. Following are the techniques which could be helpful to reduce the conducted EMI [3]:

- Grounding technique is a kind of traditional EMI mitigation techniques. It can be applied as either single-point grounding or multi-point grounding; it depends on the noise frequency intended to be reduced. Grounding technique is used to reduce the ground impedance, there by minimizing the potential of ground loop from the circuit consisting of a number of devices/ equipments.

- Shielding is absorbing or reflecting electromagnetic energy via all kinds of shielded material, to prevent external interference or restricting devices emitting electromagnetic energy, preventing interference with other devices. Shielding is commonly a barrier, a thin piece of metal, placed between circuit boards or electronic equipment.

- Filtering is the most effective and common measure to suppress conducted EMI. Design and Implementation of Radio Frequency Filter (RFI) with X and Y capacitors and choke are used in power supply circuits to reduce the CE level within limits.

- The wiring connection to and from the power supply should be reliable and as short as possible to minimize wiring loops.

- Implementation of shielded cables with shield grounded at one end of the equipment.

VI. Results For Conducted Emission Testing With Filter

To reduce the Conducted Emission level, design and implementation of RFI filter has been proposed and implemented. A line filter is made up of capacitors and inductors which form the basic elements. The inductive part is designed to act as a low frequency pass device and as high frequency blocking device whereas the capacitors are used to shunt the unwanted high frequency noise. The basic property of EMI filter is the Insertion Loss characteristics which is basically frequency dependent. It refers to the attenuation offered by the EMI filter. Higher Insertion Loss means increased level of attenuation. Insertion Loss (IL) is the ratio of the signal level, testing without filter (v1) to the signal level with filter (v2) [4, 5].

$$IL\ (dB) = 20 \log_{10} [v1/v2] \quad (1)$$

The required attenuation can be calculated by substracting the limit from the value obtained while tested without filter.

$$(A_{req,\,CM}) = (A_{CM})_{dB} - (A_{Limit})_{dB} \quad (2)$$

$$(A_{req,\,DM}) = (A_{DM})_{dB} - (A_{Limit})_{dB} \quad (3)$$

From attenuation, the value of corner frequency can be calculated by drawing a 40db/dec slope which is tangent to the required attenuation for DM and CM. Ideally a second order filter provides 12dB per octave of attenuation after the cutoff frequency f_0.

$$f_0 = 1/[(2*3.14)\sqrt{(LC)}] \quad (4)$$

Where f_0 is corner frequency, L is the choke value and C is the capacitance value. Its transfer function is given as:

$$f(s) = 1/[1+LS/R_{load} + LCS^2] \quad (5)$$

Now in terms of radians:

$$F(w) = 1/[1+jwL/Rload + j2w2LC] \quad (6)$$

$$\text{Since cutoff frequency } f0 = 1/ [(2*3.14) \sqrt{(LC)}] \quad (7)$$

$$\text{Hence in radian } w_0 = 1/ [\sqrt{(LC)}] \quad (8)$$

and

$$\text{Damping factor} = 1/ 2R [\sqrt{(LC)}] \quad (9)$$

The damping factor describes gain at the corner frequency. As it becomes smaller, the gain at corner frequency becomes larger. From design point of view, minimum damping factor is 0.707, which provides 3dB attenuation at corner frequency. Component values can be calculated as:

CM components: C_y is limited to 3300pF because of safety reasons and the corner frequency $f_{R,CM}$ can be calculated as mentioned in above steps so we get the common mode inductor

$$L_{CM} = [1/2*3.14* f_{R,CM}]^2 * [1/2 C_y][6] \quad (10)$$

DM components: The corner frequency $f_{R,DM}$ has been found in previous steps thus the DM capacitors are

$$C_{X1} = C_{X2} = [1/2*3.14* f_{R,DM}]^2 * [1/L_{leakage}][6] \quad (11)$$

By putting the values of X and Y capacitors alongwith the corner frequency, choke value can be estimated.

Filter Specification: As far as GPS based system is concerned, following are the values for:

Rated Current: 1A
Leakage Current: 2 x 0.3 mA
(X = 0.1uF, Y= 3000pF, L= 30mH, T= 1mH)

Here P.S. = Power Supply, Eqp. = Equipment

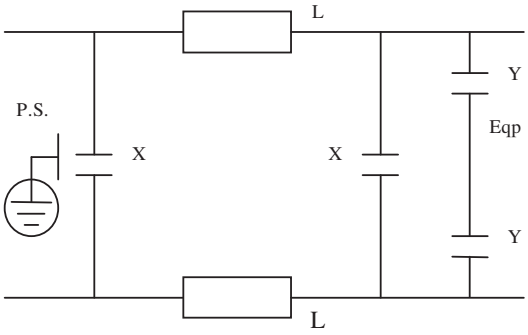

Fig. 4: Schematic of RFI Filter

Figure 4 is the schematic of RFI filter, whereas figure 5 is showing the testing of GPS system with filter [7].

Fig. 5: GPS based positioning system with Filter

TABLE IV: FINAL SCAN RESULTS FOR GPS BASED SYSTEM WITH FILTER

Frequency MHz	Avg. Level dBuV	Avg. Limit dBuV	QP Level dBuV	QP Limit dBuV
0.1640	55.00	66.00	58.82	79.00
0.2150	53.20	66.00	55.29	79.00
0.2210	47.51	66.00	50.59	79.00
0.3250	49.28	66.00	51.45	79.00
11.0570	23.67	60.00	31.63	73.00
16.5920	30.21	60.00	38.10	73.00
22.1180	49.64	60.00	51.28	73.00

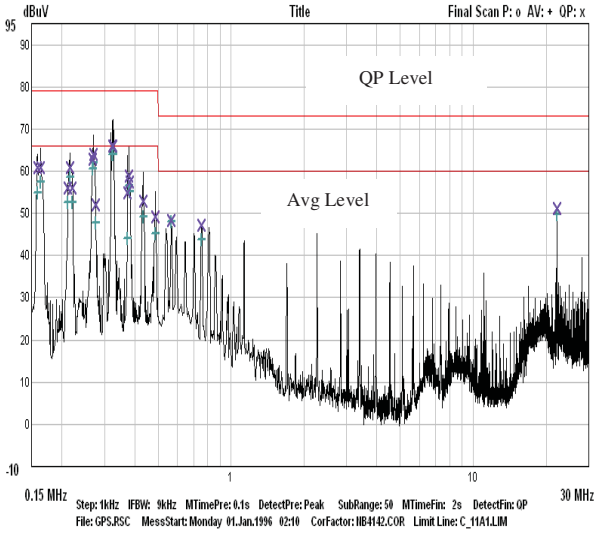

Fig. 6: Graph of Frequency vs. Conducted Emission for GPS based positioning system with Filter

The proposed EMI filter for the mitigation of conducted EMI for the GPS based Vehicle Tracking System has been designed and implemented. After re-testing the system with this filter, the Conducted Emission was found to be within safer limits making the system compatible with the EMC requirements. The average levels with filter, for the frequencies 22.1180 MHz, 0.3250 MHz and 11.0570 MHz have been observed as 49.64 dBuV, 49.28 dBuV and 23.67 dBuV respectively. From the graph shown in the figure 6 and readings as per Table IV, it is clear that peaks are reduced to the safer limits as per CISPR EMI/EMC Standard.

VII. Conclusion

The analysis of Conducted Emission from the GPS based vehicle positioning system has been performed. It was found that the CE level was exceeding the limits, specifically at the frequency of 22.1180 MHz and some of the peaks were at the boundary level of specified limits of the standard. The RFI Filter has been designed and implemented to meet specific requirements of GPS based positioning system. With incorporation of RFI Filter in power supply section, reduction in Conducted Emission level was found to be about 20dB. Results of experimentation indicate the effectiveness of the proposed EMI filter making the GPS based positioning system meeting compatibility requirements as per CISPR EMI/EMC Standard.

Acknowledgement

The authors wish to sincerely thank Dr. R.K. Jain, Principal Dr. D.Y. Patil Institute of Engineering and Technology, Pimpri, Pune, Savitribai Phule Pune University and also to Shri Krishna Murari and Shri Chetan Kathalay from Centre for Electronics Test Engineering (CETE), Pune for their valuable help for this research proposal.

References

[1] Chetan Kathalay, Book on “A Practical Approach to Electromagnetic Compatibility”, EMC Publications, Pune, Edition 1.

[2] Shreenivas Jog, M. S. Sutaone, Bhushan Joshi, Vrushali Bahirat, Jinesh Nair, and Astitva Karunesh, “Implementation of a System for Localization and Positioning of Vehicles using GPS and GPRS Technology”, International Journal of Future Computer and Communication, Vol. 3, No. 1, pp.18-21,February 2014.

[3] Schneider, Matthew J., "Design Considerations to Reduce Conducted and Radiated EMI" (2010). College of Technology Masters Theses. Paper 4, 4-21-2010.

[4] B. Keiser, “Principles of Electromagnetic Compatibility” 3rd edition Artech House, 1987.

[5] Daryl Sugasawara and Jens Paetau, “Safety, EMI and RFI Considerations”, Application note 42007, June 1996, REV. 1.0 10/25/2000.

[6] Nidhal Y. Nasser, “Practical Approach in Designing Conducted EMI Filter to Mitigate Common Mode and Differential Mode Noises in SMPS”, Journal of Engineering and Development, Vol. 16, No.1, March 2012.

[7] Shreenivas Jog, M. S. Sutaone, and Vishweshwar Badawe, "Analysis and Minimizing Strategies for Conducted Emission from Power Supply Cable of GPS Based Vehicle Tracking System”, Journal of Automation and Control Engineering Vol. 1, No. 4, pp.290-295, December 2013.

THE 5TH INTERNATIONAL CONFERENCE ON WIRELESS COMMUNICATIONS, VEHICULAR TECHNOLOGY, INFORMATION THEORY, AEROSPACE & ELECTRONIC SYSTEMS (WVITAE-2015)
December 13-16, 2015, Hyderabad, India

Design Of Low Voltage Bandgap Reference Circuit Using Subthreshold MOSFET

Sushma S Sangolli,Rohini Hongal,Ramesh Karmungi
M.Tech (VLSI Design and Testing) student, B.V.B College of Engineering and Technology, Hubli, India.
Professor, Dept. of Electronics and Comm. Engg. B.V.B College of Engineering and Technology, Hubli, India.
Manager in Analog domain, SmartPlay Technology, Banglore, India.

***Abstract*—In this paper we present design of a low voltage bandgap reference (LVBGR) for supply voltage of 1.2V which can generate an output reference voltage of 0.363V. Traditional BJT based bandgap reference circuits give very precise output reference but power consumed and area consumed by these BJT devices is larger so for low supply bandgap reference we chose MOSFETs operating in subthreshold region based reference circuits. LVBGR circuits with less sensitivity to supply voltage and temperature are used in both analog and digital circuits like high precise comparators used in data converter, phase-locked loop, ring oscillator, memory systems, implantable biomedical product etc. In the proposed circuit subthreshold MOSFETs temperature characteristics are used to achieve temperature compensation of output voltage reference and it can work under very low supply voltage. A PMOS structure 2stage opamp which will be operating in subthreshold region is designed for the proposed LVBGR circuit whose gain is 89.6dB and phase margin is 74°. Hence a LVBGR is designed which generates output voltage reference of 0.364V given with supply voltage of 1.2 V with 10 % variation and temperature coefficient of 240ppm/°C is obtained for output reference voltage variation with respect to temperature over a range of 0 to 100°C .The output reference voltage exhibits a variations of 230μ with supply range of 1.08V to 1.32V at typical process corner.The proposed LVBGR circuit for 1.2V supply is designed in Mentor Graphics Pyxis tool using 130nm technology with EldoSpice simulator. Overall current consumed by the circuit is 900nA and also the power consumed by the entire LVBGR circuit is 0.9 μW and the PSRR of the LVBGR circuit is -70dB.**

***Index Terms*—Bandgap reference circuit, PTAT, CTAT, temperature coefficient**

I. INTRODUCTION

Bandgap reference (BGR) is a circuit which provides a stable output voltage reference which is temperature and supply insensitive. A precise and stable reference voltage is used in analog to digital (A/D) and digital to analog (D/A) converters, voltage regulators, DRAM etc. As the demands for smaller area, low power consumption and low sensitivity to the supply voltage and temperature are increasing it becomes very essential that we design low voltage bandgap reference circuit.Traditional bandgap reference which use bipolar transistors (BJT) temperature characteristic produce output voltage of 1.2 V which is very precise but the drawback of this BGR is power conumed is very larger so for low supply and current we prefere CMOS transistors which will be made to operate in subthreshold region so that its characters are comparable to that of BJT because MOSFETs operating in subthreshold will operate at very low power supply levels[1].In BGR circuits output reference which is less sensitive can be obtained by adding (PTAT) proportional to absolute temperature voltage and complementary to absolute temperature (CTAT) voltage where PTAT voltage has positive temperature coefficient and CTAT voltage has negative temperature coefficient .In traditional BGR circuits PTAT voltage can be derived from the difference between the base to emitter voltages of the two BJT devices and CTAT voltage can be derived from base to emitter voltage of single diode connected BJT device.The traditional BGR circuits performance was very good because there power supply was large i.e 3V to 5V but this BGR will not be suitable for low supply voltage in proposed circuit i.e 1.2V so in order to obtain a stable refernce voltage at low supply and current we use MOSFETs which are operate in subthreshold region because these transistors operate near threshold voltage Vth so MOSFETs operating in subthreshold minimize power supply voltage.In the proposed circuit PTAT voltage is obtained by taking the difference between the gate to source voltage of two MOSFETs which will be operating subthreshold and CTAT voltage is taken from gate to source voltage of single MOSFET which is also operating subthreshold region and finally by adding the two voltage we get output reference of 0.364V.

The section II describes the traditional bandgap reference circuit, section III describes the proposed bandgap reference circuit, section IV operating principle of proposed bandgap reference circuit, section V includes analysis of simulation results of proposed BGR circuit and section VI concludes the designed bandgap reference circuit.

II. TRADITIONAL LVBGR CIRCUIT

Current-mode bandgap architecture was proposed so that it can works for low supply voltage as shown in Figure. 1.In this architecture addition of currents is done so that it operates for low supply voltages and advantage of this architecture is that it is can provide good PSRR. But the drawback of this current mode architecture is that its output voltage is only temperature compensated current of output resistor so this output voltage can be more sensitive to power supply noise and resistor mistatches as compared to traditional BGR. There are some more disadvantages in this current mode architecture i.e these PNP transistors are process dependent. So in order to over come these disadvantages we chose voltage mode architecture for low voltage bandgap reference circuit.

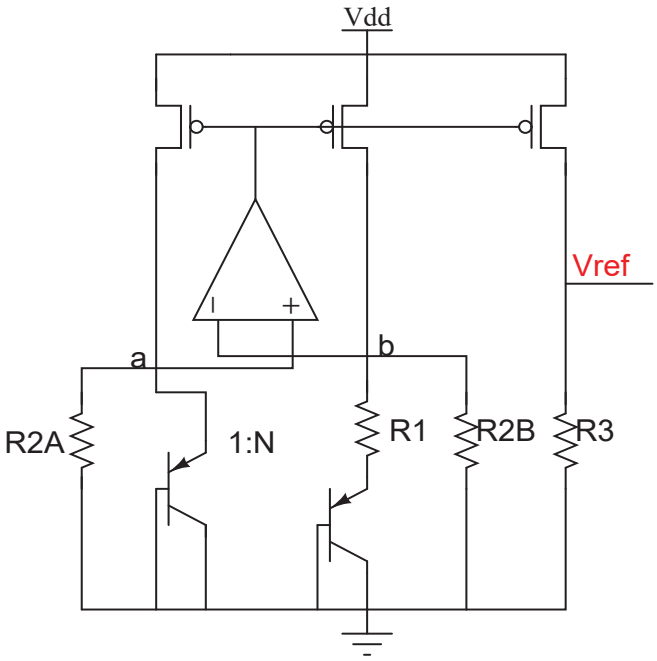

Fig. 1. Traditional Current Mode Bandgap reference circuit

III. PROPOSED LOW VOLTAGE BANDGAP REFERENCE CIRCUIT

The proposed low voltage bandgap reference (LVBGR) circuit uses voltage mode architecture with subthreshold CMOS devices for low power. The LVBGR circuit has 2 main blocks:

A. Startup circuit

Startup circuit is used to ensure that all the device start working correctly in known states during power up. The devices M7, M8 and M9 form a startup circuit and devices M8,M10,M11,M12 and M13 are used to weaken the M8 device. M7 and M8 form an inverter which is a part of startup circuit as shown in figure 3. Initially when supply is off there is no current in core circuit which makes top PMOS M4 and M5 turn on and input to inverter M7 and M8 is logic one and inverter output is zero. The zero output of inverter which turns on the PMOS M9 device whose output initiates the current in core circuit. Once the core LVBGR turns ON startup will turn off and carrying very less current (12pA). The devices M9 will be in subthreshold region, M7 in triode and M8 in saturation region for the proper operation of startup. Also M14 is used to avoid startup problem for Iref generation in opamp.

B. Ireference Generation Circuit

Current Reference for 2stage opamp is obtained from LVBGR P-MOS current M5 and by properly varing the aspect ratio of M15,M16 and M17 device we can obtain the required reference current i.e 50nA for 2stage opamp as shown in figure2 and Vbias for this current reference circuit is taken from Startup circuit in order to over come startup problems.

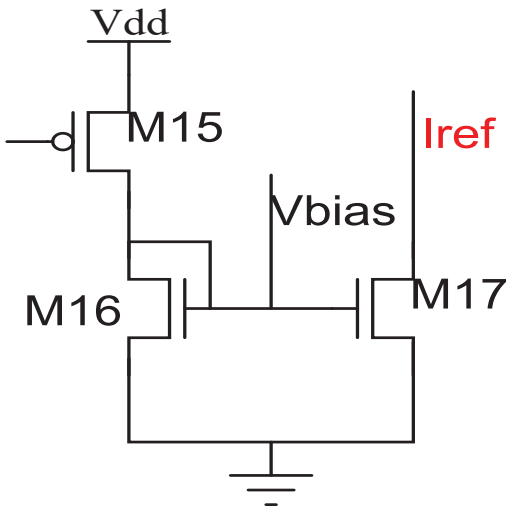

Fig. 2. Ireference generation circuit

IV. OPERATIONAL AMPLIFIER

A two stage Op-amp operating in subthreshold region is chosen to meet the low supply voltage and gain requirement is as shown in figure 2 and Miller-compensation capacitor is used to get good Phase Margin[2]. First stage of 2stage opamp has PMOS differential pair with NMOS current mirrors and second stage has common-source amplifier. The PMOS input pair of 2stage opamp operating in subthreshold is chosen in order to meet the low supply voltage requirement and input common mode range. The devices M4 and M5 are input pair of 2 stage opamp, the inputs of opamp is driven by LVBGR circuit a and b nodes as shown in figure 4. MOSFETS M2 to M6 and M1 and M8 are operate in subthreshold region and are implemented as first and second amplifier stages. TheMiller compensation capacitor Cc provides frequency compensation required to achieve closed-loop stability of the 2stage opamp. Thus entire 2stage opamp is designed to operate in subthreshold region i.e. Vgs $<$ Vth, where reference current carries current of 0.05μA which is generated from LVBGR circuit as explained above and the entire opamp consumes current of 0.45 μA. Load capacitance of opamp is taken from adding all capacitance associated with M4 and M5 devices of LVBGR circuit figure3. The approximated gain, poles and zero of 2stage opamp are given as

$$A_v = A_{v1}.A_{v2} = g_1R_1.g_2R_2 \quad (1)$$

where g1=gm5, g2=gm8, R1=r4,5 || r6,7 and R2=r1 || r8

$$P_1 = \frac{1}{cc.gm2.r1.r2} \quad (2)$$

$$P_2 = \frac{cc.gm2}{c1.c2 + c2.cc + 2(cc)^2} \quad (3)$$

$$Z_1 = \frac{gm2}{cc} \quad (4)$$

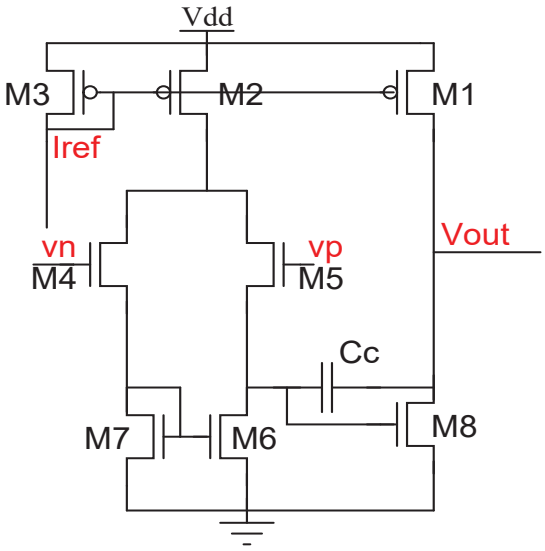

Fig. 3. 2stage opamp operating in subthreshold region

A. OPERATING PRINCIPLE

The CTAT voltage is obtained from gate to source voltage of MOSFET which is operating in subthreshold region which is given as [3]

$$V_{gs} = V_{vth} + \eta V_T[lnC - ln\frac{W}{l} + (\gamma - 2)lnT] \quad (5)$$

Where and n represents MOS constants which are related to the process and C represents Subthreshold MOSFET current. The first-order derivative of equation (1) is a negative value [4] i.e. gate to source voltage of MOSFET which is operating in subthreshold region has negative temperature coefficient. PTAT voltage is obtained by taking the difference between the gate to source voltage of two MOSFETs which will be operating subthreshold with same current flowing through them but with different ascept ratios

$$\Delta V_{gs} = V_{gs1} - V_{gs2} = \eta\frac{V_T}{R_1} + ln\frac{\frac{W_2}{L_2}}{\frac{W_1}{L_1}} \quad (6)$$

if (W/L)2>(W/L)1, then ΔV_{gs} has positive temperature coefficient so with device sizes M2 four times of M1 we get PTAT voltage and from M3 device Vgs3 we get CTAT voltage. Devices M4 and M5 will have the same size to make sure that M1 and M2 will have the same Id drain current flowing through them.Since the input impendence of 2stage opamp in subthreshold is very large so current flowing through M2 is same as current flowing through R1 which is ΔV_{gs} divided by R1.

$$I_2 = \frac{\Delta V_{gs}}{R_1} = \eta\frac{V_T}{R_1}ln\frac{\frac{W_2}{L_2}}{\frac{W_1}{L_1}} \quad (7)$$

M6 mirrors I2.The output voltage reference of LVBGR can written as:

$$V_{out} = V_{gs3} + I_3R_2 = V_{gs3} + \eta\frac{V_T}{R_1}ln\frac{\frac{W_2}{L_2}}{\frac{W_1}{L_1}}.R_2 \quad (8)$$

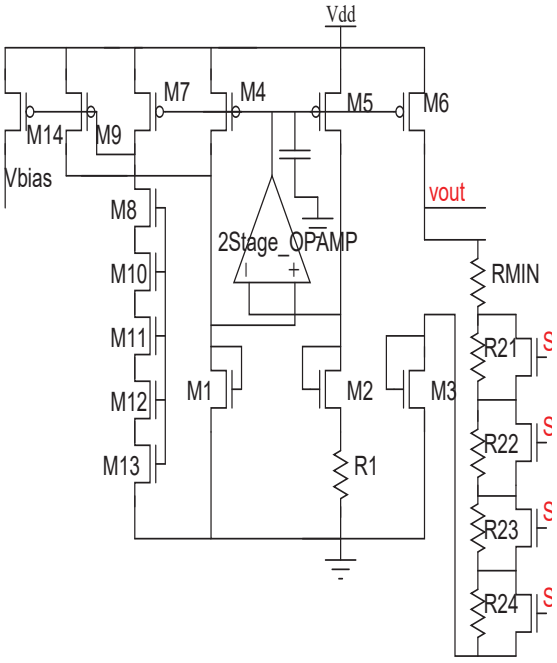

Fig. 4. Proposed low voltage Bandgap reference circuit

Hence the output voltage of LVBGR circuit is obtained by adding the gate to source voltage of M3 device which has negative temperature coefficient and the voltage drop across R2 i.e. the trimming resistors which gives positive temperature coefficient and the effects of positive temperature coefficient and negative coefficient cancells by adding in order to get stable output voltage reference which is less sensitive to supply and temperature. Since the output voltage is taken across both resistor and MOSFET it is less prone to resistor mismatches. R2 is obtained from trimming circuit such that the Vref output is having very less temperature coefficient.

B. Trimming circuit

The trimming circuit is used to reduce the temperature coefficient of output reference voltage of LBGR circuitfor different supply and process corners. A 4 bit series trimming circuit has resistors [10], whose values are chossen by calculating fine and coarse variations of resistors at different supply and process corners. The fine resistor value will be used for minute variations and coarse resistor value will be selected for large variation of resistors for different supply variations and process corners.

R_{MIN0}, R_{MIN1} and R_{MIN2} are minimum resistor values obtained at SS, TT and FF corners in order to get required LVBGR output voltage.Coarse resistors are selected by using the following equations

$$R_{coarse0} = R_{MIN1} - R_{MIN0} \quad (9)$$

and

$$R_{coarse1} = R_{MIN2} - R_{MIN1} \quad (10)$$

and fine resistors are used to make minute variations of resistance value which is require at different process corners and supply in order to get proper LVBGR output.From the figure R_{MIN0}=R_{MIN},$R_{coarse0}$=R21,$R_{coarse1}$=R22, R23 and R24 are fine resistors.These resistors are chosen by NMOS switches by their turn on and turn off which is driven by digital circuit [10].

V. SIMULATION AND RESULTS

Simulations have been carried out using MentorGraphics Pyxis tool with EldoSpice simulator in 130nm CMOS technology with supply of 1.2V with 10 % variations. The operational amplifier used in the proposed LVBGR is 2 stage opamp operating in subthreshold, which gives gain of 89.6db and phase margin of 74 ° as shown in figure 5.

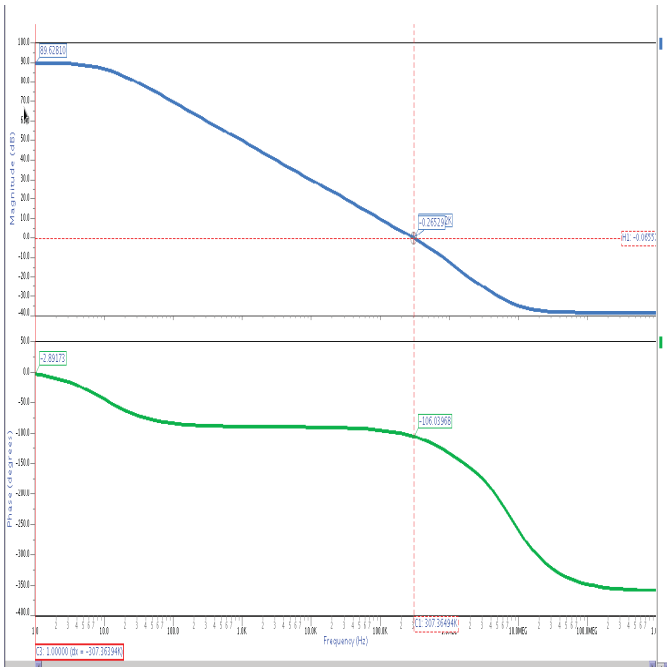

Fig. 5. Gain and Phase plot of 2stage opamp in subthreshold region

Figure6 Shows startup behavior of LVBGR output with supply variation. The time required for LVBGR to produce a stable output is 50μ (27C) and settles at 0.385V. The simulation is carried out using transient analysis.

Figure 7 shows the Vref variation with respect to temperature without trimming circuit and figure 8 shows the Vref variation with respect to temperature with trimming circuit for all the process and supply variation. The output of LVBGR with trimming circuit for supply voltage of 1.2V for TT,SS and FF process corners has variation of output voltage of 230μ with trimming circuit and without trimming circuit it was 132mV. With trimming circuit in LVBGR the temperature coefficient(TC) for all the process corner and supply variation

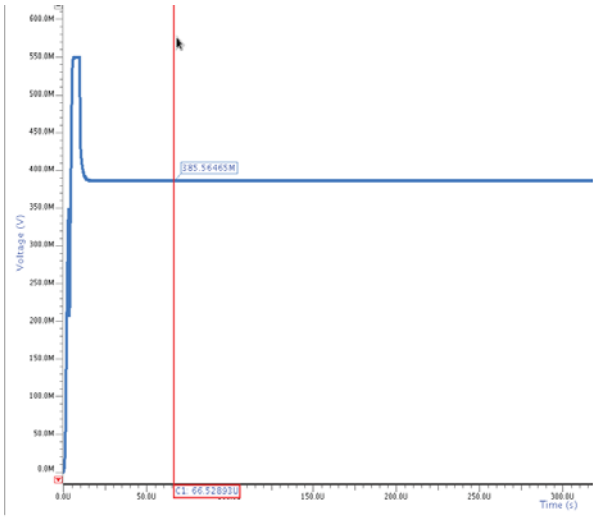

Fig. 6. Start-up behavior of the BGR output voltage with VDD ramp

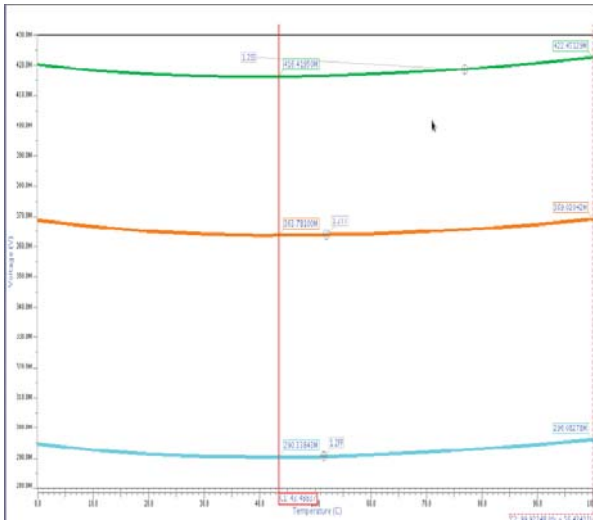

Fig. 7. Vref Vs Temperature for different process corners in LVBGR without trimming cicrcuit

TABLE I
SIMULATION RESULTS OF 2 STAGE SUBTRESHOLD OPAMP

Supply	Process corners	DC gain(dB)	UGB(KHz)	PM(degree)
1.08	TT	89.5	303	74
1.08	SS	90.1	282	75
1.08	FF	87.73	307	74
1.2	TT	89.6	307.36	73.9
1.2	SS	90.16	286.2	74.96
1.2	FF	87.76	316.76	73.7
1.32	TT	89.6	306.6	75
1.32	SS	90.2	294	75.2
1.32	FF	87.79	311	75

is 827ppm/ °C. Hence the output voltage variation of LVBGR is reduced with the help of trimming circuit.

The performance metric of different architectures of low

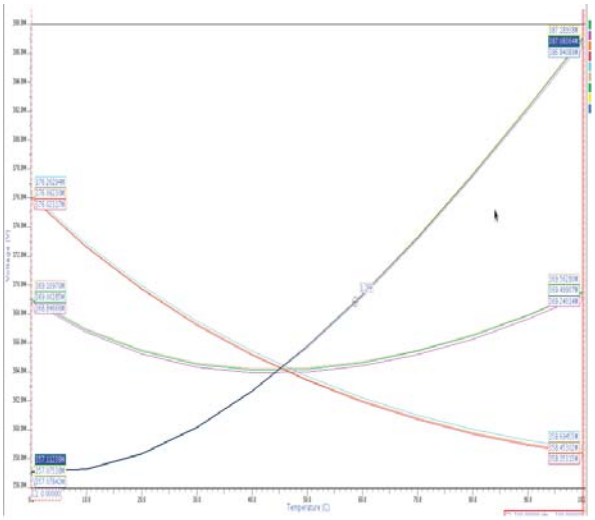

Fig. 8. Vref Vs Temperature for different process corners in LVBGR trimming cicrcuit for all the process and supply variation

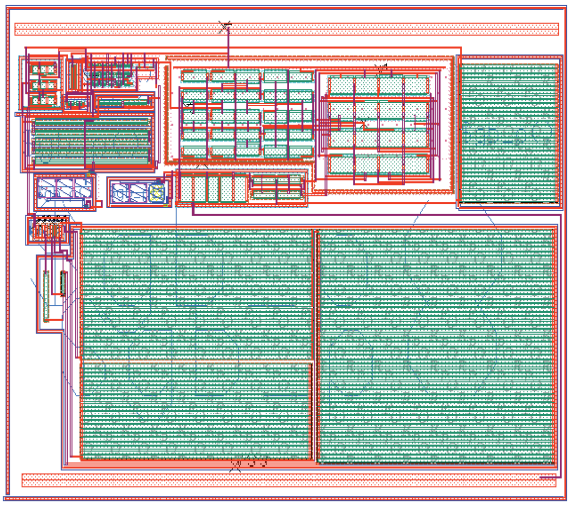

Fig. 9. Layout of proposed LVBGR circuit

TABLE II
PERFORMANCE COMPARISON OF LOW POWER BANDGAP REFERENCE CIRCUITS

Parameters	[5]	[6]	[7]	[8]	[9]	Proposed Design
CMOS Tech.	0.35	0.18	0.18	0.45	0.13	0.13
Vdd (V)	0.87	1	0.9 to 2.5	0.8	0.6	1.2
Vref(V)	0.611	0.630	0.22	0.310	0.429	0.34
Temp. range °C	-10 to 70	-20 to 70	-20 to 120	0 to100	20 to 80	0 to 100
TC ppm/ °C	20	93.33	-	14.62	25.6	240
Power μW	45	86.19	3.3	13.73	-	0.9

voltage bandgap reference are shown in table1. From the table it can be seen that the proposed LVBGR circuit has got a VREF output of 0.364V with subthreshold MOSFETS. By using voltage mode architecture the proposed circuit achieved temperature coefficient of 240ppm/ °C. Layout of proposed LVBGR circuit is as shown in figure9 which occupyies an area of 100μmx80μm.

VI. Conclusion

A bandgap reference with low supply voltage is presented by using the characteristics of subthreshold MOSFET. It can work under supply voltage of 1.2V with 10percentage variation which gives temperature coefficient of 240ppm/ °C. Compared with traditional current-mode BGR for low voltage application, the proposed LVBGR circuit is less sensitive to resistor mismatchs. Output variation is reduced from 132mV to 230μV with the help of trimming circuit.Simulations are done using MentorGraphics Pyxis tool with EldoSpice simulator in 130nm CMOS technology and the entire circuit of LVBGR consumes 9nA of current and total power consumption of 0.9W and this LVBGR circuit is used for low dropout reference(LDO) application which will be having a supply of 3.3V and must produce an output voltage of 1.8V.

VII. Acknowledgment

The authors would like to thank the SmartPlay Technology for their support in designing the low voltage bandgap reference circuit.

References

[1] E. A. Vittoz and J. Fellrath “CMOS analog integrated circuits based on weak inversion operation”, IEEE J. Solid-State Circuits, vol. SC-12,pp. 224231, June 1977.
[2] Behzad Razavi ”Design of analog cmos integrated circuits”McGraw-Hill, 2001.
[3] Y. Tsividis ”Operation and Modeling of The MOS Transistors”2nd ed.,McGraw Hill, 1999.
[4] A. H. Adl, K. El-Sankary and E. El-Masry ”Bandgap Reference with Curvature Corrected Compensation Using Subthreshold MOSFETs”IEEE International Symposium on Circuits and Systems, 2009.
[5] Yeong-Tsair Lin, Mei-Chu Jen, Dong-Shiuh Wu, and Huan-Ren Cheng ”A Low-Variation, Low-Voltage CMOS Bangap Reference Circuit” International Journal of VLSI design & Communication Systems (VLSICS) Vol.3, No.5, October 2012.
[6] Christian Jesus B.Fayomi“Novel Approach to low voltage low power band gap reference voltage in std CMOS process ’ International Journal of Innovative Technology and Exploring Engineering (IJITEE) ISSN: 2278-3075, Volume-2, Issue-5, April 2013
[7] Po-Hsuan Huang, Hongchin Lin, Member, IEEE, and Yen-Tai Lin“A Simple Sub threshold CMOS Voltage Reference Circuit With Channel-Length Modulation Compensation” International Journal of VLSI design & Communication Systems (VLSICS) Vol.4, No.2, April 2013
[8] Sonal Singhal“Design and Optimization of a Low Power Voltage Reference Generator Circuit in 45nm CMOS Technology” IEEE Journal of Solid -State Circuits, vol. 39, no 3, March 2004, pp469-475
[9] Yilei Li*, Yu Wang, Na Yan, Xi Tan and Hao Min“A Subthreshold MOSFET Bandgap Reference with Ultra-Low Power Supply Voltage”, International Journal of Soft Computing and Engineering, vol.2, Issue-2, May 2012, pp 88-92.
[10] Juan Martinez Brito, Sergio Bampi, H. Klimach*“A 4-Bits Trimmed CMOS Bandgap Reference with anImproved Matching Modeling Design”*,supported by the National Science Foundation.

THE 5TH INTERNATIONAL CONFERENCE ON WIRELESS COMMUNICATIONS, VEHICULAR TECHNOLOGY, INFORMATION THEORY, AEROSPACE & ELECTRONIC SYSTEMS (WVITAE-2015)
December 13-16, 2015, Hyderabad, India

Swarm Optimization based on Genetic Algorithm & Relevance Feedback Technique for Data Clustering

G. Malini Devi,
Asst. Professor, Dept. of CSE,
GNITS, Hyderabad-8, India.
gmalini12@gmail.com

Dr. M.Seetha
Professor, Dept. of CSE, GNITS,
Hyderabad-8, India
seetha.maddala@gmail.com

Dr. K.V.N.Sunitha
Principal, BVRIT Hyderabad,
College of Engineering for women,
India. k.v.n.sunitha@gmail.com

***Abstract**: Clustering is a group of patterns, classes or concepts .The main goal of clustering is to represent large datasets by a fewer number of clusters or prototypes. The ease of modeling data plays a central role in the process of knowledge discovery of data (KDD). We propose a PSO based relevance feedback & GA approach for data clustering to improve the accuracy of the results. First to implement the concept of relevance feedback for clustering based on parameters like mean, standard deviation, minimum value, maximum value, rank & accuracy. RFB uses the number of nearest neighbors from different classes of dataset for a particular query point using various similarity metrics like camberra distance, chebyshev distance etc. Second by implementing particle swarm optimization, this is a computational method for finding the best global optimum solution. Genetic Algorithms, being global search technique, have been widely applied for discovery of clusters. It aims to enhance the accuracy by incorporating PSO in the results presented to the user for analysis. Combining RFB with PSO & GA with PSO is the third method. Finally it can be ascertained that combined approach i.e., GAPSO gives better accuracy compare to RFBPSO algorithm.*

Keywords: RFB, GA, PSO, accuracy, similarity metrics, RFBPSO & GAPSO.

I.INTRODUCTION

Data mining is a detection process that allows users to comprehend the substance and relationships amid the data. Data clustering is the technique of consorting of data objects into dissimilar groups or clusters, which is the main task in data mining. Objects have utmost similarity, within the cluster. Outside the cluster, other objects are divergent to each other. Based on the attribute values the objects similarities and dissimilarities are assessed. Data clustering is a method in which we make cluster of objects that are somehow similar in distinctiveness [6, 7].

Relevance feedback is a feature of some information retrieval systems. The connotation of feedback is to obtain the user vector values and use the information to analyze whether the results are relevant to a new query.

Darwin's theory inspired Genetic algorithms development. GA is evolved to resolve solution to this problem [2, 3, 4, and 5]. Algorithm starts with a set of solutions (chromosomes) known as population. Outcomes from a population are taken and used to structure a new population. This is aggravated by optimism, and the new population will better the old. Chosen solutions are used to form new solutions (offspring) which are selected according to their fitness values- the more apposite will lead to more chances of reproduction.

Particle Swarm Optimization (PSO) is a population based algorithm [1]. Even though the search process is not random it searches for optimum solution. RFB is a type of correlation analysis and to perceive attributes which do not bestow to the clustering attribute subset assortment can be used. Genetic algorithm, were in each 'individual' of the generation represents a feasible solution to the problem, coding distinct algorithms/parameters should be evaluated by a fitness function.GA operators cause mutation (change of random position of the chromosome) and crossover (change of slices of chromosome between parents).

Relevance feedback supports for the general quadratic distance metrics. Similarity measure is defined such that relevance degrees between objects are respected when they are ranked according to their pair wise similarity [8, 9, 10, and 11]. A novel particle swarm optimization with genetic algorithm is an optimization task which runs after the genetic algorithm, later terminates in order to improve the value of fitness function. Final point from the genetic algorithm is taken as initial point in this function. Particle Swarm Optimization (PSO) is a swarm intelligence method for global optimization. Each unique object of the population adjusts its path to its own prior finest pattern, and towards the preceding finest position attained by any member of its topological vicinity in classical PSO. To trace the exact place of the cluster centers, a cluster center movement RF & GA is combined with PSO.

II.RELEVANCE FEEDBACK ALGORITHM

One among the adopted solutions was to directly take benefit of the human proficiency in the retrieval process, known as Relevance Feedback (RF). For a certain retrieval objects, user has to offer feedback by spotting the results as relevant or non- relevant data objects. With this information, the system then repeatedly computes an enhanced depiction of

the information desired and also retrieval is further refined. Relevance feedback (RFB) is a technique that helps searchers improve the accuracy of their query statements and has been shown to be effective in non-interactive experimental environments. RFB ppseudo-code can be represented as:

[1]In the clustering phase, *k* is a user-defined constant, and an unlabeled vector (a query or test point) is classified by calculating the distance between the cluster seed point and all the points in the dataset.

[2]The loop repeats until all the points in the dataset are completed.

[3]The obtained distances are then sorted and according to the k value, those neighbors are plotted on the graph.

[4]The user preferences are then taken into consideration.

[5]Distances are calculated between the cluster seed point and points in the user vector.

[6] These distances are also sorted and according to the k value, those neighbors are marked or plotted on the graph in addition to the already retrieved neighbors.

[7]If the neighbor lies in a particular class, then it is considered as true positive otherwise it is taken as true negative.

[8]Accuracy is calculated based on the true positive and true negative value the.

A. Similarity Metrics

In most algorithms, the dataset to be classified is represented as a set of objects X={x1, x2, …., xn}, where the object *xi* corresponds to a single object and predicts to which class label it belongs[1]. Over the years, two prominent ways have been proposed to compute the similarity between objects m_p and m_j

B. Camberra Distance

The Camberra distance *d* between objects **x** and **y** in an *m*-dimensional object space is given by:

$$D(x,y)=\sum_{i=1}^{m}\left|\frac{(x_i-y_i)}{(x_i-y_i)}\right|$$

Where $x=(x_1,x_2,...,x_m)$ and $y=(y_1,y_2,...,y_m)$ are two points in Camberra *m*-dimensional space[5].

C. Chebyshev Distance

The two dimensional manhattan distance also has circles in the form of squares, with sides of length $\sqrt{2}r$, oriented at an angle of $\pi/4$ (45°) to the coordinate axes, the planar Chebyshev distance can be viewed as equivalent by rotation and scaling to the planar manhattan distance. The Chebyshev distance between two objects x and y, with standard coordinates xi and yi, respectively in m-dimensional object space, is specified by:

$$D(x,y)=\max_{i=1}^{m}\left|(x_i-y_i)\right|$$

where $x=(x_1,x_2,...,x_m)$ and $y=(y_1,y_2,...,y_m)$ are two points in Chebyshev *m*-dimension space.

D. Chi-square Distance

The Chi-square distance *d* between objects **x** and **y** in an *m*-dimensional object space is given by:

$$D(x,y)=\sum_{i=1}^{m}\left(\frac{1}{sum_i}\right)*\left[\left(\frac{x_i}{size_x}\right)-\left(\frac{y_i}{size_y}\right)\right]^2$$

sum_i is the sum of all values for attribute *i* taking place in the training dataset, and $size_x$ is the sum of all values in the object ***x***.

E. Cityblock Distance

City block distance is also called as manhattan distance

$$D(x,y)=\sum_{i=1}^{m}|xi-yi|$$

City block distance is a exceptional case of the minkowski metric where p=1.

F. Kendall Rank Correlation

The Kendall Rank Correlation distance *d* between objects **x** and **y** in an *m*-dimensional object space is given by:

$$D(x,y)=1-\left(\frac{2}{n(n-1)}\right)*\sum_{i=1}^{m}\{\sum_{j=1}^{i-1}[(x_i-x_j)*(y_i-y_j)]\}$$

Where $x=(x_1,x_2,...,x_m)$ and $y=(y_1,y_2,...,y_m)$ are two points in object *m*-space and n is the number of observations in the given dimension space.

G. Kulczynski distance

The Kulczynski distance *d* between vectors **x** and **y** in an *m*-dimensional real vector space is given by:

$$D(x,y)=\sqrt{\frac{\left(\sum_{i=1}^{m}|x_i-y_i|\right)}{\min(x_i,y_i)}}$$

where $x=(x_1,x_2,...,x_m)$ and $y=(y_1,y_2,...,y_m)$ are two points in vector *m*-space.

H.Sorensen distance

The Sorensen distance *d* between vectors **x** and **y** in an *m*-dimensional real vector space is given by:

$$D(x,y)=\sqrt{\frac{\left(\sum_{i=1}^{m}|x_i-y_i|\right)}{\sqrt{\left(\sum_{i=1}^{m}|x_i-y_i|\right)}}}$$

where $x=(x_1,x_2,...,x_m)$ and $y=(y_1,y_2,...,y_m)$ are two points in vector *m*-dimensional space.

III.GENETIC ALGORITHM

Conceptual representations of realistic solutions are represented by GA work with a population of individuals. Performance of the solution it represents is measured by individuals assigned fitness function. Fitness function of each individual is measured in each generation. To form a new population individuals are stochastically elected from a current population (based on their fitness), and customized by means of operators mutation and crossover.

Genetic Algorithms Operators

The fundamental genetic algorithm operators are crossover and mutation. These two operators are work together to explore and exploit the search space by creating latest variants in the chromosomes. Many experimental studies have been carried out on the similarities between crossover and mutation. It is confirmed that mutation operator play the similar important role as that of the crossover.

A. Crossover

Fundamental role of the genetic algorithms is that crossover (recombination) plays best design and implementation of vigorous evolutionary systems. Through GA, individual are epitomized by fixed-length strings and crossover operates on pairs of individuals (parents) to construct new strings(offspring)by exchanging segments from the parent strings. Traditionally, the number of crossover points (which determines how many segments are exchanged) has been stable at a very low constant value of 1 or 2.

B. Mutation

Mutation is a common operator which is used to evaluate and preserve diversity in the population by finding new points in the search space. A random change is made to the values of some locations in the chromosome, when a chromosome is chosen for mutation. Single point mutation is the commonly used method. This type of special mutation is used for various kinds of problems and encoding methods.

IV. PSO ALGORITHM

PSO is an evolutionary based computation method that performs robust and efficient optimization. It's a population-based optimization procedure, where in a population is termed as a swarm. The fundamental thought depicts, each particle represents a prospective resolution which it updates according to its own experience and that of its neighbors. The PSO technique searches in analogous via group of individuals. Individuals in as swarms, surface to optimum solution through the current velocity, prior experience and the experience of its neighbors. PSO will search the problem domain when trajectories of moving points are adjusted in multi-dimensional space. For optimal solution, the activity of individual particles is governed through the interactions. The connectivity among individual particles is established by the position, velocity, best performance of individuals and their neighbors.

Notations for PSO

1.The position of the i^{th} particle of a swarm of size n, is projected by the D-dimensional object space, xi= (xi1, xi2, ..., xiD).

2.The best previous position (i.e., the position giving the best function value pBest) of the i^{th} particle is recorded and represented by pi= (pi1, pi2, ..., piD).

3.The position change (velocity) of the i^{th} particle is Vi=(Vi1, Vi2, ..., ViD) .

4.The position of the best particle of the swarm (i.e., the particle with the smallest function value) is denoted by index gBest.The particles are then manipulated according to the following equations.

$$V_{id}(t+1) = V_{id}(t) + C_1*rand*(pBest(t) - x_{id}(t)) + C_2*rand*(gBest(t) - x_{id}(t)); \quad (1)$$

$$x_{id}(t+1)=x_{id}(t)+V_{id}(t+1) \quad (2)$$

where d=1,2,…..D and i=1,2,…..n.

V: Velocity

C1, C2: positive constant parameters =1.49

rand: random numbers between (0,1)

V.RELEVANCE FEEDBACK WITH PARTICLE SWARM OPTIMIZATION (RFBPSO)

Relevance feedback success depends on positive assumptions. Initially, the user must have ample knowledge to make first seed point, proximity to the object they covet. Anyhow greatly needed for victorious information retrieval in the essential case, but it is vital to observe the kinds of problems that relevance feedback cannot work alone Relevance feedback can also have realistic problems. The seed point that is generated by straightforward application of relevance feedback techniques is inefficient for a typical IR system. Good performance will incur for this fallout and also result in potentially long response times for the user.

Pseudo-code of RFB when combined with PSO:

- Using RFB alone gives less accuracy and the performance is low.
- It overcomes the drawbacks of RFB Algorithm.
- The output obtained by Relevance Feedback technique is given as input to the PSO. Thus the best algorithm can be found which can do efficient retrieval. Thereby, efficient results are obtained.

VI. GENETIC ALGORITHM WITH PSO

Information sharing is notably dissimilar when compared with genetic algorithms in PSO. In GAs, sharing of information among chromosomes takes place which triggers a complete population movement resembling single group movement to best possible solution space. With PSO, information can be passed to other objects by gbest (or lbest) solution. In local version of most cases, all the particles tend to converge to the best solution rapidly when compared with GA. Degrade in regulation of its speed and direction indicates PSO algorithm suffering from the partial optimism.

Procedure for PSO with GA

1. Apply GA on the datasets for clustering.
2. The results are passed to the PSO for execution.
3. PSO is applied on the output obtained from GA.
4. Repeating step 2 and 3 until the convergence is achieved

VII.RESULTS & DISCUSSION

The experiments results have been carried out to authenticate the accuracy of the proposed model. The properties of the dataset are described as:

A. Data sets

Examining the conduct of the respective clustering methods, Iris data sets are used.

Iris plant data set: Which is comprised of 150 data points, include 50 instances of all the three types of iris plant.

B. RFB Algorithm Results

An assortment of similarity metrics like are camberra distance, chebyshev distance, chi-square distance, cityblock distance , kendall rank correlation, kulczynski distance & sorensen distance are analyzed for the number of nearest neighbour from different classes of dataset for a particular seed point.

C.Figures and tables

Attributes	Min	Max	Mean	StdDev
Sepal Length	4.3	7.9	5.848	0.829
Sepal Width	2	4.4	3.054	0.436
Petal Length	1	6.9	3.774	1.761
Petal Width	0.1	2.5	1.206	0.76
Sepal Length	4.3	7.9	5.848	0.829

Table-1: Comparison of min, max, mean and standard deviation of each attribute for iris dataset.

For each attribute of iris dataset four different measures min, max, mean, standard deviation are specified.

Table-2: Selection of attributes for iris dataset based on rank priority

ATTRIBUTES	RANK
Sepal Length(1)	0.43
Sepal Width(2)	0.73
Petal Length(3)	1.351
Petal Width(4)	1.427

Above table-2 states that the rank value is better for third and fourth attributes i.e., petal length and petal width compare to other attributes.

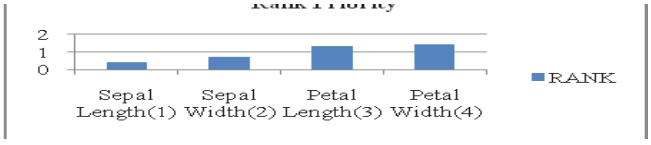

Figure-1: Selection of attributes for iris dataset based on rank priority

The figure-1 depicts that the rank value is better for third and fourth attributes with utmost values (1.351, 1.427) compare to other dimensions.

Table-3: Accuracies of iris dataset for different metrics in RFB.

Metric	Accuracy
Camberra	66.666
Chebyshev	33.333
Chi-square	33.333
Cityblock	66.666
Kendall	33.333
Kulczynski	66.666
Sorensen	66.666

The table-3 states that the accuracy is better for Camberra, Cityblock, Kulczynski and Sorensen distances on iris dataset when compared to other similarity measures.

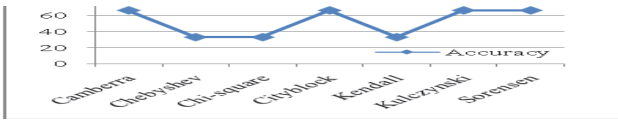

Figure-2 Comparison between the accuracies of Iris dataset for different metrics for RFB.

D.PSO

Comparison of PSO is done between the OFV and CPU time with the clusters. By taking various cluster values the comparison is done between cluster and time and also between cluster and OFV for PSO algorithm.

Table-4: Analysis of PSO Algorithm based on OFV and Time for iris datasets

DATASETS	OFV	TIME
Iris	-107.0286	33.1000 sec

Time exhausted on relevance analysis along with the time spent on learning from the resulting reduced dimensions (or feature) subset, must be lesser than the time that would have been spent on learning from the original set of attributes. Hence, these results are able to better clustering accuracy and scalability.

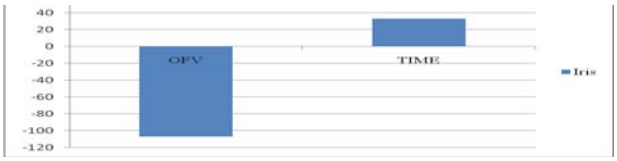

Figure-3: Comparison between the OFV and Time for iris datasets with PSO

E.RFB with PSO:

Relevance feedback lets the user guide the system.Various similarity metrics like Camberra distance, Chebyshev distance etc are being used for analysis. The output matrix obtained after applying RFB on the datasets is given as input to the PSO algorithm and thus we get RFBPSO algorithm.

Table-5: Comparison of distance metrics for Iris dataset for fitness and time

Algorithm	OFV	Time
Camberra	-82.6139	11.912
Chebyshev	-14.4605	12.357

Chisquare	-82.6139	12.193
Cityblock	-14.4655	12.359
Kendall	-154.3372	11.983
Kulczynski	-82.6139	12.691
Sorensen	-82.6139	11.961
Euclidean	-14.4605	12.595810

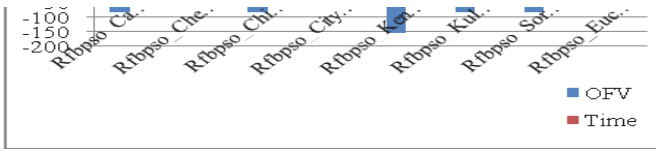

Figure-4: Comparison of distance metrics for Iris dataset for fitness and time

The table-5 & figure-4 depicts that Kendall distance is better for iris dataset compared to other similarity measures since it has the low OFV value and low CPU time.

F. Genetic Algorithm Results

In order to show the results there has been a comparison done between the OFV and time with the clusters. By taking various cluster values the comparison is done between cluster and time and also between cluster and OFV for PSO algorithm for all the datasets.

Table-6: Analysis of PSO_GA algorithm on four datasets based on OFV & time.

Datasets	PSO	GA_PSO
PSO_GA based on OFV		
IRIS	-107.8089	-147.2694
PSO_GA based on time in seconds		
IRIS	32.928	34.084

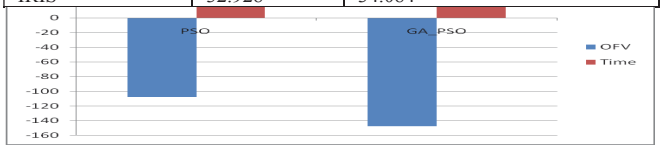

Figure-5: Analysis of PSO & GA_PSO algorithm on iris datasets based on OFV & time.

From table-6 and figure-5 it can be stated that GA_PSO is better algorithm in terms of OFV and it takes slightly more time than PSO but the difference in OFV compensates the time factor. Faster convergence rate because when stagnation of PSO occurs, even though the solution is worse GA diversifies the particle position which makes PSO_GA extra flexible and robust. Distinct to standard PSO, PSO_GA is extra consistent in giving better fitness solution with reasonable computational time. Experimental results are examined with benchmarks functions and outcomes specify proposed PSO_GA model betters the standard PSO.

VIII.CONCLUSION

PSO with combination of techniques for its relevance feedback & GA convey gleaming clustering results. Using RFB approach difficulties may arise if the data set is very large and incorrect assumption of seed point results in a more overheads for retrieval and potentially long response times for the user. Relevance feedback success depends on certain assumptions. The user must have generous knowledge to make an initial seed point which must have close proximity to the data objects they aspire. For exultant information retrieval in the fundamental case these are desired, also vital to observe various problems that relevance feedback cannot solve alone. RFB is used to compensate the semantic gap between low level attributes, high level attributes and also accuracy improvement. Solving optimization problems on the natural selection is the best method to defeat this GA. GA endeavours best point in population which later reaches to optimal solution with rapid convergence rate. The end results are the fusion of PSO_GA whose performance is notably enhanced when compared to former algorithms for these data sets.

REFERENCES

[1] M. Imran, R. Hashim, and N. E. A. Khalid, “An overview of particle swarm optimization variants,”Procedia Engineering, vol. 53, pp. 491–496, 2013.

[2] A.Sibil, N. Godin, M. R’Mili, E. Maillet, G. Fantozzi Optimization of Acoustic Emission Data Clustering by a Genetic Algorithm Method, Springer-Verlag, Journal of Nondestructive Evaluation,June 2012, Volume 31, Issue 2, pp 169-180.

[3] AnutoshPratap Singh , JitendraAgrawal , Varsha Sharma An Efficient Approach to Enhance Classifier and Cluster Ensembles Using Genetic algorithms for Mining Drifting Data Streams, International Journal of Computer Applications (0975 – 8887) ,Volume 44– No.21, April 2012.

[4] Santhosh Peddi, Alok Singh ,Grouping Genetic Algorithm for Data Clustering, Springer Berlin Heidelberg ,Swarm, Evolutionary, and Memetic Computing, Lecture Notes in Computer Science Volume 7076, 2011, pp 225-232.

[5] M. Imran, H. Jabeen, M. Ahmad, Q. Abbas, and W. Bangyal, “Opposition based PSO and mutation operators,” in Proceedings of the 2nd International Conference on Education Technology and Computer (ICETC '10), pp. V4506–V4508, June 2010.

[6] P. Melin and O. Castillo, “A review on type-2 fuzzy logic applications in clustering, classification and pattern recognition,” Applied Soft Computing Journal, vol. 21, pp. 568–577, 2014.

[7] Muza.M , BitLit Media Inc., Vancouver, BC, Canada , Lowe, D.G. Scalable Nearest Neighbor Algorithms for High Dimensional Data, IEEE Transcations on Pattern analysis and machine intelligence, vol-36,Issue-11,2014-November,pg-2227-2240.

[8] Hwanjo yu, Selective sampling techniques for feed back database retrieval ,Springer,vol-22,Issue-1,JANUARY 2011,pg no 1-30.

[9] M. Broilo and F. G. B. De Natale, “A stochastic approach to image retrieval using relevance feedback and particle swarm optimization,” IEEE Transactions on Multimedia, vol. 12, no. 4, pp. 267–277, 2010.

[10] Niall Rooney, A relevance feedback mechanism for cluster-based retrieval, Information Processing and Management: an International Journal archive Volume 42 Issue 5, September 2006 ,Pages 1176 - 1184

[11] S.H. Huang, Q.J Wu, S.H. Lu, ”Improved AdaBoost-Based Image Retrieval with Relevance Feedback via Paired Feature Learning”, ACM Multimedia Systems,12(1), pp. 14-26, 2006.

THE 5TH INTERNATIONAL CONFERENCE ON WIRELESS COMMUNICATIONS, VEHICULAR TECHNOLOGY, INFORMATION THEORY, AEROSPACE & ELECTRONIC SYSTEMS (WVITAE-2015)
December 13-16, 2015, Hyderabad, India

Self Configurable Intelligent Distributed Antenna System for Resource Management in Multilayered Dense-nets

Ambuj Kumar [*1], *Albena Mihovska* [*2], *Ramjee Prasad* [*3]
[*]Center for TeleInFrastruktur (CTIF),
Department of Electronics Systems,
Aalborg University,
Aalborg, Denmark,
{[1]in_kumar, [2]alb, [3]Prasad}@es.aau.dk

***Abstract*— Since its dawn in mid-1980's, till the present time, the Mobile Cellular Communication (MCC) has been following a common silhouette of the network architecture. In every generation of the mobile cellular technology, the final radiating elements or antennas are exclusively mapped to their respective Base Stations (BS). Moreover, in earlier generations of MCC, antennas were deemed collocated with their respective BSs. Later, the concepts like Distributed Antenna Systems (DAS) and Cloud RAN (C-RAN) made it possible to place these antennas distant from their respective BSs. However, being mapped with their respective base stations, spectrum pooling and management at antenna end is not efficient. The situation worsens in Heterogeneous and Dense-net conditions in an Area of Interest (AoI). In this paper, we propose a DAS based intelligent architecture referred to as Self Configurable Intelligent Distributed Antenna System (SCIDAS) that can simultaneously accommodate multilayer communication environment over a common BS.**

Keywords—Distributed Antenna Systems; Cloud RAN; Intelligent Networks;

I. INTRODUCTION

This section describes those challenges and limitations that are in present Mobile Cellular Networks (MCNs) and have motivated the idea discussed in this paper.

A. Background

The upswing in MCC evolved in steps of technological advancements that we call as "generations" of mobile communications [1]. With every new generation, the service providers demand better spectrum utilization and approachability with more control over the Capital and Operational Expenses (CAPEX and OPEX). However, when viewed in the background of the present overwhelming growth rate of potential subscribers and data based services [2], this demand is still bewailing for parity. The transfiguration of the mobile user equipment from a mere communication device to a personalized access and media center was the primary reason for the booming rise in capacity demand per subscriber. Ergo, technologies and architectures have been transmogrified over the time to satisfy these ever overwhelming demands, especially, the subscribers' capacity demand. This growth expectancy is lucidly mentioned in "The Mobile Economy 2014" report [3], which nicely shows the collaborative and individual transitional growth of the various technologies.

Like any other transient evolution, the existing technologies are bound to overlap with upcoming technology/ies in the same length of time and form a composite network environment. And, as newer technologies involve a more recent style of network planning, it is taking considerable time for the service providers to upgrade the network. As an example, by the time some service providers upgraded their network from 2G/2.5G to 3G (LTE), the newer technology LTE –Advanced (4G) knocked the door. Therefore, the technological overlap is a long lasting event before a technology becomes the solo MCC platform. Till then, it is required to have a multi-layered network that has backward compatibility with the previous generations. Therefore, the newer technologies like 5G [4] will be bound to maintain this hierarchical polymorphic network approach. Hence, the *coexistence* of the various generations in same time span is one of the major challenges in present and future wireless networks.

Another "hard to swallow" problem in the present and future times of the MCN is the approachability (coverage). As in previous generations, the lower capacity demand enabled higher spectrum reuse, certain carrier bands such as 900 MHz (mostly used for GSM technology) proved to be sufficient in the covering PAN areas by traditional discrete base station subsystems (BSSs). However, in the aeon of high capacity demanding subscribers, it is imminent to disseminate the carriers in every corner of the service area. Following these demands, the network architecture of 4G LTE is significantly trimmed as compared to its previous generations(such as removing the Base Station Controller from the conventional architecture) to fit into the Area of Interest (AoI) or service area [5]. However, such architecture is not ample enough to beat the whooping network requirements. Hence, an advanced architecture that is easy to deploy and manage the scarce spectrum resource efficiently is required. Next we discuss the limitations of LTE that raises the motivation to look for more.

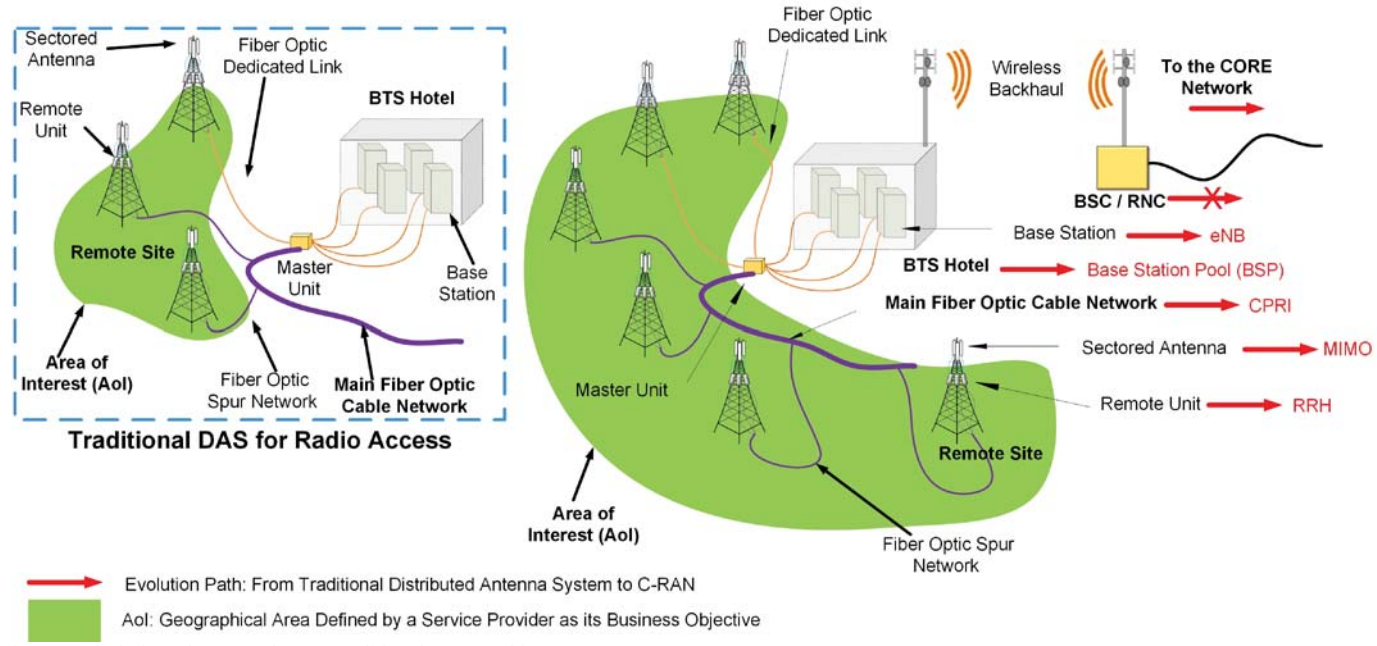

Figure 1: Evolution of C-RAN from a Traditional DAS Architecture

B. Motivation: Evolution and Limitations of LTE

Figure 1 shows the evolution of LTE architecture, where the Base Station (BS) is evolved as a clever amalgamation of the Radio Network Controller (RNC) and the Base Stations (BS) of the previous generation architectures. Therefore, an LTE BS, known as evolution-NodeB (e-NodeB or eNB) is directly connected to the core network and is simpler to deploy as compared to the previous mobile generations. The radio access part of LTE technology is known as Evolved UMTS Terrestrial Radio Access Network (E-UTRAN) [6][7]. One of the unique features of the EUTRAN that has revolutionized the deployment efficiency is the distributed BSs. This feature uses the conventional Distributed Antenna System (DAS) concept, as also shown in Figure 1, to separate the serving base stations from the radiating elements.

The distributed BS architecture of LTE allows antennas to reside near the vicinity of the strategic positions whereas; the corresponding BS may reside distant apart which saves the cost of BS equipment (as in discrete architecture) and infrastructure. Like a usual DAS, in LTE, the conversion of optical bits to RF is handled by the Remote Radio Head (RRH). The RRH receives the optical signal, converts it to digital and then to analog sinusoidal waves and feeds it to the serving antenna. The eNB-RRH concept is extrapolated to the larger context and evolved to what we know as the Cloud Radio Access Network (C-RAN) [8][9]. As discussed in [9] and [10], that, in a C-RAN the eNBs collocate at a central location that we call here as Base Station Pool or BSP (also known as Master Base Station, Centralized Base Band Unit, etc., see, figure 1) and the remote antennas are connected with RRHs for further feeding to antenna/s.

In spite of a very efficient architecture, the C-RAN is still a BS centric solution; just like any conventional architecture. This is because even though a service provider may enjoy better spectrum management using C-RAN due to better spatial carrier distribution, however, this flexibility is limited to the BS to which the RRHs belong. Thus, a subscriber in C-RAN network is still tied to a particular BS, although, the roaming space is considerably increased. Consequently, it can be observed that every antenna in the C-RAN (as in traditional DAS network) has a strong belongingness towards the feeding eNBs (also known as Baseband Unit or BU) at BSP. This leads many limitations, and the following are relevant to the present paper:

1) Just like traditional DAS network, all RRHs are exposed to all carriers of BSs at BSP. As the received signal at the user end is the superimposition of the signal levels from all the surrounding nodes, in an ultra dense network (Dense-net), this may lead to high interference situations.

2) Infrastructures convolve around respective technologies and are not considered as an independent concept. Therefore, much of the investment in an infrastructure is worthless once a newer technology takes over.

3) It is practically unviable to lay a high capacity fiber network at every possible place in AoI. Therefore, C-RAN architecture has limited scope.

4) Although, being placed on the user ends, RRHs along with their antennas do not have any idea about subscriber behavior at the particular location in AoI.

5) Also, remote units do not participate in the holistic physical restructuring of the network for the betterment of the network environment and subscriber needs in the AoI.

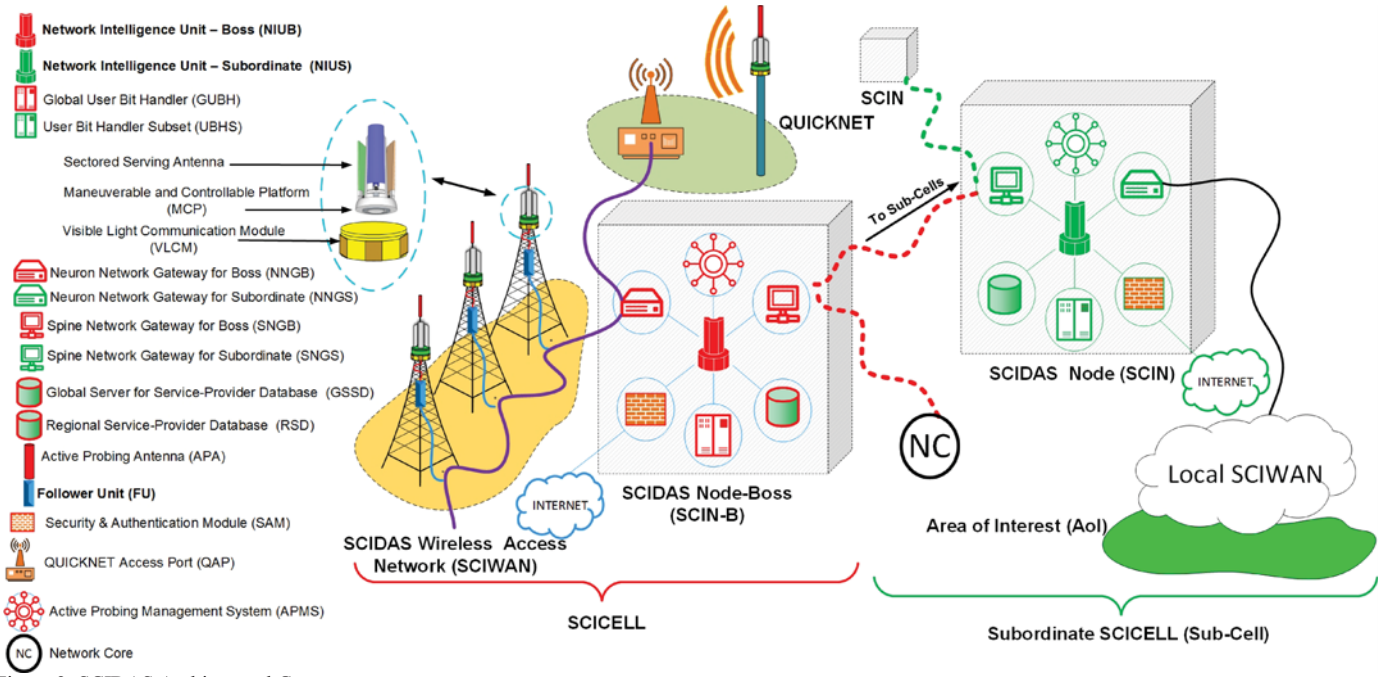

Figure 2: SCIDAS Architectural Components

6) RAN sharing (multiple service providers on common RAN infrastructure) will only distribute the additional resources over the existing infrastructure and not over the actual areas in need.

7) The existing networks respond to on-demand basis and are not proactive to the dynamic network environment.

8) Newer technologies will require overhauling of entire network elements and infrastructure as well.

9) Coexistence of new and old layers is a challenge in the present environment. Sharing RAN and CORE is only limited to basic infrastructural elements such as tower, shelter, rooms, power line, etc.

Our previous work [11] identified the challenges that wobble up when subscribers density vary significantly from place to place in AoI. [11] focuses on the significant variation in the network behavior even though the subscribers' count is constant in AoI, which means that the capacity requirement is dependent not only on the subscribers' count but also their movement and position. This phenomenon was termed as *Place Time Capacity* [11].

II. SCIDAS CONCEPT

Figure 2 shows the basic components of the *Self-Configurable Intelligent Distributed Antenna System (SCIDAS)*. The SCIDAS has an intelligence layer over the DAS-based C-RAN network for intuitive, proactive and efficient spectrum utilization. By intelligence, we mean the *ability to respond to dynamic network conditions at each and every remote unit distinctively, exclusively and simultaneously*. This is possible only when there is a common intelligent unit that generates location-specific instructions, and there are intelligent followers at each remote unit to receive and respond to these instructions. Also, please see legends of Figure 2 to refer the abbreviations used this point onwards. The major components of SCIDAS (see Figure 2), are the following (other components will be explained as they appear during discussion):

1) SCIDAS adopts a hierarchy in its architectural elements that we distinguish in two categories, the Boss and Subordinate/s (or *Sub/s*) (see figure 2). At the Boss level, processes like gathering, planning, deciding and configuring the global and respective local network functions will be carried out for the SCIDAS Network level, whereas, Sub functions are strictly local.

2) BTS Hotel or BSP equivalent in SCIDAS is the SCIDAS Node (*SCIN*). The type of SCIN, which will encapsulate the Boss elements, is the *SCIN-B*.

3) The *Network Intelligence Unit (NIU)* is a component residing in the SCIN. This entity adds technology independent intelligence functionality layer on the top of the present DAS paradigm. We distinguish between two types of NIUs, Boss (*NIUB*) and Sub (*NIUS*), based on the roles they perform (discussed later in this paper).

4) The *Follower Unit (FU)* is the equivalent of RRH in C-RAN; it differs from the RRH by its wide multi-technological support. As RRHs are responsible for feeding the antennas with carriers, in SCIDAS, we propose the radio part to reside only in FU (rather than BS, as in conventional architectures). This will enable NIU to select the individual carriers/subcarriers and to feed individual antenna differently. FU performs according to instructions from NIU rather than the Base Band Unit (*BBU*) thereby making SCIDAS more

5) suitable for the multi-technology and dense-net environment.

6) Unlike the usual DAS/C-RAN, SCIDAS has two layers of the distribution network. First one, the *Neuron Network (NuN)*, will fan out from respective NNGB/S to connect the FUs (*SCIWAN*). This will be done through fiber optic network/s or the wireless access port/s, QAP. The QAP is an easy deployment option for inaccessible areas (in terms of laying optical fiber) and/or sporadic network scenarios as a sub-network system (branched expansion) that we call as *QUICKNET*. We call a SCIN with its respective SCIWAN as a *SCICELL*. This SCICELL is building-block that will repeat in entire AoI.

7) The second network layer, the *Spine Network (SpiN)*, will connect the SCICELLs with each other through a high capacity network (Fiber or wireless) via respective SNGB/S.

8) The *Maneuverable and Controllable Platform (MCP)* is the docking station for the antennas and resides at the FU. MCP, as shown in figure 2, handles the physical conditioning of the network by orienting and tilting the antenna of every sector of the remote unit. MCP is controlled by the NIU via the FU by sending instructions to the FU.

9) *The Global User Bit Handler (GUBH)* is a type of BS/eNB with its RF and modulation techniques separated out from the module. Thus, a GUBH will process the user/subscriber bits in terms of handling the user packets (such as addressing, sending and receiving, etc.) and security/parity coding.

III. SCIDAS IMPLEMENTATION

The concept has been conceived to address the following grass root challenges that are considered obvious in architectural design of a network technology:

i) How will the network accommodate the "*Place Time Capacity"* challenge?

ii) Why do the antennas need to be dedicatedly associated to a BTS/eNB or BTS/eNB pool and cannot dynamically choose the portion of resources? Currently, RRHs may choose the carriers among the available resources. However, the total available resource is measured by available eNBs to which RRHs are connected

iii) When the end RF feeders are RRH (or similar), why BBUs should bother about the radio access technology at all? The answer to this question will allow multiple technologies at air interface end to be accommodated on the same platform.

iv) How can a single C-RAN architecture be smeared across AoI? This will benefit in terms of easy to deploy and manage.

A. Spectrum Mangement and Utilisation

The service providers' database of the allocated bands in each technology will be updated in the Global Server for Service-Provider Database module (GSSD). Based on the GSSD, the GUBH is configured to set out the traffic in the network. Once the network is deployed and FUs are distributed in the AoI, the APMS module, with the help of Active Probing Antennas (APA), will gather the information about the network environment and the subscriber concentration at each and every site location iteratively. By site, we mean the infrastructure that holds necessary equipment at a distant location that needs to be served. The NIU-B will segregate the information received from APMS in the following categories:

i) The capacity that is predominantly static to the respective location. Such traffic is generated from the slow or static subscribers.

ii) Capacity generated due to individual subscriber motions.

iii) Capacity due to excessive subscriber gathering

iv) SINR at each site location

Depending upon the user concentrations at each site locations, the NIUB will allocate the carriers for each FU and the carrier table is propagated to every FU via the NNGB. In this way, the same carries can be reused after a suitable distance as the baseband is not directly associated with radiated carriers. Also, based on the SINR, the serving channels and sub-channels can be individually selected by the NIU for every FU. Hence, the user bits can ride over any subcarrier and NIUB will map the subcarrier with the respective user data stream. Therefore, the processes such as carrier aggregation, carrier selections, etc., will be performed at the utmost basic level without affecting the user connectivity at all.

B. Subscriber Mobility in Multi-technology Environment

When FUs are considerably far from the respective NIUB, commutation of bits between the NIU and the FU will observe a significant delay. To overcome this situation, we have proposed the concept of Subordinate SCICELL or Sub-cell. Once the user/s will move significantly away from the NIU-B in the SCICELL, it will copy the user profile from GUBH to the User Bit Handler Subset (UBHS), which is similar to the GUBH with limited resources to manage.The UBHS will start performing as if the BS itself has moved from the initial to the final location. Also, the NIUB will instruct NIUS to imitate the portion of itself (NIUB) while the user/s roam in its (NIUS) vicinity. The user data packets will now be mapped onto the SUBH, and Sub-cell FUs will serve the user/s. In this way, a subscriber can roam in the AoI from one SCICELL to another and one Sub-cell to another without realizing the background management. In the case of an optimized network, the user/s may be served by a certain definite group of carriers thereby reducing the spectrum need. For the intra-SCIDAS calls, the GUBH and the UBHS can manage the calls by directing the user packets within or in between the

SCICELLS. However, for the calls that are made out of a SCIDAS network, the Network Core (NC) will be in use.

For the user packets to freely float across this kind of solutions, they must have a universal address for it to be transmitted securely and collected reliably. This we term as the *Universal Packet Addressing Scheme* (UPAS) that may embed the packet headers with the source and destination subscribers' user device address/information. UPAS will allow the multi-technology to ride on the same platform. Whereas the old technologies like 2G can be accommodated with SCIDAS performing as a usual DAS, the future technologies like Visible Light Communication (VLC) may need only a VLC module to be installed at the remote end for the user packets to float over it.

C. Handling the Place Time Capacity (PTC)

When a huge subscriber group moves from one place to another, they generate huge capacity burst that wobbles from place to place. The usual BSs are planned and deployed for normal subscriber density, and these bursts generate capacities that crave for the capacity beyond the serving capacity of the BS. Hence, such cases are undoubtedly a severe situation for all service providers as they often lead to network congestion and poor SINR (due to high uplink/downlink communication). The proposed SCIDAS will handle the PTC in more efficient way. Firstly, the accumulated users will be layered depending on the technologies they use by illuminating the area in congestion with multi-technology. This will spread the traffic in various layers. Then, for each layer, each FU, that handles the area, will be allocated individually with a maximum number of carriers to consume the generated traffic. As GUBH and UBHS will have the only responsibility to handle the user bits and not the technology of operation, the frequency reuse at the remote end can be done rigorously and dynamically without affecting the user bit flow.

As the total number of subscribers in a given AoI is predominantly constant, the neighboring FUs can be downgraded in their carrier allocation to avoid interference without losing subscriber connectivity. The APMS continuously monitors the entire spectrum related activity without imposing any burden on the user layer by using unused carriers for active probing. Finally, as the group moves in a pattern, the APMS follows and predicts the next affected zone; the FUs in that area will prepare themselves by loading the same carrier configuration as what it would be in the previous set of FUs. When the subscribers move to the next area, the FUs of the previous area will downgrade their carriers to avoid interference in the next area. In this way, the PTC burst is dissolved by SCIDAS.

IV. Conclusions and Future Work

This paper addressed the need for a novel type of architecture to handle the ever increasing number of mobile subscribers and their service demands. The paper builds on the concept of Place Time Capacity as the "motion with accumulation" and is the main challenge for the service providers. We have investigated how C-RAN are accommodated to handle some of those challenges but are not close enough. To overcome these challenges, we proposed SCIDAS, as an architecture that overlays intelligence over the conventional DAS architecture. We discussed the ease of deployment of SCIDAS where the FUs can be connected by a regular fiber optic network or by QUICKNET, which is a wireless port to connect FUs where fiber cannot reach. We also discussed MCP, another unique feature of SCIDAS that allows remote antennas to alter their physical parameters according to the dynamic network conditions. We have also discussed that why baseband unit should not bother about modulation techniques. We have promoted the role of an antenna from a passive radiator to a more active participant in carrier segregation. We have introduced a unique Active Probing Concept that will allow a network to have a panoramic view of the network and predict the future subscriber behavior. Lastly, we have discussed how the PTC is handled in SCIDAS with lesser interference and congestion.

The proposed SCIDAS concept contemplates about the need for a holistic paradigm shift in communication architecture. Separating the user data from the Radio Access technology will allow us to investigate radio part and data part as separate entities and to accommodate multi-technology on the same user bits. The proposed work also allows us to work on non-conventional communication techniques like VLC to be adopted into the mainstream communication.

References

[1] V. Gazis, N. Houssos, A. Alonistioti, and L. Merakos, "Evolving perspectives of 4th generation mobile communication systems," in *The 13th IEEE International Symposium on Personal, Indoor and Mobile Radio Communications, 2002*, 2002, vol. 1, pp. 201–207 vol.1.

[2] "Mobile marketing statistics 2015," *Smart Insights*, 2015. .

[3] "The Mobile Economy 2014." The Mobile Economy, 2014.

[4] R. Prasad, *5G: 2020 and Beyond*. River Publishers, 2014.

[5] Per Beming, Lars Frid, Göran Hall, Peter Malm, Thomas Noren, Magnus Olsson, and Göran Rune, "LTE-SAE architecture and performance." Ericsson, 2007.

[6] 3gpp, "UTRA-UTRAN Long Term Evolution (LTE) and 3GPP System Architecture Evolution (SAE)." 3gpp, 2008.

[7] F. Courau, M. Baker, S. Sesia, and I. Toufik, "Beyond LTE," in *LTE – The UMTS Long Term Evolution*, S. S. P. D. technical leader W. G. T. Officer, I. T. P. D. Telecommunications Engineering Research Engineer Research and Development Engineer, and tthew B. E. and E. inventor C. E. Member, Eds. John Wiley & Sons, Ltd, 2009, pp. 585–590.

[8] J. Huang, R. Duan, C. Cui, and I. Chih-Lin, "Overview of cloud RAN," in *General Assembly and Scientific Symposium (URSI GASS), 2014 XXXIth URSI*, 2014, pp. 1–4.

[9] Y. D. Beyene, R. Jantti, and K. Ruttik, "Cloud-RAN Architecture for Indoor DAS," *IEEE Access*, vol. 2, pp. 1205–1212, 2014.

[10] H. Niu, C. Li, A. Papathanassiou, and G. Wu, "RAN architecture options and performance for 5G network evolution," in *2014 IEEE Wireless Communications and Networking Conference Workshops (WCNCW)*, 2014, pp. 294–298.

[11] A. Kumar, P. L. Mehta, and R. Prasad, "Place Time Capacity- A novel concept for defining challenges in 5G networks and beyond in India," in *2014 IEEE Global Conference on Wireless Computing and Networking (GCWCN)*, 2014, pp. 278–282.

THE 5TH INTERNATIONAL CONFERENCE ON WIRELESS COMMUNICATIONS, VEHICULAR TECHNOLOGY, INFORMATION THEORY, AEROSPACE & ELECTRONIC SYSTEMS (WVITAE-2015)
December 13-16, 2015, Hyderabad, India

Embedded Video Processing and Data Acquisition for Unmanned Aerial Vehicle

Vrunal Mhatre
Fr. Conceicao Rodrigues College of Engineering
Mumbai, India
vrunal1994@gmail.com

Akshay Patil
Fr. Conceicao Rodrigues College of Engineering
Mumbai, India
patil2658@yahoo.in

Siddhesh Chavan
Fr. Conceicao Rodrigues College of Engineering
Mumbai, India
sid_coolkid33@yahoo.in

Ashish Chittimilla
Fr. Conceicao Rodrigues College of Engineering
Mumbai, India
chittimilla_ashish@hotmail.com

Aaron Samuel
Fr. Conceicao Rodrigues College of Engineering
Mumbai, India
aaronksamuel@gmail.com

***Abstract*— Drone technology has advanced to aid applications in field of defense, emergency, disaster relief and digital imaging. Inheriting all such applications for Unmanned Aerial Vehicle (UAV) in low cost scale to make system for ubiquitous for all domains is the motive for our system. Hence, embedding high quality video feed and controlling flight data characteristics to execute several applications. Our system has been devised specifically for air navigation and hence, seamless performance of all the components placed on-board is maintained with high compactness in form factor. First Person View (FPV) is provided for pilots for to achieve long distance mission execution along with image processing for accurate data analysis of flight characteristics. Along with this, the telemetry data procured from Arduino integrated with sensors viz., GPS, Altimeter, IMU assists the pilot for maintaining steady flight characteristics. Our system has been rigorously tested and has also been presented for Society of Automotive Engineers (SAE) Aero Design competition to accomplish humanitarian relief operation. The low-cost general processing boards like Raspberry Pi and Arduino facilitates versatility in embedding various sensors based on requirements of the pilot. Along with the on-board the telemetry system, the Ground Control System (GCS) provides first person visual aid on base station. The JavaFx interface is platform independent with features like FPV video streaming in real-time, representation of UAV's altitude, orientation and position at every instance of time. Moreover, the trans-receiver communication allows controlling flight characteristics from the interface, increasing the scope of applications with UAV.**

Keywards— Arduino, Rasp pi, pi camera, Image Processing, FPV, Ground Control Station (GCS), Java FX, Video Processing

I. INTRODUCTION

Aerospace has advanced with the advent of drone technology, to add the inclusion of Unmanned Aerial Vehicle (UAV) in artillery , the air borne application have increased multi folds. Citing these applications, we devised a system which could help supplement such applications using low cost components with capability of video processing and data telemetry with platform independence in hardware requirements. Our system was successfully tested in the Society of Automotive Engineers' (SAE) [1]. Collegiate Aero Design Competition in March 2015, which had humanitarian rescue mission application, in which we burgeoned with premier accolade for the Design and the system of the UAV. The use of on-board processors, camera and telemetry system yields robust performance for long ranges navigated with the help of Ground Control Station(GCS). The GCS is a javaFX application which can run on any standard web browser, serves as a platform independent interface for planning missions from the base station. And also, recording of the real-time data telemetry of sensors and video feed of the on-board camera is embedded in the GCS interface. On-board image processing algorithms intelligently enables the pilots to derive accurate data analysis of flight data in real-time. These features provide plethora of air surveillance applications like search and rescue, aerial farming and product delivery.

II. BLOCK DIAGRAM

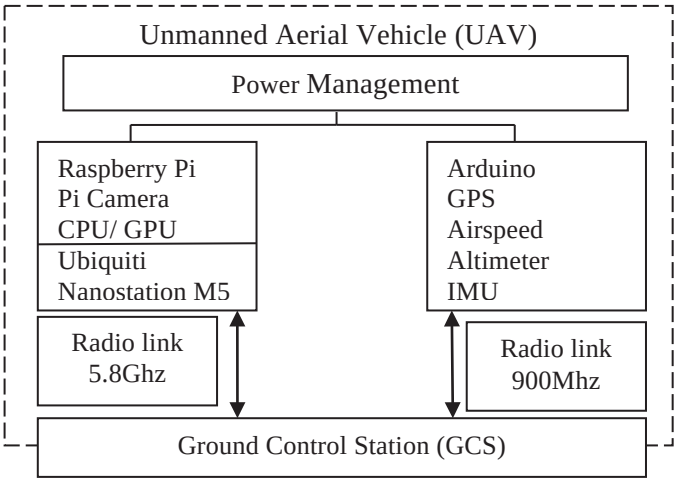

While implementing Video processing and Data Acquisition from the sensors we used a combination of Arduino and Raspberry Pi[2]. The advantage this combination is exploiting all functionalities from these two components which facilitates real-time data transmission with web Controlled Connectivity from multiple sensor data and also video streaming on variable operating systems with highly functional GUI. The Data Acquisition system consists of a sensor mesh which acquires data and sends it through a radio link to the ground station. We make use of a pair of X-bee Pro 900 HP radio.

In order to deploy successfully we need to have sizeable data at the ground station. Thus we have the GPS which gives us accurate location of our drone, the Inertial Measurement Unit (IMU) which gives the orientation of the drone, altimeter which helps get height above ground level and the air speed sensor which gives us the speed of the drone. The data acquired from this system is then processed at real time on the ground station which in-turn will direct the secondary pilot for deployment. [3]

III. VIDEO PROCESSING

First-person view (FPV) is an aid used by pilots to facilitate control of the remote-controlled vehicle from its view point. Most commonly it is used to pilot an unmanned aerial vehicle (UAV). In our system, Raspberry pi [5]along with Pi camera is used for HD live stream at maximum resolution of 1080x720 in real-time latency. This system gives a bird eye view for the UAV which is controlled remotely using the GCS interface. Thus, FPV enables UAV pilots to fly beyond the Line of Sight range and can execute missions with the aid of on-board processed video. To help enhance features of video feed, image processing at maximum rate of 12 Frame per Seconds was implemented using MATLAB[4] and FFMPEG. Algorithms like Feature Extraction, Shape detection, Object detection were implemented on raspberry pi using MATLAB raspberry pi support library. The video stream quality is maintained for long ranges due to the use of 5.8Ghz transmission frequency, as 5.8Ghz allows minimum interference and high bandwidth channel. Transmission of the video is achieved through Ubiquiti Nanostation M5, which serves as an Access point for the router ie. Ubiquiti Rocket M5 on the base station.

IV. HARDWARE

A. Raspberry Pi

A Single Computer processor with compact and light form factor, large processing power and with up to 24 GFLOPS becomes ideal for on-board image processing and flight characteristic sensor integration. Raspberry pi along with the Pi camera serves as the FPV system for the UAV. Image processing algorithms are implemented using python language and its simpler integration with the Pi Camera CSI interface provides better processing than USB camera.

Fig. 1 Raspberry Pi

B. Pi Camera

To achieve high quality FPV streaming with light weight components with digital streaming The Raspberry Pi camera module is used to take high-definition video; it has a 5 megapixel fixed-focus camera that supports 1080p30, 720p60 and VGA90 video modes. The Raspberry Pi camera board transfers data through an extremely fast camera serial interface (CSI-2) bus directly to the system-on-chip (SoC) processor. It does this through a 15-pin ribbon cable, also known as flexible flat cable (FFC), and connects to the surface mount ZIF 15 socket in the Raspberry Pi board. Owing to its low weight, small dimensions and high resolution, the Pi camera was found to be suitable for use in the UAV as compared to USB camera.

C. Arduino Uno microcontroller

The features of Arduino microcontroller are as follows:

Microcontroller	ATmega328
Operating Voltage	5V
Clock Speed	16 MHz
Digital I/O Pins	14 (of which 6 provide PWM output)
Weight	28 grams

The Arduino[6] is an inexpensive, easy-to-use microcontroller board. Its flexible programming environment provides the user the freedom to program either in Java, C++ or C language. With various libraries available online, the Arduino is one of the most sought after microcontroller boards available in the market.

Fig. 3 Arduino Uno Microcontroller

D. U-blox LEA-6H GPS Module

The GPS module has been incorporated into the system to obtain the real-time location co-ordinates of the UAV with respect to a set reference point. The on-field GPS coordinates of the target helps in determining the course of UAV to the drop point. The module has been selected for the following features:

- 5Hz update rate
- High precision-2.5m accuracy
- Super Sense® Indoor GPS: -160 dBm Tracking Sensitivity
- Dimensions: 37x37x9mm
- UART, USB and DDC (I2C compliant) interfaces

Fig.4 GPS module consisting of U-Blox LEA 6-H

The GPS module can also be used in weak signal environments. The antennae should be exposed to the sky to get proper locking of the GPS module.[7]

E. Inertial Measurement Unit- MPU6050

The InvenSense MPU-6050 sensor incorporates an MEMS accelerometer and a MEMS gyro on a single chip. It is very accurate, as it contains 16-bits analog to digital conversion hardware for each channel. Therefore it captures the x, y, and z channel at the same time. The sensor gives 6 Degree of Freedom (DOF), 3 DOF for the accelerometer and 3 DOF for the gyroscope. The sensor uses the I2C-bus to interface with the Arduino.

Fig. 5 IMU MPU-6050

The MPU 6050 was selected as a part of DAS because of its precise reading and updating process. It gives the Yaw Pitch and Roll of the UAV with respect to a predefined point. This helps us in understanding the flight in a 3-dimensional manner.

F. Altimeter – Parallax MS-5607 Altimeter Module

The DAS design objective states the use of a Data Acquisition System (DAS) to record the altitude (in feet) with a precision of at least 1 feet. The altitude must also be recorded at the time of release of the expellable cargo. The following requirement was implemented using the Parallax altimeter module MS5607[8]. The MS5607 module includes a pressure sensor and a temperature output and can be used for implementing an altimeter. [8]

The features of the module are given as:

- High resolution : 20cm Pressure range : 10 to 1200 mbar
- Supports I2C and SPI communications
- Power requirements : 3.3 to 6.5 VDC
- Dimensions : 0.85 in x 0.80 in
- Weight : 5 grams Fig. 2: Parallax MS-5607

Fig. 6. Parallax MS-5607 Altimeter Module

Altimeter Module Owing to its low weight, small dimensions and high resolution, the particular module was found to be suitable for use in the UAV.

G. Radio Communication

To channelize for the optimum bandwidth usage for transmission of large video feeds, we decided to choose 5.8 GHz frequency band. It is very advantageous to use machines that are functional at a 5.8 GHz frequency because it provides a wider coverage than that of with the 2.4 GHz frequency. Compared to the 5.8 GHz devices, 2.4 GHz 802.11g hold only about three channels, which are not overlapping. Since a number of routers may be present on ground station, using 5.8 GHz will prevent any overlapping with other channels while transmitting video streams. For video streaming we employed Ubiquity M5 rocket and Ubiquity M5[8] nanostation.

Establishing point to point connection via the Ubiquiti rocket M5 and nanostation M5 routers, ensured long range proximity for FPV streaming. Transmission of telemetry data is controlled by Arduino. We used Zigbee Transmitters for this purpose. Telemetry data like Altitude, latitude, longitude, airspeed etc are obtained by microcontroller using two digital pins, programmed as software serial ports. Programs are written to process the data from all the sensors in standard Arduino language. After processing this data, data is parsed, cleansed and then sent to Zigbee at the receiving end. We use 900 MHz for transmission of these data. 900MHz can go a lot farther with a high gain antenna (up to 15miles for the Pro modules and a high gain antenna). Also the lower the frequency the greater penetration the signal has. Also, trying to squeeze in these various components in compact weight and size forms was essential considering the aerodynamic features for any UAV. All the sensors and routers at the UAV end are of pocket size hence reducing the overall size and weight of the hardware components on UAV.

H. X-bee Pro 900-HP

The rulebook states that the telemetry system should not use 2.4GHz frequency. For this reason, we have chosen X-Bee Pro 900 HP.[9]

- Frequency band: 902 to 928 MHz
- Data Rate: 10 Kbps or 200 Kbps
- Data Interface: UART (3V), SPI

The processed data obtained from the Arduino is transmitted to the base station via the XBee modules. The X-Bee usually sends data to the computer terminal. But when the package is to be deployed i.e., the "Fire" button is pressed on the GUI, the X-Bee module works in full duplex mode.

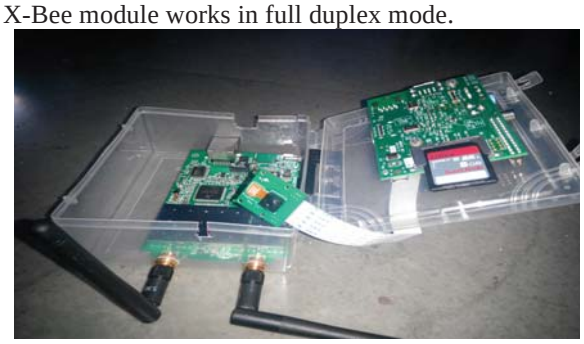

Fig. 7 Raspi+ Pi camera+ Ubiquiti NanoStation m5 with Linear Antenna

V. POWER MANAGEMENT

The most crucial part of any electronic mobile device is its battery life, in our case flight time of our system. We have used the Raspberry pi and Arduino for accurate and optimum results. In order to achieve optimum results a flight time of 45 min to 1 hour is a must. Hence battery selection at this stage is paramount, we have to select a battery which is conducive to the Arduino, Raspberry pi and the Ubiquiti router. The Raspberry pi works on 5V DC, Arduino Uno works on 9V DC supply and the Ubiquiti router works on 14.8 V. To tackle this problem we have made the use DC-DC buck converter.
The concept of DC-DC buck converter is; input power = output power, unlike the normal voltage regulator the excess power doesn't get dissipated but instead gets utilised. We have used a 14.8 V 2.5A Lithium Polymer batter (LiPo) and two DC-DC buck converters. One pertaining to the Raspberry pi of the rating and the other to the Arduino with the rating.
The below table and pie chart depicts the power distribution in our system.

Sr.No	Voltage	Current	Power
1. Ubiquiti	14.8V	1A	14.8W
2.Rasp. pi	5V	.8A	4W
3.Arduino	9V	1.3A	11.7W

From our LiPo battery of rating 14.8V 2.8 A battey we get 37 W/hour and the actual power required is 30.5 W. This wouldn't have been the case if we had used anything but DC-DC convert. With the obvious approach of voltage regulator the system wouldn't have lasted half the time as that with DC-DC converter.

Sr.No	Power consumed with DC-DC converter	Power Consumed with Voltage Regulator
1.Ubiquiti	14.8	14.8W
2.Rasp pi	4W	11.84W
3.Arduino	11.7W	19.42W

As we can evidently see that with the use of voltage regulatorwe would have consume 45.52 W instead of 30.5 W.

A. DC-DC converts

We make use of two LM2596 DC-DC buck converters.
The DC-DC converter is used in order to enhance the efficieny of the system. The DC-DC converter is an essentail tool for optimising battery usage. Specifications:

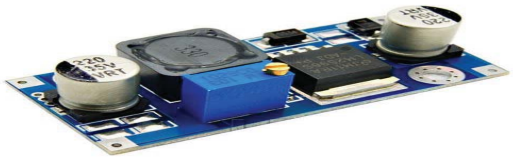

Fig.8. DC-DC Converter.

- LM2596 DC-DC Buck Converter Step Down Module
- Output: DC 1.5V to 35V voltage continuously adjustable, high-efficiency maximum output current of 3A.

VI. GRAPHICAL USER INTERFACE (GUI)

In order to present all the telemetry data and real time video streaming at the base station, platform independent single window GUI is made. GUI is made using cross-platform JavaFX API. In order to incorporate visual navigation and to

help UAV drop the package at perfect instant, various features have been added to GUI.[10]Live http streaming is achieved by establishing point-point bridge connection over the Ubiquiti rocket M5 router mounted on UAV and the Ubiquiti nano-station router at the base station. A full-fledged FPV with textual overlays using JASON(JavaScript object notation)is then embedded in GUI. This is achieved using JXBrowser API which allows chromium based browsers to be integrated into Java AWT/Swing/FX applications. With JXBrowser you can embed a lightweight Swing/JavaFX component into our Java application to display web pages, supporting the latest web standards such as HTML5, CSS3, and JavaScript etc.GPS coordinates obtained from Arduino are parsed and displayed on the GUI. But coordinates in it are not sufficient for navigation; hence UAV co-ordinates are represented on a map embedded in a GUI using Leaflet API. This JavaScript mapping library allows us to asynchronously plot the co-ordinates on the map without the need of refreshing it. Readings from MPU 6050 i.e., yaw, pitch and roll are used for getting the real time orientation of the UAV. Using these readings, aerial time simulation of a UAV is modelled using a processing sketch which is embedded in JavaFX GUI. The processing language itself builds on Java hence can be easily integrated in our GUI. Equipped with the data such as UAV's GPS co-ordinates and yaw, pitch and roll of UAV obtained from MPU 6050, precise package dropping at a specified target can be achieved. Using projectile motion equations , instantaneous package drop location is calculated at each instant of time ,having known the yaw and pitch of the UAV at that instant. Package is dropped at the instant when package drop location calculated at that instant coincides with the target location. Fire button on the GUI is pressed so that the package can be released. This is achieved using Java RXTX library which allows us to read and write data on a COM port. Xbee trans-receiver connected to the COM port then sends command to release package to the Xbee trans-receiver mounted on UAV. When the fire button is pressed; latitude, longitude and altitude at that instant are also shown on the text fields in the GUI. For representation of Altimeter and Airspeed data, Gauges are made using library of gauges.

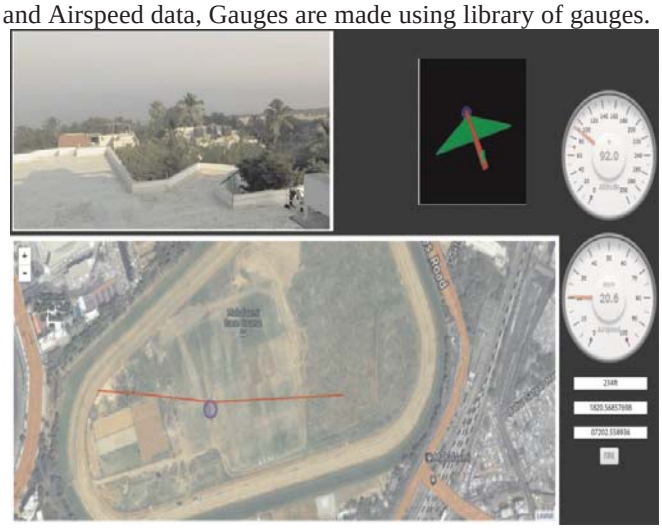

Fig.9 Graphical User Interface (GUI) application in JavaFX.

VII. FUTURE SCOPE AND CONCLUSION

Our system consists of two general purpose processing boards, Arduino Uno and Raspberry Pi as we intended to maintain redundancy in the case of failsafe situations. However, similar system can be also embedded on Raspberry Pi alone with video processing through Pi Camera and telemetry data interfaced through GPIO ports. Such system could be processor optimized and compact, but may be unreliable in the event of failure.Also, similar hardware components could be executed in Software In The Loop mechanism to achieve autonomous capabilities. To implement autonomous UAV flight PID controller can be programmed using the IMU sensor.The system designed is highly reliable in natural disaster environments because in the event of signals getting lost from one bandwidth we can still receive signals from another bandwidth which makes it possible to have atleast basic information about the area. The system can be used in Nuclear Disaster area and can be embedded with radiation sensors and one can have live video surveillance of the fatal prone area. The stability of the Drone is high in which this system is used which makes it to be used in harsh environments. One can attach robotic arms to collect samples of area where human intervention is nearly impossible.

REFERENCES

[1] About SAE AERO International, https://www.sae.org/about/

[2] "FPV setup with raspberry Pi", Blog by Philip from DIY Drones

[3]"Data Acquisition System for an Unmanned Aerial Vehicle" http://www.ijste.org/index.php?p=Archieve&v=1&i=11

[4] MATLAB Computer Vision Toolbox, "Object Detection in a Cluttered Scene Using Point feature Matching"

[5] Raspberry Pi- setup and Pi camera libraries, https://www.raspberrypi.org/learning/python-picamera-setup/

[6] Arduino - Introduction, http://arduino.cc/en/Guide/Introduction.

[7] GPS U-Blox Module http://www.u-blox.com/en/gps-modules/pvt-modules/previous-generations/lea-6-family.html

[8] Interfacing Altimeter Module http://learn.parallax.com/KickStart/29124

[9] XBee-Manual.pdf, http://www.digi.com/pdf/ds_xbeemultipointmodules.pdf

THE 5TH INTERNATIONAL CONFERENCE ON WIRELESS COMMUNICATIONS, VEHICULAR TECHNOLOGY, INFORMATION THEORY, AEROSPACE & ELECTRONIC SYSTEMS (WVITAE-2015)
December 13-16, 2015, Hyderabad, India

Automatic Household Power Measurement & Control System based on Wireless Sensor Networks

Sarah Shamsi[a], Ashutosh varshney[b], Mirza Salim Beg[c], *Jameel Ahamed[d], Rehan Muzammil[e]

[a,b,c]Department of Electronics Engineering, Students, ZHCET AMU, Aligarh-202002
[c]Department of Electronics Engineering, Professor and Chairman, ZHCET AMU, Aligarh-202002
[d]Department of Electronics Engineering, Guest Faculty, ZHCET AMU, Aligarh-202002
*Presently working as Assistant professor, Department of Computer Science and I.T, MANUU, Hyderabad-500032

Abstract

This paper deals with the electricity theft control system and an initiative to save power. The growing electricity theft in the form of overloading in the houses has motivated us to design such a system for household electricity supply which will work to solve the problem of overloading and voltage fluctuations. We have developed the prototype system based on wireless sensor network (WSN) of sensor motes installed with the prototype circuit of household electricity circuit. The WSN is formed among the houses having sensor motes attached with their electricity meter. The household load and power are measured and controlled with these sensor motes. Moreover, the gateway which is the sync node in the network is placed in the power house control room attached with the computer. In this work real time measurement and controlling of current, voltage and power of the prototype circuit is done through Crossbow wireless sensor motes using Moteworks 2.0 environment and displayed on Mote View software. The relay in the sensor mote is used to control the sensed parameters. The network health is also indicated using health packets containing received signal strength indication and retransmissions displayed via Mote View.

Keywords: WSN, Electricity

1. Introduction

This Electricity theft is becoming a growth theft. Electricity theft drags down not just the power sector but the entire nation. This work is the initiative to control this growing problem of electricity theft. We have developed such a prototype system which will work to stop electricity theft by controlling the household overloading issue. We have implemented the wireless sensor nodes for automatically controlling the load at the houses. These sensor nodes are forming the Wireless sensor networks. This technology in recent years is acquiring importance as a promising technology, as using WSN real time monitoring and controlling of the sensed parameters can be done.

The gradual improvement in Micro-Electro-Mechanical Systems (MEMS) technology has alleviated the development of smart sensors. The research in wireless sensor networks (WSNs) is gradually increasing in recent years as these sensors are small with limited processing, computing resources, and cheap compared to traditional sensors. These sensor nodes can sense, measure, and gather information from the environment and based on some local decision process, nodes can transmit the sensed data to the user [1,2].

The concept of wireless sensor networks is based on a simple equation: Sensing + CPU + Radio = Thousands of potential applications

Smart sensor nodes consist of sensors, a processor, memory, a power supply, a radio, and an actuator. Sensor nodes may be attached to a variety of mechanical, thermal, biological, chemical, optical, and magnetic sensors to measure properties of the environment. The radio part is very crucial and it is implemented for wireless communication to transfer the data to a base station (e.g., a laptop, a personal handheld device, or an access point to a fixed infrastructure), as the sensor nodes have limited memory and are typically deployed in difficult-to-access locations. In a sensor node, battery is the main power source[2,3].

2. Electricity Theft: Motivation behind the Work:

In several countries electricity theft has some kind of endemic character. Here are the following ways in which electricity theft can be done:

a. Bypassing the feeder.
b. Another way of theft of electricity is to invert the meter (pull the meter out of the socket and plug the meter back in upside down).
c. A popular way to slow down a meter is the use of strong permanent magnets like rare earth neodymium.

3. Software

The sensor nodes in WSN are described as little computers capable of doing different tasks of sensing, tracking and data acquisition. Therefore these nodes need an operating system to measure and send data to base station. An important step towards attaining the vision behind wireless sensor networks is the design of a software architecture that links the hardware capabilities and a complete system. There are numerous restraints placed on the software of WSN. It must be effective in terms of processor, memory and power so it meets firm application requirements. It must also permit multiple applications to concurrently use system resources such as communication, computation and memory. The operating system designed particularly for networked sensors is TinyOS. Figure 2 shows the architectural layout of WSN where operating

systems exist in between the actual sensor hardware and application. The wireless sensor nodes utilize less complex operating systems and event driven programming models because of its design restriction and limited resources [4].

In WSN an operating system hides the low level facts of the sensor node by giving virtual access to the device.

The key characteristics an operating system must provide in WSN are power management, memory management and bandwidth [5].

The software platform used for this work was Mote Works 2.0F, provided by Crossbow Technology Inc. and Microsoft Visual C++ Studio 2008. Mote Works 2.0F includes:

- **TinyOS and Mote WorksTool**: An event-driven OS for wireless sensor network and tools for debugging
- **nesC compiler**: An extension of C-language designed for TinyOS.
- **Programmer's notepad**: IDE for code compilation and debugging
- **MoteConfig**: GUI environment for Mote Programming and OTAP
- **MoteView** : An interface ("client tier") between a user and a deployed network of wireless sensors.

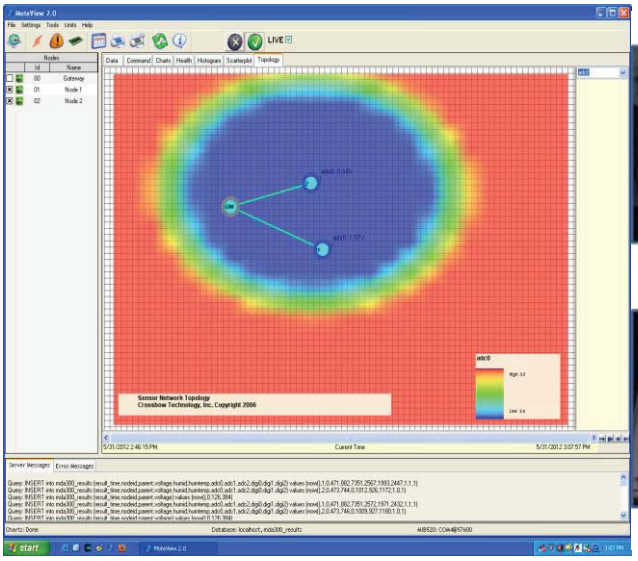

Figure 1: Showing Topology of node 1, node 2 & gateway in terms of ADC "0" voltage.

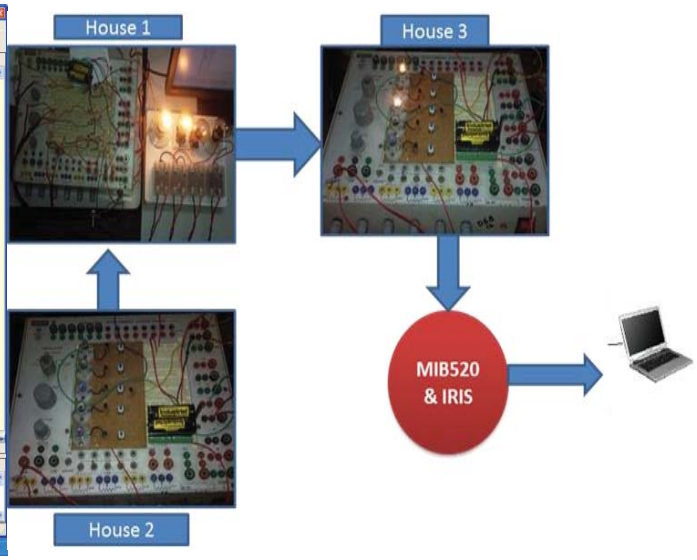

Figure: 2 Prototype System

4. Automatic Household Power Measurement & Control System

I. Experimental Setup.

To control electricity theft we have developed a prototype system based on wireless sensor networks to measure and control household power. Hence our system will perform following functions:

- Monitors and measures the household power
- Cuts power supply to houses if exceeds threshold load
- Gives back power if load is reduced
- E-mail the user of the house about the disconnection
- E-mail the user total Electricity bills

These are operations which our system will perform in order to control the problem of electricity theft in India. The prototype system is shown in the figure 2.

Figure 1 shows the nodes are attached to the electricity circuit developed and it senses the voltage as the current changes in the circuit through the ADC "0" line of the sensor board. Hence the nodes are communicating in multi hop fashion and transmitting their information to the gateway then to PC as shown in figure 2 in the moteview software. This forms the wireless Sensor Network of the motes kept in houses which will work together to control overloading problem in that area.

The prototype system developed will disconnect the supply of house 1 if ADC"0" >=1.8V and of house 2 if ADC"0" is 0.65V and connects the supply back of the load of the house or prototype circuit is reduced.

II. Circuit Design

There are two circuit designs in our system:-

- The Prototype circuit of household electricity network
- The circuit developed to generate pulse for billing application

III. Prototype: Household Electricity Network

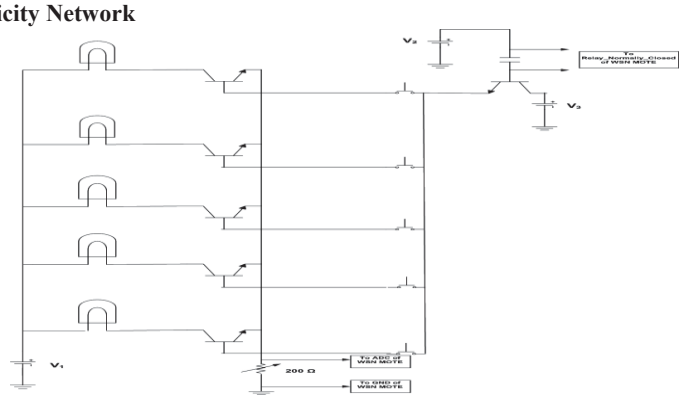

Figure 3: Prototype circuit diagram of household electricity.

Prototype circuit diagram of household electricity circuit is shown in figure 3. The specifications of the circuit are written below:

- V1 = 5volts
- V2= V3 = 7.5 volts
- Bulbs of 3.6 volts
- Transistors BC147
- Variable Resistance, R1 = 200 ohms
- Resistance, R2 = 100 ohms
  R1 || R2, hence
  R nearly 50ohms
- Current by V1 = IR
- I=2. 5/50=50mA

IV. Counter Circuit

A counter circuit is shown in figure 4 and counter pulse is shown in figure 5. A high quality Multivibrators can be generated using 555 timer IC adding external resistors and capacitors.

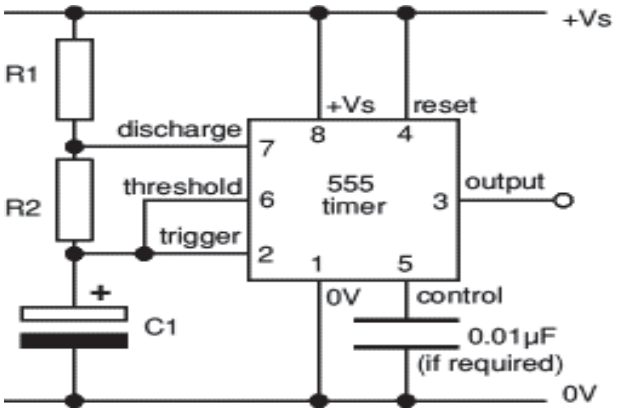

Figure 4

This circuit is used here to generate square pulse to operate Counter terminal in MDA300 sensor mote. As the counter is rising edge triggered, we need to implement the timer for rising edge. For pulse of (>50% duty cycle).

- By 555 Timer IC
- Supply voltage = 6V
- RA = 10K, RB = 10k (POT)
- C1 = 5 micro F
- C2= 0.1 micro F
- Time period= 0.1sec

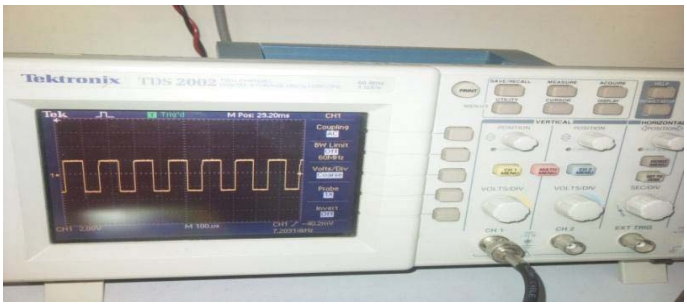

Figure 5: Square pulse for counter

5. Working

I. To Control Power Overloading

The prototype developed is common emitter based configuration with emitter Resistance. As we give load the current across R changes and hence voltage across R changes which goes to ADC line of sensor mote. When the load increases above the threshold the relay normally closed is opened which disconnects the electricity supply. When the load is reduced below the threshold the electricity supply is connected back. In our program we have set our threshold ADC0 line value = 1.8Volts so as we turn on the switches to increase the load in the circuit simultaneously the voltage across resistance (R) changes and hence ADC line input increases then when the value of voltage passes 1.8V the power cuts and ADC line displays zero volts this power cut can be reverted back if load is reduced in the circuit hence power will come back and ADC voltage will vary from 0 volts.

II. Readings:

The readings using the prototype are tabled below in table no. 1 which shows the ADC Voltage against the load connected. As shown in figure 6 the ADC Voltage when one bulb is connected is 0.34 and so on. When the load is greater than threshold load then there occur power cuts as shown in figure 6 and figure 7.

Table 1

LOAD (bulbs)	ADC_0 voltage
0	0V
1	0.34
2	1.15
3	1.2
4	1.56
5	2.19 (Power Cuts)
NO bulb ON	0V
4 (after reducing load)	1.7V (Power back)

Therefore the user has to turn off the load to bring back the electricity. The prototype circuit developed:

- It is based on common emitter based configuration with emitter Resistance.
- As we give load the current across R changes and hence voltage across R changes which goes to ADC line of sensor mote.
- When the load increases above the threshold the relay normally closed is opened which disconnects the electricity supply.
- When the load is reduced below the threshold the electricity supply is connected back.
- The amount of electricity used is also monitored and stored in a variable such that billing is done automatically using that variable.

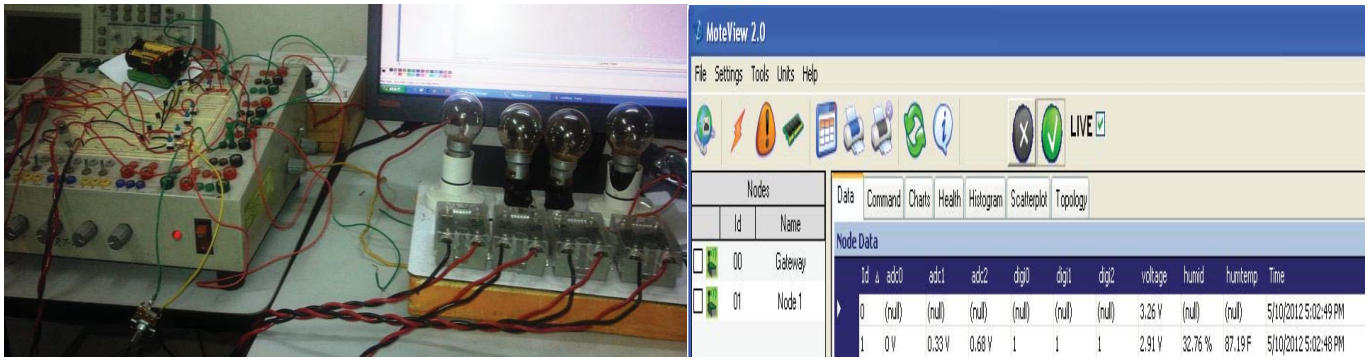

Figure 6: When NO bulb is ON and corresponding ADC voltage.

Figure 7: When "1" bulb is ON and corresponding ADC voltage.

Generate Bill

Then billing is a very significant part it is done with the help of counter port in the sensor board. To use the counter port the square pulse of 0.1sec is given to the ports counter is a rising edge triggered. The pulse was generated with the help of 555 timer circuit as shown in Fig 5. The pulse is of >50% duty cycle. The counter used is positive edge triggered and it counts 10 times in every second. The counter will count only when the ADC0 line voltage in mote view is not zero that is the when the supply is given to the circuit which means the house is not overloading. Hence when there is no overloading condition the counter counts 10 times per sec and calculates power at every instant according to the variable voltage value in adc line.

$$E = \sum_{v=1}^{N} P_v$$

Where, E is the energy used in N sec.

$$P_v = \frac{V^2}{R}$$

Where V is variable ADC0 line voltage at different counting instants , R is 50 ohm. E is the total Energy in watts sec. Pv is the instantaneous power at ADC "0" as voltage changes at different count instants. N is the total number of counts (10 per second).

Hence, E=E/10

Total Bill= E*(rate in rupees for per watt sec)

Future Work

Hence the bill will be emailed to the user's email address through MIB600 Ethernet interface board which is connected to the hub/switch/router and also the message of electricity disconnect will be emailed to the user as the power cuts due to overloading.

But unfortunately due to the lack of technical support from the developers of the sensor motes, Crossbow Technology and MEMSIC the billing of the electricity does not shape up into reality. Moreover, we have developed the logic and made the suitable changes in the program to do the billing of the electricity used in each houses but due to the programmed Mote view display, the value of the counter was not displayed in the Moteview. Hence the calculation for evaluating bill is incomplete. The email from the Mote View was also not sent due to the server issues in our working environment.

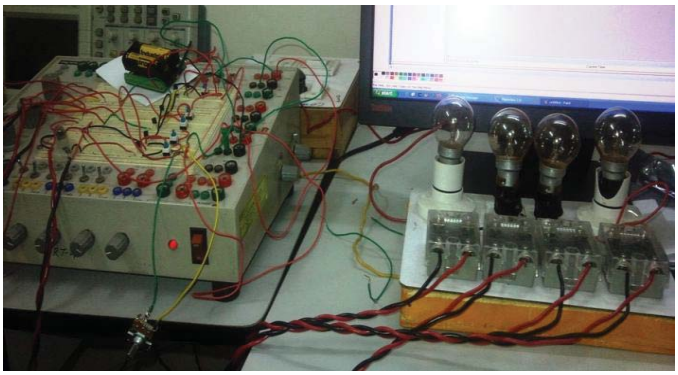

Figure 8: ADC "0" voltage is >1.8V condition of overloading, hence Electricity is disconnected.

6. CONCLUSION

This work is the first step towards the future for saving power by preventing power overloading and hence preventing voltage fluctuation, this has also reduced cables and configuration issues. The measurement of the voltage drawn from the prototype circuit (of houses) is done through Crossbow wireless sensor motes using Mote Works environment through ADC"0" line and displayed on Mote View. The charts & topology plots of ADC "0" line of both nodes have been displayed. Wireless Sensor Network health is also indicated using health packets containing path cost, RSSI and retransmissions displayed via Mote View. Variation of received signal strength and retransmissions with different antenna orientations and inter mote distances have been demonstrated. The current state of the work is the platform on which design enhancements can be made and real time power management & controlling can be done. The system developed has constant sampling rate of 10 samples per second, low latency and high reliability because of XMesh. Network Route Update Interval is 36 seconds. The route update interval can be increased to lower power consumption and increase the lifetime of node. Electricity billing is automatic and is received at the user end through e-mails and payment can be done online and hence no paper work is required.

7. REFERENCES

[1] Rizwana Ahmad, Anukrati Singh, Rehan Muzamil, M Salim Beg, Jameel Ahamed, "Use of WSN for Detection of Metal Landmines Using Unmanned Vehicle" Proceedings of the 9th INDIACom; INDIACom-2015; IEEE Conference ID: 35071 2015 2nd International Conference on "Computing for Sustainable Global Development", 11th– 13th March, 2015.

[2] MIT Study on the Future of the Electric Grid http://mitei.mit.edu/publications/reports-studies/future-electric-grid, 2011.

[3] Kazem Sohraby, Daniel Minoli and Taieb Znati "Wireless Sensor Networks Technology, Protocols, and Applications" John Wiley & Sons, Inc., Hoboken, New Jersey, 2007.

[4] Catalogue "Cylindrical Compact Inductive Proximity Sensor Amplifier Built-in GX SERIES" www.yumpu.com.

[5] Jason Hill et.al,"System Architecture Directions for Networked Sensors", Proceedings of the ninth International conference on architectural support for programming languages and operating systems, pp: 93-104, November 2000, Cambridge, Massachusetts, USA.

[6] Crossbow MPR-MIB Users Manual Revision A, June 2007 PN: 7430-0021-08

[7] Crossbow MoteWorks Getting Started Guide Revision D, March 2007 PN: 7430-0102-01

[8] Crossbow XMesh User's Manual Revision C, March 2007 PN: 7430-0108-01

[9] Crossbow XServe Users Manual Revision D, March 2007 PN: 7430-0111-01

THE 5TH INTERNATIONAL CONFERENCE ON WIRELESS COMMUNICATIONS, VEHICULAR TECHNOLOGY, INFORMATION THEORY, AEROSPACE & ELECTRONIC SYSTEMS (WVITAE-2015)
December 13-16, 2015, Hyderabad, India

Service Interaction through Gateways for Inter-Cloud Collaboration within the Arrowhead Framework

Pál Varga
Dept. of Telecommunications and Media Informatics
Budapest University of Technology and Economics
2 Magyar Tudósok krt., Budapest, Hungary, H-1117
Email: pvarga@tmit.bme.hu

Csaba Hegedűs
AITIA International Inc.
Telecommunication Division
48-50 Czetz János str., Budapest, Hungary, H-1039
Email: hegeduscs@aitia.ai

***Abstract*—Service oriented architectures (SOA) provide functional and configuration flexibility in closed communication environments, where security and service-related orchestration issues are controlled within the local network. For automation systems, these SOA-based networks can have core services, such as Service Registry, Orchestration, Authorization, and so on. A set of such core services are defined, implemented and made available through the Arrowhead framework. Since the Core Services are distributed resources available for all systems that wish to consume them, these networked services can be considered a cloud. As one cloud cannot serve for all, there is a need for such automation system clouds to interact with each other: use the services of one from another. This paper presents a solution for providing inter-cloud servicing capabilities in the Arrowhead framework by introducing a gatekeeper concept. The main idea is to extend the service discovery functionality outside the boundaries of a single cloud, and solve the security and orchestration issues in a way that fits into the general Arrowhead concept. This paper also introduces the methodology of creating secure connections between service consumers and producers situated in different clouds.**

I. Introduction

The purpose of this work is to introduce a gateway, or rather, a Gatekeeper as a new optional Core System for handling interactions between Arrowhead Local Clouds. Arrowhead is a joint collaboration project within the EU, with the grand challenge of enabling interoperability between systems that are natively based on different technologies. This enabler includes design and development methodologies, implemented Core Systems and Services, and a documentation structure to support the common understanding of the experts from various fields. It targets five business domains: production (processing and manufacturing), smart buildings and infrastructures, electro mobility, energy production and the virtual markets of energy.

The integration of the projected, very large collaborative automation systems requires that the participating systems can dynamically exchange information during run-time. This raises issues – among others – of service discovery, orchestration and security. For the use case scenarios of very large system-of-systems – i.e. whole cities – the present solutions do not scale favorable. Thus SOA (Service Oriented Architecture) approaches have been investigated to address large scale automation systems [1], [2], [3], [4].

These Arrowhead Framework compliant system-of-systems will be called Arrowhead Local Clouds. By definition, one Arrowhead Local Cloud consists of various Systems and their Services and are governed through the use of mandatory (and optional) Core Services provided by the locally involved Core Systems – the manner of the realization of the Framework is depicted in Fig. 1.

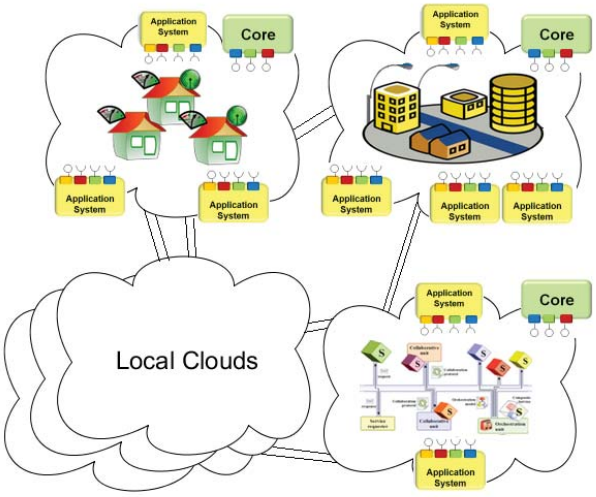

Fig. 1. Interconnected local collaborative clouds

II. The Arrowhead Framework and Related Work

The objective of the Arrowhead Framework is to efficiently support the development, deployment and operation of interconnected, cooperative systems based on the SOA approach. The building elements of the Framework are *Systems* that provide and consume *Services*, and cooperate as a larger *Systems of Systems* (SoS) called *Local Clouds*. There are three mandatory Core Services that are required to create a minimal working SOA Local Cloud based on the Arrowhead Framework. These Services are namely the Service Discovery (from the group of Information Assurance services), Authorization (Infrastructure services) and Orchestration (System Management services). Other (optional) Core Services have been also created to further enhance the capabilities of Local Clouds, such as System Configuration and Service Metadata Stores or Event Handler Services. These Core Systems are the central entities of the Local Clouds and can provide their capabilities IT cloud-based, as well.

1) Services: A Service within the Arrowhead Framework is the exchange of information between a provider System and a consumer System, as seen in Figure 2. In a service, capabilities are grouped together if they share the same context [5]. As an example, a service in a REST [6] architecture can be constituted by all interfaces which are related to the same REST resource (meaning an information source). In the context of Arrowhead, a resource might be a temperature sensor or a power consumption reading from a power meter. The same approach also applies to the other technologies being used in Arrowhead, such as COAP [7], XMPP [8] or OPC-UA [9].

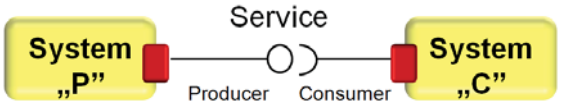

Fig. 2. Services produced and consumed by Systems

The Arrowhead Framework also implies the usage of a number of service orientation principles derived from high level objectives and properties. By definition, a Service can be realized by an arbitrary number of producers and consumers, therefore insuring its *reusability*. An Arrowhead Service might also support different kinds of *non-functional requirements* such as security, real-time constrains or different levels of reliability. Systems should also be capable of sequentially providing and consuming different types of Services with the help of the Orchestration in order to fulfil a more complex task – *composability of Services*.

Finally, in relation to Service development and maintenance, a Service has its own group of appointed stakeholders with an interest in the Service by being responsible for its governance (definition, development, deployment and maintenance). However, Services are not limited to a specific type (or instance) of a System and might not even share the same stakeholders with any System.

2) Systems: A System is what is providing and/or consuming Services (see Fig. 2). A System can be the Service Provider of one or more Services and - at the same time - the Service Consumer of one or more other Services. It normally includes software executing on (often constrained) hardware. It might support different protocol implementations of Services associated with it. A System can be a user interface display, a complete HVAC sytem within a house, but it can also be a small temperature sensor that complies with the Framework.

3) System-of-systems: When Arrowhead compliant systems collaborate, they become a System-of-Systems (SoS), see Figure 3. There are five main characteristics that differentiates these SoS realizations from other very large and complex, but monolithic systems [10], [11], namely (i) the operational and (ii) management independence of its Systems, (iii) evolutionary development, (iv) emergent behaviour, and (v) geographic distribution. Since these System-of-Systems should also collaborate, the Arrowhead framework becomes a natural enabler of further, complex solutions.

As an example, Systems A1, A2 and A3 are grouped together to create *System-of-Systems "A"*. This SoS then can be bundled together with other Systems (such as B1, C1 and D1, also depicted in Fig. 3), since they are Arrowhead

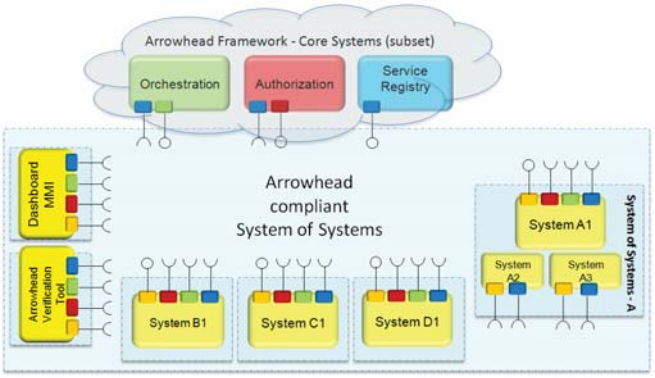

Fig. 3. Arrowhead core components support the system-of-systems - an example

compliant as well. The Arrowhead Framework provides Core Systems, such as *Orchestration*, *Authorization* and *Service Registry*, which help on establishing the most adequate and secure connections between the players. All these Application Systems are consumers of the Services of these Core Systems, which then forms this Arrowhead Local Cloud. The *Dashboard MMI* (Man-Machine Interface) allows interaction with this SoS; whereas the *Arrowhead Verification Tool* provides means for testing Arrowhead compliancy.

A. Requirement against gateways in various domains

Gateways serve various purposes in the different communication domains. They stand at the border of a subnetwork, a service area, or an operator. Their purpose is to provide means of connection and data exchange between the internal and external worlds. There could be very specific requirements against gateway functionalities, but in general, the following challenges can be dedicated to gateways:

- protocol and data format conversion or translation,
- addressing translation,
- security and AAA features,
- access control with content filtering,
- in- and outbound link control and their resource management.

These are not always solved by the gateways themselves; some methods of inter-domain communications handle these issues through specialized protocols, or have designated nodes to handle some of the above mentioned functionalities. A brief summary of gateway requirement and solution approaches within various domains are is given in Fig. 4. General interoperability issues and their handling are covered in [12], where the authors raise the performance and QoS issues regarding gateways as well. There are further, less general requirements and solutions listed for IPv6-based Internet of Things solutions in [13], for ad hoc vehicular military systems in [14], and for IT services in [15] and [16]. In the following Sections, we will heavily depend on these requirements when designing the enriched gateway concept as a Gatekeeper System, and describe its functionality. (Gatekeepers are special gateways, equipped with some decision-making functionalities – not merely on the network layer.)

	Protocol and data conversion	Address translation, Addressing issues	Access control, content filtering	Security & AAA	Link & Resource management
Managed Internet Services	-	Network Address Translation (NAT)	firewall, proxy	separate AAA servers; secure VPNs	queue management, QoS solutions (IntServ, Diffserv); Content Delivery Networks (CDN)
VoIP service	signaling conversion, dialing tone regeneration, media codec conversion	ISDN GT <-> SIP, H323 addresses	central access control, or Private Branch Exchange (PBX)	separate AAA servers	separate management for outgoing lines to PSTN, PLMN
Cellular mobile networks	-	multihoming of network nodes (transparent redundancy); roaming addresses for endpoints	Access control by Home Location Register	Ciphered communication; Separate nodes for AAA: Authentication Center, Equipment Identity Register; Charging server	handled through network layer protocols
IT Cloud solutions	cloud technology drivers (e.g. Azure - amazon conversion)	public address and NAT management (exposure issues); injecting routing info to partner cloud	Cloud Networking Gateway	secure VPNs between clouds	Virtualization; Grid resource management

Fig. 4. Requirements for various gateways and their solution approaches within different domains

III. Gatekeeper Services for Inter-Cloud Collaboration

In this Section, we introduce the Gatekeeper as a new Core System concept – as shown in Fig. 5 – for providing inter-cloud servicing capabilities in the Arrowhead framework. All inter-cloud preparations are to be handled by these Gatekeepers until the System (that requested the Service) enters the new, "Partnering Cloud", in order to create the desired producer-consumer connection. However, these modules are not involved in the data path as they operate on the control plane, see in Section III-E. In the followings we will discuss the processes and the issues involved and need to be addressed in this architecture.

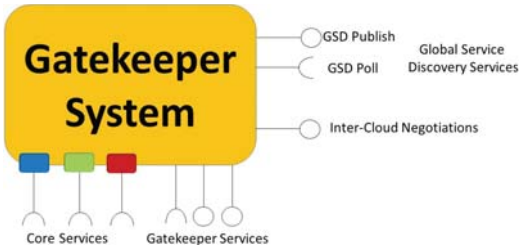

Fig. 5. The proposed gateway service module.

A. General requirements

There is a valid need for inter-cloud servicing, as one single Arrowhead cloud cannot serve for all demands. Here are some examples (use cases) when inter-cloud relations are necessary or simply better than handling requests at a local level:

- Servicing is not possible: no service provider locally.
- Service provider is not available: is in out-of-order status or registered, but not found at the time.
- Servicing is currently not possible: no free resources or the QoS expectations cannot be met locally.
- Servicing within the home cloud is not optimal (e.g. geographically a different cloud is closer or better).

One of the major philosophical questions here is about data ownership, whether the command over servicing belongs to the System (e.g. it can choose its partners) or to the managing central entities of the Local Clouds (and these Core Systems pair up Systems for servicing). As various intelligent decision-making processes (e.g. resource management) are implied here, in our primary scenario we assume that

- data ownership belongs to the Local Clouds (but this is not a necessity of the Gatekeeper Services concept),
- one identity of an Arrowhead SoS Cloud is requesting a service that cannot be fulfilled in the local cloud and therefore
- it might be viable to look for clients in other Arrowhead clouds.

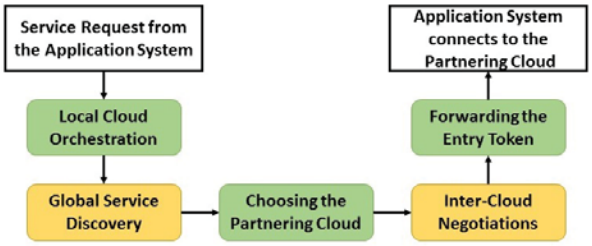

Fig. 6. Creating inter-cloud consumer-producer relationship methodology.

This Core System will provide the following functionality (see Figure 6):

1) *Global Service Discovery*: Finding other Arrowhead Local Clouds with suitable providers for the requested purposes.
2) *Inter-Cloud Negotitations*: authentication, identity verification of the chosen Partnering Cloud, authorizing transactions and establishing secure connections by managing the dialogs ("negotations") between the Clouds for establishing the inter-cloud producer-consumer relationship.

B. Security Issues

Interactions in a closed Arrowhead Local Cloud are secured by the central entities (Core Systems). As one Local Cloud might be a whole cyberphysical system (e.g. smart cars), we face serious security concerns when Service procurement goes outside the boundaries of the Cloud. One Cloud has to be

absolutely certain that it can completely trust its Partnering Cloud when redirecting its System there. For this reason, AAA will play a key role. Since a central *Authentication Service* (e.g. Certificate Agency) might not be available in an ad hoc and volatile inter-cloud environment, these issues might require new approaches like decentralized certificate management [17] or trust management [18]: as trust can also be built on previous experience or the partner simply being a trustworthy contact of my contacts. In this concept, *authorization* and *accounting* (the remaining A-s in AAA) can still be handled on the Local Cloud level with the proper Core Systems, see Section III-E.

C. Global Service Discovery

In this section, we provide approaches that would extend the Service Discovery functionality between Arrowhead Clouds. In our proposition, the Gatekeeper Systems have the ability to look for resources outside the boundaries of their Clouds. They are capable of searching for specific types of Services that are available somewhere else (in different Arrowhead Clouds) and provide the Local Cloud with options for redirection. There is *no* authentication or identity checking at this phase, but tracking the trustworthyness of the "advertisers" might be viable in some cases.

There are several approaches to this tracking of available service locations. These approaches are suitable for different environments and requirements depending on the regularity of inter-cloud interactions, the volatility of service availability in the different Clouds and the flexibility required from the collaborating Arrowhead System-of-Systems.

1) Strict rules on possible gatekeeper connections: The most basic approach is hardwiring – and manually configuring – information about a certain set of other Gatekeepers into each Gatekeeper where they can turn to, see Fig. 8. This can be based on the Service type, time of day, geographical requirements (choosing a physically close partner), etc. This concept brings several advantages and limitations as well. In this scenario, Cloud operators have strict oversight of their Arrowhead Clouds and can easily log the interactivity, set up billing and access control between operators (fits business purposes). It is also highly secure: no need for authentication, identity control or trust management in any phase. However, there is the need for manual edition of configuration and hence there is absolutely no option for scaling automatically.

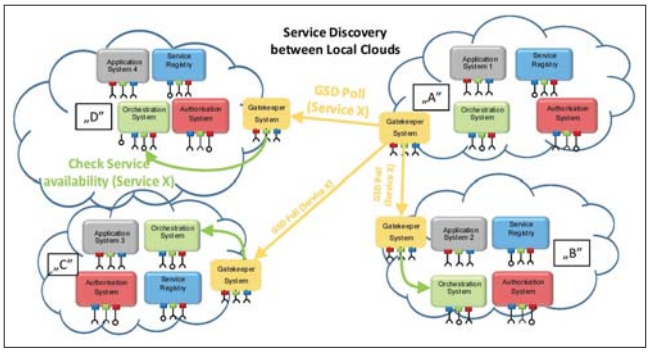

Fig. 7. Service Discovery in a hardwired inter-cloud scenario.

2) Ad hoc neighborhoods: The second approach is still based on per-transaction polling of neighbors, but letting the Gatekeepers automatically detect and poll their neighborhood. The ad hoc peer-to-peer detection of neighbors can provide adaptivity for volatile environments (e.g. moving cars looking for charging stations along the road). However, it will also pose a high administrative overhead (for Gatekeeper components) and cause scaling issues. This methodology will also present a limited list of available resources to the Local Cloud (just from the current contacts). There are several problems to solve here, such as the tracking, trust management and authentication of a rapidly changing neighborhood.

3) Cloud-of-Clouds: The third approach is pointing towards the creation of a dedicated inter-cloud system, where the "demand and supply" of inter-cloud requests can meet. The main purpose of this is to take off the computational overhead from the Arrowhead Cloud Gatekeepers and local Core Systems in a stock-market like environment (see Fig. 8). This centralized entity could provide global matchmaking for the participants of the Cloud-of-Clouds and could also centralize resource allocation and trust management. This can be achieved by tracking the reliabilitiy of the parties and providing the requester Clouds with only the globally optimal Partnering Cloud.

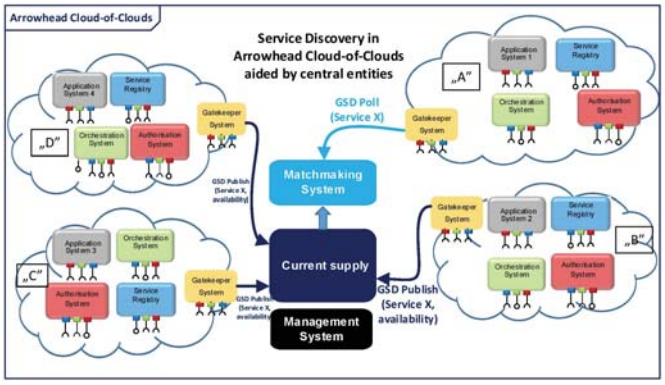

Fig. 8. The Cloud-of-Clouds concept.

D. Inter-Cloud Negotiations

After the requesting Cloud decides for a Partnering Cloud, the Gatekeepers of these Clouds will have to perform negotiations to settle the different aspects of the transaction. At the end of this phase, the requesting System gets a token that will authenticate and navigate it in the Partnering Cloud (using the local Service Discovery data). During this process, the following issues are to be handled:

1) protocol negotiations (Arrowhead Framework version and protocol matching),
2) mutual authentication and identity checking of the parties,
3) actual admission control (authorization and resource allocation for the transaction in the Clouds),
4) establishing a secure connection between the Gatekeepers, therefore the Arrowhead Clouds (creating the data path),

5) sharing the local Service Discovery data of the Partnering Cloud (addressing the Partnering Cloud from the outside),
6) injecting temporary authorization information into the Authorization System in the Partnering Cloud (access control of the ”foreigner” System),
7) the Partnering Cloud Gatekeeper issues a token for the requester with temporary entry and shares it with the requesting Gatekeeper,
8) the requesting Local Cloud forwards this token to the requesting System,
9) the System connects to the producer using the Partnering Cloud’s Core Systems.

E. Requirements for local Core Systems and Services

The proposed inter-cloud servicing methodology will require new functionalities from the Core Systems of the Arrowhead Framework. These new functionalities must include the followings.

- *Authorization:* inter-cloud transactional rights management (access rights from and towards external Clouds)
- *Authentication:* identity verification of other Local Clouds and their Systems
- *Orchestration:* intelligent resource management and Service matchmaking capabilities based on the current local and inter-cloud situation in a scalable but robust manner
- *Additional services* for supporting the inter-cloud activity (e.g. logging, status reporting) the hosting cloud Orchestrator could instruct the foreigner System to contact the Core Services from both Clouds for these purposes. This way everyone will be notified properly of the happenings.
- *QoS Management:* the Global Service Discovery response can also take into account the requested QoS parameters
- *Security System:* the creation of the data path between the Clouds require specialized Systems that handle all the network configurations required for the transaction

IV. A CASE STUDY

In an average situation the sequence depicted in Fig. 9 would lead to System 1 (from Arrowhead Cloud A) connecting to Arrowhead Cloud B for getting Service X from a System in that SoS. This sequence consists of the following logical steps:

1) Normal service orchestration procedure begins (with the help of Cloud A’s Core Service components).
2) In case the request cannot be fulfilled locally, the Orchestrator A will turn to the Gatekeeper A and initiate a Global Service Discovery (see III-C).
3) Gatekeeper A provides a list to the local Orchestrator on Arrowhead Clouds where Service X is currently available.

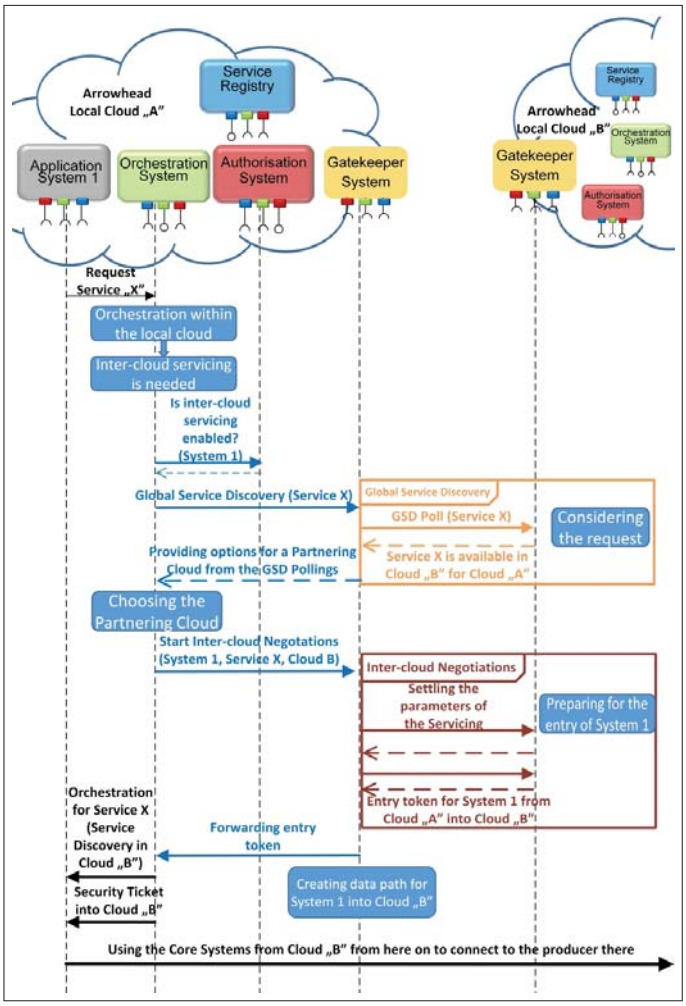

Fig. 9. An example inter-cloud servicing sequence diagram.

4) Cloud A will decide where it will redirect System 1 for Service X (in this case: Cloud B).
5) If there is a suitable Arrowhead Cloud, where Service X is optimally available, Cloud A will check for the requesting s (System 1s) AAA status and rights (e.g. if it has right to use outside resources).
6) Gateway A will start negotiating with Gateway B for access to Cloud B (Inter-cloud Negotiations) as in Fig. 10. Cloud B will also prepare for System 1’s entry.
7) When access to Cloud B has been granted for System 1 (from Cloud A), Gateway B will share the Cloud B access data (e.g. Service Discovery address) and send the transaction token via Gatekeeper A. This token will enable System 1 to access Cloud B.
8) The local cloud of System 1 (Cloud A) will orchestrate these information back to System 1 and redirect it to discover the Services in Cloud B.
9) With the help of the token, System 1 will enter Cloud B to perform Service X using the normal orchestration process of Cloud B.

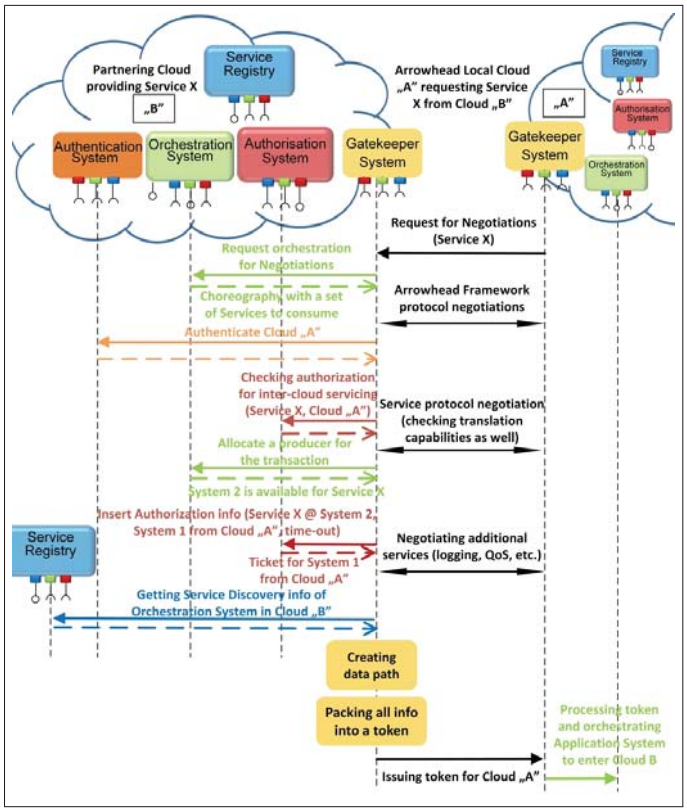

Fig. 10. An example Inter-Cloud Negotations process.

V. Further Work

The intention of the authors with this paper is to ignite discussions about (not just high-level) SOA and inter-cloud architecture designs and methodologies. We have proposed several possible ways and listed the major prospects and issues of those paths. This field requires serious further work on all design level but might be rewarding in the long term as the applications for a robust and intelligent collaboration between automation systems are endless.

VI. Summary

While the current Arrowhead Framework provides means for Systems to collaborate in a service oriented way, the Core Services can merely solve issues within the borders of a given Local Cloud– so far. These System-of-Systems form servicing realms with the help of their instance of Core Systems – and there is demand appearing for inter-cloud collaboration. The concept of Gatekeeper as a new Core System introduced in this paper can solve many of the arising issues, including security, service discovery, orchestration, and other requirements set by the Local Clouds. We described methods for the interworking with the help of such Gatekeepers, and presented a case study of a service consumer System connecting to a service consumer from a different Arrowhead Cloud.

Acknowledgment

This work is supported by the EU ARTEMIS JU funding, within project ARTEMIS/0001/2012, JU grant nr. 332987 (ARROWHEAD).

The authors would like to thank Jerker Delsing and Hasan Derhamy at LTU, as well as Fredrik Blomstedt and Per Oloffson at BNearIT for the initial discussions on the inter-cloud issues within the Arrowhead Framework.

VII. References

References

[1] S. Karnouskos, A. W. Colombo, F. Jammes, J. Delsing, and T. Bangemann, "Towards an architecture for service-oriented process monitoring and control," in *36th Annual Conference of the IEEE Industrial Electronics Society (IECON-2010), Phoenix, AZ.*, 7–10 Nov 2010.

[2] A. W. Colombo, T. Bangemann, S. Karnouskos, J. Delsing, P. Stluka, R. Harrison, F. Jammes, and E. Jose L. Martinez Lastra, *Industrial Cloud-Based Cyber-Physical Systems - The IMC-AESOP Approach*. Springer, 2013.

[3] N. Kaur, C. McLeod, A. Jain, R. Harrisson, B. Ahmad, A. Colombo, and J. Delsing, *Design and Simulation of a SOA-based System of Systems for Automation in the Residential Sector*. IEEE, 2013.

[4] R. Kyusakov, J. Eliasson, J. Delsing, J. van Deventer, and J. Gustafsson, "Integration of wireless sensor and actuator nodes with it infrastructure using service-oriented architecture," *IEEE Transactions on Industrial Informatics*, vol. 9, no. 1, pp. 43 – 51, 2013.

[5] T. Erl, *SOA Principles of Service Design (The Prentice Hall Service-Oriented Computing Series from Thomas Erl)*. Upper Saddle River, NJ, USA: Prentice Hall PTR, 2007.

[6] R. T. Fielding, "Architectural styles and the design of network-based software architectures," Ph.D. dissertation, University of California, Irvine, 2000.

[7] Z. Shelby, K. Hartke, and C. Bormann, *The Constrained Application Protocol (CoAP)*, IETF RFC 7252, 2014.

[8] P. Saint-Andre, *Extensible Messaging and Presence Protocol (XMPP): Core*, IETF RFC 6120, 2011.

[9] OPC Foundation, *OPC Unified Architecture Specification*, Standard IEC 62 541, 2010.

[10] F. Blomstedt, L. Lino Ferreira, M. Klisics, C. Chrysoulas, I. Martinez de Soria, B. Morin, A. Zabasta, J. Eliasson, M. Johansson, and P. Varga, "The arrowhead approach for soa application development and documentation," in *IEEE IECON*, 2014.

[11] M. W. Maier, *Architecting Principles for Systems-of-Systems*, ser. 4, 1998, vol. 1, pp. 267–284.

[12] P. Kalyanasundaram and A. S. Sethi, "Interoperability Issues in Heterogeneous Network Management," *Journal of Network and Systems Management*, vol. 2, no. 2, pp. 169–193, 1994.

[13] S. Ziegler and C. Crettaz, "IPv6 as a global addressing scheme and integrator for the Internet of Things and the Cloud," *Advanced Information Networking and Applications Workshop (WAINA)*, pp. 797–802, May 2014.

[14] L. A. DaSilva, S. F. Midkiff, J. S. Park, G. C. Hadijichristofi, and N. J. Davis, "Network Mobility and Protocol Interoperability in Ad Hoc Networks," *IEEE Communications Magazine*, vol. 42, no. 11, pp. 88–96, 2004.

[15] Y. Demchenko, C. Ngo, C. de Laat, and C. Lee, "Federated Access Control in Heterogeneous Intercloud Environment: Basic Models and Architecture Patterns," in *IEEE International Conference on Cloud Engineering (IC2E)*, March 2014, pp. 439–445.

[16] M. Mechtri and D. Zeghlache, "Inter-Cloud Networking Gateway Architecture," in *IEEE International Conference on Computing Technology and Science (CloudCom)*, vol. 2, no. 5, 2013, pp. 188–194.

[17] B. Aslam and C. Zou, "Distributed Certificate and Application Architecture for VANETs," in *IEEE Military Communications Conference (MILCOM)*, 2009, pp. 1–7.

[18] B. Shand, N. Dimmock, and J. Bacon, "Trust for Ubiquitous, Transparent Collaboration," in *IEEE International Conference on Pervasive Computing and Communications (PERCOM)*, 2003, pp. 153–160.

THE 5TH INTERNATIONAL CONFERENCE ON WIRELESS COMMUNICATIONS, VEHICULAR TECHNOLOGY, INFORMATION THEORY, AEROSPACE & ELECTRONIC SYSTEMS (WVITAE-2015)
December 13-16, 2015, Hyderabad, India

Cancellation of Inter-Cell Interference in Downlink with No Backhaul Information Exchange

Shuvabrata Bandopadhaya[1], Jibendu Sekhar Roy[2]
[1]Silicon Institute of Technology, Bhubaneswar, Odisha, India.
[2]School of Electronics Engineering, KIIT University, Bhubaneswar, Odisha, India.
[1]shuva_bandopadhaya@rediffmail.com, [2]drjsroy@rediffmail.com

***Abstract*—: In orthogonal frequency division multiplexing (OFDM) systems, the implementation of full frequency reuse (FFR) scheme to attain capacity upper bound of cellular system is limited due to inter-cell interference (ICI). To combat ICI, long term evolution system-advanced (LTE-A) employs the coordinated multi-point (CoMP) transmission where exchange of instantaneous channel state within the cluster is essential for joint processing. The major challenge in practical implementation of CoMP is huge backhaul overhead and latency due to congestion. This paper proposes a novel technique for downlink in ICI dominating region where the need of exchange of information through backhaul has been eliminated. In this technique, the number of antennas used in each enhanced nodeB (eNB) per user equipment (UE) is same as the number of signals received by the UE above the interfering threshold level. To pre-cancel the interference, the proposed technique generates an interference aware precoding vector at each eNB based on the instantaneous channel associated with the same eNB.**

***Keywords*-: LTE, OFDM, Inter-cell interference, CoMP cluster, Joint Processing, Backhaul Information.**

I. INTRODUCTION

To optimize the spectral efficiency, the next generation networks employ full frequency reuse (FFR) scheme, where each cell uses the total available bandwidth. Though with this scheme the capacity upper bound of cellular system is attained, a significant degradation in the performance of orthogonal frequency division multiplexing (OFDM) systems is being registered due to inter-cell interference (ICI). The cell-edge user equipments (UEs) experience a poor signal power to interference plus noise power ratio (SINR) compared to the UEs closer to the servicing enhanced node B (eNB) as the powers of interference signals at the cell-edge are comparable with the power of signal from the servicing eNB. This issue has been addressed by Third Generation Partnership Project (3GPP) with coordinated multi-point (CoMP) transmission which has been included in the features of long-term evolution – advanced (LTE-A) standard. Here, coordination is being established among more than one geographically separated eNBs connected through reliable backhaul forming a CoMP cluster [1-6]. This concept was initially discussed in release 10 and further developed with subsequent releases, release 11 and release 12 [7-8]. The CoMP with joint processing (CoMP-JP) promises a significant performance gain where the received signal quality and throughput of the cell-edge UEs is improved by jointly transmitting the intended data of a particular UE from multiple eNBs. In the information theory paradigm, the capacity upper bound is achieved as the different locations of transmitters provide uncorrelated independent paths.

Though theoretically, a significant performance improvement and capacity enhancement for cell-edge UEs is achieved with COMP-JP, its practical implementation faces major challenge with heavy backhaul traffic due to information exchange between eNBs within the CoMP cluster and the latency involved with it [9-10]. The backhaul architecture of LTE can be realized as a tree where multiple eNBs are connected with advanced gateway (aGW) having two logical interfaces; the user data moves from the aGW to each eNB through S1 interface and the mutual information exchange between the cells is made through X2 interface. In CoMP-JP, the preprocessing for interference cancellation has to be carried out at a centralized processing unit (CPU) which is either located at independent location or co-located with any one of the eNBs in the cluster which requires the information data intended for all UEs as well as instantaneous channel state information (CSI) of all paths within the CoMP cluster [11-12]. Hence the performance is limited with significantly high backhaul traffic. The delay in the exchange of instantaneous CSI due to the latency in backhaul causes a sever degradation in system performance [13]. The precise synchronization within the participating eNBs is also a critical issue [14-15].

This paper proposes a novel downlink technique for the UE present in ICI dominating region that completely eliminates the need of any information exchange through backhaul. This technique exploits the recent development in large scale MIMO where the number of antenna present in eNB is much larger than number of UEs is being served in one channel [16]. To pre-cancel the interference, the proposed technique generates an interference aware precoding vector at each eNB based on the instantaneous channel associated with the same eNB. The simulation results show the proposed technique works as good as the CoMP-JP. The organization of the paper is as following: downlink techniques for cell-edge UEs in LTE system are presented in section II, the proposed downlink technique with no backhaul information exchange is presented in section III, performances of different systems with

estimated channel are analyzed in section IV, the simulation result with discussion is provided in section V and section VI concludes the paper. [*Notations*: The bold faced letter $\mathbf{A}$ and bold faced letter with curly bracket $\{\mathbf{A}\}$ represents vector and matrix respectively, $\mathrm{E}\{.\}$ represents the time expectation operation].

II. DOWNLINK FOR CELL-EDGE UEs

Consider an interference region where the UE receives signal from N_T different eNBs with strength above the threshold. The air interface technique in the downlink of LTE system is considered as OFDM due to its robustness against the frequency selectivity of the multipath wireless channel; each OFDM symbol is spreaded over N sub-carriers. The number UE to be served per time-frequency resource per cell site is considered as one. The superscript k is the index of the sub-carrier. The power control in each eNB is assumed to be perfect to normalize the large-scale fading coefficients. In this section the following cases are being considered:

A. Interference system with no CoMP

Here there is no coordination among the eNBs and each eNB transmits its own precoded signal. The signal received at *l-th* UE is given by

$$\begin{aligned} Y_l^k &= \sum_{i=1}^{N_T} H_{i,l}^k \widetilde{X}_i^k + N_l^k \\ &= H_{l,l}^k \widetilde{X}_l^k\big|_{i=l} + \sum_{i=1,i\neq l}^{N_T} H_{i,l}^k \widetilde{X}_i^k + N_l^k \end{aligned} . \quad (1)$$

where $\widetilde{X}_i^k$ is the signal transmitted by *i-th* eNB, $H_{i,l}^k$ is the frequency domain channel gain between *i-th* eNB and *l-th* UE and N_l^k is the frequency domain noise at *l-th* UE, $\mathrm{E}\{|N_l^k|^2\} = \sigma^2$.

B. Ideal case with no interference

This is the ideal case introduced for reference; the interference is considered to be null. Hence the equation (1) reduces to

$$Y_l^k = \sum_{i=1}^{N_T} H_{i,l}^k \widetilde{X}_i^k + N_l^k = H_{l,l}^k \widetilde{X}_l^k\big|_{i=l} + N_l^k . \quad (2)$$

The spectral efficiency per cell site is given by

$$\eta_{\mathbf{no_int}}(\sigma) = \mathrm{E}\left\{ \frac{1}{N} \sum_{k=1}^{N} \log_2\left(1 + \frac{1}{\sigma^2}\left|H_{l,l}^k \widetilde{X}_l^k\right|^2\right)\right\}. \quad (3)$$

C. CoMP-Joint Processing:

In the downlink of CoMP-JP, a virtual spatial multiplexing environment is created where the information symbol for each cell-edge UE is transmitted from all eNBs in the cluster. With all eNBs are equipped with single transmitting antenna, the number of UE in same time-frequency resource per cell site is one. As the transmitters are geographically separated, the preprocessing for interference cancellation has to be carried out at CPU which needs the information symbol of all servicing UEs as well as instantaneous channel information associated with each path through X2 interface. The signal received at *l-th* UE is given by

$$\begin{aligned} Y_l^k &= \sum_{i=1}^{N_T} H_{i,l}^k . \widetilde{X}_i^k + N_l^k = \sum_{i=1}^{N_T} H_{i,l}^k \sum_{q=1}^{N_T} B_{i,q}^k . X_q^k + N_l^k \\ &= \underbrace{\sum_{i=1}^{N_T} H_{i,l}^k B_{i,l}^k X_l^k\big|_{q=l}}_{\text{Signal}} + \underbrace{\sum_{i=1}^{N_T} H_{i,l}^k \sum_{q=1,q\neq l}^{N_T} B_{i,q}^k . X_q^k}_{\text{Interference}} + \underbrace{N_l^k}_{\text{Noise}} \end{aligned} . \quad (4)$$

where X_q^k is the intended signal for *q-th* receiver and $B_{i,q}^k$ is the $(i;q)$ entry of precoding matrix $\{\mathbf{B}^k\}$ generated at CPU. The terms in the r.h.s. are associated with signal, interference and noise respectively. The condition for zero interference is obtained by setting the precoding matrix as

$$\{\mathbf{B}^k\} = \{\mathbf{H}^k\}^{-1} . \quad (5)$$

Here $\{\mathbf{H}^k\}$ is the frequency domain channel matrix with its $(i;l)$-*th* entry is $H_{i,l}^k$. Hence the knowledge of the channels corresponds to all paths in the cluster are essential at CPU which propels instantaneous CSI exchange in the cluster through X2 interface. The high backhaul load and the latency involved in this process limit the performance of CoMP-JP in its practical deployment. With perfect knowledge of channel state, the interference at all UE reduces to zero and the SINR is

$$\left(SINR_l^k\right)_{\mathbf{JP_Ideal}} = \frac{1}{\sigma^2}\left|\sum_{i=1}^{N_T} H_{i,l}^k B_{i,l}^k X_l^k\right|^2 . \quad (6)$$

The spectral efficiency per cell site for CoMP-JP technique is given by

$$\eta_{\mathbf{JP_Ideal}}(\sigma) = \mathrm{E}\left\{ \frac{1}{N} \sum_{k=1}^{N} \log_2\left(1 + \frac{1}{\sigma^2}\left|\sum_{i=1}^{N_T} H_{i,l}^k B_{i,l}^k X_l^k\right|^2\right)\right\}. \quad (7)$$

III. PROPOSED DOWNLINK TECHNIQUE WITH NO BACKHAUL INFORMATION EXCHANGE

Unlike CoMP-JP, the proposed technique eliminates the need of information exchange between eNBs through backhaul and the cell-edge UE gets its information only from the servicing eNB. Consider an interference region

where the UE receives signals above the interference threshold is N_T and hence same number of UEs being served in one channel. With this technique, the number of antenna used in each eNB per UE in each cell site is also N_T. Each eNB receives complex information symbol for its own UE through S1 interface and generates an (N_TX1) interference aware precoding vector; for *i-th* eNB it is $\mathbf{P}_i^k$. Hence the signal transmitted from its *j-th* antenna is given by $\widetilde{X}_{(i,j)}^k = P_{(i,j)}^k X_i^k$ where $P_{(i,j)}^k$ is the *j-th* element of $\mathbf{P}_i^k$. The signal received by *l-th* UE is given

$$\begin{aligned} Y_l[k] &= \sum_{i=1}^{N_T}\sum_{j=1}^{N_T} H_{(i,j),l}^k.\left(X_i^k.P_{(i,j)}^k\right)+N_l^k \\ &= \underbrace{\sum_{j=1}^{N_T} H_{(l,j),l}^k.\left(X_l^k.P_{(l,j)}^k\right)\Big|_{i=l}}_{\text{Signal}} + \underbrace{\sum_{i=1,i\neq l}^{N_T}\sum_{j=1}^{N_T} H_{(i,j),l}^k.\left(X_i^k.P_{(i,j)}^k\right)}_{\text{Interference}} + \underbrace{N_l^k}_{\text{Noise}}. \end{aligned} \quad (8)$$

The terms in the r.h.s. are associated with signal, interference and noise respectively. The condition for zero interference is

$$\sum_{j=1}^{N_T} H_{(i,j),l}^k.P_{(i,j)}^k = \begin{cases} 1 & for\ i=l \\ 0 & for\ i\neq l, \end{cases} \quad \forall i,j \le N_T. \quad (9)$$

In vector notation,

$$\{\mathbf{H}_l^k\}\mathbf{P}_l^k = \mathbf{0}_l, \quad (10)$$

where $\{\mathbf{H}_l^k\}$ is the (N_T X N_T) channel matrix for *l-th* eNB and $\mathbf{0}_l$ is a (N_T X 1) column vector whose *m-th* element is given by

$$\mathbf{0}_l(m) = \begin{cases} 1 & for\ \ m=l \\ 0 & for\ \ m\neq l. \end{cases} \quad (11)$$

The equation (20) makes *l-th* participating eNBs in the cluster aware of the interference caused by others and generates interference aware precoding vector. The precoding vector for *l-th* eNB is

$$\mathbf{P}_l^k = \{\mathbf{H}_l^k\}^{-1}.\mathbf{0}_l. \quad (12)$$

The precoding vector used at *l-th* eNB is identical with the *l-th* column of the inverse of the channel matrix associate with same eNB. Hence no knowledge of CSI associated with other interfering eNB is required resulting no need for exchange of information between eNBs through backhaul. The expression for SINR with precoding vector calculated from exact channel knowledge is given by

$$\left(SINR_l^k\right)_{\text{Prop_Ideal}} = \frac{1}{\sigma^2}\left|\sum_{j=1}^{N_T} H_{(l,j),l}^k.\left(X_l^k.P_{(l,j)}^k\right)\right|^2. \quad (13)$$

The spectral efficiency per cell site for the proposed technique is given by

$$\eta_{\text{Prop_Ideal}}(\sigma) = \mathrm{E}\left\{\frac{1}{N}\sum_{k=1}^{N}\log_2\left(1+\frac{1}{\sigma^2}\left|\sum_{j=1}^{N_T} H_{(l,j),l}^k.\left(X_l^k.P_{(l,j)}^k\right)\right|^2\right)\right\} \quad (14)$$

IV. SYSTEMS WITH ESTIMATED CHANNEL

In practical scenario, the CSI of all involved path has to be estimated. The LTE supports TDD system where the channel reciprocity is exploited; the downlink CSI is estimated via uplink training and the process is called channel sounding [17]. In the training phase, each UE of the cluster broadcasts their respective pilot sequence; to combat transmit diversity problem at the estimation end, the sequences have to maintain orthogonality among each other. The estimation process generates the estimate of channel gain H^k as $\hat{H}^k$ with estimation error given as

$$\delta^k = \hat{H}^k - H^k, \quad (15)$$

The error in the estimation process is assumed to be bounded in a spherical uncertainty region defined as [18]

$$\Re = \{\delta^k : \|\delta^k\| \le \varepsilon\}, \quad (16)$$

where ε is the radius of uncertainty sphere. Hence the SINR at the *l-th* receiver for CoMP-JP and the proposed technique are respectively given as

$$\left(SINR_l^k\right)_{\text{JP_Est}} = \frac{\left|\sum_{i=1}^{N_T}\hat{H}_{i,l}^k B_{i,l}^k X_l^k\right|^2}{\sigma^2 + \left|\sum_{i=1}^{N_T}\delta_{i,l}^k \sum_{q=1,q\neq l}^{N_T} B_{i,q}^k.X_q^k\right|^2} \quad (17)$$

$$\left(SINR_l^k\right)_{\text{Prop_Est}} = \frac{\left|\sum_{j=1}^{N_T}\hat{H}_{(l,j),l}^k.\left(X_l^k.P_{(l,j)}^k\right)\right|^2}{\sigma^2 + \left|\sum_{i=1,i\neq l}^{N_T}\sum_{j=1}^{N_T}\delta_{(i,j),l}^k.\left(X_l^k.P_{(i,j)}^k\right)\right|^2}. \quad (18)$$

And the corresponding spectral efficiencies per cell site are

$$\eta_{JP_Est}(\sigma)=\mathrm{E}\left\{\frac{1}{N}\sum_{k=1}^{N}\log_2\left(1+\frac{\left|\sum_{i=1}^{N_T}\hat{H}_{i,l}^{k}B_{i,l}^{k}X_{l}^{k}\right|^2}{\sigma^2+\left|\sum_{i=1}^{N_T}\delta_{i,l}^{k}\sum_{q=1,q\neq l}^{N_T}B_{i,q}^{k}.X_{q}^{k}\right|^2}\right)\right\} \quad (19)$$

$$\eta_{Prop_Est}(\sigma)=\mathrm{E}\left\{\frac{1}{N}\sum_{k=1}^{N}\log_2\left(1+\frac{\left|\sum_{j=1}^{N_T}\hat{H}_{(l,j),l}^{k}.\left(X_{l}^{k}.P_{(l,j)}^{k}\right)\right|^2}{\sigma^2+\left|\sum_{i=1,i\neq l}^{N_T}\sum_{j=1}^{N_T}\delta_{(i,j),l}^{k}.\left(X_{l}^{k}.P_{(i,j)}^{k}\right)\right|^2}\right)\right\} \quad (20)$$

V. SIMULATION RESULTS AND DISCUSSION

In this section, the downlink for cell-edge UE has been simulated. Hexagonal cellular structure is considered as shown in Fig 1, where the number of eNBs from which a UE receives signal with significant strength is three.

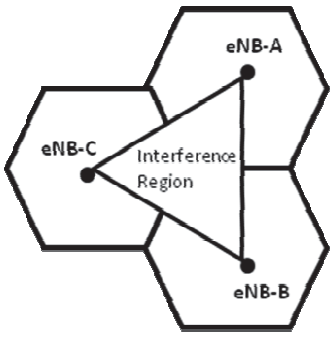

Fig.1. Region of interference in hexagonal cellular structure

A perfect power control in each eNB is assumed so that the received powers of all signals in the cluster are same. The following systems are simulated and performances are compared. (1) A system having no CoMP; the UE receives signal from its servicing eNB as well as from the other two interfering eNBs. (2) An ideal scenario with no interference; the UE receives signal only from its servicing eNB. (3) A CoMP-JP system with UE being served in same time- frequency resource equals to the cluster size. A perfect backhaul with zero latency is assumed. (4) The proposed system where the numbers of antennas present in each eNBs is equal to the number of signals received by the UE above the threshold level. The simulation includes an ideal system where perfect CSI of all paths assumed to be present at transmitting end along with the estimated system where each eNB estimates the channels associated with them using channel sounding technique. For estimated system, type-1 frame structure for LTE is considered where each sub-frame is of duration 1ms, consists of 14 symbols where in every seventh symbol dedicated estimation slot is present [19]. Details of simulation specifications are given in table-1.

Table-1 Simulation Specification

Parameters	
System Specification	
Signals received by the UE above interfering threshold level	03
No of UE/channel in interfering region	03
Transmission Specification	
Air interference	OFDM
FFT size	512
Length of cyclic prefix	16
Types of modulation	QPSK
Channel Specification	
Type of channel	6 tap, COST 207 Typical Urban
Maximum Doppler shift	5Hz

Cumulative distribution function (CDF) of spectral efficiency per cell site (Bit/sec/Hz/cell site) at SNR=10dB is shown in Fig. 2 and the spectral efficiency per cell site (bits/sec/Hz/cell site) vs SNR performance is plotted in Fig. 3.

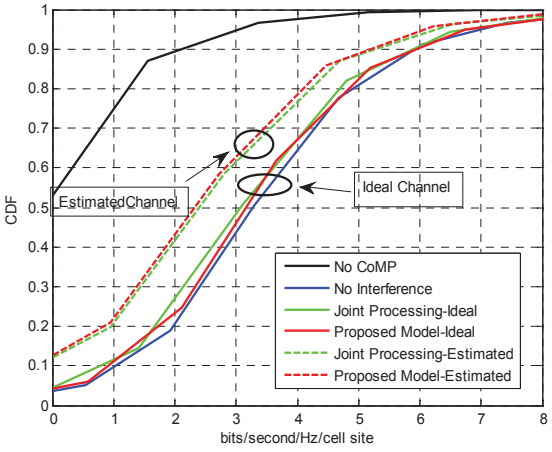

Fig. 2 Cumulative distribution function (CDF) of spectral efficiency per cell site (Bit/sec/Hz/cell site) at SNR=10dB for UE receiving signal with same power from all the immediate neighboring eNBs

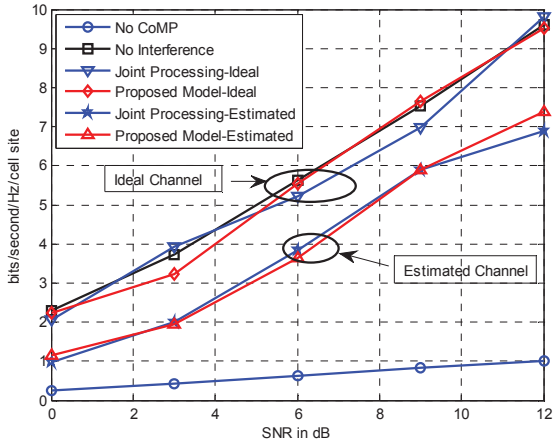

Fig. 3 Spectral efficiency per cell site (Bit/sec/Hz/cell) site performance for UE receiving signal with same power from all the immediate neighboring eNBs

Fig. 4 provides the uncoded BER vs SNR performance for UE receiving signal with same power from all the immediate neighboring eNB with different CoMP systems.

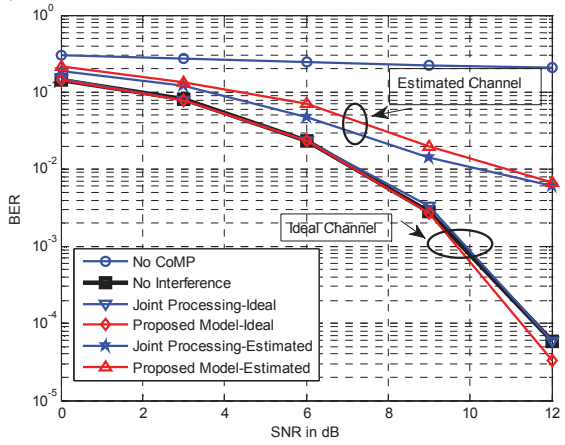

Fig. 4 Uncoded BER performance for UE receiving signal with same power from all the immediate neighboring eNBs

The performance of the system with no CoMP is too poor to be used as the signals from other two eNBs are considered as noise. It is observed that the proposed technique performs equally well as the CoMP-JP for both ideal and estimated CSI cases; for the former case with true knowledge of channel state, complete interference cancellation takes place and its performance approaches that of the system with the no interference. As the proposed technique matches with the performance of CoMP-JP, its implementation for interference cancellation at cell-edge UE has a significantly upper hand. In the proposed technique, no real-time information exchange between eNBs of the cluster is essential. Unlike the CoMP-JP, all the participating eNBs in the CoMP cluster are aware of the interference and generate their respective precoding vector by using only the channel matrix associated with the same eNB.

VI. CONCLUSION

This paper proposes a novel downlink technique for cell-edge UEs to combat ICI with no information exchange through backhaul. The proposed technique shows almost identical performance, in both ideal and estimated cases, with CoMP-JP technique which has huge backhaul overload. Using this technique, the challenge of practical implementation of FFR scheme in OFDM system, to achieve upper bound of capacity, has been reduced significantly.

References:

[1] M. Karakayali, G. Foschini, R. Valenzuela, "Network Coordination for Spectrally Efficient Communications in Cellular Systems," *IEEE Wireless Communications*, vol. 13, no. 4, pp. 56 –61, Aug. 2006.

[2] V. Jungnickel, S. Jaeckel, L. Thiele, L. Jiang, U. Kruger, A. Brylka, and C. von Helmolt, "Capacity Measurements in a Cooperative MIMO Network," *IEEE Transactions on Vehicular Technology,* vol. 58, no. 5, pp. 2392 –2405, June 2009.

[3] A. Daeinabi, K. Sandrasegaran, and X. Zhu, "An inter-cell interference coordination scheme in LTE downlink networks based on user priority and fuzzy logic system" *International Journal of Wireless & Mobile Networks,* Vol. 5, No. 4, pp.49-63, 2013.

[4] I. F. Akyildiz, D. Gutierrez-Estevez, E. C. Reyes, "The evolution to 4G cellular systems: LTE-Advanced," Elesvier Journal of Physical Communication, vol. 3, pp.217-244, 2010

[5] I. F. Akyildiz, D. Gutierrez-Estevez, R. Balakrishnan, E. C. Reyes, "LTE-Advanced and the evolution to Beyond 4G (B4G) systems," *Elesvier Journal of Physical Communication,* vol. 10, pp.31-60, 2014.

[6] D. A. Basnayaka, P. J. Smith, P. A. Martin, "Performance analysis of macro diversity MIMO systems with MMSE and ZF receivers in flat Rayleigh fading," *IEEE transactions on wireless communications*, vol. 12 (5), pp. 2240-2251, 2013.

[7] 3GPP RP-111117, "Coordinated Multi-Point Operation for LTE," 3GPP TSG RAN meeting 53, Fukuoka, Japan, Sep. 2011.

[8] 3GPP TR 36.819, "Coordinated multi-point operation for LTE physical layer aspects", V11.0.0.

[9] D. Lee, H. Seo, B. Clerckx, E. Hardouin, D. Mazzarese, S. Nagata, K. Sayana, "Coordinated multipoint transmission and reception in LTE-advanced: deployment scenarios and operational challenges," *IEEE Communications Magazine*, vol.50 (2), pp. 148-155, 2012.

[10] R. Irmer, H. Droste, P. Marsch, M. Grieger, G. Fettweis, S. Brueck, H.-P. Mayer, L. Thiele, and V. Jungnickel, "Coordinated Multipoint: Concepts, Performance, and Field Trial Results," *IEEE Communications Magazine*, vol. 49(2), pp. 102 –111, Feb. 2011.

[11] D. Samardzija and H. Huang, "Determining Backhaul Bandwidth Requirements for Network MIMO," *EUSIPCO*, 2009.

[12] J. Robson, "Guidelines for LTE Backhaul Traffic Estimation," *NGMN White Letter*, pp. 1–18, Jul. 2011.

[13] K. Manolakis, L. Thiele, C. Oberli, T. Haustein, and V. Jungnickel, "Impairment Modeling for Joint Transmission CoMP," *in Proc. 2nd Int. Conf. Wireless Comm., Vehic. Techn., Inf. Theory and Aerospace Electronic Systems (Wireless VITAE),* March 2011.

[14] Jungnickel, V., Wirth, T., Schellmann, M., Haustein, T., Zirwas, W., "Synchronization of Cooperative Base Stations," *in Proc. IEEE ISWCS*, 2008, pp. 329–334.

[15] H. Imlau, H. Droste, and S. Malla, "Impact of Synchronization Impairments on CoMP Joint Transmission Performance," *in Proc. ITSF Time & Synch in Telecoms*, 2012.

[16] T. L. Marzetta, "Massive MIMO: An Introduction", Bell Labs Technical Journal, vol. 20, pp. 11-22, March 2015.

[17] Z. Chen, X. Hou, S. Han, and C. Yang, "Low complexity channel estimation in TDD coordinated multi-point transmission systems," *IEEE Wireless Comm. & networking conf.*, pp. 3128-3133, 2013.

[18] R. Mochaourab, E.A. Jorswieck, "Roboust beamforming in interference channels with imperfect transmitter channel information" *journal of signal processing*, vol. 92, pp. 2509-2518, 2012.

[19] 3GPP, TR 25.814. Physical Layer Aspects for Evolved UTRA

THE 5TH INTERNATIONAL CONFERENCE ON WIRELESS COMMUNICATIONS, VEHICULAR TECHNOLOGY, INFORMATION THEORY, AEROSPACE & ELECTRONIC SYSTEMS (WVITAE-2015)
December 13-16, 2015, Hyderabad, India

Efficient Filtering Technique for Chronic Wound Image Processing under Tele-Wound Network

Chinmay Chakraborty
Dept. of Electronics & Communication Engineering
Birla Institute of Technology
Jharkhand, India
cchakrabarty@bitmesra.ac.in

Bharat Gupta
Dept. of Electronics & Communication Engineering
Birla Institute of Technology
Jharkhand, India
bharatg@bitmesra.ac.in

Abstract – This paper investigates efficient filtering techniques for chronic wound (CW) image pre-processing under Tele-wound network. In CW healing progress knowing the status of the wound is important as the status of the wound is the indicator of amount of healing. Hence, it is required for the doctors to check the status of CW periodically to track the healing process. But this becomes difficult for the patient who has to visit the doctors again and again. The objective of this research work is to accurately access the healing status of CW with improved image processing techniques with help of proper filtering. Efficient filtering techniques help to reduce the noise for CW images. The experimental results are presented by comparing different parameters. Performance parameters are peak signal to noise ratio (PSNR), mean square error (MSE), signal to noise ratio (SNR) and mean absolute error (MAE). Results shows Median filtering provides better performances with respect to high PSNR and reduced MSE between original and filtered image.

Keywords – Median filtering; Chronic wound; Wound images; Image processing

I. INTRODUCTION

An accurate and systematic CW assessment is the important task of wound care. Wound healing takes longer duration and regular check-up with certain interval is one of the big obstruct in wound caring [1]. Efficient screening of CW images is important for prognostic and therapeutic intervention. Visual assessment by medical people is time-consuming; subjective; and inconsistent whereas computerized analysis of wound images will be rapid and efficient approach; which requires appropriate image processing techniques and experts' domain knowledge for improved screening. A CW not only affects the individual but entire family gets suffered due to the enormous cost of wound care. Furthermore, it should be noted that without intensive medical care and treatment, a CW will most likely never heal. The effects of wounds are mainly delayed to repair or suspended skin re-growth, slow older cell proliferation rate, social isolation, depression, and a decrease in productivity, long-term and costly treatment. Five types of open wounds are abrasion (topmost layer of the skin is removed; painful), incision (smooth edges), laceration (irregular edges), puncture (deep; narrow wound) and avulsion (bleed heavily) respectively. The acquired CW images have been processed over wireless medium. The color changes of CW's gives important implication of the wound healing status to the patients, so proper filtering is required to remove the random or impulse noise. The image noise is the variation of color information randomly in images produced by image sensor with smartphone's and digital camera. The morphological filtering is used to preserve edge information of an image and eliminating the noise [3]. Wild et al. [4] developed digital wound measurement system where quality of the pictures has been maintained by filter of the device.

Tele-wound network (TWN) is defined as the delivery of medical health care services and sharing of clinical information over a distance using telecommunication platform [1, 2]. The aim is to provide better healthcare service to any place wherever and whenever required. TWN system offers reliable and efficient diagnostic aids to patients at affordable cost. TWN allows new technologies in sensing, medical imaging and wireless data communications with much lower cost, enabling the development of new widespread remote medicine initiatives. An optical imaging system is used for the TWN system for capturing skin wound images of a patient. Skin's abnormal conditions are common in the developing countries where symptoms of skin diseases are observed.

Christos et al. [5] has been taken 77 color wound photographs through Nikon digital SLR camera and used polarized filters to reduce the light reflection from CW surface. Lie et al. [6] captured wound images by the smartphones camera and used Gaussian smoothing filter to minimize the noise. Barone et al. [7] used SCIELab spatial filters for original CW image. Ederson et al. [8] applied anisotropic diffusion filtering to avoid the undesirable effects on segmentation for dermatological ulcers. Marina et al. [9] used difference of Gaussians (DoG) filter for wound segmentation. In the help of DoG filtering, local intensity variations has been equalized. Dorra et al. [10] used Gabor filtering technique for multispectral imaging. In this paper, the objective is to investigate best filter amongst all used filters on the basis of image quality assessment. The camera images

mostly suffer from independent impulse noise that can be introduced on a CW image may be salt and pepper or random-valued impulse noise. The best filtering technique is required to remove the noises for better quality of image.

The organization of paper is as follows: Section II describes the system architecture of tele-wound system. In section III comparative measures are defined. Section IV provides the experimental results for filtering and their effect on performance evaluation parameters. Finally section V describes conclusions.

II. System Architecture

TWN system is used to processing and monitoring the wound images. TWN has been proposed for this case could be efficiently used in remote location where specialists' services are not readily available. TWN system is used for characterizing wound tissue accurately and deals with large number of wound affected patients. TWN would reduce the problem of repeated and timely visits to doctors by remote monitoring and controlling. TWN minimizes the burden of health care unit and decreases the patient concerns. This TWN system consists of three modules namely image acquisition, tele-medical hub (TMH) and doctor's feedback. The portable, handheld device like smartphones can be used to capture high-quality red-green-blue (RGB) wound images and acquire patient's demographic information and send it to the TMH [11] [12] through wireless medium viz. 2G to 2.5G (iDEN 64 kbps, GPRS 171 kbps, EDGE 384 kbps), 3G (WCDMA, CDMA2000, TD-CDMA), SATELLITE, WLAN and 4G systems where the provision of faster physiological data transfer rate remotely. Wound healing process is totally depended on time i.e. may be required lengthy and several appointments with a clinician. The wound image quality can be enhanced at pre-processing stage by filtering techniques. Fig. 1 represents the TWN system for wound status monitoring. The processed CW image goes to image processing in TMH for pre-processing purpose. The wound image filtering technique is required to remove the noise. The CW image is smoothed by a median filtering for noise reduction by providing well-defined and continuous edge information. Wireless communication supported TWN system reduces the need to transport patents for physical consultation from the doctor, avoiding physical and mental stress, time and expense. This framework is effective for both rural as well as urban people; it gives good performance in terms of CW data monitoring and advanced diagnostic. Fig. 2 depicts the schematic diagram for wound image processing.

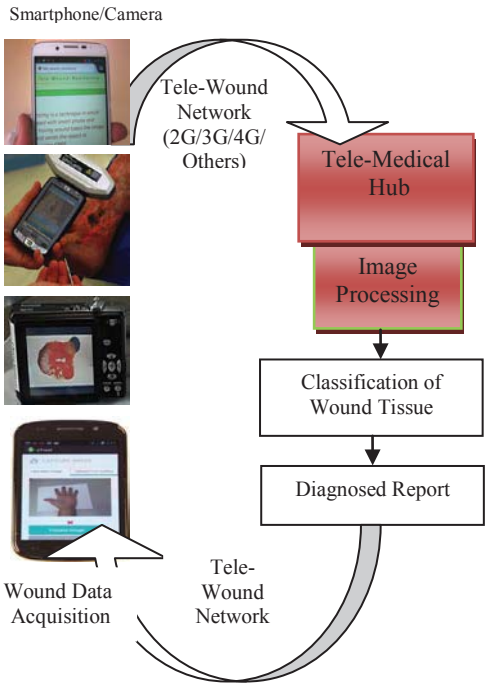

Fig. 1. Tele-wound network system

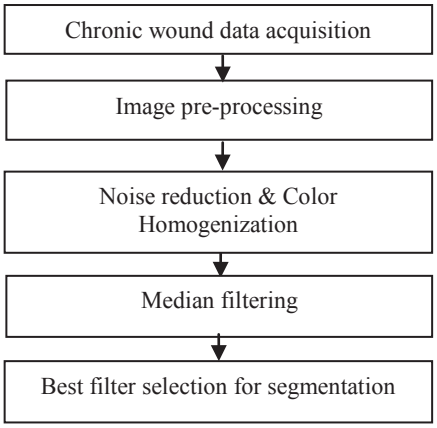

Fig. 2. Schematic diagram for wound image processing

III. Denoising Filters for Wound Imaging

The image denoising is a significant medical imaging task that is able to remove noise while preserving edges. In this paper, ten different filters have been considered and a comparative study is presented below.

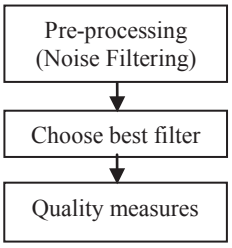

Fig. 3. Steps for quality measures

These important filters are as follows: Mean filter, Average filter, Min filter, M3 filter, Max filter, Log filter, Laplacian filter, Midpoint filter, Gaussian filter, and Median

filter respectively. The quality measure step is shown in Fig. 3. The $f(x,y)$ is represented as filtered image and $g(s,t)$ is the original corrupted image.

Mean filter – This filter is belongs to linear filtering scheme. This filtering is used to smoothing the images, mainly reducing the intensity variation between pixels. It is useful for removing Gaussian noise but preserving criteria is poor. The statistical model of the noise is swown in below.

$$p(x) = \frac{1}{\sigma\sqrt{2\pi}} e^{-\frac{(x-\mu)^2}{2\sigma^2}} \quad (1)$$

$$\textit{Mean filter } (x_1 \ldots . x_N) = \frac{1}{N}\sum_{i=1}^{N} x_i \quad (2)$$

Where, $x_1 \ldots . x_N$ is the pixel range of image.

Average filter – It is non-linear smoothing filter. This filter is used to avoids the edge blurring by searching the homogenity of current pixel neighbourhood and sharpend resulting image.

Min filter – This filter is used to fine darkest point in an image and also reduces the salt noise.

$$\textit{Min filter } \hat{f}(x,y) = \min_{(s,t)\in S_{x,y}} \left[g(s,t) \right] \quad (3)$$

M3 filter – This is the smoothing and hybrid of mean and median filter and used to remove the noise.

$$\textit{M3 filter } f(x,y) = \max\left[\underset{(s,t)\in S_{xy}}{mean}\{g(s,t)\}, \underset{(s,t)\in S_{xy}}{median}\{g(s,t)\} \right] \quad (4)$$

Max filter – This filter is used to findout the brightest point in an image and reduces the pepper noise.

$$\textit{Max filter } \hat{f}(x,y) = \max_{(s,t)\in S_{x,y}} \{g(s,t)\} \quad (5)$$

Log filter – This filter is smoothing the imageand are very sensitie to noise.

Laplacian filter – It is used to sharpening and calculates the second derivatives of an image and also measures the rate of change the first derivatives.

$$\textit{Laplacian filter } g(x,y) = f(x,y) + c\left[\nabla^2 f(x,y) \right] \quad (6)$$

Midpoint filter – This filter is very much useful or gaussian and uniform oise. It is the average of highest pixel and the lowest pixel with respect to intensity within the window size.
Midpoint filter

$$\hat{f}(x,y) = \tfrac{1}{2}\left[\max_{(s,t)\in S_{x,y}} \{g(s,t)\} + \min_{(s,t)\in S_{x,y}} \{g(s,t)\} \right] \quad (7)$$

Gaussian filter – This filter is responsible for corrects the spectral coefficient and aplitude spectrum officients within filter window.

Median filter -

The Median filter is used in pre-processing stage for providing the image color identification. The bright white spot arises on the wound image due to reflection. Median filter [13] with 5×5 window size is employed to eliminate the salt and pepper noise in wound images. The median filter can smooth noisy regions, enhance the low-contrast wound region and better preserve the structure of the edges. It considers each image pixel and looks at its close by neighbors to choose whether or not it is representative of its environs. Median filter replaces the value of central pixel with the median of all the surrounding neighborhood pixel values. The median is intended by first categorization the entire pixel values from the neighboring neighborhood into numerical categorize and then restoring the pixel being measured with the middle pixel value. The average of two middle pixel values is taken when the neighborhood under consideration contains an even number of pixels. The Median filter is represented as:

$$\textit{Median filter } (x_{1} \ldots x_N) = \textit{Median } [||x_1||^2 \ldots\ldots ||x_N||^2] \quad (8)$$

The two major advantages of median filter [14] over mean filter are: (a) the median is more robust averages than mean and as such, a single very unrepresentative pixel in a neighborhood will not significantly affect the median value and (b) as the median value is actually the value of one of the pixels in the neighborhood, it does not generate new improbable pixel values when the filter straddles an edge. Hence, the median filter is much superior at preserving sharp edges than mean filter.

A. Color homogenization

CWs are having complex mixture of colored tissues with varied intensity. Anisotropic diffusion filtering [15] is used for homogenization of color along with preservation of edges, only smoothing between edges. The objective of this method is to reduce image noise without eliminating significant portion of the image. The color homogenization is used in this work using combined Gray world assumption and Retinex theory [16].

IV. Simulation Results

The outcomes of the different filters are presented in this section. Total ten filters were implemented and output images are represented in Fig. 3. Most of them use mathematical morphology operations. 5×5 square structuring elements were used. These filters were applied on set of fifty five randomly selected wound images from our developed wound database as well as an online wound image database. The number was significantly reduced to the best five to have an automatic filter selection. In order to access the quality of image, four

different quantitative performance measures are defined as MSE; PSNR; SNR; MAE respectively.

(a) MSE – It is the most important image quality measuring method. It is basically squared error between enhanced image and original CW image. Mathematically, defined as:

$$MSE = \frac{1}{M \times N} \sum_{x=0}^{M-1} \sum_{y=0}^{N-1} \left[F(x,y) - F_{fltr}(x,y) \right]^2 \quad (9)$$

where, $F(x,y)$ and $F_{fltr}(x,y)$ are the input and filtered output images.

(a) PSNR – It is used to calculate the ratio between maximum possible intensity value of the CW image and MSE. PSNR is defined as:

$$PSNR = 10 \log_{10} \left[\frac{R^2}{\frac{1}{M \times N} \sum_{x=0}^{M-1} \sum_{y=0}^{N-1} \left[F(x,y) - F_{fltr}(x,y) \right]^2} \right] \quad (10)$$

Here, R is the maximum possible peak intensity value of the image.

(b) SNR – It is the ratio between signal i.e. enhanced image and noise in the spatial domain. In this case, noise is the difference between input image and filtered image.

$$SNR = \left[\frac{\sum_{x=0}^{M-1} \sum_{y=0}^{N-1} \left[F_{fltr}(x,y) \right]^2}{\sum_{x=0}^{M-1} \sum_{y=0}^{N-1} \left[F(x,y) - F_{fltr}(x,y) \right]^2} \right] \quad (11)$$

(c) MAE – This method is used to measure how close predictions are to the eventual outcomes. The MAE is given by

$$MAE = \frac{1}{n} \sum_{i=1}^{n} |f_i - y_i| = \frac{1}{n} \sum_{i=1}^{n} |e_i| \quad (12)$$

where, MAE is an average of the absolute errors, $e_i = |f_i - y_i|$, f_i is the prediction and y_i is the true value, n is the number of observations.

The four important parameters have been analyzed for the quality of images. Lower value of MSE indicates that there is very small change between original and filtered image. On the other hands, higher value of PSNR, SNR reports that there is very small change. From Fig. 5-8, we observe that median filter is the best choice for visualization because it provides good PSNR (67.28), SNR (54.56), MAE (0.22) and MSE (3.29). This filtering technique improves the segmentation performance with the maintaining proper homogeneity of the image. The median filtering technique provides better visualization after observing the all filtered image results.

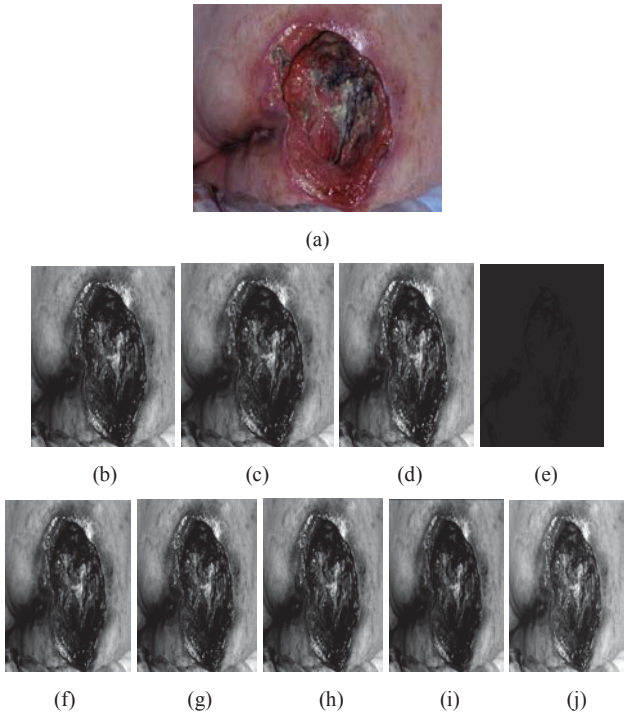

Fig. 4. (a) Original CW image; (b) Median filtered; (c) Average filtered; (d) M3 filtered; (e) Max filtered; (f) Mean filtered; (g) Min filtered; (h) Log filtered; (i) Midpoint filtered; (j) Gaussian filtered

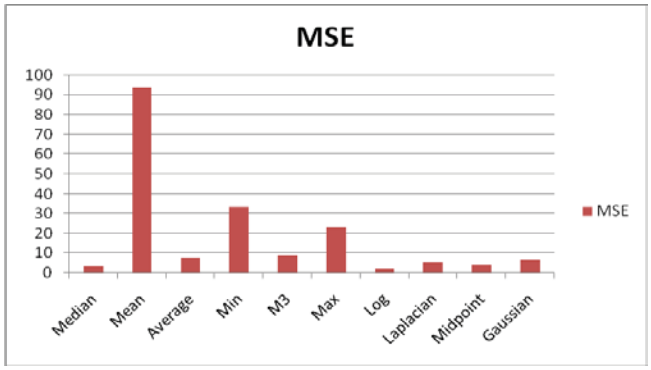

Fig. 5. MSE parameter measurement with image quality

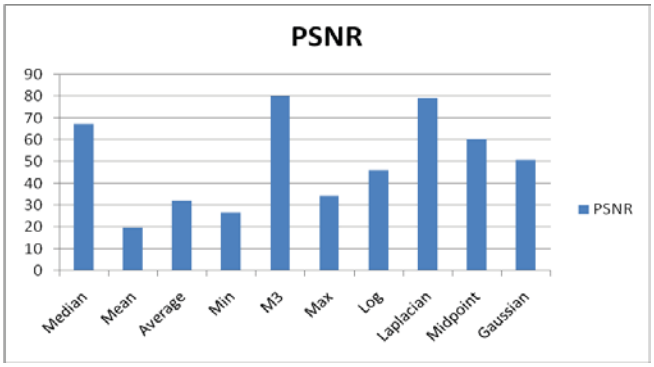

Fig. 6. PSNR parameter measurement with image quality

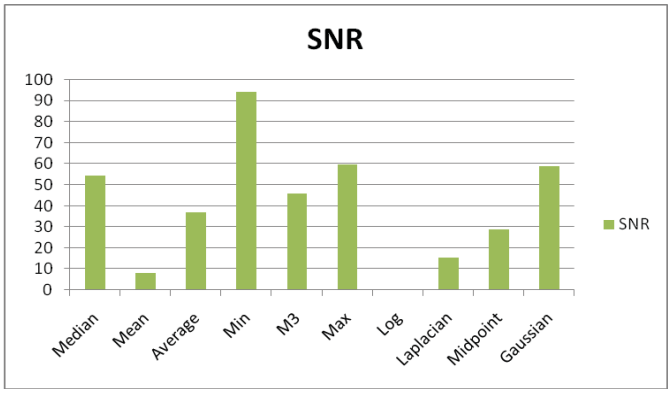

Fig. 7. SNR parameter measurement with image quality

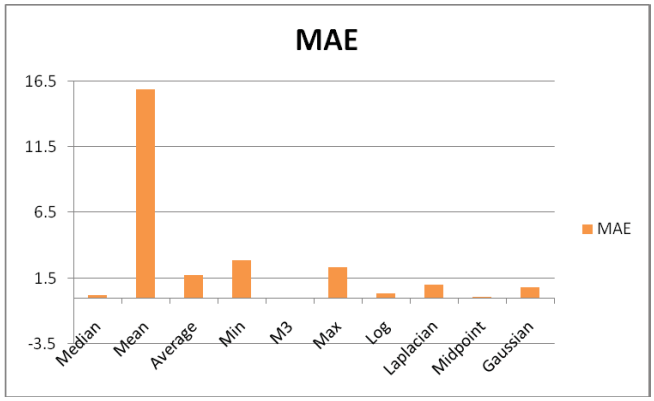

Fig. 8. MAE parameter measurement with image quality

V. Conclusion

In this paper, we have discussed about the different filtering techniques for chronic wound analysis under tele-wound network. The acquired CW image undergoes filtering scheme to remove the noise from the CW image. It is observed that median filter performs well for noise removal out of others filters with respect to different performance parameter like PSNR, MAE, SNR and MSE. We have done a comparative studied with all the filters and taking best filter selection based on average values of set of images. Results shows Median filtering provides better performances with respect to high PSNR and reduced MSE between original and filtered image. The outcome obtained manifests a system has greater scope of utilization in the field of evaluation through tele-wound network.

References

[1] Chakraborty C., Gupta B., Ghosh S.K., "Identification of Chronic Wound Status under Tele-Wound Network through Smartphone, IGI Global International Journal of Rough Sets and Data Analysis," Special issue on: Medical Image Mining for Computer-Aided Diagnosis, vol. 2, no. 2, pp. 56-75, 2015.

[2] Chakraborty C., Gupta B., Ghosh S.K., "Tele-wound monitoring through smartphone," IEEE: Int. Conf. on Medical Imaging, m-Health and Emerging Communication Systems (MedCom), pp.197-201, 2014.

[3] Gonzalez R., Richard W., "Digital Image Processing," Addison-Wesley Publishing Company, 2001.

[4] Wild T., Prinz M., Fortner N., Krois W., Sahora K., Stremitzer S., Hoelzenbein T., "Digital measurement and analysis of wounds based on colour segmentation," European Surgery, pp. 1-6, 2008.

[5] Christos P.L., Takis K., Michalis P., "Evaluation of wound healing process based on texture image analysis," Journal of Biomedical Graphics and Computing, vol. 3, no. 3, pp. 1-13, 2013.

[6] Lei W., Peder C.P., Diane S., Bengisu T., Emmanuel A., "Wound image analysis system for diabetics," Medical Imaging, Proc. of SPIE, vol. 8669, pp. 1-14, 2013.

[7] Barone S., Paoli A., Razionale A.V., "Assessment of chronic wounds by three-dimensional optical imaging based on integrating geometrical, chromatic, and thermal data," Proc. of IMechE, vol. 225, no. 181, pp. 1-14, 2011.

[8] Éderson. A. G. D., Marco A. C., Frade1, Rangaraj M., Rangayyan, Paulo M., Azevedo M., "Segmentation and analysis of the tissue composition of dermatological ulcers," 23rd Canadian Conf. on Electrical and Computer Engineering (CCECE), pp. 1-4, 2010.

[9] Marina K., Ales F., "Segmentation of wounds in the combined color-texture feature space," SPIE, pp. 1-8, 2004.

[10] Dorra N., Yves L., Sylvie T., Jolivot R., Marzani F., "Color and multispectral imaging for wound healing evaluation in the context of a comparative preclinical study," Medical Imaging, pp. 1-10, 2013.

[11] Chakraborty C., Gupta B., Ghosh S., "Mobile metadata assisted community database of chronic wound," Int. Journal of Wound Medicine, Elsevier, vol. 6, pp. 34-42, 2014.

[12] Chakraborty C., Gupta B., Ghosh S.K., "A Review on Telemedicine-Based WBAN Framework for Patient Monitoring," Int. Journal of Telemedicine and e-Health, Mary Ann Libert inc., vol. 19, no. 8, , pp. 619-626, 2013.

[13] Gonzalez R.C., Woods R. E., "Digital image processing," Prentice Hall, New York, NY, USA, 2nd edition, 2002.

[14] Arias-Castro E., Donoho D.L.,"Does median filtering truly preserve edges better than linear filtering," Annals of Statistics, Vol. 37, No. 3, pp. 1172, 2009.

[15] Perona P., Malik J., "Scale-space and edge detection using anisotropic diffusion," IEEE Transactions on Pattern Analysis and Machine Intelligence, Vol.12, No.7, pp. 629-639, 1990.

[16] Brainard, D.H., Wandell, B.A., "Analysis of the retinex theory of color vision," JOSAA, Vol. 3, pp. 1651-1661, 1986.

THE 5TH INTERNATIONAL CONFERENCE ON WIRELESS COMMUNICATIONS, VEHICULAR TECHNOLOGY, INFORMATION THEORY, AEROSPACE & ELECTRONIC SYSTEMS (WVITAE-2015)
December 13-16, 2015, Hyderabad, India

Performance Analysis Of Interference Cancellation In MIMO-FBMC

V.Padmapriya [1] and N.Venkateswaran[2]
Department of Electronics and Communication Engineering
SSN College of Engineering
Chennai,India

***Abstract*— FBMC has been researched as an heir to OFDM with the aim of enhancing bandwidth of the physical layer in conventional wireless communication techniques. Its application in new age systems like cognitive radio and MIMO has been a topic of great interest in recent times. MIMO systems built on FBMC modulation promise very high data rates in terrestrial wireless communication. Data streams from multiple antennas can cause serious interference at the receiver. De-correlating these streams is necessary to ensure accurate detection of the transmitted symbols. In this paper we analyse the performance of three interference cancellation techniques in FBMC based MIMO systems, namely-FBMC-ZF, FBMC-MMSE and FBMC-SVD based signal de-correlation. Simulation results show that FBMC SVD signal de-correlation is superior to the other two de-correlation techniques.**

I. Introduction

OFDM has been widely accepted as a successful modulation format for nearly two decades [1].However it does have its share of limitations. It requires the transmission of cyclic prefix and it uses a rectangular window to shape the signals, which inturn degrades the stopband attenuation. These limitations cost heavily interms of the required spectrum . In [1] OQAM based FBMC system,which uses well contained waveforms to shape the signals, is suggested as an alternative to OFDM. Also [1] asserts that FBMC systems are a superior choice for many applications like cognitive radio, DSL and uplink of multi user multicarriersystems. This techniqe is the brainchild of Saltzberg [2].

In recent times the demand for high data rates has increased significantly.Both the number of users and the kind of data that is being transmitted on the wireless channel has placed heavy demands on the available spectrum. MIMO has emerged as a promising solution to requisite.In [3],[4] the performance of FBMC-MIMO system is analysed .In [4][5] [6] it is show that FBMC's performance is as good as that of OFDM. Though it has been argued that FBMC is more demanding in terms of complexity it is suggested in [3] that this can be overlooked when compared to the complex signal processing required for synchronization in the case of uplink OFDM-MIMO systems.

The MIMO scheme can characterised by $y = Hx + n$ Where y and x are the received and transmitted vectors respectively. H is the MIMO channel matrix. In the single user scenario the transmit vector x consists of several parallely encoded data streams. The multiple subcarriers transmitted by each antenna are of the same frequency. These parallel data streams superimpose at the receiver antenna array. The interference presented by the neighbouring data streams may cloud the decisions at the receiver. It is necessary to separate these signals to achieve an acceptable BER performance. This paper considers three techniques which can be deployed to mitigate multi-antenna interference in FBMC-MIMO systems. Their performance has been compared under the assumption of a flat-rayleigh fading channel.

The paper is organized as follows: The basic FBMC-MIMO system is presented is section-II. The zero forcing based inter antenna interference cancellation technique is discussed in section-III.A. This is followed by a description of MMSE based interference cancellation in section III.B. The application of SVD for signal decorrelation is discussed in section II.C. The simulation results have been provided in section IV. Conclusions drawn based on these results have been presented in section V.

II. FBMC OQAM-MIMO System Model

The overall architecture for FBMC based MIMO transceiver is shown in Fig.1.The input bits are first subject to OQAM pre-processing. These symbols are then mapped to multiple carriers by the synthesis filter bank. The independent data streams from each antenna is passed through the MIMO channel. The inference caused by the data streams from the neighbouring antennas is then cancelled using any of the interference mitigation techniques discussed in section III. The independent data streams are filtered using analysis filter bank. The output is finally recovered by subjecting the received stream to OQAM post-processing.

This paper focuses on a multiantenna configuration consisting of N_T transmit antennas and N_R receiving antennas. The signal at the output of n^{th} transmit antenna is given by

$$S_n(k) = \sum_{i=-\infty}^{\infty} \sum_{m=0}^{M-1} V_{nm}(i) f_m(k - \frac{iM}{2}) \quad (1)$$

where,

$$f_m(k) = p(k) e^{j(\frac{2\pi m}{M}(k - \frac{L_p - 1}{2}))} \quad (2)$$

$$m = 0, 1, 2, ...M - 1, k = 0, 1, 2, ...L_p - 1$$

Here $Lp = Mg - 1$ denotes the length of the filter.The parameter g denotes the overlapping factor which gives the number frequency co-effecients introduced in between the FFT filter co-effecients[8],[9]. f_m is used to construct the analysis and synthesis filter bank. M denotes the number

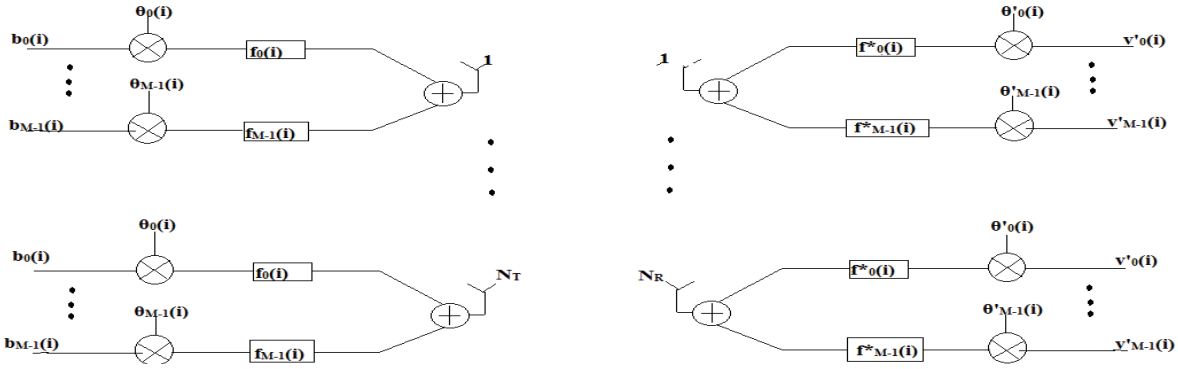

Fig. 1: Overall architecture of a MIMO-FBMC system

Table 1. COMPARISON OF PHASE CHANGE BETWEEN ADJACENT SYMBOLS IN QAM AND OQAM

Period	QAM			OQAM		
	Inphase Component	Quadrature Component	Resultant Phase	Inphase Component	Quadrature Component	Resultant Phase
T/2	1	1	180	1	0(assumed)	270
T	1	1	180	1	1	180
3T/2	0	0	0	0	1	90
2T	0	0	0	0	0	0
5T/2	-	-	-	0(assumed)	0	0

of carriers and V denotes the OQAM symbols.A detailed description of each of the various sub-bolcks is as follows.

A. OQAM Preprocessing

Offsetting the in phase and quadrature phase carriers alleviates the problem of phase noise. This is because the maximum change in phase between two consecutive symbols is restricted to be 90^0.This can be comprehended from Table.1 which compare the phase of the transmitted signal for the QAM and OQAM.The bit stream considered in the tabulation is 1100.

The transmitted OQAM symbols can be expressed as the product of the real valued PAM symbols $b_m(i)$ and the phase term $\theta_m(i)$ .The transmitted OQAM symbols can be expressed as

$$v_m(i) = b_m(i)\theta_m \tag{3}$$

Where,

$$\theta_m(i) = \begin{cases} 1, \ if \ m+i \ is \ even \\ j, \ if \ m+i \ is \ odd \end{cases} \tag{4}$$

B. The Analysis And Synthesis Filter Banks

The filter bank used is based on the complex modulated - overlapped filters designed in [7].It uses FIR filters which are designed to have superior stopband attenuation. The impulse response of the prototype filter is give by

$$p(k) = \begin{cases} \frac{1}{N}\left(C_o + 2\sum_{l=0}^{g-1} C_l cos(\frac{2\pi lk}{N}), & 0 < k < N-1 \\ 0, otherwise \end{cases} \tag{5}$$

Where $N = gM$ .The fourier transform of $p(k)$ consists of the fourier transform several overlapping rectangular windows which are shifted in frequency by $\frac{2\pi}{M}$.The proper choice of filter co-efficients C_l can be used to achieve filters with excellent stop band attenuation. It ensures that the spectrum of each subcarrier is well contained within the specified bandwidth. In this paper uses a filter with an overlapping factor of four is considered. The values of C_l used in this paper are obtained from [7] tabulated in Table.2.The complex modulated filter bank can be obtained by localizing the prototype LPF over different frequencies. The filter bank can be obtained using the expression (2). The frequency response of the first five analysis fillters is shown in Fig.2. The Analysis filter bank is matched to the synthesis filter bank and is thus denoted as $f_m^*(k)$. A FFT based implementation of these filter banks is followed as depicted in Fig.1.

C. The MIMO System

The MIMO configuration transmits N_T parallel filtered data streams. It is necessary to render these streams to be independent of one another as they propagate through the

TABLE 2. FILTER COEFFICIENTS

Coefficients	Corresponding Value For g=4
C_o	1
C_1	-0.97195983
C_2	0.70710678
C_3	-0.23514695

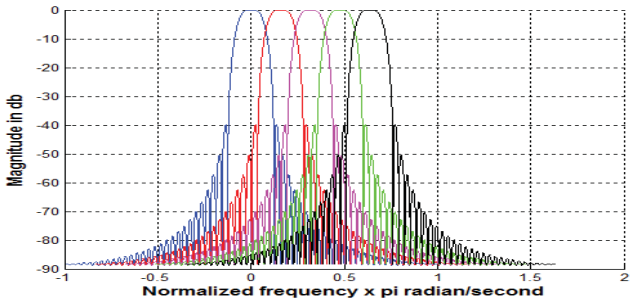

Fig. 2: Frequency response of first five subcarrier analysis filters

MIMO channel. Assigning a different set of carrier frequencies to each antenna might be an easy way out. However this becomes impractical when the number of transmit antennas grows to be large. Same set of carrier frequencies is assigned to each of these antennas to override this difficulty. The composite signal is passed through the MIMO channel. The signal at the input of the q^{th} receiving antenna is given by

$$r_q(k) = \sum_{n=1}^{N_T} S_n(k) h_{nq}(k) + w_q(k) \tag{6}$$

Where, h_{nq} represent the elements of the MIMO channel matrix H. The received signals are the de-correlated using any of the techniques discussed in section III. The independent streams are filtered using the analysis filter bank.

D. OQAM Post Processing

The filtered outputs from the analysis filter bank are subject to OQAM post-processing. The filtered output is first processed to compensate for the phase term θ_m given by (3).The output of OQAM post-processing is given by

$$v'_m(i) = b'_m(i)\theta^*_m \tag{7}$$

where b'_m represents the interference subsided, filtered stream on the m^{th} subcarrier. The antenna index is dropped for simplicity. The input bit stream is recovered by subjecting the real part of v'_m to PAM demodulation.

III. INTERFERENCE MITIGATION TECHNIQUES

In the following section we present three techniques that are employed for signal de-correlation in the multi-antenna scenario.

A. Zero Forcing Decorrelator

The zero forcing decorrelation is implemented by multiplying the received data streams by the following weighing matrix

$$W_{ZF} = (H^H H)^{-1} H^H \tag{8}$$

It functions by inverting the effects of the channel.

$$r_{ZF} = r_q W_{ZF} \tag{9}$$

$$r_{ZF} = r'_q + (H^H H)^{-1} H^H \tag{10}$$

$$r_{ZF} = r'_q + noise_{ZF} \tag{11}$$

The resultant signal r'_q is independent of inter antenna interference. Zero forcing however suffers from the problem of noise enhancement[10].This can be overcome by the MMSE based technique discussed in the following section.

B. MMSE Decorrelator

In this case square of difference between the transmitted symbols and the detected outputs is take as the performance metric. This technique looks to strike a balance between interference cancellation and noise enhancement. The MMSE weighing matrix is given by

$$W_{ZMMSE} = [H^H H + (\frac{1}{varience(noise)})]^{-1} H^H \tag{12}$$

From (12) it can be observed that at high values of SNR the MMSE based technique is equivalent to the ZF decorrelator.

C. SVD Decorrelator

Singular value decomposition is another technique to decorrelate signals from multiple antennas. The task of interference cancellation is jointly performed both at the transmitter as well as receiver. The SVD of the channel matrix H is given by

$$H = U \Sigma V^H \tag{13}$$

Where U and V are unitary matrices. They contain the eigen vectors of HH^H and $H^H H$ respectively. Σ is a diagonal matrix containing the singular values of H. The transmitted data stream is precoded by multiplication with the matrix V. The post processing is carried out by multiplication of the received streams with U^H. Fig.3 provides a pictorial overview of the signal processing at the transmitter as well as the receiver. As a result received stream is thus transformed into independent parallel data streams.

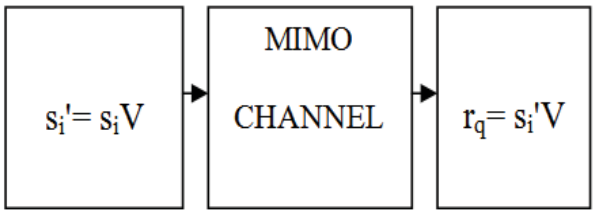

Fig. 3: SVD based precoding and receive antenna shaping

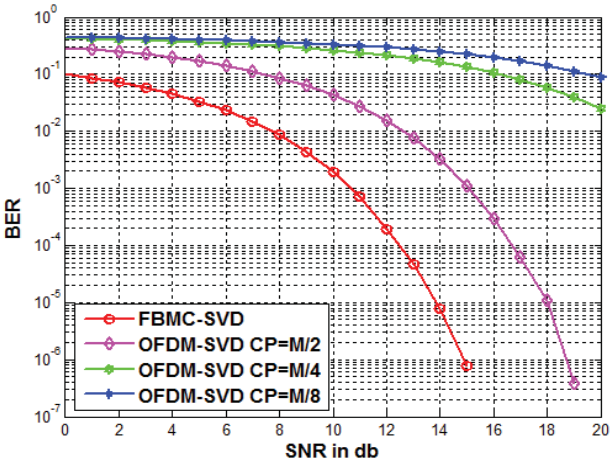

Fig. 4: Comparison of the BER performance of FBMC-SVD and OFDM-SVD signal decorrelators

IV. SIMULATION RESULTS

A 2X2 MIMO FBMC system was considered. The architecture shown in Fig.1 was simulated assuming a MIMO Rayleigh flat fading channel.The filter co-efficients used are those suggestes in [7].Due to the sharp sidelobe fall off rate an overlapping factor of 4 is chosen . Perfect CSI is assumed at the transmitter as well as the receiver.Fig.4 compares the performance of FBMC-SVD and OFDM-SVD signal decorrelators.Since FBMC uses filter banks which produce a sharp fall of rate, there is no need to transmit redundant bits as cyclic prefix.In the case of OFDM the number of bits allocated to serve as cyclic prefix is assumed to be a fraction of the number of carriers.The number of carriers is taken to be 128.Fig.4 confirms that the performance of OFDM-SVD signal decorrelator improves when the number of cyclic prefix bits increases.However it is also observed the FBMC-SVD performs better when compared to OFDM-SVD.

Fig.5 provides a comparison of the three interference cancellation techniques presented in this paper,namely,FBMC-SVD,FBMC-ZF and FBMZ-MMSE.It also provides a comparison of the corresponding OFDM counterpart.The number of cyclic prefix bits considered in this case is $M/8$. It is observed that at low values of SNR MMSE based decorrelator performs better than Zero-forcing based detecter. This is because the channel inversion is accompanied by noise enhancement in the case of zero forcing based interference

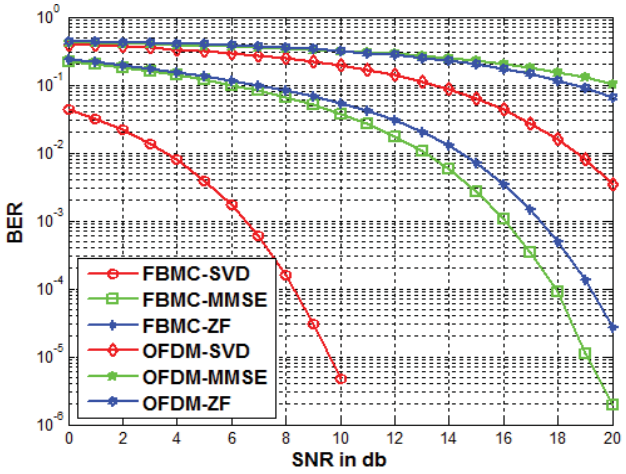

Fig. 5: Comparison of the BER performance of multi-antenna interference mitigation techniques

cancellation.The superior performance of SVD based interference cancellation can be credited to the fact that both U and V are unitary matrices. Hence the channel noise remains unaffected when the signal is subjected to receiver based signal shaping.Despite the fact that FBMC does not require the transmission of cyclic prefix, its performance is superior when compared to OFDM.This is clearly refflected in Fig.5.

V. CONCLUSION

In this paper we presented three techniques for multiantenna interference rejection in FBMC-MIMO systems.From the simulation results obtained it can be concluded that SVD based precoding and receive shaping outperforms ZF and MMSE based interference cancellation in a multi antenna scenario.The simulation results also confirm the superiority of FBMC over OFDM based MIMO systems.FBMC based MIMO systems promise high data rates while making efficient use of the available spectrum.

REFERENCES

[1] B. Farhang-Boroujeny, OFDM versus filter bank multicarrier, IEEE Signal Process. Mag., vol. 28, no. 3, pp.92-112, May 2011.
[2] B. Saltzberg, Performance of an efficient parallel data transmission system, IEEE Trans. Commun. Technol., vol. 15, no. 6, pp.805-811, Dec. 1967.
[3] I. Estella,A. Pascual-Iserte, andM. Payaro, OFDM and FBMC performance comparison for multistream MIMO systems, in Proc. Future Netw. Mobile Summit, pp.1-8,Jun. 2010.
[4] M. Caus and A. I. Perez-Neira, Transmitter-receiver designs for highly frequency selective channels in MIMO FBMC systems, IEEE Trans. Signal Process., vol. 60, no. 12, pp.6519-6532,Dec. 2012.
[5] Paolo Banelli ,Stefanzo Buzzi, Giulio Colavolpe, Andrea Modenini, Fredrik Rusek and Alessandro Ugolini, Modulation formats and Waveforms for 5G Networks: Who Will be the Heir of OFDM,IEEE Signal processing Magazine, pp.80-93,Nov. 2014.
[6] Marius Caus and Ana.I.Perez-Neria, Multi-Stream Transmission for Highly Frequency Selective Channels in MIMO-FBMC/OQAM Systems, IEEE Transactions on Signal Processing,VOL.62,No.4, pp.786-795,Feb 2014.
[7] Shahriar Mirabbasi, Ken Martin,Overlapped Complex-Modulated Trans-multiplexer Filters With Simplified Design and Superior Stopbands,IEEE transactions on circuits and systems-II:Analog and Digital Signal Processing,Vol.50 ,no.8, pp.456-468 ,Aug 2003.

[8] M. Bellanger, FBMC Physical Layer: a primerPHYDYAS, crowncom, pp.1-31,2010
[9] A. Viholainen, M. Bellanger, M. Hutchard, report on Prototype filter and structure optimization, work package 5, phydyas doc. No. PHYDYAS-007, pp.1-102, 2009.
[10] Christoph Windpassinger, Robert F. H. Fischer, Toms Vencel, and Johannes .B. Huber, Precoding in Multiantenna and Multiuser Communications,IEEE transactions on wireless communications",Vol.3,No.4, pp.1305-1315,July 2004.

THE 5TH INTERNATIONAL CONFERENCE ON WIRELESS COMMUNICATIONS, VEHICULAR TECHNOLOGY, INFORMATION THEORY, AEROSPACE & ELECTRONIC SYSTEMS (WVITAE-2015)
December 13-16, 2015, Hyderabad, India

End-to-End Delay Analysis of IEEE 802.15.6 Standard for WBAN Medical Paradigm

Vivek Kumar, *Member, IEEE*, and Bharat Gupta, *Senior Member, IEEE*

***Abstract*— In recent years, a very rigorous researches are focused towards the development of Wireless Body Area Networks (WBAN) for health monitoring. WBAN impels to make use of wearable and implanted sensor devices for monitoring various physiological sign. The standard specification is projected to achieve a vast scope for implementation possibilities for WBAN in order to gain high performance, ultra-low power consumption and high quality of service with variable data rates from few kbps to mbps. In this paper, we present a brief discussion on IEEE 802.15.6 UWB PHY specification. Moreover, we have calculated the end-to-end delay (D_{E2E}) performance of IEEE 802.15.6 Carrier Sense Multiple Access with Collision Avoidance (CSMA/CA) mechanism. The simulated results shows that the maximum end-to-end delay is less than WBAN medical healthcare application requirement of 250 ms.**

***Index Terms*— WBAN, IEEE 802.15.6, CSMA/CA, UWB PHY, Delay**

I. INTRODUCTION

Advances in wireless technology with supporting infrastructure provide unprecedented opportunity for ubiquitous real-time healthcare and wellness monitoring. WBAN based remote and ubiquitous healthcare monitoring services have proved to be a great success in this context. WBAN emerge as a subcategory of wireless sensor network (WSN) [1, 2]. They provide novel and unlimited possibilities for medical and non-medical application. [3, 4]. A WBAN comprises of miniaturized and lightweight sensor nodes mainly employed to monitor numerous body functions. Such type body-centric communication system are enamoring considerable attention from research and industrial communities. Medical application make use of tiny sensor nodes in, on, or around human body for various vital sign monitoring. These devices provides a scalable, robust, long term and real-time health monitoring of individual personal without encumbering daily life activities. Non-medical applications includes personal assistance, ambient intelligence, gaming, entertainments, social networking, environments monitoring, military, sports and consumer electronics [5-9].

Small size, flexibility, and seamless connectivity are the important issues of WBAN for providing real-time healthcare monitoring. However, the energy efficiency is the prime constraint of this field. In fact, WBAN's nodes have limited power source (battery driven) and replacing or recharging of battery is undesirable due to implanted node. Thus, an efficient power management to reduce energy consumption is the key towards prolonging WBAN life-time in order to provide long time healthcare monitoring. Moreover, for real-time healthcare monitoring, most of collected information are sensitive to the latency, and end-to-end delay must be restricted to 250 ms, since the large traffic load may give rise to unendurable latency. Thus, it very important to categories the information based on priority level and traffic pattern, so that significant information can always communicated prior to others. Hence, an energy-efficient context-aware and traffic-aware MAC protocol is essential requirement for such lifesaving application.

Therefore, in this paper, we have investigated and evaluated the end-to-end delay performance analysis of IEEE 802.15.6 CSMA/CA protocol for medical healthcare application of WBAN. We have developed a discrete-time Markov chain (DTMC) to analyze the performance of mentioned standard. We model DTMC for CSMA/CA technique under non-saturation state. We present a simple and accurate simulation model in order to evaluate end-to-end delay of proposed protocol for different data rates. A few similar Markov chain based analytical works have been proposed earlier [10, 14]. The rest of the paper is organized as follows. Section II provides brief discussion about IEEE 802.15.6 standard. Section III present IEEE 802.15.6 CSMA/CA MAC protocol end-to end delay analysis. Section IV present simulated results and related discussion. Finally, section V concludes our work and future scope.

II. ANALYSIS OF IEEE 802.15.6 STANDARD

The IEEE 802.15.6 is a standard optimized for ultra-low power miniature devices that are deployed in, on, or around human body to serve numerous medical as well as non-medical application [15]. The IEEE 802.15 Task Group 6 (TG 6) launched standard back in 2007 but final version of standard came later in February 2012 [16]. The IEEE 802.15.6 standard defines PHY layer into three frequency bands namely Narrowband, Ultra-Wideband (UWB) and Human Body Communication (HBC) in order to address variable data rate imposed by medical and consumer applications. Fig. 1 shows the available frequency spectrum for WBAN [17]. IEEE 802.15.6 standard supports two types of access mechanism at the MAC sub layer. These two techniques are contention access and contention free access. In contention access phase the standard incorporate either CSMA/CA or slotted ALOHA based medium access techniques. While in contention free

phase, the standard utilize polling based access mechanism as well as scheduled based access mechanism.

There is only one coordinator node (CN) in WBAN which manages the medium access and power management of respective node. The number of nodes in a WBAN is varied between 0 to *mMaxBANSize*. The medium access is scheduled in time, where the time axis is divided into beacon period (superframe boundary) of equal length.

The PLCP construct the PHY layer Protocol Data Unit (PPDU) by concatenating PHY layer Header (PHR), Synchronization Header (SHR), and the PHY layer Service Data Unit (PSDU). The UWB PHY offer 11 channels (each channel having 499.2 MHz bandwidth) with central frequencies starting from 3494.4 MHz for channel number 0 to 9984 MHz for channel number 10. These channels are categorized into two bands: Low band (from channel number 0 - 2) and High band

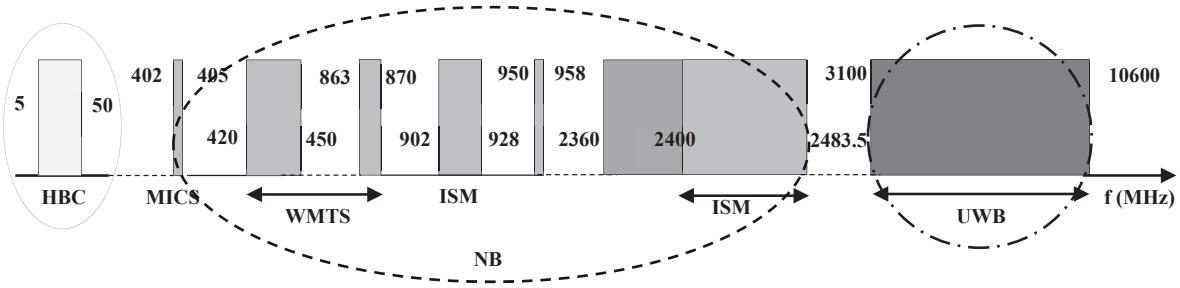

Figure 1. IEEE 802.15.6 frequency bands allocation

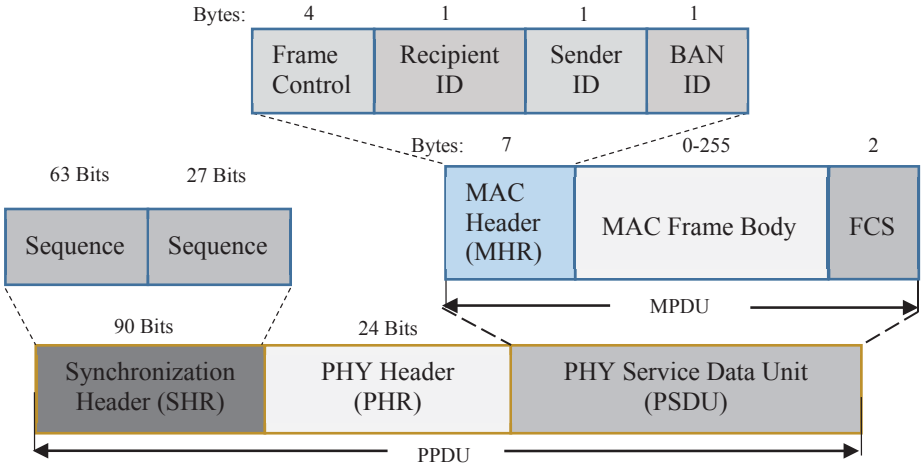

Figure 2. IEEE 802.15.6 Standard PPDU Frame Format for UWB PHY

Each superframe constitute of allocation slots of equal length and numbered from 0 to *s*, where $s \leq 255$. The coordinator broadcast beacons to specify the superframe boundaries and slots allocation. The coordinator transmit beacon in every superframe except those that are inactive. In this paper, we focus on the end-to-end delay analysis for UWB PHY with CSMA/CA based MAC access mechanism.

A. IEEE 802.15.6 UWB PHY Specifications:

The UWB PHY specification is projected to achieve a vast scope for implementation possibilities for WBAN in order to gain high performance, low complexity, and ultra-low power consumption. Furthermore, the UWB's signal power level is similar to MICS band signal power limit. Thus, providing the safe power levels for human body exposure and limiting the interference from other devices. The data interface provided by UWB PHY, which is governs by Physical Layer Convergence Protocol (PLCP).

(from channel number 3 - 10). The standard provides 2 UWB technologies namely, Impulse Radio (IR-UWB) and Frequency Modulation (FM-UWB). In WBAN, a coordinator shall implement either IR-UWB or FM-UWB but a device can implement either IR-UWB or FM-UWB or both. UWB PHY support two modes of operation: Default mode and High Quality of Service (H-QoS) mode. The default mode is utilized for both medical and non-medical application while the H-QoS mode support only high priority medical application. The minimum coded data rate offered by standard for on-off signaling is 397.8 Kbps, 202.5 Kbps by FM-UWB, and 243 Kbps by IR-UWB having DBPSK/DQPSK modulation scheme.

B. IEEE 802.15.6 UWB PHY Frame Structure:

UWB PPDU structure or UWB PHY frame format is formed by adding SHR, PHR, and PSDU as shown in Fig. 2. PSDU contains the MAC Protocol Data Unit (MPDU). The MPDU

includes MAC Header (MHR), a variable MAC frame body, and Frame Check Sequence (FCS). Moreover an additional BCH parity bits are available in H-QoS mode. The data bits of MPDU are first scrambled in order to eliminate possible long string of 1s and 0s. Than a BCH Encoder followed by Pad bits, and a Bit interleaved to generate PSDU for transmission.

The channel code BCH (n = 63, k = 51) and BCH (126, 63) are used for default mode and H-QoS mode. The number of code words in a frame is given as:

$$N_{CW} = \left\lceil \frac{N'_{PSDU}}{k} \right\rceil \quad (1)$$

Where N'_{PSDU} is the number bits in PSDU that comprised of MHR, MAC frame body, and the FCS.

$$N'_{PSDU} = 8(N_{MACHeader} + N_{MACFrameBody} + N_{FCS}) \quad (2)$$

The BCH (126, 63) encoder can be utilized according to Hybrid Automatic Repeat Request (HARQ). In UWB PHY, during default mode of operation, the maximum number of retransmissions (NR) is set to four as compared to seven in case of IEEE 802.15.4 standard. HARQ stores packets when an error packets are arrived at transmitter or receiver and authenticate the certain packets repetition. Thus, it require the interaction between UWB PHY and MAC during retransmission which is given as H_0 and H_1 in PHR.

Moreover, a systematic bits (*D*) at MHR and MAC frame body to perform error detection encoding at UWB MAC and error correction encoding at UWB PHY. When erroneous packets arrived it stored at receiver and no ACK is sent at the transmitter. A parity bits *P* of same size and *D* is added to FCS in order to construct the transmitted PSDU. Thus repetition of Both *P* and *D* bits are utilize to reconstruct the original packets using BCH coding. This repetition continues until *D* bits received successfully or a maximum number of retransmission is reached. Finally interleaving is applied prior to modulation in order to provide robustness against error propagation.

Fig. 3 shows the IEEE 802.15.6 superframe structure. In beacon mode with superframe boundaries, the coordinator is broadcast a beacon frame during each beacon period except inactive superframe. The superframe formed by concatenating nine phases namely as: beacon, exclusive access phase 1 and 2 (EAP1 and EAP 2), random access phase 1and 2 (RAP1 and RAP2), managed access phase 1 and 2 (MAP1 and MAP 2), and the contention access phase (CAP).

The beacon frame transmitted by CN to provide network management. It sent in first slot of each superframe. Beacon provide the device synchronization, medium access, and power management to the nodes in WBAN. The CN provide a specific time in a beacon period of each superframe to transfer the traffic of the highest user priority (UP). time in a beacon period of each superframe to transfer the traffic of the highest user priority (UP). This time span is termed as EAP1 and EAP2. These time slot carry the life sensitive information such as, emergency and medical implant event data. RAP1, RAP2, and CAP are provided to transfer traffic with low UP such as normal or routine traffic. The managed access phase dedicated for managing the uplink, downlink, and bi-link allocation interval. Whereas the 2nd beacon which precede CAP is utilized for grouping the ACK, beginning and the end of CAP, and information related to other device existence.

The coordinator generally employ a slotted ALOHA or CSMA/CA techniques for each access phase except managed access phase. The network CN divide time into superframe which initialize by a beacon frame. For data traffic with highest UP (UP_7), only EAP1 and EAP2 periods are utilized.

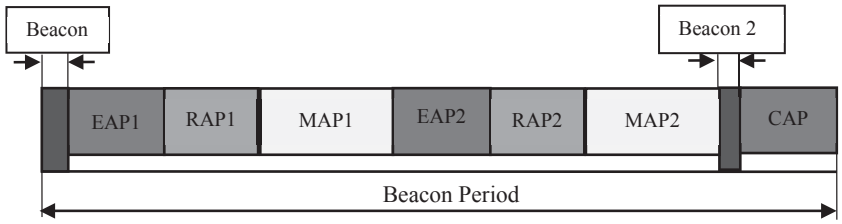

Figure 3. IEEE 802.15.6 Superframe structure

Table 1. IEEE 802.15.6 PHY PARAMETERS

UP	CW_{min}	CW_{max}	Traffic
0	16	64	Background
1	16	32	Best Effort
2	8	32	Excellent
3	8	16	Video
4	4	16	Voice
5	4	8	Medical data
6	2	8	High priority medical data
7	1	4	Emergency report

While in case of slotted ALOHA mechanism, the whole random access phase 1 and 2 are replaced by another exclusive access phases. Table 1 provides the information of Ups depending upon the CW bounds used for CSMA/CA. The detail discussion of MAC access mechanisms are as follow:

i. *CSMA/CA:* In order to obtain a new contended allocation, the nodes initialize its backoff counter to a random integer number distributed uniformly over interval [1, CW]. The CW values belong to (CWmin, CWmax). The values of CWmin and CWmax can be chosen in accordance to UPs. Whenever node sense an idle CSMA slot having length equal to *pCSMASlotLentgh*, it decrement its backoff counter by one. The data frame is transmitted when the counter values reaches to zero. The node freezes its backoff counter when it

sense the channel is busy and the CW is doubled for each failure until it reaches CWmax.

ii. *Slotted ALOHA:* In order to obtain contended allocation, a node uses predefined UPs based on contention probability threshold. These CPs values remain freeze for every consecutively odd number of failures and node halved its CPs for every consecutively even number of failures.

III. End-to-End Delay Analysis

In this analysis, we have calculated the maximum permissible D_{E2E} of IEEE 802.15.6 beacon mode with superframe boundaries for healthcare application under real-time constraints. The calculation is done for UWB PHY over frequency band of 3.1 – 10.6 GHz. Fig. 4 shows the basic data transfer models for normal and emergency or on demand traffics. Depending upon user priority CN allocates an available channel to WBAN nodes. The D_{E2E} for CSMA/CA algorithm can be defined as

$$D_{E2E} = macMaxFrameRtx \times (T_{DIFS} + T_{CW} + T_{Frane} + T_{TA} + T_{ACK} + T_{IFS}) \quad (3)$$

T_{DIFS} , is the longest wait time for medium access. If node sense medium idle for at least DIFS (Distributed Coordination Function Inter Frame Space) period, it can access the medium at once. T_{DIFS} is expressed as follow:

$$T_{DIFS} = T_{pSIFS} + 2 * T_{pCSMASlotLength} \quad (4)$$

$$T_{pCSMASlotLength} = T_{pCCATime} + pCSMAMacPHYTime \quad (5)$$

The expression for T_{CW} can be given as:

$$T_{CW} = CW_{\min} * T_{pCSMASlotLength} \quad (6)$$

Transmission time of one frame T_{Frame} , for maximum payload length is given as:

$$T_{Frame} = T_{Preamble} + T_{PLCPHeader} + T_{PSDU} \quad (7)$$

Where $T_{Preamble} = \frac{N_{SHR}}{Datarate}$, $T_{PLCPHeader} = \frac{N_{Header} \times S_{Header}}{Datarate}$ and

$$T_{PSDU} = \frac{N_T \times S_{PSDU}}{Datarate} = \frac{[N_{PSDU} + (n-k) \times N_{CW} + N_{Pad}]2}{Datarate} \quad (8)$$

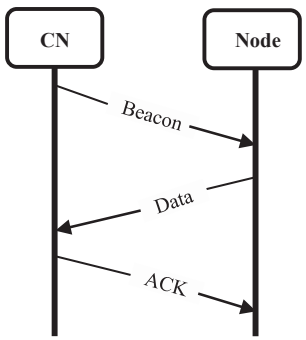

Figure 4. Data transfer model for normal traffic

The UWB PHY offer the least coded data rate of value 0.3978 Mbps for on-off modulation. The turnaround time can be given as:

$$T_{TA} = T_{pSIFS} + T_{pExtraIFS} \quad (8)$$

The expression for T_{ACK} is given as

$$T_{ACK} = \frac{(MHR + FCS) \times 8 + PHR}{Bitrate} \quad (9)$$

Thus, we can calculate the end-to-end delay for maximum payload of 255 bytes having data rate of 397.8 Kbps with *macMaxFrameRetries* = 3.

IV. Simulation Results and Discussions

In this section we have simulated end-to-end delay of IEEE 802.15.6 CSMA/CA mechanism. In section III, we evaluated the expression for end-to-end delay under ideal channel condition. But, in actual channel condition is non-ideal. Thus, to analyze the significant performance, we have calculated probability of collision and packet discarded probability based on our DTMC model under non-ideal channel condition. The packet has been either discarded due to clear channel access (CCA) failure or maximum retry limit reach.

The UWB PHY layer support minimum coded bit rate of 397.8 Kbps. In order to calculate end-to-end delay, we have taken three data rates having values 397.8, 789.7, and 1263.6 Kbps. Also, we have analytically modelled the average wait time possessed by a node to receive acknowledgement after packet transmission. Depending upon the equations as discussed in section III, we calculate end-to-end delay of IEEE 802.15.6 CSAM/CA MAC mechanism for 5 nodes.

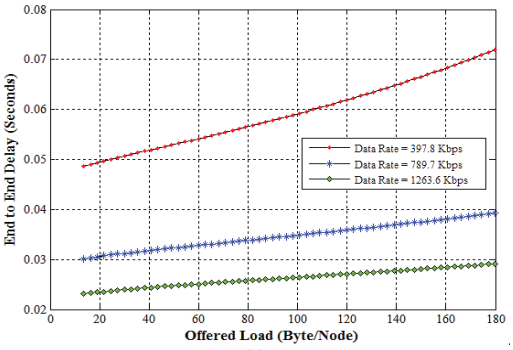

(a)

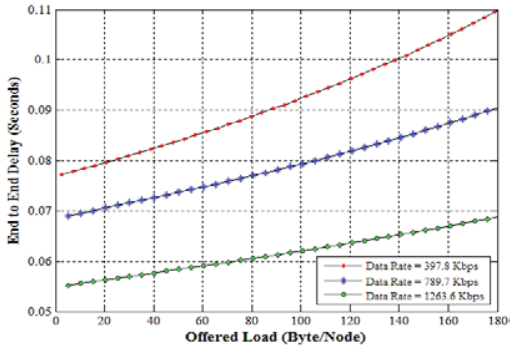

(b)

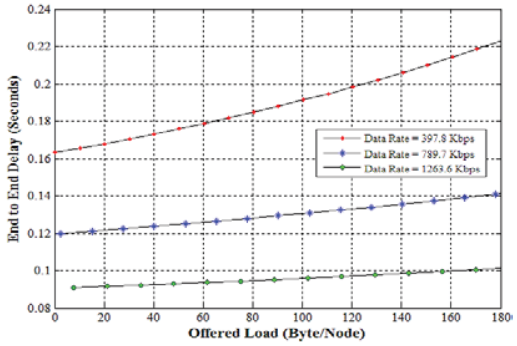

(c)

Figure 5. End to end delay evaluation for different frame length a) 2 bytes b) 75 bytes and c) 255 bytes with number of nodes = 5

We have simulated end-to-end delay for three variable payload of size 2 bytes, 75 bytes, and maximum payload of 255 bytes offered by standard as shown in Fig. 5. We have simulated maximum delay of 220 ms for minimum coded rate of 397.8 kbps for maximum payload of 255 bytes as shown in Fig. 5(c). While much low end-to-end delay of 140 ms and 100 ms have been examined for higher data rate of 789.7 kbps and 1263.6 kbps for maximum payload. In conclusion we can summarize that the end-to-end delay is proportional to traffic load and the number of nodes operated in a WBAN. Depending upon application type and proper traffic management, we can limit end-to-end delay as per requirement.

Fig. 6 shows the end-to-end delay performance of standard with number of node variation of 5, 10, 15 nodes. We have simulated for minimum payload size of 2 with data rate of 397.8 Kbps. Similarly, we can plot number of nodes variation against different data rate at different payload size.

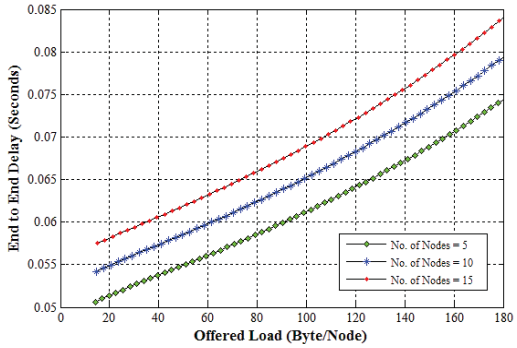

Figure 6. End to end delay evaluation of frame payload of 2 bytes with data rate of 397.8 kbps with number of nodes variation of 5, 10, 15

CONCLUSION

WBAN are the premature promising technology that has the ability to revolutionized next-generation healthcare monitoring system. WBAN enables the precise remote healthcare monitoring for a longer time period along with real-time feedback to the medical personnel. Though the WBAN technology emerges as an outstanding future e-health solution but diversified uses assign the limitation. The multiple collocated WBAN within a close proximity still hinder the full potential deployment of WBAN.

A brief discussion about IEEE 802.15.6 standard has been overviewed and we have evaluated the end-to-end delay performance of IEEE 802.15.6 CSMA/CA mechanism. We have calculated end-to-end delays of 100, 140, and 220 ms with data rates of 1263.6, 789.7, and 397.8 kbps with 5 nodes. We have concisely discussed the medium access approaches and the frame structure of IEEE 802.15.6 MAC protocols. The calculated result shows that IEEE 802.15.6 MAC is highly suitable for WBAN medical healthcare application. The least delay is the most desirable for such real-time healthcare monitoring system which is very sensitive to latency (250 ms).

REFERENCES

[1] I. F. Akyildiz, W. Su, Y. Sankarasubramaniam, and E. Cayirci, "Wireless Sensor Networks: A survey", Computer Networks, vol. 38, issues 4, pp. 393–422, March 2002.

[1] R. MacRuairi, M. T. Keane, G. Coleman, "A Wireless Sensor Network Application Requirements Taxonomy", 2nd International Conference on Sensor Technologies and Applications (SENSORCOMM '08), Cap Esterel, France, pp. 209–216, August 2008.

[2] M. Patel, J. Wang, "Applications, Challenges, and Prospective in Emerging Body Area Networking Technology," *IEEE Wireless Communication*, pp. 80-88, February, 2010.

[3] S. Ullah, H. Higgins, B. Braem et al., "A Comprehensive Survey of Wireless Body Area Networks: on PHY, MAC, and Network Layers Solutions," *Journal of Medical Systems*, vol. 36, no. 3, pp. 1065–1094, 2012.

[4] M. Chen, "Body area networks: a survey", *Mobile Networks and Application*, vol. 16, no. 2, pp. 171-193, 2011.

[5] B. Latre, B. Braem, I. Moerman, C. Blondia, and P. Demeester, "A Survey on Wireless Body Area Networks," *Wireless Networks*, vol. 17, no. 1, pp. 1–18, 2011.

[6] V. Kumar, S. Kumar, and B. Gupta, "Wireless Body Area Networks towards Empowering Real-time Healthcare Monitoring: A Survey", *International Journal of Sensor Networks*, 2015. (In Press)

[7] S. Ullah, P. Khan, N. Ullah, S. Saleem, H. Higgins and K. S. Kwak, "A Review of Wireless Body Area Networks for Medical Applications", *International Journal of Communications, Networks and System Sciences*, vol. 2, no. 8, pp. 797-803, August, 2009.

[8] N. Bradai, L. Chaari, and L. Kamoun, "A Comprehensive Overview of Wireless Body Area Networks", *International Journal of E-Health and Medical Communications (IJEHMC)*, vol. 2, issues 3, pp. 1-30, September 2011.

[9] M. R. Yuce, "Implementation of Wireless Body Area Networks for Healthcare monitoring", Sensors and Actuators A: Physical, vol. 162, issue 1, pp. 116-129, July 2010.

[10] S. Ullah and K. S. Kwak, "Throughput and delay limits of IEEE 802.15.6", *IEEE Wireless Communications and Networking Conference*, pp. 174-178, March 2011.

[11] S. Rashwand and J. Misic, "Performance evaluation of IEEE 802.15.6 under non-saturation condition", *IEEE GLOBECOM*, 2011, pp. 1-6, 2011.

[12] S. Ullah, M. Chen, and K. S. Kwak, "Throughput and delay analysis of IEEE 802.15.6-based CSMA/CA protocol", *Journal of Medical Systems*, vol. 36, pp. 3875-3891, May 2012.

[13] S. Rashwand, J. Misic, and H. Khazaei, "Performance Analysis of IEEE 802.15.6 under Saturation Condition and Error-prone Channel", *IEEE Wireless Communication and Networking Conference,* pp. 1167-1172, March 2011.

[14] S. Rashwand and J. Misic, "Effects of access phases lengths on performance of IEEE 802.15.6 CSMA/CA", *Computer Networks*, vol. 56, no. 12, pp. 2832-2846, August 2012.

[15] S. Ullah, M. Mohaisen, and M. A. Alnuem, "A Review of IEEE 802.15.6 MAC, PHY, and Security Specifications", *International Journal of Distributed Sensor Networks (IJDSN)*, vol. 2013, pp. 12, 2013.

[16] IEEE 802.15 WPAN, "Task Group 6 (TG6) Body area networks documents," http://www.ieee802.org/15/pub/TG6.html.

[17] A. W. Astrin, H. B. Li, and R. Kohno, " Standardization for Body Area Networks", IEECE Transactions on Communications, vol. 92, no. 2, pp. 366-372, 2009.

THE 5TH INTERNATIONAL CONFERENCE ON WIRELESS COMMUNICATIONS, VEHICULAR TECHNOLOGY, INFORMATION THEORY, AEROSPACE & ELECTRONIC SYSTEMS (WVITAE-2015)
December 13-16, 2015, Hyderabad, India

Relevance of signal processing of the voice in diagnosing human tuberculosis

Giovanni Saggio
Dept. of Electronic Engineering
University of Rome "Tor Vergata"
Rome, Italy
saggio@uniroma2.it

Santosh Bothe
Dept. of MCA, IMED
Bharati Vidyapeeth University
Pune 411038, India

***Abstract*— The objective of this work was to reveal the tuberculosis condition of human patients by means of the voice recording and processing, in order to evidence deviations, if any, with respect to the voice parameters of healthy people. Comprehensive voice signal recording was obtained with low-cost apparatuses, and voice signal processing was realized using very low-computational effort parameters. A total of 312 patients were engaged, 284 tuberculosis diagnosed and 28 in healthy status as an age- and sex-matched control group.**

We demonstrated that the voice can be used as a discriminating source of information between healthy subjects and tuberculosis patients, since evidence of alterations founded in some of the voice features.

Keywords*— *human voice; voice analysis; voice signal processing; tuberculosis

I. INTRODUCTION

Historically, sounds from the body have been clinically evaluated for diagnostic purposes. We can refer to the act of auscultation (in general using a stethoscope) for examining the heart, the breath and the gastrointestinal sounds. Aside from sounds revealed from traditional auscultation, in the latest years the sound of the voice has been considered [1], in particular for determining voice pathology [2-4] or voice disorder [5-7]. Since the voice is the result of sounds, produced by modulation of pushing out air flow, related basically (but not exclusively) to glottis, larynx and lungs, the voice signal processing has been useful to reveal diseases [8-10], disorders [11] or pathology [12] of larynx, inflammation of the lungs [13], and obstructive airway disease [14] or sleep apnea [15].

Within this frame, we considered the possibility that the voice analysis could lead to more intriguing possibilities in diagnosing [16], so that we performed the current study with the aim to determine the relevance of voice signal processing, if any, in diagnosing the laryngeal/lungs tuberculosis.

Recently, the World Health Organization referred of epidemiological burden of tuberculosis (TB) of about 7 million people every year [17], especially focused in developing countries. This really huge number has to be reduced as low as possible and, in such a view, the diagnosis plays a fundamental rule. Currently, the diagnosing tests leave millions undiagnosed and untreated [18], being the high-tech high-cost ones confined to industrialized countries and not still implemented in high-burden developing countries to any significant degree. This is why any technology or tool, useful for diagnosis purposes, which can result affordable, convenient, robust and reliable is welcome. In such a frame, the voice signal processing can potentially furnish an answer, being low-cost, easy manageable, safety and non-invasively recorded.

In general, the voice signal processing have been performed in the *time domain* [15, 19], in the *frequency domain* [6, 11], and in the *quefrency domain* (by means of cepstrum analysis, related to the inverse Fourier transform of the logarithmic amplitude Fourier spectrum) too [11, 20]. Different domain analysis can be convenient to evidence different aspects and parameters related to the voice sounds. In addition, a class discrimination of the speech waveform can be performed [19], and this has been done by means of classification algorithms such as Hidden Markov Models [2], Neural Networks [8], Prototype Distribution Map [8], Self-Organizing Map [8], Support Vector Machine [3, 4, 10, 12, 20], Gaussian Mixture Model [20], Linear Discriminant Analysis [4, 15], and Random Forest [12].

Regardless the so many different possibility to explore, we established to work in time and frequency domain, but limiting our attention to the most common, known and used statistical tools, in order to avoid to work with sophisticated algorithms which can be effective but can result as a step ahead towards complexity. This is to make results easily intelligible for the most part of people potentially involved in clinical treatments.

As far as we know, this is the first work addressing the relevance of the signal processing of the human voice in diagnosing tuberculosis on the basis of hundreds of evaluated subjects, with a unique prior work that considered the change in the quality of the voice of only one subject, a 28-year-old female with laryngeal and pulmonary tuberculosis [21].

II. 2. SUBJECTS, MATERIALS AND METHODS

A. Subjects

Voice data present noteworthy age-related [22], gender-related [23, 24] and ethnics-related differences. Therefore, it was fundamental to compare patients within a no meaningful difference in age, of the same gender, and members of the same ethnicity. It is reasonable to believe that also weight, height, smoking, alcohol consumption, social surrounding and culture can have some impacts on the production of voice,

nevertheless we did not considered these variables, so leading to a certain degree of uncertainty, but at this stage empirically esteemed to have a second order influence in diagnosing tuberculosis.

We had 312 male subjects who undertook this study, 28 of them were healthy and 284 of them was lung tuberculosis diagnosed. The 284 subjects diagnosed for tuberculosis claimed no other diseases differently related. The common symptoms like cough, fever, weight loss and loss of appetite were observed. The mean age of the subjects was 39.67 year, within 25-58, all subjects coming from Mumbai (India).

The voice recordings were performed at Tata Memorial Hospital (ACTREC, Sector 22, Kharghar, Navi Mumbai - 410208, India.), D.Y.Patil Hospital (Sector 5, Nerul Navi Mumbai, Maharashtra 400614), Sharma Hospital (Sector 11, Kharghar Navi Mumbai 410210 India), Navjeevan Hospital (Sector 17, Kharghar Navi Mumbai, Maharashtra 410210) and Sanjeevani Hospital (Sector 2 CBD Belapur Navi Mumbai, Maharashtra 400614). The local ethical guidelines were followed for each institution, and a written consensus was obtained for all the subjects.

Every patient was asked to phonate a predefined text in local language. In particular, we considered the Marathi and English alphabets for constructing the words of speech text. Each type of pronunciation [25-28] were related with different letter, words and phrases of spoken language. Consequently, the recruited subjects phonated: "Aai Aai Ye Ekade, Aapn Doghe Milun Jaun Tikade, Sundar Maze Gaon, Sunder Maze Ghar. Salgale Miluni Aankhi Banavu Aapn Tayala Aankhi Sunder. Swatch Asel Aapule Gaon Aani Ghar Thr Aaajar Aapnhun Jail dur. Tar Mag Maja Mothi Karu, Mayene Mazya, Msatine Mulayam Karu. Aapli Maja Aanel Rangat, Sagele Houn Jau Aandi Aani Kamat Dang". (The not fundamental translation is: "Mother, Mother come here, we together will go there, Beautiful home, will make beautiful village, We all together can make it more beautiful, If our village is clean, disease will automatically run away. Then we will enjoy a lot, our fun will bring joy, we all can focus on work.").

This text was considered to have phonetics useful to the extraction of the "voice signature" for tuberculosis. For example, the words having maximum phonetic similarity with English alphabet "U" were chosen to extract the information of lungs and chest area. In addition, the text was designed to give the sensation of a poem about cleanliness and healthy, to generate the interest of the patients.

B. Materials

In order to record the voice, we used a unidirectional microphone (8-28000Hz,-59dBV/µBar,-39 dBV/Pa+/-4dB, by Logitech, Lausanne, Switzerland) hold 6-8cm from the patient's mouth (2cm of possible oscillation). The frequency range considered was limited to an audible range, in particular 200-18000Hz.

The time recording was 30sec, so that all the voice parameters could be exhaustively expressed. Every patient was asked to avoid any high-volume talk to prevent electrical saturation of the microphone.

The output signal from the microphone was fed to a pc running our home-made software termed "Audalysis", capable to record and process the voice parameters. Audalysis is a modular, user-friendly and graphics-driven software (a block diagram reported in Figure 1) useful to avoid any special training to use it. The software allows selecting the sample rate (6000Hz, 8000Hz, 11025Hz, 22050Hz, or 44100Hz), the number of the audio channels (1 or 2) and the resolution in bits (8 or 16). For the current work we selected 44100Hz, 2 channels and 16bits. Audalysis stores the subject's voice in a .wav-format file and can compute up to 12 voice parameters. Anyway, for further simplification purposes, we limited our attention to the 6 parameters we empirically believed as fundamentals: the peak frequency, the peak amplitude, the signal to noise distortion (SINAD), the inter modulation distortion (IMD), the signal-to-noise ratio (SNR), and total harmonic distortion (THD), all in their absolute values.

Collected data were analyzed by means of suitable statistical analysis techniques and results were stored both in excel and in notepad files.

C. Methods

Body Conditions:

Body parts play important roles in production of the voice, so that it is fundamental to avoid unnatural body postures and constrains. Particular body conditions, such as abdominal cramping, bowel disorder, musculoskeletal problems, etc. may have an impact on the voice production. In addition, the diaphragm and abdomen conditions are important in supporting the voice that is stronger when the body is in the upright position. Even the psychological conditions are important in the confidence one has in the voice, as can be seen by the fluttering of the voice when a person is nervous or anxious.

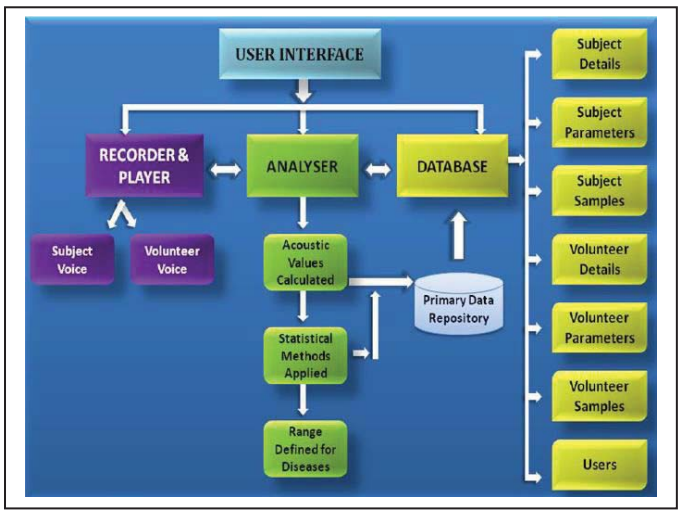

Fig. 1. Audalysis is the home-made software used to record, store and process the signal voice parameters. Its modular architecture consists of three main blocks: the recorder/player, the analyzer and the database ones.

Therefore, we paid particular attention to the mentioned conditions, so to make the voice's recording as strong as

possible to express all the detectable characteristics. Each patient was relaxed, seated on a comfortable chair, the elbows forming a 90° angle, the arm placed on a front table, and the microphone 6-8cm apart from the mouth.

Statistics:

Determination of a statistically significant difference in voice variable values between the control group and the patient group was achieved using one-way analysis of variance (1-way ANOVA). If a statistically significant difference in a voice variable was detected, a threshold value was assigned as the upper limit of the 95% confidence interval (mean +1.96 standard deviation) of the control group value. It was then used to assess the statistical significance of the distribution of the data.

ANOVA was used as a statistical method for comparing acoustic measurements because of its useful characteristics. In particular, ANOVA was most appropriate as our sample size (312 subjects), removes random variability (so significant differences can be easily found), allows to evidence interactions between factors. In order to adopt the 1-way ANOVA we assumed that (1) the observations were dependent on the parameters (acoustic measurements) involved; (2) the sampling distribution was normally distributed; (3) the samples, and their populations, had equal variance.

III. Results and Discussion

There was significant difference in the acoustic parameters between the two states (healthy and unhealthy) in all subjects. For instance, the voice peak frequency for TB conditions showed a mean value of 158.922Hz with a 95% confidence interval in mean with upper bound of 166.869Hz and lower bound of 150.977Hz, rather different from that of healthy conditions, within the 472.714-427.693Hz range. The IMD values significantly change in diseased ranging from 80.815 to 89.322 with respect to the "healthy" interval found to be 511.971 to 565.861. We revealed these as the most significant deviations in percentage for patients suffering from tuberculosis. The overall frame of the obtained results is summarized in Table 1.

TABLE I. Comparison of 6 different parameters between control healthy people and patients suffering from TB. The most relevant variations regards the peak frequency and the inter modulation distortion (IMD).

	Peak Freq. [Hz]	**Peak Amp. [dB]**	**SINAD**	**IMD**	**SNR**	**THD**
Healthy	427.693 to 472.714	65.751 to 70.041	1.9093 to 1.9285	511.971 to 565.861	3.1991 to 3.5361	122.081 to 134.932
TB	150.977 to 166.869	52.020 to 65.917	1.7503 to 1.9346	80.815 to 89.322	3.1391 to 3.4694	124.527 to 137.635

Functioning of all systems and subsystem of human body are dependent on oxygen supply it receives during the breathing process and way they adapts to the changing input of the oxygen. Organ having direct role in oxygen supply and breathing pattern are lungs and heart. We are aware of the trivial fact that, breathing and heart rhythm changes if there is change in need of oxygen by various system of human body. It means lungs and heart functions as per the need of other system of human body. The detail biological explanation is beyond the scope of this paper, but we can conclude that heart and lungs can alters their functioning to suite the various conditions e.g. diseased, health, ideal etc. It means there is an association between functioning heart and lungs to normal and diseased conditions. (This does not require any proof as it is well accepted fact by Modern Medicine, Ayurveda: "Nadi Pariksha" and all branches of diagnosis & treatment.) Now, the sound production process here means converting the steady pressure of lungs into nonlinear acceleration of air flow. The capacity of lungs to exert the pressure on vocal track to produce the voice will change as per the phase and "magnitude of activity level" of various organs and systems of human body. Claims made by authors that, "changes in biochemical parameters of measuring health status can be mapped to corresponding changes in magnitude of voice parameters". This is evident in case of lungs tuberculosis, as stated in Table 1. The reason for variation in peak frequency, peak amplitude and IMD in case of tuberculosis is probably due to a resonance of vocal tract that directly affects the peaks in the output signal.

IV. Conclusions

We evaluated the possibility that the human voice could furnish a cost-effective reliable tool in view of non-invasive safety diagnosis of human tuberculosis. Our intent was to develop a system for voice signal acquisition and processing which could be easily usable and intelligible for the most part of people potentially involved in clinical treatments.

In such a frame, we proved how the tuberculosis affects voice production to significant extents. The most significant parameters, among the six we examined, were found to be the Peak Frequency and Inter Modulation Distortion, which showed a major deviation in control group with respect to subjects suffering from tuberculosis.

The proposed technology can be made as a portable battery-operated voice sample analytics system for diagnosis purposes, which can be used in remote areas where access to robust diagnostic health care facilities is not available, and which can be adopted in high-burden developing countries.

Further investigations will be focused on revealing at what stage the tuberculosis can be usefully revealed, so to understand if the "early" stage can be revealed to help for better cure and infection control, by making subject aware about the disease.

Acknowledgment

The authors like to acknowledge the contribution of project students Ms. Priyanka Chauhan, Ms. Rashmi Chakraborti, Ms. Priya Garg, physicians of various hospitals who allowed us to collect the voice samples; Dr. S B Muley for his support for statistical analysis of data; Ms. Monali Bobade for her guidelines for designing the text to extract the information; Mr. Virupaksha Bastikar and Dr. L. H. Kamble for their help in understanding the biochemistry behind voice production.

REFERENCES

[1] H. Pasterkamp, S. S. Kraman, and G. R. Wodicka, "Respiratory sounds: advances beyond the stethoscope," American journal of respiratory and critical care medicine, vol. 156, no. 3, pp. 974-987, 1997.

[2] J. D. Arias-Londoño, J. I. Godino-Llorente, N. Sáenz-Lechón et al., "An improved method for voice pathology detection by means of a HMM-based feature space transformation," Pattern recognition, vol. 43, no. 9, pp. 3100-3112, 2010.

[3] V. Uloza, A. Verikas, M. Bacauskiene et al., "Categorizing normal and pathological voices: automated and perceptual categorization," Journal of Voice, vol. 25, no. 6, pp. 700-708, 2011.

[4] M. K. Arjmandi, and M. Pooyan, "An optimum algorithm in pathological voice quality assessment using wavelet-packet-based features, linear discriminant analysis and support vector machine," Biomedical Signal Processing and Control, vol. 7, no. 1, pp. 3-19, 2012.

[5] J. I. Godino-Llorente, N. Sáenz-Lechón, V. Osma-Ruiz et al., "An integrated tool for the diagnosis of voice disorders," Medical engineering & physics, vol. 28, no. 3, pp. 276-289, 2006.

[6] G. Niedzielska, "Acoustic analysis in the diagnosis of voice disorders in children," International journal of pediatric otorhinolaryngology, vol. 57, no. 3, pp. 189-193, 2001.

[7] A. Alpan, J. Schoentgen, Y. Maryn et al., "Assessment of disordered voice via the first rahmonic," Speech communication, vol. 54, no. 5, pp. 655-663, 2012.

[8] B. Boyanov, and S. Hadjitodorov, "Acoustic analysis of pathological voices. A voice analysis system for the screening of laryngeal diseases," Engineering in Medicine and Biology Magazine, IEEE, vol. 16, no. 4, pp. 74-82, 1997.

[9] A. Gelzinis, A. Verikas, and M. Bacauskiene, "Automated speech analysis applied to laryngeal disease categorization," Computer Methods and Programs in Biomedicine, vol. 91, no. 1, pp. 36-47, 2008.

[10] A. Verikas, A. Gelzinis, M. Bacauskiene et al., "Combining image, voice, and the patient's questionnaire data to categorize laryngeal disorders," Artificial intelligence in medicine, vol. 49, no. 1, pp. 43-50, 2010.

[11] P. Mitev, and S. Hadjitodorov, "Fundamental frequency estimation of voice of patients with laryngeal disorders," Information Sciences, vol. 156, no. 1, pp. 3-19, 2003.

[12] E. Vaiciukynas, A. Verikas, A. Gelzinis et al., "Fusion of voice signal information for detection of mild laryngeal pathology," Applied Soft Computing, vol. 18, pp. 91-103, 2014.

[13] R. L. Murphy, A. Vyshedskiy, V.-A. Power-Charnitsky et al., "Automated lung sound analysis in patients with pneumonia," Respiratory care, vol. 49, no. 12, pp. 1490-1497, 2004.

[14] Z. Wang, S. Jean, and T. Bartter, "Lung sound analysis in the diagnosis of obstructive airway disease," Respiration, vol. 77, no. 2, pp. 134-138, 2008.

[15] J. Solé-Casals, C. Munteanu, O. C. Martín et al., "Detection of severe obstructive sleep apnea through voice analysis," Applied Soft Computing, vol. 23, pp. 346-354, 2014.

[16] S. A. Bothe, M. D. Bobade, V. V. Alaspure et al., Processo di analisi di campioni di voce di un individuo per verificare il suo stato di salute, Italy, 2012.

[17] W. H. Organization, Global tuberculosis control: WHO report 2010: World Health Organization, 2010.

[18] J. Cunningham, and M. Perkins, "Diagnostics for tuberculosis: global demand and market potential," 2006.

[19] R. Murphy, "Development of acoustic instruments for diagnosis and management of medical conditions," Engineering in Medicine and Biology Magazine, IEEE, vol. 26, no. 1, pp. 16-19, 2007.

[20] X. Wang, J. Zhang, and Y. Yan, "Discrimination between pathological and normal voices using GMM-SVM approach," Journal of Voice, vol. 25, no. 1, pp. 38-43, 2011.

[21] E. Özüdogru, H. Cakli, E. Altuntas et al., "Effects of laryngeal tuberculosis on vocal fold functions: case report," Acta otorhinolaryngologica italica, vol. 25, no. 6, pp. 374, 2005.

[22] H. Goy, D. N. Fernandes, M. K. Pichora-Fuller et al., "Normative Voice Data for Younger and Older Adults," Journal of Voice, vol. 27, no. 5, pp. 545-555, 2013.

[23] V. Gross, A. Dittmar, T. Penzel et al., "The relationship between normal lung sounds, age, and gender," American journal of respiratory and critical care medicine, vol. 162, no. 3, pp. 905-909, 2000.

[24] J. Abitbol, P. Abitbol, and B. Abitbol, "Sex hormones and the female voice," Journal of Voice, vol. 13, no. 3, pp. 424-446, 1999.

[25] A. Yadollahi, and Z. M. Moussavi, "Acoustical respiratory flow," Engineering in Medicine and Biology Magazine, IEEE, vol. 26, no. 1, pp. 56-61, 2007.

[26] S. S. Kraman, G. A. Pressler, H. Pasterkamp et al., "Design, construction, and evaluation of a bioacoustic transducer testing (BATT) system for respiratory sounds," Biomedical Engineering, IEEE Transactions on, vol. 53, no. 8, pp. 1711-1715, 2006.

[27] A. Mendes, M. Alves-Pereira, and N. A. Castelo Branco, "Voice acoustic patterns of patients diagnosed with vibroacoustic disease," Revista Portuguesa de Pneumologia (English Edition), vol. 12, no. 4, pp. 375-382, 2006.

[28] R. Tahamiler, D. T. Edizer, and S. Canakcioglu, "Nasal expiratory sound analysis in healthy people," Otolaryngology--Head and Neck Surgery, vol. 134, no. 4, pp. 605-608, 2006.

THE 5TH INTERNATIONAL CONFERENCE ON WIRELESS COMMUNICATIONS, VEHICULAR TECHNOLOGY, INFORMATION THEORY, AEROSPACE & ELECTRONIC SYSTEMS (WVITAE-2015)
December 13-16, 2015, Hyderabad, India

A P2P architecture for Mobile Assisted Logistic Operations

Pierpaolo Loreti*, Lorenzo Bracciale*, Francesco Zampognaro*, Massimo Povia†, Gianluca Gargiulo‡
*NITEL - University of Rome Tor Vergata Via del Politecnico 1, Rome, Italy Email: firstname.lastname@uniroma2.it
†Technosky Via del Casale Cavallari 200, Rome, Italy Email: m.povia@technosky.it
§NAIS Via Andrea Noale 345, Rome, Italy Email: gianluca.gargiulo@nais-solutions.it

***Abstract*—Logistic and maintenance operations play a prominent role in several enterprise asset management systems. Thanks to the progress in technology, these tasks can be executed in an easier and more efficient way, by mean of solutions that combine system integration with new service models. Real scenarios present several challenges such as the unavailability of Internet connection in the maintenance area, the harsh conditions in which some apparatuses are installed or difficulties in identifying the apparatus on which they operate. The paper details the identified architecture, technologies and best practice derived as part of activities in the frame of the LogICoS project, opening the way to additional definition and implementation activities as future works.**

Keywords*—Maintenance Operations, Logistics, Augmented Reality, Ambient Intelligence, Peer-to-peer.

I. Introduction

Asset maintenance is the most complex sub process of asset management [1]. Indeed the overall maintenance process involves specialized personnel and complex procedures and the cost associated to such operations during the entire life-cycle of a device can easily exceeds the mere cost of the asset itself. Unfortunately there is not a "silver bullet", as the maintainability heavily depends on an underlying wide set of different factors such as the equipment type, vendor, state of deployment and configuration; hence the correct set of operations to cope with everyday real problems dramatically varies case by case. For this reason, industrial and the academic communities [2] studied and developed different systems and tools to efficiently cope with such complexity [3], [4], automating whenever possible some procedures, and, whenever this is not possible, providing the maintainer with the right set of tool to limit the possibility of making errors while, on the other hand, to minimize the duration of the maintenance operation and the required skills.

Among the various ICT technologies that are changing the world of asset maintenance, the diffusion of mobile devices such as tablets, smartphones, etc. arouse a strong interest since they represents a great opportunity providing advanced interfaces and with a small cost thanks to the wide market. However several challenges must be addressed to cope with real needs of operation procedures: in many cases the personnel shall perform operations in complete lack of connectivity (e.g., underground data centers, isolated environments due to security constraints, etc.), or partial connectivity to the Internet (e.g., remote areas, high EM interference ICT rooms, etc.) and thus to the main logistics and maintenance system.

A fundamental problem today is that asset management systems collect a lot of information through continuous monitoring several different parameter of systems that are more and more complex. This information must be made available during the operations of scheduled/unscheduled maintenance in an efficient way, so that the *relevant* information of a given failure must be given to the maintainer, possibly in a as simple as possible form. The overall management framework has been studied by researchers from industry and academy in the framework of the Logistics Innovative Coordination Suite project (LogICoS) [3]. In this context, starting from the expertise of the industrial partnership, we selected as use case the maintenance operation on an airport data network comprising several different devices (routers, switch, etc.) spatially distributed in a relatively wide area. The data network is a base asset that enables the proper functioning and monitoring of other systems.

This paper described the study and development of an architecture and a mobile oriented solution to support logistics activities by ambient intelligence technologies also designed for partially connected environments. The proposed solution, the proper architecture and technological details will be described in the paper. Our goal is to introduce an efficient workflow that minimizes the intervention time, the possibility of mistakes, while introducing logistics automation and a centrally controlled connection-less operation environment. The main feature of the proposed solution are outlined herein and detailed in the rest of the paper: i) self-sustained solution for mobile-to-device interaction; ii) tag based augmented reality (AR); iii) visual content description with standard web technologies; iv) peer to peer local communications, and visual procedures display.

Practical use-cases will be described, with the detailed architecture proposed and screenshots from a demo Android App developed on purpose. Specifically, two intervention will be detailed: the first one addresses the troubleshooting of a network printer, and the second one covers the maintenance and issue-solving of network router/switch within a rack including many network devices.

II. Related Work

A. Advanced IT for maintenance

The commercial systems for managing the logistics and maintenance of company assets such as SAP EAM, IBM Maximo AM or Oracle EAM are increasingly based on the technologies of the ICT world. In past years several experiments have been conducted introducing new IT technologies in order to enhance the usability of these systems.

In this field, one of the main challenges, it is to integrate with previous enterprise data management solutions that in turn usually store a large amount of information. Various IT technologies have been considered to contextual data that can be searched or filtered out by using RF or visual tags as in [5] or in [6]. Another challenge is the presentation of that information to the operator while she/he is on the maintenance site. Accessing to manuals and other documentation using the smartphone/tablet can present severe usability issues and other presentation forms have to been investigated. For example [7] uses context aware and augmented reality technologies to enhance the data presentation to the operator on mobile devices.

Similar technological assets have been successfully applied also in the constructions and building management, [8] where is fundamental to deliver information directly on-site. These applications however present specific problems of data visualization that are usually solved using GIS technology [9]. Finally, the training of the operators using AR technologies has growing in importance day by day. Recent studies [10] demonstrate how the learning experience can have a dramatic impact on the operation efficiency itself.

B. Augmented reality for smartphone

Currently the use of AR on mobile terminals exhibits specific problems not yet fully addressed. Although today there are several open and commercial solutions [12], there is not a clear reference model as severe user experience and applicability problems come out when these solutions are used the real field [11]. These impairments can be related to the characteristics of the smartphones that are clearly designed with a different goal in mind. A game changer in this field can be represented by the introduction of smart glasses that allows hands-free operations [15].

For what concern the adopted technologies, web technology have been widely used to describe the augmented reality. That description with HTML5 and JS is implemented in large framework e.g. Wikitude [12] or tool open as jartoolkit [13]. Moreover specific markup languages have been defined such as ARML [14] that is derived from the popular KML.

III. SCENARIO

As the introduction already stated, the variability and configuration of maintenance and logistic operations may be very diverse and with an high degree of complexity. Furthermore, such operations shall be carried out under different connectivity conditions and even within critical infrastructures. Within this context, IP connectivity that may be already available on the remote site (e.g., WiFi, LAN, 3G), can not be assumed available as well to the maintenance personnel for different reason, among which: remote location or room shielding, use of existing network for internal and secure communications, firewalling and IT restrictions, network access control and authentication.

A reference scenario shall be been identified, so that it can allow to tailor the system definition, the architecture, the technological aspects (e.g., communication protocols, standards, existing APIs and libraries, etc.) and the implications to a realistic use case. Out of the may applicable scenarios, we decided to focus (also considering project needs) on airport facilities and their associated ICT equipment.

We assume then as reference scenario, within the distributed critical infrastructure represented by many airports managed by the same service-maintenance company, an underground data center where air traffic control data is received. The focus then is to define the application criticality and propose a solution (architecture and software for a demonstration activity) for an effective support to the personnel.

In this specific case, the facility to maintain include at least (among several other equipment) network-specific device (i.e., router) workstations and general purpose network device (i.e., network printer). This Data Center is assumed within a local LAN without external connectivity.

This reference scenario is represented in figure 1.

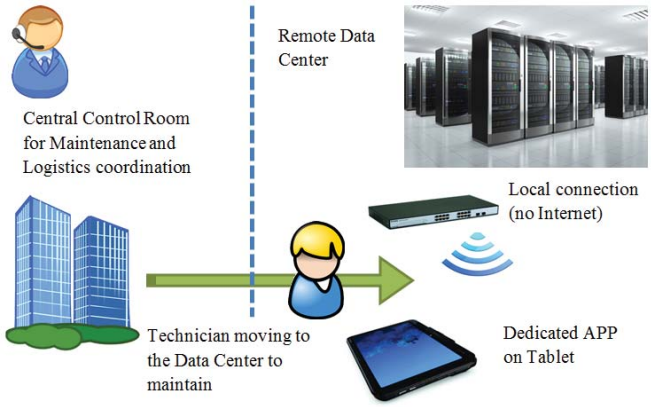

Fig. 1. Reference Scenario

It is proposed as solution, through interactions with the players involved in this scenario, an integrated and autonomous platform making use of commercial tablets and local interconnections with ad-hoc hardware. Through an augmented reality interface, the operator should identify the target object among many others present of similar aspect, and perform mobile-assisted operations to identify its status and perform the correct recovery operations. The augmented reality interface shall be provided locally by a dedicated server, to avoid the need of receiving live data by the control room. The interface is updated with tracking mechanism and part of data pre-loaded on the define according to the planned maintenance operation foreseen.

A relevant use case to drive the system requirements, the system definition and outline main technical issues is described. It consists in the recovery of a generic network device. It can be further split in the following operations: i) Ticket download at the control room through the app on the tablet of the maintenance personnel. This include all required offline data to re-establish the functioning of the required devices; ii) The personnel travels to the remote premise, at the underground data center (where connectivity to the internet and the Central control room is not guaranteed) with guidance of the App; iii) Identify through tagging and with support of the tablet pre-installed App the ICT devices to assess; iv) Establish peer-to-peer communication with the device identified; thanks to the ticket downloaded in advance and realtime data, the

troubleshooting of the device shall be straightforward and easily traceable; v) The tablet may upload new permanent data to the device after intervention; When back to the main control room, the operations performed and state update shall be pushed to the system.

The main challenges and user requirements can be inferred starting from the previously defined use-case, and different technologies shall be integrated to propose an effective solution. A preliminary analysis outlined the following principal technical and architectural aspects to solve for.

Initially, the definition of permanent data and content to be available within the mobile tablet the support in the logistics and planning activities (i.e. which tickets have higher priority? in which order to perform operations? on which devices? which aspects shall be monitored and where the malfunction may be identified?). Secondly, a key aspect, the device tagging (i.e., use of visual tagging or e.g., RFID) to allow a direct relation without interacting live with the Control Room,to relate the alert and the intervention on the target device. Then, the establishment of local peer to peer communication by means of a dedicated mediation device (called DIM and described in the following part) in between the mobile tablet and the target hardware. Finally, the implementation of effective supporting Augmented Reality views, paired with straightforward troubleshooting ambient intelligence interfaces.

These key aspects will be addressed in the following section, before discussing the test performed on two specific use cases on real and emulated devices.

IV. Proposed architecture and technology

A. Architecture

With reference to figure 2, the proposed architecture is composed essentially by two main components:

1 - an **Ambient Intelligence Application (AIA)** running on the maintainer mobile device (tablet/AR glasses/smartphone). More technically the application can i) scan QR code; ii) automatically connect to a given network; iii) fetch an HTML page and display them through a fullscreen webview displayed on top of the camera input. The page presents a transparent background to show the augmented information on top of the ”reality” displayed by the camera

2 - a software module called **Device Interconnection Module (DIM)** that runs on an embedded device called Interconnection Device. This device is capable to on one side to interact with the tablet using a suitable and supported wireless technology (e.g. bluetooth, wifi, wifi direct) and on the other side to interface with the maintained hardware through its specific communication protocol (e.g. serial cable, infrared etc). The role of this device is to decouple the application interface from the specific operating protocol of the object to be maintained or repaired. Moreover this device contains all the interface and logic to inspect and operate on the hardware. This information is stored as HTML pages and served by a web server installed on the Interconnection Device. Specific server side programs give the access for interacting with the device through web API for instance to turn on/off the device or visualize data.

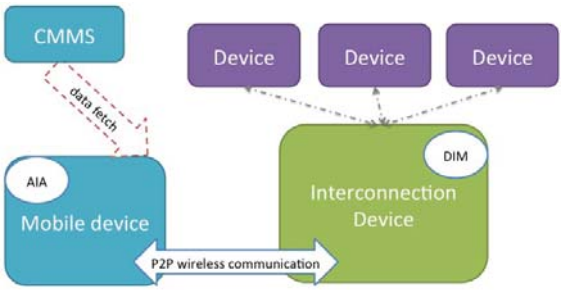

Fig. 2. Architectural representation of the proposed solution

B. Rescaled web interface

The heart of this solution is the rescaled web interface. All the augmented information displayed on top of the reality is represented through web graphic objects where standard web technologies (HTML5, css style and javascript dynamic behaviour) can be applied. Through an interaction between the tablet operating system and the web page, the size of the page is adjusted to cope with different resolutions of screen and camera. Then, parts of the page can be rendered with a “fixed” position (e.g. a side bar), while other parts can be bounded to a specific point (e.g. an arrow on a physical button of the maintained device). Differently to other literature approaches, these second part (technically html div container marked with a class), are dynamically *rescaled* real time to maintain proportions between augmented object and the reality. The information needed for this rescaling is obtained by the QR code whose dimensions must have a fixed size ($3cm \times 3cm$ in our case). A continuous QR scanning operation permit to move, rotate and rescale the bound object according to the new position of the maintained object so that the augmented data will be always bound to a specific place. This is a key point of the proposed solution as it allows on one side to pinpoint some specific part of the device (e.g. an arrow that point to a device button), and on the other side this solution does not rely on object recognition, allowing the maintenance of several (almost) identical devices such as a specific router inside a rack with other routers.

The content of this webpage as well as the possible interactions with the maintained device are defined inside the pages contained in the DIM so that, by browsing different pages, the maintainer can have different views of the status of the maintained device. With this architecture, the same AIA can operate on different devices. In turn, different maintained devices must have different web pages and different server side script to make these pages dynamical, feeding them with device information or providing API to handle common operation on the device to be maintained (e.g. turn on and off the device). In this way we re-use all the existing web technologies. The interface between the web and the device is performed by the DIM module that converts a web request in some operations on the maintained device and bring back the results in standard web format.

C. Example of operations

The proposed solution allow these typical usage model. Everything started with the retrieval of a ticket from the a Computerized maintenance management system (CMMS) by a maintainer though its ambient intelligence application (AIA). When she/he goes on the physical place, the maintainer identifies the right object to maintain by scanning a QR code displaced on the object itself. Querying a local yet asynchronously synchronized database, the AIA retrieves the information needed to automatically connect her/his terminal to the interconnection device (e.g. WiFi parameters such SSID, Channel, WPA password etc) as well as the entry point of the web page to visualize (i.e. the URL of the index page such "/"). Then the AIA visualizes the html page located at the entry point on a full screen webview. Since this moment, the operator can interact with the device, visualize contextual information, perform the most frequently used commands.

This flow is represented in figure 3.

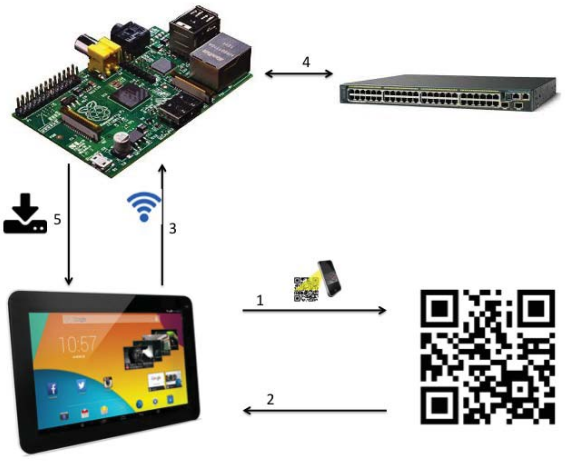

Fig. 3. Example of work flow: the mobile device scans the QR code (1. and 2.), then connects to the Interconnection Device (3. 5.) that in turn communicates with the maintained device (4.)

D. Addressed challenges

The proposed solution address several challenges presented by the proposed scenario such:

offline communication: relying on peer-to-peer wireless communication, no internet access is needed during the maintenance procedure. All the guides, manuals can be stored inside the DIM module and retrieved by the application using the peer to peer wireless connection. This is particularly important when the device to be maintained is located in the basement or in a shielded or rural area where 3G network is unavailable. Moreover this ease the deployment of the Interconnection Devices.

distinguish between similar items: object recognition algorithms can easily fail when there are several identical objects in the nearby, for instance in a rack there are several routers/switches of the same type. Hence, the detection of the right object must be performed in a different way. We choose the visual tag (QR-code) that is on one side very economical choice, and on the other give us a reference measure for applying the augmented interface with a known proportion (see next point).

pointing object parts: The presented solution allow to identify a part of the object for instance by placing an arrow on buttons, plugs, cables. This is done by re-scaling the web page according to the size information read on the visual tag as explained in sec IV-C.

interoperability with propriety solutions: air conditioning system, routers, SCADA devices typically use proprietary protocol and/or require specific hardware to communicate with. The Interconnection Device can be equipped with the required hardware to perform such communication while the DIM module can transform the interaction on the web page in proprietary commands for the maintained device.

usability and context information: Maintaining a complex object typically require to perform complex operations (e.g. router configuration) that an augmented interface is not designed to perform. However, by visually analyzing the most important parameters with a simple interface where only contextual information are shown, brings the benefit of quickly having a picture of the status that can improve efficiency in troubleshooting.

V. Description of the test cases

The practical operations of maintenance with regard to a server PC and a printer are illustrated herein. App screenshots and the sequence of operations are described in details. Both devices maintenance operational data are downloaded to the App at the control room. Details on their location and the position to the CED are uploaded as well. Other maintenance tickets may be uploaded as well by the system, in case multiple intervention are foreseen. When reaching the designated area, the App starts its AR interfaces, after that a manual scan of the QR-code tag have been done by the operator.

A. Printer

A first test case for the proposed solution is the maintenance of a printer.

Fig. 4. Printer maintenance interface: the augmented reality shows relevant information about the networking status, the toner level and provides an easy access to the documentation

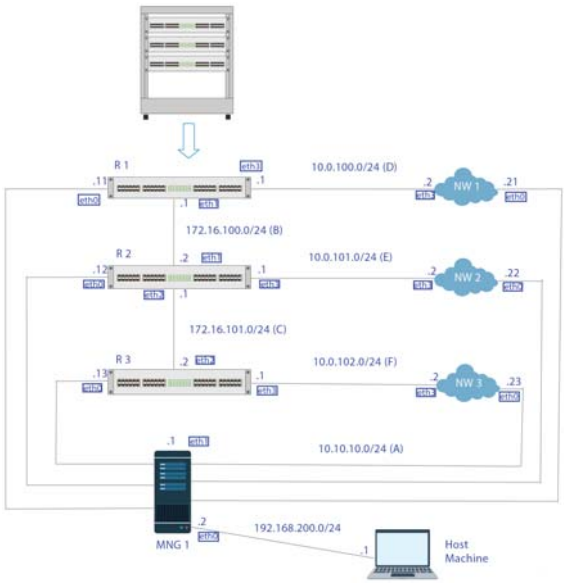

Fig. 5. Representation of the simulated topology. R1 is the router upon which we want to perform maintenance.

Fig. 6. Augmented reality interface to maintain and control the status of a switch. The interface is composed by a fixed part (side and bottom bar) and a mobile part that tracks the port of the router/switch.

These devices indeed require physical operation to be performed in order to replace the toner, or feed the paper tray as well as information monitoring for the status of the toner, out of paper messages or paper jam in the tray. A sidebar and a bottom bar are fixed as shown in figure 4 while contextual information on how to open the paper feed are displayed when needed by arrows that point to the unlocking button for opening the tray.

B. Router

A second test case has be done for router/switch maintenance in a rack. As the previous case, this one requires both physical operation (e.g. connect a cable to a Ethernet plug) as well as the observation of important parameters such as the traffic incoming/outgoing to/from a specific port. To better simulate the real characteristic of the environment, the Interconnection Device is connected to a network emulator (netkit: www.netkit.org) to emulate the topology represented in figure 5 and to simulate hardware and software malfunctioning. The augmented interface represented in figure 6 displays a side and bottom fixed bar, the status of CPU and RAM, information about the hardware and access to specific guides and documentation. The four small squares displayed on the switch ports display the status of the port. When the user click on them, the in/out bandwidth graphs related to the specific port are shown. The Interconnection Device can get those information for instance by connecting the the console port of the switch.

VI. Conclusion and future works

The architecture proposed, paired with a simple App exploiting peer to peer communications and ticket store-and-forward, allowed to illustrate the benefits to maintenance and logistics for ICT equipments. At present the implementation is at a prototypal stage, with the aim to preliminarily validate the solution and technologies identified. As continuation of this activity and future works, the App visual interface will be enhanced, with the possibility of building at the control room simplified wizard-like procedures for maintenance, with better usability and user interface. At the same time, additional development efforts are required trying to define an high level API to be used within future systems based on this concept. Finally, the platform will be migrated from tablets to Google Glass, in order to exploit at best the advantages of Augmented Reality for ambient intelligence and maintenance/logistic operations.

References

[1] Abrar Haider, Andy Koronios *ICT Based Asset Management Framework* ICEIS 2005, Miami, USA, May 25-28, 2005

[2] AREA, *Augmented Reality for Enterprise Alliance*, online at http://thearea.org.

[3] *LOGICOS Project*, online at http://logicos-project.it

[4] *FMSTAR project* online at http://fmstar.de

[5] Lin Y. C., Cheung W. F. and Siao F. C., *Developing mobile 2D barcode/RFID-based maintenance management system*, Automation in Construction, Vol. 37, 110-121., 2014.

[6] S. Lien, C. Wang; JP. Su, C.H. Wu, *Logistical Remote Association Repair Framework Using Smartphones Based on the Android Platform*, IS3C 2014

[7] Gtze, Janek, et al. *FM Knowledge Modelling and Management by Means of Context Awareness and Augmented Reality* 13th EuroFM Research Symposium. 2014.

[8] Bae, Hyojoon, Mani Golparvar-Fard, and Jules White. *High-precision vision-based mobile augmented reality system for context-aware architectural, engineering, construction and facility management (AEC/FM) applications.* Visualization in Engineering 1.1 (2013): 1-13.

[9] Schall, Gerhard, et al. *Handheld augmented reality for underground infrastructure visualization.* Personal and ubiquitous computing 13.4 (2009): 281-291.

[10] Westerfield, Giles, Antonija Mitrovic, and Mark Billinghurst. *Intelligent Augmented Reality Training for Motherboard Assembly.* International Journal of Artificial Intelligence in Education 25.1 (2015): 157-172.

[11] Jain, Puneet, Justin Manweiler, and Romit Roy Choudhury. *OverLay: Practical Mobile Augmented Reality.* Proceedings of the 13th Annual International Conference on Mobile Systems, Applications, and Services. ACM, 2015.

[12] Madden, L. *Professional augmented reality browsers for smartphones: programming for junaio, layar and wikitude.* John Wiley Sons, 2011.

[13] Geiger, Christian, et al. *Jartoolkit-a java binding for artoolkit.* IEEE Augmented Reality Toolkit, 2002.

[14] Lechner, Martin. *Arml-augmented reality markup language.* Ginzkeyplatz 11 (2010): 5020.

[15] Pal, Rohit Kumar, and Nitish Kumar Sharma. *Optical head mounted display using augmented reality.* International Journal of Research in Engineering and Applied Sciences 4.7 (2014): 1-10.

THE 5TH INTERNATIONAL CONFERENCE ON WIRELESS COMMUNICATIONS, VEHICULAR TECHNOLOGY, INFORMATION THEORY, AEROSPACE & ELECTRONIC SYSTEMS (WVITAE-2015)
December 13-16, 2015, Hyderabad, India

Hard-combined Cooperative spectrum sensing using Time-frequency method

S M Hiremath, Sarat Kumar Patra
Dept.of.Electronics & Communication
National Institute of Technology
Rourkela, Odisha 769008, India
Email:(hiremaths@nitrkl.ac.in,skpatra@nitrkl.ac.in

Amit Kumar Mishra
Electrical Engineering Department
University of Cape Town, South Africa
Email:akmishra@ieee.org

***Abstract*—Cognitive radio is the emerging standard for spectrum efficient wireless systems. Heart of cognitive radio is spectrum sensing, which requires the detection of the primary user in worst environmental condition and make the way for the secondary user to use the unused spectrum efficiently. More recently time-frequency based spectrum sensing techniques are examined for simultaneous detection of unused spectrum in time and frequency domain. Time-frequency distribution of received signal is obtained using time-frequency tool to enhance the information preserved in the noisy signal. This paper investigates the cooperative spectrum sensing using modified Wigner-Ville detection, called S-method time-frequency distribution. The paper uses the S-method detector as local spectrum sensing unit and hard-combining at fusion center to make the global decision. Performance of the time-frequency based cooperative sensing is quantified using ROC curve.**

Keywords- Cognitive radio, Time-Frequency Representation (TFR), S-method, Cooperative spectrum sensing

I. INTRODUCTION

Main function of CR is to efficiently detect the primary licensed users and make use of unused spectrum by allocating secondary users leading to high throughput. Spectrum sensing is considered to be the most prominent function,that has been well researched in the last decade[1]. Because of highly time-varying nature of wireless medium, primary user detection becomes very challenging task in the CR. Due to fading and shadowing, primary signal would be attenuated to very low value and causing the low Signal-to-Noise Ratio (SNR) scenario. So this demands need for powerful spectrum sensing techniques. In cognitive radio scenario, primary users (PU) parameters and noise environment parameters are unknown. It makes the need for spectrum sensing techniques, that are robust to low SNR and ability to detect the PU blindly. Energy Detection (ED) is one of the most researched, simple, blind spectrum sensing technique that is used for coarse sensing. But it suffers from low SNR limit[1]. So semi blind techniques like cyclostionary and feature based detections have been re investigated for spectrum sensing. These method work robustly at low SNR, but they need information about type of modulation used and are complex in implementation[1]. Statistical covariance based methods are proposed that are blind in nature. But these are suitable for correlated signals only and hardware implementability is also complex [1][2].

Some recent work on Time-Frequency based spectrum sensing have been explored [3][4], that take advantage of time and frequency dimension to separate the signal form weak noise. Time-frequency distribution are widely used for detection and estimation weak signals in non-stationary scenario [5]. So Wavelet transform (WVT), Wigner-ville distribution (WVD), Gabor transform and Short Time Fourier Transform (STFT) based spectrum sensing techniques have been seen to performing well compared to previously mentioned semi-blind and blind techniques [3, 4, 6, 7]. Guibene *et.al* used the WVD distribution and arithmetic detection for spectrum sensing and shown that, it works well at low SNR around -35 dB [7]. Biagi *et.al* converts the noisy signal into two-dimensional image using WVD and use the pattern recognition method for finding the vacant spectrum [3]. Similarly in Tian *et.al* Wavelet transform based edge detection for wide band spectrum sensing. Most of time-frequency method employ the WVD because of its good time-frequency resolution and highly concentrated energy density of signal, but it suffers from cross-wigner energy density terms that may be mistakenly depicted as signal, though it may not be signal. So in our recent work, we proposed the modified WVD based SS called S-method time-frequency spectrum sensing [8]. S-method previously used in radar detection [9], when employed for spectrum detection found to be performing better than energy detection.This method combines the advantage of STFT and WVD , extending same for hardware implementation is also seen to be simple [9].

Last decade research on spectrum sensing shows that single CR receiver have a certain limitation on sensing due to shadowing and fading. Hidden node problem, that occur due to shadowing causes large interference to the primary user [10, 11]. So Cooperative sensing or distributed sensing that are previously used in radar and acoustic signal processing are investigated for spectrum sensing. Because of space diversity, it overcomes the ill effects of single user receiver due to shadowing and fading. Cooperative sensing are well explored using basic detection techniques which are mentioned previously [11].This paper proposes the cooperative spectrum sensing based on S-method based time-frequency distribution. Paper considers all three dimensions time, frequency and space to explore the vacant spectrum. In this paper hard decision based cooperative spectrum sensing is analyzed using the time-frequency based spectrum sensing. It is first of this kind, where spatial, time and frequency dimensions have been used for spectrum detection. The paper uses the Monte Carlo simulation approach to show the detection performance. Spectrum sensing performance is justified by using Receiver Operation Char-

acteristics (ROC) curve for of cooperative decision methods. Sensing performance is analyzed by varying the number of antennas. Results are tested for both Additive White Gaussian Noise (AWGN) and Rayleigh fading channels.

Following this introduction, the remaining part of the paper is organized as under. Section II describes the importance of time-frequency distribution and S-method based Time-frequency detector. In Section III Cooperative spectrum sensing and system model are discussed. Simulation results and analysis are presented in section IV. Conclusion is given in section V.

II. Time-frequency distribution and local spectrum detection using S-method TFR

Time-Frequency tools are mainly used in analysis, processing, detection and parameter estimation of non stationary signals. First of this STFT, is derived from traditional Fourier analysis also called windowed Fourier transform. Other important important TF tool is Wigner distribution derived from quantum mechanics [5][9]. Though STFT suffers from poor time-frequency resolution, but it is free from cross terms. Whereas, Wigner distribution produces concentrated energy distribution at the cost of cross-terms. S-method TF representation combines the good properties of STFT and Wigner distribution. STFT as previously said windowed Fourier transform, that is obtained by applying Fourier transform to localized signal $x(t)$ using the sliding window function $w(t)$ [9]. STFT is defined in continuous domain as [9]

$$X(t,\omega) = \int^{\infty} x(t+\tau)w(\tau)e^{-j\omega\tau}d\tau. \quad (1)$$

In discrete domain it is defined at an instant n and frequency k as

$$X_N(n,k) = \sum_{m=-\frac{N}{2}}^{\frac{N}{2}-1} x(n+m)w(m)e^{-j\frac{2\pi}{N}mk}. \quad (2)$$

In the above case it is assumed that the number of discrete frequency points is equal to window length. In (2) wide window covers the large signal samples over wide time interval, that increases the frequency resolution at cost of time resolution [9]. Reverse phenomena can be found in the case of narrow window.
To improve the TF concentration of non stationary signals quadratic distribution are introduced. Most basic quadratic distribution is Wigner distribution, that was well defined in quantum mechanics and was reintroduced to signals by Ville, so it is called Wigner-Ville distribution (WVD). Modified Discrete pseudo Winger distribution (WD) is defined as

$$WV(n,k) = \sum_{m=-\frac{N}{2}}^{\frac{N}{2}-1} w(m)w(-m)x(n+m)x^{\star}(n+m)e^{-j\frac{4\pi}{N}mk}. \quad (3)$$

in which *w(m)* is time window. WD due to quadratic product it exhibits the cross-terms and that limits its application to multi-component signals [9]. So to overcome the cross-terms in WD, variant quadratic distribution with limitation on signal concentration are introduced [5][9]. Concentration of auto terms and appearances of cross-terms are contradicted to each other. Stankovic *et.al* [9] discussed the novel method called S-Method (SM), that preserves the concentrated auto-terms as in WD and reduces significant cross terms as in STFT. SM derived using relationship between the STFT and pseudo WD, which is given as

$$WV(n,k) = \sum_{i=-\frac{N}{2}}^{\frac{N}{2}-1} STFT(n,k+i)STFT^{\star}(n,k+i). \quad (4)$$

Using (3) SM time-frequency distribution is defined[9]

$$SM(n,k) = \sum_{i=-L_d}^{L_d} P(i)STFT(n,k+i)STFT^{\star}(n,k+i)$$
$$= |STFT(n,k))|^2 +$$
$$2Re\left[\sum_{i=1}^{L_d} P(i)STFT(n,k+i)STFT^{\star}(n,k+i)\right]. \quad (5)$$

Where $P(i)$ is a finite window, $P(i) = 0$ for $|i| > L_d$, with L_d being its width. By setting $P(i) = \delta(i)$ spectrogram is obtained and $P(i) = 1$, pseudo WD is obtained. It can produce the TF representation of a multi component signal such that the distribution of each component is its pseudo WD, avoiding cross-terms, if the STFTs of each component do not overlap in frequency plane [9].

A. Time-frequency based spectrum sensing

In case of single user detection, decision regarding availability spectrum is tested based on two hypothesis.

$$H_0 : \mathbf{y}[n] = \mathbf{w}[n], n = 1, ..., N \quad (6)$$
$$H_1 : \mathbf{y}[n] = \mathbf{x}[n] + \mathbf{w}[n], n = 1, ..., N$$

where $x[n]$ represents a primary signal, $w[n]$ is noise and n represents time, where $y[n]$ is received signal. If there is presence of primary user in received noisy signal than it is referred as hypothesis H_1 and absence of PU considered as hypothesis H_1.

First step in TFR based sensing is to find time-frequency based energy density using S-method. Here (5) used to find TF representation of $\mathbf{y}[n]$. Next is to calculate the test statistic for spectrum sensing using the energy density obtained in previous step. Last step is to compare the test statistic using predefined threshold to carry out likelihood ratio test to know the presence and absence of PUs. Difficult task is to find the test statistic and predefined threshold based on fixed probability of false alarm. In this work, test statistic is obtained using procedure given in the [9]. Path of maximum energy density is found by scanning along time and frequency plane and maximum of that path is used as test statistic for decision making. Test statistic is found by following steps as mentioned in [9].

1) $SM(n,k)$ is time-frequency representation of $\mathbf{y}[n]$,where $k = 0, 1, ..., M-1$ and $n = 0, 1, ..., N-1$.

2) Considering that instantaneous frequency of a primary signal s(n) is continuous, define a path in time-frequency plane as an array of N frequency indices *w(n)*, with $0 \leq w(n) \leq M$ for every n.
3) Obtain ensemble of W_D of such paths of having the property $|w(n) - w(n-1)| \leq D$, for some specified value of D for all n. Where D is maximum allowed frequency step for two consecutive time instants.
4) $w_m(n)$ is one observed path belonging to W_D and sum the T-F representation along this path, that results as

$$J_m = \sum_{n=0}^{N-1} SM(n, w_m(n)). \tag{7}$$

5) Same calculation done for all ensemble paths of W_D and maximum of them represented by J_{max}, which is used as test criteria for hypothesis testing. J_{max} is defined as

$$J_{max} = \max_{w(m) \in W_D} J_m = \sum_{n=0}^{N-1} SM(n, w_{max}(n)). \tag{8}$$

Primary signal is detected if

$$J_{max} > \gamma_{TF}$$

where γ_{TF} is predefined threshold value, that is obtained using same statistic procedure for only noise case by Monte simulation. Fig.1 shows the variation of J_{max} versus the number iteration for noise only case. This plot shows that magnitude of J_{max} versus iteration in ascending order and threshold set based on required probability of false alarm. This procedure is called Monte-Carlo based thresholding, which is used in radar signal detection[9]. Threshold is estimated based on best path determined for noise only case with $\sigma_w^2 = 1$. For example fixed P_{fa}=0.01, threshold is set as $M_i * P_{fa}$=10, where $M_i = 1000$, is the number iteration Monte-Carlo simulation is run. Finally for noisy signal threshold is found by multiplying the previously obtained threshold for noise only case with variance of noise in received signal.

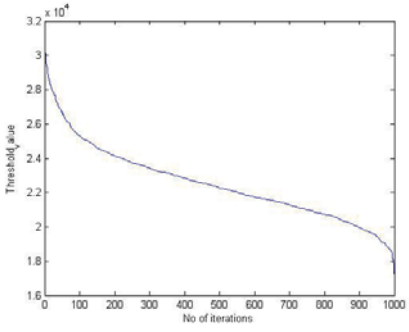

Fig. 1. Threshold estimation curve

III. Cooperative Spectrum Sensing and System Model for Time Frequency Detector

Some of the limitations in single CR receiver are as follows. limitation of sensitivity due to energy constraints, as the different primary user will be employing different modulation schemes, data rates and transmission powers [1, 12]. Due to shadowing and deep fading, effect of hidden node problem and missing of primary receiver is predominant. Hidden node phenomena occurs when path between the primary transmitter to secondary receiver is shadowed by tall building or large obstacles, while primary user may be at the vicinity of CR, than CR may fail to notice the PU and access the licensed channel and causes the significant interference to the primary user. This scenario is depicted in the Fig.2. To over come the problem of deep fade and hidden node problem in single node based receivers CR system, widely used distributed detection methods in Radar signals is incorporated as cooperative spectrum sensing in Cognitive radio scenario. Cooperative sensing enhance the robustness of detector to the fading and shadowing by using the diversity concept. In cooperative sensing, multiple CR sensors are scattered in network and they individually sense the spectrum and sensed information is sent to fusion centre, where decision is made [1][10].

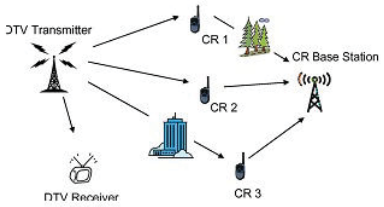

Fig. 2. Coopertive enviornment scenario in shadowing and fading effect shown[12]

Cooperative sensing is classified into soft combining (Data fusion) and hard combing (decision fusion) [1]. In Soft combining also called data fusion method, some M cognitive receivers collect the raw data from primary user and process or amplify and send it to the fusion center. In fusion center simple combining techniques based on diversity, like maximal ratio combining (MRC), square law combining (SLC) and equal gain combining (EGC) are used in decision making at fusion center. Recently weighted optimal linear combining techniques based on convex optimization are proposed in [1] [13]. In this case CR receivers does not require complex detection process. But, the bandwidth of communicating channel between CR and fusion center should be at least same bandwidth as of primary user and CR.

Hard combining or data fusion method, each cooperative CR receivers, make the binary decision based on local observation and each user sends the single bit or multi-bit decision to the fusion center (FC). Then the fusion rule at the FC user OR, AND or Majority logic combination in decision making [1][14]. This method requires low bandwidth control channel. However it performance is better, only if the control channel is error free, as only hard decision like 0 or 1 are sent. And also assumed that, SNR statistics is known at local CR sensors.

A. System model for cooperative sensing [1]

In Cooperative sensing, it is assumed to consist of M CR nodes and then hypothesis test is given as

$$H_0 : \mathbf{y_m} = \mathbf{w_m}, n = 1, ..., N \tag{9}$$
$$H_1 : \mathbf{y_m} = \mathbf{x_m} + \mathbf{w_m}, n = 1, ..., N$$

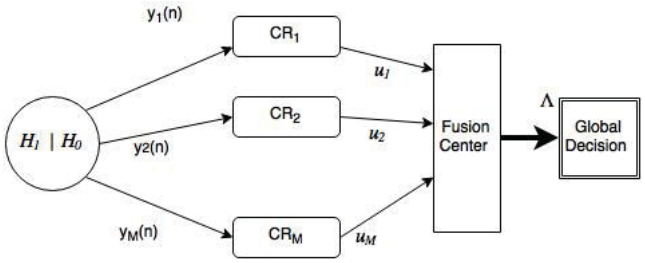

Fig. 3. System model for coopertive sensing

Above case, received signals at different CR are supposed to be independent of each other and $\mathbf{y}$ is defined as $\mathbf{y} = [\mathbf{y}_1^T, \mathbf{y}_2^T, ..., \mathbf{y}_m^T]$, then test statistics based on log-likelihood ratio is defined as

$$\sum_{i=1}^{m} u^{(m)} = log \prod_{m=1}^{M} \left(\frac{p(\mathbf{y_m} \mid H_1)}{p(\mathbf{y_m} \mid H_0)} \right) v \tag{10}$$

In above case, $u^m = log(\frac{p(\mathbf{y_m}|\mathbf{H_1})}{p(\mathbf{y_m}|\mathbf{H_0})})$ is the log-likelihood ratio(LLR) for mth receiver [1][15]. Because received data for all secondary receivers are assumed to be independent, optimal fusion rule tends to sum local LLRs. By considering noise vectors are independent $\mathbf{w_m} \sim \mathbb{N}(0, \sigma_m^2 I)$ and primary signal vector are also independent $\mathbf{x_m} \sim \mathbb{N}(0, \gamma_m^2 I)$. After neglecting the constants than LLR is written as

$$\sum_{m=1}^{M} \frac{\|\mathbf{y_m}\|^2}{\sigma_m^2} \frac{\gamma_m^2}{(\sigma_m^2 + \gamma_m^2)} \tag{11}$$

The statistic $\frac{\|\mathbf{y_m}\|^2}{\sigma_m^2}$ may be considered to be soft decision from time-frequency distribution detection of mth CR receiver. Optimal strategy like ECG, MRC and linear weighted optimal sum can used for detection. As paper uses the time-frequency based local detectors discussed in previous case, so large data handling becomes difficult and require large bandwidth, if soft-decision methods are used. In this paper only hard combining methods used for global decision making, as it is simple to implement and require low bandwidth.

In case of Hard combining individual receiver makes its own decision and sends the binary decision to fusion center. The test statistic of the local time-frequency detector can be represented as

$$J_{max} = \max_{w(m) \in W_D} J_m = \sum_{n=0}^{N-1} SM(n, w_{max}(n)). \tag{12}$$

Let local statics $u^m \in (0, 1)$ of the mth receiver. At the common fusion center, all single bit decisions are fused together according to following logic rule. Above (12) depicts that PU signal presence, when there exists at least n out of m CRs inferring as H_1. Otherwise it decides as absence of PU. OR rule corresponds to $n = 1$ and AND rule corresponds to $n = M$. Suppose all decision are independent, than the probability of false alarm for and Probability of detection for OR, AND and N out of M (majority) rule is given as

OR rule:

$$P_d = 1 - \prod_{m=1}^{M} (1 - P_{d,i})$$

$$P_{fa} = 1 - \prod_{m=1}^{M} (1 - P_{fa,i}) \tag{13}$$

And rule:

$$P_d = \prod_{m=1}^{M} (P_{d,i})$$

$$P_{fa} = \prod_{m=1}^{M} (P_{fa,i}) \tag{14}$$

IV. SIMULATION RESULTS AND ANALYSIS

Primary signals used for testing performance are taken from signals used in Project 25(P25) which is suite standards for digital radio communications used by federal, state, province and local public safety agencies in North America[16]. Fig.4 shows the time frequency representation of two types of TETRA signals, one is Compatible 4 level frequency modulation (C4FM) that transmit digital data over a 12.5 kHz channel other is Compatible quadrature phase shift keying (CQPSK), that transmits signal over 6.25KHz channel. For both signals settings are done as for the P25 standard. Fig 4 (a-d) are the time-frequency plots of clean primary signals and noisy primary signals at -10 dB SNR. Using S-method with $L = 16$ and hamming window of size of 32 with Primary signal samples of $N = 512$ are used to plot the T-F representation. Clean primary signal without any additive noise are represented by Fig.4 (a) and (c), clearly shows the concentrated plot of pure C4FM and CQPSK. Fig.4 (b) and (d) shows the noisy primary signals in which noise is spread over all the time-frequency plane. Joint time-frequency based sensing overcomes noise uncertainty problem encountered in ED, as noise equally spread in both the plane.

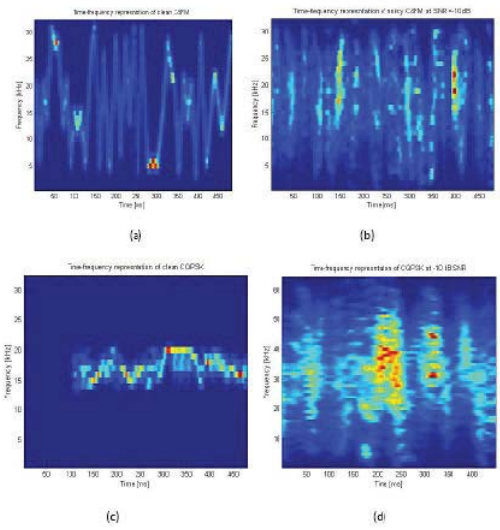

Fig. 4. Time-frequency representation of Primary signals

For simulation of cooperative scenario, environment shown in Fig.3 is considered. Previously mentioned CQPSK is used as

primary signal. Simulation are done for AWGN and Rayleigh fading case with number of receiver $M = 1, 3$ and 5 average of SNR=-5 dB. For S-method detectors, number of samples taken as N=256, window length W=32 and L=16. Fig 5(a) and(b) shows the ROC curves for hard combing based OR and AND logic cooperative sensing using the S-method based detection for both AWGN and Rayleigh Channels . As the number of receiver increased from $M = 1, 3, 5$ in case of OR logic probability detection for both channel type increases and for the case of AND probability detection decreases. From previous discussion it is known OR logic more conservative towards detection, but some time it may lead to false detection of noisy signals as primary signal. Where as AND logic is more biased towards the probability of false alarm, at the cost of low probability of detection. Most of the case OR logic is preferred over the AND logic, because of high probability of detection capability, which is stringent condition in case of Cognitive radio. So results are phenomenon, in which space, time and frequency dimension are considered to find vacant spectrum, because spectrum can be vacant in any of three dimension, this is first that kind approach. Results are validated based on simulation and still it requires the proper mathematical model. This type of detectors are very suitable for the wide band time-varying spectrum scanning. With respect to complexity requirement hard combining method are simple, but requires the individual receiver to have good signal processing capability of detection.

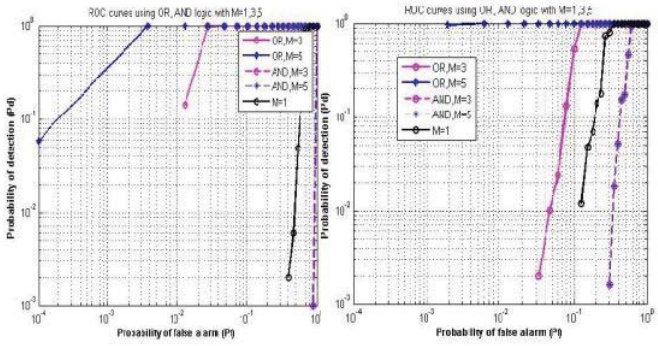

Fig. 5. ROC curve using OR, AND Logic with M=1,3,5 (a) AWGN Channel (b) Rayleigh Channel

V. CONCLUSION

Paper investigates cooperative sensing based on time-frequency detectors. This is first of the kind, where time, frequency and space dimension simultaneously used to detect the spectrum. S-method, which is combines the good characteristics of STFT and WD overcomes the problem of cross-terms appearing in time-frequency representation used as tool for detection. As S-method is obtained from STFT, hardware implementation is feasible compared to quadratic WD. All our results are based on monte-carlo simulation, so proper mathematical model for time-frequency based cooperative sensing need to be investigated.

small

REFERENCES

[1] E. Axell, G. Leus, E. Larsson, and H. Poor, "Spectrum sensing for cognitive radio: State-of-the-art and recent advances," *Signal Processing Magazine, IEEE*, vol. 29, no. 3, pp. 101–116, 2012.

[2] Y. Zeng, C. L. Koh, and Y.-C. Liang, "Maximum eigenvalue detection: theory and application," in *Communications, 2008. ICC'08. IEEE International Conference on*. IEEE, 2008, pp. 4160–4164.

[3] M. Biagi, S. Rinauro, S. Colonnese, G. Scarano, and R. Cusani, "Wivcora: Wigner–ville cognitive radio access for secondary nodes," *Vehicular Technology, IEEE Transactions on*, vol. 63, no. 9, pp. 4248–4264, 2014.

[4] Z. Tian and G. B. Giannakis, "A wavelet approach to wideband spectrum sensing for cognitive radios," in *Cognitive radio oriented wireless networks and communications, 2006. 1st international conference on*. IEEE, 2006, pp. 1–5.

[5] B. Boashash, "Time-frequency signal analysis," 1991.

[6] F. Javed and A. Mahmood, "The use of time frequency analysis for spectrum sensing in cognitive radios," in *Signal Processing and Communication Systems (ICSPCS), 2010 4th International Conference on*. IEEE, 2010, pp. 1–7.

[7] W. Guibene and A. Hayar, "Joint time-frequency spectrum sensing for cognitive radio," in *Applied Sciences in Biomedical and Communication Technologies (ISABEL), 2010 3rd International Symposium on*. IEEE, 2010, pp. 1–4.

[8] S. M. Hiremath, S. K. Patra, and A. K. Mishra, "Spectrum sensing for cognitive radio using s-method based joint time-frequency representation," in *INDICON 2015. IEEE International Conference, accepted for publication*. IEEE, 2015.

[9] L. Stankovic, M. Daković, and T. Thayaparan, *Time-frequency signal analysis with applications*. Artech House, 2013.

[10] E. Ghasemi, A.and Sousa, "Spectrum sensing in cognitive radio networks: Requirements, challenges and design trade-offs," *IEEE Communications Magazine*, vol. 46, no. 4, pp. 32–39, 2008.

[11] I. F. Akyildiz, B. F. Lo, and R. Balakrishnan, "Cooperative spectrum sensing in cognitive radio networks: A survey," *Physical Communication*, vol. 4, no. 1, pp. 40–62, 2011.

[12] K. B. Letaief and W. Zhang, "Cooperative communications for cognitive radio networks," *Proceedings of the IEEE*, vol. 97, no. 5, pp. 878–893, 2009.

[13] Z. Quan, S. Cui, and A. H. Sayed, "Optimal linear cooperation for spectrum sensing in cognitive radio networks," *Selected Topics in Signal Processing, IEEE Journal of*, vol. 2, no. 1, pp. 28–40, 2008.

[14] J. Ma, G. Zhao, and Y. Li, "Soft combination and detection for cooperative spectrum sensing in cognitive radio networks," *Wireless Communications, IEEE Transactions on*, vol. 7, no. 11, pp. 4502–4507, 2008.

[15] P. K. Varshney, "Distributed detection theory and data fusion." DTIC Document, Tech. Rep., 1995.

[16] T. Guide, "P25 radio systems," *Online]: http://www. danelec. com*, 2004.

THE 5TH INTERNATIONAL CONFERENCE ON WIRELESS COMMUNICATIONS, VEHICULAR TECHNOLOGY, INFORMATION THEORY, AEROSPACE & ELECTRONIC SYSTEMS (WVITAE-2015)
December 13-16, 2015, Hyderabad, India

Measurement and Identification of White Space using Low Cost SDR for Rural Wireless Broadband

Vinit Sharswat, Pradeep Godara, Abhijeet Bishnu, Vimal Bhatia
Discipline of Electrical Engineering
Indian Institute of Technology Indore-453446, India
Email: {ee1200240, ee1200223, phd1501102014, vbhatia}@iiti.ac.in

***Abstract*—This paper aims at identifying available free space (White band) for transmission of data, by measuring the spectrum using commodity software defined radio (SDR). Measurements are taken using low cost SDR over a wide spectrum, at different locations and during different time of the day. Standard energy detection based spectrum sensing technique is used on both GNU radio and MATLAB to test the validity of the obtained results. For measurements, an automatic framework is developed and implemented on commodity hardware. The analysis of spectrum from 400-900 MHz shows that in sub-urban areas, 92% of band in underutilized and maximum 17-18% of band is utilized in the evening (7 PM-8 PM). In rural areas, 96% of band is underutilised and maximum 13-14% of band is utilized in morning (10 AM-11 AM). This is also the first ever measurement based identification in the Central India region.**

***Index Terms*—White spaces, TVWS, GNU radio, spectrum sensing, energy detection**

I. Introduction

Increase in data volume due to rising domestic demand and ongoing Govt. of India initiatives such as Digital India is expected to fuel the telecom networking market in India [1]. Microsoft, Google and Facebook are planning to bring WhiteFi technology in India that can provide internet connectivity to a large section of the Indian population, thus, giving a boost to the Digital India initiative [2]. Cost effective connectivity to rural India has been well recognized by Governments around the world and other stakeholders for addressing the digital divide and explore new business opportunities [3].

One such white space band, the Television white space (TVWS) refers to the frequencies made available for the unlicensed use at locations where the spectrum is not being used by the licensed TV services [4]. TVWS can provide potentially low cost solution and connectivity that makes it appropriate for rural applications. It is time to start exploring the spectrum present in India and find the white spaces at different locations and at different times. The high penetration and free space propagation of the lower ultra high frequency (UHF) band in the range of 400-860 MHz is ideal for long range transmission. In other parts of the world, the overall usage of the spectrum in the range of 470-590 MHz is as low as 4.54% in Singapore [5], 6.2% in Auckland [6], 17.4% in Chicago [7] and 22.57% in Barcelona [8]. Hence, it is appropriate to do measurement based studies in India.

In India, according to the Indian National Frequency Allocation Plan (NFAP), 2011 [9], the spectrum band from 400-900 MHZ is mainly used for Fixed, Mobile and Broadcasting services. The digital broadcasting services is operated in the 585-698 MHz. Currently 470-590 MHz band is used in analog TV transmission [10]. Currently state broadcaster, Doordarshan has more than 1400 terrestrial transmitters [11]. The operating frequency of Doordarshan is characterized in three bands : VHF Band-I, VHF Band-II and UHF Band-IV [11]. Doordarshan plans to completely convert its transmission from analog to digital by the end of 2017 [12]. This will complete India's digital switchover. These bands are likely to be either unlicensed like in the UK [13] and in Africa, where the regulators have made these bands unlicensed, or lightly licensed.

In the Indian context, an investigation of TVWS has been done in Delhi [11] and Southern India [14]. IIT Bombay research group and Tata Teleservices in association with the WhiteSpace Alliance will implement test bed at several parts in India for broadband in TVWS [15]. Feasibility and applicability of IEEE 802.22 for TVWS transmission over COST-207 channel models has been studied at IIT Indore [16]. In this paper, frequency spectrum from 400-900 MHz is analyzed at different times. The readings were taken at sub-urban and rural areas around Indore (India), which represents significant area of Central India. There are about 650 villages and rural communities which are sparsely populated in distributed communities over a coverage area of 4500 square kilometre. Thus this region is appropriate for adoption of survey of white space, with Indore serving the nearby villages and rural communities using TVWS.

In order to measure and identify spectrum availability, some of the popular techniques for detection of the spectrum are energy detection, cyclostationary detection and locking detection [17]. In this paper, an energy detection based approach is used due to its low complexity and simplicity. Spectrum sensing is done in two ways; using MATLAB and by using GNU Radio to test the validity of obtained results. For both MATLAB and GNU radio implementations, we used SDR (Software Defined Radio) as a receiver. In this work, an RTL-SDR is used since, it is a commodity low cost SDR and commercial devices for TVWS are expected to have similar low cost devices.

The rest of the paper is organized as follows: Section II describes the spectrum sensing and overview of RTL-

SDR. Section III describes experimental set up for spectrum measurement including algorithm for PSD calculation and measurement locations. Section IV provides analysis of spectrum utilization at different locations and at different time, and finally conclusion are drawn in section V.

II. Spectrum Sensing and Overview of RTL-SDR

The objective of spectrum sensing in this paper, is primarily for measurement and identification of white space in particular frequency bands. However, the findings can also be used for licensed band for cognitive radio (CR). In CR, there is one primary user or licensed user, who can use band at any time instance, and the secondary user or unlicensed user can use the band when it is not being used by the primary user. The technique of energy detection involves calculation of power spectral density (PSD) of a set of samples in a determined frequency band. The PSD shows the strength of the variation of signal as a function of frequency. For our setup, the samples are taken in an interval of 2-MHz spacing. After collecting the samples, the PSD of the samples is calculated.

RTL-SDR is a popular, low cost hardware in the range of INR 2000 that can receive wireless signals. The RTL-SDR dongle features the Realtek RTL2832U chip, which provides I-Q samples through the USB interface [18]. It can receive and demodulate various wireless signals across a broad frequency range. Thus, it is used as a receiver which has specifications as follows:

- SDR frequency: 24-1700 MHz
- SDR bandwidth: 3.2-MHz (better to use 2.4-MHz)
- Antenna input: 50 ohms

The low cost of RTL-SDR is also one of the reasons to use it for the spectrum detection purpose. With Communication System Toolbox™ support package for RTL-SDR Radio, one can use MATLAB to design and prototype systems that process real time wireless signals. Using MATLAB, one can measure the spectrum at a center frequency and for a smaller bandwidth. In this paper, we have proposed a method by which we can use MATLAB to obtain the spectrum for a range of frequencies based on users need. GNU Radio is an open source software development tool kit that provides signal processing blocks to implement software radios. It is also used to obtain the spectrum for the same range of frequencies as it is used for MATLAB and hence we reconfirm our finding from two independent measurement processes.

III. Background Preparations

In this section, we describe the experimental setup, automation for spectrum measurement, algorithm for calculation of PSD of received signal in MATLAB and GNU radio, and measurement locations.

A. Experimental setup

We used RTL-SDR as a receiver which is a low cost hardware that provides I-Q samples through the USB interface. It has a maximum bandwidth of 3.2-MHz. We used laptops with 2.5-GHz Intel Core i5-3210M microprocessor with 4 GB 1600 MHz DDR3 RAM and AMD Radeon HD 7670M (1 GB DDR3 dedicated) video graphics for processing of received data from RTL-SDR. Fig. 1 shows the experimental setup.

Fig. 1. Experimental setup

B. Automation

The PSD of received samples in the band of 400-900 MHz at different time duration requires automation of code. We created a function which performs scanning of spectrum for 1-hour duration and again the code will restart after 3-hour to get the desired spectrum. The code runs at 3 different times so as to get the analysis of the spectrum has done in morning, afternoon and evening. The results from both MATLAB and GNU radio are stored in a file or file on host machine.

C. Algorithm for PSD calculation in MATLAB and GNU radio

In MATLAB and GNU radio, using a loop, center frequency is changed after taking 500 readings for the same center frequency with the bandwidth of 2-MHz ensuring that not many samples are lost. The next scanning is therefore done after an interval of 2-MHz ensuring that the whole range of 400-900 MHz is covered. Scanning of 2-MHz bandwidth at a center frequency, on our setup, takes about 0.8 seconds. An ensemble of 500 readings has been taken at a particular centre frequency and averaged to get the data at their center frequency. The code is run again and the data is stored for different centre frequency and thus we obtain PSD of the received signal. The pseudocode for PSD calculation is given in Algorithm 1.

D. Measurement location

Regions selected for our measurement are the sub-urban area and rural area located in outskirts of Indore and around Indore. The locations are sub-urban Mundla Nayta (Indore) where some residential area is located including Silver Spring township, rural Harnya Khedi village where IIT Indore is located and another rural Simrol village where IIT Indore permanent campus is located. The experimental locations are shown in Fig. 2. These locations form a triangle and are approximately 20 KM away from each other.

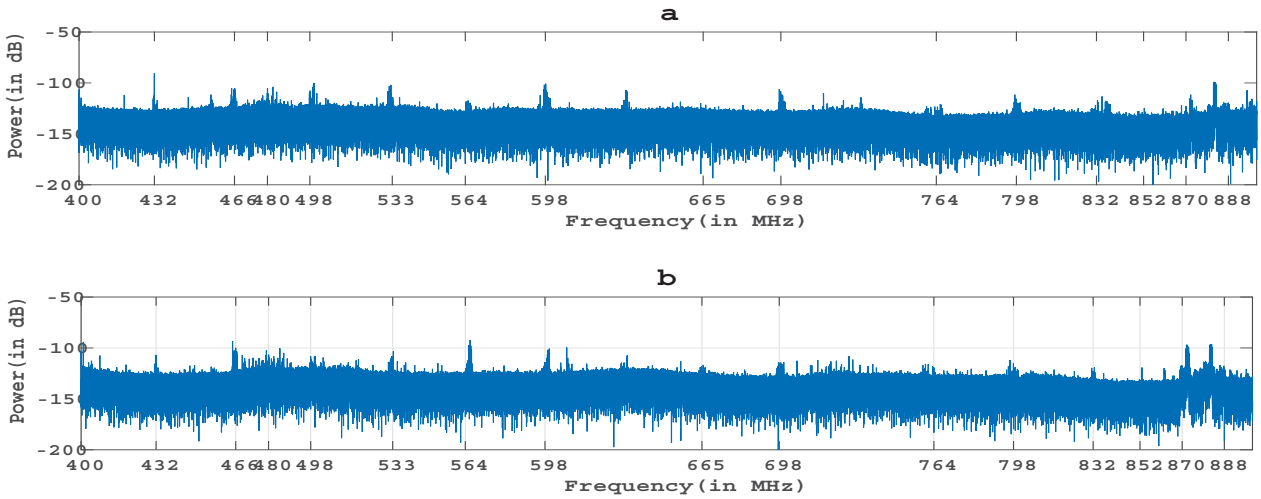

Fig. 3. a) Morning (10 AM-11 AM) and b) Afternoon (2 PM-3 PM) measurement using MATLAB in Simrol

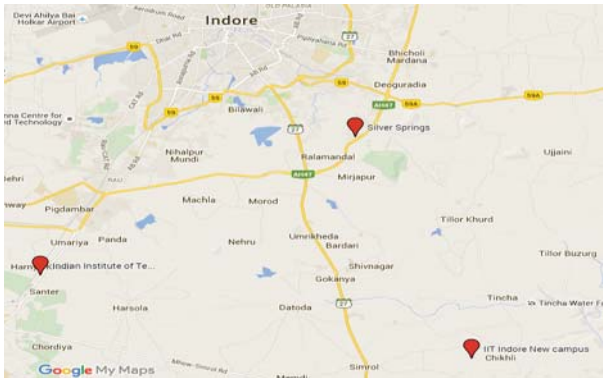

Fig. 2. Locations for measurement (courtesy: Google maps)

Algorithm 1 Pseudocode for PSD calculation in MATLAB and GNU radio

```
intialize: maxfreq=900 MHz, minfreq=400 MHz, fspan=2 MHz, ensemble=0, nxtfreq=0, count=0;
while nxtfreq < maxfreq
  count ← count+1;
  nxtfreq ← minfreq+span;
  while ensemble < 500
    scan minfreq to nxtfreq;
    save data in temp(ensemble);
    ensemble ← ensemble+1;
  end
  temp ← average(temp);
  P(count) ← PSD(temp);
  minfreq ← nxtfreq;
  ensemble ← 0;
end
```

IV. Observation and Analysis

In this section, we analyze the spectrum usage of 400-900 MHz at different locations and at different time in terms of PSD. We choose -110 dB as the noise threshold for our measurement by repeated measurements in known bands.

A. Spectrum utilization in Simrol

Fig. 3 (a) and (b) show the spectrum utilization measurement in morning (10 AM-11 AM) and afternoon (2 PM-3 PM) respectively with the help of MATLAB. The band ranges from 870-890 MHz is throughout occupied as it is a GSM band and rest of the band is sparsely occupied in compliance. Hence, on an average 10-11% and 11-12% of band is used in morning and afternoon. It has been observed that the spectrum utilization calculation by using MATLAB and GNU radio gives same results which validate our analysis of spectrum utilization. As MATLAB has higher precision as compared to GNU radio, we used MATLAB analysis for rest of the measurements. Fig. 6 (c) shows the contiguous bandwidth (maximum 160 MHz) available for Simrol. Fig. 7 shows the cumulative distribution power, which shows that 96% of bandwidth is available.

B. Spectrum utilization in Harnya Khedi

Fig. 4 (a) and (b) show the spectrum utilization measurement in morning (10 AM-11 AM) and evening (7 PM-8 PM) respectively with the help of MATLAB. The figures show that the band between 870-890 MHz band is less occupied as compared to sub-urban location and rest of the band is equally occupied as in sub-urban location. On an average 13-14% and 10-11% of band is used in morning and evening respectively. Fig. 6 (b) shows the contiguous bandwidth (maximum 110 MHz) available for Harnya Khedi. Fig. 7 shows the cumulative distribution power, which shows that 98% of bandwidth is available.

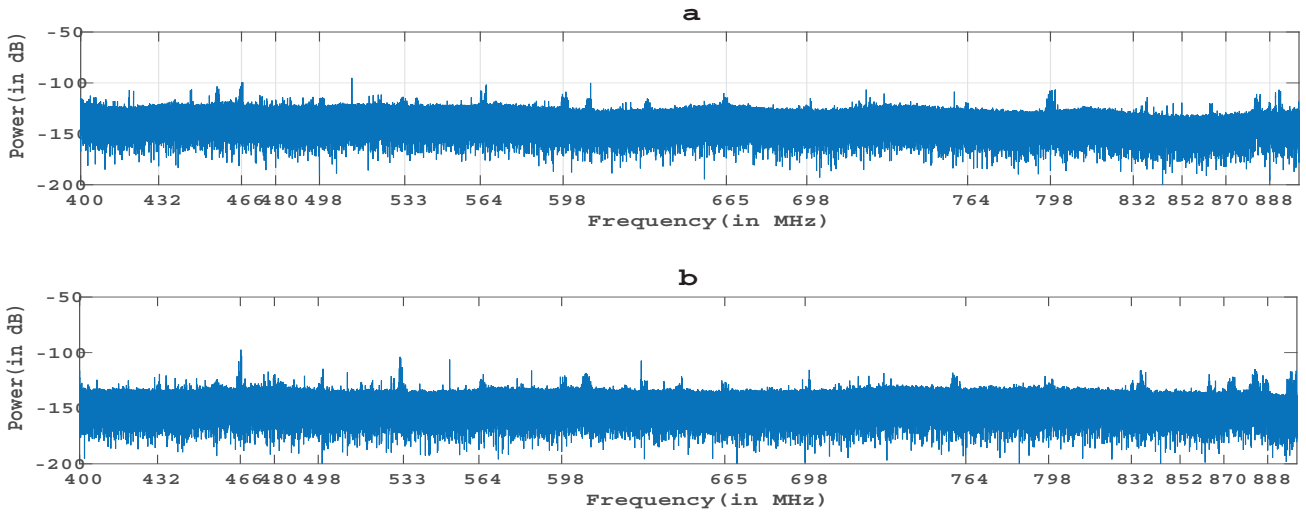

Fig. 4. a) Morning (10 AM-11 AM) and b) Evening (7 PM-8 PM) measurement using MATLAB in Harnya Khedi

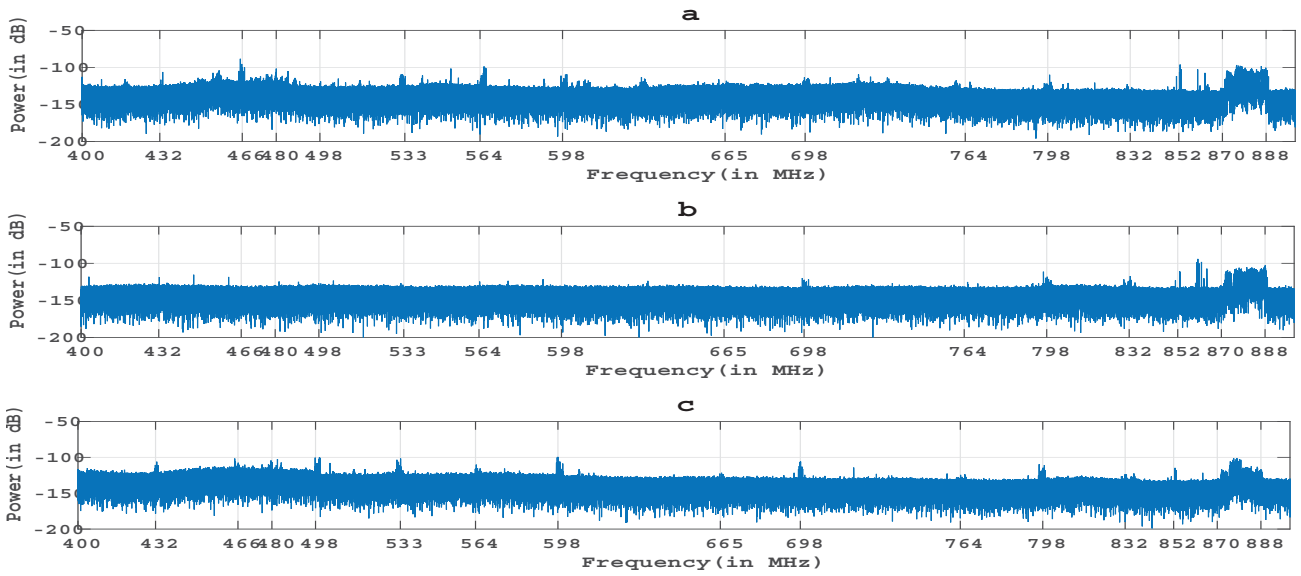

Fig. 5. a) Morning (10 AM-11 AM), b) Afternoon (2 PM-3 PM) and c) Evening (7 PM-8 PM) measurement using MATLAB in Mundla Nayta

C. Spectrum utilization in Mundla Nayta

Fig. 5 (a), (b) and (c) show the spectrum utilization measurement in morning (10 AM-11 AM), afternoon (2 PM-3 PM) and evening (7 PM-8 PM) respectively with the help of MATLAB. Figures show that again the band between 870-890 MHz is occupied and rest of the band is sparsely occupied. On an average 13-14%, 7-8% and 15-16% of band is used in morning, afternoon and evening respectively. Fig. 6 (a) shows the contiguous bandwidth (maximum 140 MHz) available for Mundla Nayta. Fig. 7 shows the cumulative distribution power, which shows that 92% of bandwidth is available.

V. Conclusion

In this paper, we measured and analyzed the spectrum utilization of band range from 400-900 MHz in sub-urban and rural area of Indore. The analysis show that in sub-urban regions 92% of band is unutilized and maximum use of band is in the evening. However, in rural areas 96% of band is unutilized and maximum use of band is in the morning. The analysis also show that the band except 870-890 MHz

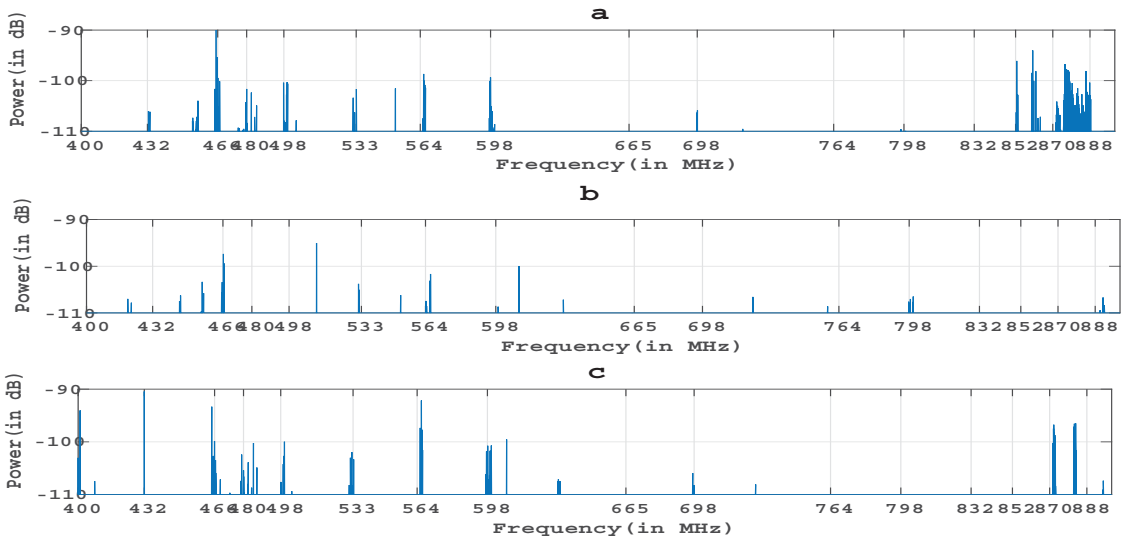

Fig. 6. Contiguous bandwidth available for a) Mundla Nayta, b) Harnya Khedi and c) Simrol

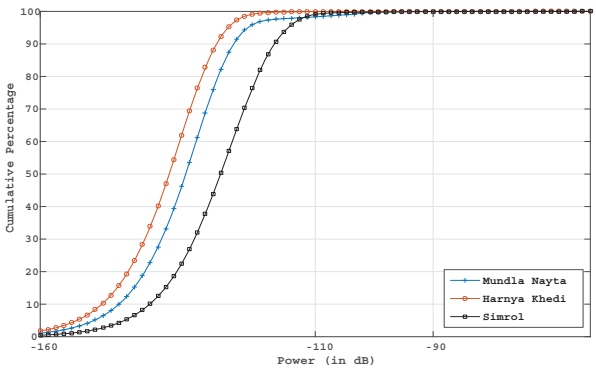

Fig. 7. Cumulative distribution of power

is not occupied contiguous. The largest value of maximum available contiguous band in sub-urban and rural region is 140 MHz and 160 MHz respectively. Hence, there is a vast availability of white space bands, that may be utilized for wireless communication for rural broadband.

ACKNOWLEDGEMENT

The authors would like to thank IIT Indore and Department of Electronics and Information Technology (DeitY), Govt. of India.

REFERENCES

[1] A. Shah, N. Jain, S. Bajpai, "A Report on INDIA@DIGITAL.BHARAT: CREATING A $ 200 BILLION INTERNET ECONOMY," Jan. 2015.
[2] "Digital India: Microsoft bats for White-Fi technology to offer free connectivity," [Online]. Available: telecom.economictimes.indiatimes.com.
[3] B. Ramamurthi, "Broadband wireless technology for rural India," *Indian Journal of Radio Space Physics*, vol. 36, pp. 168-171, Jun. 2007.
[4] A. K. Mishra, D. L. Johnson, "White Space Communication: Advances, Developments and Engineering Challenges (Signal and Communication Technology)," *Springer Publication*, 2015.
[5] M. H. Islam, "Spectrum Survey in Singapore: Occupancy Measurements and Analyses," *IEEE International Conference on Cognitive Radio Oriented Wireless Networks and Communications*, pp. 1-7, May. 2008.
[6] R. I. C. Chiang, "A Quantitative Analysis of Spectral Occupancy Measurements for Cognitive Radio," *IEEE Vehicular Technology Conference*, pp. 3016-3020, Apr. 2007.
[7] M. McHenry, "Chicago Spectrum Occupancy Measurements & Analysis and a Long Term Studies Proposal," *ACM International Workshop on Technology and Policy for Accessing Spectrum*, pp. 1-12, Aug. 2006.
[8] M. L. Benitez, A. Umbert and F. Casadevall, "Evaluation of Spectrum Occupancy in Spain for Cognitive Radio Applications," *IEEE Vehicular Technology Conference*, pp. 1-5, Apr. 2009.
[9] "National Frequency Allocation Plan 2011, WPC, Department of Telecommunication, Government of India".
[10] G. Naik, S. Singhal, A. Kumar and A. Karandikar., "Quantitative Assessment of TV White Space in India," *National Conference on Communications*, pp. 1-6, 2014.
[11] P. Kumar et. al., "White Space Detection and Spectrum Characterization in Urban and Rural India," *IEEE International Symposium and Workshops on a World of Wireless, Mobile and Multimedia Networks*, pp. 1-6, Jun. 2013.
[12] [Online]. Available: http://en.wikipedia.org/wiki/Doordarshan.
[13] "Regulatory Requirements for White Space Device in the UHF TV Band," OFCOM, Jul. 2012.
[14] S. N. Merchant and M. Z. A. Khan, "High Performance Cognitive Radio Networks," Project Report submitted to the PRSG Review.
[15] "Research paper on White Space for Digital India", Dec. 2014.
[16] A. Bishnu and V. Bhatia, "On Performance Analysis of IEEE 802.22 (PHY) for COST-207 Channel Models," *IEEE Conference on Standards for Communications and Networking*, Oct. 2015.
[17] A. F. Molisch, "Wireless Communications," *Wiley Publication*, 2e, 2011.
[18] [Online]. Available: www.rtl-sdr.com.
[19] V. S. Tomar and V. Bhatia, "Low Cost and Power Software Defined Radio using Raspberry Pi for Disaster Effected Regions", *Elsevier Journal on Procedia Computer Science*, vol. 58, pp. 401-407, 2015.

THE 5TH INTERNATIONAL CONFERENCE ON WIRELESS COMMUNICATIONS, VEHICULAR TECHNOLOGY, INFORMATION THEORY, AEROSPACE & ELECTRONIC SYSTEMS (WVITAE-2015)
December 13-16, 2015, Hyderabad, India

Modified RAR and PLSR-based artifact removal for stroke detection in UWB radar imaging

E. Ricci, A. Colucciello, S. Di Domenico, E. Cianca, T. Rossi
Electronic Engineering Department
University of Rome "Tor Vergata"
Rome, Italy

***Abstract*— This paper focuses on the use of UWB radar imaging for stroke detection. In particular, we optimized the use of the RAR algorithm, originally proposed for breast cancer, to the case of stroke detection. Moreover, we extend it to the multistatic case. Both modified RAR and multistatic RAR are then combined with a novel artifact removal algorithm based on PLSR (Partial Least Square Regression) processing. The paper shows the effectiveness of the proposed solution in terms of improved stroke localization accuracy and number of false positives.**

Keywords—beamforming algorithms; UWB radar imaging; PLSR; brain stroke detection

I. INTRODUCTION

Brain stroke is one of the main causes of disability in the world. Detecting a stroke as soon as it occurs (for example, after a trauma) would be extremely important to better manage the emergency (for instance, by optimizing the priorities in case of more than one patient) and in reducing the number of unnecessary high resolution imaging diagnoses. This would be possible with a stroke detection device that is low cost and transportable so that it can be carried on site by first response paramedical teams or in the ambulance. More traditional high resolution medical imaging tools such as CT (Computed Tomography) and MRI (Magnetic Resonance Imaging) scanners, are not compatible with these requirements (portable and low cost). Microwave imaging (MWI) is an emerging diagnostic branch based on the observation that different tissues, or the same tissue in different functional conditions (i.e. cancerous and healthy) have different dielectric properties in the microwave band. MWI allows to design less complex and costly devices, which might be transportable. Moreover, it is less invasive with no risk associate to patient exposure to ionizing radiations.

Currently, there are two main MWI approaches: microwave tomography and UWB radar. The microwave tomography determines morphological (location, size and shape) and electromagnetic characteristics (permittivity, conductivity and magnetic permeability) of any abnormal examined tissue. The output is the reconstruction of the complete dielectric profile of the crossed tissues. One limitation of this technique is that the tissue reconstruction requires the solution of a very complex mathematical inverse problem. Relevant works on stroke detection via a MWI tomographic approach has been done by a research group at Chalmers University [1], [2].

In this paper we focus on the UWB radar approach, [3]. A lot of work on the use of UWB radar imaging has been done for breast cancer detection [4]-[7]. If a low complexity beamforming algorithm, such as the Delay & Sum (DAS), was first proposed in [4], more complex and powerful beamforming algorithms have been proposed more recently, such as the MIST (Microwave Imaging Space-Time) proposed in [5] and optimized for a multistatic approach in [6]. An important recent work is [8], in which authors propose the RAR (Robust and Artifact Resistant) algorithm, based on an adaptive weighted sum via correlation exploration. The backscattered signals exhibiting high correlation are combined, reducing the algorithm sensitivity to clutter.

Recently several works have started to consider the application of UWB radar imaging also to stroke detection, [9]-[12]. Processing and pre-processing algorithms proposed for breast cancer cannot be applied in a straightforward way to stroke detection for two main reasons: 1) Requirements are rather different: for breast cancer accuracy is more important than device complexity and response-time. In case of stroke detection, a fast response, the low complexity and cost of the device are more important than accuracy; 2) The scalp generates strong artifacts to backscattered signals and attenuates wave penetration inside the brain.

Works on UWB radar for stroke detection has mainly focused on antenna design [9]-[10] or anatomical head phantom [11]. In most of these works the DAS algorithm is used [11]-[12], which allows to keep the complexity low. However, DAS offers limited capability for discrimination against clutter. As it has been shown in [13], artifact removal algorithms, such as the one based on Wiener filters, which are effective when combined with a more complex processing algorithms (such as the MIST applied for breast cancer detection in [5] and for our application in [14]) are not applicable to DAS. Therefore, in [13], the use of a novel approach for artifact removal, based on PLSR processing, has been proposed and its effectiveness has been shown.

In this paper, we propose the combination of this artifact removal algorithm with a modified version of the DAS algorithm, namely the RAR [8], which has been originally proposed for breast cancer. As it will be shown in the paper, the direct application of the original RAR algorithm and a state-of-the-art artifact removal algorithm such as the one based on Wiener filter [5] to stroke detection does not provide good results. Therefore, we have first optimized its use to the

stroke detection. Then, we have extended it to a multistatic case to further improve the achievable performance. Modified RAR, multistatic RAR, combined with the PLSR-based artifact removal algorithm, are compared with the DAS algorithm in terms of accuracy of stroke localization, presence of false positives and also computational complexity, using backscattered signals acquired by a FDTD (Finite-Difference Time-Domain) applied onto a 3D and 2D head model.

The paper is organized as follows: Section II presents the system environment; Section III describes the considered artifact removal algorithm, while in Section IV the proposed processing algorithms are presented; performance results are reported in Section V.

II. System Model

In this study the backscattered signals are generated by FDTD software and are assumed to be noiseless, which is an acceptable assumption for the purposes of this paper. We have considered 8 UWB antennas, located in different positions along head surface. Each antenna transmits a UWB pulse into the tissue and receives signals transmitted by all antennas and backscattered by the tissue discontinuity, according to a multistatic approach.

The transmitted pulses have a bandwidth that extends from 1 to 4 GHz, a good trade-off between radar spatial resolution and waves attenuation inside the human brain.

The head has been modeled as a 3D multilayered structure, considering the stratification in different layers, simulating the actual biological head structure, and the dispersive properties. The 3D model consists in the layer of the skin, the skull and the brain matter. The dispersive properties are incorporated in the FDTD model, based on 2th order fit to Cole-Cole model.

We have also assumed the presence of a coupling medium between the antenna system and the head, in order to ease wave propagation inside the tissues. The coupling medium is a mixture of different liquid substances with dielectric constant similar to skin. This liquid increases electromagnetic energy transmission inside the skull and reduces the reflection contribution.

Table I shows the main parameters of the different head tissues considered in the model for the computation of the backscattered signals, at center frequency of 2.5 GHz.

TABLE I. Head Tissue Properties At Center Frequency of 2.5 GHz [15]

Tissue	Dielectric constant	Loss tangent	Conductivity (S/m)
Skin	37.952	0.28184	1.4876
Bone	11.352	0.25597	0.40411
White Matter	36.107	0.24699	0.24699
Coupling Medium	43		

For validation of our methods we start with a 2D (planar) elliptical head model. Fig.1 shows a planar section of the head model and the antennas system around it.

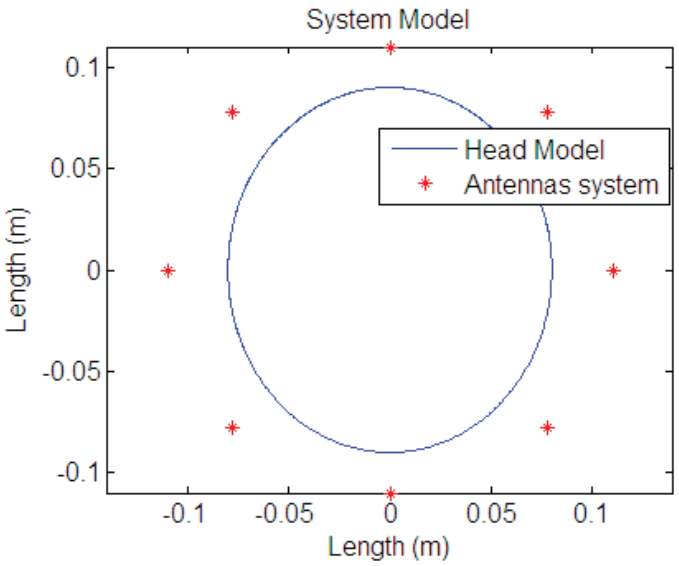

Fig 1. System model. The ellipse represents planar section of the 3D head model. The antennas, in red, are arranged along the head surface

III. PLSR-based Artifact Removal Algorithm

The UWB backscattered signals contain a lot of useless information (artifacts), including the reflected signal from the skin-coupling medium interface, coupling between antennas, antennas mismatch and clutter. Artifacts have magnitude larger than lesion contribution, leading to false positives or negatives. Therefore, they must be removed, by an artifact removal algorithm, before applying any image reconstruction algorithms.

In [13], an artifact removal algorithm based on statistical regression technique, PLSR, has been proposed. As shown in [13], the PLSR processing allows to achieve better performance compared to artifact removal algorithm originally proposed in [5], with a drastically reduced computational complexity. To apply PLSR, the artifact on each channel was estimated as a linear combination of the artifact in all other channels, utilizing the maximization of correlation as constraint and relying on the assumption that the artifacts are similar, but not identical.

Before passing the backscattered signals to the pre-processing algorithm, a first "cleaning" of the signals is performed by a simple low pass filter, because the stroke response is mainly on low frequencies of the spectrum, [13].

IV. Processing Algorithm

In this paper, we have considered the RAR algorithm, proposed in [8], for processing the backscattered signals. RAR is a modified version of the DAS. The idea is to introduce a weight factor that gives more relevance to the most significant signals, i.e. those signals with the greatest information content.

This allows to reduce the effect of the artifacts that have not been removed by the artifact removal algorithm.

The algorithms build a map of backscattering energy, applying a beamformer to each return signal. The head is divided in focal points, which are associated with the intensity

of corresponding pixel in the energy map. The signals are time-shifted to align them so that, if a scattering object exists at focal point, the energy will be relatively high, since signals are summed coherently. Conversely, if lesion is not in focal point, i.e. focal point is a healthy tissue, signals are summed incoherently, leading to low energy value.

A. RAR algorithm

Let N be the number of antennas and L the number of focal points. The steps described below are repeated for each focal point, thus the energy map is achieved by L loops, involving 4 steps.

Step 1: Preprocessed signals are time-shifted to align them approximately in time. Then, a windowing truncation is provided to eliminate useless information while preserving stroke response.

Step 2: A coherent summation of these time-shifted signals is calculated as in (1):

$$Sum(n,l) = \sum_{i=1}^{N} X_i(n,l) \tag{1}$$

where $n=1,\ldots k$ is the sample number and X_i is the i^{th} signal, after previous step.

Step 3: A weight factor is introduced, adaptively combining neighboring pairwise Pearson's correlation coefficients, calculated as follows:

$$c_i(l) = \sum_{n=1}^{k} X_i(n,l) X_{i+1}(n,l) / \sqrt{\sum_{n=1}^{k} X_i(n,l)^2 \sum_{n=1}^{k} X_{i+1}(n,l)^2} \tag{2}$$

The weight factor in [8] is calculated as:

$$wf(l) = \prod_{i=1}^{M} c_i(l) \tag{3}$$

where M is the number of relevant correlation coefficients normalized between *0-1*.

In the original algorithm proposed in [8], $M=N/2$, i.e. only half of the correlation coefficients, among the ones with higher values, are considered in (3). However, as it will be shown in the next Section, in our case we need to consider $M=N$, at least for the monostatic version of the algorithm. In the calculation of the weight factor all the correlation coefficients, normalized between *0-1*, are considered. In the following, we will refer to "modified RAR" to the algorithm that has this slight modification. Note that the last correlation coefficient is calculated between X_N and X_1 signals, because the antenna array is circular.

High correlation is expected at stroke location. The neighborhood pairwise correlation ensures that the correlation between two antennas, for each location, measures the reflection from the same scatterer.

Step 4: Finally, the energy of l^{th} focal point is

$$I(l) = \sum_{n=1}^{k} wf(l) \cdot Sum(n,l) \tag{4}$$

A high value of *wf* occurs when a stroke is in a l^{th} focal point, increasing the energy related to this focal point and giving more relevance to the stroke.

Conversely, when there is no stroke in l^{th} focal point, *wf* is low, decreasing the energy associated to the artifact.

B. Multistatic RAR

In this Section we present the multistatic extension of the RAR algorithm.

When a multistatic approach is used, we have *NxN* channels. We consider $C<NxN$ channels, selected a priori, according to distance between the i^{th} transmitting antenna and j^{th} receiving antenna. We use N mono-static channels Xij with $i=j$, when the transmitter coincides with the receiving antenna, and $2N$ multi-static channels between each transmit antenna i and nearest neighboring antennas $i+1$ and $i-1$.

Step 1- Step 2: These steps are the same of the monostatic case.

Step 3: Correlation coefficients for monostatic channels are calculated by (2), whereas for multistatic channels ($i \neq j$) we use (5) for $j=i+1$ and (6) for $j=i-1$.

$$c_{ij}(l) = \sum_{n=1}^{k} X_{ij}(n,l) X_{i+1,j+1}(n,l) / \sqrt{\sum_{n=1}^{k} X_{ij}(n,l)^2 \sum_{n=1}^{k} X_{i+1,j+1}(n,l)^2} \tag{5}$$

$$c_{ij}(l) = \sum_{n=1}^{k} X_{ij}(n,l) X_{i-1,j-1}(n,l) / \sqrt{\sum_{n=1}^{k} X_{ij}(n,l)^2 \sum_{n=1}^{k} X_{i-1,j-1}(n,l)^2} \tag{6}$$

The normalized correlation coefficients are sorted in descending order in a vector, called P vector.

The weight factor is achieved by multiplying correlation coefficients of neighboring pairwise transmitting-receiving antennas in the P vector and selecting the N higher values. The N higher values are chosen as a good trade-off between complexity and reliable performance. A lower number of the selected correlation coefficients would involve a worst discrimination between stroke and other scatterers, increasing the false positives. Whereas, a greater number of the selected correlation coefficients would lead to information loss.

Step 4: Finally, the energy of l^{th} focal point is given by (4).

V. Results and Final Remarks

In this section, the performance of the different beamforming algorithms namely the RAR algorithm in [8], modified RAR (as explained in Section IV), multistatic RAR and DAS algorithm are shown.

The performance has been evaluated considering a spherical bleeding (hemorrhage) with a diameter of 20 mm, placed in different positions of the head.

The metrics used for performance assessment, in terms of accuracy of stroke localization and amount of clutter versus stroke intensity, are:

- the absolute distance between the actual location of the stroke and the location of the maximum energy value in the

backscattering energy map, used to assess the localization accuracy. The stroke is localized with more precision when this distance is low.

- Signal-to-mean-ratio *SMR*, to validate if the stroke energy is high enough to classify it as a detected stroke, written as follow:

$$SMR = 10 \log_{10} \frac{mean\,(P_{stroke_region})}{mean\,(P - P_{stroke_region})} \quad (7)$$

where P_{stroke_region} is the average energy value of the stroke region and P-P_{stroke_region} is the average energy value of the remaining tissues. A higher value of this metric implies that stroke intensity is stronger than background region and results in a low amount of clutter.

Furthermore, an important aspect to take into account is the algorithms computational complexity.

The RAR complexity and the modified RAR complexity are comparable. Whereas, the complexity increases by introducing the multistatic RAR, since more channels are considered.

Table II reports the complexity as magnitude order, in terms of basic mathematical operations. As shown, the multistatic RAR complexity is higher than DAS complexity, due to the weight factor calculation.

TABLE II. ALGORITHMS COMPLEXITY

Metrics	**Processing algorithms**			
	RAR [8]	***Modified RAR***	***Multistatic RAR***	***Multistatic DAS***
Complexity	10^4	10^4	10^5	10^4

First of all, we assess the performance of the modified RAR and multistatic RAR using a state-of-the-art artifact removal algorithm based on Winer filter [5].

Fig. 2 shows the energy map, in a planar section, obtained with this frame. In Fig. 2, the external ellipse is the head contour, while the internal black circumference is the bleeding extension. The energy output is represented as colored pixel, according to values in dB scale.

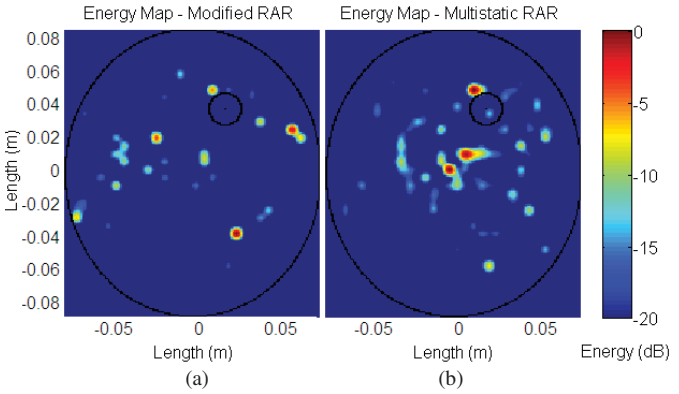

Fig. 2. Energy map obtained with the artifact removal algorithm based on Wiener filter and the (a) Modified RAR algorithm and (b) Multistatic RAR algorithm.

Fig. 2 clearly shows that, even if the RAR algorithm has been proposed for breast cancer detection to make the DAS processing less sensitive to the clutter, its performance are still poor when combined with a typical artifact removal algorithm also used for breast cancer. Therefore, we propose the use of the an artifact removal algorithm based on PLSR as described in Section III.

Fig. 3-4 show the backscattering energy map, in a planar section, obtained with different processing algorithms considering two different positions of the stroke. Table III-Table IV summarize the metrics values achieved for each of the compared algorithms, where Distance represents the absolute distance metric.

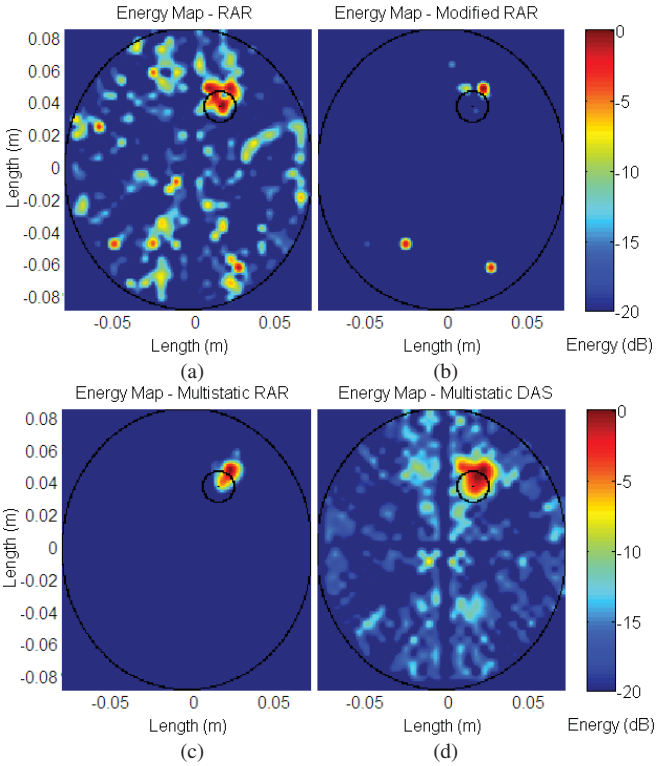

Fig. 3. Energy map obtained with the artifact removal algorithm PLSR and the (a) RAR algorithm proposed in [8], (b) Modified RAR algorithm, (c) Multistatic RAR algorithm and (d) Multistatic DAS algorithm.

TABLE III. METRICS PERFORMANCE FOR FIG. 3

Metrics	**Processing algorithms**			
	RAR [8]	***Modified RAR***	***Multistatic RAR***	***Multistatic DAS***
Distance [mm]	$2.7614 \cdot 10^{-4}$	11.1806	11.1806	5.0003
SMR [dB]	7.3667	18.1606	28.1348	9.8408

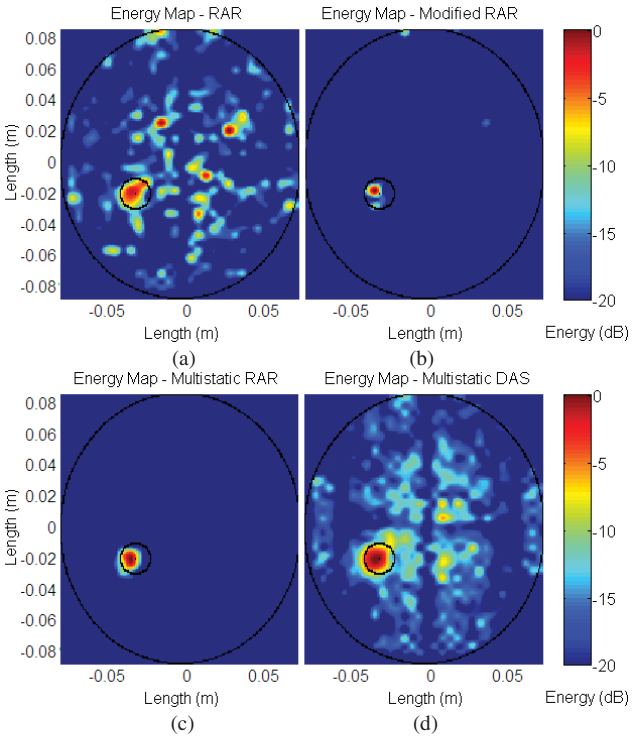

Fig. 4. Energy map obtained with the artifact removal algorithm PLSR and the (a) RAR algorithm proposed in [8], (b) Modified RAR algorithm, (c) Multistatic RAR algorithm and (d) Multistatic DAS algorithm.

TABLE IV. METRICS PERFORMANCE FOR FIG. 2

Metrics	**Processing algorithms**			
	RAR [8]	***Modified RAR***	***Multistatic RAR***	***Multistatic DAS***
Distance [mm]	72.1113	4.9999	4.9999	4.9999
SMR [dB]	6.8847	21.4698	32.353	8.8298

From Figs. 3-4 and Table III-IV, we can conclude the following:

The original RAR algorithm cannot be directly applied to our case of stroke detection. The stroke is effectively located, but the number of false positives is unacceptable. By considering all the correlation coefficients in the weight factor, as in the modified RAR, it is possible to greatly reduce the number of false positives. It is worth noting that in the case of breast cancer application of RAR, 48 antennas were considered. In our scenario, only 8 antennas are considered. Therefore, considering all correlation coefficients do not lead to a dramatic increase of the complexity as it would be in case of breast cancer.

The multistatic extension of RAR algorithm is able to locate the stroke with high accuracy and the number of false positives is extremely low. This is expected as the multistatic approach allows to acquire more information about the target, avoiding strong reflections from undesired scatterers, as clearly shown in Fig. 3. On the other hand, the multistatic approach is computationally heavier. However, it is also worth noting that in our proposed extension of the RAR, we consider a number of correlation coefficients lower than the total number of correlation coefficients, as opposite to the monostatic case where all coefficients are needed.

Finally, with respect to a multistatic DAS algorithm, the accuracy in stroke localization of the multistatic RAR is the same, but the multistatic RAR can drastically reduce the number of false positives, leading to more precise information. Moreover, this performance improvement is achieved with a low increase of the computational complexity, as previously shown in Table II.

In conclusion, the results show the effectiveness of the proposed combination, artifact removal algorithm based on PLSR and a multistatic RAR, for stroke detection.

REFERENCES

[1] A. Fhager, Y. Yu, T. McKelvey, M. Persson, “Stroke diagnosis with a microwave helmet”, 7th European Conference on Antennas Propag. (EUCAP 2013), pp. 845-846, 2013

[2] M. Persson, et al., “Microwave-based stroke diagnosis making global prehospital thrombolytic treatment possible”, IEEE Trans. Biomed. Eng., vol 61, no. 11, pp. 2806-2817, Nov. 2014

[3] C. N. Paulson, J. T. Chang, C. E. Romero, J. Watson, F. J. Pearce and N. Levin, “Ultra-wideband radar methods and techniques of medical sensing and imaging”, SPIE 6007, Smart Med. and Biomed. Sensor Technology, III

[4] X. Li and S. Hagness, “Confocal microwave imaging algorithm for breast cancer detection”, IEEE Microw. Compon. Letter. vol. 11, no. 3, pp. 130-132, Mar. 2001

[5] E. Bond, X. Li, S. Hagness, B. D. Van Veen, “Microwave imaging via space-time beamforming for early detection of breast cancer”, IEEE Trans. Antennas Propag., vol 51, no. 8, pp 1690-1705, Aug. 2003

[6] M. O’Halloran, E. Jones, M. Glavin, “Quasi-multistatic MIST beamforming for early detection of breast cancer”, IEEE Trans. Biomed. Eng., vol 57, no.4, pp. 830-840, Apr. 2010

[7] Y. Xie, B. Guo, L. Xu, J. Li, P. Stoica, “Multistatic adaptive microwave imaging for early breast cancer detection”, IEEE Trans. Biomed. Eng., vol 53, no 8, pp. 1647-1657, Aug. 2006

[8] T. Yin, F. H. Ali, C. C. Reyes-Aldasoro, “A robust and artifact resistant algorithm of ultrawideband imaging system for breast cancer detection”, IEEE Trans. Biomed. Eng., vol 62, no 6, pp. 1514-1525, Jun. 2015

[9] H. Trefna, M. Persson, “Antenna array design for brain monitoring”, Antennas Propag. Society Int. Symp, San Diego, CA, USA, 2008

[10] B. J. Mohammed, A. M. Abbosh, D. Ireland, M. E. Bialkowski, “Compact wideband antenna immersed in optimum coupling liquid for microwave imaging of brain stroke”, Progress in Electromagn. Research, 27, pp. 27-39, 2012

[11] B. J. Mohammed, A. M. Abbosh, S. Mustafa and D. Ireland, “Microwave system for head imaging”, IEEE Trans. Instrum. Meas., vol. 63, no. 1, pp. 117-123, Jan. 2014

[12] D. Ireland and M. Bialkowski, “Microwave head imaging for stroke detection”, Progress in Electromagn. Research M, vol. 21, pp. 163-175, 2011

[13] E. Ricci, S. Di Domenico, E. Cianca and T. Rossi, “Artifact removal algorithms for stroke detection using a multistatic MIST beamforming algorithm”, in press in 37th Annual Inter. Conf. IEEE Engineering in Medicine and Biology Society (EMBC 2015)

[14] E. Ricci, F. Maggio, T. Rossi, E. Cianca and M. Ruggieri, “UWB radar imaging based on space-time beamforming for stroke detection”, 6th Europ. Conf. Inter. Feder. for Medical and Biological Engineering IFMBE Proceedings, 45, pp. 946-949, 2015

[15] Dielectric properties of body tissues in the frequency range 10Hz-100 GHz at http://niremf.ifac.cnr.it/tissprop/

THE 5TH INTERNATIONAL CONFERENCE ON WIRELESS COMMUNICATIONS, VEHICULAR TECHNOLOGY, INFORMATION THEORY, AEROSPACE & ELECTRONIC SYSTEMS (WVITAE-2015)
December 13-16, 2015, Hyderabad, India

Participation of Optical Backbone Network in Successful Advancement of Wireless Network

Rajarshi Mahapatra, *Senior Member, IEEE*
Dept. of ECE, CVR College of Engineering
Email: rajarshim@ieee.org

***Abstract*—Recent survey predicts that the number of smart phone users will cross two billion worldwide by early 2016. In order to support high QoS requirements, ITU proposed IMT-2020, which is setting the stage for 5G wireless technologies. The 5G technologies aim to support broadband data rate more than 5 Gbps, latency less than 1 ms for high mobile user. Establishing and maintaining a successful wireless communication link among the users with simultaneously achieved all objectives becomes challenging. The backhaul of nearly all wireless access networks is fiber-optic. In order to support these tremendous amounts of data, optical network has been evolved in respective way. These technological advancements and deployments are creating a new landscape in access networks, with an integration of wireless and optical technologies. As optical fiber has penetrated the access network and the latest wireless standards have demanded smaller, higher bandwidth cells, fiber connectivity has become key. This paper studies the various wireless technologies to support high QoS and the impact of optical backbone network correspondingly. In particular, the development of optical networks will be discussed with advancement of wireless networks to support high performance communication. In this study, participation of both the networks will be considered to understand several efficient mechanism (*e.g.* spectral, energy, deployment, routing, transport etc.) of networks.**

***Index Terms*—Green communication, optical network, cognitive network,**

I. Introduction

Recent survey predicts that the number of smart phone users will cross two billion worldwide by early 2016. The usage of number of smart terminals (smart phones and tablet PCs) has proliferated the mobile Internet applications, which explored mobile traffic. It is predicted that mobile data traffic will grow more than 1000 times compared with the end of 2010 beyond 2020. In early 2012, in order to support high quality-of-service (QoS) requirements, ITU proposed IMT-2020, which is setting the stage for 5G wireless technologies [1]. The focus of 5G technologies is to enable a seamlessly connected society in the 2020 time frame and beyond that brings together people along with things, data, applications, transport systems and cities in a smart networked communications environment.

Network densification, miscellany of node types, split of control and data plane, network virtualization, heavy and localized cache, infrastructure sharing, concurrent operation at multiple frequency bands, simultaneous use of different medium access control and physical layers, and flexible spectrum allocations can be envisioned as some of the potential ingredients of 5G [2]. The prominent technologies of 5G includes massive MIMO, cloud computing, software-defined network, cognitive radio, distributed antenna system and others technologies, which are differ in their characteristics, operation, application, requirements, purpose etc. These technologies are diverse in nature and coexist in the same environment to provide ubiquitous network coverage. Users can connect to any available wireless network depending on their requirements. With the increased drive from the industry for a fully connected network, there is also a need to design heterogeneous wireless network (HetNet) architecture to interconnect these different wireless networks. These interworking mechanisms are of prime importance to achieve ubiquitous access and seamless mobility in HetNet environment.

The data produced at wireless access network are transported through optical fiber link. Thus, optical networks are facing increased levels of heterogeneity, from types of services to the types of transmission technologies. Over the years, capacity of optical network increases from 10 Gbps to 100 Tbps and more. Like wireless networks, optical network is also evolved to fifth generation. During this evolution, optical network incorporated several technologies such as enhancement mechanism (rate, bandwidth, wavelength), transmission mechanism (dense wavelength-division-multiplexing (DWDM), optical CDMA (OCDMA), Coarse WDM (CDWDM)), architecture (time-division-multiplexing passive-optical network (TDM-PON), long reach PON, Ethernet PON (EPON), WDM-PON), switching (optical circuit switching (OCS), optical burst switching (OBS), optical packet switching (OPS)) and other techniques. Figure 1 shows a typical service architecture of wireless network with optical backbone, where all the 5G wireless technologies are connected directly with the optical network.

The successful development of wireless network depends on the successful transmission of data traffic through optical fiber *i.e.* optical network. Thus, optical network is responsible for transmission of data traffic and make available for usage of wireless user. In this paper, we will discuss the participation of optical backbone network for successful wireless communication.

II. Participation of Optical Network in 5G Technology Development

In this section, we will discuss several 5G wireless network technologies, which are proposed to improve QoS and quality of experience (QoE) of application. Simultaneously, we will provide the details of participation or importance of optical

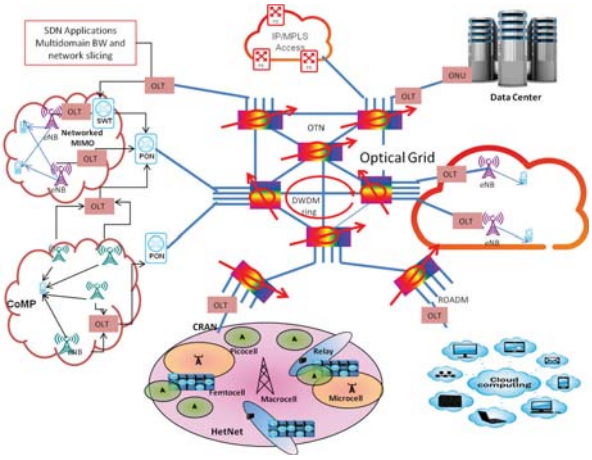

Fig. 1. A typical service architecture of wireless network with optical backbone.

network component to enable the services/applications by improving quality of transmission (QoT).

A. Coordinated Multipoint Transmission Technique

Intercell interference is one of the reason by which wireless users experience outage. Coordinated multipoint (CoMP) transmission technique exploits this scenario to improve the performances of the user, first developed for LTE Advanced. Its aim is to enhance the overall system performance, utilize the resources more effectively and improve the end user service quality by dynamic coordination or transmission and reception with multiple geographically separated eNBs. They dynamically coordinate to provide joint scheduling and transmissions as well as proving joint processing of the received signals [3]. To enable CoMP, very close and highly detailed feedback is required on the channel properties in a fast manner. It should be able to provide a very low level of latency, as required by 5G standard. Expected traffic load and and participation of more number of eNBs required additional processing, which increase delay. For deployments with the same sites topology, backhaul latency and capacity, and scheduling and processing capabilities, the configuration of the processing also has an impact on the performance of CoMP. To achieve physical layer cooperation, high speed and delay sensitive communications channels are required between eNBs [4]. Time synchronization is particularly critical in time division duplexing (TDD) systems to avoid interference between the downlink and uplink of adjacent cells and enable enhanced features such as enhanced inter-cell interference coordination (eICIC) in CoMP.

To enable CoMP, the backhaul network must fulfill stringent capacity requirements (several Gbit/s backhauling capacity per eNB) and latency requirements (round-trip latencies between eNBs less than 1 ms). It turned out that even standard future optical technologies, like WDM-PON, do not allow CoMP in a satisfactory way [5]. Optical network units (ONUs) (and hence eNBs) are attached to one optical line terminal (OLT) via a remote node (RN). The eNBs/ONUs are assigned to OLTs based on their proximity and the RN is positioned such that the fiber lengths between the ONUs and the RN are minimized in each PON (Fig. 1). Thus, fiber propagation delay for a fiber of length, link capacity of WDM, wavelength tuning time (influences the actual link capacity and link delay) and inter-ONU data exchange are the main parameters of optical network which influence the CoMP performance. More eNBs under cooperation are limited by backhaul performance.

B. Massive MIMO & Networked MIMO

Networked MIMO has been proposed to increase wireless efficiency. It is also consider as multi-user MIMO, which has ability to reduce inter-cell interference (ICI) and improve the system spectral efficiency by coordinating multiple eNBs. In a networked MIMO system (Fig. 1), each BS is equipped with a smaller number of antennas, but interference cancellation is realized by significant data and channel state information (CSI) sharing across the cooperating eNBs over the backhaul links and joint downlink transmission to the scheduled users. Performance of networked MIMO system bottleneck with out of cell interferences, feedback overhead, control channel overhead (increased reference signal overhead), backhaul link latency (delayed CSI and data sharing) and etc [6].

In case of massive MIMO, very large antenna array is used at each eNBs to serve large number of users simultaneously. Excess antennas simplified multiuser processing, reduce transmit power and minimize the effect of fast fading. It generally uses time division duplexing to enable channel estimation. The gain of massive MIMO system limited by pilot contamination (need more coordination), interference, spatial correlation (it reduces effective DoFs as increasing number of antennas) and channel aging affects (energy-focusing ability of narrow beams) [7].

C. Small Cells

Recent study shows that the data traffic generated from the indoor user is two-third of the total wireless traffic. Thus, to increase coverage and data rate at low-power for indoor users, wireless networks introduced a new type of access technology, named femtocell (HeNB). HeNBs are a low-cost, low-power base-station deployed by the end-users [8].

Femtocell needed backhaul to connect with the core network. HeNBs are deployed on an already existing and working cellular infrastructure, and may use same licensed spectrum of macrocell BS (MeNB). Due to this, HeNB users suffer interference from the serving MeNB and the neighbouring MeNBs. Femtocell backhaul needs QoS for delay-sensitive traffic and provides enough capacity. Femtocells backhaul are local ISP networks, which are controlled by same or different service provider. Femtocells are prone to backhauling energy costs and delay limitations. Frequency and time synchronization are essential to guarantee that transmitted signals use their specific allocated channels and comply with license regulations and system requirements [9].

Gigabit passive optical network (GPON) uses passive splitters within the fiber network and allows one single feeding optical fiber to provide service to multiple network nodes. WDM is used in GPON to allow the use of a single optical fiber

for both uplink and downlink. WDM-PON utilizes specific wavelengths for specific optical network components or links, while they all use the same physical infrastructure. X-GPON or 10-GPON as the next generation of GPON can achieve data rates of 10 and 2.48 Gbps for downlink and uplink, respectively. However, fiber may not always be available or the associated installation and/or operating costs may be much higher than that of DSL. It is also important to note that considering the need to keep up with the increasing traffic demands, installing wired backhaul in all new small cell sites may not be cost-effective.

D. Distributed antenna system (DAS)

DAS is a single facility system usually in a large building, sports facility or other places where cell signals cannot penetrate like tunnels for cars or mass transit. A smaller DAS may pick up cell signals from an outdoor antenna to connect indoor antennas to the cellular systems of various carriers through a network of coax cables and amplifiers. That might work for small systems, but not for systems with large numbers of users. These systems generally connect to fiber backhaul like a cell tower and distribute signals inside the facility digitally over fiber.

Radio over Fiber technology (RoF) is an integration of wireless and fiber optic networks. A fiber based DAS installations are being increasingly used in a variety of locations including public buildings, airports, stadiums and subways. In these in building wireless systems a base station (BS) includes the centralized equipment where the radio signals are converted to optical signals, which are then transmitted via optical fiber to specific remote node locations [10].

E. Cloud-assisted radio access network

Cloud computing is becoming increasingly important in todays business due to benefits such as greater flexibility, increased security, scalability, and low cost [11]. Hetnet (Fig. 1) consists with densely installed small cells such as micro/pico/femto along with macrocells. The network operator and the end users or third parties can deploy small cells with open and closed access modes. Here, it mainly focuses on operation, maintenance, and management of cells to provide services by efficiently using network resources instead of sending users' and small cell data to cloud for processing, which is generally the case in cloud RAN (C-RAN).

Cells are connected to the cloud through high-speed optical fiber. Monitoring, configuration, optimization, and mobility control operations are generally centralized in the cloud. This centralized nature allows the network operators to manage the networks in a more efficient way. Since, the traffic demand vary dramatically, the cloud based architecture helps the network operator to allocate resources on demand and coordinate cells efficiently to provide services with seamless coverage, high data rates, and low latency. Effective joint optical and radio resource management can be implemented in order to satisfy the stringent delay requirements of the emerging mobile cloud computing applications and increase the overall cell throughput [12]. The flexibility and efficiency of the underlying optical network infrastructure as well as the cloud computing infrastructure become more and more crucial. In order to achieve required flexibility and efficiency, coordinated provisioning of data centers (DCs) and optical network interconnection among DCs is essential. Performance of the fiber (guaranteed for immediate and ongoing performance for the life of the network) is critical to deliver user experience in cloud computing promises. For guaranteed performance of fiber, 0.4 dB losses per km should not be good enough in todays demanding world. Many vendors that have built their data centers for optimal performance are delivering guaranteed 0.2-dB loss.

F. Software Defined Network

Software defined networking (SDN) is a new networking paradigm where the forwarding plane is decoupled from the control plane. In SDN, network intelligence is logically centralized in the control plane, and the forwarding plane is abstracted from the control plane to perform service delivery. This separation provides user more control over network and supports more flexibility in the deployment of new services and protocols at a much faster rate, higher network utilization, lower energy consumption, better QoS and higher revenue. Moreover, SDN has triggered significant interest in network functions virtualization (NFV), which decouples network functions from proprietary hardware appliances. Therefore, network functions run flexibly in software to accelerate service innovation and provisioning. Both SDN and NFV aim to advance a software-based approach for more manageable, agile, utilize and innovative networks [13].

This require dynamic backhaul configuration in order to configure and control the routing and transport data across the BSs. Due to provisioning of network visualization, the topology of network will need to be dynamically configured. The required flexibility and capacity in the backhaul network for our approach can be provided by optical backhaul networks based on WDM-PON [14]. In this direction, software-defined optical network (SDON) has been proposed, which composed of WDM equipments, optical transport network (OTN) switches, reconfigurable optical add-drop multiplexer (ROADM), and their supporting fiber network with the help of are flexible grid and elastic rate transponders [15].

G. Load balancing, Infrastructure & Data Sharing

With all the above 5G technologies, networks can support different kinds of traffic of diverse requirements. The users (UE) can be categories as static-indoor UE with high QoS, static-outdoor UE with high QoS, low mobility outdoor UE, high mobility outdoor UE and etc. In order to support these different kinds of traffic without outage and service blocking, network needs to provide coverage with required QoS. Virtually, UE should not be outside of coverage and services at any point of time. The network should successfully communication with anyone at anytime, anywhere with anything.

Today's network is a heterogeneous one and several service providers exist in the environment operating on same/different spectrum. It is very difficult for a particular service provider to

support UE satisfactory, since user's location is random. Thus, to provide better service to UE, different service provided needs to cooperate each other. With the cooperation, they can share each other networks and can also maintain proper balancing on traffic load. However, these tasks are huge and complex, and need a proper understanding and agreement among the service providers. Therefore, network needs to configure themselves accordingly to support UE. This configuration can happen simultaneously at UE and network side, which can change time to time depending on requirements, network, location etc. Thus, reconfigurability is an important requirement in future generation network.

III. Reconfigurability in Both the Network

In the previous section, we have discussed several issues of 5G technologies, where both the networks participated differently. The requirements of networks specification varies widely with applications. To supports a particular application or service, network has to configure themselves based on the service's QoS. Since, different application has different QoS, network has to reconfigurable themselves. Thus, reconfigurability is the key in next generation network.

In wireless network, software defined radio (SDR) emerges to support reconfigurability. SDR is is a radio communication system where components that have been typically implemented in hardware (e.g. mixers, filters, amplifiers, modulators/demodulators, detectors, etc.) are instead implemented by means of software on a personal computer or embedded system. SDR is needed for next generation network. Since, spectrum is scarce resources and studies say the allocated resources are very much under-utilized, cognitive radio technology has been proposed to use this underutilized spectrum. A cognitive radio is an intelligent radio that can be programmed and configured dynamically with the help of SDR based transceiver. Its transceiver is designed to use the best wireless channels in its vicinity. Such a radio automatically detects available channels in wireless spectrum, then accordingly changes its transmission or reception parameters to allow more concurrent wireless communications in a given spectrum band at one location. This process is a form of dynamic spectrum management [16].

In a similar manner, optical networks have also evolved continuously, increasing their capacity due to the growing of internet traffic demand, thus setting the path for new approaches that allow them to become more dynamic and flexible. Such reconfigurable optical networks have the capability of being dynamically programmable by software thus enabling, among other features: configuration of different bit rates in the same optical transponder, selection of different modulation formats and forward error correction (FEC) algorithms, reconfiguration of the optical equipment parameters, depending on the quality of the transmission, and dynamic adjustment of the optical channel bandwidth. In a similar way, software defined optics (SDO) was introduced in optical network to enables cross-layer interactions through the construction of application-specific protocol stacks out of small reusable services. The dynamic reconfigurability of multiple modulation and ability to adapt various transponder provides software-defined optical transmission (SDOT). To extend this idea, cognitive optical network (CON) has been proposed to enables high data rate lightpaths and to compensate a variety of dispersion impairments and to enable more agile optical networking, [17]. The impairment compensation and transmission performance monitoring/ measurement (e.g., optical signal-to-noise ratio (OSNR), chromatic dispersion (CD), polarization-mode-dispersion (PMD), and bit error rate (BER)) to improve QoT can be done efficiently in CON. It also supports unified signaling to address different application's bandwidth reservation requirements and also able to provision dynamic wavelength services with a rate adaptive optical reach and flexible subwavelength services with rapid mesh restoration [18]. The state-of-play for optical telecommunication equipment contributes with either rigid passive-optical multiplexing devices that do not offer the required degree of flexibility and dynamicity, or, in the other extreme, highly complex networking subsystems such as ROADM as found in metro-core networks, whose high cost and energy consumption is prohibitive for metro-access [19].

IV. Energy efficient communication

Over the year, energy efficient (EE) communication has earned tremendous interest in recent years due to ever increasing number of devices operating in dense cells, while demanding high data rates with high QoS and QoE. Ever increasing demand of data traffic in recent year forced everyone to redesign the network. According to some estimates, the global information communications technology (ICT) ecosystem consumes around 1100 to 1800 Terawatt-hours of electricity annually, which is roughly equal to the electricity used by Germany and Japan combined. Worldwide telecommunication networks (which include wire-line, wireless and core networks) are responsible for more than one third of this energy consumption due to increased coverage and user subscriptions. To meet these challenges, green evolution is becoming an urgent need for wireless networks. It should be noted that the word Green has been coined to focus on reducing CO2 emission and energy efficient systems are considered as green as long as they introduce less gas emissions. A study by GreenTouch indicates that despite the data traffic growth in the next decade, wireless networks can be made Green by reducing their overall energy consumption by almost 90% in the year 2020 with significant economic and environmental impact [20].

Wireless network is a heterogeneous one, where it is ranging from technologies characterized by networks for few UEs with small coverage area (e.g. bluetooth) to networks with larger coverage and hundreds of users (e.g. LTE), which are diverse in nature and coexist in the same environment to provide ubiquitous network coverage. Energy saving mechanisms are comparatively easier for homogeneous environment than heterogeneous environment. This is mainly due to conflicting design goals of different spectrums. In HetNet, establishing and maintaining a successful wireless communication link to simultaneously achieve all the QoS objectives becomes challenging since the energy consumption requirements of

the user and network are different for different objectives. Thus, there is a need for tradeoff techniques to achieve energy efficiency in each protocol layer [21]. A green framework has been proposed for energy-efficient communication in wireless network with energy-cognitive cycle, where the awareness are categories as network awareness and access point awareness module [22].

Similarly, EE issue have been a current topic in optical network. There is no easily defined bound on the energy consumption of optical transmitters and receivers. In determining the bound on energy consumption in transport systems, it is necessary to consider the energy of the optical transmitters and receivers used in the end terminals and in intermediate repeaters. Second-generation optical systems using optical amplifiers have enabled the energy per bit to be reduced to approximately 10 nJ/b/1000-km. In optical network, the energy per bit in the system is determined by the total power consumption of each item of equipment is divided by the number of wavelengths (40) and by the bit rate (40 Gb/s) [23]. The transmission system comprises n identical optically amplified links. Each link has length L and the overall length of the system is nL. A WDM transmitter/receiver (TX/RX) pair at the interface between each link provides regenerated signals at each wavelength for injection in the next link of the system. Energy consumption exist at many levels in optical transmission systems, from inefficiencies at the device level in optical amplifier pump lasers and their cooling systems, at the circuit level in the tradeoff of efficiency for speed in high-speed electronic circuits used in transmitters and receivers, and at the system level in terms of multiplexing and management overheads. The key strategies for reducing energy consumption include improving the energy efficiency of switching, devising methods to reduce the quantity of switching infrastructure in the network, development of low-energy transport technologies, and reducing the energy consumption of the access network [24].

OFDM is a promising technique is used for transmission in wireless network. Similarly, optical OFDM [25] is used in optical network. Therefore, immense amounts of research upon OFDM-based elastic optical networks with fine granularity spectrum splitting mechanism. Subcarrier multiplexing and WDM-PON [26] is a promising solution to support RoF for the convergence of optical and wireless networks [27].

V. Conclusion

The heterogeneity in network is required to support, secure and sustain users. These needs motivate networks to be reconfigurable, flexible, adaptable dynamically to the various components of the networks in both optical and wireless domain. In any situation, the network should transparent to the user. Recent research efforts show that the developments in both the networks are looking for common platform to converge and easily transform from one domain to another domain.

References

[1] http://www.itu.int/en/ITU-R/study-groups/rsg5/rwp5d/imt-2020/Pages/default.aspx, accessed on October 16, 2015

[2] A. Imran and A. Zoha, "Challenges in 5G: how to empower SON with big data for enabling 5G," *IEEE Network,* vol.28, no.6, pp.27-33, Dec. 2014.

[3] P. Chand, R. Mahapatra and R. Prakash, "Energy efficient radio resource management for heterogeneous wireless network using CoMP," Wireless Network, Springer, July 2015.

[4] John E. Mitchell, "Integrated Wireless Backhaul Over Optical Access Networks," *Journal of Lightwave Technology,* vol 32, no.22, pp.3373-3382, Oct. 2014.

[5] T. Biermann *et. al.*, "CoMP clustering and backhaul limitations in cooperative cellular mobile access networks," Elsevier Pervasive and Mobile Computing, 2012.

[6] A. Lozano, R. W. Heath, Jr., and J. G. Andrews, "Fundamental Limits of Cooperation," *IEEE Transactions on Information Theory,* vol. 59, no.9, pp. 5213-5226, Sept. 2013.

[7] T. L. Marzetta, "Noncooperative cellular wireless with unlimited numbers of base station antennas," *IEEE Transaction on Wireless Communications,* vol. 9, no. 11, pp. 35903600, Nov. 2010.

[8] V. Chandrasekhar and J. G. Andrews, "Femtocell networks: A survey," *IEEE Communication Magazine,* 46(9):5967, September 2008.

[9] Amir H. Jafari *et.al.*, "Small cell backhaul: challenges and prospective solutions," *EURASIP Journal on Wireless Communications and Networking,* August 2015.

[10] D. Wake, A. Nkansah and N. J. Gomes, "Radio over Fiber Link Design for Next Generation Wireless Systems," *Journal of Lightwave Technology,* vol.28, no.16, pp.2456 - 2464, March 2010.

[11] Ning Zhang *et.al.*, "Cloud Assisted Hetnets Towards 5G Wireless Networks," *IEEE Communications Magazine,* pp.59-65, June 2015.

[12] Milos Milosavljevic, "Self-organized Cooperative 5G RANs with Intelligent Optical Backhauls for Mobile Cloud Computing," *IEEE ICC 2013; Workshop on Optical-Wireless Integrated Technology for Systems and Networks* , Budhapest, Hungary, 9-13 June, 2013.

[13] Y. Kyung *et.al.*, "Software Defined Service Migration through Legacy Service Integration into 4G Networks and Future Evolutions," *IEEE Communications Magazine,* vol.53, no. 9, pp.108-114, September 2015.

[14] Martin Draxler and Holger Karl, "Dynamic Backhaul Network Configuration in SDN-based Cloud RANs," arXiv preprint arXiv:1503.03309

[15] P. Bhaumik *et.al.*, "Software-defined optical networks (SDONs): a survey," *Photonic Network Communications,* vol. 28, no. 1, pp 4-18, August 2014.

[16] S. Haykin, Cognitive radio: brain-empowered wireless communications, *IEEE Journal on Selected Areas in Communications,* vol. 23, no.2 pp. 201220, Feb. 2005.

[17] W. Wei, C. Wang and J. Yu, "Cognitive Optical Networks: Key Drivers, Enabling Techniques and Adaptive Bandwidth Services," *IEEE Communication Magazine,* pp.106-113, January 2012.

[18] T. R. Tronco, M. M. Feres, A. C. Csar and M. de L. Rocha, "Self-Configuration and Self-Healing for Cognitive Optical Networks," *Journal of Microwaves, Optoelectronics and Eletromagnetic Applications,* vol. 12, no. 2, pp. 193-205, July 2013.

[19] B. Schrenk *et. al*, "Passive ROADM Flexibility in Optical Access with Spectral and Spatial Reconfigurability," *IEEE Journal on Selected Areas in Communications,* September 2015 (early access journal).

[20] "GreenTouch Green Meter Research Study: Reducing the Net Energy Consumption in Communications Networks by up to 90% by 2020," June 2013.

[21] R. Mahapatra *et. al.*, "Energy Efficiency Tradeoff Mechanism Towards Wireless Green Communication: A Survey," *IEEE Communication Survey and Tutorial*, available online.

[22] R. Mahapatra *et. al.*, "Green framework of future heterogeneous wireless network," *Computer Network, Elsevier,* vol.57, no.6, pp.1518-1528, April 2013.

[23] Rodney S. Tucker, "Green Optical CommunicationsPart I: Energy Limitations in Transport & Part II: Energy Limitations in Network," *IEEE Journal of Selected Topics in Quantum Electronics,* vol. 17, no.2, pp.245-274, March-APril 2011.

[24] Rodney S. Tucker, "Green Optical CommunicationsPart II: Energy Limitations in Network," *IEEE Journal of Selected Topics in Quantum Electronics,* vol. 17, no.2, pp.245-260, March-APril 2011.

[25] W. Shieh, H. Bao, and Y. Tang, "Coherent optical OFDM: theory and design," *Optics Express,* vol. 16, No. 2, pp. 841-859, 2008.

[26] D. V. Caballero, "SCM/WDM-PON within-service base band embedded OTDR monitoring," *Optics Communications,* pp.250255, August 2015.

[27] Takuya Murakawa *et. al.*, "Fractional OFDM based Transmitter and Receiver for Time/Frequency Multiplexing in Gridless, Elastic Networks," *Optical Fiber Communication Conference* 2015.

THE 5TH INTERNATIONAL CONFERENCE ON WIRELESS COMMUNICATIONS, VEHICULAR TECHNOLOGY, INFORMATION THEORY, AEROSPACE & ELECTRONIC SYSTEMS (WVITAE-2015)
December 13-16, 2015, Hyderabad, India

On 5G Cellular Backhaul Networks

Mahima Mehta
Intel Mobile Communications, Bangalore, India
Email: mahima.mehta@intel.com

***Abstract*—There is an upsurge in bandwidth-intensive and data-centric applications in cellular wireless networks, witnessing a shift in focus from voice to data services. 5G cellular networks are envisaged to provide very high data rates, high reliability, reduced latency and stringent quality of service, while supporting a diverse range of services. To satisfy these requirements, 5G systems will involve new innovative methods on the Radio Access Network (RAN) and Core Network side. With this, there will also be tremendous impact on the backhaul network to connect the RAN nodes to the Core. This paper reviews 5G wireless network requirements and the wireless backhaul concepts, and discusses the evolving technologies and protocols that can meet the 5G backhaul network challenges.**

I. Introduction

According to Cooper's law [1], the maximum number of "conversations" (voice or data) that can theoretically be conducted over a given area in all of the useful radio spectrum will get doubled every 30 months. Witnessing the trend (Figure 1), there are plethora of bandwidth hungry applications which makes the traffic transition from voice-centric to data-centric [2] quite evident. According to industry estimates, the global mobile data traffic is expected to reach 11.2 Exabyte per month by 2017 [2], [3], as shown in Figure 2. This is due to two reasons: a) increase in the number of Internet-connected devices such as smartphones, tablets etc., which is expected to be more than 4.2 billion by 2017 (Figure 2) and b) deployment of Machine to Machine devices in very large numbers.

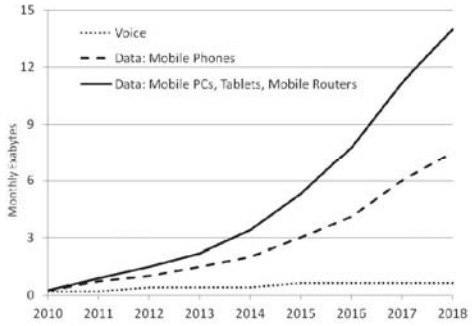

Fig. 1. Global Mobile Traffic (Source: Ericsson Mobility Report [2])

According to the Next Generation Mobile Networks (NGMN) Alliance, 5G networks are envisaged to enable fully mobile and connected society [4]. To attain this objective with billions of connected devices, Gigabit-level traffic will be generated. It is predominantly because 5G networks are expected to support diverse range of applications like Internet of Things (IoT), tactile internet, smart wearable, ultra-reliable communications like automated traffic control/driving, public safety, e-health, and many more real-time applications. Interestingly, there will be distinct and much more stringent quality

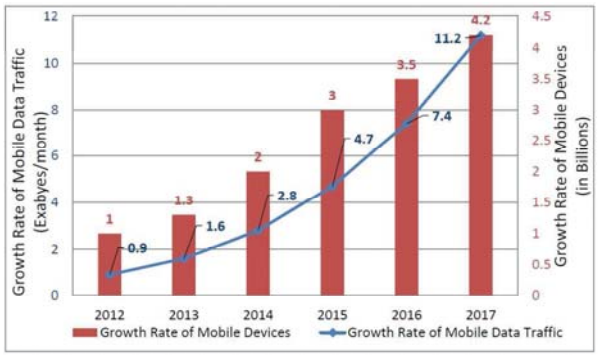

Fig. 2. Growth Rate of Mobile Data Traffic and Mobile Devices [3]

of service requirement for each application, in terms of latency, reliability and energy consumption, compared to 4G networks.

Ultra-Dense Network deployment is one of the technology enablers to meet the 5G requirements. It has several heterogeneous serving nodes, belonging to different Radio Access Networks (RANs). However, increased number of cell edges and significant variation in traffic density in both spatial as well as temporal domain leads to complex interference and mobility management [5]. Therefore, 5G networks need extremely robust and self-organized coordination mechanisms [6], [7] for efficient resource allocation, interference and mobility management. This calls for significant changes to be made in not only access and core network, but also backhaul. As revenues are not growing in proportion to the traffic growth, both cost minimization and capacity improvement are crucial. We review the mobile backhaul concepts and the 5G requirements which makes the backhaul issues crucial. We also discuss the candidate solutions, i.e., evolving technologies and protocols, to meet the backhaul challenges in this paper.

II. Backhaul Technologies

While *Access Network* is the communication link between mobile devices and the transmitting node, *Backhaul Network* (also known as "last mile" network) provides connection between the transmitting nodes i.e., Base Station (BS) and the *Core Network*, i.e., switching nodes as Radio Network Controller (RNC) and Packet Data Gateways.

In Global Systems for Mobile Communication (GSM) network (2G), backhaul link is between BS Transceiver Station and BS Controller, while in Universal Mobile Telecommunications System (UMTS) network (3G), it is between NodeB and RNC. In case of Long Term Evolution (LTE), i.e., 4G, network controller functionality is embedded in eNodeB due to the flat architecture and therefore, backhaul is between eNodeB and Evolved Packet Core nodes including Mobility Management Entity, Serving Gateway (S-GW) and Packet Gateway (P-GW).

Initially, mobile backhaul networks were rolled out as Time Division Multiplexed (TDM) based leased lines and microwave radio links. However, these are issues like: low bandwidth support, high installation costs and inefficient performance for converged data services. Most importantly, they are not scalable, specifically when required to support 1000-fold traffic. Table I summarizes the evolution of cellular technology with supported data rate and backhaul technology. Next, we review the popular wired and wireless backhaul technologies.

TABLE I. EVOLUTION OF BACKHAUL WITH THE EVOLUTION OF CELLULAR TECHNOLOGIES[1] (ADAPTED FROM [8])

Time Frame	Generation	Standard	Peak Data Rate	Backhaul Technology
Before 1999	1G	GSM	10 kbps	TDM
1999	2G	EDGE	200 kbps	TDM
2002	3G	WCDMA	384 kbps	ATM
2005	3G	HSDPA	3-21 Mbps	ATM
2009	3G	HSPA+	42 Mbps	ATM/IP
2010	4G	LTE	>60 Mbps	IP

A. Wired Backhaul

The physical transmission medium for wired backhauling could be either copper or optical fiber.

1) Copper, DSL: Technologies like E1/T1 and Digital Subscriber Line (DSL) widely use copper as the data transmission medium. DSL is predominantly deployed for residential broadband services and is suitable for delay insensitive cellular traffic backhaul for indoor scenarios. Very High Speed DSL2 (VDSL2) is one variant of DSL which provides data rate around 100 Mbps over short distances.

2) Optical Fiber: Optical fiber outperforms copper based backhaul in terms of capacity. A Passive Optical Network (PON) is a point to multipoint fiber based architecture which deploys an Optical Line Terminal (OLT) at service provider's end and a number of Optical Network Units (ONUs) near end user. Passive optical splitter near OLT enables single fiber to serve multiple termination points. Downlink signals are broadcasted, while uplink signals are TDM. Driven by passive components such as unpowered splitters and filters, PON offers high reliability and low cost compared to active networks. The PON data stream is converted to Ethernet/Wi-Fi at the subscriber's location and its range is about 20 kms.

Gigabit PON (GPON) and Ethernet PON (EPON) are two prominent standards. GPON uses optical Wavelength Division Multiplexing (WDM) so that a single fiber can be used for both downlink and uplink data. The latest version, Next Generation PON2 (NG-PON2) [9] uses Time and WDM and unlike other variants, uses active filters and tunable lasers in the ONU. It offers 40 Gpbs and 10 Gbps for downstream and upstream respectively. EPON is fully compatible with Ethernet standard. Its extension 100 GbEPON can support 100 Gbps data rate. Thus, Ethernet networking technology being scalable, turns out to be a carrier grade transport technology for mobile backhaul.

[1] EDGE: Enhanced Data for Global Evolution; WCDMA: Wideband Code Division Multiple Access; HSDPA: High-Speed Downlink Packet Access; HSPA: High-Speed Packet Access; ATM: Asynchronous Transfer Mode; IP: Internet Protocol

B. Wireless Backhaul

Compared to wired backhaul, it is easier and faster to deploy. The operational frequency distinguishes the different wireless backhaul options. Different frequency bands have different channel characteristics, which classifies the use cases and deployment scenarios for wireless backhaul options.

1) Satellite Backhaul: Satellite network is expected to evolve to provide terabit/sec of throughput. It is useful for broadcast/multicast services and can provide ubiquitous and reliable connectivity for non-real-time services, especially in remote/rural areas. Higher delay is one issue when real-time services are considered. It is due to long round trip time over a geostationary satellite, which can be improved with medium earth orbit satellite solutions. Very Small Aperture Terminal (VSAT) technology supports delay sensitive as well as IP based multicast applications. Thus, the technological advancements are expected to reduce cost and latency constraints to ensure the feasibility of satellite backhaul.

2) TV White Space Backhaul: It is the unused part of the TV band transmission, typically lying in the range 470-698 MHz. This allows radio signals to traverse distances of about 10 kms, which is much more than conventional mobile bands that starts at 800 MHz. Hence, the deployment costs are less. TV white space backhaul is an ideal candidate to provide rural broadband services at low cost.

3) Free Space Optics (FSO): It is a Line-of-Sight (LoS) technology that uses invisible beams of light (using LED/LASER) to provide optical bandwidth connections that can send/receive voice, video, and data information [10]. This optical connectivity does not require expensive fiber-optic cable or radio frequency spectrum licensing, which reduces the deployment cost and time. It is upgradable and has open interfaces, which allows using equipments from any vendor. FSO is immune to interference due to very narrow beam transmission, and offers speed of about 2.5 to 10 Gbps using WDM for short range, 20 meters to 8 kms. However, FSO communication gets severely affected by fog and atmospheric turbulence, which may cause scintillation and beam wander.

4) Microwave: Traditional microwave backhaul operates on carrier frequencies between 6 GHz and 42 GHz, which is a licensed spectrum, and offers data rates upto 1 Gbps. It is specifically useful for remote locations, where physical links are not feasible. While its operational cost is low, initial deployment cost is high. Microwave radios can support native Ethernet transport, statistical multiplexing and adaptive modulation. Long range transmission of about 10 kms is possible with highly directive antennas, due to moderate pathloss.

5) mmWave: Millimeter wave is a new generation of point-to-point microwave radio, operating in 60, 70/80 and 90 GHz bands, where each band offers up to 9 GHz spectrum. 60 GHz band is unlicensed, while its inexpensive to obtain license for other two bands. Therefore, faster and low cost deployment is feasible. These high frequency signals undergo heavy path loss and attenuation due to atmospheric absorption and rain. High signal attenuation results in reduced interference between mmWave transmissions. Path loss compensation can be achieved by either increasing transmit power (hardware and regulation constraints) or using highly directional antennas (improves security and is feasible). However, due to highly

directional antennas with small beamwidth, multipath benefits like diversity cannot be exploited. Hence, it is difficult to implement spatial diversity multiplexing techniques like MIMO and LoS is essentially required. Yet, mmWave backhaul can support data rate up to 10 Gbps, over 10 km range and is suitable for dense urban scenario.

III. Towards 5G

Massive growth in mobile data demands, number of wireless devices, diverse range of applications, ubiquitous connectivity and drastic changes in end user's expectation are the key factors driving the 5G technological advancements [4]. Additionally, very high data rates, energy efficiency, high reliability and very low latency requirements are predominant. In addition to integration of these characteristics, flexibility to adapt to the changing scenarios is required. This section discusses the key enablers for 5G and the evolving technologies which will play a significant role in the 5G roll out.

A. Key Enablers

Ultra-Dense Deployment involves several low power BSs (small cells), complementing the existing macro cell network, to meet the high traffic demands. These low power BSs can be pico cell, femto cell (for indoor scenarios), Remote Radio Heads (RRHs) or WiFi Access Points (APs). Such infrastructure, also known as Heterogeneous Network (HetNet) provides 1) efficient spectrum utilization, due to aggressive spectral reuse across multiple cells and 2) higher area spectral efficiency, due to reduced distance between users and serving nodes and the availability of dense network of BSs. The coexistence of both networks is preferred over complete replacement because both have their use case specific beneficial attributes. For instance, while macro cell network manages connectivity with high-speed users to ensure minimum handovers, small cells connects with low/medium speed users to provide higher data rates and efficient resource utilization.

Flexible Centralized Processing: With ultra-dense HetNet deployment, there are overlapping cellular footprints and each user lies in the coverage area of more than one BS, which makes association as well as mobility decisions crucial [11]. Also, the increased number of cell edges makes multi-cell interference management complicated. Additionally, temporal and spatial variation is user traffic density requires mechanisms for adaptive load balancing and interference-aware resource allocation. This calls for flexible and adaptive self-organized mechanisms [7] to be implemented in a centralized manner, which can be beneficial for both RAN as well as network [13]. At RAN level, joint Radio Resource Management (RRM) and Inter Cell Interference Coordination (ICIC) algorithms can be implemented by centralized processing. At network-level, centralized processing can enable dynamic resource allocation and network configuration based on the variation in user traffic demands. Additionally, BSs can be turned off during low load conditions to achieve energy efficiency. Hence, network operators can perform use case specific optimizations on a large scale to meet network-centric objectives.

B. Cloud Based Mobile Networks

Self-Organized Networking (SON) solutions typically operate at coarse time scales and optimize RAN performance by control plane coordination without impacting fine time scale scheduling in data plane. Significant gains are obtained using SON algorithms for RAN optimization in cellular networks [12]. Considering 5G requirements, more sophisticated RAN optimization can be performed by data plane coordination across BSs at fine timescales. Coordinated Multi-Point (CoMP) transmission is one such approach, where BSs from multiple cells coordinate their data transmissions such that interference is minimized and throughput gains are maximized. Performance gains now depend on how efficiently the centralized coordination is implemented.

Cloud-RAN (C-RAN) [13] enables efficient implementation of centralized coordination by decoupling processing from transmission, within the data plane. In C-RAN, all BSs (i.e., BaseBand processing Units (BBUs)) are aggregated in a centralized data centre (cloud), where all baseband processing is performed, while the Radio Frequency (RF) transmission is handled by RRHs which are distributed in a region to meet coverage requirements. RRHs or set of RRHs are generally referred to as Radio Access Units (RAUs). Centralized processing in C-RAN provides higher capacity due to aggressive reuse of resources, enhanced cooperative gains, better interference management, green infrastructure, reduced capital and operational expenses, easier traffic load balancing and flexibility through software defined virtualization of communication networks and protocols. Note that HetNet with cloud computing is known as Heterogeneous C-RAN (H-CRAN).

The communication link between BBU pool and RAUs is known as *fronthaul* which is required to support high data rates. At present, only fiber links support about 10 Gbps for TD-LTE with a 20 MHz bandwidth. Optical fiber coupled with WDM and/or TDM is used for signal distribution from BBU to RAU with high reliability and low latency. Signals can be transported in two ways: 1) digitized radio signals through Common Public Radio Interface (CPRI) [15], or 2) analog radio signal through Radio-over-Fiber (RoF) [16] technology. Digitized radio signal transmission experiences less degradation and can transport signals over longer range compared to RoF. However, it requires large backhaul bandwidth to carry the sampled radio signals of the order of 10 Gbps.

C-RAN decouples BBU pool from RAUs in terms of physical connectivity, but there are two issues adversely affecting the performance gains. First, there is a one-to-one logical mapping between a BBU and an active RAU. Thus, distinct radio frame for each cell is required. It enables techniques like CoMP and dynamic Fractional Frequency Reuse (FRR) to be used for capacity enhancement. However, such schemes are applicable only for static users. For non-stationery users, traditional Distributed Antenna System (DAS) technique can be used to allow transmission of the same radio signal to multiple small cells and provide increased coverage and diversity gain, while avoiding frequent handovers. Second, a single BBU is capable of managing load of multiple cells by serving them via a DAS, in case of sparse traffic. However, this will require mapping a BBU to a set of RAUs. Thus, to serve both static and mobile users, and handle variable load conditions in an energy-efficient manner, flexible backhaul is required which can also support "one-to-many" logical mappings between BBUs and RAUs. Authors in [14] propose a C-RAN system with flexible backhaul architecture, where the physical backhaul remains

the same but logical connectivity between BBUs and RAUs is configurable to adapt to varying user and traffic load profiles, and uses RoF technology for backhaul.

C. SDN in Cloud-Based Mobile Network

Performance of cloud based mobile network can be further enhanced by using Software Defined Networking (SDN). Traffic and energy optimization can be achieved by dynamically using SDN concept on backhaul/fronthaul. SDN enabled network [17] decouples data and control plane and uses OpenFlow Application Programming Interface (API) for interaction between the two. A software based controller aggregates the control plane functions, maintains an abstract view of the network topology and provides API to network operators. The operators can control the data traffic flow and handle congestion by effective traffic management and optimized resource allocation. Thus, SDN makes network devices (switches/routers) programmable and enables segregation of traffic flows, routing of flows to specific services and efficient resource management.

With the introduction of switching hardware in the fronthaul and flexible mapping between BBUs and RRHs, traffic optimization in RAN and energy optimization in BBU pool can be achieved jointly. Emerging SDN approaches facilitate transition from source-to-destination traffic routing to context-aware traffic routing and manage the complex traffic management, by providing programmable data plane. Most of the SDN related works consider wired networks and gradually, SDN concepts are being implemented in wireless networks, specifically backhaul segment. It is being investigated that unified control of radio interfaces via SDN [18] can enable flexible spectrum and capacity management.

D. RAN as a Service (RANaaS)

There is a trade-off between centralized processing requiring high capacity fronthaul links as in C-RAN, and decentralized processing using traditional backhaul. This trade-off can be exploited by the novel *RAN as a Service* concept [13], which provides flexibility in centralizing RAN functionalities based on the requirement and network characteristics. Figure 3 shows the flexible functional split of radio protocol stack between RANaaS platform and RAUs. The left side shows conventional LTE implementation where all functionalities up to admission and congestion control are implemented at BS (RAU). On the right side, C-RAN approach is shown where only radio front end is implemented at RAU, while all other functions are centralized. RANaaS is a midway approach which centralizes only some of the functionalities. For instance, when high capacity backhaul is available, lower layer functions can be shifted to RANaaS platform to achieve higher degree of centralization. However, implementation of such a functional split [13] is challenging for RAN, due to various constraints like latency, backhaul, etc. Latency issues may arise due to virtualization of RAN resources.

IV. Heterogeneous Backhaul for Cloud-Based Mobile Networks

A typical backhaul for 5G network may have a combination of one or more of the components discussed in Section III.

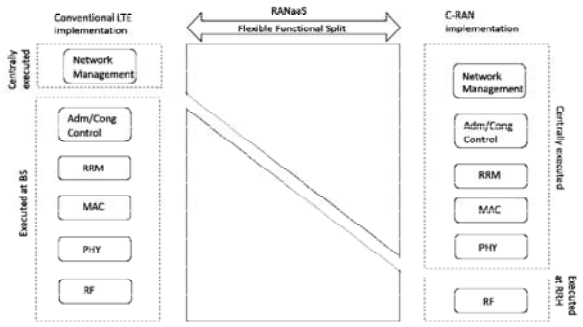

Fig. 3. Flexible Functional Split (Adapted from [13])

Backhaul for cloud based ultra dense HetNet must be able to handle different types and degrees of centralized processing, from conventional LTE to RANaaS platform to C-RAN implementations. The envisaged architecture for 5G networks with heterogeneous backhaul and RANaaS is shown in Figure 4. This section discusses the concerns and crucial aspects involved in provisioning heterogeneous backhaul [19], which is envisaged to enable 5G.

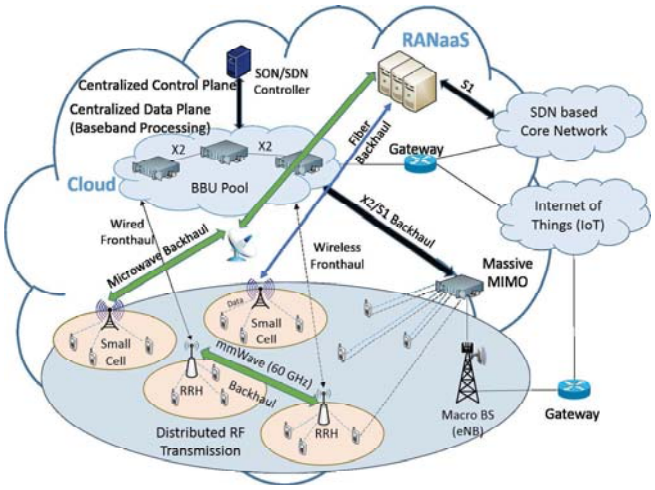

Fig. 4. Envisaged 5G Architecture with RANaaS, SDN-based C-RAN and Heterogeneous Backhaul

A. Heterogeneous Backhaul Challenges

The main challenges identified in design and optimization of backhaul are as follows:

Heterogeneity: In an ultra-dense network with diverse deployment scenarios, heterogeneous backhaul is required because different technologies discussed in Section II are suitable for different deployments. At the same time, it is not feasible to have a completely unified backhaul deployment throughout. Considering the data rate requirement and transmission range, fiber based backhaul seems to be the best choice. However, with deployment cost and geographical location considerations, it is not feasible to lay down fiber everywhere. Easy availability makes DSL backhaul a suitable option for indoor backhaul. TV white space and satellite backhaul seems to be the perfect choice for rural broadband services. FSO and

Millimeter wave backhaul/fronthaul is suitable for road side lamp posts, river side and inter-site connections. The non line of sight coverage can be ensured and transmission range can be increased by multihop concatenation of these links, at the cost of additional latency.

Data Rate: The data rate support expected from backhaul will depend on the degree of centralization in RANaaS. In case of full centralized processing like C-RAN, very high bandwidth backhaul will be required. Due to the heterogeneity of backhaul options and variable capacity, the flexible functional split in RANaaS needs to give consideration to the data carrying capacity of the available backhaul.

Latency: Latency is a function of the distance between user and RANaaS, the number of nodes in the end-to-end link and the amount of processing at each node. Processing and protocol latency can be reduced by improving the processing capabilities at each node.

B. Joint Access and Backhaul Design

5G networks are evolving towards an ultra-dense network, where small cells connected to RANaaS platform, may be deployed at unconventional locations. There will lead to different deployment scenarios, each requiring a different backhaul solution, resulting in heterogeneous backhaul infrastructure. It is crucial to ensure that backhaul does not become a bottleneck in meeting the end-to-end requirements in terms of throughput and latency. While RANaaS provides flexibility in sharing the functionalities between small cells and RANaaS, it makes sense to explore access and backhaul design issues jointly.

One instance, when centralized processing is shifted from RAU towards RANaaS. This is likely to happen when high capacity backhaul like fiber, mmWave etc is available. Let the use case be of uplink data transmission, which typically requires decoding at BS to reduce bandwidth requirement and re-encoding for transmission towards RANaaS. In such case, decoding process can be skipped at small cell and the received samples can be forwarded to RANaaS directly. This reduces the hardware requirement, reducing the deployment costs. In addition, latency and energy consumption will reduce.

Another instance, when centralized processing is shifted from RANaaS towards BS or RAU. Let the use case be frequency domain RoF approach for downlink. In a typical RoF architecture, time domain signals from multiple users along with overhead are transmitted from centralized controller to RAU. With the FFT/IFFT functionality shifted to RAU, it is possible to transmit data in frequency domain on per-user basis. This reduces overhead and hence, the capacity requirement on backhaul. User specific transmission also makes the implementation of adaptive beamforming easier.

V. Conclusion

To support multitudes of data-centric applications, demanding high reliability and very low latency, 5G networks are expected to deploy ultra-dense HetNet with cloud-RAN, which mitigates inter-tier interference efficiently and improve cooperative processing gains. Corresponding upgradation in capacity and latency is expected from backhaul network, to ensure a sustainable end-to-end user experience. With SDN implementation, the data and control plane decoupling enables efficient traffic and energy optimizations, which is useful for both RAN and backhaul. We review different backhaul technologies and their suitability for different deployment scenarios. We discuss the backhaul related challenges in cloud-based architecture and infer that heterogeneous backhaul solutions will meet the 5G requirements. With the implementation of *RAN as a service*, degree of centralization will vary, impacting the data rate and latency requirements for backhaul. This calls for a flexible functional split and joint optimization of access and backhaul, so that backhaul dose not pose any constraint and end-to-end performance is achieved.

References

[1] Cooper's Law, [Online] Available: http://www.arraycomm.com/technology/coopers-law/.

[2] Ericsson, "Ericsson Mobility Report"', Technical Report, June 2013. [Online] Available: http://www.ericsson.com/res/docs/2013/ericsson-mobility-report-june-2013.pdf.

[3] Cisco, "Cisco Visual Networking Index: Global Mobile Data Traffic Forecast Update", Technical Report, 2012-2017. [Online] Available: http://www.cisco.com/en/US/solutions/collateral/ns341/ns525/ns537/ns705/ns827/white_paper_c11-520862.html.

[4] NGMN Alliance, "5G White Paper", Feb. 2015. [Online] Available: .

[5] M. Mehta, "Radio Resource and Mobility Management Techniques in Heterogeneous Cellular Network", PhD Thesis, IIT Bombay, 2014.

[6] M. Mehta, N. Rane, A. Karandikar, M. A. Imran, B. G. Evans, "A Self-Organized Resource Allocation Scheme for Heterogeneous Macro-Femto Networks", Wireless Communications and Mobile Computing, 2014. [Online] Available: http://www.wileyonlinelibrary.com.

[7] O. A. Glenn, M. Mehta, M. A. Imran, A. Karandikar, B. G. Evans, "A New Cellular Automata based Self-Organized Fractional Frequency Reuse Scheme", IEEE Transactions on Vehicular Technology, Vol. 64, No. 4, pp 1535-1547, April 2015.

[8] S. Chia, M. Gasparroni, P. Brick,"The Next Challenge for Cellular Networks: Backhaul", IEEE Microwave Magazine, Vol.10, No.5, pp.54-66, Aug. 2009.

[9] PT Inovacao White Paper, "Evolution of FTTH Networks for NG-PON2", July 2013.

[10] Free Space Optics; http://www.freespaceoptics.org/

[11] M. Mehta, N. Akhtar and A. Karandikar, "Enhanced Mobility State Estimation in LTE HetNets", National Communications Conference (NCC), pp.1-6, 2015.

[12] O.G.Aliu, A.Imran, M.A.Imran and B.G. Evans, "A Survey of Self-Organisation in Future Cellular Networks", IEEE Communications Surveys and Tutorials, vol.15, no.1, pp.336-361, 2013.

[13] P. Rost, C. J. Bernardos, A. D. Domenico, M.D. Girolamo, M. Lalam, A. Maeder, D. Sabella, D. Wubben, "Cloud Technologies for Flexible 5G Radio Access Networks", IEEE Communications Magazine, pp.68-76, May 2014.

[14] L. Cheng, K. Sundaresan, J Meilong, S. Rangarajan, C. Gee-Kung, "The Case for Re-configurable Backhaul in Cloud-RAN based Small Cell Networks," pp.1124-1132, INFOCOM, April 2013.

[15] Common Public Radio Interface, http://www.cpri.info/

[16] M. Sauer, A. Kobyakov, J. George, "Radio Over Fiber for Picocellular Network Architectures", Journal of Lightwave Technology, vol.25, no.11, pp.3301-3320, Nov. 2007.

[17] M.Y. Arsian, K. Sundaresan, S. Rangarajan, "Software-Defined Networking in Cellular Radio Access Networks: Potential and Challenges", IEEE Communications Magazine, pp 150-156, January 2015.

[18] C. Niephaus, O.G. Aliu, M. Kretschmer, S. Hadzic, G. Ghinea, "Wireless Back-haul: a Software Defined Network Enabled Wireless Back-haul Network Architecture for Future 5G Networks", IET Networks, 2015, IET Digital Library: http://digital-library.theiet.org/content/journals/10.1049/iet-net.2015.0009.

[19] J. Bartelt, G. Fettweis, D. Wubben, M. Boldi, B. Melis, "Heterogeneous Backhaul for Cloud-Based Mobile Networks", Vehicular Technology Conference (VTC Fall), pp.1-5, 2013.

THE 5TH INTERNATIONAL CONFERENCE ON WIRELESS COMMUNICATIONS, VEHICULAR TECHNOLOGY, INFORMATION THEORY, AEROSPACE & ELECTRONIC SYSTEMS (WVITAE-2015)
December 13-16, 2015, Hyderabad, India

Cybersecurity for M2M Smart Grid

Sarmistha De Dutta, Prof. Ramjee Prasad
sd56@columbia.edu, prasad@es.aau.dk

Abstract –
The Smart Grid is the next-generation electrical power system that combines OT (Operations Technology) and IT (Information Technology) for the efficient generation, delivery, and consumption of electrical energy. More and more utility companies around the world have started to evaluate, plan, and implement Smart Grid technologies by deploying Advanced Metering Infrastructure (AMI) and other electronic communications technologies that enable the utility to monitor and analyze their networks and provide customers with a more reliable and efficient power system both at the smart grid level and micro grid level. Data that is generated by the Smart Grid is now referred to as 'big data' - data that is high in volume, velocity, variety or a combination of all three. This data is very useful as it allow utilities to gather higher resolution consumer energy usage data compared to the legacy centralized electrical power plant and distribution grid.
As Smart Grid implementation gains momentum and utilities are collecting high-volumes of data, consumer concerns about the security and privacy of this data are forcing utilities to identify and address the increasingly important issue of securing this data without compromising the efficient delivery of electricity. We aim to provide a brief overview M2M communication and its history, its application in the Smart Grid, security issues affecting M2M data on the Smart Grid and some available solutions to detect and prevent cyber threats.

Index Terms – Smart Grid, M2M, Cyber Security, AMI

INTRODUCTION

With the start of the new millennium, the term Machine to Machine (M2M) communications has become increasing prevalent in our everyday lives. However, the concept of M2M has its roots in the term 'Telemetry' which originated over 150 years ago. Telemetry in its original form was the collection, transmission, and monitoring of data, over wires. The first official occurrence of data telemetry dates back to 1845 when live data was transmitted between the Russian Tsar's Winter Palace and the army headquarters. Another breakthrough application of telemetric data was in 1912 when the Commonwealth Edison implemented a telemetry system using telephone lines to transmit operational data on electric power plants throughout the city and use this data to monitor electrical loads on Chicago's power grid.

We have made great strides in the field of telemetry over the past century and nowadays telemetric data is used in solutions across a wide-range of fields such as medicine, meteorology, aerospace communications, and managing retail sales transactions. [1] Another notable application of data telemetry came in the 1980's with the introduction smart homes. By the 1990s', a new business model evolved out of the basic concept of telemetry, M2M. [2]

Figure 1: Evolution of M2M

While telemetry was typically limited to the use of radio signals, M2M was able to transmit and measure sensor data from remote sources harnessing newer technologies such as wireless sensors, mobile devices, wireless networks, and the Internet. [2]. With the advent of this decade, M2M communications has become synonymous with another evolving concept, the Internet of Things (IoT). The IoT is a system of devices such as sensors, smart appliances or intelligent electronic devices (IEDs) installed at strategic locations on the M2M communications network that transmit and receive data which is then collected, analyzed, and accessed through a gateway such as the Internet.

M2M communications is used in a whole slew of industries ranging in such diverse fields as transportation and medicine. An increasingly popular application of M2M communications technology is in the energy sector, namely the Smart Grid (SG). The Smart Grid allows utility companies to integrate two-way M2M communication and electricity flows. Sensors and advanced control mechanisms are used to capture then analyze real-time data on power delivery, generation, and consumer usage. This information allows utility companies to manage energy supplies and demand as well as customer billing more efficiently. However, along with all these undeniable benefits comes the realization that this advanced communications and OT/IT infrastructure which is responsible for the enhanced Smart Grid is also its Achilles heel by increasing susceptibility of the power grid to destructive cyber events. The underlying technology that empowers the SG also

makes it vulnerable to cyber attacks which can also be detrimental to the health of a nation's power delivery system. [16]

M2M COMMUNICATION ARCHITECTURE

Machine to Machine (M2M) communication is the flow of data from a machine, over a wire line or wireless network, and through a gateway to another machine where it can be collected, analyzed, and these results be used for informed decision-making and applied to a wide range of services. [3]

A high-level overview of the M2M communication architecture, as per the European Telecommunications Standards Institute (ETSI) model, considers three main domains:

- M2M Device Domain – connects intelligent M2M devices to M2M gateways
- M2M Network Domain – connects M2M gateways to M2M applications
- M2M Application Domain – provides the middleware layer where the M2M data is used in business software applications

An M2M device can range from a simple temperature sensor to a highly intelligent computer system. The M2M communication is initiated by extracting data from a remote data collection device either in response to a request or automatically. Refer to Figure 2 for a simple visual depiction of the M2M architecture. [4, 15]

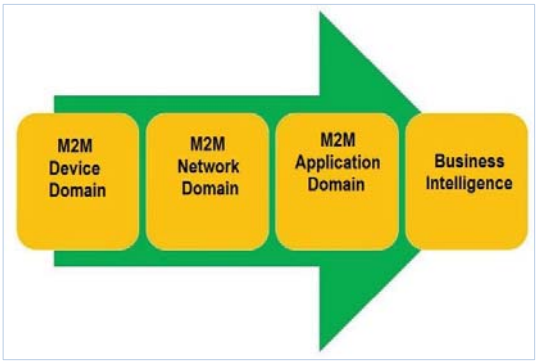

Figure 2: M2M Architecture

After the data is extracted from the remote device, it is then transported using a wired/wireless network, PLC (power line communications) lines, or communication satellites, to the M2M application where it undergoes processing. Meaningful information is extracted from these results which is in turn utilized by different business services.

Though telephone lines may be used if a line is readily available and satellites are practical for monitoring equipment in remote areas, cellular networks provide the best, cost-effective method of M2M communication in today's increasingly mobile environment. [3]

As the M2M ecosystem expands and industry leaders are jumping on the M2M bandwagon, there is an increasing need to bring standardization to this new area. The wireless standard groups such as IEEE, 3GPP, and ETSI are already studying the effects of increasingly wide-scale usage of M2M devices on existing networks.

SMART GRID CONCEPTUAL MODEL

The Smart Grid, a popular application of M2M communications, is the next-generation electrical power system that integrates OT (computers/network for power delivery) with IT (computers/network for business processes). The OT platform allows utilities to manage energy resources, plan for emergencies, and maintain the grid load based on data received from among other sources, the Supervisory Control and Data Acquisition (SCADA) system. While the IT platform is used by utilities to manage their business and administrative processes. [17] This grid infrastructure utilizes increased use of telecommunications and digital technology for an automated, decentralized, consumer-interactive but also environmentally sustainable generation, delivery, and consumption of electrical energy. In a nutshell, the SG is a more efficient electricity delivery system. [5]

The National Institute of Standards and Technology (NIST) Smart Grid Conceptual Model defines the Smart Grid as consisting of seven distinct domains: Bulk Generation, Transmission, Distribution, Customers, Operations, Markets, and Service Providers. The first four domains, cover the generation, storage, delivery of electricity, and support bi-directional flow. The latter three domains manage this electricity flow and provide data or services to power utility companies and their customers.

The IEEE-based Smart Grid model [6] shown in Figure 3 displays the two-way data and electricity flow between each domain and demonstrates how they are inter-connected to create an intelligent and dynamic power grid. [7]

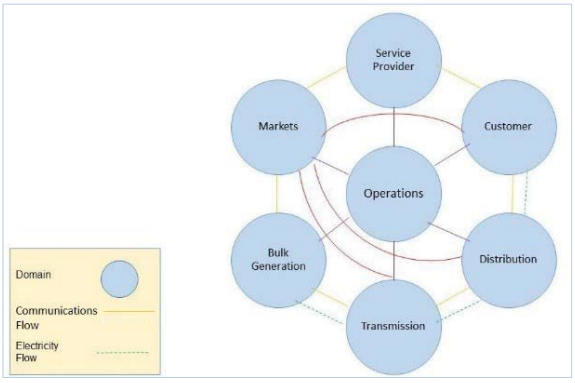

Figure 3: Smart Grid Conceptual Model

Energy is generated in the Bulk Generation domain from both centralized, traditional sources as well as distributed energy resources (DER): renewable variable sources - solar, wind; renewable non-variable sources - hydro, biomass, geothermal;

non-renewable and non-variable sources such as nuclear, coal and gas.

In the Distribution domain, electricity is distributed to utility customers (home, commercial, industrial) who are connected to the electric distribution network through intelligent M2M field devices such as smart meters. The Advanced Metering Infrastructure (AMI) is an integrated system of smart meters, meter data management systems, and gateways that allows communication between the customer and utility company. Using a real-time, two-way communications network, customers can sell back unused energy to the power grid, thus helping balance the supply and demand of power usage. The SCADA system remotely controls, monitors, and acquires real-time data every 2-5 seconds from distributed substations. This data is then used by utilities to evaluate the condition of the power delivery network every few minutes and take the necessary actions to ensure a reliable supply of power. [17]

Through the Operations domain, information such as energy consumption data collected from the consumer is further processed and provides key business intelligence. Integrating the AMI with the traditional distribution infrastructure has led to a more efficient power grid. In the Service Provider domain**,** third-party service providers such as web portals allow end-customers to exchange data with their utility company and empowers the consumer to better manage their energy consumption. [7]

The first 'smart meter' was publicly deployed in the 1990s' and since then utility companies around the world have started evaluating, planning, and implementing Smart Grid technologies by deploying Advanced Metering Infrastructure (AMI) and other digital communication technologies. This allows the utility to monitor and analyze their distribution networks and provide customers with a more reliable, available, and efficient power system whether at the smart grid level or micro grid level.

The sources of data [14] generated by this intelligent Smart Grid are as follows:

- AMI (Smart Meters)
- Distribution automation (Grid)
- Third-party Data (Data external to Grid)
- Asset Management (Firmware for smart device or Operating System)

A key component of the SG is the "smart meter". Metering is just one of the many M2M business application that utilities are using to exploit the full potential of the Smart Grid. The smart meter is a device that is used to store data related to power consumption and provides insight into the trends in electricity usage. Data from smart meters is now collected at 5-15 minute intervals as opposed to the monthly readings of the past. [9]. This is just one of the sources responsible for the explosive growth in Smart Grid data is shown in Figure 4, provided by the Electric Power Research Institute. This graph helps us better visualize the vast volumes of data that the utility must be able to analyze in order to realize the full potential of the Smart Grid.

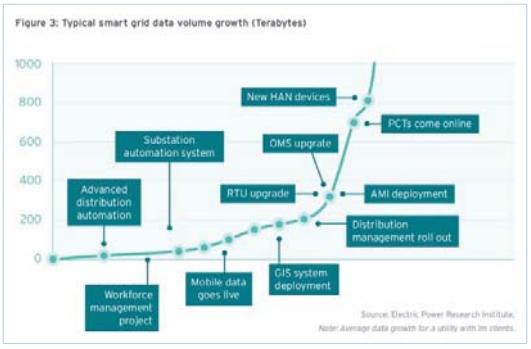

Figure 4: Smart Grid Data Growth
(Source: Electric Power Research Institute)

SECURING THE SMART GRID

The widespread blackout affecting parts of the US in August 2003, though not a result of a cyber attack, still gave us our first experience of the fallout from a possible attack. The Smart Grid is a much more complex system compared to its predecessor, the legacy power grid. The very components that are responsible for its 'intelligence" also make it more vulnerable to cyber threats. Improving cyber security, power system security, and protecting consumer data while being able to balance power grid performance with cost is a tightrope that utility companies will have to learn to manage if they wish to fulfill the true potential of the Smart Grid.

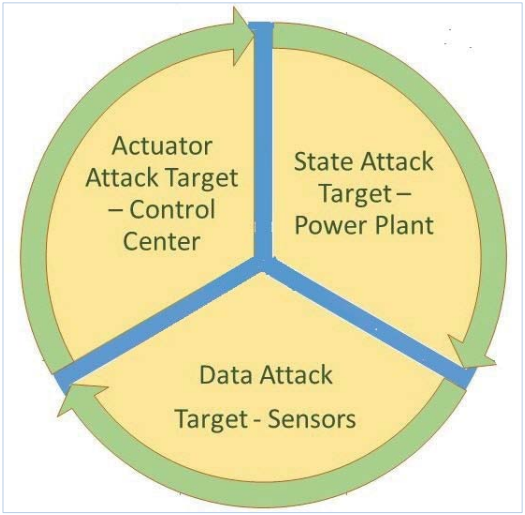

Figure 5: Smart Grid Security Cycle

Vulnerabilities in the Smart Grid range from access to and manipulation of smart devices such as IEDs with malicious intent, proliferation of malware, denial of Service (DoS) attacks, hacked smart meters, deliberately modified sensor and SCADA systems data, to the unauthorized modification of routing in wireless networks and these can all disrupt grid operations. Concerns about customer data protection and privacy are also equally important. As utility companies plan

to expand their Smart Grid operations, they must also address the problem of data security. Security controls must be correctly designed and implemented in order to provide consumers with an efficient yet secure power delivery system. In order to be truly effective these security controls will have to satisfy the unique needs of both the OT and IT platforms. [10, 11]

As Smart Grid implementation progresses around the world, the OT/IT platforms are increasing overlapping and utilities are collecting increasing volumes of Smart Grid data. Applying big data analytics to smart meter data, network sensor data and operational voltage load SCADA data will allow utilities to detect cases of electricity theft, anomalous behavior, and even predict malicious events that can lead to the disruption of power delivery. [11, 15]

Utility companies are also working with agencies such as NIST, NERC CIP (North American Reliability Corporation – Critical Infrastructure Protection), US Dept. of Energy (Office of Electricity Delivery and Energy Reliability), and IEEE among others to develop a Smart Grid security framework which will encompass remote access, authentication, encryption, and privacy of meter data and customer information thus ensuring that Smart Grids provide consumers with an efficient but safe and secure energy supply chain. [12]

BIG DATA ANALYTICS FOR THE SMART GRID

As the volume of data from the SG grows over time, utilities will have to collect, store, and mine data, then apply predictive analytics for utilities to further develop their business and manage both their operations and customer base more efficiently and effectively.

Utilities can analyze this data using the following types of Smart Grid analytical tools:

- Meter Analytics
- Grid Analytics
- Asset analytics
- Renewable Energy Integration

Utilities will increase their budget for Smart Grid data analytics as shown in the Pike Research report [Figure 6] and demand is expected to increase globally by $34 billion through 2020 with maximum growth in the Asia Pacific region. [8]

Data that is generated by the Smart Grid is now referred to as ‘big data’ which simply means data that is high in volume, velocity, variety or a combination of all three. The data generated is very useful as it allows utilities to gather consumer energy usage data at a more granular level compared to the legacy centralized electrical power plant and distribution grid. This is beneficial to the entire energy sector including energy retailers, distributors and generators as it not only allows consumers to have a better understanding of their own energy consumption, but also allows energy companies to interpret the detailed consumption patterns of their consumers and plan more accurately for future energy needs while also incorporating alternative energy sources such as wind, hydro, and solar energy, as well as the impact of micro grids on the power infrastructure. [9]

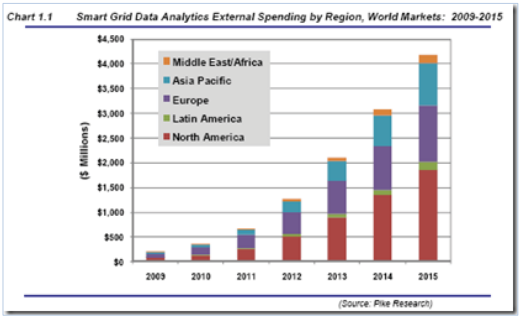

Figure 6: Smart Grid Analytics Market Distribution (Source: Pike Research)

Only if we can effectively collect and analyze these volumes of grid data generated by smart meters, sensor captures, appliances, and electric cars and then act upon the results in real-time, can we exploit the full potential of the Smart Grid. However, this requires building statistical models that extract useful information and identify patterns hidden within the generated M2M data, allowing the grid operator to use these results and forecast future grid behavior. [15]

These predictive models can help utilities optimize the Smart Grid. The field of Smart Grid data analytics, both traditional and cloud-based analytics is just evolving and applying predictive analytical techniques to mine and analyze Smart Grid data and then make intelligent decisions has not yet been fully exploited. An analytical tool can play an important role in analyzing the data generated by the Smart Grid and ensure that it operates at peak performance. [15]

However, along with optimizing performance, data-mining tools can also be used to secure the SG and prevent potential cyber attacks. A crucial M2M security application for securing the Smart Grid is authentication. For example, a lack of proper security controls for authentication can easily compromise the integrity of smart meters, a key component of the Smart Grid.

Key industry players such as ABB, NIKSUN, eMeter (Siemens), IBM, General Electric to name a few have recognized the global market demand for Smart Grid data security analytics solutions and each are a making their own niche in this rapidly expanding market are shown in Figure 7. Each vendor is developing their own technology to effectively and efficiently transform the data generated by the various components of the Smart Grid into data that is useful to utilities who would like to ensure a secure Smart Grid for its customers. [13]

However, it is important to note that these same techniques that are supposed to protect the SG can also be used by individuals for personal and illegal gain. For example,

statistical models for tracking home energy consumption can also be used to detect unusual behavioral patterns which can then by exploited by criminals.

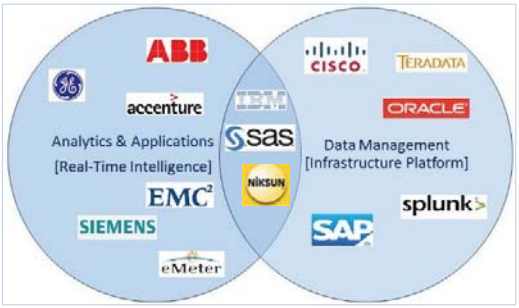

Figure 7: Top Vendors - Smart Grid Data Analytics

Some of the analytical tools offered by these vendors are listed in Table 1 below:

Vendor	Analytics Tool
ABB	ABB Utility Analytics
Capgemini	SES Platform
EMC	Smart Grid Analytics
eMeter	EnergyIP
GE	Grid IQ Insight
IBM	Netezza data warehouse appliance
Oracle	Utilities Meter Data Analytics
NIKSUN	NetDetector, NetVCR, NetMobility, NetOmni
SAP	Smart Meter Analytics
SAS	SAS®Analytics
Siemens	PSS®ODMS
Teradata	Active Smart Grid Analytics (ASA) Platform

Table 1: Analytical tools for Securing the Smart Grid

CONCLUSIONS

This paper has provided a brief overview of the evolution of M2M communication, its application in the Smart Grid, and the importance of M2M data analytics to ensure an optimally performing and secure power distribution system. For the Smart Grid to benefit from M2M communications and the IoT, it is paramount that security controls are deployed without compromising consumer privacy.

In our next paper, we plan to survey the security analytics currently available for M2M data across different components of the Smart Grid and help better understand the tradeoff between Smart Grid security and consumer privacy.

ACKNOWLEDGMENTS

We would like to thank NIKSUN Inc., one of the leading lights in the cyber security industry, for providing support while writing this paper.

REFERENCES

[1] Infographic - The History of M2M infographic

[2] 'Basic principles of Machine-to-Machine communication and its impact on telecommunications industry': co-written by Faculty of Electrical Engineering an Computing, University of Zagreb and Ericsson

[3] 'M2M - Concept and Architectural Overview': CSI Communications August 2013

[4]ETSI (European Telecommunications Standards Institute)

[5] 'Cyber security in the Smart Grid: Survey and Challenges': co-written by Wenye Wang, Zhuo Lu, Department of Electrical and Computer Engineering, North Carolina State University, Raleigh, NC 27606, USA.

[6] IEEE Smart Grid (http://sgpubs.ieee.org/publications/interactive-search-tool)

[7] US Department of Energy (www.smartgrid.gov)

[8] http://www.navigantresearch.com/research/smart-grid-data-anaytics

[9] http://www.energycentral.com/gridtandd/metering/articles/2678/Big-Data-Analytics-in-MDM-and-Smart-Grid/

[10] http://www.informationweek.com/software/business-intelligence/oracle-says-utilities-botch-smart-meter/240158743

[11] Evaluating Electricity Theft Detectors in Smart Grid Networks: Daisuke Mashima(Georgia Institute of Technology) and Alvaro A. Cardenas(Fujitsu Laboratories of America)

[12] Edison Electric Institute (EEI)

[13] The Soft Grid 2013-2020: Big Data and Utility Analytics for Smart Grid (http://www.sas.com/news/analysts/Soft_Grid_2013_2020_Big_Data_Utility_Analytics_Smart_Grid.pdf)

[14] Data Management and Analytics for Utilities (http://www.smartgridupdate.com)

[15] The Power of Data: Data Analytics for M2M and Smart Grid'- by Zhong Fan, Qipeng Chen et al: IEEE PES Innovative Smart Grid Technologies Europe (ISGT Europe), Berlin, 2012

[16] Cyber Security and Privacy issues in Smart Grids - by Jing Liu, Yang Xiao et. al; 2012 3rd IEEE PES Innovative Smart Grid Technologies Europe (ISGT Europe), Berlin

[17] Cybersecurity and the Smarter Grid- by Carol Hawk, Akhlesh Kaushiva

THE 5TH INTERNATIONAL CONFERENCE ON WIRELESS COMMUNICATIONS, VEHICULAR TECHNOLOGY, INFORMATION THEORY, AEROSPACE & ELECTRONIC SYSTEMS (WVITAE-2015)
December 13-16, 2015, Hyderabad, India

Persuasive Technology and Business Models - Profiting from Big Data

Morten Karnøe Søndergaard • Peter Lindgren • Niels Einar Veirum [1]

Abstract Recently, there has been growing interest in research on Big Data since more and more information is becoming available to us every day. This is caused by the concurrent rise of new mobile technologies and social networks, which allow us to virtually share everything, with everybody, everywhere – and anytime. These smart technologies might also be used to persuade human beings to change their behavior. The following article aims at presenting an easily understandable way to approach these new developments. Since Big Data can be used to measure specific behavior, this results to the ability of designing for specific changes. Businesses use different persuasive technologies to persuade users, customers and network partners to change behavior. Operating more than one value proposition, both tangible and intangible value proposition, in combination seems to be crucial to the success of a persuasive business model. We will give a short introduction into the area of persuasive technology and business models. Based on our experience with persuasive technologies we then conclude that it is key for all agents to relate to ownership, since enabling an intervention to the benefit of the public or to a private company, might result in spin-offs.
Keywords Persuasive Technology • Business models •Big Data • Interventions

1 Background

Big Data has been buzzing in the last decade. The term in itself describes any voluminous amount of structured or unstructured data that has the potential to be mined for information. Big Data, despite of a long history, has become a current top priority on the agenda, simply, because more information is becoming available to us every day. Mostly, this is caused by the concurrent rise of new smart technologies (mobile phones, tracking devices, sensors etc.) and social networks which allow us to virtually share everything, with everybody, everywhere – and anytime. The new reality of Big Data and its accompanying technologies has created feeding grounds for new integrative business models, which target behavior and design in a

Morten Karnøe Søndergaard - morten@peaceinnovation.dk,
Peter Lindgren - peterli@auhe.au.dk,
Niels Einar Veirum - nielseinar@auhe.au.dk.

[1] Stanford Peace Innovation Lab, Department of Business Development and Technology, Aarhus University, Denmark

whole new manner. This article present a clear-cut and easily understandable way to approach this new scene.

2 An introduction to persuasive technology

A subset of Big Data is data closely related to human behavior. It can be indicators on consumer trends or any kind of workflows or life style habits individuals perform on a daily basis. This means that you can use Big Data to measure specific behavior and as you can measure them, you can also start designing for specific changes.

Persuasive technology design is a promising discipline when trying to move from rather abstract levels of data mining to concrete interventions that can influence human actions and change the reality behind the data. Persuasive technology can, for example, take the form of a smartphone app, a web app or an embedded functionality in tools or appliances, often backed by cloud services and data sources.

In the persuasive technology design loop you define the target behavior you want to change, the technology platform you want to use and the data metrics that will indicate your failure or success. You then quickly build and deploy technology prototypes, measure the impact of various approaches and start optimizing on the most promising solutions. Behavior design is of course about motivating individual human beings to do the target behavior in question. Often you will fail if this is the only path you follow. In most cases it is smart to design interventions with the aim to make it easier for the individual to do what she is already motivated to do. However, the most crucial part is building technology such as mobile apps that can trigger her just in the right moment, when she is motivated and has the ability to perform the desired action.

In order to make behavioral changes persistent you will strive to incorporate the new actions in tiny habits, that closely connect to familiar situations in your target group's daily life. And you will try to invoke social amplifiers within the target group, like engagement and good emotions communicated within the group. It is very important for a sustainable impact that the individual and the group find the achievements meaningful. In that respect, you furthermore need sustainable business models inviting to engage by paying forward the gained benefits of the intervention to stakeholders and also by paying back rewards to support continuous improvements.

3 Persuasive technology and business models

The huge possibilities of designing persuasive business models embedded with persuasive technology were introduced in 2013. [2] Increased competition and diminishing life cycles of business models force business to think out of the box and find new ways of business – especially for those business that are locked in increasing red ocean business model ecosystems. However, in order to rapidly develop a persuasive business model ecosystem both the businesses and their business models are forced to become even more agile, dynamic and smart in bundling technics.

In this context the persuasive business model becomes highly related to the multi business model approach [3] as most businesses using the persuasive technology need a combined bundle of two or more business models. We found in earlier research that persuasive technology is especially deeply anchored in the competence dimension of the business models either in the business' own business models or in the users', customers' or network partners' business models. While most persuasive business models seem to come with a kind of tangible value proposition – a product, a service or a process of products and services – they are often coupled to "intangible" value propositions related to human activity, in particular socio-economic activity. [1]

Operating more than one value proposition, both tangible and intangible value proposition, in combination seems to be critical to the success of a persuasive business model but it can easily become blurred in the perception of the user, customer or network partner. However, if persuasive business models are constructed with smart and easy to operate technology embedded they have higher potential for success. Also, it seems persuasive business models that make the user, customer and network partner personally involved in the moment of action have higher possibilities of success.

While persuasive business models can make for a better world [2], they also have to engage in business model ecosystems that make profit in order to be sustainable. In fact, this raises significant challenges and ethical questions in relation to persuasive business model leadership and management. It is crucial that business models are clearly communicated as for-profit business models to avoid misunderstandings when entering business domains, which are largely influenced by charity organizations and others that flag different values.

4 Perspectives

We admit that we are just starting to see the contours of this vast possibility space and that we are still exploring the best methods for cultivating it.

A promising future perspective is to build a more integrated innovation process that concurrently analyze Big Data, innovate business models and implement persuasive technology. But how could that be orchestrated?

The possibility that – at least at this stage – seems to be most aligned with our experimental ambitions to act agile and learn along the way, is the loosely coupled set of methods we identified, which can act on the same entities and models from different perspectives.

Still the interconnections in a business ecosystem rapidly grow to a complexity level incomprehensive for the human brain. Therefore, the possibility which immediately comes to mind, is to carefully link all sub-processes to one giant design loop, ensuring that every aspect gets the appropriate awareness in all iterations. We are working towards this direction through our standardization efforts [4] and hopefully they will pave the way for an integrated digital business-modeling environment.

An effect might even be methods cross-fertilizing each other. For example, machine learning strategies that initially were introduced to discover patterns in Big Data sources might also be able to reveal a superior combination of business model components, when the business models and their elements over time become part of the common data repository as well.

Until now, it is a great challenge to make these generic methods grasp the complexity of a special case in a specific domain and local context. Last but not least it should be underlined that using the same methodology over a variety of cases in different urban contexts might eventually spark the cross-domain solutions that are greatly needed today.

5 Conclusions

Aiming to roadmap the way from abstract notions of Big Data to concrete positive business-models, this article has outlined a number of key elements. The first key is to grasp and map the possibility space. Translated into the company's or public entity's everyday setting this means a focus on available data combined with present and urgent issues should be a top priority. As example, if a municipality has the opportunity to harvest and collect data on potential heart patients, systemizing and

monetizing this data might prevent heart failures from occurring at the same rate, which means saved lives, optimized health quality and money saved. Before such concrete results are obtained, a phase of implementation is indispensable, which includes finding the right triggers to hit. Providing the right set-up can be learned or the service can be bought and implemented. Nevertheless, it is a possibility at hand to all agents, private as well as public, if equipped with ample visions. Finally, and perhaps, most vitally, if we judge from or cases, it is key that all agents relate to ownership. Doing an intervention to the benefit of the public or to a private company, might result in spin-offs. The intervention in its own right becomes a business, and the legal issues this might entail should be dealt with in the very early stages of intervention. The most pivotal issue with Big Data is not making a business out of it, rather it is ensuring that business fits into the existing landscape.

References

[1] Allee, Verna, and Oliver Schwabe. *Value Networks and the True Nature of Collaboration*. Edited by Marilyn Krause Babb. Meghan-Kiffer Press, 2011.

[2] Lindgren, Peter, Morten Karnøe Søndergaard, Mark Nelson, and B.J. Fogg. "Persuasive Business Models." *Journal of Multi Business Model Innovation and Technology* 1 (2013).

[3] Lindgren, Peter, and Rasmus Jørgensen. "Towards a Multi Business Model Innovation Model." *Journal of Multi Business Model Innovation and Technology* 1, no. 1 (2012): 1–22.

[4] "Value Delivery Modeling Language (VDML)," May 2015. http://www.omg.org/spec/VDML/.

THE 5TH INTERNATIONAL CONFERENCE ON WIRELESS COMMUNICATIONS, VEHICULAR TECHNOLOGY, INFORMATION THEORY, AEROSPACE & ELECTRONIC SYSTEMS (WVITAE-2015)
December 13-16, 2015, Hyderabad, India

GET IoT- Green computing and Energy harvesting Technology in Internet of Things (IoT)

Jetendra Joshi, Anshumali Singh, Lakshya Gourav Moitra and Manash Jyoti Deka
Dept. of Electronics and Communication engineering
NIIT University, Neemrana, Alwar, Rajasthan-301705

Abstract— **The Internet of Things (IoT) refers to a system of future where every day physical objects are connected by the Internet in one form or the other. The promise of the Internet of Things (IoT) becomes a part in our everyday lives, but there are many challenges regarding the security issues and also we are concerned about the low energy consumption solutions that support the pervasive components at play in IoT. The security and energy efficient approach will really play an important role in the Internet of Things. We conducted a literature review about IoT, which includes features, architecture, and security aspects in IoT. This paper aims to study and use the relevant green computing and energy harvesting methods and select the most likely candidates for IoT use.**

Keywords— Green Networking; Data Center; Virtualization; Intelligent transport systems (ITS); V2X communications; Cloud computing (key words)

I. INTRODUCTION

With the swift development of Internet technology and communications technology, our lives are gradually leading a world full of hypothetical space present in a virtual world. Activities like chatting, shopping, work, etc. can be done easily in virtual world provided by network. Since we live in a real world, all our activities cannot be fully implemented through the services in the imaginary space. It is the constraint of imaginary space that limits the development of Internet to provide better services. To eradicate these constraints, a new technology is required to accommodate imaginary space and real-world on a same scaffold. We name this platform as IoT or Internet of Things. Now-a-days, the sensor network technology is demanding new internet technology derived from low-cost sensors and wireless communication. It will bring huge changes to the future society, change the way of life and business models [1]. In section II we have taken a brief description on the concept of IoT architecture and applications. In section III, the system security and privacy issues has been discussed. In section IV, we have used the various green computing techniques in IoT. Energy harvesting techniques in IoT is given in section V lastly we have Section VI that concludes this paper and gives a glance of future work. Lastly, we have given the references used.

II. IOT: ARCHITECTURE AND APPLICATIONS

The developing network of physical objects that constitute of an IP address for connection of internet, in order to build a communication channel for communication between these objects and other devices which are internet enabled, is known as IoT or Internet of Things. Any physical object, for example a person with a heart monitor implant, a biochip transponder inside a farm animal or a built-in sensors inside an automobile, etc. or any other natural or man-made object ,to which an IP address is assigned and provided with the intelligence to transmit data over a network, can be referred as a thing in IoT. The Internet of Things most closely related with machine-to-machine (M2M) communication in manufacturing and power, oil and gas utilities, as products with M2M capabilities are referred as smart.

A. Architecture of IOT

IoTs can be divided into three important layers [1] Viz; Perception, Network and Application. Perception layer or recognition layer collects data/information and analyses the physical world. Middle layer is known as Network layer or wireless sensor networks, which is liable for the early preparation and transmission of data, collection and polymerization. The application layer bids these overhauls for all the industries. Central Nervous system role was played by the network layer that handles overall services in the IoTs, as it aggregates with upward application layer and makes the link downward of perception layer. Various basic networks including, mobile/ private network, wireless/wired network allow the elementary connection. Business applications constitute of this new network of IoTs [2].

B. Applications

A survey done by the IoT-I project in 2010[3] identified IoTs application scenarios which are gathered in various domains and they are: Smart Home and city, transportation, Lifestyle, Retail, Agriculture, Smart Factory. This survey had its foundation on 270 responses from 31 countries and the schemes which got the most interest were: smart home, smart city, transportation and health care[3] .In this paper, the focus will be briefly on the IoTs applications in medical (health care) [4], smart home[5], intelligent community security system (smart city)[6].

- *IoT in Medical Application*

  Remote Monitoring and Management Platform of Healthcare information (RMMP-HI) [4] facilitates monitoring and management of the diseases for their prevention and early detection. In spite of restrictions of

location, time, and user' movement, RMMP-HI can gather human body medical information timely with the help of different body medical sensors laden in the human body or neighboring space and excerpt useful information by data encryption, storage, comparative analysis and transformation. When exceptional sight is found, users are notified to take early treatment; this allows the early detection and prevention. Short range wireless communication sensor module will gather the various information about the human body parts and transmit this information to 3G mobile phone or home gateway. This medical information is notified and transmitted to data storage and processing center timely. Then the important health guidance will be given back to the patient, family members of patients or medical institutions after systematical preparation of trained system or the scrutiny of professional medical staff in health service center. In the case of emergency, first-aid notification is communicated to a nearby medical institution by health service center to provide faster and better emergency services to the patients.

- *IoT in Smart Home*
  Reading of remote meters can be achieved through these smart home systems. That means, the data related with home power, telecommunications, gas and water can be transmitted automatically to their corresponding utility company to enhance the efficiency of the work. In addition, by virtue of smart home systems, windows, home ventilation, doors, lighting, air conditioning etc., can be operated and controlled remotely. Entertainment equipment's like radios and televisions can be connected to common channels which are distant.
- *Intelligent Community Security System*
  The intelligent community security system (ICSS) [7] controls several subsystems, such as Vehicle Management Subsystem (VMS), Surrounding Security Subsystem (SSS), Central Information Processing System (CIPS), Property Management Subsystem (PMS), Fire and Theft Prevention Subsystem (FTPS) etc. The Vehicle Management Subsystem [7] in ICSS adopts IPR, technologies in sensor network and RFID. Image recording can be done by RFID card and video camera which is provided to the vehicles. The vehicle license knowledge will be transmitted to the CIPS, when it enters the communities. The visitors are provided with the temporary parking places. The SSS (Surrounding Security Subsystem) contains electronic access controls, electronic fences and rotatable monitoring cameras. It can be used to avoid illegal enter or intrusive behavior into communities. The subsystem can find the exact location of the accident by making use of sensing terminals which can automatically omit untrue signals. The rotatable cameras will track the people or objects by IPR technology; simultaneously they triggers alarm to the handheld devices of the security personnel and CIPS through the sensor network [6].
- *M2M*
  Machine-to-Machine (M2M) communications illustrate machinery, algorithms and technologies that enable networked devices (wireless/wired) and facilities to interchange information or control data seamlessly, without explicit human intervention. M2M communications are expected to reform telecommunication operators business due to emergence of new networked applications, which will draw in new clients and increase the data flowing in their networks, producing more billing opportunities. The Internet of Things (IoT) with its wide dimension of applications that rely on everyday objects becoming intelligent connected devices [9] is a major driver for M2M applications. The National Intelligence Council predicts that food packages, furniture, and even paper documents can have internet connectivity by 2025 [10]. IDC envisions 212 billion "things" by the end of 2020, where 30.1 billion are expected to be connected autonomously [11]. On the other hand, the sensing and connectivity abilities of smart phones and their pervasiveness in people's lives make them critical pieces of this IoT and future applications.
- *ITS*
  Cooperative intelligent transport systems (ITS) are treated very important for enabling technology to improve road safety, traffic competency and driving practicality. There is in circulation a trend to deploy this new technology in vehicles to enable them to transmit information/data through hotspots with other nearby entities by direct short-range communications (DSRC), such as vehicle-to-vehicle (V2V), vehicle-to-infrastructure (V2I), vehicle-to-pedestrian (V2P) and vehicle-to-anything (V2X). Indeed, new market predictions [12] clearly indicate that the connected vehicle market will be worth 39 billion USD in 2018, and that more than 50% of the vehicles sold worldwide in 2015 will have communication efficiency. It is envisage that every new vehicle will be connected in multiple ways by 2025. This new reality of intelligent transport systems will ascend different types of vehicular communications (VC) and telematics services to the emergence of innovative rapid road safety operations, driver convenient services, smart mobility and traffic management services.
  Certainly, this technology dejectedly depends on wireless communications, several threats and attacks can cause an impact on its functioning and entertain the safety of the compound ITS entities and users. Typical attacks on ITS consist denial of service (DoS) attacks, Sybil attacks. Subsequently, various security

requirements should be established to abide these attacks, including reliability, confidentiality, integrity, non-approval and data entrustment in order to empower the materialization of future autonomous (or driverless) vehicles [13].

- *Smart Grids*
  The Smart Grid (SG) [14], the intelligent power grid, can be seen as the largest realization of the IoT network in the next future. The whole power grid chain, from the energy power plant generation to the final electricity consumers, which consists of conveyance and circulation of power networks, will be filled with comprehension and two-way communication capacity to monitor and regulate the power grid anywhere, at a fine granularity and a very high accuracy. The aim of the Smart grid is to keep a real time balance between energy formation and utilization, by allowing an exquisite examining and control over the power chain, thanks to the large number of the two-way communicating smart objects (smart meters, smart appliances, sensors, actuators, etc.)[15]

III. SECURITY CONCERNS IN IOT

Internet of Things virtually is a network of real world systems with real-time interactions. The development of the initial stage of IoT, is M2M (Machine to Machine), having unique characteristics, deployment contexts and subscription. Unattended operation without human intervention is possible for long periods of time by the wireless area network (WAN) or WLAN. Though providing improvements in social efficiency it creates an array of new problems concerning breach of privacy and that information security [16]. Front-end sensors and equipment receives data via the built-in sensors. They then transmit the data using modules or M2M device, thus achieving networking services of multiple sensors. This methodology involves the security of machines with business implementation and node connectivity [16]. Machine or perception nodes are mostly distributed in the absence of monitoring scenarios. An intruder can easily access these devices which imply damage or illegal actions on these nodes can be done. Possible threats are analyzed and are categorized to unauthorized access to data, threats to the Internet and denial of service attack. Back-end IT systems form the gateway, middleware, which has high security requirements, and gathering, examining sensor data in real time or pseudo real-time to increase business brilliance. The security of IoT system has seven major standards viz; privacy protection, access control, user authentication, communication layer security, data integrity, data confidentiality and availability at any time.

IV. GREEN COMPUTING

Green Computing can be defined in various frame of references. Green computing helps environmentally, socially and politically with respect to adequate and productive use of energy. In order to accomplish competitive edge in terms of an energy-cost saving strategy, and reduction to carbon discharge. Green computing represents environmentally possible ways to recede power and environmental e-waste [17]. Various goals of green computing are to reduce the use of lethal and harmful materials. Green computing also helps to build the energy efficient environment and also recycling of factory waste. Such practice includes the productive utilization of server and its constituents as well as reduces the power consumption [18].
Advantages of Green Computing:

1. Lower energy utilization from green computing techniques which also help to reduce the content of carbon dioxide discharge.
2. Less energy is required to produce, use, and dispose of products in order to preserve energy and resources.
3. Saving energy and resources saves capital.
4. Green computing contributes in changing government policy to strengthen recycling and lowering energy use by individuals and businesses.

There are a number of approaches for green computing. Some approaches illustrate as:

1) *Product longevity*: The PC manufacturing process is one of the important process that accounts for 70% of the natural resources used in the life cycle of a PC. The biggest contribution to green computing is to increase the equipment's lifetime.
2) *Data center design:* Data center facilities consume a lot of energy. The U.S. Department of Energy calculates that data center energy requirements for their facilities are 100 to 200 times more energy than standard office buildings.
   According to the U.S. Department of Energy, the primary areas on which energy efficient data center form best practices are given below:
   Information technology(IT) systems
   Environmental conditions
   Air management
   Cooling systems and Electrical systems.
3) *Software and deployment optimization*: It consists of algorithmic efficiency, resource allocation, terminal servers and virtualization. With feature of virtualization, a system administrator could add up several physical systems into virtual machines on one single and powerful system. The effect of virtualization will help in unplugging the original hardware and decreasing power and cooling consumption.
4) *Power management*: The ACPI or Advanced Configuration and Power Interface, is an open industry standard, which allows an operating system to directly dominate the power-saving aspects of its underlying hardware. When the system is inactive for longer time then the system automatically turn off peripherals such as monitors and hard drives after set

intervals. In addition, a system may hibernate, when majority of the components are turned off.

Various techniques can be classified at different levels:

1) Hardware and Firmware Level
2) Operating System Level
3) Virtualization Level
4) Data Center Level

Hardware and Firmware level techniques implemented at the manufacturing time of a machine. These techniques consist of all the optimization methods that are applied at the initial phase when the designing of the logic, circuit, architectural and system levels is done. Next level is Operating System level mechanisms which consists of methods that take care about programs at operator level. Finally the Virtualization level techniques are enhanced to use the concept of Virtual Machines (VMs) to manage power. In this number of VMs are generated on a physical server, so that reduce the amount of hardware in use and improve the utilization of resources. Data Center level mechanisms are taken into effect at various data centers and these centers consist of different methods which are used to manage workload across physical nodes.

V. ENERGY HARVESTING

Ambient energy harvesting or power harvesting, is the phenomenon of deriving usable energy from natural and human-made sources that surround us in the everyday environment. From the previous calculations we can conclude that the low end of power usage for an IoT node that remains useful is at 124μW. This means the node hibernates for a second and is activated by an outside trigger for processing and data communications that will not last longer than one tenth of a second. We need to scrounge for ambient power sources that can fulfill this energy requirement [19].

A. Small Solar Cell Outdoors

A small solar cell fixed outdoors can easily give 150mW [20]. It will need a battery to function in night time or cloudy days. It has to be installed into a visible place that is free from shadow. This means it will have to survive in different weather conditions from snow to direct rain and withstand dust accumulation.

Solar cells in inside use are often overlooked as toys or completely ignored. A small unit in unfavorable angle to an incandescent lamp can create 51μW [21]. If we install three of these we hit our power target of 124μW. This is very promising. But we cannot assure that the lamps will be on all the time. So we will have to install some kind of battery or capacitor that charges from the solar cell and powers the IoT node when lamps are off. This might lead to considerable problems in buildings that become empty for longer periods of time.

B. Magnetic coupling with a nearby power line

A very simple power source is to gather energy from power lines that are embedded inside walls. They offer high power when the IoT node is directly on top of the power line. This solution can easily feed even a high power processor. Unfortunately this solution suffers from the square distance law. When there is a small increase in the distance from the power line that reduces the power available for the magnetically coupled node. Also rather unexpectedly this solution suffers from a version the same problem as the indoors solar cells.

C. Harvesting Radio Singnals

Most of the available radio signals need a huge antenna to be gathered efficiently. That naturally is not a realistic option for an IoT device. The most realistic case is a smallish (10x5 cm antenna) 10 m from Wi-Fi antenna. This gives roughly 4 μW if the base station is transmitting continuously. This is not enough unless we either go up with the signal strength or use a really large antenna. If we go up in size of the antenna we also start creating shadows behind us where the Wi-Fi signal is weaker for other listeners. This becomes quickly a problem when the number of IoT nodes goes up. It is also hard to create a design that won't create problems for other IoT nodes by damping their transmissions. Even though there are some products on offer that might be used for IoT power use, it seems the solution is not feasible with the current processor technology.

D. Magnetic capture of vibration

A very promising technology is the magnetic capture of vibration. The principle is simple. A magnet is hung from a spring or similar structure and placed inside a coil. When the magnet vibrates due to outside forces it will create alternating current in the coil surrounding it. An example installation produced from a 0.85 mm movement over 180μW [22] of power. This fulfills the requirement set earlier nicely. This kind of energy harvesting has been used to power measurement systems in bridges. The vibration created by trucks passing powered the measurement nodes in the bridge.

E. Piezo capture of vibration and strain

Energy in piezoelectric elements is captured from vibration as well as compression. For example, [22] a human walking over a large piezoelectric plate can easily produce 8W during the passing. If we expect the human to pass the plate in half a second producing 4 J and our energy needs derived from 124μW are 0.446 J per hour leads to conclusion that we need one human every 9 hours to pass the plate to keep the IoT device running. This is a very reasonable expectation. As there is so much excess energy available from the piezo plate it is logical to pair the plate with a small NiMH battery. This can be kept topped from the element to compensate for the self-discharge current.

F. Thermoelectric capture

In thermoelectric capture the idea is to gather energy from a temperature difference or more specifically heat flow. The elements are small and the output is a simple DC current. As an example Seiko wristwatch produced 22 μW @ 1.5 °C from human body heat [24]. Scaling that up by 10x surface or 10x

temperature difference we can easily get 220μW which compares favorably with our target of 124 μW. This would be continuous power. Unfortunately buildings are usually designed to minimize places where there can be heat flow between large temperature differences. So finding places where there units can be positioned will prove troublesome.

G. Air Movement

Air movement does not need to be gathered with large and visible propellers. Piezoelectric wind turbines can gather energy from passing air rather innocuously. This kind of turbine can be inside ventilation ducts and it can gather energy from the random air current inside building. Small piezoelectric wind turbines can easily get 200μW from random air movements. Leaving sufficient extra energy to keep a battery topped. Currently available models are designed for larger energies and are unfortunately bigger than an AA battery, but there is no reason why the technology could not be scaled down and some manufacturers seems to be experimenting with the small turbines.

VI. Conclusion

In the first part we concluded that the IoT architecture and application are explained in details. Later we study the various application scenarios and also study the various security concerns in IoT then at last we study the various green computing techniques in the IoT. We also demonstrate multiple ambient energy harvesting solutions and list their power output and their problems. From these it becomes evident that ambient vibration and light are the most likely sources to use for true IoT devices. Next step would be to build a demonstration system to measure the power output from vibration and light sources and to gather better insight into how these kinds of systems operate and what are their limitations in true IoT use.

References

[1] G J. Satish Kumar, Dhiren R. Patel, “A Survey on Internet of Things: Security and Privacy Issues”,March 2014.. (*references*)

[2] G. Gang, L. Zeyong, and J. Jun, “Internet of Things Security Analysis,” 2011 International Conference on Internet Technology and Applications (iTAP), 2011, pp. 1-4.

[3] O. Vermesan, P. Friess,and A. Furness, The Internet of Things 2012, By New Horizons, 2012. [Online]. Available: http://www.internet-of-things-research.eu/pdf/ IERC_Cluster_ Book_2012_WEB.pdf.

[4] W. Zhao, C. Wang, and Y. Nakahira, “Medical Application On IoT,” International Conference on Computer Theory and Applications (ICCTA), 2011, pp. 660-665.

[5] K. Bing, L. Fu, Y. Zhuo, and L. Yanlei, “Design of an Internet of Things-based Smart Home System,” 2nd International Conference on Intelligent Control and Information Processing, 2011, pp. 921-924.

[6] J. Liu, and L. Yang, “Application of Internet of Things in the Community Security Management,” Computational Intelligence, Communication Systems and Networks,Third International Conference on IEEE, 2011, pp. 314-318.

[7] D. Jiang, and C. ShiWei, “A Study of Information Security for M2M of IoT,” 3rd International Conference on Advanced Computer Theory and Engineering (ICACTE), 2010, pp. 576-579.

[8] Carlos Pereira, and Ana Aguiar,”Towards Efficient Mobile M2M Communications: Survey and Open Challenges”, October 2014.

[9] Giusto, D.; Iera, A.; Morabito, G.; Atzori, L. The Internet of Things; Springer-Verlag:Berlin/Heidelberg, Germany, 2010.

[10] National Intelligence Council (NCI). Disruptive Civil Technologies—Six Technologies with Potential Impacts on US Interests Out to 2025 - Conference Report CR 2008-07, 2008. Available online: http://fas.org/irp/nic/disruptive.pdf (accessed on 15 March 2014)

[11] IDC. Press Release—The Internet of Things Is Poised to Change Everything, Says IDC. Available online: http://www.idc.com/getdoc.jsp?containerId=prUS24366813 (accessed on 15 March 2014).

[12] GSM Association (GSMA). Connected Car Forecast: Global Connected Car Market to Grow Threefold within Five Years; Technical Report; GSM Association (GSMA): London, UK, 2013.

[13] Elyes Ben Hamida , Hassan Noura andWassim Znaidi,” Security of Cooperative Intelligent Transport Systems:Standards, Threats Analysis and Cryptographic Countermeasures”,Electronics 2015.

[14] NIST, Introduction to NISTIR 7628 Guidelines for Smart Grid Cyber Security. http://www.nist.gov/smartgrid/upload/nistir-7628_total.pdf (lastaccessed April 10th, 2014)

[15] Chakib BEKARA,”Security Issues and Challenges for the IoT-based Smart Grid”, International Workshop on Communicating Objects and Machine to Machine for Mission-Critical Applications (COMMCA-2104),2014.

[16] P.-L. Ismael, “ITU internet report 2005: The Internet of Things,” Int.Telecommun. Union (ITU), Geneva, Switzerland, 2005. architecture and network characterization,” Comput. Netw., vol. 56, no. 16, pp. 3594–3608, 2012.

[17] B. Priya, E. S. Pilli and R. C. Joshi, (Eds.), “A Survey on Energy and Power Consumption Models for Greener Cloud”, Proceeding of the IEEE 3rd International Advance Computing Conference (IACC), (2013), February 22-23; Ghaziabad.

[18] “A Study about Green Computing” Pushtikant Malviya, Shailendra Singh, International Journal of Advanced Research in Computer Science and Software Engineering, Volume 3, Issue 6, June 2013.

[19] Mikko Lampi,” Internet of Things. Ambient Energy Harvesting.”

[20] “Small solar panel 1.5v 50ma.” [Online]. Available: http://www.amazon.com/Small-Solar-Panel-1-5V-50mA/dp/B002MAWOSW

[21] “Sc-01 indoor solar cell.” [Online]. Available: http://www.imagesco.com/solar/solar-cells.html

[22] H. A. Sodano, D. J. Inman, and G. Park, “A Review of PowerHarvesting from Vibration Using Piezoelectric Materials,” The Shockand Vibration Digest, vol. 36, no. 3, pp. 197–205, 2004. [Online] Available: http://dx.doi.org/10.1177/0583102404043275

[23] G. J. Snyder, “Small thermoelectric generators,” The Electrochemical Society Interface, 2008. [Online]. Available: http://www.electrochem.org/dl/interface/fal/fal08/fal08 p54-56.pdf

THE 5TH INTERNATIONAL CONFERENCE ON WIRELESS COMMUNICATIONS, VEHICULAR TECHNOLOGY, INFORMATION THEORY, AEROSPACE & ELECTRONIC SYSTEMS (WVITAE-2015)
December 13-16, 2015, Hyderabad, India

Communication Framework for Tele-rehabilitation Systems with QoS Guarantee

Plamen Semov, Nikolay Dandanov, Georgi Balabanov, Krasimir Tonchev and Vladimir Poulkov
Faculty of Telecommunications
Technical University of Sofia, Faculty of Telecommunications, Sofia 1756, Bulgaria
p_semov@abv.bg, {n_dandanov, grb, k_tonchev, vkp}@tu-sofia.bg

***Abstract*— Nowadays, there is great interest in developing telemedicine technologies. These technologies will provide health care from distance swiftly and lightly, as well as reduce the expenses for activities, such as rehabilitation. Telemedicine applications are possible due to the advances in information technologies and the ever-expanding communication network infrastructure. The network characteristics bandwidth, packet loss, latency, jitter and policies are crucial for the performance of tele-rehabilitation systems. Because in tele-rehabilitation human lives are at stake, guaranteeing the Quality of Service (QoS) is important. In this paper, an approach for assuring the QoS for information transmission in tele-rehabilitation systems is proposed.**

Keywords—capacity; communications; delay; jitter; networks; policies; protocols; telemedicine; tele-rehabilitation; quality of service;

I. INTRODUCTION

In the recent years, a great advancement in the development of technological and rehabilitation methods was observed. By combining rehabilitation and the advancements in Information and Communications Technologies (ICT), tele-rehabilitation arises. This is a subpart of telemedicine, consisting of a system for controlled rehabilitation "via the Internet" – an actual application possibility with a promising development in the future. A tele-rehabilitation system is a bilateral system, consisting of master and slave devices, which interact through a bidirectional communication channel, as shown in figure 1.

Various communication media can be used in tele-rehabilitation: transmission lines, wireless transmission or the Internet. Depending on the different environments, based on their performance, a decision for using TCP (Transmission Control Protocol) or UDP (User Datagram Protocol) for transporting the information has to be made.

TCP provides reliable two-way communication and guarantees data delivery at the cost of retransmissions and long timeouts that are detrimental to the performance of real-time applications, such as teleoperation. UDP does not require reception acknowledgments, eliminating unnecessary waiting time, which makes it appealing for teleoperation.

In tele-rehabilitation, improved quality video-assisted telecommunication services and devices, such as videoconferencing, webcams and telepresence, assist in treatments. Sensors and body monitoring data, voice, sounds, medical images and information related to telehaptics (the sense of touch), as well as virtual reality, can also be transmitted for rehabilitation purpose. Moreover, with the massive utilization of portable smart terminals, such as smartphones, laptops and tablets, web-based approach and mobile applications are becoming ever more common and can potentially be used for tele-rehabilitation.

In tele-rehabilitation, human lives are at stake. Hence, the consequences of an error or delays in information transmission could be serious. This is the reason why reliable techniques of networking must be developed and applied [1]. Particular stress should be laid on the importance of availability and reliability of the communication networks. Interruptions in network operation, e.g. introduced by a power cut, could cause errors or delays in the transmitted data. These specifics pose strong requirements for the bandwidth, delay, jitter, reliability and availability of the network connection for tele-rehabilitation.

Five fundamental network characteristics are crucial for the performance of tele-rehabilitation systems. Bandwidth is a fundamental requirement that there is enough capacity in a network path for all of the packets to get through unimpeded. Packet loss is the amount of packets, which do not arrive correctly at their destination, and it should be less than 1-2%. Latency is the time delay between an event occurring on one site and the remote end seeing it. For a voice transmission with good quality, a latency of less than 150 ms is needed. Jitter is the time variation of latency among the packets, which can result in packets arriving in different order than transmitted. Jitter should be under 50 ms. Policies are introduced by network elements like firewalls and Network Address

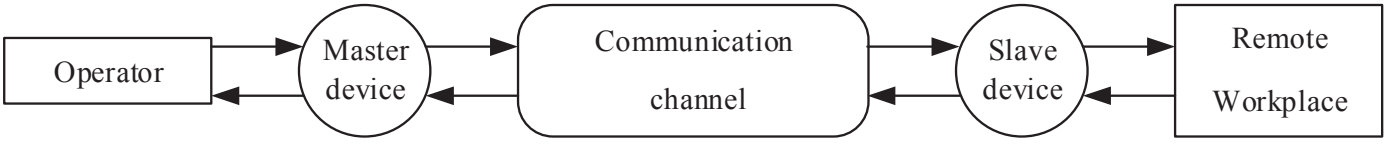

Fig. 1. Tele-rehabilitation concept

Translation (NAT) devices. If the traffic is encrypted for security, some additional aspects should also be considered.

The rest of the paper is organized as follows. In the next section, some telecommunication approaches for tele-rehabilitation purposes ensuring the required QoS are considered. In addition, in this section the problem definition and motivations are presented. In section III, various categories of telemedicine data and their Quality of Service (QoS) requirements are described. The proposed approach for assuring the QoS for information transmission in tele-rehabilitation systems is described in section IV. Finally, we conclude the paper in section V.

II. State of the art

In this section, some telecommunication approaches for tele-rehabilitation purposes guaranteeing the required QoS are considered.

In [2] to overcome instability, caused by unknown and varying time delay, an event-based teleoperation system is employed for synchronization of the robot and the operator. The developed teleoperation system could be easily adjusted to be useful for a tele-rehabilitation robot. UDP is used for sending operator commands and forcing feedback. Additionally, the size of packets for UDP compared to TCP puts less load on the communication channel. To avoid breakings in the control cycle, a server application monitors the control cycle's duration.

The effect of time delay can be reduced with latency tolerant control methods as presented in [3]. The proposed architecture is evaluated with three models of the system components: a master device, a slave device and a communication system. The master includes a controller and the human operator, which are connected via a high-delay medium to the slave model. The master side is where the "human operator" or the replacing automatic control device is located. The surgical staff can be found here, providing the control signals for the actuators of the slave. The communication system includes a transmitter, a receiver and a communication medium. In the deriving cascade setup, the time delay can be partially alleviated using appropriate predictive controllers, tuned to the master and slave systems [3].

In [4], the authors discuss the importance of provisioning QoS and information security in the field of medical care, focusing on the use of data communications, Internet, cloud and Smart Ubiquitous Computational Devices (SUCDs). They present possible scenarios, related to remote control of Medical Surgical Robots via the Internet. The main idea is to lay stress on the importance of QoS provisioning and cyber security in the field of telemedicine, which also applies to tele-rehabilitation.

To assess the convenience of the remote tele-laboratory technique, different configuration architectures have been tested in [5]. For each of these configurations, experiments have been performed, consisting of 400 remote movements of a robot. These experiments use TCP and UDP protocols. Performance details, obtained from these experiments, show that the configuration with UDP is fastest and the most convenient one for traditional tele-robotic applications. A new software protocol, called Interoperable Telesurgical Protocol (ITP), has been developed, which is open and meant for sharing. The first data interface in ITP is a packet of 84 bytes, using the UDP network protocol for fast transmission. The small size of the ITP packet makes it suitable for high packet rates.

In [6], the Secure ITP enciphers communications between the master and slave. The communications use TLS (Transport Layer Security), DTLS (Datagram TLS) protocols and the AES (Advanced Encryption Standard) cipher.

Analysis of the possibilities for providing real-time services for bilateral teleoperation systems on existing wireless infrastructures, using only application layer measurements without any information from the network layer, is presented in [7]. Since teleoperation systems should have a video feedback channel, the influence of video transmission on the transmission quality in the other two periodical channels is analysed. Based on the delay variation measurements of the two opposite directions, data channels identify WLAN (Wireless Local Area Network) problems.

The packet latency is observed and analysed in [8]. Teleoperation latency becomes noticeable to human users for delays above about 200ms, starts to be annoying at around 500ms, and significantly impacts the performance of tasks at 1s and longer. In order to provide true telesurgical care, software systems need to be in place to protect the integrity of the signal and minimize the latency of data transmission between the surgeon and the patient. One way to protect remote surgery's connectivity is to send information over multiple communication pathways or routes.

An investigation into the use of SIP (Session Initiation Protocol) protocol for a telemedicine transition system was proposed in [9]. According to standard computing platforms and operating systems, it is easier to integrate SIP protocol into the application program. Second, SIP is an extensible protocol. Therefore, it is able to run a wide range of applications with a variety of media formats and loads. In the SIP protocol, a number of criteria have been developed for instant messaging, resource management, media streaming (video) and online friend management applications.

In [10], a robotic tele-rehabilitation system has been developed to perform both interactive and cooperative bilateral rehabilitation. The system has been evaluated using four computer games, each with different specification of the data transmission and event management. In addition, robotic teleoperation techniques have been implemented to evaluate the performance and stability of the force reflecting strategy in the cooperative bilateral configuration. The internet communication between the robots has been performed through sockets, using the TCP/IP protocol stack.

A classification of the security threats against mobile surgical tele-robotic systems is presented in [11]. Communication networks security is an active research area and many existing strategies may be also applicable to tele-rehabilitation systems. Identifying those, as well as developing

novel, specialized mitigation strategies, and analyzing their impact on system's performance, security and safety, is an emerging research question.

III. Problem definition

Based on the specifics of tele-rehabilitation and the resulting requirements on the network performance and QoS, a method for conforming to these demands for information transmission in tele-rehabilitation systems should be provided. The approach has to satisfy the requisites for bandwidth, latency, packet loss, jitter, policies, reliability and availability of network connection.

IV. QoS requirements

The data for telemedicine, which is transferred through a communication channel, can be divided into five main categories with different QoS demands:

- Voice;
- Video;
- Data from sensors;
- Teleoperation;
- Virtual reality.

A. Voice over IP (Internet Protocol)

In order to digitize human voice effectively, a sampling rate of 8 kHz with 8 bits per sample is needed, which results in a minimum data transfer rate of 64 kbps (kilobits per second). The delay must be less than 100 – 150 ms. Some notable low bit rate compression algorithms used are ITU G.723.1 and G.729A. It is common to use silence compression to reduce the payload dramatically.

B. Video

The type of video, which is most important in telemedicine, is the video, which is transmitted in real-time. The throughput in raw format, without compression, varies depending on three main features – resolution, frame rate and bits per pixel. For video with resolution 1920×1080 pixels, 30 frames per second, RGB (Red, Green and Blue) color components and 8 bits per pixel per color, a total video stream with data rate of 1.5 Gbps in raw format is produced. Techniques, which compress individual frames, have been developed. In addition, motion prediction is used to compress the data even further. Most of the time, the throughput for video transmission is dependent mainly on the motion within the images. Factors, such as resolution and scanning rates, are not so relevant. A full-resolution HDTV (High-Definition TeleVision) stream, compressed with the MPEG2 method, requires 19.3 Mbps of data bandwidth. For online video streaming with 720p resolution, a 2.4 Mbps channel is required.

Every computation for compressing and decompressing the video adds delay to the total transmission delay. The greater the compression ratio used, the greater the latency introduced. The total delay requirement for video transmission is less than 150 ms.

C. Data from sensors

For this type of information, the requirements for throughput and delays are not so stringent. However, high requirements for data integrity are set. Efficient transport protocols are needed to provide correctly received sensors' data.

D. Teleoperation and Virtual reality

This category includes a mix of video, voice, text, sensors data and remote device commands, which are to be multiplexed and transferred through the communication channel simultaneously in real-time. A list of provisional network requirements for teleoperation and virtual reality can be identified. These QoS requirements include [1], [4]:

- reliability and integrity;
- an acceptable end-to-end delay;
- multiplexing of various data rates resulting in high network bandwidth;
- low data error rate (BER – Bit Error Rate);
- low latency;
- constant jitter.

Studies show that the acceptable limit of time delay in terms of a surgeon's perception of safety is roughly 330 ms [1]. A study in [1] shows how the interactive Internet gaming is affected by the end-to-end delay. The results are presented in table 1.

TABLE I. Perception of interactive Internet gaming as a function of end-to-end delay [1]

End-to-end delay	***< 50 ms***	***50-100 ms***	***100-150 ms***	***100-150 ms***	***> 200 ms***
Perception	Excellent gameplay	Good gameplay	Noticeably decreased gameplay	Significantly effected gameplay	Intolerable gameplay

V. Approach for assuring QoS for information transmission in tele-rehabilitation systems

Because of the various transport protocols and telemedicine technologies existing, we propose adaptable and scalable framework for tele-rehabilitation. Its main functions are:

1) providing abstraction and generalization of the transmitted data among telemedicine devices from different vendors. This way, the network infrastructure is transparent;

2) Data Tunneling for meeting various QoS requirements;

3) M2M communication capabilities for tele-rehabilitation devices from different vendors;

4) General and scalable application software for all telemedicine technologies;

5) Adaptation of the transport layer for reaching target QoS requirements.

The proposed framework is illustrated on figure 2.

The layer "Generalization" has the main responsibility to set the parameters for each data stream generated by a tele-rehabilitation device. It controls tele-rehabilitation devices, or more specifically – their output data streams. Another main responsibility is to adapt or translate different teleoperation and

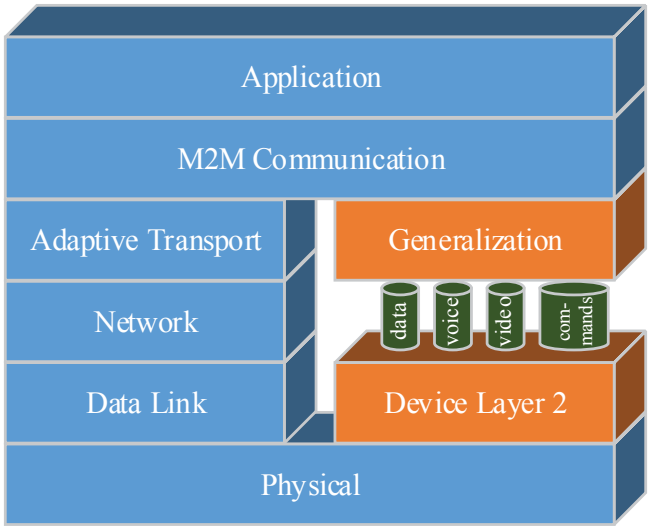

Fig. 2. Proposed framework for assuring QoS for information transmission in tele-rehabilitation systems

sensors data streams, which are sometimes unique for the device itself. The layer gives a compatibility function for all tele-rehabilitation devices to work together.

The main responsibility for the "M2M Communication" layer is to give tele-rehabilitation devices abilities to share and request data from each other, which is needed for taking an overall decision by a given tele-rehabilitation device. This functionality can be realized as a sublayer of the Application layer.

"Application" layer is the man-machine interface, which sets QoS requirements for the data streams. It works also like a SIP server to negotiate data stream parameters between different vendor-specific or technology-specific devices. Another function is to track communication KPIs (Key Performance Indicators), such as delays, throughput, error rate, latency, etc. This acts as a feedback for the "Generalization" and "Adaptive Transport" layers, so they can further modify data and communication parameters and thus meet QoS requirements.

The "Adaptive Transport" layer has the task to fulfill the QoS requirements for every data stream on the transport layer by using various transport protocols – existing or novel. For transporting information, which is insensitive to delays but should be received with no errors, TCP can be used, for example for controlling a remote workplace or receiving measurements from sensors.

Because of the broad development of the Internet and associated IP networks and protocols, this is one of the candidates for providing such transport. In this case, one appropriate protocol for transporting media in real-time is SIP in addition with Session Description Protocol (SDP) and Real-time Transport Protocol (RTP) or Secure RTP (SRTP). For a transport protocol, either TCP, UDP, Stream Control Transmission Protocol (SCTP) or any other suitable implementation can be leveraged.

By implementing this multilayer framework, we separate the communication channel functions from the tele-rehabilitation devices functions. Hence, tele-rehabilitation technologies can be developed independently from the network infrastructure. This method will be a common interface for all tele-rehabilitation technologies, providing network communication capabilities.

With the use of data tunneling, QoS requirements for the transmission of different information types are met. For meeting stringent QoS requirements, a tailored protocol on the transport layer can be developed. The M2M communication capabilities assure compatibility between tele-rehabilitation devices from different vendors. This unity enables general and scalable application software for all telemedicine technologies.

The information with particular requirements for network performance can be separated into different traffic flows. Each of these flows should use a distinct stack of protocols, tailored to fulfilling the requirements posed by this type of information.

As the technologies and services in the networks evolve, backward compatibility should be maintained, so that devices from both newer and older generations can interoperate together.

VI. Conclusions and Future Work

The proposed communication framework for tele-rehabilitation systems with QoS guarantee provides abstraction and generalization of the transmitted data among various tele-rehabilitation devices. Hence, the network infrastructure is transparent to the communicating devices. Data tunneling is leveraged for meeting various QoS requirements. M2M communication capabilities are added for interoperability. Adaptation in the transport layer protocols is a means to reach target QoS requirements.

As a result, the framework can serve to develop generalized and scalable application software for all tele-rehabilitation technologies.

The communication between tele-rehabilitation systems has to be designed in such way, so that it allows compatibility between devices from different vendors and of various generations, and provides openness of the underlying protocols and methods.

The next steps in the development of the common communication framework for tele-rehabilitation systems would include a more elaborate selection and design of the protocols in each layer should be performed. After a protocol stack has been chosen, the integrity of the whole stack shall be tested and evaluated. This can be done by simulating the interoperation of separate protocols and devices or by implementing the stack in tele-rehabilitation systems and devices.

Acknowledgment

This work was carried out in the scope of the EC funded project eWALL (FP7-610658).

REFERENCES

[1] Marescaux J., Leroy J., Gagner M., Rubino F., Mutter D., Vix M., Butner S., Smith M. K. Transatlantic Robot-Assisted Telesurgery. Nature, 413, 2001, pp. 379–80

[2] Petrović I., Kolonić F., Korondi P. Internet Based Teleoperation for Cooperative Navigation and Manipulation. Journal of Mechanical Engineering, 2009, 6:356-368

[3] Jordán S., Takács A., Rudas I., Haidegger T., Modelling and Control Framework for Robotic Telesurgery, 2013

[4] Smithwick, M. Network Options for Wide-Area Telesurgery. Journal of Telemedicine and Telecare 1(3):131-38, 1995

[5] Marín R., Sanz P. J., Nebot P., Wirz R. A Multimodal Interface to Control a Robot Arm via Web: A Case Study on Remote Programming. IEEE Transactions on Industrial Engineering, Vol.52, No.6: 1506-1520

[6] Lee G., Thuraisingham B. Cyberphysical systems security applied to telesurgical robotics. Computer Standards & Interfaces 34, 2012, 225–229

[7] Haller P., Vajda T., Szanto Z., Marton L. Communication Performance Evaluation of Bilateral Teleoperation systems Implemented over WLAN. 2013, http://www.ms.sapientia.ro/~martonl/Research_TE_Documents/WLAN_Meas.pdf

[8] Lendvay T, Rosen J., Hannaford B. Telerobotics: Its Future in Clinical Application. Pediatric Robotic and Reconstructive Urology: A Comprehensive Guide, 2012, Blackwell Publishing Ltd., 314-327

[9] Long T. Telemedicine Transmission System Design Research Based on Session Initiation Protocol. Journal of Software Engineering, 2015, 9: 298-307

[10] Siqueira A. A., Michmizos K. P., Krebs H. I. Development of a robotic system for bilateral telerehabilitation. In Proceedings of 22nd International Congress of Mechanical Engineering (COBEM 2013), November 3-7, 2013, Ribeirão Preto, SP, Brazil. ABCM, Rio de Janeiro, Brazil, 8427--8436

[11] Bonaci T., Chizeck H. J. Surgical Telerobotics Meets Information Security. RSS 2012 Workshop on Algorithmic Frontiers in Medical Robotics: Manipulation in Uncertain, Deformable, Heterogeneous Environments. Sydney, Australia. July 2012

THE 5TH INTERNATIONAL CONFERENCE ON WIRELESS COMMUNICATIONS, VEHICULAR TECHNOLOGY, INFORMATION THEORY, AEROSPACE & ELECTRONIC SYSTEMS (WVITAE-2015)
December 13-16, 2015, Hyderabad, India

An Energy Efficient Adaptive Wireless Link for Farms based on IoT technologies

T. Blaszczyk
CWSA, DTU Diplom,
Technical University of Denmark
Ballerup, Denmark
tomb@dtu.dk

P. Lynggaard
CMI, Aalborg University Copenhagen
Copenhagen, Denmark
perlyn@es.aau.dk

***Abstract* — There is a huge demand for automation infrastructures that increase the efficiency and the commercial potential for the agricultural sector. One approach to achieve these objectives is deploying Internet of Things including its embedded wireless sensor network platform. However, deploying wireless sensors in the fields far from the farms provide some challenges in terms of transmit power, path loss, and lack of power. This paper explores the possibility to deploy an efficient low power adaptable wireless link which interfaces the Internet of Things infrastructure located on the farm. This new adaptable link element offers many benefits such as adaptable transmit time, powered from a sustainable source, and a variable size payload based on the farmers need.**

Keywords—IoT; WSN; adaptive wireless links; solar power in WSN

I. INTRODUCTION

Nowadays, there is huge demand from the agriculture business to incorporate Internet of Things (IoT) based on Wireless Sensor Networks (WSN) into the farming infrastructure to automate, control and monitor most of the agricultural aspects. These aspects includes elements such as crop production monitoring, detect and control diseases, unmanned animal farm production, and food transportation and distribution. Especially, in the area of detecting and controlling diseases it is important that the IoT nodes and their embedded resource-constrained sensors are able to send selective messages. Each message must contain crucial information for one particular disease or insect attack in order to detect it at an early stage and thereby handle it in time. A study which shows the importance of this approach has been carried out in cooperation with the Research Centre for Cultivar Testing (COBORU) [*1*].

Today's wireless communication infrastructure enables fast and reliable message exchange between nodes even at a long distance. However, for the farm infrastructure the most crucial and important element is to keep the system running with limited power options. Hence, most of the agriculture applications cover large areas where there is no power infrastructure, i.e. the farming applications use resource-constrained sensor network types which are powered from sustainable sources such as solar power and wind power. The challenges for the solar based system are: the size of the solar panel, the size of sensor enclosures, and the sizes of the antennas. These parameters need to be minimized; however, small solar panels means less power and small antennas means its radiation efficiency is reduced. Important factors to minimize these parameters are the choice of network topology and the number of packets sent and received. Thus it is important to cooperate with the plant disease forecasting experts to proper design the protocols and packet types which minimize the link budget. It is noted that the transmission energy cost primarily depends on distance between the IoT devices and the size of packet to be transmitted, whereas the receiver energy costs primarily depends on packet size.

The main focus for this paper is to provide a solar powered IoT system which is able to stay alive for a long time without any maintenance or service. To provide such viable and sustainable system, an adaptive approach is taken where the parameters of the WSN link adapts the needs for a particular agriculture application.

II. RELATED WORKS

A similar work has been published by Hancke et al. Their work explores smart systems to improve and automate many of the processes such as collect rainwater and control intelligent buildings in smart cities. They discuss deployment of a ZigBee WSN in the smart city and they elaborate over the limited range problems [*2*]. A paper from Z. Nakutis et al. presents an idea of RF-169 utilization in IoT Infrastructure, but no detailed link budget calculation and system life-time span in relation to the node energy consumption. However, they studied network infrastructure including system architecture, redesign of protocol (type of packets) and regulations for the 169 MHz ISM band [*3*].

III. THE CONCEPT AND THE CHALLENGES

In this section the challenges for long range coverage is discussed in the light of minimizing the energy consumption, deploying IoT technologies, and adding adaptive link behaviour. The discussion and exploration is elaborated by a case study. A typical farm equipped with IoT technology is illustrated in Fig. 1. The farmhouse contains a collection of IoT devices which monitor and control their environments.

An example could be the grains contained in the barn are monitored for vital parameters such as temperature, moisture, and light exposure. The measured data are transferred (wireless) to the coordinator (gateway) that stores and processes these. To be able to access these data the coordinator offers an interface to a user management system (e.g. based on a Cloud IoT system).

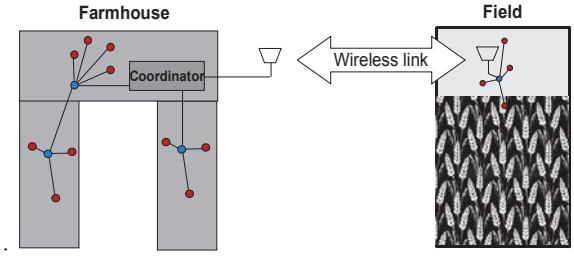

Fig. 1.A typical farm equipped with IOT's

In general, such systems are implemented by deploying a simple Wireless Sensor Network (WSN) like e.g. a ZigBee network and run the IoT devices on top of this [2]. However, the IoT devices deployed in the fields cannot be part of such a network because the WSN network is not able to cover the huge distance from the farmhouse to the fields. As discussed, to overcome this challenge an efficient adaptive wireless link is needed which adjusting the radio parameters, selects the information to be transmitted intelligently, and deploys new power sleeping technologies for the processing part. These aspects will be elaborated in the coming sections.

A. A case study regarding a common disease in vegetable farming

This section provides a selected case that elaborates over the possible choices for the adaptive link parameters. One of the most common destructive diseases in vegetable farming is the "leaf spot" disease which is caused by the Cercospora beticola Sacc. foliar pathogen. It attacks sugar beet leafs. This infection happens when a spore in a process of germination is formed on the leaf. And this process can occur only when propitious favourable weather conditions like warm and a high humidity level exists. The spores in the process of germination enter the respiration plant cells. After a few days they form small spots with a red border, visible black spots and gray coating conidia. Those conidia, which are a major dispersal diseases factor, spread from parts of leaf when it rains. Especially, when the temperature is above 17°C (optimum 27°C), the disease spreads very quickly to the neighbour leafs and plants which results in all the vegetable crop fields is infected in a few days. Thus, selective temperature, humidity, and rain conditions in the fields must be monitored frequently to handle this disease in time. Thus, this is an example of selecting important selective information to be repeated with just the right repetition interval.

B. Radio and sensor hardware choices

To relate the simulations performed in this paper to the real world settings tiny transceivers have been explored and hardware RF test modules have been build [*4*]. Parameters from these circuits are used as input for the simulations.

A transceiver module has been build with the CC1120 device (from Texas Instruments). It has a programmable transmit power up to +15dBm and sensitivity limit of -120 dBm at 1200 bps (Fig. 1 left side). To increase transmission range between two communicating nodes an external PA [*4*] with up to +30dBm transmit output power has been explored and assembled as shown on Fig. 2 right side.

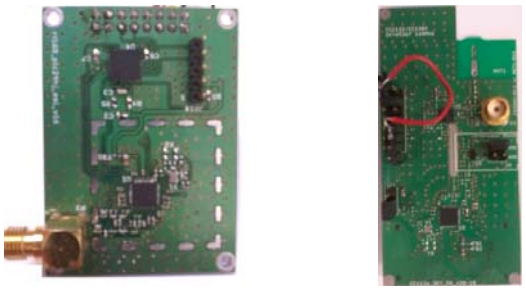

Fig. 2 A hardware RF modules based on the wireless CC1120 device

IV. AN ENERGY EFFICIENT ADAPTIVE WIRELESS LINK

The main challenges for creating an energy efficient link between a receiver and a transmitter are to overcome the path loss and to be able to supply power from a sustainable source. These challenges are explored and elaborated in the following sections.

A. Path loss

One of the most significant contributions to a wireless link loss is the path loss or free space loss, which accounts for the spreading of the transmitted energy as a function of distance. A commonly used formula that takes this into consideration is the Friis transmission formula (1).

$$\frac{P_r}{P_t} = G_r G_t \left(\frac{\lambda}{4\pi R} \right)^2 \quad (1)$$

Where: Pr and Pt are the received and the transmitted power respectively. Gr and Gt are the antenna gain for the receiver and the transmitter. λ is the wavelength and R is the distance between the receiver and the transmitter. Fig. 3 shows the formula (1) plotted with the path loss expressed in dB.

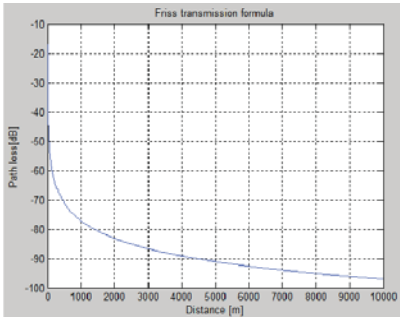

Fig. 3. Friis transmission formula with path loss on the y-axis and distance on the x-axis

As illustrated (Fig. 3) the path loss can be as large as 100 dB if the distance between the receiver and the transmitter is 10 km. However, the path loss is also a function of the Line of Sight (LoS) condition between the transmitter and the receiver. If an object is blocking the LoS it has impact on the path loss. Especially if the object is inside the first Fresnel-zone (Fig. 4) it has a considerably impact on the path loss [5] [*5*].

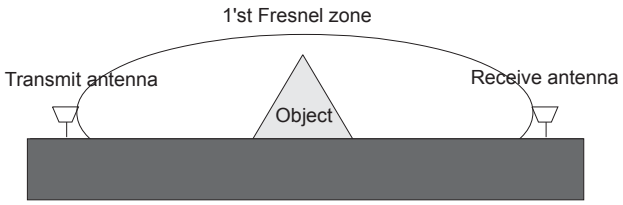

Fig. 4. The first fresnel zone with an attenuating object

Finally the curvature of the earth can disrupt the LoS condition. The distance where LoS is possible is stated in equation (2) as an approximation.

$$D \approx 4120\left(\sqrt{h_r} + \sqrt{h_t}\right) \quad (2)$$

Where: D is the LoS distance between the transmitter and the receiver in meters. The heights hr and ht are the antenna-heights in meters for the receiver and the transmitter over ground, respectively.

B. *Power source*

Many types of power sources exist; however, for low form factor IoT devices located in the field sources based on solar and wind power are attractable because they are cheap, they are available most of the time, and they are sustainable. An alternative could be batteries, but they need to be changed over time and the weather conditions have impact on their efficiency and lifespan. Nevertheless, re-chargeable batteries are needed to store the solar and wind power in non-productive periods such as at night time and under conditions with no wind.

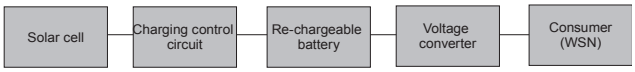

Fig. 5. A solar power system which interfaces a WSN

Focusing on a solar power system (Fig. 5) it has a solar cell which converts the solar energy into electricity. However, this process provides some challenges in form of low efficiency and it often provides an incompatible voltage for the battery and the WSN node. The efficiency for most consumer, market available solar cells is in the range of 17 - 20 percent and the produced power is approximately 15 mW/cm^2 [6][*6*]. Nevertheless, future solar cells expect a maximum efficiency of 46% [7][*7*].

Regarding the voltage incompatibility a charging circuit is often deployed as illustrated in Fig. 5. This circuit transforms the solar cell voltage and current to fit the battery parameters for the cost of an efficiency of approximately 60 percent [*8*][8]. The re-chargeable battery stores the power received from the charging control, but approximately 34 percent are wasted, i.e. the re-chargeable battery efficiency is approximately 66 percent [8]. Finally, the voltage converter adjusts the voltage so it fits the needs for the consuming IoT node (WSN) for the costs of approximately 50 percent [8] energy loss. Adding all the losses the final energy loss is given in equation 3.

$$E_{loss} = E_{solar} + E_{ch\,\mathrm{arg}\,econtrol} + E_{battry} + E_{votageconverter} \quad (3)$$

To be able to predict the produced energy from a solar cell data for the average sun hours and the energy intensity are needed. The PVGIS database [*9*] is a source that provides these information's. Assuming that the solar cell is mounted horizontal the solar radiation (Wh/m2/day) can be looked up in the database. An example for Copenhagen is illustrated in Table I.

TABLE I.

	Month			
	March	***August***	***September***	***December***
Wh/m2 /day	2810	4440	3170	384

C. *A simulation model*

A simulation model has been developed in a mathematical tool to be able to experiment and explore the most vital parameters in the adaptive wireless link. This model is primarily based on the equations discussed earlier in his paper in combination with some parameters as illustrated in Fig. 6.

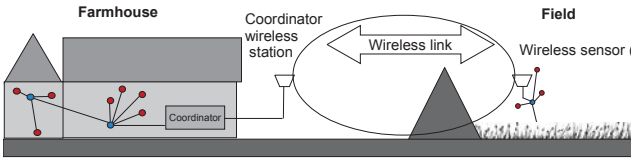

Fig. 6. The simulation model settings

The coordinator (and its user) communicates and exchange data with the farms IoT devices which are interconnected by a WSN network (Fig. 6). To be able to communicate with the external IoT devices located in the fields an energy efficient adaptive wireless link is established. In this model it is assumed that this link is attenuated by an object, which ranges into the first Fresnel zone.

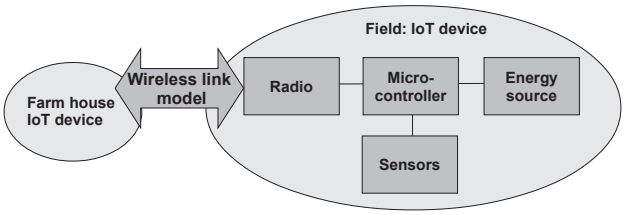

Fig. 7. Schematic of the simulated iot device

A block schematic of the simulated IoT device is presented in Fig. 7. The wireless link model implements equation 1 and 2 together with the attenuation provided by the object in the Fresnel path (Fig. 4). The following parameters are used for the model (Table II):

TABLE II.

Parameter	*Value*
Distance from the field to the farmer house	9 km
Height (over ground) of farm house antenna	4 m
Height of the antenna - the field IoT device	1 m
Attenuation of object in first Fresnel zone	20 dB
Antenna gain (Rx+Tx)	0 dB

The radio model (Fig. 7) covers a CC1120 device inclusive an external Power Amplifier (PA). The parameters for the radio and the power amplifier are given in Table III.

TABLE III.

Parameter	*Value*
Operating frequency	169 MHz
Sensitivity	-120dBm @ 1200 bps, BER=10E-2
Sensitivity (approximated)	-110dBm @ 1200 bps, BER=10E-5
Modulation	2-GFSK
Power amplifier output power	Max. 1 Watt
Radio consumed power RX	69 mW
Radio consumed power TX	150 mW
Microcontroller consumed power	3 mW
PA efficiency	50 %

The energy source (Fig. 7) is based on a solar cell with belonging components (Fig. 5). The data used in the simulation has been discussed previously and are summed-up in Table IV.

TABLE IV.

Parameter	*Value*
Solar cell (SZGD6030) area	60*30 mm (10 mm rim)
Solar cell efficiency	17 %
Solar power system efficiency (Fig. 4)	3.4 %
Solar radiation	Data from Table I

Regarding the wireless transmission protocol it approximates the popular ZigBee framework which is often used as the backbone in many IoT systems. Thus, each frame has an overhead of 31 bytes and a maximum payload of 127 bytes. These individual frames are combined into a super-frame that contains 16 of these. Additionally, it is assumed that the microcontroller provides a power saving mode (sleep mode) when no traffic takes place and it is assumed that the sensors have a very low power-consumption (i.e. it is ignored).

D. Elaborated simulation results

This section discusses and elaborates the elements in designing an energy efficient adaptive wireless link by using the previously discussed simulation settings. By focusing on the path parameters including the Friis transmission formula (1), the transmit power, the blocking object attenuation (Fig. 4), and the compensated receiver sensitivity (10 dB for changing the BER to 10E-5, Table III) the total received power can be estimated (Fig. 8).

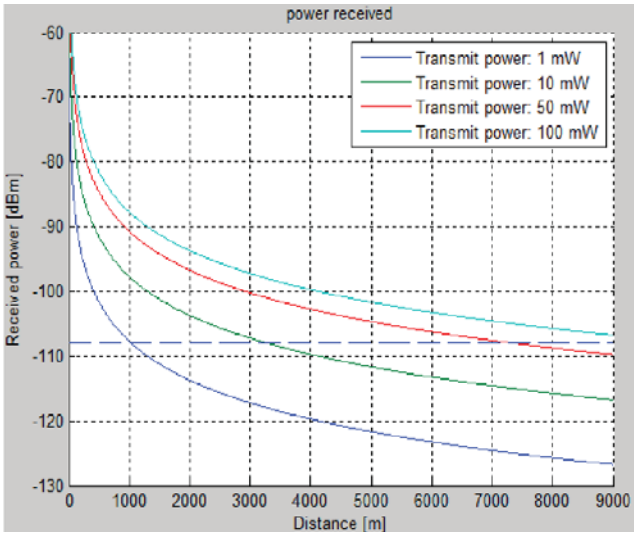

Fig. 8. The received power as a function of transmitted power and distance (a link margin of 12 db is included). The dashed line indicates the receiver sensitity level

From Fig. 8 it is notable that the received power (including the 12 dB link margin) allows a range of 1,2 km when the transmitted power is 1 mW (0dBm) and similarly, the range can be extended to 9 km when the transmit power is 100 mW (20 dBm).

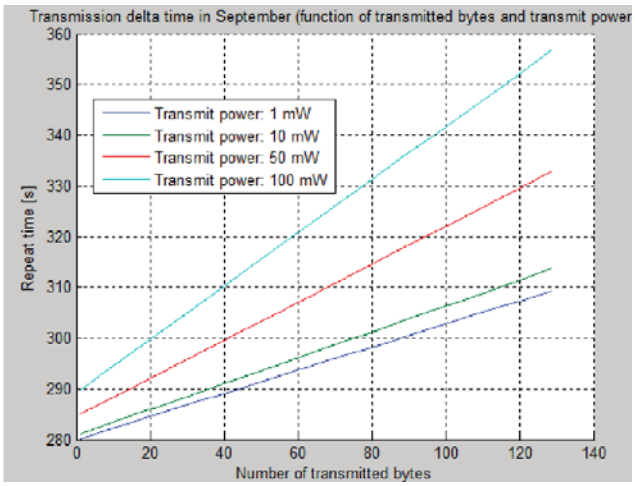

Fig. 9. The time between each transmission as a function of message length, transmit power and solar power available in september month (Denmark)

By using the average energy level provided by the solar cell to drive the IoT device it is possible to simulate the Repeat Message Time (MRT), i.e. how often a message can be send as a function of Message Length (ML) and the Transmit Power of the Field IoT Device (TPFID). This simulation result is presented in Fig. 9 where it is noted that it is possible to trade the MRT for ML. Some examples of this are provided in Table V.

TABLE V.

	TPFID [mW]	*ML [bytes]*	*MRT [s]*	*Comment*
1	100	127	356	Long range application, 9km (Fig. 7), long message
2	100	1	290	Long range application, 9km (Fig. 7), short message
3	1	127	310	Short range application, 1,2km (Fig. 7), long message
4	1	1	280	Short range application, 1,2km (Fig. 7), short message

As presented in Table V it is possible to trade ML versus MRT for a wireless IoT sensor located in the field, i.e. an adaptive link can be established. This can be very usable, e.g. if some overcast days limit the harvested solar energy it is possible to reduce the MRT and/or the ML to compensate for this, hence the link becomes adaptive. However, trading ML means sending a shorter message. Often this is possible as illustrated in the scenario (III.A) where only data about temperature, wind, and humidity are needed. These parameters occupy less than 10 bytes.

In general, the behaviour of an IoT device can be programmed into its embedded microcontroller, i.e. it behaves pseudo-intelligently. This behaviour can be programmed by the farmer remotely or the farmer can decide to overrule the pseudo-intelligence behaviour, i.e. manually setup the parameters for the IoT device. An example could be the time before harvest (September for many grain types in Denmark) where the farmer decides to monitor the humidity in the grain and therefore program the field IoT device to only transmit these data with a fixed time interval. Alternatively, the pseudo-intelligence system in the IoT device could monitor the available battery-power and transmit all data with some MRT. If the power drops (e.g. long period with overcast days) the pseudo-intelligence system could adjust the ML and the MRT to adapt to the new level of harvested power. So, if the field IoT devices has been running for some time without any harvested power the MRT and the ML can be adjusted so the battery last longer and when the solar energy is back on the parameters can be adjusted so the battery charges between the transmissions.

V. Conclusion

An energy efficient adaptive wireless link for farms based on IoT technologies has been explored and elaborated by using a simulation model. The model simulates the vital parameters in a wireless IoT link that is based on ZigBee-WSN technologies and real world hardware in form of the transceiver module CC1120 from Texas Instruments and a small form factor solar panel (SZGD6030). It has been found that it is possible to place a wireless IoT device far from the farm-controller by using the elaborated adaptive technologies. Hence, an IoT device placed 9 km from the farm-controller is able to transmit periodic messages every 6 minutes with a payload length of 127 bytes. This amount of payload is sufficient to transmit vital data like those presented and discussed in the disease scenario. Additionally, the presented simulation results support and enable the future design of an adaptive algorithm for IoT nodes. This algorithm could be able to scale the ioT node power consumption according to weather conditions and thereby behave adaptive with respect to the sustainable power available.

References

[1] M Koziol, (2015) COBORU. [Online]. www.coboru.pl

[2] P Jain, A Noor, and V Sharma, "The role of advanced sensing in smart cities," *Sensors*, pp. 393-425, 2013.

[3] Z Nakutis, A Ronkainen, and B Andersen, "Remote Agriculture Automation using Wireless Link and IoT Gateway Infrastructure," in *DEXA Workshop on Integrated Processing, Control an Knowledge Systems for Sustainable Production in Farms and Forests*, 2015. [Online]. www.nrel.gov

[4] T Blaszczyk. (2015) CWSA. [Online]. www.cwsa.dk

[5] A Johnson, T Agbinya, and K Ryszard, *4G Wireless Communication Networks: Design Planning and Applications*, 1st ed. Aalborg: River publisher, 2013.

[6] S Roundy. (2003) Energy scavenging for Wireless Sensor Nodes with a Focus on Vibration to Electricity Conversion. Ph.D. dissertation UC Berkely.

[7] NREL. (2015) NREL. [Online]. www.nrel.gov

[8] J Taneja and D Culler, "Design, Modeling and Capacity Planning for Micro-Solar Power Sensor Networks," in *Proceedings of the 7th international conference on Information processing in sensor networks*, 2008.

[9] EC europe. (2015) Photovoltaic Geographical Information System - Interactive Maps. [Online]. http://re.jrc.ec.europa.eu/pvgis/apps4/pvest.php

THE 5TH INTERNATIONAL CONFERENCE ON WIRELESS COMMUNICATIONS, VEHICULAR TECHNOLOGY, INFORMATION THEORY, AEROSPACE & ELECTRONIC SYSTEMS (WVITAE-2015)
December 13-16, 2015, Hyderabad, India

Enlarged QR-LRL Based Massive MIMO Detector for Soft Output Generation

Sukriti Garg
Electronics and Communication Engineering Department
The LNMIIT
Jaipur, India 302031
Email: sukriti@lnmiit.ac.in

Krati Mittal
Electronics and Communication Engineering Department
The LNMIIT
Jaipur, India 302031
Email: krati23jun@gmail.com

Divyang Rawal
Electronics and Communication Engineering Department
The LNMIIT
Jaipur, India 302031
Email: divyang.rawal@lnmiit.ac.in

***Abstract*—The vowed gain in capacity within the available spectrum and power consumption provided by the Multiple Input Multiple Output (MIMO) systems make it appropriate for current day technologies. The massive MIMO system provides orders of magnitude enhancement in capacity and spectral efficiency. Earlier work shows number of detection techniques[1][8] for MIMO systems. In this paper, previous work of QR-LRL with the enlarged candidate vector set based MIMO detector i.e. Enlarged QR-LRL detector has been extended to Enlarged QR-LRL based massive MIMO detectors for hard/soft output detection. The problem of Empty Vector Set (EVS)[1][2][3] procured during the soft output generation has been worked out by earlier methods but they were inefficient in terms of complexity. Enlarged QR-LRL proposed in previous work solved the EVS problem with less complexity for the MIMO systems and achieves hard as well as soft ML performance. In this paper we have extended this algorithm for the massive MIMO systems where soft as well as hard output of proposed algorithm has been compared with the conventional schemes for the large number of antennas in terms of complexity as well as performance.**

***Keywords* - Massive MIMO; Soft output; Empty vector set; OSIC; QR-LRL; Enlarged QR-LRL.**

I. Introduction

To accomplish the increasing demand of high data rate, link capacity, reliability and spectral efficiency, various new technologies, like 5G, LTE, LTE-Advance, WiMax, etc, are using MIMO systems. In order to increase the throughput, these technologies require large number of antenna system. The systems using tens or hundreds of antennas are known as large/massive MIMO systems. Large antenna array bequeath surplus degree of freedoms and also scales down the power consumption at the base station thus generating essentially less electromagnetic interference. Beam forming, due to the large number of antennas, shun the fading dips in the transmitted signal. [5] discusses how massive MIMO act as a stockpile for number of research problems.

In the massive MIMO systems, the proper detection of transmitted symbols is a major call out due to the large number of antennas on the single terminal. Till now, number of detection techniques have been developed. ML detection[11] is known as optimal detection scheme but has highest complexity. Linear detection techniques, like ZF[6] and MMSE[7], shows degraded performance due to inefficient signal processing. Non linear detection techniques, like VBLAST[8] and QR-MRL[9], uses Ordered Successive Interference Cancellation (OSIC)[10] to mitigate the problem of interference through which linear techniques undergo. However, the later techniques show degraded performance due to error propagation, if the detection of first symbol is erroneous. To abstain from this error propagation in the detection of further symbols, QR-LRL[17] detection technique was introduced where Least Reliable Layer (LRL) is detected first by applying all the constellation points at LRL.

QR-LRL algorithm almost achieves hard ML performance but its complexity increases with the number of antennas. Layered Tabu Search (LTS) algorithm introduced in [18], approaches to ML performance and have low complexity in the massive MIMO systems even for the higher order modulations. These detectors suffer from EVS while generating soft output more firmly at lower order modulations. Various techniques like threshold based, multiple QR decomposition of channel matrix, transforming QR matrix and joint iterative detection and decoding[2][3][15][14] have been developed to mitigate EVS.

In this work, we are proposing the deployment of Enlarged QR-LRL in the massive MIMO systems for the generation of hard/soft output. This work, along with the proficiency of fixing the problem of EVS in case of soft output detection, also has less complexity for the massive MIMO systems than that of the conventional schemes[17][18]. With the enlargement of candidate vector set of QR-LRL, the problem of EVS is resolved while generating soft output and achieves almost hard/soft ML performance. At the same time it avoids multiple QR decomposition and also retains low computational complexity notably in the lower order modulation for the massive MIMO systems.

Rest of the paper is organised as follows. In section II, system model for the massive MIMO systems is introduced. Section III deals with EVS problem in the conventional detection schemes for the soft output generation in MIMO systems. Conventional schemes have been discussed in section IV. Soft output detection using Enlarged QR-LRL for large number of antennas is discussed in section V. Section VI cover the simulation results and complexity is analysed in section

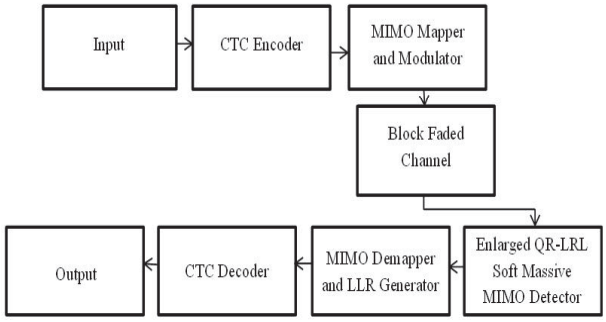

Fig. 1. Massive MIMO system model

VII. Paper has been concluded in section VIII.

II. System Model

The block diagram of massive MIMO system model for soft output generation is depicted in Fig. 1. Consider a system with N_t transmitting antennas at the base station and N_r receiving antennas at the receiver end[4][1][18]. $\mathbf{H}$ denotes the $N_r \times N_t$ block faded Rayleigh channel matrix. Here it is assumed that the complete channel state information is known at both transmitter and receiver end. The received signal $\mathbf{y}$ at the user end is given by

$$\mathbf{y} = \mathbf{Hx} + \mathbf{z} \tag{1}$$

$\mathbf{y} = [y_1, y_2, ..., y_{N_r}]$ denotes the received sequence, $\mathbf{x} = [x_1, x_2, ..., x_{N_t}]$ is the transmitted data sequence and $\mathbf{z} \sim CN(0, \sigma^2)$ denotes the circular symmetric Gaussian noise. Modulation alphabet, C, decides the order of modulation. MIMO mapper in Fig. 1, maps the single stream of data into N_t data streams. MIMO Demapper and LLR generator maps the modulated N_r data streams back to single stream of LLR values. In order to encode the input sequence and decode the soft detected sequence, Convolutional TURBO Code (CTC) Channel Encoder and Decoder has been used.

III. EVS Problem

In order to obtain the Log Likelihood Ratio (LLR) value for k^{th} bit of j^{th} symbol, where, $k = 1, 2, \ldots, log_2|C|$ and $j = 1, 2, \ldots, N_t$, distances $D^+(x) = \frac{1}{\sigma^2}||y - Hx^+||$ and $D^-(x) = \frac{1}{\sigma^2}||y - Hx^-||$ are calculated. x^+ and x^- belongs to the candidate vector set $P(k,j)^-$ and $P(k,j)^+$, corresponding to the k^{th} bit i.e. $b(k,j) = -1$ or $b(k,j) = +1$, respectively. σ^2 is the power of the transmitted signal. Therefore, LLR value can be calculated as follows:

$$LLR(b(k,j)|y) = \min_{x^- \in P(k,j)^-} D^-(x) - \min_{x^+ \in P(k,j)^+} D^+(x) \tag{2}$$

The problem of empty vector set arises when either $P(k,j)^+$ or $P(k,j)^-$ is an empty set. Due to this, LLR values cannot be obtained, thus curbing the generation of soft output values. Previously, multiple methods have been employed to overcome the problem of EVS. Best possible method to mitigate the problem of EVS is by applying all the constellation points at each layer.

TABLE I
QR-LRL Algorithm

$function[\hat{x}_{ordered}] = QrLRL(\mathbf{H}_{ordered}, \mathbf{y})$
$[Q, R] = qr(\mathbf{H}_{ordered})$
$\hat{y} = Q^H \mathbf{y}$
$for\ j = 1 : |C|$
$\hat{x}_{(4)} = C(j)$
$\hat{x}_{(3)} = M\left(\frac{\hat{y}_3 - R_{34}\hat{x}_{(4)}}{R_{33}}\right)$
$\hat{x}_{(2)} = M\left(\frac{\hat{y}_2 - R_{23}\hat{x}_{(3)} - R_{24}\hat{x}_{(4)}}{R_{22}}\right)$
$\hat{x}_{(1)} = M\left(\frac{\hat{y}_1 - R_{12}\hat{x}_{(2)} - R_{13}\hat{x}_{(3)} - R_{14}\hat{x}_{(4)}}{R_{11}}\right)$
$\hat{x}(:, j) = [\hat{x}_{(1)}, \hat{x}_{(2)}, \hat{x}_{(3)}, \hat{x}_{(4)}]^T$
$dis(:, j) = ||\mathbf{y} - \mathbf{H}_{ordered}\hat{x}(:, j)||^2$
end
$[val, ind] = min(dis)$
$\hat{x}_{ordered} = \hat{x}(:, ind)$
$end\ function$

IV. Conventional Schemes

A. LTS Massive MIMO Detector[12]

LTS algorithm was developed specifically for the massive MIMO system by employing layering approach with the Tabu Search (TS) algorithm. In this algorithm, local neighbourhood is explored to detect a sub-vector that act as an initial solution for the detection of the further layers. The complete algorithm has been discussed in [18]. The complexity of this algorithm mainly depends upon i) Total number of local neighbours considered (maximum value depends on order of modulation) ii) δ, a constant ($0 \leq \delta \leq 0.5$) which is responsible for the switching between the OSIC detection and TS detection (OSIC and TS if $\delta > 0$ and pure TS if $\delta = 0$). As δ tends to 0, performance improves but leads to high computational complexity.

As this algorithm in case of the soft output detection, does not involves application of all the constellation points at any layer for the symbol detection, thus it diversifies the scope of formation of the empty vector sets. To resolve this problem, the detected vector $d = [\hat{x}_1, \hat{x}_2, \ldots, \hat{x}_{Nt}]$ is mapped to bit vector $b_i = [b_{i,1}, b_{i,2}, ..., b_{i,k}]$, where $k = log_2|C|$ and $b_{i,j} \in [-1, 1]$, $i = 1, 2, ..., N_t$ and $j = 1, 2, ..., k$. d_i^{j+} and d_i^{j-} are the detected vectors with j_{th} bit of i_{th} symbol forced to be +1 and -1, respectively. Now, if

$$||\mathbf{y} - \mathbf{H}d_i^{j-}||^2 - ||\mathbf{y} - \mathbf{H}d_i^{j+}||^2 > 0 \tag{3}$$

then j^{th} bit of i^{th} symbol is likely to be +1, otherwise -1. In order to shun the unbounded increase with the increase in number of antennas, authors in [18] introduced a normalization factor $(\frac{\lambda_{i,j}}{2})^2||h_i||^2$.

B. QR-LRL MIMO Detector[17]

QR-LRL detection technique employs OSIC method for detection but in order to mitigate the problem of error propagation in OSIC, it tries all the constellation points at the least reliable layer. For 4×4 MIMO system, the complete algorithm is summarized in Table I. The channel matrix $\mathbf{H}$ is ordered

TABLE II
ENLARGED QR-LRL ALGORITHM

$function[V_{1,2}Dist_{1,2}] = V_{LRL,MRL}(\mathbf{y}, \mathbf{H}_{ordered})$
$[Q, R] = qr(\mathbf{H}_{ordered})$
$\hat{y} = Q^H\mathbf{y}$
$for\ j = 1 : |C|$
$\hat{x}_{(4)} = C(j)$
$\hat{x}_{(3)} = M\left(\frac{\hat{y}_3 - R_{34}\hat{x}_{(4)}}{R_{33}}\right)$
$\hat{x}_{(2)} = M\left(\frac{\hat{y}_2 - R_{23}\hat{x}_{(3)} - R_{24}\hat{x}_{(4)}}{R_{22}}\right)$
$\hat{x}_{(1)} = M\left(\frac{\hat{y}_1 - R_{12}\hat{x}_{(2)} - R_{13}\hat{x}_{(3)} - R_{14}\hat{x}_{(4)}}{R_{11}}\right)$
$V_{LRL} = [\hat{x}_{(1)}, \hat{x}_{(2)}, \hat{x}_{(3)}, \hat{x}_{(4)}]^T$
$dis_{LRL}(:, j) = ||\mathbf{y} - \mathbf{H}_{ordered}V_{LRL}(:, j)||^2$
end
$for\ j = 1 : |C|$
$\hat{x}_{(3)} = C(j)$
$\hat{x}_{(4)} = M\left(\frac{\hat{y}_3 - R_{33}\hat{x}_{(3)}}{R_{34}}\right)$
$\hat{x}_{(2)} = M\left(\frac{\hat{y}_2 - R_{23}\hat{x}_{(3)} - R_{24}\hat{x}_{(4)}}{R_{22}}\right)$
$\hat{x}_{(1)} = M\left(\frac{\hat{y}_1 - R_{12}\hat{x}_{(2)} - R_{13}\hat{x}_{(3)} - R_{14}\hat{x}_{(4)}}{R_{11}}\right)$
$V_{MRL} = [\hat{x}_{(1)}, \hat{x}_{(2)}, \hat{x}_{(3)}, \hat{x}_{(4)}]^T$
$dis_{MRL}(:, j) = ||\mathbf{y} - \mathbf{H}_{ordered}V_{MRL}(:, j)||^2$
end
$V_{1,2} = [V_{LRL}V_{MRL}]$
$Dist_{1,2} = [dis_{LRL}dis_{MRL}]$
$end\ function$

using post detection SINR, i.e. $||\mathbf{G}||^2$ (where $\mathbf{G} = \mathbf{H}^{-1}$). Therefore, the ordered channel matrix is given as

$$\mathbf{H}_{ordered} = [\hat{h}_{(N_t-1)^{th}RL}, ..., \hat{h}_{MRL}, \hat{h}_{LRL}] \tag{4}$$

In table, M is a mapping function which maps the detected symbols to the nearest constellation point. BER performance of this algorithm approaches to ML performance for hard detection. Post detection SINR based ordering of $\mathbf{H}$ involves matrix inversion which results in higher complexity (of the order of $O(N_t^3)$ for the large antenna systems. Since all the constellation points are applied only at LRL, therefore the problem of EVS may perceived in the detection of further layers.

In order to get rid of this problem , threshold value is derived at LRL where the candidate vector set corresponding to each bit cannot be empty. This threshold value is used to derive LLR values for the further layers suffering from EVS. After calculating LLR at LRL using (4), threshold value is given by

$$Thres = \frac{1}{log_2|C|}\sum_{k=1}^{log_2|C|} Th(k) \tag{5}$$

where, Th is evaluated as

$$Th(k) = max[Th^+(k), Th^-(k)] \tag{6}$$

given, $Th^+(k) = \min_{\mathbf{x}\in P(k,(m))^+} D^+(x), m = 1, 2, \ldots, |C|$ and $Th^-(k) = \min_{\mathbf{x}\in P(k,(m))^-} D^-(x), m = 1, 2, \ldots, |C|$.

TABLE III
ENLARGE VECTOR SET AT 3^{rd} LAYER DETECTION

$function[V_{S3}] = QrLRL(\mathbf{y}, \mathbf{R}, V_{1,2}, Dist_{1,2})$
$V_{1,2} = sort(V_{1,2})$
$\hat{y} = Q^H\mathbf{y}$
$V_{new} = V_{1,2}(:, 1 : U)U \leq |C|$
$for\ k = 1 : U$
$for\ j = 4 : 3 : -1$
$\hat{x}_{(j)} = V_{new}(j, k)$
end
$for\ i = 1 : |C|$
$\hat{x}_{(2)} = C(i)$
$for\ ind_1 = 2 : 1 : -1$
$\hat{x}_{(2)} = M\left(\frac{\hat{y}_{(ind_1-1)} - \sum_{ind_2=2}^{4} R_{(ind_1-1),ind_2}\hat{x}_{(ind_2)}}{R_{(ind_1-1),(ind_1-1)}}\right)$
end
$V_3(:, k, i) = [\hat{x}_{(1)}, \hat{x}_{(2)}, \hat{x}_{(3)}, \hat{x}_{(4)}]^T$
$Dist_3(:, k, i) = ||\mathbf{y} - \mathbf{R}V_3(:, k, i)||^2$
end
end
$V_{cand,3}(:, 1 : C) = (min(V_3(:, 1, :)).....min(V_3(:, C, :)))$
$V_{S3} = [V_{1,2}V_{cand,3}]$
$end\ function$

V. PROPOSED SCHEME

Consider the system model mentioned in section III. Likewise in QR-LRL scheme, Enlarged QR-LRL also utilises ordered $\mathbf{H}$ that tends to mitigate the interference. Therefore, the received vector is given by:

$$\mathbf{y} = \mathbf{H}_{ordered}\mathbf{x}_{ordered} + \mathbf{z} \tag{7}$$

where, $\mathbf{H}_{ordered}$ is the ordered channel matrix (given by (4)) and $\mathbf{x}_{ordered}$ is ordered transmitted vector represented as follows:

$$\mathbf{x}_{ordered} = [\hat{x}_{(N_t-1)^{th}RL}, ..., \hat{x}_{MRL}, \hat{x}_{LRL}] \tag{8}$$

Instead of applying strict post detection SINR based ordering criteria to $\mathbf{H}$, since almost all the constellation points are applied at each layer, this algorithm employs simply SNR based ordering. This reduces the complexity to some extent as it avoids inverse of $\mathbf{H}$ matrix. The complete algorithm for Enlarged QR-LRL has been discussed in Table II and Table III. For the simplicity, 4×4 MIMO system has been considered.

For the detection purpose, first the ordered channel matrix is decomposed using QR decomposition method. Application of each constellation point at LRL and MRL is possible due to the upper triangular structure of R matrix obtained from QR decomposition of $\mathbf{H}$. V_{LRL} and V_{MRL} denotes the two vector set obtained by applying all constellation points at LRL and MRL respectively. These vector sets will not suffer from the problem of EVS as all the constellation points have been applied here. $V_{1,2}$ is the combined vector set defined as $([V_{41}....V_{44}], [V_{31}.....V_{34}])$ and the combined distance vector $Dist_{1,2}$ consists of the distance values for $V_{1,2}$.

For the detection of third layer, $V_{1,2}$ act as the enlarged vector set. U vectors from the enlarged vector set with the

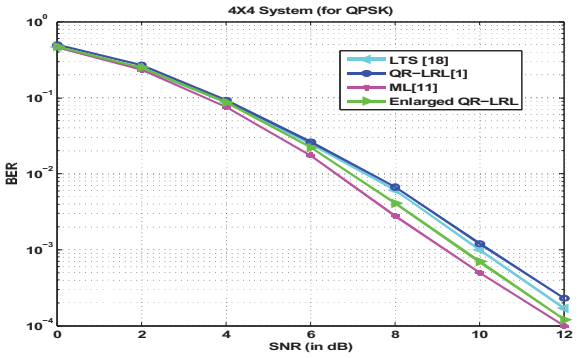

Fig. 2. BER Performance for 4x4 system with QPSK Modulation scheme

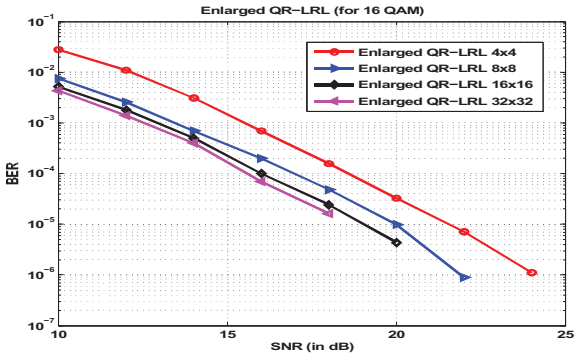

Fig. 3. BER comparison for different diversity order with 16-QAM modulation scheme

least distances in distance vector $Dist_{1,2}$ are chosen in order to avoid error propagation, where U$\leq |C|$.

$$V_{1,2}(i,j) = [\hat{x}_{(3^{rd}RL)}, \hat{x}_{(2^{nd}RL)}, \hat{x}_{(MRL)}, \hat{x}_{(LRL)}] \quad (9)$$

Considering these U vectors, detection of third layer (2^{nd}RL) is carried out by applying each constellation point at 2^{nd}RL, while $\hat{x}_{(4)}$ and $\hat{x}_{(3)}$ are symbols chosen same as x_{LRL} and x_{MRL}. V_3 denotes the resultant candidate vector set corresponding to the third layer detection. Now, V_3 is arranged by grouping vectors that uses same constellation point at 3^{rd} layer and than $V_{cand,3}$ is formed by choosing group wise minimum distance vectors from V_3 according to $Dist_3$. Again for the detection of further layer the candidate vector is enlarged by combining $V_{cand,3}$ vectors with that of $V_{1,2}$ and whole process is repeated until the last layer is detected.

After the detection of each layer, LLR values are raised in the same way as discussed in section III and then these LLR values are fed to TURBO decoder to retrieve the input symbols in case of soft output detection. The value of U is generally chosen small (here, $U = 1$) due to the least error propagation property of QR-LRL. The complexity of this algorithm increases with the higher order modulation. We have implemented this algorithm for the massive MIMO systems.

VI. Simulation Results

The massive MIMO system taken into account for the simulation purpose consists of different order of transmitting and receiving antennas i.e. 4, 8, 16 and 32. It is assumed that the perfect channel information is known at both transmitting and receiving end. The system model considers that the channel is Rayleigh block faded. 1/2 rate Convolutional TURBO code (CTC) has been used as channel encoder and CTC decoder is used to decode the detected soft output.

Fig. 2 evaluates the BER performance of 4×4 MIMO system with QPSK modulation. ML detector shows 10^{-3} BER at 9.2 dB (apx.) SNR while LTS, QR-LRL and Enlarged QR-LRL provide same BER at SNR of 10 dB, 10.2 dB and 9.6 dB respectively. This verifies that BER curve of Enlarged QR-LRL overlaps the ML curve. Fig. 3 shows the comparison of the system using Enlarged QR-LRL with 16-QAM modulation for the different diversity orders. From the

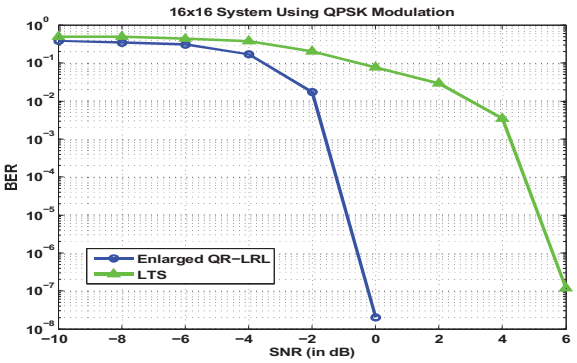

Fig. 4. Soft output BER comparison of 16x16 system with QPSK as modulation scheme

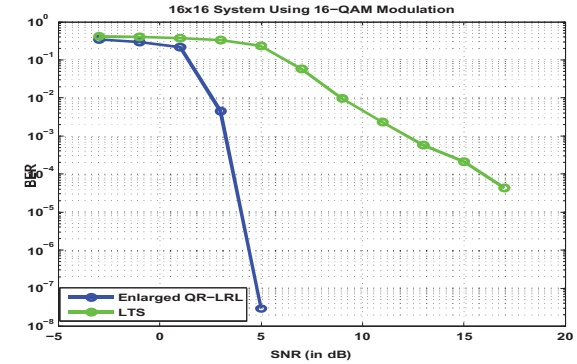

Fig. 5. Soft output BER comparison of 16x16 system with 16-QAM as modulation scheme

TABLE IV
Complexity Comparision of different detection schemes for MIMO systems of different diversity order(Real operations)

Method(with 16 QAM)	8×8	16×16	32×32
QR-LRL	9056	52,148	3,35,744
LTS(with ordering)	24,644	1,35,082	7,64,297
Enlarged QR-LRL	11,648	52,736	2,72,384

TABLE V
COMPLEXITY OF $N_t \times N_r$ ENLARGED QR-LRL ALGORITHM

Operation	No. of **M**
$\|\|h_i\|\|^2_{i=1,2...N_t}$	$2N_r$
$QR_{decomposition}$	$4N_t^2N_r$
$Q^H y$	$4N_tN_r$
$\|\|d-Rx\|\|^2@LRL$	$8(N_t(N_t+1)/2)$
$\|\|d-Rx\|\|^2@MRL$	$8(N_t(N_t+1)/2)$
.	
.	
$\|\|d-Rx\|\|^2@N_t^{th}RL$	$8(N_t(N_t+1)/2)$
$s=(6N_tN_r+4N_t^2N_r+8(N_t(N_t+1)/2)\|C\|(\sum_{i=3}^{N_t}L_i+2))$	

curves it is perceived that as the diversity order of the system increases, the BER performance of the system gets refined.

The comparison of Soft BER performance of LTS and Enlarged QR-LRL with QPSK modulation scheme is shown in Fig. 4 and with 16-QAM modulation scheme in Fig. 5. The figures distinctly show that Enlarged QR-LRL attains BER of 10^{-4} at SNR of -1.5 dB (for QPSK) and 3.5 dB (for 16-QAM) while LTS attains same BER at SNR of 4.5 dB (for QPSK) and 12 dB (for 16-QAM). Hence, the proposed scheme shows the gain of around 6 to 8.5 dB than that of LTS.

VII. COMPLEXITY ANALYSIS

Table IV and V shows the complexity analysis of MIMO system with different detection schemes in terms of number of M Multiplications[13][16]. $|C|$ denotes the number of constellation points and m indicates the QR-m. QR decomposition is used in the algorithm in order reduce the complexity as R matrix is used for multiplication with constellation points instead of taking inverse of H.

Table V gives the complexity analysis for $N_t \times N_r$ system using Enlarged QR-LRL and Table IV shows complexity comparison for 8×8, 16×16 and 32×32 MIMO system using 16-QAM modulation scheme which clearly shows that the QR-LRL becomes more complex as diversity of the system increases in comparison to Enlarged QR-LRL due to the inverse of H involved in QR-LRL. Similarly, a huge complexity difference can be observed between Enlarged QR-LRL and LTS detection scheme.

VIII. CONCLUSION

In this paper, detection algorithm of Enlarged QR-LRL has been implemented for the massive MIMO system for hard as well as soft output detection. The proposed method outperforms the conventional detection schemes both in terms of BER performance and complexity. The problem of EVS, encountered while performing soft output detection, has been mitigated by applying all the constellation points at every layer. In simulation results we have compared hard/soft BER performance of proposed scheme Enlarged QR-LRL with LTS which clearly shows that the proposed scheme gives near ML performance along with low complexity for different modulation schemes.

IX. ACKNOWLEDGEMENT

The work has been carried out as a part of the activity under the project Mobile Broadband Service Support over Cognitive Radio Networks sponsored by Information Technology Research Agency (ITRA), Department of Electronics and Information Technology (DeitY), Govt. of India.

REFERENCES

[1] S. Bahng, Y. K. Park, and J. Kim," QR-LRL signal detection for spatially multiplexed MIMO systems," *IEICE transactions on communications*, vol. E91-B, no. 10, pp. 3383-3386, Oct. 2008.

[2] H. Kawai, K. Higuchi, N. Maeda, M. sawahashi, T. Ito, Y. Kaakura, A. Usihirokawa, and H. Seki, "Likelihood function for QRM-MLD suitable for soft-decision turbo decoding and its performance for OFCDM MIMO multiplexing in multipath fading channel," *IEICE Trans. Commun.*, vol.E88-B, no.1, pp.47-57, Jan. 2005.

[3] J. Kim, Y. K. Park, and S. Bahng, "Efficient soft output generation method for spatially multiplexed MIMO systems," *IEICE Trans. Commun.*, vol.E92-B, no.11, pp. 3512-3515, Nov. 2009.

[4] D. Rawal, V. Chakka, Y. O. Park, S. Bahng and H. S. Park, "Enlarged QR-LRL based SM-MIMO detector for efficient soft output generation," *TENCON IEEE Region 10 Conference*, pp. 1-6, Oct. 2014.

[5] E. G. Larsson, F. Tufvesson, O. Edfors, and T. L. Marzetta, "Massive MIMO for next generation wireless systems," *IEEE Commun. Mag.*, vol. 52, no. 2, pp. 186195, Feb. 2014.

[6] C. Siriteanu, X. Shi, and Y. Miyanaga, "Analysis and simulation of MIMO zero-forcing detection performance for correlated and estimated Rician-fading channel," *In Communications Theory Workshop (AusCTW), Australian*, IEEE, pp. 182-187, 2011.

[7] Y. S. Cho, J. Kim, W. Y. Yang, and C. G. Kang, *MIMO-OFDM Wireless Communications with MATLAB,* by John Wiley and Sons(Asia) Pte Ltd., IEEE Press, 2010.

[8] P. W. Wolniansky, G. J. Foschini, G. D. Golden, and R. Valenzuela, "V-BLAST: An architecture for realizing very high data rates over the rich-scattering wireless channel," *In Signals, Systems, and Electronics, ISSSE, URSI International Symposium on*, IEEE, pp. 295-300, Sept. 1998.

[9] J. Kim, D. Kim, and S. Yun, " Mitigating error propagation in successive interference cancellation," *IEICE Trans. Comm.*, vol. E89-B, no. 10, pp. 2956-2960, Oct. 2006.

[10] S. Bahng, Y. O. Park, and K. Jaekwon, "QR-LRL signal detection for spatially multiplexed MIMO systems," *IEICE transactions on communications* vol. 91, no.10, pp. 3383-3386, 2008.

[11] K. Su, "Efficient maximum likelihood detection for communication over multiple input multiple output channels," *Department of Engineering, University of Cambridge*, Feb. 2005.

[12] N. Srinidhi, T. Datta, A. Chockalingam, and B. S. Rajan, " Layered tabu search algorithm for large-MIMO detection and a lower bound on ML performance," *In Global Telecommunications Conference (GLOBECOM)*, IEEE, pp. 1-5, 2010.

[13] D. Rawal, V. Chakka, Y.-O. Park, S. Bahng, and H. S. Park, "Mitigating Empty Vector Set Using Enlarged QRLRL-M Soft SM-MIMO Detector," *Wireless Personal Communication, Springer Jrnl*, pp. 1-18, 2015.

[14] D. Rawal, Y.-O. Park, S. Bahng, H. Lee, C.-J. Pil, and V. Chakka, "Efficiently using extrinsic gain for candidate vectors selection in QR-LRL based IDD MIMO receiver," *In ICT Convergence (ICIC), International Conference on*, IEEE, pp. 221-224, 2012.

[15] K. Kim, Y. Jung, S. Lee, and K. Jaekwon, "Efficient list extension algorithm using multiple detection orders for soft-output MIMO detection," *IEICE Tran. Commun.*, vol. E95-B, no. 3, pp. 898-912, March 2012.

[16] P. Salmela, A. Burian, H. Sorokin, and J. Takala, "Complex-valued QR decomposition implementation for MIMO receivers," *In Acoustics, Speech and Signal Processing, ICASSP 08, IEEE International Conference on*, pp. 1433-1436, 2008.

[17] W. Hou, F. Tadashi, and K. Toshiharu, "Low complexity MIMO detection using OSIC with conditional list generation," *IEICE Communications Express*, vol. 2, no. 10, pp. 447-452, 2013.

[18] N. Srinidhi, T. Datta, A. Chockalingam, and B. S. Rajan, " Layered tabu search algorithm for large-MIMO detection and a lower bound on ML performance," *Communications, IEEE Transactions*, vol. 59, no. 11, pp. 2955-2963, 2011.

THE 5TH INTERNATIONAL CONFERENCE ON WIRELESS COMMUNICATIONS, VEHICULAR TECHNOLOGY, INFORMATION THEORY, AEROSPACE & ELECTRONIC SYSTEMS (WVITAE-2015)
December 13-16, 2015, Hyderabad, India

Service and Big Data business model in a world of persuasive technologies

Troels Christian K. Andersen* | *E-mail: troelsck@auhe.au.dk
Torben Cæsar Bisgaard Bjerrum** | **E-mail: torben_bisgaard@yahoo.dk

Aarhus University, AUHE - BTECH 7400 Herning, Denmark

ABSTRACT

Purpose

The ability to make business model innovation has been known for more than a decade. The support and the ability of BMI provides for companies wanting to push their business can be seen in increasing number of cases, in the literature. The technology now provides the next phase of BMI with persuasive technology. The purpose with this paper is to explore the possibilities and challenges that arise with the servitization, BMI and persuasive business models, in relation to understanding, development and implementation.

Design/methodology/approach

This paper is based on a qualitative case study using a deductive approach. This is combined in a participatory action research and insider-as-researcher framework. The point of view in the case is from both the business and the researchers point of view. The discussion section is fully from the researchers' side.

Findings

The ability to find and work with new business models are matured in both technology and business organizations. The competences in the business requires structure through a more visible generic framework for SMEs' to follow. New frameworks and competences are needed to maintain a required pace of implementation for all sizes of businesses.

Keywords: Business model innovation, Servitization, persuasive business models, Big Data.

INTRODUCTION

Emerging trends indicates that the aftereffect of globalization has changed how manufacturing organizations operate and expand their businesses on a global scale. This can be explained by looking at how the competitive situation is forcing these manufacturing organizations to shift their business models towards differentiating away from commoditization that arises from development countries with low labor costs [1, 2]. The difficulty on competing against the exportation of low cost commodity products is typically associated with fixed costs that are bound to operations. Meanwhile manufacturing organizations from development countries are more flexible and able to expand their market share by competing on exporting low costs products [1, 3].

In addition to this, the ripple effect of globalization indicates that the manufacturing organizations has removed boundaries between countries, economies and industries, resulting in technologies that are ever fast changing. At the same time, the requirement of processes needed to be redesigned and communication to become faster and available at any given place and time [3]. Another perspective shows customers changing how they interact with technology, requiring organizations to rethink their way of approaching how value is offered to their customers [1, 4].
In an effort to counteract, this requires manufacturing organizations in the industrialized countries to rethink their way of doing business in order to survive, be competitive and create profit [5, 6].

The historical events indicate that organizations that have focused on delivering desirable tangible products, on a transactional basis have met the specific needs of the customer. However, the value delivered through the goods-dominant view has changed, to a more service-dominant view [7], were intangible values, exchange processes and relationships are primary factors to consider in the long-term strategic perspective for organizations to be successful [6, 8]. In addition, the increasing trend and use of the terminology; the

service-dominant view has been influenced by changes in the customers´ demand through requested goods and services in integrated solutions [5]. This new transactional view has changed the way, in which manufacturing organizations focus less on manufacturing products and more on adding value to their customers through service. Some of the aspects related to this are technology improvements, intellectual property, etc., that the manufacturing organizations differentiate and diversify their value propositions after [9].

Recent literature reveals new ways to gain revenue streams on improved product-service offerings for traditional manufacturing organizations by focusing on system solutions [10]. Relating this to the globalization effect only highlights the importance of innovating on the service offerings with the customers centered in the development process, hence escaping commoditization, whereas goods-dominant focused manufacturing organizations spread to low-labor countries to survive [11].

Another way to diversify businesses to avoid the commoditization is to focus on identifying new trends occurring within the ecosystem. The literature study conducted in relation to this article suggests that data is one of these new trends, in which the data plays an important part on identifying value to the customers [12]. More so, data acts as the gateway to optimize service business models, create new business models and to better understand what customers' value [13].

Research shows that up to 64 per cent of organizations in 2013 are heavily investing, or planning to invest in big data technology [12]. According to this study, there are challenges with adopting big data, and it is not concerning the technology, but rather about where and how big data creates value. According to [12], the synthesis of current literature on big data suggests two areas as for how big data creates value. The first idea, concerns big data used for the incremental improvement and optimization of existing services, and second, new products and business models can be innovated based on the use of data.

Recent trends indicate that organizations are actively focused on redefining their value offerings to the customers, through the use of business models innovation [14]. This typically results in incremental improvements and cost reduction to the current products or services offered. However, on rare occasions it happens that organizations decide to conduct significant changes to their business model with a focus that extends further beyond the value proposition including more aspects of the business e.g. Ryanair, IBM, and Apple etc. [15]. Further research indicates that Business Model Innovation (BMI) is important and relates this to the organizations ability to create breakthrough and game-changing business models that redefines markets [15]. These business models usually commercialize new ideas and technologies. [16] argues that business models play an important role regarding technology, its success and ability to transfer value to the customer.

The purpose with this paper is therefore to describe how to counteract commoditization through business model innovation by shifting between business models of a European Electronics Manufacturer that follows a product-oriented logic towards service-oriented logic offering solutions for their customers, using persuasive service-business models.

METHODOLOGY

The applied research method for this research, has been participatory action research (PAR). The data collection and timing is considered a cross-sectional study with qualitative data gathered from primary, secondary and tertiary sources from unstructured and semi-structured interviews.
There is no single definition on action research (AR), but the definition by [17] is adopted as an approach in which the action researcher and the client collaborate in the diagnosis of a problem and in the development of a solution, based on the diagnosis.
The researchers participated in the companies daily routine from a management perspective, with the purpose to describe and change the behavior. The ontology is seen as an idealist approach that produces a reality created by the researchers, but with the AR being almost instantly is tested and shared with actors for a common understanding towards issues, that in turn creates a snowball effect of new issues and insights. This bottom up effect creates an abductive strategy to understand more complex problems that at first

glance not is revealed through qualitative data collection. This approach compliments the AR research strategy with the iterations for thicker data collection and deeper understanding.

The implications from the AR research method, is that the researchers have to be more rigorous in documenting the research, and look for the theoretical justification on the action part of the research. The close collaboration with management of the company allowed for this less linear approach to the problem where the action part of the research related to more knowledge sharing of the possibilities of persuasive business models, than the more direct approach of an end-product within a certain time-frame and budget.

Throughout the different phases of the research, described as fact finding and analysis, coordination of the action planning, action taken of implementing the knowledge etc., and the evaluation, great care was taken in order to avoid the over involvement of the researchers. This was done by confronting in an informal way with findings, before sharing on workshops etc., and thereby avoiding the consulting role of the researchers. Therefore, no action the researchers has taken throughout the study, has been based on time- or budget goals. This in turn also lengthen the research period due to ownership issues within the organization.

CASE STUDY OF A EUROPEAN ELECTRONICS MANUFACTURER

The following section deals with the case study of a European Electronics Manufacturer (EEM) in relation to the emerging trends presented above. In addition to this, the business model cube and process of business model innovation is also related to the case study with the purpose of drawing parallels to the transformation process from a product-oriented logic towards service-oriented logic. However, the purpose of the research conducted on this case company was to introduce the concept of service business models as complementary to the current business model.

The EEM, founded in 1933 is an international manufacturing organization of advanced power management controllers, power control units and protection equipment for both land and marine. Today, the EEM employs over 600 employees in 11 subsidiaries, half of these placed in the headquarters with a turnover reaching in the access of 85 mio. EUR.
One of the strategy goals besides increasing the turnover by a fixed percentage each year is to avoid increasing the fixed costs, which is approximately half of their turnover.
Another strategic goal is to increase their market share by investing resources in business model innovation.

The current concern in the organization is to limit the costs meanwhile expanding their business. This proves to be difficult at times regarding projects at certain sizes in which some departments do not have the necessary resources to handle, and therefore must decline requests from customers.

The competitive situation on the market is changing with emerging new manufacturing organizations from development countries starting to develop and match products for power management solutions. This situation is therefore seen as a great indication for the EEM to change their current business model. However, internally in the organization it is not a concern for most employees due to the mindset that the EEM is able to provide better service, know-how and quality than its competition. In contrast to this some employees acknowledge that it is only a matter of time before this is no longer the case, and therefore change is necessary for the EEM to gain a better and stronger position on the market.

The EEM describes their customers as being conservative towards change to technology, whereas some customers are not interested in this. Although, it can be argued if the customers do not know what effect new technology can have on their products or if they simply do not need it. In either case, it is a mental barrier for the EEM to sell their newest products, meanwhile they are forces to prolong the life cycle of old products. This means that retrofitting and aftersales are very difficult to accomplish even though, the newest products hardware provide great efficiency in relation to the old products.
The customer base is consisting of above 6000 customers with a Pareto rule (20 percent of the customers stands for 80 percent of the revenue).

The service perception prior and after the Turnkey System Solution projects (TSS), was characterized as a sidekick to the actual physical products. Service had been an Achilles heel for EEM, where increasingly more complex products ends up at customers fixed on price. This combined increases the support workload on the organization and a dedicated unit now functions as a barrier for the developers. This increases the fixed

cost and questions the ability for the EEM to deliver products that fits the needs for their customers.
The mantra for the organization has been to select partners that mount and integrate the EEM products and maintain the products after the installation is done. These partners are closely related to the EEM and are trusted partners. Managers in the organization therefore sees service as something that the "others" should do and not the core competence at the EEM.

One service that the company is aware of and is not that proud of is the old products and the ability for the customers to always have the opportunity to order old and in some cases technical obsolete products. These old products also demand special customization, and this customization demands resources and the service does only in large scale products come with a fee.

The administration at the EEM has a hard time tracking the efficiency of the support department and lacks transparency of the time spend on service and support

DISCUSSION - THE EEM'S TRANSFORMATION PROCESS

This discussion will focus on the capabilities and process of getting to acknowledge and use service for more than "just" basic service and support to customers.
The first step is to establish an ambidextrous service organization that has the responsibility to handle all of the EEMs service and support and to create service business models that are complementary to the current business model. Although this seems to be the challenge for the EEM to realize due to their internal misalignment between departments with different agendas. The internal research provided the researchers with several barriers towards the terminology of service, mostly related to current culture, hinted at a product-oriented logic, but also towards resistance in not knowing what changes might have as influence on the employees' daily activities.
It is therefore seen as problematic to align the service organization with the current, AS-IS business model at the EEM, because of existing sub-cultures.

In order to reach scalability on the service organization and have simplicity of the structure, it is important that the departments can agree on both the level of service that is delivered and the technological platform to develop from. The standardization is a natural step for the EEM in relation to their evolvement into a larger organization, having to control a larger fleet of employees and products.

THE EEM ON SERVITIZATION

The terminology of service at the EEM is defined and understood as relation to basic support of products and in rare occasions as intermediate services [18] provided as complementary to technical project support. However, service is not defined or agreed upon internally among the different departments and therefore the service offerings varies from department to department, what kind and what level of service is provided by the EEM. In some cases, service is seen as an opportunity to close a deal with new customers, meanwhile experiencing customers approaching the EEM for specific services as solutions.
In relation to the product-oriented perspective, the EEM is not capable, to fully understand the concept of Servitization and certainly not aware of what possibilities there exists beyond basic service and support on their own or customers' products.

THE EEM ON DATA GATHERING TECHNOLOGY

At the current state, the EEMs products allow for data gathering technology to be applied, but it does not currently play an important role regarding intermediate services, also in relation to provide consultancy in complex and technical environments. To specify, the EEM has awareness on the need for data to create new opportunities, hence to start doing business model innovation. However, they need the technology to do so. The new technology also has to accommodate for future services and old ones currently present at the EEM. Therefore, the technologies related to both products and services has to be managed through a technological platform as support for the activities in the PSS to provide value through service business models. Such a technology platform can be viewed as the Smart Monitoring (Remote Monitoring – system/Conditioned monitoring) that consists of different hardware and software components allowing the organization to receive and send data with the outcome of delivering valid and reliable information to

customers that value this. This will require the organization to have a data management system that can capture and categorize data, then transform this into values, either visual (graphs or diagrams), or as numbering tables.

It is essential for the EEM to invest resources into technology, as this is the key driver for creating service business models using data. In addition to this, it is also important that the EEM have the capabilities through human resources to maintain the business intelligence unit that sorts and analyzes data into usable and decision making information to act on.

THE EEM ON NEW BUSINESS OPPORTUNITIES

The EEM has experienced a new opportunity to shift from being sub-supplier towards entering the role of project entrepreneur in high-scaled projects interacting with the high-end and decision making customers. This shift, demands more of the EEM in terms of resources required to fulfill the role of project coordination, product specifications, power systems design etc.

As the project entrepreneur of these large scale projects, it provides the EEM with an opportunity to expand the scope of supply to more than products, because they are also responsible for part of service and support. This is what the EEM defines as Turnkey System Solutions (TSS).

Although, these type of projects does not come without challenges. To specify, the organization do not have the necessary training or understanding of what possibilities follows selling TSS projects, and to the extent of what value the customers can receive from services that becomes available from this.

There is also the issue regarding TSS projects that changes the market situation in which the EEM competes against own customers, bidding on the same projects.

CONCLUSION

The case study clearly indicates that there is a need for establishing a framework to structure and maintain service business models at the EEM. The researchers' will argue that such a framework will help create a functioning service organization to offer not only customized solutions for their customers, but the standardization of service, which is needed. It will also be an opportunity for the EEM to merge their technology platform with such a framework to ensure alignment between developing persuasive technologies and transform this into value for the customers through service business models. To specify, the EEM will need to invest resources into the data gathering technology in order to enable the receiving, storing and analyzing of data. This data has the potentiality to visually explain the customers' behavioral patterns that in turn can be useful to create or update the value proposition with new knowledge on how the customers' actually use the EEMs products. By modifying the value proposition, new opportunities might arise that leads to new services to offer the customers, hence the persuasive service business model approach.

The EEM stands as the only organization on their market to act and focus on service business models using data as the source of value creating activities. It is therefore an important first step in the transformation process for the EEM to not only understand the importance of avoiding commoditization by evolving into another way of doing business and delivering value to customers, but also to act on clear defined issues within and outside the organization that needs attention. This is not only of great concern but it is also vital for the survival of the EEM to start readjusting their organization to create the necessary alignment and shared understanding on what is needed to successfully go through such a transformational journey as proposed in this article.

THE 5TH INTERNATIONAL CONFERENCE ON WIRELESS COMMUNICATIONS, VEHICULAR TECHNOLOGY, INFORMATION THEORY, AEROSPACE & ELECTRONIC SYSTEMS (WVITAE-2015)
December 13-16, 2015, Hyderabad, India

vNet Zero Energy for Radio Base Stations- Balearic Scenario

Pere Sabater Frau, Albena Mihovska, Ramjee Prasad
Center for TeleInFrastruktur (CTIF)
Aalborg University, Denmark
email: psabater7@ono.com

Xavier Canals Solé
Telefonica España S.A.,
Palma de Mallorca, Spain

Andreu Moia Pol and Angel Igelmo Ganzo
Universitat Illes Balears (UIB)
Palma de Mallorca, Spain

Jaume Ochogavia Colom
Balearic Islands Government
Palma de Mallorca, Spain

Abstract*— The Balearic Islands have one of the best telecommunications infrastructures in Spain, with more than 1500 Radio Base Stations (RBS) covering a total surface of 4.991,66 km². This archipelago has high energy consumption, with high CO_2 emissions, due to an electrical energy production system mainly based on coal and fossil fuels which is not an environmentally sustainable scenario. The aim of this study is to identify the processes that would reduce the energy consumption and greenhouse gas emissions, designing a target scenario featuring "zero CO_2 emissions" and "100% renewable energies" in RBS. The energy costs, CO_2 emissions and data traffic data used for the study are generated by a sample of RBS from the Balearic Islands. The results are shown in terms of energy performance for a normal and net zero emissions scenarios.

Keywords*— renewable energy; efficiency; net zero; radio base stations; CO2; DVB; Balearic Islands.

I. INTRODUCTION

The energy model of the Balearic Islands is based on imported fossil fuels; almost 97% comes from imported fossil fuels, and the rest comes from *renewable energy sources*, which include the biomass and waste materials and products. Estimating the solar and wind energy they prove to occupy only the 1 % of the total energy production. Transportation has got the biggest impact on the energy consumption – about 54% goes to transportation and 23% of the total energy consumption is destined for air transport [1].

The electricity production requires 46% of the gross energy production, with a global efficiency of 37%. The Balearic Islands energy generation and distribution system is composed of two independent electrical networks, Mallorca-Menorca and Eivissa-Formentera. The Mallorca-Menorca system has been recently connected to the mainland with 2 submarine cables 250 kV High Voltage Direct Current (HVDC) with a maximum power capacity of 400 MW, covering a total distance of 250 km. This provides about 23% of the energy. The main generation system is composed of two thermal power plants responsible for, respectively, 43% and the 23% of the demand on each of the two island subdivisions and a combined cycle central that started last year. The rest is generated in 4 small distributed generation plants [2]. The principal thermal coal power plant, with a nominal power of 510 MW, constitutes the basis of the system. The other power plants assume the peaks of demand in the islands. The described *production model* produces a high amount of CO_2 emissions, because it is based on a coal power plant steam-cycle. The government's Energy Planning Project intends to reduce the *global energy consumption* by 3%, and increase by 10% the use of renewable energy sources (RES) [3].

This paper analyzes the energy consumption for the Balearic radio base stations (RBS) employed to support voice, video and data traffic.

II. CURRENT RBS SCENARIO IN THE BALEARIC ISLANDS

Currently, there are three types of RBS in the Balearic Islands serving the urban, tourist, and rural scenarios. These can be fed by connection to power grid, or isolated powering by a set generator and a set of batteries. An exceptional type of BS serves the island of Cabrera and is powered by a mix of renewable energy sources (RES) with a set of batteries. Finally, there are up to 3 DVB-T stations that lack the infrastructure and are isolated from the power grid and powered by a set generator instead.

A. Mobile and DVB Communications: Data & Energy

Figure 1 shows the time distribution for the load on the three types of RBS analyzed for urban, rural, and tourism voice traffic in the high season period. Figure 2 shows the mobile data traffic for the same period and the same categories. A similar

intensity of traffic per hour can be observed for all three types of traffic. While, the voice traffic is more abundant during the day, tourism mobile data has larger peaks during the night hours.

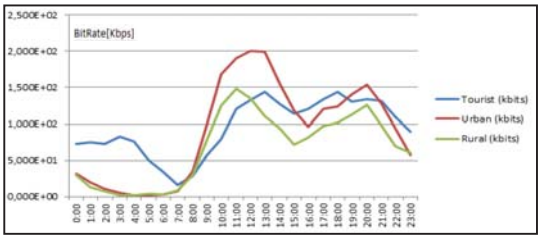

FIGURE 1. Distribution of voice traffic within a day

FIGURE 2. Distribution of traffic Data within a day

[7] provides information about the voice-video-HSDPA annual traffic for the three types of users in the period from 13 May to 14 June. The distributions and variations are shown in Figure 3.

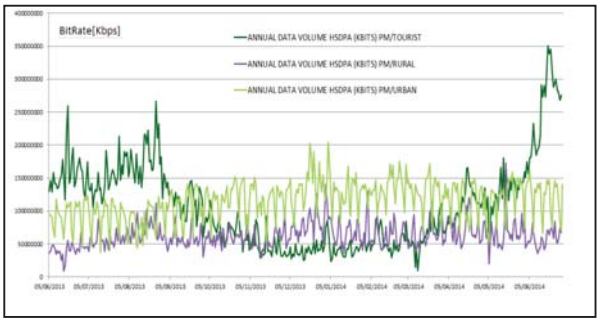

FIGURE 3. Distribution of annual all traffic data downlink at RBS

The rural traffic is more or less uniform throughout the year, while the urban traffic decreases slightly in the summer. During the tourist season, the traffic increases following a parabolic function and then decreases for the rest of the year. The distribution of the annual uplink traffic at the RBS is available in [14]. It follows the same pattern as the downlink traffic, but the data are an order of magnitude smaller. Figure 4 shows the mobile traffic fluctuations in terms of annual energy consumption at the RBS. The energy consumption due to rural mobile traffic stays at the same level throughout the year. The energy consumption due to tourist mobile traffic is higher during the summer months, with an increase in energy consumption for urban mobile traffic during the winter months.

Table 1 shows an estimate of the order of reference variables of mobile telephony, with an annual consumption of up to 58.7 GWh. The RBS consumption depends largely on the number of carriers holding the station by sector; typically rural stations often have up to one, while tourism and urban stations usually have 3 carriers per sector.

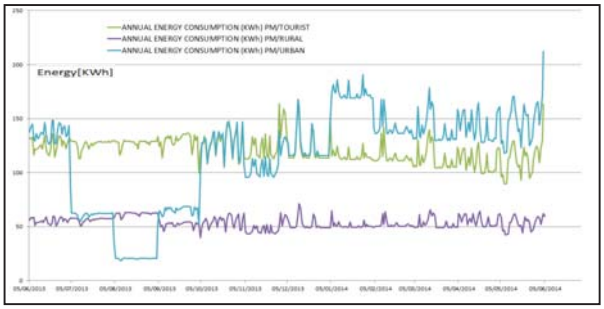

FIGURE 4. Estimation of annual Energy Consumption at RBS

Table 1 shows that tourism traffic during the summer season is the highest consumer of RBS energy. The number of RBSs at the Balearic archipelago is approximately 1586 for mobile communications, and for DVB-T is 64 [7], [8]. Table 2 shows the annual energy consumption of the DVB-T BSs for the various types of traffic. It shows that the rural traffic makes the larger consumer of DVB-T base station energy.

Table 1. Mobile Communications: Data & Energy.

	Annual Data (PBitps) Mobile Communications	Annual Consumption (GWh) Mobile Communications
Urban Station	21,1	28,8
Tourist Station	35,8	32,5
Rural Station	9,4	7,4

Table 2. Digital TV & Radio annual energy consumption.

	Annual Consumption (MWh) TV DVB-T/S
Urban Station	-
Tourist Station	249,616
Rural Station	593,059

The annual curve consumption of the rural DVB-RBS is shown in Figure 5. The DVB-T stations are running 7 x 24 hours constantly.

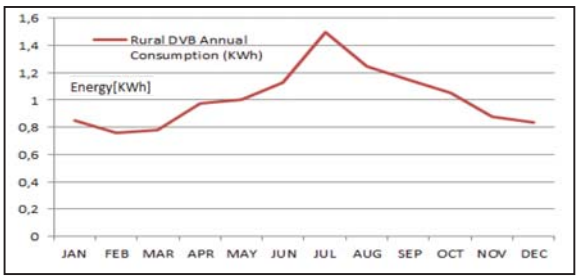

FIGURE 5: Estimated Annual Energy Consumption at DVB- RBS.

III. MODEL RBS VS ENERGY CONSUMPTION

Eq. (1) defines a model for the estimation of the RBS energy consumption. There is a linear correlation, quite similar to the one featured by the energy management systems used for buildings and industrial applications. We can relate the energy consumption to the unitary production, or to a climate variable. Then the linear function model can be defined by two independent variables, $Z\ (x, y)$, which reflect the amount of

datatraffic and the temperature on the days of the region where the study was done (Balearic) [9], [10].

$$Z(x,y) = M \cdot x + N \cdot y + C \quad [1]$$

Where, Z is the electric energy consumption in kWh; M is the unitary consumption in kWh per Gbps; x is given in Gbps; N is a factor defined by the cooling requirements in (18ºC) [kWh/ºC]; y is the temperature averaged for the days (18º) [ºC]; C is a constant in kWh.

There would be a direct relation between the energy consumption and the temperature for the DVB-RBS, which has a constant data traffic throughout the year. The cooling requirements, are known as cooling degree-days (CDDs). We assume that the need for cooling of the RBS would be on the days when the average temperature is above 18ºC. We have made some linear approximations with a polynomial of first order. The correlation index is quite good, however, there are some factors that influence more the temporary energy consumption (e.g., weather, data traffic) [7]. We can improve the approximation by adjusting slightly (1) to achieve (2).

$$Z(y) = N \cdot y + C \quad [2]$$

Eq. (2) does not satisfy the scenario of variable data traffic with variable consumption. We propose instead an alternative variable **α**, which is the *efficiency unitary*, to define the relationship between the electric energy consumption and data traffic vectors. Consequently, we redefine the model efficiency as in (3):

$$\alpha(x,y,z) = M \cdot x + N \cdot y + G.z + C \quad [3]$$

Where, α is in kWh/GBitps; M is the unitary consumption; x is the energy consumption in kWh per month; N is unitary consumption in kWh per Gbps; y is the data traffic in Gbps; Z is the CCD factor in (18ºC) [kWh/ºC] per month; C is a constant in kWh/Gbps. The consumption can then be estimated as in (4):

$$Z[kwh] = \alpha . Y \quad [4]$$

The coefficients $M, N, G, and\ C$ are obtained using the *least squares method* on the empirical data by using Eq. (1) and Eq.(2). When there are more than two explicit variables, the best option is to choose a matrix solution. We calculate the coefficients of a regression for the general matrix case as per the matrix in Table 3.

Table 3. System variables theoretical analysis

$\propto_i$	X_i	Y_i	Z_i	$\propto'_i$	e_i
$\propto_1$	X_1	Y_1	Z_1	$\propto'_1$	e_1
$\propto_2$	X_2	Y_2	Z_2	$\propto'_2$	e_2
.	.	.	.	.	.
.	.	.	.	.	.
$\propto_N$	X_N	Y_N	Z_N	$\propto'_N$	e_N

Where $\alpha'_i = M \cdot X + N \cdot Y + G \cdot Z + C$ is the theoretical efficiency of our model and $\emptyset = \alpha_i - \alpha'_i$ obtains the residuals. The squares function of the residuals is:

$$\emptyset = \sum_{i=1}^{N} e_i^2 = \sum_{i=1}^{N} (\propto_i - M \cdot X - N \cdot Y - G \cdot Z - C)^2 \quad [5]$$

M, N, G and C are calculated so that $\emptyset$ yields minimal empirical values for X, Y, Z. We calculate the derivative and equate to zero the result. For lack of space the elaborate calculations are omitted from the paper. Details can be found in [17].

IV. Simulation Analysis

The expressions for calculating the coefficients are used as the basis for generating the simulation data that is summarized in Tables 4, 5, 6, and 7. The data was processed by the Application Mathematical Software utility Language R.

Table 4. Urban Scenario : Mobile

Coefficients:	M	N	G	C
	0,0002653	-0,0002471	-0,0002056	0,94762
Equation:	α= 0,0002653.X −0,0002471.Y-0,0,0002056.G+0,94762 Z[KWh] = α.Y			
Multiple R-squared:	0.9829	Adjusted R squared:	0.9766	p-value: 2.067e-7

Table 5. Tourist Scenario: Mobile

Coefficients:	M	N	G	C
	0,0007316	-0,0003171	-0,0011118	-0.1240318
Equation:	α= 0,0007316.X −0,0003171.Y-0,0011118.G-0,1240318 Z[KWh] = α.Y			
Multiple R-squared:	0.8958	Adjusted R squared:	0.854	p-value: 0.0002984

Table 6. Rural Scenario: Mobile

Coefficients:	M	N	G	C
	0,0007369	-0,0004460	-0,0004112	0.5340732
Equation:	α= 0,0007339.X −0,0004460.Y-0,0004112.G+0,5340732 Z[KWh] = α.Y			
Multiple R-squared:	0.9632	Adjusted R squared:	0.9494	p-value: 4.43e-6

Table 7. Rural Scenario: Dvb – t/s

Coefficients:	M	N	G	C
	-	-	1,975	846,552
Equation:	α= 1,975.G+846,552 Z[KWh] = α.Y			
Multiple R-squared:	0.8101	Adjusted R squared:	0.7911	p-value: 6,623e-5

Eq. (4) shows that the model of energy consumption is equal to the alpha model for the total transmitted data (voice, video and data). We can then define the transmission efficiency as:

$$\propto_{effic} = \frac{Energy\ Consumption}{bits\ transmitted} =$$

$$\frac{Transmision\ Consumption + Cooling\ Consumption}{bits\ transmitted} =$$

$$\frac{Transmision\ Consumption}{bits\ transmitted} + \frac{Cooling\ Consumption}{bits\ transmitted} =$$

$$\propto_{effic} = \propto_{TC} + \propto_{CC} \quad \textbf{[6]}$$

Note, that the lower the numerical value of α, the greater the efficiency of the transmission system. Eq. (5) is a generic definition to establish the standard operating conditions for the transmission stations under study. The coefficients $(M, N, G, and\ C)$ are obtained by the method of least squares, carrying out the process of calculating the statistical values with language R [11], [12].

The DVB-T model shows that there is only variability in the consumption of the RBS depending on the weather, since this effectively only depends on the temperature. In fact, only the constant term is affected by the maximum amount 1.98Gd 547 kWh better compared to the constant term 860 kWh. Figure 6 shows that the distribution of residuals is very homogeneous in urban and rural stations, whereas it is fluctuant in tourism RBS and therefore a loss of homogeneity can be deducted.

	Median Residuals:	p-value:	Multiple R-squared
Urban MT-RBS	-0.00048	2.067e-7	0.9829
Tourist MT-RBS	0.02093	0.0002989	0.8938
Rural MT-RBS	0.000421	4.436e-6	0.9632
Rural MT-DVB	-27.54	0.001905	0.6354

The model then would be most appropriate to describe the urban or rural RBS, where there is more efficiency in the data transmitted per energy unit. In strict statistical terms, the overall mean of the residuals in the tourist stations is bigger than the rural and urban RBS taking a bigger *p value* and, therefore, a lower value determination.

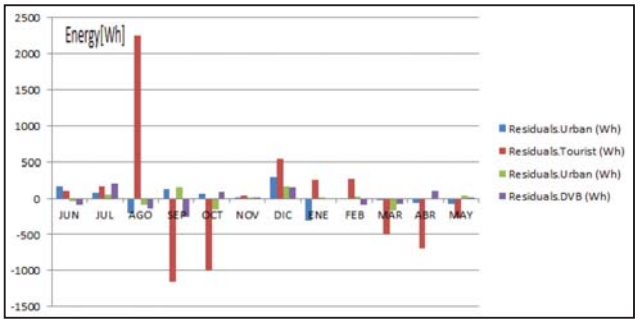

FIGURE 6: Residuals of data processing from the case study.

Table 8 shows a summary of the *correlation index* or determination referred Multiple R - Squared and as this should be inversely proportional to the level of significance or p-value and have a value of the Median Residual value close to 0.

TABLE 8. Statistics Summary from the case study.

	Median Residuals:	p-value:	Multiple R-squared
Urban MT-RBS	-0.00048	2.067e-7	0.9829
Tourist MT-RBS	0.02093	0.0002989	0.8938
Rural MT-RBS	0.000421	4.436e-6	0.9632
Rural MT-DVB	-27.54	0.001905	0.6354

Eq. (3) is the point statistical estimate of an RBS with regard to its efficiency: energy consumption, traffic data (voice-video-data) and the meteorological conditions (cooling degree days 18°C). This same argument applies to the Eq. (1) and Eq. (2) in their respective cases. Eq. (4) can be used for obtaining the punctual efficiency on the DVB RBS, setting the parameter *Y* as a function of the number of Gap fillers, and the bit rate. For example, for 7 MUX Gap Fillers, the monthly total data is Y = 361.065 Gbits.

V. NET ZERO ENERGY IN BALEARIC ISLANDS

A sustainable system can be achieved if the RBS is powered by renewable energy [1, 2]. The total number of RBSs in the Balearic islands is about 1586 - only two of these are not connected to the power grid, whereas out of the total of DVB-T RBS about 63 are connected to the power grid. That means that only one DVB-T RBS is isolated from the power grid. Photovoltaic and wind energy, incorporated in the RBS powering may contribute to the electrical system energy balance. A proposed configuration for both types of RBS would be a combination of *photovoltaic and wind micro turbine* with a storage capability of dual energy backup. Optionally, if space would be available, a set generator may be installed in the RBS for the case when the power grid would be a bit unreliable. For the isolated RBS, the dual energy backup may be implemented by an electrochemical battery as the primary energy backup, while the secondary energy backup may depend on use of a Fuel Cell, or bio fuels such as bio diesel or bio gas. The RBSs are almost in all cases located on the top of the roofs of the highest buildings or in windy sun-exposed isolated areas, which gives a good basis for the use of renewable energy an RBS power source.

By using the same methodology as in previous studies [3,13], according to the hourly simulation, we can determine the future net zero energy in the entire Balearic telecommunication system. The archipelago has areas with more than 2,000 hours equivalent peak wind and photovoltaic panels integrated architecturally with over 1250 equivalent peak solar hours (PSH) per year [14]. On the other hand, statistically the micro cuts duration of power grids in urban areas are about half hour whereas in rural areas is about 6 hour so we sized battery for a time duration of two times the minimum required that is 12 hours with a depth of discharge of the batteries of 25%. Figure 7 shows the energy import and export period for the first quarter of the year. There is a positive balance of annual renewable energy.

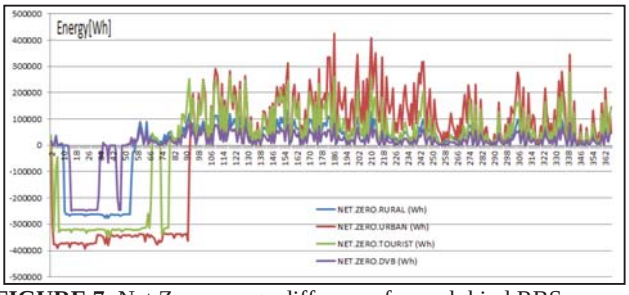

FIGURE 7: Net Zero energy difference for each kind RBS.

Table 9 shows the parameterization zero balance for each type of station, and the result of the minimum possible set balance, based on the installed capacity with commercially available solutions. If all types of stations were fed by renewable energy, the balance model will be under zero from a positive balance of the RES and the distributed energy. Moreover this would affect the environment with no shedding up to 51233.85 tons of

carbon per year, 50526 Tons of CO2 for the Mobile RBS and 707 for the DVB RBS. These statistics are shown in Table 10.

Table 9. Net Zero Energy features for each kind RBS

	Wind Power Install [KW]	Solar Power Install [KWp]	Battery Store Install [KWh]	Energy Import [KWh]	Energy Export [KWh]	Energy Balance [KWh]
Urban MT-RBS	36	9,6	87,840	34,693	35,312	+0.693
Tourist MT-RBS	30	8,5	87,840	23,69	23,712	+0.022
Rural MT- RBS	12	7,4	87,840	12,594	14,252	+1.658
Rural DVB-RBS	9	3,2	15,420	6,019	8,313	+2.294

Table 10. Net Zero energy global features and effect to power grid.

	Global Wind Power Install [KW]	Global Solar Power Install [KWp]	Annual Net Zero Energy [MWh]
Urban MT-RBS	19116	5066	+328,7
Tourist MT-RBS	20790	5877	+15,2
Rural MT- RBS	4092	2530	+565,4
Rural DVB-RBS	576	203	+146,8

VI. CONCLUSIONS

This paper described a model for calculating the dependency between data traffic and energy consumption of the RBS for a scenario on the Balearic Islands. The goal was to present a net zero balance model that can lead to sustainable telecom infrastructure of environmentally friendly nature. The model can be applied universally but the values for the variables would be based on the regional specifics.

Promoting and investing on renewable energies to combat CO_2 emissions is the way to go forward. A setup of a mix of wind micro turbines, and photovoltaic and distributed energy, would stop the discharge of more than 50,000 tons of emissions per year. The overall *zero balance* in the Balearic archipelago is overall positive in the order of 1 GWh as if it were a distributed micro generation, which strengthens the own power grid provide to it some stability. Accordingly, the transmission efficiency is due to be constant since the RBS-DVB would transmit uniformly and the system efficiency would only depends significantly on the efficiency of the cooling of the station itself. This would require an efficient as possible cooling system.

Mobile communications operators with more than 500 RBS in Balearic archipelago could make use of a bidirectional flow of electricity by a dual smart meter so instead that it plays role of net zero agent, it would perform the role of a producer and consumer agent. This opens the road to new business possibilities.

The result of the energy zero net balance would be a saving in primary energy costs or electrical energy coming from the conventional central generator per kWh in electrical renewable energy at the exit point and also a decrease in CO_2 emissions given the CO_2 gr per kWh embedded by the conventional central generator since these would start to be generated by renewable energies.

VII. ACKNOWLEDGMENTS

We would like to acknowledge Mr. Antoni Font Bauza from *Comunitat Autonoma Illes Balears* (CAIB) for the information about DVB-T Radio Base Stations. Special thanks to Mr. Jaime Homar Ferrer de Sant Jordi from Telefonica Spain delegation Baleares for the support during the paper elaboration. Finally, we would like to thank the Spanish Institution Colegio Oficial de Ingenieros de Telecomunicación COIT (Madrid) and the Technical department.

REFERENCES

[1] DG Industria i Energia. Govern de les Illes Balears
[2] REE, Red Eléctrica Española. "El suministro de la electricidad," (2012), http://www.ree.es/es/publicaciones/educacion/el-suministro-de-la-electricidad-un-equilibrio-entre-generaci%C3%B3n-y-consumo.
[3] P. Sabater, A. Moia Pol, and R. Prasad, "DC Power System for Radio Base Station by Renewable Energy Sources," in Proc. of ISABEL 2010, Rome, Italy, 2010.
[4] Informe de penetración de servicios finales de infraestructuras de Telecomunicaciones. Comisión Mercado Telecomunicaciones CMT (2011).
[5] Ministerio de Industria, Energía y Turismo. Gobierno de España. http://www.ontsi.red.es/ontsi/es/
[6] Ericsson Mobility Report, "On the pulse of the networked society," June 2013, http://www.ericsson.com/res/docs/2013/ericsson-mobility-report-june-2013.pdf.
[7] Telefonica, España S.A, http://www.telefonica.com/.
[8] Ministerio de Industria, Energía y Turismo. Gobierno de España. Espectro Radioeléctrico http://www.minetur.gob.es/telecomunicaciones/Espectro/
[9] Energy Audit Guide. Part A: Methodology and Technics. European Commission, Athens, Greece, May 2000, www.cres.gr/kape/pdf/download/guide_a_uk.pdf
[10] A. Moià-Pol, "Diagnosis and Innovation in the Energy Management at Balearic Hotel Industry," Ph.D. Thesis, UPC, 2012.
[11] J. Mac Donald and J. Braun, "Data Analysis and Graphics Using R. An Example-Based Approach," Cambridge University Press, 2007.
[12] The R book, Michael J. Crawley, Willey (2007).
[13] P. Sabater, et al, "Net Zero Emissions in Radio Base Stations Operating at different Conditions," in Proc. of the Global Wireless Summit (GWS), May 2014, Aalborg, Denmark.
[14] European Statistics, 2013, http://ec.europa.eu/eurostat/
[15] European Association for Storage of Energy (EASE), European Energy Storage Technology Development Roadmap towards 2030: Technical Annex, EERA, the European Energy Research Alliance, 2013, http://www.ease-storage.eu/.
[16] F. Dincer, "The analysis on photovoltaic electricity generation status, potential and policies of the leading countries in solar energy," in Renewable and Sustainable Energy Reviews, Volume 15, Issue 1, January 2011, Pages 713–720.
[17] S. Dowdy, S. Wearden and D. Chilko, "Statistics for Research," Third Edition, Willey Interscience, ISBN: 978-0-471-26735-5, February 2004.

THE 5TH INTERNATIONAL CONFERENCE ON WIRELESS COMMUNICATIONS, VEHICULAR TECHNOLOGY, INFORMATION THEORY, AEROSPACE & ELECTRONIC SYSTEMS (WVITAE-2015)
December 13-16, 2015, Hyderabad, India

Interference Management in Heterogeneous and Small Cell Networks

M. Bala Krishna
University School of Communication and Technology
Guru Gobind Singh Indraprastha University
New Delhi, India
E-Mail: mbalakrishna@ipu.ac.in

Puneet Bansal
University School of Communication and Technology
Guru Gobind Singh Indraprastha University
New Delhi, India
E-Mail: pbansal771@gmail.com

***Abstract* - Cloud Radio Access Network (C-RAN), Multiple Input and Multiple Output (MIMO) and Heterogeneous and Small Cell Networks (HetSNet) support on-demand network bandwidth, heterogeneous device connectivity and optimal usage of network resource operators. The traditional architecture of radio access network supports signal processing and radio frequency functions at the cell sites. This incurs an additional installation and maintenance cost that is not eco-friendly to the environment. Cloud Radio Access Network (C-RAN) combines the features of cloud computing and radio access network where the centralized baseband units are responsible for signal processing and Remote Radio Heads (RRHs) deployed at cell sites are responsible for operations of radio frequency. C-RAN supports Green Technology in which the base station reduces the percentage emission of Carbon Dioxide (CO_2). This article provides a comparative analysis of interference management in HetSNets.**

Keywords: HetSNet, Macro cell, Femto cell, Interference Management, Spectrum Management

I. INTRODUCTION

C-RAN and MIMO technologies have been proposed for future wireless networks along with Heterogeneous and Small Cell Network (HetSNet) where small cells deployed to facilitate Cell On Edge (COE) mobile users [1]. Due to the constraints in radio resources, the mobile users in COE area increase the transmitting power to communicate with the macro cell, otherwise it could lead to call drop. Handoff latency and rate of call drop indicate the performance parameters used by network operators. Small cells are less expensive, easy to install and eco-friendly that support low power transmission. Heterogeneous cells use micro, femto and pico cells [2] [3] with existing macro cell sites to increase the coverage and connectivity in the network. Heterogeneous cell structure depends on cell size, and the antenna position [1]. MIMO technology uses multiple antennas at the transmitter and receiver to increase the coverage area and mitigate multipath fading. The advantages of Heterogeneous and Small Cell Network are as follows:

(i) The deployment of small cells reduces the distance between COE mobile users and micro Base Stations (BS). This reduces the transmission or reception power of mobile users
(ii) Flexible deployment enables the HetSNet to adapt with efficient spectrum management
(iii) Uses power control mechanisms to save the energy and bandwidth constraints [4] in the network

II. INTERFERENCE MANAGEMENT IN HETSNETS

Heterogeneous and Small Cell network of different sizes are installed to enhance and expand the network capacity. The deployment of femto cells in heterogeneous networks not only reduces the cost of installation [5] but also minimizes the micro cellular interference effect on MUE. In HetSNet, the spectrum allocation for small cells [6] and macro cells are same, and this leads to Interference between the cells. There are two types of interference in HetSNets [3] – (i) Cross-Tier interference and (ii) Intra-Tier Interference. Cross-Tier Interference [7] exists between the femto cell and macro cell whereas Intra-Tier Interference exists between the femto cells in the same tier due to densely deployed cells at smaller distance. Separate spectrum allocation for each cell avoids interference but reduces the network capacity and increases the control channel overhead [3]. Table 1 provides the comparative analysis of three spectrum sharing access modes (Open, Closed and Hybrid) in HetSNets. Intra-tier interference is more harmful in closed access mode due to leakage from walls or windows the small cell causes interference to nearby small cell [3] and only a sub-set of subscribed user's access the network.

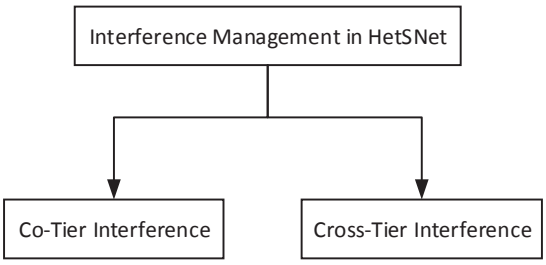

Figure 1. Types of Interference in HetSNet

Table 1. Comparative analysis of Open, Closed and Hybrid spectrum sharing access modes in HetNets [3]

Feature	Open Access Mode	Closed Access Mode	Hybrid Spectrum Sharing
Resource Usage	In Open Access mode, any user can use the resources from small cell.	In Closed Access mode, users can use the resources from the small cell that have subscribed to that particular cell. It is sometimes called Closed Subscriber Group.	This is a combination of Open and Closed Access modes. On demand certain users from outside are allowed to use the network facility. The allocation of subscription is handled by the operator with an approval from the subscriber [3].
Security	Security is the major concern in this method as this mode is open to use for any subscriber	This mode provides better security as only subscribed users are allowed to exploit the services.	This mode also provides better security services as subscribed and certain allowed subscriber from outside are all handled by the operator.
Cost Factor	Easy to install and less expensive.	Expensive compared to Open Access Mode.	Complex and expensive.

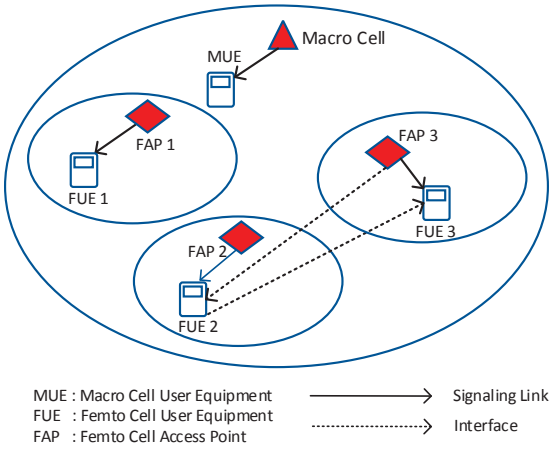

Figure 2. Intra-Tier Interference (Co-Tier)

In Figure 2, FUE 2 causes interference at FUE 3 in the uplink, and FAP 3 causes interference at FUE 2 in the downlink. To mitigate uplink interference the transmit power of FUE should be controlled by the serving Femto cell. Thus, the FAPs should automatically sense the surrounding environment and interfering Femto cells. If the power of FUE is more than the threshold limit, then it should be minimized to avoid interference with the adjacent Femto cell UE or FAPs. Similarly in the downlink, the Femto cell FAP should be able to control its power adaptively. Intra-tier interference for uplink power from femto cell is given as follows:

$$P(femto) = P(UE) + P_{Loss} + D \quad \ldots\ldots\ldots\ldots (1)$$

$P(UE)$ = Power transmitted by Femto UE
P_{Loss} = Path Loss between FAP and FUE
D = Distance between FAP and FUE

Power in femto user equipment is given as follows:

$$P(FUE) = \left(\frac{P(Interference,\ Max)}{No.\ of\ Users_{Femtocell}} \right) + P_{Loss} + WP_{Loss} \quad \ldots\ldots\ldots\ldots (2)$$

Where WP_{Loss} = Wall Penetration Loss.

Cross-Tier interference is due to the interference between the components of macro cell and femto cell networks.

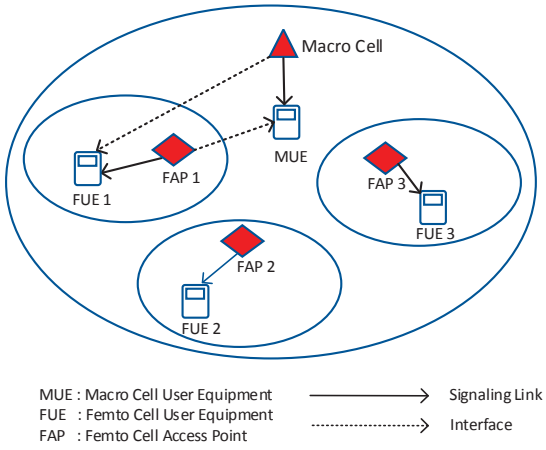

Figure 3. Inter-Tier Interference (Cross-Tier)

The cross-tier interference occurs due to the high power downlink transmission of the femto cell, and the macro cell user is in the vicinity of FUE. Hence, it becomes difficult for MUE to choose the optimal network path. Similarly, if the macro cell user at Cell on Edge (COE), transmits at high power in the uplink channel, then the interference occurs in the nearby femto cell

UE. Inter-tier interference can be reduced by using separate spectrum for macro cell base station and femto cell, but it results in reduced spectral efficiency and spatial reuse. Two schemes that primarily control the power transmission in High Speed Downlink Packet Access for Femto cells [3] are:

(i) Geostatic Power Control Scheme
(ii) Adaptively Power Control Transmission

In Geostatic Power Control Scheme, the power of the network element(s) is controlled from the cell location. In Adaptively Power Control Scheme, the power is controlled with respect to the data rate transmitted by the network element [3]. If more data is to be transmitted, then the power of network element is increased, otherwise the power is reduced to avoid interference. OFDMA femto cells can also be used to mitigate inter-cell interference since the carriers allocated to macro cell base station and femto cells are orthogonal to each other, and hence the interference is avoided. In cross-tier interference, the power transmitted [7] by femto cell base station in downlink channel is given as follows:

$$P(femto) = P(macro) + G + PathLoss\left(f_{FemtoBS}^{MacroBS}, g_{FUE}^{FemtoBS}\right)$$

$$where\ f\ and\ g \in \left(\gamma_{fading}, \zeta_{noise}, \alpha_{attenuation}\right) \quad \ldots\ldots\ldots\ldots (3)$$

$P\ (femto)$ = Downlink power from Femto BS
$P\ (macro)$ = Transmit Power from Macro BS
G = Transmitter Antenna Gain

The power transmitted by femto UE in uplink channel [7] is given as follows:

$$P(FUE) = \frac{P\left(Intfr_{Max}\right)}{No.\ of\ Users_{Femtocell}} + PathLoss\left(f_{FemtoBS}^{MacroBS}\right) \quad \ldots\ldots\ldots\ldots (4)$$

$P\ (Intfr_{Max})$ = Maximum Allowed interference or power to be transmitted from femto cell users to macro base station

The signal to interference and noise ratio gets affected due to interference. Ideally it should be high but due to path loss, wall penetration and interference between cells reduces the interference and noise ratio.

$$SINR = P \Big/ \sum_{i=1}^{n} Interference_i + N \quad \ldots\ldots\ldots\ldots (5)$$

P = Signal Power, $Interference_i$ is the interference for n users,
N = Noise Signal

III. INTERFERENCE MANAGEMENT TECHNIQUES

In HetNets, there are various interference management schemes to enhance the network performance. To handle interference, the messages are shared between the macro cell and nearby small cells with respect to time and frequency domains. Different cells in HetNets deployment are connected to the core network via different backhaul interfaces. Macro cell is connected via S1 interface, pico cell via X2 interface and femto cell via Internet IP [8]. Synchronization between the macro cell and the nearby small cell is taken into consideration to access frequency channel carrier, otherwise contention occurs in the same channel. In X2 interface, the narrowband transmit power, overload indicator and interference indicator messages are shared. In RNTP, the active cell informs the nearby cells to lower the transmit power for certain channel interval so that there is no conflict between the accessing cells. In overload indicator, the information SINR is shared between cells, and in high interference indicator the users cannot use the same channel and cause interference since the advance channel allocation is fixed within the time interval. The messages are not shared at Internet IP that is used for femto cell [8]. The distributed antenna system is used to avoid interference. Here, the spatial antennas are placed at *2*Pi /N* where *N* is the number of sectors. However, the hardware installation is expensive, hence the network operators usually use the coordination mechanisms [9] to minimize interference.

The cloud radio access network needs to function in coordination with the small cells, which reduces the handover delays during the peak traffic hours. The effect of cooperative interference [6] is significant in the deployment and defining the baseband pool matrix of the HCSNets.

Table 2 gives the comparison between the interference management techniques in HetNets. Recently, Heterogeneous Cloud Small Cell Network has been proposed to improve further and revolutionize the small cell network technology. In HCSNet, the small cells are centralized at BBU pool to handle the signal processing tasks. This approach improves latency and spectral efficiency in the cellular network. Synchronization reduces interference that is controlled by BBU pool. Hence, HCSNet provides enhanced and utilization of radio resources in the network. In low traffic conditions, the BBUs are enabled to sleep mode to save the energy in Heterogeneous Cloud Radio Access Network (H-CRAN). Spectrum allocation is the key feature to reduce interference in Heterogeneous and Small Cell Network. If the spectrum is allocated in shared mode, then the major part of allocation is utilized by macro cell, and the minor part of allocation is used by femto cell. To attain improved spectral efficiency, frequency reuse factor is considered [6].

In H-CRAN, the frequency allocation is handled by the centralized BBU pool. This avoids interference between the multi-tier cells of the network. In order to cancel interference in C-RAN and H-CRAN, Inter-cell interference (ICIC) and Coordinated Multipoint (CoMP) schemes are used. Fractional frequency reuse at the edge of cells reduces the rate of interference and transmission power to establish the communication channel.

Table 2. Comparison between the Interference Management [3] [10] Techniques in HetNets

Interference Cancellation	Interference Avoidance	Distributed Interference Management
This method is applied at the receiver side. After decoding the signal, the interference will get subtracted from the desired Signal.	This method focuses on intelligent networking and sharing the information between the small cell and macro cell. This could either reduce or increase the power and serve the end user.	This technique provides distributed mechanism to mitigate interference. Adaptive power control or selecting the small cell with high SINR and lowering the small cell power induces the interference.
As the number of users increase, interference cancellation of becomes tedious.	This technique is complex to implement on small cells.	Time consuming and complex.

For the cell edge users, the macro cell transmits at higher power to communicate with adjoining components through the air interface. This further causes interference at femto cell base station. Cell Range Extension (CRE) is applied where the edge user is in proximity to femto base station instead of macro cell base station.

In recent developments, inter-cell interference is reduced at a satisfactory margin level by using Almost Blank Sub frames (ABS). This method extends ICIC, where the multi-tier cells share messages pertaining to frequency usage prior transmission in the time domain. A sub-set of channel frames are free so that the small cells can transmit in the domain network. This reduces the cross-tier interference. Macro cell synchronizes with user equipment so that interference is reduced at a minimum level [11]. Coordinated Multipoint avoids cross-tier interference. Here, the multiple cells coordinate with each other based on geographic location. This enables the cells to adapt and schedule the transmission and reception of signals to enhance the coverage and connectivity in the network [12]. In LTE-A and 5G communications, this feature is being considered to minimize the interference in the network.

IV. SIMULATIONS

Simulations are performed for a small heterogeneous network consisting two macro base stations, six femto base stations and 200 number of heterogeneous user nodes. We assume that each macro base station supports an average of 60 Macro UE nodes. Each Femto base station is associated with 10 Femto UE nodes. Figure 4 and figure 5 represents the average downlink throughput rates with respect to the average transmission powers of the macro and femto base stations. The throughput levels of the femto UEs increases with time and increasing the transmission frequency of the femto base station.

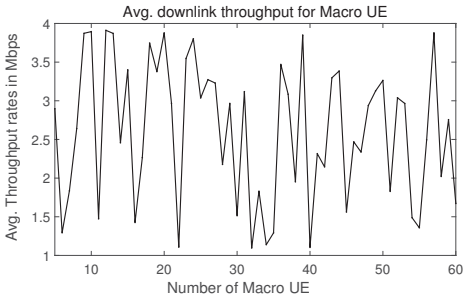

Figure 4. Average throughput rates for Macro UE

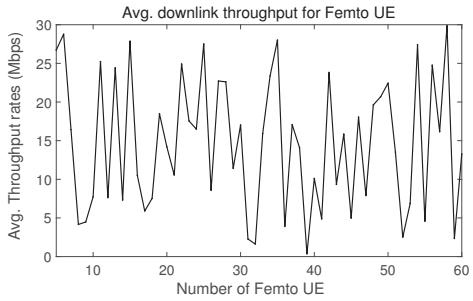

Figure 5. Average transmission power of the Femto UE

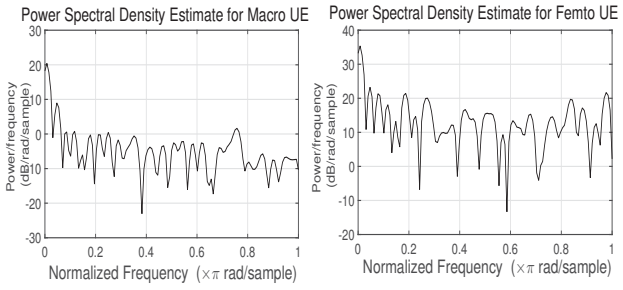

Figure 6. Macro UE and Femto UE transmission power levels

Figure 6 illustrates the macro UE and femto UE transmission power levels which are currently connected to reduce the cell outage and reduces the interference levels at the cell-edge. Femto cells configured using in-band and out-band frequencies. The macro BS transmits the signals with a strength of 46 dBm. It has been observed that that the performance of femto BS is high when it transmits the signals at the same frequency of the adjacent macro base station.

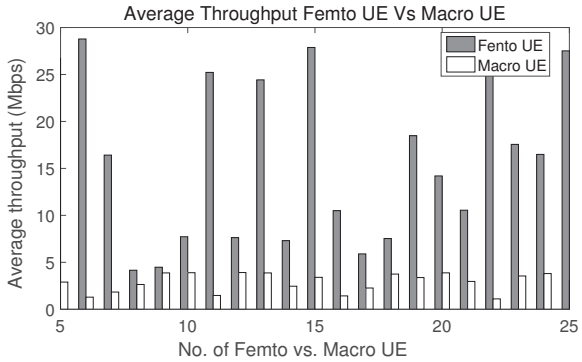

Figure 7. Comparison of Average Throughput rates for the Macro and Femto UEs

The comparison of average throughput rates for the adjacent macro and femto UEs using the in-band and out-band frequencies has been provided in figure 7. It has been observed that the femto base stations increases the throughput rates for the adjacent femto UEs by selecting the appropriate frequencies as per the density of macro UEs in the neighborhood. This technique reduces the effect of interference between the macro-macro UEs, femto-macro or macro-femto UEs.

V. CONCLUSIONS

Heterogeneous Cloud and Small Cell Network (HCSNet) has been proved to improve and revolutionize the small cell network. Since, HetNet is not a centralized approach, there arises delay, low latency and less spectral efficiency in the network. In HCSNet, the centralized BBU pool handles the signal processing tasks for small cells. This approach further improves the latency and spectral efficiency. Synchronization improves as the BBU pool handles the active cells in the network. Since, interference reduces the channel allocation, the HCSNet provides superior functionality and utilization of radio resources and thus helps to reduce undesired behavior of the network. In the emerging technology of LTE-A and 5G multi-cellular networks, HCSNet enhances the network performance.

REFERENCES

[1] Zhang H, Chen S, Li X, Ji H and Du X, “Interference Management for Heterogeneous Networks With Spectral Efficiency Improvement”, *IEEE Wireless Communications*, April 2015, Vol. 22, Issue 2, pp. 101-107.

[2] Ahuja K, Xiao Y and Schaar Mv, “Distributed Interference Management Policies For Heterogeneous Small Cell Networks”, *IEEE Journal on Selected Areas in Communications*, June 2015, Vol. 33, Issue 6, pp. 1112-1126.

[3] Zahir T, Arshad K, Nakata A, et al., “Interference Management in Femtocells”, *IEEE Communications Surveys & Tutorials*, First Quarter 2013, Vol. 15, Issue 1, pp. 293-311.

[4] Shakir M Z, Qaraqe K A, Hina Tabassum, et al., “Green Heterogeneous Small-Cell Networks: Toward Reducing the CO2 Emissions of Mobile Communications Industry Using Uplink Power Adaptation”, *IEEE Communications Magazine*, June 2013, Vol. 51, Issue 6, pp. 52-61.

[5] Chandrasekhar V, Andrews J G and Gatherer A, “Femtocell Networks: A Survey”, *IEEE Communications Magazine*, September 2008, Vol. 46, Issue 9, pp. 59-67.

[6] Zhang H, Jiang C, Cheng J, Leung VCM, “Cooperative Interference Mitigation and Handover Management for Heterogeneous Cloud Small Cell Networks”, *IEEE Transactions on Wireless Communications*, June 2015, Vol. 22, Issue 3, pp. 92-99.

[7] Shakhakarmi N, “Optimization of Cellular Resources Evading Intra and Inter Tier Interference in Femto cells Equipped Macro cell Networks”, *International Journal of Computer Science Issues (IJCSI)*, March 2012, Vol. 9, Issue 2, pp. 1-10.

[8] Lopez-Perez D, Guvenc I, De la Roche G, Kountouris M, Quek TQS and Zhang J, “Enhanced Intercell Interference Coordination Challenges In Heterogeneous Networks”, *IEEE Wireless Communications*, June 2011, Vol. 18, Issue 3, pp. 22-30.

[9] Lopez-Perez D, Valcarce A, De la Roche G and Zhang J, “OFDMA Femtocells: A Roadmap on Interference Avoidance”, *IEEE Communications Magazine*, September 2009, Vol. 47, Issue 9, pp. 41-48.

[10] Mhiria F, Sethomb K and Boualleguec R, “A survey on interference management techniques in femtocell self-organizing networks”, *Elsevier Journal of Network and Computer Applications*, Vol. 36, Issue 1, January 2013, pp. 58–65.

[11] Hughes Systique, "Current Trends In ICIC: Inter Cell Interference Coordination in LTE for Capacity Enhancement", [online] *http://hsc.com/Blog/Current-Trends-In-ICIC-Inter-Cell-Interference-Coordination-in-LTE-for-Capacity-Enhancement-1*, August 14, 2014.

[12] Nigam G, Minero P and Haenggi M, "Coordinated multipoint in heterogeneous networks: A stochastic geometry approach", *IEEE Globecom Workshop - Emerging Technologies for LTE-Advanced and Beyond-4G*, Atlanta, GA, USA, 9-13 Dec. 2013, pp. 145-150.

THE 5TH INTERNATIONAL CONFERENCE ON WIRELESS COMMUNICATIONS, VEHICULAR TECHNOLOGY, INFORMATION THEORY, AEROSPACE & ELECTRONIC SYSTEMS (WVITAE-2015)
December 13-16, 2015, Hyderabad, India

Implementation Of Internet Of Things Using Near Field Communication For Parking Automation

Aishwarya Sanjay Ikhe, Sagar Jayant More, Priyanka Sanjay Suranglikar, Prashant S Dhotre
Department of Computer Engineering,
Sinhgad Institute of Technology and Science,
Pune, India
{ikheaishwarya, sagarmore.22, psuranglikar, prashantsdhotre}@gmail.com

Abstract— **With the rapid escalation of vehicles and their usage in recent years, finding a vacant car parking space in most efficient manner and to save customers' time is becoming more and more difficult. Parking problems are becoming omnipresent and increasing at an alarming rate in every city. Lots of research and development is being done all over the world to implement efficient parking management systems. This project proposes a fully automated parking system which does not require any new infrastructure. It aims to provide optimum solution for parking management in minimum cost which will help parking owners as well as the customers. The project describes the overall system architecture from hardware to software implementation.**

Keywords— Internet Of Things (IOT), Near Field Communication (NFC), Parking Automation, Precise Payment, QR Code.

I. INTRODUCTION

Automation is necessary while we are trying to survive in the Era of smart world. Automation provides perfection and efficiency. In this paper, we are focusing on parking automation, as the current parking system is facing many problems. Here we are considering problems faced by both, users and the parking owner which will lead us to a hassle free automated parking system. [2]

A user has to deal with numerous problems like long parking queues, high rates, waste of time and energy in search of an empty parking slot, manual mistakes during payment etc. On the other side, even the parking manager faces issues; he has to recruit more and more people to handle huge traffic especially at rush hours of the day and has to maintain a database manually which is a very tedious job. [3][6]The solution to these problems is parking automation; it allows a vehicle to communicate directly with the parking system without any human interference which thus provides an efficient parking system that benefits both, user and the owner. [2]

We use the concept of IOT (Internet of Things) for the interaction between two objects. Internet of things is defined as a conceptual network of anything and everything in this world. [9] Using IOT as a base concept, attempts are being made worldwide to develop an automated parking system which will help in reducing the human error involved in the process and also save the time and fuel of the customers looking for a parking in malls, theatres, companies, etc.

In our project, we are trying to implement parking automation based on the concept of the Internet of things using NFC (Near Field Communication) to reduce the overheads in current systems. NFC allows two devices to communicate with each other using radio frequency. NFC connection is established by bringing two devices together for less than a second. NFC varies in ranges but typically it is favourable for distances less than 10 cm. [1]

Another cost effective technology that we are using in our project is the technology of QR codes. QR codes are nothing but machine readable symbols which can be described as array of white and black squares typically which can be used for storing some information. [10]

II. MOTIVATION

The incident described below is a real time situation faced by all of us. It motivates us to develop an automated system for parking to overcome all the problems.

It was a Sunday. Mr. Joshi decided to visit a mall along with his family in the evening. They started around 5 p.m. for the mall which was 8 kilometres away and reached at the entrance in 20 minutes. Mr. Joshi saw that about 4 cars were standing in front of his car and thus was a bit disappointed as he had to wait in the queue. They realised that the cars were not moving the reason being - no person attending the increasing queue. After around 10 minutes, the attendant arrived, made entries in a register specifying the time and vehicle number and let them enter the parking.

After entering this 3 storied parking, they had to now search for an empty parking slot which was indeed a challenge. Mr. Joshi's wife suggested that they should try searching for a parking slot near the lift as it will be easier to carry bags once they are done with their shopping. There were others too who

wanted the same, hence it led to congestion and he ended up wasting more time and fuel.

Finally they found an empty slot, but before they could park their car, another car driver parked his vehicle in that slot. This further led to a greater disappointed and they had to then search for another empty slot and park there. The only way to find their car after they were done shopping was by remembering the pillar number near the car, which if forgotten would've led to hours of searching all over again. The amount Mr.Joshi paid did not consider the no of hours he was in the mall moreover it was a manual cash transaction which obviously could have been prone to human errors.

III. Literature Survey and Current Issues

Various solutions have been presented as a prototype for automatic parking till date. In the following section, we will introduce some solutions and summarize them based on the themes of implementation.

A. Mechanical Parking Using Microcontrollers

This is the most popular prototype for automation of parking. Various international papers suggest building multi-storeyed mechanical parking system for automation purpose which will be then controlled using microcontrollers.

Use of rack and pinion model along with Bluetooth is suggested in the method by Harmeet Singh, Chetan Anand, Vinay Kumar and Ankit Sharma [3]. Here, the parking process starts when driver turns his Bluetooth on. The Bluetooth reader fetches the owner's unique number and then microcontroller is fed with appropriate commands, thereafter, assigns an empty parking slot. The mechanical system which consists of rack and pinion lifts the car and transports it to a predetermined parking space in the parking garage.

Harsh Kotak, Prithvish Mamtora, Dhruv Mehta and Grishma Vithalani suggest using a rack and pinion model along with NFC. [6] The user establishes communication by tapping his NFC enabled smart phone against an automated terminal nearby. The NFC Reader terminal fetches UID of the NFC enabled smart phone then commands the microcontroller and the microcontroller assigns an empty parking slot. The mechanical system which consists of rack and pinion lifts the car and transports it to a predetermined parking space in the parking garage.

Mr. John Nair, Mr. Nimesh Gupta, Ms. Rakhee Mahadik and Mr. Chintan Chauhan are also using a rack and pinion model along with NFC. [8] The driver taps his NFC enabled smart phone at an automated terminal nearby. The NFC Reader terminal fetches UID of the NFC enabled smart phone then sends the commands to microcontroller and microcontroller assigns an empty parking slot. The mechanical system which consists of rack and pinion lifts the car and parks it to a predetermined parking space in the parking.

B. Parking automation using Bluetooth

Bluetooth technology is used for improving the prototype of automated parking. Here in one of the paper by Harmeet Singh, Chetan Anand, Vinay Kumar and Ankit Sharma Bluetooth is used as a communication channel between parking and user. [3] The Bluetooth reader fetches the owner's unique number and then commands the microcontroller which, thereafter, assigns an appropriate parking slot.

C. Parking automation using NFC

To further improvise over Bluetooth technology, NFC (Near Field Communication) is introduced where communication between parking facility and user is allowed using NFC enabled devices. Harsh Kotak, Prithvish Mamtora, Dhruv Mehta and Grishma Vithalani suggest using NFC. [6] The driver taps his NFC enabled smart phone at an automated terminal nearby. The NFC Reader terminal fetches UID of the NFC enabled smart phone then commands the microcontroller and microcontroller assigns an empty parking slot.

Mr. John Nair, Mr. Nimesh Gupta, Ms. Rakhee Mahadik and Mr. Chintan Chauhan suggest an approach using NFC. [8] The driver establishes communication by tapping his NFC enabled smart phone against an automated terminal nearby. The NFC Reader terminal fetches UID of the NFC enabled smart phone then commands to microcontroller and microcontroller provides an empty parking slot.

D. Parking automation using GPS

GPS technology is used to allocate a parking slot to the user. On a forum discussion author proposes to use GPS (Global Positioning System) to locate the user and then allocate a vacant parking space near to the user with the help of Bluetooth. [4]

TABLE I. Issues In Current Automated Parking Systems

No.	Theme of Implementation	No.	Issues
1.	Mechanical parking using microcontrollers	i.	The database has to handle large amount of data.
		ii.	As the mechanical components used are quite slow, at rush hours, it would lead to congestion at the entrance.
		iii.	The setting up of a new infrastructure involves a lot of cost.

		iv.	Maintenance of the mechanical components is costly too.
		v.	There is no mention of a manual override for the mechanical system.
2.	Parking automation using Bluetooth	i.	When compared to other wireless communication technologies like NFC, Bluetooth consumes relatively more power.
		ii.	Bluetooth has trouble dealing with interference while the data is being shared especially when several other devices are in proximity.
		iii.	Setting up of connection manually every time some data has to be sent consumes a lot of time.
		iv.	In the proposed solutions so far, directions to the allocated parking slots are not provided, thus, the problem of time wastage in finding the allocated parking slot along with the wastage of fuel still remains.
3.	Parking automation using NFC	i.	Once the parking slot is allocated there is no mechanism mentioned which would ensure that no other car would be parked before the user himself parks the car in his allocated slot.
		ii.	There are no directions provided to reach the allocated slot.
		iii.	Generally, people prefer having a parking that is closer to the entrance of the mall, there is no solution mentioned yet which would address this requirement.
		iv.	As there is no redirection provided at the entrance,the parking manager ends up hiring lot of people who then guide the cars to their respective allocated parking slots.
4.	Parking automation using GPS	i.	This technology is very power hungry,lasts only 8-12 hours before needing a recharge.
		ii.	The GPS signal does not pass through solid structures effectively, thus, it might create problems for basement parkings.
		iii.	Absolute miniaturisation is not possible whilst maintaining positioning accuracy.
		iv.	Factors like Inconsistencies of atmospheric conditions, multipath issues, clock errors and man-made electromagnetic interference cause a 5m-10m error in GPS.
		v.	There is a demand of continuous internet connection.

IV. PROPOSED SYSTEM AND RECOMMENDATIONS

We are using NFC technology to register vehicle user with automated parking system. Every time a user enters the parking, he has to tap his NFC enabled smart phone against the NFC reader available at the parking entrance. Once the communication link is established, system transfers a file to the user which contains suggested available parking slots along with the date and time stamp. For example:

Available Slots: A1, B13, C8.
15 August 2015, 13.56.

Now the user is given all the liberty to park at any parking space. He may or may not choose from the suggested list. All he has to do is scan the QR code pasted on the wall of parking slot which he will be choosing. As soon as the customer will scan the QR code, the parking number encoded in QR code will be sent to parking system using the internet available with user's smart phone. This parking slot will be marked as occupied by system till the time the vehicle exits.

Now while leaving the building or mall, user can check their car's current location by a kiosk machine after tapping the phone on it. While leaving the parking premises, user has to tap his phone on a cash counter to pay the parking fees. To calculate parking fees, entry timestamp will be compared with the current system time and accordingly the amount to be paid would be deduced from the account. Here, account used for the transactions will be any e-wallet which user wishes to use. [5]

Once the user exits, the parking slot will be marked as empty. If at all the internet connectivity fails and system is not prompted with the parking slot ID, at the exit point NFC readers will fetch this data and the parking slot will be treated empty there onwards.

The highlights of system proposed in this project are no need of new infrastructure and minimum setup cost. This system can be implemented in any parking within the span of 3 to 4 days. This system does not involve any kind of human interference. Aim of our proposed system is to achieve full automation using minimum resources. This proposed solution resolves the issues discussed above.

The flowchart for proposed parking automation system is as given in Fig.1:

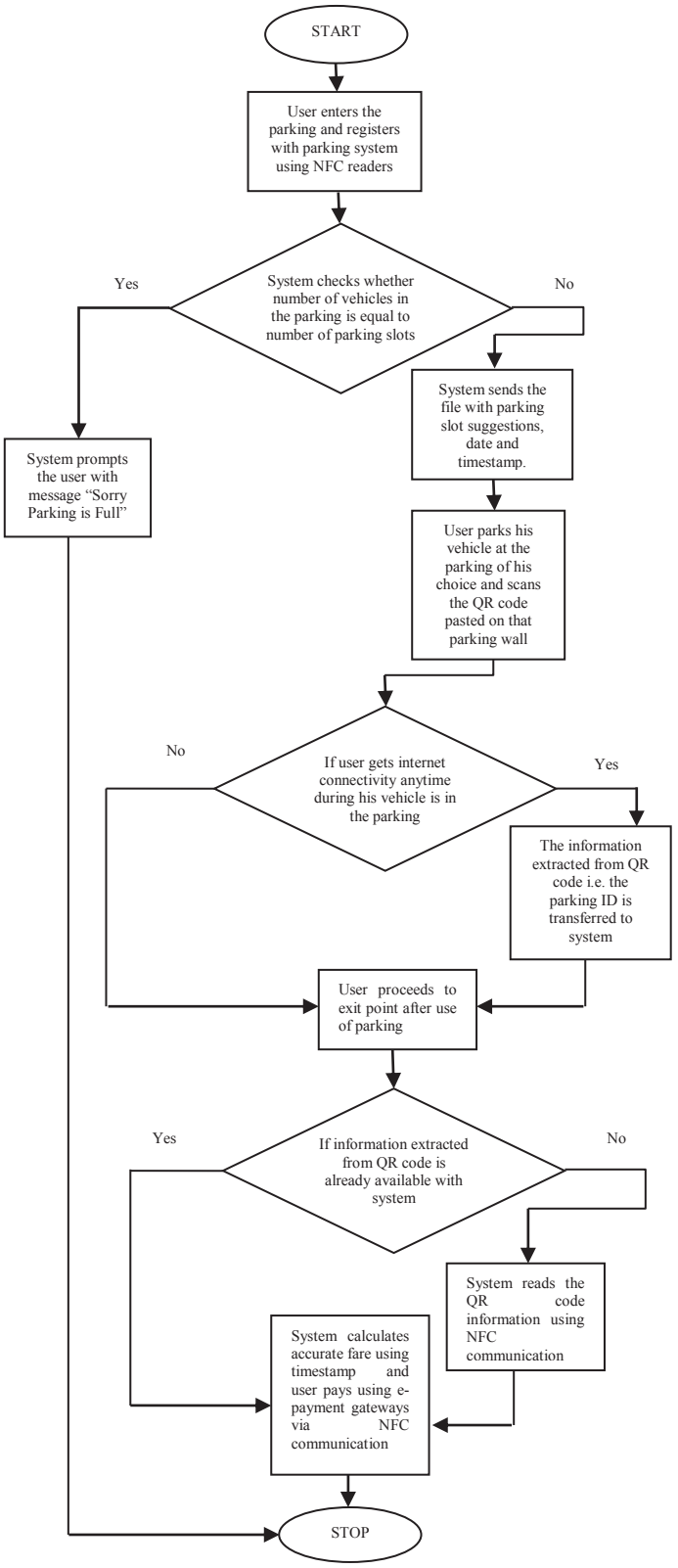

Fig. 1. Flowchart for proposed parking automation system

V. CONCLUSION

Thus, we have presented a detailed description of our Automated Parking System. It helps overcoming the shortcomings of the current parking systems. The biggest challenge that one faces in a system is the high cost involved in building new mechanical infrastructures. In this system, we have provided an automated parking without introducing any mechanical system in the existing infrastructure. Also, using NFC for suggesting parking spaces minimizes the system errors and makes it hassle-free for users as there is no need for them to wait in long queues. Precise payment with trouble free redirection to parking spaces gives this system an edge over other current systems. Being a low setup cost system, it provides an efficient way of optimizing space and performance.

VI. REFERRENCES

[1] https://en.wikipedia.org/wiki/Near_field_communication
[2] https://en.wikipedia.org/wiki/Automated_parking_system
[3] Harmeet Singh, Chetan Anand, Vinay Kumar, Ankit Sharma "AUTOMATED PARKING SYSTEM WITH BLUETOOTH ACCESS" published in International Journal Of Engineering And Computer Science ISSN:2319-7242 Volume 3 Issue 5, May 2014
[4] Near Field Communication and the NFC Forum: The Keys to Truly Interoperable Communications. NFC Forum, 2007
[5] Proximity Mobile Payments: Leveraging NFC and the Contactless Financial Payments Infrastructure. Smart Card Alliance, 2007.
[6] Harsh Kotak, Prithvish Mamtora, Dhruv Mehta, Grishma Vithalani "AUTOMATED CAR PARKING SYSTEM WITH NFC ACCESS" published in International Journal of Electronics and Communication Engineering & Technology (IJECET), ISSN 0976 – 6464(Print) ISSN 0976 – 6472(Online) Volume 4, Issue 5, September – October, 2013, pp. 201-206
[7] "An Intelligent Car Park Management System based on Wireless Sensor Networks," V.W. S. Tang, Y. Zheng, and J. Cao, Proceedings of the 1st International Symposium on Pervasive Computing and Applications, Aug 2006.
[8] Mr. John Nair, Mr. Nimesh Gupta, Ms. Rakhee Mahadik, Mr. Chintan Chauhan "Innovative Smart Car Parking System with NFC Access" published in International Journal of Engineering and Technical Research (IJETR) ISSN: 2321-0869, Volume-3, Issue-4, April 2015
[9] https://en.wikipedia.org/wiki/Internet_of_things
[10] https://en.wikipedia.org/wiki/QR_code

THE 5TH INTERNATIONAL CONFERENCE ON WIRELESS COMMUNICATIONS, VEHICULAR TECHNOLOGY, INFORMATION THEORY, AEROSPACE & ELECTRONIC SYSTEMS (WVITAE-2015)
December 13-16, 2015, Hyderabad, India

Wireless Mesh IP Video Surveillance System – A Systems Perspective

M. E. Dlodlo[1]; S. C. Lubobya[2]; O. Osanaiye[3]; E. Okumu[4]; H. Ohize[5]
Department of Electrical Engineering
University of Cape Town
Cape Town, South Africa

[1]mqhele.dlodlo@uct.ac.za; [2]LBBSMA001@myuct.ac.za; [3]OPYOSA001@myuct.ac.za; [4]okmeli001@myuct.ac.za; [5]ohzhen001@myuct.ac.za.

***Abstract*—This paper presents an overview and review of major issues involved in wireless mesh IP video surveillance systems. These include but are not limited to security, signal degradation and diversity, and quality of service. Finally, we share research directions the team is taking. The pivotal system of this discussion paper has been proposed elsewhere [1] as a model for the Internet Protocol (IP) mesh video surveillance systems complete with the performance evaluation of AODV and OSPF routing protocols in a wireless mesh video surveillance system. The discussion highlights past and current research, and reveals some scope for further collaborative research.**

Keywords—IP mesh video surveillance, security, QoS, dynamic spectrum access, MIMO, antenna selection,

I. Introduction

In recent times, internet has hosted applications from diverse sectors from telecommunications to commerce. Video surveillance has taken a cue in harnessing the benefits of transmitting information over the Internet. Relative to most applications that use the internet as a transmitting medium, emphasis is always placed on the quality of service (QoS) while security has not enjoyed as much attention. Internet being an open architecture is built on standard interfaces, protocols and basic data format. When used as a medium for transmitting IP video surveillance data, it is exposed to security threats, especially when embedded in wireless mesh networks.

Wireless mesh networks (WMN) have the advantage of extending network services to areas where wired networks or conventional wireless networks cannot be installed. WMN are mainly made up of mesh routers and mesh clients, but they are capable of providing network access to both mesh and conventional clients. An example of a network service that has traditionally been deployed on wired networks is the surveillance video system. Wired surveillance video systems have their advantages, but they also suffer from challenges which can be overcome by deploying the surveillance video system on a wireless mesh network. The performance of mesh surveillance video systems can be severely affected if a large number of nodes are placed in close proximity, this is because the bandwidth available for supporting the nodes will now be limited.

Another area of concern in wireless mesh IP video surveillance quality of service provision involves dynamic spectrum access (DSA). Video surveillance has earned high relevance globally, due to recent trends in security and the need to gather visual information for decision making. The need to get real-time video data with high resolution is a key consideration in all IP video surveillance systems. However, this is degraded by congestion in wireless networks. This congestion is attributed to the recent surge in the deployment of wireless communication technologies, introduction of various bandwidth demanding multimedia services and the current paradigm of spectrum allocation i.e. the static spectrum allocation technique. [2]

The rest of the paper discusses the issues under study, the directions envisioned and scope for possible collaboration. Section II discusses the IP video surveillance system from an Internet security point of view. Aspects of related quality of service provisioning approaches are the subject of Sections III and IV. In Section V we take a bold step and propose a game theoretic take on the deployment of IP cameras linked to mesh routers and access gateways.

II. IP Security

A. A Security Perspective on Surveillance Modelling

Much research focuses on quality of service (QoS) provisioning without paying any attention to security. The Internet being an open architecture is built on standard interfaces, protocols and basic data format. When used as a medium for transmitting IP video surveillance data, it is exposed to security threats. These are threats to confidentiality, integrity and availability in IP-based video surveillance systems.

A security assessment of the proposed mesh IP video surveillance system [1] can be guided by the CIA triad model

This work is a re-look at aspects of the concurrently published work by C. S. Lubobya [1] from the multiplicity of perspectives represented in the wireless communications laboratory. His work is supported by the University Science, Humanities and Engineering Partnerships in Africa (USHEPiA) Fund.

C. S. Lubobya is investigating wireless Internet-based crime monitoring and traffic control systems from a unified perspective. This is a joint research project between UCT and the University of Zambia.

O. Osanaiye interests himself in multi-stage security boosting for service availability in cloud computing. His work has opened up collaborations with the UCT Department of Computer Science as well as the University of South Australia

E. Okumu is developing a novel cross-layer approach to antenna selection in cognitive radio MIMO systems.

H. Ohize is developing a new MAC protocol for optimal spectrum identification, co-ordination and scheduling in Ad Hoc cognitive radio networks.

V. Moyo is improving cognitive radio energy efficiency by using game theory enhanced distributed cooperative sensing.

[2]. CIA being confidentiality, integrity and availability are the critical components of security that must be considered during the design and implementation of the system.

B. *Confidentiality*

Rajpoot & Jensen [3] describe confidentiality as the ability to protect data and information transmitted over a network against unauthorized access. It involves taking control and ownership of packets which are always at risk from attackers capable of monitoring to capture sensitive data packets. Information sent from the IP cameras to both the local and remote servers therefore needs a high level of confidentiality. Eavesdropping is a common attack against confidentiality of IP information.

C. *Integrity*

It is essential that data sent in the mesh network remains unaltered by an unauthorized user. The wireless links in the network can be used by an attacker to compromise the system through altering of configuration to achieve virtually any aim. According to Sayyad et al. [4], authentication of communication links between two parties is not a guarantee that messages transmitted cannot be altered; therefore the mesh IP video surveillance system must be protected to maintain the integrity of its data system and configuration.

D. *Availability*

Availability in this context is the ability to access the resources in form of information from the local and remote servers when needed. Several malformed packets can be used to disrupt, damage or disable network functionality [5] to the detriment of the proposed system design objectives. DDoS attack has been identified as one of the major cause of unavailability of service while congestion leads to delay in accessing resources [6].

TABLE I.

Attack	Features	Mitigation
DDoS	Flooding service with malicious packets using compromised vulnerable nodes on the internet.	Firewall, NIDS
Unauthorized access	Illegal access to system components due to non-centralized authentication in meshed ah-hoc network.	Access Control List (ACL), Password security
Eavesdropping	Intercepting or viewing IP video over without the knowledge of the administrator	Encryption of traffic, Virtual Private Network (VPN)
Masquerading	Pretense of an entity to be another entity e.g. illegal IP camera or server in the network.	Device authentication
Man-in-the-middle- attack	Secretly relays or alter communication between two nodes.	Encryption, VPN.

III. Diversity Approach

The surveillance video system is an example of a network service that has traditionally been deployed on wired networks. Wired surveillance video systems have their advantages, but they also suffer from challenges that can be overcome by deploying the surveillance video system on a wireless mesh network. However, the performance of wireless mesh surveillance video systems quickly gets severely bandlimited as the density of nodes in a geographic area increases. Incorporating cognitive capability in mesh routers, for instance, can alleviate the problem.

This will enable the mesh routers to access radio spectrum in frequency bands not assigned to them, availing more bandwidth for transmission purposes [7]. The main challenge now is how to meet the QoS requirements for the surveillance video system. This can be accomplished by deploying multiple input multiple output (MIMO) antenna systems.

A. *MIMO*

The cognitive mesh routers can be equipped with multiple antennas, and MIMO techniques can be used to improve the spectral efficiency and diversity [8] [9]. There is a hardware complexity and cost factor in this approach. Antenna selection techniques then address the latter difficulty.

B. *Cross Layer Antenna Selection*

Hardware complexity and cost reduction requires astute antenna selection that maintains the gains of MIMO [10] – [12]. Cross layer antenna selection that uses information from the data link and physical layers offers performance benefits when compared to physical layer based antenna selection which uses only information from the physical layer [13]. Throughput based antenna selection, which uses information from the data link and physical layers can be used to select cognitive mesh router antennas and optimize the link throughput. In turn, throughput based antenna selection results in increased performance of the surveillance video system in the following areas. This approach optimizes the system throughput for the mesh IP video surveillance system, and reduces packet re-transmissions, which results in lower end-to-end delay. In addition, throughput based antenna selection reduces the error rate, resulting in less jitter as packets are more likely to maintain the correct arrival sequence.

IV. DSA in Mesh IP Video Surveillance

There is a need to get real-time video data with high resolution, a key consideration in all IP video surveillance systems. However, this is mitigated by congestion in wireless networks. This congestion is attributed to the recent surge in the deployment of wireless communication technologies, introduction of various bandwidth demanding multimedia services and the current paradigm of spectrum allocation, i.e. the static spectrum allocation technique. [14]

Static spectrum allocation is rather inefficient in congested networks [15], as it hamstrings the recovery of any and all

disuesed spectral bands. Additionally, this technique fails to identify underutilized though active bands thereby resulting in apparent pseudo-spectrum scarcity [15]. Consequently, a dynamic spectrum access (DSA) approach for Mesh IP video surveillance system is proposed as a work in progress. DSA is made feasible with Cognitive Radio (CR) technology.

The CR prototype aims at devising spectrum sensing and management techniques, thereby allowing the IP cameras to intelligently locate and use frequencies other those in the 2,4 GHz ISM band. DSA concept is receiving the most attention among researchers and industry players as a more lasting and sustainable resolution to the challenge of spectrum scarcity [17-19]. This will in turn increase spectrum usage efficiency and reduce congestion currently being experienced in certain frequency bands e.g. ISM bands. However, canvassers of this technology are currently confronted with the complexities involved in the development of a fully functional CR system. This is attributed to the complex requirements for the integration of the major building blocks of CR namely Spectrum Identification (Sensing), Spectrum Access, Spectrum Sharing and Spectrum Management [20]. Therefore, in this paper, we propose an intelligent frequency-shifting self-managed IP Mesh video surveillance systems**.**

This is realized in two ways: (1) A new approach for spectrum sensing is devised without alteration to the de facto Mesh IP video surveillance systems design. (2) We propose distributed MAC protocol design. This will enhance self-organization and co-ordination for spectrum access in the Mesh IP network.

A. A new approach for spectrum sensing for Mesh IP video surveillance systems.

The success of our Mesh IP video surveillance systems model design, is pegged on the ability of the CR to accurately make spectrum occupancy decision based on it spectrum sensing results. The conventional energy detector is best suited for our Mesh IP video surveillance applications but its performance is greatly deteriorated under noise fluctuation and low SNR regimes [21]. This can be attributed to its fixed threshold approach and its lack of prior knowledge of the noise variance. In this design, we adopt an adaptive threshold energy detection technique with noise variance estimation based on the recursive one-side hypothesis test (ROHT) algorithm and the constant false alarm rate (CFAR) principle, as seen in the work of Nixon and Dlodlo in [21]. Simulation results indicate that this technique improves spectrum occupancy detection as seen in the receiver output characteristic curve (ROC) of [21].

B. Proposed Distributed MAC protocol design for DSA Mesh IP video surveillance systems.

The proposed mesh IP network consist of video cameras organised in a mesh topology or wireless ad-hoc network topology. The mesh IP network co-exist with the licensed users network also known as primary users (PU). In the spirit of improving channel access, we propose an efficient MAC protocol for enhancing spectrum access, thereby avoiding co-tier and cross-tier interference. Existing Medium Access Protocols (MAC) such as the 802.11 and others were designed for homogenous spectrum access. The introduction of DSA technique has, however, compounded the realization of an efficient MAC protocol. With respect to known solution the use of dynamic common co-ordination channel DCCC is the most patronized solution. DCC facilitates a variety of co-ordination operation such as transmitter-receiver handshake, channel access negotiation, topology change, routing information updates to cooperation among the Mesh IP videos [22]. The contribution here is the proposed dynamic control channel selection scheme. We develop an Ant Colony System (ACS) based control channel selection scheme. By ACS we make reference to the mimicry of pheromone laying behaviour of real ants to find the shortest route between their nest and a food source. ACS technique is popular in literature as Ant Colony optimization [23]. By drawing similarities, we propose the use of such technique in achieving the goal of coordination among the IP video cameras.

V. SENSING POWER: A GAME THEORY VIEWPOINT

For a case where the IP cameras, the mesh routers (MRs) and the mesh gateways (MGs) are within buildings with easy access to power, the amount of energy spent on sensing the ISM bands that the devices use for communication may not be a factor worth consideration. However, where there is no steady source of power, such as in ad hoc wireless networks, it becomes important to reduce the amount of power spent on sensing. In such a scenario, for the IP cameras to ensure reliable communication with the MRs and also on the communication between the MRs and the (access point (AP) with reduced power requirements, there is need for performance enhancing algorithms and protocols to be in place.

A Game Theory [24] based algorithm can be used to improve the energy used for sensing idle spectrum between the IP camera and the MR and between the MR and the AG. The IP cameras connecting to a single MR can be modelled as players with a number of strategies each. A strategic form game is a tuple (A, S, u) for multi IP cameras. Where: A = {1,2,…,a} is the set of IP cameras from the first IP camera to the ath IP camera shown in Figure 2 ; S = {S1,S2,…,Sa} where Si is the set of actions available to IP camera i; u = {u1,u2,…ua} where ui is the utility function for IP camera i [25]. The objective of the game would be establish a strategy that would result in each IP camera use less time and energy for sensing, if the sensed information is shared. The algorithm used by the IP cameras can be extended to the MRs if there is a number of MRs that need to connect to an MG.

VI. The Networking Viewpoint

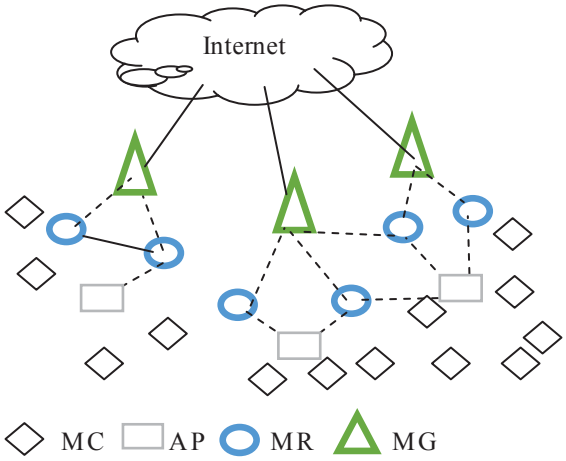

Fig. 1. Wireless Mesh Network Infrastructure [26]

A previous paper [24] analyzed and simulated the performance analysis of video surveillance applications through Wi-Fi networks, using three network topologies: wireless tree, star and wired tree topologies. It was shown there that the wireless tree topology had the best throughput performance of 100% better than star and wired tree topologies. It reduced packet losses to less than 5%. The wireless tree is is assumed in the concepts presented here. This is good news for remote as well as congested built-up areas, or for increasing the capacity of a backbone network. The next step is to investigate its performance in other IEEE 802.11 family of standards and cases where mobility introduces stochastic fading and shadowing.

A concurrent paper from this lab [26] presents an mesh IP video surveillance model that stipulates routing protocols that optimize throughput, reductions in packet loss, end-to-end delay and jitter. The routing protocol of choice is found to be OSPF. A concerted investigation of the effect of mesh topologies and routing algorithms on these metrics is also proposed.

VII. The 5G Prospect for IP Video Surveillance

The wireless communications research laboratory in the Communications Research Group (CRG) takes a multifaceted view of the questions in wireless mesh IP video surveillance systems. This paper discussed some of them, highlighting briefly what has been identified as problems, some solutions recently tested, those under investigation, as well as challenges that open up areas of collaborative research.

A systems engineering approach has been illustrated by this discussion as one approach to tackling the complicated challenges involved. The approach involves teaming together from diverse schools of thought that are collectively brought to bear on the problem at hand. It is viewed as the surest way to realize system-wide optimization of wireless mesh IP video surveillance systems embedded in the emerging 5G heterogeneous environment.

Other perspectives that the laboratory is investigating include the big question as to how much autonomy we want our networks, their components, and user devices to have. The question quickly brings up the Internet of Things and the Internet of everything paradigms in the heterogeneous 5G environment. To what extent must wireless mesh IP video surveillance systems make decisions about security issues and traffic conditions? When decisions regarding suspected crime are made by a network of things, who would take responsibility for the crime report and verification in a court of law? Our interest in this area has opened up avenues for collaboration with the Council for Scientific and Industrial Research (CSIR) in South Africa.

Acknowledgment

Our thanks go to the following colleagues: G. de Jager (UCT) and A. Zulu (UNZA) for valuable discussions on video surveillance, R. Choo (UniSA) and A. Kayem (UCT) for insights into Internet security, as well as L. Coetsee and Q. Williams (both at the CSIR).

References

[1] C. S. Lubobya, M .E. Dlodlo, G. De Jager and A. Zulu; "Mesh IP Video Surveillance Systems Model Design and Performance Evaluation"; Wireless Communications, Vehicular Technology, Information Theory and Aerospace & Electronic Systems (VITAE), 2015 5th International Conference on, Hyderabad, India, (in press)

[2]Y. Cherdantseva, J. Hilton, A reference model of information assurance & security in: Proceedings of 8th IEEE International Conference on Availability, Reliability and Security (ARES), Regensburg, Germany, 2013, pp. 546-555.

[3] Q. Rajpoot, C. Jensen, Security and Privacy in Video Surveillance: Requirements and Challenges, in: Proceedings of 29th IFIP TC 11 International Conference (SEC 2014), Marrakech, Morocco, 2014, pp. 169-184.

[4] M. Sayyad, A. Chatterjee, S. Nalbalwar, Proposed Model for SIP Security Enhancement, Communication and Network, 2(10) (2010) 69-72.

[5] F. Huang, Y.Yang, A flow-based network monitoring framework for wireless mesh networks, IEEE Wireless Communications, IEEE 14(5) (2007) 48-55.

[6] O.Osanaiye, M. Dlodlo, TCP/IP header classification for detecting spoofed DDoS attack in Cloud environment in: Proceedings of 16th IEEE International Conference on Computer as a Tool (EUROCON 2015), Salamanca, Spain, 2015, pp. 1-6.

[7] K. R. Chowdhury and I. F. Akyildiz, "Cognitive Wireless Mesh Networks with Dynamic Spectrum Access", *IEEE J SAC*, January 2008

[8] E. Telatar, "Capacity of Multi-antenna Gaussian Channels", *AT&T Bell Labs, Internal Technology Memo*, June 1995.

[9] S.M. Alamouti, "A Simple Transmit Diversity Technique for Wireless Communications", IEEE, 1998

[10] A. F. Molisch and M. Z. Win, "MIMO Systems with Antenna Selection", IEEE Microwave Magazine, 2004.

[11] Zhang N., Xu Y. and Gao X., "A New Antenna Selection Algorithm in Cognitive MIMO Systems", Journal of Selected Areas in Telecommunications, November Edition, 2011.

[12] M. F. Hanif, P. J. Smith, D. P. Taylor, and P. A. Martin, "MIMO Cognitive Radios with Antenna Selection", IEEE Transactions on Wireless Communications, November 2011.

[13] J. L. Vicario, M. A. Lagunas and C. Anton-Haro, "A Cross-Layer Approach to Transmit Antenna Selection", IEEE Trans. Wireless Commun., Aug. 2006.

[14] Valenta V., Marsalek R., Baudoin G., Villegas M., Martha S., & Fabien R., 2010. "*Survey on Spectrum Utilization in Europe: Measurement,*

Analyses & Observations." Proceedings of the 5th international Conference on Cognitive Radio & Oriented Wireless Networks & Communications. 9- 11 June 2010. Cannes. Pp 1-5.

[15] Cisco. (2011). "Cisco Visual Networking Index: Global Mobile Data Traffic Forecast Update 2010-2015." Cisco White Paper

[16] Tjelta, T., & Struzak, R. (2011). "*Physical, Technical, Practical, Economical and Regulatory Aspects of Spectrum Management*." General Assembly and Scientific Symposium, (pp. 1-4).

[17] Nekovee, M. (2010). "*Mechanism Design for Cognitive Radio Networks*." Conference on Complexity in Engineering, (pp. 12-18).

[18] Zhou, R., Han, Q., Cooper, R., Chakravarthy, V., & Wu, Z. (2010). "*A Software Defined Radio Based Adaptive Interference Avoidance TDCS Cognitive Radio*." International Conference on Communications (ICC), IEEE, (pp. 1-5).

[19] Chowdhury, K.R. and Akyildiz, I.F. (2008) "*Cognitive Wireless MexhNetworks wih Dynamic Spectrum Access*." IEEE Journal on selected areas in Communications, vol. 26, No. 1, January 2008. Pp. 1-5.

[20] Cabric, D., Mishra, S., & Brodesen, R. (2004). "*Implementation Issues in Spectrum Sensing for Cognitive Radios*." In Asilomar Conference on Signals, Systems and Computers, (pp. 772-776). Pacific Grove, USA.

[21] Ng'ethe N., Dlodlo, M. E. (2015). An Adaptice Threshold Energy Detection Techniwue with Noice Variance Estimation for Cognitive Radio Sensor Networks. Submitted to ICC 2016 kulala lumpa, Malysia, unpublised

[22] C. Cormio and K. Chowdhury, (2010). "An adaptive multiple rendezvous control channel for cognitive radio wireless ad hoc networks," in 8th IEEE International Conference on Pervasive Computing and Communications.

[23] Qian H., Ping Z., 2012. "Dynamic Channel Assignment using Ant Colony Optimization for Cognitive Radio Networks" Vehicular Technology Conference (VTC Fall), 2012 IEEE Conference. Pp 1-5.

[24] E. Yaacoub, A. Imran, Z. Dawy, and A. Abu-Dayya, "A game theoretic framework for energy efficient deployment and operation of heterogeneous LTE networks," 2013 IEEE 18th Int. Work. Comput. Aided Model. Des. Commun. Links Networks, CAMAD 2013, pp. 33–37, 2013.

[25] D. Fudenberg and J. Tirole, Game Theory, 1st ed. Cambridge, MA: MIT Press, 1991

[26] Lubobya, S. C., Dlodlo, M. E., de Jager, G.; "Performance Evaluation of the Wireless Tree Wi-Fi Video Surveillance System"; Computer Modelling and Simulation (UKSim), 2014 UKSim-AMSS 16th International Conference on, Cambridge, 26-28 March 2014, pp. 511-516. Publisher: IEEE. Print ISBN: 978-1-4799-4923-6. INSPEC Access Number: 14934037. DOI: 10.1109/UKSim.2014.40.

[27] Adeleke, J. A.,Dlodlo, M. E., Onime, C. E.; "Video Traffic Prioritization in WLANs Using Single Queue Priority Scheduler"; Computer Modelling and Simulation (UKSim), 2015 UKSim-AMSS 17th International Conference on, Cambridge, 25-27 March 2015, pp. 557-564. CD ISBN 978-1-4799-8712-2.

[28] S. C. Lubobya, M. E. Dlodlo, G. de Jager, A. Zulu; "Mesh IP Video Surveillance Systems Model Design and Performance Evaluation"; accepted for publication in Proceedings of the Fifth International Conference on Wireless Communications, Vehicular Tehnology, Information Theory, Aerospace & Electronic Systems (WirelessVITAE 2015), 13-16 December 2015, Hyderabad, India.

THE 5TH INTERNATIONAL CONFERENCE ON WIRELESS COMMUNICATIONS, VEHICULAR TECHNOLOGY, INFORMATION THEORY, AEROSPACE & ELECTRONIC SYSTEMS (WVITAE-2015)
December 13-16, 2015, Hyderabad, India

Preliminary performance evaluation of the FBMC based future IEEE 1900.7 Standard

D. Noguet, J.-B. Doré and B. Miscopein
Minatec Campus
CEA Leti
17, rue des Martyrs – 38054 Grenoble Cedex 9, France
dominique.noguet@cea.fr

***Abstract*—White space communications have attracted a particular interest after some national regulators have authorized TVWS unlicensed secondary usage. The IEEE 1900.7 working group has defined a specific air interface tailored to these applications. The standard, expected for publication in 2016, is based on an Filter Bank Multi Carrier (FBMC) physical layer and a CSMA-CA MAC sublayer. To our knowledge, this is the first time a radio standard is based on FBMC technology. This paper provides a brief description of the technology considered by the IEEE 1900.7 working group, providing also a more global perspective related to White Space research and standardization. Then, the paper provides preliminary simulation results of the IEEE 1900.7 system and uses more usual Cyclic Prefix-Othogonal Frequency Division Multiplex (CP-OFDM) technology as a comparison baseline.**

Keywords—IEEE 1900.7; white space; dynamic spectrum access; physical layer; MAC; use cases

I. INTRODUCTION

In the recent years, there has been a worldwide concern related to spectrum shortage. As an example, in June 2010, the White House issued a Presidential Memorandum stating that the National Telecommunications and Information Administration (NTIA) shall collaborate with FCC to make available a total of 500 MHz of Federal and non-federal spectrum over the next 10 years, suitable for both mobile and fixed wireless broadband use. One of the means to make new spectrum available is through sharing, and the Digital Switch Over (DSO) in TV bands, which has resulted in making the so-called TV White Space (TVWS) UHF spectrum available, was the first actual example where such a mechanism has been allowed. TVWS availability depends on TV broadcast frequency usage profile, thus changing across time and space. TVWS usage relies on unlicensed secondary Dynamic Spectrum Access (DSA) under the principle on a non-harmful interference with incumbent users [1].

In the USA, the FCC proposed rules for the Unlicensed Operation in the TV Broadcast Bands [2], with the final set of rules in 2009 [3] and an additional notice in 2011 [4], along with additional memorandum [5][6]. In Japan, MIC has published rules for secondary operation in TV white space [8]. In Europe, the Ofcom UK was the first regulator to establish rules for TVWS usage [8] [9]. Subsequently, Ofcom organized a nation-wide trial where several technologies were assessed [10]. Following up the approval of the European Parliament and Council the first Radio Spectrum Policy Programme (RSPP) in March 2012 [11], the European Commission released a Communication [12] in which shared use of TV White Spaces in the 470-790 MHz band is identified as a major opportunity. Then, regulatory actions have taken place in this area. In a first report, European Regulation (CEPT) has defined technical considerations for TVWS operation in Europe [13]. Then, ECC Report 159 established technical and operational requirements for the possible operation of cognitive radio systems in the "white spaces of the [470-790] MHz band" [14]. CEPT thoroughly addressed the way forward in European TV White Spaces, assessing both geolocation database and spectrum sensing as enabling technologies and setting out technical requirements for the use of TVWS. Finally, ETSI established some requirements for TVWS equipment in answer to the R&TTE Directive and delivered the EN 301 598 Harmonized EN [15].

Alongside these regulatory harmonization initiatives, a set of bodies developed technology standards to enable the implementation of TVWS radios. First, the CogNea consortium developed the ECMA392 TVWS standard for WLAN-like application [16]. Then, IEEE802.22 [17], and more recently in IEEE802.11af [18] issued standards for WRAN and WLAN applications respectively. Finally, IEEE802.15.4m has been developed to address WPAN operation in the TVWS [19].

All broadband TVWS standards (ECMA392, IEEE802.22, IEEE802.11af) are based on Cyclic Prefix - Orthogonal Frequency Division Multiplexing (CP-OFDM) physical layer (PHY), often inherited from previous standard developments such as IEEE 802.16e or IEEE802.11a. These standards have been adapted to make them suitable for TVWS operation. However, because of the very stringent requirement on Adjacent Carrier Leakage Ratio (ACLR) to ensure interference free operation for incumbents, and the dynamic nature of DSA, it was shown in the literature that CP-OFDM was probably not the best choice for TVWS PHY, although probably the fastest in terms of market readiness [1]. For this reason, IEEE DySPAN Standards Committee (formerly known as SCC41) created an ad hoc group on White Space (WS) Radio in March 2010 "to consider interest in, feasibility

Authors would like to acknowledge the support of the European FP7-318563 CRS-i project.

of, and necessity of developing standard defining radio interface (medium access control and physical layers) for white space radio system". Subsequently, the 1900.7 working group on "Radio Interface for White Space Dynamic Spectrum Access Radio Systems Supporting Fixed and Mobile Operation" [20] was created.

The IEEE 1900.7 standard, which is aimed at being issued in 2016, is the result of a clean slate analysis where the working group tried to identify the most suitable technology for TVWS. The standard is based on a Filter Bank Multi Carrier (FBMC) PHY and a contention based CSMA-CA MAC. [21] describes the scenarios and approaches followed by the IEEE 1900.7 working group.

In this paper, a first set of performance evaluation of the IEEE 1900.7 draft standard is carried out though simulation. Simulations are performed considering some parameters of the draft standard. First, the principles of IEEE 1900.7 FBMC PHY are recapped. Then, section III explains the MAC mechanisms of the IEEE 1900.7 standard. Then, in section IV, some performance evaluations are described.

II. Physical Layer

The rules established by regulators, like in the US [4][6], in the so-called TV white space allow opportunistic unlicensed operation in the UHF TV bands. These rules aim at ensuring opportunistic communication systems (white space devices) to coexist with TV broadcast signals and wireless microphones (referred to as 'incumbent systems' hereafter). The coexistence scheme is enforced with a priority mechanism where opportunistic systems must guarantee that no 'harmful interference' will be incurred to the incumbents. In this context, harmful interference is defined in a twofold way. Firstly, co-channel communication between incumbent and opportunistic systems is prohibited. This means that opportunistic systems must be able to assess the presence of incumbent signals and access only channels vacant from any incumbent. Besides, opportunistic systems have a limited amount of time to evacuate the channel when an incumbent is switched on. Secondly, adjacent channel leakage ratio (ACLR) is limited in order to prevent an opportunistic system from interfering with an incumbent operating in another channel, and in particular in adjacent ones. In [6], ACLR is restricted to be at least 55dB. Similar requirements are considered in other countries (e.g. in the UK [8]). Such a high ACLR requirement is specific to the TVWS context. For instance, ACLR requirement is 10dB stronger than required for LTE systems [22].

CP-OFDM has proven to be very effective for mobile wireless communications and is a first guess when broadband wireless PHY is at stake. By dividing a frequency selective fading channel into a large number of narrow-band flat fading sub-channels, CP-OFDM systems can easily compensate the effects of the channel using a simple one-tap frequency domain equalizer. However, CP-OFDM cannot meet the ACLR requirements unless the transmitter flexibility is sacrificed or spectral efficiency is compromised. This is due to the square temporal filter of CP-OFDM, or in other words the sinc kernel function in the frequency domain, which has very high sidelobes (-13dBc). On the other hand FBMC modulation has shown very good simulated ACLR performance in the context of TVWS [1]. Through an implementation on a flexible hardware TVWS transmitter, [23] shown that FBMC modulation can meet ACLR levels prescribed by the FCC's coexistence requirements. The actual implementation was aimed at assessing the performance under real hardware impairment conditions, such as limited dynamic Digital to Analog Convertors (DAC) [24].

Another way of comparing ACLR performance of FBMC vs CP-OFDM, is to measure respective power levels for a given interference level in adjacent channels. This was performed in [24] where the power of FBMC was 9dB higher than with CP-OFDM to meet quasi-error free video reception in the adjacent channel. The benefit of this 9dB margin can be estimated in terms of range (or coverage). For instance, considering a fixed station TX power of 36dBm (4W), a 12dB reception SNR, a -86dBm receiver sensitivity, the transmission range when using 470 MHz central frequency is given in Table I.

TABLE I. Range comparison for equivalent -55dBc ACLR

Propagation condition	FBMC 36dBM	CP-OFDM 27dBm
Okamura-Hata (Urban)	0,93 km	0,53 km
Okamura-Hata (Suburban)	1,56 km	0,89 km
Free Space Loss	63,72 km	22,61 km

FBMC was introduced in the 60s by [25][26]. It is a multi-carrier approach, but unlike CP-OFDM where the *sinc* kernel filter ensures subcarriers orthogonality with respect to the FFT operator, FBMC uses a prototype filters that filters each sub carrier. A proper design of the prototype filter enables to trade time and frequency localization, and thus to control ACLR. Because the prototype filter's response spreads each subcarrier over several adjacent subcarriers, another dimension is used to 'restore' orthogonality. In the framework of IEEE 1900.7, the offset QAM (OQAM) approach was used. OQAM consists in a complex to real conversion where real and imaginary parts of each complex symbol are multiplexed in consecutive time samples into Pulse Amplitude Modulation (PAM) symbols (Fig. 1). In order for this pre-processing not to impact data rate, the PAM symbols are up-sampled by a factor of 2.

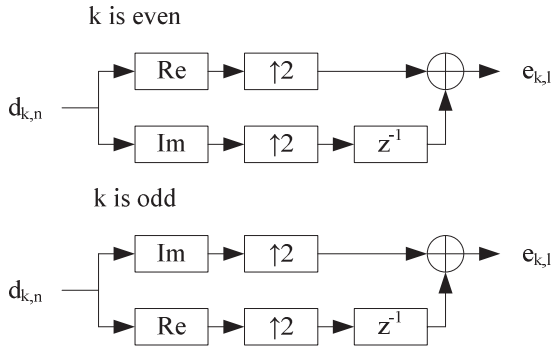

Fig. 1. OQAM pre-processing.

Then, the output real numbers are multiplied by an offset QAM sequence to form a new complex symbol: $h_{k,l} = (-1)^{kl}(j)^{k+l} e_{k,l}$. These symbols are consequently filtered through a polyphase network *G(z)*. The FBMC modulator and demodulator are shown in Fig. 2.

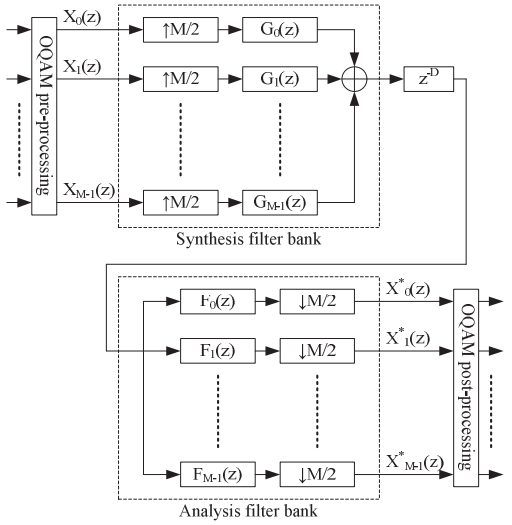

Fig. 2. FBMC modulator and demodulator using a polyphase network.

One of the main shortcomings of FBMC was supposed to be its implementation complexity. However, recent results have shown that a flexible approach was possible with very limited complexity overhead. First, on the transmitter side, it has been shown that an additional filter is required on top of CP-OFDM and shall be implemented as a digital filter for the sake of flexibility. In this context, [24] concluded that the complexity of the filtered CP-OFDM TX could be as high as or even higher than the one of the FBMC TX, which does not require this additional filtering. Similarly, the complexity of an FBMC receiver has been compared to the one of CP-OFDM. [27] has shown that the computational complexity of the FBMC receiver was only around 30% higher than the one of the CP-OFDM RX. In addition, the proposed block-wise processing approach requires FBMC symbols to be stored, which impacts the size of the memory (2.5x the one of an equivalent CP-OFDM RX). However, such memory sizes can be implemented at a very limited footprint and cost on current silicon technology nodes.

TABLE II. IEEE 1900.7 PHY MODES

Mode	*N*	Intercarrier spacing	Channel 2MHz	Channel 8MHz
4K	4096	3.75 *KHz*	504 (1.86MHz)	2016 (7.56MHz)
1K	1024	15.00 *KHz*	124 (1.86MHz)	504 (7.56MHz)
0.5K	512	30.00 *KHz*	64 (1.92MHz)	252 (7.56MHz)
0.25K	256	60.00 *KHz*	32 (1.92MHz)	124 (7.44MHz)

The IEEE 1900.7 standard specifies two different sizes for the prototype filter: K=3 or K=4 governing the level of protection of adjacent channels. Also, for the sake of flexibility, several modes are proposed. They consider different number of carriers, and two channelization modes (2 or 8MHz). Thus, IEEE 1900.7 can be used in any country authorizing TVWS operation and can cover medium to broadband channels.

The block diagram of the IEEE 1900.7 transmitter is shown in Fig. 3. The transmitter architecture is composed of two main elements: forward error correction block and data mapping and modulation block. Forward error correction (FEC) is implemented using a standard convolutional encoder. The code may be punctured to support variable encoding rates. The convolutional code is segmented by blocks of fixed size. The trellis is closed at the beginning and the end of each FEC block. The output of the encoder is forwarded to a bit interleaver of size multiple of the output length of the encoder.

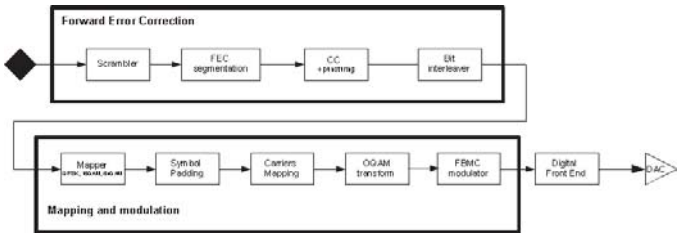

Fig. 3. Block diagram of IEEE 1900.7 baseband transmitter.

The second block maps and modulates the encoded bits to the multicarrier modulation. The coded data are mapped to QPSK, 16QAM or 64QAM modulation symbols, depending on the desired data rate. Symbols are then padded to make the transmitted burst length an integer multiple of multicarrier symbols. The generated block of QAM symbols is mapped to active carriers and modulated to an offset-QAM before being transformed into a time domain signal using FBMC waveform. A modulation and coding scheme (MCS) index is defined to describe the combination of the modulation and coding schemes that are used when transmitting data.

III. MAC SUBLAYER

The MAC sublayer is based on a Carrier Sense Multiple Access with Collision Avoidance (CSMA-CA) approach using "Request To Send" and "Clear To Send" (RTS/CTS) handshake mechanism. A basic network operates in a master-slave mode. In the master-slave mode, a device is designated as master (network coordinator) and others are associated with the master as slaves. The master coordinates channel access in the master-slave mode.

A. CSMA/CA RTS/CTS

With CSMA/CA each user can access the channel with equal priority through contention at each time instant. It is the access protocol adopted for IEEE 802.11 [23].

A node with a packet to transmit should first sense the channel. If the channel is sensed to be idle for a time period greater than the distributed inter-frame space (DIFS) time, the node sends a RTS packet. If the RTS packet is received without collision, a CTS is sent back to inform all nodes in the cell that the channel is reserved. All nodes defer their transmissions for the duration specified by the RTS: this mechanism is called virtual sensing.

If the channel is sensed as busy, a backoff procedure is invoked. Under the hypothesis of an error free transmission, collisions may only occur on RTS packets and transmission of data packets can proceed without interference from other nodes. The frame transaction of IEEE 1900.7 consists of a RTS/CTS frame exchange, a single frame, and the associated acknowledgement frame if requested by the ACK policy as shown in Fig. 6. When the I-ACK mode is invoked, an immediate acknowledgement frame is requested after the data packet (if it is decoded correctly). Otherwise, data frames are transmitted successively without acknowledgement (N-ACK mode).

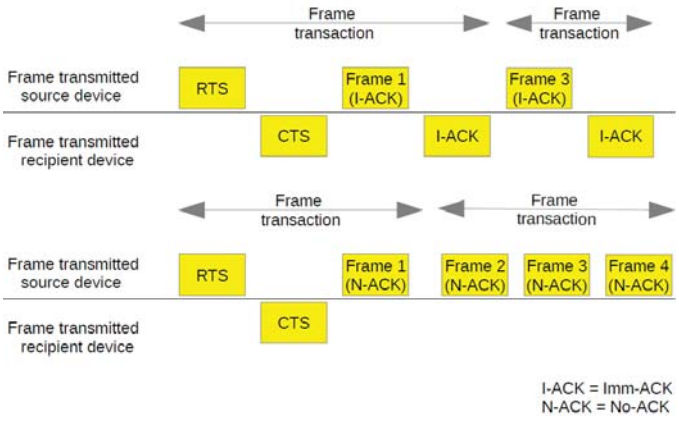

Fig. 4. Frame transaction examples.

B. Time structure of a MAC frame

The basic timing structure for a frame exchange is a superframe. The superframe is composed of 256 medium access slots (MASs) as shown in Fig. 7. Each superframe starts with a beacon period (BP). The BP is composed of 16 beacon slots. All nodes which share the same channel follow the same superframe structure.

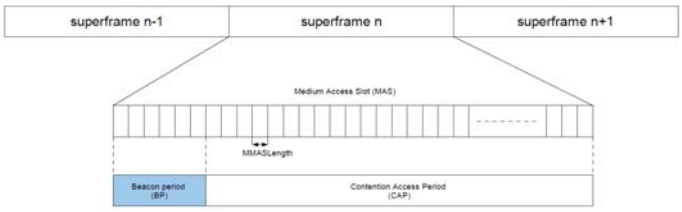

Fig. 5. Time structure of MAC frame.

The network coordinator device indicates its presence in a network to other devices by transmitting beacon frames. This allows other devices to perform the network coordinator discovery and network join procedures.

TVWS operation requires that before the completion of the master discovery procedure, a device does not know the operating channels. This results in a channelization combinatorial far too large to be discovered through blind scanning. In IEEE 1900.7 the data carried by a beacon frame is designed to speed up the discovery process. Additionally an optimized channel switching mechanism is implemented to maintain the connectivity when a new channel map is requested by higher layers.

IV. Performance Evaluation

A. PHY Layer

The IEEE 1900.7 PHY has been specified to be very flexible in terms of spectrum profile allocation. For instance, the 2MHz profile (see TABLE II. was designed to cope with 6MHz and 8MHz TV channelization in order to fit best to regulation worldwide. This profile also enables narrower spectrum allocation. Fig. 6 shows an example of 2 fragments of 2MHz each separated by an unused 2MHz fragment, using the IEEE 1900.7 FBMC PHY (0.25K and 1K profile as per TABLE II.). LTE CP-OFDM spectrum profile is given as a reference. The reference system uses 1024 carriers and a guard interval (GI) of 72 samples, similar to 10MHz LTE signal. The figure illustrates the much focalised spectrum localization of IEEE 1900.7 vs CP-OFDM based systems in the edges of the spectrum and in the gap.

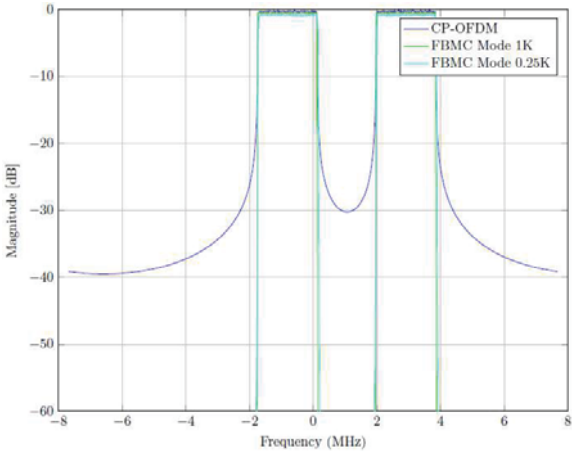

Fig. 6. IEEE 1900.7 spectrum profile example

Fig. 8 and Fig. 8 give PHY layer complete (TX-RX) performance evaluation considering a Frequency Spreading FBMC (FS-FBMC) architecture of the receiver [28][29]. With such a receiver the whole RX processing, including channel estimation and equalization is performed in the frequency domain. Performance evaluation are provided for a static LTE "Extended Typical Urban" channel model which is a 9 tap channel (delay spread of 5*us*) as defined in TABLE III. Results are given for a QPSK considering a coding rate 1/2 (Fig. 8) and 64QAM (Fig. 8) considering a coding rate 2/3 under a perfect channel estimation assumption.

TABLE III. LTE "EXTENDED TYPICAL URBAN" CHANNEL

Tap index [samples]	**0**	**1**	**2**	**3**	**4**	**8**	**25**	**35**	**77**
Relative power [dB]	-1	-1	-1	0	0	0	-3	-5	-7

The Mode 1K gives significant performance gain compared to CP-OFDM (~1.5dB). It can be explained by the high performance offered by the Frequency Spreading RX scheme demonstrated in [29]. When the size of the FFT is reduced (carrier spacing is increased), a good performance level compared to LTE CP-OFDM is maintained. This suggests that carrier spacing could be significantly reduced when FBMC is considered giving the waveform a significant advantage for resilience to Doppler shift.

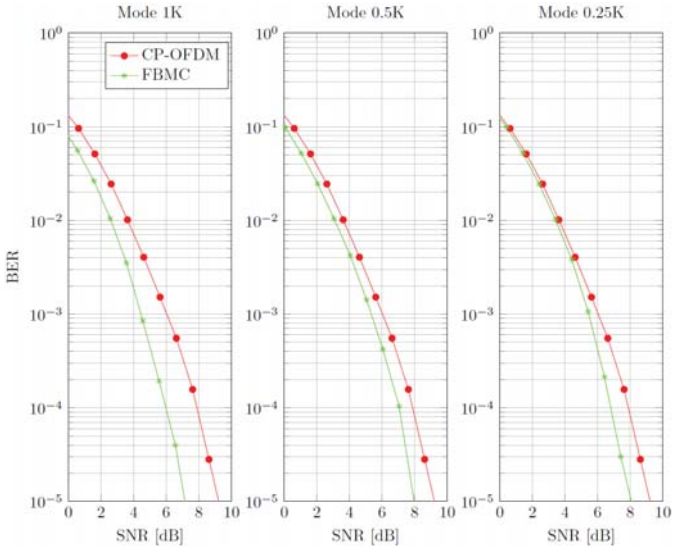

Fig. 7. IEEE 1900.7 QPSK 1/2 vs CP-OFDM

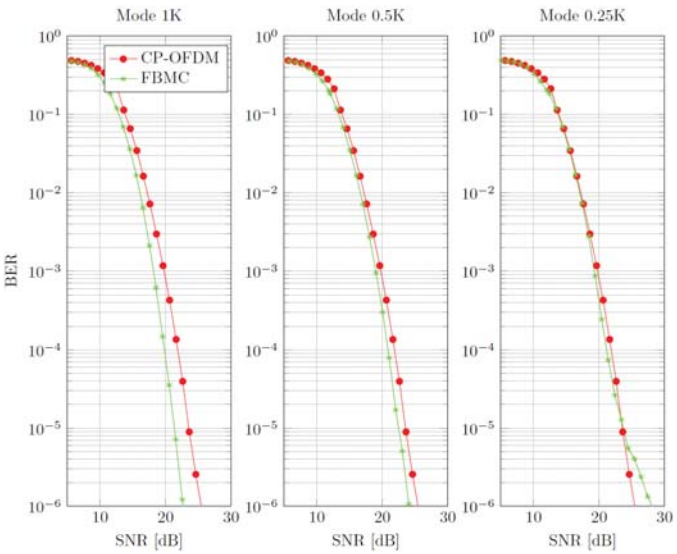

Fig. 8. IEEE 1900.7 64QAM 2/3 vs LTE CP-OFDM

B. MAC sublayer

Performance evaluation of CSMA/CA RTS/CTS MAC sublayer can be analytically derived from the Markov chain model of [30] under the following assumptions:

- No hidden nodes and capture effect.
- Failed transmissions only occur as a consequence of a collision.
- All nodes are saturated and always require to send packets.
- For any given user, the probability of collision, is constant and independent of the past collision history.
- The probability of collision does not depend on the backoff stage at which the transmission is made.
- All nodes have the same data rates and the same amount of time to transmit.

The closed form of the saturation throughput is given in [30]. Based on these assumptions, we evaluate the performance of the proposed PHY-MAC sublayers. The saturation throughput of the IEEE 1900.7 access method is estimated by considering perfect channel conditions for the PHY (no noise, no fading): failed transmissions only occur as a consequence of a collision. The evaluated MAC-PHY saturation throughput is an upper bound that gives the maximum achievable throughput on a shared channel with a given configuration. We assume that the MCS configuration for the acknowledge frame is the same as the MCS configuration used for the data payload transmission. As far as signaling packets like RTS or CTS are concerned, the MCS index 1 (QPSK, Coding rate ½) is used. As these messages serve for virtual carrier sensing, they should be decoded by all the nodes within the cell.

The achievable throughput in the case of two packet sizes 1500 bytes and 8x1500 bytes for various network load and PHY mode has been evaluated for 8MHz bandwidth. Assumption is made that the payload packets are sent using the MCS index 4 (16QAM coding rate ¾). The load of the network varies from 1 to 20 nodes trying to simultaneously access the channel. Results are depicted in Fig. 9.

Significant performance improvement is achieved when payload size is large. Indeed in case of large packet size, the overhead introduces by the handshake mechanism becomes more and more negligible. The 0.25K mode is the most efficient due to the small size of the FFT. This mode is particularly interesting for small packet size as the duration of the burst is shorter than with the 1K mode and the number of padding bits to fill a multicarrier symbol is reduced. Conversely, the 1K mode is more robust to large delay spread making this configuration interesting for long range scenarios while 0.25Kmode would be better for medium to small cell size.

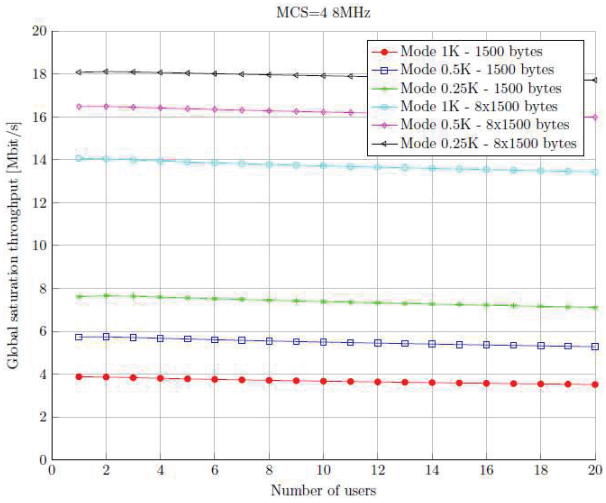

Fig. 9. Achievable throughput in Mbit/s for various mode aussming 8MHz bandwith.

V. Conclusions

In this paper, preliminary performance evaluation of some IEEE 1900.7 profiles has been provided. It was shown that the FBMC PHY used in the standard outperforms classical multicarrier PHY such as LTE 10MHz CP-OFDM. Thanks to the properties of FBMC, the IEEE 1900.7 standard has very good ACLR performance, and is well suited to fragmented spectrum operation. The steep roll-off of the FBMC spectrum also allows higher transmit power, when considering FCC spectrum masks, resulting in larger coverage. The standard is aimed as being published in early 2016.

References

[1] D. Noguet, M. Gautier, V. Berg, "Advances in opportunistic radio technologies for TVWS", EURASIP Journal on Wireless Communications and Networking 2011, 2011:170

[2] FCC proposed rule, "Unlicensed Operation in the TV Broadcast Bands", US Federal Register Vol. 69, No.117, pp 34103-34111, June 18 2004.

[3] FCC final rule, "Unlicensed Operation in the TV Broadcast Bands", US Federal Register Vol. 74, No.30, pp 7314-7332, Feb. 17 2009.

[4] FCC notice, "Unlicensed Operation in the TV Broadcast Bands", US Federal Register Vol. 76,No.26, pp 6789-6792 , Feb 8 2011.

[5] FCC, "In the matter of unlicensed operation in the TV broadcast bands: additional spectrum for unlicensed devices below 900 MHz and in the 3 GHz band," second memorandum opinion and order, September 2010.

[6] FCC, "In the matter of unlicensed operation in the TV broadcast bands: additional spectrum for unlicensed devices below 900 MHz and in the 3 GHz band," third memorandum, opinion and order, April 2012.

[7] H. Harada, Status Report on Usage of TV White Space in Japan, 802.11-12/677r0, May 2012.

[8] Digital dividend: cognitive access, statement on licence exempting cognitive devices using interleaved spectrum, OFCOM, July 2009.

[9] Ofcom, "TV white spaces - approach to coexistence," September 2013.

[10] http://stakeholders.ofcom.org.uk/spectrum/tv-white-spaces/white-spaces-pilot/

[11] Official Journal of the European Union (2012). Decision No 243/2012/EU of the European Parliament and of the Council of 14 March 2012 establishing a multiannual radio spectrum policy programme Text with EEA relevance. http://eur-lex.europa.eu/LexUriServ/LexUriServ.do?uri=OJ:L:2012:081:0007:0017:EN:PDF/20120510_inventory_workshop_invitation.pdf

[12] Official Journal of the European Union (2012). Communication from the Commission to the European Parliament, the Council, the European Economic and Social Committee and the Committee of the Promoting the shared use of radio spectrum resources in the internal market (COM/2012/0478). http://eur-lex.europa.eu/LexUriServ/LexUriServ.do?uri=COM:2012:0478:FIN:EN:HTML

[13] CEPT, CEPT Report 24: "Technical considerations regarding harmonisation options for the Digital Dividend", 1 July 2008, http://www.erodocdb.dk/Docs/doc98/official/pdf/CEPTREP024.PDF[

[14] CEPT, ECC Report 159: "Technical and Operational Requirements for the possible operation of Cognitive Radio Systems in the "White Spaces" of the Frequency Band 470 – 790 MHz", January 2011, http://www.erodocdb.dk/Docs/doc98/official/pdf/ECCREP159.PDF

[15] ETSI EN 301 598, "White Space Devices (WSD); Wireless Access Systems operating in the 470 MHz to 790 MHz frequency band; Harmonized EN covering the essential requirements of article 3.2 of the R&TTE Directive," v1.1.1, April 2014.

[16] ECMA-392 standard, "MAC and PHY for operation in TV white space," December 2009.

[17] IEEE standard 802.22, "Cognitive wireless RAN medium access control (MAC) and physical layer (PHY) specifications: policies and procedures for operation in the TV bands," July 2011.

[18] IEEE standard 802.11af, "Wireless LAN medium access control (MAC) and physical layer (PHY) specifications: television white spaces (TVWS) operation," December 2013.

[19] IEEE standard 802.15.4m, "Low-rate wireless personal area networks (LR-WPANs): TV white space between 54 MHz and 862 MHz physical layer," March 2014.

[20] IEEE P1900.7 PAR, Radio Interface for White Space Dynamic Spectrum Access Radio Systems Supporting Fixed and Mobile Operation, Jun. 2011.

[21] S. Filin, D. Noguet, J-B. Doré, B. Mawlawi, O. Holland, M. Zeeshan Shakir, H. Harada, F.Kojima, "IEEE Standard 1900.7 for White Space Dynamic Spectrum Access Radio Systems", IEEE CSCN, Oct. 2015.

[22] ETSI TS 136 141, "LTE; Evolved Universal Terrestrial Radio Access (E-UTRA); Base Station (BS) conformance testing (3GPP TS 36.141 version 10.1.0 Release 10)."

[23] D. Noguet, V. Berg, X. Popon, M. Shuehler, M. Tessema, "T-FleX: a mobile SDR platform for TVWS flexible operation", IEICE Technical Report - Software Radio, SR2012-51, Fukuoka, Oct. 2012.

[24] V. Berg, J-B. Doré, D. Noguet, "A Flexible Radio Transmitter for TVWS based on FBMC", Euromicro Digital System Design (DSD), Sept. 2013.

[25] R. W. Chang, "Synthesis of Band-Limited Orthogonal Signals for Multichannel Data Transmission", Bell Syst. Tech. J., vol. 45, pp.1175-1796, December 1966.

[26] B. R. Saltzberg, "Performance of an efficient parallel data transmission system", IEEE Trans. Comm. Tech., vol.COM-15, pp.805-813, December 1967.

[27] V. Berg, J-B. Doré, D. Noguet, "A flexible radio transceiver for TVWS based on FBMC", Microprocessors and Microsystems Journal (MICPRO), Elsevier, 38, 2014.

[28] M. Bellanger, "FS-FBMC: A flexible robust scheme for efficientmulticarrier broadband wireless access," in Globecom Workshops (GCWkshps), 2012 IEEE, Dec 2012, pp. 192–196.

[29] V. Berg, J-B. Doré and D. Noguet, "A Flexible FS-FBMC Receiver for Dynamic Access in the TVWS", CROWNCOM, June 2014.

[30] G. Bianchi, "Performance analysis of the IEEE 802.11 distributed coordination function," Selected Areas in Communications, IEEE Journal on, vol. 18, no. 3, pp. 535 –547, march 2000.

THE 5TH INTERNATIONAL CONFERENCE ON WIRELESS COMMUNICATIONS, VEHICULAR TECHNOLOGY, INFORMATION THEORY, AEROSPACE & ELECTRONIC SYSTEMS (WVITAE-2015)
December 13-16, 2015, Hyderabad, India

Reliable Frame Selection for Speaker Identification under Voice Disguise Scenario.

Swati Prasad[1,2] and Ramjee Prasad[1]
[1]Centre for TeleInfrastruktur (CTIF)
Department of Electronic Systems
Aalborg University, Aalborg, Denmark 9220
[2]Department of Electronics & Communication Engineering
Birla Institute of Technology, Mesra, Ranchi, India 835215
Email:{in_sp, prasad}@es.aau.dk

***Abstract*—Identifying the person utilizing voice / speech utterance or Biometric based on voice is gaining importance in recent scenarios, for applications like, access to shared machine from a distance through phone. Here, the person is first identified among a list of people and then a personalized service is provided by the machine. But this research area, faces threats from the attackers, who utilizes voice disguise, to steal personal information / resources of a target. Therefore, this paper studies the effect of three types of voice disguises, along with the normal speaking on speaker identification performance. Out of the three voice disguises, two are variants of imitative type, namely, Synchronous and Repetitive Synchronous speaking, and one is the Fast speaking type. A method has been proposed to measure the reliability of the test speech data, which helps in the selection of reliable speech part from the total test speech data, and which will then participate for identification process. Experimental results showed the overall better performance of the proposed method over the conventional speaker identification method.**

***Index Terms*—Reliable Frame Selection, Robust Speaker Identification, Biometric Based on Voice, Voice Disguise.**

I. Introduction

Determining the person who has spoken a given speech utterance from a group of people is referred to as *speaker identification*. It is also known as Biometric based on voice. It falls under the broad *speaker recognition* area, which in general, deals with finding out the speaker of the given speech utterance [1], [2], [3]. Speaker identification can be classified as *closed* or *open*. It is termed as *closed*, when it is known in advance that the given test speech utterance has been spoken by one amongst the N group of people. On the other hand, when the speaker of the given test speech utterance can be one, not belonging to the N group of people, it is referred to as *open*. In an open speaker identification, the task is to first determine whether the speaker belongs to the group of N people or not, if yes, then the speaker identification process is continued, otherwise the test speech utterance is discarded. Speaker identification can be further classified as *text-dependent* or *text-independent*. When the speech data utilized during the training of speaker models is different from the test speech data, it is referred to as *text-independent* and *text-dependent* otherwise. It is not difficult to understand that the open speaker identification is tougher than the closed and text-independent is more difficult than the text-dependent speaker identification [4], [5]. In this work, closed text-independent speaker identification system has been studied and for simplicity, will be referred to as just speaker identification in the rest of the paper.

With the rapid advancement in technology, speaker identification research has the potential to capture the current consumer electronics market. It can be combined with the mobile phones to gain access to information from remote places. Here, the person is first identified from a group of people and then a personalized service/information is given to him/her. In an office/home environment, a person can be uniquely identified by a shared machine, like robot or television to give customised services to the user. But this research faces challenges due to the mismatched training and test conditions, which greatly decreases its performance [5], [6], [7]. "Non-electronic voice disguise" is one, out of many factors, like environmmental noise and electronic voice disguise (a typical example is the "voice changer" software [8]) which contributes to the mismatched problem.

Non-electronic voice disguise (referred to as, simply, voice disguise in the rest of the paper) occurs when a person deliberately modifies his/ her own voice, either to sound like a target so that target's personal information or resources can be stolen, or to hide his/her own identity. It is very commonly utilized in crime scenes [9]. Therefore, researchers are now trying to develop robust speaker identification system against voice disguise. A new speech feature based on the AM/FM approximation of the speech signal, called *pykfec* (Pyknogram Frequency Estimate Coefficient) has been proposed in [10], and it has shown an overall better performance over the famous MFCC feature for voice disguise. Glottal and vocal tract characteristics of voice impersonators were studied in [11] to detect voice disguised speech data. The effects of different types of human voice modifications/voice disguise on the speaker identification performance has been investigated in [12], [13]. Frame selection has been carried out in speaker identification research for improving identification efficiency under mismatched conditions [14], but frame selection of the test speech data under voice disguise scenario has not been studied. Therefore, in this study reliable frame selection from

the voice disguised test speech data has been carried out. Here, instead of finding out the speaker of the given test speech data, speaker for each test frames were determined. The decision about the reliability or non-reliability of the frame is found out by the distance between the probability score of the selected speaker and other enrolled speakers and a threshold value. Finally, only selected reliable frames participated in the identification process using maximum likelihood rule[15]. Experimental results showed the favourable performance of this method over the conventional method for voice disguise.

The rest of the paper is organized as follows. The next Section describes the proposed frame selection method. Experimental results and discussions are decribed in Section 3. Finally, Section 4 concludes the paper with future directions.

II. Frame Selection Method.

The conventional Gaussian Mixture Model (GMM) based speaker identification system make a decision about who spoke a given test speech utterance $\vec{X} = \{\vec{x_1}, \vec{x_2}, \vec{x_3}, ..., \vec{x_T}\}$ amongst the S registered speakers using the following maximum log liklihood rule [15] :

$$\widehat{S} = \arg \max_{1 \leq k \leq M} \sum_{t=1}^{T} \log p(\vec{x_t}|\lambda_k) \tag{1}$$

In the proposed system, the decision about the speaker is calculated in the following steps:

1) Each frame is viewed as a classification problem and the speaker is found out on a frame by frame basis:
$$\widehat{S} = \arg \max_{1 \leq k \leq S} p(\vec{x_t}|\lambda_k) \tag{2}$$
2) To calculate the reliability/degree of confidence measure of the decision of the frame, the distance between the probability score of the selected speaker and other speakers were found out:
$$D_k = |p(\vec{x_t}|\lambda_{\widehat{S}}) - p(\vec{x_t}|\lambda_k)| \qquad k = \{1, 2, 3, ..., S\} - \{\widehat{S}\} \tag{3}$$
The larger the distance D_k between the selected speaker for the frame and the other speakers, the more is the confidence in the decision and vice versa.
3) In this step, each D_k is compared with a $threshold$, if $D_k \leq threshold$, the frame is discarded.
4) After the step 3, the less reliable frames will be discarded and the remaining frames will participate in the final decision about the speaker using the conventional maximum likelihood rule [15].

III. Experimental Setup and Results

A. Database and Speaking Styles

CHAINS corpus has been selected for this study. It is specifically developed for the speaker identification research [17]. It provides different speaking styles from the same speaker. This corpus gives an opportunity to capture the unique characteristics of the person, which remain intact in a variety of speaking styles and also facilitate the study of voice disguise.

It consists of approximately 36 person's voice recordings. Out of which, a bulk of people i.e. 28 (14 male and 14 female) were from the same dialect belonging to eastern part of Dublin, which raised the identification difficulty level and 8 (4 male and 4 female) were from different dialect belonging to either UK or USA. People's voice were recorded in 6 speaking styles. For this study, the following speaking styles were utilized:

1) Normal Speaking (Norm)
The speakers adopted their day-to-day speaking style for recording the text (fable/sentence).
2) Synchronous Speaking (Sync)
Speakers spoke a given text (fable/sentence) in synchronization with a co-speaker. It showed marked reduction in inter speaker variabilities for global timing and phrasing parameters.
3) Repetitive Synchronous Imitation (Rsi)
In this a person has been selected per sex, whose normal voice recordings (fable) served as a target for other speakers. The whole fable reading of the target has been broken into 19 sentences. Each sentence recording has been played repeatedly for 8 times with a gap of 0.5 sec. The speakers listened to the target and joined the repeating loop after the 2nd instance, speaking it for 6 times. The penultimate recording of the speakers were kept. It produced a very close match between the speaker and the target in prosody.
4) Fast Speaking (Fast)
Speakers listened to two sentences which has been spoken at a very fast rate from the normal speaking. Speakers then recorded their voice at approximately this fast rate. It produced complex changes in the speaker's voice.

,

Out of the above four speaking, two falls under the category of imitation, namely, Sync and Rsi. The Fast speaking falls under the non-imitative speaking styles. The Norm and Sync speaking has been recorded in a professional recording studio using Neumann U87 condenser microphone, whereas, Fast and Rsi speaking has been recorded in a quiet office environment using a shure SM50 head-mounted microphone. The spectrogram of the Norm, Sync and Fast speaking for a sentence is shown in Fig. 1, in the next page. From the Figure, it can be observed that Fast speaking shows good spectral differences from the Sync and Norm speaking of the same speech utterance.

B. Speaker Identification Experiments

Speaker identification experiments were conducted for the Baseline (Conventional GMM method [18]) and the proposed method. For both the Baseline and the proposed method, speech data were cut into smaller frames of frame size 25ms with a frame shift of 10ms. This can be done because, speech is a non-stationary signal and cutting it into smaller frames make it quasi-stationary. Features were then extracted

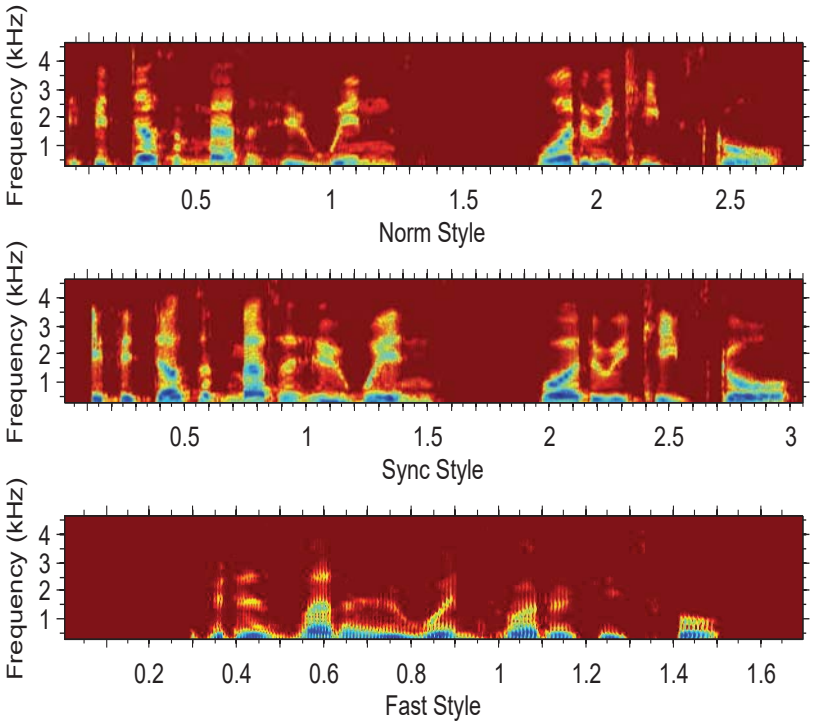

Fig. 1. *Spectrogram of the Norm, Fast and Sync speaking for the speech utterance If it doesnt matter who wins, why do we keep scores? [16]*

from these frames utilizing 12 liftered Mel-Frequency Cepstral Coefficients (MFCC), excluding the 0^{th} coefficient. Liftering is used to re-scale the lower and higher magnitude's cepstral coefficients to similar magnitudes. Cepstral mean removal method was also applied to compensate for channel variations. Speakers were then modelled utilizing 64 components GMM.

For training the speaker models, $\sim$ 70 sec of Norm speaking speech data were utilized. For testing, $\sim$ 30 sec of Sync, Fast, Rsi, along with the Norm speaking speech data were utilized. For this, the 30 sec of speech data were first segmented into 5 sec sentences, and $\sim$ 5 sentences per speaker were then utilized for testing.

The identification accuracy of the speaker identification system is found out using the following equation:

$$\frac{No.\ of\ correctly\ identified\ test\ utterances}{Total\ no.\ of\ utterances\ tested} \times 100\% \quad (4)$$

C. Results and Discussions

The identification accuracies obtained for the Baseline and the Proposed system were tabulated in Table 1. From the table, it can be observed that, the Proposed system showed similar performance for the Norm and Sync speaking test data for the threshold value of 0.03. For Fast speaking test

TABLE I
IDENTIFICATION ACCURACY (%) FOR BASELINE AND PROPOSED METHOD UNDER VOICE DISGUISED AND NORMAL TEST SPEECH.

Test Speech	Baseline(Conventional GMM)	Proposed	Threshold
Fast	80.75	81.22	0.1
Rsi	74.54	76.85 / 77.31	0.1 / 0.3
Sync	96.76	96.76	0.03
Average	84.02	84.94 / 85.10	NA
Norm	100	100	0.03

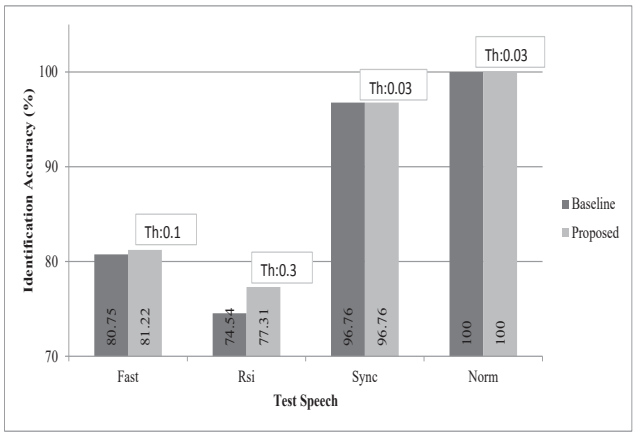

Fig. 2. Identification accuracy (%) of the Baseline and the Proposed method for voice disguised and normal speech test data.

data, the Proposed system showed a relative improvement of 0.58% for the threshold value of 0.1 over the Baseline system. For Rsi speaking test data, the Proposed system showed a relative improvement of 3.10% for the threshold value of 0.1 and a relative improvement of 3.72% for the threshold value of 0.3 over the Baseline system. The average of the identification accuracies across the different voice disguised test speech data also indicate the overall better performance of the Proposed System over the Baseline. For this initial study, the selected threshold value for frame selection has been chosen on a trial and error basis. Change in the threshold value also affects the identification accuracy as can be seen for the Rsi test data, where a threshold value of 0.1 yielded an identification accuracy of 76.85% and a threhold value of 0.3 yielded an identification accuracy of 77.31%. This suggests that, a careful selection of the threshold value can enhance the performance of the speaker identification system. The identification accuracies of the Baseline and the Proposed System for voice disguised and normal speaking test data is also plotted in Fig. 2. Here, for Rsi test speech, only the threshold value of 0.3 is used. It also confirms the better performance of the Proposed System for Fast and Rsi test speech data over the Baseline.

IV. Conclusion

A frame selection method for test speech data has been proposed in this paper. Here, instead of finding out the true speaker of the whole test speech utterance, the true speaker for each frame is determined. A degree of confidence measure is then calculated, using the distance between the probability score of the true speaker and the remaining enrolled speakers. The greater the distance, the higher is the confidence in the identification decision. Using this distance and a threshold value, frames were then categorized as reliable and non-reliable. Finally, only reliable frames participated in the identification of the test speech data using the conventional maximum liklihood rule.

Experimental results on voice disguised test speech data showed an overall better performance of the proposed system compared to the conventional GMM based method. However, for normal speaking test data, the proposed system has shown similar performance. In this study, the threshold value utilized for frame selection has been selected on a trial and error basis. However, an algorithm for careful selection of the threshold value can enhance the speaker identification performance and will be a subject for future study.

Acknowledgment

This study is supported by the Erasmus Mundus Mobility for Life project. It comes under the Erasmus Mundus External Cooperation Window Programme (EMECW11) and is funded by the European Commission.

References

[1] D. O'Shaughnessy, "Speaker Recognition," *IEEE ASSP Magazine*, pp.4-17, Oct. 1986.
[2] G. R. Doddington,"Speaker Recognition- Identifying People by their Voices", *Proc IEEE*, vol.73, no. 11, pp.1651-1664, Nov. 1985.
[3] H. Gish and M. Schmidt,"Text- Independent Speaker Identification",*IEEE Signal Process. Mag.*, pp.18-32, Oct. 1994.
[4] T. Kinnunen, H. Li,"An Overview of Text-Independent Speaker Recognition: From Features to Supervectors ", *Speech Comm.*, vol. 52, no. 1, pp.12-40, Jan. 2010.
[5] R. Togneri and D. Pullela, "An Overview of Speaker Identification: Accuracy and Robustness Issues," *IEEE Circuits Syst. Mag.*, vol.11, no. 2, pp. 23-61, May. 2011.
[6] K. Kim and M. Y. Kim, "Robust Speaker Recognition Against Background Noise in an Enhanced Multicondition Domain," *IEEE Trans. Consum. Electron.*, vol. 56, no. 3, pp. 1684-1688, Aug. 2010.
[7] X. Zhao and Y. Wang and D. L. Wang, "Robust Speaker Identification in Noisy and Reverberant Conditions," *IEEE/ACM Trans. Audio, Speech, Language Process.*, vol. 22, no. 4, pp. 836-845, 2014.
[8] AV Voice Changer Software Diamond 7.0 of AVSOFT CORP. [Online]. Available: http://www.audio4fun.com/voice-over.htm.
[9] R. Rodman and M. Powell, "Computer Recognition of Speakers Who Disguise their Voice," in *Proceedings of the International Conference on Signal Processing Applications and Technology (ICSPAT2000)*, Dallas, Texas, USA, Oct. 2000.
[10] M. Grimaldi and F. Cummins, "Speech Style and Speaker Recognition: A Case Study," in *INTERSPEECH*, Brighton, UK, Sept. 2009.
[11] T. B. Amin, P. Marziliano and J. S. German, "Glottal and Vocal Tract Characteristics of Voice Impersonators," *IEEE Trans. Multimedia*, vol. 16, no. 3, pp. 668-677, Apr. 2014.
[12] C. Zhang and T. Tan, "Voice Disguise and Automatic Speaker Recognition," *Forensic Sci. Int.*, vol. 175, no.3/5 pp. 118-122, 2008.
[13] S. S. Kajarekar, H. Bratt, E. Shriberg and R. de Leon, "A Study of Intentional Voice Modifications for Evading Automatic Speaker Recognition," in *Speaker and Language Recognition Workshop, IEEE Odyssey*, Menlo Park, CA, 2006.
[14] C. -S, Jung, M. Y. Kim and H. -G. Kang, " Selecting Feature Frames for Automatic Speaker Recognition using Mutual Information," *IEEE/ACM Trans. Audio, Speech, Language Process.*, vol. 18, no. 6, pp. 1332-1340, Aug. 2010.
[15] D. A. Reynolds, " Speaker Identification and Verification using Gaussian Mixture Speaker Models," *Speech Comm.*, vol. 17, no.1-2, pp. 91-108, 1995.
[16] S. Prasad, Z. -H. Tan, R. Prasad, "Multistyle training and fusion for speaker identification of disguised voice", *1st International Conference on Communications, Connectivity, Convergence, Content and Cooperation (IC5)*, Mumbai, India, Dec. 2013
[17] F. Cummins, M. Grimaldi, T. Leonard, and J. Simko, "The CHAINS Corpus: CHAracterizing INdividual Speakers, in *Proc. SPECOM*, St. Petersburg, Russia, 2006.
[18] D. A. Reynolds and R. C. Rose, "Robust Text-Independent Speaker Identification using Gaussian Mixture Models, IEEE/ACM Trans. Audio, Speech, Language Process., vol.3, no.1, pp. 72-83, 1995.

THE 5TH INTERNATIONAL CONFERENCE ON WIRELESS COMMUNICATIONS, VEHICULAR TECHNOLOGY, INFORMATION THEORY, AEROSPACE & ELECTRONIC SYSTEMS (WVITAE-2015)
December 13-16, 2015, Hyderabad, India

GeoLocation Aware Dynamic Spectrum Sensing in Cognitive Radio Networks

K. Usha Bhargavi
University School of Information and Communication Technology
G G S Indraprastha University
New Delhi, INDIA
E-Mail: kmushabhargavi@gmail.com

R. L. Ujjwal
University School of Information and Communication Technology
G G S Indraprastha University
New Delhi, INDIA
E-Mail: ujjwal_rl@rediffmail.com

Abstract: **The foremost challenging issue in Cognitive radio networks (CRN) is spectrum sensing and allocation. Cognitive radio network consists of a collaborated frame of layer-wise multiple cognitive radios dynamically responding to the surrounding radio environment. The primary concern of dynamic spectrum sensing is identifying the number of primary users (PUs) and the spectral bandwidths currently used, to address the issues of harmful interference of secondary users (SUs) with the primary spectrum, co-existence of hidden primary nodes. In this article, we present a geolocation aware dynamic sensing (GLADS) scheme that defines a spectral sensing and management scheme based on the location of the primary users and the bandwidths of current usage to (i) detection of number of active primary users on the channel, and (ii) using this information to predict the number of hidden primary nodes on the channel.**

Key words: Cognitive radio networks, Dynamic spectrum sensing (DSS), dynamic spectrum accessing (DSA), angle of arrival (AoA),

I. INTRODUCTION

Cognitive radios (CRs) a disruptive technology that provides promising solutions to the spectral scarcities of the ever increasing network traffic in heterogeneous wireless networks. CRs adapt dynamic spectrum sensing (DSS) and dynamic spectrum accessing (DSA) techniques [1], with the support of multiple antenna systems of the secondary users. Cognitive radio technology is upgraded and enhanced from the existing basic Software Defined Radio with smart antennas technology. CRs are capable of sensing and identifying the unutilized parts of the licensed spectrum by the primary users (PUs) and provide an opportunistic and non-harmful interfering access to the secondary user nodes (SUs). These white spaces are the guard bands defined in space, time and frequency domains to resist the potential interference in the air space. DSA techniques preferred to enhance the spectrum agility aspects of the cognitive radio networks (CRNs). CRs use DSS technology to detect spectral holes to provide services at low prices thus empowering the network operators with increasing commercial benefits. Spectrum sensing techniques not only identify and protect the spectral bands used by the primary user nodes (PUs) but also detect the spectral holes to manage the secondary user nodes (SU) traffic. The *underlay* approaches allow simultaneous packet transmissions of the primary and secondary user nodes separated by protective masks while limiting the interference of the secondary user nodes merely to the floor level noise. The *overlay* approaches allow the secondary user nodes to act partly as the relay nodes and the other as the transmitting nodes. The *interweave* approaches use the opportunistic spectral access schemes (i.e.) to allocate if only if the channel is vacant.

Spectrum opportunity discovery techniques try to determine the exact geolocation of the primary users along with their signal strengths and the number of bandwidths they availed per each session. The mobile databases of PU nodes are used to detect the geolocation as these nodes are non-stationary entities. As the signal-to-noise ratio (SINR) values highly differ from primary and secondary nodes, the complexity lies in the proper selection of backup channels. The beacon periods are used to estimate the duration of quiet periods, reservation periods to allotted for packet transmission over multiple spectral channels. The conventional spectrum sensing algorithms concerning the frequency, space and time are being upgraded to use the code dimensions, frequency hopping schemes of the spectral bands [1]. The parameters such as angle of arrival (AoA) that differ with the space dimension radios and their signals from the primary and secondary antenna can better define the spectral opportunities. The work of [2] implements the particle swarm optimization algorithm to accurate the positions of primary transmitters in CRNs.

We present a geolocation aware dynamic sensing (GLADS) and cooperation scheme that defines a spectral sensing and management scheme in terms the location and the bandwidths of current usage by PUs to (i) detection of number of active primary users on the channel, and (ii) using this information to predict the number of hidden primary nodes, which suddenly tune their radios. CRs need to sense immediately such primary node activity and alert the secondary users availing these bands to switch immediately to the next available band.

II. RELATED WORK

Localization algorithms are optimized one at the local level within a small group of cluster/mesh and the other at the global scale for large size wireless network level. Since the cognitive network consists of one or many wireless regional area networks we implement global optimization for an entire region of the network. A two level collaborative spectral sensing scheme has been proposed in [3] which uses the sensing parameters obtained from the cognitive sensor nodes that are grounded to define the real-time parameters for PU and SU nodes with higher degrees of accuracy. The information from the ground nodes is updated at regular intervals with priorities as per their frequencies. The analysis of [4] sequential and probabilistic sensing models has been performed by which states that the random hopping algorithms perform better to sequential sensing models. The concept of client-base network of secondary users has been implemented in [5] that performs non-contiguous orthogonal frequency division multiplexing technique to evaluate the spectral accessibilities with a high degree of fairness.

The enhanced version of designing a network of cognitive radio nodes [6] which are mapped in terms their interference temperatures highly evaluated from multiple domains of the radio environment. The works of [7] consider the power constraints of communication and the resulting interference levels and proves that the hazardous interference between the primary and secondary nodes can be mitigated to consider levels. The positions of PUs and SUs are estimated in terms of binary detection indicators estimate [8] the error probabilities between the actual and measured distances. A technique of awarding grades based on the performance of the nodes using the weighted sequential probabilities has been proposed in [9] which addresses the sensing dysfunctional features at the secondary user node levels. An interference based resource allocation technique has been introduced in [10] that restricts the constraints of position estimations to pre-defined limits to enhance the sensing capabilities of the cognitive radio networks. The signal strengths received from the radio transmitters, the path loss and fading parameters are used to define the [11], actual positions of the nodes. Installation of multiple access points increases the hardware and computational complexity and cost of installation also.

The work of [12] implements the technique of localization using a single point in wireless networks. Multiple channel switching during the packet transmissions increases packet delays and packet drop rates in cognitive radio networks. To address this issue a three-way solution based on the cost, [13] delay and the hybrid techniques. Another way of efficient localization scheme has been proposed by [14] which improvises a technique of configuring the primary and secondary base stations in proper positions so as to all the cognitive radios as well as the primary users present at any part of the given network.

The concept of leader and follower has been used to judge the unused spectral bands in an effective manner so as to allocate to the secondary user nodes. The secondary user nodes that want to communicate are only allowed to scan the radio environment [15] and use the sidebands of the carrier signal so as to minimize the interference. The localization in cognitive radio networks supporting cooperative methods is defined in terms of the primary user based noise levels using Bayesian technique has been provided in [16]. The received signal strength parameters are used to implement constrained localization technique [17] to estimate the location of primary user nodes. Parameters such as the receiver signal strength, direction-of-arrival with some pre-defined bounds are implemented in [18]. The channel allocation scheme that preserves the rights of primary users with a constant rate of secondary node assignment rates has been proposed in [19]. The localization method based on the evaluations of linearization of RSS parameters has been proposed in [20]. The localization method based on the time of arrival rates of the communication (request-to-send, clear-to-send) messages, data and acknowledgement have been proposed in [21] that updates these parameters in a cyclic manner.

III. SYSTEM MODEL

Geo-location aware dynamic spectrum sensing (GLADS) technique is based on the parameters such as the RSS parameters, Distance or Time (DoA or ToA). The primary and secondary user nodes are assumed to be associated with the respective base stations. The works of [17] assume that the transmission powers of the primary nodes are unknown and each primary node can be heard by a minimum of four secondary user nodes. We extend this idea and introduce the concept of defining a primary grid with a primary base station (PBS) positioned at the origin, and two primary user nodes as access points to improve the efficiency of our estimations. The basic assumptions of GLAD protocol are given as:

(i) Primary beacon node or Primary base station located at a known fixed position in the grid transmits signals of equal strength in all directions.

(ii) The positions and transmission powers of the primary users are unknown excluding the immediate two neighbors.

(iii) The secondary user nodes are assumed to know their one-hop, two-hop and three-hop neighbor (if required) nodes and this information is periodically updated to the secondary base stations.

A. GLAD Setup Phase

Let P_{BS} be the primary base station be kept at the origin and it initiates the session by the beacon and let PU_1 be the first nearest primary user node (TV_{TX}) located at the distance R obtained by using the time of arrival method. A data that exists

in the database of the primary base station. PU_2, be the second nearest primary user node (TV_{TX}) located at a distance $\frac{4R}{3}$ from the first primary user node. These two primary user nodes are assumed to be the primary access points based on which the positions of other member nodes static/mobile and PU/SU member nodes are estimated. We consider the network to be a square grid and the first secondary user node be positioned at a distance $\frac{2R}{3}$ from the primary node.

(i) We define the following conditions: The primary node exists in the middle of the diagonal of the square consisting of four secondary user nodes situated at the four corners of the square grid.

(ii) The transmission range of second primary user node, PU_2 is assumed to be equivalent to the distance $\frac{2R}{3}(i.e.)TX_{SU} \approx \frac{2R}{3}$. For larger networks, the secondary user node mesh consists of two-hop and three-hop neighbors.

A Bayesian-based covariance channel occupancy model has been designed in [22] that estimates the theoretical and spatial covariance techniques to evaluate the states (active/sleep) of the primary antennas or nodes in CRNs.

Hidden Primary node Problem: GLADS addresses the issue of Hidden PU by obtaining the a maximum of two adjacent secondary nodes identifying the activities of the PU then a search algorithm for second hop neighbors of the respective PU is performed. If at least one secondary user/primary user identifies any activity, then the conformity of hidden primary node is made and located in the grid.

B. GLAD Functional Phase

We obtained the square grid of such secondary user nodes, one hop neighbors for each secondary user and this grid is extended for two hop and three hop neighbors as per the distance of the secondary user node from one another. This procedure is over the entire region of the network.

Let $\left(x_{PU_1}, y_{PU_1}, z_{PU_1}\right), \left(x_{PU_2}, y_{PU_2}, z_{PU_2}\right)$ represent the coordinates of PU_1 and PU_2, $\theta_{11} and \theta_{22}$ be the angles at the P_{BS} and PU_2 respectively. By applying the basic laws of vector analysis, the distance between the primary base station and second primary access point PU_2 is obtained as $2.021R$. R is the diagonal vector joining the distances cognitive radio nodes. To obtain the position of secondary user SU_i at some $\left(x_i, y_i\right)$, and SUj at some $\left(xj, yj\right)$, angles of arrival being $\theta_1 and \theta_2$ we define the distances using RSS,

$$d_i = \sqrt{\left(\left(x_{PU1} - x_i\right)^2 + \left(y_{PU1} - y_i\right)^2\right)} \text{ and}$$

$$d_j = \sqrt{\left(\left(x_{PU2} - x_j\right)^2 + \left(y_{PU2} - y_j\right)^2\right)} \quad \ldots\ldots\ldots\ldots (1)$$

And by using DOA methods are obtained as:

$\tan(\theta_1) = \frac{y_i - y_{PU1}}{x_i - x_{PU1}}$, the distance of the secondary user node SU_i from the primary node PU_1 $\tan(\theta_2) = \frac{y_j - y_{PU2}}{x_j - x_{PU2}}$, the distance of the secondary user node SU_j from the primary node PU_2.

Each secondary node individually and exhaustively searches for the transmission signals of the primary users in close by. If for any two secondary user nodes SU_i, SU_j the probabilities for finding a primary node obtained as $P\left(SU_i\right)$ and $P\left(SU_j\right)$ for the same primary node in the neighborhood, then by applying Bayes' conditional probability we have,

$$P\left(SU_i \mid SU_j\right) = \frac{P\left(SU_i, SU_j\right)}{P\left(SU_j\right)} \text{ and}$$

$$P\left(SU_j \mid SU_i\right) = \frac{P\left(SU_i, SU_j\right)}{P(SU_i)} \quad \ldots\ldots\ldots\ldots..(2)$$

$$\Rightarrow P\left(SU_i \mid SU_j\right) = \frac{P\left(SU_j \mid SU_i\right) P(SU_i)}{P\left(SU_j\right)} \quad \ldots\ldots\ldots\ldots.. (3)$$

By applying the Bayes chain rule for the given set of secondary nodes SU_i, SU_j in determining the probabilities of finding the same set of primary nodes as $\left\{X_{PU1}, X_{PU2}, \ldots\ldots\ldots X_{PUN}\right\}$ we have,

$$\begin{aligned} &P\left(X_{PU1}, X_{PU2}, \ldots\ldots\ldots X_{PUN}\right) = \\ &P\left(X_{PU1} \mid X_{PU2}, \ldots\ldots\ldots X_{PUN}\right) * \\ &P\left(X_{PU2} \mid X_{PU2}, \ldots\ldots\ldots X_{PUN}\right) * \\ &P\left(X_{PU3}, \ldots X_{PUN}\right) \end{aligned} \quad \ldots\ldots\ldots\ldots (4)$$

Above equation can also be written in the form

$$P\left(\cap_{k=1}^{n} X_{PUk}\right)=\prod_{k=1}^{n} P\left(X_{PUk} \mid \cap_{m=1}^{n} X_{PUm}\right) \quad \ldots\ldots\ldots\ldots (5)$$

where '$\cap$' represents the joint probability of finding the primary node, by applying the law of probability we marginalize the probability of the primary nodes as:

$$P\left(SU_i\right)=\sum_{m=1}^{k} P\left(SU_i \mid SU_j=SU_m\right)P\left(SU_j=SU_m\right) \ldots (6)$$

The net probability of each primary user node is measured from the probability estimation of at least four number of secondary user nodes. Application of conditional probabilities for this frame of SUs, the active/sleep states of the PUs can be determined. The size of the contention window is defined as per the obtained results to the SUs seeking the access to use the communication channel for packet transmissions.

Table1. Conditional probabilities truth table for locating PU

	$P(SU_i)$	**$P(SU_j)$**	**$(P(SU_i) \cap P(SU_j))$ = P(PU) detection**
$P(SU_i)$	T	T	T
$P(SU_j)$	F	T	F
$P(SU_i)$	T	F	F
$P(SU_j)$	F	F	F

IV. SIMULATIONS

In the proposed protocol we estimate and verify the positions of primary user nodes with respect to a minimum of four secondary nodes present in the immediate neighborhood of the primary node. Simulations have been performed by using MATLAB and the proposed protocol has been analyzed. Based on the conditional probabilities obtained from simulations, if the state of the primary node is true with respect to three at least and four immediate neighbors of a primary node, then that position is selected as the optimum center for the primary node as shown above.

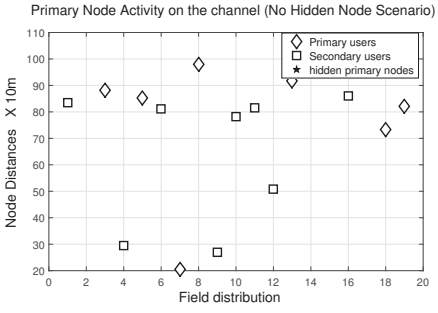

Figure 1 Distribution of PUs, Hidden primary users and Secondary users in a CRN

Figure 1 describes the distribution of nodes (PUs, hidden PUs and SUs) in a cognitive radio network. The primary and hidden primary nodes are located by the proposed GLADS technique, and the secondary nodes adjacent to such nodes are allowed to monitor the channel cautiously and increase their contention window from [0, 4] to [0,8]. The secondary users between the regions 6 -10 can use the communication channel for transmission and the secondary nodes nearer to the active primary channels are allowed switch to a contention window size to [0,8].

The following figure 2 shows the comparison of the proposed protocol with the existing location based and state based protocols.

(a) Finding the optimum centers for Primary and Hidden Primary user nodes in the GLADS Cognitive Radio Network

The primary user nodes are detected by considering the pairwise combination of conditional probabilities for four immediate neighbors as mentioned above.

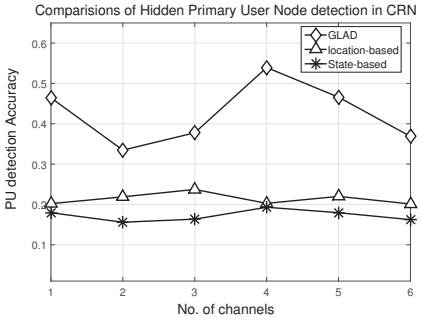

Figure 2 No hidden primary nodes Scenario in the proposed protocol

But for the identification of hidden primary node PU_h , we assume that between the four adjacent nodes $\{SU_i, SU_j, SU_k, SU_l\}$, if only two of the secondary nodes discover an active signal from the hidden primary node, then we consider the probabilities of the immediate second hop neighbor nodes which can listen and sense the activities of the primary node.

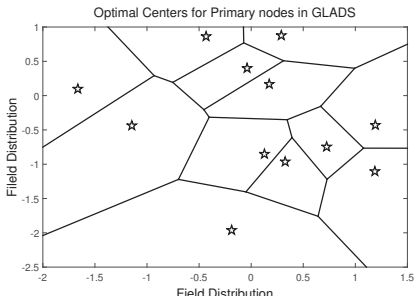

Figure 3 Optimal centers for Primary nodes in the proposed Protocol

If any one of the secondary nodes identifies a signal from this node alone and not by a different primary node towards PBS, then we assume such a node to be hidden primary node and is mapped on the field. The secondary nodes increase their contention windows to again [0, 8] to prevent the harmful collisions with the primary nodes. The field distribution is obtained as shown in the figure 3.

VII. CONCLUSIONS

Spectral sensing and intelligent based decision making is the fundamental aspect of cognitive radio networks. In this regard, this work defines the approaches for dynamic spectral sensing aspects of cognitive MAC. The geo-location aware spectral sensing technique is defined in terms of SINR and probability factors obtained from the grid of secondary nodes. The future work can be extended by including the parameters such as packet losses/communication channel. Inclusion of energy efficient spectrum sensing and access algorithms is required as the sensors have limited energy and memory resources.

REFERENCES

[1] T. Yucek and H. Arslan, "A Survey of Spectrum Sensing Algorithms for Cognitive Radio Applications", *IEEE Communications Surveys & Tutorials,* First Quarter 2009, Vol. 11(1), pp. 116-130.

[2] J. K. Nelson, M. U. Hazen and M. R. Gupta, "Global Optimization for Multiple Transmitter Localization", *IEEE Military Communications Conference (MILCOM)*, Washington, DC, 23-25 October, 2006, pp. 1-7.

[3] C. Hsieh-Chung, H. T. Kung, D. Vlah, Daniel Hague, M. Muccio and B. Poland, "Collaborative compressive spectrum sensing in a UAV environment", *In Proceedings of Military Communications Conference (MILCOM)*, Baltimore, MD, 7-10 November, 2011, pp. 142-148.

[4] J. Misic and V. B. Misic, "Probabilistic vs. Sequence-Based Rendezvous in Channel-Hopping Cognitive Networks", *IEEE Transactions On Parallel And Distributed Systems,* 2014, Vol. 25(9), pp. 2418 - 2427.

[5] A. Zubow, M. Doring and A. Wolisz, "Distributed Spectrum Allocation for Autonomous Cognitive Radio Networks", *In Proceedings of IEEE European Wireless Conference*, Barcelona, Spain, May, 2014, pp. 1-7.

[6] H. B. Yilmaz and T. Tugcu, "Location estimation-based radio environment map construction in fading channels", *Wiley on line Journal of Wireless Communications And Mobile Computing,* 25 February, 2015, Vol. 15(3), pp. 561–570.

[7] S. Stotas and A. Nallanathan, "Optimal Sensing Time and Power Allocation in Multiband Cognitive Radio Networks", *IEEE Transactions On Communications,* 11 November, 2010, Vol. 59(1), pp. 226 - 235.

[8] Z. Ma, K. B. Letaief, W. Chen and Z. Cao, "A Semi Range-Based Iterative Localization Algorithm for Cognitive Radio Networks", *IEEE Transactions on Vehicular Technology,* 03 November, 2009 Vol. 59(2), pp. 704 - 717.

[9] R. Chen, J.-M. Park and K. Bian, "Robust Distributed Spectrum Sensing inCognitive Radio Networks", *In the proceedings of IEEE INFOCOM*, 2008, pp. 31-35.

[10] L. B. Le and E. Hossain, "Resource Allocation for Spectrum Underlay in Cognitive Radio Networks", *IEEE Transactions On Wireless Communications,* December, 2008, Vol. 7(12), pp. 5306-5315.

[11] B. L. Mark and A. E. Leu, "Local Averaging for Fast Handoffs in Cellular Networks", *IEEE Transactions On Wireless Communications,* March, 2007, Vol. 6(3), pp. 866-874.

[12] A. Mariakakis, S. Sen, J. Lee and K.-H. Kim, "SAIL: Single Access Point-Based Indoor Localization", *ACM MobiSys*, Bretton Woods, New Hampshire, USA, June 16–19, 2014.

[13] J. Zhao, W. Gao, Y. Wang and G. Cao, "Delay-Constrained Caching in Cognitive Radio Networks", *IEEE INFOCOM*, Toronto, ON, April 27 2014-May 2, 2014 pp. 2094 - 2102.

[14] S. Iellamo, E. Alekseeva, L. Chen, M. Coupechoux and Y. Kochetov, "Competitive location in cognitive radio networks", *Springer Journal of 4 OR: A Quarterly Journal Of Operational Research* March, 2015, Vol. 13(1), pp. 81-110.

[15] B. H. a. D. Turgut, "Link Rendezvous Protocol for Cognitive Radio Networks", *In the proceedings of 2nd IEEE International Symposium on New Frontiers in Dynamic Spectrum Access Networks (DySPAN 2007)*, Dublin, 17-20 April, 2007 pp. 444-447.

[16] S. Kandeepan, S. Reisenfeld, T. C. Aysal, D. Lowe and R. Piesiewicz, "Bayesian Tracking in Cooperative Localization for Cognitive Radio Networks", *In proceedings of IEEE 69thVehicular Technology Conference (VTC)*, Barcelona, 26-29 April, 2009 pp. 1 - 5.

[17] S. Kim, H. Jeon and J. Ma, "Robust Localization with Unknown Transmission Power for Cognitive Radio", *In proceedings of IEEE Military Communications Conference*, Orlando, Florida, 29-31October , 2007, pp. 1 - 6.

[18] J. Wang, J. Chen and D. Cabric, "Cramer-Rao Bounds for Joint RSS/DoA-Based Primary-User Localization in Cognitive Radio Networks", *IEEE Transactions on Wireless Communications,* 2013, Vol. 12(3), pp. 1363 - 1375.

[19] A. A. El-Saleh, M. Ismail, M. A. M. Ali and A. N. H. Alnuaimy, "Capacity Optimization for Local and Cooperative Spectrum Sensing in Cognitive Radio Networks", *International Journal of Electrical and Computer Engineering,* 2009, Vol. 4(11), pp. 679-685.

[20] L. Lin and H. C. So, "Best Linear Unbiased Estimator Algorithm For Received Signal Strength Based Localization", *19th European Signal Processing Conference (EUSIPCO 2011)*, Barcelona, Spain, August 29 - September 2, 2011, pp. 1989-1993.

[21] C. Hoene and J. Willmann, "Four-way TOA and Software-Based Trilateration of IEEE 802.11 Devices", *IEEE 19th International Symposium on Personal, Indoor and Mobile Radio Communications (PIMRC)*, Cannes, France, 15-18 September, 2008, pp. 1 - 6.

[22] J. Manco-Vasquez, M.Lazaro-Gredilla, D.Ramirez, J.Via and I.Santamaria, "A Bayesian approach for adaptive multi antenna sensing in cognitive radio networks", *Elsevier Journal of Signal Processing,* 2014, Vol. 96, pp. 228–240.

THE 5TH INTERNATIONAL CONFERENCE ON WIRELESS COMMUNICATIONS, VEHICULAR TECHNOLOGY, INFORMATION THEORY, AEROSPACE & ELECTRONIC SYSTEMS (WVITAE-2015)
December 13-16, 2015, Hyderabad, India

Technical Background for Quality Long-Term Care Services in Europe

Ana Koren[1], Dina Šimunić[1], Ramjee Prasad[2]
[1]Faculty of Electrical Engineering and Computing, University of Zagreb
Unska 3 / XII, HR-10000 Zagreb, Croatia
[2]Center for TeleInfrastruktur (CTIF), Aalborg University
Niels Jernes Vej 12, 9220 Aalborg Ø, Denmark
E-mail(s): {ana.koren, dina.simunic} @fer.hr, prasad@es.aau.dk

***Abstract* - The number of older people in need of long-term care and assistance is increasing. It is estimated that by 2025 more than 20% of Europeans will be 65 or over, with a particularly rapid increase in the number of over 80s. Due to physical or cognitive impairment, many need assistance in their activities of daily living (ADL).**
One of the key challenges for Europe is to transform this longer life expectancy into longer active and healthy life years. Building on the existing European norms for quality long-term care services, it is necessary to develop an integrated quality framework for long-term care services which would cover very different types of care: all healthcare (both preventive and rehabilitative), social services, care for cognitive diseases, services delivered at home as well as support for carers as an integral part of the quality improvement process. The priority should be to develop a "person-centered" approach, creating a comprehensive system that would offer easily accessible and affordable continuous services allowing the users to enjoy a decent quality of life, independence and the chance to remain active in society.

Keywords: Smart Homes; eWALL; Wireless Sensor Networks; Person Centered Approach

I. INTRODUCTION

This paper looks at the impact of demographic ageing within the European Union (EU), which is likely to be of major significance in the coming decades [1]. It shows a clear shift towards a much older population structure that is already becoming apparent in several EU Member States. In response to the growing issue of ensuring the adequate care for the elderly people, European Commission has financed WeDO[2] project ("For the Wellbeing and dignity of Older people: European Quality Framework for long-term care services") which developed Quality care training package [2] with the aim of promoting quality long-term care services in Europe[3]. Based on the concepts of active ageing, everything should be done to enable the person to live autonomously for as long as possible.

The proposed and developed eWALL framework within eWALL project (project no. 610658: "eWALL for Active Long Living") described in this paper follows the norms and standards described in the two documents: "The European Quality Framework for Long-term Care Services"[3] and "The European Charter of the rights and responsibilities of older people in need of long-term care and assistance"[4] and focuses on providing outcome oriented and evidence based services for quality long-term care [2-4]. This way, elderly people in need of care and assistance stay involved and are empowered to define how their needs are met. At the same time, their caregivers are also given support in order to maximize the quality of the services provided.

This is planned to be done by creating a "Caring Home" environment, meaning an environment that "senses" intuitively the wishes and needs of the person that lives in the house, providing unobtrusive daily support, notifying informal and formal caregivers when necessary and serving as a bridge to supportive services in areas such as risk management and home safety, e-Health and lifestyle management and Activities of Daily Living (ADL) [5].

II. eWALL FRAMEWORK: ARCHITECTURE

Architecture of eWALL system involves an ecosystem of sensing devices, computing resources and display. It consists of two main subsystems: Sensing Environment and eWALL Cloud [6].

a. Sensing Environment is a smart environment centered on its human users in which a set of embedded networked artifacts, both hardware and software, collectively realize the paradigm of Ambient Intelligence, mainly by providing for context-awareness and personalization, adaptive reactivity, and anticipatory pro-activity. It can be Home or Mobile.

b. eWALL Cloud is a cloud environment that includes a set of hardware and software components used for aggregation of data coming from sensors, analyzing them and transforming them into specific formats suitable for the user/system that needs them and infers new higher-level knowledge by applying advanced reasoning on data.

Below, Figure 1 depicts the eWALL high-level architecture along with its main building blocks:

a. eWALL Devices are responsible for all explicit (direct interaction via audio/video devices) and implicit (collecting data) interaction with the end user in Sensing Environment.

b. Sensing Middleware is responsible for connecting, configuring, querying and reporting data from end user devices, for interconnection of Sensing Environment and eWALL Cloud, and for basic data storage [6].

c. Local Context Manager is responsible for handling low-level context data and processing, (indexing and adaptation, analysis of humans and non-A/V perception processing) [6].

d. Cloud Middleware is responsible for providing (1) all cloud communication infrastructure, (2) data abstraction and all data handling in cloud taking into account privacy and security concerns, and (3) for hiding the heterogeneity and distribution of cloud hardware environment and management of physical resources and the provisioning of virtual resources [6].

e. Horizontal Platform Services is a generic reusable set of services which eases the development of personalized services and applications (e.g. profiling, notification support, intelligent decision making, lifestyle reasoning provisioning and configuration) [6].

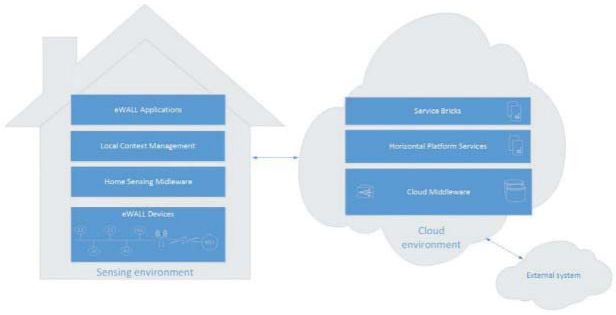

Figure 1: eWALL main building blocks [6]

f. Service Bricks are eWALL intelligent context aware service components, which together with applications act as a bridge between the end users and the eWALL back-end services [6].

g. eWALL Applications provide the interface between the user and the eWALL system. The eWALL Applications extract relevant data from Service Bricks and take care of visualization aspects of the data [6].

The most important components of eWALL system functionality are:

a. Intelligent Decision Support System (IDSS) is a software component responsible for decision-making activities in eWALL system. It uses inference to discover new relationships, automatically analyses the content of the data, and manages knowledge (i.e. perform reasoning based on corresponding or appropriate rules). It consumes low-level data (e.g. sensor data), or medium level data (e.g. processed data from service bricks) from multiple sources and makes high level, semantically meaningful data [7].

b. Lifestyle Reasoners (LR) are software components that process and store long-term data

that follows certain patterns or routines that define the lifestyle of the user. The aim of these components is to predict behavior and to detect (slow or fast) changes that might indicate a change in the user's health status. To do so, the lifestyle reasoners consume medium level data from multiple sources and derive semantically meaningful patterns [7].

c. Notification Manager (NM) is a software processing component that manages (i.e. storing, forwarding or deleting) all eWALL notifications. It is a single central block where all notifications are being managed, so the user is not overloaded by all information coming randomly from independent notification sources. The main role of the notification manager is to manage the notifications (alarms) and messages that originate from a specific set of processing blocks, e.g. service bricks [7].

III. eWALL FRAMEWORK: SERVICES

Using the data captured by the wearable and ambient environment sensors as well as user input information, several services are offered to cover the needs of our three primary target user groups: Elderly users with Age Related Impairments (ARI), patients suffering from Chronic Obstructive Pulmonary Disease (COPD) and elderly suffering from Mild Dementia (MD). Figure 2 below shows the spectrum of cognitive and physical impairments we aim to cover in the eWALL project. The proposed applications are shown to cover this entire spectrum. Daily Physical Activity (DPM) is beneficial for every individual and is the most general application. Cognitive Training (CT) is a preventive application for the ARI population and more a rehabilitation application for the MD population. Physical Training (PT) is similarly a preventive application for ARI and a rehabilitation application for COPD. Daily Functioning Monitoring (DFM) is targeted at MD patients, supporting independent living and peace-of-mind for informal caregivers. Healthcare Support (HS) is always present for COPD and in a later stage for MD patients. Each application has a number of possibilities for demonstrating personalization and intelligence in the eWALL platform [5]:

a. Daily Physical Activity application enables the system to learn the activity patterns of the user over time. Based on this, personalized goals will be set for each day of the week, which grow and change. Motivational messages will be provided based on the user's preferences and knowledge, current context (time, season, weather), and disease characteristics.

b. Daily Functioning Monitoring enables the system to learn a "normal" lifestyle pattern for the user, e.g. regarding sleeping, eating, social contacts. The system can warn informal caregivers in case of deviations from these normal values, based on the preferences of the informal caregiver (configurable).

c. Healthcare Support is a service that provides connections to professional care services and automatically initiates communication with a professional if certain events are detected.

d. Physical Training is a tool that provides exercise support to the user (e.g. video follow-along exercise). The system can follow progress over time, recommend exercises that the user likes and set the difficulty of exercises automatically based on progress and disease characteristics.

e. Cognitive Training is a tool that provides cognitive exercise support. Personalization and intelligence functions are similar to physical training (automatic selection of exercises, difficulty setting, automatic coaching or hints).

From the target end user perspective, the eWALL system consists of a set of messages, recommendations, reminders and suggestions delivered to him/her on a big screen (installed in the home) or on a portable device. From the caregivers' perspective, the system allows them to control the health status of their assigned end users, leveraging a set of technologies that allow collection of meaningful information on the target end user, to analyze them and to take actions accordingly. The ideal way to provide the above

mentioned functionality is by means of a web portal, which allows access from everywhere in a modality which is independent from the client operating system used [5].

IV. PERSON-CENTERED DESIGN

Articles [20] and [21] explain the importance of "person-centered" design in home care environments. Following the "Quality principles and Areas of Action" stated in WeDo guide [3], characteristics of eWALL are:

a. eWALL is customizable, accessible and easy to use. Different services can be "plugged in" using the concept of app market; the users define which applications they need and what they will do [8].

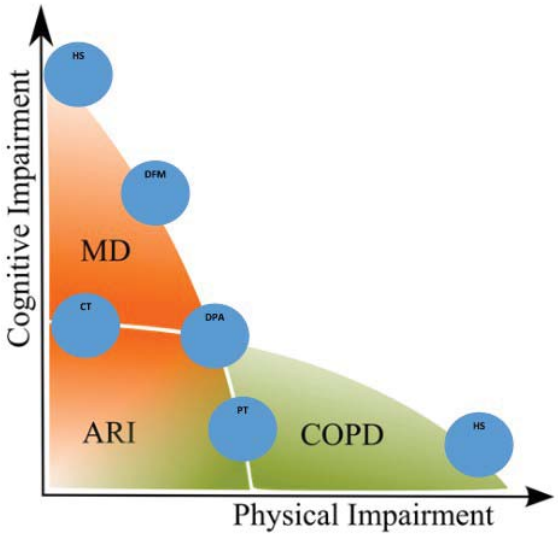

Figure 2: The spectrum of cognitive and physical impairments and the associated primary target populations with the proposed services: DFM (Daily Function Monitoring), CT (Cognitive Training), PT (Physical Training), Daily Physical Activity (DPA), and Healthcare Support (HS) [5]

b. eWALL provides adaptability since each of the services provided can be fine-tuned to correspond to the requirements of a specific user based on their cognitive and physical abilities or on their needs [8].

c. eWALL is unobtrusive: messages the platform delivers are clear and prioritized and should interrupt the personal flow of a user only when it is absolutely necessary [8].

d. eWALL provides continuous and reliable service, which is a prerequisite for a functional system and is mainly validated by technical partners [8].

e. eWALL is outcome oriented and evidence based, meaning it is oriented towards monitoring and improving a person's health, wellbeing and independence based on the information collected and the user's feedback.

f. eWALL is person-centered and respectful of human rights and dignity. Faced with impairment, many people seem to lose trust in their cognitive or physical abilities and they gradually abandon their former activities. As a result, their confidence and mood are affected and they often succumb in isolation [8]. This has an impact on their overall health and social life [22]. Among eWALL's main goals as a person-centered system is to attempt to restore these two emotional parameters, self-trust and motivation and empower the end users on a psychological level [9].

Overcoming the psychological obstacles described and empowering the end users to face their life and responsibilities by supporting independent living of senior citizens and compensating for prevailing age-related physical and cognitive impairments is certainly the utmost goal of eWALL and therefore, constitutes the most important high level goal.

V. CHALLENGES AND FUTURE WORK

In this paper, we proposed eWALL framework that provides long-term care for the elderly and assistance to their caregivers. Challenges faced were: (1) developing a comprehensive, ambient aware and dynamical system that would serve the elderly and their caregivers and (2) empowering older people and creating opportunities for participation using a person centered design.

Future work would continue to work on fostering human rights and dignity of elderly people. This can be achieved by expanding the existing system with services focused on preventing and fighting elder abuse and neglect which has been a growing issue [23].

Acknowledgement - We thank our colleagues from the eWALL project who provided insight and expertise that greatly assisted the work presented in the paper.

REFERENCES

[1] Eurostat - European Commission, "Population structure and aging", June 2015
[2] WeDO^2, "Quality Care Training Manual", June 2015
[3] WeDO, "European Quality Framework for long-term care services", December 2012
[4] European Charter of the rights and responsibilities of older people in need of long-term care and assistance
[5] The eWALL Consortium, "D2.9 Task forces COPD, MCI and ARI", eWALL for Active Long Living, November 2014
[6] The eWALL Consortium, "D2.7 Final user and system requirements and architecture", eWALL for Active Long Living, February 2015
[7] The eWALL Consortium, "D5.3.2, Intelligent context-aware services & applications", eWALL for Active Long Living, May 2015
[8] The eWALL Consortium, "D4.4.1, eWALL platform", eWALL for Active Long Living, October 2014
[9] The eWALL Consortium, "D2.6 Evaluation and Validation Methodology", eWALL for Active Long Living, November 2013
[10] The eWALL Consortium, "D6.1, Integration report", eWALL for Active Long Living, October 2014
[11] The eWALL Consortium, "D2.5, Patient Pathways and Clinical Workflows", eWALL for Active Long Living, July 2014
[12] The eWALL Consortium, "D4.1.1, Semantic model of eWALL middleware services", eWALL for Active Long Living, October 2014
[13] The eWALL Consortium, "D4.3.1, Cloud middleware services for eWALL", eWALL for Active Long Living, October 2014
[14] The eWALL Consortium, "D2.2, Initial scenarios and use cases", eWALL for Active Long Living, February 2014
[15] The eWALL Consortium, "D2.3, Preliminary system architecture", eWALL for Active Long Living, April 2014
[16] The eWALL Consortium, "D2.1, Preliminary user and system requirements", eWALL for Active Long Living, February 2014
[17] The eWALL Consortium, "D7.4, Standardization plan", eWALL for Active Long Living, October 2014
[18] The eWALL Consortium, "D6.3, Technical evaluation report", eWALL for Active Long Living, July 2015
[19] The eWALL Consortium, "D7.1, Website", eWALL for Active Long Living, November 2013
[20] Kurnianingsih, Nugroho L. E., Widyawan, Lazuardi L., Ferdiana R., Selo, "Perspectives of Human Centered Design and Interoperability in Ubiquitous Home Care for Elderly People", Electrical Engineering and Informatics (MICEEI), November 2014, pp. 118-123.
[21] Balakrishnan S., Salim S.S.B., Jer Lang Hong, "User Centered Design Approach for Elderly People in Using Website", Advanced Computer Science Applications and Technologies (ACSAT), November 2012, pp. 382-387.
[22] Hildebrand C., Taylor M., "Elder self-neglect: The failure of coping because of cognitive and functional impairments", Journal of the American Association of Nurse Practitioners, August 2013, pp. 452-462.
[23] Lindert J., de Luna J., Torres-Gonzales F., Barros H., Ioannidi-Kopolou E., Melchiorre M. G., Stankunas M., Macassa G., Soares J. F. J., "Abuse and neglect of older persons in seven cities in seven countries in Europe: a cross-sectional community study", International Journal of Public Health, February 2013, pp. 121-132.
[24] Prasad R., Velez F. J., "WiMAX Networks: Techno-Economic Vision and Challenges", Springer, October 2010
[25] Prasad R., Deneire L., "From WPANs to Personal Networks: Technologies and Applications", Archtech House, November 2005

Sponsors

Proceedings for the Joint Conference of the 3rd Global Wireless Summit, The 5th International Conference On Wireless Communications, Vehicular Technology, Information Theory, Aerospace & Electronics Systems (WVITAE), The 3rd International Conference On Communications, Connectivity, Convergence, Content & Cooperation (IC5), and 18th Wireless Personal Multimedia Communications on December 13-16, 2015, Hyderabad, India

Proceedings Co-edited by :

Dr. Ambuj Kumar

Department of Business Development and Technology,
School of Business and Social Sciences
Aarhus University, Herning,
Denmark

Prof. Peter Lindgren

Department of Business Development and Technology,
School of Business and Social Sciences
Aarhus University, Herning,
Denmark

and,

Prof. Ramjee Prasad

Knight ("Ridder") of the order of Dannebrog, a distinguished award by the Queen of Denmark

FELLOW IEEE, IET, IETE, WWRF
Founder President, CTIF GLOBAL CAPSULE
Founder Chair, GISFI
Founder Chair/Co-Chair, GWS/ WPMC Steering Board
Founder President, VISHWANIKETAN

Founder Editor-in-Chief, Int. J. Wireless Personal Communications (Springer)

Distinguished Professor, Department of Clinical Sciences and Translational Medicine, University of Rome "Tor Vergata", Italy

Professor, Future Technologies for Business Ecosystem Innovation (FT4BI), Aarhus University, Herning, Denmark

About Wireless Personal Multimedia Communications (WPMC)

The Wireless Multimedia Personal Communications (WMPC) was inaugurated as a global platform which aims at enabling collaboration in the field of wireless information and multimedia communications. The Wireless Multimedia Personal Communications (WMPC) International Symposium was started way back in 1998, with about 200 participants and about accepted 100 papers. Thereafter, in four years span, the number of participants has reached and exceeded 400 and the number of papers more than 300 for each Symposium. In every WPMC International Symposium, high-quality technical sessions, workshops, tutorials as well as product exhibitions are organized. Since the first WPMC in YRP (Japan), seventeenth WPMCs were held through the world in Asia, Europe, North and South Americas.

In the year 2007, this event was held in Jaipur (India). The quality of the presentations is also very high. It is indisputable that WPMC has become one of the major international conferences in the field of wireless Communications. Some of the themes of earlier Symposia were (i) Communications, Networking and Applications for the Internet of Things, (ii) Autonomous Communication and Networking for Promoting Human Living, and (iii) Orchestrating Wireless Personal Multimedia Communications for Digital Services etc.

Every year is witnessing rapid change in the field of wireless communications with the development and deployment of new technologies and solutions in the field of wireless technologies. Every aspect of wireless communications right from physical layer, resource management including alternative methods of spectrum management, interference management, IoT & M2M, smart antenna, MIMO, multimedia QoS & traffic management, visible light communications, cloud computing, security & privacy, vehicular networks, radio propagation & channel modelling, cognitive radio & SDR, mobile multimedia & mobile TV, wellness & health care, ICT for energy efficiency etc. WPMC is becoming more and more important every year. Against such a backdrop, it was truly gratifying that the 18th International Symposium of WPMC was held in Hyderabad during December, 2015. This Symposium was supported by National Institute of Information and Communications Technology (Japan), and YRP (Japan).

About Global Wireless Summit

The Global Wireless Summit (GWS) had been conceptualized in bringing together wireless media communication/personal communication, etc. The First GWS was successfully held in Princeton (USA), in 2013, followed by the Second one in Aalborg (Denmark), in 2014. As has been the tradition for this Summit, it continues to feature a high-quality technical program across a wide range of research in the wireless communications and related areas. Under the theme "Democratizing Communications", the GWS-15 brought together academia, industry and standardization bodies working on green and secure communication. The conference explored activities, trends and future challenges towards ICT globalization including energy and security issues in existing and future wireless technologies. The Global Wireless Summit-15 presented high-level technical sessions; tutorials, and special sessions on advance topics; workshops; and panel discussions.

Under the theme of 'Democratizing Communications,' the 18th International Symposium on Wireless Personal Communications (WPMC), and the 3rd Global Wireless Summit (GWS) are jointly organized, encompassing the 5th International Conference on Wireless Communication, Vehicular Technology, Information Theory and Aerospace & Electronics Systems (WirelessVITAE), The 12th World Wide Security and Mobility Conference (WWSMC), and the 3rd International Conference on Communications, Convergence, Content and Cooperation (IC5).

About Wireless VITAE

The Wireless Vehicular Technology, Information Theory Aerospace & Electronics Systems (VITAE) is the only international conference broadly addressing the wireless developments in the world by merging the communities from four different IEEE societies. The 1st Conference was held in 2009 in Aalborg (Denmark) followed by 2nd in 2011 in Chennai (India). The 3rd was held in 2013 at Atlantic City, NJ, USA. The 4th was co-located with GWS-2014 in 2014 at Aalborg (Denmark). The primary event in Aerospace, Information Technologies and Databases & Information Systems category centerpieces to Aerospace, Wireless Communication, Information Theory, Vehicular Technology and Electronics Systems issues. Wireless VITAE joined hands with GISFI to provide a platform to gather the different facets of the wireless into a single event and to exchange ideas and knowledge among the different research communities that address the various aspects of the wireless theme. The International Wireless VITAE conference is Global one that addresses the trends, challenges and future roadmaps within a conglomerate of existing and novel wireless technologies, including cellular, short-¬range, sensor and embedded ones. Cognitive and self-¬organizing networks, nano-sensors, positioning and localization, Internet of Things (IoT), positioning and localization, recent advances in information theory and its applications, space technology for very high data rates, and techno-¬economic aspects of telecommunications are part of the scope, among others.

Committee Members

RAMJEE PRASAD,

- Steering Board Chair/Co-Chair of WPMC, GWS, and Wireless VITAE;
- Founder Director, CTIF Global Capsule (CGC), Aarhus University, Herning, Denmark;
- Founder Chairman, Global ICT Standardisation Forum for India (GISFI).

RATNAM VARADA RAJAKUMAR,
General Chair, Global Wireless Summit 2015
Director, Indian Institute of Technology,
Bhubaneswar, Odisha, India

ASHOK CHANDRA,
Executive Chair, TPC , Global Wireless Summit 2015
Former Wireless Adviser to the Government of India

Masao Sakauchi,
President, National Institute of Information and Communications Technology, Japan
WPMC Organizing Committee

Mitsutoshi Hatori,
Chairman, YRP R&D Promotion Committee, Japan
WPMC Organizing Committee

Shingo Ohmori
Co-chair of WPMC Steering Board
President, YRP International Alliance Institute, Japan
Vice President, YRP R&D Promotion Committee, Japan
WPMC Organizing Committee

NEELI R. PRASAD,
TPC Co-Chair, Global Wireless Summit 2015
International Technological University (ITU), USA

ERNESTINA CIANCA,
Publication Chair, Global Wireless Summit 2015
University of Rome Tor Vergata, Italy

AMBUJ KUMAR,
Web Co-chair, Global Wireless Summit 2015
Aarhus University, Denmark

Welcome Speeches

On behalf of the Steering Committee of the WPMC 2015, Global Wireless Summit (GWS) 2015, and Wireless VITAE 2015, it is my great pleasure to bid you all a warm welcome to these highly renowned events in the beautiful historic city of Hyderabad, India.

Under the theme of '**Democratizing Communications**,' the 18th International Symposium on Wireless Personal Communications (WPMC) and 3rd Global Wireless Summit (GWS) are jointly organized, encompassing the 5th International Conference on Wireless Communication, Vehicular Technology, Information Theory and Aerospace & Electronics Systems (Wireless VITAE), The 12th World Wide Security and Mobility Conference (WWSMC), and the 3rd International Conference on Communications, Convergence, Content and Cooperation (IC5).

Wireless communications have evolved over the years to open great potential for monetizing on multimedia data and diversified user-generated content, making them a ubiquitous means of connecting people and businesses. Democratization of hardware, software and connectivity is the necessary enabler to benefit all stakeholders and provide a stable platform for creating profits out of technology disruption.

The setting of WPMC 2015 jointly with GWS2015 was in the heart of the City of Pearls, as Hyderabad historically been known for its blooming pearl industry. Today, Hyderabad is also a major center for the technology industry. The WPMC and GWS2015 program featured an unusually distinguished group of keynote and invited speakers, as well as a strong technical program with novel research contributions from the relevant thematic areas from all over the world. In addition, an extensive list of social events were scheduled to allow for a break from the exciting technical sessions. Please, take the advantage of the many opportunities to network and expand your technical and cultural horizons.

I would like to extend my appreciation to my global colleagues for their dedication and effort to put together a strong event.

Ramjee Prasad,

Steering Board Chair/Co-Chair of WPMC, GWS, and Wireless VITAE

It is my great pleasure to host the 18th International Symposium on Wireless Personal Multimedia Communications (WPMC'15) in Hyderabad, India.

The WPMC symposia series first commenced in 1998, as a unique international conference dedicated to wireless multimedia communications aiming for global collaboration. In cooperation with YRP, we hold the symposium in a location in Asia, Europe, America or Australia each year.

This year's host country, India, has shown remarkable developments in the information and communications technology (ICT) field, in particular, in mobile phones, since the 10th WPMC Symposium held in Jaipur in 2007. During that time attention to wireless technology has also increased and a broad range of R&D activities have been advanced. Against such a backdrop, it is truly gratifying that the WPMC Symposium is being held here.

As Japan's sole national research institute in the field of ICT, the National Institute of Information and Communications Technology (NICT), promotes research and development in fundamental technologies in the fields of networks, including wireless communication, universal communication, advanced ICT, and electromagnetic sensing. Through these technologies, we aim to contribute to improving and resolving various challenges that society faces.

In particular, NICT positions big data of a public nature that helps to contribute to society as "Social Big Data." We focus on R&D of such Social Big Data, with the goal of having it used throughout society as social infrastructure, and ensuring that the knowledge and information gained from it is further disseminated. Additionally, efforts leading to the Internet of Things (IoT) and Internet of Everything (IoE), where all things and all data become connected, are advancing, and NICT is actively contributing to the IoT Acceleration Consortium, which represents Japan's efforts in this area, and its technology development working group, the Smart 'IoT Acceleration Forum'. Furthermore, learning from the response to the Great East Japan Earthquake that devastated Japan in March 2011, we are also engaging in research and development to swiftly deploy a wireless telecommunications network in the aftermath of a disaster.

For this symposium, NICT has set up a Wi-SUN workshop, 5G workshop, and Resilient Wireless Network Technologies workshop as themes related to such areas of research and development at this symposium. Currently, data gathering through networks using wireless technology is being conducted in various fields and industries across the globe. At the same time, the diversification of ICT had made wireless communications technology increasingly available to people. Given this situation, I believe that holding

this ICT workshop here in India will be extremely effective and holds great significance.

Lastly, I sincerely hope that WPMC'15 will be a significant forum that promotes extensive collaborations and interchanges among those engaged in the R&D of wireless communications, towards the realization of a society where people can live with a sense of security and comfort.

Masao Sakauchi,

President, National Institute of Information and Communications Technology, Japan

On behalf of YRP R&D Promotion Committee, one of the co-organizers of the 18th International Symposium on Wireless Personal Multimedia Communications (WPMC 2015), it is my great pleasure to welcome you in Hyderabad, India.

Since the first WPMC was held in our Yokosuka Research Park (YRP), Japan, in 1998, this symposium had been held in various cities in the world every year providing researchers of wireless communications with opportunities to gain new knowledge and information and also to exchange with each other. We are excited that this year the WPMC is held in India for the second time after the WPMC 2007 held in Jaipur owing to the great cooperation of Global ICT Standardization Forum in India (GISFI), Indian Institute of Technology Bhubaneswar and Kharagpur, Jawaharlal Nehru Technological University Hyderabad, and other Indian colleagues, and we truly appreciate hard work and great efforts of all people concerned. YRP has developed as an international R&D hub for radio and telecommunications technologies since its establishment in 1997. Currently, about 58 organizations with 5,200 researchers and engineers gather in YRP, and the member of our Committee, one of the promoting bodies of YRP, has reached to around 150. We have also concluded memorandums of understanding for research exchange with research parks and ICT institutions, totaling 51 organizations in 15 countries and one region.

Now, in YRP, in addition to the R&D of the 4th generation mobile communication systems, discussions and studies on the 5th generation mobile communication systems that are to be introduced in 2020 are under way. In Broadband Wireless Forum, which was established in our Committee in 2009, discussions on practical application of wireless power transmission technologies are going on, and last year in May, we also established a new Committee to promote application of Wireless Smart Utility Network, Wi-SUN. YRP intends to use the fruits of these activities as a foothold to lead the world's R&D in ICT and further enhance YRP's function. We also would like to further strengthen wide-ranging international collaboration encompassing Europe, America, Asia and Oceania, and other regions, and we expect WPMC to be the very important platform for international exchange.

I hope that this WPMC2015 will be fruitful and enjoyable to all participants.

Mitsutoshi Hatori,

Chairman, YRP R&D Promotion Committee, Japan

At the outset, as the Executive Chairman of the Technical Program Committee (TPC) of the third Global Wireless Summit (GWS-2015), it gives me an immense pleasure to heartily welcome you to this Summit being held in the City of Hyderabad, India during December 13-16, 2015.

The Global Wireless Summit (GWS) has been conceptualized in bringing together wireless media communication/personal communication, etc. The First GWS was successfully held in Princeton (USA), in 2013, followed by the Second one in Aalborg (Denmark), in 2014. Under the theme "Democratizing Communications", the GWS-15 brings together academia, industry and standardization bodies working on green and secure communication. The conference will explore activities, trends and future challenges towards ICT globalization including energy and security issues in existing and future wireless technologies.

Global Wireless Summit 2015 is hosting 18th International Symposium on Wireless Personal Multimedia Communications (WPMC); 5th International Conference on Wireless Communications, Vehicular Technology, Information Theory Aerospace & Electronics Systems (WirelessVITAE) 2015, IC5 and World Wide Security & Mobility Conference (WWSMC). The WPMC-15 and WirelessVITAE 2015 are the major events and both are held second time in India. The 1st International Symposium on WPMC was held in 1998, and since then it is held every year with an objective of providing a 'global platform' for discussions on the latest trends in the wireless multimedia communications. In the year 2007, this event was held in Jaipur (India). Wireless VITAE is the only international conference broadly addressing the wireless developments in the world by merging the communities from four different IEEE societies. The 1st Conference was held in 2009 in Aalborg (Denmark) followed by 2nd in 2011 in Chennai (India).

The Global Wireless Summit-15 presented high-level technical sessions; tutorials, and special sessions on advance topics; workshops; and panel discussions. All the submitted contributions received for technical and special sessions have been thoroughly reviewed by the TPC including other leading experts and only the best quality of papers have been accepted for presentations. It may be mentioned that each paper was reviewed by at least three experts. TPC of GWS-15 has 15 Co-chairs and over 70 members, from a wide variety of academic, industrial, and research organizations around the globe.

As has been the tradition for this Summit, it continues to feature a high-quality technical program across a wide range of research in the wireless communications and related areas.

I would like to take this opportunity to profoundly thanks the TPC Co-chairs; TPC members; Chairpersons of Special Sessions, Workshops; reviewers; and authors.

I request you all to take the advantage of this grand Summit and have thought provoking 4 days in the City of Hyderabad.

Ashok Chandra

Technical Program Committee (TPC) Executive Chair, WPMC 2015 and GWS 2015

Former Wireless Adviser to the Government of India

Welcome to Hyderabad, India to join WPMC2015.

On behalf of the Steering Board of WPMC, I would like to express my deep gratitude to all the delegates for coming from all over the world, and expect you will be having exciting experiences at WPMC2015 in Hyderabad.

The WPMC2015 is the 18th WPMC held for the second time in India, one of the most fantastic and attractive countries in the world.

The WPMC was inaugurated in 1998 to establish a global platform for mutual cooperation and discussions in the field of wireless multimedia communications with a strong financial supports by National Institute of Information and Communications Technology (NICT). The first WPMC was held at Yokosuka Research Park (YRP) in Japan in honor of the opening of YRP in 1997.

Since the first WPMC in YRP, seventeenth WPMCs were held through the world in Asia, Europe, North and South Americas.

With the continued and close support by numerous organizations and human relationships, the WPMC has grown into an international symposium widely recognized by industries and academic societies.

I wish to take this opportunity to thank all supporting committee members and staffs of WPMC2015, especially for General Chair, Prof. R.V Rajakumar, Director IIT Bhubaneswar, India, and TPC Chair, Dr. Ashok Chandra, Former Wireless Advisor, to the Government of India.

Shingo Ohmori

Co-chair of WPMC Steering Board

President, YRP International Alliance Institute, Japan

Vice President, YRP R&D Promotion Committee, Japan

Venue Map

Central Events

09:30-11:30

December 14-16, 2015

Workshops and Special Sessions

11:30 until End of the day

December 14-16, 2015

1.1 & 1.2

HICC
GROUND FLOOR PLAN

Technical Papers, 11:30 until End of the day, **December 14-16**

Workshops and Special Sessions, 11:30 until End of the day, **December 14-16**

Rooms: MRG .01 to MRG .06

ENTRANCE TO THE HICC & CONFERENCE HALL

Please Contact GWS Event Management Personnel or HICC Reception for queries and guide to HALLS/ Rooms

Program at a Glance

Sunday, December 13

Day 1

“Tutorials”

Time Slot	Day1: Sunday, December 13| Tutorials	
08:30-19:00	Registration	
	Morning Tutorial Session	
09:00-13:30 Coffee Break 11:00-11:30	**WPMC Tutorial Session on "TV White Space for Affordable Broadband Access "** **Kentaro Ishizu**, *National Institute of Information and Communications Technology*, **Japan; Abhay Karandikar,** *Indian Institute of Technology Bombay*, **India; Takeshi Matsumura,** *National Institute of Information and Communications Technology*, **Japan**	**MR 2.01**
	WPMC Tutorial Session on "Optimal Filtering and Parameter Estimation Techniques for Statistical Models" **Laxminarayana Pillutla,** *Dhirubhai Ambani Institute of Information and Communication Technology*, **India**	**MR 2.02**
	WPMC Tutorial Session on " Antennas for Millimeter-wave Wireless Communications" **T Rama Rao,** *SRM University*, **India**	**MR 2.03**
	WVITAE Tutorial Session on "IoT and Low Voltage Analog Design for Wireless Applications" **Sudhanshu S. Jamuar,** *University Malaysia Perlis*, **Malaysia**	**MR 2.04**
	WVITAE Tutorial Session on "Energy-Spectral Efficiency in Cooperative Cognitive Radio Network with Challenges in Security" **Santi Prasad Maity,** *Indian Institute of Engineering Science and Technology, Shibpur*, **India**	**MR 2.05**
13:30-14:30	**LUNCH**	
	Afternoon Tutorial Session	
14:30-18:30 Coffee Break 16:30-17:00	**WPMC Tutorial Session on "Road to 5G Wireless Systems: Challenges Ahead vis-à-vis Progress Made "** **Amitava Mukherjee,** *IBM Pvt. Limited*, **India; Debashis Saha,** *Indian Institute of Management Calcutta*, **India**	**MR 2.01**
	WPMC Tutorial Session on "Wireless Channel Impairments Removal Techniques" **Sanjay Kumar,** *Birla Institute of Technology*, MESRA , **India**	**MR 2.02**
	WVITAE Tutorial Session on "Transmission Technologies for 5G" **Suvra Sekhar Das,** *Indian Institute of Technology, Kharagpur*, **India**	**MR 2.03**
	WVITAE Tutorial Session on "Visible Light Communication for Road Safety in the Intelligent Transportation Systems" **Navin Kumar,** *Amrita University & School of Engineering*, **India**	**MR 2.04**
	WVITAE Tutorial Session on "ICT for Health Care" **Vishwanath Sinha,** *M. N. National Institute of Technology, Jaipur,* **India**	**MR 2.05**
19:00-20:00	Welcome Reception in Foyer/ Pool Side Lawns	

Monday, December 14 Day 2

"Workshops, Special Sessions, Contributed Papers"

Time Slot	Day2: Monday, December 14 | Grand Opening Program		
08:30-19:00	**Registration**		
09:00-10:00	**GRAND OPENING**		**HALL 1**
	Ceremony	**Lighting of the Lamp Ceremony: Presided by B.N. Bhandari, Local Organizing Chair, WPMC/ GWS 2015**	
	Welcome Speech	**Ratnam Varada Rajakumar**, *General Chair*, WPMC/GWS 2015	
	Inaugural Speech	**Ramjee Prasad**, *Steering Board Chair/Co-Chair of WPMC, GWS and Wireless VITAE; Founder Chair, GISFI*	
	Introduction Speech	**Ashok Chandra, TPC Executive Chair, WPMC/ GWS 2015**	
	Opening Speech-1	**Fumihiko Tomita**, Vice President, *NICT*, **Japan**	
	Opening Speech-2	**Mitsutoshi Hatori**, Chairman, *YRP*, **Japan**,	
	Opening Speech-3	**Smriti Dagar**, *President, IETE*, **India**	
	Round Table Discussions: "India Knowledge Economy- Transformation through Digitization and Innovation"		
10:00-11:00	**Discussion**	Moderator:-**Sudhir Dixit**, WWRF, **USA**, **Anand R. Prasad**, NEC Corporation **Japan,** **Dina Simunic,** *University of Zagreb***, Croatia** **Ashok Chandra,** *TPC Executive Chair, WPMC/ GWS 2015*, **India** **Kiritkumar Lathia, GISFI/CTIF, Denmark,**	
	Vote of Thanks	**Sandip Inamdar**, Finance Chair, **WPMC/ GWS 2015**	
11:00-11:30	**Coffee Break**		
11:30-19:00		**Technical Sessions**	
19:30-22:30	END of DAY 2 || Cultural Program (Mridangam and Kuchipudi Group Dance Recital), GALA DINNER & Best Paper Award: HALL1		

Time Slot	Day2: Monday, December 14 || HALL 1.1 Activities || Workshops & Special Sessions (I-A)		
08:30-19:00	Registration		
09:00-11:00	**GRAND OPENING**		**HALL 1**
11:00-11:30	**COFFEE BREAK**		
11:30-13:30	**WPMC Special Session on "Mobile applications for Management of the Digital Business, Implications for the Infrastructures and Organisations"** **Session Organizer and Chair: Zoran Veljovic,** *University of Montenegro,* **Montenegro**		HALL 1.1
	Invited Talk	Manufacturing and Standardization in India**, Arun Golas**, *former DDG, Ministry of Communications, Government of India, New Delhi,* **India**	
	1570231052	Dynamic Pathloss Model for Future Mobile Communication Networks; **Ambuj Kumar, Albena Mihovska, Ramjee Prasad**; *CTIF, Aalborg University,* **Denmark**	
	1570228076	Challenges and Opportunities for Enhancing User Privacy and User Empowerment; **Prashant Dhotre, Samant Khajuria , Henning Olesen**; *Center for Communication, Media and Information Technologies (CMI),Aalborg University Copenhagen,* **Denmark (***)**	
	1570228069	Sensitive Association Rules Hiding Methods: A Survey; **Geeta Navale, Suresh Mali**; *Sinhgad Institute of Technology and Science, Pune,* **India**	
13:30-14:30	LUNCH		
14:30-16:30	**WPMC Workshop on "Vision and research activities toward the Fifth Generation Mobile Systems (5G)"** **Workshop Organizer and Chair: Kentaro Ishizu,** *Association of Radio Industries and Businesses (ARIB) & National Institute of Information and Communications Technology (NICT),* **Japan**		HALL 1.1
	Activities on 5th Generation Mobile Communications System in Japan ;**Kohei Sato;** *Association of Radio Industries and Businesses (ARIB),* **Japan**		
	5G Prospects in India; **VikramTiwathia**; *The Cellular Operators Association India (COAI),* **India**		
	5G research activities and key enabling technologies ;**Haesik Kim**; *VTT,* **Finland**		
	Small-cell Structured Wireless Networks for 5G: Centralized vs Decentralized Architecture ;**Fumiyuki Adachi**, *Tohoku University,* **Japan**		
	The Unified 5G Platform; **J. VinoshBabu James**, *Qualcomm,* **India**		
16:30-17:00	COFFEE BREAK		
17:00-19:00	**WPMC Special Session on "Combedded Systems"** **Session Organizer and Chair: Abhay Gandhi,** *Viswesarayya National Institute of Technology, Nagpur,* **India**		HALL 1.1
	1570227356	Artificial intelligence auto-mobility in material handling & fork-lift manufacturing; **Ajinkya Vasant Nichit①, Kedar S. Joshi①, Sachin B. Rao ②, Sushant S. Gaidhani ①, Shrinivas Vasantrao Shinde③**; ①*Sandip Institute Of Engg, & Management, Nashik,* ②*G.H. Sapat College Of Engg., Nashik,* ③*Jawahar Institute Of Technology, Nashik;* **India**	
	1570227801	Interference Analysis and Mitigation Techniques in Wireless Body Area Network; **Subhojit Moitra, P.H.Ghare, A.G. Kothari**; *VNIT, Nagpur,* **India**	
	1570227808	Implementation of Low Cost IoT Based Smart Home using Open Source Platform; **Varun Tiwari, Avinash Keskar** □; *Visvesvaraya National Institute of Technology, Nagpur,* **India**	
	1570227846	Performance Comparison of DCT based Entropy Coding Techniques; **Samruddhi Y. Kahu, Kishor M. Bhurchandi**; *Visvesvaraya National Institute of Technology, Nagpur,* **India**	
	1570227857	UWB Sensing antenna, Reconfigurable transceiver and antenna based Cognitive Radio Test bed; **S. Manoj, Sumin. D. Joseph**□, **Chetan. Waghmare, Nandakumar. K., Ashwin Kothari**; *Department of Electronics VNIT, Nagpur,* **India**	
	1570227987	Methods of Frequency Offset Estimation in OFDM Based System; **A. P. Rathkanthiwar①, A.S.Gandhi②**; ①*Priyadarshini College of Engineering Nagpur,* ②*Visvesvaraya National Institute of Technology, Nagpur* , **India**	
19:30-22:30	END of DAY 2 || Cultural Program (Mridangam and Kuchipudi Group Dance Recital), GALA DINNER & Best Paper Award: HALL1		

Time Slot	Day2: Monday, December 14 || HALL 1.2 Activities || Workshops & Special Sessions (I-B)		
08:30-19:00	Registration		
09:00-11:00	**GRAND OPENING**		**HALL 1**
11:00-11:30	**COFFEE BREAK**		
11:30-13:30	**WVITAE Special Session on " mHealth and Medical Informatics"** **Session Organizer and Chair: Albena Mihovska, Aalborg University, Denmark**		HALL 1.2
	Opening Talk	**Shyam Chakrabortty,** *Oy Trinnect Ltd.,* **Finland**	
	Invited Talk	Role of ICT for the Advancement of Dentistry **, Gianpaolo Sannino,** *University of Rome, Tor Vergata,* **Italy**	
	Invited Talk	Patient centered learning and Early clinical exposure of medical students to 'Diabetes and Metabolic syndrome**, Yogesh Sharma①, Ankur Joshi②, Dept of Medicine③, Rakesh Biswas;** *①LNMCH,②dept of Medicine, GMC,③dept of Medicine, LNMCH;* *Bhopal Madhya Pradesh*, **India**	
	Invited Talk	Review of telemedicine technologies in India**, Sumit Gautam***①***, Shyam Chakraborty②;** *① IIIT Hyderabad, India;* ***②****Trinnect Ltd.,* **Finland**	
13:30-14:30	LUNCH		
14:30-16:30	**WPMC Workshop on "Resilient Wireless Network Technologies" (I)** **Workshop Organizer and Chair: Ryu Miura,** *National Institute of Information and Communications Technology (NICT)*, **Japan**		HALL 1.2
	1570213366	On-going Field Experiment of NerveNet in Shirahama Town for Resilient Town Network; **Masugi Inoue, Yasunori Owada , Kiyoshi Hamaguchi** *; Resilient ICT Research Center,* *National Institute of Information and Communications Technology (NICT)*☐, **Japan**	
	1570213263	Pilot testing and demonstration of self-management network and applications by NerveNet; **Yasunori Owada , Kiyoshi Hamaguchi, Masugi Inoue;** *Resilient ICT Research Center,* *National Institute of Information and Communications Technology (NICT)*☐, **Japan**	
	1570213055	Development and Field Experiment of Distributed Peer Aware Communication Networks; **Lin Shan, Huan-Bang Li, Takashi Matsuda, Ryu Miura**; *Wireless Network Research Institute, National Institute of Information and Communications Technology (NICT)*☐, **Japan**	
	1570213332	A hybrid multi-hop network by small-unmanned aircraft and satellite telecommunication systems; **Fumie Ono①**; **Byeong-pyo Jeong②, Yasunori Owada②, Shan Lin ①, Ryu Miura①**; *①Wireless Network Research Institute,* ***②****Resilient ICT Research Center, National Institute of Information and Communications Technology (NICT)*☐; **Japan**	
16:30-17:00	COFFEE BREAK		

16:30-17:00	(Continued: Hall 1.2 Activities) COFFEE BREAK		
17:00-19:00	**WPMC Workshop on "Resilient Wireless Network Technologies" (II)** **Workshop Organizer and Chair: Ryu Miura,** *National Institute of Information and Communications Technology (NICT)***, Japan**		HALL 1.2
	1570213462	QZSS SS-CDMA Location and Short Message Communication System; **Noriharu Suematsu, Suguru Kameda, Yuji Miyake, Tomohide Takahashi , Akinori Taira, Tadashi Takagi, Kazuo Tsubouchi**; *Research Institute of Electrical Communication, Tohoku University*, **Japan**	
	1570213016	Disaster Countermeasure Experiments using WINDS; **Takashi Takahashi①, Kazuyoshi Kawasaki①, Akira Akaishi①, Toshio Asai①, Maki Akioka①, Tomoshige Kan①, Morio Toyoshima①, Byongpyo Jeong②, Hajime Susukita②, Shuji Murakami②**; ①*Wireless Network Research Institute,* ②*Resilient ICT Research Center; NICT,* **Japan**	
	1570195491	A Path Ordering and Reference Selection Method for the Differential Delay Tomography; **Takehiro Otsuka① , Shinsuke Hara①②, Takahiro Matsuda③②, Kenichi Takizawa③, Fumie Ono‡ , Ryu Miura‡**; ①*Graduate School of Engineering,* ②*Osaka City University,* ③ *Graduate School of Engineering, Osaka University*; **Japan**	
	1570205987	Experimental Evaluation on Wireless Tomography with Compressed Sensing in a Three-Dimensional Space**; Kengo Yokota; Kengo Yokota① , Shinsuke Hara① , Takahiro Matsuda②, Masaki Mukamoto②, Yuki Uemura②, Kenichi Takizawa③, Fumie Ono④, Ryu Miura④** □; ①*Graduate School of Engineering, Osaka City University ,Sugimoto, Sumiyoshi-ku, Osaka,* ②*Graduate School of Engineering, Osaka University 2-1 Yamadaoka, Suita, Osaka,* ③*Strategic Planning Office, National Institute of Information and Communications, Koganei, Tokyo ,* ④*Wireless Network Research Institute, National Institute of Information and Communications Technology ,Kanagawa*; **Japan**	
19:30-22:30	END of DAY 2 || Cultural Program (Mridangam and Kuchipudi Group Dance Recital), GALA DINNER & Best Paper Award: HALL1		

Time Slot	Day2: Monday, December 14 || MRG .01 Activities || Contributed Papers: Cognitive Radio Networks and Spectrum Management (I)		
08:30-19:00	Registration		
09:00-11:00	**GRAND OPENING**		**HALL 1**
11:00-11:30	COFFEE BREAK		
11:30-13:30	**Cognitive Radio Networks and Spectrum Sensing & Management (I-A) | CRN, Relay and Routing : WVITAE & WPMC || *Session Chair: K.T.V. Reddy, TPC Chair, IETE, India***		MRG .01
	1570213275	C2R2M: Cluster-based Cognitive Radio Routing Mechanism; **Shriram Kulkarni, Shriram Markande**; *University of Pune*, **India**	
	1570209919	Adaptive Cooperative Spectrum Sensing and Access in Cognitive Radio Networks; **Kayalvizhi G;** *SSN College of Engineering*, **India**	
	1570212756	Evaluation of Channel Assembling Strategies with Single-Class Users in Cognitive Radio Networks; **Ebenezer Esenogho, Tom Walingo**; *University of KwaZulu-Natal*, **South Africa**	
	1570188607	Evaluating the Effect of Selfishness on Flooding Based DTN Routing Algorithms; **C Sobin**, **Vaskar Raychoudhury**; *IIT Roorkee*, **India**	
	1570213104	**WPMC:** Throughput of Secondary User in Underlay Cognitive Relay Network with Energy Harvesting; **Binod Prasad, Sanjay Dhar Roy, Sumit Kundu**; *National Institute of Technology, Durgapur*, **India**	
	1570207535	**WPMC:** Quality of Service Enforcing Centrally Optimized Routing for Delay Tolerant Networks; **Abhishek Thakur, Chittaranjan Hota**; *BITS Pilani, Hyderabad Campus* , **India**	
13:30-14:30	LUNCH		
14:30-16:30	**Cognitive Radio Networks and Spectrum Sensing & Management (I-B): WPMC || *Session Chair: Masahiro Umehira, Ibaraki University, Japan***		MRG .01
	1570193943	A Compressive Sensing-based Channel Estimation via GAMP in FBMC/OQAM System; **Meng Lin, Yunzhou Li, Limin Xiao, Yan Zhang, Xibin Xu, Jing Wang**; *Tsinghua University*, **China**	
	1570206001	New Pricing Model for Dynamic Dual-operator Spectrum Sharing in GSM; **Meghan Saitwal, Yuva Kumar, Brij Mohan Baveja, Mohammed Zafar Ali Khan, Uday B Desai;** *Indian Institute of Technology, Hyderabad*, **India**	
	1570192957	Improved p-norm Energy Detector with Soft Combining in AWGN Channel for Spectrum Sensing; **Vaibhav Kumar, Deep Kandpal, Ranjan Gangopadhyay, Soumitra Debnath;** *L.N.Mittal Institute of Information Technology, Jaipur*, **India**	
	1570213925	Selective Sensing Framework for Opportunistic Mobile Phone Sensing Networks; **Thejaswini M, Pachamuthu Rajalakshmi, Uday B Desai**; *Indian Institute of Technology, Hyderabad*, **India**	
	1570193867	Investigation on Listen-Before-Talk Mechanism of Licensed-Assisted Access to Unlicensed Spectrum; **Yu Jiang①, Hiroki Harada②, Liu Liu①, Huiling Jiang① ,Satoshi Nagata††**; ① *DOCOMO Beijing Communications Laboratories Co., Ltd*, **China**, ② *NTT DOCOMO, INC*, **Japan**	
	1570213278	CDF Based Spectrum Occupancy Rate Measurement Using Least Square Estimation of Gaussian Noise Period; **Shota Rachi, Akira Saito, Masahiro Umehira, Shigeki Takeda;** *Ibaraki University*, **Japan**	
16:30-17:00	COFFEE BREAK		

16:30-17:00	(Continued: MRG .01 Activities) COFFEE BREAK		
17:00-19:00	**Cognitive Radio Networks and Spectrum Sensing & Management (I-C): WPMC** ***||Session Chair: Sumit Kondu, NIT DurgapurA Leti, France***		MRG .01
	1570208599	Detection Performance of Soft Data Fusion in Rician Fading Channel for Cognitive Radio Network; **Srinivas Nallagonda[1][2], V Chandra Sekhar[1], Aniruddha Chandra[3][4], Sanjay Dhar Roy[4], Sumit Kundu[4];** *[1]M V S R Engineering College ,[2]Osmania University,[3]Brno University of Technology, [4]National Institute of Technology, Durgapur, WB*;**[1][2][4]India, [3]Czech Republic**	
	1570213378	Evaluation of permutation entropy detection for cognitive radio networks; **Srinu Sesham, Amit Kumar Mishra**; *University of Cape Town, Cape Town*, **South Africa**	
	1570208853	Optimization of Cooperative Spectrum Sensing in Cognitive Radio over Erroneous Reporting Channel; **Narasimha Rao Banavathu, Mohammed Zafar Ali Khan**; *Indian Institute of Technology, Hyderabad*, **India**	
	1570213111	Distributed Token Based MAC for Multi-Channel Multi-Interface Cognitive Radio WMN; **Mohammed A R Quadri, Ramesh Babu Battula, Manoj Singh Gaur, Dinesh Gopalani, Meenakshi Tripathi**; *Malaviya National Institute of Technology Jaipur*, **India**	
	1570209789	Path and Load Aware Routing Algorithm for Cognitive Radio Wireless Mesh Network**; Ramesh Babu Battula, Manoj Singh Gaur, Dinesh Gopalani, Emmanuel Shubhakar Pilli**; *Malaviya National Institute of Technology, Jaipur*, **India**	
	1570213374	Fractal dimension of spectral estimates for spectrum sensing under noise variance uncertainty; **Srinu Sesham[1], Amit Kumar Mishra[1], Siba Kumar Udgata [2], Samrat Sabat[2]**; *[1]University of Cape Town, Cape Town* ,**South Africa,** *[2]University of Hyderabad, Hyderabad*, **India**	
19:30-22:30	END of DAY 2 || Cultural Program (Mridangam and Kuchipudi Group Dance Recital), GALA DINNER & Best Paper Award: HALL1		

Time Slot	Day2: Monday, December 14 || MRG .02 Activities || Contributed Papers: Next Generation Networks & Internet of Things (I)		
08:30-19:00	Registration		
09:00-11:00	**GRAND OPENING**		**HALL 1**
11:00-11:30	COFFEE BREAK		
11:30-13:30	**Next Generation Networks (I-A) | 5G and Device to Device Communications: WPMC || *Session Chair: Sri Ganesh Rao, Tata Consultancy Services, Bangalore, India***		MRG .02
	1570194953	The impact of Network Neutrality on the OTT Service of 5G WISDOM; **Yapeng Wang, Ramjee Prasad**; *Center of TeleInFrastrukur, Aalborg University,Aalborg*, **Denmark**	
	1570206855	Efficient Device-to-Device (D2D) Offloading Mechanism in LTE Networks; **Bighnaraj Panigrahi, Rashmi Ramamohan, Hemant Kumar Rath, Anantha Simha**; *Tata Consultancy Services*, **India**	
	1570208181	Survey of Device-to-Device Communications Infrastructure-less in IEEE 802.15.8 Task Group; **Marco Hernandez, Ryu Miura**; *NICT*, **Japan**	
	1570208909	Link Adaptation Strategies for Cellular Downlink with low-fixed-rate D2D Underlay; **Afonso Eduardo, Ivo Sousa, António J. Rodrigues**; *Instituto de Telecomunicações (IT) Instituto Superior Técnico (IST), Universidade de Lisboa Lisbon*, **Portugal**	
	1570210057	A Pattern Division Multiple Access Scheme for 5G wireless communication systems; **Zhang Kai, Jin Xu**; *Beijing University of Posts and Telecommunications*, **China**	
	1570213212	Coexistence of Systems with Different Multicarrier Waveforms in LSA Communications; **Mirza Golam Kibria, Gabriel Porto Villardi, Kentaro Ishizu , Fumihide Kojima**; *Wireless Network Research Institute, National Institute of Information and Communications Technology*, **Japan**	
13:30-14:30	LUNCH		
14:30-16:30	**Next Generation Networks (I -B) | Spectrum Issues and Intelligent Approach: WVITAE || *Session Chair: S.K. Agarwal, Former Director, DIETY, Government of India, India***		MRG .02
	1570213573	Spectrum Scarcity at the Extensive and Intensive Edges: From White Space to 5G; **Benoît Pierre Freyens**; *University of Canberra*, **Australia**	
	1570210051	Real Time Evaluation of Energy Detection and Covariance based Spectrum Sensing Algorithms; **Sunil Devanahalli, Samrat Sabat**; *University of Hyderabad*, **India**	
	1570213985	Self Configurable Intelligent Distributed Antenna System; **Ambuj Kumar, Albena Mihovska, Ramjee Prasad**; CTIF, *Aalborg University*, **Denmark**	
	1570209885	Distributed Forward-Backward Pursuit Algorithm for Distributed Compressive Sensing; **Suchithra Sudhakaran, Neelakantan PC**; *Adi Shankara College of Engineering and Technology*, **India**	
	1570210103	Spectrum for 5G Services; **Purnendu Shekhar Mani Tripathi①②, Ramjee Prasad②**; ①*Ministry of Communications* & IT, **India**, ②*Centre for TeleInFrastructure(CTiF),Aalborg University, Aalborg*, **Denmark**	
	1570209977	On Performance of Eigenvalue based Detectors for Spectrum Sensing under Different Fading Conditions; **Ashwini Deshmukh①, Madhukar Deshmukh②, Flemming Bjerge Frederiksen②, Ramjee Prasad②③**; ①*Trinity College of Engineering Research Pune*, **India**, ②*RATE, Department of Electronic Systems,* ③*CTIF; Aalborg University*, **Denmark**	
16:30-17:00	COFFEE BREAK		

16:30-17:00	(Continued: MRG .02 Activities) COFFEE BREAK		
17:00-19:00	**Next Generation Networks (I- C) | Future Vision and IoT: WVITAE & WPMC ||*Session Chair: Raja Rajeswari, IETE, India***		MRG .02
	1570213430	Access for Internet of Things using Smartphone as a Gateway utilizing LTE and WiFi; **Prateek Mathur[1], Rasmus Hjorth Nielsen[2], Neeli Rashmi Prasad[3], Ramjee Prasad[1]**; *[2]Cisco Systems* , **USA,** *[3]Center for TeleInFrastructure (CTIF)*, **USA**, *[1]Center for TeleInFrastructure (CTIF), Aalborg University*, **Denmark**	
	1570213454	Cognitive framework for flexible queuing strategy in Next Generation Networks; **Hanuma Chitti[1], Neeli Rashmi Prasad[2], Knut Ovsthus[3], Ramjee Prasad[1]**; *[2]Center for TeleInFrastructure (CTIF)*, **USA**, *[3]Bergen University College*, **Norway**, *[1]Center for TeleInFrastructure (CTIF), Aalborg University*, **Denmark**	
	1570215979	Service Interaction through Gateways for Inter-Cloud Collaboration within the Arrowhead Framework; **Pál Varga[1], Csaba Hegedus[2]**; *[1]Budapest University of Technology and Economics, [2] AITIA International Inc.*; **Hungary**	
	1570191635	Single Thing Sign On Identity Management for Internet of Things; **Vanya Zdravkova, Mihail Mihaylov, Albena Mihovska, Ramjee Prasad**; *Department of Electronic Systems, Center for TeleInfrastruktur, Aalborg University*, **Denmark**	
	1570191687	**WPMC:** Towards Internet of Services - SDN-enabled IMS Architecture for IoT Integration; **Anton Katov[1], Bayu Anggorojati[1], Sofoklis Kyriazakos[1], Albena Mihovska[1], Neeli Rashmi Prasad[2]**; *[1]Center for TeleInFrastructure (CTIF), Aalborg University*, **Denmark,** *[2]Center for TeleInFrastructure (CTIF), Aalborg University*, **USA**	
	1570195595	**WPMC:** Packet Scheduling Scheme to Guarantee QoS in Internet of Things; **Reema Sharma[1], Navin Kumar[2], Namratha Gowda[1,3], Srinivas Talabattula[4];** *[1]The Oxford College Of Engineering, [2]Amrita University & School of Engineering, [3]Visvesvaraya Technological University, Karanataka, [4]Indian Institute of Science, Bangalore*; **India**	
19:30-22:30	END of DAY 2 || Cultural Program (Mridangam and Kuchipudi Group Dance Recital), GALA DINNER & Best Paper Award: HALL1		

Time Slot	Day2: Monday, December 14 || MRG .03 Activities || Contributed Papers: Vehicular & Mobile Ad-hoc Networks (I)		
08:30-19:00	Registration		
09:00-11:00	GRAND OPENING		HALL 1
11:00-11:30	COFFEE BREAK		
11:30-13:30	**Vehicular & Mobile Ad-hoc Networks (I-A)| Aerial and Sensor Ad-Hoc Networks: WVITAE|| *Session Chair: Sanjay Kumar, Birla Institute of Technology, Ranchi, India***		MRG .03
	1570214001	Embedded Video Processing and Data Acquisition for Unmanned Aerial Vehicle; **Vrunal Mhatre, Akshay Patil, Siddhesh Chavan, Ashish Chittimilla, Aaron Samuel;** *Fr. Conceicao Rodrigues College of Engineering*, **India**	
	1570194189	HANET: Millimeter wave based intelligent radio architecture for serving place time capacity issue; **Purnima Lala Mehta[①②③④], Troels B. Sørensen[①③], Ramjee Prasad[①②③]**; *[②]Center for TeleInFrastructure (CTIF),* **Denmark**; *[③]Department of Electronic Systems, [①]Aalborg University,* **Denmark**; *[④]HMRITM, New Delhi,* **India**	
	1570195421	GSHMAC: Green and Secure Hybrid Medium Access Control for Wireless Sensor Network; **Pranav Pawar[①], Rasmus Hjorth Nielsen[②], Neeli Rashmi Prasad[③], Ramjee Prasad[①]**; [②]Cisco Systems , **USA**; [③]Center for TeleInFrastructure (CTIF), **USA**; [①]Center for TeleInFrastruktur, Aalborg University, Aalborg, **Denmark**	
	1570214751	Automatic Household Power Measurement & Control System based on Wireless Sensor Networks; **Jameel Ahamed;** *Aligarh Muslim University, Aligarh,* **India**	
	1570213872	Conducted EMI Analysis of Vehicle Positioning System and Strategies to Reduce Conducted EMI; **Shreenivas Ramesh Jog, Nidhi Chaturvedi**; *D. Y. Patil Institute of Engineering & Tech.*, **India**	
	1570213870	Study of Radiated Emission from Wireless Positioning System and the strategies to minimize it; **Shreenivas Ramesh Jog, Suvidha Chitnis**; *D. Y. Patil Institute of Engineering & Tech.*, **India**	
13:30-14:30	LUNCH		
14:30-16:30	**Vehicular & Mobile Ad-hoc Networks (I-B) |Wireless Sensor Networks: WPMC || *Session Chair: Vishwanath Sinha, M N National Institute of Technology, Jaipur, India***		MRG .03
	1570210123	An Interdependent Source-Channel Coding for Energy Efficient Communication in WSNs**; Resmi N C, Sonali Chouhan**; *Indian Institute of Technology Guwahati,* **India**	
	1570194199	Impact of Network Coding on Distributed Indoor Target Tracking using Wireless Sensor Networks; **Laxminarayana Pillutla, Shourya Gupta, Dushyant Singh**; *Dhirubhai Ambani Institute of Information and Communication Technology (DA-IICT)*, **India**	
	1570195119	Mobility-aware Hybrid Synchronization for Wireless Sensor Network; **Dnyaneshwar Mantri, Neeli Rashmi Prasad, Ramjee Prasad**; *Center for TeleInFrastructure (CTIF), Aalborg*, **Denmark**	
	1570195013	Characterization for Reporting Rate of Adaptive Sectoring Scheme to Improve Reliability in WSN; **Manohar S. Chaudhari [①], Vivek Shankar Deshpande[②], Ramjee Prasad[③]**; *[①]Sinhgad Institute of Technology, Pune University,* **India**; *[②]University of Poona & MIT College of Engineering,* **India**; *[③]Center for TeleInFrastructure (CTIF), Aalborg University,* **Denmark**	
	1570195063	Q-MOHRA:QoS Assured Multi-Objective Hybrid Routing Algorithm for Heterogeneous WSN; **Nandkumar Kulkarni[①], Neeli Rashmi Prasad[②], Ramjee Prasad[①]**;*[①]Center for TeleInFrastructure (CTIF),* ***Denmark****; [②]Center for TeleInFrastructure (CTIF),Aalborg University*, **USA**	
	1570213289	Performance Analysis of Total Power Consumption in Linear Multi-hop Networks; **Satoshi Yamazaki[①], Kouji Ohuchi[②]**; *[①]Numazu National College of Technology & Department of Control & Computer Engineering, Numazu, Shizuoka, [②]Shizuoka University Johoku, Hamamatsu, Shizuoka;* **Japan**	
16:30-17:00	COFFEE BREAK		

16:30-17:00	(Continued MRG .03 Activities) COFFEE BREAK		
17:00-19:00	**Vehicular & Mobile Ad-hoc Networks (I-C)|Vehicular and Mobile Ad-Hoc Networks: WPMC || *Session Chair: Vladimir Poulkov, Technical University of Sofia, Bulgaria***		MRG .03
	1570188641	Transmission Capacity Analysis for Linear Vehicular Ad Hoc Networks; **Xinxin He, Weisen Shi, Tao Luo;** *Beijing University of Posts and Telecommunications*, **China**	
	1570199753	Trust based Detection and Elimination of Packet Drop Attack in the Mobile Ad-hoc Networks; **Vishvas Kshirsagar[1][2], Ashok Kanthe[1][3], Dina Simunic[3]**; *[1]Sinhgad Institute of Technology, Lonavala,* **India**, *[2]Savitribai Phule Pune University,* **India,** *[3]Faculty of Electrical Engineering and Computing (FER), University of Zagreb*, **Croatia**	
	1570199757	The Behavioral Based Gray Hole Attack Detection in Mobile Ad-hoc Network (MANET); **Parineet Shukla[1][2], Ashok Kanthe[1][3], Dina Simunic[3]**; *[1]Sinhgad Institute of Technology, Lonavala,* **India**, *[2]Savitribai Phule Pune University*, **India**, *[3]Faculty of Electrical Engineering and Computing (FER), University of Zagreb*, **Croatia**	
	1570194567	On Supporting Integrated Multimedia Traffic in TDMA based Mobile Ad hoc Networks; **Mallesham Dasari[1], Himanshu Sindhwal[1], Naresh Vattikuti[1], Bheemarjuna Reddy Tamma[2]**;*[1]Uurmi Systems Pvt. Ltd. Hyderabad, [2]IIT Hyderabad, Hyderabad;* **India**	
	1570194813	Intrusion Detection System Against Colluding Misbehaviour in MANETs; **Pragya Mishra, Karm V Arya, Hardev singh Pal**; *ABV-Indian Institute of Information Technology & Management, Gwalior*, **India**	
	1570195073	Two-Party Key Agreement Protocol for MANETs based on Verifiable Secret Sharing Scheme; **Cheruku Asha Jyothi, Narsimha Gugulotu**; *Jawaharlal Nehru Technological University College of Engineering, Jagtial, Karimnagar, Telangana,* **India**	
19:30-22:30	END of DAY 2 || Cultural Program (Mridangam and Kuchipudi Group Dance Recital), GALA DINNER & Best Paper Award: HALL1		

Time Slot	Day2: Monday, December 14 || MRG .04 Activities || Contributed Papers: Technology Applications (I)		
08:30-19:00	Registration		
09:00-11:00	**GRAND OPENING**		**HALL 1**
11:00-11:30	COFFEE BREAK		
11:30-13:30	**Technology Applications (I-A) | Human Applications : WVITAE & WPMC || *Session Chair: Vladamir Poulkov, Technical University of Sofia, Bulgaria***		MRG .04
	1570213423	Behavior State Feature Extraction through Single Channel EEG Device for Medical Application; **Sravanth Kumar Ramakuri, Vivek Kumar, Bharat Gupta**; *Birla Institute of Technology Mesra, Ranchi*, **India**	
	1570206439	Real-time Detection of EEG Electrode Displacement for Brain-Computer Interface Applications; **Giulia Cisotto, Silvano Pupolin**; *University of Padua*, **Italy**	
	1570213165	Remote Heart Rate Evaluation by Variational Mode Decomposition**; Bogdan Gavriloaia[1], Octavian Fratu[1], Simona Halunga[1], Gheorghe Gavriloaia[2], Constantin Mara[2], Radu Vizireanu[1]**; [1]University Politehnica of Bucharest, [2]University of Pitesti; **Romania**	
	1570210205	Speech Feature Analysis and Selection for Emotion Classification; **Angel Manolov, Ognian Boumbarov, Agata Manolova, Vladimir K. Poulkov, Krasimir Tonchev**; *Technical University of Sofia*, **Bulgaria**	
	1570213386	Public Auditing and Data Dynamics in Cloud with Performance Assessment on Third Party Auditor; **Snehal Sawant[1,2], Aaradhana Arvind Deshmukh[1,2], Albena Mihovska[1], Ramjee Prasad[1];** [1]*CTIF, Aalborg University*, **Denmark,** [2]*Smt.Kashibai Navle College of Engineering, Vadgoan BK, Pune*, **India**	
	1570195309	**WPMC:** Non Audio-Video gesture recognition system; **Razvan Craciunescu[1,2], Cristian Ionut Dita[1], Albena Mihovska[1], Octavian Fratu[2], Sofoklis Kyriazakos[1], Ramjee Prasad[1]**; [1]*CTIF, Aalborg University*, **Denmark**, [2]*University Politehnica of Bucharest*, **Romania**	
13:30-14:30	LUNCH		
14:30-16:30	**Technology Applications (I-B) | Human Applications : WPMC || *Session Chair: fred Harris, San Diego State University, USA***		MRG .04
	1570207155	Fuzzy Logic based Human Detection in Video; **Manojkumar M Gawali, Dipti R. Pawar**; *Sinhgad College of Engineering, Pune*, **India**	
	1570207563	Improving Segmentation Accuracy for Motion Detection using Bidirectional Video Processing**; Abhishek Thakur, Ankesh Kumar**; *BITS Pilani , Hyderabad Campus*, **India**	
	1570194919	Automatic Speaker Detection and Recognition in a multi classroom E-Learning System; **Amitha Vijayan, Balaji Hariharan**; *AMRITA Vishwa Vidyapeetham Amritapuri, Kollam*, **India**	
	1570213262	Real-time EEG Monitoring and Transmission over Low Bandwidth Wireless Networks; **Kaushik Lahiri[1], Amitava Mukherjee[1], Mrinal Kanti Naskar[2]**; [1]*IBM India Pvt Ltd;* [2]*Jadavpur University*; **India**	
	1570194425	Adaptive priority based network bandwidth throttling for a Virtual Classroom System**; Jobina Varghese, Balaji Hariharan**; *AMRITA Vishwa Vidyapeetham Amritapuri, Kollam*, **India**	
	1570213445	Minimal Error IEEE 802.15.4 Communication Module for Heart Monitoring Data Transmission in IoT; **Subrahmanyam Vuddagiri, Mohammed Abdullah Zubair, Ajay Yadav, Pachamuthu Rajalakshmi**; *Indian Institute of Technology Hyderabad*, **India**	
16:30-17:00	COFFEE BREAK		

16:30-17:00	(Continued MRG .04 Activities) COFFEE BREAK		
17:00-19:00	**Technology Applications (I-C) | Multiple Areas: WVITAE || *Session Chair: Hiroshi Harada, Kyoto University, Kyoto, ICT, Koganei,* Japan**		MRG .04
	1570207041	Design of Amateur Radio Wireless Transceiver to Reduce the Impact of Natural Calamities; **Ashwini Shingate[1], Rushikesh Borse[2], Shubham Tiwari[3], Arvind Jawale[4]**; [1][2]*Savitribai Phule Pune University*, [2]*Savitribai Phule Pune University*, [2]*Shubhra Energy*, [4]*Scout Satara*; **India**	
	1570210199	Deep Sea Exploration Recovery and Transport [DESERT] Vehicle and its Modes of Communication; **Aileen Sengupta[1], Pavel Sengupta[2]**; [1]*Techno India College of Technology, Rajarhat,* [2]*Dr. Sudhir Chandra Sur Degree Engineering College, Dum Dum, Kolkata* □; **India**	
	1570208685	Energy Efficient Lighting System for Indoor Parking with Ubiquitous Communication; **Mahesh Jha[1], Navin Kumar[2]**; [1]CMRIT, VTU, [2]Amrita University & School of Engineering; **India**	
	1570210063	Recent Progress in Radioclimatological Modeling in Equatorial and Tropical Africa; **Thomas Afullo, Akintunde Alonge**; University of Kwazulu-Natal, Durban, **South Aftrica**	
	1570210261	Digital door lock using fingerprint, webcam and GSM - a novel approach for smart homes; **Ashish Patwari, Karuna Yepuganti, Arpit Omar, Shekhar Thakur, Kaushik Kumar**; *VIT University, Vellore*, **India**	
	1570209921	Marine Vessel Detection Comparing GPRS and Satellite Images for Security Applications; **Sajan Ambadiyil[1], Dintu Thomas[2], V P Mahadevan Pillai[3]**; [1]*Optical Image Processing Division, C-DIT,* [2]*SCMS School of Engineering and Technology,* [3]*University of Kerala, Thiruvanthapuram, Kerala*; **India**	
19:30-22:30	END of DAY 2 || Cultural Program (Mridangam and Kuchipudi Group Dance Recital), GALA DINNER & Best Paper Award: HALL1		

Time Slot	Day2: Monday, December 14 || MRG .05 Activities || Special Sessions on WWRF & GISFI and; Contributed Papers: Physical and Fundamentals (I)		
08:30-19:00	Registration		
09:00-11:00	**GRAND OPENING**		**HALL 1**
11:00-11:30	COFFEE BREAK		
11:30-13:30	**WPMC Special Session on "Selected Topics"** **Session Organizer and Chair: Shinsuke Hara,** *Osaka City University*, **Japan**		MRG .05
	Invited Talk	"Home neuro- rehabilitation: an ICT near Future Service", **Silvano Pupolin**, *University of Padua*, **Italy**	
	Invited Talk	" **Lakhshmi Mukunkutla**, *USA/Aalborg University*, **Denmark**	
	Invited Talk	"Convergence Techniques for Future Communications", **M. Jankiraman**, *Larsen & Toubro Ltd. (L&T), Bangalore*, **India**	
	Invited Talk	" Making a Safe and Secure 4 G World", **Debu Nayak**, *Huawei Telecommunications India Pvt. Ltd*, **India**	
13:30-14:30	LUNCH		
14:30-16:30	**Physical and Fundamentals (I-A) | LTE and Multiple Access Techniques (OFDMA/OFDM/SC-FDMA, MIMO, SISO): WPMC & WVIATE || *Session Chair:* ", M. Jankiraman, *Larsen & Toubro Ltd. (L&T), Bangalore, India***		MRG .05
	1570196365	Joint Transceiver Design for QoS-Constrained MIMO Two-Way Non-Regenerative Relaying; **Rohit Budhiraja, Bhaskar Ramamurthi**; *Department of Electrical Engineering, IIT Madras*, **India**	
	1570190883	New virtual 8x1 MISO scheme with QOSTBC; **Ugljesa Urosevic, Zoran Veljovic, Milica Pejanovic-Djurisic**; University of Montenegro, Podgorica, **Montenegro**	
	1570212700	Limited Feedback Scheduling For MIMO-OFDM Broadcast Network; **Prabina Pattanayak, Preetam Kumar;** *Indian Institute of Technology, Patna*, **India**	
	1570193823	An Efficient Deterministic Scheme for Blind CFO Estimation in SC-FDMA; **Vinay Kumar Trivedi, Vidya Sagar, Preetam Kumar**; *Indian Institute of Technology, Patna*, **India**	
	1570209997	**WVIATE:** Capacity Analysis of MIMO BC Channels in Presence of Spatial Correlation; **Ashok Panda①, Swadhin Kumar Mishra②, Ajit Kumar panda②**; ①IIIT Bhubaneswar,② *NIST Berhampur*; **India**	
	1570212704	**WVITAE:** Error Rate Performance for Multiuser scheduling in MIMO downlink system with imperfect CSI; **Prabina Pattanayak, Diwakar Pandey, Preetam Kumar;** *Indian Institute of Technology, Patna*, **India**	
16:30-17:00	COFFEE BREAK		
17:00-19:00	**WVITAE Special Session: Wireless World Research Forum (WWRF):** **Knud Erik Skouby,** Aalborg University **, Denmark and Sudhir Dixit,** WWRF**, USA**		MRG .05
	Theme : **Mobile History of India**		
	Opening Speech	**Knud Erik Skouby,** *Aalborg University* **, Denmark**	
	Keynote Speech	**Sudhir Dixit,** *WWRF*, **USA**	
	Invited Talk	**Krishna Sirohi,** *NIKSUN*, **India**	
19:30-22:30	END of DAY 2 || Cultural Program (Mridangam and Kuchipudi Group Dance Recital), GALA DINNER & Best Paper Award: HALL1		

Time Slot	Day2: Monday, December 14 || MRG .06 Activities || Second International Workshop on Innovation and Entrepreneurship(IWIE) (I)			
08:30-19:00	Registration			
09:00-11:00	**GRAND OPENING**			**HALL 1**
11:00-11:30	COFFEE BREAK			
11:30-13:30	**Second International Workshop on Innovation and Entrepreneurship(IWIE) :(I-A) || Entrepreneurship Contest** Second International Workshop on Innovation and Entrepreneurship(IWIE) | (I –A) Organizer and Chair: Sofoklis Kyriazakos, CTIF, Aalborg University, Denmark **Introduction to the Workshop and Entrepreneurship Contest**			MRG .06
	Mayank Kumar Mittal, **SaleYourBooks.com** Mayank Semwal , **Genralsorts** Shilpa Chaudhary, **Car security Systems** Meenakshi Gupta, **MNY PRO** Jafar Mapara, **Identity Management System** Akskay Radke, **Smart Indian railways**	Mayank Semwal, **App for professional Help** Deepak Sharma, **Instant Presentation and Converter** Mukesh Wadile, **SecureChip** Heramb Pawar, **Clear Vision** Naman Vashishth, **Find ME!!!!** Darshan Vyas, **CLOTH TESTER using IMAGE PROCESSING** Shashank Roy, **Electronic Refigerator**	Adarsh Mishra, **Virtual PPM-1** Utkarsh Trivedi, **Service Providers Support** Irram Patharwat, **Methane Extraction Digester** Manoj Radadiya, **Gesture and Voice based Television Control System** Nikhil Prabhu, **Smart Electric Car using AMR7** Jafar Mapara, **Connected Homes** Madhukesh Heggannavar, **Design and Development of Magnetron Power Source**	
13:30-14:30	LUNCH			
14:30-16:30	**Second International Workshop on Innovation and Entrepreneurship(IWIE) :(I-B) || Entrepreneurship Contest** Second International Workshop on Innovation and Entrepreneurship(IWIE) | (I –B) Organizer and Chair: Sofoklis Kyriazakos, CTIF, Aalborg University, Denmark IWIE Activities			MRG .06
16:30-17:00	COFFEE BREAK			
17:00-19:00	**Second International Workshop on Innovation and Entrepreneurship(IWIE) :(I-C) || Entrepreneurship Contest** Second International Workshop on Innovation and Entrepreneurship(IWIE) | (I –C) Organizer and Chair: Sofoklis Kyriazakos, CTIF, Aalborg University, Denmark **Results and Discussion of Entrepreneurship Contest of the IWIE Workshop Day -1**			MRG .06
19:30-22:30	END of DAY 2 || Cultural Program (Mridangam and Kuchipudi Group Dance Recital), GALA DINNER & Best Paper Award: HALL1			

Tuesday, December 15

Day 3

"Workshops, Special Sessions, Contributed Papers"

Time Slot	Day3: Tuesday, December 15 || HALL 1.1 & 1.2 Activities || Workshops & Special Sessions (II-A)			
08:30-19:00	Registration			
09:00-11:00	**Keynote Speech || Chair: Ashok Chandra, TPC Executive Chair, WPMC/ GWS-2015** **Lars Kiekegaard**, Teracom, **Denmark** **Ramesh Rao**, University of California, San Diego, **USA**			**HALL 1**
11:00-11:30	**COFFEE BREAK**			
11:30-13:30	**WPMC Special Session on "Smart Village 'Rural Model': Basic Unit for a Digital India" || Session Organizer and Chair: Mayur Dave,** *IETE*, **INDIA**			HALL 1.1
	1570227716	Demonstrating SWiFiIC - Sustainable WiFi for Rural Communication; **Abhishek Thakur, Aarthi J, Amit Chawla, Chittaranjan Hota**; *BITS Pilani, Hyderabad Campus,Hyderabad*, **India**		
	1570234273	"IoT" based Smart Village: An Indigenous step towards 'Digital India'; **Madhukant Patel①, Piyush Yadav②**; *①MD, Reve Automation LLP, ②Green Cloud iSoft P. Ltd., Dehradun*, **India**		
	1570234316	Rurbanisation of India; **Bipin Pradeep Kumar**, *Gaia Smart Cities*, **India**		
	WVITAE Special Session on "Persuasive Multi Business Model Innovation in a World of Persuasive Technologies" **Session Organizer and Chair: Peter Lindgren,** *Multi Business Model Innovation and Technology, Aarhus University*, **Denmark ||Session Co-organizers: Troels Christian, K. Andersen, Torben Bjerrum, Annabeth Aagaard, Ole Horn Rasmussen, Morten Karnøe Søndergaard** *Aarhus University*, **Denmark; Theodoor van Dongen,** *VDMBee, Veenendaal*, **The Netherlands**			HALL 1.2
	1570228216	Persuasive Technology and Business Models; **Morten Karnøe Søndergaard, Peter Lindgren, Niels Einar Veirum;** *Stanford Peace Innovation Lab, Department of Business Development and Technology, Aarhus University*, **Denmark**		
	1570228627	Service and Big Data business model in a world of persuasive technologies; **Troels Christian K. Andersen, Torben Cæsar Bisgaard Bjerrum**; *Aarhus University, Herning*, **Denmark**		
	1570228634	Secure Persuasive Business Models and Business Model Innovation in a World of 5G; **Peter Lindgren, Katharina Wuropulos**; *Aarhus University*, **Denmark (###)**		
13:30-14:30	LUNCH			
14:30-16:30	**WPMC Workshop on " Advanced Technologies and Promotion Strategies for Wi-SUN and the Wireless Grid Systems" || Workshop Organizer and Chair:** *Fumihide Kojima*, **Japan**			HALL 1.1
	Wi-SUN Alliance -Promoting open interoperable industry standards for smart utility networks; **Hiroshi Harada**, NICT, Japan		NICT's R&D, Standardization and Promotion Avtivities on Wi-SUN and the wireless grid systems; **Fumihide Kojima**, NICT, Japan	
	Wi-SUN RLMM Profile for Sensor Network Application; **Ryota Yamada**, Omron, Japan		Wi-SUN Alliance Activity in India; **Amarjeet Kumar**, Wi-SUN Alliance, India	
	WVITAE Workshop on "Wearable and Nearable Internet of Things (WaNIOT 2015)"|| Workshop Organizer and Chair: Balamuralidhar P, *Tata Consultancy Services (TCS)*, **Bangalore, India**			HALL 1.2
	Introduction by the workshop chair: Dr. Balamuralidhar P., TCS Innovation Lab, Bengaluru Wearables for Newborns": Prof. Bharadwaj Amrutur, Indian Institute of Science, Bengaluru Wearables for Safety: Mr. Ganesh Suryanarayanan, GTIO, Tata Group, Bengaluru		Data-driven Healthcare using Affordable Sensing", Dr. Arpan Pal, TCS Innovation Lab, Kolkata RF based Sensing of Cardiopulmonary Vital Signs": Mr. R.P.Pinto, SAMEER, Mumbai IoT in healthcare: Applications to neurology: Dr. Jayavardhana Gubbi, TCS Innovation Labs, Bengaluru	
16:30-17:00	COFFEE BREAK			

16:30-17:00	(Continued Hall 1.1 and 1.2 Activities) BREAK				
17:00-19:00	**Matchmaking session – Indian industry meets Global Industry || Organizer and Chair: Krishnal Sirohi,** *GISFI*, **India**				HALL 1.1
	Lars Kierkegaard, *Teracom*, **Denmark**	**Srinivasa Gutta, INVECAS,** *Hyderabad,* **India**	**Sivabalan Arumugam,** *NEC* **, Japan**	**Kiritkumar Lathia, GISFI/CTIF, Denmark**	
	Sandip Inamdar, *WISDOM Pvt. LTD.*, **India**	**Balaji Kanigicherla,** *Ineda Systems, Hyderabad,* **India**	**Gangadhar Gude, SoCtronics,** *Hyderabad,* **India**	**Subbarangaiah,** *VEDA IIT, Hyderabad*, **India**	
	WVITAE Special Session on " Fiber-Wireless Convergence for broadband Connectivity in 5G perspective" || **Session Organizer and Chair: Jayashree Ratnam,** International Institute of Information Technology, *Hyderabad*, **India**				HALL 1.2
	Invited Talk	Journey to World Wide Wireless and its Deployment Challenges**, D.S. Rao**, Tata Communications Ltd, Hyderabad, India			
	1570228022	Participation of Optical Backbone Network in Successful Advancement of Wireless Network; **Rajarshi Mahapatra**; *CVR College of Engineering*, **India**			
	1570228026	On 5G Cellular Backhaul Networks; **Mahima Mehta**, *Intel Mobile Communications India Pvt. Ltd., Bangalore*, **India**			
	1570228029	Telecom Regulatory Issues in Converged Era; **G. Muralidhar , Robert Ravi**; *Telecom Regulatory Authority of India*, India **(***)**			
19:30-22:30	END of DAY 3 || NETWORKING DINNER: FOYER				

Time Slot	Day3: Tuesday, December 15 || MRG .01 Activities || Workshops & Special Sessions (II-B)		
08:30-19:00	Registration		
09:00-11:00	**Keynote Speech**		HALL 1
11:00-11:30	COFFEE BREAK		
11:30-13:30	**WVITAE Special Session on" Internet of Things (IoT)"** **Session Organizers: Birger Andersen①, Knud Erik Skouby②, ② Samant Khajuria,** ①*Technical University of Denmark, Copenhagen*, ②*Aalborg University, Copenhagen*, **Denmark** **Session Chair: Birger Andersen,** *Technical University of Denmark, Copenhagen*, **Denmark**		MR G.01
	Keynote Talk	IoT in Theory and Practice**, Birger Andersen,** *Technical University of Denmark, Copenhagen*, **Denmark**	
	1570227404	Heuristic Trust in IoT; **Bipjeet Kaur①, Henrik Tange②;** ①*Denmark Technical University* , ②*Wireless Center CTIF Copenhagen*; **Denmark (###)**	
	1570228109	Cyber security for M2M Smart Grid; **Sarmistha De Dutta①, Prof. Ramjee Prasad②**; ①*NIKSUN, Inc.*, **USA** ②*Center For TeleInFrastruktur , Aalborg University*, **Denmark**	
	1570228247	GET IoT- Green Computing and Energy Harvesting technology in Internet of Things (IoT); **Jetendra Joshi, Anshumali Singh, Lakshya Gourav Moitra , Manash Jyoti Deka**; *NIIT University, Neemrana, Alwar, Rajasthan*, **India**	
	1570228361	An Energy Efficient Adaptive Wireless Link for Farms based on IoT technologies**; T. Blaszczyk①, P. Lynggaard②**; ①*Technical University of Denmark,* ②*CMI, Aalborg University Copenhagen*; **Denmark**	
	1570231008	Implementation Of Internet Of Things Using Near Field Communication For Parking Automation; **Aishwarya Sanjay Ikhe, Sagar Jayant More, Priyanka Sanjay Suranglikar, Prashant S Dhotre;** *Sinhgad Institute of Technology and Science, Pune*, **India**	
13:30-14:30	LUNCH		
14:30-16:30	**WVIATE Special Session on "Spectrum Management and Networking for Multi-link Satellite and Terrestrial Communication Systems"** **Session Organizers and Chairs: Preetam Kumar, Vinay Kumar Trivedi, Akash Agarwal;** *Indian Institute of Technology Patna*, **India**		MR G.01
	Invited Talk	Vimal Bhatia, *Associate Professor, IIT Indore*, **India**	
	Invited Talk	Preetam Kumar, *Assistant professor, IIT Patna*, **India**	
	1570221151	Cancellation of Inter-Cell Interference in Downlink with No Backhaul Information Exchange; **Shuvabrata Bandopadhaya①, Jibendu Sekhar Roy②**; ①*Silicon Institute of Technology, Bhubaneswar, Odisha,* ②*School of Electronics Engineering, KIIT University, Bhubaneswar, Odisha*.; **India**	
	1570226980	Performance Analysis Of Interference Cancellation In MIMO-FBMC; **V.Padmapriya , N.Venkateswaran**; *SSN College of Engineering, Chennai*,**India**	
	1570227724	Measurement and Identification of White Space using Low Cost SDR for Rural Wireless Broadband; **Vinit Sharswat, Pradeep Godara, Abhijeet Bishnu, Vimal Bhatia;** *Indian Institute of Technology Indore*, **India**	
16:30-17:00	COFFEE BREAK		

16:30-17:00	(Continued MRG .01 Activities) COFFEE BREAK		
17:00-19:00	**WVITAE Special Session on " eWALL"** **Session Organizer and Chair: Sofoklis Kyriazakos, CTIF,** *Aalborg University***,** *Aalborg,* **Denmark**		MR G.01
	1570224200	Improving the Trustworthiness of Ambient Assisted Living Applications; **Elias Z. Tragos①, Pavlos Charalampidis①, Alexandros Fragkiadakis①, George Lambropoulos②, Sofoklis Kyriazakos②;** ①FORTH-ICS,② Converge SA**; Greece**	
	1570224206	Requirements and Challenges in Evaluation of Systems for Independent Living of Senior Citizens; **Antun Kerner, Antonija Marinčić, Ana Koren, Dina Šimunić ,Ramjee Prasad**; *Faculty of Electrical Engineering and Computing, University of Zagreb,* **Croatia**	
	1570224166	Virtual sensing environment for care at home; **Aristodemos Pnevmatikakis;** *Athens Information Technology, IRIS Laboratory, Athens,* **Greece**	
	1570224167	Expression recognition using graph based feature selection; **Krasimir Tonchev, Nikolay Neshov, Agata Manolova ,Vladimir Poulkov**; Technical University of Sofia, **Bulgaria**	
	1570213206	Participatory Heuristic Evaluation of the First Iteration of the eWALL Interface Application**; Clara Schaarup①, Louise Bilenberg Pape-Haugaard①, Stine Veje Hangaard①, Albena Mihovska② ,Ole Hejlesen①; ①Department of Health Science and Technology, ②Center for TeleInfrastruktur □;** *Aalborg University, Aalborg,* **Denmark**	
	1570195309	Non Audio-Video gesture recognition system; **Razvan Craciunescu, A. Mihovska ; Center for TeleInfrastruktur □;** *Aalborg University, Aalborg,* **Denmark**	
19:30-22:30	END of DAY 3 || NETWORKING DINNER: FOYER		

Time Slot	Day3: Tuesday, December 15 || MRG .02 Activities || Workshops & Special Sessions (II-C)		
08:30-19:00	Registration		
09:00-11:00	**Keynote Speech**		HALL 1
11:00-11:30	COFFEE BREAK		
11:30-13:30	**WPMC Special Session on "Manufacturing Engineering"** **Session Organizer and Chair: Dnyandeo Dattatray Shinde,** *Sandip Foundation, Sandip Institute of Engineering & Management, Nashik, Maharashtra*, **India**		MR G.02
	Invited Talk	Total Productive Maintenance (TPM) an overview; **Rajendra G. Tated**; *Sandip Foundations, Sandip Institute of Engineering and Management, Nashik*, **India**	
	Invited Talk	Application of KK pillar of TPM – An Industrial Case study; **J. P Yavalkar;** *TPM-Learning center, Bajaj auto ltd. Waluj Aurangabad*, **India**	
	Invited Talk	Lean Six Sigma - Success Story of Kavach; **Jadhav Ganesh A.;** *Gabriel India Ltd. Pune*, **India**	
13:30-14:30	LUNCH		
14:30-16:30	**WPMC Special Session on "Manufacturing Engineering" (Contd.)** **Session Organizer and Chair: Dnyandeo Dattatray Shinde,** *Sandip Foundation, Sandip Institute of Engineering & Management, Nashik, Maharashtra*, **India**		MR G.02
	1570226974	Identifying Root Causes for Students Problems in Technical Education using Fishbone Diagram; **Dnyandeo Dattatraya Shinde①, Shwetambari Sanjay Ahirrao①, Prachi Dilip Shinde①, Rajendra G. Tated①, Morten Falch②**; ①*Sandip Foundations, SIEM, Nashik, India,* ②*Center for Communication, Media and Information Technologies (CMI), Aalborg University Copenhagen*, **Denmark**	
	1570226994	Effect of Newly Designed Burnishing Tool on Surface Micro hardness of AA6351; A. S. Maheshwari①, Dr. R. R. Gawande②; ①*Sandip Institute of Technology & Research Centre, Nashik. (Maharashtra),* ②*Bapurao Deshmukh College of Engineering, Wardha (Maharashtra)*; **India**	
	1570228066	Application of Principal Component Analysis to Magnetic Abrasive Finishing**; Sandip B. Gunjal, P. J. Pawar**; *K.K.W.I.E.E. & R, Nasik*, **India**	
	1570227495	Metric Based Efficiency Analysis Of Educational ERP System Usability - Using Fuzzy Model; **Anil Kumar, Reza Tadayoni, Lene Tolstrup Sorensen**; *Department of Electronic Systems, Aalborg University*, **Denmark**	
	1570227534	A Brief Review on Process Parameter Optimization of GMAW Process and Grey-based Taguchi Method; **U. V. Patil, G. R. Naik**; *KIT's College of Engineering, Shivaji University, Kolhapur*, **India**	
	1570227977	Vehicle Monitoring and controlling system using CAN protocol; Mosam Sangole□, **Vicky Chaudhary, Vishakha Nighute, Priyanka Satpute;** *Sandip Foundation Nashik, Maharashtra*,**India**	
16:30-17:00	COFFEE BREAK		

16:30-17:00	(Continued MRG .02 Activities) COFFEE BREAK		
17:00-19:00	**WPMC Special Session on "Manufacturing Engineering" (Contd.)** **Session Organizer and Chair: Dnyandeo Dattatray Shinde,** *Sandip Foundation Sandip Institute of Engineering & Management, Nashik, Maharashtra,* **India**		MR G.02
	1570227004	Application of Real Coded Genetic Algorithm to Dynamic Layout Benchmark Problem; **Kailas V. Chandratre, P.J. Pawar**; *, K.K.W.I.E.E. & R, Nasik*, **India**	
	1570227011	Model Development for Preventive Maintenance and Replacement Policy; **Anand S. Relkar, Keshav N. Nandurkar**; *S. I.T.R.C., Nashik, K.K.W.I.E.E.R, Nashik*; **India**	
	1570227290	Vacuum Gripper Design For An Industrial Handling System; **Ajinkya Vasant Nichit, Suraj Ramesh Jadhav, Anirudh Arun Desai, Vishal Eknath Patil,Vishal Sonowane**; *Sandip Institute Of Engg. & Mangt. Nashik*, **India**	
	1570228555	Automatic Ration Distribution System-A Review; **Swapnil R. Kurkute, Dipak P. Patil, Chetan Medhe, Ashwini Kshirsagar, Ashlesha Revgade** □; *SIEM Nasik*, **India**	
	1570227469	Self -Balancing Platform for Personal Transport; **Yogesh Risodkar , Ganesh Shirsath, Monali Holkar, Mayur Amle**; *SIEM, Sandip Fondation, Nashik*, **India**	
	1570228052	Decommissioning of Nuclear Facilities and Dose Rate Calculations for Nuclear Power Plant Staff; **Pushkar Prashant Lachake, Dnyandeo Dattatraya Shinde**; *Sandip Institute of Engineering and Management, Nashik*, **India**	
19:30-22:30	END of DAY 3 || NETWORKING DINNER: FOYER		

Time Slot	Day3: Tuesday, December 15 || MRG .03 Activities || Contributed Papers: Physical and Fundamentals (II-A)		
08:30-19:00	Registration		
09:00-11:00	**Keynote Speech**		**HALL 1**
11:00-11:30	COFFEE BREAK		
11:30-13:30	**Physical and Fundamentals (II-A-1) | Antenna & Circuit Design, Analysis and Investigation: WPMC || *Session Chair: Laxminarayana Pillutla; Dhirubhai Ambani Institute of Information and Communication Technology, India*** 1570213114	Design Optimization and SAR Evaluation of SS-UWB Patch Antenna for WBAN; **Vivek Kumar, Sravanth Kumar Ramakuri**; **Bharat Gupta**; *Birla Institute of Technology Mesra, Ranchi,* **India**	MRG .03
	1570210207	Radar Range and Range Resolution Enhancements; **Uma S Jha, Erik Chowdhury**; *Space & Airborne Systems, Raytheon Co, El Segundo, California,* **USA**	
	1570209793	SIW based Antipodal Linear Tapered Slot Antenna for Inter-Satellite Communication Links at 60 GHz; **Nishesh Tiwari, T Rama Rao, Purva Shrivastava**; *SRM University,Chennai,* **India**	
	1570192429	SAR and Thermal effects of a Body Wearable Microstrip Antenna at UHF and UWB frequencies; **Varshini Karthik, T Rama Rao**; *SRM University,Chennai,* **India**	
	1570213460	Antenna Radiation Pattern Based 3D Localization Technique; **Amarlingam Madapu[1], Pachamuthu Rajalakshmi[1], Vinod Kumar Netad[1], Masaya Yoshida[2], Kiyohito Yoshihara**; [1]Indian Institute of Technology Hyderabad, Hyderabad, **India,** [2]*KDDI R&D Laboratories Inc., Green and M2M Application Laboratory Iidabashi,* **Japan**	
13:30-14:30	LUNCH		
14:30-16:30	**Physical and Fundamentals (II-A-2) | LTE & Multiple Access Techniques (OFDMA/OFDM/SC-FDMA, MIMO, SISO): WPMC || *Session Chair: Uma S. Jha, Raytheon Co., California, USA*** 1570213429	Distributed Spatial Modulation-OFDM in Uplink Relay-assisted Cellular Network; **Kunal Sankhe, Rama Garimella**; *International Institute of Information Technology, Hyderabad,* **India (***)**	MRG .03
	1570213444	Simultaneous Transmission of Information and Energy in OFDM Systems; **Sumit Gautam, P. Ubaidulla**; *International Institute of Information Technology-Hyderabad,* **India**	
	1570210151	Blind Channel Length Estimation for OFDM Systems using Cumulant Features; **Ajay Kambhampati, Udit Satija, Baratram Ramkumar, M Sabarimalai Manikandan**; *IIT-Bhubaneswar,* **India**	
	1570213302	A Feasibility Analysis of LTE-CommSense; **Amit K. Mishra[1], Mohammed Zafar Ali Khan[2], Santu Sardar[3]**; [1]*Department of Electrical Engineering, University of Cape Town,* **South Africa**, [2]*Department of Electrical Engineering, IIT Hyderabad,* **India,** [3] *ANURAG, Defence Research & Development Organization*, **India**	
	1570167111	An Efficient Resource Block Allocation Algorithm in LTE-Based Systems with User Rate Constraints; **Vijay Gutta, AmruthMuddana, T K Ramesh**; *Amrita VishwaVidyapeetham,* **India**	
	1570213529	LTE-Advanced Radio and Network Optimization: Basic Coverage and Interference Constraints; **Fernando J. Velez, Sofia Sousa, Jessica Acevedo ,Daniel Robalo**; *Instituto das Telecomunicações - DEM Universidade da Beira Interior,Faculdade de Engenharia, Covilhã,* **Portugal**	
16:30-17:00	COFFEE BREAK		

16:30-17:00	(Continued MRG .03 Activities) COFFEE BREAK		
17:00-19:00	**WPMC Special Session on " Selected Topics in Physical & Fundamentals-1"** **Session Organizer and Chair** : **T Rama Rao,** SRM University, **India**		MRG .03
	1570160791	Performance of MIMO Detection Techniques with Spatial Multiplexing**; Soma Umamaheshwar①, Tipparti Anil Kumar②, K Srinivas Rao③**; ①*SR Engineering College,* ②*SVS Group of Institutions,* ③*TRR College of Engineering, Telangana*, **India (###)**	
	1570213390	Reducing memory consumption with a lossless image compression algorithm based on predictive coding; **Rupali S. Vairagade**; *Sinhgad Institute of Technology and Science, Pune*, **India (***)**	
	1570209839	Enhancement in Spectral Efficiency using Circular Convolution in MIMO FBMC towards Wireless Network 5G; **Payal P. Tayade, Vandana M. Rohokale**, *SKNSITS, Lonavala*, **India (###)**	
	1570209843	Performance Analysis of Group based Cooperative Sensing Schemes; **K Jyostana①, N. Vandana②, Swathi Roja②, B. N. Bhandari②**; ①*VNR Vigana Jyothi Institute of Engineering and Technology,* ②*Jawaharlal Nehru Technological University*; Hyderabad, **India (###)**	
	1570238199	A Comparative Study of Channel Estimation for MIMO-OFDM system; **G Surendher**, Sree Chaitanya *Institute of Technological Sciences, Karimnagar,* **India (###)**	
19:30-22:30	END of DAY 3 || NETWORKING DINNER: FOYER		

Time Slot	Day3: Tuesday, December 15 || MRG .04 Activities || Contributed Papers: Physical and Fundamentals (II-B)		
08:30-19:00	Registration		
09:00-11:00	**Keynote Speech**		**HALL 1**
11:00-11:30	COFFEE BREAK		
11:30-13:30	**Physical and Fundamentals (II-B-1) | Channel Fading and Selection :WVIATE || *Session Chair-Ernesthina Cianca, University of Rome, Tor Vergata, Italy***		MRG .04
	1570208291	Joint Channel Estimation and CCI Cancellation for STBC-OFDM System in Fast Fading Channel; **Jyoti P Patra, Prasanta Kumar Pradhan,, Poonam Singh, Sarat Kumar Patra**; *National Institute of Technology Rourkela*, **India**	
	1570210195	Rate Independent Multicarrier Variable Rate Scheme over Frequency Selective Channel; **Akash Agarwal**, **Vijay Mukati**, **Preetam Kumar**; *Indian Institute of Technology, Patna*, **India**	
	1570210219	Performance of Amplify-and-Forward Cooperative Diversity under Ricean Fading; **Maja Delibasic, Milica Pejanovic-Djurisic, Zoran Veljovic**; *University of Montenegro*, **Montenegro**	
	1570213163	Performance of a space-time coded MC-CDMA system in a Rayleigh fading channel; **Olanrewaju B Wojuola**, **Stanley H. Mneney**, **Viranjay M Srivastava**; *University of KwaZul-Natal*, **South Africa**	
	1570194569	A new shaping code for PAPR Reduction in Single-Carrier Modulation; **Yonathan Tate, Dan Raphaeli;** *Tel Aviv University*, **Israel**	
	1570207637	PAPR Reduction Comparison of the MC-CDMA System with Various Companding Techniques; **Sarala Beeram①, Bhagya sree Vonguru②, BN Bhandari③, Dronam Raju Venketeswarlu③**; *①M V S R Engineering College, Hyderabad & Osmania University*; *②B E & Osmania University, Hyderabad*; *③JNT University Hyderabad;* **India**	
13:30-14:30	LUNCH		
14:30-16:30	**Physical and Fundamentals (II-B-2) | Physical Channel: WPMC || *Session Chair-Thomas J. O. Afullo, University of KwaZullu-Natal, South Africa***		MRG .04
	1570213381	On Detection Improvement in MC-CDMA Image Watermarking on Fading Channel; **Santi Prasad Maity①, Seba Maity②**; ①Indian Institute of Engineering Science and Technology, Shibpur, ②CEMK, Kolaghat, **India**	
	1570213387	On the Backhaul Reduction in Joint Transmission Network with Channel Uncertainty; **Zhangxing Liu, Hui Tian, Cheng Qin** ; *Beijing University of Posts and Telecommunications*, **China**	
	1570212327	Variable Encoding and Sequencing Pattern Driven Multiple Image Bit Watermarking for Wireless Domain; Soumit Chowdhury①, Nabin Ghoshal ②; ①Govt. College of Engineering & Ceramic Technology, Kolkata, ② University of Kalyani, India	
	1570177831	Improving Performance of Impulsive Noise Canceller Under Class A Impulsive PLC Channel; **Hirotomo Yasui, Akira Nakamura, Makoto Itami**; *Tokyo University of Science*, **Japan**	
	1570211271	A Generic and Compatible Implementation for 2D and 3D Geometry-based Stochastic Channel Models; **Zhenzi Liu, Tian Lei, Yuming Bi, Pan Tang, Wei Chen, Jianhua Zhang**; *Beijing University of Posts and Telecommunications*, **China**	
	1570209407	Low Rate Common Control Channels with Distributed Cross-Layer Optimization via Genetic Algorithm; **Pranoti Balki, Kishor P. Patil**; *Sinhgad Academy of Engineering, Pune*, **India**	
16:30-17:00	COFFEE BREAK		

16:30-17:00	(Continued MRG .04 Activities) COFFEE BREAK		
17:00-19:00	**Physical and Fundamentals (II-B-3) Performance, Analysis and Ranking: WPMC || *Session Chair- Mqhele Dlodlo, University of Cape Town, South Africa***		MRG .04
	1570194241	Analysis of Data Transmission Management through Software Defined POX Controller; **Vaishnavi Moorthy, Revathi Venkatraman**; *SRM University, Chennai*, **India**	
	1570193591	Design and Performance Analysis of a Penta-band Spiral Antenna for Vehicular Communications; **Ramya R, T Rama Rao;** *SRM University, Chennai*, India	
	1570194537	Performance Analysis of Energy Detector in Correlated Log-normal Fading Channels for IR-UWB Systems; **S. Josephine, Anil Mahanta, P. R. Sahu**; *IIT Guwahati*, **India**	
	1570208727	Performance Comparision of Various Detection Methods for QO-STBC over Time Selective Channel; **Jyoti Patra, Poonam Singh**; *National Institute of Technology Rourkela*, **India**	
	1570211595	Design and Data Analysis of a Signal Measurement System Based on Variable Signature Sequences; **Ji-Hyun Moon, Jeong-Ho Kim, Na-Hyung Kim, and Bing Yuan Chen**; *Ewha Womans University*, **Republic of Korea**	
	1570191499	Ranking of Total Productive Maintenence pillars using Analytical Hierarchy Process; **Dnyandeo Shinde[1][2][3], Morten Falch[2], Rajendra Tated[3], Ramjee Prasad[4];** [1]*Center for Communication, Media and Information Technologies (CMI), Aalborg University Copenhagen,* **Denmark**, [2]*Aalborg University Copenhagen,* **Denmark,** [3] *Sandip Foundations, Nashik***, India,** [4]*CTIF, Aalborg University*, **Denmark**	
19:30-22:30	END of DAY 3 || NETWORKING DINNER: FOYER		

Time Slot	Day3: Tuesday, December 15 || MRG .05 Activities || Contributed Papers: Efficient Wireless Communications		
08:30-19:00	Registration		
09:00-11:00	**Keynote Speech**		**HALL 1**
11:00-11:30	COFFEE BREAK		
11:30-13:30	**Efficient Wireless Communications (A) | Energy Harvesting: WPMC || *Session Chair- Sudhanshu S. Jamuar, University of Malaysia Perlis*, Malaysia**		MRG .05
	1570213231	Energy-Efficient Resource Allocation for Hybrid Services with QoS Requirements in Cellular Network*;* **Yuhao Zhang, Ning Wang, Baoling Liu***; Beijing University of Posts and Telecommunications*, **China**	
	1570192925	DEAR: An Energy-centric Adaptive Region of Interest Mechanism for Wireless Mobile Devices; **Hrishikesh Venkataraman①, Ting Bi②, Ting Wu②, Gabriel-Miro Muntean②;** ①*Center for Smart Cities, Indian Institute of Information Technology (IIIT), Chittoor, Sricity, AP,* **India,** ②*Performance Engineering Laboratory, Dublin City University (DCU), Glasnevin, Dublin 9,* **Ireland**	
	1570192965	EDAS- Energy-Efficient Device-based Adaptive Cross-Layer Scheme for Wireless Multimedia Transmission; **Hrishikesh Venkataraman①, Shen Wang②, Gabriel-Miro Muntean②;** ①*Center for Smart Cities, Indian Institute of Information Technology (IIIT), Chittoor, Sricity, AP,* **India,** ②*Performance Engineering Laboratory, Dublin City University (DCU), Glasnevin, Dublin 9,* **Ireland**	
	1570194465	Energy Efficient Scheduling Algorithm for the Real-time Multicast and Unicast Services; **Min Wang①, Qiaoyun Sun①, Shuguang Zhang①, Yinlong Liu②, Yu Zhang②;** ①*Information School, Beijing City University;* ②*Institute of Information Engineering Chinese Academy of Sciences, Beijing;* **China**	
	1570213117	Secrecy Outage of a Cognitive Relay Network with Energy Harvesting and Imperfect CSI; **Pranabesh Maji, Binod Prasad, Sanjay Dhar Roy, Sumit Kundu;** National Institute of Technology, Durgapur, **India**	
	1570213446	Analytical Model of Relay Node Integrating IEEE 802.15.4 MAC and Energy Conserving State Behaviour; **Rajavaraprasad Yerra, Malyala Pavana Ravi Sai Kiran, Pachamuthu Rajalakshmi**; Indian Institute of Technology Hyderabad, **India**	
13:30-14:30	LUNCH		
14:30-16:30	**Efficient Wireless Communications (B) | Security, Trust, Privacy and Authentication: WPMC || *Session Chair- Vandana Rohokale , SIT, Lonavala, India***		MRG .05
	1570194123	Elliptic Curve Cryptography based Key Management for the M2M Local Cloud Platform; **Bayu Anggorojati①, Neeli Rashmi Prasad②, Ramjee Prasad①;** ①*Center For TeleInFrastruktur , Aalborg University*, **Denmark**; ②*Center For TeleInFrastruktur*, **USA (***)**	
	1570210161	Privacy-Preserving Friend Matching Protocol approach for Pre-match in Social Networks; **Shubhangi S.Ople①, Aaradhana A. Deshmukh②, Albena Mihovska②, Ramjee Prasad②;** *Savitribai Phule Pune University*, **India,** ②*CTIF, Department of Electronics Systems Aalborg University, Aalborg*, **Denmark**	
	1570195039	A certificate-driven Approach to Access Control in Future Internet; **Nancy Ambritta①, Poonam Railkar②, Parikshit Narendra Mahalle①;** ①*Sinhgad Institute of Technology and Sciences & Smt. Kashibai Navale College of Engineering,* ②*Smt. Kashibai Navale College of Engineering of Engineerin, Pune University*; **India (***)**	
	1570195141	A Modified RFID Authentication Protocol Using Elliptic Curve Cryptography; **Rajesh Dochania, Nirmal Roberts, Karm V Arya***; ABV-Indian Institute of Information Technology and Management, Gwalior*, **India**	
	1570213335	Secure and Privacy Enabled Anonymous Computing for Heterogeneous (SPEACH) IoT; **Meena Singh, Rajan M A, Shivraj Vl , P. Balamuralidhar**; *Tata Consultancy Sevices Limited*, **India**	
16:30-17:00	COFFEE BREAK		

16:30-17:00	COFFEE BREAK		
17:00-19:00	**Efficient Wireless Communications (C)	Security, Trust, Privacy and Authentication: WVITAE || *Session Chair-K.V. Arya, AVIIITM, Gwalior, India***		MR5 .05
	1570213434	Architectural Integration for Security in Advanced Metering Infrastructure; **Priyanka D.Halle[1], Vandana Rohokale[1], Ramjee Prasad[2]**; [1]E&TC SKNSITS, Lonavala, **India** [2] *Center For TeleInFrastruktur , Aalborg University*, **Denmark**	
	1570194669	Trustbook: A Trust-based access control in Online Social Networks; **Vedashree Takalkar, Parikshit Narendra Mahalle**; Savitribai Phule Pune University, STES, Pune, **India**	
	1570210113	Daubechies Wavelet based Effective Data Authentication in Wireless Domain; **Anirban Goswami[1], Nabin Ghoshal[2]**; [1]*Techno India*, [2]*University of Kalyani*; **India**	
	1570211897	Mesh IP Video Surveillance Systems Model Design and Performance Evaluation; **Smart Lubobya[1], Mqhele E. Dlodlo[1], De Jager Gerhard[1], Ackim Zulu[2]**; [1]*University of Cape Town*, **South Africa**; [2]*University of Zambia*, **Zambia**	
	1570210201	Secret Transmission through Audio Signal with Reduced Distortion for Wireless Communication (STASRD); **Dipnkar Pal[1], Nabin Ghoshal[2]**; [1]*Techno India*, [2]*University of Kalyani*; **India**	
	1570209931	Secure E- Voting System with integration of NFC, Biometrics and Cloud Computing; **Amol Potgantwar[1], Tejas Upasani[2]**; [1] *Sandip Foundation*, [2]*Savitribai Phule*,[1][2]*Pune University*; **India**	
19:30-22:30	END of DAY 3 || NETWORKING DINNER: FOYER		

Time Slot	Day3: Tuesday, December 15 || MRG .06 Activities || 23rd GISFI Standardization Series Meeting Meeting on Security and Privacy/ WWSMC	
08:30-19:00	Registration	
09:00-10:30	**23rd GISFI Standardisation Meeting on Security and Privacy/ WWSMC:** *Session Chair:* ***Anand R. Prasad****, NEC Corporation* ***Japan****; Session Organiser:* ***Anand R. Prasad,*** *NEC Corporation* ***Japan****;* ***Krishna Sirohi****, NIKSUN,* ***USA;*** ***Sivabalan Arumugam,*** *NEC Mobile Network Excellence Centre(NMEC), NEC India Pvt Ltd,* ***India*** Opening by Co-Chairs: **Anand R. Prasad**, Chief Advanced Technologist, Executive Specialist, NEC Corporation ; **Krishna Sirohi**, Senior Advisor, Niksun **Session 1: Cyber Security ||** Moderator**: Krishna Sirohi**, NIKSUN Topic: Cyber Security**, Ramamurthy Gemini,** *Chairman , Cyber security & privacy foundation***, India** **Session 2: IoT Security ||** Moderator: **Krishna Sirohi**, NIKSUN Topic: Internet of Things – Security**; Sivabalan Arumugam,** NEC Mobile Network Excellence Centre(NMEC), NEC India Pvt Ltd	MRG .06
10:30-11:00	COFFEE BREAK	
11:00-13:00	**GISFI Special Session on Security and Privacy/ WWSMC-1** **Session 3: Communication System Security ||** Moderator: Anand R. Prasad, NEC Corporation Topic: Telecom Security **; Vijay Madan,** Chief Mentor - IT & Technology, Network Operation, Tata Teleservices Limited Topic: Telecom Security **; Alf Zugenmaier,** Professor, Munich University of Applied Sciences Topic: Mobile PKI , **Zia Saquib**, Scientist, CDAC, Hyderabad Topic: Wired & Wireless Security **G.K. Satyanarana;** Head, Telecom, ECIL, Hyderabad	MRG .06
13:00-14:00	LUNCH	
14:00-16:00	**GISFI Special Session on Security and Privacy/ WWSMC-1** **Session 4: Cloud & Platform Security ||** Moderator: Sivabalan Arumugam, NEC India Pvt Ltd Topic: Information Security - Cloud Environment ; **Gopala Rao Jammi**, Professor , MEC (A Group of TechM), Hyderabad Topic: Personal Safety: Next Frontier in Mobile Security ; **Kulkarni Dattatraya**, Intel Security Group, Bangalore Topic: NFV Security**; Prabhu T**, NEC India, Chennai, **India** Topic: Monitoring Aspects**; Krishna Sirohi,** Senior Advisor, NIKSUN	MRG .06
16:00-16:15	COFFEE BREAK	
16:15-17:15	**GISFI Special Session on Security and Privacy/ WWSMC-2** **Session 5: Panel Discussion "What are the pains? What is needed?" ||** Moderator: **Anand R. Prasad**, NEC Corporation, **Japan** **Vijay Madan,** Chief Mentor - IT & Technology, Network Operation, Tata Teleservices Limited **G.K. Satyanarana,** Head, Telecom, ECIL, Hyderabad **Krishna Sirohi,** Senior Advisor, NIKSUN **Alf Zugenmaier,** Professor, Munich University of Applied Sciences	MRG .06
19:30-22:30	END of DAY 3 || NETWORKING DINNER: FOYER	

Wednesday, December 16

Day 4

"Workshops, Special Sessions, Contributed Papers"

Time Slot	Day4: Wednesday, December 16 || HALL 1.1 & 1.2 Activities || Workshops & Special Sessions (III-A)		
08:30-19:00	Registration		
09:00-11:00	**Keynote Speech || Session Chair : Ramjee Prasad, Center for TeleInFrastructure , Aalborg University, Denmark** **fred Harris**, San Diego State University, **USA** **Harish Mysore**, *IEEE*, **India** **Dinesh Chand Sharma,** *SESEI*, **India**		HALL 1
11:00-11:30	COFFEE BREAK		
11:30-13:30	**Second International Workshop on Innovation and Entrepreneurship(IWIE)- III** **Workshop Organizer and Chair: Sofoklis Kyriazakos,** CTIF, Aalborg University, **Denmark**		HALL 1.1
	WVITAE Special Session on "Communication, Navigation, Sensing and Services (CONASENSE)" - I **Session Organizers and Chairs: *Leo Ligthart, Tu-Delft, the Netherlands; Ernestina Cianca, University of Rome Tor Vergata, Italy***		HALL 1.2
	1570227732	Modified RAR and PLSR-based artifact removal for stroke detection in UWB radar imaging; **E. Ricci, A. Colucciello, S. Di Domenico, E. Cianca, T. Rossi**; University of Rome "Tor Vergata",Rome, **Italy**	
	1570228263	Communication Framework for Tele-rehabilitation Systems with QoS Guarantee; Plamen Semov, **Nikolay Dandanov, Georgi Balabanov, Krasimir Tonchev and Vladimir Poulkov**; *Technical University of Sofia*, **Bulgaria**	
	1570230189	vNet Zero Energy for Radio Base Stations- Balearic Scenario①; Pere Sabater Frau①, Albena Mihovska①, Ramjee Prasad①, Andreu Moia Pol② ,Angel Igelmo Ganzo②, Xavier Canals Solé③, Jaume Ochogavia Colom④; *Center for TeleInFrastruktur (CTIF) Aalborg University, **Denmark**; ②Universitat Illes Balears (UIB), ③Telefonica España S.A., ④Balearic Islands Government*, **Spain**	
	1570236132	Reliable Frame Selection for Speaker Identification under Voice Disguise Scenario; **Swati Prasad, Ramjee Prasad**; *Centre for TeleInfrastruktur (CTIF), Aalborg University, Aalborg*, **Denmark**	
	1570228151	Performance Analysis of SOFDM Transmission Scheme over Integrated Satellite/Terrestrial Network; **Akash Agarwal□①, B. M. Bhaveja②, Preetam Kumar①**; ①*Indian Institute of Technology Patna□*, ②*Department of Electronics & Information Technology (DeitY) New Delhi*, **India (***)**	
13:30-14:30	LUNCH		
14:30-16:30	**Second International Workshop on Innovation and Entrepreneurship(IWIE)- III (Contd)** **Workshop Organizer and Chair: Sofoklis Kyriazakos,** CTIF, Aalborg University, **Denmark**		HALL 1.1
	WVITAE Special Session on "Communication, Navigation, Sensing and Services (CONASENSE)" -II **Session Organizers and Chairs: *Leo Ligthart, Tu-Delft, the Netherlands; Ernestina Cianca,** University of Rome Tor Vergata, **Italy***		HALL 1.2
	1570226963	Efficient Filtering Technique for Chronic Wound Image Processing under Tele-Wound Network; **Chinmay Chakraborty, Bharat Gupta**; *Birla Institute of Technology Jharkhand*, **India**	
	1570227100	End-to-End Delay Analysis of IEEE 802.15.6 Standard for WBAN Medical Paradigm; **Vivek Kumar, Bharat Gupta**; *Birla Institute of Technology Jharkhand*, **India**	
	1570227212	Relevance of signal processing of the voice in diagnosing human tuberculosis; **Giovanni Saggio①, Santosh Bothe②**; ①University of Rome "Tor Vergata",Rome, **Italy, ②***Bharati Vidyapeeth University , Pune*, **India**	
	1570227247	A P2P architecture for Mobile Assisted Logistic Operations; **Pierpaolo Loreti* , Lorenzo Bracciale* , Francesco Zampognaro* , Massimo Povia† , Gianluca Gargiulo‡;** **NITEL - University of Rome Tor Vergata, †Technosky Via del Casale Cavallari, §NAIS Via Andrea Noale; Rome*, **Italy**	
	1570238200	GeoLocation Aware Dynamic Spectrum Sensing in Cognitive Radio Networks; **Usha Kurumaddali,** *GGS Indraprastha University*, **India**	
17:30	END OF WPMC-2015 & GWS-2015		

Time Slot	Day 4: Wednesday, December 16 || MRG .01 Activities || Contributed Papers: Wireless Communications		
08:30-19:00	Registration		
09:00-11:00	**Keynote Speech**		**HALL 1**
11:00-11:30	COFFEE BREAK		
11:30-13:30	**Wireless Communications (A) | Spectrum for Future Radio Networks: WPMC || *Session Chair: Albena Mihovska, CTIF, Aalborg University, Denmark***		MRG .01
	1570235616	Preliminary performance evaluation of the FBMC based future IEEE 1900.7 Standard; **D. Noguet, J.-B. Doré and B. Miscopein**; *Minatec Campus CEA Leti 17, rue des Martyrs – 38054 Grenoble Cedex 9*, **France**	
	1570213121	Long-haul Communication Trial in London TV White-space with IEEE 802.11af-based High Power Prototype; **Takeshi Matsumura[1] , Kentaro Ishizu[1] , Keiichi Mizutani[2], Tran Ha Nguyen[1], Homare Murakami[1][3], Fumihide Kojima[1][3], Hiroshi Harada[2][3]**; *[1]NICT, Yokosuka, [2]Kyoto University, [3]Kyoto, ICT, Koganei*, **Japan**	
	1570192849	Outage Analysis of Cellular Two-Way Relaying with Spectrum Sharing in Nakagami-m Fading; **Ronshee Chawla, M. Mounika Reddy, Prabhat Kumar Upadhyay**; *IIT Indore*, **India**	
	1570213448	Field Experiments for Broadband Mesh Network Operating in TV White Space; **Kentaro Ishizu, Fumihide Kojima**; *National Institute of Information and Communications Technology*, **Japan**	
	1570210145	TVWS Regulations and the first IEEE 802.11af indoor experiments in Singapore; Dien Vinh Hoang[1], Takeshi Matsumura[2], Kentaro Ishizu[2], Homare Murakami[2], Fumihide Kojima[2]; [1]*Singapore Smart Wireless Lab, National Institute of Information and Communications Technology* (NICT), **Singapore**, [2]*NICT*, **Japan**	
	1570194697	Novel Closed form Expression for Multi Cell Cooperation using MHCP to Reduce Interference; **Suman Yadav, S Pratap Singh**; *Galgotia College of Engineering and Techolongy*, **India**	
13:30-14:30	LUNCH		
14:30-16:30	**Wireless Communications (B) | Algorithms and Innovative Approach: WVITAE || *Session Chair: Sri Chandrasekaran, IETE, India***		MRG .01
	1570210211	Classification Based Automatic Assessment for Web Based Learning; Wacharawan Intayoad, Punnarumol Temdee; Mae Fah Luang University, **Thailand**	
	1570188921	Comparative analysis of load balancing algorithms for LTE/LTE-A Hetnets; **Diego Castro-Hernandez**, **Raman Paranjape**; *University of Regina*, **Canada**	
	1570208745	Fuzzy based Moving Object Detection and Classification in Video; **Manojkumar M Gawali**, *Sinhgad College of Engineering*, Pune, **India**	
	1570213914	Swarm Optimization Based on Genetic Algorithm & Relevance Feedback Technique for Data Clustering; **Gandamalla Malini, M.Seetha, K.V.N.Sunitha**; *GNITS, Hyderabad*, **India**	
	1570212950	Downlink Joint Processing for Non Orthogonal Multiple Access; **Islam Atef, Essam Sourour;** *Alexandria University, Alexandria*, **Egypt**	
	1570197177	The Studies of Millimeter Waves at the frequencies of 60 GHz in Outdoor Environments- A Survey; **Hitesh Singh**; *HMRITM, Delhi*, **India**	
16:30-17:00	COFFEE BREAK		
	Networking		
	END OF WPMC-2015 & GWS-2015		

Time Slot	Day 4: Wednesday, December 16 || MRG .02 Activities || Contributed Papers: Physical and Fundamentals (III)		
08:30-19:00	Registration		
09:00-11:00	**Keynote Speech**		**HALL 1**
11:00-11:30	COFFEE BREAK		
11:30-13:30	**Physical and Fundamentals (III–A) | Signal Processing-1: WPMC & WVITAE || *Session Chair: Navin Kumar, Amrita University, Bangalore, India***		**MRG .02**
	1570194245	Blind Image Quality Assessment Based on Phase Congruency and Spatial-spectral Entropies; **Maozheng Zhao, Yanping Lu, Cuiwei Li, Ran Gao, Qin Tu, Bo Yang, Aidong Men**; *Beijing University of Posts and Telecommunications*, **China**	
	1570195699	Opinion-unaware blind image quality assessment based on sparse representation; **Maozheng Zhao[1], Xiaoqiang Guo[2], Ran Gao[1], Bo Yang[1], Aidong Men[1]**; [1]*Beijing University of Posts and Telecommunications*, [2]*Academy of Broadcasting Science*, **China**	
	1570208027	QoE Based Pseudo Heartbeat Message Compression Mechanism for Wireless Networks; **Zhiqun Hu, Xiangming Wen, Zhaoming Lu, Zhaoxing Li**; *Beijing University of Posts and Telecommunications*, **China**	
	1570213506	**WVITAE**: On CS Reconstruction Images using LDPC code over Radio Mobile channel; **Ankita Pramanik, Santi Prasad Maity**; *Indian Institute of Engineering Science and Technology, Shibpur*, **India**	
	1570210061	Modeling of Modified Erlang-k Distribution for Raindrop Size Distribution over South Africa; **Akintunde Alonge, Thomas Afullo**; *University of KwaZulu-Natal, Durban*, **South Africa**	
	1570192393	Enhanced Turbo Equalizer Using 2 Dimensional Iterative Soft Decision Interference Cancellation; **Doron Shinbox, Dan Raphaeli**; *Tel-Aviv University*, **Israel**	
13:30-14:30	LUNCH		
14:30-16:30	**Physical and Fundamentals (III –B) | Design and Development: WPMC & WVITAE || *Session Chair: Venkatapathy Prithviraj, Rajalakshmi Institute of Technology, Chennai, India***		**MRG .02**
	1570209863	Modeling & Simulation for complex System of systems design, test, and verification; **Uma Jha, Jon Wada**; *Space & Airborne Systems, Raytheon CoEl Segundo, California* , **USA**	
	1570213885	Design Of Low Voltage Bandgap Reference Circuit Using Subthreshold MOSFET; Sushma Sangolli, Rohini Hongal; *B.V.B College of Engineering and Technology, Hubli*, **India**	
	1570194201	Eight-Path Harmonic Rejection Mixer for Full Band Mobile TV; **Kiran B, Roy P Paily**; *Indian Institute of Technology Guwahati*, **India**	
	1570209947	Database Assisted Automatic Modulation Classification Using Sequential Minimal Optimization; **K. Pavan Kumar Reddy, Lakhan Shiva, Kadiri Abhilash, Yoganandam Yeleswarapu**; *Birla Institute of Technology and Science, Hyderabad Campus*, **India**	
	1570212671	Design and Development of a Mobile Wireless Video Streaming Mote; **Bhuvanesh D, Manjunath Hegde, Manikandan J**; *PES Institute of Technology*, **India**	
	1570213484	Design of BiCMOS based low temperature coefficient bandgap reference; **Deepa Talewad, Anilkumar Nandi, Ramesh Karmungi**; *B.V.B College of Engineering and Technology, Hubli*, **India**	
16:30-17:00	COFFEE BREAK		
	Networking		
	END OF WPMC-2015 & GWS-2015		

Time Slot	Day 4: Wednesday, December 16 || MRG .03 Activities || Contributed Papers: Wireless Networks		
08:30-19:00	Registration		
09:00-11:00	**Keynote Speech**		**HALL 1**
11:00-11:30	COFFEE BREAK		
11:30-13:30	**Wireless Networks | WPMC & WVITAE || *Session Chair: G S Tomar, MIR Labs, Gwalior, India***		MRG .03
	1570184143	A Fine Grained Position for Modular Core NoC; B. **Naresh Kumar Reddy, M.H.Vasantha, Y.B.Nithin Kumar, Dheeraj Sharma**; *National Institute of Technology, Goa*, India **(***)**
	1570191965	Analytical Evaluation of Frequency Reuse For Hybrid Full-/Half-Duplex Cellular System; Wenping Bi, Limin Xiao, Xin Su, Shidong Zhou; *Tsinghua University*, **China**
	1570192715	A New Approach for Crossed Sector Detection in Live Mobile Networks based on Radio Measurements; David Duarte①②, Pedro Vieira①②, António J. Rodrigues③, André Martins, Nuno Silva③; ①*Instituto Superior de Engenharia de Lisboa (ISEL),* ②*Instituto de Telecomunicac¸˜oes (IT), Lisbon,* ③*Instituto Superior T´ecnico (IST), Lisbon,* **Portugal**
	1570213280	A Revolutionary Rural Agricultural Participatory Sensing Approach Using Delay Tolerant Networks; **Prateek Gupta, Bhushan Gurmukhdas Jagyasi, Bighnaraj Panigrahi, Hemant Kumar Rath, Srinivasu Pappula, Anantha Simha**; *Tata Consultancy Services*, **India**
	1570213277	**WVITAE:** Performance Analysis of EPC with IMS Network Architecture; **A Bagubali①, Prithiviraj Venkatapathy②, Pathak Mallik①**; ①*VIT University, Vellore,* ②*Rajalakshmi Institute of Technology , Chennai,India,* **India**
	Invited Talk	Role of Cyber Security for Digital Business; **T. R. Dua**, *GISFI*, **India**
13:30-14:30	LUNCH		
14:30-16:30	**Wireless Networks | WPMC || *Session Chair: Hrishikesh Vankataraman, Indian Institute of Information Technology, Chittoor, India***		MRG .03
	1570213596	IEEE802.15.4g based Wide Area and Mobile Wi-SUN Communication Systems; **Hiroshi Harada, Keiichi Mizutani, Kentaro Mochizuki, Kentaro Obata**; *Kyoto University*, **Japan**
	1570207517	Hierarchical Mesh Based Energy Efficient Multicast Routing on IEEE 802.15.4 based networks; **Verotiana Rabarijaona①, Fumihide Kojima①, Hiroshi Harada②**; ①*National Institute of Information and Communication Technology,* ②*Kyoto University & Graduate School of Informatics,* **Japan**
	1570192635	Efficient Visibility Modeling for Free-Space Optical Systems Design; **Ivo Sousa①③, António J. Rodrigues②, Maria Paula Queluz②**, ①*Instituto de Telecomunicac¸˜oes (IT), Lisbon,* ②*Instituto Superior T´ecnico (IST), Lisbon,* **Portugal**
	1570187749	Reliable Link Layer Packet Reconstruction for Rotating Polarization Based Radio Communication; **Ritesh Kumar Kalle**, *HITACHI*, **India**
	1570213414	SUN-RAN Orchestrating Resource Management using Superframe Division Data Aggregation Technology; **Fumihide Kojima, Chang-Woo Pyo, Masayuki Oodo**; *National Institute of Information and Communications Technology(NICT),* **Japan**
	1570176791	Green Indoor Network In A Passive Way; Yu Liu, *Jiangsu Automation Research Institute*, **China**
16:30-17:00	COFFEE BREAK		
	Networking		
	END OF WPMC-2015 & GWS-2015		

Time Slot	Day 4: Wednesday, December 16 || MRG .04 Activities || Workshops & Special Sessions (III-B); IC5		
08:30-19:00	Registration		
09:00-11:00	**Keynote Speech**		**HALL 1**
11:00-11:30	COFFEE BREAK		
11:30-13:30	23rd GISFI Standardization Meeting- 5 G Innovation in India **Session Chair: Ashutosh Dutt**		
	Presentation1	5G Framework for a Personalised Network; **Nitish Mittal**, *5G Company, Vishawaniketan*, **India**	
	Presentation2	5G Model in WISDOM; **Sounak Moulik**, *5G Company, Vishawaniketan*, **India**	
	Presentation3	Security Challenges in a 5G Network; **Nidhi** , *5G Company, Vishawaniketan*, **India**	
	Presentation4	5G Concept; **Sandeep Mukherjee**, *,5G Company, Vishawaniketan*, **India**	
13:30-14:30	LUNCH		
14:30-16:30	**IC5: Third International Conference on Communications, Connectivity, Convergence, Content and Cooperation** **Session Chair: Swrana Ravindra Babu, IETE, India**		MRG .04
	1570213308	Survey on Service Discovery Mechanisms; **Gitanjali Shinde Henning Olesen**; *Center for Communication, Media and Information Technologies (CMI) Aalborg University Copenhagen*, **Denmark**	
	1570191301	Multislotted Microstrip Patch Antenna for Dual Band and UWB Applications; **Shailendra Kumar Dhakad, Dr. Neeraj Kumar, Keshav Kumar, Swapnil Mengade, Rohit Gupta**; *Birla Institute Of Technology and Science Pilani, Goa*, **India (***)**	
	1570194207	An application of Internet of Things in Transportation System; **Ganesh Balaraman, Harisudha Kuresan**; *SRM University*, **India (***)**	
	1570195047	Analysis of Audio Watermarking Techniques for Cyber Security in Copyright Infringement; **Sushma Ambekar① □, Vandana Rohokale①, Ramjee Prasad②;** ①SKNSITS, Lonavala, **India**, ②CTIF, Aalborg University, **Denmark**	
	1570208707	30-Second Integration Time Power Law Conversion Model for Rainfall Attenuation in South Africa; **Mary N. Ahuna,, Thomas J. Afullo, , Akintunde A. Alonge**; *University of KwaZulu Natal Durban*, **South Africa**	
	1570209327	Illumination, Indoor Localization and Very High Speed Data Communication using VLC; **Anusha Addanki, Navin Kumar**; *Amrita Vishwa Vidyapeetham (University) Bangalore*, India	
16:30-17:00	COFFEE BREAK		
	Networking		
	END OF WPMC-2015 & GWS-2015		

Time Slot	Day 4: Wednesday, December 16 || MRG .05 Activities || Workshops & Special Sessions (III-C)		
08:30-19:00	Registration		
09:00-11:00	**Keynote Speech**		**HALL 1**
11:00-11:30	COFFEE BREAK		
11:30-13:30	**WVITAE Special Session on " Wireless Communications"** **Session Organizer and Chair** : *Mqhele Dlodlo, University of Cape Town, South Africa*		MRG .05
	1570227491	Hard-combined Cooperative spectrum sensing using Time-frequency method; **S M Hiremath①, Sarat Kumar Patra①, Amit Kumar Mishra②;** ①*National Institute of Technology Rourkela, Odisha,* **Indiadlodlo,** ②*University of Cape Town*, **South Africa**	
	1570228229	The Implementation of the Modified AODV Routing Protocol in Mobile Ad-Hoc Networks; **Vekani Reviet Baloyi, Lesiba Kola**; *University of Limpopo*; **South Africa (###)**	
	1570228530	Enlarged QR-LRL Based Massive MIMO Detector for Soft Output Generation; **Sukriti Garg, Krati Mittal, Divyang Rawal**; *LNM Institute of Information Technology, Jaipur*, **India**	
	1570230967	Interference Management in Heterogeneous and Small Cell NetwPerorks; **M. Bala Krishna, Puneet Bansal**; *Guru Gobind Singh Indraprastha University , New Delhi,* **India**	
	1570233114	Mesh IP Video Surveillance System - A System Perspective and Performance Evaluation; **M .E. Dlodlo, C. S. Lubobya, S Lubobya, O Osanaiye, E Okumu, H Ohize,** *University of Cape Town*, **South Africa**	
13:30-14:30	LUNCH		
14:30-16:30	**WPMC Special Session on " Selected Topics in Physical & Fundamentals -2"** **Session Organizer and Chair** : ***Bharat Gupta, Birla Institute of Technology, Ranchi, India***		MRG .05
	1570210153	An ingenious framework for solving cold start problem in recommender system; **Pankaj Chaudhary① , A. A. Deshmukh②**; ①*Smt. Kashibai Navale College of Engineering, Pune* **India**, ②*Department of Electronics Systems, Aalborg University*, **Denmark (***)**	
		Area-Power Analysis of Carry Selected Adder using Transmission Gates; **Ch. Rajendra Prasad①, T. Anil Kumar②**; ①*SVS Institute of Technology*, ②*SR Engineering College*; Warangal, **India (###)**	
		Privacy Preserving Friend Matching Protocol for Pre match in Social Networks; **Shubhangi Ople, Aradhna Deshmukh**; *Smt. Kashibai Navale College of Engineering, Pune* **India (###)**	
		Self-Programmable Variable Digital Filter (VDF) Design Based of FPGA; **T. Anil Kumar;** *SR Engineering College,* Warangal, **India (###)**	
		Design of High Performance Phase Locked Loop for Clock Synchronization; A. Rajesh①, B.L. Raju①, K. Chenna Kesava Reddy②; ①ACE, Engineering College, ②*Jawaharlal Nehru Technological University College of Engineering*; Hyderabad, **India** (###)	
	1570237867	Object Detection, Passive tracking and Active Tracking; **Shreeya Shevade**, *Government College of Engineering, Aurangabad, Maharashtra,* **India (***)**	
16:30-17:00	COFFEE BREAK		
	Networking		
	END OF WPMC-2015 & GWS-2015		

Time Slot	Day 4: Wednesday, December 16 || MRG .06 Activities || Workshops & Special Sessions (III-C)	
08:30-19:00	Registration	
09:00-11:00	**Keynote Speech**	**HALL 1**
11:00-11:30	COFFEE BREAK	
11:30-13:30	**Networking Meeting**	MRG .06
13:30-14:30	LUNCH	
14:30-16:30	**GISFI Future Strategy Meeting**	MRG .06
16:30-17:00	COFFEE BREAK	
	Networking	
	END OF WPMC-2015 & GWS-2015	

Note:

***** paper withdrawn and/or resubmitted with different title**

paper was not presented by authors

Index of Papers
WPMC-2015

INDEX OF PAPERS SUBMITTED IN WPMC 2015

Conference	Paper #	Title	Page #
WPMC 2015	1570167111	An Efficient Resource Block Allocation Algorithm in LTE-Based Systems with User Rate Constraints	66
WPMC 2015	1570176791	Green Indoor Network In A Passive Way	70
WPMC 2015	1570177831	Improving Performance of Impulsive Noise Canceller Under Class A Impulsive PLC Channel	75
WPMC 2015	1570187749	Reliable Link Layer Packet Reconstruction for Rotating Polarization Based Radio Communication	80
WPMC 2015	1570188641	Transmission Capacity Analysis for Linear Vehicular Ad Hoc Networks	85
WPMC 2015	1570190883	New virtual 8x1 MISO scheme with QOSTBC	90
WPMC 2015	1570191499	Ranking of Total Productive Maintenance pillars using Analytical Hierarchy Process	95
WPMC 2015	1570191687	Towards Internet of Services - SDN-enabled IMS Architecture for IoT Integration	100
WPMC 2015	1570191965	Analytical Evaluation of Frequency Reuse For Hybrid Full-/Half-Duplex Cellular System	105
WPMC 2015	1570192429	SAR and Thermal effects of a Body Wearable Microstrip Antenna at UHF and UWB frequencies	110
WPMC 2015	1570192635	Efficient Visibility Modeling for Free-Space Optical Systems Design	115
WPMC 2015	1570192715	A New Approach for Crossed Sector Detection in Live Mobile Networks based on Radio Measurements	120
WPMC 2015	1570192849	Outage Analysis of Cellular Two-Way Relaying with Spectrum Sharing in Nakagami-m Fading	125
WPMC 2015	1570192925	DEAR: An Energy-centric Adaptive Region of Interest Mechanism for Wireless Mobile Devices	130
WPMC 2015	1570192957	Improved p-norm Energy Detector with Soft Combining in AWGN Channel for Spectrum Sensing	135
WPMC 2015	1570192965	EDAS- Energy-Efficient Device-based Adaptive Cross-Layer Scheme for Wireless Multimedia Transmission	140
WPMC 2015	1570193591	Design and Performance Analysis of a Penta-band Spiral Antenna for Vehicular Communications	145
WPMC 2015	1570193823	An Efficient Deterministic Scheme for Blind CFO Estimation in SC-FDMA	150
WPMC 2015	1570193867	Investigation on Listen-Before-Talk Mechanism of Licensed-Assisted Access to Unlicensed Spectrum	155
WPMC 2015	1570193943	A Compressive Sensing-based Channel Estimation via GAMP in FBMC/OQAM System	160
WPMC 2015	1570194199	Impact of Network Coding on Distributed Indoor Target Tracking using Wireless Sensor Networks	165
WPMC 2015	1570194201	Eight-Path Harmonic Rejection Mixer for Full Band Mobile TV	170
WPMC 2015	1570194241	Analysis of Data Transmission Management through Software Defined POX Controller	175
WPMC 2015	1570194245	Blind Image Quality Assessment Based on Phase Congruency and Spatial-spectral Entropies	180
WPMC 2015	1570194425	Adaptive priority based network bandwidth throttling for a Virtual Classroom System	185
WPMC 2015	1570194465	Energy Efficient Scheduling Algorithm for the Real-time Multicast and Unicast Services	190
WPMC 2015	1570194537	Performance Analysis of Energy Detector in Correlated Log-normal Fading Channels for IR-UWB Systems	195
WPMC 2015	1570194567	On Supporting Integrated Multimedia Traffic in TDMA based Mobile Ad hoc Networks	200
WPMC 2015	1570194697	Novel Closed form Expression for Multi Cell Cooperation using MHCP to Reduce Interference	205

WPMC 2015	1570194813	Intrusion Detection System Against Colluding Misbehaviour in MANETs	210
WPMC 2015	1570194919	Automatic Speaker Detection and Recognition in a multi classroom E-Learning System	215
WPMC 2015	1570194953	The impact of Network Neutrality on the OTT Service of 5G WISDOM	220
WPMC 2015	1570195013	Characterization for Reporting Rate of Adaptive Sectoring Scheme to Improve Reliability in WSN	224
WPMC 2015	1570195063	Q-MOHRA: QoS Assured Multi-Objective Hybrid Routing Algorithm for Heterogeneous WSN	229
WPMC 2015	1570195073	Two-Party Key Agreement Protocol for MANETs based on Verifiable Secret Sharing Scheme	234
WPMC 2015	1570195119	Mobility-aware Hybrid Synchronization for Wireless Sensor Network	239
WPMC 2015	1570195141	A Modified RFID Authentication Protocol Using Elliptic Curve Cryptography	244
WPMC 2015	1570195309	Non Audio-Video gesture recognition system	248
WPMC 2015	1570195491	A Path Ordering and Reference Selection Method for the Differential Delay Tomography	253
WPMC 2015	1570195595	Packet Scheduling Scheme to Guarantee QoS in Internet of Things	258
WPMC 2015	1570195699	Opinion-unaware blind image quality assessment based on sparse representation	263
WPMC 2015	1570196365	Joint Transceiver Design for QoS-Constrained MIMO Two-Way Non-Regenerative Relaying	268
WPMC 2015	1570199753	Trust based Detection and Elimination of Packet Drop Attack in the Mobile Ad-hoc Networks	273
WPMC 2015	1570199757	The Behavioral Based Gray Hole Attack Detection in Mobile Ad-hoc Network (MANET)	277
WPMC 2015	1570205987	Experimental Evaluation on Wireless Tomography with Compressed Sensing in a Three-Dimensional Space	282
WPMC 2015	1570206001	New Pricing Model for Dynamic Dual-operator Spectrum Sharing in GSM	287
WPMC 2015	1570206855	Efficient Device-to-Device (D2D) Offloading Mechanism in LTE Networks	292
WPMC 2015	1570207155	Fuzzy Logic based Human Detection in Video	297
WPMC 2015	1570207517	Hierarchical Mesh Based Energy Efficient Multicast Routing on IEEE 802.15.4 based networks	302
WPMC 2015	1570207535	Quality of Service Enforcing Centrally Optimized Routing for Delay Tolerant Networks	307
WPMC 2015	1570207563	Improving Segmentation Accuracy for Motion Detection using Bidirectional Video Processing	312
WPMC 2015	1570208027	QoE Based Pseudo Heartbeat Message Compression Mechanism for Wireless Networks	317
WPMC 2015	1570208181	Survey of Device-to-Device Communications Infrastructure-less in IEEE 802.15.8 Task Group	322
WPMC 2015	1570208599	Detection Performance of Soft Data Fusion in Rician Fading Channel for Cognitive Radio Network	327
WPMC 2015	1570208727	Performance Comparision of Various Detection Methods for QO-STBC over Time Selective Channel	332
WPMC 2015	1570208853	Optimization of Cooperative Spectrum Sensing in Cognitive Radio over Erroneous Reporting Channel	337
WPMC 2015	1570208909	Link Adaptation Strategies for Cellular Downlink with low-fixed-rate D2D Underlay	342
WPMC 2015	1570209407	Low Rate Common Control Channels with Distributed Cross-Layer Optimization via Genetic Algorithm	347
WPMC 2015	1570209789	Path and Load Aware Routing Algorithm for Cognitive Radio Wireless Mesh Network	352
WPMC 2015	1570209793	SIW based Antipodal Linear Tapered Slot Antenna for Inter-Satellite Communication Links at 60 GHz	357
WPMC 2015	1570209863	Modeling & Simulation for complex System of systems design, test, and verification	362

WPMC 2015	1570209947	Database Assisted Automatic Modulation Classification Using Sequential Minimal Optimization	367
WPMC 2015	1570210057	A Pattern Division Multiple Access Scheme for 5G wireless communication systems	372
WPMC 2015	1570210123	An Interdependent Source-Channel Coding for Energy Efficient Communication in WSNs	377
WPMC 2015	1570210145	TVWS Regulations and the first IEEE 802.11af indoor experiments in Singapore	382
WPMC 2015	1570210151	Blind Channel Length Estimation for OFDM Systems using Cumulant Features	387
WPMC 2015	1570210161	Privacy-Preserving Friend Matching Protocol approach for Pre-match in Social Networks	391
WPMC 2015	1570210207	Radar Range and Range Resolution Enhancements	395
WPMC 2015	1570211271	A Generic and Compatible Implementation for 2D and 3D Geometry-based Stochastic Channel Models	400
WPMC 2015	1570211595	Design and Data Analysis of a Signal Measurement System Based on Variable Signature Sequences	405
WPMC 2015	1570212700	Limited Feedback Scheduling For MIMO-OFDM Broadcast Network	409
WPMC 2015	1570213016	Disaster Countermeasure Experiments using WINDS	414
WPMC 2015	1570213055	Development and Field Experiment of Distributed Peer Aware Communication Networks	419
WPMC 2015	1570213104	Throughput of Secondary User in Underlay Cognitive Relay Network with Energy Harvesting	424
WPMC 2015	1570213111	Distributed Token Based MAC for Multi-Channel Multi-Interface Cognitive Radio WMN	429
WPMC 2015	1570213114	Design Optimization and SAR Evaluation of SS-UWB Patch Antenna for WBAN	434
WPMC 2015	1570213117	Secrecy Outage of a Cognitive Relay Network with Energy Harvesting and Imperfect CSI	439
WPMC 2015	1570213121	Long-haul Communication Trial in London TV White-space with IEEE 802.11af-based High Power Prototype	444
WPMC 2015	1570213206	Participatory Heuristic Evaluation of the First Iteration of the eWALL Interface Application	449
WPMC 2015	1570213212	Coexistence of Systems with Different Multicarrier Waveforms in LSA Communications	454
WPMC 2015	1570213231	Energy-Efficient Resource Allocation for Hybrid Services with QoS Requirements in Cellular Network	459
WPMC 2015	1570213262	Real-time EEG Monitoring and Transmission over Low Bandwidth Wireless Networks	464
WPMC 2015	1570213263	Pilot testing and demonstration of self-management network and applications using NerveNet	470
WPMC 2015	1570213278	CDF Based Spectrum Occupancy Rate Measurement Using Least Square Estimation of Gaussian Noise Period	475
WPMC 2015	1570213280	A Revolutionary Rural Agricultural Participatory Sensing Approach Using Delay Tolerant Networks	480
WPMC 2015	1570213289	Performance Analysis of Total Power Consumption in Linear Multi-hop Networks	485
WPMC 2015	1570213302	A Feasibility Analysis of LTE-CommSense	490
WPMC 2015	1570213332	Hybrid multi-hop network by small-unmanned aircraft and satellite telecommunication systems	494
WPMC 2015	1570213335	Secure and Privacy Enabled Anonymous Computing for Heterogeneous (SPEACH) IoT	498
WPMC 2015	1570213366	On-going Field Experiment of NerveNet in Shirahama Town for Resilient Town Network	503
WPMC 2015	1570213374	Fractal dimension of spectral estimates for spectrum sensing under noise variance uncertainty	508
WPMC 2015	1570213378	Evaluation of permutation entropy detection for cognitive radio networks	513
WPMC 2015	1570213381	On Detection Improvement in MC-CDMA Image Watermarking on Fading Channel	518
WPMC 2015	1570213387	On the Backhaul Reduction in Joint Transmission Network with Channel Uncertainty	523

WPMC 2015	1570213414	SUN-RAN Orchestrating Resource Management using Superframe Division Data Aggregation Technology	528
WPMC 2015	1570213444	Simultaneous Transmission of Information and Energy in OFDM Systems	533
WPMC 2015	1570213445	Minimal Error IEEE 802.15.4 Communication Module for Heart Monitoring Data Transmission in IoT	538
WPMC 2015	1570213446	Analytical Model of Relay Node Integrating IEEE 802.15.4 MAC and Energy Conserving State Behaviour	543
WPMC 2015	1570213448	Field Experiments for Broadband Mesh Network Operating in TV White Space	548
WPMC 2015	1570213460	Antenna Radiation Pattern Based 3D Localization Technique	553
WPMC 2015	1570213462	QZSS SS-CDMA Location and Short Message Communication System	558
WPMC 2015	1570213529	LTE-Advanced Radio and Network Optimization: Basic Coverage and Interference Constraints	563
WPMC 2015	1570213596	IEEE802.15.4g based Wide Area and Mobile Wi-SUN Communication Systems	568
WPMC 2015	1570213925	Selective Sensing Framework for Opportunistic Mobile Phone Sensing Networks	573
WPMC 2015	1570224166	Virtual sensing environment for care at home	578
WPMC 2015	1570224167	Expression recognition using graph based feature selection	583
WPMC 2015	1570224200	Improving the Trustworthiness of Ambient Assisted Living Applications	587
WPMC 2015	1570224206	Requirements and Challenges in Evaluation of Systems for Independent Living of Senior Citizens	592
WPMC 2015	1570226974	Identifying Root Causes for Students Problems in Technical Education using Fishbone Diagram	597
WPMC 2015	1570226994	Effect of Newly Designed Burnishing Tool on Surface Micro hardness of AA6351	601
WPMC 2015	1570227004	Application of Real Coded Genetic Algorithm to Dynamic Layout Benchmark Problem	605
WPMC 2015	1570227011	Model Development for Preventive Maintenance and Replacement Policy	610
WPMC 2015	1570227290	Vacuum Gripper Design For An Industrial Handling System	615
WPMC 2015	1570227356	Artificial intelligence automobility in material handling & fork-lift manufacturing	620
WPMC 2015	1570227469	Self -Balancing Platform for Personal Transport	625
WPMC 2015	1570227495	Metric Based Efficiency Analysis Of Educational ERP System Usability - Using Fuzzy Model	630
WPMC 2015	1570227534	A Brief Review on Process Parameter Optimization of GMAW Process and Grey-based Taguchi Method	635
WPMC 2015	1570227716	Demonstrating SWiFiIC - Sustainable WiFi for Rural Communication	640
WPMC 2015	1570227801	Interference Analysis and Mitigation Techniques in Wireless Body Area Network	645
WPMC 2015	1570227808	Implementation of Low Cost IoT Based Smart Home using Open Source Platform	650
WPMC 2015	1570227846	Performance Comparison of DCT based Entropy Coding Techniques	654
WPMC 2015	1570227857	UWB Sensing antenna, Reconfigurable transceiver and antenna based Cognitive Radio Test bed	659
WPMC 2015	1570227977	Vehicle Monitoring and controlling system using CAN protocol	664
WPMC 2015	1570227987	Methods of Frequency Offset Estimation in OFDM Based System	668
WPMC 2015	1570228025	Drum handling device for industrial	673
WPMC 2015	1570228052	Decommissioning of Nuclear Facilities and Dose Rate Calculations for Nuclear Power Plant Staff	678
WPMC 2015	1570228066	Application of Principal Component Analysis to Magnetic Abrasive Finishing	683

WPMC 2015	1570228069	Sensitive Association Rules Hiding Methods: A Survey	687
WPMC 2015	1570228555	Automatic Ration Distribution System-A Review	692
WPMC 2015	1570231052	Dynamic Pathloss Model for Future Mobile Communication Networks	697
WPMC 2015	1570234273	"IoT" based Smart Village: An Indigenous step towards 'Digital India'	702
WPMC 2015	1570234316	Rurbanisation of India	707

Technical Papers
WPMC-2015

THE 18TH INTERNATIONAL SYMPOSIUM ON WIRELESS PERSONAL MULTIMEDIA COMMUNICATIONS
(WPMC-2015)
December 13-16, 2015, Hyderabad, India

An Efficient Resource Block Allocation Algorithm in LTE-Based Systems with User Rate Constraints

Vijay Gutta
Department of ECE
Amrita School of Engineering
Bengaluru, India
guttavijay.amritha@gmail.com

Amruth Muddana
Department of ECE
Amrita School of Engineering
Bengaluru, India
amruth11015@gmail.com

T K Ramesh
Department of ECE
Amrita School of Engineering
Bengaluru, India
tk_ramesh@blr.amrita.edu

***Abstract*— In this paper we proposed an Efficient Resource Block Allocation Algorithm (ERBAA). The Base Station will allocate resource blocks to users in LTE-Based systems. Resource block establishes the communication channel between base station and corresponding user. The selection and allocation of this resource block is critical in all LTE Based systems with respect to Quality of Service, in order to increase the QoS ERBAA uses an efficient algorithm in selection process i.e., it use the Channel State Information (CSI) which describes the quality and fading details of the channel. CSI will be computed among all the possible users and available resource blocks. Once it computes complete CSI matrix, algorithm find out which resource block needs to be allocated for which user. The selection is based on both user to resource block and resource block to user CSI values. By using this process, ERBAA will have better QoS across all the various network dynamic scenarios and also our simulation results shows, ERBAA has improved average CSI of the network in comparison with Greedy Based Sub-channel Processing (GBSP).**

Index Terms*— *Long Term Evaluation, 4G, MIMO-OFDMA, Resource Allocation, Resource Block (RB)

I. INTRODUCTION

In recent years the excessive growth of user requirements on ubiquitous access and high data rate multimedia traffic, QoS is becoming difficult to be maintained in LTE Based systems of wireless communication industry.

The radio transmissions in LTE are based on the Orthogonal Frequency Division Multiplexing (OFDM) modulation scheme. In particular, the Single Carrier Frequency Division Multiple Access (SC-FDMA) and the OFDM Access (OFDMA) are used in uplink and downlink transmissions, respectively. Differently from basic OFDM, they allow multiple access by assigning sets of sub-carriers to each individual users [3].

To develop an efficient resource allocation scheme applicable for LTE systems, some important factors have to be considered. First, an RB to be full considered for sub-channel assignment. The basic unit for sub-channel assignment is stipulated as the RB, which consists of a set of subcarriers that need to be identically allocated, in LTE systems. This indicates that the sub-channel assignment by individual subcarrier as in [5], [6], [9] is not allowed, and each RB should be assigned according to the aggregate channel state information (CSI) of all the subcarriers it includes rather than that of some individual subcarriers. Second, as the basic structure of LTE systems, MIMO-OFDMA should be jointly considered when carrying out resource allocation. Since multiple spatial wireless channels can be provided by MIMO transmission to achieve spatial multiplexing gain, the CSI of these spatial links should also be aggregately considered as the sub-carriers within one RB in frequency. Therefore, this work integrates these two important factors and develops an energy-efficient resource allocation algorithm that is more applicable in LTE systems. Specifically, with both RBs and MIMO-OFDMA being considered, the proposed algorithm may optimize the energy efficiency effectively, as well as fully satisfy user's rate requirements. Moreover, it is equipped with polynomial complexity and is thus favorable for practical application. With all these advantages, this work may function as a more promising candidate for the energy-efficient design of LTE systems, compared with most of the existing related works [4].

To maintain the Quality of Service we have considered scheduling process, which plays a very important role in the resource allocation to user according to a request in LTE Based systems. Resource allocation plays a very important role where resource blocks allotted to users according to their need and the priority and to increase the system performance and the throughput of the system. Scheduling takes place as follows to a particular user which is having best channel conditions for a given

time-frequency resource block should be allotted for transmission [5].

Round Robin (RR), Proportional Fair (PF) and Best Channel State Information are various types of scheduling algorithms. Some users are never been scheduled for transmission because of their degraded channel quality in comparisons with others. Because of this the QoS can be affected [10]. Here in our paper we considered Best CSI algorithm which results in the better throughput and it totally ignore the fairness.

To perform scheduling, the terminal sends channel state information to base station. Better channel condition means best CSI value. Resource blocks will be allotted to users with best channel quality.

II. RELATED WORKS

Xiao, Xiaoming Tao and Jianhua Lu proposed an algorithm GBSP (Greedy Based Channel Preprocessing) where they first considered to calculate the channel state information as follows. When there are m (1, 2, 3…..m) number of users and n (1, 2, 3, 4….n) number of resource blocks considering always m < n. The channel state information is calculated for user1 with respect to each and every resource block and the resource block which provides best CSI value is assigned to that user and remove that allocated RB from consideration. For next user again the CSI is calculated with respect to resource blocks left and the resource block which provides next best CSI is assigned, this process will continue till each user is assigned with one resource block. Here in case of last few users there might be an issue which leads to a scenario where they will be left with resource blocks which might even not suitable for channel allocation which leads to service outage but they might show some better CSI for the users which were allotted before . This point is considered in our paper and we made an algorithm which reschedules the resource block by consider each and every resource block to each and every user till every user is left with one resource block assigned [4].

Will Jeng-Ji Huang, Wei-Keng Lin and Hung-Hsiang Ko has proposed an algorithm by assigning scheduling blocks (SBs) to the UEs based on channel information. Here instead of assigning two resource Blocks (one SB) to each user, our proposed algorithm will assign one resource block to each user initially and thereafter depending on the user requirement remaining resource blocks will be assigned which improves spectral efficiency [3]. In this paper we have considered CSI matrix values in the allocation process of resource blocks, along with this in order to improve the QoS considered the need of a particular resource block to user and users demand for a particular resource block.

In our work to improve transmission rate, for each sub-channel we mainly considered the point to point MIMO transmission, for complete utilization of spatial multiplexing gain of MIMO. Thus, a specific user will be allotted with a sub-channel considering Single User (SU) MIMO transmission, and in frequency domain multiple access is realized by OFDMA.

III. CSI CALCULATION

CSI matrix between the BS and user m on subcarrier $k(n)$ at each resource allocation time is $H_{\boldsymbol{m,k(n)}} \in C_{A_{\boldsymbol{m}}*\boldsymbol{A}}$ where $A_{\boldsymbol{m}}$ represents the antennas at the mobile station and the base station has A antennas. $S_{\boldsymbol{m,k(n)}} \in C_{\boldsymbol{A,1}}$ is the input vector emitted from the multiple antennas of the BS, and $n_{\boldsymbol{m,k(n)}} \in C_{A_{\boldsymbol{m}}*\boldsymbol{1}}$ is the complex Gaussian noise vector with zero mean. We considered a block fading model and a static channel is assumed within the duration of each RB. Then the output vector $\boldsymbol{y}_{\boldsymbol{m,k(n)}} \in C_{A_{\boldsymbol{m}}*\boldsymbol{A}}$ received by user m from $H_{\boldsymbol{m,k(n)}}$ can be expressed as

$$\boldsymbol{y}_{\boldsymbol{m,k(n)}} = H_{\boldsymbol{m,k(n)}} \boldsymbol{s}_{\boldsymbol{m,k(n)}} + \boldsymbol{m}_{\boldsymbol{m,k(n)}} \quad (1)$$

Via singular value decomposition,

$$H_{\boldsymbol{m,k(n)}} = U_{\boldsymbol{m,k(n)}} \Lambda_{\boldsymbol{m,k(n)}} V^{*}_{\boldsymbol{m,k(n)}} \quad (2)$$

Where $U_{\boldsymbol{m,k(n)}} \in C_{A_{\boldsymbol{m}}*A_{\boldsymbol{m}}}$ and $V^{*}_{\boldsymbol{m,k(n)}} \in C_{\boldsymbol{A,A}}$ are both unitary matrices and $\Lambda_{\boldsymbol{m,k(n)}} \in C_{A_{\boldsymbol{m}}*\boldsymbol{A}}$ is a rectangular matrix whose diagonal elements are non-negative real numbers and whose off-diagonal elements are zero. The diagonal elements $\boldsymbol{\lambda}^{(\boldsymbol{1})}_{\boldsymbol{m,k(n)}} \geq \boldsymbol{\lambda}^{(\boldsymbol{2})}_{\boldsymbol{m,k(n)}}) \geq, \ldots, \boldsymbol{\lambda}^{(\boldsymbol{J_m})}_{\boldsymbol{m,k(n)}}$ are the ordered singular values of the matrix, where $\boldsymbol{J}_{\boldsymbol{m}} = \min \{A, A_{\boldsymbol{m}}\}$[4].

IV. EFFICIENT RESOURCE BLOCK ALLOCATION ALGORITHM (ERBAA)

Our proposed algorithm allocates the resource block to the users with maximum and suitable CSI values. We considered both user to resource block and resource block to user demand, by using this we can

improve the average CSI value in the entire network through which overall quality of service of the network can be improved.

Step 1: Base station gets the information of newly requested users (M) and available resource blocks (N) information.
User Matrix M = {1,2,3,4……..…M}
Resource Block Matrix N = {1,2,3,4…….N}

Step 2: For MIMO transmission, average CSI of all KJ_m channels is formulated below

$$h_{m,n} = (1/KJ_m) \sum_{k=1}^{K} \sum_{a=1}^{Jm} \left| \lambda_{m,k(n)}^{(a)} \right|^2$$

$$m^* \in M, n^* \in N$$

Step 3: Get the resource block number {n*} for user {m*} where the CSI (m*, n*) value is maximum.

Step 4: If the resource block is not allocated to any user then go to Step 10.

Step 5: If the resource block is allotted for some other user then compute the CSI difference between current user and previously allotted user.

Step6: If the difference is lesser than 10% of its value, then compute the next non allocated resource block where CSI value is maximum, update the resource block number and go to Step 10.

Step 7: If the difference is higher than 10% then get the next maximum CSI (m*, n*) value of non-allocated resource block for both the users. Compute the difference of current resource block and next maximum resource block for both the users.

Step 8: If the difference value of already allotted user is higher than current user then update the next maximum resource block to current resource block and go to Step 10.

Step 9: If the difference of current user value is higher, then re-allocate the next maximum resource block for the already allotted user and go to Step 10.

Step 10: Allot the resource block for the current user and update the user and resource block information table.

Step 11: Repeat Step 3 to 10 till all the users gets one dedicated resource block.
Step 12: Remaining resource blocks will be allocated as per user requirement by repeating Step 3 to Step 10.

V. SIMULATION RESULTS

We have studied the performance of our proposed algorithm an Efficient Resource Block Allocation Algorithm (ERBAA) and compared its performance with GBSP (Greedy Based Channel Pre-processing) by using MATLAB (R2013a) simulation software.

Table I: Simulation parameters

Simulation parameter	Value
Users	20-50
Resource Blocks	50-80
Sub-carriers	12
Antennas	4X4

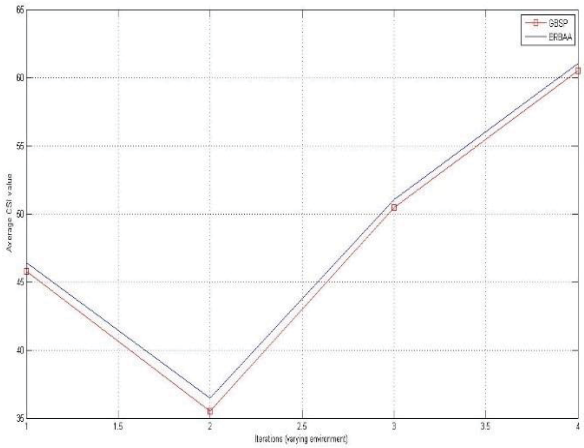

Fig.1: Average CSI value for ERBAA Vs. GBSP

For study and analysis purpose we considered a network model where the number of users and number of available resource blocks will be changed in each iteration or observation. In each instance first we allotted RB's to users based on GBSP and computed its Average CSI value across the network and in the same instance allotted RB's to users by using ERBAA and computed average CSI value. In all conditions/scenarios our experiment showed that ERBAA average CSI value is better that GBSP as shown in fig.1. Various simulation parameters are as mentioned in Table I. Improved average CSI shows that the Quality of Service in the network is improved by using ERBAA in comparison with GBSP. Because CSI value is computed based on the communication channel performance between user and base station which shows that lower CSI value means poor channel communication and which has more fading.

VI. CONCLUSION

In this paper we have proposed An Efficient Resource Block Allocation Algorithm (ERBAA) by using the concept of Channel State Information. CSI will be computed among all the possible users and available resource blocks. CSI matrix will be updated dynamically at regular events, whenever a user needs a resource block it will be allocated as per the CSI based resource block allocation algorithm. In this resource block to user requirement and users to resource block demand are taken into consideration. By using this our MATLAB simulated results shows that our proposed algorithm has improved performance in average CSI value of the LTE-Based systems network in various dynamic scenarios. This Average CSI represents the quality of the user communication channel and fading information, we have improved the quality of channel and reduced fading by using best and suitable CSI technique which leads to the improved Quality of Service.

REFERENCES

[1] Patrick Hosein,"Resource Allocation for the LTE Physical Downlink Control Channel" in 2009,IEEE.

[2] Mohamed A.Abd El-Gawad, Mohsen M. Tantawy and Mohamed El-Mahallawy, "LTE QoS Dynamic Resource Block Allocation With Power Source Limitation and Queue Stability", International Journal of Computer Networks & Communications (IJCNC) Vol.5, No.3, May 2013.

[3] Jeng-Ji Huang, Wei-Keng Lin and Hung-Hsiang Ko,"A Resource Allocation Algorithm for Maximizing Packet Transmissions in Downlink LTE Cellular Systems",in TENCON 2011, IEEE.

[4] Xiao Xiao, Xiaoming Tao, and JianhuaLu,"Energy-Efficient Resource Allocation in LTE-Based MIMO-OFDMA Systems With User Rate Constraints", IEEE TRANSACTIONS ON VEHICULAR TECHNOLOGY, VOL. 64, NO. 1, JANUARY 2015.

[5] C. Xiong, G. Y. Li, S. Zhang, and S. Xu, ―Energy- and spectral-efficiency tradeoff in downlink OFDMA networks,‖ *IEEE Trans.Wireless Commun.*, vol. 10, no. 11, pp. 3874–3886, Nov. 2011.

[6] C. Xiong, G. Y. Li, S. Zhang, Y. Chen, and S. Xu, ―Energy-efficient resource allocation in OFDMA networks,‖ *IEEE Trans. Commun.*, vol. 60, no. 12, pp. 3767–3778, Dec. 2012.

[7] Wonjong Rhee, John M. Cioffi, “Increase in Capacity of Multiuser OFDM System Using Dynamic Sub-channel Allocation”, VTC 2000, pp.1085-1089.

[8] G. P. Fettweis and E. Zimmermann, ―ICT energy consumption—Trends and challenges, in *Proc. 11th Int. Symp. WPMC*, Lapland, Finland, 2008, pp. 1–4.

[9] G. Miao, N. Himayat, G. Y. Li, and S. Talwar, ―Low complexity energy efficient scheduling for uplink OFDMA,‖ *IEEE Trans. Commun.*, vol. 60, no. 1, pp. 112–120, Jan. 2012.

[10] Rupinder Kaur, Manoj Kumar, "An Efficient Resource Block Allocation in LTE System", Volume 3, Issue 10, October 2013.

THE 18TH INTERNATIONAL SYMPOSIUM ON WIRELESS PERSONAL MULTIMEDIA COMMUNICATIONS
(WPMC-2015)
December 13-16, 2015, Hyderabad, India

Green Indoor Network In A Passive Way

Yu Liu
Jiangsu Automation Research Institute, Lianyungang 222061 P. R. China
Email: {liuyu@jari.cn

***Abstract*—With the explosive growth in the number of wireless users and the data traffic needs, how to improve coverage and provide ubiquitous broadband access causes a great challenge for operators. This paper presents a green wireless channel concept for the indoor coverage enhancement. The whole system is composed of the donor antenna, the service antenna and the coaxial cable. These antenna prototypes have good features of minimization, high gain etc. To verify its real applications, we have demonstrated the coverage enhancement under the real commercial 3G WCDMA network through multi-antenna passive energy harvesting and forwarding without any additional power consumption. When users are in the poor coverage, over 20 dB receiving power improvement can be achieved by employing the proposed passive antenna system. Finally, we proposed an interference cancellation algorithm which can further improve the receiving SINR.**

I. Introduction

A wireless cellular network is made up of a number of radio cells, each served by at least one fixed-location transceiver known as a cell site or base station. [1] Hundreds of cell sites are deployed in a typical large city to create a coverage in 95% or more of the targeted areas, so that a variable number of portable transceivers can be used in any cell and moved through more than one cell during transmission.

Coverage hole is an area within the radio coverage footprint of a wireless system in which the Radio Frequency (RF) signal level is below the designed threshold, which is usually caused by physical obstructions such as buildings, foliage, hills etc. It also occurs in places where there are no nearby base stations. In these areas, service quality can drop off sharply, resulting in slow data rates and poor voice quality. Improvements on the quality of service are always pursued by wireless service providers for competitive reasons, so a solution which offers uninterrupted access to wireless services can be very compelling. On the other hand, the poor indoor wireless coverage is now recognized globally as one of the biggest communication obstacles for mobile subscribers today. This is particularly prominent with data service and with LTE licenses being issued in frequencies as high as 2.6 GHz with a promise of 100 Mbps download and 50 Mbps upload speeds per cell. [2]

Although power boosting [3] at base station could extend coverage range of its cell, it is cost-ineffective for operator and will cause strong interference to neighboring cells. More importantly, power-inefficient solutions can not meet the operators demands in terms of cost reduction and environmental impact targets. Therefore, more power-efficient and cost-effective solution is desired to deliver better coverage and larger capacity to these hard-to-reach places.

Relay stations [4], [5] are introduced in IEEE 802.16 and 3GPP LTE-A, and other solutions such as picocell and femto cell can also be deployed in the existing network for coverage extension and throughput enhancement. However, the adoption of those solutions means more power consumption due to new active components introduced into the network, which also results in a complicated network topology, a great deal of signalling exchange and higher requirement for backhaul link etc.

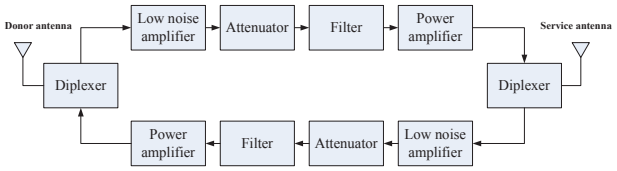

Fig. 1. Typical structure of a repeater.

Another traditional solution to coverage problems is the repeater [6]. As illustrated in Fig. 1, a repeater is typically a combination of a radio receiver and a radio transmitter that receives a weak or low-level signal and retransmits it at a higher level or higher power, so that the signal can reach a longer distance or fill in coverage holes without degradation. Although simpler and lower cost compared to the above solutions, unfortunately it has the following drawbacks:

- Power consumption by low noise amplifier and power amplifier
- Amplifying and forwarding the heat noise
- Restricted to electric power supply

Green wireless communications has recently attracted a lot of attention by researchers and engineers. [7] In radio access networks, most of the green related research focuses on the transmitter and receiver with hardware or procedure optimization for energy saving. Actually, for signal radiation, we have found that a great deal of energy is wasted during the propagation. Our research is trying to make wireless channel more energy-efficient through changing or optimizing radio propagation. The remaining part of this paper is organized as follows. The concept of green wireless channel is introduced in Section II. An implementation case with a demonstration system in the real 3G WCDMA communication network is presented in Sections III. Finally, concluding remarks are offered in Section IV.

II. Concept of green wireless channel

Green wireless channel takes good advantage of electromagnetic characteristics of radio signal for indoor or blind spot coverage, through special metal/non-metal material usage, building surface or structure optimization, or introduction of passive devices / antennas, etc.

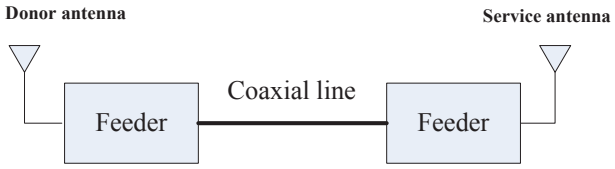

Fig. 2. Structure of passive relay system (DL).

For the purpose of further reduction of energy consumption and deployment cost, a kind of passive relay technique is employed for the coverage enhancement.

The proposed structure is described in Fig. 2. It is basically made up of a pair of donor antenna and service antenna, a basic antenna feed system and a coaxial cable to connect the receiving and the transmitting parts.

Considering the case of downlink, the donor antenna is deployed in a favorable position to harvest radio energy from donor eNode B and forward it through coaxial cable to the service antenna. The transferred energy is served as the excitation to drive the service antenna. The service antenna is typically deployed to make up the coverage hole or cover buildings for indoor coverage enhancement.

The prominent feature is that all the components are passive devices and no any power supply is required, so it is very energy efficient and suitable for power supply limited scenarios such as remote places or emergency communications.

Here, we actually proposed an implementation example of a passive relay technique. Considering a scenario of the urban wireless communication, line-of-sight (LOS) signals from donor eNB are easily blocked or attenuated by high buildings, the penetration loss of transmit signals after going through the buildings may result in a sharp degradation of receiving signal strength at mobile users.

To deal with this kind of coverage hole, we can firstly choose a favorable position for deploying donor antenna, such as the top of high building, so that LOS or near LOS path from eNB can be available. Generally, a highly-directional antenna is used with its main lobe pointed to the donor eNode B to guarantee a strong power reception. As a matter of fact, in the dense urban areas, most of eNBs are invisible to the terminal users, because there may be buildings or other obstacles (i.e. there is no direct wave) between them. In this case, the donor antenna needs to have a high gain and a relatively wide beam in order that the electromagnetic waves can be harvested from multiple directions. To ensure an effective energy receiving and conversion via antenna, a matched antenna feed system is also required.

Again, we consider the downlink (DL) communication. The energy harvested by donor antenna will be transferred to the antenna feed system of service antenna via the coaxial cable, which is used as an excitation to drive service antenna. The service antenna is normally with an omni-directional radiation pattern. It is useful for a good coverage of the indoor environment as most of WiFi access points do nowadays. The service antenna can be typically a directional antenna, and the antenna gain and beam width can be carefully designed according to the distance and size of the coverage hole.

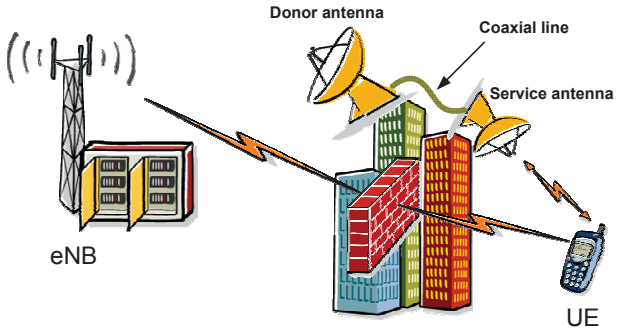

Fig. 3. Reception enhancement of UE behind tall buildings that block LOS path (DL).

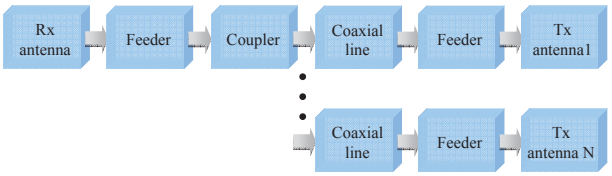

Fig. 4. Structure of downlink with multiple service antennas.

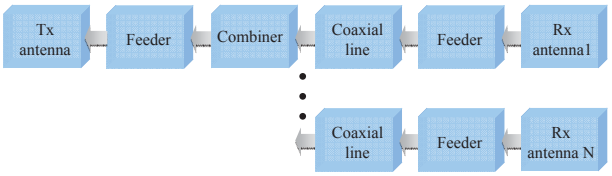

Fig. 5. Structure of uplink with multiple service antennas.

If only one service antenna exists, as shown in Fig. 3, the receiving energy at donor antenna will be transferred totally to service antenna. In real environment, there may simultaneously exist several coverage holes around buildings, so a low-cost and power efficient solution is to deploy several service antennas each covering one coverage hole, while only one donor antenna is deployed. As shown in Fig. 4, the total energy received at donor antenna will be divided equally or unequally into several portions by a coupler, each used to excite one service antenna. Correspondingly, when it works on the uplink, energy from different service antennas is combined via a combiner and then transmitted through the donor antenna (illustrated in Fig. 5).

III. An Implementation Case

We have demonstrated the green indoor coverage by employing a passive relay system.

A. Demo setup

The demonstration is composed of a monitoring module, a console module and an emulation module as shown in Fig. 6. A box covered with semi-shielding net to attenuate part of electromagnetic waves, is used to emulate the indoor environment. In such emulated indoor environment, there is a common smart phone with Andorid operation system which is connected to live WCDMA base station provided by China Unicom Co., Ltd. For a better observation, we display the

Fig. 6. The configuration of demo setup.

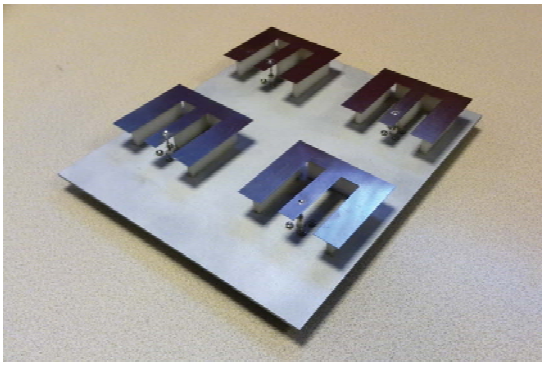

Fig. 7. E-shaped antenna array as donor antenna deployed outside of buildings.

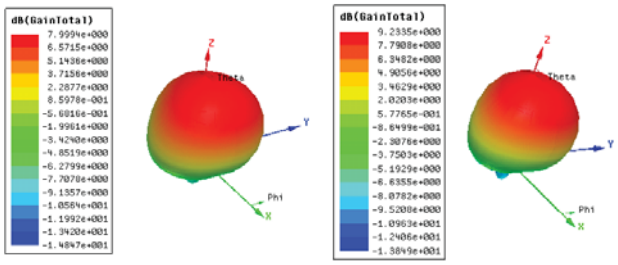

(a) 1940MHz (b) 2130MHz

Fig. 8. Normalized radiation patterns at the center frequency.

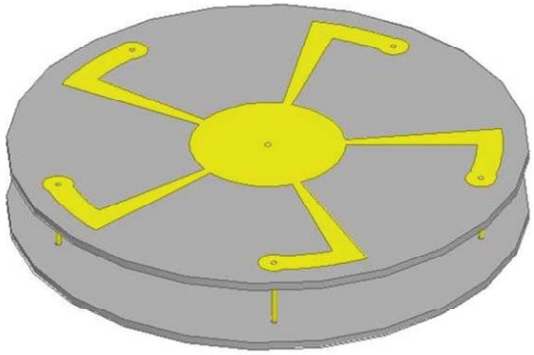

Fig. 9. Circularly polarized antenna as service antenna deployed inside of buildings.

contents of mobile phone onto a high definition monitor via a HDMI cable and control the mobile phone by a laptop via a USB cable outside of the box.

1) E-shaped antenna: For the outdoor deployment, we have designed an E-shaped antenna array which is given in Fig. 7. It has a large gain in order to convert more power from the outside to the inside building. It has a relatively wide frequency band to support both uplink and downlink transmission at least, and it also needs to be adaptive to multi-standards in order to support different operators. It has a wide beam to better harvest the wireless signal from various directions, because in the dense urban area there may be a lot of obstacles between the base stations and the user terminals. The -10 dB operational frequency bands can cover China Unicom 3G ($1940-1955$, $2130-2145$ MHz) bands. The simulated radiation patterns of the proposed antenna at 1940 MHz and 2130 MHz are illustrated in Fig.8. The simulated results are obtained using the Ansoft HFSS (High Frequency Structure Simulator) version 13 [9], and similar results of the simulation and measurement are obtained.

2) Circularly polarized antenna: The overall structure shown in Fig. 9 mainly consists of two layers of printed spoke-like metal strips on two planar substrates, respectively. The center of the upper strip is connected to the elongated inner conductor of the feeding coaxial cable; and the center of the lower strip is connected to the outer conductor. Several metal vias around the circumference connect the ends of the upper and lower strips. The current flows from the inner conductor of the feeding coaxial cable, then through the elongated inner conductor, upper strip, via and lower strip, and returns to the outer conductor of the feeding coaxial cable. The currents on them are some in phase due to half wave resonance.

All axial parts of the spoke-like metal strips, together, act as a loop with in-phase current; while the radial parts work as transmission lines for the axial parts, since the currents on each pair of them are same in amplitude and reversed in phase. A far-field similar to that generated by a small loop can thus be obtained. Elongated inner conductor of the feeding coaxial cable works as a short dipole; meanwhile, it, together with the radial parts of the metal strips, also works as the feeding structure for the axial parts of the strips.

A prototype working at 2 GHz has been designed. The goal of the design is to maintain a low axis ratio in the azimuthal plane, simultaneously, maximize the impedance and axis ratio bandwidths. The axis ratio in elevation and azimuthal planes at the center frequency, normalized radiation patterns at the center frequency is given in Figs. 10 to 11, respectively. As can been seen, (1) -10 dB impedance bandwidth is 12.2% and the 3dB axis ratio bandwidth is 95%, hence the overlapped bandwidth is only determined by the impedance bandwidth; (2) the radiation pattern is omni directional and donut shaped. The radiation is right-handed circularly polarization (RHCP); (3) the axis ratio is around -2dB within the whole space at the center frequency. The gain is 1.2 dBi at the center frequency in the elevation plane.

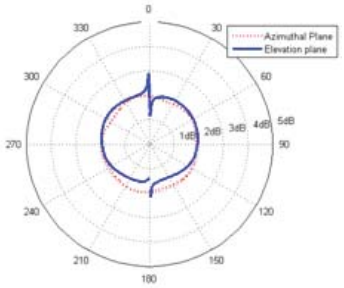

Fig. 10. Axis ratio in azimuthal and elevation planes at the center frequency.

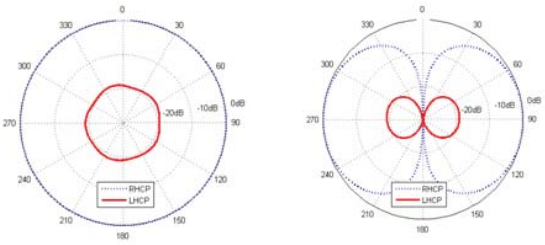

(a) Azimuth Plane (b) Elevation Plane

Fig. 11. Normalized radiation patterns at the center frequency.

Fig. 12. Performance enhancement after employing the proposed passive system.

B. Demo procedures

Firstly, the smart phone is put in the poor coverage box and is inserted a 3G WCDMA (provided by China Unicom [8]) SIM card. Without any other measures aided, the receiving signal strength on the mobile phone is very weak and if we open some online videos, the video quality is not fluent at all. After connecting the designed donor and service antennas, the signal strength is significantly improved by more than 20 dB. And if we open the online video again, it is observed that the videos can be played very fluently and clearly as shown in Fig. 12.

C. Discussion

This demonstration shows that when users are in the poor coverage, over 20 dB receiving power improvement can be achieved by employing the proposed passive antenna system. Naturally, we must raise a question: will it achieve more receiving gain if we employ higher gain antennas? To a certain extent, it is right because higher gain antennas can naturally deliver more power. As a matter of fact, the achieved 20 dB

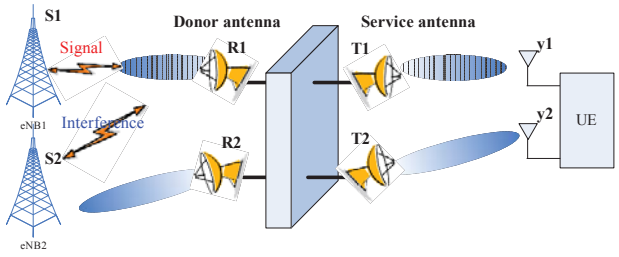

Fig. 13. Interference cancellation with two passive relays.

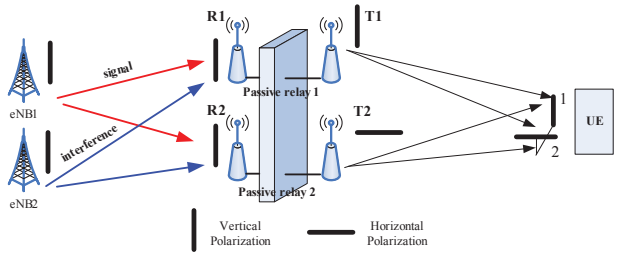

Fig. 14. Multi-polarization passive relays.

in this example is highly determined by the penetration loss of the buildings/obstacles. In other words, the more loss caused by the building, the more receive gain is capable to be obtained by the mobile terminals.

IV. Green Channel with Interference Cancellation

Assuming that there is a strong interference eNB2, one of passive relays (R1-T1 in Fig. 13) is mainly used to transfer signal to UE, and the other passive relay (R2-T2 in Fig. 13) is used to deliberately collect as much interference as possible and transfer it to the antenna 2 of UE. In the meanwhile, T2 dose not introduce more interference to antenna 1 of UE. The collected interference signal at antenna 2 of UE is used to cancel the interference received at antenna 1 of UE.

In order to improve the performance of interference cancellation, we can further utilize the polarization characteristics of antennas. In Fig. 14, horizontal polarization is used at T2 of passive relay 2 and antenna 2 of UE to let much interference and little signal reach at antenna 2 of UE, and in the meanwhile, avoid extra interference arriving at UE antenna 1. In order to describe the interference cancellation algorithm, the received signals at y_1 and y_2 are

$$y_1 = \alpha_1 \cdot s_1 + \beta_1 \cdot s_2 + n_1; \quad (1)$$

$$y_2 = \alpha_2 \cdot s_1 + \beta_2 \cdot s_2 + n_2, \quad (2)$$

and the interference cancellation is as bellow,

$$\begin{aligned} y &= y_1 - \gamma y_2 \\ &= (\alpha_1 - \gamma\alpha_2)S_1 + (\beta_1 - \gamma\beta_2)S_2 + (n_1 - \gamma n_2). \quad (3) \end{aligned}$$

Here γ is obtained by making $\beta_1 - \gamma\beta_2 = 0$ for cancellation of the interference in y_1. The parameters α, β can be obtained through channel estimation at UE. Because β_2 is much larger than β_1, γ is far less than 1, there is little impact on S_1 in y_1.

We have tested the function of the above interference cancellation algorithm in our demo platform through video communication. We first create a NLOS (LOS path is blocked) scenario that a reliable communication only can be ensured with help of passive relay. Secondly, we add a new transmitter as interference to test our interference cancellation algorithm. In the demo, it can be observed that with help of passive relay and interference cancellation algorithm, the video quality can be improved greatly at receiver and the SINR can be increased by about 20 dB.

V. CONCLUSION

From the above sections, the proposed concept of green wireless channel is a promising means to make up the coverage hole or enhance the poor indoor coverage without any external power supply. We also provide an algorithm of interference cancellation in green wireless channel for further SINR improvement.

The optimization of wireless channel for power saving probably leads to new RF structure design in eNB or UE, new signal transmission or reception mode, even new channel coding technique. These may have significant impact on green communication in various emerging mobile wireless standards and technologies, and enable a new paradigm in green networking design.

With possible introduction of new artificial passive devices into the existing system, the original network deployment and optimization may be changed accordingly. Even building material and architecture design may be reconsidered after green wireless channel research.

REFERENCES

[1] A. Goldsmith, *Wireless Communications*, USA: Cambridge university press, 2005.

[2] S. Sesia, I. Toufik and M. Baker, *LTE-The UMTS Long Term Evolution: from theory to practice*, 2nd ed., UK: John Wiley & Sons Ltd, 2011.

[3] J. Liu, R. Love, K. Stewart and M. E. Buckley, "Design and Analysis of LTE Physical Downlink Control Channel," *Vehicular Technology Conference, VTC Spring 2009. IEEE 69th*, pp. 1-5, 26-29 April 2009.

[4] A. Ghosh, R. Ratasuk, B. Mondal, N. Mangalvedhe and T. Thomas, "LTE-advanced: next-generation wireless broadband technology [Invited Paper]," *IEEE Wireless Communications Magazine*, vol. 17, no. 3, pp. 10-22, June 2010.

[5] Y. Yang, H. Hu, J. Xu, G. Mao, "Relay technologies for WiMax and LTE-advanced mobile systems," *IEEE Communications Magazine*, vol. 47, no. 10, pp. 100-105, October 2009.

[6] P. Lahdekorpi, T. Isotalo, S. U. Khan, J. Lempiainen, "Implementation aspects of RF-repeaters in cellular networks," *2010 IEEE 21st International Symposium on Personal Indoor and Mobile Radio Communications (PIMRC)*, pp. 2511-2516, 26-30 September 2010.

[7] J. Wu, "Green wireless communications: from concept to reality [Industry Perspectives]," *IEEE Wireless Communications Magazine*, vol. 19, no. 4, pp.4-5, August 2012.

[8] China Unicom Co., Ltd., "http://www.chinaunicom.com.cn".

[9] Ansoft Corporation HFSS [Online]. Available: http://www.ansoft.com/products/hf/hfss/

Improving Performance of Impulsive Noise Canceller Under Class A Impulsive PLC Channel

Hirotomo Yasui, Akira Nakamura, Makoto Itami
Department of Applied Electronics
Tokyo University of Science
6-3-1 Niijuku, Katsushika, Tokyo, 125-8585 Japan
Email: koputo@itamilab.te.noda.tus.ac.jp

***Abstract*—OFDM (Orthogonal Frequency Division Multiplexing) is a technique used for many modern applications. However, in using OFDM transmission system such as PLC (power line communication), the performance is strongly influenced by the impulsive noise with very large magnitude and short time duration. Therefore, many schemes have been proposed to reduce the influence of the impulsive noise in OFDM systems. In this paper, the algorithm for impulsive noise suppression in OFDM receivers improving time sample replacement scheme is proposed and investigated. Simulation results are provided to show the improvement in bit error rate.**

Keywords—OFDM; Impulsive Noise; PLC; Class A Noise;

I. INTRODUCTION

The OFDM (Orthogonal Frequency Division Multiplexing) is the modulation scheme that the sub-carriers are orthogonally arranged and multiple data symbols are transmitted simultaneously. The frequency band can be used effectively in OFDM system because the shape of the spectrum is nearly rectangle. Therefore high-speed communication is possible in limited frequency band [1], [2]. In addition, the addition of a GI (Guard Interval) can reduce the interference between OFDM symbols under multi-path channel as long as the maximum delay spread of the channel is shorter than the guard interval length. The OFDM system is widely studied and applied to high speed data transmission systems such as digital television broadcasting, wireless LAN, PLC (power line communication), and so on.

In PLC system that operates in the high frequency band, the multi-path by the reflected waves generated at the multiple branches and ends of power line exists. Moreover, the impulsive noise is frequently generated in the power line channels by switching operations of the appliances connected to the power line and ON-OFF noise of the power source. Impulsive noise has short time duration and very high magnitude. The performance of the OFDM system is degraded by the impulsive noise, because it has very wide frequency band width and data symbols on many OFDM sub-carriers may be severely influenced as shown in Fig. 1 [3]-[7]. Therefore, it is necessary to reduce the influence of the impulsive noise under multi-path channels.

Many schemes such as clipping and nulling scheme [8], [9], time sample replacement scheme [10], [18] and frequency domain noise reduction scheme [11] have been proposed to reduce the influence of the impulsive noise in OFDM systems.

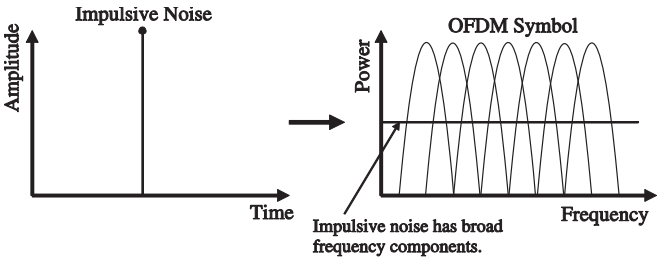

Fig. 1. The influence of the impulsive noise

In this paper, time sample replacement scheme is improved. This method is high quality in the case of low modulation scheme such as QPSK and 16QAM. However, in high density modulation scheme such as 64QAM, performance is degradation. In this paper, improving the time sample replacement scheme is shown. The performance of the proposed scheme is evaluated under the class A noise environment by using computer simulation.

This paper consists of the following sections. In section 2, OFDM transmission and the influence of the impulsive noise on OFDM signal are briefly described. In section 3, the impulsive noise mitigation schemes are described. The results of simulation are shown in section 4. Finally, this paper is concluded in section 5.

II. SYSTEM MODEL

In this section, the system model is explained. Fig. 2 shows the block diagram of the OFDM transmission system that is considered in this paper. In Fig. 2, transmitted signal at time t, $s(t)$, is expressed as

$$s(t) = \frac{1}{\sqrt{N}} \sum_{n=0}^{N-1} S_n e^{j2\pi(f_c + nf_0)t}, \qquad (1)$$

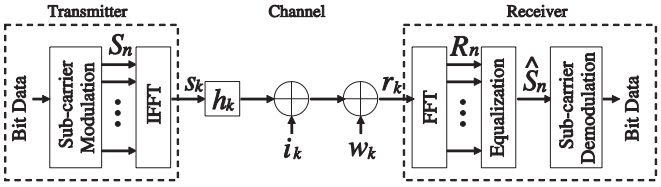

Fig. 2. System Model

where N denotes the number of sub-carriers and S_n denotes the complex data symbol transmitted on the n-th sub-carrier. Lowest sub-carrier frequency and sub-carrier spacing are denoted by f_c and f_0 respectively. If it is assumed that s_k is generated by sampling $s(t)$ with the sampling frequency of $1/(Nf_0)$, received OFDM sample, r_k, which is affected by the multipath channel and additive noises is expressed as

$$r_k = h_k \otimes s_k + w_k + i_k \qquad (k = 0,1,\dots,N-1), \quad (2)$$

where h_k denotes the impulse response of the transmission channel, $\otimes$ denotes convolution operation. In this paper, it is assumed that delay spread of the transmission channel is shorter than the guard interval length. w_k denotes the additive white Gaussian noise and it is the random variable that follows the Gaussian distribution. i_k denotes the additive impulsive noise that is added to the specific samples randomly. Generally, i_k has a high magnitude and a random phase.

In the receiver, by applying the fast Fourier transform (FFT) to r_k, the symbol transmitted on the n-th sub-carrier, R_n, is obtained by the following formula.

$$R_n = \frac{1}{\sqrt{N}} \sum_{k=0}^{N-1} r_k \left(e^{-j\frac{2\pi}{N}}\right)^{kn} = H_n S_n + W_n + I_n, \quad (3)$$

where H_n denotes the channel transfer function corresponding to the n-th sub-carrier, W_n denotes the complex Gaussian noise obtained by applying FFT to w_k, I_n denotes the complex impulsive noise obtained by applying FFT to i_k.

In order to equalize R_n in (3) and Fig. 2, zero forcing equalization is performed by dividing received OFDM symbol, R_n, by the channel transfer function, H_n, as

$$\hat{S}_n = \frac{R_n}{H_n} = S_n + \frac{W_n}{H_n} + \frac{I_n}{H_n}, \quad (4)$$

where $\hat{S}_n$ denotes the estimation of transmitted data symbol that contains the influence of the additive Gaussian noise and impulsive noise. In (4), first term, S_n, denotes actual complex data symbol transmitted on the n-th sub-carrier and the second term and later contain influence of additive noise. In (4), influence of additive impulsive noise appears on whole symbol because the additive impulsive noise consists of broad frequency components as shown in Fig. 1. We propose a method which reduces the influence of the impulsive noise as represented by 3rd term in (4). In the next section, impulsive noise mitigation schemes under multi-path channel are described.

III. Impulsive Noise Reduction Schemes

In this section, conventional impulsive noise reduction schemes and proposed scheme are explained. Conventionally "clipping and nulling scheme" and "time sample replacement scheme" have been proposed. In the following sub-sections, these schemes are explained.

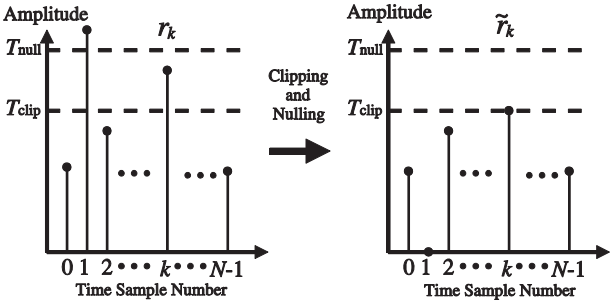

Fig. 3. Clipping and Nulling Scheme

A. Clipping and Nulling Scheme

Clipping and nulling is the scheme which combines clipping scheme and nulling scheme [8]. Clipping and nulling can be applied to the received signal, r_k, to reduce the influence of the impulsive noise by limiting and zeroing the amplitude of the signal exceeding the threshold as shown in Fig. 3. Against the received signal, r_k, received signal after impulsive noise reduction, $\tilde{r}_k$, are given as

$$\tilde{r}_k = \begin{cases} r_k, & \text{if } |r_k| \le T_{\text{clip}} \\ T_{\text{clip}} e^{j\arg r_k}, & \text{if } T_{\text{clip}} < |r_k| \le T_{\text{null}}, \\ 0, & \text{if } |r_k| > T_{\text{null}} \end{cases} \quad (5)$$

where T_{clip} and T_{null} denote the clipping threshold and nulling threshold that are defined by $T_{\text{clip}} = 2.2\sigma_s$ and $T_{\text{null}} = 3.08\sigma_s$, respectively [8]. σ_s denotes the standard deviation of OFDM signal. Conventional OFDM demodulation is performed against $\tilde{r}_k$.

B. Time Sample Replacement Scheme

In this sub-section, conventional time sample replacement scheme is described [10]. The purpose of this method is to replace the sample influenced by impulsive noise with sample that impulsive noise is reduced by re-generated. The block diagram of this scheme is shown in Fig. 4.

At first by applying the FFT to r_k in (2), the symbol transmitted on the n-th sub-carrier, R_n, is obtained in (3). After that, zero forcing equalization is performed by dividing received OFDM symbol, R_n, by the channel transfer function, H_n, in (4). After that, $\hat{S}_n$ in (4) is remapped to nearest positions in constellation plot as shown in Fig. 5. Re-modulated signal $\tilde{s}_k$ is generated by the IFFT (Inverse FFT) to $H_n\tilde{S}_n$ as

$$\tilde{s}_k = \frac{1}{\sqrt{N}} \sum_{n=0}^{N-1} H_n \tilde{S}_n \left(e^{-j\frac{2\pi}{N}}\right)^{-kn}. \quad (6)$$

If the influence of noise is small enough, $\tilde{s}_k$ is assumed to be approximately equivalent to the transmitted symbol, s_k. Therefore, in the difference signal, $D = |r_k - \tilde{s}_k|^2$, between the received signal, r_k, and the re-generated time domain signal, $\tilde{s}_k$, the influence of additive noise appears especially if there is an

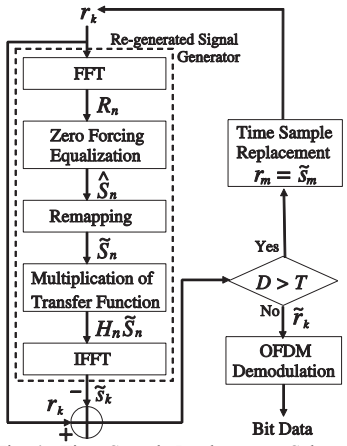

Fig. 4. Time Sample Replacement Scheme

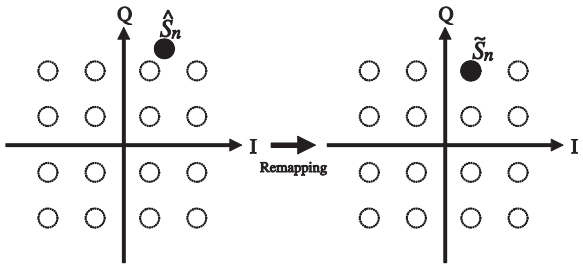

Fig. 5. Remapping

impulsive noise in r_k. By analyzing the difference signal, it is possible to detect additive impulsive noise. In this scheme, the additive impulsive noise is searched from the magnitude of the difference signal based on the pre-defined threshold value, T. In this research, the threshold value is defined as [12]

$$T = 0.01\Gamma \cdot \sigma^2, \tag{7}$$

where σ^2 denotes the average power of the additive noise, where Γ denotes impulse to Gaussian noise ratio. If the impulsive noise is detected by the threshold value, r_m is replaced by $\tilde{s}_m$ as shown in Fig. 6. m denotes the time sample number where the largest peak was detected in the difference signal.

The same procedure is repeated against replaced r_k to reduce the influence of the next largest impulsive noise until no impulsive noise is detected. If no impulsive noise is detected, conventional OFDM demodulation is performed.

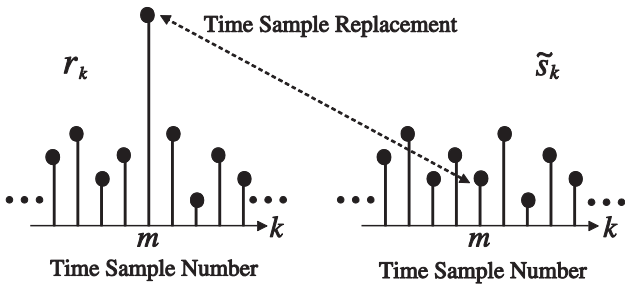

Fig. 6. Time Sample Replacement

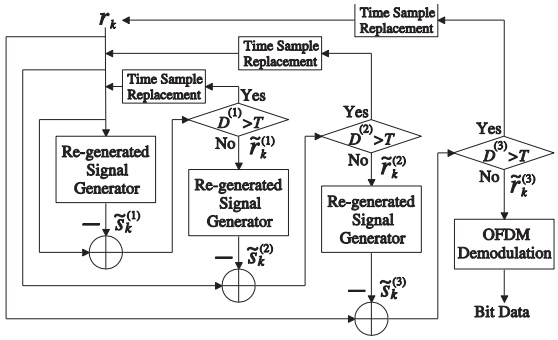

Fig. 7. Proposed Impulsive Noise Mitigation Scheme

C. Proposed Scheme

This scheme is method improved time sample replacement scheme. The BER (bit error rate) of the time sample replacement scheme is better than the clipping and nulling scheme in the low constellation modulation such as QPSK or 16QAM. However, in the high constellation modulation such as 64QAM, decision error occurred continually in the remapping process as shown in Fig. 5 because the number of signal points grows dense. Therefore, BER of the time sample replacement scheme is degraded in the high constellation modulation such as 64QAM.

In proposed scheme, BER characteristics are improved by reducing the decision error of the remapping process in the case of high order modulation scheme. The block diagram of the proposed scheme is shown as Fig. 7. In the problem of the time sample replacement scheme, decision error occurs continually in the remapping process as shown in Fig. 5 because remapping process is performed by using signal, r_k, including the influence of the impulsive noise. In the proposed scheme, in accordance with time sample replacement scheme, $\tilde{r}_k^{(1)}$ is generated as shown in Fig. 7. Against $\tilde{r}_k^{(1)}$, Re-generated signal process is performed again. Consequently, decision error is reduced by using signal that impulsive noise is mitigated, $\tilde{r}_k^{(1)}$. On the basis of this concept, it is considered that reception characteristic is improved by repeating the above process such as $\tilde{r}_k^{(2)}$ or $\tilde{r}_k^{(3)}$ as shown in Fig. 7.

IV. Results of Simulation

In this section, BER characteristics of the proposed scheme are evaluated by using the computer simulation. It is assumed that channel characteristics are time-invariant.

A. Impulsive Noise Model

In this paper, Middleton's class A impulsive noise model [13] is used to evaluate BER characteristics by using the computer simulations. This is a model which represents the Gaussian noise and impulsive noise simultaneously. It is known that class A noise well expresses the noise generated in the actual PLC systems [14]-[16], [18]. Probability density function of Middleton's class A noise model is shown as

$$p(x) = \sum_{u=0}^{\infty} \frac{e^{-A}A^u}{u!} \cdot \frac{1}{\sqrt{2\pi}\sigma_u} \exp\left(-\frac{|x|^2}{2\sigma_u^2}\right)$$
$$= \sum_{u=0}^{\infty} P_{P,A}(u) \cdot p_{G,0,\sigma_u^2}(x), \quad (8)$$

where A denotes the probability where the impulsive noise is added to each sample, $P_{P,A}(u) = \frac{e^{-A}A^u}{u!}$ denotes the probability density function of the Poisson distribution whose average value is A. $p_{G,0,\sigma_u^2}(x) = \frac{1}{\sqrt{2\pi}\sigma_u} \exp\left(-\frac{|x|^2}{2\sigma_u^2}\right)$ denotes the probability density function of the Gaussian distribution whose average value and variance are 0 and σ_u^2 respectively. If it is assumed that the number of impulsive noise sources is denoted by u, σ_u^2 is expressed as

$$\sigma_u^2 = \frac{\sigma^2\left(\frac{u}{A} + \Gamma\right)}{1+\Gamma} = u \cdot \frac{\sigma_I^2}{A} + \sigma_W^2, \quad (9)$$

$\Gamma = \sigma_W^2/\sigma_I^2$ denotes the ratio of the power of the Gaussian noise, σ_W^2, against the average power of the impulsive noise, σ_I^2. Total noise, σ^2, is defined by $\sigma_I^2+\sigma_W^2$.

B. Bit Error Rate Characteristics

In this section, the reception characteristics of the proposed scheme are compared to those of conventional schemes. Parameters used in the simulation for BER characteristics are shown in Table 1. In this paper, the values of A and Γ that are introduced in the previous researches [14]-[17] are used.

Fig. 8~10 show the BER characteristics against CNR (Carrier to Noise Ratio) under three different class A noise parameters. As shown in the figures, "w/o Impulsive Noise" denotes additive noise is only Gaussian noise without impulsive noise. In the following legends, class A noise is used for the computer simulation. "No Reduction" denotes the reduction of impulsive noise is not performed. "Clipping and Nulling" and "Time Sample Replacement" denote clipping and nulling scheme and time sample replacement scheme are respectively performed to the reduction of the additive impulsive noise. "Proposed Scheme (2)" denotes proposed scheme in the case of using $\tilde{r}_k^{(2)}$ as shown in Fig. 7. "Proposed Scheme (3)" and "Proposed Scheme (4)" are also the same as above. As shown in the figures, it is possible to much improve the performance with an increase in repeat count. As shown in the above results, the proposed impulsive noise mitigation scheme can achieve more BER performance than the conventional schemes under different class A noise parameters.

V. Conclution

In this paper, the impulsive noise reduction scheme under the impulsive PLC channel was proposed. The performance of the proposed scheme is compared to the conventional impulsive noise mitigation schemes using the clipping and nulling and time sample replacement scheme under the Middleton's class A noise environment. As the result of simulations, the BER performances against data symbols were compared and it was confirmed that the proposed scheme can achieve better performance in the high constellation modulation such as 64QAM. In the further researches, complexity reduction and theoretical optimization of the proposed scheme are studied.

TABLE I. Simulation Parameters

Number of Sub-carriers(N)	1024
Modulation Scheme of Sub-carriers	64QAM
Carrier Interval(f_0)	20.0(kHz)
Lowest Sub-carrier Frequency(f_c)	2.0(MHz)
Channel Model	Two-Path Multi-path Channel
DUR (Desired to Undesired Ratio)	10(dB)
Delay Time of Second Path	3.0(μs)
Impulse Index(A)	0.01
Impulse to Gaussian Noise Ratio(Γ)	0.01, 0.05 and 0.1

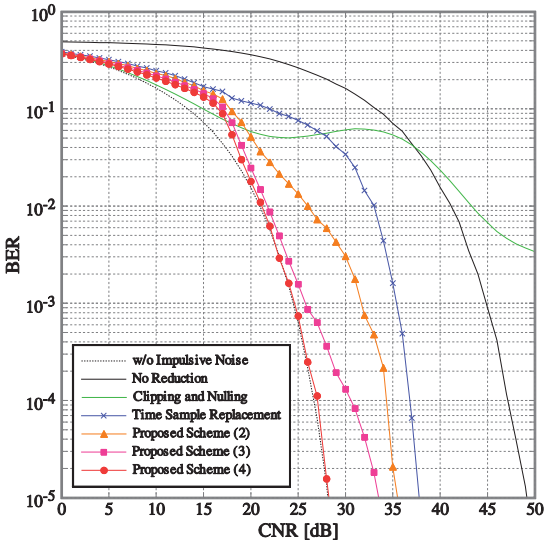

Fig. 8. BER characteristics against CNR (Γ=0.01)

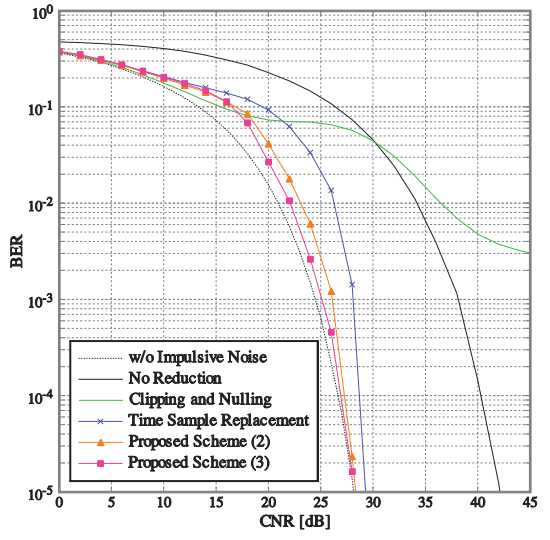

Fig. 9. BER characteristics against CNR (Γ=0.05)

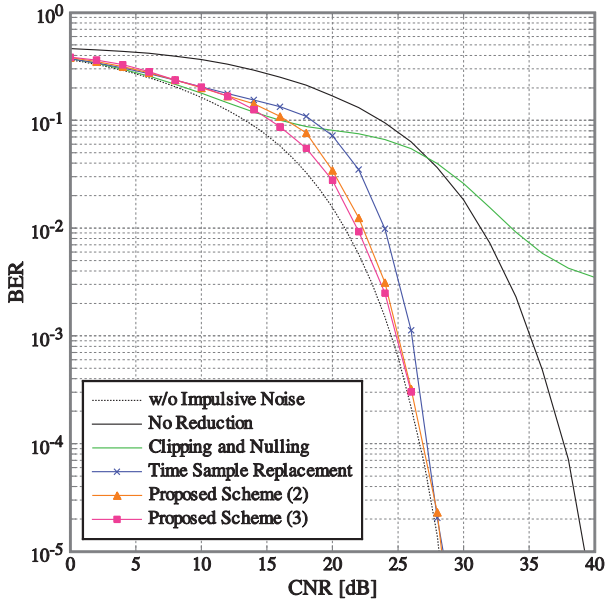

Fig. 10. BER characteristics against CNR (Γ=0.1)

REFERENCES

[1] Chang, R. and Gibby, R., "A Theoretical Study of Performance of an Orthogonal Multiplexing Data Transmission Scheme," IEEE Trans. on Communications, vol. 16, pp.529-540, 1968

[2] Weinstein, S.; Ebert, P., "Data Transmission by Frequency-Division Multiplexing Using the Discrete Fourier Transform," IEEE Trans. on Communications, vol. 19, pp.628-634, 1971

[3] D. Middleton, "Statistical-physical models of electromagnetic interference," IEEE Trans. Electromagn. Compat., vol. EMC-19, pp. 106–127, Aug. 1977.

[4] D. Middleton, "Canonical and quasi-canonical probability models of class A interference," IEEE Trans. Electromagn. Compat., vol. EMC-25, pp. 76–106, May 1983.

[5] K. L. Blackard, T. S. Rappaport, and C. W. Bostian, "Measurement and models of radio frequency impulsive noise for indoor wireless communications," IEEE J. Sel. Areas Commun., vol. 11, no. 9, pp. 991–1001, Sep. 1993.

[6] M. G. Sanchez et al., "Impulsive noise measurements and characterization in at UHF digital TV channel," IEEE Trans. Electromagn. Compat., vol. 41, no. 2, pp. 124–136, May 1999.

[7] W. R. Lauber and J. M. Bertrand, "Statistics of motor vehicle ignition noise at VHF/UHF," IEEE Trans. Electromagn. Compat., vol. 41, no. 3, pp. 257–259, Aug. 1999.

[8] Anil Mengi and A. J. Han Vinck, "Successive Impulsive Noise Suppression in OFDM," IEEE International Symposium on Power Line Communications and Its Applications (ISPLC), pp. 33-37, Mar. 2010

[9] Sergey. V. Zhidkov, "Analysis and Comparison of Several Simple Impulsive Noise Mitigation Schemes for OFDM Receivers," IEEE Transactions on Communications, vol. 56, pp.5-9, Jan. 2008

[10] Tatsuya Hirakawa, Makoto Itami, Kohji Itoh, "An Iterative Scheme to Reduce Influence of Impulse Noise in OFDM Transmission," ICCE2007 Conference, pp. 1~2, Jan. 2007.

[11] Sergey. V. Zhidkov, "Impulsive Noise Suppression in OFDM Based Communication Systems," IEEE Trans. on Consumer Electronics,vol. 49, pp. 944-948, Nov. 2003

[12] Takuya Kitamura, Hiroshi Ando, Kohei Ohno, Makoto Itami, "The Impulsive Noise Reduction Using It's Replica Signal Under Class-A Impulsive Channel," WPMC2012 Conference, pp.460-464, Sept. 2012

[13] D. Middleton, "Procedures for Determining the Parameters of the First-Order Canonical Models of Class A and Class B Electromagnetic Interference," IEEE Trans. Electromagn. Compat., vol. EMC-21, No.3, pp.190-208, Aug. 1979

[14] Stephen W. Lai and Geoffrey G. Messier, "The Wireless/Power line Diversity Channel," IEEE ICC2010 Conference, pp.1-5, May 2010

[15] Yu-Zhong Jiang, Xiu-lin Hu, Xu Kai, and Zhai Qi, "Bayesian Estimation of Class A Noise Parameters with Hidden Channel States," IEEE ISPLC2007 Conference, pp.2-4, Mar. 2007

[16] Hiroki Nakagawa, Daisuke Umehara, Satoshi Denno, and Yoshiteru Morihiro, "A Decoding for Low Density Parity Check Codes over Impulsive Noise Channels," ISPLC2007 Conference, pp.85-89, Apr. 2005

[17] Nikoleta Andreadou, "Modeling the Noise on the OFDM Power-Line Communications System," IEEE Trans. on Power Delivery, vol. 25, pp. 150-157, Jan. 2010

[18] Hirotomo Yasui, Akira Nakamura, Kohei Ohno, and Makoto Itami, "Reducing Impulsive Noise in OFDM Transmission Using Higher Order Modulation," ICCE2015 Conference, pp. 422-423, Jan. 2015.

Reliable Link Layer Packet Reconstruction for Rotating Polarization Based Radio Communication

Ritesh Kumar Kalle, *Member IEEE*
Hitachi India Pvt. Ltd., Bangalore, India
ritesh@hitachi.co.in

***Abstract*— Rotating polarization wave based radio has been proposed for enhanced wireless communication using optimum polarization(s) to transmit and receive data in multiple reflection prone environments. The transmitter expands data by orthogonal codes that divide the polarization angle space into well-distinguished regions. However, harsh radio environments to which the waves are subjected to, result in erroneous bits at the receiver. Techniques proposed in this paper provide reliable communication through link layer combination of packets received over independent polarization angles. Analytical result shows that the proposed mechanism provides higher reliability.**

Keywords*— *M2M, wireless network, rotating polarization, orthogonal code, packet combination, error correction

I. INTRODUCTION

Social infrastructure systems require periodic maintenance, failure prediction, and remote diagnosis that need reliable communication network. Due to the very nature of these systems (generation, distribution and consumption of electric power, water etc.) and the backbones of urban societies (petroleum, steel, transportation etc.), the communication network that integrates these elements should be robust, secure, and simple to deploy as well as manage. Wireless communication technologies that provide machine to machine (M2M) services in industrial scenario are viewed as the most suitable candidates for such application. However radio technologies in unlicensed band based on the existing Wireless Personal Area network (WPAN) standards perform poorly in the presence of large number of metallic reflectors which are characteristic of social infrastructure deployments.

In this context, a novel radio technology has been proposed in [1] that uses polarization angle diversity to mitigate the effects of multiple reflections. In this method, the receiver determines an optimum transmit polarization that maximizes the sum power of the received waves. The transmitter expands data by orthogonal codes that divide the polarization angle space into well-distinguished regions [2]. Further digital signal processing techniques are applied to combine the received signals and decode the information. These wireless communication systems are expected to provide better resilience against multiple reflections in industrial environments especially when operated in sub-GHz frequencies. It may be noted that the transmitted information signal may still be affected by radio interference noise due to other sources such as co-channel interference by other similar devices in vicinity, electro-magnetic (EM) emissions from high-power sources such as electric power transformer partial discharges etc. Under such circumstances, erroneous bits may be received, leading to failure of communication.

It is important to note that M2M services deployed to monitor or control social infrastructure may have varying degrees of tolerance towards erroneous received data or latency of communication. In certain cases, the application may impose strict reliability and latency requirements. In other cases, the requirements may be adequately met through higher layer protocols for error correction through retransmission and data approximation. The performance cost (space, energy, redundancy) of introducing an error control code to the original information signal can be traded off with latency of retransmissions. In order to reduce the number of packet retransmissions and for reliable reception, several packet combination techniques [4-9] have been proposed in literature. These techniques have been designed to work with multiple received packet copies through means such as antenna diversity, time diversity or code diversity reception etc. In this paper, a novel link layer packet combination scheme for rotating polarization wave (RPW) based communication system is proposed that provides reliable communication along with lower overhead. Not only is the proposed scheme feasible to be implemented on low complexity wireless devices, but also applicable to transmit-only sensors that periodically transmit sensed information and are gathered at remote nodes.

The proposed method can achieve highly reliable link layer packet reconstruction without explicit retransmission requests in case of erroneous packets. Additionally this technique can be applied without support of any explicit automatic repeat request (ARQ) and forward error correction code (FEC) and is suitable for RPW based communication system. Furthermore, it can be applied to receivers that are unable to combine signals received over the multitude of polarization angles and time instants for coherent demodulation. From the numerical result, it can be observed that the proposed technique provides up to 13% gain in packet reconstruction probability without retransmissions at BER of 10^{-3} for packet sizes varying from 10 to 100 bits used in M2M networks.

This paper is organized as follows. Section II provides a detailed overview of RPW communication system. Section III describes existing protocols for packet combination in M2M networks and key challenges faced. Section IV provides details of the proposed algorithm for packet combination and analytical results. Finally, Section VI provides key conclusions.

II. ROTATING POLARIZATION WAVE COMMUNICATION

A. *Generation, Propagation and Reception of RPW*

In [1], the proposed RPW radio transmits signal with a rotating frequency lower than those of the two carrier frequencies composing the wave using two spatially perpendicular antennas. The transmitter expands very low rate information signal by orthogonal codes at high chip rate that divide the polarization angle space into well-distinguished regions. The receiver radio can potentially use the optimum combination of transmitting and receiving polarizations to enhance communication quality. Fig. 1 depicts an example of the generation, propagation and reception of RPW radio signal.

1) Generation:

The RPW consists of two distinct narrowly spaced carrier frequencies that rotate at a frequency equal to half of the difference between the two frequencies. The occupied bandwidth is equal to the product of the frequency of the polarization-rotation and the number of bits in the chip code. Mathematically the output of the above arrangement would be,

$$Y_v(t) = x(t)\left[\cos(2\pi f_1 t) - \cos(2\pi f_2 t)\right]$$

$$= 2x(t)\left[\sin\left(2\pi\frac{\delta_1}{2}t\right).\sin\left(2\pi\frac{\delta_2}{2}t\right)\right] \quad (1)$$

$$Y_h(t) = x(t)\left[\sin(2\pi f_1 t) + \sin(2\pi f_2 t)\right]$$

$$= 2x(t)\left[\sin\left(2\pi\frac{\delta_1}{2}t\right).\cos\left(2\pi\frac{\delta_2}{2}t\right)\right] \quad (2)$$

Where, $Y_v(t)$ and $Y_h(t)$ are the outputs of the vertical and horizontal antennas respectively and the frequencies $\delta_1/2$ and $\delta_2/2$ correspond to the carrier frequency and the polarization rotating frequency respectively. $x(t)$ is the chip sequence.

2) Propagation:

The RPW changes the direction of its polarization-rotation when it is reflected from a reflector surface. The sum of waves arriving at a receiver consists of right and left handed RPWs as these waves experience reflections of odd or even numbers. The differentiation of polarization is achieved by the use of (semi-) orthogonal codes both at the transmitter and receiver.

3) Reception:

To obtain a receiving wave on an arbitrary polarization, the receiver has two spatially perpendicular antennas. The outputs from the two antennas are amplified and down-converted using the local carrier frequency (difference between the averages of two carriers) and the intermediate frequency. This signal is later decoded by block codes to recover the information.

There are several advantageous effects of using the polarization diversity for transmission and reception of information in industrial environments with multiple reflectors. This includes greater control in exploiting the path diversity using the phase angle approach, avoiding situations where receivers are permanently in deep fade condition etc. However, challenges exist with respect to achieving accurate frame synchronization, stable operational BER (< 10^{-5}) conditions etc. Also, the practical data rates achieved in conventional channels are less than 100 kbps. This motivates the design of low overhead, high reliability link layer protocols.

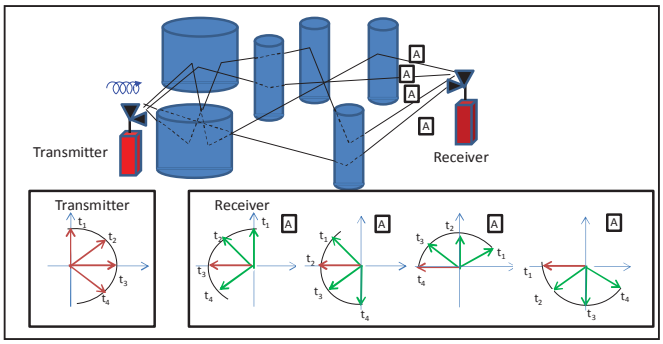

Fig. 1. RPW propagation in well defined polarization regions

III. RELIABILITY IN M2M COMMUNICATION

As described in previous sections, link layer protocol to supplement the RPW communication holds the potential to achieve higher reliability. In practice, the RPW prototype can achieve BER of 10^{-5} in the ideal scenario, but this may deteriorate in non-ideal channel conditions. Conventional methods to achieve higher reliability are compared below:

i. Forward Error Correction (FEC):

The tradeoff between the achieved coding gain due to FEC codes and energy consumed is significant for M2M applications. However, FEC codes are not suitable for low rate communication since the protection offered is proportional to the redundancy of information encoded. Also, it is essential to distinguish between bit-flips and bit-erasures in the wireless channel, FEC being suitable for the former error condition.

ii. Automatic Repeat Request (ARQ):

ARQ schemes using positive, negative acknowledgements (ACKs) and its variants with timeouts have been successfully used in low rate wireless networks for reliable transfer of information at the cost of increased latency. Variants of ARQ that weigh all the received copies of information signal before additional retransmission can be suitable for M2M application.

iii. Diversity techniques:

Packet-level diversity complements the use of radio diversity techniques. In case of wireless local area networks, packet-level diversity gain achieved by combining the received information from adjacent access-points is shown in [9]. More complex diversity techniques exploiting space, time and code space can be overwhelming for simple M2M devices.

Packet combining techniques proposed in multi-hop networks and for wireless local area networks enhances the BER performance when applied in conjunction with modified ARQ and FEC codes. However, in case of RPW, FEC and ARQ may not be best suited due to their higher overhead. A survey of packet combination methods proposed in research literature is provided in the following sub-section:

A. *Survey of techniques proposed in literature*

1) Diversity packet combining extended ARQ (EARQ) [3]: In the EARQ protocol, erroneous copies of the same packet are combined using bitwise logical XORs to locate errors in a combined copy. A brute force search method with a cyclic redundancy check (CRC) at every step is used to recover the correct copy. EARQ does not require coherent detection. Even if all the blocks received over the diversity branches are corrupt, they may be combined to retrieve the correct packet. However, the latency is high due to retransmissions and extensive CRC evaluation.

2) Simple packet combining(SPaC) [4]*:* The *SPaC* method exploits the broadcast medium and spatial diversity of a multi-hop wireless network by using overheard packets at any node, in addition to the next-hop destination of the packet. If these corrupt copies correspond to identical transmissions of the same packet, then combining them corresponds to decoding a repetition code. In a multi-hop low rate wireless network, overheard packets can be combined either having the same original information or in other cases with additional redundancy to improve the error recovery.

3) Packet merging [5]*:* For packet merging, the destination accepts two packets of the same type and creates a merged error mask also known as "Ambiguity Vector, VA". Once VA is obtained, it is then used with one of the packets, and the Frame Check Sequence (FCS) to obtain the original packet. This is achieved by modifying each bit position where there is a potential error (as indicated by V_A), and checking whether the resulting packet matches the FCS. Method to select the packet and the algorithm to search through bit combinations has been proposed to match the FCS.

4) Destination packet combining (DPC) [7]*:*

In DPC scheme, the receivers store successive received corrupted packets and use a majority voting strategy on these packets to reconstruct the original packet. The value of each bit of the determined packet depends on the values of the corresponding bit in all the corrupted packets. It was originally proposed for under water sensor networks with possibility of multipath transport or routing.

B. *Key challenges*

The retrieval process described in literature fails if there is at least one bit position where both copies have an error (hidden error). The probability of occurrence of hidden error increases with the increase of BER, thereby causing a downgrade in recovery speed. However, none of the above schemes address the issue of hidden errors and potentially led to inconclusive execution of algorithm. Furthermore, none of the schemes have been designed for the polarization diversity transmission applicable to the RPW communication. In the next section, a novel packet combination scheme for RPW is proposed that enhances the reliability of packet reconstruction.

IV. PROPOSED RPW PACKET RECONSTRUCTION TECHNIQUE

On point-to-point links, packet combining is treated equivalent to a class of coding techniques known as Hybrid ARQ (HARQ). However, the proposed scheme does not necessarily require an FEC code to protect the packet; and may be extended to support such supplementary code. Also, unlike the previously described schemes, this method does not use explicit notification to request retransmission on receipt of packets with bit errors. However, multiple packet copies with the same information content are received at the receiver node.

A. *Overview of the packet reconstruction scheme for RPW*

As depicted in Fig. 1, the transmitter encodes the same information (marked as A) with partially orthogonal periodic codes and transmits at different time points (t_1, t_2, t_3 and t_4). This scheme not only exploits the polarization diversity, but also the time diversity due to the staggered transmission that traverses different radio path owing to the nature of reflectors in the vicinity. At the receiver, therefore multiple (at least four) copies of the transmitted information (A) is received. In the hardware implementation, the FCS sequence of each packet can be checked at receiver. The packet reconstruction scheme follows only if all the copies fail to satisfy the FCS.

In Fig. 2, a six step procedure has been outlined to reliably reconstruct the transmitted packet at the receiver without explicit request for retransmissions. It may be noted that implementation specific details of the algorithm and the receiver architecture are not included due to lack of space.

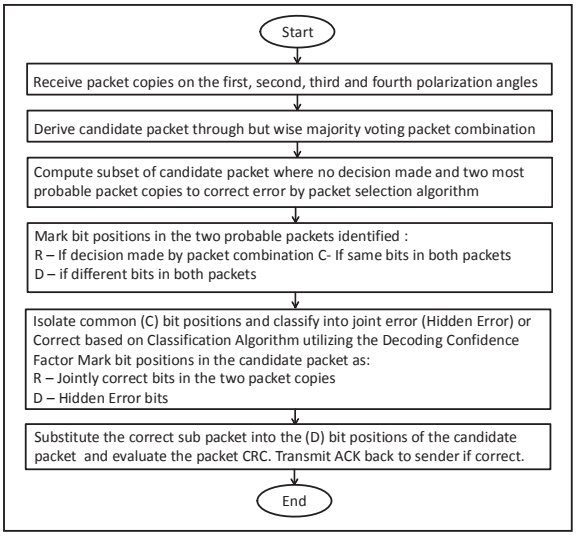

Fig. 2. Overview of steps for the proposed packet reconstruction algorithm

Step 1 describes the first stage in which the four packet copies are received over the four distinct polarization angles and passed on to the Link Layer packet processor. Note that the use of four packet copies is for illustration only and the scheme described in this paper may be applied to lower or higher polarization angles too. The packet reconstruction is only required when none of the multiple copies of packets received are deemed to be correct.

In Step 2, a candidate packet is derived through bit wise majority voting based packet combining technique. The candidate packet is stored in an appropriate structure such as the packet buffer, which may be later utilized by the packet correction unit of the packet processor. The candidate packet

is a temporary structure that holds the estimate of the final packet derived through majority vote mechanism. This mechanism (majority voting) for even number of packet copies is inconclusive when equal number of 0s and 1s are found at the same position in the packets to be combined or the number of error bits is more than the correct bits at the same position. Such errors are recovered in the Step 5.

Step 3 computes the subset of candidate packet where no decision could be made. It also selects two most probable packets amongst the multiple copies by packet selection algorithm described in Fig. 3. This algorithm first computes the pairwise Hamming distance (h_{ab}) for each of the packet copies. It also computes the pairwise function (e_{ab}) of the received packet's energy profile. This can be based on the Received Signal Strength Indicator (RSSI) signal profile (correlation characteristics, weighted average etc.). By maximizing the utility function ($\max\left(e_{ab}/h_{ab}\right)$), a pair of packets that are nearest to each other and having the highest received energy can be selected for further processing.

In Step 4, bit positions in the two probable packets are marked as: (i) Recovered (R) if decision made and assigned to candidate packet, (ii) Common (C) if bits match amongst the packets, (iii) Different (D) if bits don't match. Both (C) and (D) positions indicate the possibility of hidden error.

Step 5 isolates Common (C) positions and classifies into jointly correct or error bits (hidden errors that cannot be identified in both packets) based on classification algorithm described in Fig. 3 utilizing the Decoding Confidence metric. Decoding confidence metric is fed to the packet processor as cross layer information from the physical layer. The bit position with High decoding confidence is marked as '1' and the position with Low decoding confidence is marked as '0'. Positions where the one or both of the packets has low decoding confidence, a decision is not made and the bit position is marked 'D'. Decision is made at (C) marked positions with high decoding confidence in both copies and corresponding bits substituted in candidate packet. The packet candidate with highest number of high decoding confidence bits is utilized for the next step.

In a hard decision block decoder, such as that used for RPW system, the recovered codeword is mapped to nearest valid codeword. A threshold based classification (as High or Low) of the Hamming distance between the two can serve as one of the decoding confidence metric. In case of soft decoding, an analogous metric may be computed based on correlation between the received samples (Y) and each codeword (C_i).

$$C(Y, C_i) = \sum_{j=1}^{n} y_j c_{ij} \quad (3)$$

In Step 6, bit combinations of the selected packet (or sub-packet) are successively evaluated to satisfy the FCS. The packet is decoded to be the right packet if the FCS check is satisfied and an ACK is transmitted back to the sender. The packet candidates are evaluated in the order of increasing Hamming distance from the initial candidate packet. Also, the order of bit evaluation is dependent on pool of bit positions having low decoding confidence vector first and later with high decoding confidence vector. In case the FCS is satisfied by one of the combinations, the evaluation is terminated. Once the packet FCS is satisfied, the receiver transmits the ACK.

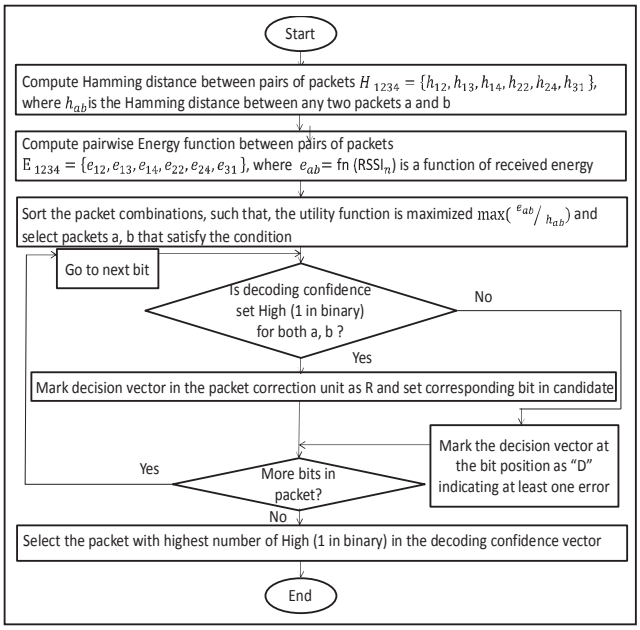

Fig. 3. Packet selection and error classification algorithm

In the worst case, if decisions could not be made at any of the n bit positions, the cost of evaluation of all possible packet candidates is prohibitively large (2^n). But in practice for RPW communication system, for small packet sizes (10 – 100 bits) and moderate BER (10^{-5} to 10^{-3}), the proportion of error bits is reasonably small and can be easily recovered by the above proposed algorithm. In the following subsection, a simple analytical model to compare the probability of decoding success is proposed.

B. Analysis and numerical results

Let p_e denote the operating BER of the wireless link. The Packet Error Rate (PER) can therefore be expressed as $B(p) = 1-(1-p_e)^n$ where n is the packet size. Consider the combination of at least two erroneous packets to generate a candidate packet without our proposed algorithm. The procedure would fail, when at least one position in which both copies have error – hidden error scenario. Further, this procedure would fail as long as additional copies of packets also contain one or more hidden errors. The probability of success in at the reception of L^{th} packet copy would be:

$$P(L) = \left[1 - \sum_{r=1}^{L-1} P(r)\right].\left[(1-p_e)^n + (1-(1-p_e)^n)(1-\alpha_d(L))\right] \quad (4)$$

where, $\alpha_d(L)$ is the probability of hidden error with all preceding L-1 copies in the packet buffer. It can be shown from [3] that,

$$\alpha_d(L) = \frac{\sum_{K_1=1}^{n} \cdots \sum_{K_L=1}^{n} P(K_1 \ldots K_L) \prod_{1 \le i,j \le L, i<j} P_{i,j}}{(1-(1-p_e)^n)^L \prod_{l=2}^{L-1} \alpha_d(l)} \quad (5)$$

where, based on assumption independent occurrence of errors

$$P(K_1 \ldots K_L) = P(K_1).P(K_2) \ldots P(K_L) \quad (6)$$

is the joint probability of the L copies having $K_1 \ldots K_L$ errors respectively. $P(K_i) = \binom{n}{K_i} p_e^{K_i} (1-p_e)^{n-K_i}$ being the probability of a copy having K_i error.

Further, $P_{i,j}$ is the probability that two copies with K_i and K_j errors, have a hidden error:

$$P_{i,j} = 1 - \frac{(n-K_i)!(n-K_j)!}{n!(n-K_i-K_j)!} \quad (7)$$

It can be considered that, the proposed algorithm in this paper eliminates the probability of occurrence of hidden error ($\alpha_d(L) \to 0$). Therefore from Eq. (3),

$$P_{proposed}(L) = \left[1 - \sum_{r=1}^{L-1} P(r)\right] \quad (8)$$

The relative benefit in terms of decoding success probability can therefore be expressed in percentage as

$$\left(P_{proposed}(L) - P(L)\right) * 100 / P_{proposed}(L) \quad (9)$$

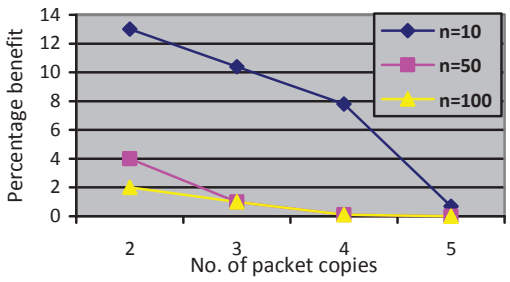

Fig. 4. Relative benefit in decoding success for varying packet sizes (n= 10, 50, 100) expressed in percentage at BER of 10^{-3}

This measures the advantage of the proposed algorithm w.r.t schemes using ARQ for packet combination such as [3], [5]. Fig. 4 depicts the numerical result of relative benefit in decoding probability w.r.t number of packet copies combined for varying packet sizes. It may be noted that the relative benefit reduces from a peak of 13% with the increasing number of packet copies through retransmissions. This however adds an additional latency proportional to the round trip time of the wireless link. Also, the proposed mechanism is most suitable for small packets on low rate wireless networks such as RPW system, where FEC and EARQ are infeasible.

There is still a small probability of false positive in which case, the packet reconstruction algorithm results in an incorrect packet that satisfies the FCS checksum. The probability of false positives is never zero, because a checksum cannot detect every possible error pattern. For a packet size of 320 bits, experimental observations in [5] indicate 0.06% of false positive for a 16-bit CRC polynomial in bad channel state. The elimination of hidden errors from the packet candidate in the proposed packet reconstruction algorithm minimizes the false positives. In RPW system, packet size of up to 100 bits is considered for packet reconstruction based link layer protocol as the probability of false positive reduces with lower packet size for any given FCS polynomial.

V. CONCLUSIONS AND FUTURE WORK

In this paper, a novel link layer mechanism to reliably combine multiple copies of the packet received at distinct polarization angles of the RPW communication system has been described. Analysis and numerical result indicates that the proposed cross layer method provides distinct feature of negating the effect of hidden errors, thereby enhancing the probability of success in packet reconstruction and minimizing the false positives. In future, it is proposed to evaluate the performance of the algorithm along with the hardware prototype of RPW communication system in field conditions.

REFERENCES

[1] Takei, K., "Polarization angle diversity for highly-reliable machine-to-machine radio," Circuits, Power and Computing Technologies (ICCPCT), 2013 International Conference on , 20-21 March 2013.

[2] Takei, Ken, "Balanced orthogonal code for polarization angle diversity," Microwave Conference (APMC), 2014 Asia-Pacific, 4-7 Nov. 2014.

[3] Chakraborty, S.S.; Yli-Juuti, E.; Liinaharja, M., "An ARQ scheme with packet combining," Communications Letters, IEEE , vol.2, no.7, pp.200,202, July 1998.

[4] Henri Dubois-Ferrire, Deborah Estrin, and Martin Vetterli. 2005. Packet combining in sensor networks. In Proceedings of the 3rd international conference on Embedded networked sensor systems (SenSys '05). ACM, New York, NY, USA, 102-115.

[5] O'Rourke, D.; Brennan, C., "Practical packet combining for use with cooperative and non-cooperative ARQ schemes in resource-constrained wireless sensor networks," Ad Hoc Networks Volume 10, Issue 3, May 2012, Pages 339–355.

[6] Vukovic, V.; Petrovic, G.; Trajkovic, L., "Packet Error Probability in Multi-Path Diversity Scheme with Majority Combining," Communications Letters, IEEE , vol.17, no.9, pp.1684,1687, Sep. 2013

[7] Sheng-Shih Wang , Pei-Chun Lee , and Kan-Yen in., "Performance Comparison of Packet Combining Based Error Recovery Schemes for Wireless Sensor Network," Lecture Notes on Information Theory Vol. 1, No. 1, March 2013

[8] Uhlemann, E.; Willig, A., "Hard decision packet combining methods for industrial wireless relay networks," Communications and Electronics, 2008. ICCE 2008. Second International Conference on , pp.104,108, 4-6 June 2008.

[9] Shi Cheng; Valenti, M.C., "Macrodiversity packet combining for the IEEE 802.11a uplink," Wireless Communications and Networking Conference, 2005 IEEE , vol.1, no., pp.88,93 Vol. 1, 13-17 March 2005.

THE 18TH INTERNATIONAL SYMPOSIUM ON WIRELESS PERSONAL MULTIMEDIA COMMUNICATIONS
(WPMC-2015)
December 13-16, 2015, Hyderabad, India

Transmission Capacity Analysis for Linear Vehicular Ad Hoc Networks

Xinxin He, Weisen Shi, and Tao Luo, *Senior Member, IEEE*
Beijing Key Laboratory of Network System Architecture and Convergence, Beijing University of Posts and Telecommunications, Beijing, 100876, P.R.China
E-mail: { hxx_9000, wilsonsws, tluo }@bupt.edu.cn

***Abstract*—In this paper, the transmission capacity of highway vehicular ad-hoc networks (VANET) is analysed based on a one-dimensional line model in topology and CSMA/CA protocol in MAC, which is described from the perspective of geometric relationship between simultaneous transmitters. The desired channel and interfering channels are assumed experience the same amount of path-loss and Rayleigh fading. Based on the proposed model, we analyse the attempted transmission probability of each active transmitter and the maximum intensity of active transmitters, followed by their theoretical values. After the outage probability is obtained, we derive the upper bound of transmission capacity of VANET, which is defined as the average spatial density of successful transmissions in the networks. Finally simulation results validate that the theoretical value offers a good bound of the network capacity.**

Keywords—VANET; Transmission Capacity; Line model; CSMA/CA

I. INTRODUCTION

Vehicular Ad Hoc Networks (VANETs) have recently become an intense research topic in the field of Intelligent Transportation Systems. VANETs assume that all or a subset of all vehicles is equipped with radio devices, treating driving vehicles as moving wireless nodes and moving routers, and forming a wide range of wireless mobile networks that take advantage of brief communication between vehicles. IEEE802.11p [1] (also referred to Wireless Access in Vehicular Environments, WAVE) was standardised to support these communications. This standard inherits many properties of IEEE 802.11, but defines enhancements to 802.11 in order to adapt to the vehicular environment.

Typically, VANET applications are categorised into safety, transport efficiency, and information/entertainment applications. Safety applications are the most important applications. Periodic messages, such as location, speed, traffic, or alert messages (accident signals), may be exchanged in VANET to help drivers navigate and adjust their vehicle to avoid dangerous situations[2-4]. Transport efficiency and information/entertainment applications are directly used by the users, such as enabling voice or communications between vehicles, analysing exemplarily enhanced route guidance and navigation, green light optimal speed advisory, and so forth. As soon as an emergency occurred, a lot of vehicles are jammed suddenly. Hence, the more frequencies for communication or entertainment is increasing. However, network capacity is limited, and not all messages can be transported effectively. Therefore, research on improving VANET capacity is crucial.

Gupta and Kumar [5] conduct a large-scale study on the asymptotic capacity of wireless ad hoc networks and prove that the per-node throughput capacity of $O\left(1/\sqrt{n}\right)$ is feasible. When the network contains n nodes, a capacity of $\Omega\left(1/\sqrt{n\log n}\right)$ is feasible. In [6], S. Weber and J.G. Andrews develop this theory and deduced the expression of transmission capacity. Numerous works [7–9] improve this bound in different scenarios and environments; however, all of these works do not prove the precise estimates, and only ALOHA protocol is used in these papers. Furthermore, the topology of networks and behaviors of nodes in these works are always described as a Poisson process in a 2-dimiensional (2D) plane, which cannot be directly applied in VAENT.

Because the vehicles are limited along the street roads or highways, and the radio range in 802.11p is much longer than the road width, the 1-demiensional (1D) lines or grids are appropriate for modelling VANET topologies. Some capacity results have been achieved based on those models [10-14]. In [10-11], the authors model the area of urban vehicular networks as a scalable grid and only intuitively analysed the asymptotic capacity performance by utilizing the protocol model without detailed theoretical results or simulation analysis. In [12-13], the authors propose an asymptotic bound of transmission capacity in linear networks. However, their model is unrealistic because the impact of interference and outage probability are ignored. In [14], the VANET capacity is estimated with interference in a straight long road. However, the model of MAC mechanism does not exactly mimic the impacts of CSMA/CA, and the interference is considered only from the two neighbor nodes. Meanwhile, only path-loss is considered while small-scale fading is ignored, and the outage probability has not been considered. Therefore the estimation of VANET capacity is not valid enough. In this paper, a 1D line model and CSMA/CA protocol are used to discuss the capacity of a linear VANET. Furthermore, all

interferences among all simultaneous transmitters are taken into account. After intuitively describe the CSMA/CA, we analyse the attempted transmission probability of each active transmitter and the maximum intensity of active transmitters, followed by their theoretical values. Then, we derive the outage probability and upper bound of transmission capacity of the networks under Rayleigh fading. Finally, we use the Matlab simulator to perform the model and validated our theoretical results.

This paper is organised as follows. Section II introduces the system model. Section III analyses the upper bound of network transmission capacity. Section IV presents the simulations and analytical results. Finally, we conclude the paper in Section V.

II. System Model

A. Proposed Model

Our model is built on the basis of a highway scenario with sufficiently great length L $(L \to \infty)$ in Fig.1. All transmitting vehicles share a same transmitting data-rate R and a same transmitting power P . Each transmitter is equipped with a dedicated receiver within its transmission range. In IEEE 802.11p standard, the transmission range D of a vehicle is about 500 to 1000 meters, which is much longer than the highway width. Therefore, we simplify the 2D strip-shaped network area into a 1D straight line.

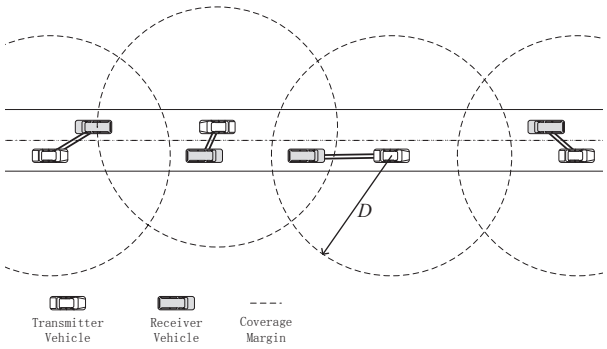

Fig.1. Basic highway scenario

As represented in Fig. 2, the line road is divided into G equal segments of length $r(d \le r < D)$, that is, $L = Gr$ where d is the average effective distance between each transmission group. We assume that a pair of vehicles can communicate only when they are on the same road segment at the same time slot. With all vehicles equipped with only one single-channel transceiver, a maximum of one transmission can occur on each road segment at each time slot. In this scenario, all the vehicles move independently along the straight line. We consider unicast flows to exist concurrently in the network, and the source and destination vehicles of each unicast flow are spatially close to each other.

The MAC protocol in this study follows the typical CSMA/CA, and it distinguishes the priorities of different businesses by setting distinct parameters. In the CSMA/CA protocol, a candidate node will sense the channel before sending the messages. In [15], whether the channel is busy or not is determined by a sensing power threshold θ , which can be translated to an exclusive region (ER) with radius R_s centered at the reference transmitter T , and $R_s = (\theta / P)^{-1/\alpha}$, where α is the path-loss exponent. With the postpone working procedure, there is no other simultaneous active transmitters in the ER. In spite of certain collisions are avoided, not every transmission is successful due to the noise and interference. Thus another interest is the outage probability, which is introduced as followed.

B. Definitions of Outage Probability and Transmission Capacity

Definition 1: The outage probability q is the probability the SIR experienced by the reference receiver at the origin is below the threshold [6]

$$q = \Pr\left(\frac{P_r}{I} < \beta\right) \tag{1}$$

where P_r is the received signal power at reference receiver, I is the total measured interference at reference receiver, the ambient noise is neglected in this interference-limited environment.

Definition 2: The transmission capacity C_T is defined as the average spatial density of successful transmissions in the networks [6]

$$C_T = \lambda(1-q)R \tag{2}$$

where λ is the maximum intensity of active transmitters, and R is transmission data rate.

III. Network Transmission Capacity Analysis

In this section, we first propose a transmission scheme mimics the CSMA/CA, and derive the attempted transmission probability of each road segment and the maximum intensity of active transmitters. After that, we obtain the outage probability and transmission capacity of the network.

As shown in Fig. 2, we partition the line into equal-sized sub-areas. Each sub-area contains M road segments, and each road segment is assumed to have a probability to transmit at a time slot. The average length of R_s around each active transmitter is about Mr , and we have

$$M = R_s / r = \left\lceil (\theta / P)^{-1/\alpha} / r \right\rceil. \tag{3}$$

The highlighted green segments in each sub-area comprise one active transmission group, that is, the measured interference on the active transmitter is no more than the predefined threshold θ . As each one sub-area contains M road segments, there are M transmission groups over the line collectively. With transmitting iteratively, each group becomes active every $1/p = M$ time slots, which means that a vehicle on one specific road segment can have an opportunity to transmit with probability p at a random time slot.

Corollary 1: The maximum density of simultaneous active transmitters over the line is given by

$$\lambda = Gp/L = p/r = 1/r\left\lceil (\theta/P)^{-1/\alpha}/r \right\rceil. \tag{4}$$

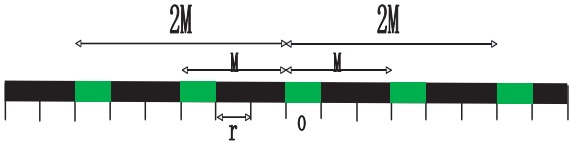

Fig.2. A line-like highway layout

In this work we treat the road as infinite and ignore the endpoints' impacts. As shown in Fig. 2, we assume the reference transmission group is on segment O. As the length of the line is sufficiently great, it can be supposed that there are both K ($K \to \infty$) simultaneous active transmitters on each side of the reference node on highlighted green segments. According to the physical model in [5], the total measured interference I at reference receiver R_0 can be defined as

$$I = 2\sum_{i=1}^{K} \frac{PH_{io}}{(iMr)^{\alpha}}. \tag{5}$$

According to definition 1, the outage probability q is the probability the SIR experienced by the reference receiver at the origin is below the threshold β. We have

$$q = \Pr\left\{ \frac{PH_{oo} r^{-\alpha}}{2\sum_{i=1}^{K} PH_{io} (iMr)^{-\alpha}} < \beta \right\}$$
$$= \Pr\left\{ H_{oo} < \beta r^{-\alpha} I \right\} \tag{6}$$

where H_{io} is the channel power gain of the interfering link from the interference vehicle to the reference receiver, and H_{oo} is the channel power gain of the desired link. All the channels are subject to Rayleigh fading and thus the channel power gain H is exponentially distributed, that is $f_H(x) = \tau \exp(-\tau x)$. Hence, formula (6) can be converted as

$$q = E\left[\int_0^{\beta r^{\alpha} I} \tau \exp(-\tau x) dx \right]$$
$$= 1 - E\left[\exp\left(-\tau \beta r^{\alpha} I\right) \right]$$
$$= 1 - L_I\left(\tau \beta r^{\alpha}\right). \tag{7}$$

Corollary 2: Under Rayleigh fading of both desired signal and interfering signals, an lower bound on the outage probability is given by

$$q_{lb} = = 1 - \left(\frac{1}{2\beta r^{\alpha} (L/4)^{-\alpha} + 1} \right)^{L/4r\left\lceil (\theta/P)^{-1/\alpha}/r \right\rceil}. \tag{8}$$

proof: Under Rayleigh fading of both desired signal and interfering signals, the Laplace transform of aggregate interference I is derived as

$$L_I(s) = E\left[\exp\left(-2s \sum_{i=1}^{K} H_{io} (iMr)^{-\alpha} \right) \right]$$
$$\le \left\{ E\left[\exp\left(-2(Mr)^{-\alpha} s H_{io} \left(\frac{K}{2}\right)^{-\alpha} \right) \right] \right\}^{\frac{K}{2}}$$
$$\underline{\underline{(a)}} \left\{ \int_{x=0}^{\infty} \tau \exp(-\tau x) \exp\left(-2s \left(\frac{MrK}{2} \right)^{-\alpha} x \right) dx \right\}^{\frac{K}{2}}$$
$$= \left\{ \int_{x=0}^{\infty} \tau \exp\left(-\left(2s \left(\frac{MrK}{2} \right)^{-\alpha} + \tau \right) x \right) dx \right\}^{\frac{K}{2}}$$
$$= \left\{ \frac{\tau}{2s \left(\frac{MrK}{2} \right)^{-\alpha} + \tau} \right\}^{\frac{K}{2}}$$
$$\underline{\underline{(b)}} \left\{ \frac{\tau}{2s \left(\frac{L}{4} \right)^{-\alpha} + \tau} \right\}^{\frac{L}{4Mr}} \tag{9}$$

where (a) follows by $f_H(x) = \tau \exp(-\tau x)$, (b) follows by $K = L/2Mr$. Therefore, we have $L_{I_{ub}}(s) = \left\{ \tau / \left(2s \left(\frac{L}{4} \right)^{-\alpha} + \tau \right) \right\}^{\frac{L}{4Mr}}$, and this upper bound can be used to obtain a low bound on the outage probability by substituting (9)and(3) into (7) as follow

$$q_{lb} = 1 - L_I\left(\tau \beta r^{\alpha}\right) = 1 - \left(\frac{1}{2\beta r^{\alpha} (L/4)^{-\alpha} + 1} \right)^{L/4r\left\lceil (\theta/P)^{-1/\alpha}/r \right\rceil}.$$

Corollary 3: Under Rayleigh fading of both desired signal and interfering signals, an upper bound on the transmission capacity is given by

$$C_{T_{ub}} = \lambda(1 - q_{lb}) R$$
$$= \frac{R}{r\left\lceil (\theta/P)^{-1/\alpha}/r \right\rceil} \left(\frac{1}{2\beta r^{\alpha} (L/4)^{-\alpha} + 1} \right)^{L/4r\left\lceil (\theta/P)^{-1/\alpha}/r \right\rceil} \tag{10}$$

where q_{lb} is obtained in corollary 2 and λ is obtained in (4). This upper bound limits the maximal possible value of transmission capacity for the linear VANET.

IV. SIMULATION RESULTS

In this section, in order to validate the upper bound of network transmission capacity, we used the simulator Matlab to build a highway environment where the highway is modeled as a line with distance of 4km, and vehicles' distribution and data transmission mechanisms were simulated in 802.11p. All vehicles in these simulations transmit frames to a neighbor with a constant bit rate, and the moving pattern of all potential transmitting vehicles is described as the classic Car-Following Model [16], which claims that the mean distance X between any two neighbor vehicles on a linear road follows a log-normal distribution parameterized by μ and σ :

$$D_X(x) = \frac{1}{\sqrt{2\pi}\sigma x}\exp\left(\frac{-(Inx-\mu)^2}{2\sigma^2}\right). \qquad (11)$$

This Car-Following Model is mainly used to simulate more realistic behaviors of vehicles in VANET. The instantaneous distribution of all transmitters in any timeslot is obtained from the model. The capacity is computed as the average spatial density of successful transmissions in the networks, and the intensity of transmitters is computed as the total number of simultaneous transmitters at a given time during the simulation. All the channels experience the same amount of path-loss and Rayleigh fading, and the value of path-loss exponent is 2. All parameters set in our simulation are shown in TABLE I.

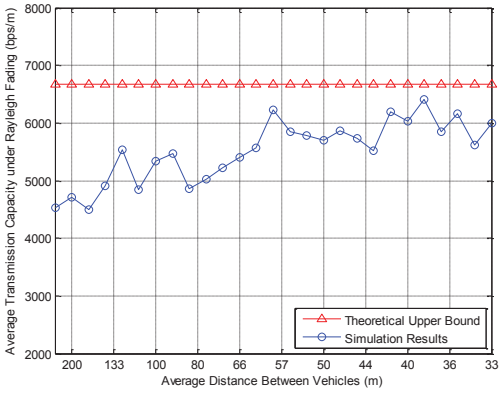

Fig. 3. Average transmission capacity and upper bound under Rayleigh fading.

Fig.3 shows the simulation results of average transmission capacity over the 2km-long central part of the road and its upper bounds. The circle-dotted curve depicts the relation between distance of neighbor vehicles and average transmission capacity under Rayleigh fading. In this paper, we set and , and the upper bound of transmission capacity equals 6583.03bps/m by solving equation (10) with parameters aforementioned in TABLE I. This upper bound is plotted as the triangle-dotted line and it constrains simulation results tight enough. Fig.4 illustrates the simulation results of successful simultaneous transmitters' average density (circle-dotted curve), and the upper bound (triangle-dotted line) is calculated by solving equation (10) without considering transmission data rate .Our result still performs well.

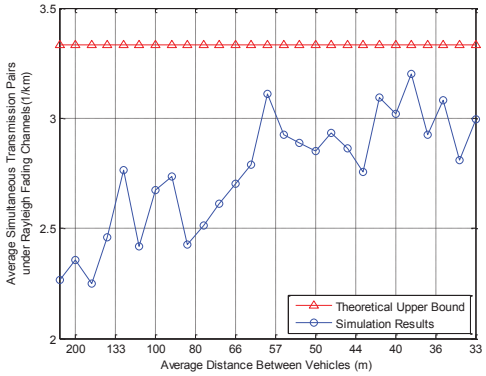

Fig.4. Average density of simultaneous transmitters and maximal density under Rayleigh fading .

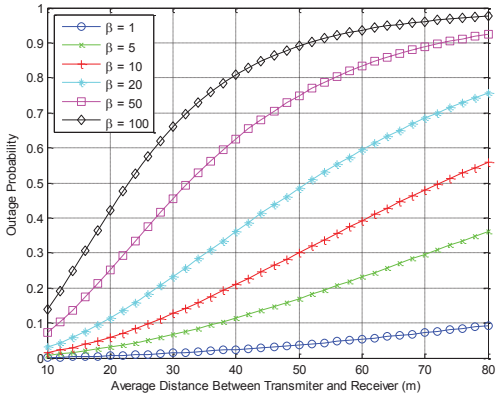

Fig.5. Outage probability vs. average distance between each transmission group under Rayleigh fading. Different colours represent different threshold β .

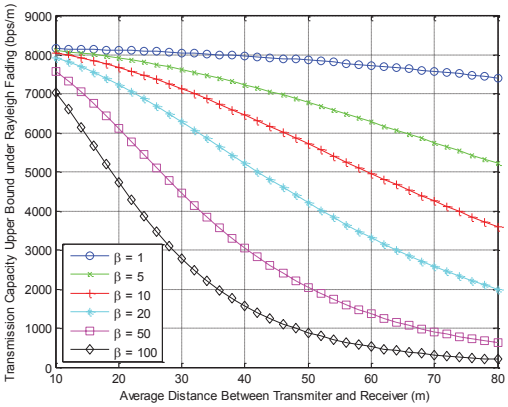

Fig.6. Transmission capacity upper bound vs. average distance between each transmission group under Rayleigh fading. Different colours represent different threshold β .

We also present numerical results based on the above analysis and give some interpretations. In fig.5, the outage probability vs. distance between each transmission group under Rayleigh fading is illustrated with different threshold β . Generally, when the distance between transmitter and receiver r is increased, the outage probability is also increased. This could be explained as that, as other parameters are fixed, the increased signal transmission distance will decrease the received signal power, which represented as the declined SIR comprehensively. It is also clear that, the outage probability is increased with the increasing of β . Fig.6 illustrates opposite change trend of Fig.5, the transmission capacity upper bound is decreased with the increasing of distance between transmitter and receiver. It is clear that larger distance will increase the outage probability, thus the transmission capacity is decreased.

TABLE I. SIMULATION PARAMETERS

Simulation Parameter	**Numerical Value**
IEEE 802.11std	802.11p
CCA mode	CCA mode 1
Carrier Wavelength	0.051 m
Packet Length	7680 byte
DCF Inter-frame Space (DIFS)	50 μs
Short Inter-frame Space (SIFS)	1 μs
Transmission Power P_t	33 dBm
Transmission Gain G_t	34 dBm
Receiving Gain G_r	33 dBm
Threshold θ	-50 dBm
Path-loss exponent α	2
Transmission Data-rate R	2 Mbps
Transmission Radium D	500m
Road Length L	4km
Duration of Simulation t_s	3 seconds

I. CONCLUSION

In this paper, we built our model on the basis of a highway scenario, and the proposed model mimics the CSMA/CA used in IEEE802.11p from the perspective of geometric relationship between simultaneous transmitters. After intuitive describe the CCA mechanism, we derive the upper bound on network capacity of VANET. Finally, we use the network simulator Matlab to perform our model and validated that the theoretical result offers a well bound on the network capacity.

ACKNOWLEDGMENT

This work is supported in part by program for National Natural Science Foundation of China under Grant No.61271184, 61571065; 863 Program of China under Grant No. 2013AA013301; National Great Science Specific Project of China under Grant No. 2015ZX03003012..

REFERENCES

[1] Chair: Wayne Fisher editor: Lee Armstrong. Status of projrct IEEE 802.11 task group p. wireless access in vehicular environments (wave). http://grouper. ieee. org / groups / 802 // 11/Reports/tgp_update.htm.

[2] Keney, B. John, “Dedicated short-range communication (DSRC) standards in the United States.” in Proceedings of the IEEE, pp. 1162-1182, 2011.

[3] F. Bai, B. Krishnamachari, “Exploiting the wisdom of the crowd: localized, distributed information-centric VANETs,” IEEE Communications Magazine, pp.138-146, 2010.

[4] R. Lu, X. Li, T. Luan, X. Liang, and X. Shen, “Pseudonym changing at social spots: An effective strategy for location privacy in VANETs,” *IEEE Transactions on Vehicular Technology*, vol 60, no. 1, 86-96, 2011.

[5] P. Gupta and P. R. Kumar,” The capacity of wireless networks.” IEEE Trans. Infor,. Theory, vol 46, no. 2, pp. 388-404, 2000.

[6] S. Weber, and J. G. Jeffrey, “Transmission Capacity of Wireless Networks,” Foundations and Trends in Networking, vol. 5, no. 2-3, 2012.

[7] M. Franceschetti, O. Dousse, and P. Thiran, “Clsing the gap in the capacity of wireless networks via percolation theory,” IEEE Trans. Infor,. Theory, vol 53, no. 3, pp. 1009-1018, 2007.

[8] V. Mhatre, C. Rosenberg, and R. Mazumdar, “On the capacity of vehicular ad hoc networks under random packet losses,” IEEE Trans. Infor,. Theory, vol 55, no. 6, pp. 2494-2498, 2009.

[9] S. P. Weber, X. Yang, J. G. Andrews, “Transmission capacity of wireless ad hoc networks with outage constraints,” Information Theory, IEEE Transactions on, vol.51, no.12, 4091-4102, 2005.

[10] N. Lu, T. H. Luan, M. Wang, X. Shen, and F. Bai, “Capacity and delay analysis for social-proximity urban vehicular networks,” INFOCOM, IEEE Proceedings, pp. 1476-1484, 2012.

[11] Y. Huang, X. Guan, Z. Cai, and T. Ohtsuki, “Multicast capacity analysis for social-proximity urban bus-assisted vanets,” In Communications (ICC),IEEE International Conference on , pp. 6138-6142, 2013.

[12] P. Jacquet and P. Muhlethaler, “Mean number of transmissions with csma in a linear network,” IEEE Vehicular Technology Conference Fall (VTC), pp. 1-5, 2010.

[13] L. Du, S. Ukkusuri , F. Wilfredo, et al. “Optimization models to characterize the broadcast capacity of vehicular ad hoc networks”. Transportation Research Part C, Emerging Technologies, pp. 571-585, 2009.

[14] A.T. Giang, A. Busson, D. Gruyer, et al, “A packing model to estimate VANET capacity” IEEE Wireless Communications and Mobile Computing Conference (IWCMC), pp. 1119-1124, 2012.

[15] S. P. Weber, J. G. Andrews, X. Yang, “Transmission capacity of wireless ad hoc networks with successive interference cancellation,” Information Theory, IEEE Transactions on, vol. 53, no. 8, pp. 2799-2814, 2007.

[16] Brackstone, Mark, and Mike McDonald. "Car-following: a historical review. "Transportation Research Part F: Traffic Psychology and Behaviour, pp. 181-196, 1999.

THE 18TH INTERNATIONAL SYMPOSIUM ON WIRELESS PERSONAL MULTIMEDIA COMMUNICATIONS
(WPMC-2015)
December 13-16, 2015, Hyderabad, India

New virtual 8x1 MISO scheme with QOSTBC

Ugljesa Urosevic
Faculty of Electrical Engineering
University of Montenegro
Podgorica, Montenegro
ugljesa@ac.me

Zoran Veljovic
Faculty of Electrical Engineering
University of Montenegro
Podgorica, Montenegro
veljovic@ac.me

Milica Pejanovic-Djurisic
Faculty of Electrical Engineering
University of Montenegro
Podgorica, Montenegro
milica@ac.me

***Abstract*— In this paper, we propose new scheme for creating virtual 8x1 multiple input-single output (MISO) channel with quasi orthogonal space time block coding (QOSTBC). This scheme includes one base station (BS), two relay stations (RS), and one mobile station (MS). BS and RSs are equipped with two antennas, while MS is equipped with one antenna. In our previous work we have proposed schemes for virtual 4x1 MISO channel with QOSTBC or OSTBC. Here we assumed more antennas per each RS, so the new coding procedure was necessary. The simulation results show SNR gains obtained with the new proposed virtual QOSTBC scheme.**

Keywords*— *BER; MISO, Relay; QOSTBC

I. INTRODUCTION

High data rates followed by appropriate quality of service (QoS) are becoming one of the major features in the future wireless communication systems regarding increasing demands for multimedia services and web-related content and applications. Creating reliable wireless connections in all possible environment types, where plethora of new applications will be realized, is the most challenging task in design of communicational part of future wireless networks. Among the many solutions proposed for addressing impairments introduced by wireless fading channels, special place belongs to relaying and multiple-input-multiple-output (MIMO) systems. These techniques improve the reliability of wireless communications, enhance the capacity and extend the coverage area of different wireless networks.

Relaying assumes resource sharing among the cooperative nodes which behaves as RS in information transmission from source to destination terminal. In this way, long wireless links can be separated into two, or more, shorter ones for performance improvement and coverage extension of wireless network, or RSs can cooperatively transmit the toward destination in order to achieve diversity gain, i.e. to realize a sort of distributed (virtual) MIMO system.

Traditional MIMO concept, also known as collocated MIMO, assumes implementation of multiple antennas at transmitter and/or receiver in order to attain spatial diversity gain. MIMO architectures are effective in improving bit error rate (BER), system capacity, spectrum efficiency, etc., of wireless communication systems, [1]-[3]. Benefits of collocated MIMO may be combined with advantages brought by relaying systems, if the RSs may implement multiple transmit and/or receive antennas, [4]-[9]. However, in some situations it is not easily feasible to implement multiple antennas on nodes, with enough separation among them in order to provide uncorrelated diversity branches. Thus, the concept of distributed, or virtual MIMO system, has gained significant research attention in recent period.

In this paper we propose new distributed QOSTBC scheme for creating virtual 8x1 MISO channel. The proposed scheme assumes one BS, two RSs, and one MS. BS and RSs are equipped with two antennas, while MS is equipped with one antenna. In this 2-hop scheme, the procedure at the RS is reduced due to omitting the decoding process. There is no need for detection and space-time decoding at RS. The procedure at RS is just permutation and forwarding of the signal sequences. This new coding procedure is extension of our previous proposed virtual QOSTBC schemes, [10]-[12]. The simulation results show the SNR gains obtained with the proposed scheme, i.e. the BER performance improvements by adding one more antennas per each RS. This paper is composed in the following order. After describing the virtual QOSTBC for creating 4x1 MISO channel and the proposed scheme for creating 8x1 MISO channel in Sect. II and III the simulation results are presented in Sect. IV. Finally, conclusions are drawn in Sect. V.

II. VIRTUAL QOSTBC FOR CREATING 4X1 MISO CHANNEL

QOSTBC for system with four transmit antennas is defined with next relation, [13]-[15]:

$$\mathbf{QOSTBC}_4 = \frac{1}{\sqrt{4}}\begin{bmatrix} a_1 & -a_2^* & -a_3^* & a_4 \\ a_2 & a_1^* & -a_4^* & -a_3 \\ a_3 & -a_4^* & a_1^* & -a_2 \\ a_4 & a_3^* & a_2^* & a_1 \end{bmatrix} \quad (1)$$

Here, a_i, i=1,…,4, are input symbols in QOSTB encoder. Average power spent per data symbol is fixed with scaling factor of $\frac{1}{\sqrt{4}}$. As it can be seen, for every four input symbols there are four output symbols at every antenna, i.e. the code rate is 1.

This code can be virtually realized [10]-[12]. The system model for the cooperative relaying with virtual QOSTBC, defined with (1) is presented in Fig. 1. The system includes one BS, two RSs and one MS. BS is equipped with two antennas, while the RS and MS are equipped with one antenna. BS transmits symbol sequences and the MS receives symbol sequences via two RSs.

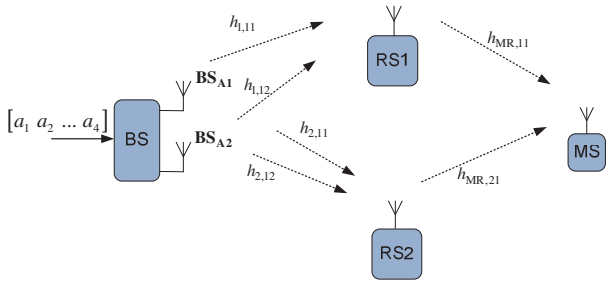

Fig. 1. Cooperative relaying scheme for virtual QOSTBC$_4$

For every four data symbols a_i, i=1,…,4, BS generates two symbol sequences:

$$\mathbf{BS_{A1_QOSTBC4}} = \frac{1}{\sqrt{2}}\left[a_1 \quad -a_2^* \quad -a_3^* \quad a_4\right]$$
$$\mathbf{BS_{A2_QOSTBC4}} = \frac{1}{\sqrt{2}}\left[a_2 \quad a_1^* \quad -a_4^* \quad -a_3\right] \tag{2}$$

Transmitted symbol sequences consist of four symbols while the average power spent per data symbol is fixed with scaling factor of $\frac{1}{\sqrt{2}}$. It is assumed that all the symbols in a single sequence suffer from same fading condition.

The channel coefficient between the i-th RS and the j-th antenna at BS is $h_{i,1j}$, i=1,2; j=1,2.

Received symbol sequence at i-th RS is:

$$\mathbf{RS_{Ai_in_QOSTBC4}} = \sum_{j=1}^{2} \mathbf{BS_{Ai_QOSTBC4}} \cdot h_{i,1j} + \mathbf{N_{Ri_QOSTBC4}} \tag{3}$$

$\mathbf{N_{Ri_QOSTBC4}}$ is additive white Gaussian noise (AWGN) matrix at i-th RS:

$$\mathbf{N_{Ri_QOSTBC4}} = [n_{Ri1_QOSTBC4} \quad n_{Ri2_QOSTBC4} \quad n_{Ri3_QOSTBC4} \quad n_{Ri8_QOSTBC4}] \tag{4}$$

Here, $n_{Ris_QOSTBC4}$, j=1,…,4 represents AWGN at i-th RS at s-th time slot.

RS1 generates the symbol sequence:

$$\mathbf{RS_{A1_out_QOSTBC4}} = \frac{1}{\sqrt{2}}\mathbf{RS_{A1_in_QOSTBC4}} \tag{5}$$

RS2 permutes the received symbol sequence, and generates output symbol sequence:

$$\mathbf{RS_{A2_out_QOSTBC4}} = \frac{1}{\sqrt{2}}\left[-\mathbf{RS}^*_{\mathbf{A2_in_QOSTBC4}}(3) \quad -\mathbf{RS}^*_{\mathbf{A2_in_QOSTBC4}}(4) \quad \mathbf{RS}^*_{\mathbf{A2_in_QOSTBC4}}(1) \quad \mathbf{RS}^*_{\mathbf{A2_in_QOSTBC4}}(2)\right] \tag{6}$$

Average power spent per data symbol is fixed with scaling factor of $\frac{1}{\sqrt{2}}$.

The channel coefficient between the i-th RS and MS is $h_{\mathrm{MR},i1}$. The received symbol sequence at MS is:

$$\mathbf{MS_{in_QOSTBC4}} = \sum_{i=1}^{2} \mathbf{RS_{Ai_out_QOSTBC4}} \cdot h_{MR,i1} + \mathbf{N_{MS_QOSTBC4}} \tag{7}$$

$\mathbf{N_{MS_QOSTBC4}}$ is AWGN matrixes at MS:

$$\mathbf{N_{MS_QOSTBC4}} = [n_{MS1_QOSTBC4} \quad n_{MS2_QOSTBC4} \quad n_{MS3_QOSTBC4} \quad n_{MS4_QOSTBC4}] \tag{8}$$

With this relaying virtual 4x1 MISO channel is created between BS and MS, i.e.:

$$\mathbf{MS}^T_{\mathbf{in_QOSTBC4}} = \frac{1}{\sqrt{4}}\begin{bmatrix} a_1 & -a_2^* & -a_3^* & a_4 \\ a_2 & a_1^* & -a_4^* & -a_3 \\ a_3 & -a_4^* & a_1^* & -a_2 \\ a_4 & a_3^* & a_2^* & a_1 \end{bmatrix}^T \begin{bmatrix} H_{1_QOSTBC4} \\ H_{2_QOSTBC4} \\ H_{3_QOSTBC4} \\ H_{4_QOSTBC4} \end{bmatrix} + \mathbf{N}^T_{\mathbf{QOSTBC4}} \tag{9}$$

where:

$$\begin{aligned} H_{1_QOSTBC4} &= h_{1,11} h_{MR,11} \\ H_{2_QOSTBC4} &= h_{1,12} h_{MR,11} \\ H_{3_QOSTBC4} &= h^*_{2,11} h_{MR,21} \\ H_{4_QOSTBC4} &= h^*_{2,12} h_{MR,21} \end{aligned} \tag{10}$$

and:

$$\mathbf{N_{_QOSTBC4}} = \mathbf{N_{MS_QOSTBC4}} + \frac{1}{\sqrt{2}}\mathbf{N_{R1_QOSTBC4}} \cdot h_{MR,11} + \frac{1}{\sqrt{2}}\left[-n^*_{R23_QOSTBC4} \quad -n^*_{R24_QOSTBC4} \quad n^*_{R21_QOSTBC4} \quad n^*_{R22_QOSTBC4}\right] \cdot h_{MR,21} \tag{11}$$

III. Proposed virtual QOSTBC scheme for creating 8x1 MISO channel

QOSTBC for system with eight transmit antennas is defined with [13]-[15]:

$$\mathbf{QOSTBC}_8 = \frac{1}{\sqrt{8}}\begin{bmatrix} a_1 & -a_2^* & -a_3^* & a_4 & -a_5^* & a_6 & a_7 & -a_8^* \\ a_2 & a_1^* & -a_4^* & -a_3 & -a_6^* & -a_5 & a_8 & a_7^* \\ a_3 & -a_4^* & a_1^* & -a_2 & -a_7^* & a_8 & -a_5 & a_6^* \\ a_4 & a_3^* & a_2^* & a_1 & -a_8^* & -a_7 & -a_6 & -a_5^* \\ a_5 & -a_6^* & -a_7^* & a_8 & a_1^* & -a_2 & -a_3 & a_4^* \\ a_6 & a_5^* & -a_8^* & -a_7 & a_2^* & a_1 & -a_4 & -a_3^* \\ a_7 & -a_8^* & a_5^* & -a_6 & a_3^* & -a_4 & a_1 & -a_2^* \\ a_8 & a_7^* & a_6^* & a_5 & a_4^* & a_3 & a_2 & a_1^* \end{bmatrix} \quad (12)$$

Here, a_i, i=1,…,8, are input symbols in QOSTB encoder. Average power spent per data symbol is fixed with scaling factor of $\frac{1}{\sqrt{8}}$. As it can be seen the code rate is 1, as in Sect. II.

Here we proposed new cooperative relaying scheme for creating virtual 8x1 MISO channel. The system model includes one BS, two RSs and one MS. BS and RSs are equipped with two antennas, while the MS is equipped with one antenna. BS transmits symbol sequences and the MS receives symbol sequences via two RSs. The system model is presented in Fig. 2.

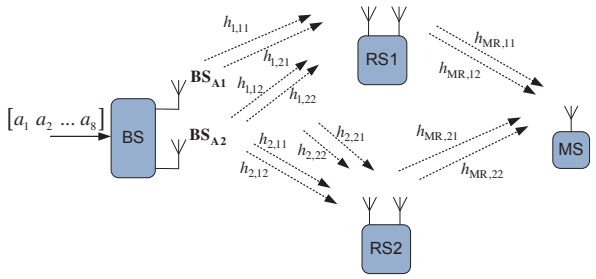

Fig. 2. The first proposed cooperative relaying scheme for virtual QOSTBC_8

We proposed that for every eight data symbols a_i, i=1,…,8, BS generates two symbol sequences:

$$\mathbf{BS_{A1}} = \frac{1}{\sqrt{2}}\begin{bmatrix} a_1 & -a_2^* & -a_3^* & a_4 & -a_5^* & a_6 & a_7 & -a_8^* \end{bmatrix}$$
$$\mathbf{BS_{A2}} = \frac{1}{\sqrt{2}}\begin{bmatrix} a_2 & a_1^* & -a_4^* & -a_3 & -a_6^* & -a_5 & a_7 & a_8^* \end{bmatrix} \quad (13)$$

Transmitted symbol sequences consist of eight symbols while the average power spent per data symbol is fixed with scaling factor of $\frac{1}{\sqrt{2}}$. It is assumed that all the symbols in a single sequence suffer from same fading condition.

The channel coefficient between the i-th, i=1,2, antenna at k-th RS, k=1,2, and the j-th, j=1,2, antenna at BS is $h_{k,ij}$.

Received symbol sequence at i-th antenna at k-th RS is:

$$\mathbf{RS}k_{\mathbf{A}i_\mathbf{in}} = \sum_{j=1}^{2} \mathbf{BS}_{\mathbf{A}j} \cdot h_{k,ij} + \mathbf{N}_{\mathbf{R}k,i} \quad (14)$$

$\mathbf{N_{Rk,}}_i$ is AWGN matrix at i-th antenna at k-th RS:

$$\mathbf{N}_{\mathbf{R}k,i} = [n_{Rk,i1}\ \ n_{Rk,i2}\ \ \ldots\ \ n_{Rk,i8}] \quad (15)$$

Here, $n_{Rk,is}$, s=1,…,8 represents AWGN at i-th antenna at k-th RS at s-th time slot.

At the first antenna RS1 generates the symbol sequence:

$$\mathbf{RS}1_{\mathbf{A}1_\mathbf{out}} = \frac{1}{\sqrt{4}}\mathbf{RS}1_{\mathbf{A}1_\mathbf{in}} \quad (16)$$

At the second antenna RS1 permutes the received symbol sequence, and generates output symbol sequence:

$$\mathbf{RS}1_{\mathbf{A}2_\mathbf{out}} = \frac{1}{\sqrt{4}}\Big[-\mathbf{RS}1^*_{\mathbf{A}2_\mathbf{in}}(3)\ \ -\mathbf{RS}1^*_{\mathbf{A}2_\mathbf{in}}(4)\ \ \mathbf{RS}1^*_{\mathbf{A}2_\mathbf{in}}(1)$$
$$\mathbf{RS}1^*_{\mathbf{A}2_\mathbf{in}}(2)\ \ -\mathbf{RS}1^*_{\mathbf{A}2_\mathbf{in}}(7)\ \ -\mathbf{RS}1^*_{\mathbf{A}2_\mathbf{in}}(8)\ \ \mathbf{RS}1^*_{\mathbf{A}2_\mathbf{in}}(5)\ \ \mathbf{RS}1^*_{\mathbf{A}2_\mathbf{in}}(6)\Big] \quad (17)$$

At the first and second antenna RS2 generates the symbol sequences:

$$\mathbf{RS}2_{\mathbf{A}1_\mathbf{out}} = \frac{1}{\sqrt{4}}\Big[-\mathbf{RS}2^*_{\mathbf{A}1_\mathbf{in}}(3)\ \ -\mathbf{RS}2^*_{\mathbf{A}1_\mathbf{in}}(4)\ \ -\mathbf{RS}2^*_{\mathbf{A}1_\mathbf{in}}(1)$$
$$-\mathbf{RS}2^*_{\mathbf{A}1_\mathbf{in}}(2)\ \ \mathbf{RS}2^*_{\mathbf{A}1_\mathbf{in}}(7)\ \ \mathbf{RS}2^*_{\mathbf{A}1_\mathbf{in}}(8)\ \ \mathbf{RS}2^*_{\mathbf{A}1_\mathbf{in}}(5)\ \ \mathbf{RS}2^*_{\mathbf{A}1_\mathbf{in}}(6)\Big] \quad (18)$$

$$\mathbf{RS}2_{\mathbf{A}2_\mathbf{out}} = \frac{1}{\sqrt{4}}\Big[\mathbf{RS}2_{\mathbf{A}2_\mathbf{in}}(3)\ \ \mathbf{RS}2_{\mathbf{A}2_\mathbf{in}}(4)\ \ -\mathbf{RS}2_{\mathbf{A}2_\mathbf{in}}(1)$$
$$-\mathbf{RS}2_{\mathbf{A}2_\mathbf{in}}(2)\ \ -\mathbf{RS}2_{\mathbf{A}2_\mathbf{in}}(7)\ \ -\mathbf{RS}2_{\mathbf{A}2_\mathbf{in}}(8)\ \ \mathbf{RS}2_{\mathbf{A}2_\mathbf{in}}(5)\ \ \mathbf{RS}2_{\mathbf{A}2_\mathbf{in}}(6)\Big] \quad (19)$$

Average power spent per data symbol is fixed with scaling factor of $\frac{1}{\sqrt{4}}$.

The channel coefficient between the i-th antenna at k-th RS and MS is $h_{\mathrm{MR},ki}$. The received symbol sequence at MS is:

$$\mathbf{MS}_{\mathbf{in}} = \sum_{k=1}^{2}\sum_{i=1}^{2} \mathbf{RS}k_{\mathbf{A}i_\mathbf{out}} \cdot h_{\mathrm{MR},ki} + \mathbf{N}_{\mathbf{MS}} \quad (20)$$

$\mathbf{N_{MS}}$ **is** AWGN matrixes at MS:

$$\mathbf{N}_{\mathbf{MS}} = [n_{MS1}\ \ n_{MS2}\ \ \ldots\ \ n_{MS8}] \quad (21)$$

With this relaying virtual 8x1 MISO channel is created between BS and MS, i.e.:

$$\mathbf{MS}_{\mathbf{in}}^{T}=\frac{1}{\sqrt{8}}\begin{bmatrix} a_1 & -a_2^* & -a_3^* & a_4 & -a_5^* & a_6 & a_7 & -a_8^* \\ a_2 & a_1^* & -a_4^* & -a_3 & -a_6^* & -a_5 & a_8 & a_7^* \\ a_3 & -a_4^* & a_1^* & -a_2 & -a_7^* & a_8 & -a_5 & a_6^* \\ a_4 & a_3^* & a_2^* & a_1 & -a_8^* & -a_7 & -a_6 & -a_5^* \\ a_5 & -a_6^* & -a_7^* & a_8 & a_1^* & -a_2 & -a_3 & a_4^* \\ a_6 & a_5^* & -a_8^* & -a_7 & a_2^* & a_1 & -a_4 & -a_3^* \\ a_7 & -a_8^* & a_5^* & -a_6 & a_3^* & -a_4 & a_1 & -a_2^* \\ a_8 & a_7^* & a_6^* & a_5 & a_4^* & a_3 & a_2 & a_1^* \end{bmatrix}^{T}\begin{bmatrix} H_1 \\ H_2 \\ H_3 \\ H_4 \\ H_5 \\ H_6 \\ H_7 \\ H_8 \end{bmatrix}+\mathbf{N}^{T} \tag{22}$$

where:

$$\begin{aligned} H_1 &= h_{1,11}h_{\mathrm{MR},11} \\ H_2 &= h_{1,12}h_{\mathrm{MR},11} \\ H_3 &= h_{1,21}^{*}h_{\mathrm{MR},12} \\ H_4 &= h_{1,22}^{*}h_{\mathrm{MR},12} \\ H_5 &= h_{2,11}^{*}h_{\mathrm{MR},21} \\ H_6 &= h_{2,12}^{*}h_{\mathrm{MR},21} \\ H_7 &= h_{2,21}h_{\mathrm{MR},22} \\ H_8 &= h_{2,22}h_{\mathrm{MR},22} \end{aligned} \tag{23}$$

and:

$$\begin{aligned} &\mathbf{N}=\mathbf{N}_{\mathbf{MS}}+\frac{1}{\sqrt{4}}\mathbf{N}_{\mathbf{R1,1}}\cdot h_{\mathrm{MR},11}+ \\ &\frac{1}{\sqrt{4}}\left[-n_{R1,23}^{*}\ -n_{R1,24}^{*}\ n_{R1,21}^{*}\ n_{R1,22}^{*}\ -n_{R1,27}^{*}\ -n_{R1,28}^{*}\ n_{R1,25}^{*}\ n_{R1,26}^{*}\right]\cdot h_{\mathrm{MR},12}+ \\ &\frac{1}{\sqrt{4}}\left[-n_{R2,13}^{*}\ -n_{R2,14}^{*}\ -n_{R2,11}^{*}\ -n_{R2,12}^{*}\ n_{R2,17}^{*}\ n_{R2,18}^{*}\ n_{R2,15}^{*}\ n_{R2,16}^{*}\right]\cdot h_{\mathrm{MR},21}+ \\ &\frac{1}{\sqrt{4}}\left[-n_{R2,23}\ -n_{R2,24}\ -n_{R2,21}\ -n_{R2,22}\ n_{R2,27}\ n_{R2,28}\ n_{R2,25}\ n_{R2,26}\right]\cdot h_{\mathrm{MR},22} \end{aligned} \tag{24}$$

IV. SIMULATION RESULTS

In this section the proposed scheme for creating virtual 8x1 MISO channel (QOSTBC$_8$) and the scheme for creating virtual 4x1 MISO channel (QOSTBC$_4$) are compared, regarding BER performance. The simulation results are presented under assumption that the propagation conditions are defined with Rayleigh fading statistics. Also, perfect estimation of channel coefficients and no direct link between BS and MS are assumed.

For the QPSK, 16QAM and 64QAM modulations BER performance in function of signal to noise ratio (SNR) per bit, of the proposed scheme and of the scheme with virtual QOSTBC$_4$ are presented in Fig. 3, 4 and 5, respectively. As it was expected it can be seen that the proposed scheme outperform scheme with QOSTBC$_4$, regarding BER performance.

For example, in the case of QPSK modulation and BER value of 10^{-5} we can see from Fig. 3 that for the proposed scheme the required SNR is smaller for 4.7dB in comparison with scheme with virtual QOSTBC$_4$. In the case of 16QAM modulation and BER value of 10^{-4} we can see from Fig. 4 that for the first proposed scheme the required SNR gain equals 3.8dB. In the case of 64QAM modulation and BER value of 10^{-3} we can see from Fig. 5 that for the first proposed scheme the required SNR is smaller for 2.4dB in comparison with scheme with virtual QOSTBC$_4$.

Obtained SNR gains are results of adding one more antenna per each RS in comparison with virtual QOSTBC$_4$.

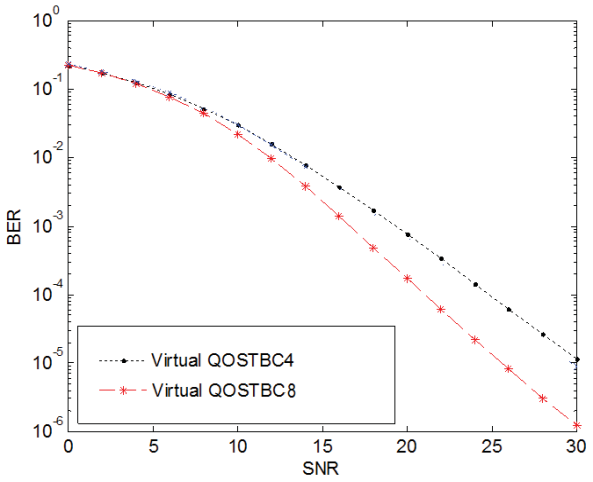

Fig. 3. BER performance of the proposed virtual QOSTBC$_8$ and virtual QOSTBC$_4$, QPSK modulation

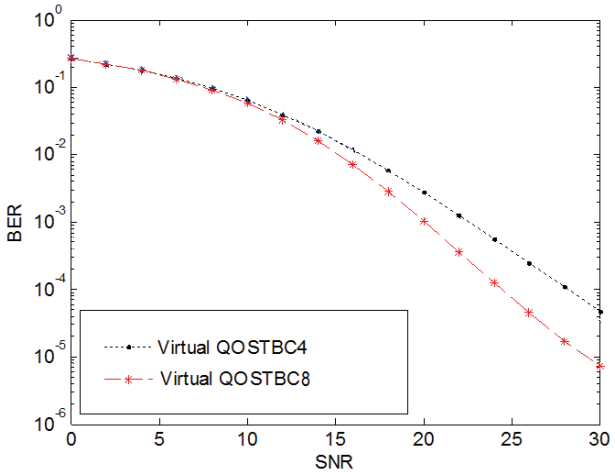

Fig. 4. BER performance of the proposed virtual QOSTBC$_8$ and virtual QOSTBC$_4$, 16QAM modulation

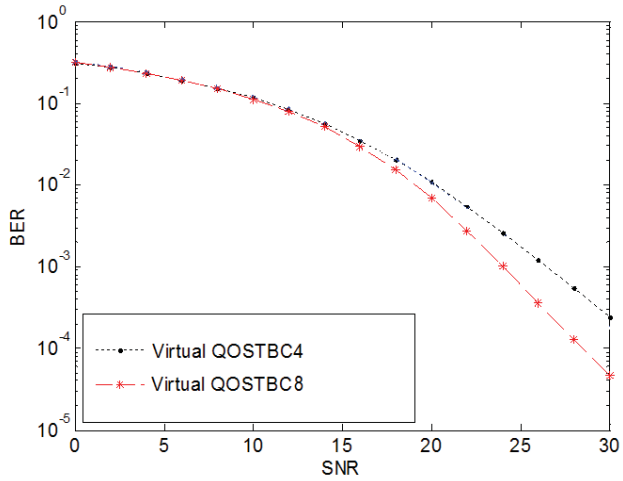

Fig. 5. BER performance of the proposed virtual QOSTBC$_8$ and virtual QOSTBC4 scheme, 64QAM modulation

V. CONCLUSIONS

In this paper we propose new distributed QOSTBC scheme for creating virtual 8x1 MISO channel. The proposed scheme assumes one BS, two RSs, and one MS. BS and RSs are equipped with two antennas, while MS is equipped with one antenna. The procedure at the RS is reduced due to omitting the decoding process. There is no need for detection and space-time decoding at RS. The procedure at RS is just permutation and forwarding of the signal sequences. There is no need for detection and space-time decoding at RS. The proposed scheme and the scheme for creating virtual 4x1 MISO channel are compared, regarding BER performance. It is assumed that the propagation conditions are defined with Rayleigh fading statistics. The simulation results show obtained BER performance improvements, i.e. SNR gains provided by proposed scheme.

ACKNOWLEDGMENT

The results presented in this paper are part of the "Improving the concept of MIMO communications in cellular networks of the next generations" research project, funded by Montenegrin Ministry of Science. Also, work is funded by European Union project Fore-Mont as a part of Seventh Framework Programme (Grant Agreement No. 315970 FP7-REGPOT-CT-2013) http://www.foremont.ac.me. Also, this work has been supported by the Ministry of Science of Montenegro and the HERIC project through the BIO-ICT Centre of Excellence (Contract No. 01-1001).

REFERENCES

[1] U. Urosevic, Z. Veljovic, M. Pejanovic-Djurisic, "MIMO Solution for Performance Improvements of OFDM-CDMA System with Pilot Tone," Wireless Networks, Volume 19, Issue 8, pp. 2021-2028, Springer, November 2013.

[2] A. J. Paulraj, R. U. Nabar, H. Bolcskei, "An overview of MIMO communications - a key to gigabit wireless," Proceedings of the IEEE, Volume 92, Issue 2, pp. 198 - 218, February 2004.

[3] F. Boccardi, B. Clerckx, A. Ghosh, E. Hardouin, G. Jöngren, K. Kusume, E.Onggosanusiand Y. Tang, "Multiple-Antenna Techniques in LTE-Advanced," IEEE Communications Magazine, Volume 50, Issue 3, pp. 114-121, March 2012.

[4] C. Woong, "Performance of amplify-and-forward cooperative networks with differential unitary space time coding," Wireless Networks, Volume 17, Issue 3, pp. 621-627, Springer, April 2011.

[5] M. R. Islam, J. Kim, "On the cooperative MIMO communication for energy-efficient cluster-to-cluster transmission at wireless sensor network," Annals of telecommunications - annales des télécommunications, Volume 49, Issue 5-6, pp. 325-340, Springer, June 2010.

[6] C. He, B. Sheng, P. Zhu, D. Wang, Xiaohu, "Energy efficiency comparison between distributed and co-located MIMO systems," International Journal of Communication Systems, Wiley, March 2012, DOI:10.1002/dac.2345.

[7] D. Wang, J. Wang, X. You, Y. Wang, M. Chen, X. Hou, "Spectral Efficiency of Distributed MIMO Systems", IEEE Journal on Selected Areas in Communications, Volume 31, Issue 10, pp. 2112 - 2127, October, 2013.

[8] Truong, K.T. ; Sartori, P. ; Heath, R.W., "Cooperative Algorithms for MIMO Amplify-and-Forward Relay Networks," IEEE Transactions on Signal Processing, Volume 61, Issue 5, pp. 1272–1287, March 2013.

[9] Y. Nam, L. Liu, J. Zhang, "Cooperative communications for LTE-advanced—relay and CoMP," International Journal of Communication Systems, Wiley, August 2012, DOI: 10.1002/dac.2423.

[10] Z. Veljovic, U. Urosevic, "Increasing Code Rate of the Cooperative Relaying with Virtual OSTBC", Wireless Personal Communications, ISSN: 0929-6212 (Print Version), ISSN: 1572-834X (Electronic Version), Vol. 83, Issue 1, pp. 399-410, Springer, July, 2015.

[11] U. Urosevic, Z. Veljovic, M. Pejanovic-Djurisic, "A New Solution for Simple Cooperative Relaying", Wireless Personal Communications, Vol. 75, Issue 2, pp. 1235-1250, Springer, March 2014.

[12] Z. Veljovic, U. Urosevic, "Performance Improvement of OFDM based virtual QOSTBC", Proceedings of Global Wireless Summit - Wireless Vitae 2014 Conference, Aalborg, Denmark, May 2014.

[13] V. Kühn, Wireless Communications over MIMO Channels - Applications to CDMA and Multiple Antenna Systems, pp. 283–288, Wiley, 2006.

[14] V. Tarokh, H. Jafarkhani, A. R. Calderbank, "Space–Time Block Codes from Orthogonal Designs," IEEE Transactions on Information Theory, vol. 45, no. 5, pp. 1456-1467, July 1999.

[15] T. Yamaoka, Y. Hara, N. Fukui, H. Kuboand T. Yamazato, "A Simple Cooperative Relaying with Alamouti Coded Transmission," IEICE Trans. Commun., Vol. E95–B, No.2, pp. 643-646, February 2012.

THE 18TH INTERNATIONAL SYMPOSIUM ON WIRELESS PERSONAL MULTIMEDIA COMMUNICATIONS
(WPMC-2015)
December 13-16, 2015, Hyderabad, India

Ranking of Total Productive Maintenence pillars using Analytical Hierarchy Process

[1]Dnyandeo D. Shinde , [2]Morten Falch
[1]Sandip Foundations,
[1]Sandip Institute of Technology and Research Center, India
[2]Center for Communication, Media and Information
[2]Technologies (CMI), Aalborg University Copenhagen
[1]dds@es.aau.dk, [2]falch@cmi.aau.dk

[3]Ramjee Prasad, Dr.[4]Rajendra G. Tated
[3]Director CTIF, Aalborg University, Denmark
[4]Principal, Sandip Foundations,
[4]Sandip Institute of Engineering and Management, India
[3]prasad@es.aau.dk, [4]rgtated@yahoo.com

***Abstract*— Total Productive Maintenance (TPM) is widely being used in industries for manufacturing excellence. TPM is based on eight pillars. Successful Implementation of TPM depends on in-depth knowledge of these pillars. The purpose of the paper is to understand the importance of these pillars mutually in terms of Quality, Cost, Delivery in time and Productivity (QCDP). In this work, ranking of TPM pillars is done by a questionnaire-based review by using Analytic Hierarchy Process (AHP), a multiple criteria decision-making (MCDM) methodology. A pairwise comparison of TPM pillars is done by survey considering a case of automotive industries in India. Ranking of TPM pillars is proposed to guide the management to decide the weightage of each pillar in terms of major factors to improve Overall Equipment Efficiency (OEE). This in terms will guide them to give proper preference and allocate fund at proper time to proper pillar. The ranking suggested suites for automotive sector and assembly lines. By varying the judgemental rating according to type of industrial sector the new ranking can be obtained from the suggested guidelines on similar basis.**

Keywords— Analytical hierarchy process (AHP); Total productive maintenance(TPM); TPM pillars

I. INTRODUCTION

In today's competitive world, it is a great challenge for industries to achieve World class excellence. To cope up with the globalized economy, manufacturers are facing stiff competition. It is a tedious task to produce maximum with minimal resources and finances available, with eminent quality and timely deliverance. Proper production planning and timely maintenance with zero defects can cause the system pull through. Proper implementation of Total Productive Maintenance (TPM) will lead the industries towards manufacturing excellence.

TPM is based on eight pillars with the foundation of 5S (Sort, Set in order, Shine, Standardize, and Sustain)[1]. It is not an easy task to understand and implement TPM, as if a set of standard procedures which, when implemented will give the results[2]. TPM is widely used to improve effective use of equipment's and to obtain world class manufacturing system in terms of Quality and Cost[3]. Successful implementation of the TPM is a team work in which individuals from each and every department should work together, it is employee focused. Due to experience and expertise operator knows more about his machine and process. In most of the case studies, barriers in implementing TPM are discussed[4][5]. It is reflected that successful implementation of TPM is difficult without the support of top management. Financial constraints are more important as per the management is concerned. If management is convinced properly, then the major hurdle in the TPM implementation will be taken away. To merge the gap it is needed to present the analytical approach, to formulate a quantitative analysis of the TPM process to focus on the most important pillar. Top management can lead discussions as per budgetary provision or can allot extra fund for TPM implementation. Detailed review of the Industries shows that only some of the areas are being focused. Survey in Indian industries reflects the limitations of TPM implementation[6]. It is mainly due to lack of knowledge and fear of investments in terms of returns.

Considering all these factors, it is important to identify the priority of the TPM pillar analytically so that the management is convinced to implement the changes step by step and monitor the returns and see the improvement in OEE to make the industry to achieve world class excellence[7].

This paper thus proposes ranking of the eight TPM pillars, as per their significance in terms of four major parameters Quality, Cost, Delivery in time and Productivity (QCDP). A pairwise comparison is done showing their hierarchy, by using Analytic hierarchy process (AHP). AHP makes it possible to assess the criteria's based on the experience [8]. Based on the survey conducted in Indian industries, the ranking of pillars is made in hierarchical order. This makes it easy to focus on the particular task of comparatively higher priority and the judgmental forecast can be done with saving plans. As per hierarchy of pillars, priority can be given to the critical maintenance activities, with optimum use of the resources, which will increase Overall Equipment Efficiency (OEE).

II. LITERATURE REVIEW

TPM plays vital role in making the industry world class, measured by Overall Equipment Efficiency (OEE). TPM kick-off takes place in many industries but very few are able to successfully implement it. To the best of author's knowledge, most of the literature discusses the failures due to improper implementations of the TPM. Review of TPM implementation in the Indian Service sector shows a tendency of people react to

implement new things, approach of top management to curb down the budget for several activities, problem of purchase and replacement of material, visionary approach and management support, are some of the factors bearing on effective implementation of TPM in Indian industries[7].

Significant review of TPM implementation in Indian industries is addressed by Ahuja & Khamba[1][9], Gupta and Vardhan[10]. TPM initiatives in steel plant, highlights how TPM implementation improved the production facilities in terms of four major criteria's – QCDP. In typical Indian industry, holistic approach for TPM needs to be implemented successfully. Team work, motivation and continuous improvement are necessary factors for positive results.

It is discerned that Indian industries are facing challenges because of many reasons like – sluggish response to change with the current market scenarios, traditional organizational structure, low quality and productivity, lacking in employee skill, education, motivation and safety, low automation, more wastage, failure to delivery in time, costumer complaints, taxes and infrastructural lacunas. According to Attri[5] et al. barriers to implementation of TPM in Indian industry can be classified as : Behavioral, Technical, Human and Cultural, Strategic and operational. Whereas Ahuja[4] has classified the barriers as : i) Organization – inability to change managerial & cultural approach, inability to convince unions, wrong focus on TPM, improper communication from top to bottom, ii) Cultural – resistance to change traditional approach, lack of consistency, iii) Behavioral - resistance from employees to adopt new changes, iv) Technological – little effort to improve design, reliability, lack of training and skills, v) Operational – acceptance of high rejection, lack of implementing standard procedures, absence of planned maintenance, vi) Financial – additional fund required in beginning to implement TPM, financial constraints from top management. vii) Departmental – poor team work.

For successful implementation of TPM it is important to find proper hierarchy of TPM pillars with respect to QCDP.

This can be done through pairwise comparison by Multi Criteria Decision Method (MCDM). Martin et al.[11] summarized various MCDM methods with its application. AHP suits for ranking the pillars, as pairwise comparison between the pillars with respect to the criteria's can be easily done. Lot of improvements are been done through TPM in Indian industries by using AHP. But only the importance of TPM verses Traditional maintenance system (TMS) is analyzed[12]. Similar attempts are being made by other researchers to justify TQM by using AHP[13]. Proper application of AHP or any other analytical method for hierarchy of TPM pillar is missing.

Use of AHP is found in various Production/manufacturing applications, N. Buyurgan presented a framework in advanced manufacturing[14], Madu implemented it for improving maintenance float system[2]. Ishizaka and Labib described its use for process ordering method[15]. This technique is applied in many areas social, personal, education, engineering, manufacturing, banking, sports, government[16] and many more fields and showed good results. No attempt has been made to use it for TPM. Attempt has been made to rank the TPM pillars by using AHP.

III. BACKGROUND

Brief regarding the TPM pillars and AHP process is given herewith:

A. TPM Pillars: Abbrivations used

TPM pillars and abbreviations used are shown in Fig. 1

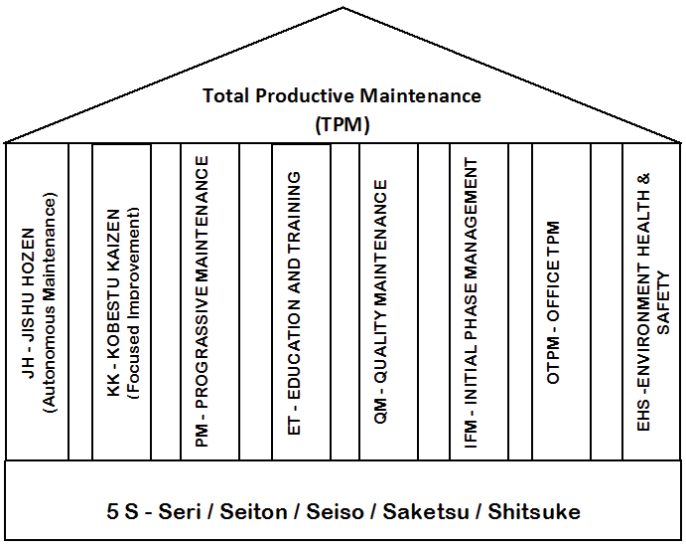

Fig. 1. TPM Pillars

TPM is based on eight pillars with a base of 5S. The goal of 5S is to create a clean and well-organized work environment.

Pillar 1: JH is mother pillar. It brings the ownership approach in the operator. Cleaning and maintenance is taken care by the the operator himself.

Pillar 2: KK aims to identify and minimize waste, quality and manufacturing losses. Elimination of losses helps improving OEE.

Pillar 3: PM pillar deals with Preventive break down (Time Base Maintenance). It establish Preventative and Predictive Maintenance systems for equipment and tooling. Effectiveness of maintenance department is increased to the point where 8 big losses are not generated.

Pillar 4: ET boost the moral and expertise of the operators and persons involved by to providing soft skill training and technical training.

Pillar 5: QM pillar monitors the factors affecting variability in product quality. It focus to accomplish zero quality defects.

Pillar 6: IFC establish systems to shorten new product or equipment development prototyping lead time. Achieve stable commissioning of new product and equipment vertical start up.

Pillar 7: OTPM goal is to achieve zero functional losses, create highly efficient offices and provide effective service and support to other departments. Administrative and support departments can be seen as process plants whose principal tasks are to collect, process, and distribute information. Process analysis should be applied to streamline information flow

Pillar 8: SHE Assures safety and prevents adverse environmental impacts which are important priorities in any

TPM effort. EHS achieve and sustain zero accidents, creates healthy, rewarding and pleasant workplace.

B. *Analytic Hierarchy Process*

Analytic Hierarchy Process (AHP) was developed by Thomas L. Saaty in 1970's[8]. It is used for multi criteria decision making in which the factors are arranged in a hierarchic structure. An advantage of the AHP over other MCDM methods is that AHP is designed to incorporate tangible as well as intangible factors, especially where the subjective judgments of different individuals constitute an important part of the decision process.

A pairwise comparison method is used to calculate relative values between each TPM pillar with respect to each other for four criteria's QCDP. A scale of judgments ranging from 1 to 9 (equal to extreme) is used for rating.

The methodology of AHP consists of following steps[17]:

Step 1: Statement of Problem having Attributes and Criteria.

Step 2: Represent problem in form of tree.

Step 3: Pairwise comparison of alternatives

Step 4 Formation of square matrix of above comparison.

Step 5: Normalization matrix is formed from eigenvalues and eigenvectors (weights)

Step 6: Check Consistency of the matrix by calculating the Consistency Index, CI. The value of CI should be less than 0.1 as recommended by Saaty.

Step 7: Obtain local & global ratings.

Step 8: Priorities or overall goal.

IV. OBJECTIVE

The objective of the research paper is to rank TPM pillars in terms of their importance in contributing to the factors QCDP of Industrial excellence using AHP developed by Thomas L. Saaty[8] for the excellence of Indian industries. Pairwise comparison of each pillar considering each criteria is done. Influence of Moral and Safety is equal with respect to each pillars, there contribution is not significant as compared to other criteria's. So analysis is carried out by considering QCDP criteria's only.

This research is based on providing the best possible solution with an analytical approach to the present theoretical concept of TPM. The study focuses on Indian industries where the TPM is not effectively implemented. During the survey for ranking of the pillars, it was clear that the TPM kick off takes place, but it is not implemented properly and over a period of time it stops. Failure occurs due to one or more constraints and barriers as discussed. The main reason is involvement of management and availability of fund for implementing the things at right time in right place. If the management is convinced by proper grading of the pillars it will be easy to allocate the fund at proper time. Ranking will give the proper focus and set the priorities for the budget. This will help in successful implementation of TPM, in terms increase in OEE.

V. METHODOLOGY

A survey was conducted based on the questioner using 9 point rating scale of Saaty for AHP[8]. Companies from Automobile and assembly sectors were considered for the survey. Following points were considered while selecting the company for survey:

a) The industry should have 5S culture, ensuring environmental cleanliness, safety and comfort. Thus the role of the criteria's Safety and Moral shall not be reckoned in determining hierarchy based on QCPD.
b) This will be more rational if the Industry happens to be an engineering Industry of Assembly type instead of a Process plant where dust and contamination of air, water etc. is dominant.

A. *Collection of Data*

Analysis is based on the data collected from Indian industries. As a part of research methodology the paired comparison data is collected in consultation with the management representatives of some companies or other persons responsible for TPM implementation. The management representatives have overall responsibility of TPM planning and implementation and they are appointed by the CEO of the company. Apart from them, consult of various pillar heads of the industry are taken to make the data more authentic. Each of these pillar heads is an experienced senior manager aware of all the pillars and their impact on QCDP. A questioner is designed based on 9 point rating scale for AHP.

B. *Ranking of TPM Pillars*

Analytical Approach: A study of literature on TPM reveals that most of reported information describes the eight pillars in a QUALITATIVE manner without resorting to utilize mathematical modelling. Most of the literature available gives an account of how a certain industry applied TPM and achieved increased productivity, quality, etc. at reduced cost. It is almost a monotonous repetition of the eight pillars. There is a need to make a proper attempt to rank the pillars in a QUANTITATIVE way so as to be a helpful guideline for research into Total Productive Maintenance.

Analysis is carried out by using paired comparison of each of the eight pillars with the objectives: Quality, Cost, Productivity and Delivery on time. The paired comparison helps in calculating the relative score of each of the TPM pillars on the four criteria. Next the four criteria are compared with each other through paired comparison to find the weightage of each of the criteria. Finally, on multiplying the scores of the eight TPM pillars, the summed, weighted score of these pillars is calculated. This helps in identifying the most important pillar on the overall ranking.

C. *AHP for Ranking of the pillars*

For the objective to rank eight pillars of TPM with respect to their importance towards QCPD, AHP process is used to find the hierarchy of the pillars as follows:

1. *Criteria and Attributes*

For ranking of the TPM pillars, its eight pillars are criteria's and Quality, Cost, Delivery in time and Productivity (QCDP) are considered as attributes.

2. *Hierarchy of Decision*

The hierarchy of the attributes and criteria are shown in Fig. 2.

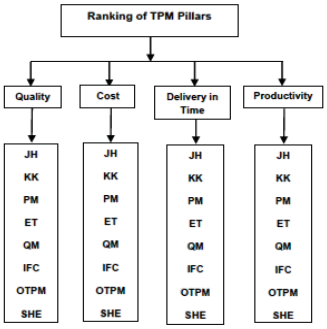

Fig. 2. Hierarchy of Decision

3. *Pairwise comparison scale*

Scale for AHP: Standard 9 point rating scale proposed by T.L. Saaty[18] is used for rating the pillars.

4. *Pairwise comparison matrix*

A questioner was generated to rate the pillars with respect to each other, sample shown in Table I. Nine point Linkert scale is used for rating the pillars with respect to each other.

TABLE I. SAMPLE VALUES FROM QUESTIONEER

Factor	Factor weighting Score - Quality																Factor
	More important than								Equal	Less important than							
JH	9	8	7	6	5	4	3	2	1	2	3	4	5	6	7	8	9	PM
JH	9	8	7	6	5	4	3	2	1	2	3	4	5	6	7	8	9	OTPM

Based on the ratings given a pairwise comparison matrix is prepared for each criteria. Table II shows rating of various pillars considering Cost as the criteria.

TABLE II. CRITERIA QUALITY: PAIRWISE COMPARISON

	JH	KK	PM	ET	QM	IFC	OTPM	SHE
JH	1.00	6.00	1.00	4.00	1.00	6.00	8.00	8.00
KK	0.17	1.00	0.50	0.50	0.50	1.00	6.00	8.00
PM	1.00	2.00	1.00	4.00	0.50	6.00	8.00	8.00
ET	0.25	2.00	0.25	1.00	0.50	6.00	8.00	8.00
QM	1.00	2.00	2.00	2.00	1.00	8.00	8.00	8.00
IFC	0.17	1.00	0.17	0.17	0.13	1.00	1.00	4.00
OTPM	0.13	0.17	0.13	0.13	0.13	1.00	1.00	4.00
SHE	0.13	0.13	0.13	0.13	0.13	0.25	0.25	1.00

Similarly, based on the data from questionner, matrix are obtained for other criteria. Table III, IV and V shows rating for Cost, Delivery in time and Productivity respectively.

TABLE III. CRITERIA COST: PAIRWISE COMPARISON

	JH	KK	PM	ET	QM	IFC	OTPM	SHE
JH	1.00	1.00	1.00	4.00	1.00	4.00	0.50	4.00
KK	1.00	1.00	1.00	6.00	1.00	6.00	1.00	6.00
PM	1.00	1.00	1.00	6.00	1.00	6.00	1.00	6.00
ET	0.25	0.17	0.17	1.00	1.00	1.00	0.50	1.00
QM	1.00	1.00	1.00	1.00	1.00	4.00	1.00	6.00
IFC	0.25	0.17	0.17	1.00	0.25	1.00	0.50	4.00
OTPM	2.00	1.00	1.00	2.00	1.00	2.00	1.00	8.00
SHE	0.25	0.17	0.17	1.00	0.17	0.25	0.13	1.00

TABLE IV. CRITERIA DELIVERY IN TIME: PAIRWISE COMPARISON

	JH	KK	PM	ET	QM	IFC	OTPM	SHE
JH	1.00	2.00	1.00	4.00	1.00	8.00	6.00	4.00
KK	0.50	1.00	4.00	6.00	4.00	8.00	6.00	6.00
PM	1.00	0.25	1.00	4.00	1.00	8.00	6.00	6.00
ET	0.25	0.17	0.25	1.00	0.50	6.00	4.00	4.00
QM	1.00	0.25	1.00	2.00	1.00	8.00	6.00	6.00
IFC	0.13	0.13	0.13	0.17	0.13	1.00	0.50	0.50
OTPM	0.17	0.17	0.17	0.25	0.17	2.00	1.00	4.00
SHE	0.25	0.17	0.17	0.25	0.17	2.00	0.25	1.00

TABLE V. CRITERIA PRODUCTIVITY: PAIRWISE COMPARISON

	JH	KK	PM	ET	QM	IFC	OTPM	SHE
JH	1.00	2.00	1.00	4.00	1.00	8.00	6.00	4.00
KK	0.50	1.00	4.00	6.00	4.00	8.00	6.00	6.00
PM	1.00	0.25	1.00	4.00	1.00	8.00	6.00	6.00
ET	0.25	0.17	0.25	1.00	0.50	6.00	4.00	4.00
QM	1.00	0.25	1.00	2.00	1.00	8.00	6.00	6.00
IFC	0.13	0.13	0.13	0.17	0.13	1.00	0.50	0.50
OTPM	0.17	0.17	0.17	0.25	0.17	2.00	1.00	4.00
SHE	0.25	0.17	0.17	0.25	0.17	2.00	0.25	1.00

5. *Normalization*

Table VI gives the calculations for normalization matrix for various pillars with respect to Quality as a criteria.

TABLE VI. CRITERIA QUALITY: NORMALIZATION MATRIX

	JH	KK	PM	ET	QM	IFC	OTPM	SHE
JH	0.261	0.420	0.194	0.336	0.258	0.205	0.199	0.163
KK	0.043	0.070	0.097	0.042	0.129	0.034	0.149	0.163
PM	0.261	0.140	0.194	0.336	0.129	0.205	0.199	0.163
ET	0.065	0.140	0.048	0.084	0.129	0.205	0.199	0.163
QM	0.261	0.140	0.387	0.168	0.258	0.274	0.199	0.163
IFC	0.043	0.070	0.032	0.014	0.032	0.034	0.025	0.082
OTPM	0.033	0.012	0.024	0.010	0.032	0.034	0.025	0.082
SHE	0.033	0.009	0.024	0.010	0.032	0.009	0.006	0.020

Normalization matrix for other criteria can be obtained similarly.

6. *Consistency Check*

Saaty[18] proposed that the consistency index should be less than 10%, if not the priorities does not make any sense and the judgements may need to be revised for various pillars with respect to Quality as a criteria. Consistency check is conducted after normalization matrix.

Table VII shows the Consistency check for the above normalization results.

TABLE VII. CRITERIA QUALITY: CONSISTANCY CHECK

	Weights	Products	Ratio
JH	0.2544	2.3963	9.4196
KK	0.0910	0.7891	8.6750
PM	0.2033	1.9168	9.4296
ET	0.1292	1.1859	9.1787
QM	0.2312	2.0604	8.9131
IFC	0.0416	0.3625	8.7180
OTPM	0.0315	0.2622	8.3282
SHE	0.0179	0.1498	8.3547
		CI =	0.1253
		CI / RI =	0.09

As consistency ratio CR is less than 10% the matrix can be considered as having an acceptable consistency.

Similarly weightage are found for cost, delivery in time and productivity.

7. Ratings

After comparing all the pillars with respect to different criteria's, the criteria's are also compared with respect to each as per the priority. Weightage for QCDP are tabulated below. The comparison matrix for QCDP is in Table VIII.

TABLE VIII. PAIRWISE COMPARISM OF QCDP

	Q	C	D	P
Q	1.00	4.00	2.00	1.00
C	0.25	1.00	0.50	0.17
D	0.50	2.00	1.00	0.50
P	1.00	6.0	2.00	1.00

8. Overall Goal

Finally the percentage weightage are calculated in Table: IX. The graphical representation of the hierarchy obtained by AHP is shown in Fig. 3.

TABLE IX. SCORE OF THE PILLARS

Pillar	% Weightage				
	Q	C	D	P	Overall %
JH	25.44	15.18	11.44	21.43	**20.581**
KK	9.10	19.15	22.29	28.73	**19.903**
PM	20.33	19.15	19.31	16.92	**18.722**
ET	12.92	5.71	10.50	8.14	**10.048**
QM	23.12	15.28	13.96	15.51	**17.899**
IFC	4.16	5.29	5.82	1.96	**3.682**
OTPM	3.15	17.36	13.84	4.29	**6.620**
SHE	1.79	2.87	2.84	3.03	**2.545**

VI. RESULTS AND DISCUSSION

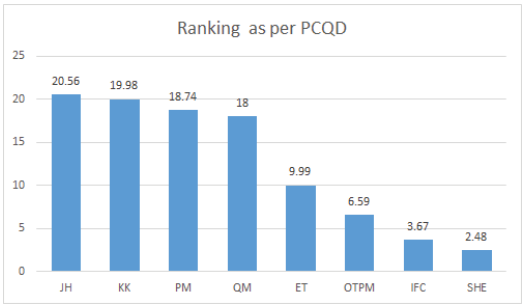

Fig. 3. Ranking of TPM pillars as per contribution towards criterias PCQD

In case of TPM implemented industries it can be seen that out of eight pillars JH and KK are used more number of times than other six. JH & KK pillars has the maximum weightage, with marginable difference. JH focus on improvement of Quality which enhances productivity whereas KK has high impact on Productivity by reducing various losses, increased production rate maintaining prompt delivery schedule followed by reduction in manufacturing cost. It is recommended to start implementing TPM with JH pillar followed by KK. After that the focus on PM & QM pillars. Once all these are in action, it will be enhanced with ET & OTPM pillar activities. IFC and SHE can be followed thereafter.

VII. CONCLUSION AND FUTURE SCOPE

The results obtained helps to categorize the pillars according to priority as: top priority (JH and KK), medium (PM and QM) and low priority (ET, OTPM, IFC and SHE). It will be easy for the managers to convince the top management and attract attention on the pillars with top most priority. However the results obtained will work for particular set of companies, it should not be treated as universal. The survey results are for automobile components manufacturing industries. According to the type of industries the rating can be varied and the new hierarchy can be obtained easily. For chemical industry top priority may go to pillar SHE, whereas for service industries it may be OTPM.

REFERENCES

[1] I.P.S. Ahuja and Khamba J.S., "TPM: literature review and direction," J. Qual. Maint. Eng., vol. 25, no. 7, pp. 709–756, 2008.

[2] C. N. Madu, "On the total productivity management of a maintenance float system through AHP applications," Int. J. Prod. Econ., vol. 34, no. 2, pp. 201–207, 1994.

[3] R. Attri, S. Grover, N. Dev, and D. Kumar, "Analysis of barriers of total productive maintenance (TPM)," Int. J. Syst. Assur. Eng. Manag., vol. 4, no. 4, pp. 365–377, 2013.

[4] I.P.S. Ahuja and Khamba J.S., "Strategies and success factors for overcoming challenges in TPM implementation in Indian manufacturing industry," J. Qual. Maint. Eng., vol. 14, no. 2, pp. 123–147, 2008.

[5] R. Attri, S. Grover, and N. Dev, "A graph theoretic approach to evaluate the intensity of barriers in the implementation of total productive maintenance," Int. J. Prod. Res., vol. 52, no. 10, pp. 3032–3051, 2014.

[6] A. T. Bon and M. Lim, "Total Productive Maintenance In Automotive Industry : Issues And Effectiveness," Proc. 2015 Int. Conf. Ind. Eng. Oper. Manag. Dubai, United Arab Emirates, vol. March, 2015.

[7] Narender and Gupta A.K., "A Review of Total Productive Maintenance System," Int. J. Mech. Prod. Eng., vol. 1, no. 1, pp. 10–18, 2012.

[8] T. L. Saaty, Analytic Hierarchy Approach. 1980.

[9] I. P. S. Ahuja and J. S. Khamba, "An evaluation of TPM implementation initiatives in an Indian manufacturing enterprise," J. Qual. Maint. Eng., vol. 13, no. 4, pp. 338–352, 2007.

[10] P. Gupta, S. Vardhan, and S. Al Haque, "Study of Success Factors of TPM Implementation in Indian Industry towards Operational Excellence : An Overview," in Industrial Engineering and Operations Management (IEOM), 2015 International Conference, 2015.

[11] M. Aruldoss, "A Survey on Multi Criteria Decision Making Methods and Its Applications," Am. J. Inf. Syst., vol. 1, no. 1, pp. 31–43, 2013.

[12] R. Kodali and S. Chandra, "Analytical hierarchy process for justification of total productive maintenance," Prod. Plan. Control, vol. 12, no. 7, pp. 695–705, 2001.

[13] G. Wang, "Research on Total Quality Management Based on AHP," in 2010 Second Pacific-Asia Conference on Circuits, Communications and System (PACCS), 2010, pp. 245–248.

[14] N. Buyurgan and C. Saygin, "Application of the analytical hierarchy process for real-time scheduling and part routing in advanced manufacturing systems," J. Manuf. Syst., vol. 27, no. 3, pp. 101–110, 2008.

[15] A. Ishizaka and A. Labib, "Selection of new production facilities with the Group Analytic Hierarchy Process Ordering method," Expert Syst. Appl., vol. 38, no. 6, pp. 7317–7325, 2011.

[16] O. S. Vaidya and S. Kumar, "Analytic hierarchy process: An overview of applications," Eur. J. Oper. Res., vol. 169, no. 1, pp. 1–29, 2006.

[17] R. W. Saaty, "Strategic Decision Making and The Analytic Hierarchy Process.," 1980.

[18] T. L. Saaty, "How to make a decision: The analytic hierarchy process," Eur. J. Oper. Res., vol. 48, no. 1, pp. 9–26, 1990.

THE 18TH INTERNATIONAL SYMPOSIUM ON WIRELESS PERSONAL MULTIMEDIA COMMUNICATIONS
(WPMC-2015)
December 13-16, 2015, Hyderabad, India

Towards Internet of Services – SDN-enabled IMS Architecture for IoT Integration

Anton N. Katov, Bayu Anggorojati, Sofoklis Kyriazakos, Albena Mihovska, Neeli R. Prasad
Center for Teleinfrastruktur (CTIF)
Aalborg University, Denmark
{annka,ba,sk,albena,np}@es.aau.dk

***Abstract*—The Internet of Things (IoT) paradigm is gaining tremendous popularity and the number of connected devices, or "things", is continuously growing, aiming to transform our everyday life. In order to address the real needs of the end user, the capabilities of the individual "things" have to be combined and offered as "services". The use of a local cloud of gateways that aggregate and analyze the data of different heterogeneous IoT devices and expose unified service oriented interfaces in support of machine-to-machine (M2M) applications has been presented in earlier works. This paper proposes a novel software-defined networking (SDN)-enabled IP Multimedia Subsystem (IMS) architecture that aims to facilitate the provision of IoT-based services over an all-IP telecom service provider's network. The architecture combines the advantages of reduced network complexity and improved efficiency of network utilization that SDN brings with the standardized approach of service deployment and management over all-IP networks, offered by IMS.**

Keywords—IoT, SDN, IMS, fog computing, BETaaS

I. INTRODUCTION

The concept of Internet of Things (IoT) incorporates the vision of ubiquitous virtual connectivity of billions of physical objects or "things" through a global network infrastructure with interoperable, self-configuring and scalable capabilities. "Things" might be part of various application domains and therefore are represented by different types of devices that have heterogeneous technical parameters and communication capabilities. This imposes various technical challenges in terms of adaptation, context awareness, device discovery and management, scalability, managing a large data volumes, privacy, and security.

The "Building the Environment for Things as a Service" (BETaaS) paradigm is the outcome of a successful research initiative [1] that leverages the concept of fog computing, and introduces the novel concept of 'Things as a Service' (TaaS) in support of machine-to-machine (M2M) applications. Fog computing [2] was introduced as a concept to cut down the amount of data that needs to be transported to the cloud and, thus, to reduce the processing burden of cloud systems, by implementing data processing, storage, analytics and networking closer to the network edge. BETaaS extended the fog computing paradigm by introducing a local cloud of M2M gateways that aggregate and analyze the data of different heterogeneous IoT devices and expose unified service oriented interfaces that can be used to access the things connected to the local cloud, thus introducing the concept of TaaS. This approach offers distinct benefits such as reduced network complexity, reduced amount of transported data, generated by the things and homogeneous service oriented interfaces that can provide access to different types of devices that have heterogeneous technical parameters and communication capabilities. In order to fully exploit the benefits of the exposed IoT services, however, an efficient mechanism for service deployment, management and delivery to the end users is needed.

The current paper addresses the main challenges for IoT integration and proposes a novel Software Defined Networking (SDN)-enabled IP Multimedia Subsystem (IMS) architecture that aims to offer a possible solution. IMS is a technology that manages session establishment, management and termination via SIP (Session Initiation Protocol) protocol in order to enable service deployment over all-IP networks. IMS provides common IP interface that simplifies signaling and application development and facilitates handling of multiple sessions that might be used by different applications. Furthermore, IMS enables access control and billing handling, which allows consistent management of the different applications on the network [3, 4]. The benefits of introducing IMS to the IoT domain have already been examined by several research teams. In [5] a generic IMS framework for integration of IoT networks and cloud computing networks is described and the implementation issues of such integration are examined. A cloud-based implementation of the generic framework is later described in [6], where the core IMS components are virtualized into a resource pool and provided as Infrastructure as a Service (IaaS). The framework concept is further extended in [7], where a mechanism for object management and naming, based on IMS uniform resource identifiers (URI) is proposed. The paper introduced a naming delivery agent that utilized SIP 'MESSAGE' messages to assign specific URIs to the 'things'. In [8] the integration of IoT devices into a SIP-IMS platform is considered in context of WLAN-3GPP networks. Different SIP message flows are designed to provide different IoT functions, such as registration, transmission of streaming data and notifications, based on query/report messages. Finally, in [9] a carrier class IoT service-oriented architecture that integrates IMS with wireless sensor networks (WSN) is prototyped. The architecture utilizes sensor web enablement (SWE) framework to tackle the heterogeneity of IoT devices, by introducing two main components – an enabler that introduces IoT services to the telecom operation platform, and a gateway that interconnects the enabler and the WSN. As a proof of concept the proposed design was implemented in an application scenario with 20 WSN nodes and the network load

was evaluated, showing that the introduction of the M2M gateway effectively reduces the generated data traffic.

The current paper proposes an architecture for the provision of IoT-based services over an all-IP telecom service provider's networks, while facilitating the development and implementation of innovative networking solutions. We take the IoT IMS integration a step further by introducing SDN-based virtualization of the IMS core elements as a solution to meet the challenges of increased traffic and network complexity. SDN is defined by the Open Network Foundation as a technology where "network control is decoupled from forwarding and is directly programmable".

Previously related work, proposed an implementation of various software modules that can exert dynamic control on the network functions, for support of the network expansion and innovation and for more efficient utilization of network resources [10]. One of the main advantages of SDN is believed to be its capability to route efficiently the traffic flows, thus facilitating the support of quality of service (QoS) differentiation. In [11], an SDN and IMS converged infrastructure is presented, which incorporates an OpenFlow controller that communicates with IMS application servers via RESTful application programmable interfaces (APIs). This allows application-based QoS classification and data flow routing. OpenFlow integration within IMS is also proposed in [12], where a research SDN IMS testbed is designed.

The rest of the paper is organized as follows: Section II summarizes the challenges for IoT integration within the existing network infrastructures and outlines how the novel design tackles these issues. Section III gives a short overview of the enabling functionalities for the exposure of IoT-based services. Furthermore, a deeper inside on the mechanisms for SDN IMS convergence is proposed. Section IV describes the component and features of the proposed architecture. Finally, Section V concludes the paper and outlines the direction of the future research.

II. CHALLENGES FOR IOT INTEGRATION

ITU define IoT as "a global infrastructure for the information society enabling advanced services by interconnecting (physical and virtual) things based on existing and evolving, interoperable information and communication technologies." In order for this futuristic vision to become reality, however, a range of technological challenges are yet to be overcome. Some of the main enabling technologies and the corresponding research issues have been discussed in [13] and [14] and briefly summarized below. The proposed technologies to address these issues are also outlined.

Architecture – an open architecture that will enable interoperability and of a large number of heterogeneous devices and distributes resources is needed. Moving the intelligence at the edge of the network is identified as a possible approach to address these issues. The current paper proposes an architecture that combines two novel technologies, SDN and IMS, which offer access to an agnostic environment for the creation, deployment and management of converged telecommunications services. Furthermore, the design integrates the M2M development and execution platform – BETaaS – which tackles the heterogeneity of IoT devices and leverages the concept of fog computing to bring some of the intelligence to the edge of the network.

Identification - creating a digital identity of the 'things', defined by a digital name and the relationships between things in the digital domain is vital for realizing the IoT vision. The identities should be globally unique, offer significant consistency and enclose the multiple existing identifiers, such as identifiers, assigned by the manufacturer and network IPv6 addresses. A possible solution, proposed in [7] and adopted in the current design, is the utilization of IMS/SIP uniform resource identifiers (URI).

Communication Technologies – the utilized communication technologies should allow efficient communication between things, between things and human users, between things and the Internet. Furthermore, access to distributed units for data collection, data mining and information processing should be provided. In the proposed architecture, the powerful capabilities for session management of IMS, combined with the SDN techniques for flow control provide an efficient communication environment for the creation and deployment of IoT services.

Network Technologies – should provide ubiquity of access of almost anything, anywhere, offering scalability and reliable identification and tracking of the various objects in the IoT domain. The implementation of IPv6 over SDN, combined with IMS URIs, can bring the required scalability and consistency of identification of the expected huge number of interconnected IoT objects.

Service Discovery – automated discovery and mapping mechanisms will be essential for the efficient network and communication management and the utilization of the IoT resources. The discovery mechanisms need to be dynamically adaptable and continuously evolving to accommodate changing topologies or changing user needs. The IMS service discovery mechanisms, integrated by the Service Capability Interaction Manager (SCIM), might offer an efficient solution for service composition and service interaction.

Data and Signal Processing – the expected massive number of interconnected devices will generate huge amounts of data traffic. In order to utilize efficiently these resources, different mechanisms for edge processing, filtering and aggregation, semantic interoperability, data sharing and collaboration, QoS and streaming processing are needed. The concept of fog computing, realized by BETaaS local cloud, offers implementation of such capabilities closer to the network edge.

Network Management – the huge number of devices and the increasing complexity of communication networks predetermine the need of improved resource allocation techniques, which incorporate traffic and congestion management and resource reservation for time-critical and life-critical data flows. SDN concentrates the network intelligence in software-based central controllers, provides more efficient control, customizability and adaptability.

Security, Trust and Privacy – the high penetration of the interconnected devices that will expose even more information about our environment, habits and needs will pose new security and privacy problems in terms of confidentiality, authenticity and integrity of data. Efficient mechanisms that

prevent unauthorized identification and tracking will be of primary importance. The BETaaS platform implements security mechanisms that monitor the environment and retrieve and impose security policies in order to prevent malicious behavior or unauthorized access. Additionally, the IMS framework provides the means for user authentication and IPsec association with the IMS terminal.

Standardization – in order to ensure high degree of interoperability between a large number of heterogeneous devices and systems the definition and use of standard interfaces and data models is needed. IMS technology specifications are defined by 3GPP's Services and System Aspects group. Regarding SDN, the Open Networking Foundation is responsible for the technology's promotion, adoption and open standards development.

III. Enablers of IoT-Based Services

A. M2M development and execution platform: BETaaS

BETaaS is an M2M development and execution platform based on a distributed runtime environment made of a so-called local cloud of nodes that allows accessing things connected to the platform regardless of their access technology and location. It creates a horizontal runtime platform. Its distributed architecture also allows for the computation (i.e. M2M application) to run in close proximity to the physical thing, which is a crucial enabler for the M2M applications that require fresh information from the physical thing [1].

The BETaaS high level architecture consists of three main layers: Adaptation, TaaS (Things as a Service), and Service, which is shown in the left hand side of Fig. 1. This structure guarantees the proper level of abstraction to the applications at the top and the flexibility in integrating different M2M systems at the bottom. At the bottom layer, BETaaS integrates heterogeneous M2M systems at the physical layer into a unified M2M system thanks to the Adaptation layer. The adaptation layer allows plugins to be dynamically added and deployed into the platform to accommodate different M2M systems, e.g. ETSI M2M, CoAP, and even some proprietary systems, within the platform. The plugins provide interfaces to the higher layer components and convert the request from the later into their respective M2M systems. On top of the adaptation layer, the TaaS layer provides an abstract and uniform description of the underlying M2M systems regardless of the technology, communication protocol, and physical location. The TaaS paradigm defines a service for each thing connected to the platform; a thing service is created to represent the basic service(s) that can be exposed to the applications in a content-centric manner. the TaaS layer is implemented in a distributed fashion to cooperatively share resources among gateways. This approach allows for the application to transparently access thing services irrespective of the gateway that provides the physical thing connection. On top of the TaaS layer, the Service layer is designed to define the platform interface to the external applications. In general, the Service layer exposes all of the available thing services in the platform as basic services allowing the applications to interact with the things connected to the platform. In addition to the basic services, this layer also allows for the dynamic deployment of a so-called extended service, from a third party

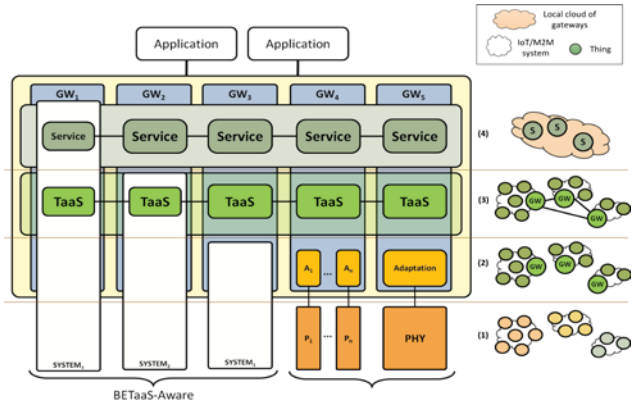

Fig. 1. BETaaS high level architecture

[1], which opens the opportunity to establish a marketplace of extended services that can be installed on demand by users [18].

B. SDN-based IMS implementation

IMS is identified in [4] as the enabling technology for the creationof a service environment over disparate all-IP networks and a step towards the Service Oriented Architecture (SOA). It provides a mechanism for session management of services, such as video conferencing and voice over IP, and open APIs for third-party access and web services integration. Furthermore, it aims to ensure relevant QoS parameters for different classes of services and to enforce the service level agreements (SLAs). In these aspects, the SDN-enabled implementation of the IMS core can be particularly beneficial, because of the powerful capabilities of adapting the network flow to the bandwidth and traffic changes and the management of virtualized resources. Such implementation will provide a synergic environment for the development and the deployment of innovative services.

Several open source implementations of the IMS core have been proposed. Two of the notable examples include the OpenIMS [15] and the Project Clearwater [16]. Project Clearwater proposes a cloud-oriented design that claims to be extremely suitable for deployment in network functions virtualization (NFV) environments. It is based entirely on open source components and supports all standardized interfaces related to the IMS core. The OpenIMS, on the other hand, offers an open source implementation IMS Call Session Control Functions (CSCFs) and a lightweight Home Subscriber Server (HSS). It does not target carrier grade deployments, but rather aims to accelerate the IMS development and adoption. It has served as the basis of the SDN-based OSIMS open source IMS experimentation platform [11].

IV. Proposed Architecture

The proposed architecture leverages the TaaS concept, defined by the BETaaS paradigm, in order to facilitate the provision of IoT-based services over an all-IP telecom service provider's network. The main purpose of the design, described in the current paper, is to offer not only an open environment for the development and deployment of innovative user-centered services, but also an architecture that targets provider

related issues, such as improved resource utilization, simplified network management, billing and access approval for the provided services. In order to address the aforementioned requirements and to tackle the various IoT-related technological challenges, described in Section II, the proposed design combines the advantages of two novel technologies - SDN and IMS - which both focus on making the network infrastructure horizontal and on the service exposure to third parties. The architecture design, shown in Fig.2, follows a layered approach distinguishing between an access layer, a transport layer, a control layer and an application layer. The current paper focuses mainly on the SDN and IMS integration, service creation, deployment and management and therefore the access and transport layers' functionalities will only be briefly mentioned.

A. Access Layer

IMS provides a standardized framework for service creation and deployment over all-IP networks, independent of the access technology, supporting mobile, wireless and wireline telecommunication environments. From the IoT device perspective, the BETaaS Adaptation Layer (described in Section III) integrates heterogeneous M2M systems at the physical layer into a unified M2M system, thus addressing the challenge of interoperability between the existing IoT technologies.

B. Transport Layer

SDN decouples the control plane and the data plane and concentrates the data forwarding decisions into a centralized software controller. A common standardized protocol that defines the communication between the control and the data forwarding plane is the OpenFlow. In the current architecture, the transport layer directly corresponds to the SDN's data forwarding plane, which consists of OpenFlow switches. Each OpenFlow switch contains one or more flow tables and an abstraction layer that communicates with the controller.

C. Control Layer

In the SDN scenario the data forwarding decisions and higher level control functions are performed by a logically centralized software controller. The network configuration is performed on a simplified network abstraction and the data flow configurations are communicated to the data forwarding devices via the OpenFlow protocol. The control plane is implemented using the SDN Network Operating System (NOS) and a set of software modules that perform the various network control functions. The NOS exposes the open APIs (northbound APIs) to allow for the development of various applications that can interact with the network and provide an improved network management. In such a scenario, the IMS core elements can be implemented as software modules that communicate with the NOS via the northbound open APIs. Several possible open source IMS solutions were mentioned in Section III. The core IMS components functions are described below.

The IMS Call Session Control Function (CSCF) server – provides the registration of the endpoints, routing of the SIP signaling messages and QoS. We distinguish the following:

- *Serving CSCF* – this is the central session control entity for the endpoint devices; it maintains the session state; stores the public user identity and the contact address of each subscriber of the network and retrieves the user profiles from the Home Subscribe Server.
- *Proxy CSCF* – this is the IMS entry point for the devices; it forwards the SIP messages to the user's home S-CSCF; provides the user authentication, the device control interworking security; and provides the QoS management, based on policy rules. The policy-based QoS control mechanism is implemented by two main entities – the Policy Decision Point (PDP) and the Policy Enforcement Point (PEP) [17]. The PDP is the logical entity that stores and retrieves the predefined policy rules and performs policy decisions, based on static or dynamic information from the network. In the current architecture, the PDP is implemented by the policy and charging rule function (PCRF) IMS component. PEP is responsible for enforcing the policies by communicating with the corresponding network elements. In the current scenario, the PEP entity is implemented by the policy and charging enforcement function (PCEF) that communicates with the SDN controller's NOS via the exposed northbound APIs.
- *Interrogating CSCF* – it maintains the session state; forwards the SIP request to the correct S-CSCF; retrieves the information regarding the correct S-CSCF from the HSS or assigns an S-CSCF if information is not available.

The Home Subscribe Server (HSS) - manages the subscriber database for the home network; grants or restricts access to the users, based on their subscriber information; and communicates with the S-CSCF.

D. Application Layer

The IMS control layer utilizes several interfaces to communicate with the service layer, which offer the capability of providing applications implemented by heterogeneous resources and application servers (AS). The ASs are the entities that host and execute the services provided by the IMS. These communicate with the S-CSCF using SIP in order to realize service the session control. These also communicate with the HSS via DIAMETER in order to retrieve or update the subscriber's profile information. The SIP ASs are the most common type of application servers used in IMS scenarios. They support SIP-based applications and respond to requests with SIP messages in order to enable the further processing of the user requests at the S-CSPF. The SIP applications might include the presence service or sessions involving multimedia elements such as voice, video, chat, gaming, etc. The proposed here architecture focuses on enabling the integration with third-party services, and particularly web services and the IoT-based services exposed by BETaaS local clouds. Such integration is enabled by the Open Service Access Gateway (OSA-GW) and the Open Service Access/Parlay Application Server (OSA/Parlay AS) components. The main purpose of these components is to allow for the integration of the underlying network assets with the third party services. This would allow for the network providers to employ a superior service access control and the QoS differentiation, which will result in an

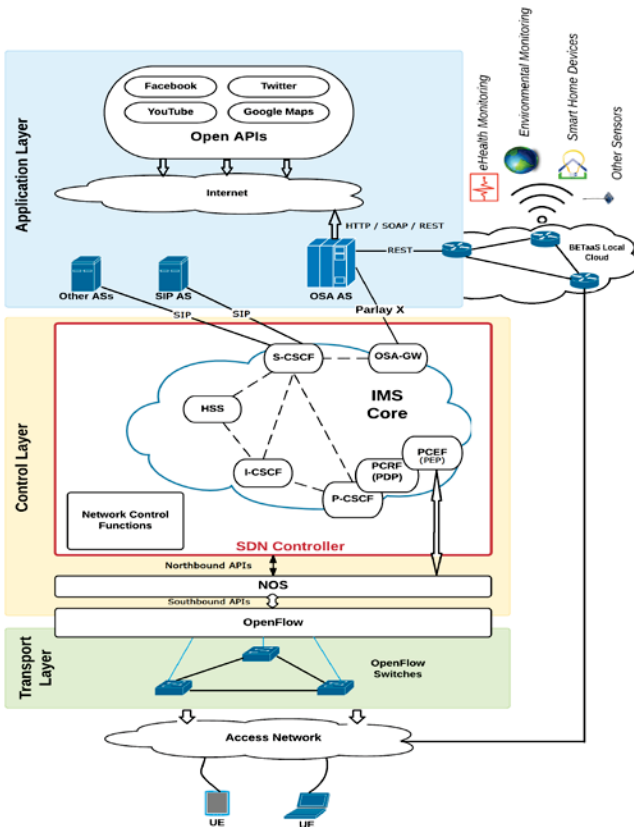

Fig. 2. SDN-based IMS architecture for IoT integration.

enhanced security and reliability of the provided services and improved quality of experience for the end-user. A set of standard web service APIs – Parlay – has been developed by The Parlay Group in collaboration with ETSI and 3GPP to allow such interoperability. The OSA/Parlay AS main purpose is to host a variety of applications that can access standard web services (via HTTP/SOAP/REST) and IoT-based services exposed by BETaaS (via REST APIs) and can communicate with the underlying network assets (via Parlay X interfaces). The OSA-GW is the session mediation gateway that defines the control flow of the established service sessions and implements the Parlay APIs and SIP protocol mapping mechanism.

V. CONCLUSION

The paper proposed a conceptual design that integrates the BETaaS M2M development and execution platform and an SDN-based IMS architecture in order to provide an open environment for the development and the provisioning of IoT services. The required technologies and the corresponding challenges for the service deployment in such a scenario were outlined and the main functional components to address these issues are described. The proposed architecture is the foundation for the planned future research on inter-cloud communication mechanisms and QoS classification and management in SOAs.

REFERENCES

[1] C. Vallati, E. Mingozzi, G. Tanganelli, N. Buonaccorsi, N. Valdambrini, N. Zonidis, B. Martnez, A. Mamelli, D. Sommacampagna, B. Anggorojati, S. Kyriazakos, N. Prasad, F. Nieto, and O. Rodriguez, "Betaas: A platform for development and execution of machine-to-machine applications in the internet of things," WPC, pp. 1–21, 2015.

[2] I. Stojmenovic and S. Wen, "The Fog computing paradigm: Scenarios and security issues," *Federated Conference on Computer Science and Information Systems (FedCSIS)*, 2014, pp. 1–8.

[3] "IMS Tutorial | IP Multimedia Subsystem | Radio-Electronics.Com." [Online]. Available: http://www.radio-electronics.com/info/telecommunications_networks/ims-ip-multimedia-subsystem/tutorial-basics.php. [Accessed: 07-Jul-2015].

[4] L. Saleem, S. Mohan, "A Complexity Analysis of IP Multimedia Subsystems (IMS)," *First International Symposium - (ANTS).* December 2007, Mumbai, India.

[5] C.-Y. Chen, H.-C. Chao, T.-Y. Wu, C.-I. Fan, J.-L. Chen, Y.-S. Chen, and J.-M. Hsu, "IoT-IMS Communication Platform for Future Internet:," *International Journal of Adaptive, Resilient and Autonomic Systems*, vol. 2, no. 4, pp. 74–94, 34 2011.

[6] H.Liao, K. Chang, C.Chen, J. Chen, H.Chao, T.Wu, "IoTIMS Communication Platform for Future Internet Implementation," *The 11th Conference on Information Technology and Applications in Outlying Islands*, Taiwan, May 25-26, 2012.

[7] K.-D. Chang, C.-Y. Chang, H.-M. Liao, J.-L. Chen, and H.-C. Chao, "A Framework for IoT Objects Management Based on Future Internet IoT-IMS Communication Platform," in *2013 Seventh International Conference on Innovative Mobile and Internet Services in Ubiquitous Computing (IMIS)*, 2013, pp. 558–562.

[8] W.-E. Chen and S.-Y. Cheng, "A SIP/IMS Platform for Internet of Things in WLAN-3GPP Integration Networks," in *Intelligent Data analysis and its Applications, Volume II*, J.-S. Pan, V. Snasel, E. S. Corchado, A. Abraham, and S.-L. Wang, Eds. Springer International Publishing, 2014, pp. 437–447.

[9] D. Xie, C. Shang, J. Chen, Y. Lai, and C. Pang, "A Carrier Class IoT Service Architecture Integrating IMS with SWE," *International Journal of Distributed Sensor Networks*, vol. 2014, p. e930472, May 2014.

[10] A. Katov, A. Mihovska, and N. R. Prasad, "Hybrid SDN architecture for resource consolidation in MPLS networks," *WTS*, 2015, 2015, pp. 1–8.

[11] C. Tranoris, S. Denazis, N. Mouratidis, P. Dowling, and J. Tynan, "Integrating OpenFlow in IMS Networks and Enabling for Future Internet Researchand Experimentation," in *The Future Internet*, A. Galis and A. Gavras, Eds. Springer Berlin Heidelberg, 2013, pp. 77–88.

[12] C.-S. Tang, C.-Y. Twu, J.-H. Ju, and Y.-D. Tsou, "Collaboration of IMS and SDN to enable new ICT service creation," in *APNOMS*, 2014 16th Asia-Pacific, 2014, pp. 1–4.

[13] Sundmaeker, H.; Guillemin, P.; Friess, P. & Woelfflé, S., ed. (2010), Vision and Challenges for Realising the Internet of Things , *Publications Office of the European Union* , Luxembourg.

[14] Vermesan, Ovidiu, and Peter Friess, eds. *Internet of Things Applications - From Research and Innovation to Market Deployment*. Place of publication not identified: River Publishers, 2014.

[15] "OpenIMSCore.org | The Open Source IMS Core Project." [Online]. Available: http://www.openimscore.org/. [Accessed: 14-Jul-2015].

[16] "Project Clearwater." [Online]. Available: http://www.projectclearwater.org/. [Accessed: 14-Jul-2015].

[17] M. Mani and N. Crespi, "Inter-Domain QoS Control Mechanism in IMS based Horizontally Converged Networks," in *Third International Conference on Networking and Services, 2007. ICNS*, 2007, pp. 82–82.

[18] B. Anggorojati, S. Kyriazakos, N. Prasad, C. Vallati, E. Mingozzi, G. Tanganelli, N. Buonaccorsi, B. Martinez, F. N. De-Santos, N. Zonidis, G. Labropoulous, A. Mamelli, and D. Sommacampagna, "Betaas platform–a things as a service environment for future m2m marketplaces," EAI Endorsed Transactions on Cloud Systems, vol. 15, no. 1, 2 2015.

THE 18TH INTERNATIONAL SYMPOSIUM ON WIRELESS PERSONAL MULTIMEDIA COMMUNICATIONS
(WPMC-2015)
December 13-16, 2015, Hyderabad, India

Analytical Evaluation Of Frequency Reuse For Hybrid Full-/Half-Duplex Cellular System

Wenping Bi, Limin Xiao, Xin Su, Shidong Zhou
Tsinghua National Laboratory for Information Science and Technology
Department of Electronic Engineering, Tsinghua University, Beijing, China

***Abstract*—Full-duplex (FD) communication has drawn more and more attention due to the potential to double the spectral efficiency. Dense cellular network is one of the possible application scenarios. However, the severe inter-cell interference may largely degrade the system performance, especially for the cell-edge users. In this paper, we focus on the hybrid full-/half-duplex (HFHD) cellular network, which is composed of a mixture of base-stations (BS) working either in half-duplex (HD) or FD mode. Frequency reuse (FR) is introduced into HFHD cellular system to deal with the serious inter-cell interference. The considered FR schemes include the traditional full FR and two main categories of Fractional Frequency Reuse (FFR) named Strict FFR and Soft FFR. Instead of assuming the base-stations are placed based on deterministic grid, we utilize stochastic geometry approach to model the base-station locations. Through the analytical results, we observe that FR is more effective used in FD system than HD network. We also study the relationship between the system spectrum efficiency and the proportion of FD BSs under different residual self-interference (SI). The simulation result shows that if the residual SI is not very large, operating all the BSs in FD mode can achieve the best performance, otherwise, it is better to operate all the BSs in HD mode.**

I. Introduction

Full-duplex (FD) communication is one of the most promising solutions to enhance the spectral efficiency (SE) in the 5th generation (5G) wireless communication system. Compared with traditional half-duplex (HD) transceiver operating either in frequency division duplex (FDD) mode or time division duplex (TDD) mode, FD radios can simultaneously transmit and receive signals over the same frequency, offering the potential to double the spectral efficiency. However, the self-interference (SI) caused by the transmitted signal at the receiver may overwhelm the desired signal and is a main obstacle to build a FD transceiver. Advanced and effective SI cancellation technologies [1] have been proposed to make the FD radios feasible. FD radios have been applied to several fields [1], including FD cognitive radio system , FD relay, FD bi-direction communication system and FD cellular system. Among all the applications, FD cellular system is an important research issue, especially in the small cells, where the transmission power is low and the distance between the base-station (BS) and user equipment (UE) is short.

This work was supported by National Basic Research Program of China (2012CB316002), National Natural Science Foundation of China (61201192), China's 863 Project (2014AA01A703), the Keygrant Project of Chinese Ministry of Education (No.313005), Science Fund for Creative Research Groups of NSFC (61321061), Tsinghua University Initiative Scientific Research Program (2011THZ02-2), National S&T Major Project (2013ZX03003003-003) and Huawei Technologies.

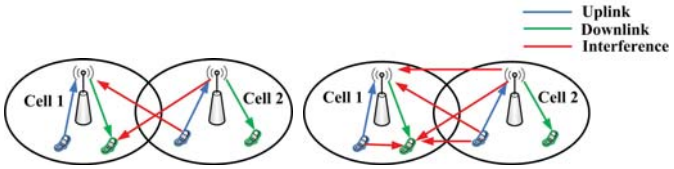

(a) HD Cellular Network (b) FD Cellular Network

Fig. 1. An Exemplary Interference Scenario Of HD/FD Cellular Network

In this paper, we focus on Orthogonal Frequency Division Multiple Access (OFDMA) based cellular network with hybrid duplex BSs and HD UEs. In other words, FD and HD BSs co-exist in the network. In FD cells, a FD BS simultaneously serves two HD UEs with one in downlink and the other in uplink direction over one sub-band. Unfortunately, extra inter-cell and intra-cell interference may largely degrade the system performance.

As illustrated in Fig. 1, for simplicity, we take two neighboring cells as an example. As shown in Fig. 1(a), in HD network, the BS in cell 1 only suffers the interference from the transmission of the uplink UE in neighbor cell. In the same way, the downlink UE in cell 1 only gets interference from the downlink signal of neighbor BS. While, as to FD cells in Fig. 1(b), besides the interference discussed in HD cells, the BS receives two extra interference: the SI and the downlink transmission of the neighbor BS. The downlink UE in FD cells also suffers two extra interference: the inter-cell and intra-cell inter-user interference.

With the cellular network becoming denser, the inter-cell interference will be more destructive, especially for the cell-edge UEs. In this paper, frequency reuse (FR) methods are applied to deal with the inter-cell interference. The focused FR schemes include the traditional full FR and Fractional Frequency Reuse (FFR) [2].

We analyze the hybrid duplex system with stochastic geometry approach, in which the BS locations are distributed based on a spatial Poisson Point Process (PPP). The authors in [3] evaluated the performance of the one tier FD network with perfect SI cancellation using stochastic geometry method. The performance of heterogeneous networks with FD bi-directional transceivers was studied in [4]. However, none of

them considers interference suppression technologies, which is impractical in the interference limited FD cellular system.

The contributions of this paper are as follows. Firstly, the primary contribution of our work is the analytical evaluation of the hybrid duplex cellular system with FR. Secondly, we analyze the impact of the proportion of FD BSs on the system spectrum efficiency (SE) under different residual SI. The results show that FR is more effective in FD system and the more FD BSs we deploy, the higher SE we can achieve, if the SI is cancelled properly.

The rest of the paper is organized as follows. In section II, we introduce the system model and the adopted FR technologies. In section III, the coverage probability is derived for different FR schemes. Simulations are conducted in section IV. Section V is the conclusion of the paper.

II. System model and relevant technologies

A. System Model And Assumptions

In this paper, we consider an OFDMA-based cellular network with hybrid duplex BSs and legacy HD UEs. The BSs are distributed in the space based on a homogeneous spatial PPP with density λ. The proportions of FD BSs and HD BSs working in the uplink and downlink direction are p_f, p_{hu} and p_{hd} , respectively. Obviously, $p_f + p_{hd} + p_{hu} = 1$. Therefore the locations of FD BSs and HD BSs working in the uplink and downlink direction are also distributed based on independent spatial PPP with density λp_f, λp_{hu} and λp_{hd}, respectively. UEs are assumed to communicate with their closest BSs, which follows the association principle of maximum average received power. The UEs uniformly distribute in each Voronoi cell formed by the BSs and we randomly select only one UE to work in one specific transmission direction over one sub-band. Based on the assumptions above, the density of active UEs is the same as their serving BSs'. We should note that the locations of the active UEs no longer follow the spatial PPP [5]. However, as confirmed in [5], the actual distribution of the active UEs' locations is almost the same as the spatial PPP. Therefore, in this paper, the locations of the active UEs are also assumed to be based on the spatial PPP. Then, the probability density function (pdf) of the distance r between the BS and its serving UE can be derived as [6]:

$$f_r(r) = 2\pi\lambda r e^{-\lambda\pi r^2} \tag{1}$$

The residual SI I_s after interference cancellation is assumed to be a gaussian random variable with zero mean and variance depending on the transmission power of the BS P_b . Then I_s can be written as:

$$I_s \sim \mathcal{N}(0, {\sigma_I}^2), \quad {\sigma_I}^2 = P_b |h_I|^2 \tag{2}$$

Where $|h_I|^2$ reflects the capability of SI cancellation.

In FD cells, the transmission of uplink UE will cause interference to the downlink UE working in the same sub-band. A bin-and-cancel (BC) strategy was proposed in [7] to mitigate the intra cell inter-user interference (IUI) and the results showed that the IUI was effectively removed. Therefore, in this paper, the IUI is ignored. Then the received signal-to-interference-plus-noise-radio (SINR) at the BS and UE can be uniformly derived as follows:

$$SINR_m = \frac{P_t G_m {r_m}^{-\alpha}}{\sigma^2 + I_m + \delta_{fb} I_s} \tag{3}$$

Where the subscript $m \in \{b, u\}$ denotes the type of receiver. b and u represent the receivers of BS and UE, respectively. G_m and r_m denote the small scale fading and distance between the focused receiver and its transmitter, respectively. We assume the small scale fading of all the channels to be Rayleigh fading, i.e. $G_m \sim \exp(1)$. $\alpha > 2$ is the path loss exponent and we assume the path loss exponents for all the channels are the same. P_t represents transmission power and it is P_u in the uplink and P_b in the downlink transmission direction. δ_{fb} is 1 only when the FD BS receiver is considered, otherwise δ_{fb} is 0. I_m denotes the received inter-cell interference. Inter-cell interference will generate from all the cells that use the same sub-band. Then the received inter-cell interference I_m can be formulated as follows:

$$\begin{aligned} I_m = &\sum_{z_b \in \mathcal{Z}_f} P_b G_{z_b,m} D_{z_b,m}^{-\alpha} + \sum_{z_u \in \mathcal{Z}_f} P_u G_{z_u,m} D_{z_u,m}^{-\alpha} \\ &+ \sum_{z_{hb} \in \mathcal{Z}_{hd}} P_b G_{z_{hb},m} D_{z_{hb},m}^{-\alpha} + \sum_{z_{hu} \in \mathcal{Z}_{hu}} P_u G_{z_{hu},m} D_{z_{hu},m}^{-\alpha} \end{aligned} \tag{4}$$

Where $\mathcal{Z}_f$, $\mathcal{Z}_{hu}$ and $\mathcal{Z}_{hd}$ denote the interfering cell sets working in FD-mode, HD-mode in the uplink and downlink direction, respectively. z_k and z_{hk} ($k \in \{b, u\}$) represent the interfering nodes in FD and HD cells. b and u denote the interfering nodes are BS and UE, respectively. $G_{z_k,m}$(or $G_{z_{hk},m}$) $\sim \exp(1)$ is the small scale fading between the interfering node z_k (or z_{hk}) and the interested receiver $m \in \{b, u\}$. $D_{z_k,m}$ (or $D_{z_{hk},m}$) denotes the distance between interested receiver m and interfering node z_k (or z_{hk}).

In a FD interfering cell, both the BS and the uplink UE will generate interference to the interested receiver. According to the association principle, the interfering UE is located in the Voronoi cell formed by the FD BS. Therefore these two interfering distance $D_{z_b,m}$ and $D_{z_u,m}$ are correlated together. Fortunately, authors in [4] demonstrated that, in dense cellular system, these two distances are almost the same. That is to say:

$$D_{z_b,m} \approx D_{z_u,m} \tag{5}$$

Here, we also adopt this approximation. Then the inter-cell interference can be re-presented as follows:

$$\begin{aligned} I_m = &\sum_{z \in \mathcal{Z}_f} G_{fz} D_{z,m}^{-\alpha} + \sum_{z_{hb} \in \mathcal{Z}_{hd}} P_b G_{z_{hb},m} D_{z_{hb},m}^{-\alpha} \\ &+ \sum_{z_{hu} \in \mathcal{Z}_{hu}} P_u G_{z_{hu},m} D_{z_{hu},m}^{-\alpha} \end{aligned} \tag{6}$$

Where $G_{fz} = P_b G_{z_b,m} + P_u G_{z_u,m}$.

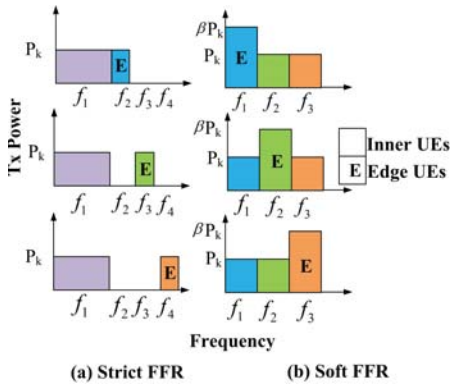

Fig. 2. Strict FFR and Soft FFR With frequency reuse factor $\Delta = 3$ for cell-edge UEs

B. Frequency Reuse

It is well known that, traditional full FR scheme is to allocate $\frac{1}{\Delta}$ of the total sub-bands to each cell randomly. By utilizing traditional full FR, inter-cell interference is well managed, but the spectrum efficiency is very low.

The adopted FFR [2] schemes will be introduced. As shown in Fig. 2, it is an example of Strict FFR (StFFR) and Soft FFR (SoFFR) with reuse factor $\Delta = 3$. The basic idea of StFFR is that, the frequency allocated to the cell-inner UEs is shared by all the inner-UEs overall the network, while the sub-bands reserved for the cell-edge UEs are reused with factor Δ.

SoFFR uses a different frequency partition scheme. All the sub-bands can be used by each cell, while the sub-bands partitioned to the cell-edge UEs are still reused according to the reuse factor Δ. The transmission power of cell-edge UEs boosts by factor β and the typical value of β is 2-20.

In order to apply StFFR and SoFFR, we should first define the cell-edge UE and cell-inner UE. We pre-define a SINR threshold value T_{FR} and the UE whose SINR is larger than the threshold is classified into cell-inner UEs, otherwise the UE is regarded as cell-edge UEs.

III. Coverage Probability and Rate

In this section, the coverage probabilities for both uplink and downlink UEs are derived. The coverage probability is defined as the probability that the received SINR of a receiver is larger than the threshold T:

$$\bar{F}(T) = \mathbb{P}(SINR > T) \tag{7}$$

It is the complementary cumulative distribution function (CCDF) of the SINR equivalently. We can also observe that $F = 1 - \bar{F}$ gives the outage probability.

A. Coverage Probability For Full FR With Reuse Factor Δ

In this section, the coverage probability of the cellular system applying traditional full FR with reuse factor Δ is studied. Based on the assumptions above, the coverage probabilities of the uplink and downlink UEs in the same cell can be solved independently and the uniform results can be given. Since each cell is assigned one of Δ sub-bands, the interference is generated from $\frac{1}{\Delta}$ of all the cells. Then we can derive the coverage probability as follows.

Theorem 3.1: When the BSs are distributed based on the spatial PPP with density λ, the coverage probability of a typical UE employing traditional full FR with reuse factor Δ can be derived as:

$$\begin{aligned}&\bar{F}_{\Delta,m}(\Delta, T, \lambda, P_t, P_b, P_u)\\ &= \pi\lambda \int_{v=0}^{\infty} \left(e^{-2\pi\lambda v \frac{1}{\Delta}\left(\sum_q p_q \psi_{s,q,m}\right) - \frac{T v^{\frac{\alpha}{2}} (\sigma^2 + \delta_{fb} I_s)}{P_t}} \right) dv\end{aligned} \tag{8}$$

Where p_q $(q \in \{f, hu, hd\})$ represents the proportion of q interfering cell set defined in section II. $\psi_{s,q,m}$ is defined as:

$$\begin{aligned}&\psi_{s,q,m}(T, P_t, P_b, P_u) =\\ &\mathbb{E}_{G_{qm}}\left(-\frac{1}{\alpha}\left(\frac{T}{P_t}G_{qm}\right)^{\frac{2}{\alpha}}\Gamma\left(-\frac{2}{\alpha}\right) + \frac{1}{\alpha}\left(\frac{T}{P_t}G_{qm}\right)^{\frac{2}{\alpha}}\Gamma\left(-\frac{2}{\alpha}, \frac{TG_{qm}}{P_t}\right)\right)\end{aligned} \tag{9}$$

Where $\Gamma(x, a) = \int_x^{\infty} t^{a-1}e^{-t}dt$ and $\Gamma(a) = \int_0^{\infty} t^{a-1}e^{-t}dt$ denote incomplete gamma function and standard gamma function, respectively. G_{qm} is defined as:

$$G_{qm} = \begin{cases} P_b G_{z_b,m} + P_u G_{z_u,m} & \text{if } q = f \\ P_u G_{z_{hu},m} & \text{if } q = hu \\ P_b G_{z_{hb},m} & \text{if } q = hd \end{cases} \tag{10}$$

Proof: Starting from the definition of the coverage probability and based on the property of expectation we have,

$$\begin{aligned}\bar{F}_{\Delta,m}(T, \lambda, P_t, P_b, P_u) &= \mathbb{P}\left(\frac{P_t G_m {r_m}^{-\alpha}}{\sigma^2 + \delta_{fb} I_s + I_m} > T\right)\\ &= \mathbb{E}_{r_m, I_m}\left(\mathbb{P}\left(\frac{P_t G_m {r_m}^{-\alpha}}{\sigma^2 + \delta_{fb} I_s + I_m} > T | r_m, I_m\right)\right)\\ &\overset{(a)}{=} 2\pi\lambda \int_{r=0}^{\infty} \left(r e^{-\frac{T r^{\alpha}(\sigma^2 + \delta_{fb} I_s)}{P_t} - \pi\lambda r^2} L_{I_m}\left(\frac{T r^{\alpha}}{P_t}\right)\right) dr\end{aligned} \tag{11}$$

(a) follows the fact that $G_m \sim \exp(1)$. $\mathcal{L}_{I_m}(s)$ is the Laplace transform of the received inter-cell interference I_m and based on the definition of the Laplace transform we can get:

$$\begin{aligned}L_{I_m}(s) &= \mathbb{E}(e^{-sI_m}) \overset{(b)}{=} \prod_q \mathbb{E}\left(\exp\left(-s\sum_{z \in \mathcal{Z}_q} G_{z,m} D_{z,m}^{-\alpha}\right)\right)\\ &\overset{(c)}{=} \prod_q \exp\left(-2\pi\lambda_q \frac{1}{\Delta}\int_r^{\infty} \mathbb{E}_{G_{qm}}\left(1 - e^{\left(-sG_{qm}D^{-\alpha}\right)}\right) D dD\right)\\ &= \prod_q \exp\Big\{ -2\pi\lambda_q \frac{1}{\Delta}\mathbb{E}_{G_{qm}}\Big[-\frac{1}{\alpha}(sG_{qm})^{\frac{2}{\alpha}}\Gamma\left(-\frac{2}{\alpha}\right) - \frac{1}{2}r^2\\ &\quad + \frac{1}{\alpha}(sG_{qm})^{\frac{2}{\alpha}}\Gamma\left(-\frac{2}{\alpha}, \frac{sG_{qm}}{r^{\alpha}}\right)\Big]\Big\}\end{aligned} \tag{12}$$

Where (b) follows from the fact that the BSs working in different mode are distributed independently. (c) follows from

the probability generating functional of PPP. Substitute Eq. (12) into Eq. (11) and we can get Theorem 3.1. ■

B. Coverage Probability For Strict FFR

We first focus on the cell-edge UEs when using StFFR. The cell-edge UEs, whose SINR is less than a pre-defined threshold T_{FR} when using the frequency shared by all the cells, are assigned a reserved sub-band that is reused according to a reuse factor Δ. Then the cell-edge UE experiences new channel fading $\tilde{G}_m$ and inter-cell interference $\tilde{I}_m$. As discussed above, $\tilde{I}_m$ is generated from $\frac{1}{\Delta}$ of all the other cells. Then the coverage probability of the system with StFFR can be derived as follows.

Theorem 3.2: When using StFFR scheme, the coverage probability of a cell-edge UE is defined as follows:

$$\begin{aligned}&\bar{F}_{strict,e,m}(T,T_{FR},\Delta,\lambda,P_t,P_b,P_u)\\&=\frac{\bar{F}_{\Delta,m}(\Delta,T,\lambda,P_t,P_b,P_u)}{1-\bar{F}_{\Delta,m}(1,T,\lambda,P_t,P_b,P_u)}\\&\quad-\frac{\pi\lambda\int_{v=0}^{\infty}\left(e^{-2\pi\lambda v(\sum_q p_q\psi_{j,q,m})-\frac{(T_{FR}+T)v^{\frac{\alpha}{2}}(\sigma^2+\delta_{fb}I_s)}{P_t}}\right)dv}{1-\bar{F}_{\Delta,m}(1,T,\lambda,P_t,P_b,P_u)}\end{aligned} \tag{13}$$

Where

$$\begin{aligned}&\psi_{j,q,m}(\Delta,T_{FR},T,P_t,P_b,P_u)\\&=\frac{\Delta-1}{\Delta}\psi_{s,q,m}(T_{FR},P_t,P_b,P_u)\\&\quad-E_{\Omega_{qm}}\left(\frac{(\Omega_{qm})^{\frac{2}{\alpha}}}{\Delta\alpha}\left(\Gamma(-\frac{2}{\alpha})-\Gamma(-\frac{2}{\alpha},\Omega_{qm})\right)\right)\end{aligned} \tag{14}$$

Where $\Omega_{qm}=\frac{T_{FR}}{P_t}G_{qm}+\frac{T}{P_t}\tilde{G}_{qm}$. $\psi_{s,q,m}$ is defined by Eq. (9). G_{qm} and $\tilde{G}_{qm}$ are defined by Eq. (10) and denote the small scale fading of the interfering channel before and after assigned the reserved sub-band, respectively.

Proof: Starting from the definition, we can get:

$$\begin{aligned}&\bar{F}_{strict,e,m}(T,T_{FR},\Delta,\lambda,P_t,P_b,P_u)\\&=\mathbb{P}(\frac{P_t\tilde{G}_m{r_m}^{-\alpha}}{\sigma^2+\tilde{I}_m+\delta_{fb}I_s}>T|\frac{P_tG_m{r_m}^{-\alpha}}{\sigma^2+I_m+\delta_{fb}I_s}<T_{FR})\\&=\frac{\mathbb{E}\left(\mathbb{P}(\frac{P_t\tilde{G}_m{r_m}^{-\alpha}}{\sigma^2+\tilde{I}_m+\delta_{fb}I_s}>T,\frac{P_tG_m{r_m}^{-\alpha}}{\sigma^2+I_m+\delta_{fb}I_s}<T_{FR}|r,\tilde{I}_m,I_m)\right)}{\mathbb{E}_{r,I_m}(\mathbb{P}(\frac{P_tG_m{r_m}^{-\alpha}}{\sigma^2+I_m+\delta_{fb}I_s}<T_{FR}|r,I_m))}\end{aligned} \tag{15}$$

Then following the steps of the proof in Theorem 3.1, we can get Theorem 3.2. ■

Now, we pay our attention to the cell-inner UEs when StFFR is used.

Theorem 3.3: The coverage probability of a cell-inner UE with StFFR is given by:

$$\begin{aligned}&\bar{F}_{strict,i,m}(T,T_{FR},\lambda,P_t,P_b,P_u)\\&=\mathbb{P}(\frac{P_tG_m{r_m}^{-\alpha}}{\sigma^2+\delta_{fb}I_s+I_m}>T|\frac{P_tG_m{r_m}^{-\alpha}}{\sigma^2+\delta_{fb}I_s+I_m}>T_{FR})\\&=\frac{\bar{F}_{\Delta,m}\left(1,\max(T,T_{FR}),\lambda,P_t,P_b,P_u\right)}{\bar{F}_{\Delta,m}(1,T_{FR},\lambda,P_t,P_b,P_u)}\end{aligned} \tag{16}$$

Proof: Its proof is similar with that of Theorem 3.2. ■

C. Coverage probability for Soft FFR

In the case of SoFFR, each cell can reuse all the sub-bands and $\frac{1}{\Delta}$ of the whole sub-bands are allocated to the cell-edge UEs. The cell-edge UEs transmit signals with power βP_t. Then in each interfering cell, $\frac{\Delta-1}{\Delta}$ of all the sub-bands apply power P_t and the rest sub-bands use power βP_t. Therefore, the effective inter-cell interference can be denoted as ηI_m, where $\eta=\frac{\Delta-1+\beta}{\Delta}$ and I_m is defined by Eq. (6) . Now we also first consider the cell-edge UEs with SoFFR.

Theorem 3.4: The coverage probability of a cell-edge UE with SoFFR is given as follows.

$$\begin{aligned}&\bar{F}_{soft,e,m}(T,T_{FR},\eta,\lambda,\beta,P_t,P_b,P_u)\\&=\bar{F}_{strict,e,m}(\frac{T}{\beta},T_{FR},1,\lambda,P_t,\eta P_b,\eta P_u)\end{aligned} \tag{17}$$

Where the $\bar{F}_{strict,e,m}$ is defined by Eq. (13).

Proof: Please refer to the proof of Theorem 3.2. ■

Then, in the same way as StFFR, we can get the coverage probability of a cell-inner UE with SoFFR.

Theorem 3.5: The coverage probability of a cell-inner UE with SoFFR can be given as follows.

$$\begin{aligned}&\bar{F}_{soft,i,m}(T,T_{FR},\eta,\lambda,\beta,P_t,P_b,P_u)\\&=\bar{F}_{strict,i,m}(T,T_{FR},1,\lambda,P_t,\eta P_b,\eta P_u)\end{aligned} \tag{18}$$

Where $\bar{F}_{strict,i,m}$ is given by Eq. (16).

Proof: Please refer to the proof of Theorem 3.2. ■

D. Average User Rate

In order to evaluate the spectrum efficiency of the network, we define the average user rate as follows:

$$R=\mathbb{E}\left(\ln(1+SINR)\right)=\int_{t>0}\bar{F}\left(e^t-1\right)dt \tag{19}$$

Then, according to Eq. (19) and the coverage probability we have already solved, we can get the average user rates of the cellular systems utilizing different FR methods.

IV. Performance Evaluation

In this section, we apply the analytical results derived in Section III to evaluate the system performance. Unless otherwise specified, the parameters used in the simulations are presented in Table I.

Firstly, the coverage probabilities of cell-edge UEs utilizing different FR methods are compared. Without loss of generality, we just focus on the downlink transmission. As shown in Fig. 3, we can observe that the analytical results match the simulation results perfectly, which identifies the effectiveness of the analytical results presented in Section III. We can also observe that, FFR can largely improve the performance of cell-edge UEs and the StFFR outperforms other schemes from the point of cell-edge UE coverage probability as expected.

Next, we evaluate the sum throughput with respect to the sub-bands allocated to the cell-edge UEs. As shown in Fig. 4, the sum throughput has been normalized according to the sum throughput of the system using full FR with reuse factor

TABLE I
SIMULATION PARAMETERS

α	Band width	Thermal noise	P_b	P_u
3	10MHz	-174dBm/Hz	0.2W	0.2W
Δ	λ	T_{FR}	$\|h_I\|^2$	β
3	$10^{-3}/m^2$	0dB	$-90dB$	2

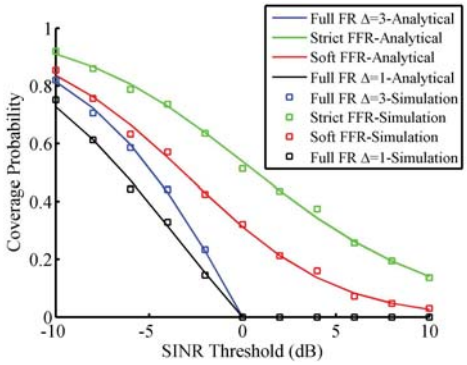

Fig. 3. Cell-Edge UE Coverage Probability. Here, $p_f = 1$.

$\Delta = 1$. We can observe that the SoFFR always outperforms other schemes at the expense of booting the cell-edge UEs' transmission power by β. Under the same assumption parameters, we also compare the relative sum throughput in FD and HD cellular system in Table II. The sub-bands allocated to the cell-edge UEs are 6. We can observe that the FR technologies are more effective in FD system.

At last, we analyze how the sum SE of uplink and downlink transmission varies along the proportion of FD radios. In the simulation, full FR with reuse factor $\Delta = 1$ is applied. As shown in Fig. 4, SE is a monotonic function with respect to the proportion of FD BSs. We can observe that there is a critical point of the SI cancelation capability. When the SI cancellation capability is larger than the critical point, the more FD BSs is deployed, the higher SE is achieved, otherwise, operating all the BSs in HD mode is better. So this point can guide the deployment of the FD BSs in the future.

V. CONCLUSION

In this paper, the analytical evaluation of the hybrid duplex system with different FR methods is conducted. The results are based on the stochastic geometry approach. Tractable expressions of coverage probability for different FR schemes are given. We also compare the system performance when utilizing different kinds of FR methods. The results show that, from the point of cell-edge UEs' coverage probability, StFFR is the best, while, SoFFR outperforms others when considering the SE. In addition, FR technologies are more effective in FD cellular network. At last, we analyze the relationship between SE and the proportion of FD BSs under different residual SI. Simulation results show that when residual SI is not very strong, operating all the BSs in FD mode is better, otherwise, it is better to operate all the BSs in HD mode.

TABLE II
RELATIVE SUM THROUGHPUT

	Full FR $\Delta = 1$	Full FR $\Delta = 3$	StFFR	SoFFR
FD	1	0.61	1.44	1.90
HD	1	0.56	1.15	1.49

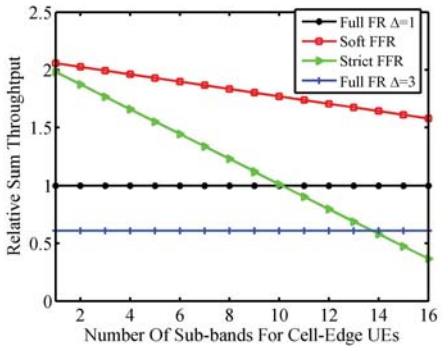

Fig. 4. Sub-bands Allocated To The Cell-Edge UEs. Here, the total number of sub-bands is 48, $p_f = 1$.

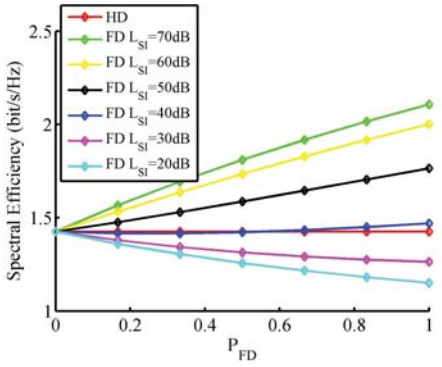

Fig. 5. Spectrum Efficiency Along Proportion Of FD BSs Under Different SI Cancellation Capacity. Here, L_{SI} denotes the SI cancellation capacity, ${\sigma_I}^2 = P_b 10^{-L_{SI}/10}$

REFERENCES

[1] A. Sabharwal, P. Schniter, D. Guo, D. W. Bliss, S. Rangarajan, and R. Wichman, "In-band full-duplex wireless: Challenges and opportunities," *IEEE Journal on Selected Areas in Communications*, vol. 32, no. 9, pp. 1637–1652, 2014.

[2] N. Himayat, S. Talwar, A. Rao, and R. Soni, "Interference management for 4g cellular standards [wimax/lte update]," *IEEE Communications Magazine*, vol. 48, no. 8, August 2010.

[3] S. Goyal, P. Liu, S. Hua, and S. Panwar, "Analyzing a full-duplex cellular system," in *2013 47th Annual Conference on Information Sciences and Systems (CISS)*, March 2013.

[4] J. Lee and T. Quek, "Hybrid full-/half-duplex system analysis in heterogeneous wireless networks," *IEEE Transactions on Wireless Communications*, vol. PP, no. 99, 2015.

[5] T. Novlan, H. Dhillon, and J. Andrews, "Analytical modeling of uplink cellular networks," *IEEE Transactions on Wireless Communications*, vol. 12, no. 6, June 2013.

[6] J. Andrews, F. Baccelli, and R. Ganti, "A tractable approach to coverage and rate in cellular networks," *IEEE Transactions on Communications*, vol. 59, no. 11, November 2011.

[7] J. Bai and A. Sabharwal, "Distributed full-duplex via wireless side-channels: Bounds and protocols," *IEEE Transactions on Wireless Communications*, vol. 12, no. 8, pp. 4162–4173, August 2013.

THE 18TH INTERNATIONAL SYMPOSIUM ON WIRELESS PERSONAL MULTIMEDIA COMMUNICATIONS
(WPMC-2015)
December 13-16, 2015, Hyderabad, India

SAR and Thermal Effects of a Body Wearable Microstrip Antenna at UHF and UWB Frequencies

Varshini Karthik
Department of Biomedical Engineering
SRM University, Chennai, India
varshinikps@gmail.com

T.Rama Rao
RAMS, Department of TCE
SRM University, Chennai, India
ramaraotr@gmail.com

***Abstract*—Microstrip based Multiband Antenna for Body Wearable Wireless Devices (BWWD) is proposed and investigations on the thermal effects caused by the interaction of the antenna with human tissues are done in this research work. Ultra high frequency (UHF) and Ultra wide band (UWB) spectrum effectively meet power, size and distance considerations for Wearable Wireless Communication Networks (WWCN) utilizing BWWDs. The antenna designed works at quad-bands, resonating at 1.8 GHz, 2.4 GHz, 5.0 GHz and 8.9 GHz when placed on human body. The electromagnetic (EM) effects in terms of Specific Absorption Rate (SAR) and thermal effects of the antenna when placed on different sites on the body are analyzed analytically and experimentally using Infra-red thermography (IRT). A simplified, human body tissue layer model that is frequency dependent in its properties is used for simulations. Simulated and experimental results are compared and are found to be in good agreement. The rise in temperature is found to be compliant with international safety regulations, favoring the use of the antenna for wearable wireless devices.**

***Keywords*— Body Wearable Wireless Devices , Infrared Thermography, Microstrip Antenna, Quad band, Human tissues, Body Interaction, UHF, UWB, Wireless Communications**

I. INTRODUCTION

The aim of wearable technology is to create convenient, portable access to information in real time and use of this Body Wearable Wireless Devices (BWWD) finds wide-ranging applications in health care, fitness, augmented reality, ambient assisted living setups, smart entertainment and many more in all walks of life via Wearable Wireless Communication Networks (WWCN). Antennas connecting these wearable devices at UHF and UWB frequencies offer high performance, ultra-low power and safe operations on human body complementing other longer range radio technologies. The human body is inhomogeneous with high loss and permittivity that are frequency dependent and which affect the properties of an antenna. The site of an antenna on the body has major control on the size and shape of the antenna being used, therefore constraining the designer. The power usage, heating effects on the body should be taken into account in BWWD antenna design. A good antenna design is essential for limited Specific Absorption Rate (SAR) values as the SAR depends on directivity, orientation and gain of the antenna [1].

In recent years, the electromagnetic (EM) effect of antennas on the human body has been an area of great interest [2]. With an extensive use of wearable wireless devices at greater proximity to the body, the concern about biological effects due to the interaction of human tissues with the RF waves is of pronounced importance. The amount of exposure of the human tissues to EM radiations is indexed in terms of SAR that gives the amount of energy absorbed by tissues when exposed to EM signals. The biological manifestation of SAR is the temperature rise. It is observed from literature that an increase of temperature greater than 1˚C would be hazardous [3]. In this context, a temperature-based technique for the evaluation of safety compliance when millimeter wave devices are used very close to the body has been proposed by [4].

In this work, a quad-band based microstrip antenna operating at UHF (30 – 3000 MHz) and UWB (3.1-10.6 GHz) frequencies is proposed for wearable wireless applications. The SAR and thermal effects of the proposed antenna when used at different places on the body is analyzed analytically and experimentally using infrared thermography (IRT) to find out the suitability of the antenna to be used as a wearable one despite its descent gain and efficiency values using 3D EM tools of HFSS and Sim4Life. Sim4Life is used for on-body simulations for the designed antenna at various body sites utilizing its high-fidelity computable human phantoms with advanced tissue models and HFSS (based on FEM) used for antenna design and fabrication

II. MODELING HUMAN TISSUES AND ANTENNA DESIGN

A. *Phantom model of human tissues*

A three layered rectangular biological tissue model made up of skin, fat and muscle is chosen as it represents the outermost body tissues. The designed antenna is proposed to be placed over the stacked tissues with an average thickness of 2 mm, 3.5 mm and 10 mm for skin, fat and muscle layer respectively as shown in Fig.1. The electrical properties of the tissues at UWB frequencies of the antenna designed are referred from [5].

Fig. 1. Layered model of human tissue with antenna

B. *Microstrip antenna design*

It is critical that the antenna has a compact design for use on the human body. The antenna design requirements differ from that of a conventional antenna that is designed for free space because of the tissue environment. Fig.2 shows the simulation model of the proposed staircase microstrip antenna. Microstrip model design equation [6] was used to design the antenna. The antenna has dimension of 35 x 32 x1.57mm^3 and is made of Rogers RT/Duroid 5880 substrate with relative permittivity of 2.2 and loss tangent of 9x10^{-3}. The selection of the substrate is due to its low electric loss along with low moisture absorption. An optimized design of the antenna with a partial ground plane and staircase rectangular patch is used. The step size of 1mm followed by 1.5mm from both the top and bottom edges is used for the staircase pattern. Horizontal slots each measuring 6 mm in length and 0.5 mm in width are used on the right and left sides of the radiating patch. A 50Ω microstrip line feeds the radiating patch. Good impedance matching is achieved by a tapered microstrip line.

Strips of conducting material at top and bottom provide a partial ground plane. The design is optimized to make the antenna work at four bands with return loss less than -10 dB at all the bands. A quad-band operation is chosen to offer better EM compatibility with existing unlicensed wireless communication technologies, such as GSM, Wi-Fi, and unlicensed UWB spectrum at low and high data rate wireless applications.

III. Simulations and Measured Results

A. *Antenna simulations, measurements in free space and on-body*

The antenna is simulated as well measured for its performance in free space and on-body. Measurements of return loss were made for the prototyped antenna shown in Fig.3.using RS-ZVL Vector Network Analyzer of frequency range 9 KHz-13.6 GHz. Placement of the antenna in direct contact with the body decreases the gain and radiation efficiency with due effects on the impedance matching due to the dielectric loading provided by the lossy human tissues. A frequency shift in the resonating frequency of 100 MHz from 1.8 to 1.9 GHz, 80 MHz from 2.4 to 2.48 GHz, 140 MHz from 5.0-5.14 GHz, 100 MHz from 8.9 to 8.8 GHz was observed between simulated and measured results in the four bands respectively. The designed antenna is kept on the human body with cotton padding of 5 mm between them. The performance of the antenna on body is enhanced due to the bio and electromagnetic compatibility nature of the chosen fabric which makes it realizable for real time use when compared to the few mm of air gap used in previous designs.

A good agreement between the simulated and measured results is seen as observed from Fig.4. Quasi-omnidirectional radiation pattern of the antenna considering the thickness of the layers of skin, subcutaneous fat and muscle as 2, 3.5, 10 mm respectively at the four bands are shown in Fig.5 for theta at 90^0. The performance of the quad bands is studied and tabulated in Table I. It is seen from table that the upper band performs well when compared to lower band. This is important while considering the EM waves (thus also antennas) interaction with body [7]. Major reflections occur due to the wave impedance mismatch between low (fat) and high water content (skin, muscle) tissues. This effect can cause an increased specific absorption rate (SAR) [8].

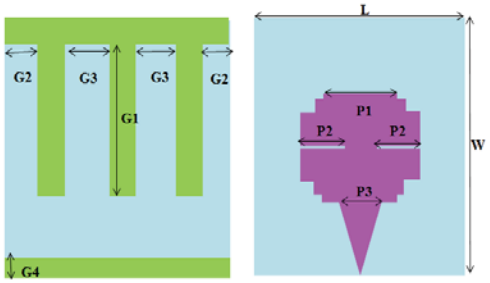

Symbol	G1	G2	G3	G4	P1	P2	P3	L	W
Dimension (mm)	22	4	6	0.5	10	6	4.4	32	35

Fig. 2. Design of staircase microstrip antenna with the dimensions for (a) Ground plane (b) Radiating patch respectively

Fig. 3. Prototype of the microstrip antenna showing the ground plane (left) and the radiating patch (right) respectively

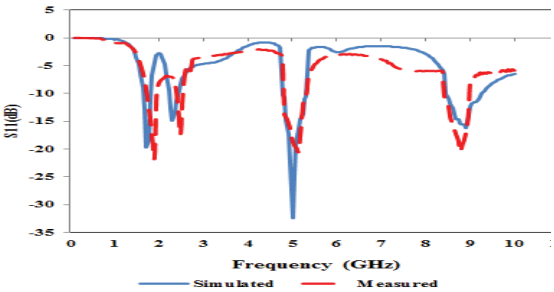

Fig. 4. Simulated and measured return loss when the antenna is placed on body

TABLE I
PERFORMANCE OF QUAD-BANDS IN FREE SPACE AND ON BODY

Performance Metrics/Quad Band	Total Gain (dB)		Radiation efficiency (%)	
	Free Space	On Body	Free Space	On Body
Band I	2.7	-6.4	99	9.0
Band II	3.2	-2.1	99	14.7
Band III	8.1	6.9	98	56.4
Band IV	11.7	9.9	98	41.5

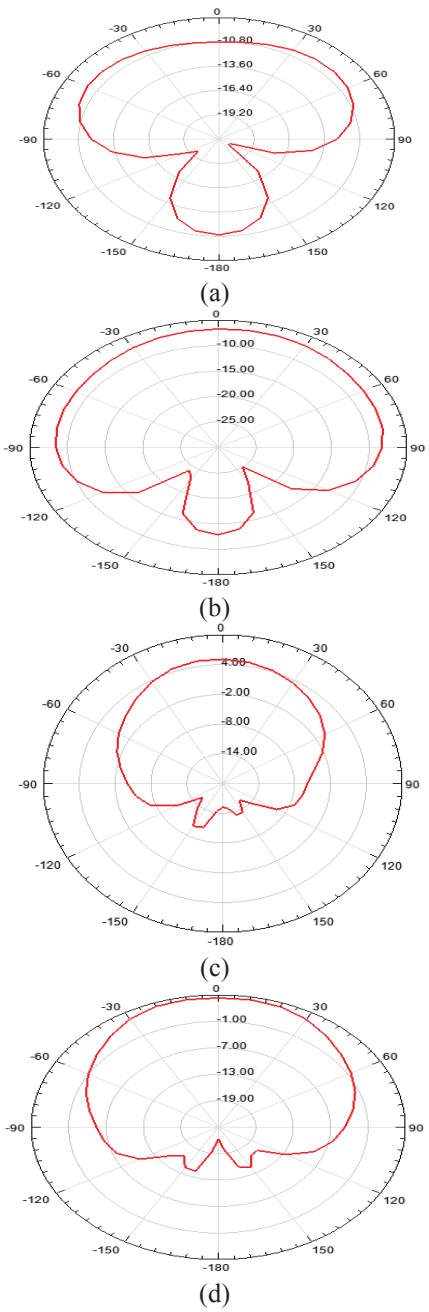

Fig. 5. Radiation pattern of the antenna showing gain (dB)for the quad bands (a) 1.8 GHz (b) 2.4 GHz 9(c) 5GHz (d)8.9 GHz when the proposed antenna is placed on body

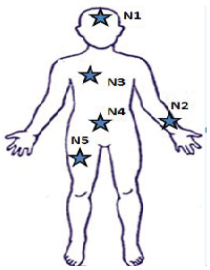

Fig. 6. Anatomical sites of the body considered for simulations

B. SAR and thermal effectts at different body sites

SAR is a good dosimetric quantity that measures the rate of energy absorption by human body when exposed to radio frequency EM field. SAR is calculated as:

$$SAR = \frac{\sigma.|E|^2}{\rho_m} \qquad (1)$$

Here, E is the RMS value of induced field in (V/m), σ is the conductivity of tissue in (S/m), ρ_m is the mass density of tissue in kg/m^3.The antenna is analyzed for its SAR on body through simulations for the four bands for the various tissues at five different anatomical sites on the body and are shown in Fig.6 and are tabulated in Table II. In order to obtain the relation between rise in temperature and time, in the case of long time exposures, the Pennes Bio Heat equation has been used [2]. Simplifying the Bio heat differential equation yields (2) that gives the Maximum temperature rise over a long period of time in the order of minutes [9]. In the equation, S is average SAR in W/kg, ρ is the mass density of tissue in kg/m^3, K is thermal conductivity of the tissue, ρ_b is mass density of blood, c_b is the heat capacity of blood and w is blood perfusion rate in ml/g/min, λ is the wavelength of the EM wave in m. The maximum temperature rise for the different tissues at all the four bands is tabulated using (2) in Table III.

$$Tmax = \frac{q}{\lambda'}[1 - (\sqrt{\lambda'}\,A + 1)e^{-\sqrt{\lambda' A}}\,] \qquad (2)$$

where, $q = \frac{\rho S}{K}$; $\lambda' = \frac{w\,c_b}{K}$; $A = \frac{\lambda}{4}$

Transient analysis of the temperature rise in the time domain is the most interesting part. There are two different approaches depending on whether the distance (radius) of the tissue at a body region is smaller or greater than the wavelength considered. When the equation above is plotted, considering the different body tissues and the different parameters, the evolution time of the rise of temperature for long time exposure is obtained. To take a closer look at the long term thermal effect of the designed antenna, the transient analysis is done for a scenario when the antenna is placed on the forearm and excited at 1.8 GHz with an input power of 1 mW. The rise in temperature with time is plotted using Matlab tool using (3) from [9], which is the second approach of the transient case where distance is greater than quarter wavelength. The graphs for skin, fat and muscle are shown in Fig.7 and Fig.8.

$$T(t) = \frac{q}{2\lambda'}\frac{\rho}{r}\left\{\frac{e^{(r-\rho)}}{2}\left(1+\frac{1}{\rho}\right).erfc\left(\frac{r-\rho}{2\sqrt{\pi}}\right) + \frac{e^{-(r-\rho)}}{2}\left(1-\frac{1}{\rho}\right).erfc\left(\frac{r-\rho}{2\sqrt{\pi}} - \sqrt{\pi}\right) + \frac{e^{(r+\rho)}}{2}\left(1-\frac{1}{\rho}\right).erfc\left(\frac{r+\rho}{2\sqrt{\pi}} + \sqrt{\pi}\right) - \frac{e^{-(r+\rho)}}{2}\left(1+\frac{1}{\rho}\right).erfc\left(\frac{r+\rho}{2\sqrt{\pi}} - \sqrt{\pi}\right) + \frac{r}{\rho}e^{-\tau}\left[erfc\left(\frac{r+\rho}{2\sqrt{\pi}}\right) - erfc\left(\frac{r-\rho}{2\sqrt{\pi}}\right) + \frac{2}{\rho}\sqrt{\frac{\tau}{\pi}}\left(exp - \frac{(r-\rho)^2}{4\tau} - exp - \frac{(r+\rho)^2}{4\tau}\right)\right]\right\} \qquad (3)$$

Where,

$\rho = \sqrt{\lambda'}\,A$; $\tau = \frac{\lambda'}{\mu}$ t; $r = \sqrt{\lambda'}\,R$;erfc(x)=1-$\frac{2}{\sqrt{\pi}}\int_0^x e^{-t^2}\,dt$

TABLE II
AVERAGE SAR VALUE AT QUAD BANDS AT DIFFERENT BODY SITES

Average SAR e^{-2} (W/kg)												
Tissue/ Nodes	***Skin***				***Fat***				***Muscle***			
	I	***II***	***III***	***IV***	***I***	***II***	***III***	***IV***	***I***	***II***	***III***	***IV***
N1-Forehead	22	20	17	15	2.5	2.1	1.7	1.5	5.4	3.4	1.6	0.8
N2-Forearm	25	16	15	11	1.5	1.3	1.2	1.0	4.4	3.9	1.4	0.4
N3-Chest	17	14	13	10	1.3	1.2	0.9	0.9	4.4	3.2	1.5	0.4
N4-Abdomen	22	17	16	9.0	1.1	0.9	0.9	0.6	1.2	1.2	0.3	0.1
N5-Thigh	21	17	13	10	1.1	1.1	1.0	0.8	2.8	2.6	0.8	0.3

TABLE III
MAXIMUM TEMPERATURE RISE AT QUAD BANDS AT DIFFERENT BODY SITES
(BIO HEAT EQUATION)

Maximum temperature rise e^{-2} (°C)												
Tissue/ Nodes	***Skin***				***Fat***				***Muscle***			
	I	***II***	***III***	***IV***	***I***	***II***	***III***	***IV***	***I***	***II***	***III***	***IV***
N1-Forehead	13.4	12.2	10.4	9.1	1.25	1.05	0.85	0.75	3.3	2.10	0.98	0.53
N2-Forearm	15.0	9.61	9.19	6.74	0.75	0.75	0.60	0.50	2.71	2.40	0.86	0.28
N3-Chest	10.4	8.58	7.97	6.13	0.65	0.60	0.48	0.47	2.79	1.97	0.92	0.27
N4-Abdomen	13.1	10.0	9.8	5.5	0.55	0.49	0.48	0.33	0.74	0.74	0.20	0.06
N5-Thigh	12.8	10.4	7.9	6.1	0.55	0.55	0.55	0.40	1.71	1.60	0.51	0.21

C. Experimental validation of the on- body thermal effect of the antenna

Infrared Thermography (IRT) is an imaging modality using which the variations in temperature in human beings can be measured. An experimental setup to validate the safe thermal effects of the designed antenna was made with comfortable subjects with the region of interest at a distance of 1m from the IR camera. Thermograms were taken against a dark non-reflecting background using FLIR A305SC series IR camera and analyzed using FLIR R&D research IR software tool. The images were captured and analyzed under normal body condition of the subject with no special regards to hormonal, metabolic, digestive and drug effects. Thermograms were taken for the marked area of interest on the forearm giving skin temperature before placing the antenna and exciting it. The antenna was excited at 1.8, 2.4 and 5 GHz at 1.0 mW power level by Agilent's N5182A MXG vector signal generator. Images were obtained after duration of 10, 20, and 30 minutes emission from the antenna placed on body and a sample of the thermograms is shown in Fig.9. Temperature rise in degree Celsius was analyzed on skin as it is the tissue that has maximum temperature rise as found out from Table III and using the relevant software to process thermograms it is tabulated in Table IV. It is observed that the maximum temperature rise is only a fraction of a Celsius and is within safe limits of 1°C.

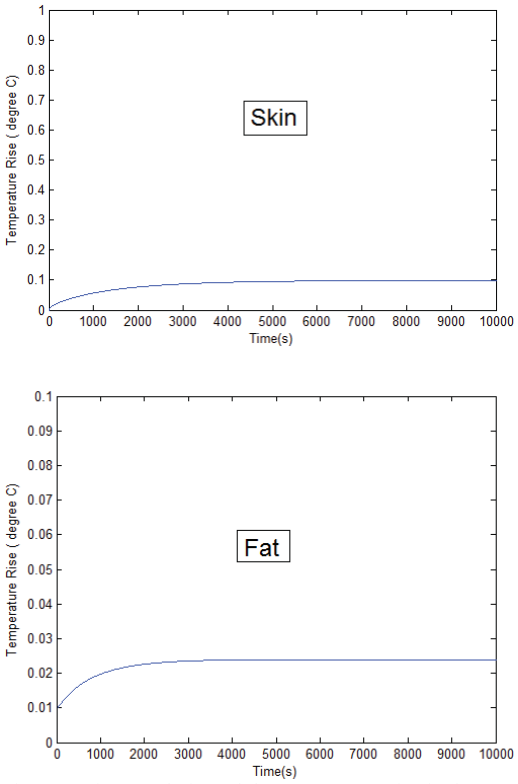

Fig 7. Time evolution of the temperature rise in forearm skin and fat tissue at 1.8 GHz

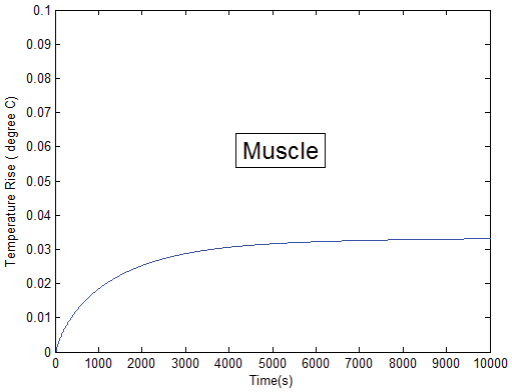

Fig 8. Time evolution of the temperature rise in forearm muscle tissue at 1.8 GHz

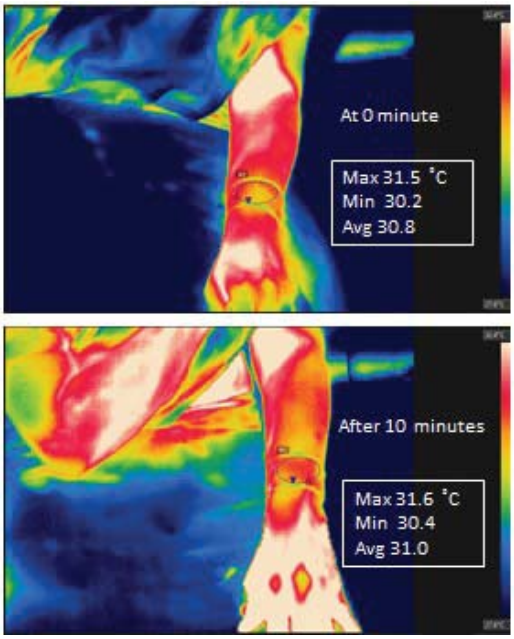

Fig.9. Sample thermo gram at 0 and 10 minutes of emission from the wearable antenna on the forearm at 1.8 GHz

TABLE IV
THERMAL EFFECT OF THE ON BODY ANTENNA FOR VARIOUS TIME DURATION FROM THE THERMOGRAMS

Tissue	Frequency	Average temperature rise(°C) for 1mW power level		
		10 minutes	*20 minutes*	*30 minutes*
Skin	1.8 GHz	0.2	0.6	0.6
	2.4 GHz	0.1	0.4	0.4
	5.0 GHz	0.1	0.3	0.3

IV. DISCUSSION AND CONCLUSION

The performance of a human tissue model based quad-band microstrip patch antenna for BWWDs was investigated in free space and on body. The antenna's return loss satisfies S_{11}< -10 dB in free space and on body simulations at all the four bands. Less value of gain at lower bands is due to the more omnidirectional radiation pattern at these bands. The performance was also studied in terms of SAR and thermal effects for different sites on the human body at all quad-bands. It is observed from Table II that the SAR at the various body sites considered was more in lower band than the upper band. This is due to the decrease in permittivity as frequency increases, leading to better reflections away from the body, lesser SAR and decreased thermal effects, improving the performance of the antenna. It is analytically analyzed that the highest temperature rise was found on skin, the outermost tissue, irrespective of the body sites. The temperature increase was found to be indeed less of about fractions of a degree Celsius for all bands at all body sites. The time evolution of temperature for the three tissues obtained show that after an initial increase in temperature, there is saturation in the graph owing to the physiological aspects of the thermoregulation of the body. Thermograms taken for several minutes of exposure also showed that the maximum temperature rise was well within limits making the antenna compliant with international safety regulations, favoring the use of the antenna for wearable devices for variety of wireless applications.

REFERENCES

[1] Kasun M.S.Thotahewa, Jean-Michel Redoute, Mehmet Rasit Yuce, " SAR, SA and Temperature variations in the Human head caused by IR-UWB Implants operating at 4GHz", *IEEE Transactions on Microwave Theory and Techniques*, pp.2161-2169, 2013.

[2] Francesc Soler, "Radiation effects of wearable antenna in human body tissues ", M.S. thesis, University of Colorado Springs , 2014.

[3] "Guidelines for limiting to time varying electric, magnetic, and electromagneticfields," ICNIRP,Oberschleissheim,Germany, 1997.

[4] Ting Wu, Theodore S. Rappaport, Christopher M. Collins ,"The Human Body and Millimeter-Wave Wireless Communication Systems: Interactions and Implications", *IEEE Microwave magazine*, March 2015.

[5] Italian National Research Council, Institute for Applied Physics, homepage on Dielectric properties of body tissues. [Online]. Available: http://niremf.ifac.cnr.it.

[6] Garg Ramesh, Prakash Bhartia, Inder Bahl, Apisak Ittipiboon, "Microstrip antenna design handbook," Artech House, 2001.

[7] C Gabriel, S Gabriely and E Corthout, "The dielectric properties of biological tissues: I. Literature Survey*," Phys. Med. Biol.,* vol . 41, pp. 2231–2249, 1996.

[8] M. Klemm and G. Troester, "EM energy absorption in the human body tissues due to UWB antennas," *Progress In Electromagnetics Research, PIER 62*, pp. 261–280, 2006

[9] H.N.Kritikos, Herman P. Schwan, "Potential Temperature Rise Induced by ElectromagneticField in Brain Tissues", *IEEE Transactions on Biomedical Engineering* ,vol .BME-26, No 1, pp. 29-34, Jan 1979.

THE 18TH INTERNATIONAL SYMPOSIUM ON WIRELESS PERSONAL MULTIMEDIA COMMUNICATIONS
(WPMC-2015)
December 13-16, 2015, Hyderabad, India

Efficient Visibility Modeling for Free-Space Optical Systems Design

Ivo Sousa, Maria Paula Queluz, António Rodrigues
Instituto de Telecomunicações / Instituto Superior Técnico
University of Lisbon, Portugal
email: [ivo.sousa, paula.queluz, antonio.rodrigues]@lx.it.pt

***Abstract*—Free-Space Optical (FSO) systems are greatly affected by fog conditions, which cause very high attenuation over considerable amounts of time. Therefore, some models have been adopted by the designers of FSO links, which take into account visibility values in order to compute the attenuation due to fog. However, the visibility distribution for an FSO link site may not be available. In this paper we propose a simple but reliable framework that estimates the visibility distribution and has a single statistical input: the number of foggy hours per year. The proposed tool is evaluated using real visibility data from a large variety of sites within the Portuguese territory. The results show that the predicted visibility distributions considerably agree with the real data for all sites, proving that the simple metric proposed herein is an easy-to-use and valid tool to take into account when designing FSO systems.**

Keywords*—Free-Space Optical (FSO) Communications; Visibility Modeling; Wireless Links Design.

I. INTRODUCTION

Over the last two decades, Free-Space Optical (FSO) links have become an attractive solution to be taken into account when designing high bandwidth wireless communication links [1]. Historically, this technology started being used in satellite communications as well as by military forces, due to a number of interesting characteristics [2]: fast installation, operation in the infrared spectrum (780–1550 nm, which is unlicensed), high data rates and high immunity to electromagnetic interference. Moreover, FSO links ensure high security of the transmitted data due to the low diffraction of the optical beam generated by a laser equipment, i.e., an interceptor would need to have its receiver perfectly aligned with the transmitted optical beam in order to receive the signal. FSO systems can also be used as an alternative to microwave links, e.g., they can be used in the mobile backhaul last-mile in order to connect base stations to the core network and provide broadband internet access to rural areas. Some of other possible applications are video teleconferencing, real-time medical imaging transfer, enterprise networking, work-sharing capabilities and high speed interplanetary internet links [3].

Nevertheless, the use of optical signals raises some challenges that must be taken into account when adopting FSO systems. Since the propagating channel for wireless optical communication is the atmosphere, factors like rain, snow, clouds, smoke, fog and mist have a negative impact on the system performance, as these atmospheric attenuators not only absorb but also cause scattering of optical beams [4]. In addition, scintillation, caused by atmospheric turbulence, also gives rise to fluctuations in the received signal power (e.g., the twinkling of the stars). Scintillation effects can be mitigated using several techniques proposed in the literature [5]. However, the major concern of terrestrial FSO links is fog, since it causes very high attenuation over considerable amounts of time [4].

Some statistical models for fog have been proposed [6], [7], [8], which yield a better understanding of the attenuation caused by fog, namely the continental fog. On the other hand, International Telecommunications Union (ITU) issued recommendations for the design of terrestrial FSO links [9], [10], in which the attenuation coefficient due to fog is easily computed by taking into account the visibility – the technical definition of visibility is the distance at which light decreases to 2% of the original power; in terms of human perception, visibility is the distance at which it is just possible to distinguish a dark object against the horizon [9]. The method adopted by ITU allows a geo-local performance evaluation of FSO systems if the visibility distribution is known.

The ITU recommendations regarding the characteristics of precipitation for propagation modeling [11] provide a simple metric to compute the rainfall rate exceeded for any given percentage of the average year and for any location on Earth. However, neither the ITU recommendations for FSO systems design nor the fog statistical models proposed in the literature have an equivalent metric for the visibility distribution. Although the visibility parameter is usually available in meteorological stations or airports databases, for many sites the only statistical information at the disposal of an FSO link designer is the average number of foggy hours per year.

The goal of this work is to provide a simple but reliable framework that estimates the visibility distribution and has the number of foggy hours per year as its single statistical input. The innovative tool proposed here is, to the best of our knowledge, the first one that adopts a straightforward metric to provide reliable estimates of visibility values for different locations. This paper is organized as follows: after this introduction, Section II describes the visibility influence on FSO links design; Section III introduces the visibility measurements data of various sites over ten years, which were used to propose the visibility distribution estimation models discussed in Section IV; Section V provides some results regarding the framework assessment; finally, Section VI concludes the paper.

The authors would like to thank FCT for the support by the project UID/EEA/50008/2013.

II. Visibility Influence on FSO links design

Fog is a type of atmospheric attenuator whose particles size is comparable to the FSO beams wavelength, hence the induced attenuation can be described as a Mie scattering process [9], [10]. This kind of attenuation is a function of frequency and visibility, and visibility is related to the particle size distribution. As mentioned in the introduction, fog constitutes the most restrictive factor to the deployment of FSO systems at long distances. The attenuation in the optical wave region can reach 300 dB/km, in contrast to the millimeter wave region, where rain attenuation is typically a few dB/km [10].

The designers of FSO links have adopted empirical models to compute the attenuation due to Mie scattering, since an analytical approach is often impractical. One of these models, known as Kruse relation [12], is part of the ITU recommendations for FSO systems design [9]; it computes this specific attenuation, $\gamma_{fog}(\lambda)$ (in dB/km), as

$$\gamma_{fog}(\lambda) = \frac{3.912}{V_{[\text{km}]}} \left(\frac{\lambda_{[\text{nm}]}}{550} \right)^{-q}, \quad (1)$$

where V stands for the visibility, λ corresponds to the FSO beam wavelength and q denotes a coefficient dependent on the size distribution of the scattering particles. In the Kruse relation, this coefficient is given by

$$q = \begin{cases} 1.6 & V > 50 \text{ km} \\ 1.3 & 6 \text{ km} < V < 50 \text{ km} \\ 0.585\, V^{1/3} & V < 6 \text{ km} \end{cases}, \quad (2)$$

while a more recent study, known as Kim relation [12], proposes the following expression for the parameter q:

$$q = \begin{cases} 1.6 & V > 50 \text{ km} \\ 1.3 & 6 \text{ km} < V < 50 \text{ km} \\ 0.16\, V + 0.34 & 1 \text{ km} < V < 6 \text{ km} \\ V - 0.5 & 0.5 \text{ km} < V < 1 \text{ km} \\ 0 & V < 0.5 \text{ km} \end{cases}. \quad (3)$$

Al Naboulsi et al. developed simple relations that allow the evaluation of the attenuation for two types of fog: advection fog and convection fog [12]. Advection fog is formed by the movement of wet and warm air masses above colder maritime or terrestrial surfaces; convection fog appears when the ground starts cooling by releasing the heat that is accumulated during the day and the air is sufficiently cool and becomes saturated. The attenuation by advection fog is expressed by

$$\sigma_{adv}(\lambda) = \frac{0.11478\, \lambda_{[\text{m}]} + 3.8367}{V_{[\text{m}]}}, \quad (4)$$

while the attenuation by convection fog is given by

$$\sigma_{conv}(\lambda) = \frac{0.18126\, \lambda^2_{[\text{m}]} + 0.13709\, \lambda_{[\text{m}]} + 3.7502}{V_{[\text{m}]}}. \quad (5)$$

The specific attenuation $\gamma_{fog}(\lambda)$ (in dB/km) for both types of fog is computed as

$$\gamma_{fog}(\lambda) = \frac{10}{\log_e(10)} \sigma(\lambda). \quad (6)$$

Regarding FSO links design, the previous expressions can be used to easily compute the attenuation due to fog if the visibility values are known. Furthermore, an FSO link is also characterized by the unavailability due to fog that it can afford. This means that the respective visibility distribution is also required, namely the value of the visibility that is not exceeded for a given percentage of time p, in order to obtain the attenuation value exceeded for this percentage p.

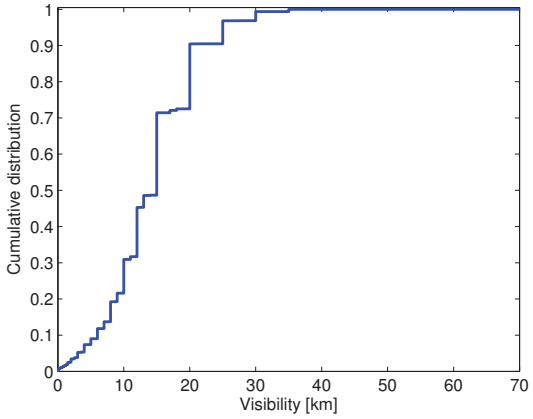

Fig. 1. Cumulative distribution of the visibility for site #7 (Lisboa).

By definition, one is in the presence of fog when water droplets suspended in the atmosphere reduce the visibility to less than 1 km [13]. However, this definition is not enough to make a correspondence between the average number of foggy days per year and a certain value of the visibility distribution; the average duration of a fog event is also required, so as to compute the average number of foggy hours per year. In other words, and assuming that a day is reported as a foggy day when part of that day has visibility below 1 km, the percentage of time (in a year) in which the visibility does not exceed 1 km is given by

$$p_{(1\,\text{km})\ [\%]} = \frac{\overline{N_{fd}}}{365.25} \times \frac{\overline{D}_{[\text{h}]}}{24} \times 100, \quad (7)$$

where $\overline{N_{fd}}$ denotes the average number of foggy days per year and $\overline{D}_{[\text{h}]}$ represents the average duration of fog in hours, which means that the product of these two variables corresponds to the average number of foggy hours per year.

III. Visibility Measurements Data

In order to obtain reliable visibility distributions, real visibility measurements samples from 17 different sites were acquired from the Portuguese Sea and Atmosphere Institute (IPMA). These sites are located across the Portuguese territory (cf. Fig. 2): the archipelagos of the Azores (3 sites) and Madeira (1 site), and mainland Portugal (4 coastal and 9 inland sites).

The visibility samples were obtained everyday during ten years (between January 1st of 1991 and December 31st of 2000), they have a high degree of resolution (the visibility values range from 100 m to 70 km) and they were taken many times per day (in some cases every hour). With these data, it is possible to build the cumulative distribution of the visibility for each different site (an example is depicted in Fig. 1).

The IPMA also provided additional data for the sites under study (regarding the ten years evaluation period), namely the

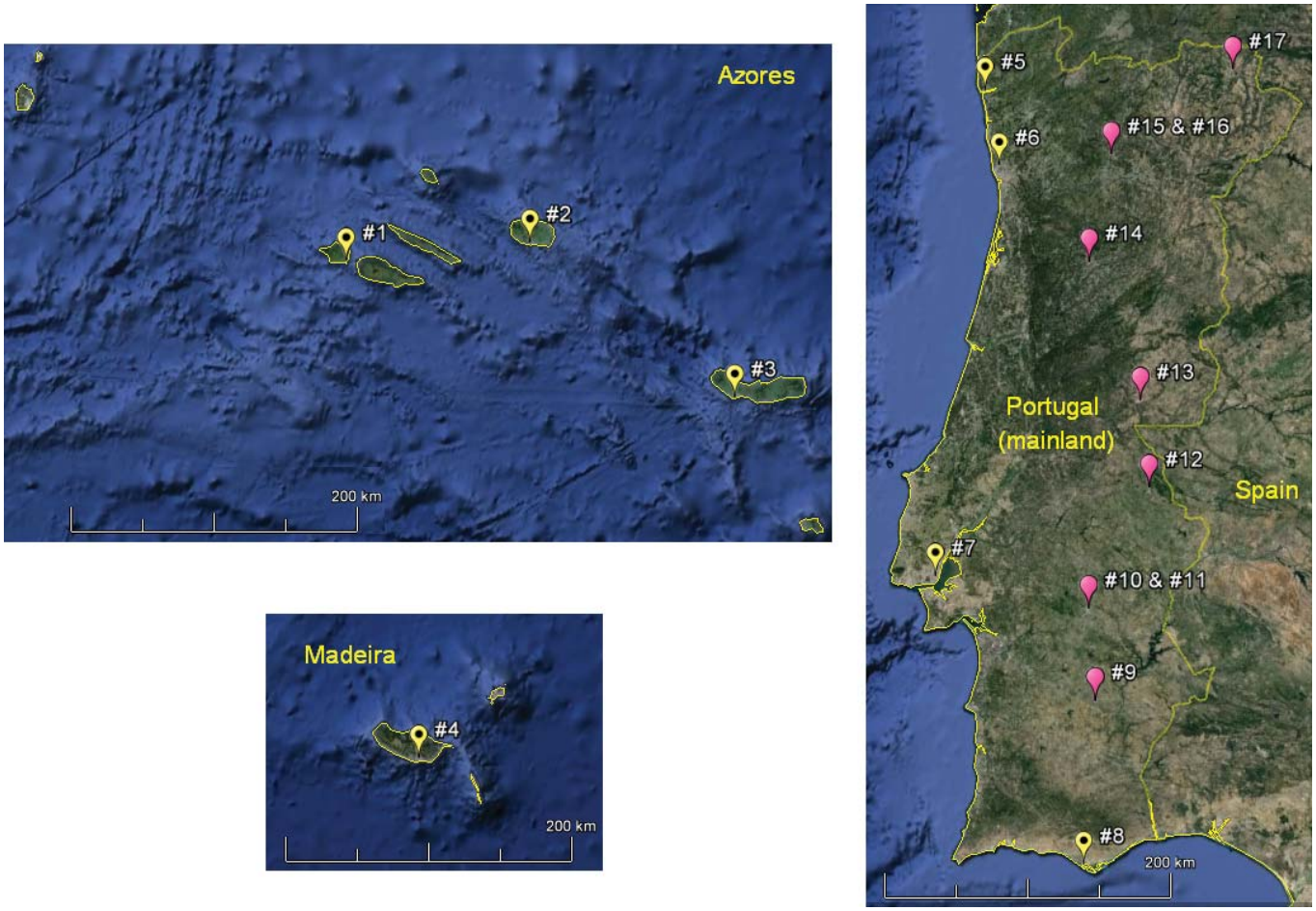

Fig. 2. Portuguese territory (map data: Google, Landsat).

TABLE I. AVERAGE NUMBER OF FOGGY DAYS PER YEAR AND AVERAGE DURATION OF FOG.

Site	$\overline{N_{fd}}$	$\overline{D}_{[\mathrm{h}]}$	Site	$\overline{N_{fd}}$	$\overline{D}_{[\mathrm{h}]}$
#1 (Horta)	5.0	6.7	#9 (Beja)	57.8	4.7
#2 (Angra do Heroísmo)	7.0	5.5	#10 (Évora *i*)	44.4	5.2
#3 (Ponta Delgada)	12.5	5.4	#11 (Évora *ii*)	35.7	3.8
#4 (Funchal)	0.3	5.7	#12 (Portalegre)	107.3	7.0
#5 (Viana do Castelo)	51.1	5.2	#13 (Castelo Banco)	25.1	6.4
#6 (Porto)	66.2	3.5	#14 (Viseu)	65.3	7.2
#7 (Lisboa)	23.3	5.9	#15 (Vila Real *i*)	32.3	7.1
#8 (Faro)	7.0	3.4	#16 (Vila Real *ii*)	24.2	7.3
			#17 (Bragança)	44.3	9.5

number of days that were considered as foggy days and the duration of these fog events. With this information, it is possible to compute the average number of foggy days per year and the average duration of fog – these values are presented in Table I.

IV. PROPOSED MODELS

As mentioned in Section II, an FSO link is characterized by the unavailability due to fog that it can afford, i.e., the measure of downtime of an FSO system allowed by the Service-Level Agreement (SLA). The availability index (measure of uptime rather than downtime) is usually expressed as a percentage per year, typically ranging from 90% (i.e., 36.5 days of downtime per year) to 99.9999999% (i.e., 31.6 milliseconds of downtime per year). Thus, and from an FSO link designer perspective, the most interesting part of the visibility distribution is the one corresponding to percentages of the time ranging from 0 to 10%. Henceforth, the work in this paper focus on providing a simple but reliable framework which estimates this specific portion of the visibility distribution.

By analyzing the visibility measurements data, we first noticed that the visibility distributions under study presented two different types of behavior, depending on whether it refers to coastal or inland sites, as exemplified in Fig. 3. Therefore, we split the study of the visibility distribution into two cases: coastal sites versus inland sites.

Considering the examples presented in Fig. 3 for coastal sites, both visibility distributions seem to follow a curve that resembles the charge on a capacitor versus time when it is charging. Taking this into account, we propose to model the coastal visibility distribution as

$$V_{coastal\ [\mathrm{km}]} = \alpha \left[1 - \exp\left(-\beta \frac{p_{[\%]}}{100}\right)\right], \quad 0 \leq p \leq 10\%, \tag{8}$$

where p stands for the percentage of time (independent vari-

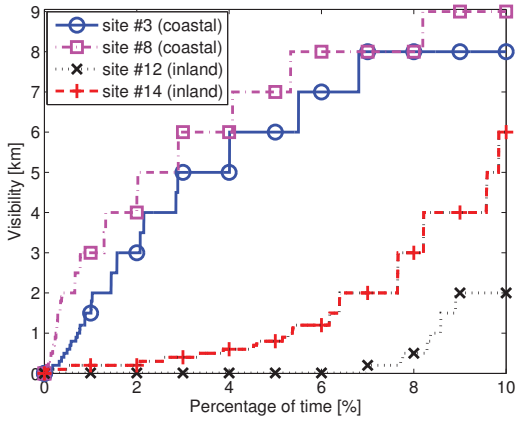

Fig. 3. Visibility values that were not exceeded for a given percentage of time – typical examples for coastal and inland sites.

able) while α and β denote the parameters of this model. To compute these parameters, first we assume that the visibility distribution stabilizes at some point, which is equal for all coastal sites, i.e., α is fixed. Afterwards, we force the proposed visibility distribution model (8) to pass through a particular point, namely the one related to the percentage of time for which the visibility does not exceed 1 km ($p_{(1\,\mathrm{km})}$, which can be obtained using (7)). Consequently, the relationship between α and β is given by

$$1 = \alpha\left[1 - \exp\left(-\beta\frac{p_{(1\,\mathrm{km})\ [\%]}}{100}\right)\right] \Leftrightarrow$$
$$\beta = \frac{-\log_e\left(1-\frac{1}{\alpha}\right)}{p_{(1\,\mathrm{km})\ [\%]}/100}. \quad (9)$$

Therefore, the proposed visibility distribution model for coastal sites is tuned by varying α (a value for this parameter is proposed in the following section).

As for inland sites, the visibility distribution examples presented in Fig. 3 resemble exponential functions that pass through the origin. For this reason, we propose to model the inland visibility distribution as

$$V_{inland\ [\mathrm{km}]} = \mu\left[\exp\left(\delta\frac{p_{[\%]}}{100}\right) - 1\right], \quad 0 \le p \le 10\%, \quad (10)$$

where μ and δ represent the parameters of this model. For inland sites, we noticed that as $p_{(1\,\mathrm{km})}$ increases, the more rapidly the visibility values grow after crossing the 1 km mark. In other words, we propose to model δ as

$$\delta = \eta\frac{p_{(1\,\mathrm{km})\ [\%]}}{100}, \quad (11)$$

where η is assumed to be a fixed value. Likewise the coastal case, we force the proposed visibility distribution model (10) to pass through the point related with $p_{(1\,\mathrm{km})}$, which means that the relationship between the different parameters can be expressed as

$$1 = \mu\left[\exp\left(\delta\frac{p_{(1\,\mathrm{km})\ [\%]}}{100}\right) - 1\right] \Leftrightarrow$$
$$\mu = \frac{1}{\exp\left(\eta\frac{p^2_{(1\,\mathrm{km})\ [\%]}}{100^2}\right) - 1}. \quad (12)$$

TABLE II. TUNED VALUES OF α AND η.

Parameter	Value
α	13.1
η	560

TABLE III. COEFFICIENT OF DETERMINATION.

Site	R^2	Site	R^2
#1 (Horta)	0.55	#9 (Beja)	0.81
#2 (Angra do Heroísmo)	0.76	#10 (Évora *i*)	0.87
#3 (Ponta Delgada)	0.89	#11 (Évora *ii*)	0.83
#4 (Funchal)	0.47	#12 (Portalegre)	0.85
#5 (Viana do Castelo)	0.92	#13 (Castelo Banco)	0.82
#6 (Porto)	0.95	#14 (Viseu)	0.94
#7 (Lisboa)	0.92	#15 (Vila Real *i*)	0.86
#8 (Faro)	-0.39	#16 (Vila Real *ii*)	0.89
		#17 (Bragança)	0.87

Therefore, the proposed visibility distribution model for inland sites is tuned by varying η (a value for this parameter is proposed in the following section).

V. RESULTS

As seen in the previous section, the proposed visibility distribution models require, as main input, the percentage of time for which the visibility does not exceed 1 km. Even though the data acquired from IPMA provided us direct access to this percentage value for each site through the respective cumulative distribution of the visibility, we want to evaluate the performance of the proposed models as if the number of foggy hours was the only statistical information available. Thus, the estimated visibility results presented hereafter are obtained by first estimating $p_{(1\,\mathrm{km})}$ using (7) and the values presented in Table I.

The coefficient of determination R^2 is adopted in this work as a measure of the goodness of fit of the proposed models to the real visibility data; it is defined as

$$R^2 = 1 - \frac{\sum_{k=1}^{N}(O_k - P_k)^2}{\sum_{k=1}^{N}(O_k - \overline{O})^2}, \quad (13)$$

where O and P correspond to the observed and predicted visibility values, and N stands for the total number of samples. Hence, the coefficient of determination ranges from minus infinity to one, with higher values indicating better agreement, while negative values indicate that the observed mean $\overline{O}$ provides a better fit to the outcomes than the prediction model, according to this particular criterion.

In order to tune the visibility distribution models proposed in this work (cf. Section IV), we first varied the value of α and then we selected the one that yielded the highest average fitness value $\overline{R^2}$ concerning coastal sites. The same procedure was adopted for the parameter η regarding inland sites. Table II contains the tuned values of α and η, while Table III presents the coefficient of determination obtained for the different sites under study.

The results show that the average coefficient of determination value concerning coastal sites is equal to 0.63, where

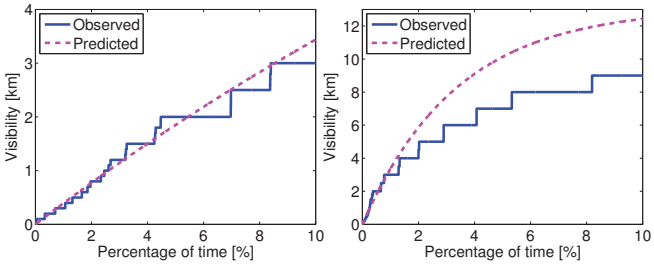

(a) Site #6 (Porto, $R^2 = 0.95$) (b) Site #8 (Faro, $R^2 = -0.39$)

Fig. 4. Analysis of the proposed visibility distribution model for coastal sites.

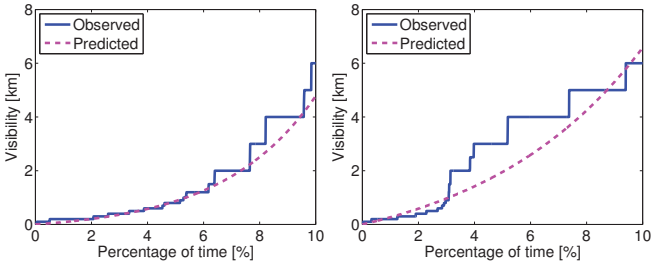

(a) Site #14 (Viseu, $R^2 = 0.94$) (b) Site #9 (Beja, $R^2 = 0.81$)

Fig. 5. Analysis of the proposed visibility distribution model for inland sites.

the best performance was obtained for site #6 with a suitable fit, Fig. 4(a). On the other hand, the worst performance was obtained for site #8, although the predicted visibility distribution has an adequate fit for values of the percentage of time below 1%, Fig. 4(b) – this last behavior was observed for all sites under study (not shown here due to the lack of space), meaning that the proposed models not only show a good fit but also they are specially efficient in estimating the visibility distribution for percentages of time below 1%, which is useful when designing FSO systems with availability indexes over 99%.

As for inland sites, the average coefficient of determination value is equal to 0.86, where the best performance was obtained for site #14 with an appropriate fit, Fig. 5(a). Moreover, even the worst inland case, which was obtained for site #9, presented a satisfactory fit, Fig. 5(b).

VI. Conclusions

In this work we presented a simple framework that estimates the visibility distribution for any given percentage of time below 10% and has as single statistical input the number of foggy hours per year. The proposed visibility distribution models were assessed using real data from 17 different sites in Portugal, with a wide diversity of environments: sites in islands, costal and inland sites in mainland Portugal. The main goal was to provide a straightforward and reliable tool that can be used by the designers of FSO systems.

Based on the obtained results, which showed a suitable correspondence between observed and predicted data for all sites under study, the adoption of the simple metric proposed herein can provide reliable estimates for visibility values just by knowing the number of foggy hours per year. Furthermore, even when the real visibility distribution is known, the proposed models can be used to somewhat enhance the resolution of the visibility information, e.g., to determine the visibility value that yields a 99.999% availability of an FSO link using real data that have a percentage resolution of only 1%.

References

[1] E. Leitgeb *et al.*, "Current Optical Technologies for Wireless Access," in *10th International Conference on Telecommunications (ConTEL 2009)*, Zagreb, Croatia, 2009, pp. 7–18.

[2] B. F. R. Sakamoto, W. Fegadolli, and J. E. B. Oliveira, "Emprego Militar de Comunicação Óptica em Espaço Livre–FSO," *IX Simpósio de Aplicações Operacionais (IX SIGE)*, pp. 1–6, 2008.

[3] A. Acampora, "Last Mile by Laser," *Scientific American*, pp. 48–53, 2002.

[4] B. R. Strickland, M. J. Lavan, E. Woodbridge, and V. Chan, "Effects of fog on the bit-error rate of a free-space laser communication system," *Applied Optics*, vol. 38, no. 3, pp. 424–431, 1999.

[5] X. Zhu and J. M. Kahn, "Free-space optical communication through atmospheric turbulence channels," *IEEE Transactions on Communications*, vol. 50, no. 8, pp. 1293–1300, 2002.

[6] E. P. Shettle, "Models of aerosols, clouds, and precipitation for atmospheric propagation studies," in *Atmospheric Propagation in the UV, Visible, IR, and MM-Wave Region and Related Systems Aspects*, vol. 454, Copenhagen, Denmark, 1989, pp. 15.1–15.13.

[7] M. Khan, M. Awan, E. Leitgeb, F. Nadeem, and I. Hussain, "Selecting a distribution function for optical attenuation in dense continental fog conditions," in *International Conference on Emerging Technologies (ICET 2009)*, Islamabad, Pakistan, 2009, pp. 142–147.

[8] M. S. Khan *et al.*, "Probabilistic model for free-space optical links under continental fog conditions," *Radioengineering*, vol. 19, no. 3, pp. 460–465, 2010.

[9] ITU, "Prediction methods required for the design of terrestrial free-space optical links," Recommendation ITU-R P.1814, 2007.

[10] ——, "Propagation data required for the design of terrestrial free-space optical links," Recommendation ITU-R P.1817, 2012.

[11] ——, "Characteristics of precipitation for propagation modelling," Recommendation ITU-R P.837, 2012.

[12] A. Naboulsi, H. Sizun, and F. De Fornel, "Propagation of optical and infrared waves in the atmosphere," in *XXVIIIth URSI General Assembly*, New Delhi, India, 2005.

[13] US Government, *Federal Meteorological Handbook Number 1*. Office of the Federal Coordinator for Meteorology, 2005, ch. 8, pp. 8.1–8.8.

THE 18TH INTERNATIONAL SYMPOSIUM ON WIRELESS PERSONAL MULTIMEDIA COMMUNICATIONS
(WPMC-2015)
December 13-16, 2015, Hyderabad, India

A New Approach for Crossed Sector Detection in Live Mobile Networks based on Radio Measurements

D. Duarte*‡, P. Vieira*‡, A. Rodrigues*†, A. Martins§, N. Oliveira§
*Instituto de Telecomunicações (IT), Lisbon, Portugal
‡Instituto Superior de Engenharia de Lisboa (ISEL), ADEETC, Lisbon, Portugal
§CELFINET, Consultoria em Telecomunicações Lda., Lisbon, Portugal
†Instituto Superior Técnico (IST), Lisbon, Portugal

***Abstract*—One of the most usual implementation errors that occurs when deploying radio access base-stations for mobile networks is to erroneously swap the antenna cables of two sectors, creating a crossed sector scenario. When this happens, the two swapped sectors still provide radio coverage, but not in the desired cell area. Hence, this paper proposes an enhanced approach for crossed sector detection, taking into account radio signal strength measurements, network topology, and also antennas' radiation pattern and orientation. The algorithm was applied to a live 2^{nd} Generation (2G)/3^{rd} Generation (3G)/4^{th} Generation (4G) mobile network, for accuracy and validation purposes. Large-scale analysis was set in UK and Portugal areas, and 16 crossed sectors were detected within a universe of 883 sites.**

***Index Terms*—Wireless Communications, Mobile Networks, Self-Organizing Networks Crossed Sector Detection.**

I. Introduction

According to a recent traffic report published by Cisco®, global mobile data traffic reached 4.2 exabytes per month at 2015, and up to 2.5 exabytes per month at 2014. In addition, in 2014, a 4G connection generated already 10 times more traffic on average than a non-4G connection. Although 4G connections represent only 6 percent of mobile connections today, they already account for 40 percent of mobile data traffic [1].

The Long Term Evolution (LTE) [2] is just one of the latest steps in an advancing series of mobile telecommunications systems. To support data traffic changes in mobile networks, in order to boost performance and deal with the increasing complexity within the operating 3G/4G networks, the Self-Organizing Networks (SON) concept was introduced as one of the main features of LTE. The main goal of SON mechanisms are to incorporate auto-configuration and self-optimization capabilities in evolved NodeBs (eNBs), where automatic crossed feeder detection and creating optimized neighbor cell lists [3] are some good examples.

Inside SON improvements, the network should auto-detect if the sectorized antennas are connected to the wrong transceivers, which can happen due to human implementation error. This erroneous implementation degrades user performance, since radio resource planning and reuse strongly depend on antenna directivity and orientation.

The aim of this paper is to present an enhanced crossed sector detection algorithm, taking into account signal strength measurements, antenna radiation patterns, and antenna orientation. The algorithm performance was validated using data from live networks.

The paper is organized as follows. Section II overviews the crossed sector issue, presenting its definition and related problems. Section III highlights the proposed algorithm. Section IV discusses results when applied to a live network, followed by the conclusions in section V.

II. Crossed Sector Issue

One of the most common implementation errors when deploying base-stations is to accidentally swap cables of two sectors, creating a crossed sector scenario, as shown in Fig. 1. Each triangle represents an antenna sector (S), connected to the respective transmitter (T).

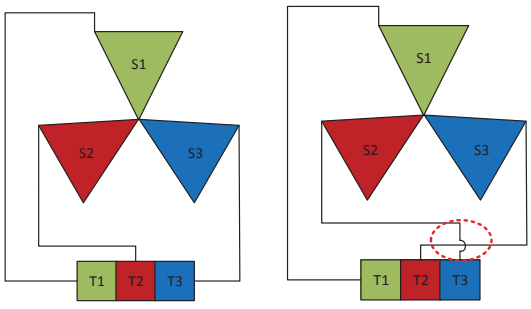

(a) Correct configuration. (b) Swapped cables of S2 and S3.

Fig. 1. Crossed sector illustration.

When it occurs, the two swapped sectors still provide coverage but not in the desired cell area. Therefore, orientation dependent configuration parameters like Physical Cell Identity (PCI), carrier frequency and Neighbour Cell List (NCL) are not the most suitable to the area covered by the sector, which can lead to performance degradation. A crossed sector

situation can generate several problems, such as high-level interference, leading to high dropped call ratio and poor data connectivity. Additionally, handover performance can be highly degraded, due to erroneous neighbor definition. Nowadays, this situation is manually detected by the radio engineer [4]. Some network statistics like Handover Sucess Rate (HOSR) help to detect probable crossed sector situations, which are confirmed in the following by Drive Testing (DT) and signal strength analysis [5].

Fig. 2 presents a detected crossed sector situation from a DT, where the colored slices represent the base station sectors, and the small filled circles present the DT samples, being mapped with the color from the best server sector.

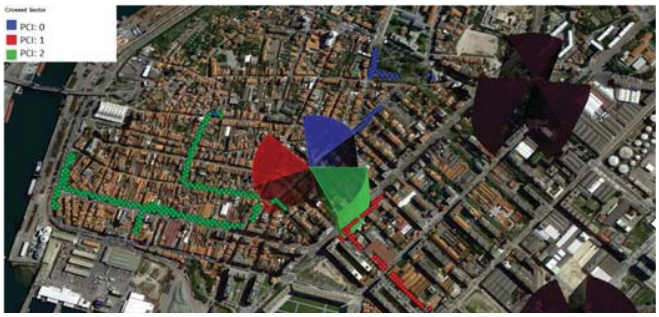

Fig. 2. A crossed sector thematic example based on drive-test best server data.

Fig. 2 shows that the samples which are supposed to be served by the red sector (PCI:1) are located on the opposite side of the site. Similarly, the samples which are supposed to be served by the green sector (PCI:2) are located on the "red" area, suggesting a crossed sector situation.

III. The Proposed Algorithm

The algorithm's aim is to detect crossed sectors based on signal strength measurements and antenna radiation pattern. The implemented concept correlates the difference between the received signal strength from two given sectors at a certain position, and the associated antenna gain prediction from these two sectors. The algorithm is composed by two modules: detection and decision module.

A. Detection Module

The detection module assures that appropriate samples are taken and examined by the decision module, so that only samples in dominant areas should be used, *i.e.*, only the samples which are in the area delimited by the sites coverage area will be considered. These dominant areas are delimited in azimuth and distance and consider the Half Power Beamwidth (HPBW) and the distance to the 1^{st} tier. This approach filters out ambiguous samples located in the central region between the two sectors. This approach is illustrated in Fig. 3, where a bisectorized site is considered. Red crosses and green squares represent ignored and considered samples, respectively.

The algorithm can be summarized as per the following pseudo code, where n is the number of the samples which will

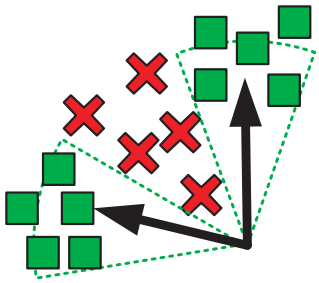

Fig. 3. Ignored and considered samples to be used in detection module.

be analysed. $\Delta P(i)$ and $\Delta G(i)$ are the difference between the received signal strength from sectors A (Pr_A) and B (Pr_B), and the difference between antenna gains from the same sectors (G_A and G_B), respectively. $crossed$ is a boolean array with the analysis results from each analysed sample. If $\Delta P(i)$ and $\Delta G(i)$ have the same signal, the boolean $crossed$ returns *false*, and the sample indicates that the sector is well defined. Otherwise, the boolean $crossed$ is affected with *true*.

repeat
  for $i \leftarrow 1, n$ **do**
    $\Delta P(i) \leftarrow sign(Pr_A - Pr_B)$
    $\Delta G(i) \leftarrow sign(G_A - G_B)$
    if $(\Delta P(i) \oplus \Delta G(i))$ **then**
      $crossed(i) \leftarrow true$
    else
      $crossed(i) \leftarrow false$
    end if
  end for
until all sectors are not compared

B. Decision Module

For the decision module, a statistical hypothesis test is applied to the detection module result, in order to classify the scenario as a function of all the analysed samples. With the difference between the received signal strength from two sectors at a given position *i*, and the difference between the antenna gains from these two sectors, α_i must be calculated as,

$$\alpha_i = \begin{cases} +(|\Delta G_i| + |\Delta P_i|), & if(\Delta G_i \otimes \Delta P_i) == 1 \\ -(|\Delta G_i| + |\Delta P_i|), & if(\Delta G_i \otimes \Delta P_i) == 0 \end{cases} \quad (1)$$

From this, the so called empirical probability density function of α is introduced and defined by

$$f(\alpha) = \begin{cases} P_i & if \quad \alpha = \alpha_i \quad (i = 1, 2...) \\ 0 & otherside \end{cases} \quad (2)$$

where,

$$P(\alpha = \alpha_i) = P_i \quad (3)$$

and

$$\sum_{i=1}^{max(i)} f(\alpha_i) = 1. \quad (4)$$

From this, a histogram based on α_i will be built, which will support the decision algorithm. The negative side of the histogram indicates the probability function that does not contribute to the crossed sector for the analysed pair. Moreover, the positive side, gives the probability density that contributes to the crossed sector decision.

Consider now two complementary sets of data so that,

$$\begin{aligned} \alpha_j &= \alpha_i \quad if \quad \alpha_i \geq 0 \\ \overline{\alpha_j} &= |\alpha_i| \quad if \quad \alpha_i < 0 \end{aligned} \tag{5}$$

and let,

$$\begin{aligned} \beta_c &= \frac{\sum_{j=1}^{max(j)} \alpha_j f(\alpha_j)}{\sum_{i=1}^{max(i)} |\alpha_i| f(\alpha_i)} \\ \beta_{\overline{c}} &= \frac{\sum_{j=1}^{max(j)} \overline{\alpha_j} f(\overline{\alpha_j})}{\sum_{i=1}^{max(i)} |\alpha_i| f(\alpha_i)} \end{aligned} \tag{6}$$

where β_c and $\beta_{\overline{c}}$ are the crossed and not crossed sample weight, respectively. The two values will be considered in the detection algorithm by direct comparison.

IV. Simulation Results and Analysis

This section describes the simulation outcomes. Extensive radio signal strength measurements from a 2G, 3G and 4G live networks were fed to the algorithm, in order to detect possible crossed sector cases. An extensive set of tests was done in UK and Portugal areas, and some crossed sectors were detected, according to the Table I.

TABLE I
Leeds and Oporto cluster analysis.

Area	Technology	Number of Sites	Crossed Sectors
Leeds, UK	2G	276	8
Leeds, UK	3G	259	2
Leeds, UK	4G	192	3
Oporto, PT	4G	156	3

Three specific case studies will be analysed in the following. Firstly, a trisectorized site with a double crossed sector, then a bi-sectorized site single crossed sector situation and finally a trisectorized site but with missing radio signal strength measurements from one of the sectors.

A. Scenario 1 - Trisectorized Site

In this scenario it will be analysed a 4G trisectorized site, in Oporto, with two crossed sectors. The third sector is well configured. The main site topology and color description is defined in Table II. Fig. 4 presents the crossed sector thematic map.

As can be seen in Fig. 4, the green samples are in the correct area service, hence, the sector (PCI:8) is well defined.

TABLE II
Scenario 2 - Analysed site details.

Cell Name	Antenna azimuth	PCI	Color
CELL A	80°	6	Blue
CELL B	170°	7	Red
CELL C	350°	8	Green

Fig. 4. Best server thematic for scenario 1.

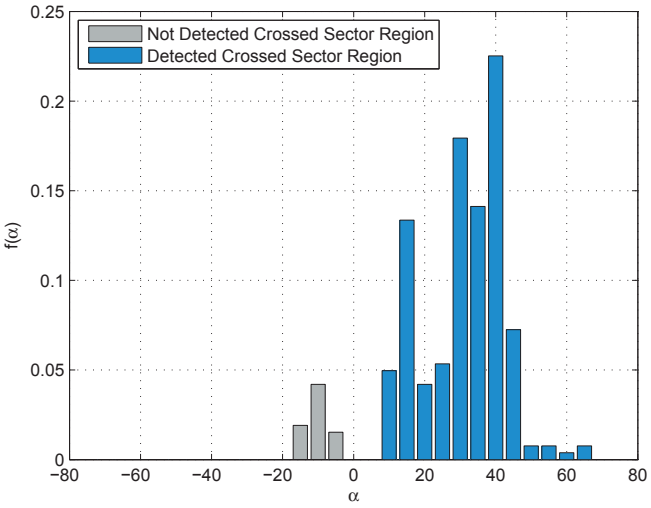

Fig. 5. α empirical probability density function for scenario 1.

Nevertheless, for the remaining sectors, the samples for each service area, do not correspond to the considered sector.

According to Section III, the empirical probability density function is presented in Fig. 5. From the histogram analysis it

is easily seen that most of the samples indicate crossed sector existence between blue (PCI:6) and red (PCI:7) sectors, since the occurrences are located in the positive side. Even so, there are also samples that indicate otherwise. These samples are located in the respective sector area service, but in smaller number. In order to decide and applying (6), the β_c and $\beta_{\overline{c}}$ distribution is created, see Fig. 6. It clearly suggests a scenario in which the blue sector is crossed with the red. In fact, the algorithm indicates that the blue sector is serving in a red sector area service. Additionally, the reverse process must be applied, *i.e.*, to verify if also the red sector is serving in the other area. In this scenario, as the green sector is well configured, the samples in its service area belong to the expected PCI. Finally, from Fig. 6, the β_c distribution suggests a probability of 0.97 in crossed sector detection, based on the available radio signal strength measurements.

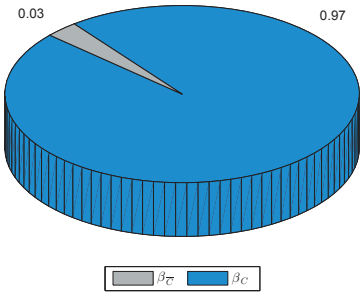

Fig. 6. β_c and $\beta_{\overline{c}}$ distribution function for scenario 1.

B. Scenario 2 - Bisectorized Site

In this scenario it will be analysed a 3G bisectorized site, in Leeds, with two crossed sectors. The site configuration, as antenna azimuth and Primary Scrambling Code (PSC), can be found in Table III.

TABLE III
SCENARIO 2 - ANALYSED SITE DETAILS.

Cell Name	Antenna azimuth	PSC	Color
CELL D	70°	184	Blue
CELL E	320°	185	Red

As in Fig. 7, the available samples in each service area do not match the corresponding sector. It is then expected that the algorithm can identify both crossed sectors. For the empirical probability density function of α visualization, see Fig. 8.

Most of the samples indicate a crossed sector situation between red (PSC:185) and blue (PSC:184) sectors, since most of the occurrences are located in the positive side. Contrary to the previous scenario, the analysed sectors are oriented in opposite azimuths, with a difference of 110°. Therefore, the difference between antenna gains and the difference between the received signal strength from sectors are greater. So, the α amplitude is is much higher. It is concluded that the red sector

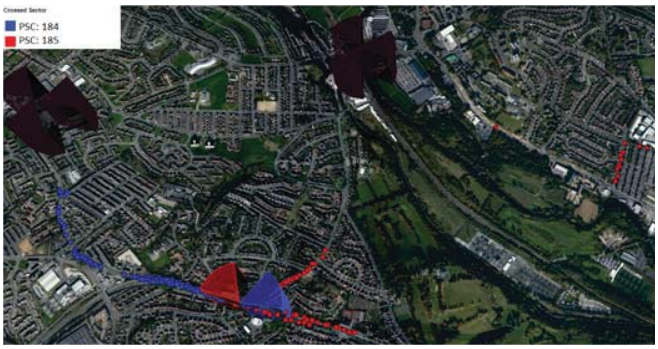

Fig. 7. Best server thematic for scenario 2.

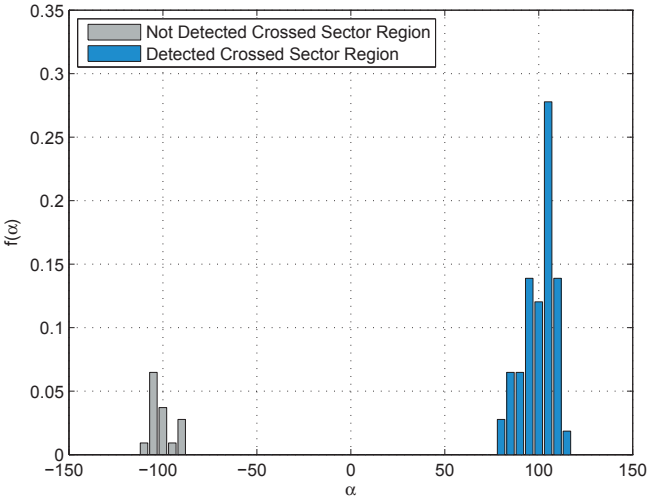

Fig. 8. α empirical probability density function for scenario 2.

is serving in the blue sector area service and vice-versa, as illustrated in Fig 9. The algorithm estimates a probability of 0.85 for a crossed sector scenario.

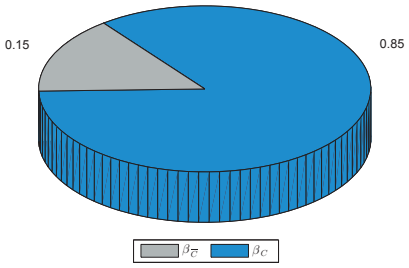

Fig. 9. β_c and $\beta_{\overline{c}}$ distribution function for scenario 2.

C. Scenario 3 - Trisectorized Site Without Samples

In this last scenario a 4G trisectorized site, also in Leeds, will be analysed, with two possible crossed sectors. However, one of them doesn't contain signal strength measurements, since a rural area with no roads exists through the northern

part of the site, see Fig. 10. The site configuration is displayed in Table IV.

TABLE IV
SCENARIO 3 - ANALYSED SITE DETAILS.

Cell Name	Antenna azimuth	PCI	Color
CELL F	0°	65	Green
CELL G	120°	63	Blue
CELL H	240°	64	Red

Fig. 10. Best server thematic for scenario 3.

According to Fig. 10, the samples in each service area do not correspond to the due sector. Furthermore, there are no available samples of the blue sector. Applying the algorithm, the usual decision chart is presented, in Fig. 11.

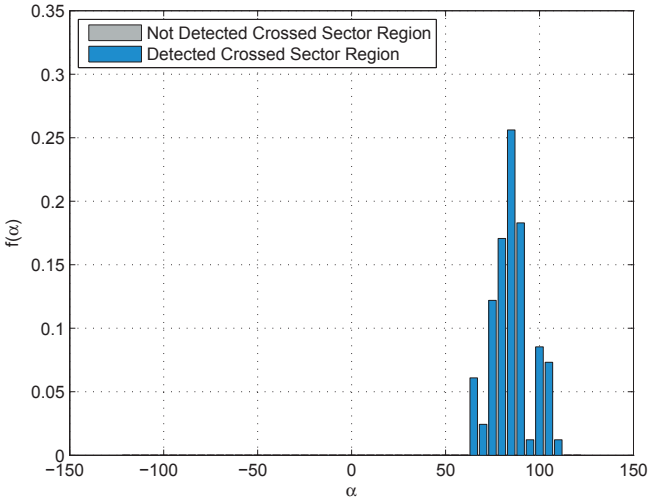

Fig. 11. α empirical probability density function for scenario 3.

All samples indicate the crossed sector between blue and red antennas, since the occurrences are located in the positive side. In other words, the algorithm stresses out that the red sector is dominant in the blue service area. However, unlike previous scenarios, the opposite does not occur. As there are no blue sector (PCI:63) samples, it is not possible to be sure that this is an effective crossed sector.

V. CONCLUSIONS

In this paper, an algorithm to detect crossed sectors is proposed. In order to identify these undesired cases, the algorithm uses strength signal measurements from DT, and information from mobile network operator topology, with the purpose of determining the antenna patterns.

The algorithm considers a statistical analysis, which supports the crossed sector detection with a certain degree of probability from empirical probability distribution functions. The algorithm performance was tested in real scenarios, both for bisectorized and trisectorized sites, as demonstrated in three scenarios above. Large-scale analysis was set in UK and Portugal areas, and 16 crossed sectors were detected within a universe of 883 sites. It is important to note that, the detected situations were reported to operators which did take the necessary correcting measures.

VI. ACKNOWLEDGEMENTS

This work was supported by the Instituto de Telecomunicações and the Portuguese Foundation for the Science and Technology (FCT) under GOLD (PEst-OE/EEI/LA0008/2013).

REFERENCES

[1] Cisco, "Cisco Visual Networking Index: Global Mobile Data Traffic Forecast Update, 2014-2019," Cisco, Tech. Rep., February 2015.
[2] 3GPP, "LTE; Evolved Universal Terrestrial Radio Access (E-UTRA) and Evolved Universal Terrestrial Radio Access Network (E-UTRAN); Overall description; Stage 2," 3rd Generation Partnership Project (3GPP), TR 36.300, Jul. 2010.
[3] D. Duarte, P. Vieira, A. Rodrigues, A. Martins, N. Oliveira, and L. Varela, "Neighbour List Optimization for Real LTE Radio Networks," in *Wireless and Mobile, 2014 IEEE Asia Pacific Conference on*, Aug 2014, pp. 183–187.
[4] "How to Analyze Crossed Feeder Issue by DT," Huawei Technologies Co., LTD., Tech. Rep., November 2008.
[5] F. Nascimento and P. Vieira, "A Field Measurement Approach for LTE (4G) Wireless Networks Performance Monitoring," in *Proc. Ibero-American Congress on Sensors - IBERSENSOR 2012*, Oct. 2012.

THE 18TH INTERNATIONAL SYMPOSIUM ON WIRELESS PERSONAL MULTIMEDIA COMMUNICATIONS
(WPMC-2015)
December 13-16, 2015, Hyderabad, India

Outage Analysis of Cellular Two-Way Relaying with Spectrum Sharing in Nakagami-*m* Fading

Ronshee Chawla, M. Mounika Reddy, and Prabhat K. Upadhyay
Discipline of Electrical Engineering
Indian Institute of Technology Indore
Indore, 452020, Madhya Pradesh, India
Email: rcronshee@gmail.com, maddhulamounikareddy@gmail.com, pkupadhyay@iiti.ac.in

***Abstract*—In this paper, we consider a cooperative spectrum sharing system in which primary communications take place bidirectionally with the assistance of one of the best-selected among multiple secondary users (relays) by using two-phase analog network coding protocol. Hereby, the primary system realizes a two-way cellular communication between a multi-antenna base station and a single-antenna mobile station. The best relay is selected based on minimizing the overall outage probability of the primary system. As such, we derive a tight expression for the overall outage probability of the primary system over Nakagami-*m* fading channels. We corroborate our analysis through numerical and simulation results, and provide valuable insights about the relay positioning and power allocation factor to ensure spectrum sharing.**

I. Introduction

Cognitive radio has emerged as a potential candidate to improve spectrum utilization efficiency in wireless networks [1]. Without causing any deleterious effect on primary transmissions, the unlicensed secondary users (SUs) are allowed to share the spectrum leased to primary users (PUs). Recently, cooperative spectrum sharing systems have been proposed by integrating relaying techniques with cognitive radio, and they have been shown to offer significant performance improvement under limited power and spectrum resources [2]-[4].

In an effort to further improve the efficiency of cooperative spectrum sharing systems, two-way relaying (TWR) approach [5] has been considered in [6]- [9], whereby one or more SUs can serve as relays to assist the primary communications. The authors in [6] have investigated a spectrum sharing system model with a decode-and-forward based TWR protocol. Recently, the concept of relay selection has been exploited in [7]-[9] to enhance system performance in combination with spectrum sharing. Moreover, in some of these works, analog network coding (ANC) [10] based TWR protocol has been used that allows bidirectional primary message exchange with spectrum sharing through an amplify-and-forward (AF) relay processing. More specifically, the authors in [9] have investigated the overall outage performance of a two-phase (2P) ANC-based spectrum sharing protocol with SU selection diversity in the absence of a direct link between two end PUs. Whereas, the authors in [11] and [12] have conducted single-user outage analysis of PUs by removing self-interference and mutual interference of the known primary signal and secondary signal respectively, followed by characterizing the spectrum sharing regions. However, all of these works have focussed on employing single-antenna devices at all nodes and their analyses are restricted to Rayleigh fading case only. Some of the earlier works have considered deploying multiple antennas at one of the end nodes to boost the performance of one-way relay [13], [14] and two-way relay [15] systems without spectrum sharing. To the best of our knowledge, the performance of 2P ANC-based cooperative spectrum sharing system with deployment of multiple antennas at the end-PU has not yet been analyzed, even for the case of Rayleigh fading. We emphasize hereby that such performance investigation over versatile Nakagami-*m* fading channels is mathematically more involved and important to understand the system behavior.

In this paper, we evaluate the performance of a 2P ANC-based cooperative spectrum sharing system under cellular scenario, wherein the bidirectional communication between a multi-antenna base station and a single-antenna mobile station is facilitated by one of the best selected among several SUs. Moreover, considering Nakagami-*m* fading channels, we derive a tight approximation for overall outage probability (OOP) of the primary system. Numerical and simulation results validate our theoretical analysis and provide useful insights about the relay location and power allocation factor to ensure spectrum sharing.

Notations: We use boldface lowercase letters to denote vectors, superscripts $(\cdot)^T$ and $(\cdot)^\dagger$ to denote transpose and complex transpose, respectively. $\mathbf{I}_N$ denotes the $N \times N$ identity matrix. $f_{\mathrm{X}}(\cdot)$ denotes the probability density function (PDF) of X. $\mathcal{CN}(\mu, \sigma^2)$ denotes a circular symmetric complex Gaussian random variable with mean μ and variance σ^2. $||\cdot||$ and $|\cdot|$ denote respectively the Frobenius norm and the absolute value, and $\binom{\cdot}{\cdot}$ denotes the binomial coefficient. $\Upsilon(\cdot,\cdot), \Gamma(\cdot,\cdot)$ and $\Gamma(\cdot)$ respectively represent the lower incomplete, the upper incomplete and the complete Gamma functions [16, eq. 8.350].

II. System and Channel Model

We consider a cooperative spectrum sharing system as shown in Fig. 1, where two end PUs T_a and T_b communicate bidirectionally with each other with the help of K SUs (relays) $S_k, k = 1, ..., K$, and S_e is secondary destination. The primary system may correspond to a cellular scenario, wherein T_a is a base station (equipped with N_a antennas) and T_b is a single-antenna mobile user. All the nodes are assumed to operate in

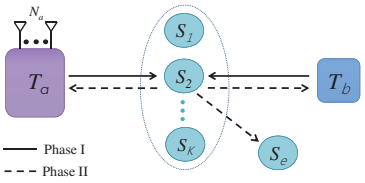

Fig. 1. Cellular two-way relay system with spectrum sharing.

a half-duplex manner and there is no direct link between T_a and T_b. We further assume that all channels are reciprocal, quasi-static and subject to independent block Nakagami-*m* fading. Let $\mathbf{h}_{a,k} = [h_{a,k}^1 h_{a,k}^2 ... h_{a,k}^{N_a}]^T$ denote the $N_a \times 1$ channel vector from T_a to S_k, $k = 1, ..., K$, where $\{h_{a,k}^l\}_{l=1}^{N_a}$ are independent and identically distributed (i.i.d.) Nakagami-*m* random variables with fading severity parameter m_a and average fading power Ω_a. Similarly, $h_{b,k}$ denotes the channel coefficient for the link between T_b and S_k, $k = 1, ..., K$, where $\{h_{b,k}\}$ are i.i.d. Nakagami-*m* random variables with fading severity parameter m_b and average fading power Ω_b. We also assume additive white Gaussian noise (AWGN) in each link with mean zero and variance unity. The transmit powers for T_a and T_b are assumed to be same and denoted by P.

The bidirectional communication between T_a and T_b occurs in two time phases by employing 2P ANC protocol with a single relay selection (say S_k). In the first phase, T_a and T_b simultaneously transmit their signals to the relay node S_k and the received signal is given by

$$y_k = \sqrt{P}\mathbf{h}_{a,k}^T \mathbf{w}_a x_a + \sqrt{P} h_{b,k} x_b + n_k, \tag{1}$$

where x_a and x_b are unit-energy transmit signals at T_a and T_b respectively, $\mathbf{w}_a$ is the transmit weight vector, chosen to be $\left(\frac{\mathbf{h}_{a,k}^\dagger}{||\mathbf{h}_{a,k}||}\right)^T$ for maximum-ratio-transmission at T_a, and n_k is the AWGN at S_k. During the second phase, the SU S_k allocates its transmit power P_R to combine its own signal x_e with the received signal y_k to generate

$$x_k = \beta_k y_k + \sqrt{(1-\mu)P_R} x_e, \tag{2}$$

where x_e has unit-energy and $\beta_k = \sqrt{\frac{\mu P_R}{P||\mathbf{h}_{a,k}||^2 + P|h_{b,k}|^2 + 1}}$, such that a fraction μ of power P_R is allocated for relaying primary signals and the rest for secondary transmission. Then, the S_k broadcasts this x_k signal to the primary and secondary terminals. The $N_a \times 1$ received signal at T_a can be given as

$$\mathbf{y}_a = \mathbf{h}_{a,k}\Big[\beta_k(\sqrt{P}||\mathbf{h}_{a,k}||x_a + \sqrt{P}h_{b,k}x_b + n_k) + \sqrt{(1-\mu)P_R}x_e\Big] + \mathbf{n}_a, \tag{3}$$

where $\mathbf{n}_a \sim \mathcal{CN}(\mathbf{0}, \mathbf{I}_{N_a})$ is the AWGN vector at T_a. For maximum-ratio-combining, the received signal $\mathbf{y}_a$ is multiplied by a $1 \times N_a$ receive weight vector $\mathbf{w}_a^T = \frac{\mathbf{h}_{a,k}^\dagger}{||\mathbf{h}_{a,k}||}$ and the resultant signal after self-interference cancellation is given by

$$\tilde{y}_a = \Big[\beta_k\sqrt{P}||\mathbf{h}_{a,k}||h_{b,k}x_b + \beta_k||\mathbf{h}_{a,k}||n_k + \sqrt{(1-\mu)P_R}||\mathbf{h}_{a,k}||x_e\Big] + \tilde{n}_a, \tag{4}$$

where $\tilde{n}_a = \frac{\mathbf{h}_{a,k}^\dagger \mathbf{n}_a}{||\mathbf{h}_{a,k}||} \sim \mathcal{CN}(0,1)$. Similarly, the signal received at T_b (after self-interference cancellation) is obtained as

$$\tilde{y}_b = \Big[\beta_k\sqrt{P}||\mathbf{h}_{a,k}||h_{b,k}x_a + \beta_k h_{b,k}n_k + \sqrt{(1-\mu)P_R}h_{b,k}x_e\Big] + \tilde{n}_b, \tag{5}$$

where $\tilde{n}_b \sim \mathcal{CN}(0,1)$ is the AWGN at T_b.

Thus, the resultant end-to-end signal-to-noise ratio (SNR) for transmission from T_b to T_a via S_k is given by

$$\gamma_{ba,k} = \frac{\mu P_R \mathrm{XY}}{(1-\mu)P_R\mathrm{X}^2 + (1-\mu)P_R\mathrm{XY} + \epsilon\mathrm{X} + \mathrm{Y}}, \tag{6}$$

and for transmission from T_a to T_b via S_k is given by

$$\gamma_{ab,k} = \frac{\mu P_R \mathrm{XY}}{(1-\mu)P_R\mathrm{Y}^2 + (1-\mu)P_R\mathrm{XY} + \epsilon\mathrm{Y} + \mathrm{X}}, \tag{7}$$

where $\mathrm{X} = ||\mathbf{h}_{a,k}||^2$, $\mathrm{Y} = |h_{b,k}|^2$ and $\epsilon = \left(\frac{P_R}{P} + 1\right)$.

III. Performance Analysis of the Primary System

In this section, we first derive a closed-form expression of overall outage probability (OOP) for the primary transmissions under Nakagami-*m* fading, and then investigate the condition for cooperative spectrum sharing.

A. Overall Outage Probability (OOP)

For the ANC protocol under consideration, the primary system is said to be in outage when either T_a or T_b is in outage. Therefore, the OOP for the bidirectional primary transmissions through the relay S_k can be given as

$$\mathcal{P}_{\mathrm{out},k}(\gamma_{\mathrm{th}}) = \Pr\left[\min\left(\gamma_{ab,k}, \gamma_{ba,k}\right) < \gamma_{\mathrm{th}}\right], \tag{8}$$

where γ_{th} is a predetermined threshold. Hereby, the relay can be chosen to maximize the worse of the two end-to-end instantaneous SNRs and is tantamount to minimize the OOP. As such, we can employ the best relay selection criteria as

$$k^* = \arg \max_{k \in \{1,2,...,K\}} \min\left\{\gamma_{ab,k}, \gamma_{ba,k}\right\}. \tag{9}$$

Based on the above formulation, we can apply order statistics to compute system OOP with best relay selection as

$$\mathcal{P}_{\mathrm{out}}(\gamma_{\mathrm{th}}) = \prod_{k=1}^{K} \mathcal{P}_{\mathrm{out},k}(\gamma_{\mathrm{th}}). \tag{10}$$

Hence, we first need to find $\mathcal{P}_{\mathrm{out},k}(\gamma_{\mathrm{th}})$ which can be splitted effectively into two parts as

$$\mathcal{P}_{\mathrm{out},k}(\gamma_{\mathrm{th}}) = \Pr\{\gamma_{ab,k} < \gamma_{\mathrm{th}}, \gamma_{ab,k} < \gamma_{ba,k}\} + \Pr\{\gamma_{ba,k} < \gamma_{\mathrm{th}}, \gamma_{ab,k} > \gamma_{ba,k}\}. \tag{11}$$

Using the expressions of $\gamma_{ba,k}$ and $\gamma_{ab,k}$ from (6) and (7) respectively, it can be readily shown that $\gamma_{ab,k} < \gamma_{ba,k}$ when $\mathrm{X} < \mathrm{Y}$ and vice-versa. Therefore, to proceed further with the analysis, the above expression becomes

$$\mathcal{P}_{\mathrm{out},k}(\gamma_{\mathrm{th}}) = \underbrace{\Pr\left\{\gamma_{ab,k} < \gamma_{\mathrm{th}}, \mathrm{X} < \mathrm{Y}\right\}}_{\mathcal{P}_1} + \underbrace{\Pr\left\{\gamma_{ba,k} < \gamma_{\mathrm{th}}, \mathrm{Y} < \mathrm{X}\right\}}_{\mathcal{P}_2}. \tag{12}$$

Let us now derive the expressions for $\mathcal{P}_1$ and $\mathcal{P}_2$. Starting with $\mathcal{P}_1$, we have

$$\mathcal{P}_1 = \Pr\left\{\mu P_R \mathrm{XY} < \gamma_{\mathrm{th}}(1-\mu)P_R \mathrm{Y}^2 + \gamma_{\mathrm{th}}(1-\mu)P_R \mathrm{XY} + \gamma_{\mathrm{th}}\epsilon \mathrm{Y} + \gamma_{\mathrm{th}} \mathrm{X}, \mathrm{X} < \mathrm{Y}\right\}, \tag{13}$$

which, after some simplifications, can be expressed as

$$\mathcal{P}_1 = \Pr\{X(Y\xi - \gamma_{\mathrm{th}}) < \gamma_{\mathrm{th}}(1-\mu)P_R Y^2 + \gamma_{\mathrm{th}}\epsilon Y, X < Y\}, \tag{14}$$

where $\xi = \mu P_R - \gamma_{\mathrm{th}}(1-\mu)P_R$. The evaluation of (14) can be performed under two feasible cases based on the power allocation factor μ as follows:

Case 1: If $\xi < 0$ or equivalently $0 < \mu < \frac{\gamma_{\mathrm{th}}}{1+\gamma_{\mathrm{th}}}$, the first inequality inside the curly brackets in (14) holds true irrespective of the values of X and Y (as X and Y are always positive) and hence, $\mathcal{P}_1$ for this case is given by

$$\mathcal{P}_1 = \Pr\left\{0 < \mathrm{Y} < \infty, 0 < \mathrm{X} < \mathrm{Y}\right\}. \tag{15}$$

Case 2: If $\xi > 0$ or equivalently $\mu > \frac{\gamma_{\mathrm{th}}}{1+\gamma_{\mathrm{th}}}$, the following two separate events can be formulated over X and Y:

- if $\mathrm{Y}\xi - \gamma_{\mathrm{th}} < 0$, the first inequality inside the curly brackets in (14) holds true regardless of the values of X and Y (always positive) and thus, the corresponding event is described by $\{0 < \mathrm{Y} < \delta, 0 < \mathrm{X} < \mathrm{Y}\}$, where $\delta = \frac{\gamma_{\mathrm{th}}}{\xi}$.
- if $\mathrm{Y}\xi - \gamma_{\mathrm{th}} > 0$, the first inequality inside the curly brackets in (14) reduces to $\mathrm{X} < \mathrm{g(Y)}$, where $\mathrm{g(Y)} = \frac{\gamma_{\mathrm{th}}(1-\mu)P_R \mathrm{Y}^2 + \gamma_{\mathrm{th}}\epsilon \mathrm{Y}}{\mathrm{Y}\xi - \gamma_{\mathrm{th}}}$. The joint event in this case is given by $\{\delta < \mathrm{Y} < \infty, 0 < \mathrm{X} < \lambda(\mathrm{Y})\}$, where $\lambda(\mathrm{Y}) = \min\{\mathrm{Y}, \mathrm{g(Y)}\}$.

Thus, for Case 2, the expression for $\mathcal{P}_1$ can be given by

$$\begin{aligned}\mathcal{P}_1 &= \Pr\{0 < \mathrm{Y} < \delta, 0 < \mathrm{X} < \mathrm{Y}\} \\ &\quad + \Pr\{\delta < \mathrm{Y} < \infty, 0 < \mathrm{X} < \lambda(\mathrm{Y})\}.\end{aligned} \tag{16}$$

We can further simplify $\lambda(\mathrm{Y})$ in (16), as it is either equal to Y or $\mathrm{g(Y)}$ depending upon the values of Y and the power allocation factor μ. So, after performing certain manipulations, $\lambda(\mathrm{Y})$ can be expressed as

$$\lambda(\mathrm{Y}) = \begin{cases} \mathrm{Y} & \text{for Case 2.1,} \\ \begin{cases} \mathrm{Y} & \text{for } \mathrm{Y} < \vartheta \\ \mathrm{g(Y)} & \text{for } \mathrm{Y} > \vartheta \end{cases} & \text{for Case 2.2,} \end{cases} \tag{17}$$

where Case 2.1: $\frac{\gamma_{\mathrm{th}}}{1+\gamma_{\mathrm{th}}} < \mu < \frac{\gamma_{\mathrm{th}}}{\frac{1}{2}+\gamma_{\mathrm{th}}}$, Case 2.2: $\frac{\gamma_{\mathrm{th}}}{\frac{1}{2}+\gamma_{\mathrm{th}}} < \mu < 1$, and $\vartheta = \frac{(\epsilon+1)\gamma_{\mathrm{th}}}{\mu P_R - 2\gamma_{\mathrm{th}}(1-\mu)P_R}$. Consequently, $\mathcal{P}_1$ for Case 2 can be obtained by substituting each of these sub-cases one-by-one in (16). On invoking Case 2.1 in (16), $\mathcal{P}_1$ reduces to

$$\begin{aligned}\mathcal{P}_1 &= \Pr\{0 < \mathrm{Y} < \delta, 0 < \mathrm{X} < \mathrm{Y}\} \\ &\quad + \Pr\{\delta < \mathrm{Y} < \infty, 0 < \mathrm{X} < \mathrm{Y}\} \\ &= \Pr\left\{0 < \mathrm{Y} < \infty, 0 < \mathrm{X} < \mathrm{Y}\right\},\end{aligned} \tag{18}$$

which coincides with the same result as presented in (15) for Case 1. Therefore, based on the conditions on μ, Case 1 and Case 2.1 can be combined together. Thereby, we can re-define the two cases and formulate the $\mathcal{P}_1$ accordingly as

Case 1: For $0 < \mu < \frac{\gamma_{\mathrm{th}}}{\frac{1}{2}+\gamma_{\mathrm{th}}}$, the expression of $\mathcal{P}_1$ can be presented using (15) and (18) as

$$\begin{aligned}\mathcal{P}_1 &= \Pr\left\{0 < \mathrm{Y} < \infty, 0 < \mathrm{X} < \mathrm{Y}\right\} \\ &= \int_{y=0}^{\infty}\int_{x=0}^{y} f_{\mathrm{X}}(x) f_{\mathrm{Y}}(y)\,\mathrm{d}x\,\mathrm{d}y.\end{aligned} \tag{19}$$

Case 2: For $\frac{\gamma_{\mathrm{th}}}{\frac{1}{2}+\gamma_{\mathrm{th}}} < \mu < 1$, the expression of $\mathcal{P}_1$ can be obtained by invoking Case 2.2 from (17) into (16) as

$$\begin{aligned}\mathcal{P}_1 &= \Pr\{0 < \mathrm{Y} < \vartheta, 0 < \mathrm{X} < \mathrm{Y}\} \\ &\quad + \Pr\{\vartheta < \mathrm{Y} < \infty, 0 < \mathrm{X} < \mathrm{g(Y)}\} \\ &= \int_{y=0}^{\vartheta}\int_{x=0}^{y} f_{\mathrm{X}}(x) f_{\mathrm{Y}}(y)\,\mathrm{d}x\,\mathrm{d}y + \int_{y=\vartheta}^{\infty}\int_{x=0}^{\mathrm{g}(y)} f_{\mathrm{X}}(x) f_{\mathrm{Y}}(y)\,\mathrm{d}x\,\mathrm{d}y.\end{aligned} \tag{20}$$

Now, we first evaluate $\mathcal{P}_1$ for Case 2 using (20). However, computation of the second integral term in (20) is not so straightforward since $\mathrm{g}(y)$ is a non-linear function in y. Therefore, in order to make the analysis tractable, we simplify $\mathrm{g}(y)$ for the case of large P_R as

$$\begin{aligned}\mathrm{g}(y) &= \frac{\gamma_{\mathrm{th}}(1-\mu)P_R y^2 + \gamma_{\mathrm{th}}\epsilon y}{y\xi - \gamma_{\mathrm{th}}} = \frac{\frac{\gamma_{\mathrm{th}}(1-\mu)P_R y^2}{\xi} + \frac{\gamma_{\mathrm{th}}\epsilon y}{\xi}}{y - \frac{\gamma_{\mathrm{th}}}{\xi}} \\ &\approx \delta(1-\mu)P_R y + \epsilon\delta,\end{aligned} \tag{21}$$

where $\delta = \frac{\gamma_{\mathrm{th}}}{\xi} << 1$ for large values of P_R.

Since the channel coefficients $\{h_{a,k}^l\}_{l=1}^{N_a}$ are assumed i.i.d. Nakagami-m random variables, the $\mathrm{X} = ||\mathbf{h}_{a,k}||^2$ follows Gamma distribution and hence the PDF of X is given by $f_{\mathrm{X}}(x) = \left(\frac{m_a}{\Omega_a}\right)^{m_a N_a} \frac{x^{m_a N_a - 1}}{\Gamma(m_a N_a)} e^{-\left(\frac{m_a}{\Omega_a}\right)x}$, $x \geq 0$. Likewise, the PDF of $\mathrm{Y} = |h_{b,k}|^2$ is given by $f_{\mathrm{Y}}(y) = \left(\frac{m_b}{\Omega_b}\right)^{m_b} \frac{y^{m_b-1}}{\Gamma(m_b)} e^{-\left(\frac{m_b}{\Omega_b}\right)y}$, $y \geq 0$. On substituting these PDFs along with approximation of $\mathrm{g}(y)$ from (21) into (20), and then simplifying with the aid of [16, eqs. 3.351.1, 3.351.2], we obtain $\mathcal{P}_1$ for Case 2 as

$$\mathcal{P}_1 = 1 - \mathcal{A}_1 - \mathcal{B}_1, \tag{22}$$

where

$$\mathcal{A}_1 = \frac{\left(\frac{m_b}{\Omega_b}\right)^{m_b}}{\Gamma(m_b)} \left[\sum_{m=0}^{m_a N_a - 1} \frac{\left(\frac{m_a}{\Omega_a}\right)^m}{m!} \left(\frac{m_a}{\Omega_a} + \frac{m_b}{\Omega_b}\right)^{-(m+m_b)} \times \Upsilon\left(m + m_b, \vartheta\left(\frac{m_a}{\Omega_a} + \frac{m_b}{\Omega_b}\right)\right)\right], \tag{23}$$

and

$$\mathcal{B}_1 = \frac{\left(\frac{m_b}{\Omega_b}\right)^{m_b}}{\Gamma(m_b)} e^{-\left(\frac{m_a}{\Omega_a}\right)\epsilon\delta} \sum_{m=0}^{m_a N_a - 1} \frac{\left(\frac{m_a}{\Omega_a}\right)^m}{m!} (\epsilon\delta)^m \times \sum_{l=0}^{m} \binom{m}{l} \left[\frac{(1-\mu)P_R}{\epsilon}\right]^l \frac{\Gamma(l + m_b, \vartheta\Theta_{ab})}{(\Theta_{ab})^{l+m_b}}, \tag{24}$$

with

$$\Theta_{ij} \triangleq \frac{m_i}{\Omega_i}\delta(1-\mu)P_R + \frac{m_j}{\Omega_j}, \tag{25}$$

for $i, j \in \{a, b\}$ and $i \neq j$.
Thus, from (19) and (22), $\mathcal{P}_1$ can be given as

$$\mathcal{P}_1 = \begin{cases} \int_{y=0}^{\infty}\int_{x=0}^{y} f_{\mathrm{X}}(x) f_{\mathrm{Y}}(y)\,\mathrm{d}x\,\mathrm{d}y & \text{for Case 1,} \\ 1-\mathcal{A}_1-\mathcal{B}_1 & \text{for Case 2,} \end{cases} \tag{26}$$

where Case 1: $0 < \mu < \frac{\gamma_{\mathrm{th}}}{\frac{1}{2}+\gamma_{\mathrm{th}}}$ and Case 2: $\frac{\gamma_{\mathrm{th}}}{\frac{1}{2}+\gamma_{\mathrm{th}}} < \mu < 1$.

Proceeding in a similar manner as for $\mathcal{P}_1$, we derive the expression for $\mathcal{P}_2$ which is given by

$$\mathcal{P}_2 = \begin{cases} \int_{x=0}^{\infty}\int_{y=0}^{x} f_{\mathrm{Y}}(y) f_{\mathrm{X}}(x)\,\mathrm{d}y\,\mathrm{d}x & \text{for Case 1,} \\ 1-\mathcal{A}_2-\mathcal{B}_2 & \text{for Case 2,} \end{cases} \tag{27}$$

where

$$\mathcal{A}_2 = \frac{\left(\frac{m_a}{\Omega_a}\right)^{m_a N_a}}{\Gamma(m_a N_a)}\left[\sum_{m=0}^{m_b-1}\frac{\left(\frac{m_b}{\Omega_b}\right)^{m}}{m!}\left(\frac{m_a}{\Omega_a}+\frac{m_b}{\Omega_b}\right)^{-(m+m_a N_a)} \times \Upsilon\left(m+m_a N_a, \vartheta\left(\frac{m_a}{\Omega_a}+\frac{m_b}{\Omega_b}\right)\right)\right], \tag{28}$$

and

$$\mathcal{B}_2 = \frac{\left(\frac{m_a}{\Omega_a}\right)^{m_a N_a}}{\Gamma(m_a N_a)} e^{-\left(\frac{m_b}{\Omega_b}\right)\epsilon\delta}\sum_{m=0}^{m_b-1}\frac{\left(\frac{m_b}{\Omega_b}\right)^{m}}{m!}(\epsilon\delta)^m \times \sum_{l=0}^{m}\binom{m}{l}\left[\frac{(1-\mu)P_R}{\epsilon}\right]^{l}\frac{\Gamma(l+m_a N_a, \vartheta\Theta_{ba})}{(\Theta_{ba})^{l+m_a N_a}}. \tag{29}$$

Finally, on substituting (26) and (27) into (12), and the result into (10), we get the required expression for OOP as

$$\mathcal{P}_{\mathrm{out}}(\gamma_{\mathrm{th}}) = \begin{cases} 1 & \text{for Case 1,} \\ [(1-\mathcal{A}_1-\mathcal{B}_1)+(1-\mathcal{A}_2-\mathcal{B}_2)]^K & \text{for Case 2.} \end{cases} \tag{30}$$

It is worthwhile to mention that our derived expression for OOP reduces to the result as presented in [9] for the special case of Rayleigh fading ($m_a = m_b = 1$) and single antenna at the base station ($N_a = 1$). Thereby, our analysis is more generalized and applicable over versatile Nakagami-*m* fading.

B. Spectrum Sharing Region

For the system under consideration, it requires that the OOP of the primary system must be lower than or equal to that for the direct transmission in order to facilitate spectrum sharing. That is,

$$\mathcal{P}_{\mathrm{out}}(\gamma_{\mathrm{th}}) \leq \mathcal{P}_{\mathrm{out}}^{\mathrm{DT}}(\gamma_{\mathrm{th}}), \tag{31}$$

where $\mathcal{P}_{\mathrm{out}}^{\mathrm{DT}}(\gamma_{\mathrm{th}})$ represents OOP of the primary system without spectrum sharing (direct transmission only). Let us consider that the direct link between T_a and T_b follows Nakagami-*m* distribution with fading severity parameter m_0 and average fading power Ω_0. Therefore, the OOP $\mathcal{P}_{\mathrm{out}}^{\mathrm{DT}}(\gamma_{\mathrm{th}})$ can be given by

$$\mathcal{P}_{\mathrm{out}}^{\mathrm{DT}}(\gamma_{\mathrm{th}}) = \frac{1}{\Gamma(m_0 N_a)}\Upsilon\left(m_0 N_a, \frac{m_0\gamma_{\mathrm{th}}}{\Omega_0 P}\right). \tag{32}$$

The condition for spectrum sharing in (31) can be re-expressed using (30) and (32) as

$$[(1-\mathcal{A}_1-\mathcal{B}_1)+(1-\mathcal{A}_2-\mathcal{B}_2)]^K \leq \frac{\Upsilon\left(m_0 N_a, \frac{m_0\gamma_{\mathrm{th}}}{\Omega_0 P}\right)}{\Gamma(m_0 N_a)}, \tag{33}$$

wherein $\frac{\gamma_{\mathrm{th}}}{\frac{1}{2}+\gamma_{\mathrm{th}}} < \mu < 1$. As evident from (22), (27) and (33), it is difficult to obtain the exact solution for optimal power allocation factor μ^* to ensure spectrum sharing and therefore, it should be computed using standard numerical methods.

IV. Results and Discussions

In this section, we carry out numerical studies for the outage performance of the primary system as described previously and substantiate our analysis with Monte Carlo simulations. We adopt the path loss model with the exponent $\nu = 4$ and consider the distance between T_a and T_b as d_0, the distance between T_a and S_k as d_1, and that between T_b and S_k as d_2, for all k. Thus, we have $\Omega_a = d_1^{-4}$, $\Omega_b = d_2^{-4}$, and $\Omega_0 = d_0^{-4}$. Also, the distances d_0, d_1, and d_2 are normalized such that $d_0 = d_1 + d_2 = 1$. For all the analytical plots (except the curve marked with $\triangleleft$ sign), we have considered $P_R = P$.

Fig. 1 plots the outage performance of the primary system as a function of SNR (P/σ^2) for various values of N_a. Here, we set $K = 4$, $m_a = m_b = 1$, and $\gamma_{\mathrm{th}} = 2$ dB. As can be observed, our analytical and simulation results are in well agreement with each other, especially in the mid to high SNR region. Though, a slight gap exists in the low SNR region due to the approximation of integral limit in (20) with a large P_R assumption. Further, the curves are shown to attain outage floor at high SNRs, suggesting an absence of diversity. Also, it can be seen that reliable communication is sustained when N_a is increased from 1 to 2. However, the outage performance degrades when N_a is increased to 3. Thus, we have two ways to improve outage performance, that is either to increase P_R or to allocate more power to primary transmissions by increasing μ. It is evident that there is little improvement in the outage performance when P_R is increased by 10 times, whereas the OOP reduces drastically when μ is increased from 0.9 to 0.95. Based on these observations, one can infer that the power allocation factor μ plays a critical role for the considered 2P ANC-based spectrum sharing system.

Fig. 2 shows the variation of OOP with power allocation factor μ for different pairs of distances, where we have fixed $K = 3$, $N_a = 1$, $P_R = P = 10$ dB, $m_0 = 1$, and $\gamma_{\mathrm{th}} = 2$ dB. As can be seen, the analytical curves match with the simulation results. All the solid plots corresponding to $m_a = m_b = 1$ are the same as [9, Fig. 2] and have been reproduced here for making comparison with our results. It can be observed that keeping other parameters fixed (comparing all the solid lines), the system attains the lowest OOP when the selected

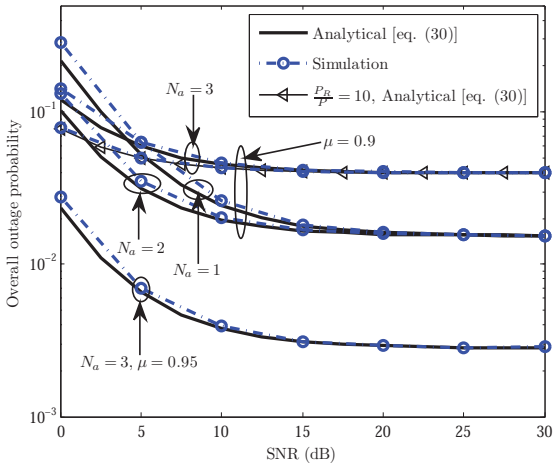

Fig. 2. Overall outage performance versus SNR for different values of N_a.

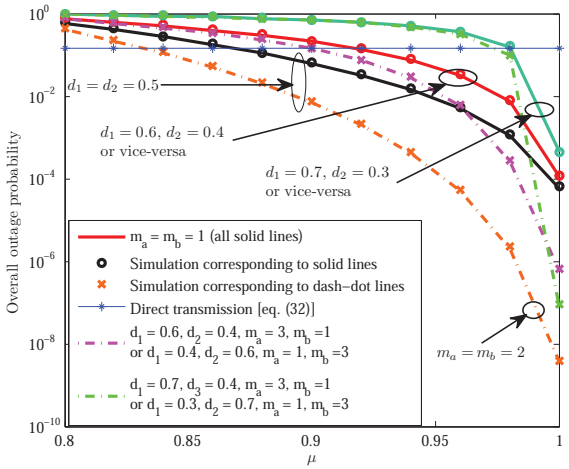

Fig. 3. Overall outage performance versus power allocation factor μ.

relay is placed at the middle of T_a and T_b, which can be further reduced as the fading severity reduces (referring to $m_a = m_b = 2$). Also, there exists an optimal power allocation threshold μ^* for all pairs of distances, which can be fetched at the intersection point with direct transmission curve. For instance, the optimal allocation threshold when $d_1 = d_2 = 0.5$ and $m_a = m_b = 2$ is $\mu^* \approx 0.832$, suggesting that the considered primary system (with spectrum sharing scheme) can achieve better performance than the direct transmission (without spectrum sharing) when $\mu^* < \mu < 1$. Furthermore, it is clearly visible that for $d_1 = d_2 = 0.5$, μ^* reduces from 0.868 when $m_a = m_b = 1$ to 0.832 when $m_a = m_b = 2$. In other words, the spectrum sharing region is increased when the fading severity gets reduced for both the links ($T_a \rightarrow S_{k^*}$ and $S_{k^*} \leftarrow T_b$) in this case. Moreover, for unbalanced cases, when the relay is not exactly at the middle of the two primary nodes, spectrum sharing region is enhanced if there is a reduction in fading severity over the longer link. As an example, when $d_1 = 0.6, d_2 = 0.4$, the outage performance is limited by the link $T_a \rightarrow S_{k^*}$. Thus, when $m_a > m_b$, the OOP is reduced and the spectrum sharing region is increased.

V. Conclusion

We evaluated the performance of a 2P ANC-based cooperative spectrum sharing system under cellular scenario. Specifically, a tight approximation to overall outage probability for the primary system is derived for Nakagami-*m* fading channels. Our results showed that an outage floor appears in the high SNR regime. The multiple antennas at one end PU help improving the outage performance when the relay allocates sufficiently high power for primary transmissions. Moreover, we have attained valuable insights for relay positioning and power allocation factor to ensure spectrum sharing under various fading conditions.

Acknowledgment

This research work was supported by SERB, DST, Govt. of India (Project no. SERC/ETA-0325/2012).

References

[1] S. Haykin, "Cognitive radio: Brain-empowered wireless communications," *IEEE J. Sel. Areas Commun.*, vol. 23, no. 2, pp. 201-220, Feb. 2005.

[2] Y. Zou, J. Zhu, B. Zheng, and Y. Yao, "An adaptive cooperation diversity scheme with best-relay selection in cognitive radio networks," *IEEE Trans. Signal Process.*, vol. 58, no. 10, pp. 5438-5445, Oct. 2010.

[3] Y. Han, S. H. Ting, and A. Pandharipande, "Cooperative spectrum sharing protocol with selective relaying system," *IEEE Trans. Commun.*, vol. 60, no. 1, pp. 62-67, Jan. 2012.

[4] P. K. Sharma, S. Solanki, and P. K. Upadhyay, "Outage analysis of cognitive opportunistic relay networks with direct link in Nakagami-m fading," *IEEE Commun. Lett.*, vol. 19, no. 5, May 2015.

[5] B. Rankov and A. Wittneben, "Spectral efficient protocols for half-duplex relay channels," *IEEE J. Sel. Areas Commun.*, vol. 25, no. 2, pp. 379-389, Feb. 2007.

[6] Q. Li, S. H. Ting, A. Pandharipande, and Y. Han, "Cognitive spectrum sharing with two-way relaying systems," *IEEE Trans. Veh. Technol.*, vol. 60, no. 3, pp. 1233-1240, Mar. 2011.

[7] S. Yadav and P. K. Upadhyay, "Performance analysis of cognitive spectrum sharing with time division broadcast protocol," *IEEE Commun. Lett.*, vol. 18, no. 2, pp. 305-308, Feb. 2014.

[8] K. B. Fredj and S. Aïssa, "Performance of spectrum-sharing constrained two-way relaying," in *Proc. IEEE WCNC*, Istanbul, Turkey, Apr. 2014, pp. 845-850.

[9] L. Yang, M.-S. Alouini, and K. Qaraqe, "On the performance of spectrum sharing systems with two-way relaying and multiuser diversity," *IEEE Commun. Lett.*, vol. 16, no. 8, pp. 1240-1243, Aug. 2012.

[10] S. Katti, S. Gollakota, and D. Katabi, "Embracing wireless interference: Analog network coding," in *Proc. 2007 ACM SIGCOMM*, pp. 397-408.

[11] Y. Li, H. Long, M. Peng, and W. Wang, "Spectrum sharing with analog network coding," *IEEE Trans. Veh. Technol.*, vol. 63, no. 4, pp. 1703-1716, May 2014.

[12] Y. Li, T. Wang, M. Peng, and W. Wang, "On the outage probability of cognitive two-way relaying based on superposition coding," *Proc. IEEE VTC-Spring*, Seoul, May 2014, pp. 1-5.

[13] S. S. Ikki and S. Aïssa, "A study of optimization problem for amplify-and-forward relaying over Weibull fading channels with multiple antennas," *IEEE Commun. Lett.*, vol. 15, no. 11, pp. 1148-1151, Nov. 2011.

[14] L. Sun, T. Zhang, H. Niu, and J. Wang, "Effect of multiple antennas at the destination on the diversity performance of amplify-and-forward systems with partial relay selection," *IEEE Signal Process. Lett.*, vol. 17, no. 7, pp. 631-634, Jul. 2010.

[15] P. K. Upadhyay and S. Yadav, "On the performance of cellular two-way relay systems with analog network coding and multiuser diversity," *Wireless Pers. Commun.*, vol. 72, no. 4, pp. 2705-2720, Oct. 2013.

[16] I. S. Gradshteyn and I. M. Ryzhik, *Tables of Integrals, Series and Products*, 6th ed. New York: Academic Press, 2000.

THE 18TH INTERNATIONAL SYMPOSIUM ON WIRELESS PERSONAL MULTIMEDIA COMMUNICATIONS
(WPMC-2015)
December 13-16, 2015, Hyderabad, India

DEAR: An Energy-centric Adaptive Region of Interest Mechanism for Wireless Mobile Devices

Hrishikesh Venkataraman[1], Ting Bi[2], Ting Wu[2] and Gabriel-Miro Muntean[2]
[1] Center for Smart Cities, Indian Institute of Information Technology (IIIT), Chittoor, Sricity, AP, India
[2] Performance Engineering Laboratory, Dublin City University (DCU), Glasnevin, Dublin 9, Ireland
Email: [1] hvraman@iiits.in [2] gabriel.muntean@dcu.ie

Abstract— **Multimedia-centric and graphic-intensive applications running on a mobile device consume high amounts of energy, resulting in shorter battery life. Importantly, there is still not enough work done in developing energy-aware solutions to prolong the battery life of devices without affecting the quality of the distributed video/multimedia content. In this context, this paper proposes *DEAR* - a device energy-centric adaptive region-of-interest quality-based mechanism, whereby the displayed video quality is varied dynamically depending on both user interests in the content and device battery level. Notably, user region-of-interests in video frames and device screens are considered and different quality levels are associated by altering dynamically both the video content properties (data-rate) and device display characteristics such as brightness and backlight. The energy consumption is measured using an Arduino board while video quality is analyzed using extensive subjective tests. The results indicate that up to 53% energy could be saved in the device while retaining above average perceptual video quality.**

Keywords - ***Bit-rate, brightness, backlight, region-of-interest, video streaming***

I. INTRODUCTION

Over the last years, with the advent of mobile Internet and smart-phones, there has been an exponentially increasing demand by the mobile users to support real-time multimedia delivery to their wireless mobile devices. However, multimedia and graphic-intensive applications consume significant amounts of energy when running on these devices, thereby resulting in reducing their overall battery life. There have been some efforts on finding different possible and efficient solutions for decreasing the energy consumption, while playing video and also at the same time, maintain video stream quality at high levels [1-4].

A particularly interesting concept that has been introduced is the region-of-interest (RoI)-awareness for video content. RoI indicates a specific video-frame region that is of greater interest to the viewers as compared to other frame regions [5]. In reality, it is very difficult to judge the exact RoI, though it is held that the viewer's eyes focus changes from the center of the screen to the screen edge. The goal of our research is to minimize the energy consumption in the device, without affecting the overall video perceived quality.

This work proposes **DEAR - a device energy-centric adaptive region-of-interest quality-based mechanism** which adjusts energy consumption in wireless mobile devices. This energy adjustment is based on adaptively varying RoI display properties in both device screen and video content in such a way that it remains largely imperceptible to the end-user.

The paper is organized as follows. Section II discusses related works on different aspects of RoI. Section III introduces the proposed DEAR algorithm and explains its different aspects in detail. Further, section IV describes testing methodology and scenarios, and presents the results of different tests. Finally, section V concludes the paper and provides some future research directions.

II. RELATED WORK

Recent noteworthy techniques in optimizing energy consumption of video applications consider different aspects of RoI. Among these are RoI-based video adaptive solutions whose essential idea is to display the region of the screen where the user is more likely to focus on at higher quality than the surrounding areas. For example, while watching a tennis match, the viewer may be most interested in looking at the area around the ball (though this may not be the case for all videos). However, in reality, there are always regions in every video frame on which users focus more, as compared to other frame areas. It has been shown in [6] that by adapting a high-resolution window at the point-of-gaze and low-resolution window in the peripheral areas, the users had longer initial saccadic latencies in peripheral areas as compared to the scenario wherein a low resolution was uniformly displayed across the whole screen of the device. Importantly, it was found in [7] that in order to maintain a particular user-perceived video quality, if the degradation is increased in the peripheral areas, the size of the adapted high-resolution window would also have to be increased at the point of gaze. Recently, a scalable RoI (SROI) was proposed which supports fine grained granularity adaptation in RoI with low computing complexity [8]. Further, a RoI adaptive delivery scheme (ROIAS) is proposed and a detailed objective and subjective assessment and analysis has been carried out for RoI-aware adaptive streaming [9, 10]. However, the adaptation focused mainly on network-related aspects to control RoI quality adaptation. The adaptations are done in order to realize better video quality both objectively and subjectively. In principle, there are numerous techniques for discovering RoI in a video including eye-tracking (with cameras),

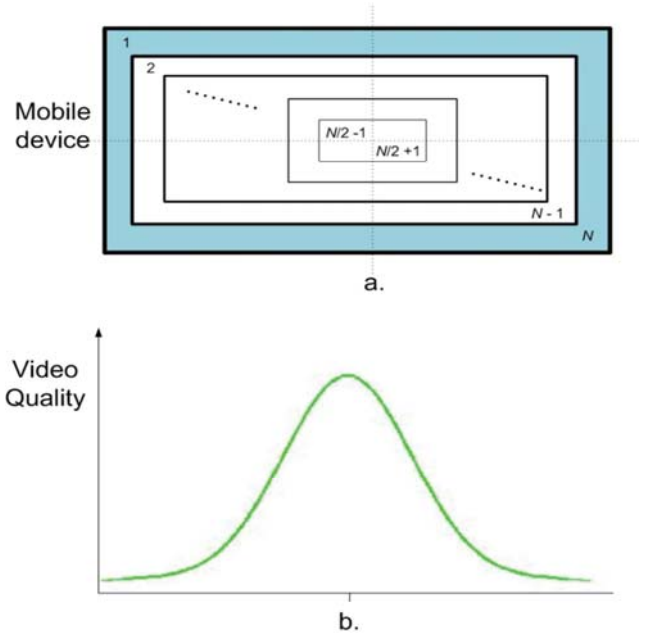

Fig. 1 Region of Interest (RoI) adaptation in screen
(1a) A *N*-step RoI in the mobile screen
(1b) Variation in video quality from the centre of screen

video processing and analysis. However, most of these mechanisms add significant complexity to the solution, focus on a single RoI, are network delivery-oriented or involve additional hardware. To the best knowledge of the authors, there has been no work on adaptively varying the number of RoI considered and investigating from the energy perspective. The next section proposes an adaptive RoI mechanism and discusses the associated potential energy savings in the device.

III. DEAR – RoI-based Video Adaptive Solution

This section describes the proposed DEAR - a novel dynamic adaptive video mechanism for real-time adjustment of the energy consumption in the mobile device. This involves having a RoI-based video adaptation in the device, wherein certain highly interesting regions of the video frame are displayed with the best video quality whereas other less-interesting regions are provided at a reduced video quality. Fig. 1 illustrates the mechanism. In this case, it is assumed that the viewer's area of most interest is in the centre of the video frame and hence, the highest quality video is shown at the centre of the device screen. Further, as the distance from the centre of the screen is increased, an ideal scenario would be to gradually decrease the video quality using a normal distribution, as shown in Fig. 1b. This is done by changing several parameters in both the device and in the video/multimedia content transmitted to the device. In order to realistically achieve a gradual degradation in the video quality, multiple-RoIs are considered for the device screen and multimedia frame, as shown in Fig. 1a. The multiple RoIs approach has as main advantage the fact that each RoI can be considered independently. This enables treating and adjusting different parameters (brightness, backlight/colour, etc.) across each region independently. Notably, multiple RoI control provides support for smoother video quality adjustments that would be almost imperceptible to the user. There are two major aspects in the design of DEAR: setting the RoIs and setting the parameters to adjust across the RoIs. Both these aspects play a major role in determining the real-time energy consumption of device.

3.1 Setting RoIs: Typically, the video played in RoI screen areas is at higher quality than that played in non-RoI zones. This result in the video played in RoI areas consuming higher energy as compared to that played in non-RoI zones. DEAR considers multiple RoIs with different quality levels. Consequently they will have different energy readings. The overall energy consumed by mobile device employing DEAR can be adjusted by varying two major parameters: the number of RoIs (N) and the area (A_x) of each RoI x of the N RoIs.

3.2 Parameters to Adjust across Different RoIs Several parameters related to both the video content and device screen affect the energy consumption of the device. They include:

i. Data rate of the video/multimedia content (R)
ii. Brightness/gamma of the screen (G)
iii. The backlight intensity of the device screen (B)
iv. The colour displayed in the screen (C)
v. Frame rate of the video/multimedia content (F)

The energy consumed in the device can be altered by adjusting the values of one or more of these parameters. As DEAR considers multiple RoIs, DEAR adaptation requires that each RoI be considered and controlled independently in terms of data rate, brightness, colour, backlight, etc. As changing some of these parameters for areas within a frame, particularly frame rate and the colour of the video content is either extremely challenging or very complex, DEAR adjusts only the first three variables (R, G, B) per RoI in real-time.

The principle of DEAR adaptation algorithm can be understood from the detailed flowchart shown in Fig. 2. The initial values of parameters are first set. Subsequently, the video quality is measured and ensured to be above the fair value (3.0 as per ITU-T P. 913 standard [13], refering to user subjective quality), Further, a two-step approach is adopted. In the first step, the actual video quality is measured; while in the second step, the energy consumption in each RoI is varied. To begin with, only one RoI is considered and different parameters associated with this RoI are varied. Depending on the situation, the following is carried out:

i. If the energy consumption of the screen is very high (above a threshold) relative to the current device battery level, then the number of RoIs is changed (increased or decreased). The parameters associated with the RoIs are modified to reduce energy consumption and the energy consumption is then measured again. This process is repeated iteratively.

ii. If the energy consumption of the screen is low (below a threshold) relative to the current device battery level, the values of the different parameters are such varied to increase the quality of RoIs in the order **o**f increasing their distance to the centre of the video frame. If two RoIs have

the same values for the parameters, they will be merged and the number of RoIs decreases.

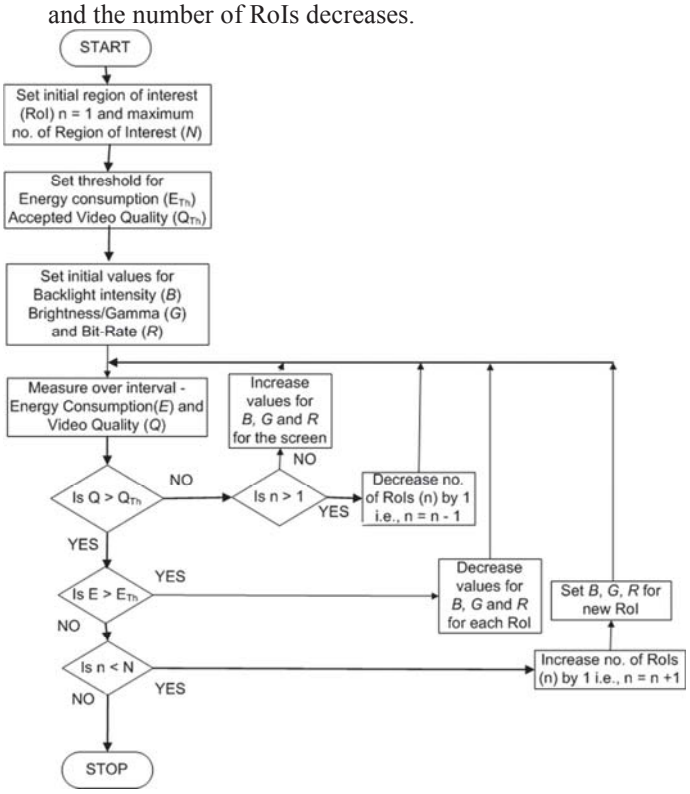

Fig. 2 Overview of the DEAR algorithm

3.3 Energy Consumption Analysis: For DEAR with N RoIs (shown in Fig. 1a), energy consumption of each RoI x is Es_x where $x \in \{1, N\}$. If As_x is the area of RoI x, the total energy consumption relative to entire screen size (divided in RoIs) is:

$$E = \sum_{x=1}^{N} Es_x \, As_x \qquad (1)$$

Further, the energy consumption for each RoI (Es_x) is a function of the above mentioned different variables. This could be written as in equation (2) or as in equation (3) when considering the parameters most feasible to be adjusted only:

$$Es_x = f(Rs_x, Gs_x, Bs_x, Gs_x, Cs_x, , Fs_x) \quad (2)$$
$$Es_x = f(Rs_x, Gs_x, Bs_x) \qquad (3)$$

In equations (2) and (3), Rs_x, Gs_x, Bs_x Cs_x and Fs_x represent the video bit rate, brightness, backlight intensity, display colour and video frame rate associated with a particular RoI x. In case of non-RoI zones, the energy consumption is the same across the whole area and can be written as in (4) or (5) if only the selected parameters are considered.

$$Es = f(Rs, Gs, Bs, Cs, Fs) \qquad (4)$$
$$Es = f(Rs, Gs, Bs) \qquad (5)$$

In equations (4) and (5), Rs, Gs, Bs, Cs and Fs represent video bit rate, brightness, backlight intensity, display colour and video frame rate associated with non-RoI. If the non-RoI adaptive approach is considered, the energy consumption across the entire non-RoI video frame could be written as:

$$E_{non\text{-}RoI} = N \, Es \qquad (6)$$

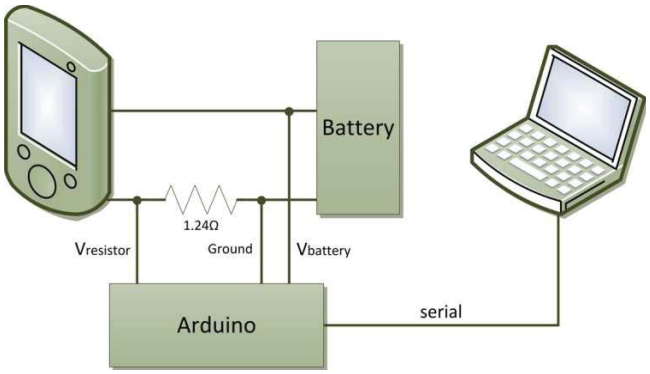

Fig. 3 Schematic representations for measuring energy consumption in mobile device

It should be noted that a change in any variable results in a change in the energy consumption of the device screen (in fact, of the area of the screen affected). Hence, considering the energy consumption modification due to each variable change to be independent, the difference in the energy consumption in the screen due to DEAR (as compared to a non-RoI approach) could be written as:

$$\Delta E = \Delta E_R + \Delta E_G + \Delta E_B \qquad (7)$$

In order to investigate the potential amount of energy savings due to RoI, the different parameters that affect the design are considered separately. Further, varying each parameter individually, the effect on the energy consumption is studied along with the effect on the overall video quality. In the next section, non-RoI and multiple RoIs approaches are considered with changes in only one parameter and the difference in the energy consumption is then measured.

IV. Scenarios, Testing and Results

The goal of the experimental tests is to adjust the video display at the mobile device using DEAR algorithm. However, in order to assess both the energy consumption and the video quality, only one parameter is varied at a time and its effect is measured. Further, the energy consumption in the mobile device is measured and compared with a non-RoI approach. Notably, for each experiment, the average video quality is observed using a subjective method. This is done in order to ensure that in the process of optimizing the energy consumption in the device, the video quality is maintained at an acceptable level.

4.1 Experimental Set-up: The experimental set-up employed is shown in Fig. 3. The device used is Samsung Galaxy GT-I5500 mobile phone, (Android 2.3, 2.8 inch LCD touch screen with 320 x 240 pixels, battery capacity of 1200mAh). The reason for selecting a low-end smart-phone is because, it is expected that all smart-phone users will have this or a better smart-phone. The energy consumption of the device is measured using Arduino – an open source micro-controller board [11]. The Arduino board can receive multiple types of input signals and can be connected between the device and device battery. Arduino board supports USB connections and hence all measurements are logged onto a laptop via USB. The Arduino board measures the energy consumed while playing a video only. Hence, in order to calculate the energy saved due

to the use of the proposed DEAR algorithm, the energy consumption is first measured for the idle state/flight mode. Once the baseline consumption of device is known (E_{base}) and the energy consumption of device during the video playing is measured (E_{play}), the energy cost of video playing can be calculated as $E_{play} - E_{base}$. The set-up for carrying out the energy measurements is based on a similar set-up for measuring the energy of different components in the device, as explained in [12, 13].

There are two different video clips considered in the experimental set-up. The first video clip *video1* is a 15-second trailer of the movie *Toy-Story* that is encoded using MPEG4 at 301 kbps. The second video clip *video2* is an 18-second trailer of the movie *Harry Potter* which is also encoded using MPEG-4 at a rate of 180 kbps. It should be noted that *Toy-Story* has a lower contrast ratio, higher brightness, higher gamma level and higher data rate as compared to *Harry Potter*. The reason for selecting the second video is to test the difference in the energy consumption, especially if and when the energy savings is considerably higher for variation in DEAR design.

The tests measure the energy consumed in the device for different videos and for different scenarios. For each scenario, the average video quality is determined by a subjective analysis on a scale of 1-5 (mean opinion score, standardized by ITU-T) that provides a scale for perceived video quality from user's perspective [14].

4.2 Scenarios and Results

Table 1 Variation in energy consumption and average video quality for different data rates

Sr. No.	No. of RoIs	Data Rate (Kbps)	Energy (mW)	Quality (1-5)
1.1	No RoI (Full screen)	180	251.88	4.93
1.2		128	243.76	4.35
1.3		64	241.03	3.02
2.1	1 RoI (Pixel Area: 160x90)	RoI: 180 Non-RoI: 128	245.97	3.93
2.2			241.97	3.70
3.1	1 RoI (Pixel Area: 90x90)	RoI: 180 Non-RoI: 128	246.13	3.65
3.2			241.36	3.50

4.2.1 Varying Data-Rates: This test is performed with 90% device brightness. A multiple concurrent RoI area is considered with different data rates across different RoIs. The RoIs are assumed to be concentric at the centre of the screen. Given the screen size of hand-held device (320x180 pixels), two different situations are considered. The first situation sees a RoI bounded by a rectangle of size 160x90 pixels, whereas in the second case, the RoIs are bounded by a square of 90x90 pixels area. Further, two different data rates are considered for the out-of-RoI area of the screen. The first data rate considered is 128 kbps while the second data rate considered is 64 kbps.

Table 1 shows the results of the energy consumption and the subjective video quality, across both a complete frame and a frame having both RoI and non-RoI areas. As the data rate is decreased, the overall quality also decreases (e.g. scenario 1.1 and 1.3). Importantly, this pattern remains consistent even when there are different data rates across different RoIs in the frame. Notably, if one compares a non-RoI frame with 64 kbps (scenario 1.3) with two frames containing two different RoIs patterns (128 kbps across non-RoI area, scenario 3.1), it can be observed that a reduction in data rate across non-RoI area gives the same energy consumption, while the quality of the video is slightly improved (3.5 instead of 3.02). Notably, only up to 4% savings in energy consumption could be obtained while still retaining quality above 3.0.

Table 2 Variation in energy consumption and average video with variation in brightness/gamma

Sr. No.	No. of RoIs	Brightness@ RoI & non-RoI	Energy Consumed (mW)	Video Quality
1.1	No RoI	100% brightnes	266.15	4.15
1.2	No RoI	80% brightness	258.93	3.71
1.3	No RoI	60% brightness	253.93	3.32
1.4	No RoI	40% brightness	248.53	2.71
2.1	1 RoI	RoI: 100% Non RoI: 80%	256.79	3.82
2.2	1 RoI	RoI: 100% Non RoI: 60%	253.03	3.42
3.1	4 RoIs	RoI:(100,75,50,25)% Non RoI: 1%	241.34	4.11
4.1	9-RoIs	RoI: (100,90,.., 20)% Non-RoI: 10%	249.76	4.04
5.1	19-RoIs	RoI:(100,95,....,10)% Non-RoI: 5%	243.43	3.96

4.2.2 Varying Brightness/Gamma: In these tests, DEAR algorithm with different brightness/gamma levels for different RoIs is considered. The brightness/gamma decreases from 100% for RoI at the centre of the screen to low levels at RoIs further from the centre, with a minimum value of screen brightness at the screen edge. Table 2 shows the effect of this reduction on the energy consumption and resulting video quality levels when DEAR with multiple RoIs and different brightness/gamma levels is employed; in comparison with non-RoI adjustment of the brightness across whole screen area. A non-RoI video with 100% brightness across entire screen has a very high video quality (4.15) and consumes 266.15 mW. On the other hand, a non-RoI video with 40% of maximum brightness value reduces energy consumption by roughly 7% (248.53 mW) only, while it decreases the video quality drastically by more than 33%. Hence, reducing brightness across the whole screen is not a good option. Hitherto, a RoI-based reduction in brightness/gamma results in significant decrease in energy consumption, while maintaining good video quality. For example, having 19 RoIs with decreasing brightness levels (100 to 10 in steps of 5%) for different RoIs and even lower brightness (5%) for non-RoI area results in energy consumption of 243.43 mW (9% decrease in energy consumption as compared to non-RoI approach with 100% brightness), and the video quality reduces by less than 4%. This shows that device energy consumption could be reduced by employing DEAR-based variation focusing on the brightness with negligible effect on quality.

4.2.3 Varying Backlight: The wireless devices/smart-phones that exist today do not allow variable backlight across different regions of the device. In order to investigate the potential benefit of varying backlight across different *regions,* the energy consumption of the device was measured for different backlight intensities. In order to measure the effect of different backlight levels on the energy consumption of the device and the overall video quality, a linear reduction in the device backlight is considered in the tests. The backlight is reduced from 100% to 25%. Table 3 shows the energy consumption and average subjective video quality when the brightness of the device is varied from 100% to 25%. It can be observed from Table 3 that in case of video1, decreasing the backlight to 50% reduces the energy consumption by 30% while decreasing the backlight to 25% reduces the energy consumption by 36%. The video quality reduces by only 1.6% and 9.4% respectively. This represents a significantly high energy savings as compared to varying the data-rate and the brightness levels in the device screen. In order to verify the large energy savings obtained by varying the backlight in the case of *video1*, *video2* with darker background was used.

The tests for *video2* showed that decreasing the backlight to 50% and 25% reduces the energy consumption by 29.6% and 35.4% while reducing the video quality by 14.5% and 21.3% respectively. Given that *video2* was already a 'dark' video, the reduction in energy consumption also resulted in important decrease in the video quality. Further, if the results of two videos are extrapolated till the video quality drops to an average of 3.0, then for these two videos, an energy saving of up to 40% could be obtained by employing DEAR focusing only on screen backlight adaptation.

4.2.4 Overall Energy Savings: The three test results indicate that having multiple adaptive RoI-based mechanism with variation in three parameters (bit-rate, brightness/gamma and backlight intensity) across different RoIs could result in significant energy savings. Notably, the tests indicate that up to 53% energy can be saved in total – bit-rate variation (atleast 4%), brightness/gamma variation (at least 9%) and variation in device backlight intensity (at least 40%).

V. CONCLUSIONS

This paper proposed an adaptive multiple region-of-interest mechanism, DEAR, for adjusting energy consumption in video-centric mobile devices while maintaing good video quality levels. Three main parameters: video bit-rate, display brightness/gamma levels and the screen backlight intensity were identified and the achievable energy savings due to each of these factors were studied in context of DEAR. The measurement of energy consumption and the subjective video assessment test results indicated that, using the proposed DEAR algorithm, it was possible to save upto 53% of energy in the wireless device while still maintaining above average video quality level; with the actual saving being also depending on the nature of the selected video.

There are two major research tasks envisaged for further enhancement of DEAR. The first aspect is to investigate the amount of variation in the three parameters that would optimally reduce the energy consumption in the device. Secondly, since the amount of energy savings depends on the number of RoIs and the variation across parameters, a future work would be to develop an analytical framework for investigating the number of RoIs that would provide maximum savings in the energy consumption in the device.

Table 3 Variation in energy consumption and average video quality with variation in device backlight

Device Backlight	Energy Consumption(mW)		Video Quality(1–5)	
	Video 1	Video 2	Video 1	Video 2
100%	260.89	265.75	4.76	4.66
75%	214.75	220.37	4.76	4.33
50%	182.32	187.01	4.68	3.98
25%	166.07	171.04	4.31	3.62

ACKNOWLEDGEMENT

The authors thank IIIT Sricity Start-up Grant and Enterprise Ireland (Grant No: EI/CF/2011/1037) for their support.

REFERENCES

[1] G. P. Perrucci, F.H.P. Fitzek and J. Widmer, "*Survey on Energy Consumption Entities on the Smartphone Platform*", 73rd IEEE Vehicular Technology Conference (VTC), Yokohoma, Japan, 1-5 May 2011.

[2] M. Kennedy, H. Venkataraman and G.-M. Muntean, "*Battery and Stream Aware Adaptive Multimedia Delivery for Wireless Devices"*, IEEE Local Computer Networks, Colorado, Denver, USA, 22-24 October 2010.

[3] S. Chen, Z. Yuan, G.-M. Muntean, "*An Energy-aware Multipath-TCP-based Content Delivery Scheme in Heterogeneous Wireless Networks"* IEEE Wireless Comms. and Networking Conf., 2013, pp. 1291-1296

[4] A.N. Moldovan, C. H. Muntean, "Subjective Assessment of Bitdetect-A Mechanism for Energy-aware Multimedia Content Adaptation", IEEE Trans. on Broadcasting, Vol. 58, No. 3, pp. 480-492

[5] G.-M. Muntean, G. Ghinea, T. N. Sheehan, "*Region of Interest-Based Adaptive Multimedia Streaming Scheme*", IEEE Trans. on Broadcasting, Vol. 54, No. 2, June 2008.

[6] E. M. Reingold and L. C. Loschky, "*Reduced Saliency of Peripheral Target in Gaze-Contingent Multi-Resolution Displays: Blended versus Sharp Boundary Windows*" in Proceedings of Eye Tracking Research and Applications Symposium, New Orleans, Louisiana, USA, 2000.

[7] B. A. Watson, N. Walker, L. F Hodges and A. Warden, "*Managing Level of Detail through Peripheral Degradation: Effects on Search Performance with a Head-Mounted Display,*" ACM Transactions on Human-Computer Interaction, Vol. 4, No. 4, pp. 323–346, 1997.

[8] J. H. Lee and C. Yo, "*Scalable RoI Algorithm for H.264/SVC-Based Video Streaming*", IEEE Trans. on Consumer Electronics, Vol. 57, No. 2, May 2011.

[9] B. Ciubotaru, G.-M. Muntean and G. Ghinea, "*Objective Assessment of Region of Interest-Aware Adaptive Multimedia Streaming Quality*", IEEE Trans. on Broadcasting, Vol. 55, No. 2, pp. 202-212, June 2009.

[10] B. Ciubotaru, G. Ghinea and G.-M. Muntean, "*Subjective Assessment of Region of Interest-aware Adaptive Multimedia Streaming Quality*", IEEE Transactions on Broadcasting, Vol. 60, No. 1, pp. 50-60, June 2014

[11] Arduino Team, "Arduino, HomePage", http://www.arduino.cc/ Last accessed: 12th Oct. 2015.

[12] M. Kennedy, H. Venkataraman, G.-M. Muntean, "*Energy Consumption Analysis and Adaptive Energy Saving Solutions for Mobile Device Applications*", in Green IT: Services and Applications, Springer-Verlag, Oct. 2011.

[13] M. Kennedy, H.Venkataraman and G.M. Muntean, "*Dynamic Stream Control for Energy Efficient Video Streaming*", IEEE Broadcasting and Multimedia Symposium (BMSB), Nuernberg, Germany, 6-8 June 2011.

[14] ITU-T, "*Methods for the subjective assessment of video quality, audio quality and audiovisual quality of Internet video and distribution quality television in any environment*", Recommendation P.913, Jan. 2014.

THE 18TH INTERNATIONAL SYMPOSIUM ON WIRELESS PERSONAL MULTIMEDIA COMMUNICATIONS
(WPMC-2015)
December 13-16, 2015, Hyderabad, India

Improved p-norm Energy Detector with Soft Combining in AWGN Channel for Spectrum Sensing

Vaibhav Kumar*, Deep Chandra Kandpal†, Ranjan Gangopadhyay‡, Soumitra Debnath§
Department of ECE, The LNM Institute of Information Technology, Jaipur, 302031, India
*vaibhav@lnmiit.ac.in, †deepkandpal.lnmiit@gmail.com, ‡ranjan_iitkgp@yahoo.com,§soumitra_deb@yahoo.com

***Abstract*—Energy detection is a well-known method for spectrum sensing in cognitive radio (CR) systems. Classical energy detection (CED) algorithm suffers from detection performance limitations in the presence of Gaussian noise. Improved energy detection (IED) algorithm has been suggested recently that outperforms the CED algorithm in AWGN channel. Further, generalized p-norm detector exists which performs better than the CED algorithm for the detection of random signals in the presence of Gaussian noise. The present paper highlights the combined benefit of IED algorithm and the generalized p-norm detector with multi-antenna assisted soft combining in AWGN channel to achieve a higher performance gain.**

***Index Terms*—Cognitive radio, Spectrum sensing, Energy detection, p-norm detector**

I. Introduction

Cognitive radio (CR) refers to an intelligent wireless communication device that has emerged since last decade to mitigate the spectrum scarcity problem by the efficient use of radio spectrum. It can sense its operational radio environment and can dynamically and autonomously adjust its operating parameters [1]. Dynamic spectrum access (DSA) is the key concept which allows a CR device to opportunistically access the frequency band allocated to an incumbent/primary user (PU), when the PU is not using the band. For DSA, the CR devices has to sense the radio environment licensed to the PUs. Various methods for spectrum sensing have been reported in the literature [2], [3], which include Energy detection, Cyclostationary detection, Matched filtering, etc. Among all aforementioned techniques, the classical energy detection (CED) is the most preferred one because of its low computational requirement and implementation cost. The main drawback of CED is that the detection threshold is highly susceptible to the changing background noise and the interference.

In order to improve the performance of energy detection based spectrum sensing systems, an improved energy detection (IED) algorithm has recently been suggested [4] which outperforms the CED in AWGN channel with almost identical complexity. Another interesting improvement strategy for energy detection based on p-norm detector was first proposed by Chen [5], where the CED is modified by replacing the squaring operation of signal amplitude by arbitrary positive power p. The application of p-norm detector in the fading channel and for diversity reception has been well investigated recently [6].

In [7], maximal ratio combining (MRC) based soft-combining scheme for CED has been investigated in which the accurate energy values observed by the different CR antennas are combined to make a better decision for spectrum occupancy, assuming the perfect reporting channels. In the present work, we aspire to evaluate the achievable performance gain in a multi-antenna assisted spectrum sensing system taking the combined benefit of the IED and the p-norm energy detector. Here the energy value (power p operation) calculated by each antenna is combined at the fusion center (FC) using the MRC and then the decision about the presence/absence of PU is made according to the improved energy detection algorithm. It is difficult to obtain analytically the optimized p-value for a given target performance criterion and therefore a numerical evaluation is adopted.

The organization of the rest of the paper is as follows: Section II provides the mathematical details of CED, IED, p-norm detector and the improved p-norm detector with soft combining scheme. Section III provides the detailed theoretical results as well as practical design guidelines. Finally the conclusion is drawn in section IV.

II. System Model

In CR, the secondary user (SU) looks for the PU in the band of interest and try to sense the surrounding spectrum space. Consider a CR sensing node with N receiving antennas. The observed normalized energy value at the j^{th} antenna is given by [7]

$$Y_j = \begin{cases} \frac{1}{M}\sum_{i=1}^{M} w_{ji}^2 & : H_0 \\ \frac{1}{M}\sum_{i=1}^{M} \left(h_{ji}s_{ji} + w_{ji}\right)^2 & : H_1 \end{cases} \quad (1)$$

where, s_{ji}, h_{ji} and w_{ji} denote the i^{th} sample of the PU signal, channel fading coefficient and the zero-mean additive white Gaussian noise with unit variance at the j^{th} antenna with $i = 1, 2, \ldots, M$ and $j = 1, 2, \ldots, N$. H_0 denotes the null hypothesis and H_1 denotes the alternate hypothesis corresponding to the vacant and the busy spectrum respectively. Fig. 1 shows the corresponding system model.

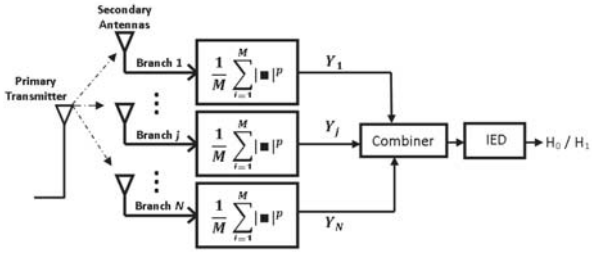

Fig. 1. The system model

For $M \gg 1$, Y_j will be Gaussian distributed as:

$$Y_j \sim \begin{cases} \mathcal{N}(1, 2/M) & : H_0 \\ \mathcal{N}\left((1+\gamma_j), 2/M\,(1+\gamma_j)^2\right) & : H_1 \end{cases} \tag{2}$$

where, γ_j is the instantaneous signal-to-noise-ratio (SNR) at the j^{th} antenna.

A. CED with Soft Combining

In soft combination, the weighted normalized energy from each antenna is added and this weighted sum of energy is then compared with the predefined threshold to decide the presence/absence of the PU. The weighted summation for the m^{th} sensing event is given as [7]:

$$\mathcal{T}_m = \sum_{j=1}^{N} \mathcal{W}_j Y_j \tag{3}$$

where, $\mathcal{W}_j$ is the weight coefficient for the j^{th} branch. The decision rule can be adopted as:

$$\begin{aligned} H_0 &: \mathcal{T}_m \leq \lambda \\ H_1 &: \mathcal{T}_m > \lambda \end{aligned} \tag{4}$$

where, λ is the decision threshold. Assuming Y_j's and $\mathcal{W}_j$'s to be independent for different j's, $\mathcal{T}_m$ will be Gaussian with

$$\mathcal{T}_m \sim \begin{cases} \mathcal{N}\left(\sum_{j=1}^{N}\mathcal{W}_j, \frac{2}{M}\sum_{j=1}^{N}\mathcal{W}_j^2\right) & : H_0 \\ \mathcal{N}\left(\sum_{j=1}^{N}\mathcal{W}_j(1+\gamma_j), \frac{2}{M}\sum_{j=1}^{N}\mathcal{W}_j^2(1+\gamma_j)^2\right) & : H_1 \end{cases} \tag{5}$$

For analyzing the performance of the spectrum sensing system, the probability of false alarm, P_{fa} and probability of detection P_d need to evaluated. A high value of P_d and a low value of P_{fa} is always desirable for an accurate spectrum sensing system. The parameters are defined as:

$$\begin{aligned} P_{fa} &= P[H_1|H_0] \\ P_d &= P[H_1|H_1] \end{aligned} \tag{6}$$

where, $P[\cdot|\cdot]$ denotes the conditional probability. In the case of CED with soft combining, the probability of false alarm and the probability of detection are given as [7]:

$$P_{fa} = Q\left(\frac{\lambda - \sum_{j=1}^{N}\mathcal{W}_j}{\sqrt{\left(\frac{2}{M}\right)\sum_{j=1}^{N}\mathcal{W}_j^2}}\right) \tag{7}$$

$$P_d = Q\left(\frac{\lambda - \sum_{j=1}^{N}\mathcal{W}_j(1+\gamma_j)}{\sqrt{\frac{2}{M}\sum_{j=1}^{N}\mathcal{W}_j^2(1+\gamma_j)^2}}\right) \tag{8}$$

where, $Q(x) = \int_x^\infty e^{-t^2}dt$ represents the Gaussian tail probability function and can be evaluated easily using the command *qfunc(x)* in MATLAB. From (7), the threshold λ can be given as:

$$\lambda = \sqrt{\left(\frac{2}{M}\right)\sum_{j=1}^{N}\mathcal{W}_j^2}\; Q^{-1}(P_{fa}) + \sum_{j=1}^{N}\mathcal{W}_j \tag{9}$$

where, $Q^{-1}(x)$ is the inverse-Q function and can be easily evaluated using the command *qfuncinv(x)* in MATLAB. From (8) and (9), P_d can be expressed as [7]:

$$P_d = Q\left(\frac{Q^{-1}(P_{fa}) - \sqrt{\frac{M}{2}}\sum_{j=1}^{N}\alpha_j\gamma_j}{\sqrt{\sum_{j-1}^{N}\alpha_j^2(1+\gamma_j)^2}}\right) \tag{10}$$

where, α_j is the normalized weight coefficient, given as:

$$\alpha_j = \frac{\mathcal{W}_j}{\sqrt{\sum_{k=1}^{N}\mathcal{W}_k^2}} \tag{11}$$

The optimal weight coefficients can be evaluated by maximizing P_d in (10), subject to

$$\sum_{j=1}^{N}\alpha_j^2 = 1; \quad 0 < \alpha_j \leq 1, \ \forall\ j \tag{12}$$

For low SNR conditions i.e., $\gamma_j \ll 1$, (10) can be approximated as [7]:

$$P_d = Q\left(Q^{-1}(P_{fa}) - \sqrt{\frac{M}{2}}\sum_{j=1}^{N}\alpha_j\gamma_j\right) \tag{13}$$

The optimal weight coefficients subject to (12) is given as [7]:

$$\alpha_j^* = \frac{\gamma_j}{\sqrt{\sum_{k=1}^{N}\gamma_k^2}} \tag{14}$$

which is identical to the maximal ratio combining (MRC) scheme [7]. Hence the optimal weight coefficients are given as:

$$\mathcal{W}_{mrc_j} = \alpha_j^* \tag{15}$$

B. IED with Soft Combining

The improved energy detection (IED) is the modified version of CED, as it gives better detection results with nearly identical complexity. In IED, the decision for the presence of the PU is done based on the average of last L test statistic $\mathbb{T}_m^{avg}$ at the m^{th} sensing interval defined as [4]:

$$\mathbb{T}_m^{avg}(\mathcal{T}_m) = \frac{1}{L}\sum_{l=1}^{L}\mathcal{T}_{m-L+l} \tag{16}$$

Out of these last L sensing events, $P \in [0, L]$ is the total number of events in which the primary signal was actually present. In IED algorithm, two additional checks are aimed to improve the detection probability as well as the probability of false alarm.

If $\mathcal{T}_m \leq \lambda$, the first additional check for $\mathbb{T}_m^{avg}(\mathcal{T}_m) > \lambda$ would improve the detection probability and the second additional check for $\mathcal{T}_{m-1} > \lambda$ would prevent the significant false alarm degradation. Since $\mathbb{T}_m^{avg}(\mathcal{T}_m)$ is the average of independently and identically distributed Gaussian random variables, it is also normally distributed:

$$\mathbb{T}_m^{avg}(\mathcal{T}_m) \sim \mathcal{N}\left(\mu_{avg}, \sigma_{avg}^2\right) \tag{17}$$

where, μ_{avg} and σ_{avg}^2 for the multi-antenna case is obtained as:

$$\begin{aligned}\mu_{avg} &= \frac{P}{L}\sum_{j=1}^{N}\mathcal{W}_j(1+\gamma_j) + \frac{L-P}{L}\sum_{j=1}^{N}\mathcal{W}_j \\ \sigma_{avg}^2 &= \frac{P}{L^2}\left[\frac{2}{M}\sum_{j=1}^{N}\mathcal{W}_j^2(1+\gamma_j)^2\right] + \frac{L-P}{L^2}\left[\frac{2}{M}\sum_{j=1}^{N}\mathcal{W}_j^2\right]\end{aligned} \tag{18}$$

Based on the above assumption, the probability of false alarm P_{fa}^{IED} and the probability of detection P_d^{IED} can be given as:

$$\begin{aligned}P_{fa}^{IED} &= P_{fa}^{CED} + P_{fa}^{CED}\left(1 - P_{fa}^{CED}\right) Q\left(\frac{\lambda_{IED} - \mu_{avg}}{\sigma_{avg}}\right) \\ P_d^{IED} &= P_d^{CED} + P_d^{CED}\left(1 - P_d^{CED}\right) Q\left(\frac{\lambda_{IED} - \mu_{avg}}{\sigma_{avg}}\right)\end{aligned} \tag{19}$$

C. p-norm Detector with Soft Combining

In the case of p-norm detector, the observed normalized energy value at the j^{th} antenna is given by:

$$Y_j = \begin{cases} \dfrac{1}{M}\displaystyle\sum_{i=1}^{M} w_{ji}^p & : H_0 \\ \dfrac{1}{M}\displaystyle\sum_{i=1}^{M}\left(h_{ji}s_{ji} + w_{ji}\right)^p & : H_1 \end{cases} \tag{20}$$

where, $p > 0$. It may be noted that $p = 2$ in (20) leads to the CED case. For $M \gg 1$, $\mathcal{T}_{m,p}$ will be Gaussian distributed as [5]:

$$\mathcal{T}_{m,p} \sim \begin{cases} \mathcal{N}\left(\mu_{0,p}, \sigma_{0,p}^2\right) & : H_0 \\ \mathcal{N}\left(\mu_{1,p}, \sigma_{1,p}^2\right) & : H_1 \end{cases} \tag{21}$$

where,

$$\mu_{0,p} = \frac{2^{p/2}}{\sqrt{\pi}}\Gamma\left(\frac{p+1}{2}\right)\sum_{j=1}^{N}\sqrt{\mathcal{W}_j^p}$$

$$\mu_{1,p} = \frac{2^{p/2}}{\sqrt{\pi}}\Gamma\left(\frac{p+1}{2}\right)\sum_{j=1}^{N}\sqrt{\mathcal{W}_j^p\left(1+\gamma_j\right)^p}$$

$$\sigma_{0,p}^2 = \left[\frac{2^p\Gamma\left(\frac{2p+1}{2}\right)}{M\sqrt{\pi}} - \frac{2^p}{M\pi}\left\{\Gamma\left(\frac{p+1}{2}\right)\right\}^2\right]\sum_{j=1}^{N}\mathcal{W}_j^p$$

$$\sigma_{1,p}^2 = \left[\frac{2^p\Gamma\left(\frac{2p+1}{2}\right)}{M\sqrt{\pi}} - \frac{2^p}{M\pi}\left\{\Gamma\left(\frac{p+1}{2}\right)\right\}^2\right] \times \sum_{j=1}^{N}\mathcal{W}_j^p\left(1+\gamma_j\right)^p \tag{22}$$

In (22), $\Gamma(\cdot)$ denotes the gamma function. The probability of false alarm and the probability of detection for the p-norm detector with soft combining scheme is given by:

$$\begin{aligned}P_{fa,p} &= Q\left(\frac{\lambda_p - \mu_{0,p}}{\sigma_{0,p}}\right) \\ P_{d,p} &= Q\left(\frac{\lambda_p - \mu_{1,p}}{\sigma_{1,p}}\right)\end{aligned} \tag{23}$$

D. Improved p-norm Detector with Soft Combining

Replacing the squaring operation of the signal amplitude in IED by an arbitrary positive power p, $\mathbb{T}_m^{avg}(\mathcal{T}_{m,p})$ may be well approximated by the Gaussian distribution as:

$$\mathbb{T}_m^{avg}(\mathcal{T}_{m,p}) \sim \mathcal{N}\left(\mu_{avg,p}, \sigma_{avg,p}^2\right) \tag{24}$$

where,

$$\begin{aligned}\mu_{avg,p} &= \frac{P}{L}\mu_{1,p} + \frac{L-P}{L}\mu_{0,p} \\ \sigma_{avg,p}^2 &= \frac{P}{L^2}\sigma_{1,p}^2 + \frac{L-P}{L^2}\sigma_{0,p}^2\end{aligned} \tag{25}$$

Modifying (19) to the present case, one obtains the probability of false alarm and the probability of detection in the following form:

$$\begin{aligned}P_{fa}^{IED,p} &= P_{fa,p} + P_{fa,p}\left(1 - P_{fa,p}\right) Q\left(\frac{\lambda_{IED,p} - \mu_{avg,p}}{\sigma_{avg,p}}\right) \\ P_d^{IED,p} &= P_{d,p} + P_{d,p}\left(1 - P_{d,p}\right) Q\left(\frac{\lambda_{IED,p} - \mu_{avg,p}}{\sigma_{avg,p}}\right)\end{aligned} \tag{26}$$

III. Results and Discussion

In this section, the results for the combined benefit of the improved algorithm and the p-norm detector are highlighted for the multi-antenna assisted spectrum sensing in AWGN channel. For a given target false alarm probability, the threshold, λ is chosen and for a given SNR, γ the optimal value of p is determined which yields the highest value of the probability of detection.

To provide practical design guidelines for a spectrum sensing system with improved p-norm detector, Fig. 2 and Fig. 3 provide the surface plots for the probability of detection with the variation of p and the probability of false alarm for AWGN channel. The optimal value of p is determined from the surface plot. The number of samples per sensing event M is considered as 30 and number of antennas N is 4 with SNR γ_j = - 10 dB $\forall$ j.

In Fig. 4, a comparison of receiver operating characteristics (ROCs) for multi-antenna assisted CED and IED with $p = 2$ and optimal p has been depicted. The ROC for single antenna CED ($p = 2$, $N = 1$) has also been drawn in order to show the

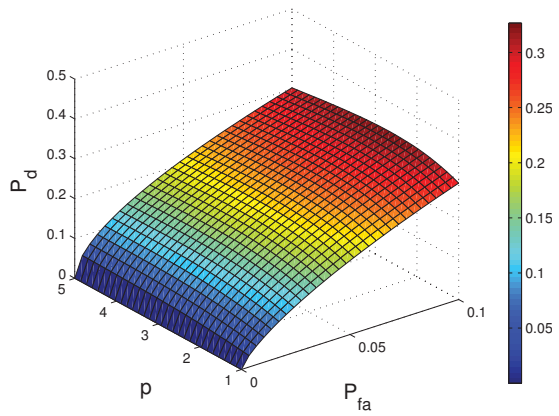

Fig. 2. Surface plot for detection probability using CED in AWGN channel with $M = 30$, $N = 4$ and $\gamma_j = -10$ dB $\forall\ j$.

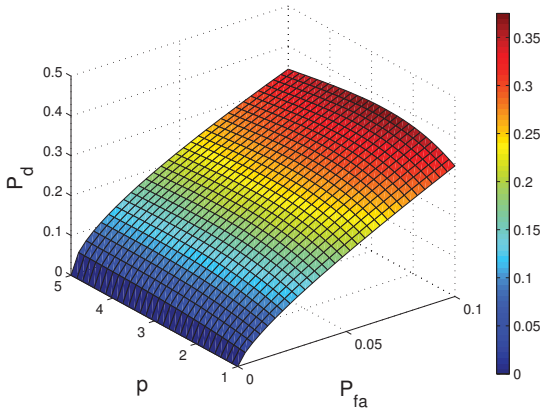

Fig. 3. Surface plot for detection probability using IED in AWGN channel with $M = 30$, $N = 4$ and $\gamma_j = -10$ dB $\forall\ j$.

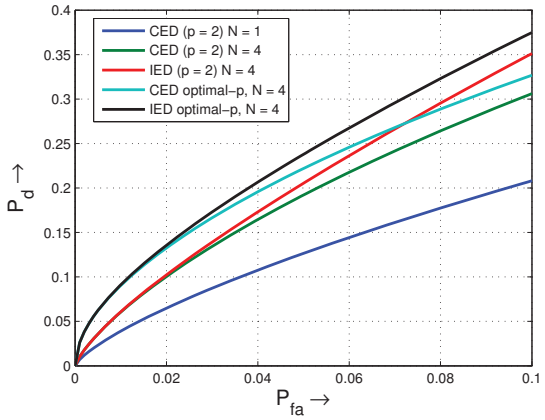

Fig. 4. Comparison of ROCs for multi-antenna assisted CED and IED in AWGN channel using $p = 2$ and optimal-p with $M = 30$, $N = 4$ and $\gamma_j = -10$ dB $\forall\ j$

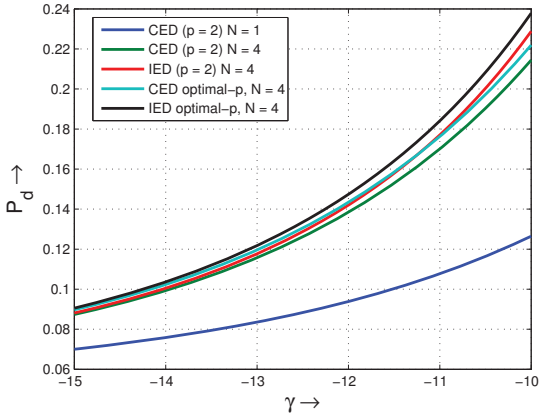

Fig. 5. Probability of detection versus SNR for multi-antenna assisted CED and IED in AWGN channel using $p = 2$ and optimal-p with $M = 30$, $N = 4$ and target $P_{fa} = 0.05$.

achieved diversity gain in other cases ($N > 1$). The optimal p-value for CED and IED is determined from Fig. 2 and Fig. 3 respectively, such that for a given target false alarm probability and SNR, the probability of detection becomes maximum. It is clearly evident from the figure that multi-antenna assisted improved-p norm detector outperform all the other schemes considered here.

The variation of detection probability against SNR at a fixed target false alarm probability of 0.05 has been shown in Fig. 5 with the number of samples per sensing event $M = 30$, and number of antennas $N = 4$. In addition, the result for the single antenna CED ($p = 2$, $N = 1$) has also been shown.

IV. Conclusion

We have analyzed the performance of a multi-antenna assisted improved-p norm energy detector in the AWGN channel for spectrum sensing. Theoretical results confirm significant gain over that of the multi-antenna assisted CED and IED algorithms. Results confirm that there exist an optimal value p (> 0), other than 2 for which the detector gives the best performance under low SNR conditions. The performance gain is not much significant if the number of samples per sensing event, M is considerably high, but for a low value of M, the p-norm detector works well for IED as compared to CED which in turn may lead to improve the total throughput of the secondary network. By combining both, the IED and the p-norm detector under multi-antenna assisted soft combining scheme, one can achieve a considerable performance gain.

Acknowledgment

The work has been carried out under the project, "Mobile Broadband Service Support over Cognitive Radio Networks," sponsored by Information Technology Research Academy (ITRA), Department of Electronics and Information Technology (DeitY), Govt. of India.

REFERENCES

[1] S. Haykin, "Cognitive radio: brain-empowered wireless communications," *Selected Areas in Communications, IEEE Journal on*, vol. 23, no. 2, pp. 201–220, Feb 2005.

[2] A. Wyglinski, M. Nekovee, and Y. Hou, *Cognitive Radio Communications and Networks: Principles and Practice*. Academic Press, 2009.

[3] V. K. Bhargava and E. Hossain, *Cognitive Wireless Communication Networks*. Secaucus, NJ, USA: Springer-Verlag New York, Inc., 2007.

[4] M. López-Benítez and F. Casadevall, "Improved energy detection spectrum sensing for cognitive radio," *Communications, IET*, vol. 6, no. 8, pp. 785–796, May 2012.

[5] Y. Chen, "Improved energy detector for random signals in gaussian noise," *Wireless Communications, IEEE Transactions on*, vol. 9, no. 2, pp. 558–563, February 2010.

[6] V. Sharma Banjade, C. Tellambura, and H. Jiang, "Performance of p-norm detector in AWGN, fading, and diversity reception," *Vehicular Technology, IEEE Transactions on*, vol. 63, no. 7, pp. 3209–3222, Sept 2014.

[7] J. Ma and Y. Li, "Soft combination and detection for cooperative spectrum sensing in cognitive radio networks," in *Global Telecommunications Conference, 2007. GLOBECOM '07. IEEE*, Nov 2007, pp. 3139–3143.

THE 18TH INTERNATIONAL SYMPOSIUM ON WIRELESS PERSONAL MULTIMEDIA COMMUNICATIONS
(WPMC-2015)
December 13-16, 2015, Hyderabad, India

EDAS– Energy-Efficient Device-based Adaptive Cross-Layer Scheme for Wireless Multimedia Transmission

Hrishikesh Venkataraman[1], Shen Wang[2] and Gabriel-Miro Muntean[2]
[1] Center for Smart Cities, Indian Institute of Information Technology (IIIT), Chittoor, Sricity, AP, India
[2] Performance Engineering Laboratory, Dublin City University (DCU), Glasnevin, Dublin 9, Ireland
Email: [1]hvraman@iiits.in [2]gabriel.muntean@dcu.ie

Abstract—**Next generation wireless networks are poised to support real-time video-on-demand and high quality multimedia streaming applications. In order to support them, several adaptation strategies have been proposed at different layers of the OSI network stack. Also, certain cross-layer strategies across physical/data link and transport/application layers have been proposed over the years. However, given the battery constraints of a smart-phone, it is imperative that new cross-layer design be developed that would bring into account an energy-oriented mechanism from a device perspective. In this paper, a new adaptive solution, EDAS – *energy-efficient device oriented adaptive cross-layer scheme* for multimedia transmission in wireless network environments is proposed. Importantly, *EDAS* provides a novel framework spanning across several OSI layers that would dynamically vary the energy consumption in mobile devices while maintaining a high peak signal to noise ratio (PSNR) in order to ensure a good video quality. It has been observed that *EDAS* significantly outperforms other schemes in terms of PSNR, loss-rate and importantly, the energy consumption in device.**

Keywords—Adaptive scheme, cross-layer design, energy-efficiency

I. INTRODUCTION

Over the last years, there has been a phenomenal increase in the demand by the mobile device users to have delivered real-time multimedia content at high quality. However, achieving high quality real time multimedia streaming is very challenging, mainly because it is delay sensitive, and requires high bandwidth for continuous high quality transmission. At the same time, multimedia and graphic-intensive applications consume high amounts of energy in the mobile device, thereby resulting in significant reduction of the overall device battery life.

There have been different works [1] that have proposed rate adaptation based protocols for high quality multimedia transmissions. However, most of these are deployed at a single layer of Open System Inter-connection (OSI) network stack. Although acceptable in case of a wired network where each layer treats the other layers as black boxes, in case of a wireless network, the OSI layer working cannot be optimized without being aware of other layers. For example, a network layer protocol could be optimized only if it has real-time information about instantaneous delivery channel conditions. Additionally, some research works have focused on adapting existing algorithms and protocols for multimedia compression and transmission to the rapidly changing wireless channel. However, many-a-times, these solutions do not necessarily provide adequate support for multimedia applications in areas of high interference. This is because the resource management and the available adaptation and protection strategies in the lower layers of the stack are optimized without the particular characteristics of multimedia applications being considered [2]. It should be noted that this "layered" optimization in the past led to a simple and independent implementation and to a non-optimal multimedia delivery performance. With the ability of the networks to process complex information and computational intelligence today, it is imperative to have cross-layer strategies in order to optimize the adaptation process for efficient multimedia delivery.

This paper proposes **a novel cross-layer energy-efficient device-oriented adaptive scheme (EDAS).** EDAS is active at *four* layers - physical layer, link layer, transport layer and application layer. EDAS is mainly a device-oriented energy-adaptive mechanism which adjusts the video bit-rate at the application layer dynamically, according to real time statistics of battery level of mobile device, effective network throughput and user perceived video quality, monitored at the receiving side at different network layers.

The paper is organized as follows. Section II describes the related work on cross-layer adaptive video delivery solutions, while section III describes *EDAS*. The simulation set-up and results are presented in section IV, while section V concludes the paper.

II. RELATED WORK

A medium access control (MAC) layer protocol proposed for rate adaptation at low network layers is the receiver based auto-rate (RBAR) protocol. Using RBAR results in high overall throughput, especially in wireless LANs. Over the years, the authors proposed a feedback-based Quality Oriented Adaptive Scheme (QOAS) [3, 4] for efficient multimedia transmission in wireless networks. QOAS is an application layer solution which employs end-user perceived quality estimation in the feedback loop and outperforms other protocols such as the TCP Friendly Rate Control Protocol (TFRCP) [5] and the enhanced Loss-Delay-based Adaptation

Algorithm (LDA+) [6] in a wireless environment, in terms of perceived quality, loss rate and the achievable throughput [7]. However, QOAS does not have any in-built energy-saving mechanism. Hence, a significant addition was required to be incorporated across the layers for energy-efficient cross-layer wireless multimedia transmissions [8]. Further, in case of real-time multimedia transmission, not only the system throughput, but also other parameters like delay, packet loss and overall quality of service (QoS) should be considered. In addition, the fluctuations in the wireless channel, limited bandwidth, contention among several subscribers and dynamic topology make QoS a very significant issue.

Recently, the authors have carried out a detailed analysis of a joint optimization of user experience and energy efficiency of wireless multimedia broadcast receivers with varying display and energy constraints [9]. This work focused mainly on the physical and link layer aspects, wherein the solution combined user composition aware source coding rate optimization, optimum time slicing for layer coded transmission and a low-level cross-layer adaptive modulation and coding scheme. However, this solution did not integrate the higher layers in the cross-layer design. Other works include an energy-quality-cost tradeoff solution for mobile video delivery [10], a battery power-aware adaptive multimedia delivery scheme for wireless mobile devices [11], energy-aware mobile learning solutions [12], an energy-aware multipath content delivery scheme [13] and a mechanism for energy-aware multimedia content adaptation. [14].

III. System Model of EDAS

This section describes the design of the proposed cross-layer energy-efficient device-oriented adaptive scheme *EDAS*. The design comprises of two aspects: the system architecture and the energy-efficient mechanism. The cross-layer *EDAS* is designed to optimize those parameters that affect the most the video delivery process, and consequently end-user perceived quality *Q*: loss rate, delay, jitter, bit rate and throughput. *EDAS* acts at various layers, from physical and MAC layers to transport and application layers. It should be noted that the proposed solution takes into account the system architecture while designing joint delivery improvement strategies across the layers. This is achieved by making use of information from layers such as physical layer on bit error rate for each link and data link layerto learn about the current network conditions and therefore quality of each link.

A. *Architecture of EDAS*

EDAS is an adaptive, information-centric solution spread across four layers. Its main characteristic is that it adapts its operation depending on the requirements of multimedia data traffic. In addition, a completely localized data management framework is presented in *EDAS* that helps capture information about traffic patterns in the network. Simultaneously, it deals with the end user perceived quality for multimedia streams at the receiver end. This information is subsequently used by application/transport layer scheme at the sender to modify its operation accordingly. The backbone of this scheme is the shared centralized database, as illustrated in the framework presented in Fig. 1. The database contains network parameters that affect individual layers or more than one layer, as well as parameters that get affected or modified by different layers. After accessing this cross layer information, each layer makes modifications of the parameters that they are concerned with applying the best adaptation strategy they can in order to imkprove delivery performance from their point of view. Note how the interaction between layers not connected directly takes place through the centralized database.

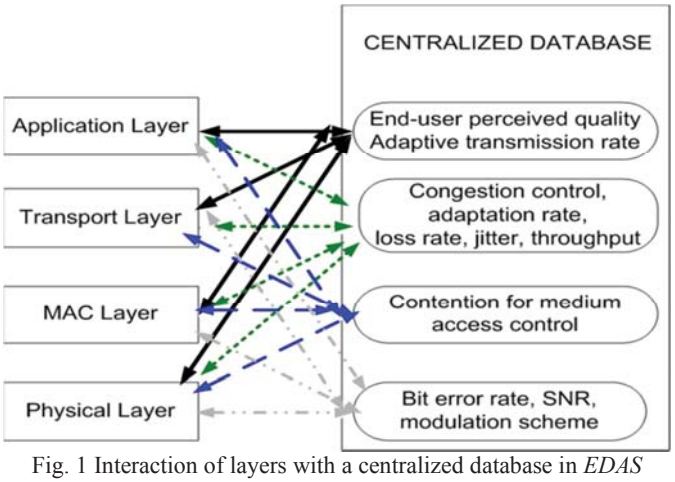

Fig. 1 Interaction of layers with a centralized database in *EDAS*

As part of this process, the physical layer provides adaptive rates to transport layer and also helps the MAC layer to select the best contention strategies for efficient delivery of traffic i.e., choosing a non-interfering set of senders and receivers at a particular time. Importantly, in the design of *EDAS*, instead of carrying the duration of the reservation as done in a non-adaptive protocol, the information on the modulation rate and size of data packets is stored in this database and only updates are being carried by packets. This serves the dual purpose of providing a mechanism by which the receiver can communicate the chosen rate to the sender, while still providing neighboring nodes with enough information to calculate the duration of the requested reservation. Hence, for e.g., the MAC layer would not only choose a modulation rate that would maximize the throughput, but also communicate the same to the server, thereby developing a continuous interactive mechanism. This considerably reduces the overhead. Further, at application layer *EDAS* extends the QOAS's client-side multimedia quality of delivery monitoring mechanism Quality of Delivery Grading Scheme (QoDGS) and uses QOAS's server-side Server Arbitration Scheme (SAS) [3] as described next.

B. *Energy-Efficient Mechanism in EDAS*

As already mentioned, *EDAS* uses SAS at sever side and a cross layer quality of delivery grading scheme (CR-QoDGS), which extends the QoDGS, at the client.

The most important feature of CR-QODGS is the calculation of a score based on the parameters from the Physical and MAC layers. These include: *bit error rate* (BER), *signal-to-noise ratio* (SNR), *modulation scheme* and *contention mode at MAC layer*. A higher BER or lower SNR would lower the CR-QODGS score which-in-turn would suggest to reduce the bit rate transmitted by the sender.

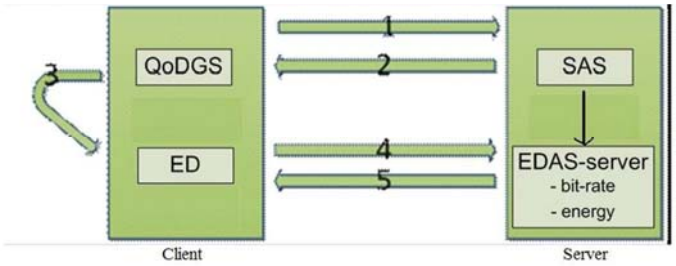

Fig. 2 Client-server model for energy-efficient bit-rate selection mechanism in EDAS

Further, a significant aspect of EDAS is to reduce the energy consumption. Regularly, the EDAS component at the client side monitors continuously the battery level of the device and request adjustments of the bit-rate based on the most recent readings. This is done in a process which includes six steps. The tasks in each step are repeated until the full video is played.

1. The client sends a video streaming request to the server. The video bit-rate in this request is at the highest possible level given the battery power readings.
2. The sever checks the receiving request and sends the video streaming at the corresponding rate.

3a. The device receives the information and while displaying the video, also finds out the remaining battery level of the device.

3b. Further, the client calculates the CR-QoDGS score based on the video quality displayed and also an ED (energy of device) score that is calculated based on the remaining battery level of the device. The ED score is calculated based on the remaining battery life ('b') and the set battery threshold level ('B_T'); explained in section 3.1

4. Both these scores are sent back to the server.
5. The EDAS mechanism at the server first calculates the bit-rate based on the CR-QoDGS score and then the actual bit-rate depending on the ED score. This is such computed in order to enable complete playout of the video content given the battery power levels at the client device. The server then transmits the video content at the data rate that is adapted to both delivery conditions and client device energy level.

C. *Instantaneous Battery Level*

The "instantaneous battery level" in the device indicates the battery of the device at the instant when the client has just received the latest video data from the server. A battery coefficient 'b' is defined as the ratio of the current energy level to the initial energy level of the device [15].

$$b = \text{Ec/Ei},$$

where Ec is device's current energy level and Ei is device's initial energy level.

'b' shows the instantaneous energy level of the device and decreases monotonically from 100% to 0%. Further, a battery threshold level, 'B_T' is considered which defines the level below which the energy-efficient mechanism of *EDAS* would be applied. 'B_T' can be set dynamically depending on user preference regarding trading-off between video quality and multimedia content duration. For instance, 'B_T' = 0.5 implies that the bit-rate reduction in the device would apply only when the value of 'B' reaches below 'B_T' = 0.5. If 'B_T' = 0.75, then the energy-efficient bit-rate adaptation mechanism is applied only when 'B' drops below 'B_T' = 0.75'. In order to alter the data rate, a 5-state bit-rate level L_i, is defined for each video content relative to its highest bit-rate level, where $i \in \{1, 2, 3, 4, 5\}$. Iteratively, when b drops below a certain value during an iteration, during the next iteration the bit-rate is reduced by half its previous level, i.e., $L_{i+1} = \lfloor L_i/2 \rfloor$. If the last decided bit rate does not have adverse effect on the network performance, the next session bit-rate is either kept at same level or increased by one-step, i.e., $L_{i+1} = L_i$ or $L_i + 1$, depending on the instantaneous user-experienced video quality. If the quality-level is above a satisfactory level (set by threshold Qt), the bit-rate level is maintained; else the rate is increased by one level. The B_T and Qt can be set in the device.

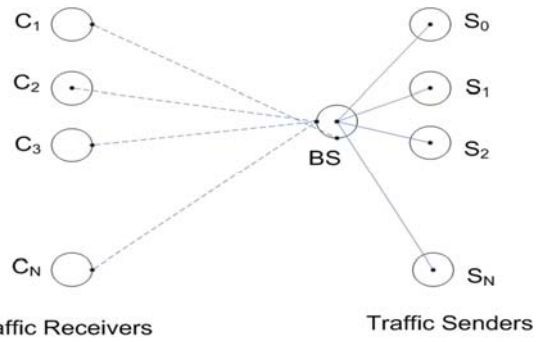

Fig. 3 Network topology for traditional multimedia wireless network architecture

D. *Experimental Set-up*

The tests involved a Samsung Galaxy Nexus One device as the client, as it is anticipated that most of the users today would have a smart-phone with at-least the capabilities of this model. The test system comprises of the phone and a video server streaming content over a wireless IEEE 802.11g network. The phone is connected to an external measurement setup that monitors and logs its power consumption during the execution of various tests. A shunt resistor (0.22 Ω; ± 1%) is inserted between the phone and battery to allow calculating the current by measuring the voltage drop across the resistor. The low-value shunt resistor of 0.22Ω ensures that energy is not wasted during the measurement phase. The instantaneous energy consumed is measured using an Arduino board as shown in Fig. 4.

In order to test the energy efficiency of the proposed *EDAS* mechanism and to investigate the impact on potential energy savings in the device, the system is simulated for an IEEE 802.11g based wireless network, with a single-hop communication between the client (device) and server (base station). The simulation setup consists of a number of mobile nodes distributed in a circular coverage area of 1 square km. There is a sender located at centre of the area. The server communicates directly with all wireless terminals in the network, as shown in Fig. 3. There are a number of sources (i.e. S_0 is the video source multimedia and S_1, S_2,…, S_N are the background traffic senders) connected to the server (BS) that transmits multimedia content to N clients - C_0, C_1, C_2.., C_N. The links between S_0, S_1, S_2…, S_N and the server are sufficiently provisioned, so as not to cause any delay or loss. The performance of EDAS scheme is evaluated in terms of four parameters: *average bit rate*, *loss rate, energy consumption* and *peak signal-to-noise ratio* (PSNR).

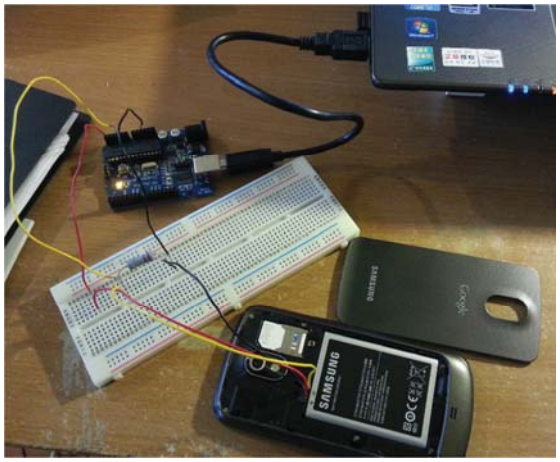

Fig. 4 Set-up for measuring energy consumption in mobile device

In order to test the performance of EDAS during multimedia streaming, the original version of test video were downloaded with bit-rate of 2657kbps and 145 seconds length. It is compressed by WisMencoder 2.3.0 (with built-in FFMPEG) into 5 different bit-rates videos: 180kbps, 500kbps, 900kbps, 1200kbps, 1600kbps respectively. Notably, different video levels were assigned for the different bit-rates. These include: 180 kbps (L1), 500 kbps (L2), 900 kbps (L3), 1200 kbps (L4) and 1600 kbps (L5). Further, the performance of EDAS is evaluated for different instantaneous battery levels. Four instantaneous battery levels are considered: 100%, 75%, 50% and 25%. The four scenarios are simulated from the same video starting point.

Fig. 5 to Fig. 8 show the results of the cross-layer based EDAS scheme for different battery threshold ('B_T') and the results are compared to QOAS. Fig. 5 shows the remaining battery level of the device while Fig. 6 shows the average PSNR of four different cases of EDAS and QOAS. It can be observed from Fig. 5 that EDAS with B_T = 1.0 has a much longer battery life as compared to other B_T levels. For instance, the remaining battery at 14,400s, i.e., at 4 hours is 0.38 in case of B_T = 1.0; only 0.097 in case of B_T = 0.25 and 0.2 in case of QOAS. In fact, this battery improvement is consistent throughout the simulation. This shows the significant battery improvement of EDAS. Notably, Fig. 6 shows that the resulting PSNR is also the highest for B_T = 1.0 as compared to other schemes. Interestingly, PSNR of EDAS for all four considered thresholds as well as that of QOAS are considerably good. This shows that application of EDAS does not result in a degradation of video quality in the network.

E. Results

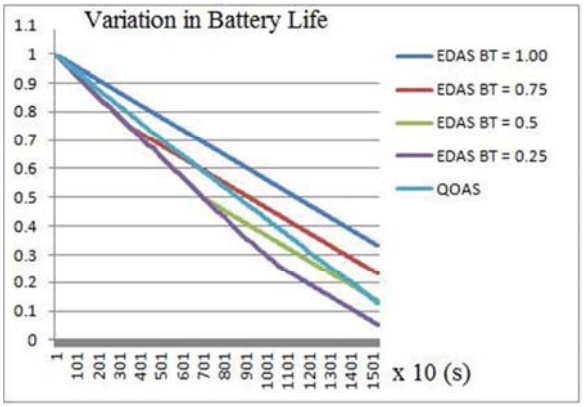

Fig. 5 Variation of battery level with time for EDAS (different threshold, B_T) with the QOAS scheme

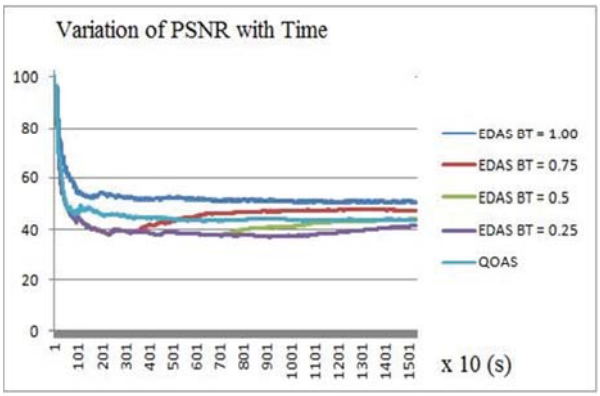

Fig. 6 Variation of PSNR with Time for EDAS (different threshold, B_T) mechanisms with the QOAS scheme

The variation of bit-rate with time in Fig. 7 gives a very interesting result. It can be observed that EDAS results in considerably higher variation in the instantaneous bit rate at for different B_T thresholds. Notably, B_T = 1.0 results in a very low bit rate; which in turn indicates a lower average video quality transmitted from the network itself. On the other hand, EDAS with low B_T values implies a higher transmission rate in the initial stages from the network itself, till the battery of the device reaches the B_T threshold value. Once this threshold is reached, the bit-rate decreases rapidly; as the primary focus is now on saving the battery life and extending the device life. In particular, the bit-rate of EDAS is higher than that of QOAS until the threshold; after which it degrades sharply. This indicates a significant feature of EDAS. Firstly, the bit-rate offered by the transmitter in case of EDAS is adaptive yet

significantly higher than that of QOAS; especially until the threshold B_T is reached. Secondly, when the battery level is low, the EDAS decreases the transmission bit rate itself, so as to reduce the overall energy consumption and also to have a smooth degradation in video quality not to be perceptible to end-users, while increasing the battery life.

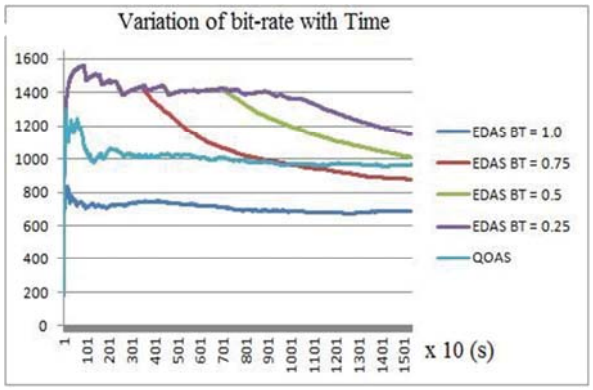

Fig. 7 Variation of Bit-Rate with time for EDAS (different threshold, B_T) with the QOAS scheme

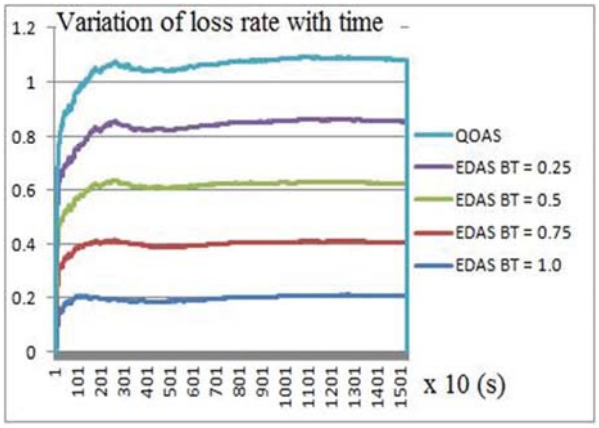

Fig. 8 Variation of Loss-Rate with time for EDAS (different threshold, B_T) with QOAS

Finally, Fig. 8 shows the variation in loss rate in percentage, for four scenarios in EDAS as compared with QOAS. It can be observed that the loss rate of all the schemes are less than 1%, resulting in good video quality level. Note how EDAS results in an extremely low value of 0.2% when the battery threshold is set at B_T = 1.0. This shows that the cross-layered EDAS provides a flexible solution to adapt the bit rate and extend the battery life while maintaining good quality level.

IV. Conclusions and Future Work

A novel cross-layer energy-efficient device-oriented solution *EDAS* was proposed in this work for efficient multimedia streaming to wireless mobile devices. The functionality of EDAS spans across four layers of the OSI network stack: physical, MAC, transport and application. EDAS provides a flexible mechanism for dynamically reducing the energy consumption of mobile devices and thereby extending their battery life, without affecting user perceived video quality. Future work will focus on developing an analytical framework to reflect closer interaction between the four network layers. This framework should also consider a comprehensive mathematical analysis that would indicate the relation between energy savings and the resulting bit-rate in order to better support the adaptation decisions. Another further work in this direction is to enhance this cross-layer design over all layers of OSI stack and considering more parameters, taking into account the current deployed network architectures.

Acknowledgment

The authors thank Prof. Swades De from IIT Delhi for the extensive discussions. Further the authors acknowledge the IIIT Sricity Research Start-up Grant, the Indo-Irish (DST-DCU) Research Funding grant scheme and the Irish Research Council (IRC) for their support.

References

[1] S. Chen, M. Shyu, I. Gray, H. Luo, "*An Adaptive Multimedia Transmission Protocol for Distributed Multimedia Applications*", In Proc. of 23rd Intl. Conference on Distributed Computing Systems, USA, May 2003.

[2] V. Srivastava and M. Motani, "*Cross-Layer Design: A Survey and the Road Ahead*," IEEE Communication Magazine, Vol. 43, No. 12, pp. 112–119, December 2005.

[3] G-M. Muntean and N. Cranley, "*Resource Efficient Quality-Oriented Wireless Broadcasting of Adaptive Multimedia Content*," IEEE Transactions on Broadcasting, Vol. 53, No. 1, pp. 362–368, March 2007.

[4] H. Venkataraman, P. Kalyampudi and G.-M. Muntean, "*CASHeW: Cluster-based Adaptive Scheme for Multimedia Delivery in Wireless Networks*", Springer Wireless Personal Communications, January 2012.

[5] D. Sisalem and A. Wolisz, "*LDA+ TCP-Friendly Adaptation: A Measurement and Comparison Study*," in Proceedings of ACM NOSSDAV, Chapel Hill, NC, USA, 26-28 June, 2000.

[6] J. Padhye, J. Kurose, D. Towsley, and R. Koodli, "*A Model Based TCP Friendly Rate Protocol*" in Proceedings of ACM NOSSDAV, Virginia, USA, 3-5 June 1999.

[7] G. Holland, N. Vaidya, and V. Bahl. "*A Rate-Adaptive MAC Protocol for Multihop Wireless Networks*", In Proceedings of ACM MOBICOM, Rome, Italy, 16-21 July 2001.

[8] H. Venkataraman and G.-M. Muntean, "*Dynamic Time Slot Partitioning Algorithm for Multimedia Transmission in Two-Hop Cellular Networks*", IEEE Transactions on Mobile Computing, Vol. 10, No. 5, April 2011.

[9] C. Singhal, S. De, R. Trestian and G.-M. Muntean, "*Joint Optimization of User Experience and Energy Efficiency in Wireless Multimedia Broadcast*," IEEE Trans. Mobile Computing, vol. 13, no. 7, pp. 1522-1535, July 2014.

[10] R. Trestian, O. Ormond, G.-M. Muntean, "*Energy–quality–cost Tradeoff in a Multimedia-based Heterogeneous Wireless Network Environment*", IEEE Transactions on Broadcasting, Vol. 59, No. 2, pp. 340-357

[11] M. Kennedy, H. Venkataraman, G.-M. Muntean, "*Battery and Stream-aware Adaptive Multimedia Delivery for Wireless Devices*", IEEE Local Computer Networks (LCN), 2010 pp. 843-846

[12] A. N. Moldovan, S. Weibelzahl, C. H. Muntean, "*Energy-aware Mobile Learning: Opportunities and Challenges*", IEEE Communications Surveys & Tutorials, Vol. 16, No. 1, pp. 234-265

[13] S. Chen, Z. Yuan, G.-M. Muntean, "*An Energy-aware Multipath-TCP-based Content Delivery Scheme in Heterogeneous Wireless Networks"* IEEE Wireless Comms. and Networking Conf., 2013, pp. 1291-1296

[14] A.N. Moldovan, C. H. Muntean, "*Subjective Assessment of Bitdetect-A Mechanism for Energy-aware Multimedia Content Adaptation*", IEEE Trans. on Broadcasting, Vol. 58, No. 3, pp. 480-492

[15] M. Kennedy, H.Venkataraman and G.M. Muntean, "*Dynamic Stream Control for Energy Efficient Video Streaming*", IEEE Broadcasting and Multimedia Symposium (BMSB), Nuernberg, Germany, 6-8 June 2011.

THE 18TH INTERNATIONAL SYMPOSIUM ON WIRELESS PERSONAL MULTIMEDIA COMMUNICATIONS
(WPMC-2015)
December 13-16, 2015, Hyderabad, India

Design and Performance Analysis of a Penta-band Spiral Antenna for Vehicular Communications

R. Ramya and T. Rama Rao
RADMIC, Department of Telecommunication Engineering,
SRM University, Chennai, India.
vijaramya@gmail.com; ramaraotr@gmail.com

Abstract— **Developments in automotive industries attempt to deliver secured and enjoyable journey by exchanging information among the vehicles, inside vehicles, between vehicle and infrastructure utilizing wireless communication networks (WCN). In order to meet the requirements, a new printed spiral antenna with tapered feed is proposed to cover the navigational frequencies viz., 1.2 GHz, 1.5 GHz and WCN frequencies viz., 2.45 GHz, 3.3 GHz and Dedicated Short Range Communication (DSRC) frequency 5.8 GHz for vehicular network communications. 3D Electromagnetic (EM) tool is used for design and validated with Radio Frequency (RF) equipment. Further, path loss analysis for different vehicular environments are simulated using EM propagation tool and compared the simulated results with empirical model viz., ITU, Two-ray reflection, Dual slope model and COST 231 Walfisch Ikegami model.**

Keywords— Multiband; circular plarization; spiral antena; propagation model; vehicular communication.

I. INTRODUCTION (*HEADING 1*)

Today's transport systems are quite tricky and emerging vehicles are smart due to the rapid developments of technology. This requires effective reliable communication systems and speedy communication among vehicles for wireless automotive applications. Several researches have been dedicated to provide such communication between vehicles and with infrastructure and regarded as a vital part of upcoming Intelligent Transportation Systems (ITS) [1]. Dedicated Short Range Communication (DSRC) technology [2] is a part of ITS used for empowering wireless communication between vehicles and outside world. Currently in addition to the DSRC, ITS looking out for the vehicles with multi band capability to address various applications like navigation and wireless communications (Wi-Fi, Bluetooth) [3].

Several research works has been carried out for resonating multiple frequencies with single radiating element. This comprises fractal antenna [4-5], slot antenna [4], inverted F antennas [6-7], and Microstrip patch antenna [8]. The European standard EN 12253 [9] delivers the requirement for vehicular communication antenna. As per standard vehicular antenna need to be omni directional with left hand circular polarization (LHCP). The omnidirectional radiation pattern covers the wide range of communication area and circular polarization reduces the interference caused by reflection and provides independent antenna orientation. Currently, printed monopole antenna became prevalent for automotive systems because it could meet above-mentioned characteristics, i.e. omnidirectional pattern, compact size, low cost and ease to fabricate [10]. A dual band omnidirectional vertical polarized, coplanar monopole (cactus shaped) antenna is proposed [11] to meet vehicular antenna characteristics. In [12], two – hook facing opposite side in one plane and cross shaped monopole at the back plane is introduced to operate at 2.4 GHz, 5.2 GHz and 5.8 GHz. In [13], a thin ferrite rod is inserted between a patch and ground plane to reduce the antenna height. However, due to the magnetic loss gain is reduced. A 0.062λ wire-patch antenna gives an omnidirectional radiation pattern, but operates at a single frequency with vertical polarization [14]. The antennas observed in literature does contain omnidirectional pattern with linear polarization.

A key to miniaturize the antenna is maximizing the current flow in the conducting element. This is can be easily achievable with spiral structure. Several spiral monopole antenna are proposed to achieve multi band, circular polarization and omnidirectional radiation pattern [15 - 18]. Impedance matching is not uniform in spiral structure. A tapered feed helps to have smooth current flow from feed to patch, which improve the impedance matching. Hence, In this work we propose, a multiband single- arm spiral antenna with tapered feed which supports wireless communication services along with navigation services operates at IRNSS (1.2 GHz), GPS (1.5 GHz), Wi-Fi (2.4 GHz), WiMax (3.3 GHz) and DSRC (5.8 GHz). In spiral antenna, impedance matching is not uniform in all bands. To address this issue we introduced tapered feed line.

Furthermore, the awareness of propagation channel plays a vital role for vehicle-to-vehicle (V2V) and infrastructure - to – vehicle (I2V) communication systems since their property speaks system performance. Of precise curiosity, the path loss is the most important property of any wireless channel. Reflection, diffraction and scattering are the three basic propagation mechanisms which impact the propagation in any wireless communication system. Path loss for V2V communications that are in the literature [19-21] similar to other wireless systems and are depends on environment. Hence, we took different environments to understand the performance of the proposed antenna with respect to V2V and I2V communication systems. EM propagation simulation tool is utilized to analyze the performance of the proposed antenna. Also, we compared our simulated result with empirical model like ITU [22], two-ray reflection, COST 231 Walfisch Ikegami model [23] and dual slope model [24].

The paper is arranged as, in Section II outlines the design of the proposed antenna and simulation model for propagation analysis followed by Section III, the results and discussions on performance of the antenna.

II. Antenna Design and Characterization

A. Antenna Design

The proposed single arm multiband planar spiral antenna with tapered feed is constructed on the Rogers's 5880 substrate with permittivity of 2.2 and loss tangent of 0.0009 is shown in Fig. 1. The size of the dielectric substrate is calculated using microstrip patch antenna design formula [25]. In spiral antenna, the inner and outer radius decides frequency bands. In our work, for desired multiband operation, we modified the general spiral antenna design equation [26] such that the circumference of the inner circle radius as one fourth of the wavelength of lower frequency and outer circle radius as one fourth of the wavelength of upper frequency. The strip line dimensions are calculated using strip line equation [25]. In order to achieve better impedance matching, we introduced tapered microstrip feed line. The slope of the tapper is optimized to get better impedance matching.

Fig. 1. Prototype of the proposed antenna

B. Simulation Model

A large-Scale propagation model predicts the received power as a function of distance between transmitter and receiver. The propagation characteristics of V2V communication vary significantly based on surroundings. Reflection, diffraction and scattering are the three basic factors which impact the propagation of EM waves.

Propagation study is carried out using Remcom's Wireless InSite EM propagation tool [27]. It is a suite of ray- tracing model and EM solver for the examination of site-specific radio propagation. In this model, the straight road and buildings on both sides of the road are considered. Multiple reflections from the building surfaces and the road are considered. Minimum of single diffraction at buildings corner are taken into account. Though, it is assumed that the propagation paths have no shadowing by any other obstacles. The three different scenarios taken into account for our simulation model.

- Scenario 1 for V2V: The transmitter - receiver vehicles with proposed antenna system on the rear roof-top travelling on same direction with same velocity on the road with no buildings and other obstructions on each side.
- Scenario 2 for V2V: The transmitter - receiver vehicles with proposed antenna system on the rear roof-top travelling on same direction with same velocity on the road with buildings of uniform height and spacing and no obstructions on each side.
- Scenario 3 for V2V: The transmitter - receiver vehicles with proposed antenna system on the rear roof-top travelling on same direction with same velocity on the road with buildings of different height, uniform spacing and no obstructions on each side.
- Scenario 1 for I2V: The receiver vehicles with proposed antenna system on the rear roof-top travelling away from the transmitter on the road with no buildings and other obstructions on each side.
- Scenario 2 for I2V: The receiver vehicles with proposed antenna system on the rear roof-top travelling away from the transmitter on the road with buildings of uniform height and spacing and no obstructions on each side.
- Scenario 3 for I2V: The receiver vehicles with proposed antenna system on the rear roof-top travelling away from the transmitter on the road with buildings of different height, uniform spacing and no obstructions on each side.

The simulation parameters used for V2V and I2V are listed in Table I.

TABLE I. Simulation Parameters

Parameters	**V2V Values (units)**	**I2V Values (units)**
Maximum Reflection	10	10
Minimum Diffraction	1	1
ε_r, σ (Concrete Building)	7 , 0.015 S/M	7 , 0.015 S/M
ε_r, σ (Road) (S/M)	5.72, $5x10^{-4}$	5.72, $5x10^{-4}$
Antenna	Proposed	Proposed
Frequency	5.8 GHz	2.4/3.3/5.8 GHz
Transmitter Antenna Gain (G_T) (dB)	5.48	0
Receiver Antenna Gain (G_R) (dB)	5.48	1.88/1.52/5.48
Transmitted Power (P_t)	24 dBm[10]	30 dBm[28]
Polarization	LHCP	LHCP
Road Width	30 m	30 m
Transmitter Height	1.6 m	1.6 m
Receiver Height	30 m	1.6 m
Building Height	5 – 15 m	5 – 15 m

III. Results and Discussions

Keysight's Vector Network Analyzer (N9925A) is used to validate the antenna performance. The measured return loss is shown in Fig. 2. It has a good agreement with simulated result. The result shows that the proposed antenna resonates at desired multi bands. Table II gives the performance of the proposed antenna. Further, in this work we considered V2V communication at 5.8 GHz and I2V communication at WCN frequencies, 2.4 GHz and 3.3 GHz and DSRC, 5.8 GHz for further analysis. Table II gives the performance of the proposed antenna.

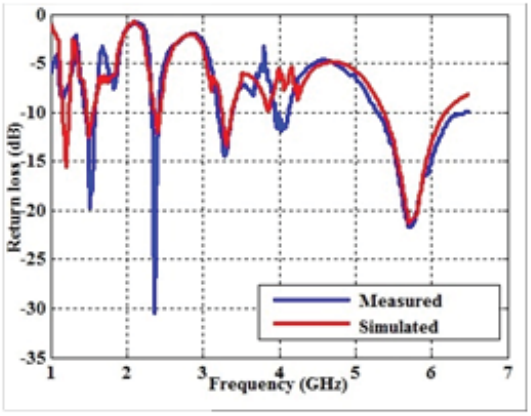

Fig. 2. Return loss of the proposed antenna.

TABLE II. Antenna Performance

Parameters	Frequency in GHz				
	1.2	*1.5*	*2.4*	*3.3*	*5.8*
Impedance BW(GHz)	0.17	0.11	0.09	0.19	1.10
Return loss (dB)	9.8	15.43	13.85	14.2	20.4
Gain (dB)	1.07	1.75	1.88	1.52	5.48
AR BW (%)	4.16	4.0	4.58	5.15	6.37
Radiation Efficiency (%)	82.1	89.7	89.8	85.0	94.7

Further, compared the performance of our work with recent multiband antennas on vehicular communications. Table III gives the performance comparison of proposed antenna with recent works. It shows that proposed antenna has better ARBW with reasonable gain.

For the analysis of V2V communication, initially two vehicles of 1.6 m height with proposed antenna systems moving on the same direction maintaining the separated distance as 10 m are considered and obtained the received power. By varying the separated distance in steps of 10 m observed the received power. This is carried out for all three V2V scenarios. For the analysis, the road's permittivity and building permittivity are considered.

TABLE III. Antenna Performance Comparisons

Ref.	Operating Frequencies (GHz)	Radiation Pattern	Gain (dB)	ARBW (%)
This Work	1.2 1.5 2.4 3.3 5.8	Omni directional with circular polarization	1.07 1.75 1.88 1.52 5.48	4.16 4.00 4.58 5.15 6.37
[6]	1.575 2.5 5.8	Omni Directional with circular polarization	** 2.1 3	1.26 2.40 5.00
[8]	1.8 2.4 3.5 5.8	Omni directional with linear polarization	2.6 2.3 3 2	NA
[9]	1.57 3.7 5.9	Directional with linear polarization	5.5 8.0 9.0	NA

For the analysis of I2V communication, at first the receiver vehicle of 1.6 m height with proposed antenna system on the rear roof – top at a distance of 10 m from transmitter is considered and obtained the received power. By moving the receiver vehicle received signal is observed. This is carried out for all three I2V scenarios. For further understanding, we considered empirical models like ITU® M 2135, COST 231 Walfisch Ikegami and Dual slope models and Two-ray reflection model.

We modified the Two-ray model equation according to circular polarization by applying superposition concept. The path loss is calculated for mentioned empirical models considering simulation parameters specified in Table I using path loss formula [22-24]. The received power is calculated using the general Friis equation,

$$R_R = T_P + G_T + G_R - L \qquad (1)$$

Where, L is path loss obtained from empirical models, T_P is the transmitted power, R_R is the received power and G_T and G_R are the transmitter and receiver gain.

The Fig. 3, Fig. 4 and Fig. 5 shows the comparison of I2V simulated and calculated received signal strength at 2.4 GHz, 3.3 GHz and at 5.8 GHz.

We infer that in I2V communication the surrounding building height does have less impact on propagation. Though the same transmitter and receiver height is considered in all scenarios, irrespective of frequency the received signal strength is of range -40 dBm to -50 dBm. Simulated received power is closer to the received power calculated through dual slope model. Whereas in V2V the environment has significant impact in propagation, shown in Fig. 6. We could infer that due to presence of buildings of same height there is a reduction of around 20 dB in received power is observed. In scenario 3 in the presence of different height comparatively slight increment in received power than received power without buildings. The received power obtained is closer to the COST 231 Walfisch Ikegami model.

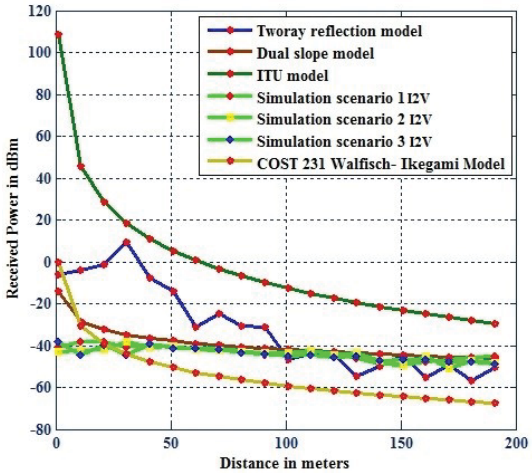

Fig. 3. Comparison of simulated I2V received signal strength with emperical models at 2.4 GHz.

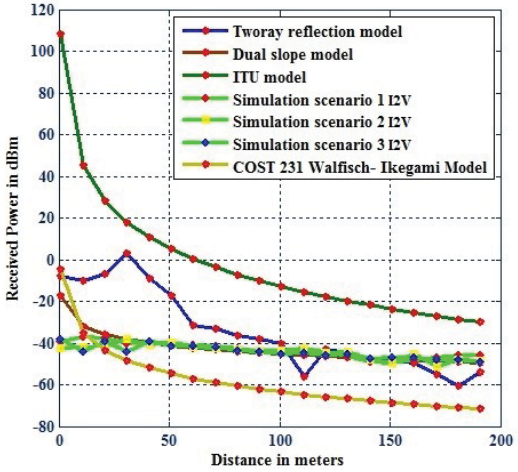

Fig. 4. Comarison of simulated I2V received signal strength with emperical model at 3.3 GHz.

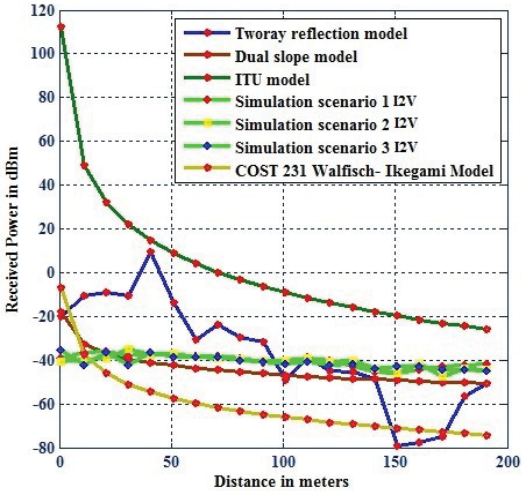

Fig. 5. Comarison of simulated I2V received signal strength with emperical model at 5.8 GHz.

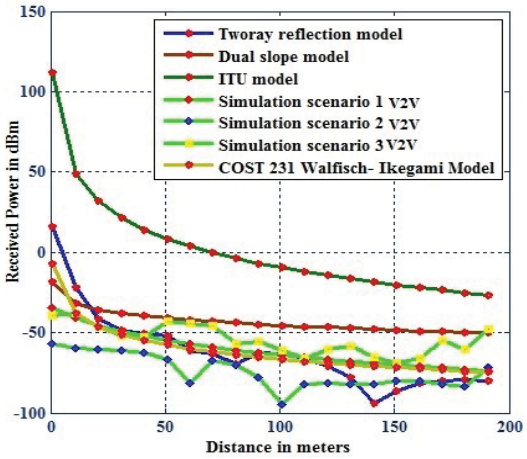

Fig. 6. Comparison of simulated V2V received signal strength with emperical model at 5.8 GHz.

IV. Conclusions

The design of a circularly polarized penta-band, single arm spiral antenna is presented with a compact size of size 51 x 35 x 1.574 mm3 to address Vehicular Wireless Applications for Navigational Communications and Terrestrial Wireless Network Communications. By introducing tapering in the feed line, better impedance matching is achieved at all desired bands. Further, path loss for V2V communications at different scenarios are analyzed and compared with empirical model. Through analysis, we infer I2V has less impact on propagation due to environment, whereas in V2V propagation has significant impact due environment. With the proposed antenna it is predicted that it is possible to have more than 200 m of line of sight communication. Thus the penta-band, omnidirectional pattern and circular polarization and good gain make the proposed antenna an appropriate applicant short range vehicular communications.

References

[1] ITS project website, http://www.its.dot.gov/index.htm, February 2007.

[2] “Standard Specification for Telecommunications and Information Exchange Between Roadside and Vehicle Systems–5GHz Band Dedicated Short Range Communications (DSRC) Medium Access Control (MAC) and Physical Layer (PHY) Specifications,” ASTM Std. E2213-03, 2003.

[3] C.H. Wang and X.Cheng “Vehicle-to-vehicle channel modeling and measurements: recent advances and future challenges”, IEEE Communications Magazine,Vol. 47, Issue 11, Nov. 2009.

[4] Mondal, Tapas, S. Samanta, R. Ghatak, and S. R. B. Chaudhuri. "A Novel Tri-Band Hexagonal Microstrip Patch Antenna Using Modified Sierpinski Fractal for Vehicular Communication." Progress In Electromagnetics Research C 57 : 25-34,2015.

[5] Raj, V. Dhana, A. M. Prasad, M. Satyanarayana, and G. M. V. Prasad. "Implementation of printed microstrip apollonian gasket fractal antenna for multi band wireless applications." IEEE International Conference on Signal Processing And Communication Engineering Systems (SPACES), , pp. 200-204., 2015.

[6] Wen-bo, Zeng, L. Xiang-yang, and L. Ji-xiang. "A dual-band RFID slot tag antenna for ITS application." In Consumer Electronics,

Communications and Networks (CECNet), 2013 3rd International Conference on, pp. 5-7. IEEE, 2013.

[7] M. T. Le, Q. C. Nguyen, T. P. Vuong, and C. Defay. "New metamaterial structure for the design of a high gain antenna at 5.8 GHz." In 2012 IEEE International Conference on Wireless Information Technology and Systems ,2012.

[8] Hossain, Md Robiul, and D. K. Karmokar. "Dual-band Inverted-F Antenna for Military and Intelligent Transportation System Applications." International Journal of Advancements in Research & Technology, Volume 1, Issue 6, November-2012 .

[9] Lee, Woncheol, Y.K. Hong, J.J. Lee, J.H. Park, and W. Seong. "Omnidirectional Low-Profile Multiband Antenna for Vehicular Telecommunication." Progress In Electromagnetics Research Letters 51: 53-59,2015.

[10] CEN, "Road Transport and traffic telematics – dedicated short range communication – physical layer using microwave at 5.8 GHz, 2004.

[11] N. Koch, Antennas for Automobiles. INTECH Open Access Publisher,2012.

[12] Gamage, K. H. Jagath , M. Engjom, and I. A. Jensen. "Design of a low profile multi-band antenna for vehicular communication system" IEEE 7th European Conference on Antennas and Propagation (EuCAP), , pp. 1273-1277., 2013.

[13] Rahman, Toyobur, Y. Zhaowen, and H. Youcef. "A dual band monopole microstriop printed antenna for WLAN (2.4/5.2/5.8 GHz) application." InMicrowave Technology & Computational Electromagnetics (ICMTCE), 2013 IEEE International Conference on, pp. 204-207. IEEE,2013.

[14] Moon, H., G.-Y. Lee, C.-C. Chen, and J. L. Volakis, "An extremely low-profile ferrite-loaded wideband VHF antenna design," IEEE Antenn. Wireless Propag. Lett., Vol. 11, 322–325, 2012.

[15] H., T. Lee, W. Jang, and J. Lee. "Miniaturization of planar spiral monopole antennas with parasitic elements for terrestrial DMB application." In IEEE Int. Symp. Antennas and Propag.(ISAP), pp. 573-576.

[16] Zhang, Fu-Shun, Yang-Tao Wan, Dan Yu, and Bing Ye. "A Microstrip-Fed Multiband Spiral Ring Monopole Antenna with Improved Radiation Characteristics at Higher Resonant Frequencies." Progress In Electromagnetics Research C 41 , 97-109., 2013.

[17] Haridas, T. Nakul, Arslan, and A. T. Erdogan. "Multiband Antenna for Space Based Reconfigurable Satellite Sensor Node." In Wideband, Multiband Antennas and Arrays for Defence or Civil Applications, 2008.

[18] Zhang, Yangjun, T. Nakata, and T. Miyashita. "A miniature circular disc monopole UWB antenna with a tapered feed line and a circular ground." In Microwave Conference, 2008 China-Japan Joint, pp. 411-414. IEEE, 2008.

[19] Viriyasitavat, Wantanee, M. Boban, H.M. Tsai, and A. Vasilakos. "Vehicular Communications: Survey and Challenges of Channel and Propagation Models." IEEE Vehicular Technology Magazine, 10, no. 2 : 55-66,2015.

[20] Boban, Mate, J. Barros, and O. Tonguz. "Geometry-based vehicle-to-vehicle channel modeling for large-scale simulation." IEEE Transactions on Vehicular Technology, 63, no. 9: 4146-4164,2014.

[21] Molisch,F. Andreas , and F. Tufvesson. "Propagation channel models for next-generation wireless communications systems." IEICE Transactions on Communications 97, no. 10 :2022-2034,2014.

[22] https://www.itu.int/pub/R-REP-M.2135.

[23] Wireless Communications: Principles and Practice,Rappaport,Pearson Education India, 2009.

[24] Karedal, Johan, N. Czink, A. Paier, F. Tufvesson, and F. Andreas Molisch. "Path loss modeling for vehicle-to-vehicle communications." Vehicular Technology, IEEE Transactions on 60, no. 1 : 323-328,2011.

[25] Microstrip and Printed Antenna Design", Randy Bancroft, Second Edition, Institution of Engineering and Technology, 2009.

[26] "Antenna Theory Analysis and Design", Constantine A.Balanis, Second Edition, Jon Wiley & Sons, Inc. Publication, 2005.

[27] http://www.remcom.com/wireless-insite.

[28] http://www.air802.com/files/FCC-Rules-and-Regulations.pdf.

THE 18TH INTERNATIONAL SYMPOSIUM ON WIRELESS PERSONAL MULTIMEDIA COMMUNICATIONS
(WPMC-2015)
December 13-16, 2015, Hyderabad, India

An Efficient Deterministic Scheme for Blind CFO Estimation in SC-FDMA

Vinay Kumar Trivedi, *StudentMember*, *IEEE*, Vidya Sagar and Preetam Kumar, *Member*, *IEEE*
Department of Electrical Engineering
Indian Institute of Technology Patna
Bihar 800013, India
Email: {vinay.pee14, vidya.mtee13, pkumar}@iitp.ac.in

***Abstract*—Single Carrier Frequency Division Multiple Access (SC-FDMA) is becoming popular compared to Orthogonal Frequency Division Multiple Access (OFDMA) on uplink transmission because of its low peak to average power ratio (PAPR), however SC-FDMA is more sensitive to carrier frequency offset (CFO). This paper proposes an efficient blind CFO estimation algorithm for SC-FDMA scheme. In this method two folded oversampled SC-FDMA symbol with cyclic prefix (CP) is used to generate two SC-FDMA symbols with time difference.Using these two SC-FDMA symbols, a cost function is modelled that can be expressed as a cosine function. The property of this cosine function is used to derive an expression for estimating CFO. Unlike Maximum Likelihood (ML) method, there is no need to search all frequency offset range for CFO estimation. In the proposed method, only three cost function values are required at three different values of frequency offsets. The proposed algorithm is best suited for wireless applications as it only requires one SC-FDMA symbol for reliable blind estimation of CFO. The simulation results show that the proposed algorithm for CFO estimation outperforms ML method at high SNR, and it is also seen that accuracy of proposed algorithm is independent of the searching step size.**

***Index Terms*—Carrier frequency offset, Single Carrier Frequency Division Multiple Access (SC-FDMA), Blind Deterministic (BD), Maximum Likelihood (ML).**

I. Introduction

Over the last decade, the demand for higher data rates has increased rapidly making the channel frequency selective and resulting into Inter Symbol Interference (ISI) [1]. In order to mitigate this effect, multi-carrier modulation technique is used. Orthogonal Frequency Division Multiplexing (OFDM) is one of the efficient multi-carrier modulation technique in which the bandwidth of sub-carrier is designed to be smaller than the coherence bandwidth of the channel, resulting into frequency flat channel and thus simplifying the equalization process. Long Term Evolution (LTE) adopt SC-FDMA for uplink transmission due to its low Peak to Average Power Ratio (PAPR), as power is an important concern for Mobile Station (MS). But SC-FDMA is more sensitive to CFO compared to OFDMA [2]. If CFO is present between transmitter and receiver, the orthogonality between sub-carriers is destroyed which results into inter-carrier interference (ICI) and multi-user Interference (MUI).

Several schemes has been proposed to estimate the CFO from last two decades, still there is a need of an efficient and less complex scheme for CFO estimation of SC-FDMA and thereby correcting its effect. A frequency domain Compensation scheme for SC-FDMA using pilot signal has been proposed in [3] also a blind deterministic CFO estimation using oversampling has been proposed for OFDM [4].

This paper proposes an efficient blind deterministic CFO estimation algorithm for SC-FDMA.This work is the application of solution presented in [5] for OFDM in a new scenario i.e. SC-FDMA. In this method two folded oversampled SC-FDMA symbol with cyclic prefix (CP) is used to generate two SC-FDMA symbols with time difference. These two SC-FDMA symbols are then used to model a cost function in terms of cosine function which is used to estimate CFO. This paper is organised as follows, the system model for SC-FDMA scheme is introduced in section II. In section III a novel deterministic algorithm is proposed for blind estimation of CFO. In section IV simulation result is discussed. Finally, in section V conclusions are presented.

II. Proposed Deterministic Algorithm for Blind CFO Estimation

A. System Model

System model for SC-FDMA with interleaved sub-carrier allocation has been considered, where N is number of sub-carriers that can support a maximum of U users, therefore number of sub-carriers that can be allotted to each user is $R = N/U$ and only one user is active at a time (uplink situation). The data of each user is mapped to QPSK symbols which is given to M point DFT block. The l^{th} sample after DFT operation is represented as ,

$$X_k(l) = \sum_{m=0}^{M-1} x_u(m) e^{-j2\pi ml/N}, \quad 0 \le l \le R-1 \qquad (1)$$

where $x_u(m)$ represents modulated source symbols of u^{th} user. The M point DFT produces M frequency domain symbols that modulate orthogonal sub-carriers. The sub-carrier index of u^{th} user after mapping is $I_u = \{v_u + lU\}$, where l represents the l^{th} sample of symbol after DFT block and v_u denotes the starting sub-carrier index of the u^{th} user. After that IDFT is applied to $S_u(k)$,which is frequency domain samples after sub-carrier allocation at k^{th} sub-carrier produces transmitted time domain

channel symbols s_u.

$$s_u(m) = \frac{1}{N}\sum_{k=0}^{N-1} S_u(k) e^{j2\pi km/N}, \quad 0 \le k \le N-1 \tag{2}$$

where, $S_u(k) \neq 0$, for $k \in I_u$. A cyclic prefix (CP) of length N_{cp} is inserted at the beginning of each transmitted SC-FDMA frame. CP length should be large as compared to channel impulse response(CIR) length.

B. Cost Function for CFO Estimation

This paper proposes an algorithm to estimate the fractional part of the normalized CFO in SC-FDMA transmission scheme [5]. In absence of CFO the two folded oversampled received SC-FDMA symbol can be expressed as,

$$r_u(q) = \frac{1}{N}\sum_{k=0}^{R-1} H(k) X_u(k) e^{j2\pi(v_u+kU)q/2N} \tag{3}$$

where, $X_u(k)$ and $H(k)$ denotes the transmitted SC-FDMA symbol and channel impulse response for k^{th} sub-carrier in frequency domain respectively and R denotes the number of sub-carriers allocated to each user. The normal received SC-FDMA symbol $r_u(2m)$ is obtained from $r_u(q)$ by removing CP and considering even samples as shown in Fig.1.

$$r_u(2m) = \frac{1}{N}\sum_{k=0}^{R-1} H(k) X_u(k) e^{j2\pi(v_u+kU)m/N} \tag{4}$$

The early received SC-FDMA symbol $r_u(2m-2i-1)$ can be

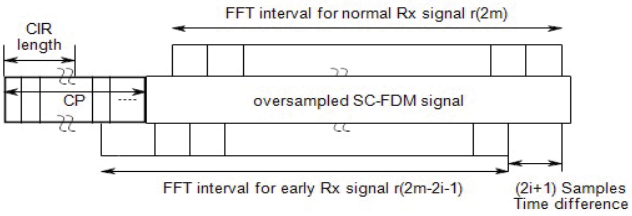

Figure 1: Normal and early Rx-SC-FDMA symbols from two folded oversampled received SC-FDMA symbol

obtained by shifting the starting point of the normal received SC-FDMA symbol to $(2i+1)$.

$$r_u(2m-2i-1) = \frac{1}{N}\sum_{k=0}^{R-1} H(k) X_u(k) e^{j2\pi(v_u+kU)(m-i-1/2)/N} \tag{5}$$

Here the time difference factor i is an integer that is used to overcome ISI, given $N_{cp} - CL \ge i$, where N_{cp} and CL denotes the CP length and channel impulse response (CIR) length. In the absence of CFO, the normal and early received SC-FDMA symbol holds the time invariant property in frequency domain and that can be written as,

$$\begin{aligned} R_u(k) &= \frac{1}{N}\sum_{m=0}^{R-1} r_u(2m) e^{-j2\pi(v_u+kU)m/N} \\ &= H(k) X_u(k) \end{aligned} \tag{6}$$

Similarly,

$$R_{ui}(k) = H(k) X_u(k) e^{-j2\pi(i+1/2)(v_u+kU)/R} \tag{7}$$

If the phase shift due to time shifting is compensated then both the signals are identical in frequency domain.

$$R_u(k) = R_{ui}(k) e^{j2\pi(i+1/2)(v_u+kU)/N} \tag{8}$$

On the other hand, if CFO (ε) is present, then phase shift of $e^{j2\pi\varepsilon/2R}$ comes in each sample of the received oversampled symbol $r_u(q)$. Therefore, the normal and early received SC-FDMA symbol can be obtained as,

$$r_u(2m) = \frac{1}{N}\sum_{k=0}^{R-1} H(k) X_u(k) e^{j2\pi(v_u+(k+\varepsilon)U)m/N} \tag{9}$$

and

$$r_u(2m-2i-1) = \frac{1}{N}\sum_{k=0}^{R-1} H(k) X_u(k) e^{j2\pi(v_u+(k+\varepsilon)U)(m-i-1/2)/N} \tag{10}$$

This CFO now results in ICI due to which $r_u(2m)$ and $r_u(2m-2i-1)$ does not hold time shift invariant property anymore. Therefore, before DFT operation CFO should be compensated, and to do this a trial CFO $\hat{\varepsilon}$ is introduced. The compensation is done by multiplying $e^{-j2\pi\hat{\varepsilon}m/R}$ and $e^{-j2\pi\hat{\varepsilon}(m-i-1/2)/R}$ with $r_u(2m)$ and $r_u(2m-2i-1)$ respectively. The CFO compensated signal in frequency domain can be expressed as,

$$D(l,\hat{\varepsilon}) = \sum_{m=0}^{R-1} \left\{ r_u(2m) e^{-j2\pi m\hat{\varepsilon}/R} \right\} e^{-j2\pi m(v_u+lU)/N} \tag{11}$$

and

$$\begin{aligned} D_i(l,\hat{\varepsilon}) = \sum_{m=0}^{R-1} &\left\{ r_u(2m-2i-1) e^{-j2\pi(m-i-1/2)\hat{\varepsilon}/R} \right\} \\ &\times e^{-j2\pi m(v_u+lU)/N} \end{aligned} \tag{12}$$

The CFO is exactly compensated when $\hat{\varepsilon} = \varepsilon$.

$$D(l,\hat{\varepsilon}) - D_i(l,\hat{\varepsilon}) e^{j2\pi(i+1/2)(v_u+lU)/N} = 0 \tag{13}$$

Using equation (13), a least square function or cost function can be defined as,

$$\xi(\hat{\varepsilon}) = \sum_{l=0}^{R-1} \left| D(l,\hat{\varepsilon}) - D_i(l,\hat{\varepsilon}) e^{j2\pi(i+1/2)(v_u+lU)/N} \right|^2 \tag{14}$$

Therefore, the estimated CFO $\hat{\varepsilon}$ for which cost function (14) can be minimized is

$$\begin{aligned} \hat{\varepsilon} &= arg \min_{\hat{\varepsilon}} \xi(\hat{\varepsilon}) \\ &= arg \min_{\hat{\varepsilon}} \sum_{l=0}^{R-1} \left| D(l,\hat{\varepsilon}) - D_i(l,\hat{\varepsilon}) e^{j2\pi(i+1/2)(v_u+lU)/N} \right|^2 \end{aligned} \tag{15}$$

To estimate the CFO, we iteratively calculate the cost function by gradually increasing the value of $\hat{\varepsilon}$ with predetermined resolution step size, which should be kept very small for better accuracy but on the other hand computation increases with decreasing resolution step size. To solve this problem, an

efficient blind deterministic CFO estimation method has been proposed in which there is no need to search for all the values of $\hat{\varepsilon}$.

C. Evaluating the Cost Function in terms of Cosine Function

1) In the Absence of Noise: In presence of CFO ε, the normal received SC-FDMA and the early received SC-FDMA symbols in time domain become $r_u(2m)e^{j2\pi m\varepsilon/N}$ and $r_u(2m-2i-1)e^{j2\pi(m-i-1/2)\varepsilon/N}$ respectively [5]. The normal received and early received SC-FDMA symbols in frequency domain can be expressed as,

$$R_u(l) = \frac{1}{N}\sum_{k=0}^{R-1} H(k)X_u(k)\sum_{m=0}^{R-1} e^{j2\pi m(k-l+\varepsilon)/R}, \quad (U/N = 1/R) \tag{16}$$

and

$$\begin{aligned} R_{ui}(l) =& \frac{1}{N}\sum_{k=0}^{R-1} H(k)X_u(k)e^{-j2\pi(i+1/2)(v_u+(k+\varepsilon)U)/N} \\ & \times \sum_{m=0}^{R-1} e^{j2\pi m(k-l+\varepsilon)/R} \end{aligned} \tag{17}$$

If $\varepsilon \neq 0$, the phase difference between $R_u(l)$ and $R_{ui}(l)$ can be compensated by multiplying $e^{j2\pi(i+1/2)(v_u+lU)/N}$ with $R_{ui}(l)$.

$$\begin{aligned} & R_{ui}(l)e^{j2\pi(i+1/2)(v_u+lU)/N} \\ & = \frac{1}{N}\sum_{k=0}^{R-1} H(k)X_u(k)e^{-j2\pi(i+1/2)(k-l+\varepsilon)/R} \\ & \times \sum_{m=0}^{R-1} e^{j2\pi m(k-l+\varepsilon)/R} \end{aligned} \tag{18}$$

Now,

$$\begin{aligned} & R_u(l) - R_{ui}(l)e^{j2\pi(i+1/2)(v_u+lU)/N} \\ & = \frac{1}{N}\sum_{k=0}^{R-1} H(k)X_u(k)\frac{1-e^{j2\pi\varepsilon}}{1-e^{j2\pi(k-l+\varepsilon)/R}} \\ & \times (1-e^{-j2\pi(i+1/2)(k-l+\varepsilon)/R}) \\ & = \frac{1}{N}\sum_{k=0}^{R-1} H(k)X_u(k)\ \mu(l,k,\varepsilon)\ (1-e^{j2\pi\varepsilon}) \end{aligned} \tag{19}$$

where,

$$\mu(l,k,\varepsilon) = \frac{1-e^{-j2\pi(i+1/2)(k-l+\varepsilon)/R}}{1-e^{j2\pi(k-l+\varepsilon)/R}} \tag{20}$$

The function $\mu(l,k,\varepsilon)$ is independent of ε [5]. So, $\left|R_u(l) - R_{ui}(l)e^{j2\pi(i+1/2)(v_u+lU)/N}\right|^2$ will be sinusoidal with respect to ε and independent of k and l. Therefore, equation (20) can be written as,

$$\mu(k,l,\varepsilon) = \mu_R(k,l) + j\mu_I(k,l) \tag{21}$$

Substituting the value of $\mu(k,l,\varepsilon)$ in equation (19),

$$\begin{aligned} & R_u(l) - R_{ui}(l)e^{j2\pi(i+1/2)(v_u+lU)/N} \\ & = \frac{1}{N}\sum_{k=0}^{R-1} H(k)X_u(k)\left\{\mu_R(k,l) + j\mu_I(k,l)\right\}(1-e^{j2\pi\varepsilon}) \\ & = (\alpha(l) + j\beta(l))(1-e^{j2\pi\varepsilon}) \end{aligned} \tag{22}$$

where,

$$\alpha(l) = Re\left\{\frac{1}{N}\sum_{k=0}^{R-1} H(k)X_u(k)\left\{\mu_R(k,l) + j\mu_I(k,l)\right\}\right\} \tag{23}$$

and

$$\beta(l) = Im\left\{\frac{1}{N}\sum_{k=0}^{R-1} H(k)X_u(k)\left\{\mu_R(k,l) + j\mu_I(k,l)\right\}\right\} \tag{24}$$

Using equation (22),

$$\begin{aligned} & \left|R_u(l) - R_{ui}(l)e^{j2\pi(i+1/2)(v_u+lU)/N}\right|^2 \\ & = (\alpha^2(l) + \beta^2(l)) \times 2(1-cos2\pi\varepsilon) \end{aligned} \tag{25}$$

Therefore, the cost function given in equation (14) can be formulated in terms of cosine function as,

$$\begin{aligned} \xi(\hat{\varepsilon}) =& \sum_{l=0}^{R-1}\left|D(l,\hat{\varepsilon}) - D_i(l,\hat{\varepsilon})e^{j2\pi(i+1/2)(v_u+lU)/N}\right|^2 \\ =& S(1-cos2\pi(\varepsilon-\hat{\varepsilon})) \end{aligned} \tag{26}$$

where, $S = 2\sum_{l=0}^{R-1}(\alpha^2(l) + \beta^2(l))$.

2) In Presence of Noise: The received two folded oversampled signal in presence of noise can be expressed as,

$$r_u(q) = \frac{1}{N}\sum_{k=0}^{R-1} H(k)X_u(k)e^{j2\pi(v_u+(k+\varepsilon)U)q/2N} + w(q) \tag{27}$$

where, $w(q) = w_R(q) + w_I(q)$ is complex Gaussian noise with mean and variance of both real and imaginary part to be zero and $\sigma_w^2/2$ respectively. As complex Gaussian noise is present, let us define $W(l,\hat{\varepsilon})$ and $W_i(l,\hat{\varepsilon})$ as,

$$W(l,\hat{\varepsilon}) = \sum_{m=0}^{R-1}\left\{w(2m)e^{-j2\pi m\hat{\varepsilon}/R}\right\}e^{-j2\pi m(v_u+lU)/N} \tag{28}$$

$$\begin{aligned} W_i(l,\hat{\varepsilon}) = & \sum_{m=0}^{R-1}\left\{w(2m-2i-1)e^{-j2\pi(m-i-1/2)\hat{\varepsilon}/R}\right\} \\ & \times e^{-j2\pi m(v_u+lU)/N} \end{aligned} \tag{29}$$

Again $D(l,\hat{\varepsilon}) - D_i(l,\hat{\varepsilon})e^{j2\pi(i+1/2)(v_u+lU)/N}$ with noise component can be evaluated as,

$$\begin{aligned} & D(l,\hat{\varepsilon}) - D_i(l,\hat{\varepsilon})e^{j2\pi(i+1/2)(v_u+lU)/N} \\ & = \left\{\alpha(l) + j\beta(l)\right\}(1-e^{j2\pi(\varepsilon-\hat{\varepsilon})}) + \eta_R(l,\hat{\varepsilon}) + j\eta_I(l,\hat{\varepsilon}) \end{aligned} \tag{30}$$

Where,

$$\eta_R(l,\hat{\varepsilon}) = Re\left\{W(l,\hat{\varepsilon}) - W_i(l,\hat{\varepsilon})e^{j2\pi(i+1/2)(v_u+lU)}\right\}$$

and

$$\eta_I(l,\hat{\varepsilon}) = Im\left\{W(l,\hat{\varepsilon}) - W_i(l,\hat{\varepsilon})e^{j2\pi(i+1/2)(v_u+lU)}\right\}$$

respectively, and assumed to have i.i.d. (independent identical distribution) with zero mean and $\sigma_n/2$ variance. Therefore, the cost function with noise can be expressed as,

$$\begin{aligned}\xi(\hat{\varepsilon}) &= S(1-cos2\pi(\varepsilon-\hat{\varepsilon}))\\ &+\sum_{l=0}^{R-1}\eta_R(l,\hat{\varepsilon})\{\alpha(l)(1-cos2\pi(\varepsilon-\hat{\varepsilon}))+\beta(l)sin2\pi(\varepsilon-\hat{\varepsilon})\}\\ &+\sum_{l=0}^{R-1}\eta_I(l,\hat{\varepsilon})\{\beta(l)(1-cos2\pi(\varepsilon-\hat{\varepsilon}))-\alpha(l)sin2\pi(\varepsilon-\hat{\varepsilon})\}\\ &+\sum_{l=0}^{R-1}\left\{\eta_R^2(l,\hat{\varepsilon})+\eta_I^2(l,\hat{\varepsilon})\right\}\end{aligned} \tag{31}$$

D. Blind Deterministic CFO Estimation

The cost function shown in equation (31) can be represented as,

$$\xi(\hat{\varepsilon}) = S(1-cos2\pi(\varepsilon-\hat{\varepsilon}))+V \tag{32}$$

where,V is the DC component of noise, which comes due to $\sum_{l=0}^{R-1}\left\{\eta_R^2(l,\hat{\varepsilon})+\eta_I^2(l,\hat{\varepsilon})\right\}$. Using which,

$$\xi(0) = S(1-cos2\pi\varepsilon)+V \tag{33}$$

$$\xi(0.25) = S(1-sin2\pi\varepsilon)+V \tag{34}$$

and

$$\xi(0.5) = S(1+cos2\pi\varepsilon)+V \tag{35}$$

Using equation (33) and equation (35), we get,

$$S+V = \frac{\xi(0)+\xi(0.5)}{2} \tag{36}$$

Therefore,

$$Scos(2\pi\varepsilon) = \frac{\xi(0.5)-\xi(0)}{2} \tag{37}$$

$$Ssin(2\pi\varepsilon) = \frac{\xi(0.5)+\xi(0)}{2}-\xi(0.25) \tag{38}$$

using equation (37) and (38), a complex variable y is defined to estimate CFO ε as follows,

$$\begin{aligned}y &= Scos(2\pi\varepsilon)+jSsin(2\pi\varepsilon)\\ &=\left\{\frac{\xi(0)-\xi(0.5)}{2}\right\}+j\left\{\frac{\xi(0)+\xi(0.5)}{2}-\xi(0.25)\right\}\end{aligned} \tag{39}$$

Therefore, the deterministically estimated CFO is,

$$\hat{\varepsilon} = \frac{1}{2\pi}tan^{-1}\angle\, y \tag{40}$$

Since, the phase of y is in the range $[-\pi,\pi)$. The above expression can be used to estimate the CFO between the range $-0.5\le\hat{\varepsilon}<0.5$. It is to be noted that the proposed algorithm is independent of step size taken.

E. Cramer-Rao Lower Bound (CRLB) for the Proposed Deterministic Estimator

The Cramer-Rao lower bound can be used to obtain the asymptotic variance of the blind estimator [5]. In equation (30) the additive Gaussian noise is normally distributed, and the large sample variance of least square estimator and maximum likelihood estimator coincide in the equation (30). The log likelihood function using equation (30), after neglecting the constant terms can be written as,

$$\begin{aligned}&lnF(\varepsilon,\alpha(l),\beta(l))\\ &\quad=\frac{1}{P}\sum_{e=-P/2}^{P/2-1}-\frac{1}{\sigma_n^2}\times|k(l,p/P)-\left\{1-e^{j2\pi(\varepsilon-p/P)}\right\}|^2\end{aligned} \tag{41}$$

Here constant terms are omitted and P denotes the total observation that has been taken and $k(l,p/P)=D(l,p/P)-D_i(l,p/P)e^{j2\pi(i+1/2)l/N}$.

In equation (41) $(\varepsilon,\alpha(l),\beta(l))$ are unknown parameters, so the (3×3) Fisher information matrix is obtained as

$$\begin{aligned}E\left[\frac{\partial^2 lnF}{\partial\varepsilon^2}\right] &= -\frac{8\pi^2\left\{\alpha^2(l)+\beta^2(l)\right\}}{\sigma_n^2}\\ E\left[\frac{\partial^2 lnF}{\partial\varepsilon\partial\alpha(l)}\right] &= \frac{4\pi\beta(l)}{\sigma_n^2}\\ E\left[\frac{\partial^2 lnF}{\partial\varepsilon\partial\beta(l)}\right] &= -\frac{4\pi\alpha(l)}{\sigma_n^2}\\ E\left[\frac{\partial^2 lnF}{\partial\alpha(l)\partial\beta(l)}\right] &= 0\\ E\left[\frac{\partial^2 lnF}{\partial\alpha^2(l)}\right] &= -\frac{4}{\sigma_n^2}\\ E\left[\frac{\partial^2 lnF}{\partial\beta^2(l)}\right] &= -\frac{4}{\sigma_n^2}\end{aligned} \tag{42}$$

Therefore, from equation (42) the asymptotic variance of estimated CFO for the l^{th} sub-carrier frequency index can be derived as

$$Var(\hat{\varepsilon}) \ge \frac{\sigma_n^2}{4\pi^2\left\{\alpha^2(l)+\beta^2(l)\right\}} \tag{43}$$

The above equation can also be derived for total sub-carriers $0\le l\le R-1$ as

$$Var(\hat{\varepsilon}) \ge \frac{\sigma_n^2}{4\pi^2\sum_{l=0}^{R-1}\left\{\alpha^2(l)+\beta^2(l)\right\}} \tag{44}$$

III. Simulation Result and Discussion

In this section BER performance of ML(Maximum Likelihood), BD(Blind Deterministic), CRLB(Cramer-Rao Lower Bond for BD), and PE(Perfect estimation) frequency offset

estimation algorithm is discussed. The six independent multi-path rayleigh fading channel has been considered. Table I shows the delay profile for multi-paths with 29 samples CIR length. The SC-FDMA symbols are transmitted at 25 *ksps* with symbol duration of 40 μsec. The duration of cyclic prefix is 8 μsec. Normal sampling interval is 0.25 μsec in such a way that one SC-FDMA symbol consists of 160 sampling points in which 32 sampling points are for CP ($N_{cp} = 32$). The total number of sub-carriers is 128. It is considered that every user uses 32 sub-carriers with interleaved sub-carrier allocation and for simulation purpose, normalized CFO is assumed to be 0.212.

Table I: Multi-path Delay Profile

	1st Tap	2nd Tap	3rd Tap
Relative delay	0.0	5.5	11.5
Initial complex gain	1.05-j0.82	0.71+j0.45	0.63-j0.72
	4th Tap	5th Tap	6th Tap
Relative delay	17.0	23.5	29.0
Initial complex gain	0.53+j0.62	0.41+j0.37	0.20-j0.34

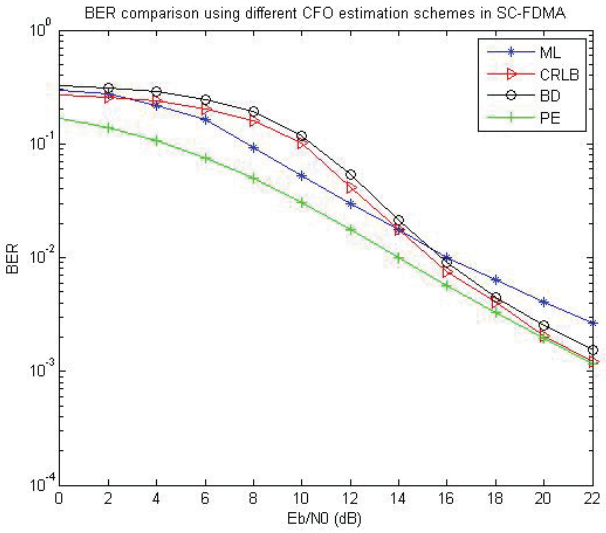

Figure 2: BER performance comparison in SC-FDMA system using ML, Blind Deterministic,CRLB and Perfect Estimation.

Fig.2 shows the BER performance comparison using QPSK modulation with different CFO estimator. It is considered that channel frequency response at the receiver is known. and a time difference factor of $i = 3$ has been considered. Notice that the BER using blind deterministic method and ML method is approximately same at 15 dB. The proposed scheme outperforms ML estimation method by approximately 1.5 dB with searching step size 0.024 at 10^{-3} BER. Fig.3 shows comparison of mean square error performance of different estimation schemes.The proposed scheme outperform approximately 3 dB at 10^{-4} mean square error. The complexity of ML method is large compared to blind deterministic method. The performance of ML method gets improved if the step size

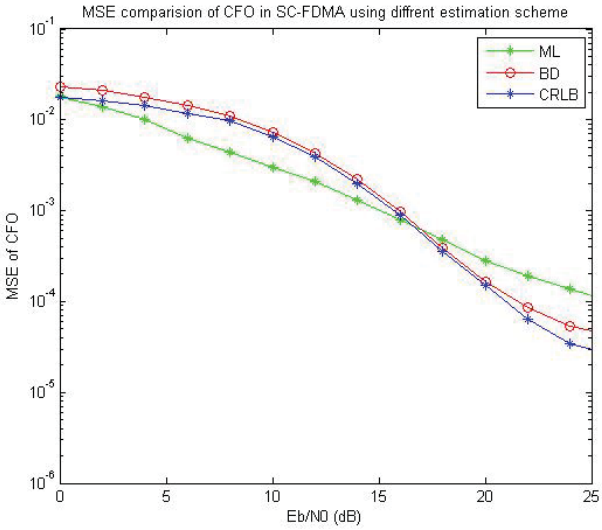

Figure 3: Mean square error performance comparison in SC-FDMA system using ML, Blind Deterministic,CRLB Estimation.

reduces also it is shown that Blind deterministic estimation is suitable to be use in high SNR environment.

IV. CONCLUSION

In this paper, an efficient deterministic algorithm for blind CFO estimation has been proposed for SC-FDMA. Unlike ML scheme, the proposed scheme does not require solution of higher order polynomial equation and only requires two SC-FDMA symbols with a time difference, which is obtained by using oversampling and CP. These two SC-FDMA symbols are then used to calculate a cost function. In proposed scheme a closed form expression is derived which requires only three values of cost function to estimate CFO. The simulation result shows that the proposed scheme out performs ML estimation scheme.

ACKNOWLEDGMENT

This work has been supported by the Centre of Excellence on Advanced System Engineering, IIT Patna vide project no. R&DINT/EE/CAS/PED/2014-15/90

REFERENCES

[1] T.Hwang, C. Yang, G. Wu,S.Li, and G. Y. Li, "OFDM and its wireless applications: A survey,"*IEEE Trans. Veh. Technol.,* vol. 58, no.4, pp. 1673-1694, May 2009.

[2] Raghunath, K., Chockalingam, A., "SC-FDMA Versus OFDMA: Sensitivity to Large Carrier Frequency and Timing Offsets on the Uplink," *Global Telecommunications Conference, 2009. GLOBECOM 2009. IEEE,* vol., no., pp.1,6, Nov. 30 2009-Dec. 4 2009

[3] A. Cao, G. Wang, Yi Ma, P. Xiao, Tafazolli, R., "Frequency domain pilot-based carrier frequency offset estimation in SC-FDMA system," *Wireless Communications Systems (ISWCS), 2014 11th International Symposium on* , vol., no., pp. 27-32, Aug. 2014.

[4] B. Chen and H. Wang, "Blind estimation of OFDM carrier frequency offset via oversampling,"*IEEE Trans. Signal Process.,* vol. 52, no.7, pp. 2047-2057, July 2004.

[5] H.G. Jeon, K.S. Kim, and E. Serpedin "An Efficient Blind Deterministic Frequency Offset Estimator for OFDM Systems,"*IEEE Trans. Commun.,* vol. 59, no.4, pp. 1133-1141, April 2011.

THE 18TH INTERNATIONAL SYMPOSIUM ON WIRELESS PERSONAL MULTIMEDIA COMMUNICATIONS
(WPMC-2015)
December 13-16, 2015, Hyderabad, India

Investigation on Listen-Before-Talk Mechanism of Licensed-Assisted Access to Unlicensed Spectrum

Yu Jiang†, Hiroki Harada††, Liu Liu†, Huiling Jiang† and Satoshi Nagata††
† DOCOMO Beijing Communications Laboratories Co., Ltd, China
{jiangy, liul, jiang}@docomolabs-beijing.com.cn
†† NTT DOCOMO, INC, Japan
{hiroki.harada.sv, nagatas}@nttdocomo.com

***Abstract*—Lack of available spectrum has severely restricted the increase of network capacity. In 3rd Generation Partnership Project (3GPP) Release 13, Licensed-assisted access to Unlicensed Spectrum (LAA) has been proposed to explore the spectrum in unlicensed band and to meet the rapidly increasing demands of data service. Listen-before-talk (LBT) is regarded as a feasible mechanism for LAA to fairly co-exist with other radio access technologies (RATs) in unlicensed spectrum, such as Wi-Fi. There are two typical LBT mechanisms, Frame-Based-Equipment (FBE) and Load-Based-Equipment (LBE), according to the European regulatory requirements. FBE can achieve frequency reuse among cells by applying simultaneous clear channel assessment (CCA) for channel occupancy every fixed period. Due to the periodic CCA, it does not have much opportunity to utilize the channel. On the other hand, LBE achieves higher probability of channel access as it senses the channel continuously until the channel becomes available. However, its transmit efficiency is low since it is hard to obtain frequency reuse. In this paper, we propose an enhanced LBT mechanism based on FBE to decouple the period of CCA and transmission burst by applying short CCA interval. Thus, it achieves both frequency reuse and high probability of channel access. System level evaluations show that the proposed LBT scheme for LAA ensures the efficiency of intra-operator co-existence of LAA and provide high throughput performance for both Wi-Fi and LAA in inter-operator co-existence between Wi-Fi and LAA.**

Keywords—Listen-before-talk, LAA, Wi-Fi, LBE, FBE, frequency reuse

I. INTRODUCTION

In recent years, Long-Term Evolution (LTE), which is standardized by 3rd Generation Partnership Project (3GPP) and regarded as 4th generation (4G) cellular networks, has been deployed in the most areas of the world. However, lack of available spectrum has severely restricted the increase in network capacity to cope with rising mobile data traffic demand. Unlicensed spectrum is more and more considered by cellular operators as a complementary tool to augment their service offering. In that case, Licensed-Assisted Access to unlicensed spectrum (LAA) has been studied [1] and will be specified [2] in 3GPP Release 13 to achieve more efficient use of unlicensed spectrum and better user experience.

Carrier Aggregation (CA) between a licensed carrier and an unlicensed carrier is considered to support LAA, where one or multiple Secondary Component Carriers (SCells) on unlicensed band and a Primary Component Carrier (PCell) on a licensed band are configured. In such a deployment, PCell in licensed band is targeted to ensure the quality of service (QoS) for user equipments (UEs) and SCells in unlicensed band is used to offload the traffic from licensed spectrum. As LAA is targeted to use the unlicensed spectrum such as 5GHz band, the design of LAA should fulfill the regulatory of the unlicensed spectrum and satisfy the fair co-existence with other Radio Access Technologies (RATs), e.g. Wi-Fi.

Co-existence issue of legacy LTE using unlicensed spectrum, especially the LTE and Wi-Fi co-existence, can be found in literature [3]-[5]. In [3], the authors address the problem that Wi-Fi channel is often blocked by LTE interference and suffer from significant user throughput degradation when Wi-Fi co-exist with LTE. Investigation on semi-static resource sharing mechanisms between LTE and Wi-Fi in either frequency [4] or time domain [5] shows that it is not a flexible approach to utilize the spectrum, since one system could not use the resource dedicated to the other system even there is no transmission from the other system.

Wi-Fi like Listen-before-talk (LBT) mechanism for LAA could ensure fair co-existence and flexible resource utilization. There are two typical LBT mechanisms, Frame-Based-Equipment (FBE) and Load-Based-Equipment (LBE), according to the European regulatory requirements [6]. FBE-based LBT mechanism seems to be aligned with LTE frame structure and easy to achieve frequency reuse among synchronized transmission nodes. But the problem is relatively lower channel access probability when it co-exists with Wi-Fi. On the other hand, LBE-based LBT mechanism senses the channel all the time before seizing the channel. LBT mechanism in Wi-Fi can be categorized into LBE-based LBT mechanism. When LAA co-exists with Wi-Fi, LBE-based LBT for LAA can achieve the same level of opportunity as Wi-Fi to seize the channel. However, since transmission timings of neighboring LAA cells would not be aligned, thus it is hard to obtain frequency reuse and the transmit efficiency of LAA would be low compared with FBE-based LBT case. In this paper, we proposed an enhanced FBE-based LBT mechanism for LAA to increase the channel occupancy probability while keep high frequency reuse among LAA cells. We perform exhaustive system level simulations to investigate the frequency reuse in intra-operator co-existence scenario of LAA and fairness in inter-operator co-existence scenario between Wi-Fi and LAA.

The paper is organized as follows. Section II describes the co-existence scenarios for LAA and Wi-Fi in unlicensed band.

Conventional FBE and LBE based LBT mechanisms are introduced in Section III. Section IV presents and analyzes the proposed LBT mechanism. In Section V, simulation environment and key assumptions are provided. The system level simulation results of proposed LBT mechanisms are also presented in this section. Finally, the conclusions are summarized in Section VI.

II. Deployment Scenarios

Unlicensed spectrum has been widely used by Wi-Fi. Many operators have deployed operator-managed Wi-Fi systems in public areas. Once LAA is introduced, several deployment scenarios could be considered.

Fig. 1 provides the deployment of co-existence scenarios. In each scenario, macro cell with licensed band provides coverage for the UEs in the area and Wi-Fi access points (APs) and/or LAA small cells (SCs) are deployed as a cluster to provide large volume data service for a high traffic area. Fig.1 (a) shows the normal co-existence scenario of LTE network where the distance between cells is appropriately designed by careful cell planning. However, as depicted in Fig.1 (b) to (d), due to lack of cell planning across different operators, small cells in unlicensed spectrum may be planted very close to each other, which introduces severe inter-operator interference.

The LBT mechanism is an effective way of solving the severe interference problem. In the design of specific LBT method for LAA system, we should consider both the high LAA transmission efficiency as well as the fairness between LAA and Wi-Fi system.

III. Conventional LBT Mechanisms for LAA

In this section, we discuss the details of FBE-based and LBE-based LBT mechanisms used for LAA and analyze their advantages and disadvantages.

In FBE, the clear channel assessment (CCA) is performed every fixed frame period, as shown in Fig. 2(a). If the energy detected in CCA duration is larger than a threshold, the channel is confirmed as busy, otherwise the channel is idle. Once idle channel is detected, LAA could occupy the channel for transmission. But if busy channel is detected, it should not use the channel until next CCA occasion. It is specified in [6] that the channel occupancy time, i.e., the maximum burst length shall be in the range 1 ms to 10 ms, and the minimum idle period including CCA duration shall be at least 5% of the channel occupancy time. FBE-based LBT could easily achieve frequency reuse of an operator by aligning the CCA and transmission period among synchronized cells within one operator. Compared with Wi-Fi, LAA with FBE-based LBT has lower probability to seize the channel since CCA can only be performed for one time every fixed frame period.

In LBE, if the equipment finds an operating channel occupied, it shall perform an extended CCA (ECCA), as shown in Fig. 2 (b). The ECCA can be repeated until the equipment finds the operating channel is idle when N idle CCA slots are observed. The value N shall be randomly selected in the range 1 to q every time an ECCA is required and the value is stored in a counter. The counter is decremented every time an ECCA

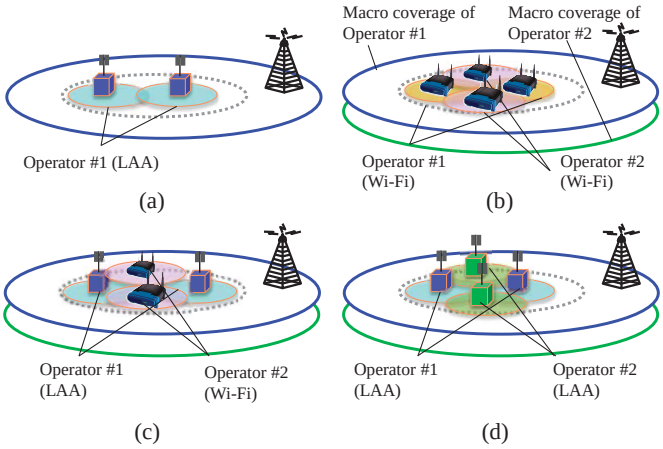

Fig.1 Deployment scenarios: (a) intra-operator LAA co-existence (b) inter-operator Wi-Fi-Wi-Fi co-existence; (c) inter-operator LAA-Wi-Fi co-existence; (d) inter-operator LAA-LAA co-existence

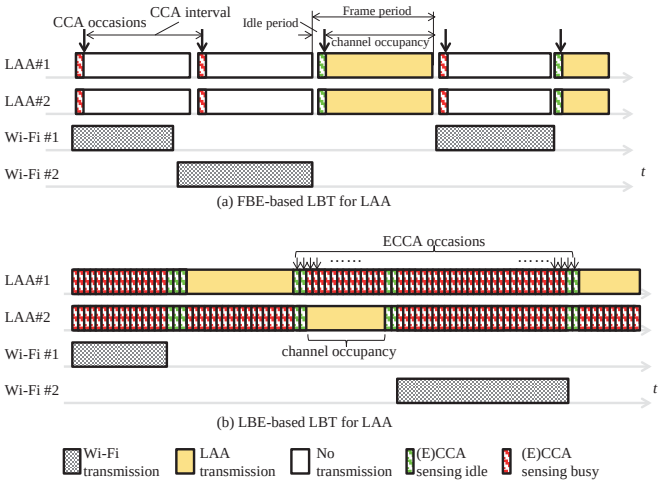

Fig.2. FBE-based LBT and LBE-based LBT for LAA

occasion is confirmed as idle. When the counter reaches zero, the equipment may transmit. The maximum channel occupancy time is limited to $13/32 \times q$ ms. A node equipped with LBE-based LBT can seize a channel immediately after the channel becomes idle, while a node with FBE-based LBT needs to wait next CCA timing and may miss the channel access opportunity due to the interception by other RAT, e.g., Wi-Fi. Therefore, LAA with LBE-based LBT would achieve comparable channel access with Wi-Fi since Wi-Fi is also equipped with a kind of LBE-based LBT. However, even if nodes within one operator are tightly synchronized, it would be difficult to realize frequency reuse since CCA and transmission timings may be unaligned due to diverse interference condition among cells. Such cell within one operator may block each other once CCA timings of cells become unaligned.

IV. Proposed LBT Mechanism for LAA

As in cellular network, such as LTE, frequency reuse is an important property to achieve high network capacity. Based on this fact, we propose FBE-based LBT with Short CCA Interval

(SCI-FBE) mechanism to increasing the channel access probability while ensuring the frequency reuse of LAA.

Fig. 3 shows the CCA timing and frame period of SCI-FBE mechanism. CCA is performed in a shorter interval than frame period when LBT result at the previous subframe is busy, while CCA is not performed during transmission burst after which it is confirmed that LBT result is idle. The transmission burst length should be configurable to fulfill the regulatory requirement of different regions. The SCI-FBE mechanism absorbs the advantages of FBE and LBE. In intra-operator co-existence of LAA, SCI-FBE mechanism helps LAA cells to transmit data bursts in the shared unlicensed carrier simultaneously. Thus transmission efficiency of LAA is improved by realizing frequency reuse. In inter-operator co-existence scenario of Wi-Fi-LAA, the channel occupancy ratio of LAA is increased as the CCA interval becomes shorter than the frame period.

V. Evaluation Results

A. Simulation assumption

In intra-operator co-existence of LAA, LAA cells are deployed in one cluster. In inter-operator co-existence scenario, two operators deploy same number of Wi-Fi or LAA cells in the cluster. There are total 7 hexagonal 3-cell macro sites are deployed with ISD of 500 meters. One cluster is randomly distributed for each macro cell with the minimum distance from macro to cluster center of 105 meters. Each LAA/Wi-Fi operator deploys four SCs/APs in each cluster with the radius of 50 meters. The minimum distance between cells of the same operator is 20 meters, while the minimum distance between cells of different operator is 10 meter. UEs of each operator are randomly and uniformly distributed in the area within 20 meters from each SC/AP. Table I summarizes the simulation parameters for both LAA and Wi-Fi.

Although there are many frequency channels in the unlicensed band, we assume the worst co-existence environment that a single channel is shared by multiple cells of different operators. Single channel of 20MHz in 5.0GHz band is assumed for LAA/Wi-Fi operators. For LAA, only downlink packet throughput is evaluated in unlicensed band as uplink control signaling is carried by licensed band. For Wi-Fi, downlink packet throughput is evaluated as well, and ideal uplink transmission without resource occupation is assumed. For LAA, Channel state information (CSI) is reported in the time granularity of 10ms for link adaptation. Chase combining with maximum 3 re-transmission time is assumed for LTE Hybrid Automatic Repeat request (HARQ). In the evaluation of LBE-based LAA, initial CCA is needed before the procedure of ECCA counter decrement is resumed.

B. Evaluation results

System level evaluations are performed to verify the effectiveness of the proposed LBT mechanisms introduced in Section IV. The co-existence scenario of intra-operator of LAA and inter-operator of Wi-Fi-Wi-Fi and Wi-Fi-LAA is evaluated. In the evaluation, FTP traffic model with Poison distribution of packet arrival rate [5] is considered. Traffic load refers as the

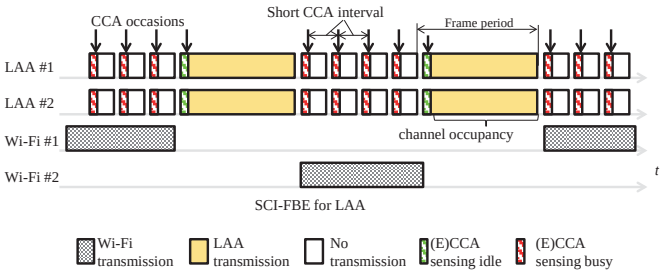

Fig.3 SCI-FBE mechniasm for LAA

Table I Simulation Parameters

Basic parameters	**Value**
Cellular layout	Hexagonal grid, 7 sites, 3 cell per site
Bandwidth	20 MHz per channel, single channel
Frequency	5.0 GHz
DL Tx Power	18 dBm
SC/AP dropping	Random and uniform within 50 m cluster radius
Mini. dist. b/w SC/AP	20 m of same operator, 10 m of different operator
SC/AP # per cluster	4
Cluster # per macro	1
UE dropping	Random and uniform within 20ms from each cell
Indoor UE/STA ratio	0.8
Cell selection	Best RSRP-based with 0dB handover margin
Antenna configuration	2D, 2x2 CPA, Omni-directional
Antenna gain	5 dBi at cell, 0 dBi at UE
Antenna height	10 m for cell, 1.5 m for UE
MIMO	Up to 2 streams
UE/STA receiver	MMSE
Traffic model	FTP model 1 [7] with packet size of 0.5 Mbytes
Channel model	ITU UMi [8] with 3D distance
LAA parameters	**Value**
Simulation step	1 ms (FBE)/8us (LBE)
Link adaptation	Subband CQI and wideband PMI of 10ms periodicity
HARQ	Chase combine
Max. ReTx. times	3
(E)CCA duration	24 us (for both FBE and LBE)
Initial CCA duration	32 us (for LBE)
q	10/25 for 4/10 ms burst length
CCA-ED	-62dBm
Scheduler	Proportional fairness
Wi-Fi parameters	**Value**
Simulation step/slot	8 us
MCS	802.11n
Channel coding	BCC
DIFS	32 us
RTS/CTS	N/A
Contention window	Min: 15 slot; Max: 1023 slot
Max burst length	4 ms
Frame aggregation	A-MPDU
MPDU	1.5 K Byte size
Link adaptation	Open loop using ACK
CCA-CS (Wi-Fi)	-82 dBm
CCA-ED (other RAT)	-62 dBm
Scheduler	Round-robin

arrival UE number per cluster per second. For example, traffic load 2 means the average 2 UEs arrived in the cluster area per second. Total simulation time of 25 seconds, i.e. 25,000ms, is assumed for each evaluated case. A 0.5 M bytes packet is assumed for each new generated UE. In low traffic load, some of the cells have traffic for transmission. In high traffic load, there is probably more than one UE stay in the buffer of the cell simultaneously. The evaluation is performed in traffic loads from low to high.

1) Intra-operator LAA co-existence

In order to comparing the LBT schemes of FBE, LBE and SCI-FBE, maximum 4 ms burst length is assumed.

Fig.4 shows the average, 5% and 95% UE throughput of LAA in different traffic load in scenario of intra-operator LAA co-existence. UE throughput is derived as the number of packet bits successfully transmitted to the sojourn time of the packet in node buffer. Fig.5 shows the averaged cell waiting time ratio and transmit time ratio in different traffic load in scenario of intra-operator LAA co-existence. For one cell, there are three statuses in the evaluation: no buffer, waiting due to LBT and transmission. Before UE arrival, the cell stays in no buffer status. After UE arrival, the cell tries to seize the channel for transmission by performing LBT. Its status would switch between waiting and transmission corresponding to LBT and data transmission procedure. The waiting and transmission time ratio observation in Fig.5 could help to analyze the throughput tendencies in Fig.4.

There are several observations on the throughput results in Fig.4. Firstly, average UE throughput is decreased with the increasing of traffic load, since averaged scheduling probability of each UE is low and interference is severe in high traffic load scenario. Secondly, FBE and SCI-FBE based LAA achieves higher average UE throughput than LBE-based LAA. As we discussed in section III, owing to unaligned CCA timing and data transmission in LBE-based LAA, LAA cells within one operator will block each other. Hence, significant higher waiting time ratio of LBE than other LBT schemes is observed in Fig.5 (a). Thus UE throughput of LBE-based LAA is relatively small. Thirdly, by comparing FBE and SCI-FBE, SCI-FBE based LAA has larger throughput in low traffic load and smaller throughput in high traffic load, in terms of averaged and 95% UE throughput. It is because that SCI-FBE could seize channel immediately by executing CCA in each subframe when new packet arrives, thus less waiting time compared to FBE especially in low traffic load. On the other hand, SCI-FBE achieves lower frequency reuse compared FBE due to CCA of SCI-FBE is not fully aligned among cells of one operator. Then waiting time ratio of SCI-FBE is relative high especially in high traffic load.

In summary of intra-operator co-existence, it is observed that SCI-FBE could achieve comparable performance and similar frequency reuse as FBE for LAA cells of the same operator.

2) Wi-Fi-LAA co-existence

There are two operators deployed within a clustered area in Wi-Fi-LAA co-existence. LBT mechanism for LAA should firstly ensure that LAA is a good neighbor for Wi-Fi. It means that the Wi-Fi performance in Wi-Fi-LAA co-existence should be equal or better than the performance of the same Wi-Fi operator in Wi-Fi-Wi-Fi co-existence. Second, the LBT mechanism of LAA should ensure the high efficient LAA transmission when LAA co-exist with another system.

Fig. 6 shows the average UE throughput performance of Wi-Fi-LAA co-existence by considering the maximum burst length for LAA of 4ms. The baseline is the Wi-Fi throughput in Wi-Fi-Wi-Fi co-existence. From Wi-Fi throughput in Fig. 6(a), it is found that Wi-Fi could achieve higher throughput if it co-exists with LAA instead of another Wi-Fi, thanks to more efficient transmission of LAA due to some advanced technologies such as close-loop link adaptation (CLLA) and HARQ. From LAA

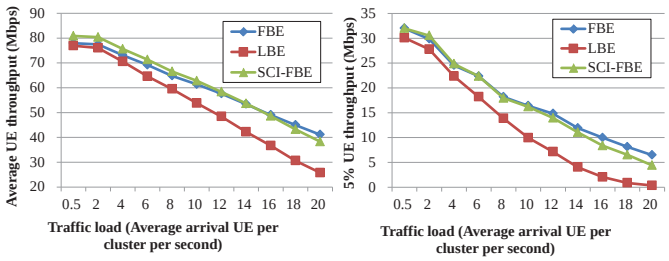

(a) Average UE throughput of LAA (b) 5% UE throughput of LAA

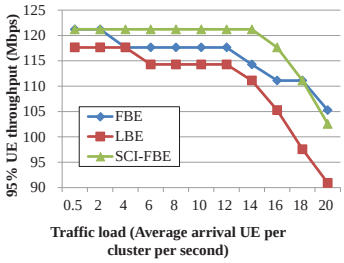

(c) 95% UE throughput of LAA

Fig.4 Average, 5% and 95% UE throughput of LAA in different traffic load in scenario of intra-operator LAA co-existence

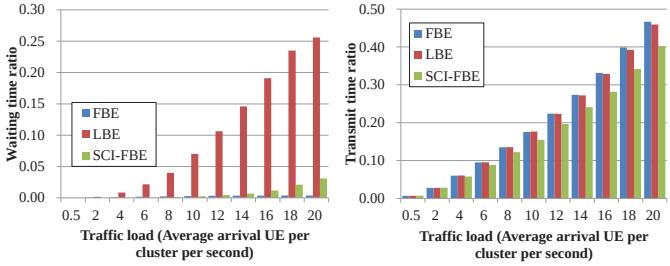

(a) Waiting time ratio of LAA (b) Transmit time ratio of LAA

Fig.5 Waiting and transmit time ratio of LAA in different traffic load in scenario of intra-operator LAA co-existence

throughput in Fig.6 (b), several points are further observed. First, FBE achieves lower performance in low traffic load and higher performance in high traffic load than LBE. As it is already observed in evaluations of intra-operator co-existence, benefits from frequency reuse by applying FBE are obvious in high load scenario but negligible in low load scenario. Thus FBE has higher performance than LBE in high traffic load. When co-existing with Wi-Fi, LBE-based LAA has higher channel access probability than FBE-based LAA, it helps LBE achieve higher throughput than FBE in low load case. The other observation is that SCI-FBE achieves higher throughput than FBE and LBE in both low and high traffic load. This is because that both intra-operator frequency reuse and higher carrier seizing ratio could be achieved by fixed and more frequent CCA timing design of SCI-FBE, respectively.

Fig.7 shows performance of Wi-Fi-LAA co-existence with maximum 10ms burst length for LAA. The LAA performance is improved comparing to 4ms burst length in Fig.6, since it allows longer continuous transmission time transmission without LBT after single CCA procedure. SCI-FBE still achieves higher throughput than FBE and LBE.

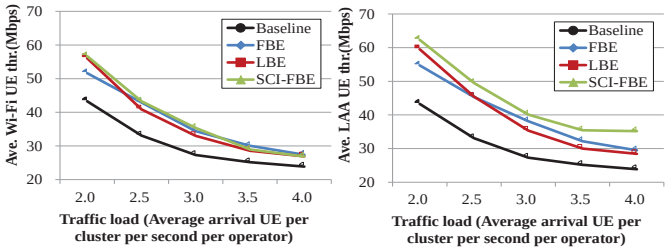

(a) Average UE throughput of Wi-Fi (b) Average UE throughput of LAA

Fig.6 Throughput of Wi-Fi-LAA co-exitence, 4ms max. burst length for LAAs

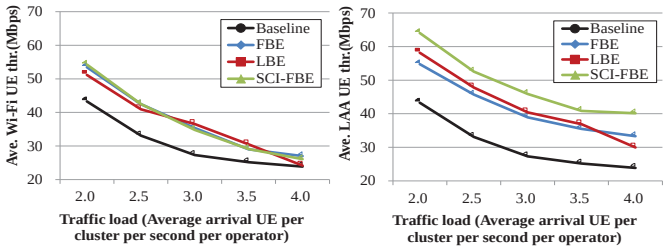

(a) Average UE throughput of Wi-Fi (b) Average UE throughput of LAA

Fig.7 Throughput of Wi-Fi-LAA co-exitence, 10ms max. burst length for LAAs

Fig.8 shows performance of SCI-FBE based LAA with maximum burst length of 1, 4 and 10ms co-existed with Wi-Fi. It is found that LAA throughput is increased with the increasing of maximum burst length. Since the longer burst length allows longer continuous transmission time without LBT after single CCA procedure. Then the waiting time of LBT needed for LAA is shorter, which is also showed in Fig.9 (a), and throughput performance is larger. For Wi-Fi, it is observed that waiting time ratio is decreased with the increasing of LAA maximum burst length. While the throughput performance difference between burst length of 1ms and 10ms is relative smaller than that of LAA. Although longer waiting time will degrade the Wi-Fi throughput, fast LAA transmission would benefits Wi-Fi.

VI. Conclusion

LBT mechanism is regarded as an essential technology for LAA to fairly access the unlicensed carrier when co-exist with other systems. In this paper, we analyze and figure out the problem of conventional LBT mechanisms of FBE and LBE. The proposed SCI-FBE mechanism absorbs the advantages from FBE and LBE, where frequency reuse and fair channel access with coexistence system such as Wi-Fi could be achieved at the same time.

System level evaluations are performed to investigate the throughput performance of FBE, LBE and SCI-FBE mechanisms used for LAA in both intra-LAA operator co-existence and Wi-Fi-LAA co-existence. Throughput results show that the proposed SCI-FBE mechanism achieves comparable performance as FBE by achieving frequency reuse in intra-LAA operator co-existence. More important observation is that SCI-FBE could provide better throughput

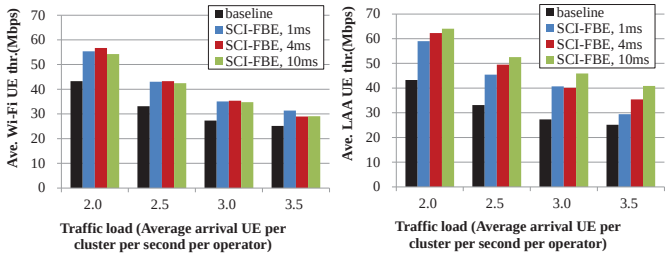

(a) Average UE throughput of Wi-Fi (b) Average UE throughput of LAA

Fig.8 Throughput of Wi-Fi-LAA (SCI-FBE) co-exitence with 1, 4, 10ms burst length

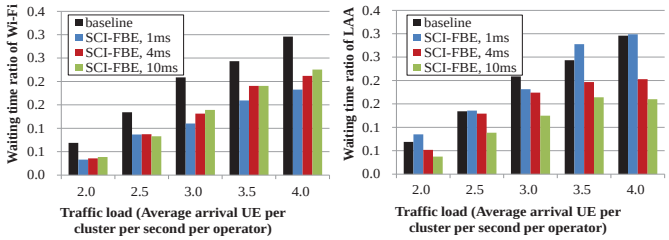

(a) Waiting time ratio of Wi-Fi (b) Waiting time ratio of LAA

Fig.9 Waiting time ratio of Wi-Fi-LAA (SCI-FBE) co-exitence with 1, 4, 10ms burst length

performance of Wi-Fi and LAA than mechanisms of FBE and LBE in Wi-Fi-LAA co-existence due to high efficiency of LAA and comparable channel access capability as Wi-Fi. Furthermore, longer burst length of SCI-FBE, such as 10ms, could improve the throughput of LAA significantly while introduce negligible degradation on Wi-Fi.

References

[1] 3GPP RP-141817, “Study on Licensed-Assisted Access to Unlicensed Spectrum,” Dec. 2014.

[2] 3GPP RP-151045, “Work Item on Licensed-Assisted Access to Unlicensed Spectrum,” June 15 - 18, 2015.

[3] A. M. Cavalcante, E. P. L. Almeida, R. D. Vieira, F. S. Chaves, R. C. D.Paiva, F. M. Abinader Jr., S. Choudhury, E. Tuomaala, and K. Doppler,“Performance evaluation of LTE and Wi-Fi coexistence in unlicensedbands,” in Proc. VTC’2013-Spring, IEEE Vehicular Technology Conf., Dresden, Germany, Jun. 2013.

[4] T. Nihtila, V. Tykhomyrov, O. Alanen, M. Uusitalo, A. Sorri, M. Moisio, S. Iraji, R. Ratasuk, and N. Mangalvedhe, “System performance of LTE and IEEE 802.11 coexisting on a shared frequency band,” in Proc. WCNC’2013, IEEE Wireless Communications and Networking Conf., Changhai, China, Apr. 2013, pp. 1056–1061.

[5] E. Almeida, A. M. Cavalcante, R. C. D. Paiva, F. Chaves, F. M. Abinader Jr., R. D. Vieira, S. Choudhury, E. Tuomaala, and K. Doppler, “Enabling LTE/WiFi coexistence by LTE blank subframe allocation,” in Proc. ICC’2013, IEEE Int. Conf. Communications, Budapest, Hungary, Jun. 2013.

[6] ETSI EN 301 893 v1.8.1, Mar. 2015.

[7] 3GPP TR 36.814 “Evolved Universal Terrestrial Radio Access (E-UTRA); Further advancements for E-UTRA physical layer aspects (Release 9)”, V9.0.0, Mar. 2010.

[8] ITU-R M.2135 “Guidelines for evaluation of radio interface technologies for IMT-Advanced”, 2008.

[9] Part 11: Wireless LAN Medium Access Control (MAC) and Physical Layer (PHY) Specifications, Amendment 4: Enhancements for Very High Throughput, IEEE Standard 802.11n, 2009.

THE 18TH INTERNATIONAL SYMPOSIUM ON WIRELESS PERSONAL MULTIMEDIA COMMUNICATIONS
(WPMC-2015)
December 13-16, 2015, Hyderabad, India

A compressive sensing-based channel estimation via GAMP in FBMC/OQAM system

Meng Lin*†, Yunzhou Li*, Limin Xiao*, Yan Zhang*, Xibin Xu*
and Jing Wang*
*State Key Laboratory on Microwave and Digital Communications
Tsinghua National Laboratory for Information Science and Technology, Beijing 100084, China
†Department of Electronic Engineering, Tsinghua University
Email: m-lin12@mails.tsinghua.edu.cn

***Abstract*—Compared to the cyclic prefix orthogonal frequency division multiplexing (CP-OFDM), filter bank based multi-carrier with offset quadrature amplitude modulation (FBMC/OQAM) is more suitable for asynchronous access applications and cognitive radio scenarios in the fifth generation (5G) communication by using synthesis and analysis filter banks composed of well time-frequency locationed (TFL) prototype filters. However, real orthogonality instead of complex orthogonality makes the channel estimation in FBMC/OQAM system challenging. In this paper, an effective and low complexity compressive sensing based channel estimation method via Generalized Approximate Message Passing (GAMP) algorithm was proposed, when it was compared with several other popular methods presented for FBMC/OQAM in the literatures, analysis and simulation results demonstrate this method is more robust to channel frequency selectivity and always works well even in underdetermined cases, in virtue of utilization of the prior probability and the sparsity property of the channel impulsive response (CIR) coefficients.**

I. Introduction

In the future 5G wireless communication, asynchronous access [1] will be an important scenario because machine-to-machine communication needs relaxed synchronization to reduce constant exchange of control signaling. Furthermore, massive machines will aggravate fragmentation of spectrum. Physical layer scheme with confined waveform and relaxed synchronization is needed to satisfy the asynchronous access and cognitive radio communications [2]. FBMC/OQAM [3] has been regarded as a candidate alternative multicarrier scheme to CP-OFDM, because of its lower sidelobe leakage, higher spectral efficiency without CP and the insensitivity to the synchronization errors. But Balian-Low theory [4] tells us, the complex orthogonality, well time-frequency locationed prototype filters and the maximal spectral efficiency cannot achieve simultaneously, and then real orthogonality instead of complex orthogonality makes the channel estimation of the FBMC/OQAM system challenging.

Organizations such as Mobile and wireless communications Enablers for the Twenty-twenty Information Society (METIS) [5] and 5th Generation Non-Orthogonal Waveforms for Asynchronous Signalling (5GNOW) [6] under European Framework 7 has been devoted to the key techniques of the FBMC/OQAM. [7] and [8] use an auxiliary pilot to cancel the interference coming from the imaginary term. [9] proposed Pairs of Pilots method (POP) and Interference Approximation Method (IAM), the latter frequency domain estimation method regards the desired time-frequency grid plus the pure imaginary interferences coming from the neighborhood grids as a pseudo pilot, but it is under the assumption that symbol interval is much longer than the maximum channel delay spread, which leads to an error floor of performance when the channel frequency selectivity increases. [10] and [11] developed a time domain channel estimation method in terms of the channel impulse response (CIR), but it is not spectral efficient to transmit all the frequency domain pilots for the sparse channel estimation, and linear estimation methods have higher complexity. In recent years, applications of compressive sensing [12] to sparse channel estimation have saved the spectral sources and increased the performance. [13] demonstrated a greedy algorithm called Orthogonal Matching Pursuit (OMP), [14] proposed a compressive sensing method based on Basis Pursuit (BP). GAMP [15] was presented that not only provides the low complexity of iterative threshold algorithm but also the strong reconstruction ability of BP. [16] and [17] applied GAMP into multiuser detection for uplink massive MIMO and massive spatial modulation MIMO. In this paper, considering the special time-frequency structure in FBMC/OQAM system, we proposed a compressive sensing based channel estimation method using GAMP algorithm.

This paper first analyzed the time domain channel estimation model and the input-output expression of FBMC/OQAM system explicitly. To further improve the performance and decrease the computation complexity of the estimation method, a GAMP based method was proposed, the prior probability and sparsity of the channel impulse response coefficients were also utilized to achieve a better performance.

The rest of this paper is organized as follows. Section II depicted the FBMC/OQAM system model. Section III described the problems of channel estimation exist in the FBMC/OQAM system, followed by the detailed design procedure of compressive sensing based channel estimation via GAMP in Section IV. The simulation results are given in Section V. Finally, Section VI concludes the whole paper.

II. System model

In FBMC/OQAM system [18], a set of parallel data symbols are transmitted through a bank of synthesis and analysis filters. The selection of prototype filters decides the localization in spectrum of the generated waveform [19]. OQAM modulation combined with Nyquist constraints on the transmit and receive prototype filter is used to guarantee real orthogonality between adjacent symbols and adjacent carriers. Meanwhile,

no use of CP provides maximum spectral efficiency. In order to decrease the processing complexity of this system, a feasible and efficient implementation of FBMC/OQAM transmit and receive processing is obtained using the Fast Fourier Transform (FFT) and Polyphase Network (PPN) in [20] and is used in this paper. The output vector of transmit synthesis filter bank $s[n]$ is given by

$$s[n] = \sum_{k=-\infty}^{\infty} \sum_{m=0}^{M-1} d_m[k]\theta_m[k]p[n-k\frac{M}{2}]e^{j\frac{2\pi}{M}m(n-k\frac{M}{2}-D)} \tag{1}$$

where $d_m[k]$ are the real transmit data extracted from the complex QAM symbols, $\theta_m[k] = j^{m+l}$ is used to keep the real orthogonality between adjacent grids, $p[n]$ is the prototype filter [21] used in the synthesis filter bank, such as (physical layer for dynamic spectrum access and cognitive radio) PHYDYAS [22], half cosine, root raised cosine (RRC), Isotropic Orthogonal Transfer Algorithm (IOTA) and Extended Gaussian Functions (EGF), all of the prototype filters have well time-frequency location (TFL) properties and guarantee the confined spectrum of the FBMC/OQAM. Delay term $D = \frac{L_g-1}{2}$, L_g is the length of prototype filter.

The output vector of transmit synthesis filter bank $s[n]$ is first affected by the CIR $h[l]$, whose length is L_h, K is the number of non-zero taps. When $K \ll L_h$, the channel can be recognized as sparse channel.

The input vector of receive analysis filter bank

$$r[n] = h[l] * s[n] + w[n] \tag{2}$$

where $w[n]$ is Gaussian white noise with variance σ^2.

On the receiver side, take a desired time-frequency grid into account, the decoded signal at the qth subcarrier and kth time instance is

$$y_q[k] = \sum_{l=0}^{L_h-1} h[l] * A_{m,l} + W_q[k] \tag{3}$$

$$A_{m,l} = \sum_{m=0}^{M-1} \sum_{n=0}^{L_g-1} d_m[k]\theta_m[k]p[n-l]*p[n]e^{j\frac{2\pi}{M}m[(n-D)(m-q)-l]} \tag{4}$$

$$W_q[k] = \sum_{n=k\frac{M}{2}}^{L_g-1+k\frac{M}{2}} w[n]p[n-k\frac{M}{2}]e^{-j\frac{2\pi}{M}q(n-k\frac{M}{2}-D)} \tag{5}$$

III. Problem description

The key issue of our paper is to estimate the channel coefficients, we use time domain model which is more robust to channel frequency selectivity and then channel impulse response coefficients will be estimated. In order to compare our proposal with other estimation methods, we also use frequency domain pilots, which is the same with IAM method. Three symbol are used as the frequency domain pilot with the first and the third is all zero, the pilot in the subcarriers of the middle symbol is repeated as 1,1,-1,-1.

A. IAM method

As mentioned in the FBMC/OQAM system before, the channel frequency response $H_{q,k}^{(c)}$ is complex but the transmit data $d_{q,k}$ is real, so IAM take the non-zero pilot and the pure imaginary interference $d_{q,k} + j \sum_{(q_0,k_0)\neq(0,0)} (d_{q+q_0,k+k_0} < g >_{q+q_0,k+k_0}^{q,k})$ as a complex pseudo pilot based on the assumption of $H_{m_0+p,n_0+q}^{(c)} \approx H_{m_0,n_0}^{(c)}$. The estimated channel frequency response is

$$H_{q,k}^{(c)} = y_{q,k}^{(c)}/d_{q,k} + j \sum_{(q_0,k_0)\neq(0,0)} d_{q+q_0,k+k_0} < g >_{q+q_0,k+k_0}^{q,k} \tag{6}$$

B. Time domain estimation method

When channel frequency selectivity increases and the symbol duration is not much longer than the maximum channel delay excess, IAM will suffer from severe performance degradations. Similar as [10] and [11], we consider our method in time domain to improve robustness of our method. We put equation (3) into the matrix form

$$Y = A * h + W \tag{7}$$

Y is the received signals of the middle non-zero pilots, A is a matrix with dimension $M * L_h$, the elements of A is decided by the pilot and mutual ambiguity function of the prototype filters. $h = [h_0 h_1 ... h_{L_h}]^T$ is the unknown parameters to be estimated.

Particularly, W is color noise filtered by the analysis filter bank and therefore the elements of it are not independent any more. Considering the whiten of noise, we firstly obtain the covariance coefficient of the color noise

$$\mathrm{cov}[w_{q_1} w_{q_2}] = \sigma^2 \alpha_{q_1,1}^{q_2,1} \tag{8}$$

where $\alpha_{q_1,1}^{q_2,1}$ means coherence degree between two subcarriers q_1 and q_2 on the middle pilot time instance. The $\alpha_{q_1,1}^{q_2,1}$ can be simplified to be

$$\alpha_{q_1,1}^{q_2,1} = \begin{bmatrix} 1 & \mathrm{j}\beta & 0 & ... & 0 & \mathrm{j}\beta \\ -\mathrm{j}\beta & 1 & \mathrm{j}\beta & ... & 0 & 0 \\ & & & ... & & \\ \mathrm{j}\beta & 0 & 0 & ... & -\mathrm{j}\beta & 1 \end{bmatrix} \tag{9}$$

then (7) is changed to be

$$Y' = A' * h + W' \tag{10}$$

after the whiten process, where

$$W' = (\alpha_{q_1,1}^{q_2,1})^{-1/2}/\sigma) * W \tag{11}$$

and the elements of it follow independent Gaussian white noise with variance σ^2. The key issue is to estimate the CIR h from the observation Y'.

IV. Compressive sensing based channel estimation via GAMP

In this paper, GAMP based compressive sensing channel estimation is used in the FBMC/OQAM system. Firstly, in order to model the sparsity of the channel, the CIR coefficients $\{h_l\}$ are regarded as random variables with independent Bernoulli-Gaussian prior distribution, the probability density function

$$p_{h_l}(h) = \frac{K}{L_h} CN(h; \mu_l, \sigma_l) + (1 - \frac{K}{L_h})\delta(h) \tag{12}$$

where $\frac{K}{L_h}$ is the sparsity rate which means the non-zero probability of the CIR coefficients.

$$CN(h; \mu_l, \sigma_l) \triangleq (\pi\sigma_l)^{-1} \exp(-{\sigma_l}^{-1}|h - \mu_l|^2) \tag{13}$$

means complex Gaussian probability density function.

Considering the sparsity property of CIR coefficients, it is not spectral efficient to using all subcarriers for transmit pilots, so we pick P pilot observations from N subcarriers. Equation(10) is further changed to be

$${Y_p}' = {A_p}' * h + {W_p}' \tag{14}$$

where ${Y_p}' = Y'(1 : I : M)$, we assume the pilot observations follow uniform distribution and I is the distance between neighbor observations. ${A_p}'$ is a matrix with dimensions $P * L_h$, whose elements are a_{ij}, $i \in [P]$, $j \in [L_h]$.

Our goal is estimating CIR coefficients $\{h_l\}$ from P pilot observations, the estimated values of elements is

$$\{\hat{h}_j = \sum_{h_j} h_j p(h_j|Y_p)\}_{j \in [L_h]} \tag{15}$$

where $p(h_j|Y_p)$ is the posterior probability density function of $\{h_l\}$.

By the literature[15], it can be known that Loopy Belief Propagation [23] can be used to compute $p(h_j|Y_p)$ approximatively, but the computation complexity is very high because it involves high dimensional integral and should maintain a large number of messages. GAMP algorithm proposed in [15] is a simplified algorithm based on the Central limit theorem (CLT) and Taylor expansion. The channel estimation is computed as follows,

A. Initialization

Let the initial iterative number $t = 0$, with $i \in [P]$ and $j \in [L_h]$, the initial mean and variance of $\{h_l\}$ is $\hat{h}_j(0) = 0$ and $\tau_j^h(0) = 1$, and set $\hat{s}(-1) = 0$.

B. Output linear step

For each i, compute:

$$\tau_i^p(t) = \sum_j |a_{ij}|^2 \tau_j^h(t) \tag{16}$$

$$\hat{p}_i(t) = \sum_j a_{ij} \hat{h}_j(t) - \tau_i^p(t) \hat{s}_i(t-1) \tag{17}$$

C. Output nonlinear step

For each i, compute:

$$\hat{s}_i(t) = (Y_i - \hat{p}_i(t))/(\tau_i^p(t) + \sigma^2) \tag{18}$$

$$\tau_i^s(t) = 1/(\tau_i^p(t) + \sigma^2) \tag{19}$$

D. Input linear step

For each j, compute:

$$\tau_j^r(t) = 1/\sum_i |a_{ij}|^2 \tau_i^s(t) \tag{20}$$

$$\hat{r}_i(t) = \hat{h}_j(t) + \tau_j^r(t) \sum_i a_{ij} \hat{s}_i(t) \tag{21}$$

E. Input nonlinear step

For each j, compute:

$$\hat{h}_j(t+1) = E(h_j|\hat{r}_j(t), \tau_j^r(t)) \tag{22}$$

$$\tau_j^h(t+1) = var(h_j|\hat{r}_j(t), \tau_j^r(t)) \tag{23}$$

F. Decision

Increment $t = t + 1$ and return to step 2 until a sufficient number of iterations have been performed, or

$$\frac{||\hat{h}_j(t+1) - \hat{h}_j(t)||_2^2}{||\hat{h}_j(t+1)||_2^2} < tol \tag{24}$$

is satisfied.

Equation (22),(23) are the expectation and variance of $\{h_l\}$ at the $(t+1)th$ iteration which are evaluated with respect to $CN(h_j; \hat{r}_i(t), \tau_j^r(t))p(h_j)$, where $p(h_j)$ is the Bernoulli-Gaussian probability distribution function.

The result is

$$\hat{h}_j(t+1) = \sum_{l \in [K]} b_l p_l \tag{25}$$

and

$$\tau_j^h(t+1) = \sum_{l \in [K]} |b_l|^2 p_l - |\hat{h}_j(t+1)|^2 \tag{26}$$

where b_l is the non-zero coefficients,

$$p_l = \phi(b_l; \hat{r}_j(t), \tau_j^r(t))/KP \tag{27}$$

$$P = (1 - \frac{K}{L_h})\phi(0; \hat{r}_j(t), \tau_j^r(t)) + \frac{1}{K} \sum_{l \in [K]} \phi(b_l; \hat{r}_j(t), \tau_j^r(t)) \tag{28}$$

$$\phi(u; \hat{r}_j(t), \tau_j^r(t)) = exp(-|u - \hat{r}_j(t)|^2/\hat{r}_j(t)) \tag{29}$$

Through the iterative computation above, the ultimate result $\hat{h}_j(t+1)$ is the estimated values of CIR coefficients.

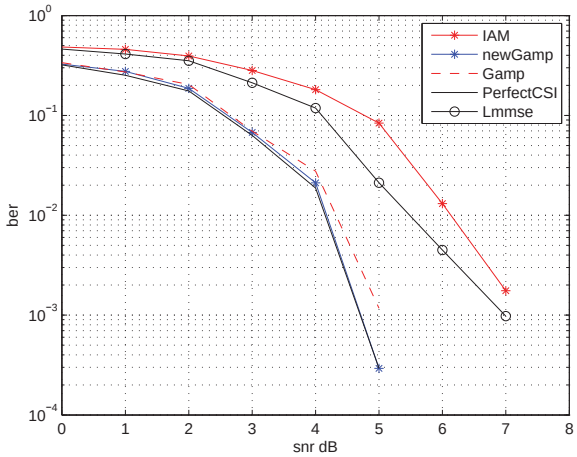

Fig. 1. BER performance of different channel estimation methods in FBMC/OQAM under full utilization of pilots

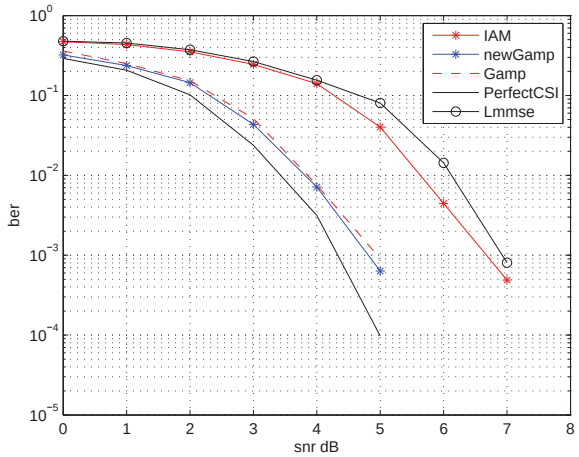

Fig. 2. BER performance of different channel estimation methods in FBMC/OQAM under less pilot observations

V. Simulation Results

In this section, we compared the proposed GAMP based channel estimation with several other methods under different number of pilot observations. To make comparisons, we use the same frequency domain pilot of three time instance, and PHYDYAS prototype filter with the overlapping factor 4 is employed. We use IEEE802.22 standard channel model which aims at constructing Wireless Regional Area Network (WRAN) utilizing free TV bands. The main channel parameters of the system used are given below: Sampling frequency is 9.14 MHz, CIR length is $L_h = 129$, Number of paths is 6, Power profile (in dB) of the 6 paths are -6.0, 0.0, -7.0, -22.0, -16.0, -20.0 and Delay profile (μs) of the 6 paths are -3, 0, 2, 4, 7, 11 respectively. QPSK modulation and convolutional channel coding (K =7 with generation polynomial (171, 133) and code rate 1/2) are used, Frame length is 41 symbols.

In the simulations, we compared four different methods, which are 'Gamp' (without noise whiten), 'newGamp' (with noise whiten), 'IAM' and 'Linear minimum mean square error (Lmmse)', the BER curve of 'PerfectCSI' assumption is also ploted to be a performance limitation reference. Firstly, We set number of subcarriers in FBMC/OQAM system to be 256, pilot observations is also 256, which means complete use of frequency domain pilots. In Fig.1, we can see the 'newGamp' method is the best and approach the performance under 'PerfectCSI'. At the position of $BER = 10^{-2}$, the newGamp is about 2.3db better than IAM, 1.5db better than Lmmse, and 0.5db better than the Gamp method. This coincides with our analysis above, GAMP based methods utilized the sparsity of CIR coefficients. When pilot observations on all subcarriers are used to construct the CIR coefficients, subcarriers are relevant because of FBMC/OQAM system's characteristic. Therefore newGamp can improve estimation performance through whitening the color noise.

Secondly, we set the number of subcarriers to be 512, pilot observations interval is 4 and the number of pilot observations is 128, which is smaller than the CIR length. In Fig.2, we can see Lmmse method rapidly deteriorates, however GAMP based methods is only about 0.4dB worse than the PerfectCSI

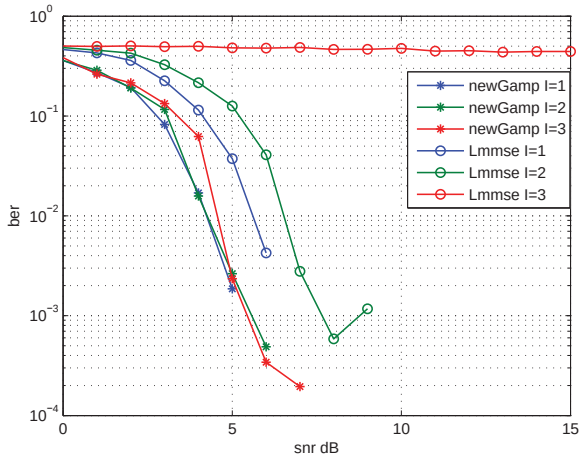

Fig. 3. BER performance comparison between GAMP and Lmmse under different cases

case at the position of $BER = 10^{-2}$. There is an interesting phenomenon that 'Gamp' and 'newGamp' method are almost the same in this situation, this is because the well time-frequency location of the prototype filters in FBMC/OQAM system. When the pilot observations are picked up apart, the pilot observation subcarriers are approximatively independent.

Thirdly, we compare the GAMP and Lmmse based methods under different number selections of picked pilot observations. We set number of subcarriers to be 256, and picked pilot interval $I = 1, 2, 3$ respectively, which means pilot observations are 256, 128 and 85 respectively, responding to using larger, equal and less number of observations to reconstruct the variables to be estimated. Fig.3 tells us, with the decrease of observations, GAMP based methods varies slowly, however, Lmmse based method deteriorates quickly. GAMP based method remains well even in underdetermined case because it utilizes the sparsity of the variables to be estimated, however, linear estimator cannot tackle the underdetermined problem because a prior probability and sparsity of the variables are not been

utilized.

VI. Conclusions

In this paper, several popular channel estimation methods used in the FBMC/OQAM system are reviewed and compared, a compressive sensing based channel estimation method via GAMP algorithm was proposed, simulation results reveal that GAMP based method is better than Lmmse method and IAM method no matter how much pilot observations are selected to reconstruct the CIR coefficients, which saved the pilot overhead and is important for asynchronous multiuser access applications in FBMC/OQAM. Secondly, GAMP based method reduces the computational complexity due to avoidance of matrix inversions of the linear estimations. Furthermore, benefiting by the time-frequency location of prototype filters in the FBMC/OQAM, when pilot observations are selected with interval larger than one, the subcarriers can be regarded as approximately independent and noise whiten process can be omitted for further lower complexity. In a word, the compressive sensing based channel estimation method via GAMP is proved to be an effective and low complexity method to tackle the channel estimation difficulties in FBMC/OQAM system.

Acknowledgment

The authors would like to thank the reviewers for their elaborative reviews and constructive suggestions, which have helped improve the quality of this paper. This work was supported by National Basic Research Program of China (NO. 2013CB329002), Chinas 863 Project (NO.2014AA01A703), National Major Project (NO.2014ZX03003002-002), Program for New Century Excellent Talents in University (NCET-13-0321) and Tsinghua-Qualcomm Joint Research Program.

References

[1] D. L. R. Y. Medjahdi, M. Terr'e and D. Roviras, "A new model for interference analysis in asynchronous multi-carrier transmission," *IEEE Trans. Veh. Technol*, vol. 1006, no. 4278, 2011.

[2] B. Farhang-Boroujeny, "Ofdm versus filter bank multicarrier," *IEEE Signal Processing Magazine*, 2011.

[3] C. S. P. Siohan and N. Lacaille, "Analysis and design of systems based on filterbank theory," *IEEE Transactions on Signal Processing*, vol. 50, no. 5, pp. 1170–1183, 2002.

[4] I. Daubechies, "The wavelet transform, time-frequency localization and signal analysis," *IEEE Transactions on Information Theory*, vol. 36, no. 5, pp. 961–1005, 1990.

[5] METIS. [Online]. Available: http://www.metis2020.com/

[6] 5GNOW. [Online]. Available: http://www.5gnow.eu/

[7] D. L. J.-P. Javaudin and A. Rouxel, "Pilot-aided channel estimation for ofdm/oqam," *Proc. IEEE Semiannu. Conf. Veh. Technol*, pp. 1581–1585, 2003.

[8] R. L. C. Ll and P. Siohan, "Channel estimation with scattered pilots in ofdm/oqam," *Proc. IEEE Workshop Signal Process. Adv. Wireless Commun*, pp. 286–290, 2008.

[9] R. L. A. S. C. Ll, J.-P. Javaudin and P. Siohan, "Channel estimation methods for preamble-based ofdm/oqam modulations," *Proc. Eur. Wireless Conf*, pp. 59–64, 2007.

[10] D. Q. D. Kong and T. Jiang, "Time domain channel estimation for oqam-ofdm systems: Algorithms and performance bounds," *IEEE Trans. Signal Processing*, vol. 62, no. 2, p. 59C64, 2014.

[11] E. Kofidis, "Preamble-based channel estimation in ofdm/oqam systems: A time-domain approach," 2013.

[12] D. Donoho, "Compressed sensing," *IEEE Trans. Inf. Theory*, vol. 52, no. 4, pp. 1289–1306, 2006.

[13] J. Tropp and A. Gilbert, "Signal recovery from random measurements via orthogonal matching pursuit," *IEEE Transactions on Information Theory*, vol. 12, pp. 4655–4666, 2007.

[14] D. L. D. S. S. Chen and M. A. Saunders, "Atomic decomposition by basis pursuit," *SIAM Rev*, vol. 43, no. 1, pp. 129–159, 2001.

[15] S. Rangan, "Generalized approximate message passing for estimation with random linear mixing," 2010.

[16] Y. Z. L. S. C. Wang and J. Wang, "Low-complexity multiuser detection for uplink massive mimo," *IEEE Wireless Commun. Network. Conf. (WCNC)*, 2014.

[17] J. W. S. C. Wang, Y. Z. Li and M. Zhao, "Low-complexity multiuser detection in massive spatial modulation mimo," *IEEE Global Communications Conference (GLOBECOM)*, 2014.

[18] C. RW, "High-speed multichannel data transmission with bandlimited orthogonal signals," *Bell System Technical Journal*, vol. 45, pp. 1775–1796, 1966.

[19] S. B, "Performance of an efficient parallel data transmission system," *IEEE Transactions on Communication Technology*, vol. 15, no. 6, pp. 805–811, 1967.

[20] B.Hirosaki, "A northogonally multiplexed qam system using the discrete fourier transform," *IEEE Transactions on Communications COM*, vol. 29, pp. 982–989, 1981.

[21] I. G. A. Sahin and H. Arslan, "A survey on multicarrier communications: prototype filters, lattice structures, and implementation aspects," *IEEE Communications Surveys and Tutorials*, vol. 16, no. 3, pp. 1312–1338, 2013.

[22] M. Bellanger, "Fbmc physical layer: A primer," 2010.

[23] S. Tatikonda and M. Jordan, "Loopy belief propogation and gibbs measures," *UAI 2002*, 2002.

THE 18TH INTERNATIONAL SYMPOSIUM ON WIRELESS PERSONAL MULTIMEDIA COMMUNICATIONS
(WPMC-2015)
December 13-16, 2015, Hyderabad, India

Impact of Network Coding on Distributed Indoor Target Tracking using Wireless Sensor Networks

Laxminarayana S Pillutla, Shourya Singh Gupta and Dushyant Singh
Dhirubhai Ambani Institute of Information and Communication Technology (DA-IICT)
Gandhinagar - 382007, Gujarat, India
Email:{laxminarayana_pillutla@daiict.ac.in, shouryasgupta@gmail.com and dushyant.singh.work@gmail.com }

***Abstract*—We consider the problem of distributed indoor target tracking using a wireless sensor network (WSN) based on received signal strength indicator (RSSI) values. To facilitate distributed tracking of targets by various nodes we consider an approach based on *random linear network coding (RLNC)* for dissemination of quantized RSSI values. Our simulation results show that the root mean square (RMS) tracking error obtained with the approach based on RLNC is strictly lower than that of the competing scheme owing to its rapid dissemination capability. Finally we observe that with the RLNC based scheme, RMS value of tracking error in a strongly connected network grows much slowly with noise variance in comparison with that of a weakly connected one.**

I. Introduction

Target tracking using wireless sensor networks (WSNs) is one of the important applications both on the domestic and defence fronts. Indoor target tracking based on WSNs is found to be a viable alternative to the global positioning system (GPS) based target tracking system, since the latter lacks desired accuracy in indoor environments [1]. Among various metrics used for tracking, RSSI is the most preferred for building a simple and inexpensive tracking system, since unlike other metrics it does not require synchronization among various network nodes [2] [3]. The target tracking system based on WSNs has to be distributed in which the sensor nodes run the tracking algorithm without help from any centralized entity like a base station. This requirement warrants the nodes to exchange their respective observations with minimal transmissions and latency.

Network coding (NC) has been shown to maximize throughput and/or minimize latency (or delay) for many different network topologies, especially for broadcast and multicast transmissions [4]. We refer interested readers to [5] for a survey on NC and its applications in internet and wireless networks. A specific instance of NC known as random linear NC (RLNC) has been found to be suitable for implementation in networks where computation across various network nodes happens in a distributed fashion. Implementation of a distributed target tracking algorithm at a given node of a WSN requires access to observations made at the other nodes [1]. It is highly desirable to ensure that the communication complexity scale linearly with the number of nodes in the network. To this end the authors in [3] propose a mechanism in which the leader node for a given target collects observations from its localized neighborhood, which is determined by an aggregation radius. It was shown using simulations that for a sufficiently large aggregation radius the performance of such a scheme comes close to the scheme in which observations from all the sensor nodes are used for target tracking. In this paper we evaluate tracking performance of the particle filter bank based tracking algorithm with RLNC mechanism as a means for information dissemination among various nodes.

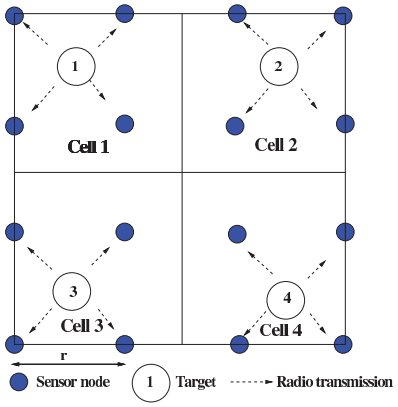

Fig. 1. The figure shows a WSN deployed on a uniform square grid for indoor target tracking.

II. Topology of WSNs, Targets' Maneuver Model and RSSI Observation Model

A. System Model

Consider a two dimensional uniform square grid of side S metres shown in Fig. 1 that is deployed with N number of nodes to track M targets moving inside it. Let r denote the common spacing between adjacent nodes. We assume each node makes RSSI measurements based on the periodic beacon frames sent by active RFID tags mounted on targets. The measured RSSI value is quantized, converted into message and encoded with messages of *same generation* received from other nodes to produce a NC packet. The RLNC mechanism used to produce the NC packet is described in Section III. The NC packet is then transmitted by each node by observing the CSMA protocol mechanism. We assume that all the nodes are synchronized to the same clock and the network to be slotted such that in a given slot only one NC packet is transmitted by a node.

B. Targets' Maneuver Model and RSSI Observation Model

Denote $X^t_{m,d}$ and $V^t_{m,d}$ as the position and velocity of m^{th} target in d^{th} dimension at time instant t. The total state of the m^{th} target at time instant t, comprising of position and velocity in each of the D dimensions, is given by $\mathbf{z}^t_m = \left[X^t_{m,1}, V^t_{m,1} \cdots, X^t_{m,D}, V^t_{m,D}\right]'$ (the operator $'$ denotes matrix transpose). We denote the total system state comprising of positions and velocities of M targets in D dimensions at time instant t as $\mathbf{z}^t$. If we assume the total system state to evolve according to a first order Markov chain, then the total system state at time instant $(t+1)$ in terms of total system state at time instant t can be written as

$$\mathbf{z}^{t+1} = A\mathbf{z}^t + B\mathbf{u}^t \ , \tag{1}$$

where A is a block diagonal matrix of size $2MD \times 2MD$ with the sub-matrix $\begin{bmatrix} 1 & T \\ 0 & 1 \end{bmatrix}$ repeated along the diagonal (T denotes the maneuver interval). The matrix B of size $2MD \times MD$ is another block diagonal matrix with $[\frac{T^2}{2}, T]'$ repeated along the diagonal. The vector $\mathbf{u}^t$ of size $MD \times 1$ represents the random acceleration that the M targets are subjected to in D dimensions. It is assumed to be Gaussian distributed of mean vector $\mathbf{0}$ and covariance matrix $\sigma^2_S I_{MD}$.

The RSSI value recorded at the n^{th} sensor node located at $\mathbf{r}_n$ corresponding to the m^{th} target whose true location is $\mathbf{x}^t_m$ at time instant t, is given by the following equation [3]

$$Y^t_{m,n} = \Phi^t_m + \Gamma^t_{f(\mathbf{x}^t_m).n} - \rho 10 \log\left(||\mathbf{x}^t_m - \mathbf{r}_n||\right) + W^t_{m,n} \ , \tag{2}$$

where Φ^t_m denotes transmission power of the target m at time instant t, Γ denotes gain of the channel from target m to the node n at time instant t, $f(.) : \mathbb{R}^D \rightarrow \{1, 2, \cdots, L\}$ denotes the cell location quantization function which maps a given location in the tracking region to one of the L possible cell values and $W^t_{m,n}$ denotes the measurement noise that is assumed to be both *spatially* and *temporally* independent across the various sensor nodes and time instants. It is assumed to be Gaussian distributed of zero mean and variance σ^2_W.

At every observation time instant t each sensor node $n\ (= 1, 2, \cdots, N)$ quantizes the observation $Y^t_{m,n}$ made about every target using a uniform quantizer. Let Y_{max} and Y_{min} denote the upper and lower limits of the quantizer. In uniform quantization the entire range of $(Y_{max} - Y_{min})$ is broken down into q equal quantization levels of width $\Delta \triangleq \frac{Y_{max} - Y_{min}}{q}$. The resulting quantization noise variance is given by $\sigma^2_q = \frac{\Delta^2}{12}$. The quantized observation is then sent using the RLNC described in next Section.

III. Random Linear Network Coding (RLNC) for Information Dissemination in WSNs

The quantized RSSI value (which is encoded over a binary alphabet) at a given observation time instant t available at a given node is converted into a packet suitable for dissemination the various fields of which are described subsequently. The following fields namely node ID and target ID are self explanatory. The field *NC coefficient* contains the encoding vector used for producing the data that goes into the *NC message* field. The NC message at a given node is generated using its quantized RSSI value for that target and NC messages for the corresponding target received from all the other nodes. The field *generation id* helps in combining of NC messages belonging to the same generation. Packets with same generation IDs essentially contain encoded quantized RSSI values for the same observation time instant t. We shall next describe as how NC messages can be produced by various nodes in the network.

Let $G(V, E)$ denote the network graph with $|V| = N$ nodes and links $E \subset V \times V$. Let $\{\mathbf{q}_n\}_{n=1}^N$ denote the set of quantized RSSI values at the N network nodes for a given observation instant corresponding to a given target (for convenience we suppress the target index m and the observation instant t). Note that each $\mathbf{q}_n$ is a binary encoded vector of length l for each node $n \in V$. For convenience we assume the field size k divides l the length of quantized RSSI value, otherwise zero padding is applied to ensure the same. At the beginning of some transmission time slot τ, an arbitrary node $n \in V$ contains a set of coded messages (as exchange of quantized RSSI values happens among various nodes):

$$Q_n(\tau) = \left\{\mathbf{u}_1, \mathbf{u}_2, \cdots, \mathbf{u}_{|Q_n(\tau)|}\right\} \ . \tag{3}$$

Each message $\mathbf{u}_i$ is generated as a linear combination of the underlying quantized RSSI values $\{\mathbf{q}_n\}_{n=1}^N$. Thus,

$$\mathbf{u}_i = \sum_{n=1}^{N} c_{i,n}\mathbf{q}_n, \ \text{(for } i = 1, \cdots, |Q_n(\tau)|) \ , \tag{4}$$

where $c_{i,n} \in \mathbb{F}_{2^k}$ denote NC coefficients which are made available using the packet header. Note that if $\mathbf{q}_n$ for a given n is not available then the corresponding $c_{i,n}$ is set to zero. The arithmetic operations involved in computation of $\mathbf{u}_i$ are performed over $\mathbb{F}_{2^k}$.

Let $\mathbf{c}_i \triangleq [c_{i,1}, \cdots c_{i,N}]^T \ (i = 1, \cdots, |Q_n(\tau)|)$, $\mathbf{q} \triangleq \left[\mathbf{q}_1^T, \cdots, \mathbf{q}_N^T\right]^T$, then one can write

$$\begin{bmatrix} \mathbf{u}_1^T \\ \vdots \\ \mathbf{u}^T_{|Q_n(\tau)|} \end{bmatrix} = \underbrace{\begin{bmatrix} \mathbf{c}_1^T \\ \vdots \\ \mathbf{c}^T_{|Q_n(\tau)|} \end{bmatrix}}_{\triangleq C_n(\tau)} \mathbf{q} \ . \tag{5}$$

From the encoded messages $\{\mathbf{u}_i\}_{i=1}^{|Q_n(\tau)|}$ the node n will be able to recover $\mathbf{q}_1, \cdots, \mathbf{q}_N$ when the rank of $C_n(\tau)$ equals N with the knowledge of NC coefficients vector $\{\mathbf{c}_i\}_{i=1}^{|Q_n(\tau)|}$.

The node n if it captures the channel at transmission time slot τ creates a vector $\mathbf{s}_n(\tau)$ by linearly combining the messages in the set $Q_n(\tau)$ (defined in Eq. (3)) with the encoding coefficients $b_i \in \mathbb{F}_{2^k}$ $(i = 1, \cdots, |Q_n(\tau)|)$. Thus

$$\mathbf{s}_n(\tau) = \sum_{i=1}^{|Q_n(\tau)|} b_i \mathbf{u}_i \ . \tag{6}$$

Note that the node n inserts the quantity $\sum_{i=1}^{|Q_n(\tau)|} b_i \mathbf{c}_i^T$ in the NC coefficient field of the transmitted packet (it just does not put $\sum_{i=1}^{|Q_n(\tau)|} b_i \mathbf{1}^T$).

IV. Particle filter based distributed target tracking

A. Target Tracking using Particle Filters

Each node once in possession of the quantized RSSI values (corresponding to M targets) from the remaining $(N-1)$ nodes computes position estimates for the underlying targets. We use a sampling importance resampling (SIR) based particle filter bank for tracking the M targets. The superior performance of particle filters for non-Gaussian and non-linear state space models over other approaches like extended Kalman filter is well known and we refer interested readers to [6] for a detailed exposition on particle filters. The SIR particle filter based tracking algorithm is given in Algorithm 1. Unlike the algorithm used in [3], in the Algorithm 1 we do not allow any interaction between the various sub-filters used for tracking of individual targets. This is because we assume the targets move independently which is unlike what was assumed in [3], where the authors assumed targets to move in a correlated fashion. In Algorithm 1 the estimates $\hat{\Phi}_m(t)$ and $\hat{\Gamma}_{l,n}(t)$ are computed incrementally using the approach given in next sub-section. Note that we have approximated the noise, introduced due to quantization of observations, to be Gaussian. Consequently, in the Step 5 of Algorithm 1, the measurement noise variance σ_W^2 is indeed augmented by the quantization noise variance σ_q^2.

B. Radio Environment Estimation

The incremental estimator is based on stochastic expectation and maximization (EM) algorithm. EM algorithm is used to compute ML estimates of unknown parameters [7]. The EM algorithm comprises of two main steps namely the E-step which involves computation of the *auxiliary likelihood function* and the M-step which involves maximization of the auxiliary likelihood function. It is used extensively in models where the observations depend on hidden or unknown random variables. In the current case the quantized observations $\left\{\left\{S_{m,n}^t\right\}_{m=1}^M\right\}_{n=1}^N$ depend on the unknown total state vector $\mathbf{z}^t$. To derive EM algorithm in the current case we introduce $\Theta^t \triangleq \left[\left\{\Phi_m^t\right\}_{m=1}^M, \left\{\left\{\Gamma_{l,n}^t\right\}_{l=1}^L\right\}_{n=1}^N\right]$. The quantized observation vector at any arbitrary time instant $t^{'}$ is denoted as $\mathbf{s}^{t^{'}} \triangleq \left[\mathbf{s}_1^{t^{'}}, \cdots \mathbf{s}_M^{t^{'}}\right]$ where $\mathbf{s}_m^{t^{'}} \triangleq [S_{m,1}^{t^{'}} \cdots S_{m,N}^{t^{'}}]$ $(m = 1, \cdots, M)$. We denote $p(\mathbf{y}_{1:t}, \mathbf{z}_{1:t}|\Theta)$ as the joint PDF of observations and total state until time t given the unknown parameter Θ. Using the fact that observations across different time instants are independent given $\mathbf{z}^t$ and Θ one can compute the auxiliary likelihood function $\mathbb{E}\left[\ln\left(p\left(\mathbf{s}_{1:t}, \mathbf{z}_{1:t}|\Theta\right)\right)\right]$ (where $\mathbb{E}(.)$ is with respect to the filtered PDF $p\left(\mathbf{z}_{1:t}|\mathbf{s}_{1:t}\right)$) and maximize it using the following recursion to compute estimate for $\Theta^{t^{'}+1}$ given the past estimate $\widehat{\Theta}^{t^{'}}$: $\widehat{\Theta}^{t^{'}+1} = \widehat{\Theta}^{t^{'}} + \epsilon \mathbf{f}\left(\widehat{\Theta}^{t^{'}}; \mathbf{s}^{t^{'}}\right)$, where $\epsilon \ll 1$ denotes a constant step size (constant step size would help us track slow time variations in parameter values), $\mathbf{y}^{t^{'}}$ as defined before denotes the vector of all observations at time instant $t^{'}$ and $\mathbf{f}\left(\widehat{\Theta}^{t^{'}}; \mathbf{s}^{t^{'}}\right) \triangleq \nabla_\Theta \sum_{m=1}^M \int_{\mathbb{R}^{2D}} \ln p\left(\mathbf{s}_m^{t^{'}}|\mathbf{z}_m^{t^{'}}, \Theta\right) p\left(\mathbf{z}_m^{t^{'}}|\widehat{\Theta}^{t^{'}}, \left\{\mathbf{s}_m^l\right\}_{l=1}^{t^{'}}\right) d\mathbf{z}_m^{t^{'}}$ ($\nabla_\Theta(.)$ denotes the gradient operator with respect to Θ).

Algorithm 1 : SIR based Particle Filter for Target Tracking

1: For each $m = 1, \cdots, M$ do steps 2 through 6:
2: **Particle Initialization:** Initialize $\left\{\tilde{\mathbf{z}}_{m,i}^t, i = 1, 2, \cdots, \Pi\right\}$ using a uniform distribution over the finite tracking area of interest. Then for each $t = 1, 2, \cdots$ execute the following steps:
3: **Creation of full-state particles:** Using the Π sub-state particles of all M targets corresponding to time instant $t-1$ i.e. $\left\{\tilde{\mathbf{z}}_{m,i}^{t-1}, i = 1, 2, \cdots, \Pi\right\}$, create Π full-state particles $\left\{\tilde{\mathbf{z}}_i^{t-1} = \left[\tilde{\mathbf{z}}_{1,i}^{t-1}, \tilde{\mathbf{z}}_{2,i}^{t-1}, \cdots, \tilde{\mathbf{z}}_{M,i}^{t-1}\right], i = 1, \cdots, \Pi\right\}$.
4: **Importance Sampling from Transitional Prior:** Generate samples for the current time instant t (i.e. $\tilde{\mathbf{z}}_i^t$) by sampling from the (sub-optimal) transitional prior $p(\mathbf{z}^t|\mathbf{z}^{t-1})$ which is done as follows: $\tilde{\mathbf{z}}_i^t = A\tilde{\mathbf{z}}_i^{t-1} + B\mathbf{u}^t$.
5: **Computation of particle weights corresponding to each target and their normalization:** (a)$w_{m,i}^t = \exp\left(-\frac{1}{2\left(\sigma_W^2+\sigma_q^2\right)} \sum_{n=1}^N term\ 1(n)\right)$, where $term\ 1(n) = (S_{m,n}^t - \hat{\Phi}_m^t - \hat{\Gamma}_{f(\tilde{\mathbf{z}}_{m,i}^t),n}^t + \rho 10\log_{10}||\tilde{\mathbf{z}}_{m,i}^t - \mathbf{r}_n||)^2$ (where $S_{m,n}^t$ denotes the quantized version of $Y_{m,n}^t$). (b)**Normalization of weights:** $\tilde{w}_{m,i}^t = \frac{w_{m,i}^t}{\sum_{i=1}^\Pi w_{m,i}^t}$, $i = 1, \cdots, \Pi$.
6: **Resampling step:** Draw Π numbers from 1 to Π with replacement using the distribution $\left\{\tilde{w}_{m,i}^t, i = 1, \cdots, \Pi\right\}$. Use these indices to select Π particles from the pool $\left\{\tilde{\mathbf{z}}_i^t, i = 1, \cdots, \Pi\right\}$. Denote these resampled particles as $\left\{\tilde{\mathbf{p}}_i^t\ i = 1, \cdots, \Pi\right\}$.
7: **Extraction of sub-state particles:** The sub-state particles $\left\{\tilde{\mathbf{z}}_{m,i}^t\ i = 1, \cdots, \Pi\right\}$ can be extracted from $\left\{\tilde{\mathbf{p}}_i^t\ i = 1, \cdots, \Pi\right\}$ by discarding all the components other than those that of m.
8: **Computation of state estimate of target** m**:** $\hat{\mathbf{z}}_m^t = \frac{1}{\Pi}\sum_{i=1}^\Pi \tilde{\mathbf{z}}_{m,i}^t$.

The various components of $\mathbf{f}\left(\widehat{\Theta}^{t^{'}}; \mathbf{s}^{t^{'}}\right)$ can be computed for $m = 1 \cdots, M)$ and $(l = 1, \cdots, L), (n = 1, \cdots, N)$ as follows:

$$f_{\Phi_m}\left(\widehat{\Theta}^{t^{'}}; \mathbf{s}_m^{t^{'}}\right) \approx \sum_{n=1}^N \frac{1}{\Pi} \sum_{p=1}^\Pi (term\ 2(n,p)) \tag{7}$$

$$f_{\Gamma_{l,n}}\left(\widehat{\Theta}^{t^{'}}; \mathbf{s}^{t^{'}}\right) \approx \sum_{m=1}^M \sum_{n=1}^N \frac{1}{\Pi} \sum_{p=1}^\Pi term\ 3(m,n,p) \tag{8}$$

where $term\ 2(n,p) = \frac{S_{m,n}^{t^{'}} - \widehat{\Phi}_m^{t^{'}} - \widehat{\Gamma}_{f(\tilde{\mathbf{z}}_{m,p}^{t^{'}}),n}^{t^{'}} + \rho 10\log\left(\left\|\tilde{\mathbf{z}}_{m,p}^{t^{'}} - r_n\right\|\right)}{\sigma_W^2+\sigma_q^2}$ and

$term\ 3(m,n,p) = \frac{\left(S^{t^{'}}_{m,n} - \widehat{\Phi}^{t^{'}}_{m} - \widehat{\Gamma}^{t^{'}}_{f(\tilde{\mathbf{z}}^{t^{'}}_{m,p}),n} + \rho 10\log\left(\|\tilde{\mathbf{z}}^{t^{'}}_{m,p} - r_n\|\right)\right)}{\sigma^2_W + \sigma^2_q}$
$\mathbb{I}_l\left[f(\tilde{\mathbf{z}}^{t^{'}}_{m,p})\right]$.

Notice the difference between expressions given in Eq. (7) and Eq. (8) to similar expressions in [3]. This can be attributed to the fact that in [3] the authors compute estimates so that the likelihood function is maximized, while in our case we maximize the auxiliary likelihood function as usually done in the EM algorithm. We believe our approach has the advantage of computing the estimates of parameters contained in the state transition equation given in Eq. (1)

V. Simulation Study of Indoor Target Tracking using WSNs with RLNC

A. Simulation scenario and Localized Aggregation Method

We simulate movement of $M = 8$ targets in a uniform square grid of side 30 metres thereby implying a total target area of 900 square metres. We assume the spacing $r = 10$ metres between adjacent nodes. Thus we have deployed around 16 targets to track the 8 targets of interest. The entire tracking area is assumed to be divided into $L = 4$ cells. The time-invariant transmit power values $\{\Phi^t_m\}^8_{m=1}$ of the 8 targets are set to random values as $\Phi_m = \phi_{nominal} + 3 \times \mathcal{N}(0,1)\ \ (m = 1, \cdots, 8)$, where we have set $\phi_{nominal} = 5$. The time-invariant gain(s) experienced by a transmission from cell l to node n, denoted as $\Gamma_{l,n}$, are set as $\Gamma_{l,n} = \lambda_{wall} d_{l,n} + \alpha_{l,n}\left(1 - \mathbb{I}_l(r_n)\right)$, where $d_{l,n}$ denote the number of walls crossed by a transmitted signal in straight line path from cell l to node n, $\alpha_{l,n}$ denote random values generated from the $\mathcal{N}(0,3)$ distribution and $\mathbb{I}_l(x)$ denotes an indicator function which is equal to 1 only when $x \in l$ and 0 otherwise. The parameters set as per the above procedure are kept constant for throughout the simulation. As in [3] one may consider varying the parameters slowly and the parameter estimation recursion should still be able to track the changes. For the purpose of particle filtering we assume the number of particles $\Pi = 128$. We measure the tracking performance in terms of root mean square error (RMSE) which is given by $\text{RMSE} = \frac{1}{M}\sum_{m=1}^{M} \mathbb{E}\left[||\mathbf{x}^t_m - \hat{\mathbf{x}}^t_m||^2\right]$ (where $\hat{\mathbf{x}}^t_m$ denotes the position estimate of the target m). In practice since it is not possible to compute the ensembled mean therefore we replace it by the corresponding time average. For the RLNC part we assume the observations are quantized by using a uniform quantizer with $q = 256$ levels and Y_{max} and Y_{min} are set to be 10 and -20 respectively (the upper and lower limits of uniform quantizer used at various nodes). The size of the finite field k is set equal to 8 i.e. the NC coefficients are generated over the finite field $\mathbb{F}_{2^8}$. We performed the simulation in MATLAB (for target tracking and generation of finite field) and JProwler an open source network simulator (for RLNC and CSMA mechanism).

In the localized aggregation method (against which we shall compare the proposed approach based on RLNC) every target that is to be tracked is associated with an owner node [3]. The node that is closest to a given target is chosen as the owner node. Once target owner is selected then all the nodes within a given aggregation radius of say $r^{'}$ meters will send their RSSI value to the owner node. Using the observations sent by nodes in the neighbourhood the target tracking algorithm given in Algorithm 1 is run.

B. Results and Discussion

The Fig. 2 shows plots of RMSE versus the noise variance for the cases of local aggregation scheme with radii 10 and 20 metres respectively and the scheme based on RLNC. As can be seen from the figure the RMSE obtained with RLNC scheme is strictly below that of the RMSE obtained with the aggregation scheme. From the Fig. 2 it can also be noted that the rate at which RMSE grows with noise variance is much slower than what can be seen for the localized aggregation scheme (for lower values of measurement noise variance). This can be attributed to two reasons: firstly the dissemination is much faster with RLNC a fact corroborated by the results in Fig. 3. Secondly each node in RLNC has access to a greater number of observations in comparison with the localized aggregation scheme.

The Fig. 3 shows the plot of RMSE versus the total number of transmission time slots taken for information dissemination in the localized aggregation scheme and RLNC. We assume the measurement noise variance to be fixed and equal to 1 dB. The RMSE achieved by the scheme based on RLNC is much lower than for the localized aggregation scheme. From this we can conclude that for a given RMSE the RLNC scheme would require lower number of transmission time slots than the localized aggregation scheme.

Finally in Fig. 4 we compare the tracking performance of RLNC scheme for two cases. In the first case connectivity among nodes is very strong and in the second case the connectivity is much weaker than the first. In the former case less number of time slots are required for dissemination than the latter one to achieve the same amount of RMSE. In general as measurement noise variance increases RMSE increases. However in the strongly connected case the observations from other nodes reach much faster than in the weakly connected case thereby causing the RMSE to grow much slower with the measurement noise variance compared to the weakly connected case.

VI. Conclusion

We considered distributed indoor target tracking using WSNs based on RSSI measurements. RLNC is used by various network nodes for dissemination of their respective quantized RSSI values to each other. We compared the tracking performance of the distributed target tracking algorithm with RLNC based dissemination against the scheme that aggregates observations only from the a given target neighborhood. The distributed tracking algorithm based on RLNC based information dissemination resulted in a lower RMS value of the tracking error compared to the localized aggregation scheme. This can be attributed to the rapid dissemination capability of the RLNC scheme. Our simulation results also showed that

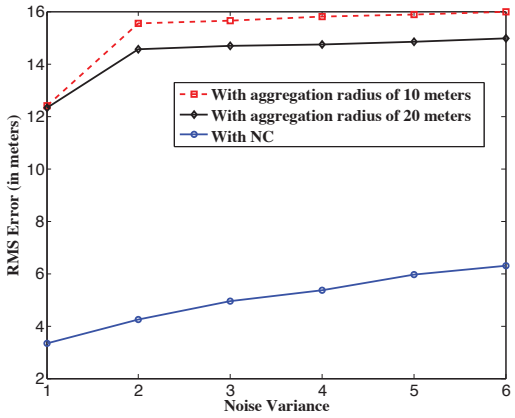

Fig. 2. The figure shows plots of RMS versus the noise variance in dB for RLNC and localized aggregation schemes.

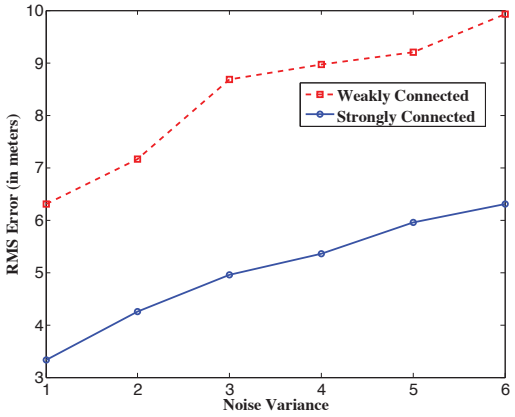

Fig. 4. The figure compares the plot of RMS versus the noise variance in dB for two contrasting network scenarios in which information is disseminated using RLNC.

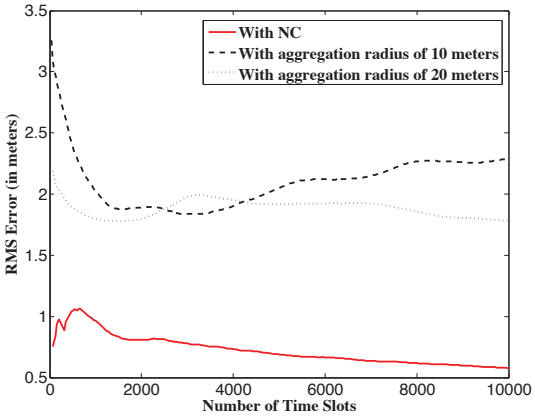

Fig. 3. The figure shows plots of RMS versus the total number of time slots used in information dissemination for the cases of RLNC and localized aggregation scheme.

in strongly connected networks the growth of RMS value of tracking error with measurement noise variance is much slower in comparison with the weakly connected case.

VII. Acknowledgement

The research of first author was supported by DST-SERB, Govt. of India, under the FAST track scheme for young scientists.

References

[1] N. Patwari, J. N. Ash, S. Kyperountas, A. O. Hero III, and N. S. Correal, "Locating the Nodes: Cooperative Localization in Wireless Sensor Networks," *IEEE Signal Processing Magazine*, vol. 22, no. 4, pp. 54–69, July 2005.

[2] A. Boukerche, H.A.B.F. Oliveira, E.F. Nakamura, and A.A.F. Loureiro, "Localization Systems for Wireless Sensor Networks," *IEEE Wireless Communications Magazine*, vol. 14, no. 6, pp. 6–12, Dec. 2007.

[3] A. Oka and L. Lampe, "Distributed Target Tracking Using Signal Strength Measurements by a Wireless Sensor Network," *IEEE Journal on Selected Areas in Communications*, vol. 28, no. 7, pp. 1006–1015, Sept. 2010.

[4] R. Ahlswede, N. Cai, S. Li, and R. Yeung, "Network Information Flow," *IEEE Trans. Inform. Theory*, vol. 46, no. 4, pp. 1204–1216, April 2000.

[5] P. A. Chou and Y. Wu, "Network Coding for Internet and Wireless Networks," *IEEE Signal Processing Magazine*, vol. 24, no. 5, pp. 77–85, Sept. 2007.

[6] M. Arulampalam, S. Maskell, N. Gordon, and T. Clapp, "A Tutorial on Particle Filters for Online Non-linearNon-gaussian Bayesian tracking," *IEEE Trans. Signal Proc.*, vol. 50, no. 2, pp. 174–188, Feb. 2002.

[7] A.P. Dempster, N.M. Laird, and D.B. Rubin, "Maximum likelihood from incomplete data via the EM algorithm," *Journal of the Royal Statistical Society, B*, vol. 39, pp. 1–38, 1977.

THE 18TH INTERNATIONAL SYMPOSIUM ON WIRELESS PERSONAL MULTIMEDIA COMMUNICATIONS
(WPMC-2015)
December 13-16, 2015, Hyderabad, India

Eight-Path Harmonic Rejection Mixer for Full Band Mobile TV

Kiran B
Department of EEE, Indian Institute of Technology
Guwahati, Assam - 781039, email: 4work.kiran@gmail.com

Roy P Paily
Department of EEE, Indian Institute of Technology
Guwahati, Assam - 781039, email: roypaily@iitg.ernet.in

***Abstract*—In this work, a harmonic rejection mixer with Local Oscillator (LO) frequency programming facility is proposed. The virtual LO frequency programming facility in this mixer enables it to cover VHF III, UHF and L bands of mobile TV communication with very relaxed master LO frequency requirement. This also uses simple frequency divider circuit to generate multi phase LO signals from master LO wave, unlike other universal mobile TV receiver front ends. The proposed circuit has other advantages like current reusing single MOS pole-zero filtering, which reduces the power consumption and offers faster roll offs, noise cancellation facility and virtual RF filtering provided by passive mixer feedback. The frequency programming facility achieves virtual LO frequencies of $2f_{LO}$, $3f_{LO}$ and $4f_{LO}$ from an actual frequency of f_{LO}. The simulation studies show a peak gain of 10.51dB, an IIP2 of 63.47dBm, IIP3 of 2.44dBm and a NF of 18.4dB. The circuit consumes 7.5mW power when operated with a supply voltage of 2.5V.**

I. Introduction

Mobile television integrates two of the most popular customer products ever: television and mobile phone. The co-existence of numerous standards defined for mobile TV transmission demands the integration of hardwares supporting multiple standards and multiple frequency bands. Mobile TV bands reside in 3 frequency bands, VHF-III (174 to 248 MHz), UHF (470 to 862 MHz) and L (1.4 to 1.7 GHz) [1]. The function of a mixer is to down-convert the desired RF input to an IF output, but, in this wide range of operating frequencies, the mixer down converts blockers around LO harmonics to required IF frequency band. Hence the receiver requires bulky external Surface Acoustic Wave (SAW) filters to eliminate the blockers. To avoid down-conversion of blockers around harmonics to baseband, wideband receivers often use a poly-phase down-converter. The use of poly-phase (N-Phase) mixers for harmonic rejection demands N poly-phase LO signals of frequency f_{LO}, phase shifted to each other by (360/N) degrees. If a simple frequency divider circuit is used to generate these N number of LO waves, then a master LO frequency of Nf_{LO} is required to drive it. This high frequency operation of master local oscillator consumes high energy and demands complex Phase Locked Loop (PLL) and Voltage Controlled Oscillator (VCO) designs.

Fujian et al [2], realized mobile TV receiver front end covering from 0.15GHz to 0.85GHz without any off chip SAW filters or separate internal RF filter. This circuit has an 8-path active mixer in the forward path with passive mixers as feedback. The mixer is stacked with a current mode single-MOS pole-zero LPF. The fed back passive mixers frequency translate the low pass ($Z_{in}(\Delta\omega)$ LPF input impedance to

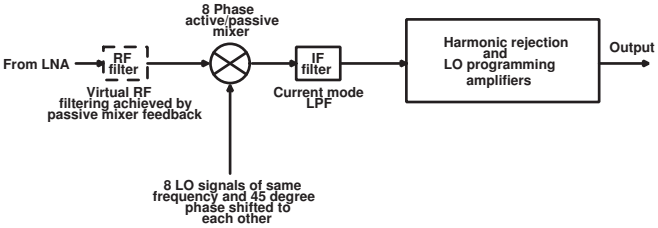

Fig. 1: Block diagram of the proposed system

$Z_{in}(n\omega_{LO} + \Delta\omega)$) at the RF input port. This LO defined input matching helps in stop-band rejection right at the mixer input. This extra filtering feature helps in avoiding the need or in relaxing the properties of external SAW filters. This circuit also has a noise cancellation property because of the feedback included. This system uses a digital divided-by-8 circuit to generate the 8-phase clock required for the 8-phase mixer. A master LO frequency of $8f_{LO}$ is required at the frequency divider circuit's clock to generate 8-phase LO waves of frequency f_{LO}. For achieving effective f_{LO} of more than 1.7GHz in 8-phase mixer case, one need to generate a master LO frequency greater than 13.6GHz. This much high frequency requirement in master local oscillator makes the VCO and PLL designs complex [3]. These drawbacks makes the system unable to cover the L (1.4-1.7GHz) band of mobile TV [1].

Pui et al [1], developed a unified receiver front end covering all 3 specified TV bands. It uses a complex direct injection-locking 4/8 phase LO generator instead of a much simpler frequency divider circuit. Direct injection circuit needs a master LO which is equal to the f_{LO} required for the multi-phase mixer. This relaxation in master LO frequency requirement enables it to cover the higher L band frequencies unlike the receiver in [2]. But this direct injection circuit, which is used to generate poly-phase LO waves, consumes larger power and area, and is complex as compared to much simpler and better, frequency divider circuit used in [2]. This receiver also needs 3 separate bulky external SAW filters unlike [2] since it lacks any passive mixer feedback, for frequency translation of base band LPF impedance to RF input.

In this work, a mixer covering all the mobile TV bands is developed by using LO programming cum Harmonic rejection circuits based on modified version of the architecture put forwarded by Travis et al [4]. This new LO programming cum HR circuit can replace the normal harmonic rejection circuits in [2] and makes it able to operate in higher L band mobile

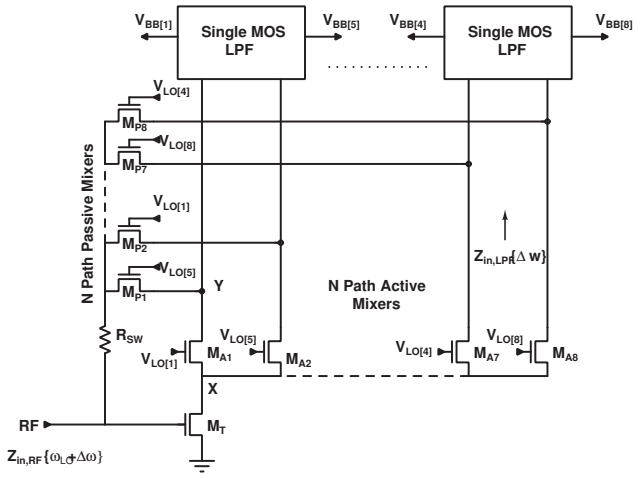

Fig. 2: 8-phase mixer with current mode LPF [2]

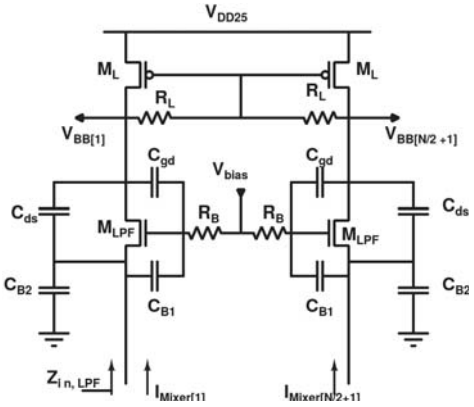

Fig. 3: Current mode single-MOS LPF[2]

TV spectrum. The tunable LO facility is able to produce the effect of 2LO, 3LO, 4LO frequencies from an 8-phase LO frequency fed 8-path mixer. This enables it to cover all the mobile TV band with a much lower maximum 8-phase f_{LO} of 850 MHz. This frequency requirement is same as that of [2], which can cover frequencies up to UHF band only. The simpler frequency divider circuit can be employed to generate these 8-phase waveforms from a master frequency of 6.8GHz. This master frequency is not a big challenge as far as the VCO and PLL designs are concerned. Additionally, this architecture needs no external SAW filters unlike [1].

II. Blocks and circuits

The block level architecture of the work is shown in the Figure 1. The mixer used here is based on the parallel 8 path active passive mixer from [2]. The 8 outputs from mixer are given to the proposed harmonic rejection cum LO programming amplifiers. Different sets of amplifiers are used for different modes of operation. The 8-phase active/passive mixer is driven by 8, LO signals with 12.5% duty cycle and 45 degree phase difference to each other. These eight LO signals can be obtained from a frequency divider circuit, which is driven by a frequency 8 times the frequency of LO signals,$8f_{LO}$. The mixer is stacked with a current mode LPF to eliminate the unwanted frequencies. The combined harmonic rejection and LO frequency mode selection circuit allow the system to obtain effective local oscillator frequencies of $f_{LO}, 2f_{LO}, 3f_{LO}, 4f_{LO}$, from an actual LO frequency of f_{LO}. This is achieved by employing different set of gains for different phase outputs of 8 phase mixer [4].

The passive mixer feedback in this circuit helps in noise cancellation and LO based frequency translation of low pass LPF input impedance to RF input node. This frequency translation effect results in a virtual RF filtering at the input of the mixer. This feature can also be used in the higher modes of operation which are obtaining the effective frequencies equal to the harmonics of the LO wave. This observation proves that the HR cum LO programming architecture proposed by Travis et al [4] can be used in [2] as well. A simple set of amplifier circuit with current mode signal summing is proposed, which can be attached to [2] to realize the architecture proposed in [4].

A. Mixer and LO defined LPF base band impedance translation to RF input[2]

The 8 path mixer circuit is shown in Figure 2. The transconductor MOS M_T convert the RF voltage at V_{in} to current. The switching action of M_A transistors down convert the V_{in} at node Y. The passive mixer switches (M_P transistors) up-convert the voltage at Y to the input RF node by same amount. In effect this loop act like a positive feedback. The equivalent input impedance from RF input of this N-path mixer can be proved as expression (1), from theory suggested by [5].

$$Z_{in}(\omega) = \frac{R_{\mathrm{SW}} + N\sum_{n=-\infty}^{+\infty} |k_n|^2 Z_{\mathrm{BB}}(\omega - n\omega_{\mathrm{LO}})}{1 - G_{\mathrm{loop}}}. \quad (1)$$

Where G_{loop} is the loop gain is

$$G_{\mathrm{loop}} = \frac{1}{N} \cdot g_{\mathrm{m,CS}} \cdot Z_{\mathrm{in,LPF}}\{\Delta\omega\}, \quad (2)$$

According to (1), the input impedance seen from the RF input is the frequency translated value of low pass input impedance of current mode LPF, shifted to the integer harmonics of the f_{LO} along with a scaling factor of $N|k_n|^2 = 1/Nsinc^2(n/N)$ at $n\omega_{LO}$. So at the RF input node, frequencies around f_{LO} and its harmonics experience a high impedance, while all other frequencies experience low impedances. This achieves a filtering at the RF input node itself for all modes of operation since the virtual LO frequencies achieved at higher modes are the harmonics of the fundamental LO frequency f_{LO}. Since $k_1 > k_2 > k_3 > k_4$, gains will be lesser for higher modes of operation.

B. Proposed replacement of the normal Harmonic Rejection (HR) in [2] with HR and LO programming circuit

1) Concept: In this work, new harmonic rejection (HR) cum LO programming circuits are proposed using the architectural idea put forwarded by Travis et al [4]. In N path HR mixers, as in [2] the out put is generated by scaling and

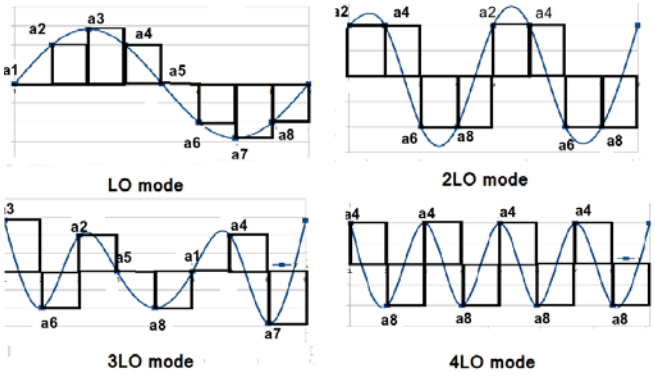

Fig. 4: Effective sinusoid LO achievement in different modes of operation

combining each of N equally phase shifted and (1/N) duty cycle LO waves. The scaling coefficients are scaled versions of samples of a sine wave of frequency f_{LO} with a sampling frequency of Nf_{LO}. These samples are given by,

$$a_k = G \sin\left\{\frac{2\pi k}{N}\right\} \tag{3}$$

where $0 \leq k \leq N$, and G is a scaling factor. In an 8 path mixer, these scaling coefficients ratios $a_1 : a_2 : a_3 : a_4 : a_5 : a_6 : a_7 : a_8$ are equal to $0 : 1 : \sqrt{2} : 1 : 0 : -1 : -\sqrt{2} : -1$.

It can be mathematically proven that, the sampling of a sinusoid of frequency nf_{LO} results in the same sampling values as obtained from a sine wave of frequency f_{LO}, where n is an integer. If the sampled values of $\sin(2\pi f_{LO}t)$ are represented as $[a_k]$ and sampled values of $\sin(2\pi n f_{LO}t)$ is represented by $[a_k^n]$, then $[a_k^n]$ will be a subset of $[a_k]$ if n is even and $[a_k^n]$ will be a permutation of $[a_k]$ if n is odd. So by rearranging the scaling coefficients in normal N path harmonic rejection mixer, the virtual effect of integral multiples of LO frequency, nf_{LO} can be obtained. The frequency spectrum of effective nf_{LO} obtained is given by

$$X(f) = \frac{1}{2} \sum_{m=-\infty}^{\infty} \delta(f - (mN \pm n) f_{\mathrm{LO}}) \mathrm{sinc}\left(\frac{n\pi}{N}\right) \tag{4}$$

It is evident from equation (4) that, while achieving virtual frequency of nf_{LO} from an actual frequency of f_{LO} using an N path mixer outputs, the first unattenuated harmonic appears at (N-n)f_{LO}. This limits the number of modes that can be achieved. If $n > N/2$ the first unattenuated harmonics will be higher in magnitude than that of required frequency. So maximum number of modes possible with 8 path mixer is 4. The pictorial representation of effective LO wave achievement in different modes is shown in Figure 4.

2) Circuit Implementation: In the current mode filter in Figure 3, which is a stacked above all the 8 branches of the mixer, the transistor M_L is diode connected. So the outputs from the 8 paths $V_{BB[1]}$ to $V_{BB[8]}$ can be used to mirror the current flowing through each of these signal paths. For achieving different modes of operation i.e. different effective LO frequencies, each of these outputs should be amplified with different amplification factors and then combined to form an approximate sinusoidal wave. Here the amplification and addition is done in current mode since the outputs from mixer can be used easily to mirror the current. The amplification is achieved by varying the width of the mirroring transistor. Separate set of amplifiers are used for different modes of operation. If the receiver is working in one mode of operation, power to all other amplifiers can be cut-off to reduce power conception.

TABLE I: Harmonic Rejection of Different Modes

Mode	HRR2 (dB)	HRR3 (dB)	HRR4 (dB)	HRR5 (dB)	HRR6 (dB)
LO	39	44	66	55	61
2LO	38	21	90	29	56
3LO	24	41	22	49	39
4LO	95	18	98	24	106

The amplifying circuits used for the four modes of circuit operation is shown in Figure 5. Here PMOS transistors preferred to have thicker gate oxide as is the case of transistor M_L used in LPF. It can be observed that the scaling factor i.e. size of mirroring transistor for each mixer output is different for different mode.

III. SIMULATIONS AND RESULTS

The harmonic rejection mixer (HRM) is tested for all the 4 modes of operation. All these results are subsequently compared with similar works reported in the literature.

A. Harmonic Rejection (HR)

The harmonic rejection for different modes of operation is listed in the Table I. In Figure 4, it can be observed that in LO mode, the equivalent LO signal is approximately a sine wave. Thereby, high rejection for both even and odd harmonics are obtained in this mode. In 2LO and 4LO modes, the equivalent LO signals are perfect square waves. This makes these modes to have no odd harmonic rejection and it is reflected in the measurements. A 16-phase mixer based HR and frequency programming can avoid this problem. In 3LO mode the imperfect shape of the effective LO wave is causing lower values of even HRRs, but the absence of DC value enables it to have a higher values of odd HRR. Low HRR does not cause much problems in 2LO, 4LO and 3LO modes, since the higher order harmonics are away from the frequency of interest.

B. Gain and NF

Maximum gains obtained in different modes are given in the Table II. As can be seen in Figure 4, the effective LO in modes 2LO and 4LO are not good sinusoidal waves and this cause the fundamental component to have lesser gain. This can also be observed from Table II. Figure 6 shows the gain variation with frequency in LO mode. The reduction in gain with frequency is due to action of the current mode LPF. Noise figure obtained is slightly worser in the higher modes of operation. This is mainly because of the reduction in gain of mixer LPF combination.

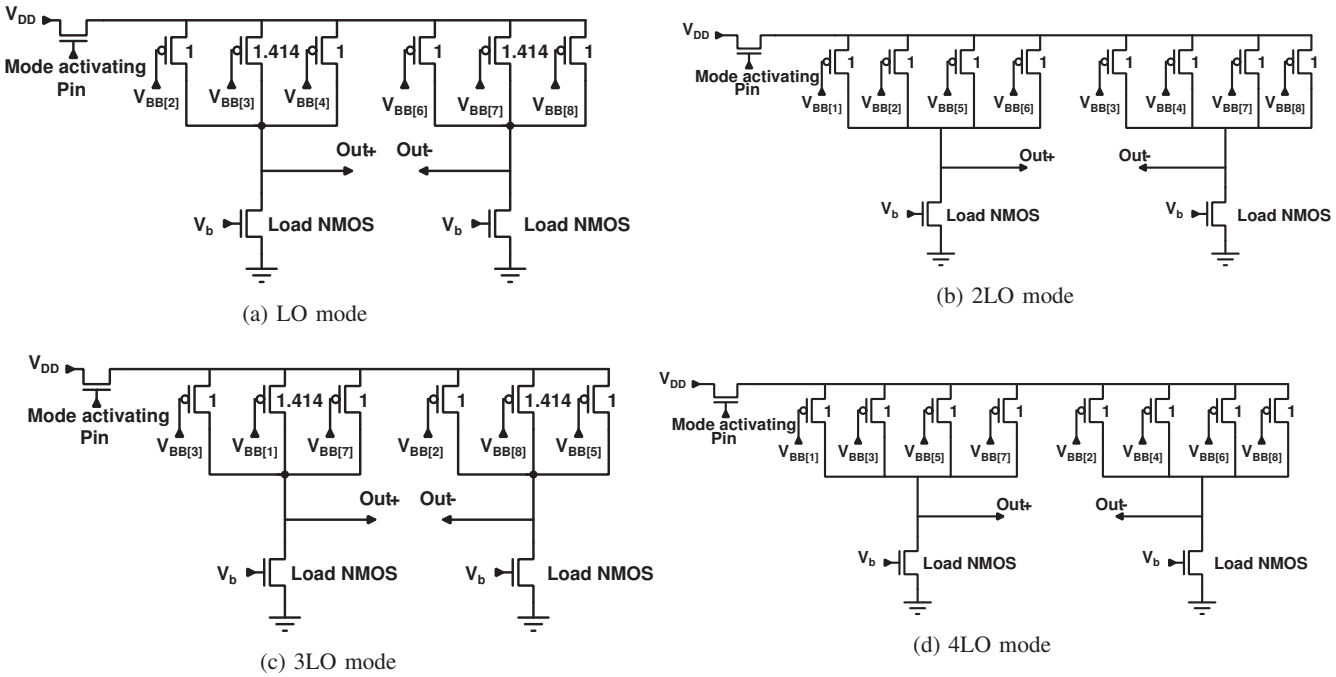

(a) LO mode

(b) 2LO mode

(c) 3LO mode

(d) 4LO mode

Fig. 5: HR and LO programming circuits for different modes of operation

TABLE II: Gain and NF in Different Modes

Mode	Gain(dB)	NF(dB)
LO	10.51	18.03
2LO	9.27	20
3LO	8.34	22.3
4LO	9.3	20.6

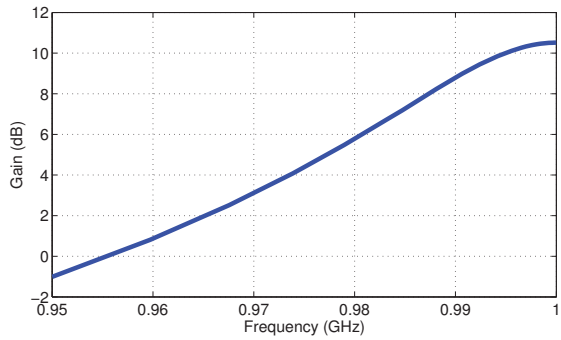

Fig. 6: Gain variation with input RF frequency(LO mode), f_{LO}= 1GHz

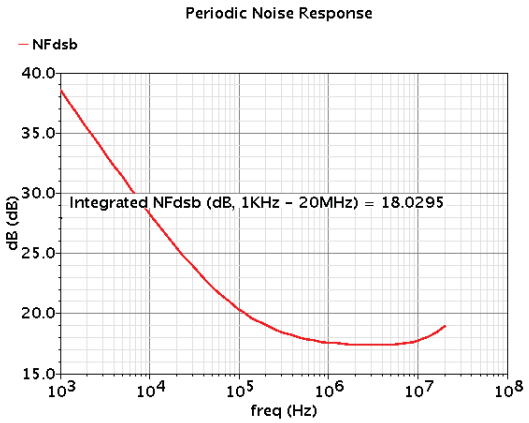

Fig. 7: NF variation with output BB frequency(LO mode)

TABLE III: IIP2 and IIP3 in Different Modes

Mode	IIP2(dBm)	IIP3(dBm)
LO	63.47	2.44
2LO	67.77	2.04
3LO	27.71	-0.78
4LO	63.64	-0.74

C. IIP2 and IIP3

The IIP2 and IIP3 values obtained for different modes of operations are summarized in Table III. With a worst case NF of 22dB and worst case IIP3 of -0.78dBm for the mixer, the LNA which is to be used prior to the mixer stage, demands a gain of 15dB to 20dB, NF less than 3dB and an IIP3 more than 3dBm. These are easily achievable with a standard LNA. So mobile TV receiver front end requirements are easily achievable with this work.

TABLE IV: Comparison with Recent Works

Feature	This work	[1]	[2]	[4]	[7]	[8]	[9]
Implementation	Mixer	Receiver	Receiver	Mixer	Receiver	Receiver	Receiver
Down conversion	Active/Passive	Passive or Active	Active/Passive	Passive	Passive	Passive	Passive
RF input style	Single ended	Single ended	Single ended	Single ended	Single ended	Differential	Single ended
RF range(GHz)	0.174-1.7	0.174-1.7	0-0.85	0.05-0.83	0.7-1.6	0.48-.86	0.04-1
Power(mW)	7.5	55	16.2	-	12	144	440
DSB NF(dB)	18.43	4	4.6	11	10.5	6	3
IIP3(dBm)	2.44	-3.4	-12	5.4	10	-13	-15
IIP2(dBm)	63.47	32	61	54	26.6	51	20
External Parts	nil	3SAWs	nil	SAW	nil	nil	inductor
HRR 3,5(dB)	44,55	35,39	53,51	72,71	34,34	70,70	65,65
RF-IF Gain(dB)	10.51	35	51	12	37	42	40
Supply(V)	2.5	1.2,2.5	1.2,2.5	1.2	1.3	1.8	1.8
CMOS Technology	65nm	65nm	65nm	130nm	65nm	180nm	80nm

D. Power

The maximum power consumption is approximately 7.5mW among all the modes of operation. This is very low in comparison with reported mobile TV receiver front ends. The gain and NF are traded-off to attain such a low power operation. Since mobile phones and portable electronic equipments have a very stringent requirement of battery backup, the proposed circuit has potential to be employed in mobile TV applications.

E. Comparison

Table IV tabulates a comparison of this work with recent works. As expected only [1] and [7] can cover all the mobile TV bands like this work, but those have complex circuits. In addition to this, circuit in [1] demands three external SAWs for blocker rejection at input. The LO programming facility employed in our work affected the harmonic rejection slightly, but when compared with others, only [4], [8] and [9] has a better HR than this work in LO mode of operation. This work is carried in 65nm technology as opposed to the 130nm, 180nm and 80nm in [4], [8] and [9] respectively.

IV. Conclusion and future scope

A wideband mobile-TV mixer, which covers all the mobile TV bands are designed. This work contains an 8-path active/passive mixer stacked with current mode LPF and a harmonic rejection cum LO programming facility. The LO programming facility of the circuit allows the system to cover a wide range of frequency using a comparatively low master LO frequency. This makes the use of simple PLL, VCO and frequency division based 8-phase LO generator possible. In this work a single stage harmonic rejection amplifier circuit is used instead of two stage circuits as in [2], to make the hardware simple, but the system becomes more prone to the bad effects of device mismatches [6]. As different circuits are employed for current mode scaling and summing for different modes of operation, they can be isolated from power supply for saving power, when not in use. A more advanced digitally assisted circuit which performs all the modes of operation with single set of amplifiers is possible. This digital circuit can direct the 8 path mixer outputs to different transistors in different modes. If a 16-phase multi-path harmonic rejection mixer is used, modes of operation up to 8LO will be possible. This higher number of paths in mixer can be utilized to make more harmonic rejection in higher modes of operation.

References

[1] Pui-In Mak and Rui P. Martins, *"A 0.46-mm 4-dB NF Unified Receiver Front-End for Full-Band Mobile TV in 65-nm CMOS"*, IEEE J. Solid-State Circuits, vol. 46, no. 9,pp 1970-1984, Sept 2011.

[2] Fujian Lin, Pui-In Mak and Rui Martins, *"An RF-to-BB-Current-Reuse Wideband Receiver With Parallel N-Path Active/Passive Mixers and a Single-MOS Pole-Zero LPF"*, IEEE J. Solid-State Circuits, vol. 49, no. 11,pp 2547-2559, Nov 2014.

[3] Z. Ru, E. Klumperink, G. Wienk, and B. Nauta,, *"A software-defined radio receiver architecture robust to out-of-band interference"*, in IEEE ISSCC Dig. Tech. Papers, Feb. 2009, pp. 230-231.

[4] Travis Forbes, Wei-Gi Ho and Ranjit Gharpurey , *"Design and Analysis of Harmonic Rejection Mixers With Programmable LO Frequency"*, IEEE J. Solid-State Circuits, vol. 48, no. 10,pp 2364-2374, Oct 2013.

[5] A. Mirzaei, H. Darabi, D. Murphy *"Architectural Evolution of Integrated M-Phase High-Q Bandpass Filters"*, IEEE Transactions on circuits and systems-1:regular papers, Vol. 59, No. 1, Jan. 2012

[6] J. Weldon, R. Narayanaswami, J. Rudell, L. Lin, M. Otsuka, S. Dedieu, L. Tee, K.-C. Tsai, C.-W. Lee, and P. Gray, *"A 1.75-GHz highly integrated narrow-band CMOS transmitter with harmonic-rejection mixers"*, IEEE J. Solid-State Circuits, vol. 36, no. 12, pp. 2003-2015, Dec. 2001.

[7] C. Andrews et al, *"A wideband receiver with resonant multi-phase LO and current reuse harmonic rejection baseband"*, IEEE J. Solid-State Circuits, vol. 48, pp. 1188-1198, May 2013.

[8] D. Im, H. Kim, and K. Lee, *"A broadband CMOS RF front-end for universal tuners supporting multi-standard terrestrial and cable broadcasts*, IEEE J. Solid-State Circuits, vol. 47, no. 2, pp. 392-406, Feb. 2012.

[9] J. Greenberg, F. De Bernardinis, C. Tinella, A. Milani, J. Pan, P. Uggetti, M. Sosio, S. Dai, S. Tang, G. Cesura, G. Gandolfi, V. Colonna, and R. Castello, *"A 40MHz-to-1GHz fully integrated multistandard silicon tuner in 80nm CMOS"*, IEEE International Solid-State Circuits Conference Digest of Technical Papers (ISSCC), Feb 2012, pp. 162-164.

THE 18TH INTERNATIONAL SYMPOSIUM ON WIRELESS PERSONAL MULTIMEDIA COMMUNICATIONS
(WPMC-2015)
December 13-16, 2015, Hyderabad, India

Analysis of Data Transmission Management through Software Defined POX Controller

Vaishnavi Moorthy
Assistant Professor: dept. of CSE
SRM University
Kattankulathur (Tamil Nadu), India
vaishnavi.m@ktr.srmuniv.ac.in

Revathi Venkataraman
Professor: dept. of CSE
SRM University
Kattankulathur (Tamil Nadu), India
revathi.n@ktr.srmuniv.ac.in

Abstract— **The current networking methodologies need a change because the users are being compromised with the already defined networking features. The flexibility in extending the network nodes simplifies the network management, thereby facilitating network evolution. Recently, introduced Software Defined Networking (SDN) concept facilitates the intelligent decision-making, flexibility, operational simplicity, and improved security across a defined infrastructure. The objective of this paper is to analyze the networking management by the software defined controller, which provides the flexibility and agility of data transmission in the data plane according to the user's requirements at any instant. The controller is informed about the transmission discrepancies, like a failure or malfunctioning in the transmitting nodes. The controller can redefine the data transmission path during such unexpected networking situations automatically, according to the predefined Open Flow table rules in the controller. Else, the authenticated user can change the data path between the other existing nodes and continue the data transmission through the controller depending upon the permitted access. Also, the performance of the implemented SDN model is analyzed by increasing the number of switches and the corresponding nodes. The paper highlights the idea of implementing the firewall in the controller over the simple topology. The firewall implemented in the test scenario will analyze and permit the data packets through the controller with respect to their arrival time. The comparative analysis of applying the firewall in the controller and the switches is done in terms of latency and throughput of data transmission.**

Keywords—***Data transmission; firewall, latency; Open-Flow table; Software defined controller; throughput***

Introduction

Today, Software Defined Networking (SDN) [1], [2] has paved a way towards the next-generation networking. It is spawning an innovative research and promoting advances in networking scalability, flexibility, performance of data communicating devices and architectures, for dependability and security in data transmission [3]. SDN blends the historical and real-time network state with performance data, to decouple the network control from the forwarding functions in a data transmission. This initiates the centralized control over the data transmission in the network [4], [5].

Current networking applications implicitly and indirectly describe their network requirements, involving a number of user processing steps, like, to negotiate if there are any sufficient resources and policy controls to support the particular application [4], [5]. So these networks do not inculcate the capability of expressing the full range of user requirements, such as throughput, delay variation or network availability in dynamic runtime [4], [5]. Some networks try to infer the user's requirements on their own, which incurs additional setup cost and sometimes leads to misclassification. Besides, these networks do not expose the information of network state to the applications using them at any point of time [6].

Network misconfigurations and related errors are extremely common in traditional networks. A single misconfigured device can be a big issue for the network operators and may have extremely severe consequences [1], [7]. To alleviate the lack of in-path functionalities within the network, a myriad of middle-boxes, which are special components like deep packet inspection, firewalls and intrusion detection systems, proliferate the current traditional networks [7]. Though the middle-boxes support the in-path functionalities, the complexity in network design and its operations have increased considerably.

SDN is a network architecture where the control plane manages the data forwarding operations in the data plane [6]. This characteristic feature enables the flexibility in implementing and customizing the networking policies in the controller. The topology for the data transmission can be decided upon in the data plane according to the user's convenience. Thus, the software defined controller acts as the networking brain of the constructed architecture [3].

The functions such as topology, statistics, notifications, transmission management, shortest data path forwarding and security mechanisms, are essential networking control functionalities, which are possible through the controller [1], [2], [3]. As the networks undergo the customization for evolutionary technologies, securing the data transmission becomes the top-most priority and a must. There are many related works [8], [9], [10], which focus on securing the data plane by implementing firewalls in the switches. It was found that firewall implementation in the data plane switches, increases the communication overhead, thus reducing the overall efficiency of the software defined data transmission Moreover, securing the controller is considered as utmost

importance because of its intelligence for controlling the data plane [11]. Hence, in this paper, a novel approach to analyze the data traffic by the transmission nodes through the controller is done. Also, a single firewall is implemented in the control plane, to reduce the communication overhead of the entire networking infrastructure.

The organization of the paper is as follows. Section II defines the emergence of Software Defined Networks. Section III describes the functional layers of SDN topology considered for the test scenario. Section IV illustrates the SDN data transmission management done through the software defined POX controller, over a simple networking topology. The section also deals with the Open-Flow table showing the failure of data transmission node over the constructed topology. It illustrates the idea of implementing the firewall in the controller instead of the switches over the default topology. Section V concludes the paper with the ideas, to enhance the implementation of the same in different scenarios in the near future

I. How Software Defined The Networks?

Emerging technologies in the field of networks have led to the creation of a digital society, where everything is connected and is accessible from everywhere. Their widespread implementation is on traditional IP networks, which involves complexity in their network management [2].

In the current dormant IP networks, a new routing protocol takes 5 to 10 years to get fully designed, tested and deployed [12]. Likewise, a clean-slate approach to change the Internet architecture (e.g., replacing IP), is regarded as a tantalizing task. Ultimately, this situation has inflated the capital and operational expenses of running an IP network [12], [13]. This growing complexity further demands novel approaches to future computer networks in which the complexity can be managed [13].

Conventional routers and switches embody a strong integration between the control and the data planes. This coupling made various network-management tasks, such as, debugging configuration, predicting or controlling routing behavior, to be extremely challenging. To address these challenges, various efforts to separate the data and control planes began to emerge [4], [5].

The 1990s saw the evolution of Internet to diverse the applications usage through active networks. The researchers developed capsule and programmable router/switch models to standardize their protocol implementation in these networks. The DARPA (Defense Advanced Research Projects Agency) stimulated these active networking concepts enforcing the ‘technology push and use pull’. The technology introduced concepts like the programmable functions in a network, virtualization, demultiplexing software programs based on packet headers and a vision for middle-box orchestration for unified network architecture. Though, innovative concepts were introduced in active networks, their practical performance upgradation in the routers, configuration management, definite routing path deployment, and network security remained unaddressed.

The early 2000s focused on the idea of widespread networks deployment, by separating the functional (data) and the management (control) planes. The ForCES (Forwarding and Control Element Separation) [3] working group, proposed a standard, open interface to the data plane to enable innovation in control-plane software. The SoftRouter [14] used the ForCES API, to allow a separate controller to install forwarding-table entries in the data plane, enabling the complete removal of control functionality from the routers. Unfortunately, ForCES was not adopted by the major router vendors, which hampered incremental deployment. Instead, the vendors started to use an existing standard control-plane protocol (Border Gateway Protocol) to install forwarding-table entries in legacy routers, enabling immediate deployment [5], [15].

In mid 2000s, the ideas pertaining SDN faced a tensed environment between the vision of fully programmable networks and pragmatism that would enable the real-world networking deployment. The Open Flow concept enabled more functions to be implemented than the earlier route controllers, which were built on-existing switch hardware [13], [16]. But, relying on existing switch hardware, has limited the flexibility of network extensibility. The development of the Open-Flow API [17], [18] was followed quickly by the design of controller platforms like NOX [19] that enabled the creation of many new controller applications.

NOX was the first controller implemented in the SDN based on OpenFlow environment [19]. Sooner, with the fast growing user requirements and the idea of network expandability, has led to the introduction of controllers like POX, OpenDaylight, Floodlight, Ryu and so on [3], [4], [5].

Then, focus shifted to the need of identifying and controlling the data attacks in the network architecture. Algorithms for performing the change-impact analysis of firewall policies, highlighted that a firewall administrator can verify a proposed change on the network before committing it [20]. The proposed algorithms can be practically used in the iterative process of firewall policy design and data packets maintenance.

A firewall application was developed over an Open-Flow based SDN controller to show that most of the firewall functionalities are able to be built on software, without the aid of a dedicated hardware [21].

Using POX controller, implementation of the firewall was tried over the default topology of the Mininet. The firewall implementation was done in OpenvSwitches in the data plane. The presence of firewall using the metrics - latency and throughput was analyzed. [9].

In this work, the concept of managing the data transmission over the simple topology is highlighted. The novel idea is to prove the flexibility of customizing the data transmission through the software defined controller, according to the users’ needs. The network performance is analyzed using throughput and latency, by customizing the network topology and with firewall in the controller. It is implied that, implementing the firewall, in the controller,

improves the communication efficiency, compared to the firewall implementation in the data plane switches.

II. SDN ARCHITECTURE

Current networking concept does not satisfy the user's day-to-day requirements completely because of their rigid networking policies. Complexity is increased, by trying to reconfigure the network according to the predefined policies, and their response to faults, load, and changes. The SDN enables the users to incorporate abstractions in the networking policies, to ease the network management [3]. Fig.1 depicts the simple default topology to describe the SDN based architectural model layers. It consists of a single POX controller. The POX controller is made to interface with transmitting nodes, which are being operated through corresponding OpenvSwitches for data transmission. The SDN architecture contains the basic functional planes- Control (Management) Plane and Data (Functional) Plane.

A. Data Plane (Infrastructure Layer)

The transmitting nodes are connected to the controller through a compatible version of Linux OS based open-source OpenVSwitch software. The forwarding devices are the transmitting nodes (h_1-h_{125}) as represented in fig.1. This occupies the bottom most infrastructure layer i.e., the Data plane. The choice of OpenvSwitch is for the extensibility into network virtualization in n for the adoption of a SDN based Open-Flow Protocol [17].

B. Control Plane

The control plane is a software stack, which consists of SDN based controller POX/Floodlight/Ryu/ OpenDaylight (open source). The controller is to monitor the data transmission and to enforce policies like control flow, infrastructure security, authenticated access control or firewalling for securing the data transmission over the implemented set of networks.

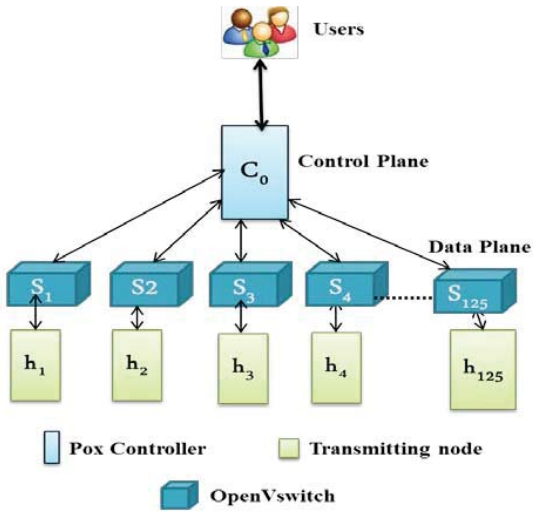

Fig. 1. SDN Architecture

The controller plane configures the data plane to respond autonomously to events such as network failures. The controller will do the maintenance of the data nodes at the data level according to the rules implemented in the open flow table tables The secured sub-policies can be implemented using open flow standard programming languages such as FLOG, Merlin [20].

The authenticated users can enforce the networking policies in the controller for the data transmission management like topology decision, en-routing data transmission path in case of any failure transmission node and firewall policies.

C. Open-Flow Standard

Vendors offer varying degrees of user programmability on their routers and switches, can lead to limited functionality for traffic engineering and management. Open-Flow design [16] is to provide consistency in network management and engineering by making it control-function independent of the hardware. Open-Flow based SDN technologies enable the users to address the high-bandwidth; dynamic nature of applications, adaptation of the network to the ever-changing business needs, and significantly reduce the operations and management complexities [17].

Controllers communicate to the switches via the Open-Flow protocol and impose policies on the flows. The controller could set up paths through the network, optimized for specific characteristics, such as speed, fewest number of hops or reduced latency [18].

III. ANALYSIS OF SOFTWARE DEFINED DATA TRANSMISSION

A. Data Transmission Management

The data transmission nodes in the data plane can be organized into different topologies like the simple, single, tree, bus, mesh, and hybrid**.** The topology selection is flexible unlike the traditional networking where only fixed topologies can be opted. The Fig.1 topology is a basic topology available in the Mininet, which has each node connected to a single switch. The switches will communicate to the single POX controller.

The topology is flexible for customization according to the users' requirements. Here, the architecture is customized by increasing the number of transmitting nodes and the corresponding switches. In this test scenario, the simulation trials for 10, 25, 50, 75 and 100 switches are considered for the performance analysis.

It is inferred from the Fig. 2, that, as the numbers of switches are increasing in the topology, there is no much difference in the throughput. This suggests that the number of forwarding devices can be increased according to the network implementation and the user needs. Simultaneously, latency for the same simulations is calculated. From Fig. 3, it is deduced that there are increasing variations in the latency as the number of data packets are increased, during the transmission for each simulation.

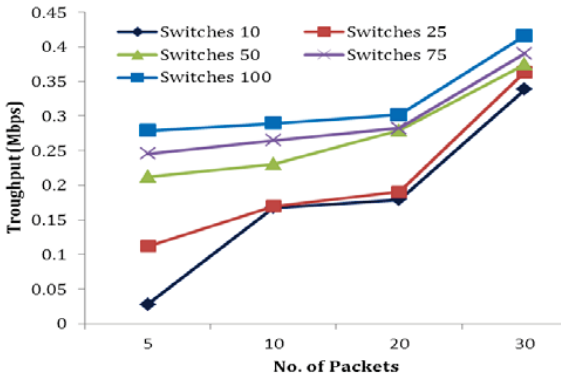

Fig. 2. Throughput vs. No. of Packets Transmitted

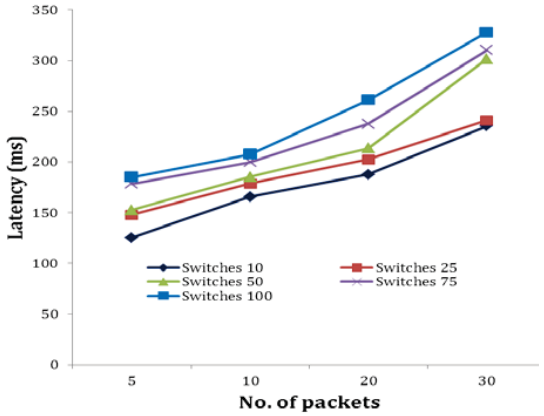

Fig. 3. Latency vs. No. of Packets Transmitted

Also, the latency rate increases, as the number of switches increases. It is estimated that, there is a difference of approximately 60ms between the simulations of 10 and 100 switches. The fig.2 & 3 analyses show that there is flexibility in scaling the network infrastructure i.e. the data transmitting nodes through software defined networking concepts.

B. Failure Node Detection

Fig. 4 shows that, if any networking node is not transmitting data packets at that point of instance, it will be communicated to its immediate SDN controller. The communication will be done, if there is any packet delay between the transmitting nodes as shown in Table II. Here, the packet delay is identified through a mismatch in the predefined priority column of the Open-Flow table.

In Table II, the priority field has null values because; the particular node is not transmitting any data packets. This is contradictory to the Table I priority column, where there is no match to the predefined Openflow rules. The priority column will be incremented only, if there is a data transmission between the nodes and the controller without any hindrance. Tables I & II analysis signify that the software defined concept eases the node failure detection and management in a network.

TABLE I. OPENFLOW TABLE FOR DATA TRANSMISSION THROUGH THE CONTROLLER

Match Field	Priority	Counter	Ins	Timer	Cookie	Delay (ms)
00	00	01	00	00	01	10.71
00	01	01	00	00	01	09.14
00	02	01	00	00	01	08.43
00	03	01	00	00	01	10.33
00	04	01	00	00	01	07.67

TABLE II. OPENFLOW TABLE FOR FAILURE NODE DETECTION

Match Field	Priority	Counter	Ins	Timer	Cookie	Delay (ms)
00	00	01	00	00	01.0	377
00	00	01	00	00	01.2	268
00	00	01	00	00	01.3	160
00	00	01	00	00	01.1	84.6
00	00	01	00	00	01.2	85.2

C. Firewall Implementation Analysis

Though the SDN concept provides the flexibility of changing the topology of a networking infrastructure, network node failure detection and management, the efficiency of the network lies in securing the controller. Firewall is always the first tool to be considered for securing a data transmission against any data attacks. SDN provides the liberty of formulating rules in the default controller firewall.

Initially, the firewall was implemented in the data plane switches. Each packet will be filtered by the firewall during the transmission between the switches and the controller [9]. This was increasing the communication overhead, while processing and transmitting large number of data packets. In order to reduce the transmission overhead, a single firewall was implemented in the controller, instead of implementing the firewall in each switch. Fig.5 shows the firewall implementation in the controller is more efficient than the switches, as the data packets filtering is done only once during the controller-switch communication.

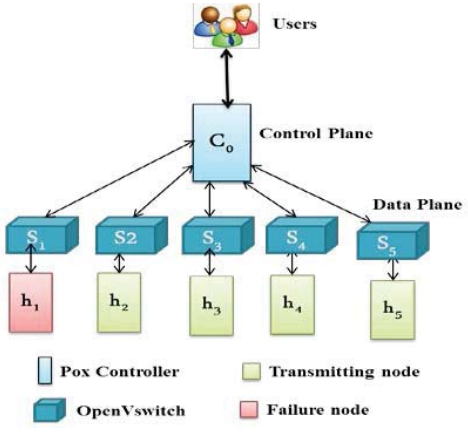

Fig.4. Failure node detection

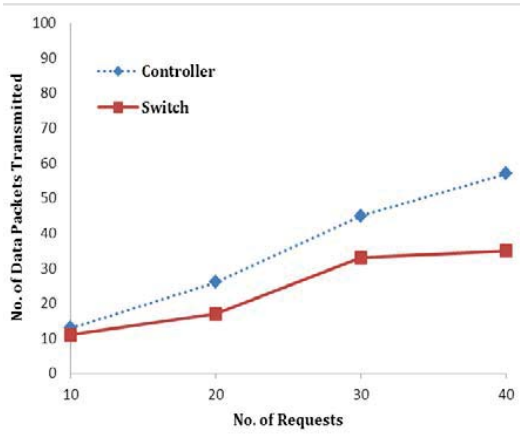

Fig. 5. Firewall Implementation Efficiency in Controller and Switches

IV. Conclusion & Future Work

The telecommunication world is witnessing new heights in data transmission technologies. There is a growing demand for personalized data transmission between the users irrespective of the application usage. The Software Defined Networking innovates the network infrastructure according to the user needs. This paper shows the data transmission management by the Software defined controller on the simple available topology in the Mininet. Also highlighted is the implementation of firewall in the controller. The presence of firewall secures the architecture from any malicious attacks causing the delayed data transmission. The same analysis can be experimented in other customized topologies like the Single-switch, tree, bus, mesh and hybrid. The Software Defined controller implementation can be extended to heterogeneous networks instead of homogeneous networks. Networking polices can be customized for improving the scalability and security of the network. The topology customization can be done by connecting more than one controller, to set up distributed or logically centralized controller in distributed environment. This can be efficiently possible by implementing Floodlight controller instead of POX controller in the proposed networking architecture.

Acknowledgement

We acknowledge the support extended by SRM University for providing the necessary infrastructure facilities to carry out this research work.

References

[1] N. Mckeown, ‘‘How SDN will shape networking,’’ Oct. 2011.
[2] S. Schenker, ‘‘The future of networking, the past of protocols,’’ Oct. 2011.
[3] D. Kreutz, F. Ramos, P. Esteves Verissimo, C. Esteve Rothenberg, S. Azodolmolky and S. Uhlig, 'Software-Defined Networking: A Comprehensive Survey', Proc. IEEE, vol. 103, no. 1, pp. 14-76, 2015.
[4] N. Feamster, J. Rexford and E. Zegura, 'The road to SDN', Queue, vol. 11, no. 12, pp. pp. 20:20-20:40, 2013.
[5] N. Feamster, J. Rexford and E. Zegura, 2015, https://www.cs.princeton.edu/courses/archive/fall13/cos597E/papers/sdnhistory
[6] W.Stallings,“Software-DefinedNetworks and OpenFlow,” The Internet Protocol Journal, vol.16, no.1, 2013
[7] Y. Jarraya, T. Madi and M. Debbabi, 'A Survey and a Layered Taxonomy of Software-Defined Networking', IEEE Commun. Surv. Tutorials, vol. 16, no. 4, pp. 1955-1980, 2014.
[8] A. Hakiri, A. Gokhale, P. Berthou, D. Schmidt and T. Gayraud, ‘Software-Defined Networking: Challenges and research opportunities for Future Internet', Computer Networks, vol. 75, pp. 453-471, 2014.
[9] K. Kaur, K. Kumar, J. Singh and N. Ghuman, 'Programmable firewall using Software Defined Networking', pp. 2125 - 2129.
[10] M. Jammal, T. Singh, A. Shami, R. Asal and Y. Li, 'Software defined networking: State of the art and research challenges', Computer Networks, vol. 72, pp. 74-98, 2014.
[11] S. Hayward, G. O’Callaghan and S. Sezer, 'SDN Security: A Survey', in IEEE SDN for Future Networks and Services (SDN4FNS), Trento, Italy, 2013, pp. 1 – 7
[12] Network Computing, 'SDN Limitations - Network Computing', 2014. Q. Zuo, M. Chen, G. Zhao, C. Xing, G. Zhang And P. Jiang, 'Research on OpenFlow-Based SDN Technologies', Journal of Software, vol. 24, no. 5, pp. 1078-1097, 2013.
[13] T. V. Lakshman, T. Nandagopal, R. Ramjee, K. Sabnani, and T. Woo. The SoftRouter Architecture. In Proc. 3nd ACM Workshop on Hot Topics in Networks (Hotnets-III), San Diego, CA, Nov. 2004.
[14] M. Caesar, N. Feamster, J. Rexford, A. Shaikh, and J. van der Merwe. Design and implementation of a routing control platform.In Proc. 2nd USENIX NSDI, Boston, MA, May 2005..
[15] A. Rosen, et.al, 2013. http://Open vSwitch. openvswitch.org.
[16] Open Networking Foundation. https://www. opennetworking.org/.
[17] N. Gude et al., ‘‘NOX: Towards an operating system for networks,’’ Comput. Commun.Rev., vol. 38, no. 3, pp. 105–110, 2008.
[18] A.X.Liu, 'Change-Impact Analysis of Firewall Policies', Springer-Verlag Berlin Heidelberg, 2007. https://www.cse.msu.edu/alexliu/publications/ChangeImpact/Change ImpactAnalysisOfFirewalls
[19] S. M, S. Park, B. Lee and S. Yang, '1. Building Firewall over the Software-Defined Network Controller', in Advanced Communication Technology (ICACT), 2014 16th International Conference, Pyeongchang, 2015, pp. Pages: 744 - 748.
[20] Xia, W., Wen, Y., Foh, C., Niyato, D. and Xie, H. (2015). A Survey on Software-Defined Networking. IEEE Commun. Surv. Tutorials, 17(1), pp.27-51.
[21] Z. A. Qazi, C.-C. Tu, L. Chiang, R. Miao, V. Sekar, and M. Yu, Simplifying middlebox policy enforcement using SDN, in Proceedings of the Conference on Applications, technologies, architectures.

THE 18TH INTERNATIONAL SYMPOSIUM ON WIRELESS PERSONAL MULTIMEDIA COMMUNICATIONS
(WPMC-2015)
December 13-16, 2015, Hyderabad, India

Blind Image Quality Assessment Based on Phase Congruency and Spatial-spectral Entropies

Maozheng Zhao, Yanping Lu, Cuiwei Li, Ran Gao, Qin Tu, Bo Yang, Aidong men

School of Information and Communication Engineering
Beijing University of Posts and Telecommunications
Beijing, 100876, China
{*maozhengzhao, luyanping, lcwhxzljj, gaoran, tuqin, boyang, menad*}*@bupt.edu.cn*

***Abstract*—We develop an efficient general-purpose blind image quality assessment (IQA) algorithm. It utilizes curvelet domain features of phase congruency (PC) values, local spatial entropy values and local spectral entropy values of distorted images as quality relevant features for quality prediction. A 2-stage framework including classification of distortion types and distortion specific quality assessment is utilized for mapping the quality relevant features to predictive scores. The classifier is implemented by a support vector machine (SVM) and the regression model is implemented by a support vector regression (SVR) model. The proposed approach which is named Phase Congruency and Spatial-Spectral Entropy based Quality (PCSSEQ) index can assess image quality blindly with out knowing the distorted type of the testing image and the predictive results of the proposed approach correlates well with human subjective scores. The performance of PCSSEQ on LIVE database is competitive with some state-of-the-art general-purpose blind image quality assessment (BIQA) approaches and some full-reference (FR) image quality assessment (IQA) approaches. We also prove that PCSSEQ has a good database independence characteristics.**

I. Introduction

Blind image quality assessment (BIQA) aims to build computational models that can evaluate image quality consistently with human perception without the undistorted version of the testing image. With the easier availability of digital images from the internet and the popularization of digital imaging devices such as smart phones with big screens and digital cameras, digital images have been becoming one of the most important way of representing and transmitting information in our everyday life. However, the perceptual quality of digital images may be declined by the process of acquisition, transmission, compression, restoration, etc. And in most cases the undistorted version of the observed image is not available, thus assessing image quality blindly has becoming increasingly important [1].

In terms of whether specifying the distortion types of testing images, the current BIQA methods can be classified as distortion specific methods [2], [3] or general purpose methods [4], [5], [6], [7], [8]. The application of distortion specific BIQA methods is limited by the necessity of knowing distortion types of testing images before quality assessment while the general-purpose BIQA approaches aim to predict quality of an image without any prior knowledge of the distortion type. Most general-purpose BIQA approaches proposed are based on training and learning. Moorthy and Bovik proposed a two-stage framework for BIQA [7] which first compute the probability of occurrence of each distortion type and then compute quality score on each distortion type, the two-stage framework performs well. They later proposed the DIIVINE index [6] which is also based on the two-stage framework and achieves better performance by utilizing natural scene statistics (NSS) features from wavelet domain. The BRISQUE index proposed by Mittal *et al.* extracts NSS features from the spatial domain which results in very low time complexity and superior performance [4]. L.Liu *et al.* proposed SSEQ [9] which applies curvelet domain statistical features, i.e. mean values and skew values of histograms of block-based spatial entropy and spectral entropy, as features. The 2-stage framework is also used for mapping features to quality scores, the performance of SSEQ is comparable to state-of-the-art BIQA methods.

However, the spatial entropy features (mean values and skew values of histograms of block-based spatial entropy) used in SSEQ performs poorly when utilized to the two-stage framework [7], [6]. In our work, we propose some new curvelet domain statistical features that performs significantly better for BIQA than spatial entropy features used in SSEQ. The new features are the mean values and the skew values of phase congruency (PC) histogram of an image. Although PC has already been applied for image quality assessment (IQA) in the literature [10], [11], [12], few of them utilize the curvelet domain statistical features of PC. Adding the proposed features to SSEQ framework results in a new BIQA which we call phase congruency and spatial-spectral entropy based quality (PCSSEQ) index. We thoroughly evaluated PCSSEQ on LIVE IQA database [13] and proved that PCSSEQ performs significantly better than SSEQ and its performance is comparable to several top-performing BIQA methods such as DIIVINE and BRISQUE, it also outperforms the two classical full reference (FR) IQA method PSNR [14] and SSIM [15] on LIVE database.

The rest of the paper is organized as follows. Section 2 describes details about the framework of PCSSEQ. In Section 3, we analyzed the power of quality prediction of each feature

This work is supported by the National Science Foundation of China (61271190).

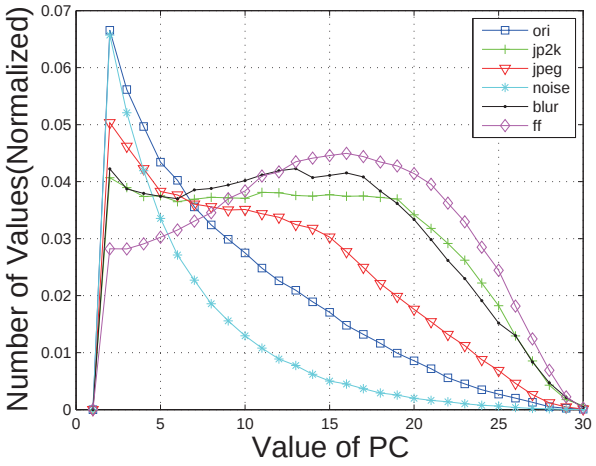

Fig. 1. Histograms of PC for different distortion types. The 6 curves correspond to the image "sailing4.bmp" and its distorted counterparts. "ori" (DMOS = 0), "jp2k" (DMOS = 64.7259), "jpeg" (DMOS = 64.6264), "noise" (DMOS = 63.7033), "blur" (DMOS = 53.3056), "ff" (DMOS = 71.6422).

subset used in PCSSEQ and evaluated the performance of PCSSEQ by several experiments. Finally, Section 4 concludes with a summary of our work.

II. BIQA BASED ON PHASE CONGRUENCY AND SPATIAL-SPECTRAL ENTROPIES

A. Phase congruency features

The physiological and psychophysical evidences had proved that visually discernable features coincide with points where the Fourier waves have congruent phases at different frequencies [16], [17], i.e., at points of high PC values. Besides, PC also have the characteristic of contrast invariance. Thus, the PC theory provides a simple but biologically plausible model of how mammalian visual systems detect and identify features in an image.

In this paper, we adopt the method of computing PC developed by Kovesi [17], which is widely used in literature. We adopt logarithmic Gabor filters [18] for wavelet transform and adopt Gaussian function as the spreading function for the log-Gabor filters to extend to 2D ones. The 2-D log-Gabor filters extended by Gaussian function have the following transfer function:

$$G_2(\omega,\theta_j)=\exp\left(-\frac{\left(\log(\frac{\omega}{\omega_0})\right)^2}{2\sigma_r^2}\right)\cdot\exp\left(-\frac{(\theta-\theta_j)^2}{2\sigma_\theta^2}\right), \tag{1}$$

where ω_0 is the filter's center frequency, and σ_r controls the filters bandwidth, $\theta_j = j\pi/J$, $j=\{0,1,...,J-1\}$ is the orientation angle of the filter, J is the number of orientations, and σ_θ determines the filter's angular bandwidth.

Denoted by M^e_{n,θ_j} and M^o_{n,θ_j} the even- and odd-symmetric filters of the 2-D log-Gabor filters on scale n and orientation θ_j, and they form a quadrature pair. By modulating ω_0 and θ_j and convolving G_2 with an image, we get a set of responses at each point x as $\lfloor e_{n,\theta_j}(x), o_{n,\theta_j}(x)\rfloor$, where $e_{n,\theta_j}(x)$ and $o_{n,\theta_j}(x)$ are responses of the quadrature pair on scale n and orientation θ_j at location x. The local amplitude on scale n and orientation θ_j is $A_{n,\theta_j}(x)=\sqrt{e_{n,\theta_j}(x)^2+o_{n,\theta_j}(x)^2}$, and the local energy along orientation θ_j is $E_{\theta_j}(x)=\sqrt{F_{\theta_j}(x)^2+H_{\theta_j}(x)^2}$, where $F_{\theta_j}(x)=\sum_n e_{n,\theta_j}(x)$ and $H_{\theta_j}(x)=\sum_n o_{n,\theta_j}(x)$. The 2-D PC at x is defined as follows:

$$PC(x)=\frac{\sum_j E_{\theta_j}(x)}{\lambda+\sum_n\sum_j A_{n,\theta_j}(x)} \tag{2}$$

where λ is a small positive constant to keep the fraction stable when all the Fourier amplitudes are very small. $PC(x)$ is a real number within $0-1$.

B. Phase congruency and spatial-spectral entropy based quality index

One reference image in LIVE database and its five distorted counterparts of different distorted types are chosen for showing their histograms. The histograms are shown in Fig. 1, numbers of zeros of histograms are excluded. We can see that the mean and skew values of PC histograms change with different distorted types and distorted extents. From the experiments in section III, we can prove that mean and skew values of PC histograms are strong features for BIQA.

The mean and skew values of spatial entropy histogram and spectral entropy histogram of a natural image would also change with different distorted types and distorted extents in a similar way. The process of computing spatial and spectral entropies are as follows.

The spatial entropy is

$$S=-\sum_x p(x)\log_2 p(x), \tag{3}$$

where x are the pixel luminance values, $p(x)$ is the empirical probability density of x.

The spectral entropy is

$$F=-\sum_i\sum_j P(i,j)\log_2 P(i,j), \tag{4}$$

where

$$P(i,j)=\frac{C(i,j)^2}{\sum_i\sum_j C(i,j)^2}, \tag{5}$$

where $P(i,j)$ is the spectral probability of normalized DCT coefficients $C(i,j)^2$,$i\neq 1$,$j\neq 1$ (DC is excluded).

We extracted mean and skew values of histograms of pixel based PC values, mean and skew values of histograms of block based spatial entropy values and mean and skew values of histograms of block based spectral entropy values as the feature vector of an image for quality assessment, the 2-stage framework proposed in [7], [6] is utilized to map feature vectors to predictive scores. The proposed BIQA method is

named Phase Congruency and Spatial-Spectral Entropy based Quality (PCSSEQ) index.

The proposed PCSSEQ can be divided into four steps:

1) Down sampling. Each incoming distorted image is down sampled twice with a factor of 2 yielding 3 scales of the incoming image, in our experiments we found that this multi scale strategy can enhance the overall performance.

2) Feature computing. PC values PC on pixels, spatial entropy values S and spectral entropy values F on 8×8 nonoverlapping neighboring blocks are computed for each scale.

3) Feature pooling. For each scale, by sorting PC, S and F values of an image in ascending order, the ordered sets $PC = (pc_1, pc_2, ..., pc_m)$, $S = (se_1, se_2, ..., se_n)$ and $F = (fe_1, fe_2, ..., fe_n)$ are yielded. Here pc_i, se_j and fe_k are PC values, local spatial entropies and local spectral entropies, m and n are the number of pixels and blocks respectively within each scale. Then percentile pooling is applied to PC, S and F based on the assumption that distortions only occur in a subset of pixels or blocks. Extracting the central 60% elements from PC, S and F yields $PCp = (pc_{\lfloor 0.2m \rfloor}, pc_{\lfloor 0.2m \rfloor+1}, ..., pc_{\lfloor 0.8m \rfloor})$, $Sp = (se_{\lfloor 0.2n \rfloor}, se_{\lfloor 0.2n \rfloor+1}, ..., se_{\lfloor 0.8n \rfloor})$ and $Fp = (fe_{\lfloor 0.2n \rfloor}, fe_{\lfloor 0.2n \rfloor+1}, ..., fe_{\lfloor 0.8n \rfloor})$. The mean values of PCp, Sp, Fp and the skew values of PC, S, F make up the final features of each scale:

$$f = (mean(PCp), skew(PC), mean(Sp), skew(S), mean(Fp), skew(F)). \quad (6)$$

4) Prediction. Each distorted image has a feature vector of $3 \times 6 = 18$ dimensions. A two-stage framework for BIQA is utilized to map the feature vector to the final image quality score. The two-stage framework used here is the same as that in [7], [6]. The first stage of the framework is to compute the probability of occurrence of each distorted type of the testing image. The second stage is to map feature vector to a quality score on each distorted type. Then the the dot product between the vector of the probability of occurrence of each distorted type and the vector of quality score on each distorted type is the final predictive score. We use a support vector machine (SVM) for classification and support vector regression (SVR) for regression [19], [20]. The SVM and SVR are implemented by the LIBSVM package [21] and the radial basis function (RBF) is used in both implementations.

III. Experiments and results

We tested the performance of PCSSEQ on the LIVE database [13], which consists of 29 reference images and their distorted versions. The database offers five different types of distortion, i.e., JPEG2k (JP2K), JPEG, white noise (WN), Gaussian blur (BLUR) and fast fading (FF). For each distortion type, distorted images of 5 to 6 different distorted levels of each reference image are offered. Difference Mean Opinion Score (DMOS) values of those images are available.

Two evaluation indexes are used to evaluate the performance of our model. The first one is the Spearman Rank Order Correlation Coefficient (SROCC) which is related to prediction monotonicity of a model. The second one is the Linear Correlation Coefficient (LCC) after non-linear mapping. LCC is considered as a measure of prediction accuracy of a model. The non-linear mapping function used in our experiments is the same as the one in [22]. A value close to 1 for SROCC and LCC indicates good performance.

TABLE I
Meaning of features.

Features	Feature description
f1-f3	Means of PC values for 1-3 scales
f4-f6	Skews of PC values for 1-3 scales
f7-f9	Means of spectral entropy values for 1-3 scales
f10-f12	Skews of spectral entropy values for 1-3 scales
f13-f15	Means of spatial entropy values for 1-3 scales
f16-f18	Skews of spatial entropy values for 1-3 scales

TABLE II
SROCC between feature values and DMOS.

	JP2K	JPEG	WN	BLUR	FF
f1	0.8638	0.7190	0.9510	0.9183	0.8104
f7	0.9052	0.9432	0.9462	0.9408	0.8323
f13	0.1081	0.6914	0.6392	0.4832	0.3234
f4	0.8720	0.7061	0.7970	0.9132	0.8244
f10	0.8405	0.8429	0.3768	0.8405	0.7671
f16	0.0630	0.6129	0.1453	0.3138	0.1807

A. Comparison of feature prediction power

We conducted two experiments to investigate the prediction power of the three feature subsets, i.e. phase congruency feature subset, the spectral entropy feature subset and the spatial entropy feature subset. The first experiment is to investigate the correlation between each feature subset and DMOS on LIVE database. The meaning of features are shown in Table I. The absolute values of SROCC between those feature values and the DMOS for distorted images in LIVE database are shown in Table II. We only computed the SROCC between DOMS and the features extracted from the original scale of images ($f1$,$f7$,$f13$,$f4$,$f10$ and $f16$) since the SROCC on other two scales shows similar regularity.

For mean values (f_1, f_7 and f_{13}), the mean value of spectral entropy of images (f_7) correlates best except on "WN" while the mean value of spatial entropy of images (f_{13}) correlates worst on each distorted type and the mean value of PC of images (f_1) correlates much better than mean value of spatial entropy (f_{13}). For skew values (f_4, f_{10} and f_{16}), the skew value of PC of images (f_4) correlates best except on "JPEG" distorted type while the spatial one (f_{16}) correlates worst on each distorted type. We can conclude that PC features (f_1, f_4) correlate much better than spatial entropy features (f_{13}, f_{16}) and is competitive with spectral entropy features (f_7, f_{10}).

We also applied each feature subset, i.e. phase congruency feature subset, the spectral entropy feature subset and the

TABLE III
MEDIAN SROCC AND LCC ACROSS 1000 TRAIN-TEST TRIALS FOR EACH FEATURE SUBSET.

	SROCC	LCC
f1-f6	0.7644	0.7770
f7-f12	0.8763	0.8757
f13-f18	0.7205	0.7211

spatial entropy feature subset, to the 2-stage framework respectively. 80% of the reference images and their distorted counterparts were randomly selected as the training set and the remaining 20% of the reference images and their distorted counterparts were used as the testing set, the median experimental results over 1000 iterations across all distortion types are shown in the first two columns of Table III. We use the realigned DMOS scores [22] of the LIVE database.

From Table III, we can observe that the spectral entropy features ($f_7 - f_{12}$) perform best while the spatial entropy features ($f_{13} - f_{18}$) perform worst and the PC features ($f_1 - f_6$) perform significantly better than the spatial entropy features ($f_{13} - f_{18}$).

B. Comparison with other IQA approaches

PCSSEQ utilizes all three feature subsets which are phase congruency features, spectral entropy features and spatial entropy features. We tested PCSSEQ on LIVE database and compared the performance of PCSSEQ with three FR IQA methods (PSNR[14], SSIM[15] and FSIM[11]) and three other BIQA methods (SSEQ[9], DIIVINE[6], and BRISQUE[4]). The SSEQ [9] compared here only utilize the spatial entropy feature subset and the spectral entropy feature subset to the 2-stage framework. For BIQA methods in our experiments, median results of 1000 train-test trails by randomly selecting 80% of reference images and their corresponding distorted versions as the training set and the rest images in the database as the testing set. For FR IQA methods, a random 20% test set selection for 1000 times is also performed for a fair comparison, and the median results of 1000 trials are reported. Only the distorted images in the database are used for training and testing in our experiments. The results are shown in Table IV. The top three values of SROCC and LCC across all distortion types ("ALL") are shown in boldface.

The SROCC and LCC of PCSSEQ are higher than that of SSEQ on each distortion type and across all distortion types ("ALL") except the LCC value on "JPEG". The SROCC values in the column indexed by "ALL" are higher than that of FR IQA methods PSNR and SSIM and higher than that of BIQA method DIIVINE. But it is lower than that of FSIM and BRISQUE noting that FSIM is a full-reference approach and BRISQUE is one of the state-of-the-art blind IQA approaches. The LCC values in the column indexed by "ALL" shows consistent results. Although the overall performance of the proposed PCSSEQ is slightly inferior than that of BRISQUE, it is significantly better than that of SSEQ because of utilizing extra PC features. The results also demonstrate that PC map of an image has great potential for blind IQA while most extant literatures only focus on its application for FR IQA.

TABLE V
RESULTS OF THE PAIRWISE T-TEST CONDUCTED BETWEEN SROCC VALUES OF 1000 TRAIN-TEST TRAILS OF DIFFERENT METHODS.

	PSNR	SSIM	FSIM	DIIVINE	BRISQUE	SSEQ	PCSSEQ
PSNR	0	-1	-1	-1	-1	-1	-1
SSIM	1	0	-1	1	-1	1	-1
FSIM	1	1	0	1	1	1	1
DIIVINE	1	-1	-1	0	-1	-1	-1
BRISQUE	1	1	-1	1	0	1	1
SSEQ	1	-1	-1	1	-1	0	-1
PCSSEQ	1	1	-1	1	-1	1	0

TABLE VI
MEDIAN CLASSIFICATION ACCURACY ACROSS 1000 TRAIN-TEST TRIALS.

	JP2K	JPEG	WN	BLUR	FF	**ALL**
SSEQ	65.7	86.5	100.0	66.7	46.7	72.8
PCSSEQ	71.4	91.9	100.0	66.7	43.3	74.7

C. Statistical significance and hypothesis testing

The student t-test results between compared BIQA methods for SROCC values of 1000 iterations are listed in Table V. A value of "1" in the table means that the mean value of SROCC of row method is statically higher to the column method, while a "-1" means that the mean value of SROCC of row method is statistically lower than the one in the column. A value of "0" means that the mean values of SROCC of row and column are statistically equivalent.

D. Classification accuracy

The median classification accuracy of 1000 train-test trails of SSEQ and PCSSEQ are listed in Table VI. From the table we can see that introduction of PC features slightly enhances the overall classification accuracy.

E. Database independence

TABLE VII
SROCC OBTAINED BY TRAINING ON THE LIVE IQA DATABASE AND TESTING ON THE TID2008 DATABASE.

	JP2K	JPEG	Noise	Blur	**ALL**
PSNR	0.7848	0.8585	0.9147	0.8914	0.7527
SSIM(SS)	0.9603	0.9354	0.8168	0.9598	0.9016
BRISQUE	0.9037	0.9102	0.8227	0.8742	0.8977
SSEQ	0.9112	0.8629	0.7986	0.8531	0.8501
PCSSEQ	0.9418	0.9168	0.8001	0.9106	0.9112

In order to demonstrate the degree of database independence of PCSSEQ, we trained it on the entire LIVE database and applied it to the TID2008 database [23]. The TID2008 database consists of 25 reference images and 1700 distorted images over 17 distortion categories. Of the 25 reference images only 24 are natural images, we test PCSSEQ on the 24 natural reference images only on distortions that are shared by the two

TABLE IV
MEDIAN SROCC AND LCC ACROSS 1000 TRAIN-TEST TRIALS ON THE LIVE IQA DATABASE. THE TOP THREE VALUES OF SROCC AND LCC ACROSS ALL DISTORTION TYPES ("ALL") ARE SHOWN IN BOLDFACE.

	SROCC						LCC					
	JP2K	JPEG	Noise	Blur	FF	**ALL**	JP2K	JPEG	Noise	Blur	FF	**ALL**
PSNR	0.8673	0.8843	0.9428	0.7575	0.8721	0.8633	0.8657	0.8866	0.8963	0.7855	0.8616	0.8568
SSIM(SS)	0.9395	0.9480	0.9644	0.9083	0.9413	0.9129	0.9513	0.9605	0.9828	0.9033	0.9569	0.9057
FSIM	0.9700	0.9807	0.9662	0.9711	0.9511	**0.9636**	0.9139	0.9833	0.9751	0.9681	0.9465	**0.9581**
DIIVINE	0.8907	0.8960	0.9826	0.9335	0.8396	0.9057	0.8961	0.9074	0.9765	0.9270	0.8541	0.8990
BRISQUE	0.9095	0.9647	0.9778	0.9511	0.8759	**0.9364**	0.9122	0.9735	0.9848	0.9456	0.9013	**0.9386**
SSEQ	0.8994	0.9420	0.9591	0.9172	0.8565	0.9122	0.9033	0.9609	0.9642	0.9286	0.8746	0.9158
PCSSEQ	0.9132	0.9461	0.9675	0.9246	0.8652	**0.9259**	0.9110	0.9477	0.9744	0.9377	0.8867	**0.9258**

databases: JP2K, JPEG, Gaussian noise (Noise), and Gaussian blur (Blur). The results are shown in Table VII. The SROCC between DMOS and the predictive scores of PCSSEQ is the highest compared with PSNR, SSIM, BRISQUE and SSEQ and it is even higher than that of BRISQUE. The results means that PCSSEQ has excellent database independence characteristic. The reason for the excellent database independence characteristic is probabily that the features of PCSSEQ are statistical features of histograms of an entire image, those features are not easily affected by the sizes and the contents of the distorted images.

IV. CONCLUSION

We proposed a general-purpose BIQA approach called Phase Congruency and Spatial-Spectral Entropy based Quality (PCSSEQ) index. The curvelet domain statistical PC features proposed in our work shows strong predictive ability for BIQA. The proposed approach performs significantly better than another curvelet statistical feature based BIQA method SSEQ on LIVE database. The performance of PCSSEQ is also competitive with some state-of-the-art BIQA methods such as BRISQUE, DIIVINE and some FR IQA methods such as PSNR and SSIM. PCSSEQ also has a good database independence characteristic. Moreover, our work indicate that PC map of an image has great potential for BIQA while most extant literatures only focus on its application for FR IQA.

REFERENCES

[1] Z. Wang, "Applications of objective image quality assessment methods [applications corner]," *Signal Processing Magazine, IEEE*, vol. 28, no. 6, pp. 137–142, 2011.

[2] Z. Wang, H. R. Sheikh, and A. C. Bovik, "No-reference perceptual quality assessment of jpeg compressed images," in *Image Processing. 2002. Proceedings. 2002 International Conference on*, vol. 1. IEEE, 2002, pp. I–477.

[3] L. Meesters and J.-B. Martens, "A single-ended blockiness measure for jpeg-coded images," *Signal Processing*, vol. 82, no. 3, pp. 369–387, 2002.

[4] A. Mittal, A. K. Moorthy, and A. C. Bovik, "No-reference image quality assessment in the spatial domain," *Image Processing, IEEE Transactions on*, vol. 21, no. 12, pp. 4695–4708, 2012.

[5] P. Ye, J. Kumar, L. Kang, and D. Doermann, "Unsupervised feature learning framework for no-reference image quality assessment," in *Computer Vision and Pattern Recognition (CVPR), 2012 IEEE Conference on*. IEEE, 2012, pp. 1098–1105.

[6] A. K. Moorthy and A. C. Bovik, "Blind image quality assessment: From natural scene statistics to perceptual quality," *Image Processing, IEEE Transactions on*, vol. 20, no. 12, pp. 3350–3364, 2011.

[7] ——, "A two-step framework for constructing blind image quality indices," *Signal Processing Letters, IEEE*, vol. 17, no. 5, pp. 513–516, 2010.

[8] P. Ye and D. Doermann, "No-reference image quality assessment using visual codebooks," *Image Processing, IEEE Transactions on*, vol. 21, no. 7, pp. 3129–3138, 2012.

[9] L. Liu, B. Liu, H. Huang, and A. C. Bovik, "No-reference image quality assessment based on spatial and spectral entropies," *Signal Processing: Image Communication*, vol. 29, no. 8, pp. 856–863, 2014.

[10] R. Hassen, Z. Wang, and M. Salama, "No-reference image sharpness assessment based on local phase coherence measurement," in *Acoustics Speech and Signal Processing (ICASSP), 2010 IEEE International Conference on*. IEEE, 2010, pp. 2434–2437.

[11] L. Zhang, D. Zhang, and X. Mou, "Fsim: a feature similarity index for image quality assessment," *Image Processing, IEEE Transactions on*, vol. 20, no. 8, pp. 2378–2386, 2011.

[12] Z. Liu and R. Laganière, "Phase congruence measurement for image similarity assessment," *Pattern Recognition Letters*, vol. 28, no. 1, pp. 166–172, 2007.

[13] H. Sheikh, Z. Wang, L. Cormack, and A. Bovik, "Live image quality assessment database release 2," 2006, available from: http://live.ece.utexas.edu/research/quality.

[14] Z. Wang and A. C. Bovik, "Mean squared error: love it or leave it? a new look at signal fidelity measures," *Signal Processing Magazine, IEEE*, vol. 26, no. 1, pp. 98–117, 2009.

[15] Z. Wang, A. C. Bovik, H. R. Sheikh, and E. P. Simoncelli, "Image quality assessment: from error visibility to structural similarity," *Image Processing, IEEE Transactions on*, vol. 13, no. 4, pp. 600–612, 2004.

[16] M. C. Morrone and D. Burr, "Feature detection in human vision: A phase-dependent energy model," *Proceedings of the Royal Society of London. Series B, biological sciences*, pp. 221–245, 1988.

[17] P. Kovesi, "Image features from phase congruency," *Videre: Journal of computer vision research*, vol. 1, no. 3, pp. 1–26, 1999.

[18] D. J. Field, "Relations between the statistics of natural images and the response properties of cortical cells," *JOSA A*, vol. 4, no. 12, pp. 2379–2394, 1987.

[19] B. Schölkopf, A. J. Smola, R. C. Williamson, and P. L. Bartlett, "New support vector algorithms," *Neural computation*, vol. 12, no. 5, pp. 1207–1245, 2000.

[20] C. J. Burges, "A tutorial on support vector machines for pattern recognition," *Data mining and knowledge discovery*, vol. 2, no. 2, pp. 121–167, 1998.

[21] C.-C. Chang and C.-J. Lin, "LIBSVM: A library for support vector machines," *ACM Transactions on Intelligent Systems and Technology*, vol. 2, pp. 27:1–27:27, 2011, software available at http://www.csie.ntu.edu.tw/ cjlin/libsvm.

[22] H. R. Sheikh, M. F. Sabir, and A. C. Bovik, "A statistical evaluation of recent full reference image quality assessment algorithms," *Image Processing, IEEE Transactions on*, vol. 15, no. 11, pp. 3440–3451, 2006.

[23] N. Ponomarenko, V. Lukin, A. Zelensky, K. Egiazarian, M. Carli, and F. Battisti, "Tid2008-a database for evaluation of full-reference visual quality assessment metrics," *Advances of Modern Radioelectronics*, vol. 10, no. 4, pp. 30–45, 2009.

THE 18TH INTERNATIONAL SYMPOSIUM ON WIRELESS PERSONAL MULTIMEDIA COMMUNICATIONS
(WPMC-2015)
December 13-16, 2015, Hyderabad, India

Adaptive Priority Based Network Bandwidth Throttling for a Virtual Classroom System

Jobina Mary Varghese.
Amrita Center for Wireless Network and Applications
Amrita Vishwa Vidyapeetham
Amritapuri, Kollam, 695525
Jobz1991@gmail.com

Balaji Hariharan
Amrita Center for Wireless Network and Applications
Amrita Vishwa Vidyapeetham
Amritapuri, Kollam, 695525
balajih@am.amrita.edu

Uma G
Amrita Center for Wireless Network and Applications
Amrita Vishwa Vidyapeetham
Amritapuri, Kollam, 695525
umag@ am.amrita.edu

***Abstract*— Virtual classroom is an online learning environment which is similar to the real world classroom, where the students and professors are at different location and they interact with each other through internet with the help of audio and video data. So the students in the remote location will get the same experiences as if they are in the same classroom and there will be a full interactivity between the students and teachers. Under high bandwidth congestion, for the continuous delivery of video data between the main class room and virtual classroom, an optimized way of video streaming is required. This optimization can be achieved by dynamically changing the frame rate, bit rate, resolution and quantization parameter. During the time of congestion, streaming the same quality video across all the classrooms will result in poor end user experience. Overall experience of the classroom can be improved by dynamically changing the priority of the various video feeds in the system. The proposed system will help us to continuously deliver the optimized video stream between the classrooms based on the priority level.**

Keywords—Remote Classroom; Local Classroom; Quantization Parameter; Peak Signal to Noise Ratio

I. INTRODUCTION

Transmission of video packets through internet exposes the media packets to variable bandwidth, loss of packets and delay as they are travelling through the network. Due to the variation in the bandwidth and less reliability of wireless medium the transmission of video over the internet is a very difficult task. Wireless transmission will always have variable bandwidth. Also the wireless medium is very prone to interferences.

Video streaming is important in all aspect of life like education, work, entertainment etc. The main requirement of streaming a video are, it should have enough quality, quick response to users and continuity. Late arrival of video packets causes poor end user experience and early arrival of video packets also doesn't help. Live streaming is always very risky. As the number of users who try to watch an online video at the same time increases, there will be a great problem in the quality of the stream. A fixed bandwidth should be available for the reliable delivery of video. So we want to accurately measure the available bandwidth. Adjusting the quality is one of the optimum solutions to deliver the audio and video during the time of network congestion. But it should be smooth enough; sudden fluctuations in video quality should be avoided. Human vision will get adapt to a specific quality after a few second. So care should be taken to avoid rapid fluctuation since it is too annoying to the users.

The rest of the paper has been structured as follows. Section II introduces the related work. Section III details the system architecture. In Section IV we present the software implementation and the result obtained. Finally we present our conclusion and future work in section V.

II. RELATED WORK

The paper of Vamseedhar R. Reddyvari et. al. [2] provides a method to enhance the end user experience by means of a video scheduling policy. This will ultimately help to solve the troubles related with scalable H.264 video scheduling.H.264 will improve the video quality by utilizing the video scalabilities like temporal video scalability, quality video scalability and space based scalability. Temporal scalability adjusts the GOP size by the creation or deletion of video layers. In quality video scalability, different quantization parameters are given to different video layers.

Yen-Fu Ou et.al. [3] explains a method to find out the effect of frame rate and quantization step size on quality. The work provides an idea of reduction in quality with the

decrease in frame rate . Quality of a video can be expressed with two factors for a given frame rate and quantization step size. They are the temporal quality factor and spatial quality factor. Temporal quality factor describes how the quality reduces as the frame rate decreases with fixed quantization step size. Spatial quality factor describes how the quality reduces as quantization step size increases. Also large frame rate variation induces noticeable jitter.

Arpad Huszak and Sandor Imre, [4] deals with a scheme that provides a correlation between GOP size (Group of pictures), packet loss and video quality. Group of successive pictures within a coded stream of video is called as GOP.A GOP can contain the intra coded frames, predictive coded frames and bipredictive coded frames. The length of a GOP is its GOP size. In this work the main goal is to find an optimal GOP structure. They came up with the findings that the coding efficiency and propagation distortion is highest with larger GOP size. Under high packet loss ratio, it is better to have a small GOP size to achieve better quality. The video quality increases with increase in GOP size, but after reaching the highest peak signal to noise ratio (PSNR), it starts to decrease. They found out that the optimal GOP size is not more than 10.

Yao Wang et.al, [5] explains a method to find out the effect of frame rate and quantization step size on the bit rate and quality. They have proposed a quality model and rate model. Quality model relates the quality with quantization step size and frame rate. Quality model is derived as the product of PSNR of the decoded frame and by means of a temporal correction factor for quality. Rate model predicts the rate from quantization step size and frame rate. Model is derived as the product of a metric (describes how rate changes with quantization step size) and a temporal correction factor for rate. Relative reduction in either rate or quality with the reduction in frame rate is quite independent of the quantization step size.

S.Sowmyayani and P.Arockia Jansi Rani [6] explains a method to achieve better quality and to reduce bit rate by means of adaptive GOP structure using frame comparison. If GOP size is large, quality of the video after decoding is low which would reduces the bit rate. The quality and bit rate increases with small GOP size. They have proposed an adaptive GOP algorithm which sends side information to the decoder which contains the GOP size for the entire video. Proposed method achieves high PSNR and small bit rate than with fixed GOP structure. Video quality can be optimized by adjusting the parameters like changing the GOP size, frame rate, bit rate and quantization step size. In addition to these parameters to adjust the video quality we can change the resolution. Our proposed system is a solution to optimize the video content with all the video parameters, and to stream this optimized video content based on priority under high bandwidth congestion.

III. SYSTEM ARCHITECTURE

As we have stated in our previous work [7], the system model will provide an optimal solution of multimedia content transmission in a virtual class room environment under high bandwidth congestion. In response to network condition the quality of the video stream is adjusted so as to ensure graceful and smooth continuous play out. Consider a simplistic virtual class room environment of three class rooms, consisting of a local class room and two remote class rooms as in Fig 1. Local class room is the class room in which the professor is taking the class. Local class room also consists of local class room students. Remote class room is in a different geographical location where remote students are present. In this system model we will adjust the quality of the different video streams which are going in and out from the different classrooms based on the priority. Quality adjustment is done by changing the parameters like resolution, bit rate, quantization step size and frame rate. Following are the different video streams for a 3-classroom scenario which are going in and out from different classrooms

1. Lecturing video of the professor to remote classroom-1(outgoing)
2. Lecturing video of the professor to remote classroom-2(outgoing)
3. Local classroom students video to remote classroom-1(outgoing)
4. Local classroom students video to remote classroom-2(outgoing)
5. Remote classroom-1 students video to local classroom-(incoming)
6. Remote classroom-2 students video to local class room-(incoming)

In addition to this two more video streams are there which is streaming between the remote classrooms.

1. Video stream of remote classroom-1 students to remote class room-2.
2. Video stream of remote classroom-2 students to remote class room-1

The priority making system should have the knowledge about all of the video streams. Normally when there is no bandwidth congestion all the videos will be streamed in high quality between the classrooms. Whenever network congestion happens, the priority making system will check the current priority of each of the video. For example, consider the scenario in which the professor is taking the lecture and remote students are just listening to the lecture. In this case the video feed which needs high priority is the lecturing of the professor. So to cope up with the bandwidth congestion, the priority making system will take a decision to adjust the quality of the video streams. A feedback is provided to each of the classroom. According to the decision from the priority making system one with high priority is streamed in the higher quality and video streams with least priority are streamed in a lower quality than that of the high priority video.

IV. SOFTWARE IMPLEMENTATION AND RESULTS

The system is implemented with five machines. Among that two will act as the server, which is attached to the camera. Another two will act as clients, that will perform as the display machine and the last machine will act as the central controller. The server will capture the videos of different classrooms. This raw video data will be encoded using FFmpeg (fast forward moving picture expert group) [8] which is a solution to stream audio and video data. Under normal condition, this streamed video

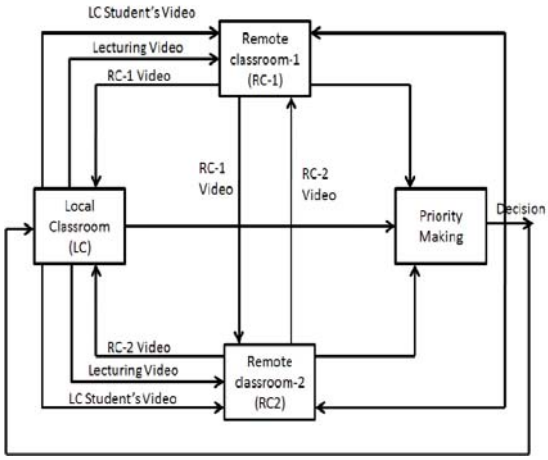

Fig 1. System Architecture

will be forwarded to the client in high quality. The client will respond with a congestion report to the central controller if there is a discontinuity in video delivery due to congestion. The congestion report carries the information to reduce the quality by adjusting the video parameters like frame rate, resolution, bit rate and quantization step size. Socket programming is used for this exchange of information between the client and the central controller. Whenever the central controller finds congestion, it will check the priority as in Fig 2. A rule based prioritization is implemented by means of keyboard input. If we pressed the keyboard input 'p' the first video stream from server-1 has treated with more importance and it will be streamed in a high quality. At the same time we will reduce the quality of the video stream from server-2. If the keyboard input is 'q' second video stream will get more importance and that is streamed in higher quality than the first. After taking the priority decision by central controller, it will request the server to adjust the quality accordingly. As a result the two servers will stream the video by adjusting the video parameters, so that the participants do not feel any perceivable change in the quality of the multimedia content presented to them. The experimentation is done with an assumption that the decoding errors are occurring only because of congestion even though interference may also lead to errors in the network. The packet drop is introduced manually using iptables[9] for creating the network congestion and Peak signal to noise ratio (PSNR) is taken into account in evaluating the quality of video in the model. Following are the result obtained for different scenarios with the system implementation.

Scenario 1: Without introducing packet drop

In the first scenario the test is conducted by not introducing any packet drop using iptable ie, the packet loss is 0%.Then the two clients will request for video files and the servers will stream a high resolution video towards the client with a bit rate of 200kb/s and a frame rate of 25fps.704*576 is taken as the high resolution value for streaming as in Table 1, beyond that the quality of the video decreases.704*576 resolution video will have a PSNR value of 30,which is of fair video quality in figure 3,4

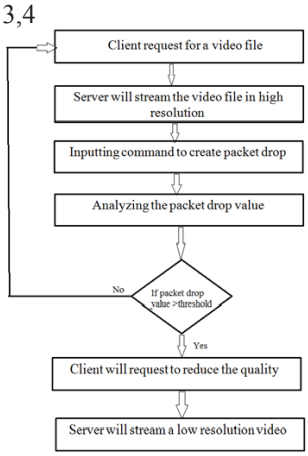

Fig 2. Flow chart of the system

Resolution	Bit rate(kb/s)	Frame rate(fps)	PSNR(dB)	Quality of Video
Sqcif,128*96	200	25	40	Excellent
Qcif,176*144	200	25	35	Good
Cif,352*288	200	25	32	Good
4cif,704*576	200	25	30	Fair

. Table 1: Parameters used for video streaming

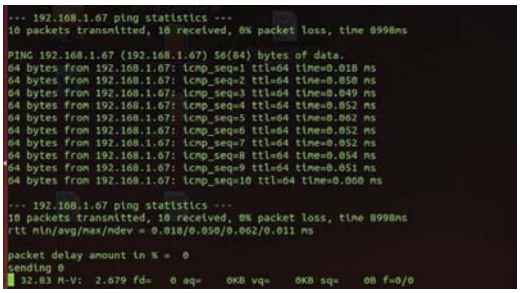

Fig 3. Packet drop is 0%

Fig.4 Video streamed without any packet drop

Scenario 2: With the introduction of packet drop

In the second scenario the test is conducted by introducing random packet drop using iptable. Then we analyze the value of packet drop. If it is less than the threshold value, the servers will stream the high resolution videos towards the clients as in fig. For the analysis purpose the threshold value of packet drop is taken as 25%.Here also a fair quality video can be streamed with a resolution of 704*576 as in Table 1.The video is streamed using a bit rate of 200kb/s and a frame rate of 25fps as in Fig 5,6.

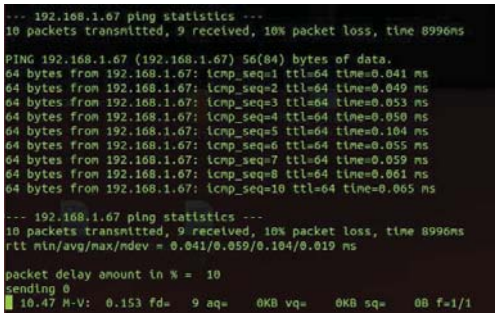

Fig.5 Packet drop is 10%

Fig.6 Video streamed at 10% packet drop

If the packet drop is greater than the threshold value the client will notify that to the central controller. Central controller will check the priority. In the priority decision, if the server 1 gets higher priority than server-2.The video from server-1 will stream in a higher resolution with fair quality. At the same time the central controller will request the server-2 to adjust the quality to have a continuous video delivery. So the video from server-2 will be streamed in a lower resolution to adjust with the packet drop introduced in the network.352*288,cif resolution can maintain a PSNR value of 32 with a bit rate of 200kb/s and a frame rate of 25fps which will help to deliver a good quality video as in fig 7,8.

If the server-2 gets higher priority than server 1, then we will stream a high resolution video to server-2 and a low resolution video to server-1 as in fig 9

If we send a video of 40 % packet drop without reducing the resolution, then the video which is delivering at the client side will be of poor quality as shown in Fig.10. In this time the video would be blocky causing irritation to the end users.

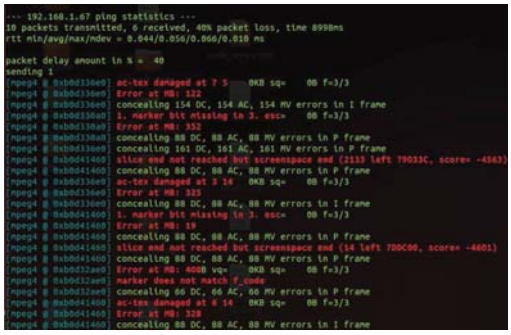

Fig.7 40% packet drop

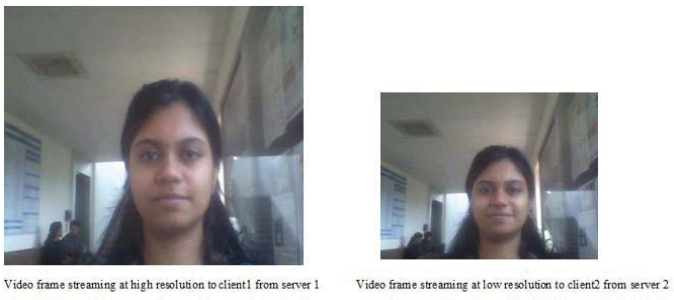

Fig.8 Video streamed when server-1 gets more priority

Fig.9 Video streamed when server-2 gets more priority

Fig.10. Video streamed without introducing our system at 40% packet drop

V. Conclusion And Futurework

A novel solution is proposed to improve the end user experience for a virtual classroom environment during congestion periods. A quality optimization and prioritization approach is introduced based on the available bandwidth by adjusting the resolution. Results indicate that the students in the main class room and remote class room will never face any noticeable change in the quality of video even in the time of congestion. Proposed system will deliver the video contents to the end-users for a virtual classroom system without any discontinuity.

In future research, the influence of decoding errors can be examined to reduce the amount of flickering. Also it is possible to implement the system with n-number of servers and n-number of clients.

ACKNOWLEDGEMENT

We would like to express our sincere gratitude to our beloved Chancellor Sri. Mata Amritanandamayi Devi (AMMA) for the immeasurable motivation and guidance for doing this work.

REFERENCES

[1] S. Krishnapriya, B. Hariharan, and S. Kumar, “Resolution scaled quality adaptation for ensuring video availability in real-time systems,” in High Performance Computing and Communication 2012 IEEE 9th International Conference on Embedded System, pp. 873–878.(2012)

[2] *Vamseedhar R. Reddyvari, Aditya K. Jagannatham*, "Optimal H.264 Scalable Video Scheduling Policies for 3G/4G Wireless Cellular and Video Sensor Networks", *Advances in Multimedia Volume 2012*

[3] Y.-F. Ou, Z. Ma, and Y. Wang, “Modeling the impact of frame rate and quantization step sizes and their temporal variations on perceptual video quality: A review of recent works,” in Information Sciences and Systems (CISS), 2010 44th Annual Conference on, March 2010, pp. 1–6. 5

[4] A. Huszak and S. Imre, “Analysing gop structure and packet loss effects on error propagation in mpeg-4 video streams,” in Communications, Control and Signal Processing (ISCCSP), 2010 4th International Symposium on, March 2010, pp. 1–5. 6

[5] Z. Ma, M. Xu, Y.-F. Ou, and Y. Wang, “Modeling of rate and perceptual quality of compressed video as functions of frame rate and quantization step-size and its applications,” Circuits and Systems for Video Technology, IEEE Transactions on, vol. 22, no. 5, pp. 671–682, May 2012. 6

[6]S.Sowmyayani and P. J. Rani, “Adaptive gop structure to h.264/avc based on scene change,” Circuits and Systems for Video Technology, IEEE Trans-actions on, vol. 22, no. 5, june 2006.

[7] Jobina Mary Varghese,Balaji Hariharan,Uma.G,Ram Kumar,Adaptive video quality throttling based on network bandwidth for virtual classroom systems-Unpublished

[8]. FFmpeg, https://ffmpeg.org/ffmpeg.html.

[9]. Iptables, http://en.wikipedia.org/wiki/Iptables.

THE 18TH INTERNATIONAL SYMPOSIUM ON WIRELESS PERSONAL MULTIMEDIA COMMUNICATIONS
(WPMC-2015)
December 13-16, 2015, Hyderabad, India

Energy Efficient Scheduling Algorithm for the Real-time Multicast and Unicast Services

Min Wang, Qiaoyun Sun, Shuguang Zhang
Information School
Beijing City University
Beijing, China
wangmin@bcu.edu.cn

Yinlong Liu, Yu Zhang
Institute of Information Engineering
Chinese Academy of Sciences
Beijing, China
liuyinlong@iie.ac.cn

***Abstract*—In order to minimize the energy consumption of the user terminal with guaranteeing the delay performance, a novel energy efficient (EE) scheduling algorithm for the real-time multicast and unicast services is proposed. According to the demand relations between the users and the services in the multicast broadcast single frequency network (MBSFN) area, the system model of the energy consumption for the user terminal is established, and the upper bound and the lower bound of the terminal energy consumption are analyzed. It adopts the idea of centralized burst transmission to realize the joint scheduling for the combination with various services, so as to achieve the minimum energy consumption of the user terminal. The simulation results show that the proposed algorithm can greatly save the energy of the user terminal by ensuring the delay performance for the real-time multicast and unicast services.**

Keywords—multicast broadcast single frequency network; energy efficient scheduling; delay; energy consumption

I. INTRODUCTION

In the LTE networks, more and more real-time multimedia services are provided for people. The single frequency network (SFN) is introduced to be a transmission mode for multicast and broadcast in the multiple cells [1]. A multicast broadcast single frequency network (MBSFN) area is a region within which all the time-synchronized base stations (BSs) send the same multicast services in a SFN fashion. On the one hand, it must satisfy the delay requirements of the real-time services. On the other hand, the energy saving of the user terminal is important for the multimedia services. The services scheduling by the centralized burst transmission is usually adopted for power saving, but it maybe leads to the delay for the real-time multimedia services. Therefore, the conflict between time delay and energy consumption is the key to the real-time multimedia services. It is essential for minimizing the energy consumption of the user terminal with guaranteeing the delay performance.

The work on energy efficient scheduling in wireless system is inherited from the burst scheduling [2] and the energy efficiency [3]. Joint packet scheduling for both multicast and unicast [4] is proposed in MAN networks. Furthermore, the energy-efficient multicast scheduling [5] is associated with the burst transmission for WiMAX networks. The problem of the battery-constrained mobile devices is focused in the wireless communication, and it takes into account energy savings for uplink cellular OFDMA transmission with low complexity [6]. Another energy-efficient scheduling in uplink OFDMA systems considers the fairness with resource allocation [7]. To guarantee the required QoS provisioning, the minimizing power consumption is adopted for the multicell cooperation networks [8]. The energy-delay trade-off for energy saving [9] is proposed in the wireless communication systems and it adopts the energy-efficient scheduling with individual packet delay constraints. The limited feedback for the delay constrained traffic [10] is introduced in the energy-efficient transmission strategies. However, to our best knowledge, there is no energy efficient scheduling for the real-time multicast and unicast services in MBSFN.

In order to minimize energy consumption of the user terminal, a novel energy efficient (EE) scheduling based on the centralized burst transmission is proposed for the real-time multicast and unicast services in MBSFN. With assuring the delay performance, the system model of the energy consumption for the user terminal is formulated. The proposed algorithm adopts the joint scheduling by the services combination, and then it achieves the minimum energy consumption of the user terminal for the real-time multicast and unicast services.

The remainder of this paper is organized as follows: the system model is introduced in Section II; the proposed energy efficient scheduling algorithm is given in Section III; Section IV provides the simulation results; and Section V concludes with the paper.

II. SYSTEM MODEL

According to the transmission energy consumption and the conversion energy consumption of the user terminal, the total energy consumption of the terminal is almost determined. Let P_{T} be the transmission energy consumption per unit time of the user terminal, and P_{S} be the conversion energy consumption of each state change between work and sleep. It is assumed that K, J and I are the number of the users per cell, the number of the multicast services and the number of

the unicast services in the MBSFN area, respectively. Let t_k denote the services delivery time of the user terminal k, and n_k denote the number of state transition in the services delivery. Then the energy consumption P_k of the user terminal k can be expressed as:

$$P_k = P_T \cdot t_k + P_S \cdot n_k \quad (1)$$

Furthermore, a set K_i denotes the users which need unicast service i in MBSFN, and d_{ki} is defined for the demand relation between user k ($1 \le k \le K$) and unicast service i （$1 \le i \le I$） as:

$$d_{ki} = \begin{cases} 1 & k \in K_i \\ 0 & k \notin K_i \end{cases} \quad (2)$$

Since the demand relationship between the users and the unicast services is not the one-to-one mapping, each user can transmit multiple unicast services, but each unicast service can be only provided for one user. The expression is given by:

$$\sum_{k=1}^{K} d_{ki} = 1 \quad (3)$$

Let T_{mj} represent the delivery time of the multicast service j, and t_{mj} is the ending time of its transmission. Then the transmission time interval of the multicast service j is $m_j = (t_{mj} - T_{mj}, t_{mj})$. Similarly, T_{ui} and t_{ui} represent the delivery time and the ending time of the unicast service i, respectively. $u_i = (t_{ui} - T_{ui}, t_{ui})$ is the transmission time interval of the unicast service i. The multicast transmission is all the same time for every user. That is, the transmission time interval of the multicast service j for each user is $m_j = (t_{mj} - T_{mj}, t_{mj})$. Because the transmission time of the multicast and unicast services can not be conflict, $m_j \bigcap u_i = 0$ is given. Additionally, there is no conflict between the transmission time of unicast services each other, $u_i \bigcap u_{i+1} = 0$ is formalized.

Furthermore, the real-time multicast and unicast services have the delay requirements. Let D_{mj} and D_{ui} be the delivery deadline of the multicast service j and the unicast service i, respectively. The expression is given by $0 < T_{mj} \le t_{mj} \le D_{mj}$ and $0 < T_{ui} \le t_{ui} \le D_{ui}$.

According to the demand relationship between the user k and the multicast and unicast services, t_k can be expressed as:

$$t_k = \sum_{j=1}^{J} T_{mj} + \sum_{i=1}^{I} d_{ki} T_{ui} \quad (4)$$

Since n_k is the number of state transition in the multicast and unicast services delivery for the user k, P_k can be also formalized as:

$$P_k = P_T \cdot (\sum_{j=1}^{J} T_{mj} + \sum_{i=1}^{I} d_{ki} T_{ui}) + P_S \cdot n_k \quad (5)$$

where $P_T \cdot (\sum_{j=1}^{J} T_{mj} + \sum_{i=1}^{I} d_{ki} T_{ui})$ and $P_S \cdot n_k$ denote the transmission energy consumption and the conversion energy consumption of the user terminal k, respectively.

III. Energy Efficient Scheduling Algorithm

A. Optimization Problem

To achieve the optimization goal of minimizing the energy consumption of the user terminal, the EE scheduling algorithm is proposed for the effective energy saving. The average energy consumption of all users can be expressed as the target function, which can also provide the real-time multicast and unicast services with the delay requirements. Therefore, from Eq. (5), the object function is formulated as:

$$\min \ \frac{1}{K} \sum_{k=1}^{K} P_k \quad (6)$$

For the user k, the value of P_k is determined by the number of the state transitions n_k after it is associated with the demand for the multicast and unicast services. The case of the upper bound is that the transmission time of all the services for the user k is not adjacent to each other. Namely, there are seconds between the transmission time interval of various services and it leads to the conversion energy consumption of the state transition between work and sleep. So the value of the upper bound can be expressed as:

$$P_k = P_T \cdot (\sum_{j=1}^{J} T_{mj} + \sum_{i=1}^{I} d_{ki} T_{ui}) + P_S \cdot (J + \sum_{i=1}^{I} d_{ki}) \quad (7)$$

However, the case of the lower bound is that the transmission time of all the services for the user k is adjacent. The transmission time interval of each service is continuous and it needs the conversion energy consumption of the only one state transition between work and sleep at the beginning of service transmission. Therefore, the value of the lower bound is given by:

$$P_k = P_T \cdot (\sum_{j=1}^{J} T_{mj} + \sum_{i=1}^{I} d_{ki} T_{ui}) + P_S \quad (8)$$

Due to the delay constraints of the real-time multicast and unicast services, the scheduling for all the users needs to be coordinated with each other, which can not guarantee that every user may get the lower bound. However, in order to

minimize the energy consumption of the user terminal, P_k can be achieved as the value of the lower bound as possible with the delay requirements of the real-time services.

B. Optimization Solution

Let P be the average energy consumption of all users in MBSFN area, and it can be expressed as follows:

$$P = \frac{1}{K}\sum_{k=1}^{K} P_k \tag{9}$$

Considering the delay constraints of the real-time multimedia services, $\min P$ is expressed as the optimization objective function. Through the comparison of the average energy consumption of user terminals to choose the minimum value with the corresponding services combination, it obtains the minimum energy consumption and determines the joint scheduling for the corresponding real-time multicast and unicast services.

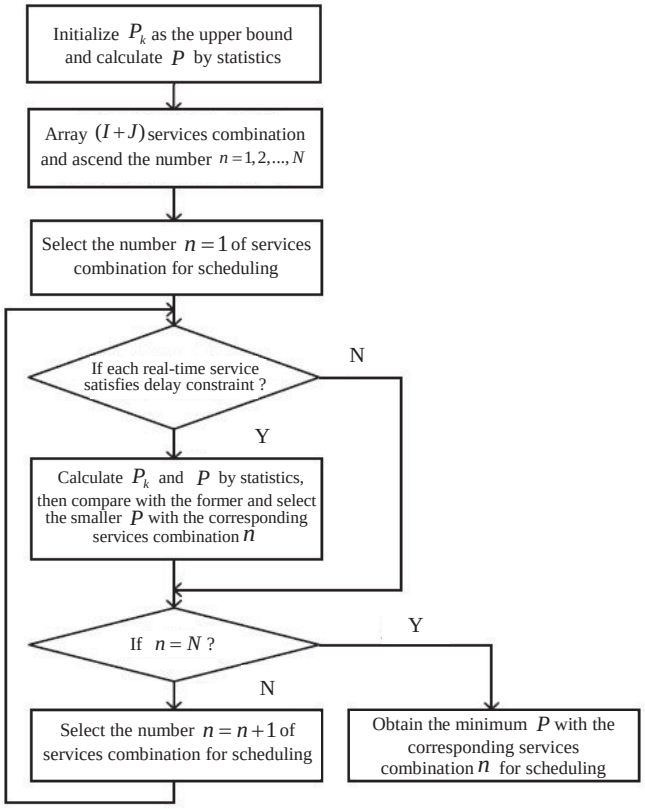

Figure 1. Minimizing energy consumption of the user terminal

As illustrated in Fig. 1, the flow of the minimizing energy consumption of the user terminal is proposed as:

Step 1: initialize the value of P_k for each user as the upper bound, and P is carried out by statistics;

Step 2: order the real-time multicast and unicast services by a full array of $(I+J)$ services combination, and code the number $n=1,2,...,N$ according to the ascending order;

Step 3: select the number $n=1$ of services combination for scheduling;

Step 4: if each real-time service satisfies the delay constraint, calculate P_k of each user at the current services combination, and then obtain P by statistics. Compare with the previous value of P and select the smaller one with the corresponding services combination n, then go into step 5; otherwise directly execute step 5;

Step 5: if $n=N$, the current value of P is the minimum average energy consumption for the user terminals. Schedule according to the corresponding services combination n, and then the algorithm is over; otherwise, turn into the implementation of step 6;

Step 6: define $n=n+1$ and select the next number of services combination for scheduling, then repeat step 4 until the ending $n=N$ of the algorithm.

IV. Performance Evaluation

To evaluate the energy saving performance of the proposed EE scheduling algorithm, the P of EE is compared with that of the upper bound and the lower bound in the different scenarios of K, J and I. As the mentioned above, K is the number of the users per cell, J is the number of the multicast services and I is the number of the unicast services in the MBSFN area, respectively. The demand relations of the user k and the unicast service i is random. However, each unicast service can be provided for only one user and each user may share different unicast services. Furthermore, the ending time of each multicast and unicast service can not beyond its deadline, which may assure the delay performance of the real-time services.

Let P_{ee} be the average energy consumption of the user terminals for the real-time multicast and unicast services in the EE scheduling algorithm. $P_{\max}$ and $P_{\min}$ denote the upper bound and the lower bound of the average energy consumption of the user terminals, respectively. The greater the difference of P between P_{ee} and $P_{\max}$ is, the higher the energy saving performance of the P in EE is.

A. Analysis of Different Number of Multicast Services

To evaluate the impact of J on $P_{\max}$, $P_{\min}$ and P_{ee}, the P of the different J with the fixed K = 30, I = 10, 30 or 60 is depicted in Fig. 2. For the same I and K, the larger J is, the more P is given by $P_{\max}$, $P_{\min}$ and P_{ee}. But the difference of P between P_{ee} and $P_{\max}$ becomes greater with the increasing J. Thus the more energy saving of the user terminals can be achieved in EE. Because the lager J leads to the less times of

the state conversion between work and sleep, the conversion energy consumption becomes smaller with the less P .

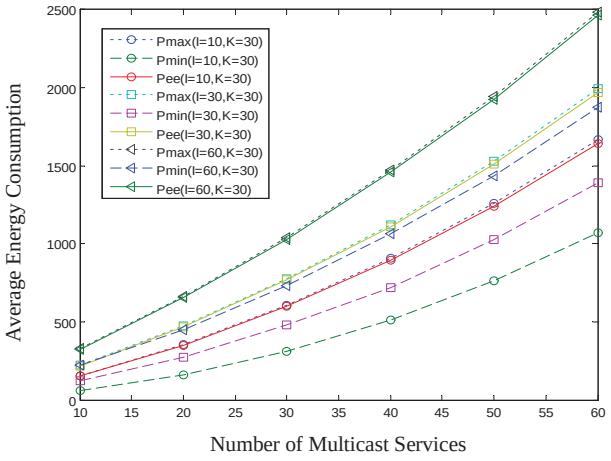

Figure 2. Impact of J on P of $P_{\max}$, $P_{\min}$ and P_{ee} (K=30)

B. *Analysis of Different Number of Unicast Services*

With the fixed K = 30, J = 10, 30 or 60, $P_{\max}$, $P_{\min}$ and P_{ee} are simulated and the impact of the different I on the P is analyzed. As shown in Fig. 3, the P of $P_{\max}$, $P_{\min}$ and P_{ee} all become more and more with the increasing I . For the fixed J = 30 and K = 30, the difference between P_{ee} and $P_{\max}$ is almost the same with the different I . However, P_{ee} can cut down the conversion energy consumption by the idea of centralized burst transmission in the EE scheduling, which may provide more energy saving for the user terminals.

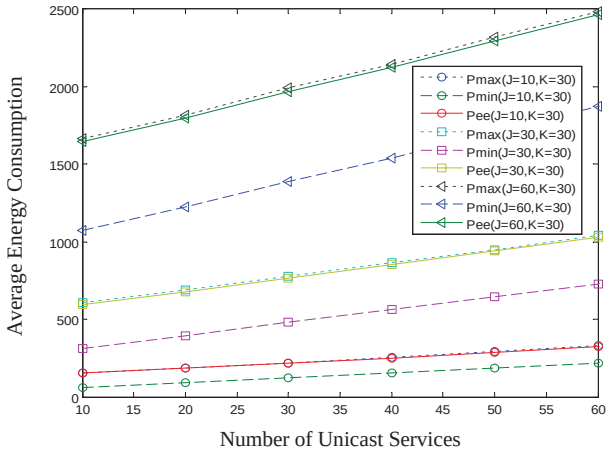

Figure 3. Impact of I on P of $P_{\max}$, $P_{\min}$ and P_{ee} (K=30)

C. *Analysis of Different Number of Users Per Cell*

To analyze the influence of K on P , P_{ee} is compared via simulation with $P_{\max}$ and $P_{\min}$ in the different K . As indicated in Fig. 4, it can be seen that P_{ee} is less than $P_{\max}$ in the different K with the fixed $I = 30$ or $J = 30$ .With the increasing K , the difference of P between P_{ee} and $P_{\max}$ becomes smaller and smaller. Thus the lager K is, the less energy saving of the user terminals is achieved in EE scheduling. Due to the increasing K , the chance to the centralized burst transmission of the real-time services becomes less and less. Therefore, it seems that there are more and more times of the state conversion between work and sleep in the EE scheduling. Then the conversion energy consumption becomes more with the less energy saving impact on the user terminals.

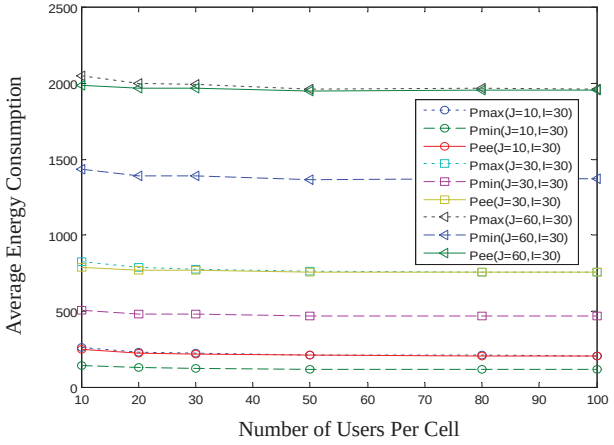

(a) Fixed $I = 30$

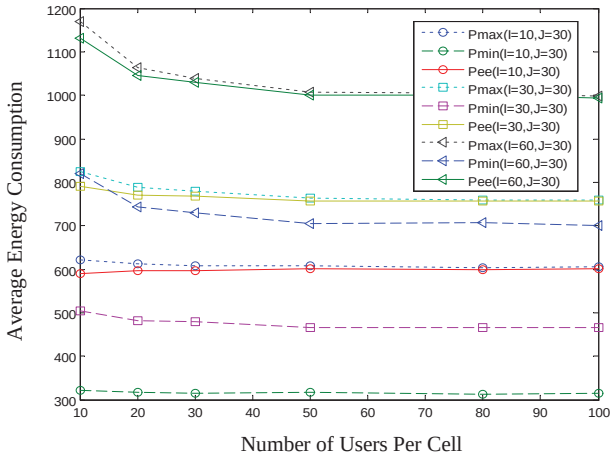

(b) Fixed $J = 30$

Figure 4. Impact of K on P of $P_{\max}$, $P_{\min}$ and P_{ee}

V. CONCLUSION

In this paper, a novel EE scheduling algorithm based on the centralized burst transmission is proposed for the real-time multicast and unicast services in the MBSFN area. It formulates the system model of the energy consumption for the user terminal and minimizes the average energy consumption for all the user terminals by joint scheduling in the services

combination. The simulation results show that the energy consumption of EE is less than that of the upper bound in the different number of multicast services, unicast services and users per cell in MBSFN.

ACKNOWLEDGMENTS

This work is supported by Beijing Natural Science Foundation (4154072).

REFERENCES

[1] 3GPP TR 36.913, "Requirements for further advancements for E-UTRAN (LTE-Advanced)," May 2008.

[2] J. Shi, G. Fang, Y. Sun, J. Zhou, Z. Li and E. Dutkiewicz, "Improving mobile station energy efficiency in IEEE 802.16e WMAN by burst scheduling," Proceedings of IEEE GLOBECOM, PP.1–5, 2006.

[3] R. Cohen and R. Rizzi, "On the trade-off between energy and multicast efficiency in 802.16e-like mobile networks," Proceedings of IEEE INFOCOM, PP.1–9, 2006.

[4] L. Tian, Y. B. Yang,G.F. Fang, J.L.Shi, and DUTKIEWICZ Eryk, "A scheduling set based integrated scheduling algorithm for unicast and multicast traffic," Journal of Software, Vol.19, No.12, PP.3196–3206, 2008.

[5] S. Sharangi, R. Krishnamurti, and M. Hefeeda, " Energy-efficient multicasting of scalable video streams over WiMAX networks," IEEE trans. on multimedia, Vol.13, No.1, PP.102–115, 2011.

[6] G. W. Miaol, N. Himayat, G. Y. Li, and S. Talwar, "Low-complexity energy-efficient scheduling for uplink OFDMA," IEEE Trans.on Communications, vol. 60, no. 1, pp. 112–120, 2012.

[7] H. N. Ye, Lim. Gubongt, L. J. Cimini, and Z. H. Tan, "Energy-efficient scheduling and resource allocation in uplink OFDMA systems," IEEE Communications Letters, vol. 19, no. 3, pp. 439–442, 2015.

[8] X. Zhang, and P. Wang, "Optimal trade-off between power saving and QoS provisioning for multicell cooperation networks," IEEE Wireless Communications, vol. 20, no. 1, pp. 90–96, 2013.

[9] Y. H. Jin, J. Xu, and L. Qiu, "Energy-efficient scheduling with individual packet delay constraints and non-ideal circuit power," Journal of Communications and Networks, vol. 16, no. 1, pp. 36–44, 2014.

[10] B. Tomasi, and J. C. Preisig, "Energy-efficient transmission strategies for delay constrained traffic with limited feedback," IEEE Trans. on Wireless Communications, vol. 14, no. 3, pp. 1369–1379, 2015.

.

Performance Analysis of Energy Detector in Correlated Log-normal Fading Channels for IR-UWB Systems

Josephine. S *Member, IEEE*, A. Mahanta *Member, IEEE* and P. R. Sahu *Member, IEEE*

***Abstract*—This work presents an analysis of the performance of an energy detector, which has the lowest hardware complexity among the suboptimal noncoherent receivers for Ultrawideband (UWB) communication. One of the major requirements among the many applications where UWB systems are used, is low complex receivers. In this communication we present a derivation of the probability density function (PDF) of the signal-to-noise ratio (SNR) at the output of the energy detector. The probability of error is numerically evaluated and plotted with respect to the number of multipath components (MPCs) and the correlation between them. The results of the paper show that a larger integration width increases the performance as the receiver input has more signal energy. In a correlated log-normal channel the correlation between the bins also affect the performance of the detector.**

***Index Terms*—Energy Detector (ED), Ultrawideband (UWB), Log normal channel.**

I. Introduction

Ultrawideband (UWB) technology, operating in the frequency range 3.1-10.6 GHz at very low power levels (-41.3dBm/MHz) is characterized by its huge achievable data rates for short range communication, using simple receiver structures [1]. UWB technology is employed in technology areas like Wireless Personal Area Networks (WPAN) and the recently standardized Wireless Body Area Networks (WBAN) for both low rate and high rate applications. In UWB communication, implementation of conventional optimum (coherent) receivers is relatively complex. Therefore, non-coherent receiver is an attractive option especially if simple and robust implementations with low power consumption is required. However, this comes at the expense of increased sensitivity to noise. Among the noncoherent receivers, energy detector (ED) is the most attractive solution for applications where low complexity is the primary motivation.

Energy detector measures the energy in the received waveform over an observation window. A typical energy detector requires a bandpass filter, a square-law device, an integrator and a decision device [2] as shown in Fig.1. The UWB ED receiver has the advantage of requiring only coarse synchronization which makes the system robust against clock jitter and triggering inaccuracy [3]. ED does not require any prior knowledge of the transmitted signal and the fading channel. However, low power design goal is challenging for UWB systems when a large number of multipath components (MPCs) have to be collected and combined at the receiver to improve the detection performance. The performance enhancement methods for energy detectors in a UWB receiver is therefor an important research topic.

Authors are with the Department of Electronics and Electrical Engineering, Indian Institute of Technology Guwahati, Assam, India (e-mail: {josephine, anilm, prs}@iitg.ernet.in).

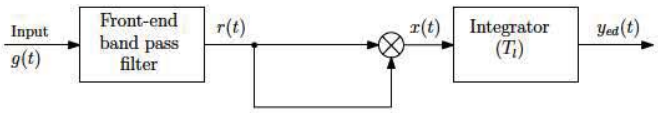

Fig. 1. Energy Detector Receiver Structure.

In this paper, an analysis of the performance of an ED in UWB communication in correlated log-normal channel, in particular, is carried out. In a UWB channel, MPCs that make up one resolvable MPC is much smaller due to the fine time delay resolution and it can change noticeably on a much shorter time scale. Due to this, it has been empirically determined that in many environments, alternative amplitude distributions are more suitable to represent the channel [4] such as Nakagami, Rice, Log-normal etc. It was suggested in [5] that the small scale fading in indoor environment follows log-normal distribution. Further, the IEEE 802.4a WPAN report on channel model for body area network in the frequency range of 2-6 GHz suggests that the best fit for the amplitude distribution measured near the body is a log-normal distribution. Thus the expressions derived in this study can be used to evaluate the performance of UWB systems over log-normal channel. Traditionally, in wireless communication, the log-normal distribution has been used to model the shadowing effect of the signal due to large obstacles. This has been studied quite extensively in the literature [6]. In this paper, we consider the small scale fading as log-normal.

The probability of detection of a deterministic signal in presence of band-limited Gaussian noise for an ED has been discussed in [7]. In [8], the probability of detection of a narrow band communication signal with random amplitudes has been presented [9] gives the performance when the detection capability is boosted by some diversity schemes. All these studies pertain to narrow-band communication. However, the propagation in UWB channel is very different from that in a narrow band channel. Several studies are also reported for the case of wideband communications using RAKE receivers [10], [12]. In the majority of the analysis of the ED, the probability of detection in an AWGN channel presented in [7] is considered, where the statistical distribution of the energy detector output is taken as a non-central chi-square random

variable. In addition to these studies, some results have been reported in the area of improving the performance of energy detector without adding much complexity to the basic structure [13]. Some results are reported describing the factors affecting the performance [14].

The goal of our work is to provide a statistical description of the performance of an ED in a UWB receiver in a correlated log-normal channel using an On-Off-Keying (OOK) modulated signal. We present the bit error rate (BER) performance of energy detector along with an exact expression for the probability density function (PDF) of the output SNR. The PDF derivation is based on the basic expression for the instantaneous output SNR. Further the bit error rate (BER) is numerically evaluated using the Gaussian approximation methods as in the case of an ED in AWGN channel presented in [15]. Eventhough this approximation is not valid for UWB environments, where the number of MPCs having significant energy is less for this approximation, we have nevertheless considered this in order to gain some knowledge as to how the error probability varies in a correlated log-normal channel.

The rest of the paper is organized as follows. The system model and the channel model are presented in Section II. We derive the exact expression for the pdf of the output SNR. In the same section, an approximate average bit error probability equation is also derived. Section III describes the Numerical results and observations and Section IV gives the conclusion.

II. System Model and Channel

The IR-UWB (Impulse Radio UWB) communication transmits information by very short pulses with durations in the range of nano seconds. For purpose of analysis, we focus on baseband UWB signals with OOK (on-off keying) modulation. In OOK UWB signaling, the binary symbols $x[n] = \{0, 1\}$ are transmitted using a train of short pulses. The pulse waveform $p(t)$ represents a single pulse of duration T_p. There are N_f frames, each of duration T_f, per symbol period with one pulse per frame. The transmitted symbol waveform is given by $x(t) = \Sigma_{j=0}^{N_f-1} p(t - jT_f)$ and has a symbol duration of $T_s = N_f T_f$ with energy normalized to unity. Thus the transmitted UWB OOK signal with energy E_w per symbol is given by

$$\mathrm{x}(t) = \sqrt{Ew} \sum_{n=0}^{\infty} x[n] p(t - nTs) \tag{1}$$

The function $p(t)$ represents the transmitted signal waveform which includes the effects of transmitting and the receiving antennas.

The impulse response $h(t)$ of a UWB channel may be expressed as [16]

$$h(t) = \sum_{i=1}^{N} \alpha_i \chi_i(t) * \delta(t - t_i), \tag{2}$$

where N is the number of MPCs that can be resolved at the receiver, α_i is the gain of the i^{th} path where $i = 1, 2, 3, .., N$. Further, t_i is the delay of the i^{th} path and χ_i(t) models the frequency selective distortion experienced by the multipath components due to its interaction with the propagation environment between the transmitter and the receiver. This is due to the variations of the averaged transfer functions caused by the different attenuations that the different frequency components of the UWB signal encounter because of its high relative bandwidth [17].

Studies on channel modeling investigations [4] reveal that the MPCs arrive in clusters and this is mathematically represented as Saleh-Valenzuela (SV) model. In specific environments where not every resolvable bin contains energy, ie., for sparse channels, the arrival times are modeled as a continuous-time stochastic point process. We consider such a sparse channel. Based on extensive channel measurements, the channel modeling subgroup of IEEE 802.15.4a proposed a modified SV model, where the number of cluster is assumed to be Poisson-distributed, while the ray arrival times are modeled as a mixture of two Poisson processes [18]. Here, the arrival times t_i has two components, T_l and $\tau_{k,l}$. T_l is the delay of the l^{th} cluster and $\tau_{k,l}$ is the delay of the k^{th} multipath component in the l^{th} cluster. The continuous-time process is converted into a tapped delay line model to simplify the analytical studies. With this simplification, the channel response $g(t)$ to the UWB pulse $x(t)$ can be obtained as [16]

$$g(t) = x(t) * h(t) = \sum_{i=1}^{N} \alpha_i p_i w(t - t_i), \tag{3}$$

where $w(t) = p(t) * \chi_i(t)$, '*' is the convolution operator and p_i is the probability whether or not the i^{th} bin is occupied with an arrival. $p_i = 1$ if there is an arrival otherwise $p_i = 0$. If the maximum excess delay of the channel is T_h and W is the channel bandwidth, then $N = T_h W$.

In this paper, we consider a base band representation of the signals. Therefore, the channel $h(t)$ and the gain are real quantities. Further, the α_i are lognormally distributed random variables and their probability density function is given as [10]

$$f_x(\alpha; \mu, \sigma) = \frac{1}{\sqrt{2\pi}\sigma\alpha} e^{\frac{-(\ln \alpha - \mu)^2}{2\sigma^2}}, \alpha > 0, \tag{4}$$

where the parameters μ and σ are the mean and the standard deviation respectively of $ln(\alpha)$. Some of the channel measurements show high correlation coefficients between adjacent bins [19].

For simplicity we assume that through proper synchronization and control methods, the integration window of the integrator collects only the energies of the different clusters, without accumulating the noise energy from the noise-only region between the clusters.

A. Energy Detector Input and Output SNR

At the input of the ED, the received waveform $g(t)$ is passed through a bandpass filter of a bandwidth W. The band limited signal after squaring, is integrated over a time window T_l. For our analysis, we have considered the received signal of one symbol duration to be consisting of only one pulse. Thus, the received signal at the ED input can be written as

$$r(t) = \sqrt{E_w} g(t) + n(t), \tag{5}$$

where E_w represents the average received energy per pulse, and $n(t)$ is the filtered noise, modeled as an additive Gaussian process with power spectral density $N_0/2$ within the double sided bandwidth W. Assuming a multipath resolvable channel, L can be written as $L = T_l W$ which represents the number of bins of width $1/W$ within the observation window. The signal at the output of the energy detector is given by

$$\begin{aligned} y_{ed} &= \int_0^{T_l} \left(\sqrt{E_w} g(t) + n(t)\right)^2 dt \\ &= x_1 + x_2 + x_3, \end{aligned} \tag{6}$$

where $x_1 = E_w \int_0^{T_l} g^2(t)dt$, $x_2 = \int_0^{T_l} n^2(t)dt$ and $x_3 = 2\sqrt{E_w}\int_0^{T_l} g(t)n(t)dt$.

The term x_1 in (6) is the 'desired signal', while x_2 and x_3 are the 'noise' and the 'signal multiplied by noise' components respectively. From the energy of the signal and the noise at the output of the receiver, the instantaneous SNR at the output (Γ_{out}) can be expressed mathematically. Noise energy can be calculated from the mean and the variance of x_2 and x_3. From (6), the signal component at the output of the energy detector is

$$x_1 = E_w \int_0^{T_l} g^2(t)dt = E_w \sum_{i=1}^{L} \alpha_i^2, \tag{7}$$

under the assumption of dense resolvable multipath channel. The various steps involved in finding the mean and the variance of noise components are shown in Appendix in detail. The mean and the variance of x_2 can be derived from the characteristic function (C.F) of the sum of the squares of $2L$ Gaussian random variables with zero mean and is given as [20, (6.24)] as

$$\Psi_x(\omega) = \left[\frac{1}{1 - 2j\omega\sigma^2}\right]^L \tag{8}$$

where σ^2 is the variance of $n(t)$. From (8), the mean of x_2 is $N_0 T_l W$ and the variance is $N_0^2 T_l W$. Similarly, the mean and the variance of x_3 is calculated from the basic definitions and are derived as zero and $(N_0/2)4x_1$ respectively [2]. Thus, the instantaneous SNR at the input of the ED is

$$\Gamma_{in} = \frac{2E_w}{N_0} \sum_{i=1}^{L} \alpha_i^2 \tag{9}$$

and the SNR at its output is

$$\Gamma_{out} = \frac{x_1^2}{2N_0 x_1 + N_0^2 T_l W + (N_0 T_l W)^2} \tag{10}$$

From (7) and (10), we can express Γ_{out} in terms of Γ_{in} as

$$\Gamma_{out} = \frac{1}{4} \frac{\Gamma_{in}^2}{\Gamma_{in} + T_l W + (T_l W)^2}. \tag{11}$$

B. Input and Output SNR Distributions

From (9), the distribution of Γ_{in} can be obtained by finding the distribution of the sum of L lognormal RVs[1]. The distribution of $Y = \sum_{i=1}^{L} \alpha^2$ is also lognormal as per the results in [21]- [23]. Several methods have been proposed for computing the parameters of the resulting log normal distribution. Among these, the method proposed by Schwartz and Yeh gives accurate estimates more accurately for the case of correlated signals with different mean and standard deviation [22]. Further,this case is more applicable for the UWB environment which we consider. Thus, applying this method the PDF of Γ_{in} can be written as

$$f_{\Gamma_{in}}(\gamma_{in}) = \frac{1}{\sqrt{2\pi}\sigma_L \gamma_{in}} e^{\frac{-\left(\ln \frac{N_0}{2E_w}\gamma_{in} - m_L\right)^2}{2\sigma_L^2}}, \gamma_{in} > 0 \tag{12}$$

where the parameters, m_L and σ_L are the mean and the standard deviation of the sum lognormal.

Thus from (11), the Cumulative Distribution Function (CDF) of Γ_{out} can be written as

$$\begin{aligned} F_{\Gamma_{out}}(\gamma_{out}) &= \Pr\left\{\frac{\frac{\Gamma_{in}^2}{4}}{\Gamma_{in} + T_l W + (T_l W)^2} \le \gamma_{out}\right\} \\ &= \Pr\left\{\Gamma_{in1} \le \Gamma_{in} \le \Gamma_{in2}\right\}, \end{aligned} \tag{13}$$

where $\Gamma_{in1}, \Gamma_{in2} = 2\gamma_{out} \pm 2\sqrt{\gamma_{out}^2 + \gamma_{out}(T_l W + T_l^2 W^2)}$ are the roots of the argument. Eliminating Γ_{in1}, which is negative, we can rewrite (13) as

$$\begin{aligned} F_{\Gamma_{out}}(\gamma_{out}) &= \Pr\left\{\Gamma_{in} \le \Gamma_{in2}\right\} = F_{\Gamma_{in}}(\varphi(\gamma_{out})) \\ &= \int_0^{\varphi(\gamma_{out})} f_{\Gamma_{in}}(\gamma_{in}) d\gamma_{in}. \end{aligned} \tag{14}$$

Then, the PDF of Γ_{out} can be derived by using the formula in [11, (3.56)]. Therefore,

$$f_{\Gamma_{out}}(y) = \frac{dF_{\Gamma_{out}}(y)}{dy} = f_{\Gamma_{out}}\left[\varphi(y)\right] \frac{d\varphi(y)}{dy}. \tag{15}$$

Thus, substituting $y = \gamma_{out}$ in (15), an expression for the PDF of Γ_{out} can be obtained as

$$f_{\Gamma_{out}}(\gamma_{out}) = e^{\frac{-(\ln(2\gamma_{out}+2K) - m_L)^2}{2\sigma_L^2}} \frac{(2K + 2\gamma_{out} + T_l W + T_l^2 W^2)}{K\sqrt{2\pi}\sigma_L(2\gamma_{out} + K)}, \tag{16}$$

where $K \triangleq \gamma_{out} + \sqrt{\gamma_{out}^2 + \gamma_{out}(T_l W + T_l^2 W^2)}$. The PDF expression given in (16) has been verified by integrating it w.r.t γ_{out} by numerical evaluation using Mathematica and has been found to be unity, i.e, $\int_0^{\infty} f_{\Gamma_{out}}(\gamma_{out}) d\gamma_{out} = 1$. For the purpose of illustration, the numerical values of integration are tabulated in Table I as a function of parameters σ, L and m. To the best of our knowledge (16) is a new expression.

C. Bit Error Rate

The bit error rate (BER) is one of the most important performance characteristic of a communication system. The detection probability of energy detector in the case of narrow-band channels as well as in the case of RAKE receivers in wideband channels has been studied extensively in literature.

[1]Since α is lognormal distributed, α^2 is also lognormally distributed [23]

Moreover, some specific cases like the bit error performance of UWB systems with RAKE receiver for a hybrid pulse amplitude and pulse position modulation scheme over an indoor lognormal fading channel using a RAKE receiver has been numerically evaluated in [10]. In [24] an analytical expression for optimum receiver bandwidth is derived and the effect of bandwidth on the bit-error-rate (BER) is quantified.

In the work presented here, the BER of energy detector in IR-UWB channel is derived by applying the approach for optical signals [15]. This method has been used in communication systems extensively [14], [24]. After filtering, the input signal to the ED can be considered to be a finite sum of L random variables, which can be gathered together in an integration window T_l. This assumption is applied to IR-UWB channel model, where a sequence of distinct pulses are received as in a tapped delay line and L is the number of MPCs which can be gathered together in the integration window. It was shown in [9] that the statistics of the ED output in an AWGN is non-central chi-square distributed.

When the receiver compares the output from the integrator with a threshold ρ, the average BER for equiprobable 0/1 can be calculated as [15]

$$P_{e|\gamma_{in}} = \frac{1}{2}\left[1 - Q_M\left(\sqrt{2\gamma_{in}}, \sqrt{\frac{2\rho}{N_0}}\right) + e^{-\frac{\rho}{N_0}} \sum_{i=1}^{M} \frac{1}{i!}\left(\frac{\rho}{N_0}\right)^i\right] \tag{17}$$

where Q_M is the generalized Marcum-Q function.

Therefore, the average error probability for an IR-UWB systems in a correlated log-normal channel can be written as

$$\overline{P_e} = \frac{1}{2} + \frac{e^{-\frac{\rho}{N_0}}}{2} \sum_{k=0}^{M-1} \frac{1}{i!}\left(\frac{\rho}{N_0}\right)^i + \int_0^\infty Q_M(\sqrt{4\gamma_{in}}, 2\frac{\rho}{N_0}) \frac{1}{\sqrt{2\pi}\sigma_L\gamma_{in}} e^{\frac{-(\ln\gamma_{in}\frac{N_0}{2E_w} - m_L)^2}{2\sigma_L^2}} d\gamma_{in} \tag{18}$$

However, as L increases, the PDF of the output of the ED can be approximated by a Gaussian PDF. With this assumption, which is called the gaussian approximation of an ED, the average BER can be written as

$$\overline{P_e} = \int_0^\infty Q\left(\frac{\gamma_{in}}{\sqrt{L} + \sqrt{L + 2\gamma_{in}}}\right) f_{\Gamma_{in}}(\gamma_{in}) d\gamma_{in}, \tag{19}$$

where $f_{\Gamma_{in}}$ is the PDF of the input SNR and

$$\overline{P_e} = \int_0^\infty \frac{1}{\sqrt{2\pi}\sigma_L\gamma_{in}} e^{-\frac{(\ln(\gamma_{in}\frac{\Omega_L}{\gamma_{in}}) - m_L}{2\sigma_L}} erfc\left(\frac{\sqrt{L+2\gamma_{in}} - m_L}{2\sqrt{2}}\right) d\gamma_{in} \tag{20}$$

III. Numerical Results

Fig. 2 shows the PDF of the SNR at the output of the energy detector for varying number of multipath components as a function of output SNR. As the number of branches increases, the pdf of output SNR increases. Further, the increment is larger in low SNR region compared to the increment in high SNR region. Also, it is observed that when the instantaneous input and output SNRs (9) and (11) are compared, the ratio is found to be very low. This is due to the multiplication of noise

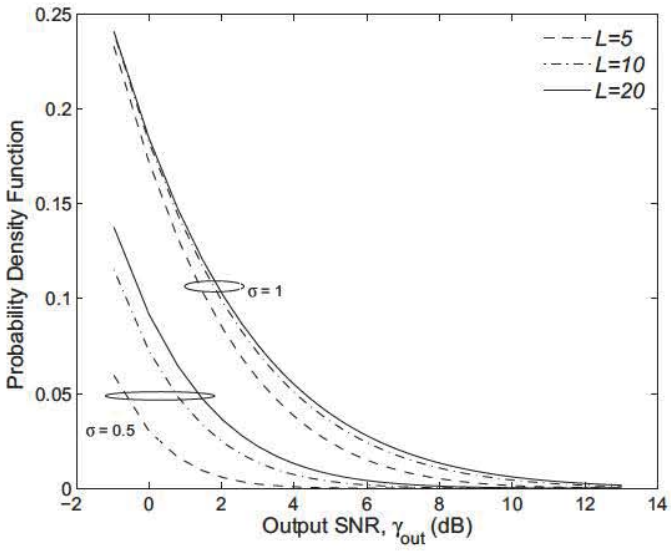

Fig. 2. PDF of output SNR.

energy. In order to capture the maximum amount of signal energy, the integration window must be kept longer than the delay spread. In the case of Wireless Body Area Networks, measurements reveal that a maximum of $L = 6$ is sufficient on all sides of the body, since in the worst cse, the average bin energy will decay by more than 20 dB after 6 bins [25].

Fig. 3 shows the gaussian approximated average probability of error for OOK modulation (20) in correlated log-normal channels. The number of MPCs are taken as $L = 4$ and $L = 6$ for a correlation of $\rho = 0.1$ and $\rho = 0.2$. From the figure, it is observed that more the integration time, lesser is the BER. As regards correlation, it is observed that as the correlation between the bins increases, the BER increases for a given L. This is due to the decrease in mean value and the increase in the variance of the sum of the log-normal components. Typical parameters for the correlated log-normal components are taken from the curves of [23]. Larger number of MPCs implies a larger integration window and thus more signal energy can be captured for conventional energy detectors without added complexity. However, in practice, the complexity will increase due to the additional synchronization circuits to receive the exact multi path energy.

IV. Conclusions

In this paper, we present a theoretical analysis of an energy detector in correlated lognormal channel, which is the best fit for some of the UWB indoor environments. Mathematical expressions for the PDF of the output SNR is derived and plotted. The numerically integrated curves for the gaussian approximated PDF are also plotted for different values of correlation among the MPCs. From these results, we conclude that L, which decides the integration time window is the most significant parameter. While implementing the energy detector in UWB, it is important to gather the MPCs that have significant energy. It is also observed that the performance improves if the bins are not correlated.

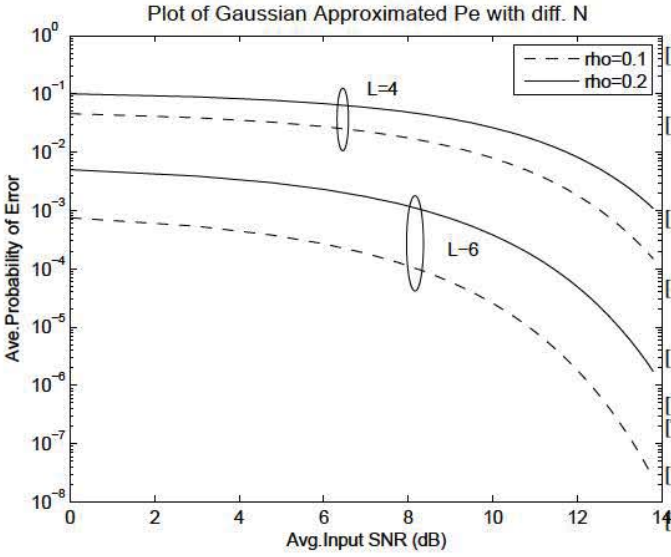

Fig. 3. Avg. Pe with different values of L.

TABLE I
VERIFICATION OF AREA UNDER THE PDF IN (16)

σ	0.5	1	2
L	4, 15, 50	2, 3	2, 10
m	1	0	0.5
$\int_0^\infty f_{\Gamma_{out}(\gamma_{out})} d\gamma_{out}$	1	1	1

APPENDIX A
MEAN AND VARIANCE OF x_2 AND x_3

A. Mean and Variance of x_2

The energy in the finite duration sample of $n(t)$ is the sum of $2L$ squares of zero mean gaussian variates all having the same variance. To find the mean and variance, the characteristic function of the product of the sum of the squres of $2L$ Gaussian random variables is taken as follows

$$\Psi_x(\omega) = \left[\frac{1}{1-2j\omega\sigma^2}\right]^L, \quad (21)$$

where σ^2 is the variance of $n(t)$. Therefore the mean of x_2 is

$$E[x_2] = \frac{d[\varphi_x(w)]}{dw}/w = 0 \quad (22)$$

and the variance can be calculated by $Var[x_2] = E[x_2^2] - E[x_2]^2$ where $E[x_2^2] = \frac{d^2[\varphi_x(w)]}{dw^2}/w = 0$. Thus, the variance of $x_2 = N_0^2 T_l W$.

B. Mean and Variance of x_3 in (6)

Mean of x_3 is $E[x_3] = E\left[\int_0^{T_l} 2\sqrt{E_w} g(t) n(t) dt\right] = 0$, since $E[n(t)] = 0$. The variance of x_3 can be derived as

$$\begin{aligned} Var[x_3] &= E\left[\int_0^{T_l} 2\sqrt{E_w} g(t) n(t) dt\right]^2 \\ &= \frac{N_0}{2} 4E_w \int_0^{T_l} g^2(t) dt = \frac{N_0}{2}(4x_1) \end{aligned} \quad (23)$$

REFERENCES

[1] L. Yang and G.B. Giannakis "Ultra-Wideband Communication:An Idea Whose Time Has Come", " *IEEE Signal Processing Magazine*, vol.21, issue.6, 2004.
[2] K. Witrisal, G. Leus, G.J.M. Janssen, M. Pausini, F. Troesch, T. Zasowski and J. Romme, "Noncohernet Ultra-Wideband Systems: An Overview of Recent Research Activities", *IEEE Signal Processing Magazine*, Jul. 2009.
[3] S. Paquelet, L.M. Aubert and B. Uguen, " An Impulse Radio Asynchronous Transceiver for High Data Rates", *Proc. IEEE Ultrawideband Systems Technology*, Kyoto, May 2004, pp.1-5.
[4] A.F. Molisch, "Ultrawideband Propagation Channels-Theory,Measurement and Modeling", *IEEE Transactions on Vehicular Technology*, vol.54, No.5, Sep. 2005.
[5] J.R. Forester and Q. Li, "UWB Channel Modeling Cotribution from Intel", *IEEE Tech.Rep.P802.15 .2/279SG3a, 2002.*
[6] J. Proakis, "Digital Communications", *4th edition, McGraw-Hill 2001.*
[7] H. Urkowitz "Energy Detection of Unknown Deterministic Signals"," *Proceedings of the IEEE*, vol.55, No.4, Apr.1967.
[8] V.I. Kostylev, "Energy Detection of a Signal with Random Amplitude," *IEEE Int. Conf. on Communications*, ICC 2002.
[9] F.F. Digham, M.S. Alouni and M.K. Simon, "On the Energy Detection of Unknown Signals Over Fading Channels", *IEEE Transactions on Communications*, vol.55, Issue:1, Jan. 2007.
[10] H. Liu, "Error Performance of a Pulse Amplitude and Position Modulated Ultra-Wideband System Over Lognormal Fading Channels", *IEEE Communication Letters*, vol.7, No.11, Nov.2003.
[11] Alberto Leon Garcia *"Probability and Random Processes for Electrical Engineering"*, 2nd Edition,Pearson Education
[12] J.D. Choi, W.E. Stark, "Performance of Ultra-Wideband Communications With Suboptimal Receivers in Multipath Channels", *IEEE Jounal On Selected Areas In Communications*, vol.20, pp.1754-1766, 2002.
[13] A.A. DAmico, and U. Mengali, and E. Arias-de-Reyna, "Energy-Detection UWB Receivers with Multiple Energy Measurements", *IEEE Transactions On Wireless Communications*, vol.6, pp.2652-2659, 2007.
[14] A. Anttonen, "Estimation of Energy Detection Thresholds and Error Probabality for Amplitude-Modulated Short-Range Communication Radios", Ph.D Thesis, University of Oulu, 2011
[15] P.A. Humblet and M. Azizoglu, "On the Bit Error Rate of Lightwave Systems with Optical Amplifiers", *J.Lightwave Technol.*, vol.9, no.11, pp.1576-1582, Nov.1991.
[16] M. Pausini and G.J.M. Janssen, "Performance Analysis of UWB Autocorrelation Receivers Over Nakagami-Fading Channels", *IEEE Journal on Selected Areas in Communications*, Vol.1, No.3, Oct. 2007.
[17] A.F. Molisch, D. Cassioli, C. Chong, S. Emami, A. Fort, B. Kannan, J. Karedel, J.Kunisch, H G Shantz, K.Siwiak and M Z Win, "A Comprehensive Standardized Model for Ultrwideband Propagation Channels", *IEEE Transactions on Anetenna and Propagation*, vol.54, No.11, Sep. 2006.
[18] A.F. Molisch, "Ultra-Wide-Band Propagation Channels", *Proceedings of the IEEE*, vol.97, No.2, Feb. 2009.
[19] A. Fort, J. Ryckaert, C. Desset, P. Doncker, P. Wambacq and L.Biesen, "Ultra-Wideband Channel Model for Communication Around the Human Body", *IEEE Journal On Selected Areas In Communications*, vol. 24, No. 4, Apr. 2006.
[20] M.K. Simon, "Probability Distributions Involving Gaussian Random Variables", Boston, MA:Kluwer 2002.
[21] J. Wu, N. Mehta and J. Zhang, "A Flexible Lognormal Sum Approximation Method", *IEEE Globecomm*, 2005.
[22] P. Cardieri and T.S. Rappaport, "Statistics of the Sum of Lognormal Variables in Wireless Communications", *Vehicular Technology Conference Proceedings*, Tokyo, 2000, vol.3, pp. 1823 - 1827.
[23] N.C. Beaulieu and Q. Xie, "An Optimal Lognormal Approximation to Sum Lognormal Distributions", *IEEE Transactions on Vehicular Technology*, vol.53, pp. 479-489, 2000.
[24] J.M. Almodovar-Faria, J. McNair and D. Wentzloff, "Optimal Receiver Bandwidth for Energy-Detection PPM UWB Systems", *IEEE Wireless Int. Wireless Communications and Networking Conf.*, 2011.
[25] A. Fort, C. Desset, J. Ryckaert, P. DeDoncker, L. VanBiesen, and P.Wambacq, "An Ultra wideband body area propagation channel model-From statistics to implementation", *IEEE Transactions on Microwave Theory and Techniques*, vol.54, No: 4, pp. 1820-1826, Apr.2006.

THE 18TH INTERNATIONAL SYMPOSIUM ON WIRELESS PERSONAL MULTIMEDIA COMMUNICATIONS
(WPMC-2015)
December 13-16, 2015, Hyderabad, India

On Supporting Integrated Multimedia Traffic in TDMA based Mobile Ad hoc Networks

Mallesham Dasari, Himanshu Sindhwal, Naresh Vattikuti
UURMI Systems Pvt. Ltd.
Hyderabad, India.
Email: {malleshamd, himanshus, vvsnaresh}@uurmi.com

Bheemarjuna Reddy Tamma
Department of CSE, IIT
Hyderbad, India.
Email:tbr@iith.ac.in

***Abstract*—In this paper, we proposed a generic Time Division Multiple Access (TDMA) based Medium Access Control (MAC) for transmitting multimedia traffic in Ad hoc Wireless Networks (AWNs). We studied the complete system with integrated services such as data, voice, audio and video flows by providing the Quality of Service (QoS) for real time traffic. The core idea behind the protocol is a novel slot distribution for different kind of flows (particularly video flows due to their huge bandwidth requirement) based on the dynamic requirement of bandwidth. We first present the slot distribution for different flows and then explain the algorithm to further optimize the slots usage with adaptive reservation based on the video compression analysis. Since the End to End (E-to-E) delay in a multi hop network is a critical factor in guaranteeing QoS for multimedia traffic, we considered the slots distribution most favourable to real time media transport over AWNs. The simulations were conducted for investigating the performance of the protocol such as E-to-E delay, packet loss ratio (PLR) and throughput by varying different types of services. The adaptive reservation of slots based on the analysis of the bit rate generated by video codec, highlights the work in evaluating the performance of the system.**

***Index Terms*—Slot Distribution, Multi-hop, Multimedia, QoS, TDMA, MAC, AWNs.**

I. Introduction

TDMA based MAC protocols are well known for providing deterministic service in AWNs. Providing the wireless communication using single Radio Frequency (RF) for control as well as actual data transfer in a multi-hop topology, leads to a challenging work. With the increasing enormous technologies such as smart phones, tablets and other mobile technologies, it requires the network to support all kinds of traffic such as data, voice, audio and video on demand, which has made the slot distribution in AWNs, much more interesting research area. Hence, we perform the application specific slot distribution by classifying the real time traffic to provide the QoS guarantee. The traffic is classified based on the bit rate generated by the application, such as Available Bit Rate (ABR), Constant Bit Rate (CBR) and Variable Bit Rate (VBR). This again divided into real time and non real time services such as CBR, rt-VBR, nrt-VBR, rt-data and nrt-data traffic as classified in [1].

In our Adaptive Slot Reservation for Integrated Media Access (ASRIMA) protocol, we considered the design of MAC system for an AWN by providing the QoS for different types of traffic. We first present TDMA slot distribution mechanism

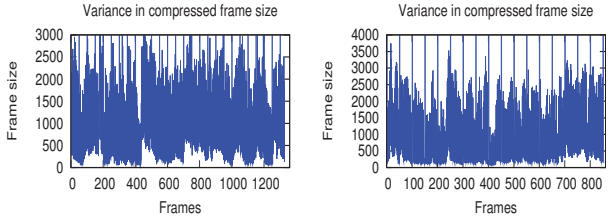

(a) (b)

Fig. 1: **Histogram for compressed bit stream variance (I, P and B frames): (a). High motion and (b). Low motion**

for different flows and then specifically talk about the real time multimedia transport over AWNs. Tremendous research has been going on in supporting data and voice traffic over an AWN. But, providing video over AWNs, is a complex problem due to its VBR nature and QoS needs. Considering High Efficiency Video Coding(HEVC) video compression known as ISO/IEC 23008-2 MPEG-H Part 2 and ITU-T H.265 [2], the frame size after compression, is highly non deterministic as shown in Fig. 1. The reason behind such phenomena is, the Group of Pictures (GOP) structure, for instance IPBPPBBBP...(where, the frames of the video are classified as I, P and B) and scene cut or high variance in motion of video. Therefore, for such kind of VBR sources, the appropriate slot distribution and frame structure is a crucial design decision for a TDMA based MAC to get the effective utilization of bandwidth. In this paper, we show the effect of VBR traffic due to its huge bandwidth requirement that effects flows with low bit rate requirements. The remaining of this paper is organized as follows: Section II presents an overview of literature in this work. In Section III, the traffic is examined for effective distribution of slots for different flows. Section IV explains the proposed TDMA MAC system particularly by studying the video transport. The simulation studies and corresponding results are evaluated in Sections V. At last, the concluding remarks are presented in Section VI.

II. Related Work

The media access protocols such as in [3][4] are not suitable for all kinds of real time traffic due to the VBR nature of video flows. These protocols works well with low bit rate CBR flows with end to end reservation of resources along the multi

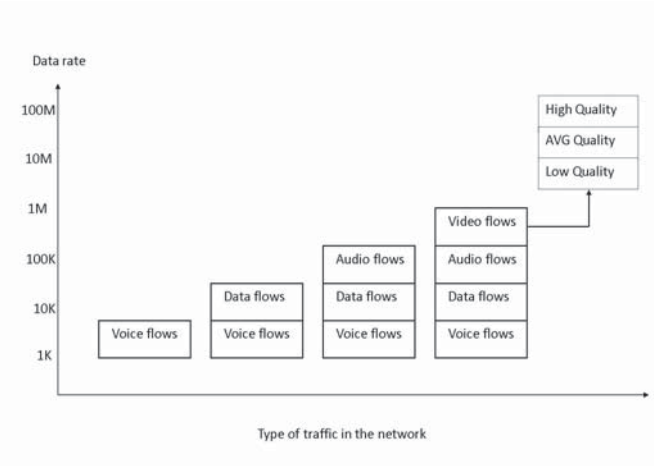

Fig. 2: **Bit rate requirement for different types of flows**

hop path. Reddy, T.B et.al [5] proposed multimedia support MAC protocol in AWNs by providing QoS. The work has well examined the VBR traffic, however it does not speak about the TDMA Frame Structure (TFS) and the slot distribution with respect to application. This also is not suitable for video flows that have high variance in the motion content. In [6][7], a cross layer approach is proposed to provide QoS for real time service. The authors have studied about the E-to-E by providing a minimal length TDMA schedule, however the video transport over AWNs and CAR performance is not well investigated. In [8], the authors have proposed the work to enhance the flow capacity of the system but were not considering the effect of TFS and VBR traffic. Many protocols were proposed as presented in [9], a comparative study of well known TDMA protocols for MAC level optimization of traffic. However, most of the protocols are not providing the full MAC layer functionality as a system with application specific slot distribution. Here, we are going to present a TDMA based MAC protocol with different kind of flows and effect of TFS on such flows.

III. Traffic Analysis

The slot distribution for different type of flows is carried out by identifying type of traffic from application, typically with Type of Service (TOS) field of Internet Protocol (IP) header. A new flow along E-to-E path, is identified with the Equation (1). The TOS field is used to detect the type of application such as voice, data, audio and video. And, the dst_id and src_id are the node identifiers of the network and dst_port is port number on the destined node, to which the application is sending data. Hence, together with TOS and, source and destination address and port number a new type of flow is identified and handled indepenent of other ongoing applications.

$$newFlow = f(TOS) \odot g(dst_port, dst_id, src_id) \quad (1)$$

First, considering the huge bandwidth requirement of video flows, the slot distribution for each video flow is handled by taking different parameters of video codecs into consideration. For instance, in HEVC video compression, Sequence Parameter Set (SPS) and Picture Parameter Set (PPS) were studied carefully to adapt the allocated slots during the session, across the E-to-E path. Second, considering low bandwidth requirement and CBR nature of voice flows as an advantage, the slot distribution for different voice flows is done in a simple approach. At the time of voice flow establishment itself, a virtual circuit for each flow is established by reserving the slots over end to end path. Suppose, for voice codec G.729 with 40ms periodic time frame and 6kbps bit rate, the size of the voice packet generated at the application is 80 Bytes per 40ms. For channel with 1Mbps data rate and slot duration 625us, one slot for each hop along the E-to-E path is enough for 40ms TDMA frame. Finally, data flows with ABR slot distribution, are established without any bandwidth reservation along the E-to-E path. Since the data traffic has high tolerance towards E-to-E delay, such flows are established with Best Effort (BE) service. Here, the queue length is analyzed for each TDMA frame and VBR extraneous slots can be used when the VBR flows are in Low Bandwidth Requirement (LBR) mode. Hence, the data traffic may also have the chance to reduce its queuing delay which is an essential requirement for data traffic such as E-mail delivery delay, text message delivery time.

IV. Proposed Work

The slot distribution for a voice traffic is illustrated in section III. We consider SDS for data and video traffic as it is a crucial factor in the effective utilization of bandwidth due to their VBR nature. First, considering the slot distribution for video calls, the design decisions are greatly dependent on the video coding algorithm. The codec parameters such as

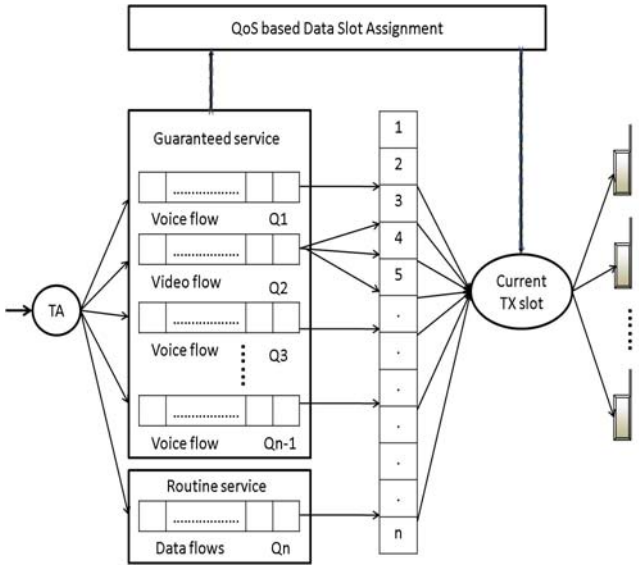

Fig. 3: **Multiple Queues handling for QoS support**

Algorithm 1 FlowSchedulingStrategy()

pkt = getPktFromNetwork();
flow_type = analyseFlow(*TOS*);
Υ_{slots} = getSlotsNeeded(Υ_{bw});
if ($flow_type == Data \| nonRealTimeMedia$) **then**
  if (isNewFlow(*port, dst, src*)) **then**
    if ($\exists \Phi_{idle} : \Phi_{idle} \in N_{ds}$ and $\Phi_{idle} \geq \Upsilon_{slots}$) **then**
      return Φ_{idle}; /* *No E-to-E reservation of slots* */
    else
      return $Null$; /* *Queue the packet*/
    end if
  else
    δ_{Ql} = getQueueLength();
    N_{vss} = getVbrSilenceSlots();
    if ($\delta_{Ql} > \delta_{dth}$) **then**
      return $\Phi_{idle} : \Phi_{idle} \in \{N_{ds}, N_{vpeak}, N_{vss}\}$
    else
      return $\Phi_{idle} : \Phi_{idle} \in N_{ds}$ /* *As packets are not experiencing queuing delay, no need of* N_{vss} */
    end if
  end if
end if
if ($flow_type == realTimeVoice$) **then**
  if (isNewFlow(*port, dst, src*)) **then**
    if ($\exists \Phi_{idle} \forall N_{hf} : \Phi_{idle} \in N_{ds}$ and $\Phi_{idle} \geq \Upsilon_{slots}$) **then**
      return Φ_{idle}; /* *Once the voice flow accepted, packets will not have queuing delay*/
    else
      return $Null$; /* *voiceCallRejected* */
    end if
  end if
end if
if ($flow_type == realTimeVideo$) **then**
  if (isNewFlow(*port, dst, src*)) **then**
    $\{\lambda_{mean}, \sigma_{var}, \Gamma_{peak}\}$ = getVbrPktRateTriplet();
    Υ_{slots} = getSlotsNeeded(λ_{mean});
    if ($\exists \Phi_{idle} \forall N_{hf} : \Phi_{idle} \in N_{ds}$ and $\Phi_{idle} \geq \Upsilon_{slots}$) **then**
      return Φ_{idle}+$peakSlotsReq$; /* $peakSlotsReq \in N_{vpeak}$ *with longer periodic reservation*/
    else
      return $Null$; /* *videoCallRejected* */;
    end if
  else
    δ_{Ql} = getQueueLength();
    if ($\delta_{Ql} > \delta_{vth}$ & $\exists \Phi_{idle} : \Phi_{idle} \in \{N_{ds}, N_{vpeak}\}$) **then**
      return $peakSlotsReq \in \Phi_{idle}$; /* *i.e, packets are coming towards* ($\lambda_{mean} + \sigma_{var}$) *or* Γ_{peak} */
    else
      Use reserved slots;
      return $Null$;
    end if
  end if
end if

mean (λ_{mean}), variance (σ_{var}), peak bit rate (Γ_{peak}) and the periodicity of I, P and B frames are considered in SDS, for each video call at the time of call establishment. For each video call, the slots required (Υ_{slots}) $\in N_{ds}$ for its λ_{mean}, are reserved along the E-to-E path. The importance of E-to-E delay analysis is detailed in [10], which is a precious factor for every packet in ensuring the QoS guarantee of an E-to-E video call. Also, from the Fig. 1, it is clearly appearing that the frame size of an I frame is very high compared to the other video frames, which however can lead to improper distribution of slots for a typical video call. As the slots allotted are based on the λ_{mean}, whenever an I frame is to be sent over the network, the allotted slots for that particular call are not enough for sending the whole I frame. This leads to an improper delay of an I frame at the receiver and may degrade the quality of the video, as the I frames are sent to provide the reliable reference for other frames. Since an I frame generates the Γ_{peak} bit rate, we model the problem as an I frame Peak bit Rate (IPR) problem. Also, we may face the IPR problem in the case of very high motion which gives very few matching macro blocks which in turn produces huge bit rate.

$$peakSlotsReq = (\Gamma_{peak} * F_d)/S_d \quad (2)$$

Therefore, we considered the periodicity of an I frame known as GOP, as an important factor in eliminating the IPR problem. Additionally, the motion (T_{mcwf}) present in the video, classified based on the DSAVC algorithm presented in [11], is also considered as a second parameter in controlling the Γ_{peak} bit rate. Allotting suitable slots for Γ_{peak} bit rate at the GOP interval or based on the motion present in the video achieves a good quality and also effective utilization of bandwidth. From the Equation (2), the slots required for sending Γ_{peak} bit rate, namely, $peakSlotsReq$ $\in N_{vpeak}$, is calculated. These $peakSlotsReq$ are used for every interval of $peakSlotPeriodicity$ which is determined based on the GOP and T_{mcwf} as shown in Equation (3). The weights $1/2 \leq \xi_1 \leq 1$ (ξ_1=1/2: if the motion is very less which does not require much bandwidth and ξ_1=1: if the motion in the video is peak stage, where the quality is highly dependent on the I frame) and ξ_2 are calculated using the motion present in the video, using DSAVC [11] algorithm.

$$peakSlotPeriodicity = \Phi(\xi_1.f(GOP), \xi_2.g(T_{mcwf})) \quad (3)$$

Initially, the $peakSlotsReq$ are used for every GOP. However, if the motion content is very less, the video call does not need much bandwidth and the Υ_{slots} goes underutilized. In this case, the reserved slots which are not used for transmission, called as $silenceSlots \in \Upsilon_{slots}$, are used for compensating the Γ_{peak} bit rate. Hence, the low motion video content eliminates the usage of $peakSlotsReq$. Further, these $silenceSlots$ are used to send the VBR data traffic (if the packets are experiencing more queuing delay i.e, $\delta_{Ql} > \delta_{dth}$). The data traffic is handled using the Best Effort (BE) service with idle slots from N_{ds} as shown in Fig. 3, without any slot reservation along the E-to-E path.

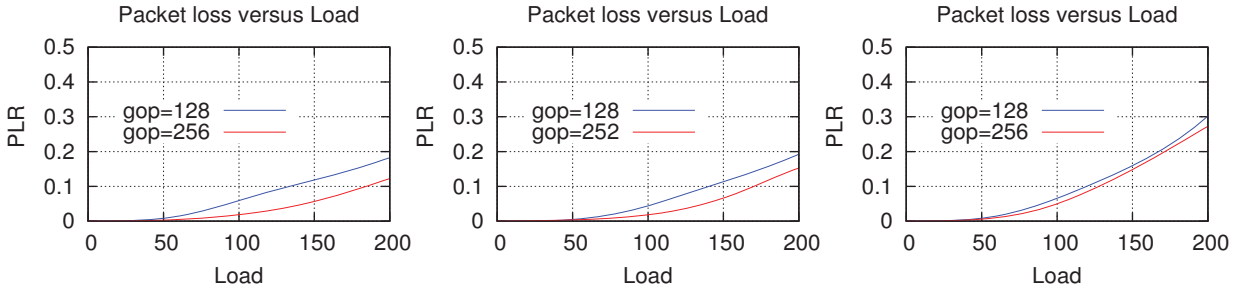

(a) ABR and CBR with 10 VBR flows (b) ABR and CBR with 20 VBR flows (c) ABR and CBR with 30 VBR flows

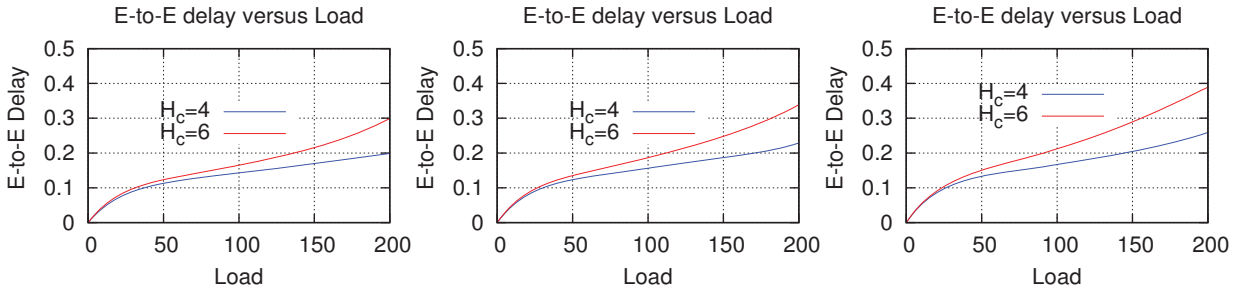

(d) ABR and CBR with 10 VBR flows (e) ABR and CBR with 20 VBR flows (f) ABR and CBR with 30 VBR flows

Fig. 4: **PLR and E-to-E delay variation of ASRIMA protocol with respect to Load (Average hop count of a flow is 6)**

V. Experimental Results

The performance of the protocol is investigated using Network Simulator-3 (NS-3) [12]. We customized NS-3 framework to support TDMA based MAC protocol. The simulation is performed by considering voice, data and video traffic in multiple scenarios. The voice source is considered as a CBR source, video source is considered as rt-VBR source and data traffic is considered as nrt-VBR source, and the slot distribution is performed according to the bit rate of the respective codecs. For transmitting the real time multimedia traffic over the network on NS-3, we used EvalVid, a framework for video transmission and quality evaluation, proposed in [13]. EvalVid evaluates the performance metrics of a video flow such as PSNR, PLR and E-to-E delay. The performance of the proposed protocol is studied by varying the GOP value of x264 video codec with respect to the PLR and the quality of the video. Also, as the performance of the protocols improves greatly with lower values of GOP, in the case of video flows, we experimented the protocol with different values of GOP for each video flow. Additionally, PLR, the E-to-E delay, CAR and throughput of the system for different types of flows, is also studied by varying the load and number of nodes. For all the experiments, we considered a $1Mbps$ link with parameters shown in Table I and 10x10 grid topology, later, we introduced mobility to investigate the performance of the protocol with respect to PLR and quality metric of video flows. For all the flows in the network, we considered the average hop count as 5 and with a hop count variance of 3.

We considered varied number of VBR video flows (10, 20 and 30) for evaluating the performance of the system combined with ABR or CBR flows. As shown in Fig. 4, as expected, the PLR and E-to-E delay changes according to GOP values and hop count respectively. From Fig. 4(a-c), it is observed that the packet loss is increasing with load as well as increase in the number of VBR video flows. The curve with GOP value 128, has higher average PLR values because of its frequent insertion of huge I frame bit rate, when compared to GOP value of 256. Also, from Fig. 4(d-f), as expected, the E-to-E delay is increasing gradually with respect to load as well as number of VBR video flows, and the average E-to-E delay with hop count (H_c) as 6, is always higher when compared to hop count as 4. The throughput of the ASRIMA protocol, as shown in Fig. 6, lies above the curve with IPR problem at almost every time frame. Here, due to the VBR traffic

TABLE I: **Simulation Parameters**

Slot information	Quantity
Number of Nodes	100
Number of Open slots	1
Number of Control slots	24
Number of Data slots	60
Open slot	100 μs
Control slot	100 μs
Data slot	625 μs
Frame duration	40 ms

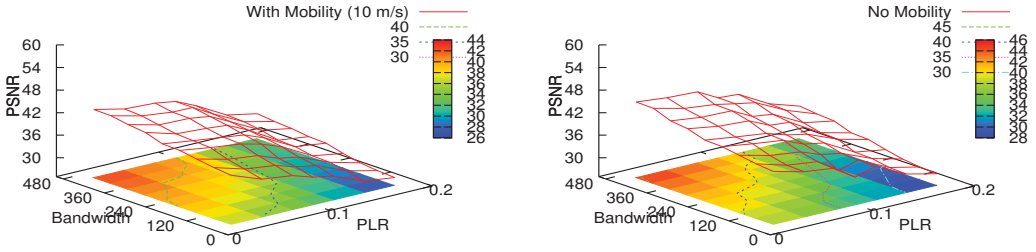

(a) No Mobility

(b) Mobility with 10m/s

Fig. 5: **VBR video flows performance: Average PSNR versus PLR and bandwidth**

induced by I frame packets, slot usage of the flow is varying over the time. By solving the IPR problem, ASRIMA protocol achieves deterministic throughput values. Additionally, we experimented the VBR video flows for evaluating the PSNR values with respect to PLR and bandwidth available at each node. In Fig. 5(a), the average PSNR values are more in the case of high bandwidth and low PLR values. The PSNR values falls below $30dB$, as the PLR value increases and bandwidth reduces. Further, as the PLR is more in the case of mobility, from Fig. 5(b), a greater fall of PSNR values is observed when compared with no mobility environment.

VI. Conclusion and Future Work

A cross layer traffic analysis should be considered as a crucial factor for QoS guarantees in TDMA based AWNs. In this paper, we studied integrated traffic support by solving the IPR problem in slot distribution of a TDMA protocol towards effective utilization of bandwidth. We experimented the system with flows such as ABR, CBR and VBR flows. From the experimental results, it is observed that the E-to-E delay is reduced marginally compared to previous algorithms. However, the PLR values and PSNR of the video flows are significantly improved. Further, the mobility environment gives poor results compared to static network, hence, the work could be extended for solving huge PLR due to mobile nodes in the network.

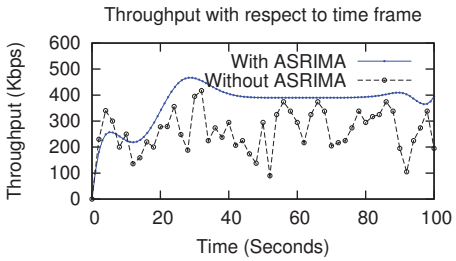

Fig. 6: **Throughput versus time frame**

References

[1] Sathaye, Shirish S. “ATM forum traffic management specification version 4.0.” In ATM Forum, pp. 95-0013. 1995.

[2] B. Bross, W.-J. Han, G. J. Sullivan, J.-R. Ohm, and T. Wiegand, “High Efficiency Video Coding (HEVC) Text Specification Draft 9”, document JCTVC-K1003, ITU-T/ISO/IEC Joint Collaborative Team on Video Coding (JCT-VC), Oct. 2012.

[3] V. Bharghavan, A. Demers, S. Shenker, and L. Zhang,“MACAW: A Media Access Protocol for Wireless LANs,” Proceedings of ACM SIGCOMM 1994, pp. 212-225, Au-gust 1994.

[4] B. S. Manoj and C. Siva Ram Murthy,“Real-Time Traffic Support for Ad Hoc Wireless Networks,” Proceedings of IEEE ICON 2002, pp. 335-340, August 2002.

[5] Reddy, T.B.; Manoj, B.S.; Murthy, C.S.R., “Multimedia traffic support for asynchronous ad hoc wireless networks,” Broadband Networks, 2004. BroadNets 2004. Proceedings. First International Conference on , vol., no., pp.569,578, 25-29 Oct. 2004.

[6] Li Yang, Han Zhiren, “A Quality of Service Supported Time Division Multiple Access Slot Assignment Protocol with Cross Layer Design,” Information Technology Journal, 11: 176-180, 2012.

[7] Byung Joon Oh; Chang Wen Chen, “A Cross-Layer Approach to Multichannel MAC Protocol Design for Video Streaming Over Wireless Ad Hoc Networks,” Multimedia, IEEE Transactions on , vol.11, no.6, pp.1052,1061, Oct. 2009.

[8] Hershey, P.C.; Davidson, S.A.; Mu-Cheng Wang, “Real-Time Communications Resource Allocation Process, Architecture, and Algorithm,” Military Communications Conference, MILCOM 2013 - 2013 IEEE , vol., no., pp.1482,1487, 18-20 Nov. 2013.

[9] Yu-Kwong Kwok; Lau, V.K.N., “A quantitative comparison of multiple access control protocols for wireless ATM,” Vehicular Technology, IEEE Transactions on , vol.50, no.3, pp.796,815, May 2001.

[10] Vergados, D.J.; Koutsogiannaki, M.; Vergados, D.D.; Loumos, V.; Pantazis, N., “Enhanced End-to-End TDMA for wireless ad-hoc networks,” Computers and Communications, 2007. ISCC 2007. 12th IEEE Symposium on , vol., no., pp.MW - 39,MW - 44, 1-4 July 2007.

[11] Dasari, M.; Sindhwal, H.; Vattikuti, N., “Efficient content-based dynamic search algorithm for motion estimation from videos,” Advances in Computing, Communications and Informatics (ICACCI, 2014 International Conference on , vol., no., pp.1004,1008, 24-27 Sept. 2014.

[12] Riley, George F., and Thomas R. Henderson. “The ns-3 network simulator.” Modeling and Tools for Network Simulation. Springer Berlin Heidelberg, 2010. 15-34.

[13] Abdel-Hady, M.; Ward, R., “A Framework for Evaluating Video Transmission over Wireless Ad Hoc Networks,” Communications, Computers and Signal Processing, 2007. PacRim 2007. IEEE Pacific Rim Conference on , vol., no., pp.78,81, 22-24 Aug. 2007.

THE 18TH INTERNATIONAL SYMPOSIUM ON WIRELESS PERSONAL MULTIMEDIA COMMUNICATIONS
(WPMC-2015)
December 13-16, 2015, Hyderabad, India

Novel Closed form Expression for Multi Cell Cooperation using MHCP to Reduce Interference

Suman Yadav[1]
Dept. of ECE
G.C.E.T.
Greater Noida, India
e-mail : sumanyadav0808@gmail.com

S Pratap Singh[2]
Dept. of ECE
G.C.E.T
Greater Noida, India
e-mail : erspratap@gmail.com

Abstract- **Ever going need of data rate and coverage can be achieved by mitigating the impairment of wireless communication system. Interference is most challenging impairment of wireless. Multi cell cooperation (MCC) is one the technique to mitigate the inter cell interference. In this paper, stochastic geometry approach is used to analyse cooperation between MCC. The positions of Base Stations (BSs) follow Matérn Hardcore Point Process (MHCP) distribution. Specifically, we derive upper and lower bounds expressions of the CCDF of SIR for MHCP distribution of base station over Chi square fading following stochastic geometry approach. To validate our model, we compare the CCDF of SIR of the Matérn hardcore topology with [6] where, a Poisson Point Process (PPP) distribution is taken in place of MHCP.**

***Key words*: MHCP, channel state information, beam forming**

I. INTRODUCTION

Base station (BS) coordination allows the cooperation among neighboring cells to improve coverage, cell-edge capacity, and/or spectral efficiency [1].The most popular approach used in modeling the BSs topology is the hexagonal grid model however these models do not accurately captures the real BSs topology and also they are not friendly to analysis. The most common information theoretic downlink model for cellular networks is the Wyner Model [2] due to its mathematical manageability. However, it is a simplified one dimensional model that sets the Signal-to-Interference ratio (SIR) as a constant. The recent witnessed evolution of cellular networks from a carefully planned deployment to more irregular, heterogeneous deployments of Macro, Pico and Femto-BSs makes the hexagonal and regular deployment models of limited utility. Which, in turn, motivates recent studies, tools and results inspired by stochastic geometry to capture the real deployment as accurately as possible. There has been growing recent interest in the use of stochastic geometry [3] to describe wireless networks. In the past ten years, stochastic geometry and related techniques have been applied and adapted to cellular systems, cognitive radio, relay networks, and many other types of wireless systems since classical methods of communication theory are generally insufficient to analyze these new types of networks. We consider the downlink of a network whose topology is modeled through stochastic geometry. For downlink topology, there are two different approaches namely, joint processing (JP) and coordinated beam forming (CB) [4]. In CB, user scheduling and beam forming are dynamically coordinated among neighboring BSs, which reduces the interference among different transmissions as well as increases the desired signal strength. Most of the stochastic geometry work on cellular networks concentrate on the case where the BS deployment follows a Poisson point process (PPP) in which the points are independent which considerably simplifies the analysis [5]. However, this is not the reality since the BSs locations are not totally independent in real cellular networks. We simplify the independent PPP analytical framework in [6] to a Matérn Hardcore Point Process (MHCP) [7], [8] which retains a minimum distance between BSs in an attempt to capture real deployments.

The remainder of the paper is organized as follows. Section II describes the proposed model for the considered MHCP scheme. The expressions are derived for the CCDF of SIR in Section III. In Section IV, we provide our numerical results. Finally, in Section V conclusions are drawn.

II.SYSTEM MODEL

We model the BS locations of a cellular network as a MHCP which is a variation of the independent PPP. A MHCP guarantees minimum distance r between BS deployment locations. In this paper, we consider a mathematically tractable type of the point processes, namely the MHCP ϕ_m of intensity λ_m and a minimum distance r between BSs. An MHCP process is generated by a dependent thinning of a stationary Poisson point process as follows:

1) A PPP ϕ_P is generated with density λ_P.

2) For each point $x \in \phi_P$ associate a mark $m_x \sim U[0,1]$ independent of any other point.

3) A point x is retained in ϕ_m if it has the lowest mark compared to all points in B(x,r) i.e. a circle centered at x with radius r.
The probability of an arbitrary point x is retained in ϕ_m is given by:

$$p = \frac{1-\exp\left(-\lambda_p \pi r^2\right)}{\lambda_p \pi r^2} \quad (1)$$

The density of the MHCP ϕ_m is $\lambda_m = p\lambda_p$, i.e.

$$\lambda_m = \frac{1-\exp\left(-\lambda_p \pi r^2\right)}{\pi r^2} \quad (2)$$

We assume that the mobile users' spatial distribution follows an independent homogeneous PPP and is connected to the nearest BS. Hence, the base stations downlink coverage areas are Voronoi tessellations. We assume the standard path loss propagation model with path loss exponent β and assume that the channel between the mobile user and the attached BS fading distribution varies according to Chi square. Moreover, since the MHCP is a stationary PP we can assume without loss of generality that the user is located at the origin.

We consider a cellular network consisting of K BSs, each equipped with N_t antennas. In dynamic clustering technique each user communicates with the K nearest BS and the set of users' locations that can be served by their K nearest BS is defined by the notion of the Kth-order Voronoi tessellation denoted by v_k. To guarantee separate encoding at each BS, an information symbol s_k (intended for the kth user) is transmitted by the kth BS through a linear beamforming vector $v_k = [v_k^1, v_k^2, \ldots, v_k^{Nt}]^T$ with unit norm $\| v_k \|$.

Our system model is illustrated in Fig.1, where r is the minimum distance between the mobile user and the serving BS at point y, v is the distance between the serving BS and any interfering BS at point x on the plane, R is the distance between the mobile user and any interfering BS at point x. Thus, the received power for a typical mobile user 1 at a distance r from the attached BS is

$$|h_{1,1}\, v_1|^2 \, \|r\|^{-\beta}$$

Where $[h^2_{1,k}, h^2_{1,k}, \ldots h^N_{1,k}] \in C^{1 \times Nt}$ represents the downlink channel between the kth BS and the user with entries that are independent and identically distributed (IID) with complex Gaussian random variables having zero mean and unit variance. The transmit power at each BS satisfies

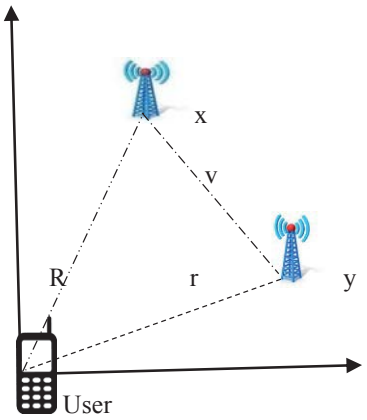

Fig.1 System Model

$E[|s_k|^2] \leq P$. Now the interference power I_k is defined as the sum of received powers from the interfering BSs which is given by

$$\mathrm{I_k} = \sum_{k=K+1}^{\infty} \left| h_{1,k} v_k \right|^2 \|R\|^{-\beta} \quad (3)$$

Hence, the corresponding SIR for the user 1 at origin is

$$SIR(K, N_t, \beta) = \frac{\left| h_{1,1} v_1 \right|^2 \|r\|^{-\beta}}{I_K} \quad (4)$$

The outage probability is defined as the probability that a typical mobile user is able to achieve some threshold SIR, denoted by γ. Hence, outage probability is the CCDF of the SIR for a typical mobile user i.e.

$$F_{SIR}(K, N_t, \beta; \gamma) = P\left[SIR(K, N_t, \beta) \geq \gamma\right] \quad (5)$$

$$P\left[SIR(K, N_t, \beta) \geq \gamma\right] = E\left[P\left[\frac{\left| h_{1,1} v_1 \right|^2 \|r\|^{-\beta}}{I_K} \geq \gamma \;\middle|\; \|r\|, I_K \right] \right] \quad (6)$$

Our aim is to characterize the outage probability under a MHCP process for which we have to derive the MHCP distance distribution.

MHCP Distance Distribution

In our model, we assume that a mobile user connects to the nearest BS. Thus, if a mobile user is at a distance r from the attached BS, then there is no interfering BS that is closer than r to the mobile user. The probability density function (PDF) of r is the distance distribution of underlying MHCP

with intensity λ_m is given by

$$f(r) = 2\pi r\lambda_m\left(\exp\left(-\lambda_m\pi r^2\right)\right) \quad (7)$$

Now to calculate this we have to derive the pdf of *r* which is given by

P [No BS is closer than *r*] = P [$N_m(B(0,r))=0$]

Here, $N_m(B(0,r))$ is the no. of points in a circle B(0,r) centered at the user at origin with radius *r* in a MHCP. Therefore,

$$P[N_m(B(0,r))=0]=\sum_{K=0}^{\infty} P[N_p(B(0,r))=K]\times$$
P [K points are eliminated in MHCP]

Where, $N_p(B(0,r))$= no. of points in B(0,r) in PPP.
Now,

$$P[N_p(B(0,r))] = \sum_{K=0}^{\infty}\frac{e^{-\lambda_p\pi r^2}(\lambda_p\pi r^2)^K}{K!}$$

P [K points are eliminated] $\approx (1-p\ )^K$

$$=\left(1-\left(\frac{\lambda_m}{\lambda_p}\right)\right)^K$$

$$P[N_m(B(0,r))] = \sum_{K=0}^{\infty}\frac{e^{-\lambda_p\pi r^2}((\lambda_p-\lambda_m)\pi r^2)^K}{K!}$$

$$P[N_m(B(0,r))] \approx e^{-\lambda_m\pi r^2}$$

Now pdf of *r* is given by

$$f(r) = \frac{d}{dr}\left(1-P\left(N_m\left(B(0,r)\right)\right)=0\right)$$

$$f(r) = 2\lambda_m\pi r\left(\exp\left(-\lambda_m\pi r^2\right)\right) \quad (8)$$

III.CCDF OF SIR

To characterize the coverage probability in terms of *K*, N_t and β we utilize a general characterization in integral form given by [6, Theorem 1]. The CCDF of the SIR can be written as

$$P\left[\frac{H_1 r^{-\beta}}{I_r}\geq\gamma \mid R\right] = P\left[H_1\geq r^{\beta}\gamma I_r \mid R\right] \quad (9)$$

Using [6, lemma 4] and applying binomial expansion we get

$$P[H_1 > x] = 1-P[H_1\leq x]$$

$$P[H_1 > x] = 1-(1-e^{-lx})^M$$

$$P[H_1 > x] = \left[\sum_{m=1}^{M}\binom{M}{m}(-1)^{m+1}(e^{-lxm})\right] \quad (10)$$

Putting (10) in (9) the conditional CCDF is upper bounded by

$$P\left[H_1\geq r^{\beta}\gamma I_r \mid R\right]\leq\sum_{m=1}^{M}\binom{M}{m}(-1)^{m+1}E\left[e^{-mlr^{\beta}I_r} \mid R\right] \quad (11)$$

Where, M =N_t-K+1 and l= $(M!)^{-1/M}$, and the expectation is over the distribution of I_r. Now CCDF can be written as

$$F_{SIR}^{c}(K,N_t,\beta;\gamma) = E\left[P\left[SIR(K,N_t,\beta)\geq\gamma \mid R\right]\right]$$

$$F_{SIR}^{c}(K,N_t,\beta;\gamma) \leq \sum_{m=1}^{M}\binom{M}{m}(-1)^{m+1}E\left[E\left[e^{-lmr^{\beta}\gamma I_r} \mid R\right]\right] \quad (12)$$

With inner and outer expectations over the distributions of I_r and R respectively. We first calculate the conditional Laplace transform of I_r to evaluate these expectations,

$$L_{I_r}(s) = E\left[e^{-sI_r} \mid R\right] \quad (13)$$

$$L_{I_r}(s) = E\left[\prod_{R\in\phi/B(0,r)} e^{-sH_k\|R\|^{-\beta}} \mid R\right] \quad (14)$$

$$L_{I_r}(s) = E\left[\prod_{R\in\phi}\frac{1}{1+s\|R\|^{-\beta}} \mid R\right] \quad (15)$$

$$L_{I_r}(s) = \exp\left(-\lambda_m\int_{R^2}\frac{1}{1+s^{-1}\|R\|^{\beta}}dR\right) \quad (16)$$

$$L_{I_r}(s) = \exp\left(-2\pi\lambda_m\int_{r}^{\infty}\frac{R}{1+s^{-1}R^{\beta}}dR\right) \quad (17)$$

Where (14) follows from the independence of R and H_k, (15) holds because H_k is exponentially distributed and unit mean, and (16) follows from the probability generating functional of the PPP [9].

Evaluating (17) at s=mlγr^{β} we will get

$$L_{I_r}\left(ml\gamma r^{\beta}\right)=\exp\left(-2\pi\lambda_m\int_r^{\infty}\frac{R}{1+(ml\gamma)^{-1}(R/r)^{\beta}}dR\right) \quad (18)$$

$$L_{I_r}\left(ml\gamma r^{\beta}\right)=\exp\left(-\pi\lambda_m r^2(ml\gamma)^{2/\beta}\int_{(ml\gamma)^{-2/\beta}}^{\infty}\left(\frac{dv}{1+v^{\beta/2}}\right)\right) \quad (19)$$

$$L_{I_r}\left(ml\gamma r^{\beta}\right)=\exp\left(-\pi\lambda_m r^2 D(ml\gamma,\beta)\right) \quad (20)$$

Where (19) follows from change of variable $v=\left[\left(\frac{1}{ml\gamma}\right)^{1/\beta}\frac{R}{r}\right]^2$ and (20) follows because of

$$D(ml\gamma,\beta)=(ml\gamma)^{2/\beta}\int_{(ml\gamma)}^{\infty}\frac{1}{1+v^{\beta/2}}dv \quad (21)$$

$$D(ml\gamma,\beta)=\frac{2}{\beta-2}(ml\gamma)\,{}_2F_1\left(1,\frac{\beta-2}{\beta},2-\frac{2}{\beta},-ml\gamma\right) \quad (22)$$

Where (22) follows by using [5] which is gauss hypergeometric function.

Now to evaluate the outer expectation of (12)

$$E\left[L_{I_r}\left(mlr^{\beta}\gamma\right)\right]=\int_{r>0}L_{I_r}\left(ml\gamma r^{\beta}\right)f(r) \quad (23)$$

$$E\left[L_{I_r}\left(mlr^{\beta}\gamma\right)\right]=\int_{r>0}\exp\left[-\pi\lambda_m r^2(D(ml\gamma,\beta)+1)\right](2\lambda_m\pi r)dr \quad (24)$$

$$E\left[L_{I_r}\left(mlr^{\beta}\gamma\right)\right]=\int_0^{\infty}\frac{e^{-x}dx}{2\pi\lambda_m r}\left(\frac{2\pi\lambda_m r}{[1+D(ml\gamma,\beta)]}\right) \quad (25)$$

$$E\left[L_{I_r}\left(mlr^{\beta}\gamma\right)\right]=\frac{1}{[1+D(ml\gamma,\beta)]} \quad (26)$$

Here (24) will be obtained by putting (7) and (20) in (23), where (25) follows from variable change $x=\pi\lambda_m r^2[1+C(ml\gamma,\beta)]$. If K=1 and N_t=1 then the above equation reduces to the case of PPP where there is no coordinated beamforming. By putting (26) into (12) we finally obtain the upper bound

$$F_{SIR}^{c,U}(K,N_t,\beta;\gamma)\le\left[\sum_{m=1}^{M}\binom{M}{m}\frac{1}{[1+D(ml\gamma,\beta)]}\right] \quad (27)$$

and by putting l=1 in this equation the lower bound of the CCDF of SIR will be obtained.

When N_t=K then the upper and lower bound will coincide, from which we obtain the exact CCDF.

$$F_{SIR}^{c}(K,K\ ,\beta;\gamma)=\left[\frac{1}{[1+D(\gamma,\beta)]}\right] \quad (28)$$

IV.NUMERICAL RESULTS

In this section numerical analysis of different closed form expressions are presented. In Fig. 2, when both no. of transmit antennas and no. of base stations is equal to 1 (i.e. N_t =K=1) then PPP and MHCP overlap with each other. After that we have compared proposed CCDF of SIR of equation (28) for different values of K and path loss exponent β=4, which is a standard value in terrestrial outdoor wireless systems, for this case $D(\cdot,\cdot)$ reduces to

$$D(\zeta,4)=\sqrt{\zeta}\,arc\cot\left(\frac{1}{\sqrt{\zeta}}\right)$$

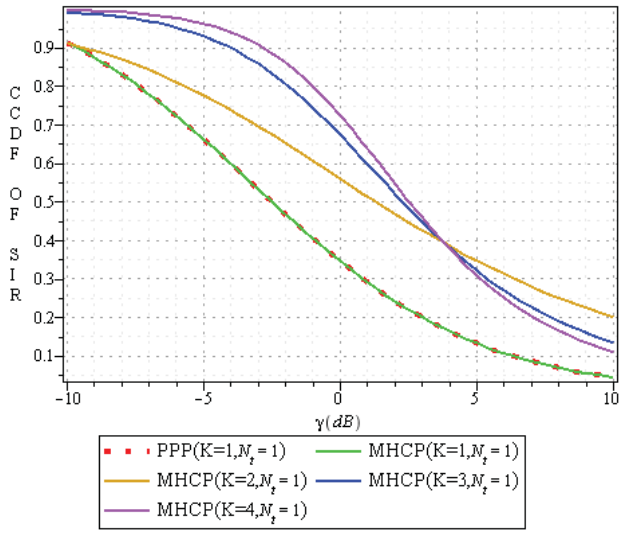

Fig. 2. CCDF of SIR of β=4 and different no. of BS

It can be noticed from Fig. 2 that as the value of *K* increases SIR of MHCP process improves.

In Fig. 3 the equation (27) for different values of transmit antennas exactly matches the exact CCDF over the entire range of SIRs of interest which clearly shows the benefits of having N_t antennas.

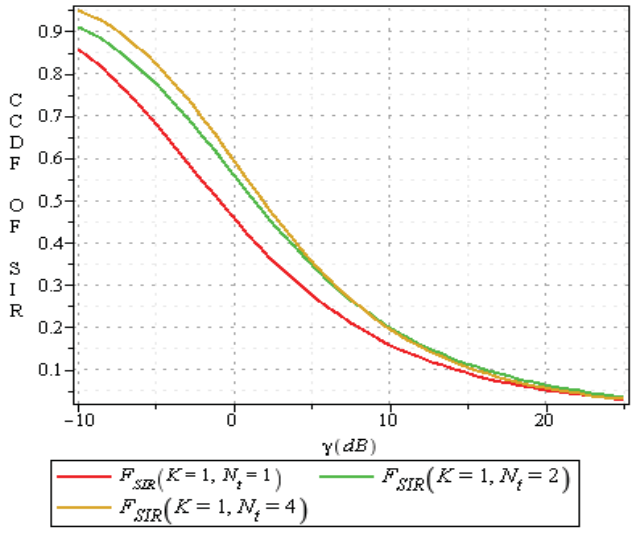

Fig. 3. CCDF of SIR of proposed model, β=4 and different number of transmit antennas

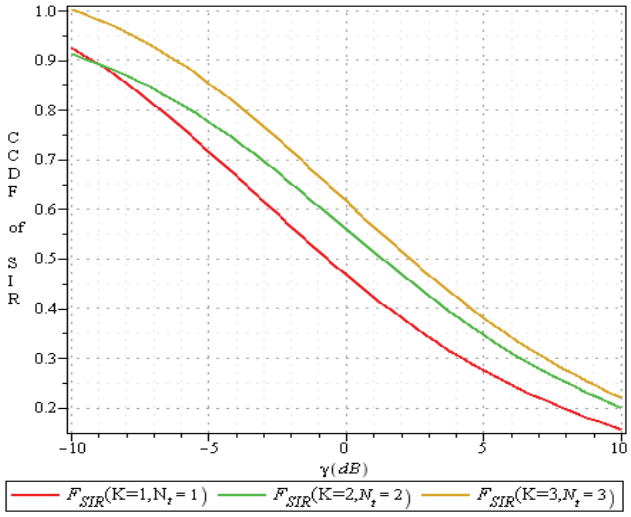

Fig. 4: CCDF of SIR of proposed model for β=4 and N_t =K

In Fig. 4 with coordinated beamforming and N_t =K the performance is simply characterized by the expression in (28), when N_t=K=2 and β=4, the SIR of MHCP improves upto γ=10dB

V.CONCLUSIONS

We presented a stochastic geometry formulation using the Matérn hardcore spatial point process to model the MCC in cellular networks. Basically, we novel closed form expression for CCDF is derived for MCC using stochastic geometry approach. In [6, 8 and 9] PPP distribution for BS distribution is assumed. However, in this paper MHCP is used in place of PPP. Also, expressions for upper and lower bounds for CCDF of SIR are presented. The results are compare with available literature; showing perfect agreement. Further, work may be extended to derive closed form expressions of the coverage probability and Ergodic capacity.

REFERENCES

[1] F. R. Farrokhi, A. Lozano, G. J. Foschini and R. A. Valenzuela "Spectral Efficiency of Wireless Systems with Multiple Transmit and Receive Antennas," *Personal, Indoor and Mobile Radio Communications, (PIMRC 2000), 11th IEEE International Symposium*, Sep 2000

[2] J. Xu, J. Zhang, and J. G. Andrews, "On the accuracy of the Wyner model in downlink cellular networks," *IEEE Trans. Wireless Communications*, vol. 10, pp. 3098 - 3109, Sep. 2011

[3] Martin Haenggi, Jeffrey G. Andrews, Francois Baccelli, Olivier Dousse, and Massimo Franceschetti, "Stochastic Geometry and Random Graphs for the Analysis and Design of Wireless Networks," *IEEE J. Select. Areas Commun.*, Sep. 2009

[4] Ya-Feng Liu*y*, Yu-Hong Dai*y*, and Zhi-Quan Luo*z*, "Coordinated Beamforming for MISO Interference Channel: Complexity Analysis and Efficient Algorithms," *Signal Processing, IEEE Transactions on* (Volume:59 , Issue: 3)

[5] J. G. Andrews, F. Baccelli, and R. K. Ganti, "A tractable approach to coverage and rate in cellular networks," *IEEE Transactions on Communications*, vol. 59, no. 11, pp. 3122–3134, 2011

[6] Namyoon Lee, David Morales-Jimenez, Angel Lozano, and Robert W. Heath Jr, "Spectral Efficiency of Dynamic Coordinated Beamforming: A Stochastic Geometry Approach," *International Conference in Communications (ICC'14)*

[7] Abdelrahman, M. Ibrahim, Tamer ElBatt2 , Amr El-Keyi, "Coverage Probability Analysis for Wireless Networks Using Repulsive Point Processes," *2013 IEEE 24th International Symposium on Personal, Indoor and Mobile Radio Communications: Fundamentals and PHY Track*

[8] Kaibin Huang and Jeffrey G. Andrews, "An Analytical Framework for Multi-Cell Cooperation via Stochastic Geometry and Large Deviations," *IEEE Globecom 2011 and IEEE Intl. Conf. on Communications 2012*.

[9] Anastasios Giovanidis and Franc¸ois Baccelli, "A Stochastic Geometry Framework for Analyzing Pairwise-Cooperative Cellular Networks," *Wireless Communications, IEEE Transactions on (Volume:14 , Issue: 2)*

THE 18TH INTERNATIONAL SYMPOSIUM ON WIRELESS PERSONAL MULTIMEDIA COMMUNICATIONS
(WPMC-2015)
December 13-16, 2015, Hyderabad, India

Intrusion Detection System Against Colluding Misbehaviour in MANETs

Pragya Mishra, K V Arya, Hardev Singh Pal
ABV-Indian Institute of Information Technology and Management, Gwalior-474015, India.
Email: pragya20691@gmail.com, kvarya@iiitm.ac.in, hardevsingh111@gmail.com

***Abstract*—Routing protocol of MANET works with the presumption that nodes will transmit the data in collaboration. This presumption is a limitation of routing protocol which gives an occasion to attackers to hinder the security of the device and data in the network. Therefore, it becomes vital to develop methods and systems which will ensure the safety, integrity and confidentiality of data in such devices and systems. Although, existing IDS are able to detect various types of attack but some misbehaviour goes undetected which potentially damage the network. Collusion attack is one such misbehaviour where nodes perform maliciously in collaboration with neighbouring nodes without being detected. In this work, Intrusion detection algorithm has been proposed that can effectively detect and isolate colluding nodes from the network so that these malicious nodes do not affect the performance of the network. Proposed detection algorithm uses in-out traffic information and overhearing statistics of nodes to identify colluding attackers. Detection algorithm works successfully for DSR routing protocol. Experimental results on NS-2 show that the proposed algorithm is capable of reducing the packet drops consequently improving the throughput of the network in presence of collusion attack.**

***Index Terms*—Mobile Ad hoc Network (MANET), Intrusion Detection System (IDS), Collusion, Misbehaviour.**

I. Introduction

A Mobile Ad hoc Network (MANET) is a self-coordinating, self-designing wireless network, where the nodes are responsible for creation, operation and maintenance of the network. Mobile system or nodes or device in the mobile ad-hoc network has a freedom for entry or exit from the network as discussed in review [1]. Trusted and co-operative behaviour of mobile nodes helps in the communication of mobile nodes in the MANET. Establishment and maintenance of connections between mobile nodes can be done with the help of existing routing protocol which have not been designed keeping security issues in mind.

The charactestics of mobile ad hoc networks raises many challenges to the security design. The main problem that hinders the security of MANET is that, it is easy for malicious attackers to reach the ad-hoc network. This is possible because of no physical protection to mobile nodes, also packets are forwarded with the assumption that nodes in the network are cooperative. This facilititate attackers to capture and compromise nodes to spoil the network security. With the increase of vulnerabilities in MANETs, raise the need of efficient and effective intrusion detection system (IDS) that indentify as well as neutralize the attacks. B. Sun [2] has demonstrated that Intrusion detection in mobile ad hoc networks is a difficult and complicated task due to the very nature of MANETs. Many IDSs are designed especially for MANETs to find out selfish or malicious nodes in the network.

In this paper, a security threat where neighbouring nodes perform malicious activity in collaboration is analyzed. Based on analysis an intrusion detection algorithm is proposed which can detect misbehaviour carried out by the collaborating neighbouring nodes.

The rest of the paper is organised as follows. Section II discusses about existing acknowledgement based IDS that how they perform against malicious activity. Section III describes collusion attack. In Section IV Intrusion detection algorithm have been proposed for detecting colluding nodes. Section V shows performance analyses of proposed detection algorithm. Finally the paper is concluded in Section VI.

II. Related Work

Transmission in MANET take place with the supposition that nodes in the network always collaborate with each other to transmit the data. This supposition makes an easy way for attackers to cause potential damages in the network by compromising one or two nodes. In order to conquer over this damage IDS is designed to intensify the safety of MANETs. Marti et al. [3] have proposed Watchdog and Pathrater techniques for mitigating the routing misbehaviour in MANETs. A Watchdog keeps an eye on the transmission of the next hop for identifying misbehaving nodes. A Pathrater then calculates the routes which avoids the misbehaving nodes. Watchdog technique is used to detect misbehaviour at the forwarding level. But this scheme fails to detect misbehaving nodes in the presence of 1) ambiguous collision, 2) receiver collisions, 3) limited transmission power, 4) false misbehaviour, 5) collusion, and 6) partial dropping.

TWOACK proposed by Liu et al. [4] is one of the approach in order to solve issues of Watchdog technique. Balakrishnan et al. [6] given a function of TWOACK to detect misbehaving links by sending a TWOACK packet for every data packet transmitted over every three consecutive nodes along the path from the source to the destination. The TWOACK scheme is able to solve the receiver collision and limited transmission power problem of Watchdog but with the disadvantage of increase in network overhead. Also there will not be any missed detections in the TWOACK scheme unless collusions between two neighbouring misbehaving nodes exist.

Pragya Mishra is M.Tech student at ABV-IIITM Gwalior, India and Dr. K V Arya is Associate Professor at ABV-IIITM Gwalior, India.

Sheltami et al. [5] proposed a hybrid scheme of TACK similar to TWOACK and end-to-end acknowledgement (ACK) scheme called AACK. AACK scheme has reduced network overhead than in TWOACK because of employing ACK scheme. As it employs TWOACK scheme so it can resolve limited transmission and receiver collision problem. AACK is able to detect misbehaving nodes but misbehaviour due to colluding attack described by Kannhavong et al. [12] is not taken into account. TWOACK and AACK suffer with the problem of false misbehaviour report.

Shakshuki et al. [7] designed EAACK to tackle false misbehaviour, limited transmission power and receiver collision problem of Watchdog scheme. It is comprised of mainly three schemes, namely, ACK, secure ACK (S-ACK), and misbehaviour report authentication (MRA). EAACK is an acknowledgement-based IDS which trust acknowledgement packets to detect malicious activity in the network. Digital signature approach is adopted to fortify integrity of IDS by sending out digitally signed acknowledgement packet. With the help of digital signature EAACK is able to authenticate false misbehaviour report. However, EAACK still suffers with the problem of collusion and partial droping.

Ghosh et al.[11] has given a mechanism to isolate malicious nodes trying to misbehave in collusion with other malicious nodes and presented a mechanism which successfully works for AODV protocol in MANET. Kannhavong et al.[12] has presented a model of collusion attack against Optimized link state routing protocol (OLSR). Simple detection mechanism has been demonstrated to detect attack but results contradicts due to frequent change in network topology. So, these techniques are not able to profitably works for existing acknowledgement based IDSs agsinst collusion. Since, these IDSs are designed over dynamic source routing (DSR) protocol. In this paper, we are designing detection algorithm against collusion attack which auspiciously works for dynamic source routing (DSR) protocol.

III. Problem Definition

The problem with existing acknowledgement based IDS like watchdog, TWOACK, AACK and EAACK is that they lack to perform well if attack occurs due to collaborative malicious nodes. Although, these IDS contributes to increase the network performance by detecting and isolating malicious nodes but fails to detect misbehaviour which occurs in collaboration of neighbouring nodes.

Consider a scenario presented in Fig. 1. Source node S sends a Packet1 to node n1 then n1 forwards this packet to n2. Since, n2 is two hop away from S it redirects S-ACK packet to S following the reverse path and forwards Packet1 to n3. By receiving S-ACK from n2, S is ensured that till node n2 there is no misbehaviour. Now, n3 is two hops away from n1 so it has to redirect S-ACK packet to n1. Node n1 is assured that there is no misbehaviour till now. But n3 instead of forwarding Packet1 further it drops the packet which n2 knows but it hides the misbehaviour of n3 and does not generate any misbehaviour report. So it is found that n2 and n3 performs malicious activity in collusion. But this goes undetected by node S. So, this how neighbouring nodes help each other in hiding their illegal actions and hamper the security of the network.

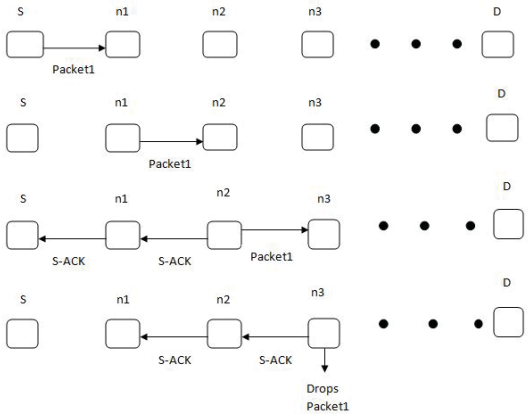

Fig. 1. Scenario presenting misbehaviour in collusion

IV. Proposed Scheme

The proposed scheme consist of two phases namely attack model and detection of attack which are described below.

Attack Model - In our system, threat occurs only when two or more nodes trying to collude with each other to simply drop the packets. These colluding nodes cooperate in the DSR Route Discovery and Route Maintenance phases, but decline to relay data packets further in the network. For example, In Fig. 2, misbehaving node n3 drops the packet rather than forwarding it to next hop with the help of node n2. Node n2 hides the misbehavior of node n3 by not reporting the misbehaviour of n3 to source node S . Node n3 upon receiving packet sends S-ACK packet to n1 through n2. Receipt of S-ACK from n3 makes n1 assured that there is no misbehaviour. This is how n2 and n3 misbehaves in collaboration.

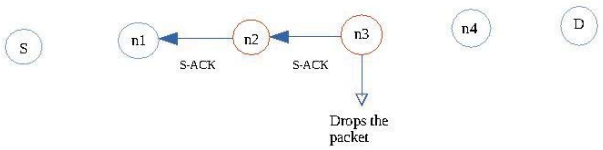

Fig. 2. Attack Model

It is required for the nodes to be in transmission range of one another in oder to collude, otherwise they have to collude through a third party. Generally, compromised neighbouring nodes are responsible to occur collusion. A node is said to be compromised when it is captured and manipulated by an attackers. Thus, when two nodes in the same neighborhood are compromised, they may be manipulated to collude. As a result of collusion, colluding misbehaving nodes hide illegal actions of each other and hamper the security of the network. A colluding attack occurs when two or more selfish or malicious nodes collaborate and gain access to certain information that

they are not authorized to have by secretly sharing their knowledge to simply destroy the secure connection in the network.

Detection of attack - In DSR protocol, source node S has information of all the routes hop-by-hop to the destination. An arrangement of continuos nodes n_i, n_{i+1}, n_{i+2},....n_k on the path from source to destination D are acting as colluding adversaries. Here promiscuous listening mode is utilized which obliges that every node keeps up the details of the sending conduct of its neighbouring nodes. Every node keeps up the data about the packets which it gets notification from its neighbour by incorporating the id of the neighbour node furthermore the timestamp at which the packet was overheard. Procedure DETECT_COLL_ATCK describes the details of the procedure adopted for identifying the colluding nodes.

Algorithm 1 DETECT_COLL_ATCK(Source S, Destination D)

Step 1: S sends random audit packet to random selected node n_i
Step 2: Node n_i sends in-out traffic T_i to S
Step 3: S sends the same audit packet to the successor node n_{i+1}
Step 4: Node n_{i+1} sends in-out traffic T_{i+1} to S
Step 5: S checks T_i and T_{i+1} and calculate threshold value

Th_i = [(no. of pkt send by S - no.of pkt received by n_i)/ no.of pkt send by S]*100

Th_{i+1} = [(no. of pkt send by S - no.of pkt received by n_{i+1})/ no.of pkt send by S] *100
Step 6: If ($Th_{i+1} >= 30\%$), is true then check threshold value of node n_i
Step 7: If ($Th_i >= 30\%$), is true then recurse the algorithm beacuse colluding adversaries present downstream ni

DETECT_COLL_ATCK(S, n_{i-1})
Step 8: Check n_{i-1} and n_i overhearing statistics If no packet is overheard at both n_{i-1} and n_i then n_i and n_{i-1} suspected.
Step 9: Else if ($Th_{i+1} < 30\%$), is true then recurse the algorithm because colluding adversaries present upstream n_i

DETECT_COLL_ATCK(n_{i+1}, D)
Step 10: Else, No colluding adversaries found

Algorithm finds out colluding adversaries if any in path segment from source to destination by checking in-out traffic of nodes and their overhearing statistics. As soon as colluding attackers detected these nodes are kept in isolation from the network so that they further not effect. The proposed intrusion detection algorithm is able to acheive network security through identifying and removing colluding attackers from the network. When colluding attackers are removed from the network the packet loss will be reduced and destination nodes will be able receive packets successfully.

V. Performance Evaluation

A. Simulation Configuration

Simulation has been done to test the performance of a network in the presence of colluding adversaries on NS-2.35 simulator. In Table I, simulation parameters are given on which simulation is performed for network size of 50, 100, 150 nodes with variable number of colluding nodes. In the simulations, a colluding node is the one that agrees to participate in forwarding packets but then indiscriminately drops all data packets that are routed through it. The percentage of the network comprised of colluding nodes is varied from 0% to 40% in step of 10%.

TABLE I
Simulation Parameters

Parameter	Values
Simulator	NS-2.35
Processor	CORE i3
RAM	4 GB
Environments size	700*700
Simulation time	100 seconds
Transmission range	250m
No. of nodes	50,100,150
Mobility speed	20m/s
Traffic type	CBR
Data payload	512 bytes

B. Experimental Results

Simulation has been done for two scenarios of collusion attack in presence and absence of detection algorithm for four performance parameters packet delivery ratio, routing overhead, throughput and average end-to-end delay described in [7] against different percentage of colluding nodes for 50, 100 and 150 nodes in NS-2.35 network simulator. By evaluating the packet delivery ratio from Fig. 3, Fig. 4 and Fig. 5 for 50, 100 and 150 nodes respectively in absence and presence of detection algorithm against 10% to 40% colluding nodes; PDR in presence of detection algorithm is higher than the PDR in absence of detection algorithm, because as soon as detection algorithm encounters the nodes misbehaving in collaboration, it report such nodes as malicious. With the increase in percentage of colluding attackers in the network, PDR acheived with detection algorithm is decreasing but with lesser rate than that of PDR acheived without detection algorithm. As the size (number of nodes) of the network is increasing, packet delivery ratio are not as much expected for both scenarios of collaborative attack but scenario in which detection algorithm is present to detect colluding nodes PDR acheived is better than the scenario in which algorithm is not present.

Similarly, By evaluating routing overhead from Fig. 6, Fig. 7 and Fig. 8 for 50, 100 and 150 nodes respectively in absence and presence of detection algorithm against 10% to 40% colluding nodes; routing overhead in presence of detection algorithm is higher than the routing overhead without detection algorithm against collaborative attack, because in detection algorithm node sends audit packet to randomly selected node and its successor node in the route, these nodes have to reply

back with their in-out traffic, so it require little more number of control packets. As the size (number of nodes) of the network is increasing, routing overhead are also increasing because more number of nodes participating in communication.

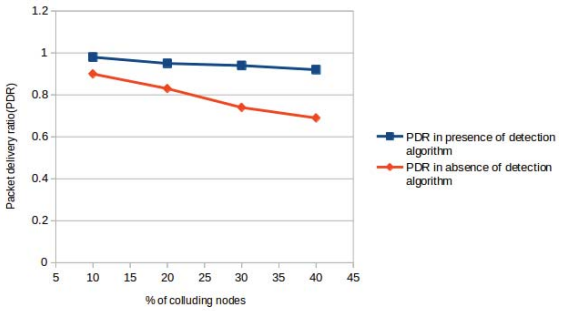

Fig. 3. PDR vs colluding nodes for 50 nodes

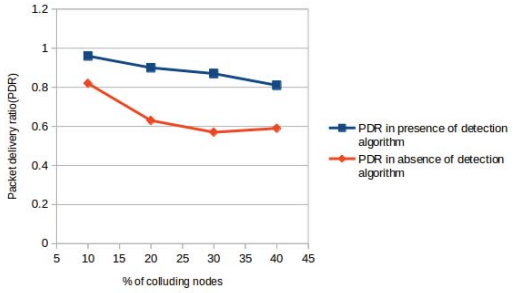

Fig. 4. PDR vs colluding nodes for 100 nodes

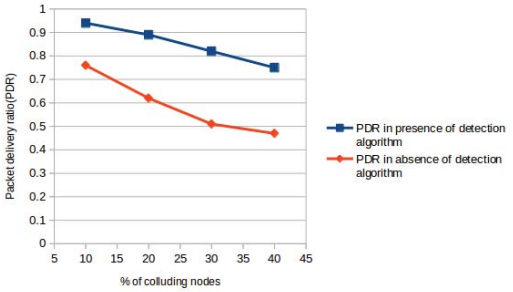

Fig. 5. PDR vs colluding nodes for 150 nodes

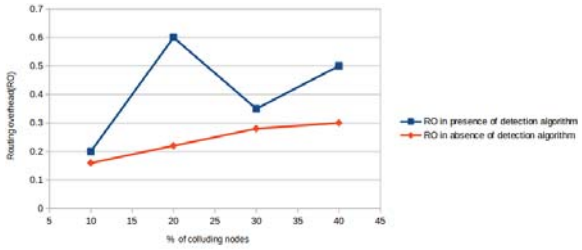

Fig. 6. RO vs colluding nodes for 50 nodes

By evaluating throughput from Fig. 9, Fig. 10 and Fig. 11 for 50, 100 and 150 nodes respectively in absence and

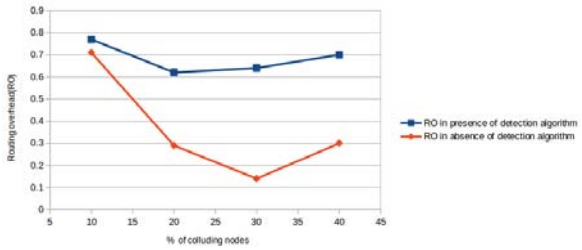

Fig. 7. RO vs colluding nodes for 100 nodes

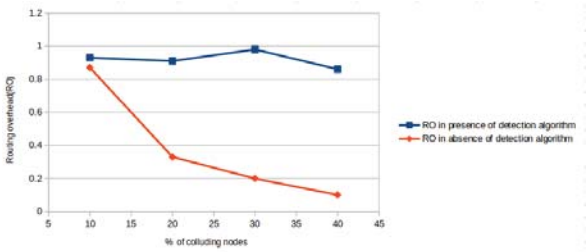

Fig. 8. RO vs colluding nodes for 150 nodes

presence of detection algorithm against 10% to 40% colluding nodes; throughput in presence of detection algorithm is higher than the throughput in absence of detection algorithm, because as soon as colluding attackers get detected that nodes kept isolated and further packet loss is controlled. We are not getting the expected throughput for both the scenarios of collaborative attack when percentage of colluding nodes is increasing. Throughput in both presence and absence of detection algorithm are slightly decreasing with the increment of colluding nodes. As the size (number of nodes) of the network is increasing, throughput are not as much expected for both the scenarios. It is decreasing with the increase in size of network.

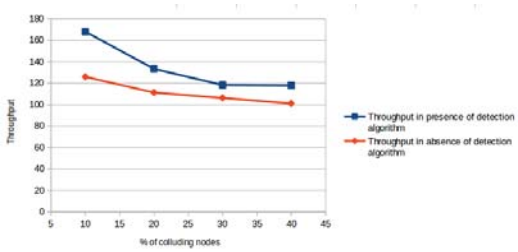

Fig. 9. Throughput vs colluding nodes for 50 nodes

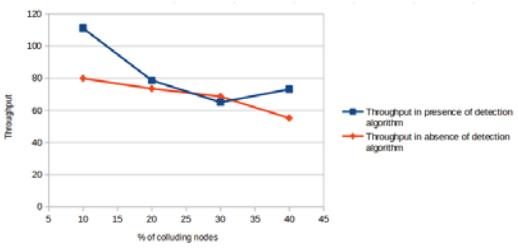

Fig. 10. Throughput vs colluding nodes for 100 nodes

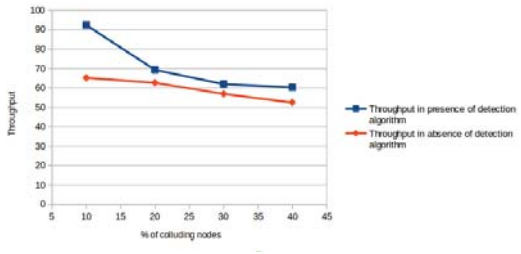

Fig. 11. Throughput vs colluding nodes for 150 nodes

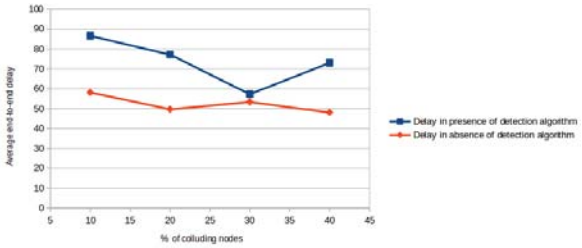

Fig. 12. Average end-to-end dealy vs colluding nodes for 50 nodes

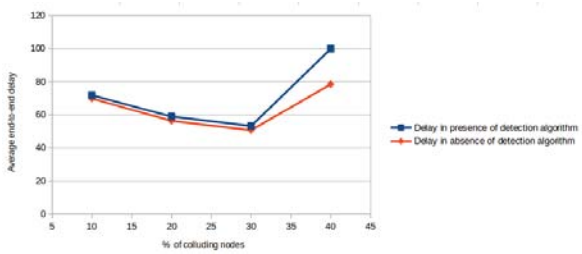

Fig. 13. Average end-to-end dealy vs colluding nodes for 100 nodes

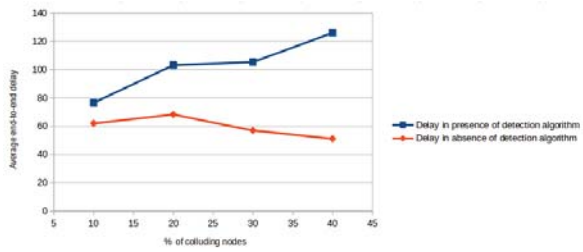

Fig. 14. Average end-to-end dealy vs colluding nodes for 150 nodes

Similarly, By evaluating average end-to-end delay from Fig. 12, Fig. 13 and Fig. 14 for 50, 100 and 150 nodes respectively in absence and presence of detection algorithm against 10% to 40% colluding nodes; average end-to-end delay in presence of detection algorithm is higher than the average end-to-end delay in absence of detection algorithm, because time taken by algorithm to detect colluding nodes adds up in time of transmitting packets to nodes. As the size (number of nodes) of the network is increasing, average end- to-end delay for both scenarios of collaborative attack are slightly increasing.

VI. Conclusion

Intrusion detection algorithm has been proposed and simulated for varying number of colluding nodes and for different sizes of network. Detetcion algorithm checks in-out traffic of selected nodes alongwith keeping an eye on the activity of neighbouring nodes. From simulation results it is observed that an improvement is visible in packet delivery ratio and throughput of the network in presence of the proposed detection algorithm which led to improved security level. Therefore, it is concluded that detection algorithm performs effectively in detecting and isolating colluding nodes from the network so that these malicious nodes do not further participate in routing consequently improves performance of the network. Although, with the increase in network size performance was not remarkable but still algorithm maintains the good network performance.

References

[1] G. Jayakumar and G. Gopinath, “Ad hoc mobile wireless networks routing protocol: A review,” J. Comput. Sci., vol. 3, no. 8, pp. 574-582, 2007.

[2] B. Sun. “Intrusion detection in mobile ad hoc networks,” Ph.D. dissertation, Texas A and M Univ., College Station, TX, 2004.

[3] S. Marti, T. J. Giuli, K. Lai, and M. Baker, “Mitigating routing misbehaviour in mobile ad hoc networks,” in Proc. 6^{th} Annu. Int. Conf. Mobile Comput. Netw., Boston, MA, pp. 255-265, 2000.

[4] K. Liu, J. Deng, P. K. Varshney, and K. Balakrishnan, “An acknowledgment-based approach for the detection of routing misbehaviour in MANETs,” IEEE Trans. Mobile Comput., vol. 6, no. 5, pp. 536-550, May 2007.

[5] T. Sheltami, A. Al-Roubaiey, E. Shakshuki, and A. Mahmoud, “Video transmission enhancement in presence ofmisbehaving nodes in MANETs,” Int. J. Multimedia Syst., vol. 15, no. 5, pp. 273-282, Oct. 2009.

[6] Balakrishnan, Kashyap, Jing Deng, and Pramod K. Varshney, “TWOACK: preventing selfishness in mobile ad hoc networks,” in Proc. IEEE Wireless Communications and Networking Conference, vol. 4, 2005.

[7] Elhadi M. Shakshuki, Nan Kang, and Tarek R. Sheltami, “EAACK- A secure Intrusion Detection System For MANETs,” IEEE Transaction On Industrial Electronics, vol. 60, no. 3, March 2013

[8] Kannhavong, Bounpadith, Hidehisa Nakayama, and Abbas Jamalipour, “A collusion attack against olsr-based mobile Ad Hoc networks,” in Proc. IEEE Global Telecommunications Conference, 2006.

[9] Nat. Inst. Std. Technol., Digital Signature Standard (DSS) Federal Information Processing Standards Publication, Gaithersburg, MD, 2009, Digital Signature Standard (DSS).

[10] R. Rivest, A. Shamir, and L. Adleman, “A method for obtaining digital signatures and public-key cryptosystems,” Commun. ACM, vol. 21, no. 2, pp. 120-126, Feb. 1983.

[11] Ghosh, Tirthankar, Niki Pissinou, and Kia Makki, “Collaborative trust-based secure routing against colluding malicious nodes in multi-hop ad hoc networks,” 29^{th} Annual IEEE International Conference on Local Computer Networks, 2004.

[12] Kannhavong, Bounpadith, Hidehisa Nakayama, and Abbas Jamalipour, “A collusion attack against olsr-based mobile Ad Hoc networks,” in Proc. IEEE Global Telecommunications Conference, 2006.

THE 18TH INTERNATIONAL SYMPOSIUM ON WIRELESS PERSONAL MULTIMEDIA COMMUNICATIONS
(WPMC-2015)
December 13-16, 2015, Hyderabad, India

Automatic Speaker Detection and Recognition in a multi classroom E-Learning System

Amitha Vijayan
Amrita Center for Wireless Networks and Applications
AMRITA Vishwa Vidyapeetham
Amritapuri, Kollam, India
amithavijayan@gmail.com

Balaji Hariharan
Amrita Center for Wireless Networks and Applications
AMRITA Vishwa Vidyapeetham
Amritapuri, Kollam, India
balajih@am.amrita.edu

Uma G
Amrita Center for Wireless Networks and Applications
AMRITA Vishwa Vidyapeetham
Amritapuri, Kollam, India
umag@am.amrita.edu

Abstract*— E-learning technology helps both students and teachers, to access the remote classroom and the professor in that classroom can interact with them efficiently. In the current scenario, the professor will view the remote classrooms in multiple screens which failed in realistic interaction. But still there are some improvements that can be done. This paper proposes a system which will help the professor to recognize the remote student who is trying to interact and thus allow him to change the flow of lecture with respect to the student interaction. Here we implement audio detection to identify the classroom and also we used a gesture recognition algorithm to switch between remote classrooms, so that the professor could access the students and continue helping the student based on the student's subject base knowledge. This will allow a more realistic feel to the virtual classroom, allowing both the student and professor to interact with ease. We can also allow this design for the interaction between students for discussions during lectures or presentations.

Keywords—E-learning; Remote classroom; Remote student; Audio detection; Gesture recognition; Virtual classroom

I. INTRODUCTION

There has been a rapid growth in the use of internet over several years. According to a recent survey, the number of Internet users worldwide reached about 2.27 billion, almost exactly twice what it was in 5 years ago which also increases the Data traffic [1]. Multimedia plays a vital role among various classes of traffic on the internet. Live video telecast, video conferencing, etc. are some of the most common applications that deliver video content over the internet. With the advancement in the internet technologies lot of applications demands interactive responses, VOIP, video streaming, etc. became our part of life.

Virtual classroom, it is one of the prominent features of the E-learning platform. As the name implies, the classes are conducted virtually, which means the students and the professors attend the class from their respective remote locations as in Figure 1.1. It is an online, web-based tool, which creates a virtual classroom environment similar to traditional classroom [2]. It is considered as an alternative to traditional, location-based classroom, as it saves the expenses of physical infrastructure [3].

Usually, professor's interaction with the local classroom-students will be more causing lack of attention and interaction with the remote classroom students. Hence, the professor fails to understand the effectiveness of his/her lectures. The proposed system focuses on improving the interaction between the professor and the students who are in different locations by adding the features like audio detection and gesture recognition

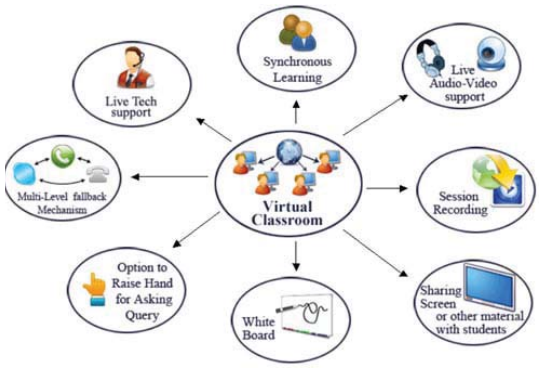

Fig. 1.1 Virtual Classroom technology [2]

The main challenge of the work is to reduce the misidentification of murmuring sound as a real sound and less audible voice as noise. The proper identification of the sound variations in the different categories like murmuring, less audible sound, surrounding noise, etc.

Hence, we propose a system which will enable an effective interaction between the professor and the students in remote classroom in multi classroom scenario. Our system will be useful in virtual classroom scenario ensuring the evident speaker detection and gesture recognition. The system filters the unwanted sounds and properly identifies the classroom in all interactive and non-interactive sessions. The professor could switch the classroom with distinct gestures without any fail.

The paper is organized as follows: Chapter 2 provides a comprehensive study and background information on existing studies. The detailed system architecture is discussed in Chapter 3, followed by Simulation Results in Chapter 4. Conclusion and future work of the presented work has been given in Chapter 5.

II. Related Work

The gesture recognition system using Kinect is described in [2]. In this system, when a student in a remote location, raises his/her hand to talk to a professor, the Kinect camera detects the student, identifies the gesture of the remote student, after identifying the gesture of the student, the student gets zoomed in with the PTZ HD camera. To zoom in the student the authors used AXIS M5014 PTZ Dome Series network cameras, i.e. the camera are accessed through its IP address. The PTZ camera, does not know to whom it has to zoom and at what angle it has to rotate to focus on the student with the raised hand. In order to solve this issue, it is imperative to map the images between both the cameras by using Homography Estimation and SIFT algorithm. From the SIFT algorithm, key points are collected and the key points are matched to estimate the Homography. The Homography Estimation determines how much the camera has to rotate and to whom the camera has to zoom.

A method to find the hand gesture by using Kinect is discussed in [4]. Initially, a gesture set is created and is compared with the hand gesture which is detected by the Kinect and, displays its meaning and the corresponding picture on the screen. The system consists of 3 phases. First phase, Hand Detection, which will detect the hand and separate it from the background. The Second phase is Finger Identification, which uses a three point alignment algorithm to detect hand contours and finger identification algorithm to identify fingers. The Last phase is Gesture recognition, where gestures are identified by passing it through some classifiers, namely finger counting classifier, finger name collecting classifier and vector matching classifier.

The detection of hand raising gestures in a meeting room and classroom environment is discussed in [5]. From the video frame the student's face is detected and the region of interest is defined. The system The system proposes a hand raising gesture in images. The hand raising gesture is identified by considering the edges of the raised arm that are parallel and close to the face that are of the same height which will determine whether the student raises the hand or not. Here, they consider the meeting room set-up in which two people face each other and the third sits in such a way that only the left side of the person is visible in the video. This type of gesture detection does not work in a messy environment.

A method for gesture recognition using depth data obtained by the Kinect sensor is discussed in [6]. Here, the proposed Gesture Recognition System consists of four steps. The Initial step is to obtain the depth map and the 3D coordinates of six joints and by using the hand coordinates the hand region is cropped. The second step is to extract the hand shape features based on the cropped hand regions gradient value. The third step is to calculate the arm movement features based on the six joint values. Finally the gesture is identified using a Hidden Markov Model. The method used in this system requires background modelling and is expensive.

III. System Architecture

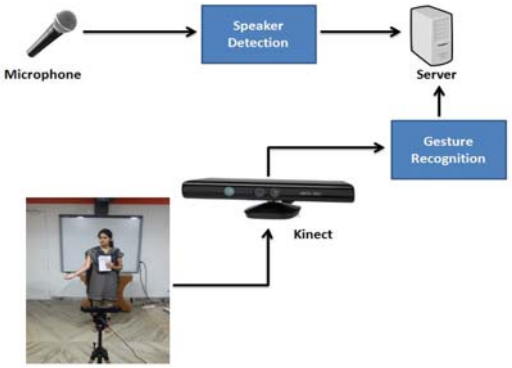

Fig. 3.1 An Overview of System Architecture

An Overview of the entire system is shown in the Figure 3.1. The system consists of microphone which capture student's interaction, and cameras for real time video streaming and a Kinect camera which identifies the gesture of the professor to switch the classroom. In our system, it consists of two main modules, speaker detection module and gesture recognition module. In speaker detection module, when a student asks doubt from any of the remote classrooms the system will capture that sound, and the input will be processed in speaker detection module and finally the system will find out the classroom from which the student asks doubts. Next is the gesture recognition module. Here, whenever the professor identifies the classroom from where the student ask doubt, the professor will give a particular gesture for that respective classroom so as to switch the classroom which is displayed on the professor side display.

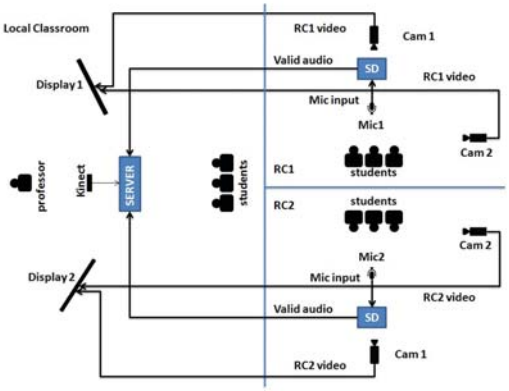

Fig. 3.2 Proposed System Architecture

The proposed system is implemented using five machines in three classrooms, i.e one local classroom and two remote classrooms. In the proposed system architecture shown in Figure 3.2 the block diagram 3.3, Among the five machines, two will act as the speaker detection (SD) module in remote classrooms, to determine whether the student's sound is valid or not. Another one will act as a server, which is attached to the Kinect camera and the rest two i.e display 1 and display 2 will act as the professor side display screens for switching the

remote classroom perspectives. From both the remote classrooms, real time videos are streamed to the professor side screens. In the remote classroom, the speaker detection module will capture the student's interaction and determines whether it is valid or not. This is performed using a speaker detection algorithm. We know that when we consider a classroom environment, it may change dynamically. So that it is a real challenge to determine whether the sound is valid or not. Initially, we will analyze the classroom for some time and at the same time we will find out the RMS (Root Mean Square) of each sample and the average of these RMS values will be set as the threshold for the remaining time. The threshold will be dynamically changed, with the variation in time. After the initial time, the calculated RMS values are compared with the threshold which is dynamically changing and whenever the RMS value is greater than the threshold the system will determine whether the sound is valid or not.

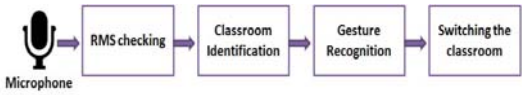

Fig. 3.3 diagram of the System

After the detection of the valid input, it is forwarded to the server. A Kinect camera is connected to the server for the gesture recognition module. In the gesture recognition module, whenever the professor identifies the classroom from which the student asks doubt by viewing the screens placed on both sides of the professor, he/she will show a particular gesture to the Kinect =camera for that respective classroom. The Kinect camera will identify the gesture and by analyzing both the inputs from the Kinect camera and the speaker detection module, i.e. valid input, the system will switch the classroom perspective displayed on the screens placed on both sides of the professor.

The flow chart of the system is shown in Fig. 3.4.

IV. Simulation Results

- Speaker Detection

The figure 4.1 shows the output of the speaker detection module in remote classroom 1 (RC1) and remote classroom 2 (RC2). The speaker detection module detects whether the captured student's voice is a valid input or not and this information is forwarded to the server.

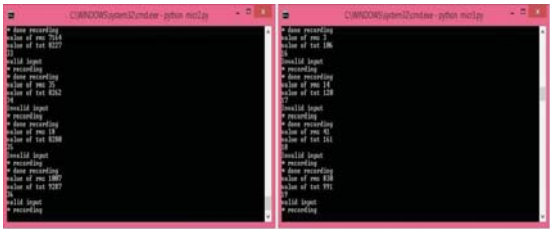

Fig. 4.1 Output of the speaker detection module in RC1 and RC2

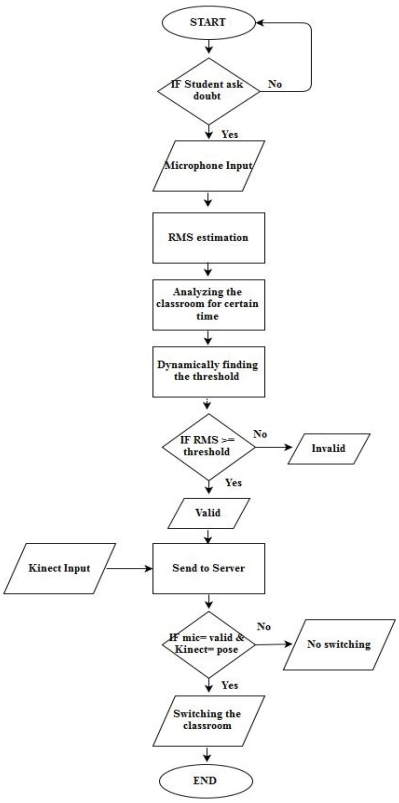

Fig. 3.4 Flow chart

- Gesture Recognition

When the professor enters the range of the Kinect camera, it will identify the professor who is in front of the camera. Initially, the calibration process has not started and it can track multiple people simultaneously and all the users have a unique ID. After that it will check to see whether the professor is in the calibration pose or not as shown in figure 4.2. If the professor has assumed to be in the calibration pose, then the skeleton detection and the skeleton drawing are initiated. The calibration process is not always successful. The skeletal drawing is initiated whenever the calibration process is successful. If the calibration process is not successful, then again the process has to be restarted to detect the calibration pose.

Fig. 4.2 Calibration of the professor when he/she is in calibration pose.

Whenever the professor identifies the classroom from which the student asks doubt by viewing the screens placed on both sides of the professor, he/she will show a particular gesture (poses) to the Kinect camera in that respective classroom. Here, we are using three different poses for each classroom. When the professor identifies the sound from the remote classroom 2 (RC2), he/she will show pose 3 as shown in figure 4.3 so as to switch to that classroom see figure 4.4.

Fig. 4.3 Pose 3 for remote classroom (RC2).

Fig. 4.4 Classroom switching after pose 3 initiated.

Similarly, pose 1 as shown in figure 4.5 will switch to remote classroom 1 (RC1) see figure 4.6.

Fig. 4.5 Pose 1 for remote classroom (RC1).

Fig. 4.6 Classroom switching after pose 1 initiated.

After the interaction from the remote classrooms, the professor will show pose 2 as shown in figure 4.7 to continue the normal classroom scenario see figure 4.8.

Fig. 4.7 Pose 2 to continue the normal classroom scenario

Fig. 4.8 Classroom switching after pose 2 initiated.

V. Conclusion and Future Work

We proposed an innovative approach to improve the interaction between the professor and the students in remote classroom in a multi classroom scenario. One of the major problems in a virtual classroom is that the remote students will not get much attention of the professor. This problem is avoided by using speaker detection and gesture recognition modules which will do the filtering of unnecessary sounds and switching of the classrooms respectively. A reliable and efficient interactive environment between teacher and student irrespective of the locations is ensured by the proposed system. As future work, we can enhance the proposed system with an added advantage of face detection and student hand raise gesture recognition modules. Whenever a student raises his/her hand, using Kinect and PTZ camera we can find that particular student and identify him/her. Details of that student can be displayed on the bottom of the screen so that the professor can vary his/her way of teaching according to the student's knowledge. Thus, the interaction of the professor and the students can be improved and some of the disadvantages in the present E-learning scenario can be solved by using this technique.

ACKNOWLEDGMENT

This project is partly funded by a grant from MPEC, National Knowledge Network (NKN), Department of Electronics and Information Technology (DeitY), Govt. Of India. We would also like to express our gratitude for the immeasurable motivation and guidance provided by Sri. Mata Amritanandamayi Devi (AMMA), Chancellor of Amrita University for doing this work. I would also like to express my sincere gratitude to Mr. Ram Kumar for the time he dedicated to help us in solving doubts at various stages of this research.

REFERENCES

[1] "World internet population has doubled in the last 5 years," April 2012. [Online]. Available: http://royal.pingdom.com/2012/04/19/world-internet-population has-doubled-in-the-last-5-years/.

[2] "Virtual Classroom Technology & Software Systems". [Online]. Available: http://www.timelesslearntech.com/virtual-classroom.php.

[3] K. S., B. Hariharan, and S. Kumar, "Resolution scaled quality adaptation for ensuring video availability in real-time systems," in 14th IEEE International Conference on High Performance Computing and Communication & 9th IEEE International Conference on Embedded Software and Systems, HPCC-ICES 2012, Liverpool, United Kingdom, June 25-27, 2012, 2012, pp. 873–878. [Online]. Available: http://dx.doi.org/10.1109/HPCC.2012.124

[4] Yi Li, "Hand gesture recognition using Kinect," Software Engineering and Service Science (ICSESS), 2012 IEEE 3rd International Conference on, vol., no., pp.196,199, 22-24 June 2012 doi: 10.1109/ICSESS.2012.6269439

[5] Nyan Bo Bo; Van Hese, P.; Van Cauwelaert, D.; Veelaert, P.; Philips, W., "Detection of a hand-raising gesture by locating the arm," Robotics and Biomimetics (ROBIO), 2011 IEEE International Conference on , vol., no., pp.976,980, 7-11 Dec. 2011 doi: 10.1109/ROBIO.2011.6181414.

[6] H.Takimoto, J.Lee, and A.Kanagawa, "A Robust Gesture Recognition Using Depth Data", 19th Korea-Japan Joint Workshop on Frontiers of Computer Vision, (FCV), 2013 International Journal of Machine Learning and Computing, Vol. 3, No. 2, April 2013 doi: 10.1109/FCV.2013.6485474.

[7] "Virtual Class Room (UNICAST)". [Online]. Available: http://www.slideshare.net/BrianNelson/virtual-class-room.

[8] "Virtual Classroom". [Online]. Available: http://whatis.techtarget.com/definition/virtual-classroom.

[9] Jared St.Jean, " Kinect hacks Tips and Tools for Motion and Pattern Detection, 1st edition,O'reilly,Make:makezine.com,2012,1-2.

[10] M. Greg Borenstein, "Making Things See", 1st edition, Makermedia ,2012, pp:1-195.

THE 18TH INTERNATIONAL SYMPOSIUM ON WIRELESS PERSONAL MULTIMEDIA COMMUNICATIONS
(WPMC-2015)
December 13-16, 2015, Hyderabad, India

The Impact of Network Neutrality on the OTT Service of 5G WISDOM

Yapeng WANG, Ramjee Prasad
Center of TeleInFrastrukur, Aalborg University
Aalborg, Denmark
yapeng@es.aau.dk, Prasad@es.aau.dk

***Abstract*—This paper presents the influence that the Network Neutrality (NN) policy may bring to the Over the top (OTT) service and 5G Wireless Innovation System for Dynamically Operating Mega Communications (WISDOM) era. It reviews the evolution of Network Neutrality, figures out the main theme of Network Neutrality and its impact to OTT services. The paper collects and analysis the opinions from different sides, including the network providers, the OTT companies, governments and researchers and points out that there are still not enough evidence to prove the long term benefit of NN policy. Let the market decide maybe a better solution.**

Keywords—Network Neutrality, Over the Top Services, 5G WISDOM, regulation, impact, long term benefit

I. INTRODUCTION

With the internet service and application develops, the debates of the "network neutrality" has continued over 'one decade. The phrase of "network neutrality" is first used in a law review article [1] by Tim WU in 2003, welcomed by those who advocate freedom, competition and innovation. Originally "Network Neutrality" was only a concept suggesting that each network protocol layer should be independent and perform their duties. With the expansion of the internet commercial-scale, the focus of the competition switch from the connection and network layer to the application and content layer which make the debate of Network Neutrality switch from technological field to commercial field. And now it is a fight among telecom operators, Internet companies and regulators, especially after the OTT services appear.

OTT implies communications carried over the physical network infrastructure using an IP protocol to reach services available on the internet. An OTT application is any app or service that provides a product over the Internet and bypasses traditional distribution. Services that come over the top are most typically related to media and communication and are generally, if not always, cheaper than the traditional method of delivery [2].

WISDOM was first proposed in February 2008[3, 4]. It is a novel concept and the evolution to 5G era. WISDOM with 4G will lead to 5G realization. WISDOM can provide the wireless link rates in short-distance burst-mode at up to1T bit/s or up to 1Tbit/s of system aggregated traffic with sustainable symmetric link rates of larger than 250 Mbps to mobile terminal at high speed.

In terms of WISDOM research, 5G will provide services and applications offered by GIMCV (Global Information Multimedia Communication Village) as shown in Figure 1 shows. National and international zones constitute the Global information village which can be divided into macro cells including suburban, regional and national network, meanwhile, micro cells which includes city centers and highway networks constitute Macro cells which further contains small pico-cell (in-house network) where there are many small personal area networks (PAN). It gives scope of WISDOM application which varies from person in home to globe from where they belong to [3, 4]. In 5G WISDOM Era, OTT will play a very important role.

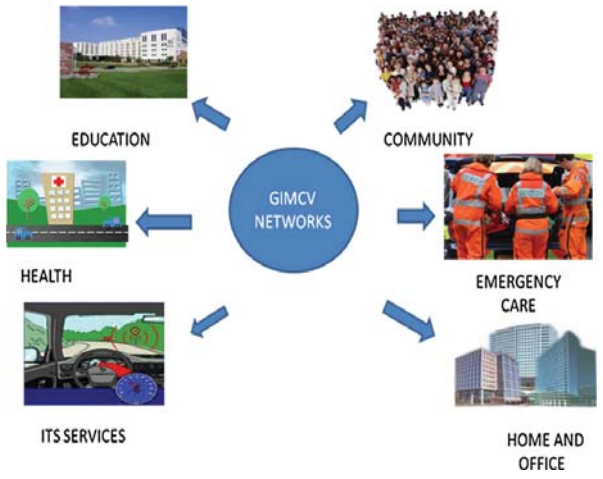

Fig 1: WISDOM in GIMCV applications

This article describes the evolution of Network Neutrality, main points of Network Neutrality, OTT services and the 5G WISDOM system. It also introduces the state of the art of OTT services, why OTT services become a focus. The article collects and analysis the opinions from different sides, including the network providers, the OTT companies, governments and researchers. Points out that at least for the long term, NN may be dangerous for the OTT Industry, 5G

WISDOM system and whole economy. The article considers that leaving the issue to market maybe a better solution.

II. NETWORK NEUTRALITY

Network Neutrality has been regarded as a hot topic for over one decade. The proponents think Network Neutrality will benefit the whole telecom market and industry, and encourage the service providers to innovate and become motivation of the society development. But the opponents think it will harm the whole telecom industry because it will aggravate the pressure on the network providers who is already in a difficult position.

A. The evolution of Network Neutrality

TABLE I

The evolution of Network Neutrality [5, 6]

Date	The evolution of Network Neutrality
February 2004	FCC called for Network Neutrality should encompass four Internet freedoms
August 2005	The FCC commanded the incumbent telecommunications carriers should share their DSL broadband connections with competitors, and approved an Internet policy statement reflecting Powell's four freedoms.
Decembe r 2010	the FCC approved three items Network Neutrality regulations including transparency, no illegal closure and no unreasonable discrimination. (mobile operator is not applicable)
January 2011	Verizon challenged to the net-neutrality rules, with the reason that the FCC did not have the authority to enforce them.
Early 2011	U.S. House of Representatives Republicans tried to overturn the FCC's net-neutrality rules without success.
Septembe r 2011	The FCC's new network neutrality rules was published in the Federal Register and originally taken effect on November 2011
Septembe r 30,2011	Verizon appeals the Open Internet Order to the D.C. Circuit challenging the FCC's authority to impose the Open Internet rules.
January 2014	The D.C. Circuit overturns the Open Internet rules, reaffirming the FCC's authority to promote the growth of the internet but telling the FCC that if it wants to treat internet access like a telecommunications service it cannot classify it as an information service.
May 2014	The FCC's proposal still tentatively concluded that it will allow fast lanes and slow lanes online, but also includes questions about Title II reclassification.
Novembe r 2014	President Obama reiterates his support for strong open internet rules and for the first time explicitly calls for those rules to be grounded in Title II authority.
February 2015	he FCC's new net neutrality rules was approved at 3-2according President Obama's recommendation
April 2015	The FCC's new net neutrality rules have been published in the Federal Register. As per normal process the rules are now scheduled to formally go into effect sixty days after publication, or June 12 of this year.
June 12 2015	The network Neutrality take effect

B. The key points of new Net Neutrality rules[7]

By the end of February 2015, the FCC approved new network neutrality rules and in mid-March has released the detailed rules and regulations. The new rule is the strongest one in the history. With that, FCC urged the network provider to treat all Internet traffic fairly. The new rule is approved at 3: 2 with three affirmative votes from Democrats and two negative votes from the Republicans.

The new network neutrality rules fold three key points, which are No Blocking, No Throttling and No Paid Prioritization and they are in detail as below:

- "No Blocking: prohibiting broadband providers from blocking lawful content, applications, services, or non-harmful devices.
- No Throttling: prohibiting broadband providers from impairing or degrading lawful Internet traffic on the basis of content, application, service, or use of non-harmful device. (including content, applications, services, or sound equipment);
- No Paid Prioritization: Prohibiting broadband provider from providing the differentiation services when they accepts payment (monetary or otherwise) to manage its network in a way that benefits particular content, applications, services, or devices and protect against "fast lanes" ."

In addition, FCC also proposed network providers " no-unreasonable interference/disadvantage" which means under which the Commission can prohibit practices that unreasonably interfere with the ability of consumers or edge providers to select, access, and use broadband Internet access service to reach one another, thus causing harm to the open Internet. This no-unreasonable interference/disadvantage standard will operate on a case-by-case basis and is designed to evaluate other current or future broadband Internet access provider policies or practices—not covered by the bright-line rules—and prohibit those that harm the open Internet. FCC claims that small operators who have less than 10 million users can exempt from these requirements.

C. The debate focus of new Network Neutrality

From the evolution of Network Neutrality, we can realize the difficulty of the approval of the Network Neutrality. And the debate focus of Network Neutrality is different at different phases of the internet development. Initially the network neutrality concerns the openness of internet and citizens' right to connect the network. The second phase is the reasonable needs of the Internet business model. By now, the focus switches to the legitimacy of the operators' network management strategy especially on OTT services management.

In recent years, Internet services develop very rapidly, especially with the emergence of OTT services, traditional

telecom services including the voice service and text message are being replaced by the OTT services. OTT services have become not only the focus of the competition between network providers and internet companies but also the debate focus of the network neutrality issue.

At this stage, the two points of "no blocking" and "no throttling" of network neutrality have reached the consensus in telecom industries. And the main debate focus is "No Paid Prioritization" which means the network providers should **not** provide differentiated services based on charges of QoS (here

the difference service means the different service qualities provided by network providers to internet companies). That is, the network providers should not charge the internet companies more money for the higher quality of broadband services, especially the OTT services such as Voice over Internet Protocol (VoIP) and video services. This paradox exist in other industry for example the highway operating. Governments charge the highway fee to construct and maintain the highway and most countries authorities charge according the size of the vehicle and the quantity of good they ferry. The current discussion is actually whether the Internet companies should pay for the high quality service and the large bandwidth consumption.

III. NN POLICY'S IMPACT ON OTT SERVICES

With the continuous emergence of the OTT services and the explosive growth of the traffic, network providers face threaten from internet companies. The industrial value is gradually transferring from pipe to content, from traditional communication network to internet and from voice services to information services. As a result, the dominate position of network providers is challenged and the traditional communication network is becoming the dumb pipe. According to the GSMA forecast, the data traffic will grow rapidly with more than 10 times than 2012 and the internet revenue will get to 290 million dollars till 2020 [8]. As an example of video services like Youtube which will occupy from 66% to 75% of the traffic on 4G network and 33% for video services and 34% for clear video. By 2020, it is estimated that the mobile volume will reach up to 2.1billion connections. [9]

But from the technical aspects, the current mobile communication cannot match OTT technology well. OTT services on the current internet not only occupy the network sources but also harm the network stability. As an example of the OTT communications services, in order to ensure instant online users, the OTT mechanism is to ask the communication system send signal frequently which make the signaling resources of the network operators been occupied constantly. Both in iOS and Android system, when the application is moved to the background, even though the user does not send any message, the signaling resource are being occupied till the application closed.

In the short term run, Network Neutrality will give the OTT services big development space, encourage more innovative applications and increase the efficiency of the society. But in the long term run, Network Neutrality will harm the enthusiasm of the investment on the network construction, make the quality of network worse gradually and weaken the connectivity of WISDOM paradigm, which also harm OTT service in the end. The reasons are as follow:

1) In technical aspect, NN will impact the quality of the OTT service because NN limits the ability to supply QoS of the network. Usually network providers guarantee the QoS of network in two ways, one is Resource Reservation Protocol (RSVP) and the second way is differentiated service (diffserv). RSVP is a signaling mechanism, which uses Integrated services (Intserv) semantics to invoke per-conversation traffic handling. RSVP simply provides a lot of resources with rich and secure equipment and it aims to cope with the expected margin in the "peak" demand. But it is expensive, and cannot cope with the scenario when peak demand is unexpected. Meanwhile, the deployment of additional resources is also time-consuming. Diffserv is an aggregate traffic handling mechanism to address scalability concerns associated with earlier approaches. The Integrated Services over Specific Link Layers (ISSLL) working group of the IETF has made a RSVP signaling model used with diffserv traffic handling to enable QoS in a scalable manner. In addition, by listening to RSVP signaling, network devices are more readily able to identify and classify traffic in order to determine the appropriate traffic handling mechanism [10]. But with NN, differentiated service is banned in public network.

2) In the original Internet, the network's objective is to provide a simple, but the best service. That is, the network makes the best-effort to deliver data packets without any guarantees for delay, bandwidth or losses. So the network operates like the default service offered by the postal service, which does not guarantee the arrival of a letter. But different applications do have different requests. Some services are very sensitive to delay, but not the packet loss and some services are sensitive to packet loss but not the delay. It is very necessary for a network to treat packets belonging to different applications differently in terms of their different requests. For instance, a network should give low-delay service to VoIP packets, but best-efforts service to e-mail packets [11]. Different OTT services also need different QoS.

3) QoS will play a very important role in 5G WISDOM network. 5G WISDOM will give us more bandwidth but QoS is also needed. As the OTT application development, the demand of the data resources will grow in geometrical progression. Over a period of time, the bandwidth demand of the network will be constantly higher than the capacity of network can provide. The network will always be a kind of scare resource. So QoS mechanism must be applied. In 5G Wisdom network, network provider should provide prioritization service to guarantee the services' quality. As we

know, video service is traffic-consuming and sensitive to delay. Packet Delay Budget(PDB), an important parameter of QoS will treat the delay with a confidence level of 98%. For example a test on requirement for delay in 3G, 4G and 5G network, if there is no quality assurance the packet delay budget of 3G, 4G and 5G are respectively undetermined, 100-300 and undetermined, but under the condition of quality assurance, the parameters change to 100-280, 50-300 and 1 respectively[9]. QoS is the guarantee of the new technology.

4) In social and economy aspect, NN may make network operators give up the investment plan on the network construction. The network cannot provide the qualified service when OTT companies overuse the network. The end result is a completely damaged network. It will reduce access to quality of services for everyone. Like the high-speed road free in holiday, it would absolutely cause congestion. Unsufficient investment on new network capacity with the increasing demand for bandwidth will result in network congestion. In order to maintain the steady operation of the network, Carriers will strictly manage the network. For example, AT&T had once blocked video applications.

5) Internet companies will also lose the incentive to improve the efficiency of content services transmission, because NN will limit the cost on content distribution on telecom Network. That easily lead to unreasonable overuse of the network resources and network operator can do little. Traffic congestion and bad QoS will be the result. China's mobile Internet, especially OTT services developed quickly in the past two years, the radio network signaling storm. It has also caused operators and Internet companies of saliva war.

6) FCC's final purpose should be prosperity and Internet innovation, not the death of traditional telecom operators. As we know, the funds usually float to the market with big profits, so it is obvious that when NN was enacted, less investments will go to the network operators and thus lead to loss of the investment incentives for the telecommunications industry, which will be a serious challenge to those traditional network constructors. That will also force those large scale internet companies construct their own networks, like Google is doing. It may be of some benefits, at least make them understand more of each other.

IV. CONCLUSIONS

The emergence of "net neutrality" debate accompanied with the new challenge and demand to traditional telecom network, business model and operation method was made by the internet economy. The attitude to NN of most regulators in worldwide except US is cautious, because NN will influence not only the internet investment, innovation and vitality but also the telecom infrastructure construction and upgradation. On the one hand, considering the rate of return on investment (ROI), in capital market, Internet applications and content services (such as OTT) attracts more funds which is significantly higher than the network infrastructure construction and maintenance. As the main role of the telecom industry chain, the ROI of the network providers is not high and the paradox of traffic growth without revenue growth becomes more and more severe. But the benefits of the network providers and investors should also be protected because the network infrastructure construction and upgradation are the basis of the healthy development of the whole telecom and Internet industry. On the other hand, we should also protect the internet companies who provide the OTT services because they are the motivation of the innovation, the source of the revenue and benefit the whole society. How to balance the interests of the two sides is a big challenge and problem to the telecom regulators. NN by now should not be considered as a final solution. It will be much better for the paradox be solved by the market and competitions, all the stake holders can find a way to ensure the prosperous development of the industry in the market on their own, especially in 5G WISDOM era.

REFERENCES

[1] Tim Wu, Network Neutrality, Broadband Discrimination, Journal of Telecommunications and High Technology Law, Vol. 2, p. 141, 2003

[2] Cory Janssen, Over the Top Application (OTT), Techopedia http://www.techopedia.com/definition/29145/over-the-top-application-ott,_2015

[3] Ramjee Prasad, 5G Revolution Through WISDOM, Springer Science+Business Media New York 2015, Wireless Pers Commun(2015) 81:1351-1357 2015 March

[4] Ramjee Prasad, 5G: 2020 and Beyond, River Publisher, Sept, 2014

[5] ALEXIS C. MADRIGAL and ADRIENNE LAFRANCE, Net Neutrality: A Guide to (and History of) a Contested Idea, The Atlantic, http://www.theatlantic.com/technology/archive/2014/04/the-best-writing-on-net-neutrality/361237/ 2014, April

[6] Michael Weinberg A Timeline of Net Neutrality, Public knowledge.com, https://www.publicknowledge.org/news-blog/blogs/net-neutrality-timeline 2013

[7] FCC, REPORT AND ORDER ON REMAND, DECLARATORY RULING, AND ORDER , 2015 March

[8] Mahanagar Doorsanchar Bhawan & Jawahar Lal Nehru Marg, Consultation Paper On Regulatory Framework for Over-the-top (OTT) services,pp. 23-26, 2015

[9] Valery Tikhvinskiy and Grigory Bochechka, Prospects and QoS Requirements in 5G Networks Journal of telecommunications and information technology, 2015

[10] Yoram Bernet, The Complementary Roles of RSVP and Differentiated Services in the Full-Service QoS Network, IEEE Communications Magazine, 2000

[11] Barbara van Schewick, the central of internet and society, Network Neutrality and Quality of Service, 2012

THE 18TH INTERNATIONAL SYMPOSIUM ON WIRELESS PERSONAL MULTIMEDIA COMMUNICATIONS
(WPMC-2015)
December 13-16, 2015, Hyderabad, India

Characterization for Reporting Rate of Adaptive Sectoring Scheme to Improve Reliability in WSN

Manohar S. Chaudhari
Department of Computer Engineering.
Sinhgad Institute of Technology,
Lonavala. Pune, India.
mschaudhari20@gmail.com

Ramjee Prasad
Department of Electronic Systems
CTIF, Alborg University
Aalborg, Denmark
prasad@es.aau.dk

Vivek Deshpande
Department of InformationTechnology
MITCOE, Kothrud.
Pune, India.
vsd.deshpande@gmail.com

***Abstract*— Wireless Sensor Network (WSN) is quickly emergent research field. The sensor is a fundamental part of WSN. IT has the bulk amount of sensor nodes which is arbitrarily deployed in given sensor field that collects, processes and sends the data back to the base station. It has the quality of service (QoS) parameters such as Congestion, energy, throughput, reliability and so on. Reliability is uniformity in calculating results. A system is said to be reliable if and only if it gives equal results constantly. To increase the reliability of a particular system, we introduce a new method called, "Adaptive Sectoring Scheme for Reliability" (ASSR). In this method, the given sensor field is divided into some sectors and at a time we activate current sector only in which an event happens. To minimize the congestion as well as increasing throughput with maximum packet delivery ratio, we ought to adjust sector dynamically to perform data transmission process effectively and efficiently. In this paper, different parameters are used for calculating reliability that gives better results in terms of packet delivery ratio, packet loss ratio, control overhead, throughput, and energy consumed.**

Keywords— Energy; QoS; Reliability; Sectoring; WSN

I. INTRODUCTION

Wireless Sensor Network consists of sink node called as a base station with unlimited energy and multiple sensor nodes with limited energy. Out of this sink, the node is secured but sensor nodes are unsecured. In WSN, sensors nodes are randomly distributed in given environment to collect the information about the changes occurred in the atmosphere of temperature, pressure, humidity, soil content, etc. and sent these noted readings back to the base station [1].WSN is most widely used in real world applications such as weather forecasting, tsunami detection, volcano sensing, and earthquake predictions and so on. It is an easy and good solution for the various applications. Since it is used to a great extent from last few years, it will be useful for future works also. It introduced a new way to perform our jobs within specific time durations. It can establish a connection between different sensor nodes across the given network [2]. The fig. 1 shows wireless sensor network. Different sensor nodes are placed in the sensor field. These sensor nodes are densely deployed in a given network. Source node collects the information from the area and sends it to sink node. The path followed by them is also shown in fig. 1

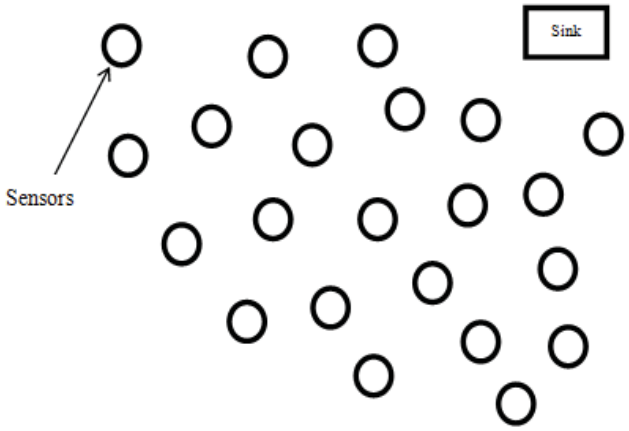

Fig. 1. Wireless Sensor Networks.

A cooperative effort of sensor nodes is one of the unique features of sensor networks. Sensor nodes use limited power and memory, and it uses broadcast communication. There are various types of sensors as seismic, magnetic, thermal, infrared, acoustic, and radar. Wireless sensor network costs efficient than wired sensor network. However, it is difficult and time-consuming in the case of the wired sensor network. As the nodes are widely distributed, it collects the respective information from surroundings and will forward this information finally to sink through the routing nodes. There may be the possibility of packets loss during transmission; hence we need to resend the packets to the destination. It creates multiple copies of single packets that result in the increase of reliability of the system [3].WSN is cost efficient than wired network because wired sensor networks are more costly to implement across the network. It is beneficial for many users to used WSN which minimizes the establishments cost of the network[3]. However, in the case of the node failure, we can replace nodes easily and quickly. However, it is difficult in the case of a wired network. As the sensor nodes are widely distributed in a given surrounding, noted down the readings and sent them back to the sink node. There may be possibilities of packet loss during this data transmission process hence we need to resend the

packets to the destination that may result in multiple copies of the single packet. It may increase the reliability of packet data[4].

Reliability is the consistency in measuring the results of any test. A test is said to be reliable if and only if it produces same results repeatedly. It is the most challenging task to send the packets with high speed and more reliability. As the number of packets reaching the destination increases, the reliability of system also increases. However, it also creates traffic or congestions in the traversed path and puts an extra load on one hop away node from the sink. It also minimizes the life of nodes. We must replace them after regular interval of times. Hence, it is a major challenge to find a way that reaches the position, where we can achieve more reliability by controlling congestion, and other parameters in wireless sensor networks like, Energy, Delay, Congestions, Throughput, and so on [3].

II. Related Work

Dukhyun Chang et al. [5] states that flooding is the mechanism in which a message sent by source node propagates throughout the complete network. The fundamental aim of flooding mechanism is to ensure that all the nodes present in given network must take delivery of that same message. This paper proposed a probabilistic and opportunistic flooding algorithm (POFA) which is used to control, rebroadcast and retransmission of data packets to attain superior target reliability. In this method, a given node will select only the subsets of its one-hop neighboring nodes called as multipoint relays (MPR) to rebroadcast the same message. While selecting the eligible neighbors to consider the link error rate. The number of retransmissions is be controlled by the sender by knowing the present states of message reception at its neighbors. Let R be network wide reliability of node, the node that received the message will forward that message, to its one-hop as well as two hop neighboring nodes for which nodes will select Reliability-aware Multipoint Relays (RA-MPR) nodes. Suppose that all of the one-hop neighbors are elect as RA-MPRs in this subsection. The first sender who is to broadcast a message will calculate an expected delivery probability (EDP). The EDP is the ratio of the expected number of close neighbors that will receive the message probabilistically to the number of all close neighbors.

Hong Luo et. al. [6] States that in wireless sensor network reliable and energy efficient data transmission process is necessary. For this data fusion process is used, in this the combination of data packets into large packet takes place that contains more correct and abundant information than individual packets. In fusion data tree, each node fuses all its incoming packets into a single packet by its own and then forwards it to its parent node. Here we use different topologies of data packets such as star, tree, chain, etc. If the packet size of the fused packet is either smaller or larger than the size of the original data packet, then this type of fusion is called as partial fusion. If the packet size of fused data is equal to the original data packet, then this type of fusion is called as full fusion. Information weight of a fusion node is the sum of all information weights of received packets including its weight. The author studied the difficulty of minimum energy reliable information gathering (MERIG) with unreliable data fusion structure. The basic idea is to allocate dissimilar transmission reliability to the packets having different information weight. They used multiple transmissions without acknowledgments that minimize latency of data packet delivery and promise the desired transmission reliability

Tien wen sung et. al. [7] states that in directional wireless sensor networks sensing angle and directionality of sensors are the two significant characteristics to calculate sensing coverage area. To study properties of Voronoi cell diagram and direction, adjustable sensing angle are used. The Voronoi cell is a geometrical structure having special properties. These Voronoi cells can be constructed by drawing a perpendicular bisector of a line that joins each sensor pair. These bisector lines form Voronoi cells boundaries called as Voronoi edges and endpoints of these edges are called Voronoi vertices. The author studied the distributed greedy algorithm to find near optimal solution. The directionality of sensors is selected and adjusted based on three criteria as firstly, to increase the area inside the Voronoi cell. Secondly, to minimize the overlapped coverage area between the sensor and its neighboring cells and finally, to reduce the sensing coverage area outside the sensing field.

Reliability is the most important factor of wireless sensor networking. The data transmitted from the source must be completely received before destination end with or without a minimum packet loss then the transmission is said to be reliable [8, 9].

III. Proposed Work

In proposed algorithm, the aim is to achieve desired reliability by using Adaptive sectoring method. In this method, the given networks are divided into N number of sectors and at a time keep current only one sector activate which helps to avoid congestion and consume less energy. After an event occurs, all data packets will send their data to their respective sector head and ultimately it is forwarded to destination sink node.

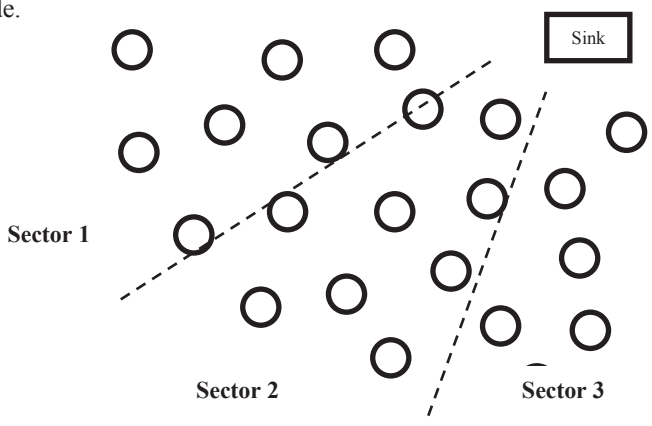

Fig. 2. Proposed Sectoring Scheme

Fig. 2 shows after sectoring method where the given sensor field is divided into three different sectors. If an event occurs in any one of these sectors, then only the current sector is activated which belongs to that event, and all other remaining nodes remains in idle conditions i.e. they do not take part in the data transmission process. Here we get better data reliability and less energy consumption in after sectoring method than before sectoring method.

As shown in the figure, after using sectoring method we divide the sensor networks in n number of sectors logically. Wherever the event occurs, the only current sector is activated, other sectors nodes are in sleep mode. Nodes, which belong to the sector in which the event occurred, transfer the packets to their respective SH within the event sector only. Finally, transfer the packets to sink.

Algorithm: Adaptive Sectoring Scheme

1. Divide given sensor node area into N number of sectors.
2. A node that is closer to sink declared as Sector Head (SH).
3. Let θ will be the angle of one sector; such that
   θ = TotalAngle / N
4. Let Δθ will be maximum angle of θ; such as max(Δθ) = θ
5. If an event occurs then, current sector nodes are activated.
6. Let dθ will be the incremental angle of the current sector.
7. Calculate Δθ = θ ± dθ
8. To find Observed reliability (Ro) and Desired Reliability (Rd) such that Ro = No. of packets received / No. of packets send.
   Rd = No. of packets received / (PD)*100.
9. (If Ro < Rd) then
   Calculate New angle of sector (θ(n) = θ(c) + dθ(n)); where θ(c) is the current angle of the sector. Adjust the sector dynamically by θ(n)
   Data packets are transferred to the sink via their receptive SH
10. End if
11. Go to statement 8.

These algorithms mainly run on each node including Source and Sink of the network with minimal functionality at the source nodes. More precisely, sensor nodes only need the following functionality.

Considering Sink node as Corner, divide given area into n number of sectors. A node that is close to sinking is declared as Sector Head (SH). If an event occurs then activated nodes present in current sectors only. Remaining sector nodes keep in the idle condition that is they neither transfer packets nor receives them. Rotate the sector dynamically accordingly to find the shortest path and avoid congestion. Data packets are transferred to the sink via their receptive sector head (SH). Firstly divide the given network area into N number of sectors by taking sink node as at a center position. Secondly, Find the node that is close to the sink node then assign it as a Sector Head (SH). Then start the data transmission process so that an event occurs in a given network area. During the data transmission process, the source node will transmit data packets to the destination. It may lead to the congestion in a given network that results in packets loss. Hence, we need to retransmit the lost data packets to the destination node.

When an event occurs, then activate nodes that are present in a given sector only. The rest of all nodes automatically goes into starvation mode means they neither transmit the packets nor receives them. The path taken by packets for data transmission process is the shortest path among all available paths. If necessary, rotate the given sector dynamically so as to transmit data packets faster. Due to the specified path, the congestion is avoided which ultimately helps us in minimizing energy consumption by nodes present in the network. Data collected by the nodes will be collected at their respective sector head and from sector head it is forwarded to sink node. AODV works within the sector. It doesn't choose the path outside of the sector. Hence within sector only shortest path is found. Route request & route reply messages are interchanged in given sector.The single hop node from the sink will be chosen as sector head. This persists as long as N/W exists. SH is rich device & has higher resources than other nodes. There is no computation performed as it is there in clustering approach; every packet must be trace passed through SH to reach to the sink. Reliability can be calculated in terms of PDR at N/W level rather than at particular Node.

IV. RESULT ANALYSIS

The testing scenario for the analysis uses Tool NS-2(Network Simulator-2). The topology used is Uniform Random. The Area of Sensor Field will be 1000*1000 m. The MAC Protocol used is IEEE 802.11 and Routing Protocol is AODV(Ad-hoc On Demand Distance Vector) used. Number of Nodes are 30 within the given field. Packet Size is 50 bytes and Reporting Rates varied from 10 to 50 packets / sec with the step of 10 packets per sec.

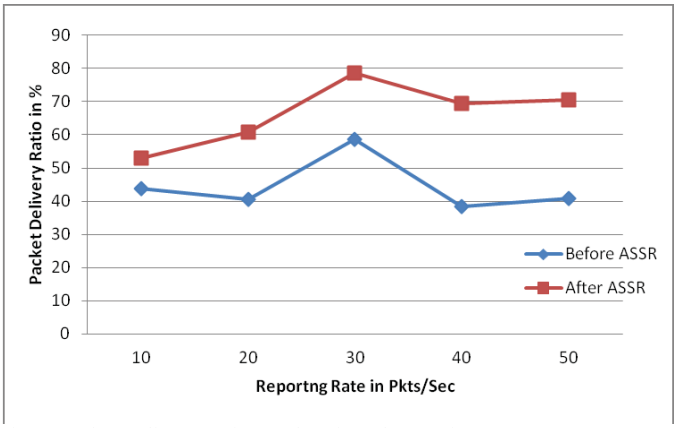

Fig. 3: Packet Delivery Ratio as a function of Reporting Rate

Fig. 3 shows the packet delivery ratio as a function of reporting rate. As the reporting rate is increasing the packet

delivery is decreasing. This is because as the reporting rate is increasing the numbers of packets in the networks are also increasing. However, the processing speed and the storage capacity of the nodes are constant. They are not increasing with respect to the reporting rate. So the packet drop also increases as we increase the reporting rate. The packet delivery ratio of After ASSR is approximately 30 percent greater for reporting rate 40 pkt/sec before ASSR was applied. The other quality of service parameter like packet loss ratio, throughput, and controls-overhead shows better performance than the Before ASM.

Fig. 4 shows the packet loss ratio as a function of reporting rate in packets/sec. As the reporting rate is increasing the packet loss ratio is decreasing. Firstly when the reporting rate is ten, then packet loss ratio is high. However, as reporting rate increases, packet loss ratio decreases. However, it is up to certain threshold point 30, after which as reporting rate increases, there is a respective increase in packet loss ratio. The packet loss ratio of After ASSR is approximately 50 percent greater for reporting rate equal to 30 packets/sec than the case for Before ASSR.

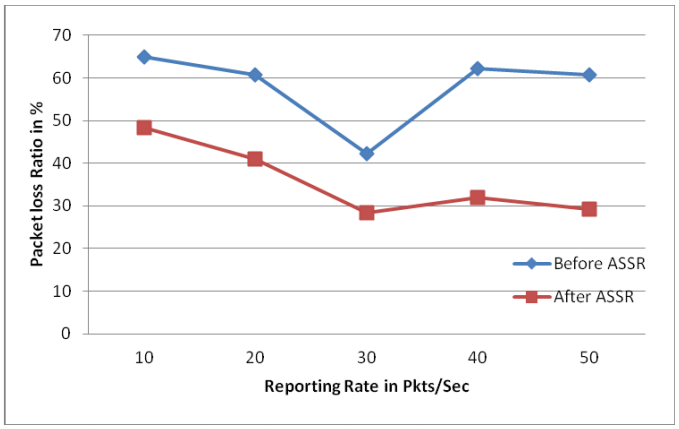

Fig. 4. Packet Loss Ratio as a function of Reporting Rate

The graph is shown in Fig. 5 is the Control Overhead variation for reporting rate. As the reporting, rate increases the Control Overhead increases. Firstly when the reporting rate is ten, then Control Overhead is small. However, as reporting rate increases, Control Overhead remains nearly constant. The packet loss ratio of After ASM is approximately constant than the Before ASSR. Control overheads can be measured at MAC as well as routing layer. RTS/CTS & other handshaking signal or messages are a part of MAC layer control overhead. Route request/route reply will be contributed as N/W layer control overhead. After sectoring scheme implementation, overall control overhead will be drastically reduced.

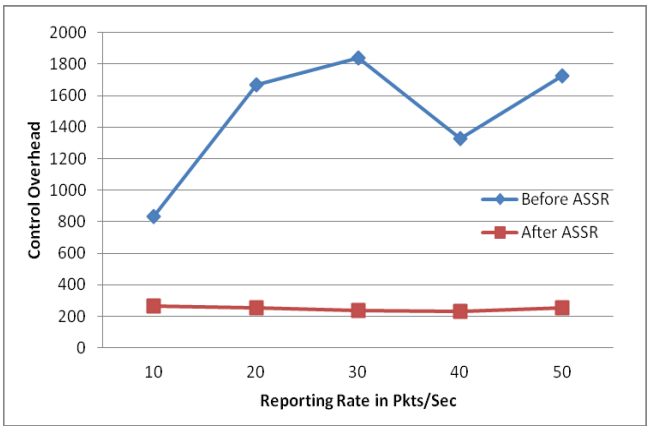

Fig. 5. Control overheads as a function of Reporting Rate

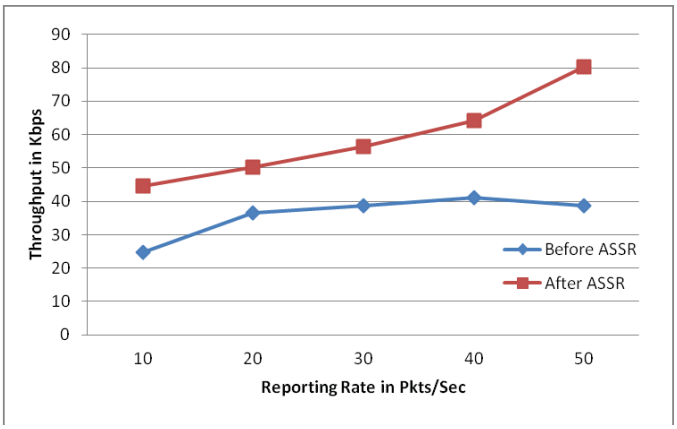

Fig. 6. Throughput as a function of Reporting Rate

The graph is shown in Fig. 6 shows the Throughput in kbps as a function of reporting rate in pkts/sec. As the reporting, rate increases the throughput increases. Firstly when reporting rate is ten then throughput is low. However, as reporting rate increases, throughput increases drastically. The throughput of After ASSR is approximately 50% greater for reporting rate 50 pkts/sec than reading before ASSR.

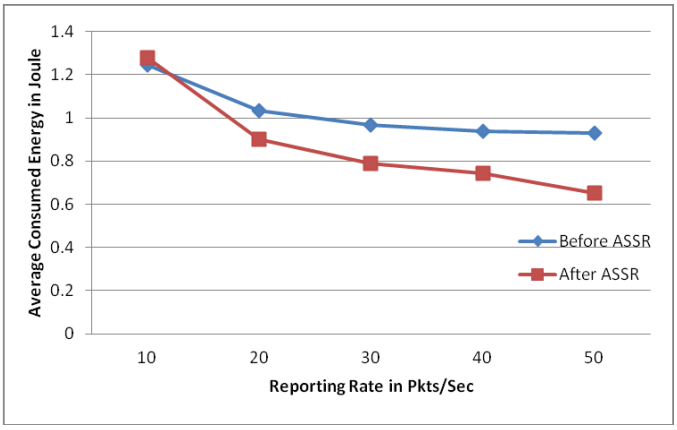

Fig. 7. Consumed Energy as a function of Reporting Rate

The graph is shown in Fig. 7 shows the Energy consumed in joule as a function of reporting rate in pkts/sec. As the reporting, rate increases the energy decreases. The energy

consumed after ASSR is approximately 30% greater for reporting rate 50 pkts/sec than before ASSR.

V. CONCLUSION

Reliability of sensor network can significantly be enlarged through the use of adaptive sectoring Scheme for Reliability (ASSR). By using Adaptive Sectoring Scheme Algorithm one can increase packet delivery ratio, minimize packet loss ratio and energy consumption, also we are successful in lowering control overhead. The proposed Adaptive Sectoring scheme gives more reliability, i.e. packet delivery ratio increase by 63.33%, packet loss ratio is minimize to 25%, throughput increases by 75% with less control overhead, and energy consumption is minimized to 20 percent when a number of nodes are 30.

VI. REFERENCES

[1] Praful P. Maktedar, Vivek S. Deshpande, "Interpretation of Reliability in Wireless Sensor Networks," 2013 IEEE CUBE International Conference on Cloud and Ubiquitous Computing and Emerging Technologies (CUBE), pp 104-107,Nov-2013.

[2] Mohammadreza Balouchestani, Kaamran Raahemifar, and Sridhar Krishnan, "Increasing The Reliability of Wireless Sensor Network With new Testing Approach Based on Compressed Sensing Theory," in Wireless and Optical Communications Networks (WOCN), 2011 IEEE International Conference on Wireless Sensor Networks, pp. 1-4, May,2011.

[3] Praful P. Maktedar, Vivek S. Deshpande, J. B. Helonde, V. M. Wadhai, "Performance Analysis of Reliability in Wireless Sensor Networks," International Journal of Innovative Technology and Exploring Engineering (IJITEE), vol 2, issues 4, pp 299-302, 2013.

[4] Hung-Ta Pai, "Reliability Based Adaptive Distributed Classification in Wireless Sensor Network," Vehicular Technology, IEEE Transactions on vol 59, issues 9, pp 4543-45, 2010.

[5] Dukhyun Chang, Kideok Cho, Nakjung Choi, "A Probabilistic and opportunistic flooding algorithm in wireless sensor networks," Elsevier International Journal on Computer Communication 35, pp 500-506, 2012.

[6] Hong Luo, M, Huixiang Huadong, and Sajal K. Das, " Data fusion with desired reliability in wireless sensor network," IEEE conference communication, PP 2819-2824, 2011.

[7] Tien Wen sung , Chu Sing yang, "Voronoi-based coverage improvement approach for wireless directional sensor networks," Elsevier Journal of Network and Computer Application, pp 1-12, 2013.

[8] Yunhuai Liu, Yanmin Zhu, Lionel Mni and Guangtao Xue, "A Reliability Oriented Transmission Service in Wireless Sensor Networks," IEEE Transactions on Parallel and Distributed Systems, Volume 22, Issue 12, PP 2100-2107,Dec 2011.

[9] D.G.Reina, S.L.Toral, P.Jonhson and F. Barrero, "A Reliable Route Selection Based On Caution Zone and Arrival Angle," IEEE Communications Letters, Volume15, Number 11, PP 1252-1255 Nov 2011.

THE 18TH INTERNATIONAL SYMPOSIUM ON WIRELESS PERSONAL MULTIMEDIA COMMUNICATIONS
(WPMC-2015)
December 13-16, 2015, Hyderabad, India

Q-MOHRA:QoS Assured Multi-Objective Hybrid Routing Algorithm for Heterogeneous WSN

Nandkumar Kulkarni
Center for TeleInFrastruktur,
Aalborg University, Aalborg,
Denmark
npk@es.aau.dk

Neeli Rashmi Prasad
Center for TeleInFrastruktur,
Aalborg University, Aalborg,
Denmark
neeli.prasad@ieee.org

Ramjee Prasad
Center for TeleInFrastruktur,
Aalborg University, Aalborg,
Denmark
prasad@es.aau.dk

***Abstract*— Quality of Service (QoS) assurance in Wireless Sensor Network (WSN) is a tough task, and it is more exciting due to the scarcity of resources. The requirement of different WSN applications running over has different constraints. In QoS, routing protocol the network has to balance the traffic. This paper presents a novel heuristic routing algorithm known as QoS Assured Multi-Objective Hybrid Routing Algorithm (Q-MOHRA) for Heterogeneous WSN. Q-MOHRA takes into account the link (energy, hop count, link quality indicator etc.) and path (jitter) metrics for optimal path selection. The performance of Q-MOHRA is evaluated through intensive simulation and equated with Simple Hybrid Routing Protocol (SHRP) and Dynamic Multi-objective Routing Algorithm (DyMORA). The metrics such as Average Energy Consumption, Residual Energy, Packet Delivery Ratio, Jitter, and Normalized Routing Load are used for comparison. The performance of Q-MOHRA has been observed to outclass SHRP and DyMORA. It improves the Packet Delivery Ratio (PDR) by 13.72% as compared to SHRP and 28 % as compared to DyMORA. Q-MOHRA outperforms SHRP and DyMORA in terms of Average Energy Consumption (AEC) by a factor of 4.2 % and 2.3 %.**

Keywords—WSN; Routing; Hybrid Routing; Multi-Objective; Cluster; Energy Efficiency; Quality of Service

I. INTRODUCTION

The significant and express advancements in the field of wireless technologies and particularly rapid growth in the area of Micro-Electro-Mechanical-Systems (MEMS) have made Wireless Sensor Networks (WSNs) part of pervasive communications for conveying, accessing and storing information across different platforms. In WSNs, huge no of sensor nodes are placed in remote target areas for collecting, processing and transmitting data to the Base Station (BS) [1]. The sensor nodes mainly characterize WSNs. The different attributes of the sensor nodes include small size, limited battery, inadequate processing capability, restricted memory and range of communication, mobility of sensor nodes, etc. [2]. WSNs have gained remarkable consideration from most of the researchers in the field of wireless due to their widespread applications. WSNs have many diversified applications such as monitoring physical or environmental conditions (vibration, pressure, temperature, sound etc.), battlefield monitoring, civilian and military applications, habitat monitoring, home automation, healthcare applications, asset tracking etc. Increasing the life of sensor node and making the WSNs energy efficient is the prime goal in all the WSNs applications due to scarcity of resources [1, 2].

Due to the shortage of energy of wireless sensor nodes in almost all applications, lot of research work has been done in the routing protocols. The requirement of all the routing protocols differs from application to application. In spite of that, the prime goal of all the routing protocols is to conserve the energy and increase the life of the network and the time of partition. The routing protocol will select the route from source to destination in the finest effort delivery manner [3].

In many traditional routing protocols, only limited number of nodes is involved in sending data packets from source to the destination while other nodes stay practically idle. The energy of the nodes those engage in the communication process depleted at a very fast rate. These nodes will quickly die out when the energy is completely drained. The dead nodes may cause partition of the network or disconnection of the link. This paper has made an effort to evade this. The prime goal of this paper is to distribute the energy uniformly across the network and to increase the network lifetime. Traditional routing algorithms use few parameters and put some conditions or threshold value for routing procedure [4, 5]. The contribution of this paper is a novel heuristic multi-objective hybrid routing with QoS assurance for heterogeneous WSNs. This protocol uses a novel weighted sum method to obtain optimal solution in order to resolve the multi-objective routing problems of existing protocols. Q-MOHRA applies multiple measures for the selection of the best route from source to destination. The various measures are (i) Reaction Time (ii) Control Overhead (iii) Average Energy consumption (iv) HOP Count (v) Link Quality Indicator. Q-MOHRA selects the energy efficient route. Packet Delivery Ratio (PDR), Average Energy Consumption (AEC), Jitter, Normalized Routing Load (NRL), etc. are the few QoS parameters used to compare the performance of Q-MOHRA. The performance of Q-MOHRA is superior compared with the state of the art solutions.

The remainder of the paper organized as follows. Section II summarizes the different multi-objective decision-making protocols. Q-MOHRA explained in section III. Section IV describes the simulation details and analysis of results. Section V concludes the work.

II. RELATED WORK

Many researchers based on various, criteria, design issues and applications in order to increase energy efficiency have proposed several multi-objective routing protocols [6].

Nevertheless, no routing protocol is ideal, which can be used for different applications and for different purposes.

The main purpose of Multi-Objective Swarm Optimization (2LB-MOPSO) [9] algorithm is to detect permanent and intermittent faults based on the multi-objective approach. It tries to find out the balance between detection accuracy and detection latency. This algorithm identifies defective sensor nodes based on the comparison of sensed data between one-hop neighboring nodes. It uses time redundancy to detect intermittent faults. This paper has demonstrated the effectiveness of the algorithm by using the multi-objective QoS parameters. The authors of the paper recommended using the parameters such as are Detection Accuracy (DA), False Detection Rate (FDR), diagnosis latency, network lifetime, and packet delivery ratio. The authors have also suggested a multi-objective optimization technique to identify an intermittent fault.

The authors in [10] proposed an innovative multi-objective routing optimization approach using evolutionary algorithms. This evolutionary algorithm tries to find out the trade-off between minimum lifetime and the average lifetime of nodes in the network. The authors have proposed a novel approach known as "k-shortest paths based search space pruning in conjunction with a new edge metric" in order to achieve faster optimization and to allow dynamic optimization. Due to scarcity of computing resources this evolutionary algorithms uses a centralized approach. The evolutionary algorithm tries to maximize the minimum lifetime of any node in the network together with the average life of all nodes in the network. The evolutionary algorithms use packet- loss ratio and QoS performance indicators as a feedback mechanism to upgrade the overall performance of the system when it declines.

Multi-Objective QoS Routing (MQoSR) [11] uses an empirical neighbor selection mechanism. It combines the geographic routing mechanism and QoS routing. MQoSR takes into account the quality of service parameters such as reliability, delay, distance to sink, energy, end-to-end delay, reliability and network lifetime. MQoSR builds multiple disjoint paths. MQoSR divides these QoS parameters into link QoS parameters and path QoS parameters. Link QoS parameters enable MQoSR to select the next hop and path QoS parameters allow to reduce the overall network resource consumption.

Multi-Objective Evolutionary Algorithm based on Decomposition (MOEA/D) [12] is designed to solve the energy conservation problem in WSN. MOEA/D solves the Multi-Objective Problem (MOP) by using problem-specific knowledge. MOEA/D divides the MOP into many sub-problems those can be optimized concurrently by using the local problem specific knowledge. MOEA/D alleviates the problem of unnecessary searches and harsh coupling, negatively affecting their overall performance. Functioning of MOEA/D solely depends on randomly generated internal population and calculation of the Euclidean distances between the weight vectors for generating more quality solutions. In MOEA/D, the optimization depends on sensors clustering with the choice of appropriate cluster-heads (CHs) and the active or inactive status of sensor nodes.

AACOCM [13] proposes a multi-objective model based on bandwidth constrained. AACOCM optimizes the route up to the destination based on multi-objective function. The multi-objective function tries to optimize multiple metrics such as energy consumption, network delay, and packet loss rate simultaneously. Each metric is associated with a weight. The algorithm adjusts well to several services by adjusting the weights. The prime goal of AACOCM is to reduce energy cost, delay, and packet loss ratio. AACOCM, defines three categories of they are, ordinary ants, greedy ants, unusual ants. In this algorithm, the progression of any ant from the source node to the destination node is a process of building a routing tree. Once the routing tree is constructed, the data is transmitted to the destination along the tree. The move probability of ordinary ant depends on the pheromone intensity trajectory and heuristic factor. Greedy ants pick the node having greatest probability as the next hop node. AACOCM uses adding positive and negative feedback mechanisms and depends on a cloud. . AACOCM is suitable for the large-scale network. The convergence rate is high in AACOCM.

For routing in WSN, the authors of [15] have proposed a framework. IT is adaptive, constraint-based, and multi-objective, and it is solely dependent on localized knowledge of each node. The authors have defined a routing task for each message m. The routing function depends on source id, single destination or a group of destination, local route constraints (LRC) and routing objective (RO). LRC applied to the current node's neighbors attribute. LRC could be avoided low-energy, hazardous areas, etc. RO depends on multiple attributes for optimizing the route. The various attributes are minimizing hop count, using the maximum energy level route, reducing hazard on the route.

Simple Hybrid Routing Protocol (SHRP) [16] is one of the energy saving protocol in WSN. SHRP selects the optimal route based on the hop count, link quality, and battery life. SHRP forwards the data only if there is a change compared with last sensed data. Among the multiple available paths, SHRP picks a route that has lesser hop count and larger available energy. If the sensed data remains unchanged during a prescribed period, SHRP forwards the data periodically to the BS. SHRP tackles the bad connection and dead neighboring problem with the help of minimum threshold.

DyMORA [16] uses the concept of Hybrid Routing Algorithm (HRP) from SHRP but it alters the mechanism with which the optimal route is selected. DyMORA is comparable with Hierarchical Routing Algorithm (HRA) that is an original version of SHRP. In terms of consistency, and time convergence DyMORA uses less energy level, but it needs more processing time. DyMORA uses multiple metrics simultaneously in order to select the best route up to the BS in critical situations or during energy crises

III. QoS Assured Multi-Objective Hybrid Routing Algorithm (Q-MOHRA)

Many everyday optimization problems have more than one trait to be considered at the same time, i.e., multiple objectives to be minimized or maximized. In multi-objective optimization domain, the researchers have identified different approaches. In scalarization approach, the multiple objective problems are

combined into a single function by using weighted sum approach. In the second approach, the domain expert might rank the objectives according to some order of preference. In this case, the domain expert access the objectives based on some predefined order. The second approach is known as lexicographical approach. In most of the real life problems, the multiple objectives are conflicting with each other. The above methods are not suitable to provide full set of optimized solutions as they introduce some prejudice. They offer few solutions, which will not often cover the entire set of objective space [8]. Unlike the scalarization and lexicographical approaches, Multi-Objective Hybrid Evolutionary Algorithms consider that all the objectives of a problem should be considered simultaneously. In order to tackle the complexity in a situation when multiple objectives are conflicting with each other, the algorithm should provide Pareto optimal solution such that the objective functions cannot be further optimized.

A. Assumptions to implement Q-MOHRA:

The entire target area is divided into small clusters. Each cluster has Cluster Heads (CH) and Cluster Member (CM). The sensor nodes are haphazardly placed in the target area and they are stationary. All the sensor nodes are heterogeneous in terms of initial energy. The CMs are liable for sensing the events in the nearby area. All the CMs harmonize themselves for selecting the CH. The CMs communicate only with the CH of that cluster or the CMs of the same cluster. They are not allowed to talk to CMs or even CH of the other cluster directly. The CHs have a second level of hierarchy. The CHs can communicate with the CHs of another cluster. The Base Station (BS) is a high-energy node situated away from the target area. The BS can communicate to any CH or CM directly. The Cluster Member (CM), Cluster Heads (CHs) and the sink node are stationary. The sensor nodes are not GPS enabled. At the outset, the density of sensor nodes in the target area very high as it helps for the cluster based routing.

B. Network model of Q-MOHRA:

As shown in Fig. 1 illustrates the WSN modeled as a graph G. Here, the vertices of the graph are nothing but sensor nodes of WSN. The graph G= (V, E) where V= {v1…..v2} is set of vertices, and E {(ni, nj) V x V | i ≠ j} is a set of edges between vi and vj. The graph G is modeled as a set of small clusters. The communication within the cluster (i.e. between the CMs and CMs or CHs) and the communication among the cluster (i.e. between the CHs and CHs is categorized into different levels of hierarchy. At the first level in the hierarchy, CMs within the cluster elect a CH based on a weighted average of multiple criteria (metrics) as mentioned in section III. The CMs will forward the data to the CH using multihop communication. The CMs will organize themselves like a pyramid. As we move, up in the pyramid the weighted average of multiple metrics increases. It is a rational organization and not physical arrangement. The node having greatest weighted average is CH. After successive rounds of communication, the role of CH is switched among the different CMs. This rotation of the role of CH among different CMs will balances the energy in the entire network. At the second layer of the hierarchy, all the CHs will organize themselves like a pyramid and the communication procedure is same as that of intra-cluster communication. The CH is elected in each round at each level. The elected CH will forward the accumulated data to the BS after applying some aggregation function to the accumulated data.

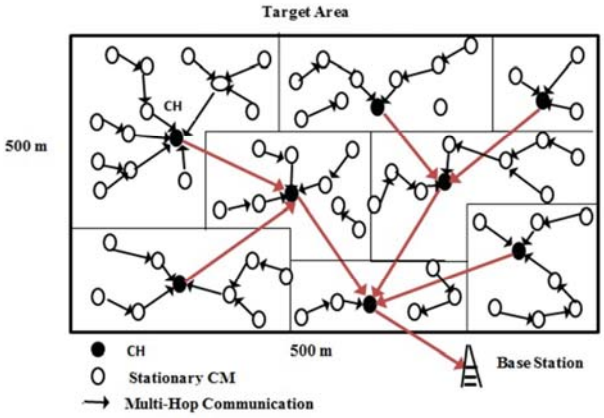

Fig. 1. A Clustered Wireless Sensor Network

C. Q-MOHRA Algorithm

Q-MOHRA is a multi-objective hybrid routing protocol based Weighted Average Method (WAM). At a high level, Q-MOHRA operations are forked into three phases.

- Establishing Neighborhood Relationships
- Routing
- Data Forwarding

1) Establishing Neighborhood Relationships

In Q-MOHRA, the routing scheme starts with Building Neighborhood Relationship. Each node has a routing table and it maintains a list called as neighborhood information. The routing table has following information for each neighbor

Neighbor ID	energy	LQI	Overhead	rtime	hops

The procedure for Building Neighborhood Relationship is as follows

- After power on a node-N in the network will broadcast a Hello Packet out to discover 1–hop neighbors.
- If a 1-hop neighbor is available then in response to the Hello packet the nodes will send a reply message.
- The reply message will contain the information about Neighbor ID, energy, LQI, Overhead, rtime and hops.
- On receipt of the reply message, the node-N will attempt to establish a neighborhood relationship with new nodes.
- Node-N will add the information about the new nodes directly into the routing table.
- All these steps are repeated periodically or whenever there is a change in the network.

2) Routing

The optimized route is calculated based on the routing table. Each node will calculate a weighted average of multiple metrics (score) as mentioned in TABLE I for each neighbor available. The score is calculated based on WAM. The CH election is based on a global parameter [7] as

$$f(n_{ij}) = \alpha.m_{energy}(n_{ij}) + (1-\alpha).\Big[\beta.m_{overhead}(n_{ij}) + (1-\beta)\Big[\gamma.m_{rtime}(n_{ij}) + (1-\gamma)\Big[\delta.m_{lqi}(n_{ij}) + (1-\delta)[\eta.m_{hops}(n_{ij})]\Big]\Big]\Big] \quad (1)$$

Where $0 \leq \alpha, \beta, \gamma, \delta, \eta \leq 1$ and $\alpha + \beta + \gamma + \delta + \eta = 1$ are weighing factors. All CM will evaluate the cost function according to the updated values in the routing table. CMs will form a pyramid (logical) and the CM with largest weighted average becomes the CH for the next iteration.

3) Data Forwarding

The data packet is forwarded up in the pyramid (forwarded to parent node in multi hop communication). The information about whom to forward is available from the routing table. The packet will get propagated up in the hierarchy. This is continued until the data packet reaches the sink node.

IV. Simulation and Result Analysis

The simulation is carried out using Network Simulator (ns2.34). The aim of the simulation is to annotate the QoS parameters and compare the Average Energy Consumption (AEC), Jitter, Normalized Routing Load (NRL) and Packet Delivery Ratio (PDR) in Q-MOHRA, SHRP, and DyMORA. To authenticate the performance of Q-MOHRA, following simulation parameters mentioned in Table II are used

TABLE I. Simulation Parameters

Parameter	Q-MOHRA	SHRP	DyMORA
Area (m)	500 * 500	500 * 500	500 * 500
Simulation time (s)	200	200	200
Initial Energy (J)	10	10	10
Rate :	0.2	0.2	0.2
Packet size (bytes)	512	512	512
Simulation Time	200 s	200 s	200 s
Number of nodes	50 -100 in step of 10		
Radio Model	TR3000		
Transmission power	24.75mW		
Receiving power	13.5mW		
Idle Power	13.5mW		
Sleep Power	15µW		

A. Packet Delivery Ratio (PDR)

PDR gives the liaison between the total number of packets received by the destination and overall packets produced by all the nodes. Fig. 2 demonstrates the packet delivery ratio of Q-MOHRA, SHRP, and DyMORA. Due to the multi-criteria mechanism, Q-MOHRA has PDR higher than DyMORA by a factor of 28.63 % and a factor of 13.8% than SHRP in various circumstances due to routing of the packets on an optimized route. The PDR confirms that the sensor nodes are used efficiently for advancing data packets. This results into increase of network life. In Q-MOHRA, PDR is higher because each node selects the optimal path based on multi-objective metrics .

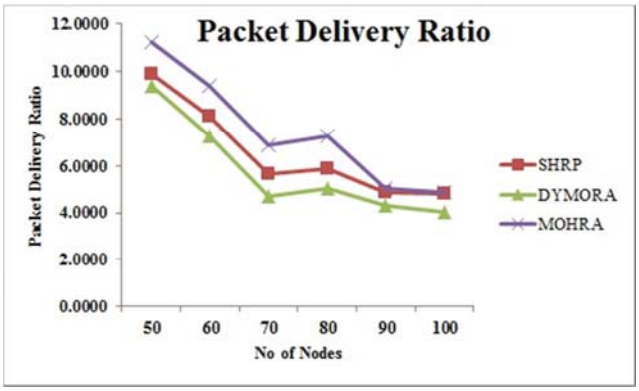

Fig. 2. Packet Delivery Ratio.

B. Average Energy Consumption (AEC)

AEC is a ratio of sum of the energy consumption of different nodes to the sum of total number of nodes. Fig. 3 shows the average energy consumption. AEC of Q-MOHRA is lesser than DyMORA and SHRP in several circumstances due to hierarchical clustering. Q-MOHRA outperforms SHRP by a factor of 2.3 % and DyMORA by 4.2 % in terms of AEC. This saving of energy extends the life of the overall system and illustrates the effectiveness of Q-MOHRA.

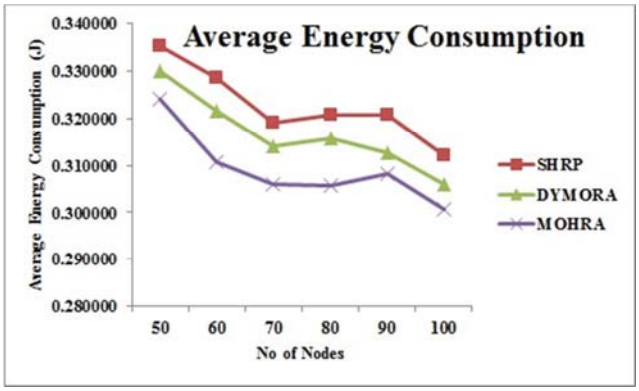

Fig. 3. Average Energy Consumption.

C. Normalized Routing Load (NRL)

Normalized Routing Load is calculated as a ratio of total number of routing packet transmitted including total no of forwarded routing packets per data packet. Q-MOHRA is a multi-objective hybrid routing protocol and it addresses QoS parameters from different layers in the WSN architecture. Q-MOHRA uses weighted average of Control Overhead, HOP Count LQI, and Average Energy consumption Reaction Time, for selecting the best path from source to sink. Routing overhead is less in Q-MOHRA by 18 % than DyMORA and 5% than SHRP. Fig. 4 gives a comparison of NRL between SHRP and DyMORA.

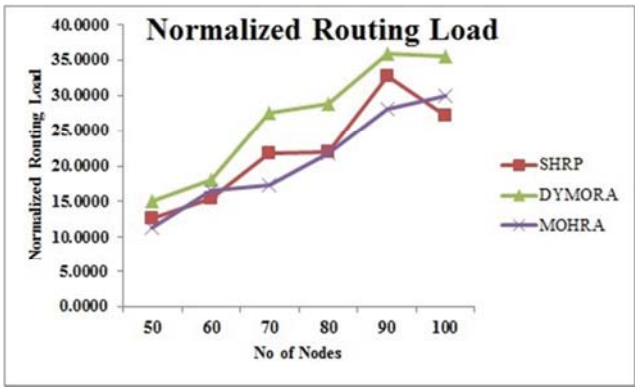

Fig. 4. Normalized Routing Load

D. Jitter

Fig. 5 illustrate the comparison of jitter. Q-MOHRA has lower jitter than SHRP and DyMORA. In WSN, the endwise one-way difference in delay between packets arrivals at destination is called as Jitter. Q-MOHRA is more efficient in routing the packets from source to destination as compared to SHRP and DyMORA. Q-MOHRA improves jitter by a factor of 19.1% and 14.7% as compared to DyMORA and SHRP respectively.

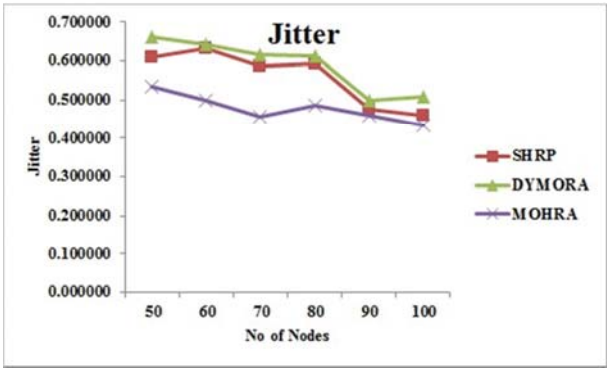

Fig. 5. Jitter

V. CONCLUSIONS AND FUTURE WORK

This paper proposes an innovative QoS assured Multi-Objective Hybrid Routing Algorithm called Q-MOHRA for WSNs. The main goal of Q-MOHRA is to assure QoS while selecting an optimal route up to sink based on multi-objective criteria. The performance of Q-MOHRA is evaluated and equated with two multi-objective hybrid routing algorithms, SHRP, and DyMORA. Q-MOHRA is energy efficient as comparing to SHRP and DyMORA. Q-MOHRA outperforms SHRP and DyMORA in terms of average energy consumption, jitter, Normalized Routing Load, and packet delivery ratio. The routing protocol can be extended taking into consideration the parameters such as heterogeneity and mobility of both sensor nodes and sink.

REFERENCES

[1] I. F. Akyildiz, W. Su, Y. Sankarasubramaniam, and E. Cayirci, “Wireless Sensor Networks:A Survey”, Computer Networks, Vol. 38, Issue 4, pp. 393–422, DOI- 10.1016/S1389-1286(01)00302-4, 2002.

[2] J. Al-Karaki and A. Kamal, “Routing techniques in wireless sensor networks: a survey”, IEEE Journal, Wireless Communications, Vol. 11 , Issue 6, pp . 6-28, DOI - 10.1109/MWC.2004.1368893, 2004.

[3] N. Pantazis, S. Nikolidakis and D. Vergados, “Energy-Efficient Routing Protocols in Wireless Sensor Networks: A Survey”, IEEE Journal, Communications Survey and Tutorials, Vol.15, Issue 2, pp. 551-591, DOI- 10.1109/SURV.2012.062612.00084, 2013.

[4] S. Ehsan and B. Hamdaoui, “A survey on energy-efficient routing techniqueswith QoS assurances for wireless multimedia sensor networks”, IEEE Journal, Communications Survey and Tutorials, Vol.14, Issue 2, pp. 265-278, DOI- 10.1109/SURV.2011.020211.00058, 2012.

[5] N. Magaiaa, N. Hortab, R. Nevesb, P. Pereiraa and M. Correia, “A multi-objective routing algorithm for Wireless MultimediaSensor Networks”, ELSEVIER Journal, Applied Soft Computing, vol - 30 pp. 104–112, DOI- 10.1016/j.asoc.2015.01.052, 2015.

[6] M. Bala Krishna and M. Doja, “Multi-Objective Meta-Heuristic Approach for Energy-Efficient Secure Data Aggregation in Wireless Sensor Networks”, Springer Journal , Wireless Personal Communication, Vol. 81, pp, 1:16, DOI 10.1007/s11277-014-2114-3, 2015.

[7] N. Kulkarni, N. R. Prasad and R. Prasad, “G-MOHRA: Green Multi-Objective Hybrid Routing Algorithm for Wireless Sensor Networks”, International Conference on Advances in Computing, Communications and Informatics (ICACCI), New Delhi, India, pp. 2185 – 2190, DOI-10.1109/ICACCI.2014.6968329, 2014

[8] D. Bucur, G. Iacca, G. Squillero and A.Tonda, “The tradeoffs between data delivery ratio and energy costs in wireless sensor networks: a multi-objectiveevolutionary framework for protocol analysis”, Proceedings of the 2014 conference on Genetic and evolutionary computation (GECCO), ACM New York, NY, USA, pp. 1071-1078, DOI-10.1145/2576768.2598384, 2014.

[9] A. Mahapatro, A. Panda, “Choice of Detection Parameters on Fault Detection in Wireless Sensor Networks: A Multiobjective Optimization Approach”, Springer Journal , Wireless Personal Communication, Vol. 78, pp, 649–669, DOI 10.1007/s11277-014-1776-1, 2014

[10] A. Rahat, R. Everson and J. Fieldsend, “Multi-Objective Routing Optimisation for Battery-Powered Wireless Sensor Mesh Networks”, Proceedings of the 2014 conference on Genetic and evolutionary computation (GECCO), ACM New York, NY, USA, pp. 1175-1182, DOI-10.1145/2576768.2598311, 2014.

[11] H. Alwan and A. Agrawal, “Multi-Objective Qos Routing for Wireless Sensor Network”, International Conference on Computing, Networking and Communications (ICNC), San Diego, CA, pp. 1074-1079, DOI-10.1109/ICCNC.2013.6504241, 2013

[12] S. Özdemir, B. Attea and Ö. Khalil, “Multi-Objective Evolutionary Algorithm Based on Decomposition for Energy Efficient Coverage in Wireless Sensor Networks”, Springer Journal , Wireless Personal Communication, Vol. 71, pp, 195–215, DOI 10.1007/s11277-012-0811-3, 2013.

[13] X. Wei and L. Zhi, “The multi-objective routing optimization of WSNs based on an improved ant colony algorithm”, 6th International Conference on Wireless Communications Networking and Mobile Computing (WiCOM), pp. 1-4, DOI- 10.1109/WICOM.2010.5601072, 2010

[14] S. Bhunia, S. Roy and N. Mukherjee, “Adaptive Learning assisted Routing in Wireless Sensor Network using Multi Criteria Decision Model”, International Conference on Advances in Computing, Communications and Informatics (ICACCI), New Delhi, India, pp. 2149 – 2154, DOI- 10.1109/ICACCI.2014.6968354, 2014

[15] D.Mahjoub and H.El-Rewini, “Adaptive Constraint-Based Multi-Objective Routing for Wireless Sensor Networks”, In Proceedings of IEEE International Conference on Pervasive Services, Istanbul, pp. 72–75, 2007.

[16] G. Valentini, C. Abbas, L. Villalba, and L. Astorga, “DyMORA :A Multi-Objective Routing Solution Applied on Wireless Sensor Networks”, IET Communications, Volume. 4, Issue. 14, pp. 1732–1741, 2010.

THE 18TH INTERNATIONAL SYMPOSIUM ON WIRELESS PERSONAL MULTIMEDIA COMMUNICATIONS
(WPMC-2015)
December 13-16, 2015, Hyderabad, India

Two-Party Key Agreement Protocol for MANETs based on Verifiable Secret Sharing Scheme

Ch. Asha Jyothi
Department of Information Technology
JNTUH College of Engineering Jagtial
Kondagattu, Karimnagar, Telangana, India
asha.prathap@yahoo.co.in

G. Narsimha
Department of Computer Science and Engineering
JNTUH College of Engineering Jagtial
Kondagattu, Karimnagar, Telangana, India
narsimha06@gmail.com

***Abstract*— The nodes of the Mobile Ad Hoc Network (MANET) are movable. This leads to unpredictable nature of node mobility and continuously changing topology there by difficulty in maintaining central control over the nodes of MANET. Secondly, the essential requirement of most of the cryptographic techniques is to share a key between the two end parties of the communication. To address the above two issues and to implement security in MANET environment, there is a basic need of sharing a key between the two communicating parties without the help of central management like Certification Authority CA or Key Generation Centre KCG or Key Distribution Centre KDC. This problem is addressed here with the help of verifiable secret sharing and bilinear pairing concepts. A verifiable secret sharing (VSS) scheme is an extension of standard secret sharing scheme with the additional property that every participant is able to validate whether the share distributed to him by a dealer is accurate. This additional property is ensured with the help of commitments created for the coefficients of a polynomial commonly used in the standard secret sharing schemes like Shamir's secret sharing. Pairings on elliptic curves initially are used as cryptanalysis tool but since 2000 they are also used to construct cryptographic systems.**

Keywords*— *Verifiable Secret Sharing, Bilinear maps, Pairings, Key Distribution protocol, Key Agreement protocol, Mobile Ad Hoc Networks.

I. INTRODUCTION

Key establishment [15] is the mechanism of sharing a secret key between two or more users. There by this secret key can be used to realize some cryptographic services like confidentiality or data integrity. Key establishment protocols are of two types namely key transport protocols and key agreement protocols. In key transport protocols, any user can choose the key and securely transmit it to the other user. In key agreement protocols both the users contribute information required to generate the shared secret key. Our key establishment protocol is especially key agreement protocol based on verifiable secret sharing scheme and bilinear pairings and very much suitable for MANETs environment due to non requirement of central authority.

A standard secret sharing scheme [2] is the process of dividing a secret into n number of shares and distributing each share to each participant of a set of n participants in such a manner that only qualified subsets of t participants can collude to construct the secret from their shares. In standard secret sharing schemes [2], the dealer and participants are believed to be honest. But dealer or participants may misbehave in real world practices i.e., dealer [3] may transmit incorrect shares to some or all of the participants during distribution phase or participants may submit incorrect shares during the reconstruction phase or the shares may be modified by the adversary during transmission of secret shares. To address all these issues, integrity service must be provided to the secret shares in the form of commitments. Such solution is provided by Verifiable secret sharing schemes. A verifiable secret sharing (VSS) [2][3] scheme is a secret sharing scheme with an extra property that every participant is capable to verify whether the share received by him from a dealer is accurate. VSS is an elementary tool of threshold cryptography and decentralized computing. VSS is a useful tool for protecting threshold cryptography schemes from malicious attackers.

A Mobile Ad Hoc Network (MANET) [4] consists of a huge number of mobile devices, moving within an unpredictable (or sometimes well specified) area, using wireless transmission channels in a hop-by-hop mode, without the help of any fixed infrastructure or centralized administration. The basic inherent characteristics [4] of Mobile Ad Hoc Networks (MANETs) are dynamic topology, absence of infrastructure and hence difficult to setup a traditional central authority for central control, limited bandwidth, limited power supply and hence the nodes may present selfishness behavior, node cooperation, self configuration etc. Such characteristics cause them to be more exposed to attacks than other types of networks. These characteristics also cause the traditional security mechanisms unsuitable for them. However, in MANETs, key distribution process is challenging as a consequence of its non-centralized structure. Obviously no user is always available; consequently no user alone can be used as a central authority. Hence we present a two-party key distribution protocol without the need of central administration and that consumes fewer resources and increases the level of security. This model makes use of pairing based cryptography and verifiable secret sharing VSS schemes. If we choose pairing friendly elliptic curves [1], the computational cost reduces to much extent and as elliptic curve cryptography is involved, it improves the intensity of security. VSS scheme avoids the attacks on integrity of the

secret shares performed either by the dealer, or participants, or attacker.

Lack of Infrastructure and dynamic topology nature of MANETs causes difficulty in establishment of Central Administrator; and key sharing between the source and destination is needed by most of the cryptographic mechanisms. So in MANET environment to provide security, certainly there is a necessity of a key distribution protocol without central administration. Our previous paper [5] proposed a model to address this requirement, but suffers from the problem of lack of integrity to the secret shares. So here we are appending the concept of verifiable secret sharing to make our previous work a complete solution. Along with the secret shares the source will also send the commitments to the destination so that the integrity of secret shares is ensured.

The paper organization is as follows. Section II briefly describes the background essentials required for understanding the proposed protocol. Section III elaborates the two major building blocks of the proposed model namely Joux's protocol and Jie and Futai's Verifiable Secret Sharing scheme. Section IV gives the detailed procedure of the proposed model. Section V gives the conclusion for the paper.

II. BACKGROUND ESSENTIALS

The proposed model uses the concepts of Pairings or Bilinear maps and Verifiable secret sharing, a specialization of threshold cryptography. So we elaborate these concepts in this section.

A. *Bilinear Pairing or Bilinear Map*

Let D_1, D_2 and D_3 be three abelian groups of the same order q, a prime. Consider D_1, D_2 as additive groups and D_3 as a multiplicative group. Assume that discrete logarithm problem (DLP) is hard in D_1, D_2 and D_3. A mapping $f : D_1 \times D_2 \rightarrow D_3$ satisfying the following properties is called a cryptographic bilinear map or bilinear pairing [7].

Bilinearity For $X_1, X_2 \in D_1$ and $Y_1, Y_2 \in D_2$

$$f(X_1+X_2, Y_1) = f(X_1, Y_1)f(X_2, Y_1)$$

$$f(X_1, Y_1+Y_2) = f(X_1, Y_1)f(X_1, Y_2)$$

Mathematically it is equivalent to $f([a]X_1, [b]Y_1) = f(X_1, Y_1)^{ab}$ for all a; b $\in \mathbb{Z}_q^*$. [a]P denotes P added to itself a times.

Non-degeneracy For all $X \in D_1\backslash\{0\}$ exists $Y \in D_2$ with $f(X, Y) \neq 1$.

For all $Y \in D_2\backslash\{0\}$ exists $X \in D_1$ with $f(X, Y) \neq 1$.

Computable There exists an efficient polynomial time computable algorithm to compute f(X, Y) for all $X \in D_1$, $Y \in D_2$.

Pairings on elliptic curves initially are used as cryptanalysis tool to attack Discrete Logarithm DL-based elliptic curve cryptography problems. Since 2000 they are also used to construct cryptographic systems. Some of them are one round tripartite key agreement [8], Identity based key agreement [9], Identity Based Encryption (IBE) [10], Hierarchical IBE [11], Short signatures [12] etc.

B. *Verifiable Secret Sharing*

The idea of verifiable secret sharing (VSS) [2] was first initiated in 1985 by Benny Chor et. al. The users that are part of VSS protocol are a dealer and set of participants; dealer is not part of the set of participants. Dealer wants to share the secret among the set of n participants by dividing the secret into n shares with each share distributed to each participant. The standard secret sharing scheme consists of two phases [3]: the distribution phase and reconstruction phase. As part of distribution phase the dealer divides the secret into n shares and distributes them to the set of n participants. As part of reconstruction phase a subset of at least t participants correlate all their shares and reconstruct the secret. Fewer than t participants can never reconstruct the key. So here the concept of threshold cryptography and especially Shamir secret sharing scheme [6] can be used for implementation. Unique to VSS, the dealer [2] broadcasts t commitments to the coefficients of the t-1 degree polynomial involved in the Shamir scheme. Once these commitments are received any party can verify their share so that the integrity of the shares can be ensured. This is called verification phase, additional phase in VSS.

The basic procedure of a VSS scheme is comparatively the same as standard secret sharing scheme expect an extra verification phase between the standard distribution phase and reconstruction phase, which can be easily implemented with the public commitments of some secret information during the distribution step. So VSS scheme consists of three different phases specifically the distribution or sharing phase, the verification or authentication phase and the reconstruction or restoration phase as shown in figure 1.

Fig. 1. Phases of Verifiable Secret Sharing Scheme

There are two types of VSS schemes: Interactive VSS and Non-interactive VSS. With Interactive VSS, interaction between dealer and participants is needed for verification. Goldwasser-Micali VSS [17], Benaloh VSS [18] are some of the interactive VSS schemes. With Non-interactive VSS, interaction between dealer and participants is not needed for verification. Feldman VSS [16], T Pedersen's VSS [19] are some of the Non-interactive VSS schemes. The proposed model is a non-interactive VSS as it is based on Jie and Futai's VSS which in turn is based on Feldman VSS.

III. BUILDING BLOCKS

The proposed model is based on Joux's protocol [8] and Jie and Futai's verifiable secret sharing scheme [13]; hence

these are the building blocks. In this section we brief the building blocks of the proposed model.

A. *Joux's Protocol*

Joux's protocol [5][8][14] is a very simple and well-designed tripartite one-round protocol. In other words it is used to establish a secret session key for three parties by just one broadcast per party. Assume A, B, and C want to share a secret key among them. Consider Symmetric pairing D1 x D1 → D3. Let P be the generator of D1. In this protocol, x, y, z ∈ Z_q^* are integers chosen at random by A, B and C respectively. The order of protocol communication messages is irrelevant and any of the three entities can initiate the protocol. In the protocol communication the symbol "→" indicates "Sends to".

Protocol Communication

A → B, C : [x]P

B → A, C : [y]P

C → A, B : [z]P

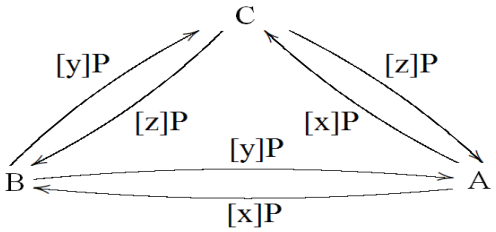

Fig. 2. Joux's Tripartite Key Agreement

Protocol Description

Once the communication is finished as shown above and in figure 2, A computes $K_A = f([y]P, [z]P)^x$, B computes $K_B = f([x]P, [z]P)^y$ and C computes $K_C = f([x]P, [y]P)^z$. From bi-linearity property of f, K_A, K_B, K_C are all equal to $K_{ABC} = f(P, P)^{xyz}$. This can act as the secret key shared by A, B and C. The security strength of Joux's protocol depends on the Bilinear Diffie-Hellman Assumption that is stated below.

Bilinear Diffie-Hellman Problem

There are several problems associated with pairings. Here we define only the BDH problem needed for our protocol. This problem is stated as follows:

Given P, uP, vP, wP with u, v and w chosen uniformly at random from Z_q^*, the computation of $f(P, P)^{uvw}$ is hard.

B. *Jie and Futai's VSS*

Jie and Futai's [13] scheme is a verifiable secret sharing scheme consisting of three phases the sharing or distribution phase, the verification phase and the reconstruction phase. This scheme considers a symmetric bilinear map $f : D_1 \times D_1 \rightarrow D_3$. Choose a random generator P from D_1. Suppose the number of participants is n and the threshold is t, the minimum number of participants that correlate to reconstruct the secret key such that $t \leq n$. The parameters in this scheme are $<D_1, D_3, f, P, f(P, P), t, n>$. The scheme functions as follows.

Distribution Phase

(1) Dealer chooses a secret K = [s]P to be distributed to n participants; s is the randomly chosen integer from Z_q^*.

(2) Dealer chooses a polynomial $p(x) = p_0 + p_1x + ... + p_{t-1}x_{t-1}$ where $p_0 = s$ and $p_1, p_2, ..., p_{t-1}$ are randomly selected from Z_q^*.

(3) Dealer calculates and broadcasts $Comm_i = f(P, P)^{p_i}$ for i = 0 to t-1 as the commitments of K and p(x).

(4) Dealer calculates the share $K_i = [p(i)]P$ mod q and sends each share secretly to participant R_i, for i = 1 to n.

Verification Phase

When participant R_i receives his share K_i from the dealer, he verifies if

$$f(K_i, P) = \prod_{j=0}^{t-1} Comm_j^{i^j}$$

If the verification is not successful, the share K_i received by R_i participant is invalid.

Reconstruction Phase

Suppose $R_1, R_2, ..., R_t$ be the t participants want to reconstruct the shared secret K. Each R_i broadcasts his share K_i to the remaining t-1 participants and every participant can check the validity of the received share using the above equation of verification phase. Once all the t shares K_i are confirmed to be legitimate, every participant can rebuild the secret K using the following equation.

$$K = \sum_{c=1}^{t} K_c \prod_{1 \leq d \leq t, d \neq c} \frac{d}{c - d}$$

IV. THE PROPOSED MODEL

The proposed model does not have dealer, and set of participants, but has only source and destination who wish to share a secret key between them because the aim of this model is to share a secret key between the two end parties of communication. Source plays the role of dealer and destination plays the role of set of participants. Source chooses the secret key to be shared with the destination, partitions the secret key into n shares using Shamir's secret sharing scheme [6], where n is the number of disjoint paths exist between source and destination. Source calculates the t commitments to the coefficients of t-1 degree polynomial and transmits the shares and commitments to the destination via n disjoint paths. Once the destination receives at least t shares and t commitments, it can verify the shares using commitments and if verification is successful, then reconstruct the secret key there by a secret key is established between the source and destination without the support of centralized trusted authority.

After the text edit has been completed, the paper is ready for the template. Duplicate the template file by using the Save As command, and use the naming convention prescribed by your conference for the name of your paper. In this newly created file, highlight all of the contents and import your prepared text file. You are now ready to style your paper; use the scroll down window on the left of the MS Word Formatting toolbar.

A. Protocol Description

If Joux's protocol is directly extended to two-party key agreement, the protocol works as below and shown in figure 3.

(1) $A \rightarrow B$: [x]P

(2) $B \rightarrow A$: [y]P

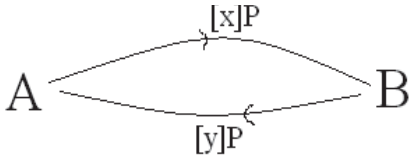

Fig. 3. Joux's protocol extension to two-party

Once [x]P and [y]P are received by B and A respectively, A calculates the key as $f(P, [y]P)^x$ and B calculates the key as $f([x]P, P)^y$ and both the calculations result in the same value $f(P, P)^{xy}$ according to the bilinear property of pairings.

But if adversary can intercept [x]P and [y]P during steps 1 and 2 above, he can also easily compute the key as f([x]P, [y]P) = $f(P, P)^{xy}$. So we cannot directly extend Joux's protocol to two-party key agreement. These issues are handled in our proposed model that is described below.

Consider the symmetric pairing $f : D_1 \times D_1 \rightarrow D_3$, where D_1 and D_3 are finite cyclic groups to same prime order q; D_1 is written additively and D_3 is written multiplicatively; $D_1 \subseteq E(Fp)$, $D_3 \subseteq (Fp\alpha)^*$ (embedding degree α = 1, 2, 3, 4, 6, 10, 12) [20]. This model can also be used with asymmetric pairing, but here we consider symmetric pairing for simplicity. Consider a random generator of D_1 as P. Let A and B wants to share a secret key K between them. The model functions as follows.

(1) A chooses $S_1 = [u]P$ where u is chosen at random from Z_q^*.

Similarly B chooses $S_2 = [v]P$ where v is chosen at random from Z_q^*.

(2) A selects a polynomial $p_1(x) = a_0 + a_1x + ... + a_{t-1}x_{t-1}$ where $a_0 = u$ and $a_1, a_2, ..., a_{t-1}$ are randomly selected from Z_q^*.

B selects a polynomial $p_2(x) = b_0 + b_1x + ... + b_{t-1}x_{t-1}$ where $b_0 = v$ and $b_1, b_2, ..., b_{t-1}$ are randomly selected from Z_q^*.

(3) A calculates $CA_i = f(P, P)^{a_i}$ for i = 0 to t-1 as the commitments of S_1 and $p_1(x)$. These values are transmitted to B via multiple paths so that they certainly reach B.

(4) B calculates $CB_i = f(P, P)^{b_i}$ for i = 0 to t-1 as the commitments of S_2 and $p_2(x)$. These values are transmitted to A via multiple paths so that they certainly reach A.

(5) A calculates the shares $U_i = [p_1(i)]P$ mod q for i = 1 to n and then sends the shares to B via n disjoint paths; one share thru each path.

B calculates the shares $V_i = [p_2(i)]P$ mod q for i = 1 to n and then sends the shares to A via n disjoint paths; one share thru each path.

(6) Once A receives at least t shares V_i and t commitment CB_i from B, he verifies the shares using the commitments as

$$f(V_i, P) = \prod_{j=0}^{t-1} CB_j^{ij}$$

Once B receives at least t shares U_i and t commitment CA_i from A, he verifies the shares using the commitments as

$$f(U_i, P) = \prod_{j=0}^{t-1} CA_j^{ij}$$

(7) Once the verification is successful, A reconstructs S_2 using the equation

$$S_2 = \sum_{i=1}^{t} V_i \prod_{1 \le j \le t, j=i} \frac{j}{j-i}$$

B reconstructs S_1 using the equation

$$S_1 = \sum_{i=1}^{t} U_i \prod_{1 \le j \le t, j=i} \frac{j}{j-i}$$

(8) A computes the secret key using the equation $f(P, S_2)^u$ and B computes the secret key using the equation $f(S_1, P)^v$. From the bi-linearity property of f, both the equations result in the same value $K = f(P,P)^{uv}$.

Among these 8 steps, steps 1-5 are part of Distribution phase, step 6 is the Verification phase and step 7 is the Reconstruction phase. By these seven steps S_1 and S_2 are exchanged between A and B, and these values are used in step8 to compute the secret key K. Hence secret key K is shared by A and B successfully.

If the shares of S1 and S2 are send via n independent paths between A and B without using commitment concept [5], the shares can be altered by the attacker during their transmission. There is no assurance to the receiver that the received shares are exact as sent by the sender. So, there is a need to provide integrity service to the shares and that is provided by the additional commitment concept of verifiable secret sharing compared to standard secret sharing schemes.

The above process for easy understanding can be simplified as follows:

(1) [u]P is transmitted from A to B by applying Jie and Futai's VSS technique on [u]P. Symbolically be represented as JF-VSS([u]P).
(2) [v]P is transmitted from B to A by applying Jie and Futai's VSS technique on [v]P. Symbolically be represented as JF-VSS([v]P).
(3) Once A receives [v]P successfully from B, computes the key $K = f(P, [v]P)^u$
(4) Once B receives [u]P successfully from A, computes the key $K = f([u]P, p)^v$. Hence key K is successfully shared between the two users A and B.

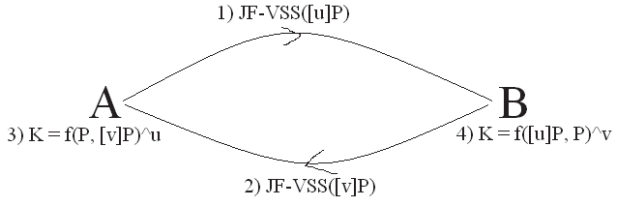

Fig. 4. Simplified Proposed Model

B. *Security Analysis*

Joux's protocol prevents the passive attacks but is vulnerable to man-in-the middle attack and active attacks. To counter these problems of Joux's protocol we appended the concept of verifiable secret sharing scheme. The man-in-the middle attack is prevented because [u]P and [v]P values are not send out directly, but are divided into shares using Jie and Futai's VSS technique. The active attacks are prevented by ensuring the integrity of secret shares using the commitments feature of verifiable secret sharing scheme. The deficiencies of Joux's protocol are addressed and also extended to two-party key agreement. As the n secret shares are transmitted via n independent or disjoint paths that exist between source and destination, the adversary or opponent [5] has to capture at least t shares by intercepting t paths at the same time, unless until he cannot recover the secret key. The cryptanalysis complexity has improved t times. As Jie and Futai's VSS is the major building block of the proposed model, the security analysis of proposed model can be inherited from Jie and Futai's VSS scheme [13].

V. Conclusion and Future Scope

We have proposed a simple and efficient model to share a secret key between the two end parties of communication without the support of central authority like certification authority, key generation centre or key distribution centre. This model is very much suitable to MANET environment due to MANET characteristics like lack of central administration and limited resources. Our model used the concepts of Joux's protocol and Jie & Futai's verifiable secret sharing. This secret that is shared between the two end-parties of communication can further be used as a secret key in Symmetric encryption algorithms. As key distribution along with encryption and signature algorithms provides a complete security solution for MANETs, we would plan to design encryption and signature pairing-based algorithms using this shared secret key.

References

[1] Paulo S. L. M. Barreto and Michael Naehrig, "Pairing-Friendly Elliptic Curves of Prime Order," In Selected Areas in Cryptography – SAC'2005, vol. 3897 of Lecture Notes in Computer Science, PP. 319–331. Springer-Verlag, 2006.

[2] Wiki web page on Verifiable secret sharing at, "https://en.wikipedia.org/wiki/Verifiable_secret_sharing".

[3] Berry Schoenmakers, "A Simple Publicly Verifiable Secret Sharing Scheme and its Application to Electronic Voting," In Advances in Cryptology—CRYPTO '99, vol. 1666 of Lecture Notes in Computer Science, Springer-Verlag, 1999, pp. 148-164.

[4] Hakima Chaouchi, Maryline Laurent-Maknavicius, "Wireless and Mobile Network Security-Security Basics, Security in On-the-shelf and Emerging Technologies," Published by ISTE Ltd and John Wiley & Sons, Inc. 2009, pp. 484-485, 525.

[5] Ch. Asha Jyothi, G. Narsimha, J. Prathap, Gorti VNKV Subba Rao,: "Two-Party Threshold Key Agreement Protocol for MANETs using Pairings," Global Journal of Computer Science and Technology (Network, Web & Security), GJCST vol. 15 Issue 5 Version 1.0 Year 2015.

[6] A. Shamir, "How to share a secret," Communications of the ACM, vol. 22(11), pp. 612–613, 1979.

[7] Youliang Tian, Changgen Peng, and Jianfeng Ma, "Publicly Verifiable Secret Sharing Schemes Using Bilinear Pairings," International Journal of Network Security, vol.14, No.3, pp. 142-148, May 2012.

[8] Antoine Joux, "A One Round Protocol for Tripartite Diffie-Hellman," LNCS 1838, pp. 385-393, Springer-Verlag Berlin Heidelberg 2000.

[9] R. Sakai, K. Ohgishi, and M. Kasahara, "Cryptosystems based on pairing," In The 2000 Sympoium on Cryptography and Information Security, Okinawa, Japan, January 2001.

[10] D. Boneh, M. Franklin, "Identity Based Encryption from the Weil Pairing," In Advances in Cryptology - Crypto '2001, LNCS 2139, Springer-Verlag (2001), pp. 213-229.

[11] C. Gentry and A. Silverberg, "Hierarchical ID-Based Cryptography," In Y. Zheng, editor, Proceedings of Asiacrypt 2002, LNCS, Springer-Verlag, 2002.

[12] D. Boneh, B. Lynn, H. Shacham, "Short Signatures from the Weil Pairing," In Proceedings of Asiacrypt 2001.

[13] Jie Zhang, Futai Zhang, "Efficient Verifiable Secret Sharing Scheme over Bilinear Groups," Advances in Information Sciences and Service Sciences(AISS) vol. 4, Number23, pp. 256-264, Dec 2012, doi: 10.4156/AISS.vol4.issue23.32

[14] S. S. Al-Riyami and K. G. Paterson, "Tripartite authenticated key agreement protocols from pairings," In IMA Conference on Cryptography and Coding, vol. 2898 of Lecture Notes in Computer Science, pages 332–359. Springer-Verlag, 2003.

[15] K Chakraborty, J Mehta, "Preventing Unknown Key-Share Attack using Cryptographic Bilinear Maps," Journal of Discrete Mathematical Sciences and Crptography, 2014.

[16] Paul Feldman, "A practical scheme for non-interactive verifiable secret sharing", In Proceeding of the 28th IEEE Symposium on the Foundations of Computer Science, pp.427-437, 1987.

[17] Benny Chor, Shafi Goldwasser, Silvio Micali, Baruch Awerbuch, "Verifiable secret sharing and achieving simultaneity in the presence of faults", In Proceeding of the 26th Annual Symposium on Foundations of Computer Science, pp.383-395, 1985.

[18] J. Benaloh, "Secret sharing homomorphisms: Keeping shares of a secret secret," In Advances in Cryptology CRYPTO '86, vol. 263 of Lecture Notes in Computer Science, pages 251–260, Berlin, 1987. Springer-Verlag.

[19] T. P. Pedersen, "Non-interactive and information-theoretic secure verifiable secret sharing," In Advances in Cryptology—CRYPTO '91, vol. 576 of Lecture Notes in Computer Science, pages 129–140, Berlin, 1992. Springer-Verlag.

[20] Dan Boneh, "Bilinear Pairings in Cryptography: Basics of Pairings. Bar Ilan Winter School. Feb. 2013, PPT.

THE 18TH INTERNATIONAL SYMPOSIUM ON WIRELESS PERSONAL MULTIMEDIA COMMUNICATIONS
(WPMC-2015)
December 13-16, 2015, Hyderabad, India

Mobility-aware Hybrid Synchronization for Wireless Sensor Network

Dnyaneshwar S Mantri, Neeli Rashmi Prasad, Ramjee Prasad
Center for TeleInFrastruktur
Aalborg University, Denmark
{dsm, prasad}@es.aau.dk, neeli.prasad@ieee.org

Abstract— **Random mobility of a node in Wireless Sensor Networks (WSNs) causes the frequent changes in the network dynamics with increased cost in terms of energy and bandwidth. During data collections and transmission, they need the additional efforts to synchronize the activities of nodes. A key challenge in maintaining the effective data collection and transmission is to schedule and synchronize the activities of the nodes with the global clock. This paper proposes the Mobility-aware Hybrid Synchronization Algorithm (MHS) which works on the formation of cluster-based spanning tree mechanism (SPT). Nodes used for formation of the network have random mobility and are heterogeneous in terms of energy with static sink. The nodes in the cluster and cluster heads in the network are synchronized with the notion of the global time scale of the network. In the initial stage, the algorithm establishes the hierarchical structure of the network and then perform the pair-wise synchronization within the cluster and then in the network. With the random mobility of the node, the network structure frequently changes causing an increase in energy consumption. To mitigate this problem, MHS aggregate data with the notion of a global time scale throughout the network. In the second phase of MHS, the aggregated data packets are scheduled level by level using time-division multiple accesses (TDMA) techniques as MAC layer protocol to reduce the collision of packets. Simulation results show that MHS is energy efficient, with increased throughput, and has less delay as compared with state-of-the-art solutions.**

Keywords— Aggregation; Delay; Energy; random mobility; Scheduling; Synchronization; WSN.

I. INTRODUCTION

Time synchronization is an important service for the collaborative and coordinated operations in WSNs. For instance, network protocols such as time division multiple access (TDMA) strictly demands synchronization among sensor nodes. Time synchronization in the WSN is mainly affected by low-cost clocks, frequent topological changes, error sources during communication, node failures and the resource constraint nature of the nodes. These factors should be considered during the design and implementation of the synchronization protocols [1]. Synchronization algorithms are required to co-ordinate the time scale of node and network, and scheduling algorithms are required to allocate the collision-free time slots to reduce the energy consumptions in the WSN[2]. For instance, if the nodes used in the sensing and collection of data is not synchronized with the global clock, it takes more time to send the packet to sink and hence consumes more energy. Also, if the activities of the nodes are provided with different schedules according to the local clock and not synchronized with the global clock, then the result will be different and uneven with more energy consumption.

This paper proposes the hybrid approach which takes care of synchronizing a local clock of the node with the global clock of the network and schedules the activities based on the present and next state of the channel. With the random mobility of the node, it is difficult to integrate and interpret the information sensed by the nodes without synchronization. The unusable network conditions and scare resources of WSN make essential to develop a time synchronized protocols. Also, the random mobility of a node causes topological variations in the network architectures, and low bandwidth restricts the multi-hopping. Hence, to deal with these challenges hybrid protocol needs to be designed taking care of scheduling and clock synchronization. The improper scheduling and synchronization of the packets generated from the lower layer of the network to the upper layer causes more energy consumption. Also, retransmission delay is caused due to the improper balancing of slot allocation during scheduling and difference in the local clock of the node and global clock of the network. The retransmission delay can be minimized by use of an efficient scheduling MAC protocol, which manages the time slots of cluster head (CH) and nodes according to the global time sync. The data propagation from node to sink may be in one–hop or multi-hop, it depends on the depth of the spanning tree formed in intra and inter-cluster communication. The packet scheduling activities of the nodes are dependent on the availability of the channel, at least equal to the synchronization time. The neighboring node will synchronize their schedules periodically to prevent long term clock drift. Timing-Sync Protocol for Sensor Networks (TPSN) [3], considers the traditional approach of two-way message exchange between sender-receiver synchronization with an increase in sync errors and energy consumption. The traditional protocols are not energy efficient and difficult to implement for WSN.

The paper focuses on a hybrid approach to minimize the energy consumption with increased throughput, hence bandwidth utilization and reduced delay with the random mobility of nodes. The nodes used are heterogeneous in terms of energy which helps to increase the network lifetime. It considers clustered architecture with the spanning tree in the presence of non-ideal clocks. The result shows that application

of spanning tree algorithm for synchronization performs better than structured as compared to scheduled-based algorithms.

The remaining part of the paper progresses with different sections as; Section II focuses on the present work related to synchronization and scheduling algorithms. Section III presents the required assumptions and network model. Section IV briefs about the MHS, Section V discusses simulation setup and results, and Section VI conclusion along with the future scope.

II. Related Works

This section explores the idea how one can use TDMA technique for scheduling and synchronization technique to improve the QoS. [2] Considers the spanning tree mechanism to improve the energy consumption as compared with TPSN. It shows the reduced sync errors. [4] Defines a time synchronization protocol based on spanning tree. A spanning tree formed by the nodes is divided into multiple sub-trees. The sub-tree synchronization process helps to match the clock time within the level. It minimizes the clock adjustment time. In [5] Clustered Time Synchronization algorithm and energy model is presented, that conserves the energy beside accuracy while synchronizing the WSNs. Reference Broadcast Synchronization Protocol [6] (RBS) uses the synchronization between the two receivers by the intermediate node within the listening range of the sender and receiver. The intermediate node sends the message for recording the time hence saves the energy in clock updates. The major disadvantage of the protocol is that the energy is wasted to synchronize the reference sender. [7] Proposes the distributed clustering algorithm for grouping the mobile nodes into the clusters. The mobility of node frequently changes the structures and accordingly not suitable to use spanning tree. [8] Addresses the issue of adopting the mobility and space division multiple accesses techniques to collect the data. Author minimized the data gathering time by moving the mobile data collector through optimal route. The errors are increased due to the improper balancing of data flows. [9] Consider the effect of mobility of a node in real life example. The author presents the energy consumption as one of the performance measures. [10] Proposes the hybrid scheme to ensure the sync accuracy with minimum energy. It considers partial scheme to calculate the time offset of few child nodes. In [11] time synchronization of node and network is done at the time of cluster tree formation. Relative time drift and phase offset are the metrics of calculation. [12] Considers the delay-sensitive approach to achieve low packet delay and high throughput by considering cycle-based sync scheduling. The proposed hybrid approach helps in reducing the delay. It has a limitation of overhead with increased network size and synchronization error. [13] Proposes the hybrid approach for scheduling the activities of mobile nodes and slots are allocated using TDMA for improving energy consumption. The mobility of node restructures the cluster and increases the energy consumption. Hybrid Green Conflict Free (H-GCF) [14] algorithm uses the node mobility to reduce the conflict-free schedule for the three hop neighbors. It improves the minimum slot sharing for reducing the energy consumption and delay. In [15] clock skew is minimized by synchronizing the local clock of the node with reference to the global clock of the network. This process takes more time for synchronization of each node and hence increases the energy consumption. [16] Presents the scheme for data aggregation under distributed algorithms with an asynchronous and synchronous time model. The delay in the network is balanced by minimizing the small clock drifts occurring during synchronization. It uses competitive analysis to assess the quality of the algorithms. It lacks in the proper balance of data to be transmitted from nodes to sink with an increase in communication cost.

The different algorithms used in the section are either work on the scheduling or synchronization technique to improve the QoS parameters. During scheduling slot allocation is the major concern to avoid the collision, when the number of aggregated packets are increased. During synchronization, if the global clock of the network is not synchronized with the local clock of the node, it results in sync errors. To minimize the energy loss and errors, this paper proposes a technique by combining the two approaches (synchronization and scheduling) which works level by level.

III. Proposed Network Model

A. *Network Model*

Consider a network tree T (V, E), where ‘V’ denotes the set of ‘n’ wireless nodes and ‘E’ denotes the set of wireless links. The network T (V, E) is divided into many sub-trees of clusters T1, T2, T3,…,Tn. Every sub-tree has one CH, which acts as a root for each sub-tree. There is one base station (sink) in the network located at the root of the tree and collects data from all CHs. Each node uses its clock for maintaining the time stamp which is synchronized with the global clock of the network for collection and send data to CH. The received data is aggregated by min, max, and average functions. It reduces the transmission time per forwarding.

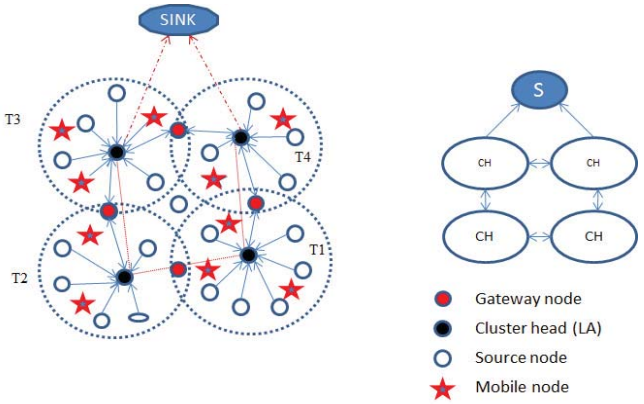

Figure 1. Cluster-based Network Model

In the first level (intra-cluster), the message ‘m’ generated by nodes within cluster, after forming tree is combined into a packet with a timestamp and forwarded to the parent node (CH). In the second level (inter-cluster), all the aggregated packets from CH are scheduled using time-slotted approach with error free channels. It benefits in achieving collision-free transmission of data packets to sink.

IV. PROPOSED MECHANISM

The main objective of proposed hybrid approach is to minimize the energy consumption with an increase in throughput. The steps in development of algorithm are as follows

- Form the cluster tree and perform level by level aggregation.
- Schedule the activities of the nodes according to free slots.
- Provide the network-wide synchronization to reduce the clock skew hence the energy consumption and increase the throughput.

A. Spanning tree formation (SPT)

In the present case WSN is considered as a connected, undirected graph G (V, E), the work considers the conversion of the graph into a minimum spanning tree. The Kruskal algorithm is used to form the minimum spanning tree of graph G (V, E). It considers the number of nodes in set A as a forest with the weight of each as one-hop.

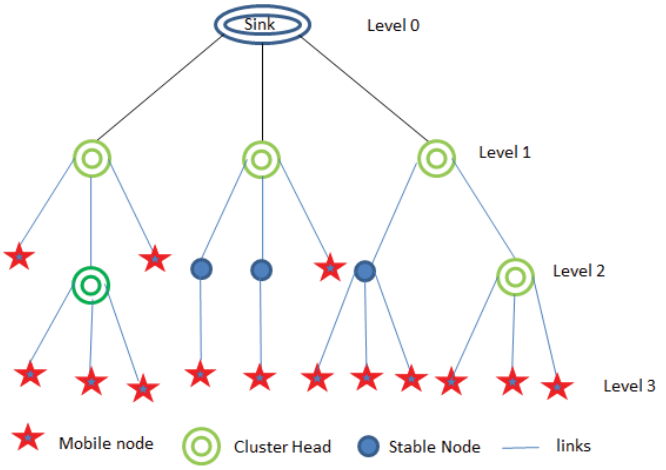

Figure 2. Structure of Proposed Spanning Tree Mechanism

In the initial stage of spanning tree as intra-cluster, nodes with random mobility are grouped into a cluster at time interval 't', a settling time, the cluster head is elected according to distributed clustering algorithms and CH is assumed to have level 0. To form a tree in the cluster, CH broadcast message and the neighbors receiving the message will be added to forest A, only the edges that are forming a loop will be discarded. The major constraint in the formation of the tree is the random mobility of node.

In the second level (inter-cluster), the CHs *v* at level 0 are grouped with a number of edges *l* connecting to CH and sink. Here, the same step like intra-cluster SPT formation is repeated; the only difference is that all the CH are static. The sink node will be assigned to level 0, and it will transfer the neighbor finding the message, the CH who will receive the message will form the spanning tree with sink node as a parent node. After connecting first level CH to sink node, the first level CH forwards the neighbor finding a message to a next CH and connect it to the spanning tree as shown in Figure 2.

B. Synchronization of nodes:

In the formation of spanning tree, different levels are maintained with sink node at level 0.The CH directly connected to sink are at level 1. The remaining CH and nodes will maintain the higher order according to the depth of spanning tree. All other nodes under CH will be assigned the next levels. The sink node, which is parent node, send clock estimation message to the direct child. The direct child is a child, who is one level distance from the parent as shown in Figure 2. The sink node maintains the global notion of time to synchronize the clocks of all nodes in the formation of spanning tree and communication of packets.

In TPSN mechanism, the global timescale is applied across the network at one time, and every node has to synchronize with global time, it introduces the clock drifts at different levels and performance decreases. It leads to increase in synchronization errors and also require more energy to keep it. But in MHS, the CH next to sink will take the global time scale from the sink while others will follow the level by level operation of synchronization with the parent node. The level by level synchronization of child and parent node reduces the clock drifts and overheads required to maintain equal time scale among all nodes at one time.

C. Energy and delay Model

In WSN, the potential source of energy consumption is in the process of communication. Typically, depending on the state of the nodes radio either in transmitting, in listing or sleep mode, energy consumption is decided. It also depends on the distance of the node to CH, CH to sink, and the number of packets transmitted by the nodes in the lower level to CH, and to 0 level by CH. According to the level of nodes in the spanning tree the energy consumption is

$$e(di) = k(e_t\, di^{\alpha} + e_0)\, t_{slots} \qquad \text{-- (1)}$$

α- path loss and depends on distance of node to CH and sink, k- number of packets, e_t- transmitter energy, e_0- initial energy. The main objective of the hybrid approach used in MHS is to increase the throughput of the network with minimum energy consumption. The radio states have different energy consumption as a transmitter (E_{tx}), receiver (E_{rcv}), listen (E_{lst}) and sleep (E_{slp}) respectively. The following assumption is made that the total time is logically divided into slots as t_{slot}, and these time slots are synchronized among nodes to avoid collision of packets. A scheduled period 'T' is composed of consecutive time slots as shown in Figure 3.

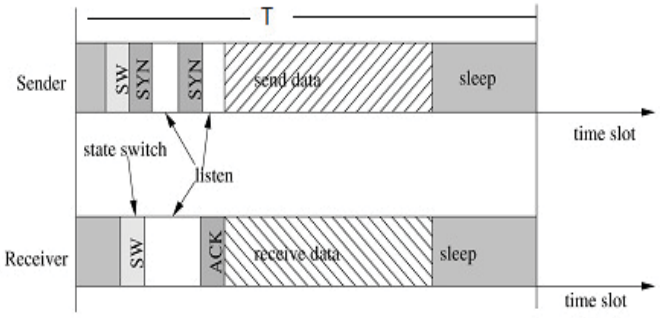

Figure 3. Structure of Synchronization Frame

Assume that a node n_i will produce r_i data packets per scheduling period T. Thus, in the one-time slot, a node can transmit multiple data packets under the ideal environment. When a node n_i is transmitting packets to a neighboring node n_j within intra-cluster, some other neighboring nodes that are in the listening state will also transmit its available data packet and consume energy. Therefore, the total energy consumption of node n_i that transmits the data packets in L slots listening to neighboring nodes is

$$\text{Energy consumption} = (E_{tx} + E_{rcv} + n * E_{lst})\ L * t_{slot}. \quad -- (2)$$

Also, the time required to schedule the 'k' packets at CH is calculated according to the number of forwardings and is

$$T_{ch} = ((N/k)-1)\ t_{slot} \quad -- (3)$$

The total time required to send the aggregated packets to sink is

$$T_{sink} = k.\ t_{slot} \quad -- (4)$$

Hence, total time required for packets to reach to sink is

$$T = [((N/K)-1) + K]\ t_{slot} \quad -- (5)$$

All the activities of each node are scheduled and synchronized in the time slot $1 \leq t_{slot} \leq T$

V. SIMULATION RESULTS

The simulation of the algorithm is performed using NS-2 (ns-2.34). The parameters considered for simulation of randomly placed mobile nodes are shown in Table I. The results are obtained by applying the spanning tree mechanism on mobile nodes. The performance of hybrid synchronization algorithm(MHS) is compared with SDA[2]using with static nodes and time synchronization (TPSN)[3], a network-wide time sync algorithm.

TABLE I. SIMULATION AND NODE PARAMETERS

Parameters	Value
Number of nodes	25,50,75 and 100
Number of sources	24, 49, 74 and 99
Number of Sinks	1
Placement of source and sink	Random and sink at center
Initial energy	100J
Idle power	14.4mW
Receive power	14.4mW
Transmit power	36.0mW
Runs of each simulation	20
Node mobility(random)	20 meters /sec

A. *Result and Discussion*

Figure. 4 represents the average energy consumption of three different synchronization mechanisms TPSN, SDA, and MHS. The average energy consumption by TPSN is more than that of MHS and SDA because TPSN tries to apply global timescale across the network at one time, while MHS uses the spanning tree based synchronization mechanism which works on level by level.

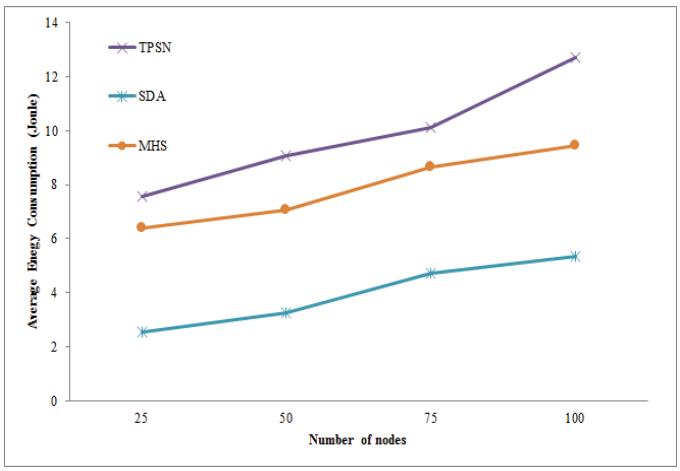

Figure 4. Comparison of Energy Consumption

Also, the distribution of global time scale across the whole network require a larger amount of energy and will be utilized from the share of nodes. Uneven time stampings of TPSN leads to increase in synchronization errors and also require more energy to keep it. At another side, SDA and MHS mechanism apply global time scale level-by-level, which gives less overhead and leads to reduced energy consumption. The energy consumption of MHS is more than SDA, due to increased overheads in finding the paths with the random mobility of nodes and updating the clock of the neighbour node used for synchronization.

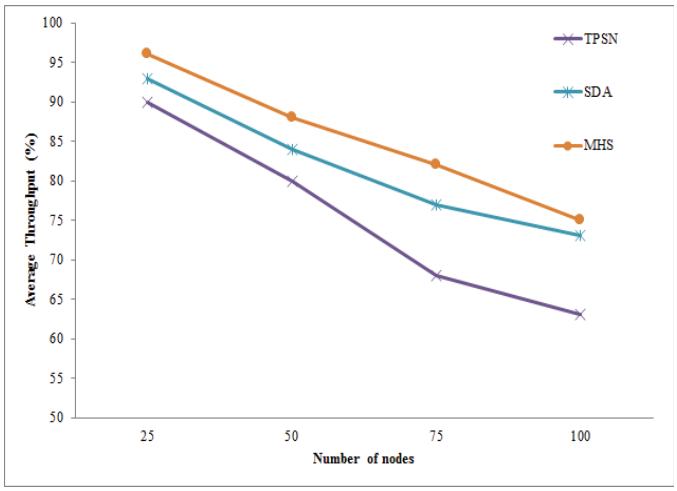

Figure 5. Comparison of Throughput

Figure. 5 shows the average throughput of the hybrid mechanism (synchronization and scheduling) applied on the three synchronization algorithms TPSN, SDA and MHS with spanning tree synchronization techniques. With an increase in the number of nodes, throughput increases by 11.73% and

4.10% in case of MHS as compared to TPSN and SDA. This improvement in the result is due allocation of collision-free scheduling slots and synchronizing clocks of parent and child node level by level. Also, data gathering time reduces due to level by level synchronization since clock drifts are minimum. However, in TPSN, it will change every time the nodes go under random mobility and need to update the global state in the whole network, hence reduced throughput.

Figure 6 shows the average delay of the hybrid mechanism. With the introduction of controlled random mobility to nodes, an avg delay in matching the local and global clock is reduced by 24.26% and 9.07% with SPT as compared to TPSN and SDA. The larger time drifts introduced in TPSN takes a large time to make a decision on schedule as compared to MHS. Also, retransmission delay is caused due to the improper balancing of slot allocation during scheduling and difference in the local clock of the node and global clock of the network. The process of exchanging a global state of information increases the overhead in the network, which leads to increased delay and reduced throughput in case of TPSN.

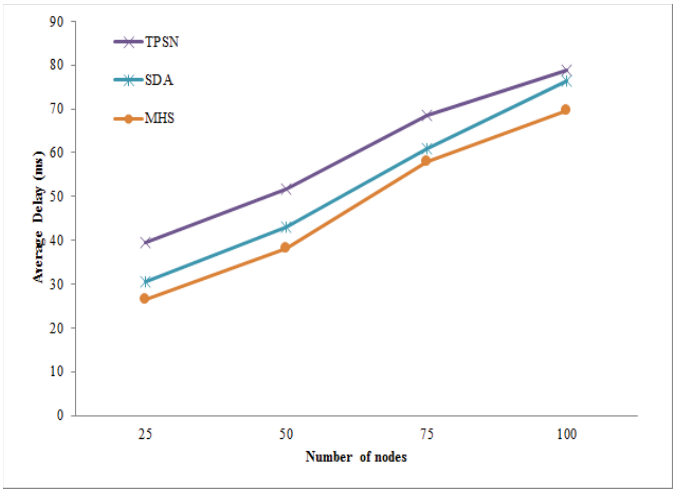

Figure 6. Comparison of Average Delay

VI. Conclusions and Future Work

The proposed mobility-aware hybrid synchronization algorithm with spanning tree mechanism shows improvement in throughput, delay, and has reduced energy consumption as compared with TPSN. The addition of heterogeneous nodes in the network along with the synchronization of local and global clock helps to increases the lifetime of the network. The clock synchronization reduces the clock drifts and hence errors which result in an increase of the throughput, and reduces the delay. It also reduces the energy consumption by 29.32%. With the introduction of random node mobility and heterogeneity, the performance of the synchronized algorithm is improved by 4%. The work can be extended by considering sink mobility in the network.

References

[1] Bharath Sundararaman, Ugo Buy, and Ajay D. Kshemkalyani, "Clock synchronization for wireless sensor networks: a survey," Elsevier Ad Hoc Networks 3 (2005) 281–323.

[2] Dnyaneshwar S. Mantri, Neeli Rashmi Prasad, and Ramjee Prasad, "Synchronized Data Aggregation for Wireless Sensor Network," 1st IEEE Global conference on wireless computing and networking, pp 263-267, December 22-24, 2014, SIT, Lonavala, India.

[3] Saurabh Ganeriwal, Ram Kumar, and Mani B. Srivastava, "Timing-sync Protocol for Sensor Networks," SenSys'03, November 5-7, 2003, Los Angeles, California, USA.

[4] LI-Ming He, "Time Synchronization Based on Spanning Tree for Wireless Sensor Network," IEEE Wireless 4th International Conference on Communication, Networking and Mobile Computing, WiCOM'08.

[5] 2008Gopal Chand Gautam, T. P. Sharma, Vivek Katiyar and Anil Kumar, "Time Synchronization Protocol for Wireless SensorNetworks using Clustering," 2011 ICRTIT, pp417-422 June 2011, India.

[6] J. Elson, L. Girod, and D. Estrin, "Fine-grained network time synchronization using reference broadcasts," Proceedings of Fifth Symposium on Operating Systems Design and Implementation (OSDI 2002), Vol. 36, pp. 147–163, 2002.

[7] Ren Qianqian, Guo Longjiang, Zhu Jinghua, Ren Meirui, Zhu Junqing, "Distributed aggregation algorithms for mobile sensor networks with group mobility model," Tsinghua Science and Technology,vol.17,no.5,pp.512,520,Oct.2012.

[8] Ma Yuanyuan Yang, "Efficient Data Gathering with Mobile Collectors and Space-Division Multiple Access Technique in Wireless Sensor Networks," IEEE Transactions on Computers, vol.60, no.3, pp.400-417, March 2011.

[9] Konstantin Mikhaylov, and Jouni Tervonen," Energy Consumption of Mobile Wireless Sensor Network's Node with Controlled Mobility," 27 IEEE, conference on Advanced Information networking and Applications Workshop,PP 1582-1587,2013.

[10] L. Schenato and F. Fiorentin, "Average timesynch: a consensus-based protocol for time synchronization in wireless sensor networks," Automatica, vol. 47, no. 9, pp. 1878–1886, 2011.

[11] Huang Hai-ping, Wang Ru-chuan, Liu Li, Sun Li-juan, Li Wen-feng, "Time synchronization algorithm of wireless sensor networks based on data aggregation tree," vol 17, pp. 24–29, July 2010.

[12] Xi Deng, and Yuanyuan Yang "Communication Synchronization in Cluster-Based Sensor Networks for Cyber-Physical Systems," IEEE Transaction on Emerging Topics in Computing, vol. 1, no.1, pp 98-110,.June 2013.

[13] Dnyaneshwar S. Mantri, Pranav Pawar, Neeli Rashmi Prasad, and Ramjee Prasad, "An Efficient Schedule based Data Aggregation using Node Mobility for Wireless Sensor Network," Wireless Vitae2013, pp1-5, May11-14, 2014, Aalborg, Denmark.

[14] Pranav M. Pawar, Rasmus H. Nielsen, Neeli R. Prasad, Shingo Ohmori, and Ramjee Prasad, "H-GCF: A Hybrid Green Conflict Free Scheduling Algorithm for Mobile Wireless Sensor Networks." 16th Internation symposium on Wireless Personal Multimedis communications(WPMC)-2013.

[15] Yildirim K.S. and A ylin Kantarci, "External Gradient Time Synchronization in Wireless Sensor Networks," IEEE Transactions on Parallel and Distributed Systems, vol. 25, no. 3, page: 633–641, march 2014.

[16] Peter Korteweg, Alberto Marchetti-Spaccamela, Leen Stougie, and AndreaVitaletti "Data Aggregation in Sensor Networks: Balancing Communication and Delay Costs," pp1-13, June 2012.

THE 18TH INTERNATIONAL SYMPOSIUM ON WIRELESS PERSONAL MULTIMEDIA COMMUNICATIONS
(WPMC-2015)
December 13-16, 2015, Hyderabad, India

A Modified RFID Authentication Protocol Using Elliptic Curve Cryptography

Rajesh Dochania, Nirmal Roberts, K. V. Arya
ABV-Indian Institute Of Information Technology And Management
Gwalior-474015, India
Email: dochaniaraj@gmail.com, nirmal@iiitm.ac.in, kvarya@iiitm.ac.in

***Abstract*—RFID is a wireless technology that uses radio frequency to transfer data. It is mostly used in tracking and identifying objects. Recently its applications are rapidly growing in health-care industry to store data related to patient's medication. Transfer of data between server and RFID tag is controlled by some protocols. If these protocols are insecure, then it is possible for an attacker to gain access and fake the report which can be harmful to patient's health. In this paper, RFID Authentication Protocol has been modified to provide enhanced security in transmission of data between server and RFID tag.**

Keywords: Radio frequency identification tag, Elliptic curve cryptography, Authentication protocol.

I. Introduction

The medical data stored in a patients tag attract increasing security and privacy concerns since its modification or damage will influence patients health. The RFID-based patient's medication system consists of tags, readers and the back-end sever [1]–[5]. The hospitals are open environments and radio waves are used for mutual communication. The adversary may read or clone the data stored in patient's tag.

Radio Frequency Identification technology is an automatic tracking mechanism that uses radio signals to detect and identify people, and other things like goods, vehicles etc., without using any physical contact. Radio Frequency Identification technology can track the objects by using radio signal over a distance of few meters to several meters.

Elliptic Curve Cryptography was proposed by **Neal Koblitz** and **Victor Miller**. It is a public-key cryptography technique which is based on the elliptic curves over finite fields of prime numbers [6]. Terms that are used in Elliptic Curve Cryptography are discuss below.

- **Prime fields**
  Let q be a prime number. The modulo q, containing a set of the integers from 0 to q - 1 with addition and multiplication modulo q, is a finite field of order of prime number q. This field is usually denoted by Z_q.

$$Z_q = \{0, 1, 2, ..., q-1\} \quad (1)$$

  eg. : Z_8 = {0 , 1 , 2 , ... , 7}

- **Additive group**
  Let q be a prime number, and let Z_q = {0, 1, 2,..., q - 1} denote the set of integers modulo q. Then (Z_q, +), where the operation + is defined to be addition of integers modulo q, is a finite additive group of prime number q with identity element 0 for addition.

- **Generator**
  The positive elements of a finite field Z_q, denoted as Z_q^* form a cyclic group including multiplication. Therefore there exist element b $\in$ Z_q^* called generator as shown below.

$$Z_q^* = \{b^i : 0 \leq i \leq q-2\} \quad (2)$$

An authentication protocol is a kind of cryptographic protocol with the aim of authenticating entities which want to communicate securely to each other. It is a main characteristic of system security in medication [7], [8]. It verifies the identity of each and every user which are trying to access network resources.

Since authentication play an important role in system security. Therefore, we need such type of authentication protocol which provide security against various security attacks as well as reduce the communication between server and tag.

This paper is organised as follows. Section I is an introduction part. Section II discuss about existing protocol i.e., Zhang and Qi RFID authentication protocol. Proposed RFID authentication protocol is discribe in section III. Then correctness of proposed protocol is included into section IV. Security analysis is presented in section V whereas section VI and section VII represent advantage of proposed protocol and conclusion part respectively.

II. Review Of Zhang and Qi RFID Authentication Protocol

An efficient RFID authentication protocol was developed by **Zhang** and **Qi** [9] to provide security in patient's online medication system. This protocol consists of two phases, i.e., setup phase and authentication phase. They have incorporated

some notations which are used in this protocols are discussed below.

q	A large prime number.
G	Additive group with order *q* consisting of points on an elliptic curve.
P	A generator of *G*.
X_i	The identifier of the i^{th} tag which is a random point in *G*.
y	The private key of the server.
Y	The public key of the server where *Y = yP*.
r,k	Two random numbers.
h( )	A secure hash function.

A. Setup phase

In setup phase, the server generates a random number as its private key and use this to computes the public key. It also selects a identifier of each tag randomly from G.

B. Authentication phase

In authentication phase, the server starts the communication with the tag. Steps of authentication phase are as follows:

1) In this step a random number r $\in Z_q$ is generated by server and assigned to C_0, i.e., C_0 = r. The value $\{C_0\}$ is sent to the i^{th} tag.

2) The i^{th} tag generates a random number k $\in Z_q$, after receiving $\{C_0\}$. Then the parameters K = kY, C_1 = kP, $C_2 = X_i$ + K and C_3 = h(X_i,K,C_0,C_1,C_2) are computed. Then this computed $\{C_1,C_2,C_3\}$ are send to server.

3) The values of $\{C_1,C_2,C_3\}$ are used by server to compute K = yC_1 and $X_i = C_2$ - K. Then the server matches the value of C_3 = h(X_i,K,C_0,C_1,C_2). If these values matches then the tag is declared as legal tag otherwise the system is rejected by the server. After that database is explored for X_i value which is then used for C_4 = h(X_i,K,C_0,C_1,C_2,C_3) and transmits $\{C_4\}$ to i^{th} tag.

4) After receiving {C4} the i^{th} tag finds whether C_4 and h(X_i,K,C_0,C_1,C_2,C_3) are equal. If they are equal then the tag confirms the server is legal otherwise rejects the session.

Server[y,Y,X_i]	Tag[P, Y, X_i,]
Generate r $\in Z_q$	
C_0 = r	
	$\{C_0\}$ $\longrightarrow$
	Generate k $\in Z_q$
	K = kY
	C_1 = kP
	$C_2 = X_i$ + K
	C_3 = h(X_i,K,C_0,C_1,C_2)
	$\{C_1,C_2,C_3\}$ $\longleftarrow$
K = yC_1	
$X_i = C_2$ - K	
Verification :	
C_3 = h(X_i,K,C_0,C_1,C_2)	
If yes, then search X_i in database	
C_4 = h(X_i,K,C_0,C_1,C_2,C_3)	
	$\{C_4\}$ $\longrightarrow$
	Verification :
	C_4 = h(X_i,K,C_0,C_1,C_2,C_3)

Zhang and Qi RFID Authentication Protocol

In this protocol, the tag, after receiving request, first sends data then verifies the user. So anyone (authorized or unauthorized user) can send the request. Therefore a lot of requests may arrive at the tag. So it increases the traffic between server and the tag. Hence, the protocol needs to be modified to reduce the communication between server and tag.

III. Proposed Modified RFID Authentication Protocol

In this section, we propose a modified RFID protocol that also has two phases, namely setup phase and authentication phase

A. Setup phase

In setup phase, the server generate a random number as it's private key and compute its public key and also selects a random point in G as identifier of each tag.

B. Authentication Phase

When interrogating a tag, the server starts the phase to authenticate each other. The details of the phase are presented as follows.

1) The server generates a random number r $\in Z_q$ and computes :
   - C_0 = rP [10]
   - C_1 = h(P, C_0)

   And send the message $\{C_0,C_1\}$ to the i^{th} tag.

2) On receiving $\{C_0,C_1\}$, the i^{th} tag check whether C_1 and h$\{P,C_0\}$ are equal or not. If they are not equal, the i^{th}

tag rejects the session, otherwise, the i^{th} tag confirms that the server is a legal one and generates a random number k $\in Z_q$ and computes :

- $K = kY$
- C_2 = kP
- C_3 = X_i + K
- C_4 = h(X_i,K,C_0,C_1,C_2,C_3)

Then the *i*th tag send the message $\{C_2,C_3,C_4\}$ to the server.

3) Upon receiving $\{C_2,C_3,C_4\}$, the server computes:
   - K = yC_2
   - X_i = C_3 - K

   Then the server checks whether C_4 and h(X_i,K,C_0,C_1,C_2,C_3) are equal or not. If they are not equal, the server rejects the session, otherwise, the server searches its database for X_i. If succeeds, the server confirms that the tag is a legal one.

Server[y,Y,X_i]	Tag[P, Y,X_i]
Generate r $\in Z_q$	
C_0 = rP	
C_1 = h(P,C_0)	
	$\{C_0,C_1\}$ $\longrightarrow$
	Verification:
	C_1 = h(P,C_0)
	Generate k $\in Z_q$ and
	Computes :
	K = kY
	C_2 = kP
	C_3 = X_i + K
	C_4 = h(X_i,K,C_0,C_1,C_2,C_3)
	$\{C_2,C_3,C_4\}$ $\longleftarrow$
K = yC_2	
X_i = C_3 - K	
Verification :	
C_4 = h(X_i,K,C_0,C_1,C_2,C_3)	
If yes then search X_i in its database.	

Proposed RFID Authentication Protocol

IV. Correctness Proof of the Proposed Authentication Protocol

Let :
q = 53
P = 1331 (let b = 11 and i = 3 in eq. 2)
X_i = 29
y = 41
Y = $y \times P$
= 41×1331
= 54571

Now,

Server[y,Y,X_i]	Tag[P, Y,X_i]
Generate r $\in Z_q$ = 31	
C_0 = rP	
= 31×1331	
= 41261	
C_1 = h(P,C_0)	
	$\{C_0,C_1\}$ $\longrightarrow$
	Verification:
	C_1 = h(P,C_0)
	Generate k $\in Z_q$ = 37 and
	Computes :
	K = kY
	= 37×54571
	= 2019127
	C_2 = kP
	= 37×1331
	= 49247
	C_3 = X_i + K
	= 29 + 2019127
	= 2019156
	C_4 = h(X_i,K,C_0,C_1,C_2,C_3)
	$\{C_2,C_3,C_4\}$ $\longleftarrow$
K = yC_2	
= 41×49247	
= 2019127	
X_i = C_3 - K	
= 2019156 - 2019127	
= 29	
Verification :	
C_4 = h(X_i,K,C_0,C_1,C_2,C_3)	

Hence we get the value of i^{th} tag i.e., 29 which we assume in the starting of this section.

V. Security Analysis

The main purpose of modified protocol is to reduce communication between server and tag as well as make the protocol secure against various security attacks. This protocol uses the generator in the start up (step 1) of the communication so that it remove the chances of any unauthorized person to take part in communication. Suppose if an attacker generate a random number and send the value without using generator value to tag, then the tag simply reject the session (step 2) on the basis of verification (verification is based on the value of

generator). This protocol is also secure against various attacks as described below.

1) **Privacy** : This protocol provide privacy, since to get the ID of each tag, Private key is required which is kept secure by server.

2) **Replay Attack** : For our protocol, the tag is identified by the tag personal ID, and the personal ID is changed after every session as the tags information is accessed by a reader.

3) **Eavesdropping** : For the proposed protocol, when the tag is actually communicating its on chip information to a reader, the information sent through a message encrypted by a session key. This ensures that an eavesdropper cannot easily obtain the information in plain text.

4) **Impersonation** : Impersonation is not possible as long as the personal ID is changed every time and the key between the server and tag is secure, since the cloned tag with the obsolete personal ID cannot be recognized by the server in the next session.

5) **De-Synchronization** : The back-end server stores both the current and previous pairs of personal IDs so that the protocol can still work even when the tag fails to update its personal ID by a de-synchronization attack between the tag and the reader.

6) **Cloning** : An adversary cannot clone the tag since the key and other secret information are used with the random number when it is transmitted in the insecure channel.

VI. Advantage of The Proposed Protocol

1) There are only 3 steps in the proposed protocol against 4 steps in the existing protocol.

2) Proposed protocol verifies server without sending any data whereas the existing protocol first sends data then verify server.

VII. Conclusion

An efficient RFID authentication protocol of Zhang and Qi provide maintain system security but it doesn't reduce the communication steps between server and tag. Therefore we need a modified RFID protocol which is more efficient than the existing protocol The modified proposed protocol is more efficient because it consists only three steps in comparison to existing protocol and it can be applied to any random tag. In this protocol the tag ID of any random tag can be easily calculated and on the basis of this ID the details of that tag can be searched in the server database. This protocol uses the benefits of both Chous protocol and Zhangs Protocol in making the RFID protocol more secure and applicable to a wide range of tags.

References

[1] Y. Hung *et al.*, "The study of adopting rfid technology in medical institute with the perspectives of cost benefit," in *International Medical Informatics Symposium in Taiwan, Taiwan*, 2007.

[2] J. E. Katz and R. E. Rice, "Public views of mobile medical devices and services: A us national survey of consumer sentiments towards rfid healthcare technology," *International journal of medical informatics*, vol. 78, no. 2, pp. 104–114, 2009.

[3] C. Yu, C. Chen, P. Liao, and Y. Lee, "Rfid-based operation room and medicare system for patient safety enhancementa case study of keelung branch," *J. Inf. Manag*, vol. 15, pp. 97–122, 2008.

[4] W. Yao, C.-H. Chu, and Z. Li, "The use of rfid in healthcare: Benefits and barriers," in *RFID-Technology and Applications (RFID-TA), 2010 IEEE International Conference on*. IEEE, 2010, pp. 128–134.

[5] P. Najera, J. Lopez, and R. Roman, "Real-time location and inpatient care systems based on passive rfid," *Journal of Network and Computer Applications*, vol. 34, no. 3, pp. 980–989, 2011.

[6] D. Hankerson, A. J. Menezes, and S. Vanstone, *Guide to elliptic curve cryptography*. Springer Science & Business Media, 2006.

[7] Z.-Y. Wu, Y.-C. Lee, F. Lai, H.-C. Lee, and Y. Chung, "A secure authentication scheme for telecare medicine information systems," *Journal of medical systems*, vol. 36, no. 3, pp. 1529–1535, 2012.

[8] Z. Zhao, "An efficient anonymous authentication scheme for wireless body area networks using elliptic curve cryptosystem," *Journal of medical systems*, vol. 38, no. 2, pp. 1–7, 2014.

[9] Z. Zhang and Q. Qi, "An efficient rfid authentication protocol to enhance patient medication safety using elliptic curve cryptography," *Journal of medical systems*, vol. 38, no. 5, pp. 1–7, 2014.

[10] J. Chou, "A secure rfid authentication protocol to enhance patient medication safety using elliptic curve cryptography," *J. Supercomput*, 2014.

THE 18TH INTERNATIONAL SYMPOSIUM ON WIRELESS PERSONAL MULTIMEDIA COMMUNICATIONS
(WPMC-2015)
December 13-16, 2015, Hyderabad, India

Non Audio-Video Gesture Recognition System

Razvan Craciunescu, Albena Mihovska, Sofoklis Kyriazakos, Ramjee Prasad
Center for TeleInfrastruktur (CTIF)
Aalborg Unviersity, Aalborg, Denmark
{razvan, albena, sk, prasad}@es.aau.dk

Cristian Ionut Dita, Octavian Fratu
Telecommunication Department, University Politehnica of Bucharest
Bucharest, Romania,
dita.cristian.ionut@gmail.com, ofratu@elcom.pub.ro

***Abstract*— Gesture recognition as a topic in computer science and language technology has the goal of interpreting human gestures via mathematical algorithms. Gestures can originate from any bodily motion or state but commonly originate from the face or hand. Current research focus includes on the emotion recognition from the face and hand gesture recognition. Gesture recognition enables humans to communicate with the machine and interact naturally without any mechanical devices. This paper investigates the possibility to use non-audio/video sensors in order to design a low-cost gesture recognition device that can be connected to any computer on the market. The paper proposes an equation that relates the distance and voltage for a Sharp GP2Y0A21 and GP2D120 sensors in the situation that a hand is used as the reflective object. In the end, the presented system is compared with other audio/video system that exist on the market.**

Keywords*— gesture recognition, infrared detectors, hand gesture detection, hand gesture recognition, motion presence;

I. INTRODUCTION

This paper presents a simple implementation of a gesture control interface that can ease the human – computer interaction. It allows the user to control various computer applications with simple hand gestures. The system we implemented uses only infrared sensors for gestures detection and an Arduino Leonardo to process them. We used a method based on the hand position detection to recognize the gestures. Different gestures can be detected based on the position and the moving direction of the hand.

The research in the field of gesture recognition is in full progress and many authors have different methods of implementation. In [1] the authors present a method of gesture recognition based on multiple sensors fusion technique: three kinds of sensors, namely surface Electromyography (sEMG) sensor, 3-axis accelerometer (ACC) and camera are used together to capture the dynamic hand gesture. In [2] and [3] the camera from the Kinect sensor is used. In [4] a hand gesture detection and classification system using two differential Pyro-electric Infrared (PIR) sensors for motion detection and a camera is introduced.

This paper proposes a non-audio/video sensor-based system comprising hardware and software components. The sensors used in the system (e.g. the sharp sensors) were properly calibrated in order to have a reliable system. The paper demonstrates that, with a good calibration of the sensors and a good software components, a low cost non-audio/video system can recognize a hand gesture in at least 95% of the cases with a low CPU usage of the microcontroller and a time of execution (from the gesture is made to the time the PC executes the command) of minimum 60 ms per gesture. Moreover the paper derives equation that shapes the interaction between the hand skin and the Sharp sensors.

This paper is organized as follows. Section II presents the hardware used for the implemented gesture control interface and the structure of the interface. Section III proposes the algorithm used for the gesture recognition, Section IV gives the conclusions regarding the implemented system.

II. THE HARDWARE

This section presents the hardware we used to implement the gesture control interface, the calibration of the sensors (where it was necessary) and the subsystems that compose the interface.

A. Arduino Leonardo Development Board

Arduino is an open source development board based on the Atmega32u4 microprocessor. The Leonardo model [5] differs from all previous Arduino boards in that the Atmega32u4 supports direct USB communication, eliminating the need for a secondary dedicated processor. This way the board can emulate different peripheral devices (mouse, keyboard) while connected to a computer.

One of the major advantages of using a single chip for code processing and USB communication is the increased flexibility in the communication with the computer. While the development board is recognized by computer's operating system as a virtual serial port, it can emulate a peripheral device. Also, using a USB communication makes the final device available for any person that has a PC with USB ports. Thus, the final system will have a worldwide audience.

B. Ultrasonic sensors - PING)))™

The ultrasonic sensors are active sensors that emits an ultrasonic wave (frequency greater than 20 kHz) and receives the signal reflected on the target object. The distance to the target object is directly proportional to the time the ultrasonic wave needs to get to the object and then back to the sensor.

The ultrasonic Parallax PING))) sensor [6] provides an accurate method for measuring distances between 2cm and 3m. The sensor emits a 40 kHz burst under the control of a microcontroller. It will generate as output signal a pulse whose width is proportional to the distance to the target. In the system, described in this paper, the PING))) sensor is part of the motion

detection subsystem. It will detect the movement inside a specified perimeter and activates/deactivates the other subsystems. Hence, we when the user is in the device area, at less than 50 cm of the device, the gesture recognition will begin. As the PING))) sensor output is influenced by the environmental temperature, the sensor output was calibrated for a temperature between 20°C -30°C.

C. *Passive infrared sensors - SE-10 PIR*

A motion detector is a device that can detect moving objects around it. In this category of sensors are included the passive infrared sensors (PIR). A PIR sensor measures infrared (IR) light radiating from objects. It can work in far infrared (FIR) and intermediate infrared (IIR) light for wavelengths between 4 and 20 µm.

The SE-10 sensor [7] can detect moving light sources whose wavelength is in the domain 7…14 µm. The human body emits infrared radiation in the wavelength interval of 8 to 14 µm. This means that the SE-10 sensor is an excellent detector for moving people. The sensor will 1-2 seconds after it is power on in order to calibrate itself to the background infrared radiation and detect motion.

In this project the SE-10 PIR sensor is used in the motion detection subsystem along with the PING))) ultrasonic sensor. If it detects a person close to the system then it will trigger the PING))) sensor.

D. *IR sensors for distance measurement - Sharp*

The IR sensors use the infrared light to detect and measure the distance to the target object. The main limitation of these sensors is the maximum distance that they can measure.

Typically, they are used to measure distances between 4-150 cm. In this project two models of IR sensors are used (both produced by Sharp company):

- Sharp IR GP2D120 [8] – can measure distance in the interval [4, 30] cm;
- Sharp IR GP2Y0A21 [9] – can measure distance in the interval [10, 80] cm.

The output voltage of these sensors is non-linear and the producer provides in the datasheets the graphics needed to convert the output voltage to the corresponding distance.

During the tests we noticed that the distance obtained using the data provided by the datasheet did not match the real one. This is because the datasheet calibration is done using a white or gray paper as the reflective object. Our system uses the hand as the reflective object (the hand skin).

TABLE I. THE EXPERIMENTAL OUTPUT VOLTAGE FOR SHARP IR GP2Y0A21

Distance[cm]	Voltage [V]	Distance [cm]	Voltage[V]
6	3.278667	45	0.700667
8	2.752000	55	0.641333
10	2.536667	60	0.622000
15	1.816667	70	0.632667
25	1.176667	75	0.627333
30	1.011333	80	0.631333

TABLE II. THE EXPERIMENTAL OUTPUT VOLTAGE FOR SHARP IR GP2D120

Distance [cm]	Voltage[V]	Distance[cm]	Voltage[V]
2	2.970	16	0.866
4	2.757	18	0.766
6	1.969	20	0.695
8	1.589	22	0.630
10	1.367	24	0.551
12	1.085	26	0.513

Thus, in order to fix this issue the sensors had to be calibrated. The calibration method was done experimentally. For different predefined distances the output voltage was measured. Based on the results, the distance-voltage variation law was determined for each sensor model.

In Fig. 1 and Fig. 2 the inverse of the measured distance, 1/L, is represented with a blue line. In this case, we observed that the inverse distance parameter could be approximated by a linear function for both sensors. Based on the red curves (Fig.1 and Fig. 2) the relations between the measured distance and the output voltage for the two sensors are given by (1) for Sharp GP2Y0A21 and (2) for Sharp GP2D120:

$$L = 6787/(V-3) - 4 \quad (1)$$

$$L = 2914/(V+5) - 1 \quad (2)$$

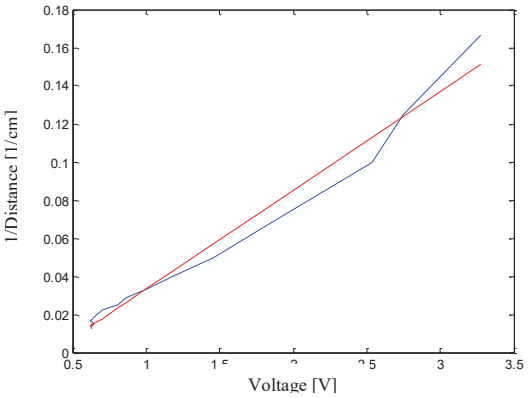

Fig.1: Linearized characteristic for Sharp IR GP2Y0A21

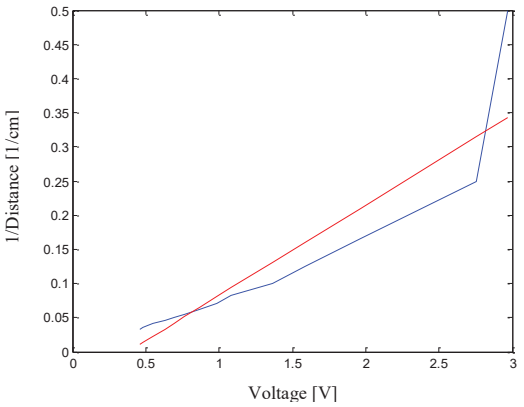

Fig.2: Linearized characteristic for Sharp IR GP2D120

Another issue that we observed at the Sharp sensors is that the output signal of the sensors is affected by noise from the power supply or from the other electronic components of the

circuit. The noise impacts the quality of the measurements as it can determine fast variations of the output voltage. To remove the effect of the noise on the output signal two capacitors, a 100nF and a 10 µF were connected between the Vcc (power supply) and GND (ground) pins of the sensor. The connection mode can be seen in Fig.3 and Fig.4.

This optimization of the Sharp sensor resulted in an increase from 80 to 95% of the gestures sensed by this sensors.

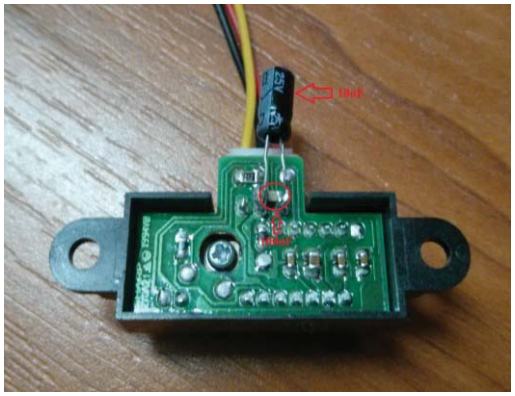

Fig. 3 Connection of the capacitors to eliminate noise in the output signal (Sharp sensor)

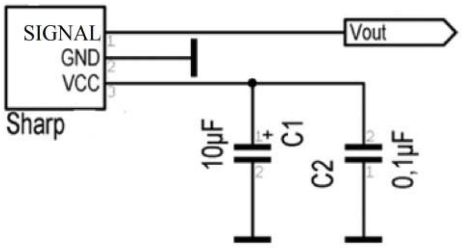

Fig. 4 Electric scheme for connection of the two capacitors

E. TFT Arduino display

The system has also a display that shows different information to the user (e.g. it can display the gesture made by the user, the state of the system).

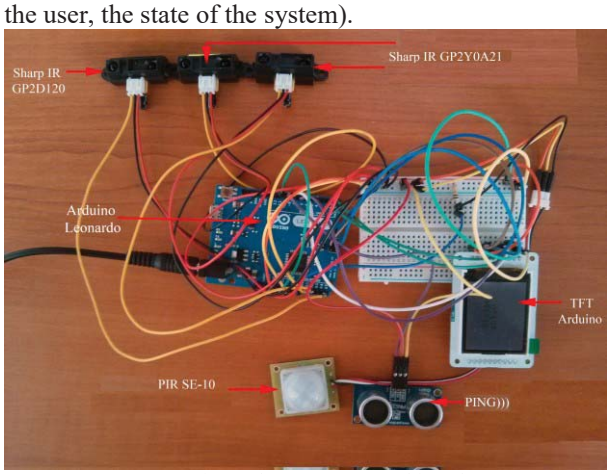

Fig. 5 The gesture control interface

We used the Arduino TFT LCD Screen [10] with a 1.77" diagonal, and 160 x 128 pixel resolution.

In Fig. 5 is the physical implementation of the gesture control interface (the first prototype). The prototype was made more user friendly (i.e. developing a PCB to integrate the Arduino board and the sensors and designing a case), as one can see in Fig. 6. The design of the final product is still under research as we want to make it smaller so that the system can be view as a small accessory.

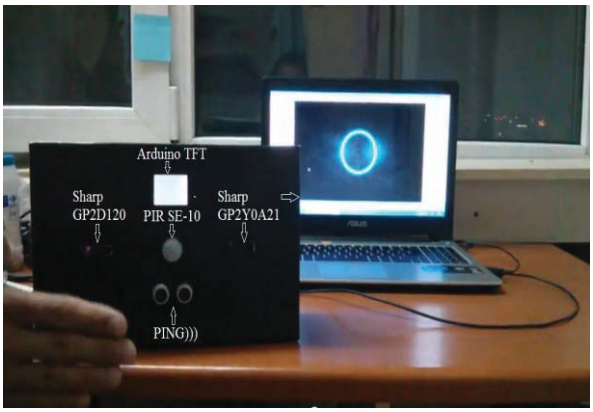

Fig. 6 The gesture control interface

III. THE LOGIC BLOCKS OF THE SYSTEM

Fig. 7 shows the diagram of the modules that we used to implement the gesture control system. All the modules are explained in the next paragraphs.

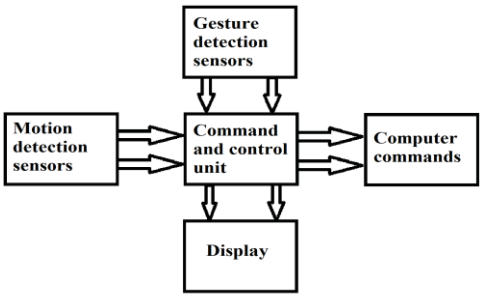

Fig. 7 The modular diagram of the gesture recognition system

A. The modules description

1) Motion detection module

It contains two sensors: the SE-10 PIR and the ultrasonic PING))).

First the PIR sensor will detect the motion of a person. Based on our work with the PIR sensor in the eWALL EU-project but also some internal projects [11][12] and the experiments with the gesture recognition system we can conclude that the SE-10 PIR sensor can sense the presence of a person from a maximum distance of 140cm.

After the PIR sensor detects that a person is in the proximity of the device the PING))) sensor will measure the distance to the person. If this distance is lower the 50 cm the gesture recognition system will start interpret the person gestures. The threshold of 50 cm distance was chosen experimental based on how far a person is sitting from the PC.

2) Gesture detection module

Three Sharp IR sensors are used to detect gestures: two GP2Y0A21 sensors and one GP2D120. If one sensor detects a gesture the others are not sensing for that period.

The GP2D120 sensor is used to detect if the hand, positioned at a maximum distance of 15 cm from the device, is not moving for a period between 300ms and 2s. If this is the case and the user is watching a movie the movie is paused or resumed (an explanatory video can be seen here: https://goo.gl/OoTSZl).

In order to determine the time from the moment the sensor sensed the hand and the moment the video is paused/resumed a time stamp, with the moment the sensor is sensed by the microcontroller, is sent alongside the command that the PC should interpret. This timestamp is compared with the timestamp from the moment the command sent is executed. The difference was of 20ms. Thus, the time from the sensing moment to the execution of the command by the PC is 60ms, regarding the fact that the typical response time of the GP2D120 sensor is 40ms. We choose a range between 300ms and 2s so that we avoid any errors caused by an accidental hand gesture. The gesture is recognized in 95% of the cases. Moreover a period of 2s, we found that is a good period for a user to feel like the action is caused by his actions.

The two GP2Y0A21 sensors are used for: one of them for detecting the right->left or left->right movement of the hand; the other one for detecting how far/close is the hand from the device. The distance rage that the hand has to be from the sensors is 4-40cm. For lower or higher distances than this one the gesture recognition decreases with 35-45%. Each sensor is used for sending a different command to the computer (e.g. scrolling, moving left/right a slideshow) an explanatory videos can be seen here: https://goo.gl/gZT9QQ ; https://goo.gl/ajwTZw). As explained, in the case of the GP2D120, a timestamp was used in order to see the reaction of the system. The time between the sensing and the PC execution of the command is 60ms.

3) Command and control subsystem

It represents the ‚brain' of the entire system. It is based on the Arduino Leonardo development board. It collects the data from all the sensors and processes it. Depending on the results Arduino can transmit to computer specific commands for controlling different applications (PowerPoint, internet browser, image viewer). In order to transmit the commands Arduino Leonardo emulates a peripheral device (either a mouse or a keyboard). The use of the Arduino Leonardo board makes the system easy to use and no additional software has to be installed. As the user receives the system and plugs it into the computer the system will interpret the predefined gestures accordingly.

4) Display subsystem

It contains the Arduino TFT LCD screen and it is used to inform the user about the state of the system or the gesture he made.

B. Comparison with other systems existed on the market

In order to evaluate the performances of our system we compared it with other gesture recognition system: the Microsoft Kinect and the Video Camera from a SonyVaio laptop with the SonyVaio gesture recognition built in software.

First of our system is a non-audio vide system. That means that the system is free from any image processing or skeleton processing algorithms, thus, making it computational light. This is shown by the fact that the process is running on a 16MHz processor with a CPU usage of 20%. The Kinect for Windows has recommended requirements of 3.1GHz [13] and the SonyVaio built in camera uses 5% CPU from a computer with a processor of 2GHz. Hence, the system that we built can be used for any computer regardless of the type or specifications. Also, our system is a plug and play one without the need of installing additional software on the user PC.

In terms of gesture recognition, the system that we described in this paper has a gesture recognition of 95% with a very fast learning curve of how to use the device. The SonyVaio built in gesture recognition is around 90% with a lot of faults especially because the system doesn't always sense the position of the hand. The KINECT has a gesture recognition percentage of 95-97% but it requires additional software to be installed. In terms of costs the Kinect is around 200 EUR and the device that we presented is less than half that amount.

IV. SOFTWARE

The software application that runs on the Arduino board is realized according to the diagram shown in Fig. 8. The code for reading the sensors and for sending commands to computer is placed inside a loop. At every iteration of the loop Arduino will read the output data from the SE-10 PIR sensor to check if a person presence is detected. If true, then the ultrasonic PING))) sensor is read to determine the distance to the person. If the person is close enough to the system then a reading cycle is started (the outputs of the Sharp IR are read in order to detect any possible gesture made by the user).

If it is possible to detect a gesture based on the output of one sensor then this sensor is kept active and the other ones are disabled. The output of the active sensor is read and interpreted (translated into a command that is sent to computer). Once there is no more gesture detected the other sensors are enabled and the reading cycle restarts. Arduino emulates the mouse and keyboard to send commands to computer. For example, if the user moves his hand from left to right/from right to left then the command sent is "press right arrow key"/ "press left arrow key". In order to do this Arduino has to emulate the keyboard. If the user moves his hand forward/backward then Arduino has to emulate the mouse and sends the command for scroll wheel movement.

The gestures that can be detected by the system are: left/right/forward/backward/motionless hand movement. With these basic commands the user can change the pictures in a slideshow, change the sides in a PowerPoint presentation, seek forward/backward in a movie, zoom in/out a picture, increase/ decrease the volume of a movie or song.

In the last part of the code is checked if the time from activation is higher than a preset value. If the measured time

interval is greater than the preset one, then the presence of the user is checked again. If the result of this checking is negative, then the system becomes inactive; otherwise, the system remains active and continues interpreting gestures made by the user.

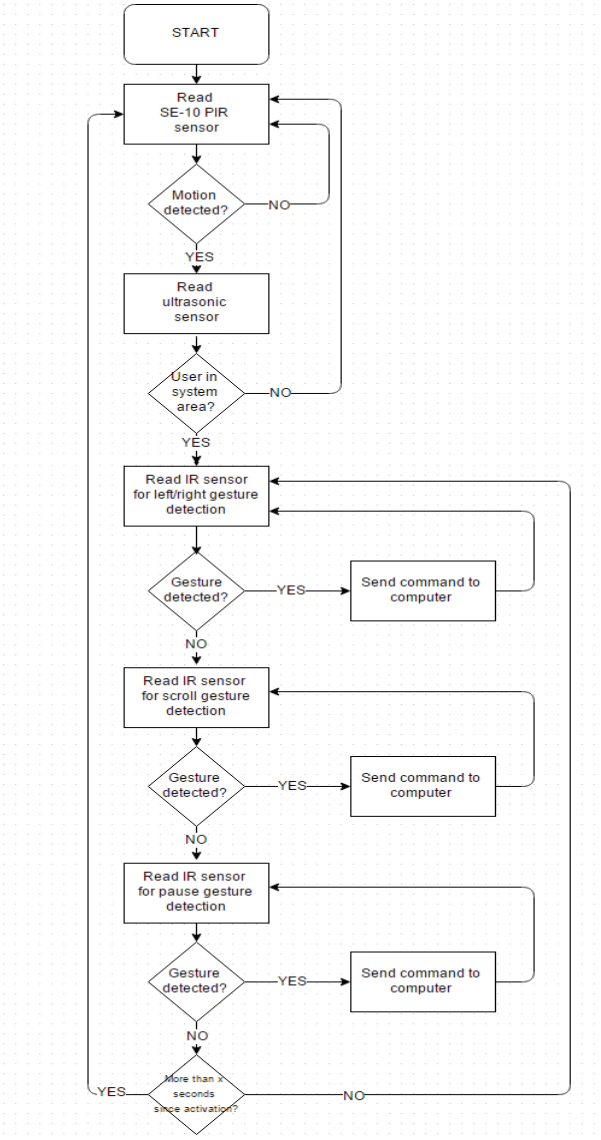

Fig. 8 Diagram of the algorithm used to detect gestures

V. Conclusions

The system presented in this paper proves the fact that a one can implement a simple gesture control interface by using only an Arduino Leonardo development board, motion detection PIR sensor and distance measurement sensors (infrared and ultrasonic sensors). The system can recognize a limited number of gestures but it can prove very useful for PowerPoint presentations, browsing photos, watching a movie etc. The cost of this system is relatively low compared to the solutions that are based on image processing to detect gestures. Also, this is a low power consumption system.

Another advantage of this gesture control interface is the fast response time. Since the amount of information processed by Arduino is small, the main cause of delays is the frequency of Sharp sensors reading.

This system is independent from the computer to which it connects. It can be connected to any computer, regardless of its operating system or specifications.

The functionality and the performance of this system can be improved by adding new sensors (for example, accelerometers) or by replacing the existing ones with more efficient ones. Using a network of IR sensors can allow the detection of more complex gestures (3D gestures).

Acknowledgment

This work has been funded by European Commission by FP7 IP project no. 610658/2013 ”eWALL for Active Long Living - eWALL” and by UEFISCDI Romania under grants no. 20/2012 “Scalable Radio Transceiver for Instrumental Wireless Sensor Networks - SaRaT-IWSN”, grant no. 262EU „eWALL” support project and by the Sectoral Operational Programme Human Resources Development 2007-2013 of the Ministry of European Funds through the Financial Agreement POSDRU/159/1.5/S/132397.

References

[1] Fan Wei; Chen Xiang; Wang Wen-hui; Zhang Xu; Yang Ji-hai; Lantz, V.; Wang Kong-qiao, "A Method of Hand Gesture Recognition Based on Multiple Sensors," Bioinformatics and Biomedical Engineering (iCBBE), 2010 4th International Conference on , vol., no., pp.1,4, 18-20 June 2010

[2] Zhou Ren; Junsong Yuan; Jingjing Meng; Zhengyou Zhang, "Robust Part-Based Hand Gesture Recognition Using Kinect Sensor," Multimedia, IEEE Transactions on , vol.15, no.5, pp.1110,1120, Aug. 2013

[3] Youwen Wang; Cheng Yang; Xiaoyu Wu; Shengmiao Xu; Hui Li, "Kinect Based Dynamic Hand Gesture Recognition Algorithm Research," Intelligent Human-Machine Systems and Cybernetics (IHMSC), 2012 4th International Conference on , vol.1, no., pp.274,279, 26-27 Aug. 2012

[4] Erden, F.; Bingol, A.S.; Cetin, A.E., "Hand gesture recognition using two differential PIR sensors and a camera," Signal Processing and Communications Applications Conference (SIU), 2014 22nd , vol., no., pp.349,352, 23-25 April 2014

[5] Arduino Leonardo specifications page. Available: http://arduino.cc/en/Main/arduinoBoardLeonardo

[6] Datasheet for Parallax PING))). Available: http://www.parallax.com/sites/default/files/downloads/28015-PING-Sensor-Product-Guidev2.0.pdf

[7] Datasheet for PIR SE-10 sensor,. Available: http://www.pololu.com/file/0J250/SE-10.pdf

[8] Datasheet for Sharp IR GP2D120. Available: http://www.sharpsma.com/webfm_send/1205

[9] Datasheet for Sharp IR GP2Y0A21. Available: http://www.sharpsma.com/webfm_send/1489

[10] Datasheet for Arduino TFT LCD Screen. Available: http://arduino.cc/en/uploads/Main/HTF0177SN-01-SPEC.pdf

[11] Kyriazakos, S.; Mihaylov, M.; Anggorojati, B; Mihovska, A; Craciunescu, R.; Fratu, O; Prasad, R., “eWALL – An intelligent caring home environment offering personalized context-aware applications based on advanced sensing”, Wireless Personal Communications Journal, pp 1-19, 2015-05-28

[12] Craciunescu, R.; Halunga, S.; Fratu, O., „Wireless ZigBee home automation system”, Proc. SPIE 9258, Advanced Topics in Optoelectronics, Microelectronics, and Nanotechnologies VII, 925826, February 21, 2015,

[13] ***, Microsoft Kinect sensor, https://www.microsoft.com/en-us/kinectforwindows/purchase/sensor_setup.aspx

THE 18TH INTERNATIONAL SYMPOSIUM ON WIRELESS PERSONAL MULTIMEDIA COMMUNICATIONS
(WPMC-2015)
December 13-16, 2015, Hyderabad, India

A Path Ordering and Reference Selection Method for the Differential Delay Tomography

Takehiro Otsuka*, Shinsuke Hara*‡, Takahiro Matsuda†‡, Kenichi Takizawa‡, Fumie Ono‡, and Ryu Miura‡
*Graduate School of Engineering, Osaka City University
Osaka, 5588585, Japan
Email:{otsuka@c., hara@}info.eng.osaka-cu.ac.jp
†Graduate School of Engineering, Osaka University
Osaka, 5650871, Japan
Email: matsuda@comm.eng.osaka-u.ac.jp
‡Wireless Network Research Institute, National Institute of Information and Communications Technology (NICT)
Kanagawa, 2390847, Japan
Email:{takizawa, fumie, ryu}@nict.go.jp

***Abstract*—Delay tomography means to estimate link delays in a network by measuring end-to-end path delays. In order to perform delay tomography accurately, strict clock synchronization is required between a transmitter node and a receiver node, but it is difficult in reality. As a delay tomography method without clock synchronization between them, a differential delay tomography using compressed sensing has been proposed and its performance has been theoretically analyzed. In the differential delay tomography, path delays are first measured between a transmitter node and a receiver node in the same way as a conventional method, and then a selected path delay is subtracted as the reference from all other path delays to eliminate the clock synchronization error between them. In this paper, taking into consideration the effects of the random delays in normal links and the clock skew between a transmitter node and a receiver node in a network, we propose a path ordering and reference selection method to reduce the effects and evaluate the performance by computer simulations.**

I. Introduction

Network tomography means to estimate internal link states by end-to-end path measurements in a network. In particular, when end-to-end path delays are measured to estimate link delays, it is called delay tomography [1], [2]. Any path delay between a transmitter node and a receiver node is the sum of the delays in all links over the path, so the delay tomography is formulated as an inverse problem to estimate unknown link delays from measured path delays. Furthermore, when we are interested in only identification of a limited number of abnormal links giving much longer delays, thanks to the sparsity of the abnormal links, compressed sensing can be efficiently applied to the identification problem [3]. Here, compressed sensing is a theory in signal/image processing for reconstructing a sparse vector based on its linear measurements of dimension smaller than the size of the unknown vector [4].

In delay tomography, when a transmitter node sends a probing packet to a receiver node though a path, the transmitter node writes the transmission time in the packet. This is because the transmitter node needs to notify the packet transmission time of the receiver node to calculate the difference between the transmission time and reception time as the transmission delay for the packet. Therefore, to perform the delay tomography accurately, strict clock synchronization is required between the transmitter node and receiver node, but it is difficult in reality. To identify abnormal links without clock synchronization in a network, a differential delay tomography with compressed sensing has been proposed [5]. In the differential delay tomography, after measuring all path delays between a transmitter node and a receiver node, the delay in a path is first selected as a reference and then the reference delay is subtracted from all the other delays to eliminate the clock offset between them.

In [5], for the differential delay tomography, the performance degradation due to differentiation has been theoretically analyzed. The performance is affected by the random delays in normal links and the clock skew between a transmitter node and a receiver node, however, their effects have not been well investigated. Therefore, in this paper, taking into consideration of the two effects, we re-formulate the problem of the differential delay tomography in detail, propose a path ordering and reference selection method for reducing the effects, and evaluate its performance by computer simulations.

II. Preliminary of Compressed Sensing

First, we define the ℓ_p norm ($p \geq 1$) of a vector $\mathbf{x} = [x_1\ x_2\ \cdots\ x_N]^\top \in \mathbb{R}^N$ as

$$\|\mathbf{x}\|_p = \left(\sum_{i=1}^{N} |x_i|^p \right), \tag{1}$$

where $[\cdot]^\top$ denotes the transpose operator.

Next, we define the mutual coherence $\mu(\mathbf{A})$ of a matrix $\mathbf{A}$, which is defined as the largest absolute inner product between any two columns $\mathbf{a}_i$, $\mathbf{a}_j$ of $\mathbf{A} \in \mathbb{R}^{M \times N}$:

$$\mu(\mathbf{A}) = \max_{1 \leq i,j \leq N, i \neq j} \frac{|\mathbf{a}_i^\top \mathbf{a}_j|}{\|\mathbf{a}_i\|_2 \|\mathbf{a}_j\|_2}. \tag{2}$$

If

$$k < \frac{1}{2} \left(1 + \frac{1}{\mu(\mathbf{A})} \right), \tag{3}$$

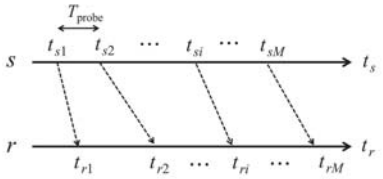

Fig. 1: Delay tomography session time chart.

then there exists at most one sparse vector $\mathbf{x}$ with k nonzero components that $\mathbf{y} = \mathbf{A}\mathbf{x}$, where a vector $\mathbf{y} = [y_1\ y_2\ \cdots\ y_M]^\top \in \mathbb{R}^M$ is a linear measurement vector.

Given a measurement vector $\mathbf{y}$ and a measurement matrix $\mathbf{A}$, compressed sensing estimates a sparse vector $\mathbf{x}$ by means of ℓ_1 optimization of the form:

$$\hat{\mathbf{x}} = \arg\min_{\mathbf{x}} \|\mathbf{x}\|_1 \quad \text{subject to } \mathbf{y} = \mathbf{A}\mathbf{x}. \tag{4}$$

ℓ_1 optimization is feasible when $\mathbf{x}$ is a completely sparse vector. However, if $\mathbf{x}$ is an approximately sparse vector, compressed sensing should estimate $\mathbf{x}$ by means of ℓ_1-ℓ_2 optimization of the form:

$$\hat{\mathbf{x}} = \arg\min_{\mathbf{x}} \left(\frac{1}{2}\|\mathbf{y} - \mathbf{A}\mathbf{x}\|_2^2 + \lambda \|\mathbf{x}\|_1 \right), \tag{5}$$

where $\lambda (> 0)$ is a constant [6].

III. System Models and Assumptions

A. System Model

Let $\mathcal{G} = (\mathcal{V}, \mathcal{E})$ denote an undirected network, where $\mathcal{V}$ and $\mathcal{E}$ denote sets of nodes and links, respectively. In the network, we select a transmitter node $s \in \mathcal{V}$ and a receiver node $r \in \mathcal{V}$ to measure the end-to-end paths delays between them. We formulate $\mathcal{E}$ as $\mathcal{E} = \{e_1, e_2, \ldots, e_N\}$, and define $\mathcal{Q} = \{q_1, q_2, \ldots, q_M\}$ as a subset of all paths from s to r, where $q_i = \{(s, v^{(i,1)}), (v^{(i,1)}, v^{(i,2)}), \ldots, (v^{(i,|q_i|-1)}, r)\} \subset \mathcal{E}$ represents the i-th path in $\mathcal{Q}$ and $v^{(i,m)} \in \mathcal{V} \setminus \{s, r\}$ are intermediate nodes in the path. We assume that link delay d_{e_j} arises independently in each link $e_j \in \mathcal{E}$ $(j = 1, 2, \ldots, N)$, and that path delay D_{q_i} is the sum of the delays in all links included the i-th path q_i.

Fig. 1 shows an overview of one delay tomography session. In the delay tomography session, the transmitter node s sends probing packets to the receiver node r to make r measure the end-to-end path delays on the pre-defined paths between them. The i-th probing packet is transmitted from s at time of t_{si} in terms of clock of s through measurement path q_i, and is received at r at time of t_{ri} in terms of clock of r $(i = 1, 2, \ldots, M)$. The i-th probing packet experiences a delay D_{q_i}, and D_{q_i} is actually calculated from t_{si} and t_{ri} as

$$D_{q_i} = t_{ri} - t_{si}. \tag{6}$$

The probing packets are transmitted with packet transmission interval of T_{probe}, and the delay tomography session repeats until all pre-defined end-to-end path delays are measured. From all the end-to-end path delays, the abnormal links in the network are finally identified based on compressed sensing.

B. Links Delay Model

We consider two kinds of links: abnormal link and normal link. The abnormal link is a link giving a constant longer delay x_A, whereas the normal link is a link giving a random shorter delay x_N which is independent and identically Gaussian distributed (i.i.d.) with average α_N and standard deviation σ_N [7]. We define a set of abnormal links as $\mathcal{E}_A \subset \mathcal{E}$.

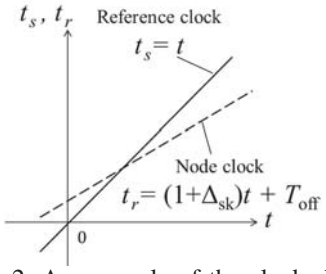

Fig. 2: An example of the clock skew.

C. Clock Error Model

Crystal oscillator (XO) is widely used as a clock generator in wireless or wired nodes. Since the oscillating frequency of XO is instable in its temperature characteristic, there is always an inevitable deviation in the oscillation frequency. Therefore, even if clock synchronizes between s and r is established at a time, the error between the clocks of s and r arises in time, which is called "clock skew."

Fig. 2 shows an example of the clock skew. On the basis of the clock of s, the clocks of s and r are respectively written as

$$t_s = t, \tag{7}$$

$$t_r = t + T_{\text{off}} + \Delta_{\text{sk}} t, \tag{8}$$

where T_{off} denotes the time offset between the clocks s and r at $t = 0$, and Δ_{sk} denotes the clock skew parameter. Assuming that the clock frequency uniformly deviates in $[-\Delta, +\Delta]$, Δ_{sk} follows the triangular distribution $[-2\Delta, 0, +2\Delta]$, so the average and variance of Δ_{sk} are respectively written as

$$E(\Delta_{\text{sk}}) = 0, \tag{9}$$

$$E(\Delta_{\text{sk}}^2) = \frac{2}{3}\Delta^2, \tag{10}$$

where $E[(\cdot)]$ denotes the ensemble average of $(\cdot)$.

IV. Conventional Delay Tomography

A. Formulation of Delay Tomography

The measured path delay over q_i is written as $(i = 1, 2, \cdots, M)$

$$y_i = t_{ri} - t_{si}, \tag{11}$$

$$= z_i + T_{\text{off}} + \Delta_{\text{sk}}(t_{si} + z_i), \tag{12}$$

$$z_i = \sum_{e_j \in q_i} d_{e_j}, \tag{13}$$

where d_{e_j} is the link delay in e_j. Defining a measured path delay vector $\mathbf{y} \in \mathbb{R}^M$, a link delay vector $\mathbf{x} \in \mathbb{R}^N$, a clock offset vector $\mathbf{x} \in \mathbb{R}^M$, and a clock skew vector $\mathbf{x} \in \mathbb{R}^M$ respectively as

$$\mathbf{y} = [y_1\ y_2\ \cdots\ y_M]^\top, \tag{14}$$

$$\mathbf{x} = [x_1\ x_2\ \cdots\ x_N]^\top, \tag{15}$$

$$\mathbf{v} = [v_i\ v_2\ \cdots\ v_M]^\top, \tag{16}$$

$$\mathbf{w} = [w_1\ w_2\ \cdots\ w_M]^\top, \tag{17}$$

where

$$x_j = d_{e_j}, \tag{18}$$

the delay tomography is formulated as

$$\mathbf{y} = \mathbf{A}\mathbf{x} + (\mathbf{v} + \mathbf{w}). \quad (19)$$

In (19), $\mathbf{A} \in (0,1)^{M\times N}$ is the binary routing matrix of $\mathcal{Q}$, whose components $a_{i,j}$ $(i = 1, 2, \ldots, M, j = 1, 2, \ldots, N)$ are 1 if $e_j \in q_i$, and 0 otherwise, and the i-th elements of $\mathbf{v}$ and $\mathbf{w}$ are written respectively as

$$v_i = T_{\text{off}}, \quad (20)$$

$$w_i = (t_{si} + z_i)\Delta_{\text{sk}}. \quad (21)$$

When we are interested in identification of a limited number of abnormal links, even for $N > M$, due to the sparsity of the abnormal links, we can solve (19) by means of the ℓ_1-ℓ_2 optimization given by (5).

B. Effect of Random Delay

Let us set $\mathbf{v} + \mathbf{w} = \mathbf{0}$ in (19) for a whole. In this case, the link delay vector $\mathbf{x}$ can be furthermore decomposed as

$$\mathbf{x} = \mathbf{x}_N + \mathbf{x}_A, \quad (22)$$

$$\mathbf{x}_A = \begin{cases} x_j - x_G & (\text{if} \quad e_j \in \mathcal{E}_A) \\ 0 & (\text{otherwise}) \end{cases}, \quad (23)$$

where $\mathbf{x}_N$ and $\mathbf{x}_A$ are the normal link delay vector and abnormal link delay vector, respectively. Thus we can rewrite (19) as

$$\mathbf{y} = \mathbf{A}\mathbf{x}_A + \mathbf{u}, \quad (24)$$

$$\mathbf{u} = \mathbf{A}\mathbf{x}_N, \quad (25)$$

where $\mathbf{u}$ is the error vector contributed from normal link delays. The average power of the normal link delays, namely, the average of the squared norm of $\mathbf{u}$ limits the performance of the delay tomography, so it can be calculated as

$$\begin{aligned} \varepsilon_{\text{delay}} &= E[\mathbf{u}^\top \mathbf{u}] \\ &= \sum_{i=1}^{M} E[u_i^2] \\ &= \sum_{i=1}^{M} (\rho_i^2 \alpha_N^2 + \rho_i \sigma_N^2). \end{aligned} \quad (26)$$

where ρ_i is the number of links through the i-th path q_i. Eq. (26) shows that the conventional delay tomography has no parameters to reduce the effect of random delays in normal links.

C. Effect of Clock Error

Now, let us set $\mathbf{u} = \mathbf{0}$ in (19) for a whole. In this case, the average of the squared norm of $\mathbf{v}$ also limits the performance of the delay tomography, so it can be calculated as

$$\begin{aligned} \varepsilon_{\text{offset}} &= E[\mathbf{v}^\top \mathbf{v}] \\ &= \sum_{i=1}^{M} E[v_i^2] \\ &= \sum_{i=1}^{M} T_{\text{off}}^2. \end{aligned} \quad (27)$$

Furthermore, the average of the squared norm of $\mathbf{w}$ limits the performance of the delay tomography, so it can be calculated as

$$\begin{aligned} \varepsilon_{\text{skew}} &= E[\mathbf{w}^\top \mathbf{w}] \\ &= \sum_{i=1}^{M} E[w_i^2]. \end{aligned} \quad (28)$$

The i-th path delay z_i is bounded by T_{probe}, so we assume that z_i is uniformly distributed in $[0, T_{\text{probe}}]$ for the sake of simplicity. In this case, Eq. (28) is calculated as

$$\varepsilon_{\text{skew}} = \frac{2\Delta^2}{3} \sum_{i=1}^{M} \left(t_{si}^2 + t_{si} T_{\text{probe}} + \frac{T_{\text{probe}}^2}{3} \right). \quad (29)$$

Eqs. (27) and (29) show that the conventional delay tomography has also no parameters to reduce the effects of the clock error, namely, there is no way except for estimating T_{off} accurately to compensate for T_{off} by $T_{\text{off}} - \hat{T}_{\text{off}}$ and employing an XO with high frequency stability for each node.

V. Reference Path Selection

A. Formulation of Delay Difference Tomography

In order to get rid of the effect of T_{off}, defining the m-th component y_m and the m-th row vector $\mathbf{a}_m \in \mathbb{R}^{M-1}$ of a reference component and a reference vector, respectively, we subtract the reference component and the reference vector from all the other components and all the other vectors. That is, defining a new measurement vector $\mathbf{y}^{(m)}$ and a new routing matrix $\mathbf{A}^{(m)} \in \{-1, 0, 1\}^{(M-1)\times N}$ as

$$\mathbf{y}^{(m)} = [y_1 - y_m \; y_2 - y_m \; \cdots \; y_M - y_m]^\top, \quad (30)$$

$$\mathbf{A}^{(m)} = \quad (31)$$

$$\begin{bmatrix} a_{1,1} - a_{m,1} & a_{1,2} - a_{m,2} & \cdots & a_{1,N} - a_{m,N} \\ a_{2,1} - a_{m,1} & a_{2,2} - a_{m,2} & \cdots & a_{2,N} - a_{m,N} \\ \vdots & \vdots & \ddots & \vdots \\ a_{i,1} - a_{m,1} & a_{i,2} - a_{m,2} & \cdots & a_{i,N} - a_{m,N} \\ \vdots & \vdots & \ddots & \vdots \\ a_{M,1} - a_{m,1} & a_{M,2} - a_{m,2} & \cdots & a_{M,N} - a_{m,N} \end{bmatrix}.$$

we have the following equation:

$$\mathbf{y}^{(m)} = \mathbf{A}^{(m)}\mathbf{x} + \mathbf{w}^{(m)}, \quad (32)$$

where the link delay vector $\mathbf{x}$ does not change by the subtraction, the time offset vector $\mathbf{v}$ disappears completely, and $\mathbf{w}$ is also changed to

$$\mathbf{w}^{(m)} = [w_1 - w_m \; w_2 - w_m \; \cdots \; w_M - w_m]^\top. \quad (33)$$

By the subtraction, although the clock skew still affects the accuracy of identifying abnormal links, it is possible to accomplish the delay tomography without the clock synchronization between the transmitter node and receiver node. The trade-off for getting rid of the clock offset is reducing the number of expressions, however, compressed sensing can estimate a unique solution from an underdetermined linear system, so it is still simply applicable in the proposed method.

Using (22), we can rewrite (32) as

$$\mathbf{y}^{(m)} = \mathbf{A}^{(m)}\mathbf{x}_A + \mathbf{u}^{(m)} + \mathbf{w}^{(m)}, \quad (34)$$

$$\mathbf{u}^{(m)} = \mathbf{A}^{(m)}\mathbf{x}_N. \quad (35)$$

Eq. (34) shows that selecting a path as a reference, $\mathbf{A}$, $\mathbf{u}$ and $\mathbf{w}$ change $\mathbf{A}^{(m)}$, $\mathbf{u}^{(m)}$ and $\mathbf{w}^{(m)}$, respectively. It is proven in [5] that, if $\mathbf{A}$ is 1-identifiable, then $\mathbf{A}^{(m)}$ is also still 1-identifiable, in other words, as long as the number of abnormal links is guaranteed to be one, we can select any path as the reference to identify the abnormal link. In the following two subsections, we discuss a path ordering and reference selection method for reducing the effects of the normal link delays $\mathbf{u}^{(m)}$ and the clock skew $\mathbf{w}^{(m)}$.

B. Reference Path Selection for Reducing the Effect of the Normal Link Delays

The average of the squared norm of $\mathbf{u}^{(m)}$ is calculated as

$$\begin{aligned}\varepsilon_{\text{delay}}^{(m)} &= \sum_{i=1,i\neq m}^{M} E\left[(u_i-u_m)^2\right] \\ &= \sum_{i=1,i\neq m}^{M} \left\{(\rho_i-\rho_m)^2\alpha_N^2+(\rho_i-\rho_m)\sigma_N^2\right\} \\ &= \sum_{i=1,i\neq m}^{M} \alpha_N^2\left\{\rho_m-\left(\rho_i-\frac{\sigma_N^2}{2\alpha_N^2}\right)\right\}^2 \\ &+ \sum_{i=1,i\neq m}^{M}\left(2\rho_i\sigma_N^2-\frac{\sigma_N^4}{4\alpha_N^2}\right). \end{aligned} \quad (36)$$

Applying the Cauchy-Schwarz inequality to the first term of (36) results in

$$\begin{aligned}\varepsilon_{\text{delay}}^{(m)} &\geq \frac{\alpha^2}{M-1}\left[\sum_{i=1,i\neq m}^{M}\left\{\rho_m-\left(\rho_i-\frac{\sigma_N^2}{2\alpha_N^2}\right)\right\}\right]^2 \\ &+ \sum_{i=1,i\neq m}^{M}\left(2\rho_i\sigma_N^2-\frac{\sigma_N^4}{4\alpha_N^2}\right). \end{aligned} \quad (37)$$

To minimize $\varepsilon_{\text{delay}}^{(m)}$, ρ_m needs to satisfy the following expression on (37):

$$\rho_m = \frac{\sigma_N^2}{2\alpha_N^2}+\frac{1}{M-1}\sum_{i=1,i\neq m}^{M}\rho_i \approx \frac{1}{M-1}\sum_{i=1,i\neq m}^{M}\rho_i. \quad (38)$$

This implies that it is better to select the path as a reference, whose number of links is closer to the number of links averaged over all the paths.

C. Reference Path Ordering for Reducing the Effect of the Clock Skew

The average of the squared norm of $\mathbf{w}^{(m)}$ is calculated as

$$\begin{aligned}\varepsilon_{\text{skew}}^{(m)} &= \sum_{i=1,i\neq m}^{M} E\left[(w_i-w_m)^2\right] \\ &= \frac{2\Delta^2}{3}\sum_{i=1,i\neq m}^{M} E\left[\left\{(t_{si}-t_{sm})+(z_i-z_m)\right\}^2\right] \\ &= \frac{2\Delta^2}{3}\sum_{i=1,i\neq m}^{M}\left\{(t_{si}-t_{sm})^2+\frac{T_{\text{probe}}^2}{6}\right\}. \end{aligned} \quad (39)$$

Applying the Cauchy-Schwarz inequality to (39) also results in

$$\varepsilon_{\text{skew}}^{(m)} \geq \frac{2\Delta^2}{3(M-1)}\left\{\sum_{i=1,i\neq m}^{M}(t_{si}-t_{sm})\right\}^2+\frac{\sigma^2(M-1)T_{\text{probe}}^2}{9}. \quad (40)$$

To minimize $\varepsilon_{\text{skew}}^{(m)}$, t_{sm} needs to satisfy the following expression on (40).

$$t_{sm} = \frac{1}{M-1}\sum_{i=1,i\neq m}^{M} t_{si}. \quad (41)$$

This implies that it is better to select the path as a reference, whose probing packet is transmitted around at the middle of the delay tomography session.

Fig. 3: Network topology.

D. Proposed Path Ordering and Reference Selection Method for Reducing the Effect of the Normal Link Delays and the Clock Skew

From the results in the above two subsections, we can conclude that, in order to jointly reduce the effect of the normal link delays and the clock skew, one method is to order the measured paths with the numbers of links in an ascending order, transmit probing packets in the order, and finally select the path as a reference whose probing packet is transmitted around at the middle order. This is because the selected path automatically has the number of links close to the one averaged over all the measured paths.

VI. Performance Evaluation

A. Computer Simulation Environment

Fig. 3 shows the network topology with 14 nodes and 29 links for the performance evaluation, where the clock of s is not synchronized to the clock of r. We constructed the routing matrix for the network topology according to the method in [8], and we obtained the 15×29 matrix (15 path measurements for 29 links). In the computer simulation, applying the delay tomography method for a wireless network, we assumed that the delay of normal link is Gaussian-distributed with $\alpha_N = 15$ msec and $\sigma_N = 3$ msec [10], whereas that of abnormal link is $x_A = 500$ msec. In addition, we assumed the clock frequency deviation of each node is $\Delta = 40$ ppm [11]. Furthermore, we set the probing packet transmission interval $T_{\text{probe}} = 1$ sec. Finally, as the algorithm of solving (5), we employed the fast iterative shrinkage-thresholding algorithm (FISTA) [9] with optimized values of λ.

The procedure of the performance evaluation is as follows: we randomly select a link as an abnormal link and identify it using the proposed delay tomography method. We define the abnormal link identification ratio R as the number of correctly identified abnormal links divided by the total number of simulation runs.

B. Effect of the Normal Link Delays

For the constructed routing matrix, the maximum and minimum numbers of links are 10 and 3, respectively, and the average of the number of links over all the paths is around 6. Fig. 4 shows the abnormal link identification ratio versus the index of the path selected as a reference, where the number of links is shown for each path index. Here, we are interested in the effect only from the normal link delays, so we set $\Delta = 0$. We can see from this figure that we should select the path with index of 9 as the reference, whose number of links is 6, that is, is close to the average number of links over all the paths, since it can give the highest abnormal link identification ratio.

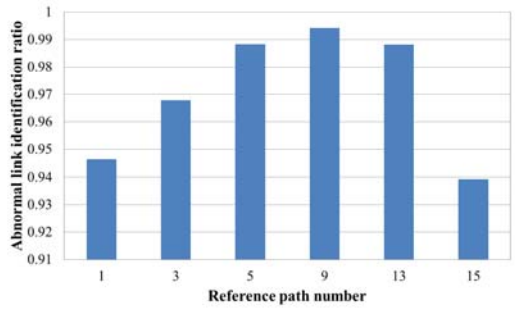

Fig. 4: abnormal link identification ratio vs. reference path number.

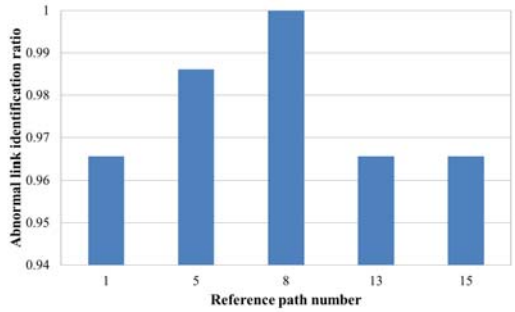

Fig. 5: abnormal link identification ratio vs. reference path number.

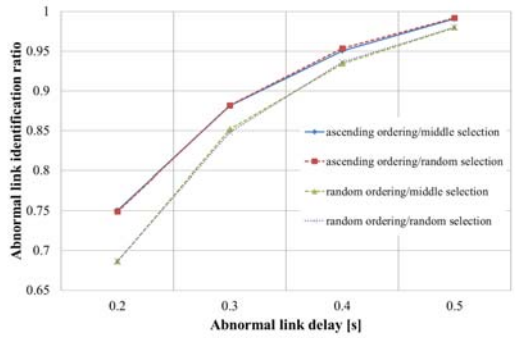

Fig. 6: abnormal link identification ratio vs. abnormal link delay.

C. Effect of the Clock Skew

For the constructed routing matrix, the number of paths is $M = 15$, so probing packets are transmitted fifteen times in a delay tomography session, so the middle order of probing packet transmission is around the 8th $(M/2) \approx 8$. Fig. 5 shows the abnormal link identification ratio versus the order of the referenced probing packet. We can see from this figure that we should select the path with order of 8 as the reference, whose probing packet is transmitted around at the middle of delay tomography session, since it can give the highest abnormal link identification ratio.

D. Performance of the Proposed Path Ordering and Reference Selectioning Method

Finally, Fig. 6 shows the performance of the proposed ascending ordering/middle selection method, which orders the paths with the numbers of links in an ascending order and selects a path with the middle order as the reference. For comparison purpose, this figure includes the performances of a random ordering/middle selection method, a ascending ordering/random selection method and a random ordering/random selection method. From the figure, we can see that the proposed ascending ordering/middle selection method performs best among the four methods. We can also see that, in the system setting, the random normal link delay is the dominant factor for determining the performance.

VII. Conclusion

In this paper, for the differential delay tomography, we analyzed the effects of the normal link delays and the clock skew on the abnormal link identification ratio, and proposed the path ordering and reference selection method for the reducing the effects. By computer simulations, we showed that the proposed ascending path ordering/middle reference selection method performs best, achieving the highest abnormal link identification ratio for smaller value of abnormal link delay.

Acknowledgment

This work was supported in part by the Japanese Ministry of Internal Affairs and Communications in R&D on Cooperative Technologies and Frequency Sharing Between Unmanned Aircraft Systems (UAS) Based Wireless Relay Systems and Terrestrial Networks.

References

[1] M. Coates, A. O. Hero III, R. Nowak, and B. Yu, "Internet tomography," *IEEE Signal Process. Mag.*, vol. 19, no. 3, pp. 47–65, May. 2002.
[2] Y. Tsang, M. Coates, and R. Nowak, "Network delay tomogrraphy," *IEEE Trans. Signal Process.*, vol. 8, 2014.
[3] M. H. Firooz and S. Roy "Network tomography via compressed sensing," *in Proc. IEEE GLOBECOM*, pp. 1–5, Dec. 2010.
[4] Y.C. Eldar and G. Kutyniok, *Compressed Sensing: Theory to Applications*. Cambridge University Press, 2012.
[5] K. Nakanishi, S. Hara, T. Matsuda, K. Takizawa, F. Ono, and R. Miura, "Synchronization-free delay tomography based on compressed sensing," *IEEE Commun. Lett.*, vol. 18, no. 8, pp. 1343–1346, Aug. 2014.
[6] M. Zibulevski and M. Elad, "L1-L2 optimization in signal and image processing," *IEEE Signal Process. Mag.*, vol. 27, no. 3, pp. 76–88, May. 2010.
[7] K.L. Noh, Q.M. Chaudhari, E. Serpedin, and B.W. Suter, "Novel clock phase offset and skew estimation using two-way timing message exchanges for wireless sensor networks," *IEEE Trans. Commun.*, vol. 55, no. 4, pp. 766-777, Apr. 2007.
[8] K. Takemoto, T. Matsuda, and T. Takine, "Sequential loss tomography using compressed sensing," *IEICE Trans. Commun.*, vol. E96-B, no. 11, pp. 2756–2765, Nov. 2013.
[9] A. Beck and M. Teboulle "A Fast Iterative Shrinkage-Thresholding Algorithm for Linear Inverse Problems," *SIAM Journal on Imaging Sciences.*, vol. 2, pp 183–202, 2009.
[10] W. Zeng, X. Chen, Y.A. Kim, and W. Wei, "Delay monitoring for wireless sensor networks: An architecture using air sniffers," in *Proc. IEEE MILCOM.*, pp. 1–8, Oct. 2009.
[11] *IEEE Standard for Local and Metropolitan Area Networks-Part 15.4: Low-Rate Wireless Personal Area Networks (LR-WPANs)*, IEEE Std. 802.15.4-2011, Rev. IEEE Std. 802.15.4-2006, Sep. 2011.

THE 18TH INTERNATIONAL SYMPOSIUM ON WIRELESS PERSONAL MULTIMEDIA COMMUNICATIONS
(WPMC-2015)
December 13-16, 2015, Hyderabad, India

Packet Scheduling Scheme to Guarantee QoS in Internet of Things

Reema Sharma
Department of ECE
The Oxford College of Engineering,
Bangalore, India
sharma80reema@gmail.com

Navin Kumar
Department Of ECE
ASE, Amrita Vishwa Vidyapeetham
Bangalore, India
navinkumar@ieee.org

Namratha B Gowda
Department Of ECE
TOCE Bangalore, India
namrathagowda25@gmail.com

T. Srinivas
Department of ECE
Indian Institute of Science,
Bangalore, India
tsrinu@ece.iisc.ernet.in

***Abstract*—In this paper, a new prediction based dynamic scheduling mechanism is proposed to ensure quality of service (QoS) especially in Internet of Things (IoT) by dynamically allocating bandwidth. The scheduling scheme is analyzed for two different applications: i) to accommodate various streaming data of IoT applications or for medical applications. Traffic is segregated based on different traffic characteristics such as bit rate, packet loss rate and tolerable delay into different classes and they are prioritized based on these characteristics; and ii) a scenario when continuous data for a long time is generated such as, from many lightweight devices like sensors. The algorithm allocates bandwidth such that its utilization can be optimized for different applications. The scheduler decision is divided into two steps: (i) calculating average increase in queue length of high priority and medium priority services at current time slot from the previous time slot and, (ii) adding these values to previous weight values for corresponding services and multiplying with a coefficient. The performance is carried out under different system loading and scenarios. The results show the improvement of the proposed scheduler with respect to end to end delay distributions, packet drop and end to end jitter values.**

Keywords— Packet Scheduler, Service Differentiation; Internet of Things; Quality of service; Queue Management.

I. INTRODUCTION

From the day of emergence, the Internet of Things (IoT) has got wide identification for its prospective applications. For the IoT applications, such as video surveillance, smart metering [1], smart homes and malls equipped with certain security devices [2], medical application (fall detection) [3] etc, devices need to report various events and streaming data to a central server over a long period of time in an efficient way. In the network of smart devices, ensuring QoS to certain delay sensitive applications is of prime importance. IoT technology also provides added value to emergency response operations in terms of obtaining efficient cooperation. The response time for such applications and QoS requirements need to be guaranteed. Kleoec and Kos [4] proposed a priority model with two queues and presented packet transit time behaviour for a delay sensitive application with minimum bandwidth constraint. The model is simple; the utilization of higher priority was shown at the cost of high data loss for low priority data. Furthermore, various approaches have been developed in order to analyze and monitor energy efficiency [1], network topologies, performance related issues [2-3] and the availability of bandwidth [5]. The solution to delay sensitive applications is not efficient as discussed in the above studies. To ensure instant communication without packet loss and queuing delay especially for the delay critical applications, an efficient packet scheduling scheme becomes necessary.

This paper proposes a round robin based packet scheduling scheme to provide QoS by dynamically allocating bandwidth. Two main important features which make this scheduler different are: (i) most of the recent round robin or rate adaptive round robin policies do not consider previous slot allocation data for allocation of current slot; and (ii) most schedulers which consider service differentiation are designed to provide precedence only to high priority packets at the cost of poor performance of medium and low priority packets. This scheduler is designed to determine the weighing coefficient of high priority queue based on the number of packets arrived in the queue in the previous cycle and allocates required bandwidth to satisfy QoS. It then determines weighing coefficient of the medium priority queue based on number of packets arrived in this queue and the weights allocated to high priority queue. Finally, weights are calculated for low priority queue and packets are accordingly scheduled.

We analyzed this scheduler for two different applications: (i) lightweight sensors which are continuously transmitting data of few kbps to few hundreds of kbps; and (ii) on biomedical data such as fall detection application which detects patient falls, for which many different services may be required with different QoS constraints. For example, one service may rely on a network of video cameras in the ceiling, while other service may use an accelerometer on the patient and yet another may use pressure sensors in the floor [3]. Different input data files are created for these applications and tested using proposed scheduling scheme to provide QoS to different services in terms of end to end delay, packet loss ratio, etc. In various applications, traffic is prioritized based on different traffic characteristics like traffic bit rate, packet loss rate and tolerable delay into different high priority, medium priority and low priority classes, stored in different buffers and scheduled to provide better QoS.

The rest of the paper is organized as follows. Section II presents a system architecture and related work. In section III, the proposed scheduling scheme for dynamic bandwidth allocation is discussed. Simulation results and performance

parameters are discussed in section IV while section V concludes the paper.

II. System Architecture and Related Work

Selection of proper architecture is very important before designing any algorithm to be implemented for the same. QoS architectures in traditional networks like DiffServ, IntServ do not satisfy the requirement of IoT which involves large number of heterogeneous devices and tasks like collection, transmission, storage and processing of complex data. QoS architectures in IoT must consider the dynamic nature of IoT otherwise it may lead to service failures. Authors in [6] presented a service modeling approach for different components in IoT framework. There are many models based on Markov chain concept to provide QoS. Markovian QoS models in traditional networks like DiffServ [7-8] do not satisfy the requirement of IoT. In [2], Markov Chain based cost-effective analytical model is proposed to ensure QoS for transmission of delay sensitive information.

Also, several devices and heterogeneous networks integrated in IoT make it complex to satisfy different QoS requirements [9]. Packet scheduling is one of the QoS mechanisms used to select the packets which should be serviced or dropped. Packet scheduling can provide service provisioning and help in differentiating emergency messages from non-critical messages. So, QoS awareness can be established in IoT by allocating traffic priorities and scheduling them with appropriate algorithm [10]. In [10] a QoS aware massage scheduling algorithm is proposed in IoT environment. The authors classified messages into two classes, high priority (emergency messages) and best effort (non critical messages) and proposed QoS scheduling algorithm. The algorithm proposed is efficient in terms of energy and waiting time however the loss and other performance parameters are not considered. In [11] a Multi-Dimensional QoS decision is proposed based on IoT estimate approach, in which each stakeholder is mapped into a single value to establish best configuration of interactions. Authors in [12] discussed a modeling approach on IoT based solutions using Human centric wireless sensor networks (WSNs). This approach supports emergency response activities which is one of the biggest challenges. We propose a QoS model at network layer to ensure QoS for emergency traffic.

III. The Proposed Scheduling Scheme and Analysis

In this section, we present dynamic bandwidth allocation prediction based scheduling scheme to optimize its utilization for different kinds of applications. The scheme includes following important features:

1.) Traffic from different applications segregated based on different traffic characteristics like traffic bit rate, packet loss rate and tolerable delay into different classes and prioritized them into high priority data, medium priority data and low priority data based on these characteristics.

2.) We assume three different queues: high priority queue, medium priority queue, and low priority queue to store packets of respective type defined above and scheduled in a round robin manner.

3.) Buffer space used for high priority queue is kept small because these services are sensitive to delay and jitter and cannot tolerate more queuing delay. But buffer space for medium and high priority queue is considered large to reduce the packet loss.

4.) Exponential Weighted Moving Average (EWMA) is used to calculate average queue size of high priority service [13]. Average queue size of medium priority queue is calculated using simple average formula.

5.) Algorithm predicts average increase or decrease in average queue length of high priority and medium priority services, and in case of high priority service, add these values to previous weight values of high priority services and then multiply with a coefficient (explained later). This helps in optimizing weights for current time slot based on this increase or decrease to allocate bandwidth required for high priority and medium priority services.

6.) For keeping delay jitter in tolerable limits for high priority traffic (<10ms), minimum and maximum thresholds are assigned which will be the indicator to assign the appropriate weights.

A. *Dynamic Weight Standardization*

To reduce the fluctuations in instantaneous queue size, we calculated the average queue size of high and medium priority services by using a low pass filter with exponential weighted moving average. Average queue length of high and medium priority queue is predicted as [13]:

$$l_avg = (1 - 0.01) * l_avg + 0.01 * l_inst \qquad (1)$$

where, l_avg is average queue size, l_inst is instantaneous queue size and 0.01 is scaling factor to reduce fluctuations in instantaneous queue size.

Threshold levels are introduced for buffer management. If average queue size is below minimum threshold, high priority weight taken is 0.3, which will provide low queuing delay, if average queue size is between minimum and maximum threshold, weights are proportionally varied with increase or decrease in the average queue length at consecutive time slots.

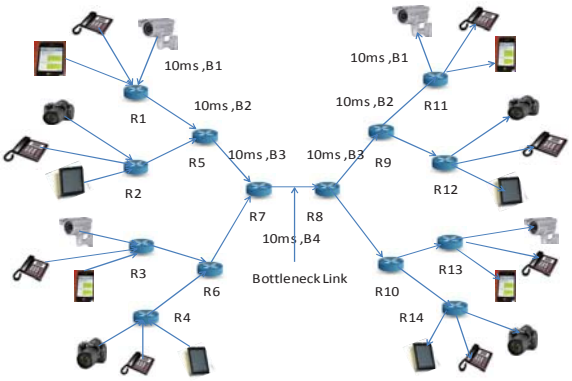

Fig 1: Network Topology used to analyze the performance of scheduling scheme

If it increases beyond maximum threshold, more but bounded to upper limit bandwidth is allocated. In this scheme, the weights are calculated in a circular fashion, starting from high, medium and then low priority queue.

Weight of high priority queue is calculated as:

$$high_{pri_{wt}} = \begin{cases} high_{wt_{init}} & l_avg \epsilon \{0,0.833\} \\ \left(C1 * high_{diff_{avg_{queue_{len}}}}\right) + high_{prev_{avg_{wt}}} & l_avg \epsilon \{0.833,3.667\} \\ high_{Upper_{bounded_{value}}} & l_avg \epsilon \{3.667,10\} \end{cases} \quad (2)$$

where, $high_{pri_{wt}}$ is $high_wt_{init}$=0.3 if average queue size is between 0 and minimum threshold, if average queue size is between maximum threshold and 10, $high_{pri_{wt}}$ is $high_Upper_{bounded_{value}}$= 0.7, i.e. a maximum of 70% bandwidth can be allocated to high priority service , C1 is a constant = $\frac{0.3}{(high_th_{Max} - high_th_{min})}$ where $high_th_{Max}$ is 3.667 and $high_th_{min}$is 0.833 which are nothing but the maximum and minimum threshold of the high priority buffer considered. Minimum threshold defines desired delay and maximum threshold covers tolerable delay. $high_diff_{avg_{queue_{len}}}$ is the difference (increase or decrease) in average queue length of high priority service queue length at current time cycle from previous cycle. The weight of medium priority queue can be calculated by:

$$med_{pri_{wt}} = \begin{cases} med_{wt_{init}} & l_avg \epsilon \{0,60\} \\ \left(1 - high_{pri_{wt}}\right) & l_avg \epsilon \{61,100\} \end{cases} \quad (3)$$

med_wt_{init} is assigned to 0.3 when the average queue size of medium priority queue is between 1 and 60, if it exceeds 60, then $med_{pri_{wt}}$is assigned as difference of total bandwidth and the bandwidth allocated to high priority service. Finally, if the bandwidth is unutilized from high and medium priority it is allocated to low priority traffic. The weight of low priority queue can be obtained as:

$$low_{pri_{wt}} = 1 - (high_{pri_{wt}} + med_{pri_{wt}}) \quad (4)$$

IV. Performance Evaluation and Simulation Results

A. Network Topology

A typical internetwork as shown in Fig.1 consists of multiple nodes. These nodes may act as sensor devices, generate data of CCTV camera or it may act as intermediate routers. We have investigated many performance measures of the proposed algorithm for different applications using different system loads. The various performance measures considered to evaluate the performance of proposed packet scheduling scheme are average end to end delay, the average delay jitter, and the average packet loss ratio for different service classes. The traffic characteristics chosen for different applications are summarized in a Table 1.

In different experiments, we analyzed average one way end to end queuing delay, average delay jitter and average packet loss ratio for high, medium and low priority service. If P is the total number of packets transmitted from *nth* source to *nth* destination, $T_n(i)$ is the time at which *ith* packet was sent by the source n, $R_n(i)$ is the time at which *ith* packet was received by the destination n, then one way end to end delay $eed_{n(i)}$is calculated as:

$$eed_{n(i)} = Rn(i) - Tn(i) \quad (5)$$

Average end to end delay Avg_{eed} for high, medium and low priority traffic is calculated as (6) where n is the source generating different traffic.

$$Avg_{eed} = (\sum_{n=1}^{S}(\sum_{i=1}^{P} eed_{n(i)})/P)/S \quad (6)$$

where, S is the maximum number of sources for each service and P is the number of packets which has been sent so for by each source.

Delay jitter is defined as the absolute difference between end to end delays of two consecutive packets. If one way end to end delay of *ith* packet from *nth* source is given by (5) then end to end Delay Jitter for packets from source n to destination n is calculated from (7):

$$Jitter = abs(eed_{n(i+1)} - eed_{n(i)}) \quad (7)$$

Also, if P_n is the total number of packets transmitted by *nth* source, R_n is the total number of packets received by corresponding *nth* receiver, then Packets lost ratio is given as::

$$Packet\ Loss\ Ratio = \frac{(P_n - R_n)}{P_n} \quad (8)$$

The simulated results obtained in different experiments are presented next. The simulation results are plotted using MatLab R2013b. Proposed scheduler is tested for two main applications under a complex topology shown in Fig.1. Traffic is prioritized based on different traffic characteristics like traffic bit rate, packet loss rate and tolerable delay into high, medium and low priority services.

TABLE I: Traffic Characteristics in Different Scenarios

Parameters	Scenario 1 with Bottleneck Bandwidth of 1.2Mbps			Scenario 2 with Bottleneck Bandwidth of 112Mbps		
Service Type (Priority)	High	Medium	Low	High	Medium	Low
Traffic Type	Poisson	Poisson	Poisson	MPEG-4	Poisson	Poisson
Packet size in bytes	100 Bytes	20 to 571 bytes	100 bytes	136 to 348250 bytes	20 to 571	100 to 500 bytes
Number of flows	12 flows at same time			12 flows at same time		
Node Topology	Random			Random		
Data rate	2Mbps			2.1Mbps to 114Mbps		
No. of Nodes	38			38		
Traffic direction	Left to right			Left to right		
No. of Packets sent	17828	499996	499996	10084	420104	420464
Link Delay	10ms			10ms		

Fig.2, 3, and 4 describe the average packet loss, average end to end delay, and the average jitter from all twelve sources which are sending a constant data of three different types as discussed in Scenario1 (Details given in Table 1). In Scenario 1, we consider sensors emergency data as high priority data. Poisson arrival process can be assumed for traffic model to each individual sensor node. So, for high, medium and low priority, Poisson traffic with variable size packets is considered. In Exp2, high priority service class in which packets are expected to be delivered in time are taken as MPEG traces. MPEG file format is considered because CCTV captured video images are normally converted into MPEG file format and is commonly used. Medium and low priority service class includes all non detrimental applications such as peer to peer applications. Query initiation model is one of the examples of peer to peer application and can be modeled as Poisson traffic. Packets are classified as high priority, medium priority and low priority packets, and are stored in different buffers of sizes 10,100,100 respectively for high, medium and low priority and finally they are scheduled using proposed packet scheduling. The results show that the average end to end delay for high and medium packets is approximately 62ms (this is the delay due to addition of all link delays in the path travelled by packets). It is increased for low priority packets by small amount but these packets are insensitive to delay. Average delay jitter for high priority packets is very less and within tolerable limits (<10ms). Delay jitter has increased for medium and low priority packets due to more bandwidth get allocated to high priority packets to guarantee its QoS performance. The no. of packets sent for high priority service is 17828 and received packets are 17500. Data rate at which high priority packets are sent from all four sources is 64000bits/sec. For a data rate less than 64000bits/sec, there is no loss for high priority packets using the scheduling scheme. For medium priority, out of 499996 packets sent 485162 packets are received successfully but for low priority out of 499996 packets, received packets are 372910. Data rate from medium priority is 0.7Mbits/s at which loss is 3% packets but for a data rate less than 0.7Mbits/sec there is no packet loss for medium priority.

Data rate for the low priority is 1.2Mbits/s at which loss is approximately 24% packets and for an overall data rate less than 1.2Mbits/sec there is no loss of any packet from any service class. All the QoS performance parameters are satisfied for all three services under the conditions mentioned in Table 1. Similarly, results for the average packet loss, the average end to end delay and the average jitter for Scenario 2 (Table 1) are described in Fig.5, 6 and 7. The results show that average end to end delay for high and medium packets is approximately 62ms for high priority and 62.12 ms for medium priority. It is increased for low priority packets by small amount but these packets are insensitive to delay.

Average delay jitter is better for all three services in Scenario 1. The no. of packets sent for high priority service is 10084 and received packets are 10020. Data rate at which high priority packets are sent from all four sources varies between 171520bits/s to 110Mbits/s.

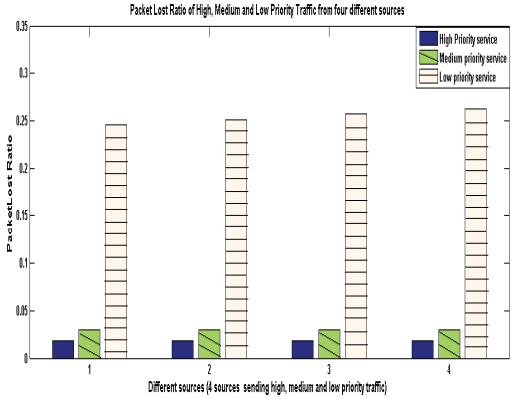

Fig. 2. Average packet lost ratio for high, medium and low priority traffic with bottleneck link bandwidth of 1.2Mbps

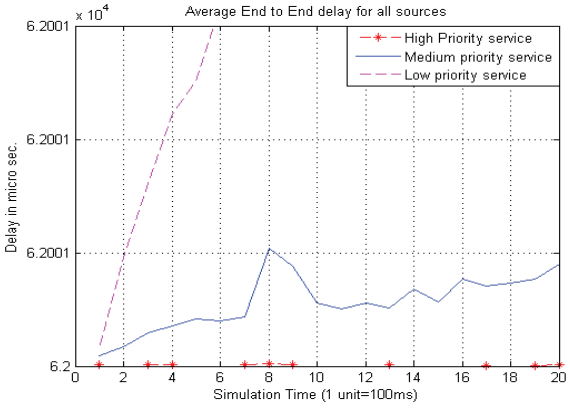

Fig. 3.Average end to end delay for high, medium and low priority traffic with bottleneck link bandwidth of 1.2Mbps

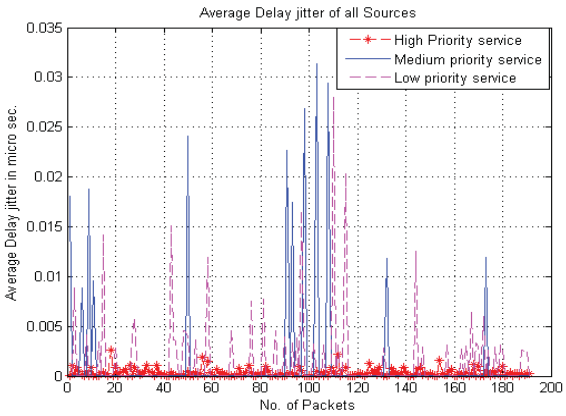

Fig. 4.Average jitter for high, medium and low priority traffic with bottleneck link bandwidth of 1.2Mbps

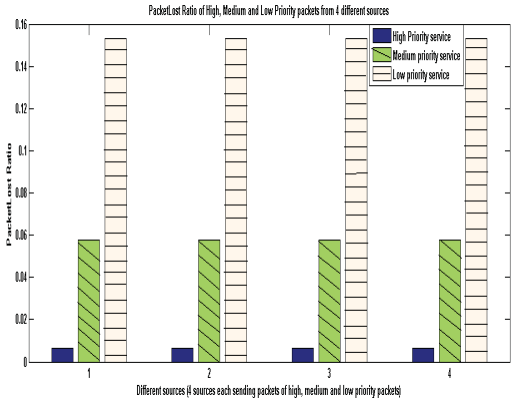

Fig. 5. Average packet lost ratio for high, medium and low priority traffic with bottleneck link bandwidth of 112Mbps

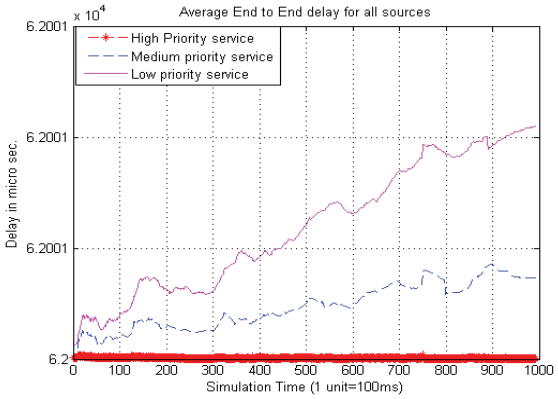

Fig. 6.Average end to end delay for high, medium and low priority traffic with bottleneck link bandwidth of 112Mbps

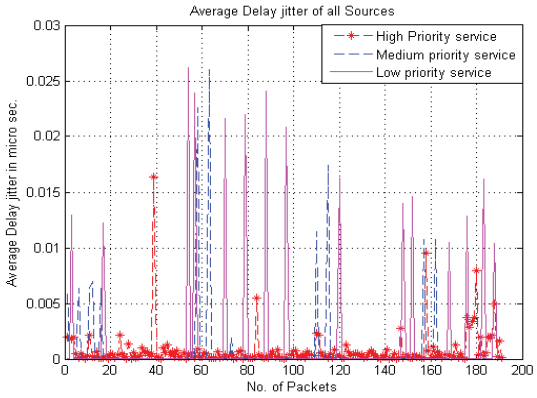

Fig. 7.Average jitter for high, medium and low priority traffic with bottleneck link bandwidth of 112Mbps

With the same data rate if simulation time is less, there is no loss for high priority packets using proposed packet scheduling scheme. The packet size varies from 136 bytes to 348250 bytes. We also observe that the high priority loss is zero if the maximum packet size is reduced to 9999 bytes and simulation time can be extended for a longer time. For medium priority out of 420104 packets sent 395904 packets are received successfully but for low priority out of 420104, received packets are 356148.

Data rate for medium priority is 0.7Mbits/s at which loss is 5.76% packets but for a data rate less than 0.7Mbits/sec there is no packet loss for medium priority provided packet size of video packets (high priority) is taken less than equal to 9999bytes. Data rate for low priority is 1.2Mbits/s at which loss is 15.0% packets and for a data rate less than 112Mbits/sec there is no loss from any service class. Even if data rate is more than 112bits/sec, packet size of video packets is <=9999bytes, simulation time is long, there is no loss for high priority, medium priority and less than 10% losses for low priority. This satisfies all the QoS requirements in IoT. Therefore, the proposed scheduler is expected to efficiently perform under many conditions.

The average delay jitter is better for all three services and is within tolerable limits. We have observed that if the number of video packets keeps on increasing as high priority packets, the lost packets will increase for low priority only if the packet size of video is more than 9999bytes but performance will be as expected for high and the medium priority in terms of all QoS parameters.

The average computation time required using this packet scheduling scheme which is calculated using profiler report generated by Matlab2013b is reported to be 2.87ms.

V. Conclusion

The proposed joint packet scheduling and dynamic bandwidth allocation scheme designed with an aim for IoT applications have been discussed. The performance results are encouraging especially guaranteeing QoS parameters. It works efficiently for continuously generated small size packets, continuously generated large packets up to 9999 bytes packet size and for 7000 packets of size 96456 bytes. Loss for BE packets is approximately up to 8% for small packet size while increases up to 12% if high priority packet length keeps on increasing. All the conditions of no loss from any differentiated service class are clearly mentioned and discussed in the results. The proposed scheme performs well in terms of all QoS parameters and is within tolerable limits.

References

[1] Jia-Ming Liang, Jen-Jee Chen, Hung-Hsin Cheng, and Yu-Chee Tseng " An Energy-Efficient Sleep scheduling with QoS consideration in 3GPP LTE advanced networks for Internet Of Things", *IEEE Journal on Emerging and Selected Topics in Circuits and Systems*, Vol 3 Issue 1, pp13-22, March 2013.

[2] Irfan Awan and Muhammad Younas, "Towards QoS in Internet of Things for Delay Sensitive Information", *MobiWIS 2013 workshops, CCIS* 183, Springer International Publishing Switzerland, pp 86-94, 2013.

[3] Chien-Liang Fok, Christine Julien, "Challenges of satisfying mulitple stakeholders:quality of service in the Internet of Things", *ACM Digital Library Proceedings of SESENA 2011*, pp55-60, 2011.

[4] Klepec B, Kos A, "Performance of VoIP applications in a simple differentiated services network architecture," *IEEE international conference Eurocon 2001* at Bratislava, Slovakia, Vol 1, pp-214-217, 2001.

[5] Xianmin Geng, Aiwen Luo, Zhinjun Sun, and Yu Cheng, "Markov Chains Based Dynamic Bandwidth Allocation in Diffserv Network" *IEEE communication letters*, vol. 16, No. 10, October 2012.

[6] Suparna De, Payam Barnaghi, Martin Bauer, Stefan Meissner, "Service Modelling for Internet of Things" Proceedings of Federated Conference on Computer science and Information Systems, pp 949-955, 2011.

[7] Long B.Le, Ekram Hossain, Aathiru S Alfa, " Service Differentiation in Multirate wireless Networks With Weighted Round Robin Scheduling and ARQ Based Error Control, IEEE Transactions on Communications , Vol 54, No.2, pp-208-215, 2006

[8] Xianmin Geng, Aiwen Luo, Zhinjun Sun, and Yu Cheng, "Markov Chains Based Dynamic Bandwidth Allocation in Diffserv Network" IEEE communication letters, Vol. 16, (10), pp-1711-1714, 2012.

[9] Ling Li, Shancang Li, Shanshan Zhao, "QoS-Aware Scheduling of Services-oriented Internet of Things, IEEE Transactions on Industrial Informatics, Vol. 10, Issue:2, May 2014.

[10] Saima Abdullah, Kun Yang, "A QoS aware message scheduling algorithm in Internet of Things environment" IEEE Online Conference on Green Communications" , pp-175-180, Oct. 2013.

[11] Chien-Liang Fog, Christine Julien, Gruia-Catalin Roman, Chenyang Lu, "Challenges of Satisfying Multiple Stakeholders: Quality of Service in the Internet of Things" SESENA ACM, Waikiki, Honolulu, USA, May 2011.

[12] Alvaro Monares, Sergio F. Ochoa, Rodrigo Santos, Javier Orozco, Roc Meseguer, "Modeling IoT- Based Solutions Using Human-Centric Wireless Sensor Networks", Open access Sensors journal, ISSN 1424-8220, pp 15687-15713, 2014

[13] Haining Wang, Chia Shen, Kang G Shin, "Adaptive Weighted Packet Scheduling For Premium Service", *IEEE Communications,* ICC Vol-6, pp.1846-1850, 2004.

THE 18TH INTERNATIONAL SYMPOSIUM ON WIRELESS PERSONAL MULTIMEDIA COMMUNICATIONS
(WPMC-2015)
December 13-16, 2015, Hyderabad, India

Opinion-unaware blind image quality assessment based on sparse representation

Maozheng Zhao, Ran Gao, Bo Yang, Aidong men

School of Information and Communication Engineering
Beijing University of Posts and Telecommunications
Beijing, 100876, China
{*maozhengzhao, gaoran, boyang, menad*}*@bupt.edu.cn*

***Abstract*—Opinion-unaware (OU) General purpose blind image quality assessment (BIQA) is an important yet difficult task in computer vision and machine learning. In this paper, we present a sparse representation based quality-unaware BIQA approach which utilizes NSS features from three different domains. At the training stage, we extract quality scores of training image blocks by full-reference image quality assessment method and NSS features of image blocks. The score-feature pairs are learned by the dictionary for sparse representation. At the testing stage, the NSS feature vector of a test image is represented via sparse coding and the final predictive quality score is obtained through weighting quality scores by the sparse coding coefficients. Experiments on the LIVE database show that the proposed algorithm has better performance than the state-of-the-art opinion-unaware method NIQE. And it also has excellent database independence.**

***Index terms*— no-reference image quality assessment (NR IQA), sparse representation, phase congruency**

I. Introduction

Thanks to the easier availability of digital images from the internet and the popularization of wireless digital imaging devices, digital images have been becoming one of the most important way of representing and transmitting information in our everyday life. However, the perceptual quality of digital images may be declined by the process of acquisition, transmission, compression, restoration, etc. For example, images could be distorted by packet loss when transmitted through a congested wireless network. Moreover, in most real life cases the undistorted version of the observed image is not available, thus assessing image quality blindly and automatically is becoming increasingly important [1].

In terms of whether specifying the distortion types of test images, the current blind image quality assessment (BIQA) methods can be classified as distortion specific methods [2], [3], [4] or general purpose methods [5], [6], [7], [8], [9]. The application of distortion specific BIQA methods is therefore limited to test images with known distortion types. Thus the general purpose BIQA methods which do not require prior knowledge of distortion types of test images are more practical in real-world applications. General purpose BIQA methods can be further classified into two categories: opinion-aware (OA) methods [6], [7], [5], [8] and opinion-unaware (OU) methods [10], [9], [11]. OA methods need subjective scores for training while OU methods can build prediction models without human opinions which is obviously a much more challenging task than OA approaches. In this paper we focus on the OU-BIQA methods.

We propose a general-purpose opinion-unaware BIQA approach based on sparse representation (SP). At the training stage of the proposed method, natural scene statistics (NSS) features of the training image blocks and their corresponding quality scores obtained by gradient magnitude similarity deviation (GMSD) [12] which is a state-of-the-art full-reference image quality assessment (FR-IQA) method are computed for dictionary learning. At the testing stage, the NSS feature vector of a test image is represented via sparse coding and the final predictive quality score is computed through weighting GMSD scores by the sparse coding coefficients. Our sparse representation based OU-BIQA approach offers the following advantages. 1) We extract NSS features from three different domains, i.e., phase congruency domain, DCT domain and spacial domain in order to fully employ the quality information of images. 2) The dictionary for sparse representation can be trained completely without human subjective scores since training quality scores are obtained from top performing FR-IQA method. 3) The quality relevant NSS features and the quality scores for constructing the dictionary are extracted from both the whole images and image blocks to make a denser dictionary. 4) By using sparse representation to constuct the dictionary, we do not have to retrain the model when samples of new distortion types are available, we just need to add new samples into the dictionary. 5) At the testing stage, NSS features of the entire image rather than image blocks are used for sparse representation which is highly efficient.

The performance of the proposed opinion-unaware BIQA metric is thoroughly validated on the LIVE IQA database [13]. The experimental results demonstrate that the proposed opinion-unaware BIQA metric is highly consistent with human opinions. It has performance which is very comparable to state-of-the-art OU-BIQA NIQE [9]. It outperforms OU-BIQA QAC [10] and FR-IQA PSNR [14] and its performance is nearly comparable to state-of-the-art OA-BIQA BRISQUE [6]. It also has good extensibility through databases.

The remainder of this paper describes SROUB (Sparse Representation based Opinion-Unaware Blind image quality assessment) in detail and is organized as follows. The details of

This work is supported by the National Science Foundation of China (61271190).

Fig. 2. Histograms of PC for different distortion types. The 6 curves correspond to the reference image "sailing1.bmp" and its distorted counterparts. "Origianl" (DMOS = 0), "JP2K" (DMOS = 67.6968), "JPEG" (DMOS = 70.5024), "Noise" (DMOS = 55.0675), "Blur" (DMOS = 68.0166), "FF" (DMOS = 64.7162).

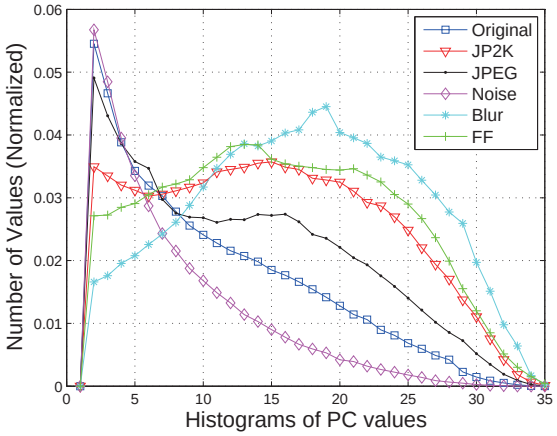

the proposed framework are described in Section 2. In Section 3, experimental results and a thorough analysis of our results are presented. Finally, Section 4 concludes our work.

II. Sparse Representation Based Opinion-Unaware BIQA

Fig. 1 is the framework of SROUB, which includes five key modules, i.e., features and GMSD scores extraction for dictionary, dictionary learning, feature extraction for quality computation, sparse representation and quality computation.

A. Features and GMSD scores extraction for dictionary

In order to get a dense overcomplete dictionary, we extract image features and image GMSD [12] scores not only from each whole image but also from image blocks in order to build a dense dictionary.

We extract image NSS features from three different domains, i.e., phase congruency [15], [16] domain, DCT domain, and spatial domain. The GMSD [12] score of each image block is also computed as the training quality labels of each image block . GMSD is one of state-of-the-art FR-IQA methods whose predictive scores correlate well with human opinions. The Spearman rank order correlation coefficient (SROCC) between GMSD scores and subjective scores on LIVE IQA database [13] is 0.960.

1) PC domain NSS features: Phase congruency (PC) [17], [16] measures the degree of congruency of image local Fourier waves frequencies. The physiological and psychophysical evidences had corroborated that visually cognizable features coincide with points of high PC values [17], [16].

Kovesi [16] proposed an efficient approach of computing PC which is widely used in literature. A 2-D extended logarithmic Gabor filters [18] is adopted for wavelet transform:

$$G_2(\omega,\theta_{\mathrm{k}}) = \exp\left(-\frac{\left(\log(\frac{\omega}{\omega_0})\right)^2}{2\sigma_l^2}\right)\cdot\exp\left(-\frac{(\theta-\theta_{\mathrm{k}})^2}{2\sigma_\theta^2}\right) \tag{1}$$

where $\theta_k = k\pi/K$, $k = \{0,1,...,K-1\}$ is the filter's orientation angle, K is the number of orientations, ω_0 is the center frequency of the filters, σ_l controls the filter's bandwidth and σ_θ determines the filter's angular bandwidth.

By convolving G_2 with an image and modulating ω_0 and θ_k, we get a set of responses at each point i as $\lfloor e_{n,\theta_k}(i), o_{n,\theta_k}(i)\rfloor$, where $e_{n,\theta_k}(i)$ and $o_{n,\theta_k}(i)$ are the real and imaginary parts of a log-Gabor filter respectively on scale n and orientation θ_k at location i. The local amplitude on scale n and orientation θ_k is $A_{n,\theta_k}(i) = \sqrt{e_{n,\theta_k}(i)^2 + o_{n,\theta_k}(i)^2}$, and the local energy along orientation θ_k is $E_{\theta_k}(i) = \sqrt{L_{\theta_k}(i)^2 + T_{\theta_k}(i)^2}$, where $L_{\theta_k}(i) = \sum_n e_{n,\theta_k}(i)$ and $T_{\theta_k}(i) = \sum_n o_{n,\theta_k}(i)$. The 2-D PC at i is as follows:

$$PC(i) = \frac{\sum_k E_{\theta_k}(i)}{\gamma + \sum_n \sum_k A_{n,\theta_k}(i)} \tag{2}$$

where γ is a small positive constant to keep the fraction stable when all the Fourier amplitudes are very small. $PC(i)$ is a real number within $[0,1]$.

We found that the histogram of PC values of one image would change with different distortion types and extents. Fig. 2 shows the histograms of PC values of the image "sailing1.bmp" of the LIVE database [13] and its 5 distortion versions, number of zeros of PC are excluded. We can see that the mean and skew values of PC histograms change with distortion types and extents.

For NSS features from PC domain, the first step is computing pixel based PC values of image blocks. Then by sorting PC values in ascending order, the ordered set $P = (p_1, p_2, ..., p_m)$ is yielded. The percentile pooling is implemented to P based on the assumption that distortions only occur in a subset of pixels. Extracting the central 60% elements from P yields $P_p = (p_{\lfloor 0.2n\rfloor}, p_{\lfloor 0.2n\rfloor+1}, ..., p_{\lfloor 0.8n\rfloor})$. Where n is the number of pixels of the relevant image scale. The mean value of P_p and the skew value of P are the NSS features of PC domain on one scale in our approach.

$$f_{PC} = (mean(P_p), skew(P)) \tag{3}$$

2) DCT domain NSS features: DCT coefficients based on 8×8 nonoverlapping patches is computed first. Then the spectral entropy F is computed based on the DCT coefficients.

The spectral entropy is

$$F = -\sum_x \sum_y P(x,y)\log_2 P(x,y) \tag{4}$$

where

$$P(x,y) = \frac{C(x,y)^2}{\sum_x \sum_y C(x,y)^2} \tag{5}$$

Fig. 1. Framework of sparse representation based opinion unaware blind image quality assessment.

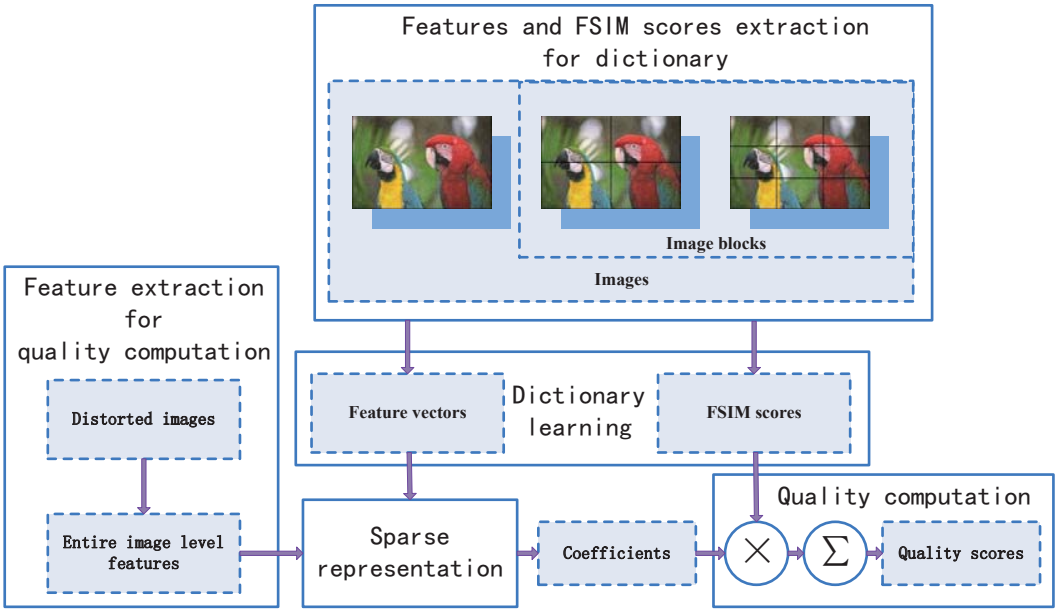

where $P(x,y)$ is the spectral probability of normalized DCT coefficients $C(x,y)^2$, $1<i\leq 8, 1<j\leq 8$ (DC is excluded).

The same percentile pooling strategy used for PC NSS features is also implemented to the ascending ordered F resulting $Fp=(f_{\lfloor 0.2m\rfloor}, f_{\lfloor 0.2m\rfloor+1}, ..., f_{\lfloor 0.8m\rfloor})$. Where m is the number of blocks within each scale. The mean values of F_p and the skew values of F are used as NSS features of DCT domain in our approach.

$$f_{DCT}=(mean(F_p), skew(F)) \tag{6}$$

3) Spatial domain NSS features: For NSS features from spatial domain, we adopt the same features used in BRISQUE [6] since they require very low time complexity and have strong representing power for image quality. 18 $(2+4\times 4)$ spatial feature vector elements in total are extrated for each scale including parameters of generalized Gaussian distribution (GGD) with zero mean of local mean subtract contrast normalization (MSCN) coefficients and parameters of a zero mode asymmetric generalized Gaussian distribution (AGGD) of products pairs of adjacent coefficients .

B. Dictionary learning

In SROUB, the dictionary learning is extremely simple by directly combining feature vectors and GMSD scores of the training blocks.

$$\begin{bmatrix} D \\ scores \end{bmatrix} \doteq \begin{bmatrix} f_1 & f_2 & ... & f_n \\ score_1 & score_2 & & score_n \end{bmatrix} \tag{7}$$

where the dictionary D is a $k\times l$ matrix ($k=44$ and l is the number of image blocks for training). Vector $scores$ is the corresponding GMSD scores of the training blocks. f_i is the NSS feature vector of the ith training image block and $score_i$ is its GMSD score.

C. Sparse representation

Sparse representation with an overcomplete basis in human perception has been strongly corroborated by studies of the human visual system (HVS) [19]. And the sparsity characteristic is one of the most important features of HVS.

The following optimizing problem can yield the sparsest and the most precise representation of the feature vector of a test image by the atoms in the dictionary $D=[f_1, f_2, ..., f_n]$.

$$\rho^*=\arg\min_{\rho\in R^N} \|\rho\|_0 \quad s.t. \quad f=D\rho \tag{8}$$

where N is the number of atoms in D, ρ^* is the sparse representation coefficients for f over the dictionary D.

The approximate solution of the above optimize problem via l_1-minimization [20] is usually used because the l_0-minimization of equation (8) is an NP hard problem. Then we have

$$\rho^*=\arg\min_{\rho\in R^N} \|\rho\|_1 \quad s.t. \quad f=D\rho \tag{9}$$

This l_1-minimization problem can be transformed into an unconstrained problem

$$\rho^*=\arg\min_{\rho\in R^N} \gamma\|\rho\|_1+\|f-D\rho\|_2 \tag{10}$$

where γ is the regularization parameter. A specialized interior-point method for solving large-scale l_1-regularized least-squares programs is used to solve the above problem [20].

D. Quality computation

Based on the assumption that image blocks with identical quality scores have similar feature distributions, the quality of a test image can be quantified by

$$Q = \frac{\sum_{i=1}^{M} \rho_i^* score_i}{\sum_{i=1}^{M} \rho_i^*} \quad (11)$$

where $score_i$ is the GMSD score of the i-th image block in the dictionary. The estimation Q is the final predictive quality score of the test image.

III. Experiments and results

In the training stage, each image is uniformly partitioned into 4 and 9 neighboring nonoverlapping blocks as shown in Fig. 1. Feature-score pairs are extracted from those blocks which means that each image for building the dictionary would contribute 15 $(1 + 4 + 9)$ feature-score pairs in total. We extract all NSS features at 2 scales to capture multi-scale characteristics via downsampling by a factor of 2 after low pass filtering. For efficiency, only the entire image NSS features are used for sparse representation in the testing stage.

A. Correlation with human opinions

We tested SROUB on LIVE IQA database [13] which consists of 29 reference images and their distorted versions with five different types of distortion, i.e., JPEG2k (JP2K), JPEG, white noise (WN), Gaussian blur (BLUR) and fast fading (FF). DMOS values of those images are offered by the database. We compared performance of SROUB with other IQA approaches. PSNR [14] and SSIM [21] are two classic FR-IQA algorithms. BRISQUE [6] is one of state-of-the-art OA-BIQA methods. QAC [10] and NIQE [9] are state-of-the-art OU-BIQA methods.

Two performance indices were used in our experiments. The Spearman rank order correlation coefficient (SROCC) between DMOS and objective scores is a measure of the prediction monotonicity. The Pearson linear correlation coefficient (LCC) is an evaluation of the prediction accuracy. LCC were calculated after a logistic non-linearity mapping [22].

Since SROUB and BRISQUE require training. We randomly chose 80% of reference images and their corresponding distorted versions in the LIVE database for training and the rest images in the database for testing. This train-test pair is performed 1000 times and the median of the results are reported. For a fair comparison, PSNR, SSIM, QAC and NIQE which do not require training are tested on 20% of randomly chosen reference images and their corresponding distorted versions of the LIVE database for 1000 iterations and the median of the results are reported.

The results are listed in Tab. I. The overall performance across 5 distortion types are shown in the columns labeled by "ALL". We can see that SROUB has higher SROCC and LCC in "ALL" than the FR-IQA PSNR and the two OU-BIQA algorithms QAC and NIQE, its overall performance is slightly inferior to FR-IQA SSIM and OA-BIQA BRISQUE.

B. Variation with dictionary size

In order to investigate the influence of dictionary size to the overall performance of the proposed algorithm, we conduct the $80\%/20\%$ train-test trails for 100 times for different dictionary sizes, the median values of SROCC on the LIVE database are reported. The median values of SROCC are shown in Tab. II, in Tab. II the subscript of a particular dictionary "D" means the number of blocks used for feature extraction, subscript of "1" corresponds to the entire image, subscript of "4" or "9" corresponds to number of adjacent uniformly partitioned blocks of an image used for dictionary construction. From Tab. II, we can conclude that a denser dictionary of the proposed approach results in better correlation with human opinions.

TABLE II
Median SROCC across 100 train-test trials with dictionaries of different sizes on the LIVE IQA database.

	D_1	D_4	D_{1+4}	D_9	D_{1+4+9}
SROCC	0.8361	0.8805	0.8863	0.9058	0.9084

TABLE III
SROCC yielded by models using different features for sparse representation on the LIVE database.

	JP2K	JPEG	Noise	Blur	FF	ALL
Curvelet features	0.7336	0.8891	0.8354	0.8554	0.6792	0.8154
Spatial features	0.4955	0.8681	0.9604	0.8590	0.8100	0.8198
Curvelet & Spatial features	0.7714	0.8683	0.9315	0.8670	0.7553	0.8495

C. Representing powers of features

We also conducted experiments with features from different domains to determine representing powers of features. Here we refer to DCT domain features together with PC domain features as curvelet features. Image blocks in D_1 were used for building dictionaries. We randomly chose 6 reference images (sailing3.bmp, caps.bmp, parrots.bmp, sailing1.bmp, statue.bmp) and their distorted versions from the LIVE database as test images, the rest images in the database are used as training images. The performance of models utilizing only curvelet features or only spatial domain features or both curvelet features and spatial domain features are reported in Tab. III.

The model utilizing both curvelet features and spatial domain features yields relatively high SROCC values on each distortion type and across five distortion types which means that our combination of NSS features from different domains has better representation power for image distortion.

D. Database independence

In order to determine the database independence degree of SROUB, we also test SROUB and the compared algorithms on the TID2008 [23] database. The SROCC values of four distortion types (JPEG2000, JPEG, WN and BLUR) and across four distortion types are listed in Tab. IV. Compared with other approaches, the correlation with subjective perception of SROUB remained consistently competitive.

TABLE I
MEDIAN SROCC AND LCC ACROSS 1000 TRAIN-TEST TRIALS ON THE LIVE IQA DATABASE. ITALICS INDICATE OPINION-UNAWARE BLIND METHODS

	SROCC						LCC					
	JP2K	JPEG	WN	BLUR	FF	**ALL**	JP2K	JPEG	WN	BLUR	FF	**ALL**
PSNR	0.8673	0.8843	0.9428	0.7575	0.8721	0.8633	0.8657	0.8866	0.8963	0.7855	0.8616	0.8568
SSIM	0.9395	0.9480	0.9644	0.9083	0.9413	0.9129	0.9513	0.9605	0.9828	0.9033	0.9569	0.9057
BRISQUE	0.9095	0.9645	0.9778	0.9511	0.8759	0.9363	0.9120	0.9733	0.9848	0.9457	0.9013	0.9385
QAC	0.8849	0.9448	0.9497	0.9181	0.8251	0.8754	0.8691	0.9579	0.9267	0.9228	0.8536	0.8710
NIQE	0.9236	0.9440	0.9720	0.9408	0.8630	0.9089	0.9359	0.9417	0.8712	0.9534	0.8873	0.9082
SROUB	0.9034	0.9592	0.9548	0.9482	0.8912	0.9206	0.9101	0.9635	0.9695	0.9367	0.9331	0.9202

TABLE IV
SROCC OBTAINED BY TRAINING ON THE LIVE IQA DATABASE AND TESTING ON THE TID2008 DATABASE. ITALICS INDICATE OPINION-UNAWARE BLIND METHODS.

	JP2K	JPEG	WN	BlUR	ALL
PSNR	0.7848	0.8585	0.9147	0.8914	0.7527
SSIM(SS)	0.9603	0.9354	0.8168	0.9598	0.9016
BRISQUE	0.9037	0.9102	0.8227	0.8742	0.8977
QAC	0.8885	0.8981	0.7070	0.8504	0.8697
NIQE	0.8940	0.8722	0.7775	0.8236	0.7970
SROUB	0.9221	0.9191	0.8212	0.8987	0.8892

IV. CONCLUSION

We presented an opinion-unaware general purpose BIQA based on sparse representation which utilizes NSS features from three different domains. The quality of a test image is expressed as a simple linear combination of training blocks' GMSD scores with sparse representation coefficients. Via comprehensive experimental validations, we could have the following conclusions. First, SROUB can be trained completely without human subjective scores. Second, SROUB can assess image quality consistently with the subjective scores across various types of distortions. Third, on the LIVE database, SROUB has superior performance to that of the state-of-the-art OU-BIQA method NIQE. Finally, SROUB also has excellent database independence.

REFERENCES

[1] Z. Wang, "Applications of objective image quality assessment methods [applications corner]," *Signal Processing Magazine, IEEE*, vol. 28, no. 6, pp. 137–142, 2011.
[2] Z. Wang, H. R. Sheikh, and A. C. Bovik, "No-reference perceptual quality assessment of jpeg compressed images," in *Image Processing. 2002. Proceedings. 2002 International Conference on*, vol. 1. IEEE, 2002, pp. I–477.
[3] J. Caviedes and S. Gurbuz, "No-reference sharpness metric based on local edge kurtosis," in *Image Processing. 2002. Proceedings. 2002 International Conference on*, vol. 3. IEEE, 2002, pp. III–53.
[4] L. Meesters and J.-B. Martens, "A single-ended blockiness measure for jpeg-coded images," *Signal Processing*, vol. 82, no. 3, pp. 369–387, 2002.
[5] A. K. Moorthy and A. C. Bovik, "A two-step framework for constructing blind image quality indices," *Signal Processing Letters, IEEE*, vol. 17, no. 5, pp. 513–516, 2010.
[6] A. Mittal, A. K. Moorthy, and A. C. Bovik, "No-reference image quality assessment in the spatial domain," *Image Processing, IEEE Transactions on*, vol. 21, no. 12, pp. 4695–4708, 2012.
[7] A. K. Moorthy and A. C. Bovik, "Blind image quality assessment: From natural scene statistics to perceptual quality," *Image Processing, IEEE Transactions on*, vol. 20, no. 12, pp. 3350–3364, 2011.
[8] M. A. Saad, A. C. Bovik, and C. Charrier, "Blind image quality assessment: A natural scene statistics approach in the dct domain," *Image Processing, IEEE Transactions on*, vol. 21, no. 8, pp. 3339–3352, 2012.
[9] A. Mittal, R. Soundararajan, and A. C. Bovik, "Making a completely blind image quality analyzer," *Signal Processing Letters, IEEE*, vol. 20, no. 3, pp. 209–212, 2013.
[10] W. Xue, L. Zhang, and X. Mou, "Learning without human scores for blind image quality assessment," in *Computer Vision and Pattern Recognition (CVPR), 2013 IEEE Conference on*. IEEE, 2013, pp. 995–1002.
[11] A. Mittal, G. S. Muralidhar, J. Ghosh, and A. C. Bovik, "Blind image quality assessment without human training using latent quality factors," *Signal Processing Letters, IEEE*, vol. 19, no. 2, pp. 75–78, 2012.
[12] X. M. Wufeng Xue, Lei Zhang and A. C. Bovik, "Gradient magnitude similarity deviation: A highly efficient perceptual image quality index," *Image Processing, IEEE Transactions on*, vol. 23, pp. 684 – 695, 2014.
[13] H. Sheikh, Z. Wang, L. Cormack, and A. Bovik, "Live image quality assessment database release 2," 2006, available from: http://live.ece.utexas.edu/research/quality.
[14] Z. Wang and A. C. Bovik, "Mean squared error: love it or leave it? a new look at signal fidelity measures," *Signal Processing Magazine, IEEE*, vol. 26, no. 1, pp. 98–117, 2009.
[15] L. Zhang, D. Zhang, and X. Mou, "Fsim: a feature similarity index for image quality assessment," *Image Processing, IEEE Transactions on*, vol. 20, no. 8, pp. 2378–2386, 2011.
[16] P. Kovesi, "Image features from phase congruency," *Videre: Journal of computer vision research*, vol. 1, no. 3, pp. 1–26, 1999.
[17] M. C. Morrone and D. Burr, "Feature detection in human vision: A phase-dependent energy model," *Proceedings of the Royal Society of London. Series B, biological sciences*, pp. 221–245, 1988.
[18] D. J. Field, "Relations between the statistics of natural images and the response properties of cortical cells," *JOSA A*, vol. 4, no. 12, pp. 2379–2394, 1987.
[19] B. A. Olshausen and D. J. Field, "Sparse coding with an overcomplete basis set: A strategy employed by v1?" *Vision research*, vol. 37, no. 23, pp. 3311–3325, 1997.
[20] S.-J. Kim, K. Koh, M. Lustig, S. Boyd, and D. Gorinevsky, "An interior-point method for large-scale l 1-regularized least squares," *Selected Topics in Signal Processing, IEEE Journal of*, vol. 1, no. 4, pp. 606–617, 2007.
[21] Z. Wang, A. C. Bovik, H. R. Sheikh, and E. P. Simoncelli, "Image quality assessment: from error visibility to structural similarity," *Image Processing, IEEE Transactions on*, vol. 13, no. 4, pp. 600–612, 2004.
[22] H. R. Sheikh, M. F. Sabir, and A. C. Bovik, "A statistical evaluation of recent full reference image quality assessment algorithms," *Image Processing, IEEE Transactions on*, vol. 15, no. 11, pp. 3440–3451, 2006.
[23] N. Ponomarenko, V. Lukin, A. Zelensky, K. Egiazarian, M. Carli, and F. Battisti, "Tid2008-a database for evaluation of full-reference visual quality assessment metrics," *Advances of Modern Radioelectronics*, vol. 10, no. 4, pp. 30–45, 2009.

THE 18TH INTERNATIONAL SYMPOSIUM ON WIRELESS PERSONAL MULTIMEDIA COMMUNICATIONS
(WPMC-2015)
December 13-16, 2015, Hyderabad, India

Joint Transceiver Design for QoS-Constrained MIMO Two-Way Non-Regenerative Relaying

Rohit Budhiraja and Bhaskar Ramamurthi
Department of Electrical Engineering, IIT Madras, India.
Email: rohit411@gmail.com, bhaskar@iitm.ac.in

***Abstract*—Transceiver designs for multiple-input multiple-output (MIMO) two-way relaying are being actively explored. Most of the state-of-the-art studies optimize a system-wide objective function subject to the transmit power constraints of the two source nodes and the relay. Transceiver designs with quality-of-service (QoS) constraints have lacked attention in two way relaying literature. In this work, we study a MIMO transceiver design, based on the generalized singular value decomposition, that incorporates per-stream QoS constraints specified as the rate required by the individual transmit streams of two source nodes. With these QoS constraints, we use geometric programming to jointly allocate power at the source and relay nodes to optimize the sum-rate. Through extensive numerical evaluations, we show that the proposed design outperforms the existing solutions not only with the QoS constraints but also without them.**

***Index Terms*—Geometric program (GP), generalized singular value decomposition (GSVD), quality-of-service (QoS).**

I. Introduction

Relaying is a well known cooperative communication technique that is used to enhance the throughput and coverage of wireless systems [1]–[3]. Two relaying protocols are widely studied in the literature – one-way [1] and two-way [2], [3]. A relay is usually assumed to be half-duplex as it is easy to implement; a half-duplex relay, however cannot simultaneously transmit and receive on the same spectral resource. This reduces the spectral efficiency of one-way relaying, as two spectral resources are now required to transmit a single data unit. This is twice the number of channel uses when two nodes communicate directly without a relay. Two-way relaying (TWR) requires two spectral resources to transmit two data units and recovers the loss in spectral efficiency.

The relay in TWR protocol is designed commonly using two different technologies – regenerative decode-and-forward [2] and non-regenerative amplify-and-forward [3]–[5]. A non-regenerative two-way relay is of special interest as it is easy to implement and has lower delay, when compared with a regenerative two-way relay. To further enhance the spectral-efficiency of non-regenerative TWR, multiple antennas are also employed in all the nodes. Many studies have investigated transceiver designs for non-regenerative TWR to explore the potential of multiple antennas [3]–[13].

The authors in [3], [4] investigated space-time coding designs for multiple-input multiple-output (MIMO) TWR. Lee *et al.* in [5] designed source and relay precoders to maximize sum-rate. In [6], the source and relay precoders are jointly constructed to minimize sum-MSE. Reference [7] developed a unified framework to optimize a broad class of Schur-convex and Schur-concave functions for MIMO TWR. Transceiver designs to minimize the MSE and maximize the sum-rate using MSE duality are recently investigated in [8] and [9], respectively. Park *et al.* in [10] proposed a transceiver based on the principles of signal alignment and uses generalized singular value decomposition (GSVD). The channel orthogonalization involves zero-forcing operation at the relay, which degrades the sum-rate for ill-conditioned channels due to noise enhancement. The design in [11] avoids zero-forcing operation at the relay but only semi-orthogonalizes the end-to-end MIMO channels for small number of antennas. This design is shown to have better sum-rate than the [10], if the residual inter-stream interference due to semi-orthogonalization of MIMO channels is ignored.

All the aforementioned references optimize a given objective function e.g., sum-rate or MSE, subject to the constraints on the transmit power of two source nodes and the relay. They, however, ignore quality-of-service (QoS) constraints which affect the user experience and are therefore crucial in practical systems. A few recent efforts have considered QoS-constrained transceiver designs for TWR [12], [13]. Leow *et al.* in [12] designed source and relay precoders to minimize the total network transmit power subject to per-stream QoS constraints expressed as the transmit rate required by the individual streams of the two source nodes. Reference [13] also jointly optimized source and relay precoders to minimize total network transmit power subject to the QoS constraints which are expressed as upper-bounds on the mean-squared error (MSE) of the signal waveform estimated at the destination nodes.

In the present work, motivated by [10], [11], we first construct a MIMO transceiver using GSVD for TWR. We then maximize sum-rate subject to the per-stream QoS constraints that similar to [12], are expressed as the transmit rates required by the individual streams of two source nodes. Optimization of these objectives, for the GSVD-based transceiver design considered herein, reduces to joint power allocation at the source and relay nodes.

We next list the **main contributions** of this paper when compared with [10]–[13].

1) We propose a novel modification to the existing GSVD-based transceiver designs in [10], [11] that overcomes two limitations: i) noise enhancement in ill-conditioned channels in [10]; and ii) residual inter-stream interference for small number of antennas in [11]. Though in this work we concentrate on

optimizing objectives with per-stream rate constraints, we also show that the proposed design yields better sum-rate than the designs in [10], [11] without the per-stream rate constraints.

2) We maximize the sum-rate, via joint power allocation at the source and relay nodes, subject to the per-stream transmit rate required by both source nodes and individual transmit power. We will show that this problem can be cast as a convex geometric program (GP). We note that both [12], [13] do not investigate this problem; it is important to analyze the effect of the per-stream transmit rate demanded by each source node on the overall sum-rate. Further, we consider more granular per-stream rate constraints unlike [13] that expresses QoS constraints in terms of upper-bounded MSE for each link (not transmit stream). *To the best of our knowledge, sum-rate maximization with per-stream rate constraints for TWR has not been considered earlier in the literature.* We show through extensive simulations that the proposed design yields significantly better performance than the state-of-the-art transceiver designs.

Notation: The symbols $\mathbf{A}$ and $\mathbf{a}$ denote a matrix and a column vector, respectively. $\mathrm{Tr}(\mathbf{A})$, $\mathbf{A}^T$, $\mathbf{A}^H$, $\mathbf{A}^\dagger$, $[\mathbf{A}]_{i,j}$ and $\mathbf{A}^*$ are the trace, transpose, Hermitian, pseudoinverse, (i,j)th element and complex-conjugate of the elements of $\mathbf{A}$, respectively. We denote the Hadamard product of two matrices $\mathbf{A}$ and $\mathbf{B}$ as $\mathbf{A} \odot \mathbf{B}$ and an $N \times N$ identity matrix as $\mathbf{I}_N$. The notation $\mathrm{diag}(x_1, \cdots, x_n)$ represents a diagonal matrix with x_1 to x_n as its diagonal elements. The notation $\boldsymbol{x} \succeq 0$ implies that all the elements of vector $\mathbf{x}$ are ≥ 0. The symbol $\mathbb{E}(\cdot)$ is the expectation operator.

II. System model

We consider MIMO TWR where two multi-antenna source nodes S_1 and S_2, as shown in Fig. 1, exchange data via a half-duplex non-regenerative multi-antenna relay. We assume that both source nodes have N_s antennas each, while the relay has N_r antennas. We also assume, as conventionally assumed in TWR literature [5], [6], that the direct links between two source nodes are absent due to high path loss and fading.

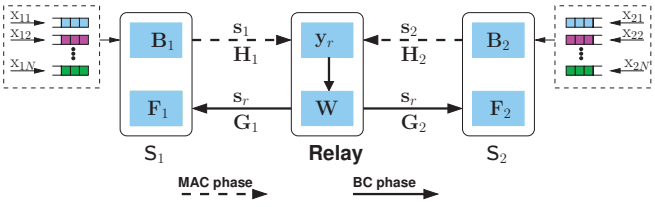

Fig. 1: QoS-constrained two-way relaying: Both source nodes have N streams to transmit, and each stream requires a particular rate.

In the first phase of TWR, commonly known as multiple access (MAC) phase, both source nodes simultaneously transmit their respective signals to the relay; the relay receives an $N_r \times 1$ signal given as

$$\mathbf{y}_r = \mathbf{H}_1\mathbf{s}_1 + \mathbf{H}_2\mathbf{s}_2 + \mathbf{n}_r. \tag{1}$$

Here the matrix $\mathbf{H}_i \in \mathbb{C}^{N_r \times N_s}$ is the MIMO channel for the $\mathsf{S}_i \rightarrow$Relay links for $i = 1, 2$,[1] and the vector $\mathbf{n}_r \in \mathbb{C}^{N_r \times 1}$ is the circularly-symmetric complex additive white Gaussian noise at the relay with $\mathbb{E}(\mathbf{n}_r\mathbf{n}_r^H) = \sigma_r^2\mathbf{I}_{N_r}$. The vector $\mathbf{s}_i \in \mathbb{C}^{N_s \times 1}$, transmit signal of the node S_i, is obtained by linearly precoding the normalized complex information data vector $\mathbf{x}_i \in \mathbb{C}^{N \times 1}$ using a precoder matrix $\mathbf{B}_i \in \mathbb{C}^{N_s \times N}$ such that $\mathbf{s}_i = \mathbf{B}_i\mathbf{x}_i$. We assume that with N_s antennas, both source nodes transmit $N = \min(N_s, N_r)$ independent source streams; therefore $\mathbb{E}(\mathbf{x}_i\mathbf{x}_i^H) = \mathbf{I}_N$. The precoded data vector $\mathbf{s}_i$ satisfies the transmit power constraint:

$$\mathrm{Tr}(\mathbb{E}(\mathbf{s}_i\mathbf{s}_i^H)) = \mathrm{Tr}(\mathbf{B}_i\mathbf{B}_i^H) = \mathrm{Tr}(\mathbf{\Xi}_i) \leq P_i, \tag{2}$$

where P_i is the maximum transmit power of the node S_i.

In the second phase of TWR, commonly known as broadcast (BC) phase, the relay multiplies its received signal with a precoder matrix $\mathbf{W} \in \mathbb{C}^{N_r \times N_r}$. The $N_r \times 1$ signal vector transmitted by the relay is $\mathbf{s}_r = \mathbf{W}\mathbf{y}_r$. The maximum transmit power of the relay is P_r, which results in the following constraint on its transmit signal

$$\begin{aligned} P_r &\geq \mathrm{Tr}\left(\mathbb{E}(\mathbf{s}_r\mathbf{s}_r^H)\right) \\ &= \mathrm{Tr}\left(\mathbf{W}(\mathbf{H}_1\mathbf{\Xi}_1\mathbf{H}_1^H + \mathbf{H}_2\mathbf{\Xi}_2\mathbf{H}_2^H + \sigma_r^2\mathbf{I}_N)\mathbf{W}^H\right). \end{aligned} \tag{3}$$

The signal received by the node S_i in the BC phase is

$$\mathbf{y}_i = \mathbf{G}_i\mathbf{s}_r + \mathbf{n}_i = \underbrace{\mathbf{G}_i\mathbf{W}\mathbf{H}_i\mathbf{s}_i}_{\text{BI}} + \mathbf{G}_i\mathbf{W}\mathbf{H}_{\bar{i}}\mathbf{s}_{\bar{i}} + \mathbf{G}_i\mathbf{W}\mathbf{n}_r + \mathbf{n}_i.$$

The term labelled BI is the back-propagating interference. The matrix $\mathbf{G}_i \in \mathbb{C}^{N_s \times N}$ is the MIMO channel for the Relay$\rightarrow\mathsf{S}_i$ link, and the vector $\mathbf{n}_i$ is the circularly-symmetric complex additive noise at the node S_i with $\mathbb{E}(\mathbf{n}_i\mathbf{n}_i^H) = \sigma_i^2\mathbf{I}_{N_s}$. We assume that all the channel matrices are frequency-flat and constant over one cycle of MAC and BC phases, but vary independently across multiple cycles as in [5]–[7]. Since S_i knows $\mathbf{s}_i$, it can cancel the back-propagating interference from its received signal with the knowledge of necessary channel state information (CSI) as in [5]–[7]. The equivalent receive signal at S_i after cancelling the back-propagating interference from $\mathbf{y}_i$ is $\widehat{\mathbf{y}}_i = \mathbf{G}_i\mathbf{W}\mathbf{H}_{\bar{i}}\mathbf{B}_{\bar{i}}\mathbf{x}_{\bar{i}} + \mathbf{G}_i\mathbf{W}\mathbf{n}_r + \mathbf{n}_i$. The node S_i recovers its desired data by processing its received signal using a decoder matrix $\mathbf{F}_i \in \mathbb{C}^{N \times N_s}$:

$$\widetilde{\mathbf{y}}_i = \mathbf{F}_i\widehat{\mathbf{y}}_i = \mathbf{F}_i\mathbf{G}_i\mathbf{W}\mathbf{H}_{\bar{i}}\mathbf{B}_{\bar{i}}\mathbf{x}_{\bar{i}} + \mathbf{F}_i\mathbf{G}_i\mathbf{W}\mathbf{n}_r + \mathbf{F}_i\mathbf{n}_i. \tag{4}$$

III. Transceiver design

We begin this section by outlining the principles of GSVD-based transceiver design. We then briefly describe two existing GSVD TWR designs in [10], [11]. We conclude this section by proposing a novel modification that will significantly improve the sum-rate of the GSVD designs in [10], [11]. For the proposed design, we assume that the relay perfectly knows $\mathbf{H}_i$ and $\mathbf{G}_i$ and that it designs the precoders/decoders and distributes them to other nodes. The perfect channel knowledge at the relay and design/distribution of precoders/decoders by it is commonly assumed in the literature on joint design [6], [7].

[1]To avoid repetition, we assume that $i = 1, 2$ throughput this paper. Further, $\bar{i} = 2$ for $i = 1$ and $\bar{i} = 1$ for $i = 2$.

A. Principles of GSVD-based transceiver design

To design a transceiver based on the GSVD, the MAC-phase MIMO channels $\mathbf{H}_1$ and $\mathbf{H}_2$ are jointly decomposed using GSVD [14]:

$$\mathbf{H}_1 = \mathbf{T}_h^H \mathbf{\Sigma}_{h_1} \mathbf{U}_{h_1} \text{ and } \mathbf{H}_2 = \mathbf{T}_h^H \mathbf{\Sigma}_{h_2} \mathbf{U}_{h_2}. \quad (5)$$

Here $\mathbf{U}_{h_1} \in \mathbb{C}^{N \times N_s}$ and $\mathbf{U}_{h_2} \in \mathbb{C}^{N \times N_s}$ are matrices with N orthonormal rows, $\mathbf{\Sigma}_{h_1} \in \mathbb{R}^{P \times N} = [\mathbf{0}_{h_1}^T \ \bar{\mathbf{\Sigma}}_{h_1}^T]^T$ and $\mathbf{\Sigma}_{h_2} \in \mathbb{R}^{P \times N} = [\bar{\mathbf{\Sigma}}_{h_2}^T \ \mathbf{0}_{h_2}^T]^T$. The matrix $\bar{\mathbf{\Sigma}}_{h_i} \in \mathbb{R}_+^{N \times N} = \text{diag}(\sigma_{h_i,1}, \cdots, \sigma_{h_i,N})$, $\mathbf{0}_{h_i} = \mathbf{0}_{N \times (P-N)}$, and $\mathbf{T}_h \in \mathbb{C}^{P \times N_r}$ is a full-rank matrix, where $P = \text{rank}([\mathbf{H}_1 \ \mathbf{H}_2]) = \min(N_r, 2N_s)$. Next, the BC-phase MIMO channels $\mathbf{G}_1$ and $\mathbf{G}_2$ are jointly decomposed using GSVD [14]

$$\mathbf{G}_1 = \mathbf{U}_{g_1} \mathbf{\Sigma}_{g_1} \mathbf{T}_g^H \text{ and } \mathbf{G}_2 = \mathbf{U}_{g_2} \mathbf{\Sigma}_{g_2} \mathbf{T}_g^H. \quad (6)$$

Here $\mathbf{U}_{g_1} \in \mathbb{C}^{N_s \times N}$ and $\mathbf{U}_{g_2} \in \mathbb{C}^{N_s \times N}$ are matrices with N orthonormal rows, $\mathbf{\Sigma}_{g_1} \in \mathbb{R}^{N \times P} = [\mathbf{0}_{g_1} \ \bar{\mathbf{\Sigma}}_{g_1}]$ and $\mathbf{\Sigma}_{g_2} \in \mathbb{R}^{N \times P} = [\bar{\mathbf{\Sigma}}_{g_2} \ \mathbf{0}_{g_2}]$. The matrix $\bar{\mathbf{\Sigma}}_{g_i} \in \mathbb{R}_+^{N \times N}$ =diag$(\sigma_{g_i,N}, \cdots, \sigma_{g_i,1})$, $\mathbf{0}_{g_i} = \mathbf{0}_{N \times (P-N)}$ and $\mathbf{T}_g \in \mathbb{C}^{N_r \times P}$ is a full-rank matrix, where $P = \text{rank}([\mathbf{G}_1^T \ \mathbf{G}_2^T]^T) = \min(N_r, 2N_s)$.

Following the decomposition, the MAC-phase transmit precoder of the node S_i is chosen as [10]

$$\mathbf{B}_i = \mathbf{U}_{h_i}^H \mathbf{\Lambda}_i. \quad (7)$$

Here $\mathbf{\Lambda}_i \in \mathbb{R}_+^{N \times N}$ is a diagonal power allocation matrix at S_i such that $\mathbf{\Lambda}_i \mathbf{\Lambda}_i^H = \text{diag}(\lambda_{i,1}, \cdots \lambda_{i,N})$. Similarly, the BC-phase decoder matrix for the node S_i is chosen as [10]:

$$\mathbf{F}_i = \mathbf{U}_{g_i}^H. \quad (8)$$

With the precoder/decoder in (7) and (8), the received signals at S_1 and S_2 in (4) can be expressed as

$$\begin{aligned} \widetilde{\mathbf{y}}_1 &= \mathbf{\Sigma}_{g_1} \mathbf{T}_g^H \mathbf{W} \mathbf{T}_h^H \mathbf{\Sigma}_{h_2} \mathbf{\Lambda}_2 \mathbf{x}_2 + \mathbf{\Sigma}_{g_1} \mathbf{T}_g^H \mathbf{W} \mathbf{n}_r + \mathbf{U}_{g_1}^H \mathbf{n}_1, \\ \widetilde{\mathbf{y}}_2 &= \mathbf{\Sigma}_{g_2} \mathbf{T}_g^H \mathbf{W} \mathbf{T}_h^H \mathbf{\Sigma}_{h_1} \mathbf{\Lambda}_1 \mathbf{x}_1 + \mathbf{\Sigma}_{g_2} \mathbf{T}_g^H \mathbf{W} \mathbf{n}_r + \mathbf{U}_{g_2}^H \mathbf{n}_2. \end{aligned} \quad (9)$$

To design the relay precoder $\mathbf{W}$, the earlier work in [10], [11] have considered two different approaches. In [10], the relay precoder orthogonalizes the end-to-end MIMO channels. To this end, the relay precoder is decomposed into a MAC precoder $\mathbf{W}_c \in \mathbb{C}^{P \times N}$, BC precoder $\mathbf{W}_b \in \mathbb{C}^{N \times P}$ and a power-allocation and permutation matrix $\mathbf{\Delta} \in \mathbb{R}_+^{P \times P}$ such that $\mathbf{W} = \mathbf{W}_b \mathbf{\Delta} \mathbf{W}_c$, where $\mathbf{\Delta}$ is an anti-diagonal matrix such that $\mathbf{\Delta} \mathbf{\Delta}^H = \text{diag}(\delta_1, \cdots, \delta_P)$. To orthogonalize the MIMO channels, precoders $\mathbf{W}_b$ and $\mathbf{W}_b$ are chosen as $(\mathbf{T}_g^H)^\dagger$ and $(\mathbf{T}_h^H)^\dagger$, respectively. The channel inversion, however, severely degrades the performance by enhancing the noise when the channels are ill-conditioned.

The design in [11] avoids channel-inversion by constructing $\mathbf{W}_b$ and $\mathbf{W}_c$ such that they have orthonormal columns and rows, respectively. This design, however, does not orthogonalizes the MIMO channels for *small* number of antennas, which leads to residual inter-stream interference between multiple transmit streams. This design ignores the residual inter-stream interference, and is shown to have better sum-rate than [10]. We will show later in Section V that the residual inter-stream interference, *if not ignored*, can significantly degrade the performance.

The objective of the relay precoder design herein, as discussed earlier, is to maximize sum-rate with per-stream transmit rate constraints. To achieve this, we do not diagonalize the end-to-end MIMO channels; we instead design the relay precoder to triangularize the MIMO channels. *This novel modification, as shown later in Section IV, is crucial in casting the optimization as a convex GP.*

The inter-stream interference due to triangular MIMO channels can be easily cancelled at the destination nodes by employing successive interference cancellation and need not be ignored as in [11]. Further, the MIMO channel triangularization is achieved by designing $\mathbf{W}_b$ and $\mathbf{W}_c$ with orthonormal columns and rows respectively. The proposed precoder, consequently, does not enhance the noise unlike [10]. Due to these two reasons, the proposed approach leads to better performance than in [10], [11]. We next discuss the proposed relay precoder design.

B. Proposed channel triangularization relay precoder

We first design the MAC-phase relay precoder $\mathbf{W}_c$ by factorizing the full-rank matrix $\mathbf{T}_h^H$ into a unitary matrix $\mathbf{Q} \in \mathbb{C}^{N_r \times N_r}$ and an upper-triangular matrix $\mathbf{R} \in \mathbb{C}^{N_r \times P}$ using QR factorization [14]

$$\mathbf{T}_h^H = \mathbf{Q}\mathbf{R} = \begin{bmatrix} \mathbf{Q}_h & \mathbf{Q}_0 \end{bmatrix} \begin{bmatrix} \mathbf{R}_h \\ \mathbf{0} \end{bmatrix}. \quad (10)$$

The bottom $(N_r - P)$ rows of matrix $\mathbf{R}$ are zeros. The matrix $\mathbf{Q}$ is therefore partitioned into $\mathbf{Q}_h \in \mathbb{C}^{N_r \times P}$ and $\mathbf{Q}_0 \in \mathbb{C}^{N_r \times (N_r - P)}$. Also, $\mathbf{R}_h \in \mathbb{C}^{P \times P}$ is an upper-triangular matrix. To reduce $\mathbf{T}_h^H$ to an upper-triangular matrix, we choose $\mathbf{W}_c = \mathbf{Q}_h^H$. Note that $\mathbf{W}_c$ is not unitary; only its rows are orthonormal. We now design the BC-phase relay precoder $\mathbf{W}_b$ by factorizing the full-rank matrix $\mathbf{T}_g^H$ into a lower-triangular matrix $\mathbf{L} \in \mathbb{C}^{P \times N_r}$ and a unitary matrix $\mathbf{V} \in \mathbb{C}^{N_r \times N_r}$ using LQ factorization [14]

$$\mathbf{T}_g^H = \mathbf{L}\mathbf{V} = \begin{bmatrix} \mathbf{L}_g & \mathbf{0} \end{bmatrix} \begin{bmatrix} \mathbf{V}_g \\ \mathbf{V}_0 \end{bmatrix}. \quad (11)$$

The last $(N_r - P)$ columns of matrix $\mathbf{L}$ are zeros. The matrix $\mathbf{V}$ is therefore partitioned into $\mathbf{V}_g \in \mathbb{C}^{P \times N_r}$ and $\mathbf{V}_0 \in \mathbb{C}^{(N_r - P) \times N_r}$. The matrix $\mathbf{L}_g \in \mathbb{C}^{P \times P}$ is a lower-triangular matrix. To reduce $\mathbf{T}_g$ to a lower-triangular matrix, we choose $\mathbf{W}_b = \mathbf{V}_g^H$. Note that $\mathbf{W}_b$ is not a unitary matrix; it only has orthonormal columns. The precoder $\mathbf{W}$ is given as

$$\mathbf{W} = \mathbf{V}_g^H \mathbf{\Delta} \mathbf{Q}_h^H. \quad (12)$$

With the above relay precoder, the received signal at S_1 and S_2 in (9) can be expressed as

$$\begin{aligned} \widetilde{\mathbf{y}}_1 &= \mathbf{\Sigma}_{g_1} \mathbf{L}_g \mathbf{\Delta} \mathbf{R}_h \mathbf{\Sigma}_{h_2} \mathbf{\Lambda}_2 \mathbf{x}_2 + \underbrace{\mathbf{\Sigma}_{g_1} \mathbf{L}_g \mathbf{\Delta} \mathbf{Q}_h^H \mathbf{n}_r + \mathbf{U}_{g_1}^H \mathbf{n}_1}_{\widetilde{\mathbf{n}}_1}, \\ \widetilde{\mathbf{y}}_2 &= \mathbf{\Sigma}_{g_2} \mathbf{L}_g \mathbf{\Delta} \mathbf{R}_h \mathbf{\Sigma}_{h_1} \mathbf{\Lambda}_1 \mathbf{x}_1 + \underbrace{\mathbf{\Sigma}_{g_2} \mathbf{L}_g \mathbf{\Delta} \mathbf{Q}_h^H \mathbf{n}_r + \mathbf{U}_{g_2}^H \mathbf{n}_2}_{\widetilde{\mathbf{n}}_2}. \end{aligned} \quad (13)$$

The lower-triangular $\mathbf{L}_g$, anti-diagonal $\mathbf{\Delta}$ and upper-triangular $\mathbf{R}_h$ result in the reflected lower-triangular structure of the end-to-end channel between $\widetilde{\mathbf{y}}_i$ and $\widetilde{\mathbf{x}}_{\bar{i}}$ as

$$\begin{bmatrix} \widetilde{y}_{i,1} \\ \widetilde{y}_{i,2} \\ \vdots \\ \widetilde{y}_{i,N-1} \\ \widetilde{y}_{i,N} \end{bmatrix} = \begin{bmatrix} 0 & 0 & \cdots & 0 & \times \\ 0 & & & \times & \times \\ \vdots & & \iddots & \vdots & \vdots \\ 0 & \times & \cdots & \times & \times \\ \times & \times & \cdots & \times & \times \end{bmatrix} \begin{bmatrix} x_{\bar{i},1} \\ x_{\bar{i},2} \\ \vdots \\ x_{\bar{i},N-1} \\ x_{\bar{i},N} \end{bmatrix} + \widetilde{\mathbf{n}}_i. \tag{14}$$

With this channel structure, the Nth transmit stream ($x_{\bar{i},N}$) does not experience inter-stream interference and is detected first. The $(N-n)$th transmit stream is then detected by successively subtracting the interference from *already-detected* streams numbered from $(N-n+1)$ to N, $n=1$ to $N-1$. After detection, the signal-to-noise ratio (SNR) of the nth receive stream of the source nodes S_1 and S_2 respectively are

$$\begin{aligned} \text{SNR}_{1,n}(\boldsymbol{\delta},\boldsymbol{\lambda}_2) &= \frac{\delta_{\widetilde{n}}\lambda_{2,\widetilde{j}}(\sigma^2_{g_1,n}\sigma^2_{h_2,\widetilde{j}}|[\mathbf{L}_g]_{\widetilde{n},\widetilde{n}}[\mathbf{R}_h]_{\widetilde{j},\widetilde{j}}|^2)}{\sigma_r^2\sum_{l=1}^{P}\delta_l[\mathbf{L}_{g_1}\odot\mathbf{L}^*_{g_1}]_{n,l}+\sigma_1^2}, \\ \text{SNR}_{2,n}(\boldsymbol{\delta},\boldsymbol{\lambda}_1) &= \frac{\delta_{n}\lambda_{1,\widetilde{j}}(\sigma^2_{g_2,n}\sigma^2_{h_1,\widetilde{j}}|[\mathbf{L}_g]_{n,n}[\mathbf{R}_h]_{j,j}|^2)}{\sigma_r^2\sum_{l=1}^{P}\delta_l[\mathbf{L}_{g_2}\odot\mathbf{L}^*_{g_2}]_{n,l}+\sigma_2^2}. \end{aligned} \tag{15}$$

Here $n=1$ to N, $\widetilde{n}=P-N+n$, $j=P-n+1$ and $\widetilde{j}=N-n+1$. Further $\boldsymbol{\delta}=[\delta_1,\cdots,\delta_P]$ and $\boldsymbol{\lambda}_i=[\lambda_{i,1},\cdots,\lambda_{i,N}]$. In the denominator of the above SNR expressions, we denote $\mathbf{L}_{g_i}=\mathbf{\Sigma}_{g_i}\mathbf{L}_g$. The above SNR expressions can be derived from (13) after simple algebraic manipulations and by noting that $\mathbf{Q}_h^H\mathbf{n}_r$, $\mathbf{U}_{g_1}^H\mathbf{n}_1$ and $\mathbf{U}_{g_2}^H\mathbf{n}_2$ have the same statistical properties as $\mathbf{n}_r$, $\mathbf{n}_1$ and $\mathbf{n}_2$, respectively. *Note that the coefficients of the power-distribution variables, δ_l for $l=1$ to P, λ_{1n} and λ_{2n} for $n=1$ to N, are non-negative. We will use this fact to prove the convexity of the optimization problems*. The complete procedure for the proposed GSVD triangularization (GSVD-TRI) design is summarized in Algorithm 1.

Algorithm 1 GSVD-TRI design.

1: *GSVD design*: Design source precoders $\mathbf{B}_i$ and decoders $\mathbf{F}_i$, as in (7) and (8), to partially diagonalize $\mathsf{S}_i\rightarrow$relay$\rightarrow\mathsf{S}_{\bar{i}}$ MIMO channels.
2: *Channel triangularization*: Design relay precoder $\mathbf{W}$, as in (12), to triangularize the end-to-end MIMO channels using LQ and QR decompositions.
3: *Power allocation*: Jointly allocate power at the source nodes and relay to maximize sum-rate (see next section).

IV. Joint power allocation

We now jointly allocate power to optimize the sum-rate subject to the per-stream transmit rate required by both source node. We next prove two lemmas that will be useful in showing that the optimization is a GP; a GP has a posynomial objective and upper-bounded posynomial constraints [15, pg. 160].

Lemma 4.1: The transmit power of the node S_i, defined in (2), is a posynomial in optimization variable $\boldsymbol{\lambda}_i$, where $\boldsymbol{\lambda}_i=[\lambda_{i,1},\cdots,\lambda_{i,N}]$.

Proof: With the transmit precoder $\mathbf{B}_i$ designed in (7), we rewrite the transmit power of S_i as $\text{Tr}(\mathbf{B}_i\mathbf{B}_i^H) = \text{Tr}(\mathbf{U}_{h_i}^H\mathbf{\Lambda}_i\mathbf{\Lambda}_i^H\mathbf{U}_{h_i}) \overset{(a)}{=} \text{Tr}(\mathbf{U}_{h_i}\mathbf{U}_{h_i}^H\mathbf{\Lambda}_i\mathbf{\Lambda}_i^H) = \sum_{j=1}^{N}\lambda_{i,j}$. In (a), we have used Tr($\mathbf{AB}$)=Tr($\mathbf{BA}$). Wee see that the constraint is a posynomial in $\boldsymbol{\lambda}_i$, as the coefficients of optimization variable $\lambda_{i,j},\forall j$ are positive [15, pg. 160]. ■

For notational convenience, the transmit power of the node S_i is henceforth denoted as $p_i(\boldsymbol{\lambda}_i)$.

Lemma 4.2: The transmit power of the relay, defined in (3), is a posynomial in $\boldsymbol{\lambda}_1$, $\boldsymbol{\lambda}_2$ and $\boldsymbol{\delta}$, where $\boldsymbol{\delta}=[\delta_1,\cdots,\delta_P]$.

Proof: This can also be proved on lines similar to Lemma 4.1. Please see [16] for details. The transmit power of the relay is now denoted as $p_r(\boldsymbol{\delta},\boldsymbol{\lambda}_1,\boldsymbol{\lambda}_2)$. ■

We next define the sum-rate as

$$R(\boldsymbol{\delta},\boldsymbol{\lambda}_1,\boldsymbol{\lambda}_2) = \frac{1}{2}\sum_{i=1}^{2}\sum_{n=1}^{N}\log_2(1+\text{SNR}_{i,n}(\boldsymbol{\delta},\boldsymbol{\lambda}_{\bar{i}})) \tag{16}$$

$$\overset{(a)}{\approx} \frac{1}{2}\sum_{i=1}^{2}\sum_{n=1}^{N}\log_2(\text{SNR}_{i,n}(\boldsymbol{\delta},\boldsymbol{\lambda}_{\bar{i}}) \tag{17}$$

$$= -\frac{1}{2}\log_2\prod_{n=1}^{N}\prod_{i=1}^{2}\text{ISNR}_{i,n}(\boldsymbol{\delta},\boldsymbol{\lambda}_{\bar{i}}) \tag{18}$$

The factor of half is due to the half-duplex constraint. The term $\text{ISNR}_{i,n}$ denotes the inverse of $\text{SNR}_{i,n}$, that is $\text{ISNR}_{i,n}=1/\text{SNR}_{i,n}$. Each $\text{ISNR}_{i,n}$ term, due to positive coefficients of power distribution variables in $\text{SNR}_{i,n}$ terms in (15), is a posynomial. The sum-rate in (16) can easily be shown as a ratio of two posynomials. As posynomials are not closed under division [15, pg. 161], the sum-rate is not a posynomial and its optimization therefore cannot be cast as a GP. We approximate the sum-rate as in (a) to cast the problem as a GP; the loss in the sum-rate due to this approximation is minor and becomes negligible in the high-SNR regime [17].

The QoS-constrained sum-rate optimization is now cast as

$$\begin{aligned} \underset{\{\boldsymbol{\lambda}_1,\boldsymbol{\lambda}_2,\boldsymbol{\delta}\}\succeq 0}{\text{Minimize}} \quad & \prod_{n=1}^{N}\prod_{i=1}^{2}\text{ISNR}_{i,n}(\boldsymbol{\delta},\boldsymbol{\lambda}_{\bar{i}}) \\ \text{subject to} \quad & \text{ISNR}_{1,n}(\boldsymbol{\delta},\boldsymbol{\lambda}_2)\le 1/(2^{r_{1n}}-1) \\ & \text{ISNR}_{2,n}(\boldsymbol{\delta},\boldsymbol{\lambda}_1)\le 1/(2^{r_{2n}}-1) \\ & p_1(\boldsymbol{\lambda}_1)\le P_1, p_2(\boldsymbol{\lambda}_2)\le P_2 \\ & p_r(\boldsymbol{\delta},\boldsymbol{\lambda}_1,\boldsymbol{\lambda}_2)\le P_r \end{aligned} \tag{19}$$

Here first two constraints, which can be equivalently expressed as $\log_2(1+\text{SNR}_{i,n}(\boldsymbol{\delta},\boldsymbol{\lambda}_{\bar{i}}))\ge r_{in}$, are on the per-stream transmit rate; here r_{in} is desired rate of nth stream of node i. The last three are transmit power constraints of different nodes. We have dropped $\frac{1}{2}\log_2$ factor from the objective as $\log(\cdot)$ is a monotonically increasing function. We see that the objective is a product of posynomials and is therefore a posynomial [15, pg. 161]. The problem is a GP as it has a posynomial objective and upper-bounded posynomial constraints.

V. Numerical results

We now investigate the effect of the per-stream QoS constraints on the sum-rate of the proposed GSVD-TRI transceiver

using Monte Carlo simulations. We assume Rayleigh flat-fading channels where the elements of $\mathbf{H}_i$ and $\mathbf{G}_i$ are independent and identically distributed complex Gaussian random variables with zero mean and variance h_i^2 and g_i^2 respectively. We fix the maximum transmit power and noise variance at all the nodes to unity and define the average SNR of the $\mathsf{S}_i \rightarrow$Relay and Relay$\rightarrow \mathsf{S}_i$ links as $\eta_i = h_i^2 = g_i^2$. We assume that both source nodes employ Gaussian signalling. The simulation results are averaged over 5000 statistically independent channel realizations.

In Fig. 2a, we plot the sum-rate of the proposed GSVD-TRI transceiver, with and without the per-stream QoS constraints for two different antenna configurations. We first focus on the scenario when each node has $N_s = N_r = 6$ antennas. The per-stream rate required by each source nodes is assumed to be 0.75 bps/Hz that is, $r_{1n} = r_{2n} = 0.75$ bps/Hz, $\forall n$. We make two key observations: 1) the per-stream rate requirement cannot be met below $\eta_1 = \eta_2 = 15$ dB; the per-stream rate requirement for $\eta_1 = \eta_2 \leq 15$ dB should therefore be reduced from the current one; and 2) the per-stream rate requirement leads to degradation in the sum-rate performance when compared with the scenario when there is no such rate requirement. This is because the system now sacrifices the overall sum-rate to satisfy the per-stream transmit rate of the individual streams. Moreover the degradation reduces at high SNR values where the probability of automatically meeting the per-stream rate requirement while maximizing the sum-rate is higher than at low SNR. For $N_s = N_r = 4$ antennas, where again $r_{1n} = r_{2n} = 0.75$ bps/Hz, $\forall n$, we see that the per-stream rate-requirement cannot be met below $\eta_1 = \eta_2 = 15$ dB. Further, similar to $N_s = N_r = 6$ antennas, the degradation due to the rate constraints reduces at high SNR values.

We now demonstrate the improved sum-rate of the proposed design over the other two GSVD-based designs: i) GSVD-ZF [Eq. (12), Eq. (13)] [10]; and ii) GSVD-HRP [Eq. (13), Eq. (15)] [11]. The improved sum-rate is because, as discussed earlier, the current transceiver overcomes the limitations of these two designs. Since both GSVD-ZF and GSVD-HRP designs do not incorporate QoS constraints, for the sake of fairness, we also maximize the sum-rate of the proposed design after dropping the QoS constraints. We also do not ignore the residual inter-stream interference of GSVD-HRP design. We see that the proposed GSVD-TRI design comprehensively outperforms both other designs.

VI. Conclusion

We investigated a GSVD-based joint transceiver design for MIMO TWR that triangularizes the end-to-end MIMO channels of the two source nodes. With MIMO channel triangularization, optimization of per-stream rate-constrained sum-rate reduce to joint optimal power allocation at the source and relay nodes, which is then cast as a convex geometric program. We analysed the impact of the per-stream rate constraints on the overall sum-rate. We also showed that the proposed design outperforms other state-of-the-art designs without rate constraints also.

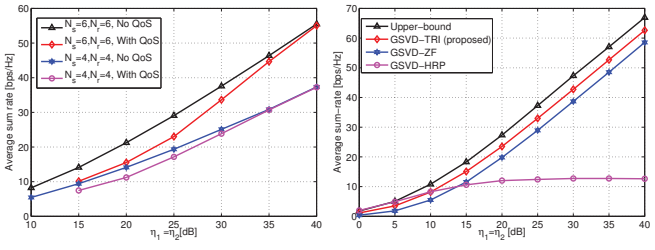

(a) (b)

Fig. 2: a) Average sum-rate of the proposed GSVD-TRI transceiver design for two different antenna configurations; and b) Average sum-rate comparison of the GSVD-TRI design with the existing GSVD-ZF and GSVD-HRP designs; here $N_s = 6$ and $N_r = 10$.

References

[1] A. Dutta, K. Hari, and L. Hanzo, "Linear transceiver design for an amplify-and-forward relay based on the MBER criterion," *IEEE Trans. Commun.*, vol. 62, pp. 3765–3777, Nov. 2014.

[2] T. Yang, X. Yuan, L. Ping, I. Collings, and J. Yuan, "A new physical-layer network coding scheme with eigen-direction alignment precoding for MIMO two-way relaying," *IEEE Trans. Commun.*, vol. 61, pp. 973–986, Mar. 2013.

[3] V. T. Muralidharan and B. Rajan, "Wireless network coding for MIMO two-way relaying," *IEEE Trans. Wireless Commun.*, vol. 12, pp. 3566–3577, Jul. 2013.

[4] M. Arti and M. Bhatnagar, "Performance analysis of two-way AF MIMO relaying of OSTBCs with imperfect channel gains," *IEEE Trans. Veh. Technol.*, vol. 63, pp. 4118–4124, Oct. 2014.

[5] K.-J. Lee, H. Sung, E. Park, and I. Lee, "Joint optimization for one and two-way MIMO AF multiple-relay systems," *IEEE Trans. Wireless Commun.*, vol. 9, pp. 3671–3681, Dec. 2010.

[6] R. Wang and M. Tao, "Joint source and relay precoding designs for MIMO two-way relaying based on MSE criterion," *IEEE Trans. Signal Process.*, vol. 60, pp. 1352–1365, Mar. 2012.

[7] Y. Rong, "Joint source and relay optimization for two-way linear non-regenerative MIMO relay communications," *IEEE Trans. Signal Process.*, vol. 60, pp. 6533–6546, Dec. 2012.

[8] W.-C. Choi, S. Choi, A. Heo, and D.-J. Park, "Joint optimization of source and relay for MIMO two-way relay networks using MSE duality," *IEEE Commun. Lett.*, vol. 18, pp. 1246–1249, Jul. 2014.

[9] A. Heo, W. Choi, J. Park, and D. Park, "Sum rate maximization of an MIMO two-way relay system using MSE duality," *IEEE Commun. Lett.*, vol. 19, pp. 863–866, May 2015.

[10] H. Park, H. J. Yang, J. Chun, and R. Adve, "A closed-form power allocation and signal alignment for a diagonalized MIMO two-way relay channel with linear receivers," *IEEE Trans. Signal Process.*, vol. 60, pp. 5948–5962, Nov. 2012.

[11] Y. Zhang, L. Ping, and Z. Zhang, "Low cost pre-coder design for MIMO AF two-way relay channel," *IEEE Signal Process. Lett.*, vol. 22, pp. 1369–1372, Sep. 2015.

[12] C. Leow, Z. Ding, and K. Leung, "Joint beamforming and power management for nonregenerative MIMO two-way relaying channels," *IEEE Trans. Veh. Technol.*, vol. 60, pp. 4374–4383, Nov. 2011.

[13] Z. He, Z. Lang, Y. Rong, and S. Qu, "Joint transceiver optimization for two-way MIMO relay systems with MSE constraints," *IEEE Wireless Commun. Lett.*, vol. 3, pp. 613–616, Dec. 2014.

[14] G. H. Golub and C. F. V. Loan, *Matrix Computations*. Baltimore, MD: The Johns Hopkins University Press, 1996.

[15] S. Boyd and L. Vandenberghe, *Convex Optimization*. Cambridge, UK: Cambridge Univ. Press, 2004.

[16] R. Budhiraja and B. Ramamurthi, "Joint transceiver design for QoS-constrained MIMO two-way non-regenerative relaying using geometric programming," *IEEE Trans. Wireless Commun.*, under first major revision.

[17] G. Caire and S. Shamai, "On the achievable throughput of a multiantenna Gaussian broadcast channel," *IEEE Trans. Inf. Theory*, vol. 49, pp. 1691–1706, Jul. 2003.

THE 18TH INTERNATIONAL SYMPOSIUM ON WIRELESS PERSONAL MULTIMEDIA COMMUNICATIONS
(WPMC-2015)
December 13-16, 2015, Hyderabad, India

Trust based Detection and Elimination of Packet Drop Attack in the Mobile Ad-hoc Networks

Vishvas Haridas Kshirsagar
Sinhgad Institute of Technology, Lonavala, Pune, India
Savitribai Phule Pune University, Pune, India
kshirsagar.vhk@gmail.com

Ashok M. Kanthe
Sinhgad Institute of Technology, Lonavala, Pune, India
Faculty of Electrical Engineering and Computing, University of Zagreb, Croatia
ashokkanthe@gmail.com

Dina Simunic
Faculty of Electrical Engineering and Computing, University of Zagreb, Croatia
Dina.Simunic@fer.hr

Abstract— **The Mobile ad-hoc Network (MANET) is a communication network of a mobile node without any prior infrastructure of communication. The network does not have any static support; it dynamically creates the network as per requirement by using available mobile nodes. This network has a challenging security problem. The security issue mainly contains a denial of service attacks like packet drop attack, black hole attack, gray hole attack, etc. The mobile ad-hoc network is open environment so; working is based on mutual trust between mobile nodes. The MANETs is vulnerable to packet drop attack in which, packets are travelers through the different node. The network while communicating, the node drops the packet, but it is not attracting to the neighboring nodes to drop the packets.**

This proposed algorithm works with existing routing protocol. The concept of trusted list is used for secure communication path. The trusted list along with trust values show how many times node was participated in the communication. It differentiates between altruism and selfishness in MANET with the help of energy level of mobile components. The trust and energy models are used for security and differentiation between altruism and selfishness respectively.

Keywords— Altruism, Blackhole attack, Denial of Service, Gray hole attack, Mobile ad-hoc networks, Packet Drop Attack, Selfishness, Trust.

I. INTRODUCTION

The MANET is an own manageable network in which, any node can participate in the communication. The network is working with limited resources like the strength of signal, power, etc. The nodes are communicating each other by using routing protocols operating at different levels of the MANET. For communication between nodes, it uses insecure media channels; they fall into malicious activity. In the MANET devices are acts as an autonomous system, so the malicious device can join the network at any time without any notification. Once a malicious node enters in the network much valuable information passed to the malicious node. A malicious node may misuse that useful information.

The MANET has different denial of service attack like gray hole attack, black hole attack, and packet drop attack, etc. In the packet drop attack, The attacker node drops all the packets passing through it similar to black hole node, but it does not attract the neighboring nodes to drop the packet.

This paper is organized as follows: Section II discusses the related work. Section III gives detailed description about proposed work. Section IV provides simulation work. Section V provides a comparision with existing work and proposed work. Section VI gives the conclusion.

II. RELATED WORK

Neelavathy et. al. [1] introduced a Novel Reputation Based Algorithm to Detect the Misbehaving nodes (NRMDM) [1]. NRMDM uses local reputation value. Each node maintains the reputation value of its k-hop neighbourhood. The maintaining reputation values of all neighbouring nodes, if neighbouring nodes are more it need more overhead. This method is excellent for small network.

S. Buchegger et. al. [2] proposes performance analysis of the CONFIDANT reactive protocol. The protocol works as an extension to a reactive protocol. Given an algorithm mainly focuses on trust relationship based on experience, observation and forwarding behavior of intermediate nodes. Given an algorithm works with dynamic source routing (DSR) protocol. This protocol has primary four pillars the monitor, the reputation, the path manager and trust manager.

A. M. Kanthe et al. [3] proposed the impact of packet drop attack and solution for the overall performance of AODV in mobile ad-hoc networks. In this paper, the reputation and trust-based mechanism is used against packet drop attack and improves the network performance in terms of throughput, packet drop rate, packet delivery ratio, normalized routing overhead and end-to-end delay.

Ing-Ray Chen et al. [4] proposed trust management in mobile ad-hoc network for bias minimization and application performance maximization. It states the trust management mechanism in the MANET and its implementation to increase the performance. This approach is an integrated social and quality-of-service trust to improve the bias and performance.

Jin-Hee Cho et al. [5] proposed on the tradeoff between altruism and selfishness in MANET trust management. In which considered the tradeoff between a node's individual welfare vs. global well-being and identify the best design condition of this behavior model to balance to selfish vs. altruism behaviors.

III. PROPOSED WORK

The MANET is a large open environment network. The mobile node can participate in the communication. The existing algorithms are available for mobile ad-hoc network security. Due to the open environment of MANET there is chance of malicious activity like purposefully dropping packets, traffic observation, etc. The existing algorithms for packet drop attack are based on local reputation of the node. The different reasons behind the packet drop like power of node, network congestion, purposefully drops the packets, and queue length etc. The hard task is to differentiate the reason for dropping of packets. If the node is purposefully dropping packets, then the node is malicious node. When node is dropping packets due other reason; the node is not malicious. The node purposefully drops the packet is known as selfish node.

The proposed works have considered two concepts, namely Trust and Energy. The mobile ad-hoc network works on mutual trust between neighboring nodes. The communication is done in the mobile ad-hoc network with help of intermediate nodes. The intermediate nodes may be unknown, they can be malicious nodes. The trust is major notion for the communication. Trust is mutual understanding between different nodes present in the MANET. Trust is used to identify the node is malicious or not. The trust management in the MANET is usually Route Request (RREQ) and Route Reply (RREP) message passing between nodes. The nodes are dropping packets because of insufficient energy or purposefully. The energy is used to distinguish between altruism and selfish node.

A. Trust

The concept of trust is as subjective degree of belief. The trust management is important to avoid the malicious activity and increase the throughput. The trust can be generated with exchanging RREQ and RREP. This proposed work deals with trust values assigned to each node. When RREP got back to source, then source node increase the trust value by 0.1. The trust value is assigned 0.5 as a trust value of a particular node, when they are communicating first time. It is threshold values [6]. The trust value varies from 0 to 1. Every RREP has made strong relationship between a source node and neighboring node. The source node creates a list of all nodes having a trust value greater than 0.5. It is known as Trusted List. The nodes in the trusted list have stronger relation as compare to other nodes. When source wants to communicate with any of the destination node, then source node can pickup intermediate nodes from the trusted list to establish a path. The selected path will be most secure path for the communication. The construction of trusted list is based on RREQ and RREP. Trust list along with trust value is also calculated, it shows that how many times that a node was participated in the communication. The trust value defines the strength of the relationship between the two neighboring nodes. The Trusted list decreases the overhead of detecting malicious node. Once all nodes can start communication by picking nodes form trusted list as intermediate node, the network communication will be free from malicious nodes.

B. Energy

The concept of trusted list is purely depends upon RREQ and RREP. The network has many problems due to which nodes unable to send RREP. The problems may be congestion in the network, inefficient energy, etc. When source node does not have RREP from neighboring node, the source node does not add into trusted list. There is no concept to know the reason for failure of the RREP. To differentiate between altruism and selfish node, proposed algorithm uses energy model. While generating trust in which node is not replied due to inefficient energy, that node is not entered into trusted list even though it is not a malicious node. The selfish node does not participate in the communication process; it decreases the performance of the network. Distinguish between altruism and the selfish node is done with the help of energy model. This model calculates the energy level of each node; it classifies lower energy node and higher energy node. If any node is not replying on RREQ, then it checks energy level. If energy level is lower then it not considered as malicious node and if it has higher energy level then it considered as a selfish or malicious node.

C. Proposed Algorithm for Trust based solution to Packet Drop Attack

Basically, this algorithm works on the trusted list along with trust value and energy of the mobile node. Initially all nodes trust value and energy level will be zero. All neighboring node details are stored in local storage. When any source wants to communicate with destination, it will start sending RREQ to all neighboring nodes. When requesting node get RREP then it will add that node to the routing table and check for the trust value. Initially trust value is zero. In beginning of communication, the trust value 0.5 is assigned when first RREP received by the source node. Otherwise add 0.1 to pervious trust value and it increments up to 1 as RREP received by the node. While creating a trusted list it will check for both trust as well as energy level. Trust value must be greater than 0.5 and energy levels must be above 20 % of total energy of a node, it will add to trust list. If trust condition is true and energy level condition is false, then it will not directly declare as malicious node. Here the algorithm creates the difference between altruism and selfishness node.

The reliable flags are used while creating a trusted list. The flags are helping while selecting a communication path between the source node and the destination node. While selecting node from the trusted list as intermediate node, it checks to reliable flag if it is 1 then select otherwise not.

The trusted list along with trust values and energy level is used to select a secure communication path between the source and the destination. This will helps in creating a difference between altruism and selfishness nodes.

This algorithm creates the trusted list. The generated trusted list contains only trusted and working energy level.

[Initialization E (Energy Level) and T (Trust Level) to 0]
Step 1 Start (send RREQ to each neighboring node)
Step 2 Check if reply from node
If yes goto step 3
If no goto step 9
Step 3: Add details of replying node into routing table
If rt=rtable.rt_lookup(rp->rp_dst)
If yes T=T + 0.1 and E=received E
If T > 1 then T=1
If no T=0.5 and E=received E
Step 4 Check if replying node is in the trust list
If yes check E < 20 then remove from trust list
If no goto step 5
Step 5 Check replying node T and E values
If T > 0.5 && E > 20 Add to trust List and
reliable = 1
If no goto step 6
Step 6: Reset the reliable flag
reliable = 0
Step 7: Check if replying node is final destination node
If yes do not add node to trust list
If no goto step 8
Step 8: Execute rests part of receivreply function
Step 9: Stop

IV. Simulation Work and Result Analysis

The proposed algorithm is simulated in Network Simulator (NS-2) [9]. NS-2 is open source network simulation tool. The 802.11 MAC layer implemented in NS-2 is used for simulation. The protocol used is AODV. The various parameters are considered to compare the results. The wireless channel type with Omni-directional antenna type is used for link. This simulation uses 802.11 MAC type. The 300 × 300 m^2 simulation area is used.

A. Effect of Speed of node on Throughput

Figure 1 shows the graphs generated between the throughput and the pause time. Figure 1 shows that when the network is under attack, the average of the packet delivery ratio is 42 % and when it's under attack with the the solution it improved up to 80 %. When we applied solution on the packet drop attack the throughput is increased because packet dropping rate is decreased. The packet dropping rate is inversely proportional to throughput. The malicious node is included in the establishment of a path. This gives a secure path for the communication.

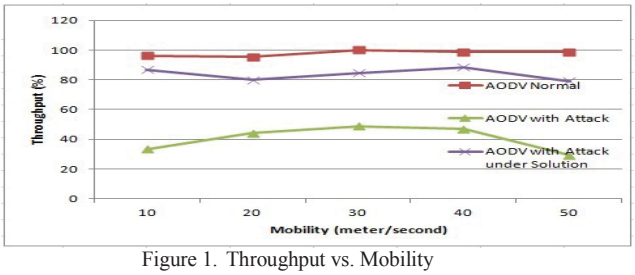

Figure 1. Throughput vs. Mobility

The throughput with an attack degrades the performance of the network. The packet dropper is dropping the packets if the packets are coming in route. The packet dropper node is not attracting the neighboring nodes. Throughput with an attack and solution improves the performance. If the packet dropper node is the busiest node in the simulation then, the performance of the network is less affected due to not attract the neighboring packets.

B. Effect of Number of node on Throughput Delay:

Figure 2 shows throughput Vs. number of nodes. Figure 2 shows, when the network is under attack, the average of the packet delivery ratio is 40% and when it under the solution it improved up to 83%. The proposed work differentiates between altruism and selfishness nodes. When any node wants to communicate with other node. There will a maximum number of secure next hops for the communication.

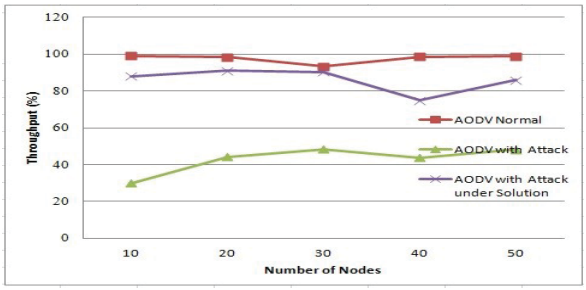

Figure 2. Throughput vs. Number of Nodes

V. Comparision of Proposed Algorithm Against Existing Work

Neelavathy [1] introduced a Novel Reputation Based Algorithm to Detect the Misbehaving nodes (NRMDM). NRMDM uses Local values are assigned for k-hop neighbouring nodes. Each node maintains all local values about its k-hop neighbourhood. NRMDM solution has large overhead when large numbers of nodes are present in the network. It is suitable for small network. Buchegger [2] proposed new protocol namely the CONFIDENT protocol, which is a solution to identify the misbehaving nodes in the MANET. The overhead of computation is more because of increase in the message exchange like ALARM messages. The effect of speed of nodes on CONFIDENT protocol is affected. Each node maintains a large table for reputation. The throughput at a law pause time is less. A. M. Kanthe [3] introduces new trust based reputation algorithm against packet drop attack is to detect a packet drop attack and improve the performance of the network. The concepts used in this dissertation are trust list and direct reputation. The node who not replied to source node it does not add into a Trust List. The node may be not replied because of energy, network issues. These existing algorithms not works with differentiated between altruism and selfishness node. Trust based detection and elimination packet drop attack in MANET, detect the packet drop attack. This proposed algorithm works on detecting and eliminating packet drop attacks with very low overhead and end-to-end delay. This

algorithm also works on the energy model to differentiate between altruism and selfishness node.

The comparative study of proposed work and existing system includes throughput, delay, overhead, technique, and packet delivery ratio and packet dropping rate [9]. The comparison of the proposed work against attack with the existing work is shown in Table I.

TABLE I. COMPARISON OF THE ALGORITHM AGAINST A PACKET DROP ATTACK WITH THE EXISTING WORK

Sr. No.	Algorithm/ Solution	Protocol	Enhancement
1.	Local values assigned based on reputation [1]	DSR	In case of a large network, numbers of possible path are available. The maintenance of all path increments overhead, it's decrement overall throughput of the network. Local value assignment increases overhead for every node, so decreases throughput. Unnecessarily paths are cached and their computation of local reputation values, it increment end-to-end delay.
2.	Trust based detection of packet drop attack [2]	DSR	DSR algorithm basically works on cache memory, maintaining local reputation, it decreases overall throughput of the networks. It uses ALARM packet with every RREQ and RREP messages. It consumes extra energy. Due which many nodes are unable to participate in the communication. So the less number of next hops available for the communication. It decreases throughput of the network.
3.	Trust List [3]	AODV	Trust based creation of trust list with the help of RREQ and RREP, gives less overhead of ALARM packet. The trust list gives the more secure node for nodes for establishing the path. Throughput will be more because malicious node cannot participate in the communication. The creation of trust list does not consider low energy node which is unable to send RREP to the source node. Many nodes from the network declared as malicious node due to inefficient energy.
4	Proposed Work	AODV	The proposed work is also depends upon the trusted list. The concept of creation of trusted list is based upon both trusts with trust values as well as the energy of the node. The trusted list includes only secure node. This will helps to increment in throughput of the network. This work considers energy to differentiate between altruism and selfishness node. So the maximum number of nodes can participate in the communication. It increases approximately 30-35 % throughput of the network.

VI. CONCLUSION

Trust based detection and elimination of the packet drop attack in MANET. This proposed work helps to detect the malicious node from the network. The trust based idea is better rather than cryptography, the cryptography increases overhead of computation. The proposed work does a considerable improvement in throughput and performance of the network. The mobile ad-hoc network with open nature of communication, security can be improved with a trust based idea.

The trust list helps to detect the malicious activity on the network and also differentiate between an altruism and selfishness nodes that avoid getting blacklisted because of the energy level of nodes. Each node maintains a list, in the local buffer that contains the list of trusted and un-trusted nodes. This helps to detect malicious node and also differentiate between altruism and selfishness node.

REFERENCES

[1] S.Neelavathy Pari,D Sridharan, "Mitigating Routing Misbehaviour in Self Organizing Mobile Ad hoc Network using K-neighbourhood Local Reputation System" IEEE-International Conference on Recent Trends Information Technology,ICRTIT ,Chennai,June 3-5,2011.

[2] S.Buchegger and J.Y.Le Boudec, Performance Analysis of the CONFIDENT Protocol, In Proc. 3rd ACM International Symposium on Mobile Ad Hoc Networking and Computing (MOBIHOC 02),Lausanne, Switzerland ,Tech. Rep. DSC/2001/001,June 2002.

[3] Ashok M. Kanthe, Dina Simunic, Ramjee Prasad, "The Impact of Packet Drop Attack and Solution on overall Performance of AODV in Mobile Ad-hoc Networks" IJRTE, ISSN: 2249-8958, Volume-2, December-2012.

[4] Ing-Ray Chen, Jia Guo, Fenye Bao, Jin-Hee Cho, "Trust management in mobile ad hoc networks for bias minimization and application performance maximization". Elsevier B. V Journal with ISSN:1570-8705, 2014.

[5] Jin-Hee Cho, Ing-Ray Chen, "On the tradeoff between altruism and selfishness in MANET", Elsevier B. V Journal with ISSN:2217-2234, 2013.

[6] Vishvas Kshirsagar, Ashok M. Kanthe, Dina Simunic, "Analytical Approach towards Packet Drop Attack in Mobile Ad-hoc Networks" ,IEEE ICCIC 2014

[7] C.Perkins,E.B. Royer, S.Das, Ad hoc On-Demand Distance Vector Routing, Proceeding of the 2nd IEEE Workshops on Mobile Computing System and Applications (WMCSA),pp.90-100,1999.

[8] Jared Cordasco, Susanne Wetzel,"Cryptographic vs. Trust-based Methods for MANET Routing Security", STM 2007

[9] http://www.isi.edu/nsnam/ns

THE 18TH INTERNATIONAL SYMPOSIUM ON WIRELESS PERSONAL MULTIMEDIA COMMUNICATIONS
(WPMC-2015)
December 13-16, 2015, Hyderabad, India

The Behavioral Based Gray Hole Attack Detection in Mobile Ad-hoc Network (MANET)

Parineet D. Shukla
Sinhgad Institute of Technology,
Lonavala, Pune, India.
Savitribai Phule Pune University,
Pune.
sh.neet11@gmail.com

Ashok M. Kanthe
Sinhgad Institute of Technology,
Lonavala, Pune, India.
Faculty of Electrical Engineering and Computing,
University of Zagreb, Croatia.
ashokkanthe@gmail.com

Dina Simunic
Faculty of Electrical Engineering and Computing, University of Zagreb,
Croatia.
dina.simunic@fer.hr

***Abstract*— The mobile Ad-hoc network does not have the fixed topology. The nodes are in moving state and participate in the communication. Due to open network it is more prone to the attack. The various attacks can be possible as any malicious node can enter into the communication. The gray hole attack is DoS kind of attack which drops the partial packets passing through them. Due changing behavior of the node from black to honest, it is difficult to detect the malicious node in the network.**

The Proposed work implements the TrueLink concept to check the link between the two intermediate nodes is valid or not. The data routing information (DRI) is used to check the behavior of the nodes which do not have a valid link between them. The primary detection is done with the help of DRI table and confirmation is done with the sequence number of the packets. The confirmation of the node being malicious or not is done using the number of packets that are forwarded by the node in particular time frame or not. The performance of the network can be improved with this proposed concept.

Keywords— gray hole attack, mobile devices, malicious, dynamic nature, security, self-configuring, Mobile Ad-hoc Network.

I. INTRODUCTION

A mobile Ad-hoc network is a collection of autonomous systems. The network is independent of infrastructure and hence it reduces the cost and deployment time [1, 2]. The MANET is highly susceptible to various routing attacks. In gray hole attack, the node drops some amount of packets and hence ultimately affects the performance of the network. The node can act in two states as an honest node and as a black hole where all the incoming packets are dropped. The node changes its state from honest to black and vice versa.

The gray hole attack is difficult to detect because some amount of packets may get dropped by the network congestion and some other issues in the network. The partial dropping of packets affects the efficiency of the network hence it's important to detect and remove the gray hole in the established network. The gray hole attack is difficult to detect because some amount of packets may get dropped by the network congestion and some other issues in the network. The partial dropping of packets affects the efficiency of the network hence it is important to detect and remove the gray hole in the established network.

This paper proposes an algorithm based on the TrueLink concept. The TrueLink is used to verify the valid link between the two nodes. Depending on the link between the two nodes, the node can be detected as a malicious node.

This paper is organized like section II discusses about related work, section III discusses about MANET and gray hole attack, section IV discusses about TrueLink, Section V discusses about the Gray hole attack detection and removal using TrueLink, Section VI discusses about simulation result and analysis and Section VII describes the conclusion.

II. RELATED WORK

This section gives the information about the previous research work done related to gray hole attack.

A. Kanthe et al. [3] have proposed a gray hole detection mechanism based on the false replies getting from the node. The counter is used to maintain the count of false replies. The proposed algorithm totally depends on the count of false replies. When the node switches from honest to black and vice versa the node produces the false replies. This information is stored in the local buffer and depending on that the malicious nodes are detected and removed from the network.

G. Wahane et al. [4] have proposed the detection of cooperative black hole and crosschecking it with TrueLink. The TrueLink is used cross check the detection of cooperative black hole attack. The DRI table entries are used to detect the black hole attack.

Payal N. Raj et al. [5] have proposed the black hole attack detection mechanism based on detection, prevention and reactive AODV (DPRAODV). The DPRAODV solution checks the Route Reply (RREP) packet sequence number which is higher than the threshold value. The threshold value is dynamically updated through simulation using the dynamic learning method. The alarm packet is sent to all the neighboring nodes to inform about the malicious nodes.

J. Eriksson et al. [6] have proposed a True-link concept for detecting the gray hole attack. Using True-link, a node can verify the existence of a direct link to an apparent neighbor. Verification of a link operates in two phases. In the rendezvous phase, the nodes exchange nonce. The TrueLink concept is totally based on the timing constraint so that the node does not enter into the network.

III. Approch for Detection of Gray Hole Attack

A. TrueLink [6]

The TrueLink is used to check the adjacency of apparent neighbor. It uses combination of timing and authentication. Truelink helps to check the authentication of the nodes participating in the communication. The reliability of the intermediate nodes is checked with the help of TrueLink. Authentication is important for communication. TrueLink performs link verification between two nodes i and j in two phases: the rendezvous phase, and the authentication phase. In the rendezvous phase, i and j exchange nonce _j and _i, where the subscript indicates the node that generated the nonce. The time constraint is an important factor to check the adjacency of the neighboring node; only a direct neighbor can respond in time. In the authentication phase, i and j each sign and transmit the message (_j, _i), mutually authenticating themselves as the originator of their respective nonce. The timing constraints of the rendezvous phase makes TrueLink immune to limits the range of attacks based on bit-by-bit or "cut-through" forwarding. TrueLink is used as an extension to the IEEE 802.11 MAC layer. TrueLink verification between two nodes i and j operates in two phases. In the rendezvous phase, i and j exchange nonces randomly generated numbers. This phase is completed as a single RTS-CTS-DATA-ACK exchange. The features of TrueLink are as follows:

Deploy ability with minimal requirements:

TrueLink does not rely on precise clock synchronization, GPS coordinates, overhearing, or geometric or statistical methods.

Backwards compatibility with IEEE 802.11:

TrueLink can be implemented using standard IEEE 802.11 hardware with a minor, backwards compatible, firmware update. TrueLink enabled terminals continued to interoperate with non-enhanced 802.11 hardware, albeit without TrueLink protection.

Compatible with most authentication methods:

TrueLink can be used equally well with asymmetric, symmetric, hash based or other authentication mechanisms.

Widely applicable:

TrueLink is independent of the routing protocol used and improves the security of both proactive and reactive routing protocols. TrueLink effectively protects the network against such attacks and the cost of protection with TrueLink is small.

B. Proposed Algorithm

The proposed work is used to detect the malicious nodes from the network. The TrueLink is used to detect whether the nodes have the valid link between the neighbors or not. When the link between the two neighbors is not valid then the confirmation is done with the help of the amount of packets forwarded by the node in particular time frame or not. The invalid link may occur between the two nodes because of the network issues so it is important to cross check the behavior of that particular node. The node forwards each and every packet coming to it. When the link between the particular node may be invalid because of the node's behavior. The behavior of the node can be checked with the help of number of packets that are forwarded by the particular node in the fixed time frame. The forwarding node forwards the packet in the form of RTS-CTS-DATA-ACK exchange. This exchange is done in single phase. The TrueLink is implemented in two phases rendezvous and authentication phase. In rendezvous phase the data is exchanged between the neighboring nodes. The authentication phase is validation of the node i.e. the node authenticates itself as an originator of the message. Depending on this the link between the two nodes is verified. When the link between the nodes is valid then the node will not drop the packet. When the link is not TrueLink, the node can drop the packet. To detect the gray hole attack the link is checked multiple times when the link is not TrueLink in multiple check at such times the node can be detected as a malicious node.

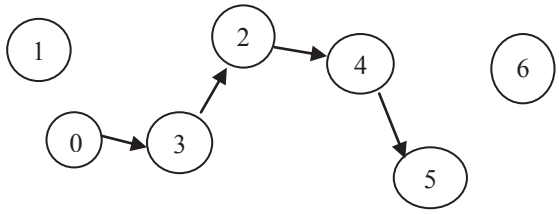

Figure 1: Scenario for Gray Hole Attack

Figure 1 shows the scenario for detection of gray hole attack. Here node "0" is Source and node "5" is destination. The path established between node "0" and "5" is 0-3-2-4-5. Here node 2 and 4 are acting as a gray hole nodes.

The TrueLink is implemented as follows:

The rendezvous phase is implemented as a single RTS-CTS-DATA-ACK exchange. We describe the operation of the protocol for each of these frames. The rendezvous operation includes following steps:

Request to Send (RTS): Node i called initiator, calls init ( ). Node i send an RTS to node j.

Clear to Send (CTS (α_j)): After receiving the RTS, node j calls HandleRTS ( ). A locally generated value α_j is included in the CTS, which is sent after a delay of one Short Interframe Space (*SIFS*), is the small time interval between the data frame and its acknowledgment.

DATA (βi): Having received the CTS, i generate value β_i. After a SIFS delay, the nonce is sent as the packet payload, together with a header, identifying the packet as a rendezvous packet.

ACK: When node j receives the payload packet containing values β_i, the HandleRTS () function sends the ACK frame, after a SIFS delay. The received packet and the locally generated values α_j are handed to the upper layer for processing. When node i receives the ACK, the init () function at i returns the pair (α_j, β_i) to its caller.

When the link is invalid between the two nodes, the nodes are checked for the malicious nature. The SEQUENCE_NUMBER is used to check the behavior.

MAX_SEQ_TH is maximum number of packets that can be used as threshold value to decide the nature of the particular

node. MAX_VALUE is used to check the threshold value for the particular node.

Comparing the MAX_SEQ_TH with SEQUENCE_NUMBER, the behavior of the suspect node can be examined. When the SEQUENCE_NUMBER is greater than the threshold the node is forwarding the packets more than that it can forward in normal scenario. The node is not malicious node.

When the SEQUENCE_NUMBER is less than MAX_SEQ_TH, the node is not forwarding the packets that it can forward in normal state. The node is detected as a malicious node and the route is dropped and new route can be selected.

Before implementing the solution to the gray hole attack, the node is created as a black hole and the results are observed. In gray hole attack the node changes its state so it is important to observe the behavior of the node when it is acting as black hole node. The black hole node is then converted into the gray hole node and the results are observed.

When the node is acting as a black hole, the node drops all the incoming packets through it. In ideal case the node forwards all the incoming packets towards destination. Hence a threshold value is considered to detect the gray hole attack.

Algorithm to detect a gray hole node from the network:

SN: Source node DN: Destination node IN: Intermediate node
α,β: nonce key DRI: Data Routing Information
Step 1: SN broadcasts the RREQ packet
Step 2: SN receives RREP
Step 3: if RREP is from any IN then
Step 4: SN verify the RREP of the node which sends RREP
Step 5: SN verify updates entry of DRI value of the intermediate node that initialized RREP
Step 6.then sendRTS();
Step 7.# recvCTS() times out after $t_{timeout}$ = SIFS
Step 8.α=recvCTS();
Step 9.if α != nil then
Step 10.β->nonce();
Step 11: # success = true if ACK received
Do reactive Link verification and routing method
Step 12 success=sendPacket([VerifyLink,β]);
Step 13.if success == true then
Step 14: Consider the route to be safe and start routing the data packets
Step 15: else Add node as suspect list
Step 16: check again for number of packets transmitted
Step 17: if SEQUENCE_NUMBERS > max_val and
max_val > MAX_SEQ_TH then
Node is not malicious node
Else
The node is malicious.

IV. Simulation Result and Analysis

The proposed algorithm is simulated in Network Simulator (NS-2) [8]. NS-2 is open source network simulation tool. The 802.11 MAC layer implemented in ns-2 is used for simulation. The protocol used is AODV. The various parameters are considered to compare the results.

The parameters used during simulation helps to analyse the network. The channel type used during simulation is wireless channel. Omnidirectional antenna is used for the communication. The Two-ray Ground propagation model is selected for simulation. The link layer type used during simulation is LL. The simulation is done on AODV protocol. The attack and solution is implemented on AODV protocol. Initially 30 nodes are created for the simulation and results are observed by varying the number of nodes. The pause time during simulation was 0.1 milliseconds and the scenario is simulated for 100 milliseconds.

The performance of the network is studied with the help of the graphs plotted by varying the number of nodes and the speed of the nodes i.e. mobility of nodes. The performance of the network is observed in terms of packet delivery ratio. Packet delivery ratio is the amount of the packets that reach to the destination.

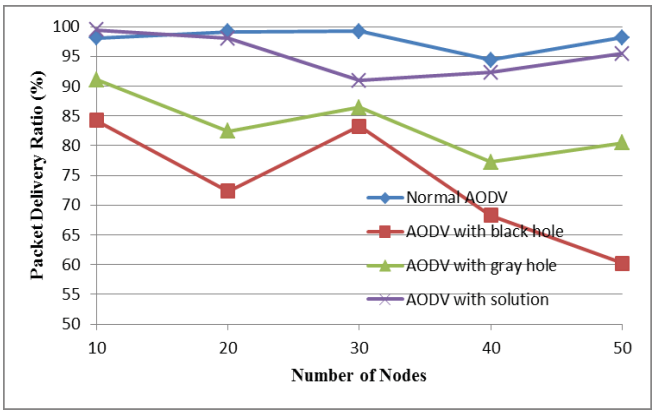

Figure 2: Packet Delivery Ratio Vs. Number of Nodes

Figure 2 shows the variation in packet delivery ratio Vs. number of nodes. When the node is acting as a black hole node, the node drops all the incoming packets to it. The packet delivery ratio is the amount of packets that reach to the destination out of the total packet sent from the source. When a black hole node is present it drops all the incoming packets through it so the packet delivery ratio will be less. When the node is acting as a gray hole, the nodes drops only few amount of packets passing through it. The packet delivery ratio will be more. When the malicious node is removed from the network the packet delivery ratio is improved approximately equal to that in normal scenario. As the malicious nodes are removed from the network, the path is established with the help of honest node only.

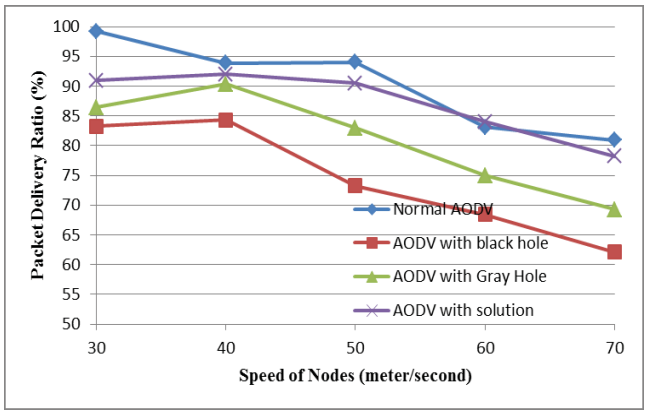

Figure 3: Packet delivery ratio Vs. speed of nodes

Figure 3 shows the variation in packet delivery ratio with respect to the speed of the nodes. The nodes in the MANET are always in moving state. The packet delivery ratio is plotted by varying the speed of nodes from 30 to 80 meter/second. It is observed from figure 3 that when the node is acting as a black hole node the packet delivery ratio decreases as the speed of the nodes increases. When the node is acting as gray hole node the packet delivery ratio is slightly greater than when the node is black hole node. When the solution is implemented the packet delivery ratio is improved.

V. Comparision of Proposed Algorithm with Existing Algorithms

The results of the proposed algorithm are compared with the existing algorithms and it is seen that the overhead is decreased as compared to the existing algorithm.

The existing algorithm proposed by A. M. Kanthe et al. [3] has used the false reply count from the particular node. The false reply count is checked for the each node so the routing overhead increases. The algorithm proposed in this paper checks the nodes for gray hole attack only if getting the invalid link from the nodes. Only suspect nodes are checked for the malicious node hence the overhead decreases.

The existing algorithm DPRAODV [5] used to detect the black hole attack from the network. Once the malicious node is detected from the network an alarm packet is sent to all the neighboring nodes. Due to alarm packets the routing overhead increases as each node checks the neighboring node is in the list of malicious nodes or not. The algorithm proposed in this paper does not send any alarm packet so the routing overhead will be less.

The proposed work is compared with existing work in terms of packet delivery ratio. Table 1 shows the comparison of existing algorithms with the proposed algorithm.

Table I Comparison with existing algorithms

Technique	Performance matric	Analysis
False reply based [3]	Overhead	False replies are calculated at each node. The counter is maintained to store the number of false replies.
DPRAODV [5]	Overhead	After detection of black hole, an alarm packet is broadcasted.
Proposed Algorithm	Overhead	The nodes which do not have valid link with neighbors are only checked for gray hole.

VI. Conclusion

The performance of the network is totally dependent on the behavior of the nodes in the network. For securing the network it is important that each node in the network must be honest node i.e. it must forward all the incoming packets to next node in the path. When a malicious node is present in the path the proper transmission of data is not possible. When a node drops some packets the data which is to be transmitted does not reach to the destination correctly. Detection of gray hole attack is important to ensure proper transmission of data. Because of partial dropping of packets, it is difficult to detect the gray hole in the network.

TrueLink is helpful for verification of the valid link between the neighboring nodes. Depending on how much packets are forwarded by the particular node the node can be detected as the malicious node. The proposed solution reduces the routing overhead by reducing the calculations at each node. Due to continuous changing state of the nodes from honest to black and vice versa the gray hole detection is difficult. So the proposed work will be helpful to keep the nodes with valid link in the network and establish the path through those nodes.

The results obtained with the proposed algorithm are compared with the results of existing algorithms. It is observed that the performance matrices are improved as compared to the previous algorithms.

References

[1] Jeroen Hoebeke, Ingrid Moerman, Bart Dhoedt and Piet Demeester, “An Overview of Mobile Ad-Hoc Networks: Applications and Challenges.” (July 2004). Journal of Communication Network, 3,60-66.0

[2] Shalini Jain, Mohit Jain, Himanshu Kandwal, “Advanced Algorithm for Detection and Prevention of Co-operative Black and Gray Hole Attacks in Mobile Ad-Hoc Networks, International journal of computer Applications (0975-8887) volume 1-No. 7, 2010.

[3] Ashok M. Kanthe, Dina Simunic, Ramjee Prasad, “A Mechanism for Gray Hole Attack Detection in Mobile Ad-Hoc Networks.” International Journal of Computer

Application (0975-8887) Volume 53-No 16, September 2012.

[4] G. D. Wahane, A. M. Kanthe, D. Simunic, "Technique For Detection Of Cooperative Black Hole Attack Using Crosschecking With True-Link In MANET " , IEEE ICCIC 2014, Coimbatore

[5] Payal N. Raj, Prashant B. Swadas, "Dpraodv: A Dyanamic Learning System Against Blackhole Attack In Aodv Based Manet", IJCSI International Journal of Computer Science Issues, Vol. 2, 2009, ISSN (Online): 1694-0784

[6] J. Eriksson, S. V. Krishnamurthy, M. Faloutsos, "TrueLink: A practical countermeasure to the wormhole attack in wireless networks", 2011. The Communications and Networks Consortium sponsored by the U. S. Army Research Laboratory under the Collaborative Technology Alliance Program.

[7] Jaydip Sen, M. Girish Chandra, Harihara S.G., Harish Reddy, P Balamurlidhar, "A Mechanism for Detection of Gray Hole Attack in Mobile Ad-Hoc Network", ICICS, IEEE, 1-4244-0983-7/07, 2007.

[8] The network simulator-ns 2.35 http://www.isi.edu/nsnam/ns/1997

THE 18TH INTERNATIONAL SYMPOSIUM ON WIRELESS PERSONAL MULTIMEDIA COMMUNICATIONS
(WPMC-2015)
December 13-16, 2015, Hyderabad, India

Experimental Evaluation on Wireless Tomography with Wireless Tomography in a Three-Dimensional Space

Kengo Yokota†, Shinsuke Hara†, Takahiro Matsuda††, Masaki Mukamoto††, Yuki Uemura††,
Kenichi Takizawa*, Fumie Ono**, Ryu Miura**

†Graduate School of Engineering, OsakaCity University 3-3-138 Sugimoto, Sumiyoshi-ku, Osaka 558-8585, Japan
††Graduate School of Engineering, Osaka University 2-1 Yamadaoka, Suita, Osaka, 565-0871 Japan
*Strategic Planning Office, National Institute of Information and Communications Technology
4-2-1 Nukuikitamachi, Koganei, Tokyo 184-8795 Japan
**Wireless Network Research Institute, National Institute of Information and Communications Technology
3-4 Hikarinooka, Yokosuka, Kanagawa, 239-0847 Japan

Email: †{yokota@c., hara@}nfo.eng.osaka-cu.ac.jp
Email: ††{matsuda@, m-mukamoto@post., y-uemura@post.}comm.eng.osaka-cu.ac.jp
Email: *takizawa@nict.go.jp
Email: **{fumie, ryu}@nict.go.jp

***Abstract*— When a disaster happens in an urban area, it is essential to localize survivors and rescue workers in burning and collapsing buildings, however, conventional localization methods do not work well for such indoor localization. One promising method is a two-layered localization using unmanned aerial vehicles (UAVs) where UAV flying outdoors, which are localized by the global positioning system (GPS), act as anchor nodes for localizing target nodes located indoors. When localizing a target node in a building by measuring the received signal strength (RSS), in order to achieve accurate indoor localization, UAVs need to know the internal architectural structure of the building, since the walls, windows and doors of the building give different attenuations for the wireless signal used for localization. However, it is impossible to know them in advance.**

In this paper, we call the distribution of the attenuation for the wireless signal ``the attenuation map,'' and propose to estimate it by wireless tomography based on compressed sensing. To explore the possibility of wireless tomography, we conducted an experiment in an anechoic chamber to estimate the three-dimensional attenuation map.

Keywords—wireless tomography; attenuation map; compressed sensing; styling; three-dimensional space

I. INTRODUCTION (*HEADING 1*)

When a disaster happens in an urban area, to search for survivors and prevent the secondary disaster, it is essential to localize survivors and rescue workers in burning and collapsing buildings. However, conventional localization methods do not work well indoors; the wireless signal from the global positioning system (GPS) cannot reach indoors, and wireless local area network (WLAN) access points and wireless sensor network (WSN) nodes with known locations are not pre-installed in buildings.

One promising method is to use unmanned aerial vehicles (UAVs) flying outdoors for indoor localization of target nodes, where the UAVs are localized by the GPS and then they act as anchor nodes for target nodes with unknown indoor locations. In this case, there are mainly two considerable techniques for the part of the indoor localization, such as time of arrival (TOA) and received signal strength (RSS). The TOA technique achieves higher localization accuracy but its realization is not easier. Therefore in this paper, we focus on the RSS technique, since almost all transceivers have a function of measuring the RSS.

When UAVs flying outdoors localize a target node in a building, the wireless signal from/to the target node experiences much attenuation when penetrating the wall and doors. The attenuation changes according to the internal architectural structure of the building, so in order to localize the target node accurately by the RSS method, the UAVs need to know it to compensate for the RSS, namely, to distinguish the attenuation by the distance for the target node from by the architectural structure. However, it is almost impossible to know the architectural structure in advance, and even when we can know it, the attenuation changes according to the carrier frequency of the wireless signal and the material of the building, so it is difficult to estimate the distribution of the attenuation for the wireless signal used for localization. One possible approach is the use of wireless tomography.

Tomography is a technique for identifying the internal structure of a monitored region by analyzing wireless waves traversed across the region or reflected in the region. The tomography using the same wireless signal as for communication thus localization is called ``wireless tomography [1],'' and the wireless tomography can be represented as a system of linear equation by using the propagation property of wireless signal [2]. Furthermore, the space of building is constructed suitably for human lives, so the

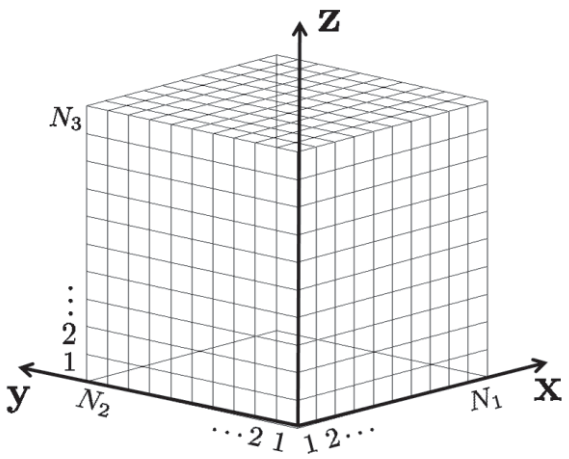

Fig. 1: Three-dimensional monitored region.

walls, windows and doors are not randomly laid out, namely, they are structured. This means that, when giving 1's to the parts with higher attenuations (such as walls and doors) and giving 0's to those with lower attenuations (such as human living spaces), the ground plan of building can be represented by a sparse matrix with the smaller number of 1's, since the human living spaces are dominant. Therefore, taking into consideration that compressed sensing [3] is a technique for solving underdetermined linear inverse problems when the solution has the sparsity, it can be successfully introduced into the wireless tomography encountered in the attenuation map estimation for the indoor localization using UAVs.

In this paper, we call the distribution of the attenuation for the wireless signal used for localization ``the attenuation map'' and in order to explore the possibility of the wireless tomography for estimating the three-dimensional attenuation map, we evaluate the performance by experiment. Three-dimensional space is represented with a tensor, so a tensor-based compressed sensing [2] can be directly applied to estimate the attenuation map, but in the paper, for the sake of simplicity, we slice a three-dimensional space into multiple two-dimensional horizontal planes and apply a matrix-based compressed sensing to estimate them.

This paper is organized as follows. Section II presents the problem formulation in the three-dimension space. Section III shows the principle of the wireless tomography based on compressed sensing. Section IV explains the confirmation experiment of the wireless tomography method and shows the results. Finally, Section V concludes the paper.

II. Principle of Three-Dimensional Wireless Tomography

As shown in Fig. 1, the attenuation map for a three-dimensional monitored region is written with a tensor as

$$\mathbf{G} = \{G_{n_1 n_2 n_3} \mid n_1 = 1,2,\ldots,N_1, \\ n_2 = 1,2,\ldots,N_2, n_3 = 1,2,\ldots,N_3\} \tag{1}$$

where N_1, N_2 and N_3 denote the numbers of grids dividing the monitored region in the x-axis, y-axis and z-axis directions, respectively, and each element of the attenuation map is defined as the amount of attenuation per unit volume of the corresponding grid. Furthermore, we define the (n_1,n_2,n_3)-th grid as $\gamma_{(n_1,n_2,n_3)}$.

Let I denote the number of combinations of wireless nodes which are deployed on the border of the monitored region, and also let us assume that a wireless signal is transmitted from a transmitter $\mathbf{T}_i = [T_{xi},T_{yi},T_{zi}]^T$ to a receiver $\mathbf{R}_i = [R_{xi},R_{yi},R_{zi}]^T$ (i = 1,2,..., I). In this case, defining P_i, d_i and L_i as the received signal power at R_i in dBm, the length of the i-th path, and the loss over the i-th path in dB, respectively, we can model the shadowing loss due to obstructions $S_i[dB]$ between $\mathbf{T}_i$ and $\mathbf{R}_i$ as

$$\begin{aligned} S_i &= L_i - P_i \\ L_i &= \alpha d_i^{-\beta} \\ d_i &= \|\mathbf{T}_i - \mathbf{R}_i\| \end{aligned} \tag{2}$$

where α and β are the propagation constants when there are no obstructions between $\boldsymbol{T}_i$ and $\boldsymbol{R}_i$. In this paper, α and β are assumed to be known in advance.

On the other hand, let us define a set of indexes of the grids which the i-th path penetrates as

$$\Gamma^i = \{(n_1^i,n_2^i,n_3^i) : \textit{the } i\textit{-th path penetrates } \gamma_{(n_1^i,n_2^i,n_3^i)}\}. \tag{3}$$

In this case, defining the length of the partial path in $\gamma_{(n_1^i,n_2^i,n_3^i)}$ as $\delta_{n_1^i,n_2^i,n_3^i}$, S_i is given by (i = 1,2,..., I)

$$\mathrm{S_i} = \sum_{(n_1^i,n_2^i,n_3^i)\in\Gamma^i} \delta_{n_1^i,n_2^i,n_3^i} G_{n_1^i,n_2^i,n_3^i}. \tag{4}$$

Therefore, defining the attenuation vector as $\mathbf{S} = [S_1,S_2,\ldots,S_I]^T$, it is written as

$$\mathbf{S} = A(\mathbf{G}) \tag{5}$$

where $A(\cdot)$ denotes a linear map $A : \mathbb{R}^{N_1N_2N_3} \rightarrow \mathbb{R}^I$. Wireless tomography means a linear inverse problem to estimate $\mathbf{G}$ from measured $\mathbf{S}$ and a given linear map A.

III. Wireless Tomography With Compressed Sensing

Buildings are generally designed suitably for human lives, so there are more empty spaces than obstructions such as walls, doors and windows. This implies that we can assume that the number of elements with exactly or approximately zero values is much larger than the number of elements with larger values in the attenuation map. Therefore, even if the number of measurements, namely, the dimension of the measurement vector I is much smaller than that of total grids $Q = N_1 \times N_2 \times N_3$ ($I << Q$), $\mathbf{G}$ can estimated from $\mathbf{S}$ using the compressed sensing theory. Measurement is always noisy, so we cannot have exactly zero values for empty spaces. In this case, we can estimate $\mathbf{G}$ using the following l_1/l_2 optimization [4]:

$$\hat{\mathbf{G}} = \arg\min_{\mathbf{G}} \left(\frac{\mu}{2}\|\mathbf{S} - A(\mathbf{G})\|_2^2 + \sum_{l=1}^{3} \|\mathbf{G}_{(l)}\|_* \right) \tag{6}$$

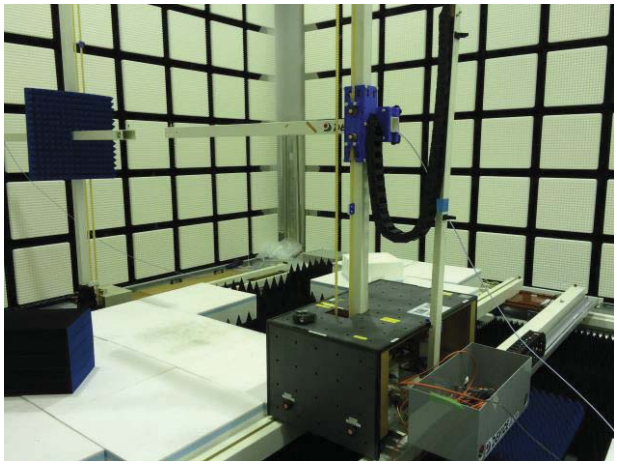

(a) A transmitter and a receiver.

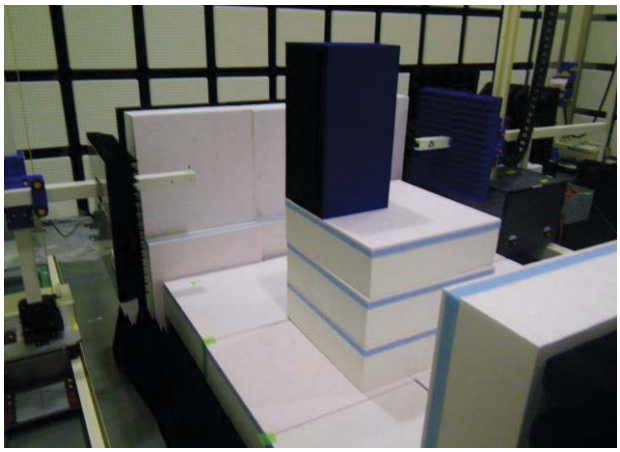

(b) An obstruction.

Fig. 2: Experimental setup.

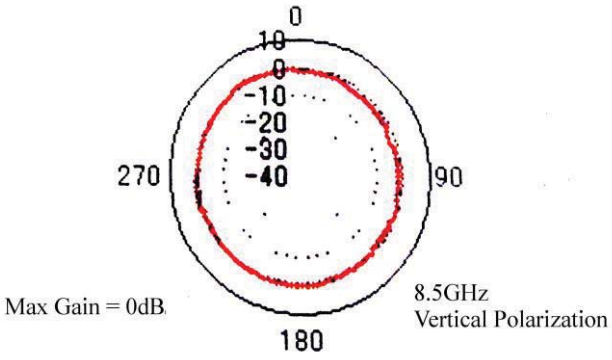

Fig. 3: Antenna radiation pattern.

where $\mathbf{G}_{(l)}$ denotes the mode-l of $\mathbf{G}$, and $\|\mathbf{G}(l)\|_*$ denotes the nuclear norm of $\mathbf{G}$, and μ ($\mu > 0$) is a regularization parameter.

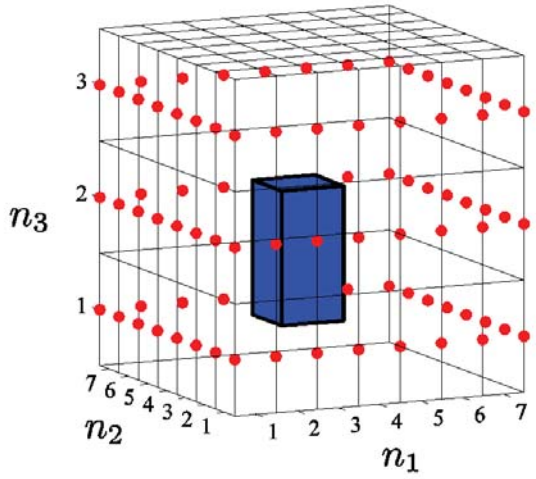

(a) Three-dimensional.

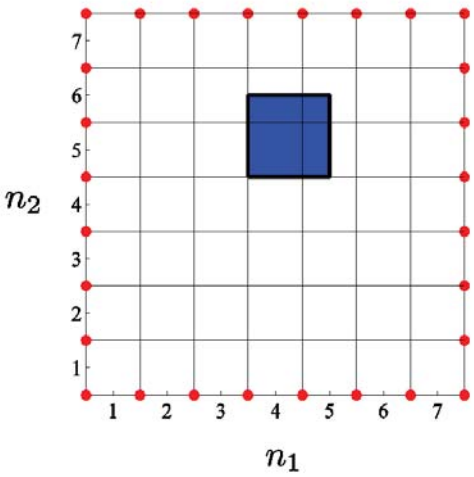

(b) x-y plane.

Fig. 4: Monitored region and placement points of wireless nodes.

In this paper, instead of directly solving the tensor-based l_1/l_2 optimization given by (6), we slice the tensor $\mathbf{G}$ into multiple matrices $\mathbf{g}_{n_3}$ on different horizontal planes under the constraint that T_{zi} and R_{zi} are located on the same plane:

$$\mathbf{G} = \{\mathbf{g}_{n_3} \mid n_3 = 1,2,\ldots,N_3\} \quad (7)$$

$$\mathbf{g}_{n_3} = \{g_{n_3} \mid n_1 = 1,2,\ldots,N_1, n_2 = 1,2,\ldots,N_2\}. \quad (8)$$

IV. Experiment on the Possibility of Wireless Tomography

A. Experimental environment

As a preliminary study to explore the possibility of the proposed wireless tomography method, we conducted an experiment in an anechoic chamber of National Institute of Information and Communications Technology (NICT)

TABLE I: Specifications of the experiment.

Location	NICT Headquarter
Anechoic chamber	840cm×720cm×660cm
Monitored region	140cm×140cm×100cm
Obstruction(Wave Absorber)	30cm×30cm×60cm
Signal emission	8GHz(CW)
RSS	-60dBm～-30dBm
Antenna	UWB antenna(Omni)
Placement points of wireless nodes	28(each plane)×3=84
Number of measurement paths	270(each plane)×3=810
Horizontal resolution	20cm
Vertical resolution	50cm

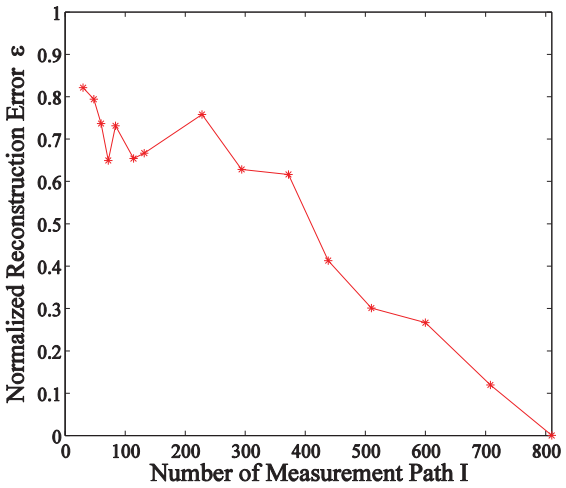

Fig. 5: Number of measurements vs the estimation error characteristics.

Headquarter. Fig. 2 shows the experimental setup with a transmitter, a receiver and an obstruction.

The wireless signal transmitted from a transmitter was a continuous wave in the 8GHz band, and its power was adjusted to be received at a receiver in -60dBm ~ -30dBm. The transmitter and receiver had the same type of antenna with almost omni-directional antenna radiation pattern as shown in Fig. 3. In addition, we used a radio wave absorber as an obstruction in the monitored region.

As shown in Fig. 4, we divided the three-dimensional monitored region to 3 slices with 50cm interval in the height direction along the *z*-axis, and in each horizontal plane, we divided the monitored space by 20cm internal along the *x*-axis and *y*-axis. Therefore, we had $N_1 = 7$, $N_2 = 7$ and $N_3 = 3$, and the number of placeable points for the transmitter or receiver was 28. As a result, the number of measurable paths was 270 on each planes, so the total number of measurable paths was $270 \times 3 = 810$.

Finally, Table I summarizes the specifications of the experiment.

B. *Experimental result*

We evaluate the estimation accuracy of the attenuation map in terms of the error using I measurements normalized by the one using the maximal number of measurements I_{max} = 810, which is defined as

$$\varepsilon(I) = \frac{1}{3}\sum_{n_3=1}^{3} \frac{\left\| \mathbf{g}_{n_3}^{I} - \mathbf{g}_{n_3}^{\max} \right\|_F}{\left\| \mathbf{g}_{n_3}^{,\max} \right\|_F} \qquad (9)$$

where $\mathbf{g}_{n_3}^{I}$ is the attenuation map matrix estimated using I, $\mathbf{g}_{n_3}^{\max}$ is the one estimated using I_{max}, and $||(\cdot)||F$ denotes the Frobenius norm of $(\cdot)$.

Fig. 5 shows the normalized estimation error versus the number of measurements (I). From Fig. 5, we can see that the normalized estimation error almost linearly decreases as the number of measurements increases. That is, if we need to achieve the 50% estimation accuracy, we can reduce the number of measurements by around 50%.

Finally, Figs. 6 and 7 compare the attenuation maps estimated using I = 114 (= 38×3) paths and I_{max} = 810 (= 270 ×3) paths, respectively. Note that the transmitter and receiver were located on the same plane, so from Fig. 4, no obstruction should appear in the attenuation map at n_3 = 3. As expected, there are no obstructions estimated in both Figs. 6 (c) and 7 (c) at n_3 = 3.

For the case of I = 114, which corresponds to around 85% reduction of the number of paths, from Fig. 5, we can see that the normalized estimation error is relatively large, but there is no large difference in these illustrative comparisons. That is, in Figs. 6 (a) and 7 (a) at n_3 = 1 and Figs. 6 (b) and 7 (b) at n_3 = 2, the obstruction is clearly estimated by the proposed wireless tomography method based on compressed sensing.

V. CONCLUSION

In this paper, we proposed the wireless tomography based on compressed sensing to estimate the attenuation map, and demonstrated the preliminary results obtained from the experiment in an anechoic chamber. Instead of estimating the three dimensional attenuation map directly by means of the tensor-based compressed sensing, after slicing the three-dimensional region into three two-dimensional regions, we estimated the three two-dimensional attenuation maps by applying the matrix-based compressed sensing to each sliced regions. In the experiment, a higher sparsity was guaranteed for the three dimensional region. Therefore, when reducing the number of measured paths by around 85%, a large estimation error was observed in the quantitative evaluation, on the other hand, no large estimation error was confirmed in the illustrative evaluation.

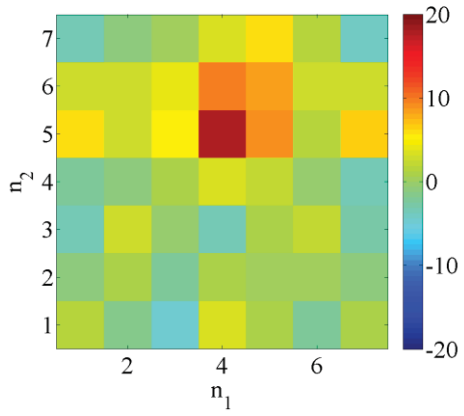

(a) $n_3 = 1$.

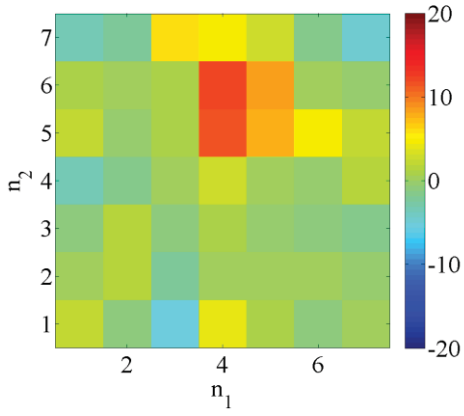

(b) $n_3 = 2$.

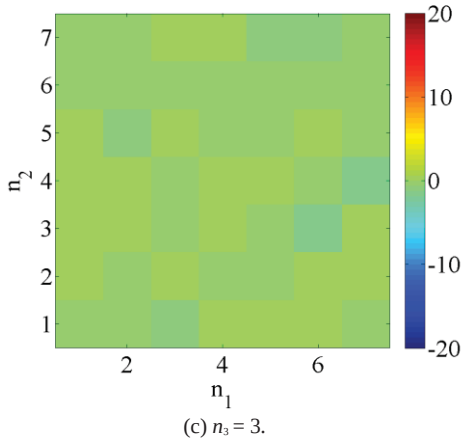

(c) $n_3 = 3$.

Fig. 6: Attenuation map estimated by using 114 paths.

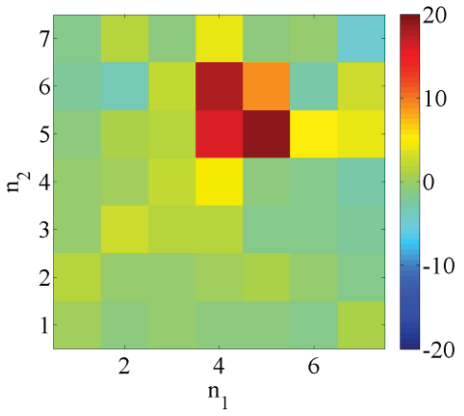

(a) $n_3 = 1$.

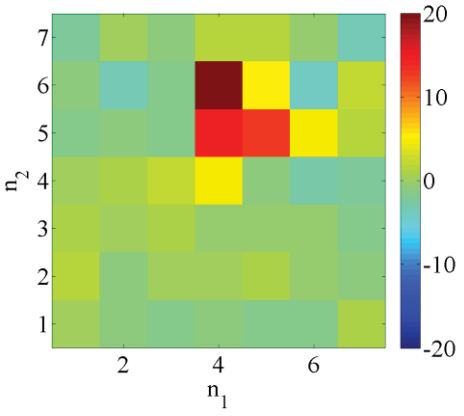

(b) $n_3 = 2$.

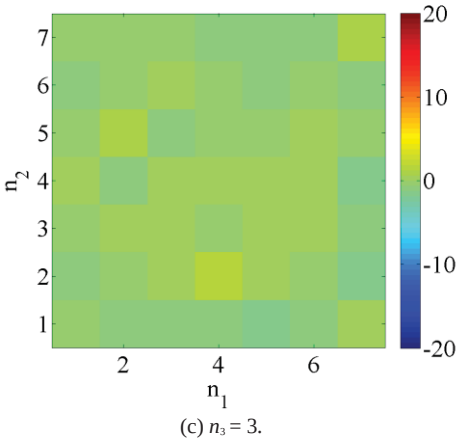

(c) $n_3 = 3$.

Fig. 7: Attenuation map estimated by using 810 paths.

ACKNOWLEDGMENT

This work was supported in parts by the Grant-in-Aid for Scientific Research, Japan Society for the Promotion of Science, No. 25289115 and No. 25330102.

REFERENCES

[1] J. Wilson, N. Patwari, "Radio tomographic imaging with wireless networks" IEEE Transactions on Mobile Computing, vol. 9, no. 5, pp.621632, May 2010.

[2] K. Takemoto, T. Matsuda, S. Hara, K. Takizawa, F. Ono, and R.Miura, "Multi-dimensional wireless tomography with tensor-based compressed sensing,"arXiv:1407.2394,Available:http://arxiv.org/pdf/1407.2394v1.pdf, July 2014

[3] K. Hayashi, M. Nagahara, and T. Tanaka, "A user's guide to compressed sensing for communications systems," IEICE Transactions on Communications, vol. E96-B, no. 3, pp. 685-712, Mar. 2013

[4] S. Gandy, B. Recht, and I. Yamada, "Tensor completion and low-n-rank tensor recovery via convex optimization," Inverse Problems, vol. 27, no. 2, Feb. 2011.

THE 18TH INTERNATIONAL SYMPOSIUM ON WIRELESS PERSONAL MULTIMEDIA COMMUNICATIONS
(WPMC-2015)
December 13-16, 2015, Hyderabad, India

New Pricing Model for Dynamic Dual-operator Spectrum Sharing in GSM

Meghan S. Saitwal, Yuva Kumar S., B. M. Baveja, Mohammed Zafar Ali Khan and U. B. Desai
Department of Electrical Engineering,
Indian Institute of Technology Hyderabad.
E-mail: {ee12m1029, yuva, ee13p0001, zafar, ubdesai}@iith.ac.in

***Abstract*—In this paper, we propose a new pricing model for Dynamic dual-operator spectrum sharing in GSM. Existing GSM pricing models will not work in case of dynamic spectrum sharing (DSS) as there is a possibility of users belonging to one operator getting served by another operator. To solve this problem, we introduce spectrum sharing co-ordinator (SSC); with database attached to it, for storing such type of entries and executing proposed pricing scheme. As GSM is expected to sustain for 15-20 years in India and other developing countries, it is important to consider spectrum sharing for GSM to improve spectrum utilization. Different DSS schemes are discussed for maximizing revenue generation, from the point of view of network operators.**

***Index Terms*—Dynamic spectrum sharing, pricing, GSM.**

I. Introduction

Measurement studies done in several parts of India [1], [2], showed in-efficient utilization of spectrum. This problem of in-efficiency in spectrum utilization can be solved by introducing dynamic spectrum sharing between mobile network operators (MNOs). We have proposed different DSS schemes between two GSM operators to improve spectrum utilization. Now, there is a need for new pricing models which suit these schemes.

Hierarchical bandwidth sharing in dynamic spectrum access networks presented in [3] gives iterative algorithms for price adaptation. The problem of profit maximization for spectrum utilization in presence of both primary and secondary users is illustrated in [4] by using stochastic dynamic programming and in this case an optimal pricing policy. Realistic pricing model for dynamic spectrum access network is given in [5] by considering factors such as reputation of sellers, incentive mechanism to attract buyers and timing requirements. Competitive pricing schemes for spectrum sharing in cognitive radion networks with the help of game theory is presented in [6]–[8].

There are many pricing models for dynamic spectrum sharing [9]–[13], but they deal in selling of spectrum licenses for short duration to secondary services which is done generally by primary service or spectrum broker/ server. Spectrum broker pools unused spectrum from MNOs and sells this spectrum on demand basis. Our proposed scheme does not deal with selling of spectrum licenses, but uses other operator's free resources based on own users requirement.

In proposed system model, spectrum sharing coordinator (SSC) is just a piece of code and not an independent entity which is responsible for carrying out spectrum sharing activities between two GSM operators. While designing pricing model for such case, we need to keep track of one operator's resources which are getting utilized by other operator users. This task is also done by SSC with the use of database where it stores all such entries.

In this paper, we propose new pricing model by considering factors such as call blocking probability, average call holding time and utilization of one operator's spectrum by other. With the focus on the maximization of spectrum utilization, the economical benefit is also equally important from proposed spectrum sharing scheme. From this point of view, we will discuss several DSS schemes.

The rest of the paper is organized as follows. The new system architecture is proposed in Section II. Section III analyses different DSS schemes between two GSM operators and gives their comparison. Section IV explains existing GSM pricing functional model. The new pricing model for DSS between two GSM operators is proposed in Section V. Conclusions and future work is given in Section VI.

II. System Architecture

The system architecture consisting of two GSM operators (OP1 and OP2) with spectrum sharing co-ordinator (SSC) is shown in Fig. 1. We can observe that both the GSM base stations are connected

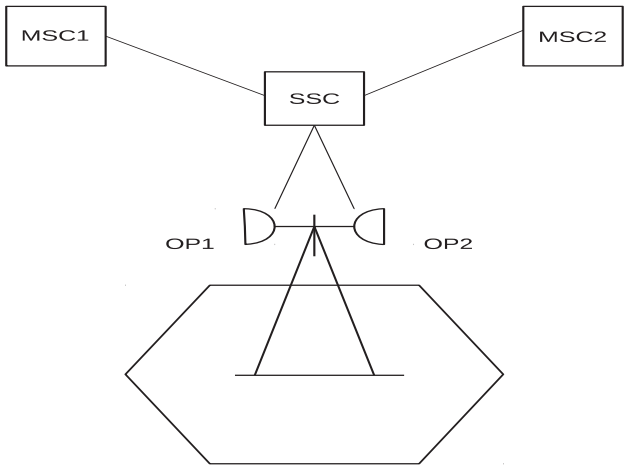

Fig. 1. Two GSM operators with spectrum sharing co-ordinator.

to their corresponding mobile switching centers (MSCs) through common SSC. BS is a combination of base transceiver station (BTS) at tower site and base station controller (BSC) which is remote radio resource management device. The SSC performs all the spectrum sharing activities such as user migration between two GSM networks and carrier allocation.

Assumption of considering both the BS to be co-located is valid, because, in many cases, we observe that location of BSs belonging to different GSM operators are on same tower or building. These BSs will be active on different absolute radio frequency channel numbers (ARFCNs) but with same coverage area. If BSs are not located at same place, then their coverage areas will be different. So, we need to consider this issue in DSS schemes. It will add complexity as well as call setup delay; and will be considered in a future study. The poisson process is used to model call arrival process and exponential distribution for call duration parameter [14].

There are many spectrum sharing approaches are discussed in [15], [16]. However, for dual-operator sharing case considered in this paper, there are mainly two approaches i.e. centralized [17], [18] and distributed [19], [20]. The centralized approach controls spectrum allocation among the operators with help of spectrum server/ broker. But, the transmitter chooses channel from available channels with the transmission power in distributed sharing approach. This paper concentrates on centralized way of sharing between two GSM operators by introducing the logical entity SSC. Many times, it can be observed that the different operators may have coinciding peak hour periods, but different peak loads. So, we can take advantage of instantaneous spectrum opportunities even during coinciding peak hour due to different call arrival rates.

III. Dynamic Spectrum Sharing between two GSM Operators

There are many different ways in which we can do dynamic spectrum sharing between two GSM operators. These ways are mainly classified based on the outcome we are expecting from sharing. Most of the papers consider two parameters such as spectrum utilization and call blocking probability or Quality of Service (QoS).

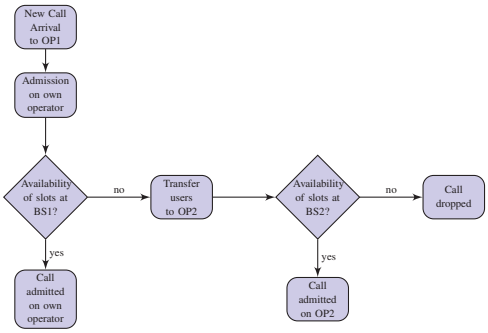

Fig. 2. DSS Scheme I flowchart

We also considered same two parameters while designing the sharing algorithm and describe it in context of DSS scheme I as shown in Fig. 2. But, when it comes to the practical deployment, the operators will be mainly focusing on the economical benefits from this type sharing. So, while designing DSS algorithm, we should consider this parameter. From an economical point of view, we can think of several different spectrum sharing techniques based on the charging schemes. The charging scheme is a vital parameter which affects the spectrum sharing algorithm. We further identify two cases i.e. DSS scheme II and DSS scheme III which are discussed in subsection III-B and subsection III-C respectively.

In these schemes, an operator is allowed to use only the free resources of another operator. An operator using other operator‘s free resources will pay less charges compared to normal call rate. To gain more economical benefit, operator will target to serve own customers preferentially as compared to other operators users. Keeping this in mind, there are two ways of spectrum sharing by considering two new parameters; call handover and QoS.

Each BS is allotted with four ARFCNs and used to transmit GSM frames. Each GSM frame of duration 4.615ms is divided into eight slots. So, each ARFCN can support seven to eight users/calls by allotting traffic channel (TCH) slots. So, each BS at any time can allow thirty one active calls.

A. DSS Scheme I

The flowchart in Fig. 2 explains DSS Scheme I between two GSM operators. This is the simplest scheme with least complexity without forced handover and call drop. For convenience, new call arrival is considered to OP1 with BS1 in all schemes.

The steps involved in DSS Scheme I are as follows:

Step 1. A new call arrives at one of the two base stations i.e. BS1 which belongs to OP1.

Step 2. OP1 tries to accommodate call by allotting free time slot.

Step 3. If call is admitted on own network, then the procedure stops as shown in flowchart in Fig. 2.

Step 4. Otherwise, user is transferred to OP2 through SSC. The call will be permitted based on the availability of free resources with OP2 at that particular time.

Step 5. If call is not admitted on OP2 also, then the call will be dropped.

B. DSS Scheme II

In this scheme, first, a new call will try to occupy TCH at its own operator. If it fails in doing that, it will check for the availability of free resources at other operator. If other operator is also not having any free TCH, then rather than dropping the call like in DSS Scheme I, it will come back to own operator. Now, it will check occupancy details of own operator. If it is serving other operator users, then one of other operator users will be forced to drop the call. Then, new call will be accommodated on own operator. But, in case, all users with active call are his own, then new call will be dropped.

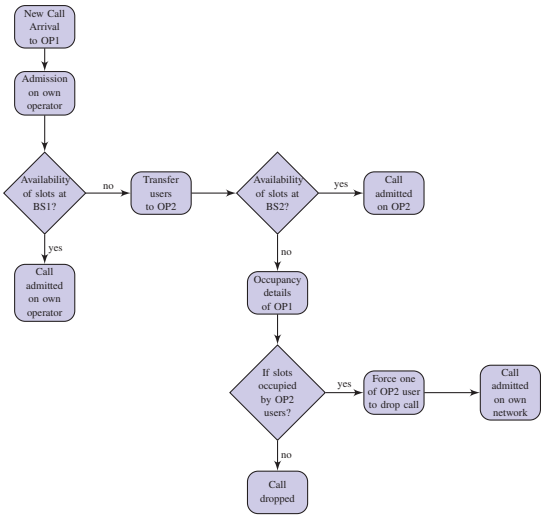

Fig. 3. DSS Scheme II flowchart

The steps involved in DSS Scheme II are as follows:

Step 1. A new call arrives at one of the two base stations i.e. BS1 which belongs to OP1.

Step 2. OP1 check for free slots and try to accommodate the call.

Step 3. If call is successfully admitted on own network/ OP1, then procedure stops as shown in flowchart in Fig. 3.

Step 4. Otherwise, user is transferred to OP2 through SSC. The call will be allowed based on slot availability with OP2 at that time.

Step 5. If OP2 also fails in serving call, then user occupancy details of BS1 (of OP1) will be checked.

Step 6. If some of BS1 resources are used by OP2 users, then one of OP2 users will be forced to drop the call and new call of OP1 user will be admitted on own network/ OP1.

Step 7. If only OP1 users are using resources of BS1, then the new call arrived will be dropped.

C. DSS Scheme III

The flowchart for DSS Scheme III is shown in Fig. 4. Similar to DSS Scheme I and II, new call will be tried to be accommodated on own operator first. If it is unsuccessful in that, then occupancy details of own operator will be checked rather than going to other operator as in previous cases. If other operator's users are not using any of resources, then new call will be transferred to other operator and based on availability of free resources, it will be served or dropped.

If operator of arrived new call is serving other operator users, then instead of simply dropping one of operator users call, handover attempt will be done. One of other operator's user will be forced to handover the ongoing call to his own operator. If handover fails due to un-availability of resources, then the call will be dropped and finally, new call will be admitted.

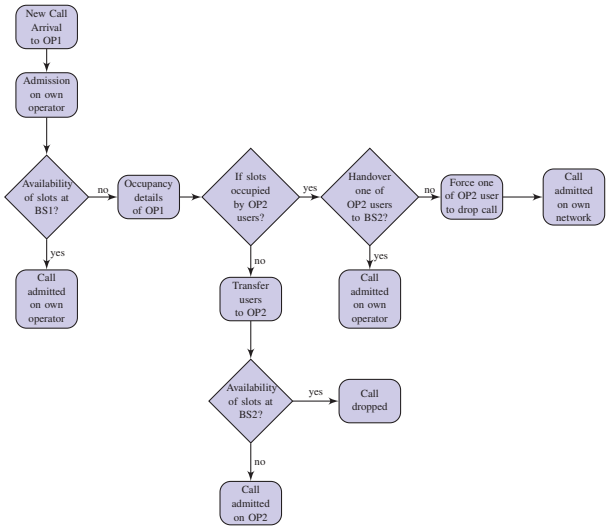

Fig. 4. DSS Scheme III flowchart

The steps involved in DSS Scheme III are as follows:

Step 1. A new call arrives at one of the two base stations i.e. BS1 which belongs to OP1.

Step 2. OP1 tries to serve his own user.

Step 3. If call is admitted on OP1, then the procedure stops as shown in flowchart in Fig. 4.

Step 4. Otherwise, user occupancy details of BS1 will be checked. If OP2 users occupied some resources of BS1, then the following subroutine will be executed.

a. One of OP2 users will opt for handover of call to BS2.

b. If handover is successful, then OP1 user will be admitted on freed resources.

c. In case of failed handover, the ongoing OP2 user call will be dropped and then OP1 user call will be admitted.

Step 5. If only OP1 users are using resources of BS1, then following subroutine is followed.

a. New call arrived at BS1 will be transferred to BS2.

b. If there are free resources with BS2 at that particular time, then call will be admitted on BS2.

c. Otherwise, the call will be dropped.

D. Comparison of the Three DSS Schemes

DSS Scheme I is the simplest sharing technique which involves lower complexity compared to DSS Schemes II and III. Even Scheme I gives exactly same spectrum efficiency gain as other two schemes and call blocking probability is less in this scheme. This is because operator is not giving preference to own customer and not forces other operator user to drop the call. But by doing this, operator looses the economical benefits; in Scheme I. That's why, even if with higher complexity, we consider other two schemes.

DSS Scheme II gives more economical benefit compared to Scheme I but less compared to Scheme III. Because, in Scheme III, new call will not go to other operator even if own operator is busy. Before going to other operator, the occupancy details of own operator will be verified. In terms of QoS, Scheme II outperforms Scheme III, because it does not involve any additional delays due to handovers. The handover considered is not normal handover but it is a forced handover as demonstrated in [21].

IV. Existing GSM Pricing

The existing GSM pricing schemes have been discussed in [22]–[24]. The functional model for GSM pricing can be divided into (mainly) three parts as shown in Fig. 5.

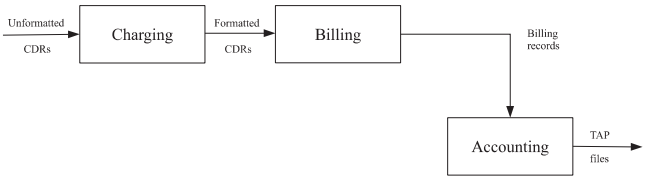

Fig. 5. GSM Pricing Model.

I. Charging

It collects information related to chargeable events which is generally structured into the form of a charging data record (CDR) from several network nodes. CDRs corresponding to all calls made are generated by the MSC's. The GGSN and SGSN produces CDRs based on Internet traffic usage done in GPRS sessions. CDR contains different fields which mainly categorized as mandatory (M) and conditional (C). Mandatory fields should be included always in the CDRs and conditional fields shall be present based on certain conditions. Some fields are operator-specific and again sub-categorized into mandatory, O_M, and conditional, O_C. The information contained in the fields categorized above as follows.

1. Mandatory (M): calling party, called party, call duration, location area code, call reference, radio channel type (full or half rate).

2. Conditional (C) : IMEI of called and calling party, Transparency indicator, Supplementary services, Event time stamps, partial record sequence number, etc.

3. Operator mandatory (O_M) : Speech version, Radio traffic channel requested by mobile, reason for connection release.

4. Operator conditional (O_C) : Roaming number, Change of service, change of radio channel, etc.

The charging functionality is carried out by a mediation system. Mediation systems collect CDRs in different formats from network elements and convert them into a format compatible for billing system. Finally, formatted CDRs will be transferred to billing system using File Transfer Protocol (FTP).

II. Billing

This function processes the CDRs arriving from mediation system based on the tariffs stored in Home Location Register (HLR) which

stores the information related to every customer. A customer can be charged based on the parameters such as local call, international call, night time calls, call per second or minute and many more.

III. Accounting

It is responsible for dividing the charges between home and serving network. The records corresponding to roaming users will be forwarded to its home network operator using transferred account procedure (TAP) in a specific format.

V. New Pricing Model

In this section, we propose a new pricing model which is combination of existing GSM pricing and an additional support for DSS scheme between two GSM operators. The proposed model is only for voice calls not for data. In existing GSM pricing, CDRs generated by MSCs will be collected by a mediation system and then forwarded to corresponding operator's billing system. Similarly, we can observe that three MSCs (MSC1, MSC2 and MSC X) have separate branch containing mediation and billing system as shown in Fig. 6. For the settlement between two GSM operators, a new branch containing series of red blocks is added.

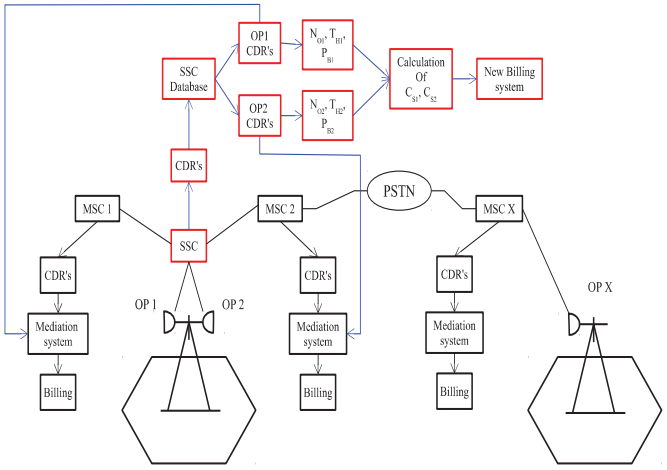

Fig. 6. New GSM Pricing Model.

As calls are getting served randomly by either OP1 or OP2 based on available free resources, we have to charge calls with variable call rates every time. This adds more complexity to pricing model. So, in our proposed model, we considered same call rates will be applied to all calls (from user's point of view) as in existing GSM pricing by operator's billing system. The CDRs for calls using other operator's resources is generated by SSC and will be stored at SSC Database. Periodically, this database separate out CDRs corresponding to different operator and send one copy to respective mediation system. Later, such CDRs will be processed by billing system to charge users accordingly.

The important point to note is that new billing system is used for the settlement between two GSM operators rather than charging users. The proposed billing system will be invisible from normal users and only operators involved in co-ordination will be aware of that. New billing system generates invoices for both GSM operators monthly or at a time interval decided by operators. This invoices shows usage of one operator's resources by another operator's users and how it is charged with variable call rates. The need of variable call rates in the proposed billing system is explained below.

Dynamic nature of DSS Schemes: There may be chances of reduction in QoS in one of the operators even if there is overall increase in spectrum utilization. By considering such a dynamic nature, variable charging scheme with time period T is adopted. The database entries at SSC will be processed with charging scheme. Now, we will define some terms which plays an important role in charging scheme and evaluated every T time period are as follows.

P_{B1}, P_{B2} : The call blocking probabilities for two GSM operators; observed during time period T.

C_{S1}, C_{S2} : The call rates to be applicable to the call entries at the database at SSC during time period T.

T_{H1}, T_{H2} : The average call holding times for each GSM operator during time period T.

N_{O1}, N_{O2} : The number of users corresponding to one operator served by another operator during time period T.

The GSM operator that observes less call blocking probability and uses more resources of other operator has to be charged more compared to other operator. This leads to following relationships.

$$C_{S1} \propto \frac{1}{P_{B1}} \propto T_{H1} \propto N_{O1} \quad (1)$$

$$C_{S1} \propto P_{B2} \propto \frac{1}{T_{H2}} \propto \frac{1}{N_{O2}} \quad (2)$$

Similar relations can be written for the C_{S2}.

Now, we will discuss how CDRs will be generated for different type of calls and how these calls will be charged in perspective of user and operator in detail below.

CASE I : Normal Call

In this case, calls will be getting served by its own operator and there is no need of routing the calls through SSC. The calls belonging to this category will be charged according to existing GSM pricing. That means, CDRs will be generated by corresponding MSCs and then collected by mediation system. After formatting CDRs, mediation system will forward them to billing system of operator. For example, suppose OP2 user initiates the call and called subscriber belongs to OP X and lies under the coverage of MSC X as shown in Fig. 6. The call will be established by finding route through PSTN. In this case, MSC2 will produce CDR which will be collected by the mediation system and finally processed by OP2's billing system. If the called party is in roaming, then it should be charged. This type of CDR will be generated by MSC X and finally will reach to OP X's billing system.

CASE II : Calls through SSC

This is an important case for dynamic spectrum sharing between two GSM operators. The calls falling in this category will be getting served by other operator not his own. The calls from one operator will be using other operator's resources and routed through SSC and then serving operator's MSC to targeted destination. This case arises only when own operator has no free resources to serve own user. In this case, MSC through which call is getting routed cannot generate CDR as it is not authorized to do that. As call is routed through SSC, we propose a new way of generating CDR by SSC, which is different from standard GSM case and is given as follows.

1. The calls which are utilizing the radio resources of other GSM operator will be routed through SSC.

2. The CDRs for such type of calls will be generated by SSC.

3. These CDRs will be stored at SSC database which will be cleared after every time period T.

4. Now, separation of these CDRs will be done based on the operator to which it belongs.

5. The separated CDRs will be sent to corresponding mediation system which further forwards it to operator's billing system. So, users will be charged accordingly.

6. Now, for settlement between GSM operators, parameters such as average call holding time, number of users served and call blocking probability will be obtained from separated CDRs as shown in Fig.6.

7. Based on these parameters and relations defined in (1), (2), calculation of call rates i.e. C_{S1} and C_{S2}, will be done.

8. The call rates decided in step 7 will be applied to corresponding operator's CDRs by new billing system to generate amount that one GSM operator should pay to another.

For example, OP1 user initiates the call to OP X subscriber under the coverage of MSC X. But, OP1 is lacking of resources and OP2 is having free resources. So, the call will be admitted on OP2 resources by routing through SSC. The call connection will be established through SSC-MSC2-PSTN-MSC X path. The CDR for this call will be generated by SSC and processed according to the procedure mentioned above.

CASE III : Calls handover to own operator

In this case, initially users will be using the radio resources of other operator. But as discussed in DSS Scheme III, some times, these progressing calls will be 'handovered' to its own operator. So, call is served partially by other operator and remaining by its own operator. In such situation, two CDRs will be generated. First CDR by SSC for the part of call served by other operator and second by own MSC for remaining part of call served by own operator.

First CDR will go to SSC database and from there, it will be forwarded to new billing system and mediation system of operator. Second CDR will directly go to mediation system and will be combined with first CDR to get complete call entry. Now, operator's billing system can charge that call entry based on total call duration.

For example, OP1 user initiates the call to OP X user. Intially, call gets accommodated on OP2 resources through SSC. After some time, OP2 user request channel to start new call. But, it comes to notice that OP2 is not having any free resources and at this time, OP1 is having free resources. So, as discussed in DSS scheme III, ongoing OP1 user call on OP2 resources will be 'handovered' to OP1 and OP2 user will allowed on its own operator. For the 'handovered' call, one CDR will be generated by SSC and other by MSC1. The user will be charged by combining these two CDRs at mediation system. But, one copy of SSC generated CDR will go to the new billing system.

VI. Conclusions and Future Work

This paper has presented new pricing model for dynamic spectrum sharing between two GSM operators. The proposed pricing model is discussed in detail for three types of calls from a user as well as an operator perspective. The three DSS Schemes between two GSM operators is presented to provide more economical benefit to operators. Future work will try to obtain generalized pricing model for dynamic spectrum sharing between any number of GSM operators.

References

[1] K. Patil, K. Skouby, A. Chandra, and R. Prasad, "Spectrum occupancy statistics in the context of cognitive radio," in *Wireless Personal Multimedia Communications (WPMC), 2011 14th International Symposium on*, Oct 2011, pp. 1–5.

[2] K. Naidu, Y. Kumar, B. Baveja, R. Naik, B. Sridhar, S. Ponnappa, M. Zafar Ali Khan, S. Merchant, and U. Desai, "A study on white and gray spaces in india," in *White Space Communication*, ser. Signals and Communication Technology, A. K. Mishra and D. L. Johnson, Eds. Springer International Publishing, 2015, pp. 49–73.

[3] D. Niyato and E. Hossain, "A microeconomic model for hierarchical bandwidth sharing in dynamic spectrum access networks," *Computers, IEEE Transactions on*, vol. 59, no. 7, pp. 865–877, July 2010.

[4] H. Mutlu, M. Alanyali, and D. Starobinski, "Spot pricing of secondary spectrum usage in wireless cellular networks," in *INFOCOM 2008. The 27th Conference on Computer Communications. IEEE*, April 2008.

[5] M. Hassan, G. Karmakar, and J. Kamruzzaman, "Realistic pricing modeling for dynamic spectrum access network," in *Communications (ICC), IEEE International Conference on*, June 2012, pp. 1838–1842.

[6] D. Niyato and E. Hossain, "Competitive pricing for spectrum sharing in cognitive radio networks: Dynamic game, inefficiency of nash equilibrium, and collusion," *Selected Areas in Communications, IEEE Journal on*, vol. 26, no. 1, pp. 192–202, Jan 2008.

[7] ——, "Market-equilibrium, competitive, and cooperative pricing for spectrum sharing in cognitive radio networks: Analysis and comparison," *Wireless Communications, IEEE Transactions on*, vol. 7, no. 11, pp. 4273–4283, November 2008.

[8] L. Yang, H. Kim, J. Zhang, M. Chiang, and C. W. Tan, "Pricing-based spectrum access control in cognitive radio networks with random access," in *INFOCOM, Proceedings IEEE*, April 2011, pp. 2228–2236.

[9] A. Subramanian and H. Gupta, "Fast spectrum allocation in coordinated dynamic spectrum access based cellular networks," in *New Frontiers in Dynamic Spectrum Access Networks (DySPAN) 2007. 2nd IEEE International Symposium on*, April 2007, pp. 320–330.

[10] P. Ahokangas, M. Matinmikko, S. Yrjola, H. Okkonen, and T. Casey, ""simple rules" for mobile network operators' strategic choices in future cognitive spectrum sharing networks," *Wireless Communications, IEEE*, vol. 20, no. 2, pp. 20–26, April 2013.

[11] M. Szydelko, "Business model analysis for spectrum sharing with the spectrum broker," in *Dynamic Spectrum Access Networks (DYSPAN), 2012 IEEE International Symposium on*, Oct 2012, pp. 378–388.

[12] K. Ryan, E. Aravantinos, and M. M. Buddhikot, "A new pricing model for next generation spectrum access," in *Proceedings of the First International Workshop on Technology and Policy for Accessing Spectrum*, ser. TAPAS '06. New York, NY, USA: ACM, 2006.

[13] O. Ileri, D. Samardzija, and N. Mandayam, "Demand responsive pricing and competitive spectrum allocation via a spectrum server," in *New Frontiers in Dynamic Spectrum Access Networks (DySPAN) 2005. First IEEE International Symposium on*, Nov 2005, pp. 194–202.

[14] J. Guo, F. Liu, and Z. Zhu, "Estimate the call duration distribution parameters in gsm system based on k-l divergence method," in *Wireless Communications, Networking and Mobile Computing (WiCom) 2007. International Conference on*, Sept 2007, pp. 2988–2991.

[15] Q. Zhao and B. Sadler, "A survey of dynamic spectrum access," *Signal Processing Magazine, IEEE*, vol. 24, no. 3, pp. 79–89, May 2007.

[16] J. Peha, "Approaches to spectrum sharing," *Communications Magazine, IEEE*, vol. 43, no. 2, pp. 10–12, Feb 2005.

[17] C. Raman, R. Yates, and N. B. Mandayam, "Scheduling variable rate links via a spectrum server," in *New Frontiers in Dynamic Spectrum Access Networks (DySPAN) 2005. First IEEE International Symposium on*, Nov 2005, pp. 110–118.

[18] O. Ileri, D. Samardzija, and N. Mandayam, "Demand responsive pricing and competitive spectrum allocation via a spectrum server," in *New Frontiers in Dynamic Spectrum Access Networks (DySPAN) 2005. First IEEE International Symposium on*, Nov 2005, pp. 194–202.

[19] R. Etkin, A. Parekh, and D. Tse, "Spectrum sharing for unlicensed bands," *Selected Areas in Communications, IEEE Journal on*, vol. 25, no. 3, pp. 517–528, April 2007.

[20] J. Huang, R. Berry, and M. Honig, "Spectrum sharing with distributed interference compensation," in *New Frontiers in Dynamic Spectrum Access Networks (DySPAN) 2005. First IEEE International Symposium on*, Nov 2005, pp. 88–93.

[21] K. Yuva, M. Saitwal, M. Khan, and U. Desai, "Cognitive gsm openbts," in *Mobile Ad Hoc and Sensor Systems (MASS), 2014 IEEE 11th International Conference on*, Oct 2014, pp. 529–530.

[22] J. Cushnie, D. Hutchison, and H. Oliver, "Evolution of charging and billing models for gsm and future mobile internet services," in *Quality of Future Internet Services*, ser. Lecture Notes in Computer Science, J. Crowcroft, J. Roberts, and M. Smirnov, Eds. Springer Berlin Heidelberg, 2000, vol. 1922, pp. 312–323.

[23] M. Koutsopoulou, A. Kaloxylos, A. Alonistioti, L. Merakos, and K. Kawamura, "Charging, accounting and billing management schemes in mobile telecommunication networks and the internet," *Communications Surveys Tutorials, IEEE*, vol. 6, no. 1, pp. 50–58, First 2004.

[24] "3gpp ts 32.205 version 5.2.0 (2002-12), 3rd generation partnership project; technical specification group services and system aspects; telecommunication management; charging management; 3g charging data description for the circuitswitched (cs) domain (release 5)."

THE 18TH INTERNATIONAL SYMPOSIUM ON WIRELESS PERSONAL MULTIMEDIA COMMUNICATIONS
(WPMC-2015)
December 13-16, 2015, Hyderabad, India

Efficient Device-to-Device (D2D) Offloading Mechanism in LTE Networks

Bighnaraj Panigrahi, Rashmi Ramamohan, Hemant Kumar Rath, Anantha Simha

CTO Networks Lab, Tata Consultancy Services, Bangalore, India,
Email:{bighnaraj.panigrahi, rashmi.ramamohan, hemant.rath, anantha.simha}@tcs.com

***Abstract*—With the increase in mobile traffic and the bandwidth demand, Device-to-Device (D2D) communication underlaying Long Term Evolution (LTE) networks has gained tremendous interest by the researchers, cellular operators and equipment manufacturers. However, the application of D2D communication has been limited to emergency services and it needs to be explored in commercial applications. In this paper, we have introduced a novel commercial D2D offloading scheme for users who may be at cell edges, inside isolated environments like basement or large buildings, etc. Our proposed scheme discovers the available idle D2D neighbors for such poor channel users and offloads its data to the D2D neighbor, which then relays the data to the eNB. We have developed a D2D offloading simulation model in MATLAB, have conducted extensive simulations and have observed that the proposed scheme can provide better efficiency to the network as well as satisfy the poor channel users significantly.**

I. Introduction

There is a huge demand for high data rate services like video sharing, online gaming, proximity-aware-social-networking, etc., in today's cellular network (2G/3G/4G). However, the vulnerability of the cellular networks significantly affects the performance of these services; not only hampers the data communication, but also adds unfairness to network usage of the users. Because of the vulnerability, cell edge users, users inside a lift or basement, etc., do not get a fair Quality of Services (QoS) experience as compared to other users in the network. Studies have been conducted by various researchers in this direction so as to ensure high data rates to poor channel users and to maximally utilize the wireless resources.

Today, Device-to-Device (D2D) communication [1], [2], in which close proximity User Equipments (UEs) can directly communicate among themselves using the cellular resources and bypassing the Evolved NodeB (eNB) is getting focus under Long Term Evolution (LTE) networks. In D2D communication, UEs directly can communicate under the control and assistance of the eNB. This helps in direct transfer of data between two close-by UEs at a higher rate with lower transmission power and delay. D2D can also be applied for many other applications; one such use-case is using D2D communications for opportunistic offload of poor channel users' data. Under opportunistic offload, whenever a poor channel user gets an idle close-proximity neighbor UE with a good channel profile to the eNB, it can offload its data to the neighbor UE using D2D communication and then the neighbor UE can relay the data to the eNB using regular cellular communication. Though this is a two hop communication, it provides higher level of assurance on the data delivery and is spectrally efficient. This kind of offloading can also be used for multi-hop relays in cellular networks, multi-casting [3], peer-to-peer communication, video dissemination, Machine-to-Machine (M2M) communication, and so on. We believe that cellular operators and the mobile users will be greatly benefited by D2D offloading and will show interest to incorporate the changes related to it.

D2D offloading requires network assistance. Therefore, appropriate modifications are required in terms of signaling, scheduling, and synchronization by the eNB. This also requires the knowledge of the location information of the UEs and channel conditions between UE-UE and UE-eNB transmissions. The location information of the UEs can be availed using the control messages and by the possible use of Global Positioning System (GPS) or any other efficient localization techniques. The eNB needs to identify if any neighbor of the poor channel UE is eligible and willing to be the D2D offloader. Once the eNB identifies the D2D offloader, it allocates resources for D2D offloading (UE-UE) and for the cellular relay (UE-eNB) serially so that UE-eNB relaying happens only after the UE-UE offloading.

In this paper, we have introduced a novel D2D offloading scheme and have extended the 3rd Generation Partnership Project (3GPP) proposed method for discovery in Proximity Services (ProSe) [4], [5] using an optimization framework. We have also proposed a 2-phase scheduling scheme to schedule D2D as well as cellular communication. The rest of this paper is organized as follows. In Section II, we provide a brief literature survey on D2D offloading. Section III describes the system model and formulation of the problem. In Section IV, we describe the offloading process, in Section V, we evaluate the performance of our scheme and conclude in Section VI.

II. Related Works

The use of cellular spectrum resources in uplink/downlink for the D2D communication is mentioned in [1], [2]. It is also proposed as a form of relaying [6]. Radio aspects of D2D discovery and communication was submitted by Qualcomm to 3GPP in 2011 [4]. The main focus of 3GPP is to design a LTE-enabled proximity service for the emergency conditions wherein two devices can communicate directly to each other without the intervention of the operator when

the network is non-functioning. Offering D2D services as a commercial service has not gained much attention due to the standardization, billing, regulatory and security related issues. In commercial case, the D2D users have to be guaranteed with better QoS than the traditional technologies such as Bluetooth, Infrared, etc., which are being offered at no cost but with lower speed and compromised security. Data offloading has been considered as one of the key solutions to handle the traffic on the networks by 3GPP.

In [7], the basic concepts of offloading methods in Internet Protocol (IP) networks are discussed. Offloading the cellular traffic to the WiFi networks are studied in [8], [9]. In a similar way, studies have also been carried out in offloading the traffic to small cells or femto cells [10]. The authors in [11] have explored offloading the cellular traffic onto the WiFi Direct links and have analyzed their performance with respect to the LTE networks. Assisted offloading has been presented in [12] where the authors have modeled the dynamic network and demonstrated the offloading process by assuming cellular users in licensed spectrum and the D2D users in the unlicensed spectrum. However, these data offloading schemes are different from D2D offloading as they follow a different network architecture; availability and reliability can not be guaranteed.

In this paper, we have proposed a novel optimal D2D offloading scheduling scheme for users with unfavorable channel conditions to eNB in LTE-based cellular networks.

III. System Model and Problem Formulation

We consider a single cell with one eNB and multiple UEs as shown in Fig. 1. The UEs are assumed to be static (full-fledged mobility of the UEs is out of scope of this paper) so that there will be minimum fluctuations in the channel conditions. The network is assumed to have technologies in place to accommodate the D2D communication with all the necessary synchronization and control mechanisms. We further assume that the following two types of communications are possible: (i) Cellular communication where the UE directly transmits to the eNB and (ii) D2D offloading where UE relays data to the eNB via another close-by UE. Based on the wireless channel condition between the UEs and the eNB, we divide the UEs into two sets: $Type-1$ users - who have a good channel to the eNB and $Type-2$ users - who have a poor channel to the eNB. Note that, while the $Type-1$ users communicate using cellular mode, $Type-2$ users use D2D offloading communication. In a typical scenario as shown in Fig. 1, UE_3 has a poor channel to the eNB, can offload its data to the close-by user UE_4 to be ultimately relayed to the eNB. Once eNB receives the request of the data offload for UE_3, it initiates the D2D offload process along with necessary scheduling and controlling methods. We further assume that the users transmit at fixed rates between the UE to eNB and UE to UE using fixed modulation scheme. However, the same model can be extended to the case of variable data rate and modulation schemes. The transmission power of the UEs can be controlled by the eNB, such that the received Signal to Noise Ratio (SNR) is above a specified threshold (SNR_{th}).

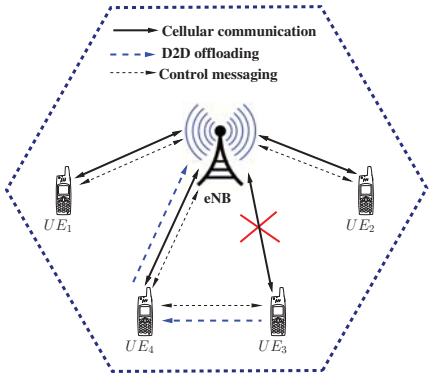

Fig. 1. Single Cell D2D Offloading

A. Frame Structure

We consider standard LTE Time Division Duplex (TDD) frame structure - periodicity: 5 ms, frame length: 10 ms and each frame consists of 10 sub-frames (1 ms each). The sub-frames can either be uplink (U), downlink (D) or special (S). As shown in the Fig. 2, six sub-frames are used for uplink scheduling. We assume that the system bandwidth is 1.4 MHz and consists of six Resource Blocks (RBs); bandwidth of each RB is 180 kHz. Each RB consists of 12 sub carriers. For D2D communications uplink frames are only preferred.

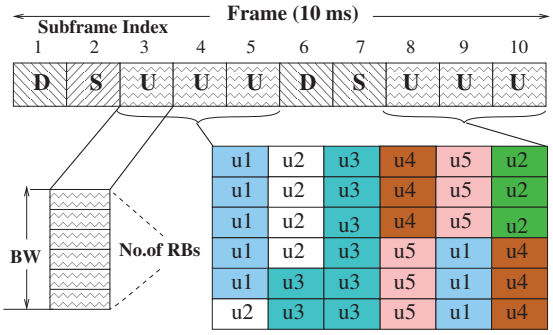

Fig. 2. LTE Uplink TDD Frame Structure

We also assume that the UEs have different amount of uplink data to transmit to the eNB. With fixed modulation scheme and fixed data rate in place, the eNB can compute the number of RBs required by each UE before hand and can schedule the number of RBs in a frame by frame basis. Note that, the performance of the network depends upon the selection of the mode of communication, i.e., using direct cellular or D2D offloading and the selection of the offloader in the possible case when multiple neighbors can act as an offloader for a particular UE. With multiple D2D offloaders available, the eNB has to choose the offloader which ensures optimal throughput as discussed below.

B. Optimal Mode and Offloader Selection

Let m be the number of D2D offloaders available for UE_i. This can be feasible in a real scenario by scanning for D2D

offloaders within a small D2D radius of r_d. Now, UE_i has one direct (cellular) and m offloading paths to choose from. Let $x_{ij}, \forall j \in (1, ..., m, e)$ be a Boolean variable which indicates whether the communication between node i and j is active or not (symbol e indicates eNB). For example, $x_{ie} = 0$ indicates that there is no direct path from node i to eNB and $x_{ij} = 0$ indicates that node j can not be an offloader for UE_i because of unavailability, mobility, etc., of the offloader. Let p_{ij} be the probability of an unsuccessful transmission of an RB between node i and j. Expected number of Hybrid Automatic Repeat reQuest (HARQ) retransmissions required per RB between node i and j can be given as $r_{ij} = \frac{1}{p_{ij}}$. Let k_{ij} be the number of RBs required to transmit the desired data from node i to j (computed by eNB as assumed earlier) and c_{ij} is the cost associated for each RB transmission. Then, the total cost associated with the transmission between node i and j is:

$$C_{ij} = \ k_{ij} \times \ r_{ij} \times \ c_{ij}. \tag{1}$$

In addition to the above, UE_j also needs to relay the data received from UE_i to eNB. The cost associated with this relay can also be calculated as in Eqn. (1). Let the cost associated with this relay be C_{je} and C_{ie} be the cost associated with the direct transmission between UE_i and eNB. Using the above costs for transmission, eNB solves the following optimization problem such that the communication mode (direct or via offloader) and the optimal D2D offloader can be selected.

$$\begin{aligned}
&\min\ (C_{ie} \times x_{ie} + \sum_{j=1}^{m} (C_{ij} + C_{je}) \times x_{ij}), \qquad \text{s.t.} \\
&(i)\ SNR_{ij} \geq SNR_{th} :\ \ \forall j \in (1, .., m), \\
&(ii)\ SNR_{ie}, SNR_{je} \geq SNR_{th} :\ \ \forall j \in (1, .., m), \\
&(iii)\ x_{ie}, x_{ij} = 0/1 :\ \ \forall j, \\
&(iv)\ x_{ie} + \sum_{j=1}^{m} x_{ij} \leq 1 :\ \ \forall j.
\end{aligned} \tag{2}$$

Constraints (i), (ii) of Eqn. (2) ensure the SNR profiles for communications. Constraint (iii) defines the Boolean variables for the possibility of a path, and constraint (iv) ensures that out of $(m+1)$ available paths, eNB selects only one. We now discuss the D2D offloading process as a solution to the above mathematical formulation.

IV. Offloading Process and Channel Model

We now explain the five-phase offloading process and power control mechanism that needs to be used for the successful data transmission.

A. Offloading Phases

1) Offloading Initiation Phase: Offloading initiation can either be made by the eNB or by the UE. In the eNB initiated type, eNB offers D2D offloading option depending on the UE's location and availability of D2D offloader. In UE initiated type, if the UE with a poor channel can send the control messages (usually transmitted at a higher power) to the eNB, then the eNB can make the necessary arrangements for D2D offloading. In case the UE is in a completely isolated environment, it can relay the offloading initiation request through a known close-by UE who has a good channel to the eNB.

2) Offloader Discovery Phase: In this phase, optimal offloader is discovered as a solution to Eqn. (2) which can be either network assisted or ad-hoc type. In network assisted type, the channel condition between the UE (UE_3 in Fig. 1) and the eNB is such that only offloading request can be communicated through control channels. The eNB which is capable of extracting information of the UE, its neighbors' locations (UE_3 and its neighbors in example), their load and channel conditions, etc., can select a suitable offloader (UE_4 for UE_3). In the ad-hoc discovery type, the $Type-2$ UE itself finds a suitable offloader among its nearest neighbors with a request/reply method and then conveys this to the eNB. In this case, the part of the optimization problem Eqn. (2) is solved by the UE itself. Although, network assisted discovery is more power consuming, it is reliable and backward compatible.

3) Handshaking Phase: In this phase, control messages are exchanged between the $Type - 2$ UE and eNB and between eNB and D2D offloader. After the finalization of the D2D offloader, eNB collects the required information like availability, channel condition, etc., and exchanges the synchronization information with the offloader UE. The handshaking mechanism is diagrammatically shown in Fig. 3.

4) Scheduling Phase: For data transmission, UE sends Scheduling Request (SR) signaling in the Physical Uplink Control Channel (PUCCH) to the eNB. The eNB then assigns RBs to the requester and the offloader. We propose a two-phase scheduling scheme; in the first phase, D2D transmission is scheduled and in the second phase the transmission of D2D offloader to the eNB is scheduled. These two phases can take place in same or in different LTE time frames without any time overlapping of a Phase-1 RB with any Phase-2 RB. The scheduling can be overlapping or non-overlapping type [2]; we have assumed non-overlapping type of scheduling in this paper, i.e., both cellular and D2D communication will use non-overlapped RBs for their communication.

5) Communication Phase: This is the actual data communication phase between D2D transmitter and offloader followed by between offloader and eNB. The control flow diagram is illustrated in Fig. 3 and the corresponding algorithm for offloading process is described in Algorithm 1. Note that, it is not necessary for all five phases to be executed serially.

B. Channel Model

The channels between the UE-eNB and UE-UE are assumed to be remain constant for at least one LTE frame duration. We assume that the channel variations follow a combination of log-normal shadowing and multi-path Rayleigh fading in addition to the variations due to distance and other factors. Let Pt_{max} be the maximum transmit power in dBm, d_{ij} be the distance between the UE_i and node j (j: eNB/UE). Received power Pr_{ij} can be expressed in logarithmic form as:

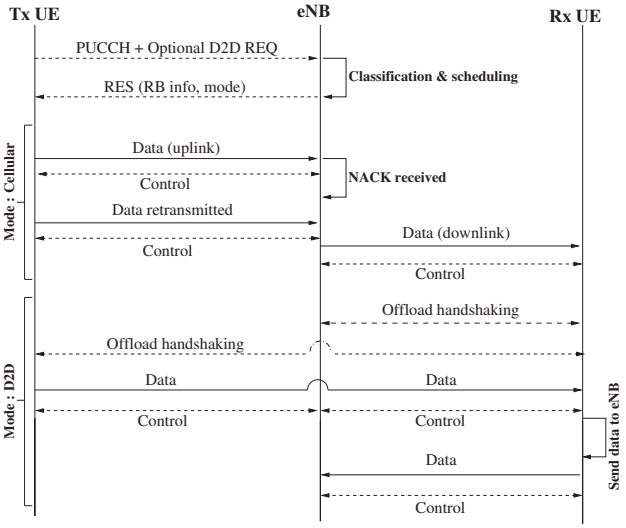

Fig. 3. Control Flow Diagram

Algorithm 1 : D2D Offloading Algorithm

1: eNB receives SR signal from UEs: {location, No. of RBs required, channel condition}
{Offloading Initiation Phase}
2: eNB computes SNR_{ie}
{Offloader Discovery Phase}
3: **if** $SNR_{ie} > SNR_{th}$ **then**
4: UE_i is a $Type-1$ user; Go to Line 8
5: **else**
6: Find the D2D offloader as a solution to Eqn. (2).
7: **end if**
{Handshaking and Scheduling phase}
8: Phase-I: Schedule the $Type-1$ cellular and D2D offload (UE-UE) transmissions
9: Indicate the RBs, transmission power and modulation scheme to be used by the UE
10: Phase-II: Schedule the D2D relay (UE-eNB) transmissions
11: Indicate the RBs, transmission power and modulation scheme to be used by the UE
{Communication Phase}
12: Starting of actual communication

$$\begin{aligned} Pr_{ij} &= Pt_{max} - P_{ij}^{loss}, \\ P_{ij}^{loss} &= \gamma log_{10}(d_{ij} + f) + L_{sh} + L_{rl} + L_a, \end{aligned} \tag{3}$$

where, f is the frequency of operation, and γ is the path loss exponent, L_{sh} and L_{rl} be the losses due to the Log normal shadowing and Rayleigh fading respectively and L_a is the location specific loss where the user is placed. Location specific loss should be factored in the path loss computation as the $Type-2$ user can be placed inside a lift or in the basement or some other place similar to this. We assume that the eNB can compute the path loss parameters and the total loss value P_{ij}^{loss}. If N_o is the Additive White Gaussian Noise power, then instantaneous $SNR_{ij} = \frac{Pr_{ij}}{N_o}$. For successful data transmission, $SNR_{ij} \geq SNR_{th}$.

1) Power Control for D2D Communication: Optimal transmission power required for D2D communication should be computed by the eNB as follows and should be informed to the UE in the handshaking phase. Since, it is difficult to have continuous values for $Pt_{c_{ij}}$, we have defined discrete levels for $Pt_{c_{ij}}$: [-5, 5, 15] mw and select the appropriate level based on the distance and SNR_{th} condition.

$$Pt_{c_{ij}} \geq \quad SNR_{th} \times N_o + P_{ij}^{loss}. \tag{4}$$

V. Experimental Evaluation

We have considered a single eNB with 100 UEs placed at random positions within a radius of 150 m. On an average maximum 50 users are assumed to be ready for transmission and termed as active transmitter UEs. The remaining users are considered to be idle and can be used as potential D2D offloaders. In order to realize a practical scenario, we have assumed on an average 40% of the active transmitter UEs as $Type-2$ users. The received power of each UE is calculated using Eqn. (3). We have considered two different scenarios: (a) cellular only communication and (b) cellular with D2D offloading. We have also implemented a simple Round Robin uplink scheduling scheme. The offloaders are assumed to have sufficient battery power. The other simulation parameters used are mentioned in Table I.

TABLE I
Simulation Parameters

Parameter	Values
Tx Power and Range	23 dBm, 150 m
Path loss component (γ)	3
Shadowing standard deviation(σ)	6 dB
Frequency of operation (f)	2300 MHz
Modulation	16 QAM
Maximum D2D distance	20 m
SNR threshold (SNR_{th})	10 dB

A. Simulation Results

Sufficient simulation runs with different UE populations have been conducted with 100 different seed values to have results with a confidence interval of $\pm 2\%$ of the mean value with a confidence level of 95%. Fig. 4 explains the average RBs utilization with varying number of active transmitters. From this figure, we observe that the average number of RBs consumed in case of D2D mode are much lower as compared to the conventional cellular mode; 40% of RBs can be saved on an average results in significant improvement in spectral efficiency. This is due to the fact that multiple retransmissions have occurred in regular cellular communications as the channel between the UE and the eNB is bad. For the very same reason the average per user delay is also less for the D2D offload case (c.f. Fig.5); improves QoS of the users.

From Fig. 6, we observe that the total energy consumption is higher in case of regular cellular mode as compared to the D2D mode. This is due to the lower transmit power usage of the UEs and higher success rate of the D2D offloading as compared to the regular ones. Energy consumption is computed by considering the maximum transmission power of UE and the transmission time interval (TTI) of an RB. Energy performance also includes the overhead energy consumption in

the D2D offloader discovery, handshaking, and control signal transmissions. System performance shown here in terms of RB utilization, delay and energy consumption only considers the Medium Access Control (MAC) level performance; further improvement is possible when higher layer parameters are taken into consideration.

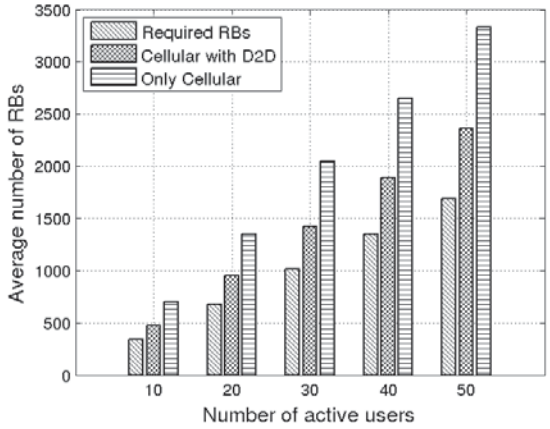

Fig. 4. Average RB utilization vs. Number of active users

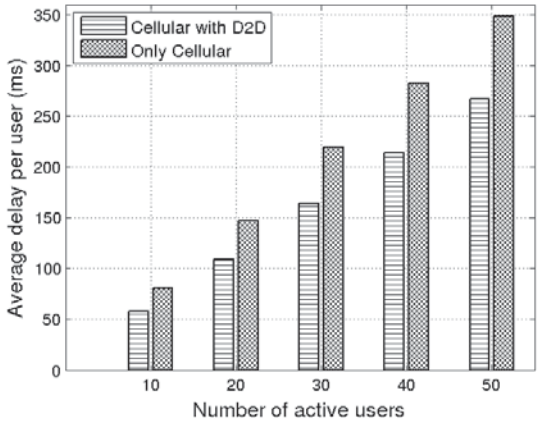

Fig. 5. Average delay per user vs. Number of active users

VI. Conclusion

In this paper, we have proposed a D2D offloading mechanism to benefit the users who are experiencing a poor channel to the eNB. We have discussed an optimization framework which selects an appropriate communication mode for uplink and also the optimal offloader in case of D2D offloading. We have also proposed a 2-phase scheduling algorithm for D2D offloading. The proposed scheme is evaluated through extensive Matlab simulations. Our simulation results exhibit that with D2D offloading technique embedded in cellular network, network performance can be improved significantly.

Implementing D2D offloading in LTE cellular networks requires appropriate signaling techniques. Moreover, the eNB should be able to compute the expected received signal strength at any UE location. Even at device level the UEs should be capable of changing their transmission powers as well as collecting their location informations. These modifications should be incorporated in the future LTE releases and should be standardized under 3GPP such that D2D offloading can be made possible seamlessly. The standardization effort should also encourage operators and vendors to adopt D2D implementation in future.

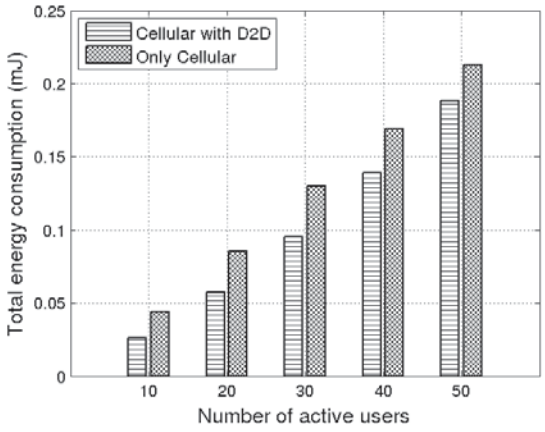

Fig. 6. Total energy consumption vs. Number of active users

References

[1] K. Doppler, M. Rinne, C. Wijting, C. B. Ribeiro, and K. Hugl, "Device-to-device communication as an underlay to LTE-advanced networks," *Communications Magazine, IEEE*, vol. 47, no. 12, pp. 42–49, 2009.

[2] B. Panigrahi, H. K. Rath, and A. Simha, "Interference-aware Discovery and Optimal Uplink Scheduling for D2D Communication in LTE Networks," in *21st National Conference on Communication (NCC), IEEE*, Feb. 2015, pp. 1–6.

[3] J. Seppala, T. Koskela, T. Chen, and S. Hakola, "Network controlled Device-to-Device (D2D) and cluster multicast concept for LTE and LTE-A networks," in *Wireless Communications and Networking Conference (WCNC), IEEE*, March 2011, pp. 986–991.

[4] 3GPP, "3rd Generation Partnership Project; Technical Specification Group SA; Feasibility Study for Proximity Services (ProSe)(Release12)," TR22.803 V1.0.0, Aug. 2012.

[5] X. Lin, J. G. Andrews, A. Ghosh, and R. Ratasuk, "An overview of 3GPP device-to-device proximity services," *Communications Magazine, IEEE*, vol. 52, no. 4, pp. 40–48, 2014.

[6] H. Wu, C. Qiao, S. De, and O. Tonguz, "Integrated cellular and ad hoc relaying systems: iCAR," *Journal on Selected Areas in Communications, IEEE*, vol. 19, no. 10, pp. 2105–2115, 2001.

[7] C. B. Sankaran, "Data Offloading Techniques in 3GPP Rel-10 Networks: A Tutorial ," *Communications Magazine, IEEE*, vol. 50, no. 6, pp. 46–53, 2012.

[8] D. Hinger and D. Kalbande, "Review of Mobile Data Offloading through Wi-Fi," in *International Conference on Circuits, Systems, Communication and Information Technology Applications (CSCITA), IEEE*, April 2014, pp. 425–429.

[9] K. Lee, J. Lee, Y. Yi, I. Rhee, and S. Chong, "Mobile Data Offloading: How Much Can WiFi Deliver?" in *IEEE/ACM Transactions on Networking*, vol. 21, no. 2, 2013, pp. 536–550.

[10] 3GPP, "3rd Generation Partnership Project;Technical Specification Group Services and SA; Local IP Access and Selected IP Traffic Offload (LIPA-SIPTO)(Release 10)," TR23.829 V10.0.1, Aug. 2011.

[11] A. Pyattaev, K. Johnsson, S. Andreev, and Y. Koucheryavy, "3GPP LTE Traffic Offloading onto WiFi Direct," in *Wireless Communications and Networking Conference Workshops (WCNCW), IEEE*, April 2013, pp. 135–140.

[12] S. Andreev, O. Galinina, A. Pyattaev, K. Johnsson, and Y. Koucheryavy, "Analyzing Assisted Offloading of Cellular User Sessions onto D2D Links in Unlicensed Bands," in *Journal on Selected Areas in Communications, IEEE*, vol. 33, no. 1, 2015, pp. 67–80.

THE 18TH INTERNATIONAL SYMPOSIUM ON WIRELESS PERSONAL MULTIMEDIA COMMUNICATIONS
(WPMC-2015)
December 13-16, 2015, Hyderabad, India

Fuzzy Logic Based Human Detection in Video

Mr. Manojkumar M. Gawali
Dept. of Computer Engineering
Sinhgad College of Engineering
Pune, India-411041
gawalimanojkumar1@gmail.com

Prof. Dipti R. Pawar
Dept. of Computer Engineering
Sinhgad College of Engineering
Pune, India-411041
dvshitole.scoe@sinhgad.edu

***Abstract*—Human detection is one of the important and fundamental steps in advanced applications like human activity analysis, gait recognition, human centric surveillance, intelligent video surveillance system, etc. Inaccurate detection of human in all these application leads to false alarms. The proposed method consists of four steps namely; moving object detection, blob detection, feature extraction and classification. Moving object detection is done by performing background subtraction technique which uses fuzzy logic approach. After performing background subtraction blobs are identified. Then blob feature extraction is done by using simple and efficient features like height, width, number of black and white pixels. These features are trained using Support Vector Machine (SVM). The Support Vector Machine is capable to learn all features of blob, and it is used for human or non-human classification. The system is tested on INRIA and PETS 2000 standard data-set.**

Index Terms*—Object Detection; Blob Detection; Feature Extraction; SVM classification

I. Introduction

Over the recent years, detecting human beings accurately from video scene of a surveillance system is attracting field due to its wide range of applications in event detection, human gait characterization, person identification, gender classification, etc. Video surveillance system having two sub-problems, one is moving objects detection and another one is determining whether moving object is human or not.

For moving object detection there are three basic approaches used: Background subtraction, Temporal differencing, and Optical flow. Background subtraction is one of the most popular approach for moving object detection. This method consists in finding the difference of current frames with respect to a background frame in order to detect pixels whose difference is greater than threshold value [1]. A popular mixture of gaussian technique for background subtraction approach consists in modeling each pixel with a Gaussian distribution [2]. The adaptive version of this algorithm works well when the background is dynamic. Temporal differencing approach for moving object detection simply takes difference between previous and next frame, if this difference is greater than threshold value, then moving object is detected [3]. Optical flow is another approach for moving object detection. This approach calculate motion of field, and flow distribution characteristics of image using different methods to estimate optical flow. Optical flow approach is sensitive against noise, and it is highly complex [4]. Lijun, Xiao proposed an approach for moving object segmentation using fuzzy logic algorithm [5]. Basically the fuzzy logic algorithm used for thresholding as well as background updation part. Object segmentation is done using background subtraction which uses fuzzy approach, that is responsible for improving segmentation accuracy and reducing under-segmentation problem. In [6] Gambhir, D and Manchando presented an algorithm that automatically segment moving object in video by creating multiplicative mask, and it contains less number of noisy, false pixels. The segmented object tracked via color features, and then position of moving object predicted using kalman filter. In [7] Kalyan Kumar, and Pankaj Kumar has presented an approach for moving object detection using simple thresholding technique for background subtraction. This scheme depends on two basic algorithms; the first algorithm models background depends on first few frames, and second algorithm extract moving object based on simple thresholding. The strength of this simple thresholding technique is lies in its simplicity, and intensity range for each pixel location define in background.

There are different methods to detect human beings from video. Template based human detection method is based on predefined template dataset defined by users. In [8] Zhujie and Yu has presented face recognition method based on eigen face technique. This face recognition method works in two part. The first part is responsible for constructing eigen faces of training images, and second part include test images that is recognized by computing the euclidean distance. In [9] Ali, Syed Sohaib and Zafar has presented method for human detection and recognition. This approach uses very effective features such as area, perimeter, centroid, principal axis of inertia for classification part. In [10] Osuna, Edgar, and Federico Girosi has presented an application for face detection using support vector machine, that is responsible for determining appropriate class, either human or non-human. Kong, Yinghui, and Lei wang [11] proposed a method for moving object classification based on feature combination and Support Vector Machine. The method for moving object classification includes various steps such as object detection, post processing, feature extraction and SVM classification. Mahapatra, Tusar Kanti Mishra [12] proposed scale and view invariant approach for human detection based on template dataset. Scale and view invariant contour features like distance, angle, and cord to arc ratio are effective for template based human detection from video. The proposed human detection approach is simple and very efficient one, because we directly worked on color video, so there will be less chances of data loss. The fuzzy algorithm for background subtraction proves it's importance compare to simple background subtraction technique, and accurately detect moving object. At last SVM classifier is classifying object class, thus the combination of fuzzy approach for background subtraction and Support Vector Machine for classification proves the effectiveness of proposed method. The human detection method requires following four steps; (a) Moving Object Detection, (b) Blob Detection, (c) Feature Extraction, (d) SVM Classification. Rest of the paper is presented as follows. Section II is the discussion about system architecture and its implementation details. Section III introduces comparative analysis and discussion. Section IV is all about

experimental evaluation part. Section V is all about conclusion and future scope of the work. Fig. 1 shows flow for proposed human detection system.

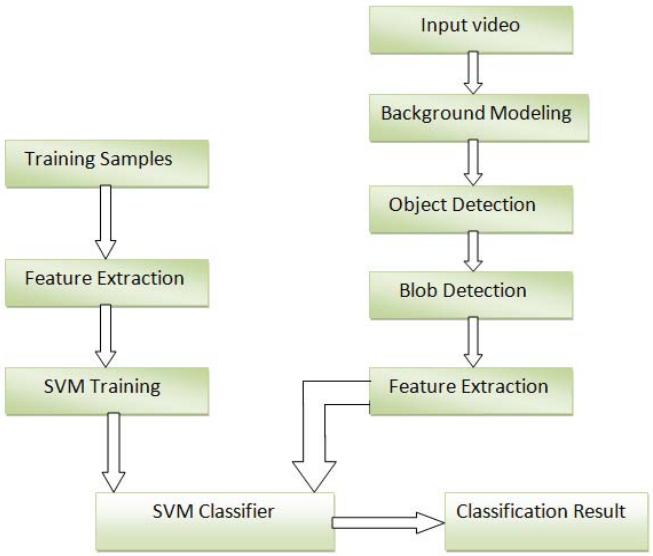

Fig. 1. Human Detection System

II. System Architecture

For human detection, the first essential step is to detect moving object from video, and then classifies it to human or non human.

A. Frame Extraction

The frame extraction module takes video as input and produces number of frames based on time delay between frames. The number of maximum frames depends on length of video and time delay between frames. Mathematically, this is shown in eq (1).

$$X_n: n>1 \ \& \ n = \text{Video length} / T_d, \ \& \ T_d > 1 \qquad (1)$$

Where,

- X_n is the n^{th} frame.
- n is the number of frames required.
- T_d represents time delay between frames.

TABLE I
Frame Extraction

Video Set	Size(MB)	Length (sec)	fps	Time delay(msec)	Number of frames
1	6.23	58	19.40	50	1161
2	6.23	58	25.0344	40	1452
3	6.23	58	33.3793	30	1936
4	6.23	58	1	1000	58
5	6.23	58	2	500	116

Table I shows number of extracted frames that mainly depends on video length and delay factor (T_d).

B. Background subtraction

Background subtraction is the process of separating out foreground objects from maintained background model. The proposed background subtraction method uses fuzzy logic approach for calculating background frames. A foreground object is an entity that is separated based on minimum and maximum frame, these two frames are calculated using fuzzy approach. For background model creation, consider first N numbers of frames are background frames, where all these background frames doesn't contain foreground objects. Apply fuzzy logic on these background frames. Let $\{F_1, F_2, ..., F_N\}$ be the fuzzified background frames, which are used for background modeling part. After getting fuzzified background frames, calculate minimum and maximum background modeling frames. When new frame comes with foreground object each pixel of frame is applied to fuzzy inference system, if pixel value is in between minimum and maximum then consider background pixel, otherwise foreground pixel. Mathematically foreground or background separation is shown below in eq (2).

$$a(i, j) - \alpha < i < b(i, j) + \alpha \qquad (2)$$

where, α is very useful parameter in variety of illumination conditions, and it's value is constant, a (i, j) is the minimum frame, while b (i, j) is maximum frame, and i is the fuzzified pixel value of current frame. The value of minimum frame a (i, j) and maximum frame b (i, j) is calculated from first N fuzzified background frames. The proposed fuzzy background subtraction approach directly works on color video, so that is the main reason, this background subtraction approach is efficient one. Using this proposed background subtraction method, there is no need for post processing of frames. Each pixel having three different values (i.e. for red, green, and blue) are given to fuzzy inference system for calculating fuzzified pixel value as shown in Fig. 2. A fuzzy inference system consists of four main parts: fuzzification, rule base, inference engine, and defuzzification.

C. Fuzzy Algorithm for Background subtraction

The basic steps required for fuzzy logic algorithm are shown in below:

1) Define the linguistic terms and variable, that comes under initialization part.
2) Then construct the membership functions, that comes under initialization part.
3) Then construct the fuzzy rules, that comes under initialization part.
4) First step is convert the crisp input data to fuzzy values using defined membership functions, that is the part of fuzzification.
5) Second step is to evaluate the rules in the rule base.
6) Third step is to combine the results of each rule, that is the part of inference engine.
7) Last step is convert the output data to non-fuzzy values, that is the part of defuzzification.

Fig. 3 shows fuzzy rules, and the abbreviation for these rules are L-Low, M-Medium, H-High, VL-Very Low, VH-Very High. There are various types of membership function such as Triangular, Trapezoidal, S, Gaussian etc. [13]. Fig. 4 shows Triangular membership function for red color. This membership function having three linguistic term Low, Medium, and High. After fuzzifying inputs, fuzzy rules in the form of (if.... then) are applied for calculating final crisp value. The proposed fuzzy background subtraction method is compared with simple thresholding technique [7]. Fig. 5 shows the result of simple background subtraction technique using thresholding method, this approach

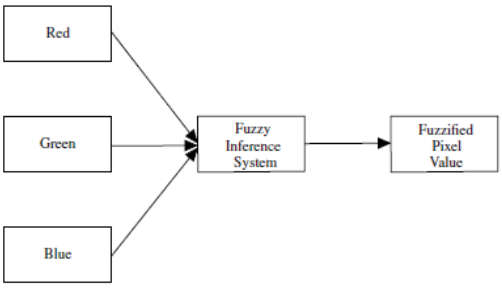

Fig. 2. Fuzzified pixel value calculation

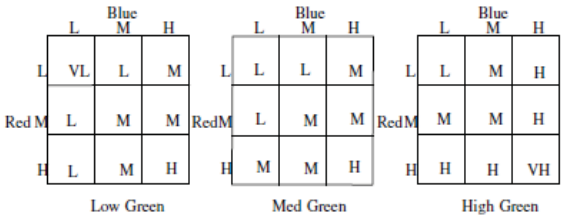

Fig. 3. Fuzzy Rules

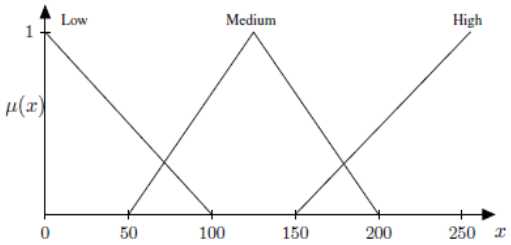

Fig. 4. Membership function for red color

(a) (b) (c)

Fig. 5. Result of Simple background subtraction technique using thresholding method. [7]

(a) (b) (c)

Fig. 6. Result of proposed fuzzy logic based background subtraction technique (without any post processing (a) with α = 5, (b) with α = 10 and (c) with α = 20).

does not give proper output as shown in Fig. 5, while Fig. 6 shows proposed fuzzy logic based background subtraction approach.

D. Blob Detection

After completion of background subtraction method, object is detected. Once moving object gets detected, then capture the blob of respective moving object as shown in Fig. 7. Blob is defined as a collection of bunch of pixels within region. Whereas blob

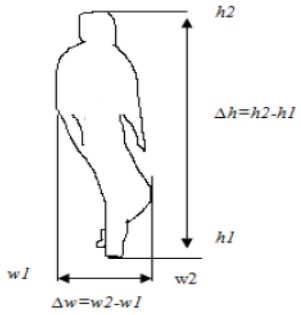

Fig. 7. Identified Blob

is analysed based on the identification of connected pixel regions from the image. The blob detection algorithm distinguishes pixels by their value and mark them in two categories: white blob (foreground) or black blob (background).

E. Feature Extraction

Feature extraction holds an important stepping stone to pattern recognition and machine learning problems. To recognize and classify an object in an image, first extract useful features out of the image. Feature extraction is necessary step for extracting image attribute, to identify or interpret meaningful object from image. Four important features like height, width, number of black and white pixels are extracted from blobs of human and car. These four features are converted into two features i.e. aspect ratio of height to width, and aspect ratio of number of black to number of white pixels.

1) Width: This feature is calculated having difference of Leftmost pixel and Rightmost pixel. Mathematically, this is shown in eq (3).

$$\Delta w = w2 - w1 \quad (3)$$

2) Height: This feature is calculated having difference of Topmost pixel and Bottommost pixel. Mathematically, this is shown in eq (4).

$$\Delta h = h2 - h1 \quad (4)$$

3) Aspect Ratio (W/H): It is the ratio of width to height. Mathematically, this is shown in eq (5).

$$\Delta w/\Delta h \quad (5)$$

4) Aspect Ratio (B/W): It is the ratio of number of black pixel to number of white pixel.

F. SVM Classification

In recent years, SVM classifier is very effective for solving classification and regression problems [14]. The features of human and non-human blobs are given to support vector machine training part. Support vector machine is capable to learn all those features. In training part these features are divided into two classes using SVM linear kernel function i.e positive and negative class.

In proposed method of human detection, SVM is based on a linear classifier in a high dimensional feature space, which has allowed the development of somewhat fast training techniques, even with a large number of input variables and training datasets. In proposed method support vector machine classifies the objects either as a human or non-human.

III. Comparative Study and Discussion

In the recent, there were several systems have been developed for human detection from videos. That are almost similar approaches, the proposed algorithm performed better in terms of detection accuracy rate. Lipton et.al. [14] used a simple multi-feature classification approach with features like dispersedness, area and detection rate of 82.8%. Kong, Lei Wang [15] had obtained 80% detection rate of human and car. Table II shows comparative analysis with existing system. See, J., Lee [16] had obtained 93.75 % detection rate of human motion. On other hand, we introduced a novel and efficient approach for moving object detection using fuzzy logic algorithm, and support vector machine classifier gives 95.29 % classification rate of human and non human.

TABLE II
Comparison of Classification Accuracy With Existing System

Sr.No	Algorithm	Detection Accuracy
1	Moving Target Classification and Tracking From Real Time Video [14]	82.80 %
2	Moving Target Classification in Video Sequences based on Feature combination and SVM [15]	80%
3	Human Motion Detection Using Fuzzy Rule base Classification of Moving Blob Regions [16]	93.75%
4	Proposed Method	95.29 %

IV. Experimental Evaluation

The proposed system uses standard dataset INRIA and PETS 2000. The dataset comprises .avi or .mp4 videos having resolution (320×240), duration 1-58 seconds, and with 2-24 frames per second. The SVM classifier was trained using 800 blobs. Among these, 500 were positive samples indicating human blobs and rest 300 were negative samples indicating car blobs for training. Table III shows classification rate of moving object. The dataset has used in this experiment is tested over 9 different videos that contain 2 objects (i.e human and car). Among these first six videos i.e (Video 1 to Video 6) contain only human and remaining three videos contain only car object class. For Video 1, first 40 frames have considered, and found total number of 48 blobs, out of that 44 blobs are correctly classified as a human. For Video 2, first 52 frames have considered, and found total number of 77 blobs, out of that 72 blobs are correctly classified as a human. For Video 3, first 42 frames have considered, and found total number of 58 blobs, out of that 55 blobs are correctly classified as a human. For Video 4, first 40 frames have considered, and found total number of 62 blobs, out of that 59 blobs are classified as a human. For Video 5, first 45 frames have considered, and found total number of 64 blobs, out of that 60 blobs are correctly classified as a human. For Video 6, first 55 frames have considered, and found total number of 80 blobs, out of that 74 blobs are correctly classified as a human. For Video 7, first 30 frames have considered, and found total number of 38 blobs, out of that all 38 blobs are correctly classified as a car. For Video 8, first 50 frames have considered, and found total number of 80 blobs, out of that 77 blobs are correctly classified as a car. For Video 9, first 40 frames have considered, and found total number of 60 blobs, out of that all 60 blobs are correctly classified as a car.

TABLE III
Classification Rate of Different Moving Objects

Sr.No	Test Video	Total number of blobs	Correctly classified blobs	Accuracy
1	Video 1	48	44	91.66 %
2	Video 2	77	72	93.50 %
3	Video 3	58	55	94.82 %
4	Video 4	62	59	95.16 %
5	Video 5	64	60	93.75 %
6	Video 6	80	74	92.50 %
7	Video 7	38	38	100 %
8	Video 8	80	77	96.25 %
9	Video 9	60	60	100 %

A. Sample output

In output part video contains human. The red line depicts detected human blob, that gives result human. Fig. 8 gives classification result of human.

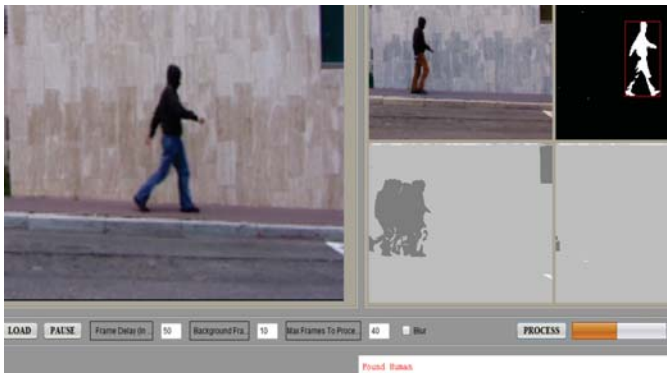

Fig. 8. Classification result of human video

Fig. 9 gives classification result of car. The red line depicts detected car blob below, that gives result car.

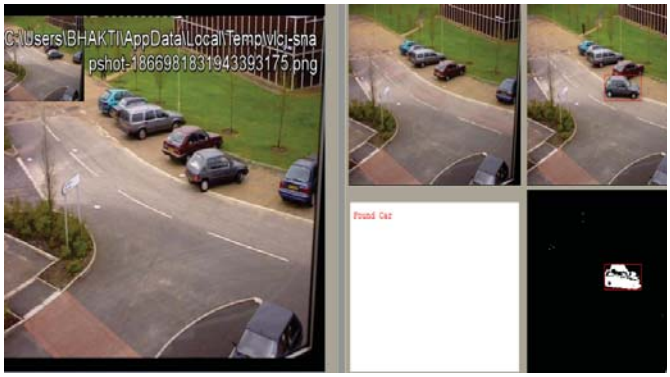

Fig. 9. Classification result of car video

V. Conclusion and Future Work

A method for human detection in video sequences is based on mainly two aspects: Fuzzy approach for moving object detection, and Support Vector Machine is used for moving object classification. In this paper, a novel and efficient approach for background subtraction using fuzzy logic has presented. Features are extracted after detecting the blobs. These features are given as input to Support Vector Machine (SVM) to classify the object, whether it is human or non-human. SVM is used as a binary classifier, means it is used for human and non-human classification. The proposed human detection method doesn't work more accurately on manual dataset (Not-Standard dataset). The proposed method will not work if there will be occlusion, and moving camera dataset i.e (works only on Non-Moving camera dataset or steady dataset). The proposed human detection system have many aspects that can be improved in future. This system will further used for object tracking and recognition purposes. The background subtraction approach for moving object detection can be extend to various image conditions (lighting or long-term scene changes), and moving camera dataset. The detected moving objects had classified for only two classes, in future this could be extended to multiple classes.

References

[1] Seki, M., Fujiwara, H., & Sumi, K. (2000).“A robust background subtraction method for changing background.” *In Applications of Computer Vision, 2000, Fifth IEEE Workshop on. (pp*. 207-213). IEEE.

[2] Stauffer, Chris, and W. Eric L. Grimson. “Adaptive background mixture models for real-time tracking.” *Computer Vision and Pattern Recognition, 1999. IEEE Computer Society Conference on*. Vol. 2. IEEE, 1999.

[3] S. Fejes, L.S. Davis, “Detection of independent motion using directional motion estimation,” *Technical Report, CAR-TR-866, CS-TR 3815, University of Maryland*, August 1997.

[4] Kinoshita, K., Enokidani, M., Izumida, M., & Murakami, K. (2006, December). “Tracking of a moving object using one-dimensional optical flow with a rotating observer.” *In Control, Automation, Robotics and Vision, 2006. ICARCV'06. 9th International Conference on* (pp. 1-6). IEEE.

[5] Lijun, X. (2011, August). “Moving object segmentation based on background subtraction and fuzzy inference.” *In Mechatronic Science, Electric Engineering and Computer (MEC), 2011 International Conference on (pp. 434-437).* IEEE.

[6] Gambhir, D., & Manchanda, M. (2014, February). Adaptive threshold based segmentation for video object tracking. In Advance Computing Conference (IACC), 2014 IEEE International (pp. 1127-1132). IEEE.

[7] Hati, Kalyan Kumar, Pankaj Kumar Sa, and Banshidhar Majhi. “Intensity range based background subtraction for effective object detection.” *Signal Processing Letters, IEEE* 20.8 (2013): 759-762.

[8] Turk, Matthew A., and Alex P. Pentland. “Face recognition using eigenfaces.” *In Computer Vision and Pattern Recognition, 1991. Proceedings CVPR'91., IEEE Computer Society Conference on*, pp. 586-591. IEEE, 1991.

[9] Ali, Syed Sohaib, M. F. Zafar, and Moeen Tayyab. “Detection and Recognition of Human in Videos Using Adaptive Method and Neural Net.” *In Soft Computing and Pattern Recognition, 2009. SOCPAR'09. International Conference of*, pp. 604-609. IEEE, 2009.

[10] Osuna, Edgar, Robert Freund, and Federico Girosi. “Training support vector machines: an application to face detection.” *In Computer Vision and Pattern Recognition, 1997. Proceedings., 1997 IEEE Computer Society Conference on*, pp. 130-136. IEEE, 1997.

[11] Soumya Varma, Sreeraj M. “Object detection and classification in Surveillance System.” *In recent advances in Intelligent computational system*, 2013 IEEE conference.

[12] Mahapatra, Ansuman, Tusar Kanti Mishra, Pankaj K. Sa, and Banshidhar Majhi. “Background subtraction and human detection in outdoor videos using fuzzy logic.” *In Fuzzy Systems (FUZZ), 2013 IEEE International Conference on*, pp. 1-7. IEEE, 2013.

[13] J.Jang and M. C-T, “Neuro-Fuzzy and Soft Computing ” . *Prentice-Hall*, 1997.

[14] Lipton, A. J., Fujiyoshi, H., & Patil, R. S. (1998, October). “Moving target classification and tracking from real-time video.” *In Applications of Computer Vision, 1998. WACV98. Proceedings., Fourth IEEE Workshop on (pp*. 8-14). IEEE.

[15] Kong, Yinghui, and Lei Wang. “Moving Target Classification in Video Sequences Based on Features Combination and SVM.” *In Computational Intelligence and Software Engineering (CiSE), 2010 International Conference on, pp.* 1-4. IEEE, 2010.

[16] See, J., Lee, S., & Hanmandlu, M. (2005). “Human motion detection using fuzzy rule-base classification of moving blob regions.” *In Proc. Int. Conf. on Robotics, Vision, Information and Signal Processing (Vol. 2005, pp*. 398-402).

THE 18TH INTERNATIONAL SYMPOSIUM ON WIRELESS PERSONAL MULTIMEDIA COMMUNICATIONS
(WPMC-2015)
December 13-16, 2015, Hyderabad, India

Hierarchical Mesh Based Energy Efficient Multicast Routing on IEEE 802.15.4 based networks

Verotiana H. Rabarijaona and Fumihide Kojima
National Institute of Information and Communications Technology
Yokosuka, Japan
rverotiana@nict.go.jp, f-kojima@nict.go.jp

Hiroshi Harada
Kyoto University
Kyoto, Japan
hiroshi.harada@i.kyoto-u.ac.jp

***Abstract*—This paper proposes a hierarchical mesh topology based multicast routing reducing energy consumption for transmission and reception. The protocol enables low complexity multicast route establishment and multicast routing and is aimed to be used in IEEE 802.15.4 based networks for various applications such as intelligent transportation systems, smart city or smart utility networks, etc. The proposal allows an implementer to fine tune the routing based on a link metric threshold to find the best tradeoff between robustness and the amount of traffic. Multicast routing can be achieved in non-promiscuous or promiscuous mode. The simulation results show that the proposed protocol significantly reduces the number of devices involved in the multicast routing to a multicast group, thus reducing the overall average energy consumption of the network while achieving high transmission delivery.**

I. Introduction

Recent technological trends have seen the demand for large scale networks as we seek to create a smart or intelligent version of everything. An increasing number of municipalities, companies, utilities, etc. seek to implement applications such as intelligent transportation systems (ITS), smart utility networks (SUN), smart city, factory and building automation networks, to name a few. These networks will comprise a large number of devices ranging from tens to thousands. Due to the limited coverage area of a device, data transmission may require multiple hops between a source and a destination. The devices may be subject to constraints such as limited transmission power or limited power supply. The IEEE 802.15.4 standard [5] has become the leading standard to deploy these networks. The standard provides a cluster tree topology rooted at the PAN coordinator, yielding increased coverage area of the network. Data frames can be transmitted up and down the cluster tree, however this does not always lead to optimized paths.

In applications such as ITS, smart city, SUN, an implementer may require communication with a set of nodes at once based on their location (block, street...), their function (lights, gas meter, motion sensor...), or other criteria. Since the information to be sent is the same for these devices, multicast groups are created and multicast routing in needed. The IEEE 802.15.4 standard provides specifications for the physical and MAC layer but does not address multicast group management or multicast routing. Multicast group management (join, leave...) has widely been addressed [10]-[13] and is out of the scope of this paper. Multicast groups may also be statically assigned. The multicast group assignments occur in layers above the MAC layer and therefore multicast addresses are unknown to the MAC layer of IEEE 802.15.4. Although routing has been addressed at the network layer[1][6], as far as multicast routing is concerned, multicast groups are managed but when multicast frames are sent through the IEEE 802.15.4 MAC layer, they are either unicast to each multicast group member or flooded through the network[2][6]. This leads to considerable waste of resources such as energy or bandwidth. Z-Cast is a multicast protocol built upon the IEEE 802.15.4/Zigbee stack[3]. However, Z-Cast is based on the cluster tree topology [4] which may create single point of failures (SPF), consequently causing all the descendants of a failing router not to receive a multicast frame. In [7], we proposed a routing protocol based on a hierarchical mesh focused on data collection and we demonstrate that a hierarchical mesh topology avoids these SPFs and enables robust routing. In this paper, we provide a hierarchical mesh topology based multicast routing that avoids the SPFs of a cluster tree as well as alleviates the resource waste from multiple unicast transmissions or broadcast flooding, thus yielding significant energy saving.

The rest of this paper is organized as follows: Section II describes the initialization of the hierarchical mesh topology. Section III details the upstream routing protocol while section IV describes the multicast route establishment and routing. Simulations results are presented in section V, and section VI concludes the paper.

II. Hierarchical Mesh (HM) Initialization

The network is organized into a hierarchical mesh (HM) rooted at a device called the HM root. The hierarchy is determined by the depth of a device representing the distance in hops to the HM root which has a depth 0. For a device T, the following definitions are used:

- *Neighbor*: a device within the coverage area of T.
- *Parent*: a neighbor one depth less than T.
- *Brother*: a neighbor of the same depth as T.
- *Child*: a neighbor one depth higher than T.
- *Next hop*: a neighbor to which a frame is forwarded on the way to the final destination

Each device holds a NT recording the address of its neighbors, their respective depth, and one metric used to select a next

[0]This work has been conducted as part of the development of the IEEE P802.15.10 recommended practice for routing packets in IEEE 802.15.4 dynamically changing wireless networks

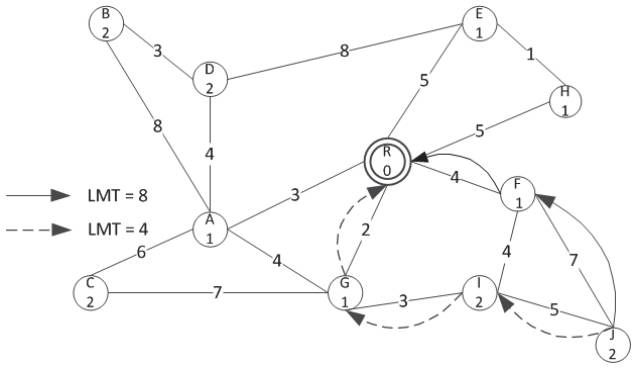

Fig. 1. Example of a HM with US routing from J to R

hop (e.g.: successful transmission ratio, error ratio, latency, etc.) The HM is constructed through the propagation of Hello frames initiated by the HM root. The HM root may fulfill different purposes such as being a center for data collection, controlling and monitoring the devices in the HM..., depending on the needs of the implementer. The Hello frame contains the address of the transmitting device and its depth. A metric field may be present if needed (some metrics such as the received power or SINR might just be measured or calculated and do not need to be exchanged[7]. The optimization of the metric selection is out of the scope of this paper. When a HM root wants to start a HM, it broadcasts a Hello frame with a depth 0. When a device receives a Hello frame for the first time, it retrieves the depth n therein and sets its depth to $n + 1$. It also records the metric information in its NT, the neighbor becomes its parent and the device starts transmitting its own Hello frame. The process continues until every device in the network has a depth. The Hello frames are transmitted after each depth update and then periodically in order to maintain the topology. A neighbor may be deleted from the NT if it has not been heard from for a prolonged period of time. Fig. 1 illustrates an example of HM where the number below each letter represents the depth of the device and the number on each link represents the metric between the devices sharing the link.

III. Upstream (US) routing

When a device wants to transmit a data frame to the HM root, it looks into its NT and finds the parent with the best metric. A link metric threshold (LMT) can be set to allow routing through the siblings while giving priority to parents to minimize the number of hops. If the LMT is set, the metric of the link shared with a parent must satisfy this threshold in order for the parent to be eligible as a next hop. If the LMT is not satisfied, a device finds the brother with the best metric. If the best brother does not satisfy the LMT, the device with the best metric between the best parent and the best brother is selected as a next hop. In order to avoid loops, a device holds a *next/previous-hop list* with the address of the devices to which it has forwarded or from which it has received or overheard a frame with a given sequence number (SN) and source address (SA). When a device forwards a data frame, it shall select a next hop that is not within the list corresponding to the (SN, SA) tuple. The *next/previous-hop list* for a given (SN, SA) tuple is deleted after a determined time. Next hop selection may be limited to parents if the LMT is not set, in this case loop avoidance is not necessary. In Fig. 1, it is assumed that a low metric value indicates a good link. The figure gives an example of US routing from device J to R. The plain arrows indicate the path when the LMT is set to 8 whereas the dashed arrows indicate the path when the LMT is set to 4. A data frame is sent along the US paths with a set of 4 addresses: the source address (SA), the destination address (DA), the transmitting address (TA) and the next hop address (NHA). In US routing, the SA is set to the address of the source of the frame and the DA, to the address of the HM root. The NHA and the TA are modified at each hop.

Transmitting address	Next hop address	Source address	Destination address	Multicast address

Fig. 2. Multicast Address Announcement frame

IV. Multicast Route Establishment and Routing

In applications such as ITS, smart city, SUN, an implementer may want to communicate with a set of nodes at once based on their location (block, street...) or their function (lights, gas meter, motion sensor...), or other criteria. Multicast groups are created and are assigned a multicast address to allow the transmission of the same information to the member devices. In the aforementioned applications, networks are relatively static and multicast group management can also be manual and fixed. Several multicast groups can be created in the same network. Multicast group management is not addressed by the IEEE 802.15.4 standard defining the MAC and physical layers, and occurs at a higher layer. As a result, the assigned multicast addresses are unknown to the MAC layer. If a device knows the MAC address of each multicast member, a multicast frame may be transmitted as a unicast frame to each member. Otherwise, the frames can be broadcast in the network and filtered by higher layers[6]. In large networks, these approaches can become very costly, especially in terms of energy consumption for transmitting and receiving. In this proposal, a set of 16-bit MAC addresses are reserved for multicast groups. The mapping between the actual multicast address, issued during the subscription procedure or manually assigned, and the 16-bit multicast MAC address is out of the scope of this paper. In the targeted applications, devices are often non mobile and 16-bit multicast addresses could be manually assigned to each members to avoid signaling for multicast group management. If a device is a member of a multicast group, it informs the HM root with a Multicast Address Announcement (MAA) frame formatted as illustrated in Fig. 2. The multicast address in the MAA frame is treated as a regular unicast 16-bit MAC address and is recorded in a route entry with the address retrieved from the *Transmitting address* field as the next hop. If another MAA frame is received announcing a multicast address that already has a route entry, the route entry is replaced only if the metric of the link shared with the transmitting device is better than that of the route entry recorded. Thus, no special multicast routing table is needed. The MAA frames are sent through the US paths according to the US routing described in section III. Multicast route establishment can be achieved in two modes: the **non-promiscuous mode** and the **promiscuous mode**.

- In **non-promiscuous mode**, only the devices receiving

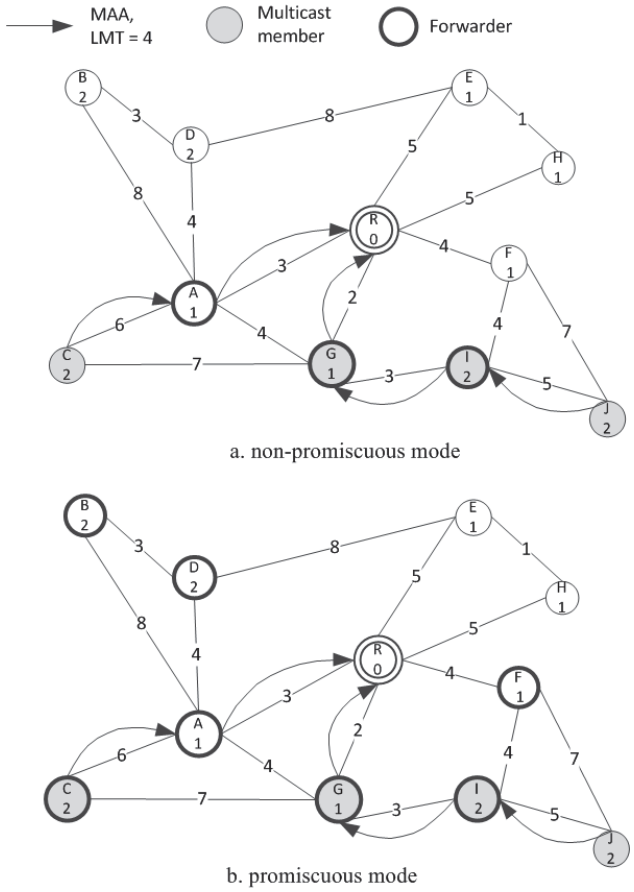

Fig. 3. Multicast route establishment in non-promiscuous and promiscuous mode

the MAA frames as next hops, i.e. with their address in the *Next hop address* field, record a route entry to the multicast address and become forwarders of any frame destined to the multicast group.

- In **promiscuous mode**, all the devices that overhear and can successfully decode the MAA frames, record a route entry to the multicast address and become forwarders, even if they are not one of the next hops on the way to the HM root.

Fig. 3 illustrates an example where the gray nodes are the members of the multicast group. The arrows represent the routes on which a MAA frame is transmitted from each member to the HM root. The nodes with bold lines represent the devices that become forwarders. In Fig. 3.a., in non-promiscuous mode, only devices A, G, I receiving the MAA frames as next hops become forwarders whereas in Fig. 3.b., in promiscuous mode, devices C, B, D and F overhearing the MAA frames also become forwarders.
When the HM root has a data frame to transmit to the multicast group, it sets the SA and the TA to its own address, the DA, to the multicast address, and the NHA, to the broadcast address so that all devices may receive the frame. When a device receives the multicast frame, the frame is forwarded only if the device has at least one route entry to the multicast address. The SA, DA and NHA are unchanged and the TA is set to the forwarder's own address. This reduces the number of transmissions needed compared to multiple unicast transmissions or flooding, especially in large scale networks based on the IEEE 802.15.4 standard, or when multiple multicast groups are present. It reduces the average energy consumption for transmitting and receiving as the number of multicast frame copies is decreased. When transmitting a multicast frame, a device records the SN and the SA of the frame. If the device receives another frame with the same SN and SA, the frame is dropped to avoid duplicate transmissions. The SN and SA records are cleared after a determined period of time.

TABLE I. SIMULATION PARAMETERS

Parameter	Value
Simulation time	24 hours
Frequency band	927MHz
Path-loss model	Two-ray
Data transmission rate	250kbps
Number of nodes	2000
Data frame size	128 bytes
Receiver sensitivity	-89 dBm
Deployment area	5000m × 5000m
Metric	SINR
LMT	5, 10
TX energy consumption (Transmission power)	16 mAh (0dBm), 15 mAh (-1dBm), 14 mAh (-3dBm)
RX energy consumption	18.83 mAh
Idle energy consumption	3.6 mAh

V. SIMULATIONS RESULTS

The proposed protocol is evaluated with extensive simulations run on version 6.1 of the Qualnet network simulator[8] with the parameters listed in Table I. The devices use the Micaz energy model provided by Qualnet. The energy consumption of a device when it is transmitting, receiving and idling is found in Table I. The devices are uniformly deployed in a 5000m×5000m square area. The HM root is placed at the center of the area and transmits a data frame to the multicast group every 5 minutes. The members of the multicast group are found in a square area in the corner of the deployment area. We compare the performance of the proposed HM based multicast routing with that of a broadcast flood, hereafter referred to as BC. The devices use CSMA/CA[9] to access the channel to transmit a frame. Four HM based multicast routing scenarios are considered:

- 5NP: LMT set to 5 in non-promiscuous mode
- 10NP: LMT set to 10 in non-promiscuous mode
- 5P: LMT set to 5 in promiscuous mode
- 10P: LMT set to 10 in promiscuous mode

The metric used for next hop selection is the SINR. The SINR measurement is provided by the Qualnet network simulator. An LMT of 5 or 10 indicates that a parent is eligible as a next hop if the SINR between the transmitting node and its parent is equal to or greater than 5dB or 10dB respectively.

In Fig. 4 and Fig. 5, the performance is evaluated when the side of the multicast group area is varied from 500m to 2500m. The transmission power of each device is set to 0dBm.

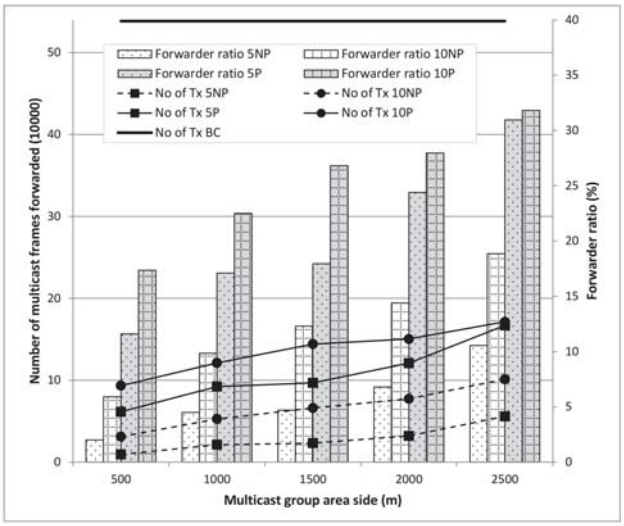

Fig. 4. Number of multicast frame forwarded and Forwarder ratio vs Multicast group area side

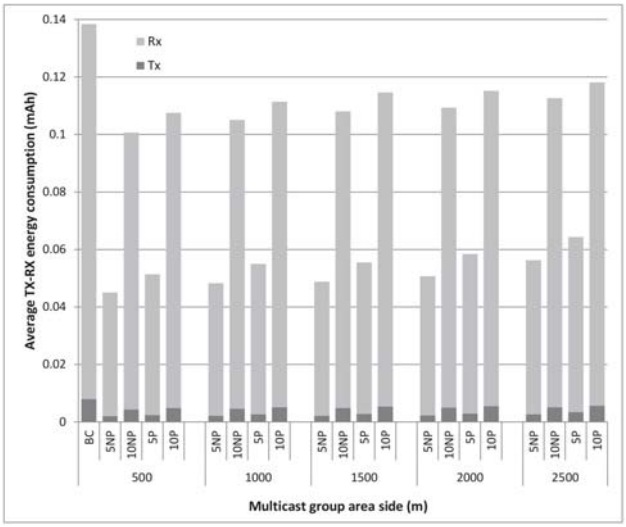

Fig. 5. TX and RX energy consumption and Forwarder ratio vs Multicast group area side

Fig. 4 depicts the number of multicast frames forwarded and the forwarder ratio. The bold line represents the number of transmissions when the multicast frames are broadcast (BC) throughout the HM, i.e. when each device forwards a multicast frame once. The dashed lines represent the number of transmissions when the HM is in non-promiscuous mode. The plain non-bold lines represent the number of transmissions when the HM is in promiscuous mode. Square markers correspond to a LMT set to 5 and circle markers correspond to a LMT set to 10. The results show that the HM based multicast routing greatly reduces the number of multicast transmissions. As the size of the area containing the multicast group widens, the number of multicast frame forwarded increases with the number of multicast members. In non-promiscuous mode, only the devices that received the MAA frame become forwarders. This explains the reduced number of multicast forwarding in non-promiscuous mode compared to that in promiscuous mode. A higher LMT results in longer paths and more devices involved in routing as seen with the plain and dashed paths in Fig. 1. Thus, the number of multicast frame forwarding is higher when the LMT is set to 10 than when the LMT is set to 5. When the side of the multicast group area is set to 2500m, this area covers a quarter of the entire deployment surface and the number of forwarders is almost the same regardless of the LMT in promiscuous mode. Consequently, the number of multicast forwarding is almost the same for both values of the LMT.

The bars represent the forwarder ratio, that is the ratio of the devices involved in the multicast routing. The dotted bars correspond to a LMT set to 5 whereas the checkered bars correspond to a LMT set to 10. The white bars represent the forwarder ratio in non-promiscuous mode, and the gray bars represent that in promiscuous mode. In all cases, less than 35% of the devices are engaged in the multicast routing. This ratio increases as the multicast group deployment area widens. At least 84% of the multicast frames are successfully delivered to the multicast members in the non-promiscuous mode of the HM based multicast routing, and 97% in promiscuous mode. This difference is due to the number of forwarders greatly reduced in non-promiscuous mode. Further, as only the devices receiving the MAA frames become forwarders, this may result in cluster-tree-like topology in some parts of the network creating single points of failures if a device only has one forwarder neighbor. The 5P scenario offers the highest frame delivery reaching more than 99%. The promiscuous mode results in a higher number of forwarders, hence a higher probability a receiving at least one copy of the multicast frame. A higher LMT in promiscuous mode further increases the number of forwarders but also increase the probability of collisions, which is why 10P does not perform better than 5P. The setting of a suitable jitter or backoff mechanism could help increase the reliability of the routing, however this is outside of the scope of this paper.

Fig. 5 represents the average energy consumption by a device for transmitting and receiving. The dark gray accounts for the average energy consumed while transmitting, the light gray accounts for the average energy consumed by a device while receiving. The graph shows that receiving consumes more energy than transmitting in average since a device forwards a multicast frame only once whereas it may receive several copies of the same frame. The first bar labeled BC represents the average energy consumption when all frames are broadcast and shows that flooding consumes more energy than any other scenario. The energy consumption in BC does not change regardless of the multicast members deployment area as all devices must forward each frame once. The energy consumption increases as the multicast members deployment area widens. This is due to more forwarders involved in the routing as seen in Fig. 4. For the same reason, the energy consumption in promiscuous mode is higher than that in non-promiscuous mode; and the increased number of forwarders when the LMT is set to 10 leads to greater energy consumption compared to when the LMT is set to 5.

Fig. 6 show the results when the devices use three different transmission power (0dBm, -1dBm and -3dBm). In all cases, at least 87% of successful frame delivery is achieved in non-

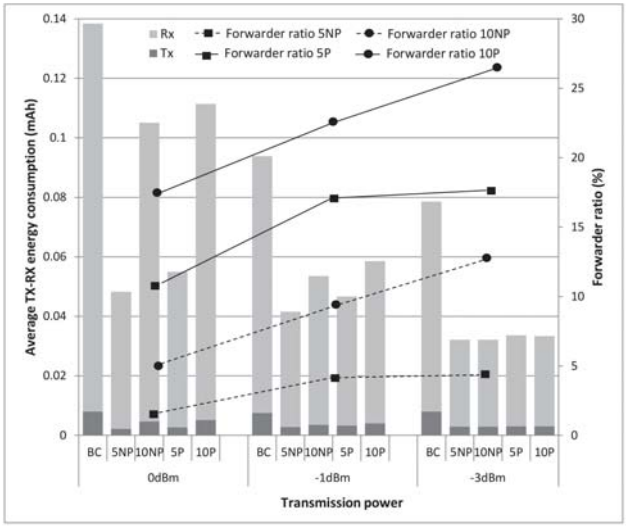

Fig. 6. TX and RX energy consumption vs Transmission power

promiscuous mode and 93% in promiscuous mode. As in Fig.4 and 5, 5P offers the highest reliability with around 99% successful frame delivery with any transmission power. A lower transmission power consumes less energy but also reduces the coverage area of a device. As a result, a MAA frame requires more hops to be transmitted to the HM root which increases the number of potential multicast forwarders as shown by the rising forwarder ratios. On the other hand, a frame is received by less devices and the energy consumption decreases with the transmission power. For the three transmission powers, the average energy consumption with BC significantly outweighs that of HM based routing especially when the transmission power is at its lowest of -3dBm. This graph demonstrates that an implementer can reduce the density of a network and save on deployment costs while maintaining a higher transmission ratio, or keep the same number of devices and reduce the transmission power to save on energy consumption.

The LMT of 5 in promiscuous mode provides the highest reliability in these simulations, however an implementer can fine tune the LMT value based on the network environment, the density or other parameters. The LMT can also be set locally on each device to allow precise MAA routing and further optimize multicast routing.

The energy consumption displayed represent that used in 24 hours. The energy saving becomes more significant as the lifetime of a network lengthens and is particularly desired in battery operated devices.

VI. Conclusion

This paper proposes a hierarchical mesh based multicast routing enabling energy saving for IEEE 802.15.4 based networks such as ITS, smart city, smart utility networks, etc. We address the need in these networks to communicate the same information to a group of devices. These devices are organised in multicast groups. The proposal enables route establishment between the HM root acting as the network controller and the members of these multicast groups. As a result, the number of copies of the same multicast frame transmitted in the network is greatly reduced compared to when the frame is flooded, yielding significant energy saving in transmission and reception. The simulation results show that the proposed protocol decreases the number of devices involved in the multicast routing, also called forwarders. This number depends on the surface of the area where the multicast members are deployed. Adequate organization of the network into several multicast groups would allow to send different information to each group while consuming less energy than when flooding is used. The proposal also maintains a high successful frame delivery percentage while reducing the transmission power to save energy. It can also reduce the number of devices deployed in the network and keeping the same transmission power to save on network deployment costs. The setting of a link metric threshold provides flexibility to an implementer to adapt to the environment globally in the entire network or locally at each device. This solution is promising to applications where a certain area of a city, a certain building of a campus, etc. needs to be controlled or reached at once.

References

[1] S. Tao, et al, *"AODVjr Routing Protocol with Multiple Feedback Policy for ZigBee Network,"* 13th IEEE International Symposium on Consumer Electronics, pp. 483-487, May 2009.

[2] G. Montenegro, et al, *"Transmission of IPv6 Packets over IEEE 802.15.4 Networks,"* IETF, RFC 4944, Sept. 2007.

[3] O. Gaddour, et al., *"Z-Cast: A Multicast Routing Mechanism in ZigBee Cluster-Tree Wireless Sensor Networks,"* IEEE 30th International Conference Distributed Computing Systems Workshops (ICDCSW), pp.171,179, June 2010.

[4] L. Hester, Y. Huang, O. Andric, A. Allen, P. Chen, *"neuRFon Netform: A Self-Organizing Wireless Sensor Network,"* in Proceedings of the 11th International Conf. on Computer Commun. and Networks, pp. 364-369, Oct. 2002.

[5] IEEE Standard for and metropolitan area networks Part 15.4: Low-Rate Wireless Personal Area Networks (LR-WPANs), 2011.

[6] T. Winter, P. Thubert et al., *"RPL: IPv6 Routing Protocol for Low-Power and Lossy Networks,"* IETF, RFC 6550, Mar. 2012.

[7] V.H. Rabarijaona, F. Kojima, H. Harada, *"Hierarchical Mesh Tree Protocol for Efficient Multi-hop Data Collection, "* in Proc. of the Wireless Commun. Networking Conf., WCNC'2014, pp.2008-2013, Istanbul, Apr. 2014.

[8] Qualnet, accessed July 31, 2015, http://web.scalable-networks.com/content/qualnet.

[9] A. Colvin, *"CSMA with collision avoidance,"* Computer Communications, Vol. 6, pp.227-235, 1983.

[10] E.M. Royer, C.E. Perkins, *"Multicast Ad hoc On-Demand Distance Vector (MAODV) Routing," http://tools.ietf.org/pdf/draft-ietf-manet-maodv-00.txt, July 2000*

[11] S. Deering, *"Host Extensions for IP Multicasting,"* IETF, RFC 1112, 1989.

[12] S. Lee, M. Gerla and C.C. Chiang, *"On-Demand Multicast Routing Protocol," in Proc. of the Wireless Commun. and Networking Conf., WCNC'99, pp.1298-1302, New Orleans, Sep. 1999.*

[13] B. Haberman, *"Allocation Guidelines for IPv6 Multicast Addresses,"* RFC 3307, Aug. 2002.

THE 18TH INTERNATIONAL SYMPOSIUM ON WIRELESS PERSONAL MULTIMEDIA COMMUNICATIONS
(WPMC-2015)
December 13-16, 2015, Hyderabad, India

Quality of Service Enforcing Centrally Optimized Routing for Delay Tolerant Networks

Abhishek Thakur, Chittaranjan Hota
Computer Science and Information Systems
BITS Pilani, Hyderabad Campus
Hyderabad, India
{abhishek, hota}@hyderabad.bits-pilani.ac.in

Abstract — **Central node(s) that collect global view on delay tolerant network performance can simplify management and ensure good quality of service. Such global view can improve DTN routing without increasing the routing complexity on individual nodes. Existing research using central nodes have explored both routing control and routing relay via central node. This paper proposes central node assisted routing where message forwarding and relay continues in pure distributed manner. Global view computed by central node augments the routing decision on individual nodes.**

Additionally this paper evaluates the extra overhead and congestion effects when all application messages are relayed though central node (for policy enforcement, management etc.).

Keywords— Delay Tolerant Networks, Quality of Service, Fairness, Adaptaton, User Generated Content

I. INTRODUCTION

Delay and disruption tolerant networks (DTN) [1] come into play when end-to-end communication using mesh or ad-hoc networks are not feasible. Node mobility is the primary enabler for DTN as it emphasizes on store-carry-forward behavior for the bundles (payload or messages for DTN).

Authors in their prior work, [2], have attempted to deploy DTN based platform for rural communication with focus on applications for intra-community communications. This is a scenario where DTN based terrestrial communication service is being provided on a long term basis for the village community. In such deployments people with low mobility or nodes in the periphery of the network are treated unfairly as they have lower delivery ratios and/or significantly higher delays.

Revenue generation is essential to make DTN rural deployment sustainable. Any revenue model mandates features like - accounting, billing, security and quality of service. When offering a commercial service, it is also important to conform to local government's rules and policies, especially with respect to the ability to do security scanning, spam control etc. In this context, challenges in pure distributed DTNs are a) lack of metering and accounting of resource usage to get a consolidated view, b) tracking and enforcement of quality of service for individual nodes, c) enforcement of policies to comply with local laws, and d) ability to do security scans (like IDS/IPS in commercial TCP/IP based networks).

To mitigate the challenges of pure distributed DTN, the authors, in prior work have explored deploying a central device to simplify user management, billing, policy enforcement etc. The owner / operator of the central device can bill the end users by demonstrating the value that the system provides. Central device, referred to as CoHub (centrally optimizing hub) in this paper, creates a global view of the community DTN nodes. Such global view CoHub can drive the routing protocols on individual nodes to target specific quality of service for end nodes.

One of the applications for this rural platform is sharing highlights from farm monitoring videos. Rather than sending complete video, only masked highlights are sent (e.g. video snippet at goo.gl/hc9MuY or goo.gl/s5XA8l). Since video generates large content (megabytes) on periodic basis (30 seconds to few minutes), hence it is important to know the DTN quality of service, so that the highlight creation and compression can be adapted to the network conditions. Information shared by CoHub can drive such decisions.

This work proposes a new routing extension "Quality of Service Enforcing Centrally Optimized Routing", referred to as QoseCo in rest of the paper. In the present work, the authors use Spray-and-Wait [3] as the base protocol, on top of which QoseCo extension is demonstrated. Performance of QoseCo + Spray-and-Wait is compared with vanilla Spray-and-Wait (SNW). Message routing is done by all nodes based on information shared by the CoHub. In absence of CoHub, QoseCo will degrade to vanilla SNW. Other protocols like PRoPHET can also be adapted with QoseCo.

An extension of QoseCo is explored where all application messages are forced to be relayed via the CoHub. This is referred to as QoseCo with Central-Relay [QoseCo-CR]. Though relaying via central nodes is expected to cause congestion and make CoHub the single point of failure, it can be used for security scanning and policy enforcements. Usage of multiple CoHub (horizontal scaling) or vertical scaling are some mitigation aspects to improve QoseCo-CR, but the same is not included in the scope of this paper. This paper only attempts to measure the impact on delivery ratios for QoseCo-CR for a single deployment of CoHub.

Structure of rest of the document is as follows: Section II provides a very brief overview of related DTN routing

protocols and quality of service related work. Section III provides overview of QoseCo and QoseCo-CR along with algorithmic details. Section IV has simulation setup, results and analysis. Section V includes conclusion and a broad overview of future work targeted by the team of authors.

II. Related Work

Massri and others in [4] provide a good overview of DTN routing. They have identified three major components in DTN routing– 1) queue management, 2) forwarding decision and 3) replication. Cao and others [5] provide a more recent survey on various DTN routing approaches. In context of [5], rural deployment can be seen as suburban networks or pocket switched networks. Routing decisions in such cases can use infrastructure approach with auxiliary nodes like mule or throw box or use participant nodes for store-carry-forward. In this paper the authors use a hybrid approach wherein "infrastructure" is used to improve routing decisions, but the actual routing is done using participant nodes in a distributed manner.

Some of the newer protocols explore human / social aspects of the person carrying the device to drive the routing decisions. This increases the computation complexity on the nodes as each node needs to have visibility beyond its own contacts to calculate social characteristics like centrality and between-ness. For DTN networks with power-law, [6] explores DTN routing via hub nodes, where the (multiple) hub nodes have higher connectivity and offload computation load from other nodes. Another set of protocols use an oracle or deterministic approach to compute the future contact probabilities and drive the routing decisions accordingly. But when these protocols are applied for pocket switched networks, especially for rural people who need not keep a strict schedule, they perform poorly.

When adding an extension to an existing routing protocol, the base protocol should be as simple as possible. Naïve Spray-and-Wait [3] was the first choice as it allows for good control on overheads and is very simple in terms of computation and storage overheads on all nodes. Origin node in SNW computes the maximum number of replicas (L) that will be created. Thereafter some replicas are given to nodes on contacts. When operating in binary mode, half the replica count will be shared with other node on contact. Eventually at max L nodes will have a copy of the message. If any of these nodes come in contact of the destination, the message is delivered.

To target fairness, QoseCo allows higher L to be used for messages with poorly served nodes as origin or destination. During forwarding QoseCo allows higher share of replicas to be given to well-connected nodes. Other than SNW, PRoPHET was also considered. Tolerance limits can be relaxed for poorly served nodes if PRoPHET is used. For brevity, it is not discussed further in this paper.

A. *Quality of Service:*

Hay and Giaccone [7] have explored QoS for DTN routing when contacts between nodes is known in advance or can be predicted in advance (e.g. Bus routes etc.). Such knowledge is used to model the DTN network as time-independent graph for optimizing QoS. Sandulescu [8] uses special messages under nominal load from the source node to destination node and collects the feedback over time. Thereafter source adapts the transmission to observed network behavior. QoseCo targets to do away with such needs by periodically updating about poorly served nodes.

B. *Fairness in DTN:*

Pujol et. al. [9] attempt to measure fairness in the share of load on individual nodes. Fan [10] et. al. measure the fairness in delivery ratios for increasing number of contacts. During relay of messages their work attempts to locally compute the utility value for each message, with delivery farness of messages as a goal. Since each node tries to compute fairness without a global perspective, the impact is limited.

Similar to [10], this paper attempts fairness in delivery ratios. To the best of knowledge of the authors, control of delivery fairness w.r.t. end nodes has not been dealt with in any prior work. QoseCo uses historical contact and delivery information to adjust the priority of nodes. Since complete graph need not be built on each node, QoseCo scales quite well, though it has a time lag in sharing the global view.

III. QoseCo Routing Extensions

QoseCo: All nodes periodically share their state information with CoHub. Based on the information received, the CoHub generates a consolidated view and updates all nodes (broadcast) with control information. This is a communication overhead (below 2%), but it helps move the computation to CoHub. CoHub periodically distributes the global context to all nodes. In absence of information from CoHub, the node degrades itself to naïve routing protocol (SNW in this case).

QoseCo-CR: If complete control of the deployment (e.g. lawful interception, virus scan etc.) is required, all traffic is relayed through the CoHub.

Major decision points are captured below.

A. *New message from origin node*

Replication count (L) for the message is set by the origin node, based on the last routing control message received from the CoHub. For poorly served nodes, higher counts are allowed.

Algorithm 1: New Message on originating node (simplified)

```
function newMessage(Message M, Host origin, Host dest)
  L = Default_Max_Replica
  if (dest or origin in poorMap)
    lowQual = MIN(getQuality(dest), getQuality(origin)
    L = L * (1+AverageQuality / lowQual)
  if(routing == QoseCo-CR)
    m.setMetadata("actualDest", dest)
    m.destination = CoHub
  m.setMaxReplica(L)
  m.setDestination(destination)
end
```

For QoseCo-CR, destination is set as CoHub and actual destination is added as metadata to the message. Once CoHub gets the message, it does the required processing and relays it to the actual destination.

B. Feedback to the CoHub

All nodes periodically send status updates to CoHub (management payload). The update message includes a) information about the nodes contacts (contact count and total duration) with other nodes; b) count of messages generated and delivered from/to end applications on the node and c) list of messages received before TTL expiry.

C. Consolidation of data (Global-View) at CoHub

When a CoHub receives status update messages from the nodes, it adjusts the metrics for the nodes. Periodically the CoHub multicasts routing updates to all the nodes. This multicast status includes a) list of poorly served nodes and their priority, b) list of nodes that are good carriers with their priority, and c) list of recent messages received by destination nodes. Poorly served nodes are identified as nodes who have reported very few contacts and/or whose packets have not been delivered (either as origin or destination). Good carriers are nodes that have had large number of contacts with different nodes. Exponential weighted moving average is used to reduce impact of really old contacts.

When nodes get multicast routing updates from CoHub, they delete all messages in their local cache that are successfully delivered to the destination nodes. They cache the details of good carriers and poorly served nodes for subsequent routing decisions and new message creation.

D. Routing decesion: Message forwarding between nodes

During contacts, nodes exchange messages with each other as per following algorithm.

Algorithm 2: Forward Message Between Nodes (simplified)

```
function startTxfr(Msg[] pendingMsgs, Host[] connList)
  if (CoHub in connList &&
       CoHub in getDestinations(pendingMsgs))
    candidateMsgs = filterOnDest(pendingMsgs, CoHub)
    sortOnOriginNodeQuality(candidateMsgs)
    transferAndDelete(candidateMsgs[0])
  else
    trgtMsgs = filterOnDest(pendingMsgs, connectedList)
    if(trgtMsgs!= EMPTY)
      sortOnOriginOrDestQuality(trgtMsgs)
      transferAndDelete(trgtMsgs[0])
    else
      txrList = sort_On_EndNodes_CopyCount_Relay(
                          pendingMsgs, connList)
      relayAndAdjustL(txrList[0].msg, txrList[0].remote)
end
```

The message transfers are attempted as follows:. A) If one of the connected nodes is a CoHub, deliver messages that have CoHub as destination. B) If node has message for one of the connected forward messages for destination. C) Relay other messages and adjust copy counts.

If there is a tie w.r.t. message or connected host, the tie is broken as follows: a) messages moving towards CoHub, b) messages with nodes as source or destination of poor quality, c) current replica values of messages, and d) relay to host which are good carriers. *relayAndAdjustL* gives higher number of copies to nodes that are in "Good Carriers" list.

E. Message deletion when buffers are full

Expired messages are deleted first. If required, further messages are deleted based on priority of end nodes.

IV. Simulation and Results

A. Implementation details

QoseCo routing and forwarding, as discussed in section III above was implemented on ONE [11]. Reporting functions were added to appropriately capture the details of management packets and include measure of fairness metric. Jain's throughput fairness index [12] is used. These metrics are captured in table 1.

TABLE I. Delivery Ratio, Overhead and Fairness

Parameter	Value
T_Delivered	Total messages successfully received at destination
T_Started	Total messages sent
T_Relayed	Count of successful forwards of messages between all nodes
N_Success	Number of messages successfully delivered for a specific node (either as source or destination)
N_Attempt	Number of messages for a node (either as source or destination)
Delivery Ratio	T_Delivered / T_Started
Overhead	(T_Relayed – T_Delivered) / T_Delivered
N_Xfactor	(N_Success/N_Attempt) / DeliveryRatio
Fairness	$(\sum N_Xfactor)^2 / \sum (N_Xfactor^2)$ for nodes that participated in attempts

Two mobility models from [11] are used - (a) Working Day Movement model – WDM; and (b) Helsinki City Scenario – HCS. WDM simulates users in home, office and shopping malls etc. in a somewhat realistic scenario based on large area of Helsinki city. HCS simulates people moving randomly (walking or in car) across a smaller area within Helsinki. For each user HCS chooses the next destination randomly based on points of interests in the map. For the chosen destination, shortest path is computed based on maps; while the speed and period of stay are randomized based on configuration settings. Readers are requested to refer Keränen's work [11] for further details about these scenarios.

B. Simulation Configuration

To target rural scenarios number of nodes were significantly reduced and simulations were run for longer

intervals. Longer duration was chosen, as compared to [11] because the rural area of developing countries will not have internet connectivity at home / office. For HCS, 37 pedestrians, 3 people with cars or two wheelers and 21 static nodes were used along with three trams. For WDM, numbers from [11] were scaled down by factor of sixteen to get 64 end user nodes. For both the scenarios static CoHub node was added. CoHub location was manually chosen near road junctions to ensure good contact opportunities.

TABLE II. DEFAULT SETTINGS FOR SIMULATION RUNS

Parameter	Value	Parameter	Value
Duration	4 days	NumCopies	64
Event Gap	8 minutes (randomized)	EWMA Alpha (QoseCo)	0.002
Event Message Size	750 KB (randomized)	NumPoorService (QoseCo)	16 nodes
Message TTL	8 hours	NumGoodCarriers (QoseCo)	8 nodes

QoseCo update messages are pretty small (typically 4-16 KB for CoHub routing updates and 1-4 KB for node status updates). They have not been included in further analysis since they are smaller by order of hundred times. For a sample run, 200 megabytes of traffic relay was caused because of QoseCo management load while application payload generated 13 gigabyte of traffic.

C. Simulation Runs

From the simulation scenarios that were executed, two reports are presented here. Results for Delivery Ratio, Fairness and Overhead are presented for simulation period. For Inter-event Gap (Congestion) the results are discussed only for fairness and delivery ratio because of space limitations. All metrics are average values for eight randomized runs.

1) Simulation Duration- low load

Execution was done for simulation periods of 0.5 days, 1 day, 2 days, 4 days, 8 days, and 16 days. The results are plotted in Figure 1 for (a) Delivery ratio, (b) Fairness and (c) overheads. As simulations run for longer interval, delivery ratios improve for all scenarios. This is because higher percentages of messages are received within the simulation time. QoseCo follows similar trajectory as SNW with a slight degradation. The degradation is observed because management messages compete with application messages during contact opportunities. QoseCo-CR has lower delivery ratios. This is because the routing via CoHub requires more hops and increases congestion in the vicinity of the CoHub.

As duration increases, fairness improves since the messages are generated with random nodes as source and destination. Both QoseCo and QoseCo-CR show significant improvements till 2-4 days, with the slope tapering off for 8 days and 16 days.

For runs of less than 2 days, lots of messages are not yet delivered; hence overheads are observed to be higher. Overheads are higher for QoseCo-CR as it first sends messages to CoHub and then CoHub relays to destination. Moreover HCS has lot more contacts; hence it creates many more copies. Overhead results for QoseCo were marginally higher as it allowed larger number of replicas for poorly served nodes. All through QoseCo had fairness which was pretty close to SNW, despite the delivery ratio being poorer for QoseCo on account of added management messages.

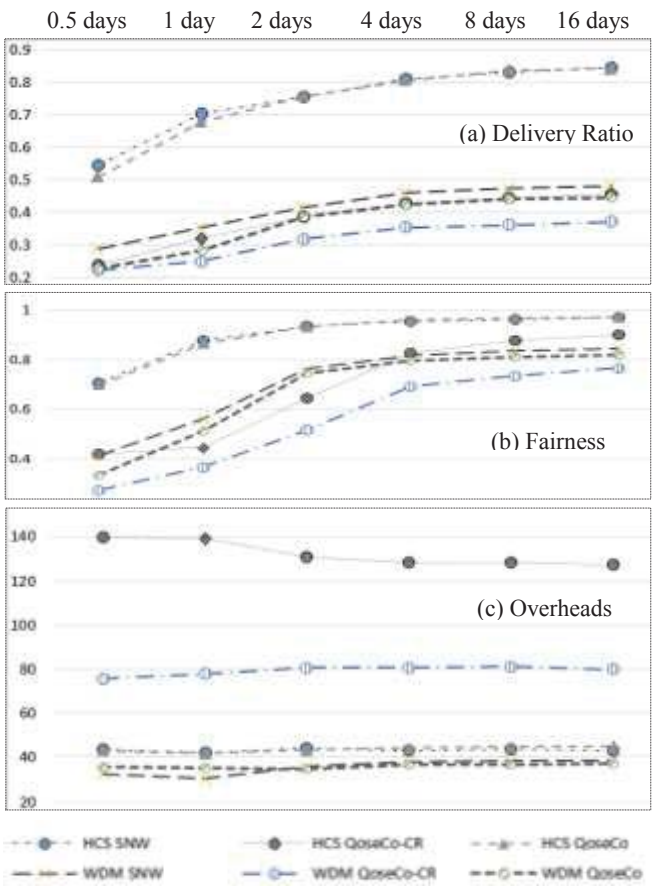

Figure 1 Simulation Duration Results

2) Inter-event Gap- Congestion

Events were randomly generated with average gap of 30 seconds, 1 minute, 2 minutes, 4 minutes, 8 minutes and 16 minutes. This scenario allows for congestion to happen in the cases where messages are generated at two minutes and below. Figure 2 plots the results for the fairness and delivery ratio for four day run.

When events are generated twice every minute, almost all nodes participate in the communication and most of them observe high losses, though the nodes on periphery will be worse off for WDM. For HCS, QoseCo does well to improve fairness in this scenario as it has values around 94% while SNW is around 90%. Similar trend is also observed for WDM (70% vs. 74% for 30 seconds). At lower frequencies since less number of nodes participate in communication, slight degradation is observed in fairness for all cases.

QoseCo-CR observes significantly higher packet loss when message frequency is high (low delivery ratio). This is because the messages get relayed via the CoHub and for all messages that get relayed, a new message is created.

D. Key Observations and Analysis

HCS scenario is completely random with respect to the mobility paths and destinations, while WDM is somewhat synchronized. With choice of 64 nodes in the simulation, and messages being randomly generated between nodes, it was observed that QoseCo improves fairness by around 4% in many scenarios.

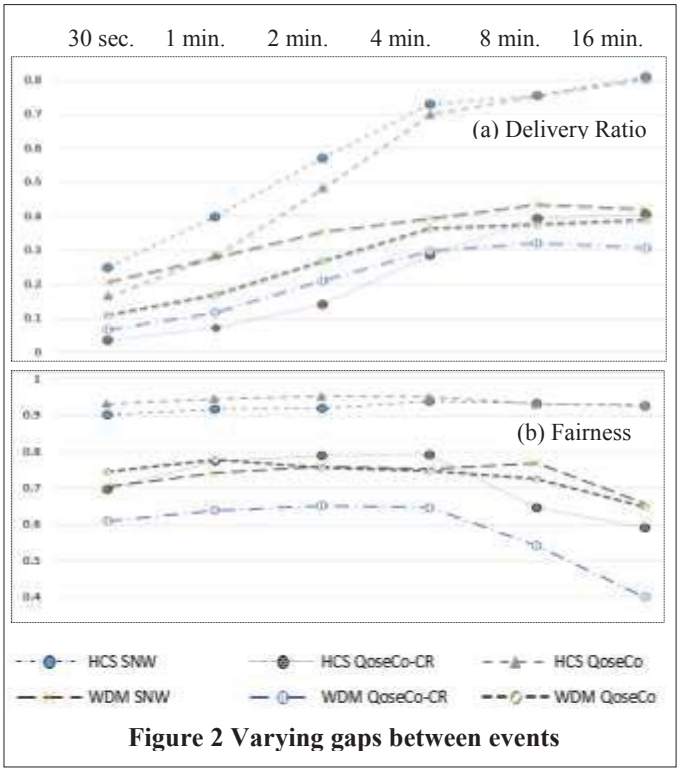

Figure 2 Varying gaps between events

Improvements for fairness in QoseCo are more pronounced when network is congested (frequently generated messages). This happens even as the overheads of QoseCo update messages are present. Poorly serviced nodes are tracked centrally. By moving this computation to central nodes, computation load for other nodes was reduced. The tradeoff was addition of QoseCo update traffic which was less than two percent for most scenarios.

QoseCo-CR is frequently worse off by a factor of about two. For 30 seconds in HCS it degraded beyond a factor of two when compared with QoseCo as severe congestion set in the vicinity of the CoHub.

V. Conclusion and Future Work

The authors proposed a new DTN routing extension and used SNW as underlying routing protocol to demonstrate centrally optimized routing. Using simulations they also showed how centralized routing extension helps improve Quality of Service under congestion. Fairness in delivery ratio was used as the quality metric to demonstrate the impact of QoseCo for real world mobility scenarios. While this work adapts SNW for centralized routing, other DTN routing protocols can also be adapted in similar manner.

This paper also studied the overheads when all messages are relayed through a central node. The cost of relaying the messages via the central nodes is found to be within 2X for most scenarios but degraded significantly as congestion sets in.

The authors are exploring the ability to include more than one location for CoHub(s) and analyze its impact. Moreover present QoseCo implementation does not explore the location and time relationships for the contact. This is another aspect that the team is exploring. Survey of real village to make the working-day-model more realistic is another area that the team is focusing on. The work is also being extended to reduce the number of copies when delivery ratio is high (e.g. above 95%).

References

[1] Fall, K. (2003, August). A delay-tolerant network architecture for challenged internets. In Proceedings of the 2003 conference on Applications, technologies, architectures, and protocols for computer communications (pp. 27-34). ACM.

[2] Thakur, Abhishek, and Chittaranjan Hota. "Designing an extensible communication platform for rural area." In Advances in Computing, Communications and Informatics (ICACCI, 2014 International Conference on, pp. 1348-1355. IEEE, 2014.

[3] Spyropoulos, Thrasyvoulos, Konstantinos Psounis, and Cauligi S. Raghavendra. "Spray and wait: an efficient routing scheme for intermittently connected mobile networks." In Proceedings of the 2005 ACM SIGCOMM workshop on Delay-tolerant networking, pp. 252-259. ACM, 2005.

[4] Massri, K., Vernata, A., & Vitaletti, A. (2012, October). Routing protocols for delay tolerant networks: a quantitative evaluation. In Proceedings of the 7th ACM workshop on Performance monitoring and measurement of heterogeneous wireless and wired networks (pp. 107-114).

[5] Cao, Yue, and Zhili Sun. "Routing in delay/disruption tolerant networks: A taxonomy, survey and challenges." Communications Surveys & Tutorials, IEEE 15, no. 2 (2013): 654-677.

[6] Ahmed, Shabbir, and Salil S. Kanhere. "HUBCODE: hub-based forwarding using network coding in delay tolerant networks." Wireless Communications and Mobile Computing 13.9 (2013): 828-846.

[7] Hay, David, and Paolo Giaccone. "Optimal routing and scheduling for deterministic delay tolerant networks." In Wireless On-Demand Network Systems and Services, 2009. WONS 2009. Sixth International Conference on, pp. 27-34. IEEE, 2009.

[8] Sandulescu, Gabriel, Aimaschana Niruntasukrat, and Chalermpol Charnsripinyo. "Guaranteed capacity bounds in intermittently-connected networks: A resource-aware, holistic evaluation." Computer Communications 59 (2015): 12-23.

[9] Pujol, Josep M., Alberto Lopez Toledo, and Pablo Rodriguez. "Fair routing in delay tolerant networks." INFOCOM 2009, IEEE. IEEE, 2009.

[10] Fan, Xiaoguang, Victor OK Li, and Kuang Xu. "Fairness analysis of routing in opportunistic mobile networks." Vehicular Technology, IEEE Transactions on 63.3 (2014): 1282-1295.

[11] Keränen, Ari, Jörg Ott, and Teemu Kärkkäinen. "The ONE simulator for DTN protocol evaluation." In Proceedings of the 2nd international conference on simulation tools and techniques, p. 55. ICST (Institute for Computer Sciences, Social-Informatics and Telecommunications Engineering), 2009.

[12] Jain, Raj, Arjan Durresi, and Gojko Babic. Throughput fairness index: An explanation. Tech. rep., Department of CIS, The Ohio State University, 1999.

THE 18TH INTERNATIONAL SYMPOSIUM ON WIRELESS PERSONAL MULTIMEDIA COMMUNICATIONS
(WPMC-2015)
December 13-16, 2015, Hyderabad, India

Improving Segmentation Accuracy for Motion Detection using Bidirectional Video Processing

Abhishek Thakur, Ankesh Kumar
CSIS department,
BITS Pilani Hyderabad Campus
Hyderabad, India
thakur@ieee.org, ankeshkumar@outlook.in

Abstract— **Most of content in video capture from static cameras consist of fixed background. Invariably the important information in such video is associated with some motion. Background Subtraction models help extract such information. Adaptive approaches of background subtraction (like Mixture of Gaussian) do not mandate prior input for object detection. But adaptive approaches suffer from misclassification during learning phase. This work extends Mixture of Gaussian to improve upon the short comings of adaptation phase. Video chunks are processed in both forward and reverse direction. Different approaches of combining the output values in both directions are analyzed. Best results are observed when different kernel sizes are used in morphological operations for forward and reverse direction, depending on the temporal offset. Experimental results for standard video data sets and farm like scenarios demonstrate improvement in detection accuracy across numerous frames.**

Keywords- ***Multimedia, Video Processing, Motion Detection, Background Subtraction, Bidirectional Processing***

I. INTRODUCTION

This work forms a significant part of object detection, highlight generation and video compression of in farm like scenarios. Large areas are monitored using cameras mounted at strategic locations. These cameras are affordable Android devices communicating over 802.11 series of protocols. In rural scenarios, actual network connectivity should be delay and disruption tolerant [1]. Continuous video is not streamed on such networks. Video must be heavily compressed to be shared over such networks within reasonable timeframe.

For such heavy compression significant portion of the video must be discarded. The challenge is to accurately segment the regions are to be discarded, from the regions to be retained. It is obvious that for such scenarios, motion is associated with portion of video to be retained. This work improves segmentation accuracy by improving motion identification.

Typical captures, for farm monitoring, involve large open areas with trees and other vegetation. The intent is to detect human / animal or inanimate objects intruding into the farm without requiring explicit human interaction. Broader work involves highlight creation and messaging using Delay Tolerant Networks [1]. Videos are stored and processed in chunks varying from tens of seconds to a few minutes, to extract key information. It is only the key extracted information that is sent over the delay tolerant network.

Accuracy can be improved by identifying regions of significant motion while discarding small movements generated by the fixed objects. For example swaying branches, tree-tops etc. show lots of small movements and do not have significance. It is assumed that the natures of objects are not known. A priori knowledge based approach could cause unknown objects to be missed. Though the wider work involves object tracking across frames, path-identification and communication mechanisms, they are not within the scope of this work. This paper focusses only on improving segmentation accuracy.

While this paper discusses farm like scenarios as primary use case, it can be applied to any scenario where video is captured using static cameras. Such applications will have impact on information extraction from archived videos, e.g. conserving storage space for archived videos.

Layout of the document: Next section provides an overview of key object detection techniques and includes an overview of Background subtraction using Gaussian Mixture Model. Section III provides the implementation details of bi-directional video processing for object detection. Section IV covers the experiment details, and metrics. Section V presents the results and related analysis. Section VI concludes the paper including a discussion of future work.

II. BACKGROUND WORK

Multiple approaches have been developed to detect motion of objects in the video. Three of the common approaches are a) Optical Flow; b) Background subtraction; and c) Color histogram based methods [2]. For brevity of this paper only background subtraction method is discussed in details. The other two approaches need prior information (histogram based) or do not scale well for large areas (optical flow).

Motion detection using background subtraction involves segmenting each video frame into background and foreground regions. The background region stays relatively static throughout the length of the video. The foreground is the region of pixels that moves across the frames while mostly maintaining its shape and color attributes. Multiple approaches have been proposed for motion detection. This work builds

upon background subtraction based object detection [3] [4]. The background subtraction approaches performs well with modern systems that have more graphical processing cores dedicated to the algorithm [5].

A. Background subtraction - Mixture of Gaussian: A brief Overview

Background subtraction methods rely on creating a model for the background. Each frame is compared with the background model to find the difference and identify regions of motion. Background subtraction Mixture of Gaussian (referred to as BGS-MOG in subsequent parts) differs from the other background subtraction methods in the way the background model is created. The background model is continuously updated for every frame that is processed. Every pixel of the background is represented as a mixture of Gaussian distributions (mean, variance and weight) [6]. This approach allows efficient handling of gradual illumination changes (e.g. shadows, clouds etc.) as well as adapts to swaying trees and branches. BGS-MOG does not require bootstrapping (externally identifying the object) or prior learning (training). It does suffer from camouflage issues (especially for slow moving objects) and does not work if camera view is not static.

For each pixel in a new frame, the pixel value is compared to the corresponding Gaussian distributions in the background model. If a match is found then the corresponding distribution is updated for mean, variance and the weight. If no match is found a new distribution is added to the mixture (if number of distributions is exceeding the maximum allowed entries then the least probable distribution is replaced by a new distribution). This new distribution is allocated the default weights and variance. All weights are normalized following updates/additions and the mixture model is sorted on descending order for weights. A learning rate (α) drives the weights applied to updates and additions.

A Gaussian mixture model is a more accurate description of the background as compared to any single distribution. The adaptive nature of the algorithm accounts for lighting changes and works even if no pristine background model was available.

If a pixel does not match, or matches against a very low weight in the mixture, it is marked as foreground in resulting mask. The mask provided by BGS MOG for a frame is generated on individual pixels without a sense of adjacency. This results in a perforated mask with varying pixel values for a given object. Morphological operations are used to smoothen out the mask.

Morphological operations are matrix based mathematical operation on images. These operations alter a pixel's value based on the values of the pixels in its neighborhood. The area and shape of the neighborhood affects the results of the operation. The operations used in this paper are erode and dilate. The erode operation reduces the thickness (shrinks) around the edges whereas dilate increases the thickness. If random small objects are present, erode tends to remove them while dilate will end up joining them. Size and shape of kernel decides how effective the removal or joining is.

B. Shortcoming of BGS-MOG

1) Spurious motion in initial frames:

The initial frames show a lot of motion since the background model is still under construction. The learning rate (α) drives the weight for pixel value in current frame. If moving objects or swinging branches are present in the first frame, the algorithm incorrectly classifies the initial region where the moving object was present, as part of the background. In subsequent frames, a lot of incorrect motion is reported where the moving body was originally present. The inaccurate motion is removed after a few frames, as the background model adjusts to the real values for background pixels. The adjustment period depends upon the learning rate α.

2) Missed trailing edges:

Trailing edges of some objects are missed, if they are narrow along their motion path. This is because mixture model has not adapted to the object.

It's difficult to ensure that initial frame does not have any motion; hence the initial frames will have false positives. To reduce this learning period, a very high learning rate (α) can be used. However a high α causes slower moving objects to be mislabeled as background. This makes tracking slower moving objects difficult. Generally a compromise is made on the learning rate and some inaccuracy in reporting motion in the first few frames is accepted. This work targets to reduce such inaccuracy.

III. BIDIRECTIONAL PROCESSING

Bi-directional processing deals with chunks of video of 30 seconds to a few minutes. The stream is individually analysed from starting to end and from end to start. The results obtained from the two analyses are then aggregated to generate a mask that that had improvements in identifying the region of motion.

The first step in the process is to create a separate reversed video of the given video chunk (last frame to first frame).

Then BGS MOG is applied on both video chunks. The result is two separate videos of masks. One is for the first-to-last frame video (henceforth called the forward stream) and the other for the last-to-first frame. The BGS MOG stream for the reversed video frame has the masks in last to first order. The two streams need to be aligned so that for a given frame number both streams provide the mask for the same frame. This is done by reversing the mask stream for the last to first frames (subsequently referred to as the reversed stream).

The two streams can be used individually to detect motion in a given frame. However both suffer from the shortcomings mentioned in II-B.

In order to improve detection accuracy, the two streams were then aggregated. Three aggregation methods were experimented upon. In all the aggregation methods dilation and erosion have been used. Three different sized square kernels were used. SMALL(3x3), MEDIUM(5x5) and LARGE(7x7).

The initial aggregation methods used were Bitwise OR and Bitwise AND. Prior to the Bitwise operation the forward and reverse stream the frames are dilated using the MEDIUM sized kernel. After the Bitwise operation the resulting mask is eroded

using LARGE kernel. This is done to minimize the addition of noise from the individual streams. This may result in loss of information. Mathematical addition and multiplication were not used since the masks are binary in nature and bitwise operations are faster.

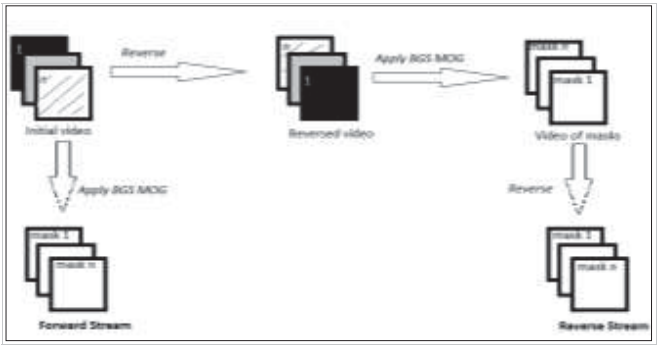

Figure 1 Creation of reverse and forward mask streams

The accuracy of the various aggregate streams was then compared to the accuracy of individual forward and reverse streams. For comparison, the individual forward and reverse streams were dilated and eroded with the same sized kernel (MEDIUM), in order to smoothen out the edges and fill in small gaps within the shapes. Figure 1 captures the processing done for individual streams (forward, reverse) and aggregated streams (AND, OR).

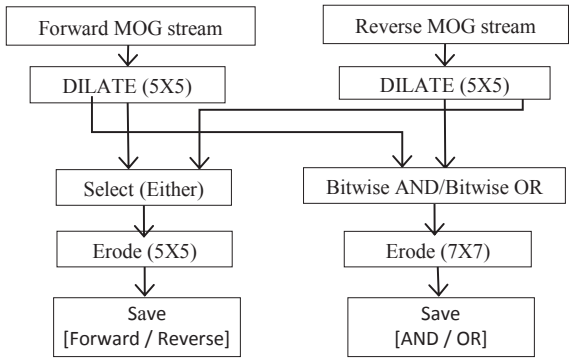

Figure 2 – Morphological operations for individual and simple aggregated streams

It was expected that the Bitwise OR aggregation method would lead to additional noise in the mask. This effect would be pronounced in the initial and terminal part of the video. Similarly it was expected that the Bitwise AND aggregation method would lead to loss of information.

To overcome these issues, a third aggregation approach based on Weighted Bitwise OR was implemented. For this method the masks from forward stream were preferred during the terminal part of the video and the masks from the reverse stream were preferred during the initial part of the video. The approach used morphological operations as weight functions for individual streams. Different sized kernels were used as function weights. The algorithm is captured below.

Algorithm 1: Weighted Bitwise OR

```
Initialization
    SMALL kernel = matrix of size (3x3) with all 1
    MEDIUM kernel = matrix of size (5x5) with all 1
    LARGE kernel = matrix of size (7x7) with all 1
    Acquire forward_MOG_stream
    Acquire reverse_MOG_stream
    Initialize output_stream
for all frames in video_stream do
    acquire forward_mask
    acquire reverse_mask
    if frame in (0 to 5% of video_stream) then
        mask1 =Dilate(forward_mask, SMALL kernel)
        mask2 =Dilate(reverse_mask, LARGE kernel)
    else if frame in (95% to 100% of video_stream) then
        mask1 =Dilate(forward_mask, LARGE kernel)
        mask2 =Dilate(reverse_mask, SMALL kernel)
    else
        mask1 =Dilate(forward_mask, MEDIUM kernel)
        mask2 =Dilate(reverse_mask, MEDIUM kernel)
    end
    combined_mask = BitwiseOr(mask1, mask2)
    final_mask = Erode(combined_mask, LARGE kernel)
    output_stream.add(final_mask)
end
```

For first 5% of the video forward stream was in learning phase. Similarly for last 5% of the video reverse stream was in learning phase. The stream that is not in learning phase was preferred in such scenarios. The preferred stream was dilated with the LARGE kernel and the other mask (corresponding less preferred) was dilated with the SMALL kernel. After the Bitwise OR operation, the resulting mask was eroded using a LAGE kernel. During the middle portion of the video (5%-95%) both the forward and the reverse stream are given equal preference and dilated by the MEDIUM kernel.

In the first 5%, since the reverse MOG stream the model is mostly accurate, hence it has better representation of actual motion. A Bitwise OR of the two dilated masks creates an aggregate that has dilated objects from both the streams, i.e. highly expanded regions from the reverse MOG and minimally expanded regions from the forward MOG stream. Subsequent erosion of the aggregate mask using the LARGE kernel diminishes the regions of motion that are only contributed by the forward MOG (as it was dilated by a smaller kernel). Most of the small random regions, contributed by forward MOG, are removed and larger regions, contributed by forward MOG, are diminished in area. For regions contributed by the reverse MOG stream, the factor of dilation is the same as the factor of erosion; hence no detail is lost for them.

Similar logic used in for frames in last 5% of the video ensures that motions identified in forward stream are prominent. For the remaining part (i.e. in the middle), both the streams are dilated by the same factor. A kernel of MEDIUM dimensions is used on both the forward and reverse MOG streams.

IV. EXPERIMENTAL SETUP

In experimental runs, Background Subtraction Model with Mixture of Gaussian is used. There were 20 mixture channels and learning rate (α) was set as 0.005. For the morphological operations square kernels were used with dimensions as 3x3, 5x5 and 7x7 for SMALL, MEDIUM and LARGE respectively.

The algorithm was implemented using OpenCV (2.4.9). "Improved adaptive Gaussian mixture model for background subtraction" implementation was used for all the experiments [7].

A. Test Videos

Two video sources were used.

- Video from within the authors' campus was chosen such that it presented challenges that were similar to the farm monitoring scenario. (From here on referred to as internal video). The video was shot in HD Ready resolution at 30 fps. Due to the large distance, the common moving objects were relatively small. The paths are such that objects are occluded by tree and shrubs. The trees and shrubs have moderate swaying motion.
- Clip from PETS 2001 video -Camera 1; from here on referred to as the PETS video [Reference: PETS2001 datasets (University of Reading, UK)]. It has motion of people and vehicles at 25 fps.

Across the video sources, series of representative frames were chosen. Each frame series consists of four individual frames (e.g. frame numbers 5, 10, 15, 20). Frame series were chosen from start, middle and end of video. The actual region of motion (Ground Truth) for the representative frames was identified manually.

For each video source, chunks of 30 seconds were used in experimental run. Sample reference frames are captured in Figure 3. The ground truth for these frames is shown in and Figure 4. Similar work was repeated for all the twenty four frames (3 series of four frames each, for both videos).

a. PETS - frame 400 b. Internal - frame 400

Figure 3 Sample Video frames

For each video the metrics were calculated for forward BGS MOG, reversed BGS MOG, Bitwise OR , Bitwise AND , and Weighted OR. The representative masks for frame 400 in PETS video is shown in each frame series are shown in Figure 5 (a. through e.).

a. PETS video b. Internal Video

Figure 4 Ground truth video frame 400

a. Forward MOG b. Reverse MOG c. Bitwise AND

d. Bitwise OR e.Weighted OR

Figure 5 Resulting motion masks for frame 400 zoomed 4x to bottom right

B. Metrics For evaluation

Accuracy of motion detection was measured by three metrics. These were 1) Missing Foreground, 2) Added Foreground and 3) Rate of Misclassification [8].

Missing foreground refers to the percentage of foreground pixels mislabeled as background pixel. It's calculated for each representative frame as

$$MF_{rel} = (\text{Missing foreground pixels in the mask}) / (\text{Number of foreground pixels in the Ground truth}) \quad (1)$$

Added foreground is a measure to determine the degree to which background pixels are mislabeled as foreground pixels.

$$AF_{rel} = (\text{Added foreground pixels in the mask}) / (\text{Number of Background pixels in the Ground Truth}) \quad (2)$$

MF_{rel} and AF_{rel} do not account for the degree of misclassification for a missed foreground pixel or added background pixel. A falsely detected pixel that is closer to the actual foreground is better as compared to a farther pixel. This measure is provided by the metric Rate of Misclassification. It's given as:

$$F_{SC}(n) = \frac{1}{F(n)} \sum_{j=1}^{F(n)} \left(\frac{d^j_{err}}{D} \right) \quad (3)$$

Where F(n) contains set of pixels in MF ∪ AF. d^j_{err} is the distance of the j^{th} misclassified pixel from the closest contour of the ground truth. D is the length of the frame diagonal.

V. RESULTS AND OBSERVATIONS

Table 1 captures the values for AF_{rel}, MF_{rel} and F_{SCrel}, across the three frame series for both video sets.

MF_{rel}: Bitwise AND is the worst performer as it missed the foreground objects consistently. This is visible in Figure 5 (c) where large part of the car is missed.

AF_{rel}: Bitwise AND, shows only those regions that are common to both the forward and reverse MOG streams. Since most noise generated by the two streams do not overlap therefore a very low AF_{rel} value is obtained. In the initial frame series reverse streams has the lowest AF_{rel} followed closely by Weighted Or approach. Correspondingly for the end frame series (of the PETS video) the reverse stream has the lowest values followed very closely by Weighted OR.

F_{SCrel}: It measures the distance of the misclassified pixel (missing foreground and added background) from the nearest contour. Bitwise AND has the best result in all cases followed closely by the remaining methods. The reason for high F_{SCrel} for Bitwise AND is due to the missing foreground pixels. Since the contours are small this effect is not prominent.

TABLE 1 RESULTS FOR INTERNAL VIDEO (MULTIPLIED BY 1000)

			Forward	Reverse	Bitwise OR	Bitwise AND	Weighted OR
Internal Video	Series 10	MF_{rel}	0	0	186	757	36
		AF_{rel}	17.56	0.25	0.14	0	0.07
		F_{SCrel}	298.02	1.98	11.47	1.11	1.65
	Series 400	MF_{rel}	3	15	265	480	265
		AF_{rel}	1.58	1.13	0.23	0.04	0.23
		F_{SCrel}	7.9	8.62	8.4	9.33	8.4
	Series 800	MF_{rel}	152	152	411	508	197
		AF_{rel}	1.02	3.66	0.41	0.07	0.43
		F_{SCrel}	9.63	86.66	21.75	3.02	17.42
PETS Video	Series 10	MF_{rel}	140	3	45	207	6
		AF_{rel}	1.62	1.16	2.64	0.36	1.60
		F_{SCrel}	29.77	3.25	51.60	2.81	13.52
	Series 400	MF_{rel}	36	138	36	271	36
		AF_{rel}	5.44	5.95	5.85	2.83	5.85
		F_{SCrel}	165.25	179.13	179.37	166.45	179.37
	Series 700	MF_{rel}	197	156	24	449	24
		AF_{rel}	10.78	13.08	13.76	4.48	13.76
		F_{SCrel}	269.28	289.20	294.46	260.27	294.46

We conclude from the above table that

- Forward and reverse MOG streams do not perform well in the initial and the final regions of the video respectively. Otherwise they have good performance (low AF_{rel} and F_{SCrel}) and moderate MF_{rel}.
- Combination approaches (both AND and OR) use larger dilate kernel hence they have lower MF_{rel} during the middle part of video. OR is better than AND.
- Near start / end of video chunks, either of forward or reverse are best, while Weighted-OR is close second (sometimes even tying for best performance).

When comparing the three aggregation approaches, Weighted OR algorithm effectively removed the noise while keeping good values for missed foreground across all parts of video.

VI. CONCLUSION AND FUTURE WORK

Efficient motion detection techniques enable creation of accurate tracking solutions. The proposed method provides a novel way to improve motion detection. The improvement comes at the cost of additional processing required to revere the video stream and analyzed the reversed video as well as the original video. For internal video dataset, the compressed output is shared at www.swifiic.in/sambv/index.html. Fourteen megabytes was compressed to below 600 kilobytes.

Experiments with bidirectional video processing showed excellent results for Weighted OR. It improved segmentation efficiency while keeping the false positives within the bounds. Authors' intend to extend this work to study the effects of different learning rates, kernel shapes and kernel sizes across different video datasets. Further the team intends to apply bidirectional approaches to other object detection and tracking approaches that do not expect static camera view (E.g. [9][10]).

Such advances can be put to use in the fields of surveillance, video compression, event generation etc. The method is not real time but is implemented in close to real time when using chunks of video. The authors are targeting to get the system to perform in real time when working in parallel on samples of 30 seconds to a minute.

ACKNOWLEDGEMENT

The authors would like to thank the anonymous reviewers whose feedback has helped improve the quality of this work.

VII. REFERENCES

[1] Fall, K. (2003, August). A delay-tolerant network architecture for challenged internets. In Proceedings of the 2003 conference on Applications, technologies, architectures, and protocols for computer communications (pp. 27-34). ACM.

[2] Yilmaz, Alper, Omar Javed, and Mubarak Shah. "Object tracking: A survey." *Acm computing surveys (CSUR)* 38, no. 4 (2006): 13.

[3] Bouwmans, Thierry. "Traditional and recent approaches in background modeling for foreground detection: An overview." Computer Science Review 11 (2014): 31-66.

[4] Sobral, Andrews, and Antoine Vacavant. "A comprehensive review of background subtraction algorithms evaluated with synthetic and real videos." Computer Vision and Image Understanding 122 (2014): 4-21.

[5] Bauer, Sebastian, Sebastian Kohler, Konrad Doll, and Ulrich Brunsmann. "FPGA-GPU architecture for kernel SVM pedestrian detection." In *Computer Vision and Pattern Recognition Workshops (CVPRW), 2010 IEEE Computer Society Conference on*, pp. 61-68. IEEE, 2010.

[6] Friedman, Nir, and Stuart Russell. "Image segmentation in video sequences: A probabilistic approach." In *Proceedings of the Thirteenth conference on Uncertainty in artificial intelligence*, pp. 175-181. Morgan Kaufmann Publishers Inc., 1997.

[7] Zivkovic, Zoran. "Improved adaptive Gaussian mixture model for background subtraction." In *Pattern Recognition, 2004. ICPR 2004. Proceedings of the 17th International Conference on*, vol. 2, pp. 28-31. IEEE, 2004.

[8] Schlögl, Thomas, Csaba Beleznai, Martin Winter, and Horst Bischof. "Performance Evaluation Metrics for Motion Detection and Tracking." In *ICPR (4)*, pp. 519-522. 2004.

[9] Kalal, Zdenek, Krystian Mikolajczyk, and Jiri Matas. "Tracking-learning-detection." Pattern Analysis and Machine Intelligence, IEEE Transactions on 34.7 (2012): 1409-1422.

[10] Babenko, Boris, Ming-Hsuan Yang, and Serge Belongie. "Robust object tracking with online multiple instance learning." Pattern Analysis and Machine Intelligence, IEEE Transactions on 33.8 (2011): 1619-1632.

THE 18TH INTERNATIONAL SYMPOSIUM ON WIRELESS PERSONAL MULTIMEDIA COMMUNICATIONS
(WPMC-2015)
December 13-16, 2015, Hyderabad, India

QoE Based Pseudo Heartbeat Message Compression Mechanism for Wireless Networks

Zhiqun Hu, Xiangming Wen, Zhaoming Lu, Zhaoxing Li
Beijing University of Posts and Telecommunications, Beijing, China
Email: huzhiqun@bupt.edu.cn, hu208, lzy_0732, fxlizhaoxing@163.com

***Abstract*—Wireless multimedia services are increasingly becoming popular, which boosts the need for better quality-of-experience (QoE). However, there are many aspects leading to the degradation of real-time video QoE, especially, a large number of always-on-line (AOL) applications existing in future wireless networks, which require massive signaling costs and overload wireless networks. To solve this problem, we propose pseudo heartbeat message compression mechanism for future wireless networks. This mechanism reduces the number of signaling loads in the radio access network by intercepting the periodical heartbeat message at a certain frequency in the proxy client. To maintain the protocol feature of the AOL applications, the heartbeat messages are reconstructed by the proxy server installed in the air interface side and sent to the application server. The simulation results show that the proposed mechanism increases the video QoE about 1.32 times with a slight lose about 0.11 of AOL application QoE.**

I. INTRODUCTION

According to Garner's [1] market estimates, global annual shipment of smartphone handsets has increased from nearly 968 million in 2013 to 1.9 billion in 2014, resulting in the sharp increase in the use of mobile applications, such as always-on-line (AOL) applications and mobile video services. A previous study [2] reports that mobile video traffic exceeded 50 percent for the first time in 2012 and that the market share is estimated to comprise two-thirds of the world's mobile data traffic by 2017. This deluge of data has been driven chiefly by video thus far, but AOL applications can reasonably be expected to materialize in the future wireless networks. However, AOL applications require to periodically send heartbeat message to maintain the always-connected capabilities, because the macro network and mobile client actively release the connection to save wireless source and electricity consumption, respectively. This permanent features occupy considerable signaling loads and overload the air interface networks. Hence, the problem of signaling overload would significantly worsen with the continued prevalence of AOL applications in wireless networks. A great deal of signaling will utilize a considerable portion of wireless resources in the network, then the available bandwidth becomes limited for video service. Thus, the QoE of video users would be degraded as the number of AOL applications increases in the network. Therefore, how to guarantee that two kind of applications quality-of-experience (QoE) is the challenge issues that we have to face in future.

To improving the efficient of resource, the solutions to solve the signaling overload problems becomes a hot research topic and has attracted the attention of many researchers all over the world [3]- [7]. The burst traffic pattern is identified as more resource efficient with respect to signaling load than periodic traffic in [3]. Different approaches to decrease the signaling are investigated in [4]- [7]. In [4], the authors recommend to use an agent to buffer the event-triggered presence updates and reduce the network access and keep mobile devices in sleep modes as much as possible. The feasibility of decreasing signaling using timer alignment to group AOL applications has been investigated in [5]. In [6], a novel architecture is proposed to offload the particular type of applications to cloud to lessen the signaling in the networks. In [7], an keep-alive message exchange process is investigated. With the usage of push server to establish connection with several application servers, the client maintains the connectivity and an alive session with only one Internet push server.

In this paper, we present a pseudo heartbeat message compression mechanism, which solves the problem of signaling overload in mobile network by intercepting the periodical heartbeat message, to improve the video QoE. However, this mechanism inevitably impairs the AOL applications QoE. Therefore, a tradeoff between the two kind of application QoE is considered to determine the optimum intercepting frequency. We construct a network framework based on software defined network (SDN) due to it global view of the network. Based on this framework, we intercept the periodical heartbeat message in the proxy client with a certain frequency and reconstruct it in the proxy server installed in the air interface side. Thus, the proxy server pretends the mobile terminal to send the heartbeat messages to the application server at the application periodicity.

The main contribution and results of this paper are summarized as follows:

- Network framework based on OpenFlow centralized control is developed in this paper. The controller contains basic functions, including radio resource management, traffic, and QoE perception. Considering that the controller has a global view of the network, evaluation parameters of QoE can be easily and timely obtained. Moreover, network applications using the programming according to the demands of the network can be added, which can bring great flexibility for network resource management.
- A pseudo heartbeat message compression mechanism that decreases the signaling in the radio access network is designed to improve the QoE for real-time video streaming in the

network. The proposed compression mechanism is simple and easy to deploy without changing the protocol feature of AOL applications.

- We use the physical resource block to analyze the improvement of the video applications, and illustrate the packet loss model of AOL application based on the proposed mechanism.

The rest of the paper is organized as follows. Section II describes the framework of the QoE based heartbeat message compression. Section III demonstrates the influence of pseudo heartbeat message compression. Subsection A and B of Section IV introduces the QoE assessment model of video and AOL applications, respectively. Section V shows the numerical results of the proposed mechanism in detail and conclude the paper in Section VI.

II. Framework of Pseudo Heartbeat Message Compression

In this section, the framework based pseudo heartbeat message compression is proposed, which makes a clear separation between a data and control plane. The data plane consists of wireless access point performing flow-based packet forwarding and proxy server implementing heartbeat message rebuilding, and the control plane consists of one controller, whose responsibility is to allocate the radio resource and dynamically determine the corresponding parameters that guarantee the best output service quality. The southbound protocol conducts communication protocol between the two planes. This framework is depicted in Fig.1.

OpenFlow controller [8] consists of network operating system and application interfaces; hence, new functions by programming without changing the underlying networks, such as the management of QoE and pseudo heartbeat message compression (PHMC) application, can be easily realized. Considering that the controller has a global view over the radio access network, the OpenFlow controller can easily obtain the parameters of the QoE assessment algorithm. Then, the PHMC application is invoked to obtain an optimum intercept frequency if one type of service exhibits an excessively poor QoE. In this way, the optimal interception frequency can be calculated on the premise that all different QoE of services are met in the current networks environment.

Based on the framework, our proposed pseudo heartbeat message compression mechanism is achieved. When the AOL applications periodically send heartbeat message to the application services, the client proxy will intercept the heartbeat messages with a certain frequency except that the first heartbeat message. And the controller can obtain the information of the heartbeat message, such as cycle information, address information, and informs the proxy server of rebuilding a list of heartbeat messages using the proprietary protocol of each AOL application. Then, the proxy server forges the user behavior to periodically send the heartbeat messages to the AOL application server at the original frequency. Therefore, from the radio access point perspective, the cycle of heartbeat messages is extended several times, but from the application

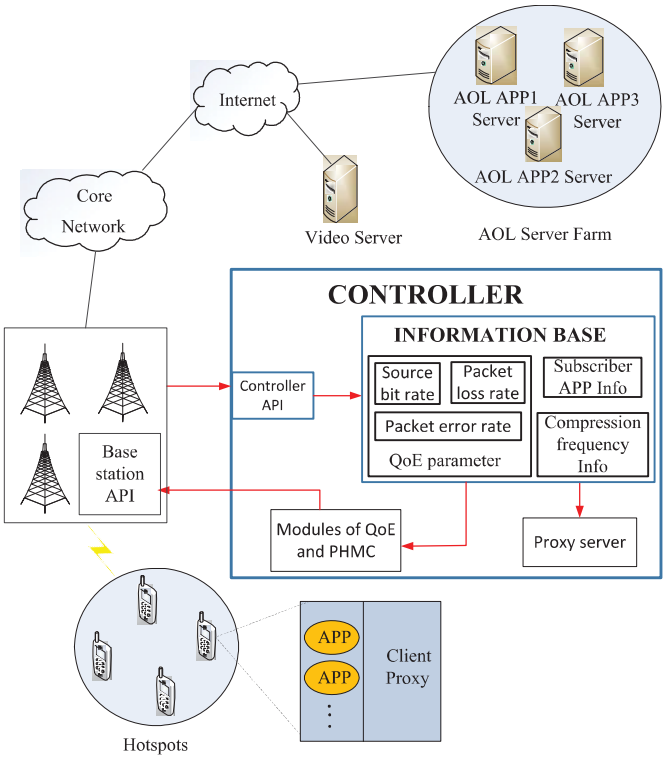

Fig. 1. Framework based pseudo heartbeat message compression.

server perspective, the periodicity of the application is not changed. This mechanism called pseudo heartbeat messages compression mechanism greatly decreases the signaling in the air interface and doesn't change the protocol feature of application. With increasing number of users with AOL applications in the networks, and enormously decreases the signaling pressure of the air interface, and more wireless resource can be saved to improve video performance.

III. Influence of Pseudo Heartbeat Message Compression

In this section, the influence of the pseudo heartbeat message compression on the video and AOL applications are presented.

A. Improvement of video application

1) Resource Saving Metric: In general, sending a heartbeat message occupies about N_b bytes of downlink (DL) resources, which consumes N_{cs} slots and every slot at least occupies N_p physical resource blocks (PRB). Therefore, the consumption of DL wireless resources for sending a heartbeat message successfully is $N_{cs} \cdot N_p$ PRBs. Supposing the compression frequency is N and the original average heartbeat message periodicity is T_h, then the average periodicity of the heartbeat message is $N \cdot T_h$ seconds according to the pesudo heartbeat message mechanism. Then, within t seconds, the number of reduced heartbeat message is equal to $\frac{t}{T_h} - \frac{t}{N \cdot T_h}$. Hence, assuming that the cell has M AOL applications running, the

number of the saved PRBs within t seconds, N_{SPRB}, can be expressed as follows:

$$N_{SPRB} = \frac{\mathrm{N}_{cs} N_p t M}{T_h}(1 - \frac{1}{N}) \quad (1)$$

2) Calculation of Transmitting Bit Rate for Real-Time Video: In this paper, the DL adapts OFDMA wherein radio resources are split into time and frequency slots, which is called resource blocks. A subframe splits into N_s slots and each slot comprises N_{OFDM} OFDM symbols. N_{CR} and N_{RS} are the number of control signal and the reference signal, respectively. N_{sc}^{RB} is the number of subcarriers in one PRB and M_{mod} is the modulation order such as QPSK, 16QAM and R_T is the coding rate. Then, the increase of the transmission bit rate ($TBR_{increase}$) within the t seconds can be written as Eq.(2) in the top of the next page.

Hence, based on the proposed pesudo heartbeat message mechanism, the TBR of video can be expressed as follows:

$$TBR_{new} = (TBR_{initial} + TBR_{increase}) * \alpha \quad (3)$$

where α denotes the factor of the current network conditions and $TBR_{initial}$ is the initial transmitted bit rate of the video.

In real-time videos, user's QoE is affected by sender bit rate (SBR), which adaptively adjusts the video coding parameters according to the available bandwidth. A high SBR in the network leads to high video quality and, ultimately, to enhance QoE of end users. Assume that the TBR is numerically equivalent to the SBR. Hence, the change of TBR can affect the video QoE.

B. Packet Loss Model of AOL application

Assume that $T = N \cdot T_h$ is the interval of the interception, which associates with the compression frequency N and the average normal frequency of heartbeat message is T_h. If the packet arrive in a Poisson manner with a mean rate u, the probability that k packets arrive in a interval T can be written as follows:

$$p(k) = \frac{(uT)^k e^{-uT}}{k!} \quad (4)$$

where uT is the average number of data arrival in a interval T.

The probability P_{loss1} is given by the probability that the packet loss occurs when the terminal drops out, i.e.,

$$P_{loss1} = P_1 \quad (5)$$

where P_1 is the probability that terminal drops out in the interval of the interception while the application server still intends to send the data to the client because the proxy server maintains the connection with the pseudo heartbeat message. Thus, the packets affirmatively loss on the fact that the terminal drops out.

Assume the observed time is $1/C$. It seems reasonable that the time of the terminal dropping should be uniformly distributed over $(0, 1/C]$. Hence, the probability that terminal drops within T can be expressed as follows:

$$P_1 = P\,(0 < x < T) = \int_0^T C dt = T \times C \qquad 0 < T < T_{\max} \quad (6)$$

Conversely, when the terminal does not drop out, the data may be lost in transmission process. Supposing that the success probability of each data packet transmission is q. The successful transmitted is defined as all packets transmit successfully. Then the average probability $Pc_{success}$ that the transmission on the channel is successful can be expressed as follows:

$$Pc(success) = \sum_{k=0}^{\infty} p(k) \cdot q^k \quad (7)$$

where $p(k)$ is the probability that k packets arrive in a time period T.

In which after rearranging yields

$$Pc(success) = e^{uT(q-1)} \quad (8)$$

Hence, let P_{loss2} be the probability that the packet loss of AOL application occurs when the terminal does not drop out, i.e.,

$$P_{loss2} = (1 - P_1)(1 - P_c(success)) \quad (9)$$

Therefore, the packet loss rate for the wireless network is approximately

$$P_{loss} = P_{loss1} + P_{loss2} \quad (10)$$

where

$$P_{loss} = N \cdot T_h \cdot C + (1 - N \cdot T_h \cdot C)(1 - e^{uNT_h(q-1)}) \quad (11)$$

IV. QoE ASSESSMENT MODEL FOR VIDEO AND AOL APPLICATION

As observed in the previous section, the framework of pseudo heartbeat message compression increases the SBR of video users as well as the packet loss rate of AOL users by intercepting the heartbeat messages. Therefore, such a situation may lead to QoE degradation for AOL users in exchange of improving the QoE of real-time video users. This section aims to introduce the assessment method of video and AOL applications.

A. Video QoE Model

In this paper, we choose a video QoE prediction model considering four most dominant factors, i.e. the video content (CT), Frame rate (FR), source bit rate (SBR), packet error rate (PER) [10]:

$$QoE = \frac{a_1 + a_2 \cdot FR + a_3 \cdot \ln(SBR)}{1 + a_4 \cdot PER + a_5 \cdot (PER)^2} \quad (12)$$

An accurate video quality assessment algorithm must consider video content because the visual quality cannot be accurately predicted by only using the bit rate and the spatial and temporal resolutions of the video streams. The video content is

$$TBR_{increase} = \frac{N_{SPRB} \cdot \left[N_{sc}^{RB} \cdot (N_s \cdot \mathrm{N}_{OFDM} - N_{CR}) - N_{RS}\right] \cdot M_{\mathrm{mod}} \cdot R_T}{t} \quad (2)$$

TABLE I
COEFFICIENTS METRIC MODELS FOR ALL CONTENT TYPES [10]

Coeff	SM	GW	RM
a_1	4.5796	3.4757	3.0946
a_2	-0.0065	0.0022	-0.0065
a_3	0.0573	0.0407	0.1464
a_4	2.2073	2.4984	10.0437
a_5	7.1773	-3.7433	0.6865

classified into three categories (Slight movement (SM), Gentle walking (GW), Rapid movement (RM)) according to video features [11]. The coefficients for all the three content types are given in Table I. Because our proposed mechanism aiming to improve the SBR of video, then we consider the source video of RM, which has great demand for wireless resource to guarantee the video quality, as our tested source, namely, the coefficients values for RM type are expressed as follow: a_1=3.0946, a_2=-0.0065, a_3=0.1464, a_4=10.0437, a_5=0.6865.

B. AOL Application QoE Model

To simplify the analysis, the QoE is assumed to be the function of a signal impairment factor. The packet loss rate is considered as the measurement of QoS. A certain amount of information is transmitted over a network simulator with variable packet loss rates.

The expression of QoE estimation model that we use in our model is the same as in [12], namely

$$QoE = 3.104 \cdot e^{(-4.472 \cdot P_{loss})} + 1.067 \quad (13)$$

where P_{loss} is the packet loss rate of AOL application.

Plugging the P_{loss}, the above Eq. (16) can be expressed as follows:

$$QoE = 3.104 \cdot e^{\left(-4.472(N \cdot T_h \cdot C + (1 - N \cdot T_h \cdot C)(1 - e^{uNT_h(q-1)}))\right)} + 1.067 \quad (14)$$

V. NUMERICAL RESULTS

In this section, pseudo heartbeat message compression among AOL applications and video applications is considered and the performance within an OFDMA communication system is tested. Assuming that M AOL applications are running in the background, and the parameters of FR and FS are 30 fps and QCIF, respectively, and the coding rate R_T is $\frac{2}{3}$. The initial TBR is set to be 100 Kbps and the average heartbeat message periodicity T_h is set to 100 seconds. The probability density function C is 1×10^{-4}. Assuming that the channel quality is stationary and the network conditions adjustment factor α is set to be 0.4. The performance analysis of the pseudo heartbeat message compression model is simulated by using matlab and the parameters are listed in table II.

TABLE II
SYSTEM PARAMETERS

System parameters	Description	Value
BW	System bandwidth	5Mhz
B_s	Bandwidth per subcarrier	15Khz
N_{sc}^{RB}	Number of subcarrier per resource block	12
N_{RS}	Number of reference signal	8
N_{CR}	Number of control signal	3
N_s	Number of slots per subframes	2
N_{OFDM}	Number of OFDM symbols per solts	7
M_{mod}	Spectral efficiency in cell	4
u	Average number of data arrival	0.006
q	The success probability of packet transmission	0.95

In Fig.2, the larger the number of AOL application users is, the higher the improvement of the QoE of video is. This result shows that the proposed scheme is quite useful to improve the QoE of video users, especially with a large number of AOL application users in the hotspot. The success of the mechanism can be attributed to the reduced number of signaling messages transmitted or received by an AOL users' device when the proposed compression scheme is used. In addition, the saved wireless resource growth for the increasing AOL users is tremendous because more signaling are intercepted, which indicates the potential of the pseudo heartbeat message compression mechanism to support large number of AOL users.

Fig.3 presents the relationship between QoE improvement of AOL application and that of video. We can obtain that the performance of real-time video users improves while the AOL user degrades as the compression frequency N increases. Fig.3 implies the evident trade-off between the QoE of AOL users and real-time video users when we choose the proper parameters of our proposed mechanism.

Fig.4 demonstrates the influence of the pseudo heartbeat message compression on the video and AOL applications. Resources saved by decreasing heartbeat messages improve the QoE of video users by 1.32 while slightly reducing the QoE of AOL users by a factor of 0.11 (from 1 to 0.89). Previous methods for solving signaling overloaded often decrease the signaling in the network by changing the network mechanism to adapt to the characteristics of the current Internet applications. However, the proposed approach, which

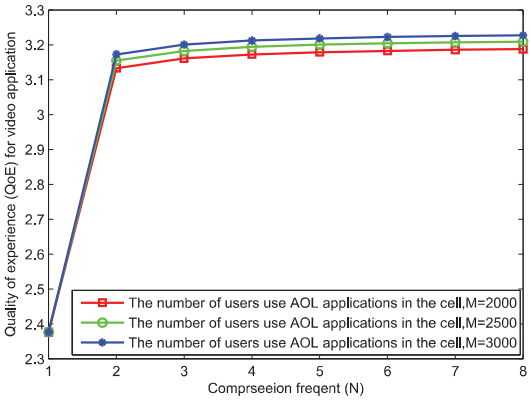

Fig. 2. Variation of QoE of video users with compression frequency N with different numbers of AOL application users in cell.

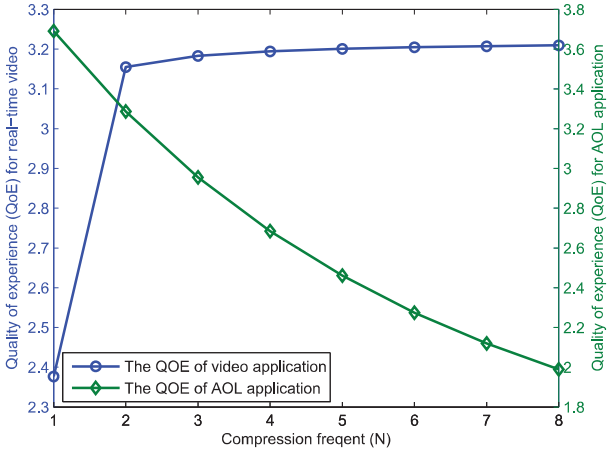

Fig. 3. Relationship between QoE improvement of AOL application and that of video.

can be considered a case of preferential treatment intercepting the heartbeat messages, is easy to deploy without changing the feature of AOL applications.

VI. CONCLUSIONS

In this paper, we proposes a pseudo heartbeat message compression mechanism to fundamentally solve the signaling overload while guarantee the QoE of services. We first construct the framework of the pseudo heartbeat message compression and then analyze the influence of the mechanism on the AOL and video services. As the prevalent of smartphone handsets and internet applications, the large number of heatbeat messages occupy the limited wireless resource, which leads to overload of network, even to paralyze the network. Simulation results show that the proposed mechanism can greatly decrease the heartbeat messages and increases the video QoE about 1.32 times with a slight lose about 0.11 of AOL application QoE. Hence, the proposed mechanism is a promising method to address the above issues. Future

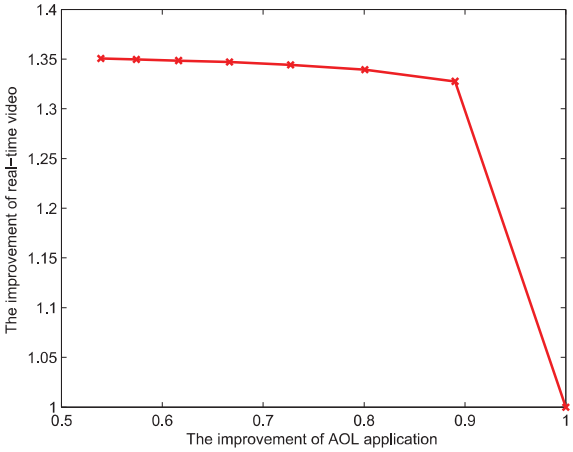

Fig. 4. Tradeoff curve between QoE improvement of AOL application and that of video.

works can involve further exploration along these dimensions by including dynamic resource allocation and considering QoE in employing offloading and load balancing techniques.

ACKNOWLEDGEMENTS

This research is supported by the WLAN achievement transformation based on SDN of Beijing Municipal Commission of Education, and the grant number is 201501001.

REFERENCES

[1] Techcrunch, "Gartner: smartphone sales finally beat out dumb phone sales globally in 2013, with 968M nits sold"[online].Available: https://www.google.com.hk/
[2] cisco."Cisco Visual Networking Index: Global Mobile Data Traffic Forecast Update, 2012-2017."[online].Available: http://goo.gl/xxLT.
[3] Signals Research Group. Smartphones and a 3g network: Reducing the impact of smartphone-generated signaling traffic while increasing the battery life of the phone through the use of network optimization techniques. Technical report, LLC, 2010.
[4] Ville Kononen, et.al.," Optimizing power consumption of always-on applications based on timer alignment." COMSNETS 2011: 1-8.
[5] Meng, Ling-San, et al. "Low power consumption solutions for mobile instant messaging." Mobile Computing, IEEE Transactions on 11.6 (2012): 896-904.
[6] Saarinen, Aki, et al. "Offloadable apps using smartdiet: Towards an analysis toolkit for mobile application developers." arXiv preprint arXiv:1111.3806 (2011).
[7] Sameh Gobriel, Christian Maciocco, et al. "EE-AOC: energy efficient always-on-line-connectivity architecture." Circuits and systems research lab, Intel labs, Intel Corporation.
[8] Pongracz, G. ; Molnar, L. ; Kis, Z.L. "Removing Roadblocks from SDN: OpenFlow Software Switch Performance on Intel DPDK" Software Defined Networks (EWSDN), Second European Workshop on, 2013.
[9] Zhai, Guangtao, et al. "Cross-dimensional perceptual quality assessment for low bit-rate videos." Multimedia, IEEE Transactions on 10.7 (2008): 1316-1324.
[10] Khan, Asiya, Lingfen Sun, and Emmanuel Ifeachor. "Content clustering based video quality prediction model for MPEG4 video streaming over wireless networks." IEEE International Conference on. IEEE, 2009.
[11] S. du Toit, A. Steyn and R. Stumpf, Cluster analysis, Handbook of graphical exploratory data analysis, ed. S.H.C. du Toit, pp.73-104, Springer-Verlag, New York, 1986.
[12] Fiedler, Markus, Tobias Hossfeld, and Phuoc Tran-Gia. "A generic quantitative relationship between quality of experience and quality of service." Network, IEEE 24.2 (2010): 36-41.

THE 18TH INTERNATIONAL SYMPOSIUM ON WIRELESS PERSONAL MULTIMEDIA COMMUNICATIONS
(WPMC-2015)
December 13-16, 2015, Hyderabad, India

Survey of Device-to-Device Communications Infrastructure-less in IEEE 802.15.8 Task Group

Marco Hernandez, Ryu Miura
Dependable Wireless Laboratory
National Institute of Information and Communications Technology
3-4 Hikarino-oka 239-0847 Yokosuka Japan
Marco@nict.go.jp Tel: +81-46-847-5439

***Abstract*—Peer-to-peer or device-to-device communications is an active field of research and development. It offers the potential of great improvement in the delivery and monitoring of ever growing data services ranging from social networking, gaming, advertisement, emergency communications (especially the case when infrastructure based systems such as base stations or access points have been knocked down by natural disasters).**

The current state of the art includes device-to-device communications for proximity services currently in development by LTE. Also, Wi-Fi Direct that aims to replace Wi-Fi ad-hoc mode, and proprietary systems such as FlashLinQ by Qualcomm. However, the mentioned systems still rely on infrastructure for network synchronization and/or discovery and management.

The IEEE 802.15.8 Peer-Aware-Communications (PAC) Task Group (TG8) aims to develop ad hoc peer-to-peer communications, infrastructure-less and with fully distributed coordination. Some PAC features include discovery of peers information without association, scalable number of devices during discovery, scalable data transmission rates, simultaneous multi-group communications, among others.

***Index Terms*—Device-to-device communications; Emergency communications infrastructure-less; IEEE802.15 Standardization.**

I. Concept and architecture

A PAC system contains the following functionalities:

- For the challenging fully distributed network synchronization, TG8 introduces a modified firefly algorithm, which allows to reach network synchronization regardless of the topology.
- Once PAC devices (PDs) are synchronized, such PDs proceed to discover or being discovered during the discovery period. In this phase, discovery information are passed to/from higher layers related to PD ID, group ID, application ID, etc.
- After discovery, PDs may request a communication link. Such next phase is association; However, as this is done in a peer-to peer basis, the process is named *peering*.
- After PDs have successfully established a communication link (authentication and security included), they proceed to communicate either contention based of contention free under a TDD scheme during the communication period.
- Power control (open loop for the CFP and close loop for CAP) aims best performance by maintaining adequate SINR.
- A measurement and report unit conducts measurements for channel information, like clear channel assessment (CCA), channel scanning, channel quality indication (CQI), etc. and it reports to upper layers. An scheduling unit controls the assessment of resources for communication based on SINR and QoS for the CFP.
- The PHY consists of FEC, scrambling, interleaving, modulation, multi-carrier modulation and multiple antennas in the form of MIMO techniques or beamforming.

II. Topology

PAC network topologies support one-to-one and one-to-many (group or multicast communications), having simultaneous communication sessions for the same or different applications as illustrated in Figure **??**.

Fig. 1. *Topology.*

III. Reference model

In accordance with the IEEE 802® reference model, PAC devices are internally partitioned into a physical layer (PHY) and data link layer (medium access control (MAC) sublayer and logical link control (LLC) sublayer). Although there is a modification respect to the OSI model as higher layers can have direct access to the MAC sublayer.

IV. MAC sublayer

A. Superframe

The MAC superframe structure is defined as illustrated in Figure **??**. The superframe is divided into 5 periods in

the following order: synchronization period, discovery period, peering period, communication period containing a contention access period (CAP), and contention free period (CFP).

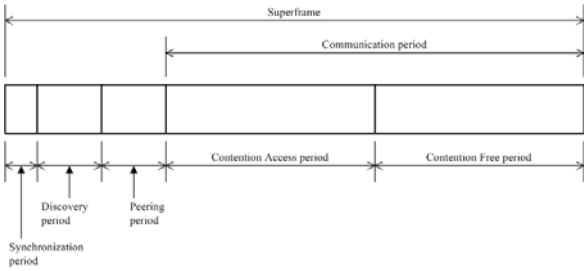

Fig. 2. *MAC superframe.*

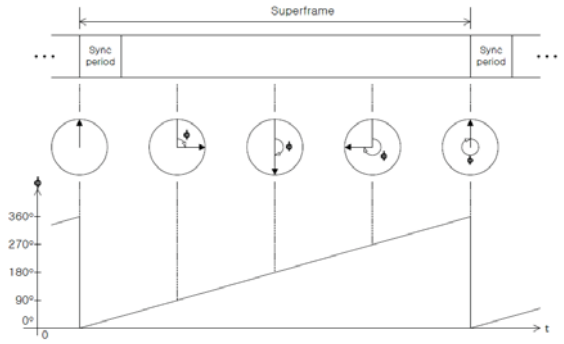

Fig. 3. *Superframe and phase of a synchronization timer.*

B. Network synchronization

The synchronization period is used to transmit a set of preambles that are used for network synchronization. In synchronized mode, PAC operates in fully distributed synchronization. Two modes of network synchronization are envisioned:

- Synchronization among PDs can be achieved by the transmission and reception of a synchronization reference signal. In case there is already synchronization among PDs, each PD may send its synchronization reference signal to maintain synchronization.
- The synchronization reference signal may be transmitted by a single PD dynamically elected from a group of PDs.

1) Transmission of synchronization signal: The synchronization signal is transmitted during the synchronization period using random access to avoid collision. The length of synchronization period is equivalent to the length of backoff slots, where one backoff slot is equivalent to the length of two OFDM symbols. The random access scheme is as follows:

a) Each PD maintains its own contention window (CW).
b) A PD selects an integer n randomly drawn from $(0, 1, 2, , CW - 1)$ and sets its backoff counter to the selected random integer n, and follows backoff procedure until its backoff counter becomes zero. Then the PD transmits a synchronization signal, and sets its backoff counter to $CW - 1 - n$, and follows backoff procedure until its backoff counter becomes zero, at which point it goes to step 3).
c) A PD updates its CW and goes to step b).

2) Adjustment of reference timing: All PDs maintain a synchronization timer whose phase ϕ varies from 0 to 360^0. Each PD does transmit a synchronization signal when its clock's phase, ϕ, reaches 360^0 and using the random access procedure described before. The relationship between the MAC superframe and synchronization timer is illustrated in Figure **??**.

When a PD receives the synchronization signal, it adjusts its reference timing by changing its phase ϕ based on the reference timing obtained from the received synchronization signal. The rule for a PD to update its phase ϕ of its synchronization timer is as follows:

1) If phase $\phi < 180^0$, then the PD does not change its reference timing.
2) If phase $\phi \geq 180^0$, then the PD adjusts such phase value to 360^0.

C. Discovery

PAC systems support the following discovery types:

- Advertisement: In this type of discovery, a PD transmits its discovery information and does not expect responses.
- Publish/Subscribe: in this type of discovery, a PD transmits its discovery information and expects responses.
- Query/Reply: in this type of discovery, a PD transmits its discovery information as response to a request to do so.

The discovery information conveys the following IDs: device ID (48 bits MAC address), peer ID (56 bits), group ID (8 bits), application ID (56 bits). The discovery procedure should support mechanisms to ensure privacy that a PD is not tracked, and protection of identity from impersonation.

D. Peering

Peering (association) is the procedure to establish a communication link among discovered PDs.

1) Random access procedure for peering for CFP: Once network synchronization and detection of discovery information are achieved, PDs may request peering to a target PD, at any time. Consequently, the random access can be requested during the peering period, in which control signals are interchanged in order to schedule the intended PDs for transmission.

E. Communication

Data packets for unicast, multicast, or broadcast are transmitted during the communication period (either CAP or CFP) as illustrated in Figure **??**. Details are still in progress in the Task Group IEEE802.15.8.

V. General PHY layer requirements

The proposed PHY layer provides a data interface to the MAC sublayer under the control of the physical layer convergence protocol (PLCP). The proposed PHYs are:

- Low mobility PHY: OFDM multi-carrier modulation with BPSK, QPSK, 16QAM and 64QAM symbols, operating in the 2.4 GHz and 5.7 GHz bands.
- High mobility PHY: OFDMA multicarrier modulation with BPSK, QPSK, 16QAM and 64QAM symbols operating in sub-GHz, 2.4 GHz and 5.7 GHz bands.
- UWB PHY: combined burts position modulation (BPM) and BPSK modulation, OOK modulation, operating in the 4.2 – 10 GHz band.

Due to the lack of space, we describe the high mobility PHY layer only.

VI. High Mobility PHY

The physical layer protocol data unit (PPDU) is formed by concatenating the synchronization preamble, the physical layer header (PHR), the discovery signal, peering signal, and the physical layer service information data unit (PSDU) signal, respectively. The PSDU is formed by N data-channels. Each data channel is sub-divided into scheduling and data frame. Each data frame consists of 10 TDD slots: two switching slots (denoted as S) and eight data slots. Each data slot consists of seven OFDM symbols with duration of 0.5 ms.

A. PSDU construction

The PSDU data is encoded by quasi-cyclic low density parity check codes (QC-LDPC), which allow performance close to turbo codes, besides that encoder/decoder enable high throughput and efficient implementation in parallel architectures. Furthermore, interleaving, scrambling, symbol modulation, MIMO layer mapping and OFDM are applied as well.

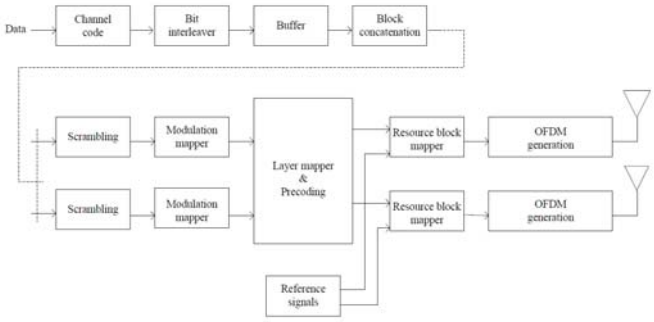

Fig. 4. *PSDU construction.*

B. QC-LDPC encoder parameters

Quasi-cyclic LDPC codes are systematic, linear codes satisfying $\boldsymbol{H}\boldsymbol{c}^T = \mathbf{0}$; where $\boldsymbol{H}_{n-k\text{x}k}$ is the parity check matrix, k is the number of information bits, n is the number of coded bits and $n-k$ is the number of parity bits.
$\boldsymbol{H}$ is constructed from a prototype matrix $\boldsymbol{H}_{p|M p\text{x}N p}$ by replacing each entry of the prototype matrix, denoted as $[H_p]_{i,j}$ with either a cyclic shift matrix, $\boldsymbol{P}_c$, or identity matrix or null matrix of size $Z\text{x}Z$. The final size of $\boldsymbol{H}$ is $MpZ\text{x}NpZ$.

$$[H_p]_{i,j} = \begin{cases} \boldsymbol{I}_{z\text{x}z} & \text{if } [H_p]_{i,j} = 0 \\ \mathbf{0}_{z\text{x}z} & \text{if } [H_p]_{i,j} = \text{"}-\text{"} \\ \boldsymbol{P}_c & \text{if } [H_p]_{i,j} = p \end{cases} \quad (1)$$

where $p > 0$ is an integer number, and "-" denotes a character. The cyclic-permutation matrix $\boldsymbol{P}_c$ is obtained by cyclically shifting the columns of $\boldsymbol{P}_0 = \boldsymbol{I}_{Z\text{x}Z}$ to the right c times. The prototype matrices are not shown for the lack of space.
The total number of coded bits in a packet is $N_{T_{cw}} = n\, N_{CW}$, where N_{CW} is the number of codewords. The coded bits are indexed as c_{nq+i} for $i = 0, 1..., n-1$ and $q = 0, 1, ..., N_{CW} - 1$.

C. Interleaver

Interleaving is based on maximum contention-free quadratic permutation interleaver. Thus, latency is minimized and the interleaver can be integrated on parallel architectures within the encoder/decoder chip implementation. A maximum contention-free quadratic permutation interleaver is defined as:

$$\Pi(i) = f_1 i + f_2 i^2 \,\text{Mod}\, N_I \quad (2)$$

where N_I is the interleaver's length. The coded bits are interleaved in blocks of N_I bits as $c_{\Pi(j \,\text{Mod} N_I)}$ for $j = 0, ..., N_{T_{cw}} - 1$.

D. Scrambler

A Gold code generator of length 63 is employed as scrambler. A scrambler is used to shape the data spectrum and randomize data across users in order to reduce interference. As the Gold code generator is formed by two PN sequences with period $L = 2^{63}$, its output remains random even for long packets. Moreover, different initialization seeds, enables a different Gold code sequence per user and consequently low correlation respect to other user using a different seed. The Gold code generator is constructed by two PN sequence generators with polynomials $x^6 + x + 1$ and $x^6 + x^5 + x^2 + x + 1$. The Gold code generator output is indicated by s_i, which is used to scramble the interleaved-coded bits as $b_i = (c_{\Pi(i \,\text{Mod}\, N_I)} + s_{i \,\text{Mod}\, L}) \,\text{Mod}\, 2$ for $i = 0, 1, ..., N_{T_{cw}} - 1$.

E. Modulation mapper

After scrambling, b_i bits are modulated with BPSK, QPSK, 16QAM or 64QAM. The modulation symbols, d_l, as function of the input bits, b_i are given in Figure **??**. The bit index $i = 0, ..., N_T - 1$ and symbol index $l = 0, ..., N_{sym} - 1$, where $N_{sym} = N_T \text{Log}_2(M)$, and N_T is the total number of bits on the air per packet. The mapping onto complex symbols $I + jQ$ for the different modulation schemes can be found in the literature.

Modulation	Complex symbol	$\text{Log}_2(M)$
BPSK	$d_l(b_l)=I+jQ$	1
QPSK	$d_l(b_i, b_{i+1})=I+jQ$	2
16QAM	$d_l(b_i, b_{i+1}, b_{i+2}, b_{i+3})=I+jQ$	4
64QAM	$d_l(b_i, b_{i+1}, b_{i+2}, b_{i+3}, b_{i+4}, b_{i+5})=I+jQ$	6

Fig. 5. *Symbol modulations.*

F. Layer mapping

Two MIMO technologies are supported: open loop spatial multiplexing and transmit diversity in the form of space-frequency block codes, for 2 and 4 antennas. The transmission in MIMO mode depends on the number of antennas that can be implemented. The complex modulation symbols for the qth codeword, for $l = 0, 1, ..., N^q_{sym} - 1$ are mapped into several layers as

$$[d^q_0, ..., d^q_{N^q_{sym}-1}] \rightarrow [x_0(i), ..., x_{\nu-1}(i)] \tag{3}$$

for $i = 0, ..., N^L_{sym} - 1$, where ν is the number of layers and N^L_{sym} is the number of symbols per layer. A layer is an independent stream of symbols in a MIMO configuration. The MIMO channel's rank is the number of layers enable.

1) Open loop spatial multiplexing: Spatial multiplexing represents the transmission of multiple parallel streams of symbols. The mapping of modulation symbols to layers is shown in Figure **??**. The number of layers is less or equal to the number of antennas, $\nu \leq P$.

No of layers	No of codewords	Mapping	Parameter
1	1	$x_0(i) = d^0_i$	$N^L_{sym} = N^0_{sym}$
2	1	$x_0(i) = d^0_{2i}$ $x_1(i) = d^0_{2i+1}$	$N^L_{sym} = N^0_{sym}/2$
2	2	$x_0(i) = d^0_i$ $x_1(i) = d^1_i$	$N^L_{sym} = N^0_{sym} = N^1_{sym}$
4	1	$x_0(i) = d^0_{4i}$ $x_1(i) = d^0_{4i+1}$ $x_2(i) = d^0_{4i+2}$ $x_3(i) = d^0_{4i+3}$	$N^L_{sym} = N^0_{sym}/4$
4	2	$x_0(i) = d^0_{2i}$ $x_1(i) = d^1_{2i+1}$ $x_2(i) = d^0_{2i}$ $x_3(i) = d^1_{2i+1}$	$N^L_{sym} = N^0_{sym}/2 = N^1_{sym}/2$

Fig. 6. *Mapping for spatial multiplexing.*

2) Transmit diversity: Transmit diversity is created by transmitting the same information from multiple antennas. The mapping of modulation symbols to layers is shown in Figure **??** (If $N^q_{sym} \,\text{Mod}\, 4 \neq 0$ add m null symbols at the end such that $N^q_{sym} + m \,\text{Mod}\, 4 = 0$).

G. Precoding

The block of symbols obtained from the layer mapping, $\boldsymbol{x}_p$, are mapped onto the block of symbols $\boldsymbol{y}_p$, to be transmitted by P antennas as illustrated in Figure **??**.

No of layers	No of codewords	Mapping	Parameter
2	1	$x_0(i) = d^0_{2i}$ $x_1(i) = d^1_{2i+1}$	$N^L_{sym} = N^0_{sym}/2$
4	1	$x_0(i) = d^0_{4i}$ $x_1(i) = d^0_{4i+1}$ $x_2(i) = d^0_{4i+2}$ $x_0(i) = d^0_{4i+3}$	$N^L_{sym} = \begin{cases} N^0_{sym}/4 & \text{If } N_{sym}\text{Mod}4 = 0 \\ \dfrac{N^0_{sym}+m}{4} & \text{If } N_{sym}\text{Mod}4 \neq 0 \end{cases}$

Fig. 7. *Mapping for transmit diversity.*

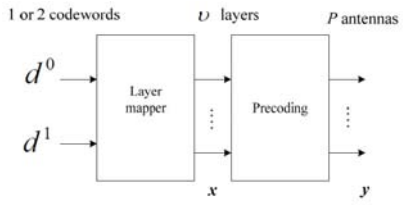

Fig. 8. *Precoding mapping.*

1) Open loop spatial multiplexing: Precoding for open loop spatial multiplexing delivers performance robustness by feeding back the channels rank. Such channels rank is indicated by 2 bits in the control channel of the TDD frame. Consequently, the transmitter can choose a pre-fixed codeword according to the channels rank.

2) Transmit diversity: Transmit diversity is aimed to increase robustness in scenarios with low SNR, low delay tolerance or no feedback to the transmitter is available or reliable. In case of 2 antennas, the space-frequency block codes (SFBC) are defined by

$$\begin{bmatrix} y_0(2i) & y_0(2i+1) \\ y_1(2i) & y_1(2i+1) \end{bmatrix} = \frac{1}{\sqrt{2}} \begin{bmatrix} x_0(i) & x_1(i) \\ -x^*_1(i) & x^*_0(i) \end{bmatrix} \tag{4}$$

where $i = 0, ..., N^L_{sym} - 1$ and $N^P_{sym} = 2N^L_{sym}$. In case of 4 antennas a combination of SFBC for 2 antennas with frequency switch transmission diversity is employed.

H. Multicarrier modulation

The multicarrier modulation parameters for OFDM are given in Figure **??**. The subcarrier spacing of 15 KHz ensures a good compromise for handling delay spread in radio channels and digital radio implementations availability.

Description	Notation
Total No of subcarriers	MFFT=1024
Subcarrier spacing	Δf=15 KHz
Sampling time	T_s=1/(Δf MFFT)=65.1 nsec
Clock rate	R_c=1/T_s=15.36 MHz

Fig. 9. *Multicarrier parameters.*

The cyclic prefix length covers 73 sampling points with duration $73Ts = 4.75$ μsec.

1) Resource block : A resource block (RB) is a set of time-frequency slots for data communication and enabling multiple access. A RB is formed by a slot time of 0.5 msec ($N_{symb} = 7$ OFDM symbols) and $N_{sc}^{RB} = 6$ subcarriers or 90 KHz spectrum. The total number of RBs is $N_{RB} = 170$ (the 2 upper and lower subcarriers are empty). Different transmission bandwidths are obtained by concatenating RBs as $BW = nN_{sc}^{RB}\Delta f$, where $12 \leq n \leq 111$.

I. Carrier aggregation

In order to have coexistence with Wi-Fi, carrier aggregation with one more channel of 10 MHz can be added to increase the transmission bandwidth to 20 MHz. Such carrier aggregation is granted by the MAC and signaled to the PHY by one bit in the control channel of the TDD frame. The aggregated channel can be considered as a single enlarged channel of 20 MHz from the RF viewpoint. Hence, the same RF front end can be used without modifications.

VII. Simulations

A. Receivers

The optimum detection of coded MIMO systems is performed in terms of joint detection and decoding. However, such optimum implementation complexity is prohibited high in practical applications. On the other hand, there are plenty of proposed suboptimum techniques that try to balance implementation complexity and performance. One popular approach is MMSE-SIC (minimum mean square error-successive interference cancelation) detection. However, the most promising sub-optimum approach with close optimum performance and [relative] low complexity implementation is iterative MIMO decoding, as illustrated in Figure **??**. The core idea is independent MIMO detection and iterative channel decoding.

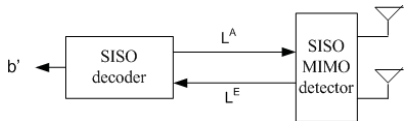

Fig. 10. *Iterative MIMO decoding.*

B. Channel models

The small scale channel models are based on the ITU and ETSI-BRAN channel models. Such models were extended to the popular correlated MIMO fading channel model as well. Details, including MatLab® scripts, can be found in [**?**].

C. Results

Figure **??** shows the PER performance with 1/2 rate CC, OFDM with 16QAM symbols and spatial multiplexing MIMO configuration for 4x4 antennas (ITU MIMO channel for low correlation and pedestrian).
Additionally, We present the PER performance for QC-LDPC(324,648), rate 1/2, OFDM with BPSK symbols for 1x1 antennas configuration and decoding with SPA=sum-product algorithm, MPA=message passing algorithm and OMS=offset min-sum algorithm, (ITU channel model for pedestrian), as it is shown in Figure **??**.

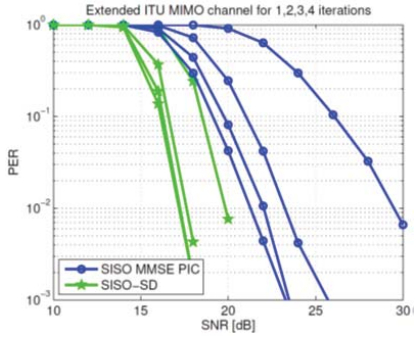

Fig. 11. *Extended ITU MIMO channel with 1,2,3,4 iterations.*

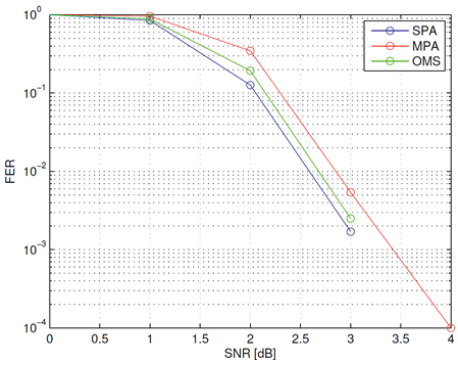

Fig. 12. *Performance of QC-LDPC with one antenna.*

VIII. Conclusions

A survey of IEEE 802.15.8 Peer-Aware-Communications (PAC) Task Group (TG8) activities towards the standardization of technologies to develop peer-to-peer or device-to-device (D2D) communications, infrastructure-less and with fully distributed coordination. Peer-to-peer communications is an active field of research and development, in particular for gaming, advertisement and emergency communications. Some performance results are presented for the high mobility PHY.

References

[1] B. Farhang-Boroujeny, "OFDM Versus Filter Bank Multicarrier," Signal Processing Magazine, IEEE , vol.28, no.3, pp.92-112, May 2011.
[2] Marco Hernandez et.al., "Channel Model Document for IEEE802.15.8 TG", IEEE 15-12-0459-07-0008, [Online] Available: https:/mentor.ieee.org/802.15/dcn/12/15-12-0459-07-0008-tg8-channel-models.doc
[3] R.E. Mirollo and S.H. Strogatz, "Synchronization of pulse-coupled biological oscillators", SIAM Journal on Applied Mathematics, Vol 50, No 6, pp. 16451662, December 1990.

THE 18TH INTERNATIONAL SYMPOSIUM ON WIRELESS PERSONAL MULTIMEDIA COMMUNICATIONS
(WPMC-2015)
December 13-16, 2015, Hyderabad, India

Detection Performance of Soft Data Fusion in Rician Fading Channel for Cognitive Radio Network

Srinivas Nallagonda and V. Chandra Sekhar
Department of ECE
M.V.S.R Engineering College
Osmania University, Hyderabad, India 501510
Email: srinivas.nallagonda@gmail.com
vadapallipadmachandrasekhar@gmail.com

Aniruddha Chandra
Department of Radio Electronics
Brno University of Technology
Brno, Czech Republic 61600
Email: aniruddha.chandra@ieee.org

S. Dhar Roy and S. Kundu
Department of ECE
National Institute of Technology
Durgapur, India 713209
Email: s_dharroy@yahoo.com
sumit.kundu@ece.nitdgp.ac.in

***Abstract*—A cooperative spectrum sensing (CSS) scheme for cognitive radio network (CRN) is proposed in this paper. The energy values from different cognitive radios (CRs) are used to perform the soft combining operation. More precisely, we analyze the performance of CSS with several soft data fusion schemes: square law selection (SLS), maximal ratio combining (MRC), square law combining (SLC), and selection combining (SC) in Nakagami-n (Rician) fading environment. Towards that, an expression of detection probability in closed-form for each soft data fusion scheme in Rician fading channel is derived. A comparative performance of soft data fusion schemes has been illustrated for different network and channel parameters. Further, the performance comparison between soft data and hard decision combining schemes (such as majority-rule, AND-rule, and OR-rule) is also investigated.**

***Index Terms*—Cooperative spectrum sensing, soft data fusion, fading channel, detection probability.**

I. Introduction

The spectrum of primary users (PUs) can be opportunistically accessed and shared by secondary users (SUs) provided it does not cause detrimental interference to the PUs [1]. Therefore, sensing the spectrum of a PU is important, since it is essential to detect the presence of PUs reliably. The operation is quite challenging when the PU signal format is unknown. In such scenarios, utilization of an energy detector (ED) is the suitable choice to detect the status of a PU [2], [3]. When compared to a single CR sensing, cooperative spectrum sensing (CSS) helps increasing the reliability of detection in the presence of uncertainties in sensing (S) channel. More precisely, in CSS, it is possible to improve the detection performance where all CRs sense the PU individually and report their sensing information to a fusion center (FC) via reporting (R) channels. Next, the FC fuses the received local sensing information to decide about the presence or the absence of the PU and reports back to the CRs. There are several soft and hard decision combining fusion schemes which can be implemented at FC to perform the fusing operation [4]. In the case of soft data fusion, CRs forward the entire sensing data (i.e., received energies at each CR) to the FC without performing any local binary decision at each CR (where '1' or '0' is forwarded to the FC in the case of hard decision fusion).

The existing literature on ED based CSS [5], assumes several fading models in S-channels such as Rayleigh, Nakagami-m, Rician, Hoyt, Weibull, and Log-normal shadowing for sensing. In these cases, the performance of CSS is evaluated only under several hard decision fusions such as majority-rule, AND-rule, and OR-rule. In contrast to hard decision fusion, it is possible to implement soft data fusion schemes (SLS, MRC, SLC, and SC) at FC to improve the performance of CSS further [6]. However, in [6], the results on the basis of simulation framework is only presented. This has motivated us to develop analytical framework and to evaluate the performance of CSS with soft data fusion schemes in fading channel. For analytical tractability, we assume that the R-channels are considered as ideal [7] where as S-channels are assumed to be noisy and Nakagami-n (Rician) fading. Rayleigh fading channels in which the reflected and scattered waves are dominated by one strong component are modeled by Nakagami-n distribution, known as the Rician distribution [8]. In this paper, we investigate the performance analysis of CSS with different soft data fusions: SLC, MRC, SLS, and SC, through complementary receiver operating characteristics (CROC) in Rician fading channel. Appropriate analytical formulations and a simulation test bed has been proposed using which our formulations have been validated. Specifically, in this paper, our contributions are as follows:

- The expressions of overall probability of detection ($\bar{Q}_d$) for different soft data fusion schemes such as SLS, MRC, SLC, and SC in Rician channel are derived analytically. To the best of our knowledge the derivation of $\bar{Q}_d$ for Rician case is not available in the literature.
- The variable substitution method (or theta approach) is proposed in this paper to solve the unsolvable expression of $\bar{Q}_d$ for SC fusion scheme in Rician channel.
- Impacts of channel and network parameters: fading parameter (K); time-bandwidth product (u); average S-channel SNR; and the number of CRs (N) on overall sensing performance is investigated.
- Qualitative performance comparison of soft data fusion schemes (SLC, MRC, SLS, and SC) with the hard decision fusion schemes has been studied.

The work is partitioned in to next three sections. The system model related to several soft schemes for CSS has been discussed in Section II. Further, the probability of detection expressions for various fusion schemes in Rician fading are derived. In Section III, simulation and analytical results are discussed. In Section IV, conclusions are presented.

II. System Model

Fig. 1 shows a proposed CSS system with N CRs, a fusion center (FC), and a primary user (PU). Each CR senses the PU individually using energy detector (ED) which is shown in Fig. 2 and send its sensing data in the form of energy values to the FC through R-channels. Next, the FC gathers these sensing data (energy values) which are coming from individual CRs. Then, FC employs any one of the soft data combining techniques such as square law selection (SLS), square-law combining (SLC), selection combining (SC), and maximal ratio combining (MRC) to make the decision of PU (presence or absence) globally. Signals from multiple CRs are combined to achieve an improved average SNR. In this paper, we assume that Nakagami-n (Rician) fading and noise affecting the S-channels while the R-channels are considered as ideal (noiseless) channels.

The received signal at k-th CR, $x_k(t)$ can be written as:

$$x_k(t) = \begin{cases} n_k(t) & : H_0 \\ h_k(t)s(t) + n_k(t) & : H_1 \end{cases} \quad (1)$$

where $s(t)$ is the PU signal with energy E_s and $n_k(t)$ is the additive white Gaussian noise (AWGN) at k-th CR. The S-channel fading coefficient for the k-th CR is denoted as h_k. Two hypotheses, denoted as H_0 and H_1 which indicates PU's absence and presence, respectively. When the PU is absent i.e. under hypothesis H_0, CR receives only the noise signal at the input of the energy detector and the noise energy at k-th CR can be approximated over the time interval $(0, T)$, following [2], [3] as:

$$\int_0^T n_k^2(t)dt = \frac{1}{2W}\sum_{i=1}^{2u} n_{k_i}^2 \quad (2)$$

where $n_{k_i} = n(i/(2W))$, $u = TW$ indicates time-bandwidth product, T indicates observation time, and W indicates PU signal's bandwidth. It can check easily that n_{k_i} is Gaussian with mean zero and variance $N_{01}W$ ($n_{k_i} \sim \mathcal{N}(0, N_{01}W); \forall i$ where $N_{01}W$ is spectral density of one-sided noise power). If we define $n'_{k_i} = n_{k_i}/\sqrt{N_{01}W}$, the received signal energy under H_0 at k-th CR, denoted as E_k, can be written as:

$$E_k = \sum_{i=1}^{2u} n'^2_{k_i} \quad (3)$$

The same approach is followed to evaluate the received signal energy under hypothesis H_1 at the k-th CR when the primary signal is present with the replacement of each n_{k_i} terms with $n_{k_i} + s_i$, where $s_i = s(i/(2W))$.

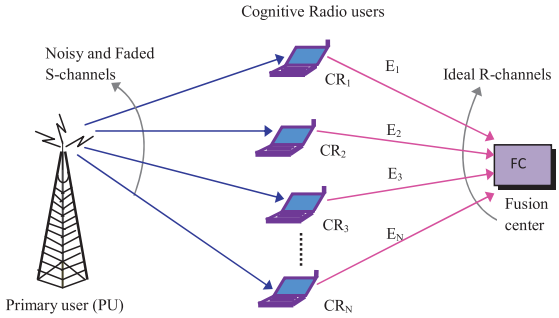

Fig. 1. Cooperative spectrum sensing scenario.

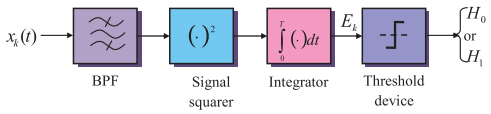

Fig. 2. Energy detector with local decision.

A. Soft Data Fusion Schemes Over Non-fading Channel

In the case of CSS with MRC fusion scheme, all CRs send their respective energy values with appropriate weighting to the FC. Then FC gathers all the data (energy values with appropriate weighting) from all CRs, and combines. The combined energy value is passed through an ED and makes a global decision about the PU. It may be noted that as we assume R-channels to be ideal (noiseless), the MRC rule at FC becomes simple summation of the received signals from all the CRs [9]. The SC scheme which selects the signal from the branch with the largest instantaneous S-channel SNR, and performs energy detection based on the signal from the selected path. The less complexities and less power consumption are offered by SC scheme as compared to MRC fusion scheme. In low SNR, a significant improvement in SNR with a limited number of branches is not guaranteed by the MRC and SC schemes. It is also noted that, MRC (a coherent combining technique) needs information on each channel status in the case of non-coherent detection, which results in high design complexity. SLC and SLS (energy-law combining techniques) are more attractive diversity techniques for energy detection [10] to overcome the drawbacks of MRC. The final test statistic can be obtained by the energy-law combining techniques which fuse the energy of each branch. Under the SLC fusion scheme, the squared and integrated energy vectors $E^1, E^2, \cdots, E^N$, from N distributed CRs are gathered at a FC, where the test statistic, $E_{lc} = \sum_{k=1}^{N} E^k$ is formed at FC. Under the SLS fusion scheme, the FC only selects the branch with the largest energy i.e. $E_{ls} = max(E_1, E_2, \cdots, E_N)$. This largest energy is compared with the threshold and final decision is taken place at FC.

Table I shows the expressions for overall detection and false alarm probabilities at FC under the SLS fusion, MRC

TABLE I
Q_d AND Q_f EXPRESSIONS FOR DIFFERENT SOFT DATA SCHEMES FOR AWGN ENVIRONMENT.

Combining Schemes	Q_d	Q_f
SLS	$1-\prod_{k=1}^{N}[1-Q_u(\sqrt{2\gamma_k},\sqrt{\lambda})]$	$1-[1-\Gamma(u,\lambda/2)/\Gamma(u)]^N$
MRC	$Q_u(\sqrt{2\gamma_{rc}},\sqrt{\lambda})$	$\Gamma(u,\lambda/2)\Gamma(u)$
SLC	$Q_{Nu}(\sqrt{2\gamma_{lc}},\sqrt{\lambda})$	$\Gamma(Nu,\lambda/2)/\Gamma(Nu)$
SC	$Q_u(\sqrt{2\gamma_{sc}},\sqrt{\lambda})$	$\Gamma(u,\lambda/2)/\Gamma(u)$

fusion, SLC fusion, and SC fusion schemes following [9], [11] under non-faded (AWGN) environment. The symbols $\gamma_{rc}=\sum_{i=1}^{N}\gamma_i$ denotes the instantaneous SNR at the output of the MRC combiner; $\gamma_{lc}=\sum_{k=1}^{N}\gamma^k$, where γ^k denotes the instantaneous S-channel SNR at k-th CR; and γ_{sc} = $\max(\gamma^1,\gamma^2,...,\gamma^N)$ denotes the instantaneous SNR at the output of the SC combiner [12]. Also one can easily observe that the expressions for Q_d and Q_f for SLC scheme can be obtained from the expressions of MRC scheme by substituting simply u with Nu as we know that $\gamma_{rc}=\gamma_{lc}$.

B. Soft Data Fusion Schemes Over Rician Fading Channel

It is seen from Table I that the expression for Q_d of any soft data fusion scheme gives as a function of the S-channel SNR (γ). Under fading scenario, by averaging Q_d of any fusion scheme, the average overall detection probability ($\bar{Q}_d$) may be derived i.e.,

$$\bar{Q}_d=\int_0^\infty Q_d f_\gamma(\gamma)d\gamma \tag{4}$$

where $f_\gamma(\gamma)$ indicates the PDF of γ under fading and it depends on type of fusion scheme. From [9] and [11], it is observed that the PDF of SLS combining scheme for Rician fading channel is same as its basic PDF of SNR under that fading and the PDF of SLC scheme for Rician channel is same as PDF of MRC of that faded channel, only is replaced γ_{rc} with γ_{lc}. The average overall false alarm probability ($\bar{Q}_f$), is same as the expressions for Q_f for all soft data fusion schemes, as given in Table I, when the S-channel is corrupted by fading due to independence of Q_f from SNR.

Assuming independent and identically distributed (i.i.d) N number of Rician faded S-channels, the average Q_d in Rician fading under SLS scheme, $\bar{Q}_{d,ls,Ric}$, can be obtained by substituting PDF of the SNR of SLS and Marcum-Q function of Q_d in the form of infinite series [5, (21)] given in Table I in (4) as:

$$\begin{aligned}\bar{Q}_{d,ls,Ric}=1-\prod_{k=1}^{N}\Bigg(1-\frac{1+K}{\bar{\gamma}_k}\exp(-K)\\ \times\sum_{n=0}^{\infty}\frac{\Gamma(u+n,\lambda/2)}{\Gamma(u+n)}\left(\frac{\bar{\gamma}_k}{1+K+\bar{\gamma}_k}\right)^{n+1}\\ \times{}_1F_1\left[n+1;1;\frac{K(1+K)}{1+K+\bar{\gamma}_k}\right]\Bigg).\end{aligned} \tag{5}$$

An alternative expression of $\bar{Q}_{d,ls,Ray}$ can be achieved by putting $K=0$. The above result is an entirely new result and is not available in the literature.

Under MRC fusion scheme, the average Q_d in Rician fading, $\bar{Q}_{d,rc,Ric}$, can be evaluated by substituting PDF of the SNR at the output of MRC combiner [6] and Q_d given in Table I in (4) i.e.,

$$\begin{aligned}\bar{Q}_{d,rc,Ric}=\exp(-NK)\left(\frac{1+K}{\bar{\gamma}}\right)\left(\frac{1+K}{NK\bar{\gamma}}\right)^{\frac{N-1}{2}}\\ \times\int_0^\infty Q_u\left(\sqrt{2\gamma_{rc}},\sqrt{\lambda}\right)\exp\left(-\frac{(1+K)\gamma_{rc}}{\bar{\gamma}}\right)\\ \times\gamma_{rc}^{(N-1)/2}I_{N-1}\left(2\sqrt{\frac{NK(1+K)\gamma_{rc}}{\bar{\gamma}}}\right)\end{aligned} \tag{6}$$

By expressing Marcum-Q function in the form of infinite series as below, the integral in (6) can be evaluated as

$$\begin{aligned}\bar{Q}_{d,rc,Ric}=NK\exp(-NK)\left(\frac{1+K}{NK\bar{\gamma}}\right)^{\frac{N+1}{2}}\\ \times\sum_{n=0}^{\infty}\frac{\Gamma(u+n,\lambda/2)}{\Gamma(u+n)n!}\int_0^\infty\exp\left[-\gamma_{rc}\left(\frac{1+K+\bar{\gamma}}{\bar{\gamma}}\right)\right]\\ \times\gamma_{rc}^{n+\frac{N-1}{2}}I_{N-1}\left(2\sqrt{\frac{NK(1+K)\gamma_{rc}}{\bar{\gamma}}}\right)d\gamma_{rc}\end{aligned} \tag{7}$$

and with the help of result given [8, (B.16)], the above integral can be solved as to obtain

$$\begin{aligned}\bar{Q}_{d,rc,Ric}=\left(\frac{1+K}{1+K+\bar{\gamma}}\right)^N\exp(-NK)\\ \times\sum_{n=0}^{\infty}\frac{\Gamma(u+n,\lambda/2)}{\Gamma(u+n)n!}\frac{\Gamma(n+N)}{\Gamma(N)}\left(\frac{\bar{\gamma}}{1+K+\bar{\gamma}}\right)^n\\ \times{}_1F_1\left[n+N;N;\frac{NK(1+K)}{1+K+\bar{\gamma}}\right].\end{aligned} \tag{8}$$

An alternative expression of $\bar{Q}_{d,rc,Ray}$ can be achieved by putting $K=0$ in (8). This is also a new result and is not available in the literature.

Under SLC scheme, the average Q_d in Rician fading, $\bar{Q}_{d,lc,Ric}$, can be evaluated by substituting Nu in place of each u in (8). Using [13], we have verified that $\bar{Q}_{d,lc,Ric}$ reduces to $\bar{Q}_{d,lc,Ray}$ for $K=0$. The expression for SLC fusion in case of Rician fading channel is also a new result. In a communication whose faded channel is diversity assisted, considering N-order SC for receivers, the CDF of N-order SC combiner output SNR is

$$F_{\gamma_{sc}}(\gamma)=[F_\gamma(\gamma)]^N. \tag{9}$$

By differentiating the CDF, it's PDF can be obtained as

$$f(\gamma_{sc})=\frac{\partial F_{\gamma_{sc}}(\gamma)}{\partial\gamma}=N\left[F_\gamma(\gamma)\right]^{N-1}f_\gamma(\gamma). \tag{10}$$

where $f_\gamma(\gamma)$ and $F_\gamma(\gamma)$ are the PDF and CDF for single fading channel, respectively [8]. For SC fusion scheme, the expression for the PDF of SNR at the SC combiner output is

obtained by substituting the basic PDF and CDF of SNR under Rician faded channel in (10). However, it becomes difficult to evaluate (4) after making substitutions of Q_d given in Table I and (10). There is an another alternative approach that states: An alternative expression for $\bar{Q}_{d,sc}$ obtained from (4) can be expressed by substituting γ_{sc} with $\tan\theta$ and $d\gamma_{sc}$ with $\sec^2\theta d\theta$ following the variable substitution approach studied by [8], [14]

$$\bar{Q}_{d,sc} = \int_0^{\pi/2} Q_{d,sc}(\tan\theta) f(\tan\theta) \sec^2\theta d\theta. \tag{11}$$

The average detection probability, under SC scheme, in case of Rician channel, $\bar{Q}_{d,sc,Ric}$ is evaluated as

$$\bar{Q}_{d,sc,Ric} = C \int_0^{\pi/2} Q_u\left(\sqrt{2\tan\theta}, \sqrt{\lambda}\right) \times \exp\left[-\frac{(1+K)\tan\theta}{\bar{\gamma}}\right] I_0\left(2\sqrt{\frac{K(1+K)\tan\theta}{\bar{\gamma}}}\right) \times \left[1 - Q_1\left(\sqrt{2K}, \sqrt{\frac{2(1+K)\tan\theta}{\bar{\gamma}}}\right)\right]^{N-1} \sec^2\theta d\theta. \tag{12}$$

where $C = N(1+K)\exp(-K)/\bar{\gamma}$. The above result is a new result.

III. Results and Discussions

In the current section, numerical results are presented and discussed for relevant values of the network parameters such as average S-channel SNR ($\bar{\gamma}$), Rician parameter (K), number of CRs (N), and time-bandwidth product (u) as well as for different soft data fusion schemes (SLS, MRC, SLC, and SC) .

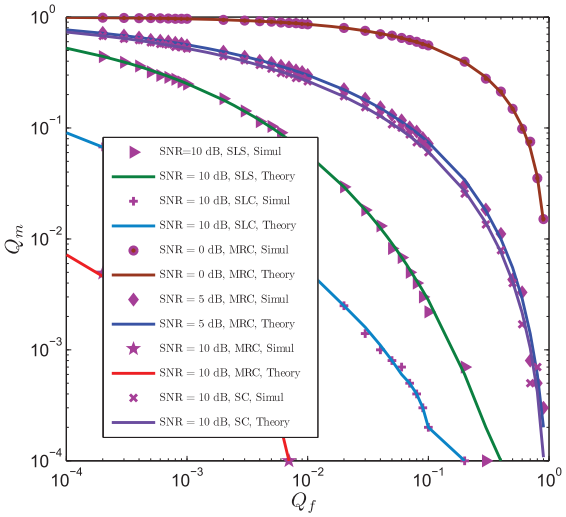

Fig. 3. Performance of soft data fusions (SLS, MRC, SLC, and SC) for various values of $\bar{\gamma}$ in AWGN channel (u=5, N=3, both simulation and analytical results are shown).

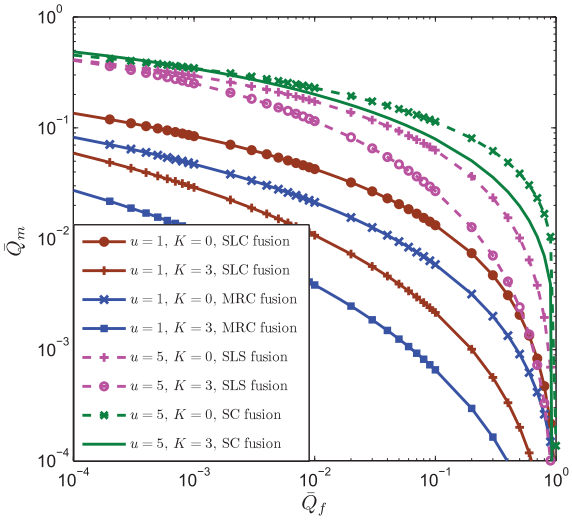

Fig. 4. Impact of Rician parameter (K) and u on performance of soft data fusions ($N=3$ and $\bar{\gamma}=10$ dB).

In Figure 3, CROC ($\bar{Q}_m$ versus $\bar{Q}_f$) in AWGN environment is shown for various soft data fusion schemes such as SLS, MRC, SLC, and SC. The impact of $\bar{\gamma}$ on performance of CSS with MRC fusion case is also shown. It is observed that $\bar{Q}_m$ reduces when any one of $\bar{\gamma}$ and $\bar{Q}_f$ increases. Higher $\bar{\gamma}$ (noise power is low) improves $\bar{P}_d$ of individual CR which further improves $\bar{Q}_d$ after cooperation i.e. overall $\bar{Q}_m$ (=1-$\bar{Q}_d$) reduces. Results based on derived expressions match with the results based on simulation testbed) under the same SNR conditions, which shows our simulation test bed and analytical approach are validated with each other. We also observe that MRC fusion based CSS performance is better as compared to the other schemes such as SLS, SLC, and SC but MRC scheme requires channel state information. The SLC fusion does not require any information about channel status and still present better performance than SLS, and SC. Thus when no channel information is available, the best scheme is SLC.

In Figure 4, the impacts of two different Rician fading parameters such as $K=0$ and $K=3$ on the CSS performance are shown. Different fusion cases such as SLS, MRC, SLC, and SC are performed at FC. For $K=0$, characteristics of Rayleigh faded channel would be obtained. Decrease in fading severity (characterized by a higher value of K) decreases the overall missed detection probability at FC. We also observe from this figure that a smaller u results in a smaller $\bar{Q}_m$ for a fixed value of $\bar{Q}_f$, K, N, and $\bar{\gamma}$ for all fusion schemes. Again MRC guarantees best performance among all fusion schemes under same network and channel parameters.

Figure 5 depicts the performance comparison between hard decision (majority-rule, AND-rule, and OR-rule) and soft data (SLS, MRC, SLC, and SC) combining fusion rules based on $\bar{Q}_d$ vs $\bar{Q}_f$ plots (ROC). In this case, the same detection threshold (λ) is assumed at each CR. The CSS performance

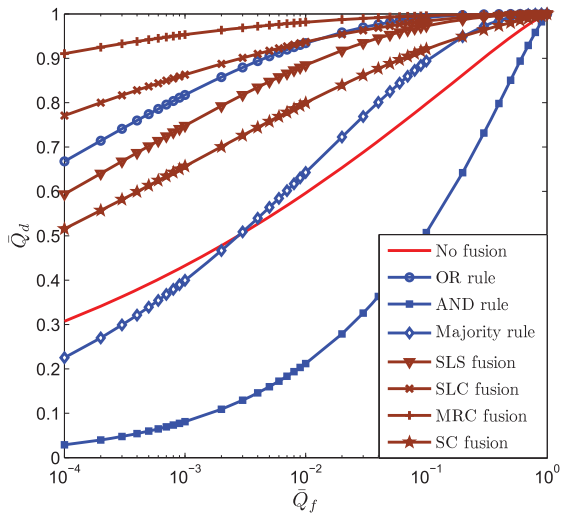

Fig. 5. Performance comparison between hard decision [5] and soft data fusions under Rician fading ($K = 3$, $\bar{\gamma} = 10$ dB, $u = 5$, and $N = 3$).

with no-fusion ($N = 1$) case is also shown for the comparison purpose. As the figure indicates, all fusion schemes outperform the single CR ($N = 1$) based sensing except AND rule. From the figure, we observe that the OR-rule performs better than the other hard decision fusion rule majority-rule or AND-rule and . The MRC soft data fusion outperforms all other soft data fusion schemes (SLS SLC, and SC) as well as all hard decision fusion rules (majority-rule, AND-rule, and OR-rule). More precisely, it is shown that all soft data fusion schemes outperform hard decision fusion rules (AND-rule and majority-rule) except OR-rule. However, these benefits are obtained at the cost of a larger bandwidth for the R-channel. The hard decision fusion rules occur with less complexity, but also with a lower detection performance than soft combination schemes. In particular, for $\bar{Q}_f = 0.0001$, $\bar{Q}_d$ is above 0.91, 0.77, 0.59, 0.51, 0.66, 0.02, and 0.22 for MRC, SLC, SLS, SC, OR-rule, AND-rule, and majority-rule, respectively. Thus MRC fusion yields the best performance among all the fusion rules.

IV. Conclusion

The performance of CSS have been evaluated with a proposed analytical framework under several soft data fusion schemes (SLS, MRC, SLC, and SC) using energy detection in Rician faded sensing channel. Missed detection performance based on our developed framework is presented under several numbers of CRs, time-bandwidth products and fading severity parameters. The CSS with soft data fusion schemes have shown excellent performance improvement as compared to CSS with hard decision fusion rules. The MRC fusion scheme has been shown to outperform other schemes such as SLS, SLC, and SC in AWGN as well as Rician fading in S-channel. To achieve better detection performance with lower number of CRs in worse S-channel fading condition, MRC can be used. The performance of CSS with any type of fusion scheme outperforms single CR based spectrum sensing (no-fusion case). Results based on derived expressions in the paper match with the results based on Monte Carlo simulations.

References

[1] A. Ghasemi and E. S. Sousa, "Opportunistic spectrum access in fading channels through collaborative sensing?," *IEEE Transactions on Wireless Communication*, vol. 2, no. 2, pp. 71-82, March 2007.

[2] H. Urkowitz, "Energy detection of unknown deterministic signals," *Proceedings of IEEE*, vol. 55, no.4, pp. 523-531, April 1967.

[3] F. F. Digham, M. -S. Alouini and M. K. Simon, "On the energy detection of unknown signals over fading channels," in *Proceedings of IEEE International Conference on Communications (ICC'03)*, Alaska, USA, pp. 3575-3579, May 2003.

[4] I. F. Akyildiz, B. F Lo and R. Balakrishnan, "Cooperative spectrum sensing in cognitive radio networks: A survey," *Physical Communication*, vol. 4, no. 1, pp. 40-62, March 2011.

[5] S. Nallagonda, A. Chandra, S. D. Roy, S. Kundu, P. Kukolev and A. Prokes, "Detection performance of cooperative spectrum sensing with hard decision fusion in fading channels," *International Journal of Electronics (Tylor & Francis)*, DOI:10.1080/00207217.2015.1036369, pp. 1-25, May 2015.

[6] S. Nallagonda, S. Bandari, S. D. Roy and S. Kundu, "Performance of cooperative spectrum sensing with soft data fusion schemes in fading channels," in *Proceedings of Annual IEEE India Conference (INDICON'13)*, pp. 1-6, IIT Mumbai, India, December 2013.

[7] V. Jamali, R. A. Sadegh Zadeh, S. Hamid Safavi and S. Salari, "Optimal cooperative wideband spectrum sensing in cognitive radio networks," in *Proc. IEEE ICUFN*, pp. 317-374, June 2011.

[8] A. Chandra, "*Performance analysis of diversity combining techniques for digital signals in wireless fading channels*," PhD Thesis, Jadavpur University, India, August 2011.

[9] D. Teguig, B. Scheers and V. Le Nir, "Data fusion schemes for cooperative spectrum sensing in cognitive radio networks," in *Military Communications and Information Systems Conference (MCC'12)*, pp. 1-7, Gdansk, October 2012.

[10] S. Atapattu, C. Tellambura and H. Jiang, "Spectrum sensing in low SNR: diversity combining and cooperative communications," in *Proc. IEEE ICIIS*, pp. 16-19, August 2011.

[11] H. Sun, A. Nallanathan, J. Jiang and C. -X. wang, "Cooperative spectrum sensing with diversity reception in cognitive radios," in *Proc. IEEE CHINACOM*, pp. 216-220, August 2011.

[12] M. K. Simon, M. S. Alouini, "*Digital Communication over Fading Channels*," John Wiley and Sons, 2nd edition, NJ, USA, December 2004.

[13] I. S. Gradshteyn and I. M. Ryzhik, "*Table of Integrals, Series and Products*," Academic Press/ Elsevier, 7th edition, San Diego, CA, USA, March 2007.

[14] S. Haghani and N. C. Beaulieu, "M-ary NCFSK with S + N selection combining in Rician fading," *IEEE Transactions on Communication*, vol. 54, no. 3, pp. 491-498, March 2006.

THE 18TH INTERNATIONAL SYMPOSIUM ON WIRELESS PERSONAL MULTIMEDIA COMMUNICATIONS
(WPMC-2015)
December 13-16, 2015, Hyderabad, India

Performance Comparision of Various Detection Methods for QO-STBC over Time Selective Channel

Jyoti P. Patra
Dept. of Electronics and Communication
National Institute Of Technology
Rourkela-769008, India
E mail[1]: jyotiprasannapatra@gmail.com

Poonam Singh
Dept. of Electronics and Communication
National Institute Of Technology
Rourkela-769008, India
E mail: psingh@nitrkl.ac.in

Abstract— The performance of Quasi-orthogonal space time block codes (QO-STBC) are generally verified by assuming that the channels remain static over the entire code word length. However, in time selective channel, this assumption does not hold good and causes severe interferences. Therefore, the simple pairwise maximum likelihood decoding scheme is not sufficient to recover original transmitted signals perfectly. Hence, in this paper, we have analyzed several detection schemes namely zero forcing (ZF), two-step zero forcing (TS-ZF), minimum mean square error (MMSE), zero forcing-interference cancellation-decision feedback equalizer (ZF-IC-DFE)and minimum mean square error-interference cancellation-decision feedback equalizer (MMSE-IC-DFE). We have also proposed two iterative detection schemes namely zero forcing iterative zero forcing successive interference cancellation (ZI-ZF-SIC) and minimum mean square error iterative zero forcing successive interference cancellation (MI-ZF-SIC). The simulation results show that the proposed detection method outperform the conventional methods for QO-STBC over time selective channel.

Keywords—QO-STBC; Detection;Time Selective; ZI-ZF-SIC; MI-ZF-SIC

I. INTRODUCTION

In recent years, the transmit diversity schemes have attracted much more attention after Alamouti [1] proposed an elegant orthogonal space-time block codes (OSTBCs) for two transmit antenna and one receive antenna because they give full diversity with low complexity ML decoding. However, it is seen that, OSTBC cannot achieve full rate and full diversity at the same time for more than two transmit antennas [2]. Hence, a full rate with partial diversity Quasi-Orthogonal Space-Time Code (QOSTBC) was introduced in [3] for flat fading channel. However, the time selective channel does exit in practice. Most research on QO-STBC assumes that the channel is quasi-static over the entire channel matrix. However, in a fast fading scenario, this assumption does not hold good and causes two interferences namely inter symbol interference (ISI) and inter antenna interferences (IAI) [4]. The ISI and IAI effect occurs due to quasi orthogonal code matrix and time selective nature of the channel respectively. Hence, a simple pairwise ML detection method is not sufficient to recover the original transmitted signal at the receiver side. In [5], a two-step ZF (TS-ZF) detector was proposed to eliminate the interferences for QOSTBC for time selective channel. This method is composed of two steps. In the first step a transform matrix is multiplied with the channel matrix to get a diagonal matrix and then a simple least square detection is performed to detect the transmitted signals. In [4], the authors propose two detection schemes ZF-IC-DFE and MMSE-IC-DFE. These detection techniques consist of three steps. In the first two steps ZF–IC or MMSE-IC is performed followed by DFE at the last step to recover the original transmitted signal.

In this paper, we propose two detection schemes to cancel the interferences based on iterative zero forcing-successive interference cancellation (I-ZF-SIC) for QO-STBC over time selective channel. Initially, either ZF or MMSE method is used to estimate the transmitted signal. Then, by using the estimated signal coming from ZF/MMSE method, the interferences are cancelled iterative followed by ZF-SIC method and soft decision. We call the proposed scheme as zero forcing iterative zero forcing successive interference cancellation (ZI-ZF-SIC) or minimum mean square error iterative zero forcing successive interference cancellation (MI-ZF-SIC) depending upon whether the initial signal is estimated by using either ZF or MMSE method.

The rest of the paper is organized as follows. In Section II, the system model for the QO-STBC is discussed. The conventional various detection methods are presented in Section III. Section IV describes the proposed detection methods. In Section V, the performance of these detection methods are compared on the basis of SER. Finally, Section VI concludes the paper.

II. SYSTEM MODEL

Consider the QO-STBC proposed in [3] with 4 transmit antennas (4Tx) and 1 receive antenna (1Rx). Four complex signals x_1, x_2, x_3 and x_4 are first grouped together and then passed through a QO-STBC encoder. The encoded output can be written as

$$X = [x_{il}] = \begin{bmatrix} x_1 & x_2 & x_3 & x_4 \\ -x_2^* & x_1^* & -x_4^* & x_3^* \\ -x_3^* & -x_4^* & x_1^* & x_2^* \\ x_4 & -x_3 & -x_2 & x_1 \end{bmatrix} \quad (1)$$

where x_{il} denotes the signal transmitted from the ith transmitted antenna at lth time slot.

After passing the encoded signal through the channel, the received signal can be expressed as

$$r = Hx + n \quad (2)$$

where $x = [x_1 \quad x_2 \quad x_3 \quad x_4]^T$ $r = [r_1 \quad r_2^* \quad r_3^* \quad r_4]^T$ and $n = [n_1 \quad n_2^* \quad n_3^* \quad n_4]^T$.

n_i is a complex additive white Gaussian noise (AWGN) with zero mean and a variance of σ_n^2. The channel matrix (*H*) can be written as

$$H = \begin{bmatrix} h_1(1) & h_2(1) & h_3(1) & h_4(1) \\ h_2(2)^* & -h_1(2)^* & h_4(2)^* & -h_3(2)^* \\ h_3(3)^* & -h_4(3)^* & -h_1(3)^* & -h_2(3)^* \\ h_4(4) & -h_3(4) & -h_2(4) & h_1(4) \end{bmatrix} \tag{3}$$

where $h_i(l)$ denotes the channel gain for the *i*th transmit antenna at the *l*th time slot. Here, we assume that all the channels undergo frequency flat and time selective channel generated from modified Jakes Sum-of-Sinusoidal (SOS) [8] model with zero mean and autocorrelation $E[h_i(l)h_i(l+m)^*] = \sigma_h^2 R_h(m)$ where σ_h^2 denotes the power of path gain and we normalize the power of path gain to unit. According to Jakes Model [10]

$$R_h(m) = J_0(2\pi f_d T_S m) \tag{4}$$

$J_0(.)$ is the zero order Bessel functions of the first kind, f_d is the Doppler frequency and T_s is the symbol period.

At first, the channel is assumed to be time invariant flat fading i.e. $h_i = h_i(l) = h_i(l+m)$ for *m* = 1,2 3. In such scenario, the pairwise maximum likelihood (ML) method proposed in [3] is applied to separate the transmitted signals. This can be performed in two steps. In the first step, matched filter operation is performed followed by a joint decoding of two symbol pair using ML method. The matched filter operation can be performed by multiplying H^H on both sides of (2) and is given by

$$\begin{aligned} r' &= H^H H x + H^H n \\ &= \Theta x + n' \end{aligned} \tag{5}$$

where Θ is the Gram matrix and is given by

$$\Theta = H^H H = \begin{bmatrix} a & 0 & 0 & b \\ 0 & a & -b & 0 \\ 0 & -b & a & 0 \\ b & 0 & 0 & a \end{bmatrix} \tag{6}$$

$$a = \sum_{i=1}^{4} |h_i|^2$$

$$b = 2\,\mathrm{Re}\left(h_1 h_4^* - h_2 h_3^*\right)$$

where Re(.) denotes the real parts of the complex. Then Pairwise ML method separates the transmitted signal into the sum of two independent terms $f(x_1,x_4) + f(x_2,x_3)$ and can be written as

$$\hat{x} = \arg\min_{x \subset \Omega} \left\| r' - \Theta x \right\| \tag{7}$$

Hence, by using pairwise ML method the transmitted signal can be perfectly recovered from the mixer of transmitted signals at the receiver side.

But, when the channel is time selective, the quasi-static assumptions does not hold well as $h_i(l) \neq h_i(l+m)$. Hence, $H^H H$ is no longer an quasi-orthogonal matrix and is given by

$$\begin{aligned} \Theta = H^H H &= \underbrace{\begin{bmatrix} a_1 & \Lambda_1 & \Lambda_2 & \beta \\ \Lambda_1^* & a_2 & \partial & \Lambda_3 \\ \Lambda_2^* & \partial^* & a_3 & \Lambda_4 \\ \beta^* & \Lambda_3^* & \Lambda_4^* & a_4 \end{bmatrix}}_{\Theta} \\ &= \underbrace{\begin{bmatrix} a_1 & 0 & 0 & \beta \\ 0 & a_2 & \partial & 0 \\ 0 & \partial^* & a_3 & 0 \\ \beta^* & 0 & 0 & a_4 \end{bmatrix}}_{\Theta_D + \Theta_{AD} = \Theta_S} + \underbrace{\begin{bmatrix} 0 & \Lambda_1 & \Lambda_2 & 0 \\ \Lambda_1^* & 0 & 0 & \Lambda_3 \\ \Lambda_2^* & 0 & 0 & \Lambda_4 \\ 0 & \Lambda_3^* & \Lambda_4^* & 0 \end{bmatrix}}_{\Theta_{ND}} \end{aligned} \tag{8}$$

where a_i denotes the desired diversity gain terms and are the diagonal entry of the Gram matrix given as Θ_D. β, ∂ and their corresponding conjugate denotes the ISI effect and are located on the anti- diagonal Gram matrix Θ_{AD}. Λ_i and their corresponding conjugate are the IAI effect occurs due to the time selective nature of the channel and are presented on the non-diagonal entry of the matrix i.e. Θ_{ND}. As the off diagonal matrix are not zeros, the pairwise ML method cannot be sufficient to recover the original transmitted signal as the likelihood function can no longer be decomposed into the sum of two pair-wise functions. Hence, in this paper, we have analyzed various detection methods and also proposed two detection methods to improve the system performance by cancelling these interferences.

III. COVENTIONAL DETECTION METHODS

In this section, we describe different conventional detection methods namely TS-ZF, ZF-IC-DFE and MMSE-IC-DFE for QO-STBC system over time selective flat fading channel.

A. TS-ZF Method

The TS-ZF method is proposed in [5] to detect the QOSTBC signal. As $H^H H$ does not give a quasi-orthogonal matrix, a transform matrix Ω is multiplied instead of H^H and then a simple least square algorithm has been performed.

[Step1] Multiply Ω matrix on both side of (2) and is given by

$$\Omega r = \Omega H x + \Omega n = D x + n' \tag{9}$$

$D = diag(\chi_1, \chi_2, \chi_3, \chi_4)$ and χ_i are the diagonal entry of ΩH.

[Step2] Apply simple LS detection scheme to estimate the transmitted signal and can be written as

$$\hat{x}_i = \arg\min_{x \in \Gamma} \left\| [\Omega]_i r - \chi_i x \right\|^2 \tag{10}$$

where $[\Omega]_i$ denotes the *i*th row of Ω. The TS-ZF performs better than pairwise ML method as it forces the two interference signals i.e. IBI and ICI to zero.

B. ZF-IC-DFE

The ZF-IC-DFE was proposed in [4]. It involves three steps in order to detect the transmitted signal. The algorithm is given below

[Step1] The ZF detection scheme [9] is used to obtain the initial estimated signal and is given by

$$\hat{x} = [H^H H]^{-1} H^H r \tag{11}$$

where $H \in C^{N_T \times N_T}$ is the channel matrix and $r \in C^{N_T \times 1}$ is the received signal.

[Step2] Use the estimated signal coming from the ZF output detector to cancel the off diagonal Gram matrix and can be written as

$$r_{IZ} = r' - \Theta_{ND}\hat{x} = \Theta_s \hat{x} + n' \tag{12}$$

where $r' = H^H r$ is the matched filter output of the received signal. Θ_{ND} denotes IAI occurs due to time selective channel and can be obtained by subtracting the diagonal and anti-diagonal of the Gram matrix given as given in (8)

$$\Theta_{ND} = \Theta - (\Theta_D + \Theta_{AD}) \tag{13}$$

[Step 3] Decompose the Θ_s using Cholesky decomposition and then apply DFE to obtain the transmitted signal

Applying Cholesky decomposition to Θ_s can be written as

$$\Theta_s = \Theta_D + \Theta_{AD} = L^H D L \tag{14}$$

where $L \in C^{N_T \times N_T}$ is an upper triangular matrix with diagonal matrix having the value one and $D \in C^{N_T \times N_T}$ is a diagonal matrix. Then DFE is performed by premultiplying the matrix $D^{-1}L^{-H}$ and is given by

$$r_D = D^{-1}L^{-H} r_{IZ} = Lx + D^{-1}L^{-H} n' \tag{15}$$

where r_{IZ} is the output of DFE and *L* is an upper triangular matrix and is given by

$$L = \begin{bmatrix} 1 & 0 & 0 & \Delta_1 \\ 0 & 1 & \Delta_2 & 0 \\ 0 & 0 & 1 & 0 \\ 0 & 0 & 0 & 1 \end{bmatrix} \tag{16}$$

where Δ_1 and Δ_2 are the coeffiecnt of feedback filter. Thus, x_3 and x_4 are detected separately and then this information is used to help make a decision about x_1 and x_2.

C. MMSE-IC-DFE

The MMSE-IC-DFE works very similar to previously mentioned ZF-IC-DFE. It employs the MMSE method [9] in the first step instead of ZF method to estimate the initial transmitted signal and is given by

$$\hat{x} = [H^H H + \sigma_n^{\ 2} I]^{-1} H^H r \tag{17}$$

where $\sigma_n^{\ 2}$ is the noise variance and *I* is the identity matrix.

The rest two steps i.e. Interference cancellation and Cholesky decomposition based DFE are same as previously mentioned ZF-IC-DFE detection method.

Both the ZI-ZF-SIC and MMSE-ZF-SIC outperform their corresponding linear detection parts i.e. ZF and MMSE, because they apply interference cancellation and DFE to further improves the system performance. However, the performances of these detection methods are not satisfactory due to the propagation of less reliable transmitted signal to estimate the other transmitted signals. Hence we have proposed two detection methods which provide more reliable information signals and are presented in the next section.

IV. Proposed Detection Method

We have proposed two detection schemes namely ZI-ZF-SIC and MI-ZF-SIC to cancel the ISI and IAI effects. In the first step either ZF or MMSE method is used to estimate the initial signal and then by using these estimated signal IAI effect are cancelled iteratively. Then by applying the IAI free received signal, the ISI effects are cancelled by adopting ZF-SIC method. Finally, the ZF-SIC output signal are soft decoded by using log likelihood ratio (LLR) and then feedback to the IAI canceller unit for the next iteration.

A. ZI-ZF-SIC

The ZI-ZF-SIC method uses ZF method to estimate the initial data symbol. Then by using the estimated signal coming from ZF output, the IAI signal are generated and then subtracted from received signal iteratively with the help of soft ZF-SIC method to get the IAI free signal. The algorithm for ZI-ZF-SIC are given below

[Step1] Set iteration number k=0 and obtain $x_i^{(0)}$ from ZF method as given in (11) and can be written as

$$x_i^{(0)} = \hat{x}_i \tag{18}$$

[Step2] Use the initial estimated signal coming from ZF output to cancel the IAI iteratively. For iteration *k=1, 2,...I*, the IAI free signal can be obtained as

$$\begin{aligned} r_{off_IAI}^{k}(i) &= r'(i) - \Theta_{ND}\hat{x}_i^{(k-1)} \\ &= \Theta_s \hat{x}_i^{(k-1)} + n' \end{aligned} \tag{19}$$

where $r_{off_IAI}^{k} = [r_{off_IAI}^{k}(1) r_{off_IAI}^{k}(2) r_{off_IAI}^{k}(3) r_{off_IAI}^{k}(4)]^T$ are the IAI free signal for the *k*th iteration.

[Step3] Separate $r_{off_IAI}^{k}$ into two groups that contain the symbol pair ($\hat{x}_1^{\,k-1}, \hat{x}_4^{\,k-1}$) and ($\hat{x}_2^{\,k-1}, \hat{x}_3^{\,k-1}$) and

$$\begin{bmatrix} r_{off_IAI}^{k}(1) \\ r_{off_IAI}^{k}(4) \end{bmatrix} = \begin{bmatrix} a_1 & \beta \\ \beta^* & a_4 \end{bmatrix} \begin{bmatrix} \hat{x}_1^{\,k-1} \\ \hat{x}_4^{\,k-1} \end{bmatrix} + \begin{bmatrix} n_1' \\ n_4' \end{bmatrix} \tag{20}$$

$$\begin{bmatrix} r^{k}_{off_IAI}(2) \\ r^{k}_{off_IAI}(3) \end{bmatrix} = \begin{bmatrix} a_2 & \partial \\ \partial^{*} & a_3 \end{bmatrix} \begin{bmatrix} \hat{x}_2^{\,k-1} \\ \hat{x}_3^{\,k-1} \end{bmatrix} + \begin{bmatrix} n'_2 \\ n'_3 \end{bmatrix} \quad (21)$$

Then, use ZF-SIC method in the first group to detect $\hat{x}_1^{\,k-1}$ and $\hat{x}_4^{\,k-1}$ signals.

[Step 4] Apply zero forcing method to obtain $\hat{x}_1^{\,k-1}$, $\hat{x}_4^{\,k-1}$ and is given by

$$\begin{aligned} \begin{bmatrix} \hat{x}_1^{\,k-1} \\ \hat{x}_4^{\,k-1} \end{bmatrix} &= \begin{bmatrix} a_1 & \beta \\ \beta^{*} & a_4 \end{bmatrix}^{-1} \begin{bmatrix} r^{k}_{off_IAI}(1) \\ r^{k}_{off_IAI}(4) \end{bmatrix} \\ &= \frac{1}{\phi} \begin{bmatrix} a_4 & -\beta \\ -\beta^{*} & a_1 \end{bmatrix} \begin{bmatrix} r^{k}_{off_IAI}(1) \\ r^{k}_{off_IAI}(4) \end{bmatrix} \end{aligned} \quad (22)$$

where $\phi = -(a_1 a_4 + |\beta|^2)$ is a scalar quantity.

[Step 5] Adopt SIC method [7] joint with ZF method to obtain more reliable data signal. The algorithm for ZF-SIC method is given in below

1. $r^{k}_{off_IAI}(1) = a_1 \hat{x}_1^{\,k-1} + \beta\, x_4^{\,k-1} + n'_1$ (23)
2. $r^{k}_{off_IAI}(4) = \beta^{*} \hat{x}_1^{\,k-1} + \alpha_4 \hat{x}_4^{\,k-1} + n'_4$ (24)
3. *if* $\alpha_1 > \alpha_4$

$$\bar{x}_1^{\,k-1} = Q(\hat{x}_1^{\,k-1}) \quad (25)$$

$$\tilde{x}_4^{\,k-1} = (r^{k}_{off_IAI}(4) - \beta^{*} \bar{x}_1^{\,k-1})/a_4 \quad (26)$$

$$\hat{x}_1^{\,k-1} = (r^{k}_{off_IAI}(1) - \beta Q(\tilde{x}_4^{\,k-1}))/a_1) \quad (27)$$

4. *else*

$$\bar{x}_4^{\,k-1} = Q(\hat{x}_4^{\,k-1}) \quad (28)$$

$$\tilde{x}_1^{\,k-1} = ((r^{k}_{off_IAI}(1) - \beta \bar{x}_4^{\,k-1})/a_1) \quad (29)$$

$$\hat{x}_4^{\,k-1} = (r^{k}_{off_IAI}(4) - \beta^{*} Q(\tilde{x}_1^{\,k-1}))/a_4) \quad (30)$$

where Q denotes the hard decision function.

[Step 6] Finally adopt the soft decision rule using the LLR method and then the soft decoded signals are feedback for next iteration.

The $\hat{x}_2^{\,k-1}$ and $\hat{x}_3^{\,k-1}$ are detected similarly by applying ZF-SIC method as given in *[Step4]-[Step6]*.

B. MI-ZF-SIC

The working principle of MI-ZF-SIC method is similar to ZI-ZF-SIC method. In MI-ZF-SIC, MMSE method is used instead of ZF method to estimate the initial signal.

V. SIMULATION RESULTS

The performance comparison of various detection methods which include Pairwise ML, ZF, TS-ZF, MMSE, ZF-IC-DFE, MMSE-IC-DFE, ZI-ZF-SIC and MI-ZF-SIC methods are carried out on the basis of symbol error rate (SER) for QO-STBC over time selective flat fading channel. Modified Jakes' model is adopted to construct the time-selective fading environment. The channel varies from symbol to symbol and perfect channel state information is assumed at the receiver side. The simulation parameters used for simulation is listed on the Table1. The simulation platform is performed using MATLAB 2010b. The SER performance of conventional and proposed detection methods for QO-STBC over mobile speed of 400km/h is shown in the figure 1. The simulation result shows that pairwise ML method suffers severe performance degradation due to time selective channel. The ZF and TS-ZF give almost similar performance and outperforms the pairwise ML method as both these method forces the interferences signals to zero. The MMSE method gives better results than ZF method as it utilizes the noise correlation properties. It has almost the same performance to ZF-IC-DFE detection method. The MMSE-IC-DFE outperforms the ZF-IC-DFE as it uses MMSE method instead of ZF method to estimate the initial data symbol. The MMSE-IC-DFE and ZF-IC-DFE give better performance than their corresponding linear detection method. However, both these methods suffer performance degradation due to error floor as less reliable data are propagated to estimate the other transmitted signal. The simulation results show that the proposed ZI-ZF-SIC method gives better result than the conventional MMSE-IC-DFE and ZF-IC-DFE method as more reliable data sequences are estimated using iterative ZF-SIC method. The MI-ZF-SIC gives better results than ZF-IC-DFE due to the implementation of MMSE rather than ZF method in order to estimate the initial data information.

Table 1 Simulation Parameters

Parameter	Value
Antenna configuration	4Tx,1Rx
Channel Model	Modified Jakes SOS
Carrier frequency	2GHz
Symbol duration	128/(3.84×10e6)
Modulation type	QPSK
Mobile velocity	400Km/h
Normalized Doppler Spread	0.025

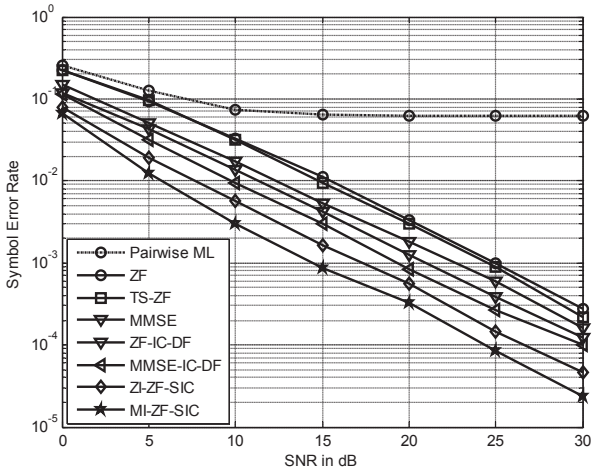

Fig.1 Performance Comparision of different detection methods for QO-STBC over mobile speed 400Km/h

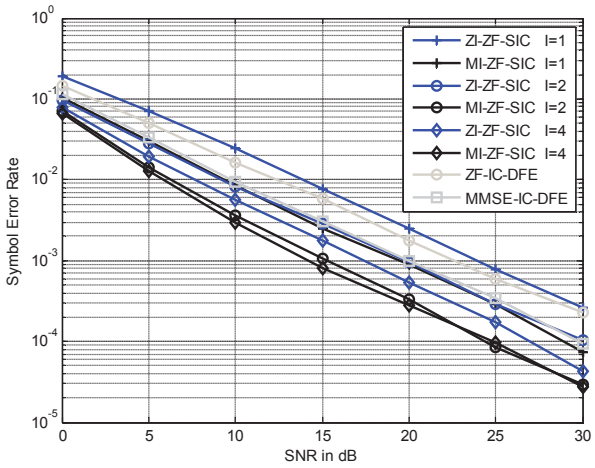

Fig.2 Performance of Proposed methods with respect to number itearion number

Figure 2 show the SER performance of the two proposed methods for different number of iteration I = 0, 2, 4. The simulation results show that as the number of iteration increases, the performance of the proposed methods improves. It is seen than, iteration I= *2* or I= *4* delivers most of the performance gain in the proposed detection schemes and thus we consider iteration I = 4 for comparison with other conventional methods as shown in Figure 1. The performance of different detection methods in the descending order are given as follows MI-ZF-SIC, ZI-ZF-SIC, MMSE-IC-DFE, MMSE, ZF-IC-DFE, TS-ZF, ZF and Pairwise ML.

VI. CONCLUSIONS

In this paper, we have analyzed various conventional detection methods and proposed two new detection methods namely ZI-ZF-SIC and MI-ZF-SIC technique methods to suppress the interferences effects for QO-STBC system over time selective channel. The various detection techniques which include TS-ZF, ZF, MMSE, ZF-IC-DFE, MMSE-IC-DFE and the proposed ZI-ZF-SIC, MI-ZF-SIC methods are compared in terms of SER. From the simulation results, it is seen that, both the proposed methods significantly outperforms the conventional detection methods.

REFERENCES

[1] S. M. Alamouti, "A simple transmit diversity technique for wireless communications," *IEEE Journal on Selected Areas of Communication*, vol. 16, no. 8, pp.1451 – 1458, Oct. 1998.

[2] V. Tarokh, H. Jafarkhani, and A. Calderbank, "Space-time block codesfrom orthogonal designs," *IEEE Transactions on Information Theory*, vol. 45, no. 5,pp. 1456 – 1467, July 1999.

[3] H. Jafarkhani, "A quasi-orthogonal space-time block code," *IEEE Transactions Communication*, vol. 49, no. 1, pp. 1 – 4, Jan. 2001.

[4] Y.Wang, J. Wang, Z. Lu, X. Liu, "Performance improvement of QO-STBC over time-selective channel for wireless network", *Journal of Network and Computer Applications (Elsevier)*, vol. 36 no.3, pp. 1018–1026, 2013.

[5] Zheng F-C, Burr AG. Signal detection for non- orthogonal space-time block over time-selective fading channels. *IEEE Communications Letters*, vol.8, no.8, pp.491–3,2004.

[6] F. Zheng and A. G. Burr, "Signal detection for orthogonal space-timeblock coding over time-selective fading channels: a PIC approach for thesystems,"*IEEE Transactions on Communication*, vol. 53, no. 6, pp. 969-972, June 2005.

[7] J. W. Wee, J. W. Seo, K. T. Lee, Y. S. Lee and W. G. Jeon, "Successive Interference Cancellation for STBC-OFDM systems in a Fast Fading Channel," *IEEE Vehicular Technology Conference*, pp. 841-844 ,2005.

[8] Y. R. Zheng and C. Xiao "Simulation models with correct statistical properties for Rayleigh fading channels", *IEEE Transactions on Communication*, vol. 51, no.6, 920-928, 2003.

[9] J.G. Proakis, *Digital communications*, New York: McGraw-Hill, 2001.

[10] W. C. Jakes, *Microwave Mobile Channels*, New York: Wiley, 1974.

THE 18TH INTERNATIONAL SYMPOSIUM ON WIRELESS PERSONAL MULTIMEDIA COMMUNICATIONS
(WPMC-2015)
December 13-16, 2015, Hyderabad, India

Optimization of Cooperative Spectrum Sensing in Cognitive Radio over Erroneous Reporting Channel

Narasimha Rao Banavathu
Indian Institute of Technology Hyderabad, India
Email: ee13p1005@iith.ac.in

Mohammed Zafar Ali Khan
Indian Institute of Technology Hyderabad, India
Email: zafar@iith.ac.in

***Abstract*—In this paper, we consider optimization of number of cognitive users (N) by minimizing global error rate of a given voting rule (k) at cognitive radio (CR) base station over erroneous reporting channel. Expressions for optimal N are derived for $k = m+1$ and $k = N-m$ voting rules. Where m is an integer ($m \geq 0$). We show that optimal N depends on m, effective probability of false alarm (P_{fe}) and effective probability of miss detection (P_{me}) of a cognitive user over erroneous reporting channel. We consider improved energy detector as an example for the analysis. Based on this analysis following observations are made;**

1) **If CR base station uses $k = m+1$ or $k = N-m$ voting rule, performance of cooperative spectrum sensing improves as m increases.**
2) **For a given m, performance of $k = m+1$ voting rule is better compared to $k = N-m$ voting rule.**

Finally, we numerically obtain the values of optimal detection threshold, optimal p of the improved energy detector and optimal N. We also compare with conventional energy detector. We show that performance using optimal values is better than conventional energy detector.

***Index Terms*—Cognitive radio, cognitive radio base station, erroneous reporting channel, optimization.**

I. Introduction

The idea of cognitive radio (CR) has evolved to overcome the spectrum shortage problem caused by the current inflexible spectrum allocation policy. A CR is an intelligent wireless communication system that monitors for the presence of the spectrum hole by changing different modulation strategies and forms the best way of communication between primary and cognitive user [1]. In many realistic environments due to multipath fading and shadowing, detection performance of a cognitive user degrades. To overcome this issue, different cognitive users may need to cooperate to enhance the performance of the cooperative spectrum sensing [2] - [3].

In cooperative CR network, each cognitive user can send the local decision to CR base station in a single time slot. As number of cognitive users increase, CR base station may take long time in deciding the decision on primary user [4]. One of the practical limitations in cooperative spectrum sensing is subject to fading and additive noise, the reporting channel between cognitive user and CR base station may also experiences errors, which results in poor performance [5]. Cooperative spectrum sensing over erroneous reporting channel is presented in [6] and it is shown that OR and AND rule are never optimal for practical cases. Optimization of number of cognitive users using OR rule at CR base station is addressed in [7].

In this paper, in lieu of OR, AND rules, in general we consider $k = m+1$ and $k = N-m$ voting rules at CR base station. Note that if $m = 0$ implies $k = 1$ (OR Rule) and $k = N$ (AND Rule). Optimal N can be obtained by minimizing the global error rate of $k = m+1$ and $k = N-m$ voting rules. We show that optimal N depends on P_{fe}, P_{me} and m. As more the number of cognitive users in the CR network does not guarantee to improve the performance of cooperative spectrum sensing. Hence, it is important to find the optimal N. Following [7], we numerically obtain values of optimal detection threshold, optimal p of improved energy detector and optimal N for $k = m+1$ and $k = N-m$ voting rules. We show performance using optimal algorithm is better compared to conventional energy detector.

The remaining part of the paper is organized as follows. In Section II we present the system model of cooperative spectrum sensing. In Section III, we obtain the expressions for optimal N by minimizing the global error rate of $k = m+1$ and $k = N-m$ voting rules at CR base station. We also discuss numerical analysis with improved energy detector. Finally, in Section IV, we draw our conclusions.

II. System Model

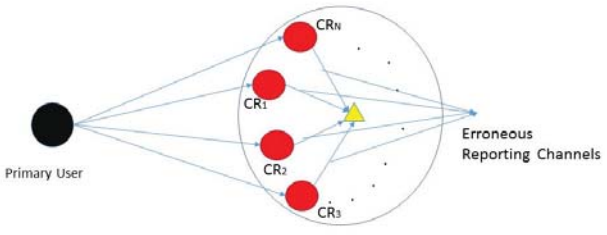

Fig. 1. Cooperative spectrum sensing model, N cognitive users communicate with CR base station over erroneous reporting channel.

We consider cooperative spectrum sensing model as shown in Fig. 1, where N CRs (cognitive users) communicate with CR base station over erroneous reporting channel. Each cognitive user identifies the primary user independently and send their local decision to CR base station over erroneous reporting channel. For the ith cognitive user with the improved energy

detector, the probability of false alarm, probability of detection and probability of missed detection are given by [8]

$$\mathrm{P}_{f,i} = \frac{\Gamma\left(n_0, \frac{T_i}{m_0}\right)}{\Gamma(n_0)}, \ \mathrm{P}_{d,i} = \frac{\Gamma\left(n_1, \frac{T_i}{m_1}\right)}{\Gamma(n_1)}, \quad (1)$$

and

$$P_{m,i} = 1 - P_{d,i}, \quad (2)$$

where

$$m_0 = \frac{2^{p/2}}{L} \frac{\sqrt{\pi}\Gamma\left(\frac{2p+1}{2}\right) - \Gamma^2\left(\frac{p+1}{2}\right)}{\Gamma\left(\frac{p+1}{2}\right)\sqrt{\pi}}, \quad (3)$$

$$n_0 = n_1 = L \frac{\Gamma^2\left(\frac{p+1}{2}\right)}{\Gamma\left(\frac{2p+1}{2}\right)\sqrt{\pi} - \Gamma^2\left(\frac{p+1}{2}\right)}, \quad (4)$$

$$m_1 = \frac{2^{p/2}(1+\gamma_i)^{p/2}}{L} \frac{\sqrt{\pi}\Gamma\left(\frac{2p+1}{2}\right) - \Gamma^2\left(\frac{p+1}{2}\right)}{\Gamma\left(\frac{p+1}{2}\right)\sqrt{\pi}}, \quad (5)$$

and where $\Gamma(.,.)$ denotes the upper incomplete gamma function, $\Gamma(.)$ denotes the gamma function, T_i is the detection threshold of the ith cognitive user, γ_i is the average *signal-to-noise ratio* (SNR) of the ith cognitive user, L be the number samples of a signal received at ith cognitive user and p is the positive power of the improved energy detector.

Following [4], we assume that distance between any two cognitive users is small, hence each cognitive user experiences identical path loss. Therefore, we can assume all cognitive users has same SNR. We also assume that all cognitive users has same thresholds i.e., $T_1 = T_2 = ... = T_N = T$. Hence they have same probabilities of detection and false alarm. Further more, we assume all reporting channels introduce identical probability of error, P_e. In summary

$$T_i = T, P_{f,i} = P_f, P_{d,i} = P_d, P_{m,i} = P_m, P_{e,i} = P_e.$$

Let P_{fe}, P_{de} and P_{me} be the effective probability of false alarm, effective probability of detection and effective probability of miss detection of a cognitive user respectively, over erroneous reporting channel as seen by the CR base station and is given by

$$P_{fe} = 1 - [(1-P_f)(1-P_e) + P_f P_e], \quad (6)$$
$$P_{de} = 1 - [(1-P_d)(1-P_e) + P_d P_e], \quad (7)$$
$$P_{me} = 1 - P_{de}. \quad (8)$$

Every cognitive user in CR network makes one bit binary decision θ_i (logic 1 denotes primary user is present, logic 0 denotes primary user is absent) and sends it to the CR base station over erroneous reporting channel. At CR base station all these one bit decisions are fused together and voting rule is applied to identify the presence or absence of primary user. i.e.,

$$Z = \sum_{i=1}^{N} \theta_i \begin{cases} \geq k, & H_1, \\ < k, & H_0, \end{cases}$$

where H_1, H_0 denotes inference drawn by CR base station that primary user is present or absent respectively. k is the voting rule. Note that we consider $k = m+1$ and $k = N-m$ voting rules.

For a, b positive integers and $0 \leq P < 1$, regularized incomplete beta function defined as

$$I_{1-P}(b-a, a+1) = \sum_{l=0}^{a} \binom{b}{l} P^l (1-P)^{b-l} \quad (9)$$

For a given voting rule (k), probability of error in the reporting channel (P_e), we define probability of false alarm and probability of miss detection at CR base station as

$$P_{F,k} = \sum_{i=k}^{N} \binom{N}{i} {P_{fe}}^i (1-P_{fe})^{N-i}$$
$$= 1 - \sum_{i=0}^{k-1} \binom{N}{i} {P_{fe}}^i (1-P_{fe})^{N-i}$$
$$= 1 - I_{1-P_{fe}}(N-k+1, k), \quad (10)$$

$$P_{M,k} = 1 - \sum_{i=k}^{N} \binom{N}{i} {P_{de}}^i (1-P_{de})^{N-i}$$
$$= I_{1-P_{de}}(N-k+1, k), \quad (11)$$

Global error rate of $k = m+1$ voting rule at CR base station can be expressed as

$$P_{GE,m+1} = P_{F,m+1} + P_{M,m+1}$$
$$= 1 - I_{1-P_{fe}}(N-m, m+1) + I_{1-P_{de}}(N-m, m+1) \quad (12)$$

Similarly, global error rate of $k = N-m$ voting rule at CR base station can be expressed as

$$P_{GE,N-m} = P_{F,N-m} + P_{M,N-m}$$
$$= 1 - I_{1-P_{fe}}(m+1, N-m) + I_{1-P_{de}}(m+1, N-m) \quad (13)$$

III. Optimization of Number of Cognitive Users in Cooperative Spectrum Sensing Over Erroneous Reporting Channels

In this section we derive the expression for optimal number of cognitive users by minimizing the global error rate of $k = m+1$ and k = $N-m$ voting rules at CR base station.

A. Optimal Number of Cognitive Users for $k = m+1$ Voting Rule

Fig. 2 shows variation of error rate with respect to detection threshold for six values of N for $k = 3$ ($k = m+1$; for $m = 2$) voting rule at CR base station. It is observed that for $N \geq 3$ there exists an optimal N for a given detection threshold. Clearly, the value of N plays an important role in describing the performance of cooperative spectrum sensing. In the following proposition we give exact solution for optimal N by minimizing the global error rate of $k = m+1$ voting rule at CR base station.

Proposition 1: Given $k = m+1$ voting rule at CR base station, the optimal number of cognitive users in CR network,

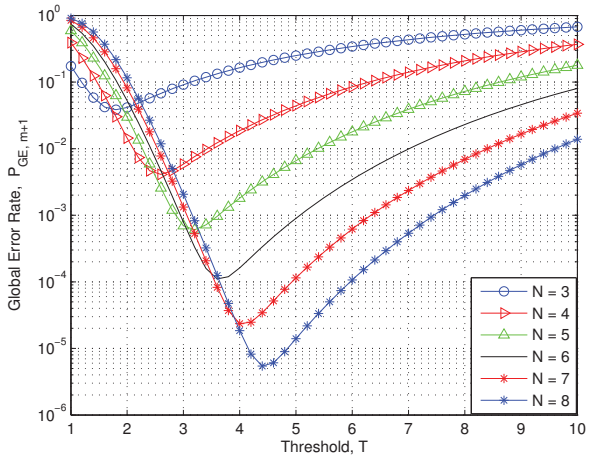

Fig. 2. Global error rate versus detection threshold, for $k = 3$ ($k = m+1$; for $m = 2$) voting rule at CR base station for p = 2, L = 5, P_e = 0, SNR = 10 dB, N = 3, 4, . . . , 8, for improved energy detector.

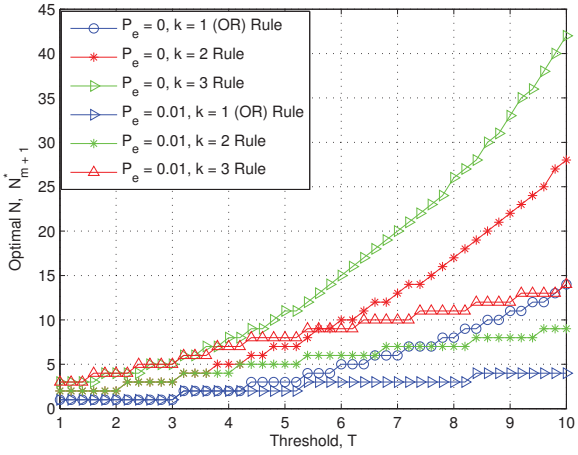

Fig. 3. Effect of reporting channel error: Optimal N versus detection threshold, T for $k = m+1$ ($m = 0, 1, 2$) voting rules at CR base station for P_e = 0, 0.01, SNR = 10 dB and p = 2, for improved energy detector.

denoted as N^*_{m+1}, that minimizes the $P_{F,m+1} + P_{M,m+1}$ is given by

$$N^*_{m+1} = \lceil (m+1)\alpha + m \rceil, \quad \alpha = \frac{\ln \frac{1-P_{me}}{P_{fe}}}{\ln \frac{1-P_{fe}}{P_{me}}}, \tag{14}$$

where $\lceil . \rceil$ indicates ceiling function.

Proof: Appendix I. ■

From proposition 1, we can make the following observations which apply to any detector (though the example plots are given for improved energy detector).

- Substituting $m = 0$ in (14), we get optimal N for OR rule ($k = 1$) and is given by $N^*_{OR} = \lceil \alpha \rceil$.
- From (14), we have

$$(m+1)\alpha + m \leq N^*_{m+1} < (m+1)\alpha + m + 1,$$

$$\Rightarrow \frac{N^*_{m+1}}{m+1} - 1 < \alpha \leq \frac{N^*_{m+1} - 1}{m+1}. \tag{15}$$

Note that $P_{fe} + P_{me} < 1$, which implies $\alpha > 0$. From (15), we draw inference as $N^*_{m+1} \geq m+1$. This means that there exists an optimal N if there exist at least $m+1$ cognitive users in the CR network.

Fig. 3 plots the of optimal N versus detection threshold of $k = m+1$ ($m = 0, 1, 2$) voting rule for various values of P_e. It is observed that for given probability of error in the reporting channel, optimal N increases as voting rule increases. However, for a given voting rule at CR base station, optimal N decreases as P_e increases. This means that error in the reporting channel deteriorates the reliability of decisions received at CR base station.

The observations we have made above are corroborated from Fig. 2 and Fig. 3

B. Optimal Number of Cognitive Users for $k = N-m$ Voting Rule

Fig. 4 plots the global error rate of $k = N-2$ ($k = N-m$; for $m = 2$) voting rule with respect to detection threshold for six values of N. It is observed that for $N \geq 3$ there exists an optimal N for a given detection threshold. Clearly, the value of N plays an important role in describing the performance of cooperative spectrum sensing. In the following proposition we give exact solution for optimal N by minimizing the global error rate of $k = N - m$ voting rule at CR base station.

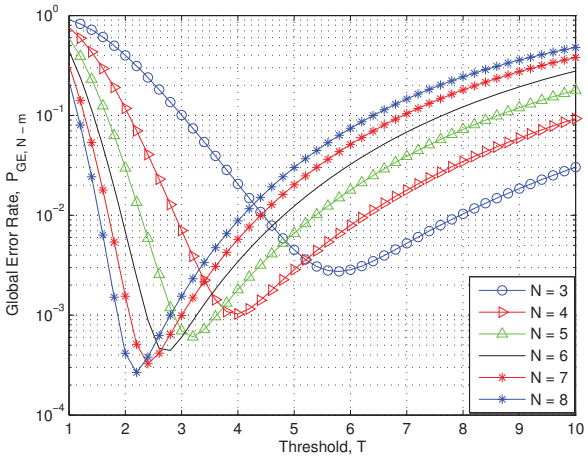

Fig. 4. Global error rate versus detection threshold, for $k = N-2$ ($k = N-m$; for $m = 2$) voting rule at CR base station for p = 2, L = 5, P_e = 0, SNR = 10 dB, N = 3, 4, . . . , 8, for improved energy detector.

Proposition 2: Given $k = N - m$ voting rule at CR base station, the optimal number of cognitive users in CR network, denoted as N^*_{N-m}, that minimizes the $P_{F,N-m} + P_{M,N-m}$ is given by

$$N^*_{N-m} = \left\lceil \frac{(m+1)}{\alpha} + m \right\rceil, \tag{16}$$

where α is given by (14).

Proof: Appendix II. ■

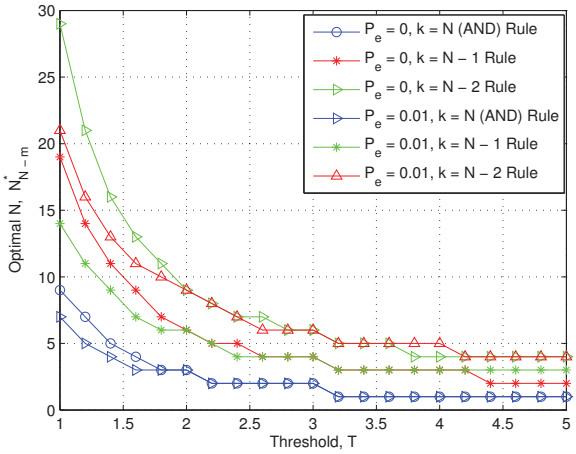

Fig. 5. Effect of reporting channel error: Optimal N versus detection threshold, T for $k = N - m$ ($m = 0, 1, 2$) voting rules at CR base station for P_e = 0, 0.01, SNR = 10 dB and p = 2, for improved energy detector.

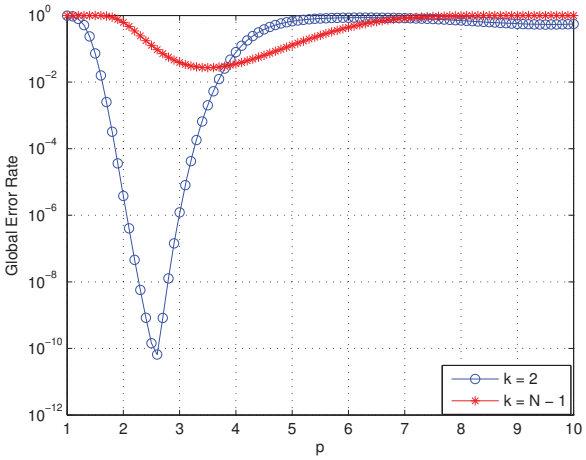

Fig. 6. Global error rate versus p, for $k = m + 1$ and $k = N - m$ (for $m = 1$) voting rules at CR base station for N = 10, L = 10, T = 10, SNR = 10 dB, for improved energy detector.

From proposition 2, we can make the following observations which apply to any detector (though the example plots are given for improved energy detector).

- Substituting $m = 0$ in (16), we get optimal N for AND rule ($k = N$) and is given by $N^*_{AND} = \lceil 1/\alpha \rceil$.
- From (16), we have

$$N^*_{N-m} - 1 < m + \frac{m+1}{\alpha} \leq N^*_{N-m},$$

$$\frac{m+1}{N^*_{N-m} - m} \leq \alpha < \frac{m+1}{N^*_{N-m} - (m+1)}. \qquad (17)$$

Since $\alpha > 0$, from (17) we conclude that $N^*_{N-m} \geq m + 1$. This means that there exist minimum $m + 1$ cognitive users in the CR network to obtain the value of optimal N.

Fig. 5 plots the of optimal N versus detection threshold of $k = N - m$ ($m = 0, 1, 2$) voting rule for various values of P_e. It is observed that for given probability of error in the reporting channel, optimal N increases as voting rule decreases. However, for a given voting rule at CR base station, optimal N decreases as P_e increases. This means that error in the reporting channel deteriorates the reliability of decisions received at CR base station.

The observations we have made above are corroborated from Fig. 4 and Fig. 5

Fig. 6 plots the global error rate with respect to p for $k = m + 1$ and $k = N - m$ voting rules. It is observed that for a given N, there exists an optimal p for each voting rule.

C. Comparison and Optimization of Improved Energy Detector for $k = m + 1$, $k = N - m$ Voting Rules

Fig. 7 shows the performance comparison of $k = m + 1$ and $k = N - m$ (for m = 0, 1, 2, 3) voting rules with respect to SNR. It is observed that for a fixed m, $k = m + 1$ rule performs better compared to $k = N - m$ voting rule. It is also observed that for a given voting rule at CR base station, as m increases global error rate decreases.

Following [7], we use optimal algorithm, i.e., we numerically obtain the values of optimal p, optimal detection threshold, optimal N with respect to SNR. Using this optimal algorithm we have plotted the error performance of $k = m+1$ and $k = N-m$ voting rules for $m = 1$. We also compare with performance of conventional energy detector (p = 2). From Fig. 8 we conclude that performance using optimal algorithm is better compare to conventional energy detector.

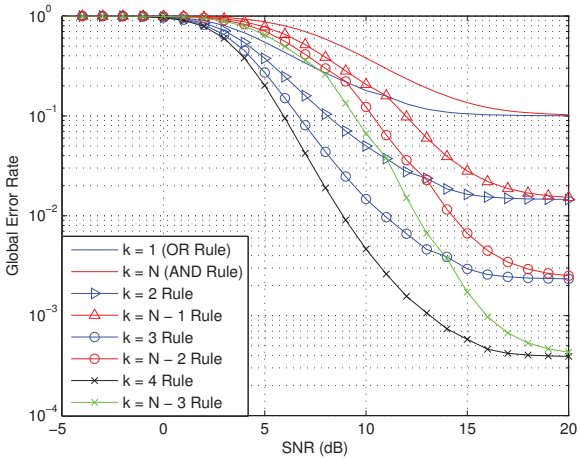

Fig. 7. Comparison of $k = m + 1$ and $k = N - m$ (for m = 0, 1, 2, 3) voting rules at CR base station for P_e = 0.05, L = 5, $p = 2$, $T = 10$, using optimal N for improved energy detector.

IV. CONCLUSION

We have derived the expressions for optimal N by minimizing the global error rate of $k = m + 1$ and $k = N - m$ voting rules at CR base station. We show that for a given m, performance of $k = m + 1$ voting rule is better compared to

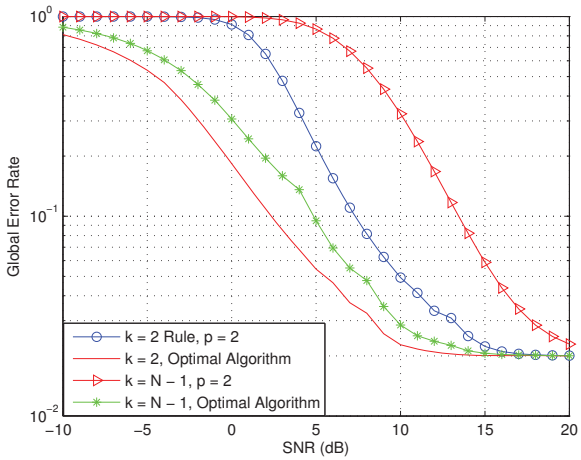

Fig. 8. Global error rate versus SNR, for $k = m + 1$ and $k = N - m$ ($m = 1$) voting rules at CR base station for P_e = 0.01, L = 5, using optimal p, optimal N, for improved energy detector.

$k = N-m$ voting rule. Finally, we use optimal algorithm, i.e., we numerically obtain the jointly optimized values of detection threshold, p of the improved energy detector and optimal N. We also compare with conventional energy detector. We show that performance using optimal algorithm is better than conventional energy detector.

Appendix I: Proof of Proposition 1

Proof: To prove proposition 1, we consider (12)

$$P_{GE,m+1} = 1 - I_{1-P_{fe}}(N-m, m+1) + I_{1-P_{de}}(N-m, m+1) = f(N)$$

Optimal value of N can be obtained when difference equation $\Delta f(N) = f(N+1) - f(N)$ equal to zero. i.e., when

$$I_{1-P_{fe}}(N-m, m+1) - I_{1-P_{fe}}(N-m+1, m+1) = I_{1-P_{de}}(N-m, m+1) - I_{1-P_{de}}(N-m+1, m+1) \quad (18)$$

For x, y are positives integers, regularized incomplete beta function can also expressed as

$$I_P(x,y) = (1-P)^y \sum_{i=x}^{\infty} \binom{y+i-1}{i} P^i \quad (19)$$

Using (19), we show that

$$I_P(x,y) - I_P(x+1,y) = \binom{x+y-1}{x} P^x (1-P)^y \quad (20)$$

Simplifying (18), using (20) and rearranging, we get

$$\left(\frac{1-P_{fe}}{P_{me}}\right)^{N-m} = \left(\frac{1-P_{me}}{P_{fe}}\right)^{m+1}$$

$$\Rightarrow N^*_{m+1} = \lceil (m+1)\alpha + m \rceil$$

where α is given by (14). ■

Appendix II: Proof of Proposition 2

Proof: To prove proposition 2, we consider (13)

$$P_{GE,N-m} = 1 - I_{1-P_{fe}}(m+1, N-m) + I_{1-P_{de}}(m+1, N-m) = g(N)$$

Optimal value of N can be obtained when difference equation $\Delta g(N) = g(N+1) - g(N)$ equal to zero. i.e., when

$$I_{1-P_{fe}}(m+1, N-m) - I_{1-P_{fe}}(m+1, N-m+1) = I_{1-P_{de}}(m+1, N-m) - I_{1-P_{de}}(m+1, N-m+1) \quad (21)$$

Using (9), we show that

$$I_{1-P}(x,y) = 1 - I_P(y,x) \quad (22)$$

Simplifying (21) by using (22) and rearranging, we have

$$I_{P_{fe}}(N-m, m+1) - I_{P_{fe}}(N-m+1, m+1) = I_{P_{de}}(N-m, m+1) - I_{P_{de}}(N-m+1, m+1)$$

Further simplifying above equation using (20) and rearranging, we get

$$\left(\frac{1-P_{me}}{P_{fe}}\right)^{N-m} = \left(\frac{1-P_{fe}}{P_{me}}\right)^{m+1}$$

$$\Rightarrow N^*_{N-m} = \left\lceil \frac{(m+1)}{\alpha} + m \right\rceil$$

■

where α is given by (14).

V. Acknowledgment

This paper has been partially supported by the IU-ATC project funded by the Department of Science and Technology (DST), Government of India.

References

[1] S. Haykin, "Cognitive radio: brain-empowered wireless communications," *Selected Areas in Communications, IEEE Journal on*, vol. 23, no. 2, pp. 201 – 220, feb. 2005.

[2] A. Ghasemi and E. Sousa, "Collaborative spectrum sensing for opportunistic access in fading environments," in *New Frontiers in Dynamic Spectrum Access Networks, 2005. DySPAN 2005. 2005 First IEEE International Symposium on*, Nov 2005, pp. 131–136.

[3] B. F. Ian F.Akyildiz and R. Balakrishnan, "Cooperative spectrum sensing in cognitive radio:a survey," vol. 4, no. 4, pp. 40–62, 12 2010.

[4] W. Zhang, R. Mallik, and K. Letaief, "Optimization of cooperative spectrum sensing with energy detection in cognitive radio networks," *Wireless Communications, IEEE Transactions on*, vol. 8, no. 12, pp. 5761 –5766, december 2009.

[5] K. Letaief and W. Zhang, "Cooperative communications for cognitive radio networks," *Proceedings of the IEEE*, vol. 97, no. 5, pp. 878–893, May 2009.

[6] N. R. Banavathu and M. Z. A. Khan, "Optimal n-out-of- k voting rule for cooperative spectrum sensing with energy detector over erroneous control channel," in *Vehicular Technology Conference (VTC Spring), 2015 IEEE 81st*, May 2015, pp. 1–5.

[7] A. Singh, M. Bhatnagar, and R. Mallik, "Optimization of cooperative spectrum sensing with an improved energy detector over imperfect reporting channels," in *Vehicular Technology Conference (VTC Fall), 2011 IEEE*, Sept 2011, pp. 1–5.

[8] Y. Chen, "Improved energy detector for random signals in gaussian noise," *Wireless Communications, IEEE Transactions on*, vol. 9, no. 2, pp. 558–563, February 2010.

THE 18TH INTERNATIONAL SYMPOSIUM ON WIRELESS PERSONAL MULTIMEDIA COMMUNICATIONS
(WPMC-2015)
December 13-16, 2015, Hyderabad, India

Link Adaptation Strategies for Cellular Downlink with low-fixed-rate D2D Underlay

Afonso Eduardo, Ivo Sousa, António Rodrigues
Instituto de Telecomunicações (IT)
Instituto Superior Técnico (IST), Universidade de Lisboa
Lisbon, Portugal
Email: afonso.eduardo@tecnico.ulisboa.pt, {ivo.sousa, antonio.rodrigues}@lx.it.pt

Abstract—**The new paradigm of Machine-to-Machine (M2M) communications poses problems in regard to the spectrum usage, arising the need to share radio resources. Downlink with low-fixed-rate Device-to-Device (D2D) underlay and Successive Interference Cancellation (SIC) are emergent solutions. The considered scenario can be described by two links: Infrastructure-to-Device (I2D) and D2D links. In this work, Long Term Evolution (LTE) physical layer, Single-Input Single-Output (SISO) mode and block flat Rayleigh fading are assumed for both links, where Link Adaptation (LA) is only performed by the Base Station (BS). In this context, this paper seeks to validate that it is possible to guarantee a certain Quality of Service (QoS) requirement, despite not being able to determine the D2D CSI in the LA process, while simultaneously addressing technical implementation problems that arise.**

Keywords—M2M, D2D Underlay, SIC, Link Adaptation, LTE

I. INTRODUCTION

Currently, the design of future 5th generation (5G) cellular networks is in the works and, within this framework, several technologies are being investigated. In [1], it is argued that a significantly better performance cannot be accomplished by simply adding new features to the existing standards and that such goal requires instead the introduction of disruptive technologies that force the deep-rooted cellular principles to be reformulated. Among those technologies, there are two that fall into the scope of this work: Device-to-Device (D2D) and Machine-to-Machine (M2M) communications.

D2D communication refers to the ability of one wireless device to communicate, via direct link, with another using the spectrum that is available for regular cellular communications. It is noteworthy that existing technologies, such as Wi-Fi and Bluetooth, already allow devices to directly communicate with each other, but the usage of unlicensed radio resources leads to several limitations given that interference levels cannot be properly controlled. On the other hand, M2M consists of a multitude of Machine-Type communications Devices (MTDs) connected to the network. These devices are often described in the context of Wireless Sensor Networks (WSNs) which are able to offer numerous applications related to data collection, ranging from environmental to health-care monitoring.

One problem that arises is related to the spectrum usage. In a situation where there is a need for a massive number of devices to communicate, efficient Radio Resource Management (RRM) algorithms are of extreme importance, reinforcing also the emergence of Interference Cancellation (IC) techniques. Indeed, if one is to interpret the interferers as yet other sources of useful information (from other devices), one can readily understand that IC techniques permit the coexistence of multiple links. Moreover, in Orthogonal Frequency-Division Multiplexing (OFDM) systems, of which LTE is part of, extracting the signal of an interferer by means of channel decoding is generally the only processing gain available [2]. It is precisely in this circumstance that the concept of Successive Interference Cancelation (SIC) arises.

The basic principle of SIC is to decode different devices sequentially, such that the interference due to the decoded devices is subtracted before decoding the others. Allied to SIC, there is also the need to adapt the transmission parameters to the channel conditions. This is referred to as Link Adaptation (LA).

Additionally, in [3], the concept of cellular downlink with low-fixed-rate D2D underlay is explored, providing insight into its relationship with SIC. In fact, it is shown analytically that "SIC is an important enabler of underlay D2D communication". In [4], this synergy is further investigated and it considers the possibility of partial Channel State Information at the Transmitter (CSIT). The noteworthy conclusion is that, in theory, there is "a positive downlink rate that can always be decoded" which leads to "zero-outage of the downlink signal".

That said, this paper seeks not only to validate, but also to evaluate in a new scenario the concept originally presented in [4] by considering a low-fixed-rate D2D underlay, the usage of SIC and partial CSIT in a LTE setting. The aim is not to achieve a zero-outage situation, but to prove that a certain QoS can be guaranteed. It is also worth emphasizing the relevance of the constraint that is associated to the knowledge of the D2D CSI in the LA process, i.e. partial CSIT. This constraint arises from the fact that, in the context of M2M communications, MTDs might exhibit intermittent activity, rather than continuous. However, the receiver is only able to report the CSI estimate if transmission occurs, given that this estimate is computed from reference signals. Thus, in such scenarios, the receiver can report an accurate Infrastructure-to-Device (I2D) CSI due to continuous transmission, but, since the D2D communication occurs intermittently, the reported D2D CSI can be fairly outdated, reporting an estimate that might be highly inaccurate.

The rest of the paper is organized as follows: Section II describes the system model; Section III focuses on the LA strategies; numerical results are given in Section IV and conclusions are drawn in Section V.

II. SYSTEM MODEL

A. Link Level Overview

Consider the topology depicted in Fig. 1 which consists of two Single-Input Single-Output (SISO) links. The link denoted by D2D refers to the transmission of the MTD data to a given UE, whereas the I2D targets the same UE but has the Base Station (BS) as the transmit entity. The D2D is considered to be a low-rate link when compared to the I2D. It is also assumed that the BS is able to dynamically adjust its rate as opposed to the MTD whose rate is fixed, i.e. fixed Modulation and Coding Scheme (MCS). Another assumption is that the system operates under non-line-of-sight conditions such that these links are characterized by two independent block flat Rayleigh fading channels whose gains remain constant over each Transmission Time Interval (TTI) and over all the assigned subcarriers. Furthermore, it is assumed that the UE has always perfect CSI knowledge during the decoding process so much so that no estimation error arises when determining both channel gain estimates and the noise power. For LA purposes, the UE computes the MCS to be reported to the BS according to a given rule (see Section III). In turn, this report is assumed to occur in an instantaneous fashion so that the BS can apply the most appropriate MCS for each instantaneous channel realization. It should be noted that, in a real scenario, rather than instantaneous, the report has a delay, but if one considers that the fading is sufficiently slow, the reports are still accurate enough, validating the simplification. That said, let the post-detection received signal on a given subcarrier be defined as

$$Y = H_M X_M + H_B X_B + w, \tag{1}$$

where X_M and X_B are the Quadrature Amplitude Modulation (QAM) symbols transmitted by the MTD and the BS respectively; H_M and H_B are the complex coefficients of the two independent channels and w represents the white Gaussian noise with variance σ_w^2. The Signal-to-Noise Ratio (SNR) of each link can then be written as

$$\gamma_i = \frac{|H_i|^2 P_i}{\sigma_w^2}, \qquad i \in \{M, B\}, \tag{2}$$

where $P_i = E[|X_i|^2]$ is the average transmitted power of the respective entity (MTD or BS). Furthermore, the corresponding Signal-to-Interference-plus-Noise Ratio (SINR) is given by

$$\eta_i = \frac{|H_i|^2 P_i}{\sigma_w^2 + |H_j|^2 P_j} = \frac{\gamma_i}{1 + \gamma_j}, \qquad (i, j) \in \{M, B\}^2, i \neq j. \tag{3}$$

B. Transmitter Model

The transmit entities are the MTD and the BS, both of which are modelled as two separate LTE downlink transmitters [5] and whose model is shown in Fig. 2.

The processing chain begins by grouping the data into chunks of variable length known as Transport Blocks (TBs),

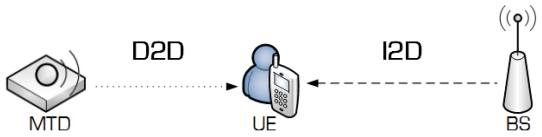

Fig. 1. Link Level Topology

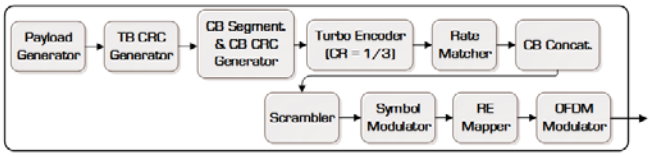

Fig. 2. LTE Downlink Transmitter Model

followed by the calculation and attachment of a 24-bit Cyclic Redundancy Check (CRC) to each TB as a means to detect errors at the receiver side. The CRC-attached TB may be split into several Code Blocks (CBs) since the turbo coder interleaver has a maximum size of 6144 bits. In such case, each CB is attached with its own 24-bit CRC (CB-CRC). Subsequently, each CRC-attached CB is rate-1/3-turbo-code encoded followed by a rate matching procedure which includes additional interleaving and produces CB Code Words (CWs) with the target code rate. The CB-CWs are then concatenated to form a TB-CW and scrambled with a unique Gold sequence based on the physical level identity of the respective transmitter. The resulting sequence passes through a symbol mapper whose modulation can be 4-, 16- or 64-QAM depending on the MCS index. Finally, the symbols are mapped to Resource Elements (REs) that form the resource grid which, in turn, serves as input to the OFDM modulator, producing the baseband time-domain signal to be transmitted. Overheads and retransmissions are not modeled.

C. Receiver Model

The considered receiver is a Hard SIC receiver based on TB CRC [6] whose model is depicted in Fig. 3. In the literature, namely where SIC is applied to LTE systems, the focus is on cancelling transmissions from multiple antennas pertaining to the same transmit entity, e.g. [6]. In such case, all the signals are encoded with the same MCS. It thus follows that the optimal order of decoding is to sort the signals according to their SINR such that the signal experiencing the highest SINR is decoded first. In the present case, this does not apply, seeing that MTD and BS generally encode their messages with different MCSs. Consequently, the rule to determine the order of decoding is not based on which link experiences the highest SINR, but rather on how great the margin between the SINR and the operation threshold associated to the given MCS is. This operation threshold is, in turn, the SINR value at which the receiver is able to decode the signal with a given target Block Error Rate Probability (BLEP).

D. Modulation and Coding Schemes

The MCSs considered in this work are the same as those in [7] and are listed in Table 1. The MTD uses the most robust MCS, i.e. MCS 1, while the BS has the ability to encode its messages with any of the listed MCSs. Additionally, in a standardized LTE system, the receiver reports a 4-bit index, Channel Quality Indicator (CQI), limited to 15 different MCSs. Therefore, in said system, the BS uses the CQI report allied to other factors, such as positive/negative acknowledgement rate, to determine the

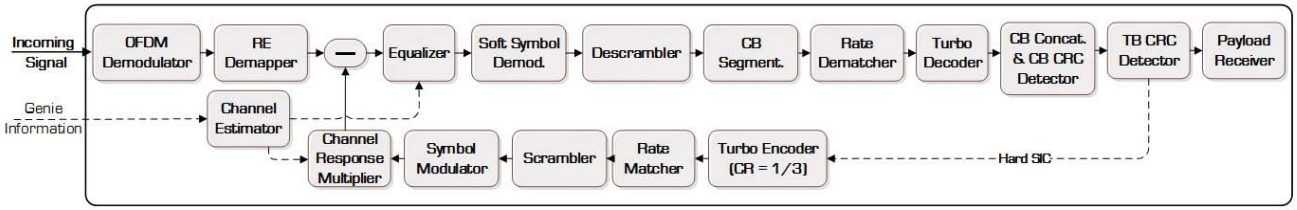

Fig. 3. LTE Receiver Model

MCS. In this work, it is assumed that the CQI is not restricted to 4 bits such that the receiver is able to report any of the available schemes, existing thus a one-to-one relationship between the CQI and the chosen MCS. In practice, this means that the MCS choice has been delegated to the receiver. Note, however, that since the CQI report is assumed instantaneous, it is analogous to the case where the BS (transmitter) is aware of the instantaneous CSI, i.e. CSIT, and chooses the MCS.

E. Operation Modes

Four operation modes are considered:

1. Orthogonal mode (Ortho): D2D and I2D links occur simultaneously, but different resources are assigned to each link. There is thus no interference, at the expense of having to allocate twice the resources.
2. Legacy mode (Legacy): D2D and I2D links occur simultaneously and share the same resources which leads to interference. The receiver (UE) does not perform SIC.
3. SIC with full CSIT (SICF): Similar to the previous mode in the sense that both links operate at the same time and share the same resources, but the UE is now a SIC-capable device. For LA purposes, both CSIs are known.
4. SIC with partial CSIT (SICP): Same conditions as the previous mode, except that the D2D CSI cannot be determined when performing LA.

Recall that the last mode is the primary focus of this work, while the other three are included for benchmarking purposes.

III. LINK ADAPTATION STRATEGIES

A. Single Link without Interference

First consider the orthogonal mode. From a LA stance, this is equivalent to the case where there is only a single link without any interference. Let k denote the index of a given MCS, $\mathcal{K}$ the set of available MCSs such that $k \in \mathcal{K} := \{1, \dots, K\}$ and that a higher MCS index corresponds to a more efficient (and less robust) MCS. Each MCS has thus its own spectral efficiency, denoted by $\mathcal{E}(k)$, and operation threshold Γ_k that corresponds to the point at which the kth MCS experiences a BLEP equal to the target Block Error Rate (BLER) given by ξ, i.e., $BLEP(k) = \xi$. Recalling that γ denotes the received instantaneous SNR, the focus is to maximize the expected instantaneous efficiency (equivalent to throughput) under the constraint that the estimated BLEP is smaller or equal than the target BLER. It is, thus, obvious that this problem can only be solved if $\gamma \geq \Gamma_1$. Provided that this condition is generally met by means of an appropriate power control scheme, the optimization problem for this scenario can be written as:

Table 1. Modulation and Coding Schemes

Index	Modulation	Code Rate	Index	Modulation	Code Rate
1	4-QAM	1/9	14	16-QAM	0.54
2	4-QAM	1/6	15	16-QAM	0.58
3	4-QAM	0.21	16	16-QAM	0.61
4	4-QAM	1/4	17	16-QAM	2/3
5	4-QAM	1/3	18	16-QAM	0.73
6	4-QAM	0.42	19	16-QAM	4/5
7	4-QAM	1/2	20	64-QAM	0.58
8	4-QAM	0.58	21	64-QAM	0.62
9	4-QAM	2/3	22	64-QAM	2/3
10	4-QAM	0.73	23	64-QAM	0.70
11	16-QAM	0.43	24	64-QAM	0.74
12	16-QAM	0.46	25	64-QAM	4/5
13	16-QAM	1/2	26	64-QAM	0.85
			27	64-QAM	0.90

$$\begin{aligned} \max_{k \in \mathcal{K}} \quad & \mathcal{E}(k).\big(1 - BLEP(\gamma, k)\big). \\ s.t. \quad & BLEP(\gamma, k) \leq \xi \end{aligned} \tag{4}$$

Assuming optimal coding and recalling that the MCS indices are sorted in terms of increased efficiency, the cost function simplifies into $f(k) = k$. Based on this approach, the only values that need to be stored are the operation thresholds Γ_k, determined from a prior calibration step [8]. The algorithm then consists in finding the highest MCS whose threshold is smaller or equal than the received SNR, i.e. SNR-MCS mapping. Lastly, it is worth pointing that the optimal coding simplification is justified by the near optimality exhibited by real coding [9] in which the BLEP decreases rapidly once the target BLER is met.

B. Single Link with Interference

Consider now the scenario where the link is also affected by interference (Legacy). In this case and assuming that the interference can be treated as Gaussian noise, the optimization problem can still be written as in (4), noting that the metric to measure the link quality becomes SINR, η, instead of SNR, γ. Following the same optimal coding simplification, the MCS is obtained by using the algorithm described in the previous subsection, but using the SINR as the metric. Also note that the problem is only solvable if $\eta \geq \Gamma_1$, which means that the system can be in outage not only due to a deep fade, but also if the interference is strong.

C. SIC with full CSIT

In this case, the goal is still to maximize the expected instantaneous efficiency of the I2D link, but under the constraint that the BLEPs of each link are smaller or equal than ξ:

$$\begin{aligned} \max_{k \in \mathcal{K}} \quad & \mathcal{E}(k).(1 - BLEP_B), \\ s.t. \quad & BLEP_M \leq \xi \\ & BLEP_B \leq \xi \end{aligned} \tag{5}$$

where the indices M and B specify the transmit entity and consequently the link, i.e. D2D and I2D links respectively.

Recalling that the D2D MCS is fixed (MCS_M), the BLEPs are given by:

$$BLEP_M = BLEP(\eta_M, MCS_M) - BLEP(\eta_M, MCS_M) \times \left(1 - BLEP(\eta_B, k)\right) \times \left(1 - BLEP(\gamma_M, MCS_M)\right), \quad (6)$$

$$BLEP_B = BLEP(\eta_B, k) - BLEP(\eta_B, k) \times \left(1 - BLEP(\eta_M, MCS_M)\right) \times \left(1 - BLEP(\gamma_B, k)\right), \quad (7)$$

where the second term results from the ideal SIC principle [2] in which the interference can be perfectly cancelled.

Assuming again the optimal coding simplification, there are only two cases to be evaluated. If $\eta_M \geq \Gamma_M$, the first constraint in (5) is automatically satisfied and the second degenerates into $BLEP(\gamma_B, k) \leq \xi$, being analogous to the single link without interference case. On the other hand, if $\eta_M < \Gamma_M$, the second constraint becomes $BLEP(\eta_B, k) < \xi$, forcing the I2D MCS to be chosen such that $\Gamma_B \leq \eta_B$. The first constraint then simplifies into $BLEP(\gamma_M, MCS_M) < \xi$ which is independent of the choice of I2D MCS, but provided that the system is well-dimensioned is satisfied for most cases, unless a deep fade occurs. Consequently, this rule can be described as follows:

Algorithm 1: SICF

```
Γ_M = get_threshold(MCS_M)
for each TTI do                    // new channel conditions
    if η_M ≥ Γ_M then              //effective I2D channel quality metric
        SINR_eff = γ_B
    else
        SINR_eff = η_B
    end if
    MCS_B = get_max_MCS(SINR_eff)  //SINR-MCS mapping
    report(MCS_B)
end for
```

D. SIC with partial CSIT

As above, the problem is expressed by (5), but now the D2D CSI is not known. Thus, the approach is to design the LA for the worst scenario. Considering again the use of optimal coding, this occurs when the MTD signal cannot be decoded without IC, i.e. $\eta_M < \Gamma_M$, which, as first derived in [4], means that

$$\eta_M = \frac{\gamma_M}{1+\gamma_B} < \Gamma_M \Leftrightarrow \gamma_M < \Gamma_M (1+\gamma_B) \quad (8)$$

and, consequently,

$$\left(\eta_B = \frac{\gamma_B}{1+\gamma_M}\right) > \left(\frac{\gamma_B}{1+\Gamma_M(1+\gamma_B)} := \widetilde{\eta_B}\right), \quad (9)$$

where $\widetilde{\eta_B}$ corresponds to the infimum and is the I2D channel quality metric ($SINR_{eff}$) used to determine the I2D MCS. It should be stressed that it is again required that $\gamma_M \geq \Gamma_M$, else the first constraint cannot be met.

Finally, note the importance of using a robust MCS_M such that Γ_M is low; otherwise, the I2D throughput is severely limited even when $\eta_B \to \infty$:

$$\lim_{\eta_B \to \infty} (\widetilde{\eta_B}) = \lim_{\gamma_B \to \infty} \left(\frac{\gamma_B}{1+\Gamma_M(1+\gamma_B)}\right) = \frac{1}{\Gamma_M}. \quad (10)$$

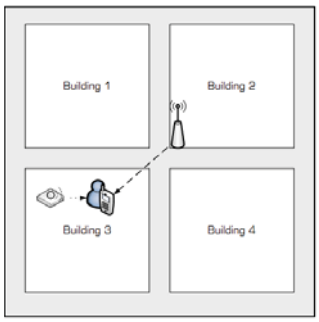

Fig. 4. Indoor on-body MTD Scenario

IV. SIMULATIONS

A. Link Level Simulator Setup

An indoor on-body MTD scenario is considered. The layout is shown in Fig. 4 and is based on "Test Case 2" of [10]: a 2x2 grid with wrap-around constituted by 120x120m 8-floor buildings whose floor height is 3.5 m and spaced apart by 18 m. The 3.5 m-tall BS is located in the southwest corner of the roof of the northeast building and it communicates with the 1.5 m-tall UE that is inside the southwest building. For each floor, the user randomly picks 500 different positions that are uniformly distributed and the I2D path losses follow the "Urban Macro Outdoor-to-Indoor" propagation model.

Additionally, this user has an on-body sensor (MTD) which directly communicates with the corresponding UE. The path loss for the D2D link is fixed and is 60 dB [11]. Each stationary measurement, in turn, has a duration of 10^5 TTIs. Other parameters include: 1.4 MHz bandwidth (6 Resource Blocks) for each link; 800 MHz carrier frequency; 9 dB UE noise figure; 0 dBi UE and MTD antenna gains; 15 dBi BS antenna gain; 0 dBm and 46 dBm transmit powers for the MTD and BS respectively [12].

Furthermore, the implemented simulator is based on a publicly available LTE link level simulator and therefore no calibration procedure had to be conducted [13]. Normal cyclic prefix, zero forcing equalization, an 8-iteration max-log-Maximum-a-Posteriori algorithm and $\xi = 10\%$ [8] are used. A full-buffer traffic model is also assumed.

B. Simulation Results

Simulations analyze the four operation modes in regard to BLER and throughput (R) per Resource Block (RB) for the D2D and I2D links, Fig. 5 and Fig. 6 respectively. Begin by noticing that only the Legacy and SICF BLER curves are shown in Fig. 5. This is due to Ortho and SICP exhibiting BLERs so low that all fall below the minimum resolution, i.e. $BLER < 10^{-5}$. Regardless, the primary goal is to evaluate if the modes meet the 10% BLER which is satisfied for all modes except Legacy, emphasizing not only that SIC is a necessity if resources need to be shared, but also attesting that SICP can indeed meet a certain QoS without full CSI knowledge during LA.

Regarding the throughput per RB, in the D2D link, the throughput is proportional to the block success rate which is given by $1 - BLER_M$. Naturally, in Legacy, a wide range of throughput rates is experienced by the user, while in the other modes the absolute throughput is practically always the

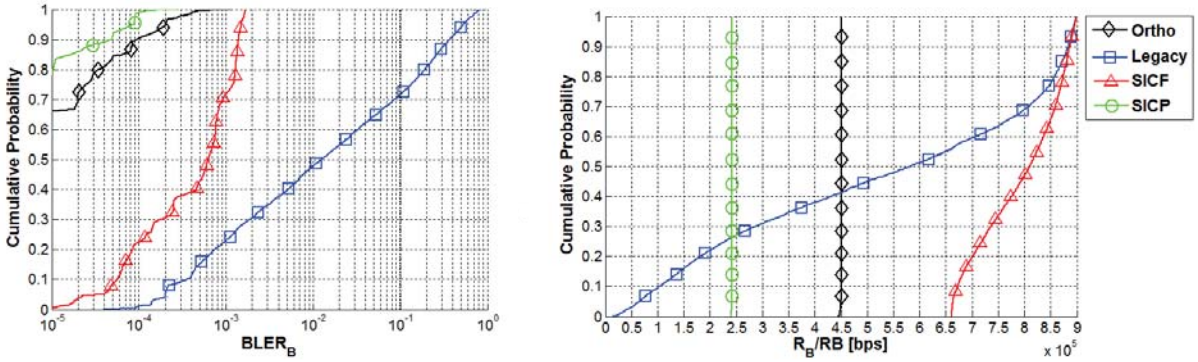

Fig. 5. BLER and Throughput per RB CDFs - D2D link

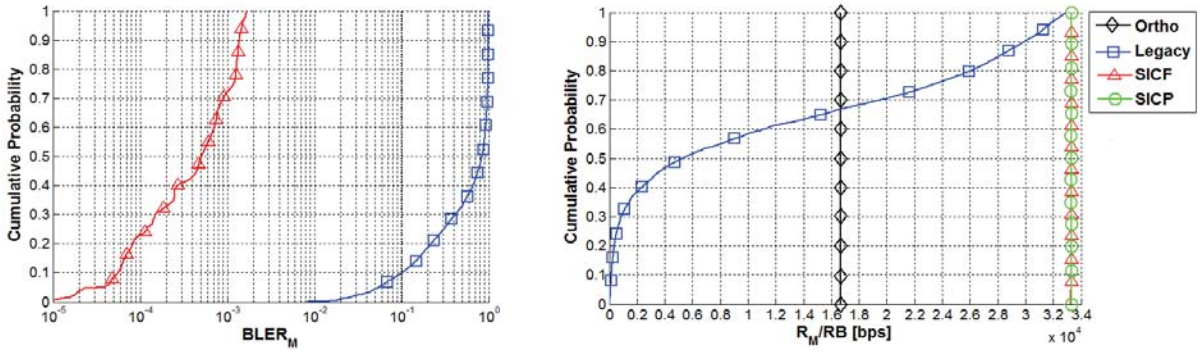

Fig. 6. BLER and Throughput per RB CDFs - I2D link

maximum. Although achieving the same absolute throughput, twice the resources are allocated in Ortho, thus the throughput per RB is halved. In the I2D link, despite using twice the resources, Ortho reaches a throughput per RB that is almost twice than that of SICP. On the other hand, Legacy experiences again a range of throughputs that covers nearly all the possible throughputs, while SICF can always guarantee a throughput per RB that is roughly 50% higher than that of Ortho and can go up to 100%.

V. CONCLUSION

This paper began by addressing technical implementation problems that arise when applying SIC LA strategies to cellular downlink with low-fixed-rate D2D underlay and whose physical layer is based on OFDM. It also validated that SICP can guarantee a certain QoS without knowledge of the D2D CSI in a LTE setting. Results show that its performance is roughly half than that of Ortho in the I2D link. To decrease this gap an even more robust D2D MCS such as Binary Phase-Shift Keying or lower coding rates, currently not standardized by LTE, ought to be used. Note that its usage should not compromise most M2M services since they are to operate at very low throughput rates.

ACKNOWLEDGEMENT

The authors would like to thank FCT for the support by the project UID/EEA/50008/2013. In addition, a word of gratitude to Nuno Pratas and Petar Popovski (Aalborg University) for their helpful and valuable contribution.

REFERENCES

[1] F. Boccardi, R. W. Heath, A. Lozano, T. L. Marzetta and P. Popovski, "Five Disruptive Technology Directions for 5G," *Communications Magazine, IEEE,* vol. 52, no. 2, pp. 74-80, 2014.

[2] E. Hardouin, M. Hassan and A. Saadani, "Downlink interference cancellation in LTE: Potential and challenges," in *Wireless Communications and Networking Conference (WCNC)*, Shanghai, 2013.

[3] N. Pratas and P. Popovski, "Underlay of low-rate machine-type D2D links on downlink cellular links," *Communications Workshops (ICC), 2014 IEEE International Conference on* , pp.423-428, 2014.

[4] N. Pratas and P. Popovski, "Zero-Outage Cellular Downlink with Fixed-Rate D2D Underlay," *Wireless Communications, IEEE Transactions on,* vol. PP, no. 99, 2015.

[5] 3GPP TS 36.212 v9.2.0 , "LTE; Evolved Universal Terrestrial Radio Access (E-UTRA); Multiplexing and Channel Coding," 2009.

[6] J. Axnas, Y.-P. E. Wang, M. Kamuf and N. Andgart, "Successive Interference Cancellation Techniques for LTE downlink," in *Personal Indoor and Mobile Radio Communications (PIMRC), 2011 IEEE 22nd International Symposium on* , Toronto, 2011.

[7] Alcatel-Lucent, "DL E-UTRA performance checkpoint," 3GPP TSG-RAN1, Tech. Rep. R1-071967, 2007.

[8] S. Schwarz, C. Mehlfuhrer and M. Rupp, "Calculation of the Spatial Preprocessing and Link Adaptation Feedback for 3GPP UMTS/LTE," in *Wireless Advanced (WiAD), 2010 6th Conference on* , London, 2010.

[9] C. Berrou and A. Glavieux, "Near optimum error correcting coding and decoding: turbo-codes," *Communications, IEEE Transactions on* , vol.44, no.10, pp.1261-1271, 1996.

[10] METIS, "Deliverable 6.1 - Simulation Guidelines," 2013. [Online]. Available: https://www.metis2020.com/documents/deliverables.

[11] K. Y. Yazdandoost and K. Sayrafian-Pour, "Channel Model for Body Area Network (BAN)," IEEE P802.15 Working Group for Wireless Personal Area Networks (WPANs), 2009.

[12] 3GPP TR 36.931 v11.0.0, "LTE;Evolved Universal Terrestrial Radio Access (E-UTRA);Radio Frequency (RF) requirements for LTE Pico Node B," Release 11, 2012.

[13] C. Mehlführer, M. Wrulich, J. C. Ikuno, D. Bosanska and M. Rupp, "Simulating the long term evolution physical layer," *Proc. of the 17th European Signal Processing Conference (EUSIPCO 2009), Glasgow, Scotland,* vol. 27, p. 124, 2009.

THE 18TH INTERNATIONAL SYMPOSIUM ON WIRELESS PERSONAL MULTIMEDIA COMMUNICATIONS
(WPMC-2015)
December 13-16, 2015, Hyderabad, India

Low Rate Common Control Channels with Distributed Cross-Layer Optimization via Genetic Algorithm

Pranoti Balki, Kishor P. Patil
Department of Electronics and Telecommunication,
Sinhgad Academy of Engineering, Pune, India
pranotibalki1@gmail.com,kppatil.sae@sinhgad.edu

Abstract— **In cognitive radio networks most of the routing protocols uses either dedicated unlicensed Common Control Channels (CCC) at 2.4 GHz or free Primary User (PU) licensed CCC for routing. In case of licensed CCC, the path selection and coordination among cognitive radio nodes takes more time. But, the problem of congestion occur at larger level in case of 2.4 GHz CCC due to interference from other wireless services and saturation which further leads to rise in link failure and routing control overhead that degrades the performance of system. In our proposed work, we have used lower unlicensed frequency as a low rate CCC since it is underutilized. Cognitive radio network routing necessitates a cross-layering approach due to close coupling and interaction between protocol layers. In this paper we presents comparative study for low (902-928 MHz) and high frequency (2.4GHz) CCC based AODV protocol with distributed optimization in cross layering via Genetic Algorithm. Assuming each node, with wireless links employing non-congestion Orthogonal Frequency Division Multiplexing (OFDM) to enable Dynamic Spectrum Access (DSA). Simulation (NS-2.32) results show that the low rate Common Control Channel performs better in terms of throughput, BER, hop count and end to end delay.**

Keywords*— *Cognitive radio; Common Control Channel; Distributed Optimization; Genetic Algorithm; OFDM.

I. INTRODUCTION

Spectrum scarcity is the major issue currently faced by the world due to rigid spectrum management policies. Unlicensed radio spectrum is the most heavily used and is occupied by a wide range of application in unlicensed Industrial, Scientific and Medical (ISM) fields that results in spectrum overcrowding. National regulatory bodies like Federal Communication Commission (FCC) [1] states that most of the allocated static licensed spectral bands is of similar type and geographical variation. Its usage is ranging from 15% to 85% in the band below 3 GHz. According to [2] Cognitive Radio (CR), is a new paradigm that provides the solution to the problem of spectrum scarcity and is capable of automatically choosing device parameters based on the prevailing operating conditions.

Many existing CR routing protocol uses 2.4 GHz band in collaboration with IEEE 802.11x for channel path selection and node coordination message transfer [3][4]. But the higher frequency band (2.4 GHz) has lower transmission range than lower frequency band. This is because of reflection, refraction, vegetation path loss, diffractions, attenuation, scattering and free space path [5]. The lower frequencies which are present at lower spectrum band (902-928 MHz) have relatively higher transmission range because of less space path loss compared with higher frequencies.

Cross-layer optimization is one of the key features of CR which enable simultaneous optimization of several operating parameters across different OSI layers of the device [6]. In addition, cognitive radio provides new proficient technology to improve the spectrum scarcity problem and increases the spectrum utilization i.e. Dynamic Spectrum Access (DSA) [7]. CR has ability to find the spectrum hole and transmit by using it without interference to the legitimate users. Genetic algorithm (GA) in combination with CR is employed in many works to achieve adoption automation and optimization in wireless networks. In [8], a population adaptation technique is presented for a GA that takes benefit of the information from prior cognition cycle, with an objective to diminish the time required to accomplish an optimal decision. According to J. F. Hauris [9] GA is used to solve the optimization of RF parameter for a wireless network to implement the adaptive process for CR on an autonomous vehicle, with chromosome structure for optimal radio communication in the varying RF environment. Distributed optimization has recently become the most active area of investigation in the wireless network. In [10], Y. Shi and Y. Hou verified that how distributed algorithm is designed for future multi hop CR network where conservative approach and aggressive approach are integrated to maximize the data rate for a set of user communication session. According to [11] it is given that a distributed channel assignment mechanism is used to plan a multiracial multi hop network where each node is outfitted with numerous IEEE 802.11 wireless transmitters and receivers.

In this paper, we proposed two Common Control Channels performing cross layer optimization via Genetic Algorithm and DSA using Cognitive Radio. Out of them, one is 2.4 GHz of CCC, and other is Low rate (902-928 MHz) CCC. The proposed approach is based on the previous work [12] where they have used low unlicensed spectrum band

(902-928 MHz) as a low rate AODV CCC for broadcasting route control messages and CR coordination message. The proposed system shows that the GA is used to route control messages by Low rate CCC and 2.4 GHz of CCC. Our simulation results show that the overall throughput of the system increases while BER, hop count and the end-to-end delay of the system decreases for low rate CCC.

The rest of the paper is organized as follows: Section II provides overview of the cross-layer design. Section III presents a brief description to our proposed scheme including multi-objective fitness function. Section IV shows the simulation results. Section V gives some concluding remark and observation.

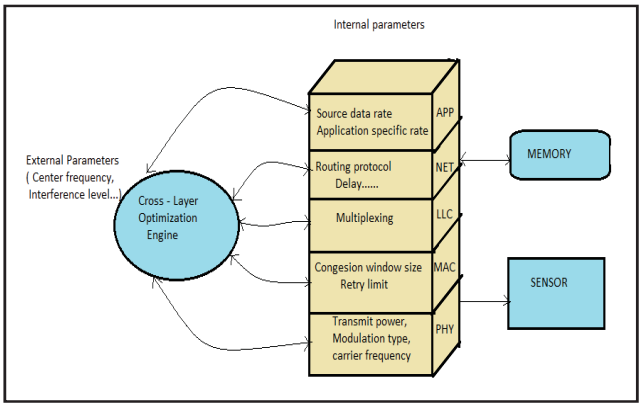

Figure 1. Framework of a generic cross-layer optimization framework

II. Cross Layer Optimization Overview

Fig.1 shows the general layout of the Cross-layer optimization architecture. The cross-layer optimization engine is provided to each node that takes the set of internal and external parameter as input by well-organized sensing methodology or via the control channel. All the sets of an internal operating parameter that are distributed across the different layer of a wireless device are decided by the optimization engine to achieve maximum performance and to coexist with another wireless device.

Some important parameter adjustments are 1) to adjust the center frequency and subcarrier number according to available spectrum. 2) to choose modulation type based on the trade-off between BER and data rate. 3) to adjust congestion window size based on data rate, 4) to set routing protocol parameter according to network stability and density. We have used Genetic Algorithm to implement optimization engine.

III. Proposed System

A. System Model

In the proposed work it is considered that all the wireless node employing non-contagious Orthogonal Frequency Division Multiplexing. This is widely considered as suitable contender for spectrally agile wireless transmission because of the advantage of subcarrier scalability and robustness to frequency fading [13]. Fig 2 shows an example of the distributed network architecture with 902 MHz and 2.4 GHz control channels. The information among different secondary nodes is exchanged by the control channels to perform distributed optimization.

In our work, we are working on four different parameters: center frequency f, normalized transmission power p, modulation index b and bandwidth w. As we are using NC-OFDM, each subcarrier has set off these four variables. Our optimization engine is used to optimize them together.

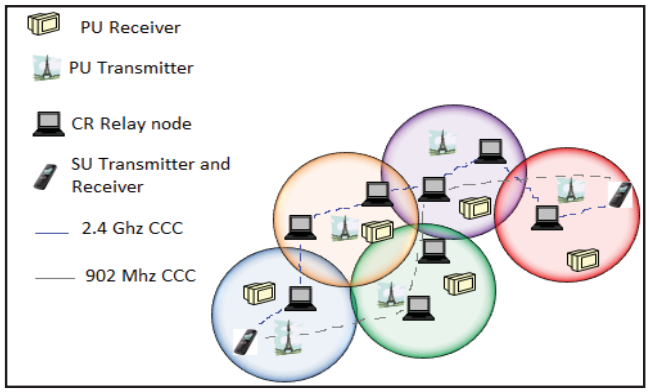

Figure 2. Schematic of distributed network architecture with 902 MHz CCC and 2.4 GHz CCC

When we consider a center frequency as 2.4 GHz, the overall bandwidth becomes high which results in the lower modulating index. Moreover, the performance of CR routing protocol has a direct effect on end-to-end network transit delay [12]. As QoS is dependent on minimal transit delay, it is essential to reduce hop count for delay sensitive application. Equation (1) explains about the possible network transit delay (D_{NT}) in between CR source and destination which include sensing delay, queuing delay, propagation delay, processing delay and medium access delay. The overall network transit delay increases as the total number of hops in between CR source and destination increases. Due to short range transmission the hop count in 2.4 GHz is higher, which results in longer end-to-end data transmission delay and additional network resource overhead [12].

$$D_{NT} = \sum_{i=1}^{p} W_i * D_i(\mathrm{c}) + \sum_{i=1}^{k} T_s(\mathrm{i}) * T_{inter-spec} \qquad (1)$$

With the fact that lower frequency gives longer transmission range, hence there is scope to reduce the total hop count and select best suitable shortest channel-path in CR sender and receiver nodes. For example in figure 2, it is clearly shown that 902 MHz CCC takes three hops to reach destination CR nodes whereas 2.4 GHz CCC takes almost seven hops to reach towards the same destination. Also with the increase in operating frequency the CR node transmission power is increases. Hence, 2.4 GHz control channels requires higher input transmission power as compared to 902 MHz Moreover, with higher input transmission power, there may be chances of interference with PU receiver signal.

B. *Fitness Function*

Following subsection presents fitness function required for cross layer optimization:

1. Overall Multi-objective Function:- Enhancing the performance of cognitive radio network using a multi-objective function for a node includes minimizing the BER, maximizing the throughput, minimizing power usage, minimizing interference with another node. The multi-objective optimization problem is solved by forcing the sum of these objectives to the optimum level. One of the disadvantages of this method is the optimum level of these objectives depends on the requirement of specific application and hence it needs to be adjust carefully. To define these function initially two thresholds has to describe i.e. lower threshold and the upper threshold.

2. Bit Error Rate Fitness Function:- If the source node needs to communicate with its destination, the average BER of all the subcarrier should be less than lower threshold for successful optimization of this function. If its value is greater than upper threshold communication is not possible. If its value is in between two thresholds it has to adjust by using these two thresholds.

3. Throughput Fitness Function:- To satisfy this function modulating index of subcarrier link between source to destination node should be maximum. If it is higher than upper threshold fitness criteria satisfies successfully. The fitness criterion is not satisfied, if its value is less than lower threshold. If it is in between the two thresholds, it has to adjust carefully with lower threshold and both the thresholds of average BER of subcarrier link between source and destination.

4. Interference Fitness Function:- Interference caused by source node to the other nodes in the network should be as minimum as possible. These values can be obtained either by estimating the environmental parameter or by control channels. Hence its value should be less than lower threshold. Otherwise it has to adjust with the receiving signal power level.

***5. Transmission Power Fitness Function*:-** When taking into consideration portable devices, whose energy supply is limited, this function is a necessary component in optimization. Its value depends upon the maximum attainable transmitting power for one subcarrier of source node and the transmitting power of subcarrier.

C. *Genetic Algorithm*

In the proposed work, we are using genetic algorithm optimization approach. Genetic algorithm is used to reflect the interplay property among all the layers by evaluating the fitness function for individual layers. Hence an effective cross layer optimization frame work is obtained which is used to find optimized power control, channel allocation and route selection in polynomial time. In this algorithm, all the input variables of the node are given to its optimization engine. Internally, it searches for an overall solution that gives the high fitness score using a fitness function. A flow chart shown in figure 3 describes the standard GA technique.

Initially, GA searches for all the channel information from the environment and selects the appropriate node. In standard GA fitness function across an entire node is calculated. After inputting all the variables of node to optimization engine, initialization of Genetic Engine takes place. Further, the fitness function for that node is evaluated, and check against the stopping criteria to check whether it satisfy the required fitness for individual layer or not.

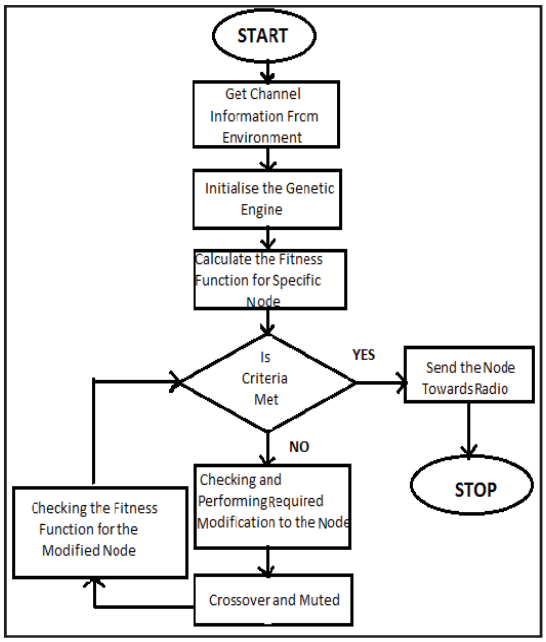

Figure 3. Flow chart of genetic algorithm

If it is found that required stopping criteria (Fitness Function) is achieved, that specific node moves towards further routing process, and the task for Genetic engine ends for that particular node. If the adequate fitness is not achieved by that node, the required modifications are performed with the help of external parameters. Moreover the fitness for the modified node is calculated and is again checks for the stopping criteria and the process repeated. When the required fitness is achieved by that node, it starts routing process and the variables of new node inputs to the engine.

IV. Result Analysis

In this section, the performance of low rate control channel is evaluated in terms of throughput achieved, Bit Error Rate, End-to-End delay of network and hop count and is compared with the performance of 2.4 GHz control channel. Experimental results are carried out using NS 2.31 simulator. The simulation results show that Low rate control channels have higher performance, and it works better in cross layering with lower central frequency. Simulation runs with the parameters shown in the following Table 1.

Fig 4 shows the graph of throughput of the network. The graph shows that initially because of higher center frequency the efficiency of 2.4 GHz CCC tends to rise and reach up to maximum value but suddenly because of higher drop-tail it

starts to go down. On another hand because of lower center frequency graph for Low rate (902 MHz) CCC takes a longer

TABLE 1.SIMULATION PARAMETER

Simulator	NS2 (ns 2.32)
Channel	Wireless channel
Propagation	Two Ray Ground
MAC	Mac/ 802_11
Ifqueue	Queue/DropTail/ProQueue
Link Layer	LL
Antenna	Omni Antenna
Ifqueue length	50
Routing	AODV
Number of nodes	34
Frequencies	902 MHz- 2.4 GHz
Flow rate	1024 Bytes
Traffic	TCP
Simulation time	2s-60s

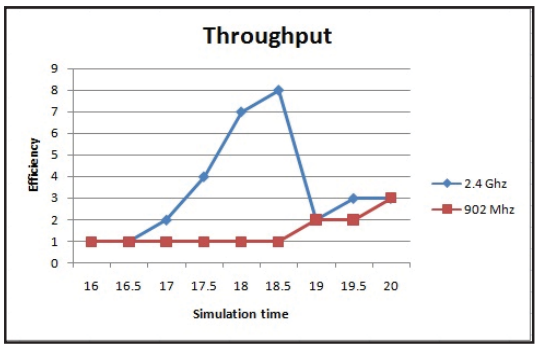

Figure 4. Graph of Throughput

time to rise but once it starts raising it provides a stable output response.

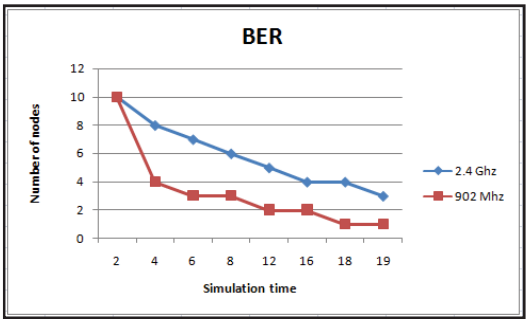

Figure 5. Graph of BER

Fig 5 shows graph for bit error rate (BER) variation. In digital transmission bit error is the number of received bits over the communication channel that is altered due to noise, interference, distortion, attenuation. Because of higher frequency such problem occurs at greater extend in 2.4 GHz of CCC. Graph shows that the BER is higher for 2.4 GHz CCC than that of low rate CCC (902 MHz).

Fig 6 Shows graph for one of the performance parameters i.e. hop count. In cognitive radio network goal is to search for the shortest path towards the destination node and this can be achieved through longer transmission range. As 2.4GHz CCC have shortest transmission range, the hop count of 2.4 GHz CCC is high while 902 MHz provides longer transmission range because of lower frequency range its hop count is low.

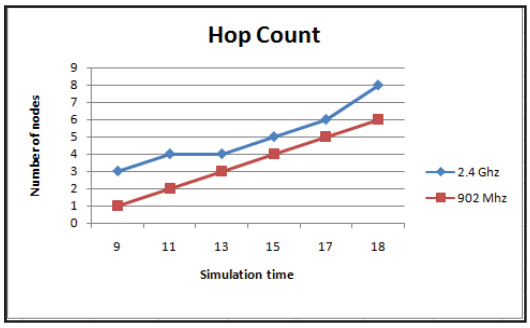

Figure 6. Graph of hop count

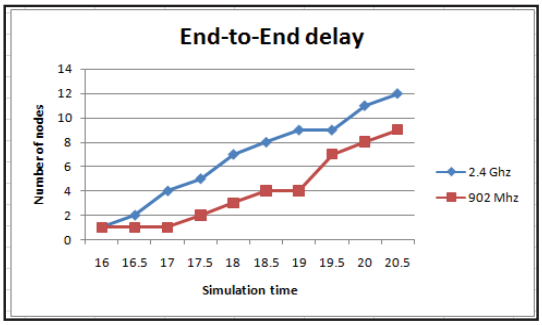

Figure 7. Graph of End-to-End Delay

End-to-End delay is the average time taken by the data packet to arrive at the destination node. It is a delay produced due to route maintenance process. Lower the value of End-to-End delay better the performance of the system. Fig 7 shows the low rate control channel has a lower end to end delay because of lower hop count.

V. CONCLUSION

This paper proposes a comparison of low rate CCC and 2.4 GHz CCC performing cross layer optimization via. GA. We have demonstrated that cross layer optimization performed with the help of GA by satisfying all the fitness criteria. Fitness function can be used to guide the wireless user to optimize coexistence with others through several tests. Our proposed work uses low rate CCC to overcome the drawback of 2.4 GHz of CCC occurs due lower transmission range. Low rate CCC with distributed optimization to gives stable throughput, low BER, hop count and the end-to-end delay. Those kind of distributed optimization passes significant potential to solve the problem of global spectrum usage in

both commercial and military application. . In future the proposed work can be implemented by using block wise Genetic Algorithm to perform cross layer optimization.

REFERENCES

[1]. FCC. Et docket no. 03-322. Notice of Proposed Rule Making and Order, December 2003.

[2] Joseph Mitola III, "Cognitive radio for flexible mobile multimedia communications," in Proc. *MoMuC'99*, San Diego, California CA,1999,pp.3-10.

[3] G. Cheng, W. Liu, Y. Li, and W. Cheng, "Joint on-demand routing and spectrum assignment in cognitive radio networks," in Proc. *IEEE ICC 2007*, Glasgow, Scotland, 2007,pp. 6499-6503.

[4] Cagatay Talay, A.; Altar, DT, "ROPCORN: Routing protocol for cognitive radio ad hoc networks," in *Proc ICUMT '09*, St. Petersburg, Florida, Oct. 2009,pp.12-14.

[5] Xiaohu Zhang; Burress, T.W.; Albers, K.B.; Kuhn W.B.; "Propagation comparisons at VHF and UHF frequencies," in Proc. *IEEE RWS'09*, San Diego, CA, Jan.2009, pp.244-247.

[6] L. U. Choi, W. Kellerer, and E. Steinbach, "On cross-layer design for streaming video delivery in multiuser wireless environments," EURASIP Journal on Wireless Commun.And Networking, vol., no., 2006.

[7] Min Song, Chunsheng Xin, Yanxiao Zhao and Xiuzhen Cheng, "Dynamic Spectrum Access: From Cognitive Radio To Network Radio," in Proc. *IEEE WC'11*, Vol.19, Issue.1,February 2011, pp. 23-29.

[8] T. R. Newman, R. Rajbanshi, A. M. Wyglinski, J. B. Evans, and G. J.Minden, "Population adaptation for genetic algorithm-based cognitive radios," in Proc. *CrownCom'2007*, Orlando, FL, USA, Aug 2008, pp. 279 – 284.

[9] J. F. Hauris, "Genetic algorithm optimization in a cognitive radio for autonomous vehicle communications," in Proc *IEEE CIRA 2007,* Jacksonville, FI, June 2007,pp. 427 – 431.

[10]Y. Shi and Y. Hou, "A distributed optimization algorithm for multihop cognitive radio networks," In Proc. *IEEE INFOCOM 2008*, Phoenix, AZ, April 2008, pp. 1292–1300.

[11] B.-J.Ko, V. Misra, J. Padhye, and D. Rubenstein, "Distributed channel assignment in multi-radio 802.11 mesh networks," In Proc. IEEE WCNC 2007, Kowloon, Hong Kong, March 2007, pp. 3978–3983.

[12] Satish Anamalamudi, Minglu IIN, "Low rate Common Control Channel based AOD routing protocol for Cognitive Radio Ad-hoc Networks", in Proc ICFN'13, Da Nang, Vietnam, July 2013, pp. 625 – 630.

[13] R. Rajbanshi, Q. Chen, A. M. Wyglinski, J. B. Evans, and G. J. Minden, "Comparative study of frequency agile data transmission schemes for cognitive radio transceivers," in Proc. Int. Workshop on Technol. Policy for Accessing Spectrum. New York, NY, USA, 2006, pp. 15.

[14] Si Chen Alexander M. Wyglinski, "Cognitive Radio-Enabled Distributed Cross-Layer Optimization Via Genetic Algorithms," in Proc. CROWNCOM'09,Hannover,June2009,pp.1-6.

THE 18TH INTERNATIONAL SYMPOSIUM ON WIRELESS PERSONAL MULTIMEDIA COMMUNICATIONS
(WPMC-2015)
December 13-16, 2015, Hyderabad, India

Path and Load Aware Routing Algorithm for Cognitive Radio Wireless Mesh Network

Ramesh Babu Battula, Dinesh Gopalani, Manoj Singh Gaur, E.S Pilli
ramsbattula@gmail.com, msgaer@gmail.com, dgopalani@gmail.com
Department of Computer Engineering, MNIT Jaipur, INDIA

***Abstract*—Cognitive Radio Wireless Mesh Networks (CR-WMNs) are reliable and promising technology to access opportunistically spectrum holes from the licensed bands with intelligible Software Defined Radio (SDR). It has the capability to revolutionize the way next generation applications having available spectrum. Multi-radio and multichannel CRWMNs are dynamic networks, which creates routing protocol design as a complex. It has a capability of assessing the spectrum availability during routing, which enhance the efficiency of the network. The proposed algorithm is a novel multipath algorithm. The path selected in this algorithm based the minimal interference information, which is useful to make this routing approach as more reliable. Channel selection has the capability to identify more suitable links for data transmission in the network. It uses a channel load metric to calculate the load throughput of available channels. The proposed algorithm has simulated in NS2. The simulation results demonstrate the efficiency of proposed channel selection and path aware routing algorithm.**

***Keywords*—Cognitive radio; Wireless Mesh Networks; Path aware; Interference ; Channel selection.**

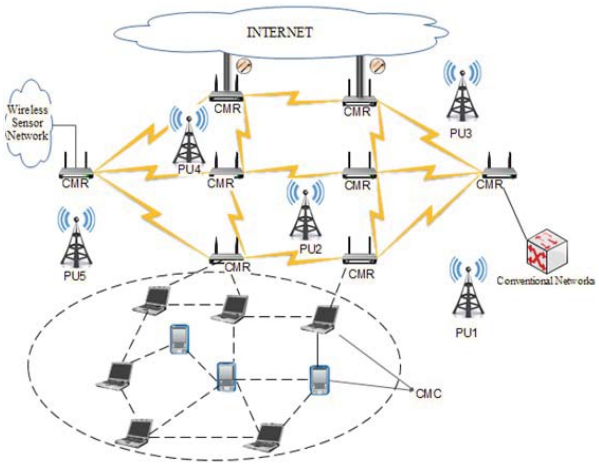

Fig. 1. Routing overhead and Number of nodes

I. Introduction

Wireless mesh networks (WMN) are highly used low cost networks. Now a days wireless mesh networks are mostly employed in local area networks (LAN), wide area networks (WAN) and metropolitan area networks (MAN). Due to their high connectivity and better performance people prefer these types of networks everywhere like broadband home networking, community and neighborhood networks, enterprise networks and building automation [1] [2]. Today entire world try to access different kinds of wireless networks, most of the wireless networks using unlicensed bands to transmit the data. The assigned wireless bands 2.4 Ghz and 5 Ghz are limited and number of users in this area are increasing day to day. It causes lot of spectrum scarcity at the unlicensed spectrum bands. To overcome this problem Federal Communication Commission (FCC) introduced the cognitive radio concept for utilizing underutilized spectrum at TV spectrum [1][2][3]. Cognitive enabled wireless mesh networks (CWMN) provide solution to spectrum scarcity for accessing broadband services. Cognitive radio enabled mesh routers (MR) or mesh clients (MC) are called as secondary users (SU). SUs are needed to identify the spectrum holes in the wireless environment and access the available spectrum without any interference with the primary user (PU). Cognitive Radio Wireless Mesh Networks architecture is showing in Fig. 1.

Most of the research has been focused on sensing, accessing, sharing and mobility of the spectrum. There are standards for direct access based medium access control (MAC) and physical (PHY) standards like IEEE 802.22. In CWMN, PU Spectrum holes behavior is in stochastic manner, this will affect the network performance of the network. During PU presence, SU quit form the occupied PU spectrum. In multi-hop cognitive wireless mesh networks, routing is a complex and distinctive problem. Establishing routes and its maintenance requires lot of information from the network [10]. Cognitive radio enabled wireless mesh network is a heterogeneous network and it has lot of problems during routing, if spectrum availability information is not considered. Multi-hop cognitive radio networks require spectrum allocation information to design better routing for the networks [8]. Routing algorithm provides information related to PU presence or absence with the help of spectrum sensing and accessing mechanisms. It will help to make network more efficient. In this paper, channel selection from the available PU spectrum and path selection has to be done with the minimum interference and maximum throughput information [18].

II. Related Work

Network performance depends on the design of routing protocol, mainly CWMN kind of networks has lot of dynamism in the network, hence it requires spectrum information from the MAC and PHY layers [10]. Licensed users has lot of spectrum under utilization, make them as use it solves the spectrum scarcity problem. Sensing a wide spectrum range, dynamically identifying currently unused spectrum

blocks for data communications, and intelligently accessing the unoccupied spectrum called Spectrum Opportunities (SOP) [8] [10]. WMN devices are enabled with cognitive radios can be networked smart wireless mesh networks called it as Cognitive Wireless Mesh Networks (CRWMN), recently gained lot of scope to improve the performance of wireless broadband services and provides a solution to limited spectrum allocations and utilization of the available spectrum at licensed users [12] [10].

In mesh networks, Routing is an extremely challenged research area and the network efficiency depends on its routing characteristics. In cognitive wireless mesh networks, routing is more complex issue than the wireless/wired mesh networks. It has lots of dynamism at spectrum identification and channel assignment. SEARCH is a distributed routing protocol; it works based on the PU activity, route optimization and awareness of the dynamic channel environment. Route optimization is purely based on the latency in the selected path. Channel assignment is defined by the mobility of the CR user [7]. End-to-End throughput for communication and optimal routing calculations based on the PU activity and path selection without any self loop paths are discussed [17]. In the presence of PU activity some of the CRs are unable to sense the available channel, so available channel identification in the presence of PU is a challenged task [16]. The available resources are identified based on the distributed routing and it has more capability to identify the end-to-end bandwidth on the available path [15]. In routing, adaptability based resource allocations and findings are useful for accurate routing solutions [14]. Primary Users are the ones who use traditional wireless communication systems with static spectrum allocation. Secondary Users are equipped with CRs and exploit Spectrum Opportunities (SOPs) to sustain their communication activities without interfering with PU transmissions. Indeed, the cognitive paradigm can be applied to different scenarios of multi-hop wireless networks including,

1) Cognitive Wireless Mesh Networks featuring a semistatic network infrastructure,
2) Cognitive radio Ad Hoc Networks (CRAHNs) characterized by a completely self-configuring architecture, composed of CR users which communicate with each other in a peer to peer fashion through ad-hoc connections [10].

Cognitive radio enabled wireless mesh networks is a heterogeneous network and it has lot of problems during routing, if spectrum availability information is not considered. Multi-hop cognitive radio networks are required spectrum allocation information to design better routing for the networks [10] [8].

Cognitive radio technology gives system the ability to operate around any interference, including any licensed traffic. This technology allows the detection of the communication channels or frequency bands which are vacant or not in use, while avoiding any occupied ones, hence improving the spectrum efficiency. This technology allows the detection of the frequency bands which are vacant or not in use, while avoiding occupied ones, resulting in spectrum efficiency [10]. There are various design challenges

1) *Channel Saturation*: The saturation problem basically occurs when the variety of nodes that are try to gain access of the control channel resulting in a high rate of packet collisions. Hence overall performance degradation.As more data channels are included in the network, the networks performance decreases gradually. The increased traffic load creates a negative impact on the overall throughput of the network that is the performance of the network worsens when more data channels are added and gradually reaches its saturation point [10].
2) *Robust PU Activity*: Unless a channel has been allocated in a primary user free frequency band, it is prone to primary user activity and interference at any time. Hence, this is another design issue that has to be taken care of.
3) *Channel Coverage*: It is not possible for all cognitive radio users to listen to the same channel; hence the coverage of a common control channel is limited to a certain area where a particular group of users are tuned in to the same channel for control message exchange. Large common control channel coverage leads to less overhead of control signaling but doing so is quite typical.

III. Path and Load Aware Routing Algorithm for Cognitive Radio Wireless Mesh Networks

In this work, all mesh routers are equipped with Cognitive Radios(CR) and Mesh Clients(MCs) also have this capability and cooperatively share the spectrum availability information without any interference.

A. Protocol Overview

Wireless mesh networks with cognitive radio capability have more scope to improve performance of wireless services. In this work, a novel approach has been introduced to find maximum throughput with minimal interference path among multiple paths. Path selection depends on the availability of PU spectrum bands in the path and its bandwidth. This algorithm considered both MAC and routing layer for implementation. Hence, it is a cross layer protocol. It has two major modules, and one provides the maximum throughput channel selection and its load from multiple channels and other module identify the minimum interference path. This approach leads to find the better path to the source and destination.

B. Working Procedure of PLRP

The proposed routing protocol using by mainly three stages, which are spectrum excerption, channel selection and load identification. In this PLRP,

C. Network Model and Assumptions

In this paper, the network consists of a set PU of primary users, set SU of secondary users, S is a set of spectrum information, set P includes all possible paths between any two or more nodes. Each primary user $(pu_1, pu_2, pu_3, ..., pu_n)$ has some fixed spectrum allocations. Spectrum holes create the opportunity for accessing spectrum, which mobile nodes equipped with cognitive radios they can access without any interference.

$$p^m_{u,v}(t) = \begin{Bmatrix} 1 & \exists m \in [1,2,.....,N] \\ 0 & Otherwise \end{Bmatrix} \quad (1)$$

Let $p_{uv}^{m}(t)$ denotes the communication channel m used to transmit data from CR enabled user u to CR enabled user v at a time t. Each channel characterized by the link throughput $\Psi_{u,v}^{m}(t)$, which calculates the number of packets conveyed in a unit time. The transmission from u to v through channel m. In this throughput calculation, several components are needed to use like bandwidth, channel spectral efficiency and the radio propagation. Let $\Psi_{u,v}^{m}$ has been worked out in this paper like in the following.

$$\Psi_{u,v}^{m} = \frac{\Psi_{A_u}\Phi_m Z_m(1-Pr_m)}{\sum_{k=0}^{n}\Phi_k Z_k(1-Pr_k)} \tag{2}$$

Ψ_{A_u} aggregated throughput at u (assumed based on IEEE 802.11).

$$\Phi_m = \frac{\omega_m \xi_m}{\sum_{m=0}^{n}\omega_m \xi_m)} \tag{3}$$

$\Psi_{u,v}^{m}(t)$ denotes the throughput at the channel m, and it uses between the CR nodes u and v at time t. In this, Φ_m represents the service probability of channel i. ω_m provides the window size at the back-off time t and ξ_m calculates channel capacity for channel m and ω_m is for maximum channel capacity, which has defined for nodes in the network [12].

$$\omega_m = \beta_m log_2\left[1 + \frac{R_{u,v}^{m}}{AW_0 + p_{I,v}^{m}}\right] \tag{4}$$

PU nodes $\in P$ such that each node has m orthogonal bandwidth frequencies, $\beta_0, \beta_1, ..., \beta_m$, R_{uv}^{m}, means received the power of the licensed channel m used for CR nodes u and v. $P_{I,v}^{m}$ is provided the interference information at node u for channel m, AW_0 is having white Gaussian noise power value. Pr_m represents the channel loss probability in the network. $\Psi_{u,v}^{m}(t)$ has the capability for calculating the maximum throughput of a channel in a particular spectrum S.

In this multipath algorithm, it has identified less interference and high throughput path among available paths with the help of a channel selection algorithm and interference aware metric. κ has to provide minimum interference with better packet delivery information and useful to select a better suitable path from available paths in the networks [3].

$$Min\lambda(p_{u,\vartheta}^{\delta}) = \frac{1}{N_l \times \varphi_{u,\vartheta}}\sum_{\delta\in p}\eta_\delta + \sum_{\delta\in p}\chi_\delta \tag{5}$$

$\lambda(p_{u,\vartheta}^{\delta})$ with this minimum interference path selection is being done in this work. If it has a value close to zero means, it has minimum interference to channel δ. N_p represents a neighbor set, which is useful to find the interfere nodes with node u during transmission with channel δ. φ has information about the expected transmission time (ETT), η has to be calculated the resource available without any interference with the channel δ.

$$\varphi_{u,\vartheta} = \frac{1}{(d_f \times d_r)} \times \frac{S}{B} \tag{6}$$

$$\eta_\delta = \varphi_{u,\vartheta} \times N_l \tag{7}$$

$$\chi_\delta = \begin{Bmatrix} W_1 & if p_u^{\delta} \neq p_u^{\delta-next} \\ W_2 & if p_u^{\delta} = p_u^{\delta-next} \end{Bmatrix} \tag{8}$$

Algorithm 1: Path Aware Routing with Channel Selection Algorithm

Input: u,v ∈ N and δ ∈ C, ϑ ∈ N p ∈ P
Output: max,p,c

PathAware(p,c)
- $\vartheta \leftarrow u_next_hop$; **while** $\vartheta \neq v$ **do**
  - $\delta \leftarrow Channel_Selection(p_{u,\vartheta})$
  - **if** $\kappa(p_{u,\vartheta}^{\delta} == 0)$ **then**
    - **if** $\vartheta = v$ **then**
      - $p_{uv}^{\delta} \leftarrow 1$;
    - **else**
      - $p_{u,\vartheta}^{\delta} \leftarrow 1$;
      - $u \leftarrow \vartheta$;
      - $\vartheta \leftarrow \vartheta_next_hop$;
  - **else**
    - $\vartheta \leftarrow \vartheta_next$;

ChannelAware(p,c)
- **Input**: m is number of channels c ∈ C, and p ∈ P ;
- $c \leftarrow 1$ **while** $c < m$ **do**
  - $\eta_1 \leftarrow \Psi(p_u^c)$;
  - $\eta_2 \leftarrow \Psi(p_u^{c_next})$;
  - **if** $\eta_1 < \eta_2$ **then**
    - $max \leftarrow \eta_2$;
    - $c = c_next$;
  - **else**
    - $max \leftarrow \eta_1$;
  - $c = c + 1$;
- **return** max, p, c;

S and B are prob packet size and bandwidth measured from the channel δ, d_f and d_r are denoted for number of successful packets delivered and receive. This protocol identifies the minimum interference path with help of path aware algorithm and channel selection algorithm identifies the maximum throughput channel.

IV. Simulations and Results

The proposed algorithm implementation performed with the help of Network Simulator(ns-2) simulator. The simulation completed with ns-2 having cognitive radio module. The simulation parameters are chosen such that they can resemble a real environment. The performance of any routing mechanism measured in terms of average throughput, Packet delivery ratio and Routing Overhead. The number of nodes used for this simulation is 10, 20,40,80 and 125. The number of CBR sources and destinations are increased based on the number of nodes and simulation area.

A. Performance parameters

1) *Routing Overhead*: The total number of control packets sent or forward to route the data packets. The ratio of control packets and data packets is called routing overhead for a protocol.

Description	Value
Total Data Channels	4
Total Simulation Area	1000 × 1000 m
Routing Protocol	PLAR, SEARCH, CRP, AODV
Number of SUs	10/20/40/80/100
Number of PUs	2/4/8/16/20
Channel Bandwidth	100, 250, 500, 650 Mbps
Packet Size	1200 Bytes
Channel Switching Delay	200μs
Mesh Routers	3/6/12/24/30μs

TABLE I. SIMULATION PARAMETERS

2) *Average Throughput* : The total data delivered at nodes in a given time unit. The average throughput measured in this simulation in kilobytes per seconds(kBps).
3) *Packet Delivery Ratio*: The number of packets that were delivered successfully in total simulation.

Performance parameters compare with number of nodes. Simulation results prove the performance of this Routing Protocol and compared with traditional routing protocols in wireless mesh networks.

B. Simulation Results

In this section, results are compared with existing protocols like Ad-hoc On-demand Modified Distance vector(AODV) [20], Cognitive Radio Ad-hoc Routing Protocol (CRP) [13] and SEARCH: A routing protocol for mobile cognitive radio ad-Hoc networks [19]. Performance parameters are here, packet loss ratio, average throughput, and average throughput throughput. Performance parameters compare with number of nodes and number of PU nodes in the simulation.

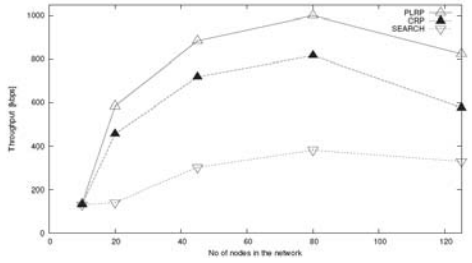

Fig. 2. Throughput and Number of nodes

In the Fig. 2 and Fig. 3, this result shows proposed algorithm dominating other two routing approaches. In the proposed approach, the channel selection method is useful to obtain the maximum throughput channel. But both SEARCH and CRP protocols are failing to reach the proposed routing approach performance related to average throughput. There is no specific approach to identify the channel selection method neither in SEARCH nor in CRP.

In the Fig. 4 and Fig. 5, the Normalized Routing Load(NRL) is very less because it uses a limited number of paths to perform routing in the network, at the same time SEARCH uses its control message more for finding routes from the available routes in the network. A mesh

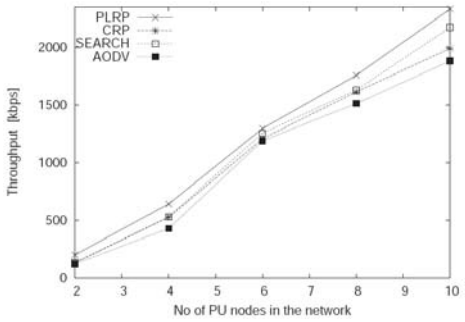

Fig. 3. Throughput and Number of PU nodes

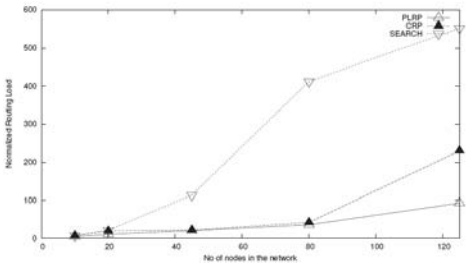

Fig. 4. Routing overhead and Number of nodes

network with multiple channels so that SEARCH required more control packets to identify the shortest path from the available paths with the help of its control packets. An error occurred during the transmission, identification path from the available spectrum it is needed many route request packets. The CRP routing protocol is better compared to SEARCH at this point, why it is doing routing based on the metric, which is helping to find the most reliable paths in the network. So that it needs very less number of control packets. In the same scenario, our proposed approach has been performed far better than the both these protocols, because of its channel and path aware concept.

In the Fig. 6 and Fig. 7, routing performance will be defined by the packet delivery ratio, as per the results proposed approach has been performed slightly better then the remaining two protocols. With the help of multi-path routing it has achieved this.

V. CONCLUSION

Now a days Cognitive Wireless Mesh Nsetworks is an emerging technology. In this paper, a new channel selection

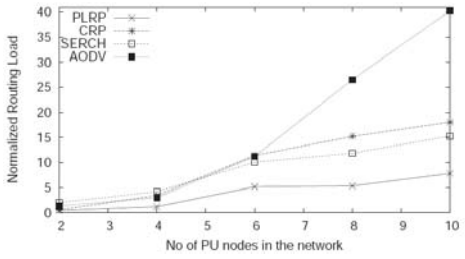

Fig. 5. Routing overhead and Number of PU nodes

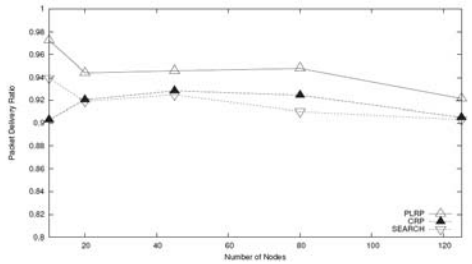

Fig. 6. Packet delivery ratio and Number of nodes

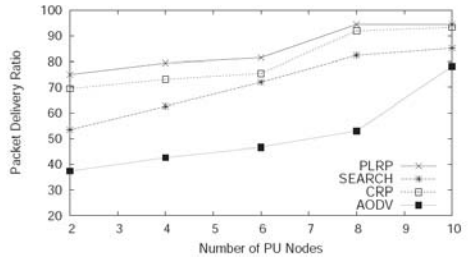

Fig. 7. Packet delivery ratio and Number of PU nodes

algorithm is designed to find the maximum throughput channel from the available spectrum. Generally in the presence of PU's, SUs are unable to identify the unused spectrum from the wireless environment. But the proposed algorithm has the capability to identify the available channels from the spectrum in the presence of PU's. It also discovers minimal interference channels in a path, so that it avoids interference with PU's. The efficiency of the proposed algorithm has been analyzed via its implementation on NS2 and it outperforms the existing routing algorithms in terms of the packet delivery ratio, normalized routing load and throughput. In future the enhancement of proposed algorithm can be performed to reduce end-to-end delay.

VI. Acknowledgment

The authors gratefully acknowledge the support from Department of Science and Technology, India for funding this project.

References

[1] Ian F. Akyildiz, Xudong Wang, Weilin Wang, Wireless mesh networks: a survey, Computer Networks, Volume 47, Issue 4, 15 March 2005, Pages 445-487, ISSN 1389-1286, http://dx.doi.org/10.1016/j.comnet.2004.12.001.

[2] Akyildiz, I.F.; Xudong Wang, "A survey on wireless mesh networks," Communications Magazine, IEEE , vol.43, no.9, pp.S23,S30, Sept. 2005 doi: 10.1109/MCOM.2005.1509968

[3] Waharte, S.; Ishibashi, B.; Boutaba, R.; Meddour, D., "Performance study of wireless mesh networks routing metrics," in Computer Systems and Applications, 2008. AICCSA 2008. IEEE/ACS International Conference on , vol., no., pp.1100-1106, March 31 2008-April 4 2008.

[4] Yanxiao Zhao, Min Song, Chunsheng Xin, and Manish Wadhwa,*Spectrum Sensing Based on Three-State Model to Accomplish All-level Fairness for Co-existing Multiple Cognitive Radio Networks* in proceedings IEEE INFOCOM 2012., pp:1782-1790.

[5] Yucek, T.; Arslan, H., "A survey of spectrum sensing algorithms for cognitive radio applications," in Communications Surveys & Tutorials, IEEE , vol.11, no.1, pp.116-130, First Quarter 2009. doi: 10.1109/SURV.2009.090109

[6] Lu Lu, Xiangwei Zhou, Uzoma Onunkwo and Geoffrey Ye Li,"Ten years of research in spectrum sensing and sharing in cognitive radio",EURASIP Journal on Wireless Communications and Networking 2012

[7] K.R. Chowdhury, M.D. Felice, "Search: A routing protocol for mobile cognitive radio ad-hoc networks, Computer Communications," Volume 32, Issue 18, 15 December 2009, Pages 1983-1997, ISSN 0140-3664, http://dx.doi.org/10.1016/j.comcom.2009.06.011.

[8] Beibei Wang; Liu, K.J.R. "Advances in cognitive radio networks: A survey", Selected Topics in Signal Processing, IEEE Journal of, On page(s): 5 - 23 Volume: 5, Issue: 1, Feb. 2011.

[9] Bourdena, A.; Mastorakis, G.; Pallis, E.; Arvanitis, A.; Kormentzas, G. "A spectrum aware routing protocol for public safety applications over cognitive radio networks", Telecommunications and Multimedia (TEMU), 2012 International Conference on, On page(s): 7 - 12

[10] Cesana, Matteo, Francesca Cuomo, and Eylem Ekici. "Routing in cognitive radio networks: Challenges and solutions." Ad Hoc Networks 9.3 (2011): 228-248.

[11] Caleffi, Marcello; Akyildiz, I.F.; Paura, L., "OPERA: Optimal Routing Metric for Cognitive Radio Ad Hoc Networks," Wireless Communications, IEEE Transactions on , vol.11, no.8, pp.2884,2894, August 2012 doi: 10.1109/TWC.2012.061912.111479

[12] Khalife, H.; Ahuja, S.; Malouch, N.; Krunz, M., "Probabilistic Path Selection in Opportunistic Cognitive Radio Networks," Global Telecommunications Conference, 2008. IEEE GLOBECOM 2008. IEEE , vol., no., pp.1,5, Nov. 30 2008-Dec. 4 2008 doi: 10.1109/GLOCOM.2008.ECP.931

[13] Chowdhury, K.R.; Akyildiz, I.F., "CRP: A Routing Protocol for Cognitive Radio Ad Hoc Networks," Selected Areas in Communications, IEEE Journal on , vol.29, no.4, pp.794,804, April 2011 doi: 10.1109/JSAC.2011.110411

[14] Soltani, S.; Mutka, M., "On transitional probabilistic routing in cognitive radio mesh networks," World of Wireless, Mobile and Multimedia Networks (WoWMoM), 2011 IEEE International Symposium on a , vol., no., pp.1,9, 20-24 June 2011 doi: 10.1109/WoWMoM.2011.5986462.

[15] Hincapie, R.; Jian Tang; Guoliang Xue; Bustamante, R., "QoS Routing in Wireless Mesh Networks with Cognitive Radios," Global Telecommunications Conference, 2008. IEEE GLOBECOM 2008. IEEE , vol., no., pp.1,5, Nov. 30 2008-Dec. 4 2008 doi: 10.1109/GLOCOM.2008.ECP.933

[16] A. Cagatay Talay and D. Turgay Altilar. 2009. "RACON: a routing protocol for mobile cognitive radio networks." In Proceedings of the 2009 ACM workshop on Cognitive radio networks (CoRoNet '09). ACM, New York, NY, USA, 73-78. DOI=10.1145/1614235.1614252 http://doi.acm.org/10.1145/1614235.1614252

[17] Mumey, B.; Jian Tang; Judson, I.R.; Stevens, D., "On Routing and Channel Selection in Cognitive Radio Mesh Networks," Vehicular Technology, IEEE Transactions on , vol.61, no.9, pp.4118,4128, Nov. 2012 doi: 10.1109/TVT.2012.2213310

[18] Shelly Salim and Sangman Moh, "On-demand routing protocols for cognitive radio ad hoc networks" EURASIP Journal on Wireless Communications and Networking 2013, 2013:102 doi:10.1186/1687-1499-2013-102.

[19] Chowdhury, K.R.; Di Felice, M., "SEARCH: A routing protocol for mobile cognitive radio ad-Hoc networks," Sarnoff Symposium, 2009. SARNOFF '09. IEEE , vol., no., pp.1,6, March 30 2009-April 1 2009 doi: 10.1109/SARNOF.2009.4850323

[20] Perkins, C. and Belding-Royer, E. and Das, S. "Ad hoc On-Demand Distance Vector (AODV) Routing", 2003 RFC Editor , United States

THE 18TH INTERNATIONAL SYMPOSIUM ON WIRELESS PERSONAL MULTIMEDIA COMMUNICATIONS
(WPMC-2015)
December 13-16, 2015, Hyderabad, India

SIW based Antipodal Linear Tapered Slot Antenna for Inter-Satellite Communication Links at 60 GHz

Nishesh Tiwari, Purva Shrivastava, and T. Rama Rao
Department of Telecommunications Engineering, SRM University, Kattankulathur – 603203, Chennai, India.
nitizaz@gmail.com, purvashrivastava09@gmail.com, ramaraot@outlook.com

***Abstract*—Future space exploration demands inter-satellite links (ISL) that allow high speed communication between two or more satellites. This paper is concerned with the antenna system capable of establishing and maintaining ISL at 60 GHz. A high gain corrugated antipodal linear tapered slot antenna (ALTSA) based on Substrate integrated waveguide (SIW) technology for inter-satellite communications at 60 GHz is proposed. SIW technology has opened-up interesting avenues in millimeter wave planar antenna and circuit development which can be fabricated with low cost printed circuit board technology. A gain of 16.2 dBi achieved with SIW based corrugated ALTSA and the 1 x 2 antenna array with dimension of 69.36 mm x 21.11 mm has a gain of 18.5 dBi with return loss below -10 dB at 60 GHz band.**

Keywords—ALTSA, intersatellite networks; millimeter wave; satellite communications; substrate integrated waveguide.

I. INTRODUCTION

The scope of specialized space communication network has increased in recent years with more space exploration scheduled in the near future. The main objective of space communication is to provide direct connectivity between two or more satellites via inter-satellite links (ISL) or cross links. Using ISL the constellation formed from clusters of several satellites can communicate with each other when necessary. To some extent this can eliminate the ground stations as the information is routed through satellites in different orbits. Several communication technologies and architectures for space networks are proposed in [1] which discusses about the international space station standard (ISS). Further in recent days low cost and small satellites have seen emerging market in earth observation application which assists in improving environmental management [2]. In these applications apart from communication with the earth station the satellite in low earth orbit (LEO) and medium earth orbit (MEO) also have to route data among themselves for fast information delivery mechanism. Therefore, a high speed ISL is necessary to interconnect the satellites in LEO, MEO and geostationary earth orbit (GEO) as well. Generally two type of ISL will be required for each satellite. They are inter-orbit ISL and intra-orbit ISL [3]. In the past 30 years ISL have been seen in large platforms [4] like TDRSS and Iridium etc. Some of them are listed in Table I.

The 60 GHz band with almost 7 GHz of bandwidth [5] is an attractive option for high speed ISL. At millimeter wave frequency band the losses in the planar microstrip circuit is high. Therefore this requires more efficient technology like the substrate integrated waveguide (SIW) to be used. It provides advantages of the traditional rectangular waveguide such as low loss, high quality factor, complete shielding and a high power handling capability [6] along with the combined advantage of planar circuit designs [7]. These have proved to be a good choice for the construction of millimeter-wave circuits. Fig. 1 shows the inter-satellite link.

TABLE I. INTER-SATELLITE LINKING SYSTEM [4]

Satellite Launch Year	Satellite Name	Frequency used for ISL
1972-1978	OSCAR 6,7,8	146 MHz
1976	LES-8 and 9	36, 38 GHz
1983-2013	TDRSS	C, Ku, Ka
1997	Iridium	23 GHz
1998	Spot-4	Optical
1994-2003	MilSTaR I/II	60 GHz
2010	AEHF SV-1	60 GHz

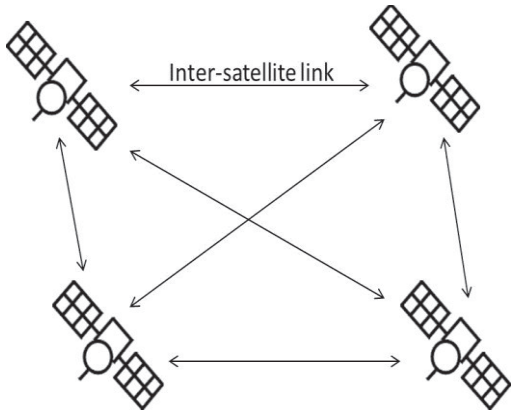

Fig. 1. Inter-satellite link.

Antenna is a vital part of any communication system. Many papers have given attention to Antipodal linear tapered slot antenna (ALTSA) for its good performance which includes high element gain and wide bandwidth. TSA antennas with corrugation structure have been used to reduce TSA width without any significant degradation in the radiation pattern [8]-[9] which helps in making the antenna array more compact. It is seen that rarely any development has been reported for the 60 GHz ISL utilizing SIW fed ALTSA array. In this paper a SIW fed ALTSA and 2-element array for inter-satellite networks at 60 GHz is proposed.

II. DESIGN AND SIMULATIONS

The ALTSA performance is sensitive to the thickness t and the dielectric constant ε_r .

$$f_{substrate} = \frac{t(\sqrt{\varepsilon_r}-1)}{\lambda_0} \quad (1)$$

where $0.005 \leq f_{substrate} \leq 0.03$. For SIW the diameter of the via is given by equation (2) and the pitch of the vias is given by equation (3).

$$D < \frac{\lambda_g}{P} \quad (2)$$

$$P \leq 2D \quad (3)$$

where λ_g is the guided wavelength. Effective width W is calculated using

$$W = W_s - 1.08\frac{D^2}{P} + 0.1\frac{D^2}{W_s} \quad (4)$$

In [10] authors have designed plain and corrugated ALTSA. The corrugated ALTSA has a gain of 16.2 dBi. The ALTSA design and fabricated antennas are shown in Fig. 2 and 3 respectively.

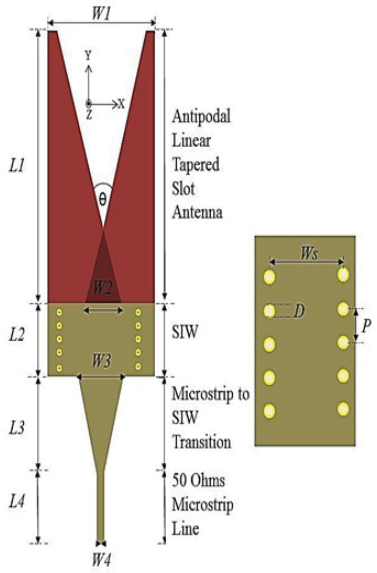

Fig. 2. ALTSA design [10].

Further the design and simulation of 1×2 planar array of the corrugated ALTSA is performed. Ansys HFSS is adopted as the main simulator for simulation of the antenna array design. Rogers RT/duroid 5880 with relative permittivity of 2.2 and thickness of 0.381 mm is used for ALTSA array design. In this design a Y-junction SIW power divider is used to feed the array. To obtain maximum gain, two antennas are fed with same phase and amplitude. Fig. 4 shows the SIW Y- junction power divider. The SIW power divider has 3 ports. Port 1 is the input port and the antennas are connected to port 2 and port 3.

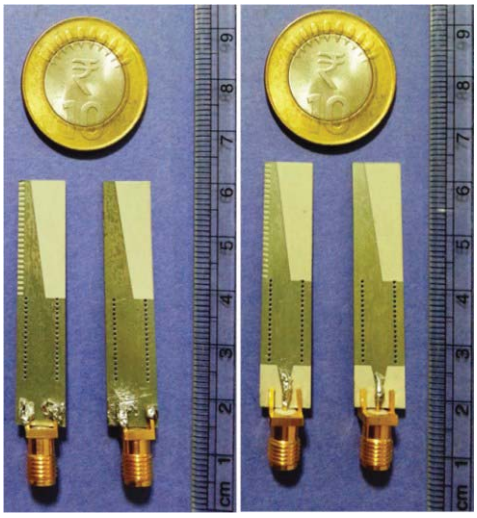

Fig. 3. Fabricated ALTSA [10].

TABLE II. DIMENSION OF ANTENNA ELEMENT [10]

Parameter	**DielectricSubstrate:RT/duriod (εr=2.20, h=0.381mm)**	
	Symbol	Value mm
ALTSA Length	L1	44.61
SIW Length	L2	22.36
Taper Length	L3	4.93
Microstrip Line Length	L4	1.5
ALTSA Width	W1	9.93
Overlapping Area Width	W2	1.8
Taper Width	W3	3.12
Microstrip Line Width	W4	0.5
SIW Effective Width	Ws	6.2
Diameter of Vias	D	0.6
Pitch of Vias	P	0.90
Corrugation Width	RCw	0.5
Space between Corrugation	RCs	0.5
Corrugation Length	RCl	1.25

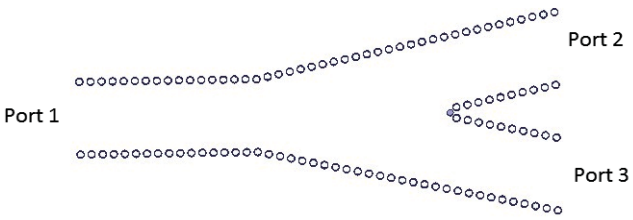

Fig. 4. SIW power divider.

Fig. 5 shows the E-field in the antenna. It shows the interaction of fields between the antipodal flares of both ALTSAs. Most E-field is observed in the linearly tapered structure. Simulated s-parameters of the power divider are shown in Fig.6. From Fig. 6 it is observed that the return loss for the power divider is below -10 dB in the entire 60 GHz band. Also, S21 and S31 are observed to have similar magnitude. Fig. 7 shows the ALTSA array design. The design consists of the SIW power divider, two corrugated ALTSA

and microstrip to SIW transition. The total dimension of the ALTSA array is 69.36 mm x 21.11 mm.

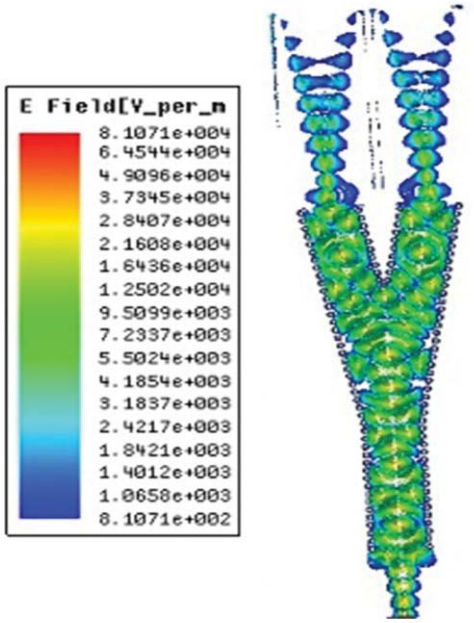

Fig. 5. E-field in the ALTSA array.

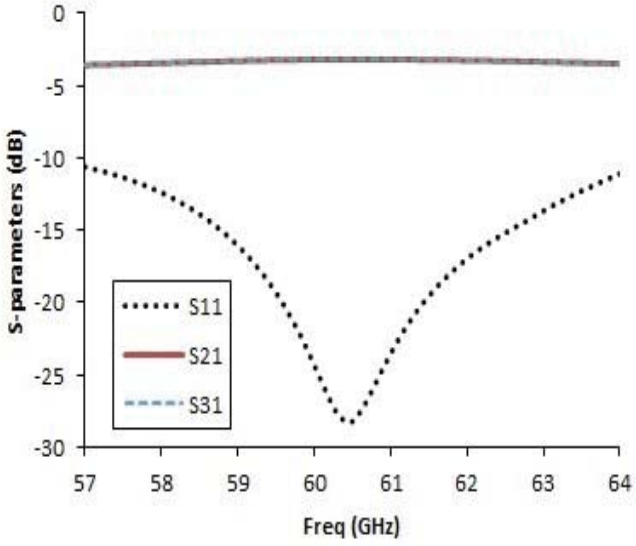

Fig. 6. S-parameters of SIW power divider.

Fig. 8 shows the return loss for the antenna array. The return loss is observed to be less than -23 dB at 59 GHz and less than -11 dB from 59-64 GHz. Fig. 9 shows the 3D radiation pattern of the antenna array. The gain of the antenna is observed to be 18.5 dBi. Fig. 10 shows the E-plane and H-plane radiation pattern of the ALTSA array. It is observed that the side lobe level in E-plane is below -18 dB. Similarly the side lobe level in the H-plane is below -10dB.

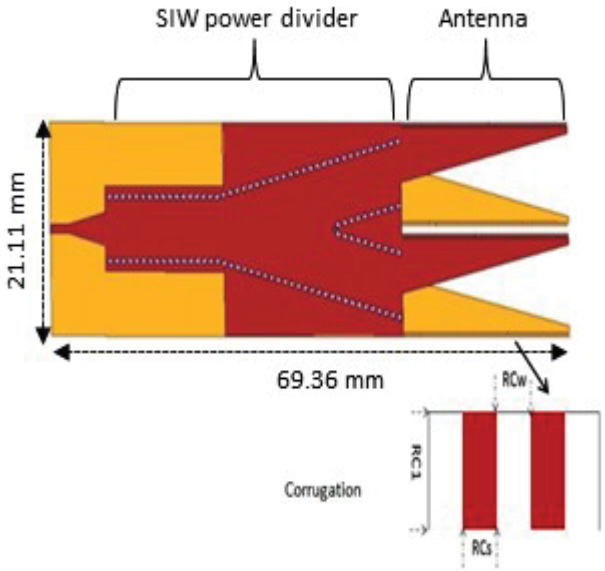

Fig. 7. Corrugated ALTSA array.

Further the 3 dB beam-width in E-plane is observed to be 34° and the 3 dB beam width in H-plane is observed to be 11°. The cross polarization level is observed to be below -17 dB. Thus, it is noted that with a compact size, high gain and large bandwidth the simulated antenna array is a good choice for the ISL network at 60 GHz. Table III lists the comparison table of the performance parameters of ALTSA array.

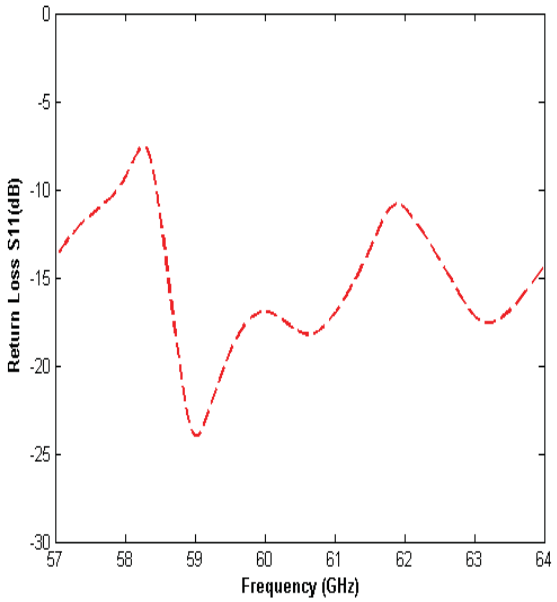

Fig. 8. Return loss of ALTSA array.

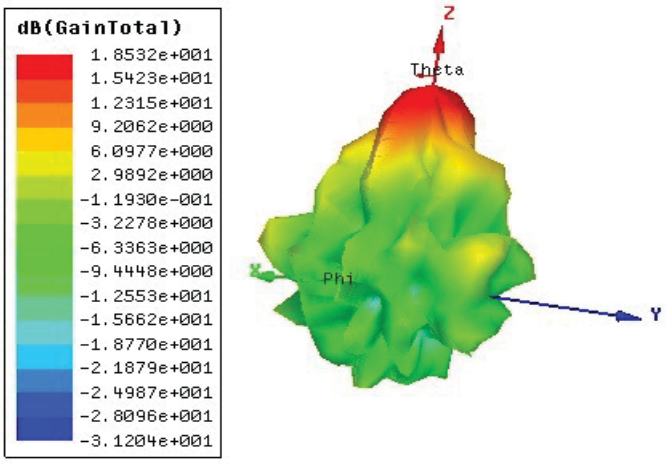

Fig. 9. 3D radiation pattern of ALTSA array.

TABLE III. COMPARISON OF ALTSA ARRAY PERFORMANCE PARAMETERS

Antenna Performance	[9]	[11]	This work
Array size	1 x 12	1 x 4	1 x 2
Gain (dBi)	19.25	19	18.5
Beamwidth (Degree)	10	-	34
Return loss(dB)	-23	-35	-17
Bandwidth(GHz)	22-30	70-100	59-64

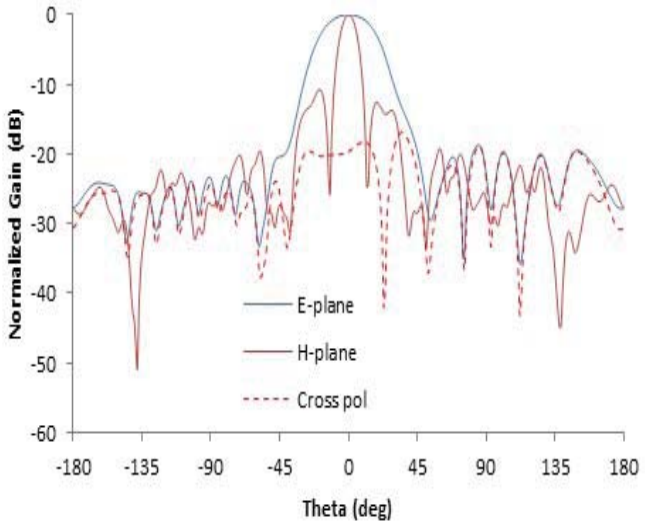

Fig. 10. E-plane and H-plane radiation pattern.

III. LINK ANALYSIS

Further link analysis is performed with the proposed antenna for ISL at 60 GHz. There are several factors that may impact the overall system performance in the inter-satellite wireless networks. Available and permitted output power, available bandwidth, receiver sensitivity, antenna gains, radio technology and environmental conditions are some of the major factors that may impact system performance. These parameters are analyzed through the RF Link budget. Table IV shows the link budget analysis. The first parameter to be discussed in an ISL is distance [12]. The distance or range between the two satellites is a function of angular separation of satellites.

$$R = 2(R_0 + H_0)\sin\left({}^{A_s}/_{2}\right) \tag{5}$$

where R is the distance, R_0 is the radius of earth, H_0 is the altitude and A_s is the angular separation. In any communication system the major issue is the transmission power. In order to transmit over a great distance sufficient transmission power is required. Further power considerations also have an impact on interference and the gain required etc. The satellite system has to be designed in such a way that it will feed the required power to the antenna. Depending on the altitude and range different power levels are used in various inter-satellite missions. ISL are operated above the earth atmosphere where the medium is vacuum. In vacuum signal propagation is faster when compared to ground based communication. In this link budget analysis it is assumed that the medium is a vacuum. No losses are considered due to fading. The path loss is given by [13],

$$PL(dB) = -10log\left[\frac{G_t G_r \lambda^2}{(4\pi)^2 d^2}\right] \tag{6}$$

Received power (P_r) is calculated as

$$P_r = P_t G_t G_r \left(\frac{\lambda}{4\pi d}\right)^2 \tag{7}$$

where, λ is the wavelength in meters and d is the distance in meters. P_t is the transmitter power, P_r is the received power, G_t is the transmitter antenna gain, G_r is the receiver antenna gain. Fig. 11 shows the received power vs distance and path loss vs. distance; reflecting the trend of increasing path loss and decreasing received power with distance respectively. Further, noise power at the input in a receiver ignoring the implementation loss is given by [13],

$$P_{noise} = 10log\left(KT_{sys}\right) + 10\log(B) + NF_{rx} \tag{8}$$

where P_{noise} is the noise power in dBm, K is the Boltzman's constant, T_{sys} is the system temperature, NF_{rx} is the noise figure of the receiver in dB and B is the bandwidth of the signal in Hz. NF_{rx} is assumed to be 6 dB. The signal to noise ratio can be calculated by the equation [13],

$$SNR(dB) = P_r - P_{noise} \tag{9}$$

where, $SNR(dB)$ is the signal to noise ratio in dB, P_r is the received power and P_{noise} is the noise power.

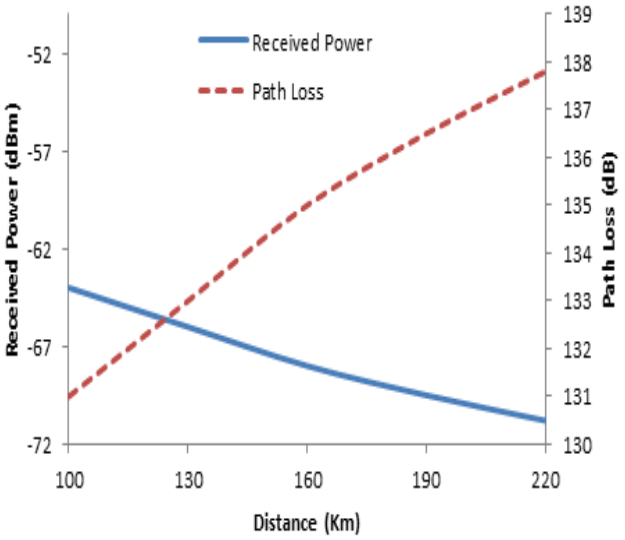

Fig. 11. Received power and path loss Vs. Distance.

TABLE IV. LINK BUDGET

Parameter	Specification
Satellite Orbit	LEO
Orbit Altitude	600 km
Satellite link Band	V-band
Carrier frequency	60 GHz
Transponder output	1W
Intersatellite Distance	220 km
Angular separation (A_s)	17 Deg
Transmitter antenna gain	18.5 dB
Receiver antenna gain	18.5 dB
Transmitted power	1 W
Path loss	137.8 dB
SNR	20.5 dB

TABLE V. SUMMARY OF LINK BUDGET ANALYSIS

Antenna performance	Single element ALTSA	ALTSA array
Transmitter and receiver antenna gain (dBi)	16.2	18.5
Received power (dBm)	-61	-64
Path loss (dB)	133.4	137.8
Estimated distance (Km)	150	220

IV. CONCLUSION

SIW based high gain corrugated ALTSA array with Y-junction power divider is designed and simulated for 60 GHz based inter-satellite wireless communications. Link budget analysis using the parameters from the designed antenna array is performed. The ALTSA array is compact in size with high gain and is suitable for the ISL at 60 GHz for high speed data transfer between the satellite communication networks.

ACKNOWLEDGMENT

Authors are very much obliged to ISRO, Government of India, for the support provided for the execution of this research work.

REFERENCES

[1] Joyeeta Mukherjee and Byrav Ramamurthy, "Communication Technologies and Architectures for Space Network and Interplanetary Internet," *IEEE Communications surveys & Tutorials* , vol.15, no.2, Second quarter 2013.

[2] Z. Yuan, Z. Liu, and J. Zhang, "Inter-satellite link design for the LEO/MEO two layered satellite network," in *Proceedings Wireless Communications, Networking and Mobile Computing*, 2005, pp. 1072-1705.

[3] Paul Muri and Janise McNair, "A Survey of Communication Sub-systems for Intersatellite Linked Systems and Cube Sat Missions," *Journal of Communications*, vol. 7, no. 4, pp. 290-308, 2012.

[4] P. F. M. Smulders "60 GHz radio: prospects and future directions," in *Proceedings Symposium IEEE Benelux chapter on communications and vehicular Technology,* 2003, pp. 1-8.

[5] M. Bozzi, L. Perregrini, K. Wu and P. Arcioni, "Current and Future Research Trends in Substrate Integrated Waveguide Technology," *Radioengineering*, vol. 18, no. 2, pp. 201-209, 2009.

[6] Yu Man Cheng, Peng Chen, Wei Hong, T. Djerafi and Ke Wu, "Substrate Integrated Waveguide Beamforming Networks and Multibeam Antenna Arrays for Low-Cost Satellite and Mobile Systems," *Antennas and Propagation Magazine, IEEE,* vol. 53, no. 6, pp. 18-30, 2011.

[7] J. Li and P. Stocia, *Robust Adaptive Beamforming* , Wiley, Hoboken, New Jersey, 2006,

[8] S. Sugawara, Y. Maita, K. Adachi and K. mizuno, "Characteristics of a mm-wave tapered slot antenna with corrugated edges," in *Proceedings IEEE MTT-S Microwave Symposium Digest*, 1998, pp. 533-536.

[9] T. Djerafi and K. Wu, "Corrugated Substrate Integrated Waveguide Antipodal Linearly Tapered Slot Antenna Array Fed by Quasi-Triangular Power Divider," *PIER C*, vol. 26,pp. 139-151, 2012.

[10] P. Shrivastava, D. Chandra, N. Tiwari, and T. Rama Rao, "Investigations on corrugation issues in SIW based antipodal linear tapered slot antenna for wireless networks at 60 GHz," *ACES Journal*, vol. 28, no. 10, pp. 960-067, 2013.

[11] N. Ghashemi, Ke Wu, "Planar high gain dielectric loaded antipodal linearly tapered slot antenna for E and W band gigabyte point to point wireless services," in *Antennas and Propagations, IEEE Transactions on* , vol. 61, no. 4, pp. 1747- 1755, April 2013.

[12] Richard S. Fuhmmann, "Intersatellite Link Design Issues," M.Sc. Thesis, University of Colorado,1986.

[13] T. S. Rappaport, J. N. Murdoch, and F. Gutierrez, "State of the art in 60 GHz integrated circuits and systems for wireless communications," *in Proc. of the IEEE*, 2011, vol. 99, no. 8, pp. 1392-1436.

THE 18TH INTERNATIONAL SYMPOSIUM ON WIRELESS PERSONAL MULTIMEDIA COMMUNICATIONS
(WPMC-2015)
December 13-16, 2015, Hyderabad, India

Scalable and Adaptable Modeling & Simulation framework key to expedited Radar System design, trade-off analysis, and verification

Uma S. Jha, Ph.D.
Space & Airborne Systems, Raytheon Co
El Segundo, California

Jon Wada
Space & Airborne Systems, Raytheon Co
El Segundo, California

***Abstract*— Modeling and Simulation (M&S) has been a key contributor to the validation of key system concepts, trade-off analysis, and dimensioning of the system performance before it could be realized in cost effective and timely manner. Leading system developers harness M&S capabilities for competitive advantage and operational/business efficiency by leveraging advances in VLSI technologies (processing horse power, memory, storage, high throughput buses), graphics, display, and networking technologies and its utility spans not only across concept development, and trade-off analysis but also in system design and development, test and evaluation, failure analysis, and, to some extent, identifying production issues.**

Keywords—Modeling, Simulation, Trade-off analysis, CONOPS, Design & development, Performance evaluation, Testing & Verification, Prototyping, Failure Analysis, Algorithm Development

INTRODUCTION

The main objective of the M&S is to make informed decisions based on use cases, systems analysis, and trade-off studies to minimize developmental glitches and to facilitate prudent programmatic decisions making. The novel goal of M&S is to support the entire product life cycle from initial concept development to design, integration, test, validation, verification, cannibalization, and follow-on products. The purpose, type, fidelity and complexity of analyses performed across the program life cycle of concept development through product realization requires an scalable M&S model, which can add value at each stages of the development process and in addition provide a collaborative and open framework to take advantage of state-of-the-art tools, technology, and process improvements.

In modeling and simulation realm all functional and behavior models of a system attributes and characteristics are represented in digital domain and can be manipulated digitally. Thus physical and behavioral models based system can be tested in a computer generated virtual, digital world in the same manner as the real systems are tested in the real world. An additional benefit of this approach is the ability to integrate multiple simulations into high-fidelity system of systems test beds. Additionally, the advancements in VLSI technology and software tools to support high-fidelity target and environment simulations as well as immersive visualization environments can be leveraged to facilitate wide variety of concept of operations (CONOPS) development and trade-off analysis.

The simulation fidelity typically grows as the system progresses towards the maturity and end-to-end system performances and interactions are validated. While initial studies often rely on analytical tools, real-time simulations are necessary for assessing complex interactions (such as the scheduling and resource loading of multimode airborne radar). These simulations will rely on lower-fidelity representations of the system since the detailed design may not be fully understood or completely developed. In addition the simulation fidelity (both all-digital and Hardware in the Loop (HWIL)) is only as good as the simulated threats and operating environments being modeled.

Due to advancements in VLSI technology, the ability to model key aspects of a system design before it is built, and to simulate that design's performance over time, has made it possible to significantly improve system performance while alleviating the need to build expensive hardware for test purposes. The enhanced offerings and capabilities of computing, networking, graphics, and storage technologies should be leveraged in architecting a simulation, which can link multiple simulations and operate them collectively towards achieving a common goal. The genesis of a Modeling & Simulation framework at large system integration house is to achieve physically distributed simulation nodes to interact in an all-inclusive simulation with human interfaces. This effort has allowed for effective utilization of the corporate wide company resources providing a very tolerant and highly available system with adequate redundancy at each level of simulation for stake holders. Today, we apply a more integrated approach that is based on rapidly configurable simulations that can grow in fidelity as a system design matures from its initial trade studies through SIL/HWIL testing. These simulation and modeling effort has reduced the risk of design and test errors, alleviated cost overruns, and improved the quality of analysis in the development of complex systems.

BACKGROUND (HISTORICAL PERSPECTIVE)

During early 80's in a complex system development environment, the constituent stake holders brought

Copyright © 2015 Raytheon Company. All rights reserved

their own favorite tools and processes, while systematic but due to the lack of the processing horse power and integrated software development environment did not allow for scalability and seamless integration. Sub-systems developed in silo did not integrate well and scale adequately to manage evolving requirements as well as lacked the capabilities to take advantage of the technological advancements to churn out the best possible solution. Requirements in general came in form of a worksheet; systems team developed their algorithm and performance compliance using mathematical tools (e.g. Matlab, Mathematica …); software team used their own code development processes and tools, and hardware team integrated, tested and sold off to the ultimate customer. The whole process was not sufficiently integrated resulting in loss of traceability and accountability through the development cycle

The cost overrun and project delay variation depended on the development stage, where the issue surfaced and whether a patch could be stitched together or not. The Figure-1 depicts the cost overrun impact [1] as a function of the project stage and its severity as it trudges towards the completion.

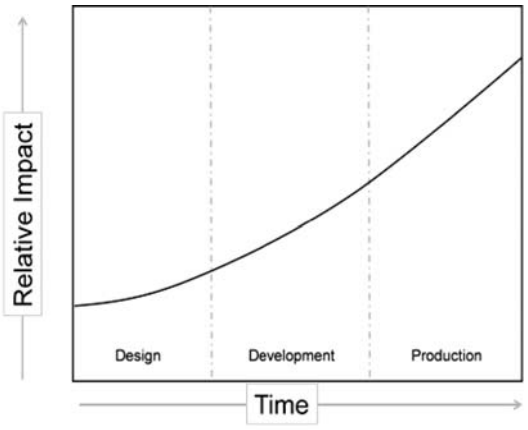

Figure – 1: Impact of system issues on cost and timeline

To overcome this, various processes and tools were considered and experimented to manage traceability from requirements to product design, testing, and sell-off phases utilizing DOORS, Ada programming language including water fall as well as agile processes. Although these showed improvements in execution of the projects from the ground up but did not solve the issues of integrating the heterogeneous complex system prevalent in most of the Department of Defense (DoD) contracts in which some subsystems lasted across the multiple generations of system of systems platform while others keep evolving to counter new threats and improved foe capabilities in the battlefield.

MODELING & SIMULATION FRAMEWORK

Modeling and Simulation capabilities are developed to benefit all stakeholders comprising of systems, test, verification, and sell-off personnel. In a complex radar system development scenario a simulation framework must accommodate and add value across its user base and be able to scale and adapt based on stakeholder's emerging requirements. Special attention is also given to the heterogeneity of the SW development processes, disparate HW capabilities and plethora of interfaces so that it is able to reuse legacy modules and HW pieces to minimize the cost and resource requirements.

MSF provides module and session management, messaging and configuration services. Modules may model processors, sensors, actuators, targets, clutters, atmospheric background, and/or environmental effects, serve as interfaces to other simulation systems.

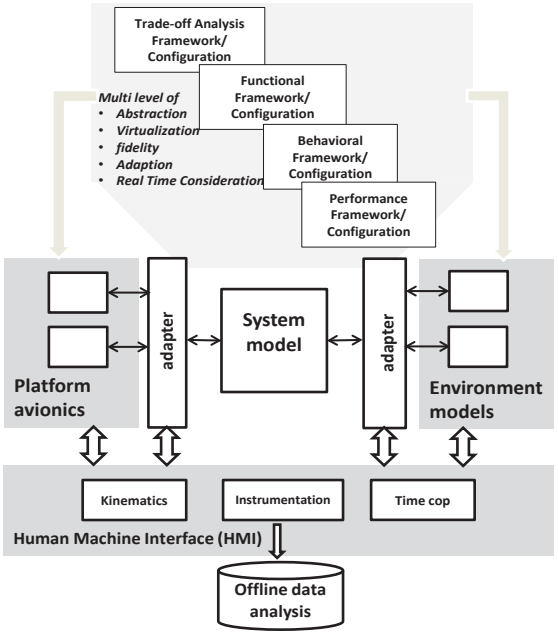

Figure – 2: M&S Architecture Framework

MSF manages session and module configuration, initialization, launch and shutdown, and provides a messaging framework for inter-module communication.

Configuration

Configuration files are an extended form of JSON [4], with extensions for file inclusion, variable substitution, and object inheritance. MSF parses configuration files into a tree, with a subtree for each module to be included in a simulation session. Each module-specific

Copyright © 2015 Raytheon Company. All rights reserved

configuration tree is used to launch its respective module, and is passed to the module's initialization function.

Modules and Messaging

MSF modules may be implemented in C++, Python or Matlab. In C++ and Python, MSF provides a Module abstract base class that's inherited by all simulation modules written in those languages; in Matlab, the framework provides a Module class that can contain function handles to implement the functionality of a Matlab simulation module.

MSF modules communicate with each other via messaging. A Message class is implemented in each of the three module languages. ZeroMQ [5] is used as the underlying messaging library. We've implemented a Messager class in Python and C++ as a wrapper around ZeroMQ, both to provide an abstraction layer and to provide some higher-level services for dispatching and handling messages. Messages are sent point-to-point; there's no central broker, to minimize network traffic and avoid bottlenecks.

Each message has:

- One "sender" (the module that sent it) and zero or more "receivers" (the modules to which it was sent).
- A string "topic"; which is used by the Messager instances in the receiving modules to dispatch message handlers. A message handler is a function, usually a method on the concrete Module subclass.
- Zero or more "payload" parts. Each payload part may have a distinct encoding; currently supported encodings are HDF5 [6] , best suited for binary and numerical data; JSON, for small-to-moderate amounts of mixed-type data, and RAW, a collection of bytes to be interpreted by the receiver.

Each message topic is associated with one "type": PUBLISH, REQUEST or ACCEPT

- PUBLISH messages are sent to any module that subscribes to that topic; no reply is returned. PUBLISH messages have no explicit receivers.
- REQUEST messages are sent to one or more explicit receivers; the sender will block until a reply is received from each receiver, and the collection of replies is returned to the caller.
- ACCEPT messages are sent to one or more explicit receivers; no acknowledgement or reply is returned.

MSF compiles a *Phonebook*, which contains a "white pages" section listing all modules running in this simulation session and the message topics they support, and a "yellow pages" section listing the union of all message topics supported by modules in this session, and which module support them. The Phonebook is distributed to all modules at session initialization.

Each MSF module runs in its own process; it may be configured to run on any host or cluster of hosts on the network or in distributed environment. Modules may be implemented in C++, Python or Matlab to accommodate a variety of needs for execution performance, use cases, ease of implementation and maintenance.

Time Management

Simulation time is maintained as a double-precision floating-point scalar, managed by a standard module called the Timecop. Simulation time moves monotonically forward, in discrete steps; the value of each time step is variable, depending on the needs of the simulation modules. The Timecop manages the process of negotiating the next time step, determines when all modules are ready for the time step to occur, then notifies modules that the time step is occurring.

MSF Modules may be Time Aware, Time Managing, or Time Agnostic. The framework provides a TimeAwareModule class derived from Module, and a TimeManagingModule class derived from TimeAwareModule.

- Time Aware Modules are notified of all time advance events. They may receive, but not send, Time-Stamped Messages.
- Time Managing Modules additionally are required to notify the Timecop when they're ready for simulation time to advance, and to specify a *lookahead*. A module's lookahead is the largest time step it can tolerate (or zero if it doesn't care); the Timecop will ensure that the next time advance is to a value less than or equal to the minimum of the lookahead values of all Time Managing Modules in the simulation. Time Managing Modules are allowed to send and receive Time-Stamped Messages.
- Time Agnostic Modules may query for the current simulation time, but are not notified of time advances. They may not send or receive Time-Stamped Messages

Before issuing a time advance, the Timecop will query all Time Aware Modules for counts of messages sent and received, and determines whether there are any messages in flight. It will wait until all in-flight messages are received before issuing a Time Advance.

Logging and Instrumentation

All simulation output for a given session is organized in a *session folder*: a single directory hierarchy in a network-mounted filesystem. This includes:

- A copy of the configuration tree;

Copyright © 2015 Raytheon Company. All rights reserved

- A copy of the environment for the session process and for each module process;
- Hashes of the executables for each module process, as well as any additional files identified by the module (so that we can ascertain whether two simulation sessions were run with identical software or not)
- Log and error messages from each process in the simulation
- Intermediate data files written by each module for debugging and analysis purposes
- Instrumentation data produced by any embedded software being exercised in the simulation

Adapters

Adapters are the system's principal mechanism for federating simulations; an Adapter is an MSF module that provides a bridge between MSF and an external system, stimuli or simulation. An Adapter to an external system is responsible for translating messages and message protocols from one system to another, and for negotiating time advances between systems.

An Adapter's Translators are responsible for translating message formats between MSF Messaging and the external system's data formats. They can also serve as abstraction layer, to isolate the two systems from local changes in data formats.

An Adapter's Scheduler and TimeSynchronizer negotiate time advances between systems. MSF was not designed to federate with real-time simulations, but was designed to allow an MSF session to be a federate in an HLA [6] simulation.

Adapters have been used, for example, to link the M&S system with Raytheon's existing Desktop Tactical Simulator (DTS), which executes embedded software in a desktop environment. Adapters are used to bridge DTS's internal messaging protocol with M&S messaging, and to keep the Timecop in sync with the DTS simulation's internal simulation clock.

Operators

Operators are MSF modules that simulate operator-in-the-loop behavior. They receive messages from other simulation modules that inform them of simulated system outputs and environmental conditions, and send messages to other simulation modules to simulate human input to simulated systems. Operators have been implemented as custom Python scripts, as well as rule-based systems using pyCLIPS [8].

Scalability

The M&S system was designed to run in a clustered environment, with multiple computers and network storage connected by a fast local-area network (LAN) [9].

This architecture was chosen to allow for load scalability, where compute or storage nodes can be added to or removed from the cluster as demand changes, or redeployed from one program to another as business needs change. Nodes within the cluster can also be updated incrementally over time, providing flexibility in (maintenance/refresh) costs. And ZeroMQ's brokerless architecture minimizes messaging bottlenecks and allows for flexibility of deployment – e.g., localizing simulation sessions to subnets without having to worry about broker placement.

Applicability Across the Product Development Cycle

The system's modular design facilitates its use throughout the product development cycle, from early conceptual studies through final Validation and Verification (V&V).

Early in the product development phase, concept studies and design tradeoffs can be performed, and system performance can be predicted using mature environment model from previous simulation efforts using MSF, augmented with new and/or specific models. Behavioral models of system behavior in Matlab or Python; as the design solidifies, models can be refined and coded in C++ for better runtime performance. As embedded software is developed, it can be introduced into the simulation via instruction-set simulators or other embedded-processor simulations, and it's expected that Adapters can be employed to introduce hardware components for Hardware in the Loop (HWIL) simulation in some applications where the hardware may not require real world operation. Finally, once the system is implemented and high-fidelity simulation models are complete, the M&S system can be used to exercise the system in situations that are difficult to realize in an actual flight test: environments requiring complex orchestration of a large number of range assets, for example, or where range assets are difficult to acquire, or tests that exhaustively cover the performance envelope, or that require a large number of Monte Carlo trials.

Federating Simulations

MSF's modular architecture was designed to facilitate the integration of external simulation systems, both legacy and evolving. We've demonstrated this by integrating Raytheon's Desktop Tactical Simulator (DTS), a system that executes airborne radar embedded software in a Microsoft Windows desktop environment. We've successfully integrated multiple instances of DTS, simulating the operation of multiple airborne radar systems, in a single target/clutter environment.

Copyright © 2015 Raytheon Company. All rights reserved

Kinematics

Six (6) Degree of Freedom (DoF) kinematics model are provided by a single MSF module in each session; this module is implemented as a wrapper around one or more kinematics sources, which can be autonomous kinematics simulations or alternatively, can be supplied by a federated simulation. The kinematics module also allows for mixed kinematics sources, so that kinematics data for different bodies can be drawn from different sources:

For example, synthetic targets can be used to

- *Augment the playback of TSPI data collected during flight test*
- *Expedite requirements development and*
- *Requirements sell-off – validate against real platform*

Operator Input(Human Machine Interface)

Operator input can be generated in a number of ways:

- MSF modules can be implemented to accept interactive input, via GUI or by presenting a command-line console. These modules can then generate messages to be sent to other simulation modules to command the desired behavior.
- Federated simulations may have operator interfaces, which directly or indirectly command MSF modules
- MSF modules can be implemented to accept messages from other modules, and to be programmed to respond to those messages. For example, a module has been implemented that accepts messages output by a DTS-simulated airborne radar system to its mission computer, correlate any reported targets to "truth" kinematics obtained from the MSF kinematics module, and command the simulated radar to initiate a high-quality track on desired targets. Other "operator" modules have been implemented using pyCLIPS [10] , to demonstrate a capability for rule-based decision-making.

CONCLUSIONS

Modeling and Simulation is one of the most versatile tools in the arsenal of the system developers, especially for complex system development. This allows for stakeholders to perform a comprehensive evaluation of system before it can be built in cost effective and timely manner. This also facilitates the customers and systems integrator to carry out the trade-off analysis, performance dimensioning, alternate design considerations, and future improvements considerations at very early stage of the program to minimize unnecessary risks and late stage surprises. The advances in technology, tools, and process have consistently enhanced the capabilities to model complex real time physical systems employing high performance distributed computers and broadband network with high fidelity input signal models and real life engagement scenario. The signal processing algorithms developed in quasi real time scenario allows system developer to design a system with right mix of cost, time, and performance offerings. These capabilities keep on improving as the digital and broadband technology continue to evolve following the Moore's law. System upgrades and performance enhancements can be established and demonstrated to key stake holders in a controlled and deterministic way without building a system. It is not farfetched that a system could be sold off solely on the basis of simulation results avoiding costly flight and real assets.

ACKNOWLEDGMENT

Authors would like to recognize the support from the Raytheon's Systems and Software group as well as their valuable suggestions during the preparation of this manuscript.

REFERENCES

The key role of business analysis in project succes and achieving business value, Alan McSweeney, June 2012

RedHat Enterprise Linux (RHEL)

SUSE Linux Enterprise Server (SLES)

http://www.json.org

Hohpe, Gregor, and Woolf, Bobby, "Enterprise Integration Patterns: Designing, Building and Deploying Messaging Solutions", Addison-Wesley Professional, 2004 http://www.zeromq.org

http://www.hdfgroup.org/HDF5/

http://www.cc.gatech.edu/computing/pads/PAPERS/Time_mgmt_High_Level_Arch.pdf

http://pyclips.sourceforge.net/web/, http://clipsrules.sourceforge.net/

http://en.wikipedia.org/wiki/Computer_cluster

http://pyclips.sourceforge.net/web/, http://clipsrules.sourceforge.net/

Copyright © 2015 Raytheon Company. All rights reserved

THE 18TH INTERNATIONAL SYMPOSIUM ON WIRELESS PERSONAL MULTIMEDIA COMMUNICATIONS
(WPMC-2015)
December 13-16, 2015, Hyderabad, India

Database Assisted Automatic Modulation Classification Using Sequential Minimal Optimization

K. Pavan Kumar Reddy, K. Lakhan Shiva, K. Abhilash, Y. Yoganandam
Department of Electrical and Electronics Engineering
Birla Institute of Technology and Science-Pilani, Hyderabad Campus
Hyderabad, Telangana State, India
Email: {pavan.kuntla,lakhanshiva,kadiri123.abhilash}@gmail.com, yogi@hyderabad.bits-pilani.ac.in

***Abstract*—In this paper, we proposed a novel algorithm for identifying the modulation scheme of an unknown incoming signal in order to mitigate the interference with primary user in Cognitive Radio systems, which is facilitated by using Automatic Modulation Classification (AMC) at the front end of Software Defined Radio (SDR). In this study, we used computer simulations of analog and digital modulations belonging to eleven classes. Spectral based features have been used as input features for Sequential Minimal Optimization (SMO). These features of primary users are stored in the database, then it matches the unknown signal's features with those in the database. Built upon recently proposed AMC, our new database approach inherits the benefits of SMO based approach and makes it much more time efficient in classifying an unknown signal, especially in the case of multiple modulation schemes to overcome the issue of intense computations in constructing features. In various applications, primary users own frequent wireless transmissions having limited their feature size and save few computations. The SMO based classification methodology proves to be over 99 % accurate for SNR of 15 dB and accuracy of classification is over 95 % for low SNRs around 5dB.**

Keywords- Automatic modulation classification, cognitive radio, Database, sequential minimal optimization, unknown signal detection, primary user, spectral based features.

I. INTRODUCTION

Cognitive Radio (CR) is a cutting edge technology on which rigorous research and Development (R&D) is occurring recently. CR enables efficient usage of radio frequency spectrum. Empty spaces in both licensed and unlicensed spectrum commonly known as white spaces are used by CR to achieve its set of objectives. The idea here is to sense for a spectrum hole and use it until its rightful owner appears. The CR then modifies its frequency to match another white space and possibly another class of modulation scheme and coding. This phenomenon supposedly may occur every now and then, imposing a heavy feedback to the receiver every time the modulation scheme and the coding changes. One possible solution to this problem is to use Digital Signal processing (DSP) analysis called automatic modulation classification. These calculations can determine the type of modulation effectively using particular feature set. But most of the work in this direction is applied to High Frequency (HF) noise and cannot be applied to Additive White Gaussian Noise (AWGN) channels. [1]

The goal of this study is to implement an automatic modulation classifier in an AWGN environment. So, we designed the database assisted AMC, analysed the need for fast classification and proposed a solution. This paper proposes Sequential Minimal Optimization (SMO) to train the Support vector machines (SVMs) to do classification by segregating a mixture of both digital and analog modulation schemes into different classes. Consequently, our contribution to Cognitive Radio research lies in classifying an unknown signal in a time efficient manner, through integration of database.

The paper is organized as follows: Section II explains sequential minimal optimization and related work. Simulation of modulated signals, feature extraction and modulation classification are presented in Section III. Section IV is about proposed database assisted design and algorithm. Results and discussions of proposed approach are presented in Section V. Conclusion is drawn in VI.

II. SEQUENTIAL MINIMAL OPTIMIZATION

Support Vector machines are built using linear kernels for classification. We make use of Sequential minimal optimization algorithm to train the SVMs. An SMO model is a representation of the data sets as points in space; they are mapped so that the data sets of the separate categories are divided by a clear gap, which is as wide as possible. New data sets are then mapped into that same space and predicted to belong to a category based on which side of the gap they fall into. It trains a support vector classifier using kernel functions such as Gaussian and Polynomial kernels. It takes minimal time in doing so [2].

The $K(x, x_i)$ are the support vectors used by SMO. α is the weight or lagrange multiplier. The output equation is given as,

$$y = f(x);\ f(x) = \sum_{k=1}^{m} \alpha_k.K(x, x_k) + b \quad (1)$$

SMO is widely used in training support vector machines (SVMs). The amount of memory required for this algorithm is linear in the training set size, due to which large training sets

are handled with very less complexity and also matrix computation is avoided. So, SMO spans somewhere between linear and quadratic in the training set size for various test problems, while the standard SVM algorithm spans somewhere between linear and cubic in the training set size. SMO's computation time is took over by SVM evaluation, hence SMO is the best algorithm for linear SVMs. On real world sparse data sets, SMO can be approximately more than 1000 times faster than the normal algorithm [2].

A. Related works

Azzouz and Nandi [3] have proposed spectral based features and algorithms to classify both analog and digital modulated signals. Popoola and Olst have extracted same set of features and proposed ANN based classification system [4]. The key features proposed by Nandi are later used in [5] [6] and many more. But in practicality, accuracy of these features depends upon noise, carrier offset error, symbol rate estimation error that affect the probability of identification. Arulampalam et al., [13] have used only digital modulation schemes using ANN and features proposed by Nandi and Azzouz, validated over non-weak segment of the incepted signal and also used maximum power spectral density of normalized instantaneous frequency of intercepted signal. When we compare our work with the study, we have obtained better results by using SMO Algorithm [8] [15] for classificaion of both analog and digital modulations at low SNRs. Our contribution is in building upon this existing work on AMC, via a database approach and classifying the unknown signal in a time efficient manner.

III. STUDY METHODOLOGY

The study flow involved three steps. The first step was extraction of the statistical features keys used as inputs to the developed classifier. The second step was development of automatic modulation classifier system. Third step was to integrate the system with the database. Satisfactory accuracy was achieved in the final step.

A. Simulation of modulated signals

Signals are generated for eleven modulation schemes, both analog and digital modulations. Modulated signals are generated using the formulae. For example, the AM modulated signal is generated using the formula,

$$Y_{am}(t) = [1 + K_a.F_t](\cos(2\pi f_c t)) \tag{2}$$

The FM modulated signal is generated using the formula,

$$Y_{fm}(t) = \cos(2\pi f_c t + k_f \sin(2\pi f_m t)) \tag{3}$$

Similarly, DSB, SSB, ASK, FSK and PSK modulated signals were generated by using their respective formulas. AWGN(Additive White Gaussian Noise) is added to the modulated signals.

B. Feature extraction

Feature extraction is a prerequisite for recognition. The motive here is to identify a pattern by using minimum number of features or attributes which are important for determining the pattern class identification. The employed classification technique was derived from the amplitude, phase and frequency instantaneous values of signal simulations. These values are obtained from the discrete time analytic signal. Hilbert transform is used for calculating the instantaneous values of a signal. The feature keys are spectral based features and had earlier been used by Nandi [3] [7].

(i) γ_{max} : This feature corresponds to maximum value of the PSD (Power spectral density) . It measures the variance in signal amplitude.

$$\gamma_{max} = \frac{max|DFT(a_{cn}[n]|^2}{N} \tag{4}$$

i.e. taking a discrete Fourier transform of the signal samples. Here $a_{cn}(n)$ is centered instantaneous amplitude at time, $t = \frac{n}{f_s}(n = 1, 2, 3...N)$ and a sampling frequency, f_s. $a_{cn}(n)$ is defined as

$$a_{cn}(n) = a_n[n] - 1 \ , \ a_n(n) = \frac{a[n]}{m_a} \tag{5}$$

Here m_a is the mean value of samples.

$$m_a = \frac{1}{N}\sum_{n=1}^{N} a[n] \tag{6}$$

All centered values refer to normalized instantaneous values.

(ii) σ_{dp} : This feature measures the variance in direct instantaneous phase. It discriminated 2PSK from other modulation schemes. This is given as σ_{dp}

$$\sigma_{dp} = \sqrt{\frac{1}{N_c}\left(\sum_{A_n > A_t} \Phi_{NL}^2[n]\right) - \left(\frac{1}{N_c}\sum_{A_n > A_t} \Phi_{NL}[n]\right)^2} \tag{7}$$

(iii) σ_{ap} : This feature corresponds to the standard deviation of the centered non-linear component of the instantaneous phase. Here we take absolute values. This is given as

$$\sigma_{ap} = \sqrt{\frac{1}{N_c}\left(\sum_{A_n > A_t} \Phi_{NL}^2[n]\right) - \left(\frac{1}{N_c}\sum_{A_n > A_t} |\Phi_{NL}[n]|\right)^2} \tag{8}$$

This is very useful in finding PSK modulation order.

(iv) P : This feature is the calculation of spectrum symmetry around the carrier frequency. This quantity is a decision factor to classify amplitude-based modulations with different properties in the frequency domain.

$$P = \frac{P_l - P_u}{P_l + P_u} \tag{9}$$

$P_l$is the spectral power of sideband (lower) and $P_u$is the spectral power of the other sideband (upper).

$$P_l = \sum_{n=1}^{f_{cn}} |F(n)|^2, \ P_u = \sum_{n=1}^{f_{cn}} |F\left[n + f_{cn} + 1\right]|^2 \tag{10}$$

Here $F(n)$ is the Fourier transform of the received signal. $(f_{cn} + 1)$ is the sample number for carrier frequency f_c . f_{cn} is defined as

$$f_{cn} = \frac{f_c N}{f_s} - 1 \tag{11}$$

(v) σ_{aa} : This feature corresponds to the standard deviation of the centered instantaneous amplitude of signal samples. N is the total number of signal samples. We take absolute and normalized values. Though this feature is similar to γ_{max}, it has the ability to discriminate 2ASK from other modulation schemes.

$$\sigma_{aa} = \sqrt{\frac{1}{N}\left(\sum_{n=1}^{N} A_{cn}^2(n)\right) - \left(\frac{1}{N}\sum_{n=1}^{N}|A_{cn}(n)|\right)^2} \quad (12)$$

(vi) σ_{af} : This feature corresponds to standard deviation of the centered instantaneous frequency. We take absolute and normalized values. It has the ability to discriminate 2ASK from 4ASK. N_c is the number of samples that meet the condition: $A_n[n] > A_t$. A_t is the threshold value.

$$\sigma_{af} = \sqrt{\frac{1}{N_c}\left(\sum_{A_n[n]>A_t} f_N^2(n)\right) - \left(\frac{1}{N_c}\sum_{A_n[n]>A_t}|f(n)|\right)^2} \quad (13)$$

(vii) σ_a: This feature corresponds to the standard deviation of the centered frequency. We take normalized values here. It has the ability to differentiate 2ASK and 4ASK.

$$\sigma_a = \sqrt{\frac{1}{N_c}\left(\sum_{A_n[n]>A_t} a_{cn}^2[n]\right) - \left(\frac{1}{N_c}\sum_{A_n[n]>A_t} a_{cn}[n]\right)^2} \quad (14)$$

(viii) μ_{42}^a: This feature is the kurtosis of normalized and centered instantaneous amplitude. It differentiates AM signal from the rest.

$$\mu_{42}^a = \frac{E\{A_{cn}^4[n]\}}{\{E\{A_{cn}^2[n]\}\}^2} \quad (15)$$

(ix) μ_{42}^f: This feature is the kurtosis of normalized and centered instantaneous frequency. It differentiates FM signal from the rest.

$$\mu_{42}^f = \frac{E\{f_N^4[n]\}}{\{E\{f_N^2[n]\}\}^2} \quad (16)$$

C. Modulation classification

Modulation can be defined as varying amplitude, frequency and phase of a carrier wave with frequency f_c with respect to modulating signal with frequency f_m[6].

While training the SVM, nominal attributes in the arff format are converted into two class (binary) ones. Coefficients in the output are based on the normalized data. The SMO algorithm will use pair wise classification considering the fact that the problem here is a multi-class one. We choose to make use of Poly Kernel i.e. polynomial kernels. Here since we have 11 classes the 11 binary SMO models have been output with one hyperplane each to support each of the possible pair of class values. In such Kernel based methods, similarity must be a kernel function satisfying some mathematical properties [11] [12].

IV. DESIGN AND ALGORITHM

The steps in design of the database assisted AMC are presented in Fig. 1.

The steps for implementing the Database assisted AMC system are divided into two phases.

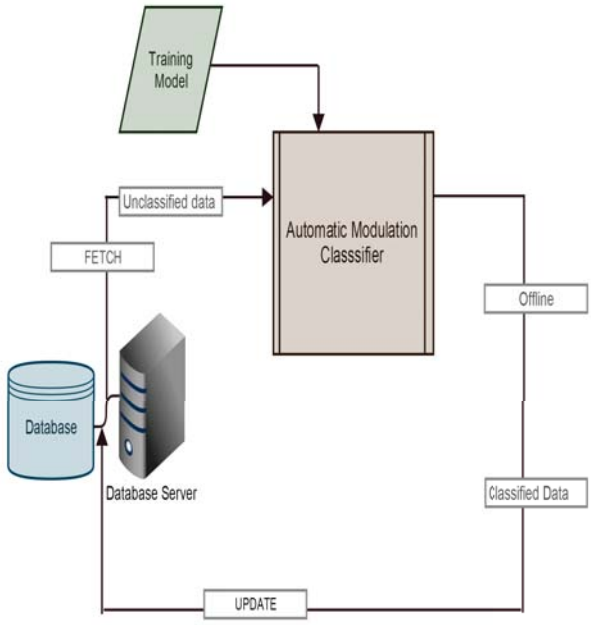

Fig. 1. Database assisted Automatic modulation classifier

1) Offline Phase:

- Firstly we had realized computer simulated signals of different modulation schemes using MATLAB codes reproducing the work of A.K. Nandi and E.E. Azzouz [3].
- Then, stored the simulated and labeled signal data into the database server.
- Thereafter we have generated reference sample data, to train the SMO model offline.
- Further saved the trained model into the file system.
- Finally evaluated by giving an unlabeled data as input to the database server (this will be used as test data that will be classified by AMC).

2) Classification Phase:

- Secondly we have connected to the database using JDBC MySQL connector/J.
- Accordingly fetched all the unlabeled data into the program.
- Next we attached arff (attribute relation file header) header format to this data in order to transform it into an arff test file.
- Then read the testing file into the program and loaded the trained SMO model.
- Afterwards we have applied the model's configuration on the test file. With this step, modulation classification is completed. In the end, updated the database server with the classified signal data.

V. RESULTS AND DISCUSSIONS

Here we have input test data (unknown signal) of 25dB SNR and applied an SMO trained model over it. The model uses

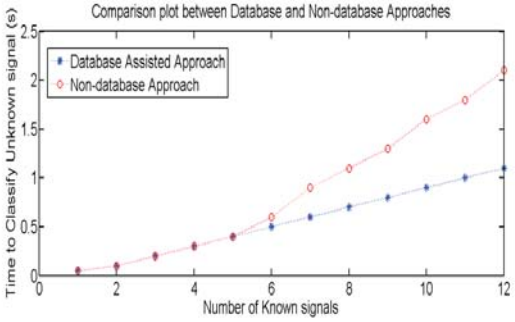

Fig. 2. Time for classification of unknown signal vs. number of known signals.

some hyper planes to divide the space to form 11 regions, each representing one modulation scheme. This has been explained in section II of this paper.

In database assisted approach, when an unknown signal's features are among the training data stored in database, an existing record in the database is selected and its modulation scheme is returned. We have first trained the SMO classifier and stored the trained model in WEKA [9] and database. Finally, we are classifying unknown signal with an assumption that it should belong to one of the known modulation schemes mentioned in section III of this paper.

In our database assisted approach, we record the features of known signals in the database system. Then, AMC monitors each incoming signal's transmitting sequence. For example, let us suppose that initially only one known signal, such as AM is present in an environment and detect the unknown signal. Then, in the next input sequence consider only two known signals such as AM, FM and compare the unknown signal's feature vectors with those in the database. In various applications, known signals have routine wireless transmissions, hence they own a limited number of feature vectors, meaning that the subsequent database is stable and limited in size. Whenever an unknown signal's feature vector does not have a match entity in the database, our approach will detect it's action as unusual by taking the stability of known signals into account and identifies it as a malicious signal, hence save some computations compared to the previous approaches in the literature. This way we realized that our proposed idea on database assisted approach for AMC is a novel work. So, we ran computer simulations and in future would like to implement this idea on a system model similar to cognitive radio scenario of known signals. Known signals are analogous to primary users' signals and an unknown signal referred as primary user is to be detected so that interference can be avoided with neighboring primary users. Therefore, we assumed all basic modulation schemes possible as the only modulation types used by authentic primary users' signals, referred as known signals. Here our research contribution is to evaluate the performance of database approach over non database in terms of efficiency, thereby solving the problem of severe computations in constructing features.

Our limitations are as follows:

1) At any instance of time, only one signal is transmitted by users' either primary, unknown or secondary.
2) Secondary users transmit at very low powers not interfering with primary and unknown users.
3) Secondary users, unknown users and primary users are utilizing the area within the same frequency band.
4) Secondary users' modulation scheme is different from primary and unknown users.
5) We cannot detect intelligent unknown users' who pretend to be primary users.
6) We have not considered other modulation schemes for transmission of unknown signal, instead used only those modulation schemes mentioned in section III of this paper.

In non database approach, we have assumed that the test signal's feature is among the training data. To match this test signal to a record in the arff format, we need to search for the record. But running a search query is not preferred in flat files (File that doesn't have any internal hierarchy). The reason is that database is a structured way of storing data, whereas flat file is unstructured way of storing data.

It is very clear from Fig. 2 that for both database and non database methods the time taken for classifying an unknown signal is surely dependent on number of known signals. When there are more known signals in the system, it consumes more time for conclusion. However, it is observed that with a larger number of known signals, the classification time increases more drastically in the case of non database approach. The database assisted approach takes linear growth, because time taken for classification is dominated only by searching time of database. Whereas, non database approach follows approximately exponential rise, due to increase in classification time with number of known signals.

At low SNRs like 5 dB, as signals are transmitted with low power, it is a challenge to classify 11 different modulation schemes, as sometimes there is confusion to classify the similar modulation schemes. Generally, we get accuracy of 80-90% at low SNRs by recent methods. But by these features we are getting around 95%.

A. *Probability of correct detection*

In multi-class prediction, the result on a test set is often displayed as a two dimensional confusion matrix with a row and column for each class. It is defined by this formula, $P = (TP+TN)/(TP+TN+FP+FN)$. Here TP means True Positives, TN means True negatives FP means False positive and FN means False negative. The error rate is one minus this [10].

TABLE I. CORRECT DETECTION RATE

Modulation Scheme	Accuracy	
	SNR = 15 dB	
	Present Work	Popoola Work [4]
2ASK	100	99.99
4ASK	100	99.98
2FSK	100	99.92
2PSK	100	99.75
4PSK	100	99.98
AM	100	99.95
DSB	99.97	99.98
FM	100	99.91
LSB	100	99.97
USB	99.97	-

TABLE II. CONFUSION MATRIX

	Confusion matrix for SNR = 15 dB					
	AM	DSB	LSB	USB	FM	2ASK
AM	1	0	0	0	0	0
DSB	0	1	0	0	0	0
LSB	0	0	1	0	0	0
USB	0	0	0.01	0.99	0	0
FM	0	0	0	0	1	0
2ASK	0	0	0	0	0	1

TABLE III. CONFUSION MATRIX

	Confusion matrix for SNR = 15 dB				
	4ASK	2FSK	4FSK	2PSK	4PSK
4ASK	1	0	0	0	0
2FSK	0	1	0	0	0
4FSK	0	0	1	0	0
2PSK	0	0	0	1	0
4PSK	0	0	0	0	1

Table I illustrates the improvement of present work with reference work by Popoola's [4] [16] feed forward neural networks [14]. Table II and III illustrate the confusion matrix for different modulation schemes at an SNR = 15 dB.

VI. CONCLUSION

In this paper, we have developed and implemented an AMC with database acting as an abettor in automating the whole process of classification. The database assisted approach gave us better results than the non database approach in terms of time taken. We have applied SMO model configuration on both labeled and unlabeled data. Firstly, SMO based classification alone gave better performance when trained and evaluated with labeled signals. The results proved to be over 98% accurate for 15 dB data. The future work of this paper includes validation of our approach through hardware implementation to show its feasibility in real life conditions.

In future, consider same modulation type during classification. Till now we are assuming that the unknown signal's modulation should belong to any one of the 11 modulation schemes generated in simulations. But, in real life we need to detect an unknown signal, which may be different from modulations stored in database. Then we consider such an unknown signal as malicious. Now as malicious users (unknown users) are intelligent they pretend modulations of primary users. So, in this case, if both primary and unknown users use same modulation type, then during the detection of unknown signals if no match is found in database, one should use methods which detect unknown signals.

REFERENCES

[1] Q. Zhang, S. Kota, V. K. Lau, W. Su, and A. Kwasinski, "Introduction to the issue on cooperative communication and signal processing in cognitive radio systems," *Selected Topics in Signal Processing, IEEE Journal of*, vol. 5, no. 1, pp. 1–4, 2011.

[2] J. C. Platt, "Sequential minimal optimization: a fast algorithm for training support vector machines. 1998," *URL citeseer. ist. psu. edu/platt98sequential. html*.

[3] A. K. Nandi and E. E. Azzouz, "Modulation recognition using artificial neural networks," *Signal processing*, vol. 56, no. 2, pp. 165–175, 1997.

[4] J. J. Popoola and R. Van Olst, "Automatic classification of combined analog and digital modulation schemes using feedforward neural network," in *AFRICON, 2011*. IEEE, 2011, pp. 1–6.

[5] A. K. Nandi and E. E. Azzouz, "Algorithms for automatic modulation recognition of communication signals," *Communications, IEEE Transactions on*, vol. 46, no. 4, pp. 431–436, 1998.

[6] E. Azzouz and A. Nandi, "Procedure for automatic recognition of analogue and digital modulations," *IEE Proceedings-communications*, vol. 143, no. 5, pp. 259–266, 1996.

[7] Z. Zhu and A. K. Nandi, *Automatic Modulation Classification: Principles, Algorithms and Applications*. John Wiley & Sons, 2014.

[8] V. Chaithanya and V. U. Reddy, "Blind modulation classification in the presence of carrier frequency offset," in *Signal Processing and Communications (SPCOM), 2010 International Conference on*. IEEE, 2010, pp. 1–5.

[9] J. R. Quinlan, *C4. 5: programs for machine learning*. Elsevier, 2014.

[10] M. Ware, "Weka documentation," *University of Waikoto*, 2000.

[11] I. H. Witten and E. Frank, *Data Mining: Practical machine learning tools and techniques*. Morgan Kaufmann, 2005.

[12] T. S. Tabatabaei, S. Krishnan, and A. Anpalagan, "Svm-based classification of digital modulation signals," in *Systems man and cybernetics (SMC), 2010 IEEE international conference on*. IEEE, 2010, pp. 277–280.

[13] G. Arulampalam, V. Ramakonar, A. Bouzerdoum, and D. Habibi, "Classification of digital modulation schemes using neural networks," in *Signal Processing and Its Applications, 1999. ISSPA'99. Proceedings of the Fifth International Symposium on*, vol. 2. IEEE, 1999, pp. 649–652.

[14] H. Guldemir and A. Sengur, "Online modulation recognition of analog communication signals using neural network," *Expert systems with applications*, vol. 33, no. 1, pp. 206–214, 2007.

[15] C.-S. Park, J.-H. Choi, S.-P. Nah, W. Jang, and D. Y. Kim, "Automatic modulation recognition of digital signals using wavelet features and svm," in *Advanced Communication Technology, 2008. ICACT 2008. 10th International Conference on*, vol. 1. IEEE, 2008, pp. 387–390.

[16] J. Popoola and R. Olst, "A novel modulation-sensing method," *IEEE Vehicular Technology Magazine*, vol. 3, no. 6, pp. 60–69, 2011.

THE 18TH INTERNATIONAL SYMPOSIUM ON WIRELESS PERSONAL MULTIMEDIA COMMUNICATIONS
(WPMC-2015)
December 13-16, 2015, Hyderabad, India

A Pattern Division Multiple Access Scheme for 5G wireless communication systems

Kai Zhang*, Jin Xu *
*The Beijing Key Laboratory Network System Architecture and Convergence,
Beijing University of Posts and Telecommunications, Beijing, China
Email: zk513@163.com

***Abstract*—Orthogonal multiple access (OMA) is widely employed in traditional cellular wireless communication systems due to a low-complexity receiver is needed. However, multiple access scheme with higher spectral efficiency and the ability of access more users than OMA scheme is preferred for future wireless communication system. In this work, a non-orthogonal transmission scheme called pattern division multiple access (PDMA) is proposed for the fifth generation (5G) wireless communication system. Two pattern matric are designed for 150% and 200% overloaded PDMA systems. Both of extrinsic information transfer (EXIT) chart analysis and simulation results show that the proposed PDMA scheme outperforms the traditional OMA system significantly. Thus PDMA scheme is a good choice for future multiple access scheme for 5G wireless communication systems.**

***Index Terms*—Pattern division multiple access (PDMA), overload, symbol-wise belief propagation, fifth generation**

I. Introduction

Orthogonal multiple access (OMA) is widely adopted in current wireless communication system due to that a low complexity detection algorithm can be employed at the receiver. In recent years, communication networks are facing the challenges of the rapid increase of mobile data growth and huge amount of access users. Overloaded non-orthogonal transmission by squeezing more users to limited number of time-frequency resource can provide both of higher spectral efficiency and large numbers of access than those of OMA scheme [1-2]. However, a new issue that we must cope with is multiple user interference (MUI) which leading to significant performance degradation. Maximum a posteriori (MAP) or maximum likelihood algorithm is known as optimal with the computational complexity increase exponential with the number of users and the order of modulation, which make it impossible for practical applications. The decorrelator and MMSE detector provide acceptable performance with much lower complexity compare to their optimum counterpart in underloaded systems. Unfortunately, they fail to achieve satisfactory performance under an overloaded condition as the desired signal sub-spaces becomes rank-deficient [3].

Belief propagation (BP) algorithm has attracted great attention due to its success in decoding theory, multiple input multiple output (MIMO) detection and other signal processing problems. In [4], degree distribution optimized low density parity check (LDPC) code with BP decoding can approach the binary input additive white Gaussian noise (BIAWGN) channel capacity with only a gap of 0.0045dB. An important feature of BP algorithm is that it can be depicted by the message passing on factor graph [5]. The extrinsic information is transferred from the leaf node to its parent node and ultimately to root node and the estimate of the transmitted symbol converge to its real value for cycle free graph. However, for full connected graph, e.g. MIMO system, the convergence cannot be guaranteed due to the error propagation [6].

Inspired by the idea of the irregularity of LDPC code and the diversity gain of multicarrier code division multiple access (CDMA) system [1,7], we propose an orthogonal frequency division multiplexing (OFDM) based non-orthogonal multiple access scheme called pattern division multiple access (PDMA) for future wireless communication systems. The features of PDMA can be summarized as: 1) For multicarrier CDMA system, every subcarrier is shared by all users, while PDMA allows every subcarrier to be used by a subset of data symbols that belongs to different users. As we will see later, the computational complexity of the BP based MUD can be reduced significantly by this way especially for high order modulation or high overloaded systems; 2) For multicarrier system, user symbols will be spread over all interested subcarriers, while a subset of subcarriers instead for PDMA system. Furthermore, the effective processing gain of each user can be different; 3) Symbol-wise BP is employed as MUD algorithm to achieve complexity and performance tradeoffs.

This paper is organized as follows: Section II presents the system model of the proposed PDMA system architecture and proposed two pattern matric with different overload factor respectively. Section III depicts the symbol-wise BP MUD algorithm of PDMA system. Numerical results and analysis are provided in Section IV. Conclusions are drawn in section V.

II. System Model and PDMA

A. System model

Consider the uplink PDMA system with N_t users with indices $k = 1, \ldots, N_t$ transmitting to the same base station where the base station and each user are equipped with a single antenna. The block diagram of an uplink PDMA system is shown in Fig. 1. Assume that each user take their symbols from the same constellation alphabet and all users have the same number of data symbols N_s which equal

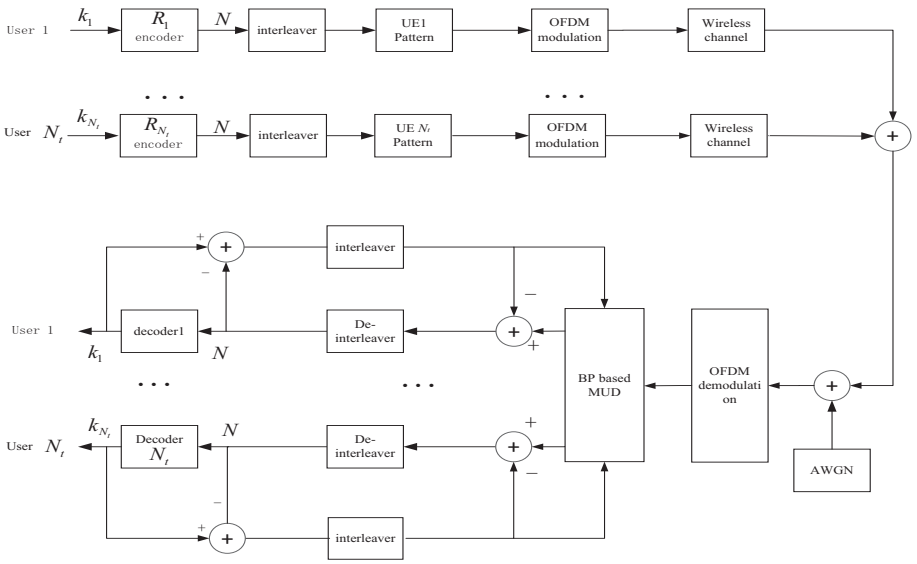

Fig. 1. The structure of the proposed transceiver

to the length of turbo code used. In the PDMA technique, the original data streams are first multiplied with their user-specific pattern sequences and then modulated on different sub-carriers. Assume that a user-specific pattern has d_v non-zero elements, we define d_v as the effective spreading factor of the specific user as in [8]. Similarly, we define d_c as the number of symbols that are allowed to interfere to each other at a specific chip. In PDMA system, d_v of each user can be different, thus d_c of all interest subcarriers can also be different. At the receiver side, after performing OFDM demodulation operations the signal is passed to a belief propagation based MUD [9], there exist two iterative processes: inner and outer iterative processing for MUD and the turbo-style processing, respectively. Considering now that two iterative processes are involved, the message update algorithm should be addressed accordingly. Define two types of supporting sets, one is row supporting set $N_c(j)$ and the other is column supporting set $N_v(i)$. Let row supporting set $N_c(j) = \{i|\mathbf{S}_{j,i} \neq 0, 1 \leq i \leq N_t\}$ denotes the subset of users that share subcarrier j, and let column supporting set $N_v(i) = \{j|\mathbf{S}_{j,i} \neq 0, 1 \leq j \leq N_r\}$ denotes the subset of subcarriers where user symbol x_i is spread. The received signal y_j at subcarrier j can be expressed as:

$$y_j = \sum_{i \in N_c(j)} h_{ji} x_i + n_j \tag{1}$$

Where $h_{j,i}$ denotes the channel fading coefficient from i-th user to j-th subcarrier, x_i is the data symbol of i-th user , n_j is the AWGN with mean zero and variance σ_n^2. The single user average bit signal-to-noise E_b/N_0 is define as in [10]

$$\left(\frac{E_b}{N_0}\right)_{dB} = \left(\frac{E_S}{N_0}\right)_{dB} + 10\log_{10}\left(\frac{1}{R_c m}\right) \tag{2}$$

where E_s denotes the symbol energy of each user, $N_0 = 2\sigma_n^2$ denotes the single side power spectral density, R_c denotes the channel coding rate, and m denotes the number of bits that mapping to a constellation point.

$$\mathbf{S}_{2,3} = \begin{bmatrix} 1 & 1 & 0 \\ 1 & 0 & 1 \end{bmatrix} \Rightarrow \begin{array}{c} \\ \text{RE1} \\ \text{RE2} \end{array} \begin{array}{c} \text{UE1} \quad \text{UE2} \quad \text{UE3} \\ \begin{bmatrix} x_1 & x_2 & 0 \\ x_1 & 0 & x_3 \end{bmatrix} \end{array}$$

Fig. 2. Proposed $\mathbf{S}_{2,3}$ pattern matrix for 150% overload

B. Proposed pattern matric for PDMA system

For example, we have design two pattern matric $\mathbf{S}_{2,3}$ and $\mathbf{S}_{3,6}$for 150% and 200% overload PDMA systems, as shown in Fig. 2 and Fig.3 respectively. The overload factor is defined as $\rho = N_t/N_r$ [11]. For $\mathbf{S}_{2,3}$, user 1 spread its symbol x_1 over RE1 and RE2 for transmission, while user 2 and user 3 spread its symbols x_2 and x_3 over RE1 and RE2 respectively. Consequently, the diversity order (effective processing gain) of user1, user2 and user3 is 2, 1,1 respectively. In addition, it is obviously that the d_c of both of RE1 and RE2 are 2. The first column of matrix $\mathbf{S}_{2,3}$ is the pattern sequence of user 1, the second and last column of matrix $\mathbf{S}_{2,3}$ are the pattern sequences of user 2 and user 3 respectively and so on.

III. Proposed symbol-wise Belief propagation based MUD

An PDMA system with N_t users and N_r chips can be described by a factor graph $\mathcal{G}(\mathcal{V}, \mathcal{C}, \mathcal{E})$ where variable nodes $x_i (1 \leq i \leq N_t)$ and function nodes $y_j (1 \leq j \leq N_r)$ representing the symbol and chip respectively and the relationship between the received chip and its constrained users are represented by edges. Fig.4 shows the factor graph of $\mathbf{S}_{2,3}$.

As shown in [6,8], the *a posteriori* LLR of i-th symbol , denoted by $\mathcal{L}_{MUD}^{D}(x_i = \chi(\alpha))$, can be written as

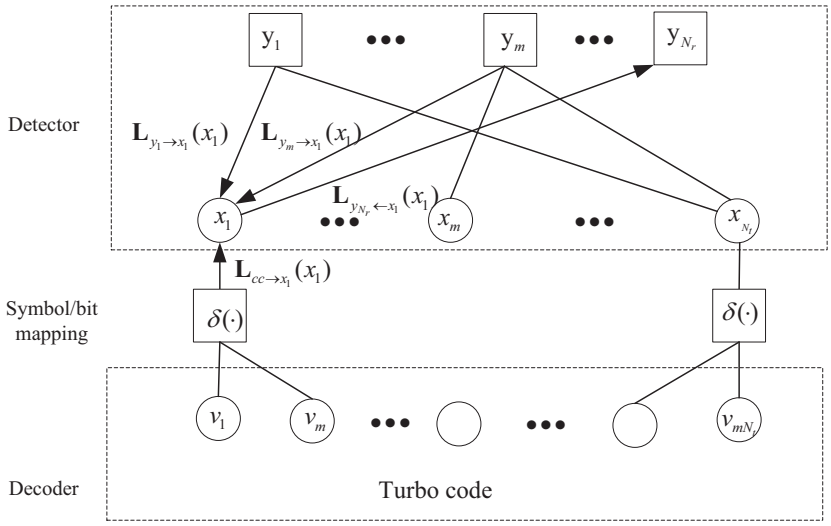

Fig. 6. Joint factor graph of the receiver

$$\mathbf{S}_{3,6}=\begin{bmatrix}1&1&1&0&1&0\\1&1&0&1&0&1\\1&0&1&1&0&0\end{bmatrix}\Rightarrow\begin{array}{c}\\RE1\\RE2\\RE3\end{array}\begin{array}{c}UE1\ UE2\ UE3\ UE4\ UE5\ UE6\\\begin{bmatrix}x_1&x_2&x_3&0&x_5&0\\x_1&x_2&0&x_4&0&x_6\\x_1&0&x_3&x_4&0&0\end{bmatrix}\end{array}$$

Fig. 3. Proposed $\mathbf{S}_{3,6}$ pattern matrix for 200% overload

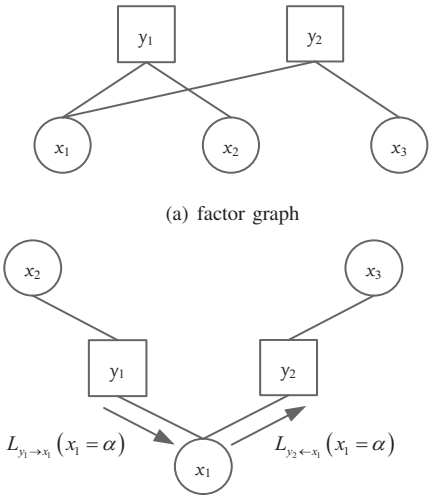

(a) factor graph

(b) Tree graph

Fig. 4. Factor graph of $\mathbf{S}_{2,3}$

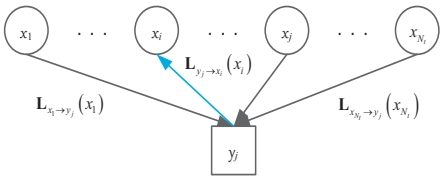

(a) Extrinsic message passing from y_j to variable node x_i

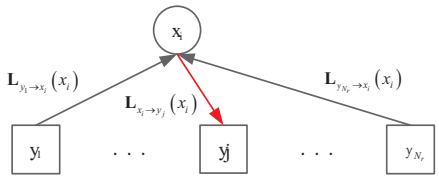

(b) Extrinsic message passing from variable node x_i to y_j

Fig. 5. Extrinsic information passing process

$$L^D_{MUD}\left(x_i=\chi(\alpha)\right))$$
$$\cong \ln\frac{\prod_{j'\in N_v(i)}\sum_{x_{N_c(j)\setminus i}}p\left(y_j|x_{N_c(j)\setminus i},x_i=(\alpha)),H\right)\prod_{\ell\in N_c(j)}p(x_\ell)}{\prod_{j'\in N_v(i)}\sum_{x_{N_c(j)\setminus i}}p\left(y_j|x_{N_c(j)\setminus i},x_i=\chi(0)),H\right)\prod_{\ell\in N_c(j)}p(x_\ell)}$$
$$=\ln\prod_{j'\in N_v(i)}\frac{\sum_{x_{N_c(j)\setminus i}}p\left(y_j|x_{N_c(j)\setminus i},x_i=\chi(\alpha)),H\right)\prod_{\ell\in N_c(j)}p(x_\ell)}{\sum_{x_{N_c(j)\setminus i}}p\left(y_j|x_{N_c(j)\setminus i},x_i=\chi(0)),H\right)\prod_{\ell\in N_c(j)}p(x_\ell)}$$
$$=\sum_{j'\in N_v(i)}\ln\frac{\sum_{x_{N_c(j)\setminus i}}p\left(y_j|x_{N_c(j)\setminus i},x_i=\chi(\alpha)),H\right)\prod_{\ell\in N_c(j)}p(x_\ell)}{\sum_{x_{N_c(j)\setminus i}}p\left(y_j|x_{N_c(j)\setminus i},x_i=\chi(0)),H\right)\prod_{\ell\in N_c(j)}p(x_\ell)} \tag{3}$$

where $0\le\alpha\le|\mathcal{A}|-1$, $\chi(\cdot)$ denotes the constellation mapping, χ^{-1} denotes the inverse mapping, $N_v(i)\backslash j$ denotes the column supporting set $N_v(i)$ except function node j. The channel transition probability function in (3) can be expressed as

$$p\left(y_j|x_{N_c(j)\setminus i},x_i=\chi(\alpha)),\cdots,x_{N_t},\mathbf{H}\right)=\frac{1}{\pi N_0}e^{-\frac{\left|y_j-\mathbf{h}^{[j]}\mathbf{x}\right|^2}{N_0}} \tag{4}$$

Where $\mathbf{h}^{[j]}$ denotes the j-th row of matrix $\mathbf{H}$, $\mathbf{x}=[x_1,\cdots,x_{N_t}]^T$, $N_0=2\sigma_n^2$. Combining (4) into (3), $\mathcal{L}^D_{MUD}(x_i=\chi(\alpha))$ can be rewritten as

$$\mathcal{L}^{D}_{MUD}\left(x_i=\chi(\alpha)\right) = \sum_{j'\in N_v(i)} \ln \frac{\sum_{x_{N_c(j)\backslash i, x_i=\chi(\alpha)}} e^{-\frac{\left|y_j-\mathbf{h}^{[j]}\mathbf{x}\right|^2}{N_0}} e^{\sum_{\ell\in N_c(j), x_\ell\neq\chi(0)} L^a(x_\ell)}}{\sum_{x_{N_c(j)\backslash i, x_i=\chi(0)}} e^{-\frac{\left|y_j-\mathbf{h}^{[j]}\mathbf{x}\right|^2}{N_0}} e^{\sum_{\ell\in N_c(j), x_\ell\neq\chi(0)} L^a(x_\ell)}} \tag{5}$$

As can be seen in (5), the $ln(\cdot)$ function following the first sum in (5) can be interpreted as chip-level Log-domain maximum *a posteriori* (MAP) detection. To calculate $\mathcal{L}^{D}_{MUD}(x_i=\chi(\alpha))$ in an iterative manner, after subtracting the *apriori* LLR $\mathcal{L}^{a}(x_i)$ from $\mathcal{L}^{D}_{MUD}(x_i=\chi(\alpha))$, the extrinsic information $\mathcal{L}_{y_j\to x_i}(x_i=\chi(\alpha))$ transferred from the function node y_j to variable node x_i, as shown in Fig. 5 (a), can be written as

$$\mathcal{L}_{y_j\to x_i}\left(x_i=\chi(\alpha)\right) = \ln \frac{\sum_{N_c(j)\backslash i, x_i=\chi(\alpha)} e^{-\frac{\left|y_j-\mathbf{h}^{[j]}x\right|^2}{N_0}} \cdot e^{\sum_{\ell\in N_c(j)\backslash k, x_\ell\neq\chi(0)} \mathcal{L}^a(x_\ell)}}{\sum_{N_c(j)\backslash i, x_i=\chi(0)} e^{-\frac{\left|y_j-\mathbf{h}^{[j]}x\right|^2}{N_0}} \cdot e^{\sum_{\ell\in N_c(j)\backslash k, x_\ell\neq\chi(0)} \mathcal{L}^a(x_\ell)}} \tag{6}$$

Similarly, the extrinsic information sent from variable node i to function node j can be divided into two cases. For the first case, i.e. symbol-wise BP without iterative decoding, as shown in Fig.5 (b), $\mathcal{L}_{y_j\to x_i}(x_i=\chi(\alpha))$ can be written as

$$\mathcal{L}_{y_j\leftarrow x_i}\left(x_i=\chi(\alpha)\right) = \sum\nolimits_{j'\in\{N_v(i)\backslash j\}} \mathcal{L}_{y_{j'}\to x_i}\left(x_i=\chi(\alpha)\right) \tag{7}$$

For the second case, i.e. symbol-wise BP with iterative decoding, $\mathcal{L}_{y_j\to x_i}(x_i=\chi(\alpha))$ can be written as

$$\mathcal{L}_{y_j\leftarrow x_i}\left(x_i=\chi(\alpha)\right) = \sum\nolimits_{j'\in\{N_v(i)\backslash j\}} \mathcal{L}_{y_{j'}\to x_i}\left(x_i=\alpha\right) + \mathcal{L}_{cc\to x_i}(x_i=\chi(\alpha)) \tag{8}$$

The basic form of chip level iterated MUD can be explained as follows. Using MPA, messages containing the reliability values of adjacent variable node are exchanged between the function nodes and the variable nodes iteratively. After appropriate number of iterations the soft output which is the calculated log likelihood ratio at each variable node, i.e. for variable node i, the *a posteriori* LLR $\mathcal{L}^{D}_{MUD}(x_i=\chi(\alpha))$ can be rewritten as

$$\mathcal{L}^{D}_{MUD}\left(x_i=\chi(\alpha)\right) = \sum\nolimits_{j'\in N_v(j)} \mathcal{L}_{y_{j'}\to x_i}\left(x_i=\chi(\alpha)\right) \tag{9}$$

After symbol/bit LLR conversion, the extrinsic LLRs of BP based MUD will be sent to the channel decoders. More details regarding the symbol/bit LLR conversion can be found in appendix. The iterative receiver of PDMA is based on iterative detection/decoding between PDMA symbol-wise MUD and users' FEC decoders. This is realized by iterative exchange of extrinsic information between detection and FEC decoding stages. The block diagram of PDMA's iterative MUD is illustrated in Fig. 6 and the BP based MUD algorithm is summarized as algorithm 1.

Algorithm 1 BP based MUD algorithm

Input: $\mathbf{y}=[y_1,\cdots,y_{N_r}]^T$.
Initialize: $1\le i\le N_t, \mathcal{L}^a_{x_i}=\chi^{-1}(0)$.
Output: $1\le i\le N_t, \mathbf{L}^D_{MUD}(x_i)=[L^D_{MUD}(x_i=\chi^{-1}(0)),\cdots,L^D_{MUD}(x_i=\chi^{-1}(q-1))]$.
while $n_iter < max_iter$ **do**
  // Vertical update;
  for $1\le i\le N_t$ **do**
    for $1\le i\le N_r$ **do**
      if $\mathbf{S}_{j,i}\neq 0$, for $1\le\alpha\le|\mathcal{A}|$ **then**
        Calculate $\mathcal{L}_{y_j\to x_i}(x_i=\chi^{-1}(\alpha))$ according to (5);
      end if
    end for
  end for
  // Horizontal update;
  for $i=1$ to n **do**
    for $i=1$ to n **do**
      if $\mathbf{S}_{j,i}\neq 0$, for $1\le\alpha\le|\mathcal{A}|$ **then**
        Calculate $\mathcal{L}_{y_j\to x_i}(x_i=\chi^{-1}(\alpha))$ according to (6);
      end if
    end for
  end for
end while
// A posteriori LLRs calculation
for $1\le i\le N_t$, for $1\le\alpha\le|\mathcal{A}|$, **do**
  Calculate $\mathcal{L}^D_{MUD}(x_i=\chi^{-1}(\alpha))$ according to (8).
end for

IV. Simulation Results

In this section, the performance of the proposed PMs are compared with that of the ones proposed in [2]. Both schemes employ turbo code of length 480 bits and rate 5/12 according to 3GPP's LTE-standard [12]. Under BPSK modulation and AWGN channel, as shown in Fig. 7, the coded BLER performance is compared between the proposed scheme the scheme proposed in [2] . The performance of the proposed $\mathbf{S}_{2,3}$ PM is superior to the $\mathbf{S}_{6,9}$ PM about 1.1dB, and the performance of the proposed $\mathbf{S}_{3,6}$ PM with about the same the performance as the $\mathbf{S}_{12,24}$. Under QPSK modulation and independent identical distribution (IID) rayleigh fading channel, simulation results are shown in Fig.8. It is need to say that the decoding complexity of both the proposed pattern matric is lower than that of the corresponding ones in [2]. For the PDMA systems employing QPSK modulation and BP-IDD algorithm, as shown in Fig. 9 and Fig. 10, the coded BLER performance of all the proposed schemes of 150% and 200% overload, outperform the OMA scheme about 2.1dB and 0.5dB respectively.

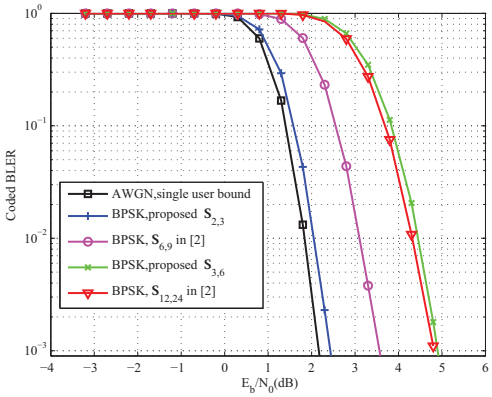

Fig. 7. Coded BLER performance comparison, AWGN channel, BPSK

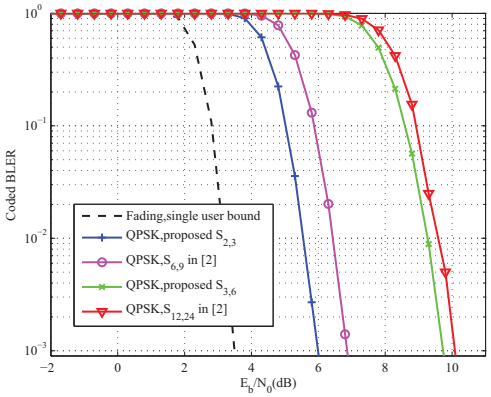

Fig. 8. BLER performance comparison, fading channel, QPSK

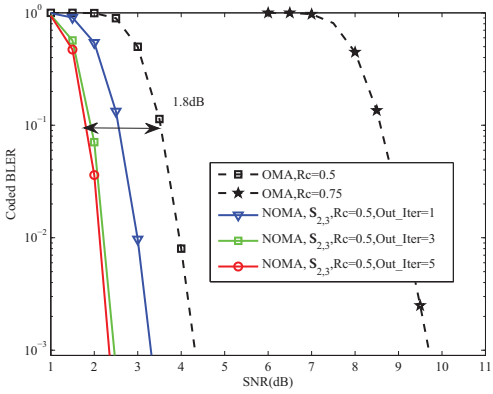

Fig. 9. BLER performance comparison between $\mathbf{S}_{2,3}$ and OMA

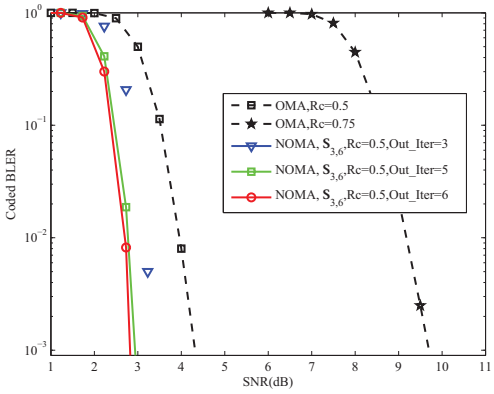

Fig. 10. BLER performance comparison between $\mathbf{S}_{3,6}$ and OMA

V. CONCLUSION

In this work, a PDMA scheme is proposed for future 5G cellular wireless communication system for the purpose of high spectral efficiency and high overload system. The proposed PMs for PDMA system achieves better performance than the existing scheme and significant performance gains than OMA scheme. It is a attractive multiple access scheme for 5G communication system.

REFERENCES

[1] J. Choi, "Low density spreading for multicarrier systems," in *proc. IEEE 8th International Symposium on Spread Spectrum Techniques and Application (ISSSTA)*, 2004.

[2] B. J. Vande , B. M. Popovic, "Multiple Access with Low-density Signatures", in *proc. IEEE Global Telecommunications Conference (GLOBECOM), 2009* .

[3] Wen L., Razavi R., Ali-Imran M, et al, Design of joint sparse graph for OFDM (JSG-OFD) system, IEEE Trans. On wireless commun. 2014, 14(4):183-1836.

[4] S.-Y. Chung, G. D. Forney, Jr. and T. J. Richardson etc, "On the design of low-density parity-check codes within 0.0045dB of the shannon limit," *IEEE Commun. lett.*, vol.5, no. 2, pp. 58-60, Feb. 2001.

[5] F. R. Kschischang, B. J. Frey, and H.-A. Loeliger, " Factor graphs and sum-product algorithm," *IEEE Trans. inf. Theory*, vol. 47, no. 2, pp. 498-519, Feb. 2001.

[6] J. Hu,T.M. Duman, "Graph-based detector for BLAST architecture,", in *proc. IEEE International Conference on Communications(ICC), 2007* .

[7] X. D. Cai, S. L. Zhang, and G. B. Giannakis, "Group-orthogonal multicarrier CDMA." *IEEE Trans. on Commun.*, vol. 52, no. 1, pp. 90-99, Jan. 2004.

[8] Razavi R., M. AL-Imari, M. AL-Imaran, et al, On receiver design for uplink low density signature OFDM (LDS-OFDM), IEEE Trans. On Communications, 2012, 60(11):3499-3508

[9] Morosi S., Fantacci R., Re D., Design of turbo-MUD receivers for overloaded CDMA systems by density evolution technique, IEEE Trans. Wireless Communications, 2007,6(10):3552-3557.

[10] S. Brink, G. Kramer, A. Ashikhmin, "Design of low-density paritycheck codes for modulation and detection," *IEEE Trans. Commun,*vol.52, no.4, pp. 670- 678, April. 2004.

[11] R. Razavi, M. Ali-Imran, R. Tafazolli , "EXIT chart analysis for turbo LDS-OFDM receivers", in *proc IEEE International Conference Wireless Communications and Mobile Computing (WCMC),* 2011.

[12] Evolved Universal Terrestrial Radio Access (E-UTRA): Multiplexing and Channel Coding (Release 8), 3GPP TSG RAN TS36.212, v8.5.0., Dec. 2008. [Online]. Available: http:// www.3gpp.org/

THE 18TH INTERNATIONAL SYMPOSIUM ON WIRELESS PERSONAL MULTIMEDIA COMMUNICATIONS
(WPMC-2015)
December 13-16, 2015, Hyderabad, India

An Interdependent Source-Channel Coding for Energy Efficient Communication in WSNs

Resmi N C and Sonali Chouhan
Department of Electronics and Electrical Engineering
Indian Institute of Technology Guwahati, Assam, India- 781039
Email: {resmi, sonali}@iitg.ernet.in

***Abstract*—Reliable data transmission is the first and foremost goal of any communication system. However, for energy constrained wireless sensor networks, the critical design constraint is energy conservation. A novel method of error control is proposed in this paper keeping reliability and energy efficiency as the prime goals. The method yields an enhanced coding gain (CG) compared to stronger codes, without any redundancy or even with savings in number of bits transmitted. Further, the upper and lower bounds on the bit error rate (BER) performance are also presented. The reliability and transmitted data savings provided are interdependent on each other and hence the name, interdependent source channel coding. Simulation results show that the proposed scheme achieves a CG of 4.093 dB in AWGN channel at BER of 10^{-5}, when there are 50 symbols in a codeword.**

***Index Terms*—WSNs, energy efficiency, coding gain, compression**

I. Introduction

A wireless sensor network (WSN) is a set of connected nodes deployed for observing a physical phenomenon and is widely used in a variety of applications. The design constraints of WSNs are very different from other traditional wireless networks because of its unique features like dense network, limited processing capability, and limited power supply. In most of the applications, sensor nodes are deployed in remote or secluded locations and are supposed to run for long time. Hence, energy conservation becomes the most important design issue of a WSN [1]. Any protocol or technique developed for WSN should be energy efficient.

Reliable information exchange is the prime motive of any communication system. Reliability is provided generally in two ways. i) Automatic Repeat Request (ARQ) and ii) Forward Error Correction (FEC). ARQ scheme is based on error detection techniques and retransmissions, while FEC on error correction at the receiver. ARQ is simpler compared to FEC schemes, and hence seems to be more suitable for WSNs, since complexity adds to energy expenditure. The authors in [2], [3] found ARQ energy inefficient for WSNs, due to the retransmissions of erroneous packets.

FEC is a good alternative to ARQ for adverse channel conditions. FEC corrects errors with help of added redundancy, and hence reduces the transmit energy required for achieving the same bit error rate (BER) of uncoded transmission. This saving is termed as coding gain (CG). This comes with the cost of additional transmit energy for parity bits and computation energy for encoding/decoding operation. If the additional energy expenditure underweighs the gain in transmit energy, FEC is energy efficient. Unlike traditional wireless networks, in a dense network, nodes are very close to each other and difference between computation energy and transmitting energy cannot be high [4]. The authors in [5] have found that FEC is an energy efficient solution for WSNs considering all the energy components of sensor nodes and encoding-, transmission-, and modulation-parameters.

There has been an extensive research in finding the optimal FEC scheme for WSNs, though none is standardized. To find an optimal scheme, both BER performance and energy consumption have to be considered. Basically, there are two types of error control codes, block codes and Convolutional codes. The block codes have been observed to be energy efficient compared to Convolutional codes. In [4], the authors have observed that to achieve the same CG, Convolutional code needs higher redundancy and complexity than Reed-Solomon (RS) code. The authors of [6] show that, even the best Convolutional codes are not energy efficient compared to BCH codes. In [7], it has been shown that the Convolutional coded channel with Viterbi decoder consumes more energy than uncoded channel and hence not suitable for WSN. The authors have also compared Hamming code, Golay code, Convolutional code, and RS codes and concluded that Hamming code is the simplest code, but has the lowest performance. Various Hamming, Convolutional, and RS codes with QPSK modulation are compared in [8] with all the energy components of a node and found an optimal code for WSNs. LDPC and turbo codes were claimed to perform well by the authors in [9]. However, these codes were incompetent in satisfying memory and timing requirement pertaining to industrial WSNs as cited in [9]. In furtherance, these codes exhibit an intense computational burden when implemented for WSNs.

Further, numerous joint source channel coding (JSCC) schemes were proposed in the literature for conventional systems. Nevertheless, these techniques are not specific for WSNs and are generally energy inefficient in WSN scenario. The existing JSCC techniques specific to WSNs, exploit the redundancy in

the measured data due to data correlation from nearby nodes for error correction [10]. This leaves scope for further research on the design of energy efficient coding technique which relaxes the strict requirement of data correlation in JSCC based methodologies.

In view of the works cited in literature, it is clear that stronger codes give better protection, but consume more computational energy, while simpler codes consume less energy. The only issue that limits the usage of existing simple codes, for example, Hamming and Repetition codes, is their poor BER performance. Therefore, the main objective of our work lies in the design of an energy efficient coding scheme for WSNs, yielding an appreciable CG.

In this paper, we propose a novel scheme for error correction as well as compression. Relative to the reported works on JSCC techniques in literature, the proposed coding scheme is prolific in the sense that it is computationally simple and neither requires source characteristics nor any data correlation information. Moreover, the methodology presented yields a coding scheme which achieves an enhanced CG exhibiting lesser computational complexity vis-à-vis existing FEC techniques. The CG and the compression ratio can be varied by varying the code parameters used.

The paper is organized as follows. In Section II, the methodology of proposed scheme is discussed. The BER performance is given in Section III. The simulation parameters and results are presented and illustrated in Sections IV and V, respectively. Finally, conclusions are drawn in Section VI.

II. Methodology

We propose a novel error control technique which gives better CG as compared to stronger error control codes. It also comes with an added advantage of compression, i.e., our method gives protection without added redundancy, or even with saving in number of bits transmitted. The basic idea is to divide the input data into some groups such that in each group the data is separated from each other by a minimum Hamming distance d_{min}. Then, the data from the same group is concatenated together, in addition to a label to identify their group, to form a codeword. For this method to apply, we need a group of data which is typical in WSN applications, e.g., temperature-, pressure-monitoring, etc.

The proposed methodology has been explained in a stepwise manner below:

Step 0: *Defining groups*

- Consider the input message of k_m bits. We split this message into k_1 and k_2 bits, where $k_m = k_1 + k_2$.
- We keep aside k_1 most significant bits from the input message.
- The remaining k_2 bits are named the SYMBOL.
- To achieve a minimum Hamming distance d_{min}, $k_2 \geq d_{min}$. In this paper, we have considered $d_{min} = 3$ for 1-bit error correction capability.
- There are 2^{k_2} possible SYMBOLs. These are divided into groups of 2^{k_1} members with $d_{min} = 3$. So we get $2^{k_2-k_1}$ such groups.
- We label these groups in order to distinguish among them. We need at least $\log_2(2^{k_2-k_1})$ bits for this Group label.

Step 1: *Coding the input data*

- For each input message, last k_2 bits belong to one of the groups defined in Step 0 and named SYMBOL, as shown in the upper branch of Fig. 1.
- The first k_1 bits of the input message, and the Group label of the SYMBOL together named as LABEL as shown in the lower branch of Fig. 1. Each LABEL has $k_L = (k_1 + log_2(2^{k_2-k_1}))$ number of bits.
- There are $L = 2^{(k_1+log_2(2^{k_2-k_1}))}$ number of LABELs in total.
- Thus each k_m bit input message is represented now as [LABEL : SYMBOL]. This consists of $\log_2(2^{k_2-k_1}) + k$ number of bits.

Step 2: *Concatenation of data*

- Since more than one SYMBOL can have the same LABEL, we can append all such SYMBOLs together, with LABEL appearing only once. This saves the number of bits transmitted. The concatenation is shown in Fig. 2.

Step 3: *Protection of LABEL*

- Each SYMBOL belongs to a group with $d_{min} = 3$. So, once the LABEL is identified correctly, each SYMBOL with the LABEL is robust to one-bit error.
- To achieve this, LABEL has to be identified correctly. Hence, the LABEL part is protected with a simple linear block code. Depending on the required error correction capability, a suitable code can be selected.
- The concatenated SYMBOLs with their corresponding protected LABEL forms a codeword.

Beyond a certain number of SYMBOLs appended with a protected LABEL, the codeword length is lesser than the total information bits. This minimum number of SYMBOLs in a codeword for achieving compression is not very large. For example, if there are minimum 6 SYMBOLs in a codeword for the case, $k_m = 7$ and $k_1 = 2$, we can achieve compression. As we append more SYMBOLs in a codeword, the compression is increased.

The definition of groups, encoding of data as SYMBOL and LABEL, and protection of LABEL by linear block code can be executed a prior and list the possible input messages and corresponding protected LABEL plus SYMBOL representation in a table. On receiving data, only comparison and concatenation need to be done. Hence, our scheme is much simpler and energy efficient compared to other schemes.

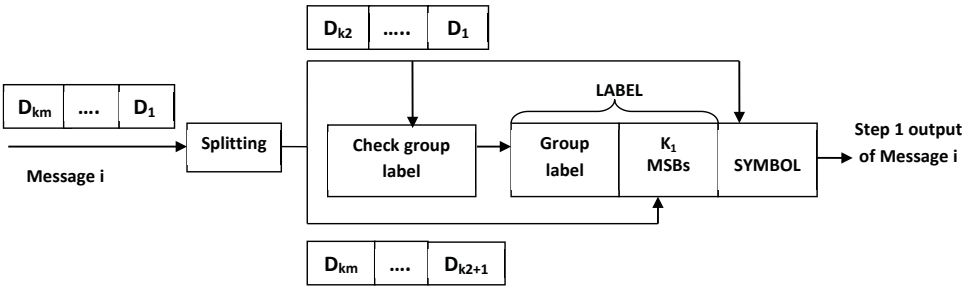

Fig. 1. Encoding of the input data as SYMBOL and LABEL (Step 1).

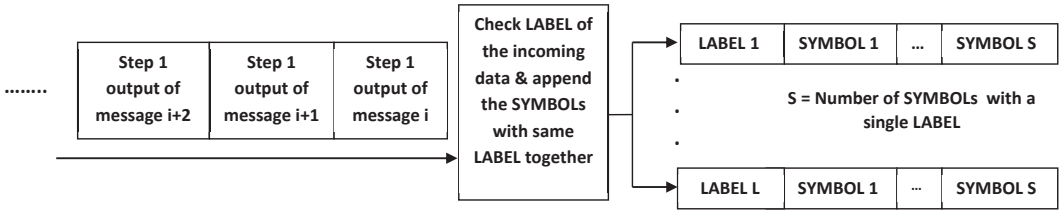

Fig. 2. Concatenation of SYMBOLs with LABEL (Step 2).

III. Bit Error Rate Performance

In this section, we present the BER performance of the proposed scheme as well as the lower and upper bounds of the BER. Probability of m errors in a block of n bits for a binary symmetric channel is upper bounded by [11]

$$P_M \leq \sum_{m=t+1}^{n} \binom{n}{m} p^m (1-p)^{n-m} \tag{1}$$

where t is the error correction capability and p is the channel transition probability given by

$$p = \frac{1}{2}\text{erfc}\left(\sqrt{R\frac{E_b}{N_0}}\right) \tag{2}$$

for binary phase shift keying (BPSK) modulation in additive white Gaussian noise (AWGN) channel, R is the rate of the code and E_b/N_0 is the signal to noise ratio per bit.

Using (1) and (2) and assigning $n = n_1$ and $t = t_1$, we can calculate the block error probability of the LABEL (P_{LABEL}), where n_1 is the length of protected LABEL and t_1 is the error correction capability of the linear block code used to protect LABEL.

When the LABEL is decoded correctly, each of the SYMBOLs have t_2 bit error correction capability. The block error probability of a SYMBOL (P_{SYMBOL}) can be calculated using (1) and (2), assigning $n = k_2$ and $t = t_2$. If the LABEL is decoded incorrectly, then entire codeword is decoded incorrectly. Hence, the error probability of the entire codeword can be calculated using,

$$P_e = (1 - P_{LABEL})P_{SYMBOL}^S + P_{LABEL} \tag{3}$$

where S is the number of symbols in a codeword. Bit error probability of a SYMBOL is calculated using the following equation from [12] as,

$$P_{bit} = \frac{1}{n}\sum_{m=t+1}^{n} (m+t)\binom{n}{m} p^m (1-p)^{n-m}. \tag{4}$$

Bit error probability of the codeword is upper bounded by the block error probability and lower bounded by block error probability divided by the number of information bits contained in the codeword [13]

$$P_{bit-upperbound} = P_e, \tag{5}$$

$$P_{bit-lowerbound} = \frac{P_e}{k_1 + Sk_2}. \tag{6}$$

IV. Simulation Parameters

For simulation, we consider an AWGN channel and BPSK modulation scheme. BPSK modulation is chosen here, because it is one of the modulation schemes defined in the standard used for specifications of WSN, IEEE 802.15.4 and the simplest. At this point, a notation for our proposed coding scheme is introduced as follows. The code is characterized mathematically by $\{S,\ k_m,\ k_1,\ k_2\}$, where, S denotes the number of SYMBOLs in a codeword, k_m defines the length of each message block, k_2 gives the number of bits in a SYMBOL and $k_1 = k_m - k_2$. Simulations have been performed using the presented coding methodology for different characterizations given by $\{S,\ k_m,\ k_1,\ k_2\}$. For instance, simulation results have been demonstrated for $\{5,\ 7,\ 2,\ 5\}$, $\{10,\ 7,\ 2,\ 5\}$, and $\{50,\ 7,\ 2,\ 5\}$, respectively. These results will help us in learning the effect of changing values of S on CG and compression. To give 1-bit error protection to LABEL (5 bits), we select the nearest possible simple linear block code, that is, rectangular (11, 6) code [14]. Since our LABEL length is 5, we add one 0-bit to the LABEL and perform rectangular (11, 6) encoding,

wherein the notation $(n,\ k)$ denotes the code length by n and the block length by k, respectively. But, while transmitting, the first bit is removed since it is known at the receiver. Finally the rectangular (11, 6) code ends up in a (10, 5) code. At the receiver the 0-bit is appended again and decoding is performed. The resulting LABEL will be one bit error corrected. Hence, the group is identified from the group label part of the LABEL. Once the group is known, each of the SYMBOLs can be corrected against 1-bit error, as there is a minimum distance restriction of 3 within the group.

The code is further simulated under various conditions with constant $S = 10$, as characterized by the following sets as given below,

$$\mathscr{R}_{k_2} := [\{10,6,1,5\},\ \{10,7,2,5\},\{10,8,3,5\}]$$
$$\mathscr{R}_{k_m} := [\{10,8,1,7\},\ \{10,8,2,6\},\{10,8,3,5\}]$$
$$\mathscr{R}_{k_1} := [\{10,6,1,5\},\ \{10,7,1,6\},\{10,8,1,7\}]$$

where, $\mathscr{R}_{k_2}$, $\mathscr{R}_{k_m}$ and $\mathscr{R}_{k_1}$ denote the cases considered for simulation purposes with k_2, k_m and k_1 held constant, respectively. Further, theoretical and simulation results are presented for $\{10,\ 7,\ 2,\ 5\}$ alongwith the upper and lower bounds on the BER.

V. Results and Discussions

In this section, the results obtained by simulating our scheme with various values of S, k_m, k_1, and k_2 are presented.

Fig. 3 plots the performance of our scheme for $\{5,\ 7,\ 2,\ 5\}$, $\{10,\ 7,\ 2,\ 5\}$, and $\{50,\ 7,\ 2,\ 5\}$; Hamming (7, 4) code; RS (31, 29) code, and uncoded transmission. We can observe that our proposed coding scheme gives significant improvement in CG compared to the simple Hamming (7, 4) code, and stronger RS (31, 29) code. It can also be observed that as the number of SYMBOLs in a codeword increases, CG also increases. The CG achieved at BER=10^{-5} is 2.833 dB for $S = 5$; 3.46 dB for $S = 10$; and 4.093 dB for $S = 50$.

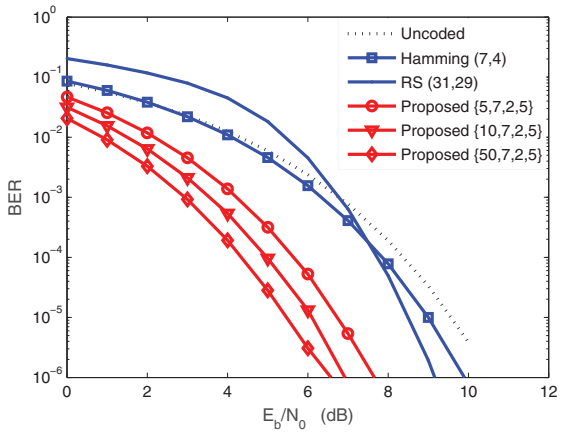

Fig. 3. BER vs. E_b/N_0 performance of the uncoded, Hamming, RS and Proposed code for $\{S,\ 7,\ 2,\ 5\}$ with $S = 5,\ 10$ and 50.

Compression can be calculated by taking the ratio of the difference in the number of input and coded bits to the number of input bits. It is found that, compression increases as S increases. Although the compression achieved for $S = 5$ is zero yet a significant CG is attained. Both CG and compression are achieved simultaneously from $S > 5$. For $S = 10$, compression achieved is 14.2857% and that for $S = 50$, is 25.7143%.

The theoretical and simulation results of the case $S = 10$, along with upper and lower bounds are plotted in Fig. 4. Using (4), BER of a SYMBOL can be calculated. This SYMBOL BER is used in (3) in the place of P_{SYMBOL}, to find the BER of the entire codeword. The upper and lower bounds of BER are calculated using (5) and (6), respectively. Theoretical and simulation BER performance fall well within the upper and lower bound curves.

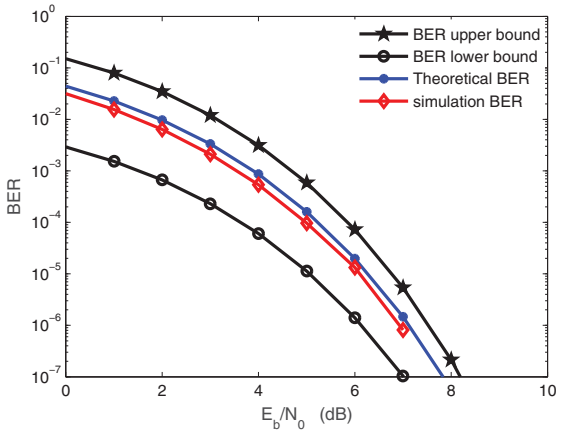

Fig. 4. Theoretical, simulation, upper bound and lower bound BER performance for $\{10,\ 7,\ 2,\ 5\}$.

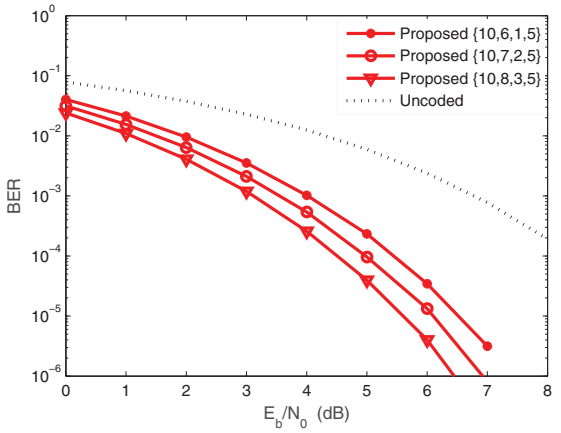

Fig. 5. BER vs. E_b/N_0 performance of the proposed code for cases contained in $\mathscr{R}_{k_2}$.

Fig. 5 shows the comparison of results for the cases contained in $\mathscr{R}_{k_2}$. An increment in the value of k_m and k_1 increases CG and compression. In each of the cases contained in $\mathscr{R}_{k_2}$, the achieved CG and compression are found as (3.045 dB, 3.33%), (3.46 dB,

14.2857%), and (3.962 dB, 23.75%). Further, results are illustrated for the cases in $\mathscr{R}_{k_m}$ in Fig. 6. As the value of k_1 increases, better CG is achieved in addition to compression, as depicted in Fig. 6. This is because as k_1 increases, our grouping improves with more members in a group with minimum distance restriction. Similarly for $\mathscr{R}_{k_m}$, the CG and compression are found as (2.796 dB, 0%), (3.393 dB, 12.5%), and (3.962 dB, 23.75%).

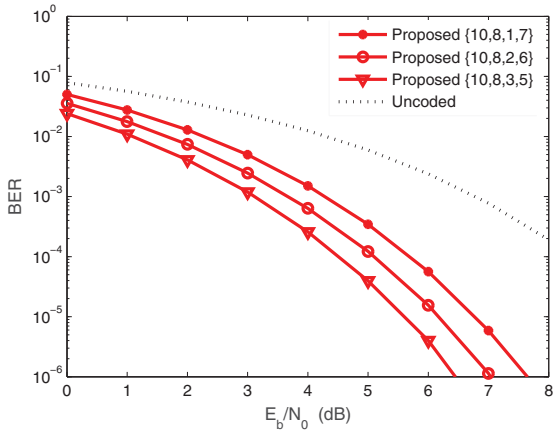

Fig. 6. BER vs. E_b/N_0 performance of the proposed code for cases encompassed in $\mathscr{R}_{k_m}$.

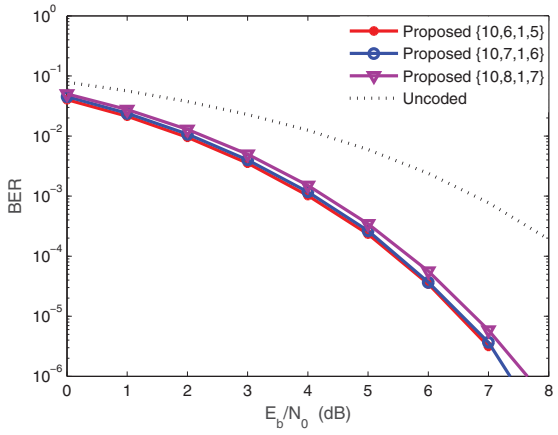

Fig. 7. BER vs. E_b/N_0 performance of the proposed code for cases contained in $\mathscr{R}_{k_1}$.

Withal, results for the cases encompassed in $\mathscr{R}_{k_1}$ are demonstrated in Fig. 7. It can be easily inferred that an increasing value of k_m leads to a marginal decrease in both CG and compression. The performance degradation with increasing message length is due to the reducing effect of grouping. In the limiting case of $k_1 = 0$, there is no grouping at all. Therefore, for $\mathscr{R}_{k_1}$, CG and compression are evaluated as (3.045 dB, 3.33%), (2.996 dB, 2.8571%), and (2.796 dB, 0%).

VI. Conclusions

In this paper, a novel technique for error correction in energy constrained WSNs is presented. The bounds of BER performance have also been derived. As evident from the theoretical and simulation results, the proposed methodology provides considerable amount of compression in addition to good coding gain. Our scheme achieves an enhanced CG with a relative enhancement factor of 3.024 dB for {50, 7, 2, 5} as compared to RS (31, 29). If the application is delay tolerant, more number of SYMBOLs can be attached in a codeword, thereby attaining a better CG and compression. Utilizing stronger codes for LABEL protection can improve the BER performance further. In addition, the proposed technique is computationally less complex relative to the existing near performance codes intuitively. Quantification of the computational complexity for the proposed coding scheme would prove to be a value addition to the presented work which is under development.

References

[1] G. Anastasi, M. Conti, M. D. Francesco, and A. Passarella, "Energy conservation in wireless sensor networks: A survey," *Ad Hoc Networks*, vol. 7, no. 3, pp. 537 – 568, 2009.

[2] V. Nithya, B. Ramachandran, and V. Bhaskar, "Energy efficient coded communication for ieee 802.15.4 compliant wireless sensor networks," *Wireless Personal Communications*, vol. 77, no. 1, pp. 675–690, 2014.

[3] J. Kleinschmidt, "Analyzing and improving the energy efficiency of ieee 802.15.4 wireless sensor networks using retransmissions and custom coding," *Telecommunication Systems*, vol. 53, no. 2, pp. 239–245, 2013.

[4] G. Balakrishnan, M. Yang, Y. Jiang, and Y. Kim, "Performance analysis of error control codes for wireless sensor networks," in *Information Technology, 2007. ITNG '07. Fourth International Conference on*, April 2007, pp. 876–879.

[5] S. Chouhan, R. Bose, and M. Balakrishnan, "Integrated energy analysis of error correcting codes and modulation for energy efficient wireless sensor nodes," *Wireless Communications, IEEE Transactions on*, vol. 8, no. 10, pp. 5348–5355, October 2009.

[6] Y. Sankarasubramaniam, I. Akyildiz, and S. McLaughlin, "Energy efficiency based packet size optimization in wireless sensor networks," in *Sensor Network Protocols and Applications, 2003. Proceedings of the First IEEE. 2003 IEEE International Workshop on*, 2003, pp. 1–8.

[7] B. S. N. Alrajeh, U. Marwat and S. Shah, "Error correcting codes in wireless sensor networks: An energy perspective," *Applied Mathematics & Information Sciences*, vol. 9, no. 2, pp. 809–818, 2015.

[8] S. Chouhan, R. Bose, and M. Balakrishnan, "A framework for energy-consumption-based design space exploration for wireless sensor nodes," *Computer-Aided Design of Integrated Circuits and Systems, IEEE Transactions on*, vol. 28, no. 7, pp. 1017–1024, July 2009.

[9] Y. Yitbarek, K. Yu, J. Akerberg, M. Gidlund, and M. Bjorkman, "Implementation and evaluation of error control schemes in industrial wireless sensor networks," in *Industrial Technology (ICIT), 2014 IEEE International Conference on*, Feb 2014, pp. 730–735.

[10] S. Pradhan and K. Ramchandran, "Distributed source coding: symmetric rates and applications to sensor networks," in *Data Compression Conference, 2000. Proceedings. DCC 2000*, 2000, pp. 363–372.

[11] J. Proakis, *Digital communications*. Boston: McGraw-Hill, 2001.

[12] T. Ha, *Theory and design of digital communication systems*. New York: Cambridge University Press, 2011.

[13] R. Wells, *Applied coding and information theory for engineers*. Upper Saddle River, N.J.: Prentice Hall, 1999.

[14] B. Sklar, *Digital communications*. Englewood Cliffs, N.J.: Prentice-Hall, 1988.

THE 18TH INTERNATIONAL SYMPOSIUM ON WIRELESS PERSONAL MULTIMEDIA COMMUNICATIONS
(WPMC-2015)
December 13-16, 2015, Hyderabad, India

TVWS Regulations and The First IEEE 802.11af Indoor Experiments in Singapore

Vinh Dien Hoang
Singapore Smart Wireless Lab, National Institute of Information and Communications Technology (NICT)
Email: hvdien@nict.go.jp

Takeshi Matsumura, Kentaro Ishizu, Homare Murakami, Fumihide Kojima
National Institute of Information and Communications Technology (NICT), Japan
Email: {matsumura, ishidu, homa, f-kojima}@nict.go.jp

***Abstract*— The demand for spectrum resource has been raising significantly all over the world with the development of the wireless communication technologies. However, spectrum resources are increasingly becoming insufficient and it is strongly required to use this limited resources wisely. Among the technologies that allow efficient use of spectrum, TV white spaces (TVWS) has been promoted as a feasible solution to address this demand in many countries. Singapore is one of those countries that have been very active in promoting the TVWS technology. This paper presents Singapore regulations regarding TVWS as well as results of the first IEEE 802.11af indoor experiment in Singapore. The prototyped IEEE 802.11af-based system and its experiment results demonstrate the promising capability and practicality of the TVWS communication system.**

Keywords— TV white-spaces (TVWS); IEEE 802.11af; field experiment; Dynamic Spectrum Access

I. INTRODUCTION

The demand for spectrum resource has been raising significantly all over the world with the development of the wireless communication technologies. The spectrum resources are limited and becoming increasingly insufficient. However, many frequencies are not fully utilized and it is strongly required to use this limited resources wisely.

White spaces (WS) refer to parts of the spectrum not used by primary users spatially or temporarily, and can be accessed by secondary users with measures in place to protect the primary users. TVWS refers to the WS in the TV bands such as the VHF and UHF bands that are unused from time to time by broadcasters or other licensees. As many countries have shifted their TV broadcasting systems from analogue TV to digital TV, frequencies in the UHF and VHF bands will be freed up. This presents huge chunk of frequencies that could be used for different scenarios and applications. Regulators will have an opportunity to examine these spectrums for full utilization.

For these reasons, regulators are carefully and actively opening TVWS for secondary usage on unlicensed basis. The FCC (Federal Communications Commission) in the U.S.A. established rules and approved the use of White Space Devices (WSD) in Nov. 2008 [8], Sep. 2010 [9] and Apr. 2012[1]. In June 2009 and Nov. 2010, the Ofcom in the U.K. (Office of Communications) permitted the use of TVWS as license-exempt access for WSDs [2]. In Japan 2013, discussions for the transmission in TVWS were finished and the standard documentation was completed by the ARIB (Association of Radio Industries and Businesses) [3]. In June 2014, IDA (Infocomm Development Authority of Singapore) in Singapore finalized the regulatory framework for WSD's accesses of TVWS [4].

Among these pioneering countries, Singapore has been very active in promoting the TVWS technology. The history of TVWS in Singapore started from 2009, when the IDA released a roadmap for innovation and adoption of TVWS and established a supporting regulatory framework. The IDA facilitated a key step by conducting proof of concept trial in the CRAVE (Cognitive RAdio VEnue) zones in 2010 with participation of five organisations. The trial showed that WSDs and traditional broadcasters could share the same spectrum band. In 2013, IDA had sent the TVWS public consultation paper to all stake holders in Singapore to get feedbacks and suggestions regarding regulation of TVWS in Singapore, then IDA finalized the TVWS regulation in 2014 [4].

This paper presents Singapore TVWS regulations in details as well as results of the first IEEE 802.11af [5] experiment in Singapore. The trial indoor experiment was successfully carried out in TeleTech Park Building located in Singapore Science Park II, in May 2015. The prototyped IEEE 802.11af-based system and its experimental results demonstrate the capability and practicality of the TVWS communication system.

This paper is organized as follows. TVWS Regulations in Singapore are presented in Section II. Section III presents the IEEE 802.11af experiment setup. Indoor experiment results are presented in Section IV. Finally, Section V concludes the paper.

II. SINGAPORE REGULATION REGARDING TVWS

With a careful but open approach, the IDA issued a consultation paper to seek comments and feedback from the industry in June, 2013 [7]. One year later on June 16, 2014, the IDA published its response to the submissions made during the consultation period on how to regulate TVWS in Singapore. These regulations [4], which came into effect on November 1, 2014, set Singapore alongside the US and the

UK as global leaders in the development and usage of TVWS on a licence-exempt basis.

These regulations allow the secondary usage of the TVWS services in the future with certainty, especially in the amount of spectrum set aside for WSDs. The regulations also specify the licensing and regulatory requirement, as well as the operating parameters of WSDs, Geo-location database, etc.

IDA's regulations specify measures to protect TV broadcasters by limiting the use of adjacent channels and placing limits on the WSD's power emissions. Existing users of wireless microphones and public mobile services are also protected through a dedicated channel and a registration process for special events.

Following is a brief overview of the regulatory framework.

A. General Regulations

- Usage of TVWS channels will be licence-exempt and not subject to spectrum usage fees, but this does not apply if public telecommunications services are offered. The use of spectrum will be on a non-exclusive and unprotected basis, and subjected to technical parameter requirements set by the IDA, such as transmission power levels, OOB (Out of Band) emission limits.
- From now until 2020, WSDs can use up to 189 MHz of spectrum when digital TV broadcasting is steadily replaced analogue TV broadcasting. This spectrum consists of 3 VHF channels and 21 UHF channels. After 2020, WSDs can use 183 MHz when some of the frequencies will be used for other services.
- Geo-location database service providers will be in charge of spectrum sensing. WSDs may also use their own spectrum sensing technologies where they do not cause interference but WSDs still need to send query to the geo-location database for available TVWS channels every 6 hours.

B. Device Regulations:

- All TVWS equipment need to comply with the general equipment registration (GER) requirements to avoid potential interference. There are 3 modes of WSD devices: *Fixed* WSDs with 4W EIRP maximum transmission power; *Mode 1* and *Mode 2* WSDs with 100mW EIRP maximum transmission power. Mode 1 devices can only operate in conjunction with Fixed or Mode 2 devices. Only Fixed and Mode 2 WSDs are required to query geo-location databases for available TVWS channels and maximum power level before operation.
- Required mobile WSDs need to query geo-location database every time before starting the TVWS communication, or when they move more than 100 metres away from their original location during the communication.
- To further protect the TV analogue broadcasting, IDA only allows low-power WSDs (Mode 1 and 2) to use adjacent channels of analogue broadcasting transmissions. In addition, WSDs are not allowed to operate on two adjacent channels of digital broadcast services. Therefore, Channels 25 and 26 will not be permitted for secondary usage by WSDs.
- Each WSD will have a unique device identifier (UDI), either ETSI/FCC authorised or regulator defined format. Geo-location database providers have to accept different UDI formats. Every WSD (portable/personal) must have antenna permanently attached. Antenna height of WSDs will be used by the geo-location database in calculation of available TVWS channels.
- Co-existence of WSDs will be left for the industry to decide. However WSD operators are expected to implement collision avoidance protocols to minimize the chances of interference arising when WSDs are in close proximity of each other.
- To protect the licence-exempt wireless microphones and not to cause excessive reduction in the number of channels available for WSDs, the two designated safe Channel 25 (502 – 510 MHz) and Channel 47 (678 – 686 MHz) will be set aside for licence-exempt wireless microphones.

C. TVWS DB - WSDB Regulations

- Geo-location database provider should use the Hata-Urban propagation model for interference computations.
- Geo-location databases can offer more services such as advance queries at multiple locations as an competitive advantage that could benefit WSD's users. These advanced services, however, are allowed for mode 2 WSDs only.
- Fixed and Mode 2 WSDs are required to obtain the position with the accuracy of at least ±50 m. They can use different kind of location technologies (GPS, etc).

D. High Priority Channels regulation

- Singapore is the first and only country until now which has the regulation for the high priority channels (HPCs). The IDA will set aside two HPCs which can be offered as a premium service by geo-location database providers to WSD users who require a higher-level of reliability and real-time transmission basis. The number of HPCs may be increased or decreased by the IDA according to the market demand.

IDA's regulations open the path to not only the commercialization of TVWS services in Singapore but also the new services in overseas markets. With this open, proactive but careful approach in TVWS regulation, Singapore has managed to groom its local TVWS market and attracted international attentions.

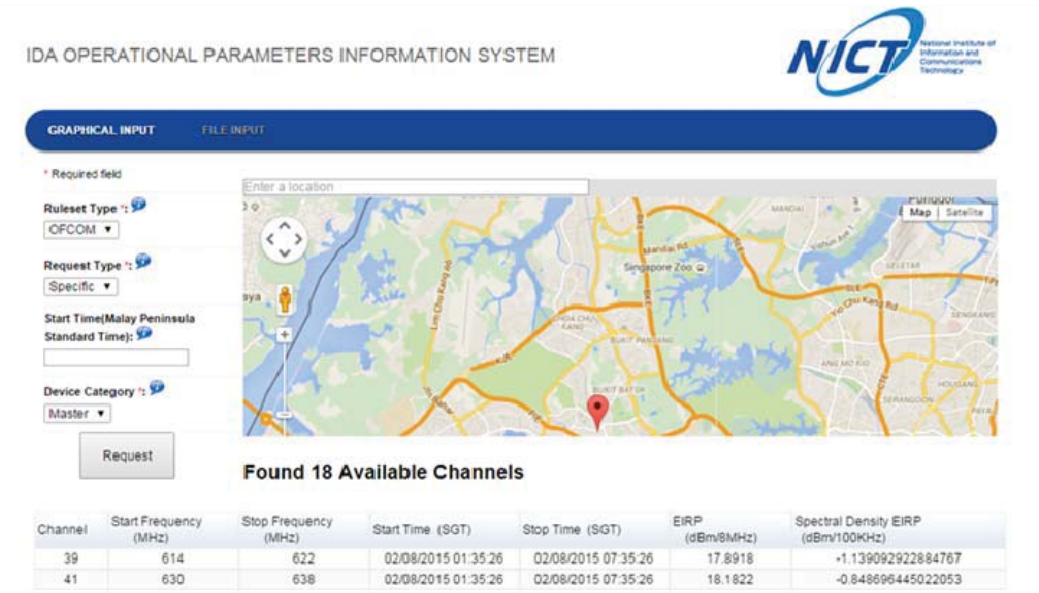

Fig. 1: The trial WSDB web page interface

III. IEEE 802.11af EXPERIMENT SETUP

IEEE 802.11af extends the IEEE 802.11 standard to allow IEEE 802.11af-based devices to operate in TVWS spectrum. It provides a framework that allows IEEE 802.11af-based WSDs to operate around the world without causing interference to primary users by using the geo-location-based white-space database (WSDB) and registered location secure server (RLSS). The WSDB will allow an IEEE 802.11af WSD to operate according to regulation requirement at its current location. The RLSS acts as a local database to distribute operation parameters to Access Points (APs) and Stations (STAs) under its control.

The IEEE 802.11af prototyped hardware used in Singapore experiment supports a high transmission power of up to +30 dBm in conformance with IDA regulations [6]. This IEEE 802.11af-based system consists of a WSD station (STA), an access point (AP), a TVWS database (WSDB) and a registered location secure server (RLSS), as shown in Fig. 2. The WSDB used in the experiment is developed by NICT and granted trial license by the IDA in Jan, 2015.

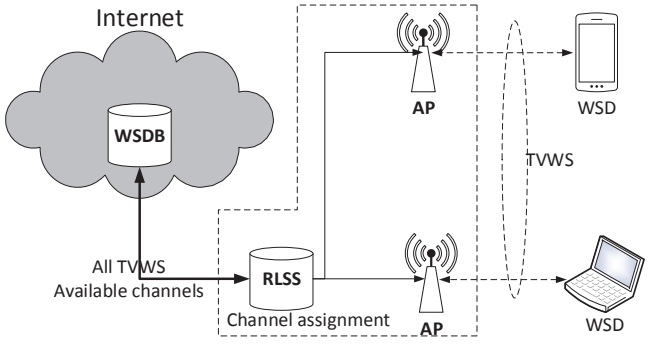

Fig. 2: IEEE 802.11af system architecture overview

A. TVWS Database WSDB

To protect the primary users, Singapore regulation requires that all WSDs need to query the WSDB for available channels and permitted transmission powers before operation. A WSDB for Singapore has been designed and developed based on the IDA regulation described in Section II. This WSDB has been granted with a trial license by the IDA in Jan, 2015. The graphical interface of the WSDB is shown in Fig. 1 On the left-hand side, users can choose different WSD types (OFCOM/FCC - fixed or mobile), and set the parameters such as antenna height. On the right-hand side is the Google map of Singapore where users can select location of the WSD and submit query to the WSDB. All the available channels in the selected location with permitted EIRP power level will be returned by the WSDB.

In addition, the RLSS is also used to avoid inter-system interference in the TVWS operating channels in the case that multiple IEEE 802.11af APs are operated in the same area. The RLSS will assign different channel to each AP from all the available channels provided by the WSDB.

B. STA and AP IEEE 802.11af system used in Singapore

The IEEE 802.11af prototyped hardware used in Singapore experiment supports a high transmission power of up to +30 dBm in conformance with IDA regulations [6]. Parameters of the prototyped devices used in Singapore experiment are shown in Table 1.

TABLE I. PHY PARAMETER

Air interface	OFDM
Operating frequency	Channel 46 (674MHz)
Operating channel bandwidth	8MHz
Modulation	MCS0 (BPSK)
Channel coding	Block convolution coding

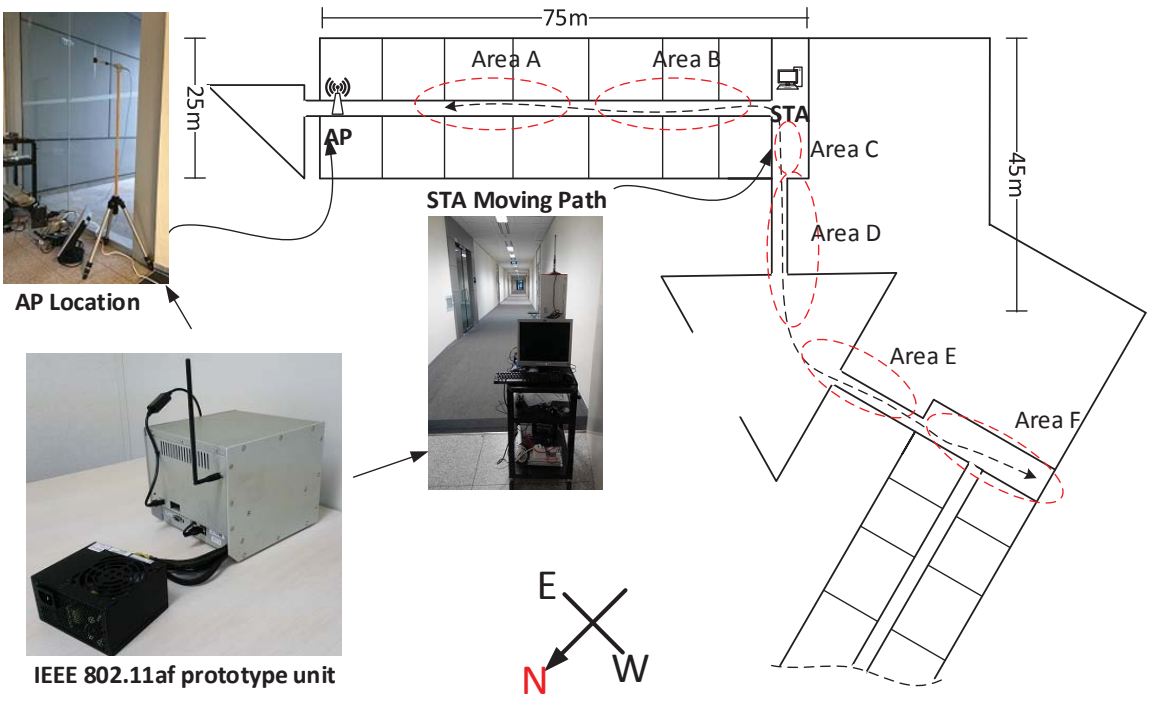

Fig.3: The indoor trial setup

The AP that was connected to the Internet was set up and fixed at the end of east wing corridor of TeleTech Park building as shown in Fig. 3.

The STA was put on the trolley with a power source that consists of a DC 12 V battery, a DC/AC inverter, and moving from Area A to Area F with a 150m distance to measure the received signal strength indicator (RSSI) and throughput around the experiment environment. The whip antenna with height of 1.5 m was connected to the STA using co-axial cable and a 10dB attenuator. The AP used dipole antenna with a 2.2 dBi antenna gain at a height of 1.7 m. TVWS channel 46 (670 −678MHz) was used for the experiment.

IEEE 802.11af TVWS_MODE_0 with MCS 0 (Max throughput of about 1.45 Mbit/s) was applied as the communication mode. Average output power was set to 20 dBm for both STA and AP.

C. *Experiment setup*

The experiment was done in the first floor of TeleTech Park Building in Singapore Science Park II. TeleTech Park Building is in the V shape with west and east wing as shown in Fig. 3. The main dimensions are summarized in Table 2. The AP was fixed at the end of east wing corridor.

TABLE II. EXPERIMENT ENVIRONMENT

West/East wing's corridor	Length: 75m, width: 2.1m
Ceiling height	2.7m
STA Moving Path	150m
AP Antenna height	1.7m
STA Antenna height	1.5m

The STA was moving around along to the 150 m moving path from east wing to west wing as shown in Fig. 3. AP was connected to the Internet for WSDB enquiry.

When the STA and AP are turned on, the RF hardware parts will do the calibration to clear the interference. Three mode of calibration was used and the throughput measurement was taken along the moving path:

- **With 50 ohm mode**: STA and AP use 50 ohm during calibration at start-up to clear the interference.
- **With Band Pass Filter (BPF) mode**: STA and AP use the BPF during calibration at start-up to suppress the interference outside the using channel.
- **Normal mode**: STA and AP use neither 50 ohm nor BPF during calibration at start-up.

IV. INDOOR EXPERIMENT RESULTS

The UDP throughput is measured by the popular iperf tool. The RSSI was measured and stored in a log file with timestamp. Throughput and RSSI were then extracted and matched together based on the timestamp. The measurement result is shown in Fig. 4.

1) RSSI: Received signal power of the STA was measured as RSSI, and is generally proportional to the distance between the AP and the STA in both cases of Line-of-Sight (LoS) and Non-Line-of-Sight (NLoS) situation along the STA 150 m moving path.

When STA moved from Area A to Area F, the RSSI level reduced from −30 dBm (Area A) to −50 dBm (Area B), −60 dBm (Area C), −65 dBm (Area D), −75 dBm (Area E) and −85 dBm (Area F). The connection was lost when STA moved

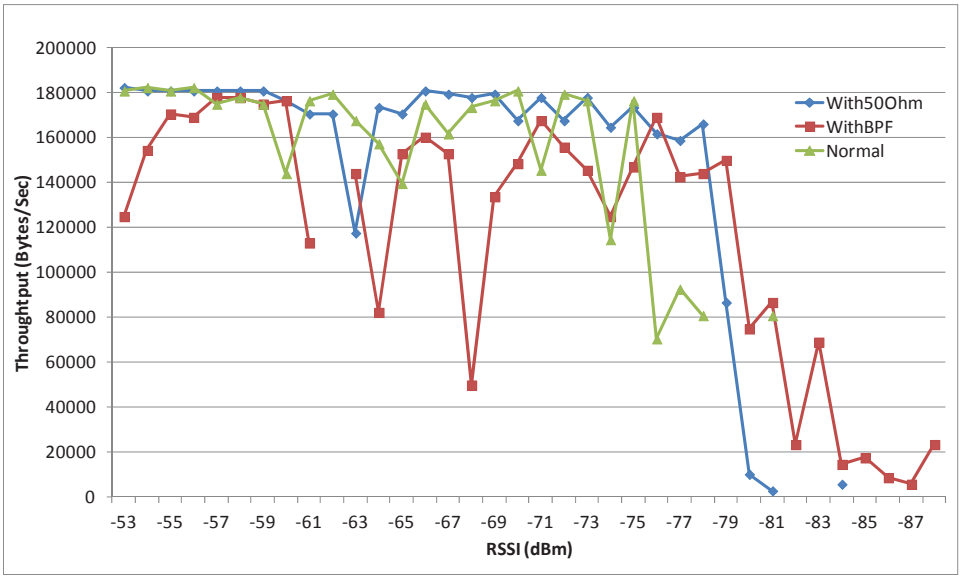

Fig. 4: Throughput vs RSSI

from LoS (Area A, B) to NLoS at the beginning of Area C. However, because the shadowing effect in the corridor, the connection was re-established at the Area D. Deflection effect was the main factor for this. In this area, the throughput was still quite high.

When STA moved to area E, the connection was lost again, because the penetration loss was higher in this area. The connection was re-established at Area F, even though the received signal power was lower than −80 dBm due to the shadowing effect. However, the throughput was severely low in this location.

2) Throughput: The measured throughput basically depends on the RSSI level. However the throughput deteriorated at Area C, Area E. The throughput was improved slightly, when 50 ohm was used during the calibration at startup as shown in Fig. 4. In addition, using BPF did not improve any throughput at all. These results indicates that the deterioration of the throughput is not mainly caused by the interference but the multi-path fading.

Based on the throughput measurement both in LoS Area A, B and NLoS Area D, F, it can be observed that in typical indoor environment, an IEEE 802.11 af AP with an output power of +20 dBm can cover a sufficiently large area (in this case 150 m) compared with normal 802.11 [10], however the prototyped WSDs need some more improvements in NLoS areas for full commercial deployment.

V. Conclusion

TVWS has been promoted as an efficient way to address the demand for spectrum resource shortage all over the world and regulators are proactively rolling out regulation for operations in TVWS spectrum. Singapore TVWS regulations has been carefully rolled out with small market share of Singapore in mind as well as the specific feature only Singapore has such as HPC channels.

Under Singapore regulation, the first IEEE 802.11af experiment had been successfully carried out in Singapore Science Park II. The IEEE 802.11af prototype system experiment results demonstrate the promising future TVWS could achieve for various practical applications.

References

[1] Federal Communications Commission, Unlicensed Operation in the TV Broadcast Bands, Third Memorandum Opinion and Order, FCC. 12-36, Apri. 5, 2012.

[2] Ofcom, “Digital Dividend: Cognitive Access, Consultation on Licence-Exempting Cognitive Devices Using Interleaved Spectrum,“ July 2009.

[3] Association of Radio Industries and Businesses, “Transmission System for Area Broadcasting,” ARIB STD-B55 Version 1.2, Jul. 2013.

[4] IDA, “Regulatory Framework for TVWS Operation in the VHF/UHF Band", June 2014.

[5] IEEE Comp. Society, “IEEE Std 802.11afTM2013”, Dec. 2013.

[6] Takeshi Matsumura, Keiichi Mizutani, Homare Murakami, Kentaro Ishizu, Hiroshi Harada and Fumihide Kojima, “Long-haul Communication Trial in London TV White-space with IEEE 802.11af-based High Power Prototype” , Proceeding of WPMC2015, India, 2015.

[7] IDA, “Proposed Regulatory Framework for TV White Space Operation in the VHF/UHF Bands", June 2013.

[8] Federal Communications Commission, “Unlicensed Operation in the TV Broadcast Bands, Second Report and Order and Memorandum Opinion and Order,“ FCC. 08-260, Nov. 2008.

[9] Federal Communications Commission, Unlicensed Operation in the TV Broadcast Bands, Second Memorandum Opinion and Order, FCC. 10-174, Sept. 23, 2010.

[10] Cassio Bento Andrade, Roger Pierre Fabris Hoefel, “IEEE 802.11 WLANs: A comparison on indoor coverage models”, Proceeding of Electrical and Computer Engineering (CCECE) 2010, pp: 1-6, 2010.

THE 18TH INTERNATIONAL SYMPOSIUM ON WIRELESS PERSONAL MULTIMEDIA COMMUNICATIONS
(WPMC-2015)
December 13-16, 2015, Hyderabad, India

Blind Channel Length Estimation for OFDM Systems using Cumulant Features

K. Ajay Babu, Udit Satija, Barathram. Ramkumar, M. Sabarimalai Manikandan
School of Electrical Sciences
IIT Bhubaneswar, India
{abk10, us11, barathram, msm}@iitbbs.ac.in

***Abstract*—Orthogonal frequency division multiplexing (OFDM) systems are now a part of all major wireless standards, because of its potential to offer high data rate. Cyclic prefix (CP) in OFDM system converts a multipath channel to a flat fading channel, thus simplifies the design of equalizer. However, there is a lot of ambiguity in choosing the length of CP. In this paper, we propose a new method for calculation of length of CP using cumulant features. The merits of proposed method are verified by computer simulation.**

***Keywords*—Orthogonal frequency division multiplexing (OFDM), Cyclic prefix (CP), Blind channel length estimation.**

I. Introduction

Increasing in the number of wireless applications and users demands for reliable, high data rate communication. High data rate can be achieved by effective utilization of the spectrum. Over the past decade, dynamic spectrum access (DSA) has been seen as a potential solution for utilizing the spectrum effectively. The research efforts in DSA are further fueled by the advent of cognitive radio (CR) [1], due to its potential platform for implementing DSA. High data rates can also be achieved by employing multiple input multiple output (MIMO) and orthogonal frequency division multiplexing (OFDM) based systems. CR combined with MIMO and OFDM has the potential to achieve reliability and high data rate. In fact, utilization of CR along with MIMO and OFDM is included in the 4G standards.

OFDM provides high data rate by exploiting the orthogonality in the frequency domain. One of the key issue in OFDM is to choose the length of cyclic prefix (CP). CP enables OFDM to convert multipath channel to flat fading channel and hence simplifies the design of equalizer. In general, the length of CP is decided greater than delay spread of the channel. For practical implementation, generally we consider CP length as one fourth of the OFDM symbol [2]. The way of choosing the fixed CP length by this traditional method leads to the wastage of transmission bandwidth. As CP does not carry any extra information, it is required to optimize the length of CP without disturbing the original data. The length of CP should be longer than the length of the channel impulse response (CIR). However, the length of the CIR is not known at the transmitter. Hence, it has to be estimated at the receiver end and then conveyed to the transmitter through some control channel (Refer Fig. 1).

Some of the existed work on calculation of channel length and CP length for OFDM system is summarized as follows: In [3], Jong Bu Lim *et al.* proposed iterative CP reconstruction procedure based on residual inter symbol interference cancellation (RISIC). In [4], D. Salvatore *et al.* introduced bit loading algorithms for an adaptive CP length to enhance the performance of system. In [5], Bin Sheng *et al.* presented blind algorithm to estimate the channel length based on minimum description length (MDL) for OFDM system.

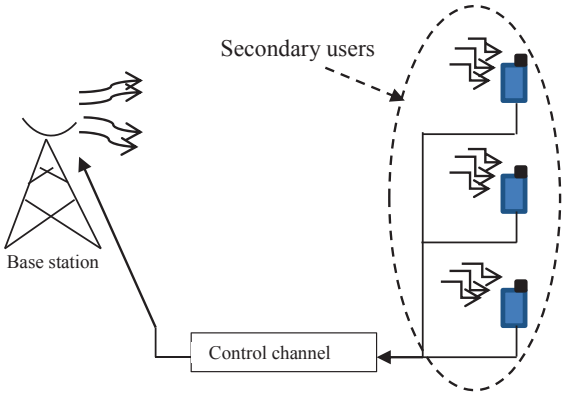

Fig. 1: Proposed system representation for OFDM transmission

In this paper, we propose a novel method to choose the CP length. The proposed approach is blind, that is no pilot or training sequence is required and hence further saves bandwidth. The proposed method is well suited for a DSA setup as illustrated in Fig. 1. In Fig. 1, the secondary users estimate the ideal CP length, and communicate it to the base station via control channel. The base station then adjusts the CP length for the future transmission. Therefore, by estimating the channel length, CP length can be adjusted. Moreover, the bandwidth can be utilized effectively by avoiding the pilot sequence transmission. In the proposed method, we first estimate the channel length and then use this information to choose the CP length. For estimating the channel length, we used the algorithm presented in our previous published work [6]. The method is based on cumulant features. Cumulant features have been widely used in the field of blind signal processing [7]–[11]. In this paper, we exploit some unique properties of cumulant features that make it suitable for channel length estimation.

The rest of this paper is structured as follows: Section II presents the problem statement. Section III introduces mathematical background on cumulant features whereas Section

IV describes the proposed method. Section V presents the simulation results followed by conclusion in Section VI.

II. Problem statement

In this paper, we consider an OFDM system with N subcarriers. The m^{th} OFDM block or symbol is denoted as $\bar{X}_m = \{X_m(0), X_m(1), X_m(2), \ldots X_m(N-1)\}$, where $X_m(k)$ is a complex valued alphabet drawn from a QAM constellation. The inverse discrete Fourier transform (IDFT) $\mathscr{F}^{-1}$ of the m^{th} block is denoted as $\bar{x}_m = \{x_m(0), x_m(1), x_m(2), \ldots x_m(N-1)\}$, i.e.,

$$\bar{x}_m = \mathscr{F}^{-1}\left\{\bar{X}_m\right\} \tag{1}$$

The transmitted symbol is subjected to multi-path fading. The multi-path channel can be modeled as a finite impulse response (FIR) filter

$$h(z^{-1}) = h(0) + h(1)z^{-1} + \ldots + h(M)z^{-M} \tag{2}$$

where M is the length of the multipath channel and $h(i)($ for $i = 0, 1 \ldots M)$ is the multi-path gains vector. CP is added before transmitting the time domain block $\bar{x}_m$. As mentioned earlier, CP is added to avoid intersymbol interference (ISI). Let, the length of CP is denoted as P, and hence the total length of the m^{th} block is $(N+P)$. The m^{th} received OFDM block after removing CP is denoted as $\bar{y}_m = \{y_m(0), y_m(1), y_m(2), \ldots, y_m(N-1)\}$. The corresponding frequency domain block is given by $\bar{Y}_m = \{Y_m(0), Y_m(1), Y_m(2), \ldots Y_m(N-1)\}$ where

$$\bar{Y}_m = \mathscr{F}\left\{\bar{y}_m\right\}, \tag{3}$$

where $\mathscr{F}$ denotes the DFT.

The relationship between the transmitted and received symbols of m^{th} block is given by

$$Y_m(K) = H(K)X_m(K), \quad K = 0, 1, \ldots N-1 \tag{4}$$

where $H(K) = H(0), H(1), \ldots, H(N-1)$ is the N point DFT of the channel impulse response in (3).

Selection of the length of CP is a challenging problem. The CP length must be greater than the length of the channel impulse response (let M) in order to avoid ISI. However, length of the channel impulse response is not known. In this paper, we propose a novel blind algorithm to estimate the CP length P at the receiver. The block diagram of the proposed method is shown in Fig. 2. In the proposed algorithm, we first estimate the channel length and then use this information to choose the CP length. The algorithm for estimating the channel length is based on exploiting the properties of n^{th} order cumulant features.

III. Background Theory on Cumulant Features

In this paper, n^{th} order cumulants features are used. For a complex random process $v(n)$, the n^{th} order moment is defined as [7], [8], [11], [12]

$$R_{v(n,m)}(\tau) = E[\prod_{j=1}^{n} v^{*_j}(\tau_j)] \tag{5}$$

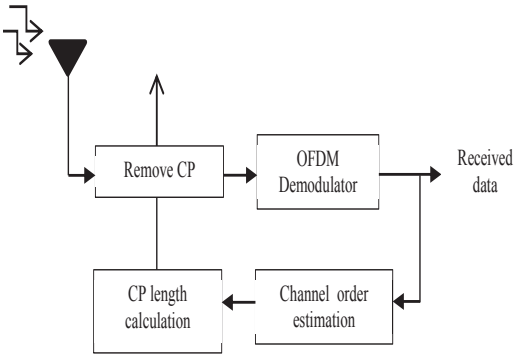

Fig. 2: Block diagram of proposed system at the receiver

where n is the order, m is the number of conjugate factors and $\tau = [\tau_1, \tau_2, \ldots, \tau_n]$ is the delay vector. The n^{th} order cumulant function is defined as [7], [8], [11], [12].

$$C_{v(n,m)}(\tau) = \sum_{pn} F(p) \prod_{j=1}^{p} R_{v(n_j,m_j)}(\tau) \tag{6}$$

where the sum is over distinct partition of indexed set $1, 2, \ldots, n$ and $F(p) = (-1)^{p-1}(p-1)!$. The normalized n^{th} order cumulant values are defined as

$$\tilde{C}_{v(n,m)}(\tau) = \frac{|C_{v(n,m)}(\tau)|}{[C^2_{v(2,1)}(0)]} \quad \text{for} \quad n = 4, 6 \tag{7}$$

The rationale behind choosing cumulant features, is the following two properties of cumulants:
Additive property: Let $x(k)$ and $y(k)$ be two independent random processes. If $z(k) = x(k) + y(k)$ then the n^{th} order cumulant value of $z(k)$ is the sum of those of $x(k)$ and $y(k)$. That is,

$$C_{z(n,m)}(\tau) = C_{x(n,m)}(\tau) + C_{y(n,m)}(\tau) \tag{8}$$

Scaling property: Let $x = ay$. Then the n^{th} order cumulant value of $x(k)$ is $|a|^n$ times the cumulant value of y(k).

IV. Proposed Method

Before illustrating the proposed approach, we first study the effect of multipath channel over n^{th} order cumulant values of the received OFDM symbols. The relationship between the transmitted and received symbols of the m^{th} block is given by $Y_m(K) = H(K)X_m(K) \quad \text{for} \quad k = 0, 1, \ldots, N-1$ where

$$H(K) = \sum_{i=0}^{M-1} h(i)e^{-}\frac{(i2\Pi k)}{N} \tag{9}$$

Using the scaling property of the cumulant features, it can be easily shown that

$$\tilde{C}_{Y_m(K)(n,m)}(\tau, M) = \beta(M)\tilde{C}_{X_m(K)(n,m)} \tag{10}$$

where $\tilde{C}_{Y_m(K)(n,m)}$ is the normalized cumulant value of k^{th} OFDM symbol in m^{th} block and

$$\beta(M) = \frac{\sum_{K=0}^{M-1} |H(K)|^n}{(\sum_{K=0}^{M-1} |H(K)|^2)^{n/2}} \quad (11)$$

where M is the order or length of channel. By observing (9) and (11), and by using the fact that $|e^{-\frac{(i2\Pi k)}{N}}| = 1$, it can be easily shown that $\beta(M) < 1$. Hence, it is clear that the length of channel is inversely proportional to the magnitude of cumulant values of the received OFDM symbols. The magnitude of the cumulant values of the received OFDM symbols shrinks by increasing the length of channel. Also, the magnitude of shrinkage depends on the value of M, i.e.,

$$\beta(M) < \beta(M') \quad \text{for} \quad M > M' \quad (12)$$

and hence

$$\tilde{C}_{Y_m(K)(n,m)}(\tau, M) < \tilde{C}_{Y_m(K)(n,m)}(\tau, M') \quad \text{for} \quad M > M' \quad (13)$$

The pseudocode of the proposed algorithm is shown as below:

Algorithm 1 Pseudocode of the proposed algorithm

Input: Received data $Y_m(K)$ with N subcarriers
Estimate the received cumulant $\tilde{C}_{Y_m(K)}$ values of the received data using the method in [7], [8], [11], [12]
for *i*=1,2, ...*M* **do**
  if $\frac{\tilde{C}_{Y_m(K)}(i+1)+\tilde{C}_{Y_m(K)}(i)}{2} < \tilde{C}_{Y_m(K)} < \frac{\tilde{C}_{Y_m(K)}(i-1)+\tilde{C}_{Y_m(K)}(i)}{2}$ **then**
    if *M*=*M'* **then**
      Terminate loop
    endif
  else
    i=*i*+1;
  endif
endfor
EndProcedure

The estimated channel length M', is used to calculate the ideal CP length. Typically, CP length P is chosen such that $P \geq M$. In this work, we choose CP length P to be

$$P = k \times M' \quad (14)$$

where k is an integer greater than two (here, k is selected as the double that of the estimated channel length). The value of P is chosen in such a way that it is at least double of the estimated channel length.

V. Simulation Results

MATLAB simulations are performed to test the proposed algorithm and the results are summarized. In this case, probability of correctness (P_c) is taken as performance metric and can be defined as P_c= prob(detection says M' is true $\mid$ M is M'). In other words, P_c = $P(M'/M')$ is the probability that the channel length is estimated as M', given the channel length is M'. Cumulant values are calculated at the output of the OFDM demodulator. For the simulations, 4^{th} and 6^{th} order cumulants $|C_{Y_m(4,0)}|$ and $|C_{Y_m(6,0)}|$ features are considered, as they are robust to phase rotation. The following experiments are performed with BPSK constellation.

Experiment-1: In this experiment, we considered fourth order cumulant features. Channel order considered as 1,2. That is the proposed algorithm has to estimate whether the tap of the channel is 1 or 2. Here, we have used $N = 1024$ bits per OFDM symbol to estimate the cumulants. The results are summarized in Fig. 3. In Fig. 3, $M = 1$ denotes the probability of correctly estimating the 1 tap channel and $M = 2$ for 2 tap channel. From Fig. 3, it can be observed that the probability of correctly estimating the channel (P_c) is more than 75% even at negative SNR (in dB scale).

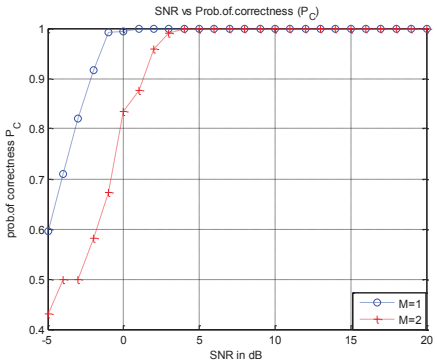

Fig. 3: SNR vs P_c with $N = 1024$

Experiment-2: This experiment is similar to previous one, except that four possible conditions are considered. That is the algorithm need to identify whether the channel is a 1 tap, 2 taps, 3 taps or 4 taps. The results are summarized in Fig. 4. In Fig. 4, $M = i$ (for $i = 1, 2, 3, 4$), has the same meaning as previous experiment. It can be seen that the algorithm performs well in estimating 1, 2 and 3 tap channel. However, in the case of 4 tap channel the performance of the method is poor. This is because, the shrinkage in the cumulant values is high and more number of bits or samples are required to estimate it. We repeat the experiment with more number of samples ($N = 4096$) and the results are summarized in Fig. 5. From the Fig. 5, it can be seen that the performance of estimating 4 tap channel is improved (70% at 0 dB) when N is increased.

Experiment-3: In this experiment, we consider the same case as experiment 1, here we considered sixth order cumulants instead of fourth order and channel length is indicated with L. From Fig. 6, it can be seen that the robustness of correct detection. The reason is sixth order cumulants are more robust than fourth order cumulants.

From the experiments, it can be seen that our proposed algorithm estimates the channel length even at low SNR, compared to MDL method [5], whose performance degrades at low SNR. In the proposed method, once the channel length is estimated the CP length is chosen to be twice the channel length. This results in a significant reduction in bandwidth as illustrated in Table I. Here, we consider $N = 1024$ subcarriers per OFDM symbol. In the traditional method, CP length is

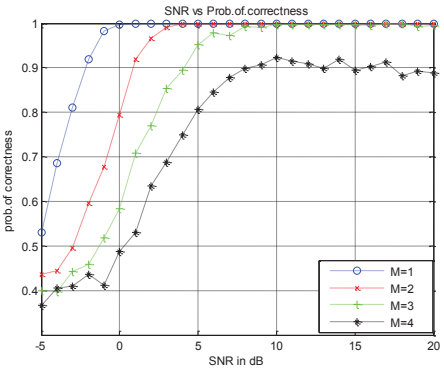

Fig. 4: SNR vs P_c with $N = 1024$

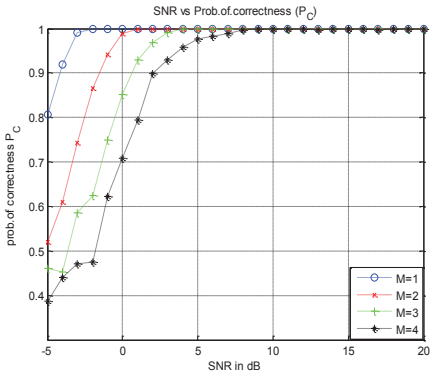

Fig. 5: SNR vs P_c with $N = 4096$

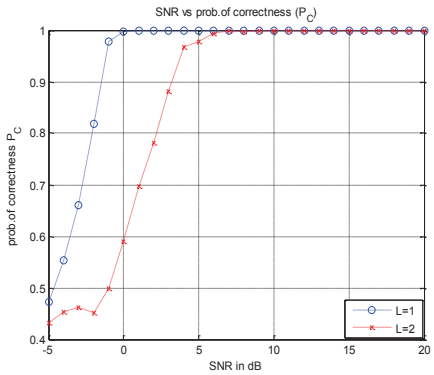

Fig. 6: SNR vs P_c by sixth order cumulants with $N = 1024$

TABLE I: CP Length Comparison

Channel order	CP length by traditional method [2] (bits per OFDM symbol)	CP length by proposed method (bits per OFDM symbol)
1	256	2
2	256	4
3	256	6
4	256	8

chosen as one fourth of the OFDM symbol length, i.e., 256 bits per OFDM symbol. However, in our proposed method CP length is chosen according to channel length.

VI. CONCLUSION

In this paper, a new method is introduced for calculating the ideal CP length in OFDM system. The significant reduction in CP length leads to bandwidth efficient OFDM system. As a part of work a novel algorithm for estimating the channel length has been proposed. The proposed algorithm is blind and does not require any training sequence to estimate channel length. Using simulation results, it was shown that the proposed algorithm outperforms other algorithms even at low SNR.

REFERENCES

[1] S Haykin, "Cognitive Radio: Brain-empowered wireless communications," *IEEE J. Select . Areas Commun.*, vol. 23, pp. 201-220, 2005.

[2] A. Goldsmith, "Wireless Communications," *Cambridge University press*, 2005.

[3] Jong-Bu Lim, Eung-Sun Kim, Cheol-Jin Park, Hui-Chul Won, Ki-Ho Kim, and Gi Hong Im, "Bandwidth-Efficient OFDM transmission with iterative cyclic prefix reconstruction," *IEEE J. Commun. and Net.*, vol.10, pp. 239-252, Sep. 2008.

[4] D. Salvatore, A. Alessandro, M. Tonello, and L. Lampe , "Bit loading algorithms for OFDM with adaptive cyclic prefix length in PLC channels," *Int. Sym. on Power Line Communications and Its Applications (ISPLC)*, pp. 177-181, 2009.

[5] B. Sheng, X. Wang, X. You and L. Chen, "Blind estimation of channel Length for OFDM systems," *Int. Conf. on Wireless Communications, Networking and Mobile Computing*, pp. 2158-2160, 2009.

[6] A. Babu K., and B. Ramkumar. "Blind algorithm for channel length estimation using cumulant features," *Int. Conf. on Signal and Image Processing (ICSIP)*, pp. 151-154, 2014.

[7] O. A. Dobre, A. Abdi, Y. Bar-Ness, and W. Su, "Survey of automatic modulation classification techniques: classical approaches and new trends," *IET Commun.*, vol. 1, pp. 137-156, Apr. 2007.

[8] C. M. Spooner, W. A. Brown, and G. K. Yeung, "Automatic radio frequency environment analysis," *Int. Conf. on Signals, Systems and Computers*, pp. 1181-1186, 2000.

[9] Y. J. Park, B. B. Ihm, and D. J. Park, "Reduction of errors in blind identification of FIR system under order over estimation," *Int. Sym. on Circuits and Systems*, vol. 3, 1999.

[10] H. Jiang, Shu-Xun Wang, Hai-Jun Lu, "An effective direction algorithm in multipath environment based on fourth order cyclic cumulants," *Int. Workshop on Signal Processing Advances in Wireless Communications*, pp. 263-267, 2004.

[11] A. Swami and B. M. Sadler, "Hierarchial digital modulation classification using cumulants," *IEEE Trans. Commun.*, vol. 48, pp. 416-429, Mar. 2000.

[12] C. M. Spooner, "Classification of cochannel communication signals using cyclic cumulants," *Int. Conf. on Signals, Systems and Computers*, pp. 531-536, 1995.

THE 18TH INTERNATIONAL SYMPOSIUM ON WIRELESS PERSONAL MULTIMEDIA COMMUNICATIONS
(WPMC-2015)
December 13-16, 2015, Hyderabad, India

Privacy–Preserving Friend Matching Protocol approach for Pre-match in Social Networks

Shubhangi S.Ople
M.E Student, Dept of Comp Engineering, SKNCOE,
Savitribai Phule Pune University
Pune
shubh.ople@gmail.com

Aaradhana A. Deshmukh, Albena Mihovska,
Ramjee Prasad
Department of Electronics Systems
Aalborg University,Aalborg, Denmark
{aad,albena,Prasad}.es.aau.dk

***Abstract* -- Social services make the most use of the user profile matching to help the users to discover friends with similar social attributes (e.g. interests, location, age). However, there are many privacy concerns that prevent to enable this functionality. Privacy preserving encryption is not suitable for use in social networks due to its data sharing problems and information leakage. In this paper, we propose a novel framework for privacy–preserving profile matching. We implement both the client and server portion of the secure match and evaluate its performance network dataset. The results show that a secure match can achieve at least one order of accuracy and better computational performance than the techniques that use homomorphic encryption.It can handle and tackle new characteristics and an environment for a particular application in a mobile social network.**

Keywords: Cloud Computing, Privacy Preserving, Friend Discovery, CRM.

I.INTRODUCTION

Mobile services have become a popular method for users to build their social relationship and share interests. The most popular mobile social networks services available allow the user to share the location, information, interests and even chat with friends. During the profile matching process, the 'users' social profiles are compared in a server owned by the social network application to find other similar social users with the same attributes (e.g. interest, location, age) in the social network. An effective profile matching process would benefit the user and the social network services. The user would enjoy more experience, while the social network providers see increased users activities in their social networks. Even through the simple public interest attributes, considered harmless by users, such as an 'interest' (or 'like'), users can reveal some basic 'private' social attributes (e.g. age, condition, interests) [1]. In social services, the user can mostly face the problem of unwanted advertisement [2] or easily crack a weak user password [3]. Hence, the privacy concerns must be addressed when developing profile matching techniques for mobile social networks [4], [5]. In social networking, through the antivirus we provide security to the network usage but to preserve the privacy on a mobile network, a more power efficient profile matching scheme is needed. To provide the privacy preserving profile matching process or techniques, homomorphic encryption [6], [7] is mostly implemented [8]. In the homomorphic encryption, certain types of computations are allowed on a plaintext and ciphertext. Here, the ciphertext preserves the information of the plaintext. Ciphertext and plaintext are encrypted by the same key. In this paper, we propose a secure match for a privacy preserving profile matching techniques for mobile network services. We identify the key sharing problems regarding the information leakage and propose verification techniques for the user to verify the profile matching result without obtaining any extra information about the other user's profile attribute. 'Friend Discovery' describes the Customer Relationship Management (CRM) database in an organization with social networks. All 'Friend Discovery' services are connected to the CRM [1] [5]. 'Friend Discovery' represents the interaction because it helps the user to find friends who also care about a particular organization and its product and services [2]. When we are developing an application according to "Friend Discovery" we have to consider/several rules, as follows:

A. Do not share any default setting.

To reduce the probability of mistakes by the user, the "do not share" rule is used to protect all information about the customer's interactions with the company.

B. Trust some selective friends more than strangers.

When sharing some information or updates on Facebook or tweet on Tweeter, some users do not wish to have visibility to the whole friend network. The second rule states that the customers need to be able to control, which friends in their social graph get access to which type of information.

C. My Relationship data is my relationship own data.

This rule enables that the 'Friends Discovery' to temporarily store the user data in the CRM database without compromising any condition in it.

D. Friend Discovery follows different formats.

Popular mobile social applications are Facebook, Twitter, Google, and LinkedIn. A few common chat-only applications are

GTalk, Whatsapp, Wechat, Hike and many more [3], [6]. Communication is mainly done between the client and the server. A different point mechanism is used for the client-server communication (e.g. client-server, centralized, decentralized, distributed, and multi-tier). The "Friend Discovery" concept has been created not only to find a friend, exchange profile, select, add and chat, but can be used in various areas such as social networking sites, and help call centers, such as a healthcare center, where secure information will get communicated.

In this paper we propose a blind transformation algorithm to protect the personal information and user privacy. The attackers of mobile social networks can directly associate the personal profiles with real persons nearby and then launch more advanced attacks. Existing research shows that the loss of privacy can expose the users to unwanted advertisement and spams/scams, cause social reputation or economic damage, and make the users victims of blackmail or even physical violence [6].

II. Related Work

The existing mobile social network systems pay little heed to the security and privacy concerns associated with revealing one's personal social networking preferences and friendship information to the ubiquitous computing environment.

[4] explored the concept of secure localization, authentication and building (SLAB) scheme for the wireless network. SLAB provides both security guarantee and performance in terms of system compromise receiving capability, and workload of the receiving broker (RB). This friend discovery SLAB scheme has been proposed for service oriented metropolitan area wireless mobile networks [4], [12].

[3] proposed a secure multilayer delay tolerant network (SMART) [3]. SMART provides low cost Internet service, e.g. to open email and send data form a source to a destination address [12].

[1] proposed 'Finding U in Privacy' preserving profile matching to use in mobile social networks. In this environment, 'friend discovery' shows various boundaries and issues. Proximity based user discovery and key establishment are two important issues for the usability of our profile matching protocols, towards designing light weight protocols [1], [12].

[2] explored a secure and privacy preserving opportunistic computing framework for mobile healthcare emergency (SPOC). The system introduced the flourish of mobile healthcare but still faces many challenges including information security and privacy preservation [2], [12].

[5] proposed topic a privacy preserving profile matching for proximity based mobile social networks. Here, a fine grained private matching protocol is used with a wide range of matching metrics at different privacy levels [5]. In this case, the private matching between two users is possible, allowing for comparison of the personal profiles without disclosing them to each other. It supports a variety of private matching metrics at different privacy levels [5], [12].

[6] Proposed a fine-grained privacy preserving friend matching protocol, used to improve the navigation effectiveness of the website, while minimizing two current structures. Further, transformation and personalization approaches are integrated. [6] [12].

III. Proposed System

With the existing mobile social networks, privacy preserving is very sensitive to whether a person is login with their secured ID or not. The 'Friend Matching' technology is unique in the sense that every person has its unique identity on a mobile social networking application. It is different even in the case of identical twins ID. Adding authentication to this will enable additional security.

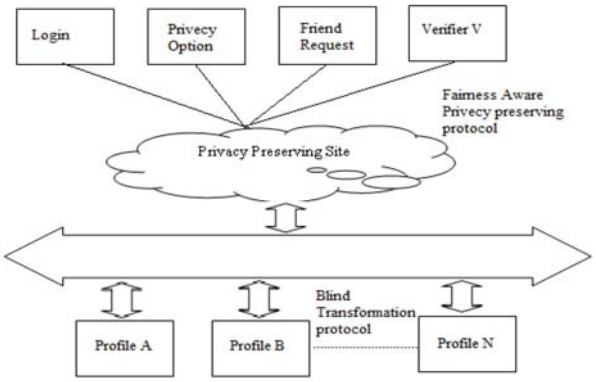

Fig. 1. System Architecture

In Figure 1, Profile A and B are two profiles one is a personal profile, composed of the fields *name*, *date of birth* (DOB), *address* and the other is an interest profile containing the fields *hobbies*, *movies*, *books*. To match the two profile fields, the process will configure the blind transformation and the fairness aware steps will add/delete requests. Here, the module contains the IF (Interest Field). The NIF (Non Interest Fields) are mandatory to fill in both profiles, i.e., the personal and the interest at the time of registration. For comparing, adding and deleting the profile, the system architecture uses the blind transformation and fairness aware protocol. From login to adding a friend in the user's friend list, each process will pass through the privacy options to be verified by the verifier *V*. Here only, the friend matching condition would decide on the user's interest profile. The personal profile is restricted to the user only. When the maximum fields (more than 60%) are matched, then the user would be able to view the other users in the finding friend list. The user has the authority to send requests, add or delete a friend. Here, the software/application controlled by file sharing, controls the access to each.

A.Blind And Fair Transformation Algorithm

The algorithm separates the personal profile and the interest profile, encrypts each user's profile with his/her public key by using the Paillier cryptosystem. It performs vector addition and shuffling, and comparison of the blind profiles. Each user's encrypted profile would be prepared for the matching phase and more matching fields to the interest profile will be added if necessary.

The proposed algorithm is based on the Paillier homomorphic Encryption.

The entity's Paillier public and private keys are $< N, g >$ and λ, where $< N, g >$ are public parameters, and λ is used to calculate a multiple of a prime integer. Here, mainly two encryption and decryption steps are used to encrypt and decrypt data, where g is public parameter, c is cipher text, d denotes the derived parameters, r is the string and n is the number of messages.

For the encryption, the cipher text could be given by,

$$E\ (m\ mod\ N, r\ mod\ N) = gm\ , rn\ mod\ N2 \quad (1)$$

E is the encryption applied on the parameters m, r, and all the public parameters combined together.

For the decryption the cipher text can be given by

$$D(c) = L\left[\frac{c\ \lambda\ mod\ N2}{L}(g\ \lambda\ mod\ N2)\right] mod\ N \quad (2)$$

Where D is the decryption.

To access and calculate the encryption key, we use the homomorphic property as below.

Given that $\{m1, m2, r1, r2\} \epsilon\ Zn$, the following homomorphic property can be satisfied:

$$E\ (m1).E\ (m2) = E\ (m1\ +\ m2), \quad (1)$$

Where, the two encryption functions are :

$$M\ \rightarrow\ gm, rn\ mod\ N2,$$

$$M\ \rightarrow\ gm\ +\ rn\ mod\ N2$$

$$D\ (E\ (m1)\ E\ (m2)\ mod\ N2)\ \ =\ km\ mod\ n, \quad (2)$$

In (4), the encrypted messages are decrypted one by one and added through the particular profile record. K is a constant. If:

$$D\ (E\ (m1)\ gm2\ mod\ n2 =\ m1 + m2\ m$$

by using the blind transformation over any cipher text, we have:

$$\forall m\ \in Zn\quad and\quad r \in N$$

$$D\ (E\ (m1)gm2)mod\ n2 =\ m \quad (3)$$

The above equations define the set of all content, which we combine through the messages. In the considered cryptosystem, the homomorphic added elements are $m = m1, m2$. Here, we use the Paillier homomorphic property for the key generation method. It works on plaintext and the ciphertext. It allows for the hash function to access large and different form of data [11], [12]. Figure 2 and Figure 3, show the accuracy and the performance obtainable through the algorithm.

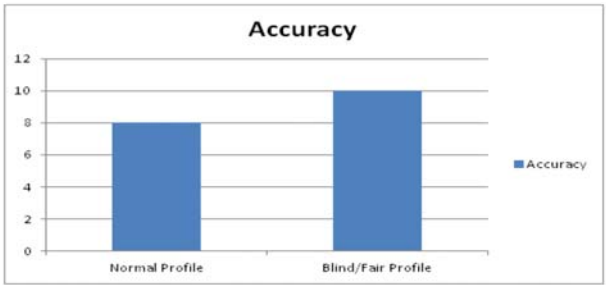

Fig. 2. Accuracy for the model

Figure 2 shows the accuracy for the profile matching for the normal profile and the blind/fairness aware profile. Here, the accuracy defines the accurate profile match. The blind/fairness aware profile is higher than the accuracy obtained than normal profile. The y-axis defines the matching level and the x-axis defines the profile methods.

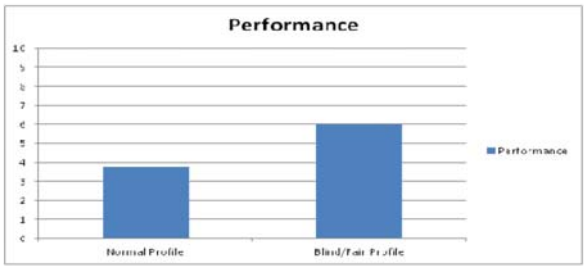

Fig. 3. Performance for the model

Figure 3 shows the performance for the profile searching and matching for a normal profile and for the blind/fair aware profile. Here, the Y-axis shows the number of profiles that were created and that performed well during the execution. The blind/fairness aware profile shows better performance for the searching. The x-axis shows profile created by different method.

Figure 4 and 5 show the time and security needed for a particular input to the model. Here, the x-axis contains the Paillier homomorphic Encrypted input and the random security access (RSA) elements. The y-axis contains the time and the calculated security factors. Figure 4 shows the key generation. It shows how the profile is searching for a particular match for the Paillier homomorphic Encryption model and the RSA. The time (in milliseconds) indicates how many matches have been generated for the combination.

As shown in Figure 4, the x-axis shows the counting of the result fetch in ms, and per process, i.e., for the existing system and for the proposed system. The y-axis shows the counting time in milliseconds per process for both systems. The result shows how the profile searches for a particular match .The Paillier homomorphic Encryption model and the RSA points are used for the cryptosystem for the key encryption and the decryption for Ciphertext and the Plaintext. The results show how many matches would be generated for the combination.

Figure 5 shows how security is provided to the Paillier homomorphic Encryption. The existing system takes more time for each process in the system and the proposed system is faster when combining the two processes. It also provides better security for each process in the system. Even the fetching time for the existing system is longer than for the proposed system.

Result Fetch in Time

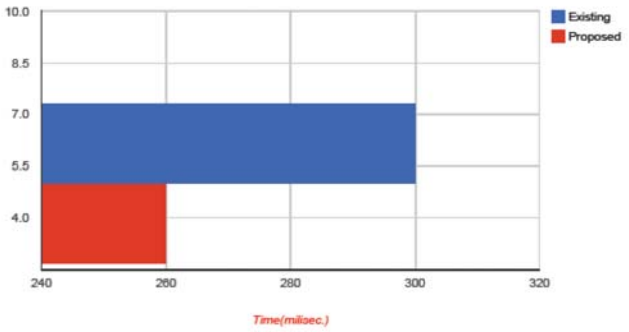

Fig. 4. Key Generation Time Graph

Figure 5 shows the use of the security parameters for the Paillier homomorphic encryption to ensure the fairness and the privacy of the privacy-preserving network. In Figure 5, the x-axis defines the security parameter for the existing and the proposed systems and the y-axis shows the provided level of security in percentage for the system and for each profile. The security for the proposed model results in more fetch per unit of time from the start to the end and it does not skip processes in between when the process is running. The security for the existing model is low through the whole process.

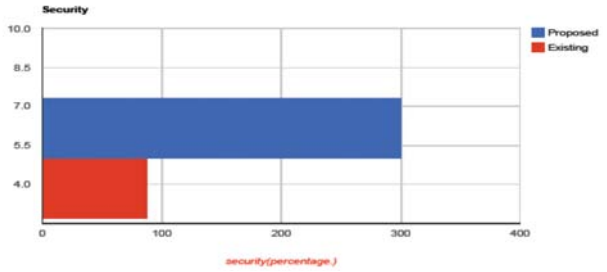

Fig. 5. Security Graph

IV. CONCLUSIONS

This paper proposed a blind transformation profile to increase security levels for the process of profile matching in in mobile social networks. The lack of sufficient security may result in the leaking of personal information. The issues to be addressed in existing mobile social networks are the slow start and the security issue. In existing systems the created profile is filtered separately by use of two separate algorithms, which leads to weakened security and confusion in between the profile matching process or in friend discovery processes. The proposed here algorithm can provide fine grained interest profile matching and can be used as a basis to investigate more security and privacy issues in mobile social networks, which can improve the negative impact of slow start of the process and the security for each profile.

Here, we combined the blind transformation and the fairness-aware algorithms. This combination allows for the filtering of each profile from the key generation technique and the fair matching process gives more secured fields to the profile. This results that only the interest profile would be visible to another user. The total security is provided to the personal profile i.e.,it is invisible for the friend and visible for the profile holder. Our future work includes how to provide fine-grained interest profile matching and investigate more security and privacy issues in mobile social networks.

REFERENCES

[1] M. Li, N .Cao, S.Yu, and W. Lou, "FindU – Privacy- Preserving Personal Profile Matching In Mobile Social Networks," *Proc. of IEEE INFOCOM 2011,* April 2011, Shanghai, China, pp. 2435 – 2443.

[2] W. Dong , V. Dave, LQiu, and Y. Zhang, "Secure Friend Discovery In Mobile Social Networks," in *Proc. of IEEE INFOCOM 2011*, April 2011, Shanghai, China, pp. 1647 - 1655

[3] H. Zhu, X. Lin, R. Lu. Fan, and X. Shen, "SMART: A Secure Multilayer credit based Delay Tolerance Network," in IEEE Transactions on Vehicular Communications, Vol. 58, Issue 8, pp. 4628 – 4639, October 2009.

[4] H. Zhu, X. Lin, R. Lu, P-H. Ho, and X. Shen, "SLAB: Secure Localized authentication and Billing Scheme for wireless mesh networks," in IEEE Transactions on Wireless Communications, Vol. 7, No. 10, October 2008.

[5] R. Zhang ,Y. Zhang, J. (Stella) Suny, and G. Yanz, "Fine-grained Private Matching For Proximity -Based Mobile Social Networking," in *Proc. of IEEE INFOCOM 2012* , March 2012, pp.:1969 - 1977.

[6] Haojin zhu, Mianxiong Dong,kao Ota,"Primatch: Fairness –aware Secure Friend Discovery Protocol In MSN", Sep-2013

[7] Ji S. Shin, V. D. Gligor, "A New Privacy-Enhanced Matchmaking Protocol," in *IEICE Transactions on Communication*, Vol. E96.B (2013) No. 8, pp. 2049-2059.

[8] B. Wang, B. Li, and H. Li," Gmatch: Secure and Privacy-Preserving Group Matching in Social Networks," in *Proc. of IEEE Global Communications Conference (GLOBECOM), S*ept 2012, DOI: 10.1109/GLOCOM.2012.6503199

[9] Q. Tang, "User-Friendly Matching Protocol for Online Social Networks," in *Proc. of the 17th ACM conference on Computer and Communications Security*, pp. 732-734, New York, USA, March 2010.

[10] P. Paillier, "Public-Key Cryptosystem Based on Composite Degree Residuosity Classes," Chapter in Advances in Cryptology — EUROCRYPT '99, Volume 1592 of the series Lecture Notes in Computer Science, pp. 223-238.

[11] S. S. Ople, A. A. Deshmukh, "Survey on Privacy Preserving Friend Matching Protocol for Pre-match in Social Networks. ISBN NO.-973-93-806886-87-9 http://www.ijcaonline.org/archives/volume118/number18/20843-3447, May 2015.

[12] P. Paillier, ``Public-key cryptosystems based on composite degree residuosity classes," in Advances in Cryptology_EUROCRYPT1999.

Radar Range and Range Resolution Enhancements using efficient binary Pseudo Random code with optimal correlation and side lobe reduction characteristic

Uma S. Jha, Ph.D.
Space & Airborne Systems, Raytheon Co
El Segundo, California

Erik Chowdhury, Ph.D.
Space & Airborne Systems, Raytheon Co
El Segundo, California

Abstract — **In Radar Intelligence, Surveillance and Reconnaissance (ISR) applications maximizing range and resolution are key objectives for the system developers. The predicament of having long range requires higher transmit power (wider pulse), which affects the range resolution adversely. This issue of range and range resolution compromise has been resolved using the pulse compression techniques such as Linear Frequency Modulation (LFM) and Coded Binary Sequences (e.g. Barker code). These techniques have served the radar community well, but with the advancements in VLSI technologies (e.g. processing power, memory, process nodes etc…) other complex techniques should be explored, especially the ones which have been tried in the commercial world with great success and differentiated offerings. Some algorithmically enhanced Pseudo Random Noise (PRN) sequences in cellular applications exhibit both good autocorrelation and low sidelobe characteristics, which are desirable for Radar ISR applications. The LFM waveform is a very common radar waveform, and has been used for the ISR application for many years. However, the pulse compressed output of the LFM signal produces an unacceptable level of sidelobes, typically only 13 dB below the mainlobe. The mainlobe to sidelobe ratio improvement is typically accomplished by applying a weighting function in conjunction with the matched filter. This results in Signal-to-Noise Ratio (SNR) reduction of 1-2 dB (depending on the weighting function), which degrades the detection range performance. The proposed PRN binary sequence codes in conjunction with the LFM waveform exhibits promising results in air-to-air and air-to-ground applications and achieve excellent range and range resolution performance at a substantially reduced sidelobe level.**

Keywords— Radar, Range, Resolution, Pulse Compression, Autocorrelation, LFM, Barker Code, Side lobes, Pulse Shaping, Pseudo Random Noise (PRN) Code, anti-jamming, antidetection, Processing Gain, 3 dB Bandwidth

I. INTRODUCTION

Typically radar systems in ISR applications transmit a pulsed electromagnetic wave and measure the returned time of the reflected echo from a distant object as shown in Figure – 1 and are used to determine the range using Eq. 1. The fundamental relationship between the radar parameters, target and received signal, is known as the radar range equation.

In general, a pulsed radar system transmits and receives a train of pulses, as illustrated in Figure – 2.

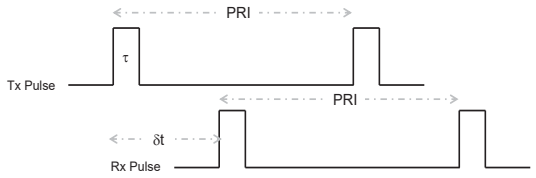

Figure -1

$$R = \frac{C * \delta t}{2} \qquad (1)$$

C - Speed of the light

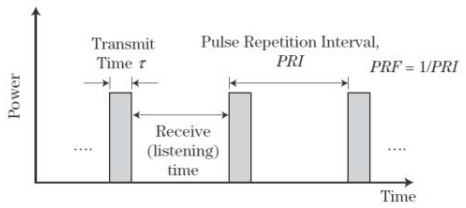

Figure -2

In a pulsed radar system, detectable range is limited by the transmit power and the range resolution by the pulse width. The design of any radar system always involves a trade-off between these two competing constraints. Pulse compression techniques have been employed extensively to achieve improved range resolution while maintaining an acceptable range capability. One of the basic types of pulse compression technique in use today is binary phase coding, which encodes the transmitted pulse with information that is known a priori to the receiver. The receiver processes the waveform of the received signals using a matched filter and depending on the length of the binary coded sequence achieves pulse compression (or processing gain) and subsequently imp roves range resolution.

By definition, range resolution is the ability of a radar system to detect targets in close proximity to each other as distinct objects. The range resolution, δR, is inversely proportional to the pulse width, i.e. the narrower the pulse width, the better the range resolution. Without pulse compression, the

Copyright © 2015 Raytheon Company. All rights reserved

instantaneous bandwidth of a radar receiver, B, is equal to pulse bandwidth. By incorporating narrower pulses of duration τ/N, the range resolution could be improved N times. Eq. 2 describes the essence of pulse compression. Resolution in the range domain, δR, corresponds to the time domain resolution, τ.

$$\delta R = \frac{C * \tau}{2} = \frac{C}{2 * B} \qquad (2)$$

Other key characteristics of a desirable radar waveform development could require a binary coded sequence to provide higher sidelobe rejection and superior autocorrelation properties. The radar community has developed many such sequences such as the Barker code which demonstrates good autocorrelation and better than average sidelobe rejection characteristics.

Autocorrelation

The cross-correlation function is the degree of likeness of one signal to another. For two identical signals the cross-correlation operation is known as autocorrelation. Mathematically, the autocorrelation function of a discrete time sequence $x[n]$, (n =1, 2..., N) is given by Eq. 3.

$$R_x(k) = \sum_{i=1}^{N-1} x[i]x^*[i+k] \qquad (3)$$

where k = 0,1,...,N -1 is the discrete time-index, the asterisk on the second term in the product of the right side of Eq. 3 denotes the complex conjugate.

Peak Sidelobe

The autocorrelation operation produces a main lobe surrounded by several sidelobes with time lags in both positive and negative sides. The autocorrelation function of a uniform Power Spectral Density (PSD) pulse is shown in Figure–3. The absolute maximum value of the secondary peaks in the sidelobes is defined as the peak sidelobe level (*PSL*) [1], which is expressed as

$$PSL = \max_{k \neq 0} \{R_x(k)\} \qquad (4)$$

This quantity is more often expressed as a value relative to the mainlobe level in decibels and defined as the peak sidelobe level ratio (*PSLR*). The *PSLR* in decibels is represented in Eq. 5 and is annotated in Figure – 3.

$$PSLR_{dB} = 20 \log_{10}\left[\frac{PSL}{R_x(0)}\right] \qquad (5)$$

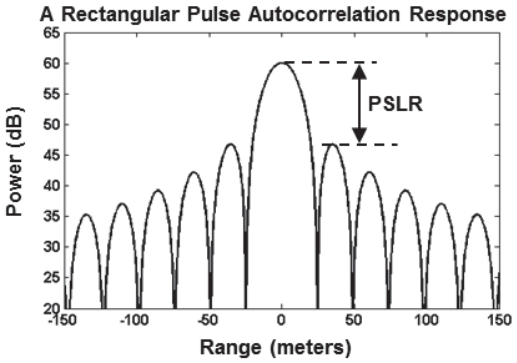

Figure -3

II. Background (Historical Perspective)

The matched filter and pulse compression concepts are the key constituents of radar pulsed signal processing. Since radar return includes noise, ground clutter and background interference in addition to the target, the receiver must be capable of differentiating a real target from accompanying noise and interference. The matched filter is widely used to decipher the signal from the noise, ground clutter and background interference.

Pulse compression is a classic radar signal processing technique used to increase range resolution without increasing the transmit power. Instead of a fixed frequency waveform, the transmitted pulse is modulated by a linearly varying frequency waveform, which broadens the bandwidth of the transmitted pulse. The receiver uses a matched filter to process returned echoes and matches the transmitted waveform at the same time to reject noise, interference and clutters. The transfer function of a matched filter is designed to maximize the attainable Signal to Noise Ratio (SNR) at the receiver output.

Linear Frequency Modulation

The Linear Frequency Modulation (LFM) waveform is the most commonly and extensively used pulse compression technique in radar systems. The bandwidth of an LFM waveform is widened using a quadratic phase coefficient (α), which varies the frequency linearly over the duration of the pulse. The LFM waveform is defined as Re{s(t)} in Eq. 6.

$$s(t) = \exp\left\{j2\pi\left(f_c t + \frac{1}{2}\alpha t^2\right)\right\}, \ -\frac{T}{2} \le t \le \frac{T}{2} \qquad (6)$$
$$= 0, \qquad elsewhere$$

Where f_c is the carrier frequency of the transmitted waveform and α is the chirp rate of the waveform and defined as

$$\alpha = \frac{B}{T} \qquad (7)$$

Copyright © 2015 Raytheon Company. All rights reserved

Where, B and T are the waveform bandwidth and the pulse width respectively of the LFM waveform. The instantaneous phase of the LFM waveform across the pulse width T is illustrated in Figure– 4.

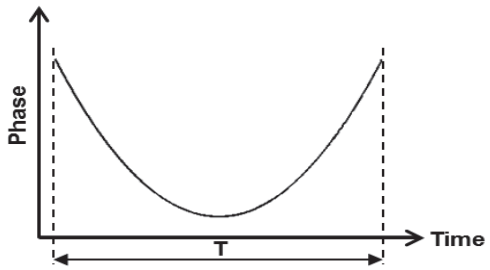

Figure -4

The instantaneous frequency *f(t)* can be obtained by differentiating the phase portion of the Eq. 6 ,

$$f(t) = \frac{d(f_c t + \frac{1}{2}\alpha t^2)}{dt} = f_c + \alpha t \qquad (8)$$

The autocorrelation function for this waveform is depicted in Figure–5. As expected it achieves a 3 meter range resolution (Eq. 2) but it has a peak sidelobe of only 13.4 dB below the mainlobe. The peak sidelobe of this level is not ideal and a weighting function may be used to reduce the sidelobes without compromising the range resolution or range performance of the system.

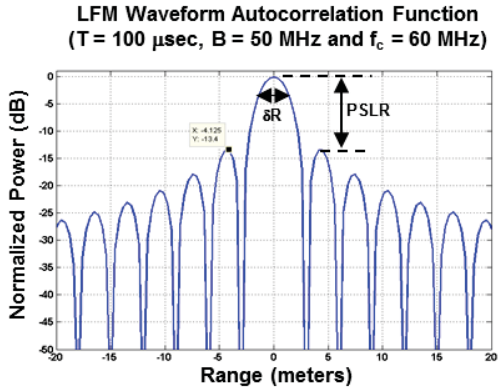

Figure -5

A commonly used Taylor [3] weighting function reduces the PSLR by 30dB as shown in Figure–6. The weighting function reduces the sidelobe peak at the expense of marginalizing the effectiveness of the matched filter as it is no longer matched precisely causing loss of SNR.

Binary Coded Barker Code

Pulse compression is also realized using binary coded sequences with good autocorrelation and sidelobe properties. The Barker code [2] is one of the most widely used binary coded sequences in radar applications, as it exhibits excellent autocorrelation characteristics as well as favorable sidelobe suppression.

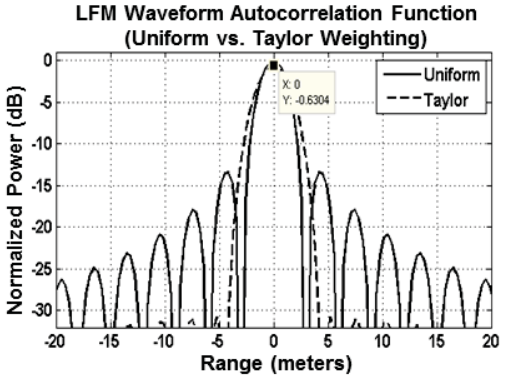

Figure -6

In order to achieve pulse compression, a binary coded wideband sequence is transmitted and the return signal is processed through matched filtering. This process results in enhancing the signal power due to the processing gain and thus improving the range resolution due to widening of the pulse bandwidth. The transmitted pulse carries the binary coded sequence of smaller chip duration, which is used to phase modulate the carrier frequency. An example of a 7-chip Barker code is shown in Figure-7. This waveform represents a carrier frequency being modulated in phase every chip between 0 and π according to the code [-1 -1 -1 1 1 -1 1] sequence, where -1 represents a phase of 0 degree and +1 represents a phase reversal of π. The amount of compression possible is equivalent to the time-bandwidth product (BT) of the code, which is the product of the signal bandwidth and the pulse duration. Bandwidth of a phase-coded signal is $B=1/\tau_c$ where τ_c is the chip duration. The returned signal power increase is proportional to the code length while the range resolution (δR) is inversely related to the bandwidth as described in Eq. 2.

The weakness of a binary coded system is the growth of sidelobe spurs, which are an artifact of the pulse compression. Figure–7 shows the matched filter output of a 7 chip Barker code. Barker codes have the property of producing mainlobe that is higher than the sidelobes by a factor of the code length. For a code length of 7 chips, the mainlobe is 7 times higher than the sidelobes.

Typically Integrated Sidelobe Level (ISL) and Peak Sidelobe Level (PSL) are used to characterize the performance of the ISL. ISL represents total power in sidelobes with respect to the main lobe, while PSL represents the peak sidelobe amplitude with respect to the mainlobe as defined in Eq. 9 & 10. In both of

Copyright © 2015 Raytheon Company. All rights reserved

these equations, x_0 refers to the mainlobe magnitude while x_i refers to all other output range sidelobes except the mainlobe.

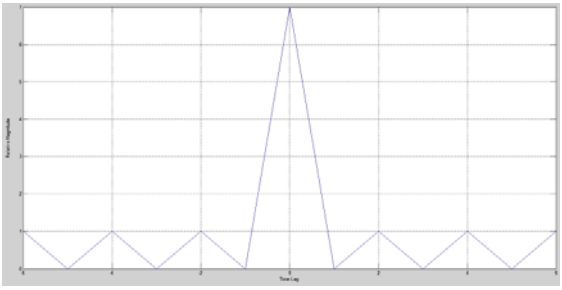

Figure -7

$$ISL = 10\log_{10}\sum_{i\neq 0}\frac{x_i^2}{x_0^2} \quad (9)$$

$$PSL = 10\log_{10}\frac{\max_{i\neq 0}(x_i^2)}{x_0^2} \quad (10)$$

III. Proposed PRN Code Framework

This section documents the detailed framework of the proposed Pseudo Random Noise (PRN) coded LFM waveform, which exhibits excellent pulse compression characteristics and subsequently better range and range resolution performance for ISR applications.

The ease of generating an LFM waveform and subsequent processing by a Matched Filter lends into an efficient hardware implementation. However, an LFM waveform is susceptible to jamming in an electronic warfare (EW) environment due to its distinguishable waveform features.

Figure–8 shows a simplified time domain design architecture which utilizes a Commercially Off-The-Shelf (COTS) LFM Direct Digital Synthesis (DDS) to incorporate a PRN phase modulated LFM waveform generator. The quadratic phase portion of LFM in φ(n) from Figure–8 can be represented by

$$\varphi_q(n) = an^2 + bn + c \quad (11)$$

Where,

n = sample number from 0, 1, 2…N,

N = number of samples generated within a transmit pulse width at the Digital to Analog Convertor (DAC) sampling rate f_s,

a = LFM chirp rate which is defined by the waveform bandwidth to pulse width ratio,

b = Intermediate Frequency (IF), and

c = a constant phase offset.

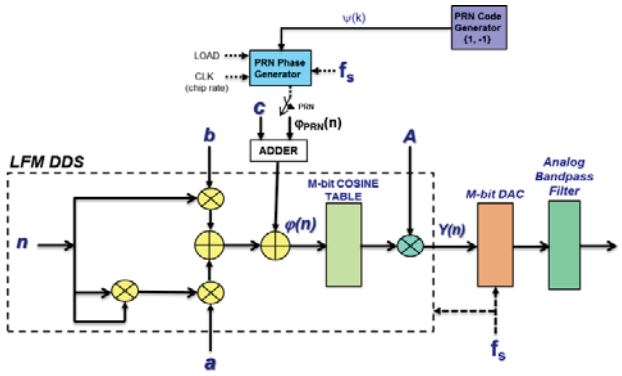

Figure -8

The modulated LFM phase φ(n) in Figure–8 is then defined as

$$\varphi(n) = \varphi_q(n) + \varphi_{PRN}(n) \quad (12)$$

Each phase sample φ(n) is then indexed into the cosine lookup table to generate the waveform samples. Each waveform sample is scaled by the control parameter (A), as shown in Figure-9, prior to the input of a Digital to Analog Convertor (DAC).

The PRN code generator in Figure–8 is a uniformly distributed binary code generator from a set $\Lambda \in \{+1, -1\}$. The code length is defined by the number of chips within a transmit pulse. Time duration of a single chip can be defined by the pulse duration divided by the length of the code. For example, a 2.5 μsec pulse with a code length of 125 has a chip time duration of 20 nanoseconds. The output PRN phase samples from the PRN Phase Generator in Figure–8 are continuous by design for any set of binary PRN codes across the transmit pulse.

The LFM quadratic samples are phase modulated by the PRN phase generator samples, as defined by Equation 12. The performance results of the proposed PRN phase modulated LFM waveform was evaluated based on a simulation developed in MATLAB. The performance of the PRN phase modulated LFM waveform generated from Monte Carlo run was compared to the same PRN phase coded waveform without the presence of LFM waveform. Figure–9 shows a comparison between the frequency spectra of the two separate waveforms generated from one of the test runs. Note that the PRN phase modulated LFM waveform exhibits a flat white noise like Power Spectral Density (PSD). On the other hand, the PRN phase coded waveform spectrum in Figure–9, without the presence of LFM waveform shows distinct spectral characteristics desirable for many other applications.

Copyright © 2015 Raytheon Company. All rights reserved

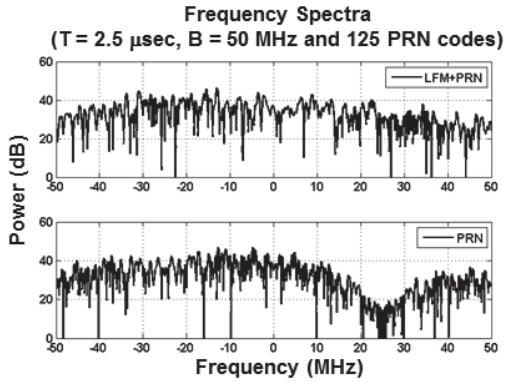

Figure -9

In addition, the target detection probability of the PRN phase modulated LFM waveform shows better performance than the PRN coded binary waveform as shown in Figure–10.

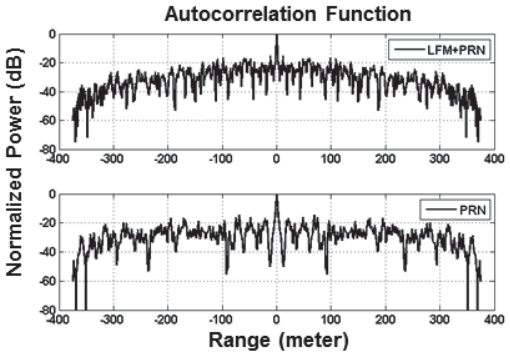

Figure -10

A comparison of the PRN phase modulated LFM waveform (solid line) shows better range resolution performance as well with respect to the PRN coded waveform as shown in Figure–11.

The autocorrelation functions (Figure–12) between LFM and PRN phase modulated LFM waveforms are also compared for a 100 μsec pulse width case. The autocorrelation results show that the PRN phase modulated LFM waveform also performed better in comparison to that LFM waveform.

IV. CONCLUSIONS

In this paper we have presented the framework of the PRN coded LFM waveform and shown that the performance of the proposed waveform matches the range performance and far exceeds the sidelobe reduction compared to widely employed LFM and Barker coded binary sequence waveforms. The simulation results also show a better range resolution in addition to having superior range and sidelobe suppression performance for ISR applications.

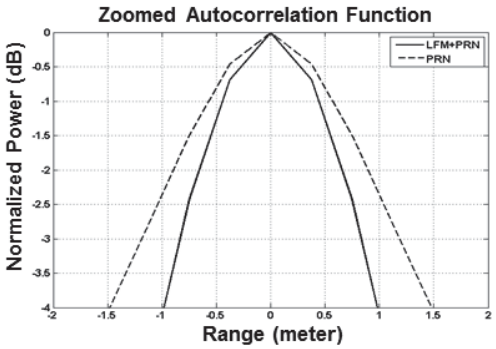

Figure -11

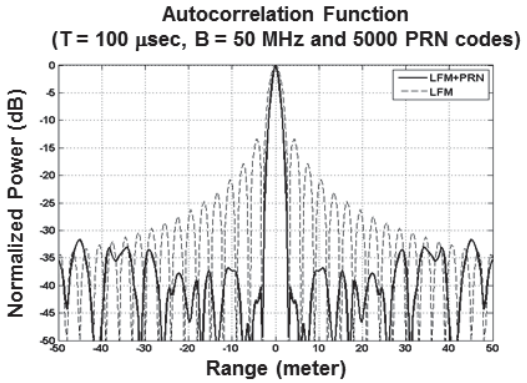

Figure-12

ACKNOWLEDGMENT

Authors would like to recognize the support from the Raytheon's RF Systems Verification group as well as their valuable suggestions during the preparation of this manuscript.

References

[1] Richards, M.A., Scheer, J. A., Holm, W.A., (2010). *Principles of Modern Radar*, Raleigh, NC: Scitech Publishing Inc., ISBN-9781891121524

[2] Barker, R.H., (1953). Group synchronizing of binary digital systems, *Communication Theory* (W. Jackson, ed.), Academic Press, New York, pp. 273–287

[3] Taylor, T.T. "Design of Line-Source Antennas for Narrow Beamwidth and Low Sidelobes", IRE Trans. Antennas and Propagation, pp. 16-28, January 1955.

[4] Fred E. Nathanson (1999); Radar Design Principles - Signal Processing and the Environment (2nd Edition); Scitech Publishing Inc., ISBN 189112109X

Copyright © 2015 Raytheon Company. All rights reserved

THE 18TH INTERNATIONAL SYMPOSIUM ON WIRELESS PERSONAL MULTIMEDIA COMMUNICATIONS
(WPMC-2015)
December 13-16, 2015, Hyderabad, India

A Generic and Compatible Implementation for 2D and 3D Geometry-based Stochastic Channel Models

Zhenzi Liu, Tian Lei, Yuming Bi, Pan Tang, Wei Chen, and Jianhua Zhang
Key Laboratory of University Wireless Communications, Wireless Technology Innovation Institute, Ministry of Education
Beijing University of Posts and Telecommunications, Mailbox NO.92, CHINA, 100876
Email: {liuzhenzibupt, tianlbupt, yumingbi, tangpan27, jhzhang}@bupt.edu.cn, chenweiw09@gmail.com

***Abstract*—Geometry-based stochastic channel model (GBSM) is an important approach for standard channel modeling, and will be a part of future 5G channel models. In this paper, we present a generic and compatible implementation for two-dimensional (2D) and three-dimensional (3D) GBSMs for both link level and system level simulations. Our approach enables a simple, flexible and scalable method for developing and simulating different GBSMs. It mainly consists of three related parts, i.e. the antenna configuration, the network layout and the channel parameters generation. We calibrate and verify our implementation by comparing several given channel parameters with reference results from other organizations, and it's in good agreement with the references. Furthermore, resulting in MIMO outage capacities are shown. The proposed implementation can be applied to simulate different GBSMs in a consistent way and to evaluate various wireless systems.**

I. Introduction

Channel models are important tools for the development of new radio systems and technologies. They allow estimation and validation of new concepts in mobile communication systems. At the same time, these concepts also motivate the development of channel models. Multiple-input multiple-output (MIMO) and 3D beamforming have been identified as key technologies for performance enhancement in communication systems, as well as in future 5G systems [1], [2]. So directional channel models that take the direction of arrival and departure in consideration are required for simulating and testing such systems [3].

There have already been several suggestions for directional channel models. Molisch *et al.* [3] have compared some of them, and selected geometry-based stochastic approach for most parts of COST-259 channel model. Since geometry-based stochastic channel model (GBSM) can keep a good balance between accuracy and complexity for simulating directional channels, it has been widely used in standard channel models, such as the 3GPP spatial channel model (SCM) [4], SCM extension (SCME) [5], WINNER model [6], [7] and IMT-Advanced model [8]. However, most of these models are based on 2D modelling approach, and not appropriate for evaluating technologies like massive MIMO and 3D beamforming which take the elevation dimension into account. This was taken up partly in WINNER II model [7] and 3GPP 3D model [9]. Recently, METIS has developed its GBSM from WINNER and IMT-Advanced channel models for future 5G communiation systems, which suppots full 3D channel simulation, spatial consistency and wide range of propagation scenarios [10].

Along with the standardization process, commercially and academic available channel simulators have been developed. The MATLAB implementations of SCM/SCME, WINNER and WINNER+ channel models developed by WINNER project partners [11] have been widely used in many systems. Ellenbeck *et. al* [12], [13] presented an efficient and fully calibrated C++ implementation of ITU-R channel model suitable for system level simulations of IMT-Advanced systems. However, to the best of our knowledge, none of these implementations is compatible with 3D channel models.

The main contribution of this paper is the generic and compatible implementation for 2D and 3D channel models. Its module-based structure results in a much more organized, understandable and maintainable implementation in which new antenna arrays filed pattern, new network layout topologies and new generation algorithms are easily added and tested. Furthermore, the proposed implementation is verified and calibrated with reference results from other organizations.

The remainder of this paper is outlined as follows. Sec. II gives an overview of 2D and 3D GBSMs. Sec. III presents our proposed implementation. Sec. IV discusses different calibration and validation approaches and presents calibration results. Finally, conclusions are drawn in Sec. V.

II. Overview of 2D and 3D GBSMs

A. MIMO Channel Realisations

Geometry-based modeling of the radio channel enables separation of propagation parameters and antennas. The channel parameters for individual snapshots are determined stochastically based on statistical distribution extracted from channel measurements. Channel realisations are generated through the application of the geometrical principle by summing contributions of rays (plane waves) with specific small-scale parameters like delay, power, angle-of-arrival (AoA) and angle-of-departure (AoD).

Considering an $U \times S$ MIMO channel, we denote the channel impulse response (CIR) of cluster n at time t to delay τ as [9]

$$\begin{aligned} h_{u,s,n}(t;\tau) = \sum_{m=1}^{M} & \mathbf{F}_{rx,u}^{T} \cdot \mathbf{X}_{n,m} \cdot \mathbf{F}_{tx,s} \\ & \times \exp\left(jk\left(\bar{r}_{rx,n,m} \cdot \bar{d}_{rx,u}\right)\right) \exp\left(jk\left(\bar{r}_{tx,n,m} \cdot \bar{d}_{tx,s}\right)\right) \\ & \times \exp\left(j2\pi\nu_{n,m}t\right) \delta\left(\tau - \tau_{n,m}\right) \end{aligned} \quad (1)$$

where $\mathbf{F}_{rx,u}$ and $\mathbf{F}_{tx,s}$ are the antenna array response matrices for the receiver (Rx) and the transmitter (Tx) respectively, $\mathbf{X}_{n,m}$ is the complex gain matrix of cross-polarisations, where n denotes a cluster and m denotes a ray within cluster n, $(\cdot)^T$ denotes the matrix transposition. Furthermore, j is the square

root of -1, k is the wave number $2\pi/\lambda$ where λ is the carrier wavelength in meters, $\bar{r}_{rx,n,m}$ is AoD unit vector, $\bar{r}_{tx,n,m}$ is AoA unit vector, $\bar{d}_{rx,u}$ and $\bar{d}_{tx,s}$ are the location vectors of element s and u respectively, and $\nu_{n,m}$ is the Doppler frequency component.

By taking a discrete Fourier transform (DFT) in the delay domain, the channel response at frequency f is given by [13]

$$H_{u,s}(f;t) = \sum_{n=1}^{N} h_{u,s}(n,t) \cdot \exp(-j2\pi\tau_n f) \qquad (2)$$

According to the existing standardized 2D fading channel models, including IMT-Advanced model and 3GPP SCM, the characteristics of the spatial domain mainly focus on the horizontal direction. Based on the elevation angles, the 2D channel model based on the IMT-Advanced channel model can be transformed into a 3D model [14].

B. Correlated Large Scale Parameters (LSPs)

At system level, all large scale fading parameters (LSPs) are fully correlated between MSs being connected to the same BS (but not between different BSs) as well as among each other for the same link. These correlations are mostly caused by some scatters contributing to different links (similarity of the environment) [7].

The procedure to achieve this stems from [6], [7] which uses a grid of locations based on MSs and a two dimensional finite impulse response (FIR) filter to generate separately the influence of LSP cross-correlations and exponential auto-correlation. Furthermore, the correlated LSPs of 2D channel models include shadow fading term, the delay spread and azimuth angular spreads and the Ricean K factor. Besides the above-mentioned LSPs, other correlated LSPs of 3D channel models include elevation angular spreads. These LSPs are used to parametrize the random distributions of the actual small scale parameters used by the spatial channel model [13].

However, correlations of LSPs between different MSs is not supported in SCM/SCME. In 3GPP SCM, shadowing fading for links from one MS to different BSs exhibits constant correlation coefficient equal to 0.5. And this correlation does not depend on distances between BSs or their relative angular positions as seen from MS [7].

C. Small Scale Parameters (SSPs)

Firstly, correlated LSPs are drawn randomly from tabulated distribution functions, then actual small scale parameters (like delay of each cluster and associated power, arrival and departure angle of each ray of each cluster) can be drawn randomly according to tabulated distribution functions and random LSPs. In order to characterize the spatial fading channel, power angle spectrum (PAS) and angular spread (AS) of the azimuth angle have been introduced. In the existing 2D channel models, PAS of the azimuth angle is well fitted by Gaussian distribution or Laplacian distribution at the BS. At the MS, it is usually assumed to be uniform distribution [14]. Similar to the horizontal domain, the basic parameters of the vertical domain, such as PAS and AS, should be studied and modelled. For scenarios defined in 3GPP 3D channel model [9], the elevation PAS at both MS and BS can be well fitted by Laplacian distribution. Furthermore, the height dependence of elevation offset angle, which is defined as the difference between the line-of-sight (LoS) direction and the mean angle of the elevation PAS, at BS observed from the ray-tracing data, is not showing a common and strong trend.

III. Compatible Implementation for 2D and 3D GBSMs

A. Implementation Framework

The block diagram of proposed compatible channel model implementation is shown in Fig. 1. Similar to other implementations [11], [13], the core part consists of: (i) the antenna configuration, (ii) the network layout and (iii) the parameters generation.

The antenna configuration part specifies separately the

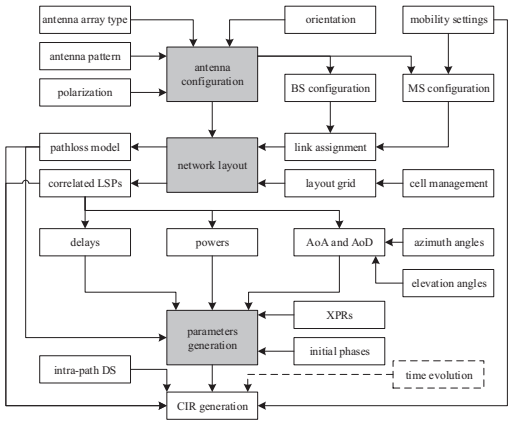

Fig. 1. Block diagram of the compatible implementation for 2D and 3D GBSMs

antenna characteristics used for generating the channel impulse responses (CIR). On the other hand, the network layout part defines the scenario layout grid type, cell management, mobility settings and locations and configurations of each BS and MS. Furthermore, the channel parameters generation part generates randomly correlated LSPs and actual SSPs of the simulated link according to tabulated distribution functions. As a mean to support bandwidth extension, intra-cluster delay spread is introduced in SCME [5]. And the dashed time evolution component depicted in Fig. 1 means that the dynamic channel simulation is not fully supported in existing channel models.

B. Implementation Workflow

The workflow of the implementation framework is shown in Fig. 2. The procedure of the proposed implementation is as follows:

Step 1: Select an appropriate channel model (2D or 3D GBSM) to start one simulation according to radio systems or technologies to be evaluated;

Step 2: Choose one deployment scenario which defined in the channel model for the evaluation, this must be done as the followed network layout configuration depend on it;

Step 3-A: Give the antenna array type (linear array or 2D planar array), polarization, position of each element and also

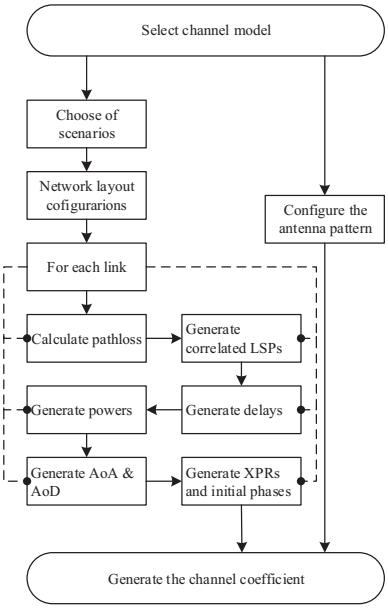

Fig. 2. Workflow of the proposed implementation

field pattern $\mathbf{F}_{tx}$ and $\mathbf{F}_{rx}$ of each BS and MS;

Step 3-B: Give the location, orientation and mobility of each BS and MS in the layout grid, assign each link with line-of-sight (LoS), non-line-of-sight (NLoS), outdoor-to-indoor (O2I) or indoor-to-outdoor (I2O) propagation condition, and calculate the line-of-sight angles of departure and arrival of each link.

Step 4: For each link which was assigned in the layout, generate the following parameters:

1) The pathloss PL;
2) Correlated LSPs include the shadow fading term σ_{SF} and the line-of-sight Rice factor K_R *et. al.*;
3) Initial delay τ_n and power P_n of each cluster n;
4) AoA and AoD of azimuth and/or elevation of each ray;
5) XPRs and initial random phases of each different polarisation combinations of each ray.

Step 5: Generate time-delay domain channel coefficients using (1), then compute the channel frequency response by discrete Fourier transform (DFT) using (2).

Generally speaking, the generation of channel parameters in *Step 4* can be done only once, because all these values stay constant during one simulation drop and independent between different simulation drops. However, on dynamic/non-stationary channel models which are channel models with time-varying channel parameters, time-evolution of channel parameters between different simulation drops should be taken.

By utilizing the framework which support both link level and system level simulations, we can simulate a number of existing channel models with a compatible implementation. It can also be applied to evaluate the performance of radio systems or technologies under different channel models. Consequently, we can simplify the channel model simulation by keeping these dominate parameters as random variables while fixing others as constants.

IV. Calibration and Simulation Results

Calibrating different simulation tools is an important requirement for obtaining comparable and reliable simulation results [13]. In this section, we calibrate the 3GPP 3D channel model implementation with reference values from other organizations. Furthermore, the outage capacities of 2D and 3D channel models are shown.

A. Standardized Calibration Phases

The phased calibration work has been agreed in RAN1 for 3D channel model [15]. The phase-1 calibration covers large scale channel characteristics including coupling loss, geometry, and LoS angle distributions with several antenna configurations. The phase-2 calibration includes fast fading channel characteristics such as distribution of elevation angular spread and singular value distribution. Further details of phase-1 and phase-2 simulation assumptions and calibration metrics are described in [16].

Phase-1 calibration: Phase-1 calibration relies on the large-scale fading parameters. The objective of this phase is to calibrate the correct scenario layout, antenna characterises, pathloss models, assignment of LoS or NLoS propagation conditions and shadow fading. The main calibration metrics of this phase are referred to as coupling loss, geometry factor and LoS elevation angles of departure (EoD).

The coupling loss measures the difference between the received signal and the transmitted signal along the LoS direction, and its computation for MS m based on reference signal received power (RSRP) is given by [17]

$$CL_m = RSRP_{k_m} - P_{TX} \tag{3}$$

where k_m is the best serving site k which maximizes the RSRP; P_{TX} is the transmitted power in dB, and the RSRP is given by

$$\begin{aligned} RSRP_{k_m} = P_{TX} &+ G_T\left(\phi_{k,m}^{LoS}, \theta_{k,m}^{LoS}\right) \\ &+ G_R\left(\varphi_{k,m}^{LoS}, \vartheta_{k,m}^{LoS}\right) \\ &+ PL_{k,m}^{LoS}(dB) - \sigma_{SF,k,m}(dB) \end{aligned} \tag{4}$$

where $\left(\phi_{k,m}^{LoS}, \theta_{k,m}^{LoS}\right)$ and $\left(\varphi_{k,m}^{LoS}, \vartheta_{k,m}^{LoS}\right)$ are the LoS direction of departure and arrival with respect to the k-th site respectively; $G_T(\cdot)$ is the antenna gain at the transmitter in dB, and $G_R(\cdot)$ is the antenna gain at the receiver in dB; $PL_{k,m}^{LoS}$ is the LoS pathloss in dB and $\sigma_{SF,k,m}$ is the shadow fading term in dB.

In Fig. 3 and Fig. 5, we present the obtained results of the coupling loss and LoS EoD for the urban macro (UMa) scenario respectively when antenna config 1 is assumed [16]. These results comply with those obtained by majority of the companies participating in the calibration process [16].

Phase-2 calibration: For phase-2 calibration, the cumulative distribution function (CDF) of small scale channel characteristics, like the azimuth and elevation angular spreads as well as the delay spread, should be given [18]. Moreover, to calibrate the channel generation procedure, CDF of the first and second largest eigenvalues of the channel should also be presented. The fact is that when the channel is known to the transmitter, spatial diversity is related to the dominant eigenmode of channel matrix [19].

Fig. 4 shows the calibration metric curves for the elevation

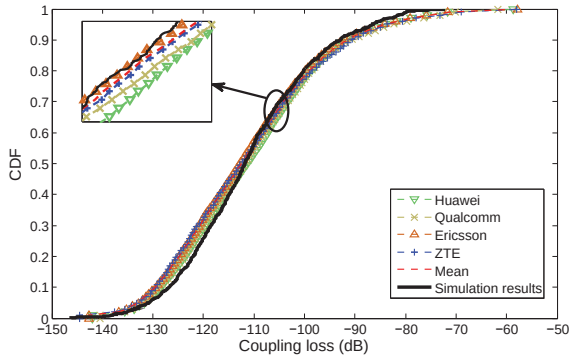

Fig. 3. Calibration of coupling loss for the UMa scenario

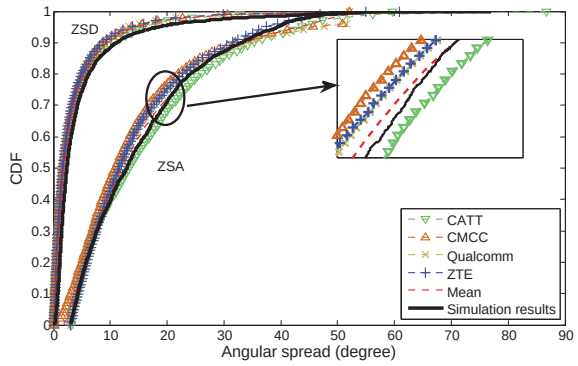

Fig. 4. Calibration of Elevation Angular Spread of Departure for the UMa scenario

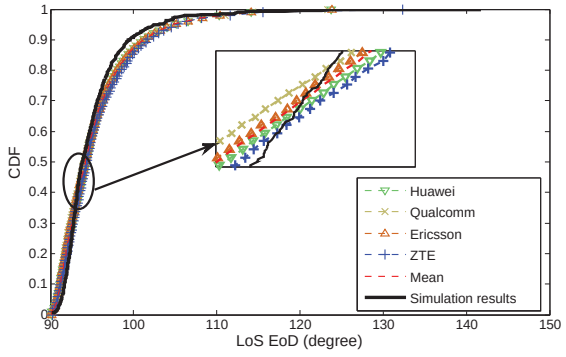

Fig. 5. Calibration of LOS ZoD for the UMa scenario

angular spread of departure and arrival which derived from the implementation of 3GPP 3D channel model for the UMa scenario in comparison with reference results from other organizations [16]. The curves closely match with the majority of reference curves thus underlining the correct implementation of our framework.

TABLE I. ASSUMPTIONS OF OUTAGE CAPACITY SIMULATION

Parameters	**Description**
Scenarios	UMa and UMi
Carrier Frequency	2.0 GHz
BS antenna configurations	2 Tx, ULA, 10.0λ H spacing
MS antenna configurations	2 Rx, ULA, 0.5λ H spacing
Polarisation	X-pol at both BS and MS
MS velocity	30.0 km/h and 3.0 km/h
Sample density	8 samples per half wavelength
No. of frequency bins	600
SNR	$\rho = 14.0$ dB

B. Further Calibration

A common way to characterize the time-frequency domain channel matrices $\mathbf{H}$ given in (2) that a channel model produces, is to consider the distribution of the resulting MIMO capacity [13]. The outage capacity, i.e. the CDF of the channel capacity, when the channel is unknown to the transmitter is preferred instead of the ergodic capacity which can be derived from the CDF. The approximation of capacity C of each channel realization t can be given by [19]

$$\tilde{C}_t(\rho) = \frac{1}{F}\sum_{f=1}^{F} \log_2 \det\left(\mathbf{I}_U + \frac{\rho}{\beta^2 S}\mathbf{H}_{ft}\mathbf{H}_{ft}^H\right) \quad (5)$$

where f and F are the discrete sample point and total sample points of the channel frequency response respectively. U is the number of receive antennas and S is the number of transmitter antennas. $\mathbf{I}$ denotes the identity matrix, ρ denotes the signal-to-noise ratio (SNR) and $(\cdot)^H$ denotes the Hermitian transpose operation. β is a common normalization factor for all channel realizations such that the average channel power gain is unitary [19], i.e.,

$$E_H\left\{\frac{1}{\beta}\|\mathbf{H}_{ft}\|_F^2\right\} = U \times S \quad (6)$$

where $E_H\{\cdot\}$ denotes the expectation operator over H; $\|\cdot\|_F$ denotes the Frobenius norm.

Fig. 6 and Fig. 7 show the outage capacity complementary cumulative distribution function (CCDF) comparing with 3GPP 3D channel model, the IMT-Advanced channel model as well as the SCM channel model against the capacity purely random Gaussian i.i.d. distributed channel matrices would yield. For all models, the values were generated assuming a configuration as Table I shows.

Obviously, the correlations considered by the different channel models yield lower than Gaussian capacities, especially for LoS conditions. From the result, we can see that the outage capacity of 3GPP 3D channel model is close or even lower than the outage capacity of IMT-Advanced channel model and SCM when linear antenna array been deployed at BS. It seems that the modelling of elevation dimension trends to increase the channel correlation and cause the loss of MIMO channel rank. However, when we consider the planar antenna arrays, Fig. 8 shows that the outage capacity of the 3D channel model is higher than 2D channel models.

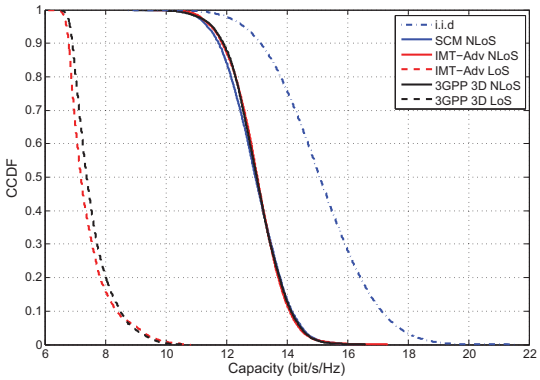

Fig. 6. The CCDF of the 2×2 MIMO wideband outage capacity in urban macro environment with fixed $\rho = 14$ dB

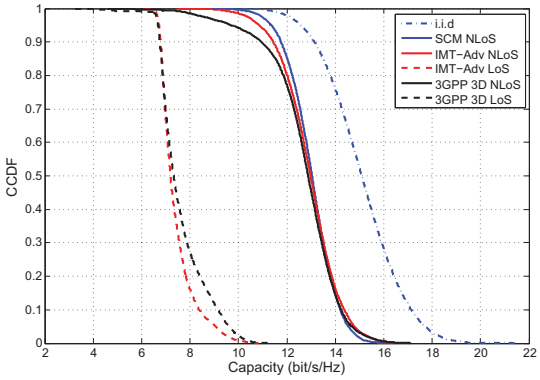

Fig. 7. The CCDF of the 2×2 MIMO wideband outage capacity in urban micro environment with fixed $\rho = 14$ dB

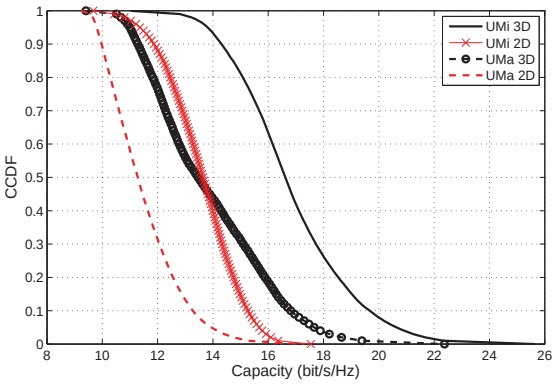

Fig. 8. The CCDF of the 32×32 MIMO wideband outage capacities with fixed $\rho = 14$ dB

V. Conclusion

In this paper we present a generic and compatible implementation for 2D and 3D GBSMs based on existing 2D channel model implementations. We discuss numerous calibration approaches from the standardization and present calibration results underlining the correctness of our implementation. It's obvious that our proposed implementation supplies a much more compatible and scalable simulation for different GBSMs.

Acknowledgment

The research is supported by National Key Technology Research and Development Program of the Ministry of Science and Technology of China (NO. 2012BAF14B01) and National Science and Technology Major Project of the Ministry of Science and Technology (NO. 2013ZX03001020-002).

References

[1] X. Cheng, B. Yu, L. Yang, J. Zhang, G. Liu, Y. Wu, and L. Wan, "Communicating in the real world: 3d mimo," *Wireless Communications, IEEE*, vol. 21, no. 4, pp. 136–144, August 2014.

[2] J. Andrews, S. Buzzi, W. Choi, S. Hanly, A. Lozano, A. Soong, and J. Zhang, "What will 5g be?" *Selected Areas in Communications, IEEE Journal on*, vol. 32, no. 6, pp. 1065–1082, June 2014.

[3] A. Molisch, H. Asplund, R. Heddergott, M. Steinbauer, and T. Zwick, "The cost 259 directional channel model-part i: overview and methodology," *Wireless Communications, IEEE Transactions on*, vol. 5, no. 12, pp. 3421–3433, December 2006.

[4] 3GPP TR 25.996, "Spatial channel model for multiple input multiple output (mimo) simulations," 3rd Generation Partnership Project, , 2014. [Online]. Available: http://www.3gpp.org

[5] D. Baum, J. Hansen, and J. Salo, "An interim channel model for beyond-3g systems: extending the 3gpp spatial channel model (scm)," in *Vehicular Technology Conference, 2005. VTC 2005-Spring. 2005 IEEE 61st*, vol. 5, May 2005, pp. 3132–3136.

[6] WINNER IST-2003-50781 D5.4, "Final report on link level and system level channel models," Wireless World Initiative New Radio (WINNER), , 2005. [Online]. Available: http://www.ist-winner.org

[7] WINNER IST-4-027756 D1.1.2, "Winner ii channel models, part i channel models," Wireless World Initiative New Radio (WINNER), , 2007. [Online]. Available: http://www.ist-winner.org

[8] ITU-R M2135, "Guidelines for evaluation of radio interface technologies for imt-advanced," International Telecommunication Union (ITU), , 2009. [Online]. Available: http://www.itu.int

[9] 3GPP TR 36.873, "Study on 3d channel model for lte," 3rd Generation Partnership Project, , 2015. [Online]. Available: http://www.3gpp.org

[10] ICT-317669-METIS D1.4, "Metis channel models," Mobile and wireless communications Enablers for the Twenty-twenty Information Society (METIS) Project, Deliverable, 2015. [Online]. Available: https://www.metis2020.com

[11] [Online]. Available: http://www.ist-winner.org

[12] [Online]. Available: https://launchpad.net/imtaphy

[13] J. Ellenbeck, O. Mushtaq, F. Sheikh, and Q. S. Shahrukh, "Calibrating an efficient c++ implementation of the itu-r m.2135 channel model for use in system-level simulations," International Workshop on Propagation and Channel Modeling for Next-Generation Wireless Networks, Lyon, France, March 2011.

[14] J. Zhang, C. Pan, F. Pei, G. Liu, and X. Cheng, "Three-dimensional fading channel models: a survey of elevation angle research," *Communications Magazine, IEEE*, vol. 52, no. 6, pp. 218–226, June 2014.

[15] 3GPP R1-140654, "Phase 1 and 2 calibration results for 3d channel model," InterDigital, RAN1 No.76, , Feb. 2014.

[16] 3GPP R1-140843, "Summary of phase-1 and phase-2 calibration results form [75-29]," NSN, Nokia, RAN1 No.76, , Feb. 2014.

[17] A. Kammoun, H. Khanfir, Z. Altman, M. Debbah, and M. Kamoun, "Preliminary results on 3d channel modeling: From theory to standardization," *Selected Areas in Communications, IEEE Journal on*, vol. 32, no. 6, pp. 1219–1229, June 2014.

[18] 3GPP R1-135087, "Initial calibration results for 3d fast fading channel modelling," CATT, RAN1 No.75, , Nov. 2013.

[19] Y. Zhang, J. Zhang, G. Liu, X. Gao, and P. Zhang, "A generic validation framework for wideband mimo channel models," in *Vehicular Technology Conference, 2008. VTC Spring 2008. IEEE*, May 2008, pp. 330–334.

THE 18TH INTERNATIONAL SYMPOSIUM ON WIRELESS PERSONAL MULTIMEDIA COMMUNICATIONS
(WPMC-2015)
December 13-16, 2015, Hyderabad, India

Design and Data Analysis of a Signal Measurement System Based on Variable Short Signature Sequences

Ji-Hyun Moon, Jeong-Ho Kim, Na-Hyung Kim, and Bing Yuan Chen

Dept.of Electronics Engineering, Ewha Womans University
11-1 Daehyundong, Seodaemungu, Seoul, 120-750, Republic of Korea.
[e-mail: jho@ewha.ac.kr]

***Abstract*—The collection of sensor data and its analysis have become more important as more smart buildings equipped with various sensors are developed. The interconnection of the wire cable through the sensors is indispensable for information collections - such as temperature, humidity, and luminance in the rooms and hallways - and the effective management of the in-building energies. However, these interconnections through the cabling are very costly, time-consuming, and high risky since they can cause some damage to the buildings. Therefore, interconnections through unwired connections are required to ensure the deployment effectiveness such as time and cost. In this paper, the design and short sequence operation appropriateness are confirmed through the simulation of a signal measurement system for in-building propagation characteristics based on short signature sequences, and the analysis of the system characteristics based on the false alarm probability are performed thereafter.**

Keywords—Signal measurement, In-building propagation characteristics, Short signature sequence, In-Building measurement

I. INTRODUCTION

This study designs a measurement system for in-building propagation characteristics and analyzes theses in-building propagation characteristics. Since the in-building propagation characteristics can vary according to the applied building materials and structures, a management system based on these characteristics is needed to develop a management system for smart buildings. To solve such engineering measurement problems, we designed and verified a reference signal generator and a system that measures and analyzes the message quality based on a short sequence according to the propagation characteristics between a transmitter and a receiver. The system operation was checked through a simulation for verifying the design validity and the in-building propagation characteristics were analyzed in the actual indoor environment. Thus, this may contribute to the exploration of the potential for a one-hop network configuration in buildings. In this respect, the propagation characteristics were analyzed and extracted from the data measured by a short-sequence system. An integrated hierarchy system was also designed to measure the in-building propagation characteristics and verified through a simulation. Based on this verified system, a one-way system that collects and analyzes actual measurement data was configured. In other words, it is necessary in an environment with noise and interference to define a short signature sequence so as to easily confirm propagation characteristics and facilitate the actual characteristics' measurement. Through this system design, more practical data may be collected than actual measurements, and thus, the measured environments may be analyzed more closely. Compared with the conventional systems [4] – [5], the proposed system can measure the indoor signal propagation characteristics more reliably due to the signature sequence based measurement procedure.

II. A SHORT-SEQUENCE SYSTEM CONFIGURATION AND ITS VERIFICATION THROUGH A SIMULATION

An in-building propagation environment refers to a setting in which signal paths are surrounded by external walls and structures and the interior of a building is separated by the corridors. The propagation environment can vary according to the basic structures of stepped and corridor buildings. The basic configuration includes the selection of proper frequency bands, choice of the signature sequence, data transfer rate and the modulation method, collection and analysis of the data and transmission power, and estimation of a proper transmitter location

A. An in-building propagation characteristics measurement system based on a short signature sequence

A distinguishable short signature sequence needs to be properly configured so as to measure the in-building propagation characteristics. This sequence should have the basic features of being easily generated and producing a number of signature sequences. In this respect, a basic pattern block needs to be developed and a certain pattern is required to be defined to confirm it even though the quality of the channel can be degraded by interference and noise. In this study, the QPSK (quadrature phase shift keying), a pattern is converted

into bit streams and a relatively high bandwidth utilization and higher order modulation through further improvement can be achieved, was applied. An RRC (root raised cosine) filter was also used to create waveforms in order to minimize the bandwidth for the channel transmission of signals from the binary I and Q channels which were generated by the two bit streams. The waveforms comprise samples of 43 taps. The measurement systems can basically work either in master or in slave mode. The master mode starts with the transmission of signature sequence without conflicts. The measuring system that will receive the signature sequence entirely will participate in the channel evaluation process by working in slave mode. The Figure 1 shows the working process of the measuring system in master mode. As shown in Figure 1, the system in master mode transmits signature sequences for measurement, gives channel numbers to them, and then collects the information of the channels to be measured at the moment. When echo back signature sequences stand by for reception and the signatures are not received normally in the slave system, retransmission procedures and timer motions are controlled. In turn, when the signatures are received normally, it transmits feedback signature sequences again, and then waits for a re-reception of echo back signatures. When the echo back signatures are not received, it delays for a certain period of time, and then transmits the feedback signature sequence again. After such procedures, channels statuses are recorded and the qualities of two-way channels are measured and collected. In the system in slave mode, the motion process is carried out as indicated in Figure 2. When the measuring system receives the signature sequence with a new channel number, it immediately enters the slave mode and then carries out a reception procedure. As shown in Figure 2, when a new signature sequence is received, a new channel number is given and then an echo back signature is transmitted. Also, it stays at the status of feedback signature receiving queue from the master mode, and whether it is received normally or not is checked up. When it is not received normally until the timer ends up, the delay timer is increased and the echo back signature sequence is transmitted again. Likewise, the qualities of new channels can be measured by measuring the delayed values that are continuously received. As indicated above, when quality evaluations of channels are carried out from the continuously received signature sequences and closing messages are received, the measurement process of the channels concerned is finished.

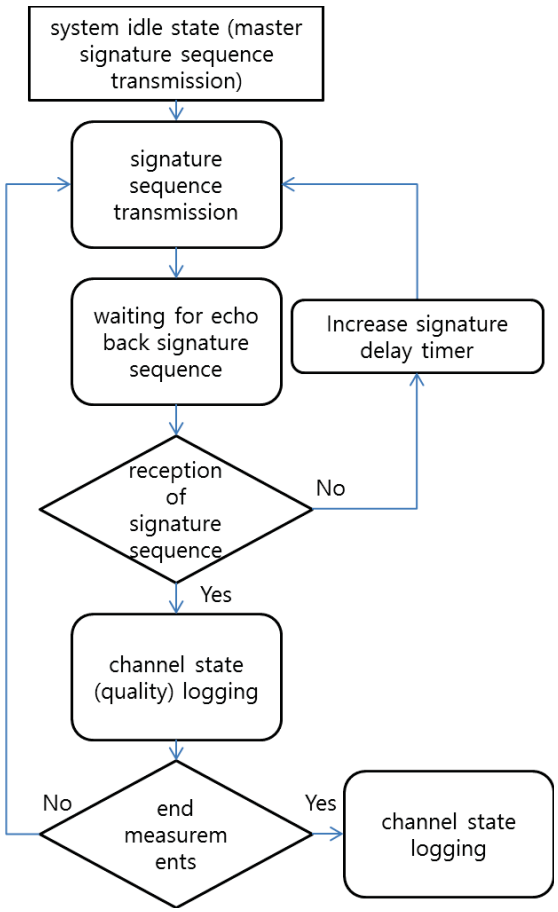

Fig. 1. Operation procedure of the measurement system [Master]

A frame structure of the system produced using the Simulink model based on Matlab is presented in Figure 2 below. After a signature sequence is selected and the transmitting end treatment is complete, the signals are transmitted to the channels. In this study, it is assumed that the noise generated in the channels at this stage is an additive white Gaussian noise (AWGN) [1].

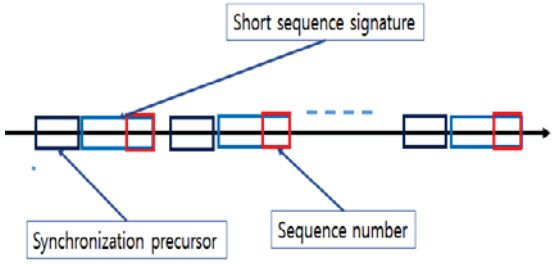

Fig. 2. Frame structure of the short signature sequence system

B. Simulation results and analysis

For the synchronization of the starting point of a frame to the message pattern, a 13-bit Barker sequence, a

synchronization precursor, was used as a basic structure of the signature sequence used in this system as presented in Figure 2. At the receiving end, the correlation value with respect to the synchronization sequence was calculated, and then, the starting point was identified. The optimum time was chosen using the 2 times over-sampled sample streams through the symbol synchronization algorithm. The correlation value was calculated from the synchronized sample with the sequence from the module which generates the Barker sequence (the sample of the QPSK demodulated I and Q channels). The highest correlation value obtained in this stage indicates the starting point of the frame. The parameters for the main system and the signal transmission band are presented in Table 1. The transfer rate can be determined according to the bandwidth available for transmitting the sensor data. When measuring the in-building propagation characteristics, the variable signature sequence (L = 12, 16, 20, 24, 28, etc.), which allows the determination of whether the signal was properly received at the measuring point, needs to be produced and then the treatment is required on the receiving point.

Table 1. Simulation parameters

Parameters	Value
Carrier Frequency	450 MHz
Bandwidth	100 kHz
Modulation	QPSK
Waveform	Raised Cosine Pulse
Message	Signature Sequence
Bit Rate	500 kbps
Oversampling rate	4
Channel Model	In-Building, AWGN

The signature sequences for classifying the different signals ar e respectively mapped to the data bits of the I and Q channels and synthesized with the QPSK modulating signals. As these s ignals are mapped to the intermediate frequency and become t he band passing signals, the frequency shift corresponding to t he RF signals occurs and then the propagation of these signals takes place in the inside of the building. Since the obtained sig nals have a wide frequency bandwidth of square waveforms, p ulse shaping is required to efficiently use the frequency band. I n terms of filters, the present study used the RRC purse shapin g filter with 41 taps [2]-[3].

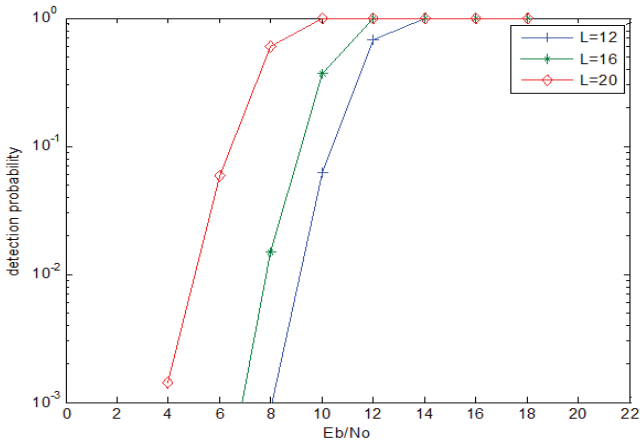

Fig. 3. Detection probability for the short signature sequence with FA = 0.01, L = 12, 16, 20

Since the RRC pulse shaping filter was used at both the transmitting and receiving ends, the signal transmission system without ISI (inter-symbol interference) can be applied. Through the simulation, it was found that when applying the RRC filter at the receiving end, no or minimal ISI can be attained and the bandwidth efficiency and the ISI minimization can be simultaneously achieved. Figure 3 shows the signal detection performances for each signal power when a variable short signature sequence is used and the false alarm probability is one percent. It suggests that a low power is required to get the same detection performances as the lengths of the signature sequence increase.

III. AN ANALYSIS OF THE PERFORMANCE CHARACTERISTICS OF THE SYSTEM

The detection threshold according to the given false alarm probability, power, and length of the short signature sequence is presented in Figure 4. As shown in the figure, as the length of the signature sequence decreases, the detection threshold needs to be higher. This is because the requirements for maintaining the given false alarm probability can be met with the higher detection threshold.

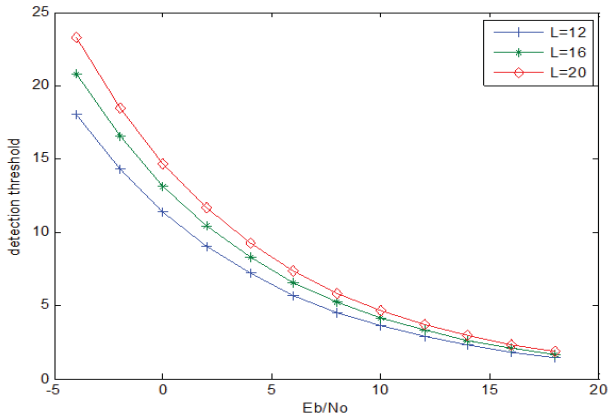

Fig. 4. Detection threshold with FA=0.01, L=12, 16, 20

Figure 5 shows the signal detection performances for each sig nal power when a variable short signature sequence of L = 12, 16, 20 is used and the false alarm probability is 5 percent.

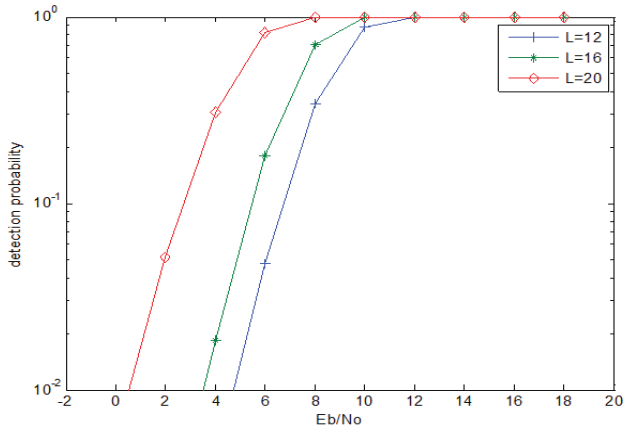

Fig.5. Detection probability for the short signature sequence with FA = 0.05, L = 12, 16, 20

IV. Conclusion

For the actual measurement of real buildings, the present study designed the measurement system based on the short signature sequence to measure the in-building propagation characteristics, produced the thresholds for the signal detection, and analyzed the detection performances. To facilitate the identification of the propagation characteristics in the indoor environment with noise and interference, the short signature sequence was defined, and thus, the practical measurement could be conducted. The identified propagation characteristics through this measurement system may contribute to the efficient configuration of an in-building smart sensor network and the accumulation of various design data. Also, a new algorithm for the two- and three-way signal transmission and reception needs to be applied so as to more efficiently measure and analyze signals.

Acknowledgment

This research is supported by the Basic Science Research Program through the NRF of Korea funded by the Ministry of Education, grant number : NRF-2014R1A1A2053294.

References

[1] Di Pu and Alexander M. Wyglinski, Digital Communication Systems Engineering with Software-Defined Radio, pp. 253-282, Artech House, 2013.

[2] Andrea Goldsmith, Wireless Communications, pp. 29-36, Cambridge, 2005.

[3] Theodore S. Rappaport, Wireless Communications - Principles and Practice 2nd Ed., pp. 227-229, Prentice Hall, 2002.

[4] X. Gao, F. Tufvesson, O. Edfors, and F. Rusek, “Measured propagation characteristics for very-large MIMO at 2.6 GHz,” in 2012 Conference Record of the 46th Asilomar Conference on Signals, Systems and Computers (ASILOMAR), 2012, pp. 295-299.

[5] J. Hoydis, C. Hoek, T. Wild, and S. Brink, “Channel behavior for very-large MIMO Systems – initial characterization,” in COST IC1004, Bristol, UK, Sep. 2012.

THE 18TH INTERNATIONAL SYMPOSIUM ON WIRELESS PERSONAL MULTIMEDIA COMMUNICATIONS
(WPMC-2015)
December 13-16, 2015, Hyderabad, India

Limited Feedback Scheduling For MIMO-OFDM Broadcast Network

Prabina Pattanayak
Department of Electrical Engineering
Indian Institute of Technology, Patna, India
Email: prabina@iitp.ac.in

Preetam Kumar
Department of Electrical Engineering
Indian Institute of Technology, Patna, India
Email: pkumar@iitp.ac.in

***Abstract*—User scheduling for downlink channel of multiple-input multiple-output orthogonal frequency-division multiplexing (MIMO-OFDM) system is studied in this paper. By utilizing the channel state information (CSI), base station (BS) selects set of users with best conditioned channel to receive data packets transmitted by transmit antennas to achieve the maximum throughput of the system. MIMO-OFDM system incurs more feedback load compared to that of single carrier MIMO systems. As the feedback load increases with number of subcarriers, per-chunk user scheduling is implemented where adjacent subcarriers are grouped together to reduce the feedback load. Signal-to-interference-plus-noise ratio (SINR) feedback model is considered in this paper for closed-loop MIMO-OFDM. A comparative study of different schemes for achievable net throughput with and without per-chunk user scheduling is carried out. Simulation results for various scenarios are presented and discussed in detail.**

***Index Terms*—MIMO-OFDM user scheduling, SINR Feedback, Per-chunk user scheduling.**

I. Introduction

Higher throughput is required for future wireless communication systems as the demand for broadband wireless services is increasing day by day. Multiple-input multiple-output (MIMO) system increases spectral efficiency of wireless channel in the presence of rich scattering and multipath fading environments [1]–[3]. Foschini *et al.* [4] presented the system capacity analysis for MIMO channels, which helped in suggesting practical structures for obtaining high spectral efficiency. This leads to the architecture called as Bell Laboratories layered space-time (BLAST) and to space-time codes discussed in [5], [6].

It has shown in [2], [3] that the system capacity of point-to-point (single user) MIMO wireless communication link increases linearly by a factor $min\{M, N\}$, where M is the number of transmit antennas at base station (BS) and N is the number of receive antennas at each user terminal (UT). Recently, multiuser MIMO (MU-MIMO) systems become more popular as this transmission strategy achieves more capacity gains in multiuser environment due to a selection diversity technique known as multiuser diversity (MUD) [7], [8].

Caire *et al.* [8] has shown that the Shannon's fundamental sum capacity limit of the MU-MIMO for broadcast channel (BC) is achieved by dirty paper coding (DPC) by serving multiple users equal to the number of transmit antennas at BS simultaneously. The encoding order of the users at BS plays a vital role in DPC as this is an interference pre-subtraction technique and it is required that the decoding order at the receiver to be the reverse order of encoding sequence at transmitter. The search space required for DPC to have the optimal precoding matrices (transmit covariance matrices) is huge. Furthermore, for implementation process of DPC, full noncausal knowledge of the interference signals of users encoded earlier are required for the users other than the first encoded user. This requirement is not practically feasible for real-time systems. Therefore, suboptimal MU-MIMO scheduling schemes with limited channel state information at transmitter (CSIT) have gathered attention as practically feasible alternatives to DPC [9]–[13]. In recent past, soft computing techniques are also used for scheduling [14], [15].

Orthogonal frequency division multiplexing (OFDM) is a technique implemented for multiuser broadcast communication over frequency-selective fading channels as its implementation is relatively less complex. Due to the combined advantages of MIMO and OFDM techniques, MIMO-OFDM is used at the background of modern wireless standards for achieving high capacity communications like LTE (Long Term Evolution) of Third-Generation Partnership Project (3GPP), WiMAX (Worldwide Interoperability for Microwave Access / IEEE 802.16e) etc..

In MU MIMO, BS schedules the best conditioned users to achieve more sum-rate. This needs to be done for each subcarrier present in MU MIMO-OFDM system to have the maximum system throughput. This kind of per-subcarrier resource allocation and scheduling is discussed in [16]. Here, each subcarrier is modulated by the data of the users selected for the corresponding subcarrier. No inter-carrier interference exists because of the orthogonality of the subcarriers. The data rate of the subcarriers are increased by exploiting spatial multiplexing by eigenbeamforming, where parallel spatial channels are created [17]. The feedback load due to MIMO-OFDM is more compared to that of MIMO as multiple subcarriers are present in MIMO-OFDM. Hence, to decrease the feedback load Pun *et al.* [18] introduced the concept of grouping of adjacent subcarriers into clusters. Due to clustering of adjacent subcarriers, the feedback load reduced significantly as compared with per-subcarrier eigenbeamforming but at the cost of system throughput. Eslami et al. in [19] discussed about grouping of adjacent subcarriers into chunks and evaluated the optimum chunk size for maximization of the net throughput for MIMO-OFDM system. It has been shown in [19] that the achievable system sum-rate obtained by chunk concept increases with user size while for other strategies it decrease

to zero.

In this paper, we calculated the system throughput of MU MIMO-OFDM system assuming a closed-loop where each user feeds back the scalar quality of the channel in terms of signal-to-interference-plus-noise ratio (SINR). Here, we evaluated three limited feedback scheduling schemes based on SINR feedback for MU MIMO-OFDM system. To reduce the feedback overhead, we have also implemented per-chunk user scheduling with these sub-optimal scheduling schemes. A comparison of feedback load incurred by these schemes is also presented.

Section II discusses about the system model considered in this paper. Three limited feedback schemes based on SINR feedback model is evaluated for MU MIMO-OFDM system in Section III. The expression for system throughput obtained by user scheduling considering grouping of adjacent subcarriers for multiuser MIMO-OFDM broadcast channel is discussed. Finally, we presented our conclusive remarks in Section IV.

II. System Model

A multiuser MIMO-OFDM broadcast cellular system is considered in this paper. The cellular system consists of a BS with M number of transmit antennas providing services to K geographically dispersed users. Each user has N number of receive antennas. A frequency selective wireless broadcast channel is assumed and this is modelled as a finite impulse response (FIR) filter of length P as discussed in [20]. The MIMO-OFDM channel bandwidth is divided into L orthogonal subcarriers. The received signal received by kth user on the lth subcarrier can be expressed as:

$$\mathbf{Y}_l^k = \mathbf{H}_l^k \mathbf{X}_l + \mathbf{W}_l^k, l = 1, \ldots, L, \tag{1}$$

where $\mathbf{Y}_l^k$ is an $N \times 1$ vector of the received signal at the user k on the lth subcarrier, $\mathbf{X}_l$ is an $M \times 1$ vector of the transmitted signal on the subcarrier l, and $\mathbf{W}_l^k$ is an $N \times 1$ vector of additive noise whose individual entries are independent and identically distributed (i.i.d) complex Gaussian with zero mean and unit variance. i.e., $\mathcal{CN}(0,1)$. $\mathbf{H}_l^k$ is an $N \times M$ matrix known as channel matrix and (n,m)th entry h_l^k(n,m) $\sim \mathcal{CN}(0,1)$ is i.i.d $\mathcal{CN}(0,1)$. Each element of this channel matrix is the complex channel gain coefficient from transmit antenna m to receive antenna n of user k on the lth subcarrier. The lth tone of the kth user's space frequency channel, $\mathbf{H}_l^k$ can be described as:

$$\mathbf{H}_l^k = \sum_{p=0}^{P-1} \sigma_p \mathbf{F}[k,p] exp\left(-j2\pi \frac{l}{L} p\right), 0 \le l \le L-1, \tag{2}$$

where exp(.) represents the exponential function, $\mathbf{F}[k,p]$ is an $M \times M$ square matrix $\forall p \in \{0, \ldots, P\}$. The channel impulse response of kth user is represented by $\mathbf{F}[k,p]$. Independent elements of $CN(0,1)$ are present in each element of $\mathbf{F}$. Further,we assume that these matrices are mutually uncorrelated. σ^2 for $p = 0, \ldots, P-1$ represents the channel power delay profile normalized by assuming $\sum_{p=0}^{P-1} \sigma_p^2 = 1$. The power delay profile of the frequency selective wireless channel is represented by $\sigma^2 \forall p \in \{0, \ldots, P\}$. The condition needs to be satisfied is $\sum_{p=0}^{P-1} \sigma_p^2 = 1$. The wireless channel characteristics do not change for one coherence time period, i.e., the channel is assumed to be quasi-static in nature as discussed in [19]. As $\mathbf{W}_l^k$ is the normalized noise vector, the average SNR is equal to ρ which defines the power constraint at BS as $\rho = (1/L) \sum_{l=0}^{L-1} Tr\left(\mathbf{E}[\mathbf{X}_l \mathbf{X}_l^H]\right)$.
The received signal at the nth receive antenna of the kth user on the lth subcarrier can be expressed as :

$$y_l^k(n) = \sum_{m=1}^{M} h_l^k(n,m) x_l(m) + w_l^k(n), \tag{3}$$

where the transmitted signal from transmit antenna m on the lth subcarrier is $x_l(m)$, the additive white Gaussian noise for nth receive antenna of the kth user on the lth subcarrier is $w_l^k(n)$.

The signal received by the user from the desired transmit antenna on the lth subcarrier is treated as the desired signal. The interference for the user comprises of the signals received from the transmit antennas other than the desired one on the subcarrier l. Let the signal $x_l(m)$ is the desired signal for the kth user and the interference signals for kth user are $x_l(m'), m' \neq m$ on the lth subcarrier. Then, the *instantaneous* SINR for $y_l^k(n)$ can be expressed as:

$$SINR_l^k(m,n) = \frac{|h_l^k(n,m)|^2}{\frac{M}{\rho_k} + \sum_{m' \neq m} |h_l^k(n,m')|^2}, \tag{4}$$

where ρ_k is the average signa-to-noise ratio (SNR) of user k. In this paper, we consider the homogeneous network, where all the users experience the same SNR, i.e., $\rho_k = \rho$ for $k = 1, \ldots, K$. We use sum-rate and throughput interchangeably throughout this paper.

III. Limited Feedback Schemes for MU MIMO-OFDM

Here, FDM is considered for per-subcarrier scheduling, i.e., the scheduling schemes are implemented for each subcarrier individually. The computation of achievable system throughput can be expressed as below:

$$T \le E\left[\frac{1}{L} \sum_{l=1}^{L} T_l\right]. \tag{5}$$

and T_l can be computed similar to [9]

$$T_l^k \le E\left[\sum_{m=1}^{M} \log_2(1 + \max_{n \in \{1,\ldots,N\}, k \in U} SINR_l^k(m,n)\right], \tag{6}$$

where $E[x]$ is the mathematical expectation value of x and U is the set of M number of users selected for receiving the data for the BS. The instantaneous throughput of the antenna selection with the feedback of SINR value can be expressed as in [10] :

$$T_l^k = \sum_{m=1}^{M} \log_2(1 + \max_{n \in \{1,\ldots,N\}, k \in U} SINR_l^k(m,n)). \tag{7}$$

We consider the below mentioned three sub-optimal feedback scheduling algorithms for closed-loop MIMO-OFDM broadcast network.

A. Limited Feedback Scheduling: Scheme I

First, each user calculates all the possible SINR values depending on all possible combinations of transmit antenna and receive antenna for a subcarrier. Then, each user selects the maximum among them and feeds back the maximum SINR value along with the index of the transmit antenna corresponding to that SINR value to BS. At BS, after receiving all the feedback data from all the users, the BS selects the users having the largest SINR values corresponding to each transmit antenna. Then after scheduling is done at BS, BS transmits the mutually independent data to the set of users scheduled for each transmit antenna as discussed in [10]. This process should be repeated for all subcarriers. Fig. 1 presents system throughput for different number of users at different system SNR values 0 dB, 5 dB, and 10 dB for MIMO-OFDM system where $M = N = 2$, number of subcarriers $L = 64$. It shows that MIMO-OFDM channel provides increased throughput with increase in system SNR value. We will model the MIMO-

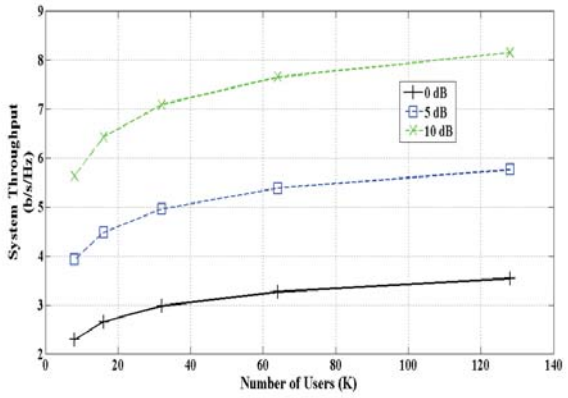

Fig. 1. System throughput of scheme I plotted for different number of users at various system SNR values of 0 dB, 5 dB, and 10 dB for $M = 2$, $N = 2$ and $L = 64$.

OFDM channel using the exponential power delay profile [21] as:

$$\sigma_p^2 = \frac{1 - exp(-1/D_{exp})}{1 - exp(-P/D_{exp})} exp(-p/D_{exp}), 0 \leq p \leq P - 1. \quad (8)$$

Throughout this section, we will use $P = 8$ and $D_{exp} = 2$.

B. Limited Feedback Scheduling: Scheme II

This scheme is similar to the previous one. But in this scheme, a threshold (λ) for SINR is being set and the users feed back their maximum SINR value along with the corresponding transmit antenna indices only if the maximum SINR value is greater than or equal to the threshold value λ as explained in [10] for a specific subcarrier. Again, this process needs to be iterated for all subcarriers. The comparison

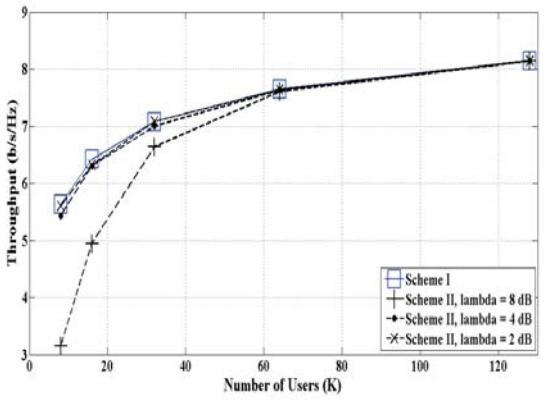

Fig. 2. System throughput of scheme II plotted for different number of users at system SNR of 10 dB for $M = 2$, $N = 2$ and various threshold values as λ= 2 dB, 4 dB, and 8 dB,$L = 64$.

of system throughput of scheme II for different values of threshold λ along with scheme I is presented in Fig. 2. It is evident that the system throughput increases and matches with that of scheme I as the threshold value λ decreases. Also, the feedback overhead increases with decrease of threshold value λ because by decreasing the threshold value λ more number of users will qualify to feedback their maximum SINR values to BS.

C. Limited Feedback Scheduling: Scheme III

In this limited feedback scheduling, each user should send an array of maximum SINR values corresponding to each transmit antenna as discussed in [**?**] for single subcarrier. Here, users do not send the transmit antenna indices like [10]. And the scheduling done at BS is similar to the above explained schemes. All subcarriers need to follow the above steps. The sum rate achieved by MIMO-OFDM by implementing this scheme is presented in Fig. 3. It shows sum rate attained by MIMO-OFDM system with M=N=3, and L=64 for different number of users at various system SNRs like 0dB, 5dB, and 10 dB. Fig. 4 shows the comparison of throughput obtained by scheme I, scheme III for MU MIMO-OFDM with M=N=3, L=64 at various system SNR values as 10 dB and 20 dB. It is shown that scheme III outperforms scheme I in utilizing the spectrum efficiently. One of the drawbacks of scheme I is that when users send only the highest SINR, some better conditioned receive antenna of some other user are not allowed to be served by BS, which could have resulted in better utilization of the spectrum. Also, scheme I may leave some of the transmit antennas idle (when none of the user's maximum SINR value is due to these transmit antennas) without sending useful data packets. This may lead to non exploitation of spatial multiplexing. But the chances of occurrence of such events get decreased with increase in number of active users due to MUD. Hence, scheme III attains better spectrum efficiency than scheme I for less number of users and both the schemes attain similar throughput for higher

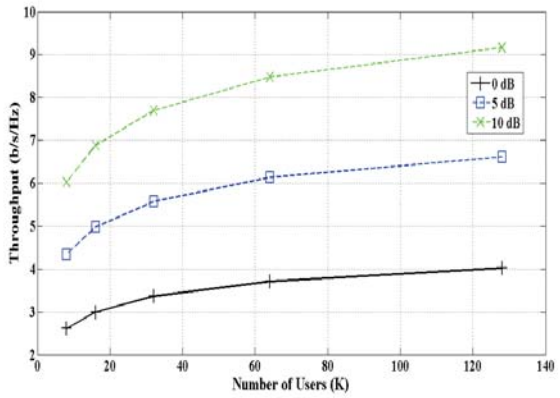

Fig. 3. System throughput of scheme III plotted for different number of users at various system SNR values of 0 dB, 5 dB, and 10 dB for M = 3, N = 3 and L = 64.

number of users.

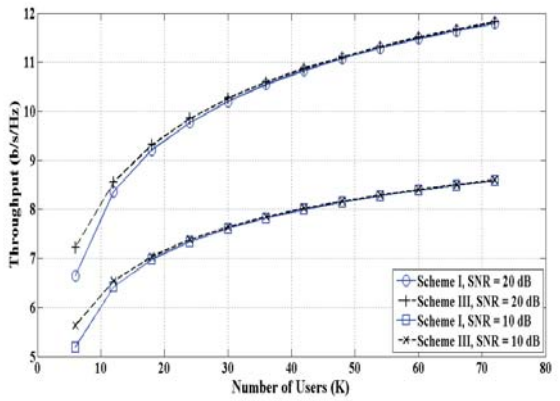

Fig. 4. Comparison of system sum rate of scheme I and scheme III for lesser number of users at various system SNR values of 10 dB, and 20 dB for M = 3, N = 3 and L = 64.

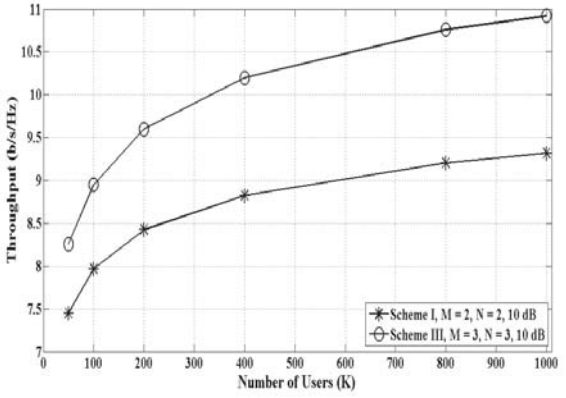

Fig. 5. Comparison of system sum rate of scheme I and scheme III for higher number of users at system SNR of 10 dB for 2×2, and 3×3 MU MIMO-OFDM system respectively with L = 2048.

In Fig. 5, it is interesting to observe that the net throughput of the system obtained by scheme I, and scheme III increase steadily with user size (unlike shown in [19]) because these schemes are able to exploit MUD. Hence, the probability of selecting receive antennas with higher SINR gets increased with number of active users. We have plotted the system throughputs obtained by scheme I and scheme III for MU MIMO-OFDM system with $L = 2048$, SNR = 10 dB for number of transmit and receive antennas are two and three respectively in Fig. 5 . Hence, this result states about the usefulness of these two user scheduling schemes.

D. Per-chunk user scheduling using scheme I and scheme III

When adjacent subcarriers are grouped into a chunk, the feedback overhead incurred by the system decreases by a factor of chunk size [19]. Hence, it is advantageous to use per-chunk user scheduling in the scheduling schemes proposed for MU MIMO system. In this section, we discuss the effect of per-chunk user scheduling in the above discussed schemes. Here, we have presented the modified expressions for system sum rate using SINR and per-chunk user scheduling. Each chunk consists of L_c adjacent subcarriers and integer number of chunks are formed out of the total subcarriers. The total achievable system throughput expressed in (5), now can be expressed by as below:

$$T \leq E\left[\frac{1}{Q}\sum_{q=1}^{Q}\max_{1<k<K} T_{chk,q}^{k}\right], \tag{9}$$

where Q is the total number of chunks in the MIMO-OFDM system and expressed as $Q = L/L_c$.And $T_{chk,q}^{k}$ is the highest instantaneous reliable rate on the chunk q for user k which is expressed in bits/second/hertz and is given by

$$T_{chk,q}^{k} = \frac{1}{L_c}\sum_{l_c=(q-1)L_c}^{qL_c-1} T_{lc}^{k}, 1 \leq q \leq Q, \tag{10}$$

where T_{lc}^{k} is expressed in (7). Comparison of system throughput obtained by user scheduling schemes like scheme I and scheme III with grouping of adjacent subcarriers is shown in Fig. 6. Here, the system throughput obtained by both the algorithms for MU MIMO-OFDM system with M=N=3, L=2048, and L_c=32 is compared. This clearly showcases the usefulness of scheme III over scheme I. This behaviour can also be explained by the explanation given for Fig. 4. But, here it is interesting to observe that the probability of non assignment of better conditioned receive antennas to transmit antennas of BS and leaving some of the transmit antennas idle without transmitting useful data packets occur for more than one subcarrier simultaneously. For this reason, the difference of throughput attained by scheme I and scheme III is more when user scheduling is implemented with grouping of adjacent subcarriers to reduce feedback overhead. It is important to observe that with implementation of per-chunk user scheduling (3×3 MIMO-OFDM system with L = 2048, L_c = 32 at 10 dB system SNR), there is a decrease in system throughput obtained by scheme I and scheme III by 64%, and

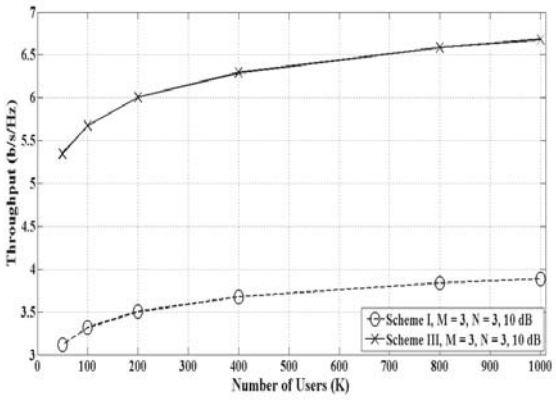

Fig. 6. Comparison of system sum rate of scheme I and scheme III for more number of users at system SNR values of 10 dB for M = 3, N = 3, L = 2048, and L_c=32.

38% respectively (as compared to the throughput obtained by these two schemes without per-chunk user scheduling) while the feedback load is reduced by a factor of 64 (i.e., $\frac{2048}{32}$). Hence, scheme III is always preferable over scheme I and scheme II for MU closed-loop MIMO-OFDM system for both with and without per-chunk user scheduling.

E. Feedback load comparison

We presented a comparison of feedback overhead incurred by these limited feedback scheduling algorithms for MU MIMO-OFDM system in TABLE I. It shows that the feedback load incurred by scheme II depends on the predefined threshold (λ) and the maximum feedback overhead is equal to that of scheme I. The scheme III incurs an insignificant increment in feedback overhead by feeding back an array of maximum SINR values, but it enjoys the advantage of not feeding back transmit antenna indices.

TABLE I
COMPARISON OF FEEDBACK LOAD INCURRED BY SCHEME I, II, AND III FOR MU MIMO-OFDM.

Scheduling Algorithms	**Number of SINR Terms**	**Number of bits representing Transmit Antenna Indices**
Scheme I without per-chunk	$L \times K$	$L \times K \times \lceil log_2(M) \rceil$
Scheme II without per-chunk	$\leq L \times K$	$\leq L \times K \times \lceil log_2(M) \rceil$
Scheme III without per-chunk	$L \times M \times K$	0
Scheme I with per-chunk	$Q \times K$	$Q \times K \times \lceil log_2(M) \rceil$
Scheme III with per-chunk	$Q \times M \times K$	0

IV. CONCLUSION

In this paper, three SINR based MU MIMO-OFDM BC scheduling algorithms are discussed with and without per-chunk user scheduling. The expression for net throughput of MIMO-OFDM system with SINR model is obtained for closed-loop feedback system with and without per-chunk user scheduling. The scheduling scheme III is proved to be better in utilizing the spectrum efficiently compared to scheme I and II for MIMO-OFDM system. Moreover, we showed that the sum-rate achieved by these user scheduling schemes increase with user size unlike the results presented in [19]. In fact, with reduced feedback load by implementing per-chunk user scheduling, scheme III produces much better net throughput than that due to scheme I.

REFERENCES

[1] J. Winters, "On the capacity of radio communication systems with diversity in rayleigh fading enviornment," *IEEE J. Select. Areas Commun.*, vol. JSAC-5, pp. 871–878, June 1987.
[2] G. J. Foschini and M. J. Gans, "On limits of wireless communications in a fading environment when using multiple antennas," *Wireless Personal Commun.*, vol. 6, pp. 311–335, 1998.
[3] E.Telatar, "Capacity of multi-antenna gaussian channels," *Eur. Transactions on Telecommunication*, vol. 10, pp. 585–596, Nov. 1999.
[4] G. J. Foschini, "Layered space-time architechture for wireless communication in fading environment when using multi-element antennas," *Bell Labs Tech. J.*, vol. 1, pp. 41–59, Nov. 1996.
[5] V. Tarokh, N. Seshadri, and A. Calderbank, "Space-time codes for high data rate wireless communication:performance criterion and code construction," *IEEE Trans. Inform. Theroyre*, vol. 44, pp. 744–765, Mar. 1998.
[6] B. Hassibi and B. Hochwald, "High-rate codes that are linear in space and time," *IEEE Trans. Inform. Theory*, vol. 48, pp. 1804–1824, July 2002.
[7] S. Vishwanath, N. Jindal, and A. Goldsmith, "Duality, achievable rates and sum-rate capacity of gaussian MIMO broadcast channel," *IEEE Trans. Inf. Theory*, vol. 49, pp. 2658–2668, Oct. 2003.
[8] G. Caire and S. Shamai, "On the achievable throughput of a multiantenna gaussian broadcast channel," *IEEE Trans. Inf. Theory*, vol. 43, pp. 1691–1706, July 2003.
[9] M. Sharif and B. Hassibi, "On the capacity of MIMO broadcast channels with partial side information," *IEEE Trans. Inform. Theory*, vol. 51, pp. 506–522, Feb. 2005.
[10] W. Zhang and K. Letaief, "MIMO broadcast scheduling with limited feedback," *IEEE J. Select. Areas Commun.*, vol. 25, pp. 1457–1467, Sep. 2007.
[11] M. Fakhereddin, M. Sharif, and B. Hassibi, "Reduced feedback and random beamforming for OFDM MIMO broadcast channels," *IEEE Trans. Commun.*, vol. 57, pp. 3827–3835, Dec. 2009.
[12] M. Min, D. Kim, H. Kim, and G. Im, "Opportunistic two-stage feedback and scheduling for MIMO downlink systems," *IEEE Trans. Commun.*, vol. 61, pp. 312–324, Jan. 2013.
[13] P. Pattanayak, K. M. Roy, and P. Kumar, "Analysis of a new MIMO broadcast channel limited feedback scheduling algorithm with user grouping," *Wireless Personal Commun.*, vol. 80, pp. 1079–1094, 2015.
[14] M. Naeem and D. Lee, "A joint antenna and user selection scheme for multiuser MIMO system," *Applied Soft Computing*, vol. 23, pp. 366–374, 2014.
[15] P. Pattanayak and P. Kumar, "A computationally efficient genetic algorithm for MIMO broadcast scheduling," *Applied Soft Computing*, vol. 37, pp. 545–553, 2015.
[16] P. Svedman, S. Wilson, L. Cimini, and B. Ottersten, "Opportunistic beamforming and scheduling for ofdma systems," *IEEE Trans. Commun.*, vol. 55, pp. 941–952, May 2007.
[17] Y. Peng, S. Armour, and J. McGeeham, "An investigation of dynamic subcarrier allocation in MIMO-OFDMA systems," *IEEE Trans. Veh. Technol.*, vol. 56, pp. 2990–3005, Sep. 2007.
[18] M. Pun, K. Kim, and H. Poor, "Opportunistic scheudling and beamforming for MIMO-OFDMA downlink systems with reduced feedback," *Proc. IEEE ICC*, pp. 688–692, May. 2008.
[19] M. Eslami and Krzymien.W.A., "Net throughput maximization of per-chunk user scheduling for MIMO-OFDM downlink," *IEEE Trans. Veh. Technol.*, vol. 60, pp. 4338–4348, Nov. 2011.
[20] H. Bolcskei, D. Gesbert, and A. Paulraj, "On the capacity of OFDM based spatial multiplexing systems," *IEEE Trans. Commun.*, vol. 50, pp. 225–234, Feb. 2002.
[21] M. McKay, P. Smith, H. Suraweera, and I. Collings, "On the mutual information distribution of OFDM-based spatial multiplexing:exact variance and outage approximation," *IEEE Trans. Inf. Theroy*, vol. 54, pp. 3260–3278, Jul. 2008.

THE 18TH INTERNATIONAL SYMPOSIUM ON WIRELESS PERSONAL MULTIMEDIA COMMUNICATIONS
(WPMC-2015)
December 13-16, 2015, Hyderabad, India

Disaster Countermeasure Experiments using WINDS

Takashi Takahashi, Kazuyoshi Kawasaki, Akira Akaishi, Toshio Asai, Maki Akioka, Tomoshige Kan and Morio Toyoshima
Wireless Network Research Institute
National Institute of Information and Communications Technology
893-1 Hirai, Kashima, Ibaraki, 314-9501 Japan

Byongpyo Jeong, Hajime Susukita, and Shuji Murakami
Resilient ICT Research Center
National Institute of Information and Communications Technology
2-1-3 Katahira, Aoba-ku Sendai, 980-0812Japan

***Abstract*—After the Great East Japan Earthquake, the National Institute of Information and Communications Technology (NICT) researched and developed resilient information and communication technologies, such as a wireless mesh and satellite network. NICT developed three types of earth stations for satellite communication, and dispatched them for use in several disaster countermeasure drills. The usefulness of satellite communication was demonstrated by establishing a temporary communication link.**

Keywords—resilient ICT, satellite commuunication, WINDS, earth station

I. INTRODUCTION

On March 11, 2011, the Great East Japan Earthquake, registering with a magnitude 9.0, struck off Japan's eastern seaboard. There was tremendous amount of damage, including damage to terrestrial networks for telephones and cell phones. This made it extremely difficult for people in the affected areas to communicate with people in other areas. Satellite communication was shown to be one of the better solutions for communication problems during large-scale disasters.

The National Institute of Information and Communications Technology (NICT) has developed resilient information and communications technology facilities. These consist of elements such as wireless mesh networks, satellite communication networks, and optical fiber networks. Three types of earth stations were developed for the disaster countermeasure experiment involving the use of the Ka-band satellite, the Wideband InterNetworking engineering test and Demonstration Satellite (WINDS) [1]. The three earth stations consist of a small mobile vehicle earth station, a large-scale in-vehicle earth station, and a fully-automatic transportable earth station, and they were designed to be easy to set up and operate.

NICT dispatched these earth stations for use in several disaster countermeasure drills. During these drills, WINDS established temporary communication network that worked in coordination with the Unmanned Aeronautical System (UAS) and the wireless mesh network. This paper introduces WINDS, the three types of earth stations described above, and disaster countermeasure drills in which they were used.

II. WINDS[1]

WINDS is an engineering test satellite developed by NICT and Japan Aerospace Exploration Agency (JAXA) to advance high-speed satellite communication network technology. WINDS was launched on February 23, 2008, and is located in a geostationary orbit of 143 degrees east longitude. It uses Ka-band (28 GHz-band for uplink and 18 GHz-band for downlink) for communication between the satellite and earth stations.

The block diagram of the WINDS transponder is shown in Figure 1. WINDS has an onboard switch (ABS) for regenerative relay mode, which demodulates uplink signals, switches, and modulates to downlink. The available data rates for uplink are 1.5, 6, 24, 51, and 155 Mbps, but only 155 Mbps is available for downlink. A time division multiple access (TDMA) system is used and multiple users can use the transponder simultaneously by means of time-slot sharing. A bent-pipe relay can also be used with a 1.1 GHz bandwidth transponder, which bypass ABS. WINDS has two types of antenna: Multi-Beam Antenna (MBA) and Active Phased Array Antenna (APAA). The MBA covers Japan and ten Asian cities, while the APAA has two receiving beams and two transmission beams that can scan around the globe. WINDS can be accessed from anywhere in Asia-Pacific region by using

TABLE I. MAJOR SPECIFICATIONS OF WINDS

Geostationary orbit	143 deg. east longitude
Launch	February 23, 2008
Frequency	Uplink: 27.5 to 28.6 GHz Downlink: 17.7 to 18.8 GHz
Antenna	Multi-beam antenna (MBA) Domestic beam: 12 beams Asian beam: 7 beams Active Phased Array Antenna (APAA): 2 beams
EIRP, G/T	MBA: > 68 dBW, > 18 dB/K APAA: > 55 dBW, > 7 dB/K
Communication mode	Regenerative relay mode Uplink: 1.5, 6, 24, 51, and 155 Mbps Downlink: 155 Mbps Bent-pipe relay mode Up to 3.2 Gbs

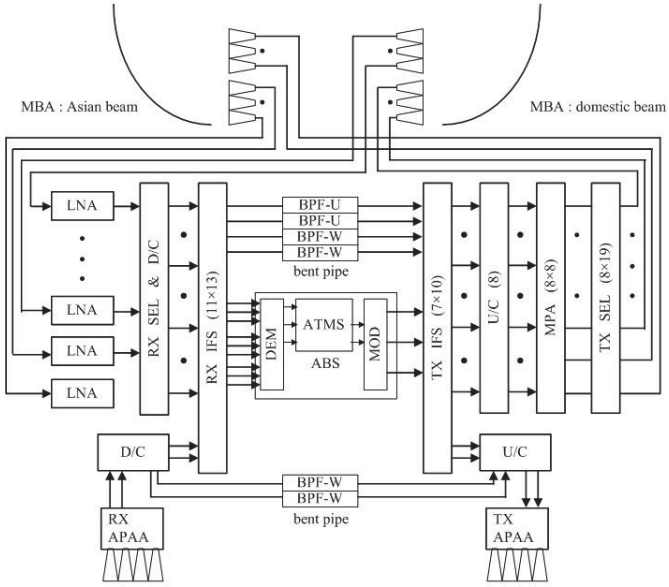

Figure 1. Block diagram of WINDS transponder.

the APAA.

The major specifications of WINDS are shown in Table I. The EIRP and G/T of the MBA are approximately 10 dB larger than the APAA.

In the area covered by the MBA, an ultra-small aperture terminal (USAT) with an antenna diameter of 45 cm can transmit at 6 Mbps and receive 155 Mbps using a regenerative relay.

III. Earth Station for Disaster Countermeasure Experiments using WINDS

The occurrence of large disaster highlighted the importance of ICT as a life line. NICT researches and develops resilient ICT networks in cooperation with universities and several companies. A resilient network should include a robust photonic network, dependable wireless and satellite network, and an anti-disaster information distribution platform. Figure 2 shows the dependable wireless mesh and satellite networks[2], [3].

NICT developed three types of earth stations for the resilient network experiment using WINDS. The three earth stations consist of a small mobile vehicle earth station, a large-scale in-vehicle earth station, and a fully-automatic transportable earth station, and they were designed to be easy to set up and operate.

A. Small mobile vehicle earth station[4], [5], [6]

A small mobile vehicle earth station was developed to communicate with the satellite while in motion so that the team dispatched to the affected area can obtain the most up-to-date

TABLE II. MAJOR SPECIFICATIONS OF SMALL MOBILE VEHICLE EARTH STATION

Tx frequency	27.5 to 28.6 GHz
Rx frequency	17.7 to 18.8 GHz
Polarization	Liner (H/V)
Antenna	0.65 m Cassegrain
HPA	20 W TWTA
Drive range	El: 20 to 90 degrees Az: Unlimited
Tracking accuracy	< +/-0.2deg.
Data rate	WINDS regenerative transponder Tx:1.5, 6, 24 Mbps Rx: 155 Mbps
Electric generator	2.8 kVA
User interface	Ethernet (1000base-T)

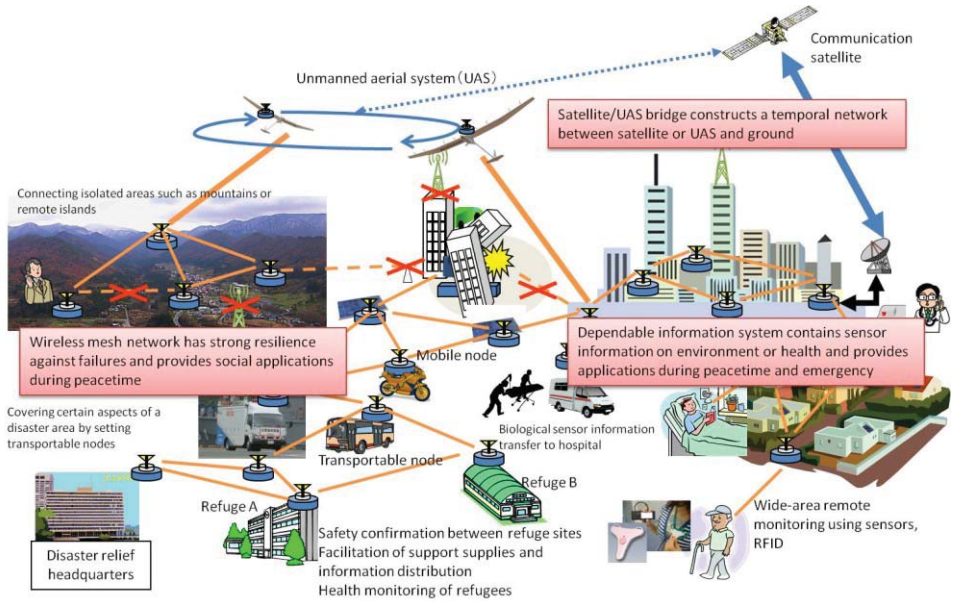

Figure 2. Dependable wireless mesh and satellite networks

Figure 3. Small mobile vehicle earth station.

information about the disaster, and modify its action plan in coordination with the dispatching agency.

This earth station is installed in a test van, such as the one shown in Figure 3, and the major specifications are listed in Table II. The antenna size is 0.65 m, and the output power of the high power amplifier is 20 W. The tracking accuracy is within +/- 0.2 deg. This earth station has an interlock function that disables transmissions when the signal to be received is small. A HDTV camera is installed on the roof, and the image can be transmitted to a satellite link.

B. Large-scale in-vehicle earth station[4], [5]

A large-scale in-vehicle earth station was developed so that it could function as a communication hub that combines the functions of satellite communication and wireless terrestrial network when it is dispatched to an affected area. This earth station is installed in a truck, such as the one shown in Figure 4, and the major specifications are listed in Table III. The antenna diameter is 2.4 m, and the output power of the high power amplifier is 175 W. The antenna is put away during transport and deployed upon arrival at the location from which it will communicate with the satellite. The earth station has an electric 8.5 kVA generator that can power the earth station and terrestrial network equipment.

C. Fully-automatic transportable earth station[4], [5]

When a disaster occurs, it may not be possible for experts

TABLE III. MAJOR SPECIFICATIONS OF LARGE-SCALE IN- VEHICLE EARTH STATION

Tx frequency	27.5 to 28.6 GHz
Rx frequency	17.7 to 18.8 GHz
Polarization	Liner (H/V)
Antenna	2.4 m offset parabola
HPA	175 W TWTA
Drive range	El: 15 to 65 degrees Az: +/-175 degrees
Tracking accuracy	< +/-0.2°
Data rate	WINDS regenerative transponder Tx:1.5, 6, 24, 51, and 155 Mbps Rx: 155 Mbps
Electric generator	8.5 kVA
User interface	Ethernet (1000base-T)

Figure 4. Large-scale in-vehicle earth station

to keep all the earth stations for satellite communications running. NICT developed a fully-automatic transportable earth station that can be installed and easily operated by individuals who are not experts.

Figure 5 shows a picture of the fully-automatic transportable earth station, the major specifications of which are listed in Table IV. The antenna diameter is 1.0 m and the power of the high power amplifier is 75 W. The earth station has a GPS compass that detects the position of the earth station and the direction of the antenna. The earth station can point the antenna in the direction of the satellite.

When using this earth station, we can transmit up to 51 Mbps and receive 155 Mbps using the WINDS regenerative transponder.

Figure 5. Fully-automatic transportable earth station.

TABLE IV. MAJOR SPECIFICATIONS OF FULLY-AUTOMATIC TRANSPORTABLE EARTH STATION

Tx frequency	27.5 to 28.6 GHz
Rx frequency	17.7 to 18.8 GHz
Polarization	Liner (H/V)
Antenna	1.0 m offset parabola
HPA	75 W TWTA
Drive range	El: 15 to 75 deg. Az: +/-95 deg.
Data rate	WINDS regenerative transponder Tx:1.5, 6, 24, and 51 Mbps Rx: 155 Mbps
Electric input power	90-132 or 180-264 V AC Power Consumption < 2 kVA
User interface	Ethernet (1000base-T)

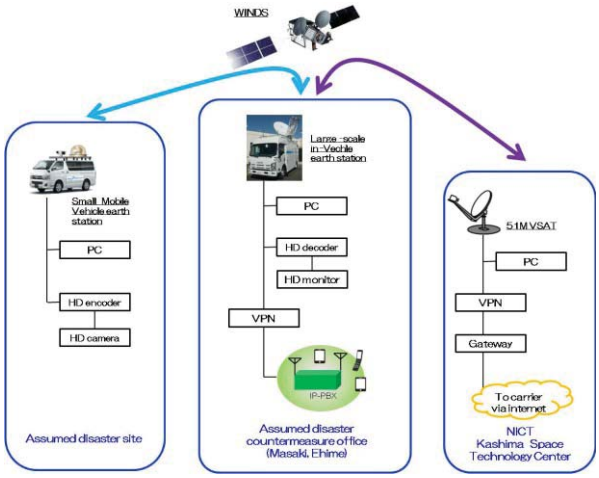

Figure 6. Network configuration of Ehime disaster prevention drill.

IV. DISASTER COUNTERMEASURE EXPERIMENTS USING WINDS

NICT participated in the disaster prevention drills conducted at various locations across Japan, providing satellite communication linkage through the use of WINDS. The following section takes a look at some of these drills.

A. Ehime prefecture disaster prevention drill

NICT dispatched a small mobile vehicle earth station and a large-scale in-vehicle earth station to participate in the Ehime disaster prevention drill. Ehime is located in the north of Shikoku, and is expected to suffer heavy damage when the next Nankai trough earthquake occurs. For this reason, the prefecture has placed emphasis on disaster prevention drills. The network configuration is shown in Figure 6. As the small mobile vehicle earth station tracked a transportation truck, it transmitted the video to the large-scale in-vehicle earth station that had been set up in the disaster countermeasure office. The large-scale earth station was connected to the NICT Kashima Space Technology Center (KSTC) via WINDS, with KSTC serving as the gateway to the Internet. In addition, the IP-PBX was installed on a large-scale in-vehicle earth station, and a demonstration of the temporary base station was given in an affected area where cell-phones could not be used. IP-PBX is a device that performs the circuit switching of the IP telephone terminal in an IP network. The data from IP-PBX was transmitted to the cell-phones carrier, enabling us to communicate with the public network.

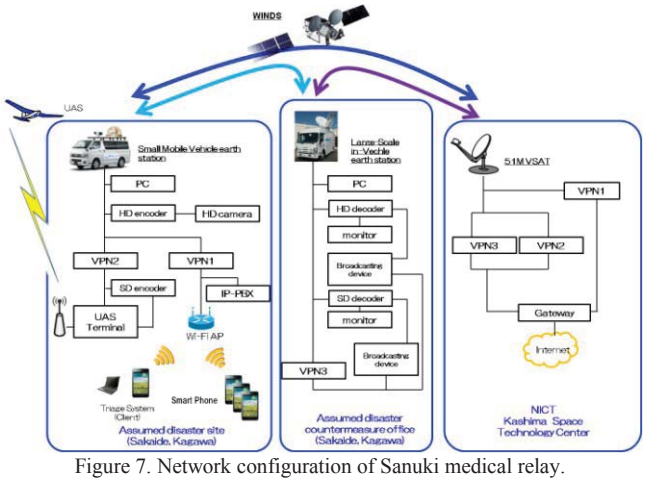

Figure 7. Network configuration of Sanuki medical relay.

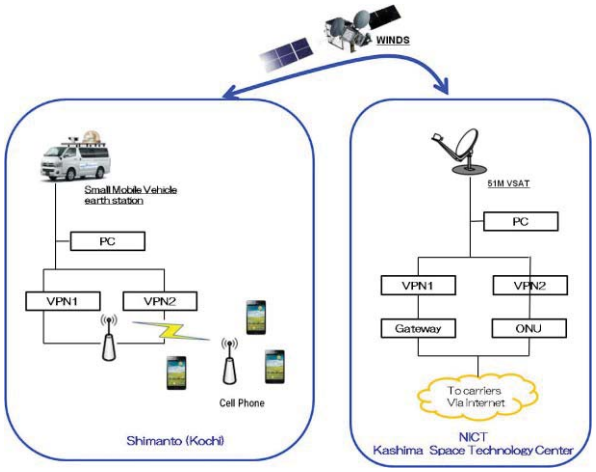

Figure 8. Network configuration of Femto-cell connection experiment.

B. Sanuki medical relay

Triage training using a satellite link and a digital triage tag system with digital pen was performed under the assumption that the terrestrial communication line would suffer damage during a large-scale disaster. NICT dispatched a small mobile vehicle earth station and a large-scale in-vehicle earth station to establish the satellite link using WINDS. The small mobile vehicle earth station was set up at the place where training was conducted, and the large-scale in-vehicle earth station was set up at the assumed disaster countermeasure office. The network configuration is as shown in Figure 7. Both earth stations were connected with KSTC, and could use Internet. The state of the training place was shot with a video camera set up on the small mobile vehicle earth station, and then transmitted to the assumed disaster countermeasure office and distributed to the Internet. An unmanned aeronautical system (UAS) served as the communication repeater and the camera from the sky. The data was transmitted to the small mobile vehicle earth station and distributed to the assumed disaster countermeasure office.

C. Femto-cell connection experiment using satellite links[7]

A femto-cell connection experiment was carried out under the assumption that temporary cell phone network would be established in an affected area where cell-phones could not be used.

The wireless mesh network was connected with the small mobile earth station and the femto-cell station. The small mobile earth station was connected with the cell-phone carriers through the KSTC via WINDS and Internet. The network configuration is as shown in Figure 8.

The delay in the satellite link was not a major concern, and good communication was established.

D. Japan Medical Association disaster prevention drill

NICT participated in Japan Medical Association (JMA) disaster prevention drill with JAXA and established a communication link using WINDS. The drill was conducted

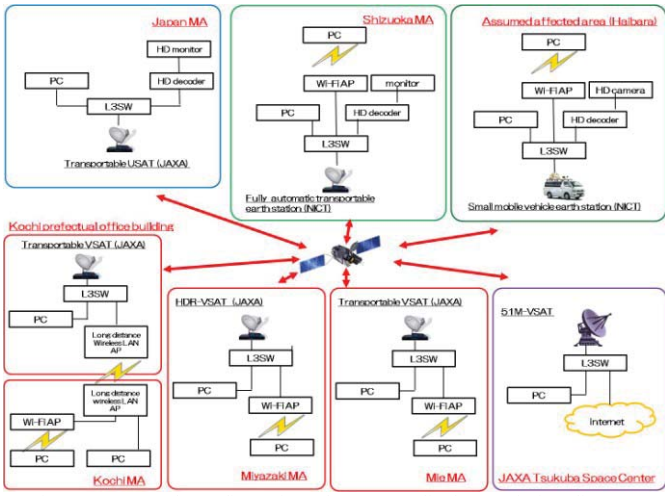

Figure 9. Network configuration of Japan Medical Association disaster prevention drill.

under the assumption that the next Nankai trough earthquake had occurred. NICT and JAXA set up WINDS terminals at five medical associations (MA), including associations in Shizuoka, Mie, Kochi, and Miyazaki Prefectures, as well as the JMA. NICT dispatched a fully-automatic transportable station to the Shizuoka MA and a small mobile earth station to Haibara in Shizuoka prefecture, based on the assumption that these two areas would be affected by the earthquake. The High-Data-Rate Very Small Aperture Terminal (HDR-VSAT) at the JAXA Tsukuba Space Center was connected to the Internet. The applications of the web meeting system used all the terminals, and HD video was transmitted from the small mobile vehicle earth station in Haibara to the Shizuoka MA and the JMA.

As a result, the effectiveness of sharing information among multiple points was demonstrated.

V. Conclusion

NICT developed resilient ICT facilities consisting of three types of earth stations for satellite communication network: a small mobile vehicle earth station, a large-scale in-vehicle earth station, and a fully-automatic transportable earth station.

These earth stations were participated in several disaster prevention drills to establish temporary communication link using WINDS. The possibility of many different applications was demonstrated by the satellite link connecting with the terrestrial network, such as the wireless mesh network. Video transmission from the small mobile vehicle earth station while moving was very useful for situation grasp and it became possible to deliver it to many points because of connecting to the internet.

An effective communication system technology will be developed when disasters occur, including the establishment of a connection with a satellite link and a wireless network between vehicles on the move.

Acknowledgment

The authors would like to thank the organizations involved with the disaster prevention drills, such as Ministry of Internal Affairs and communications, JAXA and JMA.

References

[1] Special Issue on Wideband InterNetworking engineering test and Demonstration Satellite (WINDS), Journal of the National Institute of Information and Communications Technology, Vol. 54, no. 4, December 2007.

[2] R. Miura, K. Takizawa, M. Suzuki, H. Tsuji, M. Inoue and Y. Owada, “Wireless Relay Using Small Unmanned Aerial System–For Rapid Recovery of Network Connection to Isolated Areas Under Large-Scale Disaster- ,” IEICE Technical Report SAT2012-4, Vol. 112, no. 51, pp. 17-21, 2012 (in Japanese).

[3] M. Toyoshima, N. Yoshimura, B.-P. Jeong, A. Akaishi, T. Takahashi, M. Akioka, Y. Fujino, S. Yamamoto, S. Taira and N. Kadowaki., “Concept of Satellite Communication Facility for Disaster Support in the Tohoku District,” 30th AIAA International Communications Satellite Systems Conference, 2012.

[4] T. Takahashi, B.-P. Jeong, M. Ohkawa, A. Akaishi, T. Asai, N. Katayama, M. Akioka, N. Yoshimura, M. Toyoshima, R. Miura and N. Kadowaki, “Disaster Satellite Communication Experiments using WINDSand Wireless Mesh Networks,” Proceeding of WPMC2013, 2013.

[5] T. Takahashi, Y. Fujino, A. Akaishi, N. Yoshimura, M. Akioka, M. Toyoshima and N. Kadowaki, “Development of Experimental Disaster Satellite Communications System,” 18th Ka and Communcations Navigation and Earth observation Conference, 2012.

[6] A. Akaishi, T. Takahashi, M. Ohkawa, T. Asai and B.-P. Jeong, “Ka-band Mobile Earth Station for WINDS,” 29th International Symposium on Space Technology and Science, 2013.

[7] http://www.soumu.go.jp/soutsu/shikoku/koho/teleporter/20150217.html (in Japanese)

THE 18TH INTERNATIONAL SYMPOSIUM ON WIRELESS PERSONAL MULTIMEDIA COMMUNICATIONS
(WPMC-2015)
December 13-16, 2015, Hyderabad, India

Development and Field Experiment of Distributed Peer Aware Communication Networks

Lin Shan, Huan-Bang Li, Takashi Matsuda, Ryu Miura
Wireless Network Research Institute
National Institute of Information and Communications Technology (NICT)
3-4, Hikarino-oka Yokosuka, 239-0847, Japan
E-mail: {shanlin, lee, matsuda, ryu}@nict.go.jp

***Abstract*—Applications of wireless communications to device-to-device without centralized coordination attract more and more attentions. We designed and developed a test bed of infrastructure independent wireless network that connects end devices directly without central control. Various types of end devices are implemented and used for different scenarios. There is neither conventional base station nor access point, so as to avoid the single-point-of-failure problem when accident or emergency happens. In this paper, we introduce the developed test bed of distributed peer aware communication networks. Since the MAC frame design is one of central importance for the whole system. It directly affects the delivery latency as well as system capacity. We mainly study and evaluate the system performance with different MAC frame designs using our experimental test bed.**

***Index Terms*—Device-to-Device (D2D), Peer Aware Communications (PAC), distributed control, MAC frame, solt allocation, field experiment.**

I. Introduction

To meet the ever-increasing demands on wide coverage and high capacity in wireless mobile communications, how to improve the spectrum utilization becomes more and more important. Heterogeneous network is one of the technologies that introduce multi-layer network structure in order to deal with off-load traffic [1]–[3]. On the other hand, applications of wireless communications to device-to-device (D2D) and machine-to-machine (M2M) attract more and more attentions. Moreover, in case that the existing infrastructures fail to work due to disaster like earthquake or other reasons, it is desirable that wireless devices distributedly form a network for information delivery without needing infrastructures [4]. D2D is also expected to play active roles in the Internet of Things [5] as well as in mobile social networks [6].

With the above-mentioned demand, the IEEE 802 Standardization Committee set up a task group of TG15.8 (IEEE 802.15.8) to develop a new standard for infrastructureless Peer Aware Communications (PAC). There is neither conventional base station (BS) nor access point (AP) in PAC network. Therefore, single point of failure (SPOF) due to inability of BS and AP as in conventional centralized control network will not happen. PAC can be used for information sharing and emergency communication by distributed in buses and neighbor community.

The IEEE 802.15.8 defines physical and media access control (MAC) mechanism for wireless personal area networks (WPAN) PAC with fully distributed coordination. PAC is a sort of mobile ad-hoc network (MANET) techniques and its features include (a) discovery for peer information without association, (b) discovery signaling rate, typically 100kbps, (c) the number of devices in the discovery, scalable data transmission rates, typically 10 Mbps, (d) group communication with simultaneous membership in multiple groups, typically up to 10, (e) relative positioning, (f) multi-hop relay, (g) security, (h) and operational in selected globally available unlicensed/licensed bands below 11 GHz capable of supporting these requirements [7]. The applications for PAC with multicast can support various new applications, such as social network service (SNS), local advertisement, emergency service, vehicle location service, game, audio/video streaming applications, proximity device control, P2P services, etc.

We has studied PHY and MAC mechanism and proposed MAC proposals for PAC standardization working group [8]–[11]. We focused on multiple group/network forming problem among a number of devices of proximities that are deployed in a local area, where a group operation algorithm was proposed based on distributed control [12]. In this paper, we provide a brief overview of our experimental test-bed which is deployed in two real fields: one is Odaiba area of Tokyo as a typical urban model and another is Seika Town of Kyoto as a typical rural model for field evaluation. This test bed is designed and developed as a precursor system based on the concept of PAC. Since the MAC frame design (time slot allocation) is one of central importance for the whole system. It directly affects the delivery latency as well as system capacity. We mainly study and evaluate the system performance with different MAC frame designs using the experimental test bed in this work.

The remainder of this paper is organized as follows. Sect. II describes the structure of PAC system. Sect. III describes an overview of PAC experimental test-bed and MAC frame designs. Sect. IV describes the field evaluation scenarios and experiment results. Sect. V includes our concluding remarks.

II. Peer Aware Communications (PAC) System

In the PAC system, there is no central control BS. If PAC devices come into the communication range, information can be exchanged with each other directly. The collection and

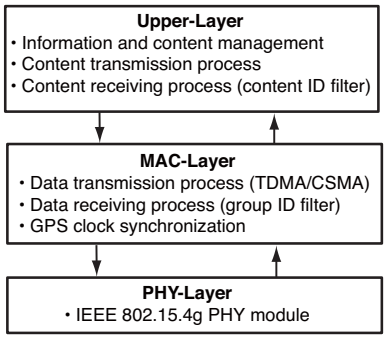

Fig. 1. Peer aware communications (PAC) system structure.

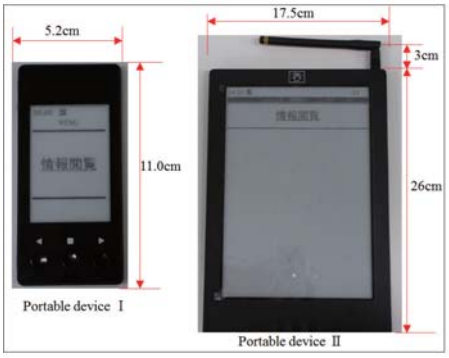

Fig. 2. Two types of portable PAC devices: Portable-I and Portable-II.

Fig. 3. Signage type PAC devices: (a) stationary version (Signage-P) and (b) vehicle-mounted version in a bus (Signage-B).

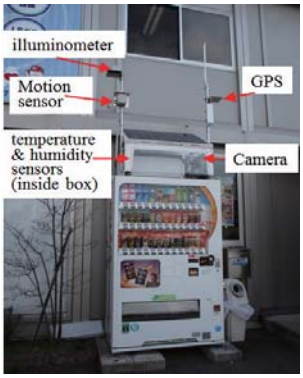

Fig. 4. Sensor type PAC device (Sensor-D) located on a vending machine.

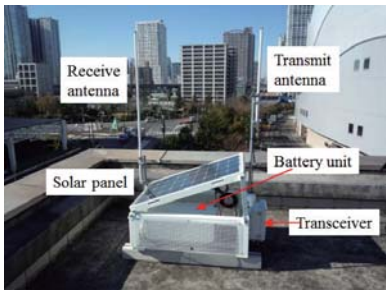

Fig. 5. High power PAC device (High-D) located on the rooftop of building.

diffusion of information are performed by either people or vehicles carrying PAC devices in fully distributed fashion. Based on the above features, we originally developed a experimental PAC test-bed. The structure of PAC system is shown in Fig. 1, where the MAC-layer protocol is designed by our original way. The IEEE 802.15.4g PHY module is applied in this PAC device.

We designed four types of PAC devices in the test bed include portable devices (type I and type II) that can be carried by person as shown in Fig. 2, signage devices that can be mounted in bus or laid in public building as shown in Fig. 3, sensor devices that are distributed in local area to gather weather and other data as shown in Fig. 4, high power device that can be mounted on the roof of a building and has a much larger coverage than the other devices as shown in Fig. 5.

All above devices have limited communication range. If a device needs to communicate with other devices exceeding the range, relay and multi-hop are necessary. It should be noted that we designed a message/data holding function for all devices. The signage device mounted in the bus (Signage-B) can directly communicate with other devices in surroundings, such as the signage devices in a hotel, in a local administration office, and/or in a shopping mall (Signage-P), sensor device (Sensor-D), portable device I (Portable-I) carried by person, as well as portable device II (Portable-II) used in houses and offices.

As bus moves, the signage-B communicates with new devices it connects to. On one hand, it diffuses information/data that it holds. On the other hand, signage-B collects data or receive message from those connected devices. In such a manner, information are collected and/or diffused gradually within the local area as buses move. This is also available with portable devices. In some case, such as the emergency alarm and bus location information, it need to be delivered in quasi-real time. To address this requirement, high power device (High-D) is used for broadcasting high-priority information to all PAC devices, of course it is operated in distributed fashion. By enabling direct link between High-Ds, the delivery latency of data can be minimized.

The devices sketched in the foregoing section are installed using a 920 MHz module. This module is implemented based

on ARIB STD-T108 [13]. It occupies 400kHz bandwidth as a single channel and achieves 115.2kbps data rate by employing binary GFSK modulation. CRC-16 is adopted for error detection. The maximum permitted equivalent-isotropically-radiated-power (e.i.r.p.) is 250mW for high-D and 20mW for other devices. It should be noted that 250mW is of the similar order of e.i.r.p. of a mobile phone. The communication range with line-of-sight (LOS) is about 900m between a pair of 20mW devices and about 3km between a 20mW devices and a 250mW device. Moreover, although there are a dozen of channels available, we use a fixed channel with a center frequency at 922.5 MHz in the test bed.

Main components of each type of device are summarized in TABLE 1. Signage devices and portable devices are installed with display and user I/O interface while Sensor-D and High-D are not. This is because that Sensor-D and High-D do not interact with users directly.

TABLE I
VARIOUS DEVICES AND THEIR MAIN COMPONENTS

Device Type	Main Components
Protable-I (2.7-inch EPD)	920MHz module, plane-type antenna, 3D motion sensor, GPS kit, user I/O interface, lithium ion battery, elctrical paper display (EPD)
Protable-II (9.7-inch EPD)	
Signage-P	920MHz module, dipole antenna, 21.5-inch display, GPS kit, user I/O interface, CF and SD.
Signage-B	
High-D	920MHz module, dipole antennas, solar power system
Sensor-D	920MHz module, dipole antennas, temperature and humidity sensor, video camera, motion sensor, illuminometer, solar power system

III. TEST-BED DEPLOYMENT AND MAC FRAME DESIGN

A. Test-Bed Deployment

We chose two different fields to experimentally deploy the developed test bed. The first field is the Seika Town in Kyoto prefecture, which is a typical rural area with scarcely scattered high buildings and small hills. The test bed is deployed alone the route of a commuter bus which is known as *Seika KURURIN*. The bus route and devices deployed in the area are depicted on a local map shown in Fig. 6. Three buses serve for this route. The second test field is the Odaiba Area in Tokyo, which is a famous tourist resort and a typical urban model with dense of high buildings. The test bed is mainly deployed alone the route of a commuter bus which is known as *Odaiba Rainbow Bus*. Route of the bus and devices deployed are depicted on a local map shown in Fig. 7.

TABLE II summarizes all devices deployed in the two areas. It can be seen that the number of Odaiba Rainbow Bus is seven to provide frequent transportation, while the bus of Seika KURURIN is three. On the other hand, sensor devices are only deployed in Seika Town, where it is convenient to find places to mount the devices. Other devices are deployed equally. A remote PC server is used in our laboratory for monitoring and analysis purposes, which is connected to particular signage devices through internet.

TABLE II

Area	Signage -B	Signage -P	Sensor -D	High -D	Portable -I	Portable -II
Seika	3	5	8	5	10	10
Odaiba	7	5	0	5	10	10

Fig. 6. Test-bed deployment at Seika-Town of Kyoto prefecture.

B. MAC Frame Design: TDMA/CSMA Channel Access

The MAC frame design is one of central importance for the whole system. It directly affects the delivery latency as well as system capacity. In this work, we design three different MAC frame patterns as shown in Fig. 8 and evaluate the system performance using our test bed at Seika-Town of Kyoto prefecture. Since our PAC system may include high-priority information such as emergency information, that must be delivered to all devices using the High-D within a super

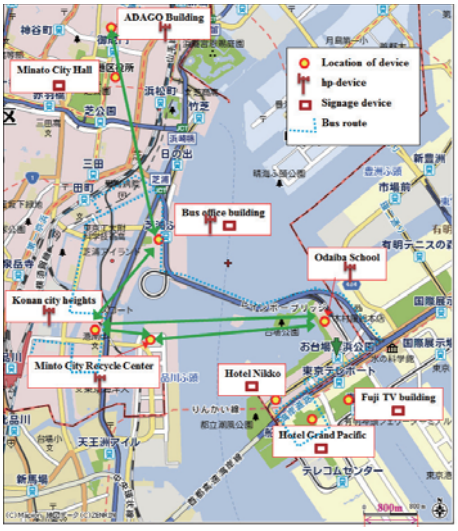

Fig. 7. Test-bed deployment at Odaiba area Tokyo.

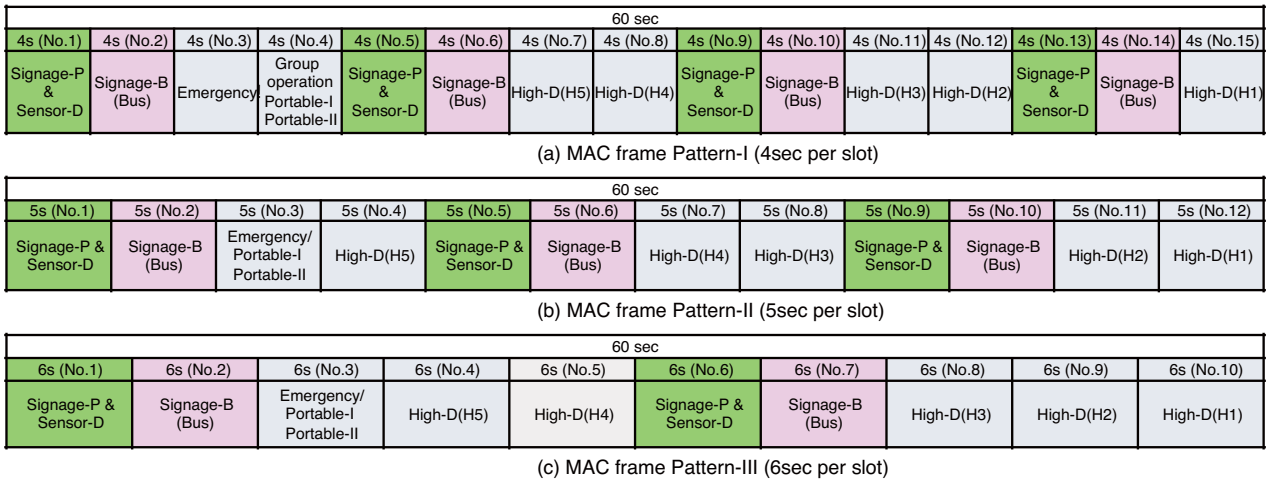

Fig. 8. Time slot allocation patterns in a super MAC frame.

MAC frame. The duration of a super MAC frame is set as 60s for all frame patterns. In each slot (4s, 5s and 6s), CSMA channel access is operated by the PAC devices.

MAC frame *Pattern-I* shown in Fig. 8 (a): there are total 15 slots in a super MAC frame and each has a length of 4s. Because that Signage-B, Signage-P and Sensor-D play more active roles, they are assigned with periodic slots in the frame, i.e., once every four slots for routine access (except the last three slots). Five slots are assigned to each High-D exclusively, that are distributed in slot no.7, no.8, no.11, no.12 and no.15. The purpose is to avoid interference between High-Ds since they have much large coverage. Slot no.3 is assigned for sending urgent message. Slot no.4 is assigned for group operation of the Portable-I and II users.

MAC frame *Pattern-II* shown in Fig. 8 (b): there are total 12 slots in a super MAC frame and each has a length of 5s. Three slots are assigned to Signage-P and Sensor-D in slot no.1, no.5 and no.9. Another three slots are assigned to Signage-B in slot no.2, no.6 and no.10. Five 5s slots are assigned to each High-D exclusively, that are distributed in slot no.4, no.7, no.8, no.11 and no.12. Slot no.3 is assigned for group operation and sending urgent message.

MAC frame *Pattern-III* shown in Fig. 8 (c): there are total 10 slots in a super MAC frame and each has a length of 6s. Two 6s slots are assigned to Signage-B. Five 6s slots are assigned to each High-D exclusively, that are distributed in slot no.4, no.5, no.8, no.9 and no.10. Slot no.3 is assigned for group operation and sending urgent message.

IV. PAC Test-bed Performance Evaluation

Since the MAC frame design is one of central importance for the whole system, we evaluate the system performance using three different MAC frame patterns at our test-bed of Seika-Town Kyoto prefecture as shown in Fig. 6. There are two scenarios considered for the PAC system performance evaluation: (i) data collection and delivery using sensor device (Sensor-D) and high power device (High-D), and (ii) data delivery using signage devices (Signage-P and Signage-B).

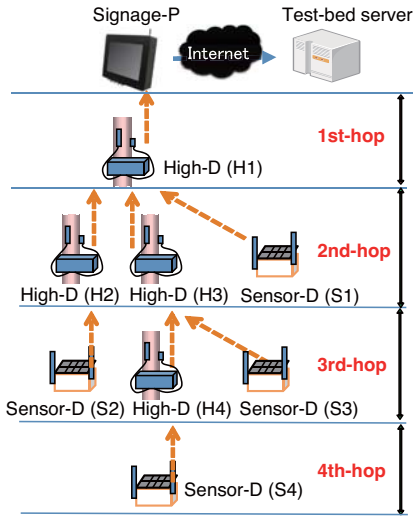

Fig. 9. Evaluation scenario of sensor device (Sensor-D) data multi-hop delivering via high power device (High-D).

A. Evaluation Scenario I: Sensor Data Multi-hop Delivery

The image of the sensor data multi-hop delivery scenario is shown in Fig. 9, where each Sensor-D delivers its data to a gate front Signage-P via High-D. For example, the Sensor-D (S4) needs four hops to deliver its data to the gate front Signage-P: Sensor-D (S4) ⇒ High-D (H4) ⇒ High-D (H3) ⇒ High-D (H1) ⇒ Signage-P. The Sensor-D (S1) needs two hops to deliver its data to the gate front Signage-P: Sensor-D (S1) ⇒ High-D (H1) ⇒ Signage-P. We measure the data necessary delivering time between Sensor-D and Signage-P using three different MAC frame patterns.

The experimental results of each Sensor-D's data delivering time are shown in Fig. 10. We observe that using MAC frame

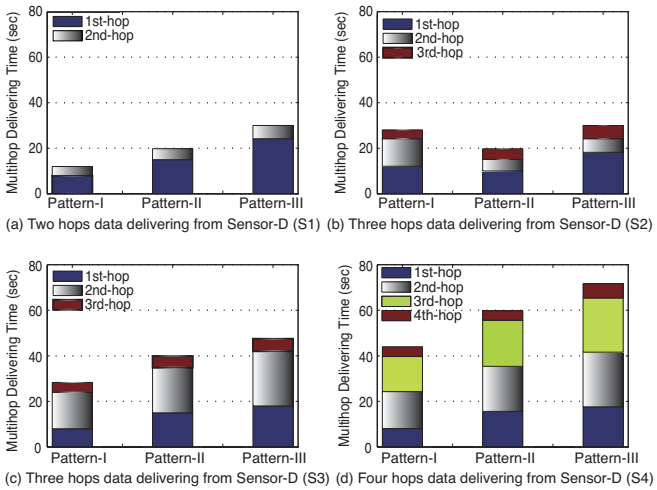

Fig. 10. Experimental results of sensor device (Sensor-D) data multi-hop delivering via high power device (High-D).

Pattern-I can achieve almost the shortest delivering time, and using Pattern-III achieves the longest delivering time. The reason is that in a super MAC frame of Pattern-I there are more chances (slots) allocated to Sensor-D to sending its data than Pattern-II and Pattern-III. Pattern-I has 4 slots allocated to Sensor-D, while Pattern-III has only 2 slots allocated to Sensor-D as shown in Fig. 8.

B. Evaluation Scenario II: Signage-P Data Relaying via Signage-B

The scenario image of the stationary signage device (Signage-P) data relaying via vehicle-mounted signage device (Signage-B) is shown in Fig. 11, where the signage data is delivered by the Signage-B from a gate front Signage-P to other Signage-Ps. In this scenario, we increase the data size by 0.2kbyte as a increment unit and measure the maximum deliverable data size per slot using different MAC frame patterns.

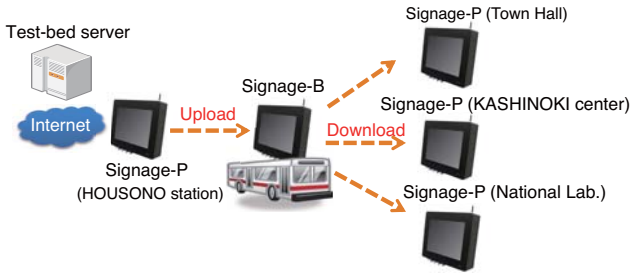

Fig. 11. Evaluation scenario of stationary signage device (Signage-P) data relaying via vehicle-mounted signage device (Signage-B).

The experimental result of scenario II is shown in TABLE III. Pattern-III can upload and download the largest data size in the designed frame patterns. Since the reliability is an important issue for the data transmission, we also find the maximum data size to secure the 90% success rate for each of the three frame patterns.

TABLE III
DELIVERABLE DATA SIZE PER SLOT FOR DIFFERENT FRAME PATTERNS.

	Pattern-I	Pattern-II	Pattern-III
Largest data size	19.8kbyte	25kbyte	30.4kbyte
Maximum data size to secure 90% success rate	19kbyte	24kbyte	29.2kbyte

V. CONCLUSIONS

We developed a test bed of infrastructure independent wireless network that connects end devices directly without central control. The test bed demonstrates a solution for PAC network, which is currently under standardization process as IEEE802.15.8. We deployed the test bed in a typical rural field as well as in an urban field respectively. Data collection and diffusion among local community are conducted and examined through the test bed. Since the MAC frame design is one of central importance for the whole system. We designed three different MAC frame patterns and evaluated the system performance using our test-bed at Seika-Town of Kyoto prefecture. Our field experiment results reveal that frame pattern directly affects the delivery latency as well as system capacity.

REFERENCES

[1] J. Andrews, "Seven ways that HetNets are a cellular paradigm shift,," *IEEE Comm. Mag.*, vol. 51, pp. 136–144, 2013.
[2] B. Bangerter, et al., "Networks and devices for the 5G era," *IEEE Comm. Mag.*, vol. 52, pp. 90–96, 2014.
[3] A. Ghosh, et al., "Heterogeneous cellular networks: From theory to practice," *IEEE Comm. Mag.*, vol. 50, no. 6, pp. 54–64, Jun. 2012.
[4] G. Fodor, et al., "Design aspects of network assisted device-to-device communications," *IEEE Comm. Mag.*, vol.50, no.3, pp. 170–177, March 2012.
[5] O. Bello and S. Zeadally, "Intelligent device-to-device communication in the internet of things," *IEEE Systems Journal*, Vol. PP, Issue: 99, pp.1–11, 2014.
[6] J. Lee, T.Q.S. Quek, "Device-to-device communication in wireless mobile social networks," *IEEE 79th Vehicular Technology Conference (VTC Spring)*, May 2014.
[7] IEEE standard for local and metropolitan area networks–part 15.8: peer aware communications (PAC) *http://www.ieee802.org/15/pub/TG8.html*
[8] H.-B. Li, M. Hernandez, I. Dotlic, and R. Miura, "NICTs MAC proposal for IEEE802.15.8 peer aware communications," *IEEE P802.15-13-0270-00-0008*, May 2013.
[9] H.-B. Li, M. Hernandez, I. Dotlic, and R. Miura, "NICT's MAC proposal with simulation results," *IEEE P802.15-13-0381-00-0008*, July 2013.
[10] H.-B. Li, M. Hernandez, I. Dotlic, and R. Miura, "NICT MAC proposal document," *IEEE P802.15-13-0396-01-0008*, July 2013.
[11] H.-B. Li, M. Hernandez, I. Dotlic, and R. Miura, "New simulation results on PAC discovery," *IEEE P802.15-13-0529-00-0008*, Sept. 2013.
[12] H.-B. Li and R. Miura, "Distributed network forming among devices of proximities," *IEICE Technical Report on Reliable Commun. and Control (RCC)*, 2014-01, Tokyo, Jan. 2014.
[13] Association of Radio Industries and Businesses (ARIB), "920MHz-Band telemeter, telecontrol and data transmission radio equipment," ARIB STD-T108 Version 1.0, Feb. 2012.

THE 18TH INTERNATIONAL SYMPOSIUM ON WIRELESS PERSONAL MULTIMEDIA COMMUNICATIONS
(WPMC-2015)
December 13-16, 2015, Hyderabad, India

Throughput of Secondary User in Underlay Cognitive Relay Network with Energy Harvesting

Binod Prasad
Department of ECE
NIT Durgapur, India
binod.ece@gmail.com

Sanjay Dhar Roy, Member, IEEE
Sumit Kundu, Senior Member, IEEE
Department of ECE, NIT Durgapur, India
s_dharroy@yahoo.com, sumit.kundu@ece.nitdgp.ac.in

***Abstract*— In this paper we study the time switching based energy harvesting (EH) and information transmission protocol for an underlay cognitive relay network where the transmit power of secondary transmitter as well as secondary relay is limited so as to maintain a constraint on QoS of primary user in terms of primary outage. We study the performance of such underlay cognitive relay network with decode and forward (DF) relaying scheme in terms of throughput. A power control law for energy harvesting secondary relay is designed so as to maintain the interference constraint at the PU receiver. The impact of allowable interference threshold (I_{th}), PU outage constraint (δ) and harvesting energy time (α) on throughput of secondary user (SU) and the average transmit power of relay is also studied. Further the impact of tolerable interference threshold, PU outage constraint on the throughput of SU is indicated.**

Keywords—Energy harvestingt;decode and forward; throughput;outage constraint.

I. INTRODUCTION

Cognitive radio has been proposed as an efficient way to strike a balance between spectrum scarcity and spectrum underutilization problem by allocating temporarily the unused spectrum to the unlicensed secondary user (SU). Underlay spectrum sharing is one of the potential techniques where both the primary user (PU) as well as secondary user concurrently utilizes the same spectral band provided the interference produced at the PU receiver due to transmission of SU is below the interference threshold of the PU [1-3]. As the transmit power of SU in underlay technique is controlled in order to protect the PU receiver, the performance of SU is limited in terms of coverage area and outage performance. Cooperative relays are the potential techniques used to enhance the system performance in terms of coverage area and as well as SINR by using spatial diversity. A combination of cooperative relay and cognitive radio is used in order to improve the secondary performance [4-5]. In the recent year there has been significant attention on the energy harvesting relays in connection with cooperative communication. The concept of harvesting energy from ambient RF signal and simultaneous information delivery by the relay has been studied in [6-8]. In [8] the performance of SU has been evaluated in terms of outage probability with energy harvesting and information transfer protocol in an underlay scenario. A general cooperative network based on decode and forward relaying has been studied in [9] where the relay is assumed to harvest energy from the RF transmission from the source. Throughput and ergodic capacity of such network is studied for two energy harvesting schemes based on time switching and power splitting respectively. It is interesting to study the network performance of cooperative network based on energy harvesting relay for an underlay cognitive network scenario. Analyzing the performance of cognitive relay network with energy harvesting under spectrum sharing approach is an important research issue. The performance of different relaying scheme, amplify and forward (AF), decode and forward (DF) in terms of outage probability under energy constraint relays are studied in [10-11]. The performance of SU with energy harvesting DF relaying in an underlay scenario has been studied in [11]. In this present paper we extend the concept of time switching based energy harvesting to an underlay cognitive relay network where the secondary relay (SR) harvests energy from the RF signal transmitted by SU and the transmit power of secondary transmitter as well as SR is limited so as to maintain a constraint on QoS of PU in terms of primary outage. The secondary relay selects its transmit power based on harvested energy and outage constraint of PU. The transmit power of the relay is chosen in any one of the two possible modes, (i) the maximum possible power level corresponding to harvested energy (ii) the maximum power level corresponding to outage constraint of PU. Throughput of underlay cognitive relay network is evaluated under such scenario. The impact of several network parameters such as QoS of PU in terms of maximum tolerable interference, outage constraint, on secondary throughput is investigated. The contributions of our paper are:

- An analytical framework is developed to evaluate performance of underlay cognitive relay network with energy harvesting relay.
- Impact of maximum tolerable interference threshold (I_{th}) at primary receiver (PU-Rx), primary outage constraint (δ) and fraction of time frame (α) allocated for energy harvesting on overall throughput of secondary network is investigated.
- Development of a simulation test bed in MATLAB to validate analytical formulation.
- Formulating a power control law for energy harvesting of secondary relay. We derive the average transmit

power of relay highlighting the impact of I_{th}, δ, and α on average transmit power.

The remainder of the paper is organized as follow: Section II describes the system model considered for this paper. In Section III, we derive the expression for throughput of the network. Section IV shows the numerical results on throughput and average power of relay . Finally, Section V concludes the paper.

II. System Model

The system model considered in our work consists of a SU transmitter (SU-Tx), a secondary relay (SR), a secondary destination (SU-Rx) and a PU receiver (PU-Rx) as shown in Fig. 1. We assume that there is no direct link between SU-Tx and SU-Rx and hence SU transmission is assisted by SR working in DF mode. We assume that the DF relay harvests energy from the source signal. The relay uses the harvested energy as a source of transmit power while maintaining the interference produced at PU receiver below a interference threshold. The relay is assumed to harvest energy for a fraction of time (αT) of the total time frame T and the half of remaining time i.e. (1-α)T/2 is used for source to relay information transmission and the other half, (1-α)T/2 for relay to destination information transmission. The relay is assumed to perform the joint task of energy harvesting and information processing [6]. In underlay the transmit power of SU and relay are controlled so as to maintain an outage constraint imposed by PU based on a given interference threshold. The harvested energy is used as a source of transmit power, ($P_r^{harvest}$) in order to forward the information from relay to destination. The transmit power of the relay is derived from harvested energy only. However there are two cases for the level of transmitted power from relay (i) in case the maximum possible transmit power based on harvested energy ($P_r^{harvest}$) is less than the maximum allowed transmit power $\left(P_r^{\max}\right)$ due to outage constraint of PU, the relay transmits with power $P_r^{harvest}$, we consider the relay to work in mode 1 and call it as *transmission in harvest power mode* otherwise (ii) if $P_r^{harvest}$ exceeds $P_r^{\max}$, the transmission power of the relay is limited to $P_r^{\max}$, and we call this as mode 2 which is *underlay constrained power mode*.

Let h_{sp}, h_{rp}, h_{sr}, and h_{rd} denote the instantaneous fading coefficients of the links from SU-Tx to PU-Rx, from SR to PU-Rx, SU-Tx to SR, and SR to SU destination respectively. All the links are assumed to be independent and identically distributed Rayleigh fading channel with zero mean and unity variance. Therefore the channel power gain, $g_{xy} = |h_{xy}|^2$ is exponentially distributed, where x,y= {s,r}or {p,d}.

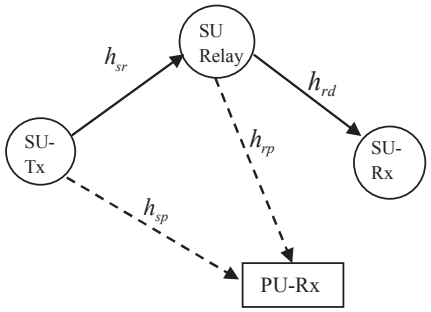

Fig. 1. (a) System model for cognitive relay network.

III. Throughput Under Time Switching Based Relaying

In this section the throughput of the network is analyzed considering a time switching based relaying (TSR) scheme of energy harvesting as in [9]. The transmission block structure in the time switching based relaying scheme is shown in Fig. 2. In the first time frame the SU transmits signal with a power evaluated under a given outage constraint of PU. The relay uses a fraction of block time α $(0 < \alpha < 1)$ for harvesting energy from the source signal. The half of the remaining time frame $(1-\alpha)T/2$ is used for source to relay information transmission and the remaining time frame, $(1-\alpha)T/2$ is used for relay to destination information transmission. However the transmit power of relay is controlled in order to protect the PU from harmful interference due to relay transmission. The relay transmits either in mode 1 with transmit power $P_r^{harvest}$ or in mode 2 with transmit power $P_r^{\max}$ depending on the interference constraint of PU as described before.

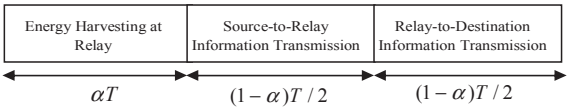

Fig. 2. Transmission block structure for energy harvesting and information transmission.

It may be noted that the relay and the SU do not transmit simultaneously. The outage probabilities of PU constrained by a maximum limit (δ) depending on QoS of PU, due to SU and relay transmissions are given as

$$P_{out-su}^{PU} = \Pr\{P_s^{\max} g_{sp} > I_{th}\} \le \delta \quad (1)$$

$$P_{out-Rel}^{PU} = \Pr\{P_r^{\max} g_{rp} > I_{th}\} \le \delta \quad (2)$$

In writing eq. (1) and eq. (2) we assume the perfect CSI between the SU-Tx and PU-Rx i.e. (g_{sp}) as well as between the SR and PU-Rx (i.e. g_{rp}) is available. The case of imperfect CSI is under investigation by us.

The maximum transmit powers of SU and relay due to underlay constraint are evaluated by equating the above eq. (1) and (2) to δ as:

$$P_s^{\max} = -\frac{I_{th}}{\log(\delta)} \quad (3)$$

$$P_r^{\max} = -\frac{I_{th}}{\log(\delta)} \tag{4}$$

The relay harvests the energy during the time, αT and uses it as a source of transmit power to forward the information during time (1-α)T/2 maintaining an outage constraint (δ) at PU-Rx. The harvested energy at the relay is given as [13]

$$E_h = \frac{\eta P_s^{\max} g_{sr}}{d_1^{\,m}} \alpha T \tag{5}$$

The maximum transmit power of relay available from the harvested energy is given as

$$\begin{aligned} P_r^{harvest} &= \frac{E_h}{(1-\alpha)T/2} \\ &= \frac{\eta P_s^{\max} g_{sr} \alpha}{d_1^{\,m}(1-\alpha)} \end{aligned} \tag{6}$$

where $0<\eta<1$ is the energy conversion efficiency and depends on the energy harvesting circuitry and 'd_1' and 'm' are distance between the source and relay; and m is the path loss exponent. Therefore the transmit power of the relay is given as

$$P_r = P_r^{harvest} \quad if\ P_r^{harvest} \le P_r^{\max} \tag{7.1}$$

$$= P_r^{\max} \quad if\ P_r^{harvest} > P_r^{\max} \tag{7.2}$$

Thus in (7.1) the relay transmits in harvest power mode, while (7.2) indicates the transmit power in underlay constrained mode. Let us assume that relay transmits in harvest power mode with probability 'p_1' while it transmits in underlay constrained mode with probability 'p_2' given as

$$\begin{aligned} p_1 &= \Pr\left\{P_r^{harvest} \le P_r^{\max}\right\} \\ &= 1-\exp\left(-\frac{P_r^{\max}}{P_s^{\max}\beta_1}\right) \end{aligned} \tag{8}$$

$$\begin{aligned} p_2 &= \Pr\left\{P_r^{harvest} > P_r^{\max}\right\} \\ &= 1-p_1 \end{aligned} \tag{9}$$

The signal to noise ratio at the relay node during time (1-α)T/2 are given as

$$\gamma_{sr} = \frac{P_s^{\max} g_{sr}}{N_0 d_1^{\,m}} \tag{10}$$

and the signal to noise ratio at the secondary receiver is given as

$$\gamma_{rd_1} = \frac{P_r^{harvest} g_{rd}}{N_0 d_2^{\,m}} \quad \text{with probability } p_1 \tag{11}$$

$$\gamma_{rd_2} = \frac{P_r^{\max} g_{rd}}{N_0 d_2^{\,m}} \quad \text{with probability } p_2 \tag{12}$$

where 'd_2' is the distance between the relay and SU receiver.

In order to find the throughput of the SU, the ergodic capacity of source to relay link and relay to destination link is evaluated as

$$\begin{aligned} C_{sr}^{\,erg} &= E\{\log(1+\gamma_{sr})\} \\ &= \int_0^{\infty} \log(1+\gamma_{sr}) d\gamma_{sr} \\ &= -\exp(-\lambda_1) Ei(-\lambda_1) \end{aligned} \tag{13}$$

where $\lambda_1 = \frac{N_0 d_1^{\,m}}{P_s^{\max}}$ and $Ei(\mathrm{x})$ is the exponential integral function given by $Ei(x) = -\int_{-x}^{\infty} \frac{e^{-t}}{t} dt$ [14].

$$\begin{aligned} C_{rd}^{\,erg1} &= E\{\log(1+\gamma_{rd_1})\} \\ &= \frac{2N_0}{P_s^{\max}\beta_1} \int_0^{\infty} \log(1+\gamma_{rd_1}) f_{\gamma_{rd_1}}(\gamma_{rd_1}) d\gamma_{rd_1} \end{aligned} \tag{14}$$

where $\beta_1 = \frac{2\eta\alpha}{d_1^{\,m}(1-\alpha)}$.

Following [9], eq. (14) can be solved as

$$C_{rd}^{\,erg1} = -\frac{2N_0}{\beta_1 P_s^{\max} \log(4)} G_{p,q}^{m,n}\left(\begin{matrix} [\{0\},\{\ \}] \\ [\{-1,0,0\},\{\ \}] \end{matrix} \middle| \frac{N_0}{\beta_1 P_s^{\max}} \right) \tag{15}$$

$C_{rd}^{\,erg1}$: indicates the ergodic capacity of SR-SU receiver link when the relay works in harvest power mode i.e. mode 1 with probability p_1.

Here $G_{p,q}^{m,n}\left(\begin{matrix} a_1 \ldots . a_p \\ b_1 \ldots . b_q \end{matrix} \middle| z \right)$ indicates meijerG function is defined as [9]

$$\begin{aligned} &G_{p,q}^{m,n}\left(\begin{matrix} [\{a_1,\ldots,a_m\},\{a_{m+1},\ldots,a_p\}] \\ [\{b_1,\ldots,b_n\},\{b_{n+1},\ldots,a_q\}] \end{matrix} \middle| z \right) \\ &= \frac{1}{2\pi l} \int \frac{\prod_{j=1}^{m} \Gamma(1-a_j-s) \prod_{j=1}^{n} \Gamma(b_j+s)}{\prod_{j=m+1}^{p} \Gamma(a_j+s) \prod_{j=n+1}^{q} \Gamma(1-b_j-s)} z^{-s} ds \end{aligned} \tag{16}$$

where $l = \sqrt{-1}$ and $\Gamma(x) = \int_0^{\infty} t^{x-1} e^{-t} dt$ is the Gamma function.

Let $C_{rd}^{\,erg2}$ indicates the ergodic capacity of SR-SU receiver link when the relay works in underlay constrained mode i.e. mode 2 with probability p_2.

$$\begin{aligned} C_{rd}^{\,erg2} &= E\{\log(1+\gamma_{rd_2})\} \\ &= \int_0^{\infty} \log(1+\gamma_{rd_2}) f_{\gamma_{rd}^{\,2}}(\gamma_{rd_2}) d\gamma_{rd_2} \\ &= -\exp\left(\frac{N_0 d_2^{\,m}}{P_r^{\max}}\right) Ei\left(-\frac{N_0 d_2^{\,m}}{P_r^{\max}}\right) \end{aligned} \tag{17}$$

The actual ergodic capacity is given by minimum of source to relay and relay destination link ergodic capacity as [15].

$$C_1 = \min\left\{C_{sr}^{\,erg}, C_{rd}^{\,erg1}\right\} \text{ and } C_2 = \min\left\{C_{sr}^{\,erg}, C_{rd}^{\,erg2}\right\} \tag{18}$$

Overall ergodic capacity is given as

$$C_{ov} = p_1 C_1 + p_2 C_2 \tag{19}$$

Now the average throughput of the network is given as

$$\tau_{avg}^{\,erg} = p_1 \tau_1 + p_2 \tau_2 \tag{20}$$

where τ_1 and τ_2 are the throughput under transmit power of $P_r^{harvest}$ and $P_r^{\max}$ respectively and given as

$$\tau_1 = \frac{C_1(1-\alpha)T/2}{T} \text{ and } \tau_2 = \frac{C_2(1-\alpha)T/2}{T} \quad (21)$$

Also the average transmit power of relay is given as

$$P_{avg}{}^{r} = p_1 \overline{P}_r^{harvest} + p_2 P_r^{\max} \quad (22)$$

where $\overline{P}_r^{harvest}$ is the average transmit power when the relay is transmitting in harvest power mode i.e. mode 1.

$$\overline{P}_r^{harvest} = E_{g_{sr}}\left[\frac{\eta P_s^{\max} g_{sr}\alpha}{d_1{}^m(1-\alpha)}\right] = \frac{\eta P_s^{\max}\alpha}{d_1{}^m(1-\alpha)\lambda_{sr}} \quad (22)$$

where $1/\lambda_{sr}$ is the average channel gain between source to relay.

IV. Numerical And Simulation Result

A simulation test bed is developed in MATLAB to evaluate the performance based on the formulation provided. The following parameters are used in the simulation d_1=0.5,1, d_2=0.5,1, path loss exponent m=2.7and noise variance, N_0=1 .

In Fig. 3 throughput of SU is plotted against energy harvesting time for different value of I_{th}. It is observed that the throughput of the SU increases as the tolerable interference threshold increases. As I_{th} increases the allowable maximum transmit power of SU as well as relay increases which yields an improvement in throughput. With increase in α, harvested energy increases which increases the throughput, however beyond a certain α, further increase in α reduces transmission time of the relay causing throughput to reduce as seen in the Fig. 3.

Fig. 4 plots the throughput of the SU against energy harvesting time for several values of PU outage constraint ($\delta = 0.01, 0.05$). It is observed that the throughput of the SU improves as the allowable outage constraint of PU increases. An increase in δ allows SU as well as relay to increase its transmit power and thereby improves the throughput.

In Fig. 5, the transmission profile of relay is plotted against α for a given value of PU outage constraint (δ) and allowable interference threshold (I_{th}). As the energy harvesting time (α) increases, the probability of transmitting in harvesting mode decreases. As α increase, the maximum possible transmit power of the relay due to harvested energy increases and exceeds the maximum allowed power due to underlay constraint. This leads to switching of the transmit power of relay to underlay constrained power imposed by cognitive constraint i.e. power of underlay. Therefore probability of transmitting in harvested mode is reduces. Simultaneously the probability of transmitting at a power level corresponding to underlay constraint increases with increase in α.

In Fig. 6, the transmit power of relay in two modes i.e. harvest mode and underlay constraint mode is plotted against α. It is observed that the relay transmits in harvest mode and increases upto $\alpha = 0.3$ for $I_{th} = 5dB$ while the probability of transmitting in harvest mode decreases and hence the average transmit power of relay decreases. Further as α increases the relay switches to underlay constraint mode and transmit in that mode with constant power while the probability of transmitting in underlay constraint mode increases which yields increase in average transmit power of relay.

In Fig. 7, the average transmit power of relay is plotted against harvesting energy (α) for different value of δ. The average transmit power of relay increases as the allowable outage constraint of PU increases. An increase in δ means relay can increase its transmit power which yields in increase of average transmit power of the relay.

In Fig. 8, the average transmit power of relay is plotted against harvesting energy (α) for different value of I_{th}. The average transmit power of relay increases as the tolerable interference threshold increase. An increase in I_{th} means relay can increase its transmit power which yields in increase of average transmit power.

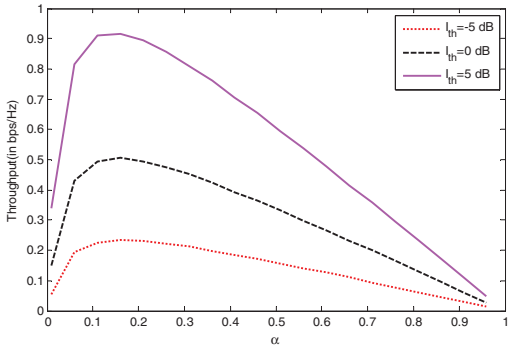

Fig. 3. Throughput at SU destination against α for different value of tolerable interference threshold,I_{th} (δ=0.05,d_1=d_2=0.5).

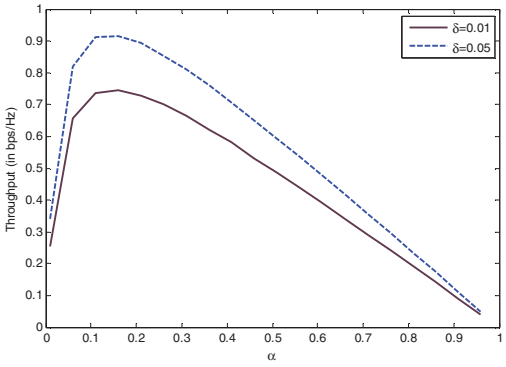

Fig. 4. Throughput at SU destination against α for different value of allowable outage constraint of PU,δ (I_{th}=5 dB,d_1=d_2=0.5).

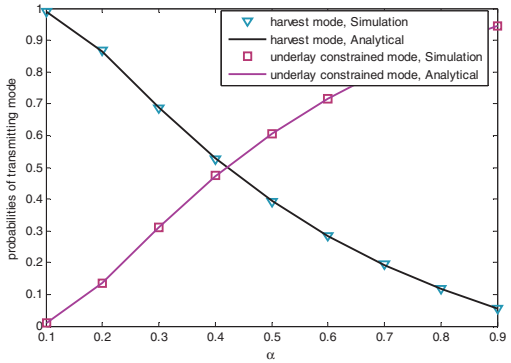

Fig. 5. Transmitting profile of relay versus α (δ=0.05, I_{th} =5 dB).

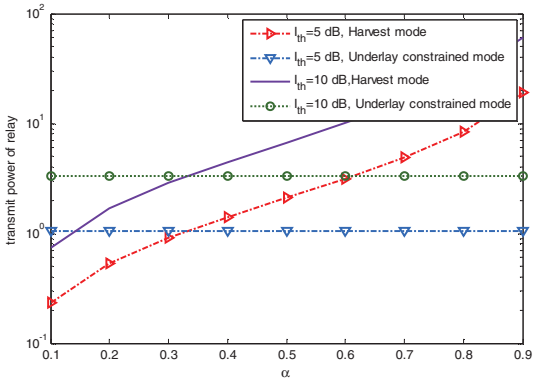

Fig. 6. Transmit power of relay versus α in two modes.

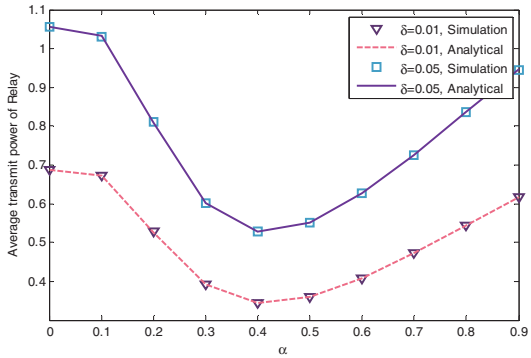

Fig. 7. Average transmit power of relay versus α for different value of PU outage constraint (I_{th}=5 dB).

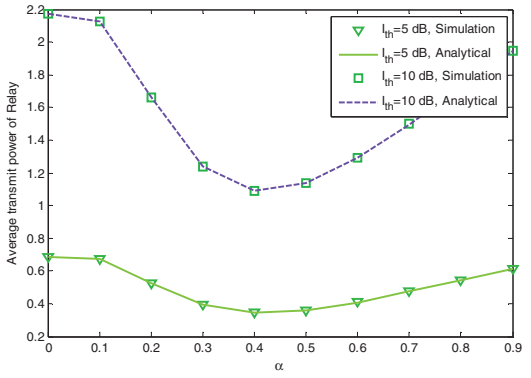

Fig. 8. Average transmit power of relay versus α for different value of PU outage constraint (δ=0.01).

V. CONCLUSIONS

In this paper the performance of cognitive relay network is evaluated under energy harvesting DF relay in terms of throughput. The impact of harvesting energy time, tolerable interference threshold, and allowable outage constraint of PU on the throughput of the system is evaluated. Furthermore the impact harvesting energy time, outage constrained and interference threshold on the average transmit power of SU relay is also indicated. It may be observed that there exists an optimal value of α which yields maximum throughput. The performance of SU improves as the allowable outage constraint of PU increases. Further the increase in allowable interference threshold also yields an improvement in throughput of SU.

REFERENCES

[1] A.Ghasemi, E. S. Sousa, " Fundamental Limits of Spectrum-Sharing in Fading Environments ," IEEE Trans. On wireless commun., vol. 6, no. 2, pp. 649-658, Feb.2007.

[2] S.Haykin, "Cognitive radio:brain-empowered wireless communications," IEEE J. Sel. Areas Commun., vol. 23, no. 2, pp. 201–220, Sept. 2005.

[3] FCC.Spectrum policy task force report,FCC02-155.Nov.2002.

[4] Q. Zhang, J. Jia, and J. Zhang, "Cooperative relay to improve diversity in cognitive radio networks," IEEE Commun. Mag., vol. 47, no. 2, pp. 111-117, Feb. 2009.

[5] I. Krikidis, S. Timotheou, and S. Sasaki, "RF energy transfer for cooperative networks: Data relaying or energy harvesting?" IEEE Commun. Lett., vol. 16,no. 11, pp. 1772–1775, 2012.

[6] L. R. Varshney, "Transporting information and energy simultaneously," in Proc. IEEE ISIT 2008.

[7] P. Grover and A. Sahai, "Shannon meets Tesla: wireless information and power transfer," in Proc. 2010 IEEE Int. Symp. Inf. Theory.

[8] Z. Wang, Z. Chen, L. Luo, Z. Hu, B. Xia, and H. Liu, " Outage Analysis of Cognitive Relay Networks with Energy Harvesting and Information Transfer," in Proc IEEE ICC,June, 2014.

[9] A. A. Nasir, X. Zhou, S. Durrani, and R. A. Kennedy, "Throughput and ergodic capacity of wireless energy harvesting based DF relaying network," in Proc. IEEE ICC, 2014, June 2014.

[10] W. Zhang and K. Ben Letaief, "Cooperative co mmunications for cognitive radio networks," Proc. IEEE, vol. 97, no. 5, pp. 878-893, May 2009.

[11] A. A. Nasir, X. Zhou, S. Durrani, and R. A. Kennedy, "Relaying protocols for wireless energy harvesting and information processing," IEEE Trans. Wireless Commun., vol. 12, no. 7, pp. 3622–3636, Jul. 2013.

[12] S.A. Mousavifar, Liu Yuanwei, C. Leung, M. Elkashlan, T.Q. Duong, "Wireless Energy Harvesting and Spectrum Sharing in Cognitive Radio," in proc. *IEEE* Vehicular Technology Conference, pp.1-5,Sept. 2014

[13] X. Zhou, R. Zhang, and C. K. Ho, "Wireless information and power transfer:Architecture design and rate-energy tradeoff," in Proc. IEEE GLOBECOM, 2012.

[14] I. S. Gradshteyn and I.M.Ryzhik, *Table of Integrals, Series and Products*, 6th ed. San Diego, CA: Academic, 2000.

[15] Y. Sun, X. Zhong, X. Chen, S. Zhou, and J. Wang, "Ergodic capacity of decode-and-forward relay strategies over general fast fading channels," IEEE Electronics Letters, vol. 47, no. 2, pp. 148–150, Jan. 2011.

THE 18TH INTERNATIONAL SYMPOSIUM ON WIRELESS PERSONAL MULTIMEDIA COMMUNICATIONS
(WPMC-2015)
December 13-16, 2015, Hyderabad, India

Distributed Token Based MAC for Multi-Channel Multi-Radio Cognitive Radio WMN

Mohammed A R Quadri, Ramesh Babu Battula, Manoj Singh Gaur, Dinesh Gopalani,Meenakshi Tripathi
Department of Computer Science and Engineering
Malaviya National Institute of Technology, Jaipur, India 302017

***Abstract*—Cognitive radio (CR) enabled secondary users (SUs) identify the spectrum white spaces opportunistically. For accessing a channel in CR network, the SU require a medium access control (MAC) protocol to select a channel that can efficiently cover the total transmission time required for its data transmission. Many MAC protocols were developed for cognitive radio networks (CRNs), most of them have not considered the opportunistic transmission length of a primary user (PU) channel in order to rank the channels accordingly depending upon the probability of successful SUs transmission. Our proposed novel MAC protocol termed as *distributed token based medium access control* (DTMAC) will address the PUs channel usage pattern estimation as minimum opportunistic transmission length metric and distribution of tokens by every mesh router/access point according to the queue size of the SUs at that time instance. Access to the control channel is coordinated by packet overhearing mechanism to pass on the token fairly among the SUs. The proposed MAC simulated using the Network Simulator (ns-2), and the simulation results demonstrate that proposed protocol improved the performance compare to the existing protocols.**

Keywords: Multi Channel,Packet Overhearing,Multi Radio,Opportunistic Transmission,Tokens.

I. Introduction

Wireless mesh network is an emerged and promising technology, it provides low cost services up-to last mile. In order to achieve the reduction of equipment cost and demand of higher capacity, wireless mesh network(WMN) router devices will have several interfaces that work on multiple channels. In these kind of networks combining the channel allocation, interface assignment, and routing can efficiently improve the network capacity and basically related to the problem of efficient network resource allocation. A WMN which works with multiple-channels consists of number of stationary wireless mesh routers which forms a wireless backbone. Each router is equipped with multiple network interface cards (NICs) and every interface of the router can operate on a distinct frequency channel [1]. In WMN, the mesh routers (MR) serve as access points (APs) for wireless mobile devices [2].

A single-interface architecture limits the whole network to operate in a single channel. This is because the subset of nodes that are using one channel for communication get disconnected from the subset of nodes which are not using the same channel . In order to perform the cross-channel communication requires either channel switching functionality within each node or have to use multiple interfaces per node each tuned to operate in different channel. Cross-channel communication can be achieved by equipping each node with multiple interfaces each operating in different channel.

II. Related Work

Research in the development of MAC protocol for CR-WMNs is still in its infancy. Some of the works [5], [7], [10]–[14] which are already existing in the current literature. Peyman, Nasser, and Ahmad have developed the DT-MAC protocol in [3], they have developed a Dual-channel Token-based MAC (DT-MAC) protocol that can provide the scalability also improve the efficiency in the case of large number of users and at high physical rates. In this work the authors have used a multi-channel model with an common control channel and a data channel. The token has been exchanged to the node which have to transmit in the packets send through the control channel. The user who is having the token is privileged to use the data channel.

Ghazale and Nitin have proposed a Token-DCF MAC protocol in [4], which is an opportunistic MAC protocol for wireless networks. In this paper they have focused on a implicit token-passing mechanism in order to reduce the idle and collision times in current 802.11 DCF MAC protocol for the WLAN. In this paper their main aim is to design the MAC protocol in such a way that the transmitting station schedules one of its neighboring stations for the next transmission in a distributed manner. They have employed the packet overhearing mechanism which is a good inspiration for our work. The same authors have also proposed a overheard ACK with token passing MAC protocol in [5] which is an advancement to the work done by them for the Token-DCF MAC protocol in [4].

In this paper they have proposed a scheme called overheard ACK where explicit ACK frame has been removed using packet overhearing mechanism.Ali, A.; Piran, M.J.; Kim, H.; Yun, J.; Suh, D.Y have proposed a PU activity aware distributed MAC protocol in [6]. They have proposed licensed channel usage pattern identification scheme, based on a two state markov chain model and estimated the future idle slots using the previous observations of the channel.

III. Estimation of Opportunistic Transmission Length and Channel Ranking Algorithm

Following are the two research contributions made in this paper

1) We propose a multi-channel and multi-radio token based MAC in accordance to the cognitive radio wire-

less mesh architecture. In this architecture every mesh client/router/access point will have this MAC protocol in them and each have to sense the licensed channels for identifying any underutilized channels and analyze the usage patterns of those channels which belong to primary users for a specific period of time T_sam.

2) A novel channel assignment solution is proposed interms of channel ranking algorithm after collecting enough data related to usage patterns of all channels. The OTL metric calculation of every channel is estimated in terms of Min_OTL(Minimum Opportunistic Transmission Length),Max_OTL(Maximum Opportunistic Transmission Length).

A. Opportunistic Transmission Length (OTL) Metric Calculation

In Algorithm 1 the initial identifier value is provided TRUE for first time say $t = t_1$. Therefore for at $t1$, the $Min_OTL^c_{t_1}$ and $Max_OTL^c_{t_1}$ will be assigned the same values as the observed IT^c_t. From the next iterations we will consider the average of the monitored IT^c_t in addition to the previously calculated idle lengths $MinIL^c_{t_{i-1}}$ in accordance to the current situation which will reflect the respective change in the PU's activity while calculating the idle slots. Once the estimation of OTL's in respective frequency channels is done, SUs can use the licensed channels without causing harmful interference with the PUs. Then based on the continues PU's activity monitoring Min_OTL and Max_OTL values are calculated. The PHY-layer monitoring scheme will monitor the licensed channels usage patterns for a sufficient amount of time. After that based on the past observations its easy to predict when a channel is idle and if it is idle then for what amount of time it will be idle means for atleast the duration of its estimated Min_OTL.

While a dedicated radio monitors all the licensed channels say C (where $c = 1, 2, 3, 4, ..., N$) in a round robin fashion it will spend a short duration of $\Delta(T) = 1ms$ for each channel to detect its current state (idle or busy). It will continue for a time duration of $Tsam = 5sec$ to collect PU's traffic samples from all the channels.

During the channel monitoring, a channel c can go through four possible transitions which are as follows:

1) when channel c is found in ON state at time instance t_1 and when the same channel is found in again ON state at t_2 time instance then utilization time can be calculated as $UT = t_2 - t_1$.
$Ch(c, t_1) = ON \rightarrow Ch(c, t_2) = ON$,then UT^c_t, $UT^c_t = t_2 - t_1$
2) when channel c is found in ON state at time instance t_1 and when the same channel is found in OFF (means the detected energy level is below 1.16 db for the duration of T_{sam}) state at t_2 time instance then utilization time can be calculated as $UT = (t_2 - \lambda) - t_1$. (where λ is the detection error).
$Ch(c, t_1) = ON \rightarrow Ch(c, t_2) = OFF$,then UT^c_t, $UT^c_t = (t_2 - \lambda) - t_1$

Algorithm 1 Calculating the Expected Min_OTL and Max_OTL times

Input:IT^c_t,$MinIL^c_t$,$MaxIL^c_t$,$Flag$=$TRUE$,C=$\{c_1,..,c_n\}$ is set of channels
Output:$Min_OTL^c_t$,$Max_OTL^c_t$
begin
for $c \leftarrow c_1$ to N **do**
  $Min_OTL^c_{t_1} \leftarrow 0$
  $Max_OTL^c_{t_1} \leftarrow 0$
  for $i \leftarrow 2$ to T_{Sam} **do**
    if $Flag == TRUE$ **then**
      $MinIL^c_{t_i} \leftarrow IT^c_{t_i}$
      $MaxIL^c_{t_i} \leftarrow IT^c_{t_i}$
      $Flag = FALSE$
    else
      if $IT^c_{t_i} \leq MinIL^c_{t_i-1}$ **then**
        $MinIL^c_{t_i} = \frac{MinIL^c_{t_i-1} + IT^c_{t_i}}{2}$
      end if
      if $IT^c_{t_i} \geq MaxIL^c_{t_i-1}$ **then**
        $MinIL^c_{t_i} = \frac{MinIL^c_{t_i-1} + IT^c_{t_i}}{2}$
        $MaxIL^c_{t_i} = \frac{MaxIL^c_{t_i-1} + IT^c_{t_i}}{2}$
      end if
      if $IT^c_{t_i} > MinIL^c_{t_i-1}$ && $IT^c_{t_i} < MaxIL^c_{t_i-1}$ **then**
        $MinIL^c_{t_i} = \frac{MinIL^c_{t_i-1} + IT^c_{t_i}}{2}$
      end if
    end if
  end for
  $Min_OTL^c_{t_i} \leftarrow MinIL^c_{t_i}$
  $Max_OTL^c_{t_i} \leftarrow MaxIL^c_{t_i}$
end for

3) when channel c is found in ON state at time instance t_1 and when the same channel is found in again ON state at t_2 time instance then IdleTime(IT) can be calculated as $IT = t_2 - t_1$.
$Ch(c, t_1) = OFF \rightarrow Ch(c, t_2) = OFF$,then IT^c_t, $IT^c_t = t_2 - t_1$
4) when channel c is found in OFF state at time instance t_1 and when the same channel is found in ON state at t_2 time instance then IdleTime(IT) time can be calculated as $IT = (t_2 - \lambda) - t_1$.
$Ch(c, t_1) = OFF \rightarrow Ch(c, t_2) = ON$,then IT^c_t, $IT^c_t = (t_2 - \lambda) - t_1$

B. Expected Transmission Time Over a Channel

Lets consider the transmission time required for a current frame of user u as t_u. To fully use the spectrum opportunity, each SU calculates the probability of successfully transmitting the current frame over channel c [9], which can be given as

P^c_u = Pr(Channel c is idle, Transmission is successful)

$$= \frac{IT_c}{UT_c + IT_c} F_k(t_{AS_u} + t_u) \quad (1)$$

where UT_c and IT_c are the utilization and idle periods of channel c, respectively, t_{AS_u} is an arbitrary sensing period selected by user u, and t_u is the transmission time of the current frame, and $F_c(x)$ is the cumulative distribution function $F_c(x) = \left(\int_0^x f_c(x)\,dx\right)$ that characterizes the usage pattern of channel c by its PU's, the derivation can be found in [8]. As we have chosen for arbitrary sensing period, so SU's transmitting simultaneously and collide with each other. If no PU appears in $t_{AS_u} + t_u$ interval then transmission is successful.

After calculating the successful transmission probability of each channel, now the SU's can determine the channel sensing sequence by simple sensing the channel that is having highest success probability after arranging them in descending order to achieve low delay and high throughput. If a channel is very less occupied by PU's, then that channel will obviously be contented by more number of SU's and will leads to high contention among the SU's which are using the same radio resources and degrades the performance. Instead of using the above said sensing model, the secondary user can select a channel based on the QoS requirement of their application.

For an instance we can consider the maximum tolerable one hop delay τ_u. The τ_u is an average value of the successive round trip times say $T = \{t_1, t_2, t_3, t_4, t_5\}$ of the five packets sent on a specific channel say c. So the average of all these round trip times will be assigned to τ_u. If we know the P_u^c, the expected transmission time over channel c can be estimated as $E[T_u^c] = \frac{(t_{AS_u}+t_u)}{P_u^c}$. So the SU will select a group of channels that satisfies the below condition

$$E[T_u^c] = \frac{(t_{AS_u} + t_u)}{P_u^c} < \tau_u \tag{2}$$

The proposed channel ranking algorithm will rank the channels in accordance to the total utilization time and total idle time. Then after collecting all these channels which fall under this estimation condition in the given algorithm 2, it will then utilization factors of all the channels and arrange these values in descending order and select a channel with maximum utilization factor as rank 1, channel with second maximum utilization factor as rank 2 and so on for all the channels in set UF^c.

C. The Channel Assignment Problem

The IEEE 802.11 DCF access method is used in WLAN [4] in this protocol each and every time when a node want to send the data it have to contend for the channel, efficient MAC protocol but not scalable. The proposed MAC protocol is a multi-channel and multi-radio token based protocol. The main limitation with all the existing protocols is that they work with a control channel in order to exchange the information from the mesh router/access point like on which channel the node have to transmit the data. While one node is using the control channel for obtaining the information regarding the possible channels for data transmission, then the other node which want to use the same control channel when it senses that the channel is busy it will immediately go to DIFS amount of waiting time plus a random backoff time. So like this it will make the nodes go on waiting for their turn to get access to the control channel.

Algorithm 2 Channel Ranking Algorithm

Require: Utilization Time of Channels,Idle Time of Channels, Set of transmission times of every Packet in Queue,C=$\{c_1, c_2, c_3, ..., c_n\}$ is set of channels

Ensure: Rank of each channel c in accordance to the calculated UF^c

for $c \leftarrow 1$ to N **do**
  TUT^c=UT_{t1}^c
  TIT^c=IT_{t1}^c
  for $i \leftarrow 2$ to T_{Sam} **do**
    TUT^c=TUT^c+$UT_{t_i}^c$
    TIT^c=TIT^c+$IT_{t_i}^c$
  end for
  And then SU will collect all the channels that satisfy the condition in equation 2 as a set of estimated transmission time over channel c
  if $E[T_u^c] = \frac{(t_{AS_u}+t_u)}{P_u^c} < \tau_u$ **then**
    $Channel_Set$=Add this Channel c to the Collection
  end if
end for

Arrange the channels in set $Channel_Set$ in ascending order to select a channel with minimum P_u^c

for $c \leftarrow 1$ to $Channel_Set$ **do**
  ETT^c=$\frac{TIT^c}{TUT^c+\sum_{i=1}^{QS_t} t_i}$
  where t_i is the transmission time required for every packet in the queue
  UF^c=BOC_t^cxETT^c
end for
Arrange the utilization factors of all channels in set UF^c in descending order.

The main drawback with this is if a secondary user has more queue size of data to send then it will not have any priority, because as it is having more queue size of data to transmit. So if a node with less queue size next time gets the chance after contending for the control channel, another node with more queue size have to starve for its turn. In order overcome this problem we can simple use packet overhearing mechanism, so that the nodes which have more data to send will get the chance to access the channel first. Lets consider that there are three mesh clients/secondary users MC1,MC2,MC3 refer Figure 1 who want to get access to the control channel and lets assume that all of the mesh clients with in one hop distance will share their respective network layer queue sizes among them selves before performing any sort of data transmission. All the three will contend for the access to the control channel and only one among them will get the chance to access the control channel. Consider MC1 is the node who won access to the control channel and sent a request to the mesh router/access point requesting for a free channel availability by embedding

three fields of information

1) Current queue size
2) Next privileged mesh client among the MC2 and MC3 who have more queue size of data to send that particular mesh client will be given the access to the control channel
3) The channels that were sensed idle for a specific time by the MC1, this information is shared with the one hope access point/mesh router of MC1 (in the wireless mesh network, every mesh client will act as mesh router/access point to perform the multi-hop transmission of data).

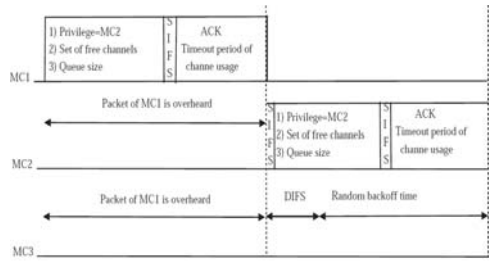

Fig. 1. Access Method of Multi-channel and Multi-radio MAC Protocol

The advantage with this kind of implicit token/privilege embedding mechanism is that, no need to send explicit token for passing the privilege of accessing the control channel to other mesh client which has more data to send in its queue. Because this control MAC frame which have been transmitted by MC1 previously will be overheard by the remaining mesh clients and they will update the queue size of MC1 in there queue size table which is maintained by every mesh client/mesh routers. After every successful access to the control channel by a mesh client, the mesh client which have received the privilege no need to go back and wait for DIFS and some random backoff time. The mesh client which have got the privilege to access the control channel will start its immediate transmission of data by just waiting for a short period of SIFS. With this it will reduce the idle time and increase the throughput of the network by implicitly transmitting the token/privilege inside the MAC header of the data packets transmitted over the control channel. The other mesh clients who don't have privilege will automatically fall back to normal 802.11 DCF mode of operation means they will wait for DIFS+Random Backoff time, so that we can reduce the collisions between the mesh clients at maximum rate.

The mesh router/access point sends request to one hop neighbors, if it receives a request for the access to a free channel depending on the queue size added to the MAC header of the data packets it will selects the channel that best suits according to the queue size requirements of the MC1 and send the best channel for data transmission from the MC1 to the access point if the destination node is in different network or a best channel for data transmission from the MC1 to the destination itself if the designated node is with in the reach of the MC1.

This channel along with the time up-to which that channel is available for transmission information is embedded in the ACK which is returned by the mesh router/access point to MC1.The need to maintain the information regarding time upto which that channel is available for transmission is considered. As the PU can't wait more than Max_OTL time, within the duration SU must be find other channel to switch. The Min_OTL gives the estimated time up-to which the allocated channel for transmission will be available without degrading the QOS provided to a primary users (PU's). So once Min_OTL expires, then the mesh router/access point which have allocated the channel will fix that channel as a free channel in its Channel Usage Table(CUT).

IV. Performance Evaluation

We will measure the performance of our MAC protocol with respect to estimated Min_OTL and Max_OTL of the primary users and SU's throughput while transmitting the data. Simulation results are performed by writing extensive C code. Figures 2 and 3 represent the observed Min_OTL and Max_OTL of the 5 licensed channels of primary users. Here the secondary users will transmit the data atleast for a minimum time of Min_OTL time. From these two graphs we can see how the values change very often due to the change in the activity of the primary users in there respective channel usage pattern. So with these two values we can estimate upto how much time for sure a SU can transmit the data without any collisions.

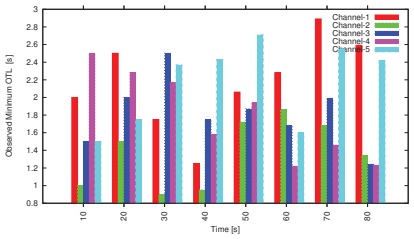

Fig. 2. Observed minimum opportunistic transmission length(OTL)

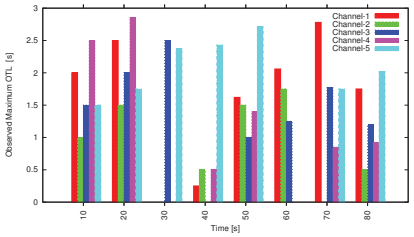

Fig. 3. Observed maximum opportunistic transmission length(OTL)

The simulations for DTMAC and PAD-MAC[6] are done in NS-2 to measure and compare the performance of these two MAC protocols. The network is a wireless cognitive radio mesh network in which the transmitting stations i.e., the secondary users are placed uniformly at random in a square area (150mx150m). The population of primary users is

considered in different numbers for every single execution of the simulation which lasted for 1020 seconds each. In each run, a different topology is considered. In our simulation by using the proposed channel ranking algorithm its possible to achieve grater throughput rates as we increase number of primary users and secondary users in the successive runs of the simulation.

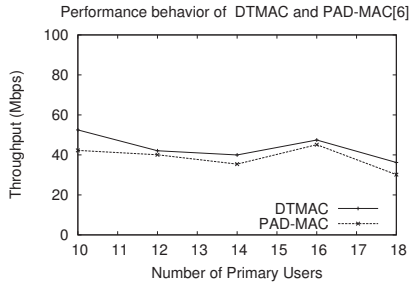

Fig. 4. Aggregate throughput (area=150mx150m)

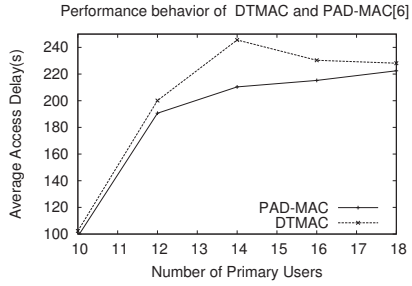

Fig. 5. Average access delay (area=150mx150m)

The aggregate throughput of PAD-MAC and DTMAC is presented in Figure 4. It can be seen that the throughput gained by DTMAC is a factor 1.2 to 1.5. Figure 5 shows the average access delay of the two protocols. It is the delay incurred between the packet at which the packet arrives at MAC layer and time at which source of the packet receives acknowledgment from the destination. It consists of the waiting time before transmitting on the channel and the time spent in packet retransmissions. Here you can see that packet delay is much smaller in DTMAC when compared to PAD-MAC. The reason is that DTMAC have much smaller idle times when compared to PAD-MAC. As a result many retransmissions are avoided my reducing the collisions.

V. Conclusion and Future Work

Our main focus in designing this MAC was on estimating the idle times of each and every channel that a secondary users/mesh clients and the mesh routers/access points can sense. And after calculating the minimum opportunistic transmission length of all the channel using the utilization and the idle time values. We have derived the equation for estimation of the channels that can be feasible for allocating to a SUs transmission. After that we have represented with an instance how the distributed token based multi-channel and multi-radio MAC protocol helps to avoid collisions among the secondary users and also how it reduces the idle and starvation times among SU's when the same control channel is accessed by multiple SU's. In the future work we will design a channel assignment and routing based distributed MAC protocol which considers the channel capacity as a metric to assign channels to SU's.

VI. Acknowledgment

The authors gratefully acknowledge the support from Department of Science and Technology, India for funding this project.

References

[1] A. Raniwala, and Tzi cker Chiueh. INFOCOM 2005. 24th Annual Joint Conference of the IEEE Computer and Communications Societies. Proceedings IEEE, 3, page 2223-2234 vol. 3. (March 2005).

[2] Ashish Raniwala, Kartik Gopalan,Tallahassee,Tzi-cker Chiueh; "Centralized channel assignment and routing algorithms for multi-channel wireless mesh networks"; ACM SIGMOBILE Mobile Computing and Communications Review; Volume 8 Issue 2, April 2004.

[3] Teymoori Peyman, Yazdani Nasser, Khonsari Ahmad; "DT-MAC: An Efficient and Scalable Medium Access Control Protocol for Wireless Networks", Wireless Communications, IEEE Transactions on Wireless Communications, Vol:12 , Issue:3, March 2013.

[4] Hosseinabadi. G. Vaidya.H.N.; "Token-DCF: An opportunistic MAC protocol for wireless networks", Communication Systems and Networks (COMSNETS), 2013 Fifth International Conference.

[5] Shegufta Bakht Ahsan and Nitin Vaidya. 2014. Poster: overheard ACK with token passing: an optimization to 802.11 MAC protocol. In Proceedings of the 20th annual international conference on Mobile computing and networking (MobiCom '14). ACM, New York, NY, USA, 345-346. DOI=10.1145/2639108.2642903 http://doi.acm.org/10.1145/2639108.2642903.

[6] Ali, A.; Piran, M.J.; Kim, H.; Yun, J.; Suh, D.Y. "PAD-MAC: Primary User Activity-Aware Distributed MAC for Multi-Channel Cognitive Radio Networks." Sensors 2015, 15, 7658-7690.

[7] Xuming Lu,Guangbin Fan,Ruibing Hao;"A dynamic token passing MAC protocol for mobile ad hoc networks", Proceeding IWCMC '06 Proceedings of the 2006 international conference on Wireless communications and mobile computing .

[8] Hyoil Kim,Kang G. Shin; "Efficient Discovery of Spectrum Opportunities with MAC-Layer Sensing in Cognitive Radio Networks";IEEE TRANSACTIONS ON MOBILE COMPUTING, VOL. 7, NO. 5, MAY 2008.

[9] Cai, L.X,Yongkang Liu ; Xuemin Shen ; Mark, Jon W,Dongmei Zhao; "Distributed QoS-Aware MAC for Multimedia over Cognitive Radio Networks",Global Telecommunications Conference (GLOBECOM 2010), 2010 IEEE.

[10] A. Hamed Mohsenian Rad,Vincent W.S. Wong; "Congestion-aware channel assignment for multi-channel wireless mesh networks",Computer Networks and ISDN Systems,Copyright 2015, Elsevier,Volume 53, Issue 14, Pages 2387-2600 (18 September 2009).

[11] Yanxiao Zhao.; Min Song.; ChunSheng Xin.; "FMAC: A fair MAC protocol for coexisting cognitive radio networks", INFOCOM, 2013 Proceedings IEEE.

[12] M. Timmers, S. Pollin, A. Dejonghe, L.V.D. Perre, and F. Catthoor, "A Distributed Multichannel MAC Protocol for Multihop Cognitive Radio Networks", ;presented at IEEE T. Vehicular Technology, 2010, pp.446-459.

[13] Duke Lee; Puri, A.; Varaiya, P.; Sengupta, Raja; Attias, R.; Tripakis, S., "A wireless token ring protocol for ad-hoc networks," Aerospace Conference Proceedings, 2002. IEEE , vol.3, no., pp.3-1219,3-1228 vol.3, 2002, doi: 10.1109/AERO.2002.1035254

[14] Battula, R.B.; Gopalani, D.; Gaur, M.S.; Kakarla, J.; "TMAC Token based MAC protocol for cognitive radio wireless mesh network"; Information and Communication Technology Convergence (ICTC), International Conference, IEEE 2014.

THE 18TH INTERNATIONAL SYMPOSIUM ON WIRELESS PERSONAL MULTIMEDIA COMMUNICATIONS
(WPMC-2015)
December 13-16, 2015, Hyderabad, India

Design Optimization and SAR Characterization of SS-UWB Patch Antenna for WBAN

[1] Vivek Kumar and [2] Sravanth Kumar
Research Scholars: dept. of ECE,
Birla Institute of Technology Mesra
Ranchi, India
[1] mr.vivek.1988@ieee.org, [2] srava2010@gmail.com

Bharat Gupta
Associate Professor: dept. of ECE,
Birla Institute of Technology Mesra
Ranchi, India
bharatg@bitmesra.ac.in

Abstract— **The proposed Swastika Slot UWB (SS-UWB) patch antenna designed specifically for body-worn applications in Wireless Body Area Networks (WBAN). Ultra-wideband (UWB) technology, standardized by IEEE 802.15.6 TG-6 for ultra-low power consumption, is one of the fastest growing technologies for short range communications. The increasing demand of compact size, portable, body-worn, and lightweight electronic devices for the WBAN applications requires the design of miniature antennas. Therefore, in this paper, we present a SS-UWB, which covers the frequency spectrum from 3.45 – 13 GHz [9.65 GHz] with a gain varied from 2.3 – 5.87 dB and total antenna efficiency varied from -0.76 to -2.67 dB (91.6% – 73.6%) over free space. Also, in this paper, we investigate the effect of antenna-body gap in terms of reflection coefficient, gain, and total antenna efficiency in free space and modeled phantom. Most importantly, we have also analyzed the effect of specific absorption rate (SAR) over modeled human phantom due to interactions between human body and the antenna.**

Keywords- Wireless Body Area Networks (WBAN), Body-worn antennas, Ultra-wideband (UWB), Specific absorption rate (SAR), Antenna efficiency.

I. INTRODUCTION

The body-worn antenna and body-centric communication systems has received much attention over the past few years for healthcare monitoring applications. Such systems are gained much concern for other applications like sports and fitness, gaming, lifestyle and entertainment [1]. Advances in microelectronics and wireless communications have enabled a way to make small and lightweight monitoring devices which consumes less (ultra-low) power. Such intelligent monitoring devices can be equipped together to configure Wireless Body Area Networks (WBAN). WBAN gather information on entities of interest by multiple distributed sensor elements, placed in, on or around human body to monitor the health condition pervasively and ubiquitously [2]–[3]. The requirements of high bandwidth with low power consumption are the key concerns for the wearable healthcare monitoring systems and applications. Since the low power consumption will significantly increases the life of battery driven devices. Therefore, the requirement of extremely low power became the necessity of such application.

Ultra-wideband (UWB) technology, standardized by IEEE 802.15.6 TG-6, is the fastest anticipating technology for such short range communications system [4]. With a very low range of effective isotropic radiating power (EIRP) emission density, less than -41.3 dBm/MHz, longer battery life for wearable and implanted health monitoring devices can be achieved. Moreover, the lesser EIRP value results in low level of interference which allows it to coexist with other system. Also it provides resistant against multipath and potential application dependent higher data transmission rate varies from few Kbps to Mbps.

Designing antenna for WBAN has several critical issues, one such issue is presence of human body in the near-field that can significantly affect antenna's performance [5]–[6]. One of the most critical issues is the size of the antenna for portable devices. Reducing antenna's size leads to various problems due to performance disfavours in antenna characteristics, such as impedance mismatch, radiation efficiency, and bandwidth. Therefore, it is quite challenging task to design a miniature antenna, which should capable of providing wide bandwidth and have reasonable performance in the vicinity of human body for impedance matching with acceptable gain.

Much exhaustive research activity has been employed on wearable antenna design and their performance modeling in presence of human body [7]–[11]. In [12], authors shown that antenna time domain characteristics are significantly improve due to presence of lossy human body.

In this paper, we have analyzed the antenna's performance in free space and in direct contact to layered human body phantom. The main objective is to study the nature of dispersive human tissues and their electrical properties, and how the antenna parameters are changed by means of the antenna-body gap. Moreover, we have performed a parametric study to observe the effects of various dimensional (notches, slot, feed width and feed gap) parameters in order to optimize antenna performance. The rest of paper is as follows. The modified SS-UWB patch antenna design and parametric study are given in section II. Section III provides the discussions related to measured and simulated results. Finally in section IV, we present conclusions of results and the future course.

II. ANTENNA DESIGN

The proposed geometry and the fabricated prototype of SS-UWB patch antenna are shown in Fig. 1.(a) and 1.(b). The reduced dimension of the antenna is 27 x 27 x 1.6 mm^3 as compared to 30 x 30 x 1.6 mm^3 in [13]. The patch and ground plane are placed on opposite sides of dielectric substrate (FR-4) having permittivity of 4.4 and loss tangent of 0.025. The radiating patch of size 13.5 x 11 mm^2 is fed by a microstrip line of width 2.8 mm. The two notches size of 1.5 x 1.5 mm^2 and 1 x 1 mm^2 are at the two bottom corners of the radiating patch. The feed gap between patch to the ground plane is 1 mm. The length of ground plane is 10.5 mm. The proposed swastika slot is printed on top of radiating patch of size 3.5 x 3.5 mm^2. Simulations of this antenna have been done by using ANSYS High Frequency Structure Simulator (HFSS) [14].

A. *Effect of the Notches at the bottom of Radiating Patch*

Fig. 2(a) and 2(b) shows the two step notches of dimensions 1.5 x 1.5 mm^2 and 1 x 1 mm^2 respectively at the bottom of patch. In addition, swastika slot with two step notches at the center of patch is shown in Fig. 2(c). Such notching techniques have been utilized for better capacitive tuning between ground plane and lower part of antenna, resulting to achieve wider impedance bandwidth.

As shown in Fig. 3, the reflection coefficient of antenna with 2 steps notches cutting at the bottom of radiating patch with swastika slot, the S_{11} curve is best, covering the frequency range from 3.45 GHz to 13 GHz. The two steps notch at bottom of patch provides a good matching bandwidth with the more peak values of reflection coefficient. While one step notch provides less matching bandwidth covers the frequency range of 6.1 GHz to 13.45 GHz.

Table I shows the effect of two notches and swastika slot at the bottom and centre of patch respectively to the antenna bandwidth. The basic rectangular patch 13.5 x 11 mm^2 ($W_P \times L_P$) provides the fractional bandwidth of 67.18%. This fractional bandwidth increases to 75.2% by cutting one notch at the bottom, while this fractional bandwidth further increases to 109.37% by cutting two notches at the bottom of patch.

Moreover, a fractional bandwidth of 116.11% is achieved by cutting swastika slot at the center of patch along with two notches at the bottom of patch. Hence, the proper selections in the size of notches and slot can lead to different UWB performance characteristics.

TABLE I.
THE EFFECT OF NOTCHES TO THE SIMULATED -10 dB BANDWIDTH OF PROPOSEED ANTENNA

Notches	f_L (GHz)	f_U (GHz)	Absolute BW (GHz)	Fractional BW (%)
0	4.35	8.75	4.4	67.18
1	6.1	13.45	7.35	75.2
2	3.75	12.8	9.05	109.37
2 & SS	3.45	13	9.55	116.11

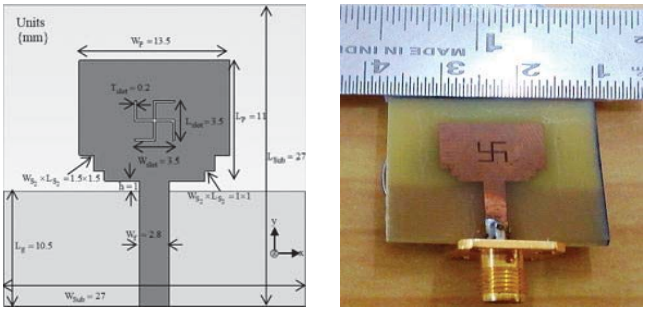

(a) (b)

Fig. 1. Geometry of proposed SS-UWB antenna

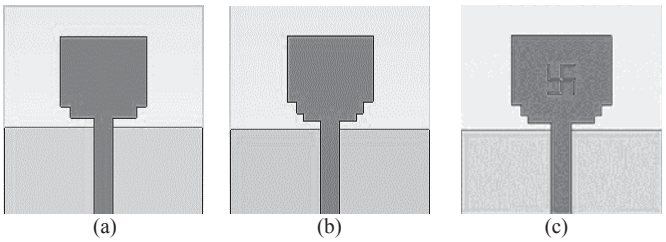

(a) (b) (c)

Fig. 2. Step notches at the bottom of patch and swastika slot at center of patch a) 1 step notch b) 2 steps notches c) 2 steps notches with swastika slot at the center of patch

B. *Effect of the Feed Gap*

The feed gap between the lower edge of the patch and the ground plane is given essential effect to the impedance bandwidth. The partial ground plane on the bottom of the substrate acted as an impedance matching element. The authors were taken four different values of feed gap of 0.5, 1, 1.5, and 2 mm in order to determine the optimum size of feed gap.

Fig. 4 shows the simulated reflection coefficient (S_{11}) curves for different feed gaps to the ground planes of SS-UWB antenna. It is shown in Fig. 4 and Table II that the -10 dB bandwidth of antenna varies with the variation of the feed gaps. The optimal feed gap from simulated result is found to be 1 mm with the fractional bandwidth of 116.11 %.

It can be clearly depicted from Table II that the -10 dB bandwidth of SS-UWB antenna does not deviate much with the variation of feed gaps below 1.5 mm. But when the feed gap value increases from 1.5 mm, it will degrade the impedance bandwidth performance. These simulated results show the dependency of antenna impedance bandwidth on feed gaps of the ground plane. Thus, the ground plane acts as the impedance matching element.

TABLE II.
SIMULATED -10 dB BANDWIDTH OF PROPOSEED ANTENNA FOR DIFFERENT FEED GAP

Feed Gaps (mm)	f_L (GHz)	f_U (GHz)	Absolute BW (GHz)	Fractional BW (%)
0.5	3.7	13.7	10	114.9
1	3.45	13	9.65	116.11
1.5	3.4	12.2	8.8	112.8
2	3.75	11.35	7.6	100.66

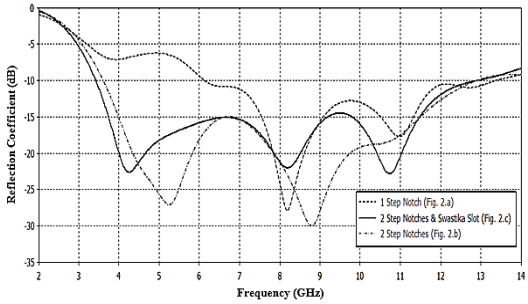

Fig. 3. Simulated S_{11} curves of various steps notches with swastika slot

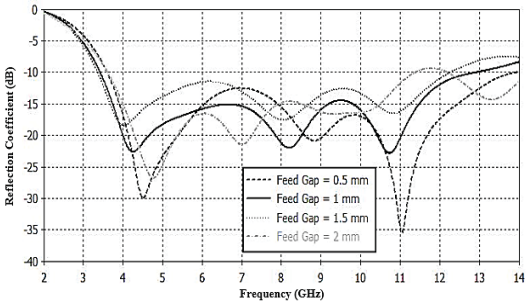

Fig. 4. Simulated S_{11} curves of proposed antenna for different feed gaps

C. *Effect of Feed Width*

Fig. 5 shows the simulated reflection coefficient curves of the proposed antenna. The authors were taken five different values of feed width of 2.6 mm, 2.8 mm, 3 mm, 3.2 mm, and 3.4 mm in order to determine the optimum size of feed width. It is shown in Fig. 6 that the -10 dB bandwidth of antenna varies with the variation of the feed widths. It can be clearly visualized that the lower edge of frequency bandwidth is quite independent of the feed widths variations, while upper edge of frequency bandwidth is much dependent on different feed width variations.

III. RESULTS AND DISCUSSIONS

In this section, we present the results obtained from full-wave electromagnetic solver. The performance of antenna was measured over free space and over modeled dispersive layered human phantom as in [15]. The antenna-body gap is introduced by using foam substrate having permittivity of 1.067, loss tangent of 0.0041. The main objective of introducing antenna-body gap is to analyze the interactions between human tissue equivalent model and the antenna. Also, this spacing is useful towards to avoid the hazardous EM absorption in soft human tissue. We examined the antenna performance over different antenna-body gaps values in the range of 0-10 mm.

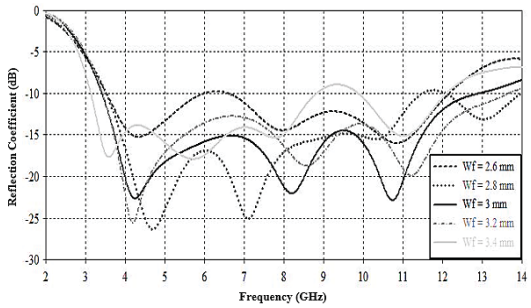

Fig. 5. Simulated S_{11} curves of proposed antenna for different feed widths

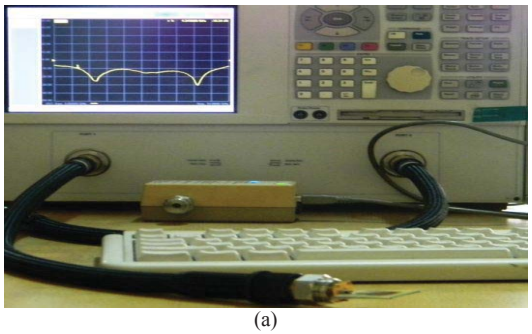

(a)

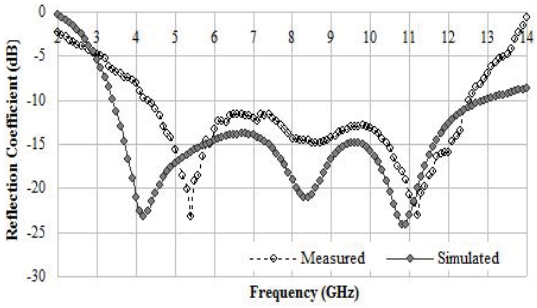

(b)

Fig. 6. Measurement of fabricated Swastika slot UWB antenna a) The VNA setup and b) Measured vs. simulated S_{11} curves

A. *Reflection Coefficient (S_{11})*

Fig. 6 shows the reflection coefficient measurement setup on L-Vector Network Analyzer (Agilent PNA series) and the measured vs. simulated S_{11} curve, respectively. In this prototype, a 50 Ω SMA connector is soldered at bottom edge of microstrip feed line which is further connected to VNA by an RF coaxial cable. The measured -10 dB bandwidth for the S_{11} results in range from 4.25 to 12.5 GHz, which is close to the simulated range from 3.45 to 13 GHz. The obtain result is acceptable; however, there is a shift of 0.8 GHz between the simulated and the measured S_{11} result at lower frequency. This shift is mainly due to the inevitable fabrication error and the amount of soldering used to attach the feeding pin. The RF cable has also some significant affects over the antenna performance. In addition, we were not taken the effect of mismatch in the simulation due to the adapter and connector used. Also, there is a slight difference between the actual dielectric properties used in the fabrication and the one used in the simulation.

B. *Radiation Pattern*

The high directivity antennas are desirable in WBAN as well as in UWB wireless communications. Since, the high value of directivity at a specific angle will lead to minimize power consumption and energy absorption within the body and most importantly minimize the path loss [16]–[17]. Fig. 7 shows the polar plot of radiation patterns (E_θ field) of the SS-UWB antenna for different antenna-body gap values.

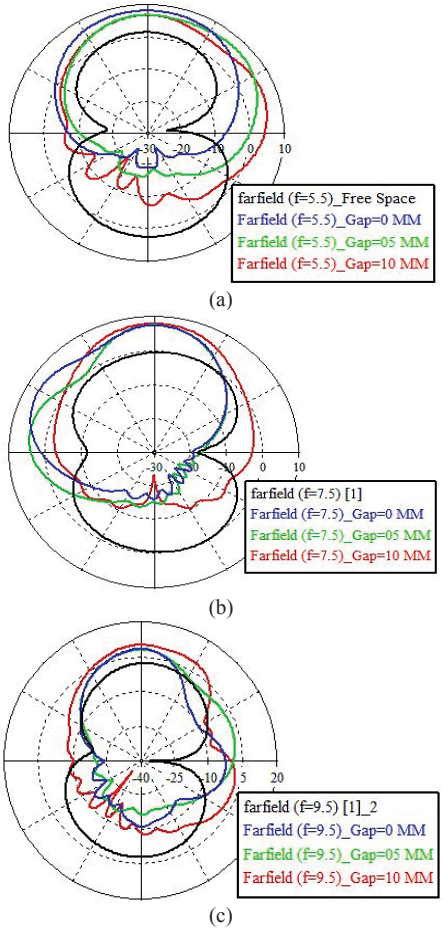

Fig. 7. The polar plot of radiation patterns of Swastika Slot antenna over modeled layered human phantom over different gap value at: a) 5.5 GHz, b) 7.5 GHz, and c) 9.5 GHz

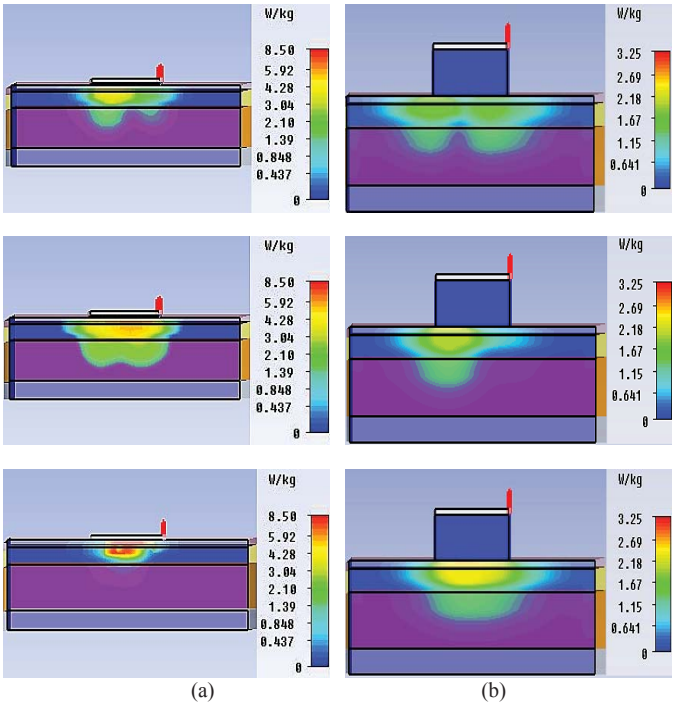

Fig. 8. SAR levels over 1g mass average layered human phantom without gaping and with 10 mm gaping at a) 5.5 GHz b) 7.5 GHz and c) 9.5 GHz

C. *Specific Absorption Rate (SAR)*

Fig. 8 shows the simulated SAR levels over layered phantom with and without antenna-body gap at frequencies 5.5 GHz, 7.5 GHz and 9.5 GHz respectively. All simulation has been done over 1g mass averaged SAR of human tissue defined as a tissue volume in the shape of cube. We observed peak SAR level of 6.26, 7.66 and 8.29 W/kg respectively over layered phantom without gaping substrate [15]. While much lower SAR values of 0.884, 0.994 and 1.54 W/Kg respectively has been observed at mentioned frequency with 10 mm antenna-body gap.

The summarize SAR results were listed in Table V. From the result, we observed that as frequency and tissue thickness increases, the SAR value also increases. The main cause for such incident is high conductivity (σ) and permittivity (ϵ_r) of skin and muscle layer, which causes severe impedance mismatch between them. That's why the fat layer possesses much absorbed power density. Also the high electric field ($\vec{E}$) value governs higher SAR value since it is related to electric field as

$$SAR = \frac{\sigma}{\rho}\vec{E}^2 \quad (1)$$

TABLE III.
SIMULATED PEAK SAR LEVEL OVER PHANTOMS

Frequency (GHz)	SAR (W/Kg) Layered Phantom without Gap (1g mass average)	SAR (W/Kg) Layered Phantom with Foam (1g mass average)
5.5	6.26	0.884
7.5	7.66	0.994
9.5	8.29	1.54

D. *Maximum Gain and Total Antenna Efficiency*

Fig. 9 shows the simulated maximum gain and total antenna efficiency over free space and over modeled phantom. From Fig. 9.(a), we can clearly depict that the deterioration of the maximum gain was occurred when antenna placed in direct contact (antenna-body gap=0 mm) to phantom. This is due to the presence of lossy human body. The antenna gain varied from 2.4 – 5.87 dB, over free space. However, the maximum gain having value of 8.43 dB has been achieved, when we increased the distance between antenna and body to the value of 10 mm. Furthermore, a constant gain of 7 dB has been observed throughout the frequency span with a 10 mm gap over modeled phantom. This is due to the reflection from the highly lossy human body tissue and the material (foam) utilized for gaping. Moreover, the maximum gain of proposed SS-UWB antenna has not increases with further increment in the antenna-body gap. Similarly, we observed that the total antenna efficiency, as shown in Fig. 9.(b), is significantly deteriorated, when antenna placed in direct contact with human tissue-equivalent phantom. Though, the highest antenna efficiency of value -0.76 dB (91.6%) has been achieved with the 10 mm antenna-body gap, which is very close to the free space efficiency. In conclusion, both the antenna gain and total antenna efficiency deteriorated close to

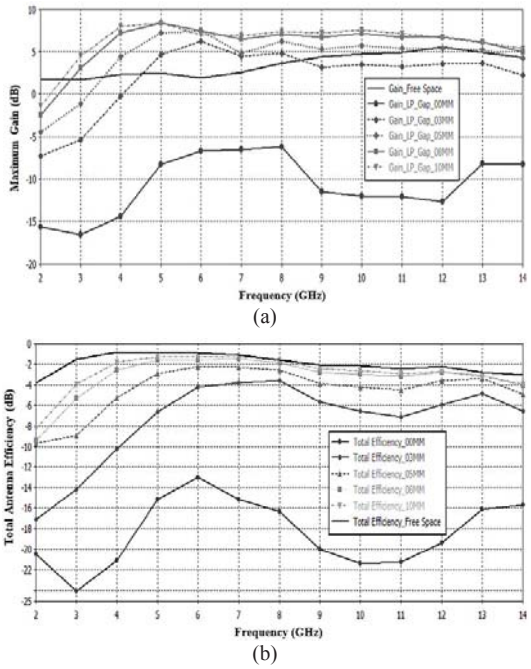

Fig. 9. Simulated a) Maximum gain, and b) Total antenna efficiency

the modeled human tissue equivalent phantom. Also, from these results, the directivity of antenna is maximum when antenna operated close to the human phantom.

IV. CONCLUSION

In this research endeavor we have investigated the performance of SS-UWB patch antenna over frequency range of 3.45 GHz – 13 GHz for antenna-body gap values of 0-10 mm. The efficiency of this design has been established by investigating the effect of antenna-body gap on the performance of antenna at three different frequencies: 5.5 GHz, 7.5 GHz and 9.5 GHz respectively. The fabricated SS-UWB antenna exhibits the wider impedance bandwidth ranging from 4.25 to 12.5 GHz over free space.

The maximum antenna gain of 5.87 dB has been achieved over free space, while a much better gain of 8.43 dB has been achieved when antenna placed at 10 mm gap. Moreover, the total antenna efficiency varied from 73.6% (-2.6 dB) to 91.6% (-0.76 dB) in the mentioned frequency span. However, a constant efficiency close to - 1 dB (89.13 %) has been achieved over frequency range from 3.1 – 7 GHz, than after deterioration in antenna efficiency (goes up to – 2.6 dB) has been observed. Also the S_{11} curve varies from -15 dB to -22 dB in the frequency range of 3.8 – 11.5 GHz.

Furthermore, most of the significant antenna results have been observed at antenna-body gap of value above 5 mm. Also, variation in the thickness of different human tissue may affect the antenna performance especially in terms of impedance mismatch. We need to study the design in different human system to modify the antenna design towards a more realistic one in application. Then it would generate a comprehensive solution to the present day wearable sensing and computing communication devices.

REFERENCES

[1] P. S. Hall, and Y. Hao, *Antennas and Propagation for Body Centric Wireless Communications Systems,* Artech House, Norwood, Mass, USA, 2006, ISBN-13:978-1-60807-376-4.

[2] B. Latre, B. Bream, I. Moerman, C. Blondia, and P. Demeester, "A Survey on Wireless Body Area Networks," *Wireless Network*, vol. 17, issue 1, pp. 1-18, January 2011.

[3] M. Patel, and J. Wang, "Applications, Challenges, and Prospective in Emerging Body Area Networking Technologies", *IEEE Wireless Communications*, vol. 17, no. 1, pp. 80-88, 2010.

[4] IEEE 802.15 WPAN™ Task Group 6 (TG6) Body Area Networks, IEEE Standard 802.15.6, 2011.

[5] T. S. P. See and Z. N. Chen, "Experimental characterization of UWB antennas for on-body communications", *IEEE Trans. Antennas Propag.*, vol. 57, no. 4, pp. 866-874, April 2009.

[6] M. Klemm, and G. Troster, "EM Energy Absorption in the Human Body Tissues due to UWB Antennas", *Progress in Electromagnetic Research (PIER),* vol. 62, pp. 261-280, 2006.

[7] M. Klemm, I. Z. Kovcs, G. F. Pedersen, and G. Troster, "Novel small-size Directional Antenna for UWB WBAN/WPAN application*", IEEE Trans. Antennas Propag*., vol. 53, no. 12, pp. 3884-3896, December 2005.

[8] X. N. Low, Z. N. Chen, and T. S. P. See, "A UWB Dipole antenna with Enhanced Impedance and Gain Performance*," IEEE Trans. Antennas Propag*., vol. 57, no. 10, pp. 2959-2966, October 2009.

[9] A. Alomainy, Y. Hao, C.G. Parini, and P.S. Hall, "Comparison between two different Antennas for UWB on-body Propagation Measurements", *IEEE Antennas Wireless Propag. Lett.,* vol. 4, pp. 31-34, June 2005.

[10] A. Rahman, A. Alomainy, and Y. Hao, "Compact Body-worn Coplanar Waveguide fed Antenna for UWB Body–Centric Wireless Communications", *IEEE 2nd European Conference on Antennas and Propagation* (EUCAP), Edinburgh, pp. 1-4, November 2007.

[11] N. Chahat, M. Zhadobov, R. Sauleau, and K. Ito, "A Compact UWB Antenna for On-Body Application*", IEEE Trans. Antennas Propag*., vol. 59, no. 4, pp. 1123-1131, April 2011.

[12] S. Licul, J. A. N. Noronha, W. A. Davis, D. G. Sweeney, C. R. Anderson, and T. M. Bielawa, "A Parametric Study of Time-Domain Characteristics of Possible UWB Antenna Architectures", *IEEE 58th Vehicular Technology Conference*, (VTC), vol. 5, pp. 3110-3114, October, 2003.

[13] V. Kumar, S. Kumar, and B. Gupta, "Performance analysis of Swastika Slot UWB antenna in Vicinity of Dispersive Human layered Tissue model", *IEEE Region 10 Symposium (TENSYMP 2014)*, pp. 219-223, 14-16, April 2014.

[14] ANSYS High Frequency Structure Simulator [Online]. Available: http://www.ansys.com.

[15] V. Kumar, and B. Gupta, "Swastika Slot UWB antenna for Body-worn application in WBAN", *IEEE 8th International Symposium on Medical Information and Communication Technology (ISMICT 2014)*, pp. 1-5, 2-4, April 2014.

[16] K.Y. Yazdandoost and K. Hamaguchi, "Very small UWB Antenna for WBAN Applications", *5th International Symposium on Medical Information & Communication Technology* (ISMICT), pp. 70-73, 2011.

[17] Y. Zhao, Y. Hao, A. Alomainy and C.G. Parini, "UWB On-Body Radio Channel Modelling using Ray Theory and sub-band FDTD Method", *IEEE Transactions on Microwave Theory and Techniques*, Special Issue on Ultra-Wideband, vol. 54, pp. 1827–1835, 2006.

THE 18TH INTERNATIONAL SYMPOSIUM ON WIRELESS PERSONAL MULTIMEDIA COMMUNICATIONS
(WPMC-2015)
December 13-16, 2015, Hyderabad, India

Secrecy Outage of a Cognitive Relay Network with Energy Harvesting and Imperfect CSI

Pranabesh Maji, Binod Prasad
Department of ECE
NIT Durgapur, India
pranabesh.nov90@gmail.com, binod.ece@gmail.com

Sanjay Dhar Roy, Member, IEEE
Sumit Kundu, Senior Member, IEEE
Department of ECE, NIT Durgapur, India
s_dharroy@yahoo.com, sumit.kundu@ece.nitdgp.ac.in

***Abstract*—In this paper the physical layer security of an underlay Cognitive Relay Network (CRN) based on wireless energy harvesting (EH) relay is studied. We consider a decode and forward (DF) relay node harvests energy from radio frequency (RF) signal transmission of secondary user (SU). We evaluate the Secrecy Outage Probability (SOP) of secondary relay network assuming that the channel state information (CSI) of the interfering links from both the SU and relay transmitter to PU receiver are imperfect. The transmit power of the SU as well as relay is controlled by the maximum tolerable interference at PU because of underlay environment and outage constraint of PU as demanded by quality of service (QOS) of PU. The impact of maximum tolerable interference threshold, energy harvesting time, imperfect CSI, and PU outage constraint on the secrecy outage of the SU network is also investigated.**

Keywords— Imperfect channel state information (CSI); Secrecy Outage Probability (SOP); Cognitive Relay Network (CRN); Energy Harvesting (EH).

I. INTRODUCTION

In the recent year there has been phenomenal growth in the field of wireless communication system which increases the demand for radio spectrum resource. Furthermore as reported by FCC, the utilization of some spectrum band is as low as 15% in the band below 3 GHz resulting in spectrum underutilization. Cognitive radio has evolved as an efficient means to strike a balance between spectrum scarcity and spectrum underutilization [1]. Underlay spectrum sharing is one of the potential techniques used to access the licensed spectrum allocated to the primary user (PU). In underlay approach, SU accesses the same band as used by the PU concurrently provided the interference produced due SU transmission is within a tolerable interference threshold limit of PU [2]. As the transmit power of SU is controlled in order to protect the PU in underlay spectrum sharing technique, the performance of SU is limited. Cooperative relay technique is one of the potential techniques used to enhance the system performance in terms of spatial diversity. A combination of cognitive radio and cooperative diversity is used to enhance the performance of Cognitive Relay Network (CRN) in terms of coverage area [3-4]. In the case of an energy constrained network, the performance is limited due to energy constraint of the relay. In the recent year wireless energy harvesting is advocated to enhance the part of energy constrained network. An energy harvesting DF relay has been analyzed where the relay is assumed to harvest energy from the RF source [5-6]. However cognitive radio networks face new privacy and security threat due to broadcast nature of wireless channel. Thus security is one of the utmost importance in this type of networks [7]. The customs way of security is based on cryptographic approaches but physical layer security is an appealing approach to achieve secured transmission [8] which gained a considerable attention over last few years. In the wiretap model introduced by Wyner [9], the source and destination try to communicate reliably while an eavesdropper tries to snoop the confidential message. Depending on the channel conditions and the bad intention of eavesdropper, a secrecy rate may not be achievable which leads to secrecy outage. Secrecy outage can be explained as a service condition and it happens when a desired secrecy falls below a threshold of acceptable performance. Using this secrecy outage parameter we can say how much securely we can forward our confidential information to the destination. This paper investigates physical (PHY) layer security in a CRN in presence of an eavesdropper. In an underlay network, SU needs to adjusts its transmit power so as to maintain a maximum interference threshold tolerable at the PU receiver. It requires the CSI of the SU transmitter and PU receiver be available at the SU transmitter. However due to practical limitations, perfect CSI may not be available at SU transmitter**.** Outage performance of a cognitive relay network with imperfect channel knowledge estimations has been analyzed in [10] without considering the security issues. A general cooperative network based on decode and forward relaying has been studied in [11] where the relay is assumed to harvest energy through the RF transmission from the source with time switching based relaying. Throughput of energy harvesting based relaying scheme is analyzed in [11] without any focus on security issues. In the present work we analyze the physical layer security in terms of SOP of an underlay cognitive relay network, where a cognitive relay harvests energy from the RF transmission of the secondary user and the CSI available at the secondary user as well as relay is imperfect. Further a QOS of the primary user in terms of maximum allowed interference threshold and an outage constraint is maintained. The major contribution of this paper can summarized as below:

- An analytical formulation is presented to evaluate SOP for an underlay CRN using a wireless energy harvesting relay in presence of imperfect CSI.
- Impact of primary QOS in terms of maximum allowable interference at primary receiver and a constraint on primary outage on SOP is evaluated.

- Impact of imperfection in CSI and energy harvesting time on SOP is indicated.
- Further, outage probability and intercept probability of SU relay is formulated for the considered network.
- A simulation test bed in MATLAB is developed following our analytical model to assess the performance of the network in terms of secrecy outage probability (SOP) of the secondary user.

The rest of this paper is organized as follows: Section II describes the system model of an underlay CRN with imperfect CSI at secondary user and relay in presence of an eavesdropper. In Section III, we derive the expression of secrecy outage probability of SU under imperfect CSI and constraint of PU QOS. Results on SOP, based on our formulation, are presented in Section IV. Finally, Section V concludes the paper.

II. SYSTEM MODEL

An underlay Cognitive Relay Network model consisting of a SU transmitter (SU-Tx), a secondary relay (SR), a SU destination (SU-Rx), an eavesdropper (Eav) and a PU receiver (PU-Rx) is considered in this paper as shown in Fig. 1. We assume that there is no direct link between SU-Tx and SU-Rx node. Thus an intermediate relay working in DF mode assists the secondary transmission. Secondary relay tries to send confidential information reliably to the destination, SU-Rx while an eavesdropper (Eav) tries to snoop that confidential information. We consider that channel state information (CSI) of the interference links i.e. both SU-Tx to PU-Rx and relay transmitter to PU-Rx are imperfect. The relay harvests energy from the signal transmitted by secondary user and uses the harvested energy as a source of transmit power as outlined in the Time Switching–Based Relaying(TSR) scheme of [11] . Further the SU as well as the relay attempts to maintain interference produced at PU-Rx below the interference threshold. The relay is assumed to harvest energy for a fraction of time (αT) of the total time frame T and the half of remaining time i.e. (1-α)T/2 is used for source to relay information transmission while the other half, (1-α)T/2 for relay to destination information transmission as shown in Fig.2. The relay is assumed to perform the joint task of energy harvesting and information processing [12]. The transmit power of SU-Tx and relays are controlled so as to maintain an outage constraint of PU-Rx. The harvested energy is used by the relay as a source of transmit power, ($P_r^{harvest}$) to send the information from relay to SU-Rx. However there are two cases for the level of transmitted power from relay such as (i) if the maximum possible transmit power based on harvested energy ($P_r^{harvest}$) is less than the maximum allowed transmit power (P_r) due to outage constraint of PU, the relay transmits with power $P_r^{harvest}$, otherwise (ii) if the maximum possible transmit power based on harvested energy($P_r^{harvest}$) exceeds P_r, the transmission power of the relay is limited to P_r. All the channels links $(h_i, i \in \{sr, sp, rd, re, rp\})$ are assumed to be independent and identically distributed Rayleigh fading channel with zero mean and unity variance i.e. $h_i \sim CN(0,1)$. The corresponding channel gains denoted as $g_i = |h_i|^2, i \in (sr, sp, rd, re, rp)$ are exponentially distributed. In a practical case, it is very difficult to acquire perfect CSI in a CRN due to mobility, feedback delay and channel estimation errors. Thus in most of the practical cases available CSI is imperfect. Therefore, following imperfect channel a model of as in [13], the estimated channel coefficient is given as follows:

$$\hat{h}_{sp} = \rho h_{sp} + \sqrt{1-\rho^2}\,\varepsilon \quad (1)$$

$$\hat{h}_{rp} = \rho h_{rp} + \sqrt{1-\rho^2}\,\varepsilon \quad (2)$$

Where h_{sp}, h_{rp} denotes the ideal channel coefficient and $\hat{h}_{sp}, \hat{h}_{rp}$ are the channel estimation available at the SU-Tx and SR respectively, ε is a Gaussian Random variable with zero mean and variance one and is uncorrelated with h_{sp}, h_{rp}. The correlation coefficient ρ $(0 \le \rho \le 1)$ is a constant that determines the average quality of the channel estimation over all channel states which reflects the degree of imperfections of CSI estimations. For example, if $\rho = 1$, the channel knowledge is perfect and the full CSI is available, while $\rho = 0$ means that CSI estimation is completely random. The estimated channel power gains $\hat{g}_{sp}$ and $\hat{g}_{rp}$ are exponentially distributed with mean λ_{sp} and λ_{rp} respectively as $g_{sp} = |h_{sp}|^2, g_{rp} = |h_{rp}|^2$.

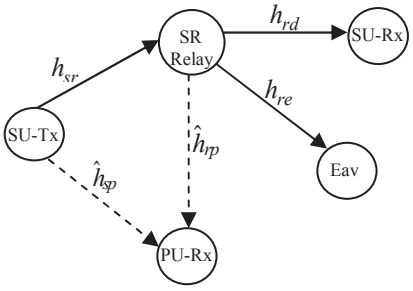

Fig. 1. System model for Cognitive Relay Network.

III. SECRECY OUTAGE PROBABILITY(SOP) OF ENERGY HARVESTING RELAY

The SOP of the CRN is analyzed where energy harvesting relay harvests energy using the time switching scheme. The transmission block arrangement in the time switching based relaying scheme as in [11] is shown in Fig. 2. Here T is the transmission block time for transmitting information from Su-Tx to SU-Rx. α indicates the fraction of T in which time the relay harvests energy from SU-Tx and uses it as a source of transmit power at relay to forward the information during time (1-α)T/2 maintaining an outage constraint on PU.

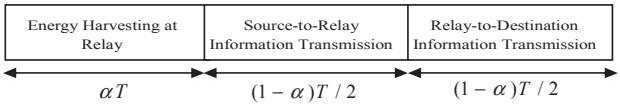

Fig. 2. Transmission block structure for energy harvesting and information transmission.

The energy harvested by the relay over a time of αT , considering a normalized distance between SU_Tx and SR as units,is given as [14].

$$E_h = \delta P_s g_{sr} \alpha T \tag{3}$$

where $0 < \delta < 1$ is the energy conversion efficiency and depends on the energy harvesting circuitry [14] and P_s is the SU transmit power. Using harvested energy E_h as a source of power for (1-α)T/2 time, the maximum transmitted power from the relay node can be written as,

$$\begin{aligned} P_r^{harvest} &= \frac{E_h}{(1-\alpha)T/2} \\ &= \frac{2\delta P_s g_{sr} \alpha}{(1-\alpha)} \end{aligned} \tag{4}$$

As explained earlier that there are two cases for the level of transmitted power from relay which is given as

$$P_{relay}^{Tx} = P_r^{harvest} \quad if\ P_r^{harvest} \le P_r \tag{4.1}$$

$$= P_r \quad if\ P_r^{harvest} > P_r \tag{4.2}$$

It may be noted that when the relay transmits as per (4.1), we call it transmission in harvesting power mode while in the case the, transmission is governed as per (4.2), we call it transmission in interference constrained mode. However it may be noted that in both the cases the transmission energy is derived from the harvested transmission energy only.

Because of imperfect CSI of the interference links from both SU-Tx to PU-Rx and SR to PU-Rx the transmit power of SU-Tx and SR are governed as below:

$$p_s = \frac{\eta P_{th}}{\hat{g}_{sp}} \quad \text{and} \quad p_r = \frac{\eta P_{th}}{\hat{g}_{rp}} \tag{5}$$

Thus equation (5) defines the maximum instantaneous transmit power of SU and SR. where η is a scaling parameter $(0 < \eta \le 1)$ used to limit the transmit power of SU and SR taking into account the effects of imperfect CSI. Further 'η' is chosen appropriately so as to maintain a constraint on primary user outage. In order to protect the PU-Rx from harmful interference of the SU-Tx and SR, the instantaneous transmit power of SU-Tx must be controlled so as to maintain a given constraint (θ) on outage probability of PU as given by [15].

$$\begin{aligned} P_{out}^{pu} &= \text{Prob}\{p_r g_{rp} > P_{th}\} \le \theta \\ &= 1 - \frac{1}{2}\left(1 + \frac{1-\eta}{\sqrt{(1+\eta)^2 - 4\rho^2\eta}}\right) \le \theta \end{aligned} \tag{6}$$

The above equation is valid for $(0 \le \rho \le 1)$ and $(0 < \eta \le 1)$ .The possible value of η for a given ρ is obtained by equating $P_{out}^{pu} = \theta$

$$or,\ 1 - \frac{1}{2}\left(1 + \frac{1-\eta}{\sqrt{(1+\eta)^2 - 4\rho^2\eta}}\right) = \theta \tag{7}$$

Now we evaluate the probability (p_1) and probability (p_2) of transmitting in harvesting mode and interference constraint mode respectively as given below.

$$\begin{aligned} p_1 &= \Pr\left\{P_r^{harvest} \le P_r\right\} \\ &= \Pr\left\{\frac{g_{sr}}{\hat{g}_{sp}} < \frac{1-\alpha}{2\alpha\delta} \cdot \frac{1}{\hat{g}_{rp}}\right\} \\ &= -\frac{1-\alpha}{2\alpha\delta}\exp\left(\frac{1-\alpha}{2\alpha\delta}\right) Ei\left(-\frac{1-\alpha}{2\alpha\delta}\right) \end{aligned} \tag{8}$$

Where $Ei(\mathrm{x})$ is the exponential integral function given by $Ei(x) = -\int_{-x}^{\infty} \frac{e^{-t}}{t} dt$ [16].

Similarly

$$\begin{aligned} p_2 &= \Pr\left\{P_r^{harvest} > P_r\right\} \\ &= 1 - p_1 \end{aligned} \tag{9}$$

Now the channel capacity of SR to SU-Rx link i.e. destination channel, is given as:

$$C_{rd} = p_1 \log_2(1+\gamma_{rd1}) + p_2 \log_2(1+\gamma_{rd2}) \tag{10}$$

Where, γ_{rd1} and γ_{rd2} are signal to noise ratio at the SU-Rx considering two different modes of relay transmit power with probabilities p_1 and p_2 respectively as given by

$$\gamma_{rd1} = P_r^{harvest} g_{rd} \tag{11}$$

$$\gamma_{rd2} = P_r g_{rd} \tag{12}$$

Here we are assuming that the noise power is normalized.

Similarly channel capacity of relay to eavesdropper link, is given as:

$$C_{re} = p_1 \log_2(1+\gamma_{re1}) + p_2 \log_2(1+\gamma_{re2}) \tag{13}$$

where γ_{re1} and γ_{re2} are SNR at the eavesdropper for two different modes of relay transmit power with probabilities p_1 and p_2 respectively as given by

$$\gamma_{re1} = P_r^{harvest} g_{re} \tag{11}$$

$$\gamma_{re2} = P_r g_{re} \tag{12}$$

The secrecy capacity C_S is expressed as, [17],

$$C_S = (C_{rd} - C_{re})^+ \tag{14}$$

Where, $[x]^+ = \max\{x, 0\}$

In presence of eavesdropping, if $C_S > R_S$ then perfect secrecy is achieved. Where, R_S is the target secrecy rate. Otherwise, in the case of $C_S < R_S$, secrecy is compromised meaning occurrence of secrecy outage. Now secrecy outage probability (SOP) can be defined as the probability that the instantaneous secrecy capacity, C_S is less than a target secrecy rate, R_S which can now be expressed as,

$$\begin{aligned} SOP &= prob[C_S \le R_S] \\ SOP &= \left(SOP_{harv}\ p_1\right) + \left(SOP_{cogn}\ p_2\right) \end{aligned} \tag{15}$$

$$SOP_{harv} = \int_0^{\infty}\int_0^{\infty} prob\left[C_s^h \le R_S\right] f_{g_{rd}}(g_{rd})\, f_{g_{re}}(g_{re})\, dg_{rd}\, dg_{re}$$

$$SOP_{cogn} = \int_0^{\infty}\int_0^{\infty} prob\left[C_s^c \le R_S\right] f_{g_{rd}}(g_{rd})\, f_{g_{re}}(g_{re})\, dg_{rd}\, dg_{re}$$

Where $f_{g_{rd}}(g_{rd})$ *and* $f_{g_{re}}(g_{re})$ are the pdf of g_{rd} *and* g_{re} respectively.

$$C_s^c = \log_2 \frac{1+\gamma_{rd1}}{1+\gamma_{re1}} \text{ And } C_s^h = \log_2 \frac{1+\gamma_{rd2}}{1+\gamma_{re2}}$$

where, C_s^h is the secrecy capacity when relay transmits in harvesting mode and C_s^c is the secrecy capacity when relay transmits in cognitive constraint mode.

Equation (15) represents SOP of an energy harvesting relay under imperfect CSI in cognitive relay network.

In addition to secrecy outage probability, intercept probability (IP) is also used to characterized the security performance of a network [18]. Further reliability performance of the network is indicated by Outage Probability (OP) [18].

Now we provide the necessary analytical expressions developed to evaluate the outage probability and probability of intercept for the network with energy harvesting relay under study. Outage probability (OP), P_{out} is defined as the probability that the capacity of source-destination (SD) link (C_{rd}) falls below a target data rate, R_d [18].

$$P_{out} = prob\left[C_{rd} < R_d\right]$$

$$= \int_0^\infty p_1\ prob\left[C_{rd} < R_d\right] f_{g_{rd}}(g_{rd})\, dg_{rd} + \int_0^\infty p_2\ prob\left[C_{rd} < R_d\right] f_{g_{rd}}(g_{rd})\, dg_{rd} \quad (16)$$

Similarly the intercept probability (IP) P_{int} is defined as the probability that the capacity of source to eavesdropper link (C_{re}) exceeds a target data rate, R_d [18].

$$P_{\text{int}} = prob\left[C_{re} > R_d\right]$$

$$= \int_0^\infty p_1\ prob\left[C_{re} > R_d\right] f_{g_{re}}(g_{re})\, dg_{re} + \int_0^\infty p_2\ prob\left[C_{re} > R_d\right] f_{g_{re}}(g_{re})\, dg_{re} \quad (17)$$

The IP and OP are used to characterize the security and reliability of the network under study. We evaluate the impact of imperfect CSI and other network parameters on IP and OP

IV. Simulation Result

We develop a MATLAB based simulation test bed on basis of our formulation to evaluate secrecy outage, intercept probability, outage probability. We now present our simulation results. Following parameter values are used in our simulation, target secrecy rate R_S =0.5 kbps/Hz, target data rate R_d =0.5 kbps/Hz, energy conversion efficiency δ =1, PU outage constraint θ =1%, 3% and 5%.

Fig.3 depicts the SOP w.r.t energy harvesting time (α), for several values of interference threshold power (P_{th}). Initially for lower and moderate values of α, we have $p_1 > p_2$ which indicates that the relay has higher probability of being in harvesting mode. With gradual increase in α, the relay is able to harvest more energy which increases the transmit power of the relay and reduces SOP gradually. However beyond a certain optimum value of α (= 0.5 in the present case), we have $p_2 > p_1$, indicating that the relay switches to cognitive constraint mode with higher probability, where its transmit power is adjusted maintaining the interference constraint. This results in dominating component of eq(15) i.e. SOP_{cogn} remains invariant w.r.t α and higher values of dominating p_2 leads to increase in overall SOP.

Fig.4 represents the effect of P_{th} on intercept probability of the eavesdropper link for several values of PU outage constraint (θ). Higher values of P_{th} allows the relay to transmit at higher power which increases the capacity C_{re}. This leads to an increase in IP. Similarly increase in θ also increases transmission power SU which in turn increases P_{int}.

Fig.5 shows the variation of outage probability of relay to SU-Rx link with interference threshold power, (P_{th}) for three different values of outage probability constraint of PU e.g. (θ =1%,3%,5%). Higher values of P_{th} allows SU-Rx to transmit at higher power which leads P_{out} to fall gradually. At a fixed P_{th}, if we increase θ i.e. SU-Tx is allowed to transmit at higher power level, P_{out} gradually reduces.

Fig.6 shows the variation of secrecy outage probability (SOP) of EH relay with interference threshold power, P_{th} for three different values of channel correlation coefficient, (*i.e.* ρ = 0.2, 0.5 and 0.8) and two values of energy harvesting parameters (α). Higher interference threshold allows SU transmitter to transmit at a higher power level. This leads SOP to gradually reduce as we increase the interference threshold which allows the relay to transmit at a higher power level. Further SOP reduces with higher ρ for a given level of P_{th} i.e. as CSI estimation moves towards a perfect case, SOP reduces. The joint impact of P_{th} and ρ on SOP is evident from this figure. It may be noted that for chosen value of $\alpha = 0.4$, the probability of transmitting in harvesting mode by the relay is more i.e. $p_1 > p_2$, which implies that we are operating in left part of the optimum value of α in Fig.3.

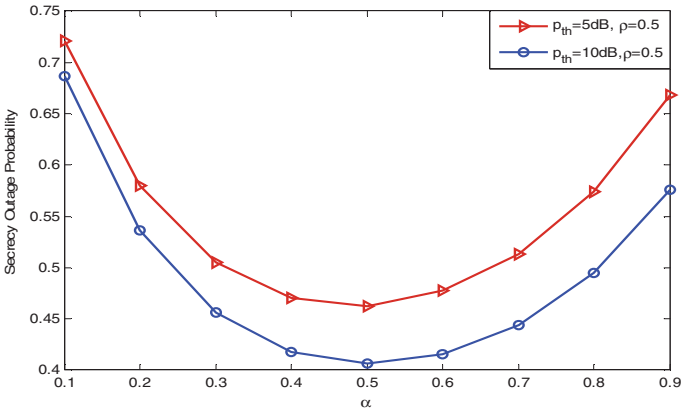

Fig. 3. SOP against α for different values of interference threshold power P_{th} (i.e. P_{th} =5,10 dB)where consider ρ = 0.5

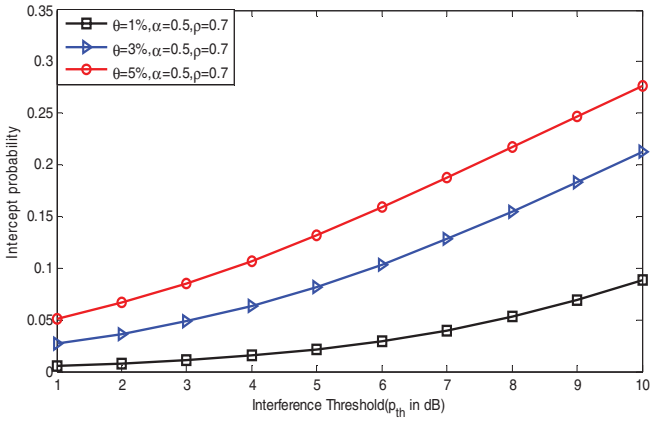

Fig. 4. Intercept probability versus P_{th} in dB for different values of PU outage constraint, θ (*i.e.* θ =1%,3%,5%) where consider R_d=0.5kbps/Hz

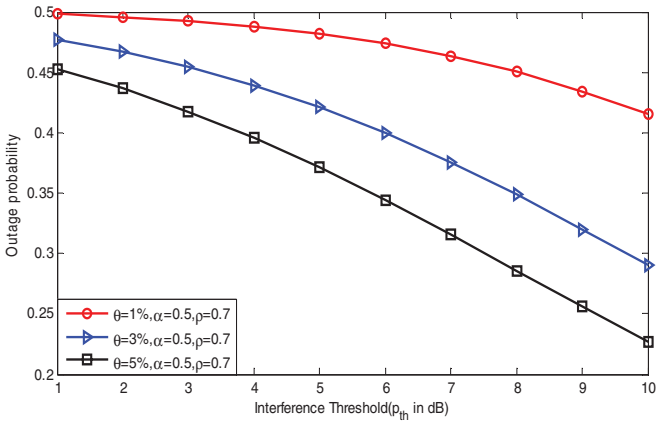

Fig. 5. Outage probability versus P_{th} in dB for different values of PU outage constraint, θ (*i.e.* θ =1%,3%,5%) where consider R_d=0.5kbps/Hz.

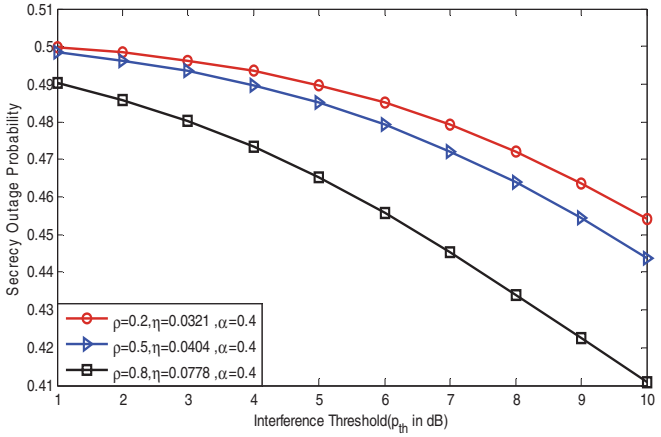

Fig. 6. SOP versus P_{th} in dB for different values of channel correlation coefficient, ρ (*i.e.* ρ =0.2, 0.5 and 0.8) for R_S=0.5 kbps/Hz.

V. CONCLUSION

An analytical model of an underlay cognitive relay network using an energy harvesting relay with imperfect CSI of the interfering links at secondary user and relay in presence of an eavesdropper is presented. The impact of QOS of PU on secrecy outage of energy harvesting based secondary relay is evaluated. The impact of harvesting time parameter in Time Switching Relay (TSR) scheme on secrecy outage is also indicated. Furthermore, the maximum tolerable interference at PU_Rx, maximum allowed outage of PU as well as imperfect CSI have significant effects on SOP. Higher interference threshold, as well as higher outage probability constraint increases intercept probability and reduces outage probability. An optimal energy harvesting time is observed which minimizes secrecy outage probability.

REFERENCES

[1] Mitola, J. "Cognitive radio: an integrated agent architecture for software defined radio". PhD thesis, Stockholm, Sweden, 2000 KTH.

[2] Haykin, S. "Cognitive radio: brain-empowered wireless communications",IEEE J. Sel. Areas Commun.,2005, 23, (2), pp. 201 – 220.

[3] I. Krikidis, S. Timotheou, and S. Sasaki, "RF energy transfer for cooperative networks: Data relaying or energy harvesting?" IEEE Commun. Lett., vol. 16,no. 11, pp. 1772–1775, 2012.

[4] Q. Zhang, J. Jia, and J. Zhang, "Cooperative relay to improve diversity in cognitive radio networks," IEEE Commun. Mag., vol. 47, no. 2, pp. 111-117, Feb. 2009.

[5] R.L.Varshney,"Transporting information and energy simultaneously."Information Theory, 2008. ISIT 2008. IEEEInternational Symposium on. IEEE, 2008.

[6] P. Grover, , and A. Sahai. "Shannon meets Tesla: Wireless information and power transfer." ISIT. 2010.

[7] Zhou, L., Chao, H.C. "Multimedia traffic security architecture for internet of things", IEEE Netw., 2011, 25, (3), pp. 29 – 34.

[8] A. Khisti and G. W. Wornell, "Secure transmission with multiple antennas—Part I: The MISOME wiretap channel," IEEE Trans. Inf. Theory , vol. 56, no. 7, pp. 3088–3104, Jul. 2010.

[9] A. D. Wyner, "The wire-tap channel," Bell Sys. Tech. J., vol. 54, pp. 1355-1387, 1975.

[10] Binod Prasad, Sanjay Dhar Roy and Sumit Kundu, "Outage Performance of Cognitive Relay Network with Imperfect Channel Estimation Under Proactive DF Relaying", in Proc. of IEEE National Conf. on Communication (NCC), IIT Kanpur, Feb 2014.

[11] A. A. Nasir, X. Zhou, S. Durrani, and R. A. Kennedy, "Throughput and ergodic capacity of wireless energy harvesting based DF relaying network," in Proc. IEEE ICC, 2014, June 2014.

[12] L. R. Varshney, "Transporting information and energy simultaneously,"in Proc. 2008 IEEE ISIT.

[13] H. A. Suraweera, P. J. Smith, and M. Shafi, "Capacity limits and performance analysis of cognitive radio with imperfect channel knowledge," IEEE Trans. Veh. Technol., vol. 59, no. 4, pp. 1811–1822, May 2010.

[14] X. Zhou, R. Zhang, and C. K. Ho, "Wireless information and power transfer:Architecture design and rate-energy tradeoff," in Proc. IEEE GLOBECOM, 2012.

[15] Xing Zhang , Jia Xing, Zhi Yan, Yue Gao, and Wenbo Wang, "Outage Performance Study of Cognitive Relay Networks with Imperfect Channel Knowledge," IEEE Communications Letters, VOL. 17, NO. 1, January 2013.

[16] I. S. Gradshteyn and I.M.Ryzhik, *Table of Integrals, Series and Products*, 6th ed. San Diego, CA: Academic, 2000.

[17] M. Bloch, J. Barros, M. R. D. Rodrigues, and S. W. McLaughlin, "Wireless information-theoretic security," IEEE Trans. Inf. Theory , vol. 54,no. 6, pp. 2515–2534, June 2008.

[18] Yulong Zou, Xianbin Wang, Weiming Shen and Lajos Hanzo," Security Versus Reliability Analysis of Opportunistic Relaying", IEEE Transactions on vehicular technology, vol.63, no.6 , July2014.

THE 18TH INTERNATIONAL SYMPOSIUM ON WIRELESS PERSONAL MULTIMEDIA COMMUNICATIONS
(WPMC-2015)
December 13-16, 2015, Hyderabad, India

Long-haul Communication Trial in London TV White-space with IEEE 802.11af-based High Power Prototype

Takeshi Matsumura[1], Kentaro Ishizu[1], Keiichi Mizutani[2], Tran Ha Nguyen[1], Homare Murakami[1,3], Fumihide Kojima[1,3] and Hiroshi Harada[2,3]
[1]Smart Wireless Laboratory, Wireless Network Research Institute, NICT, Yokosuka, Japan
[2]Dept. of Communications and Computer Engineering, Graduate School of Informatics, Kyoto University, Kyoto, Japan
[3]Social ICT Research Center, NICT, Koganei, Japan
matsumura@nict.go.jp

***Abstract*—TV white-space (TVWS) communication systems have been globally researched and developed due to its wide frequency range and superior propagation characteristics. In addition, EIRP +36 dBm is permitted as the maximum transmission power for fixed devices in some operational rules regulated in the U.S.A., the U.K., etc., and thus, the TVWS has been strongly expected to allow a long-haul backbone network at relatively low cost. On the other hand, rigorous RF characteristics such as adjacent channel power leakage are required for the WS devices not to interfere with primary users and there are some challenges in prototyping WS devices enabling high output power in conformity to such regulations. In this study, WS devices based on IEEE 802.11af communication system with a maximum output power of +30 dBm at the antenna port have been prototyped. The prototyped devices conform to the ETSI draft specification and are licensed by the Ofcom for the TVWS pilot program. Field experiment in the London urban area was also performed and resulted in a UDP throughput of about 2.2 Mbit/s with a line-on-site distance of about 3.7 km. From this result, it was confirmed that the TVWS communication system indicated the possibility of the long-haul backbone network even in a metropolis.**

Keywords—TV white-spaces (TVWS); IEEE 802.11af; high power; long-haul backbone network; field experiment

I. INTRODUCTION

The UHF band mainly allocated to TV broadcasters has possibility to provide a long-haul backbone network at low cost due to its relatively wide frequency range and superior propagation characteristics in comparison with frequency bands assigned to existing commercial networks. Therefore, white-spaces in the TV band (TVWS, TV White-Spaces) are expected not only for further accommodation of rapid-increasing mobile traffic but also for provision of broadband access in a rural area. Besides, the TVWS is also expected for the deployment of a new backbone network in the future smart city even in an urban area. For such social implementation, some international communication systems, e.g. IEEE 802.15.4 [1], IEEE 802.11af [2] and IEEE 802.22 [3], have been standardized and some rules for secondary use of the TVWS have been established in some countries such as the U.S.A. [4], the U.K. [5], Singapore [6]. In these regulations, an output power of EIRP +36 dBm is permitted as maximum transmission power for fixed devices and has boosted utilization of the TVWS for the long-haul backbone network. Furthermore, field experiment for deployment of the infrastructures utilizing the TVWS has been performed in some other countries as one of solutions for the bridge of the digital divide [7],[8].

On the other hand, rigorous RF characteristics, especially the leakage in the entire TV band outside a using channel, are required to avoid interference with the primary users such as TV broadcasters and wireless microphones. WS devices must comply with these requirements and there are still some challenges to develop hardware prototypes that are capable of transmitting a high-power RF signal with reasonable size and cost.

In this study, the authors developed hardware prototypes based on IEEE 802.11af system with the capability of transmitting a high output power of +30 dBm at the antenna port. These prototypes were licensed by the Ofcom (Office of communications) in conformity to the ETSI (European Telecommunications Standards Institute) draft specification that was adopted as a regulation in the U.K. The authors also developed TVWS communication systems including the WS database (WSDB) that also conformed to the Ofcom requirement, and participated in the TVWS pilot program operated by the Ofcom. In this trial, field experiment as a feasibility study of a long-haul backbone network was performed in London urban area and a UDP throughput of about 2.2 Mbit/s was obtained with a line-on-site distance of about 3.7 km.

The rest of this paper is organized as follows. The pilot program organized by the Ofcom in the U.K and required specification regulated by the ETSI are described in Section II and III, respectively. The prototyped device is described in Section IV and its RF performance is characterized in Section

This research was conducted under contract of R&D on “dynamic spectrum access in multiple frequency bands for efficient radio resource utilization" with the Ministry of Internal Affairs and Communications, Japan.

V. Then, the result of the field experiment in London urban area is summarized in Section VI. Finally, we conclude this paper with Section VII.

II. TVWS Pilot Program in U.K.

In the U.K., a 320 MHz frequency range from 470 MHz to 790 MHz is assigned to the DTT (Digital Terrestrial TV) and divided into 40 channels with an 8 MHz bandwidth. In addition, PSME (Programme Making and Social Events) services such as wireless microphones are operated in the TV band and permitted to preferentially utilize unused DTT channels. Therefore, secondary systems need to operate in cooperation with the WSDB to find available channels and WS devices are required to comply with the draft specification regulated by the ETSI to prevent the interference with the primary systems.

A. System Requirement

Fig. 1 shows an overview of the secondary system with the WSDB in the U.K. The interface between WS device and WSDB is properly determined and the WSDB needs to be authenticated by the Ofcom. Here, WS devices are classified into two types: *Master Device* and *Slave Device*. Before starting the communication in the TVWS, *Master Device* has to access a WSDB listing server operated by the Ofcom and acquire a list of WSDBs. Then, *Master Device* selects one WSDB from the list for parameters exchange and informs the selected WSDB of geo-location, antenna height and device parameters including *Device Emission Class*. After receiving the parameters, the WSDB calculates and provides available channels with each permitted maximum output power. After that, *Master Device* selects optimal channel to utilize and starts beacon transmission to *Slave Device.* The beacon includes permitted maximum output power, and thus, *Slave Device* optimally set its radio parameters according to the received parameter information. Eventually, *Slave Device* answers *Master Device*, and then TVWS communication is started.

During the operation in the TVWS, *Master Device* should access the WSDB and update the available channel list at least every 15 minutes, since PSME services are operated intermittently in various locations and status of available channels is frequently changed, especially in urban areas such as central London. For the WSDB, the operational schedule of the PSME service is reflected in up to 15 minutes before starting its operation. In the case that the PSME service starts to occupy the using channel of the secondary system, the secondary users must stop their operation or change the using channel to other available one. Furthermore, *kill switch* function, which allows emergency stop of the secondary system under the Ofcom's operation, must be implemented in both WSDB and WS device.

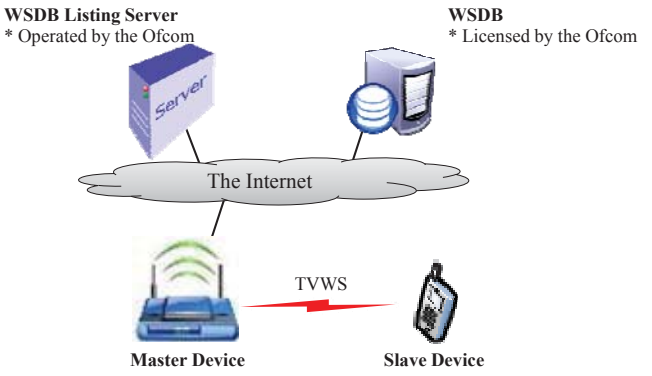

Figure 1. Overview of TVWS communication system in pilot program in the U.K.

B. Performance Requirement

Requirement for WS devices is regulated in the ETSI draft specification [9]. Particularly, adjacent channel leakage power is important to prevent the interference with primary users and stipulated as a relative value with the output power in the using DTT channel by following.

$$P_{OOB}\,(\text{dBm}/(100\ \text{kHz})) \le \max\{\,P_{IB}\,(\text{dBm}/(8\ \text{MHz})) - ACLR\,(\text{dB}),\ -84\,(\text{dBm}/(100\ \text{kHz}))\,\}, \quad (1)$$

where P_{OOB} is leakage power in a 100 kHz bandwidth outside the using channel and P_{IB} is output power in a 8 MHz BW of the using channel. Here, the *ACLR* (Adjacent Channel Leakage power Ratio) is defined by the suppression ratio of P_{OOB} to P_{IB}. Table I shows *ACLR* requirement in the ETSI draft specification and WS devices are classified into 5 *Device Emission Classes*, i.e. device classes, according to the ACLR performance. As above-mentioned, WS devices inform the WSDB of its device class before starting the TVWS communication and receive an available DTT channel list with permitted maximum power for each channel from the WSDB. At that time, availability of the TVWS varies by the device class.

III. High Power Prototype based on IEEE 802.11af

Fig. 2 shows an appearance of the prototyped WS device enabling a high output power of +30 dBm at the antenna port, based on IEEE 802.11af communication system. Overall size is 190 mm ×150 mm × 64 mm, including cooling fins. The prototype mainly consists of 6 boards as shown in Fig. 3; an I/O board for management of power supply and peripheral devices, a CPU board in which upper-layer MAC (Media Access Control) is implemented, an FPGA board for baseband processing, a DC/DC board for providing power to RF circuit, an RF board for main RF circuits including an AD/DA circuit and a transceiver IC and an high power amplifier (HPA) board for transmitting high output power. An external antenna is connected via an SMA connector implemented to the housing. According to the channel assignment of DTT in the U.K., the frequency setting of the prototype corresponds to an 8 MHz

TABLE I. ACLR for Different Device Emission Classes [9]

Where P_{OOB} falls within *n*th adjacent DTT channel	ACLR (dB)				
	Class 1	*Class 2*	*Class 3*	*Class 4*	*Class 5*
$n = \pm 1$	74	74	64	54	43
$n = \pm 2$	79	74	74	64	53
$n \ge +3, n \le -3$	84	74	84	74	64

interval.

Fig. 4 shows a block diagram of an RF part. In this prototype, direct conversion system is applied with using off-the-shelf RF IC. In the transmission part, the HPA that enables a high output power of +30 dBm is implemented with a pre-distorter circuit to reduce a distortion generated by the HPA. In the reception part, a wide-band low noise amplifier (LNA) is implemented and a variable attenuator is inserted to adjust received signal level to an acceptable level for the commercial RF IC. An RF switch is used to connect both transmission and reception circuits to the antenna port and a band pass filter (BPF) with a pass-band of 470−870 MHz is inserted between the RF switch and the antenna port to suppress unwanted signals such as harmonics in the transmission signal and image signals for the receiver circuit.

Table II shows the RF specification of the prototyped WS device. A supporting frequency range is limited to 500−710 MHz, due to the difficulty in a design of a wide-band amplifier that allows high output power in the entire TV band. In consideration of insertion loss of the BPF and the RF switch between the HPA and the antenna port, a +33 dBm output power is required for the HPA to support a +30 dBm output power at the antenna port in conformance with the ETSI draft standard. Furthermore, since at least 10 dB back-off is required to support OFDM (Orthogonal Frequency-Division Multiplexing) system in IEEE 802.11af standard, the HPA needs to support a peak output power of more than +43 dBm in the entire TV band. In the prototype, pre-distorter is implemented to suppress a distortion generated by the HPA, however, there are some challenges to sufficiently compensate the distortion in a wide frequency range of 470−790 MHz mainly due to insufficient frequency characteristics of matching circuits.

Figure 2. Prototyped WS device based on IEEE 802.11af system.

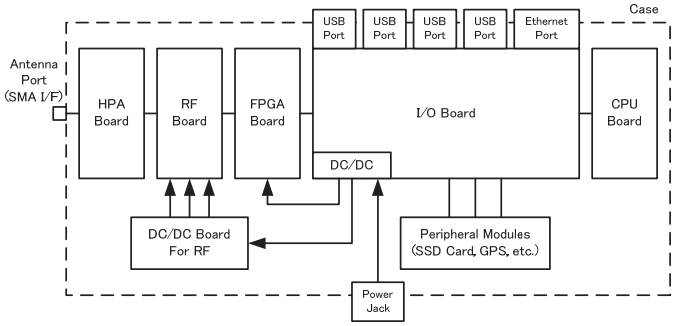

Figure 3. Hardware architecture of prototyped WS device.

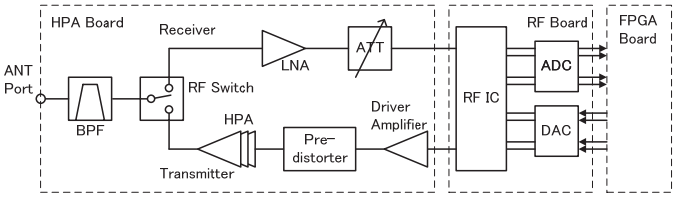

Figure 4. Block diagram of RF part.

TABLE II. RF SPECIFICATION OF PROTOTYPED DEVICE

Item	Description
Communication system	IEEE 802.11af
Supporting frequency range	500−710 MHz
Resolution of frequency setting	1 MHz
Frequency accuracy	±2 ppm
Output power	+30 dBm
Tuning range of output power	> 40 dB
Receiver dynamic range	−88 − −20 dBm

IV. RF PERFORMANCE

In this study, RF performance of the prototyped device was measured in conformity to the ETSI draft specification. Table III shows typical measured RF characteristics. All the measurement result except for *RIM3* followed measurement procedure described in the ETSI draft specification [9].

A. Transmission Power

In the ETSI draft specification, measurement procedures are stated as following. First, output power in the entire DTT band is measured by using a calibrated power meter. Then, transmission spectrum is measured by spectrum analyzer (SA) in the conditions of Table IV. All the measurement data are added together and compared with the measurement result by power meter to compensate transmission spectrum measured by SA. For instance, in the case that summation of the measurement data by SA is 1 dB higher than the result by power meter, each measured data by SA should be 1 dB reduced. After compensation of all the measurement data by SA, summation in the using DTT channel with an 8 MHz bandwidth is calculated as P_{IB}. Also, spectrum density in 100 kHz bandwidth and P_{OOB} are calculated by adding up 10 series data in each 100 kHz bandwidth. As a result of that, P_{IB} of +26.1 dBm is obtained at a center frequency of 682 MHz with a setting power of +27 dBm. Here, a 3-element ring Yagi antenna with a 7.6 dBi directivity is used in the after-mentioned field experiment, and thus, total transmission power is set to EIRP +34.7 dBm, not exceed an permitted maximum output power of EIRP +36 dBm. All other measurement results satisfy the ETSI draft specification in this measurement conditions.

TABLE III. RF CHARACTERISTICS OF PROTOTYPED WS DEVICE

Item	Conditions	Unit	Spec	Measured
Center freq.		MHz	–	682
P_{IB}	+28 dBm setup	dBm/ 8 MHz	–	26.1
Spectrum density		dBm/ 100 kHz	–	10.6
ACLR	n=−1	dB	≥43	63.2
	n=+1	dB	≥43	65.2
	n=−2	dB	≥53	73.0
	n=+2	dB	≥53	76.3
	n≤−3	dB	≥64	72.1
	n≥+3	dB	≥64	75.7
Transmitter unwanted emission outside TV band	30−47MHz	dBm/ 100 kHz	≤−36	−60.4
	47−74MHz		≤−54	−58.9
	74−87.5MHz		≤−36	−60.3
	87.5−118MHz		≤−54	−60.3
	118−174MHz		≤−36	−60.7
	174−230MHz		≤−54	−60.4
	230−470MHz		≤−36	−44.3
	790−862MHz		≤−54	−59.3
	862−1,000MHz		≤−36	−57.7
	1−4GHz	dBm/ 1 MHz	≤−30	−37.0
Transmitter intermodulation (RIM)	Lower	dB	≥45	71.7
	Upper	dB	≥45	76.0
Receiver spurious emissions	30MHz−1GHz	dBm/ 100 kHz	≤−57	−80.2
	1−4GHz	dBm/ 1 MHz	≤−47	−61.4

B. ACLR

As described in Section II, ACLR is calculated from P_{IB} and P_{OOB} measured in previous sub-section. Fig. 5 shows a typical spectrum mask in 682 MHz. Dotted line shows a limitation of the P_{OOB} calculated from the measured P_{IB} and ACLR requirement for Class 5 devices. From this result, signal level outside the using channel is sufficiently lower than P_{OOB} limitation in the entire TV band and the spectrum mask complies with the ETSI draft specification.

C. Unwanted Emissions and Intermodulation

Transmitter unwanted emissions outside the TV band and receiver spurious emissions comply with the ETSI draft specification as shown in Table III.

Transmitter intermodulation is measured by using a typical measurement system as shown in Fig. 6, in lieu of the measurement system in [9]. In this measurement, a WS device, a signal generator (SG) for unwanted signal generation and an SA are connected to each other through a power divider. Transmission frequency of the WS device is set to f_w and output power is set to maximum output power in Table III. Unwanted signal with a frequency of f_{un} is input from the SG and its signal level of P_u is set to –10 dBm, even though unwanted signal level is defined to 40 dB lower than transmission signal level in the ETSI draft specification. During the measurement with this setup, 3rd intermodulation with a signal level of *PIM3* is observed at a frequency of $2 \times f_w - f_{un}$ on the SA. Then, the third-order reverse intermodulation attenuation of *RIM3* is calculated by substitution of P_{IB}, P_u and *PIM3* to the following equation.

$$RIM3 = 2 \times P_{IB} + P_u - PIM3. \quad (2)$$

The prototypes were licensed by the Ofcom with a confirmation of these measurement method and result.

TABLE IV. MEASUREMENT CONDITIONS FOR TRANSMISSION POWER

Setting Item	Conditions
RBW (Resolution Band Width)	10 kHz
VBW (Video Band Width)	30 kHz
Start Frequency	470 MHz + RBW/2
Stop Frequency	790 MHz – RBW/2
Trace Mode	Max hold
Detector	RMS

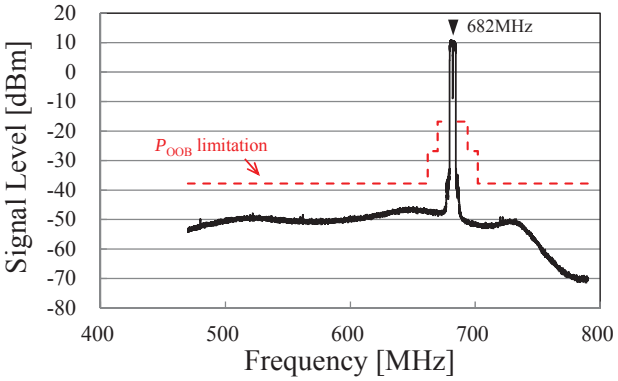

Figure 5. Spectrum mask with 682 MHz transmission signal.

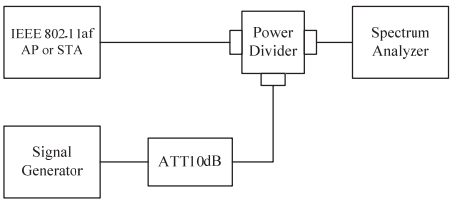

Figure 6. Measurement system for transmitter intermodulation.

V. FIELD EXPERIMENT IN LONDON

A. IEEE 802.11af-based Communication System

Field experiments in London urban area were performed with 2 prototyped WS devices; an access point (AP) and a station (STA). Fig. 7 shows overview of the communication system based on the IEEE 802.11af standard for the field experiments. The AP is connected to the RLSS (Registered Location Secure Server) installed in Japan via the Internet, and accesses the WSDB listing server operated by the Ofcom through the RLSS. Then, available channel list is obtained. After the AP selects some utilizable channels in the list according to the device performance and user's requirement,

the AP inform the RLSS of selected channels. Then, the RLSS selects one use channel in consideration with avoidance of the interference to/from nearby operating TVWS communication systems. In the field experiment in London, one of available channels with an permitted maximum power of EIRP +36 dBm is simply selected, since no other secondary system accesses the RLSS. After selecting the use channel, the AP starts to transmit beacons and the STA receives and replies them, then the TVWS communication is started.

B. Field Experiment in London Urban Area

In the field experiment in London, AP and STA were placed in Denmark Hill Campus and Guy's Campus of the KCL (King's College London), respectively, as shown in Fig. 8. A long-haul TVWS communication was performed with a line-on-site distance of about 3.7 km between the campuses. As aforementioned, output power at the antenna port is set to +27 dBm and 7.6 dBi directional antennas are connected to both devices. Therefore, transmission power of both devices is set to about EIRP +34.6 dBm with a 1.4 dB margin for the regulation. Throughput measurement was performed by using iperf with a signal bandwidth of 5 MHz, a QPSK modulation and a coding rate of 1/2. As a result, a UDP throughput of about 2.2 Mbit/s was obtained and it was confirmed that IEEE 802.11af-based communication system has the potential as a long-haul backbone network in a metropolitan environment.

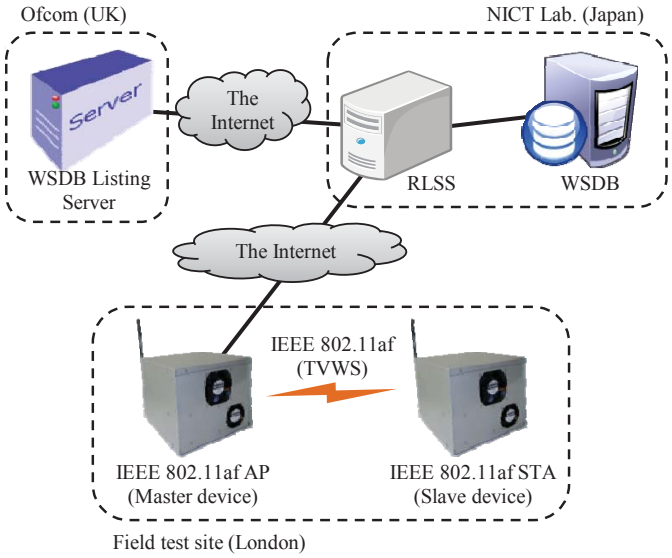

Figure 7. IEEE 802.11af-based communication systems for U.K. TVWS pilot program.

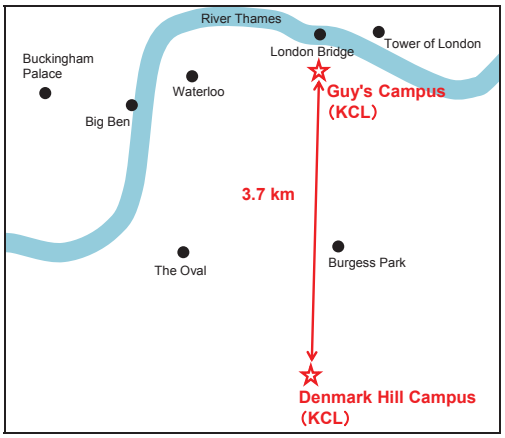

Figure 8. Location of field experiment in London urban area.

VI. CONCLUSION

In this study, the TVWS pilot program and required performance for secondary use of TVWS in the U.K. are summarized. Also, overview of the IEEE 802.11af-based prototyped device enabling a high output power of +30 dBm and its RF characteristics are presented. The prototyped WS devices comply with the ETSI draft specifications and are licensed by the Ofcom. In addition, field experiment was performed in London urban area by participating in the pilot program operated by the Ofcom.

As a result of the field experiment, a UDP throughput of about 2.2 Mbit/s with a signal bandwidth of 5 MHz was obtained with a 3.7 km line-on-site distance. Although the result of the throughput is not sufficient at present, this result indicates the potential as the long-haul backbone network based on the TVWS communication system even in the urban area where many high power TV broadcasters exist and interfere with the secondary system. For further improvement of the throughput, it is required to improve the blocking characteristics against strong interference from TV broadcasters. For the future work, these improvements will be carried out, to obtain the stability for the long-haul wireless communication in the TVWS even in the urban area.

ACKNOWLEDGMENT

Thanks for the King's College London for supporting the TVWS field experiment in the Ofcom TVWS pilot program.

REFERENCES

[1] IEEE 802.15 WPAN Task Group 4m (TG4m) TV White Space Amendment to 802.15.4, http://www.ieee802.org/15/pub/TG4m.html

[2] IEEE 802.11af Task Group. http://www.ieee802.org/11/Reports/tgaf update.htm

[3] IEEE 802.22 Working Group. http://www.ieee802.org/22/.

[4] FCC, "Unlisenced Operation in the TV Broadcast Bands, Third Memorandum Opinion and Order," FCC. 12-36, Apr. 5, 2012.

[5] Office of Communications, "Regulatory Require- ments White Space Devices in the UHF TV Band," July 2012.

[6] Infocomm Development Authority of Singapore, "Regulatory Framework for TV White Space Operations in the VHF/UHF Bands," June 2014.

[7] S. Roberts, P. Garnett and R. Chandra, "Connecting Africa using the TV white spaces: from research to real world deployments," in *Proc. IEEE LANMAN2015*, Apr. 2015.

[8] K. Patil, K. E. Skouby and R. Prasad, "Cognitive access to TVWS in India: TV spectrum occupancy and wireless broadband for rural areas," in *Proc. WPMC2013*, June 2013

[9] ETSI, "White space devices (WSD); wireless access systems operating in the 470 MHz to 790 MHz TV broadcast band; Harmonized EN covering the essential requirements of article 3.2 of the R&TTE directive," Final draft ETSI EN 201 598 V1.0.9, Feb. 2014.

THE 18TH INTERNATIONAL SYMPOSIUM ON WIRELESS PERSONAL MULTIMEDIA COMMUNICATIONS
(WPMC-2015)
December 13-16, 2015, Hyderabad, India

Participatory Heuristic Evaluation of the First Iteration of the eWALL Interface Application

Clara Schaarup; Louise Bilenberg Pape-Haugaard; Stine Veje Hangaard; Ole K. Hejlesen
Department of Health Science and Technology
Aalborg University
Aalborg, Denmark
csch@hst.aau.dk

Albena Mihovska
Center for TeleInfrastruktur
Aalborg University
Aalborg, Denmark
albena@es.aau.dk

***Abstract*—*Worldwide, the number of people having a chronic disease is increasing. Managing chronic diseases is time consuming and expensive. A need for new ways to deliver healthcare to patients with chronic diseases is urgent. Telemedicine and medical devices combined may offer several opportunities as alternative ways for healthcare to be delivered. An example of a device addressed to people with chronic disease is the device from the large-scale project "eWALL for Active Long Living", which has been tested using Participatory Heuristic Evaluation. The main results of the study showed a difference when comparing the most used heuristics given by the usability experts and the work domain professionals. When it comes to the distribution between the use of the severity grades between the usability experts and the work domain professionals, there seems to be an agreement between the two groups. For both groups the higher severity grade number 3 and 4 were more used than the lower severity grade 1 and 2. This Participatory Heuristic Evaluation of the eWALL interface application is the first iteration of the development process towards the final eWALL product. Future work includes the conduction of a second iteration, and perhaps third iteration, of Participatory Heuristic Evaluation on the eWALL interface application in order to optimize the usability of the final system.*

Keywords: telemedicine; eWALL; Participatory Heuristic Evaluation; chronic disease

I. INTRODUCTION

In the future, the correlation between a growing population of elderly people and people having two or three chronic diseases will lead to a massive organizational, economical, and professional challenge for the healthcare sector. Worldwide, the number of people having a chronic disease is increasing. In Denmark the chronic diseases such as: Chronic Obstructive Pulmonary Disease (COPD) and Mild Dementia (MD) affects more than thousands of people on a daily basis [1,2]. COPD is a lung illness characterized by a permanent blockage of airflow from the lungs [2]. The prevalence of COPD among people who have passed 35 year is approximately 14% [3]. MD is the mild form of dementia, which is the fifth frequent cause of death in Denmark [4].

Currently, the treatment of the chronic diseases is time consuming and expensive [5]. A need for new ways to deliver healthcare to patients with chronic diseases is urgent [6].

A new way of delivering healthcare service to patients with chronic diseases is to integrate telemedicine and medical devices into the standard ways that healthcare are currently delivered [6,7]. Medical devices cover a wide range of products, including wheelchairs, glasses, pacemakers, dental crowns and hip implants' [8]. The two terms, "telemedicine" and "medical devices", combined may offer several opportunities as alternative ways for healthcare to be delivered.

An example of a medical device, which is addressed to people with COPD, MD, and age related impairments, is the device from the large-scale project "eWALL for Active Long Living" [9]. The device can be used to monitor health of older adults, giving them easy access to doctors, and sensing daily activities with the aim of informing relatives in case of emergency. For the eWALL device, the overall technical and user requirements are: 1) unobtrusiveness in monitoring functions and 2) seamless interaction with primary and secondary end users (patients, healthcare professionals, and relatives).

Until now, the eWALL device has been tested using several evaluation methods, some of which are designed to provide feedback on the user-friendliness of the technology. The device is currently in the design and development phase, which means that there is still a need of removing usability issues from the system. One of the evaluation methods, which have been performed on the device with the objective to remove usability issues, is the so-called Participatory Heuristic Evaluation. In Participatory Heuristic Evaluation experts in usability perform an inspection as in a traditional heuristic evaluation followed by evaluation by work domain professionals [10]. The purpose of extending heuristic evaluation with work-domain professionals is to supplement the more theoretical knowledge of the traditional inspectors with the very specific knowledge from work-domain professionals. The Participatory Heuristic Evaluation reported in the present paper was performed as a part of the first iteration of the eWALL interface application.

The aim of the present study is to report the results and benefits of conducting a Participatory Heuristic Evaluation on the eWALL device. This paper is further organized as follows: Section II describes the materials and methods employed in eWALL and the overall layout of the interface. Section III presents the results of performing the Participatory Heuristic Evaluation. Section IV and V discuss and concludes the paper.

II. MATERIALS AND METHODS

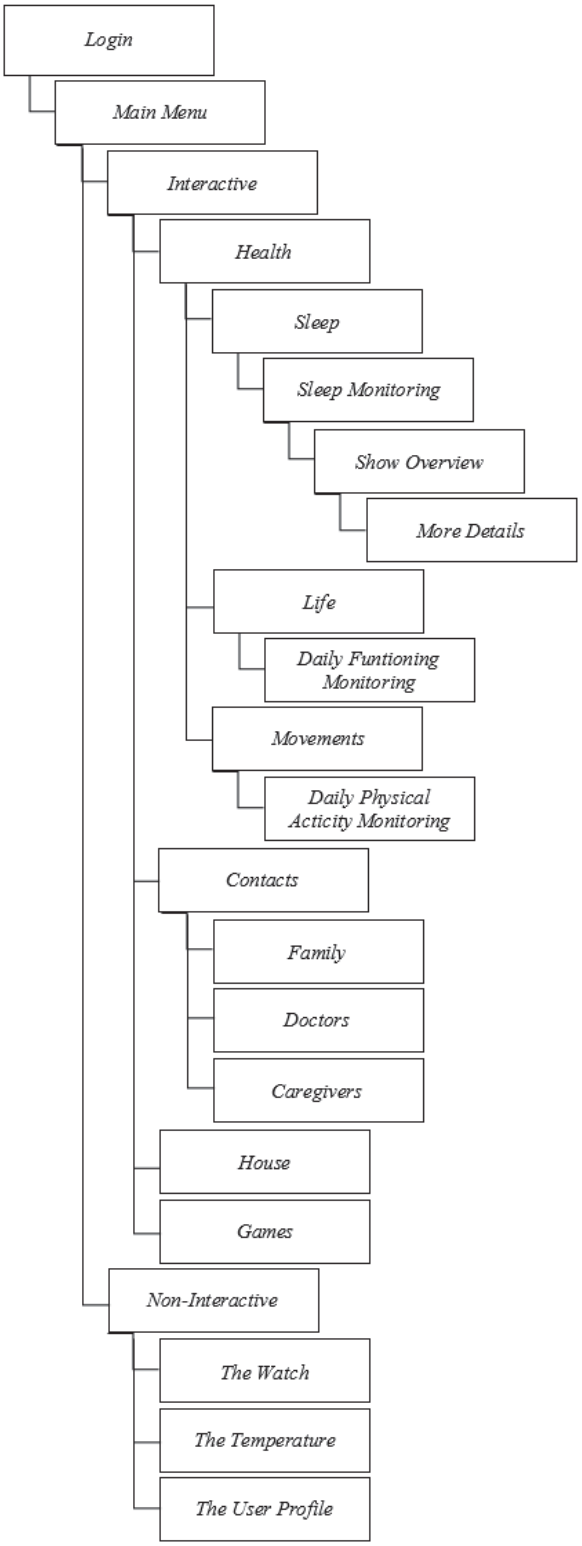

Fig. 1. *Architecture of the functionalities and features in the eWALL device*

A. The eWALL device

The eWALL interface application is an element of the final device, which is a prefabricated wall incorporating various functionalities and features for people with COPD, mild dementia, and age related impairment [9].

Fig. 1 visualizes the architecture of the functionalities and features which are integrated in the eWALL device. The figure shows that after logging in, the users have *interactive* and *non-interactive* services. The interactive services are categorized into the applications: Health, Contacts, House, and Games. Several of the applications have subgroups such as *Health* where it is possible to monitor *Sleep*, *Daily Functioning Monitoring*, and *Daily Physical Activity Monitoring*. The Non-Interactive services are *The Watch*, *The Temperature*, and *The User Profile*.

Overall, the functionalities and features of the eWALL system can be divided in three groups, namely the following: 1) Risk management; 2) eHealth; 3) Lifestyle management.

To get access to the functionalities and features in the eWALL interface application, the users have to enter a username and a password as seen in Fig. 2.

Fig. 2. *A screenshot of the front page where the users enter their username and password*

Next to the line where the users enter their username, there is a dropdown menu making it possible for the user to choose their native language as seen in Fig. 3.

Fig. 3. *A screenshot of the dropdown menu where the users choose their native language*

The non-interactive widgets include a digital watch and a weather application, which informs the users about 1) the

location, 2) the temperature of the day, 3) the cloud situation, 4) the pressure and 5) the wind speed. To make sure that the users understand everything, the information is both written and given by pictographs.

B. Participatory Heuristic Evaluation

As described in Section I, Participatory Heuristic Evaluation is a participatory inspection technique, which serves as an extension to the traditional heuristic evaluation defined by usability-expert Jakob Nielsen [11]. In the Participatory Heuristic Evaluation, five experts in usability were asked to identify and comment usability problems in the eWALL interface application. Furthermore, two work domain professionals were invited to contribute with their perspectives on the interface of the eWALL device.

a) Usability experts

To perform the Participatory Heuristic Evaluations five usability experts were recruited. All the usability experts had a MSc.in Biomedical Engineering. Three of the experts were PhD fellows and two experts were Associated Professors. The usability experts were all working at the Department of Health Science and Technology at Aalborg University. Three of them had prior experience in performing the Participatory Heuristic Evaluations. The remaining two usability experts were novices in performing a Participatory Heuristic Evaluation. All were familiar with traditional Heuristic Evaluation.

b) Work domain professionals

Two nurses were invited to participate as work domain professionals in the Participatory Heuristic Evaluations. Besides their profession as nurses, the work-domain professionals also had a MSc. in Clinical Science and Technology and were PhD fellows. The work-domain professionals were recruited from The Department of Health Science and Technology at Aalborg University. Both of the work domain professionals had experience with conducting Participatory Heuristic Evaluation.

c) Severity rating scale and 15 heuristics

The work-domain professionals and usability experts categorized and reported each usability issue using the 15 heuristics defined by Muller et al. [10]. In the following enumeration, the 15 heuristics are listed: 1) *System Status*, 2) *Task Sequencing*, 3) *Emergency Exits* 4) *Flexibility and Efficiency of Use*, 5) *Match Between Systems and the Real World,* 6) *Consistency and Standards,* 7) *Recognition rather than Recall,* 8) *Aesthetic and Minimalist Design,* 9) *Help and Documentation,* 10) *Help Users Recognize, Diagnose, and Recover from Errors,* 11) *Error Prevention,* 12) *Skills,* 13) *Pleasurable and Respectful Interaction with the User,* 14) *Quality Work,* 15) *Privacy.*

Every time a usability issue was identified, the usability experts and work domain professionals were requested to grade the usability problem using the following four level severity rating scale: 1) *Cosmetic problem only*, 2) *minor usability problem*, 3) *major usability problem*, and 4) *usability catastrophe*. By grading the usability problems, it was possible to collect information about how severe the usability problems of the eWALL interface device were.

The usability problems identified and the related severity grade were entered and categorized into columns in a Microsoft Excel worksheet. Subsequently, descriptive statistical visualizations were generated.

III. RESULTS

Fig. 4 shows the number of times each heuristic is used in total for the five experts, in total for the two work domain professionals, and in total for the usability experts and work domain professionals altogether. Heuristic no. 8, *Aesthetic and Minimalist Design* is the most used heuristic among the usability experts. The second most used heuristic is no. 6, *Consistency and Standards*, and the third most used heuristic is no. 5, *Match between the System and the Real World*. In comparison, the work-domain professionals use heuristic no. 6, *Consistency and Standards*, the most, heuristic no. 5, *Match Between the System and the Real World*, the second most and heuristic no. 13, *Pleasure and Respectful Interaction with the User*, the third most.

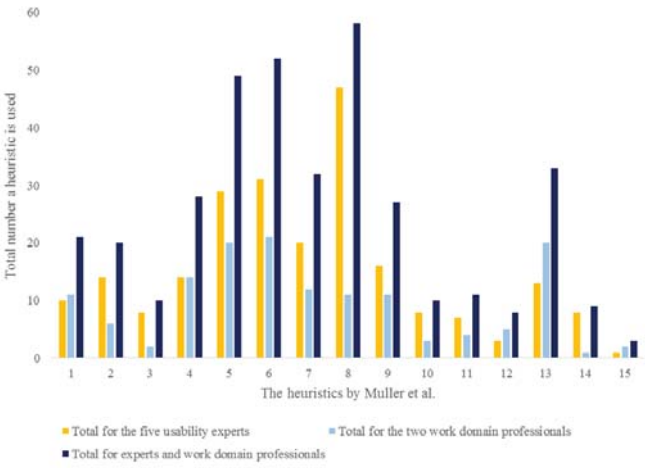

Fig. 4. *Number of times each heuristic is used in total for the five experts, in total for the two work-domain professionals, and in total for the usability experts combined and work-domain professionals altogether*

The diagram in Fig. 5 visualizes the total number of times each usability expert and work-domain professional has referred to a heuristic. Among the usability experts, the lowest total number of times a usability expert has referred to is 35 and the highest is 55. The difference between the lowest and the highest is 20 references. The work-domain professional no. 1 had the highest total use of heuristics, 91, and usability expert no. 2 had the lowest total use of heuristics, 52. The difference between the lowest and the highest is 39.

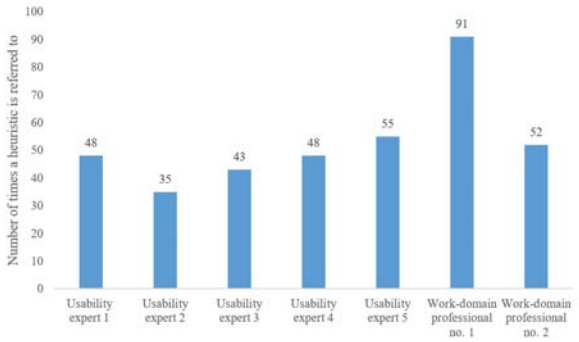

Fig. 5. *Number of times each usability expert and work-domain professional has referred to a heuristic*

Fig. 6 shows the total use of heuristics for each usability expert visualized in percent. Expert no. 2 represents the lowest, 15% of the total, and expert no. 5 represents the highest, 24% of the total.

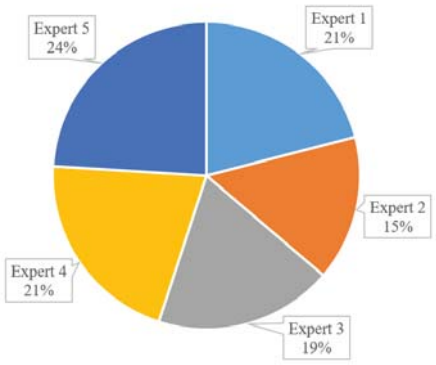

Fig. 6. *Total use of heuristics for each usability expert visualized in percent*

Figure 7 visualizes each work-domain professionals' total use of heuristics during the Participatory Heuristic Evaluation. The work-doman professional no. 1 represents 64% of the total use of heuristics. In comparison, work-domain professional no. 2 represents 36% of the total.

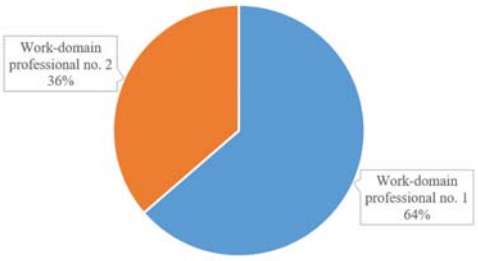

Fig. 7. *Total use of heuristics for each work-domain professional visualized in percent*

Fig. 7 shows the number of times each severity grade was used by the usability experts and by the work domain professionals.

For both groups, severity grade no. 3, *major usability problem*, was the most used and severity grade 4, *usability catastrophe*, was the second most used.

Fig. 8. *Number of times each severity grade was used by the usability experts and by the work domain professionals*

DISCUSSION

The aim of the present study was to report the results and benefits of conducting a Participatory Heuristic Evaluation on the eWALL interface application. In the Participatory Heuristic Evaluation, five usability experts and two work domain professionals were invited to participate. The five usability experts had theoretical knowledge in the field of usability and interface applications and the two work domain professionals had more practical knowledge in the domain area. The two groups of experts represented quite different perspectives when doing the Participatory Heuristic Evaluation.

The main results of the study showed a difference when comparing the most used heuristic given by the usability experts and the work-domain professionals. This might be seen as an illustration of how the work-domain professionals probably have a very strong focus on a respectful interaction with the user, where the usability experts are having a more theoretical approach, which is focused more on aesthetics and a minimalistic design.

When it comes to the distribution between the use of the severity grades between the usability experts and the work domain professionals, there seems to be an agreement between the two groups that the eWALL interface applications contains severe usability problems. 66 times did the usability experts refer to the severity grade 3 *major usability problem* and 68 times did the work-domain professionals refer to the same grade (see Fig. 8). For both groups the severity grade number 3 and 4 were more used than the lower severity grade 1 and 2.

Developing a system requires several phases of testing and rounds of iterations [12,13]. This study is the first iteration in the development phase of the eWALL interface application. The results from the study indicate that there is a need for more iterations. According to the usability expert Jakob Nielsen it is mandatory to evaluate a system during the development phase because potential usability irritations can be more easily removed and thereby help to keep the users interested in using the system [14].

In the present study, the Participatory Heuristic Evaluation was performed on the eWALL interface application. The

strength of using the extended technique is that the system will be evaluated from more perspectives – both more theoretical and more practical perspectives. Another strength of the study is that by using heuristics, it is possible to collect quantified data, because the usability experts categorize each problem into a heuristic and a severity rate. Finally, it is a strength that it is relatively straightforward to perform a Participatory Heuristic Evaluation session – it is the usability experts and work domain professionals who articulate the problems. A potential weakness of the Participatory Heuristic Evaluation is that for sure not all usability issues will be identified. A weakness of the paper is that only two work domain professionals participated. It had been more likely if five work domain professionals had participated in order to have an equal number of usability experts and work domain professionals.

IV. CONCLUSION

Performing a Participatory Heuristic Evaluation on the eWALL interface application has given very usable and relevant results. The usability experts have provided a more theoretical perspective on the eWALL interface application, and the work domain professionals have provided a more practical perspective on what is necessary to improve in the eWALL interface application.

Conducting this Participatory Heuristic Evaluation on the eWALL interface application is the first iteration of the development process towards the final eWALL product. The results indicate a second iteration of the eWALL system.

Future work includes the conduction of a second iteration, and perhaps a third iteration of Participatory Heuristic Evaluation on the eWALL interface application in order to optimize the usability of the final system.

ACKNOWLEDGMENT

The authors would like to thank usability experts and work-domain experts who participated in the Participatory Heuristic Evaluation. The work was funded by the eWALL project, which receives funding from EU's 7th Framework Programme for Research, Technological Development and Demonstration; grant no. 610658.

REFERENCES

[1] Organization WH.Chronic obstructive pulmonary disease (COPD) [Internet]. 2015. p. 2. Available from: http://www.who.int/mediacentre/factsheets/fs315/en/

[2] Lungeforening D.KOL - Kronisk Obstruktiv Lungesygdom. Anbefalinger for tidlig opsporing, opfølgning, behandling og rehabilitering [Internet]. 2007. p. 1–177. Available from: https://www.lunge.dk/kol

[3] Prevalence of COPD in Copenhagen - results from The Copenhagen City Heart Study. Ugeskr Laeger. 2007;169:3956–60.

[4] Demens NV for.Faktaark: Glemsom, men ikke dement - mild cognitive impairment [Internet]. 2014. p. 3. Available from: http://www.videnscenterfordemens.dk/faktaark/demenssygdomme-faktaark/faktaark-glemsom-men-ikke-dement-mild-cognitive-impairment/

[5] Gorst SL, Armitage CJ, Brownsell S, Hawley MS.Home Telehealth Uptake and Continued Use Among Heart Failure and Chronic Obstructive Pulmonary Disease Patients: a Systematic Review. Ann Behav Med. 2014;323–36.

[6] Epidemiology and Statistics Unit ALA. Trends in COPD (Chronic Bronchitis and Emphysema). Morb Mortal. 2013;

[7] Ho K, Cordeiro J, Hoggan B, N. Lauscher H, Grajales F, Oliveira L. et al.Telemedicine: Opportunities management. J Nurs Manag. 2008;16(173-80).

[8] Authority DH and M.Medical Devices [Internet]. 2015. p. 3. Available from: https://sundhedsstyrelsen.dk/en/medicines/medical-devices

[9] Project W, Living AL.SEVENTH FRAMEWORK PROGRAMME [Personalised health , active ageing , and independent living] Grant agreement for : Collaborative project Annex I - " Description of Work " eWALL. 2013.

[10] Muller M, Matheson L, Page C, Gallup R.Methods & tools: participatory heuristic evaluation. Mag Interact. 1998;5(5):13–8.

[11] Nielsen J.Usability Engineering. Morgan Kau. San Francisco, Calif: Elsevier Ltd; 1994. 362 p.

[12] Nielsen J.Iterative User Interface Design. IEEE Comput. 1993;26(11):32–41.

[13] Tang Z, Johnson TR, Tindall RD, Zhang J.Applying heuristic evaluation to improve the usability of a telemedicine system. Telemed J E Health. 2006;12(1):24–34.

[14] Nielsen J.Kinect Gestural UI: First Impressions [Internet]. NN/g Nielsen Norman Group. 2010. p. 1–9. Available from: http://www.nngroup.com/articles/kinect-gestural-ui-first-impressions/

THE 18TH INTERNATIONAL SYMPOSIUM ON WIRELESS PERSONAL MULTIMEDIA COMMUNICATIONS
(WPMC-2015)
December 13-16, 2015, Hyderabad, India

Coexistence of Systems with Different Multicarrier Waveforms in LSA Communications

Mirza Golam Kibria, Gabriel Porto Villardi, Kentaro Ishizu and Fumihide Kojima
Wireless Network Research Institute, National Institute of Information and Communications Technology, Japan
E-mail: {mirza.kibria, gpvillardi, ishidu, f-kojima} @nict.go.jp

***Abstract*—We study the coexistence of different multicarrier waveforms such as orthogonal frequency division multiplexing (OFDM), filter-bank multicarrier (FBMC) and universal-filtered multicarrier (UFMC) waveforms in licensed shared access (LSA) for next-generation communication systems. The fundamental changes required in the existing physical layer using OFDM towards a hybrid physical layer (either OFDM-FBMC or OFDM-UFMC) ensuring backward compatibility are discussed. We also perform mutual interference analysis for the coexisting asynchronous systems sharing the LSA frequency band. Because of the non-orthogonality between their respective transmit signals, power is spilled from a system to the other causing interference. In consideration of analyzing this interaction, power spectral densities of the multicarrier waveforms are exploited. We quantify the amount of percentage power-loss experienced by the interfering systems for not fully exploiting their available power budgets. The simulation results reveal that the interfering system with FBMC suffers the least percentage power-power loss due to its very low side-lobes while conventional OFDM-based system suffers the most. The UFMC-based system exhibits intermediary performance with respect to achieved throughput and power-loss when compared with OFDM and FBMC-based systems.**

***Index Terms*—Licensed shared access, Coexistence, Multicarrier waveforms, etc.**

I. Introduction

Radio spectrum is an extremely valuable resource. The exponential increase in demand for technologies like Wi-Fi or smart electricity grids means we must use this finite resource efficiently. But meeting that growing demand for wireless connectivity is harder in the absence of vacant spectrum. In traditional exclusive licensing systems, many spectrum bands are spatially and temporally underutilized. Due to the scarcity of the spectrum resources and to support the enormous wireless traffic explosion in future, it is important to make full use of the existing radio resources. Spectrum sharing presents a supplementary approach to conventional license-exempt and exclusive licensing schemes. Even though many applications still depend on exclusive access to spectrum, spectrum sharing is increasingly recognized as the breeding ground for wireless innovation that stimulates the development and deployment of more resilient wireless technologies. Licensed shared access (LSA) [1] facilitates dynamic and effective use of available frequency spectrum in next-generation communication networks, and it is likely to become undeniably essential to support the anticipated massive wireless traffic outburst.

The flagship of multicarrier techniques is orthogonal frequency division multiplexing (OFDM). OFDM is currently the transport mechanism base for LTE, LTE-Advanced and WiMAX systems. Although OFDM exhibits several remarkable attributes, it has two inherent shortcomings: susceptiveness to carrier frequency offset (CFO) and a large signal peak-to-average power ratio. With accurate inter-system synchronization, there is no mutual interference between the systems, when different systems use different sets of subcarriers. But if there is synchronization mismatch, the mutual interference will be very high because of the high spectral side-lobes of OFDM signals, which results in low spectral efficiency. At present, the networks of different systems are mostly not synchronized to each other. Furthermore, the OFDM access (OFDMA) based schemes require all systems to use an identical signal frame structure with alignment in time. However, 5G systems need to accommodate a large variety of devices and use cases, which require flexible frame structures. Therefore, the OFDM-based schemes cannot fulfill such 5G requirements.

Finding an appropriate substitute for OFDM is an important issue in 5G research. One basic requirement of 5G is a flexible air interface where the multicarrier attribute like subcarrier spacing is optimizable depending on specific system requirements [2]. In next-generation systems, devices could communicate based on both open-loop and closed-loop protocols that require parameter optimization, which is probable to be translated into interference. OFDM lacks the ability to address these issues. One of the contender waveforms is filter-bank multicarrier (FBMC) [3]. However, For short burst transmissions, FBMC lacks efficiency due to high time domain overheads [4]. These shortcomings exhibited by OFDM and FBMC have led some companies and organizations to transfer their focus to finding a more suitable waveform.

A new multicarrier waveform called universal-filtered multicarrier (UFMC) [3], also referred to as UF-OFDM, has attracted a great deal of attention due to its better efficiency than OFDM. UFMC can be seen as a generalization of OFDM and FBMC. The ultimate goal of employing UFMC is to combine the advantages of OFDM and FBMC while avoiding their main drawbacks. By filtering groups of adjacent subcarriers, the side-lobe levels (compare with OFDM) and the prototype filter length (compare with FBMC) can be simultaneously significantly reduced and becomes adjustable depending on types of applications. UFMC is also found to be a well-suited modulation technique for systems including option for short burst transmissions [3].

In this paper, we study the coexistence of the above men-

tioned waveforms in LSA scenario. The fundamental changes required in the existing physical layer using OFDM towards a hybrid physical layer ensuring backward compatibility are discussed. We also perform mutual interference analysis for the coexisting systems sharing the LSA frequency band.

II. System Model

We consider a co-primary LSA communication system with L systems. The LSA spectrum is licensed to multiple systems without defining distinct edge between the bands of different systems. The sharing of the spectrum is accomplished through a common entity called spectrum manager in a coordinated way. The systems have the flexibleness in employing different air-interfaces that support scalable bandwidth and discrete Fourier transnform. A common subcarrier grid of N_c subcarriers is formed as in [5]. Note that the LSA spectrum can be both contiguous and non-contiguous.

A uniform common subcarrier grid, $\mathcal{U}_{\text{grid}}$ is assumed, i.e., even if the available LSA spectrum is non-contiguous, $\mathcal{U}_{\text{grid}}$ covers the available full LSA spectrum. The spectrum assignment among the systems can be performed in two different ways, (i) subcarrier based allocations (ii) fragment based (contiguous band) allocation. Let $\{\mathcal{U}_1, \cdots, \mathcal{U}_L\}$ be the sets of indices of the subcarriers assigned to LSA compliant systems and $\mathcal{U}_{\text{grid}} = \mathcal{U}_1 \cup \mathcal{U}_2 \cup \cdots \cup \mathcal{U}_L$. In case of fragment based allocation, the subcarriers in $\mathcal{U}_l$ are adjacent in $\mathcal{U}_{\text{grid}}$. In LSA communication, the overall spectrum allocation process is achieved in two stages. In the first stage, the spectrum manager assigns sets of subcarriers or fragments to the systems and in the second stage, the systems perform resources (frequency and power) allocation optimization independently. With perfect synchronization or adequate guard bands between the fragments, each system can transmit data to its own serving users independently without causing interference to the users served by other systems.

III. Coexistence of OFDM and FBMC/UFMC Waveforms in Hybrid PHY Layer

In our waveform coexistence analysis, OFDM is fixed as the waveform of the legacy system and we discuss the fundamental changes required in the existing physical (PHY) mode using only OFDM waveform towards a hybrid PHY mode (either OFDM-FBMC or OFDM-UFMC) ensuring backward compatibility with legacy systems. Note that in 3GPP standardization there is a tendency to reduce options as far as possible for the sake of testing and implementing. We view the hybrid PHY mode as transitory that eases the migration towards the use of either FBMC or UFMC in the future. Therefore, we envisage the use of either FBMC or UFMC in a network such that the stations able to perform FBMC or UFMC should also be able to perform OFDM, at least in the transition period. Note that the stations of the legacy OFDM system do not have the capability to demodulate FBMC/UFMC signals.

Let us consider a hypothetical intra-system coexistence scenario in the transition period where the BS and some of its associated mobile stations are capable of performing FBMC/UFMC. The association of the FBMC/UFMC stations in the system is achieved by following the normal OFDM procedures such as initial ranging [6]. During the ranging process, the FBMC/UFMC stations notify the BS regarding their capabilities of performing FBMC/UFMC. The BS allocates a certain zones of the frames for FBMC/UFMC transmissions, preferable at the end of the frames, to minimize the disturbance as the stations of the legacy system cannot demodulate FBMC/UFMC signals. Both FBMC and UFMC systems are likely to coexist with OFDM systems. Since FBMC and UFMC are the evolutions of OFDM, some compatibility are expected. All these modulation techniques are based on fast Fourier transform (FFT), and they have a common core. In particular, the initialization phase can be regular to both of the hybrid PHY modes. However, presence of CP in OFDM makes the streaming of the signals different.

A. Hybrid PHY mode: OFDM-FBMC

Compatibility begins at the specifications and system parameters level. The sampling frequency is the same and the subcarrier spacing of FBMC is equal to the subcarrier spacing of OFDM or it is a sub-multiple, so that the FFT is the same, or a subset of the FFT is the same. The difference is that the IFFT is running at double speed for FBMC due to offset-quadrature amplitude modulation (OQAM). In Fig. 1 and Fig. 2, we illustrate the adjustments required to the legacy system's transmitter to implement a hybrid PHY mode: OFDM-FBMC. Here white blocks are common to both modes while blue blocks are FBMC specific, orange blocks OFDM specific. The gray blocks indicate structures needed in both modes, however, differing in implementation.

Burst generation includes the bit source, forward error coding and symbol mapping. In the multiuser case several bursts are generated. The frame generator builds the frames to be transmitted including the user bursts and the preamble. These two blocks are common between OFDM and FBMC mode. The first adjustment to the legacy OFDM transmitter is performed by adding OQAM block that transforms the QAM to OQAM symbols. This unit is specific to FBMC mode, thus gets bypassed when OFDM mode is active. Pilots are needed in both modes for channel estimation and equalization at the receiver. However, preprocessing of pilot symbols are different. In OFDM mode, pilots are binary phase shift keying (BPSK) symbols. However, in FBMC mode, pilot processing is more complicated compared to OFDM mode. As channel coefficients typically are complex (in baseband notation) the interference caused by adjacent data symbols would disturb channel estimation. To cancel this interference, auxiliary pilot method is used in PHYDYAS. The signal generation in OFDM mode is triggered by inverse FFT (IFFT) and the addition of the CP, while in FBMC mode, the synthesis filter-bank does the job. This is the most significant adjustment needs to be performed to realize hybrid OFDM-FBMC PHY mode.

The signal processing in the hybrid receiver is a bit more complicated, but can be implemented using the same principles followed in transmitter implementation. A large part of the

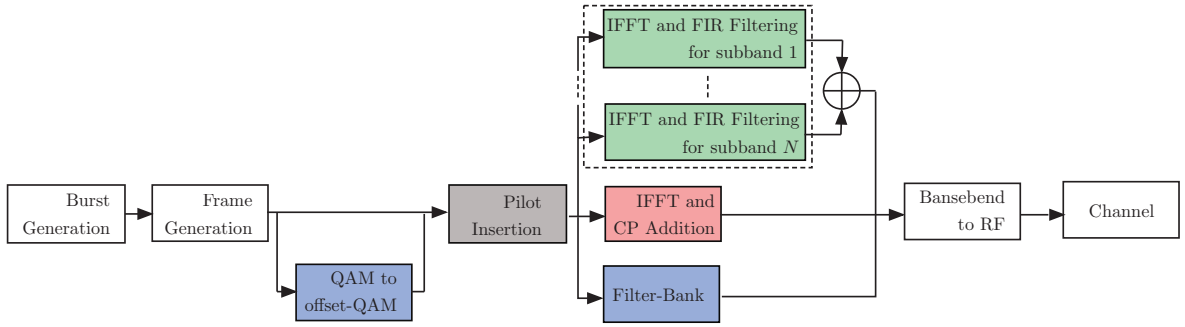

Fig. 1. Operation-flow in hybrid PHY mode transmitter including OFDM-FBMC and OFDM-UFMC modes.

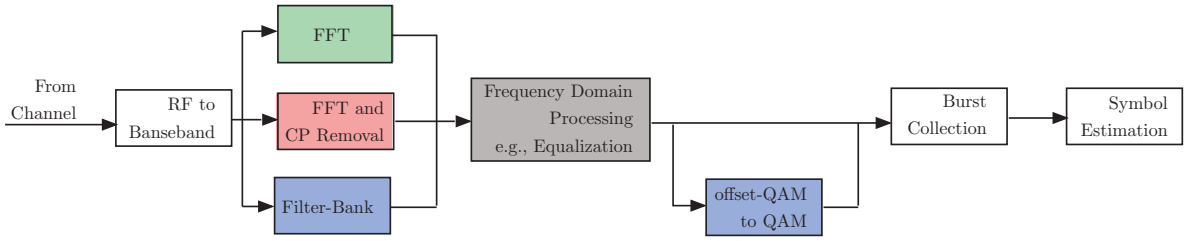

Fig. 2. Operation-flow in hybrid PHY mode receiver including OFDM-FBMC and OFDM-UFMC modes.

transmitter functions have their counterpart in the receiver. Therefore, the hybrid transmitter design can be reused in the design of a hybrid receiver. The received signal gets transformed employing an FFT after the removal of the CP, if OFDM mode is active. When the FBMC mode is active, the analysis filter-bank performs the transformation. Channel estimation, synchronization and equalization are required in both modes, differing in their implementation. Conversion from OQAM to QAM symbols is needed only in FBMC mode. Like in transmitter, this block gets bypassed if OFDM mode is active. Operations relating to burst collection and symbol estimation/detection are common to both modes.

B. Hybrid PHY mode: OFDM-UFMC

Note that UFMC is subband-wise filtered and UFMC with filter length 1 is identical to non-CP OFDM. Due to this close relationship, reusing existing OFDM transceiver parts is easy. At the transmitter, all processing leading to complex frequency-domain modulation symbols, e.g. QAM, at the multicarrier modulator input is identical. In Fig. 1 and Fig. 2, we illustrate the adjustments required to the legacy system's transmitter to implement a hybrid PHY mode: OFDM-UFMC. Here white blocks are common to both modes while green and orange blocks are UFMC and OFDM specific, respectively. The gray blocks indicate structures needed in both modes, however, differing in implementation. Since UFMC also employs QAM, the burst generation, frame generation and pilot insertion blocks are common to both modes. Triggering of signal generation for UFMC mode is a bit different from the OFDM mode. In UFMC mode, for a group of consecutive subcarriers, the IFFT operation is done deriving the corresponding set of IFFT vectors and then filtering by an FIR-filter.

Regarding the signal processing in the hybrid receiver, when UFMC mode is active, after 2-N FFT, picking each second output and dividing by the frequency response of the filter, yields the same frequency domain scalar per-subcarrier processing as in OFDM. As a result, all existing OFDM channel estimation algorithms can be directly reused by UFMC. In general, just the functionality of multicarrier modulation/demodulation has to be replaced while the rest remains the same.

IV. Mutual Interference Analysis for Coexistence of Systems with Different Multicarrier Waveforms in LSA

A. Interference Analysis of OFDM Signal

Assuming an ideal Nyquist pulse, the power density spectrum of any subcarrier in OFDM signal is written as [7]

$$\Psi_{\mathrm{OFDM}}(f) = PT_s\left(\frac{\sin(\pi f T_s)}{\pi f T_s}\right)^2, \tag{1}$$

where P amounts for transmit power on the subcarrier and T_s stands for symbol duration. Therefore, the PDS of any OFDM RB can be expressed as

$$\Phi_{\mathrm{OFDM}}(f) = \sum_{n=0}^{N_{\mathrm{RB}}-1} \delta(f - n\Delta f) P_n T_s \left(\frac{\sin(\pi f T_s)}{\pi f T_s}\right)^2, \tag{2}$$

Here N_{RB} is the number of subcarriers in a RB and δ is Dirac delta function. P_n is the amount of power allocated to the nth subcarrier. This is a sum of shifted, weighted Sinc functions.

B. Interference Analysis of FBMC Signal

In an FBMC system, we define the prototype coefficients as $h[l]$, with $l = 0, \cdots, L-1$, where $L = KM + 1$ and K is the length of each polyphase components. We define the variable $\mathcal{L} = KM/2$ and assume that the prototype has even symmetry

around the $\mathcal{L}$-th coefficient, this means that $h[l] = h[KM - l]$. The PDS of any RB in FBMC signal is given by

$$\Phi_{\text{FBMC}}(f) = \sum_{n=0}^{N_{\text{RB}}-1} \delta(f - n\Delta f)\, \overbrace{P_n \left(\sum_{k=-K+1}^{K-1} H_k \frac{\sin(\pi(f - \frac{k}{NK})NK)}{\pi(f - \frac{k}{NK})NK} \right)^2}^{\Psi_{\text{FBMC}}(f)},$$

where H_k are the polyphase components defined in [4] with $H_0 = 1$ and $H_k = H_{-k}$. $\Psi_{\text{FBMC}}(f)$ is the PDS of nth subcarrier in the RB.

C. Interference Analysis of UFMC Signal

UFMC employs Dolph-Chebyshev [8] filter as an ad hoc choice. One notable property of Chebyshev window is that side-lobes attenuation remains same at all frequencies. In UFMC, the original OFDM spectrum is filtered by Chebyshev filter. Thus, the well-known Sinc-spectrum of OFDM also plays a role, which results in the decaying side-lobes in UFMC. The filter coefficients in time-domain are defined as

$$\Psi^{(n)}_{\text{UFMC}} = \begin{cases} \left\{ \frac{1}{N} + \frac{(10^{-\alpha/20})}{N} 2 \sum_{m=1}^{M} C_{2M} \left[\kappa_0 \cos\left(\frac{\pi m}{N}\right) \right] \cos\left(\frac{2\pi mn}{N}\right) \right\}, & \text{for } |n| \le M \\ 0, & \text{for } |n| > M \end{cases}$$

where $N = 2M + 1$ is the UFMC filter length, κ_0 is a filter parameter and C_n is the nth order Chebyshev polynomial. α defines the side-lobe attenuation in dB.

Since UFMC is subband-wise filtered, to generate the PDS of any individual subcarrier of UFMC signal, we send zeros at other subcarrier positions of the RB and the UFMC filter response is shifted to the centre frequency of the RB by multiplying the l the coefficient of the filter with $e^{i2\pi(l-1)f_c \frac{1}{N_{\text{FFT}}}}$. The amplitude of any subcarrier of UFMC signal in time domain is then obtained by performing convolution between OFDM subcarrier and the centre frequency shifted UFMC filter coefficients. Let the PDS of a single subcarrier in UFMC signal is represented by $\Psi_{\text{UFMC}}(f)$. Then the The PDS of the UFMC RB is given by

$$\Phi_{\text{UFMC}}(f) = \sum_{n=0}^{N_{\text{RB}}-1} \delta(f - n\Delta f)(\Psi_{\text{UFMC}}(f))^2. \quad (3)$$

Since UFMC is RB-wise filtered, outside of the pass-band (RB width) it has a stronger side-lobe decay than OFDM. The interference from the interfering system to the other coexisting systems is defined as

$$\text{I}_n(\text{d}_n) = \int_{(\text{d}_n - 1/2)\Delta f}^{(\text{d}_n - 1/2)\Delta f + B_{\text{sys}}} \Psi_{\text{W-Type}}(f) df. \quad (4)$$

Here, d_n is the spectral distance between the nth subcarrier of the interfering system and the adjacent system. The total interference introduced to any system is a result of accumulation of interferences from all the RBs available for interfering system's transmission. In Fig. 3, power spectral densities of systems with different multicarrier waveforms are compared. It clearly shows that FBMC exhibits the best performance in terms of out-of-band emission because of very low side-lobes.

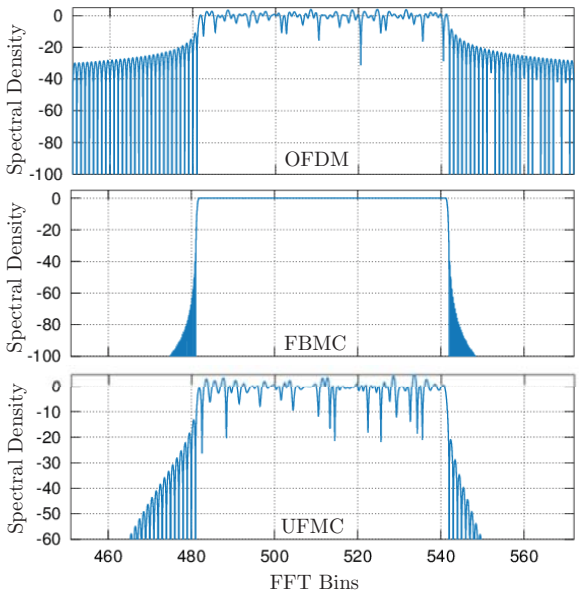

Fig. 3. Comparison of power spectral densities with 60 subcarriers.

V. Performance Analysis

Let us consider an LSA scenario with two coexisting systems operating in contiguous LSA band of 20 MHz bandwidth. We denote the systems as system-A and system-B. The effective bandwidth is taken as 18 MHz with 10% of the bandwidth assumed to be used for guardband with other nearby systems. Hence, the total number of subcarriers in the subcarrier grid is 1200, with subcarrier spacing of 15 kHz. Consequently, the number of RBs is 100, with 12 subcarriers per RB. The shared 18 MHz spectrum is partitioned into two halves, each for one coexisting system. The coexisting systems may employ different waveforms and obtain orthogonal sets of RBs for transmission. The transmit power budget for each system is taken to be P_{max}=43 dBm. Each system allocates the resources to its users independently. For simplicity, we consider that each system has one base station (BS) and supports 10 users. The interference-tolerant LSA coexisting systems have their own interference thresholds, e.g. $I_{\text{th,A}}$ for system-A and $I_{\text{th,B}}$ for system-B. For simplified performance analysis, we assume that both of the systems have equal threshold values, i.e. $I_{\text{th,A}} = I_{\text{th,B}} = I_{\text{th}}$. We vary the values of I_{th} from 10^{-6} w to 10^{-1} w. For UFMC, the filter length is 74 with $\alpha = 40$ dB.

The transmission capacity of the coexisting systems versus interference introduced to adjacent system is plotted for OFDM, FBMC and UFMC in Fig. 4. It is seen that the achievable throughput of the system can be improved by relaxing the interference threshold of the adjacent systems. OFDM-based system achieves the least downlink capacity compared to FBMC and UFMC based systems while UFMC-based system experiences intermediary performance between OFDM and FBMC-based systems. When the maximum amount of tolerable interference is very small, i.e., for non-robust systems, FBMC exhibits the best performance. Note that the achievable

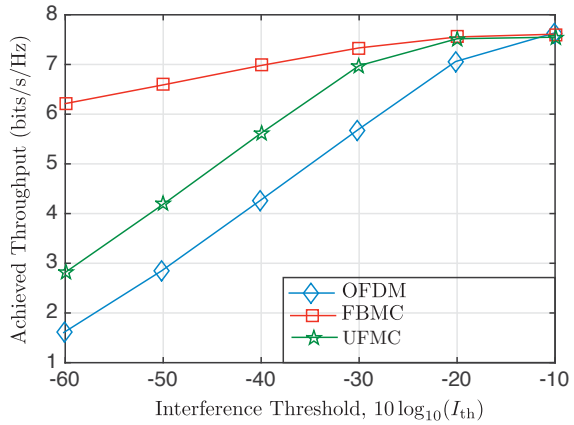

Fig. 4. Achieved throughput of system-A vs. interference threshold of system-B (or vice versa).

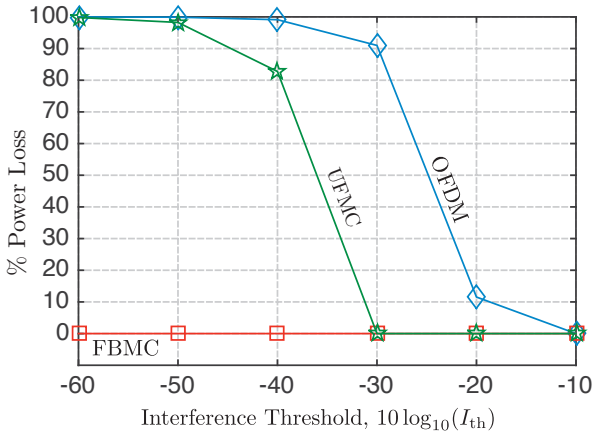

Fig. 5. Percentage power-loss of the coexisting systems. The loss is calculated as, %power-loss = $100 - P_{\text{used},I_{\text{th}}}/P_{\max} \times 100$, where $P_{\text{used},I_{\text{th}}}$ is the transmit power used by the the systems to satisfy the interference threshold I_{th}.

capacity for UFMC based system depends on the chosen value for desired sideband attenuation. Higher the value of sideband attenuation factor α, better the achievable downlink capacity. As the interference threshold values increase, therefore, for robust systems, the achievable capacity of FBMC and UFMC-based systems seem to merge depending on the chosen ripple factor and pre-specified interference thresholds. This result motivates the usage of FBMC when no accurate inter-system synchronization is available. Therefore, spectrum sharing are favored scenarios for FBMC, where either the spectrum usage policy is more stringent in terms of emission requirements (such as adjacent channel leakage ratio), or where the requirement is to be more coexistence-friendly to other systems.

In interference-tolerant coexisting systems, a practical way to manage the mutual interference between different systems is by regulating the transmit power in order to comply with the pre-specified interference threshold of different systems in LSA. As a result, the systems cannot fully exploit the maximum benefit out of their available power budget. This is clearly demonstrated in Fig. 5, where we show the *%power-loss* of the coexisting systems with different waveforms when the pre-specified interference threshold value is varied. It can be observed that OFDM-based system experiences the maximum *%power-loss*, whereas FBMC-based system does not suffer from *%power-loss* at all over the varying I_{th} values. On the other hand, UFMC based system suffers much lower *%power-loss* compared to the OFDM-based system. The characteristics of the power-loss curves depend on the spectrum usage policy whether it is more stringent in terms of some emission requirements. For example, when the spectrum usage policy is not so stringent ($I_{\text{th}} \in [-30 \; -20]$) dBw, UFMC-based system does not suffer from any *%power-loss* even with lower α. However, for non-robust systems, the *%power-loss* experienced by the UFMC based system increases.

VI. Conclusions

In this paper, we investigate the coexistence of different multicarrier waveforms in LSA communications. We discuss the fundamental changes required in the existing physical layer using OFDM waveform towards a hybrid physical layer (either OFDM-FBMC or OFDM-UFMC) ensuring backward compatibility with legacy systems. We have found that hybrid mode terminals can be designed with just a modest increase in complexity of the physical layer compared to a pure OFDM terminal. FBMC and UFMC systems are able to substitute OFDM maintaining a great amount of physical layer compatibility for the future communication networks. We also perform mutual interference analysis for the coexisting asynchronous systems sharing the LSA frequency band. Simulation results have revealed that the interfering system with FBMC suffers the least percentage power power loss due to its very small side-lobes while conventional OFDM-based system suffers the most. The UFMC-based system exhibits intermediary performance with respect to achieved throughput and power loss when compared with OFDM and FBMC-based systems.

References

[1] J. G. Andrews, S. Buzzi, W. Choi, S. V. Hanly, A. Lozano, A. C. K. Soong and J. C. Zhang, "What Will 5G Be?," *IEEE J. Select. Areas Commun.*, vol. 32, no. 6, pp. 1065-1082, Jun. 2014.

[2] F. Boccardi, R. Heath, A. Lozano, T. Marzetta and P. Popovski, "Five Disruptive Technology Directions for 5G," *IEEE Commun. Mag.*, vol. 52, no. 2, pp. 74-80, Feb. 2014.

[3] F. Schaich and T. Wild, "Waveform Contenders for 5G-OFDM vs. FBMC vs. UFMC," in *Proc. International Symposium on Communications, Control and Signal Processing*, Athens, May. 2014, pp. 457-460.

[4] M. G. Bellanger, "Efficiency of Filter Bank Multicarrier Techniques in Burst Radio Transmission," in *Proc. IEEE Global Telecommunications Conference*, Florida, Dec. 2010, pp. 1-4.

[5] J. Luo, J. Eichinger, Z. Zhao, and E. Schulz, "Multi-carrier waveform based flexible inter-system spectrum sharing for 5G systems," in *Proc. IEEE International Symposium on Dynamic Spectrum Access Networks*, McLean, USA, Apr. 2014, pp. 449-457.

[6] L. Sanguinetti, M. Morelli and L. Marchetti, "A Random Access Algorithm for LTE systemsr," *Eur. Trans. Telecomms.*, vol. 2012, no. 00, pp. 1-10, 2012.

[7] T. A. Weiss and F. K. Jondral, "Spectrum Pooling: An Innovative Strategy for the Enhancement of Spectrum Efficiency," *IEEE Commun. Mag.*, vol. 42, no. 3, pp. S8-S14, Mar. 2004.

[8] P. Lynch, "The Dolph-Chebyshev Window: A Simple Optimal Filter," *Monthly Weather Review*, vol. 125, no. 1, pp. 655-660, Apr. 1997.

THE 18TH INTERNATIONAL SYMPOSIUM ON WIRELESS PERSONAL MULTIMEDIA COMMUNICATIONS
(WPMC-2015)
December 13-16, 2015, Hyderabad, India

Energy-Efficient Resource Allocation for Hybrid Services with QoS Requirements in Cellular Network

Yuhao Zhang, Ning Wang, Baoling Liu
Key Laboratory of Universal Wireless Communication, Ministry of Education
Beijing University of Posts and Telecommunications, Beijing, 100876, China
Email: ZyhAngus@bupt.edu.cn

***Abstract*—Energy Efficiency is a key performance index for the communication networks. And with the increasing diversity of wireless services, green communication for hybrid services with less consideration has become important and drawn more attention recently. In this paper, we proposed a novel mapped water falling allocation scheme (MWF) to achieve total energy consumption minimization in cellular network. Our scheme exploits the enormous property differences of the services to complete the resource allocation while satisfying the QoS requirements which are analyzed through queuing theory. The complicated resource allocation problem that cannot be resolved with analytic solutions is separated into two subproblems, time slot selection and rate allocation, which can be solved more simple respectively and we get a closed form solution for the second subproblem. Experimental simulation results verify that our scheme outperforms the two others on energy efficiency under any circumstances.**

I. Introduction

Along with the exponential growth of mobile data traffic over the last years, it is widely acknowledged that the energy consumption of wireless network has risen considerably with the evolution of ICT [1][2]. And there is an sharply growing gap between the energy demand and the battery capacity because of the rising device power consumption and slower battery development [3]. As the result, green communication is becoming more important and getting more attentions. At this time, large capacity and high spectrum efficiency are no longer the unique target we need to concern.

For single service, various researches have been made to utilize delay to reduce the energy consumption of the system while satisfying the QoS requirements [4]-[12]. Moreover, there are variety of mathematical methods applied to analyze energy problem, including game theory [5], queuing theory [6] and convex optimization [7]. With the development of wireless network and the emersion of new services, mobile terminals will transmit or receive hybrid services simultaneously sometimes. Unlike the single service case, hybrid services need to share all the transmission resource that is limited in a system.

To settle this problem, in the scenarios where fixed and variable rate services coexist, the authors in [8] proposed a scheme that dynamically regulate the transmission bandwidth allocated to the variable rate service when a terminal can access some different networks at the same time. Paper [9] takes the utility of service fairness into account on bandwidth distribution. In [10], a cross-layer cooperative delay-energy tradeoff (CCT) scheme is presented based on energy efficiency for mixed transmission in cellular network. But little attention has been paid to the feature of different services in these papers. Moreover some schemes that they proposed like DGA of CCT are relatively complicated, which is unpractical and unfeasible.

Since the above defects we refereed, we propose a novel mapped water falling scheme for hybrid services to achieve the optimal energy efficiency in cellular network. Unlike other papers, we consider the feature of service more precisely and utilize the queue theory to analyze the QoS requirements. It can be known that the resource allocation problem combining the application and the physical layer is NP-hard and we cannot get analytic solutions with closed form. In this paper, we separate the NP-hard problem into two subproblems that can be solved more easily respectively and we get a closed form solution for the rate allocation subproblem, ingeniously. Moreover our scheme that exploiting the enormous differences of service feature between hybrid services is more effective and practical compared with other traditional schemes.

The rest of the paper is organized as follows. In section II, we describe the system model for hybrid services in cellular network. And then section III studies our proposed mapped water falling allocation scheme in details. Section IV presents the simulation experiment and analyzes the results. Finally, we conclude the paper in section V.

II. System model

In order to facilitate our analysis and without lose the generality, we assume only one mobile user exchange information with the base station over a period of time. If there are multiple mobile terminals, they can be regard as a single virtual one by gathering all the services together.

As shown in Fig.1, there are M kinds of services between the mobile terminal and the base station which have different data characteristics and QoS requirements. In this paper, we only consider the downlink transmission and uplink can be obtained in the same way. The arrival rate, the average length of data packet and the delay demand of the M services are donated by λ_1, λ_2, λ_3, $\cdots$, λ_M;L_1, L_2, L_3, $\cdots$, L_M and D_1, D_2, D_3, $\cdots$, D_M (time slot) respectively. Moreover the

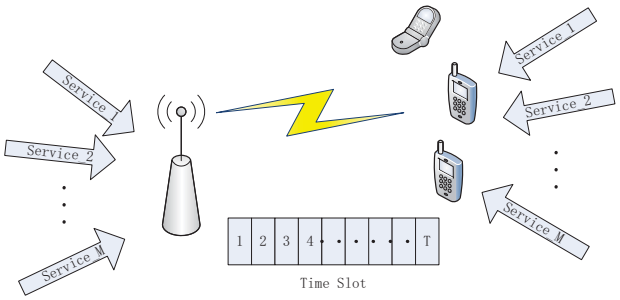

Fig. 1. Hybrid services transmission system in cellular network

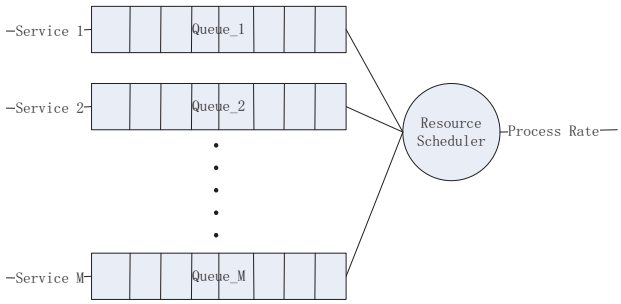

Fig. 2. The queuing model of hybrid services system (downlink)

data arrival process is a Poisson process with the parameter of arrival rate and the length of the packet obey Poisson distribution. Data packets that need to be transmitted are waiting in an infinite service queue. In other words, it can accommodate all the data packets without loss. And the resource scheduler decides when the packets will leave and the leaving rate.

It is assumed that the terminal and the base station both have full CSI and can perfectly predict the channel condition of the next T time slots. Considering the path loss and large scale fading, the channel coefficient between the two nodes can be denoted by h_t at time slot t. Furthermore, we consider a quasi-static fading channel for which the channel coefficient are constant within one slot but change independently form one slot to another. The additive white Gaussian noise is denoted by $\nu \sim \phi\ (0,\ \delta_t^2)$.

In a single time slot, the transmission power of the base station is fixed, indicating the data rate is fixed. But in different time slots, the base station can change its transmission power dynamically to achieve the rate adaption. We assume that the channel modulation and coding schemes can approach the Shannon capacity bound which can make the transmission power consumption minimum. Note that standard Shannon capacity is adopted in this paper, which represents channel capacity bound per unit bandwidth.

III. Mapped Water Falling Allocation Scheme

A. Problem Formulation

The resource for hybrid services in the system as we concern involves transmission time slots and power (rate). As we all acknowledged that service is invisible in physical layer, the rate assignment of each time slot isn't influenced by the fact that which service occupied this slot on earth. So for briefness and feasibility, the complicated resource allocation problem is divided into two subproblems as follows:

1: Select appropriate transmission time slots for each service.

2: Allocate suitable transmission rate at the time slots assigned to the service.

In this section, we first explore the QoS requirements of hybrid services. The queuing model of the system is illustrated in Fig.2. Data rate of service m at time slot t is denoted by r_m^t. Let $r_m^t = 0$ where the time slot is not selected. In each time slot, the departure of the data packets can be regarded as a non homogeneous Poisson process with the parameter of $\mu_m^t = \frac{r_m^t}{L_m}$, where μ_m^t is changing with the time slot.

A single service queue is a compound process containing a homogeneous Poisson arrival and heterogeneous Poisson departure. We propose a queue equivalent lemma to transform the heterogeneous Poisson process into a homogeneous one.

Lemma 1: In a single server queuing system where the arrival rate is fixed, the arrival and the departure process are both Poisson process. The average performance of the system is equivalent by using the two method below:

Method 1: The data packets leave with rate μ over a period time of $n \times T_{slot}$.

Method 2: The data packets leave with rate $\mu(t)$ which satisfies the following constraint:

$$n \times T_{slot} \times \mu = \int_0^{n \times T_{slot}} \mu(t)dt \tag{1}$$

The proof is so simple and apparent that we leave out it for the sake of limited space. According to lemma 1, the compound queuing process can be equivalent to a birth-death process with a fixed leaving rate $R_{mean,m}$. At this time, the queuing model is a standard $M/M/1$ model.

The paper mainly consider the average delay characteristic of service, which is statistical. In this way the QoS requirement can be expressed as:

$$Delay_m = \frac{1}{\frac{R_{mean,m}}{L_m} - \lambda_m} \leq D_m \times T_{slot} \tag{2}$$

And then we introduce the time slot assignment index C_t^m indicating whether service m occupies time slot t. Let $C_t^m = 1$ if time slot t is allocated to service m, otherwise $C_t^m = 0$. Note that each time slot can only be used by one service:

$$\sum_{m=1}^{M} C_t^m = 1, \forall t \tag{3}$$

Since based on time slot, the rate allocation is discrete in time which makes integral to summation in (1). By substituting C_t^m and (2) into (1), the constraints of the transmission rate that we must follow for service m is as follows:

$$\sum_{t=1}^{T} C_t^m r_m^t = T \times R_{mean,m} \geq T(\frac{L_m}{D_m T_{slot}} + \lambda_m L_m) \quad (4)$$

In order to reach the energy minimization, r_m^t should be as small as possible, which means the inequality on the right side must take the equal.

Combining all the time slots, we will obtain the overall energy consumption of the system:

$$\sum_{m=1}^{M}\sum_{t=1}^{T}(C_t^m \times P_{Total,t}^m)T_{slot} \quad (5)$$

Where $P_{Total,t}^m$ represents the overall power allocated to service m at time slot t, including transmission power and fixed circuit power, etc. With high data rate demand, transmission power is large enough to dominate the overall power. Closer to the actual network, we adopt the non ideal PA model, considering the influence of power amplifier that consumes the majority of energy.

Ensuring the QoS requirements of each service, the general form of this minimization problem can be formulated as follows:

$$Min \sum_{m=1}^{M}\sum_{t=1}^{T}(C_t^m \times \frac{\sqrt{\frac{\delta_t^2}{|h_t|^2}(2^{r_m^t}-1)\times P_{max}}}{\eta_{max}}) \quad (6)$$

$$Subject\ to \sum_{t=1}^{T} C_t^m r_m^t = R_{mean,m} \times T;\ \forall m \quad (7)$$

$$\sum_{m=1}^{M} C_t^m = 1;\ \forall t \quad (8)$$

$$C_t^m \in \{0,1\};\ \forall t,m \quad (9)$$

$$0 \leq r_m^t;\ \forall t,m \quad (10)$$

Here we adopt the TPA model:$P_{Total,t}^m = \frac{\sqrt{P_t^m \times P_{max}}}{\eta_{max}}$, where $P_t^m = \frac{\delta_t^2}{|h_t|^2}(2^{r_m^t}-1)$ on the basis of Shannon capacity.

We can see mapping of service and time slot is a combinatorial optimization problem, involving the 0,1 variables, and the number of optimization variables is enormous, so it is unable to give a analytical solution with closed form. For this NP-hard problem, our scheme employs genetic algorithm to iterate time slot selection and water falling algorithm to conduct rate allocation.

B. Time Slots Selection

GA is a powerful optimization technique based on the principles of genetics and natural selection and has been extensively applied to solve resource allocation problem in wireless networks which is usually NP-hard [10][13][14].

The structure of the chromosome representing slots selection scheme is described in Fig.3, where $C_m = (C_1^m, C_2^m, \ldots, C_T^m)$. As for GA's execution, we exchange

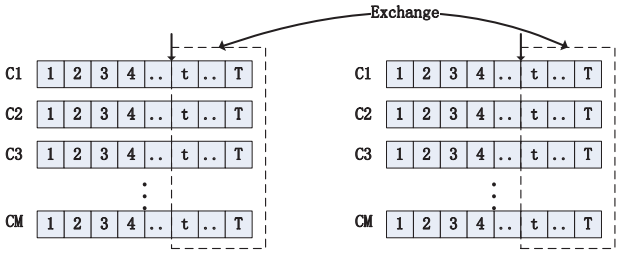

Fig. 3. Principle for crossover process of genetic algorithm in this paper

the rest sequences behind a site that is generated randomly for the crossover and the mutation is the reproduction for a chromosome. Note the constraint (8) is ensured but we cannot guarantee that every service at least have one time slot. If it happened, we need to give up this crossover and then repeat again. The better chromosome with high fitness will be more likely to be reserved according to Roulette Selection. Note that we save the best chromosome particularly before a new generation obtained.

C. Rate (Power) Allocation

Firstly, we assume that we have got a mapping relationship maybe not being the optimal through GA. Then we discuss the optimal rate allocation with the QoS constraints.

For a given mapping relationship of service m, (6) can be converted into:

$$Min \sum_{t=1}^{T}(\frac{\sqrt{\frac{\delta_t^2}{|h_t|^2}(2^{r_m^t}-1)\times P_{max}}}{\eta_{max}}) \quad (11)$$

$$Subject\ to \sum_{t=1}^{T} r_m^t = R_{mean,m} \times T \quad (12)$$

$$0 \leq r_m^t;\ \forall t \quad (13)$$

Utilize Lagrange multiplier method or convex optimization theory where:

$$J = \sum_{t=1}^{T}(\frac{\sqrt{\frac{\delta_t^2}{|h_t|^2}(2^{r_m^t}-1)\times P_{max}}}{\eta_{max}}) - \upsilon \sum_{t=1}^{T} r_m^t \quad (14)$$

Let $\frac{\partial J}{\partial r_m^t} = 0$, we can get:

$$\frac{\frac{\delta_t^2}{h_t|^2} P_{max} 2^{r_m^t} ln2}{\eta_{max}\sqrt{\frac{\delta_t^2}{|h_t|^2}(2^{r_m^t}-1)\times P_{max}}} - \upsilon = 0 \quad (15)$$

Since the demand for high data rate communication has been growing rapidly, r_m^t is fairly large, thus $2^{r_m^t} - 1 \approx 2^{r_m^t}$. So (15) can be transformed into:

$$\frac{\sqrt{\omega_t 2^{r_m^t} P_{max}} ln2}{\eta_{max}} - \upsilon = 0 \quad (16)$$

Where $\omega_t = \frac{\delta_t^2}{|h_t|^2}$, called noise-channel coefficient. If $BB = (\frac{v\eta_{max}}{ln2})^2 \frac{1}{P_{max}}$, thus $r_m^t = \log(\frac{BB}{\omega_t})$, we can get the following relationship considering constraint (12):

$$\sum_{t=1}^{T} \log(\frac{BB}{\omega_t}) = R_{mean,m} \times T \tag{17}$$

So we can resolve the water level as follows:

$$BB = \sqrt[TT]{2^{R_{mean,m} \times T} \prod_{t=1}^{T} \omega_t} \tag{18}$$

If the data rate obtained by Shannon capacity with the water level is negative, which is impossible in the actual system, we can infer that the time slot selection is wrong. It's known that the channel in poor condition will not be chosen according to the principle of water filling. So we should exclude the time slot where the data rate is negative and then recalculate the water level. Note that these excluded time slots will not be used by service m anymore.

D. Algorithm

In the algorithm, we generate the channel coefficient of each time slot randomly to simulate the real channel conditions and assume that the noise power spectral density is equal to 1, which are independent input variables. Our algorithm is described particularly as **Algorithm 1**. Note that the fitness function is designed to be the reciprocal of (6).

Algorithm 1 The mapped water falling algorithm

1: Obtain the transmission rate constraints from the QoS requirements of all services
2: **For all** $i \in (1, 2, 3, ..., Popsize)$ **do**
3: Initialize the time slot sequence of each service for chromosome i
4: **For all** $j \in (1, 2, 3, ..., M)$ **do**
5: Calculate the water level according to (18) for service j
6: Get the rate allocation according to the water level using shannon capacity formula for service m
7: **If** data rate is negative, let the rate as 0 and exclude the time slot whose allocation rate is negative. Turn to step 5
8: Calculate the fitness of the time slot sequence
9: **End for**
10: Add all the fitness together as the evaluating indicator
11: **End for**
12: Select and record the best allocation scheme
13: Obtain the next generation by crossover and mutation
14: **If** iteration reaches the threshold, end algorithm
15: **If else**, Turn to step 2 but skip step 3

IV. Simulation Results

We will get the optimal resource allocation scheme and the corresponding energy consumption by programming MWF algorithm in Microsoft Visual Studio. And then in order to evaluate the potential profit of our MWF scheme in cellular network, we adopt Monte Carlo simulation with Matlab in many cases to compare the energy performance with average rate allocation algorithm (ARA) and double genetic algorithm (DGA). ARA refers to that the data rate demand is distributed to each time slot equally, while DGA both applies genetic algorithm to finish time slot selection and rate allocation.

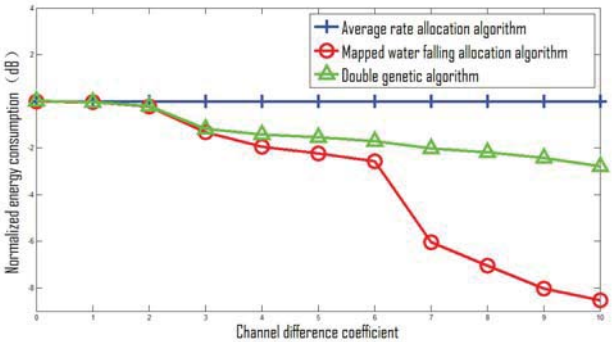

Fig. 4. Normalized energy consumption versus the channel difference coefficient (16 time slots and 2 services)

To further control the difference of channel coefficient, the channel difference coefficient $PathLossCoeff$ is also introduced. So we can get the following method:

$$|h|^2 = rand^{PathLossCoeff} \tag{19}$$

Where $rand$ is a random number between 0 and 1.

In Fig.4 and Fig.5, the vertical axis is normalized energy consumption which can be understood as the optimization degree compared with ARA scheme.

From Fig.4 we can find that the scheme we proposed has the best energy performance compared with the two others. And with the increase of $PathLossCoeff$, the optimization degree of MWF becomes better. All the three schemes reach the same performance when $PathLossCoeff$ is equal to 0 which means all the channel conditions are the same especially. The reason why appears such a phenomenon is that the channel conditions play a more and more important role in rate allocation with the increase of $PathLossCoeff$.

Fig.5 evaluates that MWF is better than the two other schemes in terms of energy. At the same time we can observe that with the increase of abscissa, MWF's performance will be getting worse while ARA's performance first will decline and then will ascend. In the end, when the service number and the time slot number are the same, only one time slot will be allocated to each service. So the performance of the three schemes are identical just depending on time slot selection. As for MWF, due to the service number increasing, the average time slots that can be allocated to a single service is reduced, i.e. the parallel channels are less, which causes the decrease of the diversity degree. As is known that each service is independent with others, the performance reduction of single service will lead to a falling of the whole scheme performance. The probability that DGA can find the optimal

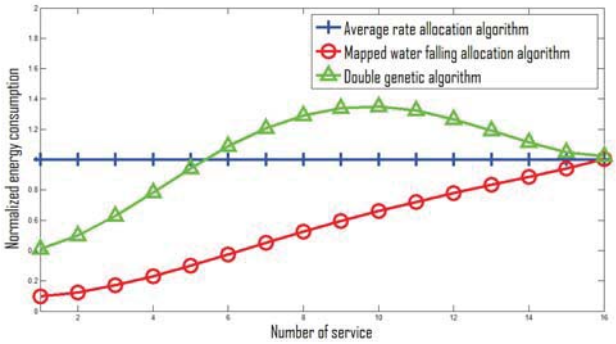

Fig. 5. Normalized energy consumption versus the number of service (16 time slots and $PathLossCoeff$ is equal to 6)

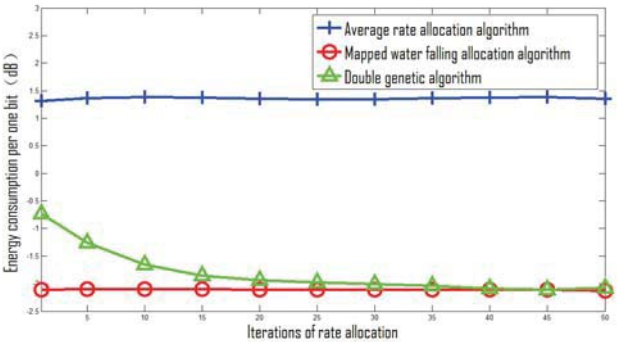

Fig. 6. Energy consumption per one bit versus the iterations of rate allocation (16 time slots, 2 services and $PathLossCoeff$ is equal to 6)

solution is determined by the number of feasible samples. According to the knowledge of permutation and combination, the mapping patterns first increase and then decrease, identical to the tendency of DGA's curve.

In Fig.6, the vertical axis is energy consumption per one bit in the form of decibel. We can see that the energy consumption per one bit of DGA are reduced and reach to the MWF's with the increase of iterations of rate allocation. The gap on the performance between DGA and MWF is getting smaller because the solution that DGA can find becomes better and better. But when the iterations exceed a certain threshold value, DGA can find a optimal solution like MWF and the performance will become stable, implying MWF is the best. Note that DGA tends to converge with evolution and iteration.

V. Conclusion

In this paper, we proposed a novel MWF scheme to separate the complicated resource allocation problem without closed form analytic solutions into two simple subproblems intelligently. Without avoiding the NP-hard problem for mapping combination between services and slots, time slot selection problem is presented by genetic algorithm rightly. Having Deduced the water falling principle under non ideal PA model, the closed form solution for the rate allocation subproblem was obtained normally. Experimental simulation results can verify the great energy performance of our proposed scheme compared with the two others, ARA and DGA.

The time slot selection adopts genetic algorithm that is randomly and complex. In the future, we will make effort to replace the method to another definite and simple one.

Acknowledgement

This work is supported by Beijing Nova Program (No. xx2012037) and National Nature Science Foundation of China Project (Grant No. 61471058).

References

[1] Daquan Feng; Chenzi Jiang; Gubong Lim et al, "A survey of energy-efficient wireless communication," *Communication Survey & Tutorials, IEEE*, vol. 15, no. 1, pp. 167-178, First Quarter 2013.

[2] Qimei Cui; Hui Wang; Pengxiang Hu; Xiaofeng Tao; Ping Zhang et al, "Evolution of Limited Feedback CoMP Systems from 4G to 5G," *IEEE Vehicular Technology Magazine*, vol.9, no.3, Pages: 94-103, 2014.

[3] G. Miao et al, "Cross-Layer Optimization for Energy-Efficient Wirelsee Communications: A Survey," *Wiley J. Wireless Commun. and Mobile Computing*, vol. 9, pp. 529, Apr. 2009.

[4] Meshkati, F.; Poor, H.V.; Schwartz, S.C. et al, "Energy-efficient resource allocation in wireless networks with quality-of-service constraints," *IEEE Transactions on Wireless Communications*, vol. 57, No. 11, pp. 3406-3414, Nov. 2009.

[5] Meshkati, F.; Poor, H.V.; Schwartz, S.C., "Energy-Efficient Resource Allocation in Wireless Networks," Signal Processing Magazine, IEEE, vol.24, no.3, pp.58,68, May 2007.

[6] Bi Zhao; Friderikos, V., "A queuing-based delay-tolerant scheme for energy efficiency over cognitive radio networks," Globecom Workshops (GC Wkshps), 2012 IEEE , vol., no., pp.326,330, 3-7 Dec. 2012.

[7] Chakraborty, S.; Yu Dong; Yan, D.K.Y et al, "On the effectiveness of movement prediction to reduce energy consumption in wireless communication," *Mobile Computing, IEEE Transactions*, vol. 5, No. 2, pp. 157-169, Feb. 2006.

[8] M Ismail; Weihua Zhuang, "A Distributed Multi-Service Resource Allocation Algorithm in Heterogeneous Wireless Access Medium," *IEEE Journal on Selected Areas in Communications*, pp. 425-432, 2012.

[9] C.Luo; H.Ji; Y.Li, "Utility based multi-service bandwidth allocation in the 4G heterogeneous wireless access networks," *Proc.IEEE WCNC*, Apr. 2012.

[10] Siqi Cao; Qimei Cui; Yulong Shi; Hui Wang, "Cross-layer Cooperative Delay-energy Tradeoff Scheme for Hybrid Services in Cellular Networks," *Vehicular Technology Conference (VTC Spring)*, Spring 2014.

[11] Qimei Cui; Tianpemg Yuan;Xiaofeng Tao et al, "Energy Efficiency Analysis of Two-Way DF Relay System With Non-Ideal Power Amplifiers," *IEEE Communications Letters*, vol. 18, no. 7, July 2014.

[12] Kolios, P.; Friderikos, V.; Papadaki, Katerina, "Mechanical forwarding for nomadic mobility in cellular networks," *Wireless Communications and Networking Conference, 2012 IEEE*, pp. 3091-3096, Apr 2012.

[13] Hua Jiang; Liping Zheng; Yanxiu Liu; Min Zhang, "Multi-constratined QoS routing optimization of wireless mesh network based on hybrid genetic algorithm," *Intelligent Computing and Integrated Systems (ICISS), 2010 International Conference on*, pp. 862-865, 2010.

[14] Xiao-Min Hu; Jun Zhang; Yan Yu; Chung, H.S.-H.; Yuan-Long Li; Yuhui Shi; Xiao-Nan Luo, "Hybrid Genetic Algorithm Using a Forward Encoding Scheme for Lifetime Maximization of Wireless Sensor Networks," *Evolutionary Computation, IEEE Transactions on*, vol. 14, no. 5, pp. 766-781, 2010.

[15] Ismail, M.; Weihua Zhuang; Ming Yu, "Radio Resource Allocation for Single-Network and Multi-Homing Services in Heterogeneous Wireless Access Medium," *Vehicular Technology Conference (VTC Fall), 2012 IEEE*, pp. 1-5, Fall 2012.

Real-time EEG Monitoring and Transmission over Low Bandwidth Wireless Networks

Kaushik Lahiri[1], Amitava Mukherjee[1], Mrinal K Naskar[2]
[1]IBM India Private Limited, Newtown, Rajarhat, Kolkata, India
[2]Dept. of ETCE, Jadavpur Univeristy, Kolkata, India
lkaushik@in.ibm.com, amitava.mukherjee@in.ibm.com,
mrinaletce@gmail.com

***Abstract*— A mobile healthcare protocol, which is capable of collecting data readings of patient's physical health parameters (e.g., EEG, ECG signals etc.) and sending them to physician through a wireless channel continuously over the service provider infrastructure network or the Internet, is of extreme importance in the case of diagnosing chronic diseases. To serve this purpose, one of the many problems arises, that is the storage of large amount of data associated with these vital readings like EEG, ECG etc., as well as their effective transmission over wireless network. In this paper, we present a mobile healthcare protocol that comprises of three different layers in which an efficient algorithm is proposed in layer II that allows near lossless compression of multi-channel electroencephalogram (EEG) signals; and the same algorithm will run in layer III in the reverse way for the perfect reconstruction of these compressed signals in the real time. As the EEG signal is highly uncorrelated in nature, the modified Run Length Encoding (RLE) and ASCII encoding techniques are used together to compress it. The EEG compression algorithm is implemented using Java. The results obtained are found to perform better when compared against existing EEG compression algorithms in terms of percent mean square difference (PRD), compression ratio (CR) and execution time.**

Keywords— Mobile; Health; Compression Algorithms; EEG; Wearable Health devices; Run-Length encoding.

I. INTRODUCTION

Mobile healthcare is fast growing in the domain of today's pervasive healthcare and wireless health monitoring. One of the main aspects of this mobile healthcare is to monitor different physical health parameters (e.g. EEG, ECG) of the patient using wearable health monitoring devices, to process them in their handheld device like smart phone and to send them to physician over wireless network infrastructure or Internet.

The mobile healthcare protocol can be divided into three major layers, which are shown in Fig. 1. The layer I consists of health monitoring devices, like ECG and/or EEG monitor and/or few other devices attached to a patient's body. These wireless health monitoring devices can build a network called wireless personal area network (WPAN). These devices can continuously send data to a registered (paired) device using a secure channel via Bluetooth.

The layer II consists of application stack which contains three components: 1) the data receiver to receive data transmitted by health monitoring devices, 2) the compression algorithm to compress data into a short ASCII message and 3) the data transmitter which sends encoded data stream to registered physician or hospital by identifying their attributes.

The layer III contains two components. The first component has two functions to receive encoded data through wireless network infrastructure and decompress them into original wave forms. The second component is a decision counter that will perform tasks based on the information extracted from decompressed data.

The main challenge to develop this architecture lies in collecting the large amount of physical health data and successful transmission of these data to the physician in real time. Compression technique is imperative to ease and solve this problem. To address the problem of compressing EEG data in real time, we propose a compression algorithm to solve this problem in the mobile healthcare protocol.

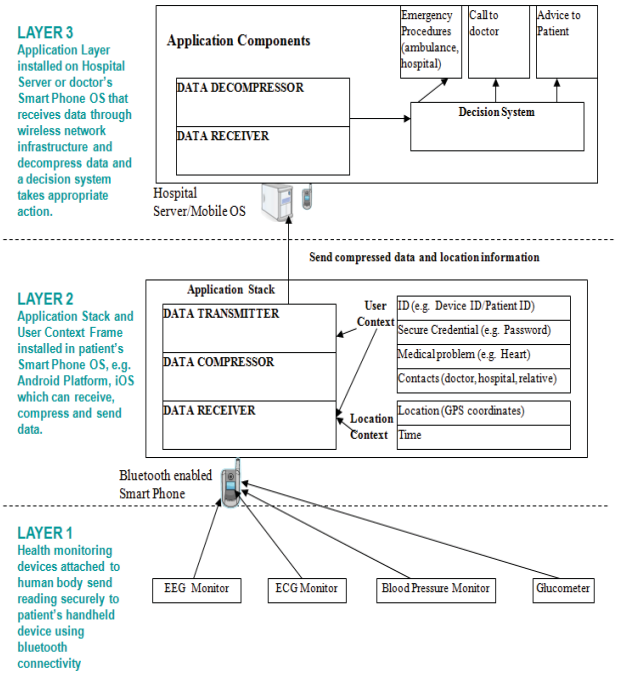

Fig. 1. Mobile Healthcare Protocol

The earlier research works had been done on ECG signal compression techniques [1], while the compression technique of EEG signal was a comparatively unexplored area. All the existing techniques [2], [5]-[7], [11]-[12] did not take into account network design parameters like

bandwidth limitation, wireless communication and packet drops, which became a design issue in our proposed protocol when EEG waveforms needed to be continuously transmitted in real time. Moreover, for highly uncorrelated signals like EEG signals, the existing techniques could not achieve high compression ratio. On the contrary our proposed compression algorithm running in layer II is capable to carry out encoded data in real time with a better compression ratio.

For ECG waveforms there is a well-defined QRS region that can be targeted for compression but for EEG there is no such corresponding feature. Also the voltage values span a much wider range for EEG. During our analysis of the EEG voltage values, we notice that the coefficients are sparse for higher orders of magnitude. We apply this feature and use an optimized combination of RLE and Digit Grouping techniques to achieve higher compression ratios. We use ASCII for encoding the compressed signals because of its narrower range of values and its ability to be sent easily over basic mobile wireless infrastructure using low network bandwidth, e.g., using simple text SMS messaging.

Section II describes the attributes of the EEG compression technique; section III describes our proposed algorithm for EEG data compression and reconstruction; section IV presents our simulation strategy and results obtained for the proposed system and compares its performance with the existing algorithms. Finally, section V concludes the paper and discusses future scope of the work.

II. ATTRIBUTES OF EEG COMPRESSION TECHNIQUE

In order to define compression algorithm stated in layer II, we need to describe few attributes of EEG.

A. EEG Overview

EEG is a graphic representation of electrical activity of brain along the scalp formed due to the constant exchanging ions by brain cells i.e., neurons with the extracellular milieu [3]. Scalp EEG activity shows oscillations at a range of frequencies [4]. The different frequency bands and their attributes are discussed below:

Delta: Its frequency range is 4Hz or below. It is highest in amplitude.

Theta: Its frequency range is between 4 Hz to 8 Hz and is classified as slow activity.

Alpha: Its frequency range is between 8 Hz to 13 Hz.

Beta: It has a frequency 13 Hz to 30 Hz and is classified as fast activity.

Per medical science, frequency bands 4Hz to 13 Hz are acceptable for clinical diagnosis. Below 4Hz and above 13Hz, the EEG readings are treated clinically normal. In our work, we will consider entire four bands for compression algorithm.

B. EEG Data Characteristics

A study of EEG Digital Data shows signal values that have a range in orders of magnitude from 10^{-6} to10^{-6} after converting to integers. Representing each number from such a large range would need at least 40 bits (41 bits considering sign bit representation). Real number representation would need even more space. In addition, EEG readings needs to be combined along with the patient's current context, location and medical information so that the health-care provider (doctor, hospital) can correctly correlate patients with EEG readings when there is transmission from multiple patients and take appropriate action specific to the patient.

In order to effectively transmit this data in real time, effective compression must be used so that a meaningful window of data can be sent in real-time along with the patient's information. Careful analysis of the EEG voltage values reveals that these are sparse in higher orders of magnitude than in lower orders. This property was used in the compression algorithm as described in the next section. An ASCII 8-bit representation is used for representing the compressed signal because of its low range of values from 0 to 256 and also the ability to easily send ASCII data over existing mobile infrastructure like SMS.

C. Parameters for Measuring Effectiveness of an EEG Compression Algorithm

The effectiveness of an EEG compression technique is described in terms of:

(a) Compression ratio (CR) is the ratio of the size of the original data (ORG) to the compressed data (CMP):

$$CR = \frac{size\ of\ ORG}{size\ of\ CMP}$$

(b) Execution time, the processing time is required for compression and reconstruction of EEG data; and

(c) A measure of error loss is often measured as the percentage mean-square difference (PRD). The PRD is calculated as follows:

$$PRD = \sqrt{\frac{\sum_{i=1}^{n}(ORG(i)-REC(i))^2}{\sum_{i=1}^{n}(ORG(i))^2}}$$

where ORG is the original signal and REC is the reconstructed signal. The lower the PRD, the closer the reconstructed signal is to the original EEG.

III. PROPOSED ALGORITHM

The *objective* of our algorithm is to encode the EEG data set in a specific format so that a high CR can be achieved (i.e., in layer II) and obtained exact reconstruction of those encoded data keeping the PRD as low as possible (i.e., in layer III). This proposed algorithm encodes the whole set of EEG data in ASCII format i.e., it maps all the EEG data into a decimal range of 0 to 255 keeping the loss as low as |.050| millivolts per sample.

The *difficulties* encountered for mapping the whole EEG data set into ASCII set are:

a) Range: EEG data sets have a long range of voltage values from microvolts to millivolts.
b) Uncorrelated dataset: The voltage values of the EEG dataset are highly uncorrelated.
c) Special ASCII characters: At the time of converting the voltage values of EEG data set, some special characters like 10 (Line feed), 13 (carriage return), 26 (substitution) or 255 (blank) occur problems. Those numbers can be printed in character form but at the time of data reconstruction of these values (13, 26 and 255) will be considered as 'End of File' by the compiler and the program will get terminated. The algorithm is designed to overcome the problem.

Careful investigation of EEG voltage values over a random period of one or two minutes reveals that the

numbers of high value data are less on the contrary, the low value data are higher in number. We have used this *sparse* nature of EEG data set to achieve high CR.

The proposed algorithm has two sections: A) the compression algorithm (i.e., in layer II) and B) the decompression algorithm (i.e., in layer III). Both of them are discussed in detail below.

A. Compression Algorithm

This *compression algorithm* consists broadly of the following steps:

1) From the continuous stream of EEG voltage values which are taken at 3-4 millisecond intervals, a window of length two seconds is picked up. This window contains multiple voltage values.
2) Let us consider −462.317 as an arbitrary sample voltage value picked up from this window. This can be expressed as
$-1 \times (4\times10^{2} + 6\times10^{1} + 2\times10^{0} + 3\times10^{-1} + 17\times10^{-3})$.

−	4	6	2	.	3	17
Sign	A3	A2	A1	_	B1	B2

Here, A3, A2, A1 and B1 denote the coefficient (1 digit each) of the 2^{nd}, 1^{st}, $0^{th,}$ -1^{th} power of 10 respectively while B2 denotes the coefficient (2-digit) for the -3^{rd} power of 10. *Sign* denotes the sign of the sample voltage. The coefficients and signs for all the voltage values in the selected window are stored in six separate arrays as described below. While the arrays for A3, A2, A1 and B1 contain the actual coefficients, the arrays for B2 and *SignBits* are binary, containing just 1 or 0 bit.

3) *Encoding SignBits and B2*: The *SignBits* and B2 arrays are 8-bit binary arrays initialized so that the last (least significant) bit is always '0' and the first two (most significant) bits are always '1'. The remaining five bits contain values for the next five voltage values.

SignBits is encoded according to the following rule.

SignBits[i] = 1 if i^{th} coefficient < 0
SignBits[i] = 0 if i^{th} coefficient ≥ 0

B2 is encoded using the following rule:
For the i^{th} voltage value,
If the coefficient B2 > 50 then B2[i]=1
Else B2[i] = 0
This ensures the maximum error per sample is .05 mV.

The 8-bit array approach ensures that the decimal equivalents of *SignBits* and B2 are always in the range 192 (11000000) and 254 (11111110). This range does not have any special ASCII characters, so it is not required to apply ASCII correction (discussed later).

4) *Encoding A3, A2, A1 and B1* arrays: These arrays (not 8-bit) are subjected to an optimized combination of *Grouping Technique* and *RLE* to convert them to their corresponding *grouped* values. Let each of the initial coefficient arrays for A3, A2, A1 and B1 be termed as *IntArr* and the corresponding grouped arrays termed as *GrpArr*. The conversion is iteratively carried out for each of the four coefficient arrays by applying either the grouping or the RLE technique as described below. Starting from 1^{st} position (1^{st} voltage value) of *IntArr* and continuing till the last but one position. Let i denote position in *IntArr* and j denote position in *GrpArr*. Both pointers start from 0 and advance as mentioned below.

(a) If the i^{th} element of *IntArr,* i.e., IntArr[i] is non-zero, then apply the *Grouping Technique*:

Grouping Technique:
If (IntArr [i] × 100 + IntArr [i+1] × 10 + IntArr [i+2]) < 256
Then
GrpArr[j] = (IntArr[i] × 100 + IntArr[i+1] × 10 + IntArr[i+2]);
Else
GrpArr[j] = IntArr[i] × 10 + IntArr [i+1];
End of if
If position (i+2) falls outside IntArr, the Else part applies.

(b) If *IntArr*[i] = 0 then apply the *Modified RLE Technique*:

Modified RLE Technique:
We count the number of *consecutive occurrences of zero* in *IntArr* starting from the i^{th} position and moving right. Let this count be *OccurZero.* Then execute the following iterative loop routine:

Label:
If (OccurZero = 1) Then
GrpArr[j] = 1; EXIT;
Else If (OccurZero = 2) Then
GrpArr[j] = 2; EXIT;
Else If (OccurZero = 64) Then
GrpArr[j] = @;
GrpArr[i+1] = 6;
GrpArr[j+2] = 4; EXIT;
Else If (2 < OccurZero ≤ 255) Then
GrpArr[j] = @;
GrpArr[j+1] = OccurZero; EXIT;
Else If (OccurZero > 255)
GrpArr[j] = @;
GrpArr[i+1] = 255;
OccurZero = OccurZero − 255;
Goto *Label*;

Since the decimal equivalent of @ is 64, so a *special treatment* is required when OccurZero is 64.

5) Once the IntArr arrays for A3, A2, A1 and B1 have been completely traversed, five grouped voltages are picked iteratively from the *GrpArr* array and *ASCII correction technique* (described later) is applied on each of them. An eight bit array named *CorrPos* having the pattern 11xxxxx0 (same as for SignBits and B2) is used to store the ASCII correction status of the five voltages based on whether they need ASCII correction or not:
CorrPos [i] = 1 if i^{th} *GrpArr* needs correction

CorrPos [i] = 0 if i^{th} *GrpArr* does not need correction.

Because of the structure of the CorrPos, B2 and SignBits arrays, no ASCII correction is needed and each can store data for five voltage values.

6) Finally, the decimal values of these seven arrays (*GrpArr*s for A3, A2, A1 and B1 and arrays for B2, *SignBits* and *CorrPos*) are converted to their equivalent ASCII characters and sent as described below:

The structure for each group of five voltages is:

GrpArr for A3	*GrpArr* for A2	*GrpArr* for A1	*GrpArr* for B1	*B2*	*Sign Bits*

The structure of the CorrPos for a group of five voltages:

CorrPos for A3	*CorrPos* for A2	*CorrPos* for A1	*CorrPos* for B1

Five such voltage values are sent serially along with the four CorrPos arrays for A3, A2, A1 and B1. The following structure is repeated for all the groups of five voltages that were picked up initially as part of the window:

1st group of 5 voltages	1st CorrPos	2nd group of 5 voltages	2nd CorrPos	…..so on for all groups

Special ASCII Correction

The ASCII correction scheme converts special characters into printable characters using the following steps:

New value = value-1 if value in {10, 13, 26, 255}
= value+32 if 128 ≤ value ≤ 159
= value otherwise

Rationale: ASCII values {10, 13, 26, and 255} are considered as end of line during program execution which therefore terminates if it encounters these. All ASCII values from 128 till 159 are interpreted as '?' or 63 when converting back to decimal and so are unusable. All the remaining ASCII values from 0 to 255 are correctly interpreted, so they *do not need* special ASCII correction.

B. Decompression Algorithm

During decompression we simply follow our proposed compression algorithm *in the reverse order.* The steps are:

1) Decomal conversion: The received ASCII characters are first converted to their decimal equivalents to get back five sets of A3, A2, A1 and B1 and the values for B2, Signbits and CorrPos.

2) Reverse ASCII Correction: The CorrPos array is used to determine whether to apply reverse ASCII correction on A3, A2, A1 and B1 and then apply the reverse correction for such cases (increment values 9, 12, 25, and 254 by 1 and decrement by 32 otherwise).

3) Ungrouping: The A3, A2, A1 and B1 GrpArr arrays are ungrouped (applying reverse grouping/RLE) to get back the initial *IntArr* values, i.e. the coefficients A3, A2, A1 and B1. Let positions in *GrpArr* be denoted as i and those of *IntArr* be j. The following reverse generation technique is applied iteratively (pointer positions are advanced by 1 for both unless otherwise mentioned.)

Reverse Grouping/RLE Technique:

- If GrpArr[i] = 1, IntArr[j] = 0
- If GrpArr[i] = 2, IntArr[j] = IntArr[j+1] = 0. Advance j by 2
- If GrpArr[i] = 64 (character '@'),
  - If GrpArr[i+1]=6 and GrpArr[i+2]=4, fill zeroes in IntArr[j] to IntArr[j+63]. Advance i by 2 and j by 64
  - If GrpArr[i+1]=255, fill 255 + GrpArr[i+2] zeroes in IntArr. Advance i by 3 and j by 255 + GrpArr[i+2]
  - Else fill GrpArr[i+1] zeroes in IntArr.. Advance i by 2 and j by GrpArr[i+1]
- If GrpArr[i] > 100 fill IntArr[j], IntArr[j+1] and IntArr[j+1] with the hundreds, tens and unit place in GrpArr[i]
- If GrpArr[i] > 10 fill IntArr[j] and IntArr[j+1] with the, tens and units places in GrpArr[i]
- Else IntArr[j] = GrpArr[i]

4) Sign Retrieval and Coefficent Conversion: Finally the SignBits array is used to get back the original signs and coefficients A1…B2 are multipled by corresponding coefficients of ten to get back the original voltage values.

.

IV. SIMULATION STUDY

In this simulation study, we test the performance of compression (layer II) and decompression (layer III) techniques described in proposed algorithm in the mobile healthcare protocol.

We assume in the simulation study that EEG data is transmitted from EEG monitor device to patent's handheld device through Bluetooth that is layer I function in mobile healthcare protocol. The compression technique part of our algorithm will run in patient's handheld device to encode the data that is the layer II Application stack function. Next, this encoded data will transmit to physician's handheld device or into hospital server through wireless service provider infrastructure or through Internet. In layer III, the reconstruction of the data will be done, that is part of our proposed algorithm, and subsequently decision system will take the next action. This study of performance for each layer of mobile healthcare protocol will be our future work.

In this work, we only validate and demonstrate the performance of compression and reconstruction technique in our proposed algorithm for EEG data that is implemented in the JAVA version 7. Next, this algorithm has been tested with ten minutes of EEG data waveform stored digitally in the MIT-BIH database [10]. The EEG signals are sampled at 256Hz (i.e., 256 samples/second). So, ten minutes of EEG data contain total 1.536×10^5 numbers of samples. After going through the compression algorithm these ten minutes of EEG long data are converted into a printable stream of ASCII characters and are printed in a file. This file has subsequently been used for the input to the decompression algorithm and EEG stream is finally reconstructed. The original EEG data stream and the reconstructed EEG data stream are then compared to calculate the loss.

To test the performance of proposed compression technique for EEG, ten datasets are randomly selected from

CHB-MIT Scalp EEG database [10] and given input to our algorithm. Subsequent to compression, the databases are reconstructed by our algorithm too. The results thus obtained are shown below in Table 1.

TABLE 1: Compression Results

Data Sets	**Compression Results**		
	Signal Record	***CR***	***PRD (%)***
chb01/chb01_01	FP1-F7	3.83	0.04
	F7-T7	3.884	0.072
	T7-P7	3.89	0.108
	FP1-F3	3.803	0.0428
	C4-P4	4.072	0.16
	P4-O2	3.89	0.0748
	P8-O2	3.864	0.0708
chb01/chb01_02	FP1-F7	3.833	0.054
	F7-T7	3.90	0.0965
	F8-T8	3.884	0.0878
chb01/chb01_03	FP2-F4	3.926	0.065
chb01/chb01_05	FP1-F7	3.821	0.033
	F7-T7	3.938	0.059
chb01/chb01_08	FP2-F4	3.826	0.0518
	P7-O1	4.02	0.185
Average		**3.892**	**0.080**

CR and PRD for different datasets are graphically shown below in Fig. 2.

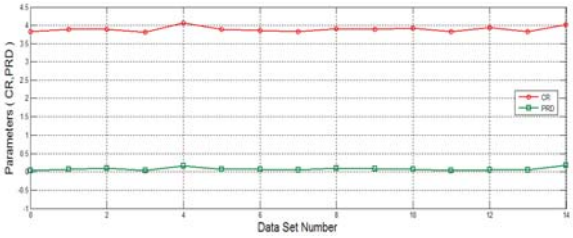

Fig. 2. CR and PRD for different datasets

The figures shown below are original signals (Fig. 3, 5) and reconstructed signals (Fig. 4, 6) using proposed algorithm.

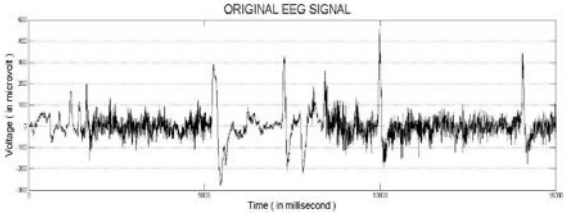

Fig. 3. Original EEG signal (Record: chb01/chb01_01 FP1-F7)

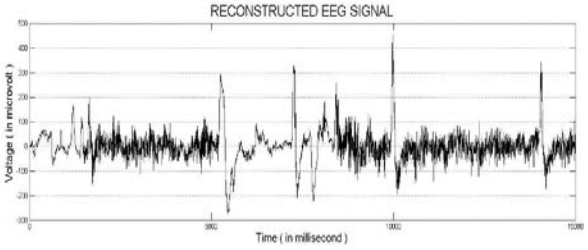

Fig.4.Reconstructed EEG (Record: chb01/chb01_01 FP1-F7)

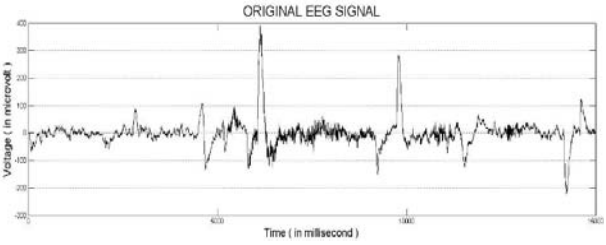

Fig. 5. Original EEG signal (Record: chb01/chb01_05 F7-T7)

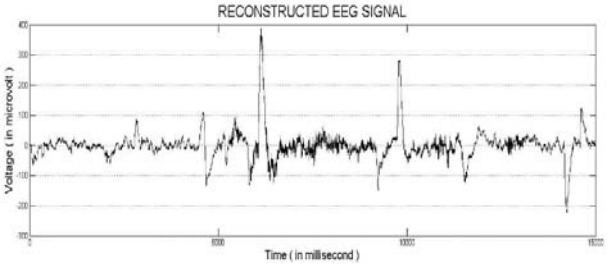

Fig. 6.Reconstructed EEG signal (Record: chb01/chb01_05 F7-T7)

We can see from the figures that for two quite different patterns of original EEG signals (Fig 3 and 5), the reconstructed EEG signals (Fig. 4 and 6) faithfully reproduce the original signals so that the doctor can make an accurate diagnosis. This is especially important for EEG signals as these can have many different patterns as opposed to ECG signals which have a relatively smoother and more consistent pattern.

TABLE 2: Performance Comparison

Algorithms	**CR**	**PRD (%)**
Vector quantization with collapsed Huffman tree [2]	2.63	~0
Adaptive error modeling scheme [8]	3.23	-
SLP predictor with error modeling and arithmetic coding[5]	2.72	-
KLT transform[6]	2.84	~0.6
Wavelet-SPIHT[7]	2.046	~0.5
SPECK[9]	1.73	0.66
BISK[9]	1.74	0.67
Our proposed algorithm	**3.892**	**0.080**

For earlier data compression techniques used for EEG compression like Huffman coding and Vector quantization [2] with collapsed Huffman tree, Linear and Adaptive predictor, RLSL filter, Artificial Neural Network predictor and other transformation techniques like KLT, DCT, DWT [5]-[7], [9], the execution time varies from medium to high as most of them require more buffer size for storing and filtering. So, it is difficult to implement them for real time applications. Whereas our algorithm has a negligible PRD (~0.1%), high CR and most importantly it can be executed on real time. Table 2 has shown the performance comparison among various compression algorithms including our proposed algorithm.

V. Conclusion and Future work

We have presented a mobile healthcare protocol comprising of three different layers with the main focus on layer II where we have proposed a near lossless compression of multi-channel EEG signals. We have used an algorithm which is a combination of a modified version of RLE and ASCII encoding techniques to compress and reconstruct the EEG signals. We used the idea of space and time management to compress a continuous stream of EEG signals and to reconstruct that stream with very low distortion. We have made an assessment of the quality of the reconstructed signal and observed that it is robust both when visually inspected and also in terms of the CR and PRD values remaining constant for multiple data sets.

In our future work we will explore the possibility of applying faster variations of compression techniques such as compressed sensing along with the use of specific templates or waveforms which can be dynamically determined and applied based on the characteristics and type of signal being compressed, e.g. EEG, ECG or EMG. We would design means of applying our three layer protocol stack in the case of large number of senders streaming signals to the same mobile device using dynamically changing, unreliable networks.

References

[1] A Comparison of Single Lead ECG Data Compression Techniques:http://www.hcs.harvard.edu/~weber/HomePage /Papers/ECGCompression/

[2] G. Antoniol and P. Tonella, ‘‘EEG data compression techniques,’’ IEEETrans. Biomed. Eng., vol. 44, no. 2, pp. 105–114, 1997.

[3] E. Nidermeyer and F. L. D. Silva, Electroencephalography:Basic Principles, Clinical applications and related fields, 5th ed. Lippincott Williams and Wilkins, 2005.

[4] Blinowska, K. and Durka, P. (2006). Electroencephalography (EEG), In: Wiley Encyclopedia of Biomedical Engineering, Ed. Metin Akay, Wyley

[5] N. Sriraam and C. Eswaran, “Context based error modeling for lossless compression of EEG signals using neural networks,” *Journal of Medical Systems*, vol. 30, no. 6, pp. 439–448,2006.

[6] Y.Wongsawat, S. Oraintara, T. Tanaka, and K. R. Rao, “Lossless multi-channel EEG compression,” in *Proceedings of the IEEE* International Symposium on Circuits and Systems (ISCAS ’06), pp. 1611–1614, May 2006.

[7] K. Srinivasan and M. Ramasubba Reddy, “Selection of optimal wavelet for lossless EEG compression for real-time applications,” Indian Journal of Biomechanics, pp. 241–245, 2010.

[8] "An Adaptive error modeling scheme for the lossless compression of EEG signals”, N.Sriraam C.Eswaran, IEEE transaction on Information Technology in biomedical, Vol.12 No.5, September 2008.

[9] K. Srinivasan, J. Dauwels, and M. Ramasubba Reddy, “Multichannel EEG compression: Wavelet-based image and volumetric coding approach,” IEEE Trans. on Inf. Technol. Biomed., vol. 17, no. 1, pp. 113–120, Mar. 2012.

[10] CHB-MIT Scalp EEG database : http://www.physionet.org/cgi-bin/atm/ATM

[11] Mahajan, R., Bansal, D., Hybrid multichannel EEG compression scheme for tele-health monitoring, 2014 3rd International Conference on Reliability, Infocom Technologies and Optimization (ICRITO) (Trends and Future Directions), Year: 2014, Pages: 1 – 6

[12] Yong-Siang Chen, Hsin-Yi Lin, Hung-Chih Chiu, Hsi-Pin Ma, "A compressive sensing framework for electromyogram and electroencephalogram", 2014 IEEE International Symposium on Medical Measurements and Applications (MeMeA), Year: 2014, Pages: 1 – 6

THE 18TH INTERNATIONAL SYMPOSIUM ON WIRELESS PERSONAL MULTIMEDIA COMMUNICATIONS
(WPMC-2015)
December 13-16, 2015, Hyderabad, India

Pilot testing and demonstration of self-management network and applications by NerveNet

Yasunori OWADA and Kiyoshi HAMAGUCHI
Resilient ICT Research Center, National Institute of Information and Communications Technology
2-1-3, Katahira, Aoba-ku, Sendai-shi, Miyagi 980-0812, Japan,
{ yowada, hamaguti }@nict.go.jp

Masugi INOUE
Resilient ICT Research Center, National Institute of Information and Communications Technology
4-2-1, Nukui-Kitamachi, Koganei-shi, Tokyo, 184-8795, Japan,
inoue@nict.go.jp

***Abstract*—An unprecedented big earthquake and tsunami happened on March 11, 2011 called Great East Japan Earthquake, more than 20,000 people passed away by this disaster. At that time, because of the communication infrastructure also damaged and congested, most people in the disaster area did not use communication system. From these lessons, the resilient, robust and early recoverable network system is required. We have developed regional resilient network system called NerveNet. In this paper, the requirements for the network at the disaster situation are organized, and NerveNet system architecture, platform and example applications are introduced. A NerveNet system pilot test has started in Onagawa town, Miyagi prefecture, hit by the tsunami. Its pilot testing and disaster drill trial using NerveNet system and applications are briefly introduced.**

Keywords— NerveNet, mesh network, disaster resilient, smart city, disaster drill, Onagawa town, information sharing.

I. INTRODUCTION

More than 20,000 people passed away by the huge earthquake and tsunami at the great east japan earthquake in March 11, 2011. The lifeline that not only electricity, water, gas, but also mobile communication and Internet communication were cut off in the affected area. Because of the damage of the communication system, people could not confirm his/her family's safety in the affected area. Emergency call was also unavailable at that time. Roads, railroads and highway also destroyed over a wide area, so that the arrival of the emergency vehicle and rescue team delayed. Food and aid and medical supplies also delayed by the transportation disruptions, it leads the secondary damage. If the disaster damage situation grasp had been accurately done and regional information sharing and communication could be available by the resilient information and communication system, secondary damage might be minimized. From this viewpoint, the communication is one of the lifeline infrastructure should not be without.

The mobile communication infrastructure is extended architecture based on the telephone system, so its network topology is tree based topology, and also centralized controlled and management system is adopted. For these reasons, if the branch nodes of the backhaul network has damaged, the whole leaf area is affected by this damage. In addition, the centralized server manages the communications, so the admission control is required when the number of communication request is over the processing capacity of the centralized server. Actually immediate after the earthquake on March 11, 2011, the mobile operators in Japan applied call restriction ratio up to 90%. For the reason of this restrictions, the mobile phone communication is hardly used not only the disaster affected area but also whole area in Japan for several days.

From this background, we have been developed disaster resilient regional area information and communication platform called "NerveNet"[1]-[4], which can provide robust network and application services without depending on the server system in the core network or the Internet. NerveNet base station can provide information sharing application service and peer to peer communication service standalone, and if two or more base stations are interconnected each other, they work together distributed manner.

II. REQUIREMENTS FOR THE EMERGENCY COMMUNICATIONS

The communication requirements for under the disaster situation is depend on the target users. Our system is targeting to the users as follows.

A. Requirements for the general users

It is the best for the general users to use ordinal mobile communication service without any inconvenience even the disaster happened. These communication infrastructures are maintained and operated by mobile service operators or mobile carriers. To increase the network redundancy and robustness, mobile carriers have to invest to the infrastructure more. But it takes large amount of costs to strengthen these infrastructures, which is over specification for general use case. The decision to construct redundant and robust network system is up to the mobile carrier's effort. Usually, enhancing the system redundancy and pursuing the profit are contrary to each other, so excessive capital investment and redundancy endurance that is not contributed to service quality improvement cannot be expected to mobile carriers.

B. Requirements for the self-managed network by local government

Some local governments construct their own self-managed regional network to ensure the communication system

redundancy. Most of their self-managed regional network infrastructure is closed network only for the local government use, and actual utilization ratio compare to its bandwidth is very low. But its maintenance fee occurs constantly. For this reasons, the effect that can be obtained from the capital investment to the private network construction is very limited in peacetime. To pay high insurance and to build a self-managed private network is equivalent. Some local governments are renting their own fiber optic cables to a network operator, which is so called public build and private operate scheme. But this scheme is limited to the physical network infrastructure construction and renting. It is demanded that the same physical network infrastructure can be isolate logically, and logical network resource can be rent to the network operator virtually to accelerate the self-managed network utilization improvement.

C. *Requirements for rescue and disaster relief team*

The ad-hoc communication system is necessary for the rescue and disaster relief tem such as fireman, police, and army. The team members have to share or report the information to the head quarter or commander, and they have to receive the instruction from head quarter without depending on an existing network infrastructure because it is not always exist in their activity area. Usually, MCA radio system is used for their communication. This system is very simple, but the communication channels are limited. So they have to care about the channel interference. Furthermore, MCA radio system is voice broadcasting, so it is useful for information sharing or one to multiple communications such as instruction message dissemination from a commander to members. But it is not suitable for the communication such as peer to peer communication and many to one communication. In addition, MCA radio system is specialized to the voice communication, and only very short data communication such as GPS data broadcasting is supported. Therefore, not only voice broadcasting but also ad hoc, peer to peer, high bandwidth data communication system is required.

When the rescue team or disaster relief team want to share photos, videos, and their location information among the team, the information sharing server system is required. Usually, most information sharing applications are depending on the specific servers on Internet. When they want to operate the same system without having a connection to Internet, some application server system has to be operated inside the ad-hoc network. But considering the ad-hoc network instability, network connectivity to the specific server might be unstable and disconnected some time. Considering this situation, information sharing system with multiple servers should be operated distributed manner to be robust to the network isolations. By employing this architecture, even when a certain disaster relief team is isolated to the other team, they can still share the information inside the team by using local information sharing server. When they merged to the other team, the sharing information also merged to the other team, and the distributed server continue working as a part of the one big information sharing system.

D. *Requirement for the network operators for the disaster recovery*

When a big disaster was happened and several network infrastructures has damaged, network operator have to recover the system as soon as possible. To recover complete system takes long-time, so temporal and early recovering technology is required even the service is conditional. For this use case, generic and reconfigurable network interface and virtualization technology are required.

III. NERVENET OVERVIEW

From the requirement above, we are designing a new regional distributed network architecture called NerveNet. NerveNet system, which is consist of several NerveNet base stations. Fig.1 shows a NerveNet base station image and specifications. NerveNet base station is consist of a VLAN intelligent switch and CPU board that has flash storage device (CF and SD card) and RAM disk. Linux OS is running on the CPU board, several distributed server and database systems are running on the OS. NerveNet base station can provide information sharing application service to mobile terminals by stand-alone. If several NerveNet base stations are interconnected each other, each base station automatically detects the neighboring base stations and they begin to co-operate with each other. Finally, individual NerveNet systems are merged to one system autonomous and distributed manner. For this characteristics, NerveNet system provides a thought of regional cloud platform which has redundant network functions, name/address resolver function, distributed storage, database, and processing functions. To be able to operate NerveNet system by stand-alone, all server functions such as DHCP, DNS, SIP, etc., are embedded inside the base station with customizing to cooperate with other base stations.

NerveNet system can use standalone network system, but if one or more base stations are connected to the Internet, NerveNet can also provide redundant Internet access backhole

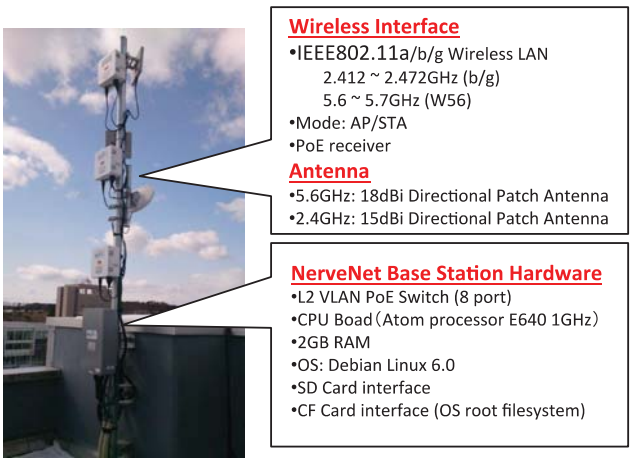

Fig.1 NerveNet base station hardware specification

network.

NerveNet system functions are categorized to two parts. One is application service platform that is including distributed

servers and database functions, database synchronization functions, and name/address resolver and P2P communication functions. The other is network service platform that is including VLAN switch controller, reliable flooding, IP address assignment, neighborhood link sensing, mesh topology monitoring and management. The architecture function block inside NerveNet base station is shown in Fig. 2, and these two service platform functions are show in table1.

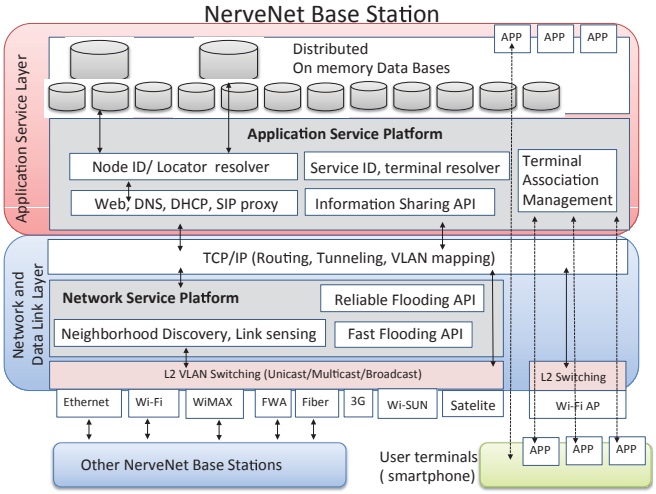

Fig. 2. NerveNet base station architecture function block

Table 1. Base station service platform functions

application service platform	IP address allocation (DHCP)
	Name resolution (DNS)
	Peer to Peer communication (SIP Proxy)
	Distributed database system
	Distributed server system(Apatche)
	Database synchronization service
	Terminal association management service
Network service platform	VLAN switch control
	Multiple VLAN path maintenance and path selection
	Traffic control and management
	Reliable flooding and multicasting
	Autonomous link sensing and path switching
	Multi-homing
	Network virtualization (L2 tunneling)

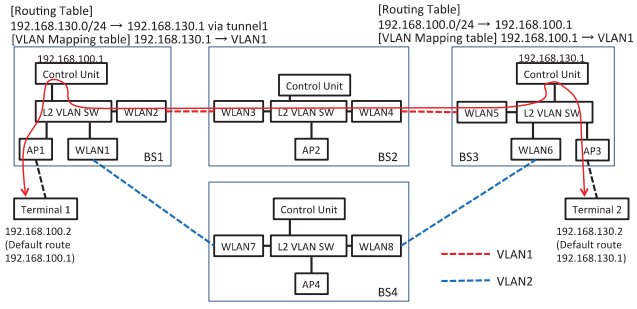

Fig. 3. NerveNet routing and switching mechanism

IV. NETWORK SERVICE PLATFORM

NerveNet network service platform provides routing, switching management and flooding functions. Total network is managed from one management PC that is called Network Manager (NM). The NM doesn't have to connect at all times. NM manages the network configuration when network topology has changed, or new base station has been installed. When a NM is attached to the NerveNet base station, whole network topology and link information can be monitored from the NM. Then, NM calculates multiple and redundant VLAN tree topology from the mesh network topology, and the multiple VLAN configuration set based on the calculation result are flooded to all base stations. All base station which is received this configuration apply to its own VLAN switch. Finally, multiple VLAN tree path is constructed over the mesh topology. NerveNet base station select minimum cost VLAN tree to communicate with each base stations.

Fig.3 shows an example of NerveNet base station routing and switching mechanism. Each base station acts as an IP router for mobile terminals. Each base station assigned different subnet, which is automatically assigned based on the base station ID. When BS1 received IP packet from a terminal, BS1 lookup its own routing table and then forward it to the BS3. At the same time, BS1 lookup its own VLAN mapping table, and VLAN 1 tag is attached to the frame and transmitted to the VLAN switch. The frame is switched through BS2 based on MAC address learning table, and reached to BS3. BS3 finally forward the IP packet to the destination terminal. When BS1 detect the link disconnection between BS2, then BS1 autonomously update VLAN mapping table to BS3 as VLAN2 without depending on the NM.

V. APPLICATION SERVICE PLATFORM

NerveNet application service platform provides many functions as API for smartphones. To explain NerveNet application service platform functions, two example applications is introduced as follows.

A. *Extension telephone application*

The extension telephone application uses NerveNet peer to peer communication functions. When a smartphone that is installed this application is connected to a NerveNet base stations, base station assigned an IP address to the smartphone by DHCP protocol. As a NerveNet base station is periodically broadcasting original beacon messages, so the application in the smartphone can notice that now it is connected to NerveNet base station, and then application register its own IP address and SIP URI to the associated base station. (When the application installation, unique SIP URI is pre-assigned to the application.) By receiving this registration massage, base station registered a pair of SIP URI and IP address to its own distributed database. Base station's distributed database is synchronized to the other base stations, so this information is shared among base stations. When a user wants to make a call using this extension telephone application, the user selects one destination SIP URI from its address book and calls up. Then "INVITE" SIP massage is transmitted to the associated base

station by caller application. Base station is act as SIP proxy, so it received INVITE message, then it looks up IP address associating to SIP URI and forward it to this IP address. When callee application received INVITE message, then "180 RINGING" message is replied and bell rings. When callee received the phone call, "200 OK" massage is transmitted to the caller, and then peer to peer voice communication starts. These IP address resolution and peer to peer session initiation API is provided to the application developer.

B. Information sharing application

Information sharing application uses distributed database inside NerveNet base station. NerveNet application service platform also provides database synchronization mechanism among smartphone applications. When the application detected a connection to NerveNet base station, the application start synchronizing its own database to the base station's distributed database. Base station's distributed database is maintained by user ID, group ID, application ID, and timestamp. So the application can only synchronize the data that have the same application ID. If several smartphone application have permit to synchronize certain group ID, the same data is synchronized among these smartphone applications through the base station's database. By using this application database synchronization scheme, the application developer can easily develop information sharing applications. The base station also maintained smartphone's connection status. Combining this status information, group-messaging application can be easily developed without using certain server system on Internet. Users don't aware of the database synchronization because all database synchronization is operated in background. In addition, user data access is only made to local database inside the smartphone, so user can send/read message at anytime even it he/she is out of communication range.

VI. NerveNet system and application demonstration at disaster drill in Onagawa town

We have cooperated with Onagawa town, Miyagi Prefecture, Japan, where is attacked by big tsunami up to 15m heights or more at the great east japan earthquake, march 11, 2011. Onagawa town location is shown in Fig.4. 55.9% evacuee died or still missing by this tsunami. Onagawa town office also hit by tsunami, and some people who went out office to check tsunami arrival after the earthquake never returned. To monitor the arrival of tsunami information remotely, or to correct and share the disaster information speedy, we installed four base stations and one IP video camera in Onagawa town. The network topology and installation location are shown in Fig.5. NerveNet base stations are connected with Wi-Fi based point-to-point communication system. Also Wi-Fi access point service is operated near base stations, so user around the base station can access to the network via Wi-Fi. High resolution IP zoom video camera system is installed in medical center to monitor sea level at any time from the town office. The video streaming image monitored from local town office is shown in Fig.6. By this system, the town officer can alert the tsunami arrival without approaching to the seashore. In addition, this IP camera is installed high location to be able to oversee whole town, so other disaster situation such as flood, the disaster situation can be quickly and easily grasped by controlling this camera. Fig.7 shows the camera image when a flood happened in Onagawa town. We have developed extension telephone application using NerveNet application service platform, and tried to use the disaster drill held in Miyagi prefecture on November 12, 2014. In this disaster drill, it is assumed that magnitude 8 level big earthquakes occurred near the sea of Miyagi prefecture, all mobile communication system was out of service at that time. Onagawa town officer correct damaged assessment information from the branch office by using extension phone application, and at the same time, they monitor the sea level in preparation for the tsunami arrival using IP video camera system. By this disaster drill, all system works well, and extension telephone application can be operated between library and town office without using Internet or other specific server system.

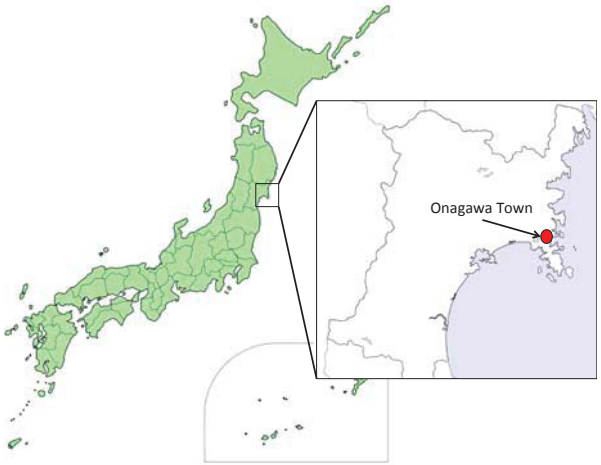

Fig. 4. Location of Onagawa town

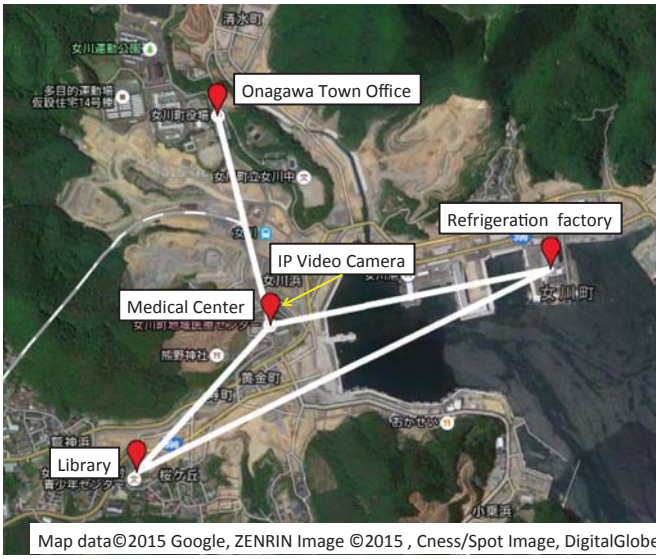

Fig. 5. NerveNet installation point and network overview

VII. Conclusion

In this paper, requirements for the communication system under disaster are organized, and NerveNet system platform and functions with original applications are introduced. Four NerveNet base stations with IP zoom video camera system are installed in Onagawa town as a pilot project for resilient regional self-managed network. NerveNet system, extension telephone application and IP camera surveillance system are used in a disaster drill, and these systems are well operated by Onagawa town officers. Utilizing these findings obtained from this trial, we are going to enhance NerveNet system to more robust, easy to user, easy to operate in future.

Acknowredgement

We would like to express the deepest appreciation to the Onagata town officers to cooperate with our pilot trials of NerveNet system.

References

[1] M. Inoue, M. Ohnishi, H. Morino, T. Sanefuji, Y. Owada “Fast Recovery from Link Failures and Blackout of Managed Wireless Mesh for NerveNet,” IEEE GLOBECOMM, Dec. 2010.

[2] M. Inoue, M. Ohnishi, C. Peng, R. Li, Y. Owada, “NerveNet: A Regional Platform Network for Context-Aware Services with Sensors and Actuators,” IEICE Trans. Commun., Vol. E94-B, No.3, pp.618-629, Mar. 2011.

[3] Y. Owada, M. Inoue, M. Ohnishi, “Regional Wireless Network Platform for Context-Aware Services and Its Implementation,” 10th international Symposium on Autonomous Decentralized Systems (ISADS), pp.539-544, 2011.

[4] R. Miura, M. Inoue, Y. Owada, H. Tsuji, S. Hara, “Disaster-tolerant dependable wireless network,” 15th International Symposium on Wireless Personal Multimedia Communications (WPMC), 2012.

Fig. 6. A snapshot image of IP video camera from Onagawa Medical Center.

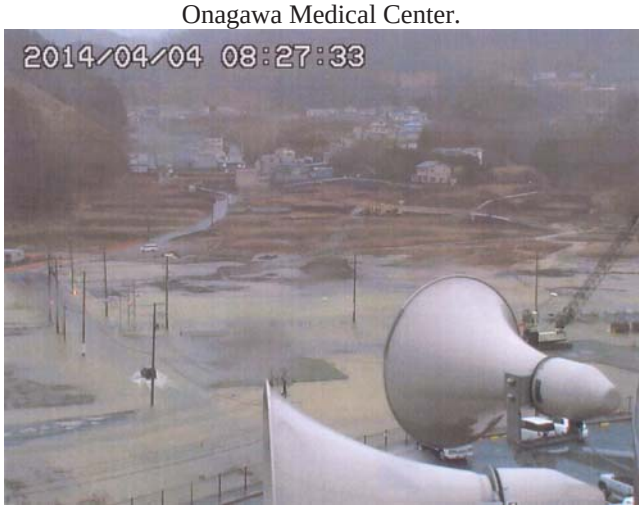

Fig. 7. A snapshot image of IP video camera when flood occurred.

Fig. 8. A picture of the disaster drill at Onagawa town office. Office worker is checking sea level at the monitor screen and talking through the extension telephone application of NerveNet

THE 18TH INTERNATIONAL SYMPOSIUM ON WIRELESS PERSONAL MULTIMEDIA COMMUNICATIONS
(WPMC-2015)
December 13-16, 2015, Hyderabad, India

CDF Based Spectrum Occupancy Rate Measurement Using Least Square Estimation of Gaussian Noise Period

Shota RACHI† Akira SAITO† Masahiro UMEHIRA†† Shigeki TAKEDA††
Graduate School of Science and Engineering
Ibaraki University
4-12-1, Nakanarusawa-cho, Hitachi-shi, Ibaraki, Japan
E-mail: †(14nm666n, 15nm659h)@vc.ibaraki.ac.jp, ††(umehira, obote)@mx.ibaraki.ac.jp

***Abstract*— Spectrum occupancy rate (SOR) is one of the most important parameters for spectrum utilization measurement. This paper proposes a novel spectrum occupancy rate (SOR) measurement method based on CDF (Cumulative Probability Distribution Function) of received signal power, by using least square estimation of Gaussian noise period, to improve SOR measurement accuracy in low SNR conditions. Computer simulation confirms that SOR measurement accuracy is improved in low SNR conditions compared with the conventional threshold based SOR measurement method and simulation results of SOR measurement performance according to SNR of received signals, packet length, and number of measured samples are presented.**

Keywords- cognitive radio , cumulative probability distribution function , least square estimation , spectrum occupancy rate , Gaussian noise

I. INTRODUCTION

As mobile traffic in cellular networks and wireless LAN is rapidly increasing in recent years triggered by wide rollout of smart phone and tablet PC, demand for frequency spectrum has been dramatically increasing. However, frequency bands below 6GHz suitable for mobile services are already allocated to various existing wireless services and no more spectrum is available for new wireless services without spectrum re-allocation. On one hand, it was reported that there exists "white space" which is allocated to primary users but spatially and/or temporally unused [1].

Cognitive radio has been drawing a great deal of attentions as a technique to make it possible secondary use of white space possible as far as no harmful interference is given to primary users. Some papers estimated available white space, however it is still a controversial issue how much white spectrum is available in terms of space and time for secondary use [2][3]. As packet based wireless systems are widely used nowadays, spectrum occupancy rate (SOR) is also an important metric to evaluate available white space in terms of time.

To the best knowledge of the authors, a standard method for SOR measurement has not been established so far. A conventional SOR measurement method measures received signal power of each frequency bin, and calculates the number of samples which have larger signal power than the pre-determined threshold relative to the noise power level. The ratio of the number of samples higher than the threshold over all samples is given as SOR, or duty cycle of designated frequency bin [4]. A problem of this threshold based method is false detection and miss detection in low SNR conditions. As well-known, setting the threshold is a trade-off issue, i.e. false detection probability increases if the threshold is too low and miss detection probability increases if the threshold is too high. Thus, the threshold based SOR measurement method cannot accurately measure SOR especially when SNR is low and a few techniques to improve SOR measurement accuracy in low SNR conditions were proposed [5][6].

In order to improve SOR measurement performance in low SNR conditions, this paper proposes a novel SOR measurement method based on CDF (Cumulative Probability Distribution Function) of received signal power employing least square estimation of Gaussian noise period. The proposed SOR measurement method assumes Gaussian distribution for noise and estimates the ratio of Gaussian noise time period which minimizes square error of probability between reference CDF of Gaussian noise and measured CDF of received signals. Then, SOR is obtained by subtracting the ratio of Gaussian noise time period from one. The proposed method needs reference CDF of Gaussian noise, but does not need threshold setting, thus it can improve SOR measurement performance in low SNR conditions, compared with the threshold based SOR measurement method. The rest of this paper is organized as follows: Chapter 2 describes the problem of the CDF based SOR measurement method using threshold. Chapter 3 describes principle of the proposed SOR measurement method using least square estimation of Gaussian noise period and Chapter 4 shows simulation results of SOR measurement performance of the proposed method. Finally, Chapter 5 concludes this paper.

II. PROBLEM OF CDF BASED SSOR MEASUREMENT METHOD UISNG THRESHOLD

A. Principle of CDF based SOR measurement method

Cumulative probability distribution function (CDF) of received signal power, x in dB is obtained by measuring a sufficient number of measured samples for each frequency bin. Using CDF of measured signal power, SOR can be obtained from the ratio of the time period of signal plus noise over all the

measurement time period. Supposing that probability density function (PDF) of thermal noise is $p_N(x)$, that of received signal plus noise is $p_S(x)$, and SOR is R at a frequency bin, PDF of received signal, $p_R(x)$ and its CDF, $P_R(x)$ are given as follows:

$$p_R(x) = Rp_S(x) + (1-R)\cdot p_N(x) \quad (1)$$

$$P_R(x) = \int_0^x p_R(y)dy \cdot \quad (2)$$

Fig.1 shows principle of CDF based SOR measurement method where CDF of $p_N(x)$ and $p_R(x)$, $P_N(x)$ and $P_R(x)$ are illustrated when SNR=20dB and R=0.5. As shown here, there is a floor at R and R can be obtained as the probability from the floor to 1. Assuming Gaussian distributed noise for $P_N(x)$, we define the threshold x_0 and $P_N(x\text{-}x_0)$ as a threshold CDF to obtain R by calculating the cross point of $P_R(x)$ and $P_N(x\text{-}x_0)$. Supposing the cross point of $P_R(x)$ and $P_N(x\text{-}x_0)$ is $(X, P_R(X))$, R is given by

$$R = 1 - P_R(X), \quad (3)$$

where $P_R(X) = P_N(X\text{-}x_0)$. $P_N(x)$ can be measured for each frequency bin before SOR measurement and stored as the threshold CDF. We assume that Gaussian noise is Gaussian distributed and CDF of $P_N(x)$ is not changed during the SOR measurement. As $P_N(x\text{-}x_0)$ is theoretically less than $P_N(x)$ for any x if x_0 is larger than 0 and number of measured samples is sufficiently large. Then, three cross points for $P_N(x\text{-}x_0)$ and $P_N(x)$ are obtained, i.e. $(X_1, 0)$, $(X_2, P_R(X_2))$ and $(X_3, 1)$ where $X_1<X_2<X_3$ and R is obtained by $1\text{-}P_R(X_2)$ according to the equation (3). Otherwise, there are only two cross points, i.e. $(X, 0)$ and $(X, 1)$ for R=0 and R=1. In this case, if median value of $P_R(X)$ is less than x_0, R=0 and if it is larger than x_0, R=1.

B. *Problem of CDF based SOR measurement method using threshold*

As described above, performance of the CDF based SOR measurement method using threshold is affected by the threshold, x_0. Fig. 2 shows simulation results of SOR error according to the threshold when SNR=20dB and duty cycle=50%. Threshold is defined as the signal power normalized by noise power. As shown here, measured SOR error increases if the threshold is less than 5dB. As it is desirable to set the threshold as low as possible for SOR measurement in low SNR conditions, threshold of 5 to 6dB seems reasonable to minimize SOR error according to Fig. 2.

The CDF based SOR measurement method using threshold is evaluated by computer simulations. Simulation model is shown in Fig. 3, where received signals are weighted by windowing function and FFT is carried out to detect signal power per frequency bin. Then, SOR is estimated after obtaining CDF of signal power per frequency bin. Major simulation parameters are shown in Table 1, where IEEE802.11n standard is employed and subcarrier spacing of OFDM signal is 312.5 kHz. Bandwidth of frequency bin is set to 1MHz to accommodate multiple subcarriers in the frequency bin. This figure, 1MHz is being used in the experiments to evaluate the SOR measurement performance by the proposed scheme. The experimental results will be reported in near future. Windowing period is 768 assuming sampling frequency of 80MHz and bandwidth of frequency bin is set at 1.05MHz,

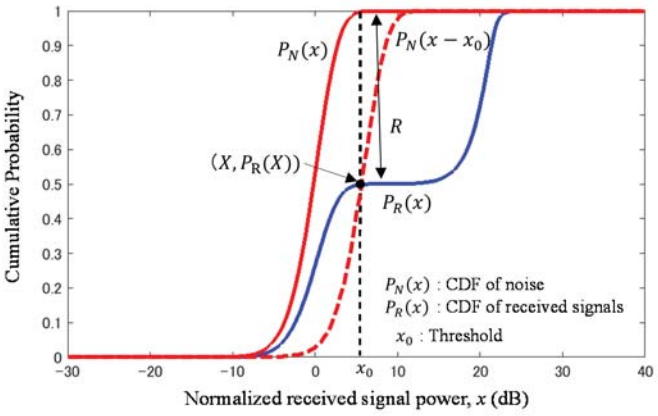

Fig.1. Principle of CDF based SOR measurement method using threshold.

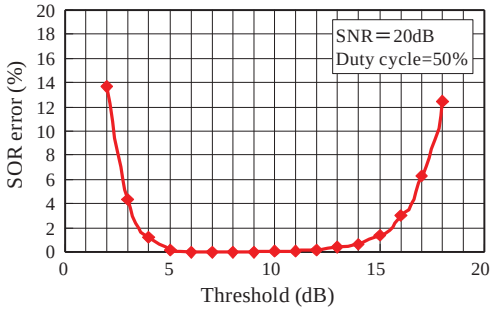

Fig.2. SOR error according to threshold.

Table 1. Major simulation parameters.

Number of subcarriers	56
OFDM symbol length	4 μs
Subcarrier spacing	312.5kHz
Modulation	QPSK
CP length	¼ OFDM symbol
Sampling frequency	80MHz
Windowing function	Hanning window, FFT length=768 samples
Frequency bin	1MHz

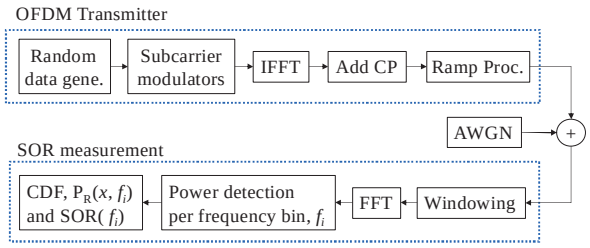

Fig.3. Simulation model for SOR measurement performance evaluation.

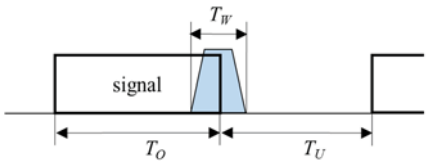

Fig. 4. Simulation scenario for SOR measurement performance evaluation.

which comprises 10 samples in frequency domain. Fig. 4 shows simulation scenario where an OFDM packet signal is transmitted periodically, where T_O is occupied time period of a packet signal, T_U is unoccupied time period or idle time period, and T_W is windowing time period. In this case, duty cycle is given by $T_O/(T_O+T_U)$.

Computer simulation has been conducted for performance evaluation of the CDF based SOR measurement method using threshold. Packet length is set at 256 OFDM symbols to avoid SOR error caused by time resolution, which is basically determined by windowing period, T_W and packet length, T_O as described later. Evaluated SOR error according to SNR is shown in Fig. 5, where threshold=6dB. As shown here, measured SOR is zero when SNR is less than 5dB, and measured SOR becomes lower than the actual duty cycle of 0.5 while SNR decreases to less than 10dB. In addition, smaller duty cycle results in more SOR error. This is because miss detection increases as SNR becomes low. However, the threshold cannot be further lower since measured SOR error increases due to false detection as shown in Fig. 2.

III. Principle of CDF based SOR measurement method using least square estimation of Gaussian noise period

A. Principle of the proposed SOR measurement method

As described in Chapter 2, SOR error of the threshold based method increases in low SNR conditions. In order to solve this problem, this paper proposes a CDF based SOR measurement method using least square estimation of Gaussian noise period.

Fig. 6 shows principle of the proposed SOR measurement method, where CDF of noise is $P_N(x)$ and that of received signal is $P_R(x)$. R is SOR to be measured from the received signals. We assume CDF of noise, $P_N(x)$ can be measured in advance and is not changed during SOR measurement, where x_1 is the minimum value, x_2 is the maximum value of the measured noise power, and 0dB is the mean value of the noise. If an appropriate range between x_{min} and x_{max} is chosen, we can assume that $P_R(x)$ is almost equal to $(1\text{-}R)P_N(x)$ since probability that signal plus noise is less than x_{max} will be sufficiently small when x_{max} is sufficiently low. With this assumption, the received signal is Gaussian noise and its CDF is $P_N(x)$ with probability of (1-R). Therefore, we can estimate R, i.e. spectrum occupancy rate which gives minimum error between $P_R(x)$ and $(1\text{-}R)P_N(x)$ within the range between x_{min} and x_{max}. As the least square error method is often used for evaluating the error, we define the square error, P_{SE} of $P_R(x)$ and $(1\text{-}R)P_N(x)$ as shown below:

$$P_{SE} = \frac{\int_{x_{min}}^{x_{max}} \{P_R(x) - (1-R)P_N(x)\}^2 dx}{x_{max} - x_{min}} \quad (4)$$

B. Optimization of estimation range, x_{min} and x_{max}

As P_{SE} is a function of x_{min} and x_{max}, it is necessary to determine, x_{min} and x_{max}. Supposing input signal is Gaussian noise only, x_1 is minimum and x_2 is maximum of measured noise power, we can assume $x_1 \le x_{min} < x_{max} \le x_2$. We optimize estimation range of x_{min} and x_{max}, which minimizes SOR error by computer simulations.

It is reasonable to set $x_{min}=x_1$ to increase number of samples for SOR estimation since larger number of samples becomes available. On the other hand, x_{max} should be as large as possible but it should not include probability of signal plus noise less than x_{max}. We introduce a parameter of noise period estimation factor, β for the proposed SOR measurement method. By using the parameter, β, x_{max} is given by

$$x_{max} = x_1 + \beta(x_2 - x_1), \quad (5)$$

where $0<\beta<1$. In a discrete system, P_{SE} is given by

$$P_{SE} = \frac{\sum_{i=N_{min}}^{N_{max}} \{P_R(x_i) - (1-R)P_N(x_i)\}^2}{N}, \quad (6)$$

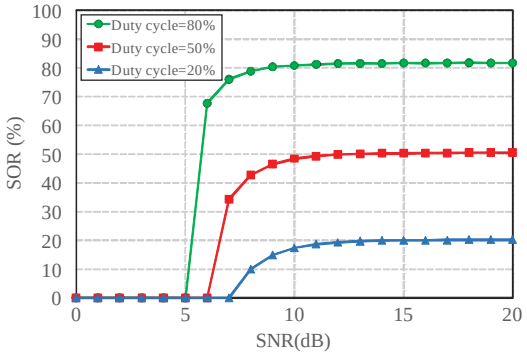

Fig.5. SOR error according to threshold.

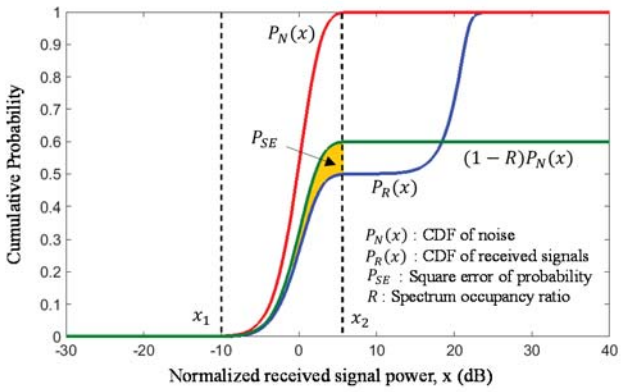

Fig. 6. Principle of the proposed SOR measurement method using least square estimation of Gaussian noise period.

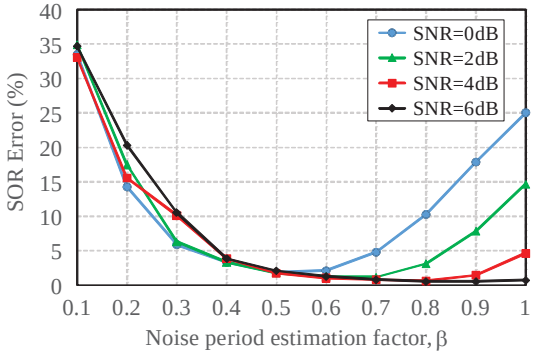

Fig. 7. SOR error as a function of noise period estimation factor, β.

where N_{min} corresponds to x_{min}, N_{max} corresponds to x_{max}, and N is total number of measured samples. Computer search has been conducted to determine β for SNR=0 to 6dB when duty cycle=50%. SOR error is evaluated for various β and SNR with the condition that P_{SE} is minimized.

Fig. 7 shows simulation results of SOR error as a function of noise period estimation factor, β. As shown here, optimal β for minimum SOR error becomes lower and SOR error increases gradually as SNR becomes lower. The results indicate that optimal β is changed according to SNR. Fig. 7 shows that β is as large as 0.9 to 1 and SOR error is be less than 1% when SNR=6dB. However, when SNR=0dB, optimal β is 0.5 to 0.6 and SOR error is 2 to 2.5%. As β=0.6 gives smaller SOR error than β=0.5 for SNR higher than 2dB, and SOR error difference is small between β=0.5 and β=0.6, β=0.6 is chosen as an optimal β in this paper. When β=0.6, almost half of Gaussian noise CDF is used for SOR estimation.

IV. Performance Evaluation of the Proposed SOR Measurement Method

A. Parameters related to SOR measurement performance

As expected from the principle of the proposed CDF based SOR measurement method, SOR measurement accuracy depends on various parameters such as bandwidth of frequency bin, windowing period, number of total measured samples, SNR of received signals, duty cycle, packet length and so on. Note that windowing period is closely related to bandwidth of frequency bin. Larger windowing period results in higher resolution in frequency domain but lower resolution in time domain. If bandwidth of frequency bin becomes smaller, detection of short packet becomes difficult. Therefore, the bandwidth of frequency bin, i.e. frequency resolution and time resolution is a trade-off issue.

Parameters shown in Table 1 are used for SOR measurement performance evaluation, and windowing period and bandwidth of frequency bin are fixed in the simulations. Then, SOR measurement performance according to packet length, SNR and total number of received samples is evaluated when duty cycle=80%, 50% and 20%.

OFDM signal is based on IEEE802.11n standard, and duty cycle of packet signal is given by $T_O/(T_O+T_U)$ as shown in Fig. 4. It should be noted that time resolution error is given by $2T_W/(T_O+T_U)$, because if a part of received packet signal is covered by windowing period, T_W, at either the head of packet or the tail of packet, or both of them, the period of $2T_W$ is regarded as occupied time when SNR is infinite. Therefore, measured SOR is given by $(T_O+2T_W)/(T_O+T_U)$ in the worst case. Note that packet length, T_O is fixed and T_U is changed according to the duty cycle of 80%, 50% and 20% in the simulation.

B. Impact of SNR

As the proposed method does not use the threshold, SOR measurement accuracy in low SNR conditions is expected to be improved. SOR measurement performance of the proposed method according to SNR is evaluated by computer simulations to confirm the validity of the proposed method and is compared

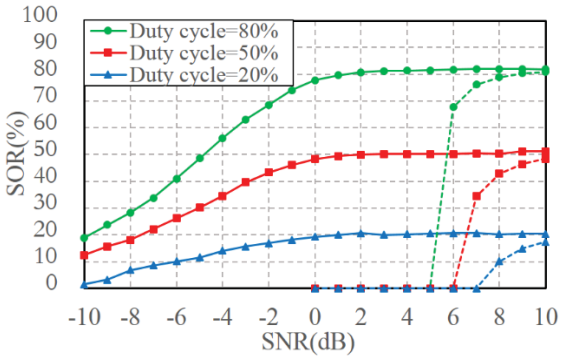

Fig.8. Simulated results of measured SOR according to SNR for duty cycle of 80%, 50% and 20% of proposed method and conventional threshold based method.

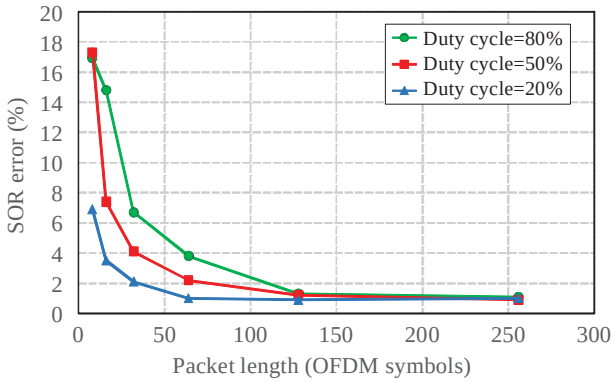

Fig.9. Simulated results of measured SOR according to packet length in OFDM symbols for duty cycle of 80%, 50% and 20% when SNR=5dB.

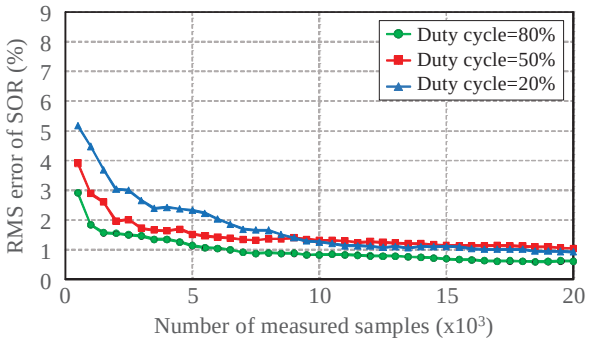

(1) SNR=5dB

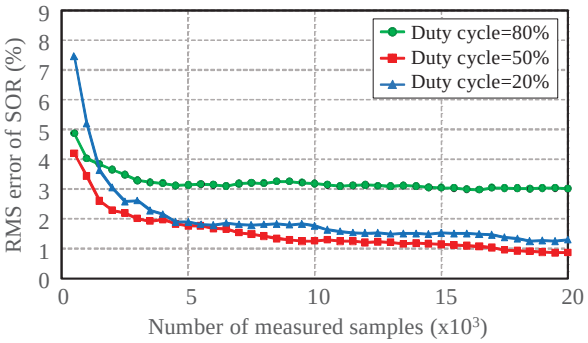

(2) SNR=0dB

Fig.10. Simulated results of measured SOR according to number of measured samples for duty cycle of 80%, 50% and 20% when SNR=5dB and 0dB.

with that of the conventional threshold based method.

Fig. 8 shows simulation results of measured SOR according to SNR when duty cycle is 80%, 50% and 20%. Measured SOR of the proposed method is compared with that of the conventional method. Packet length is 256 OFDM symbols with 10500 samples, and SNR is -10dB to +10dB. As shown here, measured SOR of the conventional threshold method becomes zero when SNR=10 dB and duty cycle=20%. On the other hand, measured SOR is almost the same as actual duty cycle of 80%, 50% and 20% and SOR error is less than 1% when SNR=2dB or higher. Furthermore, the proposed method can measure SOR even if SNR is lower than 0dB though SOR error increases. This is significant improvement compared with the conventional threshold based method.

C. Impact of packet length

Packet length is also an important parameter to affect SOR measurement accuracy because of time resolution error given by $2T_W/(T_O+T_U)$ as described earlier, where T_W is windowing period, T_O is packet length and T_U is idle time period between packets. This equation indicates that SOR measurement error increases as packet length becomes shorter. SOR measurement error for packet length of 8, 16, 32, 64, 128 and 256 OFDM symbols is evaluated by computer simulations, where duty cycle is 80%, 50% and 20%, SNR is 5dB and number of measured samples is 10500. Simulation results of SOR measurement error as a function of packet length are shown in Fig. 9. As expected from theoretical time resolution error given by $2T_W/(T_O+T_U)$, the decrease of T_O results in increase of SOR error. In addition, as duty cycle increases, SOR error increases. As T_O is constant and T_U is changed to set the duty cycle, smaller duty cycle is given by shorter T_U, which causes the increase of SOR error. SOR error less than 2% can be achieved if packet length is longer than 128 OFDM symbols.

D. Impact of number of measured samples

As the proposed method uses CDF to estimate SOR, it needs sufficient number of measured samples, especially when duty cycle is large. This means that SOR measurement error is expected to decrease as number of measured samples increases. Computer simulations have been conducted to evaluate SOR error according to the number of measured samples, where packet length is 256 OFDM symbols and duty cycle is 80%, 50% and 20%.

Fig. 10 shows simulation results of SOR error according to the number of measured samples in the case of (1) SNR=5dB and (2) SNR=0dB. As expected, SOR error decreases as the number of measured samples increases. When SNR=5dB, SOR error is 2% or less when the number of measured samples is about $5X10^3$ for duty cycle of 80% and 50%. The number of measured samples needs to be slightly larger than $5X10^3$ to achieve SOR error less than 2% for duty cycle of 20%. However, we can conclude no significant SOR measurement error is observed as far as the number of measured samples is larger than $5X10^3$ when SNR=5dB. On the other hand, in the case of SNR=0dB, SOR error of about 2% can be achieved when the number of measured samples is about $5X10^3$ for duty cycle of 50% and 20%. However, SOR error does not decrease less than 3% by increasing the number of measured samples when duty cycle=80%. This SOR error floor seems to be caused by small number of samples for P_{SE} estimation to obtain R. When duty cycle is 80% and β=0.6, only 12% of all measured samples is used for P_{SE} estimation and relatively large number of measured samples less than x_{max} during the packet signal period are counted as noise when SNR is 0dB.

V. Conclusion

This paper proposed a novel CDF based SOR measurement method using least square estimation of Gaussian noise period, to improve SOR measurement performance in low SNR conditions. The proposed method estimates SOR, R which minimizes the square error between Gaussian noise CDF and noise part of the received signal CDF. Computer simulation results have confirmed that the proposed method can improve SOR measurement performance and achieve SOR error less than 2% when SNR is up to 2dB, by optimizing the estimation range, β. Furthermore, impact of SNR, packet length and number of measured samples on SOR measurement performance has been evaluated by computer simulations and simulation results have revealed how much SOR error is resulted by SNR, packet length and number of measured samples.

The remained work is to confirm the validity of the proposed SOR measurement method by experiments. Furthermore, SOR measurement performance of the proposed method needs to be evaluated in fading environments and it needs to be further improved in lower SNR conditions.

Acknowledgement

The authors would like to thank Mr. Yilin Yao for his contributions in early stage of this work. A part of this work is supported by the Ministry of Education, Science, Sports and Culture, Grant-in-Aid for Scientific Research (C), 25420354.

References

[1] US Federal Communications Commission Spectrum Policy Task Force, Report of the Spectrum Efficiency Working Group, Nov. 2002, www.fcc.gov/sptf/files/SEWGFinalReport_1.pdf.

[2] M. Mishra, A. Sahai, "How much white space is there?," EECS Department, University of California, Berkeley, Tech. Rep. UCB/EECS-2009-3, 2009.

[3] Michael Fitch, Maziar Nekovee, Santosh Kawade, Keith Briggs, and Richard MacKenzie, "Wireless Service Provision in TV White Space with Cognitive Radio Technology: A Telecom Operator's Perspective and Experience," IEEE Communications Magazine, March 2011, pp.64-73.

[4] M. Lopez-Benitez, F. Casadevall, "Methodological Aspects of Spectrum Occupancy Evaluation in the Context of Cognitive Radio", European Wireless Conference 2009, 17-20 May 2009 pp.199-204.

[5] J.J. Lehtomaki, R.Vuohtoniemi, K.Umebayashi, MEBAYASHI J. Makela, "Energy Detection Based Estimation of Channel Occupancy Rate with Adaptive Noise Estimation," IEICE Trans. on Commun., Vol.E95-B, No.4, April 2012, pp.1076-1084.

[6] J.J. Lehtomäki, M. López-Benítez, K.Umebayashi and M. Juntti, "Improved Channel Occupancy Rate Estimation," IEEE Trans. on Commun., Vol.63, No.3, March 2015, pp.643-654.

THE 18TH INTERNATIONAL SYMPOSIUM ON WIRELESS PERSONAL MULTIMEDIA COMMUNICATIONS
(WPMC-2015)
December 13-16, 2015, Hyderabad, India

A Revolutionary Rural Agricultural Participatory Sensing Approach Using Delay Tolerant Networks

Prateek Gupta, Bhushan Jagyasi, Bighnaraj Panigrahi, Hemant Kumar Rath, Srinivasu Pappula, Anantha Simha

TCS Research India,
Email:{prateek.gupta5, bhushan.jagyasi, bighnaraj.panigrahi, hemant.rath, srinivasu.p, anantha.simha}@tcs.com

***Abstract*—To provide sustainable digital agro-advisory services to farmers, seamless flow of information from the farmers to the experts/expert systems, and vice versa is required. The query generated by the farmers, which may contain multimedia data regarding disease or pest attack in the crops is required to be transmitted to the experts for analysis. Further, after analyzing the query, an alert or advice from the expert system is required to be communicated back to the farmers within a tolerable delay. However in a country like India, network connectivity is extremely poor in several agricultural regions which makes the end-to-end connectivity between the farmers and the expert system intermittent. Therefore, providing agro-advisory services to farmers in a reasonable time becomes a challenge. In this paper, we propose a Delay Tolerant Network (DTN) based relay application model which enables agro-advisory services to farmers located in *No-network* or *Poor-network* zones. In the proposed model, end-to-end communication has been enabled with the help of Device to Device (D2D) communication and by introducing mobile relay nodes which can carry the queries (responses), from (to) the poor or no network zones to (from) the zones where communication is possible. Implementation of this model has been presented for the tea farmers of West Bengal and Assam, which can be extended for other applications in future.**

I. Introduction

In India, cellular network connectivity is very poor in several villages. Due to this, it has been observed that rural and tribal folks travel for several kilometers to make a voice call. Data connectivity of 2G/3G is even worse than the voice connectivity. From our extensive involvement in *Digital Farming* initiatives [1], the communication barrier due to the poor cellular network connectivity has been felt in several deployment locations. For instance, in remotely located tea farms and tea estates of Assam, telecommunication network is intermittent and very poor. Further, in the Araku constituency of Andhra Pradesh, which is known for its organic cultivation of coffee, rubber and spices, network is only available in selected pockets. Due to this, farmers of these regions face difficulty to get the relevant advice on their cultivation queries.

In the recent past, we have seen increasing applications of the Human Participatory Sensing in urban scenarios [2]–[4] such as traffic control, disaster information flow, epidemic monitoring, etc. In that direction, we have proposed a Rural Participatory Sensing (*RuralSense*) framework for agricultural applications [5] and have deployed the same for tea crop in West Bengal and Assam. A RuralSense mobile application has been provided to small and marginal tea growers of these areas in order to facilitate them to report various geo-tagged events from their farms. In addition, access to the web-based dashboard has also been provided to the experts to analyze the reported events and to advise back to the farmers. These events serve multiple purposes such as (a) asking queries, (b) digitization of the farm diaries, (c) self certification or tracing of the chemical applications and (d) generating contextual data for developing pest/disease/ yield/ water models for the cultivated crops. Fig. 1 illustrates a model digital farming platform; dotted lines indicate physical communication between the farmers and the expert system either through cellular or any other communication mode. The continuous lines indicate the logical flow of messages between the sensors placed in the farm and the expert system. This framework warrants a good communication network, which is the main focus of this paper. To overcome the limitations of poor network connectivity, we propose a novel Delay Tolerant Network (DTN) approach for agriculture applications. Note that throughout this paper we have used query and event interchangeably.

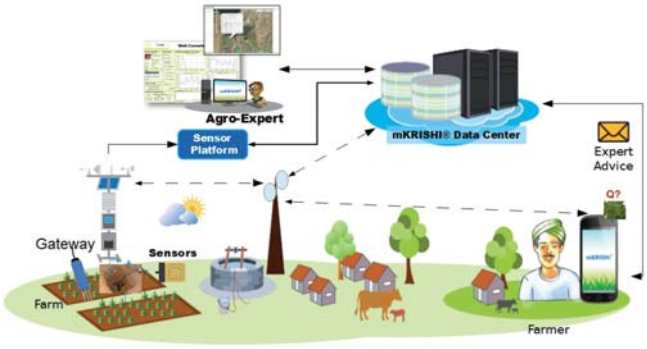

Fig. 1. Digital Farming Platform

Delay Tolerant Networks [6] has gained interest of many researchers in the last decade. It is designed for harsh and challenging conditions where continuous Internet connectivity can not be guaranteed. To compensate data loss due to frequent disconnections, a relay or DTN is required to store data packets for long time periods until connection to a forwarding node is established again. The use of this paradigm becomes critical in challenging scenarios like satellite, military, and rural applications. In countries like India DTN can be used as an alternative to provide seamless end-to-end connectivity.

In this paper, we have introduced a novel DTN-based agro-advisory framework to farmers working in a remote location with limited network connectivity. Using this we have proposed a mobile relay-based architecture which can be deployed in remote villages and provide expert advice to farmers' queries in a time bound manner. We have also provided an Android-based deployment framework to realize this. The rest of the paper is organized as follows. In Section II, we analyze the related work and in Section III, we explain the problem and our approach towards a practical solution. We then discuss the deployment framework in Section IV, and conclude this paper in Section V.

II. Related Works

Participatory Sensing [2], [3] has gained tremendous growth in the recent past and has created various innovative applications using crowd-sensing and crowd-sourcing technologies. In these technologies, huge data from the crowd workers is generated and processed for appropriate actions. We have explored crowd-sensing in our previous work on Rural Participatory Sensing [5] and Distributed Crowd Sourcing [7]. In [5], events are captured and reported with the help of a mobile application while in [7], tasks are assigned to the farmers to diagnose the plant diseases and pest classification. It is believed that for rural applications, crowd assisted sensing is an important source of data generation and the analytics performed on this big data shall serve the society for the years to come.

DTN was initially intended for Inter Planetary Networks (IPNs) [8] with a low network dynamic of satellites and rovers. In the DTN paradigm, communications can be intermittent and hence the nodes need to store the data till connection to a forwarding node is available again. By doing this, data communication can be guaranteed, even though the delay is substantial. In mobile wireless networks, the applications of DTNs have been envisioned for Vehicular Ad-hoc NETworks (VANETs) [9], Under Water Networks (UWNs) [10], Pocket Switched Networks (PSNs) [11], and suburb networks for developing regions [12], etc.

To provide Internet connectivity in rural India a Sustainable Access in Rural India (SARI) program [8], a DTN like framework has been initiated in which Internet kiosks have been distributed in different villages. However, providing and maintaining kiosks in every village is not feasible. Therefore, another project called Computers on Wheels (COW) [13] was started in 2006, in which motorcycles with Internet equipment act as mobile kiosks and travel to remote villages to collect the data from users. In this paper, we explore the feasibility of the DTNs in enabling value added services to the rural farmers in a time bound manner. We use the smartphones/mobiles with the mKRISHI® application instead of kiosks and provide DTN-based end-to-end connectivity to the farmers.

III. Problem Statement and Solution Approach

Time-bound agro-advisory services to farmers located in a remote area with either no or limited network connectivity is the challenge considered in this paper. The key goal of this paper is to remove the communication barriers due to unavailability of cellular networks.

In one of our endeavors on Rural Participatory Sensing (RuralSense) framework, farmers can collect (sense) various farming related information such as disease, pest, nutrient disorder and other activities. mKRISHI® is a Personalized Services Delivery Platform that enables two-way information exchange between farmers and expert systems that include virtual knowledge banks, Agriculture Experts and Procurement Officers (PO), etc. At the farmers' end, it uses participatory sensing (RuralSense) to collect and digitize the field data and mobile-based framework for the data communication. Each event/query generated at the farmers' end may consist of geo-tagged photographs, voice clip, meta-data, etc., and has a unique pair of Event ID (EID) bounded with the User ID (UID) which is assigned from the server. Moreover, it uses an application which can store the captured events/query in the local memory for communication at a later point of time.

At the expert system's end, it uses analytic tools and expert advisory services to evaluate the sensed data obtained from the farmers before communicating actionable advice to the farmers. This enables digitization of the farm and the farming related events. Note that, the availability of this information is extremely critical for decision makers in responding to the farmers' queries, in routing their agriculture inputs to the right location and at the right time. In poor network zones, farmers are however finding it difficult to have a seamless communication of the information. Therefore, a solution is desired which can be deployed in the mKRISHI® [1] framework such that seamless time-bounded communication can be realized. Moreover, the new solution should be easily integratable with the existing mKRISHI® framework. It should also be easy to use for the farmers.

A. Our Solution - a DTN Approach

In this section, we propose a novel solution which can be included in the mKRISHI® framework without much changes at the end points. The aim here is to provide network connectivity to the farmers in an alternative way. To realize this, we propose to use relay-based communication which can operate on the principle of DTN; an opportunistic mode that becomes critical in challenging scenarios like satellite and rural communications in emerging countries like India or Africa, where the lack of an infrastructure makes regular data communications almost impossible. DTN communications are thus the natural choice for a networking paradigm where nodes can be disconnected from the regular network for the majority of the time and exchange of data can take long time. To provide DTN-based solution, we propose a new entity into the mKRISHI® framework called *Relay Node*. A relay node can be any other smartphone which can be used by other fellow farmers, farm agents, or field executives, that comes in close proximity to the farmers at the remote locations and has the following capabilities: (i) collect the farmers' sensed data or queries using Device to Device (D2D) services [14], (ii) transmit the collected queries from one or more farmers to

the expert system using available network technologies (Wireless Fidelity - WiFi, cellular or any other) in a time-bound manner, (iii) collect and communicate the acknowledgement (ACK) and advisories from the expert system to the farmers. Fig. 2 illustrates the possible modes where multi-hop relay communication can be introduced to eliminate the network connectivity problem at the farmers' end.

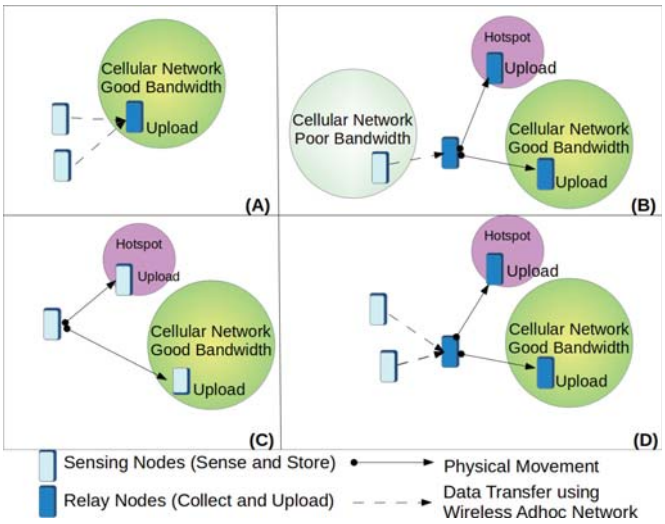

Fig. 2. Problem Cases - Need for DTN: (A) No network farmer zone, Relay with network, (B) Poor network farmer zone, Relay movement to a network zone, (C) No network farmer zone, farmer movement to a network zone, (D) No network farmer zone, Relay movement to a network zone

B. Building Blocks of our Solution

Various modules related to our architecture and the communication possibilities are explained through Fig. 3. Basic building blocks of our solution are as follows:

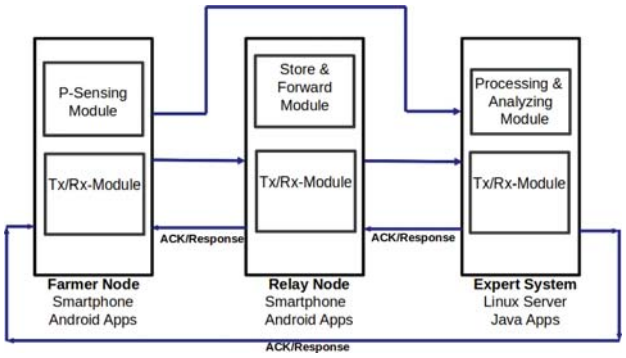

Fig. 3. Building Blocks - DTN-based Architecture

Farmer Node: In the present setup of the mKRISHI® framework, farmer node is an Android Application (App) targeted for users with Android devices having OS version not less than 3.0 and basic configurations like camera, Global Positioning System (GPS) and WiFi. The application empowers the users of remote locations to send ground scenarios in the form of 'events' that fundamentally consists of an image of the situation or surrounding, predefined textual labels and/or a voice clip. In cases where a particular farmer has a basic mobile phone instead of smartphone, he can still use any other farmer's smartphone with his own authentication to upload his queries. In this case, two different identities are assigned to the farmer - (i) physical identity, i.e., his own phone number, and (ii) logical identity, which is the phone number of the smartphone he/she uses for log-in. These events are required to be uploaded to the server over the Internet so that users can receive advices or suggestions. The application allows users to store these events, for later submission, in case of poor or no network connectivity. While uploading, the system follows DTN approach to relay the data to an agent or relay node.

Relay Node: It employs the aforementioned farmer node Android App with an additional privilege of aggregating queries from farmer nodes which are incapable of uploading events. The relay node is required to press a button in the application to create a WiFi Protected Access 2 (WPA2) secured WiFi Hotspot in the region. A limited set of farmer nodes (based on device hardware), simultaneously, could connect to the relay node and send their events to it. The relay node would then upload all the events to the server either through moving physically to a cellular network zone or connecting to the Internet through other means. The relay node can also carry the acknowledgements and the responses meant for the users provided by the expert system.

Server or Expert System: It is is a Linux powered, 16 core Xeon processor rack with 32GB RAM, hosted in a virtualized environment and capable of handling huge loads by applying standard techniques of distributed computing. It hosts the mKRISHI® server application which handles the 'events' coming from remote locations. The application is designed to maintain data integrity and has the capacity to send instant acknowledgements to the farmer nodes.

Communication between the Farmer node and the Relay node is realized through low powered ad-hoc D2D communication [14], such as WiFi Direct, WiFi Hotspot and Bluetooth, etc. It uses the licence free spectrum (ISM band) and self-initiated discovery and signalling techniques for the D2D communication initialization. At present, it uses a very low power (fixed) for the D2D communication; transmission power can be further reduced using sophisticated signalling techniques.

IV. Deployment and Evaluation

To evaluate our proposed architecture, we have extended the mKRISHI® framework with DTN functionalities. The system model is implemented to work seamlessly under all communication scenarios. The details of our implementation framework is explained as follows:

A. Scanning of Access Networks

This module is implemented in the farmer node as well as in the relay node using Android App. Once the event is sensed, the farmer node creates a message (query) and scans for an access network to communicate the same to the central expert system. The communication can be direct through the cellular network or indirect through the mobile relay node.

B. Communication Modes

Based on the availability of access networks we have implemented two modes for access network selection and communication. Mode-1 belongs to direct communication whereas Mode-2 is Relay-based communication. In this paper we focus on Mode-2 communication only.

- *Mode-1(a) - Direct:* When the Cellular or any other connectivity is available at the farmers' end, it can directly transmit the query to the central expert system.
- *Mode-1(b) Direct Periodic (P-Direct):* Under this mode, the application at the farmers' end periodically scans the signal strength of the cellular network. Upon getting good connectivity, it can transmit the query through the available cellular network. This can be applicable in scenarios where the connectivity varies between good and bad within time periods in minutes.
- *Mode-2 Periodic DTN:* This is the scenarios where the connectivity varies within time periods of hours. In such situations, if the channel is bad then most likely it will remain same for a long time. Therefore, for such situations a relay agent with a DTN enabled relaying application module will visit the farmer place and collect farmers' queries to its own device and then relay the collected queries to the server. The relay node can also collect the ACK/responses for the queries from the server and deliver to the farmer nodes through this communication mode. In this mode, the query won't be deleted from the farmer node till an ACK/response is received from the server. In case of no ACK/response received from either the server (directly) or through the relay node within a pre-defined time frame, the farmer node will restart the access scanning process for re-transmission.

C. Relay Node Communication

For query collection from the farmer nodes, the relay node creates a WPA2 secured WiFi Hotspot in the region. Farmer nodes can register with this WiFi Hotspot and send their queries to the relay node. Once registered, the farmer's authentication details are saved in the relay node and need not to register again with the same relay node. In this way, secure D2D communication is realized between the farmer and the relay node. The relay node would then transmit all the queries to the server using its own network or by physically moving to a available network zone. Multi-hop relaying is also possible but currently out of the scope of this paper. Similar to the forward direction flow of queries, the relay node can also collect the ACK/responses for the queries from the server and deliver to the farmer nodes within a permissible time bound.

D. Reverse flow of ACK/Response

The ACK/response can be sent directly to the farmers using Short Message Services (SMS) or Hyper Text Transfer Protocol (HTTP) based messaging. In case of non-availability of network ACK/response can also be sent through designated relay nodes. In case of the query came from a farmer who has two identifications as physical and logical, the ACK/Responses will be routed to the logical identity only and it is the job of the farmer to logging into the smartphone and retrieve its message. The forward and reverse flow of message between the farmer node and the server can also happen using different relay nodes. To enable this multiple relay node options, the server maintains a map of relay nodes and their registered farmer nodes. Note that, Responses are required to be received by the farmer within a specified time period (T_r) starting from the query generation time (24-hour in this paper). Else, the farmer node discards the query; new queries can be generated again. Similar to the Responses, the ACKs are also to be received by the farmer node within a smaller time period T_d ($T_d << T_r$). It is generally assumed that relay node can go online fairly quickly ($< T_d$) since it is mobile. To take care of the situation that the relay node due to some exigency is unable to connect to the server within this time period, we are having a timeout and a re-transmission to a possibly different relay node to ensure reliable message delivery to the server.

We now explain the control flow of all the events required for the end-to-end communication between the farmer node and the server. Fig. 4 illustrates the different phases and modes of the communications. Under Mode-1 communication queries can be sent directly to the server node and ACKs/Responses can be delivered to the farmer node directly. Upon receiving the ACK the query associated with the event is deleted from the farmer node. In Mode-2, two cases are possible. In the first case, i.e., when the relay node is on-line, both the query as well as the ACK/Response can be received before the expiry of the desired time; event can be deleted after the ACK is received at the Farmer node. Note that, the ACKs/responses can also be received directly using SMS. In the second possible case, i.e., when the relay node is off-line, even after collecting the queries, the relay node may not be able to transmit the queries to the server immediately due to network issues. In this case, the relay node needs to physically move to a network zone to transmit the queries. This can lead to delay in receiving the ACK/response. Hence timeout can occur at the farmer node resulting in retransmission of the queries (and possible deletion of the query). Note that, retransmission of the farmer queries can be made through another relay node; multiple retransmission attempts can be made till the Response timeout.

E. Proposed DTN-based Server Application

As discussed before, Android Apps are being designed for the farmer and relay nodes. Appropriate Java-based applications are also designed at the server end. These applications provide necessary platforms to visualize the queries, analyze them and communicate back responses or general information (advices/alerts) to the selected farmers (unicast or multicast). An SMS Gateway has been interfaced with the server in order facilitate the communication of ACKs, alerts, or responses in the form of the SMSs.

Fig. 5 shows the screen-shots of the Android Apps designed and implemented on the Farmer and the Relay nodes. These are simple and easy to use applications, which can be used by the farmers without much difficulty. Local language support is

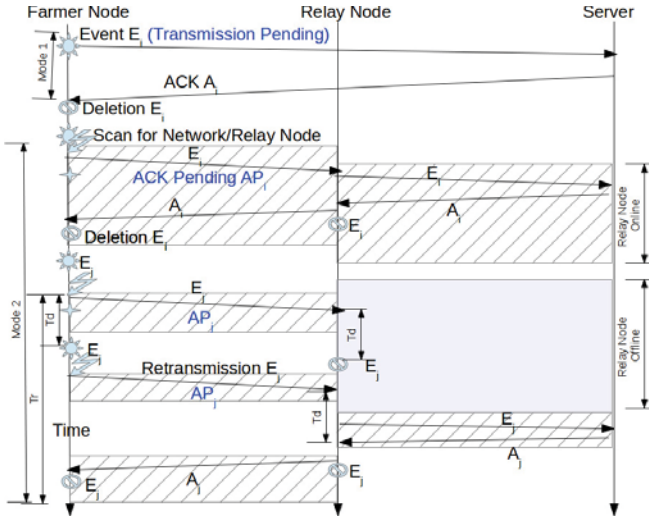

Fig. 4. Timing Diagram - DTN-based Solution

also being provided in the Apps, such that they can be adapted easily. Appropriate care has been taken by keeping security and privacy settings of smartphones intact while installing these Apps.

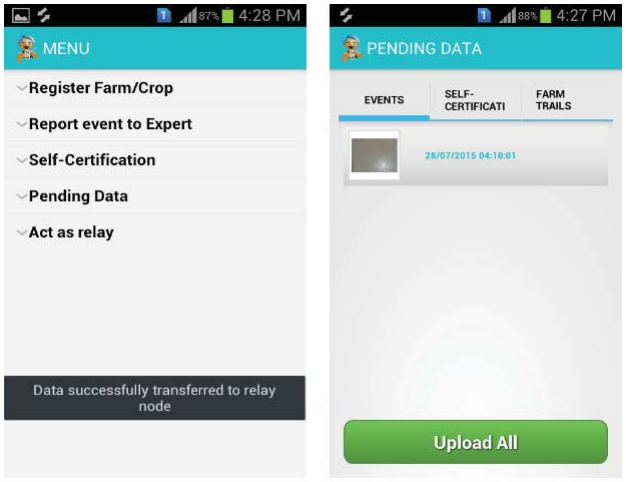

A: Android App Menus B:Data Tx. Status

Fig. 5. Android-based Deployment

F. Practical Deployment

At present laboratory prototypes are tested for (i) end-to-end data communication, (ii) ACK delivery through SMSs and through data communications, (iii) event creation, deletion, transmission and re-transmission, (iv) effect of D2D communication on interference and it's impact on throughput, (v) scalability test for the maximum number of Farmer nodes one Relay node can support, (vi) privacy and security threats which can result out of the relay-based communication, etc. Post laboratory tests, practical deployment will be considered in the Tea gardens of Assam followed by other areas in the North-East, Andhra Pradesh and Maharashtra.

V. Conclusions

In this paper, we have observed the need of a delay tolerant framework for the remote farmers with poor network connectivity and have proposed a novel DTN-based architecture for end-to-end communication. In our model, mobile relay node visits the poor channel farmers, collects their queries and transmits to the server. In future, we plan to work on estimation of the relay node's availability at a certain location. This can help us to trigger other participatory sensing applications and can also be used to initiate the sensing operation just before the relay nodes are expected to arrive in communication range of the farmer nodes. We believe that our proposed model is first of its kind to be implemented which can benefit the farming community to a large extent and can provide Digitization of the Agriculture domain in India.

Acknowledgement

We thank Arun Kumar A. V. and Narendra N. of TCS Research, India for their support in the development work.

References

[1] S. Pappula, "The concept of pride empowering farmers to live with pride," *CSI Communications*, pp. 14–18, November 2013.
[2] J. Burke, D. Estrin, M. Hansen, A. Parker, N. Ramanathan, S. Reddy, and M. B. Srivastava, "Participatory sensing," in *Workshop on World-Sensor-Web (WSW06): Mobile Device Centric Sensor Networks and Applications*, 2006.
[3] B. Thomas, F. Rembold, H. Geoffrey, W. Qihao, and R. Bernd, "Collective sensing: Integrating geospatial technologies to understand urban systems-an overview," *Remote Sensing*, vol. 3, pp. 1743–1776, 2011.
[4] B. Jagyasi, J. Mohite, and S. Pappula, "Applications of mobile sensing technologies in precision agriculture," *CSI Communications*, pp. 22–24, October 2013.
[5] J. Mohite, Y. Karale, P. Gupta, S. Kulkarni, B. Jagyasi, and A. Zape, "Rups: Rural participatory sensing with rewarding mechanisms for crop monitoring," in *PerCom Workshops, IEEE International Conference*, March 2015, pp. 378–383.
[6] K. Fall, "A delay-tolerant network architecture for challenged internets," in *ACM SIGCOMM*, August 2003.
[7] P. Singh, B. Jagyasi, N. Rai, and S. Gharge, "Decision tree based mobile crowdsourcing for agriculture advisory system," in *the 11th IEEE India Conference INDICON 2014*, Dec 2014.
[8] I. F. Akyildiz, Ö. B. Akan, C. Chen, J. Fang, and W. Su, "Interplanetary internet: state-of-the-art and research challenges," *Computer Networks*, vol. 43, no. 2, pp. 75–112, 2003.
[9] P. R. Pereira, A. Casaca, J. J. Rodrigues, V. N. Soares, J. Triay, and C. Cervelló-Pastor, "From delay-tolerant networks to vehicular delay-tolerant networks," *Communications Surveys & Tutorials, IEEE*, vol. 14, no. 4, pp. 1166–1182, 2012.
[10] T. Small and Z. J. Haas, "The shared wireless infostation model: a new ad hoc networking paradigm (or where there is a whale, there is a way," in *the 4th ACM international symposium on Mobile ad hoc networking & computing*, 2003.
[11] P. Hui, A. Chaintreau, J. Scott, R. Gass, J. Crowcroft, and C. Diot, "Pocket switched networks and human mobility in conference environments," in *the ACM SIGCOMM Workshop on Delay-tolerant networking*, 2005.
[12] A. S. Pentland, R. Fletcher, and A. Hasson, "Daknet: Rethinking connectivity in developing nations," *Computer*, vol. 37, no. 1, pp. 78–83, 2004.
[13] C. Conroy, "Telecentre initiatives in rural india: Failed fad or the way forward?" *Natural Resources Institute, University of Greenwich*, 2006.
[14] B. Panigrahi, H. K. Rath, and A. Simha, "Interference-aware Discovery and Optimal Uplink Scheduling for D2D Communication in LTE Networks," in *IEEE National Conference on Communication (NCC)*, 2015.

THE 18TH INTERNATIONAL SYMPOSIUM ON WIRELESS PERSONAL MULTIMEDIA COMMUNICATIONS
(WPMC-2015)
December 13-16, 2015, Hyderabad, India

Performance Analysis of Total Power Consumption in Linear Multi-hop Networks*

Satoshi Yamazaki
Department of Control & Computer Engineering
Numazu National College of Technology
3600 Ooka Numazu, Shizuoka, 410-8501 Japan
s-yamazaki@numazu-ct.ac.jp

Kouji Ohuchi
Department of Electrical and Electronic Engineering
Faculty of Engineering, Shizuoka University
Johoku 3-5-1, Hamamatsu, Shizuoka, 432-8011, Japan

***Abstract*— Lately, multi-hop networks which transmit data packets through some relay nodes have received much attention. We focused on the fact that the total power consumption of the whole network in multi-hop communications consists of the transmitted power and the consumed power. Our goal is to theoretically show the effectiveness of multi-hop communications in terms of total power consumption. First, we theoretically derived a closed form expression for the total power consumption in certain linear multi-hop networks. Next, we showed the validity of the derived expression using theoretical analyses and computer simulations. Moreover, we considered the predominance of multi-hop communications compared to direct communication, by theoretically examining the maximum and optimum number of hops and showing numerical examples.**

Keywords*— *Multi-hop Communications; Transmitted Power; Energy Consumption; Total Consumed Power; Theoretical Expression

I. INTRODUCTION

Recently, multi-hop networks without a fixed infrastructure, which transmit the data packets through some relay nodes, have received much attention [1],[2]. The merits of multi-hop networks are that the total transmission power decreases and the space use efficiency of radio resources improves. On the other hand, a demerit of multi-hop communications is that the end-to-end delay due to overhead by relaying is large, so time use efficiency falls. So far, theoretical approaches for linear multi-hop networks have been studied [3]-[9]. In [3], [4], maximum throughput analyses for IEEE802.11 DCF protocol multi-hop networks are shown. In [5]-[6], analyses of the optimum number of hops under various conditions are shown. In [5], analyses using coded TDMA multi-hop transmission are shown. In [6], analyses using Hybrid Automatic Repeat reQuest (HARQ) protocols in a quasi-static fading environment are shown. Also, focusing on the power consumption of relay nodes in a sensor network, the impact of some physical layer parameters on power consumption in relay nodes [8] and modeling of the relationship between the transmitted power and power consumption in relay nodes [9] are shown.

On the other hand, our research goal is as follows. A multi-hop network transmits data packets through some relay nodes. In the case of equidistant transmission, it can achieve lower transmission power than a single-hop network, because the transmission power decreases in inverse proportion to the square (or more) of the distance. It is generally known that the transmission power decreases as the number of relay nodes increases. On the other hand, the relay nodes also have their own power consumption that does not contribute to transmission. Therefore, the total power consumption, which is the transmission power of the relay nodes and their own power consumption, can be more than that of direct communications for some numbers of relay nodes and values of power consumption. So, we focus on the fact that the total power of the whole network consists of the transmitted power and the consumed power. Our goal is to theoretically show the effectiveness of multi-hop communications in terms of power consumption. In this paper, we theoretically derive a closed form expression for the total power consumption in linear multi-hop networks. Next, we show the validity of the derived expression using theoretical analyses and computer simulations and consider the predominance of multi-hop communications compared to direct (single-hop) communication. Moreover, we consider the maximum number of hops and optimal number of hops theoretically and show numerical values in areas which multi-hop communications are more predominant than direct communication. The rest of our paper is organized as follows. In section 2, we derive a closed form expression for the total power of the whole network. In section 3, we evaluate the derived theoretical performance using computer simulations. Finally, we present our conclusions in section 4.

* This work was supported by JSPS KAKENHI, Grant-in-Aid for Scientific Research (C) 15K00164.

II. CLOSED FORM EXPRESSION FOR LINEAR MULTI-HOP NETWORKS

A. Analysis Model and Assumed Conditions

Though wireless radio environment performance depends on a combination of the three phenomena: path loss, shadowing, and multi-path fading, we consider only path loss and shadowing for ease of analysis in this paper. We consider a multi-hop network whose n relay nodes are stationary and placed at equal intervals on a straight line between the transmitter and the receiver as shown in figure 1(a). Therefore, when the number of relay terminals is zero, it corresponds to direct communication (single-hop). As shown in figure 1(b), the data from the transmitter are transferred to the receiver via relay nodes. We assume the following two conditions in our analysis.

1. The path loss coefficient γ, the shadowing deviation σ and frequency band are equal among all relay nodes.
2. There is no delay in the relay nodes.

B. Derivation

The template is used to format your paper and style the text. All margins, column widths, line spaces, and text fonts are prescribed; please do not alter them. You may note peculiarities. For example, the head margin in this template measures proportionately more than is customary. This measurement and others are deliberate, using specifications that anticipate your paper as one part of the entire proceedings, and not as an independent document. Please do not revise any of the current designations.

(1) The transmitted power P_t

(A) Direct (Single-hop) communication

First, we derive the transmitted power for direct communication [10]. As the electromagnetic field strength monotonically decreases with the distance from the transmission point, the received power at a distance d, $P_r(d)$ can be expressed by (1) using the transmitted power P_t.

$$P_r(d) = P_t K\left(\frac{d_0}{d}\right)^{\gamma} \cdot \quad \text{..... (1)}$$

Here, γ is the path loss coefficient, d_0 is the reference distance and K is propagation loss at the distance d_0. The outage probability, $P_{out}(P_{r_min}, d)$, is the probability that $P_r(d)$, which is expressed by expression (1), is smaller than a threshold value, P_{r_min}. It is expressed by (2).

$$P_{out} = P(P_r(d) \le P_{r_\min}) \cdot \quad \text{..... (2)}$$

However, the value of P_{r_min} depends on the transmission environment and system. It can be expressed by (3) in both path loss and shadowing environments.

$$P_{out} = 1 - Q\left\{\frac{P_{r_\min} - P_r(d)}{\sigma}\right\} \cdot \quad \text{..... (3)}$$

Here, σ is the shadowing deviation. Also, the Q-function, $Q(z)$ is the probability of a Gaussian distributed random variable, X with a mean of 0 and a variance of 1. When X is larger than z, it is expressed by (4).

$$Q(z) = \int_z^{\infty} \frac{1}{\sqrt{2\pi}} \exp\left(-\frac{y^2}{2}\right) dy \quad \text{..... (4)}$$

Therefore, when inv_Q(z) is the inverse function of the Q-function, Q(z), the transmission power Pt which is necessary to send data to the terminal at the point at a distance d is expressed by (5).

$$P_t = P_{r_\min} K^{-1}\left(\frac{d}{d_0}\right)^{\gamma} 10^{-\left\{\frac{\sigma \times \text{inv_Q}(1 - P_{out})}{10}\right\}} \equiv P_{t_d}(d) \quad \text{... (5)}$$

(B) Multi-hop communications

As the number of times a signal is relayed from the transmitter node S to the receiver node D is n+1, the distance of one-hop, d_{hop} is expressed by (6).

$$d_{hop} = \frac{d}{n+1} \cdot \quad \text{..... (6)}$$

When the outage probability from the (k-1)-th node to the k-th node is $P_{out(k)}$ when k is larger than zero, P_{out_end} is the outage probability from the transmitter node S to the receiver node D. It is expressed by (7).

$$1 - P_{out_end} = \prod_{k=1}^{n+1}\left(1 - P_{out(k)}\right) \cdot \quad \text{..... (7)}$$

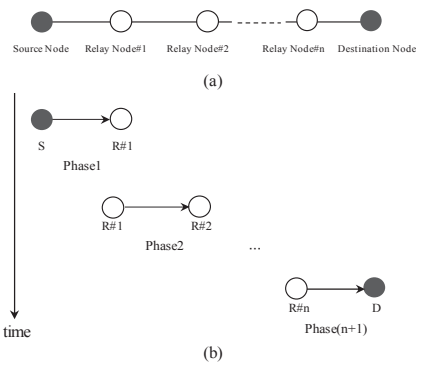

Figure 1 Linear Multi-hop Networks.

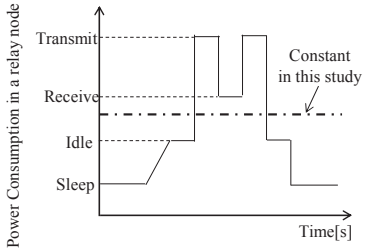

Figure 2 Power Consumption in a relay node, P_{node} [12].

If the value of the outage probability in each hops is equal, that is, $P_{out(1)}=\ldots=P_{out(n+1)}=P_{out_hop}$, (7) can be rewritten as (8).

$$1 - P_{out_end} = \left(1 - P_{out_hop}\right)^{n+1} \quad \text{..... (8)}$$

We can get (9) from (8).

$$P_{out_hop} = 1 - \sqrt[n+1]{1 - P_{out_end}} \cdot \quad \text{..... (9)}$$

By replacing P_{out} in (5) with P_{out_hop} in (9) and replacing d in (5) with d_{hop} in (6), the transmitted power per hop, P_{t_hop} is expressed by (10).

$$P_{t_hop} = P_{r_\min} K^{-1}\left(\frac{d}{(n+1)d_0}\right)^{\gamma} 10^{-\left\{\frac{\sigma \times \text{inv_Q}\left(1 - \sqrt[n+1]{1 - P_{out_end}}\right)}{10}\right\}} \quad \text{.(10)}$$

As the number of times a signal is relayed from the transmitter node S to the receiver node D is n+1, the transmitted power for the whole network, Pt is expressed by (11).

$$P_t = (n+1)P_{t_hop} = (n+1)P_{r_\min} K^{-1}\left(\frac{d}{(n+1)d_0}\right)^{\gamma} 10^{-\left\{\frac{\sigma \times \text{inv_Q}\left(1 - \sqrt[n+1]{1 - P_{out_end}}\right)}{10}\right\}} \equiv P_{t_m}(d, n)$$

.....(11)

Here, we substitute 0 for n in (11), which corresponds to (5) for direct communication. In other words, the following equat on is valid.

$$P_{t_d}(d) = P_{t_m}(d, 0) \cdot \quad \text{..... (12)}$$

Also, when we substitute 0[dB] for σ in (11), it corresponds to the case with only path loss[11].

(2) The power consumption P_{node}

In general, as shown in figure 2, the power consumption in relay nodes is changed temporally corresponding to the statu, such as idle, sleep, transmitted data and received data[12]. In [13], a mathematical analysis of power consumption in data transmission over IEEE802.11-based wireless multi-hop networks is shown. However, in this paper, we assume that

data is continuously transmitted from the source node to destination node with a constant level of power consumption in each relay node for ease of analysis.

(3) The total consumption P_{total}

The total power consumption is expressed by (13) using the transmitted power expressed by (11), the power consumption in a relay node, P_{node} and the number of relay nodes (n).

$$P_{total}(d,n) = i_{re} \cdot \{P_{t_m}(d,n) + n \cdot P_{node}\}, \quad n \geq 0 \cdot \cdots\cdots\cdots (13)$$

Here, when we substitute 0 for n, direct communication is done. When we substitute a number larger than 0 for n, multi-hop communication is done.

C. Discussion

In this section, we examine expression (13). In direct communications, the total power consumption consists of only the transmitted power in the source node S and it is constant regardless of the number of relay nodes. On the other hand, in the total power consumption in multi-hop communications, there is a trade-off between the first and second terms in (13). The former is the reduction in the transmitted power and the latter is the increase in the power consumption in relay nodes. Moreover, the latter depends on the power consumption in a relay node (P_{node}) and the number of relay nodes (n).

(A) Maximum hops h_{max}

In figure 3, we show the total power consumption as a function of hops. As shown in Fig.3, multi-hop communications is more predominant than direct communication in area-A. In area-A, we can see two areas, area-A1 which is more predominant for the first item in (13) and area-A2 which is more predominant for the second item in (13). From the point of view of total power consumption, the conditions which are more predominant for multi-hop communications than for direct communication are expressed by (14).

$$\begin{cases} P_total\ (\mathrm{d},\ \mathrm{h}) < P_total\ (\mathrm{d},\ 0) \\ 1 < h \end{cases} \cdots\cdots\cdots\cdots\cdots (14)$$

From (14), we can get the maximum hops h_{max} shown in figure 3.

(B) Optimum number of hops h_{opt}

In area-A, the number of hops which minimizes the total power consumption, h_{opt} exists. If P_{total} is considered to be continuous, the optimization condition is expressed by (15).

$$\frac{d}{dh}\{P_{total}(d,n)\}\Big|_{h=h_{opt}} = 0 \cdots\cdots\cdots\cdots\cdots\cdots (15)$$

III. Performance Evaluation

We show the validity of the derived expressions (11) and (13) using theoretical analyses and computer simulations. We used NS2 [14] as a network simulator. Moreover, we consider numerical values for expressions (14) and (15). We show our evaluation model in figure 1 and the basic simulation parameters [14] in table 1. We make the following two assumptions in our performance evaluations.

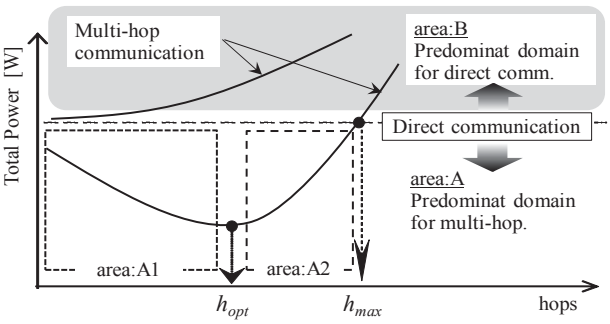

Figure 3 Analysis on total power consumption based on (13).

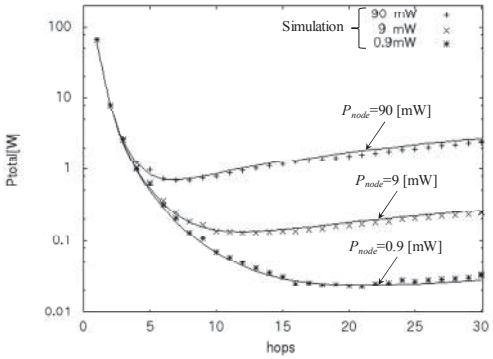

Figure 4 Relationship between number of hops and total power for some values of P_{node}. (Outage prorability P_{out}:3[%])

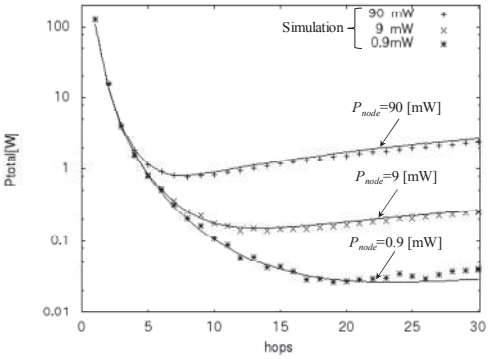

Figure 5 Relationship between number of hops and total power for some values of P_{node}. (Outage prorability P_{out}:1[%])

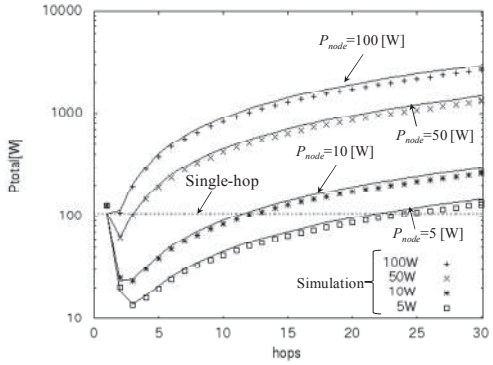

Figure 6 Relationship between number of hops and total power for some values of P_{node}. (Outage prorability P_{out}:1[%])

1. In (13), the average number of transmission times i_{re} is one, in other words, the data is sent without retransmission between relay nodes for simplification.
2. From the purpose of this study as mentioned in chapter 1, we do not consider power consumption in both the source node *S* and the destination node *D*.

A. When the number of the hops is changed and the distance between the transmitter and the receiver is fixed

We evaluate the performance for various values of outage probability, P_{out} and power consumption, P_{node}. In other words, we show the total power consumption as a function of hops. In figure 4, the result when P_{out} = 3% and in figure 5, the result when P_{out} = 1% are shown. From Fig.4 and Fig.5, as the theoretical value and simulation results are almost equal regardless of P_{out} and P_{node}, this shows the validity of the derived expression. However, when P_{node} is 0.9[mW] at P_{out} = 1%, some difference is seen between theoretical values and simulation results after about 25[hops]. In figure 6, the results for P_{node}=5, 10, 50, 100[w] are shown. As was the case for Fig.4 and Fig.5, from Fig.6, as the theoretical value and simulation results are almost equal regardless of P_{out} , P_{node}, this shows the validity of the derived expression. Here, in Fig.6, the performance of direct communication is shown using a short dashed line, and the value is 106[W] from expression (5).

(A) Maximum hops h_{max}

We verify the discussion mentioned in section 2. From Fig.6, in the case of P_{node} =5, 10, 50[W], an area in which multi-hop communications is more predominant than direct communication, area-A in Fig.3, exists. In particular, the maximum number of hops h_{max} mentioned in 2.3.1 are 21 hops (5[W]), 11 hops (10[W]), and 2 hops (50[W]). The reason is as follows. From (13), when the number of nodes *n*, i.e., hops, is larger, the value of the first term in (13) is smaller due to the effect of multi-hop communications. Therefore, if a smaller value of P_{node} is set for a fixed ~~the~~ number of nodes *n*, P_{total} can be kept smaller. As a result, the value of the maximum number of hops h_{max} is larger. On the other hand, if a larger value of P_{node} is set, the opposite can be said. Also, P_{total} is 114[W] at 2 hops when P_{node} is 100[W]. Therefore, we calculate the largest value of P_{node}, which satisfies (14) and show the result in figure 7. In Fig.7, when P_{node} is set to be more than 93[W], direct communication is more predominant than multi-hop communications.

(B) Optimum number of hops h_{opt}

If the area in which multi-hop communication is more predominant than direct communication, area-A in Fig.3, exists, the optimum number of hops h_{opt} mentioned in 2.3.2 exists. In particular, the h_{opt} are 2 hops (P_{node} = 50, 23[W]) and 3 hops (P_{node} = 14[W]). Then, the minimum values of the total

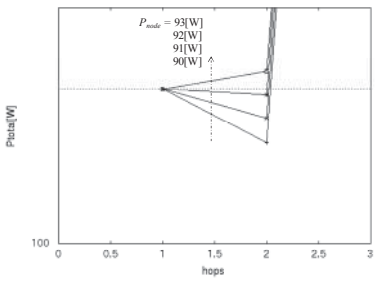

Figure 7 Relationship between number of hops and total power for some values of P_{node}. (Outage prorability P_{out}:1[%])

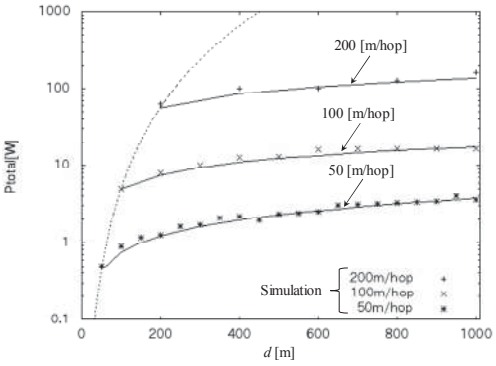

Figure 8 Relationship between distance and total power as a function of the distance per hop. (P_{node}:90[mW], P_{out}:3[%])

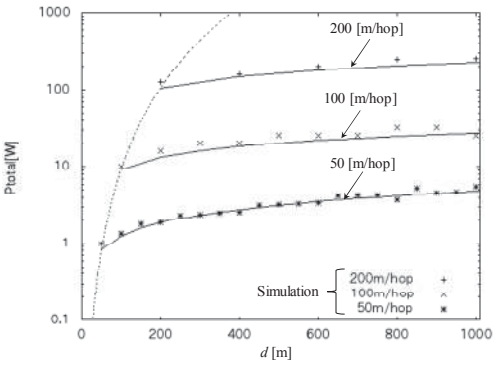

Figure 9 Relationship between distance and total power as a function of the distance per hop. (P_{node}:90[mW], P_{out}:1[%])

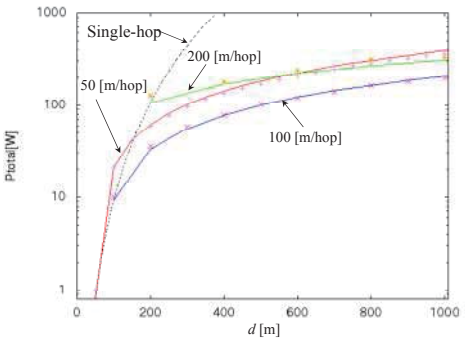

Figure 10 Relation between distance and total power for the distance per a hop. (P_{node}:20[W], P_{out}:1[%])

power consumption are 64[W], 23[W] and 14[W]. This is because if smaller values of n and P_{node} are used, we can get smaller values of P_{total}.

B. *Effect of changing the distance between the transmitter and the receiver with a fixed distance between relay nodes*

First, we evaluate the performance for P_{node}=90[mW]. In figure 8, the result for P_{out} = 3% and in figure 9, the result for P_{out} = 1% are shown. From Fig.8 and Fig.9, as the theoretical value and simulation results are almost equal regardless of P_{node} and d_{hop}, we show the validity of the derived expression. In both Fig.8 and Fig.9, we can see the following two points. Multi-hop communication is more predominant than direct communication regardless of d_{hop}. If the value of d_{hop} is larger, the total power consumption is larger regardless of the communication distance, d. Later, we consider the reasons for these results. Specifically, in Fig.9, the total power consumption P_{total} which is necessary to send data to a point at a distance d=600[m] is 3.5[W](d_{hop}=50[m/hop]), 22[W](d_{hop}=100[m/hop]) and 180[W](d_{hop}=200[m/hop]). Then, at least 11(d_{hop}=50[m/hop]), 5(d_{hop}=100[m/hop]) and 2(d_{hop}=200[m/hop]) relay nodes are needed.

Next, we evaluate the performance for P_{node}=20[W]. In figure 8, the result for P_{out} = 1% is shown. From Fig.10, the theoretical value and simulation results are almost equal regardless of the values of P_{node} and d_{hop}. Here, we can see that d_{hop} which minimizes P_{total} changes depending on the value of d and P_{node}. Specially, in Fig.10, P_{total} decreases in the following order. If d is within 600[m], the order is 100[m/hop], 50[m/hop] and 200[m/hop]. On the other hand, if d is over 600[m], the order is 50[m/hop], 200[m/hop] and 100[m/hop]. We show these reasons including the results of Fig.8 and Fig.9. For example, if the value of d_{hop} is larger for a fixed distance d, the following things can be said. First, the first term in (13), the transmitted power, is larger. Next, the number of relay nodes n is smaller. Therefore, the impact of the second term in (13) is different depending on the value of P_{node}. In Fig.10, the impact of the second term in (13) is larger as the value of P_{node} is larger than in both Fig.8 and Fig.9.

IV. CONCLUSIONS

We focused on the fact that the total power consumption of the whole network in multi-hop communications consists of the transmitted power and the consumed power. In this paper, we theoretically showed the effectiveness of multi-hop communications in terms of power consumption. First, we theoretically derived a closed form expression for the total power consumption in certain linear multi-hop networks. Next, we showed the validity of the derived expression using theoretical analyses and computer simulations. Therefore, to estimate the total power consumption in linear multi-hop communications, we could establish a method that uses a theoretical expression. This enables us to determine the required value immediately since our method does not use time-consuming computer simulations. Moreover, we considered the predominance of multi-hop communications compared to direct communication, in particular maximum hops and optimum hops theoretically and showed numerical values. In the future, we will analyze the total power consumption including resending after packetizing data and power consumption in a relay node.

REFERENCES

[1] T. Otsu, Y. Aburakawa and Y. Yamao,"Multi-Hop Wireless Link System for New Generation Mobile Radio Access Networks," IEICE Trans. Commun., vol. E85-B, no.8, pp.1542-1551, Aug. 2002.

[2] R. Pabst, etc., "Relay-based deployment concepts for wireless and mobile broadband radio," IEEE Commun. Mag., vol.42, no.9, pp.80-89, Sept. 2004.

[3] P. C. Ng and S. C. Liew, "Throughput Analysis of IEEE802.11 Multi-hop Ad Hoc Networks", IEEE/ACM Trans. On Networking, vol 15, Issue. 2, pp.309-322, Apr. 2007.

[4] Yan Gao, DahMing Chiu, John C.S. Lui, "Determining the end-to-end throughput capacity in multi-hop networks: methodology and applications", Proc. of ACM SIGMETRICS, pp.39-50, 2006.

[5] M.Sikora, J. N. Laneman, M.Haenggi, D. J. Costello and T.Fuja, "On the Optimum Number of Hops in Linear Wireless Networks", Proc. IEEE Information Theory Workshop, San Antonio, TX, Oct. 2004.

[6] I.Stanojev, O.Simeone, Y.Bar-Ness and M.Cho, "On the Optimal Number of Hops in Linear Wireless Ad Hoc Networks with Hybrid ARQ", 6th International ICST Symposium on Modeling and Optimization, Aug.2008.

[7] A.Florea and H.Yanikomeroglu, "On the optimal number of hops in infrastructure-based fixed relay networks", Proc. IEEE Globecom 2005, pp.3242-3247, Dec.2005.

[8] K.Schwieger and G.Fettweis, "Power and Energy Consumption for Multi-hop. Protocols: A Sensor Network Point of View," International Workshop on Wireless Ad-hoc Network (6 pages), IWWAN 2005.

[9] K.Schwieger, A.Kumary and G.Fettweis,"On the Impact of the Physical Layer on Energy Consumption in Sensor Networks,"Proceeedings of the Second European Workshop on Wireless Sensor Networks, pp. 13-24, 31 Jan.-2 Feb. 2005.

[10] A. Goldsmith, Wireless Communication, Cambridge University Press, 2005.

[11] T.Hironori and O.Kouji, "A Study on Power Consumption in Multihop Networks Considering power Consumption at Relay Nodes," IEICE technical report WBS2009-7, Jul.2009 (in Japanese).

[12] H.Mizuno, "Introduction of Network Simulation using NS2", MORIKITA PUBLISHING Co. Ltd, 2011 (in Japanese).

[13] W.Toorisaka, G.Hasegawa, M.Murata, "Power Consumption analysis of data transmission in IEEE 802.11 multi-hop networks", IEICE technical report NS2011-77, 103-108, 2011.8.25 (in Japanese).

[14] T. Issariyakul, E. Hossain, Introduction to Network Simulator NS2, Springer; 2nd ed, 2011.

THE 18TH INTERNATIONAL SYMPOSIUM ON WIRELESS PERSONAL MULTIMEDIA COMMUNICATIONS
(WPMC-2015)
December 13-16, 2015, Hyderabad, India

A Feasibility Analysis of LTE-CommSense

Amit K. Mishra∗, Mohammed Zafar Ali Khan† & Santu Sardar§
∗ Department of Electrical Engineering, University of Cape Town, South Africa
† Department of Electrical Engineering, IIT Hyderabad, India
§ ANURAG, Defence Research & Development Organization, India

***Abstract*—This paper describes a novel way to use the existing LTE (Long Term Evolution) communication infrastructure to monitor the change in the environment and its feasibility analysis. This system is named LTE-CommSense by the authors and can be used in many environment sensing tasks e.g. crop growth monitoring, disaster monitoring, sea state monitoring, snow avalanche monitoring, security of large unmanned landscapes etc. The key idea to this technology lies in focusing on already known signal from received signal e.g. reference symbols in the LTE communication signal frames. In the equalizer block of the receiver, the equalizer tap coefficients gets modified while training the equalizer using reference symbols, depending on the channel through which the received signal has passed through. Therefore the adaptive equalizer tap coefficients contains information regarding the channel. We propose to use these coefficients to get an estimate of change in the channel properties. Existing LTE spectrum and infrastructure will be utilized to get channel characteristics without affecting the existing communication system. After the channel information is received, this will be utilized to obtain phenomenological knowledge of the environment using ASIN (Application Specific INstrumentation) framework. We present a feasibility analysis of the novel scheme in this paper. We used LTE specific channel models from ITU (International Telecommunication Union) with AWGN noise as the dataset and nearest neighbour based classifier to validate this scheme.**
***keywords* - LTE, LTE-CommSense, adaptive equalizer, ASIN, ITU.**

I. Introduction

The first work of using Radar systems for limited amount of data communication, in the open literature is the US patent published in 1969 by Ritterbach [1]. Recently, there also has come an upsurge in activities in the field of using communication radiation for target detection and tracking using receiver only nodes. This field popularly known as passive Radar or commensal Radar ([2], [3]).

The coexistence of communication and radar systems can be broadly categorized into the following types (inspired by biological inter-species coexistence): commensal systems (one system exploits other without detrimental effect), symbiotic Systems (systems coexist and benefit from existence of each other e.g. Ritterbach patent [1], Moon-Sik patent [4] & Whitespace Radar [5]) and parasitic systems (one system affects the other in detrimental manner e.g. electronic defence & electronic warfare systems).

The proposed work will use a novel commensal radar system called CommSense [6], [7] using LTE infrastructure. We call this LTE-CommSense. The novelty of this proposed system are two fold. First of all it builds upon existing communication system to monitor the environment. This is different from any classic radar system which mainly cater to measuring the range and Doppler of a target in the scene. Secondly, and this is the major novelty of the work, LTE-CommSense does not perform correlation based processing like most existing commensal radar systems. Instead it uses the reference signal in the received communication signal to estimate the fading channels and there by predict the change in the environment.

In this paper we will show that within practicalities of simulation, this is possible and we can recognise different kinds of channels by using the channel estimation block of LTE. LTE specific six different channel models, namely ITU Pedestrian A (PA), ITU Pedestrian B (PB), ITU Vehicular A (VA), ITU Extended Pedestrian A (EPA), ITU Extended Vehicular A (EVA), ITU Extended Typical Urban (ETU) are used for this analysis. The training and recognition dataset contains multiple readings for each of these channel models each having different amount of AWGN noise added to it. Naive nearest neighbour based classifier is used to classify the recognition dataset using the training dataset as reference. The results shows promising performance of this novel scheme.

Rest of the paper is organized as follows. Section II describes the basic concept of CommSense. The feasibility analysis results of our proposed scheme is detailed in section III and conclusion & future work is provided in section IV.

II. The Concept of CommSense

In a communication system, the major thrust is on correctly estimating the received signal at the receiver. The channel model is mostly assumed to be known. Whereas in a Radar the channel is what we try to estimate. Communication systems use a range of processes and algorithms to estimate non-ergodic and fading channels in real time and try to filter out the effect of the same. Hence, the aim of CommSense will be to estimate the noise for communication systems.

Most modern communication standards and the adhering equipments cater for dynamic channel estimation. These schemes use known pilot signals in the received burst to estimate the channel and then filter the channel modulations out. Based on the above observation, we propose the Communication based Sensing or CommSense system, which will:

1) estimate the channel characteristics from the received communication signal, and
2) predict the change in the environment based on the change in the channel characteristics.

The information collected should be properly mapped from the measurements to physical events in the environment. This type of phenomenological effort is a major challenge even in conventional radar systems also [8]. To resolve this issue, different stages in the processing chain of the proposed LTE-CommSense system is shown in Figure 1. There are two sets of input and hence processing-chains in the system. The first one is a real-time system input coming from the UEs in the field. The second chain of information and processing is set by the mission control and depends on the purpose to which the LTE-CommSense will be put to for a particular time frame.

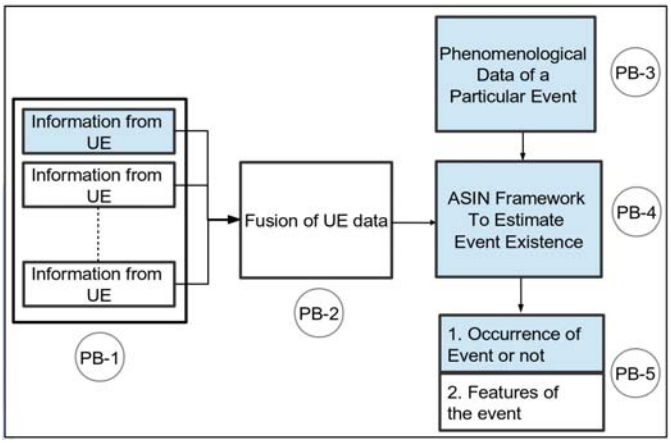

Fig. 1. Different stages in the processing chain of a LTE-CommSense system

A short description of each of the process-block (PB) are given below:

Process-block 1: Extracts information from channel equalization, done using adaptive filtering technique. In future, multiple UEs will be used to cover wider area. In that case, the adapted filter coefficients of the UE will be sent to process-block 2.

Process-block 2: Fuses all the information collected from UEs of PB-1. In this analysis single UE is considered and therefore PB-2 is bypassed.

Process-block 3: Gathers information about the event that need to be detected. This is used to train the ASIN block in PB-4.

Process-block 4: Trains and uses an ASIN block. ASIN is a pattern classification system which trains itself using the information from PB-3 and then gives prediction in real-time using information from PB-1 & PB-2.

Process-block 5: Delivers information from PB-4 to user. This information will consist of event occurrence confirmation and/or details of the event (if the event has occurred).

Bio-inspired ASIN framework [9], [10], as shown in the figure, will be utilized to obtain phenomenological knowledge about the environment. ASIN tries to estimate one or a few anomalies only instead of trying to estimate everything in the scene. Depending on what use a particular LTE-CommSense will be put into, a set of field trials will be run to gather information about the anomaly to detect and characterize. Then it can sense and characterize when that particular kind of occurrence happens in the environment. The output of the system will consist of two sets of information. First, it gives a likelihood of a particular event occurring. Secondly, given that the likelihood of that even is high enough, it gives some basic characteristics of the event also.

The proposed method will be demonstrated in indoor/outdoor environment by implementing LTE communication standard in GNURadio environment along with a software radio platform (SDR) platform. Information regarding environment changes will be extracted from very less amount of observation. Therefore, it is proposed to measure the channel from as many different locations as possible using multiple cooperative UEs. Each UE will transmit their GPS position along with the filter coefficients values. But in this initial feasibility analysis, we have considered a singe UE.

The scene of interest depends on the range of the UEs. For LTE, scene size will keep on changing and mostly will be confined to as small as the pico-cell sizes. Also, in case a LTE-CommSense system for constant monitoring of a certain area of interest, fixed UEs can be installed. The cost of such a system will be low as these will be receiver-only devices.

In LTE-CommSense, CommSense infrastructure will utilize existing LTE communication standard. The specifications for LTE was standardized in the form of Rel-8 and approved in January 2008. Target deployment started in 2010 [11]. The LTE requirements and LTE enabling technologies can be found in [12]. We are interested in LTE downlink reference signal [13] which we will use for channel estimation & equalization. In the LTE downlink, three different types of reference symbols (RSs) are provided: cell-specific RSs, UE-specific RSs and Multimedia Broadcast Single Frequency Network (MBSFN) specific RSs.

The LTE specifications don't mandate any specific channel estimation & equalization technique provided the performance requirements are met and complexity is affordable [13]. Channel estimation & equalization can be performed either in frequency domain (using channel transfer function (CTF) e.g. interpolation, least square (LS), regularized LS, minimum mean square error (MMSE), mismatched MMSE), time domain (using channel impulse response (CIR) e.g. MMSE, least mean square (LMS), normalized LMS, recursive least square (RLS), Kalman-based filtering) or in spatial domain (SD-MMSE). We will select an RS-aided channel estimation & equalization algorithm for our purpose.

III. Results & Feasibility Analysis

Six different ITU specified channel models for LTE channel analysis, namely ITU Pedestrian A (PA), ITU Pedestrian B (PB), ITU Vehicular A (VA), ITU Extended Pedestrian A (EPA), ITU Extended Vehicular A (EVA), ITU Extended Typical Urban (ETU) are used for our analysis. The multi-path profile of these six LTE channel models [13] are shown in Table I.

The highlighted blocks in Figure 1 are implemented in this feasibility analysis. In this present case, a single UE is used.

TABLE I
PROPAGATION CONDITIONS FOR MULTI-PATH FADING IN THE ITU MODELS USED FOR LTE

	Pedestrian A (PA)		Pedestrian B (PB)		Vehicular A (VA)		Extended Pedestrian A (EPA)		Extended Vehicular A (EVA)		Extended Typical Urban (ETU)	
Tap No.	Relative Delay (ns)	Relative Mean Power (db)	Relative Delay (ns)	Relative Mean Power (db)	Relative Delay (ns)	Relative Mean Power (db)	Relative Delay (ns)	Relative Mean Power (db)	Relative Delay (ns)	Relative Mean Power (db)	Relative Delay (ns)	Relative Mean Power (db)
1	0	0.0	0	0.0	0	0.0	0	0.0	0	0.0	0	-1.0
2	110	-9.7	200	-0.9	310	-1.0	30	-1	30	-1.5	50	-1.0
3	190	-19.2	800	-4.9	710	-9.0	70	-2	150	-1.4	120	-1.0
4	410	-22.8	1200	-8.0	1090	-10.0	80	-3	310	-3.6	200	0.0
5	-	-	2300	-7.8	1730	-15.0	110	-8	370	-0.6	230	0.0
6	-	-	3700	-23.9	2510	-20.0	190	-17.2	710	-9.1	500	0.0
7	-	-	-	-	-	-	-	-	1090	-7	1600	-3.0
8	-	-	-	-	-	-	-	-	1730	-12	2300	-5.0
9	-	-	-	-	-	-	-	-	2510	-16.9	5000	-7.0

Therefore, fusion of data in PB-2 is not used here. Also, Determination of occurance of the event is analyzed here. The feasibility of extracting features of the detected event will be performed in the extended work in future.

The channel profile quantifies the delays and relative powers of the multi-path components. The multi-path components in the table are not uniformly spaced in the time domain. In channel equalization, the coefficients of the used adaptive filter is dependent on the delay profile of the channel. As the channel is time-varying, each filter tap will be updated using adaptive algorithm. Depending on the changes of these channel parameters, the adaptive filter coefficients will also change. This phenomena is utilized to extract information regarding corresponding changes in the channel. The filter is be modeled as an FIR (Finite Impulse Response) filter because we receive a finite number of delayed versions of original signal at UE. We considered LMS and MMSE channel equalization method for this study.

Now, we'll analyze the feasibility to determine environment change of a noisy channel using filter coefficients of the equalizer. First we will determine equalizer tap coefficients for different LTE channel models in various channel noise conditions. This information will be used to generate training and recognition dataset for the nearest neighbour classifier. The training dataset is developed using maximum 50 images of each CIR having different amount of AWGN noise. The testing dataset also created accordingly. Given a set of adaptive filter tap coefficients, the classifier determines, to which CIR in the training dataset it best corresponds.

The analysis is performed for different values of noise variance (σ). Three different noise variances are considered: 10, 5 and 0.1 respectively. For each noise variance, accuracy is calculated for different channel lengths and two different equalizers viz. MMSE and LMS to analyze the effect of filter length on the system performance. For the LMS filter, the learning parameter (μ) is taken to be 0.004. The nearest neighbour classifier uses L_1 distance (Manhattan Distance) for distinguishing the CIRs.

The classification performance is provided in terms of performance accuracy and confusion matrix. The accuracy is the percentage of correct classification. But from the confusion matrix, we can observe in which cases incorrect classification has occurred. In this case, confusion matrix will be a $6x6$ square matrix wherein the diagonal elements corresponds to correct classification and off-diagonal elements corresponds to incorrect classification. Moreover, from the co-ordinates of these off-diagonal elements, we can determine, what is the original category of data and to what category it is classified. The recognition accuracy along with the confusion matrix for different noise variances are shown in table II, III and IV respectively.

Performance analysis of table II, III and IV proves that the idea of CommSense is feasible. Further, this limited study also showed that, MMSE is a better candidate for CommSense. For filter length more than 50, the performance accuracy of MMSE based system is consistent for the range noise condition considered. Therefore MMSE equalizer will be used in all our future experiments. Also, it can be seen that, the recognition performance improves with increase in the filter length. As the noise variance, The classification performance also increases.

As a further analysis we compared the effect of 'measure of distance' used in the nearest neighbour classifier for distinguishing the CIRs. The results are shown in table V. Here, the filter length is fixed to be 50. The noise variance of 5.0 is considered. The learning parameter (μ) for the LMS filter is taken to be 0.004. It can be observed from the result that, Euclidian distance measure is more suitable for our purpose.

IV. CONCLUSION AND FUTURE WORK

The work presented here, describes the feasibility of a novel development to the field of communication based environment sensing. It can be concluded from the analysis of the results discussed here that the proposed system is feasible in practice. CommSense being essentially a commensal radar, will not affect existing communication system in any way. Hence the required effort will be less and also it'll be a cost effective solution. Proposed LTE-CommSense will be utilized to detect

TABLE II
FEASIBILITY ANALYSIS: CLASSIFICATION PERFORMANCE AT σ = 10

	LMS Equalizer based Method							MMSE Equalizer based Method						
Filter Length	Accuracy (%)	Confusion Matrix						Accuracy (%)	Confusion Matrix					
5	19.3333	13	15	5	2	9	6	35.3333	23	22	9	5	1	1
		8	7	7	10	12	6		11	15	8	8	7	1
		10	14	8	6	5	7		12	16	5	8	8	1
		5	13	8	7	8	9		5	4	6	13	20	2
		4	3	7	10	14	12		2	7	11	8	18	4
		4	13	4	10	10	9		0	3	1	5	9	32
50	51	48	0	2	0	0	0	86	26	0	24	0	0	0
		14	14	14	6	2	0		1	47	2	0	0	0
		28	11	10	1	0	0		10	2	35	0	3	0
		0	8	8	22	10	0		0	0	0	50	0	0
		0	7	0	12	27	4		0	0	0	0	50	0
		0	0	0	7	11	32		0	0	0	0	0	50
100	41	35	7	8	0	0	0	96.3333	45	2	3	0	0	0
		8	21	10	7	4	0		1	49	0	0	0	0
		15	14	14	4	3	0		4	0	45	0	1	0
		3	10	15	11	7	4		0	0	0	50	0	0
		1	8	5	14	16	6		0	0	0	0	50	0
		0	1	1	16	6	26		0	0	0	0	0	50

TABLE III
FEASIBILITY ANALYSIS: CLASSIFICATION PERFORMANCE AT σ = 5

	LMS Equalizer based Method							MMSE Equalizer based Method						
Filter Length	Accuracy (%)	Confusion Matrix						Accuracy (%)	Confusion Matrix					
5	46.3333	43	3	4	0	0	0	82.3333	50	0	0	0	0	0
		1	14	14	7	9	5		0	28	18	4	0	0
		6	11	28	4	1	0		0	18	32	0	0	0
		0	7	4	23	10	6		0	2	0	44	4	0
		0	6	2	13	12	17		0	0	0	3	46	1
		0	4	3	9	15	19		0	0	0	0	3	47
50	52.6667	41	1	7	0	1	0	99.3333	48	0	2	0	0	0
		5	28	17	0	0	0		0	50	0	0	0	0
		23	3	23	0	1	0		0	0	50	0	0	0
		3	0	0	47	0	0		0	0	0	50	0	0
		7	4	17	5	17	0		0	0	0	0	50	0
		9	8	15	9	7	2		0	0	0	0	0	50
100	45	50	0	0	0	0	0	100	50	0	0	0	0	0
		39	0	11	0	0	0		0	50	0	0	0	0
		44	0	6	0	0	0		0	0	50	0	0	0
		18	7	7	16	2	0		0	0	0	50	0	0
		0	2	2	26	20	0		0	0	0	0	50	0
		0	0	0	3	4	43		0	0	0	0	0	50

TABLE IV
FEASIBILITY ANALYSIS: CLASSIFICATION PERFORMANCE AT σ = 0.1

	LMS Equalizer based Method							MMSE Equalizer based Method						
Filter Length	Accuracy (%)	Confusion Matrix						Accuracy (%)	Confusion Matrix					
5	93.3333	50	0	0	0	0	0	100	50	0	0	0	0	0
		0	48	2	0	0	0		0	50	0	0	0	0
		0	1	49	0	0	0		0	0	50	0	0	0
		0	0	0	50	0	0		0	0	0	50	0	0
		0	0	0	0	44	6		0	0	0	0	50	0
		0	0	0	0	11	39		0	0	0	0	0	50
50	99.3333	50	0	0	0	0	0	100	50	0	0	0	0	0
		0	50	0	0	0	0		0	50	0	0	0	0
		0	0	50	0	0	0		0	0	50	0	0	0
		0	0	0	50	0	0		0	0	0	50	0	0
		0	0	0	0	50	0		0	0	0	0	50	0
		0	0	1	0	1	48		0	0	0	0	0	50
100	96	50	0	0	0	0	0	100	50	0	0	0	0	0
		0	50	0	0	0	0		0	50	0	0	0	0
		0	0	50	0	0	0		0	0	50	0	0	0
		0	0	0	50	0	0		0	0	0	50	0	0
		0	1	2	0	47	0		0	0	0	0	50	0
		0	0	0	1	8	41		0	0	0	0	0	50

TABLE V
EFFECT OF DISTANCE MEASURE ON THE CLASSIFIER PERFORMANCE

	LMS Equalizer based Method							MMSE Equalizer based Method						
Measure of distance	Accuracy (%)	Confusion Matrix						Accuracy (%)	Confusion Matrix					
L_1 (Manhattan)	52.6667	41	1	7	0	1	0	99.3333	48	0	2	0	0	0
		5	28	17	0	0	0		0	50	0	0	0	0
		23	3	23	0	1	0		0	0	50	0	0	0
		3	0	0	47	0	0		0	0	0	50	0	0
		7	4	17	5	17	0		0	0	0	0	50	0
		9	8	15	9	7	2		0	0	0	0	0	50
L_2 (Euclidian)	57.6667	44	0	4	2	0	0	99.6667	49	0	1	0	0	0
		6	38	5	1	0	0		0	50	0	0	0	0
		22	11	15	1	1	0		0	0	50	0	0	0
		1	0	0	49	0	0		0	0	0	50	0	0
		9	6	10	3	20	2		0	0	0	0	50	0
		3	5	17	10	8	7		0	0	0	0	0	50

& characterize environment changes. In the next phase, this feasibility analysis will be extended for the case of multiple input multiple output (MIMO) scenarios, compatible with LTE standard. Then, the proposed LTE-CommSense system will be implemented using an SDR environment and validated in both laboratory (restricted/indoor) & outdoor environment.

REFERENCES

[1] O. E. Rittenbach, "Communication by radar beams," in *uS Patent 3,460,139*, Aug. 5 1969.
[2] H. Griffiths and C. Baker, "Passive coherent location radar systems. part 1: performance prediction," *Radar, Sonar and Navigation, IEE Proceedings*, vol. 152, no. 3, pp. 153–159, 2005.
[3] M. Inggs and C. Tong, "Commensal radar using separated reference and surveillance channel configuration," *Electronics letters*, vol. 48, no. 18, pp. 1158–1160, 2012.
[4] M. S. Lee, "Mimo radar apparatus and wireless communication method using the same," in *uS Patent App. 12/841,595*, Jul. 22 2010.
[5] A. K. Mishra and D. L. Johnson, *White Space Communication Advances, Developments and Engineering Challenges*. Springer, 2015.
[6] A. K. Mishra, "Commsense: Radar system using existing communication infrastructure to sense the environment," in *Radioelektronika (RADIOELEKTRONIKA), 2015 25th International Conference. IEEE*, 2015, pp. 276–279.
[7] ——, "Monitoring changes in an environment by means of communication devices," in *uK IP office, Patent Application No. GB1506665.7*, Apr. 20 2015.
[8] J. R. Huynen, "A revisitation of the phenomenological approach with applications to radar target decomposition," *DTIC Document, Tech. Rep.*, 1982.
[9] A. Mishra, G. Wilsenach, and M. Inggs, "Information sensing for radar target classification using compressive sensing," *13th IEEE International Radar Symposium (IRS)*, pp. 326–330, 2012.
[10] S. Sardar and A. K. Mishra, "Asin based uwb radar for sludge monitoring," *IEEE Access: practical innovations, open solutions*, vol. 2, pp. 290–300, April 15, 2014.
[11] $http : //www.3gpp.org/ftp/Specs/html - info/36 - series.htm$.
[12] D. et. al., "3g evolution: Hspa and lte for mobile broadband," *Academic Press*, 2007.
[13] S. Sesia, I. Toufik, and M. Baker, *LTE - The UMTS Long Term Evolution, From Theory to Practice*. Wiley, 2019.

THE 18TH INTERNATIONAL SYMPOSIUM ON WIRELESS PERSONAL MULTIMEDIA COMMUNICATIONS
(WPMC-2015)
December 13-16, 2015, Hyderabad, India

Hybrid multi-hop network by small-unmanned aircraft and satellite telecommunication systems

Fumie Ono
Wireless Network Research Institute, NICT,
3-4, Hikarino-oka, Yokosuka, 239-0847 Japan
Email: fumie@nict.go.jp

Byeong-pyo JEONG
Resilient ICT Research Center, NICT,
2-1-3, Katahira, Aoba, Sendai-city,
Miyagi, 980-0812 Japan

Yasunori OWADA
Resilient ICT Research Center, NICT,
2-1-3, Katahira, Aoba, Sendai-city,
Miyagi, 980-0812 Japan

Shan LIN
Wireless Network Research Institute, NICT,
3-4, Hikarino-oka, Yokosuka, 239-0847 Japan

Ryu Miura
Wireless Network Research Institute, NICT,
3-4, Hikarino-oka, Yokosuka, 239-0847 Japan

***Abstract*—This paper proposes a hybrid multi-hop network by the small UA-based wireless bridge system with satellite telecommunication system for a resilient wireless network. In the hybrid multi-hop network, small UA-based wireless bridge and satellite telecommunication system are concatenated serially via a vehicle mounted satellite earth station. The satellite telecommunication system is useful for ensuring a connection to the Internet since small UA-based wireless bridge system forms only a local network. This paper presents a brief overview of demonstration of the hybrid multi-hop network to collaborate with the cellular telecommunication network for disaster. It is shown that the hybrid multi-hop network is useful to telecommunication between an isolated and non-isolated area in the case of large-scale disaster in this paper.**

I. Introduction

In large-scale disaster in Japan, the most advanced and popular mobile phones becomes almost useless under large-scale disasters due to physical damage, electricity outage, and traffic congestion. In addition, many areas in mountains or islands were isolated due to the total damage of roads, harbors, and communication infrastructures. Under such situation, it is desired to monitor the situation in the whole of disaster area to judge, predict, and cope with disaster details. In addition, it is more desired to provide temporal communication lines rapidly deployable to the isolated areas until the recovery of ground infrastructures.

Based on the lessons learned from the past experiences, we have started research and development on disaster-resilient wireless system using small fixed-wing unmanned aircraft (UA) system in order to ensure the communication infrastructure between the isolated and the non-isolated areas. A typical UA is equipped with flight management system, propulsion system, energy storage, networked communication, miniaturized devices, and autonomous control [1]. In the case of the large-scale disaster, UAs serve as bridges among the isolated ground stations (GS) if UA has an on-board repeater. [2–5].

Through our initial experiment using small UA in the end of June 2013, we have succeeded in establishing wireless bridge networks. The two GSs separated by 12.5 km were able to exchange pictures through the UA that is located 15.1 km from a GS. In this experiment, the center frequency of the transmitter was chosen as 2 GHz and the transmit power was 2 W [5].

In order to improve the coverage and flexibility of the small UA-based wireless bridge network, we propose a hybrid multi-hop network by *small UA-based wireless bridge system* with *satellite telecommunication system* in this paper. In the hybrid multi-hop network, small UA-based wireless bridge and satellite telecommunication system are concatenated serially via a vehicle mounted satellite earth station. The satellite telecommunication system is useful for ensuring a connection to the Internet since small UA-based wireless bridge system forms only a local network. Therefore, by combing two systems, there is a possibility to rapidly deploy temporal communication lines to the isolated areas until the recovery of ground infrastructures. This paper presents brief overview of demonstration of a hybrid multi-hop network to collaborate with the cellular telecommunication network for disaster. The purpose of this demonstration is to operate the cellular telecommunication network even at the isolated area. In order to achieve our purpose, a femtocell of cellular telecommunication is installed in isolated area. The femtocell is a small base station of cellular telecommunication to improve cellular coverage within a house or a building. The femtocell requires the connection with core network to telecommunication operation. In this demonstration, the connection with core network is provided by the hybrid multi-hop network. This paper will provide the successful results of these demonstrations for accidents and disasters.

The rest of the paper is organized as follows: Section II describes the hybrid multi-hop network, and in Section III and IV experimental deployment and results are presented. Finally, concluding remarks and possible future work are given in Section V.

II. Hybrid multi-hop network

Figure 1 shows a overview of hybrid multi-hop network in this demonstration. This section briefly describes the small UA-based wireless bridge system and the satellite telecommunication system. Then we describes the hybrid multi-hop network for experimental demonstration.

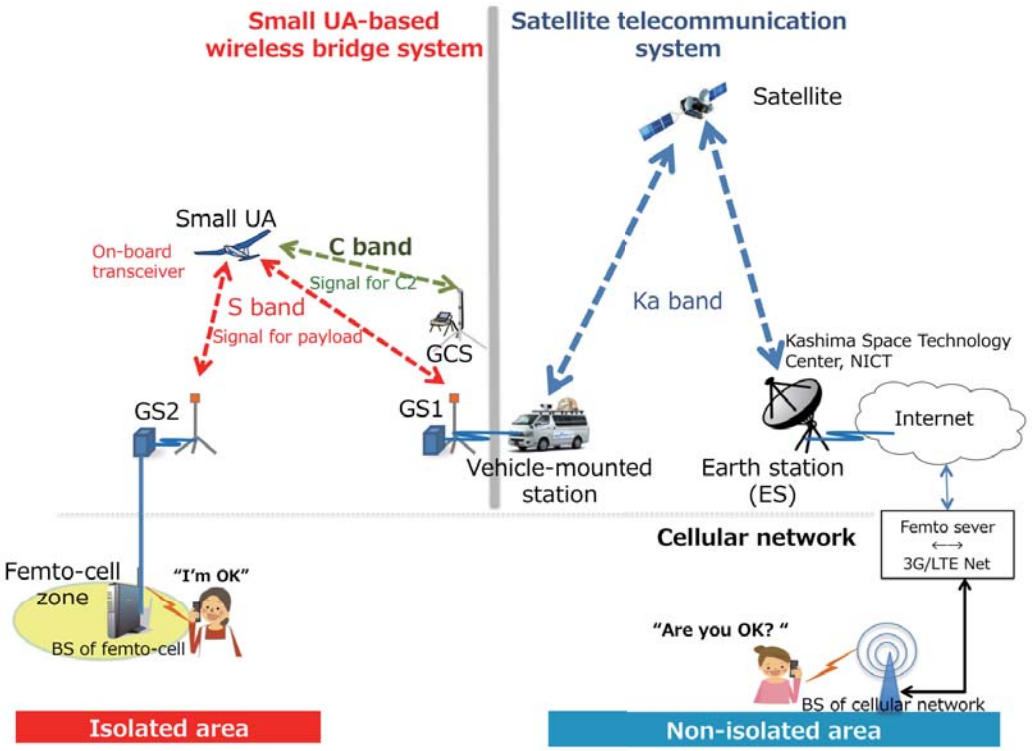

Fig. 1. Overview of hybrid multi-hop network

A. Small UA-based wireless bridge system

In the small UA-based wireless bridge system, the small UA has a on-board transceiver and relays the signal between the ground stations (GSs). The small UA circles around above the fixed area for relay communication. Table I shows the specification of small UA system. The UA system consists of a small UA and a ground control station (GCS). The payload of small UA is limited by 0.5 kg due to small airframe. The nominal endurance is about 2 or 3 hours. The control range from GCS is about 9 km. The frequency of control and non-payload communications (CNPC) is 5060 MHz and the signal power of CNPC is 1 W in this experimental measurement. The small UA can be launched by throwing and recovered by deep-stole landing. Therefore, special area such as runways is not needed for launch and landing. In addition, we can operate it even when the cars are not available due to road damage, heavy traffic jam, or gasoline shortage since the small-UA and GCS are easily hand-carried.

Table II shows the specification of transceivers for on-board and ground station (GS) for relay communication. Each transceivers for GSs and UA is equipped with a single antenna used for transmission and reception in a half duplex manner. The weight of on-board transceiver with a battery is 0.47 kg. In this experimental measurement, the frequency band of the transceiver was choose as 2 GHz and the transmit power was 2 W. The maximum range for communication between UA and GS is about 20 km. In order to relay communication, it is desired to ensure the Line-of-sight (LOS) between UA and GCs . A snapshot of small UA-based wireless bridge system is shown in Fig. 2.

Fig. 2. A snapshot of small UA-based wireless bridge system

TABLE I. SPECIFICATION OF SMALL UNMANNED-AIRCRAFT SYSTEM

Wingspan, Weight	2.8 m, 5.9 kg
Payload	Maximum 0.5 kg
Nominal endurance	about 2-3 hours
Control range	9 km
Wind speed	Maximum: 25 knots
Ceiling altitude	Maximum: 5 km
Radio frequency	5035-5085 MHz, 6 ch (experimental)
Driving power	Direct drive electric
Launch/Landing	Hand launch, Deep stall landing
Control	Manual or autonomous control

TABLE II. SPECIFICATION OF WIRELESS BRIDGE SYSTEM

Weight of GS	about 6 kg (w/o power generator)
Weight of on-board repeater	0.47 kg (w battery)
Frequency	2 GHz(experimental)
TX power	2 W
Data rate	450 kbps
Battery life	about 2 hours
Range	20 km (UA-GS)
Interface	LAN cable(1000BASE-T)
Available protocol	TCP, UDP, RTP, ICMP, ARP/RARP, etc.

B. Satellite telecommunication system

In this demonstration, we use the wideband internetworking satellite WINDS (Wideband InterNetworking engineering

test and Demonstration Satellite, also called KIZUNA). The WINDS was developed by the Japan Aerospace Exploration Agency (JAXA) and the NICT [6]. In WINDS, the frequency for communication uses Ka-band (20 GHz to 30 GHz). The WINDS includes Ka-band vehicle-mounted earth station and earth station. The earth station was installed at the NICT Kashima Space Research Center located in Kashima, Ibaraki, Japan. The user data rate of Kashima earth station is 1244 Mbps and that of the vehicle-mounted earth station is 622 Mbps. Therefore, the high-speed access to the Internet can be provided by WINDS.

C. Hybrid multi-hop network for collaboration with cellular telecommunication network

The hybrid multi-hop network consists of the small UA-based wireless bridge with satellite telecommunication systems. The small UA-based wireless bridge system provides the connection to the isolated area where broken ground infrastructures. The satellite telecommunication system proves the Internet link to the small UA-based wireless bridge system via vehicle-mounted earth station. In this experimental demonstration, we set up the femtocell at isolated area. The femtocell is the small base station of cellular telecommunication that can be installed in residential environments to provide improved cellular coverage within doors environment. In order to link the femtocells with the main core network, we uses Internet link through the hybrid multi-hop network. This configuration can provide temporal link even in a distant disaster area. However, in the case of such hybrid multi-hop network, the link quality depends on the small UA-based wireless bridge system due to the narrowband system compared with the satellite telecommunication system.

III. Experimental deployment

Figures 3 and 4 show examples of deployment and the trajectory of UA in the experimental measurement.

The area for experimental demonstration is located in the depths of mountains (1400 feet above sea level) in Kochi prefecture, Japan and it is out of coverage of cellular telecommunication network. The two GSs (denoted by GS1 and GS2) separated by about 600 m. There is no direct communication link between GS1 and GS2 such that the information can be delivered only through the relaying UA. We assumed that the area of GS2 is the isolated area and that of GS1 is non-isolated area. In the isolated area, the femtocell is located within a house close to GS2. In the non-isolated area, the vehicle-mounted earth station is located near GS1. The GS1 connects the vehicle-mounted earth station for satellite telecommunication over cable.

In Figs. 3 and 4 show two cases (denoted by case A and B) of the trajectory of UA in the experimental measurement. The flight altitude above see-level of small UA is about 2900 feet and the speed of wind is about 4 knot. In the case A as shown in Fig.3, the average of wind speed is 8 m/s, and it will be categorized as moderate breeze. On the other hand in the case B as shown in Fig.4, the average of wind speed is 2 m/s that is categorized as light breeze. In the case A, it was observed that the trajectory of is swaying due to the strong wind compared with case B. The sway of UA is one of factors that influence the communication quality.

Fig. 3. Case A: average of wind speed is 8 m/s

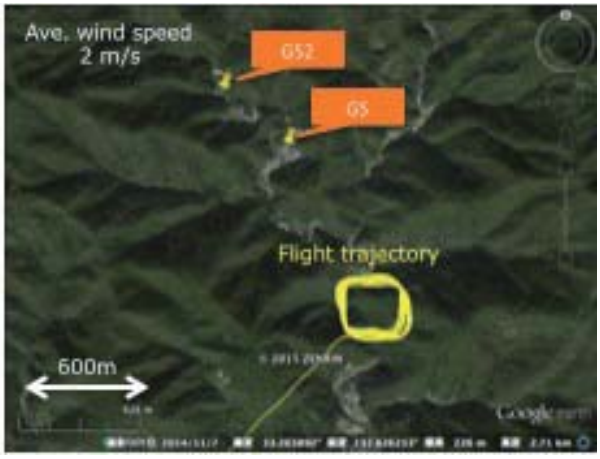

Fig. 4. Case B: average of wind speed is 2 m/s

IV. Experimental results

A. Speech quality

In this experimental measurement, we conducted voice testing using a speech quality measurement tool, such as Perceptual Evaluation of Speech Quality (PESQ) [7]. We measured the PESQ score using 3G mobile terminals, LTE mobile terminal and Skype application on LTE terminal since PESQ scores vary widely even among quality terminals.

Figures 5 and 6 show PESQ scores for various cases of mobile terminal in the demonstration system, with cases of only satellite telecommunication as a target for comparison are plotted. The 10 difference sentences of voice every terminal are inputted to the demonstration system and the scores are measured at terminal of femtocell side. Moreover, we measured PESQ scores of two cases (case A and B) for perceiving the environment influence.

From the satellite telecommunication point of view, the PESQ scores of two cases denote the same tendency and those scores depend on the mobile terminal.

On the other hand in the hybrid multi-hop network, the PESQ scores depend largely on the environment influence. In Fig. 5, the communication link between GSs often disconnects

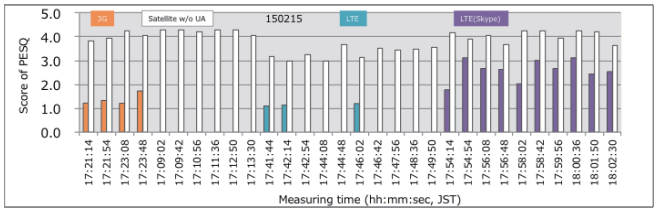

Fig. 5. PESQ scores in the case A

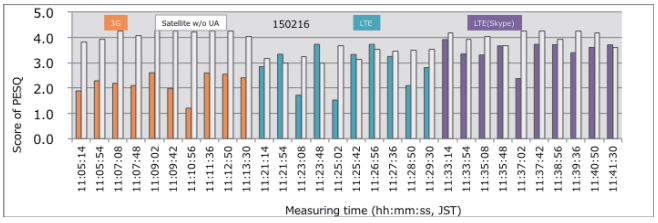

Fig. 6. PESQ scores in the case B

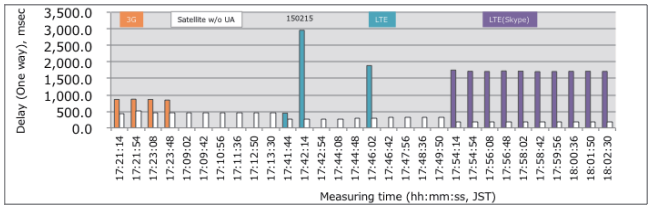

Fig. 7. One-way delay of case A

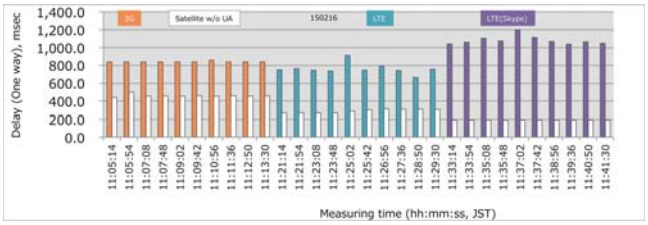

Fig. 8. One-way delay of case B

due to strong wind speed. Therefore, we could not measure all sentences of PESQ score in this case. In the case of Fig. 6, the communication link could maintain during flight. It was observed that the PESQ score of the hybrid multi-hop network exceeds 3.0 (fair) in several times. However, the variance of the PESQ score of the hybrid multi-hop network is larger than that of only satellite telecommunication system. This is because that the small-UA proves the communication link with moving relay. In order to absolutely reliability, it is necessary for the small UA-based wireless bridge system to improve the link quality.

B. Delay property

Figures 7 and 8 show one-way delay for various cases of mobile terminal in the demonstration system, with cases of only satellite telecommunication as a target for comparison are plotted. The one-way delay properties are measured at terminal of femtocell side when the 10 difference sentences of voice every terminal are inputted to the demonstration systems. Theoretically, the one-way delay of only satellite telecommunication system is below 200 msec, and the minimum delay of small UA-based wireless bridge system is 200 msec. Therefore, the minimum delay is estimated 900 msec or under at largest even if we take into account the intrinsic delay of femtocell.

In Fig. 7, we could not measure all sentences of one-way delay as with shown in Fig. 5. However, in Fig.8, it was observed that the delay of the hybrid multi-hop network varies from 740 msec to 910 msec in the case of 3G or LTE terminal. Moreover, the maximum delay of Skype application with LTE terminal reaches the edge of 1200 msec due to the addition of the processing delay of the Skype application.

V. Conclusion

We proposed the hybrid multi-hop network by small-unmanned aircraft and satellite telecommunication systems and provided overview of experiments as feasibility study of femtocell operation. The results confirm the success of the femtocell operation using the demonstration system and the validity to telecommunication between an isolated and non-isolated area in the case of disaster. The improvement of data rate and extension to multiple UAs/GSs will be left as our future works.

Acknowledgment

This work was supported in part by Shikoku Bureau of Telecommunications, the Japanese Ministry of Internal Affairs and Communications (MIC), KDDI, Softbank, docomo and TOYO corporation. The part of according to 5GHz was supported by the MIC in R&D on Cooperative Technologies and Frequency Sharing Between Unmanned Aircraft Systems (UAS) Based Wireless Relay Systems and Terrestrial Networks.

References

[1] E. Frew and T. Brown, “Airborne communication networks for small unmanned aircraft systems,” *Proceedings of the IEEE*, vol. 96, no. 12, pp. 2008–2027, 2008.

[2] D. Henkel and T. X. Brown, “On controlled node mobility in delay tolerant networks of unmanned aerial vehicles,” in *International Symposium on Advance Radio Technolgoies (ISART)*, pp. 7–9, 2006.

[3] A. Jenkins, D. Henkel, and T. X. Brown, “Sensor data collection through gateways in a highly mobile mesh network,” in *IEEE Wireless Communication Network Conference*, pp. 2786–2791, 2007.

[4] E. Yanmaz, “Connectivity versus area coverage in unmanned aerial vehicle networks,” in *Communications (ICC), 2012 IEEE International Conference on*, pp. 719–723, 2012.

[5] F. Ono, H. Ochiai, K. Takizawa, M. Suzuki, and R. Miura, “Two-way relay networks using unmanned aircraft systems,” in *Vehicular Technology Conference, 2013. VTC 2013-Spring. IEEE 77th*, 2013.

[6] T. Takahashi, H. Yukio, O. Yasuo, and K. Tomonori, “Overview of earth stations for winds overview of earth stations for winds overview of earth stations for winds experiments,” *Journal of the National Institute of Information and Communications Technology*, vol. 54, no. 4, pp. 61–63, 2007.

[7] *ITU-T Recommendation P.862.3 Application guide for objective quality measurement based on Recommendations P.862.*

THE 18TH INTERNATIONAL SYMPOSIUM ON WIRELESS PERSONAL MULTIMEDIA COMMUNICATIONS
(WPMC-2015)
December 13-16, 2015, Hyderabad, India

Secure and Privacy Enabled Anonymous Computing for Heterogeneous (SPEACH) IoT

Meena Singh, Rajan M A, Shivraj VL, Balamuralidhar P

TCS Innovation Labs, Bangalore 560 066, India
Email:{meena.s1, rajan.ma, shivraj.vl, balamurali.p}@tcs.com

***Abstract*—Secure and Privacy Enabled Computation (SPEC) for Internet of Things (IoT) system is still at nascent stage. This is an important functionality which needs to be integrated into IoT systems specifically for Cloud deployments. Further this drives designing and deploying thousands of applications to envisage smart systems and also provides an opportunity to enable dynamic, adhoc computations in a secure and privacy manner. To realize this, feasibility of applying existing SPEC technologies and underlying cryptographic schemes for IoT is essential. In this direction, we study readiness and adaptability of existing SPEC techniques for IoT systems. Further, we propose and validate a framework to envisage Secure and Privacy Enabled Anonymous Computation for Heterogeneous (SPEACH) IoT.**

I. Introduction

Recent advances in computing Internet of Things (IoT) challenge the research community with plethora of requirements. One such requirement is Secure and Privacy Enabled Computing (SPEC). Over the years, trend in the area of IoT research was targeted at achieving; how to secure device, communication and data in IoT? Moreover, future digital world envisions Internet of Everything. For this to happen, IoT systems with large number of heterogeneous devices, gateways (GWs), public and private clouds are going to be deployed across the globe. To enable this, two preliminary requirements need to be addressed: (i). Sharing of data between different GWs anonymously for various data analytics decision. (ii). Dynamic function computation in a real time in an adhoc manner,over such data. One major challenge is; how to realize the above in a secure and privacy preserving manner? In general, fundamental questions that arise here are: What are the real time computing requirements of IoT and how many of them need security and privacy? Are the existing cryptography based solutions adaptable for IoT? To address the former, there exists several computing paradigms such as Cloud and Fog Computing. However, very little work is carried out with respect to (w.r.t.) SPEC [1]. Though privacy is addressed extensively in [2], it is limited to IoT devices only and not on SPEC.

Further from the literature survey, it is found that for Cloud and Fog computing for SPEC needs to be addressed. Though security and privacy are handled in Cloud computing, there is no extensive study of these issues for Fog computing [1], [3]. Thus as part of this paper, we study feasibility of SPEC techniques for IoT in Cloud and Fog Computing paradigms. From our study, we infer that to address later, not much work is happened [1]. In this paper, we discuss analytically and experimentally, feasibility of adapting existing SPEC techniques such as searchable encryption, homomorphic encryption, multi party computation, proxy re-encryption and differential privacy for IoT.

Hence in this direction, our main contribution in this paper is to: (i). Evaluate existing SPEC technologies and underlined cryptographic schemes from feasibility, adaptability and limitations to deploy them for IoT systems under different computing paradigms. The two aspects of SPEC considered are secure and anonymously fetch data from IoT devices (searchable encryption) and perform computation in a privacy preserving manner. (ii). Propose and validate a framework to envisage Secure and Privacy Enabled Anonymous Computing for Heterogeneous (SPEACH) IoT under a hybrid cloud computation paradigm.

Paper is organized as follows. In Section II, we describe current state of the art. Various SPEC technologies and cryptography schemes which are relevant for IoT are discussed in Section III. In Section IV, we propose SPEACH IoT framework and is validated through simulations in Section V. Finally paper is concluded in Section VI.

II. Related Work

A. IoT Architecture

OneM2M architecture is proposed for Machine to Machine (M2M) communication [4]. Different architectures involving IoT devices that connect to Cloud platform (like Azure) under the umbrella of diversified industry verticals such as health care, utility, transport and enterprise are discussed in [5]. Aneka, a new Platform As A Service (PaaS) based on .Net framework was proposed and it is a hybrid model with combination of public and private clouds.

B. Secure Computing Paradigm for IoT

To envisage SPEC, several cryptographic techniques based on Functional Encryption such as Homomorphic Encryption (HE) (partial, fully, somewhat), secure Multi Party Computation (MPC), Oblivious Transaction Protocol (OTP) and Differential Privacy (DP) are applied. In HE, idea is to operate any function over an encrypted data. For instance addition of two integers is equivalent to performing addition on two encrypted integers and then result is obtained by decrypting it. Mathematically addition of two integers x and y, $x + y = D_K(E_K(x) + E_K(y))$ (where $E_K(.)$ and $D_K(.)$ are encryption and decryption operator for HE), is equivalent to decryption of sum of two encrypted integers. These schemes are either additive or multiplicative. Craig Gentry [6] proposed

a Fully Homomorphic Encryption scheme (FHE) based on lattices which is both additive and multiplicative. Brakerski et al., devised a Somewhat FHE based on intractability assumption of Learning With Errors (LWE) [7]. This scheme is practcially implementable and hence we use this scheme for SPEC. Further, secure MPC [8] schemes involves various parties with distinct inputs and computing a result such that individual inputs are not known to each other and result of the computation is shared to every party. However MPC schemes are computationally complex and is not useful for computing complex operations.

Other aspect of SPEC is Searchable encryption (SE), which is used for searching over encrypted data [9], there are two types of schemes: (i). Symmetric Searchable Encryption (SSE, searching on ones data). (ii). Asymmetric Searchable Encryption (ASE, searching others data). Search keyword is expressed in through a regular expression or a token. We implement ASE [10] scheme for searching over large data encrypted using public key encryption and search this using a regular expression. Advantage of this scheme is that it also supports partial searching.

Finally, we discuss some of these techniques which are utilized for IoT to perform SPEC. IoT is modeled as Cooperative Distributed System (CDS) in [11]. This is a computation platform wherein devices share information and capability among each other in a privacy preserving manner (achieves at least 50% of device privacy) by Differential Privacy (DP) with the help of broker. However this scheme supports partial privacy preserving computation involving many parties. Further for smart meter data analysis, DP based scheme is used in [12], [13].

III. Privacy Enabled Computing in a Nutshell

Typical characteristics of IoT are heterogeneity of (i). Devices (limited computing and battery power) (ii). Connectivity and interfaces between devices. (iii) topologies (hierarchical, random). These features causes overhead in designing and deploying applications for various purposes such as smart infrastructure (home, city, grid, ...) in a secure and privacy preserving manner. Further these applications demand real time computation for IoT systems without losing security and privacy of data and devices. Existing Cloud and Fog computing paradigms address privacy issues in a very limited way and hence SPEC frameworks needs to be augmented. In this section, we bring out some of the very important frameworks and their capabilities, strengths and weekness w.r.t. augmenting it to the existing computing paradigms for IoT.

A. Cryptography for Privacy Enabled Computation

To envisage SPEC for IoT, efficient cryptographic techniques are essential. In this section, we examine (c.f. Table I) some of these relevant techniques from: (i). utility, (ii). computation complexity, (iii). level of security and (iv). limitations perspective. Though goal of any IoT system is to achieve high utility with higher level of security and that needs to be achieved with lower computation, there is a trade off among (i), (ii) and (iii). Thus efficiency of SPEC for IoT depends on the underline cryptographic techniques employed.

From the Table I, we infer that for less complex computations, MPC schemes are better (in particularly 2PC) and mainly aggregation operation is involved. This technique is suitable for IoT, since some of the IoT systems are hierarchical in nature and computations are distributed. However malicious parties perturb the result of computations and in order to overcome this a stringent traitor tracing algorithms are needed which are computationally expensive. Further FHE schemes are useful, wherever arithmetic computations are performed. This can be used in any IoT systems such as smart meter and smart grid applications. Though theoretically, these schemes support strong security at the cost of large key size, they incur higher computational overhead when large number of successive operations are performed (due to re-linearizion technique in FHE) [7]).

For privacy enabled logical operations, Ordered Preserving Encryptions (OPE) are better than garbled circuit based approach (suitable for one time execution) for IoT in terms of computations. DP scheme is useful for statistical query processing over a large data set and in particular it is useful for offline IoT analytics. Though zero knowledge protocols are useful to verify integrity of the software (Verifiable Computation), they are computationally expensive. Hence this technique is preferred only in case of critical applications and it is not suitable for general purpose IoT applications. Private Information Retrieval (PIR) is an interactive tool applicable to retrieve data based on secret index, which is computationally expensive and hence not applicable for IoT applications. Thus the design of SPEC for IoT is greatly influenced by the underlying cryptographic techniques. In the next subsection, we analyze existing SPEC frameworks which uses some of these underlying cryptographic techniques.

B. Privacy Enabled Computation Frameworks

Some of the prominent SPEC models which are relevant for IoT systems are tabulated in Table II. We examine these models from different capabilities: (i). Different types of privacy enabled computations (searching, function evaluation). (ii). Computing point (computation done either at Device, Gateway or Cloud). (iii). Whether the computation is interactive or non interactive? (iv). Data security point (Whether data is encrypted at Device, Gateway or Cloud?). (v). Underlying cryptography technique. From IoT perspective, these factors are relevant and different types of applications or use cases need some subset of these capabilities of SPEC.

From the Table II, it is evident that Mylar and CryptDB are applicable for computation involving large databases. Limitation of these schemes are that they do not support all types of computation. Hence this is useful to perform offline data analytics for IoT. Secondly in [18] the authors have reported some frequency analysis based attacks on CryptDB wherein the identites can be inferred by matching encrypted records of CryptDB with public database. DCapBAC and UPECSI are used for authentication purpose and can be plugged to IoT framework. Mariana proposes different MPC schemes to compute and search on encrypted data. These schemes are lightweight and hence useful for IoT. In case of smart meter technology, several smart meters data are aggregated at a gateway level and there by they are suitable for IoT systems, where aggregations are required. Riposte is a secure messaging protocol which can be used for message passing during any

TABLE I: Privacy Enabled Computation Paradigms based on Cryptography

Sl No.	Crypto Primitive	Utility	Computation Complexity	Security Level	Limitation
1.	Symmetric	Encryption [14] (Xor Operation)	Medium	Medium	If secret key compromised scheme is broken
2.	Asymmetric (RSA based) (Public Key Encryption)	Encryption	Medium (Single Exponentiation)	High	Key management
3.	Multi party Computation (MPC) [8]	Computing any function	Medium (XOR in case of secret sharing)	High	Collision and Malicious parties cannot be traced
4.	FHE [7]	Computing arithmetic function	Medium	High	Errors while computing Multiplication
5.	Proxy Re-encryption [15]	Facilitates MPC	Medium (one exponentiation)	High	No practical schemes to convert to FHE
6.	Differential Privacy (DP) [16]	Computing any function	High Noise adds more computation	High	Not Fully Homomorphic
7.	Garbled Circuit	Computing Logical Operation	High	High	One time use only Re-usability not practical
8.	Order Preserving Encryption [14]	Comparison of data	High	High	Not for Computing
9.	Zero Knowledge Protocols [16]	Verifiable computing	High	High	Not practical for IoT
10.	Private Information Retrieval [17]	Secret Data Selection	High	High	Interactive and No computation
11.	Searchable Encryption (SE) [9]	Anonymized searching	Medium	High	Complexity is High for large search space

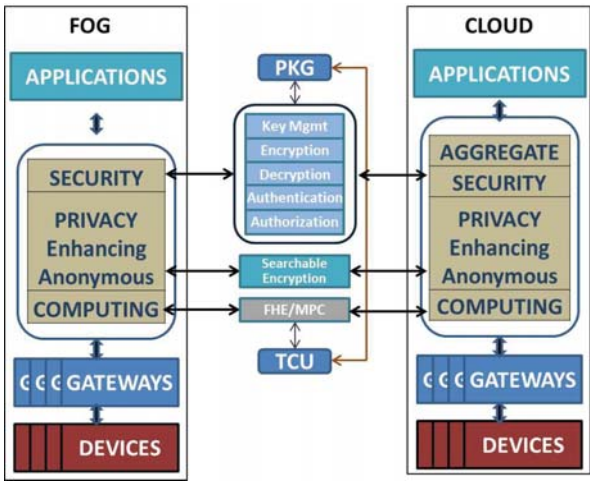

Fig. 1: Architecture diagram of SPEACH framework

computation. DJoin protocol is used for computing on distributed databases. Hence these two schemes are candidates for offline data analytics. From this analysis, we infer that, though these technologies and underlying cryptography schemes are useful in designing specific applications (for instance smart meter data analysis, large data analytics applications), they are not directly deployable for IoT systems in general. Careful integration of these technologies is very essential to envisage secure anonymous data retrieval and SPEC. Further some of these techniques are computationally expensive and don't support SPEC fully. Hence this requires a need of Trusted Computing Unit (TCU) which is capable of decoding partial results of SPEC and through which fully SPEC is enabled. Hence to address these limitations, we propose secure and SPEC for IoT under hybrid Cloud in the next section.

IV. Secure and Privacy Enabled Anonymous Computation for Heterogeneous (SPEACH) IoT

Proposed Secure and Privacy Enabled Anonymous Computation for Heterogeneous IoT is illustrated in Fig. 1. It assumes that basic functionality of security framework (Confidentiality, Integrity and Authentication) is available and on top of this, SPEACH is envisaged. Note that SPEACH framework can be augmented on existing IoT architecture such as OneM2M IoT architecture [4]. Two Important entities of SPEACH are: (i). Anonymously retrieving encrypted data (SE) from different IoT Devices, Gateway or Cloud. (ii). Securely computing over encrypted data. As discussed earlier, in case of existing SPEC techniques, certain computations cannot be performed in a privacy preserving manner fully. Hence there is a need for TCU to enable it (c.f. Fig. 1). TCU is capable of decoding partial results and facilitate computing in a privacy preserved manner. Thus flexible design of SPEACH is adaptable to support SPEC for hybrid Cloud architectures. Deployment of SPEACH for Cloud and Fog computing are similar, except that in case of Cloud computing the aggregation function is embedded at its place while in Fog the computing is pushed to the endpoints. Further at Cloud, SPEACH is capable of performing SPEC in an offline manner.

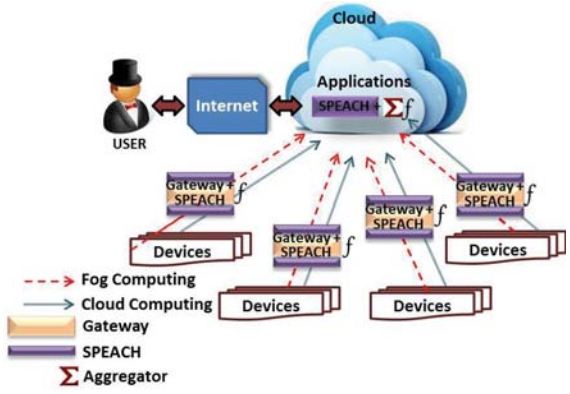

Fig. 2: Deployment of SPEACH framework

Now, we explain how SPEC can be performed for an IoT application which illustrate hybrid cloud computing through SPEACH with an example (c.f. Fig. 2). Consider a scenario, where an user invokes an application at Cloud to compute a utility function (say current power consumption). This is performed interactively in several steps. Initially the application requires data from different devices (say smart meters). Information about these devices (such as locations, relevant gateway) are stored in encrypted form at Cloud and gateway. To retrieve this information anonymously, SE algorithm of

TABLE II: Privacy Enabled Computing Frameworks

Sl No.	Scheme	Crypto Technology	Operation	Computing Entity	Interactive	Code Integrity	Authentication	Encryption
1.	Mylar [19]	Asymmetric	Search	Gateway	No	IoT Dev App Secure	IoT Device	Asymmetric
2.	CryptDB [14]	Symmetric Order Preserving Encryption	Comp Search	Gateway	No	Cloud DB Secure	IoT Device	Symmetric
3.	DCapBAC [20]	Asymmetric	None	Cloud	No	No	IoT Device	Asymmetric
4.	Mariana [8]	MPC	Comp & Search	Cloud	Yes	Yes	No	Asymmetric
5.	UPECSI [1]	Asymmetric	none	Cloud	No	Yes	IoT Device	Asymmetric
6.	Smart Metering [13]	HE	Comp	Cloud	No	No	No	Asymmetric
7.	Smart Metering [12]	HE Bit Commitment Zero Knowledge Protocol	Comp	Cloud	Yes	No	No	Asymmetric
8.	Riposte [21]	PIR	Messaging	Cloud	Yes	No	No	Asymmetric
9.	DJoin [16]	DP	Comp	Cloud	Yes	Yes	No	Asymmetric

SPEACH is invoked using the information about the devices. After obtaining relevant information, application requests relevant GWs (let us say k number of gateways among n GWs: $\{G_1, G_2, \ldots, G_k\}$) which are deployed at different locations to compute SPEC. Subsequently, each gateway (G_i) fetches encrypted data from intended devices (which are connected to them) and performs required SPEC: $f_i(D_{i_1}, D_{i_2}, \ldots, D_{i_k})$. Note that $D_{i_1}, D_{i_2}, \ldots, D_{i_k}$ are encrypted data from devices of i^{th} gateway. After this, these GWs forward encrypted result to the Cloud application. Then at Cloud, application performs SPEC based aggregation in order to compute resultant function ($f = \sum_{i=1}^{k} f_i$). Finally result is sent to user and subsequently user decrypts the end result.

V. Simulation Results

A. Simulation Setup

We validate SPEACH framework through simulation. We implemented and simulated IoT architecture deployment (c.f. Table III) as described in Fig. 2 with 100 devices, 5 GWs (20 devices per GW) and a hybrid Cloud and SPEACH is deployed at GWs and Cloud as well. We implement two major functionalities of SPEACH (i). Searchable Encryption [10]. (ii). SPEC based on and SW-FHE [7]. As part of encrypted search function, IoT devices encrypt data (about type of device, location, data model, gateway, etc.,). This data is stored at Cloud Database based on Damgard-Jurik crypto system. An User/Application initiates SE query with encrypted keywords (such as sensor location, id, etc.,) and is executed interactively between both User/Application and Cloud. Advantage of this scheme is that algorithm supports all types of encrypted search (prefix, suffix or full keyword search). We tabulate computation time at Application/GW and Cloud for different number of records. Data is encrypted using key size of 8 bits. Database and queries are prepared such that for each execution, number of search hits is 30% of total number of records.

Further to realize SPEC based on FHE, we compute $f = \sum_{i=1}^{100} a_i * b_i$ (where a_i and b_i are encrypted integers of size 8, 16, 32, 64 and 128 bits) at Cloud and GW (Fog computing). In Cloud Computing, IoT devices encrypt data and send it to the Cloud via GW. Computation is performed by the Cloud. In case of Fog Computing, each GW receives encrypted data from 20 devices and computes ($f_i = \sum_{k=1}^{20} a_{i_k} * b_{i_k} : i = 1$ to 5 and each a_{i_k} and b_{i_k} are data from sensor belong to GW G_i). Using SPEACH, all the GWs send computed values to the Cloud. At Cloud, $f = \sum_{i=1}^{5} f_i$ (aggregation function) is computed and final result is sent to user/application in encrypted format and subsequently user/application decrypts the result.

TABLE III: System Details

Hardware	Intel Core DUO CPU@3Ghz
Primary Memory capacity	2 GB
Operating System	Windows 7, 32bit
Java version	1.7
Database	MySQL 5.6

B. Performance Analysis

To enable secure and SPEC, retrieving data anonymously is achieved through SE. Performance of SE algorithm is very crucial. Hence we conduct performance analysis and Fig. 4 describes performance of SE, which involves interactions. Higher the complexity of the search query and larger the search space, more will be the number of interactions and thus more time it takes to search. This is evident from the plot and further note that time taken for client computation is less. Hence this scheme is suitable for IoT system. After determining data source locations, we perform actual SPEC computation. Performance of the computation depends on performance of data encryption, SPEC and decryption. Performance results are plotted w.r.t. computation time for various bit sizes (c.f. Fig. 5). We observe that encryption time is more than that of decryption and in case of IoT systems, encryption can be outsourced to a GW (to increase lifetime of IoT devices). Computation time w.r.t. SPEC performance is plotted in Fig. 5 for Cloud/GW(Fog) paradigm. Further we observe that computation time for a given function $f = \sum_{i=1}^{100} a_i * b_i$ is less at Fog than that of Cloud. Note that for both Cloud/Fog computing to simplify simulations, we didn't include communication overhead (which also affects performance of SPEC). From the results, we infer that for real time, dynamic and adhoc computations, where function needs to be computed in a distributed and shared manner, fog computation is better and also for predetermined computations, hybrid computation model is a better approach, wherein GWs compute the given function and aggregation is also done at GW. For offline SPEC computation in IoT systems (useful for predictive analysis), Cloud computing is preferred.

VI. Conclusion

Emerging applications for Cloud based IoT systems require secure and privacy enabled computation (SPEC). In this paper we established the fact that existing SPEC and underlined cryptography schemes cannot be directly deployed for IoT systems. Most of these techniques are computationally expensive and not fully privacy enabled. Further to envisage anonymous

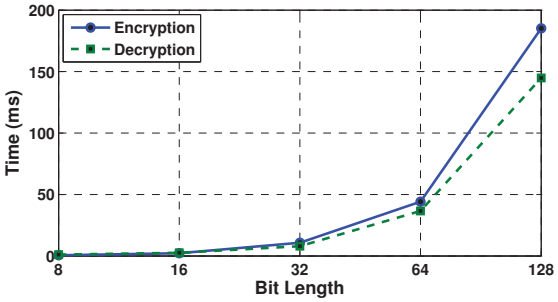

Fig. 3: Performance of Encryption and Decryption operations

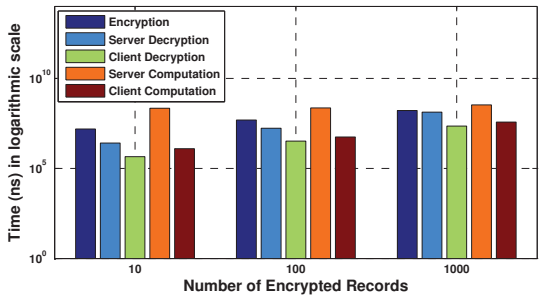

Fig. 4: Performance of Searchable Encryption Scheme

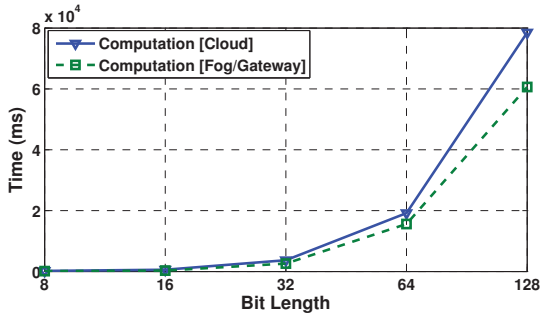

Fig. 5: Computation analysis for Cloud/Fog Computing

data sharing among different gateways in IoT and also to perform dynamic and adhoc SPEC in IoT system a secure and SPEC framework is essential. In this paper, we proposed and validated SPEACH IoT framework. As part of our future work, we will deploy SPEACH on real Cloud IoT systems and benchmark the performance and also work towards realizing robust SPEACH, which is resilient to different security attacks.

REFERENCES

[1] M. Henze, L. Hermerschmidt, D. Kerpen, R. Huling, B. Rumpe, and K. Wehrle, "User-driven privacy enforcement for cloud-based services in the internet of things," in *Proceedings of the 2014 International Conference on Future Internet of Things and Cloud*, ser. FICLOUD '14. Washington, DC, USA: IEEE Computer Society, 2014, pp. 191–196.

[2] M. V. M. Jos L. Hernndez-Ramos, Jorge Bernal Bernabe and A. F. Skarmeta, "Preserving smart objects privacy through anonymous and accountable access control for a m2m-enabled internet of things," *sensors*, vol. 15, no. 7, pp. 15 611–15 639, Jul. 2015.

[3] F. Bonomi, R. Milito, P. Natarajan, and J. Zhu, "Fog computing: A platform for internet of things and analytics," in *Big Data and Internet of Things: A Roadmap for Smart Environments*, ser. Studies in Computational Intelligence, vol. 546. Springer International Publishing, 2014, pp. 169–186.

[4] OneM2M. Function Architecture of IoT devices, OneM2M Standards for M2M and the Internet of Things. [Online]. Available: http://www.onem2m.org/technical/published-documents

[5] J. Gubbi, R. Buyya, S. Marusic, and M. Palaniswami, "Internet of things (iot): A vision, architectural elements, and future directions," *Future Gener. Comput. Syst.*, vol. 29, no. 7, pp. 1645–1660, Sep. 2013.

[6] C. Gentry, "Fully homomorphic encryption using ideal lattices," in *Proceedings of the Forty-first Annual ACM Symposium on Theory of Computing*, ser. STOC '09. New York, NY, USA: ACM, 2009, pp. 169–178.

[7] Z. Brakerski and V. Vaikuntanathan, "Fully homomorphic encryption from ring-lwe and security for key dependent messages," in *Advances in Cryptology CRYPTO 2011*, ser. Lecture Notes in Computer Science, vol. 6841. Springer Berlin Heidelberg, 2011, pp. 505–524.

[8] M. Raykova, "Secure computation in heterogeneous environments: How to bring multiparty computation closer to practice?" Ph.D. dissertation, Columbia University, 2012.

[9] C. Bösch, P. Hartel, W. Jonker, and A. Peter, "A survey of provably secure searchable encryption," *ACM Comput. Surv.*, vol. 47, no. 2, pp. 18:1–18:51, Aug. 2014.

[10] L. Wei and M. Reiter, "Third-party private dfa evaluation on encrypted files in the cloud," in *Computer Security ESORICS 2012*, ser. Lecture Notes in Computer Science, vol. 7459. Springer Berlin Heidelberg, 2012, pp. 523–540.

[11] A. Samani, H. H. Ghenniwa, and A. Wahaishi, "Privacy in internet of things: A model and protection framework," *Procedia Computer Science*, vol. 52, no. 0, pp. 606 – 613, 2015, the 6th International Conference on Ambient Systems, Networks and Technologies (ANT-2015), the 5th International Conference on Sustainable Energy Information Technology (SEIT-2015).

[12] A. Rial and G. Danezis, "Privacy-preserving smart metering," in *Proceedings of the 10th Annual ACM Workshop on Privacy in the Electronic Society*, ser. WPES '11. New York, NY, USA: ACM, 2011, pp. 49–60.

[13] Z. Erkin and G. Tsudik, "Private computation of spatial and temporal power consumption with smart meters," in *Applied Cryptography and Network Security*, ser. Lecture Notes in Computer Science. Springer Berlin Heidelberg, 2012, vol. 7341, pp. 561–577.

[14] R. A. Popa, C. M. S. Redfield, N. Zeldovich, and H. Balakrishnan, "Cryptdb: Protecting confidentiality with encrypted query processing," in *Proceedings of the Twenty-Third ACM Symposium on Operating Systems Principles*, ser. SOSP '11. New York, NY, USA: ACM, 2011, pp. 85–100.

[15] G. Ateniese, K. Fu, M. Green, and S. Hohenberger, "Improved proxy re-encryption schemes with applications to secure distributed storage," *ACM Trans. Inf. Syst. Secur.*, vol. 9, no. 1, pp. 1–30, Feb. 2006.

[16] A. Narayan and A. Haeberlen, "Djoin: Differentially private join queries over distributed databases," in *Proceedings of the 10th USENIX Conference on Operating Systems Design and Implementation*, ser. OSDI'12. Berkeley, CA, USA: USENIX Association, 2012, pp. 149–162.

[17] C. Cachin, S. Micali, and M. Stadler, "Computationally private information retrieval with polylogarithmic communication," in *Advances in CryptologyEUROCRYPT 99*. Springer-Verlag, 1999, pp. 402–414.

[18] M. Naveed, S. Kamara, and C. V. Wright, "Inference attacks on property-preserving encrypted databases," in *Proceedings of the 22nd ACM SIGSAC Conference on Computer and Communications Security, Denver, CO, USA, October 12-6, 2015*, 2015, pp. 644–655.

[19] R. A. Popa, E. Stark, J. Helfer, S. Valdez, N. Zeldovich, M. F. Kaashoek, and H. Balakrishnan, "Building web applications on top of encrypted data using mylar," in *Proceedings of the 11th USENIX Conference on Networked Systems Design and Implementation*, ser. NSDI'14. Berkeley, CA, USA: USENIX Association, 2014, pp. 157–172.

[20] J. L. Hernndez-Ramos, J. B. Bernabe, M. V. Moreno, and A. F. Skarmeta, "Preserving smart objects privacy through anonymous and accountable access control for a m2m-enabled internet of things," vol. 15, no. 7, 2015, p. 15611.

[21] H. Corrigan-Gibbs, D. Boneh, and D. Mazières, "Riposte: An anonymous messaging system handling millions of users," *CoRR*, vol. abs/1503.06115, 2015.

THE 18TH INTERNATIONAL SYMPOSIUM ON WIRELESS PERSONAL MULTIMEDIA COMMUNICATIONS
(WPMC-2015)
December 13-16, 2015, Hyderabad, India

On-going Field Experiment of NerveNet in Shirahama Town for Resilient Town Network

Masugi INOUE
Resilient ICT Research Center
NICT
4-2-1 Nukui-Kitamachi, Koganei, Tokyo 184-8795, Japan
inoue@nict.go.jp

Yasunori OWADA and Kiyoshi HAMAGUCHI
Resilient ICT Research Center
NICT
2-1-3 Katahira, Aoba-ku, Sendai, Miyagi 980-0812, Japan
{yowada, hamaguti}@nict.go.jp

***Abstract*—NerveNet is a regional-area platform network for providing resilient information sharing and communications even if the access to the Internet is impossible in emergency situations. It is composed of multiple basestations interconnected each other by a variety of Ethernet-based wired or wireless transmission systems, configuring a mesh-topological network. Database and service functions operate on each basestation in a distributed manner. In collaboration with Shirahama town in Wakayama prefecture in Japan, we deployed a NerveNet experimental network in the town as the town's resilient network. It is composed of nine basestations interconnected by 5.6GHz Wi-Fi and FWA, providing users with localized web access, voice phone, and messaging as well as ordinal Internet access via 2.4/5GHz Wi-Fi.**

Keywords—mesh network, resilient network, IoT, NerveNet

I. INTRODUCTION

The East Japan Great Earthquake and tsunami on March 11 badly damaged Japanese information and communications system. Many of the access networks and core networks in the areas were down due to link disconnections, system failures, and blackout. About 14000 cellular basestations stopped mostly due to power outage. Optical fibers, metal cables, and telephone lines were cut. These failures made it impossible for the people in the quake-hit areas to get, upload, and share information since they could not access to application servers on the Internet. People in other regions including Tokyo also could not make prompt phone calls due to the limitation of call acceptance for avoiding large-scale breakdown of their networks. Therefore, it was not easy to confirm family's safety and to figure out the extent of the disaster damages.

What we learned from those experiences is the importance of "bypass networks". See Fig. 1. Let cellular and fixed access networks be a main road. Usually, it is the best for us to use the main road for our communications. However, we learned that the main road might stop. Therefore, in order to prepare future disasters, we need to assume that the main road might stop and to prepare bypass roads besides the main road. The bypass roads composed of multiple, different networks could be better than that of a single network to increase tolerance to disasters. One of the bypass networks is disaster-resilient mesh-topological network, called NerveNet.

Figure 2 shows a concept of our bypass networks created in 2009. NerveNet, UAV radio relay system, and satellite system configure a resilient network. NerveNet covers a local-area communications while UAV radio relay and satellite systems provide communications between isolated, damaged areas and others. According to this concept, we developed and deployed a large-scale testbed network systems including the three systems in two campuses of Tohoku University March 2013 [1].

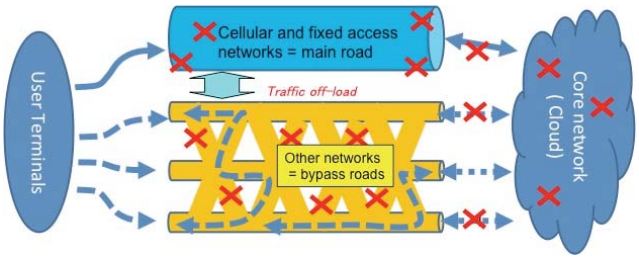

Fig. 1. A key to prepare future disaster is to build bypass networks besides main networks for increasing probability of our communications.

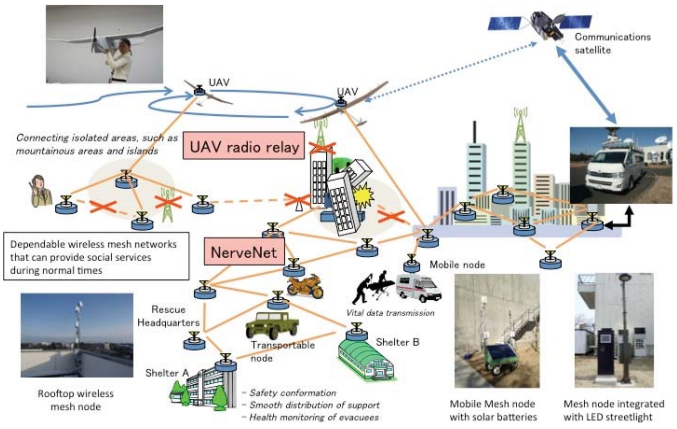

Fig. 2. Concept of bypss networks.

II. OVERVIEW OF NERVENET

A. Concept

NerveNet was originally designed as an access network of future network, future Internet or new generation network [2-4].

It is a regional network that provides various context-aware services with use of sensors and actuators. We named it as NerveNet since it works like the nervous system of the human beings.

B. *Physical Architecture*

NerveNet is composed of multiple, distributed basestations interconnected with each other by means of a variety of Ethernet-based transmission systems such as optical/metal Ethernet, WiFi, FWA, satellite, and unmanned aerial vehicle (UAV), configuring a mesh-topological network as shown in Fig. 3. A set of a basestation consists of one main unit and several pairs of a radio transceiver and an antenna. One pair is for accommodating users' WiFi appliances while others are for interconnecting basestations. Each transceiver is connected to and powered by a main unit through a PoE Ethernet cable. A typical set of basestation consumes 50 Watt or less, enabling its operation by solar power only as necessary.

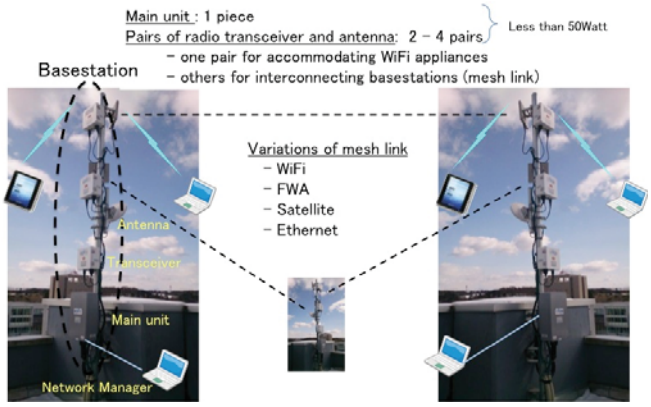

Fig. 3. Configuration of NerveNet.

A basestation main unit consists of a LAN switch and a CPU board for controlling the switch, providing packet transmission and applications using distributed database among all the basestations over a mesh network. This simple configuration promises its low price at its commercial phase. A network manager, which can be operated on a PC, is necessary to configure the network at the first stage. It is, however, not necessary after the network starts working because the network operates in a distributed manner without such central controller. As NerveNet is basically a LAN-based network system, ordinal computers and servers can be connected directly with Ethernet cables.

C. *Main Features*

NerveNet features communications and networking, and information processing as in Fig. 4.

The first is the provision of fast multihop Ethernet-frame transmission over a mesh-topological layer-2 network. Upon a request of a communication between any two users at different basestations, NerveNet assigns one of multiple virtual LANs to the communication. When the virtual LAN suffers from a link disconnection or a failure of a basestation on the route, the communication is switch over to another virtual LAN.

The CPU board in a basestation performs information processing, providing distributed database management system across all the basestations. Any data such as user data, a local map, evacuation points and routes, AED locations, and sensor data, can be data entry and shared in the network. Although the capacity of the CPU board is small, important information needed in emergency situations can be stored in the database so that users can get it even if they cannot access to the Internet.

Thus, compared with existing Internet-depend, tree-topological network systems, NerveNet is tolerant to link disconnections and system failures.

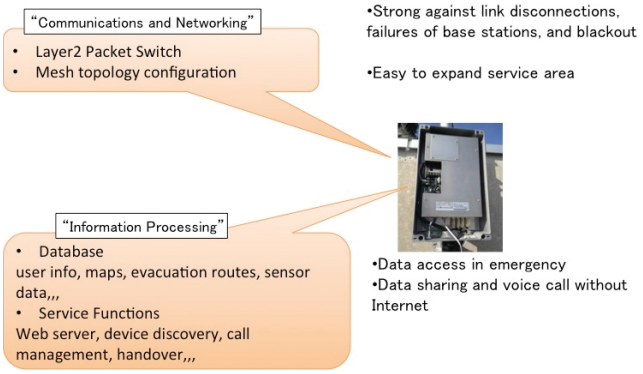

Fig. 4. Features of NerveNet: "communications and networking" and "information processing".

III. Architectural Paradigm Shift

A key of NerveNet is a paradigm shift of both networking architecture and application architecture as illustrated in Fig. 5.

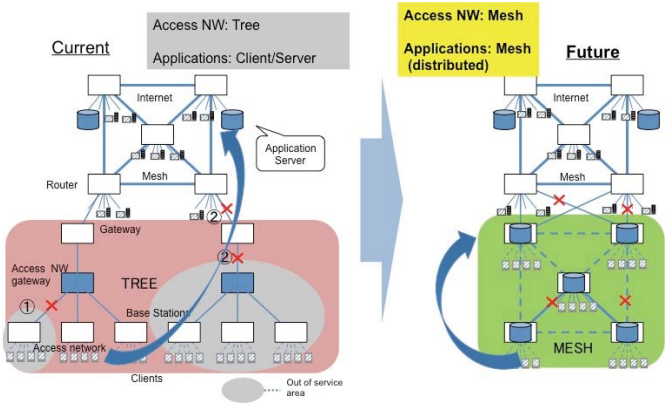

Fig. 5. Key point of NerveNet: shifting architecture of network from tree to mesh and application architecture from remote (cloud) to local.

Although tree-topological network is efficient in providing communications between remote users, it is weak against failures. Even if an access network is working and mesh-topological Internet is strong against failures, our smartphones or clients need to communicate with application servers on the Internet. Namely, this is client-server or point-to-point architecture in the application layer. This is very weak against failures and overloads of servers.

NerveNet is a mesh-topological access network and provides distributed database and information processing

functions over it. This makes the network and application services strong against failures and makes it possible to continue certain services without the user of resources on the Internet. NerveNet can also provide faster response services to end users and actuators compared to remote cloud-based architecture. This is another benefit to be emphasized.

IV. Field Experiment in Shirahama Town

A. Shirahama Town

Shirahama town is located in about the middle of Wakayama Prefecture in Japan as depicted in Fig. 6. It has a small population of about twenty-two thousands but a large number of tourists around three millions a year come for sightseeing and recreations. More than seventy thousand tourists from abroad visited last year. Shirahama town, on the other hand, has to prepare against natural disasters such as typhoons and earthquakes. In particular, it has to provide against a mega-scale earthquake and tsunami predicted by Japanese government to take place in the Nankai Trough off the Pacific coast. Several-meter to twenty-meter tsunami is predicted at the coast of Shirahama as shown in Fig. 7. This motivates the town to demand a system for ensuring safety of residents and tourists.

Fig. 6. Location of Shirahama town.

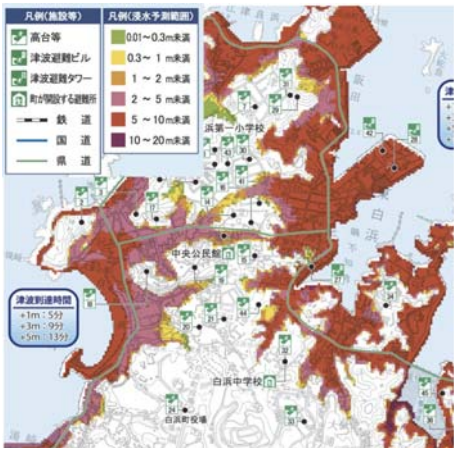

Fig. 7. Estimated tsunami heights in Shirahama.

B. Goal

Shirahama town office and NICT made an agreement of a collaborative work for resilient network in December 2014 and started preparation of a field experiment of NerveNet in the town. The goal of the experiment is to make clear the effectiveness and sustainability of NerveNet in ordinary and emergency situations in collaboration with local authorities, organizations, residents and tourists, creating a reference model “Shirahama model”. It could be applied to other regions having similarities with Shirahama such as location (coast side), topography, types of disasters, etc.

C. Setup of Experimental Network

We deployed nine basestations in total in the region and configured a NerveNet in May 2015 and started a field experiment that will last until March 2016 at least. The configuration is shown in Fig. 8. Eight basestations are in the town and another in the neighboring “Tanabe” city. Locations are Shirahama town hall, Shirahama hospital, Shirahama open-air hot-spring bath called “Shirara-Yu”, “Minakata Kumagusu” Museum, three hotels (hotel A, B, and C), a restaurant near “Senjo-jiki” in Shirahama town and Wakayama Prefectural Information Exchange Center “Big-U” in Tanabe city. Each basestation is installed on the top of each building. A commercial FWA system in the 4.9GHz (IEEE802.11j) is used for the inter-BS link between Big-U and Hotel A at a distance of about 5 km. Wi-Fi transmission systems in the band of 5.6GHz (W56) are used for other fifteen links including the link of around 2 km between Minakata Kumagusu Museum and Senjo-jiki across the sea. Basically a channel of eleven channels in W56 band is assigned to each link to avoid interference as best as possible. Connection modes of W56 links range from 6Mbps to 54Mbps depending on link distance.

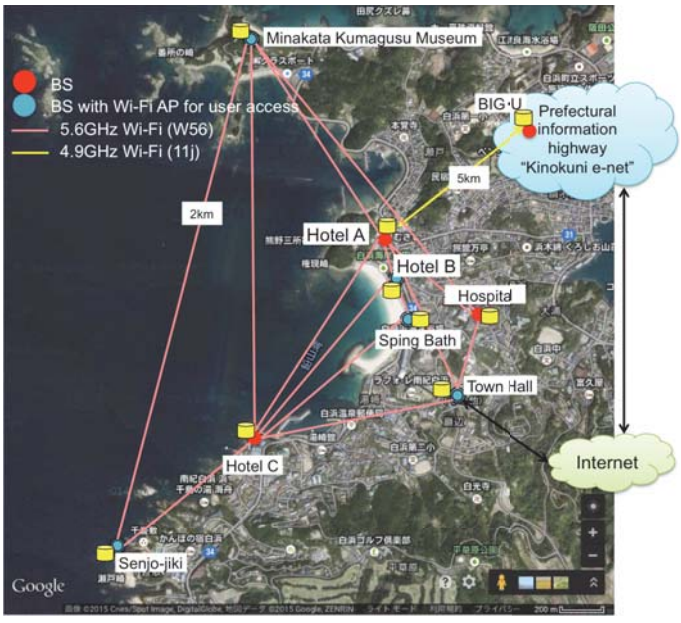

Fig. 8. Configuration of the experimental network.

It has two connections to the Internet to improve resilience. The BS at Shirahama town hall is connected to NTT’s Internet access network while another at Big-U is connected to the

Internet through Wakayama Prefectural Information Highway "Kinokuni e-net". Wi-Fi access point for user access operated in the bands of both 2.4GHz and 5GHz is also installed to provide access to this network as well as public free Internet access via Wi-Fi to residents and tourists at five BSs: Minakata Kumagusu Museum (see Fig. 9), hotel B near Shirarahama beach (see Fig. 10), Shirara-Yu near the beach, Shirahama town hall, and Senjo-jiki.

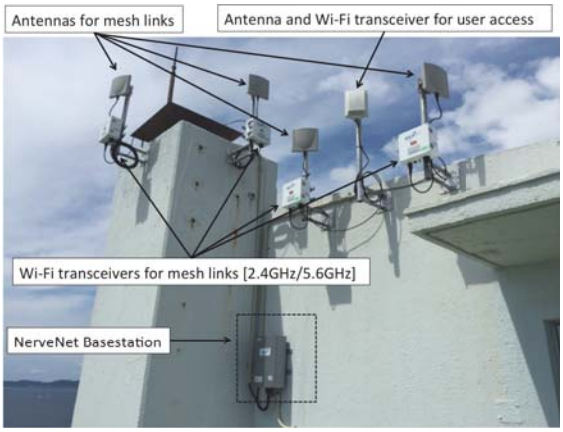

Fig. 9. Installed equipment at Minakata Kumagusu Mueseum.

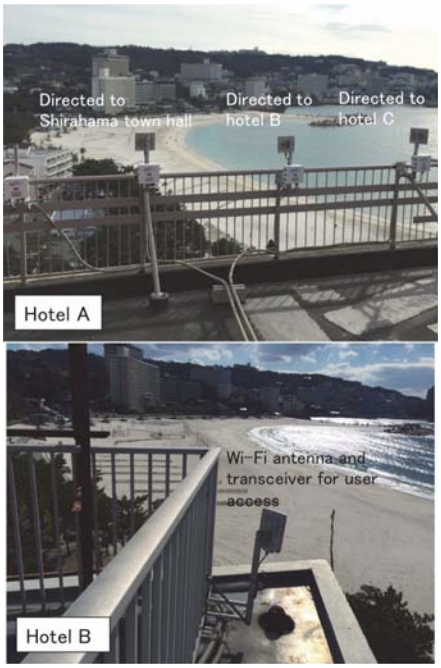

Fig. 10. Three Wi-Fi antennas and transceivers for mesh links at Hotel A (top) and the one at Hotel B for user access from the beach (bottom).

D. Applications

The experimental network provides four applications to users (Fig. 11). The first is Internet access. The second is geo-localized data access through a web server function running on each basestation. Using this functionality, potentially we can present different contents and different applications to users accessing to the network from different locations without using power-consuming GPS-based positioning. In the experiment, we provide a shelter map around the connecting basestation (Fig. 12). Furthermore, "Kokodake BBS" is provided (Fig. 12). Users can enter their notes for their memory and footprint in case of emergency. The notes stored at a basestation can be read only at the same basestation. The third and fourth are intranet voice call and intranet messaging using a dedicated application software for Android OS. Because NerveNet have call management and mobility management functions based on SIP, these applications can work without any servers on the Internet.

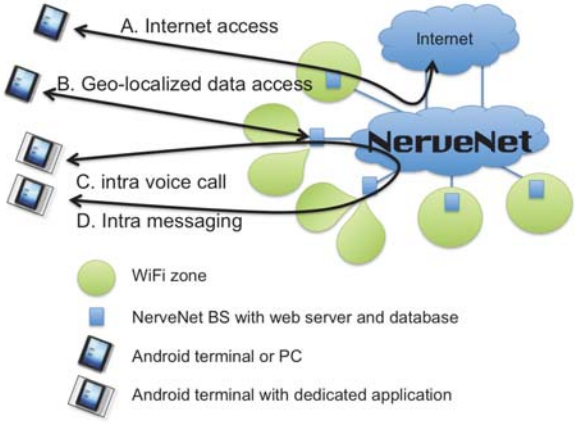

Fig. 11. Available applications in the experiment. Applications B, C, and D do not need the Internet.

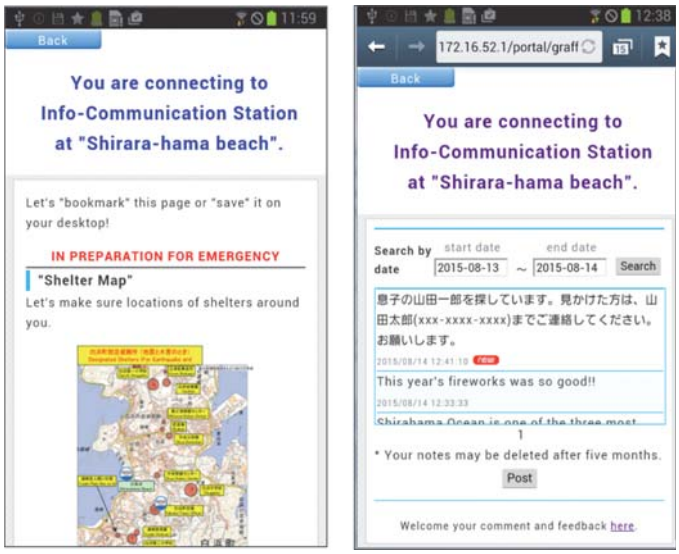

Fig. 12. Top page of a basestation's web (left) and "Kokodake BBS" where you can enter your notes (right).

V. Use Cases and Benefits of NerveNet

According to interviews conducted by NICT and companies with several tens of Japanese local governments on their needs and problems, we found that they want to provide public local services at low cost in a safe manner. They include distribution of sightseeing information, surveillance of roads and rivers, warning and alert, road traffic control, sharing of bicycles, surveillance of garbage dumps, local security such as

outdoor monitoring of children and elderly people and indoor monitoring of elderly people living alone, prevention and control of wildlife damage, and position reporting of local buses. Another interview with local governments that suffered from The Great East Japan Earthquake showed that they had needed a tool for talk or information exchange between staffs in the situation where neither cellular nor fixed networks had been available. They do not mind if it is not available anywhere. They would satisfy even if it were available at very limited locations in case of emergencies. Thus, NerveNet could be a solution to these needs and problems. Figure 13 illustrates an image of NerveNet and its use scenes in an urban area.

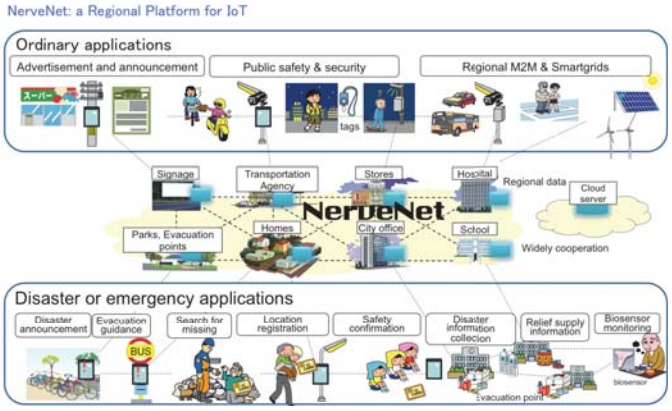

Fig. 13. Use scenes in an urban area.

Functions and benefits of NerveNet are summarized as follows.

1. It works as a regional LAN to directly interconnect a local government, authorities, companies, and residents as well as IoT devices such as digital signage and monitoring sensors, enabling two-way data communications such as collection, exchange, and distribution of any information including sensor data, voice and video, and messaging.
2. Because of resilience of both networking based on layer-2 mesh configuration and information processing based on distributed computation on each basestation, even in case where public networks and the Internet are not available, it is expected that it distributes important information on disasters, evacuation and rescue, food supply, etc., and it provides voice and message communications for government staffs and residents at a certain possibility.
3. It is possible to deploy an outdoor regional network at low initial cost and maintain it at low running cost because NerveNet can be configured with the use of variety of transmission systems including unlicensed radio systems. It is not necessary to deploy a network from the scratch. Existing fiber-based local-government network (called regional intranet in Japan) can be updated to NerveNet by installing NerveNet basestations as LAN switches and adding several new connections between basestations to obtain resilience. Commercialized wireless mesh network products cannot make such wired and wireless hybrid network because they assume to use Wi-Fi radio for mesh link and do not have enough Ethernet ports.

NerveNet applied to a rural area provides universal access for users to the Internet at low cost, gives security against disasters and sensing and alert services, and allows local communications without the outer networks such as the Internet and telephone networks, as depicted in Fig. 14. There are these demands not only in developing countries but also in Japanese rural areas.

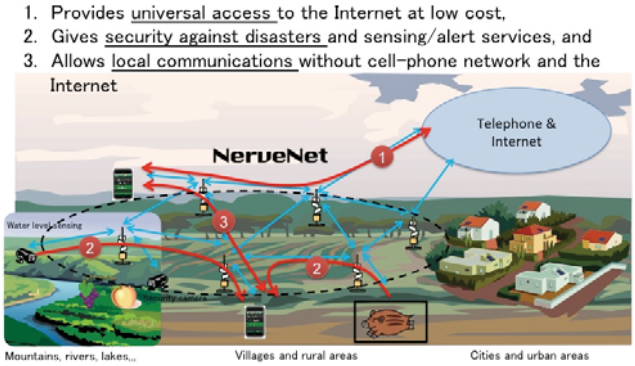

Fig. 14. Use scenes in a rural area.

VI. Concluding Remarks

NerveNet, which was originally designed as an access network of Future Network, has been developed as a resilient regional network platform. We have been gaining many attentions to this technology from IT companies, local governments, hospitals, fire departments, and authorities in ASEAN countries because probably there would be no such technology that can provide data access, data exchange, data sharing, voice call, and messaging without the Internet at low cost and low power. We will continue the experiment to obtain data to make clear the effectiveness and sustainability, creating Shirahama model for the reference to others.

Acknowledgment

We thank Mr. Makoto ITANI of the mayor of the town and Mr. Kazuhiro SAKAMOTO of the town office for their understanding and support of the experiment.

References

[1] R. Miura, M. Inoue, Y. Owada, K. Takizawa, F. Ono, M. Suzuki, H. Tsuji, K. Hamaguchi, “Disaster-resilient wireless mesh network - Experimental test-bed and demonstration,” WPMC 2013,

[2] M. Inoue, M. Ohnishi, H. Morino, T. Sanefuji, Y. Owada “Fast Recovery from Link Failures and Blackout of Managed Wireless Mesh for NerveNet,” IEEE GLOBECOMM, Dec. 2010.

[3] M. Inoue, M. Ohnishi, C. Peng, R. Li, Y. Owada, “NerveNet: A Regional Platform Network for Context-Aware Services with Sensors and Actuators,” IEICE Trans. Commun., Vol. E94-B, No.3, pp.618-629, Mar. 2011.

[4] Y. Owada, M. Inoue, M. Ohnishi, “Regional Wireless Network Platform for Context-Aware Services and Its Implementation,” 10th international Symposium on Autonomous Decentralized Systems (ISADS), pp.539-544, 2011.

THE 18TH INTERNATIONAL SYMPOSIUM ON WIRELESS PERSONAL MULTIMEDIA COMMUNICATIONS
(WPMC-2015)
December 13-16, 2015, Hyderabad, India

Fractal dimension of spectral estimates for spectrum sensing under noise variance uncertainty

Sesham Srinu, Amit Kumar Mishra
Department of Electrical Engineering
University of Cape Town, Cape Town, South Africa
Email: seshamsrinu83@gmail.com, akmishra@ieee.org

Siba K. Udgata, Samrat L. Sabat
Department of Computer & Information Sciences
University of Hyderabad, Hyderabad, India
Email: udgatacs@uohyd.ernet.in, slssp@uohyd.ernet.in

***Abstract*—Spectrum Sensing is a prime functionality that allows cognitive radio for opportunistic use of vacant bands in order to improve the radio spectrum utilization. Sensing the low signal-to-noise ratio (SNR) signal is essential to facilitate the quality of service for both licensed and cognitive users in a cognitive radio network. Though, there exist numerous sensing algorithms, their performance or reliability is sensitive to noise variance uncertainty, in particular in low SNR scenario. In this work, we propose a detection method based on fractal dimension of cyclic spectrum estimates of the received signal. Since the noise uncertainty is unknown to the detector, the noise variance uncertainty is assumed to be a random number which follows uniform distribution within the constraints. In addition, the proposed method is extended to cooperative sensing and analysed its performance by applying hard decision fusion techniques. The results reveal that the proposed method is less sensitive to noise variance uncertainty and improves the probability of detection under low SNR regime.**

***Index Terms*—Cognitive Radio, Cooperative spectrum sensing, spectral estimates, fractal dimension, Noise variance uncertainty.**

I. Introduction

The tremendous ongoing growth of wireless communication has resulted spectrum shortage which intern becomes an obstacle for growth of new wireless devices. However, recent statistical studies on radio spectrum usage have shown poor utilization of frequency bands due to rigid licensing policies. The spectrum shortage and inefficient utilization of spectrum make it necessary to develop a cognitive radio (CR) technology to exploit the existing radio spectrum opportunistically. One of the key challenges of the CR is to detect the presence or absence of the signal in a desired frequency band at low signal-to-noise ratio (SNR) with the constraint that it should not interfere with the primary user (PU) [1]. To achieve this, quite a few signal detection methods have been proposed over the last two decades, such as energy detection, entropy detection, cyclostationary detection, eigenvalue based detection, covariance based detection, and interference based detection etc.,[2], [3]. Each one of these has their own advantages and disadvantages.

Although, various detection techniques are proposed, all the methods require an estimate of the noise power a priori for fixing the value of the detection threshold. However, noise level in channel may change over time, which yields noise uncertainty. The traditional sensing algorithms are sensitive to noise variations in the received signal [4]. Nevertheless, many of the works considered energy detection due to its ability to work irrespective of signal format to detect, general applicability, and its simplicity [5], [6]. Because of the noise uncertainty, in practice, it is very difficult to obtain an estimate of the exact noise power. In the traditional sensing algorithms noise power is assumed to be known a priori and assumed to be Gaussian to design the detection threshold. In fact, real time statistical behavior of the received data at CR differs from the Gaussian approximation [4], [7], [8]. Hence, to deal with the noise uncertainty, we assume that noise uncertainty is uniformly distributed in the range as in [4]. The effect of noise uncertainty on generalized energy detector (GED) performance is studied with assumption of different uncertainty modeling [9]. The author introduced a signal detection method based on complexity of received time domain signal at cognitive radio. But, the performance of the above detectors at low SNR is very poor. In recent past, geometry of fractals and the mathematics of fractal dimension provide useful tools for a variety of scientific disciplines, in particular, the study of noisy signals [10], [11]. Many methods exist to compute the fractal dimension, each method has its own theoretic basis. The most popular methods among them are box counting method, minkowski dilation method, extended counting method, differential box counting method, a blanket method or frequency analysis, variogram method, isarithm method, and triangular prism method, etc., [12]. In this work, Higuchi Fractal Dimension (HFD) method is applied to find the roughness/complexity in estimated spectrum at one particular cyclic frequencies.

The focus of the current work is to detect the PU signal reliably in low SNR regime under noise variance uncertainty. To address the noise variance uncertainty in sensing, we propose a robust method which compute the Higuchi Fractal Dimension (HFD) of cyclic spectrum estimates of received signals. The method is based on the fact that the roughness of the spectral estimates varies as the SNR of the received signal changes. In addition, cooperative sensing performance based on proposed technique is analyzed under noise variance uncertainty by applying hard decision fusion logic [13].

Rest of the paper is organized as follows. Section II presents proposed sensing algorithm under noise uncertainty. Section III presents hard decision based fusion methods for cooperative

sensing. Simulation results are discussed in Section IV. Finally, our conclusions are presented in Section V.

II. Sensing algorithm under noise variance uncertainty

The objective of spectrum sensing is to discriminate between the following two hypotheses H_0 (PU signal active) and H_1 (PU signal inactive) in a desired frequency band.

$$H_0 : r(n) = w(n),$$
$$H_1 : r(n) = hs(n) + w(n), n = 0, 1, 2, \ldots, (N-1),$$

where $r[n] = [r(0), r(1), r(2), \ldots, r(N-1)]$ is the received signal sequence received by the CR user, N is the sample size. The channel gain (h), transmitted signal $s(n)$, and the $w(n)$ is additive white Gaussian noise (AWGN) with mean zero and uncertain variance. We assumed that the channel is time invariant during the sensing period.

In practice, the average noise power ($\hat{\sigma}_w^2$) is known [9]. But the actual noise power (σ_w^2) at fixed time and location is different from the average noise power, which is responsible for noise uncertainty. Hence, we can define noise uncertainty factor as $\beta_u = \frac{\hat{\sigma}_w^2}{\sigma_w^2}$. Let the upper bound on noise uncertainty factor in dB be φ which is defined as, $\varphi = \sup\{10\log_{10}\beta_u\}$. we assume that noise uncertainty factor β_u in dB is uniformly distributed in the range $[-\varphi, \varphi]$. This means beta is restricted in $[10^{-\varphi/10}, 10^{\varphi/10}]$. Hence the probability density function of β_u can be given by using simple transformation of random variable as

$$f(\beta_u) = \begin{cases} 0, & \beta_u < 10^{-\varphi/10} \\ \frac{2}{\ln(10)\varphi\beta_u}, & 10^{-\varphi/10} < \beta_u < 10^{\varphi/10} \\ 0, & \beta_u > 10^{\varphi/10} \end{cases} \quad (1)$$

where $ln(.)$ is the natural logarithm. The noise variance uncertainty (which follows Eqn. (1)) is included during signal generation for the decision test that can be seen in Figure.1.

A. Sensing algorithm based on HFD of spectral estimates

To compute the roughness, we consider HFD which is computationally less intense and can asses using only few samples. In this method, we construct k_n time series from the spectral estimates of fixed cyclic frequency ($S_r^{\alpha_d}(n, f)$) via sub-channels. The cyclic spectrum estimation of received signal can be formulated as [14]

$$S_r^{\alpha_c}(n, f) = \frac{1}{2N+1} \sum_{n=-N}^{N} \frac{1}{T} R_T(n, f + \frac{\alpha_c}{2}).R_T^*(n, f - \frac{\alpha_c}{2}), \quad (2)$$

where $R_T(n, f + \frac{\alpha_c}{2})$, $R_T^*(n, f - \frac{\alpha_c}{2})$ are the complex envelops of narrowband, and band pass components of the signal $r(n)$. These can be expressed as

$$R_T(n, f) = \sum_{k=-N'/2}^{N'/2} a(k)x(n-k)e^{-j2\pi f(n-k)T_s}$$

$$R_T^*(n, f) = \sum_{k=-N'/2}^{N'/2} a(k)y(n-k)e^{-j2\pi f(n-k)T_s}$$

Here $a(k)$ is a data tapering window of length $T = N'Ts$ seconds and the sampling period is Ts, N' is the number of points in the discrete FFT, k is the frequency (discrete). And the '$*$' denotes the complex conjugate, α_c is the frequency separation or cyclic frequency. N is the total number of discrete samples in the observed frame. Eventually, spectral estimates ($S_r^{\alpha_d}(n, f)$) is calculated using Eqn. (2) at desired CF whose index is estimated as $(Ceil(length(\alpha_c)/2))$.

Figure 1 shows the complete block diagram of proposed spectrum sensing method based on fractal dimension of spectral estimates under noise variance uncertainty. In this model the noise added to the PU signal have uncertain and it can take the random values whose distribution is uniform. Then, the spectral estimates are computed using FFT accumulation method at one particular cyclic frequencies (CF). The roughness of the spectrum is evaluated using HFD method and compared with a pre-defined threshold to make the decision about PU signal presence.

For i^{th} sub-channel signal with N samples, the constructed series can be expressed as [15]

$$x_{i,m}^{k_n} = \{y_i(m), y_i(m+k_n), ..., y_i(m+\psi.k_n)\}, \quad (3)$$

where $\psi = \frac{N-m}{k_n}$, k_n is an integer (called as scale size), and $m = 1, 2, 3, .., k_n$. The length of sub-series can be defined as:

$$L_{i,m}(k_n) = \frac{(N-1)\sum_{j=1}^{\varphi} |x(m+jk_n) - x(m+(j-1)k_n)|}{k_n \lfloor (N-M)/k_n \rfloor} \quad (4)$$

Then, we average $L_{i,m}(k_n)$ over m to obtain $L_i(k_n)$ and calculate logarithm of $L_i(k_n)$ for $1 < k_n < k_n\max$. The logarithm of $L_i(k_n)$ will depend on k_n in the following form.

$$\log(L_i(k_n)) = H_{fd}.\log(1/k_n) \quad (5)$$

where H_{fd} is an estimated fractal dimension. This measure can be used as a measure of complexity to sense the spectrum. Hence, in this work, we consider it as a test statistic to discriminate the hypotheses. Mathematically, the decision statistics to sense the frequency band is given as $H_1 : H_{fd} > \lambda_{fd}$ or $H_0 : H_{fd} \leq \lambda_{fd}$.

where λ_{fd} is the pre-defined detection threshold which depends on estimated fractal dimension of spectral estimates of white Gaussian noise of length N and probability of false alarm (P_f).

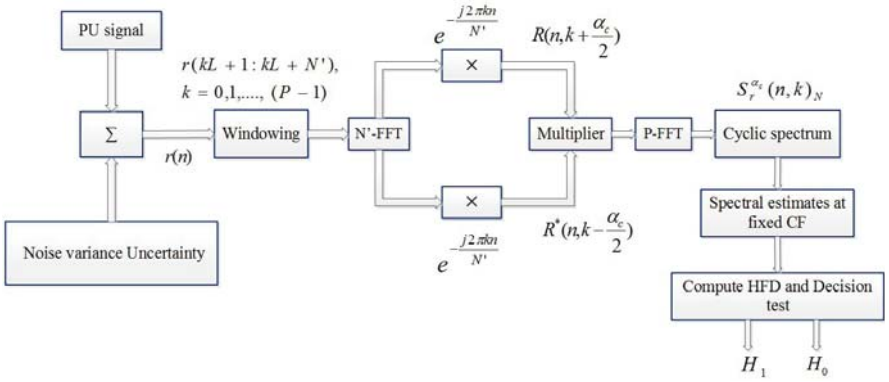

Fig. 1. Proposed sensing method based on fractal dimension of spectral estimates under noise uncertainty

III. Cooperative sensing using DS theory

In cooperative sensing, numerous fusion methods have been proposed to improve the sensing performance [16]. Among those methods, hard decision fusion techniques such as AND, OR, and MOST rules are commonly used to analyze the detector performance. Cooperative/cumulative detection probability (Q_d) of AND, OR, and MOST logics are given as [17]

$$Q_{\text{d-AND}} = \prod_{m=1}^{M} P_{d,m}, \tag{6}$$

$$Q_{d-OR} = 1 - \prod_{m=1}^{M} (1 - P_{d,m}), \tag{7}$$

$$Q_{d-MOST} = \sum_{m=n_d}^{M} \begin{pmatrix} M \\ m \end{pmatrix} P_{d,m}(1 - P_{d,m})^{M-m}, \tag{8}$$

where ($P_{d,m}$) and ($P_{f,m}$) are the detection and false alarm probability of m^{th} CR user, n_d is an integer representing decision threshold for most logic and its value is $n_d \geq M/2$, and $\begin{pmatrix} M \\ m \end{pmatrix} = {}^{M}C_m$ is a factorial function.

IV. Simulation results

In this section, we present our numerical results to describe the performance of energy detection and proposed detection method and effect of noise uncertainty on it. Quadrature Phase Shift Keying (QPSK) signal with variable SNR are considered as a PU signal. The noise uncertainty is modeled as uniform distribution. We model the fact that there is at most 'x'dB of uncertainty in the noise processes. In practical applications, the upper bound on noise uncertainty factor can be taken below 2dB [18]. The noise variance uncertainty is introduced during test which is fixed random value for one iteration and varies in each iteration in such a way that the distribution of noise uncertainty for all the iterations follows an uniform distribution. The sample length is taken as 256. In the case of energy detection, the threshold is pre-computed with noise variance one and for to achieve a tolerable (as per cognitive radio standard) false alarm probability. In the case of proposed method, the performance is evaluated based on estimated fractal dimension of spectral estimates at one particular cyclic frequency. The desired CF is evaluated as $(Ceil(length(\alpha_c)/2))$. Threshold evaluation of the proposed method depends on estimated fractal dimension of spectral estimates with noise alone in the received signal and probability of false alarm (P_f=0.1). The detection probability is estimated based on Monte Carlo simulations of 1000 iterations that mean the solutions are approximated to three decimal places. The snapshot/frame based method is considered for detecting a signal in the desired frequency band to be scanned. We extended the work to the cooperative sensing which use hard decision fusion techniques to make global decision. Number of nodes considered in cooperative network is a variable and taken up to 5. The performance of both sensing methods is presented signal strength against detection probability. Evaluation of detector performance is observed based on SNR vs. detection probability curves.

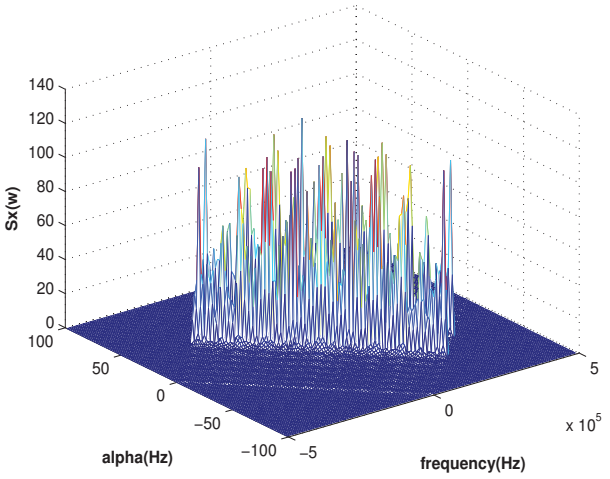

Fig. 2. Spectral estimates of WGN with different cyclic frequencies

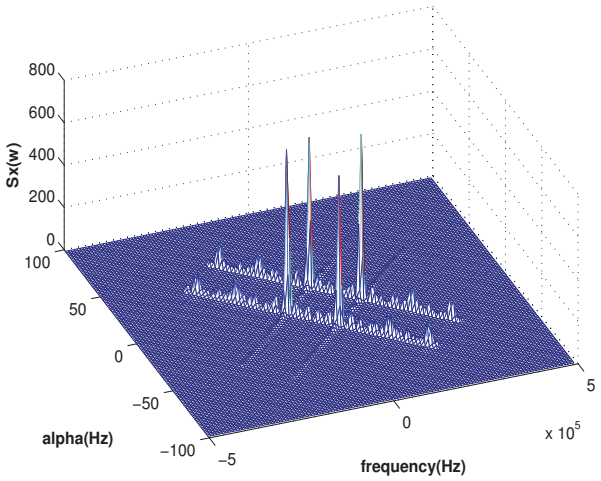

Fig. 3. Cyclic spectrum of received signal at SNR = 5dB, QPSK, N = 256

Figures 2 and 3 represents the cyclic spectrum of received signal with PU signal active and inactive at a particular frequency band, respectively. We considered rectangular windowing function to select the frame of samples. The uncertainty factor value is randomly taken within the considered range. From the figure, it can be seen that, cyclic spectrum has peaks at cyclic frequencies when the PU signal is present in the received sequence where as there is no significant peaks observable in noise (without PU signal in the channel).

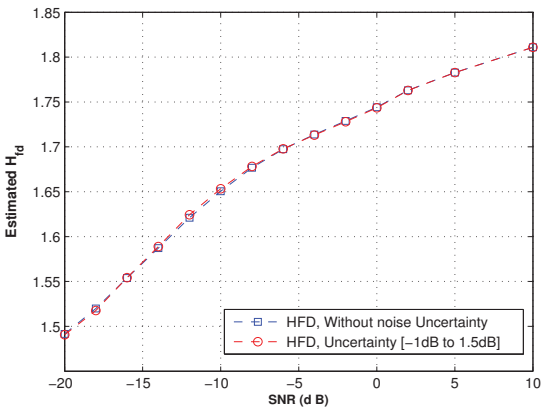

Fig. 4. Fractal dimension of spectral estimates at fixed cyclic frequency with variable SNR

Figure 4 represents fractal dimension of spectral estimates at one particular CF of received signal with different signal strength (varied from -20dB to 10dB). In the simulation, we have considered the K_n values from 4 to 10 and averaged their fractal dimension measure to improve the accuracy of the estimated HFD value. Where K_n is a number of sub-series composed from the received signal. From the figure, it is clear that the roughness of the spectrum increases as the signal-to-noise ratio of the signal increases. Hence, fractal dimension measure can be used one of the method to sense the PU signal in the band to be scanned.

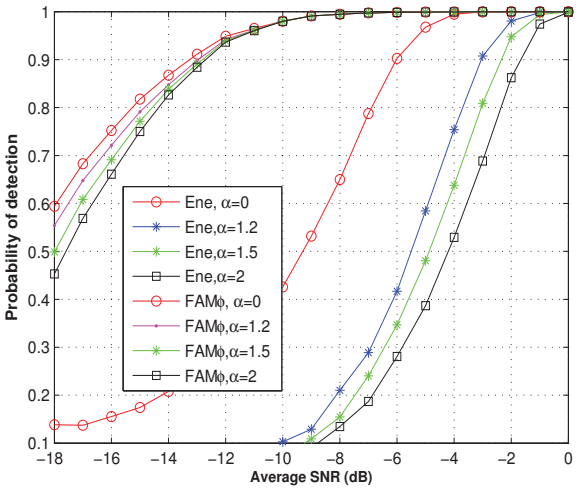

Fig. 5. Performance of proposed and energy detectors under noise variance uncertainty

Figure 5 shows the performance (SNR vs. P_d) of proposed and energy detector under various noise uncertainty factor (β_u=0.1, 1.2, 1.5, and 2). The signal strength is varied from -18dB to 0dB, N=256, and P_f=0.1. As the uncertainty increases, energy detector performance reduces significantly at all signal strengths. However, the proposed method namely fractal dimension of spectral estimates detector is less sensitive to noise variance uncertainty and its effect is negligible up to -12dB. From the figure 5, it can be seen that, the proposed detector is robust against noise variance uncertainty and is able to detect the weak signals up to -13dB as per the cognitive radio standards with respect to sensing parameters (P_d=0.9 and P_f=0.1). In contrast, the energy detector is able to detect the signal of SNR up to -6dB and and its performance further degraded with increase in uncertainty factor.

Figure 6 represents signal strength against detection probability curves with different number of CR nodes in cooperation using logical AND, OR and MOST for proposed sensing method. We considered two cognitive radio cooperative networks, one is with three nodes and the other one with five nodes. From the figure it can be observed that, detection probability increases as the number of nodes increases except for OR, which can be expected based on their logic. In addition, A close observation of these figures show that OR fusion rule gives better P_d for same P_f compared to other fusion rules (AND and MOST). Though the performance of the MOST logic is less than the OR decision, we considered because of its reliability to make the global decision. This is owing to the fact that one malicious decision can change the entire cooperative decision using OR and AND fusion logic.

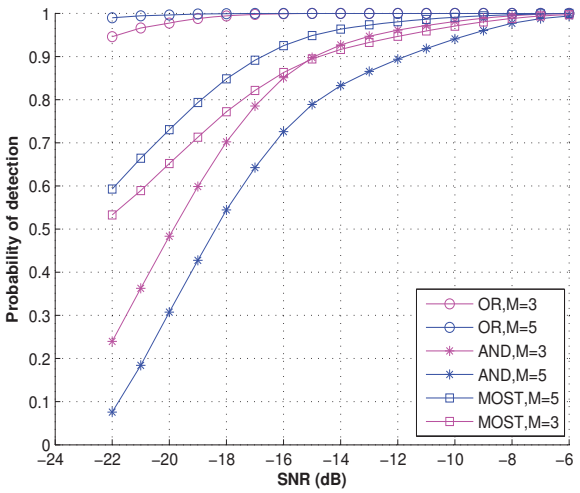

Fig. 6. Performance of proposed cooperative sensing with different hard decision fusion logic

V. Conclusions

In this work, we proposed and analyzed fractal dimension of spectral estimates sensing method under noise variance uncertainty. The notion of using the method is the fact that the fractal dimension of spectral estimates of the PU signal embedded with noise is high compared to fractal dimension of spectral estimates with noise alone. Moreover, its complexity varies as we vary the signal strength. From the simulation results, proposed method is shown to be less sensitive to noise variance uncertainty, whereas the energy detector completely depends on noise variations in the signal. The cumulative detection probability based on hard decision fusion method increases with number of nodes except for AND logic as expected. In conclusion, proposed method is robust against noise variance uncertainty up to -13dB. It shows approximately 7dB performance improvement at desired sensing probabilities, which is a significant performance improvement for cognitive radio systems. As a future work, one can improve the proposed sensing performance by selecting the optimal fractal dimension measure.

References

[1] T. Yucek and H. Arslan, "A survey of spectrum sensing algorithms for cognitive radio applications," *IEEE Communications Surveys and Tutorials,*, vol. 11, no. 1, pp. 116 –130, April 2009.

[2] E. Axell, G. Leus, E. Larsson, and H. V. Poor, "Spectrum sensing for cognitive radio : State-of-the-art and recent advances," *IEEE Signal Processing Magazine,*, vol. 29, no. 3, pp. 101 –116, 2012.

[3] A. Zoubir, V. Koivunen, Y. Chakhchoukh, and M. Muma, "Robust estimation in signal processing: A tutorial-style treatment of fundamental concepts," *IEEE Signal Processing Magazine,*, vol. 29, no. 4, pp. 61–80, July 2012.

[4] R. Tandra and A. Sahai, "SNR walls for signal detection," *IEEE Journal of Selected Topics in Signal Processing,*, vol. 2, no. 1, pp. 4–17, feb. 2008.

[5] M. Lopez Benitez and F. Casadevall, "Signal uncertainty in spectrum sensing for cognitive radio," *IEEE Transactions on Communications,*, vol. 61, no. 4, pp. 1231–1241, April 2013.

[6] M. Hammouda and J. Wallace, "Noise uncertainty in cognitive radio sensing: Analytical modeling and detection performance," in *International ITG Workshop on Smart Antennas (WSA)*, 2012, pp. 287–293.

[7] Y. Zeng, Y. C. Liang, A. T. Hoang, and E. Peh, "Reliability of spectrum sensing under noise and interference uncertainty," in *International Conference on Communications (ICC) Workshops*, June 2009, pp. 1–5.

[8] S. Srinu and S. L. Sabat, "Cooperative wideband sensing based on entropy and cyclic features under noise uncertainty," *IET Signal Processing,*, vol. 7, no. 8, pp. 655–663, 2013.

[9] S. Kalamkar and A. Banerjee, "On the performance of generalized energy detector under noise uncertainty in cognitive radio," in *National Conference on Communications (NCC)*, 2013, pp. 1–5.

[10] H. J. O Peitgen and D. Saupe., *Chaos and fractals: New frontiers of science,Volume 2*. Springer-Verlag, 2004.

[11] B. Raghavendra and D. Dutt, "Signal characterization using fractal dimension," in *IEEE Region 10 Conference (TENCON)*, Nov 2008, pp. 1–4.

[12] R. Lopes and N. Betrouni, "Fractal and multifractal analysis: A review," *Medical Image Analysis*, vol. 13, no. 4, pp. 634–649, July. 2009.

[13] S. Srinu, A. Mishra, and S. Farooq, "Cooperative sensing throughput analysis over fading channels based on hard decision," in *International Conference on Computer and Communications Technologies (ICCCT)*, Dec 2014, pp. 1–5.

[14] P. Kimtho and T. Jun-Ichi, "Signal detection based on cyclic spectrum estimation for cognitive radio in ieee 802.22 wran system," IEICE Technical Report (Institute of Electronics, Information and Communication Engineers), Tech. Rep., 2008.

[15] S. Kordan and B. Abolhassani, "Blind spectrum sensing for cognitive radio based on complexity measurement," in *19th Iranian Conference on Electrical Engineering (ICEE)*, May 2011, pp. 1–4.

[16] S. Srinu and A. K. Mishra, "Efficient elimination of erroneous nodes in cooperative sensing for cognitive radio networks," *Computers & Electrical Engineering*, pp. 1–9, July 2015.

[17] S. Srinu and S. L. Sabat, "FPGA implementation of optimum distributed sensing for cognitive radio network," in *World Congress on Information and Communication Technologies (WICT)*, 2012, pp. 897–902.

[18] ITU, "Radio Noise Measurements (SM.2055)," ITU (International Telecommunication Union), Tech. Rep., 2006.

THE 18TH INTERNATIONAL SYMPOSIUM ON WIRELESS PERSONAL MULTIMEDIA COMMUNICATIONS
(WPMC-2015)
December 13-16, 2015, Hyderabad, India

Evaluation of permutation entropy detection for cognitive radio networks

Sesham Srinu, Amit Kumar Mishra
Department of Electrical Engineering
University of Cape Town, Cape Town, South Africa
Email: seshamsrinu83@gmail.com, akmishra@ieee.org

***Abstract*—Spectrum sensing is a primary function in cognitive radio (CR) to improve radio spectrum utilization by dynamically accessing unused frequency bands while causing no interference to licensed users. In literature, many of the works considered that the noise distribution is Gaussian under assumption that the sample size is infinity to make the detector threshold. But, in real time available size of sample data at the cognitive radio to sense the spectrum is limited. Moreover, it should be as low as possible to reduce the computation complexity. Due to fixed threshold design based on prior assumption of Gaussian noise leads to unreliable spectrum decision, particularly, in low signal-to-noise ratio (SNR) environment. However, selection of appropriate detection method and framing an adaptive threshold with finite data are important to improve the detection performance of CR system. To address the above problems empirical permutation entropy (ePEn) detector with adaptive thresholding (EPEAT) method is introduced for cognitive radio system. Simulation results indicate that the proposed method is less sensitive to sample size, independent of bin width, and the dynamic thresholding according to available samples can improve the detection performance.**

***Index Terms*—Cognitive Radio, Spectrum sensing, Permutation entropy detection, Adaptive threshold, Sample size.**

I. Introduction

One of the key challenges of cognitive radio (CR) is to detect the presence or absence of the signal in a desired frequency band at low signal-to-noise ratio (SNR) with the constraint that it should not interfere with the primary user (PU) [1]. To achieve this, quite a few signal detection methods have been proposed over the years, such as energy detection, entropy detection, cyclostationary detection, eigen-value based detection, covariance based detection, and interference based detection etc.[1]. Each one of these has their own advantages and disadvantages. There are several fusion methods for co-operation spectrum sensing to improve detection performance. But, the most important process before applying fusion technique is the framing/selection of adaptive threshold for local sensing according to the distribution of available/finite samples of signal data at each sensor.

In recent past, a number of different entropy estimators have been applied in biomedical applications, meteorology, physics, statistical time series analyses, nonlinear dynamics, and economics applications to quantify the complexity of signals [2], [3]. Different entropy techniques are presented to predict the PU signal status for cognitive radio applications [4], [5], [6]. However, the authors have not consider the effect of sample size on the performance of the detectors. In addition, many of the above entropy detectors consider fixed bin width and finite number of samples which gives unreliable decision, i.e., inefficient estimation of probability distribution of received sample data during entropy estimation. This is due to distribution of data that might be sparse in the tails and more numerous in the middle. Entropy of a discrete time series can be calculated either from direct time sequence (called as embedding entropy) or from frequency domain of it (called as spectral entropy). In this work, advanced embedded entropy method such as empirical permutation entropy (ePEn) is studied and analysed their performance using small data sets to predict the signal status in low SNR regime. The motivation to consider the empirical permutation entropy is due to its ability to predict the discrete time series data periodicity with finite data and its independent property of bin width assumption.

In fact, real time statistical behavior of the received data at CR differs from the Gaussian approximation because not only due to channel noise uncertainty but also due to incomplete/finite sample of data available for test [7]. The effect of estimated noise variance using finite sample of data and deviation of true noise variance from population is given in [7]. To address the effect of limited sample data on sensing performance, one can choose an appropriate signal detection technique and make the threshold adaptive based on available data. In practice, high threshold value causes interference to the PU signal because the detector unable to detect the presence of PU signal. In contrast, low threshold value causes inefficient spectrum utilization by CR users even when opportunities are present. This is due to detector inability to detect the PU signal. There has been several research works in determining methods that select detection threshold with assumption of Gaussian noise distribution [8]. A double threshold technique to improve global decision in a cooperative spectrum sensing scheme is presented in [8]. The results show that this method improves decision making at the fusion centre, however, the authors do not address the problem of how to determine individual thresholds with finite sample size. Here, we design adaptive threshold based on noise variance of available finite data and analyses the performance using permutation entropy.

The focus of the current work is to detect the PU signal reliably in low SNR regime with finite sample of data available

at cognitive radio receiver. To achieve this, an empirical permutation entropy with adaptive thresholding (EPEAT) by estimating the noise variance based on nonparametric regression is introduced. We consider an algorithm which is shown as the best method for estimating noise variance with limited data using nonparametric regression [9]. To show the performance improvement of the proposed method, we consider spectral entropy, eigenvalue, and energy detection methods.

Rest of the paper is organized as follows. Section II presents proposed empirical permutation entropy with adaptive thresholding (EPEAT) technique as well as considered detection methods for comparative analyses. Simulation results are discussed in Section III. Finally, our conclusions are presented in Section IV.

II. Sensing algorithm

The objective of spectrum sensing is to discriminate between the following two hypotheses H_0 (PU signal is absent) and H_1 (PU signal is present) [10].

$$H_0 : r[i] = w[i], i = 0, 1, 2, \ldots, (N-1)$$
$$H_1 : r[i] = hs[i] + w[i],$$

where $r[i] = [r(0), r(1), r(2), \ldots, r(N-1)]$ is the received signal sequence received by the CR user, N is the incomplete sample of data or finite samples of signal received at sensor. The channel gain (h), transmitted signal $\mathbf{s}[i]$, and the additive white Gaussian noise (AWGN) $\mathbf{w}[i]$ with mean zero and variance σ^2 are independent of each other. We assumed that the channel is time invariant during the sensing period.

A. Detection algorithm based on Energy measurement

The test statistic for energy detector (ED) can be represented as [11]

$$\psi(r) = \sum_{i=0}^{N-1} |r[i]|^2 \underset{H0}{\overset{H1}{\gtrless}} \lambda_e, \tag{1}$$

where ψ is the energy of the received signal and (λ_e) is the threshold which depends up on the probability of false alarm P_f and number of samples.

B. Detection based on Spectral entropy

Spectral entropy is one of the measures of uncertainty using spectral properties of the received signal data. In this detection process, the spectral entropy of the received signal is estimated using the histogram method and is calculated by transforming the received signal of length N into the frequency domain [12], [5].

Thus, the entropy of frequency domain signal can be estimated as

$$SpEn = -\sum_{j=1}^{L} \frac{f_j}{N} \log_b \frac{f_j}{N} \tag{2}$$

where f_j denote the probability of samples fallen in each bin.

Based on the estimated entropy of receiving a signal and adaptive threshold (λ_ϕ) value, the detector decides H_0 : $SpEn > \lambda_\phi$ or $H_1 : SpEn \leq \lambda_\phi$.

C. Detection algorithm based on eigenvalues

In case of eigenvalue based spectrum sensing (maximum-minimum eigenvalue (MME) detection), the test statistics can be computed based on sample Covariance matrix of the received signal, can be given as [13]

$$R_r(N) \underline{\underline{def}} \frac{1}{N_s} \sum_{i=0}^{N-1} \mathbf{r}(i) \mathbf{r}(i)^\dagger, \tag{3}$$

where N is the number of collected samples and † is the Hermitian operator.

Let the ordered eigenvalues of the covariance matrix be the $\zeta_{\max} = \zeta_1 > .... > \zeta_i > ..... > \zeta_M = \zeta_{\min}$. Then, one can take the decision about PU activity in the desired frequency band based on maximum and minimum eigenvalue of the matrix $R_r(N)$, that is, $\zeta_{\max}$ and $\zeta_{\min}$. If $\zeta_{\max}/\zeta_{\min} > \lambda_{eig}$, signal exists in the band under scan. Otherwise, signal does not exist where λ_{eig} is a threshold, and is computed as

$$\lambda_{eig} = \frac{(\omega)^2}{\left(\sqrt{N} - \sqrt{ML}\right)^2} \cdot \left(1 + \frac{(\omega)^{-2/3}}{\left(N.ML^{1/6}\right)} F_1^{-1}(1 - P_f)\right) \tag{4}$$

where $\omega = (\sqrt{N} + \sqrt{ML})$, $F(.)$ is the probability density function of eigenvalues of covariance matrix with noise alone also called as Wishart random matrix.

D. Permutation entropy

Empirical permutation entropy (ePEn) was introduced to quantify complexity on the base of finite data sets [14]. It is based on the distributions of ordinal patterns, which describe order relations between the values of a discrete time series. On the one hand, permutation entropy is strongly related to Kolmogorov-sinai (KS) entropy [15]. It coincides with KS entropy for piecewise strictly monotone interval maps and is not less than KS entropy for many dynamical system. On the other hand, permutation entropy is estimated by empirical data, which is conceptually simple and algorithmically fast [16].

To calculate the ePEn of received signal $\{r(i), i = 1, 2, .., N\}$, which are embedded to an m-dimensional space can be given as

$$R_i = [r(i), r(i+l), .../r(i+(m-1)l)], \tag{5}$$

where m is the embedding dimension and l is the time lag. R_i is the i^{th} point in the m-dimensional space; $1 \leq i \leq N - (m-1)l$.

For R_i, the real values in above Eqn. (5) are arranged in an increasing order, so it can be written as follows:

$$R_i = [r(i + a_1.l) \leq r(i + a_2.l) \leq ... \leq r(i + a_m.l)]. \tag{6}$$

where $a_1 = (j_1 - 1)$. When an equality occurs, such as $r(i + (j_{n1} - 1)l) = r(i + (j_{n2} - 1)l)$, the two values $r(i + (j_{n1} - 1)l)$ and $r(i + (j_{n2} - 1)l)$ can be ordered by the values of their corresponding j. Namely, if $j_{n1} < j_{n2}$, then the order is $r(i + (j_{n2} - 1)l) \leq r(i + (j_{n1} - 1)l)$.

Hence, the vector X_i can be uniquely mapped onto: $\pi_i = [j_1, j_2, ..., j_m]$, where π_i is one of $m!$ possible permutations of m distinct symbols $(1, 2, ..., m)$.

If π_i is considered as a symbol, then all points in the m-dimensional embedding space can be expressed as a symbol sequence $\left[\pi_1, \pi_2, ..., \pi_{N-(m-1)l}\right]$. Hence, this procedure maps the original discrete time series onto a symbol sequence. The number of the distinct symbols can be most at $m!$.

Let the occurrence number of π in $\left[\pi_1, \pi_2, ..., \pi_{N-(m-1)l}\right]$ be k, then the occurrence probability of π is $k/\left(N-(m-1)\,l\right)$. Let the number of distinct symbols in $\left[\pi_1, \pi_2, ..., \pi_{N-(m-1)l}\right]$ be k, and the corresponding occurrence probabilities be $p_1, p_2, .., p_k$, then the ePEn of the discrete time series is calculated as [16]

$$H_p = -\sum_{j=1}^{k} p_j ln(p_j), \tag{7}$$

where H_p is the value of ePEn. The low values of ePEn indicate signal presence and high values of ePEn represent random noise. In practice, to detect the dynamical changes, the data is first partitioned into non-overlapping windows of suitable length. Mathematically, the decision statistics to sense the frequency band is given as $H_0 : H_p > \lambda_{pe}$ or $H_1 : H_p \leq \lambda_{pe}$.

The threshold (λ_{pe}) is calculated as.

$$\lambda_{pe} = H_{pw} + \Theta_s.(Q^{-1}(1 - P_f)) \tag{8}$$

where H_{pw} is the estimated empirical permutation entropy of standard Gaussian noise, Θ_s is the scaling parameter depends on estimated noise variance ($(\sigma_w^*)^2$) of received samples and its size (N), Q is the complementary distribution function of the standardized Gaussian.

To estimate the noise variance of received signal at CR, it is required to find the best estimate of $s[i]$. This can be achieved in two methods. One method is based on parametric regression and the another one is using nonparametric regression. The parametric regression requires a priori knowledge of the received signal in terms of an equation (also called as regression equation). But, signal data received at each cognitive radio, however, cannot be modeled/parameterized in terms of predetermined analytical function. Hence, nonparametric regression is considered and is usually the best method for estimating noise variance with considered length of sample data. To estimate the noise variance, we consider the model given by [9]. In this method, author used the fact that the model whose generalized cross validation (GCV) score is minimum can provide the standard deviation of additive white Gaussian noise.

III. Simulation results

In this section, we provide simulation results to evaluate the performance of the proposed EPEAT sensing algorithm, and compare it with that of spectral entropy detector, eigenvalue detector, and energy detector. Here, the meaning of incomplete is that the samples available for test in real time is finite. In the sequel, the desired probability of false alarm is fixed to 0.1. The two sets of finite sample size (512 and 256) of received signals at cognitive radio is taken to evaluate the sensing performance of considered detectors with proposed one . We consider a DVB-T signal which is a Matlab Simulink model that generates a signal with band width of 6MHz. The signals are sampled at a rate of 9.12 Msps. The implementation of empirical permutation entropy with adaptive threshold follows the procedure described in Section 2-D. Calculation of ePEn requires apriori values of delay (τ), embedding dimension (m), and the size of the sliding window (l). The value of m can be estimated using the calculation of false nearest neighbor algorithm. The use of sliding window is to get the permutation entropy trajectory of the captured discrete time series, which can be varied according to the application. In the simulation, we consider, τ=2, m=3, and the window size l is considered and varied between 5 to 15. The threshold for entropy detectors depends on estimated entropy of standard Gaussian noise of same length (N), desired P_f value, and the estimated standard deviation of noise using non parametric regression. In case of spectral entropy, the histogram of the received signal after FFT is evaluated based on number of bins L=15. In case of energy detection, the test statistic as per Eqn. (1) is evaluated and compared with the predetermined threshold (λ_e). In the case of eigenvalue based detector, we used tabulated values of Tracy-Widom (TW) distribution of order one due to complex nature of its function to make the threshold as per [13]. The sensing performance of each approach is quantified by the SNR versus detection probability. The detection probability is estimated based on Monte Carlo simulations of 10000 iterations that means the solutions are approximated to four decimal places. The snapshot/frame based method is considered for detecting a signal in the desired frequency band to be scanned [17].

Figures 1 and 2 illustrate the performance of spectral entropy detector and proposed permutation entropy detector with variable number of sample size (N = 256 and 512). From the figure, it can be seen that the entropy reduces as we increase the signal-to-noise ratio for both entropy detection methods. In addition, dependency of discriminate the PU signal on sample size is very less for entropy detection methods. Particularly, in the case of proposed detection method. The block color line indicates the entropy of standard white Gaussian noise of sample size equal to the signal length from which we can observe the sensing ability of considered entropy method.

Figure 3 represents the estimated ePEn values with different time lags (l) varied from 5 to 15. The sample length is considered as 256. From the figure, it can be seen that the estimated permutation entropy increase as we increase the l value. However, the ability to discriminate the signal from noise is same for all values of l. Hence, for further analyses, the least value in the considered range is taken, which is equal to 5.

Figure 4 shows the threshold values at different false alarm probabilities of proposed entropy detector with standard Gaussian random noise of length 256. In this simulation, threshold values are measured based on permutation entropy

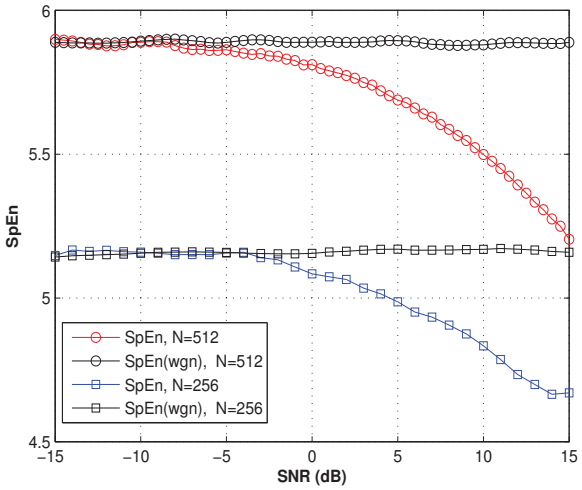

Fig. 1. Estimated entropy of captured signal and WGN using SpEn detector.

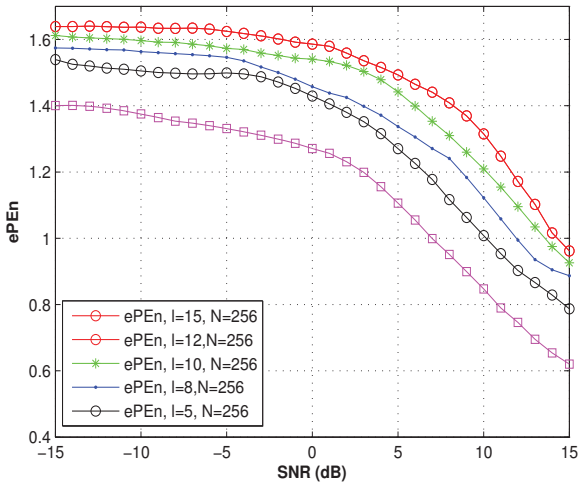

Fig. 3. Estimated entropy of captured signal and WGN using ePEn detector.

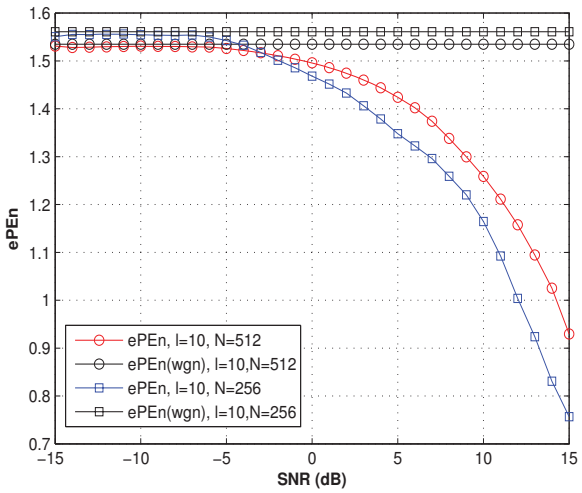

Fig. 2. Estimated entropy of captured signal and WGN using ePEn detector.

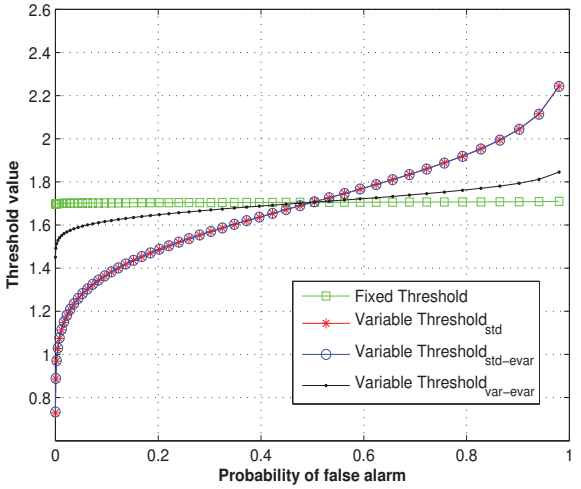

Fig. 4. Threshold value with fixed and estimated noise variance of proposed method for different P_f values

for different parameters namely fixed standard deviation, fixed variance, estimated standard deviation and estimated variance using nonparametric regression. From the figure, it can be seen that, in the case of fixed threshold detection, threshold is nearly constant for all values of false alarm probabilities. However, adaptive thresholding by estimating noise variance of the received signal vary significantly which is responsible to improve the detection probability of the detector (from P_f=0.5 to 0). From the results, threshold values are same with true standard deviation and estimated standard deviation of noise based on nonparametric regression. However, detection probability degrades compared to fixed threshold entropy detector at higher false alarm probability from 0.5 to 1. In practice, the desired values of P_f should be less than or equal to 0.1 (according to the IEEE 802.22 WRAN standard) which supports that the adaptive thresholding technique is more appropriate for real time applications of cognitive radio system.

Figure 5 illustrates the local sensing performance of proposed entropy detector with dynamic thresholding (EPEAT), spectral entropy detector with adaptive threshold, eigenvalue detector, and classical energy detector at different size of sample data (N=512 and 256). From the figure, it can be observed that the proposed EPEAT detector is less sensitive to sample size and shows its ability to predict the PU signal status even with incomplete sample of data. In general, entropy detectors have good discriminating ability with finite sample of data. However, based on the results, the proposed permutation entropy is less sensitive to sample size compared to spectral entropy detector. Moreover, the detection probability is re-

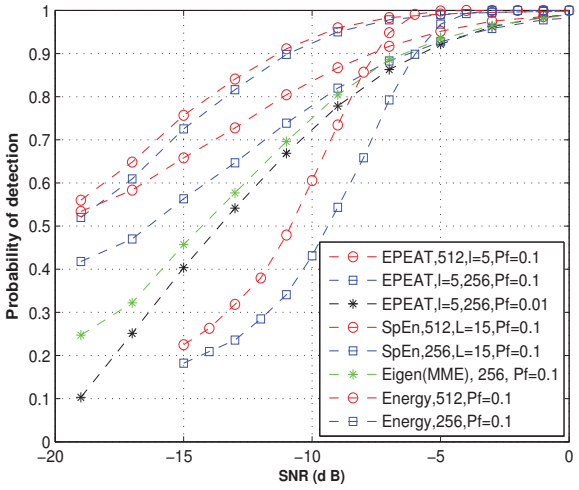

Fig. 5. Performance of EPEAT detector with considered detectors, N=256 and 512, P_f=0.1 and 0.01

duced as we reduce the false alarm probabilities from P_f=0.1 to 0.01. It can be seen that the detection probability increases as the signal strength at the sensor increases as expected. The EPEAT, eigenvalue, and spectral entropy detectors are able to detect noisy signal of SNR up to -12dB, -7dB, and -10dB, respectively with 90% accuracy. In contrast, the energy detection method is able to detect noisy signal up to -6dB using sample size of 256.

IV. Conclusions

In this work, we proposed and evaluated an empirical permutation entropy with adaptive thresholding (EPEAT) method by estimating the noise variance of the received signal using nonparametric regression. It can estimate the noise variance in the received signal with accuracy of 95% and requires no prior knowledge of the primary user signal and noise distribution. The accuracy of the estimated variance can be increased with the increase of sample size. The experimental results show that the proposed method has better performance especially with finite sample size of signal in low SNR environment. In particular, the proposed EPEAT method is shown to be less sensitive to variable sample size, whereas the energy detector completely depends on sample size available at sensor. Moreover, proposed method with variable threshold can detect the signal of SNR up to -12dB with sample size of 256. In conclusion, the detection method outperforms the recent method namely spectral entropy, eigenvalue, and energy detectors by 2dB, 5dB, and 6dB respectively, which is a significant improvement for local sensing in cognitive radio systems. The cooperative sensing with adaptive thresholding technique over fading environment is under development to improve detection performance.

References

[1] E. Axell, G. Leus, E. Larsson, and H. V. Poor, "Spectrum sensing for cognitive radio : State-of-the-art and recent advances," *IEEE Signal Processing Magazine,*, vol. 29, no. 3, pp. 101 –116, 2012.

[2] A. Garrido, "Classifying entropy measures," *Symmetry*, vol. 3, no. 3, pp. 487–496, 2011.

[3] V. A. Unakafova and K. Keller, "Efficiently measuring complexity on the basis of real-world data," *Entropy*, vol. 15, no. 10, pp. 4392–4403, 2013.

[4] W. Zhu, J. Ma, and O. Faust, "A comparative study of different entropies for spectrum sensing techniques," *Wireless Personal Communications*, vol. 69, no. 4, pp. 1719–1733, Mar 2013.

[5] S. Srinu and S. Sabat, "Optimal multinode sensing in a malicious cognitive radio network," *IEEE Systems Journal*, vol. PP, no. 99, pp. 1–10, 2013.

[6] C. Xiaojun, L. Yin, and D. Jingya, "Approximate entropy detection spectrum sensing in cognitive radio," in *IEEE International Conference on Computer and Information Technology (CIT)*, Sept 2014, pp. 865–868.

[7] R. V. Lenth., "Some practical guidelines for effective sample size determination," *The American Statistician*, vol. 55, no. 3, pp. 187–193, July 2001.

[8] H. Chen and J. Liu., "Cooperative spectrum sensing based on double threshold detection and dempster-shafer theory," in *12th IEEE International Conference on Communication Technology (ICCT)*, Nov 2010, pp. 1212–1215.

[9] D. Garcia., "Robust smoothing of gridded data in one and higher dimensions with missing values," *Computational Statistics & Data Analysis,*, vol. 54, no. 4, pp. 1167–1178, April 2010.

[10] S. Srinu, A. Mishra, and S. Farooq, "Cooperative sensing throughput analysis over fading channels based on hard decision," in *International Conference on Computer and Communications Technologies (ICCCT)*, Dec 2014, pp. 1–5.

[11] S. Srinu and S. L. Sabat., *Spectrum Sensing for Cognitive Radio Networks: White Space Communication: 1st Edition*. Springer, 2015.

[12] Y. Zhang, Q. Zhang, and S. Wu, "Entropy-based robust spectrum sensing in cognitive radio," *IET Communications*, vol. 4, no. 4, pp. 428–436, May 2010.

[13] A. Kortun, T. Ratnarajah, M. Sellathurai, and Z. Caijun, "On the performance of eigen value-based spectrum sensing for cognitive radio," in *Symposium on New Frontiers in Dynamic Spectrum*, 2010, pp. 1–6.

[14] C. Bandt and B. Pompe, "Permutation entropy: A natural complexity measure for time series," *Phys. Rev. Lett.*, vol. 88, p. 174102, Apr 2002.

[15] K. Keller, A. M. Unakafov, and V. A. Unakafova., "On the relation of KS entropy and permutation entropy," *Physica D: Nonlinear Phenomena*, vol. 241, no. 17, pp. 1477–1481, Mar 2012.

[16] Y. J. Yuan, X. Wang, Z. T. Huang, and Z. C. Sha, "Detection of radio transient signal based on permutation entropy and GLRT," *Wireless Personal Communications*, vol. 82, no. 2, pp. 1047–1057, July 2015.

[17] S. Srinu and A. K. Mishra, "Efficient elimination of erroneous nodes in cooperative sensing for cognitive radio networks," *Computers & Electrical Engineering*, pp. 1–9, July 2015.

THE 18TH INTERNATIONAL SYMPOSIUM ON WIRELESS PERSONAL MULTIMEDIA COMMUNICATIONS
(WPMC-2015)
December 13-16, 2015, Hyderabad, India

On Detection Improvement in MC-CDMA Image Watermarking on Fading Channel

Santi P. Maity
Dept. of Information Technology
Indian Instt. of Engg. Science & Tech., Shibpur
P.O. Botanic Garden, Howrah, India, 711 103
Email: santipmaity@it.iists.ac.in

Seba Maity
Dept. of Elect. & Commn. Engg.
College of Engg. & Management, Kolaghat
P.O. KTPP Township, Purba Medinipur, India, 721171
Email: sebamaity@gmail.com

***Abstract*— In this paper, an improved decoder structure on previously proposed multicarrier-code division multiple access (MC-CDMA) watermarking is proposed. To simulate attack channel, Rayleigh distribution along with the additive white Gaussian noise (AWGN) is considered. We mathematically show that the proposed decoder structure incorporates the effect of fading attack unlike the widely used correlator decoder. The concept of multiuser detection (MUD) principle which is widely used in CDMA is then explored to cancel the effect of multiple bit interference (MBI). Two variants of combined interference cancelation (CIC), namely threshold combined interference cancelation (TCIC) and group combined interference cancelation (GCIC) are then developed. Mathematical analysis with simulation results show that TCIC does not offer any bit error rate (BER) performance gain relative to CIC, while a significant improvement in BER performance and watermark payload are achieved through GCIC.**

Index words-Multicarrier code division multiple access, spread spectrum watermark, MMSEC decoder, CIC,TCIC, GCIC

I. Introduction

Spread spectrum (SS) watermarking has found to be efficient for imperceptible, robust and cryptographically secured data hiding scheme on digital media [1][2]. Despite the advantages of blind detection and robustness, its suffers from host signal interference (HSI), payload problem and poor detection for corrlator in presence of random gain operation [3]. Perceptually adaptive multi-carrier (MC)-SS is reported in [4] with minimum mean square error combining (MMSEC) decoder to design robust system against gain attack. Improved detection scheme based on statistical decision rules with probability density function [5] and multiplicative [6] SS watermarking are also reported. To increase payload, the concept of modified M-ary watermark decoding algorithm using a tree-structure with the number of correlators equal to $2log_2M$ [7] and code division multiple access (CDMA) are used [8].

In [3], [4], a MC version of SS watermarking on digital images is proposed. The host/cover image is decomposed into N-mutually orthogonal signal points and each watermark bit is embedded using a distinct code pattern. Decision variable for the embedded watermark bit is formed from the weighted average of N-decision statistics applying MMSEC strategy. We extend here this work for embedding a set of binary watermark bits using a set of orthogonal code patterns and call it MC-CDMA watermark. MC-CDMA watermarks suffer from multiple-bit interference (MBI) effect. Two variants of combined interference cancelation (CIC), namely threshold interference cancelation (TCIC) and group combined interference cancelation (GCIC) are then developed. Simulation results show that GCIC scheme offers significant gain in bit error rate (BER) for watermark decoding and consequently improved watermark payload/capacity is achieved relative to CIC and TCIC. Simulation results also show that iterative interference cancelation offers further improvement in BER subject to the relative gain achieved at initial stages.

The rest of the paper is organized as follows: Section II describes system model for MC-CDMA watermarking. Section III describes detection improvement through interference cancelation. Section IV presents performance evaluation while conclusions are drawn in Section V.

II. MC-CDMA Watermarking

Let us assume that the host signal $\mathbf{X}$ is decomposed onto N-mutually orthogonal signal points, where each signal point corresponds to a vector or signal in N-dimensional signal space. Let us also assume that the watermark is a binary valued signal i.e. $\mathbf{W} = \{b_1, b_2, b_3, ..., b_K\}$, where $b_i \epsilon \{1, -1\}$ and $i = 1, 2, ...K$. In MC-CDMA watermarking, each watermark bit is spread over N-signal points by adding each host signal point with an element of the respective bit's code pattern. Here, we consider a binary valued Walsh codes for SS watermarking. Fig. 1 shows the block diagram representation of the proposed MC-CDMA watermarking model for k-th bit embedding along with attack channel modeled as Rayleigh distribution with additive white Gaussian noise (AWGN). The watermarked signal ($X^{'}$) [3] can be written as

$$X^{'} = (X_1 \pm \sum_k \gamma P_1^k) + (X_2 \pm \sum_k \gamma P_2^k) + ... + (X_N \pm \sum_k \gamma P_n^k) = \sum_{k=1}^{K} \sum_{n=1}^{N} X_n \pm \gamma . P_n^k \quad (1)$$

where $n, k \in z$ and γ is the embedding strength for additive SS. The symbol P_n^k corresponds to the n-th binary element of the k-th code pattern. The symbol $\pm$ indicates antipodal embedding, i.e. if '+' is used for embedding '1', '-' for '-1'.

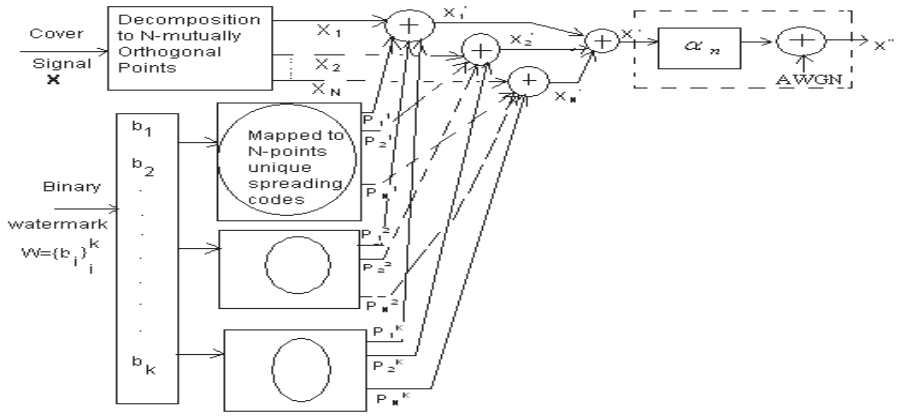

Fig. 1. MC-CDMA watermarking for k-th bit embedding

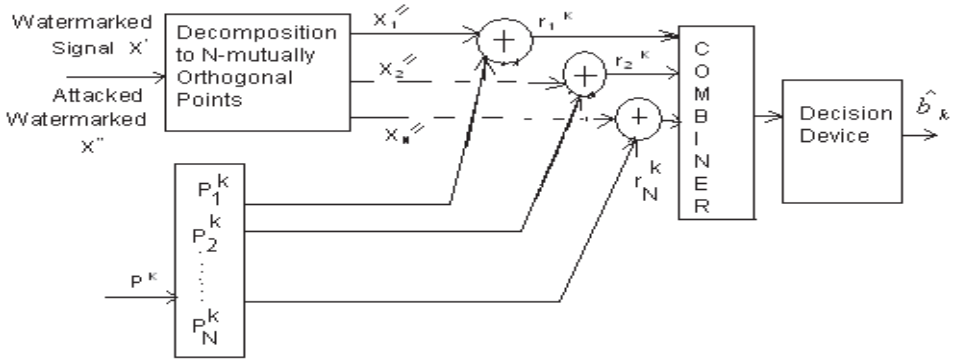

Fig. 2. MC-CDMA model of decoding for k-th watermark bit

Fig. 2 shows the block diagram representation of the k-th bit SS watermark decoding. We assume here that the watermark extraction/decoding is done with perfect synchronization. The received watermarked signal is first projected onto N-orthogonal signal points and is then correlated using j-th spreading (for decoding of j-th watermark bit) code that results in $r^j = (r_1^j, r_1^j, ...r_N^j)$ [3]. The decision variable for the j-th bit at n-th signal point is denoted by r_n^j and can be written as follows:

$$\begin{aligned} r_n^j &= < X_n^{''}, P_{nj} > \\ &= < P_{nj}, \sum_{k=1}^{K}\sum_{n=1}^{N} \alpha_n(X_n \pm \gamma.P_{nk}) + \eta_n > \\ &= \pm\alpha_n.\gamma \pm \sum_{k=1,k\neq j}^{K} \alpha_n.\gamma.\rho_{kj} + \eta_j \end{aligned} \quad (2)$$

where η_j is a Gaussian random variable with mean 0 and variance $N_0/2$. The symbol ρ_{kj} indicates the cross-correlation value due to the $j-$th and $k-$th code patterns. The expression of (2) is obtained assuming that the inner product of P_{nj} and X_n is zero i.e. HSI is assumed to be zero. The first term of (2) results in the auto-correlation value of j-th code pattern with zero lag, the second term is the sum of cross-correlation values among the different combinations of code patterns (except j-th code) and the third term is the AWGN noise component spread by j-th code pattern. The second term is called multiple bit interference (MBI) effect.

The decision variable D^j for the j-th bit obtained by MMSEC strategy [4] is

$$D^j = \sum_{n=1}^{N} r_n^j w_{nj} \quad (3)$$

where $w_{nj} = \frac{\alpha_n}{(\alpha_n^2\gamma^2\sum_{j=1}^{k} var(b_k)\rho_{kj}^2 + N_0/2)}$ and $var(b_k) = 1$. If knowledge of α_n not known, w_{nj} is calculated as in [4]. Substituting the value of the weight factors, the expression of the decision variable D^j for the j-th bit becomes

$$D^j = \sum_{n=1}^{N} \frac{\alpha_n}{\alpha_n^2\gamma^2\sum_{j=1}^{K}(var(b_k)\rho_{(kj)}^2 + N_0/2)} r_n^j \quad (4)$$

The decision variable D^j is fed to the decision device, the output of which determines the binary watermark bit pattern. Thus the correlator's outputs generate a decision vector $\mathbf{D} = [D^1 D^2 ....D^K]$ which is used to obtain an initial estimates of the embedded bits $\hat{b} = (\hat{b}_1, \hat{b}_2, \hat{b}_3, ...\hat{b}_K)$. These initial estimates are then used to evaluate the MBI.

III. Detection improvement through interference cancelation

MBI as shown in the second term in (2) greatly affects the detection performance at high payload. Analogous to

multiuser detection (MUD) in CDMA [9], nonlinear decision driven interference cancelation (IC) in watermarking can be categorized in two types- we call them here as (i) independent interference cancelation (IIC), where interference due to only one embedded bit is canceled at a time, and (ii) combined interference cancelation (CIC), where during detection of a particular watermark bit, interference due to all other group of watermark bits are estimated and canceled in one shot. While IIC takes much longer time for watermark detection to complete, CIC is attractive due to its fast speed through parallel processing but requires larger computation power. Moreover, performance improvement in CIC depends on the precise estimation of interference due to other watermark bits that leads to the relative gain achieved in interference cancelation. We briefly describe now CIC scheme along with its two variants, namely TCIC and GCIC, respectively.

A. Combined Interference Cancelation

Fig.3 shows the block diagram representation of j-th watermark detection using CIC scheme. The interfering effect, due to all embedded bits except the j-th bits, is removed to regenerate the watermarked signal containing j-th watermark bit only. The expression for this signal can be written as

$$X_j^{''} = X^{''} - \sum_{k=1, j\neq k}^{K} I_k \tag{5}$$

where I_k denotes the interference due to k-th watermark bit. This $X_j^{''}$ is then fed to the MMSEC decoder. The weights are then updated using interference cancelation as follows:

$$w_n^j = \frac{\alpha_n}{(var(b_k - \hat{b}_k)\alpha_n^2\gamma^2 \sum_{k=1}^{K} \rho_{(kj)}^2 + N_0/2)} \tag{6}$$

The weights in (6) can be calculated in two ways depending on the knowledge about the reliability of estimations.
(1) If the estimations are assumed to be correct, $var(b_k - \hat{b}_k) = var(b_k - b_k) = 0$,$\forall k \neq j$.
(2) On the other hand, if no knowledge about the reliability of the estimation for the watermark detected bits is available, $var(b_k - \hat{b}_k) = var(b_k - b_k) = 2$,$\forall k \neq j$. This value is due to the variation in the respective binary watermark embedding and decoding, thus $var(b_k - \hat{b}_k)$ as a discrete random variable with permissible possible values of 2, 0 and -2.

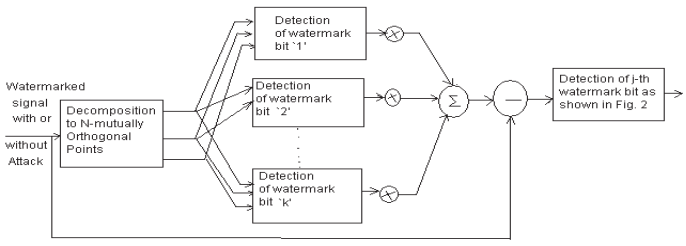

Fig. 3. CIC-SS watermark decoding for j-th watermark bit

B. Threshold combined interference cancelation

The flowchart for the implementation of TCIC watermark decoding algorithm is shown in Fig. 4. The decision variables for all the embedded watermark bits are first normalized. The normalized decision magnitudes above a specified threshold value (calculated from the conditional probability density function for a given P_e value) are assumed to belong to strong watermark bits. The expression of the normalized decision statistics for the j-th watermark bit is defined as

$$\begin{aligned} y_j &= \frac{D^j}{\sum_{n=1}^{N} \alpha_n w_n^j} = \frac{\sum_{n=1}^{N} r_n^j w_n^j}{\sum_{n=1}^{N} \alpha_n w_n^j} \\ &= \frac{\sum_{n=1}^{N} (\pm\alpha_n\gamma \pm \sum_{k=1,k\neq j} \alpha_n\gamma\rho_{kj} + \eta_j) w_n^j}{\sum_{n=1}^{N} \alpha_n w_n^j} \\ &= \pm\gamma \pm \frac{\sum_{n=1}^{N}\sum_{k=1}^{K} \alpha_n\gamma\rho_{kj}}{\sum_{n=1}^{N} \alpha_n w_n^j} + \frac{\sum_{n=1}^{N} \eta_j w_n^j}{\sum_{n=1}^{N} \alpha_n w_n^j} \end{aligned} \tag{7}$$

where $j = 1, 2, ...K$.

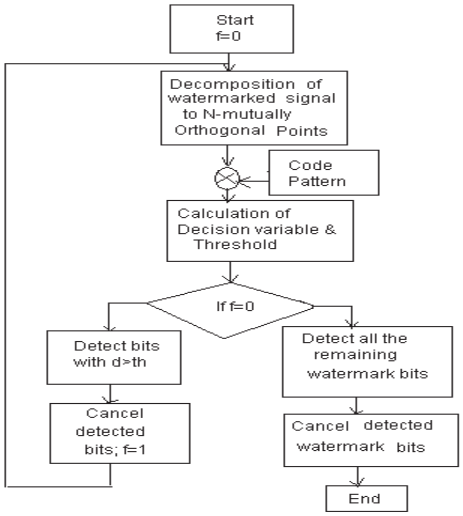

Fig. 4. TCIC algorithm for watermark decoding

If the number of embedded watermark bits are large enough (which is quite true for high payload system), the distribution of MBI i.e. the second term of (7) is Gaussian, and the third term is due to AWGN. So the total interference power is the sum of the variances of the second and the third terms in (7). Probability of bit error i.e. P_e in watermark detection can be calculated from the probability density function. The conditional probability density functions of the normalized decision statistics y_j for the given $b_j = 1$ and $b_j = -1$ are Gaussian centered at $+\gamma$ and $-\gamma$, respectively. This is symmetric in nature and the analysis can be simplified to consider only the positive values of y_j. Using Bayes rule, the

conditional probability of error is

$$P_e = P_e[b_j \neq 1/y_j] = \frac{P_e(y_j/b_j = -1)}{P(y_j/b_j = 1) + P(y_j/b_j = -1)} = \frac{1}{1 + exp^{(2y_j/\sigma_j^2)}} \quad (8)$$

The threshold value for the normalized decision statistics to determine the strong watermark group (9) as

$$Y_{th}^j = \frac{\sigma_j^2}{2} log[\frac{1 - P_e}{P_e}] \quad (9)$$

IC may sometimes cause degradation in detection performance. This is due to the inaccurate estimation of interference and its subsequent cancelation leads to further increase in interference power (i.e. variance). In the first iteration, the watermark bits with normalized decision statistics greater than the threshold are detected directly using MMSEC decoder without IC. Interference due to these watermark bits is then removed from the watermarked signal and the rest watermark bits are detected. The estimated data thus obtained for each strong watermark bit is used to cancel the interfering effect in the next iteration. Now, the normalized decision statistics of all the watermark bits are compared with the threshold and the strong bits are detected directly using MMSEC decoder. This estimated data is then used to calculate interference due to the strong bits, remove this effect from the watermarked signal and the weak bits are then detected. This process is repeated iteratively until a desired probability of error is achieved or a pre-set number of iterations are complete.

C. Group combined interference cancelation

The flowchart for the implementation GCIC is shown in Fig. 5. Here the decision magnitudes are sorted in desending order. The embedded watermark bits are then partitioned into different groups based on the magnitudes of decision statistics. In the present analysis, the watermark bits are partitioned into two groups, namely the strong and the weak watermark groups. Now, CIC is performed within the group of strong watermark bits by simultaneously canceling the interference of all other watermark bits except the desired one and the strong watermark data bits are thus estimated. Using the updated data of strong watermark bits, the interference due to these bits are removed and CIC is employed within the group of weak watermark bits. The weak watermark bits are then estimated. In the subsequent iterations, the interference experienced by each watermark bit is canceled based on the estimated data from the previous iteration. Now, all the decision magnitudes are again arranged in descending order and GCIC process is repeated iteratively until a desired probability of error is achieved or a preset number of iterations are completed.

IV. Performance Evaluation

This section presents BER performance of the proposed MC-CDMA watermarking for CIC, TCIC and GCIC schemes. Fig. 6(a)-(b) show the cover images of sizes (256×256), 8 bits/pixel, Fig. 6(c) is a binary watermark of size (32×32)

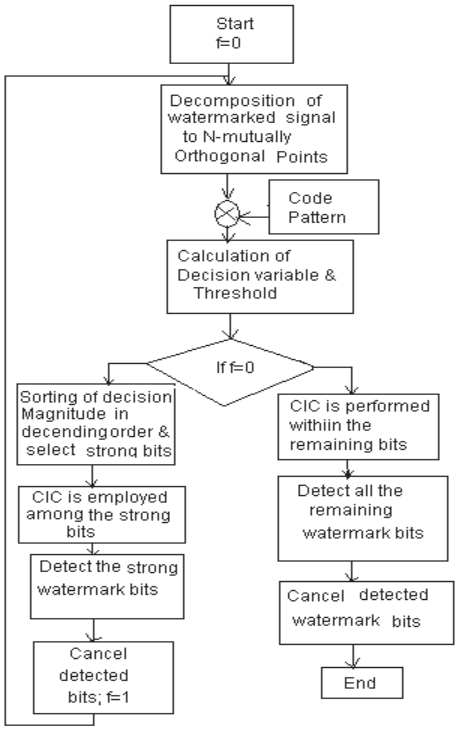

Fig. 5. GCIC algorithm for watermark decoding

and Fig.6 (d)-(e) show the watermarked images. The values for peak-signal-to-noise ratio (PSNR) and structural similarity index measure (SSIM) are $\sim 40dB$ and ~ 0.98, respectively. Fig. 7(a) shows detection performance vs watermark-to-noise ratio (WNR) for the proposed MC-CDMA watermarking using CIC, TCIC and GCIC schemes after 1st iteration (i.e after 1st stage IC). WNR is the ratio of watermark power-to-noise power, noise considered here as AWGN with zero mean and some variance. The value of probability of watermark bit detection error (P_e) is set at 10^{-2} while calculating the threshold for TCIC scheme. It is clear from Fig. 7(a) that GCIC significantly improves BER performance compared to CIC and 5dB off from MC-CDMA watermarking at a BER of 10^{-3}[8]. At low WNR, TCIC performs almost similar to MC-CDMA watermark detection without IC. This is because very few decoded watermark bits have decision values that exceed the threshold value and can be treated as strong embedded bits. On the other hand, performance of TCIC is improved with the increase in WNR. Fig. 7(b) shows performance of the MC-CDMA watermarking for the three different IC schemes at the end of 2 iterations i.e. 2nd stage IC. As expected, all three IC methods offer significant performance improvement. GCIC performance is 3.5 dB off MC-CDMA watermark performance at a BER of 10^{-3}[8]. A gain of 2dB is achieved with GCIC relative to conventional CIC at a BER of 10^{-2}.

Fig. 7(a) and Fig. 7(b) also show the effectiveness of calculating the weights in MMSEC as shown in Section III A. W1 is the weight considering the estimation is assumed to be correct, while W2 corresponds to the weight when no knowledge about the reliability of the estimation for the watermark decoded bits

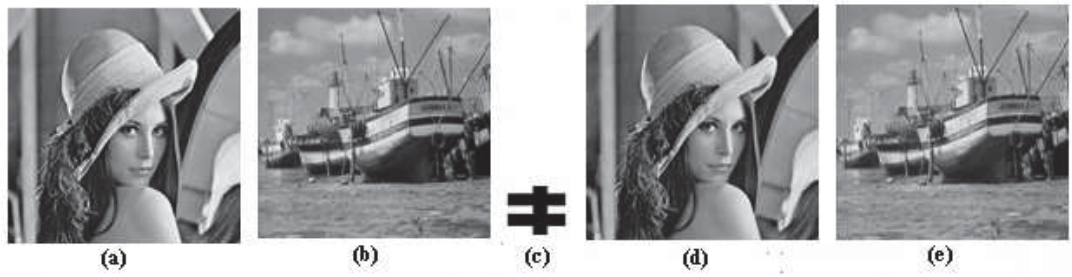

Fig. 6. (a)-(b) cover image , (c) binary watermark, (d)-(e) watermarked image

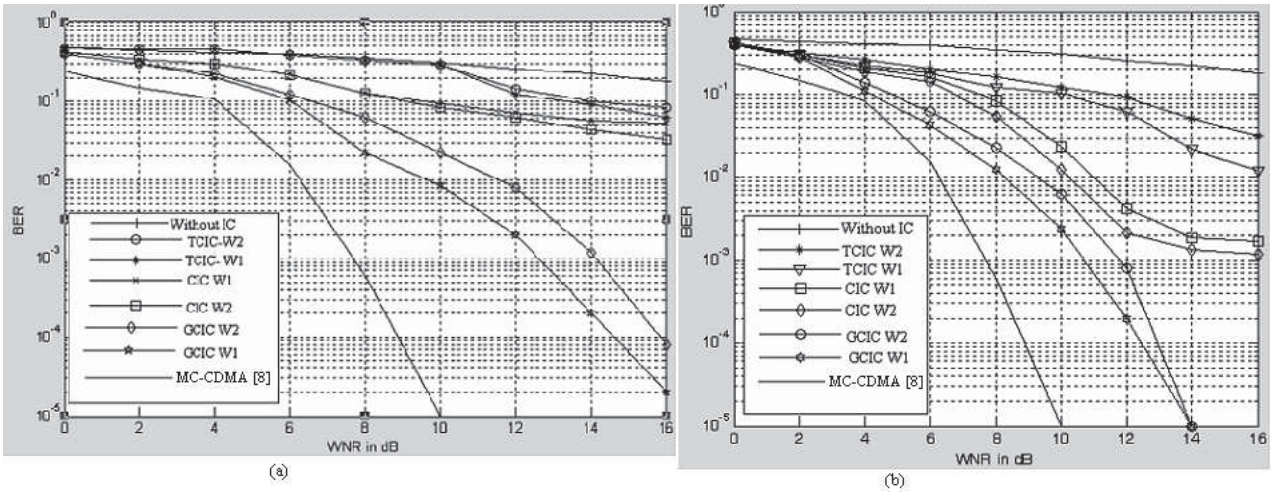

Fig. 7. BER performance through interference cancelation (a)with 1 iteration, (b) with 2 iterations

is available. Performance of the conventional CIC is better when the weights are calculated by W2, as detection of each watermark bit takes into consideration the subtraction (i.e cancelation) of interference due to every other embedded bits in one short. On the other hand, GCIC and TCIC show better performance when the weights are calculated assuming that the estimated data of the interfering bits is correct, as the strong watermark bits are detected first.

V. Conclusions and Scope of Future Work

Several versions of improved detection, namely CIC, TCIC and GCIC on MC-CDMA watermarking scheme are proposed and studied. Simulation results show that TCIC does not offer any BER performance improvement relative to CIC, while GCIC scheme offers significant improvement in BER performance and payload capacity. The proposed work may be extended for image error concealment. Extracted image digest (used as watermark) may be a representative measure of channel state information and feedback information may be sent to the receiver. This would help to design an adaptive system in terms of modulation, bit rate and power control in image transmission over fading channel.

VI. References

[1]I. J. Cox, J. Kilian, F. T. Leighton and T. Shamoon, "Secure spread spectrum watermarking for multimedia,"*IEEE Trans. on Image Proc.*, vol. 6, pp. 1673–1687, 1996.

[2]L. Perez-Freire and F. Perez-Gonzalez, " Spread spectrum watermarking security,"*IEEE Trans. on Information Forensics and Security*, vol. 4. no. 1, pp.2-24, 2009.

[3]S. P. Maity and S. Maity, "Multistage Spread Spectrum Watermark Detection Technique Using Fuzzy Logic," *IEEE Signal Proc. Letters*, vol.16, no. 4, pp. 245–248 April, 2009.

[4] S. P. Maity, S. Maity, J. Sil and C. Dlpha, "Perceptually adaptive MC-SS image watermarking using GA-NN hybridization in fading gain," *Engineering Applications of Artificial Intelligence*, vol. 31, pp.3-14,2014.

[5]Y. Bian and S. Liang, "Image watermark detection in the wavelet domain using Bessel k densities," *IET Image Processing*., vol. 7, pp.281-289, 2013.

[6]A. Valizadeh and Z. Wang, "An improved multiplicative spread spectrum embedding scheme for data hiding ,"*IEEE Trans. on Info. Forensics & Sec.*, vol. 7, pp.1127-1143, 2012.

[7]Y. Xin and M. Pawlak, "M-ary phase modulation for digital watermarking", *Int. Journal of Appl. Math. Comput. Sci.*m vol. 18, no. 1, pp. 93-104, 2008.

[8]B.-Ho Cha and C.-C. Jay Kuo," Robust MC-CDMA-Based fingerprinting against time-varying collusion attacks," *IEEE Trans. on Info. Forensics and Sec.*, vol.4, pp. 302-317, 2009.

[9]V. Thippavajjula and B. Natarajan, "Parallel interference cancelation techniques for synchronous carrier interferometry/MC-CDMA uplink," *IEEE Vehicular Technology conference*, pp.399-403,2004.

THE 18TH INTERNATIONAL SYMPOSIUM ON WIRELESS PERSONAL MULTIMEDIA COMMUNICATIONS
(WPMC-2015)
December 13-16, 2015, Hyderabad, India

On the Backhaul Reduction in Joint Transmission Network with Channel Uncertainty

Zhangxing Liu, Hui Tian, Cheng Qin
Beijing University of Posts and Telecommunications, Beijing 100876, China
Email: liuzhangxing000@sina.com

***Abstract*—Joint transmission (JT) has attracted broad attentions due to its ability to eliminate the intercell interference and to improve the system performance. JT needs to distribute the user data to the base stations (BSs) via backhaul before transmission hence it leads to consumption of backhaul links. In this paper, we consider a backhaul reduction scheme in multiple-input single-output (MISO) JT networks with incorporating the imperfect channel state information (CSI). Our goal is to design a robust procoder that minimizes the backhaul link consumption while satisfying the per-user quality of service (QoS) requirement. Due to the complexity of the original problem, we use the norm relaxation and semidefinite relaxation (SDR) to make the problem solvable. We further propose a link removal strategy based on the relaxed problem to minimize the backhaul consumption. Simulation shows that the proposed algorithm can reduce the backhaul consumption by at least 10.93% and 30.65% under different numbers of transmit antennas and users respectively.**

***Index Terms*—joint transmission, backhaul link consumption, channel uncertainty, norm relaxation.**

I. Introduction

With the increasing number of accessing equipment and data traffic volume, future networks will become more dense to provide the coverage and accommodation ability [1]. However, the dense cell deployment will incur severe inter-cell interference and deteriorate the system performance. Joint transmission (JT) is proposed to alleviate these interferences via cooperations among BSs. In JT, cooperative BSs can share the user data via backhaul links from the central processor (CP). These BSs can then transmit the desired signals to users simultaneously.

Although the JT can achieve a great improvement of system performance, the backhaul overhead becomes a main bottleneck. It is impractical for the full cooperation because of the finite capacity of backhaul. Data sharing scheme in JT is proposed in [2] in order to reduce the backhaul consumption. However, [2] only considers a information theoretical perspective. Therefore, different schemes for the reduction of the backhaul link consumption have been considered for practical systems [3]-[5]. In [3], the sum rate maximization is combined with the limited backhaul by designing beamforming. But it still concentrates on sum rate performance rather than backhaul reduction explicitly. In [4]-[5], the authors formulate the backhaul minimization problem into an ℓ_0 norm problem , which is inspired by compressive sensing. In [5], the authors uses an exponential function to approximate the ℓ_0 norm. [4] utilizes a ℓ_2 norm relaxation of the joint clustering and beamforming problem and then iteratively remove the links that correspond to the smallest link transmit power.

However, all the above literature discusses the problem with perfect CSI, which is obviously impractical. For the imperfect CSI, much literature has incorporated robustness to channel uncertainty into the formulation of the procoder design problem. [6] adopts the bounded CSI noise model and designs transceivers that optimize a worst-case QoS measure. It translates the problems into convex problems that can be solved efficiently as semidefinite programs (SDP). [7] assuming elliptically bounded CSI errors consider the worst-case robust design formulation that minimizes the weighted sum transmission powers of the BSs.

In this paper, we consider the transceiver design problem in the JT networks with limited backhaul. Our target is to minimize the backhaul consumption while providing a QoS guarantee for each user. The channel uncertainty is considered as well, which still lacks discussions in this problem to the best of our knowledge. The problem can be formulated into an ℓ_0 norm optimization, which is a non-convex and NP-hard problem. We first relax it into an ℓ_2 norm problem as [5]. Then we use the semidefinite relaxation method to transform the non-convex problem into a solvable convex SDP problem. Finally we propose a link removal method to force some beamforming vectors to zero and achieve lower backhaul consumption. The simulation results show that the proposed algorithm can significantly reduce the consumption of backhaul links, while satisfying the QoS requirement of each user.

The remainder of the paper can be organized as follows. In Section II, we provide the system model and the formulate a minimization problem of backhaul link consumption. We propose the method of link removal via semidefinite relaxation to solve the original problem in Section III. Simulation results are given in Section IV, and Section V concludes the paper. *Notation*: we use boldface letters to denote a matrix or vector. $(\bullet)^{\mathrm{T}}$ and $(\bullet)^{\mathrm{H}}$ stand for the transpose and conjugate transpose of a matrix respectively. $\mathrm{Tr}(\bullet)$ denotes the trace of a matrix. For any complex vector $\mathbf{x}$, we use $\|\mathbf{x}\|$ and $\|\mathbf{x}\|_0$ to represent the Euclidean norm and ℓ_0 norm respectivley. $\mathbf{A} \succeq \mathbf{0}$ denote the matrix $\mathbf{A}$ is semidefinite.

This work is supported by National Major Science and Technology Special Project of China (No. 2013zx03003016), the National Natural Science Foundation of China (No. 61471060), and Funds for Creative Research Groups of China (No. 61421061).

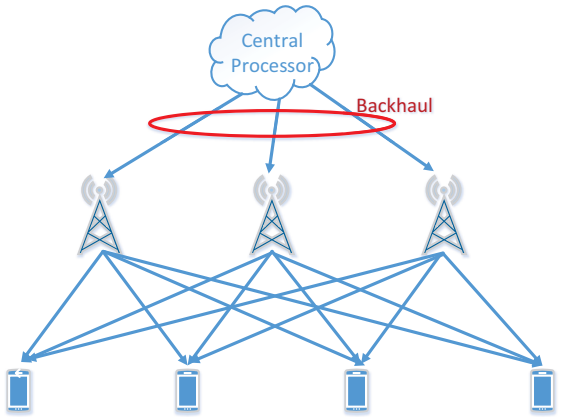

Fig. 1. Downlink joint transmission system model with the data sharing via backhaul from a CP.

II. System Model and Problem Formulation

Consider a downlink MISO joint transmission system consisted of M BSs and K single antenna users. We use $\mathcal{B}$ and $\mathcal{U}$ to denote the set of BSs and users respectively. Suppose that each BS is equipped with N_T transmit antennas. The BSs connect to a CP via limited backhaul links, as depicted in Fig. 1. Note we mainly focus on the limited capacity of the backhaul in this paper and the delay will not be considered. The CP will be responsible for the management of the network hence we can assume all user data and channel information are available at the CP.

Let $x_i \in \mathbb{C}$ be the desired signal for user i, which has a zero mean value and satisfies $\mathbb{E}\{|x|_i^2\} = 1$. Let $\mathbf{w}_{i,j} \in \mathbb{C}^{N\times 1}$ and $\mathbf{h}_{i,j} \in \mathbb{C}^{N\times 1}$ denote the transmit beamforming vector and the channel vector from BS j to user i. Here, we suppose the signal will experience a flat Rayleigh fading channel. Therefore, the received signal y_i at user i can be written as:

$$y_i = \sum_{j=1}^{M} \mathbf{h}_{i,j}^{\mathrm{H}} \mathbf{w}_{i,j} x_i + \sum_{k\neq i} \sum_{j=1}^{M} \mathbf{h}_{i,j}^{\mathrm{H}} \mathbf{w}_{k,j} x_k + n_i \qquad (1)$$

where n_i $\mathcal{CN}(0, \sigma^2)$ is the additive white Gaussian noise (AWGN) at user j.

At the receiver, each user will treat the inter-user interference as noise, thus the signal to noise plus interference ratio (SINR) of user i can be expressed as:

$$\mathrm{SINR}_i = \frac{|\sum_{j=1}^{M} \mathbf{h}_{i,j}^{\mathrm{H}} \mathbf{w}_{i,j}|^2}{\sum_{k\neq i} |\sum_{j=1}^{M} \mathbf{h}_{i,j}^{\mathrm{H}} \mathbf{w}_{k,j}|^2 + \sigma^2} \qquad (2)$$

In general cases, JT requires a full cooperation among all BSs, i.e., all BSs will transmit useful signals to the users. This feature will incur large backhaul overhead. In [4][5], the partial cooperation in JT is proposed hence some BSs can be treated as muted from the perspectives of users. Particularly, when $\mathbf{w}_{i,j} = 0$, it means that the data for user i will not be shared at BS j via the backhaul link. In this way, the backhaul overhead can be reduced since some data will not be transmitted on the backhaul. Similar to [4], we use the number of non-zero $\mathbf{w}_{i,j}$ to model the backhaul consumption. Therefore, the ℓ_0 norm is introduced and the sum backhaul link consumption for user i can be modeled as:

$$C_i = \| |\mathbf{w}_{i,1}|, |\mathbf{w}_{i,2}|, \cdots, |\mathbf{w}_{i,M}| \|_0 \qquad (3)$$

On the other hand, we assume an imperfect CSI in this paper and consider additive uncertainty channel models for the system. Therefore, the channel can be given as:

$$\mathbf{h}_{i,j} = \tilde{\mathbf{h}}_{i,j} + \mathbf{e}_{i,j}, \quad \forall i \in \mathcal{U}, \forall j \in \mathcal{B} \qquad (4)$$

where $\tilde{\mathbf{h}}_{i,j}$ is the estimated channel which is available at the BS. $\mathbf{e}_{i,j}$ is the channel estimation error which is assumed to be bounded as $\|\mathbf{e}_{i,j}\| \leq \delta_{i,j}$ for a given $\delta_{i,j}$.

Our target is to minimize the backhaul consumption of the system. Meanwhile, the QoS should be guaranteed for each specific user hence we give a SINR threshold γ_i for each user. Therefore, we formulate the backhaul link consumption minimization problem with SINR constraints as follows:

$$\begin{aligned} \min_{\{\mathbf{w}_{i,j}\}} \quad & \sum_{i=1}^{K} C_i \\ \text{subject to} \quad & \mathrm{SINR}_i \geq \gamma_i \\ & \|\mathbf{e}_{i,j}\| \leq \delta_{i,j} \\ & \forall i \in \mathcal{U}, \quad \forall j \in \mathcal{B} \end{aligned} \qquad (5)$$

The above problem is non-trivial due to two reasons. First, the QoS constraints in (5) makes the problem non-convex because the variables are coupled in the fractional expressions. Additionally, the objective function of (5) is a non-smooth function. Although exhaustive method or branch-and-bound (BB) algorithm can be used for addressing this difficulty, the complexity of these methods is too high hence they are prohibitive in practice. To handle these difficulties, in the next section, we will reformulate the non-convex constraints into a cone form and then propose a norm relaxation strategy for the non-smooth objective function.

III. Link Removal via Semidefinite Relaxation

In this section, we first propose to relax the ℓ_0 norm function into a solvable and convex function. Observe the QoS constraints, we reformulate these expressions into cone forms and use the convex toolbox to solve it. After achieving a group of solutions, we use a link removal strategy to minimize the consumption of backhaul links.

A. Problem reformulation based on relaxations

According to the definition of ℓ_0 norm, the following equation always holds:

$$\| [|\mathbf{w}_{i,1}|, \cdots, |\mathbf{w}_{i,K}|] \|_0 \triangleq \left\| \left[|\mathbf{w}_{i,1}|^2, \cdots, |\mathbf{w}_{i,K}|^2 \right] \right\|_0 \qquad (6)$$

Therefore, the sum backhaul link consumption for user i can be rewritten as given in (7):

$$C_i = \left\| \left[\mathbf{w}_{i,1}^H \mathbf{w}_{i,1}, \mathbf{w}_{i,2}^H \mathbf{w}_{i,2}, \cdots, \mathbf{w}_{i,K}^H \mathbf{w}_{i,K} \right] \right\|_0 \qquad (7)$$

For a vector, the ℓ_0 norm returns the number of non-zero elements of the vector.

Due to the non-smooth feature appears in (7), a simple approximation of ℓ_0 norm is to substitute this function by ℓ_2 norm, which is first introduced in compressive sensing [3][5]. Applying the idea of replacing the ℓ_0 norm by the ℓ_2 norm, we can first relax (5) to the following optimization problem:

$$\begin{aligned} \min_{\{\mathbf{w}_{i,j}\}} \quad & \sum_{i,j} \mathbf{w}_{i,j}^H \mathbf{w}_{i,j} \\ \text{subject to} \quad & \text{SINR}_i \geq \gamma_i \\ & \|\mathbf{e}_{i,j}\| \leq \delta_{i,j} \\ & \forall i \in \mathcal{U}, \quad \forall j \in \mathcal{B} \end{aligned} \tag{8}$$

Note the SINR constraints are still non-convex in (8). We first define $\mathbf{w}_i = \left[\mathbf{w}_{i,1}^H, \mathbf{w}_{i,2}^H, \cdots, \mathbf{w}_{i,M}^H\right]^H \in \mathbb{C}^{MN\times 1}$, which represents the downlink transmit beamforming vector from all BSs to user i, and in the same way we define $\mathbf{h}_i = \left[\mathbf{h}_{i,1}^H, \mathbf{h}_{i,2}^H, \cdots, \mathbf{h}_{i,M}^H\right]^H \in \mathbb{C}^{MK\times 1}$ and $\mathbf{e}_i = \left[\mathbf{e}_{i,1}^H, \mathbf{e}_{i,2}^H, \cdots, e_{i,M}^H\right]^H \in \mathbb{C}^{MK\times 1}$. Using the definition above, the problem (8) can be reexpressed, as given in (9):

$$\begin{aligned} \min_{\{\mathbf{w}_i\}} \quad & \sum_i \mathbf{w}_i^H \mathbf{w}_i \\ \text{subject to} \quad & \left(\tilde{\mathbf{h}}_i^H + \mathbf{e}_i^H\right) \mathbf{A} \left(\tilde{\mathbf{h}}_i + \mathbf{e}_i\right) - \sigma^2 \geqslant 0, \\ & \|\mathbf{e}_i\|^2 \leqslant \sum_{j=1}^{M} \delta_{i,j}^2, \\ & \forall i \in \mathcal{U}, \quad \forall j \in \mathcal{B} \end{aligned} \tag{9}$$

where $\mathbf{A} = \frac{1}{\gamma_i}\mathbf{w}_i\mathbf{w}_i^H - \sum_{k\neq i}^{K} \mathbf{w}_k\mathbf{w}_k^H$.

To eliminate the quadratic form of $\mathbf{w}_{i,j}$, we can use the semidefinite relaxation (SDP) method to make (9) solvable. We further let $\mathbf{W}_i = \mathbf{w}_i\mathbf{w}_i^H$ to substitute $\mathbf{w}_{i,j}$. To keep an equivalence of the transformation, we add constraints to force the rank of $\mathbf{W}_i$ to 1. Therefore, we can reformulate the problem (9) as follows:

$$\begin{aligned} \min_{\{\mathbf{W}_i\}} \quad & \sum_i \text{Tr}(\mathbf{W}_i) \\ \text{subject to} \quad & \left(\tilde{\mathbf{h}}_i^H + \mathbf{e}_i^H\right) \mathbf{X}_i \left(\tilde{\mathbf{h}}_i + \mathbf{e}_i\right) - \sigma^2 \geqslant 0, \\ & \|\mathbf{e}_i\|^2 \leqslant \sum_{j=1}^{M} \delta_{i,j}^2, \\ & \mathbf{W}_i \succeq \mathbf{0}, \text{rank}(\mathbf{W}_i) = 1 \\ & \forall i \in \mathcal{U} \end{aligned} \tag{10}$$

where $\mathbf{X}_i = \frac{1}{\gamma_i}\mathbf{W}_i - \sum_{k\neq i}^{K} \mathbf{W}_k$.

Because of the rank one constraint, the problem (10) is still non-convex. However, in SDR, we can relax the above problem by dropping the rank one constraint. If the relaxation is tight, we can always recover $\mathbf{w}_i$ from $\mathbf{W}_i$. Therefore, after the relaxation (10) becomes convex and can be easily solved by applying the following S-procedure.

Lemma 1: ([8], S-procedure) Let $f_i(\mathbf{x}) \triangleq \mathbf{x}^H\mathbf{A}_i\mathbf{x} + \mathbf{b}_i^H\mathbf{x} + \mathbf{x}^H\mathbf{b}_i + c_i$, for $i = 0, 1$,where $\mathbf{A}_i$ is a Hermitian matrix.

Algorithm 1 Link removal via semidefinite relaxation

Require: Minimizing the consumption of backhaul links
  Solve the problem (8) using semidefinite relaxation
  if not convergent **then**
    The problem (8) is infeasible. Exit to link adaptation
  else
    Sort the data streams according to $\|\mathbf{w}_{ij}\|^2$.
    Initialize $Q_{\min} = 0$, $Q_{\max} = (M-1)K$, $Q = \lfloor (Q_{\min} + Q_{\max})/2 \rfloor$.
    while $Q_{\max} - Q_{\min} \geqslant 2$ **do**
      Solve the problem (12) using demidefinite relaxation
      if not convergent **then**
        $Q_{\max} = Q, Q = \lfloor (Q_{\max} + Q_{\min})/2 \rfloor$;
      else
        $Q_{\min} = Q, Q = \lfloor (Q_{\max} + Q_{\min})/2 \rfloor$;
      end if
      Sort the data streams according to $\|\mathbf{w}_{ij}\|^2$.
    end while
    Return Q and its corresponding $\{\mathbf{w}_{i,j}\}$.
  end if

Suppose that there exists an $\bar{\mathbf{x}}$ and $f_1(\bar{\mathbf{x}}) \leqslant 0$. Then the two conditions are equivalent:

1) $f_0(\mathbf{x}) \geqslant 0$ for all $\mathbf{x}$ satisfying $f_1(\mathbf{x}) \leqslant 0$;
2) There exists a $\lambda \geqslant 0$ such that

$$\begin{bmatrix} \mathbf{A}_0 & \mathbf{b}_0 \\ \mathbf{b}_0^H & c_0 \end{bmatrix} + \lambda \begin{bmatrix} \mathbf{A}_1 & \mathbf{b}_1 \\ \mathbf{b}_1^H & c_1 \end{bmatrix} \succeq \mathbf{0}.$$

By applying *Lemma 1* to (10), we can transform (10) to the following problem:

$$\begin{aligned} \min_{\{\mathbf{W}_i\}} \quad & \sum_i \text{Tr}(\mathbf{W}_i) \\ \text{subject to} \quad & \begin{bmatrix} \mathbf{X}_i + \lambda_i\mathbf{I} & \mathbf{X}_i\tilde{\mathbf{h}}_i \\ \tilde{\mathbf{h}}_i^H\mathbf{X}_i^H & \tilde{\mathbf{h}}_i^H\mathbf{X}_i\tilde{\mathbf{h}}_i - \sigma^2 - \lambda_i \sum_{j=1}^{M} \delta_{ij}^2 \end{bmatrix} \succeq \mathbf{0}, \\ & \mathbf{W}_i \succeq \mathbf{0}, \forall i \in \mathcal{U} \end{aligned} \tag{11}$$

Now the SINR constraints are transformed to cone forms, which is convex. Hence (11) is a standard convex SDP, which can be efficiently solved via convex toolbox [9].

The optimal solution $\{\mathbf{W}_i\}$ is obtained from the rank relaxation, however, this relaxation cannot guarantee to be tight. Here we discuss two different situations: If each of the optimal solution $\{\mathbf{W}_i\}$ happens to be of rank one, which suggests a tight relaxation, we can get the optimal solution $\{\mathbf{w}_{i,j}\}$ for (8) from $\mathbf{W}_i = \mathbf{w}_i\mathbf{w}_i^H$ for all i, j. On the other hand, if the rank of $\{\mathbf{W}_i\}$ is larger than one, we can consider the idea of applying a rank-one approximation on $\{\mathbf{W}_i\}$, see [10] for the details. By using *Proposition 1* in [7], we know that the optimal solution of SDR in this paper can always guarantee to be rank one, which means that the relaxation is tight and the optimal solution $\{\mathbf{w}_{i,j}\}$ for (8) can always be obtained.

B. Link removal

The optimal solution $\{\mathbf{w}_{i,j}\}$ obtained by SDR cannot guarantee the minimum backhaul link consumption. It is because the solutions are not forced to be sparse. Therefore, we further propose to achieve sparse beamforming vectors. Note that decreasing the backhaul consumption means more $\{\mathbf{w}_{i,j}\}$ to be zero, so we can use a link removal strategy similar to [6] to deal with those non-zero solutions of $\{\mathbf{w}_{i,j}\}$.

Firstly the data streams can be sorted according to the $\|\mathbf{w}_{i,j}\|^2$, which means the transmission power allocated from BS j to user i, from the lowest to the highest, and $Num_{i,j}$ represents the sequence number. Then we can set the lowest non-zero $\{\mathbf{w}_{i,j}\}$ to be zero. It is because when $\mathbf{w}_{i,j}$ is small, the BS i will only allocate few power for user j. Similar to the idea of water-filling, it brings little improvement if BS i transmits signal to user j. Therefore, this link can be removed in order to save the backhaul resources. After the removal of the lowest $\mathbf{w}_{i,j}$, we can solve a new problem, which can be given as follows:

$$\begin{aligned} \min_{\{\mathbf{w}_{i,j}\}} \quad & \sum_{i,j} \mathbf{w}_{i,j}^H \mathbf{w}_{i,j} \\ \text{subject to} \quad & \text{SINR}_i \geq \gamma_i \\ & \|\mathbf{e}_{i,j}\| \leq \delta_{i,j} \\ & \mathbf{w}_{ij} = \mathbf{0}, \text{when } Num_{i,j} \leqslant Q \text{ and} \sum\nolimits_j \mathbf{w}_{i,j} \neq \mathbf{0} \\ & \forall i \in \mathcal{U}, \quad \forall j \in \mathcal{B} \end{aligned} \tag{12}$$

where Q represents the number of links removed from data transmission.

In the process, we must keep at least one $\mathbf{w}_{ij} \neq 0$ for each user i, which implies that keeping the link from its serving BS for data transmission. We can increase Q from 1 to $(M-1)K$ to search the optimal solution, which also leads to much complex computations. And to avoid it, we adopt the bisection method to accelerate the link removal scheme. The link removal via semidefinite relaxation method is summarized in the Algorithm 1.

IV. Simulation

In this section, we evaluate our proposed algorithm under different system configurations. We consider a network of $M = 3$. The downlink channel between the BS and each user is generated according to identically complex Gaussian distributions. Assume that the channel estimation errors δ_{ij} and the QoS requirements γ_i for different users are identical, i.e., $\delta_{ij} = \delta, \gamma_i = \gamma, \forall i \in \mathcal{U},\ j \in \mathcal{B}$. All the simulations are averaged over 100 random channel realizations. The scheme of full cooperation among all BSs in the network is used as a benchmark in the evaluations.

First we test the proposed algorithm under a fixed user number of $K = 6$. Fig.2 shows the performance of backhaul link consumption versus the various number of antennas. We also present the percentages of backhaul link reduction which are compared to the full cooperation scheme in Fig. 3. Different channel estimation errors and QoS requirements are considered as well. As we can see in these two pictures, the backhaul consumption can be remarkably reduced by using the proposed algorithm. The curves of perfect CSI provide a lower bound of the consumption. When the error of channel estimation increases, the performance will decrease because of the inaccurate channel information. From Fig. 3, it also reveals that stringent QoS will leads to more backhaul overhead because more BSs will be used for JT in order to achieve a higher SINR. On the other hand, we can see that the backhaul consumption will decrease with increasing number of transmit antennas. It demonstrates that the proposed algorithm can achieve a better performance when the BSs are equipped with large number of antennas. It should be noted that when N_T reaches a large number, e.g., $N_T = 6$ in Fig. 2, different channel error estimation or QoS will no longer affect the performance. It is because the serving BS of each user can almost satisfy the requirement alone and JT will not be used

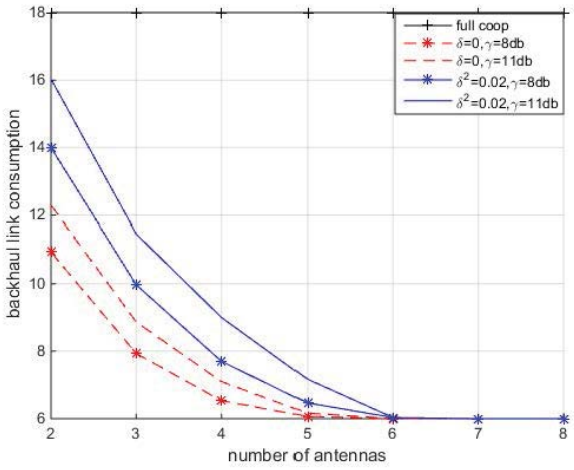

Fig. 2. Backhaul link consumption versus different number of antennas.

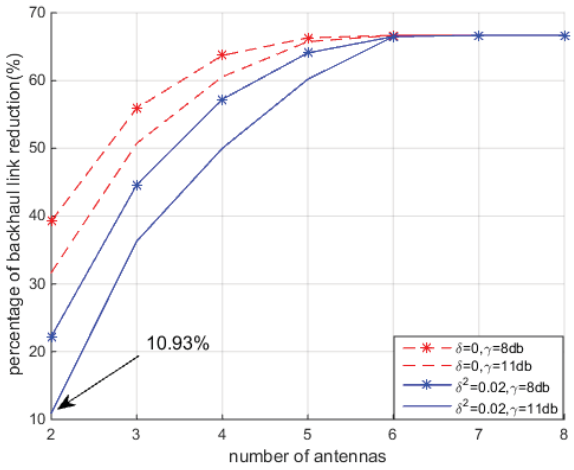

Fig. 3. Percentage of backhaul link reduction compared to full cooperation.

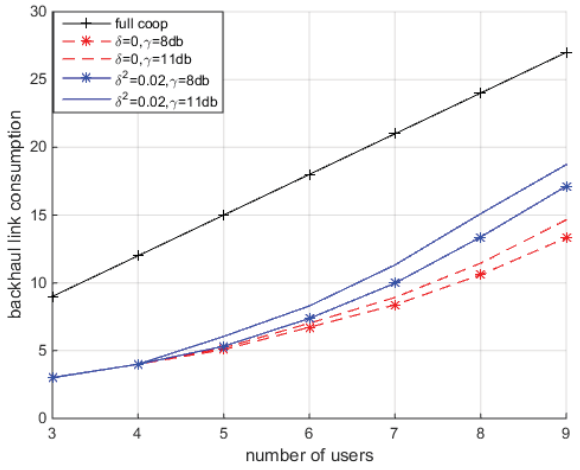

Fig. 4. Backhaul links consumption versus different number of users.

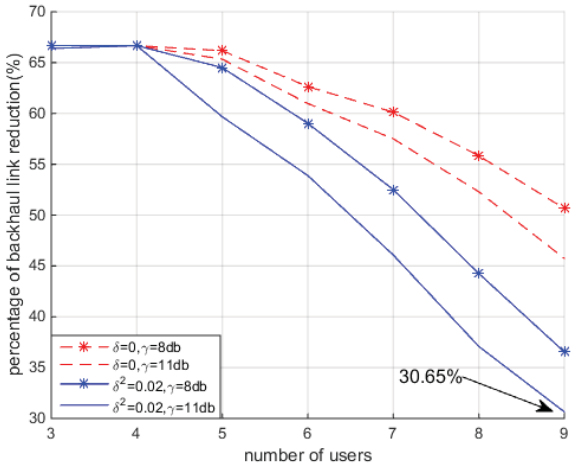

Fig. 5. Percentage of backhaul link reduction compared to full cooperation.

at this moment. Hence the backhaul consumption will reach a minimum value. As we can see from Fig. 3, the backhaul reduction will be more remarkable with an uncertain channel information or high QoS when the number of transmit antenna increases. This is because when N_T is small, the proposed algorithm will result in limited performance under imperfect CSI or stringent QoS. However, when N_T becomes larger, our strategy will become more effective and lead to a better improvement. Under the worst case (when $N = 2$, $\gamma = 11$db and $\delta^2 = 0.02$), the proposed algorithm can at least reduce the consumption of backhaul links by 10.93%.

Fig.4 shows the performance of backhaul link consumption versus the various number of users. In this figure, we set the number of transmit antennas at each BS as $N_T = 4$. We can also see that a worse channel estimation or higher QoS will lead to a performance deterioration. Fig. 4 illustrates that the channel uncertainty or QoS requirement will not affect the proposed algorithm when K is small. The reason is that the inter-user interference is much lower in this case, therefore the proposed algorithm can still keep the backhaul consumption on a substantial lower level. However, with the increasing number of users, the number of backhaul links for JT will also increase in order to satisfy the transmission requirement, as shown in Fig. 4. From Fig. 5, we can see that the percentage of backhaul link reduction compared will reduce when K is large. Particularly, this performance will drop more obvious when the channel is imperfect or the QoS is high. But the proposed algorithm can still achieve an acceptable performance improvement compared to the full cooperation. As shown in Fig. 5, when $K = 9$, $\gamma = 11$ db and $\delta^2 = 0.02$, the proposed algorithm can still substantially reduce the consumption of the backhaul links by 30.65%.

V. Conclusion

In this paper, we consider a backhaul reduction algorithm in JT systems with channel uncertainty and QoS requirement. We formulate the scheme as a non-convex and non-smooth optimization. Due to the difficulties in addressing the original problem, we use the norm relaxation and transform it to a convex SDP via SDR method. We further propose an link removal strategy based on the relaxed problem to minimize the backhaul link consumption. The imperfect CSI is incorporated therefore our algorithm can be applied in practical systems. From the simulation it can be found that the proposed algorithm can reduce the backhaul consumption remarkably while satisfying the transmission requirement comparing with the traditional full cooperation scheme.

References

[1] J. Andrews, "Seven wyas that Hetnets are a cellular paradigm shift," *IEEE Commun. Mag.*, vol. 51, no. 3, pp. 136-144, Mar. 2013.
[2] R. Zakhour and D. Gesbert, "Optimized data sharing in multicell MIMO with finite backhaul capacity," *IEEE Trans. Signal Process.*, vol. 59, no. 12, pp. 6102-6111, Dec. 2011.
[3] M. Hong, R. Sun, H. Baligh, and Z.-Q. Luo, "Joint base station clustering and beamformer design for partial coordinated transmission in heterogeneous networks," *IEEE J. Sel. Areas Commun.*, vol. 31, no. 2, pp. 226-240, Feb. 2013.
[4] F. Zhuang and V. K. N. Lau, "Backhaul limited asymmetric cooperation for MIMO cellular networks via semidefinite relaxation," *IEEE Trans. Signal Process.*, vol. 62, no. 3, pp. 684-693, Feb. 2014.
[5] J. Zhao, T. Q. S. Quek, and Z. Lei, "Coordinated multipoint transmission with limited backhaul data transfer," *IEEE Trans. Wireless Commun.*, vol. 12, no. 6, pp. 2762-2775, Jun. 2013.
[6] A. Tajer, N. Prasad, and X. Wang, "Robust linear precoder design for multi-cell downlink transmission," *IEEE Trans. Signal Process.*, vol. 59, no. 1,pp. 235-251, Jan. 2011.
[7] C. Shen, K. Y. Wang, T. H. Chang, Z. D. Qiu, and C. Y. Chi, "Worst-case SINR constrained robust coordinated beamforming for multicell wireless systems.," *in Proc. 2011 IEEE ICC*, pp. 1-5.
[8] S. Boyd and L. Vandenberghe, *Convex Optimization.* Cambridge, UK: Cambridge University Press, 2004.
[9] M. Grant and S. Boyd, "CVX: Matlab software for disciplined convex programming, version 1.21," http://cvxr.com/cvx, July 2010.
[10] Z. Q. Luo, W. K. Ma, A. M. C. So, Y. Ye, and S. Zhang, "Semidefinite relaxation of quadratic optimization problems," *IEEE Signal Process. Mag.*, pp. 20-34, May 2010.

THE 18TH INTERNATIONAL SYMPOSIUM ON WIRELESS PERSONAL MULTIMEDIA COMMUNICATIONS
(WPMC-2015)
December 13-16, 2015, Hyderabad, India

SUN-RAN Orchestrating Resource Management using Superframe Division Data Aggregation Technology

Fumihide KOJIMA, Chang-Woo PYO and Masayuki OODO
Smart Wireless Laboratory, Wireless Network Research Institute,
National Institute of Information and Communications Technology (NICT)
3-4, Hikarino-oka, Yokosuka, Kanagawa, Japan
{f-kojima, cwpyo, moodo}@nict.go.jp

Abstract— **This paper proposes an intelligent resource management scheme for multi-hop data collection that is effective for big-data management system deploying Smart Utility Network (SUN) – Regional Area Network (RAN) integrated topology where each RAN radio device plays a role of SUN Collection Station (CS) and collects data from several SUN devices in its assuming SUN area and further forward the collected data towards the RAN CS. In the proposed system, the dedicated system resources for each SUN and RAN system are flexibly and effectively allocated for date forwarding according to each topology that is seriously affected by data traffic. In order to realize such resource management, a dynamic resource management technology for each forwarding device in RAN and superframe division data aggregation technology in SUN are proposed respectively. Especially in this paper, the latter technology in SUN is investigated from the viewpoint of forwarded data traffic to RAN devices. Computer simulation results confirm that the proposed superframe division data aggregation technology achieves about 10 times improvement on the forwarded data traffic for RAN.**

Keywords—SUN; RAN; IEEE 802.15.4e; aggregation; multi-hop

I. INTRODUCTION

SUN for effective data collection from a large number of gas, water, and/or electric meters, to provide data to data-collection stations [1] would be a typical radio-based system in the smart grid structure. SUNs can reduce the labor cost in meter-reading by using radio transmission and are expected to provide comprehensive data collection free of oversight. They also appear highly effective in terms of providing safety and, moreover, they are noted for their potential to support two-way communications that can be utilized to measure intelligent energy consumption management in residences and neighborhoods. SUNs' collective benefits make them one of the most likely components in the smart grid structure. Since SUNs are seen as such promising systems, a worldwide movement for their standardization is underway. One of the most aggressive standardization organizations is the IEEE 802 committee, in which the IEEE 802.15.4g task group [2] standardized the PHY amendment for the IEEE 802.15.4 standard [3] to support SUNs. Meanwhile, the IEEE 802.15.4e task group [4] standardized the MAC modification required to realize an effective PHY amendment. Since both forms of standardization were finalized in March 2012, the world first certification body of conformance and interoperability tests on those standard-based radio devices was established – the Wireless-SUN (Wi-SUN) alliance [5] – which actively promotes popularization of SUN devices by defining Wi-SUN profile specifications based on several assumed applications. Since the Wi-SUN alliance has started its activities of certifying IEEE 802.15.4g based SUN devices according to the several expected profiles, further diversified applications employing SUN are considered. ECHONET Lite [6], the communication protocol standard for a home energy management system (HEMS), is one such application supported by the dedicated Wi-SUN profile. This profile for ECHONET Lite is already included in the Japanese standard of radio specifications for ECHONET Lite and the Japanese major ten electric power corporations including Tokyo Electric Power Corporation (TEPCO) are going to deploy it in 80 million houses. Besides ECHONET Lite, deployment of the Wi-SUN profile is also expected in further expanded applications such as the wireless sensor networks, machine-to-machine (M2M) networks or Internet of Things (IoT) with a variety of traffic in the future.

Since the assumed SUN system has a short radio range up to about 1km, another comprehensive communication measure is required in order to provide a data collection from a large area such as regional area. RAN that is also standardized in IEEE 802 as the IEEE 802.22b [7] is expected as one of good candidate because it can provide relatively longer radio link than SUN, that is more than 10km. The RAN-SUN integrated system where data in a SUN area is once collected on a RAN device and then forwarded among the RAN devices towards the RAN CS is one of the most typical systems considering the feasible data collection.

How to cope with the large amount of data is one of the most important issues for general data collection systems as well as the RAN-SUN integrated system. The issue becomes further serious for the case of big-data management using radio communication because effective data collision avoidance

technologies need to be realized by utilizing the allocated frequency resources to the system.

Therefore, in this paper we propose an intelligent resource management scheme for the RAN-SUN integrated data collection system where the dedicated system resources for each SUN and RAN system are flexibly and effectively allocated for date forwarding according to each topology that is seriously affected by data traffic. In order to realize such resource management, a dynamic resource management technology for each forwarding device in RAN and superframe division data aggregation technology in SUN are proposed respectively. Especially in this paper, the latter technology in SUN is investigated from the viewpoint of forwarded data traffic to RAN devices.

The rest of this paper is organized as follows. The next section presents an overview of the assumed system image of RAN-SUN integrated system. In section III, the concept of resource management for the RAN-SUN integrated system for data collection. Section IV explains the proposed superframe division multi-hop data collection with frame aggregation in SUN system. Section V presents computer simulation evaluation of the proposed scheme. The final section concludes the paper.

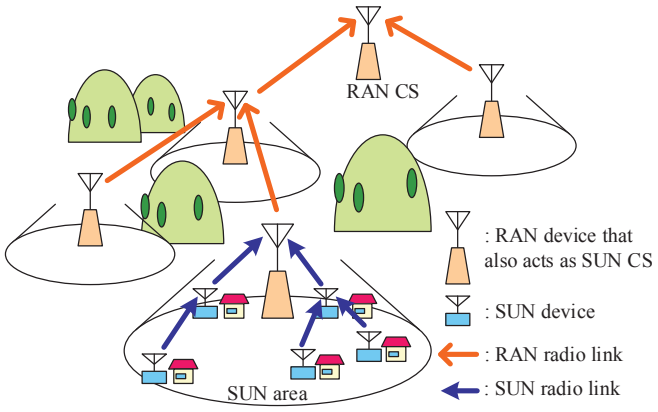

Figure 1. Assumed RAN-SUN integrated system

II. Overview of Assumed RAN-SUN Integrated System for Data Collections

Fig. 1 is a schematic of the assumed RAN-SUN integrated system for data collection. Each of more than one SUN based data collection systems is connected to the one RAN device that has a function of SUN CS. Such collected data in each SUN area is also forwarded among the RAN devices towards the RAN CS that becomes a total data collection station in the RAN-SUN integrated system.

In the SUN system that is standardized as IEEE 802.15.4g/4e, low-energy operation capability and multi-hop transmission capability are regarded as the two most important features. The former means that radio device operations under battery-driven conditions or restricted power supply conditions are required. The latter means the requirements of guaranteeing the assumed service area regardless of radio link degradations owing to pass loss or shadowing loss.

On the other hand, in the RAN system that is standardized as IEEE 802.22b, broadband radio transmission capability accompanied with the multi-hop transmission capability is considered as the key features of the system, which is also expected to work effectively for the assumed data collection system in the regional area as depicted in Fig. 1.

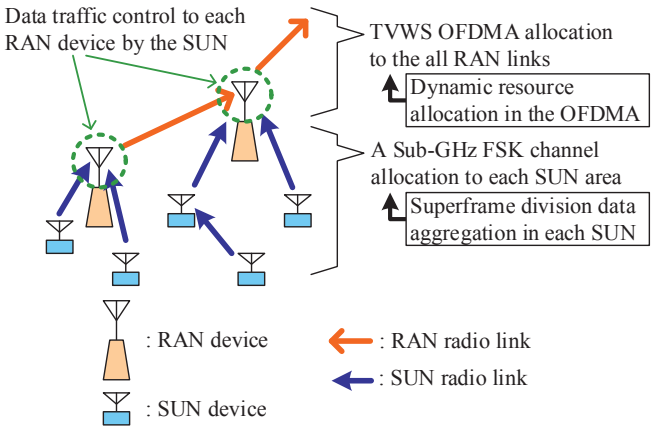

Figure 2. Concept of the resource management for the assumed RAN-SUN integrated system

III. Concept of the Resource Management for the RAN-SUN Integrated System

Fig. 2 shows the concept of the resource management for the assumed RAN-SUN integrated system. The most remarkable point here is that there are different specifications between those two systems each of them are independently standardized by employing different frequency band, modulation scheme and so on, but the two systems are also dependent on each other since they have the deal on the collected data forwarding. Therefore, there would be the possible constructive approaches from both systems to improve the total system performance.

In the SUN system, allocated frequency band for the system is different among the assumed deployed region [2], out of which 920 MHz band for Japan region or 910 MHz band for US region would be the typical allocations in the standard. Frequency Shift Keying (FSK) is most famous Physical (PHY) layer mode in the standard as the Wi-SUN alliance promotes. As for the low-energy multi-hop transmission as strongly required in the system, several research are conducted as in [8]-[13]. Among them, a control scheme that employs superframe division data aggregation technology [14] that is compliant to the IEEE 802.15.4e is considered to be effectively applied to the assumed RAN-SUN integrated system in the viewpoint of not only data flow control in the SUN but also forwarded data traffic control to the RAN. The details of the superframe division data aggregation technology is explained in the next section.

In the RAN system, allocation of TeleVision White Space (TVWS) band with employment of Orthogonal Frequency Division Multiple Access (OFDMA) are considered. Thus, dynamic subcarrier allocation according to the forwarded data traffic for each RAN device is considered as one of the most effective technologies to improve the total system performance

by harmonizing with the management in the SUN system. Since this paper is mainly focusing on the resource management in the SUN as described in the next section, the details of resource management for the RAN system and evaluation of that would become the future study.

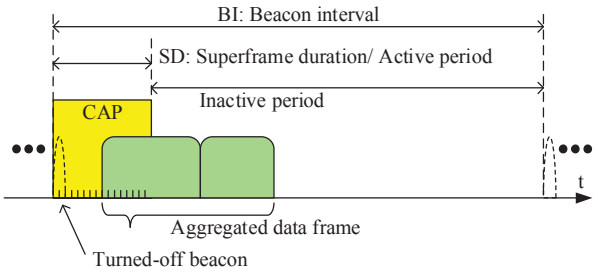

Figure 3. Superframe structure assumed in the SUN

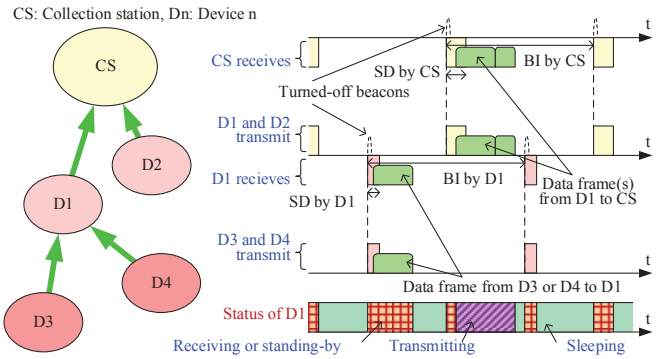

Figure 4. Example of data frame relaying to SUN CS

IV. SUPERFRAME DIVISION MULTI-HOP DATA COLLECTION WITH FRAME AGGREGATION FOR SUN

Fig. 3 shows the superframe structure as defined in IEEE802.15.4e MAC, namely a low-energy (LE) superframe [4]. As standardized in [4], Full Function Devices (FFDs) can act as coordinators in the topology and manage time slot allocation by broadcasting beacons, thus they can be referred to as superframe coordinators in this paper. A beacon interval (BI) is divided into an active and inactive period, as depicted in the figure, and associating devices can enter the sleep state during the inactive period. An active period, also denoted as superframe duration (SD) in its length, assumes a contention access period (CAP) without a contention-free period (CFP). Slotted CSMA-based contention access is adopted during the CAP. BI and SD are defined as BI = 960 *2^BO (symbols) and SD = 960*2^SO, respectively, by using parameters of BO and SO. Here, 0<=SO<=BO<=14. Especially in the LE superframe case, periodical broadcasting of the beacon can be omitted to reduce power consumption from wasted transmission by providing two options for such beacon broadcasting. The first option is where there is no beacon broadcasting except for when the beacon is clearly requested to transmit; i.e., on-demand beacon broadcasting. The other is periodical but intermittent beacon broadcasting. For this, a period of a practical beacon interval equivalent to a multiple of BI is determined and held as a parameter. In this paper, an on-demand beacon is employed in the following computer simulations and experiments. A relatively short active period without a CFP is selected to reduce unintended reception during the active period. For a shortened active period, frame transmission that starts during the period may end before the beacon period not in the current active period, as shown in Fig. 3. Devices receiving a transmitted frame continue reception until complete, even if the active period has ended. Because of this modification, devices not addressed by the frame or not interested in the frame can enter the sleeping state just after such a period, wherein not only the receiver but also all other devices should be standing by, and this helps reduce power consumption. In this paper we also assume frame aggregation [14], as in Fig. 3. The figure also depicts that the frame aggregation in the LE superframe is not restricted by an active period length and can effectively carry the aggregated frame.

Fig. 4 shows the performance of data frame relaying in the current topology. Here, the CS accommodates two meter nodes (D1 and D2), and the other two (D3 and D4) are associating meters with D1. For example, D3 and D4 operate according to the superframe defined by D1 when they send each frame to it. D1 obeys the superframe defined by its associating the CS when D1 relays the received frames to the CS. A meter such as D1 must change its own state according to both incoming and outgoing superframes, as defined in IEEE 802.15.4 MAC. Moreover, we should note that frames in the different superframes (such as those from D2 and D3) expect a very low probability of collision with LE superframe deployment. Thus, we will increase the number of superframes independently by different superframe coordinators in order to instead decrease the frame collisions.

Fig. 5 shows the concept of superframe division multi-hop data collection with frame aggregation in the tree topology constructed by a CS and meter nodes. Here, radio links grouped by the sharing superframe and expected frames on them are shown, assuming each SUN device generates one data frame addressed to the CS. Fig. 5(a) shows the basic case without superframe division or aggregation techniques. Here, a large number of frames, including relayed ones, are provided to the CS and data collection throughput degradation owing to the bottleneck problem can easily be expected. Fig. 5(b) shows the same situation except for frame aggregation. In this case, some frames, including relayed ones, are aggregated into one frame by the relaying devices, thereby decreasing the number of frames reaching the CS. However, frames on the radio links sharing the same superframe can cause collisions, as in Fig. 5(b). In the Fig. 5(c) case with superframe division with aggregation, additionally defined superframes reduce the number of links in the shared superframe, which is expected to reduce frame collision per superframe and mitigate the bottleneck. The additional superframe can be realized by restricting the number of links in a superframe that is equivalent to that for associating devices to a superframe coordinator. Though the average number of hops to the CS is also increased with such superframe division, bottleneck mitigation capability is expected to improve total throughput performance.

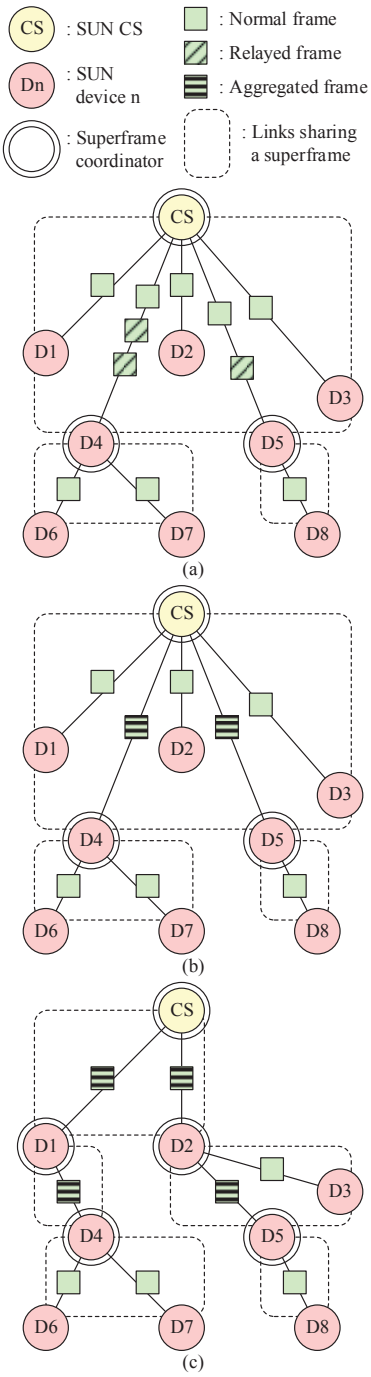

Figure 5. Concept of superframe division multi-hop data collection: a) Without superframe division or aggregation; b) Only with aggregation; c) With both superframe division and aggregation

V. COMPUTER SIMULATION RESULTS

Evaluations via computer simulation were conducted to investigate the performance of the proposed scheme. Table 1 lists the simulation conditions. A square-shaped simulation area is considered in which one collection station is located at the center and 1,000 meters are uniformly scattered. Transmission power of 20 mW in the 920-MHz frequency band is set in accordance with the IEEE 802.15.4g specifications defined for use in Japan that are also included in the Wi-SUN profile for ECHONET Lite. Such PHY parameters are proposed as the dominant transmission rate in IEEE 802.15.4g. A fixed beacon interval of 9.83 s by a BO value of 10 is assumed, which is determined according to the application type and required delay performance. The active period length is examined at 76.8 ms, employing SO values of 3, which means the active period ratio of 0.8%. In the simulation we employ payload lengths of 100 octets by assuming short data collection in SUN. In the simulation, frames periodically arrive on each meter node and all frames are addressed to the CS. In the simulations, we have two major parameters: maximum aggregation size S_{agg} and maximum radio links or devices sharing a superframe N_{DEV}.

TABLE I. SIMULATION CONDITIONS

Parameter	*Value*
Simulated SUN area	2 km x 2 km square area where CS located centered
Number of SUN devices	1,000 devices in a SUN
Frequency band	920 MHz
Transmission power	20 mW
Path loss model	ITU-R P.1411-6 [15]
Shadowing model	Log-normal with standard deviation of 4.0 dB
Receiver sensitivity	-88 dBm
Modulation scheme	100 kbps, 2 GFSK
Beacon interval	9.83 s (BO = 10)
Active period lengths	76.8 ms (SO = 3)
Frame payload length	100 octets (8 ms)
Routing scheme	Tree routing
Frame arrival	Periodical per each meter node
Frame timeout	Same as arrival interval

Fig. 6 shows the frame success probability for the superframe division data aggregation technology according to data frame interval. Several S_{agg} values are investigated in the figure where S_{agg} = 1 means the case that no aggregation is conducted. Fig. 6 shows the frame success probability is improved according to the employed aggregation size, while saturated in about S_{agg} = 16 case. The value of the other parameter N_{DEV} is set to the most effective value as shown in the following Fig. 7.

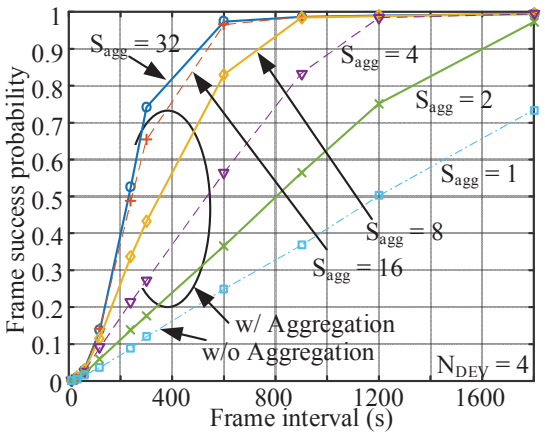

Figure 6. Frame success probability for the superframe division data aggregation according to data frame interval

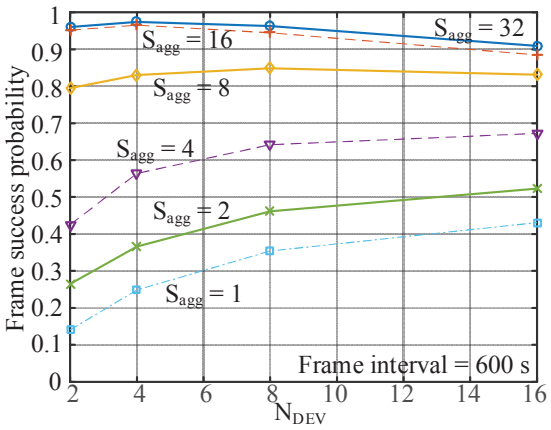

Figure 7. Frame success probability for the superframe division data aggregation according to N_{DEV}

Fig. 7 shows the performance according to N_{DEV} in the case with a 10-min. frame interval. The figure shows that the best performances are provided in the case with larger aggregation size when N_{DEV} is set to about 4. Such situation means the employed superframe division data aggregation is most effectively carried out. It confirms that performance can be improved by more than 95% with the largest aggregation size.

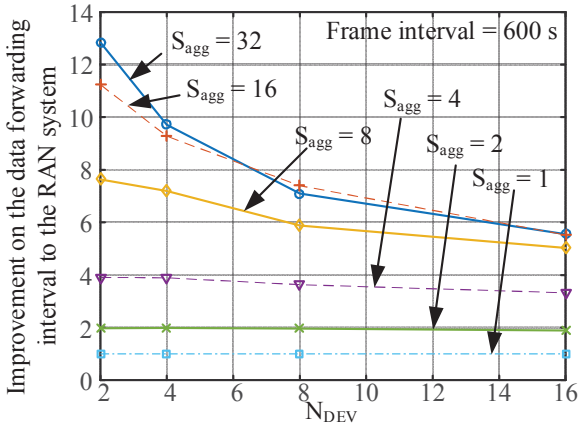

Figure 8. Improvement on the data forwarding interval to the RAN system according to N_{DEV}

Finally, improvement on the data forwarding interval to the RAN system is shown in Fig. 8. Here, the improvement is defined as the normalized forwarding interval for the aggregated data frames by that for the case no aggregation is employed. Fig. 8 shows that about 10 times improvement is possible with the suitable conditions, which results are expected to work effectively for the total system performance of the assumed SUN-RAN integrated data collection system.

VI. CONCLUSIONS

This paper proposes an intelligent resource management scheme for multi-hop data collection that is effective for big-data management system deploying SUN-RAN integrated topology In order to realize an effective resource management for each SUN and RAN system, a dynamic resource management technology for each forwarding device in RAN and superframe division data aggregation technology in SUN are proposed respectively. Furthermore, superframe division data aggregation technology for the SUN is investigated from the viewpoint of forwarded data traffic to RAN devices. Computer simulation results confirm that the proposed superframe division data aggregation technology achieves about 10 times improvement on the forwarded data traffic for RAN. Detailed resource management for RAN system and the total evaluation on the entire SUN-RAN integrated system is a topic for our future studies.

REFERENCES

[1] Y. Rachlin, R. Negi, and P. Khosla, “Sensing capacity for discrete sensor network applications,” in Conf. Rec. 2005 IEEE Information Processing in Sensor Networks, pp. 126-132.

[2] IEEE802.15.4g, “Part 15.4: Low-Rate Wireless Personal Area Networks (LR-WPANs), Amendment 3: Physical Layer (PHY) Specifications for Low-Data-Rate, Wireless, Smart Metering Utility Networks,” 2012.

[3] IEEE802.15.4, “Part 15.4: Wireless Medium Access Control (MAC) and Physical Layer (PHY) Specifications for Low-Rate Wireless Personal Area Networks (WPAN),” 2009.

[4] IEEE802.15.4e, “Part 15.4: Low-Rate Wireless Personal Area Networks (LR-WPANs), Amendment 1: MAC sublayer,” 2012.

[5] Wi-SUN alliance, “Wi-SUN alliance, ” http://www.wi-sun.org/

[6] ECHONET CONSORTIUM, “ECHONET Lite Specification Version 1.00,” 2012.

[7] IEEE802.22b, “IEEE Standard for Information Technology--Telecommunications and information exchange between systems Wireless Regional Area Networks (WRAN)--Specific requirements Part 22: Cognitive Wireless RAN Medium Access Control (MAC) and Physical Layer (PHY) Specifications: Policies and Procedures for Operation in the TV Bands Amendment: Enhancement for Broadband Services and Monitoring Applications,” 2009.

[8] J. L. Hill and D. E. Culler, “Mica: a wireless platform for deeply embedded networks,” 2002 IEEE Micro 22, pp. 12-24.

[9] W. Ye, J. Heidemann, and D. Estrin, “An Energy-Efficient MAC protocol for Wireless Sensor Networks,” in Conf. Rec. 2002 IEEE Computer and Communications Societies (INFOCOM), pp. 1567-1576.

[10] T. v. Dam and K. Langendoen, "An Adaptive Energy-Efficient MAC Protocol for Wireless Sensor Networks," in Conf. Rec. 2003 Embedded Networked Sensor Systems (SenSys), pp. 171-180.

[11] A. El-Hoiydi and J.-D. Decotignie, “WiseMAC: an ultra low power MAC protocol for the downlink of infrastructure wireless sensor networks,” in Conf. Rec. 2004 International Symposium on Computers and Communications, pp. 244-251, vol. 1.

[12] W. R. Heinzelman, A. Chandrakasan, and H. Balakrishnan, “Energy-efficient communication protocol for wireless microsensor networks,” in Conf. Rec. 2000 Hawaii International Conference on System Sciences, pp. 1-10, vol. 2.

[13] Q. Li, J. A. Aslam, and D. Rus, “Online power-aware routing in wireless ad-hoc networks,” in Conf. Rec. 2001 MOBICOM, pp. 97-107.

[14] F. Kojima and H. Harada, “Superframe Division Multi-Hop Data Collection withbAggregation on Wi-SUN Profile for ECHONET Lite,” Conf. Rec. 2014 IEEE Wireless Communications and Networking Conference Workshops, pp. 116-121.

[15] ITU-R, “Recommendation ITU-R P.1411-6: Propagation data and prediction methods for the planning of short-range outdoor radiocommunication systems and radio local area networks in the frequency range 300 MHz to 100 GHz,” 2012.

THE 18TH INTERNATIONAL SYMPOSIUM ON WIRELESS PERSONAL MULTIMEDIA COMMUNICATIONS
(WPMC-2015)
December 13-16, 2015, Hyderabad, India

Simultaneous Transmission of Information and Energy in OFDM Systems

Sumit Gautam and P. Ubaidulla
Signal Processing and Communication Research Center (SPCRC),
International Institute of Information Technology - Hyderabad (IIIT-H),
Hyderabad, INDIA.

***Abstract*—In this paper, we consider simultaneous transmission of information and energy in a wireless network with channels undergoing frequency-selective fading. The receivers can decode the information as well as harvest energy from the same received signal. The network employs orthogonal frequency division multiplexing (OFDM) for signal transmission. We consider two different problems in the simultaneous transmission of information and energy and propose algorithms for transmit and receive processing. The first problem is the optimal resource allocation for maximizing weighted sum-rate of the users while guaranteeing a minimum harvested energy at each receiver. In order to achieve this target, we propose an iterative algorithm for allocating subcarriers to each user, allocating power to each subcarrier, and computing the optimal ratio of the received signal power that goes to the information decoder and the energy harvester. The second problem is the maximization of the total harvested energy under constraints on the minimum rate achieved by each user. We propose resource allocation and receive processing algorithms as in the previous case. Numerical results are provided, and the merits of the proposed design for various operating conditions and parameters are illustrated.**

I. Introduction

Simultaneous transmission of information and energy in wireless systems have received considerable attention recently [1], [2], [3]. Such techniques enable the receivers to perform both information decoding and energy harvesting from the same electromagnetic wave. The received energy is either used to operate the receiver circuit or stored for later use. Such energy harvesting techniques hold great potential for energy-constrained networks with limited energy storage capability. Over the years, the size of batteries used to drive the wireless devices has decreased considerably. Rapid drainage of these battery sources necessitate the devices to use battery optimally by compromising on other important tasks [4]. To complement the decreasing battery size, demand for efficient and compact energy harvesters (EHs) have grown many folds [5]. In this context, the wireless transmission of power along with information holds great promise.

Conventional receiver architectures have mainly focused on increasing the data rates. These optimal receivers used for information decoding are incapable of performing both *wireless information transfer* and *wireless energy transfer* simultaneously. Therefore, this calls for a change in the receiver architecture to support *simultaneous wireless information and energy transfer*. *Time switching (TS)* and *power splitting (PS)* are two practical receiver schemes proposed by researchers to address this problem [4], [5]. In TS, the receiver is designed in such a way that for a first few symbols, it harvests all the energy from the signal power while for the remaining symbols, all of the signal power is utilized for information decoding. However, in case of PS, a fraction of the received signal power is used for harvesting energy and the remaining power is used for decoding information simultaneously.

Orthogonal frequency division multiplexing (OFDM) is a spectrally efficient multi-carrier transmission technique and it has been widely adopted in many recent standards. However, the simultaneous information and energy transmission techniques in the context of OFDM have not been widely studied [4]. In conventional OFDM, subcarriers are assigned to the users based on two main resource allocation schemes: fixed [7] and dynamic [8], [9]. When incorporated with wireless energy transfer, OFDM not only preserves its existing advantages, but it also allows multiple devices to charge simultaneously using wireless recharging. A framework for OFDM-based architecture along with power control algorithms to exploit frequency diversity that improves information and energy transfer efficiency is considered in [1].

In this paper, we consider simultaneous transmission of information and energy in the downlink of a network that employs OFDM. We address the optimal resource allocation for maximizing the weighted sum of rates and for maximizing the total harvested energy. The receivers are assumed to employ PS scheme to decode information and harvest energy simultaneously. Optimal resource allocation, which can significantly enhance the performance of OFDM systems, is well-studied in the conventional use of OFDM. Optimal subcarrier and power allocation and receive processing is a challenging problem when the additional requirement of energy transmission is taken into account. To overcome this difficulty, we propose an iterative algorithm for joint subcarrier and power allocation at the transmitter and the optimal ratio of the received signal that goes to the information decoder and energy harvester at each receiver. The algorithms reported in [9] does not consider allocation of subcarriers to each user, whereas the algorithm proposed in this paper performs the subcarrier allocation as well.

The paper is organized as follows. Section II presents a description about the system model. Section III comprises of solutions to the proposed problems involving both maximization of transmit rate and harvested energy. Section IV

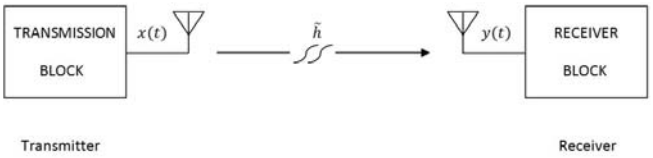

Fig. 1: System model

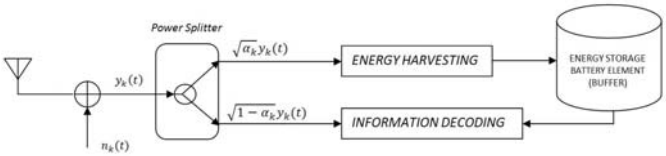

Fig. 2: Receiver architecture (for the kth user)

comprises of simulation results for the proposed algorithms. Finally, section V concludes the paper.

II. System Model

The system model considered in this paper consists of a transmitter that can transmit both information and energy to K users. Fig. 1 depicts a simple block schema of the overall model. It is considered that each user is capable of decoding information and harvesting energy simultaneously.

The transmitter considered in this paper consists of a single antenna. Let $x_k(t)$ denote the signal for kth user, η_k denotes minimum harvested energy constraint known to the transmitter, E_k is the energy harvested by kth user at the receiver and P_T denotes the total transmit power. A frequency selective fading channel is considered. Let H_k denote the channel gain matrix for the kth user, $h_{k,n}$ be the channel gain for kth user in the nth subcarrier, N_0 be the power spectral density (PSD) of additive white Gaussian noise (AWGN) and B be the overall available bandwidth in MHz range. The entire bandwidth is divided into N subcarriers and the power allocated to the nth subcarrier is denoted be p_n. Let K denote the total number of users where $k = 1, 2,..., K$. We assume that $x_k(t)$ is a narrow–band signal having a bandwidth of '$\frac{B}{N}$' MHz, and $\mathbb{E}[|x_k(t)|^2] = 1$ where $|.|$ denotes the absolute value or norm and $\mathbb{E}[.]$ denotes the statistical expectation for the kth user.

Consider a receiver model with single receiving antenna as shown in Fig. 2. Let the received signal to be denoted by $y_k(t)$ and receiver noise for kth user be denoted as $n_k(t)$. Here, the noise $n_k(t)$ can be modelled as a narrow-band Gaussian noise with bandwith equals '$\frac{B}{N}$' and centered around the frequency f_k. The complex equivalent of noise can be adopted from [5] as: $n_k = \sqrt{2}\Re\{\hat{n}_k(t)e^{j2\pi f_k t}\}$, where $\hat{n}_k(t) \sim \mathcal{CN}(0, \frac{\sigma_k^2}{2})$, where $\sigma_k^2 = N_o\left(\frac{B}{N}\right)$ which implies that $\hat{n}_k(t)$ is a circulary symmetric complex Gaussian (CSCG) RV with zero mean and variance σ_k^2.

The signal received at the kth user on the nth subcarrier can be expressed as

$$y_{k,n} = h_{k,n}x_{k,n} + n_{k,n} \tag{1}$$

At each receiver, a power splitter (PS) is employed so that an optimal fraction of the received signal is provided to the information decoder and the remaining part is provided to the energy harvester [5]. The PS ratio at the kth user is denoted by α_k, where $0 < \alpha_k \leq 1$. We can notice from Fig. 2 that PS plays a very important role in determining the efficiency of the receiver system.

Let R_k denote the kth user's rate expressed as:

$$R_k = \sum_{n \in \mathcal{S}_k} \log_2\Big(1 + (1-\alpha_k)p_n\gamma_{k,n}\Big), \tag{2}$$

where $\mathcal{S}_k$ is the set of subcarriers allocated to the kth user, and $\gamma_{k,n} = \frac{|h_{k,n}|^2}{\sigma_n^2}$. We also define

$$E_k = \alpha_k \sum_{n=1}^{N} p_n |h_{k,n}|^2. \tag{3}$$

It should be noted that each user can harvest energy from all the subcarriers.

III. Maximization of the sum-rate

We consider the problem of maximizing the weighted sum-rate of the users while ensuring that the energy harvested at each user is above a given threshold and the total transmit power does not exceed a given limit. To solve this problem, we require a mechanism that not only performs joint subcarrier and power allocation, but also find an optimal PS ratio, α_k, $k = 1, 2, \cdots, K$, at the receiver. The same α_k is applicable for all the subcarriers received by the kth user.

This problem $(P1)$ can be expressed as

$$(P1): \quad \max_{\{\alpha_k\},\{p_k\},\{\mathcal{S}_k\}} \quad \sum_{k=1}^{K} w_k R_k \tag{4}$$

$$\text{subject to}: \quad E_k \geq \eta_k, \tag{5}$$

$$\sum_{n=1}^{N} p_n \leq P_T, \tag{6}$$

where w_k is the weighting factor of the kth user's rate, η_k is the minimum energy harvested by the kth user, and P_T is the upper limit on the total transmit power. Obviously, this is a non-convex optimization problem. Since the solution to problem $(P1)$ involves joint optimization of subcarrier allocation and power, this is a mixed integer programming problem, therefore the possible solutions are not tractable. Hence, computing the optimal solution to this problem is very challenging. Therefore, we propose an algorithm to solve this problem iteratively.

The proposed algorithm (I) can be outlined as follows:

1) Initialize: $\mathcal{U} = \{1, 2, \cdots, K\}$, $\mathcal{S}_k = \phi$, $\alpha_k \in [0\ 1]$, $\Gamma_k = 0$, $k = 1, 2, \cdots, K$.
   Iterate over steps 2 to 5 until convergence
2) $\mathcal{V} = \{1, 2, \cdots, N\}$
3) for $k = 1$ to K,
   a) find n such that $|h_{k,n}| > |h_{k,m}|, \quad m, n \in \mathcal{V}$
   b) $S_k = S_k \cup \{n\}, \Gamma_k = \Gamma_k + \frac{P_T}{N}$
   c) $R_k = \log_2\left(1 + (1-\alpha_k)\Gamma_k\gamma_k\right)$
   d) $\mathcal{V} = \mathcal{V} - \{n\}$
4) While $\mathcal{V} \neq \phi$,
   a) find i such that $w_i R_i \leq w_k R_k$, $i, k \in \mathcal{U}$

b) for the i found in (4.a), find n such that $\gamma_{i,n} \geq \gamma_{i,l}$ $n, l \in \mathcal{V}$
c) $S_i = S_i \cup \{n\}$, Γ_i=Γ_i+ $\frac{P_T}{N}$
d) $\mathcal{V} = \mathcal{V} - \{n\}$
e) Use water-filling algorithm with $R_i = \sum_{n \in S_i} \log_2\big(1 + (1-\alpha_i)\Gamma_{i,n}\gamma_{i,n}\big)$ and $\sum_{n \in S_i} p_n = \Gamma_i$ to compute p_n, $\forall n \in \mathcal{S}_i$

5) Compute PS ratio $\alpha_k = \frac{\eta_k}{\sum_{\forall n} |h_{k,n}|^2 p_n}$, $\forall k \in \mathcal{U}$.

It should be noted that if $\alpha_k = 0$, then the receiver will not be able to harvest any energy at all. However, if $\alpha_k = 1$, all the power from the transmit signal can be harvested at the receiver. In step 5) of the algorithm, it is assumed that equality holds for the constraint in (5). It should be noted that the algorithm iteratively optimizes $\{p_n\}$ and $\{\alpha_k\}$, until convergence. (6) indicates that we can keep adding power until the equality is obtained, thereby maximizing the overall weighted sum rate. The proposed algorithm (I) is motivated by the resource allocation algorithm in [9], where energy transmission is not considered. In general, the subcarriers and power allocation is performed for K users involving N+K optimization parameters for an optimal solution. The proposed algorithm allocates power using water-filling for $(N-K)$ times along with the steps involved in [8].

IV. Maximization of the total harvested energy

In this section, we consider the problem of determining the optimal resource allocation and the PS ratio for maximizing the total energy harvested by the users under constraints on the rates available to each user and the total transmit power. Mathematically, this problem (P2) can be formulated as follows:

$$(P2): \max_{\{\alpha_k\},\{p_n\},\{\mathcal{S}_k\}} \quad \sum_{k=1}^{K}\Big(\alpha_k \sum_{n=1}^{N} p_n |h_{k,n}|^2\Big) \tag{7}$$

$$\text{subject to}: \quad \sum_{j \in \mathcal{S}_k} \log_2\Big(1+\Lambda_j\Big) \geq \rho_k, \ \forall k, \tag{8}$$

$$\sum_{i=1}^{N} p_i \leq P_T, \tag{9}$$

$$p_i \geq 0, \qquad \forall i, \tag{10}$$

$$0 \leq \alpha_k \leq 1, \qquad \forall k, \tag{11}$$

where $\Lambda_j = \frac{(1-\alpha_k)p_j|h_{k,j}|^2}{\sigma_j^2}$, $k = 1, 2, \cdots, K$, $i = 1, 2, \cdots, N$, the constant ρ_k is the minimum rate required by the kth user and the other variables have the same meanings as defined previously. Again, the solutions to problem $(P2)$ are not tractable as this is also a mixed integer problem involving joint subcarrier and power allocation as in the previous case. Therefore, we propose to solve this problem by alternatively computing $\{p_n\}$ for fixed values of $\{\alpha_k\}$, $\{S_k\}$ and vice versa.

Considering fixed values of $\{\alpha_k\}$ and $\{S_k\}$ to optimize $\{p_n\}$, we can rewrite the problem $(P2)$ as:

$$(P3): \max_{\{p_n\}} \quad \sum_{k=1}^{K}\Big(\alpha_k \sum_{n=1}^{N} p_n |h_{k,n}|^2\Big) \tag{12}$$

$$\text{subject to}: \quad \sum_{j \in \mathcal{S}_k} \log_2\Big(1+\Lambda_j\Big) \geq \rho_k, \forall k, \tag{13}$$

$$\sum_{i=1}^{N} p_i \leq P_T, \tag{14}$$

$$p_i \geq 0, \qquad \forall i, \tag{15}$$

where $k = 1, 2, \cdots, K$, $i = 1, 2, \cdots, N$, and other variables have same meanings as defined earlier. We can solve this problem using the *Karush-Kuhn-Tucker* (KKT) conditions for the optimal solution. The objective function and constraints can be written as:

$$f(\mathbf{p}) = \sum_{k=1}^{K}\Big(\alpha_k \sum_{n=1}^{N} p_n |h_{k,n}|^2\Big) \tag{16}$$

$$g_k(\mathbf{p}) = -\Big[\sum_{j \in \mathcal{S}_k} \log_2\Big(1+\Lambda_j\Big) - \rho_k\Big] \leq 0, \forall k, \tag{17}$$

$$r(\mathbf{p}) = (\sum_{i=1}^{N} p_i - P_T) \leq 0, \tag{18}$$

Using (16), (17), and (18), the Lagrangian is given as:

$$\mathcal{L}(\mathbf{p}; \lambda_k, \mu) = f(\mathbf{p}) + \sum_{k=1}^{K} \lambda_k g_k(\mathbf{p}) + \mu r(\mathbf{p}) \tag{19}$$

For optimality, $\nabla_{\mathbf{p}}\ \mathcal{L}(\mathbf{p}; \lambda_k, \mu) = 0$. Thus, we can represent the equation for satisfying optimality condition as:

$$\sum_{k=1}^{K} \alpha_k \sum_{n=1}^{N} |h_{k,n}|^2 + \sum_{k=1}^{K} \lambda_k g_k'(\mathbf{p}) + \mu = 0 \tag{20}$$

where $g_k'(\mathbf{p}) = -\sum_{j \in S_k}\Big(\frac{(1-\alpha_k)|h_{k,n}|^2}{\sigma_j^2 + (1-\alpha_k)p_j|h_{k,n}|^2}\Big)\frac{1}{ln2}$. The feasibility conditions can be represented as $g_k(\mathbf{p})$ and $r(\mathbf{p})$ which are expressed in (17) and (18). Complementary slackness expressions can be represented as follows:

$$\lambda_k\Big[\sum_{j \in \mathcal{S}_k} \log_2\Big(1+\Lambda_j\Big) - \rho_k\Big] = 0, \quad k = 1, 2, \cdots, K, \tag{21}$$

$$\mu\Big(\sum_{i=1}^{N} p_i - P_T\Big) = 0, \tag{22}$$

The conditions for non-negativity are: $p_j, \lambda_k, \mu \geq 0$. After further analysis, it is found that if $\lambda_k \neq 0$ and $\mu \neq 0$, then from (20) we can express p_j's as:

$$p_j = \mathcal{X} - \sum_{j \in S_k} \frac{\sigma_j^2}{(1-\alpha_k)|h_{k,j}|^2}, \forall j \in S_k, \tag{23}$$

where $\mathcal{X} = \frac{\lambda_k}{\left(\sum_{k=1}^{K}\alpha_k \sum_{n=1}^{N}|h_{k,n}|^2+\mu\right)ln2}$ and $k = 1, 2, \cdots, K$. The values for λ_k's can be expressed using (20) as follows:

$$\lambda_k = \frac{\left(\sum_{k=1}^{K}\alpha_k \sum_{n=1}^{N}|h_{k,n}|^2\right)ln2}{\sum_{j\in S_k}\left(\frac{(1-\alpha_k)|h_{k,n}|^2}{\sigma_j^2+(1-\alpha_k)p_j|h_{k,n}|^2}\right)} \tag{24}$$

The value of μ can also be obtained using (20).

Similarly, considering fixed values of $\{p_n\}$ and $\{S_k\}$ to optimize $\{\alpha_k\}$, we can reduce the problem $(P2)$ as follows:

$$(P4): \quad \max_{\{\alpha_k\}} \quad \sum_{k=1}^{K}\left(\alpha_k \sum_{n=1}^{N} p_n|h_{k,n}|^2\right) \tag{25}$$

$$\text{subject to}: \quad \sum_{j\in\mathcal{S}_k}\log_2\left(1+\Lambda_j\right) \geq \rho_k, \forall k, \tag{26}$$

$$0 \leq \alpha_k \leq 1, \qquad \forall k, \tag{27}$$

where $k = 1, 2, \cdots, K$. This is a separable problem, and hence it can be decomposed into K independent problem as follows:

$$(P5): \quad \max_{\{\alpha_k\}} \quad \alpha_k \sum_{n=1}^{N} p_n|h_{k,n}|^2, \tag{28}$$

$$\text{subject to}: \quad \sum_{j\in\mathcal{S}_k}\log_2\left(1+\Lambda_j\right) \geq \rho_k, \tag{29}$$

$$0 \leq \alpha_k \leq 1, \tag{30}$$

In order to solve this problem, we can apply line search algorithm using strong Wolfe conditions [10].

Thus, to solve the proposed problem $(P2)$, following should be repeated till desired convergence: (*i*) perform subcarrier allocation(S_k), (*ii*) solve $(P3)$ for fixed values of $\{\alpha_k\}$ and $\{S_k\}$, and (*iii*) solve $(P4)$ for fixed values of $\{p_n\}$ and $\{S_k\}$. The proposed algorithm (II) can be outlined as:

1) Initialize: $\mathcal{U} = \{1, 2, \cdots, K\}$; $\mathcal{S}_k = \phi$; $\alpha_k \in [0\ \ 1]$; $\mathcal{V} = \{1, 2, \cdots, N\}$; $\Gamma = \{p_n\}, \forall n \in \mathcal{V}$; $j = 0$; $\{g\} = \{h\}$.
2) $q_i = \sum_{\forall i}|g_{i,n}|, \quad i \in \mathcal{U}$ and $n \in \mathcal{V}$
3) Perform the following steps to obtain initial power in each subcarrier using $\{q\}$ obtained from 2):
   a) $\sum_{\forall i} q_i p_i = q^T\Gamma, \quad i \in \mathcal{V}$
   b) $\epsilon = \frac{P_T}{\sum_{\forall i} q_i}, \quad i \in \mathcal{V}$
   c) Find an optimal $\{\Psi\}$ for sub–carriers: $\Psi = \epsilon q$
   d) $\hat{g}_{k,n} = 0, \mu_k = \phi, \forall k \in \mathcal{U}$ and $\forall n \in \mathcal{V}$

   Repeat steps 4 to 6 until convergence
4) for $i = 1$ *to* N
   a) find n such that $g_{n,i} \geq g_{m,i}$, $n,m \in \mathcal{U}$
   b) increment j by 1 and set $\tilde{g}_{n,i} = g_{n,i}$ and $g_{n,i} = 0$
   c) if $\mu_j = \phi$ then $\mu_j = \mu_j + \{n\}$
      else if $\mu_j \neq \phi$ and $n \in \mu_j$, then find n again using 4(a) and 4(b) till $n \notin \mu_j$
   d) $\hat{g}_{n,i} = |\sqrt{1-\alpha_i}\tilde{g}_{n,i}|, \quad \forall i \in \mathcal{U}$
   e) if $\log_2(1+\hat{g}_{n,i}\Psi_i) \geq \rho_j$, then $\mathcal{S}_n = \mathcal{S}_n + \{i\}$
   f) if $j = K$, then set $j = 0$ and $\mu_k = \phi$, $\forall k \in \mathcal{U}$

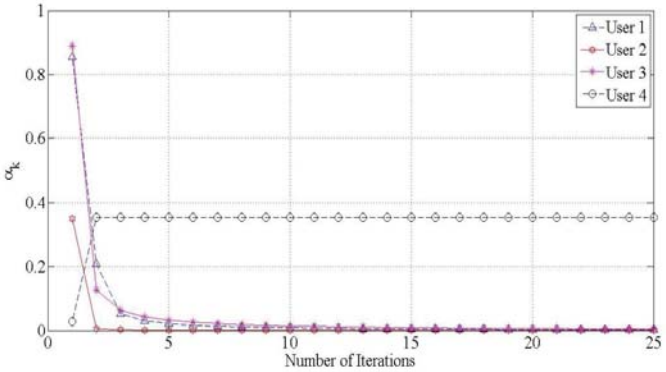

Fig. 3: Convergence of PS ratio α_k for K=4 users with $N = 256$ subcarriers and $B = 1$ MHz.

5) Fix $\{\alpha_k\}$ and $\{\mathcal{S}_k\}$ to maximize (7) over $\{p_i\}$ under the constraints (8), (9) and (10) until convergence, $\forall k \in \mathcal{U}$ and $\forall i \in \mathcal{V}$. $(Ref: (23))$
6) Fix the optimized Γ obtained, along with $\{\mathcal{S}_k\}$, to maximize (7) over $\{\alpha_i\}$ under the constraints (8) and (11) until convergence, $\forall i,k \in \mathcal{U}$. $(Ref: (28))$

In the algorithm above, step 3) is used to initialize the power of each subcarrier. It turns out that when the objective function obtains its maxima, the equality in (9) always holds. To see that, observe that if the current allocated power does not add upto the upper limit, we can always increase the power until the limit is reached without violating the rate constraint. From steps 5) and 6), we can infer that the solution to problem $(P2)$ can be found using divide and conquer mechanism by splitting $(P2)$ into two sub-problems $(P3)$ and $(P4)$ [corresponding to steps 5) and 6) respectively], and then applying the KKT conditions as described previously. The algorithm is operational for (N+K) times over a single iteration and therefore, the order of this algorithm can be expressed as a linear function of N and K for all the iterations.

V. SIMULATION RESULTS

In this section, we evaluate the performance of the two proposed algorithms using simulations. We consider $N = 256$ OFDM subcarriers, total bandwidth $B = 1$MHz, and N_0=-90dBW/Hz throughout the simulations where each user has 6-tap sample-spaced multipath channel with each tap experiencing independent Rayleigh fading. The weights w_i, $i = 1, 2, \cdots, K$ are all set to one. The lower limit of the harvested energy (η) is assumed to be the same for all users.

Fig. 3 illustrates the convergence of PS ratio (α_k) over the indicated iterations. It can be observed from results in Fig. 3 that the PS ratio (α_k), obtained from the proposed algorithm (I) converges to the optimum value within around 20 iterations for all considered scenarios. Fig. 4 depicts the performance of proposed algorithm (I) in terms of spectral efficiency, where it is compared with equal power allocation algorithm (EPA) for K=8 users with different values of total transmit power (P_T). The result indicates that maximum spectral efficiency is obtained when minimum demanded harvested energy (η) is 0 dBm. However, it can be observed that the spectral efficiency

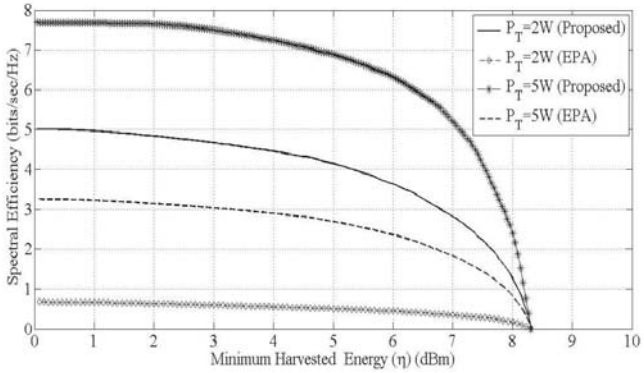

Fig. 4: Spectral efficiency versus minimum harvested energy requirement (η) for K=8 users with different P_T values.

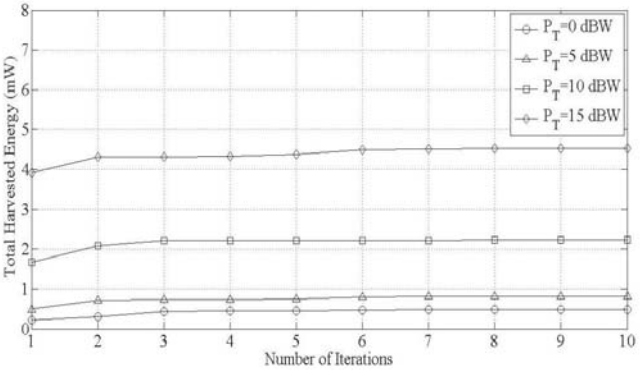

Fig. 5: Total Harvested Energy (in mW) versus number of iterations for K=4 users with different P_T values (in dBW).

is found to decrease as the demand for harvested energy is increased. It can also be noted that the spectral efficiency improves considerably as P_T increases.

In Fig. 5, performance of algorithm (II) is shown where the convergence of total harvested energy (in mW) is seen over different iterations for K=4 users and different values of P_T (in dBW). From the results, it can be observed that total harvested energy (in mW) in proposed algorithm (II) converges to the optimum value within 10 iterations for all the scenarios considered. Again, the fast convergence of proposed algorithm (II) confirms its practical implementations. Fig. 6 shows the average maximized harvested energy $\{\xi_{avg}\}$ by average rates $\{\rho_{avg}\}$ demanded by K=4 users for different P_T values. The maximized harvested energy (E_k^*) is calculated using (3) for all the K users. The average maximized harvested energy is given as, $\xi_{avg} = \frac{\sum_{\forall k} E_k^*}{K}$, $k = 1, 2, \cdots, K$. For simplicity, uniform rates (ρ_{avg}=10 Mbits/s) were considered for all the users during simulations. From the results it can be seen that, as the values of P_T increases, ξ_{avg} increases appreciably. It can be observed from Fig. 6 that ξ_{avg} decreases with increasing values ρ_{avg}.

VI. CONCLUSIONS

In this paper, multiuser OFDM environment is considered for transmission. It is assumed that channel conditions are known to both the transmitter and the receiver. Considering

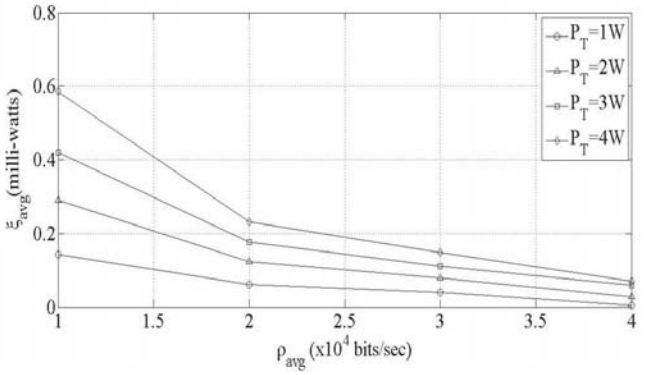

Fig. 6: Average maximized harvested energy (ξ_{avg}) versus average rate (ρ_{avg}) for K=4 users with different P_T values.

the users' frequency selective nature of the channels, we performed joint subcarrier and power allocation along with computation of a power splitting ratio, α_k. In this process, transmit rate should be kept maximum, without compromising the QoS. At the receiver, we use a power splitter (PS) for splitting the received signal power for energy harvesting and information decoding using the α_k value at the transmitter. Then, the harvested energy is maximized for each user under the constraints on minimum known rate and total transmit power. Proposed algorithm (I) is compared with equal power allocation algorithm. Moreover, it is seen that the harvested energy at energy harvester is maximized using our approach from proposed algorithm (II). This work can further be extended to many fascinating directions like addressing the design of PS, formulating an optimal approach to maximize harvested energy, and exploiting the diversities originating from time varying channels.

REFERENCES

[1] K. Huang, and E. Larsson, "Simultaneous information and power transfer for broadband wireless systems," in *IEEE Transactions on Signal Processing,* 2013.

[2] T. Le, K. Mayaram, and T. Fiez, "Efficient far-field radio frequency energy harvesting for passively powered sensor networks," in *IEEE Journal of Solid-State Circuits,* vol. 43, pp. 1287-1302, May 2008.

[3] W. C. Brown, "The history of power transmission by radio wave," *IEEE Trans. on Microwave Theory and Techniques,* vol. 32, pp. 1230-1242, Sep. 1984.

[4] X. Zhou, R. Zhang, and C.K. Ho, "Wireless information and power transfer in multiuser OFDM systems," in *Global Communications Conference,* 2013 IEEE.

[5] X. Zhou, R. Zhang, and C.K. Ho, "Wireless information and power transfer: architecture design and rate-energy tradeoff," in *Communications, IEEE Transactions on* Volume:61, Issue:11, Oct. 2013.

[6] D. Gunduz, K. Stamatiou, N. Michelusi, and M. Zorzi, "Designing intelligent energy harvesting communication systems," in *Communications Magazine, IEEE* Volume:52, Issue:1, Jan 2014.

[7] E. Lawrey, "Multiuser OFDM," in *Proc. IEEE International Symposium on Signal Processing and its Applications,* vol. 2, pp. 761-764, Aug. 1999.

[8] Jang, and K. B. Lee, "Transmit power adaptation for multiuser OFDM systems," *IEEE J. Select. Areas Commun.*, vol. 21, pp. 171-178, Feb. 2003.

[9] W. Rhee, and J. M. Cioffi, "Increase in capacity of multiuser OFDM system using dynamic subchannel allocation," in *Proc. 51st IEEE Vehicular Technology Conference*, vol. 2, pp. 1085-1089, Spring 2000.

[10] J. Nocedal, and S. J. Wright, "Numerical Optimization," chapter 3. Springer, 2nd edition, 2006.

THE 18TH INTERNATIONAL SYMPOSIUM ON WIRELESS PERSONAL MULTIMEDIA COMMUNICATIONS
(WPMC-2015)
December 13-16, 2015, Hyderabad, India

Minimal Error IEEE 802.15.4 Communication Module for Heart Monitoring Data Transmission in IoT

V. Subrahmanyam, Mohammed Abdullah Zubair, Ajay Kumar, P. Rajalakshmi
Department of Electrical Engineering
Indian Institute of Technology - Hyderabad, India
Email: ee14mtech11012, ee14mtech01003, ee15resch02002, raji@iith.ac.in

***Abstract*—With an estimation of 20 billion devices being connected to the Internet in the coming years, the accuracy and the robustness of the wireless communication modules takes the center stage. The health-care scenario, due to its critical nature, calls for an error free communication. IEEE 802.15.4 is the established standard in the Internet of Things scenario that uses Direct Sequence Spread Spectrum - Offset Quadrature Phase Shift Keying (DSSS-OQPSK) modulation. In this paper, we propose a modified minimal error IEEE 802.15.4 communication system for the IoT applications in health care. The proposed architecture uses Maximum Likelihood based frequency offset estimator that can compensate upto 80ppm of the frequency offset. The detection of the symbols is achieved by the complex correlation of the spread sequence. The Bit Error Rate (BER) performance of the proposed architecture is significantly improved compared to the standard architecture. For example, at BER of 0.01, it achieves a gain of 2db over the standard. The proposed ML estimator for frequency offset performs better in terms of error variance than the existing estimators for IEEE 802.15.4.**

***Keywords*—ZigBee, low power, Differential Encoding , synchronization , carrier offset , complex correlation**

I. Introduction

Internet of things (IoT) provides gateways to many industrial and medical applications. Healthcare applications such as patient monitoring using Body Area Networks (BAN) is being developed in IoT. Since IoT enabled devices usually transmit data on a wireless channel, there is requirement of transmitting the data such as electrocardiogram, blood pressure, temperature with less errors. Also, most of the IoT enabled devices are battery powered so the system we choose should consume less power. Healthcare includes various patient monitoring data such as Electrocardiogram (ECG), blood pressure, body temperature etc.

ECG conveys information about heart like heart rate and heart rhythm. All heart related diseases like convective heart failure, heart attack and other diseases can be diagnosed by analyzing the changes in ECG pattern. ECG signal has few key features, the PR, QRS and ST intervals that conveys critical information regarding the condition of the patient. The P wave gives information regarding the atrial contraction. The QRS interval represents the conductance and depolarization of the ventricles. The ST segment shows the time period in which the ventricles are isoelectric. There have been many wearable wireless ECG systems developed. In [1], an ECG, EEG, respiration rate and motion monitoring healthcare system was developed using IEEE 802.15.4 as communication standard. For acquiring ECG data, we have used Adaptive Rule Engine based Data Acquisition system developed at IITH [2]. Our data acquisition system has 3 lead ECG that requires 4 electrodes connected to the body.

For wireless ECG data transmission ZigBee, Wi-Fi, Bluetooth technologies have been used in the literature. In [3], the Bluetooth module has been used as an intermediate node between ECG acquisition module and smart phone in ECG monitoring system. In [4] a Wi-Fi based system with a single-chip ECG acquisition module on Concerto MCU, a simpleLink CC3000 Wi-Fi module and a smart phone was used. In [5], IEEE 802.15.4 module has been used to transmit ECG data. For our work, we are concentrating on transmission of ECG data whose maximum frequency can be 200Hz which requires minimum sampling rate of 400 samples/sec. If the resolution of the data is maintained at 16 bits, then the data rate of the ECG would be 6.4Kbps, which makes it suitable for IEEE 802.15.4 transmission which can handle upto data rate of 250Kbps. The IEEE 802.15.4 standard can be adopted for its low cost effectiveness, low power consumption and reliable self configurable capability which is the prime requirement of the ECG signal transmission.

In an IoT and WSN scenario, a node can transmit data at any time making it a random access network. The fixed preamble helps in identifying the valid IEEE 802.15.4 packet and the start of the payload. The transmitted packet format of IEEE 802.15.4 is shown in the Fig. 1, in which it has fixed preamble of length 32 bits. This preamble is used for carrier and frame synchronization.

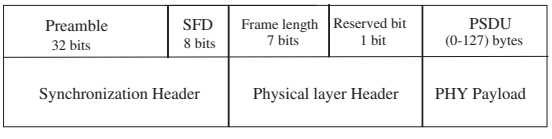

Fig. 1: IEEE 802.15.4 PHY Packet Format

Synchronization is an essential task at the baseband receiver. The received signal needs to be operated on the same clock as that of the transmitter. But in practice, oscillators differ slightly in the frequency they generate, thus creating a frequency offset at the receiver. The indoor channel effects also contributes to this offset. Frequency offset in IEEE 802.15.4

may range from 8ppm to 80ppm thus causing a maximum offset of 200KHz. The received signal may also be out of phase resulting in the phase offset. Significant amount of work is done in the field of synchronization. In [6], data aided ML estimator for joint synchronization of frequency, phase and timing offsets is used. This work is done on a preamble sequence of alternating zeros and ones that are BPSK modulated. But in IEEE 802.15.4, the baseband receiver will receive a 256 bit spreaded sequence resulted from a 32 bit preamble of all zeros. Hence, the simplifications derived from an alternating zeros and ones cannot be employed here. In [7], a simple and low complex frequency offset estimator using correlation for IEEE 802.15.4 receiver is proposed. But their estimator performance shows a significant gap between their error variance and Cramer Rao Lower Bound (CRB) for frequency estimators. In this paper we propose a joint ML estimator for phase and frequency offset working on the spreaded sequence of the preamble. The performance of the proposed estimator is significantly closer to the CRB.

Frame synchronization is achieved through correlation of the received preamble with the fixed preamble sequence. If the correlator output crosses a threshold, the packet is detected as a valid packet. In [8], authors have shown that differential encoding reduces the false and missing probabilities in Packet Detection for BPSK Signals. The authors in [9] have analyzed the packet detection with differential encoding for IEEE 802.15.4 and have shown that this method provides robust packet detection. Our receiver architecture employs symbol detection method used in [10] that correlates the received complex samples with a set of reference complex samples resulting in lesser BER.

The rest of the paper is organized as follows, the proposed architectures of transmitter and receiver are discussed under section II. The simulation results is under section III and Section IV concludes the paper with future scope.

II. Proposed System Architectures

We propose an ASIC(Application Specific Integrated Circuit) based on-chip architecture for ECG monitoring as shown in Fig.2. The System Architecture for the transmission and reception of ECG data is shown in Fig. 3. The transmitter and receiver blocks are explained in detail in the following subsections.

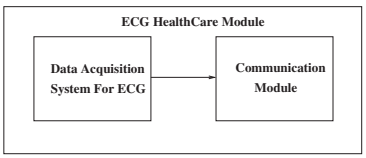

Fig. 2: ASIC chip Architecture

A. IEEE 802.15.4 Transmitter

The proposed transmitter structure is as shown in Fig. 4. The analog ECG signal is passed through the ADC in the data acquisition system and the digital output is at 500 samples/sec. This bitstream is differentially encoded as shown

$$y_k = x_k \oplus y_{k-1}$$

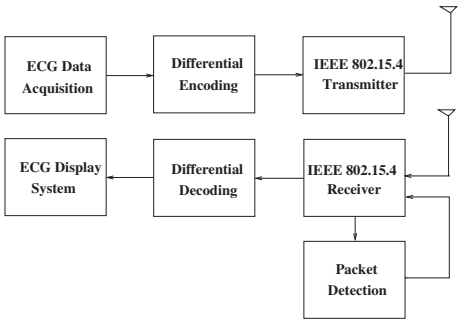

Fig. 3: Overall System Architecture

y_0 is taken as 0 at the start of the packet. The encoded bits which are at a rate of 250Kbps are mapped to symbols in the Bit to Symbol block with each symbol equivalent to 4 bits. Each symbol is mapped to a fixed 32 bit chip sequence using Direct Sequence Spread Spectrum (DSSS). These chip sequences are inherently orthogonal to each other. The output of this symbol to chip block has a data rate of 2Mbps. The signal is now modulated by using the Offset Quadrature Phase Shift Keying (OQPSK) modulation whose in-phase and out-phase component will be at a rate of 1Mbps. Each component is passed through a half sine pulse shaping filter to limit the bandwidth of the signal.

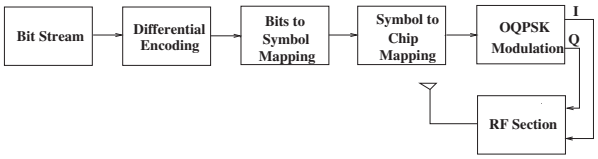

Fig. 4: IEEE 802.15.4 Transmitter with Differential Encoding

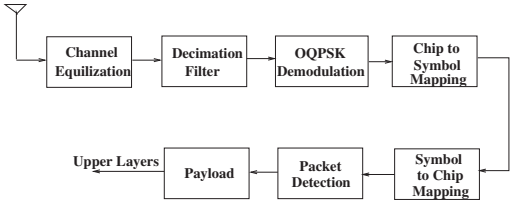

Fig. 5: IEEE 802.15.4 Receiver for ECG Data Transmission

B. IEEE 802.15.4 Receiver

1) Standard IEEE 802.15.4 Receiver: A standard receiver architecture is shown in the Fig. 5. The received signal, at the input of the baseband is filtered to remove the out of band noise. If the channel is incorporated, then corresponding equalization will be done with the help of pilot carriers. The signal is decimated and then demodulated by the OQPSK demodulation block and the chip to symbol and then symbol to bit mapping is done. The payload of the packet is detected

by the packet detection algorithm which is done by cross correlation with the fixed sequence which is 32 bit zeros. If the correlation is above the threshold value, then the payload is send to the post processing block for further processing.

2) Proposed IEEE 802.15.4 Receiver: The proposed architecture as shown in figure 6 uses a ML frequency estimator and a correlation and estimation block.

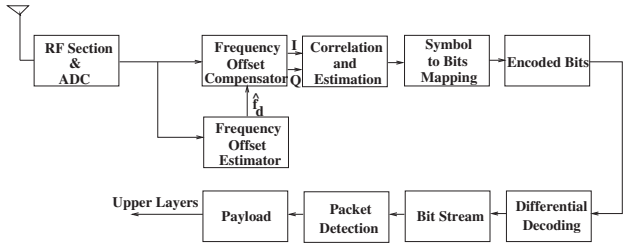

Fig. 6: Proposed IEEE 802.15.4 Receiver for ECG Data Transmission

Maximum Likelihood based carrier frequency and phase offset estimation:
The carrier frequency offset (f_d) and phase offset (θ) are manifested in the received baseband signal ($z(t)$) as:

$$z(t) = exp(j(2\pi f_d t + \theta))s(t) + n(t) \tag{1}$$

where
$s(t)$: Modulated signal $s(t) = \sum_i c_i g(t - iT_c)$
c_i is a complex symbol and g(t) is the half sine pulse shape.
T_c is the symbol period after DSSS
$n(t)$: Gaussian Noise with zero mean and variance σ_n^2

The preamble used in IEEE 802.15.4 standard contains 32 bits of zeros that corresponds to eight symbols of the integer value 0. These eight symbols each have fixed 32 bit spread sequence of $[11011001110000110101001000101110]$. This gives a spreaded sequence of length 256 bits that maps to 128 OQPSK symbols. This fixed sequence helps in data aided synchronization.
The ML estimation uses the modulated signal $s(t)$ derived from these known sequences.

The log likelihood function for the unknown carrier offset as given in [11] is:

$$\Lambda_l(\tilde{f_d}, \tilde{\theta}) = Re\left\{\left[\int_{T_0} z(t)s^*(t : \tilde{f_d}, \tilde{\theta})e^{(-i(2\pi \tilde{f_d} t + \tilde{\theta}))}dt\right]\right\} \tag{2}$$

$s(t)$: Known modulated signal of the spread sequence of the preamble.
$z(t)$: Received signal.
$\tilde{f_d}$: Frequency offset estimate.
$\tilde{\theta}$: Phase offset estimate.
The discrete time equivalent of the equation (2) when sampled at $t = kT_c/2N$, that is at twice of the chip frequency is:

$$\Lambda_l(\tilde{v}, \tilde{\theta}) = Re\left\{\left[\sum_{k=0}^{N_0-1} z[k]s^*[k]e^{(-i(\pi \tilde{v} k + \tilde{\theta}))}\right]\right\} \tag{3}$$

where
N_0 is the number of times the sequence is sampled.
$k = 0, 1, 2, 3, ...$
$\tilde{v} = \tilde{f_d} Tc/N_0$, the normalized carrier frequency offset

Rearranging the equation (3) gives :

$$\Lambda_l(\tilde{v}, \tilde{\theta}) = Re\left\{\left[e^{-i\theta}\sum_{k=0}^{N_0-1} z[k]s^*[k]e^{(-i(\pi \tilde{v} k))}\right]\right\} \tag{4}$$

Let us define

$$\Delta(\tilde{v}) = \sum_{k=0}^{N_0-1} z[k]s^*[k]e^{(-i(\pi \tilde{v} k))} \tag{5}$$

Then equation (4) becomes

$$\Lambda_l(\tilde{v}, \tilde{\theta}) = Re\{[e^{-i\tilde{\theta}}\Delta(\tilde{v})]\} \tag{6}$$

The value of $\tilde{\theta}$ that maximizes the likelihood function is given as:

$$\tilde{\theta} = arg\{\Delta(\tilde{v})\} \tag{7}$$

Now, define $q[k] = z[k]s^*[k]$
Equation (5) becomes

$$\Delta(\tilde{v}) = \sum_{k=0}^{N_0-1} q[k]e^{-i(\pi v k)} \tag{8}$$

As clearly seen, equation (8) takes the form of a Discrete Fourier Transform (DFT). The value of $\tilde{v}$ can be derived from maximizing $\Delta(\tilde{v})$.

$$\tilde{v} = max\left\{\sum_{k=0}^{N_0-1} q[k]e^{-i(\pi v k)}\right\} \tag{9}$$

The DFT can be performed efficiently using an N-point Fast Fourier Transform (FFT). The accuracy of the estimated value $\tilde{v}$ depends on the resolution of the FFT performed. The signal q[k] is zero padded to perform high resolution FFT that generates accurate value of $\tilde{v}$.

Correlation and Estimation block:

The baseband received signal passed through the channel can be expressed as:

$$z(i) = \sum_{\tau=0}^{L} h(\tau)s(i - \tau) + n(i) \tag{10}$$

where
$z(i)$: Received Signal
$s(i)$: Modulated Signal
$n(i)$: Gaussian Noise with zero mean and variance σ_n^2
$h(\tau)$: τ-th coefficient of the channel

$$h(\tau) = a(\tau)e^{j\theta(\tau)}$$

The channel is a Complex Gaussian distribution whose amplitude and phase follows Rayleigh and Uniform distributions respectively with L+1 taps.

For the k-th received signal, the correlator output is

$$J_k(l) = \sum_{n=0}^{15} |z(i)g^*(l,n)|^2$$

$$= \sum_{n=0}^{15} |g^*(l,n) \sum_{\tau=0}^{L} h(\tau)s(i-\tau)|^2 \quad (11)$$

where g(l,n) is the n-th sample of the l-th symbol's complex half sine modulated signal. Since the Gaussian noise is independent of the modulated signal, the correlation between noise and the modulated signal goes to zero.
The expectation of the output gives

$$E\{J_k(l)\} = \begin{cases} 16\sigma_g^2 \sum_{\tau=0}^{L} |h(\tau)|^2, n = i-\tau \\ 16\sigma_{xy}^2 \sum_{\tau=0}^{L} |h(\tau)|^2, n \neq i-\tau \end{cases} \quad (12)$$

where,
$\sigma_g^2 = E\{|g(l,n)|^2\}, l = k$

$\sigma_{xy}^2 = E\{g^*(l,n)g(k,n)\}, l \neq k$

The symbol can be hence estimated as:

$$\hat{l}_k = argmax_l\{J_k(l)\} \quad (13)$$

that is, the reference signal that gives maximum correlation with the received signal in the symbol duration is the estimated symbol. The flow of the block is shown in figure 7. Thus, the correlation and estimation block outputs an estimated symbol, eliminating the need of despreading. The estimated symbol is then mapped to corresponding four bits which are then differentially decoded and the payload is extracted.

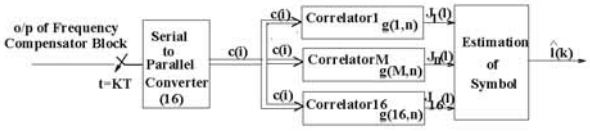

Fig. 7: Correlation and Estimation Block

III. Performance Analysis

The analysis of the proposed architectures is done with the described ECG data acquisition system. The packet is constructed with 32 bits preamble and 127 bytes of payload coming from the ECG data acquisition system. The simulation is done for 500 packets with SNR ranging from -10dB to 5dB. The architecture is analyzed under the conditions of AWGN Channel.

A. ECG signal reconstruction

The transmitted ECG signal is shown in figure 8. AWGN channel is considered. The proposed architecture faithfully recovers the ECG signal under these conditions without any loss in the features at 0dB SNR as shown in the figure.

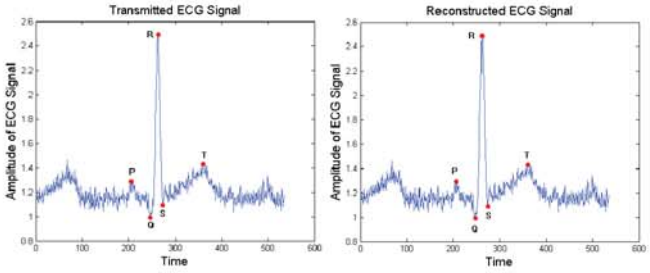

Fig. 8: Transmitted and Received ECG Signal through AWGN

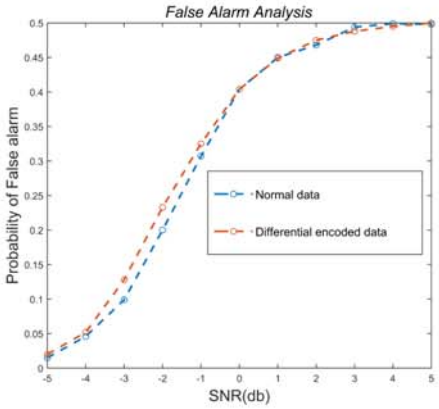

Fig. 9: Probability of False Alarm Analysis

B. Probability of False Alarm Analysis

The probability of miss and false alarm with differential encoded data for IEEE 802.15.4 was studied in [12]. It was proposed that differential encoded data performs better than the normal data. The variation probability of false alarm with SNR for both types of data for the proposed architecture is plotted in figure 9. It can be seen that the results for the normal data is as good as that of differential encoded data. This is due to the better error management of the correlation and estimation block in the proposed architecture.

C. Frequency Estimator Analysis

The Error variance of the proposed estimator is plotted in 10. The Cramer Rao Lower Bound (CRB) for the variance of a frequency offset estimator is given in [7] as:

$$var(\delta f) = 3(2\pi^2 E_b/N_0 T_c^2 N(N^2-1))^{-1}$$

where
N: sequence length
E_b/N_0: SNR in linear scale
T_c: chip interval

The simulations has been done by considering an offset of 80ppm that is approximately 200KHz which is the maximum offset in IEEE 802.15.4. As seen in figure 10, with the increase in FFT resolution, the error variance of the proposed estimator approaches the CRB. This is due to the increase in accuracy of the estimated value. We have also plotted the error variance of the estimator proposed in [7] for IEEE 802.15.4. This results shows that the performance is better than the estimator of [7] with a trade off in complexity.

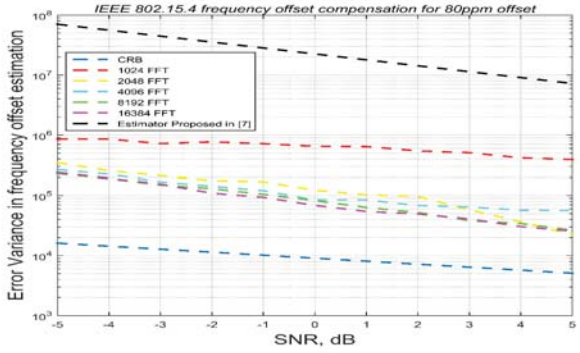

Fig. 10: Error Variance compared with CRB for 80ppm frequency offset

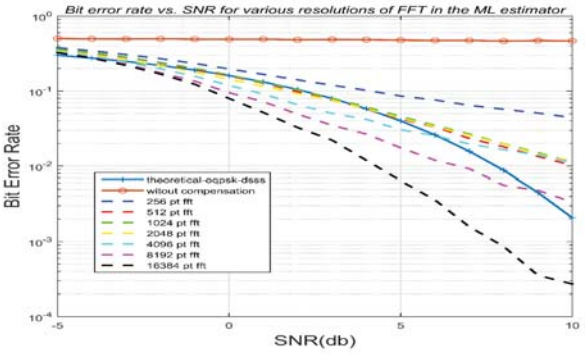

Fig. 11: Comparison of BER for different resolutions of FFT

D. BER Analysis

BER analysis as shown in figure 11 shows that the error performance has been significantly improved when compared to that of standard architecture. It has been analyzed without frequency offset compensation and with compensations under various resolution of Fast Fourier Transforms(FFT) used in the estimator. It is observed that with the increase in the resolution the BER performance significantly improves. At 512 point FFT which is relatively less complex to design, the BER performance matches with the theoretical OQPSK-DSSS BER given in [13] at low SNRs. It can be seen that the estimator with 8192 point FFT has a gain of 2db at BER of 0.01 while 16384 point FFT has more than 5db gain. This error performance is achieved due to complex correlation used for detection and accurate compensation for the frequency offsets. It is also observed that the frequency offsets, if not compensated degrades the performance severely. The frequency offset estimator improves the performance effectively even at the 80ppm of frequency offset.

IV. Conclusion

In this paper we proposed a minimal error communication module and has been tested for ECG data. The ECG signal from the data acquisition system is transmitted and faithfully reconstructed at the receiver. The proposed receiver performs considerably better than the standard architecture in terms of BER. The proposed frequency offset estimator eliminates the frequency offsets effectively and achieves error variance closer to the variance of Cramer Rao Bound. The use of correlation and estimation block eliminates the need for a despreading block which makes our system less erroneous.

References

[1] Ye Sun; Junliang Tao; Guangxi Wu; Xiong Yu, "A non-contact wearable wireless body sensor network for multiple vital signal detection," SENSORS, 2013 IEEE , vol., no., pp.1,4, 3-6 Nov. 2013.

[2] Kiran, M.P.R.S.; Rajalakshmi, P.; Bharadwaj, K.; Acharyya, A., "Adaptive rule engine based IoT enabled remote health care data acquisition and smart transmission system," Internet of Things (WF-IoT), 2014 IEEE World Forum on , vol., no., pp.253,258, 6-8 March 2014.

[3] Farid Touati, Rohan Tabish, Adel Ben Mnaouer, A Real-time BLE Enabled ECG System for Remote Monitoring, APCBEE Procedia, Volume 7, 2013.

[4] S. Shebi Ahammed, Binu C. Pillai, Design of Wi-Fi Based Mobile Electrocardiogram Monitoring System on Concerto Platform, Procedia Engineering, Volume 64, 2013.

[5] Ramu R, A. Sukesh Kumar,Real-Time Monitoring of ECG using Zigbee Technology,International Journal of Engineering and Advanced Technology (IJEAT) ISSN: 2249 8958, Volume-3 Issue-6, August 2014.

[6] MicheleMorelli .; Antonio A. DAmico., "Maximum Likelihood Timing and Carrier Synchronization in Burst-Mode Satellite Transmissions," EURASIP Journal onWireless Communications and Networking. 4 August 2006; Revised 2 March 2007; Accepted 13 May 2007

[7] Shengchen Dai.; Hua Qian .;Kai Kang .;Weidong Xiang. "A Robust Demodulator for OQPSKDSSS System", Circuits Syst Signal Process (2015) 34:231247 DOI 10.1007/s00034-014-9844-z

[8] Nagaraj, S.; Khan, S.; Schlegel, C.; Burnashev, M.V., Differential preamble detection in packet-based wireless networks, Wireless Communications,IEEE Transactions on , vol.8, no.2, pp.599,607, Feb. 2009.

[9] Son, E.; Crowley, B.; Schlegel, C.; Gaudet, V., "Packet detection for wireless networking with multiple packet reception," Military Communications Conference, 2009. MILCOM 2009. IEEE , vol., no., pp.1,5, 18-21 Oct. 2009.

[10] Soonyong Song; Kunmin Yeo; Youngil Kim; Won Ryu, "Symbol detection under multi-path fading environments for ZigBee receiver," ICT Convergence (ICTC), 2013 International Conference on , vol., no., pp.84,85, 14-16 Oct. 2013.

[11] J. G. Proakis., Masoud Salehi., Digital Communications. McGraw Hill. Fifth Edition

[12] Krishna, Y.Siva; Subrahmanyam, V.; Zubair, M.A.; Rajalakshmi, P., "IEEE 802.15.4-PHY Packet Detection and Transmission System With Differential Encoding For Low Power IoT Networks," Region 10 Symposium (TENSYMP), 2015 IEEE , vol., no., pp.1,4, 13-15 May 2015

[13] Shudong Fang; Berber, S.M.; Swain, A.K., "Energy consumption evaluations of cluster-based sensor nodes with IEEE 802.15.4 transceiver in flat Rayleigh fading channel," Wireless Communications and Signal Processing, 2009. WCSP 2009. International Conference on , vol., no., pp.1,5, 13-15 Nov. 2009

THE 18TH INTERNATIONAL SYMPOSIUM ON WIRELESS PERSONAL MULTIMEDIA COMMUNICATIONS
(WPMC-2015)
December 13-16, 2015, Hyderabad, India

Analytical Model of Relay Node Integrating IEEE 802.15.4 MAC and Energy Conserving State Behaviour

Raja Vara Prasad Y, M.P.R.S Kiran and Rajalakshmi Pachamuthu
Department of Electrical Engineering
Indian Institute of Technology Hyderabad, India
Email: [ee10p004,ee12m1021,raji]@iith.ac.in

***Abstract*—Accurate relay node model for a generic topology of multi-hop networks is still unsolved problem in the Wireless Sensor Networks (WSN) arena. Even though there are lot of multi-hop models in the literature, there is still a lot of scope for improvement in these relay node models to achieve end-to-end reliability and delay optimizing energy. In this paper a state behavioural relay node model is developed integrating IEEE 802.5.4 MAC and energy conserving states like Sleep, Idle-Listen and Active-Tx using three dimensional Markov chain framework. Novel window of reference is introduced into relay nodes to decide the wake up strategies and to improve performance of the network. Hence developed model is a combination of asynchronous and periodic protocols which is first in it's kind of nature. Developed emulation model of the MAC confirms the performance improvement with 95% confidence level. Analysis proves that random anycast routing with proposed duty cycle model extends network lifetime with efficient load sharing among all relay nodes and reduce overall active duration of a node.**

***Keywords*-Anycast clustered multi-hop network, 3D Markov chain, Analytical model of IEEE 802.15.4 MAC.**

I. Introduction

Multi-hop communication is essential for real time applications like IoT, Cyber Physical Systems (CPS) and Smart grid applications which are distributed over large area. Most of the IEEE 802.15.4 analytical models are based on 3D Markov chains. Single-hop IEEE 802.15.4 networks has been thoroughly investigated, but analytical model that can mimic multi-hop networks is still under active research.

IEEE 802.15.4 multi-hop models are inspired by IEEE 802.11 multi-hop networks in [1], [2] and [3]. Multi-hop communication is modelled for IEEE 802.11 networks for single traffic flow in [1]. Work in [1] has been extended to multiple non saturated flows in [2]. A model for saturated traffic flows in IEEE 802.11 networks is presented in [3]. However, we note that these models cannot be directly applied to IEEE 802.15.4 networks due to the different access mechanisms of IEEE 802.11 and IEEE 802.15.4. Analytical modelling of IEEE 802.15.4 multi-hop network is discussed in [4] considering heterogeneous traffic and hidden node terminal problem. Model presented in [4] analysed multi-hop considering different topologies. Even though model captured multi-hop behaviour for particular topologies due to route layer dependencies analysing a larger network without a generalized model becomes complex. Reliable and timely communication for sensors to sink is discussed in [5] with anycast multi-hop routing between relay clusters. Reliability, delay and energy of overall network are analysed with cumulative exponential wake up rate, traffic rate and number of relay clusters. Model in [5] proposed different states like sleep, idle, active and CSMA/CA for relay nodes but analytical model has fixed backoff window and lacks many network parameters.

Carrier sense multiple access with collision avoidance (CSMA/CA) scheme MultiCSMA for multi-hop WSNs is proposed in [6]. A Markov chain based analytical model for multi-hop networks is analysed with variation in traffic rate, node density, packet length, number of MAC backoff stages and retries are considered for the analysis. An analytical model for evaluating the performance of IEEE 802.15.4 multi-hop networks based on beacon-less CSMA/CA is discussed in [7]. Multi-hop tree network with sensors and relay nodes (relay node can be sensors as well) considering with and without hidden node problem was analysed in [7]. Though model in [7] captured tree multi-hop network behaviour but nodes nearer to sink have higher congestion leading to failure of nodes as well as network failure. Most of the above mentioned models could not capture multi-hop behaviour in the aspects like relay hot spots and failed to obtain generalized analytical model with network parameters like wake up rate, packet rate, packet length and node density. Above mentioned problems are answered in this paper proposing a route independent anycast routing based modified IEEE 802.15.4 analytical model. Beacon enabled slotted IEEE 802.15.4 standard is modified to model a generalized relay node in a cluster between a sensor/source node to central sink node. Relay node is modelled with three dimensional Markov chain with states like sleep, idle, active and IEEE CSMA/CA states to obtain tradeoff between application performance and energy savings.

The remainder of this paper is as follows. In Section II, proposed system model is described. Mathematical model of the proposed system is given in detail in Section III. Analytical and simulation results of proposed system is discussed in section IV. Finally, Section V concludes the paper with future scope of research.

II. System Model

We consider a generic network scenario of central sink with sensor and relay clusters shown in the Fig. 1. Sensors are distributed across large area, where data from them is forwarded using relay cluster nodes. Relay nodes in each cluster can accept data from any node and any direction in the neighborhood and forwards to it's nearest neighbor cluster which is well known as anycast routing. Relay node behaviour is captured accurately in 4 different states namely, Sleep (S_i), Idle-Listen (I_i), Active-Tx (A_i) and CSMA/CA as shown in Fig. 2. Relay node state behavioural model is briefly described as below.

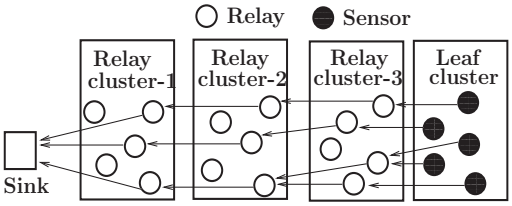

Fig. 1: Example network scenario of the proposed system

Relay node after every S_0 slot moves to Idle-Listen state with P_w probability or rolls back to Sleep state shown in the Fig. 2. Relay node after successful transition to Idle-Listen state with probability P_w waits for LI_{avg} slots to observe a packet from preceding cluster. Time intervals between beacons observed by a relay in Active-Tx are poisson distributed which determine the average waiting time LA_{avg} slots in Active-Tx state. Relay node which is successful in receiving a beacon within maximum L_a slots of Active-Tx state follows CSMA/CA flow depicted using a 3D Markov chain shown in Fig. 3 with backoff stages (*m*), backoff counter (*k*) and collision retries (*n*) as the three dimensions. Relay node spends an average LC_{avg} slots in CSMA/CA state. Finally node spends $L_{S|CSMA}$ slots in Sleep which are the remaining slots left after Idle-Listen, Active-Tx and CSMA/CA states.

Total number of slots that a relay node takes to complete all states is fixed as L_{DC}, which we termed as Duty cycle window or frame of reference window. It is assumed that only one wake-up can happen with a P_w probability, where P_w is the provability of a node to have a wake-up in first slot of L_{DC} from $1/L_{DC}$ poisson distributed wake-ups in a second. Relay node cannot wake-up in between L_{DC} slots and transmit beacon. It is also evident from above assumption that relay node can only service one packet in L_{DC} slots. The maximum capacity of a relay cluster *C* is $\frac{N}{L_{DC}}$. If number of packets to the relay cluster is more than capacity of network, then network performance surely degrade.

III. Mathematical model

We first define the required terminologies for the mathematical model and then follows the formulation of CSMA/CA model. In the rest of our discussion μ_w indicates average wake up rate per node in a cluster consisting of *N* nodes, L_a and L_i are length of active and idle slots respectively.

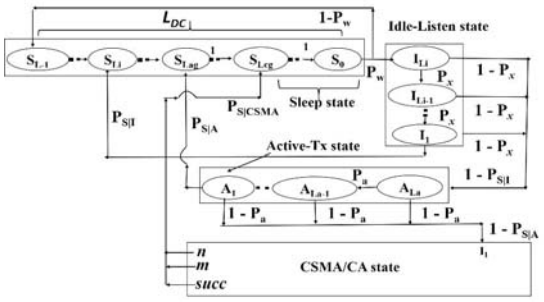

Fig. 2: Relay node model with Duty cycle frame work

In Eq. 2 , P_x gives the transition probability of a relay node to move into next Idle-Listen slot from the current, when there is no packet arrival at a given slot with an average of λ poisson arrivals and P_a in Eq. 4 indicates the transition probability of a relay node to move into next Active-Tx slot from the current, when there is no beacon arrival at a given slot with an average of λ_a poisson arrivals. The probability of a node transiting to Sleep state from last slot of Idle-Listen ($P_{S|I}$), Active-Tx ($P_{S|A}$) and CSMA/CA ($P_{S|CSMA}$) states can be obtained as shown in Eq. 13, 14 and 12 respectively.

$$\lambda_a = \mu_w * L_{DC} \tag{1}$$

$$P_x = \exp(-\lambda) \tag{2}$$

$$P_w = 1 - \exp(-\lambda_a) \tag{3}$$

$$P_a = (1 - \frac{P_w}{L_{DC}})^N \tag{4}$$

$$LA_{avg} = \sum_{i=1}^{L_a} (i) \frac{P_a^{i-1}(1-P_a)}{(1-P_a^{L_a})} \tag{5}$$

$$LI_{avg} = \sum_{i=1}^{L_i} (i) \frac{P_x^{i-1}(1-P_x)}{(1-P_x^{L_i})} \tag{6}$$

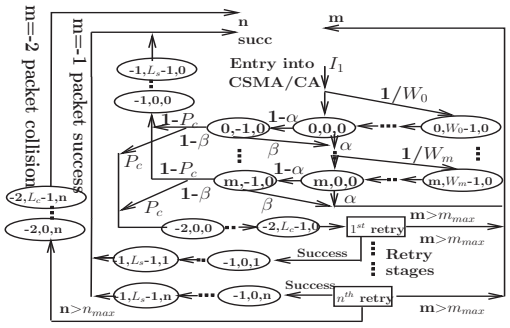

Fig. 3: 3D Markov model of IEEE 802.15.4 CSMA/CA

Relay node with proposed cyclic state framework is shown in Fig. 2. Relay node state transition starts from last slot S_{L_0} and moves to Idle-Listen state with P_w probability or rolls back to Sleep state with 1-P_w probability. P_w is the probability of a node to have a wake-up at the first slot of L_{DC} window, where wake-up of a node is assumed Poisson process with mean μ. Relay node wake-up at first slot is considered because

node is assumed to complete all its states with in L_{DC} slots and no wake-up is possible after first slot of L_{DC} window. Relay node which is wake-up at first slot follows similar Idle-Listen, Active-Tx and CSMA/CA state behaviour in the model already described. If a relay node is unsuccessful in receiving a packet it spends its rest of time in Sleep state shown in Eq. 7. Relay node after successfully receiving a packet and failing to receive a beacon in Active-Tx spends rest of time in Sleep state shown in Eq. 8. Relay node which is successful in Idle-Listen and Active-Tx states completes its CSMA/CA state in LC_{avg} which is shown in Eq. 10 and the time it spends in Sleep state after CSMA/CA is shown in Eq. 9. LC_{avg} is the average number of slots a node spends in CSMA/CA assuming CSMA/CA as gaussian distribution.

$$L_{S|I} = L_{DC} - L_i \tag{7}$$

$$L_{S|A} = L_{DC} - LI_{Avg} - L_a \tag{8}$$

$$L_{S|CSMA} = L_{DC} - LI_{Avg} - LA_{avg} - LC_{avg} \tag{9}$$

$$LC_{avg} = \frac{(n+1)(m+1)W_0}{2} \tag{10}$$

where, W_0 is the minimum backoff window (2^{m_0}), *m* is the maximum backoff stages and *n* is the maximum collision retries. It is observed that from the above expressions that relay node spends remaining time in Sleep state after it completes Idle-Listen, Active-Tx and CSMA/CA states. It is also evident that $L_{S|CSMA}$ should not exceed L_{DC} as the window size is fixed. In order to conserve energy, node should spend more time in Sleep state by adjusting other state parameters LI_{avg}, LA_{avg} and LC_{avg} considering given constraints. State probabilities and state transition probabilities of relay node with proposed framework is given in detail as below.

State transition probabilities are derived observing state behaviour model of relay node with framework shown in Fig. 2. $P_{S_{L_{DC}}}$ is the probability of a node to be in first slot of duty cycle window. $P_{S|I}$, $P_{S|A}$, $P_{S|CSMA}$ and $P_{S|L_{DC}}$ are the probabilities of a node to enter Sleep state from Idle-Listen, Active-Tx, CSMA/CA and last slot of Sleep state respectively. Expressions inter relating these probabilities are given below. P_{S_0} is the probability to enter in last slot of Sleep state.

$$P_{S_0} = P_{S|CSMA} \tag{11}$$

$$P_{S|CSMA} = P_{S|A} + b_{0,0,0} \tag{12}$$

$$P_{S|A} = P_{S|I} + P_a^{L_a} P_{A_0} \tag{13}$$

$$P_{S|I} = P_{S|L_{DC}} + P_i^{L_i} P_{I_0} \tag{14}$$

$$P_{S|L_{DC}} = (1 - P_w) P_{S_0} \tag{15}$$

$$P_{S_0} = (1 - P_w) P_{S_0} + P_x^{L_i} P_w * P_{S_0} + P_a^{L_a} (1 - P_i^{L_i}) P_w * P_{S_0} + Z_0 * b_{0,0,0}^f \tag{16}$$

Rearranging the Eq. 16, we arrive at an expression relating P_{S_0} and $b_{0,0,0}^f$. P_x and P_a are failure probabilities to receive a packet and beacon in any slot of Idle-Listen and Active-Tx states respectively from their neighbor cluster nodes. State provability equations for Sleep, Idle-Listen, Active-Tx and CSMA/CA are given in Eq. 17, 18, 19 and 20 respectively.

$$L_i * P_{S|L_{DC}} + L_a * P_{S|I} + L_c * P_{S|A} + L_{S|CSMA} P_{S|CSMA} = P_S \tag{17}$$

$$P_I = \frac{P_w * P_{S_0} * (1 - P_x^{L_i})}{1 - P_x} \tag{18}$$

$$P_A = \frac{P_w * P_{S_0} * (1 - P_x^{L_i})(1 - P_a^{L_a})}{1 - P_a} \tag{19}$$

$$P_{CSMA} = b_{0,0,0}^f * Z_1 \tag{20}$$

After substituting the above state probabilities in normalization property of Markov chain shown in Eq. 21, we can arrive at essential Markov probability $b_{0,0,0}^f$.

$$P_S + P_I + P_A + P_{CSMA} = 1 \tag{21}$$

In this paper busy channel probabilities α and β in Clear Channel Assessment (CCA1 and CCA2) states and channel sensing probability τ shown in Fig. 3 are derived considering the effect of Cyclic states Sleep, Idle-Listen and Active-Tx state probabilities along with CSMA/CA model. With basic understanding of busy probabilities in [8], [9], [10] and [11] one can derive easily $b_{0,0,0}^f$ and thereby α, β and τ using numerical methods. End-to-end Reliability, delay and energy of the proposed multi-hop model for dense traffic applications are derived in next section using mathematical expressions in previous section.

A. End-to-end Reliability Model

Performance metrics for leaf to relay cluster and end cluster to gateway cluster differ from relay to relay cluster link. All these three different links are modeled separately as follows.

$$P_f^A = \frac{P_w * (1 - P_x^{L_i}) * (1 - P_a^{L_a}) * P_{S_0}}{1 - P_a} \tag{22}$$

$$P_f^a = P_a^{L_a} \quad , P_f^m = x^{\mathrm{m+1}}(1 + \widetilde{y}) \quad , P_f^n = \widetilde{y}^{\mathrm{n+1}} \tag{23}$$

Reliability of leaf to relay link is given in Eq. 24. Reliability is derived by deriving failure probabilities of this link. Failure can happen due to channel access failure and collisions in CSMA/CA state. Packet is also discarded when leaf node cannot find a beacon in L_a slots.

$$R_S = 1 - \left(P_f^m + P_f^n + P_f^a + P_f^A\right) \tag{24}$$

$$R_k = 1 - \left(P_f^m + P_f^n + P_f^a\right) \tag{25}$$

Reliability of link between end and gateway node is shown in Eq. 26. Reliability of this link is obtained by considering CSMA/CA failure probabilities. End node doesn't have Active-Tx state due to which failure is only due to CSMA/CA is shown in the Eq. 26.

$$R_G = 1 - \left(P_f^m + P_f^n\right) \tag{26}$$

Above three links are assumed independent as shown in

Eq. 27 to obtain end-to-end performance metrics. 3D Markov modeling is used to model all three different state models.

$$R_E = R_L * \prod_{k=1}^{h} R_k * R_G \tag{27}$$

B. Delay model

End-to-end delay of the proposed model is summation of delay incurred at three types of links, shown in Eq. 28.

$$D_T = D_{SR} + \sum_{i=0}^{h} D_R(i) + D_{EG} \tag{28}$$

where D_{SR} is the delay of link between sensor and first relay cluster, $D_R(i)$ is the delay of a link between two relay nodes, D_{EG} is the delay of the link between end node and gateway/sink node. Delay models for each link are expressed in mathematical expressions and finally an end-to-end delay of the network is derived in following section.

1) Delay between Sensor and Relay: Delay of this link is composed of CSMA/CA delay and Active-Tx state delay. CSMA/CA delay of a link with *N* nodes in a cluster is similar to [11] shown in Eq. 29. Active-Tx state delay of the link is given in Eq. 30.

$$D_{\text{csma}} = (Ts + Delay_{\text{avg}}) \left(1 + \frac{y}{1-y} - \frac{(n+1) * y^{\text{n+1}}}{1-y^{\text{n+1}}}\right) \tag{29}$$

Sensor node in Active-Tx state waits for L_a consecutive slots to observe a beacon from next cluster. Sensor node may not wait for all L_a slots every time it enters Active-Tx state. Average number of slots a relay node waits to receive a beacon is the delay incurred in Active-Tx state. Broadcast of beacons from relay nodes in next cluster are Poisson distributed with mean λ_a. Active-Tx state delay D_{active} is shown in Eq. 30. Finally End-to-end delay (D_T) is sum of D_{csma} and D_{active} shown in Eq. 32. D_{SR} is shown in Eq. 31.

$$D_{active} = \sum_{i=1}^{L_a} (i) \frac{P_a^{i-1}}{\sum_{k=0}^{L_a} P_a^k} \tag{30}$$

$$D_{SR} = D_{\text{csma}} + D_{\text{active}} * S_b \tag{31}$$

D_{csma} shown in Eq. 29 is similar for relay-relay and end-gateway links. Relay-relay node link experience Active-Tx state delay as sensor node, but end-gateway link doesn't have Active-Tx state delay because gateway nodes in gateway cluster are always on to receive a packet. Relay node experience *h* number of Active-Tx state delays assuming node distribution in each relay cluster is same. End-to-end delay of the multi-hop network is shown in Eq. 32.

$$D_T = (h+2)D_{csma} + D_{active}(h+1) \tag{32}$$

C. Energy model

Energy of leaf, end and relay node models differ according to the state behaviour explained above. Energy of each node is derived from its state probabilities. State energies of leaf, end and relay nodes are calculated by accounting state transitions of each node. E_i, E_a, E_{CCA}, E_w, E_t and E_r are energy consumption in Idle-Listen, Active-Tx, CSMA/CA sensing, wake-up, transmit and receive state respectively.

1) Energy model - Leaf node: Energy spent by a leaf node can be derived considering state behaviour. Leaf node doesn't have Idle-Listen and receive states. Total energy of leaf node E_{leaf} is given in Eq. 33.

$$E_{leaf} = (E_a + E_w) + E_{\text{CCA}} + E_t \tag{33}$$

2) Energy model - End node: Energy spent by a end node is in Idle-Listen, CSMA/CA sensing, transmit and receive energies. End node Active-Tx energy is negligible as the gateway node is continuously on to receive a packet from end node. Total energy of end node E_{end} is given in Eq. 34.

$$E_{end} = (E_i + E_w) + E_{\text{CCA}} + E_t + E_r \tag{34}$$

3) Energy model - Relay node: Energy spent by a relay node can be derived by observing its state behaviour. Relay node state probabilities are derived in previous section. Total energy of leaf node E_{relay} is given in Eq. 35. Finally total energy is summation of all above node energies.

$$E_{relay} = (E_i + E_a + E_w) + E_{CCA} + E_t + E_r \tag{35}$$

IV. Analytical results

End-to-end reliability, delay and energy versus λ_g is plotted in Fig. 4(a), 4(b) and 4(c) respectively. λ_g is varied from 0.04 to 0.1 packets per slot probability. Reliability is also observed with variation in two different number of nodes in each cluster. Reliability is observed decreasing with traffic density and after certain increase in traffic variation, it decreases marginally. Increase in number of nodes from *N*=20 to 30 reduces reliability from 0.73 to 0.62 is shown in Fig. 4(a). Delay is increased marginally from 89 to 94 milliseconds with λ_g, when number of nodes are twenty. Increase in delay is justified by the fact that number of nodes increase the number of contending nodes for the channel resulting in increase in channel access delay of CSMA/CA. Energy increases with increase in λ_g due to increase in active time of relay nodes. Increase in number of nodes also increases energy as number of nodes participate in forwarding the traffic increases. Observing the plots Fig. 4(a), 4(b) and 4(c), it is observed that reliability, delay and energy respond to λ upto some extent and saturates to a value. This is due to same reason that after certain traffic levels reliability, delay and energy of networks doesn't change because the number of packets that receives with change in λ_g freezes to a value. Simulation and analytical results are in agreement with less than 4% mean error.

Congestion probability α, $b_{0,0,0}$ and Active state failure probability are observed with variation in λ_g and number of nodes in Fig. 4(d), 4(e) and 4(f) respectively. Increase in packet arrivals results in increase in α and $b_{0,0,0}$. Active state failure probability is nearly a constant value with increase in λ_g but when the number of nodes increased from 20 to 30, active failure probability reduces due to increase in number

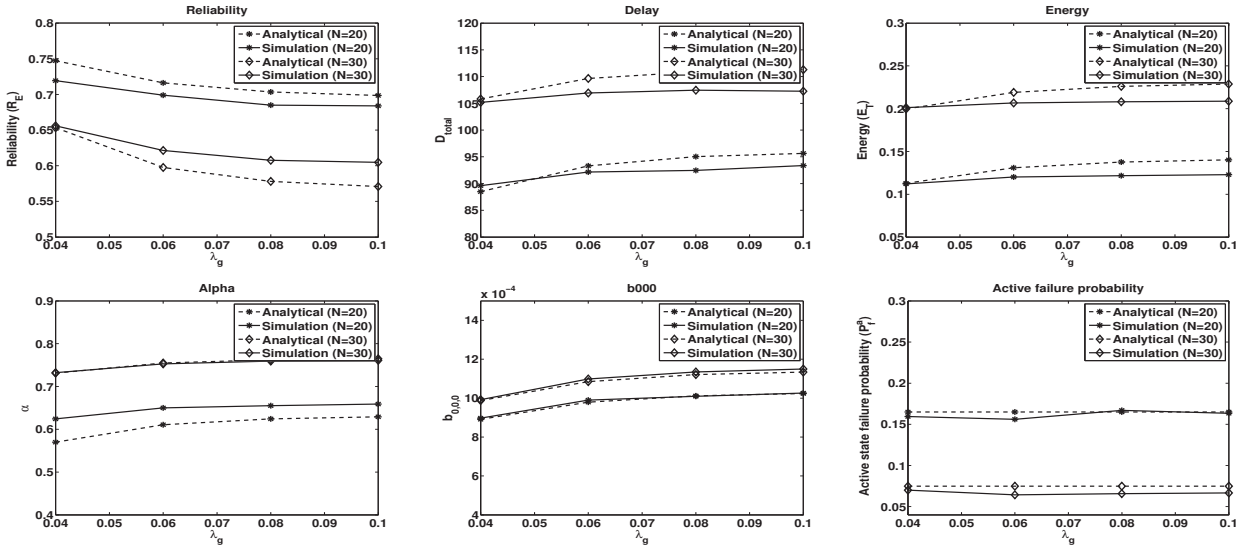

Fig. 4: Different performance metrics like R_E, D_T, E, α, $b_{0,0,0}$ and P_f^A variation with respect to λ_g and N; Fixed MAC and network parameters m_0 = 3, m = 4, L_{DC} = 500, μ_w = 6, n = 1, L_a = 70, N=[20 30], λ =[0.04 0.1], L_p = 30, L_i=100.

of beacons in L_a slots. In order to improve the performance metrics either N or μ of each relay node should be increased.

Energy of a relay node is also observed in terms of active duty cycle of relay node. Active states of a relay node are Idle-Listen, Active-Tx, CSMA/CA channel sensing, transmit and receive states. Proposed model active duty cycle is compared with existing multi-hop protocol in [5]. Results of comparison is given in Fig. 5. Parameters considered for the simulation are μ =4, N=15, m_0=3, m = 4 and n=3, L_i = 50 backoff slots, L_a = 70 backoff slots and each iteration is $4*10^5$ backoff slots. It is observed that proposed framework reduces duty cycle of nodes to 1.4%. It is observed that duty cycle of relay node is 60% lower on an average compared to the existing Breath model. Increase in energy savings is due to accurate state behaviour and anycast routing.

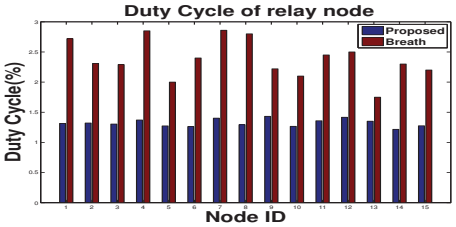

Fig. 5: Comparison of proposed and Breath models relay node duty cycle: N = 15, λ = 15 pks/sec, L_{DC} =700 slots, μ = 4

V. Conclusion

Three dimensional Markov model based analytical model for a relay node in a dense wireless multi-hop network is developed that can be part of IoT applications. Energy conserving state behaviour and generic anycast routing is integrated to IEEE 802.15.4 MAC. Results of the developed analytical and simulation models agree with each other with an accuracy of 5%. Active duty cycle of relay node is found 1.4% which is 60% less than existing models. Optimization framework at sink considering MAC and network parameters is the future scope of this work.

References

[1] M. Hira, F. Tobagi, and K. Medepalli, "Throughput analysis of a path in an IEEE 802.11 multi-hop wireless network," *in Proc. IEEE WCNC, 2007, pp. 441-446.*

[2] J. Baras, V. Tabatabaee, P. Papageorgiou, and N. Rentz, "Modelling and optimization for multi-hop wireless networks using fixed point and automatic differentiation," *in Proc. WiOPT, 2008, pp. 295-300.*

[3] M. M. Carvalho and J. J. Garcia-Luna-Aceves "A scalable model for channel access protocols in multi-hop ad hoc networks," *in Proc. ACM MobiCom, New York, 2004, pp. 330-344.*

[4] Piergiuseppe Di Marco, Pangun Park, Carlo Fischione and Karl Henrik Johansson, "Analytical Modeling of Multi-hop IEEE 802.15.4 Networks," *IEEE Transactions ON Vehicular Technology, Vol. 61, No. 7, Sep 2012*

[5] P. Park, C. Fischione, A. Bonivento, K. H. Johansson and A. Sangiovanni-Vincentelli, "*Breath: an Adaptive Protocol for Industrial Control Applications using Wireless Sensor Networks"*, IEEE Transactions on Mobile Computing, vol.10, no.6, 2011.

[6] Jianping Zhu, Zhengsu Tao and Chunfeng Lv "Performance improvement for IEEE 802.15.4 CSMA/CA scheme in large-scale wireless multi-hop sensor networks," *IET Wireless Sensor Systems, Vol.3, Iss.2, pp.93-103*

[7] Rachit Srivastava and Anurag Kumar "Performance Analysis of Beacon-Less IEEE 802.15.4 Multi-Hop Networks," *Fourth International Conference on Communication Systems and Networks (COMSNETS), pp:1-10,January 2012 Bangalore,India*

[8] P. Park, P. Di Marco, C. Fischione, and K. H. Johansson, *"Modeling and Optimization of the IEEE 802.15.4 Protocol for Reliable and Timely Communications,"* IEEE Transactions on Parallel and Distributed Systems, vol. 24, no. 3, March 2013.

[9] Prasad, Y.R.V, Rajalakshmi P. "*Analytical model of adaptive CSMA-CA MAC for reliable and timely clustered wireless multi-hop communication,*" IEEE World forum on Internet of Things (WF-IoT) conference, pp.212-217, Seoul 6-8 March 2014.

[10] S. Pollin, M. Ergen, S. C. Ergen, B. Bougard, L. Van der Perre, I. Moerman, A. Bahai, P. Varaiya, and F. Catthoor,"*Performance analysis of slotted carrier sense IEEE 802.15.4 medium access layer,*" IEEE Transactions in Wireless Communications, vol.7, no.9, pp. 3359-3371, 2008.

[11] Yerra, R.V.P, Kiran K.P.R.S, Pachamuthu R, "Reliability and Delay Analysis of Slotted Anycast Multi-Hop Wireless Networks Targeting Dense Traffic IoT Applications," *Communications Letters, IEEE* , vol.19, no.5, pp.727-730, May 2015

THE 18TH INTERNATIONAL SYMPOSIUM ON WIRELESS PERSONAL MULTIMEDIA COMMUNICATIONS
(WPMC-2015)
December 13-16, 2015, Hyderabad, India

Field Experiments for Broadband Mesh Network Operating in TV White Space

Kentaro Ishizu and Fumihide Kojima
Smart Wireless Laboratory, Wireless Network Research Institute,
National Institute of Information and Communications Technology (NICT)
3-4 Hikarino-oka, Yokosuka, Kanagawa, 239-0847, Japan

***Abstract*—This paper proposes broadband mesh network to operate in TV White Space (TVWS). Ad-hoc mode to extend IEEE 802.11af is designed to realize it. Prototype devices are implemented and field experiments using the devices in three practical scenarios are conducted. Experiment results show the feasibility of broadband mesh network operating in TVWS and that around one third of single hop throughput was achieved in two hop path. This paper also discusses deployment in large area with higher transmission power.**

Keywords— TV white space, Mesh network, Ad-hoc mode, Field experiment, IEEE 802.11af

I. INTRODUCTION

TV White Space (TVWS) is expected to expand available spectrum band for IP communications. Characteristics of the TV band include less attenuation over the air and much diffraction against obstacles compared with higher frequency bands which are much more often used for wireless broadband communications. Utilization of the TVWS can not only enhance spectrum utilization efficiency, but also increase flexibility and performance of wireless systems.

Specifications and radio regulations for TVWS that have been developed, such as IEEE 802.11af, IEEE 802.22 and FCC/Ofcom regulations [1-3], focus on perfect management of interference in order not to affect the TV broadcasts that are primary users. Therefore, basic concept of system is that White Space Database (WSDB) manages the interference from White Space Devices (WSDs) to TV broadcasts. It is required that a WSD register its GPS location to the WSDB and requests for available channels and transmission power before starting its operation. In this model, WSDs are managed centrally. The Access Point (AP) or Base Station (BS) which has interface with WSDB must exist in a network. Hence, since the WSDB is operated in the Internet, it is difficult to realize infrastructure-less or self-organized networks operating in TVWS such as point-to-point or mesh network. However, demands for such types of wireless networking are increasing recently to deploy broadband Internet to rural area or islands with less population where optical fiber network operators are reluctant to extend their business due to cost. Such networks could be possible to be realized under certain conditions of regulations. Mesh network is a typical self-organized and infrastructure-less network. Mesh network operating in TVWS will create technically new applications. Also, it is helpful in emergency situations such as recovery of networking after disasters.

Existing specifications for wireless LAN in 2.4/5 GHz allows ad-hoc network for point-to-point (P2P) connection. Moreover, IEEE 802.11s realizes mesh networking of wireless LAN. However, the link distance is limited up to several hundred meters even in good conditions. Also, there are regulations and products for long-distance P2P connection in microwave band. But, they require sharp directional antenna, therefore are not flexible. Its system becomes complicated and total cost to configure multi-hop networks is very expensive. If TVWS is used to mesh networks, the networks can be flexible, low-cost and extendable to new applications.

In this paper, we propose a broadband mesh network operating in TVWS by extending IEEE 802.11af, develop prototype system, and conduct field experiments to measure the throughput in practical scenarios.

II. MOTIVATION AND RELATED WORKS

In mesh networks, one node establishes multiple links with other nodes at the same time. This is because of topology of mesh network. As long as the topology is not daisy chain connection, some nodes must have multiple links. Another reason is that nodes have backup links which are switched to active link in case when current active link is disconnected. Fig. 1 shows a timing to switch to use a backup link as active link. The solid lines are active links and dotted line is a backup link. In the beginning, Node 3 and Node 4 established a link as backup. When the link between Node 2 and Node 4 was disconnected, the backup link becomes active.

There are two basic approaches in assignment of frequency (or channel) to links of mesh networks. The first approach is to assign different channels to different links. The second approach is to assign the same channel to all the links. The first approach require multiple channels and functions to assign them efficiently. Merit of this approach is that transmission in each link does not interfere with other links or, even when the number of available channels are not sufficient for the links, the interference can be reduced to a certain extent. However, each node of mesh networks needs to operate on multiple channels to establish links with other nodes each of which is operated in different channels. Therefore, the device needs to have rich hardware specifications for multiple channel operation resulting in complicated, large in size, and expensive devices compared with the second approach.

The second approach shares a common channel with all the nodes of a mesh network. The ad-hoc mode in IEEE 802.11

adopts this approach. Merit of this approach is that limited frequency band is not split into pieces, therefore maximum capacity of each link is kept large. Establishment of multiple links is managed in Media Access Control (MAC) layer, hence its hardware should be capable of operation in a single channel. Management of channel assignment to links are not required. However, there are issues of performance deterioration due to transmission timing such as the hidden node problem and the procedure of Carrier Sense Multiple Access / Collision Avoidance (CSMA/CA). This paper takes the second approach to elaborate the limited TVWS channel utilization.

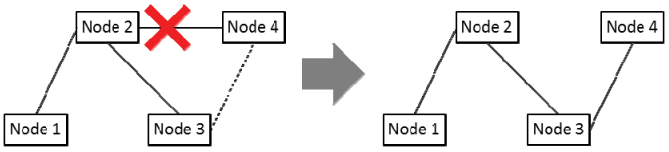

Fig. 1. Back up link in mesh networking

Major standards for wireless network system operating in TVWS are IEEE 802.11af and IEEE 802.22 [4-5]. In addition, LTE system operating in TVWS is proposed [6]. IEEE 802.11af is composed of Access Point (AP) and Station (STA). It does not assume connections between APs nor connections between STAs, therefore mesh networking is difficult with this standard. IEEE 802.22 is composed of Base Station (BS) and Consumer Premise Equipment (CPE) and has the same issue as in IEEE 802.11af to realize mesh network. LTE system is composed of evolved NodeB (eNB) and User Equipment (UE). The eNB needs to exchange management signals with Evolved Packet Core (EPC) which is typically managed carefully in a machine room and accessed via stable wired network. Therefore, LTE system is not appropriate for mesh networking.

Regarding the regulations on TVWS operation, devices are categorized into two types. One type of device needs to access the WSDB to register its location and obtain available channels, which is called Fixed or Mode II device in FCC's regulation and master device in Ofcom' regulation [1-3]. The other type of device must be under the control of the first type of devices, which is called Mode I device in FCC's regulation and slave device in Ofcom's regulation. In mesh networks, each node needs to transmit beacons so that other nodes find its existence. Therefore, all the nodes in mesh network need to be Mode II or master device. But, the nodes are not necessarily always accessible to the WSDB. The nodes must have a way to access WSDB via other wireless systems, or the regulations need to be amended to support the concept of mesh networks. How to address these issues is out of the scope of this paper.

III. Proposal to Realize Mesh Network in TV White Space

A. Approach to realize ad-hoc mode in IEEE 802.11af

IEEE 802.11af specifies specification of wireless LAN operating in TVWS. But, it has only the infrastructure mode and it is impossible that any two nodes connect each other. To realize the point-to-point (ad-hoc) connection in IEEE 802.11af, functional requirements are summarized as follows. IEEE 802.11af has two types of devices; AP and STA, but only STAs are operated in the ad-hoc mode.

- Modify MAC to conduct active scan and disable passive scan (Note that IEEE 802.11af STA does not transmit any frames without reception of Beacon from APs.)
- Modify MAC to send back Probe Response on reception of Probe Request
- Modify MAC to send back Association Response on reception of Association Request
- Remove the interface to the WSDB and implement an interface to manually configure operation frequency

B. Implementation of TVWS mesh network system

Based on the functional requirements in previous section, architecture and functions of white space device are designed. The architecture is shown in Fig. 2. The device is an integration of SDR board and CPU board. The SDR board has Field-Programmable Gate Array (FPGA) in which IEEE 802.11af PHY and low-MAC are implemented. The CPU board is operated by Linux. SDR driver is a Linux kernel module to deal with the SDR board. The mac80211 is an open source kernel module extended to have IEEE 802.11af and the functional requirements. The wpa_supplicant is also open source kernel module and manages the PHY/MAC. The use land program "olsdr" is an implementation of Optimized Link State Routing (OLSR) [7] which is a routing protocol designed for mobile ad hoc networks. OLSR configures IP routing table appropriately so that traffic from any node can reach any destination nodes via other nodes. When the device is started, it searches other devices and try to establish links with them. Then, IP routing is configured using OLSR. Overview of the developed device is shown in Fig. 3.

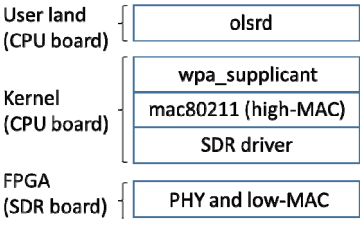

Fig. 2. Architecture of TVWS device based on IEEE 802.11af

Fig. 3. A TVWS device for TVWS mesh network

IV. Fundamental Performance Test

This section describes setup and results of fundamental performance test of the developed devices in a laboratory environment. The purpose of this test is to understand basic behavior of the multi-hop network performance with proposed extension to IEEE 802.11af.

Before the test in multi-hop configuration, sensitivity and maximum throughput were measured for different Modulation Coding Schemes (MCSs). As a result of measurements, the sensitivity was -89 dBm and -76 dBm in MCS 0 (BPSK, r=1/2) and 7 (64QAM, r=5/6), respectively. The maximum throughput was 1.45 Mbps and 6.21 Mbps in MCS 0 and 7, respectively. Note that the throughput was measured using iperf tool in UDP

mode. The throughput is averaged over 60 seconds of transmission with transmission data rate of 1500 kbps.

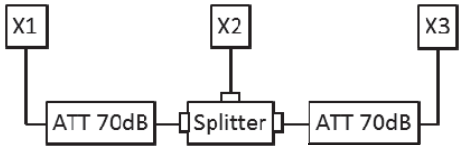

Fig. 4. System configuration of multi-hop networking for fundamental performance test

TABLE I. THROUGHPUT AND RSSI OVER RF CABLE

Direction / Link	From left to right (→)	From right to left (←)
X1-X2	870 kbps (-69 dBm)	1350 kbps (-73 dBm)
X2-X3	1450 kbps (-73 dBm)	1320 kbps (-71 dBm)
X1-(X2)-X3	328 kbps	468 kbps

Next, in order to test in the multi-hop environment, system was configured as shown in Fig. 4. X1, X2 and X3 are devices developed as described in section III. X1 and X3 are connected to the splitter via 70 dB of attenuator. There is a certain attenuation in the splitter between the two ports connected to X1 and X3. Output TX power and MCS were set to -3 dBm and 0 (BPSK r=1/2), respectively. As the sensitivity of the devices is around -89 dBm with this settings, X1 and X3 can not establish a link and X2 needs to relay both the links X1-X2 and X2-X3. The center frequency was 671 MHz (46 ch).

Table I shows throughput and RSSI for each link/path and traffic direction. The traffic direction from left to right on link X1-X2 is a direction from X1 to X2, whereas the direction from right to left on the same link is a direction from X2 to X1. Measurements were taken in two single links of X1-X2/X2-X3 and one multi-hop path X1-(X2)-X3 for both the traffic directions. The RSSI is shown in parentheses and was measured on the reception side of the traffic.

Throughput in single links (X1-X2 and X2-X3) were from 870 to 1450 kbps. Throughput in multi-hop (X1-X2-X3) was from 328 to 468 kbps. The multi-hop throughput is one third of the single link throughput. This is because the same spectrum band is shared with the two links and in addition some overhead due to the contention management of 802.11 MAC is in X2 to relay traffic over the two links.

Note that the reason why the RSSI are different in different directions and in different links is because the TX power is slightly different depending on individual device hardware. Also, due to the same reason, the throughput is partly not necessarily proportional to RSSI.

V. FIELD EXPERIMENTS

A. Environment and setup

Three scenarios are assumed for field experiments. The whole scenarios were set up at Yokosuka Research Park (YRP), Yokosuka, Japan. As shown in Fig. 5, seven points (A1-A4 and B1-B3) were specified as locations of nodes. In Fig. 5, lines in yellow are links between nodes. Numbers in yellow on the lines are the distance between the nodes. Numbers in white are altitudes above the sea at each location. Photos in red frames are taken from the locations of noted nodes.

Scenario 1 is the case where two nodes (A1 and A3) need to communicate, but they are not in line of sight due to big buildings, hence another node (A2) relays them. Scenario 2 is the case where two nodes (A2 and A4) need to communicate, but can not directly communicate due to long distance, hence another node (A3) relays them. Scenario 3 is the case where two nodes (B1 and B3) need to communicate, but they are two distant and also completely not in line of sight, hence another node (B2) on the roof of 25m height building relays them.

The devices and antennas were installed on cars except for B2, as shown in the right-top photo in Fig. 5. The antenna was mounted on the roof on cars. For B2, the device was set in a room of the building and its antenna was mounted on its roof, where the device and antenna were connected with RF cable of 50m length. Antennas are a whip type with 0 dBi gain except for B2 and co-linear type with 4.5 dBi for B2. Cable loss between the devices and antennas are 6 dB for B2 and 1.5 dB for the others, respectively.

Measurement tool and its settings are the same as described in section IV. The operation frequency, TX output power, and MCS were set to 671 MHz in center (46 ch), -3 dBm, 0 (BPSK r=1/2), respectively.

B. Measurements and discussions

The measurements of the three scenarios were conducted on July 21-22, 2015. For each scenario, it was confirmed that the target two nodes can not establish a direct link without a relay node. Measured throughput and RSSI in scenario 1 to 3 are shown in Table II (a) to (c), respectively. The notation of Table II is the same as in Table I.

TABLE II. THROUGHPUT AND RSSI IN FIELD EXPERIMENTS

(a) Scenario 1 (A1-A2-A3)

Direction / Link	From left to right (→)	From right to left (←)
A1-A2	951 kbps (-71 dBm)	1310 kbps (-71 dBm)
A2-A3	906 kbps (-77 dBm)	1090 kbps (-75 dBm)
A1-(A2)-A3	348 kbps	386 kbps

(b) Scenario 2 (A2-A3-A4)

Direction / Link	From left to right (→)	From right to left (←)
A2-A3	906 kbps (-77 dBm)	1090 kbps (-75 dBm)
A3-A4	152 kbps (-78 dBm)	277 kbps (-77 dBm)
A2-(A3)-A4	136 kbps	226 kbps

(c) Scenario 3 (B1-B2-B3)

Direction / Link	From left to right (→)	From right to left (←)
B1-B2	238 kbps (-80 dBm)	1240 kbps (-79 dBm)
B2-B3	235 kbps (-88 dBm)	235 kbps (-86 dBm)
B1-(B2)-B3	95 kbps	168 kbps

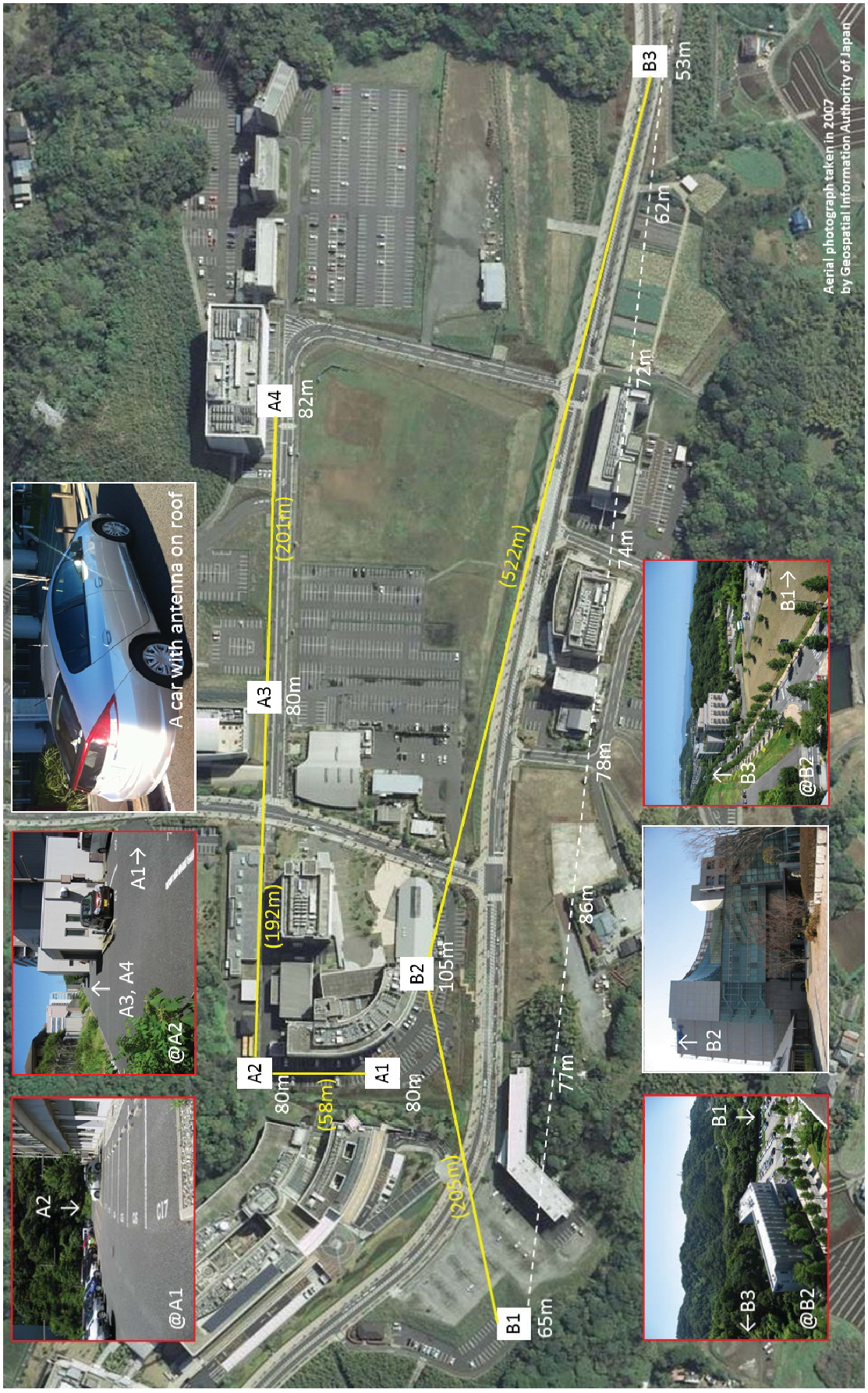

Fig. 5. Location and altitude of deployed nodes for the field experiments
(Lines in yellow are links between nodes. Numbers in yellow on the lines are the distance between the nodes.
Numbers in white are altitudes above the sea at each location. Photos in red frames are taken from the locations of noted nodes.)

1) Scenario 1 (A1-A2-A3)

The throughputs in the links A1-A2 and A2-A3 were all between 900 and 1300 kbps as in Table II (a). Throughput of the multi-hop path A1-A2-A3 are around one third of the single link throughput. This trend is the same as the laboratory environment test described in section IV.

2) Scenario 2 (A2-A3-A4)

The throughput was between 906 and 1090 kbps in link A2-A3 and between 152 and 277 kbps in link A3-A4. The reason for the lower throughput in link A3-A4 could be lower RSSI at these nodes or some spot noise around A4. Throughput of the multi-hop path A2-A3-A4 was between 136 and 226 kbps. It is observed that the multi-hop throughput was slightly lower than the lower single link throughput (A3-A4) in each traffic direction.

Compared with scenario 1, the large throughput deterioration by around one third of single link throughput was not observed. Rather, bottleneck in this scenario was in the link with lower throughput.

3) Scenario 3 (B1-B2-B3)

In link B1-B2, the throughput was 1240 kbps from B2 to B1, but around one fifth of it from B1 to B2. Note that B2 was the building roof top and B1 was lower parking area, which had 40m altitude gap over 205m horizontal distance as seen in the lower photos taken at B2 in Fig. 5. Because TV signals in other channels are stronger at B2 since the altitude is higher, the RF circuit of the device at B2 could be affected by the high power signal input in the TV band as the device has only wide band front-end filter covering just entire TV band.

In link B2-B3, the throughput was 235 kbps in both directions. Distance between B2 and B3 is 522 m and RSSI was -88 to -86 dBm that were close to the sensitivity level as in Section IV. This is the reason for lower throughput.

The multi-hop (B1-B2-B3) throughput was 95 kbps in transmission from B1 to B3 and 168 kbps in transmission from B3 to B1. From B1 to B3, throughput of the two single links were similar and the multi-hop throughput was close to one third of them, which was the same trend as scenario 1. On the other hand, multi-hop throughput from B3 to B1 was capped by the lower single link throughput (B2-B3) as in scenario 2, though the former was 70% of the latter. As seen in altitudes on the dotted line in Fig. 5, there is a quite high hill in between B1 and B3, therefore their direct link is very difficult.

4) Discussion

Our previous experiments [8] show that IEEE 802.11af system can establish a link over 3.7 km in metropolitan area with TX power of 36 dBm EIRP which is current typical regulations in the world [1-3]. Therefore, it is possible to extend length of each link of the proposed system once the TX power is increased. This means that communications over 10 km to 20 km can be achieved with 4 or 5 nodes using only one TV channel.

From the results in scenario 3, it is said that communication area of other nodes becomes extensively large like cellular networks when one of relaying node is put at high altitude. This idea can help for temporary wireless network deployment, for example, in disaster recovery activities.

The number of nodes in the experiments were just three in this paper. But, as the number of nodes increases, the spectrum utilization efficiency could increase compared with the approach to assign different channels to different links because the ratio of active links without traffic increases. Also, utilization of directional antennas can extended each single link, eliminate interference from TV signals in the same and other channels, and manage coexistence with other TVWS systems. These topics are left for future studies.

VI. CONCLUSIONS

In this paper, broadband mesh network was proposed based on IEEE 802.11af by extending to ad-hoc mode. Prototype system was developed and field experiments were conducted in three practical scenarios. Measurement showed that two hop network realizes up to one third of single hop throughput. The experiment proofed that the system can be operated in limited one TV channel. As there are large demands for long-distance wireless backhaul network operating in TVWS such as in rural area and islands, introduction of the mesh networking to broadband TVWS communications is a big progress. As future works, experiments in a large area with some practical applications are planned. Issues specific to TVWS such as difference of allowed TX power and collaboration with White Space Database need to be studied.

REFERENCES

[1] “Second report and order and memorandum opinion and order in the matter of unlicensed operation in the TV broadcast bands additional spectrum for unlicensed devices below 900 MHz and in the 3 GHz band,” FCC-08-260, FCC, Nov. 2008.

[2] “Second memorandum opinion and order in the matter of unlicensed operation in the TV broadcast bands additional spectrum for unlicensed devices below 900 MHz and in the 3 GHz band,” FCC-10-174, FCC, Sep. 2010.ETSI EN 301 598 V1.1.1, “White Space Devices (WSD); Wireless Access Systems operating in the 470 MHz to 790 MHz TV broadcast band,” April, 2014.

[3] “White space devices (WSD); wireless access systems operating in the 470 MHz to 790 MHz frequency band; Harmonized EN covering the essential requirements of article 3.2 of the R&TTE directive,” EN 301 598, ETSI, Jul 2013.

[4] K. Ishizu, et al., “Field Experiment of Long-distance Broadband Communications in TV White Space Using IEEE 802.22 and IEEE 802.11af,” WPMC 2014, Sep. 2014.

[5] K. Mizutani, et al., “IEEE 802.11af Indoor Experiment in UK Ofcom TVWS Trial Pilot Program,” IEEE VTC 2015 Spring, May 2015.

[6] K. Ibuka, et al., “Development and Field Experimet of White-spaces LTE Communication System in UK Digital Terrestrial TV Band,” IEEE VTC Spring 2015

[7] Olsr.org projects, Available: http://www.olsr.org/

[8] NICT press release, “Trials of TV White Space Communications at 40Mbps in Central London - with Qualified White Space Database under UK Ofcom Pilot,” July, 2014.
Available: http://www.nict.go.jp/en/press/2014/07/24-1.html

[9] Geospatial Information Authority of Japan,
Available: http://maps.gsi.go.jp

THE 18TH INTERNATIONAL SYMPOSIUM ON WIRELESS PERSONAL MULTIMEDIA COMMUNICATIONS
(WPMC-2015)
December 13-16, 2015, Hyderabad, India

Antenna Radiation Pattern Based 3D Localization Technique

Amarlingam M, P Rajalakshmi, Vinod kumar Netad
Department of Electrical Engineering
Indian Institute of Technology Hyderabad
Hyderabad, India
Email: ee13p1003, raji, ee13m1033@iith.ac.in

Masaya Yoshida, Kiyohito Yoshihara
KDDI R&D Laboratories Inc.
Green and M2M Application Laboratory
Iidabashi, Japan
Email: my-yoshida, yosshy@kddilabs.jp

***Abstract*—3D location knowledge of sensor node in a sensor network has many practical applications. This paper proposes a new algorithm for finding 3D location of sensor node in a sensor network by using radiation pattern of antenna with Received Signal Strength Indication (RSSI). Proposed localization algorithm is developed by considering target node equipped with half wave dipole antenna which has omnidirectional radiation pattern. The results show that proposed algorithm estimates 3D location of sensor node in a sensor network with low average error ($< 0.5m$), when compared to its actual location.**

***Index Terms*—Radiation pattern, RSSI, 3D localization.**

I. Introduction

Recent advances in micro-electromechanical systems, wireless communication technologies and digital electronics have brought us closer to the vision of pervasive Wireless Sensor Networks (WSN). Development in WSN enhanced smartness in controlling and monitoring sensors in a sensor network [1]. WSN have a number of potential applications such as sensing environment physical factors like temperature, humidity and also for monitoring and detecting chemicals, smokes etc. In most of application areas such as military, habitat sensing, target tracking, forest fire location detection and marine monitoring, knowledge of every sensor node location is very crucial to understand application context.

Authors of [2] discussed three basic advantages of having the sensor nodes location information. Firstly, location information is required to estimate the location of an event of interest for example intruder location. To deploy relief and rescue in a battlefield the location of enemy tanks is crucial. Secondly, knowledge of location information facilitates a number of application services, such as helping doctors by providing the location of nearby medical facilities in a smart hospital. Third, location information find its applications in geographical routing ([3] and [4]), network coverage checking [5] and location-based information querying [6].

For outdoor localization applications GPS is used, but in indoor environment GPS is inaccurate because of poor signal strength. Most of existing localization techniques are 2D localization techniques. In [7] and [8] RSSI based localization algorithms for 2D are discussed. In real world applications sensor nodes are deployed in 3D. To estimate 3D location of sensor node we need to develop 3D localization algorithm.

Existing localization techniques are broadly divided into two types. First one is range-based localization techniques and second one is range-free localization techniques. Range-based localization techniques are dependent on range measurement techniques (distance measurement, angle-of-arrival measurement techniques) for localization. The localization techniques which depends on RSSI and path loss modelling of environment ([9]) falls under category of range-based localization. The range-free localization techniques do not use range measurement techniques. They use topology, connectivity information for localization. Authors of [10] discuss basic centroid localization algorithm which falls under category of range-free localization algorithms.

Most of the 2D and 3D localization techniques which depend on RSSI and path loss model always consider antenna radiation pattern as isotropic i.e. antenna radiates uniform power in all directions [11]. In practice isotropic antenna does not exist. Omnidirectional antenna is used as isotropic antenna because it radiates uniform power in all azimuth directions, but it has a deep null in the orthogonal elevation direction. It radiates less power in axial direction of the antenna as shown in Fig. 1. Due to this, omnidirectional antenna or half wave dipole antenna radiation pattern gives less received power at nodes which are placed at the bottom of the antenna. In practical scenario because of the antenna radiation pattern effect localization error could increase. This motivated us to propose new radiation pattern based 3D localization algorithm, which considers radiation effect to give less error in localization.

A. Related works

In [12] authors proposed a novel centroid algorithm for 3D. Authors of [13] proposed new 3D DV-Hop Localization algorithm which is extended version traditional range-free DV-Hop algorithm in to 3D. In [14] authors described a range-free 3D azimuthally defined area localization algorithm. Authors of [15] proposed unitary matrix pencil algorithm for range-based 3D localization. It depends on time-of-arrival (TOA) estimation of ultra wideband signal using unitary matrix pencil algorithm. Paper [16] proposed a 3D positioning algorithm based on RSSI, which uses maximum likelihood estimator to estimate 3D location. Authors of [17] and [18] proposed

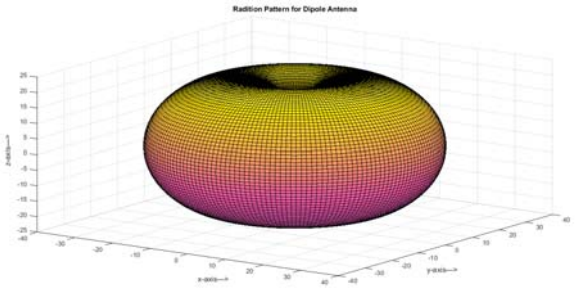

Fig. 1: 3D radiation pattern of half wave dipole antenna.

directional antenna based 2D localization techniques. These techniques depend on radiation pattern of the antenna.

In this paper we propose antenna radiation pattern based 3D localization technique by using node's omnidirectional antenna radiation pattern.

The rest of the paper is organized as follows. Section II describes proposed 3D localization algorithm. Section III describes the algorithm implementation and simulation setup for 3D localization. Section IV describes simulation results analysis. Finally, section V concludes the paper with future scope of work.

II. Proposed 3D localization algorithm

This section describes the proposed radiation pattern based 3D localization technique. We assumed that target node (the sensor node which location has to be estimated) is equipped with half wave dipole antenna, which has omnidirectional radiation pattern. In all directions, omnidirectional antenna radiation pattern is not same. It radiates less power in the axial direction of antenna. 3D radiation pattern of half wave dipole antenna is shown in Fig. 1.

A. Estimating 2D location of target node

We considered that target node is placed above the XY-plane with antenna in Z-axis direction. Omnidirectional antenna radiates power concentrically in horizontal direction with circular patterns as shown in Fig. 2. Received power from transmitting antenna at equidistant beacon locations is almost same on 2D plane (ground plane). The 2D location of the target node can be estimated by locating center of the circular patterns. To find out center of the circular patterns on 2D plane where beacon nodes are placed, the plane is divided in to circular patterns which are having arbitrary center point. These circular patterns form rings on 2D plane. Variance of received powers is computed over each ring. The mean of variances of received power where it goes to minimum, that center point of circles is regarded as 2D location of the target node.

To estimate target node 2D location (X_e, Y_e), we considered n beacon nodes in 2D plane. Location of beacon nodes are (x_i, y_i) where $i = 1, \ldots, n$ (a sensor node which is placed on mobile robot can be used as beacon node to get n beacon node locations [11]). Received power of i^{th} beacon node is Pr_i. Rn_{kl} represents l^{th} ring centered at an arbitrary point

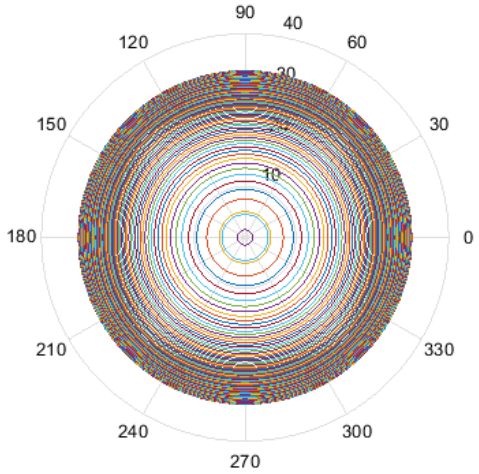

Fig. 2: Power distribution of the omnidirectional antenna in horizontal plane.

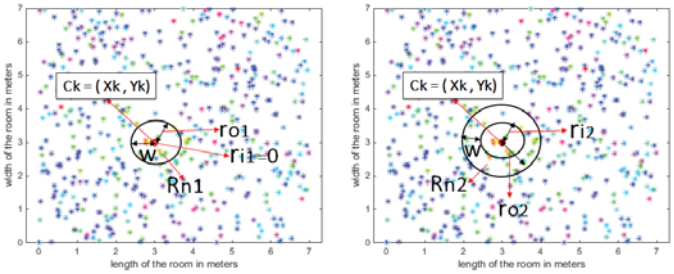

Fig. 3: The defined area is divided in circular rings.

$C_k = (x_k, y_k)$, where the radius of inner circle is ri_l, outer circle is ro_l and the width of each ring is w. Consider D_{ki} is the Euclidean distance between each points on 2D plane (x_i, y_i) and an arbitrary point $C_k = (x_k, y_k)$ which is calculated from equation (1). d_{1l} is the minimum distance between l^{th} ring's inner circle circumference and the points lying inside the ring. d_{2l} is minimum distance between l^{th} ring's outer circle circumference and points lying outside the ring i.e. points which distance $D_{ki} > ro_l$. Pt_i is the set of points of beacon node locations. Algorithm starts at an arbitrary point C_k with $ri_l = 0$ and $ro_l = w$. In next step if $d_{1l} < d_{2l}$ then $ri_l = d_{1l}$, $ro_l = ri_l + w$ else $ro_l = d_{2l}$, $ri_l = ro_l - w$. Fig. 3 shows plot of two iterations. In iterative process d_{2l}, d_{1l}, ri_l, ro_l will be update until $A_{kl} = \{\emptyset\}$.

$$D_{ki} = \sqrt{(x_i - x_k)^2 + (y_i - y_k)^2} \tag{1}$$

Here the set of points located in the ring Rn_{kl} are represented by $A_{kl} = \{Pt_i \mid Pt_i \in Rn_{kl}\}$. E_{kl} represents the mean of received power at different beacon nodes in the ring Rn_{kl} and calculated by equation (2).

$$E_{kl} = \frac{\sum_{Pt_i \in A_{kl}} Pr_i}{n_{kl}} \tag{2}$$

n_{kl} is the number of point of the set A_{kl}. Variance of received power values of each ring V_{kl} calculated using equation (3).

$$V_{kl} = \frac{\sum_{Pt_i \in A_{kl}} (Pr_i - E_{kl})^2}{n_{kl}} \tag{3}$$

$$EV_k = \frac{\sum_l (V_{kl})}{M_k} \tag{4}$$

Equation (4) is used to find the mean of the variances of the rings centered at C_k. Here M_k is the total number of rings for C_k. Finally the estimated position (X_e, Y_e) is determined using the following equation (5).

$$(X_e, Y_e) = C_k \text{ which minimizes } EV_k \tag{5}$$

B. Estimating height of the target node

The gain of omnidirectional antenna in vertical direction is lower than horizontal direction [19] as shown in Fig. 1. Thus, received power measured at the beacon nodes under the target node will be low. The average value of received power at beacon nodes from target node will decrease as target node height increases. This fact helped us to propose a new relative height estimation method for 3D localization.

To calculate average received power of beacon nodes under target node, a circle with radius r from estimated 2D location of the target node (X_e, Y_e) is considered. Set of Beacon positions M, which distance from (X_e, Y_e) is less than r is considered, i.e. $M = \{Pt_i \mid D_{ki} < r\}$. N_M is the number of beacon node in the set M. Average received power of beacon nodes P_{avg} is calculated using equation (6).

$$P_{avg} = \frac{\sum_{Pt_i \in M} Pr_i}{N_M} \tag{6}$$

Specifically, the proposed algorithm estimates the relative height Z_{ej} of target nodes N_j. Here we assumed that all target nodes heights are uniformly distributed along Z-axis with different 2D locations. First we find the average received power of all target nodes (inside the circle with radius r under target nodes). The minimum P_{avg} value is denoted by $P_{avg_{min}}$, the corresponding height of $P_{avg_{min}}$ is H_{max}. To estimate relative height of other target nodes, received average powers of all target nodes are divided in to groups. K-means clustering algorithm is used for grouping the received average powers of different target nodes with different heights. K-means algorithm will give group numbers according to received average powers. All the target nodes are classified into M groups from G_1 to G_M depending on its P_{avg}. The height of a target node in group G_h (where group number $h = 1, 2, ..., M$) is estimated by following equation (7).

$$Z_{ej} = \frac{H_{max}}{M} * h \tag{7}$$

III. Algorithm implementation and simulation setup for 3D localization

The proposed algorithm is implemented using Matlab software. Radiation pattern of the half wave dipole antenna is generated with reference of [21], [22] using Matlab. To implement the algorithm we considered beacon nodes are randomly deployed on 2D plane. Target node is considered above 2D plane (which is placed in 3D location). Received power Pr_i at randomly deployed beacon nodes (x_i, y_i) depend on gain of the antenna at respective positions. Antenna Transmit gain $G_t(\theta, \phi)$ and antenna receive gain $G_r(\theta, \phi)$ are function of azimuth angle ϕ and elevation angle θ. Transmit and receive antenna gain of beacon nodes will be different for different azimuth angle ϕ and elevation angle θ with respect to target node. Depending on these azimuth and elevation angles, antenna gains are mapped to different beacon node's location. To find received power at beacon node's location Revised Hata Okumara path loss model [20] is used (8).

$$\begin{aligned} logD_i = \frac{1}{10\eta}[P_t - Pr_i + G_t(\theta, \phi) + G_r(\theta, \phi) \\ - X_\alpha + 20log\lambda - 20log(4\pi)] \end{aligned} \tag{8}$$

Where $D_i \rightarrow$ distance between the target node to all beacon nodes (X_t, Y_t, Z_t) and i^{th} Beacon node (x_i, y_i).

$G_t(\theta, \phi)(dBi) \rightarrow$ Transmit antenna gain

$G_r(\theta, \phi)(dBi) \rightarrow$ Receiver antenna gain

$P_t(dBm) \rightarrow$Target node transmit power

$Pr_i(dBm) \rightarrow$ Measured received power at i^{th} beacon position

$\eta \rightarrow$ Measure of influence of obstacle like partitions and obstacles in indoor environment ranges from 4 to 5 and for free space it is equal to 2.

$X_\alpha \rightarrow$ Normal random variable with standard deviation of α and varies from 3dB to 20dB.

TABLE I: Path loss model parameter values used for simulation

Parameter	Value
P_t	-3 (dBm)
X_α	3 (dB)
λ	0.125 (meters)
η	2.5

A. Simulation setup

For simulation purpose we considered area of 7m*7m, number of beacon nodes are 1000 which are placed at random locations. All beacon nodes are placed on 2D plane with

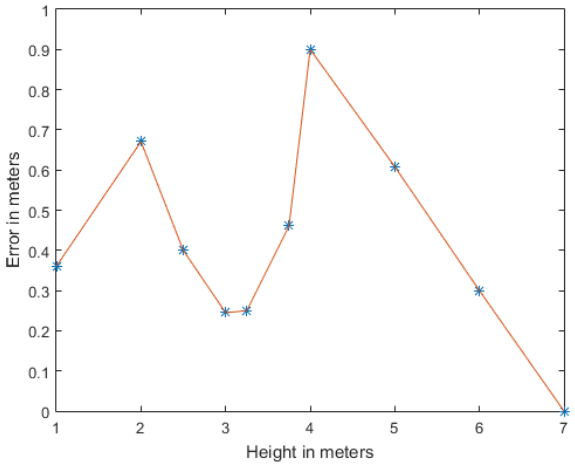

Fig. 4: Predicted location error vs height of the target nodes

random azimuth angle. We considered all target nodes and beacon nodes are equipped with half wave dipole antenna. Along with this setup 10 target nodes are considered which are placed at different 3D locations. Considered number of groups are $M = 10$ and considered maximum height is $Hmax = 7m$ which is maximum height of the considered target nodes. To calculate average received power of beacon nodes under the target node, a circle with radius $r = 0.5m$ which centered at estimated 2D location is considered. TABLE I shows path loss model parameters considered for simulation.

IV. Simulation Results analysis

Estimated location error with different heights is plotted in Fig. 4. Actual, estimated locations are tabulated in TABLE II.

TABLE II: Estimated and actual location of the sensor node at different heights

Actual locations (m)			Estimated locations (m)		
Xt	Yt	Zt	Xe	Ye	Ze
0	0	1	0.2	0	0.7
1	2	2	1	1.7	1.4
2	3	2.5	2	3	2.1
4	1	3	4.1	0.9	2.8
3	3	3.25	3	3	3.5
5	2	3.75	5.1	2	4.2
6	6	4	6	6	4.9
3.5	1.5	5	3.5	1.6	5.6
4	2	6	4	2	6.3
2	4	7	2	4	7

The error of the estimated 3D location of the target node to actual location of the target node is calculated by using equation (9).

$$E_{rr} = \sqrt{(X_t - X_e)^2 + (Y_t - Y_e)^2 + (Z_t - Z_e)^2} \quad (9)$$

Where $(X_t, Y_t, Z_t) \rightarrow$target node real location.

$(X_e, Y_e, Z_e) \rightarrow$ target node estimated location.

Estimated average error for 10 different locations with 10 different heights given in TABLE II is $0.4196m$. This result is more accurate compared to existing algorithms [11].

V. Conclusion

In this paper we proposed an antenna radiation pattern based 3D localization algorithm for estimating the 3D location of sensor node in a sensor network. The simulation results shows that the proposed algorithm gives less average error ($< 0.5m$) in estimating 3D location of target node compared to it's actual location. Our future plan is to implement proposed algorithm in real environment and test with different experimental setups.

References

[1] Seung-Ho Baeg, Jae-Han Park, Jaehan Koh, Kyung-Wook Park, Moon-Hong Baeg. "RoboMaidHome: A Sensor Network-based Smart Home Environment for Service Robots", *16th IEEE International Conference on Robot & Human Interactive Communication 26-29, Augus 2007 / Jeju, Korea.*

[2] A. Srinivasan and J. Wu, "A Survey on Secure Localization in Wireless Sensor Networks,"*Encyclopedia of Wireless and Mobile Communications,B. Furht (ed.), CRC Press, Taylor and Francis Group,2008.*

[3] J. C. Navas and T. Imielinski. "Geographic Addressing and Routing". *In Pro- ceedings of MOBICOM'97 , Budapest, Hungary, September 26, 1997.*

[4] Y.-B. Ko and N. H. Vaidya. "Location-Aided Routing (LAR) in Mobile Ad Hoc Networks", *In the Proceedings of MOBICOM'98, 1998.*

[5] N. Patwari, A. O. Hero, M. Perkins, N. S. Correal, and R. J. ODea, "Relative Location Estimation in Wireless Sensor Networks", *IEEE Transactions on Signal Processing, VOL. 51, NO. 8, AUGUST 2003.*

[6] H. Gupta, S. R. Das, and Q. Gu," Connected Sensor Cover: Self-Organization of Sensor Networks for Efficient Query Execution", *In Proceeding of MobiHoc'03, Annapolis, Maryland, June 2003.*

[7] Masashi Sugano, Tomonori Kawazoe, Yoshikazu Ohta, and Masayuki Murata. "Indoor Localization System using RSSI measurement of Wireless Sensor Network based on Zigbee standard", *Wireless Sensor Networks 2006.*

[8] Gang Wang, Kehu Yang. "A New Approach to Sensor Node Localization using RSS Measurements in Wireless Sensor Networks", *IEEE TRANSACTION ON WIRELESS COMMUNICATIONS, VOL. 10,NO. 5,MAY 2011.*

[9] Sabastin Gansemer, Uwe GroBmann, Syuzanna Hakobyan."RSSI-based Euclidean Distance Algorithm for Indoor Positioning adapted for the use in dynamically changing WLAN environments and multi-level buildings ", *International Conference on Indoor positioning and Indoor Navigation(IPIN) 2010.*

[10] N. Bulusu, J. Heidemann, and D. Estrin, "GPS-less low cost outdoor localization for very small devices", *IEEE Personal communications Magazine, 7(5):28-34,October 2000.*

[11] Amarlingam M, P Rajalakshmi, Vinod kumar Netad, Masaya Yoshida, Kiyohito Yoshihara. "Centroid Based 3D Localization Technique Using RSSI With a Mobile Robot", *Wireless Personal Multimedia Communications 2014.*

[12] Hongyang Chen, Pei Huang, Marcelo Martins, Hing Cheung, and Kaoru Sezaki, "Novel Centroid Localization Algorithm for Three-Dimensional Wireless Sensor Networks ", *IEEE 978-1-4244-2108-4/2008.*

[13] Li Wang, Jing Zhang, Dun Cao, "A New 3-dimensional DV-Hop Localization Algorithm", *Journal of Computational Information Systems 8: 6 (2012) 2463-2475, March 2012.*

[14] Guerrero E, Wang Hao, Alvarez J, Rivero L,"A Three-Dimensional Range-Free Localization Algorithm Based on Mobile Beacons for Wireless Sensor Networks", *Vol. 20 No.1 June 2010.*

[15] Chang Liu, Hong Jiang and De-Long Zeng, "Unitary Matrix Pencil Algorithm for Range- Based 3D Localization of Wireless Sensor Network Nodes", *Journal of Networks, Vol. 7, No. 9, September 2012.*

[16] Quan LIU, Ping REN, Zude ZHOU, "Three-dimensional Accurate Positioning Algorithm based on Wireless Sensor Networks". *Journal of Computers, Vol. 6, No. 12, December 2011.*

[17] Baoli Zhang, Fengqi Yu Zusheng Zhang, "A High Energy Efficient Localization Algorithm for Wireless Sensor Networks Using Directional Antenna", *2009 11th IEEE International Conference on High Performance Computing and Communications.*

[18] Baoli Zhang, Fengqi Yu , "A Feasible Localization Algorithm for Wireless Sensor Networks Using Directional Antenna", *2010 12th IEEE International Conference on High Performance Computing and Communications.*

[19] Huey-Ru Chuang and Liang-Chen Kuo, "3-d fdtd design analysis of a 2.4-ghz polarization-diversity printed dipole antenna with integrated balun and polarization-switching circuit for wlan and wireless communication applications", *IEEE Transaction on Microwave Theory and Techniques, 51:374-381, Febrary 2003.*

[20] Atreyi Bose and Chua Heng Foh."A Practical Path Loss Model for Indoor Wifi Positioning Enhancement", *ICICS 2012*

[21] Balanis, C.A., "Antenna theory: a review", *Proceedings of the IEEE , vol.80, no.1, pp.7,23, Jan 1992*

[22] Scott, W.R., Jr., "A general program for plotting three-dimensional antenna patterns", *Antennas and Propagation Society Newsletter, IEEE , vol.31, no.6, pp.6,11, December 1989.*

THE 18TH INTERNATIONAL SYMPOSIUM ON WIRELESS PERSONAL MULTIMEDIA COMMUNICATIONS
(WPMC-2015)
December 13-16, 2015, Hyderabad, India

QZSS SS-CDMA Location and Short Message Communication System

Noriharu SUEMATSU, Suguru KAMEDA, Yuji MIYAKE, Tomohide TAKAHASHI, Akinori TAIRA, Tadashi TAKAGI and Kazuo TSUBOUCHI
Research Institute of Electrical Communication
Tohoku University
2-1-1 Katahira, Aoba-ku, Sendai, Miyagi 980-8577, Japan
{suematsu, kameda}@riec.tohoku.ac.jp

Abstract—After the great east Japan earthquake, a mission of location and short message communication was added to Japanese Quasi-Zenith Satellite System (QZSS). This paper describes a novel Spread Spectrum CDMA (SS-CDMA) satellite communication system for this mission. By using long spread code, both long distance communication (high processing gain) and large capacity can be obtained. Due to the existence of long Round Trip Time (RTT) of satellite communication, a complex and real time access control method of cellular phones can't be adopted. Therefore, a novel frame slotted ALOHA with flag method and no transmit power control schemes has been proposed. The proposed access control method does not requires real time feedback or response and is applicable to huge capacity of several millions users. The design result shows the feasibility of location and short message communication system which can handle 3 million users within an hour using 2.68 MHz bandwidth.

Keywords—Satellite Communication, QZSS, CDMA, Spread Spectrum, GPS, Microwaves, Resilient Wireless Network

I. INTRODUCTION

In the event of large scale disaster, terrestrial communication infrastructure is heavily damaged. To reduce the risk of disaster, emergency/relief communication becomes important, but no wired/wireless backbone network will be left to connect the damaged area to the outside. Satellite communication has been recognized as the citadel of emergency/relief communication network [1].

After the great east Japan Earthquake, Japanese government decided to add the new mission of "location and short message service for evacuees" to QZSS (Japanese positioning system) [2]. By using this system, the data (short message of the evacuees' situation and their positioning data) can be transmitted from their mobile terminal with less than 1W RF power. This system's capacity should be more than 1,000,000 users/hour. To satisfy this requirement, we propose the SS-CDMA short message/location system [3]. By using CDMA system using long spread codes, both large capacity and long communication distance of 39,000km can be achieved. Since the round trip time (RTT) of 0.52 sec. exists, power control system with real time feedback from the base station used in the CDMA cellular systems can not be employed. We propose a novel CDMA system with no Tx power control [3],[4]. In order to realize the synchronization of the chip using positioning data and delivered GPS clock (CLK) [5]. We also propose the novel access control scheme based on frame slotted ALOHA [6]. By combining new technologies, the requirements for "location and short message service for evacuees" can be satisfied.

II. SYSTEM IMAGE AND LINK BUDGET DESIGN [3]

Figure 1 shows the system image of QZSS short message communication using SS-CDMA scheme. The satellite communication system has less near-far resistant than cellular system, because the relatively long/equal communication distance between the terminals on the earth and the satellite. By using non-directive or hemisphere beam antenna for the terminals and by transmitting same RF output power, the receiving power level from each terminal becomes almost same level. Therefore, power control which is widely used in CDMA cellular phone system is not necessary. Fig.2 shows the link budget design of proposed QZSS system. Long SS code enables both long communication distance of 39,000km and high CDMA capacity of 10,000 users. Fig,3 shows the packet structure and Table 1 shows the initial design result of QZSS short message communication in ideal case.

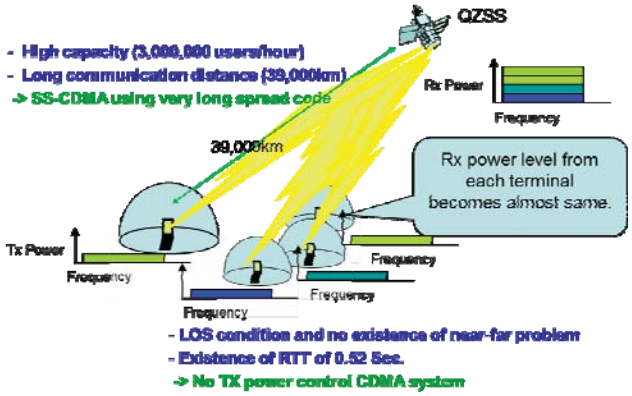

Fig.1 System image of QZSS short message communication using SS-CDMA.

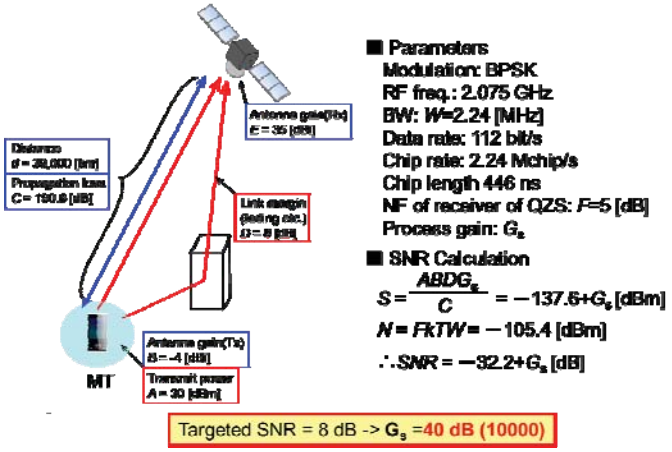

Fig.2 Link budget design of proposed QZSS system.

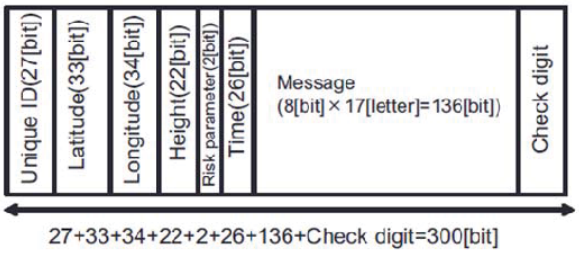

Fig.3 Packet structure.

Table 1 Initial design of QZSS short message communication in ideal case.

Process gain	dB/IR
Ideal multiplexing number	10,000
Data rate	112 bps
Packet size	300 bit
Tx time for 1 packet (1 user)	2.67 Sec.
Ideal capacity per hour	13,500,000 Users/hour

III. Code Design and Synchronization of SS-CDMA [4]-[5]

SS-CDMA communication system realizes the direct access from terminals to a satellite and accommodates several million users using long spreading codes. We design the channel which realizes the direct access from terminals to the satellite and evaluate influence of orthogonality breaking in high density CDMA using long spreading code. In the proposed system, the multiplexing rate should be set to extremely high value to accommodate several millions terminals, Therefore, keeping orthogonality among all users is very important. We selected orthogonal M-sequence for this high capacity SS-CDMA usage. "0" is added to the sequence which is obtained by cyclic shifting 1chip of M-sequence code. In the case of zero phase difference, cross correlation becomes zero. Since the single M-sequence is essentially used, any N-1 sequences can be prepared from N length code. This method is suitable to very large number multiplexing

We calculate the required accuracy of timing jitter and frequency offset by computer simulation. The simulation conditions are shown in Table 2. Due to the limitation of computer capacity for simulation, we scale down the capacity to 1/10 size. The simulated BER vs. timing accuracy is shown in Fig.4. The simulated BER vs. frequency accuracy is shown in Fig.5. The simulated results show the time accuracy is 56 ns (1/8 chip) and frequency accuracy is 0.01 ppm are required in to realize the accommodation rate of 100 % within 1dB Eb/No/Gs degradation.

Table 1 Simulation conditions (*:1/10 scaling for simulation)

Modulation scheme	BPSK
Coding	Convolutional Code (R=1/2)
Bandwidth	224 kHz *
Chip rate	224 kchip/s *
Symbol rate	220 symbol/s
Spreading code	Orthogonal M sequence
Spreading factor	1024 *
Transmit & Receiver filter	Root raised cosine filter (α=0.5)
Channel model	Adaptive white Gaussian noise

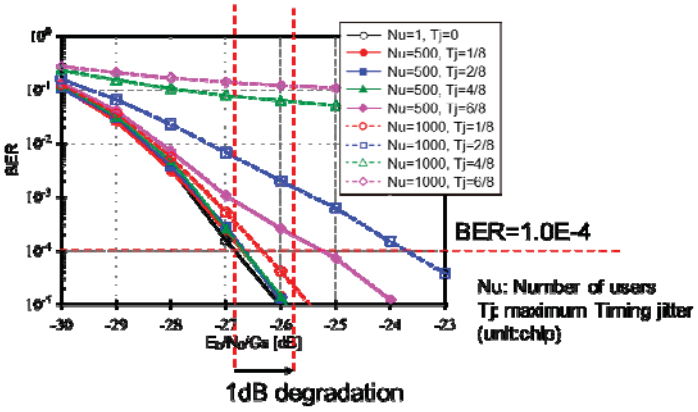

Fig.4 Calculated requirement of timing accuracy.

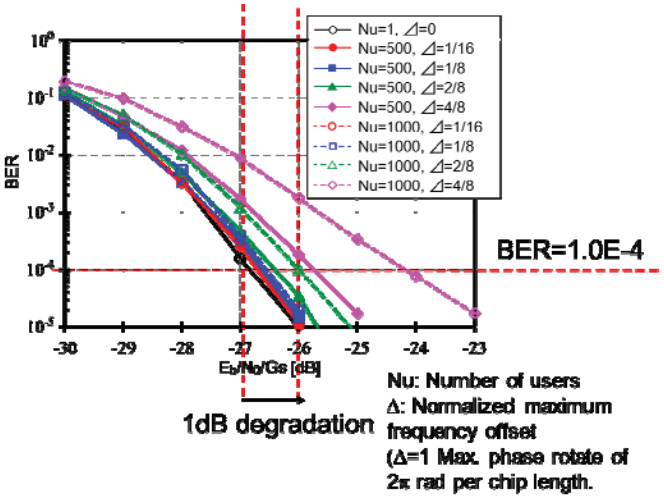

Fig. 5 Calculated requirement of frequency accuracy.

Figure 6 shows the proposed block diagram of QZSS short message communication terminals. These time and frequency accuracies can be achieved by using a high accurate positioning data and precise clock delivered from the QZSS as shown in Fig.7. We have measured the actual time and frequency accuracies by GPS locked TCXO (Furuno, GF-180TC) which can be used in the mobile terminals. The photo of measured GPS locked TCXO module is shown in Fig.6. An example of measured 1PPS Clock timing variation is shown in Fig.8. In this case, the timing error is less than 10ns. The measured time (1PPS clock) error for CDF of 99% is less than 20ns as shown in Fig. 9 and is smaller than the requirement. Frequency accuracy is also verified by the measurement.

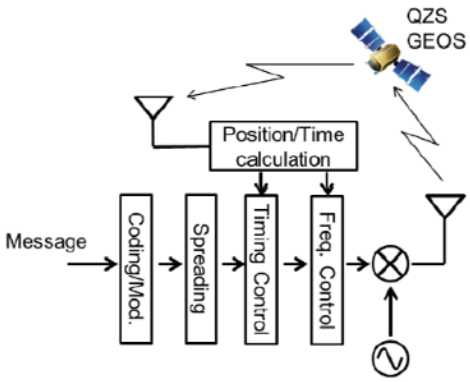

Fig.6 Block diagram of QZSS short message communication terminals.

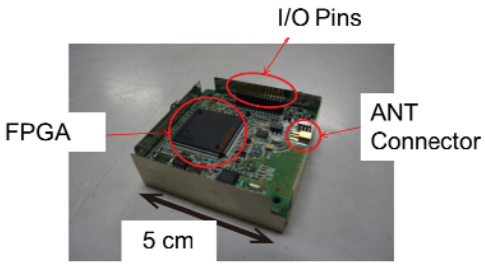

Fig. 7 Photo of measured GPS locked TCXO. (Furuno GF-180TC)

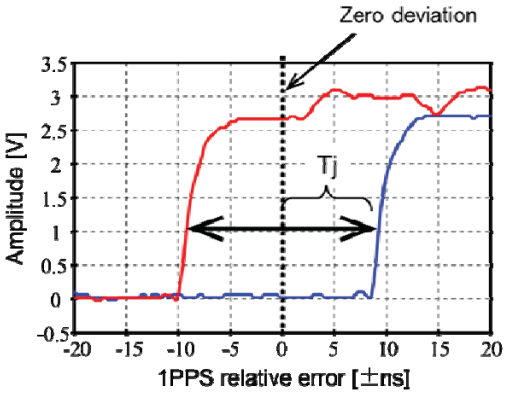

Fig. 8 Example of measured 1PPS clock timing variation.

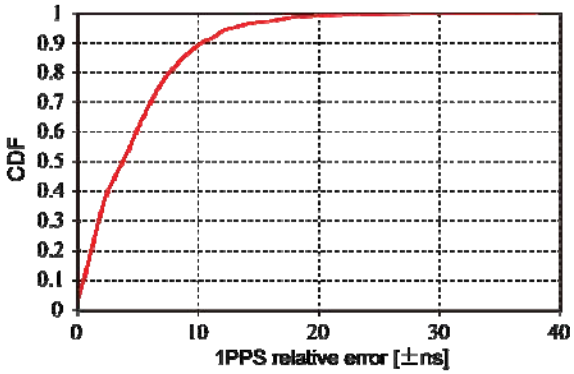

Fig.9 Measured timing error of GPS locked TCXO.

IV. Large Capacity / High Efficiency Access Control Scheme Using Flag Signal [6]

In the case of satellite communication system such as the proposed QZSS short message system, due to the existence of round trip time (RTT) and the relatively narrow control link band width, it is hard to use the access control scheme that we use for terrestrial wireless communication such as cellular phone. We propose novel/simple access control scheme which

attains high channel efficiency/capacity. In this system, all mobile terminals send flag signals compounded from multiple symbols at the same time. The approximate number of mobile terminals can be monitored by the received total power level of the added symbol, and resource can be assigned. The estimated accuracy of the number of mobile terminal is evaluated by theoretical analysis and numerical simulation. Fig.10 to Fig.12 show the proposed slotted ALOHA with flag method access control scheme. By using flag method, we can estimate the number of senders and can prepare the suitable length of frame. Fig.13 explains the concept and basic operation of proposed reservation channel (R-ch) method [6]. By adding this R-ch to the slotted ALOHA with flag method, both high capacity and high efficiency access control can be realized even in the case of very narrow control channel with RTT of 0.52s.

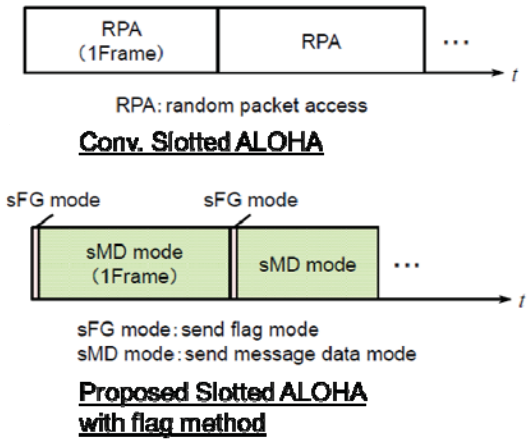

Fig.10 Proposed slotted ALOHA with flag method.

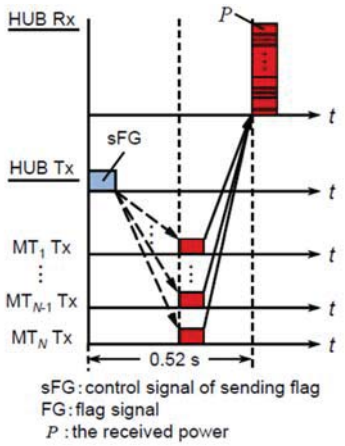

Fig. 11 Basis of proposed flag method in the sFG to estimate the number of senders. The number can be estimated from the received power level of total flag signal (P).

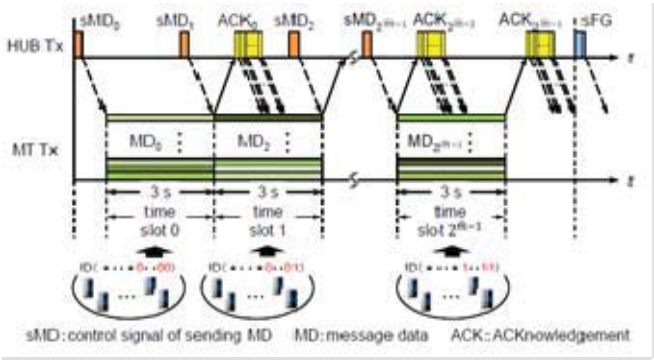

Fig. 12 Basis of proposed access control scheme using flag method.

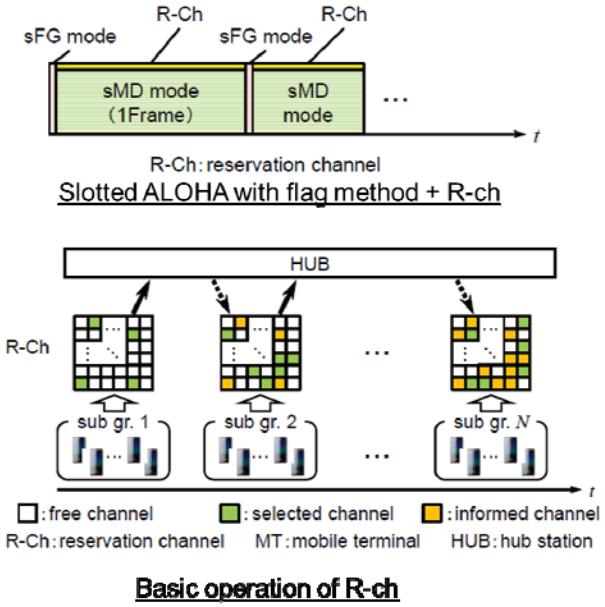

Fig.13 Concept and basic operation of proposed reservation channel (R-ch) method

Fig.14 shows the simulated results. By using proposed slotted ALOHA with flag method, 3 million users can complete their communication within an hour (3,600 sec.) By adding R-ch control scheme, time to complete will be reduced to ½. The results show that 3 million users' short message can be accommodated in an hour.

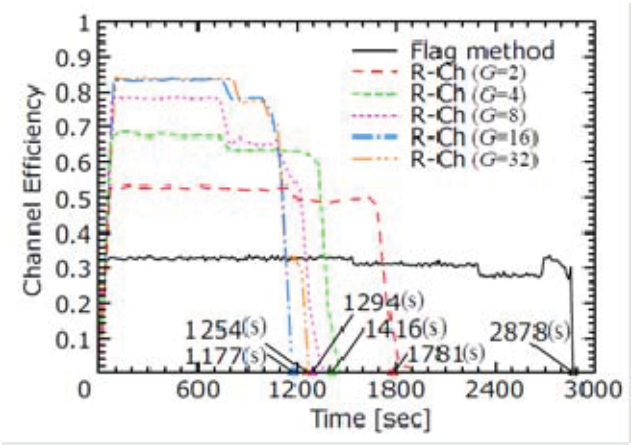

Fig.14 Time to complete 3 million users' communication .

V. Conclusion

After the great east Japan earthquake, a mission of location and short message communication was added to QZSS. For this mission, we propose a novel SS-CDMA satellite communication system for QZSS disaster relief short message communication for evacuees.

(1) Long spread code is used to obtain both long distance communication and large capacity .

(2) Due to the long Round Trip Time (RTT), a complex and real time access control method of cellular phones can't be adopted. Therefore, simple access control method is proposed.

We confirm our proposals by simulations and/or measurements.

Acknowledgment

The authors would like to thank the Core Research for Evolutional Science and Technology (CREST) program of the Japan Science and Technology Agency (JST) for fund support.

References

[1] N.Suematsu, et al., "Multi-Mode Portable VSAT for Disaster-Resilient Wireless Network," 2014 Asia-Pacific Microwave Conference (APMC2014), TH2E-4, Nov. 2014

[2] Cabinet Office, Government of Japan Home page
http://www.cao.go.jp/chotatsu/eisei/juntencho.html
(in Japanese)

[3] N.Suematsu, et al., "A study on system and link budget of location and short message communication using QZSS," IEICE technical report, MW2011-131, pp.33-36, 2011. (in Japanese)

[4] S.Kameda et al., "Feasibility Study on Wireless Access for Location and Short Message Communication System Using QZSS," IEICE technical report, SAT2012-7, pp.35-40 2012. (in Japanese)

[5] Y.Miyake et al., "Transmit Performance with Timing and Frequency Error of QZSS SS-CDMA Short Message Communication System," IEICE Trans. Comm., vol.J98-B, No.4, pp.397-405, 2015.

[6] T.Takahashi et al., "QZSS Short Message SS-CDMA Communication System: High Efficient Access Control Scheme Using Flag Signal," IEICE Trans. Comm., vol.J97-B, No.11, pp.1096-1105, 2014.

.

THE 18TH INTERNATIONAL SYMPOSIUM ON WIRELESS PERSONAL MULTIMEDIA COMMUNICATIONS
(WPMC-2015)
December 13-16, 2015, Hyderabad, India

LTE-Advanced Radio and Network Optimization: Basic Coverage and Interference Constraints

Fernando J. Velez[1,2], Sofia Sousa[1], Jessica Acevedo Flores[1] and Daniel Robalo[1]
[1] Instituto das Telecomunicações - DEM
Universidade da Beira Interior, Faculdade de Engenharia
6201-001 Covilhã, Portugal
fjv@ubi.pt, sofia.sousa@lx.it.pt, {jessik1512, robalodaniel}@gmail.com

Albena Mihovska·and Ramjee Prasad
[2] Center for TeleInfrastruktur (CTIF)
Department of Electronic Systems
Aalborg University
9220 Aalborg, Denmark
albena@es.aau.dk, prasad@es.aau.dk

***Abstract*—In cellular optimization, the UL and DL the values from carrier-to-noise-plus-interference ratio (CNIR) from/at the mobile station are very important parameters. From a detailed analysis of its variation with the coverage and reuse distances for different values of the Channel Quality Indicator (CQI) and given ITU-R propagation models, an evaluation of the possible range for the reuse factor, r_{cc}, of LTE-A is performed for the DL. By considering CQI and reference CNIR requirements recommended by 3GPP, DL peak bit rates along with the Transport Block Size assumed for single stream and bandwidths of 10 and 20 MHz, PHY and supported throughputs are analysed. HetNets with Carrier Aggregation (CA) are considered, where macro cells operating at 800 MHz provide coverage and small cells (SCs) operating at 2.6 GHz provide throughput enhancement at hotspots. A clear decrease of the supported throughput for the highest coverage distances in NLoS propagation conditions is shown. Besides, owing to existence of a breakpoint distance, d_{BP}, in the two slope model for LoS propagation, with SCs, a maximum occurs for system capacity for coverage distances, R, in the range between d_{BP}/r_{cc} and d_{BP}.**

Keywords—LTE-Advanced; CNIR; ITU-R propagation model; radio and network optimization; system capacity; HetNet

I. INTRODUCTION

In nowadays wireless cellular networks, not only mobile services and applications usage is increasing each year, leading to an expansion of mobile data traffic, but the pace at which it is growing is accelerating. According to [1], in 2013 mobile data traffic was nearly 18 times the size of the entire global Internet in 2000. One Exabyte of traffic traversed the global Internet in 2000, and in 2013 mobile networks carried nearly 18 Exabyte's of traffic. In 2013 alone, 526 million mobile devices and connections were added, the global mobile data traffic grew 81 % and mobile video represented 53 % of all mobile traffic and by 2018 it will reach 69 %. Moreover, mobile-connected devices exceed the world's population by 2014. Monthly mobile data traffic will reach 15.9 Exabyte's by 2018 and between 2013 and 2018 the annual growth rate is 61 %, i.e., mobile data traffic will increase nearly 11-fold between 2013 and 2018. These statistics show beyond the shadow of a doubt that wireless and cellular networks technologies need to be enhanced to support such demands. As such, this paper gives contributions to the basic limits of the optimization and planning of 4G cellular networks in a context of heterogeneous (HetNets) Long Term Evolution - Advanced (LTE-A) and spectrum management. LTE-A provides seamless Internet Protocol (IP) connectivity between user equipment (UE) and the packet data network (PDN), and an air interface based on Orthogonal Frequency Division Multiplexing (OFDM) in the downlink (DL) and single-carrier frequency-division multiple access (SC-FDMA) in the uplink (UL), both providing high flexibility in the frequency-domain scheduling. LTE-A has the flexibility to support time-/frequency-division duplexing (TDD/FDD) and half-duplex FDD schemes.

The main goal of cellular coverage is to offer access to mobile users in a cell, while guaranteeing quality of the received signal in both DL and UL directions, even for the users at the cell edge. As resources, e.g., radio frequency channels, need to be reused in different geographical zones (but not in the closest proximity), the impact of interference among co-channel cells needs to be evaluated in both DL e UL directions. Furthermore, this interference is heavier in users at cell edge, who may suffer from low connection quality. Therefore, a comprehensive study on the variation of the UL/DL carrier-to-noise-plus-interference ratio (CNIR) from/at the Mobile Station (MS) with different system parameters is critical in the context of LTE-A optimization. In this work, we are just considering DL. The variation of CNIR with the coverage and reuse distances is analysed for different values of the Channel Quality Indicator (CQI) and respective Modulation and Coding Scheme (MCS), considering the macro and pico cellular layers from a HetNet.

OFDM is a digital multi-carrier modulation scheme that extends the concept of single subcarrier modulation by using multiple subcarriers within the same single channel. Rather than transmit a high-rate stream of data with a single subcarrier, OFDM makes use of a large number of closely spaced orthogonal subcarriers that are transmitted in parallel. Each subcarrier is modulated with a conventional digital modulation scheme (such as QPSK, 16QAM, 64QAM.) at low symbol rate.

The goal of considering adaptive modulation is to choose the appropriate MCS for transmission in each carrier, given the local CNIR [2]. The MCS is chosen from an LTE-specific look-up table according to the provided Channel Quality Indicator (CQI) feedback [3]. The corresponding MCS value should achieve the maximum possible throughput by guaranteeing that the Block Error Ratio (BLER) is a bellow a given threshold.

Table I shows the mapping established with the MCS index and reference CNIR requirements recommended by 3GPP for DL, Los/NLoS as well as the spectral efficiency, S_{eff}. Table II presents DL peak bit rates, R_p, considered for single stream and bandwidth of 10 and 20 MHz.

TABLE I. MINIMUM CNIR, MODULATION AND SPECTRAL EFFICIENCY VERSUS MCS, FOR LTE, AND VALUES FOR THE VERTICAL ASYMPTOTE FOR DL

MCS mapping					$R_{asymptote}$ [km]					$R_{b[Mbps]}$
Mod. index	$CNIR_{min[dB]}$	Modulation	ITBS	S_{eff}	f = 800 MHz, macro		f = 2.6 GHz, pico			BW
					10 MHz	10 MHz NLoS	10 MHz	10 MHz NLoS	20 MHz NLoS	10 MHz
1	-4.63	QPSK	0	0.23	28.922	9.251	4.666	1.009	0.836	1.384
2	-3.615		1	0.31	27.281	8.714	4.401	0.947	0.784	1.8
3	-2.6		2	0.38	25.732	8.208	4.151	0.889	0.736	2.216
4	-1.36		3	0.49	23.959	7.630	3.865	0.822	0.681	2.856
5	-0.12		4	0.6	22.309	7.092	3.599	0.761	0.630	3.624
6	1.17		5	0.74	20.712	6.573	3.342	0.702	0.581	4.392
7	2.26		6	0.88	19.453	6.164	3.138	0.655	0.542	5,16
8	3.595		7	1.03	18.014	5.698	2.906	0.603	0.499	6.2
9	4.73		8	1.18	16.874	5.330	2.722	0.561	0.465	6.968
10	6.13		9	1.33	15.568	4.908	2.512	0.514	0.425	7.992
11	7.53	16-QAM	9	1.33	14.362	4.519	2.317	0.471	0.390	7.992
12	8.1		10	1.48	13.899	4.370	2.242	0.454	0.376	8.76
13	8.67		11	1.7	13.450	4.226	2.170	0.438	0.363	9.912
14	9.995		12	1.91	12.462	3.908	2.011	0.403	0.334	11.448
15	11.32		13	2.16	11.547	3.615	1.863	0.371	0.307	12.96
16	12.78		14	2.41	10.616	3.317	1.713	0.339	0.280	14.112
17	14.24		15	2.57	9.761	3.044	1.575	0.309	0.256	15.264
18	14.725	64-QAM	15	2.57	9.492	2.958	1.531	0.300	0.248	15.264
19	15.21		16	2.73	9.231	2.875	1.489	0.291	0.241	16.416
20	16.92		17	3.03	8.365	2.599	1.350	0.261	0.216	18.336
21	18.63		18	3.32	7.581	2.350	1.223	0.235	0.194	19.848
22	19.975		19	3.61	7.016	2.171	1.132	0.216	0.178	21.384
23	21.32		20	3.9	6.493	2.006	1.048	0.198	0.164	22.92
24	22.395		21	4.21	6.104	1.883	0.985	0.185	0.153	25.456
25	23.47		22	4.52	5.738	1.767	0.926	0.173	0.143	27.376
26	25.98		23	4.82	4.966	1.524	0.801	0.148	0.122	28.336
27	28.49		24	5.12	4.298	1.315	0.693	0.126	0.105	30.576
28	31.545		25	5.33	3.605	1.098	0.582	0.104	0.086	31.704
29	34.6		26	5.55	3.023	0.917	0.488	0.086	0.071	36.696

TABLE II. DL PEAK BIT RATES AND MINIMUM CNIR FOR BANDWIDTH OF 5 MHZ, 10 MHZ AND 20 MHZ - 25, 50 & 100 RESOURCE BLOCKS RESPECTIVELY

Modulation	$CNIR_{min[dB]}$	$R_{p[Mbps]}$, 5 MHz	$R_{p[Mbps]}$, 10 MHz	$R_{p[Mbps]}$, 20 MHz
QPSK/16-QAM/64-QAM	-4.63/7.53/14.725	4/7.7/18.3	7.9/15.3/36.7	15.8/30.5/75.4

Power and gains assumed in the considered LTE scenario are presented in Table III for 800 MHz/2.6 GHz LTE.

TABLE III. POWER, GAIN AND NOISE PARAMETERS

Parameters	f [GHz]	P_t[dBW]	G_t[dBi]	G_r[dBi]	BW[MHz]	N_f [dB]
Macro/Pico	0.8 / 2.6	16 / -7	17	0	10 / 20	5

The remainder of the paper is organized as follows. Section II addresses the interference, noise and frequency reuse trade-offs involved in LTE radio and HetNet optimization considering different MCSs, LoS versus NLoS propagation, comparing the behaviour of the 800 MHz and 2.6 GHz frequency bands (pico/ macro cellular layers, respectively) whilst briefly mentioning the analytical formulations. Section III presents a detailed analysis of LTE system capacity considering assumptions for different levels of MCSs, and discusses original results for the equivalent supported throughput as a function of the coverage distance. Finally, conclusions are drawn in Section IV.

II. CELLULAR RADIO AND HETNET OPTIMIZATION

In HetNets, cellular radio/network optimization must consider interference in obtaining the maximum coverage distance since it is a critical limitation in cellular systems dimensioning process. Noise is also an essential factor for the interference analysis, since it is always present in communications. Therefore, cellular optimization has to simultaneously consider carrier-to-noise and carrier-to-interference constraints. This work evaluates a 3GPP Carrier Aggregation (CA) scenario [4]. This scenario allows a flexible use of fragmented spectrum in different frequency bands. A lower frequency, 800 MHz, at the macro base station (eNB) layer provides coverage while the 2.6 GHz frequency band, at a pico-cell layer, improves throughput at hot spots. Mobility through CA is performed based on the macro eNB. The work considers LoS and NLoS propagation. Given the future reality in Portugal and Europe, the values for the evaluated bandwidth, BW, are 10 and 20 MHz both for the 800 MHz and 2.6 GHz frequency bands. The cell range at macro cellular layer varies from 150 to 3000 m, except one case, while for small cells it varies from 25 to 300 m.

In order to select the appropriate reuse pattern, K, and the appropriate frequency band, radio and network optimization aspects, like the analysis of cell coverage distance (or cell radius), co-channel reuse factor (ratio between the reuse and coverage distances), K, and supported throughput are addressed in this work for several levels of LTE MCS.

A. Analytical Formulations

If one considers the interference-to-noise ratio, M, defined by the ratio between the interference and noise powers, $M=I/N$, and the equation for the carrier-to-noise-plus-interference ratio (CNIR) to be used in the dimensioning process is the following:

$$\left(\frac{C}{N+I}\right) = \left(\frac{C}{N}\right)_{min} \quad (1)$$

equation (1) can be re-written in the two following ways:

$$\left(\frac{C}{N}\right) = \left(\frac{C}{N}\right)_{min} (1+M) \quad (2)$$

$$\left(\frac{C}{I}\right) = \left(\frac{C}{N}\right)_{min} (1+M^{-1}) \quad (3)$$

In (1) one is considering the model for CNIR from [5] while assuming that weights for noise and interference are the same. The interference-to-noise ratio is defined by

$$M(R) = \left(\frac{\left(\frac{C(R)}{N}\right)}{\left(\frac{C}{N}\right)_{min}}\right) - 1 \quad (4)$$

where $C(R)=P_R(R)$ is computed by applying, e.g., the ITU-R propagation model from [6]. Values of $M(R)$ are proportional to interference still tolerable for a given coverage distance, R, while (still) agreeing with the quality requirements for a given MCS.

With hexagonal cell topologies for the macro and pico cellular layers, in the DL, as shown in Figure 1, C/I is given by:

$$\frac{C}{I} = \frac{1}{2(r_{cc}+1)^{-\gamma}+2r_{cc}^{-\gamma}+2(r_{cc}-1)^{-\gamma}} \approx \frac{r_{cc}^{\gamma}}{6} \quad (5)$$

where r_{cc} is the co-channel reuse factor, given by $r_{cc}=D/R$, D is the reuse distance and R is the coverage distance (N.B. different Ds and Rs are defined for the macro and pico- cellular layers). In dB, the approximate equation is therefore $C/I \approx 10\cdot\gamma\cdot\log_{10}(r_{cc}/6)$.

By replacing (5) into (3), it is possible to obtain the following equation for the reuse factor in the DL:

$$r_{cc} = \sqrt[\gamma]{6\cdot\left(1+M^{-1}\right)\cdot\left(C/N\right)_{\min}} \quad (6)$$

As a horizontal asymptote arises in the analysis of the curves of r_{cc} as a function of the coverage distance, R, it is important to present the mathematical details associated to it. To compute the horizontal asymptote in the chart from $r_{cc}(R)$, one has to consider that $R \to 0$. Note that reuse pattern is given by $K=r_{cc}^2/3$.

From equation (6), if $R \to 0$ then $M \to +\infty$, and $M^{-1} \to 0$. For the DL, in the limit, one obtains:

$$\lim_{R\to 0} r_{cc} = \sqrt[\gamma]{6\cdot\left(C/N\right)_{\min}} \quad (7)$$

By considering the dependence of K on r_{cc}, it is straightforward to conclude that, for each value for the propagation exponent, apart from the dependence on the cellular interference geometry, K only depends on MCS through the corresponding minimum carrier-to-noise ratio.

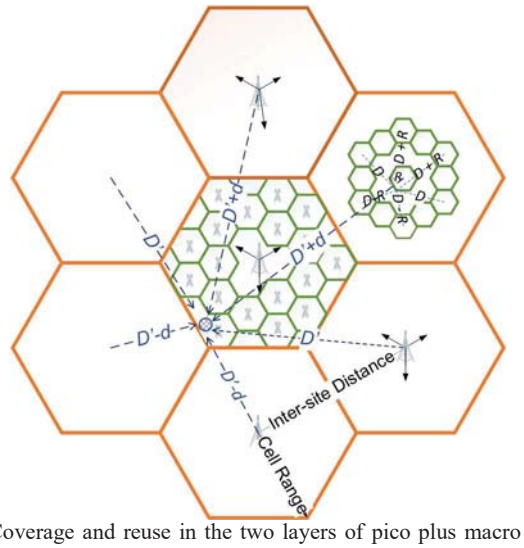

Fig. 1. Coverage and reuse in the two layers of pico plus macro HetNet, where co-channel interference s represented in the worst-case for the DL.

While the asymptotic reuse factor, r_{cc}, is associated with the upper bound for system capacity, the maximum coverage distance is associated with the carrier-to-interference-plus-noise ratio at the cell boundary when the interference is null. The vertical asymptote, $R_{asymptote}$, from $M(R)$ and $r_{cc}(R)$ represents the interference that can still be tolerated for a given R, in the limit, the maximum coverage distance for which no extra interference is tolerated.

B. Interference-to-noise Ratio and Co.channel Reuse Factor

By considering $R_{asymptote}=R_{M\to 0}$, one obtains the curves for the DL interference-to-noise ratio, considering the macro and micro/ picocellular scenarios from ITU-R model [6] for the 800 MHz and 2.6 GHz frequency bands, respectively. For the micro /picocellular scenario, the considered height from the macro base station is h_{BS}=10 m. For the macrocellular scenario, the height of the macro eNB is 25 m. The height of the mobile user is always h_{UT}=1.5 m. Variables $h'_{BS[m]}=h_{BS}$-1 and $h'_{UT[m]}= h_{UT}$-1 also stand. At 800 MHz, the breakpoint distance is $d_{BP}=4\cdot 24\cdot 0.5\cdot 800\cdot 10^6/c=$ =128m, where c is the velocity of light. For the 2.6 GHz frequency band, $d_{BP}=4\cdot 9\cdot 0.5\cdot 2.6\cdot 10^9/c$=156m. By considering these assumptions, in LoS, at 800 MHz, the path loss, PL, in dB is given by: $PL(d)=22.0\cdot\log_{10}(d_{[m]})+26.0618$, for d<128 m, and $PL(d)=40\cdot\log10(d_{[m]})-11.819$, for $d\geq$128 m. Also in LoS, at 2.6 GHz, for d<156 m, $PL(d)=22.0\cdot\log_{10}(d_{[m]})+36.29947$, while for $d\geq$156 m one achieves $PL(d)=40\ \log_{10}(d_{[m]})-3.12788$. In NLoS, the considered street width considered is 20 m while the average building height is 20 m. In the NLoS PL model there is no breakpoint. At 800 MHz, $PL(d)=39.08639\cdot\log(d_{[m]})+11.6067$ while at 2.6 GHz one achieves $PL(d)=36.7\cdot\log_{10}(d_{[m]})+33.48$.
Considering the values for P_t, G_t, G_r, BW and N_f from Table III, we obtained values for interference-to-noise-ratio, M, in the DL for f = 800 MHz. $M(R)$ depends on the CQI value and the MCS associated to it. Apart from the mapping between the MCS index and minimum CNIR, $CNIR_{min}$, Table I presents the corresponding values for the vertical asymptote, $R_{asymptote}$, for macro cells operating at 800 MHz and for pico cells operating at 2.6 GHz (LoS/NLos). At 800 MHz, one only discusses results BW=10 MHz, as the distances for the vertical asymptotes for BW=20 MHz are only slightly shorter. However, for the 2.6 GHz case, one also addresses results for BW=20 MHz. A relevant decrease of the values for the vertical asymptote (maximum R) occurs as the MCS increases because of the lowest associated $CNIR_{min}$.
Charts for the interference-to-noise ratio, $M(R)$, and reuse factor, r_{cc}, are shown in Figures 2-3 for the 800 MHz frequency band ($0\leq R\leq 3000$ m) for BW=10 MHz. Values from r_{cc} span from circa 1 up to 12 while the MCS order increases. Although charts for BW=20 MHz are not presented here, values of M are slightly lower than for BW=10 MHz, because of the highest noise power. Consequently, Rs for the vertical asymptotes are slightly shorter for BW=20 MHz. The chart of r_{cc} is also not presented because, apart from the shortest Rs for the asymptotes, the results for BW=20 MHz are very similar to the ones from Figure 3. From this analyses it is possible to conclude that the highest order MCSs can only be supported with high r_{cc} (hence high K).

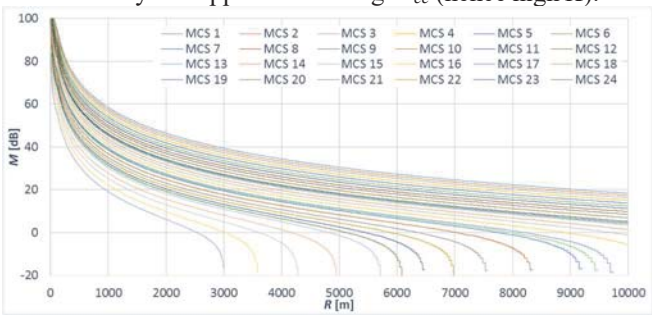

Fig. 2 Interference to noise ratio as a function of the coverage distance with MCS as a parameter for DL, in the 800 MHz band, BW = 10 MHz.

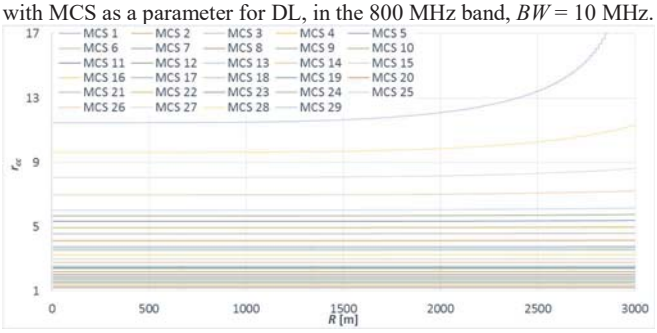

Fig. 3 Co-channel reuse factor as a function of the coverage distance with MCS as a parameter for DL, in the 800 MHz band, LoS, BW= 10 MHz.

Figures 4-5 analyse the case of 800 MHz band, NLoS, BW=10 MHz. The vertical asymptotes are clearly shorter. However, as the propagation exponent is 3.909, instead of 4, the behaviour of r_{cc} for the shortest distances is similar to the one from LoS case. Figure 6 presents the variation of $M(R)$ for the pico cellular layer, 2.6 GHz-LoS. The breakpoint is clearly visible for R=156 m. The shortest R for the vertical asymptotes occurs for R=488 m (MCS 29); hence, no vertical asymptote is visible for Rs up to 300 m.

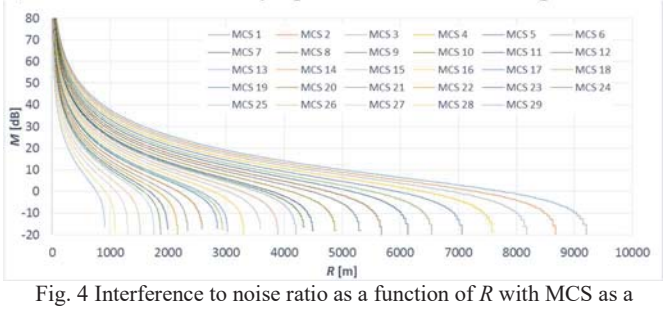

Fig. 4 Interference to noise ratio as a function of R with MCS as a parameter for DL, in the 800 MHz band, NLoS, BW = 10 MHz.

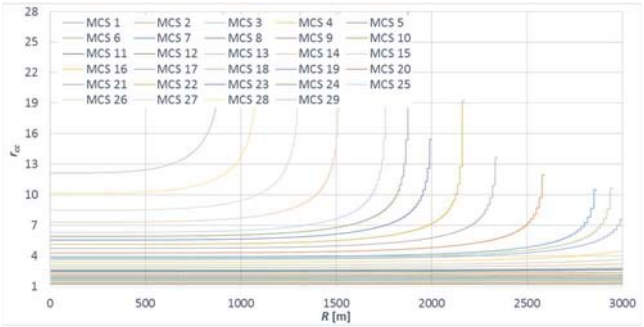

Fig. 5 Co-channel reuse factor as a function of the coverage distance with MCS as a parameter for DL, in the 800 MHz band, NLoS, BW = 10 MHz.

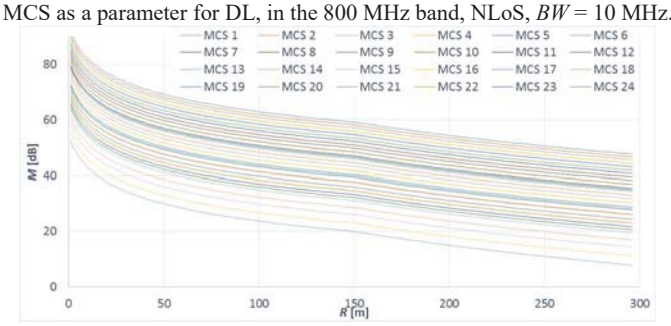

Fig. 6 Interference to noise ratio as a function of R with MCS as a parameter for DL, in the 2.6 GHz band, LoS, BW = 10 MHz.

Although the chart for r_{cc} is not presented here, the horizontal asymptotes for r_{cc} are the same as for the 800 MHz band, LoS as the propagation exponent is also γ=4. For BW=20 MHz, M is slightly lower (resulting in shorter asymptotes).

In the case of 2.6 GHz-NLoS, the propagation exponent is γ=3.67 and the path loss additive constant is higher than before. M is lower, and the asymptotes become visible in the range of Rs up to 300 m. Besides, an increase in r_{cc} exists. There are limitations in the coverage with the highest MCSs for the shortest Rs. For BW=20 MHz vertical asymptotes are slightly shorter compared to BW=10 MHz, resulting in worst coverage for short distances.

C. CNIR as a Function of r_{cc} with R as Parameter

Figure 7 facilitates to analyse the variation of the CNIR with r_{cc}, with R as parameter. Different frequency bands are considered as well as LoS versus NLoS propagation. When the interference power is much higher than noise power, the CNIR is given simply by $C/I \approx r_{cc}^{\gamma}/6$ in linear terms. In the analysis from Figure 7, this occurs in the majority of the cases, as interference, I, is always much higher than noise, N, i.e., M>8-10 dB, except for the cases "2.6 GHz-NLoS-R=300 m" and "800 MHz-NLoS-R=750 m", where M<8 dB for $r_{cc}\geq$2.85 and $r_{cc}\geq$8.75, respectively.

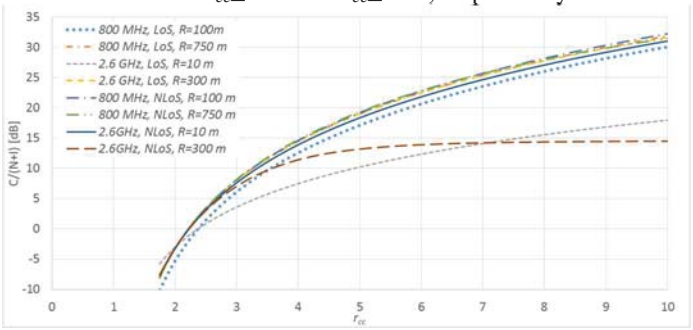

Fig. 7 Variation of the CNIR with r_{cc} for the DL in the 800 MHz and 2.6 GHz frequency band, LoS versus NLoS, and BW=10 MHz.

Hence, in the general case, the curves just follow the trend $10\cdot\gamma\log10(r_{cc}/6)$. From propagation models, one can observe that γ varies from 3.67 to 4, except for distances below the breakpoint. The exception occurs in the "2.6 GHz-LoS-R=10 m" case (purple dashed curve). In the "2.6 GHz-LoS-R=10 m" case, for the purpose of C/I computation, the value of γ is 2.2 (the lowest γ in our analysis). Also in the "800 MHz-LoS-R=100 m" case γ is considered to be 2.2 – but just for coverage purposes.

When the system is noise limited (clearly the case "2.6 GHz-NLoS-R=300 m" for $r_{cc}\geq$2.85, red wine dashed curve) $CNIR(r_{cc})$ follows a trend different from the one represented by $C/I \approx r_{cc}^{\gamma}/6$. Furthermore, if R increases for several hundreds of meters or even some kilometres, the distance considered in the computation of interference, i.e., reuse distance ($D=r_{cc}\cdot R$), considerably increases and interference decreases. Interference becomes therefore comparable to noise (not much high than noise anymore). Hence, the curves of CNIR would become lower than the upper limit curve. It is also a worth mentioning that the mapping between these values of CNIR and R_b are obtained by considering the correspondence from Table I (or Table II, in a simpler approach).

III. Detailed Analysis of System Capacity

While previous Sections analysed the individual influence of each MCS, it is also worthwhile to study the overall impact of several MCSs. Following the formulation from [7] for an implicit function procedure to compute supported throughput, the LTE system capacity is analysed for both macro (800 MHz) and pico (2.6 GHz) cellular layers from a Hetnet, considering the ITU-R propagation model [6]. The analysis considers different values of the reuse pattern, e.g., K=1, 3 and 7. One considers the values for P_t, G_t, G_r, BW and N_f from Table III. To map $CNIR_{min}$ into supported throughput one has assumed the values from $CNIR_{min}$ provided by [3], more specifically Tables 7.1.7.1-1 and 7.1.7.2.1-1. By extrapolating the gathered information it is possible to map the CNIR into MCS index, Modulation Order Transport Block Size (ITBS) index and TBS. Furthermore, by assuming TTI=1 ms the PHY throughput is obtained by multiplying the TBS by this value, and e.g., if 5 MHz bandwidth is considered, i.e., 25 PRBs, column NPRB=25 from Table 7.1.7.2.1-1 from [3] is assumed. This relation is presented in p. 122 from [7] (for BW=5 MHz), and in the last column from Table I (for BW=10 MHz), and similar relation exists for BW of 20 MHz. The maximum achievable number of coverage rings and MCSs are equal, i.e., 29, as each corresponds to different value of the PHY throughput. Figures 8 and 9 analyse the variation of CNIR and R_b with the distance d from cell centre to UE within a cell, where $0\leq d\leq R$, as shown in Figure 1. Respective cell sizes are R= 3000 and 300 m, at 800 MHz and 2.6 GHz, respectively, for BW=10 MHz, K=7;3. In "NLoS", CNIR and throughput are clearly lower than in "LoS". For the macro cellular layer, the curve for CNIR for reuse pattern 3 (r_{cc}=3) is clearly lower than for K=7 (r_{cc}=4.58) because of the much higher interference, resulting from the shortest D. This is evident both considering the LoS or NLoS propagation. The behaviour shown in Figure 9 for the pico cellular layer is similar to the one from Figure 8 (i.e., macro cellular layer).

For both (pico and macro) scenarios, by considering the mapping between $CNIR_{min}$ and R_b we clearly observe that the stepwise throughput is close to the maximum near cell centre, and gradually descends for longer distances (while UE approaches the cell edge). This decrease is more evident for NLoS propagation.

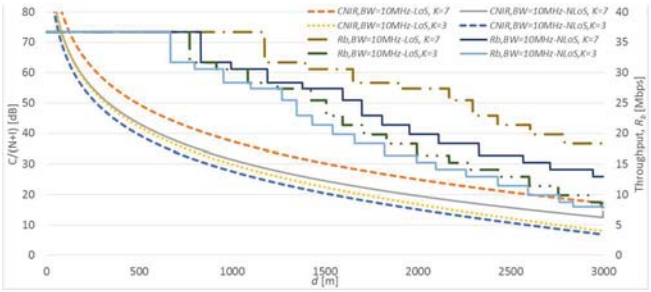

Fig. 8 Comparison of CNIR and R_b between K=7 and 3 for the macro cellular scenario (f=800 MHz), BW=10 MHz, and LoS versus NLoS.

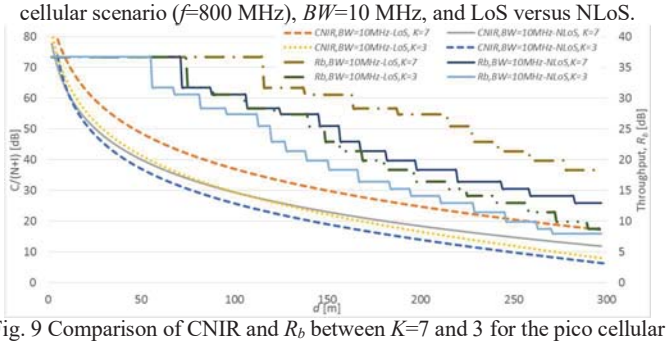

Fig. 9 Comparison of CNIR and R_b between K=7 and 3 for the pico cellular scenario (f=2.6 GHz), BW=10 MHz, and LoS versus NLoS.

Although the comparison of the behaviour between bandwidths of 10 and 20 MHz is not presented in these charts, the wider bandwidth is the lower is CNIR. From the results, this evidence is clearer for NLoS propagation but only slightly noticed for LoS propagation, as $N<<I$ and interference becomes dominant.

Figure 10 analyses the equivalent supported throughput, $R_{b\text{-}sup}$, as a function of R, for pico cells with size up to 300 m and macro cells with size up to 3000 m. $R_{b\text{-}sup}$ is determined through a weighted sum of the PHY throughput in each coverage ring throughout the cell, where the weights are the individual areas of each of the coverage rings. Bandwidth is 10 MHz. $R_{b\text{-}sup}$ is clearly superior for K=7 (blue curves) and lower for K=3 (green, red and purple curves). The curves for pico cellular scenario are the dashed ones while the continuous curves show throughput in the macro cellular scenario. At 2.6 GHz (pico cells), as there is no breakpoint in the model for NLoS, the curves (light blue and dark green) have regular behaviour. A noticeable behaviour is thus the decrease in $R_{b\text{-}sup}$ that occurs for the largest Rs, a characteristic from dynamic MCS. As the relevant model for LoS propagation at 2.6 GHz has a breakpoint at 156 m, the behaviour of CNIR changes when either the values of R or $D=r_{cc}.R$ reach d_{BP}=156 m. This means that changes in behaviour occur for $R_0= d_{BP}/r_{cc}$, i.e., R_0=52 m for K=3 and R_0=34 m for K=7, as well as for $R=d_{BP}$.

For $R<d_{BP}/r_{cc}$ the propagation exponents considered in the computation of $C(R)=P_R(R)$ and I are the same (γ=2.2), while for $R_0\leq R\leq$156 m the propagation exponent to compute I is already 4 while the coverage is still computed with γ=2.2. Hence, because of the resulting less interference in this range of Rs, a significant increase into the maximum achievable $R_{b\text{-}sup}$ is achieved, facilitating the optimization of SC networks. This analysis gives very useful hints for the optimization of CA [5], [7] between macro and pico cellular layer of a LTE-A HetNet with outdoor pico cells as trade-offs associated with the use different Ks are highlighted for LoS/NLoS propagation conditions. Although the charts do not analyse the wider values for bandwidth, the results we achieved in such analysis show that, despite the slight decrease in CNIR, circa twice of the capacity is achieved.

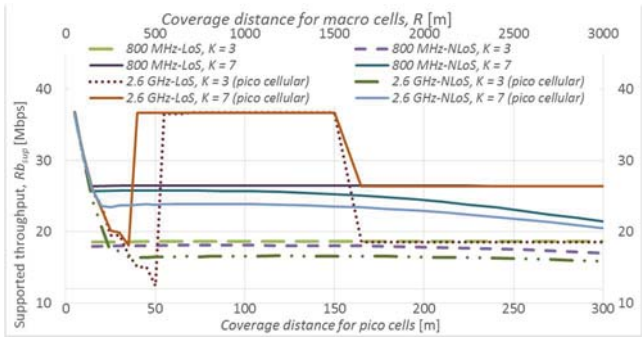

Fig. 10 Comparison of the equivalent supported throughput between K=7 and 3 for the pico/macro cellular scenarios and LoS/NLoS, BW=10 MHz.

IV. Conclusion

For cellular radio and network optimization purposes, the UL and DL carrier-to-noise-plus-interference ratios (CNIRs) from/at the mobile station are very important parameters. From a detailed analysis of its variation with the coverage and reuse distances for different LTE-A system parameters, modulation and coding schemes, in the DL, and ITU-R propagation models, an evaluation of the possible range for the reuse pattern has been performed. By considering the MCS and reference CNIR requirements recommended by 3GPP, DL peak bit rates along with the Transport Block Size assumed for single stream and bandwidths of 10 MHz and 20 MHz, an analysis of the physical and supported throughputs has been performed. One can learn that one common characteristic of the two frequency bands is the clear decrease of the supported throughput over the coverage distances with NLoS propagation. Besides, for the small cell layer, operating at 2.6 GHz, owing to the behaviour of the two slope model in LoS propagation conditions (where a breakpoint distance, d_{BP}, exists), a maximum occurs for system capacity for coverage distances, R, in the range between d_{BP}/r_{cc} and d_{BP}, a noticeable finding from this research.

Acknowledgment

This work has been partially supported and funded by CREaTION, COST CA 15104, ECOOP, UID/EEA/50008/2013, EFATraS, SFRH/BSAB/113798/2015 and ORCIP.

References

[1] Cisco Visual Networking Index: Global Mobile Data Traffic Forecast Update, 2013-2018, white paper, Feb. 2014.

[2] N. K. Noordin, B. M. Ali, N. Ismail, S.S. Jamuar, " Adaptive techniques in orthogonal frequency division multiplexing in mobile radio environment, *International Journal of Engineering and Technology*, vol. 1, no. 2, 2004.

[3] 3GPP, TS 36.212, V11.3.0. Technical Specification Group Radio Access Network; Evolved Universal Terrestrial Radio Access (E-UTRA); Multiplexing and channel coding, 3GPP Std., June 2013.

[4] 3GPP Ts 36.300, V10.8.0 Rel. 10 Evolved Universal Terrestrial Radio Access (E-UTRA) and Evolved Universal Terrestrial Radio Access Network (E-UTRAN); Overall description; Stage 2, July 2012.

[5] Jessica Acevedo, Daniel Robalo, Fernando J. Velez, "Transmitted Power Formulation for the Optimization of Spectrum Aggregation in LTE-A over 800 MHz and 2 GHz Frequency Bands," *Wireless Pers. Comms.*, June 2015.

[6] Guidelines for evaluation of radio interface technologies for IMT-Advanced, Report ITU-R M.2135-1, Dec. 2009.

[7] Daniel, Robalo, *Planning and Dynamic Spectrum Management in Heterogeneous Mobile Networks with QoE Optimization*, Ph.D. thesis, Univesidade da Beira Interior, Covilhã, Portugal, 2014.

THE 18TH INTERNATIONAL SYMPOSIUM ON WIRELESS PERSONAL MULTIMEDIA COMMUNICATIONS
(WPMC-2015)
December 13-16, 2015, Hyderabad, India

IEEE802.15.4g based Wide Area and Mobile Wi-SUN Communication Systems

Hiroshi Harada, Keiichi Mizutani, Kentaro Mochizuki, Kentaro Obata
Department of Communications and Computer Engineering, Graduate School of Informatics
Kyoto University
Kyoto Japan
{hiroshi.harada,mizutani}@i.kyoto-u.ac.jp

***Abstract*—This paper discusses key enabling technologies to realize wide area and mobile communication systems based on IEEE 802.15.4g wireless smart utility network (Wi-SUN) that is mainly used for advanced metering infrastructure. Firstly, three applications of the wide area and mobile communication systems are proposed. Then, transmission performance is evaluated by using propagation characteristic models for the three applications. Service areas of the communication systems are then estimated. Secondary, the service area calculation is validated by using actual Wi-SUN certified IEEE 802.15.4g modules. Thirdly adoption of maximum ratio combining diversity technique is proposed for the IEEE 802.15.4g based wide area and mobile communication systems. Then extension of the coverage area by the technique is evaluated by computer simulation.**

Keywords—IEEE 802.15.4g, Wi-SUN, mobile communication, , Sensor network, Smart Utility Network

I. INTRODUCTION

Currently there are increasing demands for Wi-SUN (Wireless Smart Utility Network) communication systems. In the systems, Electricity/Gas/Water meters equipping SUN (Smart Utility Network) radio devices can effectively automatically relay data frames to the collection station by expanding its service area. The SUN system also controls energy consumption according to the collected data [1]. The Wi-SUN is based on IEEE 802.15.4g that defines an alternate physical layer specification for principally outdoor Low Data Rate Wireless Smart Metering Utility Network [2][3]. It also includes additional specifications of MAC, adaptation, network, and transport layers' profiles in order to support several applications such as energy management. Currently the Wi-SUN alliance [3] has standardized its specification with interoperability between venders. One of the achievements of the Wi-SUN profile is the specification for Japanese Electricity companies. The specification is for the communication between smart meter and HEMS (home energy management system). All electricity companies in Japan have adopted the specification and the number of its subscribers is more than several tens million. After the success, new application fields for the Wi-SUN are being considered. Agriculture, disaster prevention, and intelligent transport systems have currently been proposed.

Considering new applications such as agriculture and disaster prevention, the coverage area should be as large as possible. The regulation in Japan for IEEE 802.15.4g is the following. The maximum transmission power for license-exempt is 20 mW and the operational frequency band is 920 MHz band. In this case the transmission range is at most 500 m when omni-directional antenna is used. If the range is larger than several km and the Wi-SUN supports mobile communications, a system design same as mobile phone system may be available.

This paper discusses key enabling technologies to realize wide area and mobile communication systems based on IEEE 802.15.4g Wi-SUN. Firstly, three applications of the wide area and mobile communication systems are proposed. Then, transmission performance of the Wi-SUN system under the new applications is evaluated by using propagation characteristic models for the three applications. Service areas of the communication systems are then estimated. Secondary, the service area calculation is validated by using actual Wi-SUN certified IEEE 802.15.4g modules. Thirdly adoption of maximum ratio combining diversity technique is proposed for the IEEE 802.15.4g based wide area and mobile communication systems. Then extension of the coverage area by the technique is evaluated by computer simulation.

II. CATEGORY OF WIDE AREA MOBILE WI-SUN SYSTEM

Fig. 1 and Table 1 categorize the wide and mobile communication systems based on Wi-SUN into three. Category (a) is an information sensing and monitoring system in wide area open space environment. The category is based on fixed point-to-multipoint communication and its coverage area is 1-5 km. In Fig. 1, each sensor and/or monitor communicates with access points (APs). Fig. 2 shows three configurations of APs.

AP (i) is based on a Wi-SUN certified IEEE 802.15.4g module. The module may divide into two: transmission part and reception part. The reception part may have a function of diversity such as maximum ratio combining (MRC) diversity. AP (ii) is based on several Wi-SUN certified IEEE 802.15.4g modules. Some of them may be used for diversity reception. AP (iii) is based on a software-defined radio that consists of multiband RF units for transmission and reception and a reconfigurable signal-processing unit (SPU).

Category (b) is an information sensing and monitoring system in wide area urban environment. APs are equipped on the building and communicate with sensors and/or monitors equipped in houses and/or shops by Wi-SUN. The communication is mainly non-line-of-sight and therefore the

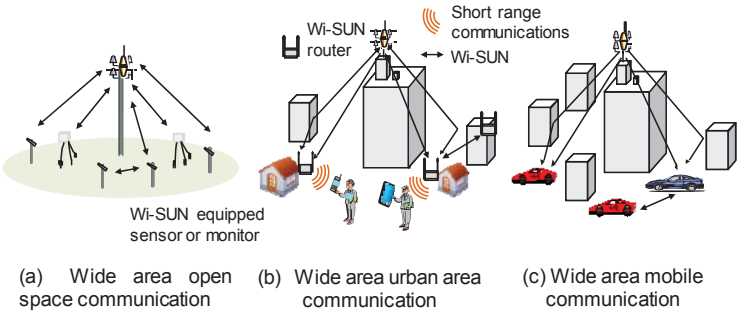

Fig. 1 Overview of wide area mobile Wi-SUN.

Table 1 Categories of wide area mobile Wi-SUN.

Category	(a) Wide area open space communication	(b) Wide area urban area communication	(c) Wide area mobile communication
Applications	• Sensor and/or monitor network for Energy management, Agriculture, disaster prevention, animal husbandry, and	• Information distribution, digital signage to building and store • Sensing and monitoring for building and store • Sensing and monitoring from smartphone via Wi-SUN router	• Collection of sensing data from vehicle such as car and bus • Control and management of vehicle
Transmission power	AP:20 mW, 250 mW Terminal: 20 mW	AP:20 mW, 250 mW Terminal, router: 20 mW	AP:20 mW, 250 mW Terminal: 20 mW
Antenna configuration	AP TX: Compliant with ARIB STD-T108 (in Japan) AP RX: Multiple antennas. Diversity reception may be used. Terminal: Compliant with ARIB STD-T108 (in Japan)		
Antenna height	> 4 m	> 30 m	
Coverage area	1 km-5 km	100 m-2 km	100 m-2 km
Radio propagation	Line-of-sight	Non line-of-sight	Non line-of sight
Path-loss model	Okumura-Hata model	Walfisch-Ikegami model	Walfisch-Ikegami model
Fading model	Multipath fading (One path Rayleigh)	Multipath fading (One path or COST207,GSM typical urban (TU) model)	
Installation method	Fixed installation	Basically fixed installation	Installation in vehicle Vehicle speed: 40-80 km/h
Multihop	May be needed to extend its coverage area and/or to keep high reliability.		

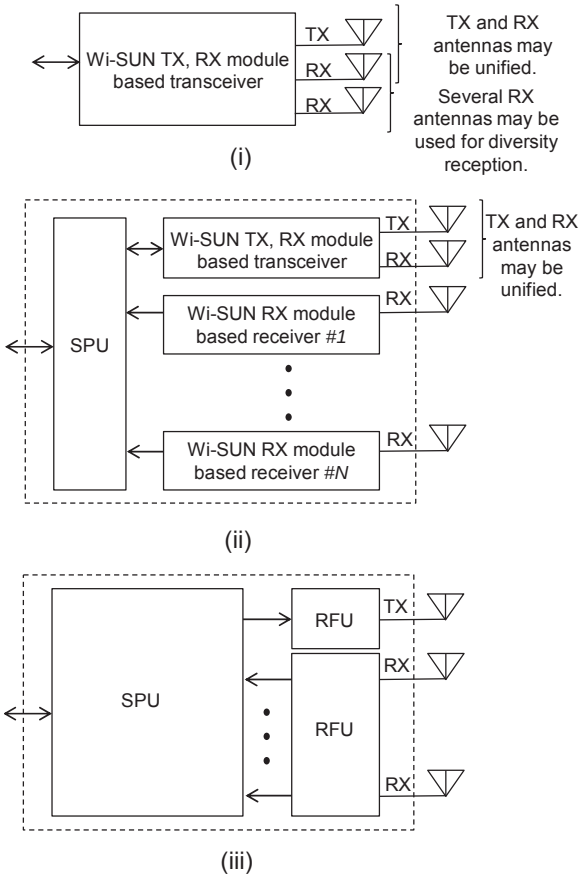

Fig. 2 Configurations of access point.

direct communication between APs and sensors/monitors may not be available. In this case, we may use Wi-SUN routers shown in Fig. 3. The router is a bridge between Wi-SUN and short-range wireless (SRW) communication systems such as Wi-SUN, Bluetooth, and NFC.

Category (c) is an information sensing and monitoring system in wide area mobile communication environment. APs are equipped on the building and communicate with sensors or monitors equipped in vehicles such as car and bus.

III. Design of Wide Area Mobile Wi-SUN Communication Systems

A. *Simulated transmission performance of IEEE 802.15.4g compliant Wi-SUN system*

Transmission performance of IEEE 802.15.4g compliant Wi-SUN system is evaluated by computer simulation. Figs. 4 and 5 and Table 2 show configuration, frame format, and specification of IEEE 802.15.4g transmitter, respectively. Table 3 shows parameters used in the computer simulation. Recursive and systematic code (RSC) shown in Fig. 6 is used in the simulation [2]. As propagation characteristic models, one path Rayleigh fading model and COST 207 GSM typical urban (TU) model shown in Table 4 are used [4]. Figs. 7 and 8 show the relationship between SNR (Signal-to-noise ratio) and PER (Packet Error Rate) under AWGN and fading environments, respectively. In Fig. 8 vehicle speeds of 0, 4, and 40 km/h are used. The required PER in IEEE 802.15.4g is 10^{-1} in the IEEE 802.15.4g standard when packet payload length is 250 octets. The required SNR to achieve the required PER is summarized in Table 5. The table shows that IEEE 802.15.4g cannot achieve the required PER when GSM typical urban model is used as fading model and the vehicle speed is 40 km/h.

Table 2 Basic specification of IEEE 802.15.4g.

Frequency	920 MHz
Transmission power	20 mW
Modulation	2GFSK (Modulation index = 1.0)
Transmission rate	50 kbps, 100 kbps, 200 kbps
Maximum data length	2047 octets

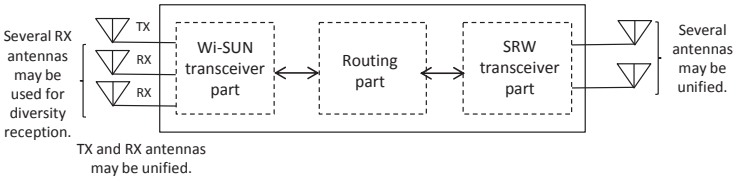

Fig. 3 Configuration of Wi-SUN router.

Table 3 Simulation parameters.

Compliant standard	IEEE 802.15.4g
Modulation	2GFSK (Modulation index = 1.0)
Preamble sync	Perfect
Modulation index	1.0
Payload size	250 octets
Transmission rate	100 kbps
Data whitening	Off
FEC	Recursive and systematic code
Multipath fading model	1 path Rayleigh fading, GSM typical urban (COST207)
Maximum Doppler freq.	34 Hz, 3.4 Hz, 0 Hz

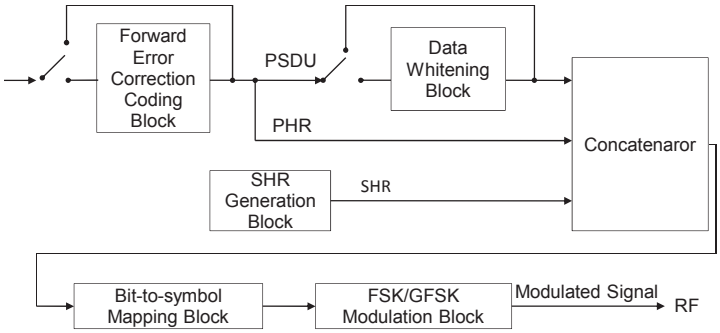

Fig. 4 Transmitter configuration of IEEE 802.15.4g (FSK).

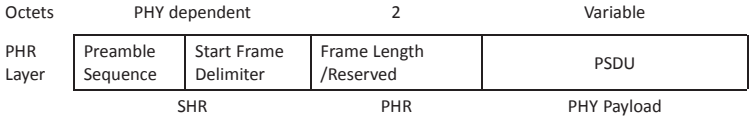

Fig. 5 Frame format of IEEE 802.15.4g (FSK).

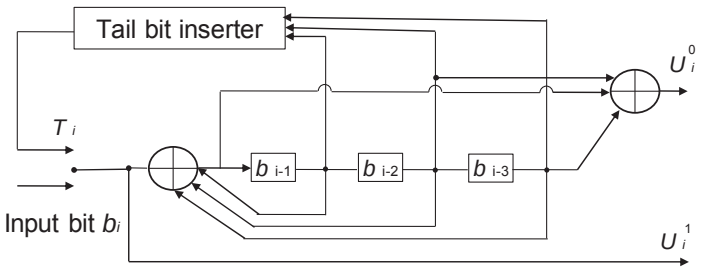

Fig. 6 Recursive and systematic code type FEC encoder.

Table 4 GSM typical urban (TU) model.

Model name		Path1	Path2	Path3	Path4	Path5	Path6
GSM Typical Urban	Delay time [us]	-0.2	0	0.3	1.4	2.1	4.8
	Relative power [dB]	-3	0	-2	-6	-8	-10

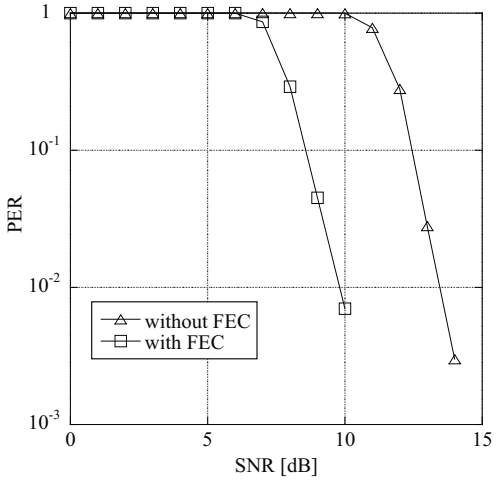

Fig. 7 PER performance (AWGN).

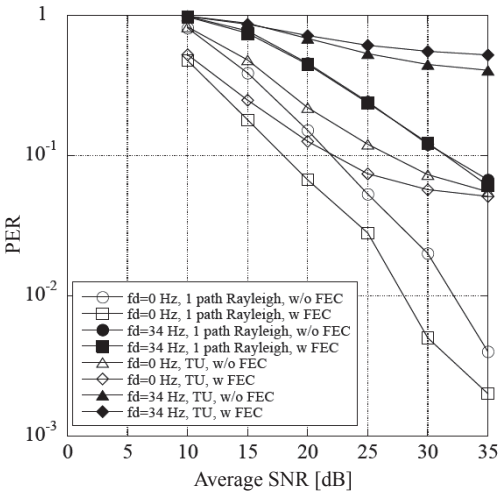

Fig. 8 PER performance (Fading environment).

B. Estimation of communication area

By using the result in Table 5, the communication area is calculated. The authorized maximum transmission power in 920 MHz band is 20 mW for license-exempt radio equipment and 250 mW for registered radio equipment. In our proposed systems shown in Fig. 1, each AP has a 250 mW radio equipment and each terminal has a 20 mW one. In this case transmission power difference between AP and terminal is 11 dB. This means that transmission distance of uplink is dominant to decide communication area. To keep same transmission distance between uplink and downlink, an AP has several directional receiving antennas as shown in Fig. 2. In this paper communication area of uplink is calculated by using parameters in Table 6. The received SNR, SNR_r at AP in uplink is calculated as following.

$$SNR_r = P_T + G_{AP} + G_T - L_f - (N_{AP} + N_s) \qquad (1)$$

where P_T, G_{AP}, G_T, L_f, N_{AP}, and N_s are transmission power of terminal, antenna gain of AP, antenna gain of terminal, propagation path loss and system noise in the receiver of AP, respectively. Table 5 also summarizes the acceptable L_f to achieve SNR_r equal to the required SNR that achieves PER= 10^{-1}.

Table 5 Required SNR and L_f to achieve PER = 10^{-1}.

Fading model	1 path Rayleigh		GSM typical urban	
Maximum Doppler frequency [Hz]	0	34	0	34
Required SNR to achieve PER of 1.0e-1 (w/o FEC)	22	32	27	N/A
Required SNR to achieve PER of 1.0e-1 (w FEC)	18	32	23	N/A
Acceptable path loss (w/o FEC) [dB] (UL)	116	106	111	N/A
Acceptable path loss (w FEC) [dB] (UL)	120	106	115	N/A

Table 6 System parameters.

	DL	UL
Transmission power of AP	24 dBm	
Transmission power of terminal		13 dBm
Antenna gain of AP	3 dBi	6 dBi
Antenna gain of terminal	3 dBi	3 dBi
Noise power (thermal noise)	−120 dBm	−120 dBm
Additional system noise level to thermal noise	+5 dB	+5 dB
Bandwidth/ch	200 kHz	200 kHz

In the case of category (a) in Fig. 1, the typical antenna height is 4 m and Okumura-Hata propagation model is adopted. The typical antenna height is 30 m in the case of categories (b) and (c) and Walfish-Ikegami propagation model is adopted. The relationship between distance and propagation path loss is shown in Fig. 9. In this calculation, the antenna height of AP and terminal is 30 m and 1.5 m, respectively. Moreover, the width of road and the interval of building and the angles of road and path between AP and terminal are 10 m, 10 m, and 0, 45, 90 degrees, respectively.

Table 5 and Fig. 9 show that the maximum communication area is 2 km and 500 m in the case of Category (a) and Category (b), respectively when the multipath model is one path Rayleigh fading.

C. *Experimental transmission performance by IEEE 802.15.4g compliant Wi-SUN module*

To do validation of estimation of communication area, transmission performances under AWGN environment and multipath fading environment are measured by using IEEE 802.15.4g compliant and Wi-SUN certified modules as shown in Fig. 10. In the laboratory experiment, two radio modules and a fading emulator are used and the PER performances are measured. Table 7 summaries parameters used in the experiment. Figs. 11 and 12 show PER performances in AWGN and multipath fading environment, respectively. Table 8 summarizes the required RSSI to achieve 10^{-1} and also summarizes the acceptable L_f to achieve SNR_r equal to the required RSSI by using noise parameters shown in Table 6. By using Table 6 and Fig. 9, the communication area is calculated.

Table 6 and Fig. 9 show that the maximum communication area is 1 km and 300 m in the case of Category (a) and Category (b), respectively when the multipath model is one path Rayleigh fading.

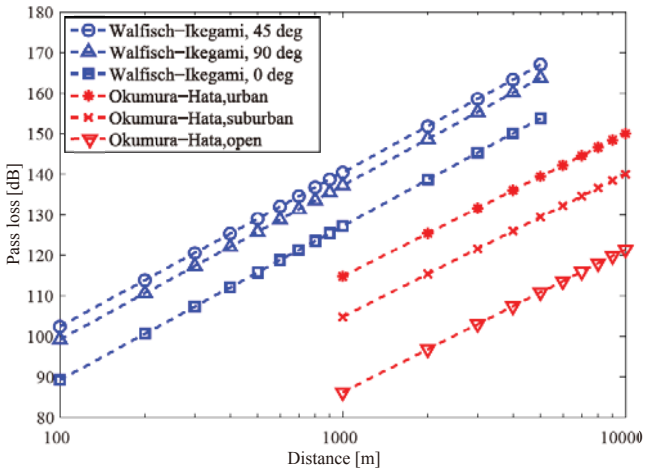

Fig. 9 Relationship between path loss and distance.

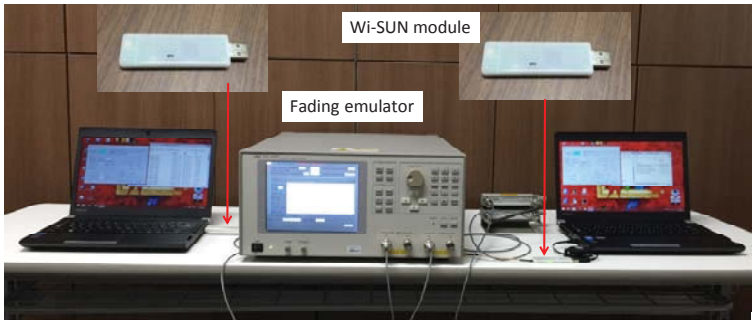

Fig. 10 Experimental environment.

Table 7 Parameters used in the experiment.

Compliant standard	IEEE 802.15.4g
Frequency band	920 MHz
Modulation	2GFSK (Modulation index = 1.0)
Preamble length	15 octets
Modulation index	1.0
Payload size	250 octets
Transmission rate	100 kbps
Data whitening	Off
CRC	CRC-32
Multipath fading model	1 path Rayleigh fading, GSM typical urban (COST207)
Maximum Doppler freq.	34 Hz, 0.4 Hz

IV. PROPOSAL FOR PERFORMANCE IMPLOBEMENT

To achieve communication area larger than 4 km, L_f must be larger than 125 dB (suburban) from Fig. 8 when Okumura-Hata model is used in the Category (a). In addition, L_f must be larger than 130 dB to achieve communication area of 1-2 km when Walfish-Ikeami model is used in the Categories (b) and (c).

To support L_f larger than 125 dB, the required SNR to achieve PER=10^{-1} must be smaller than the one in Figs. 8 and 12. The target of the required SNR is smaller than 14 dB. One of the technique is to use diversity reception, especially MRC reception. Fig. 13 shows PER performance of Wi-SUN when two-branch MRC reception is used. The figure shows that the required SNR is smaller than 14 dB when TU model is used and fd=3.4 Hz. And even if the maximum Doppler frequency is 34 Hz, the required SNR is 16 dB. This means that the communication area is expected to achieve greater than 1 km when transmission powers of AP and terminal are 250 mW and 20 mW, respectively in Category (a)-(c).

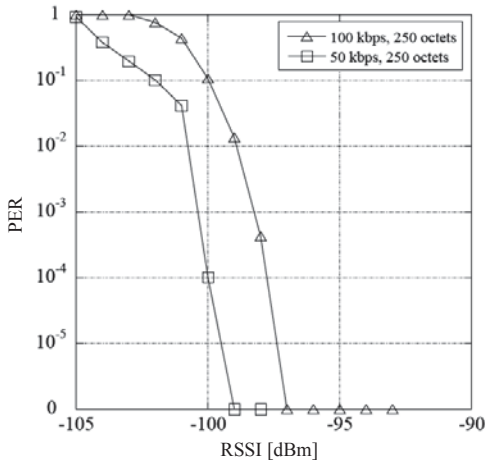

Fig. 11 PER performance in the experiment (AWGN).

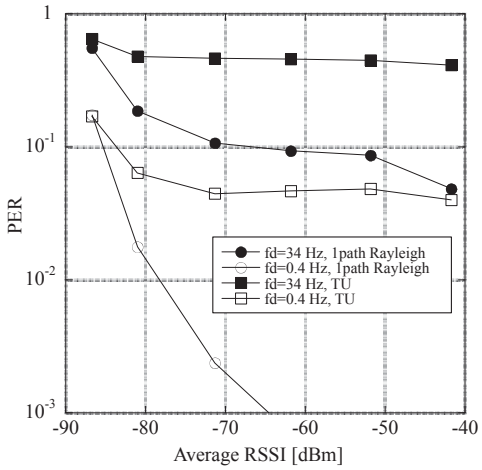

Fig. 12 PER performance in the experiment (fading).

Table 7 Required SNR and L_f to achieve PER = 10^{-1}.

Fading model	1 path Rayleigh		GSM typical urban	
Maximum Doppler frequency [Hz]	0.4	34	0.4	34
Required RSSI to achieve PER of 1.0e−1 (w/o FEC)[dBm]	−85	−67	−82	N/A
Estimated SNR to achieve PER of 1.0e−1 (w/o FEC) [dB]	30	48	33	N/A
Acceptable path loss (w/o FEC) [dB] (UL)	108	90	105	N/A

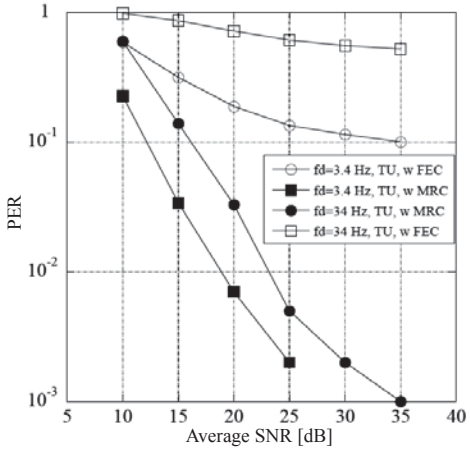

Fig. 13 PER performance when MRC is used.

Table 8 Required SNR and L_f to achieve PER = 10^{-1} (with MRC).

Fading model	GSM typical urban	
Maximum Doppler frequency [Hz]	3.4	34
Required SNR to achieve PER of 1.0e−1 (w FEC and MRC)[dB]	13	16
Acceptable path loss (w FEC and MRC) [dB] (UL)	125	122

V. Conclusion

This paper discussed key enabling technologies to realize wide area and mobile communication systems based on IEEE 802.15.4g Wi-SUN. Three applications of the wide area and mobile communication systems were proposed. Then, transmission performance was evaluated by using propagation characteristic models for the three applications. Service area of the communication systems was finally estimated. The results showed that the maximum communication area was 2 km and 500 m in the case of Category (a) and Category (b), respectively when the multipath model is one path Rayleigh fading. In the case of Category (c) and in the TU multipath fading environment it is very difficult to achieve PER=10^{-1}. But by using MRC diversity reception, the communication area was expected to achieve greater than 1 km when transmission powers of AP and terminal are 250 mW and 20 mW, respectively in Category (a)-(c). As further works, actual field experiment will be performed.

Acknowledgment

This study was carried out under support of Ministry of Internal Affairs and Communications SCOPE (No.15653992).

References

[1] H. Harada, “Smart Utility Network : Overview and Status of Standadization,” Technical Report of IEICE, SR2010-48, pp. 57-64, Oct. 2010. (in Japanese)

[2] IEEE 802.15.4g-2012.

[3] http:// www.wi-sun.org

[4] COST 207, “Digital land mobile communications,” Office for Official Publication of the European Communities, Final report, Luxembourg, 1989.

THE 18TH INTERNATIONAL SYMPOSIUM ON WIRELESS PERSONAL MULTIMEDIA COMMUNICATIONS
(WPMC-2015)
December 13-16, 2015, Hyderabad, India

Selective Sensing Framework for Opportunistic Mobile Phone Sensing Networks

Thejaswini M†, P. Rajalakshmi††, U. B. Desai††
†Department of Computer Science and Engineering
††Department of Electrical Engineering
Indian Institute of Technology Hyderabad, India
Email: (cs10p003, raji, ubdesai)@iith.ac.in

***Abstract*—The rise of opportunistic mobile phone sensing paradigm is due to ubiquitous mobile phones usage. Optimisation of battery energy consumption and achieving required spatial coverage of sensing area are important issues under opportunistic mobile phone sensing networks. Human mobility enable collection of mobile phones sensor data and sensing area coverage by forming communication network with surrounding neighbors devices (mobile phones). This paper proposes a human mobility based selective sensing framework called as HWSS (Human Walk based Selective Sensing) for sensor data collection in opportunistic mobile phone sensing networks. In proposed HWSS method, mobile phones are selected for sensing task based on users current and predicted future locations and sensing overlap area. The proposed HWSS method is compared with non-selective sensing method (NSS), where all mobile nodes are allowed for sensing during sensor data collection process, in an given application area. The simulation results show that compared to NSS method proposed HWSS method achieves reduction in energy consumption and required spatial coverage.**

***Index Terms*—Energy Consumption, Human Walk, Mobile Phones, Sensing area Coverage, Sensors**

I. Introduction

Mobile phones or smart phones which are usually carried by humans are coming with different types of scalar and multimedia sensors. For a mobile phone, sensors may be embedded externally or inbuilt, includes accelerometer, gyroscope, magnetometer, digital compass, temperature, light, proximity, barometer, humidity, heart rate, SpO2 (peripheral capillary oxygen saturation), camera, microphone and GPS (Global Positioning System) [1], [2]. Mobile phones are also come up with different types of communication technologies like 2G/3G/4G and near field communications (Wi-Fi, Bluetooth and RFID (Radio-frequency identification) [1], [2].

Mobile phone sensing applications include urban monitoring [3], [4], [5], environment monitoring, traffic monitoring [6], health care monitoring [7], intelligent transportation, disaster management [8], [9], mass education and social networking [3], [10], [9].

Human mobility enables collection of mobile phone sensor data by forming network with other device (mobile phones) in their communication range for sensing task. There are numerous open issues and research challenges to build up efficient mobile phone sensing network applications using embedded sensors and communication resources. Efficient usage of battery power, spatial and temporal sensing area coverage are challenging research issues in mobile phone sensing. Opportunistic and dynamic human mobility nature and their activities affect the performance of mobile phone sensing networks [11]. In opportunistic mobile phone sensing, mobile phones come in contact with other mobile phones and devices opportunistically [11].

For continuous environmental sensing applications using mobile phone sensors, consider high density of mobile phone users scenario, there is more possibility of spatial and temporal sensing area overlap. Mobile phone resources will be shared by many applications running on it. Sensing applications should not drain battery power and affect other applications running on it. Ensuring required minimal energy consumption and required spatial and temporal coverage of sensor data are fundamental issues in mobile phone sensing.

This paper refers to human mobility based selective sensing for efficient mobile phone sensor data collection in opportunistic sensing networks. Levy walk (LW) mobility model which depict the statistical properties of human walk patterns is considered for evaluation of proposed work. Reference [12], [13], [14], [15], [16], [17] explore LW mobility model.

Formation of communication network between mobile phones for sensing task requires regular lookup for neighbors, processing and exchange of messages, security and trust protocols. Hachem *et al.* [18] discusses reducing number of participatory users plus improving coverage by assuming that users are aware of their path. Sheng *et al.* [19] presents collaborative mobile phone sensing using cloud network. They also assume that mobile phone users path is known in advance.

In opportunistic mobile sensing applications, where users visit in the vicinity of application region is not frequent or dynamic in nature, prediction of users current location, velocity, movement direction, future location, duration of stay using mobile phone sensors is preferable [20] [21], [12], [22], [23], [24]. There is need to analyse the impact of unpredictable and opportunistic nature of human mobility on energy consumption, spatial and temporal coverage on mobile phone sensing applications.

This paper considers opportunistic mobility nature of mobile phone users and analyses the impact of dynamic human movements and patterns on energy consumption and sensing area coverage by considering proposed selective sensing method.

In proposed work, current and predicted future locations of mobile phone users used for selecting mobile phones to perform sensing task. There are many references [20], [21], [22] which explain how mobile phone users movement velocity, direction and angles can be obtained by using sensors like accelerometer, magnetometer, gyroscope and GPS in outdoor and indoor locations. In this paper, we assume that mobile phones use any method to calculate or to obtain their velocity, direction and angle of movement. The proposed work is compared with non-selective mobile phone sensing task, where all the mobile phones are involved in sensing and sending their sensed data to dedicated destination. The proposed selective sensing method achieves required spatial coverage and also shows reduction in energy consumption for mobile phone sensing activity.

The remainder of this paper is organized as follows. Section II describes system model for the proposed work. Section III gives description of proposed selective sensing algorithm for opportunistic mobile phone sensing. Section IV discusses evaluation of simulation results and Section V concludes the paper.

II. System Model

This section provides the description of models used for the development of proposed selective sensing framework for opportunistic mobile phone sensing networks.

Let A be the area of application, which consists of p number of mobile phone users. Mobile phones are also termed as mobile phone users or mobile nodes. For performance analysis of proposed work LW mobility model given in [14] is used. Mobile nodes are categorised into two types. One is mobile sensing ms nodes, which are embedded with GPS for getting location co-ordinates and other application related sensors. Another type of mobile nodes are called as volunteer mobile vm nodes, which are embedded with GPS and may or may not come with other application related sensors.

Let ms_i represent i^{th} mobile sensing node, where $i = 1, 2, ...n.$ and let vm_c represent c^{th} volunteer mobile node, where $c = 1, 2, ...m$ and n+m=p.

Let r_j be the sensing range of j^{th} sensor which is attached to i^{th} ms node, where $j = 1, 2, ...k$. We consider disk model for sensing range. Let t_j be the sampling interval of j^{th} sensor. When a mobile node moves in a straight line path with constant velocity cv and without pause or change of direction, then t_j for non-overlap sensing coverage with respect to j^{th} sensor is given by [25]:

$$t_j = 2 * \frac{r_j}{cv} \tag{1}$$

Let average or preferred human walk velocity be hwv. Under LW mobility model equation (1) is given by [25]:

$$t_j = 2 * \frac{r_j}{hwv} \tag{2}$$

III. Description of Proposed Selective Sensing Framework

It is assumed that a Dedicated Base Station (DBS) is responsible for sensor data collection from all the vm nodes and has dedicated control and sensor data collection channel. It is considered that vm nodes are programmed to send and receive query from a Dedicated Base Station (DBS). DBS broadcast query to vm nodes requesting their current location. Based on the reply from vm nodes, DBS selects specific vm node in the required application region. Multiple vm nodes can be selected but there should not be any overlap between the communication range of vm nodes for considered application time.

On receiving the command and information from DBS selected vm nodes initiate sensor data collection task with ms nodes. The pseudocode for collecting sensed data from ms nodes is given in Algorithm 1. For simplifying the performance analysis of proposed work under human mobility model, we assume collection of single sensor data from ms nodes.

For given simulation duration T, total number of sensor data collection iterations R is given by equation (3), where t_j is the sampling interval of a considered sensor (equation (2-3)). The proposed sensor data collection algorithm given in Algorithm 1 is repeated for every t_j duration until given time T. At the start of each iteration I where $I = 1, 2, ..., R$, vm computes eligible ms nodes for sensing task. The brief description of each step (Algorithm 1) is given in following subsections.

$$R = \frac{T}{t_j} \tag{3}$$

Algorithm 1 :Pseudocode for sensor data collection from ms nodes

1: **for** $I \leftarrow 1, R$ **do**
2: vm broadcast req_{info} packet to ms nodes.
3: ms nodes reply by sending requested data to vm through $replay_{info}$ packet.
4: vm computes the eligible ms nodes for sensing task and broadcast req_{sense} packet.
5: Selected ms nodes transmit sensed data within time assigned by vm.
6: **end for**

A. Broadcasting req_{info} packet

The selected vm node from DBS broadcasts req_{info} packet to ms nodes. In general, req_{info} packet consist of $[addr_{vm}, I, cur_loc_{vm}, req_addr_{ms}, req_curr_dir_info, req_sensor_info, req_velo]$. $addr_{vm}$, I and cur_loc_{vm} indicates vm node address, sampling iteration number and current vm node location respectively. req_addr_{ms}, $req_curr_dir_info$, req_sensor_info and req_velo represents address of ms, direction related sensors information, other sensors information (sensor type and range), and current velocity. These are the parameters required by vm to select the eligible ms nodes for sensing task.

B. Sending $reply_{info}$ packet by ms nodes

On receiving broadcasted req_{info} packet, ms nodes compute required data which are specified by vm node and reply by sending $reply_{info}$ packet. $reply_{info}$ packet consists of $[addr_i, I, (xc_i, yc_i), curr_dir_info_i, \{sensor_type_j, r_j\}, curr_velo_i]$.

C. Broadcast req_{sense}

On receiving $reply_{info}$ packet from ms nodes which are sent within some t_{parm} time, vm computes the eligible ms nodes. The pseudocode for selecting eligible ms nodes for sensing task is given Algorithm 2.

Algorithm 2 :Pseudocode for selection of ms nodes

```
compute current overlap between ms nodes
compute future overlap between ms nodes
if (current overlap between any pair of ms nodes > π*r_j^2/3
    and predicted future overlap > π*r_j^2/1.6) then
    remove any one ms node and mark another ms node as eligible node
else
    Mark both the ms nodes as eligible nodes
end if
```

For simulation of proposed work, direction of LW mobile nodes is calculated from their location traces.

Let (xc_i, yc_i) and (xp_i, yp_i) be the current and previous location co-ordinates at time t_2 and t_1 respectively where $t_1 < t_2$. Equation (4) gives the general formula for calculating direction angle of any i^{th} ms node.

$$\phi = \tan(yp_i - yc_i, xp_i - xc_i) \tag{4}$$

General equation to calculate future location co-ordinates for i^{th} ms node at given time t_f is given in equation (5), where $t_f > t_1$.

$$\begin{aligned} xf_i &= xc_i + curr_velo_i * t_f * cos(\phi) \\ yf_i &= yc_i + curr_velo_i * t_f * sin(\phi) \end{aligned} \tag{5}$$

By using current location, calculated future location and sensor range r_j of ms nodes, vm node calculate overlap sensing area between each and every pair of ms nodes. For any pair of ms nodes, if sensing area overlaps between them is greater than 33% when current location is considered and greater than 62% for predicted future location, then any one of ms is marked as non-eligible and another node is considered as eligible sensing node. If sensing area overlap between any pair of ms nodes is greater than 62% for predicted future location, then any one of ms is marked as non-eligible and another node is considered as eligible sensing node. After finding the eligible nodes and non eligible nodes vm broadcast req_{sense} packet. req_{sense} packet consists of information like eligible, non-eligible ms node id's of corresponding I^{th} sampling iteration, t_j and time limit to send back the sampled sensor data. By declining the assignment of sensing task to non-eligible ms nodes, overall sensing area overlap and energy consumption for proposed method is reduced.

D. Transmission of Sensor Data

It is assumed that some amount of time $t_{outrange_node}$ (equation (6)) is spent by vm node after broadcasting req_{sense} packet to collect sensed data from ms nodes. Let ls and vm_{range} be the speed of light and vm node's communication range respectively. Within $t_{outrange_node}$ time, if a ms node has not transmitted its sensor data, then it is assumed that the node has moved out of communication range of vm node.

$$t_{outrange_node} > 2 * \frac{vm_{rage}}{ls} + t_j \tag{6}$$

IV. Simulation Results and Discussion

To simplify the performance analysis of proposed work, it is assumed that base station chooses a random vm node, which is within the range of 100 meters from center of application area A at time t_{vm}. It is assumed that within t_{start} $(t_{vm} < t_{start})$ time base station completes selection of vm node and sends the required information to start the mobile phone sensor data collection task. At time t_{start} selected vm node start sensor data collection routine (Algorithm 1.). The preferred human walk velocity hwv is $\approx$ 1.0 m/s [26].

For all ms nodes, sensor range is assumed to be 20 meters. Other considered simulation parameters are given in Table 1. Term NSS is used to represent non-selective sensing which allows all the ms node for sensing. In order to represent proposed human walk based selective sensing method we use term HWSS.

For given A, T, and p values, proposed mobile phone sensing method is analysed in terms of average units of energy consumption and spatial coverage (sensing area coverage). Better performance is needed in terms of reduction of energy consumption and also in terms of required spatial coverage.

Energy consumption and sensing area coverage is calculated for every iteration. For proposed method, energy consumption and sensing area covergae is represented by $HWSS_E_I$ and $HWSS_cov_I$ respectively. For NSS method, energy consumption and sensing area coverage is represented by NSS_E_I and NSS_cov_I respectively.

Let λ_HWSS_I and λ_NSS_I be the total number of sensor data samples sent to vm node from mobile nodes by HWSS and NSS methods respectively at I^{th} iteration.

Then non-overlap sensing coverage area for HWSS and NSS methods is given by equation (7) and (8) respectively.

$$HWSS_nv_cov_I = \pi * r_j^2 * \lambda_HWSS_I \tag{7}$$

$$NSS_nv_cov_I = \pi * r_j^2 * \lambda_NSS_I \tag{8}$$

For considered sensing methods, if their sensing coverage is greater or equal to respective non-overlap sensing coverage then the method is acceptable, i.e, considered sensing method has achieved required spatial coverage.

$$HWSS_cov_I \geq HWSS_nv_cov_I \tag{9}$$

$$NSS_cov_I \geq NSS_nv_cov_I \tag{10}$$

We assume one unit of energy is consumed for sensing (both GPS and sensor) and sending a sensor sample by a mobile

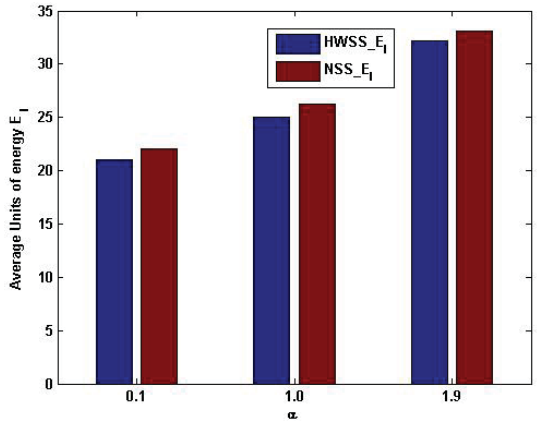

Fig. 1. Energy Consumption

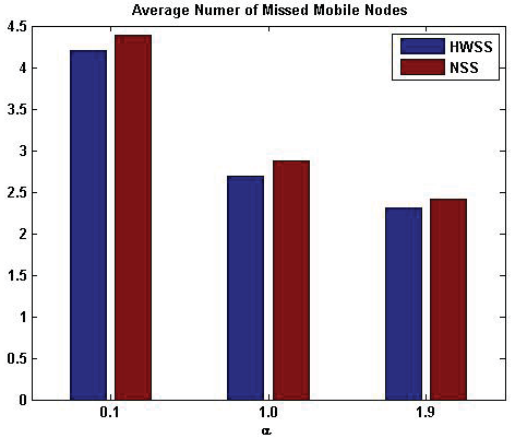

Fig. 2. Energy Consumption

node. Therefore, total energy consumed for proposed and considered sensing method is equal to the respective total number of sensor samples received by vm in I^{th} iteration.

$$HWSS_E_I = \lambda_HWSS_I \tag{11}$$

$$NSS_E_I = \lambda_NSS_I \tag{12}$$

First the impact of velocity of mobile nodes on energy consumption and sensing area coverage is analysed for both the proposed HWSS and NSS methods. Birand *et al.* [15] explore dynamic graph properties under LW mobility model. As LW mobility parameter α value decreases, $(0 < \alpha < 2)$, mobile networks become more dynamic and vice-versa [15]. For analysing the performance of proposed work α in LW mobility model is set to 0.1, 1.0 and 1.9 $(0 < \alpha < 2)$ for generating low, high and medium speed ms nodes respectively. Table 2 show average velocity of mobile nodes. For this considered simulation parameters are given in Table 1.

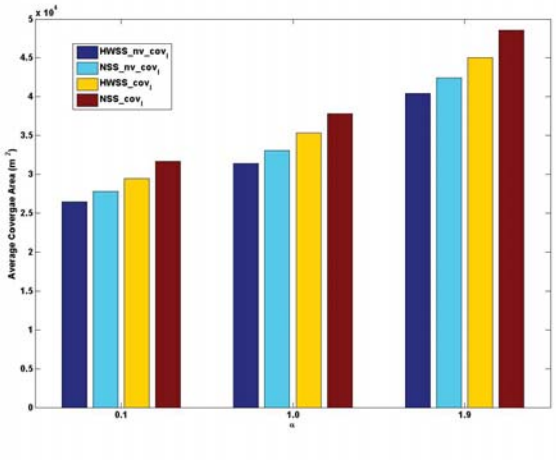

Fig. 3. Sensing Area Coverage

Figure 1 and 3 show average energy consumption and average sensing area coverage for different values of α. The simulation duration T is set to one hour, which is long enough to run many iterations. Other considered simulation parameters are given in Table 1. Dynamic network topology, i.e., when $\alpha = 0.1$, increases missing rate of mobile nodes (mobile nodes moving out of vm node range), thereby reducing number of sensor samples sent to vm node. Therefore when mobile phone nodes velocity is high i.e., for $\alpha = 0.1$ mobile nodes show very low coverage and energy consumption compared to $\alpha = 1.0$ and $\alpha = 1.9$ (Fig. 1 and Fig. 3). Low velocity mobile nodes lead to decrease in missing rate of mobile nodes (Fig. 2), as their incoming and outgoing rate within the application region is very slow. Therefore, when mobile phone nodes velocity is low i.e., for $\alpha = 1.9$ mobile nodes show very high coverage and energy consumption compared to $\alpha = 1.0$ and $\alpha = 0.1$ (Fig. 1 and Fig. 3). When mobile phone nodes velocity is equal to normal human walk velocity i.e., for $\alpha = 1.0$ mobile nodes show coverage and energy consumption in between to $\alpha = 0.1$ and $\alpha = 1.9$.

For proposed HWSS method, there is reduction of energy consumption (Fig. 1) for all the considered values of α. Because ms node are selectively chosen such that there should be less overlap between them. Both the sensing methods have achieved respective required sensing coverage area (Fig. 3). NSS covers much extra area then required and also energy consumption. In Fig. 3 the proposed HWSS method has also crossed required NSS method non-overlap sensing area coverage i.e., $HWSS_cov_I > NSS_nv_cov_I$. In each sensor data collection iteration I, simulation results show reduction in energy consumption for HWSS method. Even a single percent reduction of energy consumption for each iteration will save a lot overall network energy in long run of mobile phone sensing applications. Combining the results of Fig. 1 and Fig. 3, proposed HWSS method show better performance in terms of reducing energy consumption of mobile nodes and also

TABLE I
SIMULATION PARAMETERS

Simulation Area A	2000m*2000m
p	1000 nodes
Simulation duration	1 hours
Flight parameter α	1, 1.9, 0.1
Pause parameter β	1.0
Average flight length	5-2000m
Pause time	10-60 seconds
hwv	1 meter/second
Location sample interval t_{ls}	1 second
(future location time) t_f	13 seconds
t_{vm}	15^{th} sec
t_{start}	16^{th} sec
vm and mn nodes range	200m
Range of sensor	20
Assumed datarate	100 kbps
req_{info}, $reply_{info}$, req_{sense} packet size	100 bytes
Each mn nodes sensor data size at each iteration	200 bytes

TABLE II
SIMULATION PARAMETERS

α	average velocity (m/s)
0.1	2.1
1.0	1.3
1.9	0.4

achieving required sensing coverage.

V. CONCLUSION

Human mobility plays an active role in improving the performance of mobile phone sensing applications, if their mobility characteristics are analysed and incorporated. This paper presents an human mobility based selective sensing framework called as HWSS for sensor data collection in opportunistic sensing networks. For the given network and applications parameters the proposed HWSS method show reduction in energy consumption and also achieves required spatial coverage. Our future work involves extending the proposed selective sensing to include multiple sensor data collection for ubiquitous mobile sensing applications. The future scope also involves analysing the computation and communication (varying geographical features and network link constrains) complexities involved in experimental implementation of proposed work.

REFERENCES

[1] N. D. Lane, E. Miluzzo, H. Lu, D. Peebles, T. Choudhury, and A. T. Campbell, "A survey of mobile phone sensing," *IEEE Communications Magazine*, pp. 140–150, September 2010.

[2] W. Z. Khan, Y. Xiang, M. Y. Aalsalem, and Q. Arshad, "Mobile phone sensing systems: A survey," *IEEE COMMUNICATIONS SURVEYS & TUTORIALS*, vol. 15, no. 1, pp. 402–427, 2013.

[3] S. S. Kanhere, "Participatory sensing: Crowdsourcing data from mobile smartphones in urban spaces," *IEEE International Conference on Mobile Data Management*, pp. 3–6, 2011.

[4] N. D. Lane, S. B. Eisenman, M. Musolesi, E. Miluzzo, and A. T. Campbell, "Urban sensing systems: Opportunistic or participatory?" *HotMobile '08 Proceedings of the 9th workshop on Mobile computing systems and applications*, pp. 11–16, 2008.

[5] A. T. Campbell, S. B. Eisenman, N. D. Lane, E. Miluzzo, and R. A. Peterson, "People-centric urban sensing," *WICON'06, The 2nd Annual International Wireless Internet Conference*, August 2006.

[6] X. J. Ban and M. Gruteser, "Towards fine-grained urban traffic knowledge extraction using mobile sensing," *UrbComp '12 Proceedings of the ACM SIGKDD International Workshop on Urban Computing*, pp. 111–117, 2012.

[7] V. GAY and P. Leijdekkers, "Health monitoring system using smart phones and wearable sensors," *International Journal of ARM*, vol. 8, no. 2, pp. 29–36, June 2007.

[8] D. Yang, D. Zhang, K. Frank, P. Robertson, E. Jennings, M. Roddy, and M. Lichtenstern, "Providing real-time assistance in disaster relief by leveraging crowdsourcing power," *Personal and Ubiquitous Computing*, January 2014.

[9] H.-T. Cheng, S. Buthpitiya, F.-T. Sun, and M. Griss, "Omnisense: A collaborative sensing framework for user context recognition using mobile phones," *HotMobile*, pp. 1–1, 2010.

[10] J. Li, Y. Zhang, Y.-F. Chen, K. Nagaraja, S. Li, and D. Raychaudhuri, "A mobile phone based wsn infrastructure for iot over future internet architecture," *IEEE International Conference on Green Computing and Communications and IEEE Internet of Things and IEEE Cyber, Physical and Social Computing*, pp. 426–433, 2013.

[11] L. Pelusi, A. Passarella, and M. Conti, "Opportunistic networking:data forwarding in disconnected mobile ad hoc networks," *IEEE Communications Magazine*, pp. 134–141, November 2006.

[12] I. Rhee, M. Shin, S. Hong, K. Lee, and S. Chong, "On the levy-walk nature of human mobility," *IEEE INFOCOM*, pp. 1597–1605, 2008.

[13] I. Rhee, M. Shin, S. Hong, K. Lee, S. J. Kim, and S. Chong, "On the levy-walk nature of human mobility," *IEEE/ACM TRANSACTIONS ON NETWORKING*, vol. 19, no. 3, pp. 630–643, June 2011.

[14] Networking Research Lab. Human mobility models downloads. [Online]. Available: http://research.csc.ncsu.edu/netsrv/

[15] B. Birand, M. Zafer, G. Zussman, and K.-W. Lee, "Dynamic graph properties of mobile networks under levy walk mobility," *IEEE International Conference on Mobile Ad-Hoc and Sensor Systems*, pp. 292–301, 2011.

[16] T. Karagiannis, J.-Y. L. Boudec, and M. Vojnovic, "Power law and exponential decay of inter contact times between mobile devices," *MobiCom*, pp. 183–194, September 2007.

[17] D. Karamshuk, C. Boldrini, M. Conti, and A. Passarella, "Human mobility models for opportunistic networks," *IEEE Communications Magazine*, pp. 157–165, December 2011.

[18] S. Hachem, A. Pathak, and V. Issarny, "Probabilistic registration for large-scale mobile participatory sensing," *IEEE International Conference on Pervasive Computing and Communications (PerCom)*, pp. 132–140, March 2013.

[19] X. Sheng, J. Tang, and W. Zhang, "Energy-efficient collaborative sensing with mobile phones," *IEEE INFOCOM*, pp. 1916–1924, 2012.

[20] S. Ayub, B. M. Heravi, A. Bahraminasab, and B. Honary, "Pedestrian direction of movement determination using smartphone," *Sixth International Conference on Next Generation Mobile Applications, Services and Technologies (NGMAST)*, pp. 64–69, September 2012.

[21] N. Roy, H. Wang, and R. R. Choudhury, "I am a smartphone and i can tell my user's walking direction," *Proceedings of the 12th Annual International Conference on Mobile Systems, Applications, and Services*, pp. 329–342, 2014.

[22] T. S. Azevedo, R. L. Bezerra, C. A. V. Campos, and L. F. M. de Moraes, "An analysis of human mobility using real traces," *WCNC*, pp. 1–6, April 2009.

[23] Y.-C. Chen, J. Kurose, and D. Towsley, "Mixed queueing network model of mobility in a campus wireless network," *INFOCOM, 2012 Proceedings IEEE*, pp. 2656–2660, 2012.

[24] J. Manweiler, N. Santhapuri, R. R. Choudhury, and S. Nelakuditi, "Predicting length of stay at wifi hotspots," *INFOCOM, 2013 Proceedings IEEE*, pp. 3102 – 3110, 2013.

[25] M. Thejaswini, P. Rajalakshmi, and U. B. Desai, "Novel sampling algorithm for levy-walk based mobile phone sensing," *IEEE World Forum on Internet of Things (WF-IoT)*, pp. 496–501, March 2014.

[26] Wikipedia. Preferred walking speed. [Online]. Available: http://en.wikipedia.org/wiki/Preferred_walking_speed

THE 18TH INTERNATIONAL SYMPOSIUM ON WIRELESS PERSONAL MULTIMEDIA COMMUNICATIONS
(WPMC-2015)
December 13-16, 2015, Hyderabad, India

Virtual sensing environment for care at home

Aristodemos Pnevmatikakis
Athens Information Technology, IRIS Laboratory,
44, Kifisias Ave., 15125 Marousi, Athens, Greece
Email: apne@ait.gr

***Abstract*—This paper presents a virtual home sensing environment, where different sensors are placed throughout the home and on the body of some care recipient. The life of the care recipient is then simulated and his/her activities trigger a wealth of measurements from the virtual sensors and the resulting metadata from processing those. The metadata are stored in a database, to be used for building activity recognition and condition reasoning systems in the context of home care.**

I. Introduction

Care at home for elderly people or long-term patients that can still live independently can be provided by monitoring and reasoning systems. These aim at providing both guidance and advice, but also a sense of independence and peace of mind for the care recipients and their families. To achieve this the systems turn each room of the home into a sensing environment. They also equip the body with permanent sensors, or urge the care recipient to periodically use some medical devices. The systems can also benefit from utilising measurements from multiple care recipients, all in their own environment. Only then can the systems reason about the context of the care recipient, gamify his/her everyday life and provide hints or respond to situations. Building such systems obviously requires a large installation base of the sensing infrastructure across multiple sites. This is very difficult to achieve at the early phase of a caring home system.

A shadow user is a simulation, driven by models for the home, the weather, the sensing environment and the behaviour of the user in it. The home model is fixed at initialisation time, the weather is obtained from an external service, and the sensing environment model comprises conditional probabilities of the measurements given the user state. Finally, the user behaviour model is described by state transition probabilities that vary based on four user driving forces, as discussed at the user state section.

This paper describes a virtual sensing environment that can be used to provide the necessary metadata for developing home-care systems. It is essentially a dual simulator, simulating on the one hand the life of the care recipient and on the other hand the sensor and signal processing entities that generate the metadata from the home and the body of the care recipient. The simulations are driven by models for the home, the weather, the sensing environment and the behaviour of the care recipient in it. The home and user models are fixed at initialisation time, the weather is obtained from an external service and the sensing environment model comprises conditional probabilities of the measurements given the user state. Finally, the user behaviour is determined by state transition probabilities that vary based on context parameters of the care recipient.

The resulting metadata are formatted into the same JSON messages utilised by the actual sensing system, e.g. as in the system described in [1] for the eWALL project [2]. They are then stored in non-SQL databases in a CouchDB database system, in a way that does not discriminate them at all from the actual ones.

The remainder of this paper is organised as follows: The home model is described in section II. The care recipient model is described in section III. Sensing the care recipient and metadata generation follow in Section IV. Section V discusses the implementation of the simulators and the results. Finally, in section VI the conclusions are drawn.

II. Home model

The home model contains the rooms their names and their insulation and window factors (α_{ins} and α_{win}) that are provided at initialisation. The outside space is also modelled as a room, to allow the care recipient exiting the home. Hence a home with four rooms is modelled by 5 possible spaces where activities can happen.

The environment in each room is affected by the outside environment (via the insulation and window factors) and the activities of the user. The outside environment is sampled every hour utilising the API of a weather service.

III. Care recipient model

The care recipient model comprises the state, the state transition probabilities, and four parameters enumerating the bodily and mental context of the care recipient. These are:

- Tiredness: As it increases towards 1, the user in increasing compelled to sleep. There is also a yearly decline factor introduced, which increases the base tiredness incurred by any activity over time.
- Hunger: As it increases towards 1, the user in increasing compelled to eat.
- Boredom: As it increases towards 1, the user in increasing compelled to do have entertainment or go for a walk.
- Toilet need: As it increases towards 1, the user in increasing compelled to visit the toilet.

Note that some actions are not even attempted if any of these context parameters is outside an allowed range.

A. Care recipient states

The care recipient state is characterised by the following parameters:

- Activity: sleeping, grooming, showering, eating, doing housework, entertaining, receiving visit, going out
- Room presence: where in the home he/she is. In part dictated by the activity
- Body posture: walking, standing (moving a little bit around the home), sitting, lying. In part dictated by the activity

The three components are connected, since the one influences the other: The activity fully determines the body posture and partly the room presence. E.g. the activity sleep determines fully the body posture (lying) and partly the room (bedroom or living room).

Overall the care recipient simulator supports 25 states, depicted in Fig. 1. Each state is described by room presence, body posture, certain activity and the amount tiredness, hunger, boredom and toilet need change after remaining for 10 sec in the state.

B. State transitions and their constraints

State transitions govern the way the simulated care recipient's life evolves. The transitions are described by transition probabilities that depend on the current state (the activity and the four context parameters of the care recipient), the time of day and the weather.

The allowed state transitions can also be seen in Fig. 1. Their probabilities have a base part, modified linearly by factors depending on tiredness, hunger, boredom and toilet need. The transitions are only allowed if all these four context parameters $c = [\text{tiredness, hunger, boredom, toilet need}]$ are within certain limits. For every transition from the i-th to the j-th state, the base probability is $p_b^{(i\to j)}$, the linear factors for context parameter c_n, $n = 1, ..., 4$, are $\alpha_n^{(i\to j)}$ and the corresponding allowed ranges are $D_n^{(i\to j)}$ then the transition probabilities are given by:

$$p^{(i\to j)} = \begin{cases} p_b^{(i\to j)} + \sum\limits_n \alpha_n^{(i\to j)} c_n & \text{if } c_n \in D_n^{(i\to j)} \\ 0 & \text{elsewhere} \end{cases} \quad (1)$$

The weather only modifies the probability of the user going out or returning home: Bad weather (cold, rain) tends to keep the care recipient indoors or hasten him/her back home. Certain time intervals result into a reduction of the probability of transition into sleeping, napping, going outdoors or receiving visits.

IV. Sensing and metadata

Sensing models describe the sensors and the perceptual components in the home. These are grouped per location and function, each group providing metadata in a database in the CouchDB. These models are detailed in the following subsections. They result to metadata being written in the respective CouchDB databases.

Note that there is another database being written, containing the state of the care recipient. This is not a result of sensing, but contain valuable metadata for evaluating the performance of systems that reason about the context of the care recipient, based on the sensed metadata.

A. Environmental sensing

The readings of the environmental sensors in each room depend on the outside environment and the activities of the care recipient. The outside environment affects temperature, humidity and luminance.

The steady-state room temperature T_{ss} is modelled at an ideal temperature of $T_{ideal} = 21$ degrees Celsius, pulled towards the outside temperature T_{out}:

$$T_{ss} = \alpha_{ins} T_{ideal} + (1 - \alpha_{ins})\, T_{out} \quad (2)$$

A unity α_{ins} value renders outside conditions irrelevant, while a value of zero equates the room conditions to the outside ones.

The new steady-state room temperature is calculated every hour when the new weather data arrive. Any resulting temperature change is not applied instantly at the rooms: instead the expected room temperature T_{room} at simulation instance n is a linear combination of the expected room temperature at the previous simulation instance $n-1$ and the steady-state one:

$$T_{room}(n) = \alpha_{mem} T_{room}(n-1) + (1 - \alpha_{mem})\, T_{ss} \quad (3)$$

where α_{mem} is a memory factor. Since the simulator updates the room conditions once every 10 sec, a value of $\alpha_{mem} = 0.99$ will result to the expected conditions being fully applied in the room after about 17 minutes.

The measured room temperature deviates from the expected by some additive white measurement noise of standard deviation of 0.2 degrees.

The humidity is similarly simulated. The ideal (comfortable) level is 55%. The measurement noise standard deviation is 1.

The luminance is determined by the cloud coverage percentage, the time of day and the window factor of the room. The window factor determines how much of the outside illumination enters the room. During the night, the steady-state outside illumination value ranges from 0 lux (full clouds) to 1 lux (no clouds) plus a Gaussian component or standard deviation 1 (that is not allowed to result to negative values). During the day, the steady-state value ranges from 10 lux (full clouds) to 1010 lux (no clouds) plus a Gaussian component or standard deviation 20. The measured luminance is updated based on the product of the steady-state one times the window factor, with the usual memory factor.

The environmental sensor readings that are affected by the care recipient activities are temperature, humidity, presence, luminance, gas concentration and door status.

When the care recipient is present in a room, the probability the PIR sensor gives a positive reading increases as the user activity level increases. The PIR of any room can be active, based on the following probabilities conditioned to the user state:

- 0.01% if the care recipient is not present

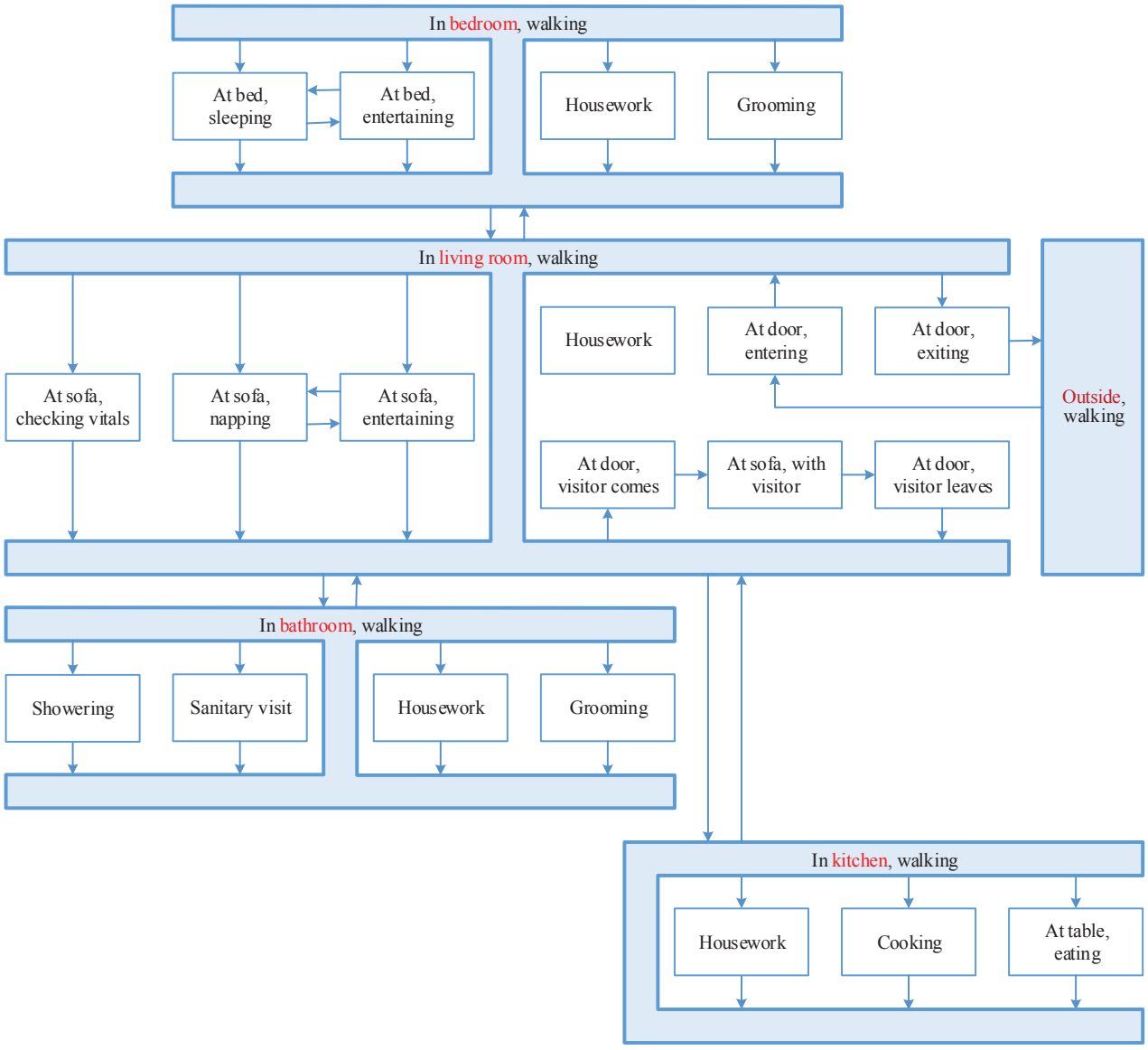

Fig. 1. The 25 states of the care recipient and their transitions. They are grouped into the five spaces (four rooms and outside) they belong to.

- 1% if the care recipient is lying
- 10% if the care recipient is sitting
- 50% if the care recipient is standing
- 90% is the care recipient is walking

If the care recipient is not lying down in a room that has luminance lower than 100 lux, then it is assumed that the lights are turned on, leading to an luminance of 100 lux plus a Gaussian component of standard deviation 2 lux.

If the care recipient is having a shower, then the humidity and temperature in the bathroom increase. The increase towards the target humidity of 90% is progressive, with a memory factor of 0.9. This factor is smaller than the one used for the change towards the environmental conditions, leading to faster humidity adaptation. The temperature target in the bathroom is 30 degrees. Similarly, if the care recipient is cooking, then the humidity and temperature in the kitchen increase. The target humidity is now 75% and the temperature target is 25 degrees.

Two gas concentrations are measured: CO and NG. If needed, LPG can be used instead of NG. Their values are simulated in parts per million (ppm), but are reported as integers between 0 and 10 in logarithmic scale. Zero corresponds to a reading at the minimum value the sensor can detect. The concentration of gases increases when the user is in the room. It increases ten times faster if the user is cooking. It decreases when the user is performing housework in the room, as the simulator assumes the windows are then open to air the room.

Only the status of the living room door (the main one towards outside) and the bathroom door is simulated, based on the activity of the user. The main door opens and closes

in two consecutive simulation steps when the care recipient or visitors enter or exit the home. The bathroom door closes when the shower or the toilet is used. The rest of the doors are always open.

B. Body sensing

Body sensing involves a wearable accelerometer. The simulation yields the number of steps and the Integral Modulus of Acceleration (IMA) depending on the care recipient state, specifically the body posture and the tiredness.

C. Visual sensing

Visual sensing employs a Kinect camera in the living room. A face tracking algorithm results to face tracks for the people present in the living room. Face analytics are employed to determine the expression, gender and age of the tracked faces. The simulation yields face tracks as follows:

- When the user is in the living room and being entertained, then it is very probable to have a single face track.
- When the user is in the living room but is walking or standing, then there is a small chance of having a face track.
- When the user has visits, then there are multiple face tracks.

The simulated expression changes between neutral, happiness and sadness based on the activity and the context parameters of the care recipient. The gender and age are fixed at initialisation for the care recipient, while for the visitors, they are randomly selected for each visit.

D. Resting surface sensing

Resting surfaces can be beds, sofas and different types of chairs. Resting surface sensing utilises a pressure sensor yielding binary values and an accelerometer yielding IMA values. A bed and a sofa are currently simulated. The simulation yields true for pressure with high probability when the user is sitting or lying on the surface, but also occasionally when the user is not. The simulated IMA is close to zero when the surface is unused, small when the care recipient is lying and moderate when sitting.

E. Socket sensing

The instantaneous power consumption, the overall energy consumption and the socket status are sensed for any necessary socket in the home. The two sockets where the living room and bedroom TVs are connected are simulated. The simulation always reports the sockets activated. Their power consumption ranges between a very small standby value when the care recipient is not entertaining, and the values specified by the particular TV models when the care recipient is entertaining. Forgetting the TV on is not supported.

F. Vital signs sensing

The vital signs being measured are the heart rate, the heart rate variation, the SPO2 and the systolic and diastolic blood pressures. The simulator assumes that all these values are made available in any vitals measuring session. All these vital parameters fluctuate around the nominal values in part randomly, and in part affected by the tiredness of the care recipient.

V. Discussion

This section discussed the implementation of the simulators for the care recipient status and the measurements conducted. It also presents results from long simulation runs.

A. Implementation

The virtual sensing system is written in Java 8. It comprises an initialisation JSON file that describes the care recipient parameters, the simulated interval, the virtual home and the states and their transitions.

The code is organised in four simulator packages and a database handling one:

- *simulator* contains the main and the graphical user interface classes
- *simulator.init* contains the classes for reading in the JSON initialisation file, obtaining the simulation parameters, the home structure in rooms, the body postures, the states and their transitions
- *simulator.models* contains the classes for the different types of sensing described in section IV
- *simulator.weather* contains the classes for obtaining the weather information
- *db* contains the class for managing metadata writing to the CouchDB

The simulators operate either in the past, in which case it runs 315 times faster than real-time (one day is simulated in 274 seconds), and in the present, in which case it waits for the next simulation epoch to actually arrive. This way both long periods of the past can be simulated in a matter of hours, and the implemented systems can be tested with the actual metadata rate in the present.

B. Results

The virtual sensing system currently is providing eight simulated care recipients, with metadata spanning 345 days (about 11.5 months, since Oct. 1st 2014). The average number of times each activity is exercised per day is shown in Table I for two care recipients: one whose base tiredness remains constant, and another who declines by 25% per year.

The average hours spent in three key activities (sleeping, walking and entertaining) and two activities that happen many times per day but at the end take up very little time (grooming and doing housework) are shown in Table II for the same two users.

The average distribution of the same activities in a day is shown in the histograms of Fig. 2. The care recipient always sleeps between 1:30 and 4:00 in the morning, with

TABLE I
AVERAGE NUMBER OF TIMES EACH ACTIVITY IS PERFORMED.

Activity	Daily avg., no decline	Daily avg., 25% decline
Toilet	3.60	3.20
Eating	4.64	4.08
Cooking	2.49	2.34
Showering	0.57	0.55
Sleeping	1.00	0.95
Napping	2.13	2.07
Outside	1.64	1.35
Visitors	0.45	0.52
Entertaining	3.76	3.54
Vitals	0.42	0.37
Grooming	5.51	4.69
Housework	4.49	3.62

TABLE II
AVERAGE TIME SPENT PER DAY DOING SOME ACTIVITIES.

Activity	Hours per day, no decline	Hours per day, 25% decline
Sleeping	11.11	12.72
Walking	2.86	2.40
Entertaining	5.95	4.80
Grooming	0.19	0.17
Housework	0.17	0.14

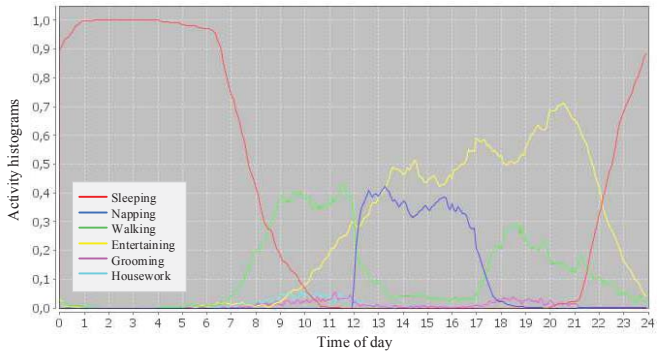

Fig. 2. Histograms of six activities showing the distribution across the day of sleeping, napping, walking, entertaining, grooming and doing housework.

the probability being above 90% from midnight to 6:40. The care recipient also rests in the afternoon, with a probability averaging 35% in the interval between 2:15 and 16:20. Comparing the results of Table I and Fig. 2, the care recipient has a single long sleeping session every night, while on average two short napping sessions every afternoon. The care recipient walks most in the morning (probability above 35% from 8:45 to noon) and again in the evening after the nap (probability above 20% from 17:45 to 20:00). Entertainment at the TV takes place mostly in the evening (probability increasingly above 40% from 13:10 to 22:00). Housework takes place in the morning, while grooming both in the morning and the evening.

Finally, the yearly decline factor is considered. The factor increases the base tiredness, forcing the care recipient to more relaxing activities. The effect of this in the average number of steps per month for the user with no decline and 25% yearly decline is examined. Both are shown in Fig. 3, together with the respective linear trends. The linear trend for the declining care recipient, projected to a complete year, is 24.5% in average steps, in line with the 25% yearly increase of the base tiredness. The linear trend for the non-declining care recipient, projected to a complete year, is 24.5% in average steps, consistent with the constant base tiredness.

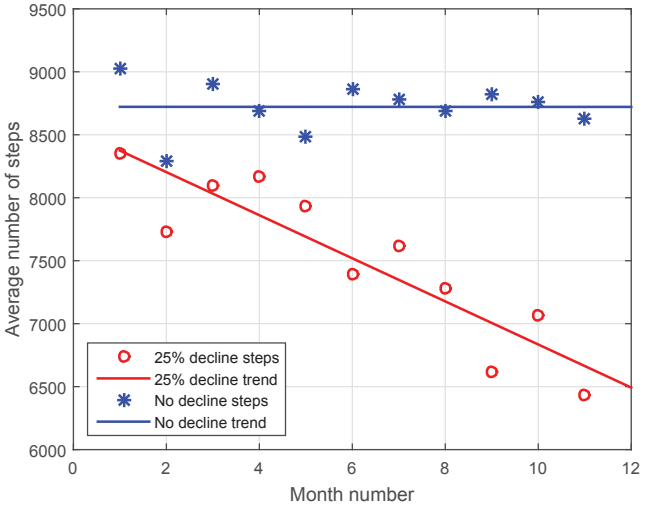

Fig. 3. Average number of steps per month for the declining and non-declining care recipients.

VI. CONCLUSION

A virtual home care environment has been implemented, comprising two simulators: one for the activities of the care recipient in the home and outside, and another for the measurements and the metadata from the systems observing the care recipients.

The virtual environment has been tested extensively, yielding plausible results, and is now in operation feeding eight home care systems with simulated metadata for about a year.

Running the virtual environments has allowed the testing of the reasoning systems of the eWALL project [2] against a wealth of situations, and the testing of the information displays both at home and at the care providers' end. Both tests would have been impossible without multiple full physical installations running for long times.

ACKNOWLEDGMENT

Part of this work has been carried out in the scope of the EC co-funded project eWALL (FP7-610658).

REFERENCES

[1] S. Astaras and A. Pnevmatikakis, "Context extraction in the caring home: Infrastructure and algorithms," in *IEEE ICC 2015 Workshop on ICT-enabled services and technologies for eHealth and Ambient Assisted Living*, London, UK, June 2015, pp. 228–233.

[2] A. Mihovska, S. A. Kyriazakos, and R. Prasad, "eWall for active long living: Assistive ICT services for chronically ill and elderly citizens," in *SMC*, 2014, pp. 2204–2209.

THE 18TH INTERNATIONAL SYMPOSIUM ON WIRELESS PERSONAL MULTIMEDIA COMMUNICATIONS
(WPMC-2015)
December 13-16, 2015, Hyderabad, India

Expression recognition using graph based feature selection

Krasimir Tonchev and Nikolay Neshov
Teleinfrastructure R&D Lab
Technical University of Sofia, Bulgaria
Email: {k_tonchev, nneshov}@tu-sofia.bg

Agata Manolova and Vladimir Poulkov
Faculty of Telecommunications
Technical University of Sofia, Bulgaria
Email: {amanolova, vkp}@tu-sofia.bg

***Abstract*—Expression recognition is a contemporary research field determining human expressions based on image data using computer algorithms. It can be used in many applications including Ambient Assisted Living where a frequent expression recognition can be used to determine human's well being. In this work we propose an algorithm for expression recognition using images of human faces. The algorithm includes a feature extraction step by log-Gabor filters and a feature selection step using sparse approximation of the graph based embedding. The algorithm is tested using a popular database and provides competitive results when compared to other approaches.**

I. Introduction

The human face plays a significant role in social communications. It is the visual representation of the human personality, emotions and thoughts. The face we look at is a mix of both physical characteristics and expressions based on feelings and emotions. As such it can be a ground for capturing the humans' internal emotional state. Regular monitoring and estimating human expressions can be used to determine the well being of human's life on a daily basis. Potential application of such a system can be in the area of Ambient Assisted Living (AAL). This new initiative is trying to build the technological foundations for improving the life of elderly by providing home automation and general assistance intelligent algorithms. Estimating the emotional state of elderly can be an important component in such systems. Frequent bad mood can serve as an alarm to trigger further actions for stimulating more activities for mood improvement, e.g. stimulate more active social behavior, music listening etc.

The goal of facial expression recognition (FER) is to imitate the human visual system in the most similar way or in other words to enable the machine to have emotional intelligence. This is a very challenging task in the area of computer vision because it not only requires efficient image/video analysis techniques but also a well-suited feature vector used in the machine learning process. The general approach to FER consists of the following five steps [1]: Image acquisition, Preprocessing of image data, Feature Extraction, Selection and Classification.

With the boom of human-computer interactive systems there are many research papers proposing different approaches to achieve FER with different levels of success [2]. A big importance is the appropriate selection of local feature extraction algorithms [3]. In the work [4] the authors used a Gabor and log-Gabor filters for feature extraction and PCA for dimensionality reduction. Classification in this work is performed by Linear Discriminant Analysis achieving results of 85% recognition rate. In another work [5], the authors performed a detailed analysis on FER using local binary patterns (LBP) for feature extraction. They noted that LBP on average perform slightly better compared to Gabor filters as the method for feature extraction on high resolution images. On the contrary, Gabor filters perform comparably or better on low resolution images.

In another work [6], the authors built a FER system by employing local information and Gabor filters. They apply Gabor filtering in the area of interests around 28 key facial point located at places such as eyebrows, nose, chin etc. They used a K-Nearest Neighbors (KNN) classifier with preliminary PCA dimensionality reduction step. The achieved recognition rate is 80% on Cohn-Kanade database [7].

The authors in [8] presented a hybrid system based on sparse representation approach, using Gabor wavelet filter for feature extraction and support vector machine for classification. They introduced sparseness as means for approximating the test sample by the Gabor dictionary built from the training set. Then the approximation is used as input to SVM classifier for expression estimation. Their algorithm achieved 89% on JAFFE database.

In [9] the authors compared the recognition rate for three different feature selection schemes: MID-mRMR, MID-mRMR and a wrapper approach based on global optimization Genetic Algorithm. The features were extracted using log-Gabor filters and the classification is done with naive Bayesian classifier. The same authors proposed another approach for FER using log-Gabor filters and feature selection in [10]. The selected feature selection algorithm is based on mutual information and for classifier KNN is chosen. They achieved 75% recognition rate on Cohn-Kanade dataset. An up to date literature survey ot FER systems using feature extraction methods can be found in [11].

In this study, we propose a novel algorithm for FER based on feature extraction followed by feature selection. The log-Gabor filters are applied to extract the localized features from the image data. The gain of this step is alleviation of lightning variations as well as detailed multi-scale and multi-angle analysis. The feature selection step consists of graph a based feature selection algorithm. The feature selection method is

of filter type utilizing sparse combination of log-Gabor filters while preserving the intrinsic manifold on which the data resides approximated by a graph. Finally features are classified by SVM classifier. The remainder of this paper provides a detailed description of the proposed system, experiments and results. Section 2 describes the feature extraction algorithm. In section 3, the feature selection is described and in section 5 the experiments on the selected image database and results are provided. Section 6 concludes the paper.

II. Log-Gabor Feature Extraction

Facial expressions cause specific changes in the pattern of the face including change or introduction of wrinkles, change of geometry of different facial parts such as mouth and eyebrows. In order to capture such changes a multi scale analysis has to be carried out, localized at the areas of change. A common choice for obtaining localized frequency information of the pattern is to apply Gabor Filters. However, they have two major drawbacks: the maximum bandwidth is limited to approximately one octave and they are not optimal if one is seeking broad spectral information with maximal spatial localization. To overcome these disadvantages, an alternative to the Gabor Filter known as log-Gabor filters was proposed by Field in 1987 [12]. They have two important characteristics to note. The first one is that by definition log-Gabor filters do not have a DC component. In contrast, the Gabor filter cannot be constructed with arbitrarily wide bandwidth while maintaining a reasonably small DC component in the even-symmetric filter. The second one is that the transfer function for the log-Gabor filters has an extended tail at the high frequency end, providing sensitivity in the high frequencies. In the frequency domain the log-Gabor filters are represented by the following transfer function $H(f,\theta)$:

$$H(f,\theta) = H_f \times H_\theta \tag{1}$$

where H_f is the radial component, which controls the frequency band of the filter. H_θ is the angular one, which controls the spatial orientation of the filter. The transfer function $H(f,\theta)$ using polar coordinates can be written as:

$$H(f,\theta) = \left\{ \frac{-[ln(\frac{f}{f_0})]^2}{2[ln(\frac{\sigma_f}{f_0})]^2} \right\} \exp\left\{ \frac{-(\theta-\theta_0)}{2\sigma_\theta^2} \right\} \tag{2}$$

where f_0 is the center frequency of the filter and θ_0 the filter direction. The parameter σ_f defines the radial bandwidth B in octaves:

$$B = 2\sqrt{2/ln2} \times \|ln(\frac{\sigma_f}{f_0})\| \tag{3}$$

while the parameter σ_θ defines the angular bandwidth $\Delta\Omega$ in radians:

$$\Delta\Omega = 2\sigma_\theta\sqrt{2ln2} \tag{4}$$

Figure (1) depicts a visual representation of log-Gabor filters in the frequency domain. In 1a and 1b are presented the two components of the filter, the radial and the angular one respectively, for an arbitrary scale and orientation. In Fig. 1c the corresponding resultant filter combining both components is presented.

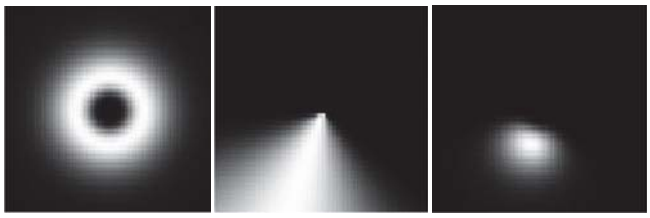

(a) Radial component (b) Anglular component (c) Resultant filter mask

Fig. 1. Log-Gabor filter in the frequency domain.

To extract the facial features we constructed Log-Gabor filters at several scales and orientations. The filtration process was carried out in the spectral domain, making it faster in comparison with the convolution in spatial domain. This process involves: 2D FFT image transformation into the spectral domain and multiplication of the resulted image by each log-Gabor transfer function. Each spectra is then transformed back to the spatial domain using 2D IFFT.

III. Feature Selection

The feature extraction process can increase the dimensionality of the data as it is with the current case of log-Gabor feature extraction. This will inevitable lead to the pronounced effect of the curse of dimensionality as well as increased computational load. For example, if the input face is of size 100×100 pixels and the selected filters scales are 5 and 4 orientations then the resultant dimensionality is $5 \times 4 \times 100 \times 100$ which is a dramatic increase of dimensionality, especially when the dataset is of size smaller than 1000 samples. To avoid this dimensionality explosion two approaches are usually used. The first one is of dimensionality reduction in which a linear or non-linear combination of features is searched. The second one is feature selection where only a small subset of the most representative features is selected.

In this work we utilize a method for feature selection based on graph embedding. The data adjacency graph is a discrete version and encodes the intrinsic data relations [13]. The data adjacency graph is represented in the form of a matrix where each coefficient is larger than zero if every two data points are related in some way, otherwise is zero. Let this matrix be $\mathbf{W}$ where each element W_{ij} encodes the data relation between points i and j. Depending on the task at hand different relations can be selected. Usually, in the supervised case an edge is placed if a couple of data points belongs to the same class. In the unsupervised case the similarity is calculated by appropriate function.

In our work we use two different ways for building the adjacency matrix. The first one is based on heat kernel similarity and every coefficient is calculated by:

$$W_{ij} = \begin{cases} \exp(-\dfrac{\|\mathbf{x}_i - \mathbf{x}_j\|}{\sigma}),\ \mathbf{x}_i, \mathbf{x}_j\ in\ same\ class \\ 0,\ otherwise \end{cases} \tag{5}$$

Given $\mathbf{W}$, let $\mathbf{D}$ is such that $Djj = \sum_i = W_{ij}$. Then, the matrix $\mathbf{L} = \mathbf{D} - \mathbf{W}$ is called the graph Laplacian and is a discrete analog to the Laplace-Beltrami operator. It can be proven [14] that the eigenvectors of this operator provide optimal embedding, preserving the adjacency of the data points in the embedding space. Hence, the eigenvectors of $\mathbf{L}$:

$$\mathbf{Lv} = \lambda \mathbf{Dv} \tag{6}$$

will provide optimal embedding, preserving the geometric structure encoded by $\mathbf{W}$. The matrix $\mathbf{V} = [\mathbf{v_1}, \mathbf{v_2}, ..., \mathbf{v_M}]$ with M eigenvectors corresponding to the smallest M eigenvalues is the optimal data embedding which preserves the geometrical structure. Clever observation that the eigenvectors $\mathbf{V}$ can be used in regression framework for learning mapping functions is developed in [15]. This framework can be used in the linear as well as in the kernel modes. Moreover different regularization schemes can be used. Since the feature selection is a sparse problem, the l_1 regularization is appropriate in our case. The regression problem in the sparse case is formalized as:

$$\min_{\mathbf{b}_m} \|\mathbf{v}_m - \mathbf{F}\mathbf{b}_m\| - \beta \|\mathbf{b}_m\|_1 \tag{7}$$

where $m = [1, 2, ..., M]$ and $\mathbf{F}$ are the log-Gabor features. The l_1 norm will zero out most of the coefficients of $\mathbf{b}_m$ and will provide means for feature selection.

We use the following criteria for feature selection [16]:

$$MCFS(j) = \max_m |b_{mj}| \tag{8}$$

where b_{kj} is the $j-th$ element of the $m-th$ vector. In other words MCFS selects the biggest weight per vector component across all vectors $\mathbf{b}_m$. The result of this operation is a vector of size M and the next step is to arrange the vector components in ascending order. Finally the features are selected by selecting the first d components.

IV. Experimental Results

A. Facial Expressions Dataset

For the experimental setup in this study we used Cohn-Kanade Extended Facial Expression Database (CK+) [7]. This database is intended for development, evaluation and comparison of algorithms for expression recognition. It contains facial photos of 123 persons in 593 image sequences. For a subset of 118 persons there is a corresponding annotation file (i.e. the ground truth data) that describes each persons expression. The following seven expressions are taken into account: anger, contempt, disgust, fear, happy, sad and surprise. The distribution of the number of images per expression is presented in Table I.

TABLE I
Number of images per class in Cohn-Kanade Extended [7]

Anger	Contempt	Disgust	Fear	Happy	Sad	Surprise
45	18	59	25	69	28	83

A sample from the database is presented in Fig. 2.

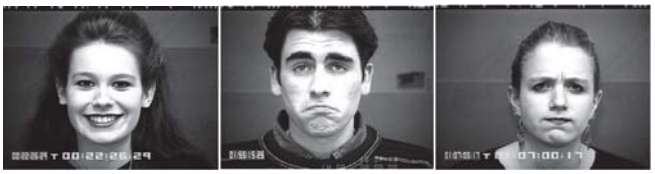

(a) Happy (b) Sad (c) Anger

Fig. 2. Log-Gabor filter in the frequency domain.

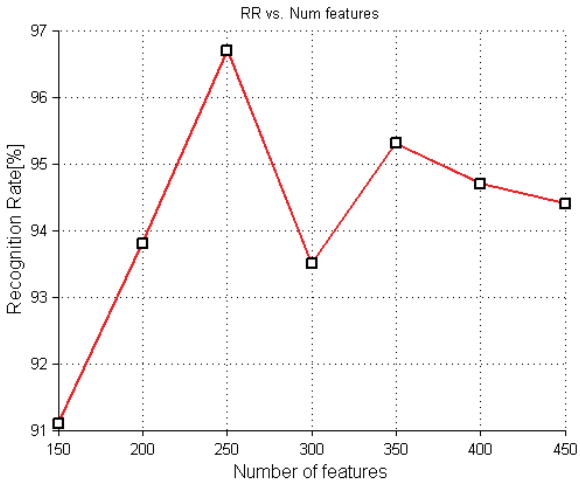

Fig. 3. Recognition rate as function of number of features.

B. Experimental setup and results

For the classifier we selected Support Vector Machines with radial basis kernel function, implemented in LIBSVM [17] and 10 fold cross validation. The value of the parameter σ of the weight matrix similarity function was experimentally chosen to be 0.1. The selected number of scales is 3 and the orientations 5. The images were resized to 60×50 pixels resulting in a feature vector with 45000 elements. The number of selected features was also selected experimentally to 250. In Fig. 3 is presented the recognition rate in % as function of the number of features. It can be observed that the peak is at around 250 features and the recognition rate is 96.7%.

The results are compared with the ones obtained in [6], [5] and [10] as shown in Table II.

TABLE II
Comparison of different algorithms

Algorithm	Recognition Rate[%]
Ou et al. [6]	80
Shan et al. [5]	92.6
Proposed	96.7

An important observation is that the Cohn-Kanade dataset is rather small and thus prone to bias when used in cross-validation setting. Thus, to validate our results we conducted tests in person independent mode (leave-one-person-out) where the images of one person are not used for training,

but only for testing. The recognition rate we achieved is 87% and is higher than the results presented in [9] where person independent tests were also performed.

V. Conclusion

The experiments carried out in this paper prove that graph based feature selection can deliver very good results even when used in filter mode. In total 250 out of 45000 features were selected which is 180 times reduction of dimensionality. The algorithm provides competitive results in cross-validation and person independent test setting when compared to others. As future work, investigation will be carried out to use the feature selection in wrapper or embedded mode. Also different adjacency matrix will be tested.

Acknowledgment

This work was carried out in the scope of the EC funded project eWALL (FP7-610658).

References

[1] A. K. Jain and S. Z. Li, *Handbook of face recognition*. Springer, 2005, vol. 1.

[2] G. Donato, M. S. Bartlett, J. C. Hager, P. Ekman, and T. J. Sejnowski, "Classifying facial actions," *Pattern Analysis and Machine Intelligence, IEEE Transactions on*, vol. 21, no. 10, pp. 974–989, 1999.

[3] Y. Tian, T. Kanade, and J. F. Cohn, "Facial expression recognition," in *Handbook of face recognition*. Springer, 2011, pp. 487–519.

[4] N. Rose, "Facial expression classification using gabor and log-gabor filters," in *Automatic Face and Gesture Recognition, 2006. FGR 2006. 7th International Conference on*. IEEE, 2006, pp. 346–350.

[5] C. Shan, S. Gong, and P. W. McOwan, "Facial expression recognition based on local binary patterns: A comprehensive study," *Image and Vision Computing*, vol. 27, no. 6, pp. 803–816, 2009.

[6] J. Ou, X.-B. Bai, Y. Pei, L. Ma, and W. Liu, "Automatic facial expression recognition using gabor filter and expression analysis," in *Computer Modeling and Simulation, 2010. ICCMS'10. Second International Conference on*, vol. 2. IEEE, 2010, pp. 215–218.

[7] P. Lucey, J. F. Cohn, T. Kanade, J. Saragih, Z. Ambadar, and I. Matthews, "The extended cohn-kanade dataset (ck+): A complete dataset for action unit and emotion-specified expression," in *Computer Vision and Pattern Recognition Workshops (CVPRW), 2010 IEEE Computer Society Conference on*. IEEE, 2010, pp. 94–101.

[8] R. S. El-Sayed and A. El Kholy, "Robust facial expression recognition via sparse representation and multiple gabor filters."

[9] S. M. Lajevardi and Z. M. Hussain, "Feature selection for facial expression recognition based on optimization algorithm," in *Nonlinear Dynamics and Synchronization, 2009. INDS'09. 2nd International Workshop on*. IEEE, 2009, pp. 182–185.

[10] ——, "Feature extraction for facial expression recognition based on hybrid face regions," *Advances in Electrical and Computer Engineering*, vol. 9, no. 3, pp. 63–67, 2009.

[11] V. J. Mistry and M. M. Goyani, "A literature survey on facial expression recognition using global features," *Int. J. Eng. Adv. Technol*, vol. 2, no. 4, p. 653À7, 2013.

[12] D. J. Field, "Relations between the statistics of natural images and the response properties of cortical cells," *JOSA A*, vol. 4, no. 12, pp. 2379–2394, 1987.

[13] M. Belkin and P. Niyogi, "Laplacian eigenmaps for dimensionality reduction and data representation," *Neural Comput.*, vol. 15, no. 6, pp. 1373–1396, 2003.

[14] ——, "Towards a theoretical foundation for laplacian-based manifold methods," in *Learning theory*. Springer, 2005, pp. 486–500.

[15] D. Cai, *Spectral regression: A regression framework for efficient regularized subspace learning*. ProQuest, 2009.

[16] D. Cai, C. Zhang, and X. He, "Unsupervised feature selection for multi-cluster data," in *Proceedings of the 16th ACM SIGKDD international conference on Knowledge discovery and data mining*. ACM, 2010, pp. 333–342.

[17] C.-C. Chang and C.-J. Lin, "LIBSVM: A library for support vector machines," *ACM Transactions on Intelligent Systems and Technology*, vol. 2, pp. 27:1–27:27, 2011, software available at http://www.csie.ntu.edu.tw/ cjlin/libsvm.

THE 18TH INTERNATIONAL SYMPOSIUM ON WIRELESS PERSONAL MULTIMEDIA COMMUNICATIONS
(WPMC-2015)
December 13-16, 2015, Hyderabad, India

Improving the Trustworthiness of Ambient Assisted Living Applications

Elias Z. Tragos*, Pavlos Charalampidis*, Alexandros Fragkiadakis*,
George Lambropoulos†, and Sofoklis Kyriazakos†

*FORTH-ICS, Greece, †Converge SA, Greece

Contact author: Elias Z. Tragos {etragos"at"ics.forth.gr}

***Abstract*—Ambient Assisted Living (AAL) systems aim to support independent living and improve the everyday quality of life of both healthy elderly and disabled people. The Internet of Things (IoT) which can really improve the performance and the efficiency of AAL applications that are built upon Wireless Sensor Networks (WSNs). The AAL applications that include getting data for the patients, monitoring their vital signs and identifying abnormal situations that need medical attention is assumed to be critical applications that have very strict Quality of Service, security and trust requirements. Regarding the latter, it is expected that the devices that are included in AAL systems are trusted and provide reliable measurements. In this work, we propose a model for calculating the trustworthiness of IoT devices and the adaptation of the model for the computation of trusted routing paths in an IoT network. For the trust model we use both statistics for the behaviour of the devices, as well as for the quality of the links in the network, in order to be able to identify the malicious or malfunctioning nodes and to increase the packet delivery ratio, thus increasing the reliability of the overall system.**

I. Introduction

The Internet of Things (IoT) aims to interconnect efficiently large numbers of physical and digital objects, e.g. cars, doors, rooms, mobile phones, etc. The goal is to create a global network infrastructure where all objects will be able to “talk" to each other. All real world objects are interconnected either directly (e.g. by attaching to them ICT devices that monitor or control them) or indirectly (by using remote devices that monitor their attributes) without any human intervention providing advanced applications to the users. These IoT-based applications span in a plethora of sectors, i.e. smart agriculture, smart food, smart buildings, smart cities, etc. [1]. Home automation is considered a broad research area for new IoT-based applications that have a direct impact on the everyday life of human users. As it has been identified lately, security, privacy and trust are main obstacles for the general acceptance of the IoT applications by the general public [2], [3].

Intelligent Building Management Systems (IBMS) can be considered as the basis for providing critical home automation applications, i.e. for smart health, monitoring the health status of the inhabitants. This can be considered as part of Ambient Assisted Living (AAL) system, which aims to provide an ecosystem for medical applications supporting user-dependent services for the disabled and the elderly [6]. The main goal of AAL systems is to allow the elderly or disabled people to live autonomously, automating most of their everyday activities and increasing the safety in their everyday lives. AAL applications include among others monitoring the vital signs of the people, tracking of their movement (mainly indoors), identifying falls and calling for assistance when health-related alarms are raised. The demographic change that results in the increase of life expectancy and the decrease in the birth rates raises the need for such applications [4].

The success of AAL applications depends on the level of trust that the users have on the system that provides these applications. It is reasonable to assume that if a user does not trust the system he will not use it. The level of trust can be affected by many factors, i.e. by personal experience that stems from previous engagement with the system, by proofs of the performance of the system or by recommendations from other known users. Assuming that there are many devices feeding data to the AAL applications, these devices have to be reliable and trusted to ensure that decisions taken by the system are not affected by malicious or malfunctioning devices. Previous works have focused on trust management in AAL applications in a very generic point of view ([5] and the references therein). Here we focus on the trust from the networking point of view, introducing trust as a routing metric in multi-hop IoT deployments, in order to compute routing paths that are formed by trusted devices when there is a need to provide sensitive AAL applications. The goal is to create a trusted routing a scheme that considers the following: (i) behavioral statistics of sensors reported by their one-hop neighbors, (ii) link quality statistics, and (iii) a fusion scheme based on the Dempster Shafer theory of evidence.

The rest of this paper is structured as follows: in section II we provide a brief overview of the state of the art. In section III, we discuss the system and trust model. In section IV we describe the trusted routing mechanism. In section V we provide the simulation setup and the performance evaluation, while in section VI we conclude the work.

II. Related Work

Node reputation has been introduced as a trust mechanism in several publications that provide classification schemes and information about how to evaluate reputation and trust, but

they are quite focused only on users' ratings. Probabilistic theory [8], Hidden Markov Model [9], ontologies [10] semantics [11] and fuzzy models have been employed in reputation calculations and modelling. Gligor and Wing [12] present a theory of trust in networks of humans and computers that consists of elements of computational trust and behavioural trust. There are two types of trust [13]: (1) social trust that is a subjective metric based on friendship, honesty, social interactions, social reputation and history, and (2) QoS trust that is a more objective metric based on QoS measurements.

Trust management has been used as an easy and efficient approach to mitigate a wide number of attacks in opportunistic routing [15] in wireless sensor networks. Nodes create trust relationships based on the expectation that their neighbours will cooperate on particular tasks (e.g. packet forwarding) and decide on routing paths based on them. In [14] a trust management protocol is applied in geographical routing for WSNs that is able to avoid attackers by routing through benevolent neighbours. In [16] the authors design a trust-aware routing framework that can cope with various harmful attacks with no time synchronization or geographic information, while [17] describes a routing scheme that expresses routing reputation by combining link quality and node behaviour. Finally, in [18] a hierarchical (social and QoS) trust management scheme for heterogeneous sensor networks is introduced.

III. System Model

A. Network Model

We follow the approach of Virtual Sensor Networks (VSNs). According to [19] a Virtual Sensor Network is formed by an appropriate subset of sensor nodes of a standard Wireless Sensor Network (WSN). This subset collaborates in order to provide a specific service as requested by an application. A virtual sensor network is basically formed by interconnecting logically (and not always physically) collaborative sensor nodes. An Overlay Sensor Network is a network that is built on top of a standard Wireless Sensor Network in a similar way that the Internet was built on top of a telephone network. The overlay network creates a virtual topology comprising nodes that are connected with virtual links that correspond to paths of the underlying network.

We model the network as an overlay bi-directed graph G(V,E) where V is the set of nodes (smart objects), including a single sink node (normally the Gateway), and E is the set of edges representing wireless links between nodes, as depicted in Figure 1. Of course IoT networks are normally in larger scale, but we can use clustering (as in [20] to divide the network into smaller parts. The sink node is normally not a constrained device, meaning that it is reasonably powerful with increased capabilities with regards to processing, memory and energy. We assume that each node of the network has a limited communication range, thus can directly communicate only with the nodes that reside inside his range, which we call them his "neighbours". Communication with the sink is possible in a multi-hop fashion with each node following a path calculated through a respective algorithm at the sink.

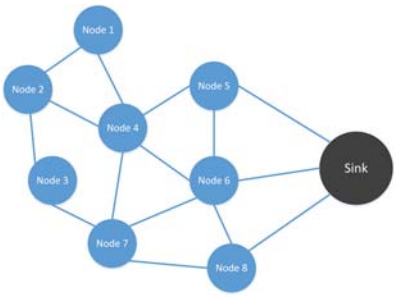

Fig. 1: Network model.

B. Trust Modeling

In this work the trust model is based on statistics that relate with the behaviour of each node in terms of dropping packets or modifying them and on the statistics of the link quality between the nodes, since the latter affects also the possibility of correct reception of the measurements at the sink.

1) Behavioural Statistics: The first part of the trust model is related with creating a metric for considering the behaviour of the nodes that are parts of the network of the devices that provide the AAL applications. We assume that there may be some devices that can be either malfunctioning (i.e. due to hardware or software failures) or tampered with by malicious third parties. The trust model is built on the evaluation of trust degree values based on the observed behaviour of a network node by its neighbours. Each node observes and records a neighbour's abnormal behaviour each time there is an interaction between them, while it also keeps track of the total amount of incoming packets. For the sake of simplicity and to keep the communication and signalling overhead low, two statistics that capture the forwarding behaviour of an node are used: (i) packet drop rate (PDR) and (ii) packet modification rate (PMR) defined as follows:

$$PDR = \frac{\#\text{of dropped packets}}{\text{total}\,\#\text{of received packets}} \tag{1}$$

$$PMR = \frac{\#\text{of modified packets}}{\text{total}\,\#\text{of forwarded packets}} \tag{2}$$

We assume that there is a sender node i and a receiver neighbour j. Each time i sends a packet to j, it enters promiscuous mode to overhear the forwarding behaviour of j and it updates accordingly the values of $PDR_{i,j}$ and $PMR_{i,j}$. Then, the aggregate MisBehaviour Rate (MBR) of node j as perceived by a node i is calculated as:

$$MBR_{i,j} = w \times PDR_{i,j} + (1-w) \times PMR_{i,j} \tag{3}$$

where $w \in [0,1]$ is a user-defined weight controlling the balance between the behavioural statistics.

2) Link Quality Statistics: Using only the behavioural statistics for evaluating the trustworthiness of a node can be indeed useful to isolate malicious nodes in the network. However, to improve the performance and allow the metric to be used as a routing metric we have to also take into consideration a link quality metric for the optimal path calculation of the routing algorithm. Here, we use the estimated transmission count (ETX) metric [21] to quantify the reliability of the link

between any two nodes within the network. ETX is one of the most widely used routing metrics due to its simplicity and computational efficiency. The ETX calculated for node i by node j is defined as:

$$ETX_{i,j} = \frac{1}{f_{i,j} \cdot r_{i,j}} \quad (4)$$

where $f_{i,j}$ is the forward delivery ratio, i.e. the measured probability that a packet sent from node i is received by node j, and $r_{i,j}$ is the reverse delivery ratio, i.e. the measured probability that the acknowledgement packet from node j will be received by node i. Thus, ETX expresses the average number of transmissions needed for a packet to successfully reach its destination in cases when there are transmission failures due to degradation of link quality.

3) Behavioural Trust Fusion: The calculation of the MBRs for each one of the nodes in the network is assumed to be a crucial step in the proposed routing scheme. For this calculation the observations and the recordings of the statistics by the interacting neighbours are utilized. However, since for this calculation we can't be sure that the observations and the reported values are accurate and reliable, we need an appropriate combination technique to fuse the neighbour views. In our framework, each node builds a local view of the neighbours' behaviour from its own observations. As a result, the reported views may be biased or intentionally wrong, leading to the existence of uncertainty. Therefore, we propose the use of Dempster-Shafer (DS) theory of evidence [22], [23] as a fusion technique. DS is a mathematical framework able to handle uncertainty of the complete probabilistic model describing the system under consideration. Essential terminology related to DS and used throughout this section is presented below to ease the reader to understand our contribution:

- Frame of discernment Θ, which is the set of all possible mutually exclusive and complete states of a system. Here, the frame of discernment is defined as Θ = trust, no-trust.
- Mass function (probability assignment) m. $m : 2^{\theta} \rightarrow [0,1]$ is a mass function if $m(\emptyset) = 0$ and $\sum_{A \subset \Theta} m(A) = 1$. A is any proposition that is a subset of Θ.
- Belief function, which measures the belief of a proposition A and computes the sum of all the nonempty subsets of A. It is given by the formula $Bel(A) = \sum_{B \subseteq A} m(B)$, where B are the nonempty subsets that compose A. Here, since the belief on a node's trust depends only on the MBR value, the belief and the mass functions are equivalent.
- Focal elements of a frame of discernment Θ, which are comprised of all hypotheses for which the observers can provide evidence. In our case, where $\Theta = \{trust, no-trust\}$, the corresponding focal elements form the set $[trust, no-trust, trust, no-trust]$, where the last element shows the uncertainty for the trustworthiness of one node.

Individual beliefs on each node's trust as reported by each of its interacting neighbours can be combined into a single belief by applying Dempster's rule of combination:

$$m_1(A) \oplus m_2(A) = \frac{\sum_{B \cap C = A} m_1(B) m_2(C)}{1 - \sum_{B \cap C = \emptyset} m_1(B) m_2(C)}$$

Belief \ MBR	$MBR < h(1-r)$	$MBR > h(1+r)$	$h(1-r) \le MBR \le h(1+r)$
b^T	$c+\lvert h-MBR \rvert / h$	$(1-b_r)/2$	1/3
b^U	$(1-b_r)/2$	$c+\lvert h-MBR \rvert / h$	1/3
b^{TU}	$(1-b_r)/2$	$(1-b_r)/2$	1/3

Fig. 2: Belief Computation

In cases where there are in total N neighbours reporting individual beliefs for a specific node, the belief functions can be combined sequentially in any order (due to the associative property of DS), as expressed by the following formula:

$$m_{1\ldots K}(A) = \bigoplus_{k=1}^{K} m_k(A) \quad (5)$$

Each neighbour produces a single belief for each focal element (b^T: belief that a node is trusted, b^U: belief that a node is untrusted, b^{TU}: belief expressing ambiguity) according to the table in Figure 2.

The uncertainty area lies between $h(1-r)$ and $h(1+r)$, where$h$ is a user-defined threshold (since every user has a different perception of trust), $0 < r < 1$ is a user-defined scalar controlling the width of the uncertainty area and c is a scalar controlling how fast trust/distrust belief increases. By combining the believes of trust reported by each node for their neighbours we calculate the trust degree of a node j, denoted as b_j^{CT} , by using Equation 5. We have to note here that the belief and the mass functions are equivalent, since node trust is characterized only by a single basic event (MBR).

IV. Trusted Routing with Link Quality

Considering both the trust degree b_j^{CT} and the link quality as quantized by $ETX_{i,j}$ a combined routing metric on a route r from a node to the sink can be defined as

$$RM_r = \sum_{i,j \in r} ETX_{i,j} \left(1 - b_j^{CT}\right) \quad (6)$$

We find the shortest path from each node to the sink using the classic algorithm of Dijkstra [24]. The "shortest path" in this context shows a path that has both a low number of retransmissions at the links and comprises of nodes that have a high trust degree. In the following, the steps of the proposed trust-based routing scheme are described.

a) Initialization: Each node measures the ETX metric by broadcasting a probe packet periodically with a fixed time interval. Additionally, it sends a packet containing the count of probe packets from its neighbours, so that all nodes can calculate the loss of probe packets on both directions of a link. Subsequently, the calculated ETX values are flooded to the sink. At this time no behavioural statistics are available and all nodes are assigned a trust degree of 0.5 (neither trusted nor untrusted). Optimal paths are computed using Dijkstra's algorithm and are broadcasted to the network.

b) Trust belief update: The behaviour of malicious (or malfunctioning) nodes is possible to change over time; as a result, it is necessary to update periodically the trust values

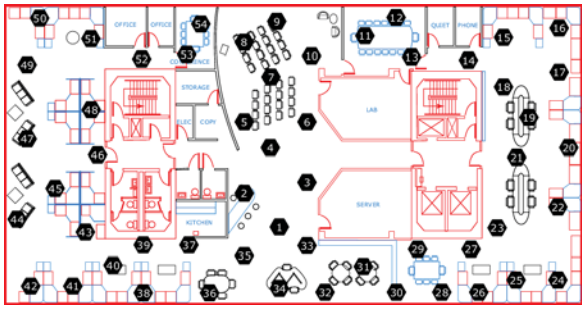

Fig. 3: Intel Berkeley lab sensor network topology.

assigned to each node. While a node interacts with its neighbours, it observes and records their behaviour and recalculates accordingly the behavioural statistics, the total misbehaviour rate and, finally, the trust belief. After a predefined trust update interval Δt we have:

$$b'^{T}_{i,j}(t+\Delta t) = \theta \times b^{T}_{i,j}(t) + (1-\theta) \times b^{T}_{i,j}(t+\Delta t)$$

where $\theta \in [0,1]$ is a weighting factor that balances current and previous estimation of misbehaviour rate. We choose to use a different weighting factor depending on whether the MBR has increased or decreased, as follows:

$$\theta = \begin{cases} \theta_1, & \text{if } b^{T}_{i,j}(t+\Delta t) > b^{T}_{i,j}(t) \\ \theta_2, & \text{if } b^{T}_{i,j}(t+\Delta t) \leq b^{T}_{i,j}(t) \end{cases}$$

with $\theta_1 > \theta_2$.

As a result, trust degree decreases quickly in case of misbehaviour but increases slowly in case of improved behaviour.

c) Routes update: After updating the trust degree, each node calculates the beliefs for the neighbours based on the Table in Figure 2. New beliefs are sent to the sink where they are fused based on Dempster-Shafer rule of combination, so that a combined trust belief b_j^{CT} and distrust belief b_j^{CU} is assigned to each node j. We use a threshold B_{mal} to detect malicious or misbehaving nodes, in other words if $b_j^{CU} > B_{mal}$, then node j is considered untrusted and it is omitted from the routing paths. Afterwards, the optimal routing paths are found through Dijkstra's algorithm, by considering the combined metric defined in Equation 5.

V. Performance Evaluation

In order to evaluate the proposed scheme we assume the indoor sensor network of Figure 3 (http://db.csail.mit.edu/labdata/labdata.html), which corresponds to a deployment of 54 Mica2Dot sensors at Intel Berkeley lab employed with weather boards to monitor low frequency phenomena (humidity, temperature, light and voltage). Both topology information (nodes' coordinates) and bi-directional link quality (probability of successful transmission that can be used to easily compute ETX values) are available online .

We choose randomly a node as the sink and we conduct simulations for data aggregation rounds. Trust belief update interval is set to 20 rounds, while we choose $c = 0.1$, $h = 0.5$, $r = 0.05$ and $w = 0.5$. In order to account for some variance of wireless channel characteristics, in each round we vary

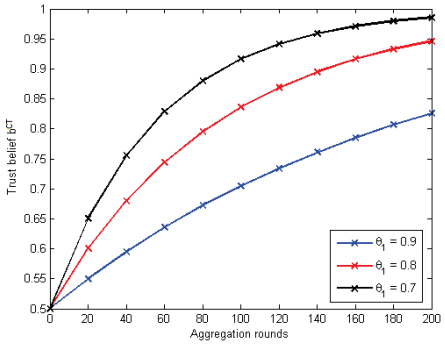

Fig. 4: Trust belief of normal node.

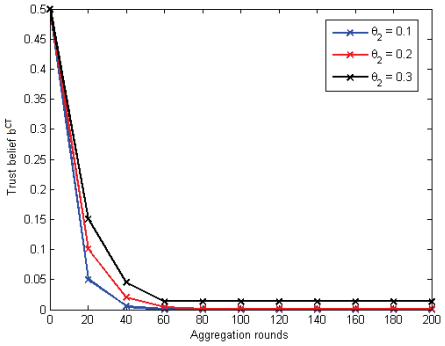

Fig. 5: Trust belief of malicious node.

randomly the ETX of all links in [90%, 110%] of their nominal values. Figure 4 and Figure 5 show the combined trust belief for a normal and a malicious node, respectively, and for various values of weights θ_1 and θ_2 . Obviously, an increase of θ_1 reduces the rate of trust belief increase, applying more significance on history data. Similarly, an increase of θ_2 causes trust belief to decrease slower. Furthermore, we can see that the disbelief for a node (who has low trustworthiness) is calculated very quickly, which means that in only a few rounds we can identify which nodes are untrusted and avoid them in future routing decisions. Generally, by choosing the appropriate values for θ_1 and θ_2 we can assure that our scheme becomes more sensitive to malicious actions, enabling the quick omission of the malicious nodes from the routing paths.

Next, we proceed by evaluating our scheme by means of

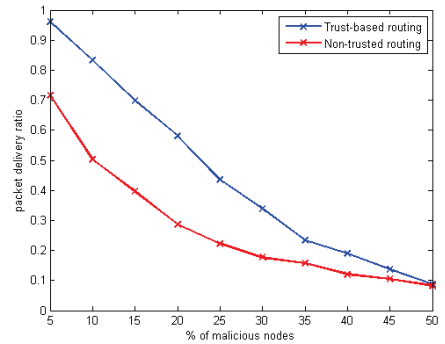

Fig. 6: Packet delivery ratio (highly malicious behaviour).

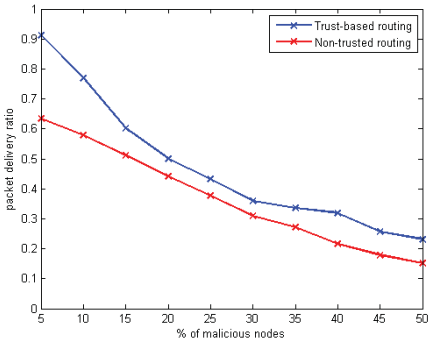

Fig. 7: Packet delivery ratio (low malicious behaviour).

packet delivery ratio at the sink. We assume two scenarios, namely highly malicious behaviour and low malicious behaviour. In first case, malicious nodes exhibit PDR and PMR with values in [0.8,1] while in second case the values vary in [0.3,0.5]. For each scenario we execute 20 Monte Carlo runs each consisting of 2000 data aggregation rounds. The proposed trust-based routing scheme is compared against a simple routing scheme with no trust management mechanism. Mean packet delivery ratio (averaged over all runs) vs percentage of malicious nodes for highly malicious behaviour and low malicious behaviour is depicted in Figure 6 and Figure 7, respectively. Observe that in both cases the trust-based scheme outperforms the simple scheme, with the difference being more profound for small number of malicious nodes and highly malicious behaviour. For example, in case of 5-20% of highly malicious nodes there is an increase of more than 30% in packet delivery ratio. Normally, as the number of malicious nodes increases the packet delivery ratio for both routing schemes is almost equal.

VI. Conclusion

In this paper we presented a trust model for evaluating the trustworthiness of nodes that are providing AAL applications. The trust scheme is based on both node behaviour (for identifying malicious or misbehaving nodes) and link quality statistics (to identify lossy links) in order to ensure that the resulting routing paths will include only trusted nodes with high reliable links so that no information will be lost or tampered with. Since AAL applications are sensitive applications that affect the quality of life and the well-being of elderly or disabled people, the measurements gathered from the devices (i.e. vitals from wearables, fall detection) are critical and have to be sent to the AAL system with the highest protection. The scheme proposed in this paper, as shown in the evaluation section, can quickly identify malicious or misbehaving nodes and can isolate them from the network routes. The percentage of delivered packets can also be significantly improved even in the case of many malicious/malfunctioning nodes in the network. Future steps include the extension of the trust model to include more trust metrics for addressing more attacks and a more formal expression of the trusted routing metric.

Acknowledgment

This work has received funding from the European Unions Seventh Framework Programme (FP7/2007-2013) under grant agreements no 609094 and 612361.

References

[1] Vermesan, Ovidiu, and Peter Friess, eds. “Internet of Things-From Research and Innovation to Market Deployment". River Publishers, 2014.
[2] Tragos, Elias Z., et al. "Enabling reliable and secure IoT-based smart city applications." Pervasive Computing and Communications Workshops (PERCOM Workshops), 2014 IEEE International Conference on.
[3] Pohls, Henrich C., et al. "RERUM: Building a reliable IoT upon privacy- and security-enabled smart objects." Wireless Communications and Networking Conference Workshops (WCNCW), 2014 IEEE. IEEE, 2014.
[4] A. Mitseva et al., “Intelligent system for independent living and self-care of seniors with mild cognitive impairment or mild dementia," Journal on Information Technology in Healthcare, vol. 7, no. 6, 2009.
[5] Sini Ruohomaa, Lea Kutvonen, “Trust Management Survey, Trust Management", Volume 3477 of the series LNCS pp 77-92.
[6] Q. Zhang, T. Yu, K. Irwin: “A classification scheme for trust functions in reputationbased trust management", in: Proceedings of ISWC Workshop on Trust, Security, and Reputation on the Semantic Web (2004).
[7] Sabater, J. and Sierra, C.: “Review on Computational Trust and Reputation Models". Artif. Intell. Rev. 24, 1, pp. 33-60 (Sep. 2005).
[8] Li, L., et.al.: “Trust-Oriented Composite Service Selection and Discovery". In Proceedings of the 7th international Joint Conference on Service-Oriented Computing (Stockholm, November 24 - 27, 2009).
[9] Malik, Z., et.al: “Web Services Reputation Assessment Using a Hidden Markov Model". 7th international Joint Conference on Service-Oriented Computing (Stockholm, November 24-27, 2009).
[10] Sabater, J. and Sierra, C.: “REGRET: A reputation model for gregarious societies". In Proceedings of the 4th Int. Workshop on Deception, Fraud and Trust in Agent Societies, AGENTS’01, pp. 61- 69, Montreal (2001).
[11] Huang, J. and Fox, M. S.: “An ontology of trust: formal semantics and transitivity". In Proceedings of the 8th international conference on Electronic commerce: ICEC ’06, ACM, NY, USA, 2006.
[12] V. Gligor and J. M. Wing, “Towards a theory of trust in networks of humans and computers," in Proc. 19th International Workshop on Security Protocols, ser. LNCS. Springer Verlag, March 28-30 2011.
[13] Jin-Hee Cho, et. al., “Modeling and Analysis of Trust Management for Cognitive Mission-Driven Group Communication Systems in Mobile Ad Hoc Networks," Computational Science and Engineering, 2009.2.
[14] K. Liu, et.al., “Location verification and trust management for resilient geographic routing," J. Parallel Distrib. Computing, vol. 67, no. 2, 2007.
[15] N. Gazoni, et. al., “A framework for opportunistic routing in multi-hop wireless networks," in Proceedings of the 7th ACM PE-WASUN, pp. 50-57, October 2010.
[16] G. Zhan, W. Shi, and J. Deng, “Design and Implementation of TARF: A Trust-Aware Routing Framework for WSNs," Dependable and Secure Computing, IEEE Transactions on , vol.9, no.2, March-April 2012.
[17] A. Rezgui, and M. Eltoweissy, “TARP: A Trust-Aware Routing Protocol for Sensor-Actuator Networks," Mobile Adhoc and Sensor Systems, 2007. MASS 2007. IEEE International Conference on, pp.1,9, 8-11 Oct. 2007.
[18] F. Bao, et.al., “Hierarchical Trust Management for Wireless Sensor Networks and its Applications to Trust-Based Routing and Intrusion Detection," Network and Service Management, IEEE Trans. on, vol.9, no.2, June 2012.
[19] Islam, Md Motaharul, et al. “A survey on virtualisation of wireless sensor networks." Sensors 12.2 (2012): 2175-2207.
[20] Karamolegkos, Pantelis N., et al. "User-profile based communities assessment using clustering methods.", 18th IEEE PIMRC 2007.
[21] Biswas, Sanjit, and Robert Morris. “ExOR: opportunistic multi-hop routing for wireless networks." ACM SIGCOMM Computer Communication Review. Vol. 35. No. 4. ACM, 2005.
[22] Dempster, Arthur P. “The Dempster-Shafer calculus for statisticians." International Journal of Approximate Reasoning 48.2 (2008): 365-377.
[23] A. Fragkiadakis, et.al., "Anomaly-based intrusion detection of jamming attacks, local versus collaborative detection", Wireless Communications and Mobile Computing 15 (2), 276-294.
[24] Noto, Masato, and Hiroaki Sato. “A method for the shortest path search by extended Dijkstra algorithm." Systems, Man, and Cybernetics, 2000 IEEE International Conference on. Vol. 3. IEEE, 2000.

THE 18TH INTERNATIONAL SYMPOSIUM ON WIRELESS PERSONAL MULTIMEDIA COMMUNICATIONS
(WPMC-2015)
December 13-16, 2015, Hyderabad, India

Requirements and Challenges in Evaluation of Systems for Independent Living of Senior Citizens

Antun Kerner, Antonija Marinčić, Ana Koren, Dina Šimunić and Ramjee Prasad
University of Zagreb
Faculty of Electrical Engineering and Computing
Unska 3, 10000 Zagreb Croatia
e-mail: antun.kerner@fer.hr

***Abstract* - One of the main concerns in the era of aging population is how to enable senior citizens to live independently. In order to solve this problem, systems for independent living of senior citizens are being developed. In process of delivering these systems to end users, evaluation plays a crucial role. In this paper evaluation and testing of the European project FP7 eWALL for Active Long Living system is presented. Different technologies that have been used in system development are listed. The emphasis is put on evaluation methodologies and challenges that were encountered during system evaluation. In addition, possibilities in improving system evaluation have been listed.**

Keywords-component; Cloud, network architecture, end to end testing

I. INTRODUCTION

The verification and the validation processes form part of the larger process of software engineering. Thus, from a process viewpoint, software testing, as a part of verification and validation can be viewed as being included within software engineering, which, in turn, is a part of systems engineering. In fact, the systems engineering, the software engineering and the verification and validation processes are all covered by corresponding standards (ISO 15288:2015 "Systems and software engineering - System life cycle processes", ISO 12207:2008 "Systems and software engineering - Software life cycle processes" and IEEE 1012 "Standard for software verification and validation" respectively). Each of these standards contains requirements relevant to the software tester. Both ISO 15288 and ISO 12207 include processes for verification and validation, and although many software developers and testers ignore the systems aspect of their work, it is impossible to deny the relevance of ISO 12207, the software life cycle processes standard. The software maintenance life cycle process begins with process implementation, where planning for maintenance is performed and ends with the retirement of the software product. It includes modification of code and documentation due to a problem or as a need for improvement. The objective of the maintenance process is to modify an existing software product while preserving its integrity. According to ISO/IEC 14764:2006 "Software Engineering - Software Life Cycle Processes - Maintenance" [1] Figure 1 shows standard steps should be performed.

a) Trace the modification request-MR/problem report-PR from requirements, to design, to code;
b) Verify testability of the code;
c) Verify conformance with coding standards;
d) Verify that only necessary software components were modified;
e) Verify that the new software components were integrated properly;
f) Check documentation to ensure that it was updated;
g) Configuration management-CM personnel build software items for testing;
h) Perform testing by an independent test organization;
i) Perform system tests on a fully integrated system;
j) Develop test report

Figure 1: Steps of maintenance process

II. EWALL SYSTEM ARCHITECTURE

According to the ISO/IEC/IEEE 42010 "Systems and software engineering - Architecture description", an international standard for architecture descriptions of systems and software, the architecture is defined as “fundamental concepts or properties of a system in its environment embodied in its elements, relationships, and in the principles of its design and evolution”. The eWALL project considers system architecture as “the conceptual model that defines the structure, behavior and more views of a system” [1].

The chosen description methodology for specification of eWALL system architecture is founded on ARCADE framework [2]; an open architectural description framework based on the IEEE 1471-2000 "Recommended Practice for

Architecture Description of Software-Intensive Systems" standards. Furthermore, as it is important to show how different selected hardware components (sensors, actuators, user interaction devices, servers) will interact with developed software components to form a unique eWALL system. Figure 2 shows the holistic Service Oriented Architecture of eWALL system. The OMG Systems Modeling Language (OMG SysML™) has been selected as the main modeling language for eWALL system architecture definition. SysML is a general-purpose modeling language for systems engineering applications and it is defined as an extension of a subset of the Unified Modeling Language (UML). Produced preliminary eWALL SysML model helped share understanding of system design, and will further assist in managing complex eWALL system development. Cloud deployment models the eWALL cloud environment infrastructure (eWALL IaaS) as an Openstack-based private cloud, which has been set up on dedicated hardware infrastructure. Figure 3 shows parallel environments in the eWALL cloud. The private cloud allows configuring and using a set of parallel environments, each one enabling a fully functional server-side eWALL system, to be used within the eWALL Consortium for a specific phase of the application management lifecycle. Four parallel environments have been set up, dedicated respectively to: development activities, integration testing activities, end-to-end testing and validation activities and production-level solution hosting. In addition to them, an application lifecycle management environment was created, which orchestrates the software artifacts management and deployment towards the parallel environments and executes the automated testing tasks.

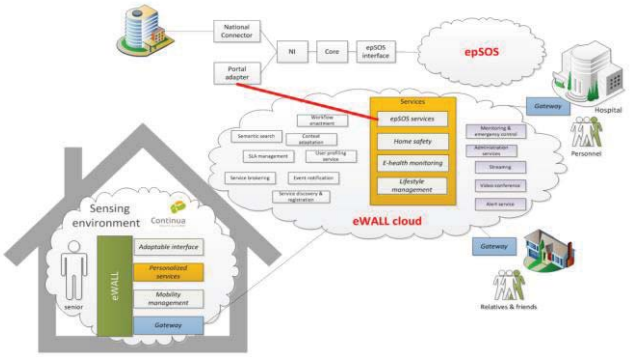

Figure 2: The holistic Service Oriented Architecture of eWALL

Within each of the parallel environments, the same set of components constituting the eWALL central system are deployed and executed. Figure 3 depicts the deployment model for one of such parallel environments (namely the integration test environment). The other ones follow exactly the same deployment pattern. The only difference between the parallel environments lies in the computational resources allocated for them (production and validation environments are assigned more resources, as they are expected to support higher usage loads). In the sample environment of Figure 4, the eWALL components are deployed on four virtual servers. One virtual server is dedicated to hosting applications and service bricks. The communication with the external world is based on http/REST. The second server is dedicated to caching. Cache server software (memcached) is installed on the server, and is accessed by the other components of the system to store in the cache or to get from the cache sets of data. This allows for optimization of network usage and response time, which directly affects the QoS of the platform. The third server is dedicated to the Horizontal services and Cloud middleware services of the eWALL platform. Since such components are responsible for data exchange with both local and remote components, they also can communicate with the external world via http/REST. The fourth server is dedicated to data storage. Such machine hosts a MongoDB server, which is accessed by the data management component of the Cloud middleware services, to store or provide data to the eWALL components.

Since the components are loosely coupled by design (they all communicate via stateless, web service protocol) the deployment model described above can be easily changed and adapted to different requirements. Additional virtual servers can be added to the deployment scenario and most of the components can be distributed on them. As an example, based on the number of applications and service bricks in the platform at a certain moment, it might be preferable to separate such components on different servers seamlessly (or, as an alternative, deploy additional ones on new servers).

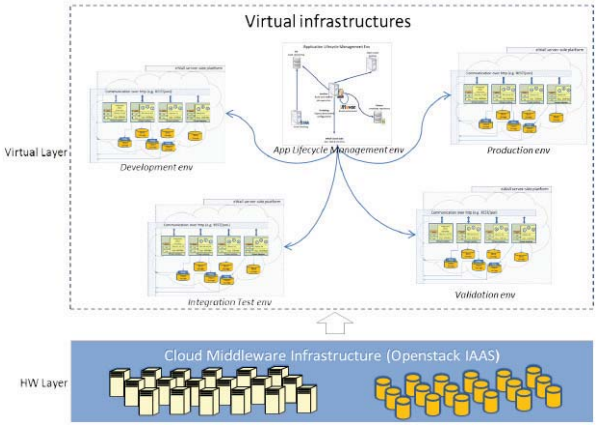

Figure 3: Parallel environments in the eWALL cloud

Within each of the parallel environments, the same set of components constituting the eWALL central system are deployed and executed. Figure 3 depicts the deployment model for one of such parallel environments (namely the integration test environment). The other ones follow exactly the same deployment pattern. The only difference between the parallel environments lies in the computational resources allocated for them (production and validation environments are assigned more resources, as they are expected to support higher usage loads). In the sample environment of Figure 4, the eWALL components are deployed on four virtual servers. One virtual server is dedicated to hosting applications and service bricks. The communication with the external world is based on http/REST. The second server is dedicated to caching. Cache server software (memcached) is installed on the server, and is accessed by the other components of the system to store in the cache or to get from the cache sets of data. This allows for optimization of network usage and response time, which directly affects the QoS of the platform. The third server is dedicated to the Horizontal services and Cloud middleware services of the eWALL platform. Since such components are responsible for data exchange with both local and remote components, they also can communicate with the external world via http/REST. The fourth server is dedicated to data storage. Such machine hosts a MongoDB server, which is accessed by the data management component of the Cloud middleware services, to store or provide data to the eWALL components. Since the components are loosely coupled by design (they all communicate via stateless, web service protocol) the deployment model described above can be easily changed and adapted to different requirements. Additional virtual servers can be added to the deployment scenario and most of the components can be distributed on them. As an example, based on the number of applications and service bricks in the platform at a certain moment, it might be preferable to separate such components on different servers.

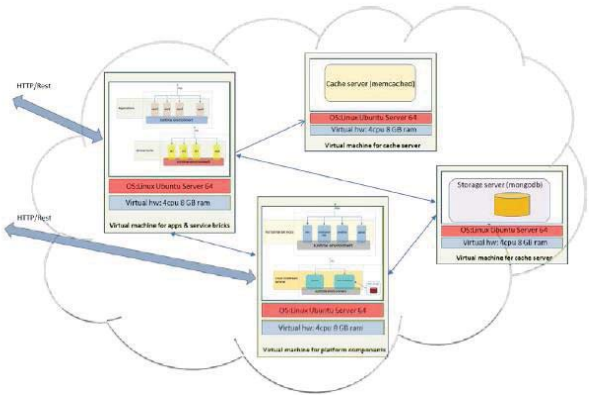

Figure 4: Sample deployment model for an eWALL cloud environment (Integration Test environment)

III. VALIDATION AND TESTING

Software testing is an important part of eWALL software development. Any incorrect human action that produces a problem in the system is called error. Deviation between expected behaviors to the actual behavior of the system is called defect. The deviation identified by end-user while using a system is called a failure. Presence of errors during software development results in defects and presence of defects results in failure of the eWALL system as a product. Figure 5 shows eWall integration work flow which consists of tools for build automation and deploy execution which should ensure error detection and avoid integration of components with errors.

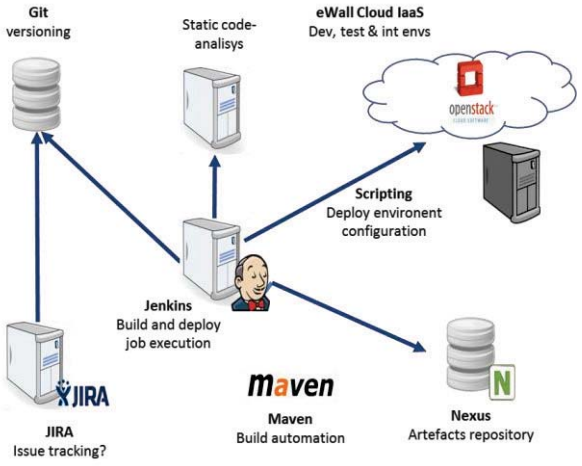

Figure 5: eWALL Integration work flow

Generally, software has defects because of incorrect requirements, wrong design, poor coding, complex logic, complex technology, work pressure or frequently changing requirements. Software testing is a process of verification, as well as of validation whether the exactly the wanted product is under development. Verification is a process known as static testing and validation as dynamic testing. Code review and unit testing are organized as part of development related work packages while integration testing and system testing are in scope of independent work group (WP6). System testing approach is based on traditional testing approach or positive testing which shows that the system does what it should. Most common defects are incorrect functionality, incorrect data edits, poor performance, poor security, incompatibility, poor user interface (UI) and poor usability. Objectives of testing are: to confirm whether the application is developed according to customer requirements or not, finding defects, to make sure all problems are resolved and close and help to deliver a quality product and risk-free product to the customer. Dynamic testing is carried out at following levels of testing: unit, integration, and system and user acceptance. The smallest separable portion in the source code of the application is called unit (functions, procedures, etc.). Testing conducted on these units (to check if the code behind the units is working as expected or not) is called unit testing. It is also called module testing or

component testing. Once all units are tested and integrated as wanted, the interactions among the units are checked, which called integration is testing. Unit testing and integration testing is collectively called white box testing. White box testing is helpful to reduce the defects as early as possible. Black box testing is conducted on the application by WP6 to check whether the application is working according to designed requirements. White box testing is conducted by a developer in a technical perception where as black box testing is conducted by test engineers with end-user perception. Programmers/developers will conduct white box testing in a positive perception whereas tester will conduct black box testing with a negative perception where there is a more chance of finding more defects. The more identified defects results in a quality system. White box testing will not cover non-functional areas. As functional requirements are also very important for production system, those are covered in the black box testing. WP6 uses functional system testing approach called smoke testing. It is a kind of quick test carried out on the application to determine whether the application is testable or not. Testing of software application by following all pre-plan procedures and proper documentation is called formal testing. Testing of the software without following any procedures and documentation is called ad-hoc informal testing. The critical functionality in the system and testing it first or conducting testing in the same order of priority is called risk based testing or priority based testing. Re-testing is testing functionality again or testing functionality repetitively. Re-testing comes in the following two scenarios: a) testing functionality with multiple inputs to confirm if the requested validations are implemented or not; b) testing functionality on the modified build to confirm that the bug fixers are made correctly. Regression testing is a process of identifying various features in the modified build where there is a chance of getting affected and retesting these features. The new functionalities added to the existing system or modifications made to the existing system or the bug fixes may introduce side effects. Regression testing helps to identify eventual side effects. End-to-end testing is testing the overall functionalities of the system including the data integration among all the modules. Testing conducted on an application unevenly or zigzag way with an intension of finding tricky defects is called monkey testing. Validating various non-functional aspects of the system such as user interfaces, user friendliness, security, compatibility, load, stress, performance, etc. is called non-functional system testing. Validation of professional design of user interfaces is called UI Testing. Check List for manual UI Testing: check if all basic elements are available in the page or not, check spelling of the objects, check alignments of the objects, check content displayed in web pages, check if the mandatory fields are highlighted, checks the consistency in the background color, font type and font size, etc. Usability testing means checking how easily the end user is able to understand and operate the application. Security testing is validating whether all security conditions are properly implemented in the software. Check list for security testing encompasses checking if the sensitive data such as password, credit card, CVV numbers are getting encrypted; checking the browser navigation after logout; checking direct URL access for the both secured and non-secured pages, checking for the session expiry; checking view source code option for secured pages; checking for the authorization; checking for authentication; checking the cookies. Performance testing is a process of measuring various efficiency characteristics of a system such as response time, throughput, load, stress transactions per minute and transaction mix. Load testing means analyzing functional and performance behavior of the application under various load conditions. Checking the application behavior under stress conditions is called stress testing; in other words, it means reducing the system resources and keeping the load as constant, while checking the behavior of the application. Checking the system ability to handle some unexpected or unpredictable situations is called recovery testing. Globalization testing is checking if the application has a provision of setting and changing languages, date and time format and currency etc. Installation testing is checking if the software was installed successfully, as per the guidelines given in installation document. Un-installation testing is checking of the software uninstallation ability from the system. Compatibility testing is checking if the application is compatible with the different software and hardware environment. Test planning is the first phase of system testing where the management plan the high level and detail testing activities to be carried out. Stakeholders responsible for validation and testing define test strategy and based on this test strategy the detail plan called test plan is prepared. Test strategy is high-level management plan and approach that provides sufficient confidence on the project being tested. Test plan is detail day-to-day work plan that explains scope, approach resources and work schedules etc.

IV. REQUIREMENTS AND CHALLENGES

Smoke testing

This type of side-effect regression testing is done with the goal of proving that a new build is not worth testing. Smoke tests are often automated and standardized from one build to the next. They test things we expect to work, and if they don't, we suspect that the program was built with the wrong file or that something basic is broken. Challenge is to find eventual errors as early as possible.

End-to-end testing

During the testing, functionalities are carefully examined. For the system to pass end-to-end testing, it needs to be functional and successfully started. The testing conducted can be divided into two different groups: deployment testing verifies successful deployment of proper versions; and functional testing verifies that every component is running and that basic functions are accessible. The main challenge is to ensure that entire eWall system is tested for critical functionalities such as communicating with the interfaces, database, network, and applications.

Usage-based Model testing
Requirement is to look at a system from the perspective of the states, transitions, events and actions that can describe its behavior. It can help identify a statistically efficient subset of those tests that might be worth running first. The automated testing process assumes to be a regular user and takes all the regular actions that a user can take on the system. Challenge is to find and define useful level of granularity.

Load and stress testing
Load testing is aimed at identifying the maximum operating capacity, detection of bottlenecks and measuring response times of a system. The tests are designed to reproduce the conditions where the system is at peak load conditions, but still fully operational. On the other hand, stress testing takes the conditions even further and tests the system above those peak conditions in order to determine the stability of the system and to detect its breaking points. The test scenarios for this group of tests are designed around repetitive tasks from a simulated number of users simultaneously using the application. It gets considerably more challenging to measure the scalability and performance of an interactive multi-user application. Doing so requires special tools and techniques, and a successful measurement and result is highly dependent upon a realistic assessment of the number of users and how they will use the application.

Automated performance tests for the Profiling Server
Screen Shot) – this can be used also for apps tests. Unlike Apache JMeter or SoapUI, these are totally web based (e.g. BlazeMeter records automatically app activity and saves it as JMeter script which can be loaded later or exported directly to Blaze Meter test).

Automated testing by Selenium IDE
Selenium IDE has been established for FireFox and Chrome. In FireFox it is useful to repeat previously recorded test cases. Challenge is to update test cases after changes on web pages and applications.
For the test, LoadStorm [3] is used (although there are plenty of alternatives such as LoadFocus [4], LoadImpact [5], Blitz [6], Loader [7], BlazeMeter [8] and ApiMetrics [9]). Also, the following performance test [10] gives a good overview (link is on results of Prof Server test, notice different fields: Summary, Details, Performance Review, Content Breakdown, Domain,

V. RESULTS OF TESTING

Testing and evaluation of the integrated prototype finished according to the plan of the eWALL project. Tests and integration become more complex and require systematic approach. List of tested applications is as follows: 0hn0 game, DFM, DPAM, HCM, memory card game, memory quiz game, memory test game, sleep, YouTube exercises portal, physical trainer application and eWALL-caregivers-web-app. Functionalities such us: fall detection, motivation messaging, presence detection, luminance, temperature, humidity, weather, notification manager, body motion, goal setting, exercising video, sleep monitoring, doors and windows, sanitary visitors services, voice and sound, messaging, admin tools and security protocols, Pulse, blood pressure and oxygen in blood are developed and implemented. The end-to-end testing finished with the OK status on 24 tests. There are 2 problems recorded in *Issue tracker* related to eWALL portal. Both recorded problems are marked with the "bug" and "minor" labels and milestone. In addition to the end-to-end testing, more than 200 tests were conducted. Requirements become complex as well as challenges. Testing becomes time-consuming work so we should implement in the next testing cycles more automated elements. In this project, we broke the myth that testing can be done by anyone.

VI. CONCLUSION

In process of delivering systems for independent living of senior citizens to end users, evaluation and testing play crucial roles. Main requirements in evaluation of the system are related to planning and execution of smoke testing, end to end testing, usage-based model testing, load and stress testing, automated performance testing. Challenge is to find eventual errors as early as possible and to ensure that entire eWall system is tested for critical functionalities such as communicating with the interfaces, database, network, and applications. In next development cycle we should consider modeling and simulation options due to some aspects of integration are complex to perform with the actual system. Pre-Configuration Management Testing and Post-Configuration Management Testing and implementation of standards for testing and documentation will enable decreasing of costs and increasing of quality of the eWALL system.

REFERENCES

[1] ISO/IEC 14764:2006. Software Engineering - Software Life Cycle Processes – Maintenance
[2] ISO/IEC/IEEE 42010. Systems and software engineering - Architecture description
[3] LoadStorm, http://loadstorm.com/
[4] LoadFocus, https://loadfocus.com/
[5] LoadImpact, https://loadimpact.com/
[6] Blitz, https://www.blitz.io/
[7] Loader, https://loader.io/
[8] BlazeMeter, https://blazemeter.com/
[9] ApiMetrics, http://apimetrics.io/
[10] http://www.webpagetest.org/result/150729_2X_DRN

THE 18TH INTERNATIONAL SYMPOSIUM ON WIRELESS PERSONAL MULTIMEDIA COMMUNICATIONS
(WPMC-2015)
December 13-16, 2015, Hyderabad, India

Identifying Root Causes for Students Problems in Technical Education using Fishbone Diagram

Shinde Dnyandeo Dattatraya
Department of Mechanical Engineering
Sandip Foundations, SIEM, Mahiravani, Trimbak Road
Nashik - 422013, India
dnyandeo.shinde@siem.org.in

Shwetambari Sanjay Ahirrao
Sandip Foundations, SIEM, Mahiravani, Trimbak Road
Nashik - 422013, India
shweta.ahirrao23@gmail.com

Prachi Dilip Shinde
Sandip Foundations, SIEM, Mahiravani, Trimbak Road
Nashik - 422013, India
shinde.prachi246@gmail.com

Prof. Dr. Morten Falch
Center for Communication, Media and Information Technologies (CMI), Aalborg University Copenhagen
A.C. Meyers Vænge 15, DK-2450 Copenhagen SV, Denmark
falch@cmi.aau.dk

Prof. Dr. Rajendra G. Tated
Principal, Sandip Foundations, SIEM, Mahiravani, Trimbak Road, Nashik 422013, India
rgtated@gmail.com

***Abstract*— Fishbone diagram is a tool used in Industries to identify the root cause of the problems. An attempt has been made in this paper to use this technique to identify problems in engineering education system in India, considering student as the stakeholder. Major problems are classified and fishbone diagram is used to analysis the root causes of each parameter.**

Keywords*— Fishbone diagram, Root cause analysis, Engineering education system, students problems.

I. INTRODUCTION

The current imbroglio in the teaching and learning process depends on the three major stakeholders; which are staff, students and the methods used to teach. In this scenario, the every stakeholder plays an equivalent role in the success or failure of the system. Thus, looking at all the three parameters this paper has initiated to do the root cause analysis in one of the most interesting parameter i.e. students. This paper deals with the problems arises in the lives of student in this circle of technical (engineering) education system. Analysis of the problems is going to be done with the help of the fishbone cause and effect diagram.

This method proves to be effective in order to reach the root cause of some issue. In this process there are major parameters; which acts as the main points or as a general term of one compiled problem and then on which further sub-issues are discussed. For example: this skeleton of a fishbone diagrams depict the causes of the problem until its root cause.

The outcomes that we expect from this analysis are we will be able to identify the ultimate or the root causes faced by the students. In this way, we will be able to propose a common solution their problems and also suggests education (Indian) system to upgrade their policies and methods. This paper makes an effort to mitigate the flaws in the technical Indian education system thus, increasing its efficiency and strengthening its position in the global education scenario.

II. LITERATURE REVIEW

A. Fishbone Diagram

The Ishikawa diagram is a tool to recognize the root causes of quality imbroglios. It was named after Kaoru Ishikawa, a Japanese quality control statistician, the man who pioneered the use of this chart in the 1960's. The Fishbone diagram is a process of breaking down the known truths that provides an orderly way of observing at result and the reason that account for those effects. Because of the intention of the Fishbone diagram, it may be delegated as a cause-and-effect diagram by Watson in 2004. Fishbone (Ishikawa) diagram mainly represents a model of suggestive presentation for the correlations between an event (effect) and its multiple happening

causes. The structure provided by the diagram helps team members think in a very systematic way[1].

Fishbone diagram is effectively used to reach the root cause of the problem. Some of the cases are discussed herewith. Jayswal et al. has used this to analysis of sustainable process of chemical/energy sector[2]. Quantification of risk assessment for FMEA analysis in processing industry[3].

Use of Fishbone in Educational sector is reflected in few cases. Reid[4] use this for categorising barriers of instructional technologies. Jih,Huang[5] used it for analysis of e-teaching. Use of 5why technique for questioning technique was done in Thiwan by Lu[6]. Problems in University colleges where analysed by Desai et al[7]. However the analysis is to be done in Indian perspective.

B. Scenario of Indian Engineering Education System

The pattern in the graduates passing every year is observed and is variable. However, this pattern changes in India. There are three variables – sanctioned intake (S), the enrolment (E) and the Output or Out-turn (O). These are defined as follows: (a) Sanctioned Intake - The AICTE approves the sanctioned intake of different engineering colleges in each state. This is for a given year. (b) Enrolment - The actual number enrolled (joining the course) may differ from the sanctioned strength. In many institutions all seats may not be filled. (c) Outturn / Output - The numbers that graduate each year. This is not reported on an all India basis. In some of the state reports (ATMRs) the annual output is reported for a few years.[8]

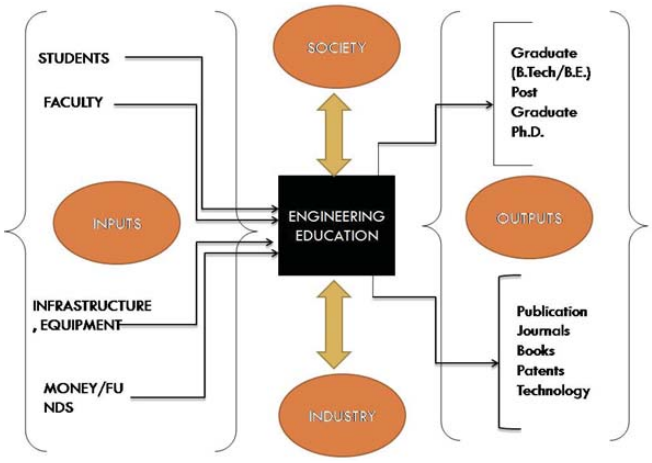

Fig. 1. Engineering Education in India[8]

The block diagram shown in Fig. 1 describes the Indian engineering education system. The four main stake holders are the society, industry, inputs and outputs. As engineering education is a professional technical degree which servers for four years course with many outcomes being either bad or good. The inputs are induced by students, faculty, infrastructure, money these are the factors which influence the engineering education system on a whole and further more joined by the society and the industry at regular intervals and all this resulting into the outputs shown in the figure namely the various degrees of graduation or the post graduation and the publications[8].

III. STUDENTS PROBLEMS WITH FISHBONE DIAGRAM

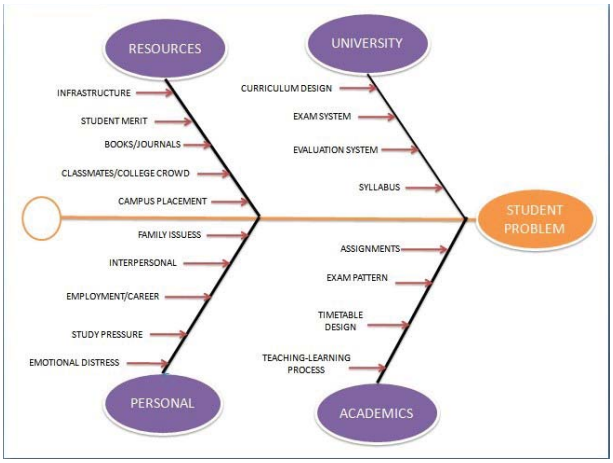

Fig. 2. Root Cause Analysis of Students Problems

The Fig.2 shows the root cause analysis of the student problems with the help of fishbone diagram. The main reasons are personal, universities, resources, academics. These main factors have sub-factors which takes us to the root cause of these problems.

A. Personal

Zhibin Chen reveals in his paper Psychological Problems and Countermeasures of College Students all the personal and psychological problems which a college student faces being in college. On further adaptation, the paper tells us that nowadays it's a very major issue in the college life to have these problems and many students are diagnosed with these disorders.

Zhibin jotted down few causes for these emotional unbalance in a student's mind. They were as follows: interpersonal tensions, Crises of employment and career prospectus, study pressure, Emotional distress, psychological expectations do not meet family, contemporary social impacts, inertia in inherent traditional educational models, family reasons, and traditional Chinese cultural factors. The above mentioned causes are relevant and do exists in the lives of student[9].

One more parameter that is to be considered is that there are no proper career councilors available for students to guide them in their journey to become a successful engineer. According to Lie Pan, Haiyan WU and Xun Wang career councilors say that access to information is the key to employment. There are various mediums to seek information like campus network, University Career Guidance Website, Job network, customized services. According to the authors student are keen to work and get employed but the only issue is they do not have the right platform to do so. They lack information and the seriousness of employment in the colleges while getting educated. Colleges should increase the propaganda of the employment issue right from the first year itself[10].

B. Academics:

The sub reasons that come under the academics as a stakeholder are as follows: 1. Assignments, 2. Exam pattern, 3. Timetable design, 4. Teaching and learning process. Now considering each pattern separately we get to know that the higher technical education demands the various assessments based to test a set of skill of a student on his problem solving skills, logic abilities, etc. The candidate has to solve these assignments and prove his worth in every assignment in order to get good grades in the term work grades and ace his exams. These assignments also reflect the student's capabilities to understand the topic. The assignments should be designed in such a way that they are good enough to test skills but not intimidate the student. However according to the author Rekha and Uma many a times home assignments are not taken seriously by the students and a lot of copying is involved thus making it unfair to grade their work[11].

Author as a student has an opinion that, students have an issue with assignments when excessive assignments are forced on them. To the point assignments which will reflect their abilities are considerable although just writing for the sake of assignments does no good. In the engineering education excessive assignments plays a key role in wasting the time of the student. However a good assignment if replaced with these unnecessary work; it will definitely help to improve the scenario of Indian engineering education. For this need of different technique to get the things done in more practical way is necessary, which can be done by Problem Based Learning (PBL).

Secondly, exam pattern is a very prime issue in understanding the difficulty to get good grades in the exam. Every student's perception of the getting adapted to the education system is different and also the estimated time for getting adjusted with the system may differ. This difference often results into the failure or a major setback for the student. Understanding the exam pattern is very important in order to write the exams. In universities over the time many patterns have changed which confuses the student to a larger extent. Students take time to understand exam pattern, which results in their gradation. They focus on scoring in exams but the actual conceptual study is missing. Thirdly, timetables play a crucial role in any academic system. A well designed timetable is always a key to more success stories in the engineering education. Timetables can be of exam as well as the daily scheduled lectures. Academic timetable should take care of basic workload as per the university guidelines, as well as it should take care of co-curricular and extra-curricular activities of the students. It should as well consider the time required for student upgrading and merging the gap between syllabus and present requirements from the recruiters. Both the timetables should be designed in such a way that they take care of all norms but are also student friendly, are designed by making student as the focus considering their study and work.

Lastly, another very important factor is the teaching-learning methods. Latest techniques of teaching-learning should be used like : PBL, e- Learning, ICT etc. In Indian education system traditional teaching method should be supplemented with these recent techniques for excellent results.

C. Resources

As like requirements of materials in industries, resources are required for education. One of the causes for student's failure is resources. This cause highlights the various shortcomings as college infrastructure, variation in students merit and tradition, books, journals etc.

The college infrastructure plays a vital role in the education of the students, if it's not well built than there will be obstacles in the overall development of the student. Some of the most basic necessary elements that a college campus should have are: well-equipped classrooms and laboratories, as the norms mentioned by the university syllabus. Library with sufficient books, journals, newspapers, magazines, e-library with access to online books and journals proves to be an important aid in education.

Classmates are also major reason for the student to be disinterested in the curriculum. If the college crowd is not good as in the students are not study oriented they affect the performance of the student as they might distract the student's focus from the studies and divert it elsewhere. This may happen if there is large difference in students merit during intake.

Campus placement also plays major role. Also access to industries through industrial visits, expert lecture series through industrial person, in-plant training, internship, projects is required for overall growth of the students. Some colleges fail to do so even they are advertising; this decays the moral of the students.

D. Universities

Role of universities is very important because the entire educational course is governed by it. Curriculum design is the most important parameter. Examination system and evaluation system also affects the output of the students. It should be taken care to match the syllabus with latest technologies.

IV. RESULTS AND DISCUSSION

By using Fishbone diagram, it is easy to reach till the root cause of the problem. Four major aspects of the source of problems are identified and causes of the same are discussed

References

[1] G. Ilie and N. Ciocoiu, C, "Application of Fishbone Diagram to Determone the Risk of An Event With Multiple Causes," *Manag. Res. Pract.*, vol. 2, no. 1, pp. 1–20, 2010.

[2] A. Jayswal, X. Li, A. Zanwar, H. H. Lou, and Y. Huang, "A sustainability root cause analysis methodology and its application," *Comput. Chem. Eng.*, vol. 35, no. 12, pp. 2786–2798, 2011.

[3] P. Taylor and T. H. Varzakas, "Application of ISO22000 , Failure Mode , and Effect Analysis (FMEA) Cause and Effect Diagrams and Pareto in Conjunction with HACCP and Risk Assessment for Processing of Pastry Products," *Crit. Rev. Food Sci. Nutr.*, vol. 15:8, no. July 2015, pp. 762–782, 2011.

[4] P. Reid, "Categories for barriers to adoption of instructional technologies," *Educ. Inf. Technol.*, vol. 19, no. 383–407, pp. 383–407, 2014.

[5] H. J. Jih and T.-Y. Huang, "e-Teaching Empowered by Knowledge Visualization :," *IEEE Conf.*, vol. 65, no. 1, pp. 6560–6564, 2011.

[6] C. Lu, "How to build a 5Why scaffolding guided questioning teaching case film ? Campus insects unit as an example," *Asia-Pacific Forum Sci. Learn. Teach.*, vol. 14, no. 1, pp. 1–16, 2013.

[7] M. S. Desai and R. A. Johnson, "Using a fishbone diagram to develop change management strategies to achieve first-year student persistence.pdf," *SAM Adv. Manag. J.*, pp. 51–64, 2013.

[8] R. Banerjee and V. P. Muley, "Engineering education in India," 2007.

[9] Z. Chen, "Psychological Problems ans Countermeasures of College Students," in *International Conference on Optics, Photonics and Energy Engineering*, 2010, pp. 129–132.

[10] L. Pan, H. Wu, and X. Wang, "Research on Employment of College Students Oriented Information Dissemination," in *2010 2nd International conference on Education Technology and Computer*, 2010, pp. 533–536.

[11] R. Ramesh and U. P. Rao, "Investigating the impact of in-class assignments on higher order thinking skills of students in engineering course," in *International Conference on Learning and Teaching in computing Engineering*, 2015, pp. 95–99.

Effect of Newly Designed Burnishing Tool on Surface Micro hardness of AA6351

A. S. Maheshwari[1]
[1] Department of Mechanical Engineering,
Sandip Institute of Technology & Research Centre,
Nashik. (Maharashtra), India
maheshwari.anil@sitrc.org

Dr. R. R. Gawande[2]
[2] Department of Mechanical Engineering,
Bapurao Deshmukh College of Engineering,
Wardha (Maharashtra), India
wsbdcoe@rediffmail.com

Abstract: ***Burnishing is a simple, cost effective surface improvement process that not only improves surface finish but also surface micro hardness of the component. In burnishing process rotating ball or roller is pressed on the surface of the work piece beyond elastic limit of the material, so that plastic deformation of the material takes place, which induce residual stresses compressive in nature on the surface of the material.*** [1] ***The newly developed cost effective ball burnishing tool can be used on conventional lathe machine. By using the designed tool Surface micro hardness of 150.2 HV is achieved. Number of passes and depth of penetration proved to be the predominant parameters among the parameters studied.***

Keywords- Burnishing tool, Burnishing, Surface micro hardness, feed rate, number of passes

I. INTRODUCTION

The functional performance of a machined component, such as load bearing capacity, fatigue strength, wear resistance depends upon surface characteristics like surface topography, residual stresses, and hardness. The functional properties can be increased either by using new material or by means of surface plastic deformation process. Conventional surface finishing methods like grinding, honing, lapping especially depends upon chip removal to attain desired surface finish, these machining chips may cause further abrasion and geometrical tolerance problem, especially if conducted by unskilled operators.[2] Accordingly surface deformation process like burnishing offers an attractive post machining alternative due to its chip less and relatively simple operations. It not only improves surface finish of the material, but also improves surface hardness and in turn it increases fatigue strength, corrosion resistance and wear resistance of the material by inducing residual compressive stresses on the surface.[3] Based on literature survey, feed, speed, depth of penetration and number of passes are chosen as burnishing parameters. Kerosene is used as lubricant, throughout the experimentation. The effect of above parameters on surface hardness is studied. The ball burnishing mechanism is shown in fig. 1.

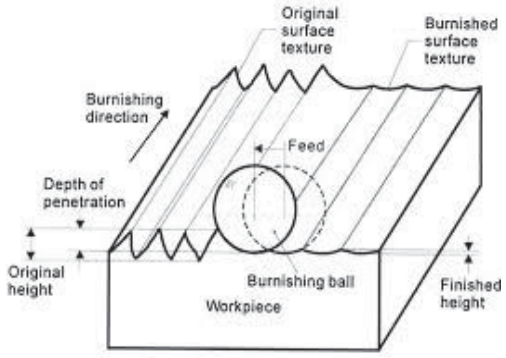

Fig 1. Burnishing Mechanism

II. LITERATURE REVIEW

N. H. Loh et al. explored effects of burnishing parameters like depth of penetration, feed, ball material and lubricant on surface hardness of AISI 1045 specimens. Based on their research the layer of maximum surface hardness lies beneath the burnishing surface. Grease gives maximum hardness of 331VHN. Hardness is increased by 68%.[4]

Fang-Jung Shiou et al used Taguchi L18 orthogonal array technique and ANOVA to investigate surface hardness value. Based on results, the hardness of the specimen, which was tested, increased to 480 on Vickers hardness scale from about 338 after ball burnishing process. The thickness of the harden layer was about 30 µm. By using the optimum values of burnishing parameters for plane burnishing to the surface finish of the freeform surface mold cavity, the surface finish improvement of the injection part on plan surface was about 62.9% and that on freeform surface was about 77.8%..[5]

N.S.M. EL-Tayeb et al. used Radial Basic Function for predicting Surface Integrity after burnishing. For prediction of surface roughness, they used artificial neural network (ANN) and radial basic function (RBF) techniques. Artificial neural networks are computing elements, which are based on the structure and function of the biological neurons. These networks have nodes or neurons, which are described by difference or differential equations. The nodes are interrelated layer-wise or intra-connected among

each other. Each node in the successive layer receives the inner product of synaptic weights with the outputs of the nodes in the previous layer when the vectors are binary or bipolar, hard-limiting non-linearity is used. When the vectors are analog, a squashed function is used.[6]

Adel Mahmood Hassan and Aiman Sharef Al-Bsharat studied the effect of burnishing process parameters on properties of material like surface roughness, hardness. It was found that surface hardness decreases with increase in feed rate and speed and increases with increase in force and number of passes. The percentage increase in surface micro hardness observed was around 60%. [7]

Aysun Sagbas analyzed effect of burnishing parameters on surface hardness of Aluminum 7178, using full factorial design nd analysis of variance. (ANOVA) Feed rate, burnishing force and number of passes were found as main burnishing process parameters to improve surface hardness. [8]

III. BALL BURNISHING TOOL

Ball burnishing tool is designed for conventional lathe machine. This tool is designed in such a way that ball can rotate freely. For this purpose instead of keeping ball on outer race of the bearing, 12 mm diameter ball is supported on 14 mm ball. Front adapter is also interchangeable, so that we can use ball of different diameters in the same tool. The spring is used to reduce sticking between ball and workpiece due to friction. To measure depth of penetration dial gauge is mounted on the tool, so that we can measure depth of penetration accurately.

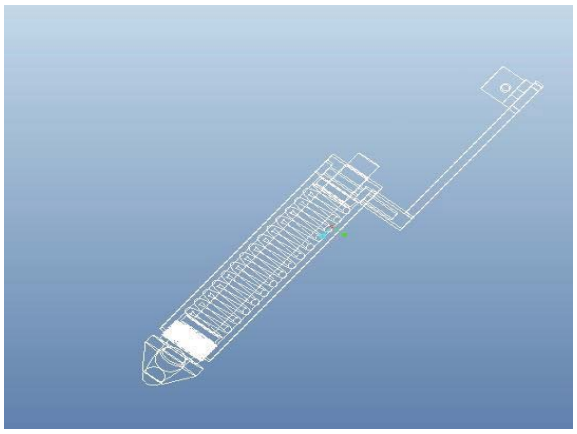

Fig. 2 Ball Burnishing Tool

IV. MATERIAL SELECTION

The experimental work is carried out to explore the effect of different ball burnishing process parameters on surface micro hardness of AA6351 alloy. Aluminum alloy is widely used in automobile and aerospace sector due to its properties like corrosion resistance, high strength to weight ratio. Aluminum alloy used for experimentation is most widely used alloy in wide variety of general applications in small scale industry as well as large scale industries. Aluminum is chosen as its weight to strength ratio is high and can be further improved by using burnishing process.

The composition of alloy and mechanical properties are given in Table 1 and Table 2 respectively.

Table 1: Composition of work material

Element	Cu	Mg	Mn	Si	Fe	Al
Weight %	0.1	0.4 - 1.2	0.4 - 1.0	0.6-1.3	0.6	Remainder

Table 2 Material Properties of work material

Density g/cc	Tensile Strength Mpa	Yield Strength Mpa	Hardness, HB	Modulus of Elasticity , GPa	Poisson's ratio
2.6-2.8	250	150	95	70-80	0.033

V. SPECIMEN PREPARATION

Solid bars of AA6351 Aluminum alloy of 26 mm are taken and turned on lathe machine as shown in fig below, keeping all process parameters same while turning all specimens.

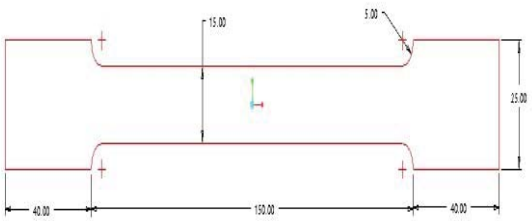

Fig.3 Specimen

VI. EXPERIMENTATION

5.1 Process Parameter Selection:

The factors and their levels are shown in table 3. Feed, speed, depth of penetration and number of passes are adopted as factors which vary during experiments. The values of the factors are decided based on pilot experiment carried out.

Table 3: Levels of factors for experiment design

Factors / Levels	Code	Low(-)	High(+)
Feed Rate (mm/Rev)	A	0.04	0.051
Speed (rpm)	B	800	900
Depth of Penetration(mm)	C	0.50	0.75
No. of tool passes	D	1	2

For each factors, two levels are deliberately chosen and set during experiments according to the DOE. Table 4 shows the selected design matrix. All these data were utilized for the analysis and evaluation of optimum parameter combination required to achieve desired surface micro hardness within the experimental domain.

Table 4: Design of Matrix and Results

Run	Actual Values				Surface Micro hardness value (After Burnishing)
	A	B	C	D	
1	0.04	800	0.50	1	142.9
2	0.04	800	0.50	2	143.4
3	0.051	800	0.50	1	144.8
4	0.051	800	0.50	2	140.6
5	0.04	900	0.50	1	142.4
6	0.04	900	0.50	2	146.8
7	0.051	900	0.50	1	144.7
8	0.051	900	0.50	2	145.9
9	0.04	800	0.75	1	147.7
10	0.04	800	0.75	2	144.8
11	0.051	800	0.75	1	143.4
12	0.051	800	0.75	2	150.2
13	0.04	900	0.75	1	145.7
14	0.04	900	0.75	2	146.9
15	0.051	900	0.75	1	142.5
16	0.051	900	0.75	2	145.7

Experiments were carried out based on experimental design matrix. The experimentation for burnishing operation is done on conventional lathe. The surface roughness measurement is done on surface tester. Table 4 shows selected design matrix based on Taguchi L16 orthogonal array consisting of 16 sets of conditions. All this data is used for conduction of actual experimental work on lathe. Experimentation is done on experimental matrix developed by Minitab 15 and results are evaluated for surface micro hardness of AA6351 Alloy. The objective of the present work is to explore the effect of feed rate (mm/rev), speed (rpm), depth of penetration (mm) and number of passes on AA6351 alloy. In this investigations "surface micro hardness" is typically chosen as response variables. The entire investigation is carried out on conventional lathe machine.

Fig. 4 Experimental Setup

Fig. 5 Burnishing Process

Table 5 Effect of Different Parameters

Factors	SS (Sum of Squares)	DF (Degree of freedom)	MS (Mean Square)	F (Variance Ratio)	% P (% Contribution)
A (feed rate)	0.0582	3	0.0160	1	1.358
B(speed)	0.1145	3	0.0378	2.37	3.263
C (depth)	2.2570	3	0.7503	46.79	64.71
D (passes)	1.0964	3	0.3588	22.48	30.88
Total	3.5241	12	1.1629		

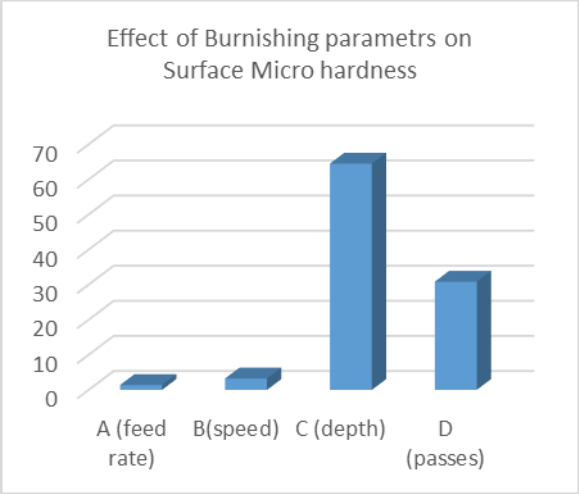

Fig. 6 Effect of Different Parameters on Surface Micro hardness

VII CONCLUSION AND DISCUSSION

1. The micro hardness value depends on burnishing parameters. Depth of penetration and number of passes are the major parameters in improving surface micro hardness of the material.
2. Depth of penetration is the predominant parameter among the parameters taken during experimentation. Its contribution is 64.717% among the parameters taken.
3. Along with depth of penetration, number of passes also plays role in improving surface micro hardness. (30.88 %)
4. It is also observed that if initial surface roughness is more, amount of plastic deformation will be more and hence surface micro hardness will be more.

VIII FUTURE SCOPE

The burnishing operation is successfully carried out on AA6351 Alloy which shows the improved results for surface finish as well as surface micro hardness. Following work can be carried out to check other properties of alloy.

1. Empirical models can be developed for surface hardness as well as other properties of material.

2. FEM analysis can be carried out, so that we can predict the surface roughness, micro hardness, residual stress etc.

3. By changing ball material and ball diameter better surface quality can be achieved.

4. Optimization of parameters can be done to improve surface integrity of material.

References:

[1] M. H. El-Axir, O. M. Othman, and a. M. Abodiena, "Study on the inner surface finishing of aluminum alloy 2014 by ball burnishing process," *J. Mater. Process. Technol.*, vol. 202, no. 1–3, pp. 435–442, 2008.

[2] A. M. Hassan, "The effects of ball- and roller-burnishing on the surface roughness and hardness of some non-ferrous metals," *J. Mater. Process. Technol.*, vol. 72, no. 3, pp. 385–391, 1997.

[3] F. Gharbi, S. Sghaier, K. J. Al-Fadhalah, and T. Benameur, "Effect of ball burnishing process on the surface quality and microstructure properties of aisi 1010 steel plates," *J. Mater. Eng. Perform.*, vol. 20, no. 6, pp. 903–910, 2011.

[4] N. H. Loh, S. C. Tam, and S. Miyazawa, "Surface hardening by ball burnishing," *Tribol. Int.*, vol. 23, no. 6, pp. 413–417, 1990.

[5] F. J. Shiou and C. H. Chen, "Freeform surface finish of plastic injection mold by using ball-burnishing process," *J. Mater. Process. Technol.*, vol. 140, no. 1–3 SPEC., pp. 248–254, 2003.

[6] N. S. M. El-Tayeb, K. O. Low, and P. V. Brevern, "Influence of roller burnishing contact width and burnishing orientation on surface quality and tribological behaviour of Aluminium 6061," *J. Mater. Process. Technol.*, vol. 186, no. 1–3, pp. 272–278, 2007.

[7] A. M. Hassan and A. S. Al-Bsharat, "Influence of burnishing process on surface roughness, hardness, and microstructure of some non-ferrous metals," *Wear*, vol. 199, no. 1, pp. 1–8, 1996.

[8] A. Sagbas, "Analysis and optimization of surface roughness in the ball burnishing process using response surface methodology and desirabilty function," *Adv. Eng. Softw.*, vol. 42, no. 11, pp. 992–998, 2011.

THE 18TH INTERNATIONAL SYMPOSIUM ON WIRELESS PERSONAL MULTIMEDIA COMMUNICATIONS
(WPMC-2015)
December 13-16, 2015, Hyderabad, India

Application of Real Coded Genetic Algorithm to Dynamic Layout Benchmark Problem

Kailas V. Chandratre
Research Scholar, Production Engg. Department,
K.K.W.I.E.E. & R,
Nasik, India
ckailas@rediffmail.com

Dr. P.J. Pawar
Professor, Production Engg. Department,
K.K.W.I.E.E. & R,
Nasik, India

Dr. K.N. Nandurkar
Principal & Professor K.K. W. I.E.E & R
Nasik, India

***Abstract*— in the current scenario of industries, the product mix and demands are very frequently changing and so the quick response is expected from industry. Layout design has a significant impact on manufacturing efficiency. A static plant layout if possible to be converted to dynamic layout may improve the efficiency of the plant significantly. Dynamic layout is a layout, which can be rearranged with respect to time as per variation in product design, quantity, and change in product mix. Dynamic layout problem is a quadratic assignment problem and is of non-deterministic polynomial-time (NP) hard problem. In this work, real coded genetic algorithm (RCGA) is applied to solve benchmark problem in dynamic layout, which gives better results than the reported.**

Keywords—Dynamic layout, Real coded genetic algorithm.

I. INTRODUCTION

Layout planning gives a significant impact on the performance of a manufacturing or service industry system, and consequently has been an active research area for several decades. Layout is the arrangement of facilities, machines, or departments in the plant, such that it makes it convenient for movement, operations of man, material and reduces the material handling. Generally, once the plant layout is finalized, it is not changed. This type of layout is called as static layout. However, in due course of time, because of change in product quantity or product mix or change in product itself, the static layout may not remain optimum. It may result in more material handling cost and more time or delay. So, to overcome this problem, if the layout is changed from time to time; with respect to change in product mix or quantity such layout is called as dynamic layout. In today's challenging conditions, frequent changes in the products, product mix, and quantity, the static layout may not be effective, as it will result into more material handling and subsequently higher material handling cost. Therefore, it is essential to consider the dynamic approach in such cases to increase the effectiveness of the plant.

Dynamic layout problem becomes more and more complex as the number of departments and the number of time periods are increasing. It is non-deterministic polynomial-time (NP) hard problem [6] and generally, this problem is formulated as quadratic assignment problem (QAP). Many times solving the complex dynamic layout problem is difficult with traditional methods of optimization [27]. Hence, the researchers are attempting metaheuristics such as Genetic Algorithm (GA), Simulated Annealing (SA), and Tabu Search (TS) etc. for solving dynamic layout problems. The dynamic layout problem has wide applications in industries where the product mix is highly prone to change according to the market demand. Developments in the materials and machine handling technology are very useful for changing the layout frequently. In this paper benchmark problems are solved using RCGA.

II. LITERATURE REVIEW

Traditionally layout planning is treated as strategic decision, which once implemented is difficult to modify. Advent of new material handling technology and materials used for manufacturing of modern machine tools has changed the perspective of layout planning. Development of mathematical models and use of recent and powerful problem solving methodologies proved to be very useful to improve the effectiveness of plant operations. Various researchers have tried to solve the dynamic layout problem using various approaches as discussed in this section.

Lenin et al. [25] have presented a genetic algorithm approach, to find out machine's linear sequence with multi products and different operation sequences for static layout. They have tried to minimize the total flow distance travelled by the product. They have generated some problems and their approach was compared with other approaches. Presented approach was found to give results that are more favorable. However, they have not considered the dynamic conditions and only virtual problems are considered. Brunese and Tanchoco [9] have studied single row machine layout problem with the within building constraints, because of which they could get improved quality of solutions in reduced time. To achieve these results authors have used nonlinear and mixed integer formulations. However, they have not considered the multi row layout and dynamic conditions. Bock and Hoberg [8] have planned layout in more detailed way, by considering

machine layout and transportation paths simultaneously. They have introduced new mathematical layout model and suggested several solution procedures to solve it. Promising results are obtained to the author when it was tested with randomly generated instances. However, the authors have used randomly generated instances and have not considered the dynamic conditions and real life industry problems. Goncalves and Tiberti [17] have proposed a new approach of genetic algorithm, for the machine cell layout design. It is working on group encoding instead simple machine encoding, also new crossover and mutation operators are suggested. The tests show that the algorithm is able to disclose the group structure. However, the authors have not considered the changing product mix and quantity. Solimanpur and Kamran [34] have assumed a shop floor with multiple products, on multiple machines; and the alternate processing routes are considered to minimize total distance travelled by material. Genetic algorithm is applied to solve this problem. The effectiveness of the approach is evaluated by numerical example and results show that applied GA is effective and efficient. However, the applied approach does not consider the changing demand.

Above review shows that most of the researchers have considered the static nature of layout for optimization. However, current scenario of industry shows the trend of changing demand, change in product mix and quantity. Therefore, to cope up with this changing scenario it is necessary to consider dynamic layout concept. Though dynamic layout is a new approach to industry, few researchers have worked on it.

Moslemipour and Lee [32] have suggested QAP formulation to solve Dynamic machine layout problem in flexible manufacturing system (FMS). They have considered the variation in product demand for changing the layout and have solved two randomly generated dynamic problems. These are solved with SA approach and have obtained satisfactory results. However, the problems they have considered are computer generated and virtual. Donga et al. [11] have studied dynamic multistage facility layout problem, in which new machines can be added or removed at different planning periods. They have proposed and used an auction algorithm, which is based on SA algorithm. To illustrate the proposed methodology an industrial case of 4 periods and 56 machines are employed. The results obtained are efficient. However, for discrete category problems, GA approach is more useful. Azimi and Charmchi [4] have suggested a new heuristic algorithm, which is developed by combining mathematical programming and simulation methods for dynamic facility layout problem with budget constraint. Proposed algorithm was tested over wide range of problems and the improved results were obtained. However, real case study needs to be solved. Mohammadi and Moghadam [31] have studied dynamic machine layout for automotive shop; and suggested a model to solve it. A problem of seven machines and seven-time periods is assumed, and satisfactory results are obtained. However, they have not considered the changing product mix. Ashthiani et al. [3] have discussed the dynamic plant layout problem. They have proposed multi start simulated annealing approach to solve this problem. To compare the performance of the approach some data sets are selected from the literature and the results show good performance. Krishnan et al. [23] have developed 'Dynamic from between chart' approach to solve dynamic plant layout problem. A case study from Aircraft Company has been considered for verification of approach. However, they have not considered machines layout. Ahin and Turkbey [2] have presented a new approach 'TABUSA' to solve the dynamic facility layout problem. The presented heuristic is based on simulated annealing approach supplemented with tabu list. The efficiency of the approach is tested against the data sets from literature. Baykasoglu and Gindy [7] have used SA to solve dynamic layout problem. Some problems from literature are solved and the results are compared. Jinde and Telsang [21] apply a genetic algorithm approach to electrical motor manufacturing company to minimize material handling cost between machines. The problem is formulated in QAP and the results show that GA approach is performing well. However, the authors have considered static layout problem only.

Above literature, review shows that most of the researchers have worked on design of plant layout, using various algorithms and various approaches. Still there is scope to consider dynamic machine layout problem. With various changing parameters, real coded genetic algorithm can also be seen as new approach for solving these problems.

III. Presented Approach

When the flow of material between departments changes during a planning horizon, the static layout problem (SLP) becomes dynamic, and this problem is known as the dynamic plant layout problem (DPLP). The DPLP is based on the anticipated changes in flow that can occur in the future. The prospective future is divided into a number of time periods and the period may be defined in weeks, months, etc. The solution for the SLP is a single layout, and the solution for the DPLP is a series of layouts, where each layout is associated with a particular period. This problem is of the category of NP hard problem. [27]

A. Mathematical Formulation

The above problem is more commonly formulated as the QAP, and it is taken from Balakrishnan et al. [6], where minimizing total material handling cost Z is the objective function, it can be expressed in terms of the variables like f, d, and t.

$$\text{Min } Z = \sum_{p=1}^{P}\sum_{i=1}^{n}\sum_{j=1}^{n}\sum_{k=1}^{n}\sum_{l=1}^{n} f_{ikl} d_{ijl} X_{ij} X_{kl} + \sum_{p=2}^{P}\sum_{i=1}^{n}\sum_{j=1}^{n}\sum_{k=1}^{n}\sum_{l=1}^{n} A_{ijl} Y_{ijl} \quad (1)$$

Subject to,

$$\sum_{i=1}^{n} X_{tij} = 1, \quad j = 1,\ldots,n, \quad t = 1,\ldots,P \qquad (2)$$

$$\sum_{j=1}^{n} X_{tij} = 1, \quad j = 1,\ldots,n, \quad t = 1,\ldots,P \qquad (3)$$

$$Y_{tijl}=X_{(t-1)ij}*X_{til}, \; I,j,l=1,\ldots n; \; t=2,\ldots,P \qquad (4)$$

Where
P : Number of time periods in planning horizon
n : Number of machines in the layout
i,k : Machines in the layout
j,l : Locations in the layout
f_{ik} : Flow cost from machine i to k
d_{jl} : Distance from location j to l
Y_{tijl} : 0,1 variable for shifting i from j to l in period t
X_{tij} : 0,1 variable for locating machine i at location j in period t
A_{tijl} : Cost of shifting from j to l in period t. ($A_{tijj} = 0$)

Equation (1) is the addition of the material flow cost and layout rearrangement cost at the planning horizon. Equations (2) and (3) state that every machine must be located and each location must be occupied in every period. Equation (4) states that the 0-1 departmental rearrangement variable takes on a value of 1, only if at the end of a period machine shifts its location.

There can be *N!* possible layout arrangements, for *N* machines. Enumeration of which is a very difficult approach to solving the QAP. However, as the problem size *(N)* increases, the number of possible arrangements (*N!)* also increases. This approach aims for good solution, which is indicated by solution obtained in shortest processing time and comparable to results obtained by other algorithms. Hence, the goodness of any solution approach is adjudged against known example problems, for which the best solutions have been claimed.

B. *Real Coded Genetic Algorithm*

Goldberg [15], has discussed the approach for binary and real coding of GA. GA imitates the mechanism of the natural selection and evolution and aims to solve an optimization problem with object function *f(x)* where $x=[x_1\ x_2\ \ldots\ldots\ x_n]$ is the N-dimensional vector of optimization parameters. For any combinatorial optimization problems, it has proved to be an effective and powerful global optimization algorithm, especially for discrete optimization parameters, non-differentiable and discontinuous object function.

Binary GA is made up of *genes* and *chromosomes*. Binary code string is used to encode the optimization parameters in conventional binary GA. A binary bit is called as a gene in GA. While dealing with continuous search spaces with large dimensions, and in the requirement of high numerical precision, Real coded genetic algorithm (RCGA) possesses many advantages over its binary coded counterpart. Each gene represents a variable of the problem in RCGA, and the size of the chromosome is kept the same as the length of the solution to the problem. Without sacrificing precision, RCGA can deal with large domains unlike the binary implementation (assuming a chromosome of fixed length). In addition, RCGA possesses the capacity for the local tuning of the solutions; it also allows integrating the domain knowledge to improve the performance of genetic algorithm (GA).

The binary GA does not operate directly on the optimization parameters but on a discretised representation of them. Discretization error will inevitably be introduced when encoding a real number. The operations like encoding and decoding also makes the algorithm more computationally expensive when the problem uses real optimization parameters. Both practical experiences and theoretical proof show that RCGA usually works better than binary GA, especially for problems having real optimization parameters. [19]

The RCGA operates on chromosome population (or creatures, individuals, etc.) simultaneously. It starts from an initial population, and randomly generated within the search space. Once initialization is completed, the population enters the main RCGA loop and performs a global optimization for searching the optimum solution of the problem.

GA has some limitations such as all offspring are accepted and their parent strings are abandoned at the end of every generation regardless of their fitness values. Because of this, there is a risk of replacing good parent strings with deteriorated child string. However, in the methodology of RCGA presented in this paper, the good parent strings are also restored with the good child strings and the care is taken that both good parent and child strings will go to the next generation. Another limitation of GA is that only good parents are given chance to produce the offspring, this is also taken care in the methodology of RCGA, as roulette wheel selection is employed the chance is given to all parent strings. Hence, the answers obtained are near optimal.

C. *Algorithm for RCGA*

Step 1:- The parameters like Probability of *Crossover (p), Probability of Mutation (q), population size and termination criteria* are defined.

Step 2: -A set of possible solutions called the *"Initial Population"* is initialized such that the values range uniformly throughout the search space.

Step 3:- The *Fitness Values* are calculated for each of the individuals and the population is sorted in the decreasing order of the fitness.

Step 4:- Using the "*Roulette Wheel*" method of *'Selection'*, few individuals are selected to undergo *crossover*.

Step 5:- According to *Crossover Probability* the *'Crossover'* between two individuals produces two '*Child Chromosomes*'.

Step 6:- Then using the '*Probability of Mutation'*, a few individuals are mutated.

Step 7: At the end of performing crossover and mutation, we obtain the crossover and the mutated child individuals. These along with the parent population form super set for the next generation population.

Step 8:- The Steps 3 to Steps 7 are repeated until the '*Termination'* condition is reached.

Step 9: The population obtained at the end of the specified number of iterations is the outcome of this process.

IV. Application of Algorithm

Here, an example is considered, which is a standard benchmark function for dynamic layout problem [33].

Example :

Standard benchmark function for dynamic layout problem with 6 machines and 5 periods given by Rosenblatt M. J.[33], is shown in Table 1. It shows the flow between the machines. The distances between the machines are assumed to be one unit and the layout is of 2 rows and 3 columns. To this problem, RCGA is iterated for 100 generations and the population size is 50. Crossover probability is 0.7 and mutation probability is 0.2.

Table 1 Standard benchmark function given by Rosenblatt [33]

Period 1

To -- From	1	2	3	4	5	6
1	0	63	605	551	116	136
2	63	0	635	941	50	191
3	104	71	0	569	136	55
4	65	193	622	0	77	90
5	162	174	607	591	0	179
6	156	13	667	611	175	0

Period 2

1	0	175	804	904	56	176
2	63	0	743	936	45	177
3	168	85	0	918	138	134
4	51	94	962	0	173	39
5	97	104	730	634	0	144
6	95	115	983	597	24	0

Period 3

1	0	90	77	553	769	139
2	168	0	114	653	525	185
3	32	35	0	664	898	87
4	27	166	42	0	960	179
5	185	56	44	926	0	104
6	72	128	173	634	687	0

Period 4

1	0	112	15	199	665	649
2	153	0	116	173	912	671
3	10	28	0	182	855	542
4	29	69	15	0	552	751
5	198	71	42	24	0	758
6	62	109	170	90	973	0

Period 5

1	0	663	23	128	119	50
2	820	0	5	98	141	66
3	822	650	0	137	78	91
4	826	570	149	0	93	151
5	915	515	53	35	0	177
6	614	729	178	10	99	0

Shifting cost for departments

887	964	213	367	289	477

Table 2 shows the analysis of above problem, when solved with presented RCGA and the results obtained for the problem provided by Rosenblatt using Dynamic programming. For the above problem, if static layout is applied then the cost obtained is $ 78,374; and as if the machines are not changing their positions, its rearrangement cost is zero. However, for all time periods, the layout is non-optimum, so the material handling cost is high. The presented RCGA approach is giving 5.56% better results as compared to the reported answer. In reported answer the material handling cost is less as compared to present approach; but the machines rearrangement cost is more in the reported answer, which is $75,384. So the total cost obtained ($ 71,187) by presented approach, is less than the reported answer.

The objective function Z, is represented by the 'Total cost', column in the above table. Above comparison shows that the dynamic layout approach is definitely saving the cost as compared to the static layout approach. In addition, it shows that machines rearrangement cost is equally important as that of material handling cost. Total cost is comprising of machines rearrangement cost and material handling cost.

Table 2 Result and analysis of optimization for dynamic layout problem [33]

Approach	Machine Positions	Machines Rearrangement Cost ($)	Material handling cost ($)	Total Cost ($) (Z)
Static	For all time periods 1 2 3 4 5 6	--- --- --- --- --- Subtotal	15,403 18,617 15,156 14,659 14,539 78,374	78,374
Dynamic (by Rosenblatt using dynamic programming)	1st time period 1 3 5 6 4 2 2nd time period 1 4 2 5 3 6 3rd time period 1 5 3 2 4 6 4th time period 1 6 4 2 5 3 5th time period 3 2 6 4 1 5 Subtotal	--- 2,310 1,833 1,346 3,197 8,686	12,822 14,853 13,172 13,032 12,819 66,698	75,384
	1st time period 1 3 5 2 4 6 2nd time period 1 3 5 2 4 6	---- ----	12,894 15,356	

	3rd time period	502	13,172	
Presented	1 5 3 2 4 6			
approach	4th time period	844	13,188	
(RCGA)	1 5 3 2 6 4			
	5th time period	1,364	13,867	
	6 5 3 2 1 4			
	Subtotal	2,710	68,477	**71,187**

V. CONCLUSION

Dynamic machine layout concept is useful in the industries where product mix and product quantity are changing with respect to time. In this work, real coded genetic algorithm (RCGA), is applied to benchmark problem and it is observed that the better answer is obtained than the reported in the literature. This clearly indicates the potential of this approach to solve dynamic layout problems.

REFERENCES

[1] G. Eason, B. Noble, and I.N. Sneddon, “On certain integrals of Lipschitz-Hankel type involving products of Bessel functions,” Phil. Trans. Roy. Soc. London, vol. A247, pp. 529-551, April 1955. (references)

[2] Ahin R. and Turkbey, O,. “A new hybrid tabu-simulated annealing heuristic for the dynamic facility layout problem”, International Journal of Production Research, pp.1-19, iFirst. 2008.

[3] Ashtiani, B., Aryanezhad, M.B., Moghaddam, B.F., ‘‘Multi start simulated annealing for dynamic plant layout problem’’, Journal of Industrial Engineering International, Vol.3, no.4, pp.44-50. 2007.

[4] Azimi, P. and Charmchi, H.R., “A new heuristic algorithm for dynamic facility layout problem with budget constraint’’, World academy of science, Engineering and Technology, Vol. 65, pp. 478-484, 2012.

[5] Balakrishnan, J., ‘‘Dynamic Layout Algorithms : A State-of-the-art Survey’’, Omega, Vol. 26, no. 4, pp.507-521, 1998.

[6] Balakrishnan, J., Cheng, C.H., Conway, D.G., Lau, C.M, ‘‘A Hybrid Genetic Algorithm for the Dynamic Plant Layout Problem’’. International Journal of Production Economics, Vol. 86, no.2, pp.107-120, 2003.

[7] Baykasoglu, A. and Gindy, N.N.Z, ‘‘A simulated annealing algorithm for dynamic layout problem’’. Computers and Operations Research, Vol.28, pp.1403–1426, 2001.

[8] Bock, S. and Hoberg, K.., ‘‘Detailed layout planning for irregularly-shaped machines with transportation path design’’. European Journal of Operational Research, Vol.177, pp.693-718, 2007.

[9] Brunese, P.A. and Tanchoco, J.M.A.. ‘‘On implied within-building constraints for machine layout’’. International Journal of Production Research, Vol. 51, No. 6, pp.1937–1952, 2012.

[10] Daskin, M. S., Hopp, W. J., Medina, B., ‘‘Forecast horizons and dynamic facility location planning’’. Annals of Operations Research, Vol.40, pp.125-151, 1992.

[11] Donga, M., Wu, C., Hou, F., ‘‘Shortest path based simulated annealing algorithm for dynamic facility layout problem under dynamic business environment’’. Expert Systems with Applications, Vol.36, pp.11221–11232, 2009.

[12] Drira, A., Pierreval, H., Hajri-Gabouj, S., ‘‘Facility layout problems: A survey’’. Annual Reviews in Control, Vol.31, pp.255–267, 2007.

[13] Gen, M., Ida, K., Cheng, C., ‘‘Multi row Machine Layout Problem in Fuzzy Environment Using Genetic Algorithms’’. Computers industrial Engineering, Vol. 29, No. 4, pp. 519-523, 1995.

[14] Golany, B. and Rosenblatt, M. J., “A heuristic algorithm for the quadratic assignment formulation to the plant layout problem”. International Journal of Production Research, Vol. 27, no. 2, pp. 293-308, 1989.

[15] Goldberg, D.E., “Real Coded Genetic Algorithms, Virtual Alphabets, and Blocking”, Complex Systems, Vol.5, pp. 139–167, 1991.

[16] Gomez, A., Fernandez, Q.I., Garcia, D., Garcia, P.J., “Using genetic algorithms to resolve layout problems in facilities where there are aisles”. International Journal of Production Economics, Vol.84, pp. 271–282, 2003.

[17] Goncalves, E.V. and Tiberti, A.J., “A group genetic algorithm for the machine cell formation problem”. International Journal of Production Economics, Vol.102, pp. 1–21, 2006.

[18] Heragu, S.S., “Modeling The Machine Layout Problem”. Computers industrial Engineering, Vol.19, no. 4, pp. 294-298, 1990.

[19] Herrera, F., Lozano, M., Verdegay, J.L., “Tackling Real coded Genetic algorithms: Operators and tools for behavioral analyses”. Artificial Intelligence Review, Vol. 12, pp. 265-319, 1998.

[20] Islier, A.A., “A genetic algorithm approach for multiple criteria facility layout design”. International Journal of Production Research, Vol. 36, no. 6, pp.1549-1569, 1998.

[21] Jinde, A.R. and Telsang, M.T., “Material handling cost reduction by redesigning layout – a genetic approach”. NCIETM held at NITIE Mumbai, pp.174-181, 2014.

[22] Kothari R. and Ghosh, D., “Tabu Search for the Single row facility layout problem using exhaustive 2- Opt and insertion neighborhoods”. European Journal of Operational Research, Vol. 224, pp.93-100, 2013.

[23] Krishnan, K. K., Cheraghi, S.H., Nayak, C., “Case study in using in dynamic from between charts to solve dynamic facility layout problems”. California Journal of Operations Management, Vol. 6, No. 1, pp 115-122, 2008.

[24] Kusiak, A. and Heragu, S.S., “The facility layout problem”. European Journal of Operational Research, Vol. 29, pp. 229–251, 1987.

[25] Lenin, N., Siva Kumar, M., Islam, M.N., Ravindran, D., “Multi-objective optimization in single-row layout design using a genetic algorithm”. International Journal of Advanced Manufacturing Technology, Vol.170, no.12, pp.4608, 2012.

[26] Levary, R.R. and Kalchik, S., “Facilities Layout, A Survey of solution procedures”. Computers & Industrial Engineering, Vol. 9, no. 2, pp.141-148, 1985.

[27] McKendall, A.R. and Hakobyan, A., “Heuristics for the dynamic facility layout problem with unequal-area departments”. European Journal of Operational Research, Vol.201, pp.171–182, 2010.

[28] McKendall, A.R. and Shang, J., “Hybrid ant systems for the dynamic facility layout problem”. Computers and Operations Research, pp.790-803, 2006.

[29] McKendall, A.R., Shanga, J., Kuppusamy, S., “Simulated annealing heuristics for the dynamic facility layout problem”. Computers and Operations Research, Vol.33, pp. 2431-2444, 2006.

[30] Meller, R. D. and Gau, K.Y., “The Facility layout problem: Recent and emerging trends and perspectives”. Journal of manufacturing science, Vol. 15, no. 5, 1996.

[31] Mohammadi, E. and Moghadam, M.A., “Design of dynamic body shop layout in automobile industry”. International Journal of Automotive Engineering, Vol. 1, Number 4, 2011.

[32] Moslemipour, G. and Lee, T. S., “Intelligent design of a dynamic machine layout in uncertain environment of flexible manufacturing systems”. Journal of Intelligent Manufacturing, Vol. 23, pp.1849–1860, 2012.

[33] Rosenblatt, M.J., “The dynamics of plant layout”. Management science, Vol. 32, no.1, 1986 .

[34] Solimanpur, M. and Kamran, M.A., “Solving facilities location problem in the presence of alternative processing routes using a genetic algorithm”. Computers & Industrial Engineering, Vol. 59, pp. 830–839, 2010.

Model Development for Preventive Maintenance and Replacement Policy

Anand S. Relkar
Mechanical Engineering
S. I.T.R.C.
Nasik-13,
anand.relkar@sitrc.org.in

Dr.Keshav N. Nandurkar
Principal
K.K.W.I.E.E.R
India Nasik-3,India
Keshav1965@gmail.com

ABSTRACT :

To increase productivity and operational efficiency maintenance management & reliability engineering, now gaining more and more importance, as upkeep of all the equipments in manufacturing industries becomes essential. It is very easy to say do maintenance, but it is really very tricky to decide the optimum policy of preventive maintenance and replacement that can result into minimum maintenance cost.

A case study in process industry is discussed to develop the model for preventive maintenance and replacement policy. FMEA analysis is done to prioritized the system with high risk. This identified high risk system further drilled down to know the root cause of failures and corrective actions to be taken.

Further a model is developed for total maintenance cost. Replacement cost and preventive maintenance cost is considered for total maintenance cost. It is optimized by using interval halving method.

I. INTRODUCTION

Due to continuous use of equipment, deterioration with age and usage is natural phenomenon. This equipment or part deterioration can take various forms such as wear, breaking, cracking or fracture etc. This ultimately results in to equipment failure and equipment could not perform its desired function. Avoiding this equipment failure and controlling its deterioration is essential.

Due to cut through competition in the manufacturing sector, no organization can afford any type of manufacturing delay or equipment failure (losses). Hence it becomes essential to focus on identification and measurement of losses and its control. One prominent area, where losses can occurred, is maintenance. Although maintenance is previously considered as secondary function, now a days it becomes important supporting function if treated properly can results in productive tool to increase production rate and reduce six big losses or equipment failure. These six big losses are breakdowns, downtime, setup and adjustments, small stops , reduced speed, start up rejects and production rejects. This six big losses can be grouped into three main subgroups. First is availability includes breakdown and downtime losses. Secondly performance considers small stops, reduced speed, setup and adjustments. Third is quality it includes startup rejects and production rejects. All these aspects can be measured with single performance measuring parameter Overall Equipment Effective Effectiveness (OEE). OEE is introduced by Nakajima in 1988 as first objective of Total Productive Maintenance (TPM). It is a single parameter indicator , that covers all six big losses. In Total Productive maintenance a key issue is to decide the frequency of PM and the time of replacement to minimize total cost of maintenance. In this paper an attempt is made to find out these optimum values. This paper is concluded with specific values of PM frequency and replacement time with minimum total maintenance cost.

II. LITERATURE REVIEW:

Yeh and Sun 2011 establish a model to maintain the key equipment in a semiconductor factory, based on its history of preventive maintenance (PM) and applying Monte Carlo simulation to predict the probability of the next PM time-point. According to the results of this study, businesses could establish an effective maintenance model, standardize a regular maintenance plan and the maintenance arrangement and prediction, provide the setting control and the alerting specifications as the referral index of maintenance time-point for the manufacture and the equipment engineering departments to achieve 85% Overall Equipment Efficiency (OEE).

Sobamowo *et al*. 2012 develops optimal preventive maintenance models using Weibull Distribution to predict maintenance models for Eglin steam turbines. They imply that it is more expensive to perform a preventive maintenance at the inception of a preventive maintenance cycle. The cost decreases as the cycle increases. It is worthy to note that there exist an inverse relationship between the total cost of replacement and the cycle length. It reveals that for an increasing cycle length, the total cost of replacement per unit

turbine becomes constant. Also, the downtime continues to decrease until it gets to a very minimal level before it becomes steady.

Chitakala and Sukumari 2014 developed the Preventive replacement strategy for determining an optimal replacement time for an automobile system that deteriorates with time is proposed and investigated, while the part of the system is in the final stages of its life span. The failure time followed the Weibull distribution and hence the optimum replacement time can be determined. This time minimizes total downtime and maximizes the proportion of time the parts of the system available.

Chang 2014 proposes the preventive replacement policy for an operating system which may continuously work for N jobs with random working times and be imperfectly maintained upon failure.

From above literature review it is clear that more focus must be given on deciding the frequency of preventive maintenance (PM) and appropriate time of replacement. In this paper an attempt is made to find out optimal frequency of PM and replacement to make the maintenance process cost effective.

III. METHODOLOGY

Case Study: A case study in process industry, engaged in manufacturing of electrodes is discussed to elaborate the nature of problem and its proposed methodology to solve the same.

The electrodes are manufactured with the raw material having particle size ranging from 5-8 cm diameter. Initially the raw material is crushed, sized and milled. The degree to which the coke is broken down depends on the grade of electrode to be manufactured. Raw material is mixed after the desired proportion in charging bins is established. The purpose of mixing is to blend the coke filler materials and to melt and distribute the pitch binder over the surfaces of the filler grains. The degree of mixing depends on factors such as time, temperature and batch size. The hot mix must be cooled to a temperature slightly above the softening point of the binder pitch. The forming and extrusion press produce a article that can withstand at high tamping pressure.

Data Collection:

Above mentioned process involved three main sub system crushing, extrusion and pitch and scrap system. Eleven moth breakdown data is collected as shown in table no 1

Thus from above table no. 1 it can be observed that out of these three system Extrusion system faces more breakdown i.e. 185.5 hours as compared to other system.

TABLE I: MEASUREMENT OF BREAKDOWN HOURS (DOWNTIME) FOR THREE SUB SYSTEMS DURING APRIL 13 TO MARCH 14

Months	Crushing System	Extrusion System	Pitch & Scrap System
April	2.5	17.25	1.75
May	1.5	16.25	1.5
June	2.5	12.75	2.5
July	3	13.5	1.5
August	5	16.25	1
September	4.75	14.75	2.25
October	3.5	17.25	1.5
November	2.25	18.75	2
December	2.5	14.25	1.25
January	4.5	20	1.5
February	3.5	11.5	0.75
March	3.75	13	1
Total Hours	39.25	**185.5**	18.5

Hence this extrusion process is further studied to know root cause of higher breakdown hours.

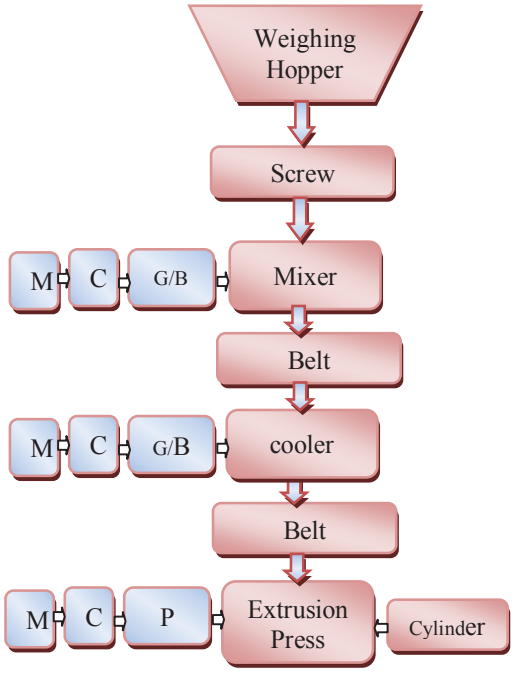

Fig.1 Block diagram of Extrusion System

In Extrusion system green electrode is extruded from press and delivers to next department for further processing. In Extrusion system CPC (Calcanide petroleum coke), Binder Pitch, Ferric oxide and oil are weighted as per recipe then through screw conveyor, the recipe means one charge weight is discharged into mixer where it is

heated and mixed up to 160 to 170° C, then from mixer it is delivered to cooler through belt conveyor where the charge is cool down up to 100 to 110° C then through belt conveyor the charge is discharged into extrusion press where electrode is extruded. Detailed breakdown hours for various components of extrusion system in weeks are given in table II

TABLE II: EXTRUSION SYSTEM COMPONENTS FAILURE (HOURS)

Month	Motor	Coupling	Gear box	Valves	Cylinder	Pump
1	6.25	4.25	3.25	1.25	2.75	3
2	6	4.5	0	2.25	2	.5
3	1.5	2.75	0	1.25	2.5	.5
4	0	4	3.75	2	4	0.25
5	5.25	2.5	1.5	0.5	0.5	1.5
6	0.75	2	3.5	1	2.5	0
7	1.75	1.75	1.5	2.75	5.75	0
8	1.25	2.5	2	3.5	0.5	1.75
9	1	0.75	0	0.75	1.5	0.5
10	0	3.75	2	0.75	2.75	1.25
11	2	4.75	2.5	1.5	1.5	3.75
12	3.5	4	2.5	0.75	2.5	0
13	2.75	4	0	1.50	2.5	1.5
Total	**28.5**	**41.5**	22.5	19.75	**31.25**	14.5

From the history of breakdown failure data in table II, it has been observed that coupling is most critical component as its breakdown hours are highest i.e. 41.5 hours as compared to other component or sub assembly .Thus coupling is identified component for further study. Failure mode and effect analysis (FMEA) is used to identify, analyze and suggest corrective actions to reduce failure of coupling. The severity of failure is measured in terms of risk priority number (RPN). Higher is RPN higher attention must be provided to reduce its risk.

TABLE III: RISK PRIORITY NUMBER CALCULATIONS

Sr. No	Component	SEV	OCC	DET	RPN
1	Coupling	8	9	7	504
2	Cylinder	7	9	7	441
3	Motor	6	8	8	384

RPN= SEV * OCC*DET

SEV= Severity, OCC= Occurrence & DET= Detection of faults

From table III, it is clear that coupling of extrusion system is more critical and risk priority of it is 504. Hence it is essential to reduce RPN of 504 to reduce the breakdown hours of the entire system. By reducing breakdown hours corresponding maintenance cost can be reduced.

IV MATHEMATICAL MODEL FOR PREVENTIVE MAINTENANCE AND REPLACEMENTS

For a new system, one need to find cost associated with a given schedule of future maintenance and replacement activities. The cost associated with all component level preventive maintenance (n) and replacement (m) actions in period (t), will be a function of the all the actions taken during that period.

1 Preventive Maintenance Cost (C_{pm})

If maintenance is performed on component ' i ' in period ' t ', a maintenance cost constant C_{pm} is incurred at the end of the period.

2 Replacement Cost C_{rj}

If component 'j' is replaced in period 't' we assume that the replacement cost is the initial purchase price of the component 'j', denoted **(C_{rj})**

3 Total Cost $f(x)$

From advantage point at the start of the planning horizon, we wish to determine the set of activities, i.e., maintenance, replacement for each component in each period such that total cost is minimized. And from definitions of each type of cost, the following total cost function is derived.

$$\textbf{Total Cost} = \sum_{i=1}^{n} \boldsymbol{Cpm_i} + \sum_{j=1}^{m} \boldsymbol{Cr_j} \quad [1]$$

This objective function computes the total cost as a summation of component costs in each period based on preventive maintenance or replacement cost and the system downtime cost.

Optimization Model

The mathematical foundation for solving models arising from the proposed modeling framework is Interval Halving technique. The algorithms described in this section can be used to solve minimization problems of the following type:

Minimize f(x), Where f(x) is the objective function and x is a real variable. The purpose of an optimization algorithm is to find a solution x, for which the function f(x) is minimum.

Interval Halving method

Figure 2, shows a region in the interval (a, b). Three points divide the search space into four regions .The fundamental rule for region elimination is used to eliminate a portion of search space based on function values at three chosen points.

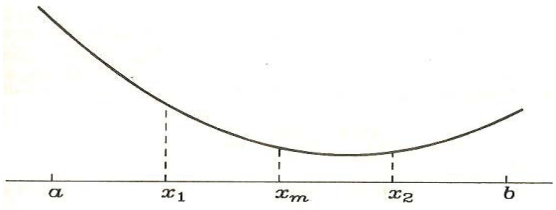

Figure 2 Three points x_1, x_2, x_m used in the interval halving

Algorithm:

1. Choose lower bound 'a' and upper bound 'b' and small value $\in$ for desired accuracy $X_m=(a+b)/2$ and $L_0= L= b-a$, compute $f(X_m)$
2. Set $X_1 = a+ L/4*(X_2)=b-L/4$ compute $f(X_1)$ and $f(X_2)$
3. If $f(X_1)<f(X_m)$, $X_m =X_1$
Set $b =X_m$ go to Step5, else go toStep4.
4. If $f(X_2)< f(X_m)$ set $a= X_m$, $X_m = X_2$ go to step 5
Else $a= X_1$, $b= X_2$ go to Step5.
5. Calculate L= b-a if $|L| < \in$ If terminates, else go to step2.

The objective function is to find out optimal Preventive maintenance and replacement frequency with minimum cost the following data is collected from SAP & Log book.

TABLE IV: NUMBER OF PM & COST OF PM

PM (n)	Cost of PM (*Cpm*) in Rs	Summation of PM cost (*Cpm*)
1	1379.8	1379.8
2	1803.13	3182.9
3	2478.9	5661.8
4	2889.45	8551.2
5	3376.35	11927.5
6	3928.6	15855
7	3685.75	19540
8	4567.25	24107

The frequency and cost of PM is as per above table. To use regression of PM and corresponding cost, above data is classified as given below.

To find PM relation between number of Preventive maintenance frequency and cost of preventive maintenance, Regression technique is used with help of Minitab software. Cost of Preventive maintenance includes Labour cost and maintenance cost. The following equation is obtained.

$$C_{pm} = 748.5 + 619.2n - 20.44n^2 \quad [2]$$

Thus by putting value of n=1 to 8 in equation [2] preventive maintenance cost is obtained as follows

Similarly regression analysis is done for number of preventive maintenance and number of replacement. Thus equation [3] show number of replacement (m) and number of preventive replacement (n) using regression in Minitab Software.

$$m = 4.371 - 0.5429n \quad [3]$$

Now put value of n=1 to 8 in equation [3] as shown in table

TABLE V: REPLACEMENT NO (m) AND COST (Cr_j)

No of PM Frequency (n)	No of replacement (m)	Cost of replacement Cr_j=6246*m
1	3.8281	23910.31
2	3.2852	20519.36
3	2.7423	17128.41
4	2.1994	13737.45
5	1.6565	10346.5
6	1.1136	6955.546
7	0.5707	3564.592
8	0.0278	173.6388

Cost of Preventive maintenance and cost of Replacement is calculated as per equation as follows Total cost $f(x)$ = Cost of PM + Cost of Replacement

$$f(x) = \sum_{i=1}^{n} Cpm_i + \sum_{j=1}^{m} Cr_j$$

The main objective is to minimize the total cost thus using interval halving method, the optimize total cost is obtain by solving the example as follow.

TABLE VI: TOTAL COST OF PM AND COST OF REPLACEMENT

PM (n)	Cost of PM (*Cpm*)	Σ(*Cpm*)	Replacement (m)	Cost of Repl. Cr_j	Total cost (*Cpm* + Cr_j)
1	1347.26	1347.26	3.8281	23910.31	25257.57
2	1905.14	3252.4	3.2852	20519.36	23771.76
3	2422.14	5674.54	2.7423	17128.41	22802.95
4	2898.26	8572.8	2.1994	13737.45	22310.25
5	3333.5	11906.3	1.6565	10346.5	22252.8

6	3727.86	15634.16	1.1136	6955.546	22589.71
7	4081.34	19715.5	0.5707	3564.592	23280.09
8	4393.94	24109.44	0.0278	173.6388	24283.08

Consider 'a' as lower bond and 'b' as upper bond, take a= 4 and b=6.
Hence X_m= (a+b)/2; putting values of a & b
X_m= (4+6)/2 , therefore X_m= 5 .
Thus initial interval length L_0=L is calculate as
L_0= L= b-a,
Therefore L_0=L= 6-4=2
Now Calculate $f(X_1)$, $f(X_m)$, & $f(X_2)$ as follows
X_1= a+L/4 & X_2= b-L/4
Thus X_1= 4+(2/4)= 4.5 & X_2= 6-(2/4)=5.5
Now put f(4.5), f(5), f(5.5), in equation [2]
f(4.5) = 3120.99, f(5)= 3333.5 , f(5.5)=3535.79
Now set b= 5 and repeat the procedure until $f(X_1)$ and $f(X_2)$ and are equal.

TABLE VII: OPTIMUM VALUES OF PM AND REPLACEMENT

PM (n)	**Cost of PM (*Cpm*)**	**Σ(*Cpm*)**	**Replace--ment (m)**	**Cost of Repl. Cr_j**	**Total cost ($(Cpm+Cr_j)$**
1	1347.26	1347.26	3.83	23910.31	25257.57
2	1905.14	3252.4	3.29	20519.36	23771.76
3	2422.14	5674.54	2.74	17128.41	22802.95
4	2898.26	8572.8	2.20	13737.45	22310.25
4.5	3120.99	11693.79	1.93	12041.98	23735.77
4.625	3175.076	14868.87	1.86	11618.11	26486.97

IV. RESULT & CONCLUSION:

The research aimed to produce an effective PM model, Considering a maintenance system that consist, number of preventive maintenance (n) and number of replacement (m) activities for a certain period (t) of identical and independent units which are put into use sequentially in time. In order to illustrate the models numerically, and the proposed solution procedure, we captured a representative data set for considered component and it is also useful to mention that for this problem, the optimization models presented above that is total cost F(x) have been solved using Interval halving technique.
The optimized values of Preventive Maintenance (PM) and replacement are 4.5 and 1.93 respectively. The minimum maintenance cost for this frequency is Rs. 23,735/-.

REFERENCES

1. Afefy, I. H. (2000). "Reliability Centered Maintenance Methodology and Application: A Case study". *Scientific Research Engineering , 2*, 863-873.
2. Ahmad, R. B. (2007). *Development of Decision Model for Maintenance analysis of nonrepairable.* University of Sains Malaysia, Master of science.
3. Armen Kiureghain, O. D. (2007). "Availability, reliability and downtime of systems with repairable components". *Reliability Engineering and System Safety* , 231-242.
4. Bagajewicz, D. N. (2010). "Optimization of Preventive Maintenance in Chemical Process Plants ". *Ind. Eng. Chem. Res., , 49* (9), 4329-4339.
5. Behera, A. S. (2011). "Optimization of replacement stocks using a maintenance programme derived from Reliability studies of production systems". *Journal of Mechanical Engineering and Computational Science–ISSN* , 2249-3468.
6. Chang, C.-C. (2014). "Preventive Replacement Policy and Imperfect Maintenance Model with Random Working Times". *International conference on Education and Modern* , 370-373.
7. Deb, K. (1995). *Optimization for Engineering Design Algorithm and examples.* Kanpur: Department of Mechanical Engineering Indian Institute of Technology.
8. Duy Quang Nguyen, C. B. (2008). "New Tool for the Evaluation of the Scheduling of Preventive Maintenance for Chemical Process Plants". *Ind. Eng. Chem. Res , 47*, 1910-1954.
9. Heidelberg, D. (2009). *"Handbook of Maintenance Management and Engineering"*. London New York: Springer.
10. J.Duarte, C. (2007). "Optimization of the preventive maintenance plan of a series components system with Weibull hazard function.". *RTA # 3-4, Special Issue* .
11. K. A. H. Kobbacy, B. B. Fawzi and D. F. Percy,. (1997). A full history Proportional Hazards model for Preventive Maintenance Scheduling. *Quality And Reliability Engineering International* , 187-198.

Vacuum Gripper Design For An Industrial Handling System.

Ajinkya Vasant Nichit (Author)
Dept. Mechanical Engg.
Sandip Institute Of Engg. & Mangt.
Nashik, India.
ajinkyanichit94@gmail.com

Jadhav Suraj Ramesh (Author)
Dept. Mechanical Engg.
Sandip Institute Of Engg. & Mangt.
Nashik, India.
suraj904jadhav@gmail.com

Desai Anirudh Arun (Author)
Dept. Mechanical Engg.
Sandip Institute Of Engg. & Mangt.
Nashik, India.
anirudhdesai99@gmail.com

Patil Vishal Eknath (Author)
Dept. Mechanical Engg.
Sandip Institute Of Engg. & Mangt.
Nashik, India.
vishalkul77@gmail.com

Vishal Ratan Sonawane (Author)
Dept. Mechanical Engg.
Late. G.N.Sapkal COE.
Nashik, India.
vishalsonawane616@gmail.com

***Abstract*— Vacuum Gripper Design For An Industrial Handling System is a device designed for handling natural stone slabs (graphite slabs). It is a simple pick and place mechanism. The handling task comprises of taking the top slab from a stack of slabs with the help of gripper, transporting it to an unload position via actuators and placing it on that position. Another aim of this paper is to check the deflection (displacement in mm) & factor of safety in the beam at full load conditions and considering all the friction parameters.**

Keywords— Graphite slabs, Gripper, Actuator, Motors, positioning, pick & place mechanism, Factor Of Safety and displacement.

I. INTRODUCTION

This paper explains the overall mechanism of the pick and place process for handling of graphite slabs as shown in figure below. This mechanism is a part of a huge system which is used in processing of graphite slabs in an industry. This paper explains the overall design of mechanism using solid works software for the below given dimensions:

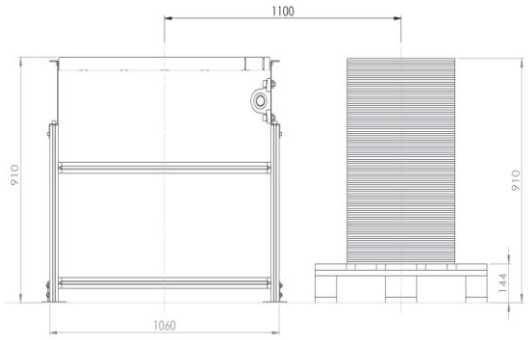

Fig.1. CAD drawing of Actual Mechanism

The dimensions of a slab are:

$W_{max} = 1{,}000\ m$ $\quad H_{min} = 0{,}020\ m$

$H_{max} = 0{,}500\ m$ $\quad T_{min} = 0{,}008\ m$

$T_{max} = 0{,}050\ m$ $\quad W_{min} = 0{,}020\ m$

where, W_{max}, W_{min} are the maximum and minimum widths of the stone slab; H_{max}, H_{min} are the maximum and minimum heights of the stone slab; and, T_{max}, T_{min} are the maximum and minimum thicknesses of the stone slab. The stone slabs are made from granite with density of $\rho = 2700\ kg/m^3$. Design for minimum cycle time for the handling operation. Optimal time (no idle time from the processing machine) $optT_{hc} \leq 4\ s$. According to above specification we have designed the manipulator under the Industrial Automation branch. In this we have considered all the factors like speed, acceleration, frictional resistance due to motion etc.

II. EASE OF USE

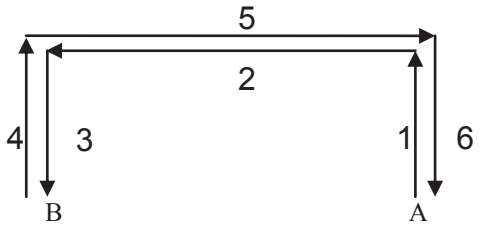

Fig.2-Operational Working

The handling cycle is decomposed to 6 parts (Fig. 3). For every part there are forces that are acting on the handling system. The maximum loading occurs when the system is handling a slab with maximum dimensions as per the assignment. The slab is picked from point A which follows path 1-2-3. Once the slab is placed on desired location B the mechanism follows reverse path 4-5-6.

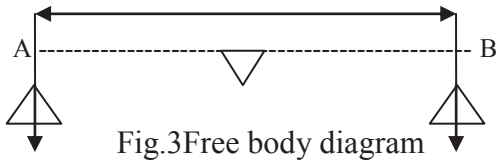

Fig.3Free body diagram

R_A (Reaction at A) R_B (Reaction at B)

The above arrangement shows the actual arrangement of the overall mechanism. In this the whole mechanism is placed on two columns as in the figure. it is the same arrangement as a simply supported beam. The gripper assembly and the sliding mechanism is rested on this simply supported beam.

III. CONSTRUCTION AND WORKING OF MECHANICAL SYSTEM:

The mechanical system consists of following components-

1. Vacuum gripper system
2. Vertical actuator for vertical movement of gripper
3. Guide ways for guiding vertical piston movement
4. Horizontal actuator for horizontal displacement
5. Main supporting frame

The vacuum gripper system consists of vacuum pads/cups (selected form SMC ZP2_Pads online pdf.), frame for holding the pads and other connecting elements. Here 14 vacuum pads are used as shown in figure for effectively lifting the slab for different conditions. The pads used are bellow vacuum pads. The bellow type pads are used because they do

not impact on the surface to be lifted and any surface irregularities can be effectively handled. The diameter of each vacuum pad is 40mm and material of pad is Urethane Rubber. The vacuum pads hold the slab when vacuum is applied to it and releases the slab as soon as the vacuum is released.

The vertical pneumatic actuator/actuator (selected online form SMC MGP-C_EU actuator for vertical catalogue) is used so as to provide a vertical lift to the vacuum gripper which is holding the slab. This is

required so that the slabs lifted do not slide over each other and damage their surfaces. For this we have assumed the vertical lift to be 50mm.

The load carried by the vertical actuator piston is considerably high. During working it may happen that the dynamic load conditions will tend it to get slightly inclined and this will result in misalignment. To avoid this we provide additional guide ways attached to piston which helps to maintain the perfect vertical movement and also prevents any deformation of piston due to dynamic loading.

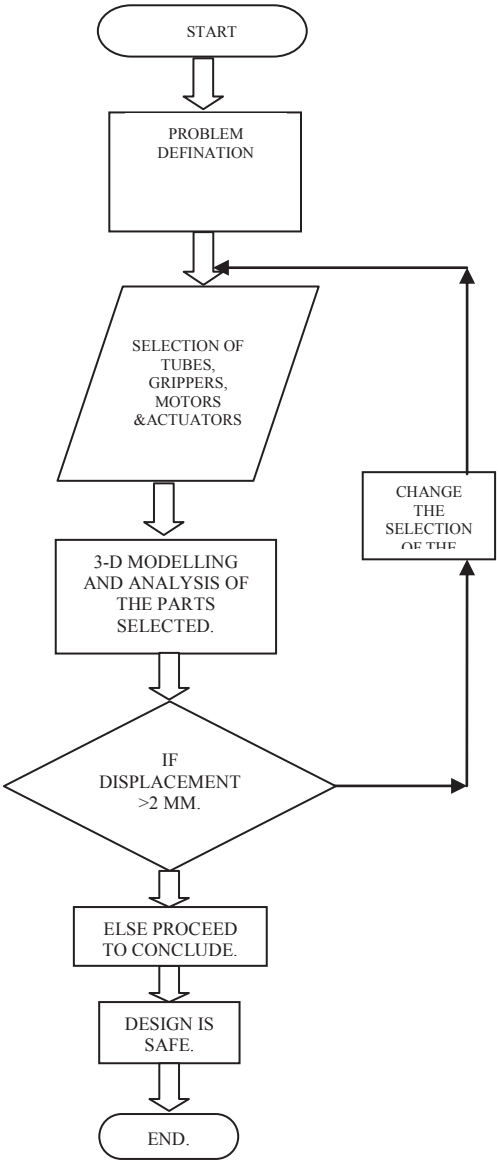

Flowchart.1- Process chart.

The horizontal actuator used is mechanically joined rod less actuator (Selected from SMC REA_REB_EU linear actuator for horizontal movement.)with high rigidity and high precision guide type with required stroke of 1100mm. Even this actuator operates on pneumatic power. The rod less piston holds the vertical actuator and gripper system. This horizontal actuator is used for the horizontal displacement of slabs from the pallet to the conveyor. So the sequence of working of different components is as follows-

1. The whole assembly is at position 1 as shown in figure. Now in this position vacuum is applied to the gripper cup. Due to which this slab is lifted.

2. Now the vertical actuator is stimulated and due to pneumatic power supplied the piston of vertical actuator is lifted up. This results in lifting of the slab and gripper system.

3. Now the horizontal pneumatic actuator is actuated so as to give horizontal movement to the rod less piston holding vertical actuator so that position 2 is achieved.

4. Now the vertical actuator is actuated in reverse direction and the gripper system holding the slab is moved downwards.

5. Dampers are attached at the end of the guide ways to avoid jerky operation. Dampers are selected from SMC RB_EU page-5 selecting damper RB 1412.

6. Once the gripper system is brought down the vacuum pressure is released and the slab is dropped on the conveyor.

7. Now the gripper system again moves from here to the original position in reverse order.

8. The above cycle mentioned in points 1 to 6 is repeated a number of times for the required number of jobs.

IV. STUDY PROPERTIES (TABLE-01):

Analysis type	Static
Mesh type	Solid Mesh
Thermal Effect:	On
Thermal option	Include temperature loads
Zero strain temperature	298 Kelvin
Include fluid pressure effects from SolidWorks Flow Simulation	Off
Solver type	FFEPlus
Inplane Effect:	Off
Soft Spring:	Off
Inertial Relief:	Off
Incompatible bonding options	Automatic
Large displacement	Off
Compute free body forces	On
Friction	Off
Use Adaptive Method:	Off
Result folder	SolidWorks document (F:\data0\Assistant\Indiitsi\Model\Gripper)

V. UNITS (TABLE-02)

Unit system:	SI (MKS)
Length/Displacement	mm
Temperature	Kelvin
Angular velocity	Rad/sec
Pressure/Stress	N/m^2

VI. MESH INFORMATION (TABLE-03)

Mesh type	Solid Mesh
Mesher Used:	Standard mesh
Automatic Transition:	Off
Include Mesh Auto Loops:	Off
Jacobian points	4 Points
Element Size	13.0275 mm
Tolerance	0.651373 mm
Mesh Quality	High
Remesh failed parts with incompatible mesh	Off

VII. MESH INFORMATION - DETAILS (TABLE-04)

Total Nodes	78176
Total Elements	40520
Maximum Aspect Ratio	60.083
% of elements with Aspect Ratio < 3	1.31
% of elements with Aspect Ratio > 10	36.4
% of distorted elements(Jacobian)	0
Time to complete mesh(hh;mm;ss):	00:01:18
Computer name:	ADP4124LAPTOP1

VIII. RESULTS:

RESULTANT FORCES (TABLE-05):

Selection set	Units	Sum X	Sum Y	Sum Z	Resultant
Entire Model	N	0.0421467	1423.69	-0.0439034	1423.69

RESULTANT MOMENTS(TABLE-06):

Selection set	Units	Sum X	Sum Y	Sum Z	Resultant
Entire Model	N-m	0	0	0	0

STUDY RESULTS:

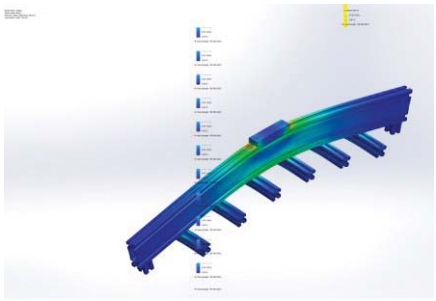

Fig.5- Shows the max deflection in the beam

The modelling and analysis of this overall mechanism is done in Solidworks hence the results indicated in the tables are directly taken from the result document obtained after analysis of the mechanism. As shown in the table the study results prove that the displacement after application of full load and after considering all the factors like friction factor, resistance of air in opposite direction to that of motion of the graphite slab etc, in the gripper holding beam is 0.293065mm which is less. Hence the beam can sustain the load of the graphite slabs effectively in both the conditions like
static & dynamic.

DISPLACEMENT IN MECHANISM (TABLE-07):

Name	Type	Min	Max
Displacement1	URES: Resultant Displacement	0 mm Node: 42	0.293065 mm Node: 44560

IX. MANUAL CALCULATIONS:

QZ= Forces acting in Newton & MY= Moments on points in N-m. Point nos.1,2,3.....7. These are the points of 6 small bars attached on the single beam whose axis are perpendicular to the axis of main beam as shown in fig. 5.

QZ1 = 91.08 N MY0 = +0
QZ2 = 273.63 N MY1 = -7.2864 Nm
QZ3 = 456.18 N MY2= -29.176 Nm
QZ4 = 638.73 N MY3= -65.6712 Nm
QZ5 = -456.19 N MY4 = -91.22 Nm
QZ6 = -273.64 N MY5=-65.6712 Nm

X. CONCLUSION-

From this paper we successfully designed a manipulator assembly for the picking & placing mechanism for graphite slabs for the further operating them for drilling. As stated above, the displacement of beam with full load is 0.293065mm. Since picking and placing is not an critical operation the calculated factor of safety is 5.28848 to 63981.1 (NOTE- FOS is as per Solidworks Results obtained.). This design satisfies the parameters and all the constrains.

XI. REFERENCES:

[1] http://www.boschrexroth.com/ue/gb/products/engineering/index
[2] http://www.boschrexroth.com/ue/gb/industries/machinery-applications-engineering/index
[3] http://www.smc.eu/portal_ssl/WebContent/corporative/products/product.jsp?tree_options==tree_products.js&tree_highlighted_node==999999
[4] http://www.smc.eu/portal_ssl/WebContent/cooperative/content/campaign/e.actuator12/E_actuator2012.jps?tree_options==tree_products.js&tree_state=2&tree_highlighted_node=51700.
[5] Solidworks software licensed version.

Artificial intelligence automobility in material handling & fork-lift manufacturing (AIA)

(*Indian Patent Reg. No.- 2929/MUM/2013*)

Ajinkya Vasant Nichit (*Author*)
Mechanical Engg., Sandip Institute Of Engg, & Management, Nashik, India
ajinkyanichit94@gmail.com

Kedar S. Joshi (*Author*)
Mechanical Engg., Sandip Institute Of Engg, & Management, Nashik, India,
joshikedars19@gmail.com

Sachin B. Rao (*Author*)
Mechanical Engg., G.H. Sapat College Of Engg., Nashik, India
sachin.rao45@gmail.com

Sushant S. Gaidhani (*Author*)
Mechanical Engg., Sandip Institute Of Engg, & Management, Nashik, India
sushantsgaidhani@gmail.com

Shrinivas Vasantrao Shinde (*Author*)
Mechanical Engg., Jawahar Institute Of Technology, Nashik, India
shreelife@gmail.com

***Abstract*— The Artificial Intelligence Automobility (AIA) is designed to make the process of stocking warehouses and material handling in industries safer and more efficient. With current manually operated fork-lifts, employees are at risk of injury. Employers also spend a lot of money on insurance and paying multiple employees to operate fork-lifts in their warehouses. The AIA will limit the need for employees to operate fork-lifts manually. This will not only cut down on long term employer costs but will reduce the chance of injury among employees as well. It takes pallets to and from the docking area and different aisles. The user chooses what they want the fork-lift to do by way of the hand-held user interface. The commands from the user are sent wirelessly to the fork-lift just by one click and the required motion of the fork-lift is achieved. It then drives itself along predetermined paths, picks up the pallet, and brings it to the desired Location. When finished, it returns "Home" where it awaits another command. "Home" is the aisle were the fork-lift parks while waiting for commands; on a full scale electric fork-lift this would also be where it pulls into its charger. For safety purposes, the fork-lift is equipped with a tilt sensor**

(Limit Switches), front and rear proximity sensors, and emergency shut off buttons.

The tilt sensor detects if the fork-lift tips over; if this happens, the fork-lift stops and tells the user via the user control that the fork-lift has tripped over. Once the fork-lift has been righted, the user may then choose to proceed, or go back home. The front and rear proximity sensors detect if an object is in the path of the fork-lift; if this happens, the fork-lift stops and the user control asks the user if it is safe to proceed. Self alignment is the new system allotted to the fork lift in order it will firstly align the job to be picked up and then it will take it to its destination.

Keywords— Artificial Intelligence, material handling, wirelessly, Home sensor, Limit Switches, proximity sensors, tilt sensor, Self alignment.

I. INTRODUCTION (*HEADING 1*)

We the students of Second year Mechanical Engineering are here to present a totally new concept of **ARTIFICIAL INTELLIGENCE AUTOMOBILITY (AIA) ON FORK LIFT MANUFACTURING AND MATERIAL HANDLING**. This Paper brings up a new face of automation world under MECHATRONICS group.

This Paper is fully self imagined and self organized by us in order to provide medium scale as well as large scale industries with some newly implemented technologies in their day to day working. A fork lift usually needs a trained person to handle it with care. But today we will be presenting in front of you a fork lift which won't need any person to handle instead it would work on a remote control(If one fork lift is used) or on computer server basis(If more than One fork-lifts are used).

Basically our aim doing this Paper is to modernize the industrial working and improve its working conditions.

This Paper comprises of some basic concepts of Mechanical Engineering and Electronics and Telecommunication in order to provide automation to the fork-lift system.

A. WORKING PROCESS AFTER AUTOMATION (ON PROTOTYPE):

The main purpose of automation was to enhance the present scenario of the material handling process in industries with a advance technology that will in turn help in increased production and reduced industrial accidents.

This fork-lift can perform all the operations like a normal fork-lift but in an automatic and in advanced form. Some of the operations are stated below-

Automatic lifting. Self-AlignmentTrack detector and self navigator. Obstacle detector and sensing.If in industries when any of the machine operators need the use of fork-lift he has to press the push button provided on his work station. Once the button is pressed via radio frequency signals the nearest fork-lift will reach the Work station, scan the job that is to be loaded via IR sensing. Then the forks will get align according to the scanned job dimensions, and once the alignment is done the forks lift the job and deliver it to its destination. While travelling if any obstacle comes in the way of fork- lift then the proxy sensors sense the obstacle and terminate the further operation.

An automized fork-lift is the one that is implemented with some of the best aspects of Different Engineering Fields.This automation is basically brought into application for a set of fork-lifts (NEARLY 35-40 Fork-lifts) in an industry operated through a strong server. The server will load its program through a computer.

If any defect is noticed by the operator in the server room through cameras, then immediately the workingof the fork-lifts is paused and the defective truck number is entered and is taken aside using a Joystick or even if it is observed that an accident is to happen then the operator can pause the system and can avoid the unexpected The above automations are achieved using MECHANICAL linkages with the help of ELECTRONIC circuits and components.

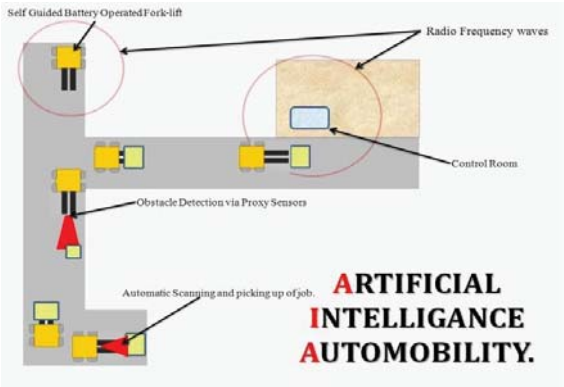

Fig.01 Animated view.

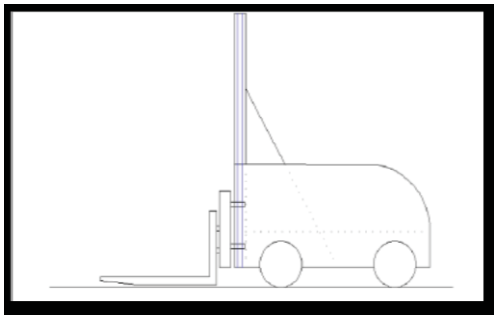

Fig.02 CAD drawing of prototype.

II. TABLE SHOWING COMPARISON BETWEEN MANUAL & AUTOMATED FORK-LIFT

MANULLY OPERATED	FORK LIFT WITH ARTIFICIAL INTELLIGENCE
1. Two persons are required, One trained for driving the truck and other person to guide the driver. Hence many labors are required.	1. It will run on its own with modern technology of self navigation. Only one person is enough to control a group of more than 40 forklifts.
2. The chances of accidents are extremely high in this	2. The accidents won't occur here because of the advancement.
3. We would not get the accuracy required at the shop floor due to manually handling.	3. Here we will attain high accuracy.
4. The person handling the fork-lift may lose control over the path to be travelled leading to instant stopping of work.	4. The self-navigator and track detector will avoid the fork-lift from losing its path thus avoiding the loss of time while doing work.

5. The job cannot be aligned to its perfect scale.	5. Use of sensors will help the fork-lift in aligning the job perfectly.
6. The maintenance for this fork lift is more.	6. It has very low maintenance due to lesser components.
5. The job cannot be aligned to its perfect scale.	5. Use of sensors will help the fork-lift in aligning the job perfectly.
6.The maintenance for this fork lift is more.	6. It has very low maintenance due to lesser components.

.

III. SALIENT FEATURES

1. It is totally automatic hence labour cost is reduced.

2. The sensors used avoid the accidents & its losses when the obstacle comes in.

3. The track detection helps in proper working of fork lift while carrying load.

4. Micro-controller is the one which controls the overall movement of the fork lift.

5. Barcode reader helps in efficient loading and unloading of the products.

6. Auto lift provides high accuracy on the shop floor.

IV. FUTURE SCOPE

1. The user may check the **Video feed** that shows the area immediately in front of the fork-lift and determine if the area is clear.

2. Emergency shutoff buttons are located on three sides of the forklift; in case all other safety options fail, Someone can push one of the buttons which physically disconnects the power to the motors.

3. The fork-lift model can be implemented with Automatic Tyre Changer so that the vehicle can operate in any atmospheric conditions by changing its wheels according to outside atmospheric conditions.

4. Automation on fuel operated forklift which are typically used in core industries the fuel going to be used it will be BIODIESEL.

V. CONCLUSION-

For our Paper, we have concluded successfully that the Artificial Intelligence Automobility installation helps both medium scale and large scale industries in their efficient working. Maintenance required is less as compared to the common fork lift. This advancement helps in improvement of working environment as well as increases the profit of industries by reducing material handling cost. This atomization finally is a boon for nearly all types of companies in and all over the world.

VIII. REFERENCE

[1] Godreg Forklifts and material handling Brochures.[1]

[2] Voltas India Ltd, Fork-lift and material handling Dept.[2]

[3] www.google/forklifts/wikipedia/automation.html.[3]

[4] Crown industries (An international manufacturer of Fork-lifts).

[5] Design data book.[5]

[6] Production engineering by Khurmi & Gupta.[6].

Self –Balancing Platform for Personal Transport

1. Yogesh Risodkar , 2.Ganesh Shirsath, 3.Monali Holkar, 4.Mayur Amle
Electronics & Telecommunication Department, SIEM, Sandip Fondation, Trimbak Road, Post Mahiravani, Nashik, Maharashtra 422213,India

Abstract*— In this paper challenges of transportation of goods and public transportation are well elaborated. The adverse effects are known and well documented. Discussions about various views of the best solutions for these problems are taking place around the world. One of these visions involves the use of advanced technology based on the public transit as the basis for all sustainable solutions. In this search for different methods, MPTDs could help to promote a modal transfer away from the automobile for short-distance trips. Electric scooters and Segways are two user friendly, "in" modes of transportation that facilitate effortless travel and could provide suitable transportation in metro cities. Our aim is to make a design and fabrication of Segway personal transporter. The Segway is based on the principle of inverted pendulum that will keep an angle of zero degrees with vertical at all times. The Segway is an intelligent vehicle which uses gyroscopic sensors to detect the motion of rider, so that it can accelerate, brake or steer the vehicle. This Segway is absolutely ecofriendly mode of transport which causes zero pollution.

Keywords—inverted pendulum; gyroscopic sensors; MPTD; segway.

I. INTRODUCTION

IT is a two-wheeled, self-balancing, battery powered electronic vehicle that maintains its own balance and that of its passenger. It is equipped with a stationary T-shaped control shaft fitted into a platform mounted on two parallel wheels. Segways are driven standing up and handle according to human body dynamics: lean forward to move forward, stand straight up to stop, and lean backward to reverse. For two-wheeled self-balancing robots, stability is vital as they cannot remain upright (balanced) without effort. As previously mentioned, their design concepts are mostly derived from classical robotic research called the inverted pendulum. An inverted pendulum, like its name suggests, is a pendulum that has its mass above its pivot point and not below like traditional pendulums. A self-balancing robot, such as a Segway, is an extended version of an inverted pendulum[1].

One of the most important tasks of autonomous systems of any kind is to be able to acquire knowledge about its environment. This can be done through the use of sensors (Ronald Siegwart et.al 2004). It uses two types of sensors where an accelerometer is an electromechanical device that measures inertial acceleration forces whereas gyroscope is a device used to measure the rate of rotation (angular velocity) of a body. Using microcontroller, the Segway continuously analyses its performance. Five gyroscopes and two sensors work together to determine the Segway's position in relation to its centre of gravity. The onboard computers analyse their measurements and compensate in real time for surface irregularities in order to control the device's movement and ensure the rider's stability[2].

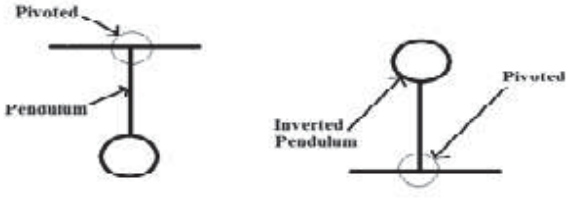

Fig.1.Normal and inverted pendulum

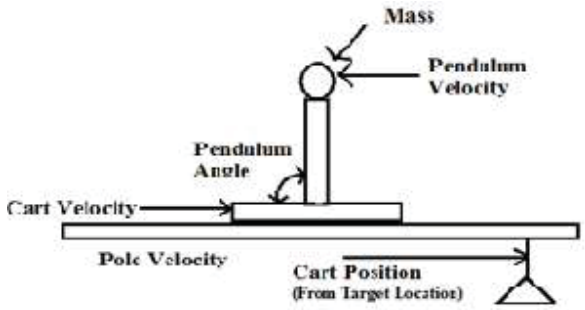

Fig.2.Inverted pendulum experiment set up

II. LITERATURE REVIEW

The United States began regulating Segways in 2002, just after the product began to be marketed and a year after a media campaign promoting the Segway HT and its inventor Dean Kamen. Most defines the Segway as an "electronic self balancing personal vehicle". Few states also resolute to redefine the phenomenon pedestrian to include "a person using a Segway". However, Senate Bill 2004, which defines the Segway as an electric transportation device with a stabilized platform between two parallel wheels, gives states and local authorities the power to pass legislation governing the use of Segways at the regional and local level. It approves the use of Segways on sidewalks under federal authority and on private property[3].

According to the Bill's wording, the device "employs advances in technology and effectiveness to fully and safely integrate the user with personal transportation;enables individuals to travel farther and carry more without use of traditional vehicles," and "promotes gains in utility;minimizes environmental impacts; and facilitates better use of public roadways."[4].

Fig.3. Segway

Segway Human Transporter (HT), which is invented by Dean Kamen, is known as the first two-wheeled, self-balancing system in the literature. Segway HT is demonstrated in fig.3. Also, Segway brings out two wheeled self balancing robotic platform which is called Robotics Mobility Platform (RMP)[5].

Two-wheeled self-balancing systems are mainly classified into two groups as robotic platforms and transporters according to their structure. Robotic platforms are generally constructed as small sized. Fig.4. is that kind of robot. Some of them are driven by an operator while rests are driven autonomously. Fully autonomous robots may also have intelligence. These robots generally have camera in order to detect the environment and path planning[6].

As a transporter system, it is driven semi-autonomously by the driver on it. The driver determines the speed and direction of movement of the vehicle by leaning forward and backward. Most of the transporters are combined of standing base and handlebar which make the driver feel comfortable . Also, steering mechanism is generally mounted on the handlebar.

Fig.4. nBot by David Anderson(Andeson 2007)

The hybrid system is the robot combined with a manipulator. Two wheeled platform is also used for actuator of a humanoid robot. Moreover, a system which is designed as both ground and aerial robot is studied in [7].

Besides the two-wheeled system, similar studies about one-wheeled (unicycle) self balancing system and balancing on ball systems exist in the literature. As a mechatronic system, it is interested by the academicians. Its stability

problem and the interaction among controller algorithm, hardware and software make it popular to study on Segway[8].

Designing controller is the crucial part of the system. The main problem stability is satisfied by the controller. It is designed and implemented . State feedback controller makes the system robust. Observer is used in order to estimate the states[9].

The main sensors of the system are accelerometer and gyroscopes which measure the angle and angular rate of the body, respectively. Most of the studies, use both of these sensors together. All processing are carried out by the embedded controller hardware. Microcontrollers are generally preferred in literature because of affordability . Microcontrollers manufactured by Microchip and Atmel are used in many researches. Digital Signal Processing (DSP) board is used for real time applications[10].

II. PROBLEM STATEMENT

1.Industries working in the field of transportation are required to put more work into building environmental friendly design and construct a fully functional two wheeled balancing vehicle which can be used as a means of transportation for a single person.

2.Design a small footprint electronic vehicle which will promote more environmentally friendly and energy efficient transportation method in metropolitan areas.

DESIGN GOALS

1.Speed should be controlled by the rider leaning forwards and backwards.

2.Turning should be controlled by tilting the handlebar.

3.Balance and transport persons weighing up to 100 kg.

4.Be strong enough to handle minor bumps and going up and down curbs at low speed.

5.Propel the vehicle safely at the maximum speed of 20 km/h.

6.Provide enough torque to balance a 100 kg rider in inclines of 20 degrees.

IV.PROPOSED SYSTEM

A. BLOCK DIAGRAM OF SEGWAY

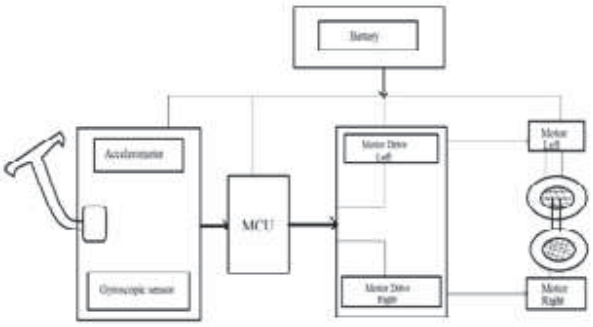

Fig.5. Block diagram

System initially takes the inertial inputs from the IMU (Inertial Measurement Unit) which comprises of the two sensors i.e. a) Accelerometer: A device capable of sensing acceleration. A modern accelerometer often includes a spring loaded structure whose deflection in response to external forces can be capacitively sensed and converted to an electrical signal. b) Gyroscopic sensor: Gyro is used to measure the angular rate of an object with respect to an inertial system.

The accelerometer and gyroscope within the IMU are mounted such that coordinate axes of their sensor are not aligned with self-balancing bot. This is the real fact that the two sensors in the IMU are mounted in two different orientations according to its orientation of the axis need.

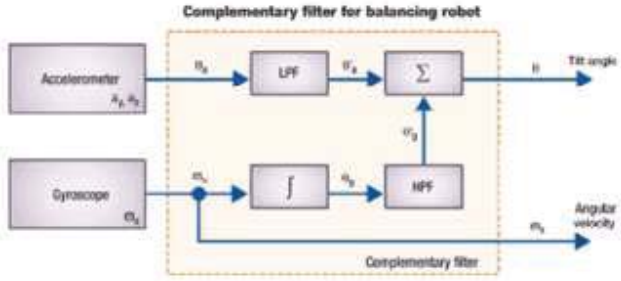

Fig.6. Complementry filter for balancing robot

B. HARDWARE REQUIREMENTS

1.Two wheels to drive the platform.

2.Two motors to drive the wheels.

3.Motor controller unit.

4.Platform to stand on, Gaffer tape and

movement controlling shaft.
5.Batteries to power everything.
6.Sensors to detect leaning.(Gyroscopic and Acelerometer sensor).
7.Electronics to drive the motors.
8.Software to drive the electronics.

C. ALGORITHM

1.Start
2.Acquire the physical parameters using the Inertial Movement Unit.
3.Use Complementary Fusion Technique to detect the corresponding change.
4.If the robot is leaning, drive the wheels in the direction of the lean.
5.If you lean more, go faster.
6.If you lean quickly, go faster.
7.Turns out to be a control systems problem:
  a.Input variable is platform angle.
  b.Output variable is motor speed.
8.By controlling the output variable, attempt to keep the input variable zero.
9.When lean zero with respect to the original vertical positions, stop driving the wheels.
10.Stop

D. FLOWCHART

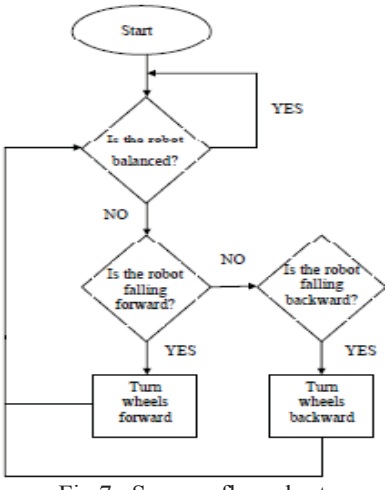

Fig.7. Segway flow chart

V. EXPERIMENTAL ANALYSIS

A complementary filter is a frequency domain filter. At the beginning of this paper it is mentioned that the accelerometer cannot follow tilts at fast motion and that the gyroscope respond better to fast motions. Therefore, this means that for motion that is greater or faster than 0.09 second time period the gyroscope's integrated tilt angle θg is weighted more. When the motion is slower than the 0.09 second time period, the accelerometer tilt measurement θa has more weight than the θg of gyroscope. This technique is chosen over Kalman filter technique because it is not mathematically extensive and simple to implement when programming the microcontroller. s

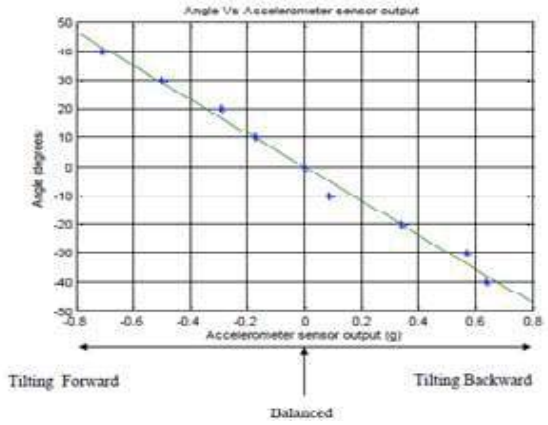

Fig.8. Accelerometer calibration graph

An accelerometer is used in this project to provide the tilt angle that the robot make relative to the balanced position or vertical position. The accelerometer was located at different angle positions along the angle protractor and the sensor output in g-forces and degrees is observed in the serial monitor of the program platform. Then the measured angle from the protractor is compared with the output in the serial monitor.

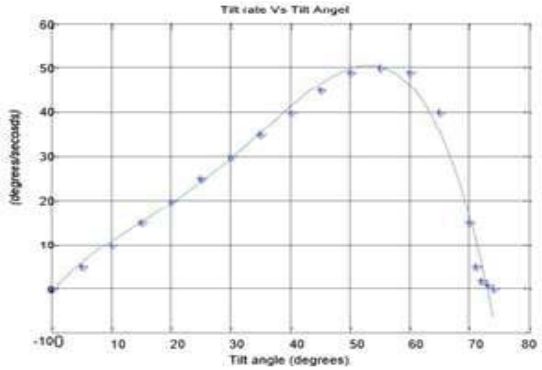

Fig.9. Gyroscope calibration graph

Figure 9 above shows the gyroscope tilt rate against tilt when the robot is made to fall forward from its upright position and caught before it hit the ground. The data is generate in the serial monitor of the Arduino platform then streamed to excel then finally plotted using matlab.

VI. CONCLUSIONS

In this paper the design of personal transporter is presented with more efficient use of energy. Along with the design an alternatives to form an eco-friendly artifice by using the relevant concepts like complementary fusion, PID action, MPTD algorithm are explored. This project is implemented with an idea to find an effective solution to transportation problem. The main objective is to achieve space utilization and minimize the fuel consumption especially for commuting over shortest distance.

From the experimental result it can be concluded that the basic objective of Segway and fuel consumption is satisfied. It is believed that idea implemented in this paper can be beneficial to reduce the future problem in MPTD.

REFERENCES

[1]D. Küçük, 2010, "Design of Two-Wheeled Twin Rotored Hybrid Robotic Platfor," M.Sc Thesis, Atılım University, Ankara.

[2]M. Kumaga and T. Ochiai, 2009, "Development of a Robot Balanced on a Ball," *2009 IEEE International Conference on Robotics and Automation,* May 12-17 2009, pp. 4106-4111, Japan.

[3]K. Pathak, J. Franch and S. K. Agrawal, 2005, "Velocity and Position Control of a Wheeled Inverted Pendulum by Partial Feedback Linearization," *IEEE Transactıons on Robotıcs*, Vol. 21, No. 3, June 2005, p. 505-513.

[4] A. N. K. Nasir, M. A. Ahmad and R. M.T. Raja Ismail, 2010, "The Control of a Highly Nonlinear Two-wheels Balancing Robot: A Comparative Assessment between LQR and PID-PID Control Schemes," *World Academy of Science, Engineering and Technology* 70, pp. 227-232.

[5]C. N. Huang, 2010, "The Development of Self-Balancing Controller for One-Wheeled Vehicles," *Scientific Research Journals of Engineering*, Vol 2, pp.212-219.

[6]M. Burkert, T. Groll, T. Lai, T. McCoy and D. Smith, 2004, "Segway Design Project," Project Report, Grand Valley State University The Padnos School of Engineering, USA.

[7]G. Chi, J. Hausbach and B Hunter, 2005, "Segbot," Senior Design Project, University of Illinois at Urbana-Champaign, USA.

[8]K. M. Goher and M. O. Tokhi, 2010, "Development, Modeling and Control of a Novel Design of Two-Wheeled Machines," *Cyber Journals Multidisciplinary Journals in Science and Technology, Journal of Selected Areas in Robotics and Control (JSRC*), December Edition.

[9]Motion planning of a balancing robot with threefold sub-task:An endogenous configuration space approach,Krzysztof Tchon.

[10]T. Vallius and J. Röning, 2007, "Embedded Object Concept: Case Balancing Two-Wheeled Robot," *Proceedings of the SPIE*, Vol. 6764.

[11] C. N. Huang, 2010, "The Development of Self-Balancing Controller for One-Wheeled Vehicles," *Scientific Research Journals of Engineering*, Vol 2, pp.212-219.

[12]Motion planning of a balancing robot with threefold sub-task:An endogenous configuration space approach, Krzysztof Tchon.

[13]M. Burkert, T. Groll, T. Lai, T. McCoy and D. Smith, 2004, "Segway Design Project," Project Report,

[14]W. Zhou, 2008, "Platform for Ergonomic Steering Methods Ġnvestigation of "Segway-Style" Balancing Scooters," M.Sc. Thesis, University of Waikato, New Zealand.

THE 18TH INTERNATIONAL SYMPOSIUM ON WIRELESS PERSONAL MULTIMEDIA COMMUNICATIONS
(WPMC-2015)
December 13-16, 2015, Hyderabad, India

Metric Based Efficiency Analysis Of Educational ERP System Usability–Using Fuzzy Model

Anil Kumar
PhD Fellow
Department of Electronic Systems,
Aalborg University, Denmark
aku@es.aau.dk

Reza Tadayoni
Associate Professor
Department of Electronic Systems,
Aalborg University, Denmark
reza@cmi.aau.dk

Lene Tolstrup Sorensen
Associate Professor
Department of Electronic Systems,
Aalborg University, Denmark
ls@cmi.aau.dk

Abstract– **Enterprise Resource Planning (ERP) systems are sophisticated information database that provide an automatic cross –functional business processes. An ERP user, however, often encounters challenges using complex ERP interfaces. Educational ERP implementation has been plagued with failure, but it to be adopted and is expanding in Indian higher education. An AICTE, UGC and others government approving bodies have made ERP system as mandatory software for all technical institutions. Educational ERP system includes almost all related modules. Despite many benefits, ERP users' recognize usability problems and these problems negatively affect the adaptability of the system in large scale. Usability is mainly making systems 'easy to use' and usability testing is a process to collect information about the usability of user interfaces. Usability test consist usability related attributes. Each usability attribute influences a specific characteristic associated with the ERP system. The impact of each usability attribute may very during usability evaluation process. These attributes are navigation, presentation, learnability, customizing, and task support. Usability metrics is generally imprecise, vagueness and ambiguous are characterized by fuzzy aspects and linguistic variables. Fuzzy logic is a branch of mathematics that allows a computer to model the real world the same way that people do. It provides a way to reason with vague, ambiguous and imprecise inputs or knowledge. This paper presents a fuzzy model for assessing the usability of ERP system usability by using these metrics. The present model uses the Mamdani fuzzy Inference approach for developing an overall measure of educational ERP system.**

Keyword–Usability Evaluation Method; Human Computer Interaction; All India Council for Technical Education (AICTE);University Grand Commission (UGC);Enterprise Resource Planning (ERP);Fuzzy Logic.

I. INTRODUCTION

Today, Software is used everywhere. It is a product itself is developed by software developers. To identify which module or part of it is working properly, we require the software testing. Software testing is an essential phase of Software Development Life Cycle (SDLC), whose main task is to provide bugs free and quality software to its users'. According to C.J. Mayers' software testing can be defined as "It is the progression of executing a program or a system by means of aiming of finding errors" [1]. Software testing activities ensures that software has been used is traceable to customer requirements as the software is developed, its GUI (Graphic User Interface) is used as means of user interaction with the software. Initially, software testers start testing its interface to find out its functionality but black box testing methods to detect as many bugs as possible. Software user generally requires a user-friendly interface. Usability is defined [2] as "The extent to which a product can be used by specified users to achieve specific goals with effectiveness, efficiency and satisfaction in a specific context of use". Usability is mainly making systems 'easy to use' and usability testing a process to collect information about the usability of user interfaces. End users always involve as participants of a usability test. It is usually divided into a number of attributes. Usability attributes play a vital role in confirming usability of the system. Usability of software can be understood as how much it is easy or hard for a user to use the software. To make software interface more user-friendly creates complexity in terms of usability and its related attributes.

An ERP is the information system, that an organization adopts to make fast the business process and Indian higher educational institutes are also using ERP system for its routine functions. Different Indian higher educational authorities force the institutes to use the Educational ERP system. Although Educational ERP system integrates many modules to organize educational related data in best ways, still it is always criticized due to complexity. ERP system is more complex only because of cohesiveness and coupling of different business application and process huge data. In spite of tremendous benefits a multifaceted educational ERP system facing usability problems and become less effective as it should be. Usability of educational ERP system can be measure using different usability techniques. Each usability technique has its benefits and drawbacks. We are using the fuzzy model on different usability attributes to find out the user perspective for ERP system. Usability of an ERP system is very important, which is basically a non-functional requirement. Software engineering requirements analysis methods do not focus on non-functional requirements faced resultants a serious problem for software adaptability. Educational ERP system negating non-function requirements are more severe than any functional requirement. Quantification of usability problems of ERP system is desirable for system adaptability. There are various usability models and techniques for assessing ERP system. These techniques aim to predict usability's problems on the bases of hands on experience on the software. Thus, a usability quantitative measurement is an essential part of ERP system. Though available usability literature uses different usability measuring

techniques but as concerned of educational ERP system usability evaluation is very less. The proposed fuzzy model uses various usability attributes and finds the best suitable solution of ERP system usability. In this model, we are using Matlab fuzzy tools for calculating of usability data.

The rest of paper is organized in following sections: Section I discusses introduction part. Section II presents related worked and various currents challenges in Indian Educational ERP system. Section III discusses the factors affecting usability and its attributes. Section IV proposed a fuzzy model. Section V elaborates fuzzy inference approach. Fuzzification process is defined in Section VI. Section VII presents Rule –based for the proposed system. Defuzzification defines in Section VIII. Section IX presents results and discussions of proposed model. Section X presents conclusion and future scope of the paper.

II. Related work

There exist different usability evaluation methods in the literature. One of the widely used methods is a manual evaluation. This method is applicable only when evaluation tool is not available. But, now a day different automatic tools are available for software usability evaluation by using various usability metrics for its evaluation. Metric values of any software can be generated.

Basili et al. in [3] presented the goal oriented data collection method for evaluation of software usability. Goal oriented questions are being formulated to collect the data from the users.

Lee et al in [4] has proposed the common dimension of web usability and verifies the result with the usability metrics. Stolz et al. in [5] used a GPI (Guidance Performance Indicator) to an extent by, which a goal driven web sites achieve its goal. In paper [6, 7] presented information visualization techniques and analyzes data with data mining techniques of website usability.

Kumar et al. [8] presented a fuzzy model for software reliability. Nielsen and Philips in [9] have illustrated inspection based usability techniques while Thmbley in [10] has designed a formal complexity measures for software usability and user experience evaluation. Most of usability evaluation techniques concentrate on isolated specific problems with user interface and widely ignore the overall figure of metrics of usability for a GUI interface of ERP system.

The above literature review, it is clearly observed that previous usability work focused on the certain area of GUI while it is now required to measure user preference and user performance experience on macro level of any software and educational ERP is not an exception from this observation.

III. Factors affecting usability of Educational ERP

Usability is a non-functional requirement, and it is used to measure the characteristics of software product like ease to use, ease of understanding. Jakob Nielson definition of the usability is composed of:

1) Learn ability: How easy is the design for new users' to accomplished basic tasks?
2) Efficiency: How quick cans an experienced user' achieve tasks with design?
3) Memorability: How easily can experienced users get back to the same task after a long period of time?
4) Satisfaction: How pleasant can users' be when they achieve the tasks with the design?

Nielson's and Schneiderman's' proposed different golden rules for usability evaluation. On the basis of these studies, we have selected only most valuable five usability evaluations attributes for our ERP System as follow:

1) Navigation: This attribute is of great important to evaluate the users' experience of the software and also contribute significantly towards usability evaluation.
2) Presentation: This attribute determines the degree of complexity of user interface's layout.
3) Learnability: This attribute focuses to determine required affordance of learning to use the system.
4) Customization: This attribute is used to determine the effort in customizing the system in order to improve the users' performance.
5) Task support: This attribute helps the user with an effective task support to complete a task with an alignment of the system.

IV. Proposed Fuzzy Model

In this paper, we proposed a fuzzy model to predict usability of Educational ERP system as shown in figure1. Input used for this model is usability factors namely Navigation, Presentation, Learnability, Customizing, and Task support and only one output i.e. Usability.

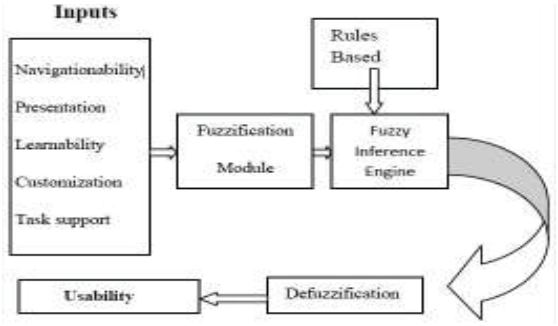

Fig. 1. Block Diagram of Fuzzy Model Predicting Usability

V. Working With Fuzzy Model

The first step is to give the input and determine the degree which they belong to each of the appropriate membership function. Fuzzification block produces the fuzzy inputs by converting the crisp values into fuzzy sets. The fuzzy rule base is a collection of attributes. A membership function associated with given fuzzy set maps as an input value to its appropriate membership function value. Fuzzy inference combines the facts obtained from the fuzzification with rule base and

condition of the fuzzy reasoning process. Fuzzy inference system is a process of formulating a mapping from given inputs to an output using fuzzy logic. Here, we are using the Mamdani fuzzy inference method, which mostly used fuzzy based analysis. Defuzzification block produces the output values to crisp values. The input of defuzzification process is a fuzzy set and the output is a single fuzzy set. Given fuzzy set. the encompasses a range of output values, one need to be returned thereby moving from fuzzy set to crisp output.

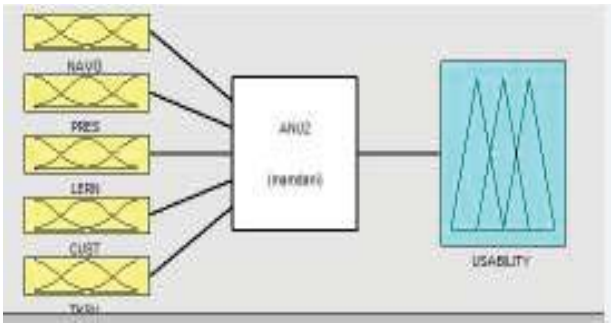

Fig. 2. Structure of Fuzzy Model

VI. FUZZIFICATION

The first step is the fuzzy inference system is to fuzzify inputs. The inputs attribute to the fuzzy system are represented as fuzzy sets. As in fuzzy methodology, the fuzzy set allows its attributes to have a degree of membership. Therefore, attributes of a fuzzy set are represented as a pair of member and degree. A linguistic variable value is used to represent a degree of favor and confidence for membership. The usability parameters Navigation is assumed values for (NAVG), Presentation is assumed values for (PRES), Learnability is assumed values for (LERN), Customizing is assumed values for (CUST), and Task support is assumed values for (TASK), and higher side of resultant value provides the higher level of Usability. All inputs values mentioned as above are defined as a fuzzy number by suitable fuzzy sets. Level of five inputs attributes i.e. Navigation, Presentation, Learn ability, Customizing, and Task support as a fuzzy set are given below:

Navigation = {VBAD, BAD, MODERATE, GOOD, VGOOD}

Presentation = {VLOW, LOW, MED, HIGH, VHIGH}

Learn ability = {LOW, AVG, HIGH}

Customizing = {VLOW, LOW, MED, HIGH, VHIGH}

Task Support = {VBAD, BAD, MODERATE, GOOD, VGOOD}

These fuzzy sets are represented by a membership function. This can be best achieved by deciding numeric range for each of the input and output variables.

TABLE I. FUZZY VARIABLE RANGE FOR NAVIGATION

Numeric Range	Linguistic Variable
0-3	VBAD
2-5	BAD
4-7	MODERATE
6-9	GOOD
8-10	VGOOD

TABLE 2. FUZZY VARIABLE RANGE FOR PRESENTATION

Numeric Range	Linguistic Variable
0-3	VLOW
2-6	LOW
5-9	MED
8-12	HIGH
11-13	VHIGH

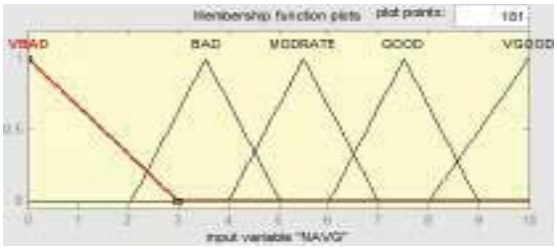

Fig.3 Fuzzification of Input variable Navigation

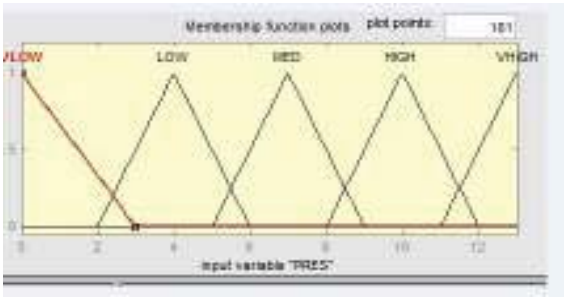

Fig.4. Fuzzification of Input variable Presentation

TABLE 3. FUZZY VARIABLE RANGE FOR LEARNABILITY

Numeric Range	Linguistic Variable
0-4	LOW
3-7	AVG
6-10	HIGH

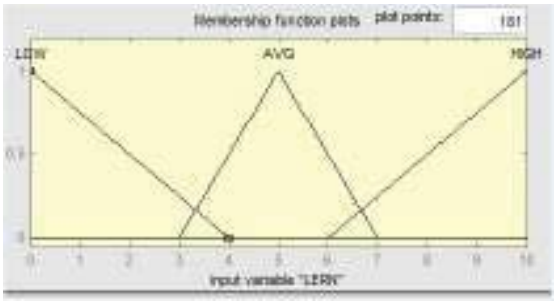

Fig.5. Fuzzification of Input variable Learnability

TABLE 4. FUZZY VARIABLE RANGE FOR CUSTOMIZING

Numeric Range	Linguistic Variable
0-3	VLOW
2-5	LOW
5-9	MED
8-12	HIGH
11-13	VHIGH

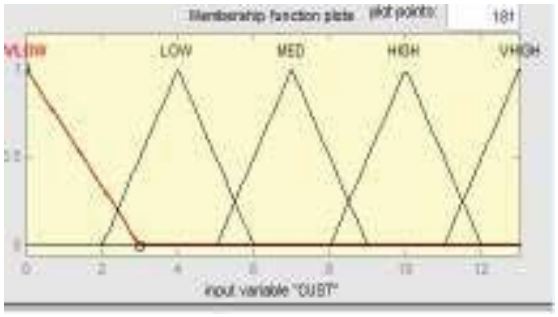

Fig.6. Fuzzification of Input variable Customizing

TABLE 5. FUZZY VARIABLE RANGE FOR TASK SUPPORT

Numeric Range	Linguistic Variable
0-3	VBAD
2-5	BAD
4-7	MODERATE
6-9	GOOD
8-10	VGOOD

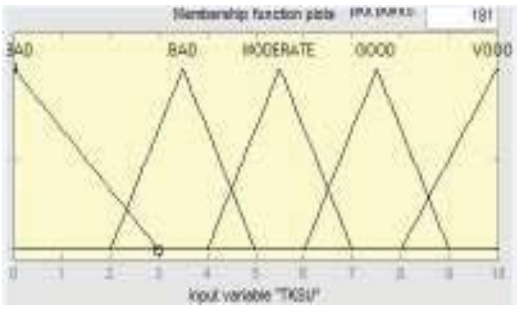

Fig.7. Fuzzification of Input variable Task Support

VII. RULE BASED FOR THE PROPOSED SYSTEM

After fuzzification of inputs, various fuzzy operations are performed to find out the usability of the system. The proposed model integrates the combined effect of NAVG, PRES, LERN,CUST and TASK of usability attributes. On the basis of these attributes, we have defined 150 rules. The sample of rule base is given below:

If (NAVG is MODERATE) and (PRES is LOW) and (LERN is AVG) and (CUST is LOW) and (TASK is MODERATE) then (USABILITY is LOW) (1)

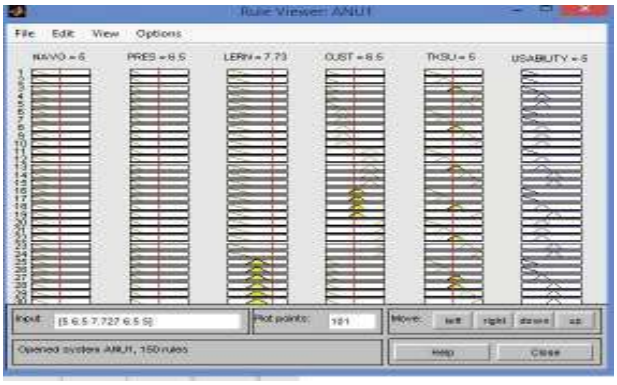

Fig.8 Rule Viewers

VIII. DEFUZZIFICATION

Defuzzification is a process of transformation of output from fuzzy domain to crisp domain. We, de-fuzzified output to get a crisp value to output variable i.e.usability. In this proposed model, we are using a centre of gravity method. In this method, finding is a centre of the area, which determined by joint membership function of fuzzy action. Overlapping area is taken only once, the 3-D surface is to display the resultant of usability variable.

In this, we show two different figures to demo the usability on the basis of rule-based. When Navigation and Presentation are high then Usability is also high for the system. The graphical analysis is shown in three respective figures namely Fig. 9 and Fig.10

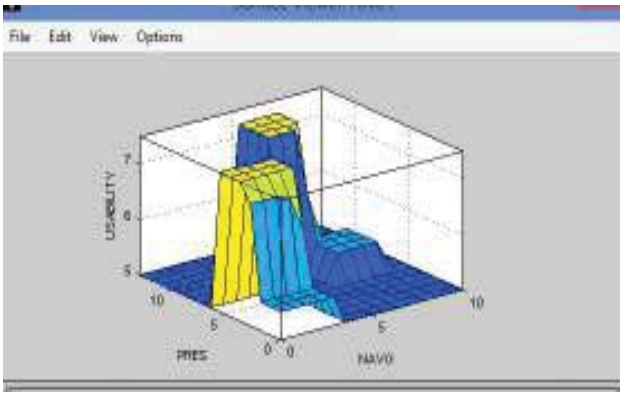

Fig.9. Defuzzification shows the relationship between NAVG and PRES

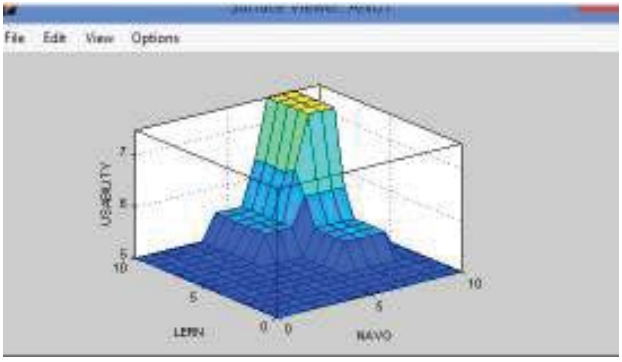

Fig.10. Defuzzification shows the relationship between LERN and NAVG

IX. RESULTS AND DISCUSSION

Suppose we have the following crisp value inputs to the model: NAVG = 5, PRES = 6.5, LERN =5, CUST = 6.5 and TASK = 6.5. These inputs are fed to fuzzification module and after fuzzification of given values the usability of the system is USABILITY = HIGH with membership function. This value has been shown in fig.8. Rule-based viewer. With these inputs values, we find that following rules were fired as given below in Table 6

TABLE 6. EDUCATIONAL ERP SYSTEM USABILITY CALCULATION FOR GIVEN INPUT SET.

NAVG	PRES	LERN	CUST	TASK	USABILITY
GOOD(5)	HIGH(6.5)	AVG(5)	HIGH(5.8)	MODERATE(5)	HIGH(5)

X. CONCLUSION AND FUTURE SCOPE

Many educational ERP systems failed due to low usability. This affects directly the adoptability of ERP system in a higher educational institute. Although, in recent years, various usability evaluation techniques have been proposed by the researchers but none of them quantify the educational ERP system usability using fuzzy model. The final crisp value of usability in this model obtained can help to identify the educational ERP system adoptability by end users'.

In future, data will be collected through online survey of educational ERP system used in Indian institute from its users and various evaluation methods will be applied on above mentioned usability attributes. Then, this fuzzy model will analyze the usability of educational ERP system and designed a new effective usability framework for educational ERP.

REFERENCES

[1] Roger S Pressman, "Software Engineering 4th Edition", McGraw-Hill

[2] Alian Abran, Adel Khelifi, Witold Suryn, Ahmed Se Ffah,"Consolidating the ISO Usability Models",Proc.11th International Software Quality Management Conference, 2003

[3] V.R. Basili and D. M Weiss, "A Methodology for Collecting Valid Software Engineering Data ", IEEE Transactions on Software Engineering,1984

[4] Younghwa Lee, Kenneth A, Kozar, "Understanding the Usability of Website" Specifying and measuring construct and their relationships", Elsevier Journal Of Decision Support System,2013

[5] Carsten Stolz, Maximilian Viemetz, and Michal Skubacz,"Guidance Performance Indicator Web Metrics for Information Driven Web Site", IEEE 2005.

[6] Victor Pascual-Cid, "An information Visualization System for the Understanding of Web Data", IEEE Symposium on visual analyics science and technology,pp.183-184,2008

[7] Sanjay K.D, Anubha G, Ajay R, "Usability Evaluation Of Software using Fuzzy MultiCriteria Approach", IJCSI,2012

[8] Kumar R, Kiran K, Arivind K, "Measuring Software Reliability: A Fuzzy Model", acm, 2011

[9] Nielsen, J. and Philips, V(1993) "Estimating Relative Usability ot Two Interfaces: Heuristic ,Formal, and Empirical Methods Compared. ACM 1993.

[10] Thmbley, H.(1991) " Formal Usability". SIGCHI Bulletin APRIL 94.

THE 18TH INTERNATIONAL SYMPOSIUM ON WIRELESS PERSONAL MULTIMEDIA COMMUNICATIONS
(WPMC-2015)
December 13-16, 2015, Hyderabad, India

A Brief Review on Process Parameter Optimization of GMAW Process and Grey-based Taguchi Method

Patil U. V.[1]
[1]*PG. Student,*
Department of Production Engineering, KIT's College of Engineering, Kolhapur
Shivaji University, Kolhapur (India)
ulhasvr@gmail.com

Naik G. R. [2]
[2] *Asso. Professor*
Department of Production Engineering, KIT's College of Engineering, Kolhapur
Shivaji University, Kolhapur (India)
girishnaik2025@gmail.com

ABSTRACT: ***The prediction and optimization of process parameters is an significant aspect in welding process. Therefore, input process parameters play an important role in determining the mechanical properties. Proposed project work aims on optimization of process parameters of bead geometry for Gas Metal Arc welding (GMAW) process. For this study application of the Taguchi approach will be followed by Grey Relational Analysis to optimize the parameters of Gas Metal Arc Welding process for AISI 446 grade of stainless steel plates.***

Keywords—: Bead Geometry, Gas Metal Arc Welding, Grey Relational Analysis, Taguchi Orthogonal Array

I. INTRODUCTION

The Gas metal arc welding processes are quickly replacing the shield arc stick electrode process because the GMAW process can easily applicable to both ferrous and nonferrous metals. GMAW processes are also popular as they can deposit a large quantity of weld metal in a relatively small period of time. GMAW plays a significant role in many industries. Welding is mainly important in heavy fabrication industry, which includes machinery, farming equipment, process tools for manufacturing and mining, and infrastructure for petroleum refining and distribution. During the welding process, input parameters influenced the weldment quality. Therefore, welding becomes as a multi-input multi-output process. To catch the preferred weld superiority in GMAW process it is necessary to study input and output process parameters interrelationships. It is necessary to control shape of weld bead geometry in determining mechanical properties. Therefore, appropriate assortment of process parameter is necessary. It is not easy task to developing mathematical models which gives relationship between input and output process parameters of GMAW process because there were some unknown nonlinear process parameters. Therefore, it is better to resolve this problem by experimental models. In Grey relational generation, the normalized data follows either lower-the-better or larger-the-better criterion according to the selected output parameters. Grey relational grade is to reveal the degree of relation between the defined sequences the reference sequence represents the best process sequence; therefore, higher Grey relational grade means that the corresponding parameter combination is nearer to the optimal. The mean response of the Grey relational grade, its grand mean state may well be calculated from this plot. By using appropriate optimization technique, it gives the optimum parameters setting which can be satisfying the multi-objective problem. The efforts taken out by several researchers are presented in table I.

II. METHODOLOGY

Systematic approach of project work is required to predict and obtain the optimum solution of process parameters and weld bead geometry for GMAW process. This approach consists of the subsequent steps for the proposed work.

A. Identification of process parameters and their levels in GMAW

The process parameters play very significant role to determine the good weld bead. In the proposed work four welding input parameters selected are the welding voltage (V), welding speed (S), wire feed rate (F) and gas flow rate (G) and the output parameters are bead penetration (BP), bead height (BH) and bead width (BW). The weld bead geometry will influence the mechanical properties of the weldment. These are key controllable process parameters and it is required to have minimum three levels of process parameters to expose the true performance of response parameters. Intermediate ranges coded value can be determined by the subsequent equation:

$$x_i = 2(2x-(x_{max}+ x_{min})) / (x_{max}- x_{min}) \quad (1)$$

Where, x_i = the required coded value of a parameter x; x is any parameter value from x_{max} to x_{min};
x_{min} = the lower level of the parameter;
x_{max} = the upper level of the parameter.

B. Development of design matrix

In the proposed work, design matrix based on Taguchi's orthogonal array is selected. Therefore the experiment will be conducted with four controllable, 3-level factors and three performance characteristics. Nine experimental runs based on the orthogonal array L9 (3^4) will be required.

C. Conducting the experiments as per design matrix.

In the proposed work, GMAW machine manufactured by ATE, Pune, INDIA will be used. It is a 3-phase, 50Hz frequency, 300A, forced air cooling semi-automatic machine. The torch is secure to the frame at 90^0 to the work specimen can be kept on trolley which will move at perfect path. Gas

Table1. Summary of literature survey

Ref No	Authors	Year	Process	Process Parameters		Technique Employed	Work Material	Remarks
				Input	Output			
1	M. Sen M. Mukherjee T.K.Pal	2015	DP-GMAW	Current Thermal pulse frequency Arc voltage Pulse frequency	Bead Width Bead Height Bead Depth Aspect Ratio Convexity Index	Response Surface Methodology	Mild Steel	A second order mathematical model was developed to predict the weld bead geometry. Reasonable accuracy found in the weld bead geometry.
2	Pathiyasseril et al.	2014	GMAW	Wire current Welding Speed Welding gun angle Contact tip to work dist. Pinch	Clad Bead Width Bead Height Bead Penetration % of Dilution	PSO-Based Neural Network	IS 2062	The proposed ANN-PSO model is found to be flexible, speedy and accurate than conventional ANN system.
3	Ramos Jaime et al.	2013	Robotic GMAW	Wire Feed Rate Welding Voltage Torch Travel Speed	Bead width Bead height Bead Depth	Radial Basis Function Neural Network	-	In this paper RBF neural network is applied and predicted the weld bead geometry using three level factorial design.
4	Ghalib Thama et al.	2012	GMAW	Weld Current Arc Voltage Weld Speed Wire Extension	fillet bead geometry	Mean Absolute Deviation (MAD)	Carbon steel	This result validates the accuracy and reliability of the calculator to predict the fillet bead geometry and welding parameter for fillet welding in 3F position.
5	Y. T. İÇ, F. ELALDI et al.	2012	GMAW	Current Arc voltage Welding speed	Tension and compression tests of welded joints	Design of Experiment Goal Programming	Armor steel	The developed approach possesses flexibility of adding new constraints, aspiration levels, improvement objectives, and modifying them whenever necessary.
6	S. W. Campbell ElaldiI et al.	2012	GMAW	Voltage Current Travel Speed	Penetration Leg Length Effective Throat	ANN	DH36 grade steel	The output from the model has demonstrated that the use of alternating shielding gases during GMAW results in a step change in the weld metal geometry.
7	M. Aghakhani et al.	2011	GMAW	Wire feed rate Welding voltage Nozzle-to-plate distance Welding speed Gas flow rate	Dilution	Taguchi Method	STEEL ST-37	The wire feed rate has the most significant effect on the weld dilution
8	Fanrong Kong et al.	2011	GMAW (hybrid laser–GMA welding Process)	welding speed	heat distribution and residual stress along the weld joint	3D thermo-elastic–plastic FEM	ASTM A36 carbon steel	The proposed thermo-mechanical FEM could be further applied to the optimization of the processing parameters of hybrid laser–GMA welding as well as other welding techniques
9	Mohammad Mousavi Anzehaee and Mohammad Haeri	2011	GMAW	Droplet size Melting rate	Detaching droplet size Detached droplet size Mean value of droplet detachment frequency	Modified force balance model and the designed estimators	-	A new method to estimate the droplet size in the projected spray mode of a gas metal arc welding process has been proposed which is based on the modified force balance model.

10	Kalenda Mutombo and Madeleine du Toit	2011	GMAW	Arc voltage Welding current Wire feed speed Wire diameter Nozzle to plate distance Travel speed Torch angle Gas flow rate	Corrosion fatigue behavior	Microstructure analysis by Corrosion fatigue testing M/C	Aluminium alloy 6061-T651	The fatigue life of 6061-T651 aluminum in the un-welded condition is significantly reduced on testing in a 3.5% NaCl solution, compared to that measured in ambient air.
11	Her-Yueh Huang	2010	GMAW	Arc voltage Welding current, Welding speed Joint gap	Weld bead geometry Angular distortion Mechanical properties	Taguchi method	AISI 1020 Carbon Steel	The fluxes Fe2O3, SiO2 and MgCO3, not only increased the weld area and weld penetration but also improved the tensile strength and hardness of the GMAW joint.
12	S. Zielin ska et al.	2009	GMAW	Shielding gas, The wire feeding speed The arc current	Precipitates Oxide gangue	Microstructural analysis	Mild steel	These investigations allow to hope a control of the metal transfer mode, taking into account the chemical reactions occurring between melted metal drops and the shielding gas.
13	K. Manikya Kanti and P. Srinivasa Rao	2008	GMA	Thickness of the plate Pulse frequency Wire feed rate, Wire feed rate/travel speed ratio Peak current	bead penetration depth and the convexity index of the bead	Back propagation neural network	--	The results obtained from neural network model are accurate in predicting the weld bead geometry.
14	Erdal Karadeniz et al.	2007	GMAW	Welding current Arc voltage Welding speed	Penetration	The spectrometric analysis	Erdemir 6842 steel	In this study, the effects of various welding parameters on welding penetration in Erdemir 6842 steel having 2.5 mm thickness welded by robotic gas metal arc welding were investigated
15	Davi Sampaio Correia et al.	2005	GMAW	Reference voltage Wire feed rate Welding speed	Deposition efficiency Bead width Depth of penetration Reinforcement	Genetic algorithms and response surface Methodology	Mild steel	It was found that the GA can be a powerful tool in experimental welding optimization, even when the experimenter does not have a model for the process
16	D. S. Correia et al.	2004	GMAW	Reference voltage, Wire feed rate Welding speed	Deposition efficiency Bead width Depth of penetration Reinforcement	Genetic Algorithm	Mild steel	Genetic algorithm had a relatively good quality with no problems of melt-through, porosity or cracks. Considering quality as closeness to defined targets, the genetic algorithm did not manage to achieve all the established targets.
17	I.S. Kim et al.	2003	GMAW	Current Welding voltage Welding speed	Bead width Bead height Penetration	Full factorial design	Mild steel AS 1204	The results obtained show that developed mathematical models can be applied to estimate the effectiveness of process parameters for a given bead geometry, and a change of process parameters affects the bead width and bead height more strongly than penetration relatively.
18	I.S. Kim et al.	2002	GMAW	Layer Current Voltage Welding Speed	Bead height	Neural network	BV-AH32 Steel	The results show that not only the proposed models can predict the bead height with reasonable accuracy and guarantee the uniform weld quality, but also a neural network model could be better than the empirical models

19	Jeongick Lee! and Kiwoan Um	2000	GMAW	Gas flow rate Contact tip to workpiece distance Current Voltage Gap Speed	Width Depth	Multiple regression analysis and artificial neural network	SS41 mild steel	The error rate predicted by the artificial neural network was smaller than that predicted by the multiple regression analysis, in terms of the width and depth of the back-bead.
20	N Murugan and S. Parmar	1994	MIG	Open circuit voltage Wire feed rate Welding speed Nozzle-to-plate distance	Penetration Width Reinforcement Dilution	Four-Factor five factorial technique	Structural steel IS 2062	Developed mathematical models to predict the weld bead geometry and also determined the factors on the weld features and presented graphically.
21	Saurav Datta et al.	2008	SAW	voltage wire feed rate Traverse speed, Electrode stick-out Creep feed	Bead height Bead width Penetration Depth of HAZ	Grey-based taguchi method	Mild Steel	The study has intended to prove the application feasibility of Grey-based Taguchi technique for solving multi-objective optimization problem in the field of submerged arc welding.
22	Chorng-Jyh Tzenga	2009	CNC turning	Cutting speed Feed rate Depth of cut Cutting fluid mixture ratios	Roughness average Roughness max. Roundness	Grey relational analysis	SKD11	The Grey relational analysis based on an orthogonal array of the Taguchi method was a way of optimizing the turning operations for SKD11.
23	C. C. Tsao	2009	Milling	Spindle speed Feed per tooth Axial depth of cut Radial depth of cut	End cutting edge Peripheral cutting edge Material removing rate	Grey–Taguchi method	Aluminum alloy	Experimental results indicate that the optimal process parameters in milling aluminum alloy can be determined effectively by using Grey–Taguchi method

flow rate can be vary and to be measured by flow meter. The mixture of argon (98%) and oxygen gas (2%) can be used as a shielding gas. The wire feed and welding voltage regulators are provided in the machine to changes the values of same. Variation of welding voltage automatically changes the current. Therefore, four process parameters welding voltage, wire feed rate, welding speed and gas flow rate can be varied in this machine. Based on design matrix, the experimentations are done by varying input parameters. AISI 446 grade stainless steel is used as work-piece material. The stainless steel filler rod of AISI 309L is recommended by American welding society (AWS) will be used for conducting the experiments. To estimate the bead geometry of the stainless steel weldment, specimens having dimension of 150mm x 100mm x 8mm with a single V shaped groove of 30^0 are to be used for each piece as per the design data on the 100 mm side of the plate using vertical milling machine. The land and root gap of 2mm will be provided between the two work pieces.

D. Measurements of the response parameters

The experiments will be conducted by single pass. The samples will be prepared as per American Society of Testing Materials (ASTM) standards and will be cut into three parts for the measurement of bead geometry parameters using water jet cutting machine. The metallurgical polishing process revealed the bead geometry for measuring the BH, BW and BP. The bead geometry parameters will be measured by optical microscope at three places and the average values will be calculated.

E. Analysis of experimental data by Grey-based Taguchi method.

The result obtained for bead width, bead height and bead penetration after experimentation will be first normalized and grey relational coefficients may be evaluated. These Grey relational coefficients for each response will be collected to calculate Grey relational grade. Grey relational grade is the total characteristic of all the features of weld quality. Thus, the multi-objective optimization problem can be transformed into a single comparable objective function optimization problem by the combination of Taguchi approach and Grey relational analysis. Maximum grey relational grade equivalents factor combination to the closer optimal parametric setting.

F. Calculation of S/N ratio

The S/N ratio of overall Grey relational grade can be determined using LB (larger-the-better) criterion by Eq. (2)

$$\text{SN (Larger-the-better)} = -10 \log \left[\frac{1}{n}\sum_{i-1}^{n} \frac{1}{yi^2}\right] \quad (2)$$

Where n = the number of measurements, and yi = the measured characteristic value.

Main effect plot for the S/N ratios can be plotted from the mean response for S/N ratio which gives the optimal parametric combination setting.

G. Confirmation experiment

After assessing the optimal parameter settings, the next stage is prediction and verifies the improvement of quality targets using the optimal parametric combination. The predictable Grey relational grade $\gamma\hat{}$ using the optimal level of

the design parameters can be determined by Eq. (3) and Grey relational grade.

$$\hat{\gamma} = \gamma_m + \sum_{i=1}^{0} (\gamma_i - \gamma_m) \quad (3)$$

S/N ratio for predictable grey relational grade can be calculated using Eq. (2). The Grey relational grade and S/N ratio for initial factor settings, predicted optimal parametric process setting and experimental optimal parametric process setting signifies the comparison of the predicted bead geometry parameters with the original by using the optimal welding conditions; improvement in overall Grey relational grade. This confirms the usefulness of the planned approach in relation to process optimization, where more than one objective has to be fulfilled concurrently. It may be noted that, the Taguchi optimization technique and the optimal parametric combination to be calculated depend on the selected response variables and their individual weight ages.

H. Analysis of variance (ANOVA)

ANOVA is a statistical technique, which can infer some important conclusions based on investigation of the experimental data. If the P-value for a term appears less than 0.05 then it may be concluded that, the effect of the factor is significant on the selected response. Using MINITAB release 15, ANOVA for overall Grey relational grade can be exposed.

III. CONCLUSIONS

From the above literature survey, it is concluded that, only few researchers had attempted the use of Grey relational analysis for the parameters optimization of GMAW process. Very few mathematical models were observed in the literature describing the relation between input and output parameters. Also, the work was not carried on AISI 446. Hence, there is an opportunity for the use of Grey based Taguchi techniques to increase the performance of GMAW process by allowing for various input parameters and trying multi-objective task of the process. Effort can also be made to obtain optimum parameters setting by using Grey based Taguchi technique. It is essential to control the shape of weld bead geometry which plays a significant role in defining mechanical properties as it is affected by weld bead geometry shape.

REFERENCES

[1] M. Sen et al., " Evaluation of correlations between DP-GMAW Process parameters and bead geometry" Welding Journal 94(2015) 265-279.

[2] Pathiyasseril Sreeraj et al., " PSO-based neural network prediction and its utilization in GMAW process" Jordon Journal of Mechanical and Industrial Engineering 8(2014) 333-342.

[3] Daniel Ramos Jaime et al., " Effect of process parameter on robotic GMAW bead area estimation" Procedia Technology 7(2013) 398-405.

[4] Ghalib Tham et al., "Predicting the GMAW 3F T-Fillet Geometry And It's Welding Parameter" Procedia Engineering 41(2012) 1794 – 1799

[5] Y. T. İç, F. Elaldi, F. Pakdil, N. E. İpek, "Design of Experiment and Goal Programming Application for the GMAW Process" Welding Journal, Vol 91 (2012) 106-112.

[6] S. W. Campbell, A. M. Galloway, N. A. Mcpherson, "Artificial Neural Network Prediction of Weld Geometry Performed Using GMAW with Alternating Shielding Gases" Welding Journal, Vol 91 (2012) 174-181.

[7] M. Aghakhani, E. Mehrdad, and E. Hayati, "International Journal of Modeling and Optimization" Vol. 1, No. 3, (2011) 216-220

[8] Fanrong Kong, Junjie Ma, Radovan Kovacevic, "Numerical and experimental study of thermally induced residual stress in the hybrid laser–GMA welding process" Journal of Materials Processing Technology 211 (2011) 1102–1111

[9] Mohammad Mousavi Anzehaee, Mohammad Haeri, "Estimation and control of droplet size and frequency in projected spray mode of a gas metal arc welding (GMAW) process" ISA Transactions 50 (2011) 409–418

[10] Kalenda Mutombo , Madeleine du Toit, "Corrosion fatigue behaviour of aluminium alloy 6061-T651 welded using fully automatic gas metal arc welding and ER5183 filler alloy" International Journal of Fatigue (2011) in press.

[11] Her-Yueh Huang, "Effects of activating flux on the welded joint characteristics in gas metal arc welding" Materials and Design 31 (2010) 2488–2495

[12] S. Zielinska et al, "Microstructural analysis of the anode in gas metal arc welding (GMAW)" journal of materials processing technology 2 0 9 (2 0 0 9) 3581–3591.

[13] K. Manikya Kanti, P. Srinivasa Rao, "Prediction of bead geometry in pulsed GMA welding using back propagation neural network", journal of materials processing technology 20 (2008) 300–305.

[14] Erdal Karadeniz , Ugur Ozsarac , Ceyhan Yildiz, "The effect of process parameters on penetration in gas metal arc welding processes" Materials and Design 28 (2007) 649–656.

[15] Davi Sampaio Correia, Cristiene Vasconcelos Gonçalves, Sebastião Simões da Cunha, Jr., "Comparison between genetic algorithms and response surface methodology in GMAW welding optimization" Journal of Materials Processing Technology 160 (2005) 70–76.

[16] D. S. Correia, C.V.Gonçalves,Sebastião, S.C.Junior,V.A. Ferraresi, "GMAW Welding Optimization Using Genetic Algorithms" J. of the Braz. Soc. of Mech. Sci. & Eng. (2004)28-33.

[17] I.S. Kim a, K.J. Son , Y.S. Yang , P.K.D.V. Yaragada, "Sensitivity analysis for process parameters in GMA welding processes using a factorial design method" International Journal of Machine Tools & Manufacture 43 (2003) 763–769.

[18] I.S. Kima, J.S. Sona, C.E. Parka, C.W. Leea, Yarlagadda K.D.V. Prasad, "A study on prediction of bead height in robotic arc welding using a neural network" Journal of Materials Processing Technology 130–131 (2002) 229–234.

[19] Jeongick Lee, Kiwoan Um, "A comparison in a back-bead prediction of gas metal arc welding using multiple regression analysis and artificial neural network" Optics and Lasers in Engineering 34 (2000) 149}158.

[20] N. Murugan and R.S. Parmar, "Effects of MIG process parameters on the geometry of the bead in the automatic surfacing of stainless steel " Journal of Materials Processing Technology, 41 (1994) 381-398.

[21] Saurav Datta, Ashish Bandyopadhyay, Pradeep Kumar Pal. Grey based Taguchi method for optimization of bead geometry in submerged arc bead-on-plate welding. International journal of Advance Manufacturing Technology (2008) 39:1136-1143.

[22] Chorng-Jyh Tzenga, "Optimization of turning operations with multiple performance characteristics using the Taguchi method and Grey relational analysis" journal of materials processing technology 209(2009)2753–2759.

[23] C.C.Tsao, "Grey–Taguchi method to optimize the milling parameters of aluminum alloy" International Journal on Advanced Manufacturing Technology (2009) 40:41–48.

THE 18TH INTERNATIONAL SYMPOSIUM ON WIRELESS PERSONAL MULTIMEDIA COMMUNICATIONS
(WPMC-2015)
December 13-16, 2015, Hyderabad, India

Demonstrating SWiFiIC - Sustainable WiFi for Rural Communication

Abhishek Thakur, Aarthi J, Amit Chawla, Chittaranjan Hota
Computer Science and Information Systems
BITS Pilani, Hyderabad Campus
Hyderabad, India
{abhishek, h2014103018, f2012412, hota}@hyderabad.bits-pilani.ac.in

Abstract — **Delay tolerant networks have not been operated for terrestrial communication on a long term basis. SWiFiIC is an effort to create an extensible platform for future applications in rural communication where delay and loss are less important as compared to cost.**

While costs are minimized, SWiFiIC targets financial sustainability by including a revenue model. As demands for infrastructure increases in rural communication with Internet of things and related applications, SWiFiIC attempts to provide a simple extensible middle-ware which is cost efficient to deploy and operate.

Keywords— Delay Tolerant Networks, Rural Communication, Wireless

I. INTRODUCTION

Delay Tolerant Networks [1] was proposed more than a decade ago with primary applications in deep space communication and other challenged environments like battlefield, underwater communication, deserted locations, post disaster communication etc. Routing and message transfer schemes for DTN are based on store-carry-forward mechanism.

In DTN, there is no end-to-end connectivity between the source and destination nodes. Instead the bundles (DTN messages) are transferred (relayed) from source nodes to other nodes when they have contact. These other nodes (also called intermediate nodes) act as custodians for the bundles. They receive a bundle from a node, physically carry the bundle from one place to another, and pass the bundle to some other node they meet. The latency of a bundle in DTN is unpredictable; it can be of the order of minutes, hours or even days depending on the deployment scenario.

For deep space communications or interplanetary networks, satellites act as custodians of the bundles. DTN has also been attempted for communication with rural communities and remote areas of developed countries [2] or semi-rural areas of developing countries [3]. In rural or remote scenarios people or vehicles moving through the area carry devices that participate in DTN. In such perspective these networks may also be termed as pocket switch networks (with people as carriers) or vehicular ad-hoc networks (with vehicles as custodians).

The author's team, in their prior work have analyzed [4] rural deployments of developing countries. It was noticed that most of the deployment have not sustained themselves without significant external funding. The primary reasons were found to be the complexity of solution and inability of the local community to generate revenue from such solutions.

To mitigate these issues the authors have designed a platform called SWiFiIC (Sustainable Wi-Fi in Indian Context) with focus on **rural** communication in developing countries like India. Over the last three years, the implementation of the design has progressed to a demonstrable proof of concept using open source DTN stack from Braunschweig University of Technology [6].

This paper is a demonstration of SWiFiIC as it exists today and has most of the implementation as proposed in [5]. Extension from [5] is related to change of some notations, usage of screen shots from running applications and discussions on challenges because of central Hub.

Structure of rest of the document is as follows: Section II provides a brief overview of the architecture components. Section III provides details of user interface for management applications. Section IV includes demonstration of a sample application on SWiFiIC. Section V includes details of challenges being observed during SWiFiIC development and deployment. Section VI includes conclusion and a broad overview of future work targeted by the team of authors.

II. ARCHITECTURE

SWiFiIC platform targets four primary goals

- Simplicity of deployment and easy management.
- Usage of "off the shelf components" to benefit from commoditization to achieve cost efficiency and minimize operational cost.
- Commercial model to drive revenue generation.
- Extensible platform with ability to add applications.

To achieve these goals, a deployment of SWiFiIC uses a Linux based hub to control the deployment. All end user devices are Wi-Fi enabled smart phones or tablets. All the

communication uses Wi-Fi (either as Wi-Fi direct or assisted by consumer grade access points).

The platform allows specific applications to have gateway / proxy capabilities extended using the Hub. E.g. broadband connectivity (like NOFN) to the village can be integrated to the Hub. In absence of wired or optical connectivity, 3G/4G can also be used for connectivity. If the cost of communication is a concern, these gateway elements can compress the information. Moreover the platform allows for integration of DTN as a transport for open source frameworks like IoTivity[7].

In this demonstration, the hub is not being used as a gateway for providing Internet based services. It only show-cases the communication within the village.

A. Physical Components

Hub: A low end laptop running Linux (2GB RAM, 250 GB hard disk, dual core). Linux has been chosen primarily to aid debugging during the initial prototyping phase. If needed, it can be moved to an Android device in future. The cost of the device was USD 200.

The software installed on the Hub is Ubuntu 14.04, IBR-DTN, MySQL, Tomcat, PHP and Apache services along with SWiFiIC components.

User terminals: End users have access to SWiFiIC platform using Android devices. All communication relies on Wi-Fi and happens using IBR-DTN service running on these devices. In addition a lightweight SWiFiIC User Terminal Application (SUTA) runs on these devices so that all SWiFiIC applications, list of users and basic billing information etc. can be made available to end users. Extensible applications make use of data provided by SUTA to further implement their functionality. E.g. Messenger gets the list of users.

Operator Terminal: With the intent that Hub need not be physically exposed, an Android device connects to services running on the Hub to provide all management and troubleshooting activities. E.g. User addition and modification, account recharge etc. are provided by the SWiFiIC Operator App (SOA) running on the Operator Terminal. SOA does not rely on DTN, instead it directly communicates with the Hub over HTTP.

B. Logical Components

There are platform specific components called SUTA and SOA. Other than these, SWiFiIC allows third party applications to be developed and deployed on the platform. Each independent App has two components – 1) Android application and 2) Hub specific code. In SWiFiIC paradigm the third party app is called Swilet. The hub component of Swilet is called Hublet, while the corresponding mobile applications are referred to as Moblets.

SUTA Moblet running on end-user device, provides access to the Swilet. As a new Swilet is deployed, the Hublet component automatically runs on the Hub. The details of the new Swilet are pushed (multicast) to all SUTA instances. Once the end user is notified, the end user may decide to install the Moblet piece through SUTA. This functionality is still under development.

Periodically, the SUTA Hublet multicasts the list of users to all SUTA Moblet instances. The SUTA Moblet also responds periodically to these heartbeat messages to provide feedback on round trip delay, node reachability etc. The response includes statistics of device like battery power, software version etc. This information is used by Hublet to update the list of active users and their device details.

The Moblet for other apps can query SUTA for SWiFiIC deployment specific information. Presently this is limited to details of Hub and the list of end-users in the SWiFiIC platform.

C. SWiFiIC communication

Except the SOA, all communication in SWiFiIC relies on unicast or multicast based Delay Tolerant Network. In the present iteration all Moblets talk to their respective Hublets (unicast). The Hublet code may relay or reply in unicast or multicast manner.

As mobile devices come in contact with each other, they exchange the messages so that they reach the destination. Because of reliance on DTN, many DTN bundles may not reach the destination or have significant delay (order of hours). The Swilets need to implement their own logic (like sequencing, acknowledgement, retry etc.) to ensure that it gets the level of quality they desire. Occasionally the end user may need to be notified, especially for people who live on the periphery of the village.

D. Cost and benefit of Centralized Hub

All messages are relayed to the Hub and then distributed back towards the recipients. This approach was necessary to ensure monitoring (and hence billing) of the setup. In future this will also help scan the messages to include IDS/IPS functionality. Further computationally heavy tasks or large storage of data can be delegated to Hublet, thus reducing the space and power needs on mobile devices. Hublets can also act as gateway/proxy to Internet.

Because of such a centralized communication, round trip delays will increase and delivery ratios may drop. In separate ongoing work, authors have done simulations to measure such impact. It was found that in the vicinity of the Hub, congestion sets in as load is increased. To mitigate this, in future design, the team intends to have multiple hubs directly connected over wire.

One benefit that the centralized design allows is the ability to measure quality of service for end users. If the SWiFiIC operator finds that some devices are having poor connectivity, she/he may decide to use dedicated ferry based mechanism to serve such nodes. For example they may hire a person to periodically visit the area where the poorly served nodes reside, or they may allow higher replicas to be created for messages originating or terminating at such nodes.

III. Base Platform Components

SOA and SUTA are two crucial parts of the SWiFiIC platform. Moreover libraries are provided for Hublet and Moblet pieces to simplify development. Figure 1 below captures the deployment for Hub. Figure 2 captures the deployment for typical end user terminal.

A. Hublet basic Logic

For each Swilet, the Hublet needs to implement the handlePayload function. This is the code that gets triggered on receipt of message from Moblets.

Algorithm 1: Handle Payload

function handlePayload(payload, context)
  Identify the *operation* within the payload
  Check account previleges of the originator of payload
  Do the necessary billing for the *operation*
  Invoke the implementation for *operation*
End

handlePayload is the single entry to process all types of operations for the specific Swilet. E.g. for Exam Swilet, it handles operations like, addStudent, sendPaper, submitAnswerScript, getAnswerScripts, getAttendance etc.

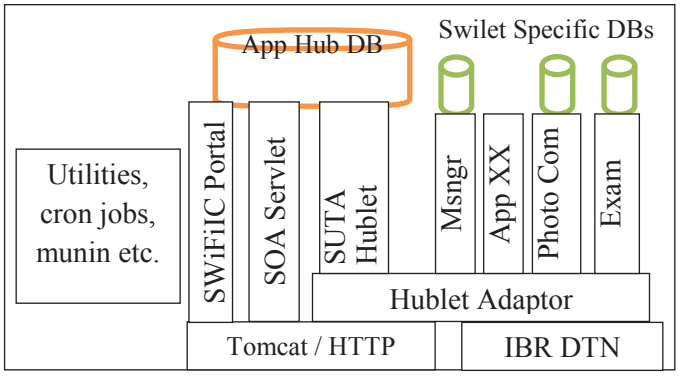

Figure 1 Deployment on Hub

A check on account privilege is necessary to verify the user and avoid impersonation. Billing aspects are optional. The implementation of operation is Swilet specific logic and generally operations such as queries to Swilet specific DBs and generation of DTN messages back towards Moblets.

Hublet code relies on functionality provided by generic code within the Hublet Adaptor so as to mask the complexity of communication.

B. Moblet basic Logic

The Moblet's in present context are Android applications. Other than implementing the logic for the user interaction and application specific requirements, the Moblet's implement a broadcast receiver to handle incoming messages from the Hublet. Further they rely on base libraries (SWiFiIC JAR) to register with the IBR DTN service and to send / receive their messages.

For getting the context of SWiFiIC deployment like Hub's DTN address, list of users etc., Moblets use content provider interface of SUTA.

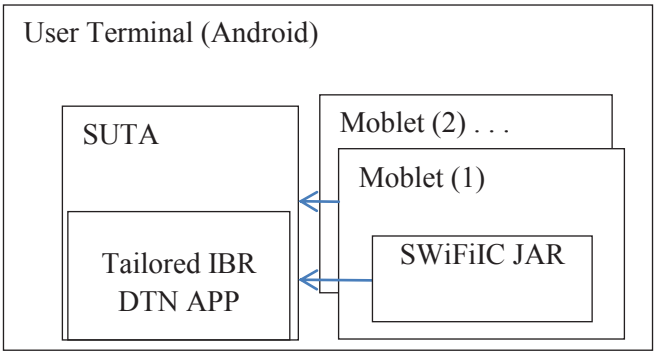

Figure 2 Deployments on User Devices

C. Screen shots

Following figures captures the screen shots for different UI components.

1) SOA

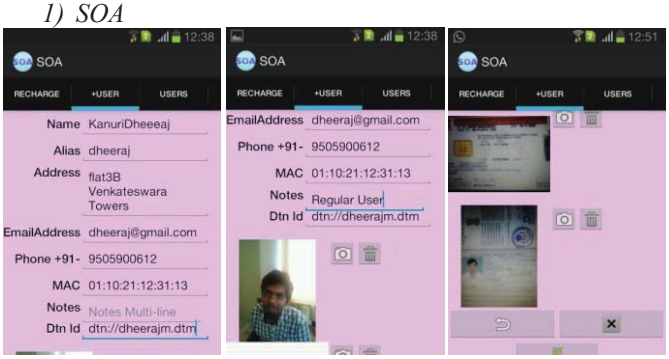

Figure 3 SOA – Add user

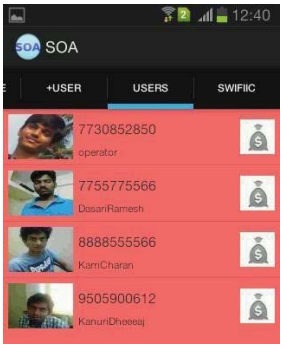

Figure 4 SOA – Other Screens

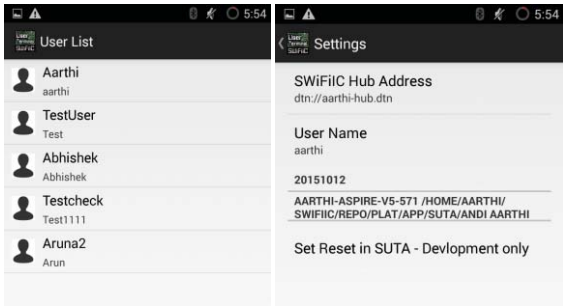

Figure 5 SUTA Moblet

The SUTA Hublet code receives the updates from the Moblets and also generates periodic updates. The figure below captured debug output for some of these scenarios.

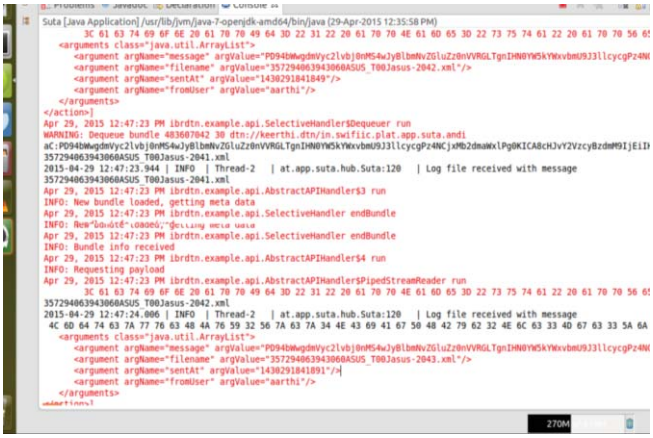

Figure 6 SUTA – Hublet – Node Updates Received

IV. Sample Application

Few applications have been developed to demonstrate the capabilities for the platform. We discuss the messenger app implementation below including a few screen captures.

A. Messenger

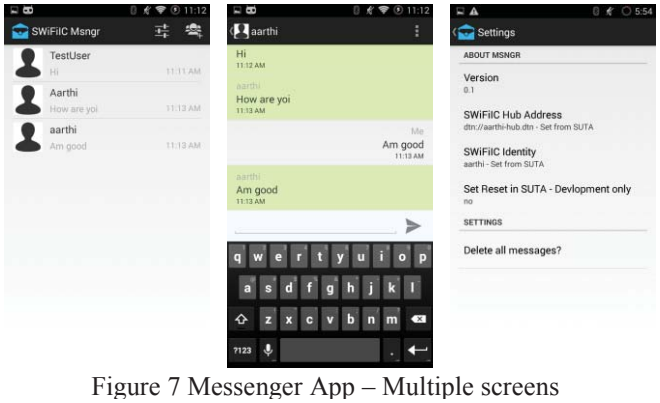

Figure 7 Messenger App – Multiple screens

Hublet: The messenger Hublet after authenticating the sender, debits (notional amount of 1 rupee presently) from their account. Thereafter it queries the DTN id for the receiver of the message and relays the message to the destination DTN node.

Moblet: Majority of the code here is related to UI and tracking of messages received in the past. In addition using the broadcast receiver the code handles incoming DTN messages. To send a new message (towards Hublet) the code uses sendAction on Helper functionality provided by the SWiFiIC JAR files.

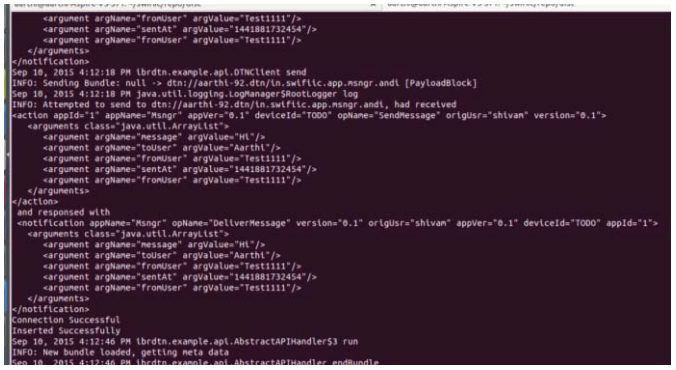

Figure 8 Messenger Hublet – Logs

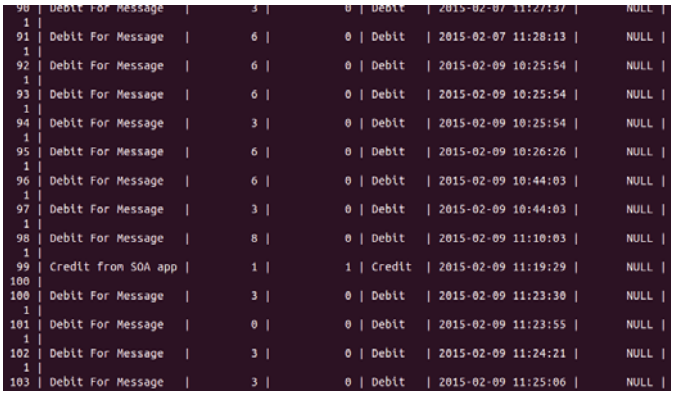

91	Debit For Message	6	0	Debit	2015-02-07 11:28:13	NULL
92	Debit For Message	6	0	Debit	2015-02-09 10:25:54	NULL
93	Debit For Message	6	0	Debit	2015-02-09 10:25:54	NULL
94	Debit For Message	3	0	Debit	2015-02-09 10:25:54	NULL
95	Debit For Message	6	0	Debit	2015-02-09 10:26:26	NULL
96	Debit For Message	6	0	Debit	2015-02-09 10:44:03	NULL
97	Debit For Message	3	0	Debit	2015-02-09 10:44:03	NULL
98	Debit For Message	8	0	Debit	2015-02-09 11:10:03	NULL
99	Credit from SOA app	1	1	Credit	2015-02-09 11:19:29	NULL
100	Debit For Message	3	0	Debit	2015-02-09 11:23:30	NULL
101	Debit For Message	0	0	Debit	2015-02-09 11:23:55	NULL
102	Debit For Message	3	0	Debit	2015-02-09 11:24:21	NULL
103	Debit For Message	3	0	Debit	2015-02-09 11:25:06	NULL

Figure 9 Hub – User transaction ledger entries

V. Development and Deployment Challenges

During the present development and trials for SWiFiIC, it has been noticed that user experience for Wi-Fi Direct is sub optimal. It confuses some of the end users who do not understand the technology in depth.

The peer discovery for IBR-DTN relies on multicast support. In many scenarios for Android devices, the peers have not been discovered even after few minutes. Restarting the Wi-Fi interface or restarting the IBR-DTN service frequently solves this issue. It was also observed that some access points allow peer discovery to happen most of the time, while a few do not.

The author's team has also surveyed a nearby village to better understand the challenges for deployment. While some villagers can afford their own devices, majority of the others still cannot afford to spend four thousand rupees to have their

own tablet. It is an unsolved challenge to create a viable model where the devices can be provided on a subsidized basis, without the fear of loss/theft.

VI. Conclusion and Future Work

SWiFiIC platform is being operated by multiple students within the campus of the authors. It is still far from production ready. Some of the pending items are

- Providing a better way to use Wi-Fi Direct.
- Improving diagnostics and reporting from SUTA.
- Developing other apps.
- Deployment in true rural scenario.
- Multiple Hub with wired connectivity so as to avoid single point of failure and reduce congestion.
- Auditing mechanisms to ensure that the Hublet does not go beyond its manifest.

The authors and the team of students continue to implement further functionality on an ongoing basis. The project code is maintained as open source at www.swifiic.in.

Acknowledgement

The authors are thankful to the development team of IBR-DTN [6]. SWiFiIC platform relies heavily on it. We also appreciate the feedback of reviewers who have helped improve the quality of this work.

References

[1] Fall, K. (2003, August). A delay-tolerant network architecture for challenged Internets. In Proceedings of the 2003 conference on Applications, technologies, architectures, and protocols for computer communications (pp. 27-34). ACM.

[2] Grasic, Samo, and Anders Lindgren. "Revisiting a remote village scenario and its DTN routing objective." Computer Communications 48 (2014): 133-140.

[3] Pentland, Alex Sandy, Richard Fletcher, and Amir Hasson. "Daknet: Rethinking connectivity in developing nations." Computer 37.1 (2004): 78-83.

[4] Thakur, A., & Hota, C. (2013, August). Sustainable wireless Internet connectivity for rural areas. In Advances in Computing, Communications and Informatics (ICACCI), 2013 International Conference on (pp. 1335-1340). IEEE.

[5] Thakur, Abhishek, and Chittaranjan Hota. "Designing an extensible communication platform for rural area." In Advances in Computing, Communications and Informatics (ICACCI, 2014 International Conference on, pp. 1348-1355. IEEE, 2014.

[6] Schildt, Sebastian, et al. "IBRDTN: A lightweight, modular and highly portable Bundle Protocol implementation." Electronic Communications of the EASST. 2011.

[7] Linux Foundation Collaborative Project , “IOT Architecture Overview” https://www.iotivity.org/documentation/architecture-overview

THE 18TH INTERNATIONAL SYMPOSIUM ON WIRELESS PERSONAL MULTIMEDIA COMMUNICATIONS
(WPMC-2015)
December 13-16, 2015, Hyderabad, India

Interference Analysis and Mitigation Techniques in Wireless Body Area Network

Subhojit Moitra
Dept of ECE, VNIT,Nagpur
moitrasubhojit@gmail.com

P.H.Ghare
Asst. Prof. Dept of ECE,
VNIT,Nagpur
phghare@ece.vnit.ac.in

A.G. Kothari
Associate Prof. , Dept of ECE
VNIT,Nagpur
agkagk72@rediffmail.com

Abstract—**Data communication in Wireless Body Area Networks can be used in the vicinity of the human body, among its other applications. Other WBANs using similar frequency bands working in the same vicinity can cause a significant amount of interference to the primary network of interest. This paper presents the analysis of the interference patterns under specific environmental parameters and conditions. Upon analyzing, this paper also suggests an algorithm and based upon it interference mitigation mechanisms to improve the interference scenario in terms of Packet Loss Ratio in WBANs.**

Keywords— Low power Wireless Sensor Network; healthcare; intelligent sensors; Body Area Network; inter-BAN interference; interference mitigation.

I. INTRODUCTION

Body Area Network is a relatively new field of wireless communication as well as remote healthcare. A BAN usually consists of micro sensors implanted inside or on the surface of human body. These sensors can be worn on clothes or worn. The sensors measure different vital parameters such as heart rate, blood pressure, cardio vascular signs, blood sugar etc. The sensors, upon collecting the relevant data, send it to a coordinator node in its network. In this way, coordinator nodes of different body area networks send it to a remotely located computer or a handheld device. It is possible to monitor the conditions of several patients from this central computer at the same time and act according to the values of the respective vital parameters.

BANs are expected to work in a hospital environment and hence, may have to co-exist with other wireless devices working in their proximity and in the same frequency band. This may cause interference. This type of interference can be characterized as Cross Technology Network Interference or CTI, because as the name suggests, different wireless devices using different technologies interfere with each other. For example, in the ISM band (from 2.4GHz to 2.5GHz) there are many sources of CTI available, such as Bluetooth, Wi-Fi, even some of the daily appliances such as microwave ovens, cordless phones etc. These sources can create enough RF interference to result in the deterioration of performance of the BAN of interest. Interference affecting the BAN performance can also occur if two or more networks happen to reside on each other's immediate vicinity. This is characterized as Intra Technology Network Interference (ITI) or Inter-Ban Interference. Furthermore, as per specifications for the IEEE 802.15.6 standard, the performance of a WBAN should remain reliable when upto 10 WBANs are co-located in a 6-by-6-by-6m space [1]. In light of all these considerations for WBANs this work focuses on interference mitigation and hence coexistence enhancement by using simple two-hop, relay-assisted cooperative communications.

The rest of the paper is organized as follows, in section II the related literature to this particular work is discussed. Section III manifests the WBAN architecture that has been used in this scenario. Section IV consists of the contribution of this work and the observations gathered from it. Section V concludes the results of this work.

II. RELATED WORKS

Wireless Body Area Network and interference modelling and analysis is a relatively new topic. Some of the works in this domain includes [2], [3], [4], [5] & [6]. In [2] Z Zhang et al. proposed an interference mitigation mechanism based upon people's social interaction information in social networks. In that particular work, inter WBAN interference is analyzed, social network interactions are detected among WBAN carrying people and then a transmission power game is developed to eradicate interference effects. Rout et al. proposed a mitigation mechanism based on the performance of modifiedand modulated hermite pulses (MHP) for narrowband interference mitigation in the 4.94-4.99 GHz in [3]. W-B Yang et al. proposed interference mitigation using variable data rates, duty cycles and modulation schemes in [4]. Here in [4], the metric of choice to measure interference and improve the interference scenario has been SINR. The proposed algorithm leads to better SINR when compared to its unmitigated scenario and Received Signal Strength Indication (RSSI) would be the most suitable parameter to indicate network performance. In [5], a time hopping code assignment strategy is used to improve Body Area Network performance and a strategy to increase the lifetime of the network is also introduced. Kim et al. proposes a distributed TDMA-based beacon interval shifting scheme to lower the level of interference in BANs in [6]. Here, active period of each BANs coinciding with other networks is avoided through career sensing, thereby reducing the chances of interference.

III. Overview of the System Architecture

A WBAN system can be set up in different ways, and based upon the set up architecture it can be of two types, namely Flat Architecture and Multi Stage Architecture.

In Flat Architecture, usually there are data sensors which collect the data (i.e the vital parameters like heart rate, pulse rate, blood sugar etc.) of a certain patient and relay it to a handheld device or a computer. This computer is comparable to a server computer or a sink node, centrally storing all the data. It is the simpler of the two architectures, shown in figure 1.

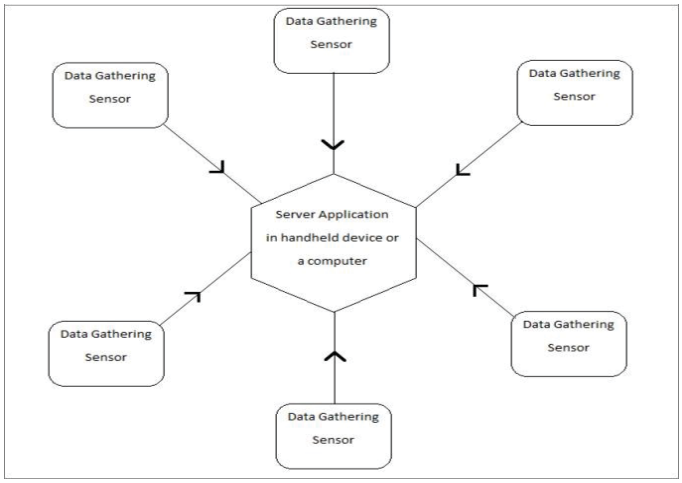

Figure 1: Flat Architecture

In multi stage architecture, devices used are classified into three stages based upon its usage. The Primary Stage is made up of data gathering sensors, which are arranged in clusters. For each cluster, a cluster head node is assigned which acts as a gateway between the server application and data gathering sensors. All the cluster head nodes make up the Secondary Stage. Finally there is the server application which receives all the collected data and this can be called as the Tertiary Stage.

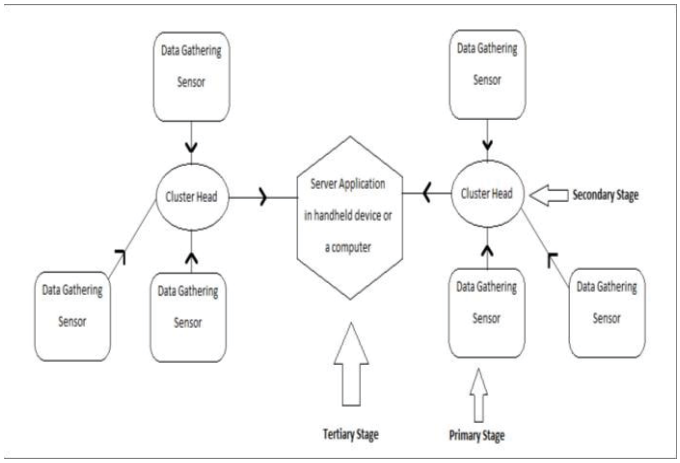

Figure 2: Multi Stage Architecture

In this work, the typical system architecture scenario used for experimentation purposes has been a multi stage architecture using a simple two hop, relay assisted packet delivery mechanism.

IV. System Design

As we have already discussed earlier in this paper, interference affecting WBANs are mainly of two types, such as CTI and ITI. In terms of interference mitigation approaches, there have been a fair amount of interest in CTI mitigation. For one particular instance, Hou et al. in [7] have characterized the effect of non-protocol compliant CTI on BAN reliability and suggested routing and power control strategies to mitigate it. In this work, Inter WBAN interference, also known as ITI has been the focus of the analysis. The mitigation mechanisms that has been proposed here also mitigates the Inter WBAN interference scenario.

A. Experimental Environment

The experimental scenario that has been created in simulator to observe the effects of interference has a few parametric considerations. They are the following,

1) An area of 25 X 20 sqm area is chosen, consisting of 6 WBANs corresponding to six patients.

2) Each WBAN consists of 9 sensors, including one sensor cum cluster head and 8 other sensors to measure vital parameters.

3) A sink node (equivalent to a server application enabled device) is placed in the same environment which receives all the data from the sensor node.

4) The default data rate of the uplink from sensor to cluster head and then to sink node is 250Kbps.The channel is centered at ISM band frequencies (2.405GHz).

5) It is unlikely that there would be many sources inside a hospital room to cause significant amount of path loss. So, the environment created here is a path loss free environment.

The values of the various parameters stated above has been taken after considering practical situations (in hospitals) and typical scenarios used in related similar works [8] [9].

B. Results of Unmitigated Scenario

The software which has been used primarily for all types of simulation regarding multiple Wireless Body Area networks environment is NetSim.

Figure 3 depicts the performance of a typical WBAN in unmitigated scenario working in the system architecture mentioned earlier. Although it is a statistic of one particular WBAN, it can be taken as the representative of typical WBANs. We can make a few observations from here and they are,

A) In a particular BAN, one or two sensor node(s) would be most heavily affected by the interference, while the other nodes in the BAN will perform better. From figure 3. We can assume that node 7 has been most heavily affected by interference and other nodes are less affected in various degrees.

B) The cluster head, receives the packets from sensor nodes, adds its own packets into it and then transmits itinto the server. Essentially it uses a Store and Forward mechanism while sending the packets to the sink node.

C) It is worth noting here that in this scenario, if one particular packet is successfully received without any error and above a pre-defined SINR, then only its corresponding acknowledgement is generated. Otherwise, no acknowledgement is generated.

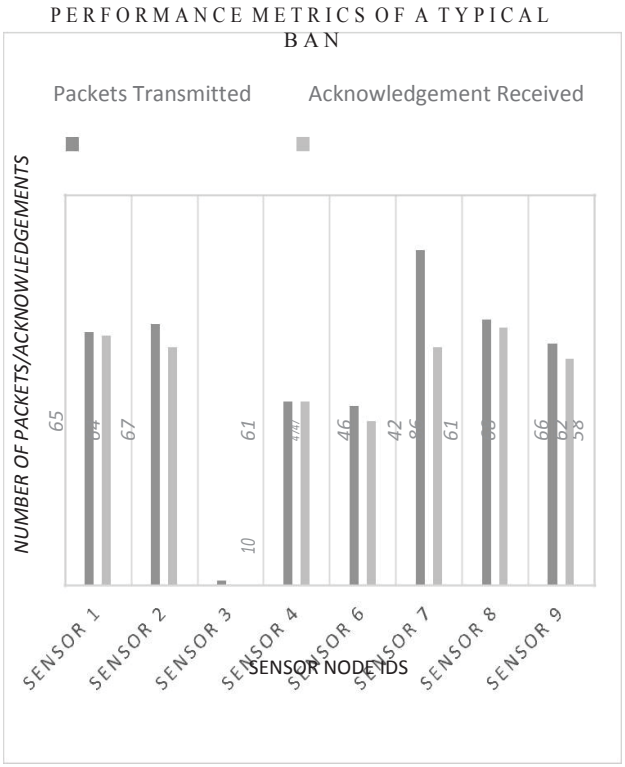

Figure 3: Performance Statistics of a Typical BAN

Packet Delivery Statistics at Sink Node/Server		
Number of Packets Transmitted	*PLR (in %)*	*System Runtime (in Sec)*
10530	3.86	100

Table 1: Packet Delivery Statistics of Unmitigated Scenario

C. Observing the Effects of Interference Using File Transfer Model

In the previous section, the quantitative amount of packets collided has been shown, in percentage terms for the sink node and individual sensor nodes. While the statistics are comprehensive, it does not show the extent of the effect of the interference in real time files, which can be sent over these sensors to the sink node, for example ECG signal of a patient. To investigate this particular case, a scenario using four sensor nodes (in 4 X 1 arrangement) which represent a cluster each (containing one node and one node only) was created. ECG signal files are sent by the sensors to the sink node through the same channel (i.e same center frequency). The signal files, after being received by the sink node, has been reconstructed there to get back the sent file. A thorough comparison of the sent file from the sensor and the reconstructed file at the sink node will depict the extent of effect of interference in this scenario.

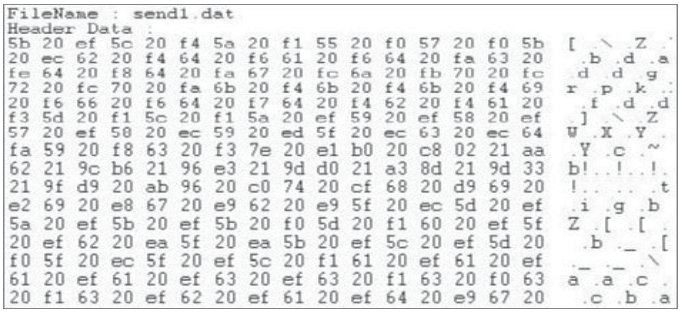

Figure 4: Sent ECG File from Sensor to Sink Node

Figure 4 depicts the sent ECG signal data file from one particular sensor to the sink node, projected in 7 bit ASCII format and converted to hexadecimal representation. At the sink node or server, the PLR in this scenario is approximately 9.09%. Due to this, a certain number of packets have been dropped. The sent file is captured at the sink node and reconstructed there, which is shown in figure 5. It can be argued that the difference between the sent and reconstructed file is obviously due to the packet loss due to unmitigated interference.

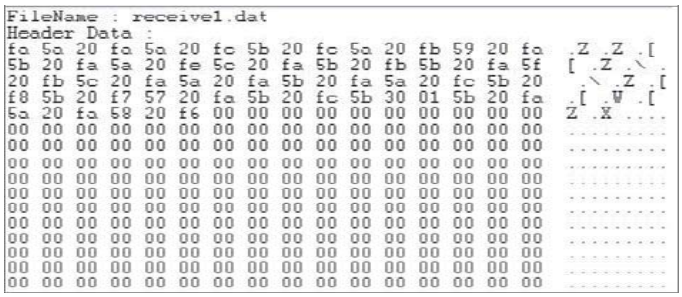

Figure 5: Reconstructed ECG File at Sink Node

D. Implementation of Interference Mitigation Techniques

In this work, two run time interference mitigation techniques are proposed based upon the Packet Loss Ratio (i.e the number of data packets a node has already dropped). Intelligent sensors are used to implement these techniques so that the transmission parameters of individual sensors can be adjusted in run time subject to fulfillment of certain pre-determined criteria. The mitigation techniques are discussed in the following part of this paper.

I. Run Time Adaptive Data Rate in Sensors

Adaptive Data Rate, usually denote the varying data rate of a particular device depending upon fulfillment of certain criteria. In this case, the sensors are having varying data rates with the criteria being the number of packets dropped by a particular sensor node or a cluster head (directly related to PLR). This whole process is carried out in runtime and the adjustment is done automatically by the sensors itself. The criteria upon which these adjustments are done are exclusively user defined so that it can be changed based upon application, environmental parameters or user expectations from the system.

To determine when, how and which data rate is going to be used in the Run Time Adaptive Data Rate mechanism, an algorithm is used. It is given below.

Algorithm: Run Time Adaptive Data Rate

Required: M data rates
Required: $\bar{u}$ (target Packet Loss Ratio)
Initial: u (current Packet Loss Ratio) = 0;
Initial: R_{max}= R1 (default Data Rate);
1. R=R1
2. $\Delta = (R_{max} - R_{min})/ M$;
3. If $u \geq \bar{u} + \delta$ and $R > R_{min}$, then
4. $R = R1 - \Delta$;
5. end if
6. Send Packet;
7. Calculate u;
8. If (Packets != Null), then
9. Go to Step 3;
10. End.

In the given algorithm, δ represents a miniscule amount and represents the step size in data rate used, in Kbps. M is defined as the number of data rate levels to be chosen for the sensor to switch upon, excluding the default data rate level. For example, in this work, 3 different data rates have been chosen to switch upon, namely 200 Kbps, 150 Kbps & 100 Kbps other than the default data rate of 250 Kbps. The range of the data rate values (e.g. from 250 Kbps to 100 Kbps) have been chosen to match the actual data rates used in different healthcare application such as ECG, EEG, and EMG etc. as closely as possible. So, in this case, M comes to be three. It is worth noting that since M, u, $\bar{u}$, R max, R min are all changeable or user defined and can be set in an application specific or user requirements based manner.

Initially, the number of data rate levels (M) and target packet loss ratio ($\bar{u}$) is required from the user. Both of these values are determined based upon hardware & software constraints of the sensor nodes, application in which it is used and required precision in terms of mitigation. The current PLR (u) is set as 0 and maximum data rate (Rmax) is equated to default data rate. The step size is calculated based on Rmax, Rmin and M. As long as the current PLR is lesser than target PLR, packets are sent at default data rate and the resultant current PLR is calculated subsequently during run-time. Now, if this PLR overhauls the target PLR, then the data rate is adjusted by decreasing it by the amount of step size ( ) as long as it is greater than pre-defined minimum data rate. The algorithm ends when the number of packets to be transmitted by a device reaches zero.

The mechanism to choose the data rates and the corresponding number of packet drops (representative of PLR) for each cases is based on optimization techniques. In each of the cases, one data rate and one packet drop ratio is chosen initially on the basis of sensor wise statistic of unmitigated scenario. As we have seen earlier, one or two rogue sensor(s) which perform worse than rest of the sensors in a particular BAN contribute a lot to the PLR of that BAN. So, if we are able to eliminate or decrease significantly the PLR from these rogue sensors, the PLR improves drastically. Primarily, the initial packet drop ratio and data rate chosen for each case is done based upon considerations regarding these rogue sensors. The next step in this mechanism is to optimize the packet drop ratio along with the data rate even more, so that the solution covers higher degrees of packet drops and thereby reducing the PLR. This two-step strategy is followed in every case mentioned, where mitigation mechanism is applied. As we move from Case 1 to Case 5, the packet drop limits for switching to a lower data rate has been made gradually more stringent. In this way, we can arrive at a more robust solution to achieve a better PLR and also compare one particular scheme with respect to its previous one in terms of PLR (as shown in Figure.6).

In this work, test cases to procure observations are obtained using the algorithm. The values of the data rates are grouped along with different target PLRs (represented in absolute number of packets dropped) for the sake of comprehensive observations.

II. Run Time Adaptive Power Level in Sensors

Run Time Adaptive Power Level at the sensors also is an effective mechanism to reduce interference in WBAN. The rationale behind the adaptive power level mechanism is that if a sensor node which is dropping packets switches its transmission power from one particular level to another one, the corresponding interfering nodes will cease to interfere. For example, in the given scenario in this work any sensor node can switch from its basic transmitting power level of 10mW to 20mW or 100mW subject to fulfillment of certain packet loss criteria. In this mechanism, the power levels at which the sensors will switch to for transmitting packets are to be decided by the user. The values of these power levels will have to be chosen after considering certain constraints. These constraints include the permissible SAR values for Body Area Applications, the initial energy and power handling capabilities of the sensors.

E. Results of Mitigated Scenario

As discussed earlier, five different test cases for observation is made by grouping various data rates with packet drop criteria of any sensor node (representing PLR) to examine the results of mitigated scenario. The respective cases are,

I. Default Scenario (250 Kbps data rate throughout)

II. Adaptive Data Rate-I (200 Kbps after 10 Packet Drops, 150 kbps after 30 packet drops by a sensor)

III. Adaptive Data Rate-II (150 Kbps after 8 Packet Drops, 100 Kbps after 15 packet drops by a sensor)

IV. Adaptive Data Rate-III (150 Kbps after 5 Packet Drops, 100 Kbps after 10 packet drops by a sensor)

V. Adaptive Data Rate & Adaptive Power Level (150 Kbps and 20mw of transmitter power after 5 Packet Drops, 100 Kbps and 100mw of transmitter power after 10 Packet Drops by a sensor)

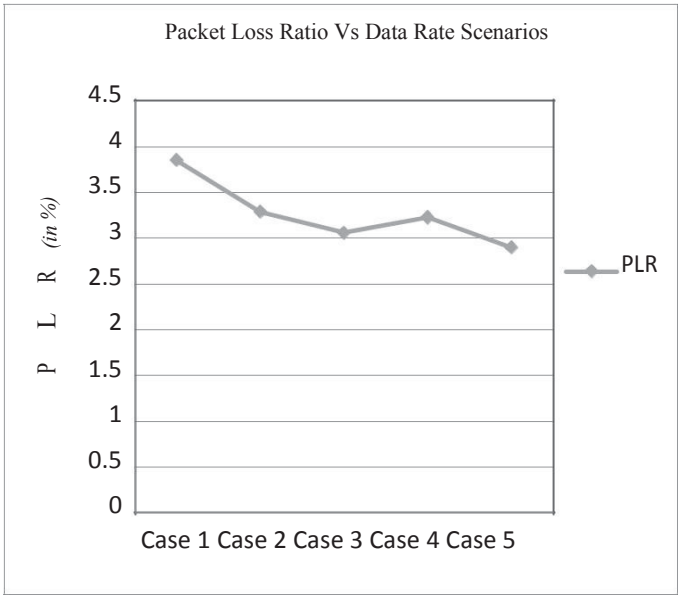

Figure 6: Improvement of PLR vs. different case scenarios

From the figure above, we can infer the comparative effect of the mechanisms on interference. It can be seen that Case2, Case 3 and Case 5 has improved the PLR from its previous scenario, but on the contrary in Case 4, PLR has deteriorated. So, it is clear that an optimization of data rate and threshold metric values are required after extensive implementation, experimentation and observation. In the order the cases has been used, it can be seen that Case 2 is the first bit of interference mitigation mechanism applied on the scenario. So, the improvement of Case-2 (14.77 %, 0.56 % of PLR) over its previous case is highest when compared to improvement of other cases over its immediate previous one. In Case 3, a marginally different and evidently improved mechanism is used. So, essentially it is nothing but an optimization technique. The improvement upon its immediate preceding case here is 9.85%, 0.23% of PLR. Then, in Case 4, the mechanism of Case 3 has been altered to optimize further and it does not improve the Packet Loss Ratio. So, after a certain point, any more change in threshold metric will result in deterioration, it can be observed from here. In this particular case, the deterioration of Packet Loss Ratio is 8.5%, 0.17% of total number of packets sent towards sink node. In Case 5, exclusively the effect of the Run Time Adaptive Power Level scheme has been shown, because while migrating from Case 4 to Case 5 the data rate related metrics are kept exactly the same. This mechanism improves the interference rate by nearly 10 percent, 0.30 % of the PLR. These two mechanisms, Run Time Adaptive Data Rate and Run Time Adaptive Power Level can be used simultaneously to reduce the packet loss rate, in this case by more than 26 percent (Almost 1% of PLR) when compared to normal unmitigated scenario.

V. CONCLUDING REMARKS

In this work, a simulation based scenario is created with respect to practical situations to analyze the patterns of inter WBAN interference, especially in healthcare domain. Furthermore, the impact of inter-WBAN interference is checked on medical signals using File Transfer Model. An interference mitigation mechanism is proposed based on Run Time Adaptive Data Rate algorithm along with a Run Time Adaptive Power Level mitigation mechanism. The mitigation techniques, when used both separately and simultaneously, improve the Packet Loss Ratio and hence the interference scenario. It is expected that the combination of common manual calibration techniques and the mitigation mechanisms would be able to completely eradicate Inter WBAN interference in these scenarios.

REFERENCES

[1] J. Dong and D. Smith, "Cooperative Body-Area-Communications: Enhancing Coexistence Without Coordination Between Networks," in *23rd International Symposium onPersonal,Indoor and mobile Radio Communications (PIMRC)*,2012.

[2] Z. ZHANG, H. WANG, C. WANG and H. FANG, "Interference Mitigation for Cyber-Physical Wireless Body Area Network System Using Social Networks," *Emerging Topics in Computing,* vol. 1, pp. 121-132, 2013.

[3] D. K. Rout and S. Das, "Interference Mitigation in Wireless Body Area Networks Using Modified and Modulated MHP," *WirelessPersonal Communications,* vol. 77, pp. 1343-1361, 2014.

[4] W.-B. Yang and K. Sayrafian-Pour, "Interference Mitigation Using Adaptive Schemes in Body Area Networks," *InternationalJournal of Wireless information Networks,* vol. 19, pp. 193-200,2012.

[5] D. Domenicali, L. D. Nardis and M.-G. D. Benedetto, "UWB Body Area Network Coexistence by Interference Mitigation," in *International Conference on Ultra-Wideband (ICUWB 2009)*,2009.

[6] S. Kim, S. Kim and J.-W. K. a. D.-S. Eom, "A Beacon Interval Shifting Scheme for Interference Mitigation in Body Area Networks," *Sensors,* vol. 12, pp. 10930-10946, 2012.

[7] Y. Hou, M. Li and S. Yu, "Surviving the RF smog: Making Body Area Networks robust to cross technology interference," in *Sensor,Mesh and Ad Hoc Communications and Networks (SECON)*, 2013.

[8] J. M. Ho, "Wireless Medium Access Control (MAC) and Physical Layer (PHY) Specifications for Wireless Personal Area Networks (WPANs) used in or around a body," IEEE P802.15.6/D01, 2010.

[9] S. B. Nji, M. Tabassum and C. H. Siang, "A SURVEY OF MAJOR INTER-USER INTERFERENCE MITIGATION," in Society for Design and Process Science,USA, 2014.

THE 18TH INTERNATIONAL SYMPOSIUM ON WIRELESS PERSONAL MULTIMEDIA COMMUNICATIONS
(WPMC-2015)
December 13-16, 2015, Hyderabad, India

Implementation of Low Cost IoT Based Smart Home using Open Source Platform

Varun Tiwari, Avinash Keskar
Department of Electronics and Communication
Visvesvaraya National Institute of Technology Nagpur, India
varun.etrx@gmail.com, agkeskar@ece.vnit.ac.in

***Abstract*— Integration of various devices and sharing of information has been the baseline of improving the human machine interaction. Internet of Things is the concept of connecting the devices to internet for sharing of information. In this work the concept of IoT is used for a home environment. A local network is formed using low cost NRF24L01 transceivers. All the local connected devices send the information to a master node which sends the collected data to the cloud. This cloud data can be accessed from any cloud connected platform. A mobile application can be developed to monitor and control the home remotely. A cloud server provides various applications that can be integrated with the system. This automated smart cloud program enables the home to act smartly under any critical conditions.**

Keywords— Internet of Things (IoT), Human Machine Interaction (HMI), Smart Home, Wireless Sensor Network

I. INTRODUCTION

With the increase in technology every device we use is becoming smarter and intelligent. Every device is designed to interact with the user more conveniently. This design includes integrating the device with sensors so that a lot of information can be known and processed. The more the information the better and smarter the device can be. In order to improve the human machine interaction the information needs to be shared and sharing this information with the user can be done using local network or a global network. Sharing the information through a global network enables the devices to be accessed from anywhere around the world, this concept of connecting various devices to the internet (global network) is referred as Internet of Things (IoT).

A lot of work has been done in the field of home automation, Zhangxing et al. [1] designed and implemented a home monitoring system with local network and computer [2]. Most of the previous work involved a centralized control unit located in the home itself. All the decision and processing were done by this control unit only. But as more and more devices are getting connected with the increase in technology a lot of information is being generated so the architecture of home central computing becomes limited. Instead of a central control unit the information can be send to a cloud server for processing. In this IoT based architecture all the information is collected and is send to the cloud. The cloud can not only receive data from the home but can also receive data of the users. This user data can be the users GPS location which the cloud server can process and find the optimum time to turn on the air condition of the user's room. Thus, this architecture of collecting and processing all the information on cloud improves the HMI.

Reference [3, 4] implements a ZigBee based network architecture. In this work IoT based home architecture is proposed using low cost NRF24L01 modules for forming local network with open source platforms. The next section discusses about the architecture design of the system.

II. ARCHITECTURE

An IoT based home can be designed using different sensing, monitoring and control devices. All these devices can be designed to be connected to internet to share the information. But designing the devices with direct internet connectivity requires more hardware and cost. So in order to reduce the cost of the overall system the devices can be designed to form a local wireless network with one or more master nodes. These master nodes can be designed to connect and share all the collected information to internet. Once the information is available on the internet it can be accessed from any mobile internet platform. Fig.1 represents the structure of the system. Different sensor nodes are connected to the master node within a local wireless network which then connects to the cloud through the master node.

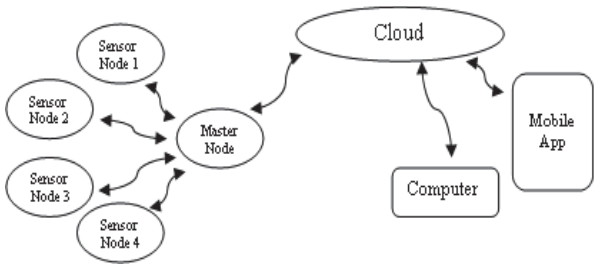

Fig.1 System Architecture

Fig.2 (a) shows the block diagram of a sensor node with one or more sensing/ control/ monitoring unit, wireless transceiver unit, a processing unit and power supply unit. A sensing unit is the interfacing of different sensors to analyze

The work was financially supported by Department of Electronics & Information Technology under Ministry of communications and IT, Government of India and Center of Excellence on Commbedded systems, Visvesvaraya National Institute of Technology, Nagpur, India.

home environment this can be a temperature, humidity, moisture, etc. A control unit can be a relay that can be used to switch on/off any home appliance. A monitoring unit can be a motion detector, proximity sensors as intruder detector, etc. Fig.2 (b) shows the block diagram of a master node with a wireless transceiver unit, internet network module, a processing unit and a power supply unit.

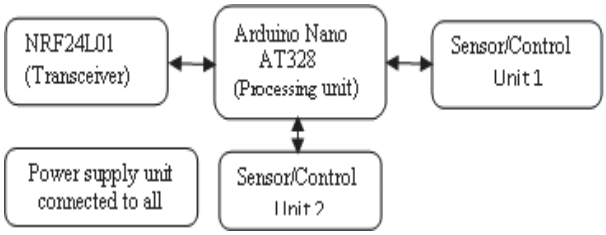

Fig.2 (a) Sensor Node block Diagram

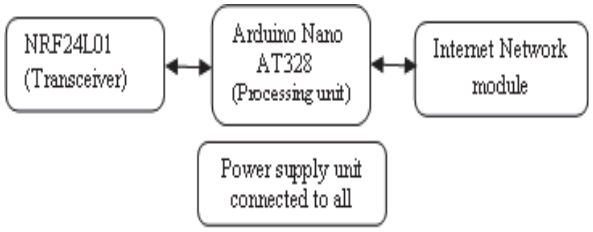

Fig.2 (b) Master Node block Diagram

Fig.3 shows general cloud architecture where a user can create his private secured account. This secured account can only be accessed with API keys, which is known to the cloud account holder only. A secured mobile application can be developed using this API keys to access and control the cloud data. The cloud server has various applications which can be programmed to respond to any critical information coming to the cloud.[5]

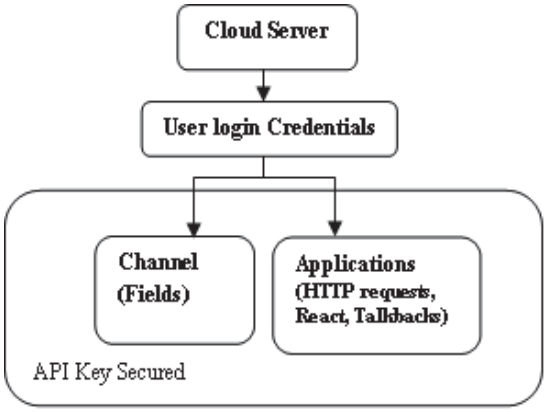

Fig.3 Cloud Architecture

III. IMPLEMENTATION

The complete system can be developed using open source platforms. The design of hardware requires the design of various sensor nodes and master node. The nodes are designed on Arduino open source platform. Atmega328 is used as the microcontroller it has inbuilt 8-channel 10-bit ADC, 23 general purpose I/O pins including 8 ADCs. It has 32KB in system programmable flash memory [6] which provides sufficient space for implementation of our application.

A. Sensor Nodes

Different sensor nodes can be designed to control/ monitor as per requirement. Table 1 shows the different sensor node configuration. Table 2 shows the sensors which can be integrated with the system. A sensor node can be designed to have multiple sensor units and control units. A sensor node should have information sending and receiving capability so the block diagram of the sensor node can be Fig. 2 (a). These sensor nodes use IC NRF24L01 as a transceiver module. It is an ultra low power 2.4GHz based wireless module [7]. It can be configured in a star or tree topology to form a large local wireless network. The nodes can be powered directly through the home power supply with AC to DC converter unit and power regulators. Some nodes which are sensing some critical information such as outdoor sensor or LPG gas leakage sensor can be provided backup power supply with batteries.

The processing unit performs the task of reading the data from the sensors, sending the data to the control units, processing of the data and communicating with the master node. The algorithm for performing the task is explained as follow:

TABLE 1

Environment	Sensor Node
Kitchen	Node with temperature, LPG gas sensor, humidity and exhaust fan control.
Bedroom	Node with temperature, humidity sensor and AC or Lights control.
Garden	Node with humidity, soil moisture sensor, and water pump control.
Outdoor	Node with proximity, Passive infra red sensor, magnetic relay sensor and intruder alarm control.

TABLE 2

Sensor	Modules
Temperature	LM35
Humidity	DHT11(also sense temperature)
Soil Moisture	Analog capacitive rods
Motion Detection	HC-SR510
LPG sensor	MQ6
Proximity sensor	IR-sensor
Door sensor	Magnetic reed relay
Appliance Control	Mechanical / Solid state Relay

Sensor Node Algorithm:

1. Initialize the sensor modules and control units.
2. Initialize and configure the transceiver module to communicate with the master node.
3. Check if any data is received from the master node. If data is received send it to the control unit to perform the operation and repeat step 3 else move to next step.
4. Get the data from the different sensors and process (apply conversions if required).
5. Send the data to the master node.

B. Master Node

A master node can be designed with local network capability and internet connectivity. A master node can receive the data from all sensor nodes and can also send control signals to the sensor nodes. IC NRF24L01 is used for local network connectivity and CC3000 can be used as a Wi-Fi module for internet connectivity. A master node needs to be configured with the addresses of the sensor nodes to form the local network. It sends the information received from the sensor nodes to the cloud so the API keys associated with the users cloud account must be known to the master. The processing unit handles the task of information exchange. The algorithm of a master node is explained as follow:

Master Node Algorithm:

1. Initialize and configure the NRF24L01 transceiver module to communicate with sensor nodes.
2. Initialize the CC3000 Wi-Fi module to connect to the internet.
3. Connect the node to the cloud server with secured user credentials.
4. Check if any data is received from the cloud server, if any control signal is generated then send the control signal to the required sensor node to perform the control task and repeat step 4 else move to next step.
5. Wait and collect the information from the sensor nodes.
6. Arrange the collected information according to the cloud channel and fields.
7. Connect to the cloud server and send the data along with the secured API keys.
8. Check if proper acknowledgement is received, if received correctly move to step 4 else move to step 7.

C. Cloud

A number of cloud servers are available which can be used for the application. The cloud service provided by thingspeak.com is used in this work. A user needs to create a cloud account on the server with proper user credentials. Then the user can create a channel which has different fields that can receive a sensor data. The channel can be made public for free access to anybody or private for secured access. A private channel should be created for secured information sharing. Every private channel generates an API key which can be used for accessing/sending the data from/to the channel. A master node should know this API key in order to send the information to the server. The server also provides various applications that can be programmed as required for e.g. It has an application REACT which can be programmed to automatically turn on the water pump of a garden when the data received from the soil moisture sensor of the garden is below a threshold value. If the API key is known to the user then the information can also be integrated with other mobile platforms through HTTP requests.

IV. Result and Discussion

The complete system has been developed on open source platform. Arduino platform is used for programming the microcontrollers. Arduino Nano is used to keep the design smaller. Open source cloud development platform provided by thingspeak.com is used for cloud application development.The modules used for the design of nodes are low power [6, 7]. For local network formation NRF24L01 module is used which is a low cost device as compared to ZIGBEE Table 3 shows the comparison of the modules. NRF24L01 has high data rate capability and supports star and tree topology which is sufficient for the system even with a large number of nodes. Both are ultra-low power modules. A ZIGBEE can be programmed easily using AT commands and the NRF24L01 needs to be programmed by updating its firmware. The firmware update requires the network configuration with source and destination address settings. The Module can also be configured as a repeater and a number of repeaters can be used to increase the network area.

TABLE 3

Parameter	**ZigBee (ProFLEX01)**	**NRF24L01**
Cost	20$ (approx.)	2$ (approx.)
Range	30m	50m
Power	Ultra Low power device (1uA at standby)	Ultra Low power device (1uA at standby)
Max Data rate	Upto-250Kbps	Upto-2 Mbps
Topology	Star, Tree & Mesh	Star & tree
Interfacing	AT commands	Firmware update

Fig.4 (a) Humidity and temperature sensor node

Fig.4 (b) Soil moisture sensor node

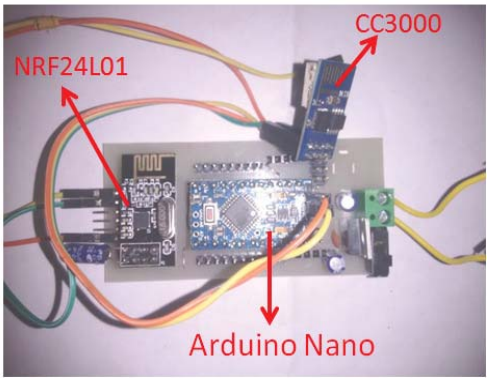

Fig.5 Master Node

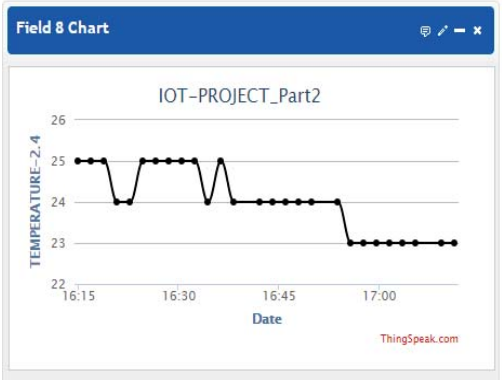

Fig.6 Channel Field of temperature sensor

Fig 4 (a)shows a battery powered sensor node with temperature and humidity sensor, Fig 4 (b) shows a solar powered sensor node with soil moisture sensor. Fig 5 shows a master node and Fig 6 shows the live temperature value on one of the field of a channel of the cloud server at different times of a day. Further the system can be easily integrated with a mobile application as the cloud supports easy information sharing using HTTP requests.

References

[1] Xing, Zhang, Fu Yao Xian, and Wang Ying Guan. "Design and implementation of smart home monitoring system based on msp430." Electrical & Electronics Engineering (EEESYM), 2012 IEEE Symposium on. IEEE, 2012.

[2] Wei, Luo, and Li Wei. "Design and Implement on Smart Home System."Intelligent Systems Design and Engineering Applications, 2013 Fourth International Conference on. IEEE, 2013.

[3] Zhang, Chunlong, et al. "Smart home design based on ZigBee wireless sensor network." Communications and Networking in China (CHINACOM), 2012 7th International ICST Conference on. IEEE, 2012.

[4] Zhang, Shuyan, et al. "Design of smart home control system based on Cortex-A8 and ZigBee." Software Engineering and Service Science (ICSESS), 2014 5th IEEE International Conference on. IEEE, 2014.

[5] Thingspeak, "Actions" Internet: https://thingspeak.com/apps, [August 10, 2015].

[6] Atmel, "Atmel 8-bit microcontroller with 4/8/16/32kbytes In-system programmable flash " Datasheet, 2014.

[7] Nordic semiconductor, "nRF24L01+ Single chip2.4GHz Transceiver" Datasheet, September, 2008.

THE 18TH INTERNATIONAL SYMPOSIUM ON WIRELESS PERSONAL MULTIMEDIA COMMUNICATIONS
(WPMC-2015)
December 13-16, 2015, Hyderabad, India

Performance Comparison of DCT based Entropy Coding Techniques

Samruddhi Y. Kahu, Kishor M. Bhurchandi
Dept. of Electronics and Communication Engg.
Visvesvaraya National Institute of Technology
Nagpur, India
samruddhikahu@gmail.com, bhurchandikm@ece.vnit.ac.in

Abstract— **Many reviews on image and video compression and topics related to it have come up in the last decade. However, a review of entropy coding techniques is a subject which has not been touched upon till now. Entropy coding is an integral part of any image or video compression technique entrusted with the task of representing information using minimum number of bits. Although a host of entropy coding techniques are available and are being developed for many applications, this paper compares and analyzes the performance of four major DCT based entropy coding techniques used for image and video compression under two different intra-coding scenarios: i) block based image data compression and ii) image compression using prediction residuals. The DCT based entropy coding techniques being compared are Huffman, CAVLC, Exponential Golomb and Binary Arithmetic (QM) coding. Two image compression frameworks (algorithms) for the two intra-coding scenarios mentioned above are considered for the comparison of these techniques. Entropy coding being a lossless technique, quality metrics such as Compression Ratio (CR) and time required for coding and reconstruction of images are sufficient for performance comparison and evaluation.**

Keywords— Image Compression, Video Compression, Entropy Coding, Huffman Coding, CAVLC, Golomb Coding, Binary Arithmetic Coding, QM coder.

I. INTRODUCTION

The word 'Entropy' means 'uncertainty' or 'unpredictability'. According to information theory, information content or energy contained in an entity is proportional to the uncertainty conveyed by it. That means, the more likely the occurrence of an event, the less the information it conveys. Thus, entropy is used as a measure of the average information content of a symbol or a source. In this sense, entropy coding can simply be defined as a technique for coding entropy of a source or a symbol using minimum number of bits. The basic principle behind entropy coding is that frequently occurring symbols are encoded using lesser number of bits whereas rarely occurring symbols are coded using a longer bit stream.

Many entropy coding techniques have been developed for data compression such as Huffman, Golomb, Arithmetic, EZW, LZW, LZ77, Wyner-Ziv, etc. All of these are not exclusively used for image/video compression. Some are used for text compression, some for compressing speech signals while some may be used for compressing more than one type of data. Besides their classification based on the application in which they are used, entropy coding techniques can be classified as either variable length or fixed length codes depending on the length of the output code words, dictionary based or non-dictionary based depending on the use of look-up table for the generation of code words, prefix or non-prefix codes depending on whether the codes are uniquely decodable or not and so on.

In this paper, we are going to compare and analyze the performance of DCT based entropy coding techniques, namely, Huffman [1], CAVLC [2], Exponential Golomb [3] and Binary Arithmetic (QM) coding [4] and also discuss their characteristic properties in brief. For effective comparison of these techniques, a common framework (algorithm) is developed using the basic image compression scheme in which all the other steps are identical except entropy coding. Hence compression ratio is sufficient to compare the performance of these four entropy coding techniques. Time required is also used as a measure to compare the computational complexity of each of these techniques. Performance of these techniques is also compared using intra-prediction based image compression algorithm using the same two performance metrics.

Outline of the rest of the paper is as follows. Section II gives a survey of the existing reviews related to image and video compression. In section III the four DCT based entropy coding techniques are discussed in brief. Section IV describes the algorithms used for comparison of these entropy coding techniques. Performance comparison results are shown in Section V while conclusion and future work are presented in section VI.

II. LITERATURE SURVEY

Image/video compression and topics related to it have been reviewed many times under different purviews. Most recent ones include a review of several generations of video coding standards by ITU-T and ISO/IEC starting from H.262 to H.265

(HEVC) [5] and a review of the recent video compression standards like H.264 (AVC), H.265 (HEVC) by ITU-T and ISO/IEC and VP9 by Google Inc. [6]. Reviews on different image compression techniques have also been done. One such analysis of the existing fractal image compression techniques have been discussed in [7, 8]. In fractal image compression, blocks of an image are represented using other smaller sized blocks of the same image which are converted into fractal codes. Much advancement has been done in this technique which is well studied and analyzed in [7, 8]. Image compression using codebook vector quantization is another prominent field which is well developed and improved over the years through constant research. [9, 10] have reviewed some of the landmark Vector Quantization (VQ) techniques whereas [11] studies some prominent advancements in image compression using residual VQ. In [9], a survey of different families of VQ such as Spatial VQ, Predictive VQ, Transform VQ, etc. is done. [10], however classifies and surveys different VQ techniques based on the design of their code books. Not only these, there are reviews comparing the performance of the various components of the basic image or video compression schemes. Such as in [12], various reversible integer-to-integer wavelet transforms are evaluated and analyzed from the point of view of image compression and various optimized non-orthogonal transforms for image compression are compared in [13]. Lossy and lossless intra-coding techniques used in image/video compression standards such as HEVC, H.264 (AVC), JPEG2000 and JPEG are evaluated and analyzed in [14]. Thus, this paper focuses mainly on how effectively spatial correlation is used in the mentioned four compression techniques. Also, all the existing block matching based motion estimation and compensation techniques are reviewed in [15]. It is clear from the above discussion that review of entropy coding techniques is a subject which has not been touched upon till now. Specifically, DCT based entropy coding techniques is chosen for review in this paper even though DWT based compression is a hot research topic these days as the performance of DCT based compression algorithms in terms of CR and PSNR is good.

III. Overview of the DCT based Entropy Coding Techniques

Not all the existing entropy coding methods are suitable to be used with the DCT based image compression algorithms. Hence, in this section, the DCT based entropy coding techniques are described in brief.

A. Huffman Coding

Origin of Huffman coding dates back to 1952 [16]. Since then lot of improvements and modifications have been done to it [17-19] with a view to improve its compression performance. Huffman coding is used in the most widely used JPEG image compression standard [4]. But the Huffman coding scheme used in this review is a modified one as proposed in [1].

Huffman coding is based on the principle that smaller code words are assigned to frequently occurring symbols and larger code words are assigned to rarely occurring symbols. Hence, in order to achieve optimal Huffman coding performance, it is necessary that probability distribution of the data source should be known beforehand. Huffman coding procedure creates an optimal code for a set of symbols and probabilities subject to the constraint that the symbols are coded one at a time.

B. Context Adaptive Variable Length Coding (CAVLC)

This is a recently developed technique for H.264/AVC video coding standard. In this scheme, VLC tables for various syntax elements are switched depending on already transmitted syntax elements. Since the VLC tables are designed to match the corresponding conditioned statistics, the entropy coding performance is improved in comparison to schemes using a single VLC table [2]. More detailed information on CAVLC can be found in [20].

C. Exponential Golomb Coding

Golomb codes were first proposed for the representation of non-negative integers, more specifically for the coding of non-negative integer inputs with exponentially decaying probability distribution [17]. Golomb codes offer a host of advantages above Huffman codes. Firstly, they don't require coding tables to provide supplemental information to the encoder. And they can be used to encode a data source with an infinite number of possible symbols [3]. Even though they are defined for encoding non-negative integers, they can be extended to code signed numbers using a suitable mapping function. Use of exponential Golomb coding as an entropy coding technique in a DCT based image compression algorithm is described in detail in [3]. This paper has adopted the [3] version of exponential Golomb coding for comparison.

D. Binary Arithmetic Coding

In arithmetic coding, a sequence of symbols is encoded into a single long code word. Like Huffman coding, for arithmetic coding also source statistics are needed to be known beforehand. Arithmetic coding is useful when coding a source with less number of symbols. Especially when coding a binary source, Huffman may not provide any compression whereas arithmetic is highly efficient in this scenario [21]. Thus, the JBIG format used for coding bi-level images uses arithmetic coding as its entropy coding technique.

Binary arithmetic coding is used as an entropy coding technique in many image or video compression techniques. Apart from its advantages over other entropy coding techniques of encoding a complete sequence of symbols at a time, thereby coding each symbol using non-integer number of bits, it suffers from the disadvantage of having very high computational complexity. This disadvantage was overcome in its adaptive multiplication-free version called Q-coder developed by W. B. Pennebaker and others [22]. QM-coder is an enhancement over Q-coder which is used with some implementations of the JPEG standard [4, 23]. Thus, in this paper QM-coder implementation of binary arithmetic coding is used for comparison.

Properties of these entropy coding techniques can be summarized as shown in Table I below.

Identify applicable sponsor/s here. If no sponsors, delete this text box (*sponsors)*.

TABLE I. COMPARISON OF THE PROPERTIES OF ENTROPY CODING TECHNIQUES

CAVLC	Exp. Golomb	Huffman	Binary Arithmetic
A complete image sub-block is coded at a time.	Only a single coefficient is coded at a time	Only a single coefficient is coded at a time	Bit sequence for the entire image is coded at a time
Variable sized code words	Variable sized code words	Variable sized code words	Single long code word for an input bit sequence
Look –up table required for encoding and decoding	No look-up table required for encoding and decoding	Look –up table required for encoding and decoding	Probability estimation look-up tables required
No need to store length of code words	No need to store length of code words	Length of code words are stored so as to separate code words at the decoder	No need to store length of code words
Encoder complexity is more as compared to decoder	Decoder complexity is more than the encoder	Encoder complexity is much higher as compared to decoder	Both encoder and decoder are complex
Requires more time	Very less time is required	Requires more time	Less time is required

IV. EVALUATION METHODOLOGY

The four entropy coding techniques are compared using the two algorithms shown in fig. 1 and fig. 2 and are discussed below.

A. Algorithm 1

The basic algorithmic framework used for the comparison of the four DCT based entropy coding techniques is shown in fig.1 below. Since, here we are concerned only about the coding gain provided by the entropy coding techniques, all the steps till quantization are same. Identical quantization matrices are used so that coding gain and image quality deterioration due to quantization will be identical in the case of all the four entropy coding techniques. Hence, Compression Ratio and time required for coding and decoding would suffice as performance metrics for comparison of these techniques. Any arbitrary quantization matrices can be used. JPEG quantization matrices resized to size 4×4 are used here. Algorithm 1 can give the comparison of the entropy coding techniques in case of any arbitrary quantization matrix used.

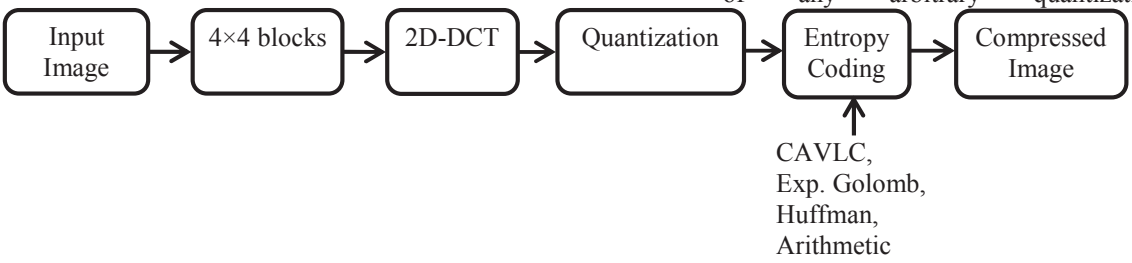

Fig. 1. Algorithm 1 used for comparison of the DCT based entropy coding techniques

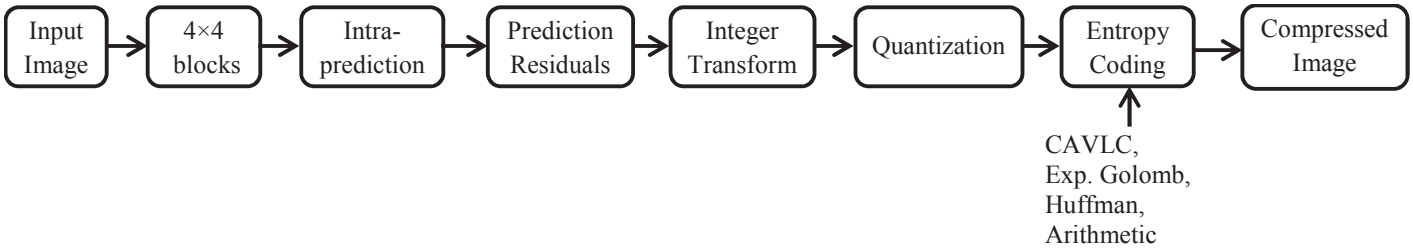

Fig. 2. Algorithm 2 used for comparison of DCT based entropy coding techniques in Intra-prediction framework

B. Algorithm 2

Second scenario considered for the analysis of the entropy coding techniques is the intra-prediction algorithm used to encode I frames in H.264 (AVC). Algorithm for this is shown in fig.2. Originally, CAVLC is used as an entropy coding technique in this algorithm. But in this paper, we have analyzed the compression gain achieved if it is replaced by some other entropy coding technique. DCT based entropy coding techniques can be used in this algorithm instead of CAVLC even though this algorithm uses integer transform as its core transform. This is because integer transform is derived from DCT itself [24]. A Quantization Parameter (QP) needs to be specified to achieve a desired CR and image quality (PSNR). To maintain uniformity of quantization, same QP is used for all four entropy coding techniques. QP of 30 is used for the purpose of comparison which is chosen arbitrarily.

V. PERFORMANCE ANALYSIS

Performance of the DCT based entropy coding techniques mentioned above have been tested on 25 standard test images using the two scenarios discussed in section IV. Parameters used for comparison are CR and time required for coding and reconstruction of an image. PSNR is deliberately not considered due to the fact that entropy coding techniques are

lossless. Hence, PSNR in case of each of the four entropy coding techniques will be same as long as a same quantization matrix in case of algorithm 1 and same QP in case of algorithm 2 is used. Out of these 25 test images, results for 5 images have been tabulated below in Table II and III.

Table II shows the comparison of the four entropy coding techniques using algorithm 1 shown in Fig. 1. From Table II, it can be seen that CAVLC requires maximum time whereas Golomb requires least time. Compression achieved by CAVLC is also very poor as compared to the other three techniques. Arithmetic (QM) gives maximum compression in this algorithm though time required is a bit more as compared to Golomb. Poor performance of CAVLC can be attributed to the fact that CAVLC was developed for entropy coding of the prediction residuals in H.264/AVC video compression system.

Table III shows the Compression Ratio achieved and time required for compression and reconstruction of 5 test images using the intra-prediction algorithm shown in Fig.2 for each of the four DCT based entropy coding techniques. As seen from Table III, CR achieved by CAVLC is the best closely followed by arithmetic coding. But the time required for compression and reconstruction of images using arithmetic is half as compared to CAVLC. Performance of Huffman is worst in terms of compression ratio. Being a non look-up table based technique, Golomb requires least time for compression and reconstruction of these images.

Images for the results tabulated in Tables I and II are shown in fig. 3 (a) to (e). Images reconstructed using the two algorithms are shown in fig. 4 (a) to (e) and fig. 5 (a) to (e) respectively along with the PSNR achieved.

TABLE II. RESULTS OF COMPARISON BY ALGORITHM 1

Image (H×W)	CAVLC		Golomb		Huffman		Arithmetic	
	CR	*Time (sec)*	*CR*	*Time (sec)*	*CR*	*Time (sec)*	*CR*	*Time (sec)*
Image 4 (960×960)	11.52	478.95	20.02	49.59	13.8	318.5	27.02	171.55
Image 7 (512×480)	12.52	79.68	17.08	13.31	11.98	76.41	21.67	45.82
Image 8 (1040×1040)	11.48	595.94	24.2	51.76	15.6	364.35	34.27	174.6
Image 14 (512×512)	11.58	84.29	22.01	11.83	14.85	63.84	30.16	36.18
Image 18 (512×512)	10.62	84.28	20.88	12.14	14.67	64.51	29.13	37.02

TABLE III. RESULTS OF COMPARISON BY ALGORITHM 2

Image (H×W)	CAVLC		Golomb		Huffman		Arithmetic	
	CR	*Time (sec)*	*CR*	*Time (sec)*	*CR*	*Time (sec)*	*CR*	*Time (sec)*
Image 4 (960×960)	21.85	4090.6	17.08	1564.27	9.98	1964.61	20.04	2179.37
Image 7 (512×480)	14.23	501.01	11.51	127.67	7.59	279.22	13.12	230.5
Image 8 (1040×1040)	29.9	4877.78	22.57	2105.53	11.75	2666.62	27.44	2577.44
Image 14 (512×512)	23.79	517.64	18.48	137.64	10.47	245.27	21.81	194.92
Image 18 (512×512)	21.01	415.67	16.71	137.92	9.69	242.78	19.17	209.75

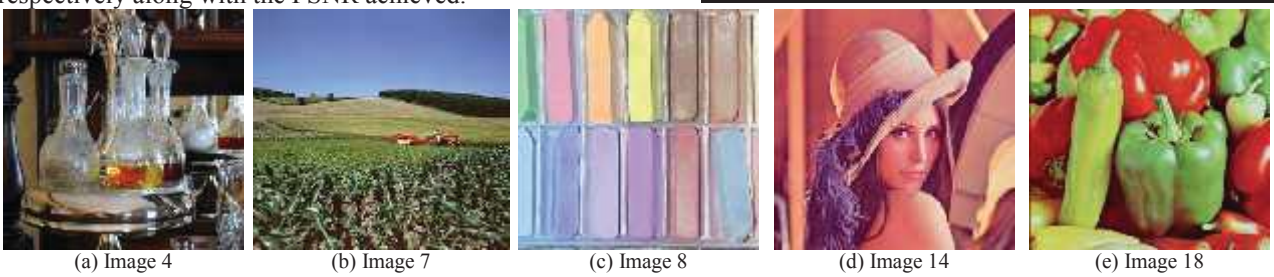

(a) Image 4 (b) Image 7 (c) Image 8 (d) Image 14 (e) Image 18

Fig. 3. Original Images

(a) Image 4 (PSNR = 35.00 dB) (b) Image 7 (PSNR = 33.89 dB) (c) Image 8 (PSNR = 36.31 dB) (d) Image 14 (PSNR = 34.9 dB) (e) Image 18 (PSNR = 33.77 dB)

Fig. 4. Images reconstructed using algorithm 1

Fig. 4 (a) to (e) show the images reconstructed using algorithm 1 using any of the four entropy coding techniques. This is because, even if entropy coding technique is varied, same quantization matrix is used in case of any of the four entropy coding techniques. Similarly, fig. 5 (a) to (e) show the images reconstructed using any of the four entropy coding techniques as QP used in algorithm 2 is same even if the entropy coding technique used in the algorithm is varied.

(a) Image 4 (PSNR = 36.52 dB) (b) Image 7 (PSNR = 35.57 dB) (c) Image 8 (PSNR = 37.44 dB) (d) Image 14 (PSNR = 35.96 dB) (e) Image 18 (PSNR = 35.07 dB)

Fig. 5. Images reconstructed using algorithm 2

VI. Conclusion and Future Work

In this paper, we have surveyed four different DCT based entropy coding techniques namely, Huffman, Exponential Golomb, Arithmetic and CAVLC. These entropy coding techniques are compared and their performance is evaluated using two different compression scenarios. Although CAVLC performs best in terms of CR in algorithm 2 for image compression using intra-prediction and performance of exponential Golomb is good in terms of both CR and time required for image compression algorithm 1, it is clearly seen that performance of QM coder version of arithmetic coding is optimal under both the scenarios with regard to both CR and time required for compression and decompression of the images. However, choice of an entropy coding algorithm is still application dependent.

Performance of these entropy coding techniques can be analyzed using different block sizes in both the algorithms discussed in this paper and also for increasing QP in algorithm 2. A new hybrid entropy coding technique can be formulated using the discussed entropy coding techniques as a future scope of this paper. Also, some other entropy coding techniques can be modified so as to be effectively used under the discussed scenarios.

References

[1] S. Kahu, R. Rahate and K. Bhurchandi, "An improved JPEG image compression algorithm," Irish Machine Vision and Image Process. Conf. (IMVIP-2014), August 2014, pp. 163-168.

[2] T. Weigand, G. Sullivan, G. Bjontegaard and A. Luthra, "Overview of the H.264/AVC video coding standard," IEEE Trans. Circuits Syst. Video Technol., vol. 13, no. 7, pp. 560-576, July 2003.

[3] J. Ding, H. Chen, W. Wei, "Adaptive Golomb code for joint geometrically distributed data and its application in image coding," IEEE Trans. Circuits Syst. Video Technol., vol. 23, no. 4, pp. 661-670, April 2013.

[4] Digital compression and coding of continuous-tone still images, CCITT ITU Rec. T-81 and ISO/IEC 10918-1, September 1992.

[5] J. Ohm, G. Sullivan, H. Schwarz, T. Tan and T. Weigand, "Comparison of the coding efficiency of video coding standards – including High Efficiency Video Coding (HEVC)," IEEE Trans. Circuits Syst. Video Technol., vol. 22, no. 12, pp. 1669-1684, December 2012.

[6] D. Grois, D. Marpe, T. Nguyen and O. Hadar, "Comparative assessment of H.265/MPEG-AVC, VP9 and H.264/MPEG-HEVC encoders for low-delay video applications," Proc. SPIE, Appl. Digital Image Process. 37, vol. 9217, September 2014.

[7] B. Wohlberg and G. Jager, "A review of the fractal image coding literature," IEEE Trans. Image Process., vol. 8, no. 12, pp. 1669-1684, December 1999.

[8] E. Zhau and D. Liu, "Fractal image compression methods: A review," Proc. IEEE ICITA, Sydney, Auatralia, July 2005, pp. 756-759.

[9] N. Nasrabadi and R. King, "Image coding using vector quantization: A Review," IEEE Trans. Communications, vol. 36, no. 8, pp. 957-971, August 1988.

[10] A. Vasuki and P. Vanathi, "A review of vector quantization techniques," IEEE Potentials, vol. 25, no. 4, July 2006.

[11] C. Barnes, S. Rizvi and N. Nasrabadi, "Advances in residual vector quantization: A Review," IEEE Trans. Image Process., vol. 5, no. 2, pp. 1716-1729, February 1996.

[12] M. Adams and F. Kossentini, "Reversible integer-to-integer wavelet transforms for image compression: Performance evaluation and analysis," IEEE Trans. Image Process., vol. 9, no. 6, pp. 1010-1024, June 2000.

[13] O. Guleryuz and M. Orchard, "Optimized non-orthogonal transforms for image compression," IEEE Trans. Image Process., vol. 6, no. 4, pp. 507-522, April 1997.

[14] Q. Cai, L. Song, G. Li and N. Ling, "Lossy and lossless intra-coding performance evaluation: HEVC, H.264/AVC, JPEG2000 and JPEG LS," Proc. IEEE APSIPA ASC, California, USA, December 2012, pp. 1-9.

[15] S. Bachu and K. Chari, "A review on motion estimation in video compression," Proc. IEEE SPACES, Guntur, India, January 2015, pp. 250-256.

[16] R. Gonzales and R. Woods, Digital Image Processing, 3rd Edition, Pearson Education Inc., 2012.

[17] G. Lakhani, "Optimal Huffman coding of DCT blocks," IEEE Trans. Circuits Syst. Video Technol., vol. 14, no. 4, pp. 522-527, April 2004.

[18] X. Kavousianos, E. Kalligeros and D. Nikolos, "Optimal selective Huffman coding for test-data compression," IEEE Trans. Computers, vol. 56, no. 8, pp. 1146-1152, August 2007.

[19] Y. Wen, G. Lin, S. Chen and Y. Hu, "Optimal multiple-bit Huffman decoding," IEEE Trans. Circuits Syst. Video Technol., vol. 20, no. 5, pp. 621-631, May 2010.

[20] T. Chen, Y. Huang, C. Tsai, B. Hsieh and L. Chen, "Architecture design of Contest-based Adaptive Variable-Length Coding for H.264/AVC," IEEE Trans. Circuits Syst. – II: Express Briefs, vol. 53, no. 9, pp. 621-631, September 2006.

[21] T. Acharya and P. Tsai, JPEG 2000 Standard for Image Compression: Concepts, Algorithms and VLSI Architectures, John Wiley & Sons Inc., New Jersey, 2005.

[22] W. Pennebaker, J. Mitchell, G. Langdon and R. Arps, "An overview of the basic principles of the Q-coder adaptive binary arithmetic coder," IBM J. Res. Develop., Vol. 22, No. 6, pp. 717-726, Novenber 1988.

[23] W. Pennebaker and J. Mitchell, JPEG Still Image Data Compression Standard, Chapman and Hall, New York, 1993.

[24] H. Malvar, A. Hallapuro, M. Karczewicz and L. Kerofsky, "Low-complexity transform and quantization in H.264/AVC," IEEE Trans. Circuits Syst. Video Technol., vol. 13, no. 7, pp. 598-603, July 2003.

THE 18TH INTERNATIONAL SYMPOSIUM ON WIRELESS PERSONAL MULTIMEDIA COMMUNICATIONS
(WPMC-2015)
December 13-16, 2015, Hyderabad, India

UWB Sensing antenna, Reconfigurable transceiver and Reconfigurable antenna based Cognitive Radio Test bed

S. Manoj
Lab Engineer, Center of Excellence
Department of Electronics
VNIT, Nagpur
manojstanley1990@gmail.com

Sumin. D. Joseph
Lab Engineer, Center of Excellence
Department of Electronics
VNIT, Nagpur
sumindjoseph@gmail.com

Chetan. Waghmare
Lab Engineer, Center of Excellence
Department of Electronics
VNIT, Nagpur
chetan170989@gmail.com

Nandakumar. K.
Lab Engineer, Center of Excellence
Department of Electronics
VNIT, Nagpur
nandu3008@gmail.com

Ashwin. Kothari
Associate Professor
Department of Electronics
VNIT, Nagpur
ashwinkothari@ece.vnit.ac.in

***Abstract*— In recent years, cognitive radio technology is emerging for efficient use of spectrum for wireless communications. In this, spectrum is shared between primary and secondary users. Secondary users also called as unlicensed users, makes use of part of spectrum which is not used by primary or licensed users. Hence secondary user systems must be capable of sensing the spectrum and should be able to reconfigure to transmit at different frequencies. For this it must consists of spectrum sensing circuit and a reconfigurable transceiver consisting of reconfigurable antenna. This paper discuss the single module of reconfigurable transceiver which dynamically allocates two different frequencies 2.4GHz and 3.1GHz for transmission. Ultra-wideband patch antenna, Spectrum sensing algorithm and reconfigurable patch antenna are also discussed. The module can be modified to transmit at more frequencies in the range 2.4GHz to 9GHz by having reconfigurable devices such as LNAs, Power amplifiers, Local Oscillators, Mixers etc.**

Keywords*— *Cognitive Radio, Energy Detection Algorithm, Ultra-wideband Patch Antenna, Dynamic Spectrum Allocation, Reconfigurable Antenna, PIFA antenna

I. INTRODUCTION

The electromagnetic radio spectrum access is a limited resource & is regulated by the government agencies all around the world. The current policy is to assign fixed frequency bands to different wireless applications i.e. fixed spectrum allocation policy. At any given time, 15%-85% of the spectrum is unused according to the geographic location. To improve the efficiency, dynamic spectrum access was proposed. Secondary or unlicensed users (SU) may be configured to transmit in the licensed bands without causing any interference to primary users (PU) [1]. Cognitive radios with the ability to adapt transmission parameters according to the environment are perfect fit for the secondary users [2].

In this paper, a novel Cognitive Radio system is proposed consisting of a UWB sensing antenna, reconfigurable transceiver and a reconfigurable antenna in section II. Then a planar micro strip UWB antenna is proposed in section III. Then in section IV spectrum monitoring is done through energy detection with modified threshold selection. In section V the reconfigurable transmitter and receiver is explained. In section VI a reconfigurable PIFA antenna has been proposed.

II. COGNITIVE RADIO SET UP

In this paper a different Cognitive Radio setup has been proposed. The flowchart of the system is shown in Fig 1. Sensing algorithm can be implemented using FPGA or host computer in NI PXI module.

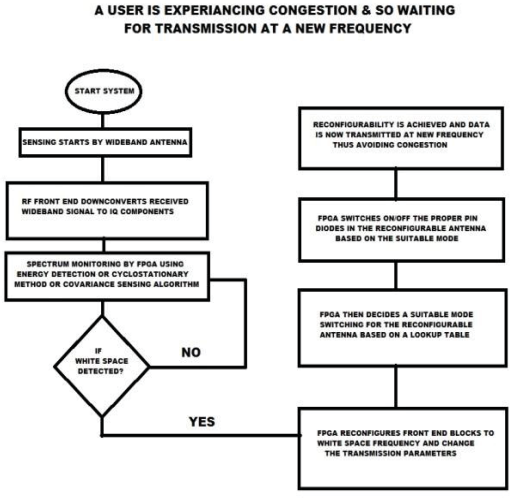

Fig 1. Flowchart of cognitive radio system

III. SENSING ANTENNA

A. Antenna Design Theory

In order to identify unoccupied spectrum bands called as "spectrum holes", an ultra-wideband antenna is required [3]. But designing an antenna giving satisfactory response over an ultra-wideband is quiet challenging. Hence using formulae's given in [4], a narrowband patch antenna is designed and then certain techniques are employed to widen its bandwidth. A rectangular patch antenna was designed and simulated using Ansoft's HFSS software (14.0). An inset feed technique is used to feed the patch for 50Ω impedance matching. An infinite ground plane is used so that maximum radiation goes into the broadside direction to get a directional radiation pattern. The simulated return loss is found to be -14.7dB at 2.4GHz. Bandwidth of patch is 83.6MHz.

The first change in achieving the wideband response is to use elliptical shape patch rather than rectangular [5]. Inset feed is removed in order to radiate patch in multiple resonant frequencies. Ground plane is made finite so that it supports multiple resonating modes. Overlapping closely spaced multiple resonant modes can achieve wide bandwidth and this is the idea of obtaining the UWB bandwidth.

The width of ground plane is determined using the parametric analysis and its optimum value is found to be 10.82mm. The gap between ground plane and patch controls the coupling of fields. This coupling causes to spread the impedance bandwidth and hence must be accurately measured using parametric analysis [6]. The optimum value of this gap is 0.9mm.A slot in ground plane is inserted in order to get better frequency response at these frequencies. The slot is optimized for its dimensions. Also current distribution of patch is studied and a rectangular slot was inserted at the place where it was minimum and its optimum dimension is decided using parametric analysis which comes to be 3.53mm*18.5mm.

B. Final Design of ultra-wideband antenna

Table 1 provides dimension of the whole geometry.

Table 1. Dimensions for ultra wideband patch antenna

Objects in Antenna	Dimensions (mm)
Substrate	45*45
Patch	29.44*38
Micro strip line	3*12
Rectangular slot in Ground	1.6*5.1
Rectangular slot in Patch	6*18.5

The gain of narrowband patch when it was radiating at 2.4GHz was found as 3.1342dB and had directional radiation pattern, Whereas the proposed UWB antenna is having gain of 3.54dB at 3.8GHz and omnidirectional radiation pattern. This gain value is acceptable in UWB communication and cognitive radio applications. Ultra Wide band antenna was fabricated with substrate as FR4 epoxy. Fig 2 shows the fabricated antenna with finite ground plane and rectangular slot in patch and ground. The antennas were connected through SMA connector. Starting frequency of 1GHz and stop frequency of 15GHz were chosen.

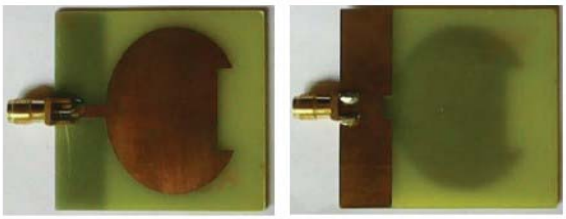

Fig 2. Fabricated antenna: top view (showing patch) and ground plane

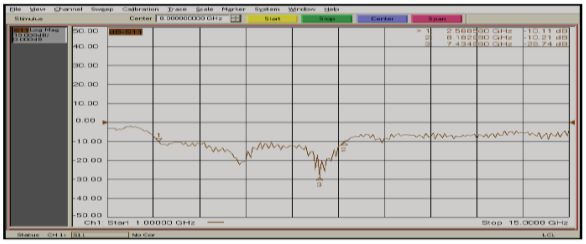

Fig 3. Return loss tested using PNA of Agilent N5230A

IV. SENSING ALGORITHM

A. Algorithm

Energy detection, matched filter detection and cyclo stationary feature detection are important spectrum sensing methods. An energy detector can be implemented by averaging frequency bins of a FFT. Increasing FFT size N improves frequency resolution which helps narrowband signal detection [7]. Longer averaging time reduces the noise power thus improves SNR. This is followed by threshold detection. If noise power is known, threshold can be set based on noise power. The proposed energy detection do not need any prior knowledge of the noise [8].Let us assume that the received signal has the following simple form

$$y(n) = s(n) + w(n) \quad (1)$$

where s (n) is the signal to be detected, w(n) is the additive white Gaussian noise (AWGN) sample, and n is the sample index. Note that s(n) = 0 when there is no transmission by primary user. The decision metric for the energy detector can be written as

$$M = \Sigma_{n=0}^{N} |y(n)|^2 \quad (2)$$

where N is the size of the observation vector. The decision on the occupancy of a band can be obtained by comparing the decision metric M against a fixed threshold λ_E . This is equivalent to distinguishing between the following two hypotheses:

$$H_0: y(n) = w(n) \quad (3)$$

$$H_1: y(n) = s(n) + w(n) \quad (4)$$

The white noise can be modeled as a zero-mean Gaussian random variable with variance σ_W^2, i.e. $w(n) = N(0, \sigma_W^2)$. For a simplified analysis, let us model the signal term as a zero-mean Gaussian variable as well, i.e. $s(n) = N(0, \sigma_s^2)$. The model for $s(n)$ is more complicated as fading should also be considered [9]. The performance of the detection algorithm can be summarized with two probabilities: probability of detection $P_D$and probability of false alarmP_F. P_D is the probability of

detecting a signal on the considered frequency when it truly is present. It can be formulated as

$$P_D = P_r(M > \lambda_E | H_1) \quad (5)$$

P_F is the probability that the test incorrectly decides that the considered frequency is occupied when it actually is not, and it can be written as

$$P_F = P_r(M > \lambda_E | H_0) \quad (6)$$

The mean value, variance and the peak value of received signal, y(n) is computed. Then the following condition is checked at every frequency bins of FFT.

Peak value of y(n) - mean of y(n) > P_F * variance of y(n) (7)

If this condition is satisfied then a signal is detected and the corresponding carrier frequency is estimated. The decision threshold $\lambda_E$can be selected for finding an optimum balance between P_D and P_F . When PF is high, probability of success is also high. This method uses only incoming data and no other prior information of channel noise is needed.

B. Hardware setup

The hardware demonstration consists of generating a QAM signal of certain carrier frequency and transmitting using an antenna. It is then received using the UWB antenna along with the noise. The spectrum sensing is performed on this received signal by energy detection algorithm. After spectrum sensing, the carrier frequency of the received signal is estimated and verified as the transmitted carrier QAM frequency. NI PXI and NI VST 5644R along with UWB antenna is shown in Fig. 4. This is capable of sensing any signal from 65MHz to 6GHz.

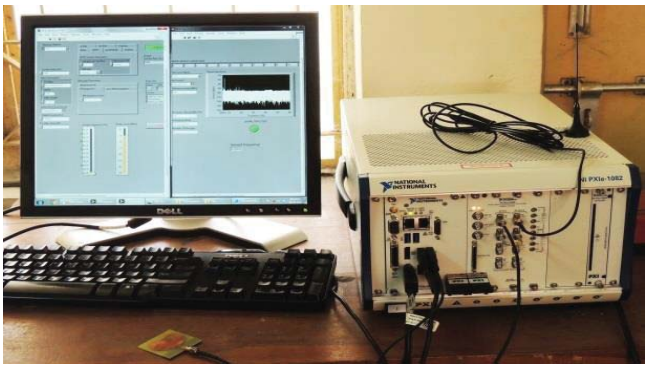

Fig 4. Spectrum monitoring using NI PXI and NI VST with UWB antenna

V. RECONFIGURABLE RF TRANSCEIVER

A. Design and simulation of RF transceiver

Cognitive radios are adaptive and programmable systems which know users preferences and automatically adjust to changes in the operating environment [10]. Before feeding to baseband processor such as FPGA or host processor, signal received through wideband antenna is processed by a re- configurable transceiver so as to down convert the signal. Receiver section is used for sensing as well as data receiving purposes by means of switching. Mode selection in reconfigurable operation is achieved mainly by filter bank and mixer sections.

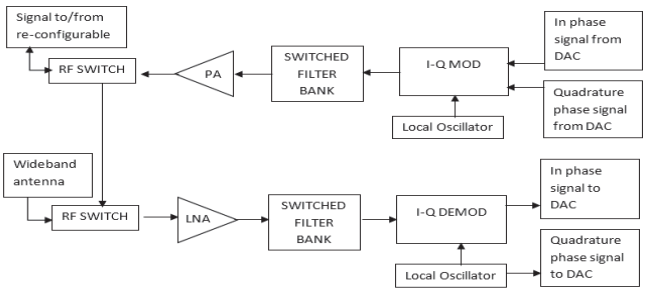

Fig 5. Reconfigurable transceiver block diagram

In order to understand the basic operation and optimization of receiver components the system is first simulated using the software Agilent ADS. Switches are manually controlled for the frequency selection.

Cognitive radio front end has a sensing part along with the reconfigurable section. Sensing network will sense the spectrum; in this case it senses the two bands i.e. 2.4GHz and 3.1GHz.and checks the output signal level. This output signal is used to trigger the control voltage of re configurable part. Sensing part always senses the spectrum to find the spectrum holes in these two frequencies. Once the vacant frequency is found the reconfigurable system will tune itself to that particular frequency. Hence sensing part will act as a control unit of re configurable section. Output of sensing network is given for energy detection and then accordingly control action takes place. The output of sensing circuit is used to drive a switch which decides the operating frequency of reconfigurable section [11]. For a control voltage of 1 V the sensing antenna is designed to be operated at 3.1 GHz and checks whether output level is high or not. If the signal level is high then the device will be re configured to 2.4 GHz. Separate IF frequencies are deliberately given to each user so as to distinguish them. 100MHz is set for 2.4 GHz user and 50 MHz for 3.1 GHz is assigned.

B. Hardware Emulation

Reconfigurable transceiver is designed by integrating different components of Analog devices and Mini-circuits. Direct conversion transceiver architecture is employed for the simplicity [12]. Individual characterization of each component is carried out using vector network analyzer, N5230A PNA (Agilent technologies), and then system design and verification is carried out. Other devices used for the verification process are E4407B Spectrum analyzer and E8267D Vector signal generator (Agilent technologies).

RF signal from signal generator which acts as the primary user signal is transmitted and a spanner shaped UWB antenna is used for receiving purpose. Output of antenna is connected to wide band LNA followed by the band pass filters. Local oscillator frequency is programmed according to the input signal frequency. ADF 4351 IC of analog devices is used as Local oscillator which is one of the main components responsible for reconfiguration. It generates signals from 400MHz to 4.4 GHz and is also programmable. Manual configuration is carried out in this work. USB port connected to the device ensures power supply as well as software interface.

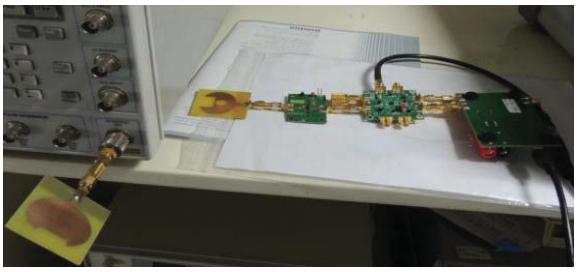

Fig 6. Reconfigurable receiver setup

When the input signal is of 2.4GHz the frequency synthesizer will be tuned to 2.6GHz resulting an IF frequency of 200MHz. Similarly for 3.1 GHz user, local oscillator is set to 3.4GHz to get an IF frequency of 300MHz. Different IF frequencies is given to distinguish between the users. IF signal is demodulated using IC ADL5380. I and Q components are fed to NI PXI module. The processing can be done either by host computer or FPGA inside NI PXI.

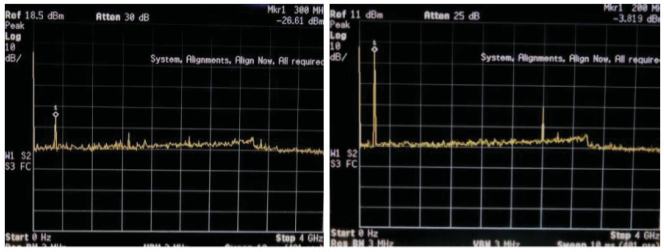

Fig 7. Output spectrum of received signal at 300MHz and 200MHz IF

If primary signal is detected, the transmitter must start transmitting at a new frequency. The transmitter circuit should be reconfigured at a new transmitting frequency by controlling LO frequency using software and changing the antenna mode in reconfigurable antenna. The mode in reconfigurable antenna can be changed by changing the switch configuration obtained from Digital I/O pins of NI VST module connected to NI PXI. The required switch configuration is estimated with the help of lookup table loaded inside the code in NI VST module. In phase and quadrature signal from the source is modulated and is transmitted using the reconfigurable antenna in this section. The transmitting secondary user signal can be generated inside an FPGA or host computer and passed on to reconfigurable transmitter stage. In this case signal demodulated by ADL5380 is given as I and Q input of modulator IC, ADL 5375-15. Output signal is then filtered and amplified by power amplifier.

Fig 8. Reconfigurable transmitter setup

The signal from processor or FPGA is normally in the form of in phase and quadrature component. So this signal is first modulated by wideband modulator IC ADL 5375-15. Tunable frequency synthesizer provides the local oscillator frequencies corresponding to each user. Wideband power amplifier is used before the antenna to amplify the signal. The modulated output signal is transmitted through a reconfigurable antenna and is observed by E4407B Spectrum analyzer. Observed spectrums for 2 different configurations are given in Fig. 9.

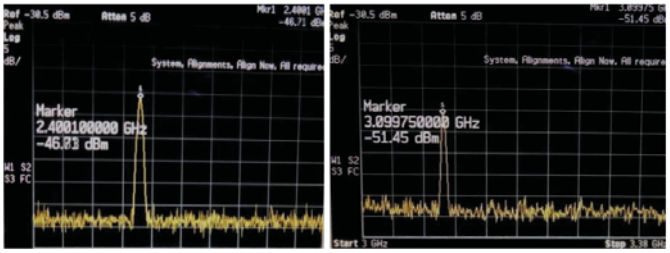

Fig 9. Output spectrum of received signal at 2.4GHz and 3.1GHz

VI. Reconfigurable Antenna

Reconfigurable antennas offer multiple functions by dynamically changing their properties. Reconfigurable antennas can be classified according to their reconfiguration techniques. It can be using lumped elements, variable capacitors, silicon photo switches, MEMS switches [13], or PIN diodes [14].The Planar Inverted-F antenna (PIFA) is resonant at a quarter- wavelength. It has good SAR properties. Since the radiation is away from the ground plane, the energy is directed away from the head. It also has a low profile and an omnidirectional pattern. The reconfigurability is achieved using the switching of PIN diodes. The simulations were done in AWR Microwave Office software. Geometrical dimensions of the antenna are specified in Fig. 10.

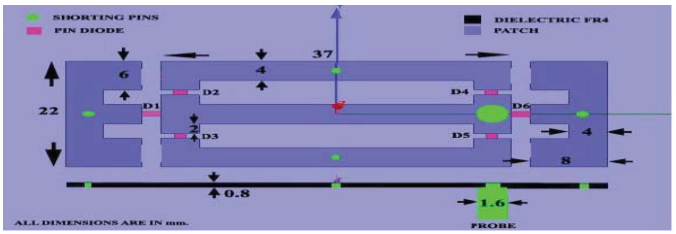

Fig 10. Reconfigurable PIFA dimensions

The S- parameter results for various modes are given below. Here 000110 correspond to PIN diode switches D1 D2 D3 D4 D5 D6. There are 6 PIN diode switches present. Hence 2^6=64 combinations of modes are possible. We have simulated some modes & stored these s- parameter results in a look up table.

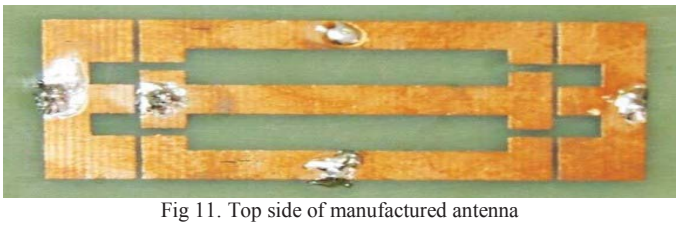

Fig 11. Top side of manufactured antenna

Table 2. Lookup table showing the major 14 modes

MODE	SWITCH CONFIG	FREQUENCY(GHz)
0	111111	1.5,4.4,4.7,5.7,6.62,7.29,7.94,8.2,9.75
1	011111	1.3,2,4.3,5.8,7.15,6.5,8.54
2	001111	2,5.78,8.4,8.76
3	000111	5.77,8.95
4	000011	5.79,6.3
5	000001	0.75,2.49
6	000000	5.66-5.83,7.87
7	101101	1.45,2.16,3.78,5.84,6.45
8	000110	.77,1.82,5.79
9	100001	1.3,2.26,5.85

PIFA antenna was manufactured using FR4 as substrate of thickness 0.8mm with ε_r of 4.4. The top patch and ground plane was shorted using shorting pins to make it act as a PIFA antenna. Fig. 12 shows the measured S-parameter result using VNA.

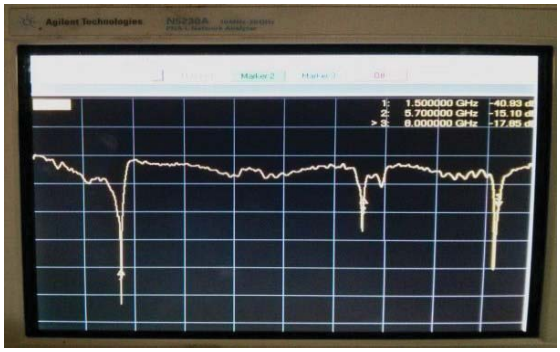

Fig 12. Measured S-parameter result for 000000 mode in N5230A VNA

VII. Conclusion

This paper has proposed a novel Cognitive Radio test bed system. A spanner shaped Ultra wideband patch antenna and frequency reconfigurable PIFA antenna has been proposed. A reconfigurable RF transceiver section has also been designed and setup. Spectrum sensing algorithm were tested using host computer in PXI module which verified the performance of sensing antenna over wide band frequencies. The UWB antenna shows a maximum power gain of [3.306dB] and has acceptable return loss for 2.23GHz-11.6GHz. The antenna is having omnidirectional radiation. Both the antennas were interfaced with a reconfigurable RF transceiver. Hence configurability has been achieved from baseband processor level to antenna level making all the components programmable. This system is not a complete design and needs future work to enhance the functionality and reliability

VIII. Futurescope

The current project has been worked on the physical layer. Suitable modifications can be made in MAC layer & Network layers to provide security, modulation data transfer & transfer of antenna mode data. Also processing time can be considerably reduced if FPGA modules are utilized for FFT computation. The performance of the reconfigurable antenna will depend on the mode chosen. Hence mode selection can be made more efficient by using fuzzy systems. Fine tuning of sub bands can be made possible using varactor diodes at suitable positions.

Acknowledgment

The project is funded through Centre of Excellence on COMMBEDDED SYSTEMS: hybridization of Communication and Embedded systems under TEQIP 1.2.1 at V.N.I.T., Nagpur. The hardware is provided by National Instruments, Bangalore

References

[1] N. Devroye, P. Mitran, and V. Tarokh, “Achievable rates in cognitive radio channels,”IEEE Transactions on Information Theory, vol. 52, no. 5, pp. 1813–1827, May 2006

[2] F. G. Awan and M. F. Hanif, “A Unified View of Information-Theoretic Aspects ofCognitive Radio,” in Proc. International Conference on Information Technology: NewGenerations, pp. 327–331, April 2008

[3] I. Akyildiz, W. Lee, M. Vuran, and S. Mohanty, “A survey on spectrum management in cognitive radio networks,” IEEE Communications Magazine, vol. 46, pp. 40-48, 2008.

[4] C. A. Balanis, Antenna Theory: Analysis and Design. 3rd ed., John Wiley & Sons, INC., 2013, pp. 727-751.

[5] Sanjeev Sharma, Bharat Bhushan, Shailender Gupta, and Preet Kaur, “Performance Comparison of Micro-strip Antennas with Different Shape of the Patch,” International Journal of u- and e- Service, Science and Technology, vol. 6, no. 3, June 2013.

[6] Swapnil S. Thorat, R.C. Jaiswal, Dr. Rajkumar, and Dr. S.D. Lokhande, “Efficient techniques for bandwidth improvement of microstrip patch antenna,” International journal of computer Networks and wireless communications IJCNWC, vol. 2 no. 6, December 2012.

[7] Takeshi Ikuma and Mort Naraghi-Pour (2008), “A Comparison of Three Classes of SpectrumSensing Techniques”, IEEE GLOBECOM proceedings.

[8] S. P. Herath, N. Rajatheva, and C. Tellambura, “Energy detection of unknown signals in fading and diversity reception,” IEEE Trans. Commun., vol. 59, no. 9, pp. 2443–2453, Sep. 2011.

[9] S. Atapattu, C. Tellambura, and H. Jiang, “Performance of an energy detector over channels with both multipath fading and shadowing,” IEEE Trans. Wireless Commun., vol. 9, no. 12, pp. 3662–3670, Dec. 2010.

[10] Costlow, T. "Cognitive radios will adapt to users Intelligent Systems”, IEEE Volume: 18 , Issue: 3 Digital Object Identifier: 10.1109/MIS.2003.1200720 Publication Year: 2003 Cited by: Papers (4)

[11] Ghouwayel, A. ; Louet, Y. “FPGA implementation of a re-configurable fft for multi standard systems in software radio context” Consumer Electronics, IEEE Transactions on Volume: 55 , Issue: 2 Digital Object Identifier: 10.1109/TCE.2009.5174479 Publication Year: 2009 , Page(s): 950 – 958

[12] Jusung Kim ; Silva-Martinez, J."Low-Power, Low-Cost CMOS Direct-Conversion Receiver Front End for Multi standard Applications” Solid-State Circuits, IEEE Journal of Volume: 48 , Issue: 9 Digital Object Identifier: 10.1109/JSSC.2013.2265781 Publication Year: 2013 , Page(s): 2090 – 2103

[13] Cetiner, B.A., et al., "RF MEMS Integrated Frequency Reconfigurable Annular Slot Antenna", IEEE Transactions on Antennas and Propagation, vol. 58, issue 3, 2010, pp. 626-632.

[14] Trong Duc, N., et al. "Novel reconfigurable 8 - shape PIFA antenna using PIN diode", International Conference on Advanced Technologies for Communications (ATC), 2011, pp. 272-275.

Vehicle Monitoring and Controlling system using CAN protocol

Mr. Mosam Sangole
E&TC department, , SIEM ,
Sandip Foundation Nashik, Maharashtra India

Mr.Vicky Chaudhary
E&TC department SIEM ,
Sandip Foundation Nashik, Maharashtra,India

Miss.Vishakha Nighute
E&TC department SIEM ,
Sandip Foundation Nashik, Maharashtra,India

Miss.Priyanka Satpute
E&TC department SIEM ,
Sandip Foundation Nashik, Maharashtra,India

Abstract- **In today's world where science has made amazing advances so has the recent cars. These cars are more advanced than ever. They have more speed, state of the art engines and are very closely to these reasons there is a need to adapt a device which can continuously monitor all the various parameters of car. We propose a system which, in case of accident will records all the parameters and also help us to prevent any accident to happen. The Data Acquisition system (DAS) interface between the real world of physical parameters, which are analog , and the artificial world of digital computation and control ,CAN bus is a message-based protocol, designed specifically for automotive applications. CAN is a standard protocol for efficient and reliable communication between sensor, actuator ,controller and other nodes in real-time applications. This paper is aimed at the design of CAN protocol using PIC Microcontroller for vehicle monitoring and controlling system. The main feature is to monitor various parameters such a presence of CO level, temperature, fuel level and rain.. This paper describes the PIC based design of CAN Bus prototype for vehicle automation. Hardware interface circuit mainly consists of MCP2551 stand alone CAN-Controller with SPI interface. MCP2551 CAN Transceiver equipment ISO-11898 standard physical layer requirements. The design of software communication module includes system initialization and CAN controller initialization unit, message sending unit, message receiving unit and the interrupt service unit.**

Keywords-Vehicle Automation, Controller Area Network(CAN), LCD display, Dc Motor, Gas sensor, etc.

I. INTRODUCTION

The protocol was developed aiming at automotive applications. Today CAN have gained wide spread use and is used in industrial automation as well as in automotives and mobile machines. The CAN protocol is implemented in silicon. This makes it possible to combine the error handling and fault confinement facilities of CAN with a high transmission speed. The method used for distributing messages to the right receivers contributes to gaining a good use of the available bandwidth. This requires a simple transmission medium. A common transmission medium is a twisted pair of wires.. The development of CAN began when more and more electronic devices were implemented into modern motor vehicles. Examples of such devices include engine management systems, active suspension, ABS, gear control, lighting control, air conditioning, airbags and central locking. So, it is important that human drivers still have some control over the vehicle. Advanced in-vehicle information systems provide vehicles with different types and levels of intelligence to assist the driver. The introduction into the vehicle design has allowed an almost symbiotic relationship between the driver and vehicle by providing a sophisticated & intelligent driver-vehicle interface through an intelligent information network. This paper discusses the development of such a control framework for the vehicle which is called the digital-driving behaviour, which consists of a joint mechanism between the driver and vehicle for perception, decision making and control system.

All this means more safety and more comfort for the driver and of course a reduction of fuel consumption and exhaust emissions. The complexities of these control systems, and the need to exchange data between them meant that more and more hard-wired, dedicated signal lines had to be provided. Sensors had to be duplicated if measured parameters were needed by different controllers. Each device can decide if a message is relevant or if it should be filtered. This structure allows modifications to CAN networks with minimal impact. Additional non transmitting nodes can be added without modification to the network.

A microcontroller based data acquisition system that uses ADC to bring all control data from analogue to digital format is used. Since the vehicle information systems are spread out all over the body of a practical vehicle, communication module that supports to implement a one stop control of the vehicle through the master controller of the digital driving system. The proposed high-speed CAN bus system solves the problem of automotive system applications, also has a certain practical value and significance. Since the vehicle information systems are spread out all over the body of a practical vehicle, a communication module that supports to implement a one stop control of the vehicle through the master controller of the digital driving system. The proposed high-speed CAN bus system solves the problem of automotive system applications, also has a certain practical value and significance.

II. LITERATURE SURVEY

Vehicle control system implementation using CAN protocol discussed in [1] emphasizes the development and implementation of a digital driving system for a Semi-autonomous vehicle to improve the driver-vehicle interface. It uses an ARM based data acquisition system that uses ADC to bring all control data from analog to digital format and visualize that through LCD. The communication module used here is an embedded networking by CAN which has efficient data transfer. It also takes feedback of vehicle conditions like Vehicle speed, Engine temperature etc.,The development of such a control framework for the vehicle which is called the digital-driving behaviour, consists of a joint mechanism between the driver and vehicle for perception, decision making and control.

Traditional electronic control system can improve a vehicle dynamics, economy and comfort. But some problems also have come up, such as the body wiring complexity, space constraints and some reliability issues. In order to solve these problems, the vehicle network technology has been created. In-vehicle networking protocols must satisfy requirements which include, significant reduction of wiring harness, reducing body weight and costs, improving the efficiency of fault diagnosis, low latency times and configuration exibility and enhancing the level of intelligent control. Sub-systems (ECU) require the exchange of particular performance and position information within defined communication latency. Therefore the requirement for each ECU is to communicate via some kind of network technology such as CAN (Controller Area Network) bus.

Parameters	CAN	RS 232	SPI	I^2C
Async/Sync	Async	Async	sync	sync
Type	Multi-master	Peer to peer	Multi-master	Multi-master
Communication (Duplex)	Half	Full	Full	Half
Max. devices	112	2	Based on bus capacitance and bit rate	Based on bus capacitance and bit rate
Max speed	1Mbps	20Kbps	› 1Mbps	3.4Mbps

Table1. Comparison of CAN protocol with existing other protocol

By Using CAN protocol we can connect multiple microcontroller and other devices to a common CAN bus. To connect it to CAN bus we require a CAN transceiver in between bus and devices which enables the communication between all thing with great speed and priority. CAN based is a message based protocol which is designed specially for automotive vehicle.

III. METHODOLOGY

Considering all the approaches for controlling and monitoring system for vehicle, we come to conclusion that the CAN based systems avoid the number of wires and complexity in the system. In the various protocol system one drawback is that, the interference of noise may damage the data and will increase the complexity. So to implement controlling and monitoring system for vehicle we are using CAN protocol

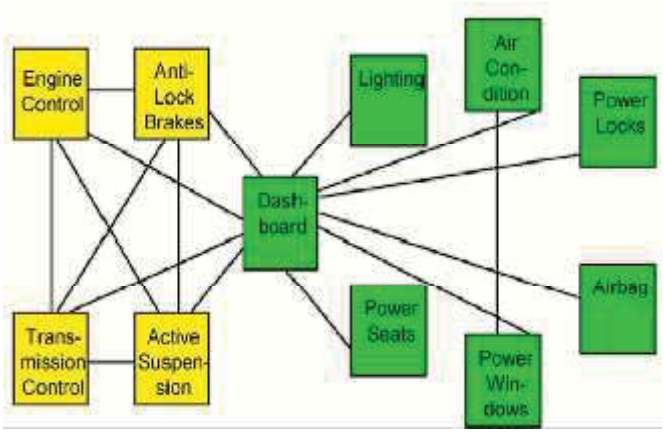

Fig 1 Existing system without CAN

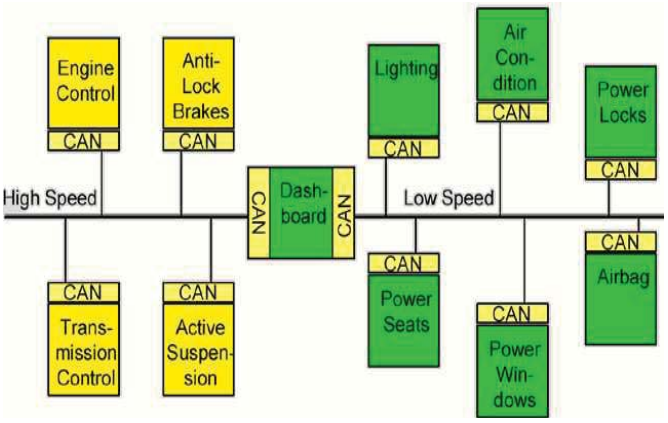

Fig 2 System using CAN

By using these methodology we are designing a system which we reduce no of wires and complexity of the system and the system is comfortable to the driver also and it will prevent many accident which got occur because of insufficient data available with the driver and it will overcome the disadvantages of analog system.

IV . ARCHITECTURE

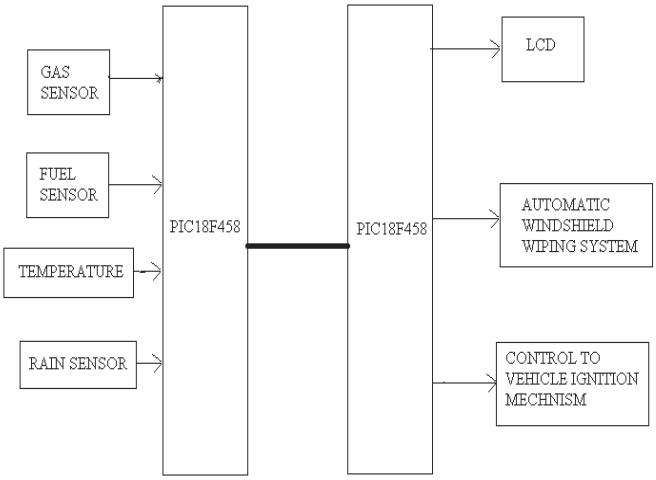

Fig 3 Proposed system architecture

A. *System architecture.*

The proposed system consists of Rain, fuel level, Gas and temperature sensor, CAN controller, motor driver circuit, PIC microcontroller, LCD.

B. *Operation*

The block diagram consists of various sensor which are continuously sensing various parameter and providing input to inbuilt ADC of PIC micro-controller. The ADC convert that analog data into the digital data and with the help of can controller sends that data to the receiving part which is another PIC microcontroller used for controlling the various parameter of vehicle. The 16*2 LCD is used to display data continuously and which is also used for indication. The motor is used to drive the windshield automatic when rain occurs. The buzzer is used for indicating when temperature crosses the threshold limit which is the maximum limit. The LED are used for indication of excessive presence of gas in vehicle.

C. *Microcontroller (PIC18F458)*

It is heart of our project. There are used various application such as automatically controlled products, remote controls, printer, scanner, office machines , appliances, toys and other embedded systems. PIC18FX58 devices have twice the Flash program memory and data RAM of PIC18F458 device (32 Kbytes and 1536 bytes vs.16 Kbytes and 768 bytes, respectively).The microcontroller circuit diagram is shown in less. The PIC18F458 devices include feature that allows the system clock source to be switched from the main oscillator to an alternate low-frequency clock source. Only PIC18F4X8 devices implement the Enhanced CCP module, analog comparators and the Parallel Slave Port. It is having a capacity of High current sink/source 25 mA/25 mA, Three external interrupt pins, Low-power, high-speed Enhanced Flash technology, Four Timer modules (Timer0 to Timer3),10-bit, up to 13-channel Analog-to-Digital Converter module (A/D) with Programmable Acquisition Time, Two External Clock modes, up to 48 MHz, Programmable Brown-out Reset (BOR) and Wide operating voltage range (2.0V to 5.5V)

D. *CAN transceiver (MCP2551)*

The MCP2551 is a high-speed CAN, fault-tolerant device that serves as the interface between a CAN protocol controller and the physical bus. The MCP2551 provides differential transmit and receive capability for the CAN protocol controller and is fully compatible with the ISO-11898 standard, including 24V requirements. It will operate at speeds of up to 1 Mb/s. Typically, each node in a CAN system must have a device to convert the digital signals generated by a CAN controller to signals suitable for transmission over the bus cabling (differential output).It also provide a buffer between the CAN controller and the high-voltage spikes that can be generated on the CAN bus by outside sources (EMI, ESD, electrical transients).

E. *Temperature Sensor*

LM-35 was Calibrated Directly in Celsius (Centigrade).It is Linear + 10 mV/C Scale Factor0.5C Ensured Accuracy (at +25C) .Rated for Full .55C to +150C Range. LM-35 is Suitable for Remote Applications. It is Low Cost Due to Wafer-Level Trimming. It Operates from 4 to 30 V and Less than 60-A Current Drain .It has Low Self- Heating 0.08C in Still Air. And Low Impedance Output, 0.1 for 1mA Load. It indicates the low level and high level temperature measurement and automotive ignition level gas exhausting, over heat when vehicle engine/motor speed was increased gradually.

F. *Rain Sensor*

The Raindrop Detection Sensor module is an easy-to-use and low cost drop recognition sensor. The sensor works through a series of exposed parallel traces on board which produces electrical variations when drops or water volume changes. By using microcontrollers or ADC ICs (Arduino and PIC) its fairly easy to convert the analog output from the sensor to digital values. This can be directly read by an Arduino or a comparator circuit if you wish to use it as a rain detection alarm. It can be used to monitor a variety of weather conditions.

G. *MQ-6 GAS Sensor*

MQ-6 gas sensor has high sensitity to Propane, Butane and LPG, also response to Natural gas. The sensor could be used to detect different combustible gas, especially Methane, it is with low cost and suitable for different application. Sensitive material of MQ-6 gas sensor is SnO2, which with lower conductivity in clean air. When the target combustible gas exist, The sensors conductivity is more higher along with the gas concentration rising. Please use simple electro circuit, Convert change of conductivity to correspond output signal of gas concentration.

H. *Power Supply*

The power supply most important for electronic circuits, which is provide the required power to microcontroller and other electronics

devices. which provide the required power to the PIC16F877A and other electronics devices. For this system we are using +5v power supply for buzzer and all different sensor which are used by us , .Also we required 3.3 v power supply for PIC microcontroller which is obtained by LM1117.For DC motor 12v supply is required which is taken from rectifiers output.

I. Buzzer

Lots of buzzers are available in the market depending upon the size and voltage range. We mostly use piezo buzzer working on 5v or 12v having a resonant frequency around 2000Hz. These buzzers are easily available in the local market and low costing. These buzzers require about 25mA-45mA current for proper sound generation if they do not get the desired current and voltage the output volume of the buzzer decreases or else we do not get any output at all. The controller cannot directly turn ON/OFF the buzzer as the output source as well as sink current of the current is below 20ma. So we have used an NPN transistor BC547 to ON/OFF the buzzer and provide the necessary current and voltage required for the buzzer.

V. CONCLUSIONS

This proposed system introduces an embedded system with a combination of CAN bus systems. Digital control of the vehicle is an important criterion of modern technology. With the rapid development of embedded technology, high performance embedded processor is penetrated into the automotive industry, which is low cost, high reliability and other features to meet the needs of the modern automobile industry. The proposed high-speed CAN bus system solves the problem of automotive system applications, also has a certain practical value and significance. With PIC as the main controller and it makes full use of the high-performance of PIC18f458, high-speed reduction of CAN bus communication control networks and instrument control. so as to achieve full sharing of data between nodes and enhance their collaborative work. This system features efficient data transfer among different nodes in the practical applications.

REFERENCES

[1] M.A Kumar. Verma and A. Srividya,, “Response time modeling of Control Area Network(CAN)”. Distributed computing and networking. Lecture Notes in computer science Volume 5408,P163-174,2009.
[2] K Tindell, A. Burns, and A.J. Wellings, “Calculating controller area network (CAN) message response times”, Control Engineering Practice, 3(8): p. 1163-1169,2005.
[3] W. Prodanov, M. Valle, and R. Buzas, “A controller area network bus transceiver behavioral model for network design and simulation”, IEEE Transactions on Indus-trial Electronics, 56(9): p. 3762-377, 2009.
[4].B.Gmbh, CAN specication vol 1 Version 2.0, 1991.
[5].Benjamin C kuo, M.Farid Golnaraghi, Automatic Control System, Eight edition, John wiley sons.Inc2003.

Methods of Frequency Offset Estimation in OFDM Based System

A. P. Rathkanthiwar
Department of Electronics Engineering,
Priyadarshini College of Engineering
Nagpur, MS, India
anagharathkanthiwar@yahoo.co.in

Sandeep Kumar Singh
sandeepraju1988@gmail.com

A.S.Gandhi
Professor and Head, Department of Electronics & Communication
Visvesvarya National Institute of Technology
Nagpur, MS, India
abhay4083@yahoo.co.in

Abstract: Orthogonal Frequency Division Multiplexing (OFDM) is a bandwidth efficient modulation scheme and has become a popular technique for transmission of signals over wireless channels. It has been chosen for several current and future communication systems all over the world because of many features. However OFDM systems are extremely sensitive to time and frequency synchronization errors. Hence one of the most important tasks in OFDM receiver is time and frequency synchronization. Synchronization errors are errors are estimated and corrected before demodulation of subcarriers. We are proposing preamble based synchronization methods for error estimation. In this paper, only frequency synchronization process is considered. Simulation results are presented to confirm the performance of the proposed methods in two different channel conditions which are AWGN and multipath fading channel.

Keywords: OFDM synchronization, Carrier Frequency Offset, Frequency synchronization.

I. Introduction

The OFDM system transmits a large number of narrowband carriers, which are closely spaced. At the central frequency of the each sub channel there is no crosstalk from other sub channels. Thus there is no interference from other sub carriers at the peak of a desired sub carrier even though the sub carrier spectrums overlap [1]. So in order to assure a high spectral efficiency the subchannel waveforms must have overlapping transmit spectra and for this subchannels need to be orthogonal. This orthogonal modulation and demodulation can be achieved with the help of IFFT at transmitter and FFT at receiver. Recent advances in Very Large Scale Integration (VLSI) technology make high speed, large size Fast Fourier Transform (FFT) chips commercially affordable. Also substantial advancements in Digital Signal Processing technology made OFDM an important part of telecommunications landscape. In the 1990s, OFDM was exploited for mobile radio FM channels, High-bit rate Digital Subscriber Lines, Asymmetric Digital Subscriber Lines and Very-high-speed Digital Subscriber Lines. The first commercial use of OFDM technology was made in Digital Audio Broadcasting (DAB) which was started in 1995. OFDM is also used in Digital Video Broadcasting (DVB) and High Definition Television (HDTV). HiperLAN2 was defined in June 1999 which also uses OFDM. OFDM is being used in wireless LAN, and also for fixed broad-band access [2]. OFDM has successfully replaced Direct Sequence Spread Spectrum (DSSS) for 802.11a and 802.11g. Perhaps of even greater importance is the use of this technology in fourth Generation (4G) wireless systems.

II. OFDM Signal Description

In OFDM, multiplexed frequencies are orthogonal to each other and hence it is possible to arrange the carriers so that the sidebands of the individual carriers overlap and the signals can still be received without adjacent carrier interference. Cyclic prefix is a crucial feature of OFDM to combat the effect of multipath. Cyclic prefix is a guard interval placed at the beginning of an OFDM symbol, which is same as the last portion of the time domain OFDM symbol. Idea behind this is to convert the linear convolution (between signal and channel response) to a circular convolution. In this way, the FFT of circularly convolved signals is equivalent to

a multiplication in the frequency domain. Another advantage with the cyclic prefix is that it serves as a guard between consecutive OFDM symbols. Although the use of the CP prolongs the duration of OFDM symbols and results in a loss in data throughput, it has become a common practice in most commercial OFDM systems because of its advantages.

The baseband OFDM symbols consist of set of physical subcarriers whose frequencies are equal to the indices multiplied by the subcarrier spacing. N is the total number of subcarriers, usually a power of 2 to facilitate the FFT and IFFT operations [3].

In OFDM, data stream is mapped into number of complex symbols in frequency domain using either Quadrature Amplitude Modulation (QAM) or Quadrature Phase Shift Keying (QPSK). These complex symbols are modulated on N subcarriers by using N-point IFFT to get time domain complex OFDM symbol. The samples of baseband OFDM signal can be expressed as

$$x(n) = \frac{1}{\sqrt{N}} \sum_{k=0}^{N-1} d_k(n)\, e^{\frac{j2\pi kn}{N}} \qquad n = 0,1,...N-1 \qquad \textbf{(1)}$$

Here $d_k(n)$ are the complex data symbols.

The total symbol duration is

$$\mathbf{T_{Total} = T_{CP} + T_{Sym}}$$

Where T_{CP} is CP duration and T_{sym} is effective symbol duration

III. Timing Error Estimation

Timing error or time offset θ occurs because of channel delay and multipath dispersion. Due to timing error the receiver's time-domain FFT window spans samples from two consecutive OFDM symbols. This results in inter-OFDM symbol interference leading to Bit Error Rate (BER) degradation [4].

Timing synchronization is performed to estimate timing error and it has two main objectives:

- Frame synchronization: The task of the frame synchronization is to identify the Preamble in order to detect a packet arrival
- Symbol-synchronization: The task of symbol timing is to identify the beginning of the symbol or symbol boundary

A. Proposed Algorithm for Timing Error Estimation

Realizable receiver structures usually follow the principle of synchronized detection i.e. synchronization parameters are first estimated and then used as if they are the true parameters. We developed method for timing error estimation which take advantage of the special structure in the training symbol and locate the start positions of OFDM bursts. The training symbol is used as preamble.

The preamble used for this algorithm has two identical halves of length N/2 and is the same used in S and C algorithm [5]. The proposed algorithm makes use of autocorrelation function (ACF) and cross correlation function (CCF) both.

We are simply multiplying both functions over certain window length. Metric of this proposed algorithm is given by

$$M(n) = P_{ACF} \times P_{CCF} \qquad \textbf{(2)}$$

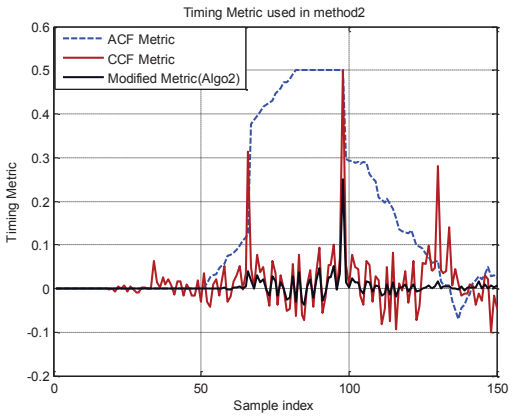

Figure 1 Timing metric of proposed algorithm without CP and with CP

Metric obtained using ACF, CCF and proposed algorithm are shown in Figure 1. Here CP is of length 16 samples. If maximum value of timing metric is higher than a predefined threshold, the peak is detected. If no peak is found, the frame is considered as empty and noise estimation is performed. From the sample right after the peak, first OFDM symbol starts.

IV. Frequency Error Estimation

In OFDM, frequency synchronization errors are actually Carrier Frequency Offsets (CFO). In a typical wireless communication system, the signal to be transmitted is up converted to a carrier frequency prior to transmission. The receiver is expected to tune to the same carrier frequency for down-converting the signal to baseband, prior to demodulation. However, due to device impairments the carrier frequency of the receiver need not be same as the carrier frequency of the

transmitter. When this happens, the received baseband signal, instead of being centered at DC (0MHz), will be centered at a frequency Δf which is equal to CFO. In general CFO is caused by unmatched local oscillators at the two ends of the communication links, Doppler shifts or phase noise introduced by nonlinear channel [6].
As the subcarriers are closely spaced in frequency compared to the channel bandwidth, the frequency offset must be kept within a small fraction of the subcarrier spacing to avoid severe bit error rate degradations.
So after timing synchronization next step is to estimate fractional carrier frequency offset (CFO) to align local oscillator frequency to the received carrier frequency.

A. Proposed Algorithms for Frequency Error Estimation

Method1

We are herewith proposing a scheme for fractional CFO estimation. Our proposed method utilizes the CCF generated for timing metric of method 2 required in timing synchronization. So no separate training symbol is required. This CCF function is shown in figure 2.
For CFO estimation, it is assumed that timing synchronization is done perfectly.
In this proposed method, we are using the fact that phase separation between two consecutive peaks of CCF function is proportional to CFO. Carrier frequency offset hence can be estimated using

$$\Delta f = \frac{\Delta\phi}{\pi T_u / 2} \quad \textbf{or} \quad \textbf{(3)}$$

$$\Delta f = -\frac{\angle y(k - N/2).y^*(k)}{\pi N/2} \quad \textbf{(4)}$$

Here $\Delta\phi$ is phase difference between two peaks of CCF function which are separated by time duration of Tu/2 or N/2. Any consecutive two peaks can be used.

Method 2

The training symbol used has two identical parts. The main difference between the two halves of this training symbol at receiver is a phase difference of

$$\varphi = \pi T \Delta f \quad \textbf{(5)}$$

The phase can be estimated by using

$$\hat{\varphi} = angle(\max(\mathrm{M(n)})) \quad \textbf{(6)}$$

Where M (n) is the timing metric of proposed algorithm2 and is shown in Figure1. Single peak is observed.

Fractional CFO is then estimated by

$$\Delta \hat{f} = \frac{\hat{\varphi}}{\pi T} \quad \textbf{(7)}$$

Method3

This method provides complete frequency synchronization and uses either method1 or method2 for estimation of fractional CFO. After timing synchronization and fractional CFO correction is done, integer frequency synchronization is performed. After N point FFT of OFDM symbols of the frame, integral shifts are carried out in all subcarriers and from this the shift for which the energy is maximum is found out. Argument of this maximum position is equal to integer frequency offset i.e.

Integer CFO = arg(max(energy)) (8)

B. Performance of Proposed method3

Fractional CFO is estimated and corrected using method1. This is coarse frequency synchronization. In the next step fine frequency synchronization is performed in which integer CFO is estimated and then corrected. For simulation in MATLAB, known value of CFO is inserted in the OFDM signal. This is done by multiplying the nth sample with

$$e^{\frac{j2\pi\varepsilon n}{N}}$$

Here ε is the normalized CFO. If the inserted CFO ε is 4.3, then the integer value of frequency offset inserted is 4 and fractional value of frequency offset inserted is 0.3. The amplitude of samples in preamble is kept such that the average power of preamble is almost equal to the OFDM symbols. There are in effect 214 non zero subcarriers having odd index with interleaved null subcarriers between successive non zero sub carriers. Major specifications used for simulation of this algorithm are depicted in Table 1.

Table 1 Simulation Parameters

FFT length N	512
Number of effective subcarriers	428
Constellation mapping	4QAM
Cyclic Prefix length	N/8=64
Number of simulation runs	100
SNR range	0 to 30 dB
Number of Symbols in frame	10

1) Performance of Proposed method3 for AWGN channel

Integer frequency offset is estimated using method3 after fractional CFO correction and performing FFT. Simulation is performed 100 times for SNR values of 30 dB and 5 dB. Histogram plots and scatterplot are generated for estimated integer CFO and scatterplot are obtained for estimated fractional CFO.

Figure 2 is a histogram plot of estimated integer CFO. This plot shows that for all 100 trials, estimated value of integer CFO is 4 which is equal to the actual inserted value. Scatterplot of estimated fractional CFO is depicted in Figure 3. This figure shows estimated values for 100 trials. All values are very close to actual inserted value which is 0.3. Total estimated CFO is calculated using

EstimatedCFO = integer_offset+fract_offset

Error is calculated for all trials using

CFOerr = ActualCFO-estimatedCFO

Mean of this error is calculated and found to be

Mean(CFOerr) = 2.4789e-005

In above discussion, value of SNR is 30dB.
Similar results are obtained for value of SNR=5dB
Mean of estimation error is found to be Mean(CFOerr) = 0.0015
It is clear that for low value of SNR, estimation error has been increased so the estimation accuracy depends on SNR value. Mean value of residual error is very less even for SNR= 5dB and is within tolerable level i.e. less than a percent of actual value.

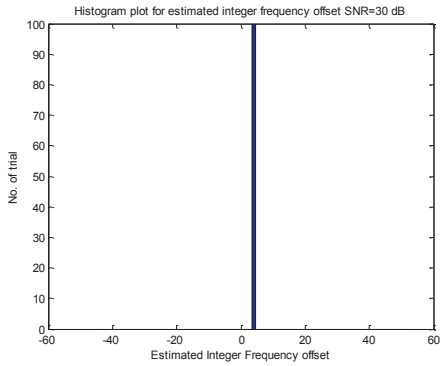

Figure 2 histogram plot of estimated integer CFO for SNR=30 dB (AWGN channel)

To demonstrate the performance of proposed methd3, reference design of Shimidl and Cox is considered. Figure 4 shows a plot of mean squared error vs SNR obtained using proposed method3 and reference method. Proposed method gives better performance than reference method. However improvement in performance is less. The mean squared error is calculated using equation (9).

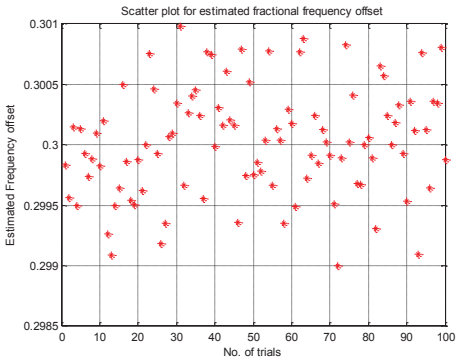

Figure 3 Scatterplot of estimated fractional CFO for SNR = 30 dB ((AWGN channel)

$$MSE = \frac{1}{n}\sum_{i=1}^{n}(EstimatedCFO - ActualCFO)^2 \quad (9)$$

Here n = Number of trials

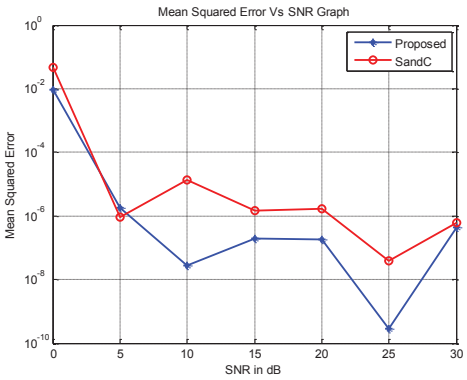

Figure 4 Mean squared error vs SNR, inserted CFO=4.3 (AWGN channel)

2) Performance of Proposed method3 for Multipath fading channel

Similar steps are performed for doing simulation of proposed method3 for multipath channel. As a multipath channel, Channel B of ITU Channel Model for Outdoor to Indoor and Pedestrian Test Environment is being considered. Initially the amplitude of samples in preamble is kept such that the average power of preamble is almost equal to that of the OFDM symbols. Inserted value of CFO is 4.3. Histogram plot is obtained and it is found that, for all 100 trials estimated value of

integer CFO is 4 which is equal to the actual inserted value for SNR=30 dB. Scatterplot of estimated fractional CFO is depicted in Figure 5. This figure shows estimated values for 100 trials. All values are very close to actual inserted value which is 0.3.

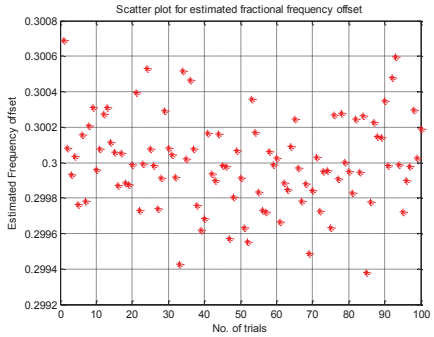

Figure 5 Scatterplot of estimated fractional CFO for SNR = 30 dB (Multipath fading channel)

Total estimated CFO is calculated and Mean of the error is found to be
Mean (CFOerr) = 1.4551e-006
Similar results are obtained for SNR=5dB
For 5dB SNR, in histogram plot it is found that, value is estimated correctly for 52 trials out of 100 trials. Mean error in CFO estimation for this case is found to be
Mean (CFOerr) = 0.3593

Residual error here is nearly 10% of the actual value which is not tolerable.
However it is found that estimation accuracy can be improved if the training symbol is boosted. After boosting of training symbol, the mean error was found to be
Mean (CFOerr) = 0.0303 for SNR =5dB

Now this residual error is less than 1% of the actual value and method gives good performance. Here value is estimated correctly for 95 trials out of 100 trials.

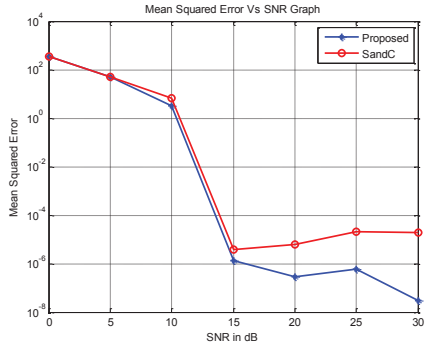

Figure 6 Mean squared error vs SNR, inserted CFO=4.3 (Multipath fading channel)

100 simulation runs are performed to evaluate the mean squared error (MSE) of CFO estimation versus SNR. In each run, the timing offset and the channel are constant. Figure 6 shows a plot of mean squared error vs SNR obtained using proposed method3 and reference method for multipath fading channel. For both Proposed method and reference method, average power in training symbol is 3dB more than the OFDM symbol. The two methods have similar performance for SNR up to 10 dB however MSE performance of Proposed method 3 is better than the reference method for SNR more than 10 dB.

V. Conclusion

Method3 of frequency error estimation is analyzed in detail. Estimation error (residual error) values for two channel conditions are summarized in Table 2. From this result, we conclude that our proposed method3 shows satisfactory performance. From MSE graph, it is clear that our proposed method3 shows performance nearly same to that of standard reference method. Performance is tested for multipath channel environment also.

Table 2 Estimation error values

AWGN Channel, SNR=30 dB	2.4789×10^{-5}
AWGN Channel, SNR=5 dB	1.5×10^{-3}
Multipath Fading Channel, SNR=30 dB	1.4551×10^{-6}
Multipath Fading Channel, SNR=5 dB	3.593×10^{-1}
Multipath Fading Channel, SNR=5 dB (Boosted training symbol)	3.03×10^{-2}

References

[1] R. P. a. F. J. Velez, "OFDMA WiMAX Physical Layer," WiMAX Networks, Aalborg, Springer Science, Business Media B.V., pp 63-135, 2010, pp. DOI 10.1007/978-90-481-8752-2_2.
[2] J. S. M. P. Van de Beek, "ML Estimation of Time and Frequency Offset in OFDM Systems"," IEEE Transaction on Signal Processing, vol. 45, no. 7, pp. 1800-1805, July 1997, 1053-587x/97.
[3] M. Ruan, "Timing and Frequency Synchronization in Practical OFDM Systems," National ICT Australia, Research School of Information Sciences and Engineering, pp.1-207, 2009.
[4] M. K. C.-C. P. M.-O. Morelli, "Synchronization Techniques for Orthogonal Frequency Division Multiple Access (OFDMA): A Tutorial Review," Proceedings of the IEEE, vol. 95, no. 7, pp. 1394-1427, July 2007, 10.1109/JPROC.2007.897979.
[5] T. M. S. a. D. C. Cox, "Robust Frequency and Timing Synchronization for OFDM," IEEE Transaction on Communication, vol. 45, no. 12, pp. 1613-1621, Dec 1997, 0090-6778/97.
[6] J. H. G. Y. W. S. Y. Y. P. L. a. G. L. B. Ai, "Frequency Offset Estimation for OFDM in Wireless Communications," IEEE Transactions on Consumer Electronics, vol. 50, no. 1, pp. 73–77, Mar. 2004, 0098 3063/04.

Drum handling device for industrial

Vishal Ratan Sonawane (Author)
Dept. Mechanical Engg.
Late. G.N.Sapkal COE.
Nashik, India.
vishalsonawane616@gmail.com

Jadhav Suraj Ramesh (Author)
Dept. Mechanical Engg.
Sandip Institute Of Engg. & Mangt.
Nashik, India.
suraj904jadhav@gmail.com

Desai Anirudh Arun (Author)
Dept. Mechanical Engg.
Sandip Institute Of Engg. & Mangt.
Nashik, India.
anirudhdesai99@gmail.com

Patil Vishal Eknath (Author)
Dept. Mechanical Engg.
Sandip Institute Of Engg. & Mangt.
Nashik, India.
vishalkul77@gmail.com

Ajinkya Vasant Nichit (Author)
Dept. Mechanical Engg.
Sandip Institute Of Engg. & Mangt.
Nashik, India.
ajinkyanichit94@gmail.com

***Abstract*—This paper presents the main use of drum handling and tilting equipment in the industries. This device is developed to reduce the human efforts and to safeguard the operator from hazardous chemicals. This results in efficient and safe operation. Also to study the effects of this device after implementation in industry.Also study the effect of material handling and tilting on the human.**

Keywords—Worm & Worm gear, sprocket with pulley, chain, Drum, paper roll, clamping device & supporting frame.

I. INTRODUCTION

In many industries the drum is handled manually. In workplace, the drum needs to be loaded, unloaded ,transported, tilted etc, manually. Manual drum handling and tilting takes much time, and requires more number of workers. It is also risky and hazardous to the operator. In chemical industries number of different chemicals are stored in drums. It is requires to handle carefully the process of loading, unloading, and tilting. Company cannot use pump to drain out the chemicals (is in liquid form) from the drum or barrels because of its cost. Company requires effective handling and tilting equipment for effective performing the given operation. This paper successfully provides an successful and a safe solution to all the industries who deal in the drum handling as a part of their daily routine.

II. EASE OF USE

When chain is pulled, the pulley rotates in anticlockwise direction hence it rotate the worm shaft in anticlockwise direction, the power is transmitted to fixed end of holding device in clockwise direction (Both worm gear and adjustable holding frame) and it tilts the drum up to 90°.

When the chain is released the pulley rotates in clockwise direction due to which the worm gear rotates in clockwise direction and both worm wheel and adjustable holding frame rotates in anticlockwise

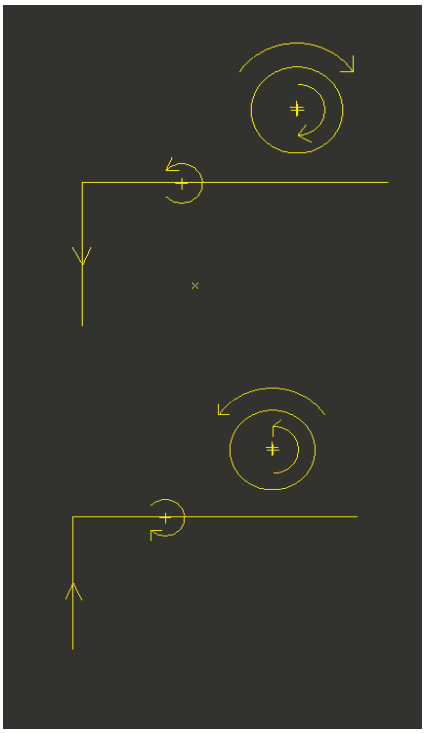

Fig.1- General operation

direction. After that the drum comes back to its original position (vertically stands).

III. CONSTRUCTION

It consist of supporting frame, holding frame, four bearings, worm and worm gear, pulley, chain etc. A holding frame is placed over the supporting frame which is to be used to hold the drum. This holding frame is adjustable and can hold drums of diameter ranging between 60 cm to 65 cm. There are four bearings used in the device two are taper roller bearings and two are ball bearing. These two taper roller bearing are attached to the both end of adjustable holding frame. Non intersecting non parallel worm and worm gears are used. Two ball bearings are attached to both ends of the worm shaft. The last part comprises of pulley which is connected to the end of the extended worm shaft. The sprocket is provided over the pulley and the chain is placed over it to pull the pulley.

A. Units

Abbreviation	Full form
Cm	Centimeter
Kg	Kilogram
N	Newton

IV. WORKING

As specified in the construction supporting frame, holding frame, four bearings, worm and worm gear ,pulley, chain etc are the working component. The working start with the Drum or paper roll which is fixed between the adjustable holding frame ranging from 60 to 65 cm in diameter and the frame can sustain 300 kg load. The frame is connected to the taper roller bearings. Taper roller bearings are used because this type of bearings can sustain more radial load. One side of the holding frame (first taper roller bearing) is fixed, another side of holding frame goes through taper roller bearing and connected to the worm gear. For this device we use worm and worm gear because this gear are self locking.

When the chain is pulled, the pulley rotates. Hence the worm shaft rotate due to Non intersecting non parallel gear the worm gear rotate and the drum is tilted up to 90°. Once the material or chemical is removed from the drum the chain is released & drum comes to its original position. The drum does not come back to its original position automatically because the gears are self locking.

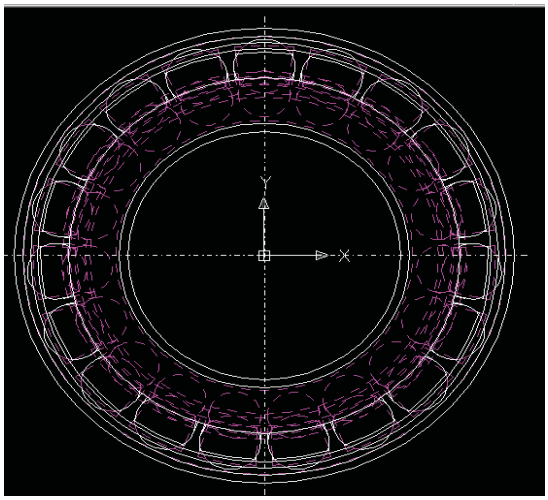

Fig.2-CAD of taper roller bearing.

Bearing selection is done according to the static and dynamic loads on the bearing. By considering the overall weight of the system of nearly 300kgs and considering 25% excess weight according to safety assumptions the bearing selected is 32006 X/Q from SKF online catalogue.

V. CALCULATIONS

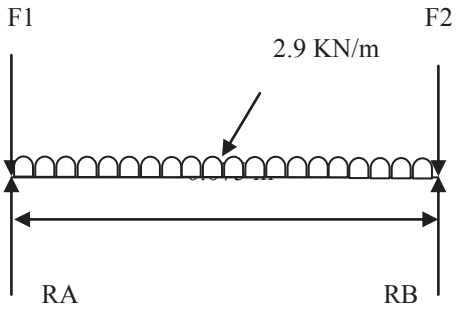

GIVEN – LOAD=300 KG A=5 CM

=300*9.81 b=65 cm

=2943 N c=5 cm

To calculate the force

F1=[w1(b+c)+w2c]/(a+b+c)]

=[2943(65+5)+(2943*5)]/(5+65+5)]

=2943 N

F2=[w1a+w2(a+b)]/(a+b+c)]

= 2943 N

F=F1+F2

=5886N =5.885 KN

Shear Force Calculations

RA-F1-(UDL*L)-F2+RB=0

RA-2.943-0.02175-2.943+RB=0

RA+RB=6.10 KN

Bending Moment Calculation

-RA*0+2.9*0.075*(0.075/2)

+F2*0.075-RB*0.075=0

$8.156*10^{-3}+0.2207=0.075*RB$

RB=3.05 KN

RA+RB=6.10 KN

RA=3.10 KN

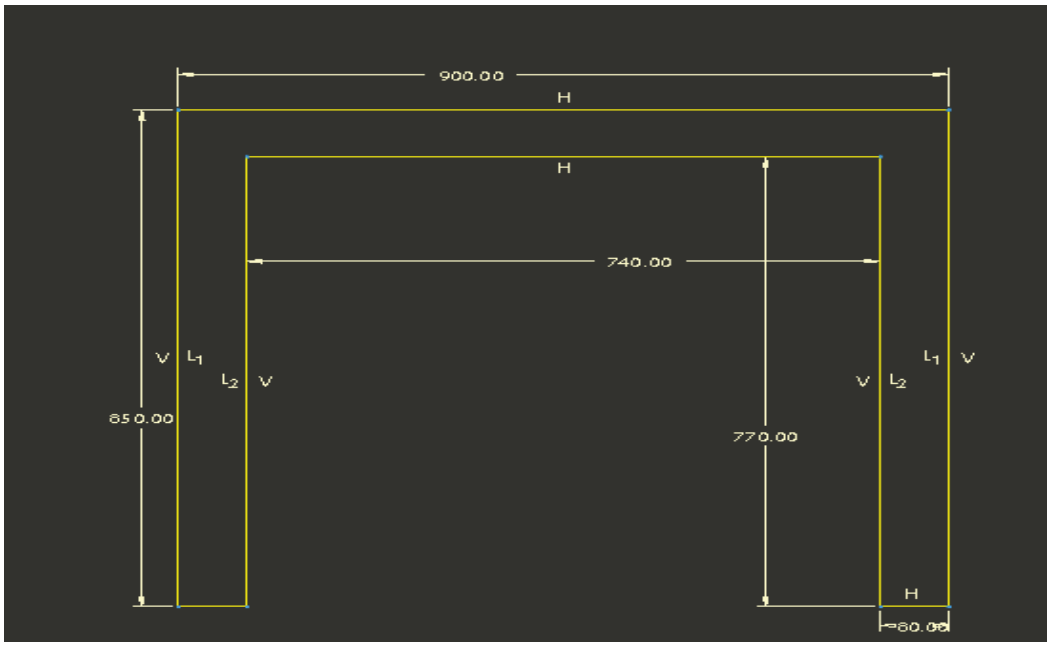

Fig. 03- CAD drawing of supporting base

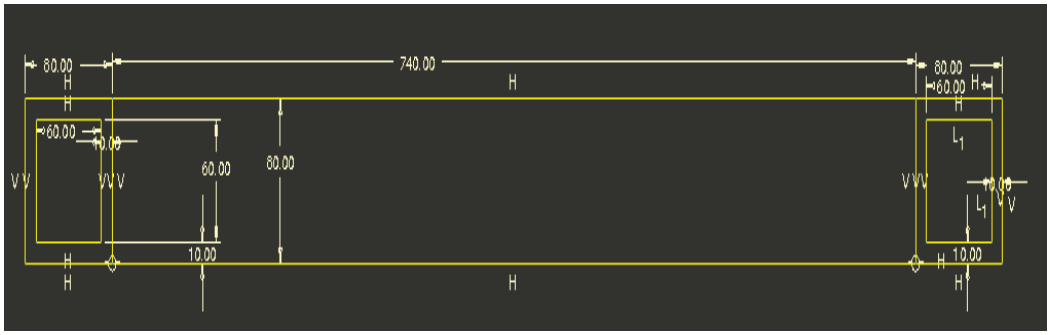

Fig. 04- CAD drawing for Calculating volume.

Shear stress Calculation

A1=A3=0.068 m^2

A2=0.0592 m^2

Total area=A1+A2+A3

=0.1952 m^2

$$\sigma = \frac{F}{A} = \frac{5.886}{0.1952} = 30.15\frac{kN}{m^2} = 0.03015\frac{N}{mm^2}$$

According to standard value- E= 211 GPa
= 211x10^3 MPa.

$$E = \frac{\sigma}{\varepsilon}$$

$$\varepsilon = \frac{0.03015}{211 * 10^3} = 1.4289 * 10^{-7}$$

$$\varepsilon = \frac{\delta V}{V} = \frac{\delta V}{6.832 * 10^{-3}}$$

$$\delta V = 9.7622 * 10^{-10}\ m^3$$

VI. CONCLUSION

From this paper we have successfully designed a Drum Handling Equipment for reducing the accidents in the industries. After implementing this mechanism in industries we claim to reduce the accident and to provide safety to the worker from hazardous chemicals. Results of this mechanism in terms of mechanical calculations are- sustainable load 300kg load, total force= 5.886 KN, Stress=0.0315 N/mm^2, Volume=$6.832*10^{-3}$ m^3, Strain =$9.7622*10^{-10}$ m^3.

References

[1] Nilesh k. Garghate, Dr S.K.Choudhary,A.P.Ninawe 'Design and Fabrication of Drum Handling Equipment' IJSRD\Vol.3,Issue04,2015\ISSN(online):2321-0613

[2] S Ramamrutham, R Narayanan 'Strength of Material' Dhanpat Rai Publishing Company eighteenth Edition

[3] V.B.Bhandari 'Design of Machine Element'-Design of bearing and change in Volume

[4] www.skf.com/in/products/bearings-units-housing/roller-bearing/tapered-roller-bearings/single-row/index.html?prodid=1310002006&imperial=false

THE 18TH INTERNATIONAL SYMPOSIUM ON WIRELESS PERSONAL MULTIMEDIA COMMUNICATIONS
(WPMC-2015)
December 13-16, 2015, Hyderabad, India

Decommissioning of Nuclear Facilities and Dose Rate Calculations for Nuclear Power Plant Staff

Lachake Pushkar Prashant
Mechanical Engineering Department
Sandip Institute of Engineering and Management
Nashik-422012, India
pushkar.lachake@gmail.com

Shinde Dnyandeo Dattatraya
Department of Mechanical Engineering
Sandip Foundations, SIEM, Mahiravani, Trimbak Road
Nashik - 422013, India
dnyandeo.shinde@siem.org.in

Abstract—**Many countries in the world are using nuclear energy to fulfill their energy requirement due to increasing demand of electricity. But the fuel used in NPP is highly radioactive & ionizing radiations emitted by these fuels is harmful for all living beings in the environment. If the exposure of these ionizing radiations is more than optimum value then it cause various health issues. Probability of ionizing radiation exposure is very high at time of Decommissioning process of NPP after completing its lifespan. Decommissioning is nothing but he administrative and technical actions taken to allow the removal of regulatory controls from a nuclear facility and typically includes dismantling the facility.**

Measure of energy deposited by radiation in a target is known as dose of radioactive element & pathway of a contaminant (Dose of radioactive element) may take to reach humans or other living organisms is called as exposure pathway like ingestion, inhalation, skin contact, etc. This paper contains detailed information of decommissioning of NPP, Ionizing Radiations Exposure due to NPP, Dose Limits of Ionizing Radiations for NPP Staff, Design Aspects for Radiation Protection in NNP & Steps for ALARA and Results of a Test Case For Decommissioning Dose Rates Calculations

Keywords—***Decommissioning; Dose Rate; Ionizing Radiations; exposure route; radioactive element***

I. INTRODUCTION

Radioactive material is handled by almost every country in the world may, for example, be in the form of a source used for medical purposesorfuel in a nuclear power plant. The facilities that use and handle radioactive material vary in size from large, complex sites, such as nuclear fuel cycle facilities andnuclear power plants, to smaller facilities such as manufacturing plants research and university laboratories. Now questions will arise regarding the effects of dose of ionizing radiation's exposure and ageing or usefulness of these facilities. Then they will require the implementation of a decommissioning strategy. Thousands of facilities in the worldhave been estimated that they will require some degree of decommissioning & currently some are undergoing decommissioning.

Both man-made and natural sources of ionizing radiation contribute to human exposure. The exposure of workers and public, to low levels of radiation from NPP have become an integral part of industrialized society. This paper consists of Planning, Strategy , Policy & techniques of decommissioning as well as dose rate calculations for NPP staff.

II. DECOMMISSIONING OF NPP

Decommissioning is an invasive process that presents industrial and chemical hazards as well as radiological ones, and indeed the non-radiological hazards generally represent greater overall risk to workers (IAEA, 2013; Jeong and Lim, 2009).

Decommissioning include both technical & administrative actions ones that must be accomplished to show that the facility can be released for unrestricted use or otherwise reused. The safety and economic considerations defined operating lifetime of nuclear facilities. NPPs are designed for an operating lifetime of several decades & it can be extended to up to 60 or more years by appropriate replacement, refurbishment or upgrading of some equipment called as “life extension”. The closure of operating life of nuclear installation & the decommissioning sequences should be planned at the design stage and may be related to termination of the design life of major components;

-Excessive operating costs compared with competing energy sources

-The conclusion of a research program that has achieved its goal and Safety issues

- Changes in government policy and accident or unplanned event requiring the final decommissioning to be performed.

A. Decommissioning Policy

It refers and includes government policy, all governmental choices, as described in laws, standards,mandatory requirements andregulations that will influence the framework in which decommissioning takes place.

B. Decommissioning Strategy

It includes all aspects of decommissioning and industrial approaches which may affect costsandprojects that are proposed to national competent authorities in the context of application for permission to decommission.

C. *Decommissioning Planning*

Careful and organized planning and clear identification of the objectives of the decommissioning is essential to ensure successful decommissioning. Before the start of decommissioning activities the regulatory body provides guidance in this respect, and reviews and approves the decommissioning plan.

Three stages of planning are as follows:

- Initial planning
- Ongoing planning
- Final planning

III. DECONTAMINATION TECHNIQUES

The removal of contamination from surfaces of facilities or equipment by heating,washing ,electrochemical orchemical action, mechanical cleaning or other techniquesis known asdecontamination.

Objectives of decontamination are as follows :

- To decrease radiation exposure;
- To salvage materials andequipment;
- To reduce the magnitude of the residual radioactive source and volume of materials requiring storage and;
- To restore site and facility, or parts thereof, to an unconditional-use situation;
- To remove loose radioactive contaminants and fix the remaining contamination in place in preparation for protective storage or permanent disposal work activities;
- To reduce the protective storage period or to minimize long-term surveillance requirements.

Some form of decontamination is required in any decommissioning program. As a minimum, the floor, walls, and external structural surfaces within work areas should be cleaned of loose contamination, and simple water rinsing of contaminated systems is performed.A decontamination program may also require a facility capable of treating secondary waste from decontamination.

The proven and emerging decontamination techniques which may be used to accomplish the goals of decommissioning activities have been discussed by the Technical Advisory Group of the Organization for Economic Cooperation and Development-Nuclear Energy Agency (OECD-NEA), a Cooperative Program on Decommissioning. International organizations which dealing with decommissioning in various roles and aiming at different goals are:-

1. UNO-IAEA (United Nations Organization-International Atomic Energy Agency)

2. OECD-NEA (Organization for Economic Cooperation & Development)

3. EC (European Commission)

4. WANO (World Association of Nuclear Operators)

5. WENRA (West European Nuclear Regulator Association)

A. *What do expert agencies say*

Several national and internationalagencies study different substances in the environment to determine if they can cause cancer. American Cancer Society looks towards these organizations to evaluate the risks based on evidence from research studies.

The International Agency for Research on Cancer (IARC) is part of the World Health Organization and plays major role in identifying the causes of cancer as well as human carcinogens.

The US Environmental Protection Agency (EPA) sets limits for exposure to x-rays and gamma rays in part because it recognizes that this form of radiation can cause cancer. For more information on the classification systems used by these agencies, see Known and Probable Human Carcinogens.

B. *Safetyconsideration during decommissioning of nuclearfacilities :*

Workers, the public and environmentshould be properly protectedat all phases of decommissioning from hazards resulting fromthe decommissioning process. During decommissioning a thorough safety assessment of thehazards involved should be conducted todefine protective measures, as part of a defense in depth system. Such measures may be different from those in place duringthe operation of the installation (IAEA, 1999).

The early stage of decommissioning of nuclear installations often involves theremovalof significant quantities of radioactivematerial, including fuel and operational waste. After this,the total contamination and activation of the installation is significantand has to be taken into account in the safety assessment(IAEA, 1999).

There is great importance for implementation of particular activities such as decontamination,cutting and handling of large equipment, and the progressivedismantling or removal of some existing safety systems. These activities have the potential for creatingnew hazards. An important objective during decommissioning is,therefore, that the safety aspects of these decommissioningactivities, such as the removal of existing safety system, beadequately assessed and managed, so as to mitigate any potentialexposure. Integrity of spent fuel, when still stored on-site in a fuelpool, should be considered and maintained. Fire protection andsuppression for the complete site should be included in thedecommissioning plan (IAEA, 1999).

IV. A TEST CASE FOR DECOMMISSIONING DOSE RATES CALCULATIONS OF NUCLEAR POWER PLANT STAFF :

Estimate the total Estimated Dose for exposure to ionizing radiation from external and internal sources on a young 19

years old male who is working in a Nuclear Power Plant which is in process of Decommissioning.

The worker is exposed to I-129 in the air at the workplace with activity concentration of 0.6 Bq/m3 and Am-241 (americium-241) in the water. The total daily ingestion rate of water is assumed to be 3 L/day with only 1/3th being consumed at the workplace. The activity concentration of Am-241 in the water is estimated at 0.008 Bq/L.

The worker is exposed also to accident ingestion of Pu-239 in the soil with ingestion rate of 20 mg over 24 hours. The Pu-239 activity concentration in the soil at the workplace was measured to 7 Bq/kg.

This young male has one meal eaten from food prepared at the workplace so that 1/3th of the average amount of food (presented in TABLE 3) is consumed in the workplace. The radionuclide activity concentration is measured in three food groups which are part from adult's meal. First food group is meat with activity concentration 1.1x10-5Bq/g from Cs-137. The second food group is dairy products with activity39 x 10-4Bq/g from Cs-137 again and the third group in the meal is vegetables with activity concentration 11 x 10-3Bq/g from Ra-226.

The radiation exposure (external) from artificial sources has been measured by instruments and estimated to be 1.4 x 10-2 mSv above the natural background radiation.Assume a 52-week work year and a 4-day work week with 10 hours work day.

GIVEN DATA:

- Age of young male = 19 years
- No. of working weeks in 1 working year = 52
- No. of working days in 1 working week = 4
- No. of working hrs. in 1 working day = 10
- Radiation Exposure (external) from Artificial Sources = ED(external)= 1.4 x 0.01 mSv
- CF = Conversion Factor: The factor of 365 days is required to convert the inhalation or ingestion rate from units/day to units/year
- EF = Exposure Factor =

$$\frac{(\text{working weeks per year}) \times (\text{working days per week})}{365 \text{ days per year}} \quad \text{.....(1)}$$

$$= \frac{52 \times 4}{365} = 0.5699$$

- Air inhalation Radiation Exposure Data:
  - Contaminat = I-129
  - Activity Concentration of I-129 = 0.6 Bq/m^3
  - Standard Value for Daily Intake of Air = 21 m^3/day
- Hence value for daily intake of air in working hrs. = Inhalation Rate (IR) =

$$\frac{\text{Standred Value for Daily Intake of Air} \times \text{No of working hrs. in 1 working day}}{\text{No of total hrs in 1 Day}} \quad \text{.....(2)}$$

= 8.75 m^3//Day

- DCF of Radionuclide I-129 for air Inhalation = 6.7×10^{-8} Sv/Bq

- Water ingestion Radiation Exposure Data:

- Contaminant = Am-241
- Activity Concentration of Am-241= 8×10^{-3} Bq/L
- Standard Value for Daily Intake of Water = 3 L/day
- Hence value for daily intake of water in working hrs. = Ingestion Rate (IR) = $1/3$ rd of Standard Value for Daily Intake of Water = 1 L/Day
- DCF of Radionuclide Am-241 for water Ingestion = 5.7×10^{-7} Sv/Bq

- Soil ingestion Radiation Exposure Data:

- Contaminant = Pu-239
- Activity Concentration of Pu-239= 7 Bq/Kg
- Standard Value for Daily Ingestion rate of Soil = 20 mg/day = 20 mg/24hrs.
- Hence value for daily Ingestion rate of Soil in working hrs.=Ingestion Rate (IR) =

$$\frac{\text{Standred Value for Daily Ingestion of soil} \times \text{No of working hrs. in 1 day}}{\text{No of total hrs in 1 Day}} \quad \text{.....(3)}$$

$$= \frac{20 \times 10}{24} = 8.33 \text{ mg/Day}$$

- DCF of Radionuclide Pu-239 for Soil Inhalation = 5.6×10^{-7} Sv/Bq

- Food ingestion Radiation Exposure Data:

<u>Food Group 1 (Meat)</u>

- Contaminant = Cs-137

- Activity Concentration of Cs-137= 1.1×10^{-5} Bq/gm
- Standard Value for Daily Ingestion of Food Group 1 = 169 gm/person/day
- Hence value for daily Ingestion of Food Group 1 in working hrs. = Ingestion Rate (IR) = $1/3$ rd of Standard Value for Daily Ingestion of Food Group 1 = 56.33 gm/person/Day
- DCF of Radionuclide Cs-137 for Food Group 1 Ingestion = 1.3×10^{-8} Sv/Bq

Food Group 2 (Dairy Products)

- Contaminant = Cs-137
- Activity Concentration of Cs-137= 39×10^{-4} Bq/gm
- Standard Value for Daily Ingestion of Food Group 2 =573 gm/person/day
- Hence value for daily Ingestion of Food Group 2 in working hrs. = Ingestion Rate (IR) = $1/3$ rd of Standard Value for Daily Ingestion of Food Group 2 = 191 gm/person/Day
- DCF of Radionuclide Cs-137 for Food Group 2 Ingestion = 1.3×10^{-8} Sv/Bq

Food Group 3 (Vegetables)

- Contaminant = Ra-226
- Activity Concentration of Ra-226 = 11×10^{-3} Bq/gm
- Standard Value for Daily Ingestion of Food Group 3 = 250 gm/person/day
- Hence value for daily Ingestion of Food Group 3 in working hrs. = Ingestion Rate (IR) = $1/3$ rd of Standard Value for Daily Ingestion of Food Group 3 = 83.33 gm/person/Day
- DCF of Radionuclide Ra-226 for Food Group 3 Ingestion = 2.2×10^{-7} Sv/Bq

SOLUTION :

Estimating Air Inhalation Radiation Exposure :

The committed dose from internal radiation exposure as a result of air inhalation can be estimated with the equation

$$\boldsymbol{ED_a} = \mathbf{C} \times \boldsymbol{IR} \times \boldsymbol{CF} \times \boldsymbol{EF} \times \boldsymbol{DCF} \quad \textbf{.....(4)}$$

= 0.073169 mSv

The estimated 50-years committed dose from I-129 , as a one year of inhalation at the workplace , is 0.073169 mSv.

Estimating Water Ingestion Radiation Exposure :

The committed dose from internal radiation exposure as a result of water ingestion can be estimated with the equation $\boldsymbol{ED_w} = \mathbf{C} \times \boldsymbol{IR} \times \boldsymbol{CF} \times \boldsymbol{EF} \times \boldsymbol{DCF}$ .....(5)

= 0.094854mSv

The estimated 50-years committed dose from Am-241 , as a one year of ingestion at the workplace , is 0.094854 mSv.

Estimating Soil Ingestion Radiation Exposure :

The committed dose from internal radiation exposure as a result of soil ingestion can be estimated with the equation :

$$ED_S = \mathbf{C} \times \boldsymbol{IR} \times \boldsymbol{CF} \times \boldsymbol{EF} \times \boldsymbol{DCF} \quad \textbf{.....(6)}$$

=0.0067951mSv

The estimated 50-years committed dose from Pu-239 , as a one year of ingestion at the workplace , is 0.0067951mSv.

Estimating Food Inestion Radiation Exposure :

The committed dose from internal radiation exposure as a result of food ingestion can be estimated with the equation := 0.043964 mSv

The estimated 50-years committed dose from Cs-137, Ra-226 , as a one year of ingestion at the workplace , is 0.043964 mSv.

Total Estimated Dose for Ionizing Radiation :

ED = 0.13888 mSv

The estimated dose from both internal & external radiation exposure to ionizing radiation at the workplace , is 0.13888 mSv.

V. Design Aspects for Radiation Protection in Nuclear Power Plant :

- Plant layout, Proper design and adequate shielding:

  Prescribedesign values for the radiation level at a specified distance from the equipment and for the general radiation fields in different areas of the plant. The plant layout is such that the areas are segregated according to their radiation levels and contamination potential. The design, layout of areas and equipment, maintenance approach and shielding, etc. are made such that the collective dose to the station personnel would be “as low as reasonably achievable” (ALARA).

- Limits of air contamination levels in different zones of the plant:

  Made provision of ventilation such that in full-time occupancy areas of the plant and the airborne contamination are maintained below 1/10 Derived Air Concentration.

- Proper selection of materials/componentsto control source:

  Select Materials which are used in plant systems in such a way that the activation products arising from the base material or the impurity content do not significantly contribute to radiation exposures.

- Design limit for collective dose:

Specify a limit on the collective dose at the design stage of each NPP that adequate provisions for radiation protection are made in the design of plant to keep radiation levels in different areas below design levels.

VI. Dose Limits of Ionizing Radiation for NPP Staff

Following are the dose limits for exposures to ionizing radiations for occupational workersprescribed by AERB :

A. Effective dose (whole body)

- 20 mSv/year averaged over 5 consecutive years, calculated on a sliding scale of 5 years. (The cumulative effective dose in the same 5-year period shall not exceed 100 mSv.)
- A maximum of 30 mSv in any year.

B. Equivalent dose (individual organs)

- Eye lens 150 mSv/year.
- Skin 500 mSv/year.
- Extremities 500 mSv/year (hands and feet).

C. Pregnant woman

- Equivalent dose limit to the surface of the woman's lower abdomen (for the remaining period of pregnancy) – 2 mSv.
- Annual Limit on Intake (ALI) for radionuclide's – 0.05 ALI. (For the remaining period of pregnancy.)

D. Apprentices and students (above the age of 16 years)

- Effective dose (whole body): 6 mSv/year.
- Equivalent dose (individual organs)

  - Eye lens 15 mSv/year.
  - Skin 50 mSv/year.
  - Extremities 50 mSv/year (hands and feet).

VII. Steps for ALARA("as low as reasonably achievable") exposures:

Working procedures and methods are examined in order to meet the objectives of the ALARA and to reduce the possibility of doses resulting from radiation jobs. The exposures are kept ALARA by implementing the following operational aspectsduring the operational stage of the NPP:

- Implementation of contamination control procedures andradiation protection.
- Use of proper protective equipment.
- Adherence to approved operating and maintenance procedures.
- Implementation of radiation protection training and qualification programs and conduct of refresher courses to impart ALARA concept and awareness.
- Proper work planning and its practical implementation through the issuance of Radiation Work Permit and dose budgeting for each operation.
- Constitution of an ALARA committee at the plant level.
- Planning and preparedness for unusual events.

VIII. Results and discussion

By studying Decommissioning of NPP & Dose Rate Calculations for NPP Staff I can able to :-

- Understand the Scope of Decommissioning as well as Decontamination Techniques & Spent-Fuel Management
- Know the dangers of Ionizing Radiations Exposure due to NPP & Dose Limits of Ionizing Radiations for NPP Staff
- Get familiar with Design Aspects for Radiation Protection in NNP & Steps for ALARA
- Calculate the Results of a Test Case For Decommissioning Dose Rates Calculations for NPP Staff
- Get the information about Safety, Health & Environment Protection as well as International Organizations for Nuclear energy.

References

1. Nuclear Site Remediation and Restoration during Decommissioning of Nuclear Installations : A Report by the NEA Co-operative Programme on Decommissioning
2. "Safe and effective nuclear power plant life cycle management towards decommissioning" IAEA
3. Investigating Human Exposure to Contaminants in the Environment: A Handbook for Exposure Calculations
4. 'Radiations , People and the Environment ' : IAEA, Austria, 2004
5. http://nuclearsafety.gc.ca/eng/resources/radiation/introduction-to-radiation/radiation-doses.cfm
6. IAEA, 1999. Decommissioning of Nuclear Power Plants and Research Reactors, IAEA Safety Standards Series No. WS-G-2.1. International Atomic Energy Agency.
7. KwanSeongJeong , Establishment of the hazard reduction methodology to be taken into account for safety assessment during decommissioning of nuclear facilities, Korea Atomic Energy Research Institute, Daedeok-daero 989-111, Yuseong-gu, Daejeon 305-353, Republic of Korea.

THE 18TH INTERNATIONAL SYMPOSIUM ON WIRELESS PERSONAL MULTIMEDIA COMMUNICATIONS
(WPMC-2015)
December 13-16, 2015, Hyderabad, India

Application of Principal Component Analysis to Magnetic Abrasive Finishing

Sandip B. Gunjal
Research Scholar, Production Engg. Department,
K.K.W.I.E.E. & R,
Nasik, India
gunjsandip@rediffmail.com

P. J. Pawar
Professor, Production Engg. Department,
K.K.W.I.E.E. & R,
Nasik, India

***Abstract*-With the development of industry manufacturing technology, fine surface finish is in high demand in a wide spectrum of industrial applications. Magnetic abrasive finishing (MAF) is one of the advanced finishing processes capable of producing excellent surface finish of the order of few nanometers. MAF process is used for fine finishing of flat surfaces as well as internal and external surfaces of tube type work pieces. The process can finish ferromagnetic as well as non-ferromagnetic materials. The MAF process is becoming popular due to its ability to give repeatable and consistent results. However, as the surface finish requirement increases, the operational cost of this process increases exponentially. Quality, cost, time and efficiency of this process can be improved significantly by choosing the optimum values of process parameters. This paper therefore presents a well-known statistical method known as Principal Component Analysis (PCA) to find the optimal combination of process parameters of MAF process for multi-objective optimization considering average normal force and average finishing torque as objectives. The results of the PCA are compared with the previously published results.**

Keywords-Magnetic abrasive finishing; multi-objective optimization; principal component analysis.

I. INTRODUCTION

Robust design is an engineering method of quality improvement that seeks to obtain a lowest cost solution to the product design specification based on the customer's requirements. The Taguchi method, which combines the experimental design techniques with quality loss considerations, is the conventional approach to achieve robustness. This method can only be used in a single-response case; it cannot be used to optimize a multi-response problem. However, a customer normally considers more than one quality characteristic in most manufactured products and the quality characteristics are usually correlated. Engineering judgment has up until now been used primarily to optimize the multi-response problem in the Taguchi method (Phadke, 1989). Unfortunately, an engineer's judgement increases the uncertainty during the decision-making process. Another approach to solve this problem entails assigning a weight for each response (Hung, 1990; Shiau, 1990; Tai *et al.*, 1992). Nevertheless, determining a definite weight for each response in an actual case still remains difficult. Another method employs the regression technique (Logothetis & Haigh, 1988; Pignatiello, 1993). However, such an approach increases the computational process complexity, and the possible correlations among the responses may still not be considered. In addition, a factor which is significant in a single-response case may not be significant when considered in a multi-response case. Therefore, a more effective approach is required to solve this complicated problem [1].

In this work, a systematic procedure via principal component analysis (PCA) is proposed for multi-objective optimization considering average normal force and average finishing torque as objectives. By using PCA, a set of original responses is transformed into a set of uncorrelated components so that the optimal factor/level combination can be found.

II. LITERATURE REVIEW

Taguchi method have been applied by many researchers for multi-objective optimization of MAF process. Yang et al. [2] performed the operations using Taguchi experimental design, considering the effects of magnetic field, pole rotational speed, feed rate, working gap, abrasive, and lubrication. The optimal parameter conditions was obtained after experimental data analysis, the quality surface roughness (R_{max} = 0.1 μm) which is similar to a mirror surface was obtained after confirmatory tests. The different optimal parameter conditions were obtained for surface roughness and material removal weight. Singh and Shan [3] studied the effect of key parameters i. e. magnetic flux density, volume flow rate and number of cycles on the material removal and percentage improvement in surface roughness using response surface methodology. Singh et al. [4] applied the Taguchi design of experiments to find out important parameters influencing the surface quality generated. Important parameters influencing the surface quality generated during the MAF are identified as: (i) voltage (DC) applied to the electromagnet, (ii) working gap, (iii) rotational speed of the magnet, and (iv) abrasive size (mesh

number). They determined the effect of process variables on the surface finish and both the forces (normal magnetic force and cutting force). Kala and Pandey [5] measured the finishing force and torque for a double disk magnetic abrasive finishing process. Investigations were made to understand the effect of process factors namely upper and lower working gap rotational speed, abrasive weight percentage on the normal finishing force and finishing torque using Taguchi L_9 orthogonal array.

However, the Taguchi approach in real sense is not optimization technique. Moreover, it can be applied only to single objective problem and in case of conflicting multi-objective optimization problem it gives different levels, thus it becomes difficult to interpret this result to achieve the best performance. Hence, this paper discusses the application of PCA to multi-response problem with a case study.

III. PRINCIPAL COMPONENT ANALYSIS

In PCA, a set of original responses is transformed into a set of uncorrelated components so that the optimal factor/level combination can be found. The PCA is a well-known unsupervised linear technique for dimensionality reduction. The central idea behind PCA is to reduce the dimensionality of a data set consisting of a larger number of interrelated variables, while retaining as much as possible variation present in the original data set. This is achieved by transforming to a new set of variables, the so-called principal components (PCs), which are uncorrelated and ordered so that the first few retain most of the original data variation. It selects a small number of components to account for the variance of original multi-response. Different steps in PCA are discussed as below,

Step (1): Calculation of S/N ratios

$$n = -10\log(MSD) \tag{1}$$

Where, MSD is the Mean square deviation and is calculated as,

$$MSD = \frac{1}{n}\sum y^2{}_i \tag{2}$$

Step (2): Normalization of S/N ratio,

$$X_i^*(j) = \frac{Xi(j) - X(j)^-}{X(j)^+ - X(j)^-} \tag{3}$$

Where

$X^*i(j) =$ Normalized S/N ratio for j[th] quality characteristic,

$Xi(j) =$ S/N ratio for jth quality characteristic,

$X^*i(j)^- =$ Minimum S/N ratio for j[th] quality characteristic in all experimental runs.

$X^*i(j)^+ =$Maximum of S/N ratios for j[th] quality characteristic in all experimental runs.

Step (3): Representation of the multi-response by matrix.

Step (4): Evaluation of Correlation coefficient of normalized multi-response matrix.

$$R_{ij} = \frac{\mathrm{cov}[X_i^*(j), X_i^*(l)]}{\sigma X_i^*(j) \times \sigma X_i^*(l)} \tag{4}$$

Where

$\mathrm{Cov}[X^*i(j), X^*i(l)] =$ Covariance of sequences Xi*(j) and Xi*(l)

$\sigma X^*i(j) and\ \sigma X^*i(l) =$ Standard deviation of sequence Xi*(j) and Xi*(l) respectively.

Step (5): Calculation of eigenvalues and the eigenvectors of the correlation matrix.

Step (6): Computation of Principle Components (PC).

$$p(i)^k = \sum_{j=1}^{m} X_i^*(j) \times v_k(j) \tag{5}$$

Where pi(k) is the k[th] PC corresponding to i[th] experimental run, v_k(j) is the j[th] element of k[th] eigen vector. The total principal component index (TPCI) corresponding to i[th] experimental run (Pi) is computed as follows.

$$p_i = \sum_{k=1}^{m} (p_i k) \times e(k) \tag{6}$$

Where

$$e(k) = \frac{eig(k)}{\sum_{k=1}^{m} eig(k)} \tag{7}$$

Where eig(k) is the k[th] eigenvalue.

Step (7): The TPCI for each experiment run is used to find out the average factor effect at each level. The optimum parameter level that corresponds to the maximum TPCI is predicted.

To validate the application of principal component analysis to multi-objective optimization of MAF process, following case study is considered.

IV. CASE STUDY

MAF is a super finishing process which uses a resilient multi point cutting tool to finish the work pieces. Blend of iron and abrasive particle forms a flexible magnetic brush (FMAB) between the work piece and the magnetic tool. The force exerted by the FMAB on the workpiece is responsible for the finishing action. By varying various process factors the finishing force and torque acting on the workpiece can be varied to finish the work pieces. Knowledge of finishing forces is important in any manufacturing process as the surface integrity of the finished surface is being affected. Fig. 1 shows the experimental setup used for the study. Fig. 2 shows the schematic view of the experimental setup and the directions along which the normal force and the finishing torque act.

This case study analyzes the effect of upper working gap (A), lower working gap (B), abrasive weight percentage (C) and rotational speed (D) on average normal force (F_n) and average finishing torque (T_f). The process factors and their levels considered by Kala and Pandey [5] to perform

experimentation is shown in Table I and the details of the experimental design based on Taguchi L9 orthogonal array and the corresponding average normal and average finishing torque is shown in Table II.

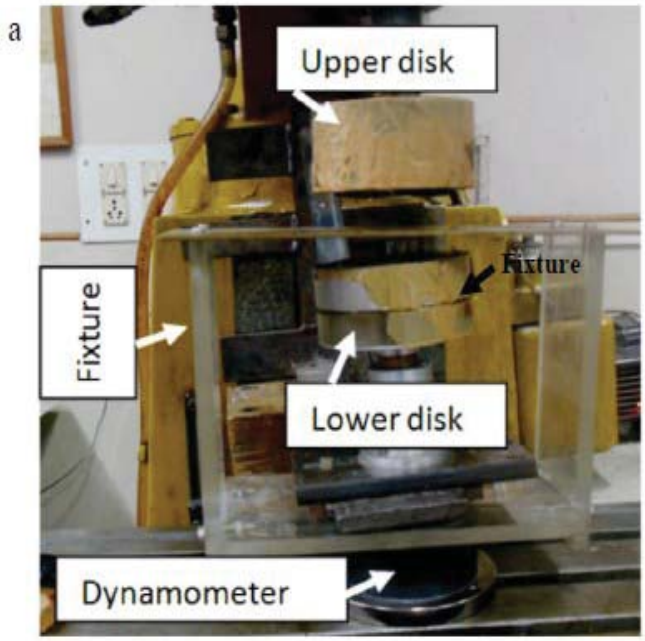

Fig. 1. Experimental setup used in the study [5]

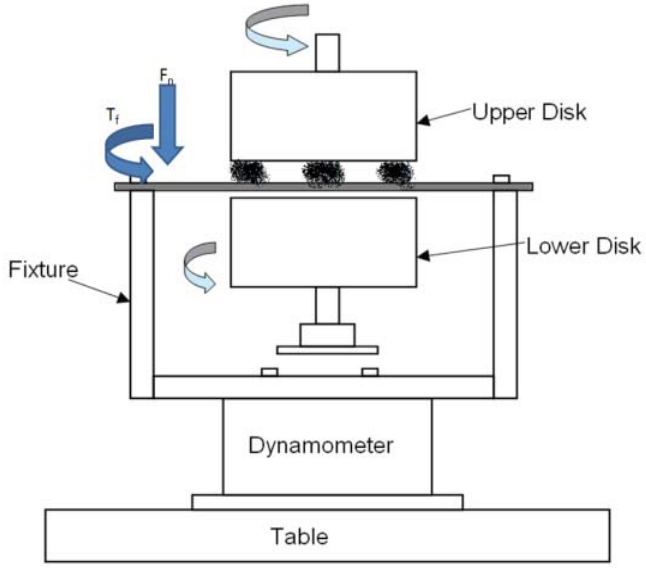

Fig. 2. Schematic representation of the setup used for measuring finishing forces for double disk magnetic abrasive finishing (DDMAF) [5]

TABLE I. PROCESS FACTORS AND THEIR LEVELS CONSIDERED TO PERFORM EXPERIMENTATION [5]

Factors	Description	Levels		
		L_1	L_2	L_3
A	Upper disk working gap (mm)	1.5	2	2.5
B	Lower dusk working gap (mm)	1.5	2	2.5
C	Percentage of abrasive	10	20	30
D	Rotational speed (rpm)	200	300	400

TABLE II. EXPERIMENTAL DATA [5]

Expt. No.	*A*(mm)	*B*(mm)	*C* (%)	*D* (rpm)	F_n (N)	T_f (N-m)
1	1.5	1.5	10	200	72.83	0.425
2	1.5	2	20	300	59.05	0.41
3	1.5	2.5	30	400	45.62	0.344
4	2	1.5	20	400	60.2	0.478
5	2	2	30	200	56.67	0.321
6	2	2.5	10	300	54.99	0.356
7	2.5	1.5	30	300	48.75	0.317
8	2.5	2	10	400	51.59	0.396
9	2.5	2.5	20	200	46.05	0.214

Table III shows the calculation of S/N ration by using the equation 1 and normalized S/N ratio by using the equation 3 for the two responses. From the normalized S/N ratio coefficient of determination (R_{12}) is calculated by using the equation 4.

TABLE III. CALCULATION OF S/N RATIO AND NORMALIZED S/N RATIO

Sr. No.	S/N Ratio		Sr. No.	Normalized S/N Ratio	
	For F_n	*For* T_f		*For* F_n	*For* T_f
1	37.24	-7.43	1	0.99	0.85
2	35.42	-7.74	2	0.55	0.80
3	33.18	-9.26	3	0	0.59
4	35.59	-6.41	4	0.59	0.99
5	35.06	-9.86	5	0.46	0.50
6	34.80	-8.97	6	0.39	0.63
7	33.75	-9.97	7	0.14	0.48
8	34.25	-8.04	8	0.26	0.76
9	33.26	-13.39	9	0.02	0
Minimum	33.18	-13.39	**SUM**	3.43	5.64
Maximum	37.24	-6.41	**MEAN**	0.38	0.62
Difference	4.06	6.98	σ	0.30	0.27
			COV(1,2)	0.055	
			R_{12}	0.67	

Table IV shows the calculation of Principal Components (PC) by using the equation 5 and Total Principal Components Index (TPCI) by using the equation 6.

TABLE IV. PRINCIPAL COMPONENTS (PC) AND TOTAL PRINCIPAL COMPONENTS INDEX (TPCI)

Sr. No.	Principal Components		TPCI	Sr. No.	Principal Components		TPCI
	PC1	PC2			PC1	PC2	
1	1.57	1.52	1.56	6	0.82	0.90	0.83
2	1.09	1.18	1.11	7	0.47	0.58	0.48
3	0.39	0.59	0.42	8	0.77	0.94	0.80
4	1.26	1.39	1.28	9	0.020	0.01	0.01
5	0.80	0.81	0.80				

Best level of responses are selected from the calculated TPCI for the four factors *A, B, C.* and *D* and three levels L_1, L_2, *and* L_3 as shown in Table V.

TABLE V. BEST LEVEL FOR RESPONSES BASED ON TPCI

Factor	*A*			*B*		
Level	L_1	L_2	L_3	L_1	L_2	L_3
	1.56	1.28	0.48	1.56	1.11	0.42
	1.11	0.80	0.80	1.28	0.80	0.83
	0.42	0.83	0.01	0.48	0.80	0.01
Sum	**3.10**	2.93	1.31	**3.34**	2.72	1.28

Factor	*C*			*D*		
Level	L_1	L_2	L_3	L_1	L_2	L_3
	1.56	1.11	0.42	1.56	1.11	0.42
	0.83	1.28	0.80	0.80	0.83	1.28
	0.80	0.01	0.48	0.01	0.48	0.80
Sum	**3.21**	2.41	1.72	2.39	2.43	**2.52**

In order to have a better understanding of the effect of process factors on finishing force and torque the multivariable regression equations were obtained by Kala and Pandey[5], as given below**.**

$$F_n = 127 - 10.4 \times A - 11.7 \times B - 0.946 \times C - 0.0302 \times D \quad (8)$$

$$T_f = 0.734 - 0.0836 \times A - 0.102 \times B - 0.00651 \times C + 0.00043 \times D \quad (9)$$

Table VI shows the calculation of average normal force (F_n) and average finishing torque (T_f) by using the equation 8 and 9.

TABLE VI. CALCULATION OF FINISHING FORCE AND TORQUE

Sr. No.	*A*	*B*	*C*	*D*	F_n (N)	T_f (N-m)
1	1.5	1.5	10	200	78.35	0.476
2	1.5	2	20	300	60.02	0.403
3	1.5	2.5	30	400	41.69	0.330
4	2	1.5	20	400	57.65	0.455
5	2	2	30	200	48.38	0.253
6	2	2.5	10	300	58.43	0.375
7	2.5	1.5	30	300	46.01	0.305
8	2.5	2	10	400	56.06	0.427
9	2.5	2.5	20	200	46.79	0.225
10	**1.5**	**1.5**	**10**	**400**	**72.31**	**0.562**

Comparison of the results obtained by Taguchi method [5] and PCA are shown in Table VII.

TABLE VII. COMPARISON OF RESULTS

Method	Responses	Optimum Levels	F_n (N)	T_f (N-m)
Taguchi	Finishing force (F_n)	1-1-1-1	78.35	0.476
	Finishing Torque (T_f)	1-1-1-3	72.31	0.562
PCA	Finishing force(F_n)	1-1-1-3	72.31	0.562
	Finishing Torque(T_f)			

Combined index for average normal force and average finishing torque is shown in Table VIII.

TABLE VIII. INDEX FOR COMBINED OBJECTIVE FUNCTION

Responses	Optimum Levels	For F_n	For T_f	Combined Index
Finishing force (F_n)	1-1-1-1	1	0.84	1.84
Finishing Torque (T_f)	1-1-1-3	0.92	1	1.92

V. CONCLUSION

In this study, PCA is applied to multi-response problems, which was solved by Taguchi method. The following are the conclusions

1. PCA results in same optimum level as for the finishing torque and although the value for average finishing force is reduced the extent with which the second objective function is improved is much more, ultimately that results into higher index value for combined objective function. Thus results obtained by PCA are always superior than individual Taguchi method.
2. It is observed that for combined objective function of average normal force and average finishing torque, the upper working gap should be set lower value i.e. at 1.5 mm, lower working gap should be set at lower value i.e. at 1.5 mm, abrasive weight percentage is lower i.e. 10 and rotational speed of the magnet should be set at higher value i.e at 400 rpm
3. Maximum possible value of average normal force and average finishing torque obtained by PCA is 72.31 N and 0.562 N-m respectively.

REFERENCES

[1] C. T. Su and L. I. Tong, "Multi-response robust design by principal component analysis", Total Quality Management, Vol. 8, pp. 409 ± 416, 1997.

[2] L. D. Yang, C. T. Lin and H. M. Chow, "Optimization in MAF operations using Taguchi parameter design for AISI304 stainless steel", Int J Adv Manuf Technol, Vol. 42, pp. 595-605, 2009.

[3] S. Singh and H.S. Shan, "Development of magneto abrasive flow machining process", International Journal of Machine Tools & Manufacture, Vol. 42, pp. 953-959, 2002.

[4] D. K. Singh, V.K. Jain and V. Raghuram, "Parametric study of magnetic abrasive finishing process", Journal of Materials Processing Technology, Vol. 149, pp. 22-29, 2004.

[5] P. Kala and P. M. Pandey, "Experimental Study On Finishing Forces In Double Disk Magnetic Abrasive Finishing Process While Finishing Paramagnetic Workpiece", Procedia Materials Science, Vol. 5, pp. 1677 – 1684, 2014.

Sensitive Association Rules Hiding Methods : A Survey

Mrs. Geeta S. Navale
Research Scholar, SKNCOE, Pune, India
Sinhgad Institute of Technology and Science
Pune, India
geetanavale@gmail.com

Dr. Suresh N. Mali
Principal
Sinhgad Institute of Technology and Science
Pune, India
snmali@rediffmail.com

***Abstract*—In today's scenario of internet world, a cloud computing and data center, a lot of importance has to be given to the security of information while sharing it with different organizations. Present advance data mining techniques gives knowledge about various relationships of itemsets which will be useful to a group of people while enhancing their businesses. However, in many cases the organizations having the source of information may not intended to share such relationships (association rules) with any other organization or they wants to have rights of information. Therefore, there is a need to hide the sensitive information in the database prior to share it among in the organizations. The focus of this work is to understand the hiding methodologies of association rules in database while maintaining the disturbance in the original database as less as possible. However, intended recipients must receive this sensitive information robustly against various intentional or unintentional attacks.**

Keywords— Association Rule Hiding; Privacy Preserving Data Mining

I. INTRODUCTION

Consider the scenario as shown in Fig 1.1. If owner of one of the organizations get an access to the database of the other organization, one can mine the database and able to get the various business secrets (sensitive association rules) of that owner and may result in loss of business. Thus, there is a need of privacy of association rules. There are various ways to achieve this privacy. However, the use of information hiding methodology for this purpose will not only enhance the privacy but also produce minimum side effects (distortion) in the given data base which otherwise creates suspects in the minds of organizations about originality of database. Also, after applying the hiding process to original database, there shouldn't be drastic increase/decrease in the size of database. Ideally, the process of hiding of sensitive association rules should give correct mining results for rest of the association rules and must hide all the sensitive association rules.

An association rule is a rule of type $X \rightarrow Y$, where X and Y are itemsets. If transaction contains itemset X, it (probably) also contains itemset Y.

Agrawal, R. et al. were the first to introduce Association rule mining[1]. Based on the concept of strong rules, Agrawal et al. introduced the problem of mining association rules from transaction data as follows: Let I = {i1,i2,...,in} be a set of n attributes called items. Let D = {t1, t2,..., tm} be a set of transactions called the database. In a database D, each transaction has an unique transaction ID and contains a subset of the items in I. A rule is defined of the form $X \Rightarrow Y$ where $X, Y \subseteq I$ and $X \cap Y = \emptyset$. The sets of items (for short itemsets) X and Y is called antecedent (left-hand-side or LHS) and consequent (right-hand-side or RHS) of the rule. Association rules give the relationships between a set of items in large datasets to be discovered. When we discover such relationships between items, we get a large number of association rules. From these large number of association rules, it is very difficult to conclude which are important one? Then there should be some way or technique or measure which will decide this. By applying this technique we will get the desired or interested association rules. Various interesting measures have been proposed by Geng L., Hamilton et al. [2] and McGarry, K [3]. G. Dong et al. [4], Lallich, S. et al.[5], A.A. Freitas [6], Michael Steinbach [7] also put a focus on interesting measures. Pang-Ning Tan et al. [8] focuses on how to select correct objective measure to find the association rules. Searching for interesting patterns will optimize the problem. To exemplify the concepts, we use a small example from the superstore domain. The set of items is I = {wheat, pulses, rice, spices} and a small database containing the items is shown in Table 1.

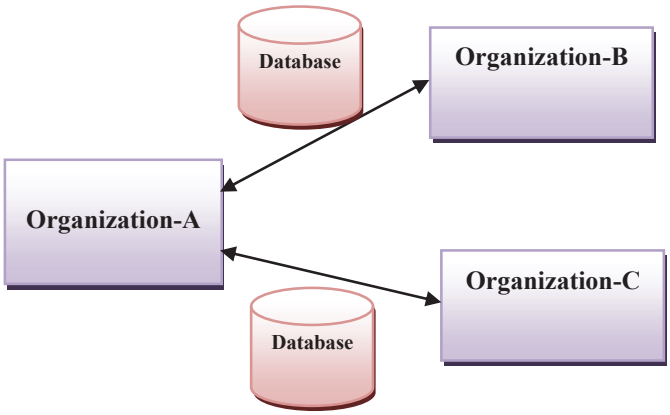

Fig. 1.1 Sharing of database

TABLE I.

Transaction ID	Items
T1	Wheat
T2	pulses, rice, spices
T3	rice, spices
T4	rice, spices
T5	pulses, rice

An example of association rule for the superstore could be {pulses, rice} ⇒ {spices} means if pulses and rice is bought, customers also buy spices. To select interesting rules from all possible rules, constraints on various measures of importance and interest can be used. The best-known constraints are thresholds on support and confidence. The support supp(X) of an itemset X can be defined as the proportion of transactions in the data set which contain the itemset. The support of rule X → Y in data D is given in (1)

$$\text{supp}(X \rightarrow Y) = \text{supp}(X \cup Y) \quad (1)$$

The support is the probability that a transaction contains X ∪ Y. In the example database in Figure 1, the rule {pulses, rice} ⇒ {spices} has a support of 1/5 = 0.2 since it occurs in 20% of all transactions (1 out of 5 transactions). The confidence of rule X → Y in data D is given in (2)

$$\text{conf}(X \rightarrow Y) = \text{supp}(X \cup Y) / \text{supp}(X) \quad (2)$$

The confidence is the conditional probability that transaction contains *Y* given that it contains *X*. For example, the rule {pulses, rice} ⇒ {spices} has a confidence of 1/2 = 0.5 in the database in Table 1, which means that for 50% of the transactions containing pulses and rice the rule is correct.

The association rule mining has many applications. To mention few- shelf management in superstore, sending SMSs to customers when superstores are executing any scheme.

If owner of one of the superstores get the database of the other store, he can mine the database and gets the various business secrets of that owner and may result in loss of business. Thus there is a need to hide association rules. The hiding process should ensure that it will produce minimum side effects. The meaning of side effects is that after applying the hiding process to original database, it shouldn't drastically increase/decrease the size of database, it should give correct mining results, must hide all the required rules.

II. SURVEY

In this section we are going to present the techniques used by the researchers to hide the association rules. The very first heuristic solution to hide association rule was proposed by Dasseni et al.[9]. They proposed three algorithms based on the measures of support and confidence. By using, the confidence measure, an algorithm could decrease the confidence and become insignificant. They looked for the transactions that partially support both the left- and the right-hand side of a sensitive rule. The confidence measure of these transactions is minimized below the confidence threshold.

Oliveira et al.[10] introduced a framework for hiding sensitive association rules. This framework scans the database either once or twice to hide the rules. They select the victim item by computing the frequencies of items in the restrictive association rules. They compute the number of sensitive transactions to hide. Then they are sorting the sensitive transactions by size, and finally hide a sensitive transaction.

Verykios et al.[11] progressed on existing techniques by establishing a distortion and a blocking algorithms. The distortion algorithm works like this- a weight is assigned to each rule in the database based on the minimum confidence threshold is its confidence. For each transaction, based on these weights a priority value is calculated. All the transactions are sorted in ascending order of priority.

Wu et al.[12] proposed an approach that classifies the valid modifications and represents each class by three attributes indicating the modification scheme, the set of items to be contained in the transactions to be modified and the item to be modified.

Sun and Yu [13] [14] proposed a border based hiding process. To have separation between sensitive and nonsensitive items, they suggested a border based approach. Their main aim was data quality. They went for minimization of side effects at the cost of degrading efficiency. An algorithm was proposed to recognize the optimal candidate item to be removed, which has a minimal impact on the border. They used the concept of the weight of a border itemset to count the impact of hiding candidates on the border.

Moustakides and Verykios [15][16] proposed approach efficient than the approach proposed by Sun and Yu. Also hiding quality was better. The proposed algorithms sorts the sensitive itemsets based on their support in an increasing order. The hiding process starts with the sensitive itemset having the minimum support. The procedure is repeated until the hiding of every sensitive itemset is done.

Menon et al. [17] were the first to introduce a Constraint Satisfaction Problem (CSP) to hide association rules. The CSP is formulated as an integer program. The authors proposed two approaches blanket approach and intelligent approach. After hiding one item is remaining from the original transaction in blanket approach. In intelligent approach some of items from the transaction were removed which will result in reducing the

support of every sensitive itemset. The integer program was used to maximize the accuracy of the shared database by minimizing the number of transactions that had to be changed to hide the frequent itemsets corresponding to the sensitive patterns.

Menon and Sarkar [18] improved the first solution methodology. They minimized the number of transactions that need to be sanitized. The authors also tried to keep the minimum number of nonsensitive itemsets lost during the hiding of the sensitive ones. Because of its high complexity, they reported that the problem could not be solved even for very small number of cases. Because of this reason, they proposed a solution that depends on two smaller solutions. First one is sanitization and the modified frequent itemset-hiding. The sanitization solution identifies how the support of sensitive itemsets can be purged from a specific transaction by removing very few numbers of items from it. Because of this fewer nonsensitive itemsets will be lost during the hiding process of sensitive itemsets. The modified frequent itemset-hiding solution will concentrate on minimizing the number of nonsensitive itemsets lost, while hiding sensitive ones.

Gkoulalas-Divanis and Verykios.[19] proposed an exact approach for association rule hiding problem. For effective hiding, the authors revised the border introduced by Sun and Yu [13][14] to find out a minimum set of itemsets without any side effects. They used the revised border to formulate a minimal integer program, which is changed into a binary integer program.

The approach proposed by Gkoulalas-Divanis and Verykios [20] proposed a two-phase iterative algorithm that developed the functionality of the ‘inline’ algorithm. The two-phase iterative algorithm comprises of two phases that iterate until either (1) an exact solution of the given problem instance is identified or (2) a prespecified number of subsequent iterations of the algorithm has been done. The first phase of the algorithm utilizes the ‘inline’ algorithm to hide the sensitive knowledge. If it succeeds, the process is terminated and the modified database is returned. If the first phase is unable to identify an exact solution, the algorithm proceeds to the second phase, in which a certain number of selected inequalities from the CSP of the first phase are removed in an ‘one-to-one’ fashion, until the underlying CSP becomes feasible. The second phase results in the expansion of the positive border, whereas the iteration through the two phases aims to approximate the optimal borderline between the sensitive and public itemsets in the sanitized database.

Gkoulalas-Divanis and Verykios[21] introduced the first exact methodology to hide sensitive frequent itemsets by extending the original database. By utilizing the revised borders as well as the cover relationships among the item sets, authors were able to minimize the set of item sets participating in the CSP, which provides a solution to the sensitive knowledge hiding. The hiding process maximizes the data utility of the sanitized database, with minimum side effects while guaranteeing the satisfaction of all the privacy constraints. The released database (the original and the extended database), can guarantee the protection of the sensitive knowledge, when mined at the same or at a higher support threshold than that used for the mining of the original database. Extending the original database for sensitive itemset hiding has confirmed to offer better solutions for an extended set of hiding problems, compared with the previously presented approaches, as well as to lead to hiding solutions of better quality.

III. PROBLEM STATEMENT

Most of the authors contributed a lot to convert original database into sanitized database to hide association rules but they didn't focus on how to get back the hidden sensitive association rules in intended usage. Also they haven't addressed the attacks by malicious users which are likely to tamper the sanitized database to disturb the hidden sensitive association rules.

Considering the survey in Section II, the main scientific challenges are:

1. How to provide the privacy to association rules?
2. How to categorize and minimize the side effects?
3. How to gain optimality of various data hiding parameters in the scalable database?

Our aim of this research work is to enhance the privacy of association rules of data mining with reduced side effects on false rules, information loss and modification degree by adaptive modification strategies of reversible information hiding in scalable database.

IV. OBJECTIVES

1. To study various association rule hiding methods.
2. To analyze the relationship between various parameters (false rules, information loss, modification) degree with respect to privacy.
3. To measure the performance of existing association rule hiding schemes and to optimize various data hiding parameters while implementing an adaptive data hiding system for robust information hiding of association rules in scalable database.
4. To evaluate and validate the proposed methodology of association rule data hiding and to test the robustness of hidden association rules under intentional or unintentional attacks.

V. PROPOSED METHODOLOGY

1. An extensive literature survey will be carried out to gain the various methods of association rule hiding and analysis of results of methodologies used by previous researchers.

2. Implementation of proposed methodology. Experimentation of proposed algorithm with scalable database to optimize the relationship between data hiding parameters such as false rules, information loss and modification degree to attain privacy as these parameters will be affected while achieving privacy.

3. The overall methodology is described in the following Fig. 1.2 The original scalable database 'D' is used by data mining tool to generate association rules. The selected association rules based on given threshold values of 'Support' and 'Confidence', eventually called Sensitive Association Rules (SARs) are considered while modifying the original scalable database 'D' to draft copy of sanitized database 'DS''. After optimizing various parameters of association rule hiding criterions, the sanitized database will get finalized as '$D^{S'}$'. The embedding function (E) will use a secret key 'K' to convert 'D' to '$D^{S'}$' as:

$$E\ (D\ X\ K) \rightarrow D^{S} \qquad (3)$$

The embedding secret key 'K' will be function of embedding methodology and going to reflect the side information used at the time of embedding and necessary while extracting the original database D. This embedding secret key has to be shared through secured channel for protecting the privacy amongst the trusted organizations.

The intended user will use the same secret key 'K' and extraction function (E-1) to get the original database 'D' as:

$$E^{-1}\ (D^{S}\ X\ K) \rightarrow\ D \qquad (4)$$

4. Various intentional attacks such as addition of noise, filtering and unintentional attacks such as data compression may disturb the sanitized data. However the intended user should get the original data as well as sensitive association rules robustly. Therefore the sanitized data will be tested for its robustness under such attacks. The robustness can be achieved by redundancy in hidden association rules and by adaptively deciding the hidden locations.

CONCLUSION

There are various methodologies of hiding the association rules in the database and optimizing support and confidence. Each methodology has its advantages and disadvantages. The outcome of the proposed research is to hide the sensitive association rules of data mining with following criterions –

i. No false rules generation
ii. No information loss
iii. Modification Degree
iv. Robustness against intentional or unintentional attacks

Apart from above three criterions, the proposed method will be adaptive for scalable database Therefore, the proposed methodology of association rule data hiding will be evaluated and validated with respect to various parameters as mentioned in criterions and also it is necessary to check the satisfaction of above mentioned criterions. The research will implement novel steps to make the proposed system complete in all respect.

ACKNOWLEDGEMENT

I am thankful to Sinhgad Institute of Technology and Science, Pune as well as to Smt. Kashibai Navale College of Engineering, Pune for technical support.

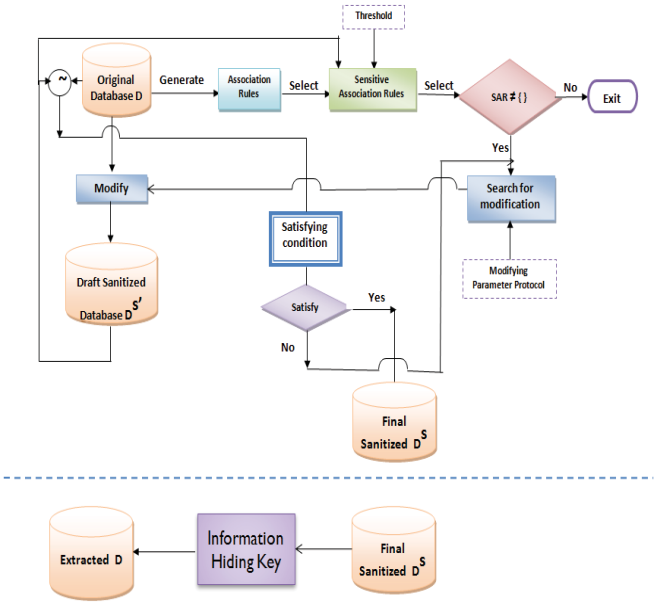

Fig. 1.2 Proposed Methodology

REFERENCES

[1] Agrawal, R., Imielinski, T., Swami, "A.: Mining Association Rules between Sets of Items in Large Databases," ACM SIGMOD International Conference on Management of Data (SIGMOD'93), Washington D.C., USA , pp. 207–216, May 1993.

[2] Geng L., Hamilton, H.J., "Interestingness Measures For Data Mining: A Survey," ACM Comput. Surv. (CSUR) 38(3), 9, 2006.

[3] McGarry, K, "A survey of Interestingness Measures for Knowledge Discovery," Knowl. Eng. Rev. 20(1), pp. 39–61, 2005.

[4] G. Dong and J. Li, "Interestingness of Discovered Association Rules in terms of Neighbourhood-Based Unexpectedness," Second Pacific-Asia Conference on Knowledge Discovery and Data Mining (PAKDD'98), pp. 72-86, 1998.

[5] Lallich, S., Teytaud, O., Prudhomme, E., "Association Rule Interestingness: Measure and Statistical Validation," Qual. Measur. Data Min. 43, pp. 251–276, 2006.

[6] A.A. Freitas, "On Rule Interestingness Measures," Elsevier, Knowledge-Based Systems 12, pp. 309–315,1999.

[7] Michael Steinbach, Pang-Ning Tan, Hui Xiong, and Vipin Kumar, "Objective Measures for Association Pattern Analysis," American Mathematical Society, pp. 1-21,2007.J. Clerk Maxwell, A Treatise on Electricity and Magnetism, 3rd ed., vol. 2. Oxford: Clarendon, 1892, pp.68-73.

[8] Pang-Ning Tan, Vipin Kumar, Jaideep Srivastava "Selecting the Right Objective Measure for Association Analysis," Elsevier Ltd, Information Systems 29, pp. 293–313, 2004.

[9] Dasseni E, Verykios VS, Elmagarmid AK, Bertino E., "Hiding Association Rules by Using Confidence and Support," In: Proceedings of the 4th International Workshop on Information Hiding, pp. 369–383, 2001.

[10] Oliveira SRM, Zaiane OR., "A Unified Framework for Protecting Sensitive Association Rules in Business Collaboration," Int J Bus Intell Data Mining, pp. 1:247–287, 2006.

[11] Verykios VS, Pontikakis ED, Theodoridis Y, Chang L., "Efficient Algorithms for Distortion and Blocking Techniques in Association Rule Hiding," Distributed Parallel Databases, pp. 22:85–104, 2007.

[12] Wu Y-H, Chiang C-M, Chen ALP., "Hiding Sensitive Association Rules with Limited Side Effects," IEEE Trans Knowledge Data Eng, pp. 19:29–42, 2007.

[13] Sun X, Yu PS., "A Border-Based Approach for Hiding Sensitive Frequent Itemsets," In: Proceedings of the Fifth IEEE International Conference on Data Mining, pp. 426–433, 2005.

[14] Sun X, Yu PS., "Hiding Sensitive Frequent Itemsets by A Border-Based Approach," JCSE, pp. 1:74–94, 2007.

[15] Moustakides GV, Verykios VS., "A Max-Min Approach for Hiding Frequent Itemsets," In: Proceedings of the Sixth IEEE International Conference on Data Mining—Workshops, pp. 502–506, 2006.

[16] Moustakides GV, Verykios VS., "A Maxmin Approach for Hiding Frequent Itemsets," Data Knowledge Eng, pp. 65:75–89, 2008.

[17] Menon S, Sarkar S, Mukherjee S., "Maximizing Accuracy of Shared Databases When Concealing Sensitive Patterns," Inf Syst Res, pp. 16:256–270, 2005.

[18] Menon S, Sarkar S., "Minimizing Information Loss and Preserving Privacy," Manage Sci, pp. 53:101–116, 2007.

[19] Gkoulalas-Divanis A, Verykios VS., "An Integer Programming Approach For Frequent Itemset Hiding," In:International Conference on Information and Knowledge Management, Proceedings, pp. 748–757, 2006,.

[20] Gkoulalas-Divanis A, Verykios VS., "Hiding Sensitive Knowledge Without Side Effects," Knowledge Inf Syst , pp. 20:263–299, 2009.

[21] Gkoulalas-Divanis A, Verykios VS., "Exact Knowledge Hiding Through Database Extension," IEEE Trans Knowledge Data Eng, pp. 21:699–713, 2009.

THE 18TH INTERNATIONAL SYMPOSIUM ON WIRELESS PERSONAL MULTIMEDIA COMMUNICATIONS
(WPMC-2015)
December 13-16, 2015, Hyderabad, India

Automatic Ration Distribution System-A Review

Swapnil R. Kurkute
Department of E &TC
SIEM Nasik, India

Dipak P. Patil
Department of E &TC
SIEM Nasik, India

Chetan Medhe
Department of E &TC
SIEM Nasik, India

Ashwini Kshirsagar
Department of E &TC
SIEM Nasik, India

Ashlesha Revgade
Department of E &TC
SIEM Nasik, India

***Abstract* – In the present days many illegal activities are taking place in ration shops, which are meant to distribute the commodities to the people who are in below the poverty line, as the distribution process is manually operated and due to which it consumes a lots of time. To overcome this problem we one can use RFID technology. In this paper RFID tags are introduced, The RFID cards are instead of ration cards, which consist of all the details about the card holder like family details, type of card and its validity etc. In this paper we are going to discuss different types of automatic ration distribution system implemented for the automatic ration distribution.**

***Keywords* – RFID, GSM module, Solenoid Control Circuits.**

I. INTRODUCTION

Government of India is issuing Ration Card to every Indian family for fulfilling their daily meal needs. Quantities of different food like rice, sugar, kerosene etc. is fixed for every month per families depending upon their income and total number of person in family. [1] Alongside this Government of India provides different facilities for ration distribution towards poor people but such facilities do not reach up to needy and poor people due to present distribution system. It is mandatory to have a valid ration card to buy the any materials from the ration shops. Presently the distribution process is following a distribution monthly pattern. There is a lacuna for monitoring the unused or balance food material at the distribution centre. And chances of misuse are more due to manual monitoring system. In this paper the solution to the problem of manual distribution system is studied and comparative analysis of three different ration distribution systems is presented. The automated system can be linked with government offices, shopkeeper and the ration card holder. The detailed review of few ration distribution systems which are implemented by using GSM, RFID and PIC Microcontroller is presented.

The remainder of the article is organized as follows. Section II presents the literature survey of different automatic ration distribution techniques and implementations. Automatic ration distribution methods such as automatic distribution system using PLC, automatic distribution system based on ARM7 and automatic distribution system using PIC controllers are described in Section III. Experimentation for automatic distribution system is illustrated in Section IV. Finally conclusions are drawn in Section V.

II .LITERATURE SURVEY

The most of people having the ration card to buy the materials from the ration shop first needs to submit the ration card. They will put the sign on ration card depend on the materials taken they will issue the materials through weighting system with help of human but there are two drawbacks weight of materials may be inaccurate due human mistakes and secondly if any card holder not buy the materials end of the months then shopkeeper buy to other and doing deception.

K. Balakarthik gives the idea under title "Cloud-Based Ration Card System using RFID and GSM Technology" [2]. This paper presents an efficient method for the user to buy the products in the ration shop by just flashing the card at the RFID reader. The user authentication is done by sending a random password text to the user mobile which has to be entered in a keypad. The purchase is validated by the employee only after the details are entered in a windows application which stores the user's personal and purchase information. This paper was published in vol.2, Issue 4, Apr 2013.

Rajesh C. Pingle, P. B. Borole gives the idea about automatic ration distribution system thorough his paper under title "Automatic Rationing for Public Distribution System (PDS) using RFID and GSM Module to Prevent Irregularities", In this automated system conventional ration card is replaced by smartcard in which all the details about users are provided including their AADHAR (social security) number which is used for user authentication. This prompted us to interface smart card reader (RFID Based) to the microcontroller (AT89C51) and PC via RS232 to develop such a system. Using such a system, Government would have all required control/monitoring over the transactions at ration shop. To involve government in the process we proposed connecting the system at ration shop to a central database (provided by government.) via GSM module (SIM900D) and RS232. Hence it is possible to prevent the corruption and irregularities at ration shop. This would bring the transparency in public distribution system and there will be a direct communication between people and Government through this. This paper was published in Volume issue by 2, pp.102-111, Mar 2013. [3]

S. Valarmathy, R. Ramani [4] the idea under title "Automatic Ration Material Distributions Based on GSM and RFID Technology", proposed to use RFID and GSM technology based Ration cards by showing the RFID tag into the RFID reader. Then the controller checks the customer codes and details of amounts in the card. After verification, these systems show the amount details. The customer need to entered the required materials by using the PC, after receiving the materials controller send the information to government office and customer through GSM technology. In this system microcontroller is used for executing the process. This paper was published in vol.2, Issue 4, Apr 2013.

The current public distribution system (PDS) involves corruptions and illegal activities of goods during manual ration distribution process. This is one of the widely controversial issues that grip the wrong information about utilization of material allotted for the card holders. Photo shows the existing Public Distribution System (PDS).

Fig.1.Manual ration distribution at Ration Shop

According to environmental conditions and government rule the prize of material varies and it is different for people according to type of ration card. Many times it is observed that the ration distributers do not disclose the rate chart with proper reference date according to which the rates are decided by government of India. Due to witch consumer are forced to pay as per rate decide by distributers. Figure shows one of the pick from ration shop who does not disclose the dated rate.

India's Public Distribution System (PDS) with a network of 4.78 Lakh Fair Price Shops (FPS) is perhaps the largest retail system in the world [6]. Major problems due to this system are the inefficiency in the targeting of benefits and the resulting leakage of subsidies food grain. The PDS system today supports over 40 Cr. Indians below the poverty line with monthly supply of subsidized food grains.

"55% of the public distribution system (PDS) food grain does not reach the intended people many drawbacks of PDS like PDS leakage, scale & quality issue, system transparency and accountability, grievance redressed mechanism are overcome by making automatic distribution system.

Fig.2. Undated Chart with prize of material in ration shop

III. Methods & Algorithms

The existing conventional ration distribution system has two basic issues one is renewing the ration card every year and corruption by the distributers or by the employees by doing malpractices like diverting food grains to open market to make profit. This can be overcome using automatic ration distribution techniques. The basic fundamental elements of such system are RFID and GSM Technology [3]. Global system for mobile communication (GSM) is a globally accepted standard for digital cellular communication. [2] The RFID reader continuously transmits a 125 kHz carrier signal using its antenna. Such system can be implemented with the different processor such as system using ARM7, PLC & PIC microcontroller.

The Public Distribution System (PDS) in the country facilitates the supply of food grains to the poor at a subsidized price. However, doubts have been raised about the efficacy and cost-effectiveness of the PDS, especially in the light of the growing food subsidy and food stocks. [7]

A. Automatic Ration distribution using ARM 7

In this system LPC2148 (ARM7) plays a vital role of actual processing unit. The 12 MHz crystal oscillator is used to provide the required clock signals to the ARM7. It takes input from power supply of 3.3V for its operation this generation introduced the thumb 16 bit Instruction set providing improved code density compared to previous design .it is versatile processor designed for mobile device and other low power electronics. In ARM7 they are combination of c and assembly language but in ARM7 architecture used more instruction set as compared PIC microcontroller

Disadvantages of ARM7

- Cost is high
- Complex instruction set

- Complicated to designs because number of pin is more

B. Automatic Ration distribution using PLC

An PLC (programmable logic controllers) is an industrial computer used to monitor inputs and outputs depending upon their decisions based on its program or logic (turn on/off) its outputs to automate a machine or process but PLC based automatic ration distribution system have some disadvantages.

Disadvantages of PLC based Automatic Ration distribution

- Difficulty with changes or replacements
- Difficulty in finding errors, requiring skilful work force
- When a problem occurs, hold-up time is indefinite, usually long.
- Cost of PLC is high.

C. Automatic Ration distribution using PIC controller

In PIC based automatic ration distribution system microcontroller plays a vital role. PIC microcontroller is a RISC based Architecture. It is low cost and is used for real time application [7]. The size and cost of the microcontroller are less as compare to PLC and ARM7. The 4 MHz crystal oscillator is used to provide the required clock signals.
As a comparative review study of different method we found that implementation automatic of ration distribution using PIC is best option as compare to others. The block diagram of an RFID and GSM Based Ration Distribution System Using PIC Microcontroller is shown in the Fig.3.This system consists of various parts such as RFID, GSM, microcontroller, motor driver, solenoid control circuits and PC.

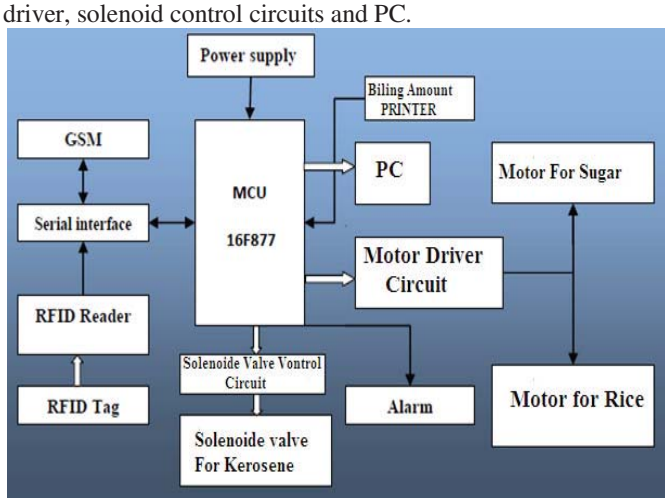

Fig.3. Block diagram of PIC based ADS

Radio-Frequency Identifications (RFID) is small electronic device that consist of a small chip with antenna. The chip is typically capable of carrying about 2,000 bytes of data. RFID has significant advantage of above the others devices, RFID device does not require to be found accurately relative to the scanner. The RFID devices will work within a 10 meter (up to 20 feet for high-frequency devices) of the scanner. The other device called RFID tag is used to read information about the customer through RFID reader. The GSM used to send the SMS to the customer as well as government authorized person for the verification of customer details, material prices, baling of materials and amount of material sanction by government according to type of ration card. Second important part of implementations is visual basic tool. Visual Basic is a tool that allows you to develop Windows (Graphic User Interface - GUI) applications. The applications have a familiar appearance to the user. GSM also plays an important role in this system GSM offers wide range of services like voice, data and internet access.[9] GSM is a low cost mobile communication used by the user to activate ON/OFF control remotely. [12] Fig.4 shows the basic flow of operation of Automatic Ration distribution using PIC controller

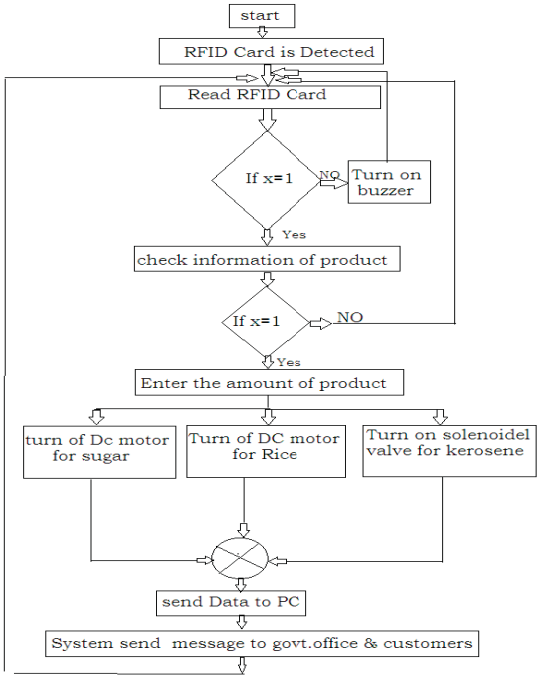

Fig.4. Flow chart of ARD System using PIC

1. Initialization of process
2. Check the tag, it is valid or not.
3. If the card is invalid card then display it as an invalid card by activating the buzzer.
4. Else if the card is valid then go to the next step.
5. Check the type of card either it is a yellow card or white card.
6: If the card detected by the reader is a yellow card then display the card holder's details on the PC screen.
7. Based on type of material chosen, the motor or solenoid valve is activated.
8. The load cell or level indicator is checked for proper quantity.

9. After collecting proper quantity material motor or solenoid is disabled.
10. GSM module will send the information in form of SMS to the user as well as PDS authority.
11. Current stock in the ration shop is displayed using PC

Advantages of PIC microcontroller

- Supports up to 32 Endpoints. (16 bidirectional)
- On-Chip USB Transceiver with On-Chip Voltage Regulator.
- Four Timer modules (Timer0 to Timer3).
- Dual Oscillator options allow microcontroller and USB Up to 2 Capture/Compare/PWM (CCP) modules
- High Performance RISC CPU Synchronous Serial Port (SSP) with SPI (Master mode) and I2C™ (Master/Slave)

IV. EXPERIMENTATION

From the above review study we wish to implement an system which is design to distribute ration material automatically so as to reduce man power as well as to control the corruption in ration distributions which is to be design should be capable of identification of users information and the amount of material allotted to him according to type of card issued by the government of India. Hardware includes the controlling unit, RFID tag, material storage, automatic billing system. Most important is GSM so as to provide legal data information to GOV of India.

V. EXPECTED RESULTS

The expected results from the system is the system should have a display which shows the following information on screen when RFID card is inserted by the customer.

User 1
Card no. 8975538244
Available material in ration shop
Rice- 100kg, Oil- 50litre, wheat-200kg
Allotted material: Rice- 5kg, Oil- 5 liter wheat-20kg

If the card is Invalided the system should shows the massage on screen as

User 2
Invalid ID

After purchasing the material allotted to the customer the massage should be deliver which includes details of bill and amount to be paid to distributor.

User 1
Card no. 8975538244
Allotted material: Rice- 5kg, Oil- 5 liter wheat-20kg
Material parches: Rice- 2kg, Oil- 2 liter, wheat-10kg
Delivered material-: 12:36pm, 05/10/2015
Total amount to be paid = Rs. 320
Balance Material: Rice- 3kg, Oil- 3 liter wheat-10kg
Available material in ration shop
Rice- 98kg, Oil- 48litre, wheat-190kg

Automatic bill should be generating after confirmation and the database should be auto update after every customer. Figure 5 shows the expected format of auto generated bill. The rates includes in bill are not actual but we expect the rate according to the governments norms. The note should be given at the end of bill which gives the idea about rate of material and related circler pass by government of India or by state government.

Distributor : 126589 **Date: 05/10/2015**

Sr. No	Material	Quantity	Rate	Amount
	Rice	2 Kg	30	60
2	Oil	2 lit	30	60
	Wheat	10 Kg	10	100
			Total	220

Note: Rates of all the materials are according to government circular it may change.

Fig.5. Expected format of auto generated bill at PSD

VI. CONCLUSION

In this paper comprehensive survey of present day automated ration distribution system is presented. The problem of existing manual ration distribution system with unusual and uneven distribution is addressed through appropriate and relevant literature. The outcome of the survey focuses on the significant issue for the sleaze in ration distribution and inappropriate or incorrect data of quantity arability at distribution center. The solution suggested in the survey for quantitive analysis of material at the distribution center. Another issue is up gradation of ration card is also discussed. As the up gradation process is quit complicated people use to continue the same card even if number of people on the card changes due to some reasons. Hence from the above study we conclude to have Automatic Ration Distribution System which overcomes all the issues stated earlier. System must be easy to install and should be economical in favor of GOV of India. It is further believed that the survey carried out in this paper can be beneficial for design and development of automatic distribution system for benefit of the needy people.

REFERENCES

[1] http://www.pdsportal.nic.in/main.aspx
[2] K.Balakarthik,"Closed-Based Ration Card System using RFID and GSM Technology,'' vol.2, Issue 4,Apr 2013
[3] Rajesh C. Pingle and P. B. Borole,"Automatic Rationing for Public Distribution System (PDS) using RFID and GSM Module to Prevent Irregularities", HCTL Open International Journal of TechnologyInnovations and Research, vol 2,pp.102-111,Mar 2013.
[4] S.Valarmathy, R.Ramani "Automatic Ration Material Distributions Based on GSM and RFID Technology" I.J. Intelligent Systems and Applications, 2013, 11, 47-54
[5] A. Parvathy, Venkata Rohit Raj, Venumadhav, Manikanta, "RFID Based Exam Hall Maintenance

System'', IJCA Special Issue on "Artificial Intelligence Techniques - Novel Approaches & Practical Applications" AIT, 2011

[6] S. Zope, Prof. Maruti Limkar, "RFID based Bill Generation and Payment through Mobile", International Journal of Computer Science and Network (IJCSN) Volume 1, Issue 3, June 2012 www.ijcsn.org ISSN 2277-5420

[7] S.Sukhumar,K.Gopinathan,S.Kalpanadevi, "Automatic Rationing System Using Embedded SystemTechnology", International Journal Of Innovative Research In Electrical, Electronics, Instrumentation And Control Engineering Vol. 1, Issue 8, November 2013

[8] MahammadShafi.,K.Munidhanalakshmi,"e RationShop An Automation Tool for Fair Price Shop under the Public Distribution System in the State of Andhra Pradesh",International Journal of ComputerApplications (0975 – 8887)

[9] Rubananth, T.Kavitha, "GSM based RFID approach to Automatic Street Lighting system", journal of theoretical and applied information technology 30th april 2012. Vol. 38 no.2, ISSN: 1992-8645.

[10] Rubananth, T.Kavitha, "GSM based RFID approach to Automatic Street Lighting system", journal of theoretical and applied information technology 30th april 2012. Vol. 38 no.2, ISSN: 1992-8645.

[11] RFID Journal, "Wall-mart begin RFID process changes ".http://www. rfidjournal.com/article/article view/1385.

[12] Hande Alemdar, CemErsoy, "Wireless sensor networks for healthcare, A survey, Computer Networks", The International Journal of Computer and Telecommunications Networking, ,pp 2688- 2710 2010.

THE 18TH INTERNATIONAL SYMPOSIUM ON WIRELESS PERSONAL MULTIMEDIA COMMUNICATIONS
(WPMC-2015)
December 13-16, 2015, Hyderabad, India

Dynamic Pathloss Model for Future Mobile Communication Networks

Ambuj Kumar [*1], *Albena Mihovska* [*2], *Ramjee Prasad* [*3]
[*]Center for TeleInFrastruktur (CTIF),
Department of Electronics Systems,
Aalborg University,
Aalborg, Denmark,
{[1]in_kumar, [2]alb, [3]Prasad}@es.aau.dk

Abstract*— Future mobile communication networks (MCNs) are expected to be more intelligent and proactive based on new capabilities that increase agility and performance. However, for any successful mobile network service, the dexterity in network deployment is a key factor. The efficiency of the network planning depends on how congruent the chosen path loss model and real propagation are. Various path loss models have been developed that predict the signal propagation in various morphological and climatic environments; however they consider only those physical parameters of the network environment that are essentially static. Therefore, once the signal level drops beyond the predicted values due to any variance in the environmental conditions, very crowded areas may not be catered well enough by the deployed network that had been designed with the static path loss model. This paper proposes an approach that incorporates the environmental dynamics factor in the propagation model for intelligent and proactively iterative networks.

Keywords—Dynamic Path Loss Model; Friis Path Loss Model; Okumura-Hata Model; COST 231 Hata Model; Intelligent Networks.

I. INTRODUCTION

In any Transmitter (T_x) and Receiver (R_x) system, the power received at the receiver end is subject to the environment composition through which the EM wave propagates from T_x to R_x. The role of any path loss model is to predict the expected values of the received signal level in absentia of T_x-R_x deployment. Therefore, such models are very crucial for network design and optimization strategies.

A. Crowd and Coverage

A lot of work has been done to manage the coverage in a dense crowded environment. Some incorporate the deployment of additional equipment such as the femto-cell in the high subscriber areas as discussed in [2] (whereas other propose serving the area though an alternative approach, such as unmanned aerial vehicles (UAVs)[3], [4], and [5]. Other research focuses on the services and applications that are crowd dependent by means of crowd sensing of the user density [6]. However, these solutions are subject to instantaneous conditions of the subscriber crowd.

B. Why gathering is problematic?

An accurate pathloss model can save loss of capital and operation expenses by avoiding over or under equipment requirements. However, existing path loss models do not consider the time-varying compositions of the propagation environment and presume the environmental characteristic as predominantly static. Therefore, in the cases when the time varying components deviates significantly, the network performance fails to perform optimally. One of the majorly occurring events is the crowd burst and accumulations.Previously published work [1], discussed the effect of the crowd on the capacity demand of the Area in Question (AiQ), which was termed as 'Place Time Capacity.' In this paper, we study the impact of the network coverage and the significance of the evolved equations. The discussion is not only limited to "human" density but any entity that may vary in numbers and can affect the electromagnetic wave (EMW) propagation.

This paper is structured as follows. Section II surveys the common current propagation models and reasons they cannot cater for the specifics of the dynamic environments. Section III proposes an accommodative path loss model. Section IV proposes a verification of the concept through an empirical approach (experiment).Section V concludes the paper.

II. STATIC PATHLOSS MODELS

For a network deployment, the size of cells and the proposed locations of the respective base stations (BSs) are predicted by path loss model. Figure 1 shows several propagation scenaria[7], [8]. The common parameters used in the path loss models associated with the propagation scenario in Figure 1, are summarized below:

- λ : Operating Carrier Wavelength of the signal,
- f : Operating Carrier frequency of the signal,
- T_x : Antenna of the Transmitting Module,
- R_x : Antenna of the Receiving Module,
- D : Distance between T_x and R_x,
- P_t : Power Transmitted from a T_x,
- P_r : Power Received by a R_x,
- G_t : Gain of T_x,
- G_r : Gain of R_x,
- h_t : Height of T_x with respect to ground,
- h_r :Height of R_x with respect to ground,
- PL(D):Total Path loss at a distance D from T_x

A. Definition of Path loss

Path loss [9], can be expressed in the terms of least square (LS) regression as in (2):

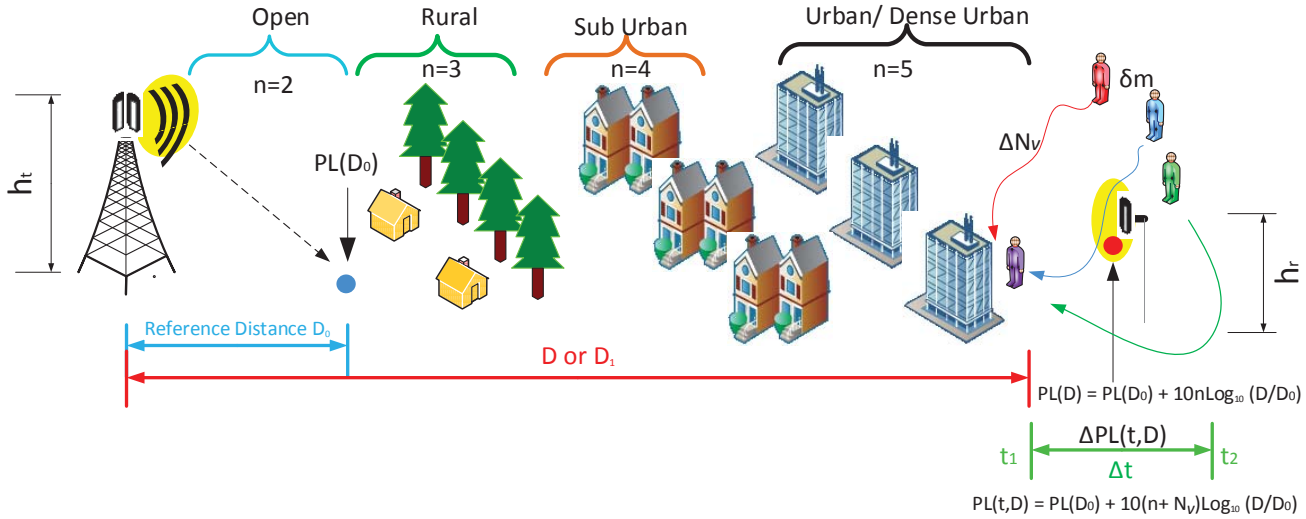

Figure 1: Factors Affecting Propagation of Signal.

$$PL(D) = PL(D_0) + 10n\log_{10}\left(\frac{D}{D_0}\right) \quad (1)$$

Here, D_0 is the reference point, which is usually obtained by empirically measuring the signal values at a unit distance from the transmitter (1km for outdoor large cell environment and 1m for indoor or pico cell environment). Usually, for a reference measurement, there is free space between Tx and Rx. The path loss exponent "n" represents the environment, in which the prediction needs to be done. For free space propagation medium between T_x and R_x, n=2 that gradually increases to 3 for flat rural, 3.5 for rolling rural, 4 for suburban, and, 4.5 for dense urban and so on.

B. Popular Pathloss Models

1) Friis Path Loss Model

The Friis path loss model [10] is the free space model that considers the loss of signal strength due to the distance between transmitter and receiver and the respective gains as mentioned below:

$$\frac{P_r}{P_t} = G_t G_r \left(\frac{\lambda}{4\pi D}\right)^2 \quad (2)$$

2) Okumura-Hata Model

Okumura- Hata [11] is one of the most rigorously used urban terrestrial propagation models for large-scale deployments:

$$P_r = P_t + G_t - 69.55 - 26.16\log_{10}(f) + 13.82\log_{10}\left(\frac{h_t}{h_0}\right)$$

$$+C(h_r) - \left[44.9 - 6.55\log_{10}\left(\frac{h_t}{h_0}\right)\right]\log_{10}\left(\frac{D}{D_0}\right) + A_\alpha$$

(3)

Where,

- A_α: Area adjustment factor,
- $C(h_r)$: Receiver antenna height correction factor,
- h_0 : BS antenna height (length) =1m,
- D_0 : Reference distance = 1 Km.
- L_{50} : Median path loss between Tx and Rx,
- L_{FS} : Free Space Path Loss,
- A_{mu}: Attenuation due to propagation in densely structured environment,
- H_{tu} : T_x antenna gain factor,
- H_{ru} : R_x antenna gain factor,

3) Cost-231Hata Model

The Cost-231 Hata Model [12]is given by (4) (in dB):

$$PL_{cost231} = 46.3 + 33.9\log_{10}(f) - 13.82\log_{10}(h_t) - aH$$

$$+\left(44.9 - 6.55\log_{10}(h_t)\right)\log_{10}(D) + C_E \quad (4)$$

Where, aH and C_E are environment dependent (Urban, rural, etc. values).

These models are inevitably static in nature and incorporate the morphological properties of the Area of Interest (AoI) such as vegetation, water bodies, concrete, etc. Therefore, these propagation models do not include environment dynamics.

Each model that has been developed is the result of the empirical fine tuning of the base path loss models through exhaustive On-field measurements. Hence, theoretically, a static user at a constant distance from the base station must experience the same signal strength for the entire duration till user resides at that distance. However, there are significant variations in the signal levels even though T_x and R_x are static in the Area of Interest (AoI).

The radio environments, investigated under macroscopic level may not show significant importance to this time-dependent variations and are comfortable in the static modeling of the radio propagation. However, future networks shall be extremely environmentally sensitive and dynamic environments may affect the performance significantly.

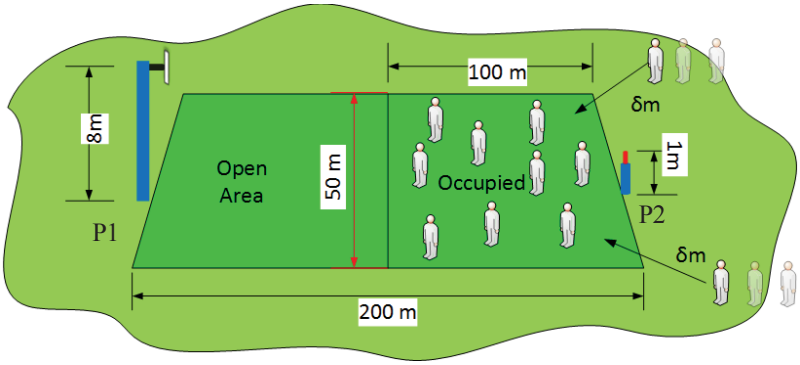

Figure 2: Study of People's Accumulation in Network Environment

Moreover, these networks will be more intelligent, and the near future may see those incorporating self-configuring properties regarding parameters and positions. In such cases, the static propagation model may not provide sufficient information for the intelligent networks to respond to the variation in the network environment and inclusion of the environmental dynamics in the path loss equation.

III. Dynamic Path Loss

Let us assume that a mobile user is static at a distance D_1 from the base station (see figure 1) which means that as per propagation model, the user at a distance D_1 must experience an unchangeable loss given by (see equation 1):

$$PL(D_1) = PL(D_0) + 10n\log_{10}\left(\frac{D_1}{D_0}\right) \quad (5)$$

Let us also assume that the user observes the signal level at the receiver end between the time intervals $[t_1, t_2]$. Incorporating this assumption in (5), we have:

$$\Delta PL(D_1)\Big|_{t_1}^{t_2} = \Delta PL(D_0)\Big|_{t_1}^{t_2} + \Delta 10n\log_{10}\left(\frac{D_1}{D_0}\right)\Big|_{t_1}^{t_2} \quad (6)$$

With all the relevant physical parameters static for this time interval, the terms in the right-hand side (RHS) of (6) reduce to zero, which means, $\Delta PL(D_0)\Big|_{t_1}^{t_2} = 0$, and,

$$\Delta 10n\log_{10}\left(\frac{D_1}{D_0}\right)\Big|_{t_1}^{t_2} = 0 \quad (7) \quad (8)$$

Therefore, from 6,7, and 8 we have:

$$\Delta PL(D_1)\Big|_{t_1}^{t_2} = 0 \quad (9)$$

This means that theoretically, the user does not experience any variation in the path loss. However, in reality this is not true, and the user does experience significant variations in the signal level which is not incorporated by the path loss models. Therefore, (9) is not true and the inequality can be written as:

$$\Delta PL(D_1)\Big|_{t_1}^{t_2} \neq 0 \quad (10)$$

In Figure 1, T_x and R_x are placed at positions P_1 and P_2, respectively, in the AoI. Rewriting equation (1) in non-logarithmic form, we have:

$$PL(D_1) = PL(D_0)\times\left(\frac{D_1}{D_0}\right)^n \quad (11)$$

Where, $PL(D_0)$ is the path loss measured at the reference distance D_0 from the T_x and is given by:

$$PL(D_0) = \left(\frac{4\pi D_0}{\lambda}\right)^2 \quad (12)$$

Where, D_1 is the distance of user receiver (R_x) from T_x (See figure 3). In case the environment between T_x and R_x is free space, the path loss exponent "n" takes an inevitable value n=2 and (11) reduces to:

$$PL(D_1) = \left(\frac{4\pi D_0}{\lambda}\right)^2 \times \left(\frac{D_1}{D_0}\right)^2 = \left(\frac{4\pi D_1}{\lambda}\right)^2 \quad (13)$$

Initially, there is a free space environment between T_x and R_x. However, the medium between them gradually densifies in small increments of "material" δm. This material may be of any kind such as metal, glass, concrete, or even humans. Now, let this small incremental material δm enters the AoI. Then, as discussed in Section I, the value of n must experience an increment from the static condition, even if it is a very small increment. Therefore, in such a case, the static path loss also experiences an increment and becomes a time dependent function. Therefore, from (11) and (12), this time dependent path loss behavior can be expressed as:

$$PL(D_1,t) = \left(\frac{4\pi D_0}{\lambda}\right)^2 \times \left(\frac{D_1}{D_0}\right)^{n+N_V(t,m)}$$

Or,
$$PL(D_1,t) = \left(\frac{4\pi D_0}{\lambda}\right)^2 \times \left(\frac{D_1}{D_0}\right)^{n} \times \left(\frac{D_1}{D_0}\right)^{N_V(t,m)} \quad (14)$$

Where, $\widehat{PL}(D_1,t)$ is the time dependent path loss at distance D_1 and at time t_1. The $N_v(t,m)$ is a variable defined as the Variant Path Loss Exponent and is the material and time dependent function that incorporates the time dependent variances in the network environment. The value of N_v at a timet defines the additional path loss due to amount of dynamic material at time t. As D_0, D_1, and n are constant, (14) can be written as:

$$PL(D_1,t) = K(n,D_0,D_1)\times\left(\frac{D_1}{D_0}\right)^{N_V(t,m)} \quad (15)$$

Where, $K = K(n,D_0,D_1) = \left(\frac{4\pi D_0}{\lambda}\right)^2 \times \left(\frac{D_1}{D_0}\right)^n$, (16)

and is time independent variable.

Therefore,

$$\frac{d}{dt}PL(D_1,t) = \frac{d}{dt}\left\{K\left(\frac{D_1}{D_0}\right)^{N_V(t,m)}\right\} \quad (17)$$

or, $$\frac{d}{dt}PL = K\frac{d}{dt}\left(\frac{D_1}{D_0}\right)^{N_V} \quad (18)$$

As we know that for any variable x and constant a,

$$\frac{d}{dx}a^x = a^x \log_e(a) \quad (19)$$

From (18) and (19) we have:

$$\frac{d}{dt}PL = \left[K\left\{\log_e\left(\frac{D_1}{D_0}\right)\right\}\left(\frac{D_1}{D_0}\right)^{N_V}\right]\frac{d}{dt}(N_v)$$

or, $$\frac{d}{dt}PL = \left[\dot{K}\left(\frac{D_1}{D_0}\right)^{N_V}\right]\frac{d}{dt}(N_v) \quad (20)$$

Where, $\dot{K} = K\log_e\left(\frac{D_1}{D_0}\right)$ (21)

As discussed before, N_v is time and material dependent variable. Therefore,

$$\frac{d}{dt}(N_v) = B(m)\frac{d}{dt}(m) \quad (22)$$

Where, B(m) is the Base Variance that depends on the type and concentration of the material. The term $\frac{d}{dt}(m)$ defines the rate at which the material densifies or rarifies in the AoI. Substituting (22) in (20), we have:

$$\frac{d}{dt}PL(D_1,t) = \dot{K}\left(\frac{D_1}{D_0}\right)^{N_V} B(m)\frac{d}{dt}(m) = \dot{K}\left(\frac{D_1}{D_0}\right)^{N_V} B(m)m' \quad (23)$$

In the case when the incremental variation in material density is due to the movement of the material entities, the term m' represents velocity $v(t)$ of the incremental entity times the volume density of the material defined as ρ_m. Therefore, (23) can be rewritten as:

$$PL'(D_1,t) = \dot{K}\left(\frac{D_1}{D_0}\right)^{N_V} B(m)\rho_m v(t) \Rightarrow PL' = \dot{K}\left(\frac{D_1}{D_0}\right)^{N_V} B(m)\rho_m v \quad (24)$$

Therefore, in the case when the material density is uniform, and the properties are not time dependent, $\widehat{PL'}$ will be a constant gradient and drop in the received signal level with be linear in the logarithmic domain.

IV. EMPIRICAL APPROACH

Rewriting (14) in dB format, we have:

$$PL_{dB}(D_1,t) = 10\log_{10}\left\{\left(\frac{4\pi D_0}{\lambda}\right)^2 \times \left(\frac{D_1}{D_0}\right)^{n+N_V(t,m)}\right\}$$

Or simply,

$$PL_{dB} = 10\log_{10}\left(\frac{4\pi D_0}{\lambda}\right)^2 + 10\log_{10}\left\{\left(\frac{D_1}{D_0}\right)^{n+N_V(t,m)}\right\} \quad (25)$$

From (12) and (25), we have:

$$PL_{dB} = PL_{dB}(D_0) + 10(n + N_v(t,m))\log_{10}\left(\frac{D_1}{D_0}\right) \quad (26)$$

Where, $PL_{dB}(D_0)$ is a dB representation of (9). Hence,

$$PL_{dB} = PL_{dB}(D_0) + 10n\log_{10}\left(\frac{D_1}{D_0}\right) + 10N_v(t,m))\log_{10}\left(\frac{D_1}{D_0}\right) \quad (27)$$

As we know from (5) that:

$$PL(D_1) = PL(D_0) + 10n\log_{10}\left(\frac{D_1}{D_0}\right)$$

Therefore, from (5) and (27) we have:

$$PL_{dB} = PL_{dB}(D_1) + 10N_v\log_{10}\left(\frac{D_1}{D_0}\right) \quad (28)$$

The equation (28) is a standard line equation known as:

$$y = gx + C \quad (29)$$

The equation 28 means that in logarithmic scale, the received signal will experience a linear drop when there is an increment in the density of the material with constant velocity, and material property does not vary with time and space keeping $B(m)\rho_m$ as constant.

To verify the mathematical model in (28), we conducted an experiment as shown in Figure 2. We selected an area of 200X100 meters in dimension from a large open ground (in Goa, India). Points P_1 and P_2 were chosen for placing T_x and R_x respectively (see figure 2). For other parameters related to the setup, please see figure 2. Firstly, the measurement was taken as free space and then people were allowed to enter in the one-half of the area. People entered the area in steps of 10,50, 100, 200, …, 1000 and signal measurements at P_2 were recorded for a duration of 20 minutes for each step. To avoid the interference from other mobile and point-to- point services, we selected a band of 1400MHz that is currently not being used for terrestrial mobile services in the selected rural areas of India. All power values are in [dB], frequencies are in [MHz] and distances are given in [m].

Figure 3 shows the significant and consecutive discrete drops in the received signal level from the receiver placed at P_1. This drop is observed for the entire duration (20 minutes or 1200 seconds) of the measurement for each set of groups of people, which means that this drop is not because of the instantaneous disturbances but due to the people gathering in the area between the T_x and R_x path.

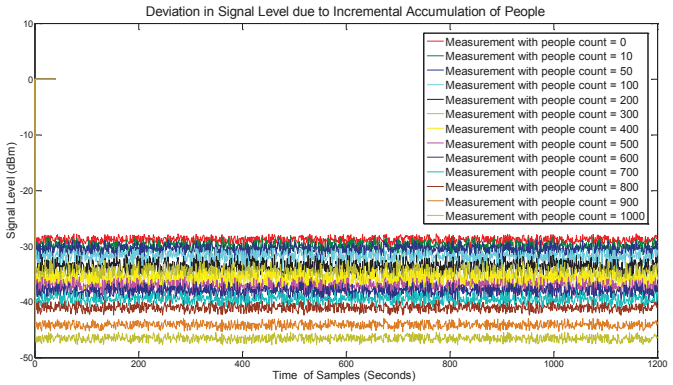

Figure 3: Received Signal Drop v/s Time (Per People Density)

Figure 4: Received Signal Drop v/s People Density

During the measurements, people were allowed to fill the path as evenly as possible by roaming in the area. Out of 1200 received signal values recorded for each group, we randomly selected measurement values at the 100th second for each group to create a data set of signal level versus people's accumulation. This data set is plotted as shown in Figure 4.Itcan be clearly seen that the drop in observed signal levels follows the regression line y=78x-29. Similar observations were made for other data sets at different times. This empirical observation also corresponds to the equation that we have derived in (29).We see that data points deviate from the regression line. This is due to other factors playing during the measurements such as Fresnel Radius, multipath losses and ground reflections, etc. that are not incorporated in the basic path loss model for the ease of representation. We also bring this to notice that the people's density was not high enough to make δm infinitesimally small so that the impact of granularity can be avoided.

V. CONCLUSIONS

In this paper, we have discussed the path loss variability due to non-static elements, (i.e., materials), entering the path between the T_x and R_x. We incorporated this time-dependent variation in the path loss model as in equation (1) equation though some assumptions and then mathematical derivation. We have introduced a Variant Path Loss Exponent (N_v) in the PL equation as in equation (1) that accommodates these instantaneous variations. Lastly, we verified this derived equation through an empirical observation that was made by signal measurements carried out when people gather in an area from 0 to 1000 in certain defined steps.

VI. FUTURE WORK

The variable path loss model $\widehat{PL}(D_1, t)$which is derived in this paper will be very useful for the intelligent networks performing in extreme dense net environments. The variability factor Nv can be used to "train" the "intelligent networks" to behave with the varying propagation environments. We have discussed the impact of people accumulation on capacity dimensioning in[1], the proposed model incorporates coverage aspect of the dynamic network environment. Further, this model has huge scope for further studies and its suitability to the intelligent network environment. This concept can be useful in the analysis of the margins for senstivity of the radio equipments that will be designed to serve the extremely congested and dynamic network conditions.

REFERENCES

[1] A. Kumar, P. L. Mehta, and R. Prasad, "Place Time Capacity- A novel concept for defining challenges in 5G networks and beyond in India," in *2014 IEEE Global Conference on Wireless Computing and Networking (GCWCN)*, 2014, pp. 278–282.

[2] O. Arafat, M. A. Gregory, and A. U. Ahmed, "Cluster-based femtocell efficiency evaluation," in *Telecommunication Networks and Applications Conference (ATNAC), 2014 Australasian*, 2014, pp. 99–104.

[3] C. Cerasoli, "An Analysis of Unmanned Airborne Vehicle Relay Coverage in Urban Environments," in *IEEE Military Communications Conference, 2007. MILCOM 2007*, 2007, pp. 1–7.

[4] Y. Chen, H. Zhang, and M. Xu, "The coverage problem in UAV network: A survey," in *2014 International Conference on Computing, Communication and Networking Technologies (ICCCNT)*, 2014, pp. 1–5.

[5] H. Chen and K. He, "U-turn optimization for three-dimensional area coverage of UAV," in *2015 IEEE International Conference on Mechatronics and Automation (ICMA)*, 2015, pp. 98–103.

[6] G. Cardone, A. Cirri, A. Corradi, L. Foschini, R. Ianniello, and R. Montanari, "Crowdsensing in Urban Areas for City-Scale Mass Gathering Management: Geofencing and Activity Recognition," *IEEE Sens. J.*, vol. 14, no. 12, pp. 4185–4195, Dec. 2014.

[7] V. S. Abhayawardhana, I. J. Wassell, D. Crosby, M. P. Sellars, and M. G. Brown, "Comparison of empirical propagation path loss models for fixed wireless access systems," in *Vehicular Technology Conference, 2005. VTC 2005-Spring. 2005 IEEE 61st*, 2005, vol. 1, pp. 73–77 Vol. 1.

[8] M. Stoffers and G. Riley, "Comparing the ns-3 Propagation Models," in *2012 IEEE 20th International Symposium on Modeling, Analysis Simulation of Computer and Telecommunication Systems (MASCOTS)*, 2012, pp. 61–67.

[9] C. C. Pu, P. C. Ooi, B. G. Lee, and W.-Y. Chung, "Analysis of path loss exponent error in ranging and localization of wireless sensor network," in *International Conference on Frontiers of Communications, Networks and Applications (ICFCNA 2014 - Malaysia)*, 2014, pp. 1–6.

[10]X. Zhang and J. G. Andrews, "Downlink Cellular Network Analysis With Multi-Slope Path Loss Models," *IEEE Trans. Commun.*, vol. 63, no. 5, pp. 1881–1894, 2015.

[11]Z. Nadir, "Empirical path loss characterization for Oman," in *Computing, Communications and Applications Conference (ComComAp), 2012*, 2012, pp. 133–137.

[12]P. Mogensen and J. Wigard, "COST Action 231: Digital Mobile Radio Towards Future Generation System, Final Report.," 1999.

"IoT" based Smart Village

An Indigenous step towards 'Digital India'

Madhukant Patel (MD, Reve Automation LLP, Former Scientist Engineer, ISRO, PhD Scholar UPES, Dehradun)

Piyush Yadav (Director, Green Cloud iSoft P. Ltd., MBA from University of St. Gallen, Switzerland)

Abstract:
With a strong vision and drive of Digital India, the first deserving audience to target is Rural India. From Darwin's day, mankind has seen the evolutions and revolutions. Each time, society has seen the changes which are affecting the way society functions. With advancement of technology and political will, the transformation is in rapid momentum and going to achieve much different milestones in terms of livelihood of rural India. The rural world has seen the dynamism of changes through means of scientific & technological revolutions, economical revaluations, green revolutions, educational effects and many more. At present, the world is experiencing the revolution in telecommunication, data communication, cloud computing and smart mobile devices. This dynamism has changed the face of urban and rural life all across. Urban areas seem to be more inclined to accept and adopt Information and Communication Technology due to advantages of literacy and better infrastructure as compared to rural areas. Such suitable circumstances of urban scenes throws great measure of achievement of this innovation as unmistakable as savvy urban areas and better occupation of residing human beings. But the problems, consequences and opportunities in urban territories are distinctive for successful use of Information and Communication Technology for reasonable improvement of provincial masses. The present research on 'rural echo system' done by our group companies is focused into the frame work or backbone for smart villages and smart cities using IoT (Internet of Things) for all segments of life; may it be comfort, safety, energy efficiency or monitoring control of functions connected with villages. The concept of "Smart Village" is to connect every individual and homes with each other and to connect them with their farms, dairies, APMCs, trade links, dispensaries, schools and governance in general. The framework will also support and spot neighbourhood business opportunities, enhancing wellbeing and welfare, improving just engagement general upgrade of rustic town inhabitants. The " Smart Village " concept aims to realize its goal through providing policymakers with insightful, bottom–up analyses of the challenges of rural development. The presentation will be accompanying live demonstration of "IoT enabled rural ecosystem".

Keywords: ***IoT (Internet of Things), IoE (Internet of Everything), Rural Eco-cycle, Smart framework, Smart sensors, Informatics, Access points, Smart HUB, Cloud Computing, APMCs***

Introduction:
As per our understanding, Internet is a network of networks that consists of millions of private, public, academic, research, business, and government networks, of local to global scope, that are linked by a broad array of electronic, wireless and wired networking technologies. Internet of Things is making an open and comprehensive network of intelligent objects that have the capacity to auto–organize, share information, data and resources, reacting and acting in face of situations and changes in the environment. Internet of Things is the latest advancement in Information and Communication Technologies, providing global connectivity and management of sensors, actuators, devices, machines, users and informatics. Things are also often interchanged with the word "Objects". IoT can be defined as "things belonging to the Internet" to supply and access all of real-world information. IoT is the biggest promise of the technology today, but still lacking a novel mechanism, which can be perceived through the lenses of Internet, things and semantic vision. Internet of things is widening to evolve as Internet of Everything (IoE).

The Internet carries an extensive range of information resources and services, IoT is the convergence of Internet with Smart sensor and Smart objects. Realizing the vision of sustainable smart city applications requires enhancing IoT technologies with new ways that will enable things and objects to become more reliable, more resilient, more autonomous and smarter. The Internet is a powerful global communication medium that provides instantaneous information across geographical, cultural, language, and time spheres. 'Thing' can be defined as an entity, an idea, a quality perceived, or thought to have its own existence in the world.

The IoT is a technology and their integration is to be implemented in Indian villages to achieve near to ideal ecosystem of a typical Indian village.

Ecosystem of typical Indian village
From ancient days, Indian villages have an 'autonomous' and self-governing system. The 'Panchayat raj' was precisely defined on this concept.

Following are the key factors to form typical Indian smart village ecosystem:

1. Education
   a. Schooling: Teachers training, quality delivery to students, attendance, effective and real-time feedback mechanism, providing general awareness about opportunities and challenges to students, making aware about local, national and international dynamism, informant of effective & efficient evaluation system, continuing motivations are few of the parameters where the present system is lacking. e-Learning, distance-learning, lab and hands-on methodology through physical and virtual laboratories, etc. are supported by smart sensors and smart framework. Adult education system can be easily augmented on the smart framework.
   b. Vocational: In recent past, the rural people (illiterate and semi-literates) have shown good amount of innovations. Through digital media and smart framework, variety of vocational trainings like crafting, carpentry, poetry, goldsmith, fabric based art, singing, dancing etc can be easily taught using modern teaching aids. Providing knowledge on trade and business aspects can motivate them and ultimately lead them to sustainable self-employment by connecting Government trade linked system.

2. Health and Medical Emergencies:

Regular and emergency health support system is lacking in villages. Using smart sensors and smart framework, each village person can be linked with primary health centres as well as 24x7 medical assistance and monitoring can be done by expert doctors working in cities. The system also supports online prescriptions and provides alerts for regular health check-up awareness, camps and follow-up from digital data (data mining).

3. Agriculture and Farming:

The biggest challenge for Indian villages is to automate agriculture, farming, irrigation, watering of plants, establishing green houses and harvesting systems. The smart system can monitor life of crops and qualifies agro products that have link with APMCs.

4. Animal Husbandry:

Animal husbandry is one of the resource to create economic reforms of village and provides regular health check-up of animals and creates eco-system in production from animal related products.

5. Rural Transport:

The smart transport is digitally linked with private and government transport service providers through e-ticketing window and booth. The system has IoT displays to show timing and schedule of local transport vehicles.

6. Governance (PUNCHAYAT):

The system has facility to lodge online complaints & grievances and is able to resolve with digital link with state & central government reporting system. Whole lot of forms and certificates may be requested through smart devices through IoT infrastructure.

7. Sahakari Mandali Reforms:

All Sahakari Mandalis have Internet working facility and are able to exchange and broadcast information. The system itself handles conferences and trainings. The economic reforms are possible to provide online trading for products. Through smart village tools and means, Sahakari can link each farmers/ members through infomatics; enabling people with handy information and alerts from time to time.

8. Energy:

The power generation and distribution network can be created for domestic, farms, hospitals, dairies and other amenities. Using smart framework and smart sensors, people can save/ optimise the energy usage by minimising wastages.

9. Eco-enterprise and self-employment:

By providing data and support, the rural people can be motivated for self-employment. The system can also help the individual to form a cluster and strengthen them to compete and venture into larger territories.

10. Natural Calamities:

The system advances to exchange and broadcast information for floods, earthquakes, fires and others to save humans and their belongings.

Literature survey:
Internet of Things and Smart Things has been going on for more than a decade and reaches back to original dream of ubiquitous computing. Recently popularized the idea of Smart Objects and the IoT, Smart Things is another paradigm shift in IT world. Smart Things are the things that are having embedded smartness or intelligence, identification, automation, Monitoring and controlling calibre. Smart Things are assisting human life a lot, nowadays without their applications life is becoming cumbersome. Systematically on Internet, Things, and then explores on Internet of Things and finally Smart Things from researchers', and corporate's Perspective. This things forward towards the Smart Things and its applications. This in turn would help the new researchers, who want to do research in this IoT

domain [1].

For the smart village we can use the existing idea of the smart city. As an example, the existing smart city application of heat and energy management. In a world of multi-stakeholder information and assets provision on top of millions of real-time interacting and communicating things, systems based on IoT technologies aim at exploiting these assets in a resilient and sustainable way allowing them to reach their full potential. The heat management aims to utilizing different resources (such as heat and electricity meters) in order to optimize use of energy in commercial and residential areas. The energy management for the cruise control of public transportation, and aims at utilizing different resources (such as environmental and traffic Sensors) in order to provide driving recommendations that aim at eco efficiency [2].

For the smart villages creating perfect business environment where work meets pleasure, using the latest technology "Internet of Things" in operational support and infrastructure, Internet of Things, in short IoT, can impact Governance. Internet of Things and Smart Services will change Society. SMART VILLAGE will become the hub of business community and the economic growth. The Internet of Things is driven by an exponential expansion of the Internet through the inclusion of physical objects combined with an ability to provide smarter services to the environment as more data becomes available [3].

Smart Villages are the need of the hour as development is needed for both rural and urban areas for better livelihood and Information technology will offer an effective solution. There are successful technologies available, which have been implemented in urban areas. There is tremendous pressure on urban landscapes due to migration of rural people for livelihood. Smart Villages will not only reduce this migration but also irrigate the population flow from urban to rural area. Smart village concept will have potential to uplift the grass-root level of the country, hence adding feather in the overall development of India [4].

Failure to utilize Information Technology tools for rural development is because of lack of strategy, unfocused planning, monitoring and execution of the activities. All these activities need to be addressed based on the varying rural situations. A specially designed suitable framework for rural areas on the grounds of Science, Technology, Engineering, Regulations and Management will play important role to build next generation smart villages. Each village is a unique example and having diverse set of problems and situations. It may be difficult to implement the same model of village development for all the villages. To address this complex problem, Public Private Partnership (PPP) may play key role for developing smart villages. Benefits of the smart village efforts are foreseen to be tremendous.

Problem Formulation:
To develop an ideal ecosystem in Indian village to provide services, alerts and interactive data exchanges & analytics based on the query messages to satisfy all needs of the citizens in various dimensions almost automatically; with end objective to upliftment of economy, education, healthcare, safety, lifestyle etc. and eventually to help rural society as part of a Digital India.

Proposed work:
The proposed work leading to development of the ideal ecosystem requires an implementation of homogeneous ICT infrastructure to provide access to data and services through pervasive devices like smart mobile phones, smart sensors, and smart framework. The citizens can get all variety of services as well as can easily control & monitor processes and devices. Design and Smart framework and smart sensors with generic protocol and interfaces are the key challenges. These will provide better safety, lifestyle, resource and energy management.
According to Cisco, IMB etc., more than 1 million devices are connected to Internet. Till today, due to limited number of devices connected to Internet, the need for middleware, embedded on Linux OS, which was not prominently there, but as number of IoT Devices increases requirement of standardization as well as middleware has increased.

The proposed middleware with following context will provide strong backbone and complete Eco cycle for a smart village:

1. Kernel which can connect different IoT devices operating on different protocols.
2. Modern applications layer like smart mobile phones which allows installations of third party applications.
3. Middleware developed on open source software resides on local HUB and interacts with shell and mobile devices.
4. Shell layer of OS resides on cloud, and does the computational work.

The Framework can be used to form a complete eco-system integrating people, process and devices. This can help to realize smart city, smart village and smart cluster etc. which helps to implement & invent on modular based framework creating the values for smart villages with complete ecosystem.

Smart Sensors
Numerous electronic devices generate huge amount of data, which are of immense importance and can be used for more than one purpose and more than one occasions at more than one locations. At present, they are in isolation and do not follow systematic protocol nor they are communicative with 'world'. These may be safety sensors at home, devices for healthcare, soil sensors, cattle tags, health bands, energy monitoring &

distribution control devices, climatic sensors, CCTV systems, entertainment systems like TV, Music system, home theatre, Lights, ACs, Fans, and many more. The present devices are operating at their respective locations. The data/ log generated are not stored in a central data repository because of lack of network integration and communication capabilities. If a proper framework satisfies this need/requirement, is expected to facilitate data to be stored in a database as well as processing of stored data to activate certain critical processes by issuing commands. This implementation will not only automate but it will be intelligent/ smart system. The proposed framework and smart sensors developed satisfies the stated need/requirements to implement smart system. The prototype provides a flexibility of developing services to be embedded to the installed middleware by simply writing a script, which is added to the library of the services. This is an innovative feature of the middleware.
The IoT enables the possibility of information discovery about a tagged object or a tagged person by browsing an internet address or database entry that corresponds to a particular active device with sensing/ actuating capability. It is a media for information exchange between the physical world to a digital/cyber world. With available wireless communication, the wireless node entities can increase their effective usage with virtue of big data, extensive analytics and informatics.

Proposed indigenous smart sensors shall 'talk' to cloud with a very generic protocol. Smart sensors form a WSN (Wireless Sensor Network) using wireless links like RF, WiFi, IR, Bluetooth, which are compatible with devices like TV, air conditioners, lights, fan, safety sensors, curtains, pumps, and other appliances; while, the cloud connectivity is achieved through smart hub. These sensors and actuators will be/are Internet compatible.

This requires device connectivity through a single hardware hub which integrates all the devices, get status of the devices also receive data from various implanted wireless sensors in the integrated network. The received data from the sensors is processed by processors in the hub and the scripts activating the services comes into action to automate the process, control the process and devices and provides intended services to the end users of the system.

Methodology
Figure-1 shows the architecture of the system topology. Server on the cloud is the heart of the system where computational work and datamining is done. Besides managing the devices, the proposed framework supports augmented reality, artificial intelligence, housekeeping and administrative support.
At individual home or office, TV screen is connected with smart Hub which links cloud, mobile devices, access points and devices virtually. The devices are configured and managed through Hub, while user interactions are done through air mouse via TV or mobile devices. The end devices (like smart sensors, lights, fans, curtains, doors, electrical gadgets etc.) are controlled through user commands, cloud events or personal profiles.

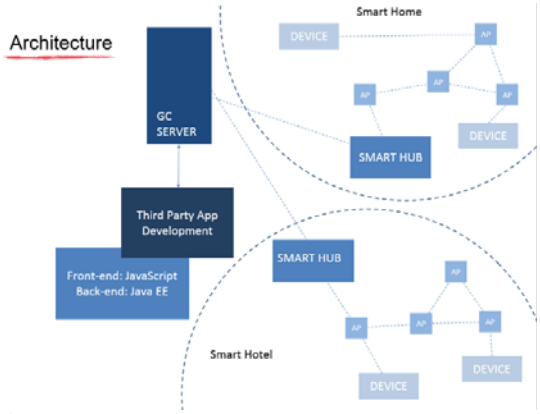

Figure-1

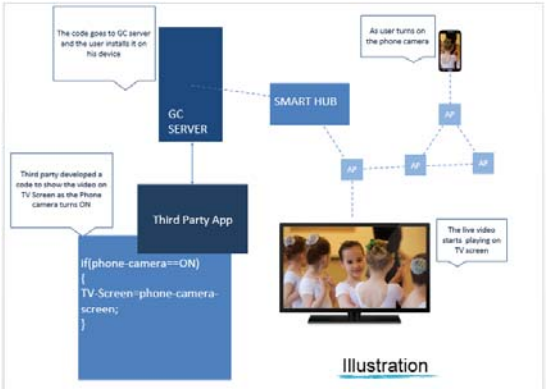

Figure-2

As shown in Figure-2, devices communicate through access points (AP). The APs are connected to HUB via WiFi and uses RF, Bluetooth, IR etc for connectivity with devices. While configuring new devices, the unknown (which is not in the local device library) 'remotes' are taught through APs.
The example of third party Apps is also highlighted in Figure-2. The simple script can be written by any individual to create 'profile' of the choice, which can be shared to other users seamlessly.

Conclusion

A complete study of village ecosystems has been done and reviewed meticulously to understand the requirements and needs of people and society for integration of smart sensor technology and framework to become part of their routine life.

The IoT based smart sensor technology can be implemented for various utilities in village to make digitally smart villages in education, healthcare, agriculture & farming, transport, e-governance, craft, local art etc. to realise better life and economic reforms for villages.

The proposed work is implemented as smart home in which all the devices are connected and control lighting, fans, window curtains for their switching ON/OFF through TV, mobile devices, or through profiles. This implantation serves as template for building smart hospital, smart schooling system, smart governance, and eventually, to form a smart village ecosystem.

References:

[1] SomayyaMadakam "Internet of Things: Smart Things",International Journal of Future Computer and Communication, Vol. 4, No. 4, August 2015

[2] DimosthenisKyriazis, Theodora Varvarigou,Andrea Rossi,Daniel White,Joshua Cooper,Sustainable smart city IoT applications: Heat and electricity management & Eco-conscious cruise control for publictransportation, IEEE.

[**3**] Jenne. Hanumanthu, Dr. A. Srinivas, Smart Grama's with Internet of Things (IoT),International journal of Research in Engineering,Science and technology,vol1,No-2,2015

[4] Pinak Ranade, Sunil Londhe ,Asima Mishra, SMART VILLAGES THROUGHINFORMATION TECHNOLOGY – NEED OFEMERGING INDIA, *International Journal of Information Technology (IIJIT), Volume 3, Issue 7, July 2015*

RURBANISATION OF INDIA
The Slow Change of Rural India, and ICT's Role and Opportunities

Bipin Pradeep Kumar, Gaia Smart Cities.

Abstract: *India has traditionally been a country of villages. Urban India had been but a shadow of its rural counterpart. But this is changing since late. There has been a slow transition under play in this traditional setting, and a more accelerated one expected. This transition brings with it its own needs and challenges in areas like public services, housing, basic utilities, marketplaces, education, health and infrastructure; services that allow societies to function and even thrive. Bringing to fore the slow upheaval and its possible impact, the role played by ICT and the new services required in this transforming landscape are areas addressed (using 2 cases of ICT in rural Karnataka as examples) in this paper.*

1. Introduction

Rurbanisation by its very approach and feature is a phenomenon that presents its effect on rural patterns. In its earliest recorded versions – Kayser, 1990[1] and Mahajan, 2010[2] it is defined as: "a process of altering rural forms with pre-selected urban patterns and lifestyles, which creates new genetically altered rurban forms". It has been adapted more recently by the Indian government as 'Villages with a rural soul but an urban feel with all urban amenities'[3]. Nonetheless, rurbanisation is a process of rural change.

The 2011 census of India classifies all places with a municipality, corporation or cantonment board and a notified town area committee, etc. as an urban unit, Town or Statutory Town. All other units of living that satisfy the following criteria are classified as Census Towns: a minimum population of 5,000; at least 75% of the male workers engaged in non-agricultural pursuits; and a minimum density of 400 people/sq. km. As such, there are 7,935 Towns, 4041 Statutory Towns and 3894 Census Towns in India[4]. All other areas that are not categorized as urban are considered as rural, of which it lists 6,40,867 villages in India

On one hand it is within this arena of urban and rural India that there is the migration from rural to urban and expansion and growth of new urban agglomerations, just as there is the evolution of rural India itself. On the other hand, there is the transformation led by the explosion of Information and Communication Technologies (ICT) and its associated services. ICT is changing the way India – both rural and urban works, socializes, lives and even draws its aspirations from and this affects rural India too. This transition and transformation, and what it can facilitate in the form of new services, more transparent operations, easier access to healthcare and education, an open democracy, visible environmental impacts, effective and productive labour and social inclusion have the potential to enable Indians to live a better quality of life.

The first section deals with the transition arena, the changes that are happening to rural India. With the figures and facts from secondary studies presented, it provides a different lens to look through and highlights the impact. The subsequent section deals with the transformational power of ICT, through networks of communication and information in rural and semi urban India and its importance. The last section, through primary research deals with a few ICT solutions in use by this new rurban populace.

2. Rurban transition

With change as the underlying theme, we can classify the urban-rural shift underplay into three broad areas -

[1] Kayser B. The rural renaissance. Sociology of campaigns in the western world. Armand Colin, Paris, 1990
[2] http://sdmahajan.tripod.com/rurbanization.htm
[3] http://vibrantgujarat.com/Portal/Event_Images/Attachment/79/3_1_Panel-Discussion-Rurbanization.pdf
[4] http://www.censusindia.gov.in/2011-prov-results/paper2/data_files/india/Rural_Urban_2011.pdf

the migration to and growth of new urban agglomerations, the evolution of rural India and the rise in Semi Urban India. Though the migration cannot strictly be called rurbanisation, it is a large rural change with considerable momentum. Combining this with the simple fact that there will be rural populace in a new urban environment, there could be large swathes of people requiring ICT solutions and services tailored to their needs. Similarly the change within rural India itself merits its own needs and solutions, just as the rise in semi urban India merits its own. The sections below illustrate why these are segments we need to address:

Migration to and growth of Urban India:

In 2011 India had a population of 68.84% living in rural India and the remaining 31.16% living in an urban setting. This is expected to reduce to 60% in villages with urbanization at 40% in 2030. Though, in some states like Karnataka, the averages are already different with urban population in 2011 estimated at 38% and the balance 62% in rural areas[5].

The population of India is expected to be 1470 million in 2030; an increase of almost 210 million in urban, and 48 million in its rural areas. The increase of 210 million people could be a combination of migration and organic growth. What isn't obvious in this same vein and probably disturbing to the burgeoning urban populace is the migration path.

Typically migration occurs to the top ten cities of India. These are Mumbai, Delhi, Bengaluru, Hyderabad, Chennai, Kolkata, Ahmedabad, Pune, Surat and Jaipur[6]. These top 10 cities, just 0.1% of India's land mass in 2011 had 8% of India's population and contributed about 15% of the GDP[7]. There is an absence of reliable disaggregated growth data for all these cities, but if we were to distribute a major portion of the 210 million among these 10, in sheer number terms, it would be an understatement to call it challenging. Even if we were to distribute a major portion of 210 million among the top 100 cities of India keeping the current population as a factor it would still imply most major cities doubling in size or growing by almost 50%. This increase puts a significant strain on the already constrained and limited resources and infrastructure.

At a national level it is a 35.9% increase in urban populace, but a meager 5.8% increase in the rural populace. This would affect various national needs such as access to water supply, sanitation, urban sprawl and a strain on institutional framework among others, not just bringing a myriad set of challenges nationally.

Evolution of Rural India

Traditionally, agriculture played a vital role in India's economy. But this is slowly beginning to change. While the migration numbers in the earlier section underline a geographic shift of people, the activities and data from present rural India cast a different view of the village ecosystem of today's India. At Independence, agriculture contributed about 60% of our GDP, but it is barely 14% now[8]. Not just as an overall factor, Agriculture as a contributor to rural income has been declining steadily from about 43% in 2000 to about 27% (estimates) in 2012. This could be attributed to the higher growth in other sectors, but it depicts the evolution of rural India to other forms of livelihood.

At the same time, 75% of all factories in India between 1999 and 2009 came up in rural India, with manufacturing creating 70% of the jobs there. This is not surprising given that there is little physical space available in cities and most factories are set up in the outskirts of cities, which are classified as rural areas

As villages start urbanising, their consumption habits change as well. In a separate study, it was stated that the rural consumption basket of 2010 in India was surprisingly similar to the urban basket of 1994. The fastest growing consumption items are durables, education and services—hitherto considered 'urban' consumption categories[9]

[5] http://www.uddkar.gov.in/
[6] https://en.wikipedia.org/wiki/List_of_cities_in_India_by_population
[7] http://iihs.co.in/wp-content/uploads/2013/12/IUC-Book.pdf

[8] Credit Suisse, "India Market Strategy.
[9] Credit Suisse, "India Market Strategy"

Rise in Semi Urban

There is a clear differentiation of India into rural and urban made by the Census 2011, but little to no literature on what constitutes semi-urban India. The Reserve Bank of India attempts to categorise semi-urban as regions with population of 10,000 and above upto 1,00,000[10] which according to the Census of India is a town and therefore urban. The UN has semi-urban as part of what constitutes a City-Region. It defines a City-Region as an urban development on a massive scale: a major city that expands beyond administrative boundaries to "engulf small cities, towns and semi-urban and rural hinterlands, sometimes expanding sufficiently to merge with other cities, forming large conurbations that eventually become city-regions." [11] This area of coverage could extend to 200 km beyond city limits. There are semi-urban pockets in large cities, but these are more a social construct than a region separate and different from the city itself.

Independent data puts the total number of semi urban households at 153 million in 2009-10, up from 135 million in 2001-02[12]. Assuming an average household of 3 people per household, it takes on massive proportions of about 459 million people. Further assuming this is growing at the same rate of 1.25% as the current (2015) population growth rate of India and if we were to consider it as steady, it translates to 198 million semi-urban households by 2030 thereby amounting to a semi-urban population of about 594 million by 2030.

One can draw different conjectures on the distribution and size of this segment, but this is beyond the scope of this document. It is sufficient to note that this requires deep analysis and insight and that we need to catalyse and facilitate the linkages of ICT solutions with semi urban users too. It will have its own challenges in water and power utilization, environmental impacts, effective and productive labour management, social inclusion, education and healthcare among others, and consequently opportunities for relevant solutions. The emerging economic importance of semi-urban India as well as their demographic presence is to be reckoned with.

3. Technology aided Transformation

The foundations of ICT are tied to Internet availability and mobile telephony. There is a need to harness the innate capabilities of the poor and complement them with capacities (information, knowledge, skills, tools, finance and collectivization) to deal with the rapidly changing external world.

The National Optic Fiber Network (NOFN) an initiative under Bharat Broadband Networks Ltd. aims to provide 100 Mbps Broadband connectivity to 2,50,000 Gram Panchayats(GPs) in the country[13]. This would ensure broadband connectivity with adequate bandwidth necessary for all kinds of use. Together with mobile telephony that telecom service companies provide, rural India will have access to video, data and Internet services in areas such as education, business, entertainment, environment, health households, e-governance services along with a plethora of government schemes. With this there is a path for rural India to achieve increased access to their rights, entitlements and public services.

The number of telephone subscribers in India at the end of Aug 2015 was 1,014.70 million. Urban subscription was 591.52 million and rural subscription at 423.18 million with an overall Tele-density at 80.44. Of this wireless (mobile) subscriber base stood at 988.69 million Mobile users in urban areas was 570.33 million and in rural areas 418.36 million[14]. Wireless tele-density in urban and rural, the former was at 145.67 and the latter at 48.09 in the month of Aug-15.

Several studies have investigated the relationship between increase in Internet penetration and mobile telephony on economic growth. In 2005 study, the London Business School found that an extra ten mobile phones per 100 people in a typical developing country

[10] https://www.rbi.org.in/scripts/bs_viewcontent.aspx?Id=2035
[11] http://www.unicef.org/sowc2012/pdfs/SOWC-2012-DEFINITIONS.pdf
[12] http://www.slideshare.net/rcmindia/rcm-towns-beyondsemi-urban-india-pdf
[13] http://www.bbnl.nic.in/
[14] http://www.trai.gov.in/WriteReadData/PressRealease/Document/PR-TSD-Aug-14102015.pdf

added 0.6 percentage points of growth in GDP per person[15]. In another, Deloitte research cites a World Bank study that shows that in developing economies a 10% increase in broadband penetration increases per capita GDP growth by 1.3%.[16]

ICT benefits and advancements are not limited to agriculture. Access to a new breed of electronics, mobile and Internet based services extend the range of business services and livelihood opportunities to rural communities. The mobile phone and the connectivity it provides is slowly becoming a means of accessing information and controlling systems, not just as a tool for communication. New services and approaches as illustrated below are arising that place the mobile as a crucial element in rural development. It aids in services, and building assets and skills such that people in rural areas can avail new opportunities for their personal enhancement, income generation and employment.

4. New ICT services in rurban India

We explore 2 novel cases of how ICT has been used in Kangandlahalli village in KGF, Kolar district, Karnataka, around 100 Km from Bengaluru. In these cases, ICT is not about having a computer, or integration with the State Wide Area Network (SWAN) or e-Governance solutions. Computers help, but these solutions are more about having a mobile phone, connectivity and some electronics. These cases also illustrate that it is not just simple agricultural solutions like weather or commodity prices in nearest markets that are sought by rural India, but that the today's rural India has a certain technological maturity and seeks a truly evolved set of new services and solutions. Similarly, solutions are not dependent on language or literacy levels, they are agnostic to both. They are supplementary to their livelihood and are looked upon as new tools, mostly oblivious to the technological complexity underneath. Most require an Internet connection and these are solutions that its urban counterparts will identify with.

Case 1: Poultry

The first one is in a fairly sized poultry that houses around 6000 birds for fertilised egg collection. Unlike a regular poultry, here the focus in on the eggs that are sold to other poultries for rearing birds. There is currently a daily output of 4000 egg, with each egg being sold for between Rs. 12 to Rs. 14. Eggs are retrieved every day and sorted, graded, packed and transported directly to their customers.

Case 1: ICT expectations

The owners are exploring video surveillance (with rudimentary video analytics). This is being considered to prevent theft and misuse of the resources and facilities. There is a need to monitor temperature regularly which is done manually at periodic intervals presently. With the aid of local students, the owners are trialing a system to automate temperature and humidity, using sensors connected to a GSM device. This sends notifications over SMS and triggers alarms in the event of anomalies, further progressing to a feature that can activate a water spray remotely for bringing the temperature down using a missed call. Also under consideration is automating water spray and feed dispensing to reduce labour costs and also reduce manpower which is increasingly becoming a scarce resource.

To summarise these in ICT terms, they are: 1) Video Surveillance with Video Analytics, 2) Remote Asset Monitoring, 3) Remote Control of Systems or Remote Asset Management. 4) Robotics or Systems Automation and 5) Temperature and Humidity sensors.

Case 2: Milk Cooperative

With an annual output of 138 MT, India is the largest producer of milk in the world[17]. More farmers are seeking other means of livelihood cause of scarcity of water, economic benefits and leveraging innovative government programs. In this village, several have procured cows with loans and subsidies provided by the government. On average each cow produces about 15-20 liters/day. This is sold for a price of Rs.20/liter, in addition to which they receive Rs.4/liter as Govt. subsidy. Typically livestock owners with 5 cows make an

[15] http://www.economist.com/node/14483872

[16] http://www2.deloitte.com/content/dam/Deloitte/in/Documents/technology-media-telecommunications/in-tmt-broadband-noexp.pdf

[17] http://www.ibef.org/blogs/india-the-largest-milk-producer-in-the-world

avg. of Rs. 15000 to 20000 every 2 weeks which is the duration of payment. There are incidents like 'Foot & mouth disease' that have caused many cows to perish, but backed by robust insurance schemes by the state, most have received insurance amount of Rs. 40K/cow. These are sometimes misused.

Case 2: ICT expectations

Small farmers are encouraged to come to the milk cooperative to use the milking facilities there, while larger ones use their own hand operated or electro-mechanical (diesel or diesel + electric) milking machines. These are preferred over hand milking as it prevents infection caused by additives used for frictionless manual process. Past experiences with diseases have taught them the benefits of machines. These machines are in the range of Rs. 10000 to Rs. 65000 and diesel ones consume only 200ml of diesel in 1 hour while pumping milk at the rate of 12ltrs/3minutes.

At the milk cooperative there is an ordinary or electronic lactometer to measure the specific gravity of buffalo and cow milk to detect contaminants. There is also an electronic butyrometer used to measure the density of milk, or the fat content in milk. While it is not a practice now, there is growing consent among livestock owners to the milk cooperatives to offer a differential fat content linked price. In this manner, livestock owners who provide better care, good feed and practice sustainable methods benefit more. Livestock owners also prefer money transfer directly into their bank accounts to prevent middleman charges and to obtain it in time. Livestock owners also request their daily supply quantity to be sent their mobile phone.

At the co-operatives end, they are tied to government insurance schemes or private insurance and banks. These institutions choose to be updated of their customers credit history, loan repayment and premium payment as well as facilitate easier methods to undertake these.

To summarize these in ICT terms, they are: 1) Electro-mechanical Systems, 2) Density and other sensors, 3) Financial services and 5) Insurance Services

5. Perspectives and Conclusion

- The massive migration to urban centers should be stemmed as it could be fraught with catastrophic consequences.
- If left unchecked the urban and semi urban population in and around the 100 or more cities will be equal or roughly equal to the population of the rest of India
- Rural India is not agriculture based anymore. Non-farm based livelihoods are making its presence felt
- Access to a new breed of electronics, mobile and Internet based services extend the range of business services and livelihood opportunities. ICT needs are not limited to agriculture.
- Rural ICT is not about having a computer, or access to state sponsored e-Governance solutions. A mobile phone, phablet or tablet have replaced large chunky computers as means of information, communication and entertainment
- The integration of electronics with computing systems and their proliferation have significant benefits in Rural India
- Literacy or language is not a barrier to benefitting from integrated electronic and computing services.

6. Acknowledgements

I'd like to express my gratitude to Mayur Dave for giving me the opportunity to write this, Shilpi Batra from M2Mpaper for igniting my thoughts on Smart villages and then keeping me engaged in the Village ecosystem, Naveen Ram of Kangandlahalli for the work he has done in his village and showing us how villages have evolved, and to Aastha Sayal for proof reading this.

7. References

Document references

Kayser B. The rural renaissance. Sociology of campaigns in the western world. Armand Colin, Paris, 1990.

Credit Suisse, "India Market Strategy.

Website references:

All websites accessed between November 6, 2015 and November 12, 2015 are listed as footnotes in the respective pages of their use.

Sponsors

Proceedings for the Joint Conference of the 3rd Global Wireless Summit, The 5th International Conference On Wireless Communications, Vehicular Technology, Information Theory, Aerospace & Electronics Systems (WVITAE), The 3rd International Conference On Communications, Connectivity, Convergence, Content & Cooperation (IC5), and 18th Wireless Personal Multimedia Communications on December 13-16, 2015, Hyderabad, India